



# TMS 2009

138th Annual Meeting & Exhibition

**Linking Science and Technology  
for Global Solutions**

## Technical Program

Program-at-a-Glance .....	2
Session Listing .....	9
Sunday PM .....	14
Monday AM .....	37
Monday PM.....	82
Tuesday AM.....	129
Tuesday PM.....	175
Wednesday AM .....	226
Wednesday PM .....	274
Thursday AM.....	323
Posters.....	360
Index .....	381
Floor Plans.....	408

	Sunday	Monday	Tuesday	Wednesday	Thursday			
	PM	AM	AM	AM	AM			
2001	Light Metals Division: Poster Session		Aluminum Reduction Technology: Environment	Aluminum Reduction Technology: Potline Performances and Vision	General Abstracts: Light Metals Division: Session I	Aluminum Reduction Technology: Process Control	Aluminum Reduction Technology: Operational Improvements	Aluminum Reduction Technology: Potroom Operation and Maintenance
2001/2003		Challenges for Sustainable Growth in the Aluminum Industry - Through the Current Crisis and on to the Future: Aluminum Plenary Session						
2002			Alumina and Bauxite: Bayer Process Safety, Environmental and Sustainability Issues	Alumina and Bauxite: Bauxite Ore Handling and Benefication	Alumina and Bauxite: Process Improvements and Experiences - Red Side	Alumina and Bauxite: Methods - Bauxite Characterization, Bayer Chemistry, Alumina Quality	State of the NSF Metallic Materials and Nanostructures (MMN) Program: Session I  Alumina and Bauxite: Alumina Precipitation	Alumina and Bauxite: Process Improvements and Experiences - White Side
2003			Electrode Technology for Aluminum Production: Environmental Issues and Raw Materials	Electrode Technology for Aluminum Production: Special Session: Coke Quality Changes and Countermeasures	Electrode Technology for Aluminum Production: Jt Aluminum Reduction Technology and Electrode Technology Session: Coping with Changes in Coke Quality	Electrode Technology for Aluminum Production: Anode Production Operations - Focus on Baking	Electrode Technology for Aluminum Production: Electrode Connections and Cathode Studies	Electrode Technology for Aluminum Production: Electrode Technology - Cathodes and Inert Anodes
2004			Aluminum Alloys: Fabrication, Characterization and Applications: Development and Application	Aluminum Alloys: Fabrication, Characterization and Applications: Processing and Properties	Aluminum Alloys: Fabrication, Characterization and Applications: Formability and Texture	Aluminum Alloys: Fabrication, Characterization and Applications: Materials Characterization	Aluminum Alloys: Fabrication, Characterization and Applications: Modeling and Corrosion	Aluminum Alloys: Fabrication, Characterization and Applications: Composite and Foam
2005		General Abstracts: Extraction and Processing Division: Session I	Cast Shop for Aluminum Production: Engineering and Industrial Developments	Cast Shop for Aluminum Production: Environment, Health and Safety	Cast Shop for Aluminum Production: Characterization and Furnace Operation	Cast Shop for Aluminum Production: Molten Metal Cleanliness	Cast Shop for Aluminum Production: Casting Structure vs. Process	Cast Shop for Aluminum Production: Casting Technology
2006	Magnesium Technology 2009: Poster Session Magnesium and Its Alloys	Magnesium Technology 2009: Alloys I: Rare Earth (Gadolinium, Neodymium)	Magnesium Technology 2009: Casting	Magnesium Technology 2009: Alloys II: Calcium	Magnesium Technology 2009: Alloys III: Rare Earth (Cerium and Other)	Magnesium Technology 2009: Refining and Surface Treatment	Magnesium Technology 2009: Alloys IV: Yttrium and Tin	Magnesium Technology 2009: Modeling

# Program-at-a-Glance

Sunday	Monday	Tuesday	Wednesday	Thursday				
PM	AM	PM	AM	PM	AM			
	Magnesium Technology 2009: Magnesium Town Hall Meeting - A Decade of Modern Magnesium in China - AND - Fatigue and Tension/Compression Asymmetry	Magnesium Technology 2009: Primary Production	Magnesium Technology 2009: Applications, Testing and Forming	Magnesium Technology 2009: Deformation	Magnesium Technology 2009: Twin Roll Casting and Semi-Solid Processing	Magnesium Technology 2009: Wrought Alloys	2007	
Microstructural Processes in Irradiated Materials: Poster Session	Microstructural Processes in Irradiated Materials: Radiation Effects I: Segregation and Modeling	Microstructural Processes in Irradiated Materials: Radiation Effects II: Advanced Characterization and Fe-Cr Alloys	Microstructural Processes in Irradiated Materials: Advanced Oxide Dispersion Strengthened Ferritic Alloys	Microstructural Processes in Irradiated Materials: Radiation Effects III: He Effects on Microstructural Evolution and Deformation	Microstructural Processes in Irradiated Materials: Ceramics and Fuels	RPV Embrittlement and Fusion Materials: Measuring, Modeling and Managing Irradiation Effects: RPV Embrittlement: Technical Contributions of Professor G. Robert Odette	RPV Embrittlement and Fusion Materials: Measuring, Modeling and Managing Irradiation Effects: Fusion Reactor Materials: Technical Contributions of Professor G. Robert Odette	2008
	Peirce-Smith Converting Centennial Symposium: Historical Foundations/Refractory Practices	Peirce-Smith Converting Centennial Symposium: Operational Aspects	Peirce-Smith Converting Centennial Symposium: Injection Techniques, Modeling and Process Control	Peirce-Smith Converting Centennial Symposium: New Converting Technologies and Panel Discussion	Materials for the Nuclear Renaissance: New Materials and Past Limitations	Materials for the Nuclear Renaissance: Materials: Applications and Characterization	Materials for the Nuclear Renaissance: Materials: Manufacturing and Testing	2009
Near-Net Shape Titanium Components: Poster Session	General Abstracts: Structural Materials Division: Session I	Aluminum Cold Rolling and Strip Processing: Session I	Aluminum Hot Rolling: Session I	Near-Net Shape Titanium Components: Casting, Welding and Beam Processes	Near-Net Shape Titanium Components: Powder Metallurgy I	Near-Net Shape Titanium Components: Deformation and Machining Processes	Near-Net Shape Titanium Components: Powder Metallurgy II	2010
	Shape Casting: Third International Symposium: Properties	Shape Casting: Third International Symposium: Processes	Shape Casting: Third International Symposium: Characterization	Shape Casting: Third International Symposium: Novel Methods and Applications	Shape Casting: Third International Symposium: Modeling			2011

	Sunday	Monday	Tuesday	Wednesday	Thursday			
	PM	AM	AM	AM	AM			
2012		Energy Conservation in Metals Extraction and Materials Processing II: Extraction Processes/ Refractories/ Modeling and Analysis	Energy Conservation in Metals Extraction and Materials Processing II: Energy Conservation and Technology	CO <sub>2</sub> Reduction Metallurgy 2009: Mechanisms and Electrolysis	CO <sub>2</sub> Reduction Metallurgy 2009: Ferrous and Titanium Metallurgy	Aluminum Reduction Technology: New Pot Technology and Pot Start-Up	Aluminum Reduction Technology: Fundamentals	Aluminum Reduction Technology: Modelling
2014		Friction Stir Welding and Processing-V: Session I	Friction Stir Welding and Processing-V: Session II	Friction Stir Welding and Processing-V: Session III	Friction Stir Welding and Processing-V: Session IV	Friction Stir Welding and Processing-V: Session V	Friction Stir Welding and Processing-V: Session VI	
2016		Materials Processing Fundamentals: Solidification and Casting	Materials Processing Fundamentals: Process Modeling	Materials Processing Fundamentals: Deformation Processing	Materials Processing Fundamentals: Smelting and Refining	Materials Processing Fundamentals: Powders, Composites, Coatings and Measurements	Materials Processing Fundamentals: Aqueous and Liquid Processing	
2018		Frontiers in Solidification Science III: Fundamentals of Solidification: Interfaces, Nucleation, Growth, and Nonequilibrium Considerations	Frontiers in Solidification Science III: Dendritic Growth Phenomena	Frontiers in Solidification Science III: Coupled Multiphase Growth Morphologies	Frontiers in Solidification Science III: Prediction and Control of Solidification Behavior and Cast Microstructures	General Abstracts: Structural Materials Division: Session II	General Abstracts: Structural Materials Division: Session III	
2020	Pb-Free Solders and Emerging Interconnect and Packaging Technologies: Poster Session	Pb-Free Solders and Emerging Interconnect and Packaging Technologies: Fundamental Properties, Interfacial Reactions and Phase Transformation	Pb-Free Solders and Emerging Interconnect and Packaging Technologies: Electromigration Reliability	Pb-Free Solders and Emerging Interconnect and Packaging Technologies: Effects of Surface Finishes and Advances in Interconnects	Pb-Free Solders and Emerging Interconnect and Packaging Technologies: Electromigration, Microstructure, and Mechanical Properties	Pb-Free Solders and Emerging Interconnect and Packaging Technologies: Reliability and Microstructure Development	Pb-Free Solders and Emerging Interconnect and Packaging Technologies: Microstructure, Modeling and Test Methods	Pb-Free Solders and Emerging Interconnect and Packaging Technologies: Tin Whisker Formation and Mechanical Properties
2022		Phase Stability, Phase Transformations, and Reactive Phase Formation in Electronic Materials VIII: Session I	Phase Stability, Phase Transformations, and Reactive Phase Formation in Electronic Materials VIII: Session II	Phase Stability, Phase Transformations, and Reactive Phase Formation in Electronic Materials VIII: Session III	Phase Stability, Phase Transformations, and Reactive Phase Formation in Electronic Materials VIII: Session IV	Phase Stability, Phase Transformations, and Reactive Phase Formation in Electronic Materials VIII: Session V	General Abstracts: Electronic, Magnetic and Photonic Materials Division: Session I	General Abstracts: Electronic, Magnetic and Photonic Materials Division: Session II
2024		Recycling of Electronic Wastes: Life Circle Analysis and Environmental Issues	Recycling of Electronic Wastes: Mechanical Recycling and Pyrometallurgical Recycling	Recycling of Electronic Wastes: Hydrometallurgical Recycling	Recycling of Electronic Wastes: General Recycling	Recycling--General Session: Session I: Metals	Recycling--General Session: Session II: Waste Utilization	Recycling--General Session: Session III: Aqueous Processing

# Program-at-a-Glance

Sunday	Monday		Tuesday		Wednesday		Thursday
PM	AM	PM	AM	PM	AM	PM	AM
	Structural Materials Division Symposium: Advanced Characterization and Modeling of Phase Transformations in Metals in Honor of David N. Seidman on his 70th Birthday: Driven Alloy Systems	Structural Materials Division Symposium: Advanced Characterization and Modeling of Phase Transformations in Metals in Honor of David N. Seidman on his 70th Birthday: Thermodynamics of Phase Transformations	Structural Materials Division Symposium: Advanced Characterization and Modeling of Phase Transformations in Metals in Honor of David N. Seidman on his 70th Birthday: Structure Property Relationships	Structural Materials Division Symposium: Advanced Characterization and Modeling of Phase Transformations in Metals in Honor of David N. Seidman on his 70th Birthday: Kinetics of Phase Transformations I	Structural Materials Division Symposium: Advanced Characterization and Modeling of Phase Transformations in Metals in Honor of David N. Seidman on his 70th Birthday: Kinetics of Phase Transformations II	Applicable Computing Technologies in Heat Treating: Numerical Modeling and Simulation for Heat Treatment	Open Source Tools for Materials Research and Engineering: Session I
	Transformations under Extreme Conditions: A New Frontier in Materials: Keynote: Melting and Solidification I	Transformations under Extreme Conditions: A New Frontier in Materials: Melting and Solidification II	Transformations under Extreme Conditions: A New Frontier in Materials: High Rate Deformation	Transformations under Extreme Conditions: A New Frontier in Materials: Extreme Deformation and Damage	Transformations under Extreme Conditions: A New Frontier in Materials: Solid-Solid Transformations and In Situ Diagnostics I	Transformations under Extreme Conditions: A New Frontier in Materials: Pressure/Stress-Induced Transformations and In Situ Diagnostics II	Transformations under Extreme Conditions: A New Frontier in Materials: Driven Reactions
	Computational Thermodynamics and Kinetics: Energy Materials	Computational Thermodynamics and Kinetics: Thin Films	Computational Thermodynamics and Kinetics: Functional Materials	Computational Thermodynamics and Kinetics: Defects	Computational Thermodynamics and Kinetics: Integrated Thermodynamic and Kinetic Modeling	Computational Thermodynamics and Kinetics: Thermodynamics	Computational Thermodynamics and Kinetics: Grain Growth and Recrystallization
Synergies of Computational and Experimental Materials Science: Poster Session	Synergies of Computational and Experimental Materials Science: Three-Dimensional Materials Science I	Synergies of Computational and Experimental Materials Science: Three-Dimensional Materials Science II	Synergies of Computational and Experimental Materials Science: Three-Dimensional Materials Science III	Synergies of Computational and Experimental Materials Science: Synergies in Nanoscience	Synergies of Computational and Experimental Materials Science: Synergies in Integrated Computational Materials Engineering	Computational Materials Research and Education Luncheon Roundtable: FiPy  Progress in Computational Materials Science and Engineering Education: Session I	Progress in Computational Materials Science and Engineering Education: Session II  Computational Materials Research and Education Luncheon Roundtable: Gibbs: A Multi-Component Thermodynamics Calculation and Visualization Suite
	Materials Issues in Additive Powder-Based Manufacturing Processes: Additive Manufacturing Applications	Materials Issues in Additive Powder-Based Manufacturing Processes: Additive Manufacturing Metals I	Materials Issues in Additive Powder-Based Manufacturing Processes: Additive Manufacturing Metals II	Materials Issues in Additive Powder-Based Manufacturing Processes: Coatings and Deposition	Solar Cell Silicon: Production and Recycling: Session I	Solar Cell Silicon: Production and Recycling: Session II	

3000

3001

3002

3003

3004

	Sunday	Monday	Tuesday	Wednesday	Thursday			
	PM	AM	AM	AM	AM			
3005		Global Innovations in Photovoltaics and Thermoelectrics: Session I	Global Innovations in Materials and Technologies for Energy Harvesting: Plenary Session	Materials in Clean Power Systems IV: Clean Coal-, Hydrogen Based-Technologies, and Fuel Cells: High Temperature Materials for Power Generation	Materials in Clean Power Systems IV: Clean Coal-, Hydrogen Based-Technologies, and Fuel Cells: Materials for Hydrogen Production and Transport - AND - Advanced Materials for PEM Fuel Cells and Batteries Session I	Materials in Clean Power Systems IV: Clean Coal-, Hydrogen Based-Technologies, and Fuel Cells: Advanced Materials for PEM Fuel Cells and Batteries Session II - AND - Solid Oxide Fuel Cell Materials, Session I: Membranes, Electrodes, and Seals	Materials in Clean Power Systems IV: Clean Coal-, Hydrogen Based-Technologies, and Fuel Cells: Solid Oxide Fuel Cell Materials, Session II: Interconnects	
3006		Manufacturing Issues in Fuel Cells: Session I	Manufacturing Issues in Fuel Cells: Session II	Diffusion in Materials for Energy Technologies: Session I	Diffusion in Materials for Energy Technologies: Session II	Diffusion in Materials for Energy Technologies: Session III	Diffusion in Materials for Energy Technologies: Session IV	
3007		Bulk Metallic Glasses VI: Alloy Development and Glass Forming Ability I	Bulk Metallic Glasses VI: Alloy Development and Glass Forming Ability II	Bulk Metallic Glasses VI: Structures and Mechanical Properties I	Bulk Metallic Glasses VI: Structures and Mechanical Properties II	Bulk Metallic Glasses VI: Fatigue and Other Properties	Bulk Metallic Glasses VI: Structures and Mechanical Properties III	
3008		Fatigue: Mechanisms, Theory, Experiments and Industry Practice: Characterization Methods for Elucidating Fatigue Mechanisms	Fatigue: Mechanisms, Theory, Experiments and Industry Practice: Theory and Simulation	Fatigue: Mechanisms, Theory, Experiments and Industry Practice: The Role of Microstructure in Fatigue	Fatigue: Mechanisms, Theory, Experiments and Industry Practice: Fatigue in Engineering Components	Fatigue: Mechanisms, Theory, Experiments and Industry Practice: Experimental Studies of Initiation and Growth in Structural Materials	General Abstracts: Materials Processing and Manufacturing Division: Session IV	
3009	Characterization of Minerals, Metals and Materials: Poster Session	Characterization of Minerals, Metals and Materials: Emerging Characterization Techniques	Characterization of Minerals, Metals and Materials: Characterization of Processing	Characterization of Minerals, Metals and Materials: Characterization of Microstructure of Properties of Materials I	Characterization of Minerals, Metals and Materials: Characterization of Microstructure of Properties of Materials II	Characterization of Minerals, Metals and Materials: Characterization of Microstructure of Properties of Materials III	Characterization of Minerals, Metals and Materials: Characterization of Microstructure of Properties of Materials IV	Characterization of Minerals, Metals and Materials: Characterization of Microstructure of Properties of Materials V



# Program-at-a-Glance

Sunday	Monday		Tuesday		Wednesday		Thursday
PM	AM	PM	AM	PM	AM	PM	AM
Materials for High Temperature Applications: Next Generation Superalloys and Beyond: Poster Session	Materials for High Temperature Applications: Next Generation Superalloys and Beyond: Future Application Requirements and Next Generation Superalloys	Materials for High Temperature Applications: Next Generation Superalloys and Beyond: Next Generation Superalloys	Materials for High Temperature Applications: Next Generation Superalloys and Beyond: Refractory Alloys I	Materials for High Temperature Applications: Next Generation Superalloys and Beyond: Refractory Alloys II	Materials for High Temperature Applications: Next Generation Superalloys and Beyond: Advanced Coatings I	Materials for High Temperature Applications: Next Generation Superalloys and Beyond: Advanced Coatings II and Intermetallics  National Academies Propulsion Materials Study Community Town Hall Meeting	Materials for High Temperature Applications: Next Generation Superalloys and Beyond: Ceramic Composites and Other Technologies
	Recent Advances in Thin Films: Process-Property Correlations	Recent Advances in Thin Films: Applications	Recent Advances in Thin Films: Metal Films and Integration Schemes	Surface Structures at Multiple Length Scales: Surface Properties in Various Length Scales	Surface Structures at Multiple Length Scales: Bio Coatings and Nanoscale Characterization	Surface Structures at Multiple Length Scales: Processing of Novel Surfaces	Surface Structures at Multiple Length Scales: Surface Deposition and Properties
	Emerging Applications of Neutron Scattering in Materials Science and Engineering: Neutron Diffraction and Structure Determination	Emerging Applications of Neutron Scattering in Materials Science and Engineering: Residual Stress Mapping and Neutron Imaging	Emerging Applications of Neutron Scattering in Materials Science and Engineering: Microstructure Control	Emerging Applications of Neutron Scattering in Materials Science and Engineering: Phase Transformation	Emerging Applications of Neutron Scattering in Materials Science and Engineering: Deformation Behaviors	Bulk Metallic Glasses VI: Mechanical Behavior of Nano and Amorphous Materials	
Biological Materials Science: Poster Session	Biological Materials Science: Implant Biomaterials I	Biological Materials Science: Biomimetic Processing	Biological Materials Science: Drug Delivery and Imaging	Biological Materials Science: Biological Materials I	Biological Materials Science: Cell-Biomaterial Interactions	Biological Materials Science: Implant Biomaterials II Scaffolds	Biological Materials Science: Biological Materials II - and - Implant Biomaterials III
	Neutron and X-Ray Studies of Advanced Materials: Resolving Local Structure	Neutron and X-Ray Studies of Advanced Materials: Diffuse Scattering	Neutron and X-Ray Studies of Advanced Materials: Small Scale and Thin Film Studies	Neutron and X-Ray Studies of Advanced Materials: Advances in Line Profile	Neutron and X-Ray Studies of Advanced Materials: Phase Transition	Neutron and X-Ray Studies of Advanced Materials: Advanced Imaging and Bio-Inspired Studies	Neutron and X-Ray Studies of Advanced Materials: Neutron Diffraction and Modeling of Materials Behavior
2009 Functional and Structural Nanomaterials: Fabrication, Properties, and Applications: Poster Session	2009 Functional and Structural Nanomaterials: Fabrication, Properties, and Applications: Low Dimensional Nanostructures I	2009 Functional and Structural Nanomaterials: Fabrication, Properties, and Applications: Low Dimensional Nanostructures II	2009 Functional and Structural Nanomaterials: Fabrication, Properties, and Applications: Nanoscale Oxides: Synthesis and Applications	2009 Functional and Structural Nanomaterials: Fabrication, Properties, and Applications: Nanoscale Fabrication and Devices: Concepts, Approaches and Scale-Up	2009 Functional and Structural Nanomaterials: Fabrication, Properties, and Applications: Bulk Nanocrystalline Materials	2009 Functional and Structural Nanomaterials: Fabrication, Properties, and Applications: Nanoscale Phenomena: Mechanics, Phase Stability and Properties	2009 Functional and Structural Nanomaterials: Fabrication, Properties, and Applications: Nanoscale Powders: Materials, Synthesis and Applications

3010

3011

3012

3014

3016

3018

		Sunday	Monday	Tuesday	Wednesday	Thursday			
		PM	AM	AM	AM	AM			
3020			Nanocomposite Materials: Nanoparticle Synthesis	Nanocomposite Materials: Polymer Nanocomposites	Nanocomposite Materials: Characterization and Modeling of Nanocomposites I	Nanocomposite Materials: Metallic Nanocomposites	Nanocomposite Materials: Characterization and Modeling of Nanocomposites II	Nanocomposite Materials: Nanocomposites for Energy Conversion and Storage	Nanocomposite Materials: Nanocomposite Processing
	3022		Dislocations: 75 Years of Deformation Mechanisms: Dislocation Structures and Effects of Material Microstructure	Dislocations: 75 Years of Deformation Mechanisms: Dislocation Ensembles and Structures	Dislocations: 75 Years of Deformation Mechanisms: Effects of Obstacles, Surfaces, and Scale on Dislocation Generation and Motion	Dislocations: 75 Years of Deformation Mechanisms: Nanostructured and Temperature Effects on Dislocations	General Abstracts: Materials Processing and Manufacturing Division: Session I	General Abstracts: Materials Processing and Manufacturing Division: Session II	General Abstracts: Materials Processing and Manufacturing Division: Session III
3024		Mechanical Behavior of Nanostructured Materials: Poster Session	Mechanical Behavior of Nanostructured Materials: Stability of Nanostructures	Mechanical Behavior of Nanostructured Materials: Nanostructures by Severe Plastic Deformation	Mechanical Behavior of Nanostructured Materials: Plasticity and Deformation Mechanisms at Small Length Scale I	Mechanical Behavior of Nanostructured Materials: Strengthening Mechanisms at Small Length Scale	Mechanical Behavior of Nanostructured Materials: Plasticity and Deformation Mechanisms at Small Length Scale II	Mechanical Behavior of Nanostructured Materials: Plasticity and Deformation Mechanisms at Small Length Scale III	
	Exhibit Hall					Peirce-Smith Converting Centennial Symposium: Short Course on Injection Phenomena in the Peirce-Smith Converter			
	2nd/3rd Floor Foyers				General Poster Session				



# Session Listing

2009 Functional and Structural Nanomaterials: Fabrication, Properties, and Applications: Bulk Nanocrystalline Materials .....	Wed AM .....	3018.....	226
2009 Functional and Structural Nanomaterials: Fabrication, Properties, and Applications: Low Dimensional Nanostructures I .....	Mon AM .....	3018.....	37
2009 Functional and Structural Nanomaterials: Fabrication, Properties, and Applications: Low Dimensional Nanostructures II .....	Mon PM .....	3018.....	82
2009 Functional and Structural Nanomaterials: Fabrication, Properties, and Applications: Nanoscale Fabrication and Devices: Concepts, Approaches and Scale-Up.....	Tues PM .....	3018.....	175
2009 Functional and Structural Nanomaterials: Fabrication, Properties, and Applications: Nanoscale Oxides: Synthesis and Applications .....	Tues AM .....	3018.....	129
2009 Functional and Structural Nanomaterials: Fabrication, Properties, and Applications: Nanoscale Phenomena: Mechanics, Phase Stability and Properties .....	Wed PM.....	3018.....	274
2009 Functional and Structural Nanomaterials: Fabrication, Properties, and Applications: Nanoscale Powders: Materials, Synthesis and Applications.....	Thurs AM .....	3018.....	323
2009 Functional and Structural Nanomaterials: Fabrication, Properties, and Applications: Poster Session.....	Sun PM.....	3018.....	14
Alumina and Bauxite: Alumina Precipitation .....	Wed PM.....	2002.....	276
Alumina and Bauxite: Bauxite Ore Handling and Benefication .....	Tues AM .....	2002.....	130
Alumina and Bauxite: Bayer Process Safety, Environmental and Sustainability Issues .....	Mon PM .....	2002.....	83
Alumina and Bauxite: Methods - Bauxite Characterization, Bayer Chemistry, Alumina Quality .....	Wed AM .....	2002.....	227
Alumina and Bauxite: Process Improvements and Experiences - Red Side .....	Tues PM .....	2002.....	176
Alumina and Bauxite: Process Improvements and Experiences - White Side .....	Thurs AM .....	2002.....	324
Aluminum Alloys: Fabrication, Characterization and Applications: Composite and Foam .....	Thurs AM .....	2004.....	325
Aluminum Alloys: Fabrication, Characterization and Applications: Development and Application.....	Mon PM .....	2004.....	84
Aluminum Alloys: Fabrication, Characterization and Applications: Formability and Texture .....	Tues PM .....	2004.....	177
Aluminum Alloys: Fabrication, Characterization and Applications: Materials Characterization .....	Wed AM .....	2004.....	228
Aluminum Alloys: Fabrication, Characterization and Applications: Modeling and Corrosion.....	Wed PM .....	2004.....	277
Aluminum Alloys: Fabrication, Characterization and Applications: Processing and Properties.....	Tues AM .....	2004.....	131
Aluminum Cold Rolling and Strip Processing: Session I.....	Mon PM .....	2010.....	85
Aluminum Hot Rolling: Session I.....	Tues AM .....	2010.....	132
Aluminum Reduction Technology: Environment .....	Mon PM .....	2001.....	86
Aluminum Reduction Technology: Fundamentals .....	Wed PM.....	2012.....	278
Aluminum Reduction Technology: Joint Aluminum Reduction Technology and Electrode Technology Session: Coping with Changes in Coke Quality.....	Tues PM .....	2003.....	190
Aluminum Reduction Technology: Modelling .....	Thurs AM .....	2012.....	326
Aluminum Reduction Technology: New Pot Technology and Pot Start-Up .....	Wed AM .....	2012.....	229
Aluminum Reduction Technology: Operational Improvements .....	Wed PM.....	2001.....	279
Aluminum Reduction Technology: Poster Session.....	Sun PM.....	2001.....	16
Aluminum Reduction Technology: Potline Performances and Vision .....	Tues AM .....	2001.....	134
Aluminum Reduction Technology: Potroom Operation and Maintenance.....	Thurs AM .....	2001.....	327
Aluminum Reduction Technology: Process Control .....	Wed AM .....	2001.....	230
Applicable Computing Technologies in Heat Treating: Numerical Modeling and Simulation for Heat Treatment .....	Wed PM.....	3000.....	280
Biological Materials Science: Biological Materials I.....	Tues PM .....	3014.....	179
Biological Materials Science: Biological Materials II - and - Implant Biomaterials III .....	Thurs AM .....	3014.....	328
Biological Materials Science: Biological Materials Science Poster Session.....	Sun PM.....	3014.....	16
Biological Materials Science: Biomimetic Processing .....	Mon PM .....	3014.....	87
Biological Materials Science: Cell-Biomaterial Interactions .....	Wed AM .....	3014.....	231
Biological Materials Science: Drug Delivery and Imaging.....	Tues AM .....	3014.....	134
Biological Materials Science: Implant Biomaterials I.....	Mon AM .....	3014.....	38
Biological Materials Science: Implant Biomaterials II - Scaffolds .....	Wed PM.....	3014.....	282
Bulk Metallic Glasses VI: Alloy Development and Glass Forming Ability I.....	Mon AM .....	3007.....	39
Bulk Metallic Glasses VI: Alloy Development and Glass Forming Ability II .....	Mon PM .....	3007.....	88
Bulk Metallic Glasses VI: Fatigue and Other Properties.....	Wed AM .....	3007.....	232
Bulk Metallic Glasses VI: Joint Session of Mechanical Behavior of Nanostructured Materials and Bulk Metallic Glasses VI: Mechanical Behavior of Nano and Amorphous Materials .....	Wed PM.....	3012.....	283
Bulk Metallic Glasses VI: Structures and Mechanical Properties I.....	Tues AM .....	3007.....	135
Bulk Metallic Glasses VI: Structures and Mechanical Properties II .....	Tues PM .....	3007.....	180
Bulk Metallic Glasses VI: Structures and Mechanical Properties III .....	Thurs AM .....	3007.....	329
Bulk Metallic Glasses VI: Structures and Modeling .....	Wed PM .....	3007.....	284
Cast Shop for Aluminum Production: Casting Structure vs. Process .....	Wed PM.....	2005.....	286
Cast Shop for Aluminum Production: Casting Technology .....	Thurs AM .....	2005.....	331
Cast Shop for Aluminum Production: Characterization and Furnace Operation.....	Tues PM .....	2005.....	182
Cast Shop for Aluminum Production: Engineering and Industrial Developments .....	Mon PM .....	2005.....	89
Cast Shop for Aluminum Production: Environment, Health and Safety .....	Tues AM .....	2005.....	137
Cast Shop for Aluminum Production: Molten Metal Cleanliness .....	Wed AM .....	2005.....	234
Challenges for Sustainable Growth in the Aluminum Industry: Aluminum Plenary Session .....	Mon AM .....	2001/2003 .....	41
Characterization of Minerals, Metals and Materials: Characterization of Microstructure of Properties of Materials I .....	Tues AM .....	3009.....	138
Characterization of Minerals, Metals and Materials: Characterization of Microstructure of Properties of Materials II .....	Tues PM .....	3009.....	183

Characterization of Minerals, Metals and Materials: Characterization of Microstructure of Properties of Materials III.....	Wed AM	3009	235
Characterization of Minerals, Metals and Materials: Characterization of Microstructure of Properties of Materials IV.....	Wed PM	3009	287
Characterization of Minerals, Metals and Materials: Characterization of Microstructure of Properties of Materials V.....	Thurs AM	3009	332
Characterization of Minerals, Metals and Materials: Characterization of Processing.....	Mon PM	3009	91
Characterization of Minerals, Metals and Materials: Emerging Characterization Techniques.....	Mon AM	3009	41
Characterization of Minerals, Metals and Materials: Poster Session.....	Sun PM	3009	18
CO <sub>2</sub> Reduction Metallurgy 2009: Ferrous and Titanium Metallurgy.....	Tues PM	2012	185
CO <sub>2</sub> Reduction Metallurgy 2009: Mechanisms and Electrolysis.....	Tues AM	2012	140
Computational Materials Research and Education Luncheon Roundtable: FiPy.....	Wed PM	3003	315
Computational Materials Research and Education Luncheon Roundtable: Gibbs: A Multi-Component Thermodynamics Calculation and Visualization Suite.....	Wed PM	3003	354
Computational Thermodynamics and Kinetics: Defects.....	Tues PM	3002	186
Computational Thermodynamics and Kinetics: Energy Materials.....	Mon AM	3002	43
Computational Thermodynamics and Kinetics: Functional Materials.....	Tues AM	3002	141
Computational Thermodynamics and Kinetics: Grain Growth and Recrystallization.....	Thurs AM	3002	334
Computational Thermodynamics and Kinetics: Integrated Thermodynamic and Kinetic Modeling.....	Wed AM	3002	237
Computational Thermodynamics and Kinetics: Thermodynamics.....	Wed PM	3002	289
Computational Thermodynamics and Kinetics: Thin Films.....	Mon PM	3002	92
Diffusion in Materials for Energy Technologies: Session I.....	Tues AM	3006	142
Diffusion in Materials for Energy Technologies: Session II.....	Tues PM	3006	188
Diffusion in Materials for Energy Technologies: Session III.....	Wed AM	3006	239
Diffusion in Materials for Energy Technologies: Session IV.....	Wed PM	3006	290
Dislocations: 75 Years of Deformation Mechanisms: Dislocation Ensembles and Structures.....	Mon PM	3022	94
Dislocations: 75 Years of Deformation Mechanisms: Dislocation Structures and Effects of Material Microstructure.....	Mon AM	3022	44
Dislocations: 75 Years of Deformation Mechanisms: Effects of Obstacles, Surfaces, and Scale on Dislocation Generation and Motion.....	Tues AM	3022	143
Dislocations: 75 Years of Deformation Mechanisms: Nanostructured and Temperature Effects on Dislocations.....	Tues PM	3022	189
Electrode Technology for Aluminum Production: Anode Production Operations - Focus on Baking.....	Wed AM	2003	240
Electrode Technology for Aluminum Production: Electrode Connections and Cathode Studies.....	Wed PM	2003	292
Electrode Technology for Aluminum Production: Electrode Technology - Cathodes and Inert Anodes.....	Thurs AM	2003	335
Electrode Technology for Aluminum Production: Environmental Issues and Raw Materials.....	Mon PM	2003	95
Electrode Technology for Aluminum Production: Joint Aluminum Reduction Technology and Electrode Technology Session: Coping with Changes in Coke Quality.....	Tues PM	2003	190
Electrode Technology for Aluminum Production: Poster Session.....	Sun PM	2001	20
Electrode Technology for Aluminum Production: Special Session: Coke Quality Changes and Countermeasures.....	Tues AM	2003	145
Emerging Applications of Neutron Scattering in Materials Science and Engineering: Deformation Behaviors.....	Wed AM	3012	241
Emerging Applications of Neutron Scattering in Materials Science and Engineering: Microstructure Control.....	Tues AM	3012	146
Emerging Applications of Neutron Scattering in Materials Science and Engineering: Neutron Diffraction and Structure Determination.....	Mon AM	3012	46
Emerging Applications of Neutron Scattering in Materials Science and Engineering: Phase Transformation.....	Tues PM	3012	191
Emerging Applications of Neutron Scattering in Materials Science and Engineering: Residual Stress Mapping and Neutron Imaging.....	Mon PM	3012	96
Energy Conservation in Metals Extraction and Materials Processing II: Energy Conservation and Technology.....	Mon PM	2012	97
Energy Conservation in Metals Extraction and Materials Processing II: Extraction Processes/Refractories/Modeling and Analysis.....	Mon AM	2012	47
Fatigue: Mechanisms, Theory, Experiments and Industry Practice: Characterization Methods for Elucidating Fatigue Mechanisms.....	Mon AM	3008	48
Fatigue: Mechanisms, Theory, Experiments and Industry Practice: Experimental Studies of Initiation and Growth in Structural Materials.....	Wed AM	3008	242
Fatigue: Mechanisms, Theory, Experiments and Industry Practice: Fatigue at High-Temperature and in Harsh Environments.....	Wed PM	3008	293
Fatigue: Mechanisms, Theory, Experiments and Industry Practice: Fatigue in Engineering Components.....	Tues PM	3008	192
Fatigue: Mechanisms, Theory, Experiments and Industry Practice: The Role of Microstructure in Fatigue.....	Tues AM	3008	147
Fatigue: Mechanisms, Theory, Experiments and Industry Practice: Theory and Simulation.....	Mon PM	3008	99
Friction Stir Welding and Processing-V: Session I.....	Mon AM	2014	49
Friction Stir Welding and Processing-V: Session II.....	Mon PM	2014	100
Friction Stir Welding and Processing-V: Session III.....	Tues AM	2014	148
Friction Stir Welding and Processing-V: Session IV.....	Tues PM	2014	194
Friction Stir Welding and Processing-V: Session V.....	Wed AM	2014	243
Friction Stir Welding and Processing-V: Session VI.....	Wed PM	2014	294
Frontiers in Solidification Science III: Coupled Multiphase Growth Morphologies.....	Tues AM	2018	149
Frontiers in Solidification Science III: Dendritic Growth Phenomena.....	Mon PM	2018	101
Frontiers in Solidification Science III: Fundamentals of Solidification: Interfaces, Nucleation, Growth, and Nonequilibrium Considerations.....	Mon AM	2018	51

Frontiers in Solidification Science III: Prediction and Control of Solidification Behavior and Cast Microstructures.....	Tues PM.....	2018.....	195
General Abstracts: Electronic, Magnetic and Photonic Materials Division: Session I.....	Wed PM.....	2022.....	296
General Abstracts: Electronic, Magnetic and Photonic Materials Division: Session II.....	Thurs AM.....	2022.....	336
General Abstracts: Extraction and Processing Division: Session I.....	Mon AM.....	2005.....	53
General Abstracts: Light Metals Division: Session I.....	Tues PM.....	2001.....	197
General Abstracts: Materials Processing and Manufacturing Division: Session I.....	Wed AM.....	3022.....	245
General Abstracts: Materials Processing and Manufacturing Division: Session II.....	Wed PM.....	3022.....	297
General Abstracts: Materials Processing and Manufacturing Division: Session III.....	Thurs AM.....	3022.....	337
General Abstracts: Materials Processing and Manufacturing Division: Session IV.....	Thurs AM.....	3008.....	339
General Abstracts: Structural Materials Division: Session I.....	Mon AM.....	2010.....	54
General Abstracts: Structural Materials Division: Session II.....	Wed AM.....	2018.....	246
General Abstracts: Structural Materials Division: Session III.....	Wed PM.....	2018.....	298
General Poster Session.....	Mon AM-Wed PM.....	Foyer.....	360
Global Innovations in Materials and Technologies for Energy Harvesting: Plenary Session.....	Mon PM.....	3005.....	103
Global Innovations in Photovoltaics and Thermoelectrics: Session I.....	Mon AM.....	3005.....	55
Magnesium Technology 2009: Alloys I: Rare Earth (Gadolinium, Neodymium).....	Mon AM.....	2006.....	57
Magnesium Technology 2009: Alloys II: Calcium.....	Tues AM.....	2006.....	150
Magnesium Technology 2009: Alloys III: Rare Earth (Cerium and Other).....	Tues PM.....	2006.....	198
Magnesium Technology 2009: Alloys IV: Yttrium and Tin.....	Wed PM.....	2006.....	300
Magnesium Technology 2009: Applications, Testing and Forming.....	Tues AM.....	2007.....	151
Magnesium Technology 2009: Casting.....	Mon PM.....	2006.....	104
Magnesium Technology 2009: Deformation.....	Tues PM.....	2007.....	200
Magnesium Technology 2009: Fatigue and Tension/Compression Asymmetry.....	Mon AM.....	2007.....	58
Magnesium Technology 2009: Magnesium Town Hall Meeting - A Decade of Modern Magnesium in China.....	Mon AM.....	2007.....	57
Magnesium Technology 2009: Modeling.....	Thurs AM.....	2006.....	340
Magnesium Technology 2009: Poster Session - Magnesium and Its Alloys.....	Sun PM.....	2006.....	20
Magnesium Technology 2009: Primary Production.....	Mon PM.....	2007.....	105
Magnesium Technology 2009: Refining and Surface Treatment.....	Wed AM.....	2006.....	248
Magnesium Technology 2009: Twin Roll Casting and Semi-Solid Processing.....	Wed AM.....	2007.....	249
Magnesium Technology 2009: Wrought Alloys.....	Wed PM.....	2007.....	301
Manufacturing Issues in Fuel Cells: Session I.....	Mon AM.....	3006.....	59
Manufacturing Issues in Fuel Cells: Session II.....	Mon PM.....	3006.....	106
Materials for High Temperature Applications: Next Generation Superalloys and Beyond: Advanced Coatings I.....	Wed AM.....	3010.....	250
Materials for High Temperature Applications: Next Generation Superalloys and Beyond: Advanced Coatings II and Intermetallics.....	Wed PM.....	3010.....	302
Materials for High Temperature Applications: Next Generation Superalloys and Beyond: Ceramic Composites and Other Technologies.....	Thurs AM.....	3010.....	342
Materials for High Temperature Applications: Next Generation Superalloys and Beyond: Future Application Requirements and Next Generation Superalloys.....	Mon AM.....	3010.....	60
Materials for High Temperature Applications: Next Generation Superalloys and Beyond: Next Generation Superalloys.....	Mon PM.....	3010.....	107
Materials for High Temperature Applications: Next Generation Superalloys and Beyond: Poster Session.....	Sun PM.....	3010.....	22
Materials for High Temperature Applications: Next Generation Superalloys and Beyond: Refractory Alloys I.....	Tues AM.....	3010.....	153
Materials for High Temperature Applications: Next Generation Superalloys and Beyond: Refractory Alloys II.....	Tues PM.....	3010.....	201
Materials for the Nuclear Renaissance: Materials: Applications and Characterization.....	Wed PM.....	2009.....	304
Materials for the Nuclear Renaissance: Materials: Manufacturing and Testing.....	Thurs AM.....	2009.....	343
Materials for the Nuclear Renaissance: New Materials and Past Limitations.....	Wed AM.....	2009.....	251
Materials in Clean Power Systems IV: Clean Coal-, Hydrogen Based-Technologies, and Fuel Cells: Advanced Materials for PEM Fuel Cells and Batteries - Session I.....	Wed AM.....	3005.....	252
Materials in Clean Power Systems IV: Clean Coal-, Hydrogen Based-Technologies, and Fuel Cells: Advanced Materials for PEM Fuel Cells and Batteries - Session II.....	Wed PM.....	3005.....	305
Materials in Clean Power Systems IV: Clean Coal-, Hydrogen Based-Technologies, and Fuel Cells: High Temperature Materials for Power Generation.....	Tues AM.....	3005.....	154
Materials in Clean Power Systems IV: Clean Coal-, Hydrogen Based-Technologies, and Fuel Cells: Hydrogen Storage Materials.....	Tues PM.....	3005.....	203
Materials in Clean Power Systems IV: Clean Coal-, Hydrogen Based-Technologies, and Fuel Cells: Materials for Hydrogen Production and Transport.....	Wed AM.....	3005.....	252
Materials in Clean Power Systems IV: Clean Coal-, Hydrogen Based-Technologies, and Fuel Cells: Solid Oxide Fuel Cell Materials, Session I: Membranes, Electrodes, and Seals.....	Wed PM.....	3005.....	306
Materials in Clean Power Systems IV: Clean Coal-, Hydrogen Based-Technologies, and Fuel Cells: Solid Oxide Fuel Cell Materials, Session II: Interconnects.....	Thurs AM.....	3005.....	344
Materials Issues in Additive Powder-Based Manufacturing Processes: Additive Manufacturing Applications.....	Mon AM.....	3004.....	61
Materials Issues in Additive Powder-Based Manufacturing Processes: Additive Manufacturing Metals I.....	Mon PM.....	3004.....	108
Materials Issues in Additive Powder-Based Manufacturing Processes: Additive Manufacturing Metals II.....	Tues AM.....	3004.....	155
Materials Issues in Additive Powder-Based Manufacturing Processes: Coatings and Deposition.....	Tues PM.....	3004.....	204
Materials Processing Fundamentals: Aqueous and Liquid Processing.....	Wed PM.....	2016.....	307
Materials Processing Fundamentals: Deformation Processing.....	Tues AM.....	2016.....	156
Materials Processing Fundamentals: Powders, Composites, Coatings and Measurements.....	Wed AM.....	2016.....	253



Materials Processing Fundamentals: Process Modeling.....	Mon PM	2016	109
Materials Processing Fundamentals: Smelting and Refining.....	Tues PM	2016	205
Materials Processing Fundamentals: Solidification and Casting.....	Mon AM	2016	62
Mechanical Behavior of Nanostructured Materials: Joint Session of Mechanical Behavior of Nanostructured Materials and Bulk Metallic Glasses VI: Mechanical Behavior of Nano and Amorphous Materials.....	Wed PM	3012	283
Mechanical Behavior of Nanostructured Materials: Nanostructures by Severe Plastic Deformation.....	Mon PM	3024	111
Mechanical Behavior of Nanostructured Materials: Plasticity and Deformation Mechanisms at Small Length Scale I.....	Tues AM	3024	158
Mechanical Behavior of Nanostructured Materials: Plasticity and Deformation Mechanisms at Small Length Scale II.....	Wed AM	3024	255
Mechanical Behavior of Nanostructured Materials: Plasticity and Deformation Mechanisms at Small Length Scale III.....	Wed PM	3024	307
Mechanical Behavior of Nanostructured Materials: Poster Session.....	Sun PM	3024	24
Mechanical Behavior of Nanostructured Materials: Stability of Nanostructures.....	Mon AM	3024	64
Mechanical Behavior of Nanostructured Materials: Strengthening Mechanisms at Small Length Scale.....	Tues PM	3024	206
Microstructural Processes in Irradiated Materials: Advanced Oxide Dispersion Strengthened Ferritic Alloys.....	Tues AM	2008	160
Microstructural Processes in Irradiated Materials: Ceramics and Fuels.....	Wed AM	2008	257
Microstructural Processes in Irradiated Materials: Poster Session.....	Sun PM	2008	28
Microstructural Processes in Irradiated Materials: Radiation Effects I: Segregation and Modeling.....	Mon AM	2008	66
Microstructural Processes in Irradiated Materials: Radiation Effects II: Advanced Characterization and Fe-Cr Alloys.....	Mon PM	2008	113
Microstructural Processes in Irradiated Materials: Radiation Effects III: He Effects on Microstructural Evolution and Deformation.....	Tues PM	2008	208
Nanocomposite Materials: Characterization and Modeling of Nanocomposites I.....	Tues AM	3020	161
Nanocomposite Materials: Characterization and Modeling of Nanocomposites II.....	Wed AM	3020	258
Nanocomposite Materials: Metallic Nanocomposites.....	Tues PM	3020	209
Nanocomposite Materials: Nanocomposite Processing.....	Thurs AM	3020	345
Nanocomposite Materials: Nanocomposites for Energy Conversion and Storage.....	Wed PM	3020	309
Nanocomposite Materials: Nanoparticle Synthesis.....	Mon AM	3020	68
Nanocomposite Materials: Polymer Nanocomposites.....	Mon PM	3020	114
National Academies Propulsion Materials Study Community Town Hall Meeting: National Academies Propulsion Materials Study Community Town Hall Meeting.....	Wed PM	3010	310
Near-Net Shape Titanium Components: Casting, Welding and Beam Processes.....	Tues PM	2010	211
Near-Net Shape Titanium Components: Deformation and Machining Processes.....	Wed PM	2010	310
Near-Net Shape Titanium Components: Poster Session.....	Sun PM	2010	31
Near-Net Shape Titanium Components: Powder Metallurgy I.....	Wed AM	2010	259
Near-Net Shape Titanium Components: Powder Metallurgy II.....	Thurs AM	2010	346
Neutron and X-Ray Studies of Advanced Materials: Advanced Imaging and Bio-Inspired Studies.....	Wed PM	3016	311
Neutron and X-Ray Studies of Advanced Materials: Advances in Line Profile.....	Tues PM	3016	212
Neutron and X-Ray Studies of Advanced Materials: Diffuse Scattering.....	Mon PM	3016	115
Neutron and X-Ray Studies of Advanced Materials: Neutron Diffraction and Modeling of Materials Behavior.....	Thurs AM	3016	348
Neutron and X-Ray Studies of Advanced Materials: Phase Transition.....	Wed AM	3016	260
Neutron and X-Ray Studies of Advanced Materials: Resolving Local Structure.....	Mon AM	3016	69
Neutron and X-Ray Studies of Advanced Materials: Small Scale and Thin Film Studies.....	Tues AM	3016	162
Open Source Tools for Materials Research and Engineering: Session I.....	Thurs AM	3000	350
Pb-Free Solders and Emerging Interconnect and Packaging Technologies: Effects of Surface Finishes and Advances in Interconnects.....	Tues AM	2020	164
Pb-Free Solders and Emerging Interconnect and Packaging Technologies: Electromigration Reliability.....	Mon PM	2020	117
Pb-Free Solders and Emerging Interconnect and Packaging Technologies: Electromigration, Microstructure, and Mechanical Properties.....	Thurs AM	2020	351
Pb-Free Solders and Emerging Interconnect and Packaging Technologies: Fundamental Properties, Interfacial Reactions and Phase Transformation.....	Mon AM	2020	71
Pb-Free Solders and Emerging Interconnect and Packaging Technologies: Microstructure, Modeling and Test Methods.....	Wed PM	2020	313
Pb-Free Solders and Emerging Interconnect and Packaging Technologies: Reliability and Microstructure Development.....	Wed AM	2020	262
Pb-Free Solders and Emerging Interconnect and Packaging Technologies: Poster Session.....	Sun PM	2020	31
Pb-Free Solders and Emerging Interconnect and Packaging Technologies: Tin Whisker Formation and Mechanical Properties.....	Tues PM	2020	214
Peirce-Smith Converting Centennial Symposium: Historical Foundations/Refractory Practices.....	Mon AM	2009	72
Peirce-Smith Converting Centennial Symposium: Injection Techniques, Modeling and Process Control.....	Tues AM	2009	165
Peirce-Smith Converting Centennial Symposium: New Converting Technologies and Panel Discussion.....	Tues PM	2009	216
Peirce-Smith Converting Centennial Symposium: Operational Aspects.....	Mon PM	2009	119
Peirce-Smith Converting Centennial Symposium: Short Course on Injection Phenomena in the Peirce-Smith Converter.....	Wed AM	Exhibit Hall	264
Phase Stability, Phase Transformations, and Reactive Phase Formation in Electronic Materials VIII: Session I.....	Mon AM	2022	74
Phase Stability, Phase Transformations, and Reactive Phase Formation in Electronic Materials VIII: Session II.....	Mon PM	2022	120
Phase Stability, Phase Transformations, and Reactive Phase Formation in Electronic Materials VIII: Session III.....	Tues AM	2022	167
Phase Stability, Phase Transformations, and Reactive Phase Formation in Electronic Materials VIII: Session IV.....	Tues PM	2022	217

# Session Listing

Phase Stability, Phase Transformations, and Reactive Phase Formation in Electronic Materials VIII: Session V .....	Wed AM .....	2022.....	265
Progress in Computational Materials Science and Engineering Education: Session I .....	Wed PM.....	3003.....	314
Progress in Computational Materials Science and Engineering Education: Session II.....	Thurs AM.....	3003.....	353
Recent Advances in Thin Films: Applications .....	Mon PM .....	3011.....	121
Recent Advances in Thin Films: Metal Films and Integration Schemes .....	Tues AM.....	3011.....	168
Recent Advances in Thin Films: Process-Property Correlations .....	Mon AM .....	3011.....	75
Recycling of Electronic Wastes: General Recycling .....	Tues PM .....	2024.....	218
Recycling of Electronic Wastes: Hydrometallurgical Recycling .....	Tues AM .....	2024.....	169
Recycling of Electronic Wastes: Life Circle Analysis and Environmental Issues .....	Mon AM.....	2024.....	76
Recycling of Electronic Wastes: Mechanical Recycling and Pyrometallurgical Recycling .....	Mon PM .....	2024.....	122
Recycling--General Session: Recycling--General Session I: Metals.....	Wed AM .....	2024.....	266
Recycling--General Session: Recycling--General Session II: Waste Utilization .....	Wed PM.....	2024.....	316
Recycling--General Session: Recycling--General Session III: Aqueous Processing .....	Thurs AM.....	2024.....	354
RPV Embrittlement and Fusion Materials: Measuring, Modeling and Managing Irradiation Effects: Fusion Reactor Materials: Technical Contributions of Professor G. Robert Odette .....	Thurs AM.....	2008.....	355
RPV Embrittlement and Fusion Materials: Measuring, Modeling and Managing Irradiation Effects: RPV Embrittlement: Technical Contributions of Professor G. Robert Odette.....	Wed PM.....	2008.....	317
Shape Casting: Third International Symposium: Characterization.....	Tues AM.....	2011.....	170
Shape Casting: Third International Symposium: Modeling .....	Wed AM .....	2011.....	267
Shape Casting: Third International Symposium: Novel Methods and Applications .....	Tues PM .....	2011.....	219
Shape Casting: Third International Symposium: Processes .....	Mon PM .....	2011.....	123
Shape Casting: Third International Symposium: Properties.....	Mon AM .....	2011.....	77
Solar Cell Silicon: Production and Recycling: Session I.....	Wed AM .....	3004.....	268
Solar Cell Silicon: Production and Recycling: Session II .....	Wed PM.....	3004.....	318
State of the NSF Metallic Materials and Nanostructures (MMN) Program: Session I .....	Wed PM.....	2002.....	319
Structural Materials Division Symposium: Advanced Characterization and Modeling of Phase Transformations in Metals in Honor of David N. Seidman on his 70th Birthday: Driven Alloy Systems .....	Mon AM.....	3000.....	78
Structural Materials Division Symposium: Advanced Characterization and Modeling of Phase Transformations in Metals in Honor of David N. Seidman on his 70th Birthday: Kinetics of Phase Transformations I .....	Tues PM .....	3000.....	220
Structural Materials Division Symposium: Advanced Characterization and Modeling of Phase Transformations in Metals in Honor of David N. Seidman on his 70th Birthday: Kinetics of Phase Transformations II.....	Wed AM .....	3000.....	269
Structural Materials Division Symposium: Advanced Characterization and Modeling of Phase Transformations in Metals in Honor of David N. Seidman on his 70th Birthday: Structure Property Relationships.....	Tues AM.....	3000.....	171
Structural Materials Division Symposium: Advanced Characterization and Modeling of Phase Transformations in Metals in Honor of David N. Seidman on his 70th Birthday: Thermodynamics of Phase Transformations .....	Mon PM .....	3000.....	124
Surface Structures at Multiple Length Scales: Bio Coatings and Nanoscale Characterization.....	Wed AM .....	3011.....	271
Surface Structures at Multiple Length Scales: Processing of Novel Surfaces.....	Wed PM.....	3011.....	319
Surface Structures at Multiple Length Scales: Surface Deposition and Properties .....	Thurs AM.....	3011.....	357
Surface Structures at Multiple Length Scales: Surface Properties in Various Length Scales.....	Tues PM .....	3011.....	222
Synergies of Computational and Experimental Materials Science: Poster Session.....	Sun PM.....	3003.....	34
Synergies of Computational and Experimental Materials Science: Synergies in Integrated Computational Materials Engineering.....	Wed AM .....	3003.....	272
Synergies of Computational and Experimental Materials Science: Synergies in Nanoscience.....	Tues PM .....	3003.....	223
Synergies of Computational and Experimental Materials Science: Three-Dimensional Materials Science I.....	Mon AM .....	3003.....	79
Synergies of Computational and Experimental Materials Science: Three-Dimensional Materials Science II.....	Mon PM .....	3003.....	125
Synergies of Computational and Experimental Materials Science: Three-Dimensional Materials Science III .....	Tues AM.....	3003.....	172
Transformations under Extreme Conditions: A New Frontier in Materials: Driven Reactions.....	Thurs AM.....	3001.....	358
Transformations under Extreme Conditions: A New Frontier in Materials: Extreme Deformation and Damage.....	Tues PM .....	3001.....	224
Transformations under Extreme Conditions: A New Frontier in Materials: High Rate Deformation .....	Tues AM.....	3001.....	173
Transformations under Extreme Conditions: A New Frontier in Materials: Keynote: Melting and Solidification I .....	Mon AM.....	3001.....	80
Transformations under Extreme Conditions: A New Frontier in Materials: Melting and Solidification II .....	Mon PM .....	3001.....	127
Transformations under Extreme Conditions: A New Frontier in Materials: Pressure/Stress-Induced Transformations and In Situ Diagnostics II.....	Wed PM.....	3001.....	321
Transformations under Extreme Conditions: A New Frontier in Materials: Solid-Solid Transformations and In Situ Diagnostics I .....	Wed AM .....	3001.....	273

## 2009 Functional and Structural Nanomaterials: Fabrication, Properties, and Applications: Poster Session

Sponsored by: The Minerals, Metals and Materials Society, TMS Electronic, Magnetic, and Photonic Materials Division, TMS Materials Processing and Manufacturing Division, TMS: Nanomaterials Committee, TMS: Nanomechanical Materials Behavior Committee

Program Organizers: Gregory Thompson, University of Alabama; Amit Misra, Los Alamos National Laboratory; David Stollberg, Georgia Tech Research Institute; Jiyoung Kim, University of Texas at Dallas; Seong Jin Koh, University of Texas at Arlington; Wonbong Choi, Florida International University; Alexander Howard, Air Force Research Laboratory

Sunday, 6:00-8:00 PM Room: 3018  
February 15, 2009 Location: Moscone West Convention Center

*Session Chairs:* Gregory Thompson, University of Alabama; Jiyoung Kim, University of Texas at Dallas; Alexander Howard, Air Force Research Laboratory; Amit Misra, Los Alamos National Laboratory; David Stollberg, Georgia Tech Research Institute; Seong Jin Koh, University of Texas at Arlington; Wonbong Choi, Florida International University

### Bending Strength of Single Crystal Silicon Micro Beams Fixed on Both Ends: *Guangping Han*<sup>1</sup>; Gaoping Wang<sup>2</sup>; Xiuhong Wang<sup>1</sup>; Kai Liu<sup>3</sup>; <sup>1</sup>Zhengzhou Institute of Aeronautical Industry Management; <sup>2</sup>Henan University of Technology; <sup>3</sup>Xi'an University of Technology

MEMS is a rapidly growing multidisciplinary technology, in which understanding of the mechanical behavior of materials and micro structures lags far behind micro-fabrication and application of micro devices, thus, accurate evaluation of the mechanical properties of material is one of the most challenging issues. Six kinds of single crystal silicon micro beams fixed on both ends with trapezoidal cross section were fabricated using photolithography technology, with dimensions of 150-1000  $\mu\text{m}$  long, 16-60  $\mu\text{m}$  wide, 6 and 20  $\mu\text{m}$  thick. The micro beam specimens were used in bending test by nano indentation method. Results show that the mean values of bending strength increase with the ratio of surface area to volume, varying from 3.24 to 10.15GPa; based on weibull analysis, shape parameters are 4.21-10.54 while scale parameters under the fracture probability of 65.4% vary from 3.26 to 10.26GPa; both the average bending strength and weibull parameters display strong size effects.

### Characteristic of the Liquid Sodium by the Dispersing Nanoparticles: *Jun-ichi Saito*<sup>1</sup>; Kuniaki Ara<sup>1</sup>; <sup>1</sup>Japan Atomic Energy Agency

The purpose of this study is to suppress the high chemical reactivity by dispersing nanoparticles into liquid sodium. An atomic interaction between the nanoparticle atom and sodium atom is harnessed to suppress the chemical reactivity. The theoretical calculation showed the atomic bonding between nanoparticle atom and sodium atom was stronger than that between sodium atoms. The charge transfer occurred to the nanoparticle atom from the sodium atom. It suggests that the fundamental and reaction properties change by the atomic interaction. The fundamental property of sodium dispersing nanoparticle changed compared to sodium. The reaction behavior with water or oxygen of the sodium dispersing nanoparticles also changed compared to sodium. The reaction heat of the sodium dispersing nanoparticles reduced. It means that there is the possibility of suppression of reactivity of liquid sodium by the atomic interaction.

### Characterization of Noble Metal Core Shell Nanostructures via Scanning Probe Microscopy and Ab Initio Calculations: *Aniketa Shinde*<sup>1</sup>; Juexian Cao<sup>1</sup>; Sangyeob Lee<sup>1</sup>; Chulsu Jo<sup>1</sup>; Ruqian Wu<sup>1</sup>; Regina Ragan<sup>1</sup>; <sup>1</sup>University of California, Irvine

Self assembled rare earth disilicide nanowires are used as templates for Pt and Au nanostructures on Si(001). We performed experimental and computational studies to investigate the adsorption of rare earth atoms on the Si(001) surface and the onset of disilicide nanowire formation. These results pave a way for understanding and eventually controlling the growth of rare earth disilicide nanowires on the Si(001) substrate. Simulated scanning tunneling microscopy (STM) and charge density difference images agree with experimental STM and Kelvin Probe microscopy contact potential difference data. Dipoles induced by RE adatoms are predicted to decrease the substrate work function, as confirmed

by KPFM. We have also explored calculations for the adsorption of noble metal atoms on YSi<sub>2</sub> nanowires. Significant charge transfer from Y to Pt drastically lowers the Pt-d band and hence new chemical and optical behaviors are expected from the Pt atom.

### Controlling the Self-Assembly of Silica-Capped Silver Nanoparticles through Hydrophobicity: *Yong-Jae Choi*<sup>1</sup>; Tzy-Jiun Luo<sup>1</sup>; <sup>1</sup>North Carolina State University

Recent progress on spontaneous metallization process associated with aminosilane was utilized to synthesize silver nanoparticles with a narrow size distribution, which were later confirmed by TEM, XRD, and UV-Vis spectroscopy. The as-synthesized nanoparticles were capped in silica structures through amine groups, and their surface charges can be modified through mole ratios of silane and silver ions. Self-assembly of silica modified silver nanoparticles was observed on hydrophobic surfaces such as polypropylene and polydimethylsiloxane. The deposited nanoparticle layer, once initiated, was found to induce accelerated growth of nanoparticles at the surface, resulting in a thicker film with a reflective metallic colors. In contrast, surface treated O<sub>2</sub> plasma was found to significantly reduce the surface deposition of nanoparticles. This surface controlled self-assembly of silver nanoparticles was later utilized to produce patterns of silver nanoparticles layer. SEM, AFM and cyclic voltammetry were also utilized to characterize the structures and properties of the film.

### Development of a Simulation Method for the Formation of Nano-Porous Anodic Aluminum Oxide: *Eun Cheol Do*<sup>1</sup>; Byeong-Joo Lee<sup>1</sup>; <sup>1</sup>POSTECH

Since the nano-porous anodic aluminum oxide is used as a template for fabrication of nanostructured materials, it is important to be able to control the structural factors of AAO such as pore diameter, interpore distance and pore alignment. As a means to provide a guide to control the structural property of AAO, we developed a simulation scheme for the formation and growth of nanopores during the anodizing. The dissolution of oxide layer on oxide/electrolyte interfaces which is the rate-determining step in pore growth was mainly focused, assuming that the strength and distribution of electric field which have effects on the pore growth rate depend on the curvature and thickness of oxide layer on the pore bottom. By calculating the direction and rate of dissolution as a function of the electric field distribution, pH and temperature, the growth and rearrangement of pores could be well reproduced in good agreement with experiments.

### Direct Synthesis of Straight SiO<sub>2</sub> Nanorods: *Guang Zhu*<sup>1</sup>; <sup>1</sup>Beijing Information Technology Institute

The straight SiO<sub>2</sub> nanorods with a diameter of about 200nm and smooth surface have been directly synthesized by high temperature vapor deposition method at 1300°. The as-synthesized samples were characterized by means of scanning electron microscopy, energy dispersive x-ray, and transmission electron microscopy. The results show that as-synthesized silica nanorods have a uniform size, well-defined shape, and smooth surface. However, the morphologies and microstructures of silica nanorods are affected by synthesis conditions, such as the concentration of the SiO<sub>x</sub> and the deposition temperature. On the basis of these experimental results, a possible growth mechanism of silica nanorods in this process is proposed.

### Effect of Ingot Microstructure on Magnetic Properties of Nd<sub>2</sub>Fe<sub>14</sub>B/ $\alpha$ -Fe Nanocomposite Magnets: *Junhua You*<sup>1</sup>; <sup>1</sup>Northeastern University

In this text, Metallographic microscope, Scanning electron microscopy (SEM) and X-ray diffraction (XRD) have been used to analyze the microstructures and phases of the cast ingots. The effect of cast ingot microstructure on magnetic properties of the bonded magnets is also investigated. The results indicated that: Both of the ingot I (1kg) and the ingot II (60g) are composed of Nd<sub>2</sub>Fe<sub>14</sub>B matrix phase,  $\alpha$ -Fe particle phase and Nd-rich phase, the microstructure of the ingot II is much finer because of its faster cooling velocity; The magnetic properties of the bonded magnets made from the ingot II are higher than that made from the ingot I, meanwhile the magnetic properties difference of the magnets made from different parts of the ingot is about 6%, it indicates that the magnetic properties of bonded magnets are not sensitive to the ingot microstructure.

### Enhanced Photoelectrochemical Degradation of Methyl Orange Using Anodized Ti Rods: *Archana Kar*<sup>1</sup>; Vaidyanathan Subramanian<sup>1</sup>; <sup>1</sup>University of Nevada, Reno

Titanium dioxide (TiO<sub>2</sub>) is widely used for heterogeneous photocatalytic waste treatment. Several studies have reported the application of TiO<sub>2</sub> slurry as well as immobilized TiO<sub>2</sub> but they are limited by difficulties in post-treatment recovery and reduction in active surface area. One approach to minimize this problem is



to utilize TiO<sub>2</sub> nanotubes formed by anodization of Ti foil backbone. To increase the photoefficiency of the TiO<sub>2</sub> nanotubes with respect to geometrical surface area we utilized Ti rods of diameter 0.5 mm for anodization. TiO<sub>2</sub> nanotubes were prepared by anodizing Ti rods in an Ethylene glycol and Ammonium fluoride electrolyte. The length and diameter of the nanotubes were found to be 700 - 800 nm and 100 - 170 nm respectively. Photodegradation experiments confirmed that anodized Ti rod shows 43% Methyl orange degradation whereas anodized Ti foil shows 20% MO degradation under the same conditions.

**Modeling the Electrochemical Interactions of Nano-Particulate Systems in Medical Devices:** *Jonathan Guyer*<sup>1</sup>; David Saylor<sup>2</sup>; James Warren<sup>1</sup>; <sup>1</sup>National Institute of Standards and Technology; <sup>2</sup>Food and Drug Administration

Nano-particulate silver systems are widely used in wound dressings, surgical masks, and catheter coatings as anti-microbial agents. We previously developed a phase field model of the electrochemical interface and demonstrated that a simple set of assumptions gives rise to a rich set of behaviors, including electrocapillary phenomena, differential capacitance curves that resemble experimental measurements, and non-linear kinetics consistent with the empirical Butler-Volmer relation. Despite these successes, numerical constraints limited the applicability of the model to dimensions of a few nanometers. Fortunately, however, the model is capable of making predictions at precisely the spatial and temporal scale that we are interested in for studying medical applications of silver nano-particles. We will discuss the impact of particle size, solution concentration, and particle aggregation on ion release and surface charge, which not only impact the anti-microbial efficacy and system stability, but may also affect biocompatibility.

**Multilayer Optical Filters Withstand Extreme Strain:** Thad Druffel<sup>1</sup>; Matt Lattis<sup>1</sup>; Omar Buazza<sup>1</sup>; *Scott Farmer*<sup>1</sup>; <sup>1</sup>Optical Dynamics

Nanocomposites composed of UV cured polymers and metal oxide nanoparticles offer highly engineered mechanical and optical properties for transparent, flexible systems. Because nanoparticles can offer high hardness and a wide range of refractive indices, their inclusion in a polymer matrix can dramatically increase wear resistance and significantly alter refractive index, while the polymer binders are allowed to control overall mechanical flexibility. We have successfully built sharp cut optical filters composed of more than 30 discrete layers that easily withstand large strains induced by mechanical loading and thermal cycling. We demonstrate a UV cured, spin applied thin-film system that can undergo strains in excess of 20 percent without failure. This novel coating system allows sophisticated thin-film filters to be used in applications and environments that were previously impractical.

**Palladium Doped TiO<sub>2</sub> Thin Films with Antibacterial Properties:** *Mehdi Rezaian Deloei*<sup>1</sup>; Mohammad Ghorbani<sup>1</sup>; Mohammad Mohsenzadeh<sup>2</sup>; <sup>1</sup>Sharif University of Technology; <sup>2</sup>Ferdowsi University of Mashhad

Thin film of TiO<sub>2</sub> and its palladium doped sample were prepared from a titanium isopropoxide precursor by particulate sol-gel processing on 316 stainless steel substrate. FTIR analysis was used to identify the chemical changes which occurred in the solution. It shows absorption peak at about 576 Cm<sup>-1</sup> correspond to Ti-O-Ti bands. The morphology of the coatings was characterized by scanning electron microscopy (SEM). X-Ray diffraction pattern showed that Palladium presence increases the transformation temperature of anatase to rutile. It was found that Pd addition contributes to an increase in the activity of thin film by the aid of UV-Vis spectroscopy and antibacterial tests against E.coli.

**Phase Formation and Mechanical Properties of Cu-Zr Based Glasses and Glass Matrix Composites:** *Simon Pauly*<sup>1</sup>; Jayanta Das<sup>1</sup>; Jürgen Eckert<sup>1</sup>; <sup>1</sup>IFW Dresden

The crystallization behaviour of Cu<sub>50</sub>Zr<sub>50-x</sub>Ti<sub>x</sub> (0 = x = 10) metallic glasses is investigated. Higher Ti contents promote the formation of metastable phases and the crystallization proceeds in multiple steps. However the phase evolution upon quenching the melt is different also indicating a distinct dependence on the Ti content. Therefore, different TTT or CCT diagrams have to be considered. Kinetic parameters like fragility, activation energy of crystallization are compared with data of Cu-Zr-Al alloys. Cu-Zr based alloys can undergo an austenite-to-martensite transformation (MT). This transformation is believed to enhance the ductility of partially crystalline Cu-Zr based bulk metallic glasses. These composites show high yield strength (up to 1753 MPa) and large plastic strain (over 15%). The high strength scales with the volume fraction of glassy matrix. The MT was investigated in a high-energy x-ray beam with respect to compositional influences and the stress levels at which the transformation occurs.

**Preparation and Characterization of Nano-Sized Polyhedron Co<sub>3</sub>O<sub>4</sub> Powder by Spray-Oxidation:** *Xueyi Guo*<sup>1</sup>; Qiusong Guo<sup>1</sup>; Qingming Feng<sup>1</sup>; Qinghua Tian<sup>1</sup>; <sup>1</sup>School of Metallurgy

Nano-sized Co<sub>3</sub>O<sub>4</sub> powder with polyhedron morphology were prepared by using single step spray-oxidation. The precursor solution was prepared by using cobalt chloride (CoCl<sub>2</sub>·6H<sub>2</sub>O) as raw material. Precursor solution was sprayed by using inner mixed air-nozzle and oxidized in a pipe resistance furnace with compressed oxygen as the carrier gas. The products were characterized by scanning electron microscope(SEM), x-ray diffraction(XRD), infrared spectrum(IR) and brunauer-emmett-teller(BET) surface area method. SEM results show that the reaction temperature strongly influences the morphology of the particles. Nano-sized powders polyhedron-Co<sub>3</sub>O<sub>4</sub> can be successfully prepared at temperature of about 800°. XRD studies and infrared spectrum(IR) revealed that the product is pure Co<sub>3</sub>O<sub>4</sub> with normal-spinel structure. The specific BET surface area was found to be 5.3m<sup>2</sup>/g, indicating that the particles have a high activity and a good prospect of application.

**Preparation of Antimicrobial Colored Sheets with Modified Silver-Doped Titanium Dioxide Nanocrystals:** Guoliang Li<sup>1</sup>; *Bing Peng*<sup>1</sup>; <sup>1</sup>School of Metallurgical Science and Engineering, Central South University

Silver-doped titanium dioxide nanocrystals were treated with several dispersant agents by wet activated technology, and sodium stearate showed the superior property to boost the hydrophobicity of silver-doped TiO<sub>2</sub> nanocrystals. Antimicrobial colored sheets were prepared with modified silver-doped TiO<sub>2</sub> nanocrystals which were treated with sodium stearate by dry activated technology. The properties of treated colored sheets were significantly affected by concentration of silver-doped TiO<sub>2</sub> nanocrystals in polyester coatings and the treatment conditions. The treated colored sheets showed fine photocatalytic activity to enhance the decolorization and degradation of methyl orange under UV light irradiation, good antimicrobial activity against *Escherichia coli*, and strong time effectiveness of photocatalytic and antimicrobial properties after water flushing. The optimal property was obtained when the colored sheets were coated with paint including 3% modified silver-doped TiO<sub>2</sub> nanocrystals which were treated with 3.5% sodium stearate.

**Preparation of Nanorods and Diamond like Carbon by High Temperature Dissociation of Silicon Carbide in a Plasma Heated Special Reactor:** *Bijan Nayak*<sup>1</sup>; B. K. Mishra<sup>1</sup>; <sup>1</sup>Institute of Minerals and Materials Technology

Silicon carbide nanorods have excellent scope in several future applications such as field emission TV, flexible thin film computers, atomic force microscope tips, quantum devices, micro and nano composites to name a few. Like wise, diamond like carbon (DLC) finds wide use in wear resistant surface coatings and electronic component packaging. The present work reports an ingenious arc plasma method to dissociate silicon carbide at temperatures above 2200°C by taking advantage of its typical non-melting property. A special plasma reactor has been designed and developed to prepare silicon carbide nanorods and DLC by controlling the retention and exit of Si vapour in the reactor. In the first case, when the dissociated Si in the form of vapour is allowed to recombine with C inside the reactor, SiC nanorod formation is observed. Assembly of rods are found to pin to SiC grains at different points. In the second case, when the Si vapour is let out of the reactor zone, the left out C on the dissociated SiC surface, grows epitaxially on the underlying SiC surface to produce DLC layer. The SiC nanorods and DLC layer were characterized by micro Raman spectra, optical microscopy, TEM and AFM for structural evaluation. The paper envisages to discuss further details about the work and results at the time of presentation.

**Preparation of Nanosized Zinc Ferrite Particles in the System of Fe(III)-Zn(II)-NH<sub>3</sub>-CO<sub>3</sub>—H<sub>2</sub>O:** *Qinghua Tian*<sup>1</sup>; Xueyi Guo<sup>1</sup>; Jun Li<sup>1</sup>; Dong Li<sup>1</sup>; <sup>1</sup>Central South University

Based on the review of technical literatures, the co-precipitation-drying-thermal decomposition was determined for the preparation of nanosized zinc-ferrite. The ammonium bicarbonate was chosen as the co-precipitation agent, and the thermodynamic analyses were done for the solution system of Fe(III)-Zn(II)-NH<sub>3</sub>-CO<sub>3</sub>—H<sub>2</sub>O. The double-jet precipitation process was proposed based on the thermodynamic analyses results. Considering the heavy aggregation among nano-sized particles, the measures were adopted by addition of dispersant in the process of co-precipitation and washing by organic solvent or azeotropic distillation. By TG-DTA analysis, the suitable thermol-decomposition temperature of the zinc ferrite precursor was determined at about 450°. Kept at this temperature for 2 hours, the pure and well crystalized ZnFe<sub>2</sub>O<sub>4</sub>



was obtained. SEM Photos of the obtained powder shows that the particles are uniform in size distribution (20nm-50nm) with good dispersivity.

**Surface Modification of Silver-Doped Nanometer Titania with Stearic Acid:** Yunchao Liu<sup>1</sup>; Bing Peng<sup>1</sup>; *Liyuan Chai*<sup>1</sup>; Liqiang Liu<sup>1</sup>; <sup>1</sup>School of Metallurgical Science and Engineering, Central South University

Organic surface modification of silver-doped TiO<sub>2</sub> with stearic acid was investigated by varying reagent amount, reagent concentration, time, temperature and pH value. The lipophilic degree was analyzed using a 37 factorial design to obtain the optimal condition. The prepared samples were characterized by FT-IR and SEM, and the antibacterial property was determined. The results showed that the lipophilic degree reached up to 64.3% under optimum condition of stearic acid amount 1%, stearic acid concentration 0.0002mol/L, modification time 90 min, temperature 80° and pH 6. The stearic acid was bonded on the surface of silver -doped TiO<sub>2</sub> by chemical bond. The dispersancy of silver-doped TiO<sub>2</sub> was improved after modification. Although antibacterial rate decreased slightly, it still achieved 99.77%.

**Synthesis and Characterization of SiO<sub>2</sub> and SiC Micro/Nanostructures:** *Guang Zhu*<sup>1</sup>; <sup>1</sup>Beijing Information Technology Institute

Silica-based nanowires, straight nanorods, straight Y-shaped silica nanorods, flower-like microstructures, and SiC/SiO<sub>2</sub> core-shell coaxial nanocables have been generated through a simple thermal evaporation method. The synthesized samples were characterized by means of scanning electron microscopy, transmission electron microscopy, high resolution transmission electron microscopy, energy dispersive X-ray spectroscopy, and Raman spectrum. Generated silica nanowires with a diameter of about 100nm and length of up to several tens of micrometers, straight silica nanorods and Y-shaped nanorods with a diameter about 50-200nm, and novel flower-like silica microstructures all are amorphous and consist only of silicon oxide, and have a neat smooth surface. Generated SiC/SiO<sub>2</sub> core-shell coaxial nanocables have a crystalline core and a surrounding amorphous layer. The results show that the present method should be possible to synthesis various micro/nanostructures under appropriate experimental conditions. These nanostructures may find applications as building blocks in nanomechanical or nanoelectronic devices.

**Synthesis and Processing of Cu-CNT Nano-Composites:** Martín Mendoza<sup>1</sup>; *Guillermo Solórzano Naranjo*<sup>1</sup>; Eduardo Brocchi<sup>1</sup>; <sup>1</sup>PUC-Rio

This work presents some structural characteristics of a Copper-2%CNT nanocomposite synthesized by chemical method. Single wall Carbon nanotubes(SWCNTs), with diameters between 5-10 nm were used. The nanocomposites powders were produced by dissociation of a homogeneous suspension containing Cu(NO<sub>3</sub>)<sub>2</sub>·3H<sub>2</sub>O, SWCNT an anionic tensoactive; followed by hydrogen reduction of the obtained CuO-SWCNT product. Thermodynamic studies provided support to the experimental procedure. X ray diffraction and Transmission Electron Microscopy have been used as characterization tools. The former confirmed the presence of metallic copper with carbon. The later allowed the observation of a good dispersion and adherence between Cu particles onto CNT. The obtained Cu powder particles were observed to be in the 150-300nm range. Bulk nano-composite pellets were produced by isostatic pressure under 150MPa. Sintering studies show a heterogeneous grain growing of copper matrix reaching a polycrystalline product of 150nm- 3µm grain size. Mechanical and transport properties measurements are currently in progress.

**Synthesis of Single-Crystalline Silicon Nitride Nanowires with Controlled Diameters by Nitriding Cryomilled Nanocrystalline Silicon Powder:** Fei Chen<sup>1</sup>; Ying Li<sup>2</sup>; Wei Liu<sup>2</sup>; Qiang Shen<sup>1</sup>; Lianmeng Zhang<sup>1</sup>; Qing Jiang<sup>3</sup>; Enrique Lavernia<sup>2</sup>; *Julie Schoenung*<sup>2</sup>; <sup>1</sup>Wuhan University of Technology; <sup>2</sup>University of California, Davis; <sup>3</sup>Jilin University

In the present work, silicon nitride nanowires (SNNWs) have been synthesized via nitriding cryomilled nanocrystalline silicon powder. The silicon powder exhibits a fine polycrystalline structure after the cryomilling process, with an average grain size of 25 to 125 nm at various cryomilling times. The SNNWs that form after the nitridation of the cryomilled silicon powder exhibit single crystal structure and are 20 to 100 nm in diameter and ~ 10 µm in length. The diameter of the nanowires is in agreement with the grain size of the cryomilled Si powder. Microstructural characterization reveals that the as-synthesized nanowires have a hexagonal structure and their primary growth direction is along the [0001] direction. The formation of the Si-N-Si bond during the cryomilling process, as investigated theoretically with density functional theory, promotes the

subsequent synthesis of the a-Si<sub>3</sub>N<sub>4</sub> nanowires. The mechanism for nanowire formation appears to be a vapor-solid (VS) reaction.

**Synthesis of Straight Si<sub>3</sub>N<sub>4</sub> Nanowires:** *Guang Zhu*<sup>1</sup>; <sup>1</sup>Beijing Information Technology Institute

The novel straight Si<sub>3</sub>N<sub>4</sub> nanowires have been directly synthesized by thermal evaporation of the mixture powders of silica and carbon nanofibers at 1300°C without assistance of any metal catalyst. The as-obtained Si<sub>3</sub>N<sub>4</sub> nanowires are generally 30-50 nm in diameter and several tens of micrometers in length, and have a smooth surface. The characteristics of the products are analyzed by various methods, results of which indicating that temperature and ambience are two key factors for the formation of Si<sub>3</sub>N<sub>4</sub> nanowires, and the possible growth mechanisms is also discussed.

## Aluminum Reduction Technology: Light Metals Division Poster Session

Sponsored by: The Minerals, Metals and Materials Society, TMS Light Metals Division, TMS: Aluminum Committee  
Program Organizers: Gilles Dufour, Alcoa Canada, Primary Metals; Martin Ifert, Trimet Aluminium AG; Geoffrey Bearne, Rio Tinto Alcan; Jayson Tessier, Alcoa Deschambault

Sunday, 6:00-8:00 PM Room: 2001  
February 15, 2009 Location: Moscone West Convention Center

**Detecting Abnormalities in Aluminium Reduction Cells Based on Process Events Using Multi-Way Principal Component Analysis (MPCA):** *Brent R. Young*<sup>1</sup>; John Chen<sup>1</sup>; Nazatul Aini Abd Majid<sup>1</sup>; Mark Taylor<sup>1</sup>; <sup>1</sup>University of Auckland

In the aluminium industry optimal production and quality products are major process targets. One way to achieve these targets is by improving the process control of aluminium reduction cells, and this is the aim of this research. This research proposes to apply an advanced multivariate control chart to aluminium reduction cells in a manner which provides new insights into process abnormalities and their diagnosis. The proposed approach uses multi-way principal component analysis to observe the movement of data towards abnormality after process events. Preliminary results showed that using the proposed approach could detect anode spikes after anode changing or tapping. Data with anode spikes present moved in a different direction than the data with anode spikes absent. An anode spike trajectory could be set up based on this discrimination. Data which move towards the anode spike trajectory have a high possibility of having anode spikes. Therefore based on this trajectory, the cell could be monitored ahead of time for spikes, and operations may take action to search for them much earlier. This will lead to a real-time fault detection system and is expected to assist process engineers in improving the process control of aluminium reduction cells.

## Biological Materials Science: Poster Session

Sponsored by: The Minerals, Metals and Materials Society, TMS Structural Materials Division, TMS Electronic, Magnetic, and Photonic Materials Division, TMS: Biomaterials Committee, TMS/ASM: Mechanical Behavior of Materials Committee  
Program Organizers: Ryan Roeder, University of Notre Dame; John Nychka, University of Alberta; Paul Calvert, University of Massachusetts Dartmouth; Marc Meyers, University of California

Sunday, 6:00-8:00 PM Room: 3014  
February 15, 2009 Location: Moscone West Convention Center

**Application of Small Angle Neutron Scattering to Quantitatively Analysis of Bony Canaliculus of Human Compact Bone:** *Yong Choi*<sup>1</sup>; Eun J. Shin<sup>2</sup>; Baik S. Seong<sup>2</sup>; Doo J. Paik<sup>3</sup>; <sup>1</sup>Sunmoon University; <sup>2</sup>KAERI; <sup>3</sup>Hanyang University

Small angle neutron scattering (SANS) was applied to quantitatively analyze of human compact bone, especially fine bony canaliculus to get important information about growth and degradation of the human bone. Two types of jaw-bone with different physiological histories such as normal and osteoporosis bones were selected. Bone density was determined by bone densitometer.

Microstructure of the compact bone was observed by transmission electron microscopy. The specimen was cut to fit and tested by SANS of HANARO in KAERI. Directional distribution of bony lacuna of the compact bone and nano-sized canaliculus interconnected in all direction were observed by SANS. The amount of canaliculus of lacuna was larger in normal bone than in osteoporosis bone. Microstructure observation by transmission electron microscopy and measurement of bone density also support the fact that SANS is one of the useful techniques to study in-situ quantitative evaluation of the very fine bony canaliculus of compact bone.

**Development of a Vascular Occluder for Use in Liver Resection Surgery:** *Michael Ashbrook*<sup>1</sup>; Prince Anyalebechi<sup>1</sup>; Timothy Fitzgerald<sup>2</sup>; John Hall<sup>3</sup>; Ken Jonkman<sup>3</sup>; <sup>1</sup>Grand Valley State University; <sup>2</sup>Saint Mary's Hospital; <sup>3</sup>Avalon Laboratories

Liver resection surgery is the procedure by which a cancerous region of a liver is removed. Unfortunately the surgery has the potential to cause high levels of blood loss. This is because nearly all of the blood returning from the lower extremities to the heart flows either through the liver or through the major vein that the liver connects to such as the inferior vena cava. Current techniques cannot seal the larger blood vessels in the liver and so do not completely eliminate bleeding. A device known as hepatic vein occluder has been designed to completely isolate the liver from blood flow during liver resection. It seals off the point where the liver joins into the inferior vena cava, while still allowing blood to flow through and into the heart. In this paper, the design, construction, and results of preliminary testing of the device are discussed.

**Electrochemical Study of Titanium Behaviour and Semiconducting Properties of Anodic Oxide Films Formed on Titanium in PBS Solutions with Different pH:** *Piotr Handzlik*<sup>1</sup>; Krzysztof Fitzner<sup>1</sup>; <sup>1</sup>AGH University of Science and Technology

The first aim of this study was to investigate the electrochemical corrosion behavior of titanium and the corrosion rate in the PBS solutions with pH=8.9, and pH=2.9. Potentiodynamic curves and Tafel plots were used to estimate  $E_{cor}$  and  $i_{cor}$  at  $t=21^{\circ}C$ . Electrochemical Impedance Spectroscopy (EIS) confirmed high corrosion resistance of Ti under imposed conditions. To obtain information about electronic properties of passive oxide films formed at various potentials Mott-Schottky plots were constructed and the flat band potential and number of donor densities were derived. However, the change of temperature to  $36.6^{\circ}C$  showed that the corrosion current increased significantly in both solutions. EIS experiments indicated that equivalent circuit must be changed which speaks for the change of the properties of the protective layer at the titanium surface. Calculated donor densities confirmed also this observation: donor densities increased. Anodic oxide films were studied by XPS technique to identify composition of the layer.

**Femtosecond Laser Micromachining of Bone Mechanical Test Specimens:** *Katrina Altman*<sup>1</sup>; Katharine Flores<sup>1</sup>; Dave Farson<sup>1</sup>; Elise Morgan<sup>2</sup>; <sup>1</sup>The Ohio State University; <sup>2</sup>Boston University

The mechanical properties of bone are highly statistical due to its anisotropic and hierarchical microstructure. For other engineering materials, testing at the microscale has been shown to provide data for individual microstructural components in an effort to understand macroscopic mechanical behavior. The application of such microscale testing to bone will permit modeling of the aggregate material to predict effects of age, disease, or injury on the mechanical properties. The femtosecond laser is presently used to produce microscale specimens in bovine cortical bone, which will be used for mechanical testing. The femtosecond laser is advantageous for micromachining of biological materials because it may be used in ambient, non-vacuum environments, making it a flexible tool for machining the bone surface while preserving its microstructure. The short pulse duration minimizes thermal diffusion and damage to the surrounding material. Microcompression pillars with diameters  $\sim 10\mu m$  have been produced. Processing and experimental results will be discussed.

**Fluoridated Hydroxyapatite Bioactive Coatings on Ti-Alloy Substrate Deposited by RF Magnetron Sputtering:** Dongyang Lin<sup>1</sup>; Xiaoxiang Wang<sup>1</sup>; Xiaoyan Liu<sup>2</sup>; <sup>1</sup>Zhejiang University; <sup>2</sup>Jiangsu University

A pure and dense hydroxyapatite  $[Ca_{10}(PO_4)_6(OH)_2]$ , HA) coating and a fluoridated HA  $[Ca_{10}(PO_4)_6(OH)_2-xFx]$ , FHA) coating are deposited on Ti6Al4V substrates by Radio frequency magnetron sputtering. Researches have been carried out in the phase composition, microcosmic appearance and growth pattern of sputtering coatings, based on XRD, SEM, FTIR and AFM.

The result indicates that magnetron sputtering coating appears in amorphous state, which could be transformed into crystalline state after annealing treatment; the microscopic surface of the sputtered coating is uneven, forming network structure. The growth pattern of the coating is lamellar accompany with island way. There isn't any pore or crackle on the coating/substrate interface and the interfacial binding strength is higher than 50Mpa. Fluorine-incorporation in HA does not generate significant influence on interfacial binding strength. However, FHA bioactive coating implant has better mechanics stabilities than HA coating implant in Simulated Body Fluid (SBF) experiment, which is significant in extending the period of validity of the coating.

**Micro-Arc Oxidization of a Commercial Purity Titanium for Biomedical Applications:** Cemil Isiksacan<sup>1</sup>; Mert Gunyuz<sup>1</sup>; Hakan Bermek<sup>1</sup>; Pinar Huner<sup>1</sup>; Murat Baydogan<sup>1</sup>; Eyup Kayali<sup>1</sup>; *Huseyin Cimenoglu*<sup>1</sup>; <sup>1</sup>Istanbul Technical University

Commercial pure titanium is an attractive material for dental implant production. Conventional titanium implants do not chemically connect to bone or actively induce bone growth compared with calcium phosphate coated implants. In this respect, micro-arc oxidation is an effective surface modification technique to enhance their bioactivity by forming functional, adherent and porous titanium oxide surface layer. In this study, the surface properties including the morphology, roughness and wettability a commercially pure titanium was investigated after. Micro-arc oxidation process was performed in " $(CH_3COO)_2Ca \cdot H_2O + Na_3PO_4$ " electrolytic solution with addition of silver in order to achieve antibacterial surface layer. Micro-arc oxidation formed a porous titanium oxide layer on the surface with small precipitates containing phosphorous, calcium and silver. Biocompatibility of the titanium was then determined by simulated body fluid and cell culture tests as well as antibacterial tests.

**Temperature Effect on the Structure and Mechanical Properties of Nacre:** Zaiwang Huang<sup>1</sup>; *Xiaodong Li*<sup>1</sup>; <sup>1</sup>University of South Carolina

Structural and mechanical characterization has been performed on nacre heat treated at various temperatures. We show that, after treated for 10 minutes at  $500^{\circ}$  and  $1000^{\circ}$  in air respectively, two phase transformations with aragonite to calcite and aragonite to calcium oxide (CaO) occur. Scanning electron microscopy and atomic force microscopy images clearly demonstrate the microstructure evolution process: the survival of sandwiched structure and occurrence of holes instead of nanoasperities on aragonite platelet surface treated from  $500^{\circ}$ , eventually, the formation of micro-scale CaO particles at  $1000^{\circ}$ . The nanoindentation testing results exhibit that nacre at high temperature has a sharp loss in elastic modulus and hardness comparing with those at room temperature. Nanoscale structural and mechanical characterization for nacre heat treated at different temperatures therefore may provide great benefits in bioinspired materials and open new avenues for exploring the origin of its unique mechanical properties.

**The Effect of Dialysis Environment on the Structural Properties of the Membranes Used for High Flux Dialysis:** *Mehmet Aksoy*<sup>1</sup>; Metin Usta<sup>2</sup>; A. Hikmet Ucisik<sup>3</sup>; <sup>1</sup>Istanbul City Health Management; <sup>2</sup>Gebze Yuksek Teknoloji Enstitüsü; <sup>3</sup>Bogazici University

High flux dialysers containing new generation of dialyser materials have been widely used for patients with chronic renal failure within the last decade. Dialyser membranes are more prone to damage to the harsh environment during high flux dialysis. Reuse of dialysers has advantages like better biocompatibility and lower cost, any damage of the dialysers membrane during reuse of the dialysers can also cause very serious clinical complications. Therefore reuse of the dialysers is an issue that has to be approached more cautiously. In this study polysulphone and polyamide dialyser membranes were being investigated in terms of mechanical properties and changes in crystallinity before and after dialysis sessions. Dialysis sessions were performed on five patients with dialysis age less than two years and without any other accompanying disease at the Hemodialysis Department of Istanbul Haydarpaşa Numune State Hospital.

**The Evaluation of Hysteresis Loop of Nickel-Titanium Orthodontic Wires:** S. Mohamad S. Aghamiri<sup>1</sup>; *Mahmoud Nili Ahmadabadi*<sup>1</sup>; <sup>1</sup>University of Tehran

NiTi wires have been used in orthodontic application because of their unique characteristics. The mechanical properties of wires should result in achieving continuous optimal forces and rapid tooth movement. Magnitude of hysteresis loop attributes to energy dissipative processes and the stress hysteresis specifies the limit of irreversible phenomena that happen during stress induced martensite (SIM) transformation. This investigation was carried out to examine stress

hysteresis behavior of nickel-titanium archwires in different temperatures. Two different brands of NiTi archwires including TrueFlex (superelastic wire) and 3M Unitek (shape memory wire) were studied by three-point bending test in 4 mm deflection. Each test was done in three clinically relevant temperatures of 22, 37 and 50°C. Differential scanning calorimetry (DSC) analysis was performed to determine the phases and transformation temperatures in wires. The results show that there are considerable and meaningful differences between the hysteresis of wires in each situation.

## Characterization of Minerals, Metals and Materials: Poster Session

Sponsored by: The Minerals, Metals and Materials Society, TMS Extraction and Processing Division, TMS: Materials Characterization Committee, TMS/ASM: Composite Materials Committee  
Program Organizers: Toru Okabe, University of Tokyo; Ann Hagni, Geoscience Consultant; Sergio Monteiro, State University of the Northern Rio de Janeiro - UENF

Sunday, 6:00-8:00 PM Room: 3009  
February 15, 2009 Location: Moscone West Convention Center

### A New Method of Cutting Blast for Vertical Shaft Excavation and Its Experimental Study: Zhang Yiping<sup>1</sup>; <sup>1</sup>Guizhou University

Based on cutting principle and technology development of vertical blasthole cut by stage and deck in vertical shaft excavation, combined with the merits of middle space charging and toe space charging, the reinforced cutting effect of central large-diameter blasthole and the method of cutting blast by stage and deck toe space charging for the vertical large-diameter blastholes is put forward and analyzed theoretically. This new cutting blast method is provided with the advantages of high blasthole using ratio, big cavity bulk, low rate of chunk, even lumpiness and relatively high energy using ratio. The parameters choice and practical effects of this cutting method were discussed after in-situ experiment. It shows that the decked delay time of 75ms-100ms is applicable.

### Analysis of the Contacting State of Specimen with Supports in Dynamic Fracture Tests by Modified Hopkinson Pressure Bar: Chunhuan Guo<sup>1</sup>; Ruitang Liu<sup>1</sup>; Yang Yang<sup>1</sup>; Yongdong Wang<sup>1</sup>; <sup>1</sup>Harbin Engineering University

Presently, problems existing in dynamic fracture experiments which are tested in Hopkinson bar are that the contacting state of specimen with supports is not very clear. In this paper, Experiments with standard Charpy specimens (10mm×20mm×100mm) of a structural steel are tested using modified Hopkinson pressure bar and strain gage techniques. The initial results indicate that the bouncing of specimen from supports in impact loading instant is observed, i.e. the contact of specimen with supports is lost and that the pre-crack in specimen is initiated under the condition of one-point-bending. The effect of span(S) on the bouncing behaviors of the specimen is important, and the critical span size in the test is obtained, that is, when  $S \leq 67.5\text{mm}$ , the specimen always keeps in contact with supports during loading process. In addition, the studies about the size effect of specimens in this test are ongoing.

### Carbon Compound as Anode Material Electrode in Super Lithium Ion Capacitor: Li Jie<sup>1</sup>; Yang Juan<sup>1</sup>; Hao Xin<sup>1</sup>; Zhang Zhian<sup>1</sup>; Lai Yanqing<sup>1</sup>; Zhou Xiangyang<sup>1</sup>; <sup>1</sup>Central South University

Series of carbon compounds as anode materials were prepared for super lithium ion capacitor using graphite and active carbon (AC) as raw materials. Their electrochemical properties were investigated by constant current charge-discharge test. The results showed that the compound anode had good capacitive performance as well as Li-ion battery performance. The potential of the capacitor could be as high as 3.5V vs Li/Li<sup>+</sup> when compared with 2.5V vs Li/Li<sup>+</sup> in the AC-AC capacitor, accordingly, the energy density increased from 21.7Wh/kg to 40.3Wh/kg. The compound anode also had excellent rate performance that as the current density increasing from 0.1A/g to 1A/g, the capacitance decreased only 1.3F/g, and good cycle performance that the capacitance holding remained 96.7% after 10 times cycles even at the highest potential of 3.5 V vs Li/Li<sup>+</sup>.

### Characterization of the SnO<sub>2</sub>:F/CdS:In Structures: Shadia Ikhmayies<sup>1</sup>; Riyadh Ahmad-Bitar<sup>2</sup>; <sup>1</sup>Applied Science Private University; <sup>2</sup>University of Jordan

SnO<sub>2</sub>:F/CdS:In bilayers were produced by the spray pyrolysis technique on glass substrates. The structures were characterized by recording and investigating their transmittance curves, I-V plots, x-ray diffractograms (XRD)

and by observing their scanning electron microscope (SEM) images. From the I-V plots it was found that the SnO<sub>2</sub>:F forms an ohmic or quasi-ohmic contact with CdS:In. XRD patterns show the polycrystalline nature of the films and show that there is a small shift in the position of the (200) line of SnO<sub>2</sub>:F without the appearance of new peaks. The morphology of the structures are compared with those of SnO<sub>2</sub>:F alone and CdS:In alone on glass substrates.

### Coating LiNi<sub>1/3</sub>Co<sub>1/3</sub>Mn<sub>1/3</sub>O<sub>2</sub> with ZnO Nano-Particles by Mechanical Solid-State-Chemistry-Reaction: Ping Yang<sup>1</sup>; Jing Zhan<sup>1</sup>; Chuan-fu Zhang<sup>1</sup>; Xi Dai<sup>1</sup>; You-qi Fan<sup>1</sup>; <sup>1</sup>Central South University

To improve the electrochemical performances, LiNi<sub>1/3</sub>Co<sub>1/3</sub>Mn<sub>1/3</sub>O<sub>2</sub> cathode materials have been coated with ZnO nano-particles by mechanical solid-state-chemistry-reaction. The structures and morphologies of the synthesized materials were investigated by XRD, SEM and TEM and the electrochemical performances of materials were studied within a voltage window of 2.75-4.3 V at current density of 170mAh/g. The results show that the surface of LiNi<sub>1/3</sub>Co<sub>1/3</sub>Mn<sub>1/3</sub>O<sub>2</sub> particles is coated with very fine ZnO composite but its structure is not affected by coated with 3% ZnO. The presence of a thin ZnO layer could suppress the reaction between the cathode and electrolyte, and remarkably decreases the charge transfer resistance, which is attributed to the improvement in the cyclic performance comparing the bare LiNi<sub>1/3</sub>Co<sub>1/3</sub>Mn<sub>1/3</sub>O<sub>2</sub>. It is proposed that surface treatment by mechanical solid-state-chemistry-reaction is a simple and effective method to improve the electrochemical performance of LiNi<sub>1/3</sub>Co<sub>1/3</sub>Mn<sub>1/3</sub>O<sub>2</sub>.

### Defects in Deformed Zircaloy 2: An Effort to Couple Observations from Different Analytical Techniques: S. Sahoo<sup>1</sup>; V. Hiwarkar<sup>1</sup>; I. Samajdar<sup>1</sup>; P. Pant<sup>1</sup>; P. Pujari<sup>1</sup>; G. Dey<sup>2</sup>; D. Srivastav<sup>2</sup>; R. Tiwari<sup>2</sup>; S. Banerjee<sup>2</sup>; <sup>1</sup>IIT Bombay; <sup>2</sup>BARC, Mumbai

Defect evolution during uniaxial cold compression and cold/warm rolling of fully recrystallized zircaloy 2 was extensively studied. An attempt has been made to correlate the observations obtained from various techniques; positron annihilation spectroscopy (PAS), x-ray diffraction (XRD), transmission electron microscopy (TEM) and electron backscattered diffraction (EBSD). Deformation twinning in compression samples had shown strong influence on positron lifetimes. Samples, where twinning was maximum had lowest positron lifetime and where twin decay was maximum had highest positron lifetime. In case of cold/warm rolled samples, the positron lifetimes decreased with increase in deformation temperature. This drop was relatively higher up to a deformation temperature of 200°C and thereafter it was lower to 400°C and 600°C. XRD estimated dislocation density and lattice strain increased with progressive compression. However for rolled samples, the results of dislocation density showed exactly similar trend as lifetime measurements and lattice strain gradually decreased with increase in deformation temperature.

### Electrical, Optical and Structural Properties of Vacuum Evaporated CdTe Thin Films: Shadia Ikhmayies<sup>1</sup>; Riyadh Ahmad-Bitar<sup>2</sup>; <sup>1</sup>Applied Science Private University; <sup>2</sup>University of Jordan

Polycrystalline CdTe thin films were prepared by vacuum evaporation on glass substrates. The I-V plots which were linear were used to find the resistivity. A value of 2.10×10<sup>6</sup> Ω.cm was obtained. The transmittance was measured in the wavelength range 400-1100 nm. The bandgap energy was found to be 1.48 eV. X-ray diffraction pattern shows that the material deposits in the zinc blend structure with one strong reflection from the C(111) plane. The scanning electron microscope image shows a uniform surface with a small density of large ( ) grains scattered on the surface.

### Influence of Particles Shape Characteristics of Galena on their Floatability Ground by Ball and Rod Mills: Mohammad Reza Aslani<sup>1</sup>; Bahram Rezaei<sup>2</sup>; Esmail Jorjani<sup>1</sup>; <sup>1</sup>Islamic Azad University, Tehran Science and Research Campus, Technical and Engineering Department; <sup>2</sup>Amirkabir University of Technology, Mining, Metallurgical and Petroleum Engineering Department

Crushing and grinding are factors that cause creation some changes in physical and chemical characteristics of processing materials such as distributions of sizes and shapes. In this research, experimental studies to determine the shape properties and floatability of galena were performed on the products of ball and rod mills. Shape properties have been stated in terms of common shape descriptors such as elongation, flatness, roundness, and relative width by measuring on the projections of particles using scanning electron microscope. The floatability characteristics of galena were determined by flotation technique using the laboratory flotation cell. Finally, some correlations were found between the shape properties and recovery rate of particles. The results have shown that



the recovery rate decreases with increasing roundness and relative width, that these particles are slow floatable, i.e., elongated and flatted particles having higher recovery rate indicated more hydrophobicity and are fast floatable.

**Liquid Metal Embrittlement of AISI 4340 Low Alloy Steel by Ga-In Eutectics:** Refael Levy<sup>1</sup>; Eugen Rabkin<sup>2</sup>; David Gorni<sup>1</sup>; Shimshon Bar - Ziv<sup>1</sup>; <sup>1</sup>RAFAEL Ltd.; <sup>2</sup>Department of Materials Engineering, Technion – Israel Institute of Technology

We studied the Liquid Metal Embrittlement (LME) of 4340 martensitic steel by liquid In-Ga eutectics. LME reduces the steel strength only in high strength notched specimens that were deformed in tension at low strain rates. The nucleation stages of LME were investigated using notched specimens that were deformed in liquid metal environment under sustained load, close to their fracture stress. After load was removed, the near-notch region was examined using SEM and AFM. A pre-fracture penetration (~10 μm) of liquid alloy along the grain boundaries associated with changes in the martensitic microstructure was observed. A significant decrease of notch tensile strength with decreasing deformation rate was found in the case of LME. The corresponding value of the deformation activation volume was in a good agreement with predictions of Nam-Srolovitz atomistic mechanism of LME [PRL vol. 99, No. 025501 (2007)].

**Mechanisms of Bioleaching of Phosphor from Phosphorous Iron Ore:** Li Qian<sup>1</sup>; Jiang Tao<sup>1</sup>; <sup>1</sup>Central South University, School of Minerals Processing and Bioengineering

The investigation on bio-dephosphorization from iron ore was conducted. The results show that there are two ways for bio-dephosphorization from iron ore, one is that thiobacillus ferrooxidans directly derive phosphorus from ore, the other is acid that metabolizing by thiobacillus ferrooxidans leaching, which is the more impotent one. Adding suitable pyrite can strengthen the process through providing nourishment and direct or indirect producing acid. From the analysis of E-pH graph of Fe-H<sub>2</sub>O system, it was concluded that Fe<sup>2+</sup> wouldn't be oxidized under sterile system in this potential and pH ranges. It obviously can conclude that the Thiobacillus ferrooxidans reduced the potential for the oxidization of Fe<sup>2+</sup> and made the oxidization would occur in the above pH and potential zone, so the bio-leaching process can proceed. From the analysis of E-pH graph of P-H<sub>2</sub>O system, it was concluded that H<sub>3</sub>PO<sub>4</sub> can exist steadily.

**Microstructure and Creep Properties of T6 Treated Ti-6Al-4V Alloy:** Bao Xianyu<sup>1</sup>; Tian Sugui<sup>1</sup>; <sup>1</sup>Shenyang University of Technology

By means of T6 heat treatment, creep properties measuring and microstructure observation, an investigation has been made into the influence of T6 treatment on the microstructure and creep properties of Ti-6Al-4V alloy. Results show that the deformation feature of the isothermal forged Ti-6Al-4V alloy during creep is that a large number of <a> dislocation slipping are activated on the basal planes, and the slipping of <a+c> dislocation is activated on pyramidal planes. After T6 treatment, the initial α phase displays an equiaxed morphology, and some of the β phase is distributed around the region of α phase, in which distributes some needle-like martensite phase, which enhances obvious the creep lifetimes of the alloy at 575 MPa and 400°C. The deformation mechanism of T6 state alloy during creep is that dislocations occur the single orientation slipping, namely, the slipping of <a+c> dislocation is activated on the pyramidal planes.

**Organic Radical Battery: Nitroxide Polymers as a Cathode-Active Material:** Yan Yuan<sup>1</sup>; Baizhen Chen<sup>1</sup>; Hui Xu<sup>1</sup>; Xichang Shi<sup>1</sup>; <sup>1</sup>Central South University

Stable nitroxyl polymers, such as poly(2,2,6,6-tetramethyl-1-piperidinyloxy-4-yl methacrylate) (PTMA), are known to be effective as cathode active materials for lithium rechargeable batteries. The nitroxide radicals displayed a reversible and very rapid redox performances. We present a new synthesized method to get PTMA powder, then a doctor-blading method was used to prepare the PTMA composite electrodes, enabling successful production of homogeneous electrodes. It was characterized through FT-IR and SEM methods. The organic radical battery consists of lithium metal anode and PTMA cathode with an active material content of 65wt.%. The best performance is achieved with a thin cathode that shows nearly 100% utilization of the active material (-111mAh/g) at 0.1C. Through the electrochemical tests, it was found that there was a stable plateau at 3.65V while discharging. Besides, the cycling stability and rate capability were measured in detail. Although they showed a certain quantity of irreversible capacity on the first cycle, the capacity stabilized after the second cycle.

**Preparation and Characterization of Porous Copper Powder by Thermal Decomposition of Complicated Copper Oxalate:** Chuanfu Zhang<sup>1</sup>; Youqi Fan<sup>1</sup>; Jianhui Wu<sup>1</sup>; Jing Zhan<sup>1</sup>; Ping Yang<sup>1</sup>; <sup>1</sup>Central South University

Based on Thermogravimetric and Differential Thermal Analysis (TG-DTA), porous copper powder is prepared by thermal decomposition of complicated copper oxalate. The effects of various conditions on the morphology, crystalline grain size and specific surface area of copper powder were investigated, including temperature, time, mixing ratio and flow rate of gas, and the heating rate. Furthermore, composition and morphologies of the products were characterized by X-ray Diffraction (XRD), Scanning Electron Microscope (SEM) and BET adsorption isotherm. It is found that porous copper powder was produced under optimal conditions. The specific surface area is over 5.74 m<sup>2</sup>·g<sup>-1</sup>, and average pore size in particles is about 30.3 nm. After comparison of SEM images, the final product Cu well inherits the morphology of the precursor, thus a mechanism of in-situ decomposition is proposed.

**Study on Deeply De-Magnesium Oxide from Phosphate Ores by Floatation:** Zhang Qin<sup>1</sup>; Chen Wei<sup>1</sup>; Qiu Yueqin<sup>1</sup>; Mao Song<sup>1</sup>; Liu Zhihong<sup>1</sup>; Tang Yun<sup>1</sup>; <sup>1</sup>Guizhou University

Dolomite is main impurity mineral in phosphate ores. In practice of phosphate ores production, the grade of concentrates is only containing P<sub>2</sub>O<sub>5</sub> 31-32%. In this study, even the increasing of floatation reagent consumption and decreasing of floatation recovery, economic performance is estimated high according to the decreasing of H<sub>2</sub>SO<sub>4</sub> consumption in subsequent production of phosphate fertilizer and the increasing of products value. In floatation stage, influence factor include the synergism impacts of floatation collector, the consumption of H<sub>2</sub>SO<sub>4</sub> and other factors such as structure of flow sheet, stages, time, concentration of ore pulp, which were discussed respectively in this paper. The samples including raw material, concentrates and tailings were characterized by mineralogy, chemical analysis, the X-ray diffraction (XRD), scanning electron microscopy (SEM). The results show that the grade of concentration can reach to P<sub>2</sub>O<sub>5</sub> 36% by deeply de-magnesium oxide from phosphate ores, which yield a high added value.

**Study on Radioactive Contamination of Fly Ash in Guizhou:** Qiu Yue Qin<sup>1</sup>; Zhang Qin<sup>1</sup>; Cao Jianxin<sup>1</sup>; <sup>1</sup>Guizhou University

In Guizhou Province, most radionuclide and content of fly ash did not analyzed and the safety requirement did not restricted. In this study, the composition and content of the natural radionuclide of the main fly ash in Guizhou Province were determined and analyzed. The results show the scope and severity of radioactive contamination of fly ash in Guizhou. The scientific and feasible countermeasures were exhibited in this paper.

**Synthesis and Characterization of Complicated Copper Oxalate Precursor Powder by Complexing Precipitation Method:** Chuanfu Zhang<sup>1</sup>; Youqi Fan<sup>1</sup>; Jianhui Wu<sup>1</sup>; Jing Zhan<sup>1</sup>; Ping Yang<sup>1</sup>; <sup>1</sup>Central South University

Complicated copper oxalate precursor powder was prepared using ammonium oxalate as precipitating agent in the Cu(II)-C<sub>2</sub>O<sub>4</sub><sup>2-</sup>-NH<sub>3</sub>-NH<sub>4</sub><sup>+</sup>-H<sub>2</sub>O system. The composition and morphology of the powder are characterized by chemical analysis, X-ray Diffraction(XRD), Scanning Electron Microscope (SEM), Infrared spectroscopy(IR), Thermogravimetric and Differential Thermal Analysis(TG-DTA). The effects of temperature, copper ion concentration, pH value, addition of ethanol are investigated. It's indicated by the experimental results that precursor of copper oxalate is prepared below a critical pH value, whereas the precursor turns to be a complicated copper salt while over the pH value. Conclusively, homogeneous belt aggregation powder is synthesized under the optimized conditions: 50~60°, 0.4 mol·L<sup>-1</sup> copper ion concentration, pH value 6.4~6.8.

**Synthesis and Electrochemical Characteristics of Li(Ni<sub>1/3</sub>Co<sub>1/3-x</sub>M<sub>x</sub>O<sub>2</sub>(M=Ti, Mg) Cathode Material by Oxalate Precursor:** Chuan-fu Zhang<sup>1</sup>; Ping Yang<sup>1</sup>; Jing Zhan<sup>1</sup>; Xi Dai<sup>1</sup>; Yin-liang Zhang<sup>1</sup>; <sup>1</sup>Central South University

Li(Ni<sub>1/3</sub>Co<sub>1/3-x</sub>Mn<sub>1/3</sub>)M<sub>x</sub>O<sub>2</sub>(M=Ti, Mg) cathode materials were prepared from LiOH·H<sub>2</sub>O and oxalate precursor. The physical and electrochemical properties were studied by XRD, SEM, cyclic volt-ampere (CV), AC impedance and constant current charge-discharge. The results show that crystal volume of Ti<sup>4+</sup> or Mg<sup>2+</sup> doped sample is increasing and the electrochemical reaction resistant R<sub>ct</sub> is decreased at high rate, improving the cyclic performance and rate capability. The effect of Ti<sup>4+</sup> doped is better than Mg<sup>2+</sup>. The sample is well crystallized and simple pure phase with a-NaFeO<sub>2</sub> layered structure when doping quantity x=0.025. The second specific discharge capacity of Li(Ni<sub>1/3</sub>Co<sub>1/3,0.025</sub>Mn<sub>1/3</sub>)Ti<sub>0.025</sub>O<sub>2</sub> is

143.2mAh/g at 1C, 128.0mAh/g at 2C in the voltage of 2.75–4.3V, and still has 140.7mAh/g and 121.7mAh/g after 20 cycles, respectively, keeping 98.25%, 95.07% capacity.

### Electrode Technology for Aluminum Production: Light Metals Division Poster Session

Sponsored by: The Minerals, Metals and Materials Society, TMS Light Metals Division, TMS: Aluminum Committee  
Program Organizers: Barry Sadler, Net Carbon Consulting Pty Ltd; John Johnson, RUSAL Engineering and Technological Center LLC

Sunday, 6:00-8:00 PM Room: 2001  
February 15, 2009 Location: Moscone West Convention Center

### Boron Salt Inhibitors of Air Reactivity of Prebaked Carbon Anodes – Literature Review and Laboratory Studies: Rafael Tosta<sup>1</sup>; Evelyn Inzunza<sup>1</sup>; Luisa Delgado<sup>2</sup>; <sup>1</sup>CVG Aleasa; <sup>2</sup>Universidad Simón Bolívar

The anode carbon consumption in a reduction cell for the aluminum production depends on many factors among those that are included the raw materials, the factory processes, the design of the cell, the current efficiency and the operations of the cell. In the protection of prebaked carbon anodes, they are something well known the kindness of the boron against the oxidation for air and although the contamination could exist in the electrolytic reduction cells on the part of the boron, the one impregnated selective of carbon anodes will reduce to the minimum the presence of boron in the molten metal. The use of a modifier of the structure of the film inhibitor will reduce even more the proportions of boron to use without reducing the resistance to the oxidation. This allowed assuring the efficiency of the boron in the protection of carbon anodes against the oxidation for air.

### Empiric Mathematical Models for Real Density of Calcined Coke Based on Industrial Data: Edinaldo Silva<sup>1</sup>; Deovaldo Júnior<sup>2</sup>; Aldo Santos<sup>2</sup>; Marco Giulietti<sup>3</sup>; Silas Derenzo<sup>3</sup>; <sup>1</sup>Petrocoque S.A. Indústria Comércio; <sup>2</sup>Santa Cecília University; <sup>3</sup>IPT - Intitute for Technological Research

The production of green coke provides additional gain to refineries due to the increase of light fractions such as LPG, gasoline, diesel oil and by reduction of sulphur and metals in these fuels. After calcination, green coke is used by aluminum, iron, re-carburizing and titanium dioxide industry. The high quality of the coke is indicated by the consistency of the real density, which is, according to the literature, function of calcining conditions of green coke. The following work has aimed at making mathematics models based on industrial data for the prediction of real density of calcined petroleum coke. For the confection of the mathematical model, it was applied the software "Table Curve 3D". The results for the proposed models indicated that the highest coefficient of correlation ( $r=0.30$ ) was obtained under following process condition: a) calcining temperature and b) feeding rate of the calcining kiln.

### Analysis of Sodium and Cryolite Bath Penetration in the Cathodes Used for Aluminum Electrolysis: Jilai Xue<sup>1</sup>; Wenli Ou<sup>1</sup>; Jun Zhu<sup>1</sup>; Qingsheng Liu<sup>1</sup>; <sup>1</sup>University of Science and Technology Beijing

Quantitative analysis of penetrated sodium and bath is very important in evaluating carbon cathode property and service life. In this work, sodium and bath components in the cathode samples used for aluminum electrolysis were analyzed using quantitative XRD, chemical titration, SEM-EDS techniques. The samples were sliced along their axis and each piece was analyzed to obtain a concentration profile of the penetrated sodium and bath components against the penetration depth. A sodium front was found ahead of the penetrated NaF and Na<sub>3</sub>AlF<sub>6</sub>, which formed a peak at 3.5% in the curve of Na concentration vs. penetration depth. The penetrated NaF and Na<sub>3</sub>AlF<sub>6</sub> also showed the peaks at 2.5 % and 20%, respectively, in their concentration curves following the Na front. Various chemical reactions within the cathode materials are discussed against their possible effects on the Na and bath penetration.

### Numerical Analysis of the Anode Voltage Drop of a Reduction Cell: Wangxing Li<sup>1</sup>; JieMing Zhou<sup>2</sup>; Yiwen Zhou<sup>1</sup>; <sup>1</sup>Zhengzhou Research Institute of CHALCO; <sup>2</sup>School of Energy and Power Engineering, Central South University

About 7~9% of the overall cell voltage of a modern Hall-Heroult cell is the anode voltage drop. It contributes a significant fraction of the cell's overall power consumption. The paper presents Finite Element Method simulation results of

anode voltage drop. The purpose of the work is to determine the constituents of the anode voltage drop and to consider possible design modifications to lower the anode voltage drop. The influences of anode carbon material, carbon shape, stub shape, and contact condition on anode voltage drop were analyzed. The paper presents the ideal design of the anode.

### Magnesium Technology 2009: Poster Session - Magnesium and Its Alloys

Sponsored by: The Minerals, Metals and Materials Society, TMS Light Metals Division, TMS: Magnesium Committee  
Program Organizers: Eric Nyberg, Pacific Northwest National Laboratory; Sean Agnew, University of Virginia; Neale Neelameggham, US Magnesium LLC; Mihriban Pekguleryuz, McGill University

Sunday, 6:00-8:00 PM Room: 2006  
February 15, 2009 Location: Moscone West Convention Center

Session Chair: Eric Nyberg, Pacific Northwest National Laboratory

### Age Hardening Response of Mg-Ce-Al Alloys: Harpreet Brar<sup>1</sup>; Michele Manuel<sup>1</sup>; <sup>1</sup>University of Florida

The aim of this paper is to characterize the age hardening response of permanent mold cast Mg-Ce-Al alloys containing various strengthening precipitates. Several compositions were designed using the PANDAT software system and a proprietary Mg alloy database to precipitate various phase fractions of Al<sub>3</sub>Ce and Al<sub>11</sub>Ce<sub>3</sub> strengthening phases. Of particular interest is the Al<sub>3</sub>Ce phase having a DO19-type ordered crystal structure, which has been shown to have a high lattice coherency with the HCP lattice. The coherency of the DO19 precipitates promotes greater strengthening of the alloy. The alloys were aged for different times and their hardness was measured to determine solution and precipitation strengthening contributions to the peak hardness.

### Crack Behavior of Magnesium Alloys Studied Using a CamScan Microscope: Dafei Kang<sup>1</sup>; Martin Crimp<sup>1</sup>; <sup>1</sup>Michigan State University

Magnesium alloys are receiving increasing attention as they are potentially good candidate materials for a range of applications, particularly in the automotive industry. Their promising properties, for instance, high specific strength and low density, make them likely substitutes for conventional heavier materials such as cast iron, steel, and at some cases even aluminum. In this paper, the crack behavior of some magnesium alloys are examined in a CamScan FE microscope equipped with EBSD/OIM capacity.

### Determination of Mushy Zone Mechanical Properties of a Magnesium Alloy: Partha Saha<sup>1</sup>; Srinath Viswanathan<sup>1</sup>; <sup>1</sup>University of Alabama

The mushy zone tensile behavior of magnesium alloy MRI 206 was determined using a Gleeble 1500D thermo-mechanical simulator. A protective atmosphere of CO<sub>2</sub> + 0.5% SF<sub>6</sub> mixed gas was used during the tests. Various specimen geometries were investigated in order to develop an isothermal zone along the specimen gauge length. It was observed that grip materials and contact area have a profound effect on the temperature profile distribution along the specimen free span. Tensile deformation tests were conducted at varying strain rates and fraction solid. The results are compared with data obtained previously for aluminum 3004 alloy.

### Effect of Grain Size on Corrosion Behavior of Squeeze Cast AJ62 Magnesium Alloy in Salt Solution and Automotive Coolant: Lihong Han<sup>1</sup>; Xueyuan Nie<sup>1</sup>; Qiang Zhang<sup>1</sup>; Zhizhong Sun<sup>1</sup>; Henry Hu<sup>1</sup>; <sup>1</sup>University of Windsor

AJ62 magnesium alloy was prepared by squeeze casting. The fine grain structure formed in the thin skin layer close to the surface of the castings while the central region of the casting exhibited coarse microstructure. The potentiodynamic polarization and the electrochemical impedance spectroscopy (EIS) experiments were performed by using EC-LAB SP-150 electrochemical apparatus to investigate the corrosion resistances of the AJ62 alloys with different grain sizes in a salt solution and automotive coolant. The electrochemical behavior of fine microstructure was compared with that of coarse-grained AJ62 alloy. The effect of grain size on the corrosion behavior including the intergranular corrosion rate and pitting corrosion resistance was analyzed, and the mechanisms of corrosion were discussed.



**Effect of Thermo-Mechanical Treatment on Texture Evolution of Twin-Roll Cast Mg Alloys with Various Second Phase Particles:** *Kyung Hun Kim*<sup>1</sup>; G. T. Bae<sup>1</sup>; J. H. Bae<sup>1</sup>; D. H. Kang<sup>1</sup>; Nack Kim<sup>1</sup>; <sup>1</sup>Pohang University of Science & Technology

Recent development of twin-roll casting technology has shown that it can efficiently produce low cost, high performance Mg alloy sheet products. They are usually subjected to thermo-mechanical treatment (TMT) such as warm rolling to modify the microstructure so that optimum combination of mechanical properties can be obtained. Among various microstructural features, grain size and texture would be mostly affected by TMT. It is of common knowledge that the poor ductility of wrought Mg alloys is due to the strong basal texture developed during TMT and thus it is important to modify the texture of Mg alloys by various TMTs. In the present study, effect of TMT on the texture evolution has been investigated. Alloy systems investigated are ZM, ZMA, and ZE alloys which have different types of second phase particles. Correlation between the texture and tensile properties will be made and the effect of TMT conditions.

**Effects of KCl on Electrical Conductivity of BaF<sub>2</sub>-LiF-MgF<sub>2</sub> Electrolyte:** *Ying Nie*<sup>1</sup>; Shaohua Yang<sup>1</sup>; Zhaowen Wang<sup>1</sup>; Xianwei Hu<sup>1</sup>; Linzhi Ma<sup>1</sup>; <sup>1</sup>Northeastern University

This paper studies on the preparation of Al-Mg alloy from MgO by molten salt electrolysis method. BaF<sub>2</sub>-LiF-MgF<sub>2</sub> is taken as electrolyte. The CVCC method was used to measure electrical conductivity of the electrolyte. The experimental results indicated that KCl as additive can obviously improve the electrical conductivity of the electrolyte. The electrical conductivity of the electrolyte was increased with the increase of temperature and also the KCl content. The electrical conductivity of electrolyte increased from 1.4500S•cm<sup>-1</sup> to 2.0272S•cm<sup>-1</sup> with the mass percentage of KCl from 0 to 11% under the temperature of 850°C, the increased value is 0.5772S•cm<sup>-1</sup>.

**Influence of Strontium Addition on Tensile Properties of Squeeze Cast AM60 Alloy:** *Shuping Wang*<sup>1</sup>; Henry Hu<sup>1</sup>; <sup>1</sup>University of Windsor

The effect of strontium content on the tensile properties of squeeze cast Mg-Al-Sr alloy was investigated. Three different strontium contents, 0, 1.5, and 3.0 wt%, were added to Mg-6 wt.% Al alloy (AM60 alloy) and squeeze casting under the applied pressure of 30 MPa. The results of tensile testing indicate that the ultimate tensile strength (UTS), yield strength (YS) and elongation (Ef) of the squeeze cast Mg-Al-Sr alloy decreased with increasing strontium content. Microstructural analysis indicated that Sr content influences a number of phases present in the squeeze cast Mg-Al-Sr alloys. Also, Sr addition decreased the grain size of the alloys with increasing the strontium content. However, the increase in porosity level by Sr addition, which seems to offset its grain refinement effect, should be responsible for the decrease in tensile properties.

**Microstructure and Properties of Mg-Al-Zn(Sm) Alloys:** *D. H. Xiao*<sup>1</sup>; <sup>1</sup>Central South University

Mg-9.0Al-0.8Zn alloys with 0.3%Sm were prepared by casting. The effects of scandium addition on the microstructure and mechanical of the alloys before and after heat extrusion have been investigated using microscopy analyzing and mechanical properties testing. It has been shown that the based alloys structure is mainly composed of α-Mg matrix, Mg17Al12 phase and MgAlSm phase when samarium was added. The samarium addition improves the morphology and distribution of Mg17Al12 phase. Such improved microstructure is accompanied by the improvement of mechanical properties of the extruded alloy at room temperature and high temperature. At this condition, the tensile strength and elongation of the alloy with Sm are 325 MPa and above 11% at the room temperature.

**Microstructures and Mechanical Properties of the Recrystallized Mg-Zn-MM-Sn Alloy Sheets:** *Beomsoo Shin*<sup>1</sup>; Heon Kang<sup>1</sup>; Donghyun Bae<sup>1</sup>; <sup>1</sup>Yonsei University

Microstructures and mechanical properties of the recrystallized Mg-Zn-MM-Sn alloy sheets, fabricated via rolling after gravity casting, were investigated. Dynamic recrystallization(DRX) occurs during hot rolling and static recrystallization(SRX) is achieved by heat treatment after cold rolling. The final grain size developed after SRX and DRX was significantly varied; the average grain sizes are measured to be 4~6 μm and 15~20 μm after SRX and DRX, respectively. Furthermore, the SRXed sample exhibits weaker crystallographic texture than the DRXed one. To investigate effects of recrystallization methods on mechanical properties, uniaxial tension tests were performed on the alloy sheets at varied temperatures and strain rates. As a result, the recrystallized Mg-

Zn-MM-Sn alloy shows superior elongations at high strain rates of 10<sup>-1</sup>s<sup>-1</sup>, 10<sup>-2</sup>s<sup>-1</sup> and elevated deformation temperatures, i.e. 150 ~ 250 °C than those of AZ31 magnesium alloys. The relation between ductility and grain morphology will be also presented in detail

**Relationship between Internal Porosity and High Cycle Fatigue Property of Die-cast Magnesium AZ91D Alloy:** *Won-Guk Kang*<sup>1</sup>; Jeoung-Han Kim<sup>2</sup>; Sang-Bok Lee<sup>2</sup>; Jung-Chul Park<sup>3</sup>; *Kee-Ahm Lee*<sup>1</sup>; <sup>1</sup>Andong National University; <sup>2</sup>KIMM; <sup>3</sup>RIST

High cycle fatigue properties for two different die-cast magnesium AZ91D alloys with different amount and size distribution of internal porosity were investigated. Mechanical fatigue tests were conducted under R=0.1 and 80Hz frequency condition at room temperature. The fracture surfaces and grip regions of selected specimens were examined with scanning electron microscopy. It was found that internal porosity highly influences the mechanical and fatigue properties, reducing significantly the values of elongation, tensile strength and especially high cycle fatigue strength. The difference in cycles to fatigue failure was mainly attributed to a drastic difference in nucleation site size, with ranged from several hundred μm's to several mm's. Fatigue cracks initiated at internal porosity cluster within the specimen and near the surface, depending on the relative cluster size and propagated primarily through the β-Mg<sub>17</sub>Al<sub>12</sub> particle laden interdendritic regions. Effects of size distribution and amount of porosity on fatigue property were also discussed.

**Tensile and Compressive Deformation behavior of Ca-containing AZ31 Extrudes:** *Chang Yim*<sup>1</sup>; Na Eun Kang<sup>2</sup>; Jeoung Han Kim<sup>1</sup>; Bong Sun You<sup>1</sup>; Hyeong Kyu Park<sup>3</sup>; <sup>1</sup>Korea Institute of Materials Science; <sup>2</sup>Metals Bank; <sup>3</sup>Korea Institute of Geoscience and Mineral Resources

The deformation behavior of Ca-containing AZ31 extrudes during tensile and compressive loading parallel to extrusion direction was characterized experimentally under various strain rates and temperatures. The ultimate tensile strength and maximum compressive strength were increased with increasing of strain rate and amount of Ca and decreasing of temperature. The shape of compressive flow curves was different from the shape of tensile flow curves. Tensile flow curves showed a typical convex shape showing strain hardening after yielding, but during compressive loading concave flow curve was observed in initial plastic deformation region due to activation of deformation twin as additional deformation mode. After peak stress, the flow stress was decreased gradually with continuing the deformation under tensile loading, but the flow stress was sustained constantly under compressive loading.

**Tracing Nucleation and Grain Growth during Static Recrystallization of Pure Mg by EBSD:** *Jianxin Zou*<sup>1</sup>; Jayant Jain<sup>1</sup>; Chadwick Sinclair<sup>1</sup>; <sup>1</sup>University of British Columbia

The "nucleation" of new grains and their subsequent growth during static recrystallization of uniaxially compressed, commercially pure Mg have been investigated using Electron backscattered diffraction (EBSD). The pure Mg samples were uniaxially compressed at room temperature and specific regions were selected from the as-deformed microstructure to follow during isothermal annealing at 573K. Our results illustrate the heterogeneous nature of recrystallization within pure Mg. This heterogeneity can be linked to the underlying deformation mechanisms operative in individual grains. As such, the recrystallization response appears to depend strongly on factors such as crystallographic orientation and starting grain size. The results gathered here clearly show the importance of local deformation state on the recrystallization process and final recrystallized grain structure within pure Mg.

**Very High Cycle Fatigue (VHCF) of Thixomolded® AZ91D Magnesium Alloy: Effect of Porosity and Aging Heat-Treatments:** *Raghavendra Adharapurapu*<sup>1</sup>; Andrew Sharp<sup>1</sup>; Chris Torbet<sup>1</sup>; J Jones<sup>1</sup>; Tresa Pollock<sup>1</sup>; <sup>1</sup>University of Michigan

The very-high-cycle-fatigue behavior of Thixomolded® magnesium alloy AZ91D in the 10<sup>6</sup>-10<sup>9</sup> cycles regime has been studied. Fatigue experiments were conducted in an ultrasonic fatigue testing machine at ~19kHz in materials with varying casting porosity and aging heat-treatments. Fatigue properties of as-cast, naturally-aged (5 years, 20° C), hot-isostatically pressed (HIP-ed)+solution-treated (ST) and HIP+ST+peak-aged material have been characterized. The HIP process removed only solidification-induced porosity, while the gas porosity remained. The porosity in the as-cast alloy was measured to be 2.33±0.30% compared to 1.64±0.76% for HIP-ed samples and 2.14±0.50% for HIP-ed+ST samples. A comparison of the fatigue behavior of AZ91D produced by different

routes, viz., die-casting and Thixomolding®, indicated a higher endurance limit for the latter due to lower internal porosity of the castings. Fractographic analysis was carried out in all cases to correlate the porosity to the overall fatigue behavior and to examine the fatigue fracture surfaces.

### Materials for High Temperature Applications: Next Generation Superalloys and Beyond: Poster Session

Sponsored by: The Minerals, Metals and Materials Society, TMS Structural Materials Division, TMS: High Temperature Alloys Committee, TMS: Refractory Metals Committee  
Program Organizers: Joseph Rigney, GE Aviation; Omer Dogan, National Energy Technology Laboratory; Donna Ballard, Air Force Research Laboratory; Shiela Woodard, Pratt & Whitney

Sunday, 6:00-8:00 PM Room: 3010  
February 15, 2009 Location: Moscone West Convention Center

### Aging Effects on the High Temperature Tensile Behavior of Inconel 718 Superalloy: Hui-Yun Bor<sup>1</sup>; Chao-Nien Wei<sup>1</sup>; Chen-ming Kuo<sup>2</sup>; Yan-Tang Yang<sup>2</sup>; Chao-Chung Tai<sup>2</sup>; <sup>1</sup>Chung-Shan Institute of Science & Technology; <sup>2</sup>I-Shou Univ

Standard heat treatment (HT1) for Inconel 718 superalloy is solid solution at 1095°C, 1h/AC, then aging at 955°C, 1h/AC + 720°C, 8h/FC 48°C/h to 620°C, 8h/AC. In order to study the aging effects of delta phase, two more conditions were studied in this research, namely, HT2 (no aging condition 955°C, 1h/AC) and HT3 (955°C, 3.5h/AC). Tensile tests using servohydraulic MTS system were performed at room temperature, 350°C, 450°C, 550°C, and 650°C. Since HT2 produces no delta phase, elongation to failure are the largest among these three aging conditions. Increasing the 955°C aging time, the UTS and yield stress raise, because platelet delta phase is more uniformly nucleated and more direction oriented at grain boundaries. The fractographics of tensile specimens show that both inter-granular and trans-granular fractures are observed in HT2 specimens, nevertheless, only inter-granular fracture is observed in the other two cases.

### Comparative Oxidation Study of High Temperature Superalloy Fibers for Turbomachinery Sealing Applications: Huseyin Kizil<sup>1</sup>; Mahmut Aksit<sup>2</sup>; <sup>1</sup>Istanbul Technical University; <sup>2</sup>Sabancı University

Demand for increased power and efficiency placed superalloys in the cornerstone of most high temperature engineering applications. Use of such materials in fiber form at elevated temperatures is not desirable due to high surface to cross-section ratio. Recently, fiber components find use in contact applications in turbomachinery due to their superior wear performance. Although oxidation behavior of cobalt and nickel based alloys is well characterized in bulk form, aggravation caused by high surface to cross-section ratio requires detailed oxidation evaluation of these fibers. Present study investigates oxidation performance of eight different cobalt and nickel based superalloy fibers. Although both cobalt and nickel based fibers show similar oxidation performance at lower temperatures, nickel based fibers exhibit superior performance as exposure temperature is raised to 1100°C. The results indicate that application of cobalt based fibers should be limited by 900°C due to poor oxidation performance.

### Crack Growth Behavior of Alloy 276 as Functions of Temperature and Load Ratio: Joydeep Pal<sup>1</sup>; Muhammad Hasan<sup>1</sup>; Ajit Roy<sup>1</sup>; <sup>1</sup>University of Nevada, Las Vegas

Austenitic nickel-base Alloy 276 has been considered as a structural material for nuclear hydrogen generation using a thermochemical cycle. In view of fluctuations in temperature during operations, this alloy may undergo thermal cyclic loading and experience crack propagation in the presence of minute flaws present in this alloy. This paper presents the results of a crack propagation study under cyclic loading (da/dN) at ambient and elevated temperatures under different load ratios (R). The data indicate that the magnitude of da/dN under a steady-state condition at all three R values (0.1, 0.2 and 0.3) was maximum at higher temperatures. Further, temperature did not influence the magnitude of threshold stress intensity range ( $\Delta K_{th}$ ) at a constant R value. However, the magnitude of  $\Delta K_{th}$  was reduced at higher R values, irrespective of the testing temperature. The overall da/dN vs.  $\Delta K$  data will be substantiated with the results of fractographic evaluations.

### Effect of Rare Earth Elements on the Isothermal Oxidation Behavior of CM247LC, a Polycrystalline Ni-Base Superalloy: Krishna Ganesan<sup>1</sup>; Gerhard Fuchs<sup>1</sup>; Cynthia Klein<sup>2</sup>; Allister James<sup>2</sup>; <sup>1</sup>University of Florida; <sup>2</sup>Siemens Power Corporation

Minor additions of Rare Earth Elements (REE) to superalloys can lead to dramatic improvements in high temperature oxidation properties by retarding oxide scale growth rate and increasing the scale adherence under thermal cycling conditions. In this work, effect of ppm level additions of REE on the isothermal oxidation behavior of CM247LC was investigated. Fully heat treated superalloy samples were exposed to oxidizing conditions at elevated temperatures for an extended time. Comparison between different REE additions was based on weight gain data which was also used to establish the oxidation kinetics. Examination of oxide scales, internal oxidation stringers and inter-diffusion zone (IZ) was done using SEM and EPMA line scans on samples exposed for varying oxidation times. XRD was performed to identify the oxide phases while detailed analysis of IZ was done using TEM for understanding the role of REE in the oxidation mechanism.

### Effects of Cyclic Loading, Temperature and Load Ratio on Plastic Deformation of Alloy 617: Muhammad Hasan<sup>1</sup>; Joydeep Pal<sup>1</sup>; Ajit Roy<sup>1</sup>; <sup>1</sup>University of Nevada, Las Vegas

Hydrogen generation is currently being considered under both Nuclear Hydrogen Initiative and Next Generation Nuclear Plant programs. The structural materials to be used in both programs will experience elevated temperatures approaching 950°C. Nickel-based austenitic Alloy 617 has been identified to be a suitable material by the United States Department of Energy for such applications. Substantial data have recently been generated on this alloy with respect to the effect of temperature and load ratio (R) on its crack propagation rate under cyclic loading (da/dN). The results indicate that the magnitude of da/dN was enhanced with a reduction in R value within the steady-state-region for all three tested temperatures. The magnitude of stress intensity range at constant R values remained identical despite a variation in testing temperature. Fractographic evaluations revealed a combination of striations and dimples on the fracture surfaces of the tested specimens. The comprehensive results are presented in this paper.

### High Temperature Oxidation Behavior of SiO<sub>2</sub> Protective Layer Coated IN738LC Superalloy Using Combustion CVD (CCVD): SeungKeun Oh<sup>1</sup>; Youngman Kim<sup>1</sup>; Sang Ryu<sup>1</sup>; YangHong Kim<sup>1</sup>; <sup>1</sup>Chonnam National University

IN738LC is a Ni-based superalloy for high temperature applications such as gas turbine blades for generator in power plants. The oxidation behavior of IN738LC is a major factor in determining the life time of material when it is exposed in air of high temperature. Protective coatings may be a solution to improve the stability of parts made of the alloy. The processing methods, such as thermal CVD, PECVD, and the combustion CVD (CCVD), may be applied for protective coatings on IN738LC. In this study, SiO<sub>2</sub> protective coating is applied to an IN738LC alloy by using CCVD. TEOs(C<sub>8</sub>H<sub>20</sub>O<sub>4</sub>Si) and HMDS (C<sub>6</sub>H<sub>19</sub>NSi<sub>2</sub>) were selected for the source material of the SiO<sub>2</sub> layer during CCVD. The oxidation resistance of the alloy was evaluated through TGA.

### Hot Cracking of Ni Based Superalloys: Joel Andersson<sup>1</sup>; Göran Sjöberg<sup>1</sup>; Aurélien Albuoussière<sup>2</sup>; <sup>1</sup>Volvo Aero Corp; <sup>2</sup>ENSICA Engineering Institute

The demand for aerospace materials that could sustain their desirable properties at even higher temperature together with processing characteristics that are better or comparable to that of alloy 718 is increasing not at least due to environmental aspects. Waspaloy which is used in the hotter sections in an aero engine because of its higher working capability compared to alloy 718 face some drawbacks as cost and processing are not as good. However, a newly developed alloy, Allvac 718Plus is claimed to have a working capability in between 718 (650C) and Waspaloy (750) with processing characteristics similar to that of alloy 718. In this study the susceptibility towards hot cracking of highly restrained welds in alloy 718, Waspaloy and Allvac 718Plus are investigated. Repair welding of machined grooves together with dsc and microscopy techniques for metallurgical investigation are performed.

### Interface Structure and Chemical Stability of Continuous Mo Wire Reinforced NiAl Composites: Jia Song<sup>1</sup>; Weiping Hu<sup>1</sup>; Günter Gottstein<sup>1</sup>; <sup>1</sup>Institute of Physical Metallurgy and Metal Physics

Refractory metal Mo has a high melting point (2617 °C), a high strength (about 500~700 MPa) associated with a good ductility (> 15% at fracture elongation) at room temperature as well as good thermal conduction and good



thermal stability at high temperatures. Due to these valuable properties it has been tried in the present study to reinforce NiAl with continuous Mo wires in order to improve the ductility at RT and enhance the creep resistance at high temperatures of NiAl. The diameter of the used Mo wire is 125  $\mu\text{m}$ . Mo wire reinforced NiAl composites were produced as following: at first, the Mo wires were coated with NiAl by PVD. The coating thickness is about 20~50  $\mu\text{m}$  that is corresponding to about 30~50% volume fraction of Mo wire. The matrix-coated Mo wires were then put into a channel die for diffusion bonding. The hot pressing parameters were at 1300°C under 40 MPa in vacuum for 1 hour. Interface structure and chemistry of the composites were characterized by means of electron microscopy (HRTEM, SEM) and microanalysis (EDX, EELS and electron diffraction). Results of micro-characterization demonstrated that a continuous brittle Mo<sub>3</sub>Al reaction layer with a thickness of about 5  $\mu\text{m}$  has been formed between Mo wire and NiAl matrix during diffusion bonding. Behind Mo<sub>3</sub>Al reaction layer inner Mo wire the Al concentration reached to about 1.6 at% that indicated an over-saturated dissolution of Al in Mo matrix. The formation of Mo<sub>3</sub>Al reaction layer and diffusion of Al into Mo caused Al-dilution in NiAl near interface and led to a deviation of matrix composition from the region far away from interface. Possible influence of the interface structure and chemistry on mechanical properties of Mo wire reinforced NiAl composites are discussed.

**Lattice Misfit Measurements of Ruthenium-Bearing Nickel-Base Superalloys:** *Jestine Ang*<sup>1</sup>; *Hon Tong Pang*<sup>1</sup>; *Vassili Vorontsov*<sup>1</sup>; *Howard Stone*<sup>1</sup>; *Catherine Rae*<sup>1</sup>; <sup>1</sup>University of Cambridge

Under intermediate creep conditions, a superalloy with a highly negative misfit will spontaneously develop a 'labyrinth' structure, rafting in all six <001> directions, irrespective of the direction of the applied stress; consequently, premature creep failure occurs. As there is generally a positive correlation between the refractory content and lattice misfit, we seek to quantify the effect of lattice misfit on creep, as this will enable us to determine the threshold of useful refractory element additions. A series of eight ruthenium-containing superalloys were designed using DoE to evaluate the effects of Co, Mo Ru and W on mechanical properties. Alloys with representative low, intermediate and high misfit values will be compared. Specimens used were interrupted at the end of primary creep. Misfit values calculated using the lattice parameters of  $\gamma$  and  $\gamma'$  measured at the high energy x-ray synchrotron facility, ESRF, will be compared to misfit values estimated by JMatPro®.

**Microstructural Analysis of Nickel Base Super Alloy, IN 738LC in Different Time Temperature Exposure:** *Babak Jahani*<sup>1</sup>; <sup>1</sup>Toos Gashtavar

Nickel base superalloys are widely used for gas turbine blading and other related parts at high temperatures. These alloys are vacuum melted and investment casted for high quality casts and heat treated to get excellent mechanical properties at high temperatures. The alloy used in this investigation was IN\_738LC and heat treatment adopted for this alloy is solution treatment at 1120 C for two hours and air cooled to the room temperature and then aged for 24 hours at 845 C. By means of scanning electron microscopy (SEM), hardness testing and EDS, the changes in characteristics during different aging times, the size of particles and characteristic of carbides have been studied. Room temperature hardness of the superalloy decreases with increasing in aging temperature. In the a specified temperature, the hardness of the alloy increases at first but after reaching to a peak, the hardness begins to decreasing.

**Microstructure and Mechanical Properties of Direct Aged 718Plus® Alloy:** *Erin McDevitt*<sup>1</sup>; *James Bentley*<sup>2</sup>; *Wei-Di Cao*<sup>1</sup>; <sup>1</sup>Allvac; <sup>2</sup>Oak Ridge National Laboratory

ATI 718Plus® alloy is a new gamma-prime strengthened Ni-based superalloy that has a 100°F increase in temperature capability compared to 718 alloy, good hot working characteristics and relatively low cost. Direct aging has been demonstrated to be effective at providing an increase in strength and a corresponding improvement in stress rupture performance. The fine scale microstructure of 718Plus in the direct-aged and solution-treated and aged conditions was characterized using analytical and conventional transmission electron microscopy. The elemental partitioning among the gamma-prime, delta, and austenite phases, the composition of the grain boundary delta-phase, and grain boundary segregation of Mo and Nb, will be discussed and compared to alloy 718. A portion of this research was conducted at the ORNL SHaRE User Facility, which is sponsored by the Division of Scientific User Facilities, Office of Basic Energy Sciences, U.S. Department of Energy.

**Oxidation Behavior of Inconel 617 Surface Treated by Al-Pack Cementation:** *Tae Sun Jo*<sup>1</sup>; *Sang Gil Park*<sup>1</sup>; *Dong-Seong Kim*<sup>1</sup>; *Ji Yeon Park*<sup>2</sup>; *Young Do Kim*<sup>1</sup>; <sup>1</sup>Hanyang University; <sup>2</sup>Korea Atomic Energy Research Institute

Inconel 617 is a candidate material for the high temperature applications such as turbine blades, structural materials for nuclear reactors, and high-temperature gas-cooled reactors. In this work, the oxidation behavior of Inconel 617 after Al-pack cementation was studied by exposure to air for 1000 hr at 950°C. Al-pack cementation was carried out at 800°C ~ 1000°C for 1 h in Ar using an Al<sub>2</sub>O<sub>3</sub> crucible containing the specimen and a powder mixture of Al : Al<sub>2</sub>O<sub>3</sub> : NH<sub>4</sub>Cl = 15g : 83g : 2g. The coating layer phase after Al-pack cementation was confirmed as NiAl and Ni<sub>2</sub>Al<sub>3</sub> by EPMA and XRD. The thickness of coating layer was increased with increasing temperature. After exposure at 950°C, the phase analysis of coating layer was carried out by TEM, SEM, and EPMA. The hardness of coating layer was measured by nanoindentation. The oxidation resistance and hardness of surface after Al-pack cementation have improved.

**Rapid Synthesis and Consolidation of Nanostructured WSi<sub>2</sub>-SiC from Mechanically Activated Powders by Pulsed Current Activated Heating:** *In-Jin Shon*<sup>1</sup>; *Jeong-Hwan Park*<sup>2</sup>; *Kee-Do Woo*<sup>2</sup>; *Jin-Kook Yoon*<sup>3</sup>; <sup>1</sup>Division of Advanced Materials Engineering, the Research Center of Industrial Technology, Chonbuk National University; <sup>2</sup>Division of Advanced Materials Engineering and the Research Center of Industrial Technology, Engineering College, Chonbuk National University; <sup>3</sup>Advanced Functional Materials Research Center, Korea Institute of Science and Technology

WSi<sub>2</sub> has an attractive combination of properties, including high melting temperature, high modulus, high oxidation resistance in air, and a relatively low density. To improve on its mechanical properties, the approach commonly utilized has been the addition of a second phase to form composite and to make nanostructured materials. Dense nanostructured WSi<sub>2</sub>-SiC composite was synthesized by pulsed current activated heating within 2 minute in one step from mechanically activated powders of WC and 3Si. Highly dense WSi<sub>2</sub>-SiC with relative density of up to 99.9% was simultaneously synthesized and consolidated under simultaneous application of a 80 MPa pressure and the pulsed current. The average grain sizes of WSi<sub>2</sub> and SiC were about 47 nm and 38 nm, respectively. The average hardness and fracture toughness values obtained were 1698 kg/mm<sup>2</sup> and 4.8 MPa•m<sup>1/2</sup>, respectively. The present fracture toughness and hardness are higher than those(3.3 MPa•m<sup>1/2</sup>, 1375 Kg/mm<sup>2</sup>) of monolithic WSi<sub>2</sub>.

**Study of the Effects of Fe and Ti Additions on the Microstructure of Nb-18Si-5Sn Based Alloys:** *Panayiotis Tsakiroopoulos*<sup>1</sup>; *Nikos Vellios*<sup>2</sup>; <sup>1</sup>The University of Sheffield; <sup>2</sup>University of Surrey

In developmental Nb silicide based alloys improvement of their environmental behaviour has been reported when alloying with Fe, Sn and Ti. In the presence of Cr and Ti and the absence of Sn in the aforementioned alloys, the addition of Fe is claimed to enhance the formation of Laves phase, and thus to be beneficial regarding oxidation. However, there is very limited literature regarding the role of Fe and Sn in the microstructure of Nb silicide alloys in the absence of Cr. The motivation for this work was to study the synergistic effects of Sn and Fe in the presence of Ti on the microstructure of Nb-18Si silicide based alloys. The paper will discuss the role of Fe in phase selection with particular reference to the niobium solid solution, Nb<sub>3</sub>Sn, the niobium Nb<sub>3</sub>Si and 5-3 silicides, alphaNb<sub>5</sub>Si<sub>3</sub> and betaNb<sub>5</sub>Si<sub>3</sub>, and Laves phase as well as the hardness of the silicides.

**TEM Observation of Ti-47Al-2Cr Alloy, Refined by Cyclic Heat Treatment:** *Hesam Shakoorian*<sup>1</sup>; *Saeed Heshmati-manesh*<sup>1</sup>; *Mahmoud Nili-ahmadabadi*<sup>1</sup>; *Hassan Ghassemi Armaki*<sup>2</sup>; <sup>1</sup>University of Tehran; <sup>2</sup>Tohoku University

TiAl intermetallics are excellent candidates for high temperature applications for their unique properties. However, they suffer from severe embrittlement and low formability at room temperature. Grain refinement could be a solution for this problem and could improve ductility and formability at low temperatures. In this research, the grain refinement of Ti-47Al-2Cr alloy was achieved by cyclic heat treatment. In each heat treatment cycle Massive transformations was formed. The microstructure was investigated by optical and transmission electron microscopy. Some defects such as stacking faults were observed in the microstructures resulted from massive transformation. It is supposed that formation of these faults play an important role during grain refinement. Finally, the optimum heat treatment route was selected and the mechanism of the grain refinement was discussed by means of electron microscopy.

**Temperature Dependence of the Lattice Misfit of Rhenium and Ruthenium Containing Nickel-Base Superalloys:** *Steffen Neumeier*<sup>1</sup>; Sigrid Schwub<sup>1</sup>; Florian Pyczak<sup>2</sup>; Mathias Göken<sup>1</sup>; <sup>1</sup>University of Erlangen-Nuremberg; <sup>2</sup>GKSS Research Centre Geesthacht

Rhenium and ruthenium in 4th generation nickel-base superalloys increase the lattice misfit between the  $\gamma$ - and  $\gamma'$ -phase. The lattice misfit varies with temperature and its magnitude determines the evolution of the  $\gamma/\gamma'$ -microstructure during creep. The lattice misfit of several experimental alloys with systematically varied rhenium and ruthenium contents was investigated at temperatures up to 1100 °C by X-ray diffraction. It was found that the lattice misfit depends strongly on the chemical composition of the alloys and the partitioning behavior of the alloying elements. The hardness of the phases  $\gamma$ - and  $\gamma'$  measured by nanoindentation in an atomic force microscope both correspond well with the partitioning behavior and X-ray results. Also the temperature dependence of the lattice misfit is modified by rhenium and ruthenium. The change of the lattice misfit with temperature is significantly smaller in rhenium-containing alloys compared to rhenium-free alloys and even less pronounced in ruthenium-containing alloys.

**Temperature Dependent Elastic Constants of Directionally Solidified Superalloys:** *Chen-ming Kuo*<sup>1</sup>; <sup>1</sup>-Shou University

Directionally solidified superalloys have been extensively used as turbine blade materials to improve creep-rupture and thermal fatigue performances. Turbine blades are subjected to fluctuant temperature changes. Precise knowledge of material behavior at various temperatures is essential in design and service life evaluation of turbine blades. In this study, Wells' averaging method is extended to consider temperature dependent engineering elastic constants. Although no existing theory predicts the temperature dependence engineering elastic constants, these constants could be estimated based upon very limited experimental data of solidification direction specimens and other temperature dependent materials data. Excellent agreement is observed between estimations and experimental data of 45° and 90° off DS direction specimens. Temperature dependent moduli and Poisson's ratios of nickel-based superalloy DS plates are also proposed.

**The Effect of Thermal Exposure on the Microstructure and Properties of a RENE-80 Superalloy:** *Saeed Farahany*<sup>1</sup>; Mehrdad Aghaie-Khafri<sup>1</sup>; <sup>1</sup>K.N.T University of Technology

The Ni-base superalloy RENE-80 is widely used in manufacturing of the first stage blades of gas turbine engines. The influence of long time heating at 800 and 850 °C for 100, 500, 750 and 1000 hr on the microstructure, hardness, stress-rupture and mechanical properties have been investigated. Test specimens for creep tests were prepared from the heat treated and aged materials according to the ASTM-E139. Creep behaviour of blade alloy are generally determined by means of a test in which a constant uniaxial load and temperatures, 191Mpa and 982°C according to GE standard. Results of microstructure study by means of optical and scanning electron microscopy showed the particle gamaprime coarsened according to LSW theory. This phenomenon caused to decrease of hardness, creep strength and creep life time.

**Theories and Computational Models for Internal Oxidation:** *John Morrall*<sup>1</sup>; Ximiao Pan<sup>1</sup>; Yali Li<sup>2</sup>; Yunzhi Wang<sup>1</sup>; <sup>1</sup>Ohio State University; <sup>2</sup>Shell Global Solutions, Inc

Internal oxidation is a well known phenomenon that results from gas-solid reactions. An example is oxygen diffusing into a Ni-Al alloy to form sub-surface alumina particles. Recent attempts to revise the classical theory based on a local equilibrium (LE) approach have suffered from a lack of experimental or modeling evidence. In this work the results of DICTRA style and phase field models of internal oxidation will be presented and compared with both the classical and LE theories. The detailed information provided from such models are a better test than most previous internal oxidation experiments which failed to measure concentration and precipitate volume fraction profiles, which are critical to distinguishing between the theories.

**Time and Temperature Dependent Deformation of Alloy 617:** *Muhammad Hasan*<sup>1</sup>; Joydeep Pal<sup>1</sup>; Ajit Roy<sup>1</sup>; Sudin Chatterjee<sup>1</sup>; <sup>1</sup>University of Nevada, Las Vegas

The heat exchangers to be used in the proposed nuclear hydrogen generation under the Next Generation Nuclear Plant (NGNP) program must withstand a maximum operating temperature of 950°C. In view of its superior high temperature deformation resistance, Alloy 617 has been identified to be a suitable candidate material for such application. Due to a variation in temperature

during operations this alloy may undergo time-dependent anelastic deformation (Creep) at different temperatures under a sustained loading condition. Classical creep curves have been generated involving Alloy 617 at 750, 850 and 950°C. While three stage plots were observed at 950°C within a short duration (300hr), testing at 750 and 850°C exhibited primary and secondary stages alone of creep deformation following 1000hr. A detailed analysis of the creep including the creep rate and activation energy will be presented in this paper.

**Mechanical Behavior of Nanostructured Materials: Poster Session**

Sponsored by: The Minerals, Metals and Materials Society, TMS Electronic, Magnetic, and Photonic Materials Division, TMS Materials Processing and Manufacturing Division, TMS Structural Materials Division, TMS: Chemistry and Physics of Materials Committee, TMS/ASM: Mechanical Behavior of Materials Committee, TMS: Nanomechanical Materials Behavior Committee  
Program Organizers: Xinghang Zhang, Texas A & M University; Andrew Minor, Lawrence Berkeley National Laboratory; Xiaodong Li, University of South Carolina; Nathan Mara, Los Alamos National Laboratory; Yuntian Zhu, North Carolina State University; Rui Huang, University of Texas, Austin

Sunday, 6:00-8:00 PM

Room: 3024

February 15, 2009

Location: Moscone West Convention Center

**3D Dislocation Dynamics Simulations of Thin Rods under Uniaxial Tension:**

*Caizhi Zhou*<sup>1</sup>; Richard Richard<sup>1</sup>; <sup>1</sup>Iowa State University and Ames Laboratory

High strength, high hardening rates and abnormal Bauschinger effects in thin films have been attributed to constraints on dislocation motion and dislocation interactions. To understand these phenomena, 3-D dislocation dynamics (DD) simulations have been used to investigate the dislocation interactions in single crystal FCC thin rods with the same dimensions and initial loading conditions as those in an experimental program employing nanoscale tensile testing. The full 3D simulations were carried out at multiple strain rates and with different initial dislocation densities under uniaxial tension in various loading directions. Simulations were compared directly with the experimental results both to validate the 3D DD simulations and to elucidate mechanisms of dislocation interactions in small-scale samples.

**Adhesion and Cohesion of Hard Transparent Coatings on Polymer Substrates:** *Ani Kamer*<sup>1</sup>; Reinhold Dauskardt<sup>1</sup>; <sup>1</sup>Stanford University

Acrylics and polycarbonates are tough and light and have replaced glass in many applications. However, the surface of plastics is prone to scratching and water absorption and hard transparent coatings with high adhesion are critical for reliable function. Sol-gel derived hybrid coatings based on polysiloxanes have proven very versatile in terms of high hardness, ease of additive incorporation and optical properties, although their adhesion to plastics is not well characterized or understood. We report on quantitative thin film techniques to characterize the adhesion energy of hard transparent coatings on elastically soft polymethylmethacrylate substrates. In addition, cohesive properties are reported using channel cracking methods. The subcritical adhesive and cohesive crack growth rates are reported for a range of temperatures and moist and chemically active environments. Implications for the reliability and service life of coated plastics are discussed.

**Analysis of Deformation Induced Lattice Defects in SPD Processed fcc Nanometals by DSC:** *Daria Setman*<sup>1</sup>; Michael Kerber<sup>1</sup>; Michael Zehetbauer<sup>1</sup>; <sup>1</sup>Physics of Nanostructured Materials

For the strength, ductility and stability of nanometals processed by Severe Plastic Deformation (SPD) the nature, distribution and density of deformation induced lattice defects is crucial. Methods of annealing resistometry and differential scanning calorimetry (DSC) have been proven well to determine these quantities, although in case of complex vacancy defects, comparisons with X-ray line profile analyses for the dislocation density are necessary. For a given peak, the variation of heating rate in DSC allows to derive the activation enthalpy which provides informations on the defect type and the diffusion mechanism involved. Measurements of the activation energy as a function of shear strain and hydrostatic pressure are presented for SPD processed Ni 99.998% and Cu 99.99%. The variation of the activation enthalpy of the dislocation peak can be interpreted by the differences in internal strains left in the samples after SPD processing, which markedly affect their ductility and stability.

**Atomistic Computer Simulations of Plasticity in Faceted Nanoparticles during Compression Test:** *Dan Mordehai*<sup>1</sup>; Eugen Rabkin<sup>1</sup>; David Srolovitz<sup>2</sup>; <sup>1</sup>Department of Materials Engineering, Technion; <sup>2</sup>Department of Physics, Yeshiva University

We report on a series of molecular dynamics simulations of the indentation process of faceted gold nanoparticles. Firstly, we employed the Winterbottom construction to determine the nanoparticle shape according to the calculated surface energies and the adhesion between the particle and the substrate, which is a tunable parameter in our simulations. Then, the particle was compressed by a rigid flat indenter at a constant velocity. For strong adhesions between the indenter and the particle, onset of plasticity occurred in tension, when the particle was attracted to the indenter as it approached. As the adhesion between them was decreased, the jump-to-contact became elastic and dislocation nucleation occurred only in compression. The first Shockley partials nucleated at the facet corners and at the topmost surface steps, propagated toward the substrate and then spread along it. We discuss our results for different nanoparticle geometries and various adhesions between the particle and the indenter.

**Characterization of a Large Plate Consolidated from Cryomilled Al 5083 Powder:** *Troy Topping*<sup>1</sup>; Byungmin Ahn<sup>2</sup>; Yonghao Zhao<sup>1</sup>; Steven Nutt<sup>2</sup>; Enrique Lavernia<sup>1</sup>; <sup>1</sup>University of California, Davis; <sup>2</sup>University of Southern California

Aluminum alloys with nanocrystalline (NC) and ultra-fine grain (UFG) size are of interest because of their high strength – typically 30% stronger than conventionally processed alloys of the same composition. But, scalability of the materials is a concern for potential commercial and military users. This study investigates the mechanical and microstructural properties of a round, 14.4 kg plate produced by quasi-isostatic (QI) forging and subsequent rolling of cryomilled Al 5083 powder. After rolling, final dimensions of the plate are ~ 60 cm diameter by ~ 1.9 cm thick. The plate exhibits ductility and strength superior to conventional Al 5083 in tensile tests conforming to ASTM E8 standards. Microstructural investigation confirms the UFG nature of the material with a grain size distribution that accommodates plastic deformation while retaining high strength. This grain size distribution allows further strengthening of the material via cold-rolling, with deformation accommodated by multiple mechanisms.

**Comparing the Texture Development during Cold Rolling of Nanocrystalline Nickel and Coarse-Grained Nickel:** *Andreas Kulovits*<sup>1</sup>; Jorg Wiezorek<sup>1</sup>; <sup>1</sup>University of Pittsburgh

We cold rolled fully dense nanocrystalline (NC) Ni (30-40nm average grain size) up to 85% thickness reduction. In this grain size regime dislocation glide mainly facilitates plastic deformation. Grains of coarse-grained (CG) metals generally exhibit simultaneous activation of multiple glide systems. For average size grains in NC metals glide activity is limited to single dislocation glide systems in the initial stages of plastic deformation and glide dislocations react with grain boundaries that act as sources and sinks. The different dislocation behavior of NC and CG metals should impact microstructure and property evolution during plastic deformation. Here we compare the microstructural responses of NC and CG Ni to cold rolling. We determined changes in texture, boundary character, grain sizes and hardness as a function of strain by combining XRD, TEM and hardness testing. Differences in the texture evolution in NC and CG Ni are discussed in relation to dislocation behavior.

**Cryomilled Commercially Pure Titanium with High Strength and Ductility:** *Osman Ertorer*<sup>1</sup>; Troy Topping<sup>1</sup>; Ying Li<sup>1</sup>; Enrique Lavernia<sup>1</sup>; <sup>1</sup>University of California, Davis

Commercially pure titanium (GradeII) was cryomilled in a liquid argon environment and consolidated at 1073K via quasi isostatic forging (commonly known as the CERACON process). A multi-modal microstructure with the grain size range of 50-2200 nm was attained, providing balanced mechanical properties in term of tensile strength and ductility. A yield strength of 840 MPa and ultimate tensile strength of 902 MPa with 27.5% elongation to failure was measured in room temperature tensile tests. Mechanical behavior was rationalized on the basis of processing history, microstructure (multi-modal grain distribution, high-angle grain boundaries, high dislocation density), and chemistry. Accordingly the obtained high strength was attributed to reduced grain size, high dislocation density and solid solution strengthening. High ductility in combination with high strength was attributed to existence of coarse grains and high angle grain boundaries. The authors acknowledge the financial support provided by the Office of Naval Research (Grant No. ARO W911NF-06-1-0230).

**Deformation of a Nano-Precipitate Strengthened Superalloy:** *E-Wen Huang*<sup>1</sup>; Peter Liaw<sup>1</sup>; Yee-Lang Liu<sup>2</sup>; Ji-Jung Kai<sup>2</sup>; Lee Pike<sup>3</sup>; Wei-Ren Chen<sup>4</sup>; <sup>1</sup>University of Tennessee; <sup>2</sup>National Tsing Hua University; <sup>3</sup>Haynes International Inc.; <sup>4</sup>Oak Ridge National Laboratory

The structural properties of a nano-precipitate strengthened alloy have been studied by the small-angle neutron scattering (SANS) and the transmission-electron microscopy (TEM). The alloy is selected because the strength of the alloy is doubled by these precipitates upon the aging treatment while keeping good ductility. The SANS patterns show pronounced inter-particle correlation peaks due to the nano-precipitates. By a stochastic phenomenological model, the structure and form factors of the precipitates are determined and used to fit the experimental SANS results. We first calculate the structural information of the undeformed alloy and then confirmed the validity by transmission-electron-microscopy experiments. The SANS results show an invariance of the precipitate size and inter-precipitate distance on the deformed alloy, which suggests the change of a precipitate shape after deformation. This microstructural information resolved by SANS is in good agreement with the results obtained from the quantitative transmission-electron-microscopy (TEM) image analysis.

**Effect of Nanocrystallization Conditions on the Structure and Mechanisms of Deformation of Amorphous Alloys:** *N. Noskova*<sup>1</sup>; A. Potapov<sup>1</sup>; <sup>1</sup>Institute of Metal Physics of UD RAS

The amorphous alloys of  $Fe_{73.5}Cu_1Nb_3Si_{13.5}B_9$ ,  $Fe_{64}Co_{21}B_{15}$ , and  $Fe_5Co_{70}Si_{15}B_{10}$  prepared by the fast melt quenching on rotational Cu disc in the ribbon form with width 6-12 mm and thick 25-40  $\mu m$  were investigated. Toroidal specimens were wound of these ribbons with an outer diameter 30 mm and inner diameter 25 mm. The studies of specimens of  $Fe_5Co_{70}Si_{15}B_{10}$  ( $\lambda S \approx 0.5 \cdot 10^{-6}$ ) and  $Fe_{60}Co_{20}Si_5B_{15}$  ( $\lambda S \approx 30 \cdot 10^{-6}$ ) amorphous alloys with different magnetostriction have been carried out. The influence of annealing temperature, rate of cooling, magnetic field frequency under thermomagnetic treatment (TMT) on the structure and deformation of  $Fe_5Co_{70}Si_{15}B_{10}$  and  $Fe_{60}Co_{20}Si_5B_{15}$  amorphous alloys samples has been studied. Amorphous-nanocrystalline alloys  $Fe_{73.5}Nb_3Cu_1Si_{13.5}B_9$ ,  $Fe_{63.5}Co_{10}Nb_1Cu_3Si_{13.5}B_9$ ,  $Fe_{53.5}Co_{20}Nb_1Cu_3Si_{13.5}B_9$  and  $Fe_{43.5}Co_{30}Nb_1Cu_3Si_{13.5}B_9$  were studied under different nanocrystallization condition. The chemical compositions of the disperse phases were determined. This work was supported by RFFI (grant -07-03-00339).

**High Strength Al-Cu Based Ultrafine Eutectic Composites with Enhanced Plasticity:** *Sung Woo Sohn*<sup>1</sup>; Jin Man Park<sup>1</sup>; Tae Eung Kim<sup>1</sup>; Won Tae Kim<sup>2</sup>; Do Hyang Kim<sup>1</sup>; <sup>1</sup>Yonsei University; <sup>2</sup>Cheongju University

Recently, ultrafine eutectic composites have received increasing attention due to their remarkable mechanical properties. In the present work, a possible way to fabricate Al-Cu based nanostructure-dendrite composites with enhanced plasticity has been investigated. Our main focus is to investigate systematically the effect of microstructure evolution on mechanical properties and the role of the third alloying elements. We prepared in-situ bulk samples with eutectic structure with ultrafine scaled lamellar spacing via an injection casting method. As a result, addition of small amount (~3at%) of the third element (Ni, Ag, Be, Sn, In, Si, Ge, Ga etc.) in Al-14at%Cu alloy effectively endows larger plastic strain reaching ~ 10% in Al-Cu-Si/Ge and notable plastic strain of ~25% in Al-Cu-Ga alloy with a reasonably high strength of ~ 1GPa due to the heterogeneities with different length-scale. Possible criteria that govern the ductile deformation behavior in Al-based ultrafine eutectic composites have also been investigated.

**Introduction of Nanotwinning Structure in Copper Thin Films by Ion Bombardment Treatment:** *Tsung-Cheng Chan*<sup>1</sup>; Chien-Neng Liao<sup>1</sup>; <sup>1</sup>National Tsing Hua University, Department of Materials Science and Engineering

An air gap structure employed in interconnect technology of integrated-circuits requires interconnecting materials of high mechanical strength and low electrical resistivity. Recently, copper with nano-scaled twins has been intensively researched due to its high yield strength, good ductility and reasonably low electrical resistivity. It has been reported that copper thin films with nano-scaled twins can be prepared by magnetron sputtering technique [1]. In this study, we have proposed a method to fabricate copper thin films with nano-scaled deformation twins by an ion bombardment treatment. Mechanical properties and microstructures of copper thin films were analyzed by nanoindentation technique and transmission electron microscopy, respectively. The effect of ion bombardment treatment on the microstructures and mechanical properties of the copper film will be discussed. Reference: 1. X. Zhang, A. Misra, H. Wang, X. H. Chen, L. Lu, K. Lu, and R. G. Hoagland, Appl. Phys. Lett. 88, 173116(2006).



**Low Temperature Strain Rate Sensitivity of the Nanocrystalline Ni-20%Fe Alloy:** *Elena Tabachnikova*<sup>1</sup>; *Aleksey Podolskiy*<sup>1</sup>; *Vladimir Bengus*<sup>1</sup>; *Sergey Smirnov*<sup>1</sup>; *Mikhail Bidylo*<sup>1</sup>; *Hongqi Li*<sup>2</sup>; *Peter Liaw*<sup>2</sup>; *Hahn Choo*<sup>3</sup>; <sup>1</sup>B.Verkin Institute for Low Temperature Physics and Engineering of the National Academy of Sciences of Ukraine; <sup>2</sup>University of Tennessee

Cryogenic mechanical properties of nanocrystalline (NC) alloys attract considerable scientific attention in last years. However, the micromechanisms of low temperature plastic deformation in NC materials are not clear yet. One of the parameters characterizing the deformation micromechanisms is the activation volume  $V$  of the process of plastic deformation. In this connection, strain dependences of  $V$  have been found in this work by measuring strain rate sensitivity of the deforming stress at temperatures 300, 170 and 77 K during uniaxial compression of rectangular specimens at initial strain rates  $3 \cdot 10^{-5} \text{ s}^{-1}$  and  $3 \cdot 10^{-4} \text{ s}^{-1}$ . It was found that values of activation volume are rather small ( $V \sim 20 \text{ a}^3$  at 300 K), and practically no strain dependence of  $V$  has been registered. The analysis carried out on this basis allowed us to suppose that controlling mechanism of plastic deformation in the NC alloy is emission of mobile dislocations from grain boundaries.

**Mechanical Properties and Nanocrystallization Behavior of Al-Ni-La Alloys:** *Rina Sahu*<sup>1</sup>; *S Chatterjee*<sup>2</sup>; *Kanai Sahoo*<sup>3</sup>; <sup>1</sup>National Metallurgical Laboratory; <sup>2</sup>Bengal Engineering and Science University

The mechanical properties and nanocrystallization behavior of rapidly solidified ribbons of Al-Ni-La alloys have been investigated in both as-melt spun and annealed condition using nano-indentation technique, Vicker's microhardness, differential scanning calorimetry and transmission electron microscopy. Microhardness, tensile strength and modulus of ribbons were examined with the variation of temperature and subsequently correlated with evolved microstructure. Significant improvement in properties with nanocrystallization (up to around 30 vol. %) occurs which are attributed to changes in microstructure. Scanning electron microscopy images of indented ribbons show pile up of materials in a semi-circular shear band. With increasing indenting load or with increasing nanocrystallization the material flow pattern changes to a radial distribution. These changes in mechanical properties, material flow behavior and the corresponding evolution of microstructure will be discussed.

**Mechanisms of Deformation of Nanocrystalline Materials:** *N. Noskova*<sup>1</sup>; <sup>1</sup>Institute of Metal Physics of UD RAS

Results of recent original studies of structure and properties of nanocrystalline metals and alloys produced by severe plastic deformation. High resolution transmission electron microscopy, scanning electron microscopy, and in situ deformation in the column of an electron microscope were used to analyze the structures and the mechanisms of plastic deformation of nanocrystalline materials. Based on the results of the investigation of deformation of fcc, bcc, and hcp nanocrystalline materials in situ in the column of an electron microscope, we can apparently assume for all types of crystal structures that, as the nanograin size decreases in a nanocrystalline material, rotational deformation modes arise upon deformation by tension, which lead to the development of mesoscopic deformation shears because of their cooperative nature. In the hcp nanocrystalline  $\alpha$ -titanium, unlike the fcc and bcc nanocrystalline materials, deformation. This work was supported by RFFI (grant -07-03-00339).

**Microstructural Evolution and Mechanical Properties in Fe-Based Nanostuctured-Dendritic Composites:** *Tae Eung Kim*<sup>1</sup>; *Jin Man Park*<sup>1</sup>; *Sung Woo Sohn*<sup>1</sup>; *Won Tae Kim*<sup>2</sup>; *Do Hyang Kim*<sup>1</sup>; <sup>1</sup>Yonsei University; <sup>2</sup>Cheongju University

In the present study, we investigated the effect of third alloying element addition on microstructural evolution and mechanical properties of Fe-Zr, Fe-Nb and Fe-Ti in-situ nano/ultrafine eutectic composites. The microstructure of suction-cast samples (diameter: 2mm) is changed significantly by choice of additional elements (Cr, C or Ni/Mn) in Fe-7Zr, Fe-11Nb and Fe-11Ti(wt%) alloys. With the addition of C, ZrC, NbC and TiC carbides form inside the primary dendrites. It is noticeable that remarkable compressive plastic strain of 23% in Fe-11Nb-0.3C and 27.7% in Fe-11Ti-0.3C together with the reasonably high strength of  $\sim 1.4 \text{ GPa}$  is obtained presumably due to the homogeneous deformation behavior with the presence of carbide. On the other hand, with the addition of Ni/Mn, lath martensitic transformation occurs in the primary phase. As a result, Fe-Nb-Ni-Mn and Fe-Ti-Ni-Mn alloys exhibit high strength ( $\sim 1.5 \text{ GPa}$ ), however plasticity is significantly low ( $\sim 8\%$ ) due to the presence of hard primary phase.

**Nano Crystal Surface Modification Technology and Its Effects on Fatigue, Wear and Friction Characteristics:** *Young Pyun*<sup>1</sup>; *Inho Cho*<sup>2</sup>; *Jin Park*<sup>3</sup>; *Chang Min Suh*<sup>4</sup>; <sup>1</sup>Sun Moon University/DesignMecha; <sup>2</sup>Designmecha; <sup>3</sup>DesignMecha Inc.; <sup>4</sup>Kyungpook National University, Daegu

UNSM (Ultrasonic Nano Crystal Surface Modification) technology will be introduced, which strikes the surface of a workpiece 20,000 or more times per second with 1,000 to 10,000 shots per square millimeter utilizing ultrasonic generating tool and thus brings severe plastic deformation to surface layers and induces nano crystal structure. The nano crystal structure of the surface layer is analyzed by XRD and TEM. UNSM also improves surface roughness and hardness and induces compressive residual stress in surface layers, which will in turn improve fatigue strength of the workpiece. UNSM creates micro dimples structure on surface, which will in turn also improve rolling contact fatigue strength and friction loss. The results of rotary bending test, tension and compression test, rolling contact fatigue test, pin-on-disc test, and friction coefficient test are carried out in order to show the UNSM effects.

**Nanocrystalline Powder Consolidation in AA2124 Using Uniaxial Compaction and Severe Plastic Deformation:** *Hanadi Salem*<sup>1</sup>; *Ahmed Sadek*<sup>1</sup>; *Moataz Attallah*<sup>2</sup>; <sup>1</sup>American Univ in Cairo; <sup>2</sup>University of Manchester

Hot and ambient compaction of AA2124 nanocrystalline powders was performed to produce bulk nanostructured materials, in combination with severe plastic deformation via warm equal channel angular processing (ECAP). Nanocrystalline powders of  $\sim 40 \mu\text{m}$  particle size and  $\sim 700 \text{ nm}$  grain size were consolidated into hot and green compacts under various compaction conditions. Hot compacts with highest densities and hardness were achieved over pressure and temperature ranges of 375-450MPa and 420-480°C, respectively. Hot compaction resulted in coarsening of the initial grain structure to  $2.2 \mu\text{m}$ . Subsequent deformation via single-pass ECAP produced uniform fully densified bulk rods, with almost no coarsening in grain size, with subgrains 100nm in size. This processing route enhanced the hardness and compressive yield strength by 23% and 43%, respectively. Ambient compaction followed by single-pass ECAP produced macroscopically uniformly deformed rods. Nonetheless, due to lack of pre-consolidation, particle rotation under shear resulted in a significant degree of structural heterogeneity (grain size 78-500nm).

**Performance Comparisons of Nanocrystalline Copper Fabricated by Room-Temperature-Molding and Vacuum-Warm-Compaction Method:** *Wei Liu*<sup>1</sup>; *Tianzu Yang*<sup>1</sup>; *Guang Chu*<sup>1</sup>; *Weifeng Liu*<sup>1</sup>; <sup>1</sup>Central South University

Nanocrystalline Cu with average grain size of 20-25 nm was fabricated by room-temperature-molding method (RM) and vacuum-warm-compaction method (VWC) respectively. Scanning Electronic Microscopy (SEM), X-ray diffraction (XRD), Positron annihilation spectroscopy (PAS) and microhardness test were utilized to characterize these as-prepared nanocrystalline copper. The thermal stability, microhardness and micro-void distribution of the as-prepared nanocrystalline copper were compared and discussed in detail. The experimental results show that, compared with RM process, the increasing of density is unremarkable while the microstrain reduced during warm-compaction process. The microhardness of nanocrystalline copper prepared by VWC (2.7GPa) is higher than that prepared by RM (1.6-1.9GPa). Also, the nanocrystalline copper prepared by VWC has better thermal stability. Positron annihilation spectroscopy analysis indicates that, compared with the specimens prepared by RM, the average micro-void size and proportion of single vacancy is a little larger in nanocrystalline copper fabricated by VWC.

**Plastic Flow Mechanisms in Ultra Fine Grained Pd and Pd-Ag Alloys Studied by In-Situ Tensile Tests:** *Kejing Yang*<sup>1</sup>; *Julia Ivanisenko*<sup>2</sup>; *Lilia Kurmanaeva*<sup>2</sup>; *Andrey Chuvilin*<sup>1</sup>; *Arnaud Caron*<sup>1</sup>; *Jürgen Markmann*<sup>3</sup>; *Ruslan Z. Valiev*<sup>4</sup>; *Hans-Jörg Fecht*<sup>1</sup>; <sup>1</sup>University of Ulm; <sup>2</sup>Forschungszentrum Karlsruhe; <sup>3</sup>Universität des Saarlandes; <sup>4</sup>Ufa State Aviation Technical University

In-situ tensile testing, as a booming technique in materials analysis, expands the conventional understanding of mechanical properties, gaining insight into the deformation evolution. Its application to a systematic investigation of HPT Pd and Pd-x%Ag (x=5,20) alloys confirms enhanced strain hardening capacity by tailoring stacking fault energy of UFG materials. The plastic flow analyzed by grey scale correlation demonstrates that the Pd-20%Ag sample with the lowest stacking fault energy manifests not only largest uniform elongation but also the best resistance against strain localization after the onset of necking. Shear banding is the primary mechanism of plastic deformation after uniform elongation has been exhausted. However, unlike other samples that failed by development of existing shear bands, Pd-20%Ag surprisingly ruptured through

the catastrophic multiplication of newly-formed shear bands. Quantitative characterization of these shear bands and tentative explanations are provided.

**Precipitation and Mechanical Behavior of an Al-Mg-Si Alloy Processed by ECAP:** *Edgar Garcia-Sanchez*<sup>1</sup>; Marco Hernandez-Rodriguez<sup>1</sup>; Edgar Ortiz-Cuellar<sup>1</sup>; <sup>1</sup>UANL-FIME

The Equal Channel Angular Pressing (ECAP) is one of the most important SPD (Severe Plastic Deformation) methods for the production of ultrafine and nanostructured metals, and has been extensively utilized. In this work a commercial Al-Mg-Si alloy has been deformed at room temperature by multi-pass equal channel angular pressing (ECAP) to obtain submicron grained structures. The mechanical behavior was analyzed by nanoindentation tests and was associated with the microstructural state. The thermal stability of microstructure and the secondary precipitation were examined by scanning calorimetry (DSC) and transmission electron microscopy (TEM). The results showed the effect of the number of passes and post-SPD thermal treatment on the microstructural evolution and the mechanical properties.

**Processing High-Strength Aluminum Alloys by ECAP at Room Temperature:** *Zhichao Duan*<sup>1</sup>; Nguyen Chinh<sup>2</sup>; Cheng Xu<sup>1</sup>; Terence Langdon<sup>1</sup>; <sup>1</sup>University of Southern California; <sup>2</sup>Eötvös Loránd University

Because of the strengthening effect of precipitates, it is often difficult or impossible to process age-hardenable Al-Zn-Mg-(Cu) alloys by equal-channel angular pressing (ECAP) at room temperature. Processing at elevated temperatures is also not satisfactory because it leads to uncontrolled precipitation and/or significant grain coarsening. This paper describes alternative approaches which may be applied to successfully press these alloys at relatively low temperatures. The experimental results demonstrate that it is feasible to achieve a significant improvement in strength after only one pass in processing by ECAP.

**Propagation of Buckling Delamination in Osmium-Ruthenium Films:** *Wen Chung Li*<sup>1</sup>; Scott Roberts<sup>2</sup>; T. John Balk<sup>1</sup>; <sup>1</sup>University of Kentucky; <sup>2</sup>Semicon Associates

Due to their high thermal stability and low work function, osmium-ruthenium (OsRu) films are used as coatings for porous tungsten (W) dispenser cathodes. The grain morphology and microstructure of the films, which exert a significant influence on dispenser cathode lifetime, are affected by in-plane film stress. Electron microscopy reveals that the OsRu films consist of nanocrystalline (15 to 50 nm) columnar grains. Depending on deposition conditions, primarily the sputtering pressure and substrate biasing power, OsRu films exhibited in-plane stresses that varied greatly (between 20 MPa and 5 GPa in compression). The high residual stresses in as-deposited films led to extensive buckling delamination, in the form of telephone cords that spread over the entire film surface. This buckling propagation was observed in-situ using optical microscopy, and proceeded at an average rate of ~165  $\mu\text{m/s}$ . The interplay of substrate biasing, in-plane stress and OsRu film microstructure will be discussed.

**Properties and Consolidation of Binderless Nanocrystalline Tungsten Carbide by Rapid Sintering:** In-Jin Shon<sup>1</sup>; *Byung-Ryang Kim*<sup>2</sup>; Min-Seok Moon<sup>2</sup>; Kee-Do Woo<sup>2</sup>; <sup>1</sup>Division of Advanced Materials Engineering, the Research Center of Industrial Technology, Chonbuk National University; <sup>2</sup>Division of Advanced Materials Engineering and the Research Center of Industrial Technology, Engineering College, Chonbuk National University

The attractive properties of WC are high melting temperature, high hardness, high thermal and electrical conductivities. Tungsten carbide find applications primarily in the cutting tool industries. In this work, we investigated the sintering of WC without the use of a binder by the high frequency induction heated sintering method. In addition, we also studied the effect of high energy ball milling on the sintering behavior, microstructure, and mechanical properties of binderless WC. The relative density of binderless WC sintered at 1240°C without high energy ball milling was about 72%, but increased with high energy ball milling time. Nearly full density (98%) of WC was obtained from high energy ball milled powder for 4 hours at the same sintering temperature. The grain size, fracture and hardness of binderless WC sintered from high energy ball milled powder for 10 hours were 87 nm, 8.1 MPa.m<sup>1/2</sup> and 3020 kg/mm<sup>2</sup>, respectively.

**Properties and Consolidation of Binderless Nanostructured TiC from Mechanically Activated Powder by High Frequency Induction Heated Sintering:** In-Jin Shon<sup>1</sup>; Byung-Ryang Kim<sup>2</sup>; *Min-Seok Moon*<sup>2</sup>; Kee-Do Woo<sup>2</sup>; <sup>1</sup>Division of Advanced Materials Engineering, the Research Center of Industrial Technology, Chonbuk National University; <sup>2</sup>Division of Advanced Materials Engineering and the Research Center of Industrial Technology, Engineering College, Chonbuk National University

Titanium carbide has a low density, relatively high thermal and electrical conductivity, high melting temperature (31000C) and high hardness. These properties have seen it used extensively in cutting tool applications and a hardening phase in composite materials. High frequency induction heated sintering is utilized to consolidate binderless nanocrystalline TiC within 3 minutes with the application of 80 MPa pressure. Nano-particle size (~25nm) of TiC is obtained by high energy ball milling for 10 hours. The relative density of TiC increases with milling time at the same sintering temperature. Nearly full density (98%) of binderless TiC is obtained using high energy ball milled powder for 1 hour at sintering temperature of 1335°C. The average grain size of the densified TiC decreases with milling time. The TiC sintered from high energy ball milled powder for 10 hours had grain size, fracture toughness and hardness values of 99 nm, 8.6 MPa.m<sup>1/2</sup> and 2209 kg/mm<sup>2</sup>, respectively.

**Reliability of Nano-Scale Au Thin Films on PDMS:** *Onobu Akogwu*<sup>1</sup>; Marcus Eleruja<sup>2</sup>; Auxillia Munhutu<sup>1</sup>; David Kwabi<sup>1</sup>; Swaminathan Midthuri<sup>2</sup>; Wole Soboyejo<sup>3</sup>; <sup>1</sup>Princeton University; <sup>2</sup>The Obafemi Awolowo University; <sup>3</sup>University of Arkansas

This paper presents the results of a combined experimental and theoretical study of the reliability of nano-scale Au thin films on poly-di-methyl-siloxane (PDMS) substrates. The loading rate dependence and creep response of PDMS are investigated in stretching experiments, before using spring dash-pot models to characterize the observed deformation response. The mechanisms of deformation and cracking are then elucidated for nano-scale Au thin films on PDMS substrates deformed under monotonic or cyclic loading. The related changes in film resistance are examined before presenting Coffin-Manson approaches for fatigue life prediction. The implications of the results are discussed for design of robust flexible electronic structures.

**Simulation and Mechanical Characterization of Open Celled Foams from MicroCT Scan Data:** Bruno Notarberardino<sup>1</sup>; Brian Walker<sup>2</sup>; Philippe Young<sup>1</sup>; *Ash Harkara*<sup>1</sup>; <sup>1</sup>University of Exeter; <sup>2</sup>ARUP

Computational simulation is a very effective and valuable tool in investigating materials behavior at the micro and nano-scale level and in assessing its influence on the overall macro-scale properties. Well established computational techniques can now be used to simulate mechanical, fluid dynamics, thermal or any combined (multi-physics) phenomena at the micro and nano-scale level. Crucial to the success of such a simulation is the ability to represent the 'micro-architecture' accurately and efficiently - which has proved to be a very challenging task so far. This paper will present an innovative image-based mesh generation technique that converts 3D images of micro and nano-structures (as provided by typical Micro/NanoCT scanners) directly into high fidelity computational models. The approach provides a deeper understanding than experimental tests, and achieves more realistic model results than via analytical approaches. Real-life applications will be presented, including the densification analysis of open celled foam.

**Study on Post Annealed Effect of SiOC(-H) Films by Inductive Coupled Chemical Vapor Deposition:** *Teresa Oh*<sup>1</sup>; <sup>1</sup>Cheongju University

Low-k materials, low dielectric constant, inter layer dielectric material, organic thin films.

**Surface Nano-Deformation of Gum Metal by In-Situ AFM Observation:** *Yoshihisa Tanaka*<sup>1</sup>; Yang Jenn-Ming<sup>2</sup>; Liu Yu-Fu<sup>3</sup>; Yutaka Kagawa<sup>3</sup>; <sup>1</sup>National Institute for Materials Science; <sup>2</sup>University of California Los Angeles; <sup>3</sup>The University of Tokyo

Gum Metal is a newly developed beta titanium alloy which, in the cold work condition, exhibits a large non-linear elastic deformation and high strength at room temperature. This study was conducted to investigate the in-situ surface nano-deformation characteristics of a cold worked Gum Metal using an atomic force microscope (AFM). Tensile test and in-situ observations were conducted using a tensile device equipped with an AFM. Surface morphologies of the Gum Metal specimen were acquired before and after the deformation at various stages of the straining. The formation of slip bands within a grain was clearly observed

when the applied strain was approximately 2.1%. The amount of slip bands and average surface roughness was found to increase with increasing applied strain. The interaction of slip bands with the grain boundaries and mechanism of deformation of the Gum Metal based on nanoscale in-situ AFM observation will be discussed.

**The Application of EBSD to Study Microstructural Development in Commercial Pure Ti Fabricated by Severe Plastic Deformation:** Yongjun Chen<sup>1</sup>; Hans. J. Roven<sup>1</sup>; Yanjun Li<sup>2</sup>; Stephane Dumoulin<sup>2</sup>; John Walmsley<sup>2</sup>; <sup>1</sup>The Norwegian University of Science and Technology; <sup>2</sup>SINTEF

High resolution electron backscatter diffraction (EBSD) in conjunction with a field emission gun scanning electron microscope (FEG-SEM) has been used to study microstructural development during Equal channel pressing (ECAP) of commercial pure (CP) Ti. The use of EBSD allows one to quantitative measure in-grain orientation gradient, subgrains or cells, boundaries and microtexture. In the present paper, the commercially pure (CP) Ti with the average grain size of 22 $\mu$ m after rolling is refined towards a nanostructured microstructure after elevated temperature ECAP up to 8 passes. The evolutions of grain size, grain boundary structure, misorientation angles, subgrains or cells and microtexture were analysed in detail. The work also aims at revealing the dominating grain refining mechanism of HPC structured Ti during ECAP.

**The Effect of Annealing on the Hardness of Electrodeposited Nanocrystalline Nickel:** Hsiao-Wei Yang<sup>1</sup>; Anna Torrents Cabestany<sup>1</sup>; Manish Chauhan<sup>1</sup>; Farghalli A. Mohamed<sup>1</sup>; <sup>1</sup>University of California

The effect of annealing on the hardness of bulk electrodeposited (ED) nanocrystalline (nc) Ni having an average initial grain size of 20 nm was investigated. Hardness measurements were conducted at room temperature on specimens after annealing at different temperatures, ranging from 323 – 693 K for various annealing times. The results showed that the hardness of the material initially increased slightly with increasing annealing temperature and then decreased rapidly with increasing temperature above 500 K. It was suggested that the increase in hardness below 500 K was most likely due to the occurrence of substructural relaxation at non-equilibrium boundaries and the formation of annealing twins. Micrographs from tunneling electron microscope (TEM) show the evidence of annealing twin structure. Statistical analysis is also applied to determine the twin density and average grain size with twinning.

**The Effect of HIP Temperature on a Cryomilled Al Alloy:** Troy Topping<sup>1</sup>; Piers Newbery<sup>1</sup>; Byungmin Ahn<sup>2</sup>; Steven Nutt<sup>2</sup>; Enrique Lavernia<sup>1</sup>; <sup>1</sup>University of California, Davis; <sup>2</sup>University of Southern California

Al 5083 powder was cryomilled to obtain a nanocrystalline structure. Samples of the powder were hot vacuum degassed, to remove interstitial contaminants, and then consolidated by hot isostatic pressing (HIPping) at six different temperatures, before being forged at a high strain rate to produce plate material. The microstructure was characterized at the different processing stages using optical, scanning and transmission electron microscopy. The compressive properties of the as-HIPped material, plus tensile properties of the final product were evaluated. Despite grain growth as a result of HIPping, an ultra-fine grain structure was retained in the consolidated material, which consequently had increased strength over conventionally processed Al 5083. As the HIP temperature was increased, the density and grain size increased and the strength decreased, with near-full density being attained at 275°C (~0.64TM). Yield strength data indicate that both work hardening and Hall-Petch mechanisms are at work in the microstructure.

## Microstructural Processes in Irradiated Materials: Poster Session

Sponsored by: The Minerals, Metals and Materials Society, TMS Structural Materials Division, TMS/ASM: Nuclear Materials Committee  
Program Organizers: Christophe Domain, Electricite De France; Gary Was, University of Michigan; Brian Wirth, University of California, Berkeley

Sunday, 6:00-8:00 PM Room: 2008  
February 15, 2009 Location: Moscone West Convention Center

Session Chairs: Brian Wirth, University of California, Berkeley; Gary Was, University of Michigan; Christophe Domain, Electricite De France

**A Three Feature Model of Irradiation Hardening in RPV Steels:** G. Robert Odette<sup>1</sup>; Takuya Yamamoto<sup>1</sup>; Erik Mader<sup>2</sup>; <sup>1</sup>University of California, Santa Barbara; <sup>2</sup>EPRI

A new physical three-feature irradiation-hardening model (3FIHM), that is applicable over a wide range of fluxes and fluences, is described. In addition to stable matrix features (SMFs) and copper rich precipitates (CRPs), the 3FIHM treats both direct hardening and indirect sink effects of thermally unstable matrix defects (UMDs) that form and anneal under irradiation. High fluxes shift hardening to higher fluences, but also add the UMD hardening contribution. Thus the net effect of flux depends on all the embrittlement variables. The 3FIHM model is validated and calibrated by microstructural as microhardness data for both as-irradiated alloys and following low temperature post irradiation annealing to recover the UMDs. The 3FIHM model rationalizes observed hardening trends over several orders of magnitude of flux up to fluences in excess of 6x10<sup>19</sup>n/cm<sup>2</sup>. New insights on the role of other hardening features, including late blooming Ni-Mn rich phases and dislocation loops are also discussed.

**Anisotropy Changes in Pyrolytic Carbon Resulting from Proton Irradiation Induced Creep:** Anne Campbell<sup>1</sup>; Rongsheng Zhou<sup>1</sup>; Gary Was<sup>1</sup>; <sup>1</sup>University of Michigan

High density pyrolytic carbon (PyC) is one of the structural materials used in the TRISO fuel particles for the Very High Temperature Reactor. Mechanical properties of PyC are dependent on the degree of anisotropy, so an understanding of the change in anisotropy caused by irradiation and irradiation-induced creep is imperative. Creep experiments were conducted on thin (<40 $\mu$ m) strip samples of high density PyC using a 2 MeV proton beam, with stresses of 20.7 and 13.8 MPa, and temperatures between 800 and 1200°C. The degree of anisotropy is characterized for samples without irradiation, after irradiation, and after irradiation creep, by analyzing the cross-sectional TEM diffraction patterns. Preliminary results show an increase in the degree of anisotropy from irradiation, and a greater increase from the addition of an applied stress. The dependence of the degree of change of anisotropy due to irradiation and stresses will be discussed along with possible mechanisms.

**Assessing Composition Dependence in the Five-Frequency Model Using Kinetic Monte Carlo:** Benjamin Swoboda<sup>1</sup>; Julie Tucker<sup>1</sup>; Dane Morgan<sup>1</sup>; Anton Van der Ven<sup>2</sup>; <sup>1</sup>UW-Madison; <sup>2</sup>University of Michigan - Ann Arbor

Diffusion of point defects play an important role in microstructural changes in irradiated materials. A widely used method for determining diffusion coefficients in materials with a dilute solute is the five-frequency model [1]. However, it is not clear over what range of compositions the dilute solute approximation is valid. Kinetic Monte Carlo is used to test the validity of the five-frequency model with increasing solute concentration. An effective Hamiltonian is defined which is equivalent to that used in the five-frequency model for dilute solute, but which can also be evaluated at all compositions. The effects of varying solute and solvent activation energies and solute-vacancy binding energies are explored. In addition, the compositional range of validity of an ab initio determined five-frequency model for the Ni-Cr and Ni-Fe system is discussed. [1] A.D. LeClaire, Solute Diffusion in Dilute Alloys, Journal of Nuclear Materials 69-70, 70 (1978).

**Atomistic Simulation of Dislocation-Dislocation Loop Interactions in BCC Fe:** Hyon-Jee Lee<sup>1</sup>; Brian Wirth<sup>1</sup>; <sup>1</sup>UC Berkeley

Ferritic steels exhibit large interstitial loops with Burgers vector  $\frac{1}{2}\langle 111 \rangle$  and  $\langle 100 \rangle$ , which can be formed by agglomeration of point defects, either interstitials or vacancies, that are produced upon irradiation, or following



plastic deformation. Notably, recent transmission electron microscopy (TEM) experiments showed that nano-meter sized prismatic dislocation loops in body centered cubic (BCC) iron (Fe) exhibit fast one-dimensional motion. These dislocation loops along with other defects, such as voids and/or small precipitates, ultimately cause hardening, loss of ductility, and flow localization upon interaction with gliding dislocations. In order to understand the microstructural process that controls the change in mechanical properties of BCC Fe, molecular dynamics (MD) and molecular statics (MS) simulations are used. The atomistic nature of interstitial loops, such as the formation mechanism, structure, mobility, and gliding behavior, as well, the interaction behavior of dislocation loops with screw dislocations will be discussed using both dynamic and static methods.

**Characterization of Ion Irradiation Defects in Glassy Polymeric Carbon and Pyrolytic Graphite - A Comparison:** *Malek Abunaemeh*<sup>1</sup>; Bopha Chhay<sup>1</sup>; Cydale Smith<sup>1</sup>; Claudiu Muntele<sup>1</sup>; Yanbin Chen<sup>2</sup>; R. Zhou<sup>2</sup>; Lumin Wang<sup>2</sup>; Gary Was<sup>2</sup>; Daryush Ila<sup>1</sup>; <sup>1</sup>Alabama A&M University; <sup>2</sup>University of Michigan

TRISO fuel that is planned to be used in some of the Generation IV nuclear reactor designs consists of a fuel kernel of UO<sub>x</sub> coated in several layers of materials with different functions. Pyrolytic carbon (PyC) is considered for two of these layers. In this study we are investigating the possibility of using glassy polymeric carbon (GPC) as an alternative to PyC. GPC is a type of polymer used for products where a lightweight material that can maintain dimensional and chemical stability in adverse environment and very high temperatures (up to 3000°C). We are looking at comparing the defects that appear in the structures of GPC and PyC after different doses irradiation with 2 MeV proton, 3 MeV N and 5 MeV Si bombardment at 600 and 800°C by using Fourier Transform Infrared spectroscopy, Raman Spectroscopy, Hall effect measurements, transmission electron microscopy and electron diffraction.

**Comparison of the Stability of Different Oxides under Electron Irradiation in Martensitic ODS Steels:** *Isabelle Monnet*<sup>1</sup>; Yann de Carlan<sup>2</sup>; Joël Ribis<sup>2</sup>; Philippe Dubuisson<sup>3</sup>; <sup>1</sup>CIMAP; <sup>2</sup>CEA/DEN/DMN/SRMA; <sup>3</sup>CEA/DEN/DMN

ODS ferritic materials are reinforced by a dispersion of oxides and nano-oxides within the matrix. Those materials are considered for different nuclear applications under irradiation but previous experimental studies have shown a partial dissolution of some oxides under neutron irradiation. In this work, electron irradiations were used to evaluate the stability of the oxides and to simulate the neutron irradiations. Four ferritic steels (Fe-9Cr-1Mo), reinforced respectively by Al<sub>2</sub>O<sub>3</sub>, MgO, MgAl<sub>2</sub>O<sub>4</sub> and Y<sub>2</sub>O<sub>3</sub>, were studied. These materials were irradiated with 1MeV or 1,2 MeV electrons in a High Voltage Electron Microscope. This technique allows to follow one single oxide and to determine the evolution of its size during the irradiation. The results show that the dissolution rate of the oxides depends on the type of the oxide, on the temperature and on the irradiation dose.

**Dilute Fe Alloys under Irradiation Modeled by an Ab Initio Based AKMC Model: Solute-Interstitial Clusters Properties:** *Christophe Domain*<sup>1</sup>; Pär Olsson<sup>1</sup>; Raoul Ngayam-Happy<sup>1</sup>; Charlotte Becquart<sup>2</sup>; <sup>1</sup>EDF R&D; <sup>2</sup>LMPGM

The evolution of the microstructure of dilute Fe-CuNiMnSiP alloys under neutron irradiation, has been modeled using a multiscale approach based on ab initio and kinetic Monte Carlo simulations. Neutron irradiation of pressure vessel steels lead to the formation of point defects and solute clusters that are responsible for the vessel embrittlement. Intrinsic properties of point defect clusters as well as their interaction with solute atoms have been studied using DFT. Our atomistic kinetic Monte Carlo (AKMC) model treats thus self interstitials in addition to vacancies. The parameters regarding the self interstitial atoms were based on ab initio predictions and adjusted on isochronal annealing data. Of special interest is the modeling of the solute – self interstitial clusters for which complex configurations has been obtained ab initio. AKMC results on irradiation using this improved parameterization will be presented and discussed.

**Effect of Vacancy Supersaturation on Curvature Driven Grain Boundary Migration:** *Moneesh Upmanyu*<sup>1</sup>; Branden Kappes<sup>1</sup>; <sup>1</sup>Colorado School of Mines

Considerable debate occurs on the effect of vacancy supersaturation on grain growth. While it is well known that grain coarsening results in vacancy generation and therefore opposes motion by mean curvature, the effect of an extrinsic non-equilibrium vacancy concentration, typically present in irradiated crystalline microstructures, on grain boundary properties is unknown. To this end, we have performed embedded-atom-method (EAM) based molecular

dynamics simulations aimed at quantifying the effect of vacancy supersaturation on curvature driven grain boundary motion in Al. A bicrystal system is employed, consisting of an embedded cylindrical grain misoriented with respect to the matrix grain so as to form a high-symmetry, high angle <111> tilt grain boundary. Randomly dispersed vacancies are introduced into the simulation cell. The dynamics of the grain boundary allows us to extract the boundary mobility and stiffness. Results on the variation of these two quantities with vacancy undersaturation and supersaturation are presented and discussed.

**Examining Lot-to-Lot Variability of HT-9 with Response to Irradiation:** *Yong Yang*<sup>1</sup>; Kevin Field<sup>1</sup>; Alicia Certain<sup>1</sup>; Todd Allen<sup>1</sup>; <sup>1</sup>University of Wisconsin-Madison

This paper studies whether the lot-to-lot variability of HT-9 is a concern that would affect the potential application as the fuel cladding material in the next generation of nuclear reactors. Three different heats of HT-9 from EBR-II, ORNL and LANL were irradiated using a proton beam with various doses at two different temperatures of 300°C and 500°C, respectively. The post-irradiation examination includes the void swelling, dislocation structures, precipitates, as well as the radiation induced segregations along prior austenite grain boundaries and the martensite lath boundaries. The microhardness measurement was performed to study the irradiation hardening effects in the different heats, which can be correlated with the irradiated dislocation structures and the pre-irradiation microstructural differences.

**Irradiation-Induced Precipitation and Dislocation Loop Formation in Ferritic-Martensitic Alloy HCM12A:** *Zhijie Jiao*<sup>1</sup>; Janelle Penisten<sup>1</sup>; Gary Was<sup>1</sup>; <sup>1</sup>University of Michigan

Ferritic-martensitic (F-M) alloy HCM12A is under consideration as cladding and structural materials for advanced reactor systems. The copper content in this alloy could lead to irradiation-induced precipitation that may alter the mechanical properties of the alloy. However, little work has been done on this subject for this alloy. In this study, HCM12A was irradiated using 2 MeV protons to doses of 3, 7 and 10 dpa at 400 and 500C. The irradiation-induced precipitation was characterized using transmission electron microscopy (TEM) as well as atom probe tomography (APT). Preliminary results show that a significant amount of Ni- and Cu- rich precipitates, a few nanometers in size, were formed when the alloy was irradiated to 7 dpa at 400C. The evolution of precipitates and loops with dose and temperature will be discussed.

**Lattice Strain and Damage Evolution of 9-12%Cr Ferritic/Martensitic during In-Situ Tensile Test by X-Ray Diffraction and Small Angle Scattering:** *Xiao Pan*<sup>1</sup>; Xianglin Wu<sup>1</sup>; Jonathon Almer<sup>2</sup>; Jan Ilavsky<sup>2</sup>; James Stubbs<sup>1</sup>; <sup>1</sup>UIUC; <sup>2</sup>Argonne National Laboratory

Radiation-induced defect structures are known to elevate material yield strength and reduce material ductility. These changes substantially reduce uniform elongation compared to the unirradiated material condition so that the small strains induce plastic instability. This process is commonly known as flow localization. Recent work by our group indicates that the tendency for embrittlement in face-centered cubic (FCC) materials is controlled by the critical stress, regardless of irradiation dose but strongly depending on temperature. It is believed that the critical stress, an intrinsic material property, is associated with the interfacial strength between particle and matrix which determines the void nucleation. In-situ tensile tests have been performed by high energy X-ray diffraction in Advanced Photon Source at Argonne National Laboratory. The lattice strain and stress evolution during deformation and corresponding damage evolution will be reported in the paper. In addition, the existed void nucleation criterion will be evaluated.

**Material Selection for Spallation Neutron Windows - Application to ADS Prototypes:** Manuel Perlado<sup>1</sup>; *Fernando Sordo*<sup>1</sup>; Alberto Abanades<sup>1</sup>; Jose Maria Martinez-Val<sup>1</sup>; Emma del Rio<sup>1</sup>; Enrique Martinez<sup>1</sup>; Antonio Lafuente<sup>1</sup>; Shalom Eliezer<sup>1</sup>; <sup>1</sup>Universidad Politécnica Madrid

High performance neutron sources are being proposed for many scientific and industrial applications: material studies, hybrids reactors and transmutation of nuclear wastes. In the case of transmutation of nuclear wastes, accelerator driven systems (ADS) are proposed as one of the main technical options for such purpose, being a high performance spallation neutron source a critical element for its operation. Inertial Fusion neutron sources will also be considered. The material selection for the window component become of paramount importance. We show an integral analysis of this spallation sources taking as reference the proposal in the framework of European projects. Our estimations show that



Titanium and Vanadium alloys are more suitable than steel as structural material for an industrial ADS beam window, mostly due to its irradiation damage resistance. An analysis of the microstructural knowledge from simulation and experiments of these materials will also close the estimation of this evaluation of materials.

**Microstructural Development in Fe-Cr Alloys upon Ion Implantation:** *Amuthan Ramar*<sup>1</sup>; Robin Schaeublin<sup>1</sup>; <sup>1</sup>CRPP - EPFL

Ferritic / Martensitic (F/M) steels shows good resistance to swelling and low defect accumulation upon irradiation relative to austenitic steels. A number of experimental studies in ferritic alloys, have shown the existence of large self-interstitial atoms loops with Burgers vector  $b = 1/2 \langle 111 \rangle$  and  $b = \langle 100 \rangle$  in the bulk, which may provide a significant contribution to the hardening caused during irradiation at lower temperatures. Ab-initio simulation results shows that, initially loops with  $b = 1/2 \langle 110 \rangle$  which is lower in energy should be formed. They would transform to loops with  $b = 1/2 \langle 111 \rangle$  with the increase in the Self-interstitial atoms and latter to loop with  $b = \langle 100 \rangle$ . One of the challenge in this field is the observation of the loops with  $b = 1/2 \langle 110 \rangle$  experimentally. The loop with  $b = 1/2 \langle 110 \rangle$  could be analyzed in the microscope using weak beam g.b analysis, but their size is at the limit of the microscope's resolution.

**Modeling of Carbon Diffusion in Ultrafine Grain Tungsten during Rapid Annealing:** *Shahram Sharafat*<sup>1</sup>; Manmeet Narula<sup>1</sup>; Aaron Aoyama<sup>1</sup>; Nasr Ghoniem<sup>1</sup>; Nalin Parikh<sup>2</sup>; <sup>1</sup>University of California Los Angeles; <sup>2</sup>University of North Carolina at Chapel Hill

The High Average Power Laser (HAPL) project is pursuing development of an IFE power reactor with a solid First Wall. Typical operation exposes the FW tungsten armor to a variety of high energy ions including carbon at 10 Hz and will raise the surface temperature to about 2400 C within 10 ns between shots. Implantation of carbon can result in formation of WCs which decrease thermo-physical properties of tungsten. To estimate WC formation rates, carbon diffusion in polycrystalline tungsten must be determined. A carbon diffusion model was set up and solved for a 3-dimensional control volume consisting of ultra-fine grain structured tungsten. The diffusion of carbon during the rapid temperature transients were modeled and compared with diffusion in single crystals. It is shown that the temperature transient assists diffusion of carbon toward the implantation surface instead of pushing the carbon deeper into the tungsten armor.

**Modeling of Point Defect Cluster Evolution under Pulse Irradiation:** *Stanislav Golubov*<sup>1</sup>; Roger Stoller<sup>1</sup>; <sup>1</sup>Oak Ridge National Lab

Nucleation, growth and coarsening of point defect clusters or secondary phase precipitates are responsible for numerous changes that occur in the physical and mechanical properties of materials during irradiation. Most of the theoretical investigations of these phenomena have focused on continuous irradiation with little attention paid to pulsed irradiation conditions. However, the problem of pulsed irradiation is quite important when one considers that pulsing is an inherent aspect of current and proposed irradiation facilities such as the MTS (LANL), SNS (ORNL), IFMIF, and ITER. Thus, it is important to develop a fundamental understanding of material behavior under pulsed irradiation conditions, and the differences between this and the continuous irradiation characteristic of fission reactors in which a substantial amount of irradiation data has been obtained. Material response to pulsed and continuous irradiation conditions has been characterized using a new numerical solution to the kinetic equations describing point defect cluster dynamics.

**On the Effects of Mechanical Alloying Ball Milling Parameters on the Grain Size and Nanofeature Distributions in Nanostructured Ferritic Alloys:** *Nicholas Cunningham*<sup>1</sup>; G. Robert Odette<sup>1</sup>; Charles Eiselt<sup>2</sup>; Michael Salston<sup>1</sup>; Anton Meoslang<sup>2</sup>; Seward Gareth<sup>1</sup>; <sup>1</sup>University of California, Santa Barbara; <sup>2</sup>Forschungszentrum Karlsruhe

A previously reported extensive study of the effect of a large matrix of ball milling parameters on the homogeneity of Y-Ti-O enriched nanofeatures (NFs) in nanostructured ferritic alloys (NFA) was based on characterizing the grain size distribution by SEM and image analysis methods. The grain size distributions were assumed act as a surrogate to the NF distributions: small grains are stabilized by high NF concentrations, while larger grains contain fewer NFs. Larger grains and lower NF concentrations are believed to result in lower NFA strength and fracture toughness. In the current study a combination of electron back scattering diffraction (EBSD), nanoindentation, tensile and strain rate jump creep tests, small angle neutron scattering and transmission electron microscopy

characterization techniques are used to refine the evaluation of the effects of ball milling parameters on the NFs and their spatial distributions, as well as the NFA grain sizes and strength levels.

**Optical and Electrical Properties of Al Doped ZnO Transparent Film Irradiated by Co-60 Radioisotope:** Ozge Ozdemir<sup>1</sup>; Huseyin Cimenoglu<sup>1</sup>; Nilgun Baydogan<sup>1</sup>; Hande Sengel<sup>2</sup>; Fehiman Akman<sup>2</sup>; Ates Parlar<sup>2</sup>; <sup>1</sup>Istanbul Technical University; <sup>2</sup>Sisecam

Al doped ZnO (Al:ZnO) thin film was prepared by sol-gel dip coating technique and deposited on soda-lime-silicate glass. After the annealing processes of Al:ZnO film, the specimens were cooled down to room temperature in air. Co-60 radioisotope was used to investigate gamma radiation effect on Al:ZnO film. The color of the Al-doped ZnO is the same as that of the undoped ZnO film. However the doping of Al ions and irradiation of the film was effected on the defect chemistry of ZnO. The effects of Al dopant on the electrical conductivity of irradiated ZnO were investigated. The doping of Al increased the electrical conductivity of ZnO. The resistivity was measured by a four point probe. The variations of the resistivity, charge carrier concentration, and carrier mobility for the ZnO:Al film were investigated.

**Point Defects as Effective Pinning Centers in High-Tc Single Crystals:** *Yuri Petrusenko*<sup>1</sup>; Alexander Bondarenko<sup>1</sup>; Ivan Neklyudov<sup>1</sup>; <sup>1</sup>National Science Center - Kharkov Institute of Physics & Technology

The effect of low-temperature 2.5 MeV electron irradiation on the critical temperature  $T_c$  and transport critical current  $J_c$  in  $YBa_2Cu_3O_{7-x}$  single crystals is reported. It is demonstrated that point defects generated by the ~MeV electron beam serve as effective pinning centers of the magnetic flux in high- $T_c$  crystals, which give a substantial rise to the critical current density of irradiated superconductors. It is also found that irradiation to a dose of  $3 \times 10^{18}$  electrons/cm<sup>2</sup> slightly decreases the critical temperature,  $\Delta T_c \approx -2$  K. At the same time, it substantially increases the  $J_c$  value (up to 30 times) and drastically changes the shape of the  $J_c(\alpha)$ -dependence, where  $\alpha$  is the angle between the magnetic field vector and the  $ab$ -plane of the crystal. These changes are caused by the transition of the vortex lattice from the ordered state to disordered, this being due to an increase in the point defect concentration.

**SANS Investigation of Irradiation-Induced Phase Separation in a Binary Fe-Cr Alloy:** *Andreas Ulbricht*<sup>1</sup>; Frank Bergner<sup>1</sup>; Cornelia Heintze<sup>1</sup>; <sup>1</sup>Forschungszentrum Dresden-Rossendorf

Ferritic-martensitic chromium steels are candidate materials for future applications in both Gen-IV fission and fusion technology. Investigations of binary Fe-Cr alloys will contribute to the understanding of the behaviour of more complex alloys. The presented SANS results are focused on a Fe-9at%Cr alloy neutron-irradiated up to neutron doses of 0.6 and 1.5 dpa. We have observed a pronounced increase of scattering cross-sections for both magnetic and nuclear scattering. The A-ratio is about 2.8 for both irradiation conditions. This value is far from a value of 1.45 corresponding to nanovoids as scattering objects. This indicates that the irradiation-induced clusters are different from pure nanovoids and must contain Cr-atoms with the same or very similar average composition for both irradiation conditions. The composition of the clusters will be discussed in more detail. The size distributions of irradiation-induced defects have been calculated. The volume fraction of clusters increases slightly with neutron dose.

**Temperature Dependence of Dislocation Loop Morphologies under Heavy-Ion Irradiation in Ultra High Purity Fe and Fe-Cr Alloys:** *Zhongwen Yao*<sup>1</sup>; Mercedes Hernandez-Mayoral<sup>1</sup>; Mike Jenkins<sup>1</sup>; Mark Kirk<sup>1</sup>; <sup>1</sup>University of Oxford

Thin foils of pure Fe and FeCr alloys were irradiated with 150 keV Fe<sup>+</sup> ions at temperatures 30-500°C in the Argonne IVEM-Tandem Facility. Dynamic observations followed the evolution of damage over doses 0-13 dpa. At low doses damage took the form of isolated dislocation loops with Burgers vectors  $b = \langle 100 \rangle$  and  $1/2 \langle 111 \rangle$ . At temperatures  $\geq 300^\circ\text{C}$  and doses  $\geq 1$  dpa, complex microstructures developed in thicker regions of the foils, involving cooperative interaction and coalescence of smaller loops. In UHP Fe irradiated at 300°C, the damage took the form of large interstitial finger-shaped loops with  $b = 1/2 \langle 111 \rangle$ . At 500°C, square-shaped interstitial loops with  $b = \langle 100 \rangle$  nucleated and grew to large sizes. Damage structures in FeCr were similar but on a finer scale. Small voids were found at both 300°C and 500°C. In this paper we will describe experiments to investigate the transition in loop types.

**The Change in the Hardness of LCAC, TZM, and ODS Molybdenum in the Post-Irradiated and Annealed Conditions:** *Brian Cockeram*<sup>1</sup>; Richard Smith<sup>1</sup>; Lance Snead<sup>2</sup>; <sup>1</sup>Bechtel Bettis Inc; <sup>2</sup>Oak Ridge National Laboratory

Hardness measurements were performed on wrought LCAC, TZM, and ODS molybdenum in the post-irradiated and annealed conditions to determine the kinetics for defect mobility. Irradiations in HFIR at 270C to 600C were shown to result in relatively large increases in hardness (54% to 100%), while small changes in hardness (-11% to 18%) were observed for irradiations at 870C to 1100C. The kinetics for recovery for the alloys irradiated at 270C to 605C were determined by performing isochronous anneals. Recovery is observed to begin at about 600C and was completed at 1100C. The activation energy for recovery was determined to be about 4 eV for LCAC and ODS molybdenum, which is comparable to values reported in literature for molybdenum self-diffusion. TZM exhibits much slower recovery kinetics.

**The Structure and Composition of Y-Ti-O Nanoclusters in Nanostructured Ferritic Alloys:** *Barbara Wang*<sup>1</sup>; Hyon-Jee Lee<sup>1</sup>; Brian Wirth<sup>1</sup>; <sup>1</sup>University of California, Berkeley

Nanostructured ferritic alloys are distinguished by a high density of Y-Ti-O nanoclusters (NCs). The presence of these NCs stabilizes ultrafine grain sizes and subgrain dislocation structures, resulting in a material with remarkable tensile strength, creep strength, and irradiation resistance. In a study by Alinger et al., lattice Monte Carlo methods were used to determine the NC composition and structure, within a model of pair interactions on a rigid body centered cubic lattice. The pair interaction potentials were parameterized using ab-initio methods, while making several simplifying assumptions. In this work, a larger set of ab-initio calculations is utilized to determine the adequacy of the assumptions and to refine the interaction potentials. The results are used to define full potential energy functions for off-lattice relaxation Monte Carlo simulations of NC formation. The obtained NC composition and structure are compared with the Alinger et al. results, as well as with available experimental data.

**Near-Net Shape Titanium Components: Poster Session**

Sponsored by: The Minerals, Metals and Materials Society, TMS: Titanium Committee  
Program Organizers: Rodney Boyer, Boeing Company; James Cotton, Boeing Co

Sunday, 6:00-8:00 PM Room: 2010  
February 15, 2009 Location: Moscone West Convention Center

**Comparison of Texture Evolution during the Extrusion of Zr-2.5Nb and CP Ti Tube:** *Konstantinos Alevizos*<sup>1</sup>; Richard Dashwood<sup>2</sup>; Martin Jackson<sup>3</sup>; David Dye<sup>1</sup>; <sup>1</sup>Imperial College; <sup>2</sup>University of Warwick; <sup>3</sup>University of Sheffield

The texture and microstructure of Zr-2.5Nb pressure tubes used in structural nuclear applications is critical to the component life attained, and to the avoidance of costly re-tubing operations. Here, we compare the evolution of texture and microstructure obtained by tube extrusion in CP Ti and Zr-2.5Nb for both sub- and super-transus extrusion conditions. The effect of low temperature aging and heat treatment high in the alpha+beta field on the textures and microstructures obtained in the extrusions are also considered. The strain path and temperature evolution of the billet during extrusion have been modelled using constitutive data generated from isothermal compression and friction test samples. The model results are used to inform the discussion of the observations made using X-ray texture analysis, SEM and TEM.

**The Effect of Plastic Strain and Applied Stress on Variant Selection during Transformation of Ti-6Al-4V:** *Michael Glavicic*<sup>1</sup>; David Furrer<sup>1</sup>; David Rugg<sup>1</sup>; Lee Semiatin<sup>2</sup>; John Almer<sup>3</sup>; <sup>1</sup>Rolls-Royce Corporation; <sup>2</sup>Air Force Research Laboratory; <sup>3</sup>Argonne National Laboratory

The effect of plastic prestrain and applied stress on variant selection during the cooling-transformation of Ti-6Al-4V was established. For this purpose, the alpha-phase variants developed in tension samples comprising two coarse beta grains which were deformed to a finite strain in the beta phase field and then cooled with or without an applied load were determined by an electron backscatter diffraction. It was found that variant selection within a given grain and at the grain boundaries themselves is strongly affected by both prestrain and the applied load during cooling from the beta phase field.

**Pb-Free Solders and Emerging Interconnect and Packaging Technologies: Poster Session**

Sponsored by: The Minerals, Metals and Materials Society, TMS Electronic, Magnetic, and Photonic Materials Division, TMS: Electronic Packaging and Interconnection Materials Committee  
Program Organizers: Sung Kang, IBM Corp; Iver Anderson, Iowa State University; Srinivas Chada, Medtronic; Jenq-Gong Duh, National Tsing-Hua University; Laura Turbini, Research In Motion; Albert Wu, National Central University

Sunday, 6:00-8:00 PM Room: 2020  
February 15, 2009 Location: Moscone West Convention Center

Session Chairs: Fu Guo, Beijing University of Technology; Iver Anderson, Iowa State University

**The Influence of Ni Content on Cracking in IMC Reaction Layers between Sn-Cu-Ni Solders and Cu Substrates:** *Kazuhiro Nogita*<sup>1</sup>; Christopher Gourlay<sup>2</sup>; Tetsuro Nishimura<sup>3</sup>; Shoichi Suenaga<sup>3</sup>; Stuart McDonald<sup>1</sup>; Hideaki Tsukamoto<sup>1</sup>; <sup>1</sup>University of Queensland; <sup>2</sup>Imperial College London; <sup>3</sup>Nihon Superior Co. Ltd.

IMC reaction layers between ball grid array (BGA) solders and Cu substrates has been investigated in Sn-Cu and Sn-Cu-Ni solders. The Ni content in the (Cu,Ni)<sub>6</sub>Sn<sub>5</sub> reaction layer depends on the bulk solder alloy composition. In this paper, it is shown that the level of cracking in the (Cu,Ni)<sub>6</sub>Sn<sub>5</sub> reaction layer varies with Ni content in the IMC. To explore this finding, DSC, SEM-EDS and XRD are used to study the influence of Ni content on phase transformations in (Cu,Ni)<sub>6</sub>Sn<sub>5</sub>. The findings are compared with a recent TEM study on the stability of hexagonal (Cu,Ni)<sub>6</sub>Sn<sub>5</sub> in Sn-Cu-Ni alloys[1]. [1] K. Nogita and T. Nishimura, Scripta Materialia 59 (2008) 191.

**Effect of Ionization Characteristics on Electrochemical Migration Lifetimes of Various Solder Alloys in NaCl and Na<sub>2</sub>SO<sub>4</sub> Solutions:** *Young-Bae Park*<sup>1</sup>; Ja-Young Jung<sup>1</sup>; Shin-Bok Lee<sup>2</sup>; Young-Sik Kim<sup>1</sup>; Young-Chang Joo<sup>2</sup>; <sup>1</sup>Andong National University; <sup>2</sup>Seoul National Univ

Higher density integration and adoption of new materials in advanced electronic package systems result in severe electrochemical reliability issues in microelectronic packaging due to higher electric field under high temperature and humidity conditions. Under these harsh conditions, metal interconnects respond to applied voltages by electrochemical ionization and conductive filament formation, which leads to short-circuit failure of the electronic package. In this work, in-situ water drop test and evaluation of corrosion characteristics for various solder alloys such as Sn, SnPb, SnAgCu alloys in NaCl and Na<sub>2</sub>SO<sub>4</sub> solutions were carried out to understand the fundamental electrochemical migration characteristics and to correlate each other. The electrochemical migration characteristics of each solder in NaCl and Na<sub>2</sub>SO<sub>4</sub> solutions will be discussed in detail.

**Effects of Pad Open Size and Bump Height on the Electromigration Lifetimes and Failure Mechanism of Flip Chip Sn-3.5Ag Bump:** *Young-Bae Park*<sup>1</sup>; Jang-Hee Lee<sup>1</sup>; Seung-Taek Yang<sup>2</sup>; Min-Suk Suh<sup>2</sup>; Qwan-Ho Chung<sup>2</sup>; Kwang-Yoo Byun<sup>2</sup>; <sup>1</sup>Andong National University; <sup>2</sup>Hynix Semiconductor Inc.

Electromigration of the flip chip Pb-free solder bump has recently been one of the most important reliability issues in flip chip packages. Effect of ever-decreasing size of solder bump on electromigration performance is very important not only in fundamental aspect but also technological point of view. In this work, the effects of pad open size and bump height on the electromigration lifetimes and failure mechanism of flip chip Sn-3.5Ag bump with Cu under bump metallurgy were systematically investigated by using both ex-situ electromigration test in an oven and in-situ electromigration test in a scanning electron microscope chamber, respectively. And, the line length effect on electromigration characteristics of Pb-free solder using the multi line-patterned specimens were correlated with the results from electromigration of Pb-free solder bump in flip chip package. Possible mechanism of size dependence of electromigration resistance will be discussed in detail.

**Environmental Effect on Interfacial Debonding Energy of Inkjet-Printed Ag Interconnects on Polyimide Substrate for Flexible Electronics:** *Young-Bae Park*<sup>1</sup>; *Sung Cheol Park*<sup>1</sup>; *Hyun Chul Jung*<sup>2</sup>; *Jaewoo Joung*<sup>2</sup>; <sup>1</sup>Andong National University; <sup>2</sup>Samsung Electro-mechanics

Inkjet printing technology is widely used as a direct writing technique for fabrication of the electronic circuits on the flexible substrates. Even though there are many advantages including low cost, low temperature process, solution processing, and rapid prototyping, the interfacial adhesion between inkjet-printed Ag film and flexible polymer substrate is known to be very poor, which can be interfacial reliability issues for flexible electronics applications. In this work, the effects of CF<sub>4</sub> plasma treatment conditions of polyimide surface on the interfacial adhesion energy are evaluated from 180° peel test for various temperature/humidity conditions. Extensive surface analysis using AES, XPS, and AFM is performed to understand the fundamental adhesion enhancement mechanism due to CF<sub>4</sub> plasma treatment and degradation mechanism due to 85°C/85%R.H. temperature/humidity conditions, respectively.

**Interfacial Adhesion and Reliability of Electroless-Plated Ni Film on Flexible Polyimide Substrate:** *Kyung-Jin Min*<sup>1</sup>; *Sung-Cheol Park*<sup>1</sup>; *Kyu Hwan Lee*<sup>2</sup>; *Yongsoo Jeong*<sup>2</sup>; *Young-Bae Park*<sup>1</sup>; <sup>1</sup>Andong National University; <sup>2</sup>Korea Institute of Materials Science

Flexible electronic substrates are increasingly adopted as future electronics packaging technology due to its merits of flexibility and performance. The applications of this technology needs high density integration process by using metal electrode on polyimide. Although these FPCB are widely used in flexible electronics application, poor interfacial adhesion between conductor metal and polymer substrate such as polyimide lead to bottleneck of its wide application due to lack of long-term interfacial reliability. In this study, we investigated the effects of the chemical pretreatment conditions of polyimide surface with KOH and Ethylenediamine combinations and also the post-baking treatment condition on the interfacial adhesion energy of electroless-plated Ni to polyimide systems in order to understand the interfacial bonding mechanism and enhance the adhesion. Extensive interface analyses using FE-SEM, AFM and XPS were performed to understand the fundamental interfacial bonding mechanism and to find the optimum conditions of wet treatment and post-baking, respectively.

**Aging-Informed Constitutive Models for Steady State Creep-Plasticity in Sn3.8Ag0.7Cu Solder Alloy:** *Kaushik Mysore*<sup>1</sup>; *Dennis Chan*<sup>1</sup>; *Sri Chaitra Chavali*<sup>1</sup>; *Ganesh Subbarayan*<sup>1</sup>; *Indranath Dutta*<sup>1</sup>; *Vikas Gupta*<sup>1</sup>; *Darvin Edwards*<sup>1</sup>; <sup>1</sup>Purdue University

Aging influences on microstructure and behavior of Sn3.8Ag0.7Cu solder alloy are shown to be significant. A modified viscoplastic Anand model and a simpler power law creep-plasticity model are developed to predict aging effects on behavior. Aging effects on primary and secondary creep under a range of applied loads and test temperatures are addressed. Procedures to compare alloys in terms of aging effects are discussed. Steady state creep strains, monotonic plastic strains and unified creep-plasticity theory are also discussed. Aging temperatures of -100 C, 250 C, 750 C and 1250 C, and aging times of 15, 30, 60 and 90 days (at each aging temperature) were selected as different levels of factors in a statistically designed experiment to study aging effects. Test specimens were selected with due pre-test considerations to joint-geometry, associated stress heterogeneity and joint-microstructures.

**Inhomogeneous Consumption of Electroless Ni-P Layer at the Solder Joint Formed with Sn3.5Ag0.7Cu Alloy:** *Yong Jun Oh*<sup>1</sup>; *Sung Yong Oh*<sup>1</sup>; <sup>1</sup>Hanbat University

The consumption behaviors of electroless Ni-P under-bump metallization (UBM) at the solder joint of Ni-P and Sn3.5Ag0.7Cu solder (SAC) alloy after reflowing and solid-state annealing are compared with those of electrolytic Ni UBM. Under the same reflow and annealing conditions, electroless Ni UBM is consumed more slowly than electrolytic Ni UBM, indicating that phosphorus (P) in Ni-P layer effectively retards the growth of intermetallic compounds (IMCs). However, the electroless Ni-P/IMC interface is highly irregular and serrated, and these irregularities become more severe with the aging time. Two reasons for this irregularity are proposed: 1) Ni-P UBM causes marked variations in the sizes and morphologies of the interfacial IMCs, and this results in different UBM consumption rates at different locations; 2) the coalesced Kirkendall voids in the Ni3P layer, particularly those formed during the annealing, facilitate the diffusion of Ni and Sn, thereby increasing the localized consumption of the Ni-P layer.

**Creep Behavior of Sn-Zn Alloys:** *Indrajit Charit*<sup>1</sup>; *Srikant Gollapudi*<sup>2</sup>; *Triratna Shrestha*; *Korukonda Murty*<sup>2</sup>; <sup>1</sup>University of Idaho; <sup>2</sup>North Carolina State University

Creep properties of three Sn-Zn solder materials (Sn-9Zn, Sn-20Zn and Sn-25Zn) were investigated using the impression creep technique in a temperature range of 323-413 K and at various stresses. Microstructures of these materials were examined using both optical and scanning electron microscopy. The Sn-Zn alloys show a typical M-type creep behavior implying the operation of a dislocation-climb controlled mechanism ( $n = 4-6$ ). However, the activation energies for creep deformation in these alloys were calculated to be ~ 50-70 kJ/mol, which is less than the lattice self-diffusion activation energies of Sn or Zn. The creep results from the present study are compared with those of various Sn-Zn alloys and other solder alloys from various literature sources.

**Failure Mode Characterization of Pb-Free Solder Joint with High-Speed Shear Test:** *Sang-Su Ha*<sup>1</sup>; *Jin-Kyu Jang*<sup>1</sup>; *Sang-Ok Ha*<sup>1</sup>; *Jong-Woong Kim*<sup>1</sup>; *Seung-Boo Jung*<sup>1</sup>; <sup>1</sup>Sungkyunkwan University

During the solder process, the components, distribution and thickness of intermetallic compound (IMC) between solder and pad can strongly affect the strength of solder joints, which will eventually determine the brittles of joints. In this paper, failure behaviors of solder joints under various aging time of high-speed shear test were investigated with an experimental and nonlinear 3-dimensional finite element modeling work. A representative Pb-free solder alloy, Sn-3.0Ag-0.5Cu, was employed in this study. The shear force further increased with shear speed mainly due to the high strain-rate sensitivity of the solder alloy. Brittle interfacial fractures can be more easily achieved by high-speed shear test, especially in higher shear speed. This was discussed with the relationship between the strain-rate and work-hardening effect and resulting stress concentration at interfacial regions.

**Solderability of Nanostructured Sn-Ag Solders:** *Guangwen Zhou*<sup>1</sup>; *Ying Sun*<sup>1</sup>; *Timothy Singler*<sup>1</sup>; <sup>1</sup>State University of New York, Binghamton

The drive for green electronics has prompted a strong interest in the development of Pb-free nanosolders. However, the properties of even the most promising Pb-free nanosolders still do not meet the target goals, primarily due to the lack of understanding the fundamental processes governing the wetting reaction. In an effort to understand the solderability of Pb-free nanosolders, we have selected the reaction of Sn-Ag nanoparticles with Cu substrates as a model system to investigate the wetting reaction over different length and mass scales by employing a unique combination of in-situ microscopy techniques and multiscale modeling. An in-situ optical microscope is used to study the reaction of large quantities of nanoparticles at the micron scale, while the in-situ TEM provides visualization of the wetting reaction of individual nanoparticles and phase transformations of intermetallic compounds at the nanometer. The results obtained from the in-situ microscopy observations will be elucidated by multiscale simulations.

**Microstructural Evolution of Interfacial Reaction Layers in Sn-3.5Ag-0.7Cu/ Electroless Ni-P Solder Joints:** *Han-Byul Kang*<sup>1</sup>; *Jee-Hwan Bae*<sup>1</sup>; *Jae-Wook Lee*<sup>1</sup>; *Min-Ho Park*<sup>1</sup>; *Cheol-Woong Yang*<sup>1</sup>; <sup>1</sup>Sung Kyun Kwan Univ

We investigated the interfacial reaction between Sn-3.5Ag-0.7Cu solders and an electroless nickel-immersion gold plated Cu substrate using analytical transmission electron microscopy (AEM). Cross sectional AEM samples were prepared by focused ion beam. Nano beam electron diffraction (NBED) technique is used for phase identification of interfacial reaction layers. The composition redistribution was analyzed by scanning transmission electron microscopy (STEM)/ energy dispersive X-ray spectrometry (EDS). The (Ni,Cu)<sub>3</sub>Sn<sub>4</sub> IMC was formed at the Sn-3.5Ag-0.7Cu/Ni (P) interface. The Ni<sub>2</sub>SnP ternary was formed between β-Sn and P-rich Ni layer and the dominant phase of P-rich Ni layer to be Ni<sub>12</sub>P<sub>5</sub> and Ni<sub>3</sub>P phase with a small amount of Ni<sub>2</sub>P phase. In particular, Ni<sub>2</sub>P phase was formed below the IMC. The Sn was found in the P-rich Ni layer, which indicates that Sn can diffuse through the P-rich Ni layer and react with the Ni-P compound to form a Ni<sub>2</sub>SnP ternary phase.

**Effect of Sn Grain Orientation on the Electromigration Behavior of SnCu0.7 Solder:** *Han-wen Lin*<sup>1</sup>; *Chih Chen*<sup>1</sup>; <sup>1</sup>NCTU

The requirement for smaller electrical devices but with much greater performance leads to a boost in current density and damage caused by electromigration. In this study, we use a sandwich structure of Cu|SnCu0.7|Cu of about 300μm wide to avoid the current crowding effect. Electron backscatter diffraction (EBSD) is used to acquire a grain orientation map before and after current stressing.



Due to the non-equiaxial crystal structure (body center tetragonal) of Sn, the electromigration behavior on grains with different orientation may appear different. It is expected that the electromigration damage prefers to occur along C axis, so the shrinkage of grain is more obvious in some particular grains. In this study, a lot of Sn grains with different orientations can be prepared. The effect of grain orientation on the electromigration behavior will be discussed in the conference.

**Effect of Al-Trace Dimension on the Joule Heating in Flip-Chip Solder Joints under Current Stressing:** *Hsiang-Yao Hsiao*<sup>1</sup>; Chih Chen<sup>2</sup>; <sup>1</sup>National Chiao Tung University; <sup>2</sup>National Chiao Tung University

Joule heating effect may occur during accelerated electromigration tests in solder joints. It induces a temperature increase inside the solder joints, resulting in a much higher temperature than the ambient temperature and it may trigger thermomigration in solder. This work uses infrared microscopy to measure temperature distributions on the solder joints with various Al-trace dimensions. In order to investigate the thermal characteristics in solder bumps, lead-free solder joints with typical dimensions were adopted. Since the major heat source for the solder joints is the Al trace, we investigated the influence of Al-trace dimension on the temperature distribution in solder joints. Solder joints with Al-traces of 40  $\mu\text{m}$  and 100  $\mu\text{m}$  wide were examined. In addition, Joule heating effect in solder joints with 2550- $\mu\text{m}$ -long, 1700- $\mu\text{m}$ -long, and 850- $\mu\text{m}$ -long Al traces were investigate. It is found that the dimension of the Al traces has significant influence on the temperature in solder bumps.

**In-situ Observation of Electromigration Failure in Pb-Free SnAg<sub>2.6</sub> Solder Joints with 2- $\mu\text{m}$  Thick Nickel under-Bump-Metallization:** *Wei-an Tsao*<sup>1</sup>; Chih Chen<sup>1</sup>; <sup>1</sup>NCTU

The failure due to electromigration is observed in Pb-free solder joints by in-situ observation. In this study, SnAg<sub>2.6</sub> solder with 2- $\mu\text{m}$  thick nickel under-bump-metallization (UBM) was stressed under 150°C with 0.8 Ampere, and the increase in resistance is monitored by using Kelvin probes. It is found that the different test condition may cause different failure mode and failure time of the solder joints. Furthermore, we can successfully obtain the details of microstructures changes during various stages of current stressing and the failure mode by in-situ observation. The detailed results will be presented in the conference.

**Mitigation of Tin Whiskers Growth by Micro-Alloying of Tin Plating:** *Aleksandra Dimitrovska*<sup>1</sup>; Radovan Kovacevic<sup>1</sup>; Dechao Lin<sup>1</sup>; <sup>1</sup>SMU

Sn serves as a key industrial material to make coatings on various components in the electronic industry. However, it was noticed that tin was prone to the development of whiskers even at room temperatures which is the leading cause for many electronic damages reported in the last several decades. One of the solutions developed was by applying Sn-Pb alloy as electroplated coating which has proven to have positive effect on the mitigation of Sn-whiskers. Unfortunately, with the European law imposed on July of 2006 all lead content is no longer permitted for use. In this study alloys such as Sn-Bi, Sn-Sb, Sn-Zn and Sn-Cu were electroplated onto the brass substrate by utilizing pulse plating technique, in order to achieve properties similar to the Sn-Pb alloy. Experimental results have indicated that this technique of the selected Sn-alloys can alter the microstructure of pure tin and could mitigate the growth of Sn-whiskers.

**Size and Substrate Effects on the Mechanical Properties of Solder Joints:** *Jenn-Ming Song*<sup>1</sup>; Guo-Wei Lee<sup>1</sup>; Cheng-Yi Liu<sup>2</sup>; <sup>1</sup>National Dong Hwa University; <sup>2</sup>National Central Univ

Due to the tremendous developments in IC and electronic packaging technologies, the size miniaturization of microelectronic interconnections has become an important trend. Since a reduction in joint size may give rise to complex mechanical and metallurgical responses, this study aimed to clarify the effect of gap size on microstructure and mechanical properties of pure Sn and Sn-Ag-Cu joints with Cu substrate. In addition, the influence of cross-sectional interaction of different substrates (Cu and Ni) on opposite side of joints was also examined. The results show that the shear strength increased and shear modulus descended with a shrunken joint gap size because of the constraining effect due to size miniaturization. Fracture mode was also affected by a change in joint thickness. For Cu/solder/Ni joints, the shear strength and its size dependence were weaker than those of Cu/solder/Cu joints. This could be ascribed to the asymmetrical structural feature.

**Structure and Properties of Grain Boundary in Cu Affected by Nano-Twins:** *Di Xu*<sup>1</sup>; Luhua Xu<sup>1</sup>; Vinay Sriram<sup>1</sup>; Jenn-Ming Yang<sup>1</sup>; K. N. Tu<sup>1</sup>; <sup>1</sup>UCLA

Cu with a high density of nanotwins have been shown to possess excellent mechanical strength and good electrical conductivity. This may lead to promising applications as interconnect material in Si microelectronic technology. The effect of nanotwin boundary on grain boundary structure and properties of Cu has been investigated. Nanoindentation study showed that hardness of copper near the grain boundaries which intersect with nanotwin boundaries is much higher than those of normal grain boundaries and bulk copper. Thermal stability study indicated that nanotwinned Cu thin films maintained good uniformity of grain size (absent of abnormal grain growth) while nanocrystalline Cu thin films with few twins underwent abnormal grain growth. We propose that the triple point where a twin intersects a grain boundary may play the key role in changing the structure and properties of the grain boundaries in Cu having a high density of nanotwins.

**Effect of Design of Wiring Traces on the Current Crowding Effect in Flip-Chip Solder Joints:** *Chien-Chih Kuo*<sup>1</sup>; Chih Chen<sup>1</sup>; <sup>1</sup>NCTU

The effect of different designs of Cu wiring traces on electromigration of flip-chip solder joints was investigated in this study using 3D finite element simulation. When flip-chip solder joints is stressed by currents, the currents flow along the path with the lowest resistance instead of distributing uniformly in the solder. The current crowding effect leads to electromigration damage and void formation in solder bumps. So how to relieve current crowding become an important issue. Four different designs of Cu wiring traces were adopted: slab trace, slit trace, 2-4 trace, 2-2-2 trace models. For the same stressing condition at 1A, the four different samples were simulated by ANSYS software. Take the slab trace sample as standard, we could find the other three models possess lower current density and better uniformity of current in solder bumps. Especially the 2-2-2 model has the lowest current crowding effect in solder joints. Thus, by changing the design of the wiring traces, we can get a uniform distribution of current in solder joints and relieve the current crowding effect.

**In-Situ Observation of Electromigration Eutectic SnPb Flip-Chip Solder Joints under Current Stressing:** *Dai-lin Wu*<sup>1</sup>; Chih Chen<sup>1</sup>; <sup>1</sup>NCTU

The eutectic SnPb flip-chip solder joints with under bump metallization(UBM) of Ti 1k / Cu 5k / Ni 2  $\mu\text{m}$  has been used for this in-situ observation. The temperature increase during electromigration test of the eutectic SnPb was investigated by Infrared (IR) Microcopy, to make sure that the Joule heating effect is taken into consideration. The experiment was conducted under 130°C and 0.8A. The structure and chemical composition were determined by Scanning Electron Microscopy (SEM) and Energy Dispersive Spectroscopy (EDS). Kelvin probes are employed to measure the total resistance of a pair of bumps and the connecting Al trace. Detailed results will be presented in the conference.

**Interfacial Reaction between the Electroless Nickel Immersion Gold Substrate and Sn-Based Solders:** *Ruihong Zhang*<sup>1</sup>; Ran Zhao<sup>1</sup>; *Fu Guo*<sup>1</sup>; <sup>1</sup>Beijing University of Technology

The electroless nickel immersion gold (ENIG) surface finish is widely used in electronic packaging. The ENIG induced Au embrittlement has been investigated in SnPb/ENIG/Cu solder joint since several years ago. However, in Sn-based lead-free solder joint, discrepancies still exist about the influence of Au finish on the reliability of the solder joint. This study investigated the effects of ENIG surface finish on the interfacial reaction and thus the mechanical property of Sn-based solder joints. Experimentally, two types of ENIG with different thickness of Au layer were fabricated. The results indicated that the Au layer dissolved into the solder matrix readily in the soldering stage, and then affected the shear strength of the solder joint significantly. The Au migration occurred in the solder joint during service. The existence of Cu in the interfacial intermetallic compounds (IMCs) promoted the Au atoms to diffuse to the interface and made the solder joint immune to embrittlement.

**Structural Analysis of Composite SnPb Whiskers Grown by Current Stressing:** *Cheng-Chang Wei*<sup>1</sup>; *Tao-Chi Liu*<sup>2</sup>; Chih Chen<sup>1</sup>; <sup>1</sup>National Chiao Tung University; <sup>2</sup>National Chiao Tung University; Integrated Service Technology

The growth of whiskers from lead-free solder is the key concern for electronic components. It is well known that adding Pb into solder can mitigate Sn growth effectively due to stress relief. In this study, an accelerated test on whisker growth is achieved by current stressing in thin solder stripes. Composite SnPb whiskers can be grown at a current density above  $5 \times 10^4 \text{A/cm}^2$  at 100°C. In some case, the diameter of a composite whisker is less than 600 nm; the length

could extend to several tens of microns. The microstructure of the composite whiskers is examined by a dual-beam focus ion beam and TEM technologies. EDS mapping is employed to examine the composition of the whiskers. The orientation relationship between the Sn and Pb whiskers were examined. The parent grains in which the whiskers grow from are also examined by TEM.

**A Phase Field Model for the Study of Microstructure Evolution in Lead-Free Solder Joints:** *An Serbruyns<sup>1</sup>; Nele Moelans<sup>1</sup>; Bart Blanpain<sup>1</sup>; Patrick Wollants<sup>1</sup>; <sup>1</sup>KU Leuven*

The presented phase field model is used to study the behavior of intermetallic compound (IMC) layers during soldering and subsequent thermal cycling in Sn-Cu systems. Thick IMCs are detrimental for the mechanical properties of the solder joint due to their brittle nature and therefore their growth has to be controlled. The microstructural evolution of IMCs is governed by diffusion, precipitation, grain growth and electromigration. All these concurrent processes are taken into account in the proposed phase field model. By varying diffusion coefficients, initial compositions, geometries, ..., it is possible to study their effect on IMC growth. By using advanced modeling techniques, this can be done faster and on a larger scale than what is possible with experiments.

**Accelerated Growth of Tin Whiskers from Evaporated Film:** *Jing Cheng<sup>1</sup>; Joe Subject<sup>1</sup>; Heather Howard<sup>1</sup>; Paul T. Vianco<sup>2</sup>; James C.M. Li<sup>1</sup>; <sup>1</sup>University of Rochester; <sup>2</sup>Sandia National Laboratories*

An acceleration method was designed to apply compressive stresses on a 1 micron thick tin film evaporated on silicon wafer with an underlayer of 20nm thick chromium. By this method, the compressive stresses are known without the complication of intermetallic compounds when tin is deposited on copper. The loaded sample was annealed at 180°C in a vacuum oven for a week. SEM observations showed a number of unexpected tin depleted areas with whiskers grown in them. The sample was annealed again for another four weeks, after each week some depleted areas seemed to shrink and sometimes disappear but other new ones appeared. However, the whiskers remained intact. Another clamping experiment showed tin whiskers grew from the interface between the substrate and the tin film. Based on these observations, the authors propose an interface fluid flow mechanism for the transport of tin atoms in the formation of depleted areas and the growth of whiskers.

**Microstructural and Mechanical Characterization of Solder Joints Fabricated by Explosively Reacting Nanolayers:** *Michael Tong<sup>1</sup>; Jenn-Ming Yang<sup>1</sup>; <sup>1</sup>UCLA*

This study focuses on characterizing the microstructure and mechanical properties of solders fabricated by reactive soldering. The microstructure of Al/Ni explosively reacted nanolayers as well as post-joining reactive foil/solder interface is characterized with XRD, SEM, and TEM, which has never been done. Additionally, the mechanical properties of reactively soldered joints have been characterized by single lap shear and nanoindentation. Single lap shear testing is used to determine the effect of thermal aging on the joint shear strength. Furthermore, fracture surface analysis provided additional information regarding the integrity of the reactive foil/solder interface. Nanoindentation is used to clarify the mechanical behavior of individual layers and interfaces across the joints. Linear arrays of indents are used to capture data at or near the reactive foil/solder interface and the composite values of modulus and hardness are discussed.

**Silver-Bismuth Alloys as High Temperature Lead-Free Solders:** *Anthony Muza<sup>1</sup>; Mark Cooper<sup>1</sup>; Carol Handwerker<sup>1</sup>; <sup>1</sup>Purdue University*

Under pressure from RoHS, microelectronics companies are exploring possible high temperature lead-free solders to replace the 95Pb-5Sn tin-lead alloy used for chip interconnects and hierarchical soldering processes. This study investigated a range of Bi-Ag binary eutectic alloys as suitable high temperature lead-free solders and as partially molten joining materials. Results will be presented describing the wetting of these alloys as a function of alloy composition, temperature, and flux type, their microstructures, and their resulting electrical and mechanical properties. Of greatest importance for use in interconnects is that, as the Ag concentration increases, the Ag dendritic primary phase provides not only a more electrically conductive path than high Bi alloys, but also improved mechanical properties.

**Constitutive Behavior of Mixed PbSn/SnAgCu Solder:** *Jonathon Tucker<sup>1</sup>; Carol Handwerker<sup>1</sup>; Ganesh Subbarayan<sup>1</sup>; <sup>1</sup>Purdue University*

At this time, in reworking legacy components, there is a need to understand the reliability of Sn-Pb components reworked with Pb-free solder. Rate-dependent

viscoplastic constitutive models for Pb-mixed solders are developed through extensive testing in this study. Three alloys of 1, 5 and 20 weight percent Pb were selected so as to represent reasonable ranges of Pb contamination expected from different Sn-Pb components reworked with Sn3.0Ag0.5Cu. Monotonic and creep tests were performed on specially designed assemblies at temperatures of 25°C, 75°C, and 125°C using a double lap shear test setup that ensures a nearly homogeneous state of plastic strain at the joint interface. The experimental data were used to fit for the parameters of the rate-dependent constitutive models.

## Synergies of Computational and Experimental Materials Science: Poster Session

Sponsored by: The Minerals, Metals and Materials Society, TMS Materials Processing and Manufacturing Division, TMS/ASM: Computational Materials Science and Engineering Committee

Program Organizers: Katsuyo Thornton, University of Michigan; Henning Poulsen, Risoe National Laboratory; Mei Li, Ford Motor Co

Sunday, 6:00-8:00 PM

Room: 3003

February 15, 2009

Location: Moscone West Convention Center

## Calculation of Forming Limit Diagrams Using a Revised Hill's Nonquadratic Yield Criterion:

*Hadi Noori<sup>1</sup>; Reza Mahmudi<sup>1</sup>; <sup>1</sup>University of Tehran*

Forming Limit Diagram (FLD) is a useful tool in analysing sheet metal formability. It has had a significant impact in both academia and industry on the determination of the maximum deformation that a material can withstand during a sheet metal stamping process. Jones and Gillis (JG) have proposed an analysis based on the idealization of sheet metal deformation into three phases: (1) homogeneous deformation up to maximum load, (2) deformation localization under constant load, and (3) local necking with a precipitous drop in load. In the present work, a revised Hill's nonquadratic flow law for sheets having planar isotropy with a high order of  $M=20$  has been used in conjunction with the JG analysis. Calculated FLDs are successfully comparable with experimentally determined results for interstitial free steel sheet. Using the revised flow law eventuates in the FLD levels independent of the plastic anisotropy parameter, similar to what happens in reality.

## Cellular Automaton Modelling of Grain Growth during Annealing of Alloy Fe-19Cr-8Ni:

*Mirza Candic<sup>1</sup>; Gerald Winter<sup>2</sup>; Baohui Tian<sup>2</sup>; Christof Sommitsch<sup>1</sup>; <sup>1</sup>University of Leoben; <sup>2</sup>Bohler Edelstahl GmbH & Co KG*

Simulation and control of grain size during heat treatments are essential for tailoring the properties of polycrystalline materials. In the present work, for the description of grain coarsening process, a deterministic two-dimensional cellular automaton model has been developed. The model simulates the grain coarsening process, from the point of variable initial microstructures and annealing temperatures with the computational time. For the validation of the presented model, the annealing of the austenitic stainless steel Fe-19Cr-8Ni with variable initial microstructures and annealing conditions was carried out. The results of the simulation have been validated by experimental results.

## CFD Characterization of an Electrochemical Cell with a Rotating Electrode:

*Jesus Gonzalez-Trejo<sup>1</sup>; Rosalba Orduña-Martinez<sup>1</sup>; Manuel Palomar-Pardave<sup>1</sup>; Luis Hoyos-Reyes<sup>1</sup>; Mario Romero-Romo<sup>1</sup>; Miriam Aguilar-Sanchez<sup>1</sup>; Cesar Real-Ramirez<sup>1</sup>; <sup>1</sup>Universidad Autonoma Metropolitana - Azcapotzalco*

Electrochemical cells with rotating electrodes (RE) are amply used to study the kinetics of charge transfer reactions. For this purpose, it is common to estimate the Reynolds number using geometrical parameters of the electrode, namely its diameter, and the applied angular velocity. Recent works have shown that many systems with the same Reynolds number but different cell boundary conditions, namely different electrode depth immersion or cell volume, are associated to totally different flow patterns. The main goal of this work is to obtain a hydrodynamic characterization of an electrochemical cell with RE using two different turbulence models ( $k-\epsilon$  and LES) to obtain with the former a general description of the system and with the latter further specificities. Moreover, we will compare the resulting turbulences models with physical simulations.



**Deformation Mode Characterization and FEM Simulation of  $\alpha$ -Titanium Deformed in a Bending:** *Leyun Wang*<sup>1</sup>; *Yiyi Yang*<sup>1</sup>; *Martin Crimp*<sup>1</sup>; *Philip Eisenlohr*<sup>2</sup>; *Darren Mason*<sup>3</sup>; *Thomas Bieler*<sup>1</sup>; <sup>1</sup>Michigan State University; <sup>2</sup>Max-Planck-Institut für Eisenforschung; <sup>3</sup>Albion College

Deformation of polycrystalline  $\alpha$ -titanium was investigated using a combination of electron microscopy characterization and crystal plasticity FEM (CPFEM) simulation. Commercially pure  $\alpha$ -titanium samples were deformed by four-point bending. Microstructural patches displaying dislocation slip bands and deformation twinning were characterized using scanning electron microscopy (SEM). Grain orientations were determined using electron back-scattered diffraction (EBSD) before and after deformation. Based on this orientation data, activated slip and twinning modes were identified in the patches using trace and misorientation analysis. Using digital image correlation (DIC) analysis to compare images of the patches in the undeformed and deformed states, heterogeneous local strain distributions were determined. To assess the ability of the computational model to describe microscale deformation processes, the experimental results were directly compared with CPFEM simulations carried out on FEM meshes based on the orientation maps of the undeformed microstructural patches. This work was supported by NSF (DMR-0710570) and DFG (EL 681/2-1).

**Dynamic Characterization of Granular Materials:** *Gregg Fenton*<sup>1</sup>; *Glenn Daehn*<sup>2</sup>; *Tracy Vogler*<sup>3</sup>; *Dennis Grady*<sup>1</sup>; *Anupam Vivek*<sup>2</sup>; *Yuan Zhang*<sup>2</sup>; *Geoff Taber*<sup>2</sup>; <sup>1</sup>Applied Research Associates Inc; <sup>2</sup>Ohio State University; <sup>3</sup>Sandia National Laboratories

The dynamic behavior of granular materials such as granular silica (sand) and other ceramics has importance to a variety of engineering applications. Structural Seismic coupling, planetary science, earth penetration mechanics, and the performance of ceramic armors are some of application areas. Although the behavior of sand has been studied extensively for several decades, its dynamic behavior remains poorly understood. High-quality experimental data is needed for computational verification of dynamic events involving sand along with the need to improve our general understanding of granular material physics. This presentation will describe a series of experiments used to measure the dynamic behavior of sand in the partially compacted state as well as show how advanced instrumentation techniques, particularly the Photonic Doppler Velocimetry (PDV) can be used to obtain model parameters for a multi-component Equation of State (EOS) of dry sand. The EOS parameters are then available for use in computational simulations.

**Femtosecond Laser Aided Tomography Applied to Titanium - Modified 4330 Steel:** *McLean Echlin*<sup>1</sup>; *Tresa Pollock*<sup>1</sup>; <sup>1</sup>University of Michigan

Femtosecond laser aided serial sectioning is a novel tomographic technique that has been developed at the University of Michigan over the past 3 years. This system utilizes a femtosecond laser to machine a sample surface, capture successive images and create a 3D reconstruction. The technique has been applied to capture 3D data for a variety of different metallic material systems. This talk will primarily focus on the acquisition, image processing, and reconstruction of micron-scale particles in a 4330 steel. Of particular interest are titanium nitrides and 3D reconstructions of the nitrides and their surrounding microvoids which will be used as direct inputs for modeling the shearing process including shear banding and shear localization in ballistic armor applications of this material. To date, this reconstruction has allowed us to verify local and global spatial distributions of nitrides within the sampled material to resolutions of 1-10 microns within near cubic millimeter volumes.

**Mechanical Behavior and Texture Evolution of AZ31 Magnesium Alloy during Uniaxial Compression:** *Shiyao Huang*<sup>1</sup>; *Mei Li*<sup>2</sup>; *John Allison*<sup>2</sup>; *Shaorui Zhang*<sup>1</sup>; *Yinghong Peng*<sup>1</sup>; <sup>1</sup>School of Mechanical Engineering, Shanghai Jiao Tong University, Shanghai 200240, P.R. China; <sup>2</sup>Research and Advanced Engineering Laboratory, Ford Motor Company, Dearborn, MI 48121, USA

The mechanical behavior has been studied in compression at temperatures ranging from 200°C~250°C and constant strain rates of 0.01~1/s. Texture analysis was carried out by EBSD. A crystal model was implemented into ABAQUS/Explicit finite element code using VUMAT. The constitutive model was then used to calculate the flow stress curves and grain orientation distributions. Challenges in matching simulation and experimental results are mainly due to the insufficient knowledge of slip and twinning mechanisms, especially the initial critical resolved shear stresses (CRSSs). In this paper, reasonable values of initial CRSSs and hardening parameters under different temperatures were obtained when the simulation results offer best agreement

with both experimental stress-strain curves and grain orientation distributions from texture analysis.

**Microstructure Based Failure Analysis of Multiphase Steel Using Damage Mechanics Modelling:** *Vitoon Uthaisangsuks*<sup>1</sup>; *Ulrich Prahl*<sup>1</sup>; *Wolfgang Bleck*<sup>1</sup>; <sup>1</sup>RWTH Aachen University

Multiphase steels have been developed for the automotive industry according to the purpose of the reduction of car body weight. These steels show excellent strength and ductility due to the coexistence of harder and softer phases in their microstructure. To describe the influence of the multiphase microstructures on mechanical properties and complex fracture mechanisms, an approach is presented using representative volume elements (RVE). Real microstructures were considered and cohesive zone was applied for the debonding of martensite-ferrite interfaces. Additionally, RVE simulations in combination with continuum damage mechanics were used to investigate local crack initiation in different sheet forming processes. At the failure moment, local strain distributions between different phases were studied, and correlated with macroscopic deformability results. The influences of material properties of the individual phases and the local states of stress on the failure behaviour were examined. A precise formability prediction based on microstructure for multiphase steels is aimed.

**Microstructures and Mechanical Properties of Extruded AZ31 Magnesium Alloy:** *Wei Qin Tang*<sup>1</sup>; *Xiaohui Fan*<sup>1</sup>; *Shaorui Zhang*<sup>1</sup>; *Dayong Li*<sup>1</sup>; *Yinghong Peng*<sup>1</sup>; <sup>1</sup>Shanghai Jiaotong University

Hot extrusion is an efficient processing technique to manufacture magnesium alloy components. In this study, AZ31 rods were extruded from casting ingots under various conditions. The mechanical properties of specimens were tested and the fracture surfaces for tensile specimens were analyzed by scanning electron microscopy. The microstructures were observed by using optical microscopy and electron back scattering diffraction. The results show that the specimen after extrusion has finer microstructure and better mechanical properties compared with the casting specimens. Furthermore, the microstructure and mechanical properties differ under different extrusion speeds and temperatures. The fracture surfaces of the casting specimens show a typical brittle fracture character while the extruded specimens exhibit a mixed mode of brittle fracture and toughness fracture. Finally, the dynamic recrystallization during hot extrusion was found to be able to change the crystal orientation, and influence the mechanical properties of the alloys.

**Modeling of Residual Stress Fields in Structural Materials: Computational, Mechanical, and Metallurgical Approaches:** *Christopher Lammi*<sup>1</sup>; *Diana Lados*<sup>1</sup>; <sup>1</sup>Worcester Polytechnic Institute

Adjusting/controlling macro residual stress fields while preserving a desired microstructure is often a challenging proposition. A novel mechanical/geometrical technique able to generate controlled residual stress fields was developed. The method is based on a "plug-and-hole" approach and was used to produce set residual stress magnitudes and distributions in rectangular coupons and compact tension specimens. Residual stress fields created through this method were first modeled computationally using ANSYS software and then reproduced using metallurgical means by adjusting the processing conditions. Long fatigue crack growth data for low and high residual stress conditions were generated and compared. High residual stresses were introduced in the testing samples using both the mechanical/"plug-and-hole" method and metallurgical/processing techniques. Effects of residual stress on crack growth thresholds and fracture toughness are presented and discussed. The developed method is proposed to facilitate the acquisition and analysis of fatigue crack growth data in the presence of residual stress.

**Schmid Factor Dependence of Deformation Twinning in Magnesium, Uranium, and Zirconium:** *Rodney McCabe*<sup>1</sup>; *Laurent Capolungo*<sup>1</sup>; *Peter Marshall*<sup>1</sup>; *Dhriti Bhattacharyya*<sup>1</sup>; *Gwenaelle Proust*<sup>2</sup>; <sup>1</sup>Los Alamos National Laboratory; <sup>2</sup>University of Sydney

Twinning is an important deformation mode in the hexagonal metals magnesium and zirconium and in orthorhombic uranium, and these three metals represent three potentially different behaviors with regard to twin Schmid factor dependence. For compression perpendicular to a strong (0001) texture, most grains in Zr and Mg have high resolved shear stresses on at least one variant of the {10-12} twin system. This is the dominant deformation mode in Mg while it competes with prismatic slip in Zr. For stress perpendicular to a strong (001) texture in U, grains are distributed approximately evenly from highly positive to

highly negative with regard to Schmid factor for the primary twin mode {130}. We use Electron backscatter diffraction (EBSD) to quantify the area fraction distribution of Schmid factors driving twin formation in textured, polycrystalline samples of Mg, Zr, and U. The results from these experiments are compared to predictions from polycrystal plasticity models.

**Study on Conductivity Change of M/SWNTs as Methane Adsorption by Density Functional Theory:** *Xuehui Zhan*<sup>1</sup>; Zhongliang Xiao<sup>1</sup>; Yan Shi<sup>1</sup>; Fei Li<sup>1</sup>; Weilian Zheng<sup>1</sup>; <sup>1</sup>Chansha University of Science and Technology

Density functional theory(DFT) is used to calculate adsorption of methane molecules in transition metal dispersed in surfaces of the single walled carbon nano-tubes(M/SWNTs). Structures of methane molecules inside the tubes have been studied by DFT for nano-tubes of diameters 0.954, 2.719 and 4.077nm at ambient temperature 300K. Then the electron structure and density of states of the different association scheme of M/SWNTs with methane molecules were investigated. The results indicate that there is a conjugative effect between M/SWNTs and methane. Which induces the change of electron distribution on the SWNTs surface. It increased the Carrier density and the electrical conductivity of SWNTs became higher.

**Study on Methane Adsorption in Single Walled Carbon Nano-Tube by Density Functional Theory:** *Xuehui Zhan*<sup>1</sup>; Zhongliang Xiao<sup>1</sup>; Yan Shi<sup>1</sup>; <sup>1</sup>Chansha University of Science and Technology

Density functional theory(DFT) is used to calculate adsorption of methane molecules in single walled carbon nano-tubes. Adsorption isotherms and structures of methane molecules inside the tubes have been studied by DFT for nano-tubes of diameters 0.954, 2.719 and 4.077nm at ambient temperature 300K. By using the grand potential, the effect of tube diameter on adsorption is discussed. We found that increasing the pore size of several nanometer is preferable for the methane adsorption.

**The Application of Bayesian Neural Network Modeling and Critical Experimentation for the Prediction of Tensile and Fracture Toughness Properties in Alpha/Beta Titanium Alloys:** *Santhosh Koduri*<sup>1</sup>; Vikas Dixit<sup>1</sup>; Peter Collins<sup>1</sup>; Hamish Fraser<sup>1</sup>; <sup>1</sup>Ohio State Univ

The development of computational tools that permit microstructurally-based predictions for tensile and fracture toughness properties of commercially important titanium alloys is a valuable step towards the accelerated maturation of materials. Modeling tools, such as Neural Network Models based on Bayesian statistics have been used to predict the yield strength, ultimate tensile strength and toughness of Ti-6Al-4V at room temperature. The development of such rules-based models requires the population of extensive databases containing compositional and microstructural information. These databases have been used to train and test Neural Network models. These models have been successfully used to identify the influence of individual microstructural features on the mechanical properties, consequently guiding the efforts towards development of more robust phenomenological models. The influence of the individual microstructural features on tensile and toughness have been subsequently probed using a variety of characterization techniques, including orientation microscopy and transmission electron microscopy. These results will be discussed.

**The Complex Formula and Capability Evaluation of Corrosion-Scale Inhibitor for Power Plant Cooling Water System:** *Daowu Yang*<sup>1</sup>; Linping Yu<sup>1</sup>; Chengfeng Wang<sup>1</sup>; Zhongliang Xiao<sup>1</sup>; <sup>1</sup>Changsha University of Science and Technology

Orthogonal and corrosion-linked methods were applied in this paper to find a higher efficient corrosion-scale inhibitor, the formula contained HEDP 3.0mg/L AMPS2.0mg/L PESA1.5 mg/L imidazole2.0 mg/L. Limit carbonate and electrochemical methods were used to evaluate the efficiency of scale and corrosion inhibition, which achieved 97.7% and 88.6% respectively. Additionally, the best pH range was found during these experiments. The inhibitor in our research shows advantages of small agent, good inhibition effect, and environment protection and so on.



## 2009 Functional and Structural Nanomaterials: Fabrication, Properties, and Applications: Low Dimensional Nanostructures I

Sponsored by: The Minerals, Metals and Materials Society, TMS Electronic, Magnetic, and Photonic Materials Division, TMS Materials Processing and Manufacturing Division, TMS: Nanomaterials Committee, TMS: Nanomechanical Materials Behavior Committee

Program Organizers: Gregory Thompson, University of Alabama; Amit Misra, Los Alamos National Laboratory; David Stollberg, Georgia Tech Research Institute; Jiyong Kim, University of Texas at Dallas; Seong Jin Koh, University of Texas at Arlington; Wonbong Choi, Florida International University; Alexander Howard, Air Force Research Laboratory

Monday AM  
February 16, 2009

Room: 3018  
Location: Moscone West Convention Center

Session Chairs: Seung Kang, Qualcomm Inc; Wonbong Choi, Florida International University

### 8:30 AM Invited

**Nanoprobes and Applications Based on Carbon Nanotubes:** *Sungho Jin*<sup>1</sup>; <sup>1</sup>University of California at San Diego

The key component of the AFM is the probe tip, the size and properties of which determine the resolution and reliability of nanoscale imaging. We have fabricated an extremely sharp probe based on carbon nanocone structure directly grown on an AFM cantilever at a predetermined tilt angle by orientation-controlled DC plasma CVD process. The high-aspect-ratio yet thermal-vibration-resistant geometry, together with excellent mechanical strength of the carbon nanocone AFM probes offer many advantages for nanoscale imaging in nanotech and biotech applications. We have also fabricated MFM probes for analysis of magnetic nanostructures, and special AFM probes with extremely low modulus, about three orders of magnitude reduced, for imaging of soft matters, living cells or delicate components. Stresses and Si cantilever beam bending introduced during CVD growth of carbon nanotubes, and techniques to prevent such undesirable geometry changes are also discussed.

### 9:00 AM

**Atomic Scale Models of Multiwall Carbon Nanotube Thermal Properties:** *Edmund Webb*<sup>1</sup>; <sup>1</sup>Sandia National Laboratories

Results will be presented for thermal conductivity of multi-wall carbon nanotubes (MWCNTs). While significant research exists on thermal transport properties of single-wall CNTs, comparatively less is known about MWCNTs. This represents a shortcoming for CNT technology since most synthesis methods currently well suited to device manufacturing produce MWCNTs, rather than SWCNTs. Furthermore, superior thermal conductivity observed for SWCNTs is expected to be impacted by phonon modes activated due to wall/wall interactions in a MWCNT. To address this, calculations were performed of the phonon density of states for two SWCNTs: (8,0) and (17,0) zigzag nanotubes. The same calculation was performed for the same two nanotubes threaded together to form a simple MWCNT. By examining differences in the density of states, predictions are made for thermal conductance changes for a MWCNT, compared to SWCNTs comprising it. Predictions are compared to thermal conductivity results from non-equilibrium (constant heat flux) molecular dynamics simulations.

### 9:15 AM

**Carbon Nanotubes for Spacecraft Harness Wiring:** *Ryne Raffaele*<sup>1</sup>; Alex Howard<sup>2</sup>; David Wilt<sup>2</sup>; John Merril<sup>2</sup>; Roberta DiLeo<sup>1</sup>; Christopher Schauerman<sup>1</sup>; Brian Landi<sup>1</sup>; Brian Moses<sup>1</sup>; Jack Alvarenga<sup>1</sup>; <sup>1</sup>Rochester Institute of Technology; <sup>2</sup>Air Force Research Laboratories

We are investigating the use of carbon nanotubes for the development of next generation of electrical harnesses for spacecraft. A prime motivation for this work is the potential for mass savings due to the outstanding current carry capability of these 1-d nanostructured materials coupled with their low mass density. There are also several other potential ancillary benefits for space power systems such as their outstanding tensile strength, flexibility and resiliency, stable thermal characteristics, and radiation tolerance. We will report on recent advances in the processing of carbon nanotube wires and their resulting electrical and mechanical properties. A comparison of these results to current state-of-the-art

wiring material will be presented and the potential of these novel nanomaterials for aerospace applications will be discussed.

### 9:30 AM Invited

**Si/Ge Nanowires: Growth, Properties, and Integration:** *S. Picraux*<sup>1</sup>; <sup>1</sup>Los Alamos National Laboratory

Semiconducting nanowires are of great interest for the realization of next generation functional electronic, photonic, and sensor devices, and the vapor-liquid-solid (VLS) synthesis technique has the potential for scalable production of such devices. While much progress has been made, improved understanding and control of VLS nanowire growth, properties, and integration onto platforms is now essential for further progress and future applications. Si and Ge, as the best understood electronic materials, provide an excellent test bed to advance this understanding. In this presentation our progress in the fabrication of Si, Ge, and SiGe alloy nanowires will be reviewed. Growth processes for monoatomic, alloy, and heterostructure nanowires will be discussed. Recent electrical and optical property studies will then be reviewed. Finally, directed assembly methods for the integration of nanowires into regular arrays will be presented.

### 10:00 AM Break

### 10:15 AM Invited

**Functional Nanoparticles: Synthesis and Potential Applications:** *Shouheng Sun*<sup>1</sup>; <sup>1</sup>Brown University

Our progress in synthesis of monodisperse transition metal nanoparticles will be presented in this talk. The major challenge in nanoparticle research is the control of particle size, shape, and composition. High temperature solution phase decomposition or reduction of metal precursors in the presence of stabilizing agents has been employed to produce well-dispersed transition metal nanoparticles with less than 5 % variation in diameter. We present our recent syntheses in solid, hollow and dumbbell-like nanoparticles with magnetic and optical functionalities. We demonstrate that monodisperse Pt- or Au-based multifunctional nanoparticles can be used to enhance the catalysis for oxygen reduction in the fuel cell reaction conditions and for CO oxidation. Self-assembled SmCo and FePt nanoparticle arrays can be made for potential information storage applications. With controlled surface functionalization, multifunctional solid and hollow nanoparticles are also promising for medical diagnostics and drug delivery applications.

### 10:45 AM

**Role of Al in Au-Catalyzed Growth of Si Nanowires:** *Suneel Kodambaka*<sup>1</sup>; Jerry Tersoff<sup>2</sup>; Cheng-Yen Wen<sup>3</sup>; Eric Stach<sup>3</sup>; Frances Ross<sup>2</sup>; <sup>1</sup>University of California, Los Angeles; <sup>2</sup>IBM T.J. Watson Research Center; <sup>3</sup>Purdue University

Using in situ transmission electron microscopy, we investigate the growth kinetics of Si nanowires using Au-Al alloy and disilane gas. We find that the Si nanowires grow via vapor-liquid-solid (VLS) process with liquid AuAl droplets at temperatures (~520°C) than are relatively higher than that required in the Au/Si system. At lower temperatures, nanowires grow in presence of a solid catalyst. Presence of Al leads to the growth of narrower wires with smoother surfaces. We expect that our results provide new insights into nanowire growth kinetics and enable synthesis of nanowires with tunable morphologies and compositions. \*work done at the IBM T.J. Watson Research Center.

### 11:00 AM

**Morphology of Epitaxial Core-Shell Nanostructures: Nanowires and Nanoparticles:** *Moneesh Upmanyu*<sup>1</sup>; Hailong Wang<sup>1</sup>; Cristian Ciobanu<sup>1</sup>; <sup>1</sup>Colorado School of Mines

We analyze the morphological stability against azimuthal, axial, and general helical perturbations for epitaxial core-shell nanowires in the growth regimes limited by either surface diffusion or evaporation-condensation surface kinetics. For both regimes, we find that geometric parameters (i.e., core radius and shell thickness) play a central role in determining whether the nanowire remains cylindrical or its shell breaks up into epitaxial islands similar to those observed during Stranski-Krastanow growth in thin epilayers. The combination of small cores and rapid growth of the shell emerge as key ingredients for stable shell growth. Our results provide an explanation for the different core-shell morphologies reported in the Si-Ge system experimentally, and also identify a growth-induced intrinsic mechanism for helical nanowire morphologies. Finally, we will also present the results of a similar analysis for the morphological stability of epitaxial nanoparticles.

11:15 AM

**MoO<sub>3</sub> Nanobelts: Lithiation and Electrochemistry:** *Liqiang Mai*<sup>1</sup>; Bin Hu<sup>1</sup>; Yuan Gao<sup>1</sup>; Yanyuan Qi<sup>1</sup>; Ying Dai<sup>1</sup>; Wen Chen<sup>1</sup>; <sup>1</sup>Wuhan University of Technology

Nanostructured molybdenum oxides have attracted much attention as the promising cathode materials for lithium batteries. MoO<sub>3</sub> nanobelts were fabricated through rheological self-assembling and lithiated MoO<sub>3</sub> nanobelts were attained by the direct and non-direct autoclave reaction. The influence of lithiation methods on the structure and electrochemistry of the nanobelts were studied by XRD, Raman, FTIR, SEM, TEM, C-V and model battery. The results show that Li<sup>+</sup> is inserted in the interlayer of the nanobelts, which takes up some space and leads to the decrease of the capacity, but lithiation can improve transport and diffusion of Li<sup>+</sup>, resulting in the enhancement of the insertion/extraction reversibility of Li<sup>+</sup> ions and the cycling properties of MoO<sub>3</sub> nanobelt cathode materials. Interestingly, it has been found that direct and non-direct lithiation can bring about the improvement of electroactivity of MoO<sub>3</sub> nanobelts which shows good promise for fundamental study and application of this kind of nanomaterial.

11:30 AM

**Zinc Phosphide Nanorods: Fabrication and Transport:** *Liqiang Mai*<sup>1</sup>; Yuan Gao<sup>1</sup>; Wen Chen<sup>1</sup>; Bin Hu<sup>1</sup>; Ying Dai<sup>1</sup>; <sup>1</sup>Wuhan University of Technology

Zinc phosphide nanomaterials have attracted much attention as theoretical optimum for solar power conversion and photovoltaic devices. In the present work, Zn<sub>3</sub>P<sub>2</sub> nanorods were fabricated via a mild solvent-thermal method using P, ZnCl<sub>2</sub> and NaBH<sub>4</sub>. The results show that the attained products are tetragonal phased Zn<sub>3</sub>P<sub>2</sub> with certain crystallinity. The nanorod with a diameter of 90 nm and length of more than 1 μm can be observed. Current-voltage (I-V) curve of single Zn<sub>3</sub>P<sub>2</sub> nanorod exhibits a novel hysteresis due to the hole trapping in the single Zn<sub>3</sub>P<sub>2</sub> nanorod. This work was supported by the National Nature Science Foundation of China (50702039, 50672071, 50672072), the Research Fund for the Doctoral Program of Higher Education (20070497012), Program for Changjiang Scholars and Innovative Research Team in University (IRT0547), MOE, China. The authors are pleased to thank the strong support of Professor ZL Wang and Dr RS Yang of Georgia Institute of Technology.

11:45 AM

**Influence of the Temperature on the Growth of Core-Shell SiC-SiO<sub>2</sub>:** *Guang Zhu*<sup>1</sup>; <sup>1</sup>Beijing Information Technology Institute

The core-shell SiC-SiO<sub>2</sub> nanowires with different diameters have been synthesized through a simple thermal evaporation of the mixture powders of silica and active carbon and condensation on Si substrate without assistance of any metal catalyst. Their microstructures were characterized by scanning electron microscopy, energy-dispersive X-ray spectroscopy, X-ray diffraction and high-resolution transmission electron microscopy. The results show that the nanowires have a crystalline SiC core and a surrounding amorphous SiO<sub>2</sub> layer, and we also have found that the thickness of the SiO<sub>2</sub> shell layer could be controlled using different synthesis temperature. The growth of the core-shell SiC-SiO<sub>2</sub> nanowires is via a vapour-solid (VS) process, on which a detailed study of both the chemical and structural composition has been carried out.

## Biological Materials Science: Implant Biomaterials I

Sponsored by: The Minerals, Metals and Materials Society, TMS Structural Materials Division, TMS Electronic, Magnetic, and Photonic Materials Division, TMS: Biomaterials Committee, TMS/ASM: Mechanical Behavior of Materials Committee

Program Organizers: Ryan Roeder, University of Notre Dame; John Nychka, University of Alberta; Paul Calvert, University of Massachusetts Dartmouth; Marc Meyers, University of California

Monday AM

Room: 3014

February 16, 2009

Location: Moscone West Convention Center

Session Chairs: Ryan Roeder, University of Notre Dame; Devesh Misra, University of Louisiana

8:30 AM Invited

**Structural Aspects of Fracture in Ultra High Molecular Weight Polyethylene and the Implications for Total Joint Replacements:** *Lisa Pruitt*<sup>1</sup>; <sup>1</sup>University of California, Berkeley

This work investigates the role of processing and microstructure on the fracture properties of medical grade ultra high molecular weight polyethylene and examines the implications for total joint replacement design. The effects of various process conditions including thermal treatments and crosslinking on the mechanical properties are evaluated. This study examines the role of crystallinity and lamellae size distribution on the deformation, yield and fracture processes of UHMWPE.

9:00 AM Invited

**Micromechanisms of Fracture in Resin Based Dental Restorative Composites:** *Jamie Kruzic*<sup>1</sup>; Minal Shah<sup>1</sup>; Jack Ferracane<sup>2</sup>; <sup>1</sup>Oregon State University; <sup>2</sup>Oregon Health and Science University

Understanding the micromechanisms of fracture is an important aspect to achieving an optimal balance between the aesthetic and mechanical performance of dental composites. The fracture behavior of two commercial dental composites (micro-hybrid and nanofill) are examined using double notched four point beam bending and pre-cracked compact-tension, C(T), specimens. The influences of water and post-cure heat treatments are also considered. Fracture resistance curve (R-curve) experiments revealed that both materials exhibit rising fracture resistance with crack extension, and that the micro-hybrid has superior fracture resistance. The latter is reasoned to give the higher observed flexural strength, as measured by un-notched four point beam bending. Optical and SEM observations reveal an interparticle crack growth mechanism independent of the environmental conditions. Crack deflection and crack bridging are both observed toughening mechanisms, and the nano-agglomerates appear to be less effective at deflecting cracks than solid particles, contributing to the lower toughness for the nanofill composite.

9:30 AM

**Indentation Deformation of Crystallized-Bioglass 45S5:** *Ding Li*<sup>1</sup>; Fuqian Yang<sup>1</sup>; <sup>1</sup>University of Kentucky

Bioactive glasses have been used as the bone replacement implants for several decades. It generally prefers that the materials remain the glass state without presence of crystallinity for the implant applications. Due to heat treatment and mechanical stresses, it is possible to have crystal phases in bioactive glasses which could alter the bioactivity and biofunctionality of the implanted materials. In this work, a bioglass 45S5 was crystallized at temperature of 650°C. Microindentation was used to examine localized mechanical deformation of the crystallized-bioglass 45S5 and the effect of crystallization on the dissolution in phosphate buffer solution. Both the indentation hardness and the fracture toughness were determined as a function of the indentation load. The crystallization had a strong effect on the indentation hardness and a less effect on the fracture toughness. The indentation hardness of the crystallized-bioglass 45S5 is less than that of the corresponding material at the glass state.

9:50 AM Invited

**Nanoporous Membranes for Medical Applications:** Jeffrey Elam<sup>1</sup>; Michael Pellin<sup>1</sup>; Shashishekar Adiga<sup>1</sup>; Larry Curtiss<sup>1</sup>; Roger Narayan<sup>2</sup>; <sup>1</sup>Argonne National Laboratory; <sup>2</sup>University of North Carolina - and - North Carolina State University

Membrane biofouling and inflammation play significant roles in instability of implantable biosensors. An ideal biosensor membrane material must both exhibit

limited protein adsorption and promote tissue-biosensor integration. Furthermore, biosensor membranes must exhibit low thickness and high porosity values in order to allow the biosensor to respond to analyte fluctuations. In this study, the use of atomic layer deposition and pulsed laser deposition to deposit biologically functional thin films on anodized aluminum oxide membranes is discussed. The nanoporous membranes were examined using several techniques, including scanning electron microscopy, atomic force microscopy, X-ray photoelectron spectroscopy, Raman spectroscopy, and platelet rich plasma testing.

## 10:20 AM Break

### 10:30 AM

**Patterned Bioactive Coatings of Ca-P and Bioglass on Ti-6Al-4V Substrate Using a Pulsed Nano Second Marking Laser:** Sameer Paital<sup>1</sup>; Narendra Dahotre<sup>1</sup>; <sup>1</sup>University of Tennessee

A key tenet of bone tissue engineering is the development of scaffold materials with both physical and chemical cues at the surface so as to stimulate cell attachment, bone regeneration and bone integration at the defect sites. In the present study a marking laser delivering nanosecond pulses was used to synthesize three different patterned coatings, each of Ca-P and Bioglass on Ti-6Al-4V substrate. XRD and EDS analysis were used to study the various kinds of phases and elemental distribution of the coated samples. Osteoblast and fibroblast like cells were cultured on both the samples to study the influence of pattern and chemistry on cell attachment, cell orientation, and cell proliferation. Microstructure and morphological evolutions of the coated samples were studied using a SEM. Phase contrast and confocal laser scanning microscopy were used to study the cell morphology, qualitative cell proliferation and focal contact of the cells with time.

### 10:50 AM

**Favorable Surface Adhesion Response of Electrodeposited Nano-Hydroxyapatite on Ultrafine-Grained (UFG)/Nano-Grained (NG) Austenitic Stainless Steel:** Sachin Mali<sup>1</sup>; Sashank Nayak<sup>1</sup>; Devesh Misra<sup>1</sup>; Mahesh Somani<sup>2</sup>; Pentti Karjalainen<sup>2</sup>; <sup>1</sup>University of Louisiana; <sup>2</sup>University of Oulu

We describe here the significance of ultrafine-grained (UFG)/nanograined (NG) structures in the electrodeposition of nano-hydroxyapatite and compare with conventional coarse-grained structures. The study demonstrates superior adhesion of electrodeposited nano-hydroxyapatite on UFG/NG structures in relation to coarse-grained austenitic stainless steel examined using nanoscratching by a nanoindenter. It is proposed that hydrophilicity (contact angle) and grain structure are the underlying reasons for the difference in nanoscratching or adherent nature of nano-hydroxyapatite coatings on coarse-grained and UFG/NG austenitic stainless steel. An accompanying aspect that emerged from the primary objective is that the amorphous calcium phosphate is a precursor to the formation of nano-hydroxyapatite.

### 11:10 AM

**Compositionally and Structurally Graded Ti-TiO<sub>2</sub> Coatings Using Laser Engineered Net Shaping:** Vamsi Balla<sup>1</sup>; Paul DeVasConCellos<sup>1</sup>; Weichang Xue<sup>1</sup>; Susmita Bose<sup>1</sup>; Amit Bandyopadhyay<sup>1</sup>; <sup>1</sup>Washington State University

Novel structures with functional gradation in composition were successfully made with Ti-TiO<sub>2</sub> combination using Laser Engineering Net Shaping (LENS). Addition of fully dense, compositionally graded TiO<sub>2</sub> ceramic on porous Ti significantly increased the surface wettability and hardness. The graded structures with varying concentration of TiO<sub>2</sub> on top surface found to be non-toxic and biocompatible. Besides the higher wettability, surfaces with TiO<sub>2</sub> can enhance their ability to form chemisorbed lubricating films and thus potentially lower the friction coefficient against ultrahigh molecular weight polyethylene liner reducing its wear rate. These unitized structures with open porosity on one side and hard, low friction on the other side can eliminate the need for multiple parts with different compositions for load bearing implants such as total hip prosthesis. The presentation will primarily focus on processing and characterization of these graded Ti-TiO<sub>2</sub> structures with special emphasis on biomedical applications.

### 11:30 AM

**Anodization of Dental Archwires and Miniscrews:** Wu Hsin Jay<sup>1</sup>; Huang Li-ling<sup>1</sup>; Chen Sinn-wen<sup>1</sup>; Liou Jein-Wein<sup>2</sup>; Lee Yueh-Tse<sup>2</sup>; <sup>1</sup>Department of Chemical Engineering, National Tsing Hua University; <sup>2</sup>Department of Orthodontics and Craniofacial Dentistry, Chang Gung Memorial Hospital

Commercial titanium and titanium-based archwires and miniscrews are anodized and examined in this study. The  $\beta$ -Ti archwires with different colors

are produced by anodization with different anodized voltages. The surface of the anodized wire is titanium oxide, and the oxidation states of Ti vary from TiO<sub>2</sub> on the surface to inwardly a mixture of TiO<sub>2</sub> and Ti<sub>2</sub>O<sub>3</sub>. For most of the anodization conditions, the oxide layers are amorphous. The thickness of the oxide layer is determined by using TEM and AES. With longer anodization time, the archwires change to milky white color. Compositional and structural analysis results of the milky white archwires indicate that it is still TiO<sub>2</sub> on the surface, but the titanium oxide layers become crystalline. Ti-6V-4V miniscrews with mesoporous surfaces are produced by anodization using electrolyte with a small amount of fluorine.

## Bulk Metallic Glasses VI: Alloy Development and Glass Forming Ability I

Sponsored by: The Minerals, Metals and Materials Society, TMS Structural Materials Division, TMS/ASM: Mechanical Behavior of Materials Committee

Program Organizers: Peter Liaw, The University of Tennessee; Hahn Choo, The University of Tennessee; Yanfei Gao, The University of Tennessee; Gongyao Wang, University of Tennessee

Monday AM

Room: 3007

February 16, 2009

Location: Moscone West Convention Center

Session Chairs: William Johnson, California Institute of Technology; Peter Liaw, University of Tennessee

### 8:30 AM Keynote

**Metallic Glass Matrix Composites; A High Performance Structural Material:** William Johnson<sup>1</sup>; Douglas Hofmann<sup>1</sup>; <sup>1</sup>California Institute of Technology

While bulk metallic glasses (BMG's) exhibit high strength and moderate fracture toughness, they lack a strain hardening mechanism and deform by highly localized shear banding. This leads to brittle failure under unconfined loading. In non-uniform stress states such as bending, shear band extension is limited by stress gradients and global plasticity becomes possible. To exploit this, one can "design" partially crystallized BMG-composites wherein inhomogeneous stress states are created by a two-phase microstructure under applied stress. Shear band initiation and propagation are then controlled by internal stress distributions created by the microstructure. To apply this strategy, one must consider the elastic/plastic properties of the glassy matrix and embedded crystals, spatial scale of the microstructure, and geometry of the crystalline inclusions. With proper design, BMG-composites can exhibit exceptional combinations of strength, toughness, and ductility. Experimental examples of successful BMG-composites will be presented.

### 8:55 AM

**Bulk Metallic Glass Foams via Equal Channel Angular Extrusion:** Suveen Mathaudhu<sup>1</sup>; Marie Cox<sup>2</sup>; Laszlo Kecskes<sup>1</sup>; K. Hartwig<sup>3</sup>; David Dunand<sup>2</sup>; <sup>1</sup>U.S. Army Research Laboratory; <sup>2</sup>Northwestern University; <sup>3</sup>Texas A&M University

To a first approximation, a ductile foam energy absorption scales with its strength. Thus, foams based on bulk metallic glasses (BMG), which have the highest strength of any metals, should be optimal. An obstacle to the use of BMG foams is the brittle behavior of BMG. However, recent demonstrations show that the thin, sub-millimeter, struts of BMG foams are ductile in compression, with outstanding energy absorption. The work presented here will demonstrate that equal channel angular extrusion (ECAE) can be used to create composites of BMG powders and metallic powders (Cu, Ni, W) which can subsequently be converted to BMG open-cell foams by leaching of the metallic second phase. These foams show excellent mechanical properties and particularly high energy absorption. Comparisons with similar melt cast BMG foams will be made. Acoustic emission measurements to assess damage accumulation will also be presented.

### 9:05 AM

**Atomic Origins of High Glass Forming Ability of a Multicomponent Bulk Metallic Glass:** Mingwei Chen<sup>1</sup>; <sup>1</sup>Tohoku University

Formation mechanism of multicomponent bulk metallic glasses (BMGs) with very low critical cooling rates has been one of the most outstanding issues in solid-state physics and materials science. Traditionally, atomic size ratios of constituent elements have been suggested to be the most important factor



governing glass forming ability (GFA), particularly in alloys only containing transition metals, and chemical effects arising from interatomic interactions have not been well assessed. In this talk we will report the atomic structure of multicomponent BMGs investigated by state-of-the-art experimental and computational techniques. The excellent GFA of the BMGs is demonstrated to be associated with chemical short- and medium-range order through the formation of extended clusters. This study uncovers the atomic origins of the excellent GFA of the multicomponent BMG and underscores the importance of chemical effect in the formation of amorphous structures in metal-metal based alloys.

#### 9:15 AM Invited

**Thermal Stability and Glass-Forming Ability of (Fe,Co)-Gd-Nb-B Glassy Alloys with Good Soft Magnetic Properties:** *Wei Zhang*<sup>1</sup>; *Fei Jia*<sup>2</sup>; *Xingguo Zhang*<sup>2</sup>; *Guoqiang Xie*<sup>1</sup>; *Hisamichi Kimura*<sup>1</sup>; *Akihisa Inoue*<sup>1</sup>; <sup>1</sup>Tohoku University; <sup>2</sup>Dalian University of Technology

The glass-forming ability (GFA) and the stabilization of supercooled liquid of (Fe<sub>0.9</sub>Co<sub>0.1</sub>)<sub>71.5</sub>-xGd<sub>3.5</sub>B<sub>25</sub>Nb<sub>x</sub> (x=0-6) glassy alloys were greatly enhanced. The large supercooled liquid region of 105 K and the highest reduced glass transition temperature of 0.57 were obtained at x=4, leading to the formation of the glassy alloy rods with diameters up to 3 mm. The new Fe-based bulk glassy alloys exhibit good soft magnetic properties and high strength. However, a distinct two step glass transition phenomenon was observed in the x=4-6 alloys, and little is known about the two step glass transition of the Fe-based alloys. With the aim of clarifying the reason for the two-stage glass transition, we further examined the structure, thermal stability and crystalline behavior of (Fe,Co)-Gd-B, (Fe,Co)-Nb-B and (Fe,Co)-Gd-Nb-B glassy alloys by XRD, DSC and TEM. In addition, the effects of Co concentration on the thermal stability, GFA and magnetic properties of (Fe,Co)-Gd-Nb-B alloys were investigated.

#### 9:30 AM Invited

**Bulk Metallic Glasses for Biomedical Applications:** *Marios Demetriou*<sup>1</sup>; *Aaron Wiest*<sup>1</sup>; *Gongyao Wang*<sup>2</sup>; *Nikolaj Wolfson*<sup>3</sup>; *Bo Han*<sup>3</sup>; *William Johnson*<sup>1</sup>; *Peter Liaw*<sup>2</sup>; <sup>1</sup>California Institute of Technology; <sup>2</sup>The University of Tennessee; <sup>3</sup>University of Southern California

Owing to a unique liquid-like atomic structure, glassy metals exhibit a combination of chemical and mechanical properties that are considered attractive for biomedical applications. These include a good corrosion resistance combined with high hardness, strength, and elasticity. There are certain features of their behavior however which from a bioengineering perspective can be regarded as inadequate, such as a near-zero ductility, a toughness that spans over a very broad range, and a fatigue performance that is at present poorly understood. More critically, most known compositions contain elements that are undesirable from a biomedical perspective (e.g. Ni and Cu), as they have been associated with adverse biological reactions. In this presentation, several new compositions designed according to a set of criteria to satisfy the requirements for chemical and mechanical biocompatibility will be introduced. Static and cyclic loading performances will be presented along with results from in vitro and in vivo cytotoxicity studies.

#### 9:45 AM Invited

**Processing of Bulk Metallic Glass:** *Jan Schroers*<sup>1</sup>; <sup>1</sup>Yale University

The sluggish crystallization kinetic of bulk metallic glass results in two fundamentally different processing opportunities. BMG can be directly cast. But even for BMGs with low critical cooling rates geometries with high aspect ratio are particularly challenging since during casting cooling and filling of the mold must occur simultaneously. This limits the complexity of the geometries that can be cast even when processing parameters are carefully balanced. Alternatively, BMG can be thermo plastically formed in the supercooled liquid region. In this case the required fast cooling and forming are decoupled. The BMG is formed in a high viscous state where it behaves very similar to plastics when compared by processing temperature and forming pressure. A measure for the formability of BMGs will be introduced. Processing potentials and challenges will be discussed and various examples will be given including blow-molding, miniature fabrication, and nano-patterning.

#### 10:00 AM Break

#### 10:10 AM

**Cooling Slope Casting Process for Synthesis of Bulk Metallic Glass Based Composites with Semisolid Structure:** *Advenit Makaya*<sup>1</sup>; *Takuya Tamura*<sup>1</sup>; *Kenji Miwa*<sup>1</sup>; <sup>1</sup>National Institute of Advanced Industrial Science and Technology (AIST)

A process combining cooling slope casting and suction casting was developed to generate a semisolid structure in a Zr-based bulk metallic glass

matrix composite. The melt was injected onto a cooling slope and subsequently vacuum-sucked into a cylindrical mould placed at the end of the slope. The structure obtained for 4-mm diameter cylindrical specimens of composition Zr<sub>66</sub>,<sub>4</sub>Nb<sub>6.4</sub>Cu<sub>10.5</sub>Ni<sub>8.7</sub>Al<sub>8</sub> consists of a dispersion of spheroidal and rosette-like crystals in a glassy matrix. The effects of parameters such as the cooling slope angle, the slope length and the casting temperature on the microstructure were studied. The obtained materials are expected to show improved mechanical properties and ductility inherent to the semisolid structure.

#### 10:20 AM

**New Low-Density, Low-Cost Glass-Dendrite Composites with Tensile Ductility:** *Douglas Hofmann*<sup>1</sup>; *Jin-Yoo Suh*<sup>1</sup>; *William Johnson*<sup>1</sup>; <sup>1</sup>California Institute of Technology

Recently, nanostructure-dendrite composites have been demonstrated which are said to exhibit enhanced mechanical properties over metallic glasses and their composites. We notice however, that these new alloys are similar to metallic glass composites where the matrix material has crystallized, creating an apparently brittle material in unconfined loading conditions. In this work, we demonstrate that by successfully freezing the matrix material of the composites as a glass and designing the inclusions to have a low shear modulus, tensile ductility and fracture toughness similar to other high performance crystalline alloys is observed. We report a new system of low density (4.9-5.2 g/cm<sup>3</sup>) glass-dendrite composites with at least 5% tensile ductility in each alloy. The new alloys have low cost, exhibit volume fractions of glass from 20-70%, and high glass forming ability. The work demonstrate that metallic glass composites can be competitive with the best crystalline alloys for real structural applications.

#### 10:30 AM

**Fabrication of Cu-Zr-Al Bulk Metallic Glasses via Spark Plasma Sintering Process:** *Zhihui Zhang*<sup>1</sup>; *Troy Topping*<sup>1</sup>; *Ying Li*<sup>1</sup>; *Yizhang Zhou*<sup>1</sup>; *Enrique Lavernia*<sup>1</sup>; <sup>1</sup>University of California

(Cu<sub>0.5</sub>Zr<sub>0.5</sub>)<sub>100-x</sub>Al<sub>x</sub> bulk metallic glasses have shown an exceptional combination of high strength and large compression ductility; however, their fabrication via conventional ingot casting methods is limited to samples of only a few millimeters (i.e., diameter ~5 mm). In this study, a series of (Cu<sub>0.5</sub>Zr<sub>0.5</sub>)<sub>100-x</sub>Al<sub>x</sub> alloys (x=0, 2.5, 5, 7.5 and 10), as amorphous precursor powders, are employed to study their consolidation behavior in the supercooled liquid region via spark plasma sintering (SPS). The SPS sintering was used to provide a fast heating rate (0-400 °C/min) and accurate control of the consolidation temperatures. X-ray diffraction indicated that fully amorphous disks were generated. In addition, partial crystallization was promoted during consolidation in order to study the in-situ formation of nanocrystalline precipitates during sintering as well as their influence on mechanical properties. The microstructure of the glassy billets was investigated using electron microscopy and differential scanning calorimetry. Mechanical properties under compression were evaluated.

#### 10:40 AM Invited

**Malleable Hypoeutectic Zr-Ni-Cu-Al Bulk Glassy Alloys with Tensile Elongation at Room Temperature:** *Yoshihiko Yokoyama*<sup>1</sup>; *Kazutaka Fujita*<sup>2</sup>; *Alain Yavari*<sup>3</sup>; *Peter Liaw*<sup>4</sup>; *Akihisa Inoue*<sup>1</sup>; <sup>1</sup>Institute of Materials Research; <sup>2</sup>Ube National College; <sup>3</sup>LTPCM-CNRS UA29, Domaine Universitaire BP 75; <sup>4</sup>University of Tennessee

Ternary Zr-TM-Al (TM: Cu, Ni or Co) bulk glassy alloys were investigated to clarify the relationship among the volume, thermal, and mechanical properties, and we tried to accomplish the alloy design of Zr-TM-Al bulk glassy alloys. Ultimately, we found that the relationship between the Young's modulus and volume-change ratio provides the suitable guide for the alloy design of bulk glassy alloys. Based on this guide, we suggested that hypoeutectic bulk glassy alloys exhibit superior ductility due to enhancement of metallic bond nature, and never show the structural relaxation embrittlement. Furthermore, we examined about more ductile and malleable cast bulk metallic glass in hypoeutectic Zr-Ni-Cu-Al alloys with high Poisson's ratio over 0.39. This hypoeutectic Zr-Ni-Cu-Al bulk glassy alloy reveals the distinct tensile plastic elongation and unlimited compressive plastic deformation at room temperature.



10:55 AM

**Synthesis and Behavior of Mg-Based Bulk Glasses via Spark Plasma Sintering (SPS):** *Baolong Zheng*<sup>1</sup>; *Zhihui Zhang*<sup>1</sup>; *Troy Topping*<sup>1</sup>; *Yizhang Zhou*<sup>1</sup>; *Chi Y.A. Tsao*<sup>2</sup>; *Enrique J. Lavernia*<sup>1</sup>; <sup>1</sup>University of California, Davis; <sup>2</sup>National Cheng Kung University, Tainan

Mg-based bulk metallic glasses (BMGs) are of interest due to their high specific strength and excellent corrosion resistance relative to those of conventional Mg alloys. In particular, the Mg-Cu-Gd alloy has a good glass forming ability (GFA) and a relatively wide supercooled liquid region, which facilitates fabrication of bulk metallic glasses via consolidation of powder precursor. Spark plasma sintering (SPS) has recently been studied as an attractive consolidation technique for amorphous powders due to its fast heating rate and consolidation cycle. In view of these factors, the primary objectives of this research are: consolidate the Mg<sub>65</sub>Cu<sub>25</sub>Gd<sub>10</sub> (at.%) amorphous powders into bulk component by using the SPS technique; investigate the microstructural evolution of Mg-Cu-Gd powder and their microstructural stability during thermal exposure of SPS processing using SEM, XRD, DSC, and TEM. Microstructural variations and mechanical properties were also investigated as a function of the initial powder size and SPS processing parameters.

11:05 AM

**A Study on the Critical Stress for Continuous Shear Banding of a Bulk Metallic Glass:** *Zheng Han*<sup>1</sup>; *Hai Yang*<sup>1</sup>; *Yi Li*<sup>1</sup>; <sup>1</sup>National University of Singapore

The serrated flow characteristic of the plastic deformation behavior of recently reported plastic bulk metallic glasses (BMGs) indicates that shear bands have been repeatedly initiated and arrested. By properly taking the instant load-bearing area into consideration, we have obtained sustained true stress of the BMG samples during plastic deformation under various distinct deformation modes. Our present work reveals that the critical stress for continuous shear banding maintains invariant on and after yielding over a large plastic strain, contrary to the previously reported assumptions of "strain-softening" and "strain-hardening". With an understanding of the mechanism of yielding and thus the origin of yield strength, we further point out that the atomic cohesive energy constantly serves to be the controlling factor of the critical stress for shear banding. On the other hand, the mechanism for arresting the propagating shear bands will be later suggested.

11:15 AM

**Preparation of Spray-Formed La<sub>62</sub>Al<sub>15.7</sub>(Cu,Ni)<sub>22.3</sub> Bulk Amorphous Alloy with Large Size:** *Bin Yang*<sup>1</sup>; <sup>1</sup>University of Science and Technology Beijing

A large sized La<sub>62</sub>Al<sub>15.7</sub>(Cu,Ni)<sub>22.3</sub> amorphous alloy was produced by melt atomization and spray deposition, and XRD proved a plate-like sample with a diameter of 340 mm and maximum thickness of 13 mm is fully amorphous. The formation mechanism of amorphous phase during the process was analyzed. The experimental results showed that there always exist some porosities in the spray-deposited La<sub>62</sub>Al<sub>15.7</sub>(Cu,Ni)<sub>22.3</sub> amorphous alloy. The densification parameters of the La<sub>62</sub>Al<sub>15.7</sub>(Cu,Ni)<sub>22.3</sub> amorphous alloy were determined by hot pressing in the undercooled liquid region of the amorphous alloy. The present results indicated that spray deposition is a potential technique to prepare bulk amorphous alloys with larger size, especially for bigger plate-shaped deposit.

## Challenges for Sustainable Growth in the Aluminum Industry - Through the Current Crisis and on to the Future: Aluminum Plenary Session

Sponsored by: The Minerals, Metals and Materials Society, TMS Light Metals Division, TMS: Aluminum Committee

Program Organizers: *David DeYoung*, Alcoa Inc; *Halvor Kvande*, Hydro Aluminium AS; *Geoffrey Bearne*, Rio Tinto Alcan; *Ray Peterson*, Aleris International Inc; *Wolfgang Schneider*, Hydro Aluminium GmbH

Monday AM

Room: 2001/2003

February 16, 2009

Location: Moscone West Convention Center

Session Chair: *David DeYoung*, Alcoa Inc

8:30 AM

**Welcome and Introduction**

8:35 AM **Keynote**

**Current Economic Situation, Comparison to Past Recessions in the Metals Industry, Future Projections:** *Dave Persampieri*, CRA

9:05 AM

*Dick Evans*, Rio Tinto Alcan

9:30 AM

*Jan Arve Haugen*, Hydro

9:55 AM **Break**

10:10 AM

*Galdino Claro*, Aleris

10:35 AM

*Bill O'Rourke*, Alcoa

11:00 AM

*To Be Announced*, Rusal

11:25 AM **Panel Discussion**

MONDAY  
AM

## Characterization of Minerals, Metals and Materials: Emerging Characterization Techniques

Sponsored by: The Minerals, Metals and Materials Society, TMS Extraction and Processing Division, TMS: Materials Characterization Committee, TMS/ASM: Composite Materials Committee

Program Organizers: *Toru Okabe*, University of Tokyo; *Ann Hagni*, Geoscience Consultant; *Sergio Monteiro*, State University of the Northern Rio de Janeiro - UENF

Monday AM

Room: 3009

February 16, 2009

Location: Moscone West Convention Center

Session Chairs: *Ann Hagni*, Geoscience Consultant; *Jian Li*, Natural Resources Canada

8:30 AM

**Synchrotron X-Ray Computer Microtomographic and Light Optical Microscopic Investigation of Strength and Microstructure of Polymer-Metal Joints Produced by FricRiveting:** *Sergio Amancio-Filho*<sup>1</sup>; *Felix Beckmann*<sup>1</sup>; *Jorge dos Santos*<sup>1</sup>; <sup>1</sup>GKSS Research Centre

The FricRiveting technique is an alternative new spot joining process developed for thermoplastic-lightweight alloy structures. In this technique a cylindrical metallic rivet is used to join one or more thermoplastic-metal components by means of plasticizing and deforming the tip of the rotating rivet through frictional heating. Advantages of this new technique are e.g. short joining cycles, minimal sample preparation, absence of environmental emissions and enhanced mechanical performance in comparison to base materials. This paper will demonstrate through qualitative and quantitative synchrotron X-Ray microtomographic and light optical microscopic analysis of a case-study joint on aircraft materials polyetherimide and aluminum 2024 - that FricRiveting joint performance under tensile loading is mainly dependent on geometrical

and microstructural features of the deformed tip of the rivet. The influence of processing on joint strength will be demonstrated in terms of rotation speed.

8:45 AM

**On the Role of Low-Concentration Elements in the Formation of Misoriented Grains in Ni-Based Superalloys: Combination of Atom-Probe Tomography and Electron-Dispersive X-Ray Spectroscopy:** *Yaron Amouyal*<sup>1</sup>; David Seidman<sup>1</sup>; <sup>1</sup>Northwestern University

Single-crystal, two-phase Ni-based superalloys are currently used for turbine blades and they represent an incredible technological achievement. Their superior properties are manifested by their high tensile strength and creep resistance up to a working temperature of 1400°C. Avoiding the formation of highly-misoriented grains (MGs) during solidification is crucial, since their boundaries are preferential sites for cracks and fast-diffusion. This goal can be achieved by characterization of the composition of such MGs. We employ both electron-dispersive X-ray spectroscopy (EDS) and atom probe tomography (APT) to determine the partitioning of elements into MGs in two-phase, multi-component (>10 elements) Ni-based superalloys. The combination of both techniques provides us with composition measurements for the large length scale of 10-100 μm, which is typical for EDS with high detectability (< ppm) typical for APT. We discuss the effect of several low-concentration (<500 ppm) elements on the formation of MGs in these alloys.

9:00 AM

**3D Atom Probe Techniques for the Atomic Scale Investigation on the Quantitative Composition of Boron in Steels:** *Jae Bok Seol*<sup>1</sup>; Ju Seok Kang<sup>1</sup>; Yo Sep Yang<sup>1</sup>; Chan Gyung Park<sup>2</sup>; <sup>1</sup>Pohang University of Science and Technology (POSTECH), Department of Materials Science and Engineering; <sup>2</sup>National Center for Nanomaterials and Technology (NCNT), Pohang University of Science and Technology (POSTECH)

It has been widely known to enhance the hardenability of any structural materials by the addition of a small amount of B due to the segregation of solute boron at austenite grain boundary. However, the analytical techniques to identify boron, such as Fission Track Etching (FTE) and Auger Electron Spectroscopy (AES), have limits on observing B in the concentration as low as a few ppm because of their poor sensitivity. Newly developed atom probe tomography (APT) can provide the highest available spatial resolution, 3D tomography imaging and resolve quantitative chemical information with a resolution better than 2nm. Therefore, the exact behavior and position of boron in steels can be investigated by the APT techniques in the sub-nanometer scale. The results obtained by 3D-APT revealed that the B atoms were mainly segregated to C enriched area rather than C depleted area, which were clearly a retained austenite and ferrite phase, respectively due to the strong attraction in the analytical volume of 35 x 35 x 96 nm<sup>3</sup>. The current results demonstrate that the state-of-art LAWATAP has made it possible to excellently identify and quantify the exact B state in steels with 3D tomography imaging and composition profile in the atomic scale.

9:15 AM

**Two and Three-Dimensional Characterization of Microstructural Evolution in Ti-550 and Ti-6Al-4V:** *Vikas Dixit*<sup>1</sup>; Santhosh Koduri<sup>1</sup>; John Sosa<sup>1</sup>; Dan Huber<sup>1</sup>; *Peter Collins*<sup>1</sup>; Hamish Fraser<sup>1</sup>; <sup>1</sup>Ohio State University

The microstructures of titanium alloys, which can significantly influence the mechanical properties, are often quite complex and span across length scales. The microstructural evolution of both a β-processed Ti-alloy, Ti-550 (Ti-4Al-4Mo-1Zr-1Sn, wt%) and an α+β-processed Ti-alloy, Ti-64, have been explored using both two-dimensional techniques, including optical microscopy, scanning electron microscopy (SEM), orientation microscopy (OM), and transmission electron microscopy (TEM), and their three-dimensional analogues (Robo. Met-3D™, DB-FIB/SEM, and (S)TEM tomography). The three dimensional datasets will be presented, and the feature size/fraction compared with the values obtained using two-dimensional stereological approaches.

9:30 AM

**Three-Dimensional Materials Characterization Using HAADF-STEM Tomography:** *Michael Sarahan*<sup>1</sup>; Daniel Masiel<sup>1</sup>; Bryant Gipson<sup>1</sup>; David Morgan<sup>2</sup>; Nigel Browning<sup>1</sup>; <sup>1</sup>University of California, Davis; <sup>2</sup>Indiana University

High-angle annular dark-field scanning transmission electron microscopy (HAADF-STEM) is a powerful technique to visualize compositional differences in a material due to its sensitivity to atomic number (Z-contrast). We have used advanced image processing techniques to derive an average structure and

the average chemical composition from HAADF-STEM images and to map variations from the average across the field of the original image. This allows us to resolve minute compositional details on the length scale of atoms. This study uses the analytical features of STEM imaging in combination with tomographic reconstruction of a tilt series of STEM images to create 3-dimensional models of nanomaterials with high-resolution compositional information. Additional high-resolution information in support of STEM images is obtained from diffractive imaging using iterative image reconstruction techniques, and STEM image-based models are refined using diffraction pattern-based models.

9:45 AM

**High Resolution X-Ray Tomography for Polymeric Structural Composites:** *Stephen Young*<sup>1</sup>; Dayakar Penumadu<sup>1</sup>; Vlastimil Kunc<sup>2</sup>; Eliot Specht<sup>2</sup>; <sup>1</sup>University of Tennessee; <sup>2</sup>Oak Ridge National Laboratory

Polymeric composites have been of significant interest in the automotive field due to their light weight and high strength. In the current research, 3-dimensional x-ray imaging techniques with high resolution are used to study the microstructure of glass and carbon fiber polymeric composites using polypropylene resin. The radiographs were reconstructed to visualize the fiber content and arrangement. In-situ tensile testing system was developed and integrated into the existing hardware for tomography equipment to study the evolution of damage and microstructural features as a function of applied mechanical stress and example results are included. This research will pave the way to quantify damage and develop new class of scale-dependent constitutive models for composites materials for immediate use in structural and transportation applications.

10:00 AM Break

10:20 AM

**In-Situ Characterization of Creep and Creep-Damage in Copper by X-Ray Microtomography:** *Federico Sket*<sup>1</sup>; Krzysztof Dzieciol<sup>1</sup>; Augusta Isaac<sup>1</sup>; Marco Michiel<sup>2</sup>; Thomas Buslaps<sup>2</sup>; *Andras Borbely*<sup>1</sup>; Anke Pyzalla<sup>1</sup>; <sup>1</sup>Max Planck Institut für Eisenforschung; <sup>2</sup>European Synchrotron Radiation Facility

Geometrical shape and microstructure evolution during high temperature creep of a copper was in-situ characterized by X-ray microtomography. It is shown that geometric information of tomographic data combined with image correlation techniques is accurate enough to characterize plastic strain within material slabs with areas equal to the sample cross section but with heights of only 10-20 μm. Imposing a constant temperature gradient along the gauge length of the sample allows for evaluating the apparent activation energy of steady-state creep on a single specimen. The slice correlation technique developed for tracking local material flow during plastic deformation showed to be an excellent tool for tracking the evolution of single damage events, too. It was possible to evaluate the volumetric growth rate of more than 10,000 cavities evolving during the creep process. The obtained growth rates are in good correlation with the "power law creep" theory of Cocks and Ashby.

10:35 AM

**Spatially Resolved Diffusivity Measurement with Thermography:** *Christian Wögerer*<sup>1</sup>; Gerhard Traxler<sup>1</sup>; <sup>1</sup>Profactor Research and Solutions GmbH

For material or process development as well as for quality checking of materials, thermal diffusivity measurement may be the tool of choice in many applications. Especially if diffusivity is measured locally resolved, a lot of information can be read out of such a "diffusivity image". This paper explains the method to measure parallelepiped specimen like plates and lists some interpretations of diffusivity images, like inhomogeneity of sintered materials, structural voids or inclusions. Diffusivity is a material property, describing transportation of heat in solids in spatial and temporal terms. With thermo cameras it is possible, to measure diffusivity of larger areas simultaneously. The result is an area of diffusivity values that may be plotted or displayed like an image. Locations with lower diffusivity values could be caused by the presents of structural differences in the material, by decomposition of the material components or by inclusions of other material like air.

10:50 AM

**In-Situ TEM Observation of Repeating Events of Nucleation in Epitaxial Growth of Nano CoSi<sub>2</sub> in Nanowires of Si:** *Yi-Chia Chou*<sup>1</sup>; King-Ning Tu<sup>1</sup>; Lih-Juann Chen<sup>2</sup>; Wen-Wei Wu<sup>3</sup>; <sup>1</sup>University of California, Los Angeles; <sup>2</sup>National Tsing Hua University; <sup>3</sup>National Chiao Tung University

CoSi<sub>2</sub> formation in Si nanowires has been investigated in high-resolution transmission electron microscopes at 800°C by point contact reactions between Co and Si nanowires. The CoSi<sub>2</sub> has undergone an axial epitaxial growth in

the Si nanowire and a stepwise growth mode was found. We observed that the stepwise growth occurs repeatedly in the form of an atomic step sweeping across the CoSi<sub>2</sub>/Si interface. It appears that the growth of a new step or a new silicide layer requires an independent event of nucleation. We are able to resolve the nucleation stage and the growth stage of each layer of the epitaxial growth in video images. The epitaxial growth consists of a repeating nucleation and a rapid stepwise growth across the epitaxial interface. This is a general behavior of epitaxial growth in nanowires. A discussion of the kinetics of supply-limited reaction in nanowire case by point contact reaction is proposed.

**11:05 AM**

**The Application of Electron Backscatter Diffraction to Study Abnormal Grain Growth and Twinning in Nanocrystalline Nickel:** *Hsiao-Wei Yang*<sup>1</sup>; Shehreen S. Dheda<sup>1</sup>; John R. Porter<sup>1</sup>; <sup>1</sup>University of California

Electrodeposited (ED) Nanocrystalline (nc) nickel, with a grain size of 20nm, has the superior properties typical of nc materials. Understanding the effect of thermal annealing on grain growth morphology and kinetics is important to fully determine the functional capabilities of these materials. Nc nickel has been observed to undergo both grain growth and the formation of twinning upon annealing. Electron backscatter diffraction (EBSD) in a scanning electron microscope (SEM) was used to measure the microstructural evolution due to heat treatment at temperatures between 0.27 and 0.43 of the melting temperature. Sequential EBSD mapping shows the change in grain size, twinning structure and overall texture of the material. Abnormal grain growth and the propensity of coherent twin boundaries (coincidence site lattice (CSL) sigma 3 boundaries) to develop were shown to increase with increasing annealing temperature. The implication of this observation for the application of nc nickel will be discussed.

## Computational Thermodynamics and Kinetics: Energy Materials

Sponsored by: The Minerals, Metals and Materials Society, ASM International, TMS Electronic, Magnetic, and Photonic Materials Division, TMS Materials Processing and Manufacturing Division, ASM Materials Science Critical Technology Sector, TMS: Chemistry and Physics of Materials Committee, TMS/ASM: Computational Materials Science and Engineering Committee

Program Organizers: Long Qing Chen, Pennsylvania State University; Yunzhi Wang, Ohio State University; Pascal Bellon, University of Illinois at Urbana-Champaign; Yongmei Jin, Texas A&M

Monday AM Room: 3002  
February 16, 2009 Location: Moscone West Convention Center

Session Chair: Christopher Wolverton, Northwestern University

**8:30 AM Introductory Comments**

**8:35 AM Invited**

**Thermodynamics and Kinetics of Phase Transformations in Hydrogen Storage Materials:** Alireza Akbarzadeh<sup>1</sup>; Hakan Gunaydin<sup>1</sup>; Kyle Michel<sup>1</sup>; Kendall Houk<sup>1</sup>; Christopher Wolverton<sup>2</sup>; *Vidvuds Ozolins*<sup>1</sup>; <sup>1</sup>University of California, Los Angeles; <sup>2</sup>Northwestern University

General adoption of hydrogen as a vehicular fuel depends on the ability to store hydrogen at high volumetric and gravimetric densities, as well as on the ability to extract and recharge H<sub>2</sub> at sufficiently rapid rates. We will show how first-principles density-functional theory (DFT) techniques can be used to gain fundamental understanding of the thermodynamic driving forces and detailed atomic-scale kinetic mechanisms of phase transformations involved in hydrogen storage reactions. The power of these techniques will be illustrated on several examples of recent work conducted in our group: (i) predicting the crystal structures and thermodynamic properties of several new solid-state borohydrides and amides/imides, (ii) calculating multicomponent phase diagrams, favored reaction pathways, and designing new thermodynamically reversible hydrogen storage reactions in borohydrides, and (iii) clarifying the atomic-scale kinetics of mass transport and hydrogen release in aluminum, sodium alanate, and lithium amide. Research supported by DOE DE-FG02-05ER46253 and DE-FG02-07ER46433, and NSF CBET-0730929.

**9:05 AM Invited**

**Ab-Initio Modeling of SOFC Cathodes:** *Dane Morgan*<sup>1</sup>; *Yueh-Lin Lee*<sup>1</sup>; <sup>1</sup>University of Wisconsin - Madison

Perovskites are the major class of materials used for modern solid oxide fuel cell (SOFC) cathodes and have the ability to catalyze the oxygen reduction reaction (ORR) on their surfaces. However, difficulties in performing *in-situ* characterization of well-controlled samples means that the rate limiting steps and structure-property relationships underlying ORR on these materials are not understood. We have used *ab-initio* based thermokinetic modeling to study (La,Sr)MnO<sub>3</sub> (LSM), which is the primary cathode catalyst used in commercial SOFCs, and developed a combined bulk and surface defect model in order to better understand surface defect structure and catalytic properties. We have also studied lanthanum transition metal oxides LaBO<sub>3</sub> (B= Fe, Co, and Ni) to understand trends of surface oxygen binding, hopping, vacancy formation, and dissociation vs. transition metal types. These studies are being used to develop molecular level models of the ORR on SOFC cathodes.

**9:35 AM**

**Hydrogen Storage on Li-Dispersed Carbon Nanotubes:** *Wei Liu*<sup>1</sup>; *Yonghao Zhao*<sup>1</sup>; *Ying Li*<sup>1</sup>; *Qing Jiang*<sup>2</sup>; *Enrique J. Lavernia*<sup>1</sup>; <sup>1</sup>University of California, Davis; <sup>2</sup>Jilin University, China

High storage capacity and a moderate binding strength are ideal for hydrogen storage materials. Inspection of the literature indicates that the highest H<sub>2</sub> storage capacity by simulation is 13 wt% obtained in the fullerene doped by 12 Li atoms. Using density functional theory, we achieved a similar high uptake capacity (about 13.45 wt%) by optimizing 8 Li on carbon nanotubes. The binding is found to be dramatically enhanced when the additional dopants are introduced. The electronic orbital analysis shows that dopants are essential for storage, whose bands overlap strongly with those of H<sub>2</sub> and the nanotube simultaneously. The presence of an electric field is demonstrated to have a significant influence on the 8-Li-doped model. The calculated adsorption energy E<sub>ad</sub> decreases dramatically to -0.58 eV/H<sub>2</sub>, which is 4.5 times lower than that of pure nanotubes. This increase is attributed to the further ionization of dopants under electric fields.

**9:55 AM**

**Role of Particle Size Distribution in Long Term Platinum Surface Area Loss in PEMFC Cathodes:** *Edward Holby*<sup>1</sup>; *Yang Shao-Horn*<sup>2</sup>; *Wenchao Sheng*<sup>2</sup>; *Dane Morgan*<sup>1</sup>; <sup>1</sup>University of Wisconsin-Madison; <sup>2</sup>Massachusetts Institute of Technology

Long-term durability of Pt catalysts in proton exchange membrane fuel cell (PEMFC) cathodes is an important issue in achieving the commercial viability of PEMFC technology. Fuel cell efficiency is decreased as Pt electrochemically active surface area (ECASA) is lost. It is important to better understand the mechanisms of Pt surface area loss in the cathode and if they can be mitigated in order to meet lifetime requirements. Currently, ECASA loss is attributed to four mechanisms: Ostwald ripening of Pt nanoparticles; Pt nanoparticle migration and coalescence; detachment of Pt particles from the carbon support; and dissolution and reduction of Pt off of the carbon support due to crossover hydrogen from the anode. By modeling these processes, the effect of the initial particle size distribution of the Pt nanoparticles and its role in long-term ECASA loss is investigated.

**10:15 AM**

**First Principles Modeling on Stability Mechanism of Cuboctahedral Clusters in UO<sub>2</sub>:** *Ying Chen*<sup>1</sup>; *Hua Yun Geng*<sup>1</sup>; *Yasunori Kaneta*<sup>1</sup>; *Motoyasu Kinoshita*<sup>2</sup>; <sup>1</sup>University of Tokyo; <sup>2</sup>Central Research Institute of Electric Power Industry

UO<sub>2</sub> is a widely used fuel materials in nuclear reactor, its performance is quite related to the defects behavior under irradiation environment which arises the deviation from stoichiometry of the compound. To clarify ambiguousness remaining for long in structure of nonstoichiometric uranium dioxide, the stability mechanism of oxygen clusters is investigated by first-principles LSDA+U method. A new physical model of thermodynamic competition between cuboctahedral cluster and point oxygen interstitials is proposed. Calculations reveal that the structural stability of the cuboctahedral cluster embedded into the crystal UO<sub>2</sub> is inherited from U<sub>6</sub>O<sub>12</sub> molecular, and the energy gain through occupying its center by one additional oxygen makes the cluster win out by competition to point oxygen interstitials at the ground state. By incorporating the temperature effect, a pseudo phase diagram of temperature and the oxygen concentration is constructed which shows that the elevation of temperature favors point interstitial over cuboctahedral clusters.



## 10:35 AM Break

## 10:50 AM Invited

**First-Principles Solid-State Kinetics:** Anton Van der Ven<sup>1</sup>; <sup>1</sup>University of Michigan

While much progress has been made in the first-principles prediction of the thermodynamics of multi-component solids, predicting the kinetics of solid-state phase transformations remains a major challenge. Both diffusion and the kinetics of first-order phase transformations in intercalation compounds (e.g.  $\text{Li}_x\text{C}_6$ ,  $\text{Li}_x\text{CoO}_2$ ,  $\text{Li}(\text{Ni}_0.5\text{Mn}_0.5)\text{O}_2$ ,  $\text{Li}_x\text{TiS}_2$  ...) play an important role during operation of modern Li-ion batteries, as a charge-discharge cycle leads to the removal and reinsertion of Li ions from the cathode intercalation compounds. Similar kinetic processes occur in hydrogen storage materials and during corrosion processes of structural materials involving hydrogen embrittlement. In this talk, I will describe how first-principles electronic structure methods combined with statistical mechanical techniques from alloy theory have elucidated complex diffusion mechanisms in intercalation compounds and how they can shed light on the mechanisms of first-order diffusional and structural phase transformations in the solid state.

## 11:20 AM Invited

**An Efficient Method to Study Ordering in Low-Symmetry Materials:** Tim Mueller<sup>1</sup>; Gerbrand Ceder<sup>1</sup>; <sup>1</sup>Massachusetts Institute of Technology

Cluster expansions are commonly used to develop effective Hamiltonians for systems with substitutional disorder. The coefficients of the linear expansion are typically fit to training data generated using *ab-initio* methods. Low-symmetry systems, such as nanoparticles and materials with crystal defects, require the determination of a large number of coefficients. A large amount of training data must be generated for such problems, and the cost calculating the energy of each training structure is high due to the low symmetry of the system. For these reasons it has been impractical to use the cluster expansion to study low-symmetry materials with the same level of accuracy as bulk materials. We address this problem by demonstrating new methods that significantly reduce the prediction error of a cluster expansion for a given training set size. Our approach makes it possible to study atomic ordering in low-symmetry systems at a fraction of the current computational cost.

## 11:50 AM

**Computer Simulation on Thermoelectric Energy of Rh-Ir Alloy:** Zhongliang Xiao<sup>1</sup>; Weilian Zheng<sup>1</sup>; Yan Shi<sup>1</sup>; Xuehui Zhan<sup>1</sup>; <sup>1</sup>Changsha University of Science and Technology

As the environment and the energy crisis, research on thermoelectric materials become a hotspot because of their no pollution, no mobile parts and transformation between electricity and thermal energy. One of the studying hotspots is how to predict thermoelectric energy of thermoelectric materials. thermoelectric energy of Rh-Ir alloy was investigated in this paper. At first the super cell models for the alloy were built by changing the composition of alloy and its crystal structure in CASTEP. Then the density of states (DOS), Fermi energy and the electronics structure can be calculated with the plane-wave pseudo potential local density algorithm (LDA) in CASTEP software package. The thermoelectric energy can be obtained according to the Onsager's relationship and DOS of alloys with different compositions. The calculated results is consistent with that from measurement.

## 12:10 PM

**Molecular Dynamics Simulations on the Inhibition of Methane Hydrate Formation by Polyesteramides:** Zhijiu Zheng<sup>1</sup>; Monica Lamm<sup>1</sup>; Richard LeSar<sup>1</sup>; <sup>1</sup>Iowa State University

Gas hydrates form in transmission pipelines as stable solid networks composed of hydrogen-bonded water molecules trapping a second group of encaged molecules, such as methane and hydrogen, leading to undesired blockages in the lines that result in both economic loss and safety risks. To control the formation of hydrates, additives can be added that inhibit hydrate plugging. In this study, we employ atomistic simulations to examine the effects of hyperbranched polyesteramides, Hybrane H1500 (1,3-isobenzofurandione, hexahydro-, polymer with 1,1'-imino-bis[2-propanol]) on hydrate formation. These systems have large numbers of hydroxyl functional groups that form extensive hydrogen bonding with water. All-atom molecular dynamics simulations were used to determine the binding energy and structure of the hydrate/hybrane systems to elucidate the fundamental mechanism for hydrate inhibition. We discuss how the structure, polarity, and size of the polymers influence the performance of these polyesteramides as hydrate inhibitors.

**Dislocations: 75 Years of Deformation Mechanisms: Dislocation Structures and Effects of Material Microstructure**

Sponsored by: The Minerals, Metals and Materials Society, TMS Materials Processing and Manufacturing Division, TMS Structural Materials Division, TMS/ASM: Mechanical Behavior of Materials Committee, TMS: Nanomechanical Materials Behavior Committee

Program Organizers: David Bahr, Washington State University; Erica Lilleodden, GKSS Research Center; Judy Schneider, Mississippi State University; Neville Moody, Sandia National Laboratories

Monday AM

Room: 3022

February 16, 2009

Location: Moscone West Convention Center

Session Chairs: Neville Moody, Sandia National Laboratories; Kip Findley, Colorado School of Mines

## 8:30 AM

**Atomistic Modeling of Low Temperature Dislocation Plasticity in  $\alpha$ -Fe:** Neeraj Thirumalai<sup>1</sup>; Youhong Li<sup>1</sup>; Michael Luton<sup>1</sup>; Ju Li<sup>2</sup>; Liu Cao<sup>3</sup>; Peter Gordon<sup>1</sup>; <sup>1</sup>ExxonMobil Research and Engineering Company; <sup>2</sup>University of Pennsylvania; <sup>3</sup>The Ohio State University

It is well-known that at low temperatures the flow stress in  $\alpha$ -Fe exhibits strong temperature dependence. This dependence arises from the motion of screw dislocations, known to be controlled by double-kink nucleation. Previous atomistic studies suggested that this temperature sensitivity is partly a consequence of the polarized core structure of the screw dislocations. However, recent *ab initio* calculations have shown the core structure of screw dislocations to be compact. We have investigated the kink nucleation pathways that control screw dislocation motion using a recently developed interatomic potential for  $\alpha$ -Fe using Nudged Elastic Band (NEB) and Molecular Dynamics (MD) simulations. In addition, we have also investigated the stability of core states using *ab-initio* calculations. In this presentation we will discuss the results of this study and its relevance towards understanding low temperature plasticity in  $\alpha$ -Fe.

## 8:50 AM

**Modeling and Dislocation Dynamics Study of Precipitation Strengthening in Steels at Low Temperature:** Ghiath Monnet<sup>1</sup>; Benoit Devincere<sup>2</sup>; <sup>1</sup>EDF - R&D; <sup>2</sup>CNRS

At low temperature in iron, dislocation mobility depends strongly on the dislocation character. Screw dislocations are known to move slowly compared to other dislocations and are found to control plastic behavior of steels. The classical picture of dislocation interaction with precipitates is no longer valid and the corresponding strengthening cannot be predicted using classical theories, based on the line tension approximation. In this work we provide a new model, supported by the results of dislocation dynamics simulations, describing the effect of temperature, the strain rate and the precipitation microstructure on the flow stress. It is shown that the difference in mobility between dislocations of different character induces a difference in the effective stress on these dislocations. This leads systematically to a decrease of the precipitation strengthening compared to that measured in the athermal regime.

## 9:10 AM

**The Effect of Microstructure on the Low Temperature Dislocation Behavior in Plate Steels:** Kimani Partin<sup>1</sup>; Kip Findley<sup>1</sup>; Chester Van Tyne<sup>1</sup>; <sup>1</sup>Colorado School of Mines

Plate steels are often used in low temperature applications such as chemical transport and naval armor. However, the strengthening mechanisms at low temperature in light of dislocation mobility are not fully understood. The focus of this study is to examine the effect of microstructure on plastic flow and strengthening behavior in steels. Noble and Hull and later Gupta and Li developed methods utilizing stress relaxation tests to determine the dislocation velocity exponent,  $m^*$ . Combined with tensile testing, the temperature independent internal stress and temperature dependent effective stress can be calculated. These methods have been used to evaluate a single steel grade, ASTM A514. Testing of green, as-quenched, and quenched and tempered conditions was performed to compare steel with the same composition but different microstructures. The activation energies to overcome the Peierls barrier for dislocation motion are

also compared, and the results provide insight into the differences in strength between microstructures.

**9:30 AM**

**Ternary Junctions and Hardening in BCC and FCC Crystals:** *Ronan Madec*<sup>1</sup>; Ladislav Kubin<sup>2</sup>; <sup>1</sup>Commissariat à l'Énergie Atomique; <sup>2</sup>CNRS/ONERA

When two dislocations cross each other, they may form a junction. When a third dislocation crosses a junction, a ternary junction may be formed. We examine the possible configurations of ternary junctions in bcc and fcc crystals and estimate their contribution to strain hardening. Two distinct families are found: axial ternary junctions are formed when three slip planes share a common axis; zigzag ternary junctions form when the binary junctions can glide to react with a third dislocation along a new direction. In bcc metals, the second type of reaction is statistically the most probable and the strongest junction is associated with a zigzag ternary junction. Ternary junctions are found to induce Taylor hardening only in bcc metals, whereas an increased strain hardening is expected to result from increased dislocation storage in both fcc and bcc metals.

**9:50 AM**

**Dislocation Dissociation and Locking in Supersaturated Co-Ni Based Superalloys Due to Aging Treatment:** *Akihiko Chiba*<sup>1</sup>; Satoshi Tadano<sup>1</sup>; Hiroaki Matsumoto<sup>1</sup>; Toyohiko Konno<sup>1</sup>; <sup>1</sup>Tohoku University

To establish high-temperature strengthening materials with excellent ductility, we have studied a new strengthening mechanism operative in Co-based alloys without  $\eta'$  precipitation. Dislocation structures in a Co-Ni-based alloy have been examined. The alloy studied is found to be a supersaturated solid solution with fcc crystal structure. With aging treatment at 973K for 10h after pre-straining the alloy at room temperature, the dislocations widely dissociate into Shockley partials bounding the stacking fault (SF), resulting from Suzuki segregation to the SF bounded by Shockley partials. It has been found that the widely dissociated dislocations is transformed into precipitations of  $\delta$  phase with crystal structure of DO19, resulting in strengthener of the Co-Ni based alloy at around 800°C. As a result, the dislocations which exhibit tendency to be widely dissociated into the Shockley partials at elevated temperatures can act as the effective strengthener of the high temperature strength of the alloys.

**10:10 AM Break**

**10:30 AM**

**Fine Structure of c-Component Dislocations Associated with Pyramidal Slip Activity in Ti3Al:** *Jorg Wiezorek*<sup>1</sup>; Andreas Kulovits<sup>1</sup>; <sup>1</sup>University of Pittsburgh

The hexagonal ordered phase Ti3Al is a minor constituent in current TiAl-based alloys, which offer potential for applications in advanced transportation system. The minority phase affects the deformation behavior of lamellar grains in promising these TiAl alloys. General plastic deformation of Ti3Al requires pyramidal plane c-component dislocation slip,  $\{2-201\}\langle 11-26 \rangle$  and  $\{11-21\}\langle 11-26 \rangle$ , which operates only for loading close to the c-axis and exhibits anomalous yielding. We use binary Ti-48at%Al model alloys to elaborate the fine structure of c-component dislocations activated during c-axis loading of lamellar grains in TiAl-alloys at ambient and elevated temperature by conventional diffraction contrast and high-resolution transmission electron microscopy. In addition to the large amounts of debris characteristically associated with pyramidal slip in Ti3Al, we have observed non-planar dissociated configurations of the c-component dislocations with atomic resolution. The results are discussed in relation to the mechanical behavior of Ti3Al and two-phase TiAl.

**10:50 AM**

**Monazite (Monoclinic LaPO4) Slip Systems at Room Temperature:** *Randall Hay*<sup>1</sup>; <sup>1</sup>Air Force Research Laboratory

Polycrystalline monazite (monoclinic LaPO4) was deformed by spherical indentation at room temperature. Dislocation Burgers vectors were identified by Burgers circuit closure in high resolution TEM images, supplemented by diffraction contrast where possible. A total of 441 b determinations were made in 97 grains. The most common slip systems were  $[001]/(010)$ ,  $[100]/(010)$ , and  $[010]/(100)$ . Slip on (001) was less common. Many other less dislocations were also identified, including  $[101]$ ,  $[10-1]$ ,  $[011]$ ,  $[110]$ , and  $[111]$ .  $[101]$  dislocations dissociate into  $\frac{1}{2}[101]$  and  $\frac{1}{2}[10-1]$  partials.  $b = [100]$  dislocations may dissociate into  $\frac{1}{4}[210] + \frac{1}{4}[2-10]$  partials. Several other partial dislocations were tentatively identified. All partial dislocations were climb dissociated. Dislocation line energies were calculated, and stacking fault structures and energies between partial dislocations were analyzed. Satisfaction of the Von

Mises criteria most likely involves  $[101]/(11-1)$  and  $\langle 011 \rangle / \{011\}$  slip. If deformation twinning is active  $\langle 011 \rangle$  slip may not be necessary for full ductility.

**11:10 AM**

**Deformation within Molecular Single Crystals:** *Kyle Ramos*<sup>1</sup>; Daniel Hooks<sup>2</sup>; David Bahr<sup>1</sup>; <sup>1</sup>Washington State University; <sup>2</sup>Los Alamos National Laboratory

Dislocations have remained relatively unexplored within molecular crystals. Lower symmetry, intermolecular degrees of freedom, and susceptibility to electron beam degradation have prohibited studies of deformation within these materials. Using the newer technological capabilities of nanoindentation and scanning probe microscopy, older etching analysis techniques have been revitalized to overcome some complications associated with molecular crystals and enable the experimental investigation of deformation at an elementary level previously unattainable. The approximate two order of magnitude increase in characterization resolution has permitted experimental observations that are near length scales attainable for molecular dynamics simulations employing fully flexible potentials. A collaborative experimental-simulation effort promises a new insight to dislocation mediated plasticity within molecular materials. Experimental data from several molecular crystals will be presented to emphasize new capabilities and future possibilities.

**11:30 AM**

**Slip Paths of  $\langle c+a \rangle$  Dislocations and Stacking Faults in HCP Metals:** *Bin Li*<sup>1</sup>; Evan Ma<sup>1</sup>; <sup>1</sup>Johns Hopkins University

The nature of the pyramidal slip of  $\langle c+a \rangle$  dislocations in HCP metals remains unclear. We present molecular dynamics (MD) simulations in single-crystal HCP magnesium, as well as TEM observations. The  $\langle c+a \rangle$  slip is found to be composed of two consecutive dislocation slips, each having a Burgers vector of only about one half of  $\langle c+a \rangle$  and gliding in a corrugated manner adjacent to the twinning plane. The constituent dislocations of the  $\langle c+a \rangle$  slip nucleate independently, leading to a wide stacking fault (hundreds of nanometers) on the twinning plane. We have indeed observed such stacking faults under TEM. This mode of deformation can be generalized to the four major twinning modes observed in HCP metals, regardless of the c/a ratio. The relationship between the  $\langle c+a \rangle$  dislocations and the twinning dislocations will also be briefly discussed, and elaborated in a separate talk.

**11:50 AM**

**Dislocation Dipole Formation and Breaking during Shear Deformation:** *Dongsheng Xu*<sup>1</sup>; Hao Wang<sup>1</sup>; Rui Yang<sup>1</sup>; <sup>1</sup>Institute of Metal Research, Chinese Academy of Sciences

Molecular simulations were carried out to investigate the formation and breaking of dislocation dipoles in some fcc metals and intermetallic compounds. Dipoles of various heights and orientations were formed and their configuration changes during shear deformation were studied. It was found that for dipoles with small height, of several interplanar spacing, due to the strong reaction among the constituent dislocations, various reacted structures formed, such as faulted dipoles, stacking fault tetrahedra and zigzagged configurations, depending on the dipole height and deformation temperature. The breaking stress of small height dipoles increased substantially due to the formation of the above products, compared with elastic calculations. Furthermore, these reacted products are hard to move or break, and will be strong obstacles to the movement of other dislocations, so as to contribute to work hardening during deformation and may serve as the anchoring point for the dislocation wall formation during fatigue process.

**12:10 PM**

**A Quantitative Model of Strength in Mg from First-Principles:** *Joseph Yasi*<sup>1</sup>; Louis Hector<sup>2</sup>; Dallas Trinkle<sup>1</sup>; <sup>1</sup>University of Illinois at Urbana-Champaign; <sup>2</sup>General Motors Technical Center

Computational modeling of solute-dislocation interactions in magnesium is essential to develop new alloys with high ductility. We present a quantitative first-principles model of plastic deformation in Mg from density functional theory calculations of basal and prismatic dislocation core geometries with and without applied stress. An ultrasoft pseudopotential for Mg with PW91 GGA accurately reproduces lattice constants, elastic constants, phonon spectra and stacking fault energies from experiment. We calculate the Peierls stress, dislocation core splitting and the activation energy for cross-slip for basal and prismatic screw, edge and mixed dislocations. To include alloying effects, we calculate dislocation-solute interaction energies and changes in the dislocation

core splitting with Al and Zn solutes. The first-principles data parameterizes a model for the motion of a dislocation in a field of solutes at finite temperature to predict the strength of Mg alloys.

## Emerging Applications of Neutron Scattering in Materials Science and Engineering: Neutron Diffraction and Structure Determination

Sponsored by: The Minerals, Metals and Materials Society, TMS Electronic, Magnetic, and Photonic Materials Division, TMS: Chemistry and Physics of Materials Committee

Program Organizers: Xun-li Wang, Oak Ridge National Laboratory; Brent Fultz, California Institute of Technology; Hahn Choo, University of Tennessee

Monday AM  
February 16, 2009

Room: 3012  
Location: Moscone West Convention Center

Session Chairs: Xun-li Wang, Oak Ridge National Laboratory; Bill David, STFC

### 8:30 AM Invited

**Scientific Opportunities at the SNS and Upgraded HFIR:** *Ian Anderson*<sup>1</sup>; <sup>1</sup>Oak Ridge National Laboratory

The Spallation Neutron Source (SNS) at Oak Ridge National Laboratory (ORNL) provides the research community with access to the most intense pulsed neutron beams in the world. ORNL is also home to the High Flux Isotope Reactor (HFIR), one of the world's most powerful research reactors. Together, the SNS and HFIR provide scientists and engineers around the world with the opportunity to carry out research at the forefront of physics, chemistry, materials science, engineering, and biology. A project to upgrade the power of the SNS accelerator from 1.4 MW to 3 MW is underway and construction of a second, long pulse target station is planned. These new facilities will extend the present capabilities of the neutron scattering techniques to high resolution studies of both the structure and dynamics of materials in a wide range of environments.

### 9:00 AM Invited

**Neutron Powder Diffraction Studies of Hydrogen Storage Materials:** *Bill David*<sup>1</sup>; Marco Sommariva<sup>1</sup>; <sup>1</sup>STFC

This presentation focusses on the use of neutron powder diffraction to study the detailed behaviour of hydrogen storage materials. Particular emphasis will be given to the combined in-situ gravimetric and neutron powder diffraction analysis that enables detailed structural and gravimetric information to be obtained as a function of both temperature and pressure. Neutrons are the ideal tool to investigate the structure of hydrogen storage materials and, in addition to discussing in-situ hydrogen absorption and desorption measurements, high resolution diffraction data will be presented that provide insights into the detailed mechanisms of lightweight hydrogen storage materials.

### 9:30 AM

**Time Resolved Neutron Diffraction Studies of Defect Structure Formation in Lithium Imide during Hydrogenation and De-hydrogenation:** *Ashfia Huq*<sup>1</sup>; Jason Hodges<sup>1</sup>; Luke Heroux<sup>1</sup>; Evan Maxey<sup>2</sup>; Dhanesh Chandra<sup>3</sup>; <sup>1</sup>Oak Ridge National Laboratory; <sup>2</sup>Argonne National Laboratory; <sup>3</sup>University of Nevada, Reno

Reversible hydrogen absorption and desorption properties of lithium imide to lithium amide at 250°C have generated a great interest in this system. The structure of lithium amide is fairly well established where as there is significant debate about the structure of lithium imide. While there is general agreement about the position of the Li and N atoms which form an antifluorite structure, several types of hydrogen positions have been proposed. In all these models, however, a common theme is the disordered hydrogen. In situ neutron diffraction measurement revealing a variation in stoichiometry of cubic lithium imide during hydrogenation and dehydrogenation at 250°C will be presented. ORNL/SNS is managed by UT-Battelle, LLC, for the U.S. Department of Energy under contract DE-AC05-00OR22725. Work at ANL supported by the U.S. DOE, Basic Energy Sciences—Materials Sciences, under Contract W 31-109-ENG-38.

### 9:50 AM

**Neutron Diffraction Experiments of Polarized Protons:** *Maths Karlsson*<sup>1</sup>; Ted Forgan<sup>2</sup>; Eddy Lelièvre-Berna<sup>3</sup>; Ken Andersen<sup>3</sup>; Christian Vettier<sup>1</sup>; Colin Carlile<sup>1</sup>; Trevor Forsyth<sup>3</sup>; Garry McIntyre<sup>3</sup>; Patrik Carlsson<sup>1</sup>; <sup>1</sup>European Spallation Source Scandinavia; <sup>2</sup>University of Birmingham; <sup>3</sup>Institut Laue-Langevin

Hydrogen atoms play a key role in many materials of high interest. X-ray and neutron diffraction are the tools of choice for structural studies, but X-rays are not very sensitive to hydrogen, and neutrons give a large background due to incoherent scattering from the hydrogen. We propose to develop a new method, with which we will exploit the strong spin dependence of the proton cross section and reduce the incoherent scattering from the hydrogen by aligning their nuclear spins. A very large increase in the signal-to-noise ratio will then result, which will enable new science and improve existing methods for studying hydrogenous materials. We aim to implement the method on a suitable instrument at ILL, with the longer term goal to install it at the forthcoming European Spallation Source. Initially though, we will investigate the key aspects of the technique. In this talk we present our first results from this work.

### 10:10 AM Break

### 10:30 AM Invited

**High-Pressure Neutron Diffraction Studies for Materials Sciences and Energy Sciences:** *Yusheng Zhao*<sup>1</sup>; <sup>1</sup>Los Alamos National Laboratory

The neutron diffraction under pressure and temperature conditions is highly valuable to condensed matter physics, crystal chemistry, materials sciences. We have incorporated a 500-ton press TAP-98 into the HIPPO diffractometer to conduct in situ high P-T neutron diffraction experiments. Recently, we have developed high-P low-T gas/fluid cells in conjunction with neutron diffraction and inelastic neutron scattering instruments. We have successfully used these techniques to study the equation of state, structural phase transition, and thermo-mechanical properties of metals, ceramics, and minerals. We have conducted researches on the formation of methane and hydrogen clathrates, and hydrogen adsorption of the inclusion compounds such as the recently discovered metal-organic frameworks. The aim of our research is to accurately map phase diagram, lattice parameters, thermal parameters, bond lengths, bond angles, neighboring atomic environments, and phase stability in P-T-X space. Studies based on high-pressure neutron diffraction are important for multidisciplinary science, particularly for the theoretical/computational modeling/simulations.

### 11:00 AM

**Investigation of the Crystallographic Structure of the  $\epsilon$  Phase in the Fe-Al System by High-Temperature Neutron Diffraction:** *Sven Vogel*<sup>1</sup>; Frank Stein<sup>2</sup>; Martin Palm<sup>2</sup>; M. Eumann<sup>2</sup>; <sup>1</sup>Los Alamos National Laboratory; <sup>2</sup>MPI für Eisenforschung GmbH

In the central part of the Fe-Al system between about 58 and 65 at.% Al, a high-temperature phase denoted as  $\epsilon$  occurs with a hitherto unknown crystallographic structure. The phase is stable between 1231 and 1095°C and disintegrates at the lower temperature by a spontaneous eutectoid reaction into a fine-scaled, lamellar FeAl (B2) + FeAl<sub>2</sub> microstructure. Because this reaction can not be suppressed even by rapid quenching, the crystallographic structure of the  $\epsilon$  phase could not be determined yet. An alloy with 60 at.% Al, i.e. approximately eutectoid composition, has been produced by crucible-free levitation melting. In order to study the crystallographic structure of the high-temperature  $\epsilon$  phase, in-situ high-temperature neutron diffraction experiments have been performed at the HIPPO instrument at Los Alamos Neutron Science Center (LANSCE) at Los Alamos National Laboratories (LANL).

### 11:20 AM

**Neutron Diffraction Study of Structure Parameters of Chemisorbed NaX and NaY Zeolite Catalysts:** *Stanislav Vratislav*<sup>1</sup>; Maja Dlouhá<sup>1</sup>; Vladimír Bosáček<sup>2</sup>; <sup>1</sup>CTU in Prague, Faculty of Nuclear Sciences and Physical Engineering; <sup>2</sup>CAS, Institute of Physical Chemistry of Jaroslav Heyrovsky

The regular structure of zeolites can be easily modified, many laboratories try therefore to "tailor" zeolitic catalysts of the requested properties. Nature of acid or basic sites, their amount and distribution in the zeolitic lattice belong to the most important problem of surface chemistry. Some organic cations like methylum or ethylium, create chemisorbed, with more or less polarized, but covalently bonded alkoxy species in zeolitic structures. Careful <sup>13</sup>C MAS NMR measurements make possible to distinguish between signals of bridging and terminal methoxy groups. Neutron powder diffraction patterns were collected from evacuated ampoules with samples at room and 7 K on the KSN-2 diffractometer



which is placed at the LVR-15 research reactor in Rež near Prague. The complete structural parameters (including chemisorbed ions at O1 and O4 in NaX and at O1 in NaY and redistribution of Na<sup>+</sup> cations) were determined by Rietveld analysis using GSAS package.

## 11:40 AM

**First Results from POWGEN: A New Neutron Powder Diffractometer at the SNS:** *Jason Hodges*<sup>1</sup>; *Ashfia Huq*<sup>1</sup>; *Olivier Gourdon*<sup>1</sup>; *Luke Heroux*<sup>1</sup>; <sup>1</sup>Oak Ridge National Laboratory

POWGEN is a fundamental departure from previous designs for a time-of-flight powder diffractometer at a spallation neutron source and may be considered a third-generation design. The instrument is optimized for both parametric studies of materials under a wide range of conditions (T, P, H, flowing gases, etc) and *ab-initio* crystal structure determinations of complex solid-state materials with asymmetric unit-cells of the order ~1500 Å<sup>3</sup>. The geometric design of the instrument allows for all detected scattered neutrons to be focused onto a single diffraction profile yielding high count rate while preserving good resolution ( $\Delta d/d = 0.0015$  at  $d = 1$  Å). The new time-event mode for data acquisition will permit stroboscopic experiments with approximately 100 ms time resolution. Early results from commissioning experiments will be presented.

## 12:00 PM

**Nested Neutron Microfocusing Optics on SNAP:** *Gene Ice*<sup>1</sup>; *Jae-Young Choi*<sup>2</sup>; *Peter Takacs*<sup>3</sup>; *Yevgeniy Puzyrev*<sup>4</sup>; *Jamie Molaison*<sup>4</sup>; *Chris Tulk*<sup>4</sup>; *Ken Andersen*<sup>5</sup>; *Terry Bigault*<sup>6</sup>; <sup>1</sup>Oak Ridge National Laboratory; <sup>2</sup>Pohang Accelerator Laboratory; <sup>3</sup>Brookhaven National Laboratory; <sup>4</sup>Oak Ridge National Laboratory; <sup>5</sup>Institut Laue-Langevin

The Spallation Neutron Source (SNS) together with large detector solid angles, now makes possible neutron experiments with much smaller sample volumes. Nested Kirkpatrick-Baez supermirror optics provide a practical and efficient way to further decrease the useable neutron sample size by focusing polychromatic neutron beams. Because the optics are nondispersive, they are ideal for spallation sources and for polychromatic beam experiments on reactor sources. Theoretical calculations indicate that nested mirrors can preserve source brilliance at the sample for small beams and for modest divergences that are appropriate for diffraction experiments. Here we describe the design, calibration and performance of a nested neutron mirror pair for the Spallation Neutrons At Pressure (SNAP) beamline at the SNS. This is an example of a general class of experiments that can benefit from spatially-resolved diffraction inside environmental chambers.

## Energy Conservation in Metals Extraction and Materials Processing II: Extraction Processes/Refractories/Modeling and Analysis

Sponsored by: The Minerals, Metals and Materials Society, TMS Extraction and Processing Division, TMS Light Metals Division, TMS: Energy Committee  
Program Organizers: Edgar Vidal, Brush Wellman, Inc.; Cynthia Belt, Aleris International Inc; Marie Kistler, Air Products and Chemicals, Inc; Mark Cooksey, CSIRO; Rob Hardin, Burner Dynamics, Inc.

Monday AM Room: 2012  
February 16, 2009 Location: Moscone West Convention Center

Session Chairs: Edgar Vidal, Brush Wellman, Inc.; Mark Cooksey, CSIRO

## 8:30 AM Introductory Comments

### 8:35 AM

**Energy and Sustainable Development in Hydrometallurgy - An Emerging Perspective:** *Katragadda Sarveswara Rao*<sup>1</sup>; <sup>1</sup>Institute of Minerals and Materials Technology (CSIR)

Any innovative approach made in non-ferrous metallurgical industry centers upon developing new processes, saving materials, improving production quality and born-again materials. Aqueous processing is commonly used to treat lean grade or more complex ore bodies. Its sustenance largely depends on energy and environmental compliance including water and wastewater management. The present paper focuses the importance of using particle size distribution and surface area measurements during ammoniacal dissolution of a Cu-Pb-Zn sulphide bulk concentrate and with an overview of the effect of water salinity

on the process chemistry and residue mineralogy. Accordingly, an effort is made here to discuss the emerging perspective and highlight the recent successes and trends in terms of energy savings in non-ferrous hydrometallurgy.

### 8:55 AM

**Copper Electrowinning Using Noble Metal Oxide Coated Titanium - Based Bipolar Electrodes:** *Krishnasamy Asokan*<sup>1</sup>; *Kandasamy Subramanian*<sup>1</sup>; <sup>1</sup>Central Electro Chemical Research Institute

Electro winning of copper by monopolar cells require common anode and cathode bus bar and cross bars to connect each electrode to the respective common bus bar. On the other hand, the bipolar configuration warrants the end electrodes only to be connected to bus bars; there is substantial reduction in copper requirement. In the present work, an electro winning cell with bipolar electrodes and end electrodes, each having an area of 1000 cm<sup>2</sup> was designed and operated. The bipolar electrode is made of mixed metal oxide coated titanium mesh welded to plain titanium sheet. Coated titanium mesh acts as anode and the plain titanium sheet acts as cathode. Environmentally unacceptable lead anode and the recurring loss of lead are done away with. Closer spacing of the electrodes, paves way for the application of higher current density leading to mass transfer enhancement. Performance of bipolar copper electro winning cell is reported.

### 9:15 AM

**Microbial Reduction of Lateritic Nickel Ore for Enhanced Recovery of Nickel and Cobalt Through Bio-Hydrometallurgical Route:** *L. Sukla*<sup>1</sup>; *N. Pradhan*<sup>1</sup>; *R.K. Mohapatra*<sup>1</sup>; *B.K. Mohapatra*<sup>1</sup>; *B.D. Nayak*<sup>1</sup>; *B.K. Mishra*<sup>1</sup>; <sup>1</sup>Institute of Mineral and Material Technology

The chromite overburden sample of Sukinda, India is lateritic, where valuable metals like Ni (1%) and Co (0.04%) are bound within goethite (α-FeOOH) phase. To recover these metals an ecofriendly biohydrometallurgical route has been developed. An anaerobic dissimilatory iron (III) reducing bacterial consortium capable of using acetate as carbon source and lateritic ore as terminal electron acceptor was used for reducing iron hydroxide to iron oxide. The initial light brown colour of the ore changed to dark brown colour. The change in colour is due to the conversion of goethite to hematite/magnetite which was confirmed by XRD and EPMA. The treated sample when subjected to bio/acid leaching, higher recovery of Ni and Co was obtained. Thus it is possible to make use of dissimilatory iron reducing bacteria for recovery of valuable metals from low grade iron ore.

### 9:35 AM Break

### 9:55 AM

**Energy Saving Strategies for the Use of Refractory Materials in Molten Material Contact:** *James Hemrick*<sup>1</sup>; *Klaus-Markus Peters*<sup>2</sup>; *John Damiano*<sup>3</sup>; *James Keiser*<sup>1</sup>; <sup>1</sup>Oak Ridge National Laboratory; <sup>2</sup>Fireline TCON, Inc.; <sup>3</sup>MINTEQ International, Inc.

This paper will present work performed by Oak Ridge National Laboratory (ORNL), in collaboration with industrial refractory manufacturers and users, to employ novel refractory systems and techniques to reduce energy consumption of molten material processing vessels found in industries such as aluminum, glass and pulp and paper. Energy savings discussed will be achieved through reduction of chemical reactions, mechanical degradation by the service environment, temperature limitations of materials, and costly installation and repair needs. Key results of several case studies resulting from Department of Energy (DOE) funded research programs will be discussed with emphasis on applicability of these results to all high temperature processing industries.

### 10:15 AM

**Energy Savings through Phosphate-Bonded Refractory Materials:** *Jens Decker*<sup>1</sup>; <sup>1</sup>Stellar Materials

In consideration of energy savings the ideal refractory furnace lining should possess the following features:- Lowest thermal conductivity possible in order to avoid heat loss. - Single component lining in order to allow freeze plane changes caused by wear, infiltration and temperature changes of the furnace. - Resistance against mechanical wear from cleaning tools and stirring in order to allow maximum output without equipment downtime due to maintenance. - Resistance against thermo-chemical attack from aluminum and alloying elements. However, refractory materials with a low thermal conductivity typically possess a higher porosity and this leads to lower strengths and resistance against chemical attack and wear. Hence, as a compromise, multi layer linings are required in order to meet energy saving standards. In this paper we present

the features of chemically phosphate-bonded dense and light weight refractories and how such refractories can contribute to energy savings.

10:35 AM

**Advanced Ceramic Composites for Improved Thermal Management in Molten Aluminum Applications:** *Klaus-Markus Peters<sup>1</sup>; Robert Cravens<sup>2</sup>; James Hemrick<sup>3</sup>; <sup>1</sup>Fireline TCON Inc; <sup>2</sup>Rex Materials Group; <sup>3</sup>Oak Ridge National Laboratory*

Degradation of refractories in molten aluminum applications leads to energy inefficiencies, both in terms of increased energy consumption during use as well as due to frequent and premature production shutdowns. Therefore, the ability to enhance and extend the performance of refractory systems will improve the energy efficiency through out the service life. TCON® ceramic composite materials are being produced via a collaboration between Fireline TCON, Inc. and Rex Materials Group; these materials were found to be extremely resistant to erosion and corrosion by molten aluminum alloys during an evaluation funded by the U.S. Department of Energy and it was concluded that they positively impact the performance of refractory systems. These findings were subsequently verified by field tests. Data will be presented on how TCON® shapes are used to significantly improve the thermal management of molten aluminum contact applications and extend the performance of such refractory systems.

10:55 AM

**Energy Efficient, Non-Wetting, Microporous Refractory Material for Molten Aluminum Contact Applications:** *Kenneth McGowan<sup>1</sup>; <sup>1</sup>Westmoreland Advanced Materials, LLC*

Result of a R&D effort addressing the need for energy efficient refractories serving the aluminum industry is the development of patented microporous refractory materials for molten metal contact applications in all furnace areas including the belly band. It has been demonstrated that this material can reduce energy consumption up to 38% in reverb and holding furnaces and significantly reduce heat loss in transfer ladles, launders and trough systems. Furthermore, the material developed is non-wetting and remains un-penetrated by metal throughout its lifetime. The material does not contribute to the formation of corundum. As a result, the energy efficiency of an older lining remains intact compared to standard refractory materials which may have an initial high insulating value (such as lightweights and board) or standard dense refractory (even with penetration inhibitors) both of which show a rapid increase in thermal conductivity as the refractory is penetrated with aluminum and formed corundum.

11:15 AM

**CFD Modeling for Optimization of Aluminum Melting Furnace Design Parameters:** *Mohamed Hassan Ali<sup>1</sup>; Zhengdong Long<sup>1</sup>; Shridas Ningileri<sup>1</sup>; Subodh Das<sup>2</sup>; <sup>1</sup>University of Kentucky; <sup>2</sup>Phinix LLC*

In order to enhance the energy efficiency of aluminum melting furnace, several models using computational fluid dynamics (CFD) have been developed. The models can be used to answer questions as to: how can the melting cycle be shortened; how does geometry and shape affect melting efficiency; what is the best shape and location of the flue gas exit as well as burners; how does the flow circulate; and how does the temperature distribute within the furnace space. The results will show the flow and temperature contours within the furnace combustion space as well as the metal load. The models will take into account the temperature dependency of the load's thermal properties, furnace burner design configuration in addition to the load shape and lining properties. The model will be validated by using real measurements from a base model then followed by a CFD parametric study.

11:35 AM

**A Study of Exergy Analysis for Combustion in Direct Fired Heater:** *Ahmed Abd Elrahman<sup>1</sup>; <sup>1</sup>Egyptalum*

Heat transfer with organic media has often been able to replace or improve the classic steam-water operation. The possibility of transferring and closely controlling temperature up to > 300°C has provided the heat transfer media technology with many new fields of application. The growing application of heat transfer plants with liquid heat transfer media other than water has made it necessary to produce complete and accurate engineering database for combustion and his devices to continuous improvement of industrial heating. Heating is an important operation in almost all industrial fields. The analysis of related combustion process and estimation of the effective coefficients is the first step toward a successful design. The process of combustion, fuel and their

combustion and combustion devices are considered in this study, direct fired heater Exergy and energy analysis are performed taking into account precisely calculation of chemical Exergy for products of combustion.

11:55 AM Concluding Comments

## Fatigue: Mechanisms, Theory, Experiments and Industry Practice: Characterization Methods for Elucidating Fatigue Mechanisms

Sponsored by: The Minerals, Metals and Materials Society, TMS Structural Materials Division, TMS/ASM: Computational Materials Science and Engineering Committee, TMS/ASM: Mechanical Behavior of Materials Committee, TMS/ASM: Nuclear Materials Committee

Program Organizers: Koenraad Janssens, Paul Scherrer Institute; Corbett Battaile, Sandia National Laboratories; Brad Boyce, Sandia National Laboratories; Luke Brewer, Sandia National Laboratories

Monday AM

Room: 3008

February 16, 2009

Location: Moscone West Convention Center

Session Chair: Luke Brewer, Sandia National Laboratories

8:30 AM Invited

**Elastic Strain and Dislocation Distributions near Fatigue Cracks Measured Using High Resolution Electron Back Scatter Diffraction:** *Angus Wilkinson<sup>1</sup>; <sup>1</sup>University of Oxford*

Over the past few years there has been a significant advance in the sensitivity of EBSD measurements so that the technique now allows determination of the elastic strain tensor and small angle rotations to a level of  $\sim 10^{-4}$ . In this presentation the basis of the technique will be briefly described before turning attention to applications in analysis of fatigued metals. Images and linescans taken near the tips and wakes of fatigue cracks in single crystal superalloy samples will be presented. Lattice curvature shows the extent of the plastic zone and quantitative analysis using Nye's dislocation tensor allows the geometrically necessary dislocation content to be assessed. Elastic strains (ie stresses) are also measured. Stresses normal to the crack plane are observed to be compressive within an inner reversed plasticity zone, while weaker tensile stresses are seen in an outer zone.

9:00 AM

**3D Characterisation of Short Cracks in Ti-6246 Using X-Ray Tomography and EBSD:** *Soran Biroscu<sup>1</sup>; <sup>1</sup>The University of Manchester*

In the present study, crack propagation was imaged non-destructively in 3 dimensions during in-situ fatigue loading of Ti-6246 using X-ray micro-tomography on beamline ID19 at the European Synchrotron Radiation Facility (ESRF), Grenoble, France. Phase contrast enabled the visualization of the two-phase microstructure but in order to obtain the crystallographic orientation of individual grains along the crack path a 3D EBSD volume was recorded subsequently. By combining both techniques it was possible to relate the crystallographic orientation of grains to crack arrest and accelerated crack propagation. It is shown that the lamellar grain orientation and morphology have a great influence on the crack direction and growth. Moreover, crack resistance property of the alloy is investigated by means of EBSD grain characterisation methodology, orientation and misorientation data evaluations.

9:20 AM

**An Electron Microscope Study of Low-Cycle Fatigue in a High Niobium Containing and Precipitation Hardened TiAl Alloy:** *Fritz Appel<sup>1</sup>; Thomas Heckel<sup>2</sup>; Hans-Jürgen Christ<sup>2</sup>; <sup>1</sup>GKSS Research Centre Geesthacht; <sup>2</sup>Universität Siegen*

The micromechanisms controlling low cycle fatigue of a Nb-bearing TiAl alloy (TNB-V2) have been characterized by conventional and high-resolution transmission electron microscopy. Fully reversed isothermal tests were performed under strain control at temperatures of 25, 550 and 850°C. Samples fatigued at 25 and 550°C exhibited dense structures of ordinary dislocations and debris that were accumulated in tangles. The dipole defects apparently serve as additional glide obstacles but may also contribute to dislocation multiplication if the local stress rises. In situ heating experiments have been performed in order to assess the thermal stability of the dipole defects. Another important low temperature

deformation mechanism is the stress-induced transformation of an orthorhombic phase, which is a significant constituent of the microstructure. The orthorhombic phase is apparently unstable under tetragonal distortion and transforms into  $\gamma$  phase. Under high-temperature fatigue the lamellar microstructure degrades by phase transformation combined with dynamic recrystallization.

## 9:40 AM

**Acoustic Effects on Cyclic-Tension Fatigue of Al-4Cu-1Mg Alloy by Ultrasonic Shear Wave Methods:** Hideki Yamagishi<sup>1</sup>; Mikio Fukuhara<sup>2</sup>; Akihiko Chiba<sup>2</sup>; <sup>1</sup>Toyama Industrial Technology Center; <sup>2</sup>Tohoku University

Cyclic-tension fatigue of aluminum alloy, Al-4Cu-1Mg, has been determined by usage of SV wave reflection and SH wave transmission methods in terms of nondestructive evaluation. Internal friction measured by SV method begins to increase rapidly from normalized fatigue ratio of about 0.5, showing dominating interaction of movable dislocations with the waves, as viscoelastic effect. Logarithmic damping ratio and propagation time in SH method decrease with increase of the fatigue degree due to acoustoelastic effect. According to SH wave flux model that SH wave energy shifts to specimen surface under crystal-lattice distortion by tensile load, the cyclic-tension induced residual-stress shift which correlates to the decreases in the damping ratio and the propagation time. These effects will provide an accurate and useful tool for nondestructive evaluation of fatigue of the alloy.

## 10:00 AM

**Measuring Micromechanical Behavior for Polycrystalline Materials Under Cyclic Loading:** Jun-Sang Park<sup>1</sup>; Matt Miller<sup>1</sup>; Alexander Kazimirov<sup>1</sup>; Ulrich Lienert<sup>2</sup>; <sup>1</sup>Cornell University; <sup>2</sup>Advanced Photon Source

Understanding the crack initiation and propagation mechanisms of a polycrystalline material under cyclic loading remains a challenging problem. Complicated crystal stresses arising from single crystal anisotropy and complex grain and phase morphologies make the prediction of crack initiation and propagation in the grain size scale difficult. In this work, oxygen free high conductivity copper specimens were cyclically loaded while x-ray diffraction experiments were performed to find the orientation-wise crystal stresses. It was found that the evolution of the crystal stress distribution over orientation space with respect to specimen life is small but not negligible. The peak widths associated with the dislocation density and the distribution of elastic strain in a material also showed small changes with respect to specimen life indicating changes in the grain size scale.

## 10:20 AM Break

## 10:50 AM Invited

**Image-Based Modeling of Crack Growth in Particle Reinforced Composites:** Nikhilesh Chawla<sup>1</sup>; <sup>1</sup>Arizona State University

The fatigue crack growth behavior of particle reinforced composites is determined by several factors, such as reinforcement volume fraction, size, and morphology. Because crack growth is significantly influenced by the morphology and spatial distribution of the reinforcement particles, it is important to adequately characterize the microstructure in simulations of crack growth. In this talk, the results of image-based simulations of crack growth in SiC particle reinforced Al matrix composites, both in two- and three-dimensions, will be described. In particular, the effect of SiC particle distribution and morphology on crack growth was studied. In addition, the effect of particle fracture on crack growth was also studied. Particle fracture ahead of the crack tip significantly alters the crack trajectory and the stress intensity at the crack-tip. Finally, it will be shown that these simulations, encompassing actual microstructures, provide an excellent basis for explaining experimental observations of crack growth in this system.

## 11:20 AM

**Observations of Fatigue Crack Initiation in 7075-T651:** John Papazian<sup>1</sup>; Robert Christ<sup>1</sup>; Joel Payne; Greg Welsh<sup>2</sup>; Joel Payne<sup>3</sup>; <sup>1</sup>Northrop Grumman; <sup>2</sup>United Technologies; <sup>3</sup>Toho Tenax

Detailed microstructural and crystallographic information on fatigue crack initiation and early stage propagation was required as part of a larger effort to model and predict the remaining life of aircraft. Commercial aluminum alloys were the materials of primary interest. In these materials, fatigue cracking is generally associated with constituent particles. Therefore, the purpose of the current study was to use direct observation (scanning electron microscopy) to establish the exact nature and timing of crack initiation in 7075-T651 with particular reference to the issues of cracking or debonding of the constituent

particles, when cracking first occurs during the fatigue process, the influence of matrix orientation on the process, the transition from a constituent particle crack to a matrix crack, and the early stage propagation of short cracks. A double edge notch specimen was designed that was small enough to be imaged in the SEM yet large enough to replicate the fastener hole geometry in actual aircraft structure. Interrupted fatigue cycling starting with fractional initial cycles (20, 40, 60 and 80% of the eventual constant amplitude fatigue load) and continuing on with 1, 3, 10, 30, etc. cycles until failure. At each interval, the crack initiation and propagation process was documented for approximately 100 constituent particles. Orientation Imaging Microscopy was used to document the crystallography of the surrounding grains. The results provide a quantitative description of the fatigue crack initiation process and document the essential characteristics of the process.

## 11:40 AM

**Effects of Microstructure on the Kinematics of Fatigue Crack Propagation in Ti-6Al-4V:** Thomas Villarreal<sup>1</sup>; Rikki Teale<sup>1</sup>; Pedro Peralta<sup>1</sup>; <sup>1</sup>Arizona State University

Opening strain fields ahead of fatigue cracks in Ti-6Al-4V were studied for two different microstructures to investigate their effects on the kinematics of fatigue crack growth. The tests were performed on standard Compact Tension (CT) specimens at constant values of  $\Delta K$  and load ratio (0.1), and the microstructure along the crack path was characterized via Electron backscattering diffraction (EBSD). In-situ loading and Digital Image Correlation (DIC) software were used to derive opening strain fields beyond the crack tip. The strain fields will be correlated to crack growth rates and the microstructure around the crack tip and will also be compared to lattice rotations obtained via EBSD. The lattice rotation, as an indirect measure of strain, will also be studied at the half thickness of the samples to investigate constraint effects. Results will assist in constructing a model of fatigue crack growth at the microscale that accounts for microstructural effects.

## 12:00 PM

**In-Situ Investigation of Residual Stresses around Cracks in Hydrided Zircaloy SENT Specimen:** Axel Steuwer<sup>1</sup>; John Daniels<sup>2</sup>; <sup>1</sup>ESS Scandinavia; <sup>2</sup>ESRF

Using high-energy synchrotron X-ray diffraction on ID15B at the ESRF, Grenoble, we investigated the residual stresses around a fatigue crack grown in 600ppm zircaloy SENT specimen in-situ. The diffraction patterns clearly reveal the matrix as well as the hydride diffraction peaks, allowing phase-specific strain information to be collected at different levels of load. The results as well as the general capabilities of the technique will be discussed.

## Friction Stir Welding and Processing-V: Session I

Sponsored by: The Minerals, Metals and Materials Society, TMS Materials Processing and Manufacturing Division, TMS: Shaping and Forming Committee  
Program Organizers: Rajiv Mishra, Missouri University of Science and Technology; Thomas Lienert, Los Alamos National Laboratory; Murray Mahoney, formerly with Rockwell Scientific

Monday AM

February 16, 2009

Room: 2014

Location: Moscone West Convention Center

Session Chair: Rajiv Mishra, Missouri University of Science and Technology

## 8:30 AM Introductory Comments

## 8:35 AM Invited

**Microstructure – Processing Relationships in Friction Stir Processing (FSP) of NiAl Bronze:** Terry McNelley<sup>1</sup>; Srinivasan Swaminathan<sup>2</sup>; Jianqing Su<sup>1</sup>; Sarath Menon<sup>1</sup>; <sup>1</sup>Naval Postgraduate School; <sup>2</sup>GE Global Research

The use of FSP for localized modification of microstructure and properties in large cast NiAl bronze components is envisioned to reduce costs and improve component service performance. As-processed stir zone (SZ) microstructures reflect transients and gradients in strain, strain rate and temperature although SZ strength and ductility values are both typically enhanced relative to as-cast properties. The evolution of SZ and thermomechanically affected zone (TMAZ) microstructures during single-pass and multi-pass FSP by rectangular and spiral raster processes will be summarized. Microstructures produced by



thermomechanical simulations will be compared to those produced during FSP. Current models for recrystallization need to be modified to include the transients and gradients in FSP in order to account for the exceptional refinement of microstructure and enhancement of mechanical properties associated with this process.

### 8:55 AM Invited

**Advancements in FSW of Hard Metals:** *Jeff Bernath*<sup>1</sup>; Nate Ames<sup>1</sup>; Brian Thompson<sup>1</sup>; Timothy Stotler<sup>1</sup>; <sup>1</sup>EWI

Friction Stir Welding (FSW) is a solid state joining process originally developed and applied on soft metals such as aluminum. As the technology has matured, much of the recent research has shifted to FSW of hard metals. Novel advancements have been achieved in FSW of hard metals including steels, titanium, and nickel based alloys. Developments have been made to improve process robustness, tool life, and microstructure. Improvements to tool materials have allowed welding of increased thicknesses of hard metals using conventional and bobbin methods. New tool geometries have been designed through finite element analysis of the FSW process. Developments in process control mechanisms have provided improved methods for microstructural control of the stir zone. These recent advancements have provided an overall improvement to the capabilities and process robustness of FSW of hard metals. A summary of the advancements to date and application the technology will be discussed.

### 9:15 AM Invited

**Microstructural Evolution during Friction Stir Welding of Near-Alpha Titanium:** *Richard Fonda*<sup>1</sup>; Keith Knipling<sup>2</sup>; <sup>1</sup>Naval Research Laboratory; <sup>2</sup>Naval Research Lab

The microstructural evolution, and the deformation mechanisms that give rise to that evolution, have been analyzed in friction stir welds of a near-alpha titanium alloy, Ti-5111. In particular, this presentation will describe the base plate microstructure, how that microstructure evolves as it becomes influenced by the deformation field surrounding the tool, and what further evolutions occur as this material is deposited in the wake of the tool and cooled to ambient temperature to produce the microstructure observed in the deposited weld.

### 9:35 AM

**Electron Backscatter Diffraction Study of Cast and Friction Stir Processed Ti-6Al-4V:** *Adam Pilchak*<sup>1</sup>; James Williams<sup>1</sup>; <sup>1</sup>Ohio State University

Electron backscatter diffraction has been used to characterize texture in the stir zone (SZ) of investment cast and friction stir processed Ti-6Al-4V. While the maximum intensities in the orientation distributions are low compared to conventional metal working processes, simple shear textures are present in both the bcc  $\beta$  phase and hcp  $\alpha$  phase. The orientation of the shear plane normal and shear direction changed as a function of position in the SZ. These observations provide insight into the strain fields that accompany this complicated deformation process. In material processed above the  $\beta$  transus, the SZ texture was correlated to a continuous dynamic recrystallization texture observed during hot torsion of interstitial-free steel and  $\alpha$ -Fe. Recrystallization of the coarse colony structure in sub  $\beta$ -transus processed material was also investigated. The mechanism appears to be based on continuous recrystallization processes where subgrain boundaries gradually evolve into high angle boundaries with increasing dislocation density.

### 9:55 AM

**Physical Simulation of Friction Stir Processed Ti-5111:** *Melissa Rubal*<sup>1</sup>; John Lippold<sup>1</sup>; Mary Juhas<sup>1</sup>; <sup>1</sup>Ohio State University

Friction stir processing (FSP) of Ti-5111 was performed above and below the beta-transus temperature, allowing for investigation of the microstructural evolution in both conditions. Each processed panel was instrumented with thermocouples to record the thermal histories in the stir zone and adjacent heat-affected zone. Single sensor differential thermal analysis (SS-DTA) was used to determine the beta transus during processing. The FSP microstructures were characterized using light and scanning electron microscopy, while the microtextures of the FSP regions were compared using electron backscatter diffraction (EBSD). FSP produced extreme grain refinement in both processing conditions – reducing the 200-500 micron base material grains to 1-20 microns. The microstructures observed in the FSP panels were simulated using a Gleeble 3800. The strain and strain rate data may be used to verify FSP modeling programs of titanium to reduce the parameter selection phases of future friction stir projects.

### 10:15 AM

**Thermal Stir Welding High Melting Temperature Materials:** *Joseph Querin*<sup>1</sup>; Judy Schneider<sup>1</sup>; Christopher Kolb<sup>2</sup>; Ray Walker<sup>2</sup>; Bryant Walker<sup>2</sup>; Robert Ding<sup>3</sup>; <sup>1</sup>Mississippi State University; <sup>2</sup>Keystone Synergistic Enterprises, Inc.; <sup>3</sup>National Aeronautics and Space Administration

Thermal stir welding (TSWing) developed by the National Aeronautics and Space Administration's (NASA) Marshall Space Flight Center (MSFC) is a solid state joining technique similar to friction stir welding (FSWing). However, unlike FSWing, the heating, stirring, and forging elements of the process are decoupled allowing independent, dynamic control of each process element. With the separation of heating, stirring, and forging elements during the joining process there are more degrees of freedom allowing greater process control. In this study the thermal stir welding (TSWing) process was used to join 1/2 in thick commercially pure titanium in a butt joint configuration. Metallographic samples have been mounted, polished, and analyzed using optical microscopy to document the microstructure.

### 10:35 AM Break

### 10:45 AM Invited

**Fatigue Crack Growth in Friction Stir Welded Ti-5111:** *Peter Pao*<sup>1</sup>; Richard Fonda<sup>1</sup>; Harry Jones<sup>1</sup>; C.R. Feng<sup>1</sup>; D.W. Moon<sup>1</sup>; <sup>1</sup>Naval Research Laboratory

The effects of weld microstructure and weld speed on the fatigue crack growth kinetics of friction stir welded Ti-5111 were investigated. The FSW weld consists of very fine recrystallized grains, in contrast to coarse basketweave grains in the base metal. The fatigue crack growth rates are significantly lower and fatigue crack growth thresholds are significantly higher through the weld than those in the base metal. As the weld speed increases, the fatigue crack growth rates are progressively higher and fatigue crack growth thresholds lower through the weld. However, after stress-relief annealing, such differences in fatigue crack growth kinetics among different weld speeds no longer exist. Fatigue crack growth rates through post stress-relieved welds are slightly higher than those in the base metal. The observed fatigue crack growth responses are discussed in terms of differences in crack tip microstructure, compressive residual stress distribution, and crack closure.

### 11:05 AM Invited

**Speed and Feed Effects on the Surface Texture and Superplastic Forming Performance of Titanium 6Al-4V Friction Stir Welds:** *Daniel Sanders*<sup>1</sup>; M. Ramulu<sup>2</sup>; Paul Edwards<sup>1</sup>; Anthony Reynolds<sup>3</sup>; Glenn Grant<sup>4</sup>; <sup>1</sup>Boeing; <sup>2</sup>University of Washington; <sup>3</sup>University of South Carolina; <sup>4</sup>Pacific Northwest National Laboratory

The purpose of this study was to investigate the speed and feed effects of the Friction Stir Welding (FSW) process on the surface texture along the top of a butt welded nugget. The test was conducted using fine grain (0.8 to 2 $\mu$ ) titanium alloy 6Al-4V with a thickness of 2.5 mm. Through additional development of the FSW process parameters, the butt welded nugget was also made to have equivalent superplastic forming (SPF) characteristics as the parent sheet material. By using special cooling techniques, the weld zone can be kept below the beta transus temperature, which enables the formation of a grain structure conducive to superplastic behavior.

### 11:25 AM Invited

**Faster Temperature Response and Repeatable Power Input to Aid Automatic Control of Friction Stir Welded Copper Canisters:** *Lars Cederqvist*<sup>1</sup>; <sup>1</sup>SKB

The Swedish Nuclear Fuel and Waste Management Company will join at least 12,000 lids to the extruded copper tubes containing Sweden's nuclear waste. To ensure that high quality welds are produced repeatedly, the need of an automated welding procedure controlling the tool temperature instead of the current procedure depending on a skilled welding operator is evident. The reliability of the automatic procedure is however limited by the time lag in the temperature responding to changes in heat input. Currently, the tool temperature takes 15-20 seconds to respond to heat input changes. New thermocouple placements have proved that the response time can be reduced to 5-10 seconds. The paper discusses how the shorter response time aid the development of the automatic procedure and how, due to the lag, PID-control algorithms using both tool temperature and heat input are used to automatically control the tool temperature within its process window.

11:45 AM

**Investigating the Effects of Pin Tool Design on Friction Stir Welded Ti-6Al-4V:** *Haley Rubisoff*<sup>1</sup>; Joseph Querin<sup>1</sup>; Judy Schneider<sup>1</sup>; <sup>1</sup>Mississippi State University

Friction stir welding (FSW), a solid state joining technique, uses a non-consumable rotating pin tool to thermomechanically join materials. Heating of the weldment caused by friction and deformation is a function of the interaction between the pin tool and the work piece. Therefore, the geometry of the pin tool is in part responsible for the resulting microstructure and mechanical properties. In this study microwave sintered tungsten carbide (WC) pin tools with tapers and flats were used to FSW Ti-6Al-4V. Transverse sections of welds were mechanically tested, and the microstructure was characterized using optical microscopy (OM) and scanning electron microscopy (SEM). X-ray diffraction (XRD) and electron back-scatter diffraction (EBSD) were used to characterize the texture within the welds produced from the different pin tool designs.

12:05 PM

**The Effect of Friction Stir Processing on the Microstructural Evolution and Mechanical Properties of Ti-6Al-4V Alloy:** *Nilesh Kumar*<sup>1</sup>; Jeffrey Rodelas<sup>1</sup>; Rajiv Mishra<sup>1</sup>; <sup>1</sup>Missouri University of Science and Technology

Friction stir processing (FSP) was applied to Ti-6Al-4V alloy to modify the microstructure and improve the mechanical properties. Experiments were carried out at three different tool rotational rates – 1200, 1000 and 800 rpm. Other parameters (traverse speed, tilt angle, etc) were kept unchanged. The material processed at 800 rpm showed very narrow HAZ. Hardness in the nugget region was higher than the parent material in each case. In case of sample processed at 1200 rpm, an improvement of approximately 33% in YS and UTS over as-received material was observed. It was 36% and 27% in the case of samples processed at 1000 rpm and 800 rpm, respectively. The best strength after FSP was 1236 MPa as compared to 910 MPa in as received material. This improvement in strengths was observed with no compromise in the ductility of the material (25% elongation for parent and 23-27% elongation for FSPed samples).

12:25 PM

**Texture and Microstructural Evolution during the Linear Friction Welding of Ti-6Al-4V:** *Elvi Dalgard*<sup>1</sup>; John Jonas<sup>1</sup>; Mohammad Jahazi<sup>1</sup>; <sup>1</sup>McGill University

The linear friction welding behavior of Ti-6Al-4V was investigated using various processing conditions of frequency (30-70 Hz), pressure (30-70 MPa) and shortening (2-3 mm). The strain and flow stress during LFW for each set of welding parameters was estimated based on known properties and behavior of the material during hot deformation. LFW samples were examined using electron backscatter diffraction (EBSD) to relate the texture and variant selection behavior to the strain and flow stress. Characterization of the welds includes analysis of the microstructure of the weld and thermomechanically affected zones (TMAZ) in relation to the parent material. Prior studies have shown that in the weld region, exposure to temperatures above the beta transus (995°C), combined with deformation and rapid cooling after joining, produced a Widmanstätten alpha-beta transformation microstructure. The relationship of the transformed structure to the prior grains was examined using EBSD and electron microscopy.

12:45 PM

**Thermohydrogen Processed Friction Stir Welding:** *Yuri Hovanski*<sup>1</sup>; <sup>1</sup>PNNL

Thermohydrogen processing parameters were developed to temporarily modify the properties of titanium sheet into conditions uniquely applicable to joining via friction stir welding (FSW). Modifications of mechanical properties and phase kinetics of commercially pure titanium that was temporarily alloyed with hydrogen created beneficial changes in the processability of the metal during FSW. Significant reductions in both the plunge forces required to seat a tool as well as the transverse loading during the traverse were demonstrated in temporary alloyed titanium sheet. In order to exhibit the increased workability of the thermohydrogen processed sheet, tests were conducted using conventional tool materials used for FSW titanium as well as lower cost materials more typical of FSW aluminum alloys. Hydrogen was successfully removed with a post processing vacuum anneal.

## Frontiers in Solidification Science III: Fundamentals of Solidification: Interfaces, Nucleation, Growth, and Nonequilibrium Considerations

Sponsored by: The Minerals, Metals and Materials Society, ASM International, TMS Materials Processing and Manufacturing Division, TMS/ASM: Computational Materials Science and Engineering Committee, TMS/ASM: Phase Transformations Committee, TMS: Solidification Committee, TMS: Chemistry and Physics of Materials Committee  
Program Organizers: Ralph Napolitano, Iowa State University; James Morris, Oak Ridge National Laboratory

Monday AM  
February 16, 2009

Room: 2018  
Location: Moscone West Convention Center

*Session Chair:* Christoph Beckermann, University of Iowa

8:30 AM Invited

**Modeling Wetting and Nucleation: Some Recent Surprises:** *James Warren*<sup>1</sup>; Daniel Wheeler<sup>1</sup>; Laszlo Granasy<sup>2</sup>; Tamas Pusztai<sup>3</sup>; William Boettinger<sup>1</sup>; <sup>1</sup>National Institute of Standards and Technology; <sup>2</sup>Brunel University; <sup>3</sup>RISSPO

The analysis a solid nuclei wetting and/or reacting with an impurity in a melt provides the basis for classical models of nucleation. Conversely, models of a liquid melt dissolving into/reacting with a solid substrate provide insight into phenomena as diverse as VLS growth and soldering. Developing a thermodynamically consistent picture of such phenomena forces a reconsideration of a number of classical assumptions. The notions of contact angle, phase boundaries, surface energies, as well as a number of kinetic phenomena must all be reevaluated in the context of these new models. In this talk I will explore several phase field models of wetting and spreading and explore some of the new metrics that might provide better predictive power in understanding these systems.

8:50 AM Invited

**Non-Equilibrium Solidification of Undercooled Melts of Al-Based Alloys:** *Dieter Herlach*<sup>1</sup>; Helena Hartmann<sup>2</sup>; Peter Galenko<sup>1</sup>; Dirk Holland-Moritz<sup>1</sup>; <sup>1</sup>German Aerospace Center; <sup>2</sup>Ruhr-University Bochum

Electromagnetic levitation is utilized to containerlessly undercool drops of metallic melts. High-speed camera technique is employed to measure dendrite growth velocities as a function of undercooling. Significant changes of the temperature dependence of the growth dynamics are observed when solute trapping and/or disorder trapping are taking place during solidification of deeply undercooled melts far from equilibrium. The experimental data are analyzed within an extended sharp interface theory of dendrite growth. The results of the measurements of growth velocity are quantitatively described over the entire undercooling range of  $\Delta T \leq 350$  K accessible by levitation experiments. The primary solidification of disordered superlattice structures of intermetallics at undercoolings exceeding a critical value for the onset of disorder trapping is confirmed by in situ energy dispersive X-ray scattering on levitation processed samples using high intensity synchrotron radiation at the European Synchrotron Radiation Facility in Grenoble.

9:10 AM

**Critically Comparing Molecular Dynamics Simulations of Nucleation with Theory:** *James Morris*<sup>1</sup>; Lujian Peng<sup>2</sup>; Rachel Aga<sup>3</sup>; <sup>1</sup>Oak Ridge National Laboratory; <sup>2</sup>University of Tennessee; <sup>3</sup>Wright State University, Department of Chemistry

We have performed critical examinations of nucleation in molecular dynamics simulations. The Lennard-Jones system and an EAM model of Al were used; in both cases, quantities that affect nucleation, particularly the solid-liquid interfacial free energy, were calculated separately, for a parameter-free comparison with theory. At higher temperatures, a reasonable comparison with classical nucleation theory is obtained, but transient effects must be accounted for. Simulation sizes affect the distribution of nucleation times. At low temperatures, the Lennard-Jones system transforms rapidly, suggesting a low barrier; however, in contrast to recent reports, there is no evidence of a spinodal at undercoolings near  $T/T_m = 0.67$ . The Al system always shows a measurable time to nucleation, with a minimum near  $T/T_m = 0.45$ , demonstrating that fast nucleation is not generic. This research has been sponsored by the Division of Materials Sciences and Engineering, Office of Basic Energy Sciences, U.S. Department of Energy under contract DE-AC05-00OR-22725 with UT-Battelle.

9:30 AM

**Morphology Evolution and Solidification Kinetics in 2D: A Phase-Field Crystal Study:** Gyorgy Tegze<sup>1</sup>; Laszlo Granasy<sup>1</sup>; <sup>1</sup>Brunel University

Using the phase-field crystal model, we address the evolution of complex solidification morphologies and the solid-liquid transformation kinetics on the atomistic scale. In single component systems, we observe a diffusion controlled growth mechanism at low supersaturations, which switches to an interface controlled mechanism at high supersaturations, a behavior reminiscent to that seen in colloidal systems. We present a morphology map that contains transitions between compact and dendritic structures and polycrystalline growth forms. Next, we use a recent model of Elder et al. (2007) to investigate morphological transitions in a binary system of ~1.6 million atoms, and determine morphological aspects of dendritic solidification including the variation of tip radius and velocity as a function of time. Finally, we address transformation kinetics of polycrystalline solidification in single component and binary systems, and compare the respective behaviors of the Avrami-Kolmogorov exponent describing the time evolution of freezing.

9:50 AM

**The Microstructural Evolution of Impulse Atomized Al-Fe Powder:** Jian Chen<sup>1</sup>; Hani Henein<sup>1</sup>; <sup>1</sup>University of Alberta

The microstructure and metastable phases in three compositions of Al-xFe (x=0.61, 1.90 and 7.98 in wt pct) droplets prepared by impulse atomization were studied by transmission electron microscopy (TEM). For Al-0.61Fe, the droplets exhibits microstructure of dendritic/cellular alpha-Al with eutectic Al<sub>3</sub>Fe/alpha-Al (m=4.0-4.4) precipitated at the dendritic/cellular wall. The non-equilibrium condition incorporated by the impulse atomization shifts hypoeutectic Al-1.90Fe to hypereutectic composition, thus it produces a similar microstructure as demonstrated in Al-0.61Fe. For Al-7.98Fe, the microstructure is more complicated comparing with those of Al-0.61Fe and Al-1.90Fe. Metastable primary Al<sub>3</sub>Fe, stable Al<sub>13</sub>Fe<sub>4</sub> with blade morphology, eutectic Al<sub>6</sub>Fe/alpha-Al and alpha-Al coexist in the microstructure in Al-7.98Fe. Based on the above results undercooling conditions are predicted and the solidification path of phases in Al-7.98Fe is proposed.

10:10 AM Break

10:30 AM Invited

**A Molecular Dynamics Simulation Study of Solute Trapping during Rapid Solidification:** Jeffrey Hoyt<sup>1</sup>; Y. Yang<sup>2</sup>; H. Humadi<sup>1</sup>; D. Buta<sup>2</sup>; M. Asta<sup>2</sup>; D.Y. Sun<sup>3</sup>; <sup>1</sup>McMaster University; <sup>2</sup>University of California, Davis; <sup>3</sup>East China Normal University

It is well known that the partitioning of solute in the solid phase increases above its equilibrium value at high solidification rates, yet very few experiments have successfully measured the relationship between the segregation coefficient and the growth velocity. In this work molecular dynamics simulations of solute trapping have been performed on a model Lennard-Jones binary alloy and the Ni-Cu system modeled with the embedded atom method. The velocity dependent segregation coefficient, as a function of driving force and crystallographic growth direction, is compared with the Kaplan and Aziz continuous growth model and the results provide estimates for the diffusive speed,  $V_D$ , which reflects the interplay between solid-liquid interface motion and atomic transport across the interface. In addition, we also compare the results to more recent sharp interface models.

10:50 AM Invited

**Molecular Dynamics Investigations of Faceted Growth at the Nanoscale:** Tomorr Haxhimali<sup>1</sup>; Dorel Buta<sup>1</sup>; Mark Asta<sup>2</sup>; Peter Voorhees<sup>3</sup>; Jeff Hoyt<sup>4</sup>; <sup>1</sup>University of California; <sup>2</sup>University of California; <sup>3</sup>Northwestern University; <sup>4</sup>McMaster University

We present results of atomistic simulations investigating mechanisms at the solid-liquid interface underlying faceted solidification in a geometry mimicking the vapor-liquid-solid nanowire growth. These simulations employ a model potential for pure Si, with the driving force for growth applied by undercooling. The simulations yield an equilibrium solid-liquid interface shape that is non-planar, with a faceted orientation bounded by curved orientations near the solid-liquid-vacuum contact line. The curved portions lead to a capillary undercooling which increases in magnitude with decreasing nanowire diameter. In growth simulations, the interface shape is preserved. Growth is observed to proceed in a layer-by-layer mode with a rate limited by the nucleation of new (111) terraces. For a given driving force, measured as the undercooling below the capillary-

corrected coexistence temperature, the growth rates are observed to increase with decreasing nanowire diameter. These results are interpreted to reflect a size dependence of the barrier for terrace nucleation.

11:10 AM Invited

**Phase-Field Modelling of Liquid Crystal Solidification:** Mathis Plapp<sup>1</sup>; Jesper Mellenthin<sup>1</sup>; Hervé Henry<sup>1</sup>; <sup>1</sup>Ecole Polytechnique

Some years ago, the nematic-isotropic transition that occurs in liquid crystals has been used as an analog for solidification. Directional "solidification" of liquid crystal alloys can be used to investigate cellular patterns for parameter regimes that are difficult to attain in experiments on metals. However, liquid crystals also exhibit a non-conventional interfacial anisotropy due to the presence of the nematic director field, the effect of which has not been studied so far. We present a phase-field model that describes the nematic ordering by a tensorial order parameter, which naturally includes the bulk dynamics of the director field and the proper anchoring condition at the nematic-isotropic interface. Numerical simulations reveal that the coupling to the director field strongly influences the linear stability of a planar front, and the shape and stability of well-developed cells. The relation of our findings to the known results for anisotropic crystals are discussed.

11:30 AM

**How Do Quasicrystals Grow?:** Aaron Keys<sup>1</sup>; Sharon Glotzer<sup>1</sup>; <sup>1</sup>University of Michigan

Using molecular simulations, we show that the aperiodic growth of quasicrystals from the liquid state is controlled by the ability of the growing quasicrystal nucleus to incorporate kinetically trapped atoms into the solid phase with minimal rearrangement. In the system under investigation, which forms a dodecahedral quasicrystal on cooling from a high temperature liquid, we show that this process occurs through the assimilation of stable icosahedral clusters by the growing quasicrystal. Our results demonstrate how local atomic interactions give rise to the long-range aperiodicity of quasicrystals. References: A.S. Keys and S.C. Glotzer, Phys. Rev. Lett. 99, 235503 (2007). P.J. Steinhardt, Nature 452, 43 (2008).

11:50 AM

**Solidification Behavior of Tin on Quasicrystalline Surfaces:** Alok Singh<sup>1</sup>; Hidetoshi Somekawa<sup>1</sup>; An Pang Tsai<sup>2</sup>; <sup>1</sup>National Institute for Materials Science; <sup>2</sup>Tohoku University

Solidification behavior of tin on quasicrystalline surfaces has been studied by embedding one micron size tin particles in Al-Cu-Fe icosahedral phase by rapid solidification followed by annealing. Another annealing treatment was carried out to obtain a microcrystalline matrix. Particle-matrix interfaces were studied by TEM, while solidification studies were carried out by DSC as well as in-situ in TEM. Tin made faceted interfaces with the icosahedral phase, matching close packed planes in various orientations. Prominent solidification peaks occurred on cooling in DSC. In the microcrystalline matrix there was a single exothermic peak, but multiple peaks occurred in the quasicrystalline matrix at a similar lever of undercooling. Three major peaks were distinguished, whose relative heights were dependent on the cooling rate. Contact angle of the solid nucleus were estimated to be 11° in the microcrystalline matrix, and 9.5°, 11° and 14° in the quasicrystalline matrix. Role of interface structures is analyzed.

12:10 PM

**Effect of the Shear Flow on Morphological Stability during Directional Solidification:** Zidong Wang<sup>1</sup>; <sup>1</sup>McGill University

The effect of a shear flow on the planar solidification process has been considered for the hypercooled pure melt. In the basic steady state solution for the flow field, there is a boundary layer for the case of small Prandtl number. A linear stability analysis shows that the morphological stability of the interface is modified by the shear flow. There are two traveling waves for the flow field along the interface paralleling to the shear flow, the solidification allows the oscillatory decay mode solution for the temperature and flow fields. As the shear flow increases, the minimum wave number that makes the flow field stable increases, the range of stability becomes smaller, then the shear flow is a destabilizing factor in this problem. If the shear flow vanishes, there is no oscillatory mode for the system, which gives the growth rate of crystal as a function of the shear flow.



## General Abstracts: Extraction and Processing Division: Session I

Sponsored by: The Minerals, Metals and Materials Society, TMS Extraction and Processing Division, TMS: Energy Committee, TMS: Hydro and Electrometallurgy Committee, TMS: Materials Characterization Committee, TMS: Process Technology and Modeling Committee, TMS: Pyrometallurgy Committee, TMS: Recycling and Environmental Technologies Committee

Program Organizer: Boyd Davis, Kingston Process Metallurgy

Monday AM  
February 16, 2009

Room: 2005  
Location: Moscone West Convention Center

Session Chair: Elli Miettinen, Outotec Oyj

### 8:30 AM

**Comparative Study of Cyanide and Acid Leaching of Gold and Silver from Deer Trail Mine Oxide Ore and Tailings:** *Edgar Blanco*<sup>1</sup>; *Charlie Madsen*<sup>1</sup>; *Michael Moats*<sup>2</sup>; <sup>1</sup>UNICO Deer Trail Mine; <sup>2</sup>University of Utah

At the Deer Trail Mine, interest in recovering noble metals from ore tailings with 1.0 g/t Au and 200 g/t Ag has led to metallurgical studies focused on finding an adequate treatment for this material. Using cyanide leaching, the silver/gold recoveries from oxide ore and sulfide tailings were 53%/95% and 30%/76%, respectively. Since these recoveries were less than desired for silver, it was decided to explore a non-cyanide leaching process that would extract silver and gold better. Based on previous research the possibility of using aqua regia in combination with sulfuric acid was evaluated. On a laboratory scale, variables such as particle size, concentration of reagents, dissolved oxygen, reaction time, pH and temperature were evaluated. Under optimal conditions it was possible to achieve >80% silver recovery and >90% gold recovery for both oxide ore and tailings.

### 8:50 AM

**Comparison of Solvent Extraction Studies on Tetravalent Platinum from Acidic Chloride Solutions Using Tri-Octyl/Decyl Amine and Bis(2,4,4-Trimethylpentyl) Monothiophosphinic Acid:** *Rajesh Kumar Jyothi*<sup>1</sup>; <sup>1</sup>Korea Institute of Geoscience and Mineral Resources (KIGAM)

The extraction equilibrium study of tetravalent platinum was carried out using tri-octyl/decyl amine (Alamine 336) and bis(2,4,4-trimethylpentyl) monothiophosphinic acid (Cyanex 302) in kerosene from hydrochloric acid media to investigate their extraction capacity, since they have different donor atoms, 'N' and 'S'. Their distribution equilibria were studied as a function of acid, extractant, diluents and temperature. The title metal shows the inverse behavior at higher acid concentrations. Extraction of tetravalent platinum increases with increase of extractant concentration. The plot of log D vs. log [Extractant], mol.L<sup>-1</sup> is linear with slopes 1±0.3, indicating the association of one mole of extractant with the extracted metal species. Stripping of metal from the loaded organic (LO) with mineral acids and bases such as hydrochloric, sulphuric, nitric acids and ammonia, hydrogen peroxide, sodium hydroxide, thio- urea were studied. Regeneration and recycling capacity of Alamine 336/Cyanex 302 and extraction behavior of associated elements was also studied.

### 9:10 AM

**Treatment of Produced Water by Electrocoagulation:** *Jewel Gomes*<sup>1</sup>; *David Cocks*<sup>1</sup>; *Kamol Das*<sup>1</sup>; *Mallikarjuna Guttula*<sup>1</sup>; *Doanh Tran*<sup>1</sup>; *Jim Beckman*<sup>2</sup>; <sup>1</sup>Lamar University; <sup>2</sup>Kascelco

Produced water (PW) is salty water trapped in the reservoir rock and brought up along with oil or gas during production. It subsists under high pressures and temperatures, and usually contains hydrocarbons and metals. Therefore, it must be treated before being discharged to surface water. Different techniques are being used to treat PW through phase separations, system control and design, and chemical treatments. In this paper, we discuss our experimental results on treating PW through electrocoagulation (EC). The performance of EC was investigated for the reduction of chemical oxygen demand (COD) and metal ions. Effects of different electrodes, residence time, current density, and pH were also studied to optimize the treatment conditions. Different kinds of cleansing agents, such as lime and borax were used to break the buffering effect encountered during treatment. FTIR, SEM/EDS, and XRD were used to characterize the EC-floc and thus to elucidate removal mechanisms.

### 9:30 AM

**Mathematical Modeling of Particle Suspension in Pachuca Tanks:** *Esperanza Rodriguez M.*<sup>1</sup>; *Alfonso Castillejos*<sup>1</sup>; *Francisco Acosta G.*<sup>1</sup>; <sup>1</sup>CINVESTAV - Unidad Saltillo

The efficient behavior of Pachuca tanks as hydrometallurgical reactors is strongly linked to the suspension of the mineral particles, which results from the motion of the liquid caused by the injected gas rising, in general, through a central draft tube. This study reports a computational investigation carried out to determine the effect of operating and design parameters on the suspension of particles. By extending the classical drift-flux model to compute the gas hold-up, the three-phase (water-air-particles) system was simulated as a two-phase system formed by a variable density-liquid plus the solid particles. The two phases were treated as interpenetrated continua using an Eulerian approach to set a turbulent recirculating flow model in 2-D and transient state. The model predicted adequately the measured critical gas superficial velocity needed for complete particle suspension in pulps with 10-50 wt% solids. Additionally, the model was used to investigate the performance of industrial size reactors.

### 9:50 AM

**The Theoretical Calculation and Validation of Burden Trajectory in Blast Furnace of Bell-less Top:** *Yu Yaowei*<sup>1</sup>; *Bai Chenguang*<sup>1</sup>; *Zhang Zhengrong*<sup>1</sup>; *Wang Feng*<sup>1</sup>; *Lv Daguang*<sup>1</sup>; <sup>1</sup>Chongqing University

Blast furnace ironmaking is a main method by which iron is efficiently reduced from iron-bearing materials with CO. Charging is one of primary systems for blast furnace control. The trajectory of materials is an important parameter in determining impact point where falling materials intersect with the stockline profile in the charging. In order to clarify the trajectory of materials and validate theoretical calculated trajectory, a 1/15 scale cold model of an actual 2500m<sup>3</sup> shaft and bell-less top charging system has been built. The results indicate that the measured trajectory is consistent with the theoretical one.

### 10:10 AM Break

### 10:30 AM

**Principle and Practice of Producing Qualified Antimony White from Lead-Antimony Alloy by Blowing Directly:** *Liu Weifeng*<sup>1</sup>; *Yang Tianzu*<sup>1</sup>; *Xia Wentang*<sup>2</sup>; *Liu Wei*<sup>1</sup>; *Huang Chao*<sup>1</sup>; <sup>1</sup>Central South University; <sup>2</sup>Chongqing University of Science and Technology

On the basis of the thermodynamic calculation of lead, antimony and arsenic about oxidating volatilization in high temperature, the possibility of separating lead, antimony and arsenic in different temperature was analyzed, and the practice of qualified antimony white through direct blowing from lead-antimony alloy was introduced in detail in this paper. The blast furnace reduction smelting was brief introduced firstly, and then alkaline refining was applied to removing arsenic from lead-antimony alloy that contains As1%, Sb39%, Pb58%, the arsenic in the treated lead-antimony alloy could be decreased to 0.008% by that method. The antimony white containing Sb2O<sub>3</sub> 99.8% could be produced by air blowing in the special furnace at 650° from the treated lead-antimony alloy. And the electrolytic lead could be achieved by electrolysis from the lead bullion which contained 83% lead.

### 10:50 AM

**Reduction Roasting Study of Greek Nickeliferous Laterites:** *Emmanuel Zevgolis*<sup>1</sup>; *Charalabos Zografidis*<sup>1</sup>; *Iliana Halikia*<sup>1</sup>; *Eamonn Devlin*<sup>2</sup>; <sup>1</sup>NTUA; <sup>2</sup>NCSR Demokritos

The reduction roasting experimental study of Greek nickeliferous laterite samples with a gaseous reducing mixture – CO:N<sub>2</sub> – is presented in the present work. The effect of parameters such as temperature, ore grain size and composition of the reductive mixture on the result of reduction, were examined. It is deduced that the reducibility of intermediate type laterite sample, where iron appears mainly in form of goethite, is considerably higher than that of limonitic type laterite samples, where hematite is the predominant iron mineral phase. Increase of temperature within the range of 750-900°C, unlike decrease of the ore grain size and more intensive reductive conditions, does not favor considerably reduction. Metallic iron phase co-exists with magnetite and hematite in all the reduced samples. Considerable increase of the specific surface area of the intermediate laterite ore type after calcination due to goethite dehydroxylation, can be regarded as critical parameter for its higher reducibility.

11:10 AM

**Thallium Extraction from Liquid Pb-Tl Solution:** *Piotr Kapias*<sup>1</sup>; <sup>1</sup>The Silesian University of Technology

The theoretical part of the paper presents the analysis of the conditions of Tl extraction from liquid Pb using different extractants: PbCl<sub>2</sub>, ZnCl<sub>2</sub> or Cl<sub>2</sub>(g). The analysis and evaluation were made of the influence of the methods of extractants introduction into a Pb-Tl solution upon the efficiency of the Tl extraction process under thermodynamic equilibrium conditions. The analysis made it possible to formulate relevant equations describing the process of Tl extraction from Pb under static as well as under the extractant stirring and injection into the liquid Pb-Tl solution conditions. In the part concerning experimental work, results are given for tests on the Tl extraction process from Pb-Tl liquid solutions of initial Tl content of approximately 0.05% mass or 0.02% mass using PbCl<sub>2</sub>, ZnCl<sub>2</sub> or Cl<sub>2</sub>(g) conducted in laboratorial scale. The idea of a reactor for thallium extraction from lead has been presented.

11:30 AM

**Thermal Conductivity and Characterisation of Copper Flash Smelting Flue Dust:** *Elli Miettinen*<sup>1</sup>; <sup>1</sup>Outotec Oyj

In Copper Flash Smelting operation disturbances may lead into dust build-up in the off-gas handling system causing reduced heat recovery efficiency and process availability. Flue dust of a Copper Flash Smelting process heat recovery boiler has been characterized and its thermal conductivity and diffusivity have been determined. Dust accretions consist of several layers possessing varying particle sizes, densities, and thermal properties, with the binding phase mostly being sulphate. All studied samples can be regarded as effective thermal insulators with thermal conductivity values of less than 2 W/mK and thermal diffusivity values of less than 0.005 cm<sup>2</sup>/s. Porosity can be regarded as a fairly good indicator of the thermal transport efficiency of these types of materials, but the material microstructure must also be considered. The results can be used in the scaling of metallurgical heat recovery boilers and they also provide accurate input data for process models.

11:50 AM

**Study on Health Risk Assessment of POPs from a Copper Smelt Enterprise:** *He Dewen*<sup>1</sup>; Du Lu<sup>1</sup>; Wang Wei-lian<sup>1</sup>; Liang Ding-ming<sup>1</sup>; <sup>1</sup>Central South University

The distribution of persistent organic pollutants in the environment is studied using the multimedia environmental fugacity model, and environmental health risk assessment of POPs nearby a copper smelt enterprise is carried out. The result indicates that all are in an agreeable risk level without exception. The annual individual chronic risk index of HCB is 7.50×10<sup>-11</sup>. The annual individual risk index of 3,3',4,4'-TCB is 1.57×10<sup>-9</sup>, and the annual individual risk index of 2,3,7,8-TCDD is 6.57×10<sup>-9</sup>.

12:10 PM

**Performance on Leaching of Antimony Trioxide with Polyhydric Organics in Alkaline Solutions:** *Wei Liu*<sup>1</sup>; Tianzu Yang<sup>1</sup>; Duchao Zhang<sup>1</sup>; Xing Xia<sup>1</sup>; Weifeng Liu<sup>1</sup>; <sup>1</sup>Central South University

Antimony trioxide was leaching in alkaline solutions containing polyhydric organics (glycerol, xylitol and tartaric acid). Experimental based on orthogonal array table (L9) was utilized to determine the optimum leaching conditions. The influences of concentrations of polyhydric organics and sodium hydroxide on the leaching efficiency were studied in detail. The reaction mechanism was also discussed. The experimental results show that the antimony trioxide could be dissolved easily in alkaline solutions containing polyhydric organics. The concentrations of polyhydric organics and sodium hydroxide have significant effect upon the leaching efficiency, while the leaching temperature and time have few effects. The leaching rate arises with increasing concentrations of polyhydric organics and sodium hydroxide. The resultant may be Sb-Na double alkoxides. The formation of the resultant could be restrained by the reactivity of hydroxyl. Under the same conditions, the react ability of antimony trioxide with glycerol is weaker than that with xylitol and tartaric acid.

## General Abstracts: Structural Materials Division: Session I

Sponsored by: The Minerals, Metals and Materials Society, TMS Structural Materials Division, TMS: Advanced Characterization, Testing, and Simulation Committee, TMS: Alloy Phases Committee, TMS: Biomaterials Committee, TMS: Chemistry and Physics of Materials Committee, TMS/ASM: Composite Materials Committee, TMS/ASM: Corrosion and Environmental Effects Committee, TMS: High Temperature Alloys Committee, TMS/ASM: Mechanical Behavior of Materials Committee, TMS/ASM: Nuclear Materials Committee, TMS: Refractory Metals Committee, TMS: Titanium Committee

Program Organizers: Robert Hanrahan, National Nuclear Security Administration; Eric Ott, GE Aviation

Monday AM

February 16, 2009

Room: 2010

Location: Moscone West Convention Center

Session Chair: To Be Announced

8:30 AM

**A Methodology for Non Destructive Evaluation of Dwell Fatigue Susceptibility of a Near Alpha Titanium Alloy:** *Amit Bhattacharjee*<sup>1</sup>; S.I. Rokhlin<sup>1</sup>; Andy Woodfield<sup>2</sup>; J. C. Williams<sup>1</sup>; <sup>1</sup>Ohio State University; <sup>2</sup>General Electric

Acoustic wave attenuation has been measured in ultrasonic range for specimens cut from a series of Ti6242 forgings. Large variation has been observed. Orientation imaging microscopy scans also was carried out using electron backscatter diffraction technique to determine the degree of microtexture in the forgings. The correlation between the microtexture and the attenuation will be presented. These data suggest that acoustic attenuation can be used to non-destructively assess the types and degree of microtexture in Ti alloy forgings. This technique has the potential to assess the degree of microtexture in existing forgings that have been processed by various routes prior to the recognition of the importance of microtexture. It has been recognized for some time that microtexture in titanium alloys leads to a debit in dwell fatigue life. Therefore, the outlined procedure may be useful to non-destructively assess the dwell sensitivity of existing titanium alloy hardware of varying processing history.

8:50 AM

**Brittle Compressive Failure: Transition from Splitting to Faulting in Ice:** *Erland Schulson*<sup>1</sup>; Carl Renshaw<sup>1</sup>; Luke Wachter<sup>1</sup>; <sup>1</sup>Dartmouth College

When loaded under compression, ice and other Coulombic materials fail by axial splitting when unconfined and by shear faulting when moderately confined. The question is: how moderate is moderate? We show from systematic experiments on columnar-grained fresh-water ice biaxially loaded across the columns that the transition from one mode to the other occurs continuously, but rapidly: once the ratio of the minor to major stress reaches  $R=0.01$ , it is complete. Moderate is thus very small indeed—so small that from a practical perspective splitting is of little importance to either ice-structure interactions or other geophysical/engineering situations. Ceramics and rock are expected to exhibit the same behavior. The transition can be understood in terms of the growth of wing cracks and the stress field ahead of them. A quantitative model will be presented.

9:10 AM

**Effects of Tantalum on the Phase Decomposition of a Model Ni-Al-Cr Superalloy on a Nanoscale:** *Christopher Booth-Morrison*<sup>1</sup>; Ronald Noebe<sup>2</sup>; David Seidman<sup>1</sup>; <sup>1</sup>Northwestern University; <sup>2</sup>NASA Glenn Research Center

The effects of a 2.0 at.% addition of Ta to a model Ni-10.0 Al-8.5 Cr at.% superalloy are assessed by atom-probe tomography. The  $\gamma(L1_2)$ -precipitate morphology that develops as a result of  $\gamma(f.c.c.)$ -matrix phase decomposition at 1073 K is found to evolve from a bimodal distribution of spheroidal precipitates, to  $\{001\}$ -faceted cuds and parallellepipeds aligned along the elastically soft  $\langle 001 \rangle$ -type directions. The phase compositions and the widths of the  $\gamma$ -precipitate/ $\gamma$ -matrix interfaces evolve temporally as the Ni-Al-Cr-Ta alloy undergoes quasi-stationary state coarsening after 1 h of aging. Tantalum is observed to suppress the mobility of Ni in the  $\gamma$ -matrix sufficiently to cause an accumulation of Ni on the  $\gamma$ -matrix side of the  $\gamma/\gamma$  interface. Computational modeling employing Thermo-Calc, Dictra and PrecipiCalc, elucidates the kinetic pathways that lead to phase decomposition in this concentrated Ni-Al-Cr-Ta alloy.

9:30 AM

**Method for Determining Dislocation Viscous Drag Coefficients:** *John Gilman*<sup>1</sup>; <sup>1</sup>University of California

In imperfect crystals, dislocation motion is of the stick/slip type so fundamental viscosity coefficients are difficult to measure. However, the maximum velocities are determined by a balance between the driving stress, and the drag. The driving stress is limited by cohesion so the drag can be determined at the terminal velocity where the motion is of the slip type alone. Fortunately, there is a reliable equation for extrapolating from intermediate velocities to the terminal velocity. Given the terminal velocity, an expression without disposable parameters yields the viscosity coefficient. The latter can be compared with values measured directly at low stresses, or derived from internal friction measurements. This method will allow values for a wide range of materials to be made and a library to be constructed that will be useful for fundamental studies.

9:50 AM

**Life Prediction and Reconstruction of Creep Curves Based on an Evaluation of Strain Rate Change in Secondary Creep:** *Hiroyuki Sato*<sup>1</sup>; Takaya Miyano<sup>2</sup>; <sup>1</sup>Hirosaki University; <sup>2</sup>Ritsumeikan University

Shape of creep curves and change of strain rate in secondary creep are quantitatively evaluated; furthermore, reconstructions of creep curves are performed by means of extrapolation of strain rate change in secondary stage. We have reported that the behavior of strain rate change in secondary creep depends on the classes of magnesium-based solution strengthened alloys; and have proposed a characteristic parameter that reflects the strain rate change quantitatively. In this report, we show that a reconstructed creep curve based on the proposed parameter fairly agree with experimental creep curves in the alloys; moreover, we propose one method of creep life prediction. It is shown that a combination of the minimum creep rate and the proposed parameter that reflects strain rate change reasonably describe creep curves. The changes in strain rate acceleration reasonably agree with the transition of creep characteristics evaluated by minimum creep rate.

10:10 AM

**Mechanical Properties and Phase Stability of Ti-Cr System Alloys:** *Yonosuke Murayama*<sup>1</sup>; Shuichi Sasaki<sup>1</sup>; Rajagopalan Srinivasan<sup>2</sup>; Daniel Huber<sup>2</sup>; Hisamichi Kimura<sup>3</sup>; Akihiko Chiba<sup>3</sup>; Hamish Fraser<sup>2</sup>; <sup>1</sup>Mechanical and Control Engineering, Niigata Institute of Technology; <sup>2</sup>Materials Science and Engineering, The Ohio State University; <sup>3</sup>Institute of Material Research, Tohoku University

Low modulus beta titanium alloys are attractive alloys for biomedical application. This work examines the mechanical properties of Ti-Cr-Sn-Zr system alloys. The elastic modulus of the alloy varies with the composition, which variation is caused from the competition between the meta-stable beta phase and the omega phase. The elastic modulus of the alloy decreases very much owing to the addition of alloy element that depresses the omega phase, which is similar to Ti-Nb system alloys. This work focuses on the effect of the varying alloy composition on the microstructure, the elastic modulus, the deformation mechanism and the deformability. The deformation modes of the Ti-Cr-Sn-Zr alloy, which are the mechanical twinning, the deformation by slip and the deformation-induced transformation, change by the composition of the alloy. We discuss the effect of the transition of the deformation modes on the mechanical properties.

10:30 AM

**Mode I Penny Shape Crack in Sandwich Multilayered Composites:** *H. Y. (Sean) Yu*<sup>1</sup>; <sup>1</sup>Naval Research Laboratory

The solution of a mode I penny shape crack at the center of a sandwich layered composite is obtained. The sandwich composite consists of any number of layers of homogeneous, isotropic materials. The upper half of the sandwich is the mirror image of the lower half. For example, if the crack is at the center of layer A, then the composite consisting of layers A, B, C, D is with the stacking sequence D/C/B/A/B/C/D. The point force Green's functions for this composites is derived first. The solution of the crack problem is formulated by integrating the Green's function over the crack surface with a given point force distribution. The dual integral equations of the unknown crack surface displacement are established by considering the boundary conditions on the crack surface of the multilayered solid, which can be converted into a Fredholm integral equation of the second kind and solved numerically.

10:50 AM

**Physical and Microstructural Characterization of TiC Reinforced Al-Cu Matrix Alloy Composites:** *Hülya Kafelen*<sup>1</sup>; Necip Ünlü<sup>1</sup>; Lütfi Öveçoglu<sup>1</sup>; Hani Henein<sup>2</sup>; <sup>1</sup>Istanbul Technical University; <sup>2</sup>University of Alberta

Aluminum - 4 wt. % copper composites containing 5-20 vol. % of TiC powders in 2 µm size were fabricated using K-Al-F type flux-assisted conventional casting method. The resulting morphologies and compositions of the composites were characterized as a function of TiC volume fraction by optical microscopy (OM), scanning electron microscopy (SEM), X-ray diffraction analysis (XRD) and microhardness tests. The microstructural investigations exhibited the reasonably homogeneous distribution of the carbides in Al4Cu matrix alloys. The XRD results of the composite samples revealed that the phases of the Al, Al<sub>2</sub>Cu and TiC were detected. In addition, the intensity of the diffraction peaks belonging to the TiC phase gradually increased with increasing of the volume fraction of the reinforcement. Increasing of the volume percent of TiC particles from 5 through 20% contributed to increase in hardness values of Al-Cu based composites.

11:10 AM

**The Dynamic Strength of a Representative Double Layer Prismatic Core: A Combined Experimental, Numerical and Analytical Assessment:** *Enrico Ferri*<sup>1</sup>; Tony Evans<sup>1</sup>; Vikram Deshpande<sup>1</sup>; <sup>1</sup>University of California, Santa Barbara

Dynamic out-of-plane compressive testing is used to characterize the dynamic strength of metal prismatic cores with double layer topology. The dynamic strength was evaluated by measuring the stresses transmitted to a Hopkinson pressure bar impacted at constant velocities up to 140 m/s. 2D plane strain, FE calculations successfully predicted the experimental results with appropriately calibrated imperfections. To infer the response of this core when included in a sandwich plate subject to blast loading, the finite element model was modified to unsupported (free-standing) back face boundary conditions. The transmitted stress is found to be modulated by the momentum acquired by the back face mass and, as the mass becomes larger, the core strength approaches that measured and simulated for stationary conditions. An analytical model that accounts for the shock effects in a homogenized core is presented and shown to capture the observations and simulated results with acceptable fidelity.

## Global Innovations in Photovoltaics and Thermoelectrics: Session I

Sponsored by: The Minerals, Metals and Materials Society, TMS Materials Processing and Manufacturing Division, TMS: Energy Committee, TMS: Global Innovations Committee

Program Organizers: Sivaraman Guruswamy, University of Utah; Joy Forsmark, Ford Motor Co; John Smugeresky, Sandia National Laboratories

Monday AM

February 16, 2009

Room: 3005

Location: Moscone West Convention Center

Session Chairs: Sivaraman Guruswamy, University of Utah; Narsingh Singh, Northrop Grumman Corp ES; Joy Forsmark, Ford Motor Co

8:30 AM Keynote

**Recent Advances in Thermoelectric Power Generation Materials, Technology and Terrestrial Application Opportunities:** *Jean-Pierre Fleurial*<sup>1</sup>; <sup>1</sup>Jet Propulsion Laboratory/California Institute of Technology

Thermoelectric power sources have consistently demonstrated their extraordinary reliability and longevity for deep space missions (67 missions to date, more than 30 years of life) as well as terrestrial applications where unattended operation in remote locations is required. The development of new, more efficient materials and devices is the key to improving existing space power technology and expanding the range of terrestrial applications. The Jet Propulsion Laboratory is leading collaborative research and development on novel advanced bulk materials capable of long term operation at temperatures up to 1300 K at more than 20% conversion efficiency. The research areas include refractory rare earth compounds and bulk 3-D nanostructures that emulate results obtained on low dimensional superlattices through "force engineering" and "self-assembling" techniques. Recent experimental results will be highlighted, and progress in transitioning thermoelectric technology to a more flexible, lower cost modular array configuration suitable for various application opportunities will be discussed.



9:15 AM

**Melt Spinning and Spark Plasma Sintering for Manufacturing of Highly Textured Thermoelectric Materials:** *Juergen Schmidt*<sup>1</sup>; Dirk Ebling<sup>2</sup>; Alexandre Jacquot<sup>2</sup>; Harald Boettner<sup>2</sup>; Thomas Weissgaerber<sup>1</sup>; Bernd Kieback<sup>1</sup>; <sup>1</sup>Fraunhofer Institute for Manufacturing and Applied Materials Sciences IFAM; <sup>2</sup>Fraunhofer Institute for Physical Measurement Techniques IPM

V-VI thermoelectric compounds are well known for room temperature applications like Peltier coolers. The anisotropic physical properties and the mechanical weakness of the crystals are a problem for the manufacturing. Polycrystalline bismuth telluride based n- and p-type thermoelectric materials were fabricated through Spark Plasma Sintering (SPS) technique. The combination of a rapidly solidified alloy and temporary liquid phase sintering by SPS allows controlling the texture of microstructure. With this technique sintered, polycrystalline  $(\text{Bi,Sb})_2(\text{Te,Se})_3$  with ZT values  $> 1$  were produced. This paper will report on the preparation by melt spinning technique and the influence of the SPS process on the texture, the thermoelectric and mechanical properties of the polycrystalline materials.

9:35 AM Invited

**Morphology of High Temperature Boron-Based Thermoelectric Materials:** *Takao Mori*<sup>1</sup>; <sup>1</sup>National Institute for Materials Science (NIMS)

The useful energy conversion of waste heat is a huge incentive to find viable thermoelectric materials. Obviously a particular need exists to develop materials which can function at high temperatures. Boron-rich cluster compounds are attractive materials for their stability under high temperature typically exhibiting melting points above 2200 K. As a synthesis method it has been found that addition of small amounts of third elements like carbon, nitrogen, and silicon can result in the formation of novel and varied rare-earth boron cluster structures.  $\text{REB}_{44}\text{Si}_2$  compounds exhibit Seebeck coefficients greater than 200  $\mu\text{V/K}$  at high temperatures and unlike most compounds, the figure of merit shows a steep increase at  $T > 1000$  K. Homologous RE-B-C(N) compounds were recently discovered to be the long awaited n-type counterparts to p-type boron carbide. The focus of the talk will be on the control of morphology of these materials in relation to their high temperature thermoelectric properties.

10:00 AM

**The Formation of Aligned  $\text{Ag}_2\text{Te}$  Precipitates in  $\text{AgSbTe}_2$ :** *Joshua Sugar*<sup>1</sup>; Douglas Medlin<sup>1</sup>; <sup>1</sup>Materials Physics Department, Sandia National Laboratories, Livermore

The thermoelectric alloy  $\text{AgSbTe}_2$  is a relatively simple alloy with a ZT as high as 1.3 at 720 K. It is also a primary constituent in the more complicated, high-performance  $(\text{AgSbTe}_2)_{1-x}(\text{GeTe})_{1-x}$  and  $(\text{AgSbTe}_2)_{1-x}(\text{PbTe})_x$  systems. The high ZT of these more complicated alloys is generally attributed to compositional heterogeneities in their microstructure, which have been inferred to contribute different mechanisms to the interfacial scattering of electrons and phonons.  $\text{AgSbTe}_2$  provides a good system for understanding the types of compositional inhomogeneities that one could expect in similar thermoelectric alloys. This study investigates the decomposition of  $\text{AgSbTe}_2$  into crystallographically aligned precipitates of monoclinic  $\text{Ag}_2\text{Te}$  in a matrix of cubic  $\text{Ag}_{22}\text{Sb}_{28}\text{Te}_{50}$ . The precipitate formation is energetically easy because of the topotactic alignment of the high-temperature  $\text{Ag}_2\text{Te}$  phase. Below 145°C, cubic  $\text{Ag}_2\text{Te}$  undergoes a displacive transformation to a monoclinic structure, which creates several symmetric orientation relationship variants and complicates the diffraction analysis.

10:20 AM Break

10:30 AM Invited

**Effect of Growth Parameters on the Quality of PbSe Nanocubes and Nanodots:** *Narsingh Singh*<sup>1</sup>; Eric Jones<sup>1</sup>; E. Jelen<sup>1</sup>; B. Wagner<sup>1</sup>; S. Mc Laughlin<sup>1</sup>; A. Berghmans<sup>1</sup>; D. Kahler<sup>1</sup>; D. Knuteson<sup>1</sup>; <sup>1</sup>Northrop Grumman Corporation

The concept is based on utilizing peaks in the solar spectrum irradiance to design materials which have bandgap very closed to those wavelengths. These can be grown as quantum dot (QD) materials to increase quantum yield which could increase efficiency due to a quantum effect called multiple exciton generation. We developed a series of lead selenide (PbSe) detector materials with different characteristics. We observed that substrate temperature and purity has pronounced effect on the morphology, resistivity and crystallinity. As the substrate temperature changed, the crystal orientation changed from (111) to (001) orientation. We grew very good quality film with full width of maxima of 0.3 degree. The virgin material showed 60.7 K Ohm-cm and annealed sample showed a resistivity value of 5.0 M Ohm-cm.

10:55 AM

**Towards Predicting Reaction Pathways in the Cu-In-Se-Ga System:** *Carelyn Campbell*<sup>1</sup>; <sup>1</sup>National Institute of Standards and Technology

To reduce the production costs of CIGS ( $\alpha\text{-CuIn}_x\text{Ga}_{1-x}\text{Se}_2$ ) photovoltaic cells, the processing time must be reduced from approximately 30 minutes to less than 2 minutes. This challenge requires finding new reaction pathways in the Cu-In-Se-Ga system to increase the synthesis rate of the CIGS absorber material. The complex chemistry of the CIGS system has limited efficient exploration of potential processing sequences. Combining CALPHAD-based thermodynamics and diffusion mobilities descriptions enables prediction of reaction pathways for prospective processing sequences. Preliminary diffusion mobility descriptions for the Cu-In-Ga-Se system, based on previously developed thermodynamic descriptions, will be presented. These mobility descriptions are derived from both measured unary, binary and ternary tracer, intrinsic and chemical diffusion data and experimentally derived activation energies. The diffusion mobility descriptions are then used to simulate a wide range of model reactions. The fundamentals of the approach and the simulations will be discussed.

11:15 AM

**Using Patterned Si Thin Foils to Build 3-D Photovoltaic Devices:** *Xiaoying Guo*<sup>1</sup>; Huan Li<sup>1</sup>; *Jimmy Hsia*<sup>1</sup>; Ralph Nuzzo<sup>1</sup>; <sup>1</sup>University of Illinois at Urbana-Champaign

Unlike flat panel photovoltaic systems, three dimensional photovoltaic devices present a promising way to harvest solar energy efficiently without requiring additional apparatus to adjust the orientation of the device. In this research, we developed a technique to fabricate 3-D photovoltaic devices using patterned Si thin foils, which make use of the self-assembly process driven by capillary forces. One key requirement for this technique, however, is the condition under which folding of the patterned thin foil occurs. A mechanics model based on the theory of thin plate has been developed to identify this critical condition. The model is capable of predicting the critical condition for thin foil folding for complicated foil shapes. Our experimental measurements of the foil folding condition agree with the model predictions beautifully. Furthermore, an intrinsic, non-dimensional material parameter has been identified in the model to be the single parameter controlling the foil folding process.

11:35 AM

**Preparation of Metallic Precursor of Cu(In, Ga)Se<sub>2</sub> Thin Film for Solar Cell Applications by Sputtering Alloyed Cu-In-Ga Target:** *Yaojun Lin*<sup>1</sup>; Paul Gilman<sup>1</sup>; <sup>1</sup>Praxair Electronics

As solar energy materials, Cu(In, Ga)Se<sub>2</sub> (CIGS) thin film is attracting considerable interest due to long-term stability and highest conversion efficiency. Among various techniques to prepare metallic precursors of CIGS thin film, sputter techniques are the most promising since they can be easily scaled up and facilitate roll to roll production on flexible substrate. This presentation reports preparation of metallic precursor of CIGS by sputtering alloyed Cu-In-Ga target, which is advantageous over co-sputtering of elemental targets in substantial compositional uniformity, and successive sputtering of elemental targets due to reduction in production time. Compositional uniformity, microstructure and phases in metallic precursor, which have dominant effects on CIGS properties, are studied in detail using EDS, XRD and SEM. The approaches to optimize compositional uniformity and microstructure of metallic precursor are discussed, including an improvement in alloyed target's metallurgical quality and modification of sputter parameters. Copyright 2008, Praxair Technology, Inc., all rights reserved.

11:55 AM

**Effect of Electric Current Assisted Thermal Treatment on Thermoelectric Properties of Bi-Sb-Te and Bi-Se-Te Based Thin Films Prepared by Sputtering:** *Kuen-Ming Liou*<sup>1</sup>; Chien-Neng Liao<sup>1</sup>; Hsu-Shen Chu<sup>1</sup>; <sup>1</sup>National Tsing-Hua University/Department of Materials Science and Engineering

In this study a novel approach of electric current assisted thermal treatment for improving thermoelectric properties of sputtered Bi-Sb-Te and Bi-Se-Te films is presented. Both electrical conductivity and Seebeck coefficient of the sputtered Bi-Sb-Te and Bi-Se-Te films were enhanced by introducing a high density of electric current through the films during thermal annealing. The electrically stressed films were found to have lower carrier concentration but much higher mobility than the films that were only thermally annealed at the same temperatures. An electromigration induced defect elimination model is proposed to explain the observed electrical transport properties and microstructure evolution of the electrically stressed thin films. The study shall lead to an effective strategy of improving thermoelectric properties of the thermoelectric films by electric current stressing.

## Magnesium Technology 2009: Magnesium Town Hall Meeting - A Decade of Modern Magnesium in China

Sponsored by: The Minerals, Metals and Materials Society, TMS Light Metals Division, TMS: Magnesium Committee

Program Organizers: Eric Nyberg, Pacific Northwest National Laboratory; Sean Agnew, University of Virginia; Neale Neelameggham, US Magnesium LLC; Mihriban Pekguleryuz, McGill University

Monday AM  
February 16, 2009  
Room: 2007  
Location: Moscone West Convention Center

Session Chair: Eric Nyberg, Pacific Northwest National Laboratory

### 8:30 AM Introductory Comments by Eric Nyberg

#### 8:35 AM

#### Overview of Advanced Magnesium Alloy Development, Forming, Welding and Corrosion Protection in IMR: *En-Hou Han*<sup>1</sup>; <sup>1</sup>Chinese Academy of Sciences

Due to the remarkable increase of energy price and the decrease of the source of the raw structural materials such as steel, aluminum, magnesium and its alloys become more and more popular in last decade. The primary magnesium production in China now becomes dominant in the world. In the meanwhile, China promotes the development and application of magnesium alloys. Institute of Metal Research (IMR) developed various advanced magnesium alloys, such as magnesium-lithium alloys, high strength high ductility cast-alloys, and high strength high toughness wrought alloys. IMR also developed various processing techniques, such as ultrasonic grain refinement, ECAP, friction stirring welding, etc. Especially various corrosion protection techniques, such as chemical conversion coatings, micro-arc oxidation, anodizing (MAO), electroless plating, electroplating, were developed. At last, future need for magnesium alloys development and application was proposed.

#### 8:55 AM

#### Global Magnesium Market Fundamentals: *Susan Slade*<sup>1</sup>; <sup>1</sup>US Magnesium LLC

The supply and demand balance in the global magnesium market continues to be dynamic based on the changing business environment in China. Magnesium production in China supplies over 80% of global demand, creating a situation in which even minor changes in the Chinese magnesium industry can have a significant impact on all markets. Factors affecting ingot supply and magnesium demand growth will be reviewed. Analyses of global supply and demand forecasts will provide an outlook for the future.

#### 9:15 AM

#### Recent Developments in the Chinese Magnesium Industry: *Liming Peng*<sup>1</sup>;

<sup>1</sup>Shanghai Jiaotong University, China

Abstract not available.

#### 9:35 AM Question and Answer Period

#### 10:00 AM Break

## Magnesium Technology 2009: Alloys I: Rare Earth (Gadolinium, Neodymium)

Sponsored by: The Minerals, Metals and Materials Society, TMS Light Metals Division, TMS: Magnesium Committee

Program Organizers: Eric Nyberg, Pacific Northwest National Laboratory; Sean Agnew, University of Virginia; Neale Neelameggham, US Magnesium LLC; Mihriban Pekguleryuz, McGill University

Monday AM  
February 16, 2009  
Room: 2006  
Location: Moscone West Convention Center

Session Chairs: Liming Peng, Shanghai Jiaotong University; Karl Kainer, GKSS Research Center

### 10:15 AM Introductory Comments

#### 10:20 AM

#### Characterization of Dynamic Strain Ageing in Mg-3.11wt.%Gd Alloy: *Lei Gao*<sup>1</sup>; *Rongshi Chen*<sup>2</sup>; *Enhou Han*<sup>1</sup>; <sup>1</sup>Institute of Metal Research Chinese Academy of Sciences; <sup>2</sup>Institute of Metal Research, Chinese Academy of Sciences

To elucidate the dynamic strain ageing behavior of Mg-Gd based alloys which were developed as high specific strength and good creep resistant magnesium alloys at elevated temperature, tensile tests were carried out for Mg-3.11wt.%Gd in the temperature range of 25-300°C and in the strain rate range from  $1 \times 10^{-4}$  to  $1 \times 10^{-2} \text{ s}^{-1}$ . At given strains, stress relaxation (SR) experiments were performed. Serrated flow, negative strain rate sensitivity, and post-relaxation effect were observed in some cases. The post-relaxation effect was sensitive to testing temperature and the strain at which the stress relaxation was performed. The critical strain for the onset of serrated flow was observed to increase with increasing strain rate but decrease with increasing temperature. In addition, activation energy for serrated flow was calculated. The results were analysed in relation to dynamic strain ageing effect (DSA) due to interactions between dislocations and solute Gd atoms.

#### 10:40 AM

#### Effect of Cold Roll on Microstructure and Mechanical Properties of Mg-8Gd-3Y-0.5Zr Alloy: *Li Dejiang*<sup>1</sup>; *Zeng Xiaoqin*<sup>1</sup>; *Dong Jie*<sup>1</sup>; *Zhai Chuanquan*<sup>1</sup>; <sup>1</sup>Shanghai Jiao Tong University

The simplest TMT process including cold roll with strain of 8%, 15%, 22% and subsequently aged at different temperatures to peak hardness were carried out to investigate the influence on microstructure and mechanical properties of heat resistant Mg-8Gd-3Y-0.5Zr alloy. The microstructure observation showed that basal plane dislocation sliding and twinings (including double twinning) were the main deformation mechanisms during cold rolling, the amount of twins were increased with increasing deformation strain. The initial hardness of the alloy specimen was increased with the increasing of strain and the aging time to peak hardness was greatly shortened for the reason of work hardening and acceleration of precipitation from the supersaturated solid solution, respectively. However, the peak hardness value of the deformed and non-deformed alloy specimens remained almost the same. TEM investigation confirmed that the precipitation in the deformed microstructure preference for the equilibrium phase was attributed to lower age hardening response.

#### 11:00 AM

#### Effects of Heat Treatments on Tensile Properties and Creep Behavior of Mg-Y-Gd-Zr Alloys: *Yan Gao*<sup>1</sup>; *Qudong Wang*<sup>1</sup>; *Jinhai Gu*<sup>2</sup>; *Yang Zhao*<sup>1</sup>; <sup>1</sup>Shanghai Jiaotong University; <sup>2</sup>Hitachi (China) Research & Development Corp., Shanghai Research Institute

We have investigated the microstructure, mechanical properties at room and elevated temperatures (250°C, 300°C), strengthening mechanisms, creep behavior and creep deformation mechanisms of Mg-10Y-5Gd-0.5Zr alloys of in the cast and T6 conditions. The results showed that the tensile properties of the cast-T6 specimen are much higher than that of the as-cast specimen and the creep resistance of the cast-T6 specimen is markedly better than that of the as-cast specimen at both conditions. The creep resistance of the Mg-10Y-5Gd-0.5Zr at T=250,  $\sigma=80\text{MPa}$  is markedly better than that at T=300,  $\sigma=50\text{MPa}$ . This means the temperature makes more effects on the creep resistance than the stress. Finally, the creep mechanism of the alloy at different condition is further analyzed.

#### 11:20 AM

#### Microstructure and Mechanical Properties of Hot Extruded Mg-3Nd-0.2Zn-0.4Zr (wt. %) Alloy: *Penghuai Fu*<sup>1</sup>; *Liming Peng*<sup>1</sup>; <sup>1</sup>National Engineering Research Center of Light Alloy Net Forming, School of Materials Science and Engineering, Shanghai Jiaotong University

The microstructure and mechanical properties of 350, 450 and 525°C hot extruded Mg-3Nd-0.2Zn-0.4Zr (NZ30K) (wt. %) alloys are investigated. The grains are significantly refined by hot extrusion and the extruded alloys show a bimodal grain distribution, in which the finer grains are less than 1 $\mu\text{m}$  and the coarser grains are several to ten micrometers in size. The lower extrusion temperature, the finer grains are got. The extruded NZ30K alloys have aging hardening ability. The higher extrusion temperature, the higher aging hardening effect  $\Delta\text{HV}$  (HV peak-aged - HV as-extruded) is obtained. After aging treatment, both yield strength (YS) and ultimate tensile strength (UTS) are significantly improved. The 350°C extruded NZ30K alloy shows the best strength after 200°C peak-age treatment. The YS, UTS and elongation are 290MPa, 317MPa

and 22%, respectively. The extruded alloys show dimple fracture pattern characterized by dimples covered all of fracture surfaces.

### 11:40 AM

**Mechanical Properties and Microstructure of Mg-Zn-Gd Alloys with Long Period Stacking Ordered Structure:** *Michiaki Yamasaki*<sup>1</sup>; Minami Sasaki<sup>1</sup>; Yoshihito Kawamura<sup>1</sup>; <sup>1</sup>Kumamoto University

Rare earth-containing Mg alloys are of interest because of the precipitation reaction that results in age hardening. In general, isothermal aging of supersaturated alpha-Mg solid solutions in these alloys has been performed at about 473 K. The hardness of alloys increases with increasing aging time, and reaches a peak value with beta' phase precipitation and then decreases with beta phase precipitation. Recently, it was found that the addition of Zn to the Mg-Gd alloys brings about the precipitation of the 14H long period stacking ordered (LPSO) structure at more than 623 K. Therefore, we have investigated the aging behavior of the Mg-Zn-Gd (at.%) alloy at temperatures ranging from 473 K to 773 K and propose a TTT diagram for beta', beta-1, beta and 14H-LPSO phase precipitation of the alloys. The relationship between the mechanical properties and the microstructure of the cast and extruded alloy will be discussed.

---

## Magnesium Technology 2009: Fatigue and Tension/Compression Asymmetry

Sponsored by: The Minerals, Metals and Materials Society, TMS Light Metals Division, TMS: Magnesium Committee

Program Organizers: Eric Nyberg, Pacific Northwest National Laboratory; Sean Agnew, University of Virginia; Neale Neelameggham, US Magnesium LLC; Mihriban Pekguleryuz, McGill University

Monday AM

Room: 2007

February 16, 2009

Location: Moscone West Convention Center

Session Chair: Sean Agnew, University of Virginia

---

### 10:15 AM Introductory Comments

### 10:20 AM

**Enhancing In-Plane Fatigue Resistance of Rolled AZ31 Magnesium Alloy by Pre-Straining:** Chong Soo Lee<sup>1</sup>; Seong-Gu Hong<sup>1</sup>; *Sung Hyuk Park*<sup>1</sup>; <sup>1</sup>Pohang University of Science and Technology

Rolled AZ31 magnesium alloy has a strong basal texture so that it favors extensive twinning under compressive loading, resulting in a low compressive flow stress compared to a tensile flow stress; this induced a tensile mean stress, which reduced the fatigue resistance during fatigue deformation. The improvement of fatigue resistance was attempted by reducing the developed tensile mean stress, which was achievable by the fact that the lattice reorientation caused by twinning during compressive loading favors detwinning in the twinned regions during the subsequent tensile reloading, leading to a significant drop in tensile flow stress. The variation of the twinning-detwinning characteristics was made by pre-compressions of 2, 5, and 8 % and their effect was evaluated at the fully reversed strain amplitude of 1% at room temperature. The enhancement of fatigue resistance was explained in the relation with the amount of pre-compression.

### 10:40 AM

**Influence of Stress Ratio on Fatigue Crack Propagation Behavior of AZ31 Alloy:** *KyoSoo Song*<sup>1</sup>; Hwa Chul Jung<sup>1</sup>; Kwang Seon Shin<sup>1</sup>; <sup>1</sup>Seoul National University

Although the resistance to fatigue crack propagation (FCP) is one of the most important design criteria for structural materials, there have been limited studies on FCP behavior of magnesium alloys, particularly in the near-threshold region. In the present study, the influence of stress ratio on FCP behavior of an AZ31 alloy was investigated in conjunction with crack closure phenomena. FCP experiments were carried out under the constant load amplitude at ambient temperature. The  $\Delta K_{th}$  value of the AZ31 alloy was affected by the change in stress ratio. The  $\Delta K_{th}$  value decreased with increasing the stress ratio, while the  $\Delta K_{th,eff}$  showed almost constant value regardless of the stress ratio. The crack closure levels were high in the near-threshold region and decreased with increasing FCP rates. It was found that the crack closure effect diminished in the high stress ratio region.

### 11:00 AM

**Comparison of Quasistatic and Cyclic Plastic Behaviour of Wrought Magnesium Alloys:** *Lenka Fuskova*<sup>1</sup>; Jan Bohlen<sup>1</sup>; Dietmar Letzig<sup>1</sup>; Karl Ulrich Kainer<sup>1</sup>; <sup>1</sup>GKSS Research Centre Geesthacht GmbH

The extrusion of magnesium alloys causes the occurrence of characteristic crystallographic textures and leads to a significant orientation dependence of the mechanical properties, as well as a distinctive tension-compression yield asymmetry. This will also affect the cyclic deformation behaviour of such profiles. The objective of this study is to investigate and compare the deformation behaviour of textured profiles from the magnesium AZ-series during static and cyclic testing. The influence of the loading condition on the microstructure and crystallographic texture evolution during testing will be shown. Fatigue tests are performed under tensile and compressive loading (stress ratio  $R = 0.05$  and  $R = 8$ ) at low frequency. A relation between the maximum stress during cyclic loading in comparison to the yield strength in tension and compression will be given. Microstructure and texture analysis before and after testing will enable a discussion on fatigue behaviour of textured samples in tension and compression.

### 11:20 AM

**Tension / Compression Test of Mg AZ31B at Elevated Temperature:** *Kun Piao*<sup>1</sup>; June Lee<sup>2</sup>; Heon Lim<sup>3</sup>; Robert Wagoner<sup>1</sup>; <sup>1</sup>Department of Materials Science and Engineering, The Ohio State University; <sup>2</sup>Department of Mechanical Engineering, The Ohio State University; <sup>3</sup>Division of Mechanical Engineering & Mechatronics, Kangwon National University

A large-strain tension/compression test for elevated temperature for in-plane continuous testing of sheet metal in the sheet plane has been designed, simulated, optimized, and constructed. Thermal and mechanical analysis was carried out using finite-element method to optimize heating system, particularly material selection and placement of heating cartridges. The result is a device that can attain a temperature of 350°C within 15 minutes, and can maintain a constant temperature throughout the gage length of specimen within 10°C. To demonstrate the capabilities of the device, testing of AZ31B Mg sheet was carried out up to 250°C. The room-temperature asymmetry between tensile and compressive deformation (inflected hardening curve in compression accompanying twinning) vanished between 125°C and 150°C. The mechanical results indicate that dislocation slip instead of twinning deformation dominates the hardening behavior of Mg AZ31B alloy sheet above 150°C. This conclusion was confirmed by metallography to reveal the presence of twins after testing.

### 11:40 AM

**Comparison of Flow Stress Anisotropy and Tension-Compression Asymmetry in Ultrafine Grained AZ31B and ZK60 Magnesium Alloys:** *Majid Al-Maharbi*<sup>1</sup>; David Foley<sup>1</sup>; Ibrahim Karaman<sup>1</sup>; Suveen Mathaudhu<sup>2</sup>; Laszlo Kecskes<sup>2</sup>; <sup>1</sup>Texas A&M University; <sup>2</sup>Army Research Laboratory

Two magnesium alloys, AZ31B and ZK60A, have been processed using Equal Channel Angular Extrusion (ECAE) to enhance their mechanical properties by introducing ultra-fine grained (UFG) structures with grain sizes less than 1  $\mu\text{m}$ . The mechanical flow anisotropy of ECAE processed samples is investigated taking into account the competition between the crystallographic texture and microstructural morphology. The flow stress anisotropy, tension-compression asymmetry, and Bauschinger effect are monitored as a function of number of ECAE passes and processing routes. The anisotropy as well as texture evolution during ECAE is predicted using a visco-plastic self-consistent crystal plasticity model. In this talk, similarities and differences between these two magnesium alloys in UFG form will be presented in terms of aforementioned properties.



## Manufacturing Issues in Fuel Cells: Session I

Sponsored by: The Minerals, Metals and Materials Society, TMS: Shaping and Forming Committee

Program Organizers: Tsung-Yu Pan, Consultant, Ann Arbor Michigan; John Bradley, General Motors Corp; Michael Miles, Brigham Young University

Monday AM  
February 16, 2009

Room: 3006  
Location: Moscone West Convention Center

Session Chair: John Bradley, General Motors Corp

### 8:30 AM

#### Failure Mechanism of Nb-Cladded Stainless Steel Sheets under Bending:

*Kamran Asim*<sup>1</sup>; *Sung-Tae Hong*<sup>2</sup>; *Scott Weil*<sup>3</sup>; *William Hosford*<sup>1</sup>; *Jwo Pan*<sup>1</sup>; <sup>1</sup>University of Michigan; <sup>2</sup>University of Ulsan; <sup>3</sup>Pacific Northwest National Laboratory

Niobium (Nb)-cladded 304L stainless steel sheets can potentially be used as bipolar plates in polymer electrolyte membrane (PEM) fuel cells. Mechanical behavior and failure mechanism of Niobium (Nb)-cladded 304L stainless steel sheets were examined. Uniaxial tensile, bend and flattening tests of as-rolled and annealed specimens were conducted. The effects of different annealing temperatures and times on the mechanical behavior and failure mechanism were investigated. A micrographic analysis of bent and flattened specimens showed that the as-rolled specimens have limited ductility. The results also show that the specimens annealed above 900°C developed a micron thick intermetallic layer. The annealed specimens failed due to the breakage of intermetallic layer and subsequent localized necking failure of Nb layer. The springback angles of these specimens can be correlated to their elastic moduli and the yield strengths of these as-rolled and annealed specimens.

### 8:55 AM

#### Failure Mechanism of Polymer-Coated Stainless Steel Sheets under Bending:

*Kamran Asim*<sup>1</sup>; *Jwo Pan*<sup>1</sup>; *Daniel Wilkosz*<sup>2</sup>; *Tsung-Yu Pan*<sup>3</sup>; <sup>1</sup>University of Michigan; <sup>2</sup>Ford Motor Company; <sup>3</sup>Consultant, Ann Arbor Michigan

Polymer-coated stainless steel sheets can potentially be used as bipolar plates in polymer electrolyte membrane (PEM) fuel cells. A polymer coating EB-815 was selected in this investigation. EB815-coated 316L stainless steel sheets were examined for their ductility and formability. Uniaxial tensile tests, bend tests and flattening tests were carried out to determine the mechanical behavior and failure mechanism of these sheets under large plastic deformation. EB815 coating failure was observed at about 15% tensile strain in uniaxial tensile tests. A micrographic analysis of bent and flattened specimens showed that these specimens have good ductility under bending. Failure of the polymer coating in bend and flattening tests depends on the bend radius and the amount of bending. The data obtained from these tests will be helpful in future modeling of these sheets for forming fuel channels in bipolar plates.

### 9:20 AM

#### Low-Cost High-Volume Production of Fuel Cell Bipolar Plates by Electromagnetic Impact Forming:

*Steve Hatkevich*<sup>1</sup>; *Glenn Daehn*<sup>2</sup>; *Shekhar Srinivasan*<sup>2</sup>; *Jason Johnson*<sup>2</sup>; *John Bradley*<sup>3</sup>; <sup>1</sup>American Trim; <sup>2</sup>Ohio State University; <sup>3</sup>General Motors Corp

Investments from American Trim, GM, The Ohio State University and the State of Ohio Third Frontier Fuel Cell Program are supporting the development of a pilot plant for the manufacture of fuel cell metallic bipolar plates using a process where a magnetic field generated from a Uniform Pressure Actuator upon capacitor discharge accelerates a conductive workpiece sheet uniformly to high velocity. It then impacts a die with the desired shape, and takes the shape of that surface. Several challenges related to the development of a robust manufacturing method from this fundamentally new method are addressed. These will include discussion of design methods and validating experiments for modeling launch efficiency of materials of varied conductivity and the development of methods to qualify, test and assure long-life actuators. The overall economics of this emerging manufacturing process will be quantitatively discussed.

### 9:45 AM

#### Formability of Thin Sheet Metals in Impact-Forming of Fuel Cell Bipolar Plates:

*Shekhar Srinivasan*<sup>1</sup>; *Glenn Daehn*<sup>1</sup>; *Geoff Taber*<sup>1</sup>; *John Bradley*<sup>2</sup>; *Steve Hatkevich*<sup>3</sup>; <sup>1</sup>Ohio State University; <sup>2</sup>General Motors Corp; <sup>3</sup>American Trim

Conventional sheet metal stamping is an attractive manufacturing process for metallic fuel cell bipolar plates. However, successful stamping of the plates can be limited by aggressive flow field channel geometries, as well as by plate material properties. High velocity impact forming using a Uniform Pressure Actuator (UPA) with capacitor bank discharge represents an alternative method to manufacture these shapes. Here, plates are formed via high velocity (100-200 m/s) impact against a properly shaped die. This work compares the formability of several candidate high strength materials formed with this process against that obtainable from quasi-static forming. Impact velocities are measured using photon Doppler velocimetry and numerical modeling of the impact forming using LS-DYNA is used to explain the improved forming limits using local failure criteria.

### 10:10 AM Break

### 10:25 AM

#### Manufacturing, Assembling and Testing of Micro-PEM Fuel Cells:

*Yuhao Lu*<sup>1</sup>; *Alton Highsmith*<sup>1</sup>; *Ramana Reddy*<sup>2</sup>; <sup>1</sup>University of Alabama; <sup>2</sup>University of Alabama

Micro-proton exchange membrane fuel cells ( $\mu$ -PEMFCs) can provide more than 10 times the energy density of a rechargeable lithium-ion battery. Thus, it has been developed as a promising electrochemical power source. In this study, the microelectromechanical system (MEMS) technology was employed to manufacture the end plates of  $\mu$ -PEMFCs with micro-channel flow field on the silicon wafers. The  $\mu$ -PEMFCs were assembled using the end plates and two kinds of membrane electrode assembly (MEA) fabricated at different pressure and temperature. The technologies of polarization and electrochemical impedance spectroscopy (EIS) were used to test the  $\mu$ -PEMFCs at different conditions. The results in this study demonstrated that the process of fabrication and integration drastically affect the performance of the  $\mu$ -PEMFCs, which provided a clear idea for further designing and optimizing the  $\mu$ -PEMFCs.

### 10:50 AM

#### Processing and Properties of Porous Metallic Sandwiches for Solid-Oxide Fuel Cell Interconnects:

*Justin Scott*<sup>1</sup>; *John DeFouw*<sup>1</sup>; *David Dunand*<sup>1</sup>; <sup>1</sup>Northwestern University

Weight and cost remain an issue in mobile applications of solid-oxide fuel cells. One approach to mitigate these problems is incorporating porosity in the interconnects. Accordingly, two types of sandwiches with porous faces and a dense core were created. First, E-Brite (Fe-Cr-Mo) sandwiches were fabricated by cold-pressing three layers of elemental powders and subsequent co-sintering. Porosity was formed in the outer layers through a NaCl placeholder, which was mixed with the metallic powders before pressing and removed upon sintering. A similar placeholder technique was used for J5 (Ni-Mo-Cr-Ti-Mn-Al-Y) sandwiches, which were prepared by casting the alloy around a sandwich scaffold consisting of permanent alumina spheres in the core and temporary sodium aluminate in the faces. Following infiltration, the sodium aluminate placeholder was leached out, resulting in porous faces around a syntactic core. Mechanical properties of both types of sandwiches were measured in three-point bending tests and compared to finite-element models.

### 11:15 AM

#### Fabrication of Ni/YSZ Anode for SOFC Application by Plasma Spraying:

*Yung-Chin Yang*<sup>1</sup>; *Yu-Chuan Wu*<sup>1</sup>; *Yung-Fu Hsu*<sup>1</sup>; *Yuh-Ruey Wang*<sup>1</sup>; *Sea-Fue Wang*<sup>1</sup>; <sup>1</sup>National Taipei University of Technology

By introducing the pore former into the composite powder, the porous structure of SOFC anode will be obtained by plasma spraying. In this study, bi-feedstock of the pure nickel powder and composite (Na<sub>2</sub>CO<sub>3</sub>/YSZ) powder were simultaneously deposited on a stainless substrate. At high temperature of plasma torch, the solid state of Na<sub>2</sub>CO<sub>3</sub> would decompose to release CO<sub>2</sub> and then eject the molten powder to induce the interconnected pores in the coatings. After cleaning and soaking in deionized water, the residual Na<sub>2</sub>CO<sub>3</sub> in the coating would dissolve to form the open pores, and the porous YSZ would exist at the inner coating. By varying the size of the composite powder, the porosity of porous coating could be varied from 20 to 40%. These results suggest that the method exhibits the potential to manufacture the porous ceramic/metal composite anode of SOFC to achieve the large three phase boundary for fuel oxidation.

11:40 AM

**Fracture of Perfluorosulfonate Polymers for Fuel Cell Proton Exchange Membranes:** *Ruiliang Jia*<sup>1</sup>; Ekaterina Kolozhvari<sup>1</sup>; Takuya Hasegawa<sup>2</sup>; Jiping Ye<sup>3</sup>; Reinhold Dauskardt<sup>1</sup>; <sup>1</sup>Stanford University; <sup>2</sup>Nissan Research Center, Nissan Motor Company, Ltd; <sup>3</sup>Research Department, Nissan Arc Ltd.

Perfluorinated sulfonic polymers are widely used as proton exchange membranes in fuel cells as the proton conductor. Fracture of the membrane is a common failure mode that limits the operational life of the cell. Surprisingly, there are no well established test methods to assess fracture properties, particularly under constrained conditions, and little is understood regarding the fracture properties of such polymer membranes in simulated operational environments. In the present work, we examine a number of novel fracture methods to assess the fracture properties of Nafion films under mixed mode loading conditions, and with varying degrees of mechanical constraint. Techniques are adapted from methods used in thin film cohesion and adhesion testing, and are used to reveal the significant effect of simulated operational environments on fracture resistance.

12:05 PM

**Novel Technology for Producing Bipolar Plates in Metal Material at High Rate:** *Katarina Franzén Byttner*<sup>1</sup>; *Bill Walczak*<sup>1</sup>; <sup>1</sup>Cell Impact AB

Cell Impact has a patented new developed technology for producing customized, highly detailed bipolar plates in metal material for fuel cells, as well as flow field plates for heat exchangers, using adiabatic forming. An impact with a piston is controlled so that the energy is transmitted into the metal during a few milliseconds. Adiabatic softening occurs at the point where the impact energy is concentrated, making the material receptive to processing. The plate is shaped from both sides at the same time. Flow fields can be oriented in any direction and any shape single or double sided can be produced. Forming takes place in a single rapid operation. The manufacturing rate of one complete plate per second reduces production costs. Production is performed in a production line with an energy level of 12.5kJ. A second production line is designed where the energy level will be increased to 146.2kJ.

## Materials for High Temperature Applications: Next Generation Superalloys and Beyond: Future Application Requirements and Next Generation Superalloys

Sponsored by: The Minerals, Metals and Materials Society, TMS Structural Materials Division, TMS: High Temperature Alloys Committee, TMS: Refractory Metals Committee  
Program Organizers: Joseph Rigney, GE Aviation; Omer Dogan, National Energy Technology Laboratory; Donna Ballard, Air Force Research Laboratory; Shiela Woodard, Pratt & Whitney

Monday AM  
February 16, 2009

Room: 3010  
Location: Moscone West Convention Center

Session Chair: Joseph Rigney, GE Aviation

8:30 AM Invited

**Beyond Nickel Based Superalloys: Materials for Advanced Military Engines:** *Dallis Hardwick*<sup>1</sup>; David Shifler<sup>2</sup>; <sup>1</sup>US Air Force; <sup>2</sup>Office of Naval Research

Advanced military engines of the future will undoubtedly operate at higher temperatures to meet performance requirements and/or environmental goals. We continue to push the limits of superalloys, both wrought and cast alloys, but other materials systems are also important for future systems. Ceramics, ceramic matrix composites and refractory alloys are all systems that are being investigated. Each of these alternatives has strengths and weaknesses that we continue to explore. We'll discuss the major issues and potential future directions for research.

8:55 AM Invited

**Fossil Energy Extreme Conditions Materials Research Program:** *Robert Romanosky*<sup>1</sup>; <sup>1</sup>NETL

One of the most difficult challenges facing the Advanced Materials Research Program of the Department of Energy, Office of Fossil Energy, is the development of materials for the extreme environments encountered in advanced power generation systems. Advanced materials are vital to higher

performance and more economic operation of fossil energy systems. The scope of the program addresses material requirements for all fossil energy systems, including materials for fossil fueled advanced power generation technologies such as gasification, turbines, combustion systems, advanced sensors, and fuel cells. Research is focused on developing high-temperature, corrosion-resistant alloys and protective coatings that are compatible with advanced power system high temperature environments, as well as materials that perform specific functions in advanced fossil energy systems. A detailed overview of the Materials Program effort will be presented with an emphasis on research efforts in development of materials for the extreme environment of advanced power generation technologies.

9:20 AM

**Materials Evolutions in Hot Parts of Aero Turboengines:** *Jean-Yves Guedou*<sup>1</sup>; *Claude Quillien*<sup>1</sup>; <sup>1</sup>SNECMA

The requirements in aero-turbo-engines regarding endless improved performances on higher overall pressure ratios, compressor discharges and turbines entry temperatures lead to more and more severe thermo-mechanical loadings in critical parts such as turbine discs and blades. The Ni base superalloys have been developed by the 80's - 90's to fulfil those challenges and they are presently at an industrial level. So the Research activities on those materials have been carried on for the last decade more for reliability improvement and cost savings purposes than properties upgrading. New grades tailored for higher performances are still being developed both for single crystals and PM alloys but the improvement capabilities appear to be more and more limited. For Future, light highly resistant and refractory materials are sought beyond Ni base alloys. Ceramics matrix composites, eutectic solidified ceramics and high temperature intermetallics such as silicides are investigated as potential breakthroughs in the 2020 aero-turbo-engines.

9:40 AM

**Materials and Component Development for Advanced Turbine Systems:** *Mary Anne Alvin*<sup>1</sup>; <sup>1</sup>US DOE NETL

Hydrogen-fired and oxy-fueled land-based gas turbines currently target inlet operating temperatures of ~1425-1760C (~2600-3200F). In view of natural gas or syngas-fired engines, advancements in both materials, as well as aerothermal cooling configurations are anticipated prior to commercial operation in 2015. This paper reviews recent technical accomplishments resulting from NETL's collaborative research efforts with the University of Pittsburgh and West Virginia University for future land-based gas turbine applications.

10:00 AM Break

10:10 AM Invited

**The Properties of New High Temperature Cobalt-Based Superalloys:** *Tresa Pollock*<sup>1</sup>; *Akane Suzuki*<sup>1</sup>; <sup>1</sup>University of Michigan

The recent discovery of Ishida and co-workers of the existence of a stable L12 phase field in the ternary Co-Al-W system suggests a path for development of a new class of high temperature alloys. The properties of quaternary and higher-order Co-Al-W base alloys with additions of Ta, Ti, Cr, Re, Mo and Ni have been investigated. Two phase microstructures with high volume fractions of the gamma prime phase have been observed over a range of composition. Single crystals of these materials have been grown using a conventional Bridgman process. In the [001] orientation, a temperature-dependent flow stress anomaly is observed. The rise in flow stress above 873K is much higher in comparison to two-phase nickel superalloys and the deformation mechanisms responsible for this behavior will be discussed along with the influence of alloy composition.

10:35 AM

**Enhanced Creep Rupture Strength in Re and Ru Containing Nickel-Based Superalloys by Addition of Minor Elements:** *Astrid Heckl*<sup>1</sup>; *Robert Singer*<sup>1</sup>; <sup>1</sup>University of Erlangen-Nürnberg

The performance of gas turbines in power plants is governed by nickel-base-superalloys, which can sustain severe thermal and mechanical stresses under extreme conditions. Alloy development to increase the gas inlet temperature is fundamental for a continuous efficiency improvement, which simultaneously leads to a cost decrease of energy production, as well as lower CO<sub>2</sub>-emissions. Important improvements in the creep rupture strength of modern Nickel-Based-Superalloys have been achieved by adding elements like Rhenium (Re) and Ruthenium (Ru). In the present work we investigate the creep rupture strength of the alloy CMSX-4 and in-house designed new alloys with different Re and Ru contents. Special emphasis is placed on the effect of minor elements like carbon

(C) and magnesium (Mg). These elements are found to affect the mechanical properties substantially. Single crystals as well as columnar grained samples are studied in order to clarify the reasons for the positive effect of minor element additions.

## 10:55 AM

**Effects of the Al Content on the Mechanical Behavior of NiAl Strengthened Ferritic Fe-Based Superalloy:** *Zhenke Teng*; Shenyan Huang<sup>1</sup>; Peter Liaw<sup>1</sup>; Chain Liu<sup>2</sup>; Gautam Ghosh<sup>3</sup>; Morris Fine<sup>3</sup>; Gongyao Wang<sup>1</sup>; <sup>1</sup>University of Tennessee; <sup>2</sup>Oak Ridge National Laboratory; <sup>3</sup>Northwestern University

For body-centered-cubic (BCC) Fe matrix, ordered B2 NiAl-type  $\beta'$  precipitates form in a coherent-coplanar orientation, providing the possibility of achieving a Fe-based analogue to the Face-centered-cubic (FCC) nickel-based  $\gamma/\gamma'$  superalloys. However, the applications of this type of alloy are restricted by the limited creep resistance at temperatures higher than 973 K and the poor ductility at room temperature. In this research, the effects of Al content on the mechanical behavior of NiAl strengthened ferritic Fe-based alloy were studied. Our results show that the optimal creep properties can be reached when the Al content is about 6.5 wt.%. The ductility at room temperature will improve with decreasing the Al content. To reach an optimal balance of creep and ductility properties, the addition of Al is estimated in the range of 5 - 7 wt.%.

## 11:15 AM

**On the Different  $\gamma-\gamma'$  Behaviors over the Dendritic Structure of the New Generation Ni-Base Single Crystal Superalloy MCNG:** *Michaël Arnoux*<sup>1</sup>; Xavier Milhet<sup>1</sup>; José Mendez<sup>2</sup>; François Vogel<sup>2</sup>; <sup>1</sup>LMPM - UMR CNRS 6617; <sup>2</sup>Turboméca - Safran Group

The capability of reaching higher operating temperature is essential in prospect of the development of a new supersonic aircraft engine or for the integrity of helicopter turbines when abrupt overheating occurs during specific operating regimes. MCNG is a new generation Nickel-base single crystal superalloy, containing both Rhenium and Ruthenium.  $\gamma-\gamma'$  microstructure evolutions were studied either after very high temperature exposures at 1200°C and 1250°C or during creep at 1050°C / 140 MPa. Drastic behavior differences are observed between dendritic and interdendritic regions. The influence of Rhenium on diffusion rates and on internal stress level (through  $\gamma-\gamma'$  lattice mismatch), coupled with its preferential partitioning in dendritic cores, are discussed to explain the differences in term of directional coarsening rates, phase ripening, raft stability and  $\gamma'$  phase dissolution. The particular creep behavior of MCNG at 1050°C / 140 MPa is also discussed regarding the continuous microstructure evolution.

## 11:35 AM

**Crack Observations during Sustained-Peak Low Cycle Fatigue in Single-Crystal René N5:** *Akane Suzuki*<sup>1</sup>; Michael Gigliotti; Michael Gigliotti<sup>1</sup>; Brian Hazel<sup>2</sup>; Tresa Pollock<sup>3</sup>; <sup>1</sup>GE Global Research; <sup>2</sup>General Electric Aviation; <sup>3</sup>University of Michigan

Crack-development during compressive sustained-peak low cycle fatigue (SPLCF) was examined in vapor phase aluminide coated single-crystal René N5. Tests were conducted at 1093°C with 0.35% total strain range. Tests were ended at selected fractions of predicted life. Crack lengths on the surfaces and crack depth in longitudinal sections were examined for each specimen. Cracks were observed on the coating surface in a sample removed at 10% of predicted life. Crack lengths into the coating increased with cyclic exposure. Cracks did not penetrate into the substrate through the interdiffusion zone until about 80% of predicted life. These results suggest that understanding crack growth behavior within the coating and inter-diffusion zone would provide important insight into SPLCF behavior. The roles of mechanical properties, environmental resistance of the coating and inter-diffusion zone, and fracture mechanics will be discussed.

## 11:55 AM

**Thermodynamical Considerations for Applying the Halogen Effect to Ni-Base Superalloys:** *Hans-Eberhard Zschau*<sup>1</sup>; Patrick J. Masset<sup>1</sup>; Daniel Renusch<sup>1</sup>; Michael Schütze<sup>1</sup>; <sup>1</sup>DECHEMA e. V.

Future power generation and propulsion concepts require an increased efficiency for saving fuel and reducing environmental pollution. Due to their wide application in high temperature technologies the Ni-base superalloys have to withstand high temperatures and extreme corrosion environments. In the present paper a concept for next generation oxidation protection is presented. Oxidation of these alloys in most cases does not form a pure continuous protective

alumina scale on the surface, but rather a complex layer structure. This structure is characterized by internal oxidation. By using the halogen effect which had successfully been applied for the TiAl-alloys the internal oxidation can be transformed into external scale formation. The thermodynamical conditions of the halogen effect in the field of Ni-base alloys are investigated and discussed.

## Materials Issues in Additive Powder-Based Manufacturing Processes: Additive Manufacturing Applications

Sponsored by: The Minerals, Metals and Materials Society, TMS Materials Processing and Manufacturing Division, TMS: Powder Materials Committee  
Program Organizers: David Bourell, University of Texas; James Sears, South Dakota School of Mines and Technology; Pavan Suri, Mississippi State University

Monday AM

February 16, 2009

Room: 3004

Location: Moscone West Convention Center

Session Chair: David Bourell, University of Texas

## 8:30 AM

**Overview: Laser Additive Manufacturing and Repair: Issues and Opportunities:** *James Sears*<sup>1</sup>; <sup>1</sup>South Dakota School of Mines and Technology

Laser Additive Manufacturing (LAM) is serving a growing number of applications. The LAM technology employs metal and composite powders as the additive material. The LAM technology serves the market segment where traditional thermal spray and welding techniques have failed to provide adequate solutions. Laser cladding is one of the most widely used LAM techniques. LAM for directly building complete structures has been limited but also seems to be growing. Lasers have been the choice when automation and low heat input are required. So how does laser technology compare to other methods (e.g., electron beam, plasma transferred arc, and ultrasonics) being used in additive manufacturing? Also, how are the other technologies being refined for additive manufacturing to fill similar requirements that previously only lasers could perform? This paper discusses the relative attributes of each of these technologies and how they compared to each other.

## 8:55 AM

**Material Issues in the Qualification of LENS® For Structural Applications Including Repair:** *David Gill*<sup>1</sup>; John Smugeresky<sup>2</sup>; <sup>1</sup>Sandia National Laboratories, Albuquerque, NM; <sup>2</sup>Sandia National Laboratories, Livermore, CA

Laser Engineered Net Shaping™ (LENS®) offers opportunities to repair and modify components by adding features to or replacing damaged one on existing parts. A simple bracket was used to qualify the LENS Process with minimal time and cost for testing. LENS deposited material was evaluated for interface strength, machinability, weldability, corrosion resistance, geometric effects, heat treatment, and repair strategy. Parts were subjected to mass analysis and structural dynamic testing including free-free and assembly-level modal tests, and Haversine shock tests. The brackets performed as well as conventionally processed brackets. The brackets were subjected to testing in actual subsystem level tests, which qualified the LENS process. This presentation will include an overview of the qualifying tests and evaluation completed, with special focus on the materials analysis comparing layer deposited material with wrought material. Work by Sandia is supported by the U. S. Department of Energy under contract DE-AC04-94AL85000.

## 9:20 AM

**Biofabrication of 3D Tissue Scaffolds and Cell-Integrated Constructs: Material and Process Issues as Well as the Effects on Biological Behavior:** *Wei Sun*<sup>1</sup>; <sup>1</sup>Drexel University

Recent cell biology and scaffold-guided tissue engineering research has increasingly explored using 3D in vitro cell culture models to study gene expression and other complicated biological phenomena that more closely simulating in vivo microenvironment. Solid Freeform Fabrication (SFF) has been proven as a promising technique to meet this demand. Although widely used for fabricating tissue scaffolds, there are many challenges in materials and in processes for SFF in biological application, including material biocompatibility, process feasibility, structural formability, and the limitation of fabricating cell-integrated biological structure. Furthermore, the material and process may also



affect the biophysical and biological function of the SFF-ed structure. This presentation will review some recent SFF enabled applications in biological and tissue engineering, with a discussion of issues and challenges, along with an introduction of our research on 3D tissue scaffold fabrication and construction of tissue analog for drug metabolism study.

**9:45 AM**

**Design and Production of Bone Scaffolds with Selective Laser Melting:** *Simon Van Bael*<sup>1</sup>; Ben Vandembroucke<sup>1</sup>; Greet Kerckhofs<sup>1</sup>; Jan Schrooten<sup>1</sup>; Jean-Pierre Kruth<sup>1</sup>; <sup>1</sup>KUL

The use of bone scaffolds for treatment of large bone defects promises a solution for all disadvantages which are present with traditional care methods. The success of these scaffolds depends on its internal structure and mechanical properties. To be able to conduct a reliable investigation on the effect of these parameters, an efficient production method is required which can produce controlled internal structures. The presented work examines the ability to produce Ti6Al4V bone scaffolds with selective laser melting. The bone scaffolds were produced with a pore size range of 400-900µm and strut size 200µm. To check the repeatability mechanical and geometrical tests were performed.

**10:10 AM**

**Computational Materials Design and Layered Fabrication of Solid Oxide Fuel Cells:** *Suman Das*<sup>1</sup>; Chan Yoon<sup>1</sup>; <sup>1</sup>Georgia Institute of Technology

Electrodes in a solid oxide fuel cell (SOFC) must possess both electronic conductivity and porosity to perform their functions in the cell. They must be porous to permit rapid mass transport of reactant and product gases and be electronically conductive to transport electrons easily. However, it is nearly impossible to control electronic conductivity and porosity simultaneously using conventional fabrication techniques. Our aims are to investigate computational materials design of SOFCs and to develop a dry powder direct-write system for controlling the distribution of SOFC materials consistent with these designs. We then aim to apply the dry powder direct-write system to the fabrication of SOFCs with higher power density and thus higher efficiency than currently attainable in state-of-the-art SOFCs. This talk will present results of our efforts on computational materials design, experimental fabrication, and performance testing of SOFCs built through a layered fabrication approach.

**10:35 AM Break**

**10:50 AM**

**Rapid Prototyping of Direct Methanol Fuel Cell (DMFC) Graphite Bipolar Plates by Indirect Selective Laser Sintering (SLS):** *Kaushik Alayavalli*<sup>1</sup>; David Bourell<sup>1</sup>; <sup>1</sup>University of Texas

Graphite bipolar plates are highly desirable due to their high electrical conductivity, low weight and resistance to corrosion. However, the poor mechanical properties of graphite lead to prohibitive machining cost. Indirect Selective Laser Sintering (SLS), involving laser sintering of graphite powders mixed with a phenolic resin binder, offers the advantage of rapid, complex part production and testing of prototype bipolar plates. Carbonizing the poorly conducting, highly porous plates at high temperature and infiltrating with a low viscosity (~5 – 10 cps) cyanoacrylate polymer improves the electrical conductivity significantly and renders the plate fluid impermeable. A CAD model for various plate configurations was optimized for methanol flow and current distribution using a Computational Fluid Dynamics (CFD) simulation tool. Optimized models were fabricated by indirect SLS and evaluated in a fuel cell test bed. This work was supported by the Office of Naval Research MURI Grant No. N00014-07-1-0758.

**11:15 AM**

**Layered Manufacturing of Metallic Cellular Materials via Three Dimensional Printing of Spray-Dried Metal Oxide Ceramic Powder:** *Christopher Williams*<sup>1</sup>; Joe Cochran<sup>2</sup>; David Rosen<sup>2</sup>; <sup>1</sup>Virginia Tech; <sup>2</sup>Georgia Institute of Technology

In this paper, the authors augment the three-dimensional printing process in an effort to address geometric, build time, and cost limitations typically found in the realization of cellular materials with direct-metal layered manufacturing technologies. Specifically, metallic cellular materials are made by selectively printing solvent into a bed of spray-dried metal oxide ceramic powder. The resulting green part is then sintered in a reducing atmosphere to chemically convert it to metal. As a result of their investigation of this process, the authors are able to create cellular materials made of maraging steel that feature wall sizes

as small as 400 µm, angled trusses and channels that are 1 mm in diameter, and have an estimated average cost of ~\$3.00 per cubic inch.

**11:40 AM**

**Investigation of New Materials for Selective Laser Sintering:** *Ruth Goodridge*<sup>1</sup>; Richard Hague<sup>1</sup>; Chris Tuck<sup>1</sup>; <sup>1</sup>Loughborough University

Attempting to exploit the dramatic advantages in design that are achieved by taking an additive approach to manufacturing, researchers at Loughborough University are investigating the potential to produce custom-fitting sports Personal Protective Equipment (PPE) using the powder-based technique, selective laser sintering (SLS). However the limited range of materials that can be processed by SLS, and their high cost compared to materials used in existing manufacturing processes, is particularly problematic for sports PPE as current SLS polymers cannot withstand the cyclic and high impact loading conditions experienced in contact sport. Attempts have therefore been made at Loughborough to process new materials, such as UHMWPE, PLA, PCNs, with varying degrees of success. This talk will address the problems that have been experienced and the knowledge that has been gained through the search for new materials that are more suitable for this and other such demanding applications.

**12:05 PM**

**Effect of Liquid Phase Migration on Extrusion Pressure in Freeze-Form Extrusion Fabrication:** *Hongjun Liu*<sup>1</sup>; *Ming Lew*<sup>1</sup>; Robert Landers<sup>1</sup>; Gregory Hilmans<sup>1</sup>; <sup>1</sup>Missouri University of Science and Technology

Freeze-form extrusion fabrication (FEF) process extrudes an aqueous ceramic paste of high solids loading to fabricate 3D ceramic green parts. Liquid phase migration (LPM) may exist in this process and influence the paste composition and extrusion pressure. This paper describes a study of the existence of LPM and its effect on extrusion pressure in the extrusion of alumina paste by the FEF process. Based on the extrusion pressure profile, the extrusion process can be divided into three stages: the compaction stage, the steady stage, and the dead zone stage. The extrusion pressure increases gradually with ram displacement in the steady stage for all the ram velocities tested. Also, the extrusion pressure increases when the ram velocity increases or nozzle diameter decreases. These observations can be explained using the Benbow-Bridgwater model. It is also found that the steady stage enlarges with increasing ram velocity or decreasing nozzle diameter.

## Materials Processing Fundamentals: Solidification and Casting

Sponsored by: The Minerals, Metals and Materials Society, TMS Extraction and Processing Division, TMS: Process Technology and Modeling Committee  
Program Organizer: Prince Anyalebechi, Grand Valley State Univ

Monday AM

February 16, 2009

Room: 2016

Location: Moscone West Convention Center

*Session Chair:* Prince Anyalebechi, Grand Valley State University

**8:30 AM**

**Influence of Strong Convection Patterns on Remelting and Species Transport in a Composite Casting Process:** *Autumn Fjeld*<sup>1</sup>; Andreas Ludwig<sup>1</sup>; <sup>1</sup>University of Leoben

In a composite casting process remelting and mixing is critical to the formation of a well-bonded, durable casting and are dependent upon the flow patterns that arise during mold filling. In the casting under investigation, a thin outer shell material is first cast inside a large cylindrical mold, which is then assembled to a lower and upper neck mold, and finally the core material is poured into the shell-mold assembly. The filling process has been simulated to investigate the effect of strong convection patterns in the liquid metal on the remelting, mixing, and species transport of the outer-shell material during filling of the inner-core material. The present numerical model captures the global convection patterns and species transport and mixing between the shell and core materials. Simulations have shown that the convection patterns that develop during filling dictate the degree of shell remelting and material transport.

8:45 AM

**Control of Microstructure in Electrical Steel with Directional Solidification by LASER:** *Jung-Ryoul Yim<sup>1</sup>; Eun-ho Choi<sup>1</sup>; Yo-Han Yoon<sup>1</sup>; Jung-Han Kim<sup>1</sup>; Kyu-Hwan Oh<sup>1</sup>; Young-Chang Joo<sup>1</sup>*; <sup>1</sup>Department of Materials Science and Engineering, Seoul National University

Electrical steel needs the control of texture for its excellent soft magnetic properties. Especially, electrical steel needs the control of <100> orientation, because <100> orientation in steel is the direction of high magnetic induction and low core loss. As the melted steel continues to solidify, the grains - which have a <100> axis parallel to the steepest temperature gradient in the liquid - quickly outgrow those grains with less favorable orientation. Using Nd:YAG pulse laser (power: 4kW), 3.04%Si steel sheet with the thickness of 0.35mm can be melted through its entire thickness. Furthermore, the direction of solidification can be controlled through the change of thermal contact with the melted region. With this laser process, <001> orientation can be effectively controlled. Using EBSD, the microstructures of the lased regions are discussed.

9:00 AM

**New Physical Phenomena: Temperature-Induced Liquid-Liquid Transition in Alloys and Its Effects upon Solidification:** *Fang-Qiu Zu<sup>1</sup>; Xian-Fen Li<sup>1</sup>; Lan-Jun Liu<sup>1</sup>; Jin Yu<sup>1</sup>; Yun Xi<sup>1</sup>; Zhi-Hao Chen<sup>1</sup>; Jie Chen<sup>1</sup>; Guo-Hua Ding<sup>1</sup>; Zhong-Yue Huang<sup>1</sup>*; <sup>1</sup>Hefei University of Technology

The knowledge on nature of liquid structures and properties remains an open problem for many fundamental and applied fields such as materials sciences & processing, condensed state physics, metallurgy etc. And as well known, there is no other defined phase line above liquidus in phase diagrams of ordinary binary systems. However, via different experimental resorts, our research results of recent years show a novel physical image: temperature induced liquid-liquid structure transition(TI-LLST)can occur hundreds of degrees above TL in over 30 metallic melts including alloys and elements. On the other hand, the solidification behaviors and structures from melts experienced TI-LLST are distinct from those from melts before TI-LLST. In this presentation, some characteristic aspects of the TI-LLST and the effects on solidification behaviors and structures are summarized, and the pertinent rules and mechanism are also theoretically analyzed.

9:15 AM

**Effects of Application of Electric Current during Solidification on the Cast Microstructure of Aluminum Alloy 7050:** *Prince Anyalebechi<sup>1</sup>*; Kathy Tomaswick<sup>2</sup>; <sup>1</sup>Grand Valley State University; <sup>2</sup>Alcoa, Inc.

The effects of application of steady and pulsed electric current on the cast microstructures of ingots of a 7050 type aluminum alloy have been experimentally investigated over a solidification rate range of 0.1-10 K/s. This involved the application of an electric current of 465-930 mA/cm<sup>2</sup> of melt surface area to laboratory-size ingots solidified in a unidirectional manner. Within the electric current density and range of solidification rate investigated, the applied electric current reduced the average dendrite, grain, and second-phase particle size. It also made the size distribution of the second-phase particles more uniform. The mechanism for the observed refinement of the cast microstructure by the applied electric current is not well understood. It is provisionally attributed to the combined effects of heat-induced local convections, shear stress-induced fragmentation of dendrites, increased temperature gradient due to Joule heating and the thermal and constitutional supercooling engendered by Peltier, Thompson, and Joule heating.

9:30 AM

**A Comparative Examination of the Tensile and Fatigue Properties of Aluminum Alloy A356 Automotive Suspension Components Produced by Different Shape Casting-Related Processes:** *Prince Anyalebechi<sup>1</sup>*; <sup>1</sup>Grand Valley State Univ

A comparative study of the mechanical properties of automotive steering knuckles produced by three different shape-casting related processes has been conducted. It involved the characterization of the tensile and fatigue properties of aluminum alloy A356 knuckles produced by the vacuum/pressure riserless casting (VRC/PRC), pressure counter pressure casting (PCPC), and the hybrid Cobapress (a casting-forging) processes, in accordance with the appropriate ASTM standards. Surprisingly, the knuckles produced by the hybrid Cobapress process exhibited the lowest strength. For example, the average 0.2% yield strength of the Cobapress knuckles was 31 MPa and 40 MPa less than that of the VRC/PRC and PCPC knuckles, respectively. However, between stresses of 150-200 MPa, the fatigue lives of the VRC/PRC, PCPC, and Cobapress knuckles

were comparable. But above 200 MPa, the Cobapress knuckles exhibited the lowest fatigue life. The observed differences in the mechanical properties are attributed to the inherently different microstructures of the different knuckles.

9:45 AM

**Optimization of Submerged Entry Nozzle of Slab Continuous Casting:** *Zhigang Liang<sup>1</sup>*; <sup>1</sup>Northeastern University

Effects of the structure of submerged entry nozzle on the flow filed in mould were investigated through a water modeling experiment. The results of physical simulation showed that there was an appreciable fluctuation of the free liquid surface in the mould with obvious exposure of liquid surface and entrapment of mould powder when the original submerged entry nozzle was applied. A stable liquid surface was obtained by increasing the immersion depth of submerged entry nozzle and enlarging the downward inclination angle, but the penetration depth of jet stream increased remarkably and the position of higher temperature zone descended, which is unfavorable for increasing the casting speed. By increasing the outlet area of the submerged entry nozzle, an even fluid field with good covering of free surface by mould powder was available without any change of other geometry parameters or immersion depth of submerged entry nozzle.

10:00 AM Break

10:15 AM

**A Study of Non-Metallic Inclusion Evolution inside Fe-Al-Ti-O Melts:** *Cong Wang<sup>1</sup>*; Sridhar Seetharaman<sup>1</sup>; <sup>1</sup>Carnegie Mellon University

In this study, non-metallic inclusions, such as alumina and titanium oxides, are systematically investigated by means of morphology examination, structure analysis as well as chemistry revelation. The investigation is carried out through sampling in a vacuum-induction furnace inside iron melts involving aluminum, titanium and oxygen. The purpose of this study is to simulate de-oxidation process of interstitial free steels through transient ladle reaction products. Based on structure analysis imparted via transmission electron microscopy, it is revealed that desired non-metallic inclusions are produced within accordingly predicted stable regions. In addition, it is found that inclusion morphology, under any thermodynamic stable circumstances, undergoes dramatic changes, which are always accompanied with statistically permanent evolution from initially spherical-dominated percentages to finally irregular-prevalent situation. It is also shown that chemistry may vary continuously within one individual inclusion, suggesting that local thermodynamic stable conditions may not be reached and that the inclusion was once viscous.

10:30 AM

**Heat-Resistance Property of Cu-3.5Ti-0.1Zr Alloy:** *Cao Xingmin<sup>1</sup>*; <sup>1</sup>Suzhou Institute of Non-Ferrous Metal Processing Research

Abstract: The effect of Zr on the heat-resistance of a Cu-3.5Ti (wt.%) alloy was investigated by mechanical tests and TEM observation. The results show that the softening temperature of the Cu-3.36Ti alloy was substantially increased by the addition of 0.11wt% Zr. The softening of the Cu-3.36Ti alloy is mainly controlled by the phase transition from TiCu<sub>4</sub> to TiCu<sub>3</sub> in the temperature range from 450° to 550°, and the addition of 0.11 wt.%Zr can retard this phase transition. The mechanism was discussed in relation to the microstructural evolution.

10:45 AM

**Friction Stir Welding Characteristics of Different Heat-Treated-State 7075 Aluminum Alloy Plates:** *Meysam Mirazizi<sup>1</sup>*; <sup>1</sup>Sharif University of Technology

Friction stir welding of 7075 al-alloys was performed to investigate the effects of the base material conditions on the FSW characteristics. The results indicated that the base material condition has a significant effect on weld morphologies, weld defects, and mechanical properties of joints. microscopy investigation showed that In the 7075-O welds, no visible interface exists between the stir zone and the ThermoMechanically Affected Zone and a weld nugget with an onion ring-like morphology not clearly exists. weld defects are formed in the lower part of the weld. In the 7075-T6 welds, there is visible interface between the SZ and the TMAZ, and a weld nugget with an onion ring-like morphology clearly exists. The defects are liable to form in the middle and upper part of the weld. The results of Shear Punch Test and tensile test showed that strength efficiency of 7075-O is greater than 7075-T6 joints (95% against 82%). The two types of joints have different fracture location characteristics.

11:00 AM

**Hybrid Laser/GTAW Welding of Galvanized High-strength Steels in Gap-Free Lap Joint Configuration:** *Shanglu Yang*<sup>1</sup>; <sup>1</sup>Research Center for Advanced Manufacturing

In this study, laser-GTAW hybrid welding was used to the lap welding of galvanized high-strength steels in a gap-free lap joint configuration. The effects of welding parameters such as the laser power, the distance between the laser beam and the electrode torch, the arc current on the quality of hybrid welds were studied. The reason for the formation of different weld defects arises from the development of the highly-pressurized zinc vapor at the interface of two metal sheets. Experimental results demonstrated that the elongated molten pool introduced by the GTAW can suppress the formation of spatters to some extent. However, the hybrid laser-arc welding process still suffers from a large amount of spatters that degrade the weld quality. Additionally, it was found that the weld quality was enhanced with the increase in the laser beam-arc distance and welding current.

11:15 AM

**Optimization of Ductile Iron Treatment by Computing the Refining Reactions in Liquid Irons:** *Simon Lekakh*<sup>1</sup>; David Robertson<sup>1</sup>; Sergey Rimoshevsky<sup>2</sup>; Vladimir Tribyshevsky<sup>2</sup>; Nikolay Bestyzev<sup>2</sup>; <sup>1</sup>Missouri University of Science & Technology; <sup>2</sup>Belarusian State Polytechnic University

Experimental work and thermodynamic simulations of cast iron refining were carried out using various additions of alkali and rare earth metals. The sequences of the refining reactions for sulfur and oxygen removal were found for melts treated with Mg, Ca, and Ce. The measured data and the results of the computer simulations were in agreement. Experimental kinetic data, together with the thermodynamic calculations, were used for optimization of the amount and sequence of the addition of nodulizers for ductile iron production.

11:30 AM

**Influence of the Submerged Entry Nozzle Geometry on the Heat Transfer inside the Continuous Casting Mold:** Jaqueline Alexander<sup>1</sup>; *Cesar Real-Ramirez*<sup>1</sup>; Manuel Palomar-Pardave<sup>1</sup>; Raul Miranda-Tello<sup>1</sup>; Jesus Gonzalez-Trejo<sup>1</sup>; <sup>1</sup>Universidad Autonoma Metropolitana - Azcapotzalco

Some of the most important phenomena which govern the continuous casting process and determine the quality of the product are the fluid flow and the heat transfer. Steel flows into the mold through the ports of a bifurcated submerged entry nozzle (SEN), which directs the jet to the mold narrow faces where the superheat contained is dissipated on the solidifying shell. Many important aspects of the fluid flow in the mold are transient and difficult to control. However, the time-averaged flow pattern in the mold is greatly influenced by the nozzle geometry, the submergence depth and the mold dimensions. The aim of this work is to analyze the relationship between the heat transfer and the fluid flow pattern inside the mold using the CFD technique at several operation conditions.

**Mechanical Behavior of Nanostructured Materials: Stability of Nanostructures**

Sponsored by: The Minerals, Metals and Materials Society, TMS Electronic, Magnetic, and Photonic Materials Division, TMS Materials Processing and Manufacturing Division, TMS Structural Materials Division, TMS: Chemistry and Physics of Materials Committee, TMS/ASM: Mechanical Behavior of Materials Committee, TMS: Nanomechanical Materials Behavior Committee

Program Organizers: Xinghang Zhang, Texas A & M University; Andrew Minor, Lawrence Berkeley National Laboratory; Xiaodong Li, University of South Carolina; Nathan Mara, Los Alamos National Laboratory; Yuntian Zhu, North Carolina State University; Rui Huang, University of Texas, Austin

Monday AM

Room: 3024

February 16, 2009

Location: Moscone West Convention Center

Session Chairs: Xinghang Zhang, Texas A & M University; Alan Jankowski, Texas Tech University

**8:30 AM Introductory Comments****8:35 AM Keynote****Thermal and Mechanical Stability of Nanocrystalline Grain Structures:** *Carl Koch*<sup>1</sup>; <sup>1</sup>North Carolina State University

This talk will review the thermal, and to a lesser extent, the mechanical stability of nanocrystalline grain structures. Since grain boundaries are not equilibrium defects in crystals, polycrystalline materials are metastable and with sufficient thermal activation the grain size microstructure will coarsen. This is particularly true for nanocrystalline microstructures where the enormous grain boundary area provides a large driving force for grain growth. However, there are kinetic and thermodynamic processes that can provide significant stabilization of nanocrystalline grain sizes. This talk will briefly review examples of grain boundary stabilization in nanocrystalline materials by kinetic approaches. The major part of the presentation will focus upon thermodynamic stabilization by solute segregation to grain boundaries from reports in the literature and from the author's laboratory. The possibility of recrystallization of nanocrystalline microstructures will be discussed. The stress-induced coarsening of nanocrystalline grains will also be considered. Author's research supported by NSF, DMR-0504286.

**9:05 AM****Evolution of Mechanical Properties during Room Temperature Grain Growth of Nanocrystalline Pd:** *Rainer Birringer*<sup>1</sup>; Markus Ames<sup>1</sup>; Manuel Grewer<sup>1</sup>; Jürgen Markmann<sup>1</sup>; <sup>1</sup>Saarland University

Nanocrystalline Pd prepared by IGC exhibits room temperature grain growth in the limit of high purity thereby bridging a size range from 10nm to 10  $\mu$ m. The growth kinetics significantly deviate from parabolic behavior. Possible scenarios that may explain this deviation are shortly addressed. The main focus concentrates on discussing results obtained from in situ measurements of mechanical properties during RT grain growth. Setting up appropriate scaling laws enables to extract interface stress and interface elastic moduli. Grain-size-dependent hardness and strain rate sensitivity will be discussed in the light of available data from non-in-situ measurements.

**9:20 AM****Thermal Stability of LIGA Nickel Composites for High-Temperature MEMS Applications:** *S.J. Suresha*<sup>1</sup>; Manel Haj-Taieb<sup>2</sup>; Jarir Aktas<sup>2</sup>; Kevin Hemker<sup>1</sup>; <sup>1</sup>Johns Hopkins University, Department of Mechanical Engineering; <sup>2</sup>Forschungszentrum Karlsruhe, Institut für Materialforschung II

LIGA Ni-W MEMS structures with 5 and 15 at% W were prepared by electrodeposition. The thermal stability of the Ni-W specimens were investigated by annealing at 400 and 700°C for different durations (1h and 4h). The microstructure and mechanical properties were analyzed with TEM, XRD, micro-tensile testing and indentation. No precipitates were observed, but in comparison to the LIGA Ni the microstructure of the LIGA Ni-W was found to be stable up to 700°C. The tensile strengths of the LIGA Ni-W were higher than for pure LIGA nickel in both as received and annealed states. The Ni-W structure exhibited brittle failure at room temperature, but the annealed Ni-W samples exhibited considerable ductility before fracture and showed higher tensile strength. Thermal stability in this system appears to come from the segregation



of W in the grain boundary and the increased ductility and strength from grain boundary strengthening in the nanocrystalline range.

**9:35 AM**

**Thermal Stability of Nanostructured Materials Created by Severe Plastic Deformation:** Christopher Saldana<sup>1</sup>; Jiazhao Cai<sup>2</sup>; Sergei Suslov<sup>1</sup>; Ravi Shankar<sup>2</sup>; Srinivasan Chandrasekar<sup>1</sup>; Eric Stach<sup>1</sup>; <sup>1</sup>Purdue University; <sup>2</sup>University of Pittsburgh

Severe plastic deformation (SPD) while offering a convenient and scalable framework for creating fully-dense nanostructured materials from a range of alloy systems significantly limits the options available for achieving high levels of thermal stability in the resulting fine-grained materials. Following traditional approaches, the stability of severely deformed materials can be improved by utilizing multi-phase alloys composed of a dense dispersion of second phases. In such multi-phase systems, we show that the overall stability of the fine-grained material is in turn determined by the stability of the second phases. Examples of precipitate stabilized nanostructured materials from aluminum and nickel alloys are utilized to illustrate stabilization criteria. Rate-dependent strengthening and related mechanical behavior of these materials are presented. Finally, an emerging interface engineering approach is discussed wherein a high-density twin of nano-lamella when introduced amongst nano-scale grain boundaries through SPD at cryogenic temperatures is shown to improve the overall thermal stability.

**9:50 AM**

**Thermal Stability of Ultra-Fine Grained Ti-6Al-4V Alloys Processed via Multi-Axis Forging:** Radhakrishna Bhat<sup>1</sup>; Richard Didomizio<sup>1</sup>; Andrew Deal<sup>1</sup>; Judson Marte<sup>1</sup>; P. Subramanian<sup>1</sup>; <sup>1</sup>GE Global Research

A near-isothermal multi-axis forging (MAF) process was used to produce ultra-fine grained (UFG) Ti-6Al-4V alloys. The thermal stability of the resulting ultra-fine grained structure was evaluated at temperatures below the beta transus under both static and dynamic conditions in order to investigate the coarsening kinetics of the primary alpha particles in the alpha+beta phase field. Specimens were heat-treated for varying durations at different temperatures within the alpha+beta phase field for the static studies, while hot compression tests were conducted to evaluate the thermal stability under dynamic conditions. The results of the characterization with scanning electron microscopy and quantitative metallography will be presented and compared with data for the conventionally processed Ti-6Al-4V material. The coarsening mechanisms and methods to stabilize the ultra-fine grain size will be discussed, especially in the context of using UFG Ti-6Al-4V for producing near-net shape Ti components via superplastic deformation.

**10:05 AM**

**Deformation Behaviour of Nanocrystalline Pd Studied in Conditions of High Pressure Torsion Loading:** Julia Ivanisenko<sup>1</sup>; Jörg Weissmüller<sup>1</sup>; Hans-Jörg Fecht<sup>2</sup>; <sup>1</sup>Forschungszentrum Karlsruhe in der Helmholtz Gemeinschaft; <sup>2</sup>Universität Ulm

We have investigated the hardening behaviour of nanocrystalline nc igr Pd with a mean grain size of 12 nm in compression-torsion mode in a wide range of shear strains (0-400). We show that in the studied shear strain range the notable changes in the microstructure, namely a strain induced grain growth of igr Pd occurs, that controls the relevant deformation mechanisms. For lower strains when the grain size is still small enough, the plastic flow is governed by twinning and probably grain boundary sliding. For this range of shear strains a rapid strain hardening observed in the shear strain vs. torque curves is conditioned by the increase of the twins density. When the grain size becomes larger and deformation is controlled exceptionally by dislocation glide a steady stage is achieved, when the grain size, dislocation density and flow stress (torque) are saturated.

**10:20 AM Break**

**10:30 AM Invited**

**Plastic Flow and Irradiation Stability of Nanolayered Composites:** Amit Misra<sup>1</sup>; <sup>1</sup>Los Alamos National Laboratory

Magnetron sputtering is used to synthesize nanolayered composites with controlled length scales in the nanometer range. These materials exhibit ultra-high flow strengths, typically within a factor of two to three of the theoretical strength limit of perfect crystals. The morphological and chemical stability of incoherent interfaces such as copper-niobium in these nanolayered composites was explored at large plastic strains via tensile tests, pillar compression and

rolling. Furthermore, ion irradiation, over a range of temperatures and ion doses, was used to examine the irradiation stability. These materials exhibit remarkable thermo-mechanical and irradiation stability due to the ability of the interfaces to attract, absorb and annihilate defects. The design of the nanostructural dimensions and interface structures to achieve both ultra-high strength and high radiation damage tolerance will be discussed. This work is supported by the U. S. Department of Energy, Office of Science, Office of Basic Energy Sciences.

**10:50 AM**

**The Effect of Layer Thickness and Volume Fraction on Structure and Mechanical Properties of Al/TiN Multilayers:** Dhriti Bhattacharyya<sup>1</sup>; Nathan Mara<sup>1</sup>; Patricia Dickerson<sup>1</sup>; Richard Hoagland<sup>1</sup>; Amit Misra<sup>1</sup>; <sup>1</sup>Los Alamos National Laboratory

Nano-scale multilayers of Al and TiN with Al layer thickness varying from 5nm to 500nm and TiN layer thickness varying from 1nm to 50nm were deposited in two different thickness ratios – Al:TiN :: 9:1 and Al:TiN :: 1:1. The hardness values measured by nanoindentation increased with decreasing layer thickness and the hardness of the multilayers with Al:TiN :: 1:1 thickness ratio was, in all cases, more than the hardness for the multilayers with the same bilayer thickness having a layer thickness ratio of Al:TiN :: 1:1. The hardness values of the two kinds of multilayers were found to be close for any given bilayer thickness, when normalized by their modulus of elasticity. These results are discussed in terms of possible dislocation mechanisms and the structure of the interfaces between the Al and TiN layers, which were characterized by Transmission Electron Microscopy (TEM).

**11:05 AM Invited**

**Is There a Future for Nanograined Steel?:** John Morris<sup>1</sup>; <sup>1</sup>University of California, Berkeley

While it is sometimes assumed that nanograined materials will come to dominate the structural, as well as the electronic applications for advanced materials, researchers who specialize in structural steels are less optimistic. While ultrafine grain size leads to exceptionally high strength, tensile ductility is lost, and it is difficult to achieve useful ductility in conventional steels with grain sizes much below 1  $\mu\text{m}$ . However, strength is only one of the important properties of steel. Ductile fracture and hydrogen resistance are also important. They are also influenced by grain size, but by different mechanisms, with the consequence "grain size" has a somewhat different meaning. Given the crystallography of coherent transformations in steel, it is possible to create steels that have submicron grain size with respect to fracture or embrittlement, while retaining excellent strength and good ductility. This is the promising path to nanostructured steels with exceptional properties.

**11:25 AM**

**Atom Probe Tomography, Small Angle Neutron Scattering and Transmission Electron Microscopy Characterization of Nano-Scale Features in MA957:**

G. Robert Odette<sup>1</sup>; Emmanuelle Marquis<sup>2</sup>; Peter Hosemann<sup>3</sup>; Pifeng Miao<sup>1</sup>; Nicholas Cunningham<sup>1</sup>; Sergio Lazono-Perez<sup>2</sup>; Matthew Alinger<sup>4</sup>; Erich Stergar<sup>5</sup>; <sup>1</sup>University of California; <sup>2</sup>University of Oxford; <sup>3</sup>Los Alamos Nat Laboratory; <sup>4</sup>GE Global Research; <sup>5</sup>University of Leoben

Nano-dispersion strengthened ferritic alloys contain a high density of thermally stable Y-Ti-O nano-scale features (NFs) which provide both high creep strength and irradiation damage resistance. The NFs have been studied by small angle neutron scattering (SANS), three-dimensional atom probe tomography (APT) and transmission electron microscopy (TEM). However, the compositions and structures of various NFs are not well understood, and they appear to range from coherent solute enriched GP-type zones (in APT studies) to stoichiometric complex oxides (Y<sub>2</sub>TiO<sub>5</sub> and Y<sub>2</sub>Ti<sub>2</sub>O<sub>7</sub>, in some SANS and TEM studies). We cross compare the APT (four groups), SANS and TEM (two groups) characterization of the NFs in MA957. The various techniques are generally in good agreement on the sizes and number densities of the NFs. However, APT studies show high Ti+Y/O and Ti/Y ratios that are inconsistent with complex oxides. The APT indicates a complex shell structures of Y-T-O enriched cores surrounded by TiO shells.

**11:40 AM**

**Deformation Behavior of High Strength Nano-Structured Ferritic Alloys:** David Hoelzer<sup>1</sup>; Jim Bentley<sup>1</sup>; Meimei Li<sup>2</sup>; Mikhail Sokolov<sup>1</sup>; David McClintock<sup>1</sup>; <sup>1</sup>Oak Ridge National Laboratory; <sup>2</sup>Argonne National Laboratory

Reducing the grain size and dispersing precipitates are classical ways for increasing the strength of bulk metallic alloys. For an advanced ferritic alloy

produced by mechanically alloying, the dispersion of nano-size oxygen-rich clusters, i.e. nanoclusters, caused nano-size grains to form. This nano-structured ferritic alloy (NFA) possesses high tensile strengths from low (196°C) to elevated (800°C) temperatures with some measure of ductility at low temperatures. Furthermore, the NFA has a low ductile-to-brittle transition temperature and shows ductile failure characteristics in tension down to -196°C. The deformation behavior of the NFA including the stability of the nanoclusters and nano-size grains during deformation at low and elevated temperatures will be presented. Research supported by the Office of Nuclear Energy, Science and Technology, by the Office of Fusion Energy Sciences, and at the SHaRE User Facility by the Scientific User Facilities Division, Office of Basic Energy Sciences, U.S. Department of Energy.

**11:55 AM Invited****Deformation Process of Nanocrystalline Materials with In-Situ TEM and Synchrotron:** *Scott Mao*<sup>1</sup>; <sup>1</sup>University of Pittsburgh

The discovery of mechanical grain growth at liquid nitrogen temperatures show such unique stress induced microstructure evolution. It is therefore necessary to study the properties of non-equilibrium boundaries effect on the dislocation storage or grain agglomeration/ growth induced by deformation. This talk focuses on stress-induced microstructure evolution of grain agglomeration in nc materials through in-situ TEM and in-situ synchrotron tests. We used in situ TEM and observe nc Ni with an average grain size of about 10 nanometers, which shows deformation-induced grain agglomeration. It has been found that grain boundary mediated processes have become a prominent deformation mode. In collaboration with Dr. Yang in Argonne National Laboratory, in situ synchrotron on nc and micron Ni under hydrostatic stress up to 57Gpa show that peak broadening increases during loading up to 45 Gpa in nc-Ni, which indicates high dislocation density storage, and no clear grain growth or texturing.

**12:15 PM**

**In Situ TEM Nanocompression Testing of Gum Metal:** *Elizabeth Withey*<sup>1</sup>; Jia Ye<sup>2</sup>; Velimir Radmilovic<sup>2</sup>; Shigeru Kuramoto<sup>3</sup>; Andrew Minor<sup>1</sup>; Daryl Chrzan<sup>1</sup>; John Morris<sup>1</sup>; <sup>1</sup>University of California; <sup>2</sup>National Center for Electron Microscopy, Lawrence Berkeley National Laboratory; <sup>3</sup>Toyota Central Research and Development Laboratory Inc

Gum Metal is a newly developed set of  $\beta$ -Ti alloys that, in the cold-worked condition, have exceptional elastic elongation and high strength. The available evidence suggests that Gum Metal does not yield until the applied stress approaches the ideal strength, and then deforms by mechanisms that do not involve conventional dislocation plasticity. In order to study the deformation behavior in more detail, in situ compression of submicron-sized pillars has been performed on solution-treated and cold-worked samples of one composition of Gum Metal. Explanation of the mechanical behavior observed was assisted through the correlation of quantitative load vs. displacement data and real-time images, along with high resolution microscopy of undeformed samples of solution-treated and cold-worked Gum Metal of the same composition used in the compression tests.

**12:30 PM**

**Role of Nanoscale Interface Diffusion in Creep Deformation and Microstructural Stability of Si-C-N Nanocomposites in High Temperature Environments:** *Ming Gan*<sup>1</sup>; *Vikas Tomar*<sup>1</sup>; <sup>1</sup>University of Notre Dame

Next generation ceramic nanocomposite coatings need to have excellent creep strength and microstructural stability at extreme operating temperatures beyond 1750 K. In the presented research atomistic analyses of microstructural stability and creep deformation in Silicon (Si) carbide (C) and nitride (N) coatings developed for this purpose are presented. The focuses is on understanding the nanoscale diffusion phenomenon in such materials and correlate the developed understanding with observed creep strength and microstructural stability characteristics. Atomistic analyses are performed using non equilibrium molecular dynamics. Such analyses are then correlated with nanoindentation creep studies on some representative samples. Analyses show that the nanoscale diffusion dominates the creep behavior of the nanocomposites. In addition by varying the nanoscale structural configuration a significant improvement in creep strength and microstructural stability could be obtained. Alternate phase arrangements based on biomimetic structures are also analyzed.

**12:45 PM**

**Change of Deformation Mechanism in Nanocrystalline Nickel at Very Low Temperatures:** *Lutz Hollang*<sup>1</sup>; Klemens Reuther<sup>1</sup>; Suhash Dey<sup>1</sup>; Werner Skrotzki<sup>1</sup>; <sup>1</sup>Dresden University of Technology

Pure nanocrystalline nickel was produced by pulsed electro-deposition without additives for grain refinement. The average grain size of the material is  $d_{\text{EBSD}} = 150$  nm and  $d_{\text{XRD}} = 30$  nm if determined by electron backscatter diffraction (EBSD) and X-ray diffraction (XRD), respectively. Tensile tests with constant deformation rate were performed at temperatures between 4 K and 320 K. The stress-strain curves are parabolic with the ultimate stress strongly decreasing with increasing temperature. Stress relaxation experiments reveal that dislocation interaction governs the plastic behaviour of the material at low temperatures. However, if the stress attains the threshold of 2400 MPa, as it is the case between 4 K and 9 K, the deformation mode suddenly changes towards "catastrophic" shear. The shear events are characterized by substantial stress drops accompanied by acoustic emission. The nature of the shear events will be discussed on the basis of microstructural investigations performed by electron microscopy.

**Microstructural Processes in Irradiated Materials: Radiation Effects I: Segregation and Modeling**

Sponsored by: The Minerals, Metals and Materials Society, TMS Structural Materials Division, TMS/ASM: Nuclear Materials Committee

Program Organizers: Christophe Domain, Electricite De France; Gary Was, University of Michigan; Brian Wirth, University of California, Berkeley

Monday AM

February 16, 2009

Room: 2008

Location: Moscone West Convention Center

Session Chairs: Charlotte Becquart, University of Lille; Christophe Domain, Electricite De France

**8:30 AM Invited**

**Phase Field Modeling for Irradiation-Induced Segregation and Precipitation in Undersaturated Solid Solutions:** *Arnoldo Badillo*<sup>1</sup>; *Daniel Schwen*<sup>1</sup>; *Robert Averbach*<sup>1</sup>; *Pascal Bellon*<sup>1</sup>; <sup>1</sup>University of Illinois

Current phase field models for diffusion-controlled evolutions in the solid state are based on phenomenological kinetic equations. The lack of absolute time and space scale raises problems when applying these models to alloys subjected to irradiation by energetic particles since this external forcing introduces new length scales and time scales. We propose here an approach that relies on a mixed continuous-discrete treatment of the evolution of chemical species and point defect concentrations. This approach makes it possible to take into account important irradiation effects, namely the production and elimination of point defects and point defect clusters and the forced chemical mixing. Examples of application of the model are given, in particular for heterogeneous segregation and precipitation reactions induced by irradiation in undersaturated solid solutions.

**9:00 AM**

**Modeling Nanocluster Formation during Ion Beam Synthesis:** *C. Yuan*<sup>1</sup>; *Diana Yi*<sup>1</sup>; *Ian Sharp*<sup>2</sup>; *Swanee Shin*<sup>1</sup>; *Christopher Liao*<sup>1</sup>; *Julian Guzman*<sup>1</sup>; *Joel Ager III*<sup>3</sup>; *Eugene Haller*<sup>1</sup>; *Daryl Chrzan*<sup>1</sup>; <sup>1</sup>Lawrence Berkeley National Laboratory; <sup>2</sup>Department of Materials Science, University of California, Berkeley; <sup>3</sup>Walter Schottky Institut, Technische Universitat Munchen; <sup>3</sup>Lawrence Berkeley National Laboratory

Ion beam synthesis (IBS) is a technologically important method to produce semiconductor nanocrystals within a solid. The process involves implanting ions into a matrix at concentrations beyond their solubility limit. During IBS, a competition between cluster growth and cluster damage evolves. A model describing the nucleation, growth and fragmentation of clusters during IBS is studied via kinetic Monte Carlo simulations and the self-consistent solution to a set of coupled, mean-field rate equations. It is found that the nanocluster size distribution approaches a steady-state profile, the shape of which depends only on the ratio of the transient enhanced diffusion coefficient to the ion volumetric flux. Fitting observed distributions to theoretical predictions allows one to determine the transient enhanced diffusion coefficient. Estimates of transient enhanced diffusion coefficients so obtained for Ag, Co and Ge in silica are

presented. This research is supported by the Directorate, Office of Science, Office of Basic Energy Sciences of the U.S. Department of Energy under Contract No. DE-AC02-05CH11231.

**9:20 AM**

**Atomistic Simulation of Diffusion on Grain Boundaries and in Irradiated Metals:** *Je-Wook Jang*<sup>1</sup>; *Byeong-Joo Lee*<sup>1</sup>; <sup>1</sup>POSTECH

The grain boundary (GB) diffusion in bcc-Fe has been investigated using molecular dynamics simulations. Attention was focused on the effect of type and misorientation of GBs on the diffusivity. A new method to avoid the difficulty in assuming the width of GB was developed, and applied to the calculation of GB diffusivity and activation energy for a wide range of GBs with different types and misorientations, including a special twin boundary. The calculated diffusivity was generally in a good agreement with experimental information. The calculated activation energy of GB diffusion was also comparable with that of bulk diffusion. No strong correlation between misorientation angle and diffusivity is observed in a range of 10~40°, but certain difference in diffusivity between planar or normal direction to the GB plane is observed. By performing the simulation using irradiated samples, the effect of irradiation could also be estimated and will be discussed.

**9:40 AM**

**Phase Field Formalism for Modeling Microstructure in Irradiated Materials: Simulation of Void Growth:** *Srujan Rokkam*<sup>1</sup>; *Anter El-Azab*<sup>1</sup>; *Paul Millet*<sup>2</sup>; *Dieter Wolf*<sup>2</sup>; <sup>1</sup>Florida State University; <sup>2</sup>Idaho National Laboratory

Void formation in irradiated materials is a subject of great technological importance for the design of high performance structures in nuclear reactors. Here we present a diffuse interface phase field model for nucleation and growth of voids in irradiated materials. The formalism developed herein treats both the nucleation and growth processes simultaneously in a spatially resolved fashion. The defect fluxes and the defect density modulations are formulated using Cahn-Hilliard type description for the vacancy and interstitial concentration fields. The dynamics of void growth are obtained in terms of the evolution of a non-conserved order parameter field, whose evolution is prescribed by a phenomenological Allen-Cahn type equation. The model also accounts for the effect of applied stress, cascade-induced and thermally-induced fluctuations, vacancy-interstitial recombination, and interaction of vacancies and interstitials with lattice sinks. Using the case of pure metals as an example, illustrative results of model capabilities are presented.

**10:00 AM**

**Dislocation Evolution in V-4Cr-4Ti:** *David Gelles*<sup>1</sup>; <sup>1</sup>Battelle Pacific Northwest National Laboratory

V-4Cr-4Ti is being considered for application in the first wall of a fusion reactor. V-4Cr-4Ti is a refractory solute strengthened body centered cubic alloy chosen in part for its low swelling characteristics. It has been subjected to a wide range of tests to determine suitability, including irradiation creep, irradiation induced swelling, post-irradiation deformation and thermal creep. A part of that effort has been to perform post-test microstructural examinations in order to better understand dislocation behavior. This report is intended to describe dislocation evolution under irradiation and/or stress along with a number of unusual observations arising from that work, including indications for the operation of the Harper-Dorn thermal creep mechanism at temperatures as high as 800°C and a novel Burgers vector found following irradiation. Recent results will be reviewed in order to provide a better understanding of dislocation evolution in this material.

**10:20 AM Break**

**10:40 AM Invited**

**Monte Carlo Simulations of Irradiated Materials on the Reactor Timescales:** *Vasily Bulatov*<sup>1</sup>; *Aleksandar Donev*<sup>1</sup>; <sup>1</sup>Lawrence Livermore National Laboratory

Irradiation produces copious quantities of atomic defects giving rise to complex diffusion-controlled processes defining the evolution of material microstructure. The time scales on which this evolution takes place range from nanosecond time intervals of fast atomic diffusion to tens of years of material work life in nuclear reactors. Here we present a new method for kinetic Monte Carlo simulations that encompasses all relevant time scales and connects the fundamental atomistic mechanisms directly to the long-term damage accumulation. The new simulation method is tested on a simple model of  $\alpha$ -iron for a range of temperatures and irradiation dose rates. The results suggest an approximate scaling relationship

by which material damage observed in accelerated irradiation tests can be extrapolated to predict how the same material would resist irradiation over the much longer time scales of nuclear reactors.

**11:10 AM**

**Atomistic Simulations of Radiation Damage in Polycrystalline Metals:** *Hanchen Huang*<sup>1</sup>; <sup>1</sup>Rensselaer Polytechnic Institute

Much has been learned about atomistic mechanisms of radiation damage in single crystalline solids. Meanwhile, grain boundaries have usually been assumed as sinks and sources of infinite strength and constant position and character, such as in typical rate theories. Such assumption is certainly unwarranted particularly when solids are nanostructured. Combining classical molecular dynamics and kinetic Monte Carlo based ADEPT simulations, this work presents atomic view of grain boundary effects to radiation damage and effects on grain boundaries from radiation-produced defects.

**11:30 AM**

**Point Defect Clusters in Zirconium and Their Influence on Radiation Damage:** *Alexandre Legris*<sup>1</sup>; *Petrica Gasca*<sup>1</sup>; *Christophe Domain*<sup>2</sup>; <sup>1</sup>University of Sciences and Technologies of Lille; <sup>2</sup>Électricité de France, Research and Development

The cladding material in Pressure Water Reactors is made with zirconium alloys that are submitted to intense neutron radiation damage in service conditions. As a consequence, the formation of dislocation loops evenly distributed in the basal and prismatic planes induce an elongation of the textured material. To understand the growth and more generally the microstructure evolution under irradiation it is crucial to know the relative stability of the point defect clusters formed which are sinks for point defects and nucleation sites for dislocation loops. The present work presents an ab initio study of small point defect clusters in zirconium including self-interstitials and vacancies. The structure (number of defects and shape) and formation energy of the clusters were determined. The results are discussed and used as input for mesoscopic simulations of radiation damage.

**11:50 AM**

**Modeling of Diffusion in Fe-Ni-Cr Alloys Using Ab-Initio Based Approach:** *Samrat Choudhury*<sup>1</sup>; *Julie Tucker*<sup>1</sup>; *Benjamin Swoboda*<sup>1</sup>; *Dane Morgan*<sup>1</sup>; <sup>1</sup>University of Wisconsin

For more than three decades materials used in nuclear reactors have been known to degrade in radiation environments. Radiation changes the materials composition through the formation and migration of large concentration of point defects to sinks. Central to the understanding of such radiation induced segregation (RIS) is explaining the complex solute-defect interaction in multi-component alloys. Prior theoretical models to study diffusion in multi-component alloys often lack adequate energetic parameters of the diffusing species. In this work, we use ab initio energetics to calculate solute-defect interaction in Fe-Ni-Cr alloys. Both ferritic and austenitic structures are considered. We observe in fcc: 1) Strong Cr-interstitial binding 2) Weak binding of Cr and Fe to vacancies and 3) Enhanced Cr diffusion compared to Ni and Fe. Diffusion coefficients for both vacancy and interstitial migration were determined from the ab initio energetic using statistical mechanics and kinetic Monte Carlo approaches.

**12:10 PM**

**Radiation-Induced Segregation in Ferritic-Martensitic Alloys HT9, T91, and HCM12A:** *Janelle Penisten*<sup>1</sup>; *Zhijie Jiao*<sup>1</sup>; *Gary Was*<sup>1</sup>; *Kwan Wong*<sup>2</sup>; *Brian Wirth*<sup>2</sup>; <sup>1</sup>University of Michigan; <sup>2</sup>University of California, Berkeley

Ferritic-Martensitic (F-M) alloys are candidates for cladding and structural material in the Advanced Burner Reactor. However, there is little understanding of radiation-induced segregation (RIS) in these alloys, although Cr segregation is of particular concern. Samples of T91 (9wt% Cr), HT9 (12wt% Cr), and HCM12A (11wt% Cr) were irradiated with 2.0 MeV protons at 400°C and 500°C to doses of 3, 7, and 10 dpa. Prior austenite grain boundary (PAGB) compositions were measured with scanning transmission electron microscopy with energy dispersive X-ray spectroscopy (STEM/EDS). Preliminary results from the 400°C irradiation series show that Cr depletes at PAGBs in both HT9 and HCM12A, and enriches in T91. These results suggest that RIS behavior in F-M alloys may depend on the Cr composition. Results of RIS analysis on PAGB and packet boundaries at multiple doses and at both irradiation temperatures will be discussed in the context of the atomistic-based models of Cr segregation.



## Nanocomposite Materials: Nanoparticle Synthesis

Sponsored by: The Minerals, Metals and Materials Society, TMS Structural Materials Division, TMS Electronic, Magnetic, and Photonic Materials Division, TMS/ASM: Composite Materials Committee, TMS: Materials Characterization Committee, TMS: Nanomaterials Committee

Program Organizers: Jonathan Spowart, US Air Force; Judy Schneider, Mississippi State University; Bhaskar Majumdar, New Mexico Tech; Benji Maruyama, Air Force Research Laboratory

Monday AM Room: 3020  
February 16, 2009 Location: Moscone West Convention Center

Session Chairs: Benji Maruyama, US Air Force; Jonathan Spowart, US Air Force

### 8:30 AM Introductory Comments

#### 8:40 AM Invited

**Synthesis and Properties of DWCNT Composites:** *David Lashmore*<sup>1</sup>; <sup>1</sup>Nanocomp

The CVD growth of dual wall carbon nanotube sheets or textiles will be described. This growth process has been shown to produce very strong stand alone sheets or non-woven textiles that can be aligned after their growth. This post alignment process has a profound effect on the electronic and mechanical properties of the sheets. For example breaking strength for the randomly aligned as grown material is about 200 to 300 MPa, but following alignment breaking strength can increase to over 1 GPa. Similar changes in electronic properties will also be presented. The fabrication of composite materials from these sheets involves a high pressure infusion of the matrix. Data on elastomeric composites that exhibit a fracture toughness of over 60 J/gram will be described along with a number of practical applications both in the electronic area and for structural components.

#### 9:05 AM

**A Comparative Study on the Morphology of Strontium Hexaferrite Nano Particles Synthesis by Co-Precipitation Method and Modified Flux Method:** *Sachin Tyagi*<sup>1</sup>; <sup>1</sup>Indian Institute of Technology Roorkee

In the present study single phase M-type Strontium Hexaferrite nano crystals that is SrFe<sub>12</sub>O<sub>19</sub> were synthesized by Co-Precipitation and Modified Flux Method. Heat treatment conditions played an important role in the formation of pure SrFe<sub>12</sub>O<sub>19</sub> hexaferrite phase. Conventional heat treatment produced  $\alpha$ -Fe<sub>2</sub>O<sub>3</sub> and M phase for the particles synthesized by Co-Precipitation Method whereas Modified Flux Method produced single pure M- phase as confirmed by the X-ray diffraction (XRD). Surface morphology of non porous ultra fine particles has been examined by SEM. The material was annealed at 800°, 900° and 1000°C for 6 hours and its effect on the particles size is also studied. Room temperature magnetic properties were investigated using a Vibrating Sample Magnetometer (VSM) and decomposition behavior therein was investigated by means of thermal analysis (DTA/DTG/TG).

#### 9:25 AM

**Nano-Aluminum Based Polymeric Composites:** *Christopher Crouse*<sup>1</sup>; Stephanie Johnson<sup>2</sup>; Jared Boock<sup>2</sup>; C. Michael Lindsay<sup>2</sup>; Jennifer Jordan<sup>2</sup>; Jonathan Spowart<sup>1</sup>; <sup>1</sup>Air Force Research Laboratory, Materials and Manufacturing Directorate, Wright-Patterson Air Force Base; <sup>2</sup>Air Force Research Laboratory, Munitions Directorate, Eglin Air Force Base

Mass transport between reacting species typically governs the reaction kinetics in most energetic systems. The kinetics can be increased by manipulating specific features of the reactant materials such as overall surface area thereby reducing the diffusion distance between reactants. Ensuing from their large surface areas, nanoparticles have become promising candidates for energetic applications. Towards this end we have explored the development of nanoparticulate based composite materials with energy stored in the form of reactive metal nanoparticles (e.g. aluminum and nickel) capable of liberating energy through either a thermite process or intermetallic formation. Specifically we have focused on developing a chemical route towards the preparation of these materials through manipulation of the nanoparticle surface to allow for physical and chemical intimacy within a polymer matrix. Our initial efforts towards the

incorporation of aluminum nanoparticles within a poly(methyl methacrylate) matrix at varying volume percentages will be presented.

#### 9:45 AM

**Microstructure and Photoluminescence of NiO/Ni Core-Shell Nanorods on a Silicon Substrate:** *Chien-Ming Liu*<sup>1</sup>; Chih Chen<sup>1</sup>; <sup>1</sup>National Chiao Tung University

One-dimensional Ni/NiO core-shell nanorods with an average diameter around 70 nm were grown using anodic alumina oxide (AAO) as a template on a silicon substrate. First, area arrays of Ni nanorods were grown by electroless plating in the AAO pores. Then the Ni nanorods were oxidized in air to grow the Ni oxide on the surface of the Ni nanorods. After the oxidation process, the Ni nanorods were capped with a thin layer of NiO shell. The oxide layer was about 2-10 nm thick and the NiO shell consists of poly-crystals. Photoluminescence spectrum shows emission peak at 375 nm, which suggests that the NiO/Ni core-shell nanorods have potential application as UV a sensor.

#### 10:05 AM

**Synthesis Routes for the Production of Nanoscale Tungsten Powder:** *K. Scott Weil*<sup>1</sup>; Curt Lavender<sup>1</sup>; Lee Magness<sup>2</sup>; <sup>1</sup>Pacific Northwest National Laboratory; <sup>2</sup>Army Research Laboratory

Bench-scale testing has shown that tungsten nanocomposites may display the type of mechanical behavior required for use in a range of applications, including use in materials processing tools such as friction stir welding tips and long-life welding electrodes, as well as in munitions. However for these materials to be seriously considered for deployment, precursor fabrication (i.e. nanoscale powder synthesis) must be validated using approaches that are scalable to high-volume production. We will present results from our recent efforts to produce nanoscale tungsten powder by three different approaches and discuss the viability for each in terms of powder purity, size, and morphology; process scalability; and high density powder consolidation practice.

#### 10:25 AM Break

#### 10:40 AM Invited

**High-throughput Nanomaterial Fabrication, Characterization, and Consolidation:** *Christopher Haines*<sup>1</sup>; Deepak Kapoor<sup>1</sup>; Darold Martin<sup>1</sup>; <sup>1</sup>US Army ARDEC

ARDEC has established a pilot-scale facility for the fabrication, characterization, and consolidation of a wide range of nanomaterials. We employ inductively-coupled plasma and inert gas condensation to synthesize nanoscale powders in the 20 – 200 nm size range and a “top-down” milling approach to fabricate nanostructured powders. The versatility and high-production rate of our systems allow us to produce kilogram quantities of nanoscale and nanostructured powders of various metals and alloys, ceramics, cermets, and energetic materials. Fully-integrated, computer control of processing parameters provides the ability to precisely control the particle size and distribution of nanoscale powders. Beyond traditional characterization techniques such as x-ray diffraction and electron microscopy, we employ both small angle x-ray scattering (SAXS) and ultra-small angle x-ray scattering (USAXS). Processing of nanoscale and nanostructured powders to fully dense bulk nanostructured materials poses a much bigger challenge; therefore, novel powder consolidation techniques are being developed to overcome this issue.

#### 11:05 AM

**Industrial Production of Nanoparticle Masterbatches:** Steffen Pilotek<sup>1</sup>; Kerstin Grosse<sup>1</sup>; <sup>1</sup>Buhler Inc.

Inorganic oxide nanoparticles may be introduced into liquid product formulations using dispersions of high concentration. Due to the large specific surface area of colloidal systems, the compatibility of particle dispersion and product formulation needs to be specifically addressed. We use the chemomechanical process to produce nanoparticle masterbatches in industrial scale. In the process, agglomerated nanostructured powders are surface modified under well defined mechanical stress conditions. It enables the production of dispersions up to 60 wt.-% with a particle size of well below 100 nm. The chemical surface modification is a key component in providing a valuable masterbatch. The approach allows for chemical functionalization of the particles. The technical challenge lies in finding the right overall process parameters to manufacture a dispersion that is compatible and thus functional with respect to the product formulation. As reaction compartment, agitator bead mills are used which ensures that the masterbatches are available in ton-scale.

11:25 AM

**Preparation of Porous Ultra-Fine Fiber Fe-Ni Alloy Powder Precursor by Coordinated Co-Precipitation-Direct Reduction Process:** *Zhang Liang*<sup>1</sup>;

<sup>1</sup>Central South University

The precursor, prepared by coordinated co-precipitation with FeSO<sub>4</sub> and NiSO<sub>4</sub> as the raw materials, oxalate as the precipitator, and ammonia as the coordinator, was direct reduced by hydrogen to obtain porous ultra-fine fiber Fe-Ni alloy powder. The effects of parameters such as the concentration of reactants, pH value, additives, and reaction temperatures for precursor preparation and the reductive temperature, the composition of reductive atmosphere amid the reduction process were systematically investigated. The structure, thermodecomposition process and surface morphologies of the alloy powder derived from thermal reduction of the precursors were characterized by FTIR, XRD, TG/DSC and SEM. The experimental study shows that using 1(wt)%PVP as additive, well-dispersed precursors with a uniform morphology can be obtained in a solution with Fe<sup>2+</sup> and Ni<sup>2+</sup> concentration of 0.8 mol/L, pH value of 6.1 at 60°.

11:45 AM

**Microscopic and Spectroscopic Characterization of Cryomilled Nanostructure of Aluminum Alloy and B4C Powder:** *Clara Hofmeister*<sup>1</sup>; Bo Yao<sup>1</sup>; Helge Heinrich<sup>1</sup>; Yongho Sohn<sup>1</sup>; Cory Smith<sup>2</sup>; Mark van den Bergh<sup>2</sup>; Kyu Cho<sup>3</sup>; <sup>1</sup>University of Central Florida; <sup>2</sup>DWA Aluminum Composites; <sup>3</sup>US Army

Extensive attention has been paid to the production of tri-modal aluminum alloy composites that possess excellent strength and impact resistance. We have examined the microscopic and spectroscopic characteristics of nanostructured Al-5083 and B4C powder blends produced via large commercial scale cryomilling in liquid nitrogen. A blend of a commercial grade prealloyed Al-5083 and a commercial grade B4C powders were used as a precursor for the cryomilling. X-ray diffraction, scanning electron microscopy, transmission electron microscopy, X-ray photoelectron spectroscopy, Auger electron spectroscopy, laser dynamic scattering, and BET measurement were employed. Results from microstructural and spectroscopic characterization are presented and discussed with respect to production of tri-modal aluminum alloy composites.

12:05 PM

**Preparation of Ultra-Fine MgO•Al<sub>2</sub>O<sub>3</sub> Spinel Powder and Its Metallurgy Behavior in Low Carbon Steel:** *Yang Li*<sup>1</sup>; Wei-Jian Li<sup>1</sup>; Liang-You Wang<sup>1</sup>; Zhou-Hua Jiang<sup>1</sup>; <sup>1</sup>Northeastern University

Micron, sub-micron and nanometer sized MgO•Al<sub>2</sub>O<sub>3</sub> ultra-fine powder were prepared by gel precipitation, solid-phase synthesis, sol-gel and flame throwing pyrogeneration methods. XRD analysis shows that all of the ultra-fine powder is pure with a single MgO•Al<sub>2</sub>O<sub>3</sub> spinel phase. The size is measured by laser granularity analyzer and the average size is 60, 505 and 1780 nm with quite uniform distribution. MgO•Al<sub>2</sub>O<sub>3</sub> spinel powder with different granularity were sprayed into molten low carbon steel in MgO crucible and MoSi<sub>2</sub> furnace at 1873 K. Quantitative microscopic examination shows that big particle inclusions are reduced and small particle inclusions increased, and the average size is reduced. Data comparison from spraying different size powders shows that spraying MgO•Al<sub>2</sub>O<sub>3</sub> of nanometer tends to cause more small inclusions. The sprayed steel samples were rolled and heat treated for the mechanical properties tests, which shows spraying nanometer MgO•Al<sub>2</sub>O<sub>3</sub> is the best way to improve mechanical property.

**Neutron and X-Ray Studies of Advanced Materials: Resolving Local Structure**

Sponsored by: The Minerals, Metals and Materials Society, TMS Structural Materials Division, TMS/ASM: Mechanical Behavior of Materials Committee, TMS: Advanced Characterization, Testing, and Simulation Committee, TMS: Titanium Committee  
**Program Organizers:** Rozaliya Barabash, Oak Ridge National Laboratory; Yandong Wang, Northeastern University; Peter Liaw, The University of Tennessee; Jaimie Tiley, US Air Force

Monday AM

February 16, 2009

Room: 3016

Location: Moscone West Convention Center

*Session Chairs:* Andrea Gerson, University of South Australia; Wolfgang Pantleon, Risoe DTU

8:30 AM Keynote

**At the Limit of Polychromatic Microdiffraction:** *Gene Ice*<sup>1</sup>; Bennett Larson<sup>1</sup>; Jonathan Tischler<sup>1</sup>; Jae-Young Choi<sup>2</sup>; Wenjun Liu<sup>3</sup>; Deming Shu<sup>3</sup>; Ali Khounsary<sup>3</sup>; <sup>1</sup>Oak Ridge National Laboratory; <sup>2</sup>Pohang Accelerator Laboratory; <sup>3</sup>Argonne National Laboratory

With a high-energy 3rd generation source like the Advanced Photon Source (APS) it is possible to push the performance of polychromatic microdiffraction far beyond current levels and to approach the intrinsic limit of the technique based on sample damage and the diffraction limit of x-rays. We describe ongoing efforts to improve the spatial, temporal and momentum transfer resolution of polychromatic microdiffraction on beamline 34-ID-E at the APS. The goal of this effort is to provide high-resolution images of 3D crystal structures over sufficient volumes and with sufficient detail to understand the underlying physics of inhomogeneous mesoscale structural evolution. The performance of a new detector system and the development of more advanced focusing optics will be described and discussed in light of the ultimate limits set by the physics of x-rays and materials and in light of opportunities to field specialized insertion devices and optics for polychromatic microdiffraction.

9:00 AM Invited

**Evolution of Deformation Structures under Varying Loading Conditions Followed In-Situ by High Angular Resolution 3DXRD:** *Wolfgang Pantleon*<sup>1</sup>; Christian Weidemann<sup>1</sup>; Ulrich Lienert<sup>2</sup>; Bo Jakobsen<sup>3</sup>; Henning Poulsen<sup>1</sup>; <sup>1</sup>Risoe DTU; <sup>2</sup>Argonne National Laboratory; <sup>3</sup>Roskilde University

With the high angular resolution three-dimensional x-ray diffraction method (established at APS), individual subgrains are detected in the bulk of polycrystalline specimen and their dynamics is followed in-situ during varying loading conditions. Analysing the intensity distribution of a single Bragg reflection from an individual grain in reciprocal space, subgrains can be distinguished by their unique combination of orientation and elastic strain. Responses to different loading conditions are presented: During uninterrupted tensile deformation the subgrain structure develops intermittently. When the traction is terminated, stress relaxation occurs and number, size and orientation of subgrains are found to be constant. The structure freezes and only a minor clean-up of the microstructure is observed. Upon unloading the subgrain structure remains unchanged, but the compressive stresses of the subgrains increase in average. When changing the strain path, a systematic correlation between changes in the dislocation structure and the degree of strain path changes is established.

9:20 AM Invited

**Friedel-Pair Based Indexing Method of Individual Grains in Polycrystals Investigated with Hard X-Rays:** Marcin Moscicki<sup>1</sup>; Haroldo Pinto<sup>1</sup>; *Andras Borbely*<sup>1</sup>; Anke Pyzalla<sup>1</sup>; <sup>1</sup>Max-Planck Institut für Eisenforschung

A new procedure for characterizing the crystallographic orientation, spatial position and average strain tensor of single grains in the bulk of a polycrystalline sample is presented. It is complementary to existing indexing methods developed within the frame of three-dimensional X-ray diffraction (3DXRD). The algorithm uses detector coordinates corresponding to Friedel reflection-pairs (hkl and -h-k-l) and requires the measurement of diffraction spots in a relatively large interval of about 180°. The advantage of using Friedel pairs resides in their symmetry properties enabling a clear separation of the contributions from grain orientation, grain position and average strain to the position of the diffraction spots measured on a 2D detector. This leads to reduced number of unknown fitting parameters that have to be simultaneously considered and consequently to their higher

accuracy. The method is exemplified on experimental data obtained during in-situ straining of steel wires with 300  $\mu\text{m}$  in diameter.

#### 9:40 AM Invited

**In Situ Single Grain Peak Profile Measurements on Ti-7Al during Tensile Deformation:** *Ulrich Lienert*<sup>1</sup>; Matthew Miller<sup>2</sup>; Joel Bernier<sup>3</sup>; Matthew Brandes<sup>4</sup>; Michael Mills<sup>4</sup>; <sup>1</sup>Argonne National Laboratory; <sup>2</sup>Cornell University; <sup>3</sup>Lawrence Livermore National Laboratory; <sup>4</sup>Ohio State University

It has recently been demonstrated that the combination of focused high energy synchrotron radiation and area detectors provides a powerful tool for the structural in situ characterization of bulk polycrystalline materials on the single grain length scale. At the APS 1-ID beamline the 3DXRD technique has been extended to high reciprocal space resolution. Thus, not only can average strain tensors of individual grains be measured, but also intra-granular strains and misorientations. Here, measurements on Ti-7Al specimens are reported. Two very different dislocation structures are produced by annealing treatments. As evidenced by TEM, ice water quenching results in a random dislocation structure, while well ordered domains form by slow air cooling. Single grain strain tensors were measured up to 2% tensile deformation, and selected peaks were mapped with high resolution at selected loads and during relaxation. The sensitivity of the technique to the different dislocation structures will be discussed.

#### 10:00 AM Invited

**Measuring Local Strains and Composition in Nickel Alloys Using Synchrotron Radiation:** *Stewart McIntyre*<sup>1</sup>; Marina Suominen Fuller<sup>1</sup>; <sup>1</sup>University of Western Ontario

To predict the onset of Stress Corrosion Cracking in Alloy 600 requires knowledge of both mechanical and chemical changes. For the strain studies we are using Laue diffraction and micron-scale xray beams from a synchrotron. Diffraction patterns for each micron-sized area are indexed to yield maps that show grain orientation, composite elastic strain magnitudes as well as their directional components. Further, streaking of the diffraction spots when present, can be used to estimate the local dislocation density and the direction(s) of the slip systems. Our applications have focussed on local strain effects in polycrystalline Alloy 600 introduced by tensile extension or by placing calibrated scratches in the surface. While our current work uses APS, we are developing the VESPERS beamline at the Canadian Light Source for simultaneous micro-nd XRF measurements.

#### 10:25 AM Invited

**X-Ray Micro/Nano-Diffraction for Studies of Individual Nano-Objects:** *Wenjun Liu*<sup>1</sup>; Paul Zschack<sup>1</sup>; Matthew Bierman<sup>2</sup>; Song Jin<sup>2</sup>; John Budai<sup>3</sup>; Gene Ice<sup>3</sup>; <sup>1</sup>Argonne National Laboratory; <sup>2</sup>University of Wisconsin-Madison; <sup>3</sup>Oak Ridge National Lab

The rapidly evolving field of x-ray micro/nano-diffraction on 3rd generation synchrotron sources opens up new frontiers in x-ray studies for nano science. Taking advantage of high brightness of the source and state-of-the-art x-ray mirror focusing optics, 3D scanning polychromatic and monochromatic diffraction microscopy developed at 34-ID beamline at the Advanced Photon source (APS) could provide detailed local structural information, such as crystallographic orientation, grain morphology, strain tensor, and lattice structure in nano-materials, with high spatial resolution of 300 nm and angular resolution of 0.2 mrad. Recent applications in nano-materials science include studies of dislocation-driven crystal growth and twist mechanism in PbS pine-tree-like and PbSe helical nanowires, and crystal structural study of ZnO and EuAlO nanorods.

#### 10:45 AM Break

#### 10:55 AM

**A Grain-Subdivision Study of a Cyclically-Deformed Nickel-Based Superalloy Using Synchrotron X-Ray Micro-Beam Diffraction:** *E-Wen Huang*<sup>1</sup>; Rozaliya Barabash<sup>2</sup>; Gene Ice<sup>2</sup>; Wenjun Liu<sup>2</sup>; Peter Liaw<sup>1</sup>; Chung-Hao Chen<sup>4</sup>; <sup>1</sup>Department of Materials Science and Engineering, University of Tennessee; <sup>2</sup>Oak Ridge National Laboratory; <sup>3</sup>Argonne National Laboratory; <sup>4</sup>Department of Electrical Engineering and Computer Science, University of Tennessee

A newly-developed nickel-based superalloy is selected to study its fatigue behavior. The current study focuses on the local microstructure changes, which are responsible for the fatigue deformation, using the micro-beam technique at Argonne National Laboratory. The atomic structures of the cyclically-deformed superalloy can be studied as a function of the distance within one grain and

from adjacent grains. The polychromatic X-ray microbeam provides the local structural information from the Laue pattern, which reflects the number of geometrically necessary dislocations (GNDs). The Laue patterns demonstrate that the plastic deformation results in the formation of the alternating regions with high and low GND densities. The inhomogeneous plastic deformation of the cyclically-deformed specimen was observed using the synchrotron X-ray. The evolution of the dislocation substructure and local texture orientations within one grain and in the adjacent grains identifies the sequence of structural changes during the cyclic loadings.

#### 11:05 AM Invited

**Synchrotron-Based White/Monochromatic Beam Micro X-Ray Diffraction at the Advanced Light Source:** *Nobumichi Tamura*<sup>1</sup>; Martin Kunz<sup>1</sup>; Kai Chen<sup>1</sup>; <sup>1</sup>Lawrence Berkeley National Lab

BL 12.3.2 at the Advanced Light Source is a recently commissioned superconducting magnet beamline entirely dedicated to white/monochromatic beam micro X-ray diffraction for the measurement and mapping of strain/stress in engineered materials. The current status of the hardware and software of the beamline will be described and a few chosen applications will be presented.

#### 11:25 AM Invited

**The Application of Synchrotron Microdiffraction to Identify 3D Strains in High Performance Steel:** *Andrea Gerson*<sup>1</sup>; Ning Xu<sup>1</sup>; Joe Cavallaro<sup>1</sup>; <sup>1</sup>University of South Australia

The excellent mechanical properties achieved by modern steels are, in most part, attributable to advances in the thermal processing. Recently, with the advent of highly focused, high flux density X-ray beams from third generation synchrotron sources the study of the phase changes which take place during the processing of steels can be studied with a high degree of spatial resolution. We report on monochromatic synchrotron microdiffraction mapping of cryogenically treated tool steel (Advanced Photon Source synchrotron, end-station 34ID-E). Significant spatial inhomogeneity is apparent. The mean of each of the martensitic diffraction peak's FWHM for the most rapidly cooled cryogenically treated sample were the smallest of the samples examined. This treatment also displayed the smallest and most narrow d-spacing distribution. These results suggest that rapid cryogenic cooling results in better formed, more ordered and denser martensitic crystallites as compared to slow cryogenic cooling or no cryogenic treatment at all.

#### 11:45 AM

**The Effect of Residual Stress on Texture and Growth of Oxide Scale on Zirconium Alloys:** *Philipp Frankel*<sup>1</sup>; Richard Moat<sup>1</sup>; Efthymios Polatidis<sup>1</sup>; Michael Preuss<sup>1</sup>; <sup>1</sup>University of Manchester

Zr alloys are extensively used in PWRs as nuclear fuel cladding and structural fuel assembly components. The performance of the cladding material is strongly affected by its corrosion properties. Therefore, better understanding of the corrosion mechanisms is key to improving the degree of "burn-up" that can be sustained. This work investigates the effect of residual stresses on the crystallographic relationship between zirconium alloys and zirconium oxide formed in steam at elevated temperatures. It is believed that this relationship is very important to the growth kinetics of the oxide. High-Energy synchrotron X-ray measurements have been carried out at the ESRF, (Grenoble, France) with a ~1 micron spot size which allowed mapping of the residual stresses and texture in cross-sectional samples across the interface between the metal and the oxide. Therefore, texture of the oxide could be related to that of the metal and the residual stresses with distance from the interface.

#### 12:00 PM Invited

**Spatially Resolved Elastic Strains within Bulk Dislocation Cell Structures: Measurements and Models:** *Lyle Levine*<sup>1</sup>; Ben Larson<sup>2</sup>; Francesca Tavazza<sup>1</sup>; Jon Tischler<sup>2</sup>; Peter Geantil<sup>3</sup>; Michael Kassner<sup>3</sup>; Wenjun Liu<sup>4</sup>; <sup>1</sup>National Institute of Standards and Technology; <sup>2</sup>Oak Ridge National Laboratory; <sup>3</sup>University of Southern California; <sup>4</sup>Argonne National Laboratory

The existence and magnitude of long range elastic strains (and thus stresses) in dislocation cell interiors and walls in deformed metals have been the subject of extensive investigation for more than 20 years. We have used depth-resolved, submicrometer X-ray beams to directly measure the axial elastic strains within numerous *individual* dislocation cell interiors and cell walls in plastically deformed copper single crystals. As previously reported, the average cell interior strains are tensile in unloaded compression specimens and compressive in unloaded tensile specimens. Recent measurements from individual, buried



cell walls show that these have the reverse average strains. Most significantly, all of these cell interior and cell wall strains exhibit large cell-to-cell variations reminiscent of the misorientations across cell walls. The experimentally determined distribution functions describing these strain fluctuations will be presented along with theoretical models that explain their origin. Finally, local spatial correlations in the elastic strains will be discussed.

## Pb-Free Solders and Emerging Interconnect and Packaging Technologies: Fundamental Properties, Interfacial Reactions and Phase Transformation

Sponsored by: The Minerals, Metals and Materials Society, TMS Electronic, Magnetic, and Photonic Materials Division, TMS: Electronic Packaging and Interconnection Materials Committee

Program Organizers: Sung Kang, IBM Corp; Iver Anderson, Iowa State University; Srinivas Chada, Medtronic; Jenq-Gong Duh, National Tsing-Hua University; Laura Turbini, Research In Motion; Albert Wu, National Central University

Monday AM Room: 2020  
February 16, 2009 Location: Moscone West Convention Center

Session Chairs: Sung Kang, IBM Corp; Jeng-Gong Duh, National Tsing-Hua University

### 8:30 AM Introductory Comments by Sung K. Kang

#### 8:35 AM Invited

**The Next Phase in Pb-Free Solder Development in Electronic Packaging:** Darrel Frear<sup>1</sup>; <sup>1</sup>Freescale Semiconductor

Electronic Packaging has undergone tremendous change as a result of legislative actions restricting hazardous materials. One of the key elements targeted is Pb in eutectic Sn-Pb solder used to attach electronic packages to circuit boards. Through extensive efforts a variety of Pb-free solder alloys were successfully implemented for board attach applications. The next challenge is the extension of Pb-free solders for flip chip and die attach applications that use Pb-rich Sn-Pb solder and are currently exempted from legislative bans because there were no identified Pb-free solutions. There are still no drop-in Pb-free replacements for Pb-rich Sn-Pb but there are a number of innovative potential solutions ranging from new conductive adhesives to composite solder alloys to the complete elimination of solder as an interconnect. An overview of these materials and their performance will be presented along with a summary of future work required to eliminate all Pb from electronic packages.

#### 8:55 AM

**Preferred Orientation Relationships between Intermetallic Compounds and Substrate Metals in Reactive Wetting Reactions between Molten Sn-Based Solders and Metals:** Jong-ook Suh<sup>1</sup>; King-Ning Tu<sup>2</sup>; Nobumichi Tamura<sup>3</sup>; <sup>1</sup>Jet Propulsion Laboratory, California Institute of Technology; <sup>2</sup>University of California, Los Angeles; <sup>3</sup>Lawrence Berkeley National Laboratory

Crystallographic orientation relationships between intermetallic compounds and substrate metals are discovered by synchrotron micro x-ray diffraction studies. Cu<sub>6</sub>Sn<sub>5</sub> has six different preferred orientation relationships with Cu, which can be categorized into two groups due to pseudo-hexagonal crystal structure of the Cu<sub>6</sub>Sn<sub>5</sub>. Ni<sub>3</sub>Sn<sub>4</sub> has two types of preferred orientation relationships with Ni. If a single crystal metal with proper orientation is used as a substrate, morphology of intermetallic compounds can be greatly altered due to the preferred orientation relationships. Amount of the misfit between Ni<sub>3</sub>Sn<sub>4</sub> and Ni is greater than the misfit between Cu<sub>6</sub>Sn<sub>5</sub> and Cu. The difference in misfit explains morphological difference between Cu<sub>6</sub>Sn<sub>5</sub> and Ni<sub>3</sub>Sn<sub>4</sub>. The present study suggests that the existence of preferred orientation relationships can be a general mechanism in intermetallic compound formation by reactive wetting.

#### 9:10 AM

**Interfacial Reaction and Thermal Cycling Reliability of Zn-Sn High Temperature Lead-Free Solders:** Seongjun Kim<sup>1</sup>; Keun-Soo Kim<sup>1</sup>; Goro Izuta<sup>2</sup>; Katsuki Saganuma<sup>1</sup>; <sup>1</sup>Osaka university; <sup>2</sup>Mitsubishi Electric Corporation

High temperature solders containing 85-97 wt.% Pb have been widely used as die-attach solders in the power electronics packaging. In contrast to the middle temperature solders such as Sn-Ag-Cu alloy, however, little research has been done on high temperature lead-free solders to replace the high Pb

bearing solders. In the previous study, we suggested Zn-xSn (x=20, 30, and 40 wt.%) solders as one of the best candidates. To evaluate the possibility of this alloy further, we have investigated the interfacial reactions and thermal cycling reliability of a Si die attached joint with Zn-xSn solders. Si die (Au/TiN/Si) attachment was carried out on the direct copper bonded (DCB) substrates and direct aluminum bonded (DAB) substrates, which are used in a variety of power electronic systems. The changes of interface microstructure and joining strength were examined throughout the thermal cycling test up to 2000 cycles.

#### 9:25 AM

**Modification of the Interface Microstructures of Sn-3.5Ag/Cu Solder Joints by Zn Electroplating:** Youngkun Jee<sup>1</sup>; Jin Yu<sup>1</sup>; <sup>1</sup>KAIST

A Cu UBM is widely used as a surface finish for lead-free solder joints, however fast consumption of Cu, rapid growth of IMC and formation of Kirkendall voids pose serious reliability concern. In our previous study, additions of Zn to Sn-3.5Ag solder increased the reliability by replacing Cu-Sn IMC by Cu-Zn IMCs. The beneficial effects of Zn can be also achieved by modifying UBM rather than the solder composition, which is simpler and cheaper. In this study, the interface microstructure of Sn-3.5Ag / Cu joint was modified by electroplating varying amount of Zn on Cu UBM. As the amount of Zn dissolved in Sn-3.5Ag solder increased with the electroplated Zn thickness, Cu-Sn IMCs such as Cu<sub>6</sub>Sn<sub>5</sub> and Cu<sub>3</sub>Sn were replaced by Zn-containing IMCs such as Cu<sub>5</sub>Zn<sub>8</sub> and Ag<sub>5</sub>Zn<sub>8</sub>, which increased the drop reliability of solder joints significantly. Then, the results were compared with those of Sn-3.5Ag-xZn / Cu solder joints.

#### 9:40 AM

**Diffusion Behaviour of Zn during Reflow of Sn-9Zn Solder on Ni/Cu Substrate:** Jagjiwan Mittal<sup>1</sup>; Shih-Ming Kuo<sup>2</sup>; Yu-Wei Lin<sup>1</sup>; Kwang-Lung Lin<sup>1</sup>;

<sup>1</sup>National Cheng Kung University

Reflow behaviour of Sn-Zn solder on Ni/Cu substrate was investigated using different reflow conditions of 230°C in SMT scope. EDX studies of the reflowed samples showed high diffusion of Zn from solder to the intermetallic compounds (IMC) layer from 9 to 41 atomic percentages with the decrease in heating rates from 180°C/min to 90°C/min. Results demonstrated high interfacial activity and affinity of Zn in the formation of IMC. Reasons of this diffusion are related to the higher reactivity and smaller size of zinc in comparison to tin, phase separation during heating and affinity of Zn to form NiSnZn and Ni<sub>x</sub>Zn<sub>y</sub> intermetallic compounds. Detailed process study, possible mechanism and other related aspects will be presented

#### 9:55 AM

**The Effect of Thickness of Cu-Zn Solder Wetting Layer on the Intermetallic Growth:** Youngmin Kim<sup>1</sup>; Changyul Oh<sup>1</sup>; Hee-Ra Roh<sup>1</sup>; Young-Ho Kim<sup>1</sup>; <sup>1</sup>Hanyang University

Cu-Zn solder wetting layers developed recently were proven to suppress the excessive growth of intermetallic compound and formation of Kirkendall voids in Sn-Ag-Cu/Cu-Zn system. In this study, the effect of the thickness of the Cu-20wt% Zn layer has been investigated by varying the thickness of Cu-Zn layers ranging 2 to 10 μm. After reflowing Sn-4.0Ag-0.5Cu solder balls onto Cu-Zn layers, these were aged. The granular-like Cu<sub>6</sub>Sn<sub>5</sub> was formed at the Sn-4.0Ag-0.5Cu/Cu-Zn interface after reflow. As the thickness of Cu-Zn wetting layer increased, the IMC growth rate decreased. A typical bi-layer (Cu<sub>6</sub>Sn<sub>5</sub> and Cu<sub>3</sub>Sn) was formed on the Cu or Cu-Zn (2 μm) layer during aging. When the 6 or 10 μm-thick Cu-Zn layer was used, it was not completely dissolved and Cu<sub>3</sub>Sn, Kirkendall voids were not formed even after aging up to 1000 hrs. Since the interdiffusion between Sn and Cu was suppressed due to Zn in the wetting layer.

#### 10:10 AM

**Effect of Amount of Cu on the Intermetallic Layer Thickness between Sn-Cu Solders and Cu Substrate:** Md. Alam<sup>1</sup>; S. M. L. Nai<sup>1</sup>; Manoj Gupta<sup>1</sup>;

<sup>1</sup>National University of Singapore

In the present study, Sn-Cu solders were synthesized using pure tin with varying volume fraction of nano size copper (0% vol., 0.2 % vol., 0.35% vol., 0.7% vol. and 1.1 % vol.) by powder metallurgy route incorporating microwave assisted sintering. Intermetallic compound (IMC) layer formation between Sn-Cu solders and Cu substrate were investigated following reflow process. Samples were prepared by heating at 250 °C using hot plate. Results revealed that IMC layer thickness decreases with the addition of nano copper up to 0.35 vol. %. Beyond 0.35 vol. % copper addition, IMC layer thickness started to increase and maximum IMC layer thickness was found for Sn with 1.1 vol. % Cu. An attempt

is made in this study to correlate the effect of nano copper addition on the IMC layer thickness.

#### 10:25 AM Break

#### 10:40 AM Invited

##### **A Mechanism of Kirkendall Void Formation in Cu/Sn-3.5Ag Solder Joint:** Jin Yu<sup>1</sup>; Jong Yeon Kim<sup>1</sup>; <sup>1</sup>KAIST

In our previous work, residual S from the SPS additive in Cu electroplating bath was shown to play critical roles in Kirkendall void formation. Segregation of S to Cu/Cu<sub>3</sub>Sn interface lowered the interface energy thereby localizing Kirkendall voids at the interface. Once nucleated, Kirkendall voids can grow without the presence of external load leading to catastrophic drop failure of joints. In this work, a quantitative model on the Kirkendall void growth is presented based on classical Darken's analysis and the diffusive growth of cavities.

#### 11:00 AM

##### **Reaction Mechanism and Mechanical Property for the Flip Chip Sn-3.0Ag-0.5Cu Solder Bump with Ti/Ni-Cu/Cu under-Bump Metallization after Various Reflows:** Chung-Nan Peng<sup>1</sup>; Jeng-Gong Duh<sup>1</sup>; <sup>1</sup>National Tsing Hua Univ

Ni under bump metallization (UBM) has been widely used as the diffusion barrier between solder and Cu pad. In order to retard the fast dissolution rate of Ni UBM, the copper was added into Ni thin film. It is expected that the Ni-Cu UBM could provide extra Cu into solders to maintain Cu<sub>6</sub>Sn<sub>5</sub> IMC in the interface. Therefore, it could significantly decrease the Ni dissolution rate. In this study, the Cu content of the sputtered Ti/Ni-Cu/Cu UBM was varied from 0 to 20 at.% in Ni-Cu UBM. Sn-3Ag-0.5Cu solder was reflowed with Ti/Ni-Cu/Cu UBM for 1, 5, and 10 times. The amount of (Cu,Ni)<sub>6</sub>Sn<sub>5</sub> increased with increasing Cu contents in the Ni-Cu film. Cu concentration of the IMC was strongly dependent on the composition of the Ni-Cu films. The relationships between microstructure and strength of the solder with various reflow times were investigated and discussed.

#### 11:15 AM

##### **Interfacial Reactions in the Au/Sn/Cu Sandwich Couples:** Ching-feng Yang<sup>1</sup>; Sinn-wen Chen<sup>1</sup>; <sup>1</sup>National Tsing-Hua University

Au bumps are commonly used in the flexible electronic products. Cu tracks on flexible substrates protected by Sn surface finish are attached to the Au bumps, and the Au/Sn/Cu three-layer structure is thus frequently encountered. Interfacial reactions in the Au/Sn/Cu sandwich couples at 210°C were examined. The thickness of the Sn layer varied from 5, 7, 27 to 31µm. At the Sn/Cu interface, the phases formed were (Cu,Au)<sub>6</sub>Sn<sub>5</sub> and Cu<sub>3</sub>Sn. The phases formed at the Au/Sn interface were affected by the Sn layer thickness. Initially, AuSn, AuSn<sub>2</sub>, and AuSn<sub>4</sub> phases were formed when the Sn layer thickness was 7µm. When the Sn layer was 27 and 31µm, (Cu,Au)<sub>6</sub>Sn<sub>5</sub> phase was observed not only on the Sn/Cu side but also on the Au/Sn side. Besides, a ternary Au<sub>25</sub>Sn<sub>50</sub>Cu<sub>25</sub> phase is found in the AuSn<sub>4</sub> matrix. Electromigration effect on Au/Sn/Cu interfacial reactions is studied as well.

#### 11:30 AM

##### **Interfacial Reactions between In-Sn Solder and Ni-Fe Platings:** John Daghfal<sup>1</sup>; J. Shang<sup>2</sup>; <sup>1</sup>Institute of Metal Research; <sup>2</sup>University of Illinois at Urbana-Champaign

Ni-Fe platings are attractive device metallizations because of their unique thermal properties and good solderability. In this study, the interfacial reactions between the eutectic In-Sn solder alloy and Ni-Fe platings were examined as a function of reaction temperature, time and Fe content. Both the type and thickness of the reaction phases were found to depend strongly on Fe content in the Ni-Fe platings. Upon thermal aging, Fe-Sn intermetallic compound showed much slower growth kinetics than Ni-Sn compound. The reaction products were analyzed by considering both nucleation and growth of intermetallic compounds.

#### 11:45 AM

##### **Application of Cu-RuN Film as a Diffusion Barrier for UBM in the Electronic Packaging:** H. Y. Chuang<sup>1</sup>; C. H. Lin<sup>2</sup>; J. P. Chu<sup>3</sup>; C. Kao<sup>1</sup>; <sup>1</sup>National Taiwan University; <sup>2</sup>Chin-Min Institute of Technology; <sup>3</sup>National Taiwan University of Science and Technology

This paper reports the dissolution behavior of the RuN-bearing Cu film deposited by cosputtering. This copper film exhibits an extremely low dissolution rate in SAC solder. The consumption of the Cu-RuN film after 120 sec. is about

10 times lower than that of pure Cu. The dissolution resistance of Cu-RuN is even better than that of the commercial Ni-P layer. Consequently, this film is potentially useful as a diffusion barrier for under bump metallization. For a better understanding of the new method, thermal aging and wettability tests are also studied in the present work.

#### 12:00 PM

##### **The Peltier Effects upon Interfacial Reactions in the Soldering System:** Chao-hong Wang<sup>1</sup>; Sinn-wen Chen<sup>2</sup>; <sup>1</sup>National Chung Cheng University; <sup>2</sup>National Tsing Hua University

Interfacial reactions in the sandwich-type Sn/Co/Sn couples at 180°C were examined with and without passage of electric current. Only the CoSn<sub>3</sub> phase was formed at both the Sn/Co and Co/Sn interfaces. The thickness of the reaction layer at the Sn/Co interface where electrons flew from Sn to Co was similar to that in the couple without current; however, it was thinner than that at the Co/Sn interface where electrons flew from Co to Sn. Since the Sn flux resulted from electromigration was not in the same direction as that caused by the chemical potential gradients, the fact that it was thicker at the Co/Sn interface could not be explained by the electromigration effect. It was found that the temperature was higher at the Co/Sn interface and its difference was caused by the Peltier effect. It should be the reason why the reaction layer was thicker at the Co/Sn interface.

#### 12:15 PM

##### **Interfaces of Tin with Al-Cu-Fe Quasicrystalline Phase and Its Effect on Solidification Behavior of Tin:** Alok Singh<sup>1</sup>; Hidetoshi Somekawa<sup>1</sup>; An Pang Tsai<sup>2</sup>; <sup>1</sup>National Institute for Materials Science; <sup>2</sup>Tohoku University

Tin particles of micron size were embedded in Al<sub>63</sub>Cu<sub>25</sub>Fe<sub>12</sub> quasicrystalline matrix by rapid solidification and annealing. Interfaces were studied by TEM. Each tin particle made faceted interfaces with several quasicrystal grains in various orientations. At least five orientation relationships were determined, which matched close packed Sn planes 200, 101, 220 or 211 with fivefold or twofold planes of the quasicrystalline phase. Solidification behavior of the tin particles was studied by DSC. Tin particles showed multiple, mainly three, solidification peaks in the range 205°C to 185°C. Solidification nucleus contact angles were calculated to be 9.5°, 11° and 14°. In contrast, when the matrix phase was transformed to a microcrystalline phase, solidification involved only one peak, at about 192°C, with a contact angle of 11°. Interface structures and solidification behavior are compared with those reported for aluminum matrix. Interface formation and its effect on solidification behavior will be discussed.

## Peirce-Smith Converting Centennial Symposium: Historical Foundations/Refractory Practices

Sponsored by: The Minerals, Metals and Materials Society, TMS Extraction and Processing Division, TMS: Pyrometallurgy Committee  
Program Organizer: Joël Kapusta, Air Liquide

Monday AM

Room: 2009

February 16, 2009

Location: Moscone West Convention Center

Session Chairs: Joël Kapusta, Air Liquide; Tony Eltringham, BHP Billiton Base Metals

### 8:30 AM Welcome Address

### 8:40 AM Keynote

#### **William Peirce and E.A. Cappelen Smith and Their Amazing Copper Converting Machine:** Larry Southwick<sup>1</sup>; <sup>1</sup>LM Southwick & Assoc

This Peirce-Smith Converting Centennial symposium is celebrating the contributions of two men, William Peirce and E.A.C. Smith, in advancing technology allowing the copper industry to realize its full potential. However, theirs is representative of a larger story: New, simpler technology releasing the stranglehold of older, more complicated technology, new developments in vessel configuration and design finding alternate routes around dead ends in operability, advances in technique and concepts removing roadblocks of cycle time and capacity, and overall innovation opening up vast new reserves around the world to those companies willing to embrace those improvements. Our story is also one of personalities, stubborn smelters versus the innovators, those inside the industry versus those from outside. It is a story of an initial borrowing from

the steel industry, but also Peirce and Smith, from the refining end of the copper business, taking the ideas of Baggaley from Pittsburgh's steel and airbrake industry, who built on what Holloway, Manhès and David, Douglas, and others had done in smelter tests, further to compete with the previous primacy and closely held expertise of the copper smelters in Wales. These advances have been well recorded in photographs taken over the last 150 years. A number were submitted especially for this symposium. Many others were published in the mining and metallurgy press of the times. Several mining schools also retained copies of photos either taken during field trips, or donated to the school by alumni and operating companies. This presentation will provide a selection and discussion from these sources of "converters in action", describing the various designs, operations and developments depicted. The focus here will be on the first roughly 60 years of copper converter development, from Bessemer's days at the dawn of this new idea, up to and slightly past the time of initial adoption of Peirce and Smith's designs.

## 9:10 AM

**Before Peirce and Smith - The Manhes Converter and the Story of Its Development and Some Reflections for Today:** Albert Pelletier<sup>1</sup>; Phillip Mackey<sup>2</sup>; Larry Southwick<sup>3</sup>; Albert Wraith<sup>4</sup>; <sup>1</sup>Late of Montreal, Quebec; <sup>2</sup>Xstrata Nickel; <sup>3</sup>LM Southwick & Assoc; <sup>4</sup>A.E. Wraith

In 1881, the first commercial pneumatic Bessemer-type converter treating copper matte was successfully introduced by Pierre Manhes at the Eguilles copper plant near Vedène in France. This development followed over a year of testing on a smaller scale at a foundry in Vedène, during which the vertical tuyeres of the conventional Bessemer converter had been successfully replaced by horizontal tuyeres in an effort to avoid the freezing of copper which had occurred in the bottom of the vessel having vertical tuyeres. The Manhes Converter, as it became known, was the first successful large-scale adaptation of the Bessemer concept of using compressed air blown into a melt for metal refining and treatment. Within a few years, Manhes Converters utilizing horizontal tuyeres in either the original type of vertical converter, or a later and more enduring horizontal barrel converter, were in operation at over a dozen copper smelters around the world. It was this process that Messrs Peirce and Smith essentially improved with the introduction of the larger converter which bears their name and the development celebrated at this Symposium. The present paper briefly traces the original development by Pierre Manhes in the early 1880s and which set the stage for the later Peirce-Smith adaptation. The paper observes that the original development by Manhes was in part driven by the need to reduce coal (energy) consumption and hence the production cost in order for Eguilles to remain competitive with the larger plants in Swansea, Wales, where a ready supply of cheap coal helped keep smelter treatment terms of the day low. These themes are eerily resonant of today where booming copper production in China has impacted the industry, and also where energy consumption, closely linked to today's more familiar theme of 'climate change' remains an important challenge currently confronting the entire industry. The paper concludes with comments on these seemingly parallel situations today and offers some thoughts for the future.

## 9:30 AM

**Conflicts over Designs, Refractories and Awards: The First 20 Years of PS Experience:** Larry Southwick<sup>1</sup>; <sup>1</sup>LM Southwick & Assoc

This paper covers technical and other developments during the first 20 years of Peirce-Smith converting. There were numerous mechanical and process ideas and concepts already being developed and used by others that had possible application within the converter that Peirce and Smith were moving ahead with. There were also other converter configurations in which the basic lining and larger size concepts could function. Finally, as awards and honors began to accumulate, there were those who felt that contributions of other early workers were being ignored. The working out of these conflicts and differing directions will be described.

## 9:50 AM

**Converting and Refining – Experience in Ferrous and Non-Ferrous Metallurgy:** Theo Lehner<sup>1</sup>; Caisa Samuelsson<sup>2</sup>; <sup>1</sup>Boliden Mineral AB; <sup>2</sup>Lulea University of Technology

Converting and refining play a central role in the extraction of metals. Sweden has a long tradition as an experimental play ground for metallurgists, chemists and alchemists, developing new methods and technologies. Presenters of papers are usually happy in recording successful developments. But reporting failures can be as great a value as the former. In the paper experiments and experience in

process development are illustrated, differences between ferrous and non-ferrous developments are highlighted and industrial learning curves are discussed.

## 10:10 AM Break

## 10:30 AM

**Chrome-Magnesite Refractory Corrosion with Olivine Slag of High Cuprous Oxide Content:** Carolina Ramirez<sup>1</sup>; Patricio Ruz<sup>2</sup>; Gabriel Riveros<sup>1</sup>; Andrzej Warczok<sup>1</sup>; Robert Treimer<sup>3</sup>; <sup>1</sup>Universidad de Chile; <sup>2</sup>RHI Chile; <sup>3</sup>RHI AG

Continuous converting of copper matte produces slag with high cuprous oxide content. The corrosion of chrome-magnesite refractories with slag of high cuprous oxide content is a major problem. Properties of olivine type of slag make the slag very attractive for matte smelting and converting. Analysis of phenomena determining the slag infiltration into the porosity of a refractory and dissolution of refractory components in the slag allowed for better understanding of the mechanisms of refractory destruction. The results of laboratory scale tests of the olivine slag infiltration into open porosity and corrosion showed dominating effects of slag temperature and cuprous oxide content. The optical and X-ray examination of slag samples permitted the definition of the mechanism of formation of new phases and refractory deterioration.

## 10:50 AM

**Development of Refractory Practices for Peirce Smith Converters:** Jan Bäckström<sup>1</sup>; Martin Johann Hansel<sup>2</sup>; <sup>1</sup>Boliden Mineral AB; <sup>2</sup>RHI AG

Starting from historic perspectives on Converting at the Rönnskär Smelter, the continuous developments of refractory practice is described. In the development the joint efforts of operators and suppliers of refractory have lead to significant achievements. This paper comprises the development of the converting process and the refractory lining as well as future prospects regarding operation and refractory lining design, especially in the face of equipment and raw material availability.

## 11:10 AM

**Wear of Magnesite and Magnesite-Chromite Bricks in Vessels of the Non Ferrous Industry:** Robert Treimer<sup>1</sup>; <sup>1</sup>RHI AG

For all high temperature processes refractory linings are used, which are influenced by a number of different factors and mechanisms causing wear of these refractory linings. In vessels of the Non-Ferrous-Industry mainly magnesite and magnesite-chromite bricks are used where the wear behaviour is influenced by a number of different chemical, thermal or mechanical factors. Chemical wear factors are e. g. corrosion through infiltrated slag, matte or metal, SO<sub>2</sub>-diffusion, redox-reactions and hydration. Thermal wear factors are the temperature level and thermal shocks and mechanical wear factors are primarily erosion due to the movement of the metallurgical bath, impacts by charging and tuyere-punching. Mostly however, not only single wear factors are dominating, but rather a combination of different factors like thermo-mechanical impacts or thermo-chemical stresses are interacting simultaneously. The detailed knowledge of the different wear factors and their impacts to the refractory material is essential for recommendations of the suitable refractory material for a great variety of applications in the Non Ferrous Industry and for a successful further development of refractory solutions. This paper presents in detail the process steps of a PS-converter and the wear and impact to the refractory lining. Based on the knowledge of these operational parameters and the single wear factors the most suitable lining concept of RHI is presented.

## 11:30 AM

**Corrosion of Refractories in Peirce Smith Converters:** George Oprea<sup>1</sup>; Waiman Lo<sup>1</sup>; Tom Troczynski<sup>1</sup>; Joe A. Rigby<sup>2</sup>; <sup>1</sup>University of British Columbia; <sup>2</sup>RHI Canada

The refractory lining of the tuyere line in Peirce Smith converters have usually much shorter life in service than the rest of the lining, above or below it. There are already recognized chemical, thermal and mechanical factors which contribute to the wear of the lining. Our study presents the experimental results on microstructural changes occurring on these tuyere line bricks in a nickel-copper converter. The experimental bricks, after use at the tuyere line, were investigated using SEM/EDS and XRD techniques, to identify the mineralogical changes due to interactions with the nickel-copper matte or fayalite type slag at the process temperatures. The microstructural changes were correlated with physical and mechanical properties of the brick before and after use and a wear mechanism was suggested. Although the matte does not theoretically react with the mineralogical components of the brick, a partial oxidation of the Ni-Cu sulphides was identified using a line analysis by SEM/EDS in the densified layer



at the hot face, which allows for mineralogical changes at the matte-refractory interfaces, with a high probability of micro-crack formation due to the thermal cycling during use. These microcracks were also identified to open through intergranular fractures parallel to the hot face, which appeared to be the main cause of lost lining during use. The reactions between the fayalite slag and refractory brick could eventually play a role in chemical dissolution of the brick only in the superficial layer at the hot face, as no slag components were identified deep into the brick.

**11:50 AM Discussion**

### Phase Stability, Phase Transformations, and Reactive Phase Formation in Electronic Materials VIII: Session I

Sponsored by: The Minerals, Metals and Materials Society, TMS Electronic, Magnetic, and Photonic Materials Division, TMS: Alloy Phases Committee  
Program Organizers: Chih-ming Chen, National Chung-Hsing University; Srinivas Chada, Medtronic; Sinn-wen Chen, National Tsing-Hua University; Hans Flandorfer, University of Vienna; A. Lindsay Greer, University of Cambridge; Jae-ho Lee, Hongik University; Daniel J. Lewis, Rensselaer Polytechnic Institute; Kejun Zeng, Texas Instruments; Wojciech Gierlotka, AGH University of Science and Technology; Yee-wen Yen, National Taiwan University of Science and Technology

Monday AM                      Room: 2022  
February 16, 2009              Location: Moscone West Convention Center

*Session Chairs:* Chih-ming Chen, National Chung-Hsing University; Sinn-wen Chen, National Tsing Hua University

#### 8:30 AM Invited

**Whisker Growth Behavior of Tin and Tin Alloy Lead-Free Finishes:** *Katsuaki Sukanuma*<sup>1</sup>; *Keun-Soo Kim*<sup>1</sup>; *Sun-Sik Kim*<sup>1</sup>; *Alongheng Baated*<sup>1</sup>; *Kyoko Hamasaki*<sup>1</sup>; <sup>1</sup>Osaka Univ

As a result of the global transition to lead-free electronics, the majorities of the electronic component manufacturers are now using pure tin or tin-rich alloys for terminal and lead finishes. Not only because of lead-free, tin whiskers have been one of the serious failure causes for electronics and aerospace equipments. Tin whiskers spontaneously grow from tin based lead-free finished surfaces even at room temperature. Recent researches have revealed the mechanisms of Sn whisker formation and growth from pure tin plating at room temperature. Comparing with pure tin plating, some tin alloy plating was found to be rather immune to whisker formation. However, the mechanism of alloying effects on whisker formation is still unclear. In this study, tin whisker growth process was examined on the various tin alloy platings at room temperature. Sn-Bi plating on Cu substrate significantly suppressed the tin whisker formation compared with pure tin plating.

#### 8:50 AM

**Whisker Growth on Sn Plating with or without Surface Treatment during Heat and Humid Environments:** *Keun-Soo Kim*<sup>1</sup>; *Sun-Sik Kim*<sup>1</sup>; *Alongheng Baated*<sup>1</sup>; *Kyoko Hamasaki*<sup>1</sup>; *Katsuaki Sukanuma*<sup>1</sup>; *Masanobu Tsujimoto*<sup>2</sup>; *Isamu Yanada*<sup>2</sup>; <sup>1</sup>ISIR, Osaka University; <sup>2</sup>C. Uyemura & Co., Ltd.

Establishment of lead-free plating technology and whisker countermeasures is one of the critical problems remaining to be solved for lead-free electronics packaging. In our previous study, we reported on mitigation method of the Sn whisker by thin metal layer formation, such as Ni, Au, Pd, on pure Sn plating. Comparing with pure Sn plating, metal layer/Sn plating was much stable against Sn whisker formation in room ambient environment. In the current work, Sn whisker growth behavior of pure Sn plating and metal layer/Sn plating samples during 55°C/85% and 85°C/85% relative humidity (RH) exposure and thermal fatigue tests were investigated. Ni, Au and Pd layers with the thickness from 50nm to 200nm were deposited on matte Sn plating by flash-coating process. Ni, Au and Pd metal layer on Sn plating significantly suppressed the Sn whisker formation under the severe thermal and humid conditions.

#### 9:05 AM

**Study of Surface Oxidation of Sn(Ni, Ag, Si, In, Cu) Alloys:** *Yan You Li*<sup>1</sup>; *Cheng-Yi Liu*<sup>1</sup>; <sup>1</sup>National Central University

Surface oxidation of molten solder plays a very important role for the soldering wettability and wave soldering. Oxidation of molten Sn-base alloys is investigated. Five different metallic elements (Ni, Ag, Si, In, Cu) were alloyed with pure Sn and form Sn(M) alloys. The M doping ranges from 0.5wt.% to 10 wt.%. Sn(M) alloys were annealed at 600° for certain times. Then, the weight gain of Sn(M) were measured, which indicate the degree of oxidation of molten Sn(M) solder. Our preliminary results show that the Ag and In additive can retard the oxidation rate of Sn (M) solder. And, Cu additive can enhance the oxidation rate of Sn(Cu) molten solders, because the surface oxide scale has larger number of voids, which encourage oxygen diffuse inward easily. In this talk, the detail oxidation mechanism of kinetics on Sn(M) molten solders will be present and discussed.

#### 9:20 AM

**Fundamental Study on the Inter-Mixing between 95/5 High Lead Solder Bump and the 37/63 Pre-Solder on Chip-Carrier Substrates:** *Chih-Chiang Chang*<sup>1</sup>; <sup>1</sup>National Taiwan University

The microstructure of solder, as well as the formation and growth of intermetallic compounds, plays a critical role in the reliability of electronic packaging. In this study, we study the inter-mixing between the eutectic solder deposited over chip-carrier substrates and 95Pb5Sn solder bump. The interfacial reactions on the bump interface and the substrate interface are also studied. The reaction conditions include aging at 100, 130, 150, 175°C for 100, 500, 1000, 1500, or 2000hr. It is found that de-wetting occurred between UBM and high lead solder interface after five reflow. After 100 hr of aging, (Cu,Ni)<sub>6</sub>Sn<sub>5</sub>, Cu<sub>3</sub>Sn, and (Ni,Cu)<sub>3</sub>Sn<sub>4</sub> IMCs formed. Micro-voids formed between Cu<sub>3</sub>Sn and Cu interface were also identified at 150 and 175°C. At 100°C, however, micro-void formed only after aging for more than 1500 hr. The activation energy values for the growth of Cu<sub>6</sub>Sn<sub>5</sub>, Cu<sub>3</sub>Sn and Ni<sub>3</sub>Sn<sub>4</sub> were found to be 116, 67, and 88 kJ/mol, respectively.

#### 9:35 AM

**Sn Concentration Effect on the Massive Spalling in High-Pb/Cu Reaction:** *M.H. Tsai*<sup>1</sup>; *C.R. Kao*<sup>1</sup>; <sup>1</sup>National Taiwan University

Massive spalling of Cu<sub>3</sub>Sn intermetallic compound in high-Pb solders on bare Cu substrate during soldering reaction was investigated to understand the spalling phenomenon of intermetallics in various Sn-containing solders. High-Pb solder alloys of four compositions (0.5Sn-99.5Pb, 1Sn-99Pb, 3Sn-97Pb and 5Sn-95Pb) were soldered at 350°C for 1 to 20 minutes. For all solder compositions only Cu<sub>3</sub>Sn was observed at the interface between the solder and the substrate during soldering. When the Sn concentrations (0.5Sn and 1Sn) were low, the massive spalling occurred. However, spalling was not observed when the Sn concentrations (3Sn and 5Sn) were high until the soldering time was more than 10 minutes. The Cu-Sn-Pb phase diagram is used to rationalize this Sn concentration effect.

#### 9:50 AM Break

#### 10:10 AM Invited

**Assessment of Electromigration Effects at Copper Wire-Bonds:** *C. Wang*<sup>1</sup>; *H. Goddin*<sup>2</sup>; *A. Greer*<sup>1</sup>; <sup>1</sup>University of Cambridge; <sup>2</sup>TWI Ltd

The interfacial reactions of Cu wire-bonds on Al-based metallization have been studied. A sequence of intermetallic phases forms, the phase selection being influenced by the limited supply of Al. Ultimately, the bond is dominated by Cu with a graded concentration of Al in solution. There is no evidence for any formation of Kirkendall voids. To investigate electromigration effects, electrical currents of 500 mA were imposed on the Cu ball-bonds. Compounds formed at the Cu/Al interface in a sequence similar to that without currents. Electromigration appears to have a negligible effect on intermetallic growth at Cu/Al interfaces, in contrast to the strong electromigration effects found for reactions at Au/Al interfaces. Computational simulations of resistance changes of the Cu ball-bonds are consistent with the experimental results.

#### 10:30 AM

**Current-Induced Growth of Reaction Phases at Electroless Nickel/Tin Interfaces:** *Q. Yang*<sup>1</sup>; *P. Shang*<sup>1</sup>; *J. Guo*<sup>1</sup>; *Z. Liu*<sup>1</sup>; *J. Shang*<sup>2</sup>; <sup>1</sup>Institute of Metal Research; <sup>2</sup>University of Illinois at Urbana-Champaign

The microstructural transformations at the electroless nickel/tin interfaces following current stress were observed by scanning and transmission electron

microscopy. A clear polarity effect was found in the growth of the interfacial reaction phases. At the cathode side, intermetallic compounds (IMC) delaminated from the electroless Ni (EN) layer and drifted into the Sn phase with the electron wind force. While the total thickness of Ni-P and EN decreased at the cathode side, the Ni-P layer grew in thickness between the EN layer and Sn. At the anode, only slight increases in the IMC and Ni-P thickness were observed. Such polarity effect is shown to result from current-driven migration of reactive species.

## 10:45 AM

**Electromigration of Sn-Zn-Based Lead-Free Solders:** *Chih-ming Chen*<sup>1</sup>; Yumin Hung<sup>1</sup>; Chi-pu Lin<sup>1</sup>; <sup>1</sup>National Chung-Hsing Univ

Sn-Zn-based alloys are promising lead-free solders. Electromigration is an important reliability issue of solder systems. Electromigration of Sn-Zn-based solders were investigated under current stressing with a density of about 105 A/cm<sup>2</sup> at 80 to 140°. Two different cooling conditions, furnace and fan cooling, were used in the cooling process of reflow, and by which different microstructures developed in the solders. The furnace and fan-cooled solders displayed distinct electromigration behaviors, where lots of Sn extrusion sites were found in the furnace-cooled solder but the fan-cooled solder displayed a nearly unchanged microstructure. The effects of Bi and Cu addition into the Sn-Zn solder on the electromigration behavior were also investigated.

## 11:00 AM

**Effect of Current Density Distribution on the Formation of Intermetallic Compounds in Pb-free Solder Joints:** *Jung-Kyu Han*<sup>1</sup>; Luhua Xu<sup>1</sup>; Shih-Wei Liang<sup>2</sup>; King-Ning Tu<sup>3</sup>; Yi-Shao Lai<sup>3</sup>; <sup>1</sup>UCLA; <sup>2</sup>National Chiao Tung University; <sup>3</sup>Advanced Semiconductor Engineering

An investigation was carried out of the role of current density distribution in determining the formation of intermetallic compounds, using Pb-free flip-chip SnAgCu solder joints. In general, Cu atoms diffuse to the anode side in solder joints due to electromigration and evenly form intermetallic compounds along the contact area. When Cu trace on the substrate side was irregularly consumed, however, the shape of intermetallic compounds was changed to arc-shape at anode side. In this case, abnormal Cu trace consumption causes current density re-distribution in solder joints. Since Cu atoms migrate faster along high current density regime than low current density regime, the change of current density distribution affects the shape of intermetallic compounds. The simulation data of current density distribution is also in good agreement with the experimental results.

## 11:15 AM

**Critical Product of Electromigration in Cu-Sn Intermetallic Compounds:** *Luhua Xu*<sup>1</sup>; *Jung-Kyu Han*<sup>1</sup>; *Shih-Wei Liang*<sup>1</sup>; *Di Xu*<sup>1</sup>; *Masaru Fujiyoshi*<sup>2</sup>; *K.N. Tu*<sup>3</sup>; <sup>1</sup>University of California, Los Angeles; <sup>2</sup>Hitachi Metal Ltd, Japan

The properties of intermetallic compound become more important with the trend in reducing solder joint size. This is because the thickness of UBM as well as the reflow temperature will remain the same while the bump size decreases. Thus the volume fraction of IMC formation in the solder joint will increase greatly. For example, when the solder joint size decreases from 100 to 50 and to 25 micron, the volume will decrease 8 to 64 times, respectively. As a result, intermetallic compound (IMC) could occupy the entire solder joint which can become a pure intermetallic joint. The properties of intermetallic (i.e., Cu<sub>6</sub>Sn<sub>5</sub> + Cu<sub>3</sub>Sn) were characterized in this study. Electromigration behavior and critical product of the intermetallic compound is investigated by employing the V-groove solder joint samples. It was found that the critical product of Cu<sub>6</sub>Sn<sub>5</sub> IMC is at least one order of magnitude higher than that of SnAgCu solder.

## 11:30 AM

**Polarity Effect of the Growth of Intermetallic Compound in SnAgBiIn Pb-Free Solder under Electromigration:** *Albert Wu*<sup>1</sup>; *Kuo-Hao Sun*<sup>1</sup>; <sup>1</sup>National Central University

The Pb-free SnAgBiIn solder strips were prepared in the Si(001) U-grooves to investigate the behaviors under electromigration. The Cu electrodes were electroplated in the grooves and the solders were consequently reflowed between the electrodes. The samples were tested under various temperatures and current densities. The thickness of the compounds at both interfaces between the solders and the Cu electrodes were measured. The changes of the thickness with times were recorded. The compositions of the intermetallic compounds were analyzed by EPMA. The kinetics of the growth of the compounds is discussed in this paper.

## Recent Advances in Thin Films: Process-Property Correlations

Sponsored by: The Minerals, Metals and Materials Society, TMS Electronic, Magnetic, and Photonic Materials Division, TMS: Thin Films and Interfaces Committee  
Program Organizers: Nugehalli Ravindra, New Jersey Institute of Technology; Gregory Krumdick, Argonne National Laboratory; Choong-un Kim, University of Texas; Narsingh Singh, Northrop Grumman, ES

Monday AM

February 16, 2009

Room: 3011

Location: Moscone West Convention Center

Session Chairs: Nugehalli Ravindra, New Jersey Institute of Technology; Choong-un Kim, University of Texas

## 8:30 AM Introductory Comments

### 8:40 AM Invited

**A Microstructural Characterization of Ta-Based Thin Films for Cu Metallization:** *Julien Nazon*<sup>1</sup>; *Marie-Hélène Berger*<sup>2</sup>; *Thierry Sauvage*<sup>3</sup>; *Jean-Claude Tedenac*<sup>1</sup>; *Nicole Fréty*<sup>4</sup>; <sup>1</sup>Institut Charles Gerhardt - Université Montpellier II; <sup>2</sup>Centre des Matériaux P.M. Fourt - Ecole des Mines de Paris; <sup>3</sup>CEMHTI - UPR3079 CNRS; <sup>4</sup>Institut Charles Gerhardt - Université Montpellier II

Advances in microelectronic and thermoelectric device technologies are dependent on the development of new barriers against the diffusion of electrical wiring copper. In the present work, the efficiency of tantalum-based thin films was investigated through a microstructural approach associated to the measurement of the electrical resistivity. The properties of TaN(75nm)/Ta(75 nm) and TaN(50 nm)/Ta(50 nm)/TaN(50 nm) multilayer thin films have been studied and compared to that of TaN(150 nm) single layers. These thin films were deposited onto silicon substrates by radio-frequency reactive sputtering. The microstructure was characterized using Glancing Angle X-Ray Diffraction, Scanning and Transmission Electron Microscopies and Rutherford Backscattered Spectrometry. The diffusion mechanisms were studied after vacuum annealing in the 773-973K temperature range using these characterization techniques. The results pointed out the interest of a multilayered thin films structure in the improvement of the diffusion barrier properties.

### 9:10 AM

**A Statistical-Thermodynamic Modeling of Behavior and Properties in Thin-Film Intermetallic L12- and D019-Structures:** *Olga Semenova*<sup>1</sup>; *Regina Krachler*<sup>1</sup>; *Sabine Knott*<sup>1</sup>; <sup>1</sup>University of Vienna

Modeling of behavior of thin films under various technological states is of paramount importance, since these compounds are fascinating group of materials, from point of view of fundamental properties and practical applications. Statistical-thermodynamic modeling based on Ising approach and Bethe-Bragg-Williams random-mixing approximations is proposed for description of thermodynamic behavior and ordering phenomena in many layers nano-crystalline materials with L12- and D019-structure. It includes description of Long-Range and Short-Range Ordering in crystal lattice. Obtained theoretical results are tested using experimental data on thermodynamic and structural properties of bulk intermetallics Ni<sub>3</sub>Ga, Ni<sub>3</sub>Al, Ti<sub>3</sub>Al. Degree of long-range order and critical transition temperatures were predicted and compared to experimental data. Proposed approach and obtained results can be applied to process of new advanced materials discovery and development, these may help address a challenge of rapid and accurate optimization in solution of many fundamental and technological problems, which are not able to be solved experimentally.

### 9:30 AM Invited

**Corrosion Properties of Chromized Tungsten Carbide Materials:** *Jyh-Wei Lee*<sup>1</sup>; *Jai-Lin Li*<sup>1</sup>; *Yu-Ting Lin*<sup>1</sup>; <sup>1</sup>Tungnan University

Tungsten carbide (WC) materials have been widely used in industries due to their high hardness and excellent wear resistance. However, poor corrosion resistance of WC material in the acid solution is found due to the selective corrosion of cobalt binder. A novel chromized thin film has been produced on the surface of tungsten carbide by pack cementation process at 900°C. A thin film mixture containing chromium nitride and chromium carbides was revealed. The corrosion resistances of untreated substrate and chromized WC materials

under various chromizing conditions in sulfuric acid solution were investigated. It is observed that the novel chromizing thin film provides excellent corrosion resistance to the cobalt contained WC substrate. Nevertheless, selective corrosion attack on the surface defects of chromizing thin film was found.

**10:00 AM**

**Crystallization Structure and Annealed Effect of Ni-Doped Sn-Al Thin Films on Electromagnetic Interference Shielding Characteristics:** *Hung Fei-Shuo*<sup>1</sup>; Fei-Yi Hung<sup>2</sup>; Chiang Che-Ming<sup>1</sup>; Lui Truan-Sheng<sup>3</sup>; <sup>1</sup>Department of Architecture, National Cheng Kung University, Tainan; <sup>2</sup>Institute of Nanotechnology and Microsystems Engineering, Center for Micro/Nano Science and Technology, National Cheng Kung University, Tainan; <sup>3</sup>Department of Materials Science and Engineering, National Cheng Kung University, Tainan

Electromagnetic interference (EMI) is a new form of pollution discovered in recent years. The elements Sn and Al not only possess EMI shield efficiency, but also have acceptable costs. In this study, sputtered Sn-Al thin films with Ni doped (0–9 at.%) were used to investigate the effect of the crystallization mechanism and film thickness on the electromagnetic interference (EMI) characteristics. In addition, the annealed microstructure, electrical conductivity and EMI of the Sn-Al films and the Ni-doped Sn-Al films were compared. The results show that Sn-Al film increased the electromagnetic interference (EMI) shielding after annealing. For the Ni-doped Sn-Al films with higher Ni atomic concentration, the low frequency EMI shielding could be improved. After annealing, the Sn-Ni and Al-Ni intermetallic compound (IMC) of thin film distributed in the matrix. This metallurgical effect not only enhanced the diffusion of atoms to the grain boundaries, but also promoted the high frequency EMI shielding.

**10:20 AM Break****10:40 AM**

**Effect of Sputtering Conditions and Post-Annealing on Internal Structure and Electrical Properties of Titanium-Oxide Thin Films:** *Masanari Tomozawa*<sup>1</sup>; Masashi Mikami<sup>1</sup>; Kimihiro Ozaki<sup>1</sup>; Keizo Kobayashi<sup>1</sup>; Toshimasa Miyazaki<sup>2</sup>; <sup>1</sup>National Institute of Advanced Industrial Science and Technology; <sup>2</sup>Tayca Corporation

Titanium-oxide thin films were deposited onto glass substrates by magnetron-sputtering. A target material consisted of TiO and Ti6O11. Deposition was carried out under various applied voltage, Ar gas pressure and sputtering time. Thickness, internal structure and electrical resistivity of the thin films were investigated. Thickness of the thin films increased with increasing applied voltage, Ar gas pressure or sputtering time under our experimental conditions. The thin films deposited under lower Ar gas pressure were mainly composed of Ti6O11. On the other hand, those deposited under higher Ar gas pressure were composed of Ti6O11 and TiO. Vacuum annealing after deposition also produced TiO phase in the thin films. Formation of TiO phase lowered electrical resistivity of the thin films.

**11:00 AM**

**Evolution of Annealing Twins in Thin Film Microstructures:** *ChangKyoo Yoon*<sup>1</sup>; David Field<sup>1</sup>; <sup>1</sup>Washington State Univ

The characteristic microstructure of a thin film affects its function in electronic applications. Modern Cu films and line structures often contain a large fraction of annealing twins that change the crystallographic texture and grain boundary character distribution in these structures. Annealing twin evolution is often overlooked or ignored in models of grain growth such as the conventional Monte Carlo simulation (Potts model). In this work, texture and grain structure evolution is modeled using Potts model according to the overall energy minimization model. Specific criteria are introduced to nucleate and grow twin boundaries. Simulation results are compared with observation of structure evolution in Cu and Ni films as a function of film thickness and annealing temperature.

**11:20 AM**

**Phase-Field Modeling of Thin Film Growth: Applications to Step and Island Dynamics:** *Zhengzheng Hu*<sup>1</sup>; Shuwang Li<sup>1</sup>; Steven Wise<sup>2</sup>; John Lowengrub<sup>1</sup>; Axel Voigt<sup>3</sup>; <sup>1</sup>University of California, Irvine; <sup>2</sup>University of Tennessee; <sup>3</sup>TU Dresden

A phase-field model is presented to simulate the dynamics of step flow and small islands during epitaxial growth. Asymmetric kinetics rates and edge diffusion are incorporated. Moreover, a modified free energy function and a corrected initial phase variable are given to efficiently capture the morphological evolution. Our recent study on step flow matches with results presented by Frank Haußer et al., based on a front tracking method. In the long wavelength

regime, we observe meandering with a wavelength being determined by the linear instability and endless growth of the amplitude. Whereas in the shorter wavelengths, we observe coarsening due to the competition between different wavelengths. We also observe mushroom formation, subsequent pinch-off leading to the formation of a vacancy island. When apply our model to the island dynamics, our simulations confirm the linear stability results of Hu et al., and reveal the possibility of shape control in nanoscale.

**11:40 AM**

**Stress-Driven Surface Instabilities in Solids with Diffusing Charged Defects:** *Steven Henke*<sup>1</sup>; P. Chung<sup>2</sup>; A. El-Azab<sup>1</sup>; M. Grinfeld<sup>2</sup>; <sup>1</sup>Florida State University; <sup>2</sup>US Army Research Laboratory

Stress-driven rearrangement instability (SDRI) theory postulates that diffusion in stressed solids can lead to surface morphological instability, an effect that is currently believed by many physicists to be real and important for elevated-temperature deposition or annealing of thin films. Both atomic surface diffusion and bulk diffusion of point defects contribute to the instabilities. The stress-driven diffusion of mobile oxygen vacancies in the bulk is especially important in ferroic perovskite films (e.g., Barium Strontium Titanate), which have desirable optical and electric properties for device and sensor applications, and often require well-controlled surfaces and interfaces. We present a continuum reformulation of the SDRI theory that includes the coupled electro-elastic diffusion of oxygen vacancies and introduce a 3D finite-element scheme to solve the equations for film surface evolution. We also explore the stability of the film boundary due to perturbations and attempt to characterize the incipient instabilities in terms of the model parameters.

---

## Recycling of Electronic Wastes: Life Circle Analysis and Environmental Issues

Sponsored by: The Minerals, Metals and Materials Society, TMS Extraction and Processing Division, TMS Light Metals Division, TMS Materials Processing and Manufacturing Division, TMS: Recycling and Environmental Technologies Committee  
Program Organizers: Lifeng Zhang, Missouri University; Fay Hua, Intel Corp; Oladele Ogunseitan, University of California, Irvine; Gregory Krumdick, Argonne National Laboratory

Monday AM

Room: 2024

February 16, 2009

Location: Moscone West Convention Center

Session Chair: Gregory Krumdick, Argonne National Laboratory

---

**8:30 AM Introductory Comments****8:35 AM**

**Closed Loop WEEE Recycling? Challenges and Opportunities for a Global Recycling Society:** *Christina Meskers*<sup>1</sup>; Christian Hagelueken<sup>1</sup>; <sup>1</sup>Umicore

End-of-life Electronic and Electrical Equipment (WEEE) is unjustly regarded as mainly a waste management problem. What is structurally overlooked is the enormous resource impact of these devices. EEE represents a tremendous metal resource, which should be utilized through effective recycling, which has a much lower environmental footprint than primary production. The actual amount of end-of-life EEE recycled today is embarrassingly low since insufficient EEE is collected and part of the collected EEE is exported to developing countries, where it is largely not entering official recycling systems. To achieve a global recycling society issues like technology, economics, life cycle structure, stakeholder awareness and legislation have to be addressed in a global, co-operative manner so that sustainable closed product cycles can be obtained. Requirements for a "global recycling society" are defined to address today's reality of global flows of used consumer products, taking into account the likely needs of the future.

**8:55 AM Question and Answer Period****9:05 AM**

**Life Cycle Analysis for Recovered E-Wastes:** *Ociléide Custódio da Silva*<sup>1</sup>; Diego Blanco<sup>2</sup>; <sup>1</sup>INdT; <sup>2</sup>UEA

The use of recovered e-waste has been evaluated in order to reach environmentally friendly solutions for the end of life of electronic products. However, to assure the performance of these recovered products is necessary to understand the critical points affecting the reliability and final characteristics



of them. This work uses life cycle assessment as methodology to evaluate the performance of e-waste from electronic devices. The following materials were evaluated: polymers and metals. The life cycle of these materials were assessed from cradle to grave. The degradability of the materials was analyzed by environmental tests to complement the evaluation of the end of life of the materials studied. According to the results, the materials analyzed may be considered to be a good option for manufacturing different products if obstacles, such as processing parameters, can be overcome.

## 9:25 AM Question and Answer Period

### 9:35 AM

#### **Toxicity Screening for Materials Selection in the Printed Wiring Board Industry:** *Carl Lam*<sup>1</sup>; Julie Schoenung<sup>1</sup>; <sup>1</sup>University of California, Davis

In order to support the decision process of toxics use reduction in manufacturing and design of product systems, it is pertinent to provide a rigorous and up-to-date method in efficiently screening and scoring a material's hazard based upon its potential human health toxicity and exposure. Similar to that of EPA's Use Cluster Scoring System (UGSS) and Risk Screening Environmental Indicators (RSEI) models, publicly available toxicity data sources are utilized in this screening model. Example analyses of metals commonly used in the printed wiring board manufacturing industry (such as lead, copper, tin, zinc and others) are presented to illustrate the evaluation methodology. Statistical analysis on the reliability of the various toxicity data will provide better insight and quantification of uncertainties in the scoring methodology. The end result has potential to expand traditional life cycle analysis in the human health effect categories to provide error reporting at its foundation.

## 9:55 AM Question and Answer Period

### 10:05 AM

#### **Engineering Environmentally-Benign Electronics: Convergent Optimization of Materials Use, Consumer Participation, and Government Regulation:** *Oladele Ogunseitan*<sup>1</sup>; Jean-Daniel Saphores; Julie Schoenung<sup>2</sup>; Andrew Shapiro<sup>1</sup>; <sup>1</sup>University of California, Irvine; <sup>2</sup>University of California, Davis

Sustainable strategies to reduce the public and environmental burden of hazardous materials associated with discarded electronic products will require coordination of efforts ranging from selective use of materials in product design, consumer behavior toward recycling, to trans-boundary regulatory incentives. Our project adopted the cellular phone for a model for addressing the knowledge gaps and policy discrepancies that contribute to continuing risks associated with electronic waste. This presentation focuses on progress and emerging solutions according to five specific objectives: (a) Development of an integrative environmental burden model (EBD) for chemicals associated with the designation of these products as post-consumer hazardous waste. (b) Identification of alternative materials to replace hazardous constituents according to the EBD and current policies. (c) Estimation of the cost and performance differentials between the alternative materials and current CE constituents. (d) Survey of consumer willingness to participate in e-waste management practices (e) Comparative assessment of regulatory policy designs.

## 10:25 AM Break

### 10:45 AM

#### **Modeling the Impact of Physical System Architecture on Recycling System Performance:** *Jeffrey Dahmus*<sup>1</sup>; Elsa Olivetti<sup>1</sup>; Susan Fredholm<sup>1</sup>; Jeremy Gregory<sup>1</sup>; Randolph Kirchain<sup>1</sup>; <sup>1</sup>Massachusetts Institute of Technology

As recycling systems for waste electronics become more widespread, understanding and characterizing the key determinants of economic and environmental performance becomes critical. One such determinant is physical system architecture, which in turn has a profound impact on material recovery rates. The work presented here examines the effect of system architecture on the economic and environmental performance of electronics recycling systems. Such architectural decisions greatly impact the economic performance, affecting costs, such as those associated with collecting and transporting end-of-life electronics, as well as revenues, such as those associated with the amount of saleable material recovered. Environmental performance, including the trade-off between the burdens of collecting and transporting waste electronics and the benefits of recovering and recycling materials, is also greatly affected by system architecture. The work presented here uses network models, process-based cost models, and lifecycle analysis tools to evaluate the impact of system architecture on recycling system performance.

## 11:05 AM Question and Answer Period

### 11:15 AM

#### **Human Health and Ecosystem Toxicity Potentials of Waste Electronic Devices:** *Seong-Rin Lim*<sup>1</sup>; Julie Schoenung<sup>1</sup>; <sup>1</sup>University of California, Davis

The objective of this study is to evaluate human health and ecosystem toxicity potentials from heavy metals in e-waste, i.e., laptop computers, LCD monitors, LCD TVs, plasma TVs, and CRT TVs. These toxicity potentials are evaluated by using heavy metal contents from the literature (California Department of Toxic Substances Control, 2004; Matsuto et al., 2004) and their toxicity characterization factors from the US EPA Tool for the Reduction and Assessment of Chemical and other environmental Impacts (TRACI). The toxicity potential from the plasma TVs are more significant than those from the LCD-related devices but less than those from the CRT TVs with the exception of ecotoxicity through water. The cancer potential is primarily from lead; the noncancer potential is primarily from lead and copper; and the ecotoxicity is primarily from copper. Therefore, e-waste management policy should focus on recycling and elimination of lead and copper.

## 11:35 AM Question and Answer Period

### 11:45 AM

#### **A Review of Electronic Waste (e-Waste) Recycling Technologies "Is e-Waste an Opportunity or Treat?":** *Muammer Kaya*<sup>1</sup>; <sup>1</sup>Osmangazi University

The electronic industry is the world's largest and fastest growing manufacturing industry. As a result of this growth, combined with rapid production obsolescence, discarded electronics or electronic waste begin a serious solid waste problem in the world. Electronic waste is the most rapidly growing waste and contains over 1000 different substances. It is a crisis not only of quantity but also a crisis born from toxic ingredients- such as Pb, Be, Hg, Cd, Cr+6 and BFRs that pose both occupational and environmental health treat upon disposal. E-waste market will exceed 11 billion \$ in 2009 in the world. This paper reviews the e-waste problem in the world, describes existing collection, dispose and recycle techniques for glass, plastics and metals and covers the legislations and finance for environmental friendly solutions and for sustainable development. Current situations of scrap automobile accumulators/household batteries recycle in Turkey are presented as a case study.

## 12:05 PM Question and Answer Period

### **Shape Casting: Third International Symposium: Properties**

Sponsored by: The Minerals, Metals and Materials Society, TMS Light Metals Division, TMS: Solidification Committee, TMS: Aluminum Processing Committee  
Program Organizers: John Campbell, University of Birmingham; Paul Crepeau, General Motors Corp; Murat Tiryakioglu, Robert Morris University

Monday AM

Room: 2011

February 16, 2009

Location: Moscone West Convention Center

Session Chair: Glenn Byczynski, Nemak Europe GmbH

## 8:30 AM Introductory Comments

### 8:35 AM

#### **Intrinsic and Extrinsic Metallurgy:** *John Campbell*<sup>1</sup>; <sup>1</sup>University of Birmingham

Physical metallurgy has been highly successful in describing the nucleation and growth of dense phases occurring during solidification of metals. The limitations of intrinsic metallurgy are seen mainly in the presence of pores and cracks that lead to various kinds of failure in materials, but which cannot be explained by intrinsic mechanisms. For instance solidification as a simple phase change is unable to nucleate a pore or a Griffiths crack (by either homogeneous or even by heterogeneous nucleation) because of the extremely high interatomic forces, as supported by much excellent theoretical and experimental evidence. Only defects entrained from the outside can explain the occurrence of volume defects such as pores and cracks, and therefore provide understanding of the fundamental causes of failures in tensile, creep, fatigue modes, and probably some types of corrosion pitting failures. An accurate metallurgical understanding of cast and wrought alloys requires both intrinsic and extrinsic contributions.

9:00 AM

**Quality Indices for Cast Aluminum Alloys:** *Murat Tiryakioglu*<sup>1</sup>; John Campbell<sup>2</sup>; <sup>1</sup>Robert Morris University; <sup>2</sup>University of Birmingham

Several indices are available in the literature to assess the structural quality of cast Al alloys, especially Al-7%Si-Mg alloys, based on tensile test results. Some of these indices, most notably the one developed by Drouzy et al. provide a number that do not necessarily have a physical meaning, while the others are a measure of what fraction of the expected tensile property is achieved. These indices are discussed and the concept of maximum potential ductility is introduced. A new quality index that uses this maximum ductility potential concept is introduced for Al-7%Si-Mg as well as Al-Cu alloys.

9:25 AM

**Use of 'Standard' Molds to Evaluate Metal Quality and Alloy Properties:** *Geoffrey Sigworth*<sup>1</sup>; Tim A. Kuhn<sup>1</sup>; <sup>1</sup>Alcoa Primary Metals

Several mold designs have been proposed as standards for aluminum castings. The two most commonly used in North America are the ASTM B108 test bar, and a 'step' casting proposed by the Aluminum Association (AA). The history of these molds is reviewed briefly and mechanical properties are presented for A356-T6 alloy castings. The B108 test bar is prone to shrinkage. Measures that help to minimize this shrinkage are discussed. The AA mold is also prone to shrinkage, but a judicious selection of sample locations avoids much of the problem. In spite of their limitations, the two molds can be used to evaluate melt treatment procedures and metal quality in the foundry. Data from casting trials are presented for both molds.

9:50 AM

**Properties of B356-T6 Aluminum Cast via Permanent Mold and Advanced Squeeze Cast (ASC) Processes:** *Gerald Gegel*<sup>1</sup>; David Weiss<sup>2</sup>; William Edney<sup>3</sup>; <sup>1</sup>Materials & Process Consultancy; <sup>2</sup>Eck Industries; <sup>3</sup>Prototype Cast Manufacturing Inc.

The mechanical properties of cast products are a function of alloy composition, solidification rate and porosity content. The tensile and fatigue properties of AA B356 cast using low pressure permanent mold and advanced squeeze casting processes are compared to illustrate the mechanical property advantages accrued as a result of solidification under pressure. The ASC method uses low pressure to fill the die and then applies squeeze pressure directly to the entire volume of the component. As this technology is new, we will describe the design and operation of this production-viable 600-ton machine. The design of the machine permits the use of the same tooling to produce both LPPM and ASC castings. This DOE sponsored research and development project has provided a production-viable machine and process technology that will improve the strength and reliability of cast components.

10:15 AM Break

10:25 AM

**The Relationship between Defect Size and Fatigue Life Distributions in Al-7% Si-Mg Alloy Castings:** *Murat Tiryakioglu*<sup>1</sup>; <sup>1</sup>Robert Morris Univ

Fatigue life of cast Al alloys is dictated by the largest defect in the casting. The size distribution of largest defects can be modeled by extreme value distributions. When the defect size statistics are combined with equations that link the failure-initiating defects with fatigue life, the statistical distribution can be estimated. This technique is demonstrated on several datasets from the literature.

10:50 AM

**Improvement of an Existing Model to Estimate the Pore Distribution for a Fatigue Proof Design of Aluminium High-Pressure Die Casting Components:** *Christian Oberwinkler*<sup>1</sup>; Heinz Leitner<sup>1</sup>; Wilfried Eichseder<sup>1</sup>; <sup>1</sup>University of Leoben, Institute of Mechanical Engineering

The estimation of the fatigue life time of aluminium high-pressure die casting components requires the knowledge of the pore distribution. A basic model was derived from a hpdc plate using Self-Organizing Maps and statistical tools to compute a statistical distribution of the porosity within a well defined area. A new component (especially designed for this project) has been used to extend the applicability of the existing model, including influences like the hydrogen content, the wall thickness, different feeding times, and the mold temperature. An example will be presented to visualize how the estimated porosity distribution can be included into the computation of the safety against dynamic loading using a simplified Monte-Carlo simulation together with the Kitagawa-Haigh diagram as a material model.

11:15 AM

**Advanced Cast Aluminum Alloys:** *Alan Druschitz*<sup>1</sup>; John Griffin<sup>1</sup>; <sup>1</sup>University of Alabama at Birmingham

A recent advancement in aluminum casting has demonstrated that complex shapes can be cast from microalloyed Al-Cu alloy in dry sand molds with chills and that these castings can be heat treated to produce mechanical and physical properties nearly comparable to wrought 2519 aluminum alloy. Given this initial level of success, further research has been focused on improving this microalloyed Al-Cu alloy so that the mechanical properties consistently meet or exceed those of wrought 2519 alloy. Further, new research has been initiated on ultra-high strength, microalloyed Al-Zn-Mg-Cu alloys with the goal of producing complex castings with properties significantly better than wrought 2519 aluminum alloy and equivalent to or better than the best 7000 series wrought alloys. The development of the appropriate chemistries, casting practices and heat treatments are described in this paper.

## Structural Materials Division Symposium: Advanced Characterization and Modeling of Phase Transformations in Metals in Honor of David N. Seidman on his 70th Birthday: Driven Alloy Systems

Sponsored by: The Minerals, Metals and Materials Society, TMS Structural Materials Division, TMS: Advanced Characterization, Testing, and Simulation Committee, TMS: Chemistry and Physics of Materials Committee

Program Organizers: Robert Averback, University of Illinois, Urbana-Champaign; Mark Asta, University of California, Davis; David Dunand, Northwestern University; Ian Robertson, University of Illinois at Urbana-Champaign; Stephen Foiles, Sandia National Laboratories

Monday AM

February 16, 2009

Room: 3000

Location: Moscone West Convention Center

Session Chair: Ian Robertson, university of illinois

8:30 AM Introductory Comments

8:40 AM Keynote

**Energy Security, Climate Change and Materials Science: Requirements and Strategies for Sustainability in the 21st Century:** *Tomas Diaz de la Rubia*<sup>1</sup>;

<sup>1</sup>Lawrence Livermore National Laboratory

Increasing energy demand and levels of CO<sub>2</sub> in the atmosphere are placing enormous pressure on natural resources, the global ecosystem, and international political stability. Alternative sources of energy are required in order to meet increased energy demand, stabilize the increase of atmospheric carbon dioxide, and mitigate the concomitant climate change. In response, governments are urgently trying to develop new economical, sustainable, and environmentally friendly energy technologies. In this talk, I will present an overview of a new approach that combines inertial confinement fusion and fission into a simple, safe, cost-effective technology that promises to provide sustainable energy while minimizing proliferation concerns and nuclear waste disposition issues and cost. I will survey some of the key research challenges associated with the accelerated development of new materials with properties tailored to meeting this energy technology.

9:20 AM Invited

**The Dislocation Network under Irradiation:** *Georges Martin*<sup>1</sup>; Dan Mordehai<sup>1</sup>; <sup>1</sup>CEA

In crystalline metals, the dislocation network is the main source of internal strain. Irradiation, steadily injects new sources of internal strain in the metal (point defects, defect clusters): as a consequence, the evolution of the dislocation network is driven by irradiation. Examples are irradiation enhanced dislocation annealing, irradiation driven re-crystallization and irradiation induced plasticity at temperatures and stress levels where plastic strain does not show up in the absence of irradiation. The atomistic mechanisms by which the forcing proceeds have long been recognized: the partitioning of defect elimination between dislocations and other defect sinks, both in stationary or transient regimes, cascade effects... As a result, under irradiation, dislocations climb "for free". However dislocation annealing requires the coordinated climb of dislocation pairs. We show that polarisability effects, at the root of SIPA creep (Stress

Induced Preferential Absorption), provide the mechanism for coordinated climb, which eases dislocation annealing.

## 9:50 AM Break

### 10:15 AM Invited

**Atom Probe Tomography Characterization of Multiple Phase Separations in PM 2000 Ferritic ODS Steels:** *Michael Miller*<sup>1</sup>; Carlos Capdevila<sup>2</sup>; Kaye Russell<sup>1</sup>; <sup>1</sup>Oak Ridge National Laboratory; <sup>2</sup>Centro Nacional de Investigaciones Metalúrgicas

Atom-probe tomography has been used to quantify the scale and composition parameters of the  $\alpha$ - $\alpha'$  and Fe(Ti,Al) phases that are produced in a PM 2000 oxide dispersion strengthened ferritic alloy during low temperature isothermal annealing between 400 and 475°C. Atom probe tomography has revealed that both the scale and concentration amplitude of the chromium-enriched  $\alpha'$  regions increase with ageing time. The morphology of the  $\alpha'$  regions also changes from an interconnected network structure to isolated particles as ageing proceeds. These fine scale phases are responsible for a significant increase in the hardness of the alloy with ageing time. The influence of aluminum on the position of the miscibility gap has also been determined. Research at the Oak Ridge National Laboratory SHaRE User Facility was sponsored by the Scientific User Facilities Division, Office of Basic Energy Sciences, U.S. Department of Energy.

### 10:45 AM

**Austenite Precipitate Kinetics and Ballistic Property of Low-Carbon Ni Steels:** *Xian Zhang*<sup>1</sup>; <sup>1</sup>Naval Surface Warfare Center

A comprehensive study on the phase transformation kinetics of austenite reversion in a series of VIM (vacuum induction melt) Low-Carbon Ni steels, containing five different Ni contents ranging from 2.5 % to 10 %, was performed to investigate key microstructural contributors to the ballistic resistance of steel. A wide range of heat treatments, static and dynamic mechanical tests, and various analytical techniques including SEM, TEM, EELS, EBSD, and X-ray diffraction, were employed to characterize microstructure and processing-structure-property correlations. This paper focuses on the control of austenite precipitate kinetics and morphology during the QLT (quenching-lamellarizing-tempering) process and its effect on FSP ballistic resistance V50. We conclude that highly dispersed fine austenite particles (on the nanometer scale) embedded in a ductile ferrite matrix appear to be the optimum microstructure for obtaining the best combination of strength, toughness, and ballistic property of Low-Carbon Ni steels.

### 11:00 AM Invited

**Synthesis of New Materials via Self-Organization Driven by External Forcing:** *Pascal Bellon*<sup>1</sup>; Robert Averback<sup>1</sup>; Pavel Krasnochtchekov<sup>1</sup>; See Wee Chee<sup>1</sup>; Brad Stumphy<sup>1</sup>; <sup>1</sup>University of Illinois

Materials, either during their processing or in service, are often subjected to sustained dynamical forcing, for instance plastic deformation during extrusion, and irradiation by energetic particles in nuclear reactors. These non-equilibrium dissipative material systems display a tendency to self-organize. Using atomistic simulations and continuum modeling, we will show that, for alloys irradiated with energetic particles, this self-organization results from the competition of dynamical processes acting at different length scales. Furthermore, the characteristic length scale of these self-organized structures, which is typically in the range of 1 to 100 nm, varies continuously as the irradiation-induced displacement rate and the temperature are varied. These predictions are tested using experiments on Cu-base alloys using transmission electron microscopy and atom probe tomography. This approach opens a new route for the synthesis of nanostructured materials with tunable scale, a property that can then be used to design radiation-resistant materials.

### 11:30 AM Invited

**Atom Probe Tomography of Materials for Energy Applications:** *Thomas Kelly*<sup>1</sup>; <sup>1</sup>Imago Scientific Instruments

Atom probe tomography (APT) produces three-dimensional structural and compositional images of materials at the atomic scale. These data have proven invaluable for a wide range of materials used in energy applications. Specimen preparation advances have made it routine now to extract and analyze specimens from bulk materials including advanced alloys, device wafers and even finished components. Major developments in atom probe technology have led to greater facility for running specimens and greater detail in quantitative analysis. In this talk, examples will be given of how this capability is having impact on metals, semiconductors, ceramics, and even synthetic organics and polymers.

### 12:00 PM

**Radiation Resistant Alloys for Use at High Temperatures:** See Wee Chee<sup>1</sup>; Brad Stumphy<sup>1</sup>; *Robert Averback*<sup>1</sup>; Pascal Bellon<sup>1</sup>; <sup>1</sup>University of Illinois

It has been known for several decades that materials that include high concentrations of nanoscale features within their microstructures provide excellent resistance to irradiation damage. Such highly non-equilibrium structures, however, are generally unstable to coarsening during exposures to long term irradiation and operation at very high temperatures. We examine here the potential for developing alloys that self organize on an ultrafine length scale during high temperature irradiation, and thus maintain their radiation tolerance. By using a combination of x-ray diffraction, transmission electron microscopy, and atom probe tomography measurements analyze a series dilute Cu alloys, we show that ultrafine microstructures can indeed be preserved at irradiation temperatures exceeding 650 °C (i.e., > 0.62 $T_M$ , where  $T_M$ =melting temperature of Cu) and to irradiation doses greater than 100 dpa. Molecular dynamics computer simulations provide a clear explanation for the stability of some of these microstructures.

### 12:15 PM

**Self Organization in Irradiated Cu-10at%Fe Alloys: An Atom Probe Tomography Investigation:** *Brad Stumphy*<sup>1</sup>; See Wee Chee<sup>1</sup>; Robert Averback<sup>1</sup>; Pascal Bellon<sup>1</sup>; <sup>1</sup>University of Illinois

Atom probe tomography (ATP), in combination with magnetization measurements, was employed to investigate irradiation-induced precipitation in dilute Cu-Fe alloys. Thin-film specimens, ~200 nm thick, were fabricated using magnetron sputtering. For the magnetization measurements, the alloys were deposited directly on heavily oxidized Si wafers, while for the APT, the alloys were deposited onto the tips of Mo wires, using a Ti layer to enhance the cohesion of the film. The ATP specimens were shaped using a focused ion beam. Irradiation at 80 K led to the complete dissolution of Fe precipitates. Between room temperature and ~ 250°C, precipitation was observed, but the sizes of the precipitates saturated with dimensions less than ~ 5nm. Solubilities of Fe in the Cu matrix and Cu in the Fe precipitates, and the interface diffuseness, were determined as a function of temperature in both the irradiated and unirradiated samples.

## Synergies of Computational and Experimental Materials Science: Three-Dimensional Materials Science I

Sponsored by: The Minerals, Metals and Materials Society, TMS Materials Processing and Manufacturing Division, TMS/ASM: Computational Materials Science and Engineering Committee

Program Organizers: Katsuyo Thornton, University of Michigan; Henning Poulsen, Risoe National Laboratory; Mei Li, Ford Motor Co

Monday AM

Room: 3003

February 16, 2009

Location: Moscone West Convention Center

*Session Chairs:* Katsuyo Thornton, University of Michigan; Henning Poulsen, Risoe National Lab

### 8:30 AM Introductory Comments

#### 8:35 AM Invited

**Microstructure Evolution and Fundamental Characteristics in Solidification of Metals and Alloys - A Comparison of Modelling and Experiments:** *Ragnvald Mathiesen*<sup>1</sup>; <sup>1</sup>NTNU

Alloy solidification processes generally evolve under non-equilibrium conditions, where the solid grows as intricate self-assembly structures controlled by complex interplays of diffusive and hydrodynamic heat and mass transport, with the solid-liquid interface both as an internal boundary and a solution to the problem itself. While modelling of solidification microstructures and fundamentals has advanced considerably over the last decades, provision of new experiments for guidance has fallen behind. In the past in-situ studies were limited to video microscopy on optically transparent model systems. However, these are severely limited as analogues to real alloys, and can only be used to realize a few cases. Recent improvements in sources and detectors have opened for X-ray investigations at spatiotemporal resolutions approaching those of



video microscopy. Here, in-situ X-ray imaging observations from solidification studies in Al-based alloys will be presented, and compared qualitatively and quantitatively with results from modelling.

### 9:15 AM Invited

**Using Experimental Data in Simulations of Grain Growth:** I. McKenna<sup>1</sup>; D. Rowenhorst<sup>2</sup>; E.M. Lauridsen<sup>3</sup>; *Peter Voorhees*<sup>1</sup>; <sup>1</sup>Northwestern University; <sup>2</sup>Naval Research Laboratory; <sup>3</sup>RISO Laboratory

Recent advances in computational and experimental techniques allows for the routine visualization of the three-dimensional grain structure of materials. This opens new routes to explore the relationship between materials processing, structure, and properties. Using experimentally measured three-dimensional grain structures we have followed the evolution of grains using a phase field model that accounts for all five degrees of freedom that determine the grain boundary energy. We show that a multiorder parameter model can be used to explore the topological changes of individual grains during grain growth. This model employs quaternions to account for the dependence of the grain boundary energy on the misorientation and a tensor gradient energy coefficient to account for the change in grain boundary energy with boundary normal. Results of the simulations and the development of the models will be discussed.

### 9:55 AM

**Modeling and In-Situ X-Ray Video Microscopy of Confined Equiaxed Grain Growth and Buoyant Motion in Al-Cu:** *Pierre Delaleau*<sup>1</sup>; Ragnvald Mathiesen<sup>2</sup>; Paul Schaffer<sup>1</sup>; Lars Arnborg<sup>1</sup>; Martin Bellmann<sup>1</sup>; Christoph Beckermann<sup>3</sup>; <sup>1</sup>NTNU, Department of Materials Science and Engineering; <sup>2</sup>NTNU, Department of Physics; <sup>3</sup>The University of Iowa, Department of Mechanical and Industrial Engineering

Equiaxed dendritic growth in grain refined Al-x%wtCu (x=15-25) has been studied in situ during directional solidification by means of synchrotron X-ray video microscopy. At these compositions, the  $\alpha$ -Al grains have a lower density than the surrounding melt and experience buoyant forces which affect their growth rates and morphologies. As the samples are concealed into a thin container, the walls severely influence grain motion. A model, based on a spherical envelope approximation to the dendrite morphology in order to simplify both the interface geometry of the growing crystals and the Stokes drag exerted upon them during motion, has been derived taking into account the influence of the sample confinement. The model is compared with the in situ experiments both to evaluate its present merits and to devise possible routes for improvement in order to develop it further to a model description for  $\alpha$ -Al dendritic growth during buoyant motion.

### 10:15 AM

**Predicting the Evolution of Interfacial Morphology during Coarsening:** *Larry Aagesen*<sup>1</sup>; Julie Fife<sup>2</sup>; Peter Voorhees<sup>1</sup>; Erik Lauridsen<sup>2</sup>; Marco Stampanoni<sup>3</sup>; <sup>1</sup>MSE Dept., Northwestern University; <sup>2</sup>Riso National Laboratory; <sup>3</sup>Swiss Light Source

The process of coarsening in two-phase systems is governed by interfacial morphology. A new method of predicting the evolution of interfaces and their morphologies was developed. The method uses a phase-field model of a binary alloy which allows for unequal diffusivities between the liquid and solid phases, and accounts for changes to interfacial morphology due to the motion of the interface itself. To validate this method, experimental data was used as input to the phase-field model, and simulation results were compared to data at later times. The experimental data was from a directionally solidified Al-Cu alloy which was coarsened just above the eutectic temperature and observed using in-situ X-ray tomography at the Swiss Light Source. This provided three-dimensional data of the microstructure throughout the coarsening process. The comparison allowed the fine-tuning of simulation parameters to more closely match experimental results, and thus improved the accuracy of the predictions.

### 10:35 AM Break

### 10:50 AM Invited

**3DXRD Characterization and Modelling of Recrystallization:** *Dorte Jensen*<sup>1</sup>; <sup>1</sup>Riso - DTU National Lab

3D x-ray diffraction (3DXRD) allows non-destructive characterizations of bulk microstructures and strains. The method is described briefly with focus on recent developments. 3DXRD results obtained so far have in particular highlighted the importance of LOCAL phenomena which are typically not at all (or incorrectly) incorporated in existing models. This is illustrated for recrystallization of metals. It is shown how 3DXRD measurements have led to

new 3D geometrical modelling and 3D MD simulations necessary to explain the experimental results and in turn how the modelling and simulations have guided new 3DXRD experiments.

### 11:30 AM

**Phase Field Simulations of Coarsening of Al6Mn Precipitates Located on Grain Boundaries in Al Alloys:** *Nele Moelans*<sup>1</sup>; Alexis Miroux<sup>2</sup>; Erica Anselmino<sup>2</sup>; Sybrand van der Zwaag<sup>3</sup>; Bart Blanpain<sup>1</sup>; Patrick Wollants<sup>1</sup>; <sup>1</sup>K. U. Leuven; <sup>2</sup>M2i; <sup>3</sup>Delft University of Technology

In-situ observations show that grain boundary movement during recrystallization in aluminum alloys is not smooth but jerky on a microscopic scale. There is experimental and theoretical evidence that the jerky motion is due to the pinning effect of small Al6Mn precipitates. The pinning precipitates are however too small to study this effect in detail from in-situ observations. Therefore phase field simulations are performed of the recrystallization in Al-alloys that account for the interaction between precipitates and grain boundaries. Model parameters are, as far as possible, determined based on experimental information. Comparison of the phase field simulations with the in-situ observations will give a better understanding of the mechanisms behind and conditions for jerky grain boundary motion.

### 11:50 AM

**Influence of Grain Boundary Misorientation on Nucleation of Twins in Textured Zr:** *Dhriti Bhattacharyya*<sup>1</sup>; Rodney McCabe<sup>1</sup>; Carlos Tome<sup>1</sup>; <sup>1</sup>Los Alamos National Laboratory

Deformation twinning is a major method of strain accommodation in hcp metals like Zr. It is well known that grain orientation with respect to the applied load (Schmid factor) has a significant effect on the formation of twins in any grain. Another important factor for the nucleation of twins in a grain may be its misorientation with neighboring grains. In this study, we have used electron-backscatter diffraction (EBSD) data to investigate the latter effect, by correlating the misorientation between the active twin and slip systems in the neighboring grains on twin-formation in a given grain. Specifically, we investigate whether dislocation or twin induced stress concentrations at a grain boundary can cause twin nucleation in a neighboring grain. Extensive studies made over hundreds of grain-boundaries indicate that misorientation with the neighboring grain is an important factor for nucleation of twins at the boundaries.

## Transformations under Extreme Conditions: A New Frontier in Materials: Keynote: Melting and Solidification I

Sponsored by: The Minerals, Metals and Materials Society, ASM International, ASM Materials Science Critical Technology Sector, TMS Materials Processing and Manufacturing Division, TMS/ASM: Phase Transformations Committee  
Program Organizers: Vijay Vasudevan, University of Cincinnati; Mukul Kumar, Lawrence Livermore National Laboratory; Marc Meyers, University of California-San Diego; George "Rusty" Gray, Los Alamos National Laboratory; Dan Thoma, Los Alamos National Laboratory

Monday AM

February 16, 2009

Room: 3001

Location: Moscone West Convention Center

*Session Chairs:* Mukul Kumar, Lawrence Livermore National Laboratory; Srikumar Banerjee, Bhabha Atomic Research Center

### 8:30 AM Introductory Comments

### 8:40 AM Keynote

**Phase Transformation Kinetics and Mechanisms in Shocked Condensed Matter: Challenges and Opportunities:** *Yogendra Gupta*<sup>1</sup>; <sup>1</sup>Washington State University

Shock wave experiments provide a unique approach to examine compression induced phase transformations in real time. Continuum measurements under shock loading (either peak state values or wave profile measurements) in conjunction with static pressure results are most commonly used to infer thermodynamic states, transformation mechanisms, and kinetics. Challenges associated with these traditional approaches will be discussed using representative examples. Understanding the role of crystal orientation, material microstructure, and stress deviators on phase transformations constitute long standing needs.

New experimental capabilities that have the potential to provide an in-depth understanding of transformation mechanisms and kinetics will be outlined. The combination of dynamic loading capabilities, recent computational developments, and new in-situ microscopic measurements presents an exciting opportunity to understand transformation of materials at extreme conditions.

## 9:30 AM Invited

**First Principles Calculations of Shock Hugoniot and Shock Induced Melting of Osmium:** Keshaw Joshi<sup>1</sup>; Satish Gupta<sup>1</sup>; *Srikumar Banerjee*<sup>1</sup>; <sup>1</sup>Bhabha Atomic Research Centre

The stability of crystal structure of osmium under application of high pressure has been examined by carrying out the first principles calculations of total energy at various compressions for hcp, bcc, omega (a three atom simple hexagonal) and fcc structures. Our analysis indicates that the ambient hcp phase remains lowest energy structure up to a hydrostatic pressure of ~ 698 GPa ( $V/V_0 = 0.58$ ). The shock Hugoniot derived from 0 K isotherm by incorporating the thermal lattice and thermal electronic contribution in conjunction with the Rankine Hugoniot relation yields  $C = 4.49$  km/s and  $s = 1.304$  in the  $U_s - U_p$  plot. The melting line has been constructed by applying the theoretically determined pressure dependent Grüneisen parameter in Lindemann criterion of melting. The intersection of melting line with the shock Hugoniot, indicating the melting of osmium under shock compression, occurs at ~ 440 GPa ( $T = 8944$  K).

## 10:05 AM

**Thermodynamics of the  $\gamma$ - $\alpha$  Transition in Cerium with Phonon Contributions:** *Yi Wang*<sup>1</sup>; L. Hector<sup>2</sup>; Hui Zhang<sup>1</sup>; Shun-Li Shang<sup>1</sup>; Long-Qing Chen<sup>1</sup>; Zi-Kui Liu<sup>1</sup>; <sup>1</sup>The Pennsylvania State University; <sup>2</sup>GM R&D Center

Thermodynamics of the  $\gamma$ - $\alpha$  transition in Cerium are investigated with a model that accounts for finite temperature mixing of the free energies of the nonmagnetic and magnetic Ce 4f-states. All model inputs are taken from first-principles density functional theory (DFT) calculations with strong correlation of the f-electrons. Vibrational free energies are computed with phonon calculations based upon the direct approach to lattice dynamics. This provides the correct phase transition thermodynamics as demonstrated in our computed free energy curves over 0 to 600 K and temperature-volume phase diagram. We find remarkably close agreement between our computed 0 GPa phase transition temperature, critical point, and 300 K  $\gamma$ - $\alpha$  volume collapse and experiment. Our model, which does not rely upon existing experimental data or other approximations outside of DFT, provides a framework for accurate prediction of the temperature-pressure behavior of other f-state systems, such as Plutonium.

## 10:25 AM Break

## 10:40 AM Invited

**Dynamic Phase Transitions Compared with Static; Flat Melting Curves and Other Mysteries:** *Robert Hixson*<sup>1</sup>; <sup>1</sup>Naval Postgraduate School

In this talk I'll show comparisons of phase transition locations for selected metals determined using static high pressure techniques with those made using shock wave compression techniques. I will in particular look at available data for melting curves measured using static high pressure techniques, and make comparisons with Hugoniot melting points determined from shock compression experiments. There are only a few metals for which shock wave Hugoniot melting points have been determined, and many of these will be discussed. One focus will be on iron. I'll also briefly review and discuss recent work that shows relatively flat melting curves determined from diamond anvil cell data.

## 11:15 AM

**Pressure Induced Solidification of Ta and Cu: A Comparison:** *David Richards*<sup>1</sup>; James Glosli<sup>1</sup>; Fred Streitz<sup>1</sup>; <sup>1</sup>Lawrence Livermore National Laboratory

Using powerful computers such as Blue Gene/L it is now possible to use classical molecular dynamics to simulate pressure induced solidification at size scales that are free of finite size effects. We present a comparison of the nucleation, growth, and coalescence of clusters during pressure induced solidification in large scale MD simulations of liquid Ta and Cu. We extract growth and nucleation rates from our simulations, as well as cluster size distributions that can be compared against the predictions of simple models. This work performed under the auspices of the U.S. Department of Energy by Lawrence Livermore National Laboratory under Contract DE-AC52-07NA27344 UCRL-ABS-2367881.

## 11:35 AM

**New Phase Diagram of Ta: Bridging Laser Heated Diamond-Anvil Cell and Shock Melting:** *Christine Wu*<sup>1</sup>; Per Soderlind<sup>1</sup>; James Glosli<sup>1</sup>; John Klepeis<sup>1</sup>; <sup>1</sup>Lawrence Livermore National Lab

Determination of the melt line of materials under high pressures is essential for establishing its phase diagrams and has important implications for geophysics, material science, and high-pressure physics. So far, melting temperatures at high pressure are primarily measured by in situ laser-heated diamond-anvil cell (DAC) or shock wave experiments. Often, these two methods yield significantly different results, particularly for non close-packed metals, such as bcc metals. For instance, anomalously flat melting slopes were reported for numerous bcc metals by laser-heated DAC. The flatness of the melting slope is in sharp contrast to the classical Lindemann behavior which shock-melting temperatures follow closely. In this presentation, we will report a novel phase diagram of Ta obtained from ab initio methods, and molecular dynamics (MD) simulations, which resolves the long-standing controversy, and has significant impact on our understanding of phase diagrams of bcc metals. This work performed under the auspices of the U.S. Department of Energy by Lawrence Livermore National Laboratory under Contract DE-AC52-07NA27344.

## 11:55 AM

**Pressure-Driven Solidification: Coupling Phase-Field Modeling with Underlying Molecular Dynamics:** *James Belak*<sup>1</sup>; Patrice Turchi<sup>1</sup>; Milo Dorr<sup>1</sup>; Bryan Reed<sup>1</sup>; David Richards<sup>1</sup>; Jean-luc Fattebert<sup>1</sup>; Michael Wickett<sup>1</sup>; Fred Streitz<sup>1</sup>; <sup>1</sup>Lawrence Livermore National Lab

Large parallel computers have enabled MD simulations of pressure-driven solidification of sufficient scale to observe the formation of realistic microstructure. Here, we calculate the coarse-grained phase-field order parameter from the local atomic coordinates within the MD. The results are represented within emerging crystallographic phase-field models and validated through overlapping MD and phase-field simulations. Results will be presented for the solidification of tantalum. F. H. Streitz, J. N. Glosli, and M. V. Patel, Phys. Rev. Lett. 96, 225701 (2006). R. Kobayashi and J.A. Warren, Physica A, 356, 127-132 (2005). T. Pusztai, G. Bortel and L. Granasy, Europhys. Lett, 71, 131-137 (2005). This work performed under the auspices of the U.S. Department of Energy by LLNL under Contract DE-AC52-07NA27344.

## 2009 Functional and Structural Nanomaterials: Fabrication, Properties, and Applications: Low Dimensional Nanostructures II

Sponsored by: The Minerals, Metals and Materials Society, TMS Electronic, Magnetic, and Photonic Materials Division, TMS Materials Processing and Manufacturing Division, TMS: Nanomaterials Committee, TMS: Nanomechanical Materials Behavior Committee

Program Organizers: Gregory Thompson, University of Alabama; Amit Misra, Los Alamos National Laboratory; David Stollberg, Georgia Tech Research Institute; Jiyoung Kim, University of Texas at Dallas; Seong Jin Koh, University of Texas at Arlington; Wonbong Choi, Florida International University; Alexander Howard, Air Force Research Laboratory

Monday PM Room: 3018  
February 16, 2009 Location: Moscone West Convention Center

Session Chairs: Seong Jin Koh, University of Texas at Arlington; William Ready, Georgia Tech

### 2:00 PM Invited

#### Ferromagnetic Nanoparticles: J. P. Liu<sup>1</sup>; <sup>1</sup>University of Texas at Arlington

Most ferromagnetic particles lose their hysteresis when their size is reduced to nanoscale, except few materials like FePt and SmCo compounds with extremely high magnetocrystalline anisotropy can hold a permanent magnetic moment at room temperature in particles of few nanometer size. By applying newly developed "salt-matrix annealing" and "surfactant-assisted milling" techniques, monodisperse ferromagnetic FePt and SmCo nanoparticles have been successfully synthesized. These first-ever-available nanoparticles display various ferromagnetic properties at room temperature which are found to be strongly size dependent. The ferromagnetic nanoparticles are used as building blocks for advanced bulk and thin film magnets, and can be also applied in biomedical technologies.

### 2:30 PM

#### Nanoscale Modeling Studies of Magnetic Flux Closure in Cobalt Nanoparticles: Prabeer Barpanda<sup>1</sup>; <sup>1</sup>Rutgers University

Soft magnetic rings are promising candidates for nonvolatile random access memory (RAM) devices due to their capacity to support bistable flux closure (FC) domains. Cobalt nanoparticles form one such soft magnetic ring system, having zero magnetostatic energy and can be closely packed for high-density data storage. Flux closure states in Cobalt nanoparticles can be rapidly (picoseconds range) switched by in-plane magnetic fields/ coaxial currents. In the current study, 3D-FFT micromagnetic modeling has been employed to examine magnetic states in nanoparticle rings that are formed from 20-nm-diameter cobalt crystals. We assess the effect of the number of particles in a ring on the formation of flux closure or 'onion' states at remanence after the rings are subjected to out-of-plane fields. We compare the simulations with experimental magnetic induction maps measured using electron holography and assess the influence on the reversal mechanism of a ring of the morphologies of the constituent crystals.

### 2:45 PM

#### B/SiOx Nanonecklace Reinforced Nanocomposites by Unique Mechanical Interlocking Mechanism: Xinyong Tao<sup>1</sup>; Jie Liu<sup>1</sup>; Goutam Koley<sup>1</sup>; Xiaodong Li<sup>1</sup>; <sup>1</sup>University of South Carolina

Necklace-like nanostructures with SiOx beads on boron strings were self-assembled via a facile environment-friendly method at atmospheric pressure. The electrical conductivity of the boron string is a thousand times higher than that of pure bulk boron (10<sup>-6</sup> O-1cm-1). Due to the unique mechanical interlocking between beads and epoxy matrix, the reinforcement effect of the nanonecklaces in epoxy is even better than normal carbon nanotubes. B/SiOx nanonecklaces are expected to exhibit unique electrical and mechanical properties for constructing nanodevices and nanocomposites.

### 3:00 PM

#### Synthesis and Magnetic Properties of FePt and FeRh Mixed Nanoparticles: Naidu Seetala<sup>1</sup>; Jessica Harris<sup>1</sup>; Joseph Buchanan-Vega<sup>1</sup>; J. W. Harrell<sup>2</sup>; Zhiyong Jia<sup>2</sup>; David Nikles<sup>2</sup>; <sup>1</sup>Grambling State University; <sup>2</sup>University of Alabama

We have examined the properties of FePt and FeRh nanoparticles for the heat assisted magnetic recording (HAMR) media applications. FePt and FeRh nanoparticles (~ 6 nm) were chemically synthesized using simultaneous polyol reduction method. The FeRh nanoparticles were annealed in salt at 800°C to avoid particle segregation and sintering. The XRD results show CsCl-type bcc (B2) phase for FeRh upon salt annealing. The temperature dependent magnetic studies of annealed FeRh nanoparticles showed anti-ferromagnetic to ferromagnetic transition at around 80°C. The high temperature synthesis of FePt nanoparticles provided L1<sub>0</sub> phase with a magnetic coercivity of ~ 2000 Oe for as-synthesized particles. The temperature dependence (20 - 230°C heating and cooling cycles) of the magnetic properties were studied individually for FePt and FeRh nanoparticles, and after physically mixing them and annealing at 400°C. Temperature dependent hysteresis behavior is observed in all the samples.

### 3:15 PM

#### Preparation of Nanostructured Iron Oxide Particles via Ultrasonic Spray Pyrolysis (USP): Burcak Ebin<sup>1</sup>; Sebahattin Gurmen<sup>1</sup>; Cuneyt Arslan<sup>1</sup>; <sup>1</sup>Istanbul Technical University

Scientific and technological attentions have focused on synthesis and characterization of nanostructured iron oxide particles in recent decades due to their interesting physical and chemical properties. Especially novel magnetic properties of nanosized particles could open new practical applications in many fields such as magnetic storage devices, ferro fluids, catalysis, magnetic drug delivery system, and cancer treatment. In this research, nanostructured iron oxide particles were prepared via ultrasonic spray pyrolysis (USP) method using iron (II) chloride solution. The dependence of iron oxide particles size and morphology to the precursor concentration, and reaction temperature were investigated under 1.3 MHz ultrasonic frequency, and 1.0 l/min air flow rate. Scanning electron microscopy (SEM) and X-ray diffraction (XRD) were used to investigate size, morphology and crystal structure of particles. It was observed that decreasing of precursor concentration and temperature cause the reducing in particle size.

### 3:30 PM Break

### 3:45 PM

#### Solution and Low Temperature Synthesis of a Conductive and Porous Metal-Silica Nanocomposite: Tsan-Yao Chen<sup>1</sup>; Yong-Jae Choi<sup>1</sup>; Tzy-Jium Luo<sup>1</sup>; <sup>1</sup>North Carolina State University

In our effort to control and synthesize metallic nanoparticles that exhibit interconnected 3-D network, we have developed a low temperature and solution procedure to fabricate a porous metal-silica nanocomposite. We used silver as a test model and successfully synthesized a metal-silica nanocomposite that is highly conductive (< 2 ohm-cm), low density (~ 2 g/mL), with low weight percentage of silver (2 ~ 5 wt%). This material is nanoporous in nature and was synthesized using polyethyleneglycol blended sol-gel matrix as structural template. It consisted of three major components: nanoporous silica matrix, pore-filled polymers, and silver ions that were later reduced to interconnected silver network at 160°C. Such material will find its applications in fuel cells, biofuel cell, and sensors. Therefore, SEM, XRD, Tapping mode AFM and cyclic voltammetry were utilized to characterize its nanostructure and properties.

### 4:00 PM

#### Study on Microstructure and Emission Properties of Scandate Cathode: Wei Liu<sup>1</sup>; Jinshu Wang<sup>1</sup>; Yiman Wang<sup>1</sup>; Meiling Zhou<sup>1</sup>; <sup>1</sup>Beijing University of Technology

The sub-micron Sc<sub>2</sub>O<sub>3</sub> doped tungsten powders have been successfully prepared by Sol-Gel and two-step reduction method for the first time. Then, the Scandia doped tungsten mixed matrix impregnated cathodes with the sub-micron structure has been also successfully prepared. 50A/cm<sup>2</sup> of Jdiv and 100A/cm<sup>2</sup> of J10% at 850°C<sub>b</sub> are obtained for the optimally activated cathodes. By using in situ AES, HRSAM and other kinds of analysis methods, it is found that BaSc and O diffuse from the interior porous body to surface simultaneously to form a uniform activator substance layer with the optimal atomic ratio. The comparison experiment between "M"-type cathode and sub-micron Scandate cathodes displays that the thickness of the activator substance layer in Scandate cathodes is larger than that in "M"-type cathodes, indicating that this uniform



activator layer has a multi-layer structure which leads to the excellent emission property of this cathode.

#### 4:15 PM

##### **Gram-Scale Synthesis of Functionalized, Highly Fluorescent, and Non-Toxic Silicon Nanoparticles:** Han Zuilhof<sup>1</sup>; <sup>1</sup>Wageningen University

Non-toxic fluorescent nanoparticles are highly desirable for a wide variety of bio-imaging studies. To this aim we developed methods to synthesize functionalized, oxide-free silicon nanoparticles. These are brightly fluorescent, with a narrow emission due to a very narrow size distribution (1.6 +/- 0.2 nm). Since they can be synthesized on a gram scale, this allows for the first time a range of optical properties (both steady state and time-resolved), bio-imaging of yeast cells using functionalized Si nanoparticles, and toxicity studies on different cell lines. The paper discusses this synthesis, opto-electronic properties, preliminary bioimaging studies and detailed quantitative studies on the (lack of) toxicity of these nanoparticles.

#### 4:30 PM

##### **Synthesis of Sb4O5Cl2 Nanobelts by Hydrolysis of Alkoxide and Thermal Decomposition Properties of the Novel Nano-Flame Retardant:** Li Feng<sup>1</sup>; <sup>1</sup>China University of Mining and Technology

Novel flame retardant of antimony oxychlorides (Sb4O5Cl2) nanobelts have been synthesized via alkoxide hydrolysis. X-ray diffraction (XRD) measurement showed that the samples were pure Sb4O5Cl2 crystals with monoclinic structure. The fibers-like structure of Sb4O5Cl2 nanobelts with 0.3-1.0 µm in length and 10-50 nm in diameter were confirmed by TEM. The thermal analysis (TG/DTG/DSC) revealed that there were three steps of mass loss of the products under nitrogen atmosphere, and the possible mechanisms for the decomposition of Sb4O5Cl2 were discussed.

## **Alumina and Bauxite: Bayer Process Safety, Environmental and Sustainability Issues**

Sponsored by: The Minerals, Metals and Materials Society, TMS Light Metals Division, TMS: Aluminum Committee

Program Organizers: Everett Phillips, Nalco Co; Sringeri Chandrashekar, Dubai Aluminum Co

Monday PM  
February 16, 2009

Room: 2002  
Location: Moscone West Convention Center

Session Chair: Pierre Ferland, Rio Tinto Alcan

#### **2:00 PM Introductory Comments**

#### **2:10 PM**

##### **The Asia-Pacific Partnership: An Important New Initiative for a Sustainable Alumina Industry:** Markus Gräfe<sup>1</sup>; Greg Power<sup>1</sup>; Craig Klauber<sup>1</sup>; <sup>1</sup>CSIRO Minerals

The Asia-Pacific Partnership on Clean Development and Climate is an inter-governmental agreement between seven countries, predominantly located around the Pacific Rim: Australia, Canada, China, India, Japan, Republic of Korea and the United States of America. Collectively these countries represent about half the world's emissions and 52% of the world's aluminium production. Aluminium is one of eight key areas covered by the APP and the Task Force is chaired by Australia and co-chaired by the United States of America. Projects within this area are focused on best practice and its deployment across the Partnership economies. Within aluminium there are seven project activities covering benchmarking and linkages to technology providers, plus per-fluorocarbon emissions, bauxite residues, high silica bauxite, fluoride emissions and aluminium recycling. The Partnership program and how it is implemented is described with a particular focus on the bauxite residue management work being undertaken.

#### **2:35 PM**

##### **Operations Support in the Alumina Industry – A Valuable Partnership:** Jason Berzansky<sup>1</sup>; <sup>1</sup>Hatch Associates Consultants

Since 2001, Hatch Associates Consultants has been involved in a highly successful engineering alliance with an alumina supplier for the client's sustaining capital program. As part of Hatch's Operations Support (OpSupport)

network, this relationship has flourished over the past seven years, as evidenced by the recent extension of the alliance agreement. While the primary focus of this engineering alliance is on the sustaining capital program, Hatch has added value to the client through a variety of other activities such as maintenance and operations support activities. This paper focuses on the sustaining capital engineering alliance concept and demonstrates how such relationships can achieve success when common goals are established, agreed upon and eventually realized.

#### **3:00 PM**

##### **Sustainable Storm Water Management:** Dana Smith<sup>1</sup>; Jaw Fu<sup>2</sup>; Amanda Ludlow<sup>3</sup>; <sup>1</sup>AWA Atlantic; <sup>2</sup>Alcoa; <sup>3</sup>Roux Associates, Inc

Alcoa's Point Comfort, Texas alumina refinery has deployed a multi-faceted Engineered Natural System (ENS) to capture and recycle bauxite ore, improve runoff water quality and reduce runoff volume from the bauxite storage area at the Site. The ENS is comprised of initial sedimentation trenches and swales to capture and recover coarse fractions of bauxite eroded from large bauxite storage piles. Decanted stormwater from the trenches is then conveyed to a staged constructed treatment wetland (CTW) for additional cleansing and retention. The staged CTW contains an initial forebay, settling pond, high marsh and low marsh areas and a terminal micropool. Clean effluent from the CTW can either be conveyed to a phytoplot for consumptive elimination or used by the refinery to reduce dependency on potable water.

#### **3:25 PM**

##### **Achieving Excellence in Liquid Effluent Treatment at Alunorte:** Jorge Aldi<sup>1</sup>; <sup>1</sup>Alunorte – Alumina do Norte do Brasil S.A

Alunorte began its operation in 1995 with a capacity of 1.1mi t/y and after three Expansions the production in 2009 will be 6.3mi tpy. As Alunorte use the dry stacking technology to dispose the red mud, the area for the red mud deposit is very big as well the pluvial index in the rain forest region. So in 2003, after the first Expansion, Alunorte have decided to build a new liquid effluent treatment station to guarantee a nominal capacity of 3,600m<sup>3</sup>/h of treated effluent, ensuring a pH around 8.0, a temperature below 40°C and a NTU below 20. This paper aims to present the concept implemented for such an effluent treatment station as well the results achieved to date after the implementation, emphasizing that all kinds of liquid effluents, no matter if it is contaminated or not, are treated before being discarded in the river.

#### **3:50 PM Break**

#### **4:05 PM Invited**

##### **Sustainability of Chinese Alumina Production from High Silica Diasporic Bauxite:** Songqing Gu<sup>1</sup>; Zhonglin Yin<sup>1</sup>; <sup>1</sup>Zhengzhou Research Institute of Chalco

The sustainable development of Chinese alumina production faces great challenges from the low grade bauxite resource, high process energy consumption, product quality and environmental issues. Improving flotation-Bayer process and developing the hydro-chemical processes to produce suitable DSP will be the key solutions for efficiently processing high silica bauxite with lower consumptions and more competitive cost. Developing new technologies for energy savings and high alumina recovery to reduce residue disposal, enhancing circulation efficiency and productivity in the various production stages for high output and low consumptions, realizing dry residue disposal and zero- waste water discharge, reusing red mud for new materials manufacture and valuable elements recovery will provide a vital basis for longer term sustainability of the Chinese alumina industry.

#### **4:30 PM**

##### **The Design of Pressure Safety Systems in the Alumina Industry:** Brady Haneman<sup>1</sup>; <sup>1</sup>HATCH Associates

The alumina refinery presents the designer with multiple challenges. For a given process flowsheet, the mechanical equipment installed must be routinely inspected and maintained. Piping systems must also be inspected routinely for signs of erosion and/or corrosion. Rapid deposits of chemical species such as lime, silica, and alumina on equipment and piping need special consideration in the mechanical design of the facilities such that fluid flows are not unduly interrupted. Above and beyond all else, the process plant must be a safe place of work for refinery personnel. This paper outlines some of the pressure safety considerations to be incorporated into the mechanical design of the digestion facilities for some alternate process flow sheets. Armed with these considerations at the process flowsheet definition stage, optimisation of the process and/or

equipment selection is possible preserving the delicate balance of process facility performance, plant operability and maintainability, and personnel safety.

**4:55 PM**

**Mercury Vapor Sensor for Alumina Refinery Processes:** Ylias M. Sabri<sup>1</sup>; Samuel J. Ippolito<sup>1</sup>; *Suresh Bhargava*<sup>1</sup>; <sup>1</sup>RMIT University

The sustainability of bauxite mining and refinery practices is reliant on attempts to reduce the environmental impacts of traditional processes. Mercury reduction targets set by industry and regulators has spurred attempts to develop technologies for evaluating the efficiency of mercury removal processes. The development of a mercury sensor suited to alumina refineries will be a significant breakthrough in controlling mercury emissions, as well as having many other applications. Gold coated Quartz Crystal Microbalance (QCM) based sensors employing enhanced nano-structured surfaces have been developed which show a substantial increase in response magnitude of at least 67% over non-modified QCMs. Additionally, the Hg-Au sticking probability calculated from the QCM data of the modified and non-modified sensors showed increased Hg affinity for the modified sensor. Furthermore, the modified QCM sensor was found to have better repeatability and stability while having 47 fold lower drift at the higher operating temperature, when compared to its non-modified counterpart.

**5:20 PM Concluding Comments**

### Aluminum Alloys: Fabrication, Characterization and Applications: Development and Application

Sponsored by: The Minerals, Metals and Materials Society, TMS Light Metals Division, TMS: Aluminum Processing Committee

Program Organizers: Weimin Yin, Williams Advanced Materials; Subodh Das, Phinix LLC; Zhengdong Long, Kaiser Aluminum Company

Monday PM  
February 16, 2009

Room: 2004  
Location: Moscone West Convention Center

Session Chair: Shridas Ningileri, Secat Inc

**2:00 PM**

**Development of Low-Cost, High-Performance AlZn4.5Mg1 Alloy 7020:** *John Chinella*<sup>1</sup>; <sup>1</sup>U. S. Army Research Laboratory

This paper reviews properties, processing, and performance of Cu-free Al-Zn-Mg alloy 7020. Comparisons are made with alternative military aluminum alloys' chemistry, material costs, properties, levels of strength and ductility, and resistance to stress and exfoliation corrosion. The approach and experimental results for development and optimization of alloy 7020 for vehicle armor or welded structures are identified and described either for the mill, solution treated quenched and aged, or high-temperature aged conditions. Advantages for military and commercial use include: (1) low thermal sensitivity of the microstructure and mechanical properties to deleterious effects either from reheat or solution-treatment quench, (2) low material cost, (3) medium strength, and (4) high levels of weld strength and ductility in the natural or artificial aged condition.

**2:20 PM**

**Aluminum Sheet Applications and Manufacturing Challenges in the Automotive Industry:** *Susan Hartfield-Wunsch*<sup>1</sup>; Jody Hall<sup>1</sup>; <sup>1</sup>General Motors Corp

Application of aluminum for mass reduction in automobiles has been a topic of discussion for several decades. Aluminum casting and extrusion applications are pervasive in powertrain and chassis components. In contrast, aluminum sheet metal has only limited application in automotive bodies, and is currently found predominantly on higher-end vehicles. New CAFÉ requirements and higher fuel costs have increased pressure on the automotive industry to improve fuel economy and reduce emissions. This paper will explore the reasons for the 'limited and slow' implementation of sheet aluminum into automotive bodies and make a prediction of how this scenario will change. It will also cover the major challenges in manufacturing aluminum sheet metal components and outline where additional research and development projects can help accelerate production applications.

**2:40 PM**

**High Strength Aluminum Sheet for Automotive Applications:** *Dirk Uffelmann*<sup>1</sup>; <sup>1</sup>AMAG Rolling GmbH

The most common aluminum alloys for automotive sheet applications are work-hardening 5000-series and heat-treatable 6000-series alloys. They are used in a wide range of structural parts, components and hang-on-parts. From a general view, the usage of these alloys results in a reasonable ratio of cost per weight saving and a good compatibility with existing production methods in terms of forming and joining. Superior yield strength and tensile strength can be achieved by heat-treatable 2000- and 7000-series alloys, commonly used for aircraft applications. For certain automotive applications, there is additional weight saving potential by use of these high-strength aluminum alloys. The purpose of this paper is to show the possibilities and limitations of weight saving by usage of high-strength aluminum alloys with respect to production (forming, joining, heat treatment) and performance (corrosion, fatigue, crash performance).

**3:00 PM**

**Development of Twin-Belt Cast AA5XXX Series Aluminum Alloy Materials for Automotive Sheet Applications:** *Pizhi Zhao*<sup>1</sup>; Toshiya Anami<sup>1</sup>; Ichiro Okamoto<sup>1</sup>; Kazumitsu Mizushima<sup>1</sup>; Kevin Gatenby<sup>2</sup>; Mark Gallemeault<sup>2</sup>; Simon Barker<sup>2</sup>; Kunihiko Yasunaga<sup>3</sup>; Akira Goto<sup>3</sup>; Hitoshi Kazama<sup>3</sup>; Noboru Hayashi<sup>3</sup>; <sup>1</sup>Nippon Light Metal Company, Ltd.; <sup>2</sup>Novelis Global Technology Center; <sup>3</sup>Honda R&D Co., Ltd

Process routes for AA5XXX series aluminum alloy sheet produced via a twin belt caster (FLEXCASTER) have been successfully trialed. The FLEXCAST AA5XXX sheet has a fine intermetallic and grain structure compared to conventional DC processed AA5XXX aluminum alloy sheet as a consequence of the high cooling rate during solidification. Optimization of composition and refinement of microstructure results in superior dome stretchability and lower susceptibility to SCC than DC AA5182 sheets. Moreover, the FLEXCAST AA5XXX aluminum alloy sheet shows good performance in coating and adhesive bonding tests, which are critical for automotive structure parts.

**3:20 PM**

**Microstructure-Property Correlation of Aluminum Alloy 2219 Produced by Electron Beam Freeform Fabrication:** *Ravi Shenoy*<sup>1</sup>; Marcia Domack<sup>2</sup>; <sup>1</sup>Lockheed Martin Mission Support; <sup>2</sup>Advanced Materials and Processing Branch, NASA Langley Research Center

Electron beam freeform fabrication (EBF3) is a layer-additive manufacturing process wherein a metal wire of required alloy composition is fed at a controlled speed into a molten pool created on a metal substrate surface, using a focused electron beam. The component geometry is achieved through the ensuing solidification, by translating the substrate with respect to the beam. In the present study, cast and precipitate microstructures unique to complex thermal histories experienced during successive layered EBF3 depositions in aluminum alloy 2219 were characterized using electron microscopy, microtexture, and thermal analysis in order to investigate the metallurgical mechanisms contributing to the observed properties. The strength level of as-deposited 2219 was between O and T4 temper wrought products and within 2% of T6 temper products after heat treatment. The results of the investigation are presented in relation to process parameters employed such as the translation speed, wire feed rate, and beam power.

**3:40 PM**

**A Novel Thermomechanical Processing Method to Achieve Fine-Grained AA6xxx Sheet:** *Shahzad Esmaeili*<sup>1</sup>; David Lloyd<sup>2</sup>; Haiou Jin<sup>2</sup>; <sup>1</sup>University of Waterloo; <sup>2</sup>Novelis Global Technology Centre

A novel thermomechanical processing method to produce fine-grained sheets of heat treatable aluminium alloys has been developed. The method, which includes a continuous cold rolling and annealing process, has been applied to an AA6xxx alloy plate and a fine-grained sheet with desirable microstructural characteristics has been achieved. The fabricated sheet has shown significantly enhanced ductility in wide ranges of temperatures and strain rates and therefore provides a potential solution to the formability issue in automotive applications of AA6xxx sheets. The present work will outline the processing route and the characteristics of the fine-grained AA6xxx alloy in comparison with the conventionally-produced coarse-grained version of the alloy.

## 4:00 PM Break

### 4:15 PM

**Re-Use of Aluminum Turning Chips by Hot Extrusion:** *Klaus Pantke*<sup>1</sup>; Dirk Biermann<sup>1</sup>; <sup>1</sup>University of Dortmund

Aluminum is the most widely used metal after steel in the manufacturing industry. Due to the convenient material properties, this material can be used in several products. The energy requirement for producing and melting aluminum is one of the major disadvantages of this material. Although the re-melting of scrap aluminum can reduce the energy requirements, the needed energy even for the melting process is still high. This article presents a process chain of direct conversion technology of aluminum chips by cutting, compaction of the chips to billets, hot extrusion to a rectangular square profile, and finally characterization of the profile properties. It is shown that, by direct conversion, a melting of the chips for secondary use can become unnecessary. Due to the fact, that this process chain doesn't need a melting process, there will be great advantage over the conventionally process chain to save ecological and economical resources.

### 4:35 PM

**Establishing Foil Stock Production through Continuous Casting Route - Our Experience in BALCO:** *P.K.N. Raghavan*<sup>1</sup>; Mousumi Kar<sup>1</sup>; Diwakar Singh<sup>1</sup>; <sup>1</sup>Bharat Aluminium Co. Ltd., (A Unit of Vedanta Resources Plc.)

Coils for the production of thin foils can also be done through continuous strip casting process which is directly cold rolled. The alloys processed in a continuous strip casting process result in foil stock which has a higher supersaturation of solute elements, and therefore has undesirable hardening and softening properties, causing difficulties in rolling the foil stock to the final gauge thickness. The various difficulties faced in production of AA 8011 foil stock through twin roll continuous strip casting process and the corrective measures taken at Balco to overcome the difficulties for producing good quality foil stock have been elaborated in this paper. Microstructural examination and structure-property correlation of foil stocks produced through DC casting and Continuous strip casting routes have also been discussed in detail. The advantages of this process viz the Direct Chill Casting route will also be discussed.

### 4:55 PM

**On the Distortion and Warpage of 7249 Aluminum Alloy after Quenching and Machining:** *Omar Es-Said*<sup>1</sup>; Eui Lee<sup>2</sup>; <sup>1</sup>Loyola Marymount University; <sup>2</sup>Naval Air Systems Command

From large extrusion plates of 7249 Aluminum Alloy with fins, T sections of length 25.4 cms (10 inches) and width 4.6 cms (1.8 inches) were cut. Three solution temperatures, two quenching media, two aging treatments, and three machine cuts were used. The objective was to determine the degree of warpage as a function of solution temperature, quenching media, and machining sequence. Two machining cuts removed the fin; one left it on. The flatness was measured on the surfaces orthogonal to the z-axis. They were then averaged together to represent the overall warpage of each sample.

## Aluminum Cold Rolling and Strip Processing: Session I

Sponsored by: The Minerals, Metals and Materials Society, TMS Light Metals Division, TMS: Aluminum Processing Committee  
Program Organizer: Kai Karhausen, Hydro Aluminium

Monday PM  
February 16, 2009

Room: 2010  
Location: Moscone West Convention Center

Session Chair: Kai Karhausen, Hydro Aluminium

## 2:00 PM Introductory Comments

### 2:05 PM Keynote

**Cold Rolling Processes to Functionalize Semi-Finished Products:** Gerhard Hirt<sup>1</sup>; *Koos van Putten*<sup>1</sup>; Reiner Kopp<sup>1</sup>; Mario Thome<sup>1</sup>; <sup>1</sup>RWTH Aachen

Sheets, strips and profiles are semi finished products, which are widely used for structural light weight components in transport systems, civil engineering and machine building. During the last years various rolling processes have been investigated and partly been introduced to industrial applications, which enable to manufacture geometrically tailored products: The so called "flexible rolling"

process is used to roll sheets with product specific thickness changes in rolling direction to produce sheet metal parts with load optimized thickness distribution. Thickness changes in width direction of thin strips can be produced by strip profile rolling using modified roll forming equipment. Riblet surface structures similar to shark skin can be rolled directly into aluminium sheet using a new roll structuring technique. The actual status of these processes and their application is presented including consequences for further processing.

### 2:45 PM

**Analytical Stress Field Modelling of Rolled Aluminium Strips under Tensile Loading:** *Holger Aretz*<sup>1</sup>; Stefan Neumann<sup>1</sup>; Kai Karhausen<sup>1</sup>; <sup>1</sup>Hydro Aluminium Deutschland GmbH

During downstream processing aluminium strips are often subjected to tensile loading. In particular, during cold rolling upstream and downstream tensile loads are imposed by the de-coiler and the coiler, respectively. The knowledge of the resulting stress field is essential for the rolling and the downstream winding process. The present contribution consists of three major parts: (1) An analytical stress field model is developed resting on the construction of an admissible stress function according to Airy's theory within the framework of plane stress linear elasticity. Application examples are provided. (2) Based on an elementary analysis the incorporation of off-flatness effects in form of residual plastic strains in the aforementioned stress field model is described. (3) A new approach based on elementary equilibrium conditions is presented that aims at calculating the across-width stress distribution in rolled strips possessing an arbitrary transversal thickness profile which are loaded by a constant remote tensile stress.

### 3:05 PM

**Recrystallization Texture Development under Various Thermo-Mechanical Conditions in Aluminum Alloys:** *Jurij Sidor*<sup>1</sup>; Alexis Miroux<sup>1</sup>; Roumen Petrov<sup>2</sup>; Leo Kestens<sup>2</sup>; <sup>1</sup>Materials Innovation Institute; <sup>2</sup>TU DELFT

The texture development during recrystallization annealing is affected by the thermo-mechanical history. A variety of hot and cold rolling parameters account for various recrystallization textures both qualitatively and quantitatively. Asymmetric rolling by a differential circumferential velocity of the top and bottom rolls is applied to the investigated aluminum alloy. The resulting shear deformation gives rise to a non-conventional texture evolution in the hot band. Introduction of intermediate annealing during cold rolling affects both volume fraction of the cube orientation as well as the total strength of the produced texture. The influence of both rolling parameters and initial textures on the development of the deformation and recrystallization textures is discussed based on experimental data and results of texture simulation with a wide variety of crystal plasticity models.

### 3:25 PM

**Experimental Procedures for Characterization of Static Recovery in Cold Rolling Processes of AlFeSi Alloys:** *Christoph Heering*<sup>1</sup>; Xiaoli Li<sup>1</sup>; Gerhard Hirt<sup>1</sup>; Markus Bambach<sup>1</sup>; <sup>1</sup>RWTH Aachen

In this paper, experiments regarding the influence of static recovery on the flow stress of AlFeSi alloys are presented. Double compression tests at different temperatures were carried out. From these tests, stress-time curves were generated that describe the static recovery. The stress time curves were used for an empirical recovery. Additionally, two series of cold rolling experiments with AlFeSi alloys were performed. One series of cold rolling tests was performed with a heat treatment at 230°C and one series of rolling experiments was performed under ideal cold rolling conditions. Subsequent to every process step the flow stress of the sheet was measured by tensile tests. Thus, the influence of static recovery on the flow stress in cold rolling processes can be compared to the flow stress development in ideal cold rolling. Finally, the rolling experiments were simulated using a physical flow stress model with an implemented empirical recovery model.

## 3:45 PM Question and Answer Period

### 3:55 PM Break

### 4:10 PM

**Innovations in Surface Quality Inspection as a Cornerstone for Production Optimization:** *Uwe Knaak*<sup>1</sup>; Elisa Jannasch<sup>1</sup>; <sup>1</sup>Isra Vision Parsytec Ag

Surface defects impair the quality of the manufactured aluminum strip; they may lead to strip breaks or to equipment damage: less ability to deliver usable quality to customers, less throughput, and higher costs are the consequences. Isra Vision Parsytec offers leading-edge solutions for surface quality inspection:



Surface Inspection Systems deliver defect information to be turned into quality data for a most efficient production optimization. The benefits for customers include highest detection sensitivity and accelerated access to relevant quality data combined with highest availability and easiest handling and maintainability of the systems. Furthermore, so-called "production decision intelligence" solutions transforming inspection data to production benefit in selected applications are available. Production optimization can be achieved by combining surface quality data with all available production and process data, as well as with customer and order information. Surface inspection thus serves two aims: increasing product quality, and turning surface quality information into production excellence.

**4:30 PM**

**Modeling of Cold Surface Rolling Process of Al 2014 T6 Alloy, Residual Stress Calculation:** *Behzad Majidi*<sup>1</sup>; <sup>1</sup>Amirkabir University of Technology

Cold surface rolling is a very important process which is performed on different parts to enhance surface quality and to generate near- surface residual compressive stresses. In the present investigation cold surface rolling of 2014 T6 aluminum alloy has been modeled by the mean of finite element method using ABAQUS/Explicit software. The effects of rolling load and speed and also number of rolling steps have been studied. Results showed that the most favorable compressive stress gradient in depth of the part corresponds to the load of 100Kgf in one step rolling. It was also found that increasing rotation speed of part during rolling has a positive effect on the residual compressive stress magnitude at surface.

**4:50 PM**

**Effects of Annealing Process on Intermetallic Compound of Carbon Steel/Al Cladding Strip:** *Guoyin Zu*<sup>1</sup>; *Wei Wang*<sup>1</sup>; *Jiuming Yu*<sup>1</sup>; <sup>1</sup>School of Materials and Metallurgy

The annealing process for carbon steel/Al cladding strip was investigated systematically, to discuss the effects of annealing temperature/time on the growth of intermetallic compound by OM, SEM, XRD measurements, the tensile strength and elongation of cladding strip was tested using electronic universal testing machine. The results show that the deformation energy during rolling process go against growth control of intermetallic compound. The critical temperature spot of intermetallic compound forming is 420°, the intermetallic compound is FeAl<sub>3</sub> phase. The tensile strength and elongation of cladding strip tended to raise first and then declined with increasing annealing duration. Based on comprehensive consideration of growth condition of intermetallic compound and the mechanical properties of cladding strip, the optimum annealing process should be at 420° for 40min. In addition, short time high temperature and single-side annealing were beneficial to inhibit the growth of intermetallic compound.

**5:10 PM Question and Answer Period**

**Aluminum Reduction Technology: Environment**

Sponsored by: The Minerals, Metals and Materials Society, TMS Light Metals Division, TMS: Aluminum Committee  
 Program Organizers: Gilles Dufour, Alcoa Canada, Primary Metals; Martin Iffert, Trimet Aluminium AG; Geoffrey Bearne, Rio Tinto Alcan; Jayson Tessier, Alcoa Deschambault

Monday PM Room: 2001  
 February 16, 2009 Location: Moscone West Convention Center

*Session Chair:* Nancy Holt, Hydro Aluminium

**2:00 PM Introductory Comments and Presentation of 2008 Best Paper Award 2008 Light Metals Paper Awards Presentation: Aluminium Reduction**

**2:05 PM**

**Global Anode Effect Performance: 2010 PFC Emissions Reduction Objective Met:** *Jerry Marks*<sup>1</sup>; <sup>1</sup>International Aluminium Institute

One of the first objectives set by the Directors of the International Aluminium Institute (IAI) as part of the global industry's Aluminium for Future Generations Sustainability Initiative was to reduce PFC emissions per metric ton aluminum produced by 80% from the 1990 baseline by 2010. To monitor progress toward this objective the IAI conducts an annual global industry survey of anode effect

performance. The 2006 survey data showed that the 2010 objective has been achieved four years early. Now that the objective has been met the Directors are considering a new PFC emissions objective. This paper discusses the details of the analysis of the anode effect survey data, the progress made to date in PFC emissions reduction, and considers what the potential might be for future PFC emissions reductions.

**2:25 PM**

**An Innovative Method for Sampling and Analysis of Tetrafluoromethane and Hexafluoroethane Emitted from Aluminium Smelter Using Sorbent Tubes:** *Josette Ross*<sup>1</sup>; *Véronique Bouchard*<sup>2</sup>; *Michel Gagnon*<sup>2</sup>; *Jean-Nicolas Maltais*<sup>1</sup>; <sup>1</sup>Rio Tinto Alcan; <sup>2</sup>UQAC

Rio Tinto Alcan has aggressive objectives regarding the reduction of CF<sub>4</sub> and C<sub>2</sub>F<sub>6</sub> (two greenhouse gases) emitted during the anode effect. Consequently, the PFC concentrations decrease during the sampling measurement campaigns. Presently, the most frequently used method to evaluate the PFC emissions in an aluminium smelter is the Fourier Transform Infra Red analysis. It is a costly method with a probably detection limit not low enough for high performing plants. The Arvida Research and Development Centre has developed a new innovative method using a thermal desorption system coupled with a gas chromatograph and a mass spectrometer for the sampling and analysis of CF<sub>4</sub> and C<sub>2</sub>F<sub>6</sub>. The sampling is easy and inexpensive to perform, the sample could easily be sent by post, and the analysis is fast and very sensitive. For a 24-hour sampling period, the detection limits were determined as being 120 and 260 pptv for CF<sub>4</sub> and C<sub>2</sub>F<sub>6</sub> respectively.

**2:45 PM**

**Initiatives to Reduce Anode Effect Frequency at Dubal:** *Arvind Kumar*<sup>1</sup>; *Ali Al Zaroni*<sup>1</sup>; *Maryam Al Jallaf*<sup>1</sup>; <sup>1</sup>Dubai Aluminium Co. Ltd.

Extensive studies have been carried out in smelters around the world to understand the fundamental cause of an anode effect. The exact nature of the onset of an anode effect is still shrouded in mystery. However, the consensus is that anode effects are detrimental to pot operation; they result in reduced energy consumption and cause emission of CF<sub>4</sub> and C<sub>2</sub>F<sub>6</sub> gases. With the intention of reducing carbon footprint, there is an excellent opportunity to reduce anode effects and the resulting PFC emissions. Occurrence of an anode effect was studied in relation to different aspects; alumina feed rate, work schedule, cathode type, operating parameters, mechanical issues, etc. Onset of an anode effect was primarily due to inability of the response strategy to deal with it efficiently. Alumina fines and pencilling of crust breaker tip were the other reasons. The paper covers strategies pursued at Dubal to reduce anode effect frequency.

**3:05 PM**

**Handling Co<sub>2</sub>EQ from an Aluminum Electrolysis Cell:** *Odd-Arne Lorentsen*<sup>1</sup>; *Are Dyroy*<sup>1</sup>; *Morten Karlsen*<sup>1</sup>; <sup>1</sup>Hydro Aluminium

The current focus on reduction of energy consumption and preserving our environment will affect a lot of industries in the coming years, also the aluminum industry. Hydro believes aluminum is a part of a sustainable future, and wants to take an active part in developing an even more environmentally friendly production process. Most of Hydro's electricity used for aluminum production is based on water power, but the plants in Kurri Kurri and Neuss are based on coal and our new smelter in Qatar will be based on gas. This paper gives an insight in Hydro's plans for reduction of their carbon footprint from their primary productions around the world by keeping their focus aiming for elimination of AE and production of CF-gases. Hydro also have developed a gas suction technology enabling CO<sub>2</sub> capture from their electrolysis pots, as well as reduction of the net gas suction volume, with promising results.

**3:25 PM Break**

**3:45 PM**

**Comparison of PFC Emission for Operating and Newly Started Pots at the Alcoa Fjardaal Point Fed Prebake Smelter:** *Neal Dando*<sup>1</sup>; *Weizong Xu*<sup>1</sup>; *Jerry Marks*<sup>2</sup>; <sup>1</sup>Alcoa Inc; <sup>2</sup>J Marks and Assoc.

Under a jointly sponsored program by the USEPA and Alcoa, PFC monitoring campaigns were performed at Alcoa's Fjardaal smelter to 1) determine Tier 3 PFC emissions rates from previously started (months earlier) operating cells, 2) determine Tier 3 PFC emissions from recently started (days earlier) operating cells and 3) determine the PFC emissions from a population of newly started cells during the initial "bathup" period and subsequent operation. The measured PFC slope terms from these three pot populations indicate that no significant difference exists between initial startup and "normal" pot Tier 3 PFC emission

coefficients when the pots are well heated prior to bath up (gas-bake pre-heating). This data also suggests that anode effect data from the initial "bath-up" period can be included in the plant's PFC reporting inventory using the same emission coefficients determined during normal pot operation, assuming that "soft" (well pre-heated cathode) pot starts are performed.

#### 4:05 PM

**Dry Scrubbing for Modern Pre-Bake Cells:** *Stephen Lindsay*<sup>1</sup>; Neal Dando<sup>1</sup>; <sup>1</sup>Alcoa Inc

The two fundamental "raw materials" for pot room gas treatment systems are alumina and the process off-gases. Modern dry scrubbing technology offers very efficient removal technology. However, increases in the amount of fluoride evolved from reduction cells and increases in fume evacuation rates can challenge the abilities of dry scrubbers. This is especially so if the goal is to provide; state of the art removal efficiency, and alumina at the pot that is low in fines content. In this paper the author discusses trends in our industry and proposes solutions that include more efficient utilization of alumina and process gas flow to meet emerging needs.

#### 4:25 PM

**Pot Gas Heat Recovery and Emission Control:** Geir Wedde<sup>1</sup>; *Anders Sorhuus*<sup>1</sup>; <sup>1</sup>ALSTOM Norway AS

Substantial quantities of heat is released to the ambient through pot exhaust and present pot gas temperature of 150-180°C also affect the operation of the Gas Treatment Centres (GTC). Standard polyester filter bags used in the GTC can only sustain gas temperatures of 135°C. A sharp rise in fluoride emissions (HF) is seen as pot gas temperatures exceed 100°C. Dilution of the pot gas with ambient air is used to achieve acceptable GTC gas temperatures (110-115°C) and emission levels. This results in a need for substantial increase in the filtration capacity of the GTC. A heat exchanger has been developed to combine heat recovery and cost efficient cooling of pot gas. The technology has been tested on pot gas in a pilot plant. Promising stable heat exchange and pressure drop over longer test periods have encouraged Alstom to continue the development into a commercial product.

#### 4:45 PM

**Development of a Jet Induced Boosted Suction System to Reduce Fluoride Emissions:** *Michel Meyer*<sup>1</sup>; Guillaume Girault<sup>2</sup>; Jean-Marc Bertolo<sup>1</sup>; <sup>1</sup>Rio Tinto Alcan; <sup>2</sup>Tomago Aluminium Company Ltd

For many aluminium smelters, reducing fluoride specific emissions is the sine qua non condition for production growth. Since they represent nearly 40% of the overall roof vent results, anode change operations are particularly targeted for improvements. A preliminary review of the available options concluded that significantly increasing the pot exhaust flow during anode change was the more promising technological option. An Alcan patented solution, the Jet Induced Boosted Suction System has been trialled successfully on AP22 pots in Tomago. The performance of the system, in terms of emission reduction, costs, operating and maintenance requirements was evaluated during the trial with the objective of extending the system to larger trial groups and AP30 pots.

#### 5:05 PM

**The Impact of Ambient Wind on the Vertical Component of Smelter Roofvent Flow Velocity:** *Michael Gershenson*<sup>1</sup>; Neal Dando<sup>1</sup>; <sup>1</sup>Alcoa Inc

This work details the correlation between ambient wind (direction and speed) and the vertical component of smelter rooftop air flow velocity. This study shows that when ambient winds are co-aligned with the long axis of a smelter building, the average vertical airflow velocity leaving the potroom roofline is reduced. This effect is especially pronounced when the building's side ventilators (basement panels) are shut during the colder months of the year. This study emphasizes the importance of examining prevailing wind patterns for assessing fugitive emissions from both existing and projected smelters, especially for geographic locations with distinct wind roses (e.g., marine regions).

## Biological Materials Science: Biomimetic Processing

Sponsored by: The Minerals, Metals and Materials Society, TMS Structural Materials Division, TMS Electronic, Magnetic, and Photonic Materials Division, TMS: Biomaterials Committee, TMS/ASM: Mechanical Behavior of Materials Committee

Program Organizers: Ryan Roeder, University of Notre Dame; John Nychka, University of Alberta; Paul Calvert, University of Massachusetts Dartmouth; Marc Meyers, University of California

Monday PM

Room: 3014

February 16, 2009

Location: Moscone West Convention Center

Session Chair: Roger Narayan, University of North Carolina

#### 2:00 PM Keynote

**Chemical Tailoring of Biologically-Derived 3-D Nanostructured Inorganic**

**Assemblies:** *Kenneth Sandhage*<sup>1</sup>; Zhihao Bao<sup>1</sup>; Eric Ernst<sup>1</sup>; Sehoon Yoo<sup>2</sup>; Yunnan Fang<sup>1</sup>; Michael Weatherspoon<sup>3</sup>; Samuel Shian<sup>1</sup>; Ye Cai<sup>1</sup>; Qingzhong Wu<sup>1</sup>; Matthew Dickerson<sup>4</sup>; Emily Malcolm<sup>1</sup>; Nicole Poulsen<sup>1</sup>; Nils Kroger<sup>1</sup>; <sup>1</sup>Georgia Institute of Technology; <sup>2</sup>Korea Institute of Industrial Technology; <sup>3</sup>Harris Corporation; <sup>4</sup>Air Force Research Laboratory

The low-cost fabrication of chemically-tailored inorganic structures with selectable morphologies, controlled over the micro-to-nanometer scales and over three dimensions, remains a significant technological challenge. Hierarchical 3-D inorganic assembly is, however, accomplished under ambient conditions by diatoms (single-celled microalgae). Each of the tens of thousands of diatom species forms a nanostructured silica microshell (frustule) with a unique, genetically-determined 3-D morphology. Sustained diatom reproduction can yield enormous numbers of frustules of similar morphology. Such genetically-precise, massively-parallel, 3-D assembly is without analog in synthetic nanofabrication. However, the silica-based frustule chemistry severely limits the range of potential applications. With the patented\* BaSIC (Bioclastic and Shape-preserving Inorganic Conversion) process, reaction-based and/or coating-based methods can be used to convert such bioclastic templates into non-natural functional chemistries, while preserving the 3-D hierarchical morphology. Recent work on conversion of diatom frustules into functional metallic and oxide chemistries will be described. U.S. Patents 7,204,971 (4/17/07) and 7,067,104 (6/27/06).

#### 2:40 PM

**Writing Fiber-Reinforced Gels for Soft Tissue Replacement: The**

**Robospider:** *Paul Calvert*<sup>1</sup>; Animesh Agrawal<sup>1</sup>; Tesfay Meressi<sup>1</sup>; Bharat Mahajan<sup>1</sup>; <sup>1</sup>University of Massachusetts Dartmouth

While large quantities of textile fiber can be readily melt-spun or solution-spun, there is no simple way to form small quantities of fiber from specialty polymers or biopolymer solution. A pultrusion system is being used to spin micron-diameter polymer fibers from solution in analogy to the spinning of a spider web. Extrusion of fibers from a moving syringe needle coupled to a sensitive force transducer was used to measure and model the process. This system is now being used to deposit fibers onto surfaces or into gels in order to build webs and fiber-reinforced hydrogels. This paper will discuss the constraints on using this approach to mimic soft tissues such as cartilage.

#### 3:00 PM

**Molecular Biomimetics - A New Paradigm in Functional Materialization:**

*Mehmet Saikaya*<sup>1</sup>; <sup>1</sup>University of Washington

Properties of engineered materials are structure sensitive and their synthesis, formation and organization take place with the control of heat that allows manipulation of atoms and molecules, providing the energy for compound formation. The TTT diagrams in Fe-C systems are ideal examples where transformation is controlled by temperature and time. In biological systems, such as hard tissues, all these processes, however, take place at ambient conditions in aqueous solutions, without the effect of heat flow. Functions of biological materials are also structure-sensitive, and are the results of evolution. In biological systems, synthesis, formation, and structuring are controlled by peptides and proteins that are evolved to bind to these solids and, in turn, manipulate their behavior. This presentation will highlight examples of materialization in biology and offer ways of how it may be possible to genetically engineer peptides for inorganics as molecular building blocks for next generation materials systems.

3:20 PM

**Feasibility of Fabricating Root-Form Implants by Electron Beam Melting:** Marie Koike<sup>1</sup>; Gilbert Chahine<sup>2</sup>; Radovan Kovacevic<sup>2</sup>; Toru Okabe<sup>1</sup>; <sup>1</sup>Baylor College of Dentistry; <sup>2</sup>Southern Methodist University

Currently, endosteal dental implants are made of titanium alloys which consist of the root-form fixture and transmucosal abutment. Traditional implants are placed in the jawbone after a socket hole is drilled to accept endosteal implants. With the advent of electron beam melting (EBM), we developed the method for micro-CT scanning of teeth in need of extraction and rapid prototyping of one-component biomimetic implants that fit within the existing root socket. These implants are expected to decrease the risk of implant failure at the root-form fixture/transmucosal abutment interface and improve osseointegration to encourage bone in-growth, leading to shorter healing time. Using EBM equipment (ARCAM A2, Sweden), molar teeth of Ti-6Al-4V (ELI) were fabricated from computerized X-ray tomography images of extracted maxillary teeth. The shape and dimension of the EBM teeth were similar to the extracted teeth. In the presentation, the mechanical properties of EBM-fabricated titanium will be reported.

3:40 PM Break

3:50 PM Student Poster Contest Short Oral Talks chaired by Ryan K Roeder, University of Notre Dame

## Bulk Metallic Glasses VI: Alloy Development and Glass Forming Ability II

Sponsored by: The Minerals, Metals and Materials Society, TMS Structural Materials Division, TMS/ASM: Mechanical Behavior of Materials Committee  
Program Organizers: Peter Liaw, The University of Tennessee; Hahn Choo, The University of Tennessee; Yanfei Gao, The University of Tennessee; Gongyao Wang, University of Tennessee

Monday PM Room: 3007  
February 16, 2009 Location: Moscone West Convention Center

Session Chairs: Akihisa Inoue, Tohoku University; Marios Demetriou, California Institute of Technology

2:00 PM Invited

**Metallic Glassy Nanowire:** Koji Nakayama<sup>1</sup>; Y. Yokoyama<sup>1</sup>; G. Xie<sup>1</sup>; Q.S. Zhang<sup>1</sup>; M. W. Chen<sup>1</sup>; T. Sakurai<sup>1</sup>; A. Inoue<sup>1</sup>; <sup>1</sup>Tohoku University

Metallic glassy nanowires were spontaneously created on the fracture surfaces that were produced by a conventional mechanical test. The presence of the nanowires is directly related to the one-dimensional meniscus configuration with a small viscosity at high temperatures and to the wide supercooled liquid region of the metallic glass. The electron microscopic observations demonstrate the diameters, the lengths, and the amorphous structural states, and the energy dispersive X-ray reveals the chemical components. In addition, we found that round ridges are constructed from nanotubes. The finding of amorphous nanostructures provides not only fundamental understanding of fracture processes but also give a new insight into nano-engineering constructions.

2:15 PM

**The Role of Friction in Measurements of the Formability of Bulk Metallic Glasses:** Sven Bossuyt<sup>1</sup>; Jan Schroers<sup>2</sup>; <sup>1</sup>Vrije Universiteit Brussel; <sup>2</sup>Yale University

Recently, a simple experiment was proposed to characterize the formability of bulk metallic glasses. It measures the total deformation of a specimen that occurred, under constant load, while heating from below the glass transition, to above the crystallisation temperature. A priori, it is not clear whether the higher deformation rate achievable with more fragile glass-formers or the larger time-temperature processing window before crystallization of stronger glass-formers is most beneficial for formability of bulk metallic glasses reheated above their glass transition temperature. The proposed measurement takes these contradictory effects into account, and directly measures this formability. We demonstrate the role of friction in these experiments, using analytical results for limiting cases and mixed numerical experimental methods for finite friction coefficients.

2:25 PM Invited

**Preparation and Characterizations of Bulk Metallic Glasses Using Spark Plasma Sintering:** Jinn Chu<sup>1</sup>; Ying Chen Tai<sup>1</sup>; Robert Aalund<sup>2</sup>; Tom C. Clappier<sup>2</sup>; Matt W. Mede<sup>2</sup>; Shian-Ching Jang<sup>3</sup>; <sup>1</sup>National Taiwan University of Science and Technology; <sup>2</sup>Thermal Technology, LLC; <sup>3</sup>I-Shou Univ

Due to many unique properties, bulk metallic glasses (BMG's) have recently generated enormous interest. Yet, some BMG's in large sizes are not readily obtained because their glass-forming ability (GFA) is not high enough to use the conventional casting technique to prepare BMG's. Spark plasma Sintering (SPS) has been reported to sinter nano-sized or amorphous powder materials into bulk forms with no or minimal crystallization and grain growth through a short and effective sintering process. In addition, SPS'ed samples with nearly 100% theoretical density and properties close to those of bulk parts make SPS an attractive technique for BMG's with low GFA. In this presentation, many BMG systems prepared using SPS are characterized by various analytical techniques including differential scanning calorimeter, X-ray diffractometer, scanning and transmission electron microscopes. This study is directed toward to establishing better understanding of SPS-prepared BMG properties, thus utilizing SPS for the large-sized BMG's with desirable properties.

2:40 PM

**High Glass Formability for Cu-Hf-Ti Alloys with Small Additions of Y and Si:** Ignacio Figueroa<sup>1</sup>; Hywel Davies<sup>1</sup>; Iain Todd<sup>1</sup>; <sup>1</sup>University of Sheffield

The effect of small substitutions of Si and Y on the glass forming ability (GFA) of the Cu<sub>55</sub>Hf<sub>25</sub>Ti<sub>20</sub> glassy alloy is reported and discussed. Fully glassy rods with diameters up to 7 mm and 6.5 mm, were produced for Cu<sub>54.5</sub>Hf<sub>25</sub>Ti<sub>20</sub>Si<sub>0.5</sub> and Cu<sub>55-x</sub>Hf<sub>25</sub>Ti<sub>20</sub>Y<sub>0.3</sub> alloys, respectively. The addition of Si enlarged the Tx considerably from 30 to 53 K for the Cu<sub>54</sub>Hf<sub>25</sub>Ti<sub>20</sub>Si<sub>1</sub> alloy. The results showed that the parameters obtained from thermal analysis, such as Trg and ΔTx are not reliably correlated with GFA, at least for these bulk glass forming alloys. The scavenging effect of the Y and Si, in particular the possibility of Y reducing the oxides, could be responsible for enhancing the GFA. The effectiveness of small additions of Si on the GFA was considered that might be enhanced by the large negative heat of mixing and the possible formation of HfSiO<sub>4</sub> as a strong network former.

2:50 PM

**New Processing Potential for Bulk Metallic Glass Matrix Composites with Tensile Ductility:** Douglas Hofmann<sup>1</sup>; Jin-Yoo Suh<sup>1</sup>; Aaron Wiest<sup>1</sup>; William Johnson<sup>1</sup>; <sup>1</sup>California Institute of Technology

Recently, metallic glass matrix composites have been demonstrated with high toughness and extensive tensile ductility. A composite with ~60% crystalline phase is demonstrated to have bending ductility in large dimensions and crack arrest in large thickness samples. For the composite, plastic forming above the glass transition temperature is demonstrated, room temperature cold rolling to strains over 100% is achieved with high reduction rates per rolling pass, and tension tests are performed on previously rolled samples. We note that yield strength and stiffness increase as a result of rolling but tensile ductility is preserved. The tests demonstrate that the new toughened glassy composites combine the best properties from metallic glasses (high strength, high elastic limit, plastic forming ability, low melting point, net shape forming ability, high hardness, etc.) with the toughest of crystalline metals. The alloys therefore represent a new paradigm in metallurgy

3:00 PM

**Influence of Bond Enthalpy on Metallic Glass Stability:** James Dahlman<sup>1</sup>; Daniel Miracle<sup>1</sup>; <sup>1</sup>Materials and Manufacturing Directorate

Metallic glasses form structures with a high degree of short range order, indicating an underlying thermodynamic criterion, as interatomic bond strength largely governs nearest neighbor interaction. While earlier empirical guidelines suggest that the enthalpy of mixing exerts a strong influence on glass stability, previous work has failed to show a correlation. This work seeks to establish a connection between nearest neighbor bond energy and glass-forming ability through evaluation of interatomic bond enthalpies. An approach to determine bond enthalpies from available thermodynamic data will be described and resulting bond enthalpies will be presented. The number and type of atom bonds that are present in a metallic glass structure are estimated as a function of metallic glass constitution using the efficient cluster packing structural model. By combining these two analyses, we estimate the enthalpy associated with glass formation, and explore correlations with experimental measurements of glass-forming ability.



## 3:10 PM Break

### 3:20 PM Invited

**Nanoglasses Synthesized by Extreme Plastic Deformation of BMG:** *Hans Fecht*<sup>1</sup>; Yulia Ivanisenko<sup>2</sup>; <sup>1</sup>Ulm University; <sup>2</sup>Forschungszentrum Karlsruhe

We present recent results on the fundamentals of extreme plastic deformation of a range of fully dense metallic glasses. By high pressure torsion it becomes possible to change the free volume of an amorphous material considerably. This method can be used to (i) fully densify a collection of metallic glass nanoparticles or (ii) tune the atomic structure of a metallic glass by the formation of a high density of primary and secondary shear bands. On this basis, the changes in structural, thermodynamic and mechanical properties will be discussed.

### 3:35 PM

**Strong Effects of Alloying Elements on the Structure, Dynamics and Glass Forming Ability of Metallic Supercooled Liquids:** *Yongqiang Cheng*<sup>1</sup>; Evan Ma<sup>1</sup>; <sup>1</sup>Johns Hopkins University

The addition of a relatively small amount of alloying element(s) can induce major changes in the viscosity, fragility and glass forming ability of supercooled liquids. A microscopic understanding of this behavior from the structural perspective has been elusive. Through comparisons between Cu-Zr-Al and Cu-Zr supercooled liquids, here we demonstrate the strong effects of Al alloying on the atomic-scale structure, in particular the evolution of icosahedral local motifs, as well as the resulting dramatic slowing down of relaxation dynamics. The composition-structure-dynamics relationship uncovered for realistic bulk metallic glass forming liquids is important for understanding the subsequent glass transition and their high glass forming ability.

### 3:45 PM

**The Prediction of Glass-Forming Compositions in Metallic Systems:** *Kevin Laws*<sup>1</sup>; <sup>1</sup>University of New South Wales

A new methodology of predicting specific compositions for glass forming ability based on elemental cluster selection, atomic packing efficiency, ab initio calculations and liquidus lines will be presented and discussed. The proposed composition selection model has led to the discovery of a number of soon to be reported transition metal-based bulk metallic glasses, some with critical casting thicknesses in excess of 7 mm and high thermal stability. The proposed model may also be used to explain high glass forming ability of known BMG compositions and to pin-point new or superior BMG compositions in existing glass forming systems. Further, the aforementioned model shows strong correlations between proposed elemental clusters, glass forming ability and BMG density, mechanical strength and ductility. This model has also shown applicable adaptation to known ceramic oxide glass forming systems.

### 3:55 PM

**Periodic Amorphous Metallic Cellular Structures:** *Joseph Schramm*<sup>1</sup>; Marios Demetriou<sup>1</sup>; William Johnson<sup>1</sup>; <sup>1</sup>California Institute of Technology

The high yield strength and ability to deform plastically at sub-millimeter sizes make amorphous metal an attractive material for strong metallic cellular structures. Additionally, softening at the glass transition allows amorphous metals to be "thermoplastically" formed. Recent work has shown that stochastic amorphous metallic cellular structures (amorphous metallic foams) deform plastically under compression at plateau stresses that correlate consistently with the yield strength of the monolithic amorphous metal. Periodic cellular structures (e.g. honeycombs) are able to inherit a significantly larger fraction of the monolithic yield strength than foams, making them substantially stronger at a given relative density. In this presentation, recent progress on honeycomb-type amorphous metallic structures will be presented. Structures with porosities in the range of 75-90% have been assembled from thermoplastically-formed corrugated sheets. Compression tests on single cores of the periodic structure reveal their ability to deform in the same manner as foams while maintaining higher plateau stress.

### 4:05 PM Invited

**Formation and Electrochemical Behavior of Mechanically Alloyed Cu-Zr-Ti-Ta Bulk Metallic Glass Composites:** *Pee-Yew Lee*<sup>1</sup>; Chien-Yie Tsay<sup>2</sup>; Chin-Yi Chen<sup>2</sup>; Hong-Ming Lin<sup>3</sup>; <sup>1</sup>National Taiwan Ocean University; <sup>2</sup>Feng-Chia University; <sup>3</sup>Tatung University

The preparation of (Cu60Zr30Ti10)90Ta10 BMG composites through a powder metallurgy route was investigated. The metallic glass composite powders were found to exhibit a super-cooled liquid region before crystallization. (Cu60Zr30Ti10)90Ta10 BMG composites were synthesized by vacuum hot pressing the as-milled (Cu60Zr30Ti10)90Ta10 composite powders

It was observed that pressure enhanced the thermal stability and suppressed the formation of nanocrystalline phases in (Cu60Zr30Ti10)90Ta10 BMG composites. The corrosion behavior of (Cu60Zr30Ti10)90Ta10 BMG composites in four different corrosive media was studied using the potentiodynamic method. The resultant polarization curves indicated lower corrosion rates, and current densities were obtained for composites measured in 1N H2SO4, NaOH, and HNO3 solutions. The XPS results revealed that the formation of Zr-, Ta-, and Ti-rich passive oxide layers provided a high corrosion resistance in 1N H2SO4 and HNO3 solutions, while the breakdown of the protective film by Cl- attack was responsible for pitting corrosion in the 3 wt% NaCl solution.

### 4:20 PM

**Characterization of Complex Geometry Amorphous Metal Structures Created by Micromolding:** *Gerald Bourne*<sup>1</sup>; Jeffrey Bardt<sup>1</sup>; Tony Schmitz<sup>1</sup>; Daniel Zeenberg<sup>1</sup>; Nickolas Ptschelinzew<sup>1</sup>; W Sawyer<sup>1</sup>; Michael Kaufman<sup>1</sup>; <sup>1</sup>University of Florida

Casting and molding are attractive options for low cost mass production. However crystallization during cooling induces shrinkage that can be on the order of several percent, resulting in poor tolerances. Additionally, molds must be fabricated from materials capable of withstanding the high temperatures associated with melting of metals. To enable molding of micro-scale devices, metallic glasses offer the potential to avoid many of the problems associated with molding of metals. The amorphous structure in metallic glasses leads to properties that may include high yield strength, hardness, strength-to-weight ratio, elastic limit, and wear resistance. In this study, we have produced complex geometries using a multilayer sacrificial Si wafer micromolding process from Zr<sub>41.2</sub>Ti<sub>13.8</sub>Cu<sub>12.5</sub>Ni<sub>10</sub>Be<sub>22.5</sub>. Scanning electron microscopy (SEM) and transmission electron microscopy (TEM) are used to characterize the net shape forming ability, surface quality, and microstructure of the molded products. Results are presented.

### 4:30 PM Invited

**Cu-Hf-Al Bulk Metallic Glasses: Compositional Dependence of Glass-Forming Ability and Compressive Plasticity:** Peng Jia<sup>1</sup>; Jian Xu<sup>1</sup>; <sup>1</sup>Institute of Metal Research, Chinese Academy of Sciences

In this talk, we will report recent progress regarding the compositional dependence of glass-forming ability (GFA) and compressive properties for Cu-Hf-Al ternary bulk metallic glasses (BMGs). Firstly, the Cu-Hf-Al BMG-forming composition region is identified to correlate with the (L-Cu<sub>10</sub>Hf<sub>7</sub>+CuHf<sub>2</sub>+CuHfAl) eutectic reaction. The fragility parameter  $D^*$  of the Cu<sub>55</sub>Hf<sub>45</sub> binary and Cu<sub>49</sub>Hf<sub>42</sub>Al<sub>9</sub> (C1) ternary supercooled liquid was determined from relaxation time measurements, indicating that Al incorporation also leads to a "stronger" liquid. Secondly, Weibull statistics was used to study the distribution of compressive yield strength ( $\sigma_y$ ) of the Cu<sub>49</sub>Hf<sub>42</sub>Al<sub>9</sub> and Cu<sub>45</sub>Hf<sub>46</sub>Al<sub>9</sub> (C2) BMGs. The  $\sigma_y$  of both BMGs exhibits high uniformity. The C2 BMG with a higher Weibull modulus ( $m=40$ ) is less brittle than C1 ( $m=53$ ). Comparison of the elastic constants and fragility between C1 and C2 indicates that the less brittle C2 shows a slightly higher Poisson's ratio and fragile feature with respect to the C1.

## Cast Shop for Aluminum Production: Engineering and Industrial Developments

Sponsored by: The Minerals, Metals and Materials Society, TMS Light Metals Division, TMS: Aluminum Committee

Program Organizers: Pierre Le Brun, Alcan CRV; Hussain Alali, Aluminium Bahrain

Monday PM

February 16, 2009

Room: 2005

Location: Moscone West Convention Center

Session Chair: Ravi Tilak, Almex USA Inc

### 2:00 PM Introductory Comments by Pierre Le Brun

2:05 PM TMS 2008 - Best Paper Award 2008 Best Paper Award Presentation

### 2:10 PM

**Hindalco Almex Aerospace Limited – A New Greenfield Aerospace Alloy Casthouse:** *Shaun Hamer*<sup>1</sup>; Lorraine Fortier<sup>1</sup>; <sup>1</sup>Almex USA Inc

Hindalco Almex Aerospace Limited, an Indian incorporated company started a new Greenfield casthouse in the third quarter of 2008. The casthouse is designed

to supply the aerospace and specialist alloy downstream operations with a billet supply option for 2000 and 7000 series alloys in billet sizes ranging from 7" to 41½". The concept for the casthouse, a joint venture between Hindalco and Almex USA has developed out of the understanding of the aerospace downstream industries and identifying the niche markets where billet supply can boost the industry's global growth. This paper describes the implementation of this casthouse from concept through to start-up and the growth steps for the coming years to realize the plant's maximum operating capacity. It further investigates the production philosophies and design criteria incorporated to ensure success of this new venture and world class metal supply to the extrusion, forging, sheet and plate industries.

### 2:30 PM

**Qatalum Cast House:** *Andrew Home*<sup>1</sup>; A. Tropeano<sup>2</sup>; <sup>1</sup>K Home International Ltd; <sup>2</sup>FATA EPC

The new smelter being built by joint venture partners Qatalum Petroleum and Hydro will set a new standard for the size of green field smelter projects. An important part of the project is the cast house producing 625 thousand tonnes per annum of value added product, making it the largest smelter cast house to be built in a single phase. This paper will discuss the concept for the project, a novel approach to the contract methodology and report the progress of the project to date.

### 2:50 PM

**CVG Venalum- Design of a 55 t Tilting Melting Furnace:** *Santiago Barry*<sup>1</sup>; Fidiás Rodriguez<sup>1</sup>; Orlando Gil<sup>1</sup>; <sup>1</sup>CVG Venalum

In this paper, the engineering design of a 55 t tilting melting furnace is described. This includes all the simulations that apply for the efficient design of this furnace, that is: Metallic structure; Refractory body; Tilting system; Foundations system; Combustion system; Control and Power system. The aim of this new tilting furnace design is to replace the current static furnaces which are coupled to a vertical DC casting machine at CVG Venalum; with an outlook of increasing the production levels, the quality of the products, as well as improving the security, ergonomic and environmental conditions of the workplace. This engineering has been developed by CVG Venalum Research and Development Center.

### 3:10 PM

**Advanced Control of a Rotary Drum Furnace in a Secondary Smelter:** *Detlef Maiwald*<sup>1</sup>; <sup>1</sup>Innovatherm GmbH

In the secondary smelter industry rotary drum furnaces are used for the remelting of various types of aluminium scrap, especially UCB's and coated scrap. The control of the rotary drum furnace is difficult due to the following circumstances: - temperature of rotary drum refractory or the aluminium bath can't be measured, only the exhaust gas temperature is measurable; - production cycle is interrupted by several repeating phases of charging, decoating and melting; - operation of this equipment is still on a high degree of manual impact. A new technology determine the process parameters indirectly by Fuzzy Logics. Additionally a new measurement is introduced, using the actual electrical current consumed by the rotary drum main motor during the entire melting cycle. The target is the optimization of the melting cycle and minimization of primary fuel usage. Also peak temperatures should be avoided to extend lifetime of refractory.

### 3:30 PM

**Fluid Modeling of the Flow and Free Surface Parameters in the Metallurgical LOTUSS System:** *Mark Bright*<sup>1</sup>; Florin Illinca<sup>2</sup>; Jean-Francois Hetu<sup>2</sup>; Frank Ajersch<sup>3</sup>; Charbel Saliba<sup>1</sup>; Chris Vild<sup>1</sup>; <sup>1</sup>Pyrotek Inc.; <sup>2</sup>National Research Council of Canada; <sup>3</sup>Fabmatek Services Inc.

The growth of aluminum product consumption has placed an emphasis on improving the efficiency of processing internally generated scrap. In the Metallurgical LOTUSS (LOW TURbulence Scrap Submergence) System, aluminum machining chips can be melted at a rate in excess of 15 tons per hour with very high recovery efficiencies. A computational fluid dynamics (CFD) model has been implemented to optimize the LOTUSS System to further enhance efficiency and maximize melting performance. Preliminary studies of the CFD modeling will be presented outlining the three-dimensional numerical algorithm for solving the turbulent and free-surface flow inside the LOTUSS system. CFD simulations were carried out for melting system conditions and verified against previous experimental studies. The results indicate that the free surface CFD model is an accurate representation of real-world conditions and the predictions

for the position and size of the vortex cone compare very well with the measured experimental values.

### 3:50 PM Break

### 4:10 PM

**Electromagnetic Stirring in Aluminum Ladles:** *Robert Stål*<sup>1</sup>; Patrick Hanley<sup>1</sup>; <sup>1</sup>ABB

Electromagnetic stirring (AL-EMS) in aluminum furnaces is now a well-established technology to enhance chemical and thermal homogeneity and to reduce cycle time, energy consumption and dross formation. This paper will discuss the benefits of using AL-EMS for ladle stirring of liquid aluminum. To become more cost efficient some foundries are purchasing liquid aluminum. The molten aluminum is stored in ladles which can be put on hold for as long as 24 hours before being delivered to the foundry. Heating and stirring will be needed to assure correct temperature during this waiting time. Experiences from industrial plant trials have shown that electromagnetic stirring can generate total thermal homogenization in aluminum ladles. Reduction of melt surface temperature by AL-EMS and how this can suppress surface oxidation and improve heat transfer to the melt is discussed in this paper. This further demonstrates the potential of AL-EMS to reduce burner running cost.

### 4:30 PM

**Optifine - A Grain Refiner with Maximized Nucleation Efficiency:** *Rein Vainik*<sup>1</sup>; John Courtenay<sup>2</sup>; <sup>1</sup>Opticast Aluminium AB; <sup>2</sup>MQP Ltd

A new grain refiner with a strong nucleation efficiency, Optifine, is presented. By optimizing the growth restriction, i.e. mainly by adding low amounts of titanium, extremely low additions of this gives the same grain size as normal additions of standard grain refiners. The efficiency is explained by a narrow range of boride particle sizes, which allows simultaneous nucleation on a large number of aluminium crystals. Furthermore, the growth restriction determined by the alloy composition and/or aided by minute additions of titanium, will allow a substantial proportion of these crystals to grow resulting in a very fine grain structure. Apart from cost savings due to much reduced application rates, a high efficiency master alloy will have a large impact on the billet and ingot quality, since only a very small amount of the hard boride particles are needed in order to produce a cast grain size resistant to ingot cracking.

### 4:50 PM

**New Grain Refiner Containing Ternary Carbide Nucleant Particles:** *Marta Suarez*<sup>1</sup>; Mauro Martin<sup>1</sup>; *Abinash Banerji*<sup>2</sup>; <sup>1</sup>Aleastur; <sup>2</sup>Microalloy

A new grain refiner, AlTiX (patent pending), has been invented for aluminum and its alloys. It is essentially an aluminum based quaternary master alloy containing ternary carbide nucleant particles. Both short and long time TP1 tests were carried out on commercially pure aluminum (99.7%) to find out the grain refining efficacy of the new refiner under different test parameters and the results have been compared with those obtained with commercially available conventional AlTiB and AlTiC master alloys respectively under similar test conditions. The paper deals with a maiden report on the newly invented grain refiner containing ternary carbide particles which are believed to nucleate aluminum grains during solidification of the inoculated melt.

### 5:10 PM

**New SiC-Graphite Castable for Molten-Metal Transfer Units:** *Claude Allaire*<sup>1</sup>; <sup>1</sup>CIR Laboratory Inc

In aluminum molten-metal transfer units, silicon carbide containing refractories should be used where maximum thermomechanical abuse resistance is required. These materials are most often used either in the form of castables or as preformed carbon or clay-bonded shapes using techniques such as ribforming, rollerforming and isopressing. Where applicable, the later materials are advantageous since they may contain graphite that contributes to increase their thermal shock and corrosion resistance due to its higher thermal conductivity and chemical inertia, respectively. To benefit of the graphite properties as well as the simple and low expensive forming method available with none shaped refractories, a new silicon carbide ultra-low cement castable containing up to 15 vol. % graphite has been developed. The formulation principles and the properties of this new SiCGraphite castable are presented in this paper.

## Characterization of Minerals, Metals and Materials: Characterization of Processing

Sponsored by: The Minerals, Metals and Materials Society, TMS Extraction and Processing Division, TMS: Materials Characterization Committee, TMS/ASM: Composite Materials Committee

Program Organizers: Toru Okabe, University of Tokyo; Ann Hagni, Geoscience Consultant; Sergio Monteiro, State University of the Northern Rio de Janeiro - UENF

Monday PM  
February 16, 2009

Room: 3009  
Location: Moscone West Convention Center

Session Chairs: Tzong Chen, CANMET-MMSL; Kazuki Morita, University of Tokyo

### 2:00 PM

**Characterization of Manganese Oxide Scales on Rolled Lead Anodes from a Commercial Zinc Electrowinning Operation:** *Tzong Chen*<sup>1</sup>; John Dutrizac<sup>1</sup>; <sup>1</sup>CANMET-MMSL

Rolled Pb-0.7% Ag anodes are porous. The manganese oxide scales, consisting mainly of MnO<sub>2</sub>, characteristically occur in a banded colloform structure which adheres to an irregular layer of PbSO<sub>4</sub> and PbO<sub>2</sub> that oxidized from the Pb anode. Hydrated Mn oxides, Mn<sub>3</sub>O<sub>4</sub> and amorphous Mn oxides are believed to be also present. Tiny particles of gypsum, PbSO<sub>4</sub>, SrSO<sub>4</sub> and AgCl are entrapped in the colloform mass. Silver originated from the anodes; strontium carbonate was added to the Zn solution to control Pb, and gypsum originated from the Zn electrolyte. Some colloform bands contain minor amounts of Pb, implying minor dissolution of Pb during electrolysis. Other colloform bands incorporate trace amounts of Zn and Ca. Colloform structures permeated with silica gel were presumably caused by the high silica content of the electrolyte.

### 2:15 PM

**Titanium Production/Coating Process by Disproportionation of Titanium Dichloride in Molten Magnesium Chloride:** *Taiji Oi*<sup>1</sup>; Toru Okabe<sup>1</sup>; <sup>1</sup>Institute of Industrial Science, the University of Tokyo, c/o Okabe Laboratory (Fw-301)

In order to establish a new titanium production/coating process, the synthesis and disproportionation of TiCl<sub>2</sub> in molten MgCl<sub>2</sub> were investigated. TiCl<sub>2</sub> was synthesized by reacting TiCl<sub>4</sub> with titanium metal in MgCl<sub>2</sub> molten salt at 1200-1273 K and titanium metal was produced by the disproportionation of TiCl<sub>2</sub> in molten MgCl<sub>2</sub> at 1273 K. The results revealed that TiCl<sub>2</sub> was successfully obtained in the synthesis experiment and that the efficiency of TiCl<sub>2</sub> formation was drastically improved by using molten MgCl<sub>2</sub> as a reaction medium. In the titanium production experiment, titanium powder of over 99% purity was produced by disproportionation of TiCl<sub>2</sub> in molten MgCl<sub>2</sub>. From these results, it was shown that the methods investigated in this study can be applied to a new titanium production process. In addition, the feasibility of a new method for titanium coating utilizing disproportionation of TiCl<sub>2</sub> is discussed from some results of preliminary experiments.

### 2:30 PM

**Fundamental Study on Recovery of Nd and Dy from Rare Earth Magnet Scrap Using Molten Salt:** *Sakae Shirayama*<sup>1</sup>; Toru Okabe<sup>1</sup>; <sup>1</sup>Institute of Industrial Science, the University of Tokyo, c/o Okabe Laboratory (Fw-301)

In order to develop a new process for the recovery of neodymium (Nd) and dysprosium (Dy) from rare earth magnet scrap, selective extraction of Nd and Dy was investigated by using metal halides. For preliminary experiments, magnesium chloride (MgCl<sub>2</sub>) was selected as an extracting agent, and molten MgCl<sub>2</sub> was reacted with Dy-containing Nd-Fe-B magnet alloys. Experimental results revealed that the rare earth elements in the magnet alloys were successfully extracted into MgCl<sub>2</sub> in high yields. After the removal of MgCl<sub>2</sub> by vacuum distillation, Nd and Dy could be separately recovered by a wet or dry process. The effectiveness of MgCl<sub>2</sub> and other metal halides as extracting agents and the feasibility of effective recycling of Nd-Fe-B magnet scrap are discussed in this paper.

### 2:45 PM

**Characterization of CO<sub>2</sub> Laser-Assisted Deposition of Diamond Thin Films by Combustion-Flame Method:** *Travis McKindra*<sup>1</sup>; Matthew O'Keefe<sup>1</sup>; <sup>1</sup>Missouri University of Science and Technology

The effect of the CO<sub>2</sub> laser irradiation and the combustion gas composition on the microstructure of diamond thin films was investigated. A continuous wave CO<sub>2</sub> laser operated at 600 W was used to irradiate the flame tip during C<sub>2</sub>H<sub>2</sub>/C<sub>2</sub>H<sub>4</sub>/O<sub>2</sub> and C<sub>3</sub>H<sub>8</sub>/O<sub>2</sub> combustion-flame deposition. The film morphology, chemical bonding, and crystal structure were characterized by scanning electron microscopy (SEM), x-ray photoelectron spectroscopy (XPS), x-ray diffraction (XRD) and Raman spectroscopy. The films were continuous with faceted diamond grains 1-2 μm in size. The CO<sub>2</sub> laser irradiation increased the diamond (111) diffraction peak intensity. These results were in agreement with the film morphology results from the SEM as the film deposited with the laser had a larger grain size which resulted in a sharper, more intense peak. The films deposited with the C<sub>3</sub>H<sub>8</sub>/O<sub>2</sub> combustion-flame contained W<sub>2</sub>O<sub>3</sub>, Co<sub>x</sub>W<sub>y</sub>O<sub>z</sub> and Co<sub>x</sub>W<sub>y</sub>C phases. The XPS results confirmed that the films had a significant amount of diamond.

### 3:00 PM

**Production of V and V-Ti Alloys from Oxide Preforms:** *Akihiko Miyauchi*<sup>1</sup>; Toru Okabe<sup>1</sup>; <sup>1</sup>Institute of Industrial Science, the University of Tokyo, c/o Okabe Laboratory (Fw-301)

In order to develop a new process for effective production of vanadium metal (V) and V-Ti alloys from V<sub>2</sub>O<sub>5</sub>, a fundamental study was conducted on a preform reduction process (PRP) based on metallothermic reduction. Feed preforms with good mechanical strength even at elevated temperatures were prepared by adding either CaO or MgO to V<sub>2</sub>O<sub>5</sub> feed powder; thus, complex oxides (Ca<sub>x</sub>V<sub>y</sub>O<sub>z</sub>, Mg<sub>x</sub>V<sub>y</sub>O<sub>z</sub>) were obtained. Reduction experiments were conducted by using either Ca or Mg vapor at 1273 K for 6 h. Vanadium metal with a purity of 99.7% was successfully obtained when Mg was used as a reductant. The feasibility of producing V or V-Ti alloys by the PRP will be discussed on the basis of fundamental experiments.

### 3:15 PM

**Characterization of β-FeSi<sub>2</sub> Film Synthesized by Exchange Reaction between Si and Molten Salts:** *Motohiro Sakamoto*<sup>1</sup>; Kazuki Morita<sup>1</sup>; <sup>1</sup>University of Tokyo

β-FeSi<sub>2</sub> is a candidate material for Si-based optical and photovoltaic devices. In order to fabricate β-FeSi<sub>2</sub> film on Si wafer, various kinds of processes have been developed. Since ultra-high vacuum atmosphere is essential for these processes, vacuum-free process is required for mass production of photovoltaic cell at low cost. In this study, β-FeSi<sub>2</sub> film was prepared on Si wafer by the cation exchange reaction between Si wafer itself and molten NaCl-KCl-FeCl<sub>2</sub> salts. Two phases of FeSi and β-FeSi<sub>2</sub> were formed by the reaction between single crystal (100) wafer and 0.1mol% FeCl<sub>2</sub> molten salts at 1173K for 1h in He atmosphere. After the sample was annealed at 1173K for 24h, the flat β-FeSi<sub>2</sub> layer was confirmed to be formed on Si wafer by X-ray diffraction and scanning electron microscopy. The band gap of this β-FeSi<sub>2</sub> was determined to be 0.85eV by infrared spectroscopy, showing good agreement with other reported values.

### 3:30 PM Break

### 3:50 PM

**FeCr<sub>2</sub>O<sub>4</sub> Spinel Formation: Relationship between Color and Magnetics Properties:** *Oscar Restrepo*<sup>1</sup>; Juan Montoya<sup>1</sup>; Ernesto Baena Murillo<sup>1</sup>; <sup>1</sup>Univ Nacional De Colombia

The compounds type spinels are oxides whose ideal formula is AB<sub>2</sub>O<sub>4</sub>, where A is a divalent cation and B is a trivalent cation. They have been the subject of scientific interest because their properties allow its use in different applications. They are used as pigments; they are usually obtained by sinterization of various oxides, where cations comply with certain characteristics of atomic ratio and oxidation number. This paper shows the results obtained in the study using iron and chromium oxides in fixed proportions, used as precursors of the compound with spinel type structure FeCr<sub>2</sub>O<sub>4</sub>. For different temperatures synthesis, a characterization for the obtained material was performed using X-ray diffraction (XRD), UV-VIS-NIR spectroscopy and Mössbauer spectroscopy. The changes in the reflectance spectra are related with the identified phases, crystallinity degree, spatial ordering of cations and magnetic behavior.



4:05 PM

**Synthesis and Production of Ni-Mo Alloys for Hydrogen Production via Mechanical Alloying:** *Maria Valero Rocha*<sup>1</sup>; Roberto Martinez Sanchez<sup>2</sup>; Jose Cruz Rivera<sup>2</sup>; Israel Rodriguez Torres<sup>2</sup>; <sup>1</sup>Centro de Investigacion en Materiales Avanzados, S.C.; <sup>2</sup>Instituto de Metalurgia

The present work studied the structural and microstructural evolution of Ni-Mo alloys (10%, 20% and 30%Wt) produced by Mechanical Alloying. Alloys production was performed in a commercial Fritsch planetary mill, the ball-to-powder weight ratio was 6:1, and the process control agent used was hexanos. Nominal compositions of original powders were 99.99% purity, the particle sizes was 2.23  $\mu\text{m}$  and 67.93  $\mu\text{m}$ , respectively. Mixtures of powders of Ni-10%Mo, Ni-20%Mo and Ni-30%Mo were milled by different times. After Milling, powders were cold compact. The sintering compacts were carried out in a resistance tubular furnace. Structural and morphological characterization of the powders and the sintering materials were performance by XRD, SEM, TEM and EDS. From characterization results it is possible to observe an increment in the parameter which suggests that during the process a solid solution and nanometric phase were formed. The results has been analyzing in cathodes for hydrogen production.

4:20 PM

**Shape-Controlled Synthesis of Porous Fibrous Cobalt Powders:** *Zhan Jing*<sup>1</sup>; Dong Chengyong<sup>1</sup>; Zhang Chuanfu<sup>1</sup>; Wu Jianhui<sup>1</sup>; Fan Youqi<sup>1</sup>; <sup>1</sup>Central South University

The fibrous precursor can be obtained by coordination precipitation process. The composition and morphology of fibrous precursor were characterized by XRD, IR, DTA/TGA and SEM analysis. The results show that XRD pattern and composition of the precursor with fibrous morphology precipitated at pH=9.0 are different from that of  $\beta\text{-CoC}_2\text{O}_4\cdot 2\text{H}_2\text{O}$  precipitated at pH=1.0. The mechanism on the thermal decomposition of fibrous precursor was addressed. The influences of various conditions in pyrolysis, including the temperature, time, atmosphere, and the morphology of the precursor, on the morphology, average size and specific surface area of the Co powders were investigated in detailed. At last, the final product-fibrous cobalt powders with about 0.3~0.5 $\mu\text{m}$  in size and 40~60 in aspect ratio were produced by thermal decomposition at 400~500 $^\circ\text{C}$  in the weak reducing atmosphere. The structure of pores in cobalt powders is capillary tube with open ports and the majority is mesoporous.

4:35 PM

**Synthesis of Nanometer Core-shelled Titanium Dioxide/Tungsten Oxide Powder:** *Daoxin Wu*<sup>1</sup>; <sup>1</sup>Changsha University of Science and Technology

With the controllability in composition, structure and property, the complex core-shelled nanoparticles have attracted both domestic and international interests in recent years. Originated from  $(\text{C}_4\text{H}_9\text{O})_4\text{Ti}$ , nano-rutile  $\text{TiO}_2$  was synthesized by low temperature hydrolytic process in this paper. After being prepared by decomposing ammonium tungstate and covering on the surface of  $\text{TiO}_2$ ,  $\text{TiO}_2/\text{WO}_3$  were characterized by means of thermogravimetric and differential scanning calorimeter (TG-DSC), X-ray diffraction (XRD), UV-vis diffuse reflectance (DRS), fluorescence spectrum (FS). Results showed that with the increase of the supported concentration of  $\text{WO}_3$  the reflectance of DRS and the fluorescence spectrum intensity of  $\text{TiO}_2/\text{WO}_3$  decreased accordingly which indicated the powder's increase in light absorbance and the decrease in luminescence respectively.

4:50 PM

**Vibration Damping of High-Chromium Ferromagnetic Steel:** *Satish Bhujang Muti*<sup>1</sup>; Mahesh Kumbeshwara<sup>1</sup>; Girish Bhujang Muti<sup>1</sup>; <sup>1</sup>East Point College of Engineering and Technology

The present work aims to study the effect of annealing on the vibration damping capacity of high-chromium (16%) ferromagnetic steel. The alloys were prepared from raw materials of 99.9% purity melted in a high frequency induction furnace under vacuum. The samples were heat-treated in vacuum temperatures (800 to 1200 $^\circ\text{C}$ ) for 1 hour followed by slow cooling (120 $^\circ\text{C}/\text{h}$ ). The inverted torsional pendulum method was used to evaluate the vibration damping capacity. A water-based magneto-fluid was used to analyze magnetic domain morphology of the alloy using optical microscopy. The results indicated that the vibration damping capacity of the alloys is influenced by annealing and there exists a critical annealing temperature after 1000 $^\circ\text{C}$ . The damping capacity increases quickly below the critical temperature since the magnetic domains move more easily. Above the critical temperature the damping capacity decreases due to the larger size of the magnetic domains leading to decrease in domain wall area.

5:05 PM

**Corrosion Mechanism of A3 Steel Induced by Chloride Ions in the Purified Water:** *Liyuan Chai*<sup>1</sup>; Haijuan Xiao<sup>1</sup>; Yunyan Wang<sup>1</sup>; Yude Shu<sup>1</sup>; Fei Pei<sup>1</sup>; Jinlong Zhang<sup>1</sup>; <sup>1</sup>Central South University

In the nonferrous metallurgical industry it is of great significance to solve the problem of resource waste and environment pollution due to the discharge of heavy metal-containing wastewater. However, there arises a question whether the water impurities with chloride ions and fluoride ions will result in the corrosion of the pipeline during the whole recycling process. In this study, the corrosion mechanism of A3 steel induced by chloride ions in the purified water had been investigated with the A C Impedance technique. The results showed that there were another two factors which determined its electrochemical corrosive rate: the electrode potential and coverage ratio of chloride ions on the surface of A3 Steel. The corrosion mechanism of A3 steel in the solution with chloride ions emendation was two steps of electrode process with the rate-determining step of  $\text{FeCl Fe}_2 + +\text{Cl}^- +\text{e}^-$ .

## Computational Thermodynamics and Kinetics: Thin Films

Sponsored by: The Minerals, Metals and Materials Society, ASM International, TMS Electronic, Magnetic, and Photonic Materials Division, TMS Materials Processing and Manufacturing Division, ASM Materials Science Critical Technology Sector, TMS: Chemistry and Physics of Materials Committee, TMS/ASM: Computational Materials Science and Engineering Committee

Program Organizers: Long Qing Chen, Pennsylvania State University; Yunzhi Wang, Ohio State University; Pascal Bellon, University of Illinois at Urbana-Champaign; Yongmei Jin, Texas A&M

Monday PM

Room: 3002

February 16, 2009

Location: Moscone West Convention Center

Session Chair: Pascal Bellon, University of Illinois

## 2:00 PM Introductory Comments

### 2:05 PM Invited

**Stress-Driven Surface Evolution during Whisker and Hillock Formation:** *W. J. Boettinger*<sup>1</sup>; T. Frolov<sup>2</sup>; V. A. Ivanov<sup>2</sup>; Y. Mishin<sup>2</sup>; <sup>1</sup>National Institute of Standards and Technology; <sup>2</sup>George Mason University

In stressed solids, surface evolution is often driven by grain boundary diffusion and can result in growth of hillocks and whiskers. Examples are whisker growth in compressively stressed Sn deposits on Cu and hillock formation in Cu conductor lines during electromigration. The mechanisms of hillock and whisker growth remain largely unknown. We present molecular dynamics simulations aimed at understanding the conditions (stress, temperature, grain boundary diffusion, surface diffusion) at which the hillock/whisker growth processes can be initiated. The simulated geometries include a single boundary normal to the surface and a tri-crystal with a wedge-shape surface grain, both under an applied stress parallel to the surface. We have also studied extrusion of materials through a nano-hole simulating a crack in an oxide layer covering a stressed film. The early stage of hillock/whisker growth is observed at high homologous temperatures when the boundary diffusion flux exceeds the lateral fluxes of surface diffusion.

### 2:35 PM Invited

**Effects of Substrate Symmetry and Patterning on the Stability of Compositional Patterns in Ultrathin Alloy Films:** *Bo Yang*<sup>1</sup>; Tejodher Mupidi<sup>1</sup>; Vidvuds Ozolins<sup>1</sup>; *Mark Asta*<sup>1</sup>; <sup>1</sup>University of California

First-principles-based computer simulations are employed to elucidate the effects of substrate symmetry and externally applied prepatterned "potentials" on directing self-assembly of ordered nanoscale compositional patterns in ultrathin films. This work focuses on alloy films as a specific example where the energetics underlying composition modulation can be accurately quantified within the framework of a hybrid model that incorporates an atomistic calculation of interatomic bonding with continuum theories of long-range substrate-mediated elastic interactions. Employing Monte-Carlo simulations based on this hybrid model for alloy energetics, we demonstrate that even relatively weak external potentials, with periodicities considerably larger than the intrinsic composition-modulation wavelengths, can be highly effective in stabilizing ordered compositional patterns at the nanoscale.

3:05 PM

**Compositional Domain Formation in Ultrathin Films: A Phase-Field Crystal Study:** *Srevasan Muralidharan*<sup>1</sup>; Mikko Haataja<sup>1</sup>; <sup>1</sup>Princeton Univ

It is well-known that materials confined in one or more dimensions may display properties which are strikingly different from those of their bulk counterparts. An illustrative example of this phenomenon is provided by a binary alloy, which is immiscible in the bulk and yet forms miscible phases when deposited on a surface as a (sub)monolayer aggregate. In this case, the mixing of the components is brought upon by the epitaxial nature of the growth processes. In addition to alloying, surface dislocations provide a mechanism for strain relaxation. In this talk we describe a phase-field crystal (PFC) model we have recently developed to study this technologically relevant process. The PFC model incorporates alloy thermodynamics, the presence and motion of free surfaces and/or grain boundaries, the presence of long-ranged elastic strains, and the nucleation and dynamics of dislocations, thus providing a physically-based picture of the domain formation kinetics at the nanoscale.

3:25 PM

**Coarsening of 3D Thin Films under the Influence of Strong Surface Anisotropy, Elastic Stresses:** *Peng Zhou*<sup>1</sup>; Steven Wise<sup>2</sup>; John Lowengrub<sup>1</sup>; <sup>1</sup>University of California Irvine; <sup>2</sup>University of Tennessee Knoxville

We develop a diffuse interface model to investigate the three dimensional coarsening in thin films. In this model, both strong surface anisotropy with Willmore regularization, elastic stresses and deposition are included. The governing equation for the phase field parameter is a sixth order Cahn-Hilliard Equation due to the presence of surface anisotropy and the Willmore regularization. The simulated system is assumed to be in mechanical equilibrium with misfit in the film generated by lattice mismatch in the substrate. Thus, the Cauchy-Navier equations are solved for elastic displacements which lead to the elastic energy. Both the Cahn-Hilliard equation and the Cauchy-Navier equations are solved with a non-stiff, adaptive nonlinear multigrid method. Simulation results of coarsening in three dimensions with different strengths of the surface anisotropy, misfit strain, and deposition rates will be shown. Comparison and analyses of these results will help to explain their influence on coarsening processes in thin films.

3:45 PM Break

4:10 PM

**Sintering and Microstructure Evolution in Columnar Thermal Barrier Coatings:** *Ramanathan Krishnamurthy*<sup>1</sup>; David Srolovitz<sup>2</sup>; <sup>1</sup>Caterpillar Inc; <sup>2</sup>Yeshiva University

Sintering of thermal barrier coatings changes their key properties, thus adversely impacting their reliability. We present a hierarchical modeling approach to study sintering-induced evolution of topcoat microstructure, wherein the sintering of individual topcoat column pairs is modeled using a thermodynamic principle, and column center-to-center approach rates calculated thence are incorporated into a discrete dynamics model of the temporal evolution of hundreds of columns. Surface, grain boundary and strain energy effects are naturally included in this framework. Varied late-time microstructures, with small clusters and random in-plane porosity, or with 50-100 columns-wide clusters separated by elongated inter-cluster channels, are observed, corresponding to small/large extents of contact among 'feathery' protrusions from columns. Statistical measures extracted from predicted microstructures reveal that cluster formation is strongly favored for large column densities and extents of the 'feathery' protrusions from columns. We compare predicted microstructures with recent experimental observations and discuss their import for thermal barrier coating processing/reliability.

4:30 PM

**Characterizing Adsorption on Metallic Surfaces: Effect of Composition:** *Baskar Ganapathysubramanian*<sup>1</sup>; Nicholas Zabaras<sup>2</sup>; <sup>1</sup>Iowa State University; <sup>2</sup>Cornell University

The enhancement of adsorption of (hydrogen) molecules on metallic surfaces is a key challenge for producing feasible fuel storage technologies. The chemistry of the surface under consideration plays an essential part in the adsorption phenomena. A reliable computational framework requires very accurate first-principle calculations of the energy of the system. We utilize the recently developed weighted multi-body expansion to accurately represent the energy of a cluster of atoms. An adaptive sparse grid collocation strategy provides the ability to effectively tessellate high dimensional surfaces. This

allows us to naturally incorporate higher order interactions (up to 5 body terms). We utilize this strategy to construct multibody potentials representing the interaction of hydrogen with various transition metals. We investigate the effect of composition variation on the absorption coefficient.

4:50 PM

**Thermodynamics of Nanoscale Binary Systems:** *Muralidharan Ramachandran*<sup>1</sup>; Ramana Reddy<sup>1</sup>; <sup>1</sup>The University of Alabama

Nanoscale materials have been considered for and been in use in a variety of industrial engineering applications. It is shown that the melting temperature decreases and the phase diagram of binary systems change with the decrease in particle size. Non-ideal or real solution characteristics were introduced into the binary system using the activity data obtained from the literature. The phase diagrams of selected nanoscale binary systems were constructed considering the non-ideality of the system, the surface effects and the variation in the particle size and shape. The availability of data on surface and interfacial tensions has limited the number of systems considered. The calculated results were compared with that of the experimental results from the literature.

5:10 PM

**Simulation of Thickness Effect on Grain Growth in Thin Films and Experimental Verification:** *Zhinan An*<sup>1</sup>; *Yonghua Rong*<sup>1</sup>; <sup>1</sup>Shanghai Jiao Tong University

Various stagnation effects of grain growth in nano materials have been found, but thickness effect has not yet been researched. This paper presents an anisotropic Monte Carlo (MC) algorithm to stimulate grain growth in thin films in annealing process. The simulation results reveal that thickness effect begins to work only when the average grain size reaches 0.8 to 1.2 times of the thickness of the film, not in the whole process of grain growth. Experimental data of grain growth in pure Co films with different thicknesses confirm the simulation results. Based on the stimulation and experiments, a modified grain growth kinetic equation is suggested to better describe the whole process of grain growth in nano-films.

5:30 PM

**Effect of Partial Failure on the Yield Strength of SiCp/Al Matrix Composites:** *Dai-hong Xiao*<sup>1</sup>; <sup>1</sup>Central South University

The SiC particles stress in aluminum matrix composites was examined according to the Eshelby's equivalent inclusion approach. A model was established to examine the influence of SiC particles failure on the yield strength of SiCp/Al composites after assumption that the SiC particles failure follows Weibull statistics. The values of tensile strength of SiCp/Al composites predicted by the model are well agreed with the experimental values. Moreover, the interface debond is the main failure way when the particle diameter is small in yielding condition, the percentage of particle fracture was found to increase with the increase of particles volume fraction and play the more important role in particle failure.

## Dislocations: 75 Years of Deformation Mechanisms: Dislocation Ensembles and Structures

Sponsored by: The Minerals, Metals and Materials Society, TMS Materials Processing and Manufacturing Division, TMS Structural Materials Division, TMS/ASM: Mechanical Behavior of Materials Committee, TMS: Nanomechanical Materials Behavior Committee

Program Organizers: David Bahr, Washington State University; Erica Lilleodden, GKSS Research Center; Judy Schneider, Mississippi State University; Neville Moody, Sandia National Laboratories

Monday PM Room: 3022  
February 16, 2009 Location: Moscone West Convention Center

Session Chairs: David Bahr, Washington State University; Lyle Levine, National Institute of Standards and Technology

### 2:00 PM Invited

**Measured Elastic Strains within Dislocation Cell Structures: Local Behavior and Statistical Distributions:** *Lyle Levine*<sup>1</sup>; Ben Larson<sup>2</sup>; Jon Tischler<sup>2</sup>; Peter Geantli<sup>3</sup>; Francesca Tavazza<sup>1</sup>; Mike Kassner<sup>3</sup>; Wenjun Liu<sup>4</sup>; <sup>1</sup>National Institute of Standards and Technology; <sup>2</sup>Oak Ridge National Laboratory; <sup>3</sup>University of Southern California; <sup>4</sup>Argonne National Laboratory

The existence and magnitude of long range elastic strains (and thus stresses) in dislocation cell interiors and walls in deformed metals have been the subject of extensive investigation for more than 20 years. We have used depth-resolved, submicrometer X-ray beams to directly measure the axial elastic strains within numerous *individual* deeply buried dislocation cell interiors and cell walls in plastically deformed copper single crystals. As previously reported, the average cell interior strains are tensile in unloaded compression specimens and compressive in unloaded tensile specimens. Recent measurements from individual, buried cell walls show that these have the reverse average strains. All of these cell interior and cell wall strains exhibit large cell-to-cell variations with magnitudes up to 50% of the flow stress. The experimentally determined distribution functions describing these strain fluctuations will be presented along with new theoretical models that explain their origin.

### 2:30 PM

**Determination of Geometrically Necessary Dislocation Distributions Using Electron Backscatter Diffraction:** *Angus Wilkinson*<sup>1</sup>; <sup>1</sup>University of Oxford

Cross-correlation based analysis of EBSD patterns has been shown to give significant improvements in angular resolution so that strains and lattice rotations can be measured at  $\pm 10^{-4}$ . This sensitivity coupled with the high spatial resolution makes the technique very attractive. Measurement of lattice curvature allows the geometrically necessary dislocation (GND) content to be assessed using Nye's dislocation tensor analysis (Nye 1953). The technique has been applied to various systems including: crack tip deformation during tensile loading in BCC metals (W and V), fatigue crack tips in Ni-based superalloy, flow fields around nanoindenters in Fe, Cu and Ti, low strain deformation of HSLA steel, martensite induced GNDs in dual phase steel, and tilt and twist mosaics in GaN layers grown on sapphire. The presentation will use some of these applications to illustrate the technique.

### 2:50 PM

**Resolving the Geometrically Necessary Dislocation Content by Conventional Electron Backscattering Diffraction:** *Wolfgang Pantleon*<sup>1</sup>; <sup>1</sup>Risoe DTU

From local orientation measurements on planar surfaces by means of electron backscattering diffraction, six components of the lattice curvature tensor can be identified. They allow determination of five components of the dislocation density tensor (thus two more than hitherto reported) and, additionally, one difference between two other components. When determining the geometrically necessary dislocation content, all available information should be utilized, i.e. all six independent components of the curvature tensor and not only the three or five components of the dislocation density tensor. With the increased number of available components, more accurate, increased lower bounds for the total dislocation density are obtained by linear optimization. The method is illustrated on deformed metals and rocks.

### 3:10 PM

**An Experimental Investigation of the Plastic Strain Evolution in Commercial Purity Ti Deformed in Bending:** *Yiyi Yang*<sup>1</sup>; Leyun Wang<sup>1</sup>; Thomas Bieler<sup>1</sup>; Gene Ice<sup>2</sup>; Wenjun Liu<sup>3</sup>; Philip Eisenlohr<sup>4</sup>; Martin Crimp<sup>1</sup>; <sup>1</sup>Michigan State University; <sup>2</sup>Oak Ridge National Laboratory; <sup>3</sup>Argonne National Laboratory; <sup>4</sup>Max-Planck-Institut für Eisenforschung GmbH

Slip system interaction with grain boundaries leading to heterogeneous deformation and damage nucleation has been studied in commercial purity Ti. In-situ SEM four-point bending was performed to develop a tensile stress state on the observable surface. Orientation-imaging microscopy (OIM) was used to characterize the orientation distributions in the microstructures and to identify deformation twinning during plastic deformation, while electron channeling contrast imaging (ECCI) was used to identify activated slip and twinning systems. Grain boundary inclinations and orientation gradients within particular grains were examined using synchrotron 3-D X-ray analysis and revealed large strain gradients developed near some grain boundaries. From these observations, conditions that facilitate or prevent slip transfer across a grain boundary are identified. This work was supported by National Science Foundation (NSF) grant DMR-0710570 and German Science Foundation (DFG) grant EL 681/2-1. Use of the Advanced Photon Source was supported by the US DOE-BES Contract No. W-31-109-Eng-38.

### 3:30 PM

**Contrasts in Hot Worked Al-Alloy Substructures from EOM, POM, XRD, TEM, STEM, SEM-EBSI and OIM:** *Hugh McQueen*<sup>1</sup>; <sup>1</sup>Concordia University

Substructure characteristics in Al alloys are important for mechanical modeling in hot forming and its products. In contrast to simple grain shape in etched-optical microscopy (EOM), polarized optical microscopy (POM) significantly confirmed subgrain presence in better detail than x-ray diffraction (XRD). Transmission electron microscopy (TEM) revealed the dislocations forming subgrain boundaries (SGB) and dispersed between them; scanning mode (STEM) provided microtextures substantiating XRD. Scanning electron microscopy with back-scattered image (SEM-EBSI) exhibited substructures more accurately than POM but much less detailed than TEM. Orientation imaging microscopy (OIM) provided microstructures as in SEM-EBSI along with detailed misorientations; however, omission of very-low angle SGB seen in TEM estimated larger subgrain sizes and misorientations. The field of view is very limited in TEM, but fairly similar in POM, SEM-EBSI and OIM with higher magnifications possible in the last two. They are affected differently by substructure scale, solute and particle distributions (partly through specimen preparation).

### 3:50 PM Break

### 4:10 PM Invited

**Void Growth by Dislocation Loop Emission:** *Marc Meyers*<sup>1</sup>; David Benson<sup>1</sup>; Sirirat Traiviratana<sup>1</sup>; Eduardo Branga<sup>1</sup>; <sup>1</sup>UC San Diego

Analytical calculations and molecular dynamics simulations show that the initiation of void formation, thought to occur by the convergent vacancy migration, takes place by the emission of shear loops from the void surface. The configurations of these loops are analysed and it is shown that reactions take place, leading to biplanar and triplanar configurations. These configurations are dependent on the tensile direction. The shear loop mechanism operates for voids as small as 0.3 nm radius, containing 13 vacancies. The density of geometrically necessary dislocations is calculated from the expansion of shear loops and is found to be consistent with observed values. The MD calculations are applied to polycrystals and it is shown that voids nucleate at grain boundaries, particularly at triple points.

### 4:40 PM

**Temporal Statistics and Coarse Graining of Dislocation Ensembles:** *Jie Deng*<sup>1</sup>; Mamdouh Mohamed<sup>1</sup>; Anter El-Azab<sup>1</sup>; <sup>1</sup>Florida State University

The theoretical modeling and numerical simulation of temporal statistics of dislocation ensembles is presented. A kinetic-equation hierarchy is established to describe the evolution of dislocation density, in which the source terms are governed by the rates of dislocation cross slip, annihilation and junction reactions. The stochastic point process and time series theories are used to model the spatial and temporal dependence of these processes and to model the source terms in the kinetic equation. The statistical properties of these processes, in both time and frequency domain, are analyzed in conjunction with dislocation



dynamics simulations. The moving average is applied to remove the trend and keep all the processes stationary. The numerical simulation of autocorrelation function and spectrum provides the preferred frequencies of different types of processes, which, together with their dependence of dislocation density, provide the better understanding of the temporal nature of those processes.

## 5:00 PM

### **Dislocation Structure and Slip Activity of PSBs in Cyclically Deformed Polycrystalline Nickel:** *Anja Weidner*<sup>1</sup>; *Werner Skrotzki*<sup>1</sup>; <sup>1</sup>TU Dresden

Cyclic deformation of metals leads to strain concentrations in so-called persistent slip bands (PSBs) which produce a characteristic extrusion/intrusion profile at the surface. The dislocation structure of these bands can be described as a ladder-like structure of dislocation dense walls and dislocation poor channels embedded in a vein-matrix structure. Beside transmission electron microscopy (TEM), electron channelling contrast (ECC) in a FEG scanning electron microscope is a powerful method to image such dislocation structures. The resolution of ECC images is comparable to that of TEM micrographs. As the ECC method is non-destructive, it is possible to investigate the development of dislocation structures during different stages of fatigue life on the same sample. Moreover, the focused ion beam technology allows visualizing the dislocation structure of individual grains in 3D. An overview on the dislocation structure and the slip activity of PSBs in cyclically deformed polycrystalline nickel will be given.

## 5:20 PM

### **Experimental and Microstructurally-Based Finite-Element Investigation of the Dynamic Compressive Behavior of High Strength Alloys:** *K. Elkhodary*<sup>1</sup>; *W. Lee*<sup>1</sup>; *Bryan Cheeseman*<sup>2</sup>; *Mohammed Zikry*<sup>1</sup>; <sup>1</sup>North Carolina State University; <sup>2</sup>Army Research Laboratory

The objective of this study is to identify the dominant microstructural and dislocation mechanisms related to the high strength and ductile behavior of 2139-Al, and how high strain-rate loading conditions would affect the overall behavior. Characterization techniques and specialized microstructurally-based finite-element (FE) analyses based on a dislocation-density based multiple-slip formulation that accounts for an explicit crystallographic and morphological representation of  $\theta$  and  $\theta'$  precipitates and their rational orientation relations was conducted. The predictions from the microstructural finite element model indicated that the precipitates continue to harden, and also act as physical barriers that impede the matrix from forming large connected zones of intense plastic strain. As the microstructural FE predictions have indicated, and consistent with the experimental observations, the combined effects of  $\theta'$  and  $\theta$ , acting on different crystallographic orientations, enhance the strength, the ductility, and reduce the susceptibility of 2139-Al to shear strain localization due to dynamic compressive loads

## 5:40 PM

### **Modelling Inhomogeneous Deformation Using a Dislocation Density Based Crystal Plasticity Finite Element Model:** *Alankar Alankar*<sup>1</sup>; *David Field*<sup>1</sup>; *Ioannis Mastorakos*<sup>1</sup>; <sup>1</sup>Washington State Univ

A dislocation density based crystal plasticity finite element model (CPFEM) has been developed in which different dislocation densities evolve. Based upon the kinematics of crystal deformation and dislocation interaction laws, dislocation generation, annihilation and flux have been modeled. Stress evolution and inhomogeneous deformation based on dislocation density evolution have been predicted. Texture evolution in plane strain deformation of polycrystalline aluminum was used to validate the crystal plasticity modeling. The framework has been implemented in ABAQUS with user interface UMAT subroutine. Dislocation strength interaction, dislocation segment length interaction, dislocation-solute interaction and dislocation velocity laws have been used as studied using dislocation dynamics (DD) simulations.

## **Electrode Technology for Aluminum Production: Environmental Issues and Raw Materials**

Sponsored by: The Minerals, Metals and Materials Society, TMS Light Metals Division, TMS: Aluminum Committee

Program Organizers: Barry Sadler, Net Carbon Consulting Pty Ltd; John Johnson, RUSAL Engineering and Technological Center LLC

Monday PM

Room: 2003

February 16, 2009

Location: Moscone West Convention Center

*Session Chair:* Frank Cannova, BP Coke

## **2:00 PM Introductory Comments 2:05 PM Presentation of 2008 Best Paper Award by Barry Sadler**

## 2:10 PM

### **Carbon Products: A Major Concern to Aluminum Smelters:** *Ulrich Mannweiler*<sup>1</sup>; *Werner Fischer*<sup>2</sup>; *Raymond Perruchoud*<sup>2</sup>; <sup>1</sup>Mannweiler Consulting; <sup>2</sup>R&D Carbon Ltd.

Since decades the world wide primary aluminum production grows continuously with a rate of five percent per year. From thirty eight million tons aluminum today over sixty eight million tons are expected to be produced in 2020. With the aluminum growth the requirement for carbon products – petroleum coke, coal tar pitch, anodes and cathodes - will grow simultaneously. For each carbon product an outlook is given regarding availability, quality, price and production facilities. China's role as important supplier and consumer for coke, pitch, anodes and cathodes will be reviewed. The impact of production technologies and product properties on the emission of green house gases will be quantified for all process steps from raw materials to aluminum production.

## 2:35 PM

### **Anode Reactivity: Effect of Coke Calcination Level:** *Marie-Josée Chollier*<sup>1</sup>; *Alexandre Gagnon*<sup>1</sup>; *Claude Boulanger*<sup>1</sup>; *Dany Lepage*<sup>1</sup>; *Gaby Savard*<sup>1</sup>; *Ghislain Bouchard*<sup>1</sup>; *Charles Lagacé*<sup>2</sup>; *André Charette*<sup>2</sup>; <sup>1</sup>Rio Tinto Alcan; <sup>2</sup>Université du Québec à Chicoutimi

Coke properties and anode performance are affected by the coke calcination level. Predictions of anode performance have traditionally been based on evaluation of coke reactivity. Using these methods, the use of a higher calcination temperature, up to the point where desulphurisation occurs, is preferred. Undercalcined cokes have, however, been shown to be beneficial to reduce anode consumption in industry. Changes in coke quality, such as increased sulphur, may affect the optimum calcination level for an individual coke. Improved laboratory techniques are required to define the industrial calcination level that will minimise anode reactivity. In this work, different methods for coke calcination, bench scale anode baking and anode reactivity testing have been compared. A procedure for the evaluation of anodes, which reproduces industrial results, has been developed. The study has also confirmed that, for the coke used, calcination at a lower level will reduce anode reactivity.

## 3:00 PM

### **Evaluation of the Necessary Amount of Quinoline Insolubles in Binder Pitch:** *John Baron*<sup>1</sup>; *Stacey McKinney*<sup>2</sup>; *Robert Wombles*<sup>1</sup>; <sup>1</sup>Koppers Industries Inc

The role of quinoline insolubles in a binder pitch has long been the topic of discussion and disagreement. Throughout the world, especially in Asia, QI levels in crude coke oven tar are decreasing. What was once thought to be the lowest acceptable amount of QI in a binder pitch will have to be adjusted. This study was conducted to determine the effect of the quinoline insoluble content of the binder pitch on the physical properties of aluminum anodes. This study used coal tar pitches having QI levels of 1 wt.%, 2 wt.%, 4 wt.% and 6 wt.%. This paper will present the results of this laboratory anode study by comparing the physical properties of the resulting anodes.

**3:25 PM Break****3:35 PM****Environmental and Operating Benefits of a New Fume Treatment System at a Paste Mixing Plant:** *Matthias Hagen*<sup>1</sup>; Ralf Forster<sup>2</sup>; <sup>1</sup>LTB; <sup>2</sup>SGL Carbon GmbH

Increasing energy prices and high labour costs made a plant manager think of possibilities to save costs. A green production plant should be optimised in order to reduce production costs, increase the output and fulfil newest emission regulations. The solution was a completely new designed system. Heated suction hoods at the mixers and a ductwork system with preheating avoided condensations. The effect was zero cleaning, which saves time and increases the availability of the whole plant. A central fume treatment was installed with a thermal oxidiser as main part. The resulting energy is used for preheating of the fumes and the production of heat for the process, which reduces the energy consumption dramatically. The paper shows the technical solution and the numbers of savings in detail.

**4:00 PM****From the "Low Caustic Leaching and Liming" Process Development to the Jonquiere Spent Potlining Treatment Pilot Plant Start-up, 5 Years of Process up-Scaling, Engineering and Commissioning:** *Ghislain Hamel*<sup>1</sup>; Raymond Breault<sup>1</sup>; Gaston Charest<sup>1</sup>; Stéphane Poirier<sup>1</sup>; Bruno Boutin<sup>1</sup>; <sup>1</sup>Rio Tinto Alcan

The LCL&L process is a hydrometallurgical route developed by researchers of Rio Tinto Alcan (RTA) to treat, both environmentally and economically, spent potlining (SPL) generated by aluminium cells. Considering local characteristics, including the low capacity of cement producers to recycle SPL, there is a high SPL inventory that has accumulated over the last 25 years. LCL&L was selected as the preferred solution for the treatment of RTA's SPL in Quebec, and as a sustainable solution for other Quebec aluminium producers. This paper describes LCL&L process characteristics, including valorization alternatives for the by-products and special chemical analysis methods developed for process control. Some technological challenges faced and managed during scale-up from laboratory and mini-pilot process development, design and construction of the industrial scale pilot plant will be discussed. Finally, preparations for the plant commissioning and start-up in April 2008 as well as some early operational highlights will be discussed.

**Emerging Applications of Neutron Scattering in Materials Science and Engineering: Residual Stress Mapping and Neutron Imaging**

Sponsored by: The Minerals, Metals and Materials Society, TMS Electronic, Magnetic, and Photonic Materials Division, TMS: Chemistry and Physics of Materials Committee

Program Organizers: Xun-li Wang, Oak Ridge National Laboratory; Brent Fultz, California Institute of Technology; Hahn Choo, University of Tennessee

Monday PM  
February 16, 2009

Room: 3012  
Location: Moscone West Convention Center

Session Chairs: Werner Wagner, Paul Scherrer Institute; Philip Withers, Manchester University

**2:00 PM Invited****Engineering the Residual State with Mechanical Surface Treatments:** *Philip Withers*<sup>1</sup>; Suzanne Clitheroe<sup>1</sup>; Mark Turksi<sup>2</sup>; Christopher Rodopoulos<sup>3</sup>; <sup>1</sup>The University of Manchester; <sup>2</sup>Magnesium Elektron; <sup>3</sup>University of Patras

Emerging mechanical treatments, such as laser peening, low plasticity burnishing and ultrasonic impact treatment can introduce residual stresses to a depth of many millimetres. In this paper we will report a study of laser peening and ultrasonic impact treatment as compared to performances of shot peened and unpeened benchmarks. In particular the capacity to overwrite previous residual stresses, as might be introduced by bending or weld stresses, will be assessed. In addition the stability of the resulting residual stresses to thermal and mechanical tests will be established, as well as the effect of the residual stresses on fatigue performance. Results for both stainless steels and titanium alloys will be reported being important for the nuclear and aerospace industries

respectively. This work paves the way for the intelligent engineering of the residual stress state in terms of depth and intensity for optimum performance for a given set of in-service conditions.

**2:30 PM****Neutron Residual Stress Mapping of Spur Gears under Applied Load:** Robert LeMaster<sup>1</sup>; Jeffrey Bunn<sup>2</sup>; Brian Boggs<sup>1</sup>; Jon Kolwyck<sup>1</sup>; William Bailey<sup>3</sup>; *Camden Hubbard*<sup>3</sup>; <sup>1</sup>University of Tennessee-Martin; <sup>2</sup>University of Tennessee-Knoxville; <sup>3</sup>Oak Ridge National Laboratory

Stresses in operating gears arise from the externally induced stresses associated with the transmission of power and from the residual stresses associated with the heat treatment and machining of the tooth profiles. Residual stresses at the surface are typically measured ex situ using x-ray diffraction. Neutrons can non-destructively measure stress within a component and can pass through associated hardware. This paper presents the special capabilities of neutron strain mapping to map stresses in situ. Total stress was measured as a function of externally applied load and at depths below the meshing gear tooth surface. Changes in d-spacing between stressed and unstressed states allow determination of strains as a function of location and load. The measurements were made using the second generation Neutron Residual Stress Mapping Facility (NRSF2) at HFIR. A Static Load Application Device (SLAD) was developed to load the gear pair while mounted on the NRSF2 instrument.

**2:50 PM Invited****In-Situ Neutron Diffraction Study of Materials Behavior under Severe Thermal-Mechanical Deformation:** Wan Chuck Woo<sup>1</sup>; *Zhili Feng*<sup>1</sup>; Xun-li Wang<sup>1</sup>; Bjorn Clausen<sup>2</sup>; Donald Brown<sup>2</sup>; Thomas Sisneros<sup>2</sup>; *Camden Hubbard*<sup>1</sup>; Stan David<sup>1</sup>; <sup>1</sup>Oak Ridge National Laboratory; <sup>2</sup>Los Alamos National Lab

The materials behavior under rapid and severe thermo-mechanical deformation is one of the most important yet least understood research areas. We have successfully demonstrated a new measurement method for the direct observation and determination of the material behaviors as they evolve rapidly under complex thermo-mechanical material synthesis environment. For this purpose, a special portable friction-stir processing system was installed inside the beam room of the Spectrometer for MAterials Research at Temperature and Stress (SMARTS) at Los Alamos Neutron Science Center and the in-situ neutron-diffraction experiments were performed during the thermo-mechanical processing of 6.5-mm thick 6061-T6 Al alloy plate. Significant improvement of the temporal resolution of neutron scattering measurements has been achieved using the quasi-steady-state phenomenon. The new measurement methodology and data analysis approach enable us to determine the transient and dynamic variations of temperature, thermal stresses, dislocation density, and subgrain size during severe thermo-mechanical process of materials.

**3:20 PM****Analysis of Residual Stress inside Complex Engineering Components Using Neutron Diffraction:** *Supriyo Ganguly*<sup>1</sup>; Jon James<sup>1</sup>; Michael Fitzpatrick<sup>1</sup>; <sup>1</sup>The Open University

Residual stress measurement using neutron diffraction is an important tool for structural engineers. A new generation of dedicated engineering strain instruments have been built, offering considerable improvements in counting time and spatial resolution. Alongside these improvements, measurements in complex geometry prototype components are increasingly in demand. Therefore, there is a strong driver towards an integrated sample positioning systems for simplified set-up and operating of experiments on such prototype components. The present study was carried out at the ENGIN-X instrument at the ISIS pulsed neutron source, on measurements in a prototype metal matrix composite aircraft wheel, forged from a billet produced through powder metallurgy route. The measurement was designed to obtain macro and misfit stresses developed in matrix and reinforcement phase during fabrication. The use of the SScanSS software for experimental design and implementation, and for precise spatial location of the measuring gauge volume inside such complex components was also demonstrated.

## 3:40 PM Break

### 4:00 PM

**Macroscopic Stress Relaxation in Complex High Performance Alloys:** *Julia Repper*<sup>1</sup>; Michael Hofmann<sup>1</sup>; Christian Kremphaszky<sup>2</sup>; Ewald Werner<sup>3</sup>; Winfried Petry<sup>1</sup>; <sup>1</sup>Forschungsneutronenquelle FRM II; <sup>2</sup>Christian-Doppler-Laboratory of Material Mechanics of High Performance Alloys; <sup>3</sup>Institute for Materials Science and Mechanics of Materials

Because of its excellent thermo-mechanical properties, the multiphase nickel based superalloy IN718 is widely used in industrial components. Macroscopic and microscopic residual stresses are induced during the production process of such components. While the effects leading to macroscopic stresses are well understood, the microscopic mechanisms of stress accumulation are less known. Neutron diffraction is a powerful technique to determine induced macro stresses by a comparison of diffraction angles of strained samples and unstrained reference samples. The identity of the micro stress state in component and reference sample is the basic assumption for macro stress analysis using neutron diffraction. For high performance alloys, like IN718, changes in the micro stress state are conceivable during macroscopic stress relaxation while cutting out reference samples. In this contribution we present the changes in phase specific strains determined by neutron diffraction resulting from a stepwise relaxation of macroscopic residual stresses measured on an IN718 pancake.

### 4:20 PM

**Comparison of Intergranular Residual Strains in Hollow Cylinder Steel Specimens Subjected to Torsion and Tension:** *Jeffery Bunn*<sup>1</sup>; Dayakar Penumadu<sup>1</sup>; Camden Hubbard<sup>2</sup>; <sup>1</sup>University of Tennessee; <sup>2</sup>UT-Battelle/ORNL

Torsion provides a unique opportunity to probe mechanical behavior of materials under pure shear stress. Two hollow cylinder 12L14 steel specimens had been subjected to two levels of torsion exceeding yield, and two other specimens were subject to two levels of tension using a combined axial-torsional testing system. Pairs of torsion-tension samples were subjected to the same magnitude of equivalent octahedral shear strain. In this study the samples were characterized with 0.5 x 0.5 mm spatial resolution. Residual strains for the Fe (110), (200) and (211) reflections were recorded for the hoop, radial and axial directions as a function of location through the hollow cylinder wall. Intergranular residual stresses for both torsion samples and for both tension samples were similar. However, major differences exist between the torsion set and the tension set. The largest differences are in the Fe (200) while the smallest differences was in the Fe (211).

### 4:40 PM Invited

**Neutron Imaging – A Promising Tool in Material Science and Technology:** *Werner Wagner*<sup>1</sup>; Eberhard Lehmann<sup>1</sup>; <sup>1</sup>Paul Scherrer Institut

At the Swiss Spallation Neutron Source SINQ, two facilities for neutron imaging are operating: NEUTRA, a radiography station at a thermal beam port, and ICON at a beam port viewing the cold moderator. Both facilities make use of different state-of-the-art imaging devices, based on imaging plates, semiconductor arrays or CCD-cameras, and specifically tailored for various types of applications. Among those are: radiography and tomography with particularly high spatial resolution (down to the 10- $\mu$ m range), real-time imaging up to 30 frames per sec, stroboscopic imaging with  $\mu$ s resolution, phase contrast imaging and energy selective imaging. One further option is imaging of highly radioactive samples for which NEUTRA is specifically equipped. The presentation will highlight the potential of these options for various applications in materials science and technology by means of selected examples.

### 5:10 PM

**A New Option for Material Characterisation by Means of Energy Selective Neutron Imaging:** Eberhard Lehman<sup>1</sup>; Gabriel Frei<sup>1</sup>; Axel Steuwer<sup>2</sup>; Winfried Kockelmann<sup>3</sup>; <sup>1</sup>SINQ PSI; <sup>2</sup>ESS Scandinavia; <sup>3</sup>STFC

In recent years neutron imaging techniques have developed significantly driven by digital imaging capabilities which enables a more efficient use of the applied neutrons and by the exploitation of scattering effects. Sophisticated techniques such as tomography and phase contrast imaging have now become available on a routine basis. A new approach based on energy selective neutron imaging was recently developed using different experimental set-ups. This option is particularly important for cold neutrons, where common engineering materials have Bragg edges due to the micro-structural behaviour of the crystals, which provides enhanced contrast. Using two different approaches, a double-crystal mono-chromatizers and the time-of-flight option at a pulsed spallation

source, scattering artefacts were identified in transmission mode of imaging for welds and otherwise treated structural materials. In this manuscript, we present and discuss first results with a view to dedicated and optimized installations are foreseen at the upcoming new spallation sources.

### 5:30 PM

**Neutron Transmission Strain Tomography:** *Shu Yan Zhang*<sup>1</sup>; Ed Oliver<sup>2</sup>; Alexander Korsunsky<sup>3</sup>; <sup>1</sup>Science and Technology Facilities Council; <sup>2</sup>Science and Technology Facilities Council; <sup>3</sup>University of Oxford

In many respects, strain mapping by neutron and synchrotron X-ray diffraction can be regarded as imaging techniques in 2D or 3D, i.e. the spatially resolved determination of a material property within the interior of an object. The aim of the study here is to present the concept of strain tomography using Bragg edge neutron transmission measurements. The principle of this novel approach is to analyze residual strain fields by de-convolution of unknown distributions of residual elastic strains from redundant sets of data collected from gauge volumes representing sections through the region of interest. Four representative samples were studied. They have demonstrated spatial resolution and shown the ability to discriminate strains in multiple phases. The strains present within the samples were successfully resolved and were showed very good agreement with the known strain field within the samples.

## Energy Conservation in Metals Extraction and Materials Processing II: Energy Conservation and Technology

Sponsored by: The Minerals, Metals and Materials Society, TMS Extraction and Processing Division, TMS Light Metals Division, TMS: Energy Committee

Program Organizers: Edgar Vidal, Brush Wellman, Inc.; Cynthia Belt, Aleris International Inc; Marie Kistler, Air Products and Chemicals, Inc; Mark Cooksey, CSIRO; Rob Hardin, Burner Dynamics, Inc.

Monday PM

February 16, 2009

Room: 2012

Location: Moscone West Convention Center

Session Chairs: Cynthia Belt, Aleris International Inc; Marie Kistler, Air Products and Chemicals, Inc

### 2:00 PM Introductory Comments

### 2:05 PM

**Catalytic Combustion of Coal and Its Application in Blast Furnace Ironmaking:** *Zhan-cheng Guo*<sup>1</sup>; <sup>1</sup>University of Science and Technology, Beijing

Catalytic combustion of coal is an energy saving technology. However, due to the low activity or high cost of catalyst or its negative impact on device and applied process, there are a few applications in industry. The present paper will introduce how to improve the activity of catalyst for pulverized coal combustion. Our experimental results show that size and surface electric property of catalyst are key factors to affect the catalytic activity, the less the volatile of the coal, the more effect of catalytic combustion. A kind of Ca(OH)<sub>2</sub> based catalysts with nano-micro size was produced, and it was applied to pulverized coal injection combustion in Blast Furnace ironmaking process. When adding the catalyst about 0.5% of coal and coal injection about 150 kg per ton iron, saving coke over 10 kg per ton iron was achieved.

### 2:25 PM

**Improving Energy Efficiency in a Modern Aluminum Casting Operation:** *C. Eckert*<sup>1</sup>; Mark Osbourne<sup>2</sup>; Ray Peterson<sup>3</sup>; <sup>1</sup>Apogee Technology, Inc.; <sup>2</sup>General Motors Powertrain; <sup>3</sup>Aleris International Inc

The theoretical melting energy requirement for a typical hypoeutectic aluminum-silicon alloy is approximately 520 BTU/lb. It has been demonstrated, however, that even a state of the art secondary processing-automated lost foam casting operation can exceed this value by at least an order of magnitude when the actual thermal energy input from melting to solidification is monitored. Metal transfer and holding operations constitutes over 65% of this expenditure. The authors present relative benchmark energy expenditure information by unit operation for an off-site melting/lost foam casting line with a daily throughput in excess of 100,000 lbs. Efficiency improvements through optimization of the current process, and anticipated energy values at the culmination of a U.S.



Department of Energy sponsored project to develop, integrate and demonstrate an advanced melting, transportation, and dispensation system will be cited.

**2:45 PM**

**Overview of the Department of Energy's Industrial Technologies Program:** *Bob Gemmer*<sup>1</sup>; <sup>1</sup>US Department of Energy

An overview of the Industrial Technologies Program (ITP) will be provided. The presentation will focus both on near-term efforts to reduce the energy intensity of American industry as well as longer-term research activities needed to maintain progress once all the "low hanging fruit" are addressed. Specific examples will be given on the approach ITP takes for helping plants through Save Energy Now assessments. In addition, recent successful development of advanced, energy efficient industrial technologies will be described. Future directions for ITP will be discussed.

**3:05 PM**

**Oxyfuel – Energy Efficient Melting:** *Thomas Niehoff*<sup>2</sup>; *David Stoffel*<sup>1</sup>; <sup>1</sup>Linde Gas; <sup>2</sup>Linde North America, Inc.

Energy in form of natural gas, oil and electricity is expensive and will continue to be a rare resource in the future. Recycling of metals instead of primary production is a logic and crucial step towards energy conservation. Greenhouse emissions and energy consumption are impacted by using advanced combustion systems for metals recycling. Airfuel combustion has been the conventional way to melt and recycle metals. Competitive pressure from global companies as well as high energy prices force melt shop operations to reduce and optimize energy usage and cost. Oxyfuel combustion and process technology can be applied in most cases. Linde Gas has converted several hundred furnaces from airfuel to oxyfuel and has extensive experience to avoid start up issues. Oxyfuel process technology does require optimization and experience in the field. This paper will describe the benefits and potential issues for conversion to oxyfuel.

**3:25 PM**

**Energy Savings and Productivity Increases at an Aluminium Slug Plant Due to Bottom Gas Purging:** *Klaus Gamweger*<sup>1</sup>; *Peter Bauer*<sup>2</sup>; <sup>1</sup>RHI AG; <sup>2</sup>NEUMAN Aluminium Austria GmbH

Gas purging systems are well established in nonferrous metallurgy at multiple steps during metal production, including melting, converting, alloying, and metal cleaning. Since the kinetics of all of these stages are positively influenced by using gas purging systems the overall process benefits are substantial. In the aluminum industry, inert or reaction gases are blown into the melt using porous plugs to achieve improved metal grades, higher productivity, and more efficient energy utilization. To enable the most effective application of the process gases a complete package, termed AL KIN, was developed by RHI that includes porous plugs, refractory expertise, gas supply technology, and gas control equipment. This paper discusses the technological and economic advantages of this system and the specific benefits of fuel reduction, production time savings, decreased process gas consumption, and improved refractory service life and maintenance are illustrated using an aluminum slug plant in Austria.

**3:45 PM Break**

**3:55 PM**

**Energy Conservation and Productivity Improvement Measures in Electric Arc Furnaces:** *Ajit Jaiswal*<sup>1</sup>; <sup>1</sup>Steel Authority of India Limited

Electric Arc Furnace (EAF) being a power-intensive equipment, EAF based industries are highly dependent on scarce electric energy. This is the reason Government of India is highly concerned about this and laid emphasis on the conservation of electric energy. This paper highlights factors contributing to reduction in specific electric energy consumption and suggests measures not only for power saving, but also for productivity improvement. To name a few, these are proper sealing of furnace, introduction of oxy-fuel burners, foamy slag practice, increased usage of hot metal/DRI, post-combustion of CO gas for preheating of scrap, improved selection & design criteria of electric, power demand management, process automation, etc. Few cases also have been cited, where the above measures have helped in reaping significant benefits.

**4:15 PM**

**Evaluating Aluminum Melting Furnace Transient Energy Efficiency:** *Edward Williams*<sup>1</sup>; *Donald Stewart*<sup>1</sup>; *Ken Overfield*<sup>1</sup>; <sup>1</sup>Alcoa

Recent increases in energy cost have led to a renewed focus on energy efficiency during aluminum melting operations to reduce fuel usage. The goals of a batch melting operation are to melt the charge using the minimum required energy,

to melt the metal to the required temperature within the required timeframe, and to avoid generating unwanted contaminants by overheating the charge. The heat transfer efficiency of a conventional hydrocarbon fired aluminum melting furnace varies over the course of the melt cycle, depending on the conditions in the furnace. The purpose of this work was to develop a method of determining the transient heat transfer efficiency throughout the furnace cycle and to take advantage of this knowledge to optimize the melting process through furnace controls and proper production operations. This furnace survey methodology has been developed and used to evaluate a number of furnaces.

**4:35 PM**

**Billions of Dollars Could be Saved with Reliability Excellence:** *Darrin Wikoff*<sup>1</sup>; *Scottie Williams*<sup>1</sup>; *Tom Dabbs*<sup>1</sup>; <sup>1</sup>Life Cycle Engineering

The data, compiled by the Department of Energy indicates that the average industrial plant could reduce its total energy cost by 14.8% by implementing effective Life Cycle Asset Management processes. The actual savings varies by industrial classification, but in all cases the potential is substantial and could have a marked impact on the operating profit of the company. Improvements geared towards improving equipment reliability have distinctive linkages to environmental performance, such as reducing the amount of product and raw material waste through routine monitoring of system parameters through predictive technologies, and preventing interruptions to production cycles with a focus on Overall Equipment Effectiveness. Alcoa successfully reduced solvent disposal costs by more than 40% and GE reduced greenhouse gas emissions by more than 250,000 metric tons. This presentation will show you how companies have successfully reduced energy and disposal costs through a focused effort on manufacturing process reliability.

**4:55 PM**

**Elements of an Energy Management Program:** *Ray Peterson*<sup>1</sup>; *Cynthia Belt*<sup>1</sup>; <sup>1</sup>Aleris International Inc

World energy prices have increased significantly in the last several years. These increasing costs impact the overall manufacturing costs of industrial operations and their ability to be profitable. At the same time, there is societal pressure to reduce greenhouse gas emissions. To address these forces, every company should have an energy management program. In this paper, the key elements of an energy management program will be addressed using examples from the Aluminum metals industry. In particular, the elements of Data Collection, Data Analysis, Project Selection, Implementation, and Communications will be reviewed. The size and degree of sophistication of such a program will be dependent upon the magnitude of the energy costs and the resources available to address the issues.

**5:15 PM**

**Understanding and Evaluating Energy Saving Options:** *William Choate*<sup>1</sup>; *Robert D. Naranjo*<sup>1</sup>; <sup>1</sup>BCS Inc

Simply put - energy efficient heating, melting, holding, transporting, and refining operations do not let energy or metal (oxidation) escape. Numerous operating practices and technologies are available that conserve energy, lower costs, and lower GHG emissions (insulation; molten metal pumps; oxy-fuel firing; preheaters; recuperators; refractories, ...). New technologies are emerging that promise even greater benefits (thermoelectric energy recovery; electron, infrared, microwave, plasma heating and melting; solar furnaces...). The challenge for manufacturers is how to evaluate a multitude of opportunities considering that each change brings new learning curves and combinations of changes have diminishing returns (i.e., benefits do not simply add together). This paper explores old technologies and practices that have new life given the price of energy today, emerging technologies, and experimental technologies. It examines lessons learned from changes and upgrades, and provides guidelines to understanding how incorporating the old, emerging or experimental technologies will impact productivity and profitability.

**5:35 PM Concluding Comments**

## Fatigue: Mechanisms, Theory, Experiments and Industry Practice: Theory and Simulation

Sponsored by: The Minerals, Metals and Materials Society, TMS Structural Materials Division, TMS/ASM: Computational Materials Science and Engineering Committee, TMS/ASM: Mechanical Behavior of Materials Committee, TMS/ASM: Nuclear Materials Committee

Program Organizers: Koenraad Janssens, Paul Scherrer Institute; Corbett Battaile, Sandia National Laboratories; Brad Boyce, Sandia National Laboratories; Luke Brewer, Sandia National Laboratories

Monday PM Room: 3008  
February 16, 2009 Location: Moscone West Convention Center

Session Chairs: Koenraad Janssens, Paul Scherrer Institute; Corbett Battaile, Sandia National Laboratories

### 2:00 PM Invited

**A Geometric, Multiscale Approach to Stochastically Modeling Microstructurally Small Fatigue Crack Formation:** *Anthony Ingraffea*<sup>1</sup>; Jacob Hochhalter<sup>1</sup>; Jeffrey Bozek<sup>1</sup>; Michael Veilleux<sup>1</sup>; Paul Wawrzynek<sup>1</sup>; <sup>1</sup>Cornell University

Recent advances in computational and experimental capabilities have provided the opportunity to model accurately fatigue damage in its entirety, from incubation to structural failure. The main thrust of the work presented here is toward the creation of a computational framework that geometrically models microstructurally small fatigue crack (MSFC) formation for a proof-test material: aluminum alloy 7075-T651. Methods are presented that generate and discretize statistically accurate microstructure geometry models, and explicitly simulate the MSFC formation stages: incubation, nucleation, and microstructurally small propagation. A multiscale approach is taken to couple a microstructural domain with the local deformation fields in a structural domain experiencing variable amplitude spectrum loading. The physics-based crack formation criteria are validated through direct comparisons to experimental observations. Thousands of simulations are computed, each for a unique statistical realization of the microstructure, to generate high fidelity, probabilistic predictions of MSFC growth rates.

### 2:30 PM

**Microstructure-Based Approach for Predicting Microplastic Ratcheting in Metals:** *Remi Dingreville*<sup>1</sup>; Corbett Battaile<sup>1</sup>; Luke Brewer<sup>1</sup>; Elisabeth Holm<sup>1</sup>; <sup>1</sup>Sandia National Laboratories

This study examines the elasto-plastic response of nickel microstructures under microplastic ratcheting conditions using a crystal plasticity model combined with experimental characterization of microstructures. The morphology and deformation behavior of polycrystals are characterized using Electron Back Scatter Diffraction (EBSD), while a non-local crystal plasticity framework with augmented kinematics is used in a computational context. The predicted cyclic behavior is compared against experimental results both at the macroscopic level and microstructural level. The examination of the macroscopic and microscopic material behavior suggests fundamental mechanisms of microplastic ratcheting at the microstructural scale, while the discrepancies between the experimental and computational observations underline the limitations of the current theoretical framework.

### 2:50 PM

**Application of Field Dislocation Mechanics to Cyclic Plasticity:** *Armand Beaudoin*<sup>1</sup>; Koenraad Janssens<sup>2</sup>; Amit Acharya<sup>3</sup>; <sup>1</sup>University of Illinois; <sup>2</sup>Paul Scherrer Institute; <sup>3</sup>Carnegie-Mellon University

In the study of cyclic plasticity, interplay between mechanisms of elasticity, anelasticity and (micro-) plasticity must be addressed. There exists a varying landscape of internal stress — due to dislocation interactions with boundaries, precipitates and solute atoms, for example. Some obstacles may be relatively soft, giving rise to a component of area swept by dislocations recoverable upon unloading. Development of local constitutive equations presents a challenge, with the variety of mechanisms at odds with the desire to maintain a tractable description. We adopt a field description, “Mesoscale Field Dislocation Mechanics” (MFDM), wherein long range stresses are developed through incompatibility and transient elastic response follows from the motion of the polar dislocation density. MFDM leverages existing models of continuum

plasticity within a non-local framework. Cyclic deformation of a polycrystal is examined, with attention given to the development of mobile polar density, internal stress and effect on the averaged stress-strain response.

### 3:10 PM

**Fatigue Mechanism and Multistage Fatigue Modeling for Wrought Mg-3Al-1Zn:** *Yibin Xue*<sup>1</sup>; Adrian Pasco<sup>2</sup>; Mark Horstemeyer<sup>2</sup>; <sup>1</sup>Utah State University; <sup>2</sup>Mississippi State University

The microstructure-fatigue properties relation is developed based on multiscale fatigue experiments and micromechanical simulations. The large intermetallic particles in coarse grains at or near the surface are identified as the fatigue damage incubation sites. The morphology of the inclusion particles, as well as the bonding strength between the particle and alloy matrix, affects the fatigue incubation life as observed in micromechanical simulations in conjunction with the modified microscale Coffin-Manson law. The microstructurally and physically small crack growths were observed using in-situ SEM fatigue testing. The crack growth rate was directly quantified as a function of applied stress amplitude weighted by the applied stress ratio. The fatigue long crack growth was modeled combining a generalized Paris law with the application of a strip-yield model at the crack tip. Finally, the multistage fatigue model was implemented to evaluate the fatigue life of a simple component in an automobile Mg-front end application.

### 3:30 PM Invited

**Microstructure-Sensitive Modeling of Rolling Contact Fatigue:** *Erick Alley*<sup>1</sup>; *Richard Neu*<sup>1</sup>; <sup>1</sup>Georgia Inst of Technology

Crack nucleation, first spall generation and spall growth in rolling contact fatigue (RCF) are known to be highly sensitive to the heterogeneity of the microstructure. Yet the current state-of-the-art in the design of high performance bearing materials and microstructures is highly empirical requiring substantial lengthy experimental testing to validate the reliability and performance of these new materials and processes. We have laid the groundwork necessary to determine the influence of microstructure in RCF and related very high cycle fatigue problems. Crystal plasticity material models provide more realistic accumulations of localized plastic strains with cycling compare to homogenized J2 plasticity. With J2 plasticity, the bearing must be overloaded to capture significant plasticity near inclusions; with crystal plasticity, realistic bench test loads can be applied with plastic strain accumulation observed near inclusions in cases where RCF failure is anticipated.

### 4:00 PM Break

### 4:30 PM Invited

**Microstructure-Sensitive Modeling of High Cycle Fatigue:** *Craig Przybyla*<sup>1</sup>; *Rajesh Prasannavenkatesan*<sup>1</sup>; *Nima Salageheh*<sup>1</sup>; *David McDowell*<sup>1</sup>; <sup>1</sup>Georgia Tech

We explore microstructure-sensitive computational methods for predicting variability of low cycle fatigue (LCF) and high cycle fatigue (HCF) processes in metallic polycrystals to support design of fatigue resistant alloys. We outline a philosophy of establishing relations between remote loading conditions and microstructure-scale plasticity/crack behavior as a function of stress amplitude, stress state and microstructure, featuring calibration of mean experimental responses for known microstructures that bound the range of virtual (digital) microstructures. Effects of process history and resulting residual stresses are considered in certain cases of subsurface crack formation. The need to characterize extreme value correlations of microstructure attributes coupled to the local driving force (i.e., features) for HCF crack formation is outlined, along with a strategy involving a set of Fatigue Indicator Parameters (FIPs) relevant to different mechanisms of crack formation.

### 5:00 PM

**Science-Based Modeling and Simulation of Fatigue Damage:** *Elias Anagnostou*<sup>1</sup>; <sup>1</sup>Northrop Grumman Corp

Probabilistic microstructurally-based models for fatigue are being developed as part of a DARPA/Northrop Grumman Structural Integrity Prognosis System (SIPS). The fatigue models are based on a fundamental understanding of the fatigue process, and trace the structural degradation caused by fatigue back to its physical origins in the microstructure of the metallic component. The objectives are to discover and link all the important damage mechanisms leading to a macroscopically observable crack and to allow defects to emerge naturally from statistically meaningful ensembles of material representations, subject to more accurate, scale-specific, damage inducing fields. An example is modeling the

interplay between the grain crystallography and crack incubation at a constituent particle. A microstructurally-based model allows estimation of the total fatigue life from incubation and nucleation at a constituent second phase particle to propagation of micro-cracks to emergence of macro-cracks all in a statistical sense to permit accurate estimation of reliability indices.

### 5:20 PM

**Small-Crack Growth Based Prediction of the Effect of Temperature on Fatigue Lifetime Distribution and Probabilistic Lifetime Limit in Ti-6Al-2Sn-4Zr-6Mo:** *Sushant Jha*<sup>1</sup>; James Larsen<sup>2</sup>; <sup>1</sup>Universal Technology Corp; <sup>2</sup>US Air Force Research Laboratory

Recently, it has been shown that the fatigue lifetime distribution can be modeled as a superposition of the crack-growth probability density and a mean-lifetime-dominating density. It has also been demonstrated, that the effect of microstructural and extrinsic factors on the lifetime distribution can be understood in terms of the different rates of response of the two behaviors with respect to these variables, thereby producing a separation (or convergence) between them. In this paper, this modeling approach is applied to predict the lifetime probability density and the probabilistic lifetime limit as a function of temperature in Ti-6Al-2Sn-4Zr-6Mo. A range of temperatures including 23°C, 260°C, and 399°C were considered. The effect on the fatigue variability and the probabilistic limit could be analyzed, almost independently of the number of experimental points, via the role of the small-crack growth regime in separation (or convergence), with respect to temperature, of the two aforementioned responses.

## Friction Stir Welding and Processing-V: Session II

Sponsored by: The Minerals, Metals and Materials Society, TMS Materials Processing and Manufacturing Division, TMS: Shaping and Forming Committee  
Program Organizers: Rajiv Mishra, Missouri University of Science and Technology; Thomas Lienert, Los Alamos National Laboratory; Murray Mahoney, formerly with Rockwell Scientific

Monday PM Room: 2014  
February 16, 2009 Location: Moscone West Convention Center

Session Chair: Murray Mahoney, BYU

### 2:00 PM Invited

**Microstructure and Properties of Friction Stir Welded 1.3wt%N Containing Steel:** *Yutaka Sato*<sup>1</sup>; Kei Nakamura<sup>1</sup>; Hiroyuki Kokawa<sup>1</sup>; Shuji Narita<sup>2</sup>; Tetsuya Shimizu<sup>3</sup>; <sup>1</sup>Tohoku University; <sup>2</sup>Daido Steel

In this study, FSW was applied to a high nitrogen steel (HNS) containing 1.3wt% nitrogen using a PCBN tool, and feasibility of FSW for HNS, and microstructure and properties of the weld were examined. FSW produced defect-free welds at several welding parameters in the HNS. The stir zone had roughly the same nitrogen content as the base material, which suggested that both the PCBN tool wear and the nitrogen desorption hardly occurred during FSW. FSW refined the grain structure in the stir zone, which resulted in the higher hardness than the base material. Simultaneously, FSW resulted in rapid formation of Cr<sub>2</sub>N precipitates on the grain boundaries in the stir zone, which caused reduction of the corrosion resistance. This study showed that FSW is an effective method to produce a defect-free weld with high hardness in the HNS, although the corrosion resistance of the stir zone is reduced.

### 2:20 PM Invited

**Friction Taper Stud Welding of Creep Resistant 10CrMo910:** Daniel Hattings<sup>1</sup>; Mark Newby<sup>2</sup>; *Axel Steuwer*<sup>3</sup>; Ian Widderburn<sup>1</sup>; Philip Doubell<sup>2</sup>; Malcom James<sup>4</sup>; <sup>1</sup>Nelson Mandela Metropolitan University; <sup>2</sup>ESKOM Holdings Ltd; <sup>3</sup>ESS Scandinavia; <sup>4</sup>University of Plymouth

Friction Taper Stud Welding (FTSW) is a novel welding technique that involves forcing a rotating consumable tool into a tapered (conical) cavity of nearly matching shape. The resultant generated heat causes a plasticised layer which bonds to the bottom of the hole and radially to the adjacent hole side. This is similar to other friction welding techniques such as linear and inertia friction welding, but involves a conical interface. Possible applications are repair welds in steel pipes. However, detailed knowledge of the residual stress distributions is essential for structural integrity interactions. This manuscript introduces the main concepts of FTSW and discusses the effects of pre and post weld heat

treatment on the triaxial residual stress field (measured by neutron diffraction) generated by FTSW in a creep resistant steel manufactured from 10CrMo910 steel.

### 2:40 PM Invited

**Friction Stir Welding of High Temperature Materials for Power Plant:** *Seung Hwan Park*<sup>1</sup>; Kazutaka Okamoto<sup>1</sup>; Satoshi Hirano<sup>1</sup>; Akihiro Sato<sup>1</sup>; <sup>1</sup>Hitachi, Ltd. Materials Research Laboratory

Friction stir welding has been applied to high temperature materials for power plant such as 12 Cr steel, Ni-base oxide dispersion strengthened (ODS) alloy and Zr alloy, to examine the microstructures and properties in the welds. All welds were conducted using polycrystalline cubic boron nitride tool. Hardness remarkably increased in the 12 Cr steel weld, which was attributed to the formation of martensite in the stir zone (SZ). The weld of Ni-base ODS alloy showed the coarsening and aggregation of Y<sub>2</sub>O<sub>3</sub> strengthening oxide particles in the SZ, which resulted in the decrease in the hardness. Remarkable hardness increase, which generally occurs due to oxygen absorption during welding, was not observed in the SZ of Zr alloy weld.

### 3:00 PM

**Exploring Geometry Effects for Convex Scrolled Shoulder, Step Spiral Probe FSW Tools:** *Carl Sorensen*<sup>1</sup>; Bryce Nielsen<sup>1</sup>; <sup>1</sup>Brigham Young University

A new tool design for FSW is the convex scrolled shoulder, step spiral probe (CS4) tool. Compared with traditional FSW tools, the CS4 tool has been demonstrated to offer larger process windows, lower operating forces, and the possibility of operating at zero tilt angle. This paper presents a parametric geometric description of the CS4 tool. Based on this description, a series of experiments has been performed to determine the effects of tool geometry on operating forces and weld surface finish. The advantages of convex scrolled shoulder tools in difficult FSW applications are presented.

### 3:20 PM

**An Analytical Investigation of Tool Deformation and Wear in FSW of Hard Metals:** Brian Thompson<sup>1</sup>; *Zak Pramann*<sup>1</sup>; Jeff Bernath<sup>1</sup>; Timothy Stotler<sup>1</sup>; <sup>1</sup>EWI

Friction stir welding (FSW) has progressed rapidly from a technology developed for joining of soft metals such as aluminum to a technology capable of joining hard metals such as steel, titanium and nickel based alloys. This advancement in technology has been possible primarily due to advancements in tool materials. There are two widely accepted tool material categories for FSW of hard metals: refractory metal based tools and composite tools. The tool technology has progressed to significantly reduce tool deformation, wear and breakage compared to early designs. However, tool deformation and tool wear and the mechanisms causing this degradation are still two very important topics in FSW. An analytical approach has been developed to study tool deformation and tool wear as two separate issues. Tool deformation will be evaluated using a thermomechanical model and tool wear will be studied using a tribological approach.

### 3:40 PM

**Precipitation Reactions in Friction Stir Welded PH15-5 Steel:** *Thomas Weinberger*<sup>1</sup>; Norbert Enzinger<sup>1</sup>; Horst Cerjak<sup>1</sup>; <sup>1</sup>Graz University of Technology

In the present study, the effect of friction stir welding on the precipitation microstructure of a martensitic precipitation hardened steel PH15-5 was investigated. Friction stir welding was performed using a tungsten based tool and different welding parameters. To analyze the temperature - stress profile in the plates, which has a significant influence on the precipitation reaction, a coupled thermo-mechanical model was used. Temperature measurements on the upper and bottom side of the plates were performed to verify the temperature distribution. To study the precipitation mechanism, advanced techniques like transmission electron microscopy and atom probe field ion microscopy were used. Additionally, the local mechanical properties of the joint were analyzed and the relationship between the precipitation and the hardness was studied. With the combination of different methods, it was possible to identify the hardening mechanism and the influence of the thermal cycle on the precipitation process.



## 4:00 PM Break

### 4:10 PM

**Friction Stir Welding of "T" Joints in HSLA-65 Steel:** *Murray Mahoney*<sup>1</sup>; Russell Steel<sup>2</sup>; Tracy Nelson<sup>1</sup>; Scott Packer<sup>3</sup>; Carl Sorensen<sup>1</sup>; <sup>1</sup>BYU; <sup>2</sup>Megadiamond; <sup>3</sup>Advanced Metals Products

Our objective is to demonstrate a practical approach for friction stir welding (FSW) "T" joints in long lengths of HSLA-65 steel. FSW of HSLA-65 steel offers challenges but achieving a defect-free weld in a "T" joint geometry in HSLA-65 steel is even more challenging. In addition to producing a sound weld nugget, the "T" fillet requires additional consideration. An excessive fillet volume can create thinning of the top sheet and an unbonded lap adjacent to the leg of the "T" where metal extrudes into the fillet cavity. Conversely, if the fillet volume is small, there is a risk of the FSW tool contacting the support tooling. Our FSW studies use both different PCBN tool designs and different "T" joint geometries in attempts to circumvent these concerns and create a practical weld approach. Metallographic results, tool designs, different "T" joint geometries, and joint properties will be presented.

### 4:30 PM

**Surface Processing, Tempering and Toughening of 4340 Steel by Friction Stir Processing (FSP) of Melt-Deposited Alloy Layer:** *Sibasish Mukherjee*<sup>1</sup>; *Amit Ghosh*<sup>1</sup>; *Harshad Natu*<sup>2</sup>; *Ashish Dasgupta*<sup>3</sup>; <sup>1</sup>University of Michigan; <sup>2</sup>POM Group, Inc; <sup>3</sup>Focus Hope

Direct Melt Deposition (DMD) of pre-alloyed 4340 steel, complemented by FSP, has been examined as a means to repair damaged areas of expensive components used by the Navy. Laser deposition process of steel 4340 steel powder leads to fully martensitic structure and high hardness but with low toughness. Surface processing of DMD 4340 steel by FSP using W-Re tool is found to provide penetration of deformation and thermal effects several millimeters into the material surface encompassing the depth of the DMD layer and converts this layer into a high toughness repaired region. In addition to processing by W-Re tool, flame softening followed by FSP by using H-13 tool steel was also found to be an adequate low-cost approach to develop a tempered and tough microstructure. Microstructural changes and mechanical property after these operations will be reviewed.

### 4:50 PM

**Microstructure and Mechanical Properties of Friction Stir Welded MA956:** *Ramprashad Prabhakaran*<sup>1</sup>; *Wei Yuan*<sup>2</sup>; *James Cole*<sup>1</sup>; *Rajiv Mishra*<sup>2</sup>; *Indrajit Charit*<sup>3</sup>; <sup>1</sup>Idaho National Laboratory; <sup>2</sup>Missouri University of Science and Technology; <sup>3</sup>University of Idaho

Oxide dispersion strengthened (ODS) steels would require good weldability for in-core applications in advanced nuclear reactors. Conventional fusion welding of ODS steels can cause undesirable effects such as coalescence of oxide dispersoids and significant porosity. In this study, friction stir welding was performed in bead-on-plate configuration on an ODS MA956 steel sheet using a cermet tool. Tensile properties of the parent and the stir zone materials were evaluated using mini-tensile testing. Interestingly, the yield and tensile strength of the stir zone showed marked improvement over the parent material with no loss in ductility. Microhardness profile of the processed material was obtained to understand the extent of microstructural gradient. Optical microscopy and transmission electron microscopy were used to evaluate changes in grain size and characteristics of the nanoscale oxide dispersoids (particle size, volume fraction, etc.) across the processed zone. This work is partly supported by the US Department of Energy.

### 5:10 PM

**Correlating Extended Plasticity Mechanisms to Final Microstructure in Friction Stir Welding of 304L Stainless Steel:** *Benjamin Nelson*<sup>1</sup>; <sup>1</sup>Brigham Young University Department of Mechanical Engineering

The formation of sigma phase (which assists corrosion) in friction stir welded (FSW) 304L stainless steel is one of the main obstacles keeping FSW 304L from being used in industry. There is evidence that sigma phase formation, in general, is a recrystallization related phenomenon. The proposed research is focused on identifying the mechanisms of extended plasticity active in producing the final microstructure in FSW 304L stainless steel. This research will give further insight into whether recrystallization plays an active role in the formation of sigma phase in FSW 304L. This characterization will be carried out for several regions within the stir zone. The mechanisms will be identified by use of EBSD. Using five FSW process parameters a central composite design will be used to

determine a relationship between extended plasticity mechanisms and process parameters. FSW will be performed using a polycrystalline cubic boron nitride convex scrolled shoulder step spiral tool.

### 5:30 PM

**Quantifying Post-Weld Microstructures in FSW HSLA-65:** *Tracy Nelson*<sup>1</sup>; *Lingyun Wei*<sup>1</sup>; *Majid Abassi*<sup>1</sup>; <sup>1</sup>Brigham Young University

A comprehensive microstructural investigation of friction stir welds in HSLA-65 steel has been undertaken. Friction stir welds were made in 6.4 mm HSLA-65 steel over a range of process parameters using a polycrystalline cubic boron nitride (PCBN) convex scroll-shoulder step-spiral (CS4) tool. The post weld microstructure was investigated by optical microscopy (OM) and Orientation Imaging Microscopy (OIM). OM revealed primarily lath upper bainite microstructures in the stir zone. OIM was used to establish quantitative measures of the prior austenite grain size, bainite packet size, and lath size. Prior austenite grain sizes in the stir zone were as large as 50µm. This new approach to acquiring quantitative microstructural data is presented.

### 5:50 PM

**Friction Stir Welding of Dual Phase Steel:** *Wei Yuan*<sup>1</sup>; *Jeffrey Rodelas*<sup>1</sup>; *Rajiv Mishra*<sup>1</sup>; <sup>1</sup>Missouri University of Science and Technology

Friction stir welding (FSW) of a dual phase (DP590) steel was evaluated with a cemented carbide tool. Different tool traverse speeds at 1000 rpm tool rotation rate were employed to compare the microstructural changes (phase transformation, grain morphology, and grain size) and mechanical properties in the nugget region. The properties of parent material and nugget regions were characterized by mini-tensile and microhardness tests. The yield strength and ductility increased in the nugget region after FSW. For these traverse speeds, the yield strength and ductility increased with the increase in traverse speed. Microhardness profiles showed that hardness in the nugget was higher than base material and the heat affected zone was the softest region. Detailed microstructure evolution and corresponding thermal history in different regions will be compared and discussed.

## Frontiers in Solidification Science III: Dendritic Growth Phenomena

Sponsored by: The Minerals, Metals and Materials Society, ASM International, TMS Materials Processing and Manufacturing Division, TMS/ASM: Computational Materials Science and Engineering Committee, TMS/ASM: Phase Transformations Committee, TMS: Solidification Committee, TMS: Chemistry and Physics of Materials Committee  
Program Organizers: Ralph Napolitano, Iowa State University; James Morris, Oak Ridge National Laboratory

Monday PM

Room: 2018

February 16, 2009

Location: Moscone West Convention Center

Session Chair: Jeffrey Hoyt, McMaster University

### 2:00 PM Invited

**Measurements of Dendrite Tip Growth in Succinonitrile-Acetone Alloys:** *Christoph Beckermann*<sup>1</sup>; *Antonio Melendez*<sup>1</sup>; <sup>1</sup>University of Iowa

Measurements are performed of dendrite tip growth of succinonitrile-acetone alloys solidifying freely in an undercooled melt. The experiments are conducted using a setup similar to the IDGE of Glicksman and coworkers. The setup allows for precise measurements of the dendrite tip velocity, radius and shape for a range of undercoolings and solute concentrations. The measurements are compared to available theories of free dendritic growth. It is found that for pure succinonitrile, the measured dendrite tip Péclet numbers and selection parameters agree well with previous theories of free dendritic growth, if the effects of melt convection are taken into account. For finite solute concentrations, however, the tip selection parameter is found to deviate significantly from the pure succinonitrile value, especially at higher undercoolings. Furthermore, the three-dimensional dendrite tip shape becomes significantly more anisotropic. In light of this new data, a re-examination of the dendrite tip growth theory for alloys is needed.

**2:20 PM Invited**

**Pattern Formation in Dendritic Directional Solidification of Al-Based Alloys: Investigation of 3D- Dendrite Shape and Dynamical Mechanical Effects by Synchrotron Live X-Ray Imaging:** *Bernard Billia*<sup>1</sup>; Henri Nguyen-Thi<sup>1</sup>; Nathalie Manginck-Noel<sup>1</sup>; Nathalie Bergeon<sup>1</sup>; Adeline Buffet<sup>2</sup>; Guillaume Reinhart<sup>3</sup>; Thomas Schenk<sup>4</sup>; Jose Baruchel<sup>5</sup>; Hyejin Jung<sup>5</sup>; Jurgen Hartwig<sup>2</sup>; Paul Tafforeau<sup>2</sup>; <sup>1</sup>CNRS - University Paul Cezanne; <sup>2</sup>ESRF; <sup>3</sup>European Space Agency; <sup>4</sup>Ecole des Mines de Nancy; <sup>5</sup>National Fusion Research Institute

Precise characterization of the dynamical formation and selection of the dendritic microstructure in alloy solidification is critical for both the understanding of fundamental aspects and the breaking of technology barriers in materials processing. Owing to a unique experimental set-up combining in situ and real-time X-ray radiography and topography at the European Synchrotron Radiation Facility, detailed investigation of the solidification progress in thin Al-based alloys solidified upwards is enabled. Beyond revealing strains and stresses of various origins (shape-induced solute segregation; gravity causing bending of secondary arms and even dynamical disorientation along the primary trunk; competitive growth with eutectic behaving as a metal-matrix composite...) that have a significant influence on the crystalline quality of dendrites, X-ray topography gives access to the 3D-morphology through the equal-thickness fringes captured in Laue 2D-images. These 3D-shapes can be compared with theoretical predictions for free growth and growth in a channel, and lateral confinement effects discussed.

**2:40 PM**

**Real Time Observation of Dendritic Solidification in Real Alloys by Synchrotron Microradiography:** *Bin Li*<sup>1</sup>; <sup>1</sup>Johns Hopkins University

The opacity of real alloys poses a challenge to the study of dendrite growth during solidification. Conventional experiments have to be performed after solidification is completed or interrupted. We present real time observations of dendrite growth in real alloys (Sn-Bi and Al-Cu) by using synchrotron radiation and the cutting-edge technology at national synchrotron facilities at CHESS and APS. Dendrite growth and coarsening in Sn-13%Bi alloy was studied in real time. Kinetics of coarsening was measured based on the real time observations. Dendrite morphology evolution during directional solidification was also studied, and we found that temperature gradient zone melting (TGZM) had a strong effect on the dendrites. These observations provided unambiguous understanding towards morphological evolution during dendritic solidification in real alloys.

**3:00 PM**

**Spatial Correlations in Directionally Solidified Dendrites:** *Amber Genau*<sup>1</sup>; Peter Voorhees<sup>1</sup>; <sup>1</sup>Northwestern Univ

Spatial correlations in directionally solidified Pb-Sn dendrites are analyzed using a recently developed technique for directly measuring the radial distribution function on complex, three-dimensional surfaces. We will discuss changes to the correlation function due to variations in the volume fraction of solid, as well as changes which occur after isothermal coarsening. At very long coarsening times, as the morphology undergoes dramatic changes to become predominantly vertically aligned tubes, long-range periodic order appears. Changes in correlation are also compared between dendrites in a typical mush and those in regions more reminiscent of free-growing dendrites. These types of spatial correlations are critical to understanding the evolution of solidification structures, as the coarsening process is driven both by local mean curvature and by diffusional interactions with surrounding interface.

**3:20 PM Invited**

**Effect of Interface Anisotropy on Spacing Selection in Constrained Dendrite Growth:** *Ingo Steinbach*<sup>1</sup>; <sup>1</sup>Ruhr-University

The selection of spacing in directional dendritic solidification is investigated numerically using the phase-field method in 2D and 3D. A criterion for the critical spacing below which no stable array growth can exist is derived from analysis of individual tip shapes. Constricted solute diffusion in the array leads to a deformation of the dendrite tip shape that competes with the deformation due to surface tension anisotropy. At the critical spacing both effects balance and a stable growth solution is destroyed. This mechanism is identified to determine the critical spacing of a dendritic array and leads to a dependence of the spacing on the anisotropy of the solid-liquid interface energy in a similar way as for the dendrite tip radius.

**3:40 PM Break****4:00 PM Invited**

**In-situ Observations of Coarsening of Dendritic Solid-Liquid Mixtures:** J.L. Fife<sup>1</sup>; L. Aagesen<sup>1</sup>; E.M. Lauridsen<sup>2</sup>; *Peter Voorhees*<sup>1</sup>; M. Stampanoni<sup>3</sup>; <sup>1</sup>Northwestern University; <sup>2</sup>RISO Laboratories; <sup>3</sup>Paul Scherrer Institute

The solid-liquid mixtures produced following dendritic solidification are morphologically complex with spatially varying mean and Gaussian curvature. To understand the manner in which these systems evolve during coarsening, we have employed in-situ three-dimensional x-ray tomography and phase field simulations. Both the experiments and simulations determine the evolution of the interface shape distribution, the probability of finding a patch of curvature with a certain mean and Gaussian curvature. The approach allows the interfacial velocities to be determined experimentally and compared directly to phase field simulations that employ the experimentally measured microstructures as initial conditions. We also determine both experimentally and theoretically the flow of the probability that governs the evolution of the interfacial shape distribution. The experiments show the importance of topological singularities in the coarsening process as well. An analysis of this process will be given.

**4:20 PM Invited**

**Ginzburg-Landau Model of Polycrystalline Solidification:** *Alain Karma*<sup>1</sup>; Robert Spatschek<sup>2</sup>; <sup>1</sup>Northeastern University, Boston, Physics Department and Center for Interdisciplinary Research on Complex Systems; <sup>2</sup>Northeastern University, Boston, Physics Department and Center for Interdisciplinary Research on Complex Systems - and - Ruhr-University, Interdisciplinary Centre for Advanced Materials Simulation

This talk will describe a Ginzburg-Landau model of polycrystalline solidification that is formally derived by a multiple scale analysis of the phase-field crystal model. The free-energy of the model is formulated in terms of complex order parameters that describe the slow spatial modulation of both the amplitude and orientation of density waves corresponding to principal reciprocal lattice vectors of the crystal lattice. This model has the advantage that it can be used to simulate efficiently polycrystalline solidification with defects and elastic interactions in the limit of small misorientation between crystal grains where the model is quantitatively valid. Fundamental insights into grain boundary premelting in pure metals obtained with this model will be discussed in the light of quantitative comparisons with phase-field crystal model predictions and atomistic simulations.

**4:40 PM**

**Real-Time X-Ray Observations of Hot Tearing in Al-Cu Alloys:** *Richard Hamilton*<sup>1</sup>; Devashish Fuloria<sup>1</sup>; Andre Phillion<sup>2</sup>; Peter Lee<sup>1</sup>; <sup>1</sup>Imperial College London; <sup>2</sup>Ecole Polytechnique Fédérale de Lausanne

Hot tearing was directly observed using an in situ, high temperature, tensile/compression tester and x-ray radiography in synchrotron and laboratory sources. This allowed the load to be measured whilst directly observing the deformation of the primary dendrites and flow of Cu-enriched interdendritic fluid. The localisation of load, followed by void formation, coalescence and final fracture was observed whilst monitor the changes in load. The effect of cooling rate and strain rate on the mechanisms of hot tears initiation, growth, and potential healing was studied. At low strains, healing by liquid flow was observed, whereas at higher strains void formation combined with liquid necking between grains was prevalent.

**5:00 PM**

**Modeling on Dendrite Growth during Slab Continuous Casting of Stainless Steels:** *Wei Guo*<sup>1</sup>; Lifeng Zhang<sup>1</sup>; Miaoyong Zhu<sup>2</sup>; <sup>1</sup>Missouri University of Science and Technology; <sup>2</sup>Northeastern University

Dendrite growth is an important phenomenon of solidification structure, which is controlled by interfacial atom deposit dynamics, interfacial tension, heat diffusion, mass diffusion, etc. In the current paper, the undercooling for AISI304 type stainless steel in both the mold and the secondary cooling zone of the continuous casting process was simulated using non-traditional methods. The radius of the dendrite tip, growth velocity and the temperature gradient in the front of S/L interface were calculated. The simulation agreed well with the experimental data published in the literature..

5:20 PM

## **Novel Periodic Diphasic Dendrite Structure in Solidified Al-35wt. %La**

**Alloy:** *Zidong Wang*<sup>1</sup>; <sup>1</sup>McGill University

By vacuum-melting and casting in metal, graphite and sand molds, Al-35wt. % La alloys with different solidification velocities were fabricated. With the help of X-ray diffraction and SEM, a novel dendrite structure has been determined to be found in Al-35wt. % La alloy. The dendrite is composed of a-Al alternating with Al<sub>11</sub>La<sub>3</sub> and thus called periodic diphasic dendrite structure. The dendrite structure, different from common dendrite of single phase, is composed of alternating two phases, so that the chemical compositions along the arms of the diphasic dendrite change in discontinuous and periodic oscillatory. The structure is somewhat similar to banded structure and possesses light and dark regions to turn up alternately; but unlike banded structure, the regions, which are of two phases, regularly arrange in dendrite shape to form the periodic diphasic dendrite structure with the chemical composition periodic variation along a dendrite growth direction.

---

## **Global Innovations in Materials and Technologies for Energy Harvesting: Plenary Session**

Sponsored by: The Minerals, Metals and Materials Society, TMS Materials Processing and Manufacturing Division, TMS: Global Innovations Committee  
Program Organizers: Sivaraman Guruswamy, University of Utah; Robert Hyers, University of Massachusetts, Amherst; Joy Forsmark, Ford Motor Co

Monday PM

Room: 3005

February 16, 2009

Location: Moscone West Convention Center

*Session Chairs:* Joy Forsmark, Ford Motor Co; Sivaraman Guruswamy, University of Utah; Robert Hyers, University of Massachusetts

---

### **2:00 PM Introductory Comments**

#### **2:05 PM Keynote**

**Harvesting Alternate Energies from our Planet:** *Bhakta Rath*<sup>1</sup>; <sup>1</sup>Naval Research Laboratory

Recent price increases at the gas pump have brought our attention to the phenomenal increase of global energy consumption in recent years. It is now evident that we have almost reached a peak in global oil production. Several projections indicate that total world consumption of oil will rise by nearly 60% between 1999 and 2020. In 1999 consumption was equivalent to 86 million barrels of oil per day, extracted from most known oil reserves. These projections, if accurate, will present an unprecedented crisis to the global economy and industry. As an example, in the US, nearly 40% of energy usage is provided by petroleum, of which nearly a third is used in transportation. An aggressive search for alternate energy sources, both renewable and nonrenewable, is vital. The presentation will review national and international perspectives on the exploration of alternate energy with special focus on energy derivable from the ocean.

#### **2:55 PM Plenary**

**Solar Photovoltaics Technology: The Beginning of the Revolution:** *Larry Kazmerski*<sup>1</sup>; <sup>1</sup>National Center for Photovoltaics, National Renewable Energy Laboratory

The prospects of current and coming solar-photovoltaic (PV) technologies are envisioned, arguing this solar-electricity source is at a tipping point in the complex worldwide energy outlook. The co-requirements for policy and technology investments are strongly supported. The emphasis of this presentation is on R&D advances (cell, materials, and module options), with indications of the limitations and strengths of crystalline (Si and GaAs) and thin-film (a-Si:H, Si, Cu(In,Ga)(Se,S)<sub>2</sub>, CdTe). The contributions and technological pathways for now and near-term technologies (silicon, III-Vs, and thin films) and status and forecasts for next-generation PV (organics, nanotechnologies, non-conventional junction approaches) are evaluated. Recent advances in concentrators with efficiencies headed toward 50%, new directions for thin films (20% and beyond), and materials/device technology issues are discussed in terms of technology progress. Insights into technical and other investments needed to tip photovoltaics to its next level of contribution as a significant clean-energy partner in the world energy portfolio. The need for R&D accelerating

the now and imminent (evolutionary) technologies balanced with work in mid-term (disruptive) approaches is highlighted. Moreover, technology progress and ownership for next generation solar PV mandates a balanced investment in research on longer-term (the revolution needs revolutionary approaches to sustain itself) technologies (quantum dots, multi-multijunctions, intermediate-band concepts, nanotubes, bio-inspired, thermophotonics, . . . ) having high-risk, but extremely high performance and cost returns for our next generations of energy consumers. Issues relating to manufacturing are explored—especially with the requirements for the next-generation technologies. This presentation provides insights into how this technology has developed—and where we can expect to be by this mid-21st century.

### **3:40 PM Break**

#### **3:50 PM Plenary**

**New Composite Thermoelectric Materials for Energy Harvesting Applications:** *Mildred Dresselhaus*<sup>1</sup>; Gang Chen<sup>1</sup>; Zhifeng Ren<sup>2</sup>; Jean-Pierre Fleurial<sup>3</sup>; <sup>1</sup>MIT; <sup>2</sup>Boston College; <sup>3</sup>Jet Propulsion Laboratory

There have recently been several important advances in both thermoelectrics research and industrial applications that have attracted much attention, increasing incentives for developing advanced materials appropriate for large scale applications of thermoelectric devices. One strategy that seems promising is the development of materials with a dense packing of random nanostructures as a route for the scale-up of thermoelectrics applications. The concepts involved in designing composite materials containing nanostructures for thermoelectric applications will be discussed in general terms. Specific application is made to the Bi<sub>2</sub>Te<sub>3</sub> nano-composite system for use in power generation. Also emphasized are the scientific advantages of the nanocomposite approach for the simultaneous increase in the power factor and decrease of the thermal conductivity, along with the practical advantages of having bulk samples for property measurements. A straightforward path is identified for the scale-up of thermoelectric materials synthesis containing nanostructured constituents for use in thermoelectric applications.

#### **4:35 PM Plenary**

**Lessons from Natural Photosynthesis for Synthetic Photosynthesis:** Graham Fleming<sup>1</sup>; <sup>1</sup>University of California, Berkeley, Department of Chemistry - and - Lawrence Berkeley National Laboratory

In this talk, I will briefly outline the design principles responsible for the remarkable efficiency of, and regulation of, natural photosynthetic light harvesting. I will then show how some of these ideas are beginning to be applied in the design of human-constructed light harvesting systems and photoconversion devices.

#### **5:15 PM Plenary**

**Integration of Manufacturing Limits to Design Methodologies:** *Stephane Renou*<sup>1</sup>; *Shu Ching Quek*<sup>1</sup>; <sup>1</sup>GE Global Research

In 2007, US capacity of wind-powered generators was estimated at a total of 5.2 gigawatts, and worldwide capacity was 94.1 gigawatts. Currently wind turbines produces less than 1% of US electricity, however, in 2007 US saw an increase in wind energy by 45% and the US government plans to supply 20% of electricity with wind power by 2030, according to American Wind Energy Association. There is a clear need to improve robustness and production cycle time in order to meet the demands of the growing market. Innovative technologies in both blade design and manufacturing processes will allow our current platforms (1-2 megawatt systems) to produce larger megawatt class machines. Although larger blades are desirable for higher efficiency, there remain challenges in material development, manufacturing, and design to make larger blades a reality. Novel polymers that are durable and have favorable processing characteristics will need to be developed. Eventually recyclability is also needed for scrapped wind turbine blades due to damage and/or replacement. Combination of material development and process improvements will result in not only more efficient blades but also cost effective, lightweight, reliable wind turbines that would allow expansion of wind sites to lower wind speed locations.

#### **5:55 PM Concluding Comments**



**Magnesium Technology 2009: Casting**

Sponsored by: The Minerals, Metals and Materials Society, TMS Light Metals Division, TMS: Magnesium Committee  
 Program Organizers: Eric Nyberg, Pacific Northwest National Laboratory; Sean Agnew, University of Virginia; Neale Neelameggham, US Magnesium LLC; Mihriban Pekguleryuz, McGill University

Monday PM Room: 2006  
 February 16, 2009 Location: Moscone West Convention Center

Session Chair: Randy Beals, Chrysler LLC

**2:00 PM Introductory Comments****2:05 PM**

**Refinement of microstructure by electromagnetic vibration process in magnesium wrought alloy and cast alloy:** Kenji Miwa<sup>1</sup>; Mingjun Li<sup>1</sup>; Takuya Tamura<sup>1</sup>; <sup>1</sup>National Institute of Advanced Industrial Science and Technology (AIST)

We have developed the refinement process of the microstructure of metallic materials by imposition of electromagnetic vibration force during solidification. This process is effective for both wrought and cast magnesium alloys. By imposition of a static magnetic field of 10 tesla under an alternative electric current of 60 A, the average grain size of the AZ31B wrought alloy and the AZ91D cast alloy was obtained about 50 micron. The grain size was affected by electric current frequency and decreased the minimum value at the special electric current frequency of 500 to 2000 Hz and 900 Hz for both wrought alloy and cast alloy, respectively. From experimental results, we suggested the mechanism of refinement of microstructure during solidification by imposition of electromagnetic vibration force. It is important the cavitation phenomenon in liquid phase and also the difference of electric conductivity between solid phase and liquid phase.

**2:25 PM**

**Melt Conditioned High Pressure Die Casting (MC-HPDC) of Mg-Alloys:** Spyridon Tzamtzis<sup>1</sup>; Huawei Zhang<sup>1</sup>; Nadendla Hari Babu<sup>1</sup>; Zhongyun Fan<sup>1</sup>; <sup>1</sup>Brunel University

The high pressure die casting (HPDC) process is characterized by low cost and high efficiency. However, HPDC Mg-alloy components have non-uniform microstructure, chemical segregation, and substantial amount of casting defects, such as porosity and hot tearing. Recently, we have developed a new shape casting process named as melt conditioned high pressure die casting (MC-HPDC) where liquid metal is conditioned under intensive forced convection provided by the MCAST unit (melt conditioning by advanced shear technology), and then transferred to a conventional HPDC machine for shape casting. Melt conditioning can be done at temperatures both above and below the liquidus of the alloy. Compared to conventional HPDC, the MC-HPDC process offers cast components with fine and uniform microstructure, much reduced cast defects and substantially improved mechanical properties. In this paper we present the microstructures and mechanical properties of MC-HPDC Mg-alloys processed under different conditions and discuss the solidification behaviour of conditioned melt.

**2:45 PM**

**Microsegregation Study of Mg Alloys and Adaptation of Directional Solidification Technique:** Rainer Schmid-Fetzer<sup>1</sup>; Djordje Mirkovic<sup>1</sup>; <sup>1</sup>Clausthal University of Technology

This paper copes with new challenges in directional solidification posed by liquid alloys containing both Mg and Al. These liquid alloys are highly reactive and attack standard ceramic as well as metallic container materials. Another novelty is an extension of the well known Scheil method to reflect solute profiles of components in all precipitating phases. It predicts the primary crystallizing Al-Mn intermetallic phase, experimentally detected in the microstructure. This prediction is also confirmed for the first time by application of an advanced processing of quantitative EPMA mapping data. Dendritic microstructures observed in longitudinal sections of the quenched mushy zone, X-ray maps of fully directional solidified cross sections and quantitative solute profiles reveal the impact of cooling rate and alloy type in a comparison of AZ31 and AM50.

This work is supported by the German Research Foundation (DFG) in the Priority Programme "DFG-SPP 1168: InnoMagTec".

**3:05 PM**

**Intermetallics Distribution in Two and Three Dimensions in High Pressure Die Cast Mg-Al Alloys:** Venkata Nagasekhar Anumalasetty<sup>1</sup>; Carlos Caceres<sup>1</sup>; <sup>1</sup>University of Queensland

The strength of Mg-Al alloys is influenced by the solute content, the grain size, and the volume fraction and distribution of intermetallics. An additional factor is that the distribution of intermetallics is a function of the casting wall thickness. Hence, in order to find the contribution of intermetallics to the strength of a given casting, it is necessary to determine in detail the distribution of intermetallics across the cross-section. The distribution of intermetallics across the cross-section has been studied in hpdc Mg-Al alloys of various thicknesses. Scanning Electron Microscope (SEM) and dual beam (FIB [Focussed Ion Beam]-SEM) system have been used for 2D and 3D characterization of the intermetallics, in selected areas near the edge and in the core regions of the castings.

**3:25 PM**

**Investigations on Hot Tearing of Mg-Al Binary Alloys by Using a New Developed Quantitative Method:** Zisheng Zhen<sup>1</sup>; Norbert Hort<sup>1</sup>; Oliver Utke<sup>1</sup>; Yuanding Huang<sup>1</sup>; Nikolai Petri<sup>1</sup>; Karl Kainer<sup>1</sup>; <sup>1</sup>GKSS Research Center

Hot tearing, also referred as hot cracking, has been widely recognized as one of the most fatal defects in casting processes. Although it has been intensively investigated for decades, most of the contributions are still based on qualitative level. In this work, a quantitative method for investigating hot tearing had been developed. The new method is based on true contraction force measuring principle, and shows very good repeatability. The recorded true contraction force can not only quantitatively evaluate hot tearing susceptibility, but also monitor the hot tear initiation and propagation. With this method, hot tearing behavior of Mg-Al binary alloys has been investigated. The results show that increasing mold temperature decreases hot tearing susceptibility. The recorded true contraction force curves also indicate that increasing mold temperature increases hot tearing initiation temperature, i.e. liquid fraction. Therefore liquid refilling has a chance to heal the initiated hot crack.

**3:45 PM Break****4:00 PM**

**Magnesium Recycling System Prepared by Permanent Mould- and High Pressure Die Casting:** Daniel Fechner<sup>1</sup>; Norbert Hort<sup>1</sup>; Karl Kainer<sup>1</sup>; <sup>1</sup>GKSS Research Center

Due to changing legislation and an increasing use of magnesium alloys in the automotive industry, magnesium recycling will get more important in future. Treating end-of life vehicles often means shredding. Separating the resulting magnesium scrap according to chemical compositions is complex and expensive. Therefore it would be useful to define alloys made from blended post consumer scrap. For creep resistant alloys the weight per component is usually high and a secondary alloy is reasonable. The scenario of blended post consumer scrap from different heat resistant magnesium alloys was realised by modifying the AM50 system with varying additions of Ca, Si and Sr. After preparing a matrix of potential recycling systems via permanent mould casting, three alloys were selected for further processing via HPDC. The materials properties are compared with regard to the processing techniques.

**4:20 PM**

**Solidification Behavior of Recyclable Mg Alloys - AZ91 and AZC1231:** Adam Gesing<sup>1</sup>; Jerry Sokolowski<sup>2</sup>; Carsten Blawert<sup>3</sup>; N. Reade<sup>2</sup>; <sup>1</sup>Gesing Consultants Inc; <sup>2</sup>University of Windsor; <sup>3</sup>GKSS

Common Mg alloys come from the Mg-Al-Mn and Mg-Al-Zn-Mn families, AM and AZ respectively. The popular AZ91 die casting alloy has a high concentration of all of the common alloying elements and hence can accommodate new scrap from any alloys coming from these families. Old scrap often contains contaminants, notably copper which cannot be refined out and contributes to corrosion of the AZ91 product alloy. Recently it was determined that the addition of 3% Al and 2% Zn to AZ91 allows the product to accept up to a 1% Cu impurity without increasing the susceptibility of the product alloy to corrosion - leading to the development of the AZC1231 alloy. The solidification behavior of the AZ91 and AZ1231 alloys was tested under various solidification rates using the UMSA Technology Platform to determine the compatibility of the new alloy with various casting technologies.

4:40 PM

**Stresses and Cracking during Direct Chill Casting of AZ31 Alloy Billet:** John Grandfield<sup>1</sup>; Vu Nguyen<sup>2</sup>; Ian Bainbridge<sup>3</sup>; <sup>1</sup>Grandfield Technology Pty Ltd; <sup>2</sup>CSIRO; <sup>3</sup>CAST CRC

The Alsim FEM model which has been applied to aluminium DC casting was applied to the problem of crack formation during vertical direct chill casting of magnesium alloys. The model is a fully coupled thermal stress model. Predictions were compared to crack incidence observed for a variety of cast start speed conditions used on AZ31 alloy, 208 mm diameter billet casting. Crack incidence was related to the principle stresses and other criteria such as the liquid pressure in the mush. The model can be used to develop improved starting head designs and cast start practices.

5:00 PM

**Refinement of Solidification Microstructures by the MCAST Process:** Z. Fan<sup>1</sup>; Mingxu Xia<sup>1</sup>; Z. Bian<sup>1</sup>; I. Bayandorian<sup>1</sup>; L. Cao<sup>1</sup>; H. Li<sup>1</sup>; G.M. Scamans<sup>1</sup>; <sup>1</sup>BCAST

MCAST (melt conditioning by advanced shear technology) is a novel technology developed recently for conditioning liquid metal under intensive forced convection before solidification. It uses twin screw mechanism to impose a high shear rate and a high intensity of turbulence to liquid metal, so that the conditioned liquid metal has uniform temperature, uniform chemical composition and well-dispersed and completely wetted oxide particles with a fine size and a narrow size distribution. The microstructural refinement is achieved through an enhanced heterogeneous nucleation rate and an increased nuclei survival rate during the subsequent solidification. In this paper we present the MCAST process and its applications for microstructural refinement in both shape casting and continuous casting of magnesium alloys. Discussions will be made on the effect of intensive forced convection on the enhanced heterogeneous nucleation. The concept of physical grain refinement will be proposed and discussed in contrast to the conventional grain refinement.

5:20 PM

**Preliminary Investigation on the Grain Refinement Behaviour of ZrB<sub>2</sub> Particles in Commercial Mg-Al Alloys:** Gerald Klösch<sup>1</sup>; Brian McKay<sup>2</sup>; Peter Schumacher<sup>2</sup>; <sup>1</sup>Austrian Foundry Research Institute; <sup>2</sup>University of Leoben

This paper investigates the effect of ZrB<sub>2</sub> particles on the grain refinement of Mg-Al and commercial AZ alloys. Samples were taken in accordance with the TP1 test procedure and the resulting grain size of the primary Mg measured using the linear intercept method. An SEM equipped with EDS was employed to elucidate the effect of the Zr. Results show that the ZrB<sub>2</sub> successfully grain refines the Mg-Al alloy resulting in ultimate grain sizes of 100 and 60 µm for the synthetic ZrB<sub>2</sub> particles respectively. Mg-Al and AZ alloys can be successfully grain refined using ZrB<sub>2</sub> heterogeneous particles and the resultant effect should be beneficial in improving the mechanical properties of the alloy.

## Magnesium Technology 2009: Primary Production

Sponsored by: The Minerals, Metals and Materials Society, TMS Light Metals Division, TMS: Magnesium Committee

Program Organizers: Eric Nyberg, Pacific Northwest National Laboratory; Sean Agnew, University of Virginia; Neale Neelameggham, US Magnesium LLC; Mihriban Pekguleryuz, McGill University

Monday PM  
February 16, 2009

Room: 2007  
Location: Moscone West Convention Center

Session Chair: Neale R Neelameggham, U.S.Magnesium LLC

### 2:00 PM Introductory Comments

2:05 PM

**Cathode Wetting Studies in Magnesium Electrolysis:** Kevin McLean<sup>1</sup>; James Pettingill<sup>1</sup>; Boyd Davis<sup>2</sup>; <sup>1</sup>Queens University; <sup>2</sup>Kingston Process Metallurgy Inc.

The effects of cathode materials and electrolyte additives on magnesium wetting were studied with the goal of improving current efficiency in a magnesium electrolysis cell. The study consisted of static wetting and electrolysis tests, both conducted in a visual cell with a molten salt electrolyte of MgCl<sub>2</sub>-CaCl<sub>2</sub>-NaCl-KCl-CaF<sub>2</sub>. The wetting conditions were tested using high

resolution photography and contact angle software. The electrolysis tests were completed to qualitatively assess the effect of additives to the melt and were recorded with a digital video camcorder. Results from the static wetting tests showed a significant variation in wetting depending on the material used for the cathode. Mo and a Mo-W alloy, with contact angles of 60° and 52° respectively, demonstrated excellent wetting. The contact angle for steel was 132° and it ranged from 142°-154° for graphite depending on the type. Improvements to the cathode wetting were observed with tungsten and molybdenum oxide additives.

2:25 PM

**Mechanism and Kinetics of Reduction of Magnesium Oxide with Carbon:** Leon Prentice<sup>1</sup>; Michael Nagle<sup>1</sup>; <sup>1</sup>CSIRO Minerals

The reaction mechanism of the gas-solid carbothermal reduction of magnesium oxide is not well known, although some kinetic evaluations have been conducted. Previous studies have reported a two- or three-stage reaction process, each with different activation energy, while others have found a catalytic effect of other metal species. The present study, conducted as part of ongoing research into the carbothermal process, found that the reaction mechanism and its kinetics may be usefully described by a phase-boundary-controlled model. The activation energy of the gas-solid reaction was found to be 222 (±20) kJ/mol. It did not exhibit multi-stage complexity, but was otherwise consistent with reported values. The data obtained are at a larger scale than previously investigated, which minimises the errors related to surface area differences. The information is useful for the scale-up and control of the carbothermal reduction process.

2:45 PM

**A Study on Influence of Fluxing Additives on Magnesium Refining Process:** Yeliz Demiryol<sup>1</sup>; Bora Derin<sup>1</sup>; Onuralp Yucel<sup>1</sup>; <sup>1</sup>Istanbul Technical University

This study aims to investigate the effect of different flux addition and time on refining of crown magnesium produced via pidgeon process. The different flux compositions (MgCl<sub>2</sub>, KCl, CaCl<sub>2</sub>, MgO, CaF<sub>2</sub>, NaCl, and SiO<sub>2</sub>) with or without B<sub>2</sub>O<sub>3</sub> additions and reaction durations (15-45 min) were selected in order to lower iron content in Mg ingot samples at 690°C. The chemical compositions of the final ingots were measured by using wet chemical analyses technique. Each final ingot was also subjected to a corrosion test to understand the influence of iron to Mg corrosion. It is found that when the flux composition with B<sub>2</sub>O<sub>3</sub> was used, iron content in the Mg ingot can be reduced from 0.080 to 0.0027 wt%. The corrosion test results showed that corrosion rates decreased with decreasing iron content in Mg ingots. The minimum corrosion rate was obtained as 0,235 mg/cm<sup>2</sup>/day.

3:05 PM

**Study on Ultrasonic Purification of Magnesium Alloy Melt:** Qichi Le<sup>1</sup>; Zhiqiang Zhang<sup>1</sup>; Jianzhong Cui<sup>1</sup>; Xue Wang<sup>1</sup>; <sup>1</sup>Northeastern University

The fluxing processing, a traditional purification method for magnesium melt, not only bears the risk of flux inclusions but also is facing more and more environmental pressure today. Therefore, the effective substitutes for fluxing processing are paid more attention recently. The mechanical effect generated by ultrasonic field in the media also called as ultrasonic agglomeration in chemical industry could conglomerate solid particulates in suspending liquid and then realize their separation. In this research, it is used to treat magnesium alloy melt with aim to promote and accelerate the separation of oxidation inclusion from melt. The effects of ultrasonic power, ultrasonic processing temperature and the holding time after ultrasonic treatment on the inclusion distribution in the billet were investigated. The results indicate that the ultrasonic conglomeration produced at low power ultrasonic field could be used to promote and accelerate the separation of oxidation inclusions from magnesium melt.

3:25 PM

**Prediction Model of Magnesium Powder Consumption during Hot Metal Pre-Desulfurization:** Dongping Zhan<sup>1</sup>; Huishu Zhang<sup>1</sup>; Zhouhua Jiang<sup>1</sup>; Zhouhua Jiang<sup>1</sup>; <sup>1</sup>Northeastern University

Based on the productive practice of a steel plant, adopted the back propagation (BP) algorithm with the network configuration of 4-12-1 and the range of normalization from 0 to 1, used Visual Basic 6.0 software, the prediction model of magnesium powder consumption during hot metal pre-desulfurization processing was established. Meanwhile, four parameters, which are the weight and temperature of hot metal, the initial and final sulfur content in hot metal, were selected as input parameters. The data of 210 heats were used as the training samples and the other 46 heats were randomly selected as the test samples. The results show that the prediction errors of magnesium powder consumption less

than  $\pm 5$  kg and  $\pm 10$  kg are 54.3 percent and 89.1 percent of the total test heats respectively. Average absolute error is 5.12 kg. Minimum absolute error is 0.02 kg. The model greatly coincides with the actual production operation.

#### 3:45 PM Break

#### 4:00 PM

**Study on Electrolysis of Magnesium Oxide on 200A Scale:** Shaohua Yang<sup>1</sup>; Fengli Yang<sup>1</sup>; Qingsheng Liu<sup>1</sup>; Xianwei Hu<sup>1</sup>; Zhaowen Wang<sup>2</sup>; Zhongning Shi<sup>2</sup>; Bingliang Gao<sup>2</sup>; <sup>1</sup>School of Materials and Chemistry, Jiangxi University of Science and Technology; <sup>2</sup>School of Materials and Metallurgy 117#, Northeastern University

Preparation of aluminum-magnesium alloy from magnesium oxide was studied by molten salt electrolysis method. Aluminum liquid as cathode and graphite as anode, the test was carried through on 200A scale in MgF<sub>2</sub>-LiF-KCl electrolyte. It was proved that the process of electrolysis was stable, range of variation for voltage cell was narrow, and the value was in 0.4V. Content of magnesium in alloy was not even, the highest and the lowest was 20%, 6%, respectively. Even alloy could be attained by re-melting the alloy, and current efficiency was about 82%. The loss of anode oxidation was not serious. The results attained by this test could provide some technical parameters for further developing test.

#### 4:20 PM

**Vacuum Thermal Extract Magnesium from Boron Mud:** Xiaolei Wu<sup>1</sup>; Naixiang Feng<sup>1</sup>; Jianping Peng<sup>1</sup>; Yaowu Wang<sup>1</sup>; <sup>1</sup>Northeastern University

Boron mud is residue from which the ascharite minerals is produced borax by carbon dioxide-soda process. It still contains a lot of magnesium and silicon. This experiment utilized the vacuum-thermal to extract most of magnesium, and the residual materials which is suitable to manufacture flat glass. The process can come to clean production. The experiment includes two parts. At first, optimum roasting conditions were determined through roasting tests at 650~700° for 0.5~1.0h. The major composition of after calcination boron mud is Mg<sub>2</sub>SiO<sub>4</sub>. Then, in the process of vacuum-thermal reduction experiment, calcium carbide was used as reductant. Fortunately the reduction rate of magnesium can reach as high as 99.6%.

#### 4:40 PM

**Study on Behavior of Anode Bubble:** Shaohua Yang<sup>1</sup>; Fengli Yang<sup>1</sup>; Qingsheng Liu<sup>1</sup>; Xianwei Hu<sup>1</sup>; Zhaowen Wang<sup>2</sup>; Zhongning Shi<sup>2</sup>; Bingliang Gao<sup>2</sup>; <sup>1</sup>Jiangxi University of Science and Technology; <sup>2</sup>School of Materials and Metallurgy 117#, Northeastern University

Behavior of anode bubble was studied by transparency cell. It was proved that anode bubble was grown up gradually at bottom of anode, and bubble generated on side of anode was smaller than that at bottom of anode. Obvious phenomena were observed that diameter of anode bubble opposite cathode was the smallest in all bubbles, some small bubbles together into big bubble were not observed in whole test, and the bubbles were separated out electrolyte as small shape, this was different with that of anode other side. Behavior of anode bubble was influenced by current density. The diameter of anode bubble at high current density was bigger than that of anode bubble at low current density, and the released velocity of anode bubble at high current density was faster than that of anode bubble at low current density.

### Manufacturing Issues in Fuel Cells: Session II

Sponsored by: The Minerals, Metals and Materials Society, TMS: Shaping and Forming Committee

Program Organizers: Tsung-Yu Pan, Consultant, Ann Arbor Michigan; John Bradley, General Motors Corp; Michael Miles, Brigham Young University

Monday PM

Room: 3006

February 16, 2009

Location: Moscone West Convention Center

Session Chair: Tsung-Yu Pan,

#### 2:00 PM

**A High-Temperature Sealing Technology for Solid Oxide Fuel Cells:** Timothy Lin<sup>1</sup>; Chunhu Tan<sup>1</sup>; Bob Liu<sup>1</sup>; Jens Darsell<sup>2</sup>; Scott Weil<sup>2</sup>; <sup>1</sup>Aegis Technology Inc.; <sup>2</sup>Pacific Northwest National Laboratory

A reliable, cost-effective high-temperature sealing technology for the joining of ceramic components to metallic structures is critical to the successful

development of solid oxide fuel cells (SOFCs). In this presentation, Aegis Technology will present its latest development of a novel reactive air brazing (RAB) technology, which is sponsored through an U.S. Department of Energy (DoE) Small Business Innovative Research (SBIR) project in collaboration with the Pacific Northwest National Laboratory. This RAB technology uses Ag-CuO as base braze compositions with a variety of additional elements. With a proper processing control, the resultant sealing technology is capable of providing a high-temperature sealing with sufficient chemical inertness, thermal reliability, and bonding strength. This presentation will report our latest studies on composition design/synthesis of braze filler material, and the characterizations including microstructure and mechanical properties, and a preliminary numerical simulation addressing the residual stress development in the joining assembly during thermal cycling.

#### 2:25 PM

**Aging Effect on the Mechanical Properties of Perfluorosulfonate Polymer for Fuel Cell Proton Exchange Membranes:** Hyun Jee Park<sup>1</sup>; Takuya Hasegawa<sup>2</sup>; Jiping Ye<sup>3</sup>; Reinhold Dauskardt<sup>1</sup>; <sup>1</sup>Stanford University; <sup>2</sup>Nissan Research Center, Nissan Motor Co., Ltd; <sup>3</sup>Research Department, Nissan Arc Ltd

Perfluorinated sulfonic polymers are widely used as proton exchange membranes in fuel cells. These polymers have high selectivity and permeability to water mediated by their sulfonic groups, and exhibit good thermal and mechanical stability. However, water sorption leads to extensive swelling and degradation of mechanical properties, which can degrade the performance and lead to early breakdown in fuel cells. In this study, we experimentally investigate the change of mechanical properties by aging at different thermal and hydrothermal conditions. Specifically, both micro-tensile tests and constrained and unconstrained swelling tests were conducted under selected environmental and exposure times. The effects of dehydration and hydration/dehydration cycling were also investigated. We shown that the membrane is highly sensitive to water content and mechanical properties significantly degraded by cycling. The work has implications for the thermal management of cells during operation and is intended to provide guidance on the long term reliability of membrane materials.

#### 2:50 PM

**Structural Information of  $\alpha$ -Alumina Supported Cobalt Nanoparticle Catalysts during Autothermal Reforming of Iso-Octane:** Mohammad Shamsuzzoha<sup>1</sup>; Earl Ada<sup>1</sup>; Ramana Reddy<sup>1</sup>; <sup>1</sup>University of Alabama

The microstructure of a nanoparticle Co catalyst supported on  $\alpha$ -alumina prior to and after the autothermal reformation were studied using Transmission Electron Microscopy, and X-ray Photoelectron Spectroscopy. The support of the fresh catalyst exhibits a homogenous aggregation of amorphous granules with sizes ranging between 10 to 20 nm. The structure of the fresh catalyst support is of hexagonal alumina phase. Cobalt in the fresh catalyst is highly dispersed and embedded in the matrix in the form of contrasted crystallites with size in the range of 5 - 20 nm. The support of the used catalyst exhibits external coating made of carbon related compound, but show very little grain growth. Co particles in the reformed sample were found to be in the mooted form. Crystallographic information in relation to this autothermal reformation of  $\alpha$ -alumina supported Co nanoparticles has been discussed in the light of the efficiency of Co as catalyst.

#### 3:15 PM Break

#### 3:30 PM

**Economic Production of Metallic Separator Plates:** Marc Decker<sup>1</sup>; <sup>1</sup>Gräbener Maschinenteknik GmbH & Co. KG

Metallic separator plates are used for building high-quality and efficient fuel cells. To produce highest-quality metallic separator plates, a new production system had to be found since theoretical calculations and practical tests have shown that the machines and systems available on the market nowadays are not able to provide highest forces on small surfaces. In search of such an efficient system Gräbener has developed a special hydraulic press. This so called PowerBoxx®, the tool technology developed by Gräbener and the sheet hydroforming process provide a perfect symbiosis for the efficient production of highest-quality metallic separator plates. The system is especially designed for pressing thin metallic sheets (foils) within shortest cycle times and with greatest evenness. Gräbener will present this symbiosis starting from the idea to its realisation, compare it with other production systems and give an outlook on the future and the developments.



3:55 PM

**Preparation and Characterization of Nano-Structured Proton Conductive Electrolytes:** *Zhigang Xu*<sup>1</sup>; Jag Sankar<sup>1</sup>; <sup>1</sup>North Carolina A&T State University

The purpose of this study was to acquire a preliminary understanding in portion conductive electrolytes through material preparation and characterizations. 20mol% ytterbium doped Barium cerates which is partially substituted with zirconate was chosen for study. At the first place, nano crystalline powders were prepared using sol-gel technique. Pellets were produced from the powder compact by high-temperature sintering. Electrolyte thin films were also made by spin-coating of the gel. The crystallographic properties of the powders and sintered pellets were determined with X-ray diffraction. The crystallite size was measure by using Scherrer method and confirmed by TEM direct observations. The morphologies of the thin films and pellets were determined on the polished and etched surfaces by TEM. The conductivity of the material was measured using ac-impedance in a temperature range from 300-800°C in the presence of 4% hydrogen in argon.

4:20 PM

**Novel Coating Process to Facilitate Traditional Solder Connection to Graphitic Fabrics for Use in Fuel Cell Assemblies:** *Ben Poquette*<sup>1</sup>; <sup>1</sup>Keystone Materials LLC

High conductivity graphite fabrics show much promise for use in future fuel cell assemblies. However, creating low resistance electrical connections with these fabrics generally requires excessive mechanical compression joints or high temperature brazing techniques which can damage other components of the fuel cell stack and require inert or vacuum processing. A novel process, to deposit a uniform coating around the individual fibers, has been developed to allow joining to graphitic fabrics by traditional soldering techniques.

**Materials for High Temperature Applications: Next Generation Superalloys and Beyond: Next Generation Superalloys**

Sponsored by: The Minerals, Metals and Materials Society, TMS Structural Materials Division, TMS: High Temperature Alloys Committee, TMS: Refractory Metals Committee  
Program Organizers: Joseph Rigney, GE Aviation; Omer Dogan, National Energy Technology Laboratory; Donna Ballard, Air Force Research Laboratory; Shiela Woodard, Pratt & Whitney

Monday PM Room: 3010  
February 16, 2009 Location: Moscone West Convention Center

*Session Chairs:* Dallis Hardwick, US Air Force; Sammy Tin, Illinois Institute of Technology

2:00 PM Invited

**Superalloys: Evolution and Revolution for the Future:** *Hiroshi Harada*<sup>1</sup>; <sup>1</sup>NIMS

Superalloys have evolved from wrought to conventionally cast, directionally solidified, and then single crystal (SC) alloys. SC superalloys have also evolved from 1st(0Re) to 2nd(2-3Re), 3rd(5-6Re), 4th(5-6Re and 2-3Ru), and then 5th (5-6Re and 5-6Ru) generation alloys. So far 1st to 3rd generation SC superalloys are used practically, e.g., CMSX-10, a 3rd generation alloy, as turbine blade materials in the latest aeroengines. The highest temperature capability, 1100°C (137MPa, 1000h creep rupture), has been reached by NIMS 5th generation alloys, typically TMS-196. In the 5th generation alloys, an interfacial dislocation network on  $\gamma$  and  $\gamma'$  phase boundary is designed to be finer (20 nm) to prevent dislocations from cutting through the interface and suppress creep deformation. In the present paper, after the introduction of historical evolution in superalloys, possible further evolution and revolution will be discussed in conjunction with advanced aeroengines and ultra-efficient gas turbines being planned to improve specific fuel consumption and reduce CO<sub>2</sub> emissions.

2:25 PM

**New Fabricable Dispersion Strengthened Cobalt Based Wrought Superalloy:** *S. Srivastava*<sup>1</sup>; <sup>1</sup>Haynes International Inc

The problems associated with the fabricability, irreproducibility of properties, and high cost of mechanically alloyed ODS alloys provided the motivation for the development of a nitride dispersion strengthened alloy. The program

goals for HAYNES® NS-163™ alloy (Nom. Comp: Co-28Cr-9Ni-21Fe-1.25Ti-1Nb) were to take a segmented approach to develop a sheet alloy that would be fabricable in the as-received condition and would achieve its high temperature creep strength as a result of a nitride dispersion strengthening (NDS) heat treatment. Specifically, the aim was to obtain a stress rupture life of > 250h at 982°C/55 MPa (1800°F/8 ksi). Based on the laboratory data, it appears that its 1000h-rupture strength at 982°C was more than twice that of HAYNES 188 and 230® alloys, the two leading solid solution strengthened gas turbine alloys. The paper will present preliminary data derived from the laboratory heats and a production heat, and briefly describe the ongoing work.

2:45 PM

**Fatigue Crack Growth Behavior of the Ni-Base Superalloy ME3:** *Jeffrey Evans*<sup>1</sup>; Ashok Saxena<sup>1</sup>; Andrew Rosenberger<sup>2</sup>; <sup>1</sup>University of Arkansas; <sup>2</sup>Air Force Research Lab

A set of crack growth tests was performed on the turbine disk alloy ME3 at 704°C (1300°F) in vacuum and in air at 0 and 10 second hold times using two microstructures developed with two different cooling rates. Fatigue crack growth tests were also conducted at 25°C (77°F) with the two microstructures. For the tests conducted in air at elevated temperature, both hold time and microstructural effects were evident while tests conducted in vacuum showed no difference regardless of microstructure or hold time. A coupling effect was also observed between the microstructure and the environment. The slow cooled samples had larger secondary gamma prime particles, slower crack growth rates, and less intergranular fracture in air as compared to the fast cooled samples.

3:05 PM

**Dwell Notch LCF Behavior of Advanced Powder Metallurgy Disk Superalloys:** Jack Telesman<sup>1</sup>; John Gayda<sup>1</sup>; Timothy Gabb<sup>1</sup>; <sup>1</sup>NASA Glenn Research Center

The lives of powder metallurgy superalloy disks in aerospace turbine engine applications can be limited by fatigue cracking at notches. The most severe limitations can sometimes occur for notched locations exposed to high temperatures and dwells at maximum stress, where cycle-dependent and time-dependent damage can each accumulate. Improvements of performance and durability in future disk applications require an understanding of what drives such damage. Several aspects of this fatigue cracking problem were examined in disk superalloys ME3 and LSHR using notched specimens. Specimens were fatigue tested at high temperatures, with dwells at maximum stress. The effects of applied stress, dwell time, and temperature on fatigue life and failure modes were examined and will be discussed.

3:25 PM

**Alloy 10 - An as-HIP Compacted Nickel Based Superalloy for High Pressure Turbine Rotor Applications:** *Derek Rice*<sup>1</sup>; Brian Hann<sup>1</sup>; Pete Kantzos<sup>1</sup>; Dan Greving<sup>1</sup>; James Neumann<sup>1</sup>; <sup>1</sup>Honeywell Engines, Systems & Services

As part of the VAATE program Honeywell evaluated the potential of PM Alloy 10 in the as-HIP super solvus heat treated condition for high pressure turbine disk applications. This report presents the high temperature mechanical properties of as-HIP coarse grain PM Alloy 10 relative to cast and wrought fine grain U720Li up to 760C. Properties presented and discussed include tensile, creep, LCF, and crack growth. Operating gas turbine disks above 700C will require sophisticated PM Ni based alloys. Utilizing these materials in the as-HIP compacted form will help mitigate component cost and risk.

3:45 PM Break

3:55 PM Invited

**Development of Pt-Modified  $\gamma$ -Ni+ $\gamma'$ -Ni<sub>3</sub>Al-Based Alloys Having Strength and Environmental Resistance at High Temperatures:** *Brian Gleeson*<sup>1</sup>; Andy Heidloff<sup>2</sup>; Zhihong Tang<sup>2</sup>; Takeshi Izumi<sup>3</sup>; <sup>1</sup>University of Pittsburgh; <sup>2</sup>Iowa State University; <sup>3</sup>Hokkaido University

Heat-treatable  $\gamma$ -Ni+ $\gamma'$ -Ni<sub>3</sub>Al-based alloys having excellent resistance to high-temperature oxidation, hot corrosion, and creep are being developed in a systematic manner using multiple alloying additions, including Pt and/or Ir, i.e., platinum group metals (PGMs). Alloys that collectively possess these high-temperature properties are highly attractive for niche applications involving extreme conditions. The results discussed in this presentation stem from a larger-scale project supported by the U.S. Air Force within the Materials for Air-Breathing Propulsion in Support of the Versatile Affordable Advanced Turbine Engine (VAATE) Program. It will be shown that PGM additions reduce the detrimental effects of "strengthening" alloying additions on oxidation and

hot corrosion. Microstructural characterization of the alloys included elemental partitioning and thermal stability, with both being compared to thermodynamic predictions using the software package PANDAT.

4:20 PM

**Gamma Prime Dissolution and Grain Growth during Supersolvus Heat Treatment of Advanced Ni-Base Disk Superalloys:** *Eric Payton*<sup>1</sup>; Gang Wang<sup>1</sup>; Yunzhi Wang<sup>1</sup>; Dan Wei<sup>2</sup>; David Mourer<sup>2</sup>; Deborah Whitis<sup>2</sup>; Michael Mills<sup>1</sup>; <sup>1</sup>Ohio State University; <sup>2</sup>GE Aviation

Grain size control is critically important for achieving desired mechanical properties in Ni-base superalloys for turbine disk applications. New jet engine designs demand increased operating temperatures for improved efficiency. To improve manufacturing processes and useful life of the turbine disks, physics-based prediction of grain size as a result of thermomechanical processing is desired. The size and volume fraction of particles of the gamma prime phase have a significant effect on the grain size during heat treatment, and can influence the final grain size of the material. Dissolution of gamma prime occurs rapidly during supersolvus heat treatment. Grain growth and gamma prime dissolution during supersolvus heat treatment have been measured experimentally. Gamma prime dissolution observations have been compared to phase field simulation results to develop a model for gamma prime dissolution.

4:40 PM

**Elemental Partitioning in Ni-Based Superalloys with PGM Additions:** *Jason Van Sluytman*<sup>1</sup>; Tresa Pollock<sup>1</sup>; <sup>1</sup>University of Michigan

Elemental partitioning in Ni-based superalloys containing various PGM additions has been investigated through use of electron probe microanalysis (EPMA). Alloys with a baseline composition of 15Al-5Cr-1Re-2Ta-0.1Hf (at%) containing various amounts of Pt, Ir, Ru, and W, have been heat treated to produce coarse two phase  $\gamma$ - $\gamma'$  microstructures. Large  $\gamma'$  particles approximately 3-4  $\mu\text{m}$  diameter were utilized to acquire EPMA scans for phase composition to determine partitioning of elements between the two phases. Limited TEM energy dispersive spectroscopy as well as local electron atom probe analysis were also utilized to compare partitioning values gathered from EPMA. These analysis indicate that Cr, Re, and W partition preferentially to the matrix  $\gamma$  phase while Al, Pt, and Ta preferentially partition to the  $\gamma'$  phase. Additions of Ir reduce the partitioning of W, as well as Re, to the matrix.

5:00 PM

**Net-Shape, Powder Metal, HIP-Bonded Surface Layers for Environmental Compatibility of Superalloys in Rocket Engine Turbines:** *Cliff Bampton*<sup>1</sup>; Victor Samarov<sup>2</sup>; Alex Lobovsky<sup>3</sup>; Daniel Matejczyk<sup>1</sup>; Mohammad Behi<sup>2</sup>; <sup>1</sup>Pratt & Whitney Rocketdyne; <sup>2</sup>Synertech Inc.; <sup>3</sup>United Materials Technologies, LLC

Net shape consolidation of powder metal (PM) by hot isostatic pressing (HIP) provides opportunities for cost, performance and life benefits over conventional fabrication processes for rocket engine structures. The method employs sacrificial metallic tooling (HIP capsule and shaped inserts), which is removed from net-shape surfaces of the consolidated part, by selective acid dissolution. Net-shape PM HIP enables fabrication of complex configurations providing additional functionalities. One example is discussed in detail: a novel HIP-Bonded Surface Layer method which has been demonstrated for provision of both smoother net-shape surfaces and robust surface layers of environmentally compatible alloys integral with a stronger, but less compatible substrate alloy.

5:20 PM

**Next Generation Materials Property Profiles for Superalloy and Refractory-Based Panels in Scramjet Combustors:** *N. Vermaak*<sup>1</sup>; L. Valdevit<sup>2</sup>; A. Evans<sup>1</sup>; <sup>1</sup>University of California, Santa Barbara; <sup>2</sup>University of California, Irvine

The operating conditions of scramjet engines require lightweight materials that withstand extreme heat fluxes and structural loads. An optimization tool has been introduced to direct the development of next generation materials that outperform existing high temperature alloys and compete with ceramic matrix composites. Performance maps reveal the relative merits of candidate superalloys and refractory-based materials over a broad operating domain. Specific results are presented for scramjet combustor liners applicable to a Mach 7 hypersonic vehicle (albeit the methodology is general). By probing the constraints that limit performance, the respective roles of the material properties and the design variables are unearthed. Based on these insights, notional materials are used to demonstrate how feasible design space can be reclaimed by tailoring critical material properties. These performance benefits are benchmarked and compared

for two of the more viable material candidates: the nickel-based superalloy, Inconel X-750 and the niobium-based refractory alloy, Cb-752.

5:40 PM

**Hot Working of Platinum Group Metal-Modified Nickel-Base Superalloys:** *Donna Ballard*<sup>1</sup>; Lee Semiatin<sup>1</sup>; Patrick Martin<sup>1</sup>; <sup>1</sup>US Air Force

Platinum- and iridium-modified  $\gamma$ - $\gamma'$  nickel-base superalloys are being evaluated for high-temperature use due to their superior oxidation resistance compared to conventional nickel-base superalloys. These materials also retain excellent strength at temperatures in excess of 1100°C due to a higher  $\gamma'$  solvus. Because of their cost and density, however, specific applications must be chosen carefully. Two product forms of interest are thin gage sheet and foil for thermal-protection-system applications. Initial research to evaluate the conversion of subscale ingots of two PGM alloys to sheet, the latter stages of which utilize conventional pack rolling, will be reviewed. Additional results on extrusion experiments on a third alloy will also be covered.

## Materials Issues in Additive Powder-Based Manufacturing Processes: Additive Manufacturing Metals I

Sponsored by: The Minerals, Metals and Materials Society, TMS Materials Processing and Manufacturing Division, TMS: Powder Materials Committee  
Program Organizers: David Bourell, University of Texas; James Sears, South Dakota School of Mines and Technology; Pavan Suri, Mississippi State University

Monday PM

February 16, 2009

Room: 3004

Location: Moscone West Convention Center

Session Chair: John Smugeresky, Sandia National Laboratories

2:00 PM

**Direct Digital Manufacturing with Layer-by-Layer Melt Deposition Processes:** *Khershed Cooper*<sup>1</sup>; Sam Lambrakos<sup>1</sup>; <sup>1</sup>Naval Research Lab

The essence of direct digital manufacturing (DDM) is developing controllable, incremental, additive processes to generate objects and components without tools, without manual assembly, at point-of-use. DDM allows manufacturing where we can know the microstructure and properties at every moment and at every point during a build. Deposition processes involving metal powder are, among others, direct laser deposition (e.g., LENS, DMD), selected laser melting (SLM) and e-beam melting (EBM). These processes involve either powder feed or powder beds. To understand the manufacturing science of these "melt deposition" processes, we need to model the spatial-temporal dynamics of materials under conditions involving short time durations and intense localized heat. In this paper, we will present examples of ongoing direct "melt deposition" research and our attempts to develop thermal models for such processes using inverse problem methodology.

2:25 PM

**Laser-Material Interaction Research in a Metal Deposition Process:** *Frank Liou*<sup>1</sup>; Zhiqiang Fan<sup>1</sup>; Hsin-Nan Chou<sup>2</sup>; Kevin Slattery<sup>2</sup>; James Sears<sup>3</sup>; Mary Kinsella<sup>4</sup>; Joseph Newkirk<sup>1</sup>; <sup>1</sup>Missouri University of Science and Technology; <sup>2</sup>Boeing Phantom Works; <sup>3</sup>South Dakota School of Mines and Technology; <sup>4</sup>AFRL/RXLMP

A laser deposition process involves the supply of metallic powders into a laser-heated spot where the powder is melted and forms a melt puddle which quickly solidifies into a bead. The development of an accurate predictive model for laser deposition is extremely complicated due to the multitude of process parameters and materials properties involved. In this work, the metal powder used in the laser deposition process is injected into the system by using a coaxial nozzle. In order to design an effective system, the laser beam, the powder beam, and their interactions need to be fully understood. This presentation summarizes the work to model a powder delivery system using non-spherical particle-wall interactions. The laser-material interaction within the melt pool is also investigated using a multi-scale model: a macroscopic model to model mass, heat and momentum transfer, and a microscopic model to model the evolution of solidification.

2:50 PM

**Maintaining Consistent Conditions over a Wide Range of Material Deposition Rates in Beam-Based Additive Manufacturing:** *Jack Beuth*<sup>1</sup>; Shane Esola<sup>1</sup>; Raymond Walker<sup>2</sup>; <sup>1</sup>Carnegie Mellon University; <sup>2</sup>Keystone Synergistic Enterprises

Significant advances have been made in the development of laser and electron beam-based freeform fabrication processes using powder injection, powder bed or wire feed systems for material delivery. Electron beam-based deposition is currently receiving serious consideration for additive manufacturing and repair applications in the aerospace industry. To be successful, these processes must work over a wide range of material deposition rates to combine affordability (requiring high deposition rates) with the ability to precisely deposit fine geometries (requiring low deposition rates). The goal of this modeling research is to identify paths through processing space yielding consistent melt pool sizes independent of material deposition rate, ultimately yielding rules of thumb useable by processing engineers. Process variables to be controlled are beam power and translational speed.

3:15 PM

**Effect of Process Parameters on Electron Beam Melted (EBM) Additively Manufactured Components in Ti-6Al-4V:** *Micheal Blackmore*<sup>1</sup>; Sinan Al-Bermani<sup>1</sup>; Iain Todd<sup>1</sup>; <sup>1</sup>University of Sheffield

Additive layer manufacturing (ALM) in metallic materials has many potential applications and offers many advantages over conventional subtractive machining practices. However, ALM machines at present are yet to be fully utilised in a production environment due to lack of validation and process maturity. An Arcam S12 EBM machine has been used to deposit near net components in titanium 6Al-4V (grade 5) alloy operating directly from CAD data. The effects of changes in various process parameters such as beam speed, power, focus and scan strategy have been investigated and related to material integrity and as deposited surface finish.

3:40 PM Break

4:05 PM

**Powder-Cored Tubular Wire Manufacturing for Electron Beam Freeform Fabrication:** *Christine Hillier*<sup>1</sup>; Marcia Domack<sup>2</sup>; Robert Hafley<sup>2</sup>; Stephen Liu<sup>1</sup>; <sup>1</sup>Colorado School of Mines; <sup>2</sup>NASA Langley Research Center

Powder-cored tubular wires exhibit great flexibility in terms of final deposit composition when used in conjunction with a heat source, whether arc, laser or electron beam. By modifying the core composition, a wide range of chemical compositions can be easily produced. With known alloy recovery, powder-cored tubular wires can be used to produce deposits of custom chemical composition. In this work, the manufacturing process of titanium-based cored tubular wires is discussed. These tubular wires are manufactured via U-O bending of CP-Ti Grade 2 strip metal, with a core of Ti-Al-V powder. By adjusting the powder composition, the aluminum loss observed in wire-based electron beam processing can be mitigated. Using a button melting technique, custom powder compositions are being developed with enhanced Al and V chemistries to account for alloy losses, as well as sheath metal compositions.

4:30 PM

**Structure-Property-Process Optimization in the Rapid-Layer Manufacturing of Ti-6Al-4V Components by Electron Beam Melting:** *Sara Gaytan*<sup>1</sup>; Lawrence Murr<sup>1</sup>; Edwin Martinez<sup>1</sup>; Daniel Hernandez<sup>1</sup>; Stella Quinones<sup>1</sup>; Francisco Medina<sup>1</sup>; Ryan Wicker<sup>1</sup>; <sup>1</sup>University of Texas

Rapid prototype (RP) manufacturing using Ti-6Al-4V powder and electron beam melting (EBM) has presented the prospects of microstructure-property control within small volumes and linear dimensions of <1 mm. Utilizing optical and electron microscopy (SEM and TEM), it has been demonstrated that alpha (hcp) acicular platelet dimensions and dislocation substructures within these platelets, composing simple build geometries, can be varied with related variations in hardness, tensile strength, and elongation. These structure-property variations occur by thermal differences as a consequence of beam current, focus, and scan rate or scan sequencing. In addition, during layer building various defects can be created by beam tripping and related phenomena. These include spherical or irregular voids ranging from a few microns to tens of microns in diameter as well as porous zones of even larger dimensions which result from non-melting or local variations in liquid-phase sintering. Examples of these build-related defects will be described.

4:55 PM

**Laser Surface Modification of 2024 Al Alloy to Enhance Thermal Conductivity:** *Amit Bandyopadhyay*<sup>1</sup>; B. Vamsi Krishna<sup>1</sup>; Susmita Bose<sup>1</sup>; W. M. Keck<sup>1</sup>; <sup>1</sup>Washington State University

With rapid advances in microelectronics particularly in the areas of miniaturization with increased power and greater functionality, innovative heat-removal materials as well as techniques are needed for thermal management of active devices for next generation military and commercial applications. Different approaches have been used to make materials with properties suitable for thermal management applications, but not via surface modification. We have examined the feasibility of enhancing thermal conductivity of 2024 Al by depositing 80Cu-20Mo using a Laser Engineered Net Shaping (LENS\153). Coatings of 667 2.5 micron thickness were formed with metallurgically sound interface. Results showed an 87% increase in the thermal conductivity of 2024 Al alloy. The coating approach in combination with LENS\153; process can also be used to deposit high TC materials in desired locations to reduce 'hot spots'. The presentation will discuss materials and manufacturing issues related to laser surface modification of 2024 Al alloy to enhance thermal conductivity.

5:20 PM

**Spheroidisation and Oxide Disruption Phenomena in Direct Selective Laser Melting (SLM) of Pre-Alloyed Al-Mg and Al-Si Powders:** *Eyitayo Olakanmi*<sup>1</sup>; Robert Cochrane<sup>1</sup>; Kenneth Dalgarno<sup>2</sup>; <sup>1</sup>University of Leeds; <sup>2</sup>University of Newcastle

Spheroidisation and oxide disruption phenomena in the direct laser melting of pre-alloyed Al-Mg and Al-Si powders had been explored. Spheroidisation is interpreted in terms of Raleigh's instability, Marangoni convection, laser absorptivity, heat conductivity, fluidity of the melt volume and the powder's oxide content. Balling occurred only in the single layer parts due to the lower thermal conductivity of the bed and possibly the difference in wettability of the powder bed and sintered layers. The existence of a high degree of thermal expansion mismatch between the oxide film and the parent metal and a uniform oxide layer thickness were found to favour the disruption of the oxide shell promoting inter-particulate melting across the layers. This was the case for Al-Si parts, whereas SLM of pure aluminium and pre-alloyed Al-Mg powders gave rise to high incidence of randomly distributed pores.

---

## Materials Processing Fundamentals: Process Modeling

Sponsored by: The Minerals, Metals and Materials Society, TMS Extraction and Processing Division, TMS: Process Technology and Modeling Committee  
Program Organizer: Prince Anyalebechi, Grand Valley State Univ

Monday PM  
February 16, 2009

Room: 2016  
Location: Moscone West Convention Center

*Session Chair:* Prince Anyalebechi, Grand Valley State University

---

2:00 PM

**Solidification Stresses in Steel for Continuous Casting Conditions:** *Matthew Rowan*<sup>1</sup>; Brian Thomas<sup>1</sup>; Robert Pierer<sup>2</sup>; Christian Bernhard<sup>2</sup>; <sup>1</sup>University of Illinois; <sup>2</sup>University of Leoben

Measuring stress development in solidifying steel is very difficult. The submerged split cell tensile (SSCT) test can measure force developed in a cylindrical shell of steel during solidification under controlled conditions identical to continuous casting. Determining the stress profile is difficult given the nonuniform temperature and strength across the shell. A computational model of thermal-mechanical behavior during solidification is applied to simulate the SSCT test. The 2-D axisymmetric elastic-viscoplastic finite-element model features different mechanical properties for delta-ferrite and austenite that vary with temperature and strain rate. The model successfully matched measurements of 1) temperature history; 2) shell thickness; 3) solidification force; and 4) failure location. The results show the effect of carbon content on critical failure strain, and stress profiles, which depend on the phase fraction history. The SSCT test and validated model together is a powerful analysis tool of hot tear crack formation and other phenomena in continuous casting.



2:15 PM

**Numerical Simulation of Continuous Casting Process of Bloom by Finite Point Method:** *Seyed Ahmad Jenabali Jahromi*<sup>1</sup>; Mostafa Alizadeh<sup>1</sup>; S. Behrouz Nasihatkon<sup>1</sup>; <sup>1</sup>Shiraz University

In this paper a meshless method called Finite Point Method (FPM) is developed to simulate the solidification process of continuously cast bloom steel in both primary and secondary cooling region. The method is based on the use of a weighted least-square interpolation procedure. A transverse slice of bloom as it moves with casting speed is considered as computational domain. The two dimensional heat transfer equation together with temperature dependent thermophysical properties is solved in the computational domain. The enthalpy method is used to calculate the latent heat. The present work is verified in the mold region by the comparison of the surface temperature simulated by FPM and finite volume method (FVM) and also comparison of solidified shell thickness simulated by FPM and measured on a breakout bloom. For secondary cooling region the validation is done by comparison of the surface temperature simulated by FPM, FVM and thermovision measurements.

2:30 PM

**Numerical Simulation of Stress Field in a Wide Slab Mold of Peritectic Steel Continuous Casting:** *Min Chen*<sup>1</sup>; Liang Zhao<sup>1</sup>; Yongkuan Yao<sup>1</sup>; <sup>1</sup>Northeastern University

A numerical simulation of the stress field of the solidified shell in the mold during continuous casting of peritectic steel slab was calculated with commercial software. The results showed that the maximal stress on wide face of the solidified shell was located at the corner and near middle of the slab, and it increased with increasing the width of slab. In addition, the stress was also influenced by operating parameters such as super heat degree, drawing speed and cooling intensity of the mold, and the maximal stress value and its position changed with these parameters. For the slab with section size of 3200mm×150mm, the proper drawing speed was around 1.2m/min, with cooling intensity of 5500L/min while the super heating rate was 15°C to 25°C in order to prevent longitudinal crack happening during peritectic steel continuous casting.

2:45 PM

**Modeling the Effects of Processing Variables in Simple Castings of Actinide Metal:** *Paula Crawford*<sup>1</sup>; Deniece Korzekwa<sup>1</sup>; <sup>1</sup>Los Alamos National Lab

The application of modern computer modeling and simulation techniques to materials processing can aid in providing valuable insight into the effects of process variables and mold design variations on the final casting product. A computer model was developed to simulate the casting process using a multi-physics computational modeling package. The effects of mold design variations on the solidification rates and final product phase stability are evaluated through modeling. Additional sensitivity analysis of various processing variables provides an indication of the process controlling variables. Combining the results of the simulation with the experimental casting results should provide a better understanding of the effect of process variables on the casting of plutonium metal.

3:00 PM

**Simulation of Microstructure Evolution during Solidification of Magnesium Alloys:** *Hebi Yin*<sup>1</sup>; Sergio Felicelli<sup>2</sup>; <sup>1</sup>CAVS, Mississippi State University; <sup>2</sup>Department of Mechanical Engineering, Mississippi State University

A coupled cellular automaton(CA) - finite element(FE) model was developed to calculate the growth of dendrites during the solidification of cubic and hexagonal metals. The model solves the conservation equations of mass, energy and solutes in order to calculate the temperature field, solute concentration and the growth morphology of dendrites, including the grain structure and the dendritic microstructure. Validation of the model was performed by comparing the simulation results with experimental data from previously published works, showing qualitatively good agreement in the dendritic morphology. Application to magnesium alloy AZ91 illustrates the difficulty of modeling dendrite growth in hexagonal systems, observed as deviations in growth direction caused by mesh-induced anisotropy. The model was applied to the simulation of small specimens with single- and multiple- equiaxed grain growths and columnar grain growth in directional solidification. The influence of cooling rate and some kinetics parameters on the grain morphology are also discussed.

3:15 PM

**Experimental and Numerical Modelling of the Flow Field in an Industrial Bronze Caster – Improving the Numerical Model:** *Sven Eck*<sup>1</sup>; James Evans<sup>2</sup>; Abdellah Kharicha<sup>1</sup>; <sup>1</sup>University of Leoben; <sup>2</sup>University of California Berkeley

In previous work the influence of the casting speed on the flow field and the shape of the solidification front in an industrial 0.82x0.25x0.8m<sup>3</sup> bronze caster had been investigated. Both numerical and experimental model represented 1:1 the real caster geometry. A comparison of the results of both numerical and experimental models for the flow during the casting process showed a good agreement in the qualitative velocity fields(flow direction and vortex formation). This work represents a parameter study of the numerical model with variations of the turbulence conditions at the inlet in order to clarify their influence on the flow field in the caster. In order to find the best boundary condition at the inlet, the numerical calculations for water have been compared with the measured flow fields in the water model. The new boundary conditions were then applied to the numerical model of the bronze casting process.

3:30 PM Break

3:45 PM

**Advances on Multiscale Design of Deformation Processes for the Control of Material Properties:** *Nicholas Zabaraz*<sup>1</sup>; *Babak Kouchmeshky*<sup>1</sup>; <sup>1</sup>Cornell Univ

We will review advances on the development of a robust design methodology for achieving desired distribution of macro-scale properties in polycrystal plasticity problems during metal forming processes. The polycrystal is represented by an orientation distribution function using the Rodrigues parameterization. Using this continuum representation of texture the underlying texture is allowed to evolve during the process. An updated Lagrangian framework is used in modeling the finite deformation processes. A multi-scale sensitivity analysis is utilized for calculating the sensitivity of the macro-scale properties with respect to the perturbation in process parameters. The multi-scale sensitivity analysis is used in a gradient optimization framework for achieving the desired distribution of the macro-scale properties. The effectiveness of the methodology is shown through controlling properties such as ductility and hardness of the product in a metal forming process. Process conditions (e.g. forging velocity, die and performs) and initial texture are used as the design parameters.

4:00 PM

**Simulation of the Filling of Moulds by the Method FEM/CV in Techniques RTM:** *Jamal Samir*<sup>1</sup>; *Hattabi Mohamed*<sup>1</sup>; <sup>1</sup>ENSEM

In the course of this study, the simulation of the resin flow in the RTM process is developed by the control volume finite element method (CVFEM) coupled with the equation of the free surface location. This location is made by means of the so called "Volume of Fluid" methods or VOF. Thus, the position of the flow front, the time-lapse and the rate of the non saturated zone are calculated at every step. Our results will be compared with the experimental and analytical models in the literature. On the whole, our study is concerned with the simulation of the thermally insulated filling of moulds in RTM process while adopting the CVFEM and VOF method, taking into account the presence of obstacles, coupled with the thickness variation effect and the reinforcement coats.

4:15 PM

**A Comparison of Gas and Low Pressure Carburization of 9310 and 8620 Steels - A Numerical Simulation Study:** *Gang Wang*<sup>1</sup>; *Mohammed Maniruzzaman*<sup>1</sup>; *Richard Sisson*<sup>1</sup>; <sup>1</sup>Worcester Polytechnic Institute

A comparative study of gas carburization and low pressure carburization processes has been performed using CHTE's numerical simulation software – CarbTool. CarbTool is a 1-D carbon diffusion model developed based on the thermodynamics and kinetics of the carburization process. The model is capable of simulating the complex boost-diffuse processes used in the industry. The output of CarbTool is the carbon concentration distribution inside the part. Two steels- 9310 and 8620 are investigated in this study. The quenching process of carburized rods is simulated using DANTE/ABAQUS FEM software. Results are compared in terms of carbon profile, microstructures and residual stresses.

4:30 PM

**A Diffusion Model for the Prediction of a-Case Depth during Heat Treatment of Ti-Alloys:** *Stephen Brown*<sup>1</sup>; *Daniel Clark*<sup>2</sup>; *Steven Tuppen*<sup>2</sup>; <sup>1</sup>Swansea University; <sup>2</sup>Rolls-Royce Plc

A Fickian model of oxygen diffusion in alpha-beta titanium alloys has been developed. It is well known that the diffusion of oxygen into the surface of Ti-alloys gives rise to a potentially harmful outer layer of a-phase. The validated

computer model of diffusion can be used to predict likely penetration depths of alpha-case for different times and temperatures. This work was carried out specifically to provide information on likely alpha-case depths that might be expected for various heat-treatments. Small amounts of oxygen within the vacuum heat treatment chambers are considered. The code has been compared to existing alpha-case experimental data and presentation of simulated results in convenient design diagram format is described. Efficiency in definition of effect can determine economics and process performance. While established codes have general predictors for given temperatures and cooling rates these do not currently allow discrimination due to the effects of diffusion with microstructural variation.

#### 4:45 PM

**Numerical Simulation of Welding Arc and Weld Shape Variations under Helium Shielded GTA Welding:** *Dong Wenchao*<sup>1</sup>; Lu Shanping<sup>1</sup>; Li Dianzhong<sup>1</sup>; Li Yiyi<sup>1</sup>; <sup>1</sup>Shenyang National Laboratory for Materials Science, Institute of Metal Research, Chinese Academy of Sciences

A numerical modeling of welding arc and weld pool is established for moving helium shielded GTA welding to investigate the effect of surface active element oxygen on the weld shapes. For different oxygen content from 20 to 200ppm, the simulation results showed that the weld shape is decided by the pool flow patterns, which are driven by the surface tension, gas shear force, electromagnetic force and the buoyancy force. The surface tension induced Marangoni convection plays an important role on the weld shape. Small addition of oxygen can change the Marangoni convection from outward to inward direction on liquid pool, and make the wide shallow weld shape become narrow deep one. The weld D/W ratio under high oxygen content decreases with increasing welding speed, but it is not sensitive to the welding speed under low oxygen content. The experimental results agree well with the predicted results by numerical simulation.

## Mechanical Behavior of Nanostructured Materials: Nanostructures by Severe Plastic Deformation

Sponsored by: The Minerals, Metals and Materials Society, TMS Electronic, Magnetic, and Photonic Materials Division, TMS Materials Processing and Manufacturing Division, TMS Structural Materials Division, TMS: Chemistry and Physics of Materials Committee, TMS/ASM: Mechanical Behavior of Materials Committee, TMS: Nanomechanical Materials Behavior Committee

Program Organizers: Xinghang Zhang, Texas A & M University; Andrew Minor, Lawrence Berkeley National Laboratory; Xiaodong Li, University of South Carolina; Nathan Mara, Los Alamos National Laboratory; Yuntian Zhu, North Carolina State University; Rui Huang, University of Texas, Austin

Monday PM  
February 16, 2009

Room: 3024  
Location: Moscone West Convention Center

*Session Chairs:* Yuntian Zhu, North Carolina State University; Michael Zehetbauer, University of Vienna

#### 2:00 PM Invited

**Using ECAP for the Processing of Magnesium and Other Similar Difficult-to-Work Alloys:** Roberto Figueiredo<sup>1</sup>; *Terence Langdon*<sup>1</sup>; <sup>1</sup>University of Southern California

Magnesium and other similar difficult-to-work alloys, such as titanium, often present challenges for successful processing by equal-channel angular pressing (ECAP). This presentation examines these difficulties and discusses possible solutions. Examples are presented showing the exceptional properties that may be achieved through the successful pressing of magnesium-based alloys.

#### 2:20 PM

**Strategies for Improving the Ductility of Nanostructure/Ultrafine-Grained Metals without Sacrificing Strength:** Yonghao Zhao<sup>1</sup>; Enrique Lavernia<sup>1</sup>; *Yuntian Zhu*<sup>2</sup>; <sup>1</sup>University of California, Davis; <sup>2</sup>North Carolina State Univ

The strength and ductility of structural materials are frequently inversely related. In other words, high strength is often accompanied by low ductility, and vice versa. Inspection of the scientific literature reveals that this is also the case for nanostructured and ultrafine-grained materials, which are usually strong, but with accompanying low ductility levels. Conventional approaches to improve ductility often yield a loss of strength. This talk presents several approaches that can be effectively implemented to increase the ductility of

nanostructured/ultrafine-grained materials while simultaneously improving or at least maintaining their strength. The fundamental mechanisms that underlie the proposed approaches are discussed in this talk.

#### 2:35 PM

**Correlations between Texture and Mechanical Properties of Mg and Cu Processed by High-Pressure Torsion:** *Bartlomiej Bonarski*<sup>1</sup>; Nariman Enikeev<sup>2</sup>; Erhard Schaffler<sup>1</sup>; Bernhard Mingler<sup>1</sup>; Borys Mikulowski<sup>3</sup>; Ruslan Valiev<sup>2</sup>; Michael Zehetbauer<sup>1</sup>; <sup>1</sup>University of Vienna; <sup>2</sup>UFA State Aviation Technical University; <sup>3</sup>AGH - University of Science and Technology, Cracow

Ultrafine grained and nanocrystalline metals processed by Severe Plastic Deformation (SPD) reveal outstanding mechanical properties, especially a considerable ductility at still enhanced strength. While the latter can be quantitatively associated to the grain refinement, the ductility is still under dispute. This work aims at clarification by investigating both the texture evolution and the hardening characteristics during and after HPT processing of Mg and Cu. Deformations by HPT (High Pressure Torsion) have been achieved up to shear strains  $\gamma = 120$  with hydrostatic pressures between 1 and 6 GPa. While HPT processed Cu exhibits marked shear textures with only little influence of hydrostatic pressure, that of Mg shows massive recrystallization which even ceases the further evolution of shear textures and of grain refinement. The extent and the nature of recrystallization depend on the prestrain, the hydrostatic pressure and the alloy content, which has a direct influence to the macroscopic mechanical properties.

#### 2:50 PM

**Mechanical Properties of Ultrafine-Grained Cu with Bimodal Grain Size Distribution:** *Yonghao Zhao*<sup>1</sup>; Troy Topping<sup>1</sup>; Ying Li<sup>1</sup>; Ruslan Valiev<sup>2</sup>; Yuntian Zhu<sup>3</sup>; Enrique Lavernia<sup>1</sup>; <sup>1</sup>University of California at Davis; <sup>2</sup>Institute of Physics of Advanced Materials, Ufa State Aviation Technical University; <sup>3</sup>Department of Materials Science and Engineering, North Carolina State University

A bimodal grain size distribution was investigated as an effective strategy to enhance the ductility of nanostructured materials. In this work, we studied the influence of a bimodal grain size distribution on the mechanical properties of ultrafine grained (UFG) Cu. The UFG Cu samples were prepared by equal-channel angular pressing, Bc, route by 2 and 16 passes, respectively. The samples were then annealed at 250 C for different times to attain a bimodal grain size distribution. We found with increasing annealing time (fraction of coarse grains), the yield strength values of both samples decreases, and the ductility increases gradually. The microstructural origin of the observed behavior is discussed in detail in the lecture.

#### 3:05 PM Invited

**Ultrahigh Tensile Ductility and High Strength in Nickel via Cryo-Milling and Quasi-Isostatic Forging:** Yonghao Zhao<sup>1</sup>; Troy Topping<sup>1</sup>; Ying Li<sup>1</sup>; John Binger<sup>2</sup>; A.M. Dangelewicz<sup>2</sup>; Peiling Sun<sup>3</sup>; Yuntian Zhu<sup>4</sup>; Yizhang Zhou<sup>1</sup>; *Enrique Lavernia*<sup>1</sup>; <sup>1</sup>University of California at Davis; <sup>2</sup>Los Alamos National Laboratory; <sup>3</sup>Department of Materials Science and Engineering, Feng Chia University; <sup>4</sup>Department of Materials Science and Engineering, North Carolina State University

The limited ductility of nanocrystalline/ultrafine-grained materials has emerged as a singular issue in the study and application of this novel class of materials. Numerous investigators have addressed this topic, with varying degrees of success, via a variety of approaches, most of which can be grouped into two general categories: microstructural design and introduction of alternative deformation mechanisms. In this talk, results are reported obtained with fine-grained Ni and bimodal grained Ni (mixture of fine grains and coarse grains) prepared by cryo-milling and subsequent quasi-isostatic forging (formerly known as Ceracon forging). In tension, the fine-grained Ni shows remarkable strength and ductility, yielding at 470 MPa with 42% elongation to failure. The bimodal Ni shows lower strength and higher ductility, yielding at 310 MPa with 49% elongation to failure. In contrast, the coarse-grained Ni, processed by annealing the fine-grained Ni at 1000 C for 10 hours, has a yield strength of 150 MPa and elongation to failure of 48%. The combination of strength and ductility of our Ni is superior to those of the nanocrystalline/ultrafine-grained Ni prepared by electrodeposition, cryo-rolling, and equal-channel angular pressing methods. The microstructural origins for such combinations of good strength and high ductility will be discussed.

3:25 PM

**Microstructure and Mechanical Properties of Cu-Al<sub>2</sub>O<sub>3</sub> Nanocomposites Prepared by High Energy Mechanical Milling and Thermomechanical Powder Consolidation:** *Deliang Zhang*<sup>1</sup>; *Aamir Mukhtar*<sup>1</sup>; *Charlie Kong*<sup>2</sup>; *Paul Munroe*<sup>2</sup>; <sup>1</sup>University of Waikato; <sup>2</sup>University of New South Wales

Cu matrix nanocomposite powders with each of the powder particles consisting of a dispersion of nanometer sized (2.5-10)vol.%Al<sub>2</sub>O<sub>3</sub> particles were synthesized by high energy mechanical milling (HEMM) of a mixture of Cu and Al<sub>2</sub>O<sub>3</sub> powders. HEMM also results in reduction of the grain sizes of the Cu matrix to submicrometer or nanometer range. Bulk nanocomposite samples were prepared by powder consolidation of the nanocomposite powders using thermomechanical processes such as hot pressing, upset forging and extrusion. The microstructure and mechanical properties of the samples were studied as a function of the consolidation conditions, with the aim of establishing a correlation between the microstructure and mechanical properties of the materials and determining the effect of consolidation defects on mechanical properties. This paper is to present an overview of the major findings from this study and discuss the effects of various factors on the mechanical properties of Cu matrix nanocomposite.

3:40 PM Break

3:50 PM Invited

**Grain Boundaries Interface Phenomena and Mechanical Properties of Ultrafine-Grained Metals:** *Ruslan Valiev*<sup>1</sup>; <sup>1</sup>UFA State Aviation Technical University

In the present report using variations of regimes and routes of severe plastic deformation (SPD) processing we show for several light alloys (Al, Mg and Ti) the ability to produce ultrafine-grained (UFG) materials with different grain boundaries, and this can have a dramatical effect on mechanical behaviour of the processed materials, particular, on their strength and ductility, fatigue or superplasticity. We demonstrate several examples of this approach for attaining superior strength and ductility as well as enhanced superplasticity at low temperatures and high strain rates in various UFG metals and alloys. The origin of these phenomena is discussed on the basis of the results of microstructural studies and observations of deformation mechanisms. Special emphasis is laid on the innovation potential and first applications of SPD-produced nanometals.

4:10 PM

**Simulation of Stress-Strain Characteristics and Microstructural Evolution of SPD Processed Nanomaterials:** *Michael Zehetbauer*<sup>1</sup>; *Nariman Enikeev*<sup>2</sup>; *Christian Holzleithner*<sup>1</sup>; <sup>1</sup>University of Vienna; <sup>2</sup>Ufa State Aviation Technical University

The composite model by Zehetbauer has proven to be successful in describing the hardening characteristics and specific dislocation densities of nanomaterials during and after SPD processing. For both cases, the model could be extended for correct simulation of the grain size and of the grain boundary thickness. Recently, at the example of Cu being processed by High Pressure Torsion (HPT), efforts were made to predict also the mean misorientation as a function of accumulated strain and applied hydrostatic pressure. The results fit best to the experimental data when a linear array of dislocation in the grain boundary is assumed. Differences left between simulation and experiment may be attributed to the failing of X-ray profile analysis which detects too small dislocation densities when the dislocation distance in the grain boundary becomes smaller than 1 nm.

4:25 PM Invited

**Development of Shear Drawing Process for the Spheroidization of Medium and High Carbon Steels: Industrial Application of ECAP:** *Dong Shin*<sup>1</sup>; *Hyun H. Choi*<sup>1</sup>; *Young G. Ko*<sup>2</sup>; *Il-Heon Son*<sup>3</sup>; *KiHo Rhee*<sup>3</sup>; *Duklak Lee*<sup>3</sup>; <sup>1</sup>Dept. of Mater. Sci. & Eng., Hanyang University; <sup>2</sup>Dept. of Mater. Sci. & Eng., MIT; <sup>3</sup>Technical Research Laboratory, POSCO

Severe plastic deformation of metals utilizing ECAP has been recognized as one of the attractive methods for tailoring the ultrafine-grained microstructures which exhibit better performance in mechanical properties than those of the traditional metals where the deformation during ECAP is simply shear in nature. Particularly, with regard to obtaining good formability, this feature is also beneficial for metals to break down lamellar structure in steel through the decomposition of pearlitic cementite phase. Therefore, it can be put to use for the industrial applications of steel-wire manufacturing when problems causing from the batch processing will be solved. The aim of this study is to

propose the new-typed ECAP termed shear drawing (SD) by modifying the design of the die in order to avoid dimensional inhomogeneity. Moreover, the deformation characteristics and the microstructural changes associated with the spheroidization of carbon steel during SD are discussed and compared to results obtained by ECAP.

4:45 PM

**Molecular Dynamics Simulations of Dislocation Activity in Single Crystal and Nanocrystalline Copper Doped with Antimony:** *Rahul Rajgarhia*<sup>1</sup>; *Douglas Spearot*<sup>1</sup>; *Ashok Saxena*<sup>1</sup>; <sup>1</sup>University of Arkansas

Recently published simulation results have indicated that high temperature grain growth in nanocrystalline copper can be suppressed by introducing dopant atoms at the grain boundaries [Millett et al., 2006]; however, the impact of grain boundary dopants on plastic behavior is still unclear. In this work, molecular dynamics simulations are used to study dislocation activity in single crystal and nanocrystalline copper with low concentrations of antimony (0.0-2.0 at.%Sb). A new interatomic potential for Cu-Sb is developed in this work and used to model the dopant/host interatomic interactions. In single crystal models, it is observed that the strained regions around the Sb atoms act as sources for partial dislocations and that the dislocation nucleation stress decreases with increasing concentration of antimony. In nanocrystalline models, antimony atoms randomly dispersed along the grain boundaries alter the stress-strain response and subsequently the grain diameter at which the maximum strength is observed (modified inverse Hall-Petch response).

5:00 PM

**The Influence of Temporary Hydrogenation on ECAP Formability and Low Cycle Fatigue Life of CP Titanium:** *Andrew Czerwinski*<sup>1</sup>; *Rimma Lapovok*<sup>1</sup>; *Dacian Tomus*<sup>1</sup>; *Yuri Estrin*<sup>1</sup>; <sup>1</sup>Monash University

Titanium has been successfully competing with other metallic materials due to its high strength-to-density ratio. UFG titanium processed by ECAP can be made 30-120% stronger than conventional structural steel. However, the increase in tensile strength is often accompanied with decrease in the low cycle fatigue (LCF) life. The new opportunities to improve the LCF life come from the use of hydrogen as a temporary alloying element, which has been shown to enhance the properties of titanium. In particular, for some Ti alloys hydrogen induced ductility is in the low temperatures range, which is directly correlated with improved formability by ECAP and increased LCF life. Typically damage initiates from the surface, and, therefore, hydrogenation and the associated enhancement of the surface properties are beneficial. The effect of hydrogenation on the improvement of ductility, formability by ECAP, and enhancement of LCF life of ultrafine grained titanium has been investigated.

5:15 PM

**Mechanical Behavior during Tensile Straining of Nano/Ultrafine-Grained Structures Formed by Reversion in Metastable Austenitic Steels:** *Sashank Nayak*<sup>1</sup>; *Sachin Mali*<sup>1</sup>; *Devesh Misra*<sup>1</sup>; *Mahesh Somani*<sup>2</sup>; *Pentti Karjalainen*<sup>2</sup>; <sup>1</sup>University of Louisiana; <sup>2</sup>University of Oulu

The deformation behavior of nano/ultrafine-grained structures during tensile deformation has been examined by transmission electron microscopy in metastable austenitic steels. Special fine-grained structures were obtained by controlled reversion annealing of strain-induced martensite. Proper gradual strain hardening by the formation of ultra-fine martensite results in excellent tensile strength-ductility property combination. Twinning and dislocation glide were identified as the primary deformation mechanisms in nano-/ultrafine-grained structures.

5:30 PM

**Grain Refinement and Mechanical Properties in Nanostructured Al and Al-Mg Alloys Subjected to Severe Plastic Deformation:** *Hans Roven*<sup>1</sup>; *Manping Liu*<sup>1</sup>; *Maxim Murashkin*<sup>2</sup>; *Ruslan Valiev*<sup>2</sup>; *Tamas Ungár*<sup>3</sup>; *Levente Balogh*<sup>3</sup>; <sup>1</sup>Norwegian University of Science and Technology (NTNU); <sup>2</sup>Ufa State Aviation Technical University; <sup>3</sup>Eötvös University

Bulk nanostructured materials can be produced by a variety of severe plastic deformation methods. The present work focuses on commercial purity Al and Al-Mg alloys subjected to high pressure torsion. The grain sizes are in the range 10-200 nm with typical average values ranging from 46 to 120 nm. The hardness and strength values as well as the dislocation densities increased, whereas, the average grain size decreased significantly with increasing Mg contents. The local dislocation densities in grain boundary and triple junction areas are two to three orders of magnitude larger than the average values. Extensive high-resolution



transmission electron microscopy observations reveal that these materials develop new nanostructures such as deformation nano-twins, stacking faults and non-equilibrium grain boundaries. The purpose of this work is to explore the impact of these nanostructures as well as Mg contents on grain refinement mechanism and mechanical behavior in these materials.

**5:45 PM**

**Effect of Microstructure on the Tensile Behavior of Ultrafine-Grained Cu:** *Pei-Ling Sun*<sup>1</sup>; *Chia-Hao Yang*<sup>1</sup>; *Chung-Yi Yu*<sup>2</sup>; *Yun-Jun Wang*<sup>3</sup>; *Po-We Kao*<sup>3</sup>; *Chih-Pu Chang*<sup>3</sup>; <sup>1</sup>Feng Chia University; <sup>2</sup>China Steel Corporation; <sup>3</sup>National Sun Yat-Sen University

Pure Cu with ultrafine-grained (UFG) structure was produced by equal channel angular extrusion (ECAE) to an equivalent strain of ~8. Different UFG structures were obtained by performing ECAE either at ambient temperature (sample A) or at 373 K (sample B). Additionally, cryo-rolling was also applied to an ECAEed specimen in order to create an UFG structure with higher dislocation density and higher fraction of high angle boundaries (sample C). Low temperature annealing (<423 K) treatments were applied to introduce various amount of microcrystalline grains into these three different UFG matrices via partial recrystallization. The microstructures of these samples were characterized by TEM and SEM. Tensile properties were measured at room temperature. The influence of the microstructure of the UFG matrix as well as of the size and amount of microcrystalline grains on the tensile properties will be presented.

**6:00 PM**

**The Effect of Milling Media and Time on Cryomilled 99.95% Pure Al:** *Troy Topping*<sup>1</sup>; *Chris San Marchi*<sup>2</sup>; *Ying Li*<sup>1</sup>; *Zhihui Zhang*<sup>1</sup>; *Rustin Vogt*<sup>1</sup>; *Osman Ertorer*<sup>1</sup>; *Julie Schoenung*<sup>1</sup>; *Richard Karnesky*<sup>2</sup>; *Nancy Yang*<sup>2</sup>; *Enrique Lavernia*<sup>1</sup>; <sup>1</sup>University of California, Davis; <sup>2</sup>Sandia National Laboratories

Aluminum powder (99.95% pure) was cryomilled in separate batches in liquid argon (LAR) and liquid nitrogen (LN<sub>2</sub>) to obtain a nanocrystalline structure. Samples were removed from the milling vessel every 4 hours to characterize the powders over a 24 hour period. Transmission electron microscopy (TEM) and x-ray diffraction (XRD) show differences in microstructural evolution during milling for the two different media. After cryomilling, powders removed after 12 and 24 hours for the LAR and 24 hours for the LN<sub>2</sub> were hot vacuum degassed and consolidated via hot isostatic pressing (HIP). After HIPping, bars were extruded for tensile testing. The extrusions were analyzed for interstitial elemental composition to determine the uptake of nitrogen in all cases, since it is believed to contribute to the mechanical behavior of the consolidated aluminum. High resolution TEM is also employed to further investigate the microstructural contributions to the properties of the respective materials.

## Microstructural Processes in Irradiated Materials: Radiation Effects II: Advanced Characterization and Fe-Cr Alloys

Sponsored by: The Minerals, Metals and Materials Society, TMS Structural Materials Division, TMS/ASM: Nuclear Materials Committee

Program Organizers: Christophe Domain, Electricite De France; Gary Was, University of Michigan; Brian Wirth, University of California, Berkeley

Monday PM

Room: 2008

February 16, 2009

Location: Moscone West Convention Center

Session Chairs: Pascal Bellon, University of Illinois; Vasily Bulatov, Lawrence Livermore National Laboratory

**2:00 PM Invited**

**State-of-the-Art Positron Annihilation Techniques to Study Embedded Nano-Clusters in Metals:** *Takeshi Toyama*<sup>1</sup>; *Yasuyoshi Nagai*<sup>1</sup>; *Koji Inoue*<sup>1</sup>; *Zheng Tang*<sup>2</sup>; *Masayuki Hasegawa*<sup>1</sup>; *Abderrahim Abderrahim*<sup>3</sup>; *Eric van Walle*<sup>3</sup>; *Robert Gerard*<sup>4</sup>; <sup>1</sup>Tohoku University; <sup>2</sup>East China Normal University; <sup>3</sup>SCK-CEN; <sup>4</sup>Tractebel Engineering

We have developed a "positron quantum-dot" method for embedded nano-clusters in metals using Coincidence Doppler Broadening (CDB) of positron annihilation. It features self-searching and gives exclusive information of atomic and electronic structures of the embedded clusters. It extends its applicability of positron annihilation other than that in the research field of vacancy-type defects

and has been successfully applied to studies of Cu nano-clusters in Fe-Cu model alloys and surveillance test specimens of nuclear Reactor Pressure Vessel (RPV) steels. Furthermore recently we developed new experimental techniques for the positron quantum-dots, (i) two dimensional angular correlation of annihilation radiation (2D-ACAR), and (ii) Age Momentum Correlation (AMOC) between positron lifetime and Doppler broadening. From smearing of 2D-ACAR momentum distributions we can estimate sizes of Cu nano-clusters and from AMOC spectra we can obtain the chemistry and number densities of the nano-clusters. Thus we clarify detailed evolution of the nano-clusters in Fe matrix.

**2:30 PM Invited**

**Imaging and Spectroscopy of Single Atoms and Point Defects through Aberration-Corrected STEM:** *Stephen Pennycook*<sup>1</sup>; *M. Varela*<sup>2</sup>; *A. R. Lupini*<sup>2</sup>; *A. Y. Borisevich*<sup>2</sup>; *W. Luo*<sup>1</sup>; *S.-H. Oh*<sup>3</sup>; *K. Van Benthem*<sup>4</sup>; *S. Rashkeev*<sup>5</sup>; *K. Griffin Roberts*<sup>6</sup>; *K. M. Krishnan*<sup>6</sup>; *J. Garcia-Barriocanal*<sup>7</sup>; *C. Leon*<sup>7</sup>; *J. Santamaria*<sup>7</sup>; *S. T. Pantelides*<sup>1</sup>; <sup>1</sup>Oak Ridge National Laboratory - and - Vanderbilt University; <sup>2</sup>Oak Ridge National Laboratory; <sup>3</sup>Korea Basic Science Institute; <sup>4</sup>University of California, Davis; <sup>5</sup>Idaho National Laboratory; <sup>6</sup>University of Washington; <sup>7</sup>GFMC, Universidad Complutense de Madrid

In recent years the probe size in the scanning transmission electron microscope has decreased more than a factor of two, bringing improved resolution both laterally and vertically. In addition, the smaller, sharper probe provides greatly increased signal to background ratio, enabling the study of single atoms inside materials for the first time. In Si nanowires individual Au interstitials are seen that match well in both atomic position and relative formation energies with density functional calculations. Single atom sensitivity has also been achieved in electron energy loss spectroscopy, which can not only positively identify the element, but also, from the fine structure, provide information on local bonding, band structure and carrier concentration. Several examples will be shown of oxide materials and heterostructures where spectroscopic analysis reveals the origin of surprising bulk properties including ferromagnetism in Co-doped anatase and colossal ionic conductivity in Y-stabilized ZrO<sub>2</sub>/SrTiO<sub>3</sub> heterostructures. This research was sponsored by the Office of Basic Energy Sciences, Division of Materials Sciences and Engineering, US Department of Energy and NSF/ECS No. 0224138.

**3:00 PM**

**JANNUS: A New Multi-Ion Irradiation Facility to Study the Stability of Nano-Oxides in ODS Materials:** *Ribis Joël*<sup>1</sup>; *de Carlan Yann*<sup>1</sup>; *Boulanger Loïc*<sup>1</sup>; *Serruys Yves*<sup>1</sup>; *Trocclier Patrick*<sup>1</sup>; <sup>1</sup>CEA

Ferritic ODS alloys are primary candidates as long life cladding materials for the Sodium Fast Reactor (SFR) developed in France in the frame of Generation IV research program. These alloys exhibit a fairly high resistance to swelling under neutron irradiation and the embedded oxide dispersion helps to preserve good mechanical properties at high temperature. Previous experimental studies have shown a partial dissolution of some oxides under neutron irradiation. However, a relative stability of the nano-oxide particles has been reported under ion irradiation experiments even at a damage level up to 200 dpa.<sup>1</sup> Then, the behaviour of ODS alloys under ion irradiation at high damage dose has to be clarified using multi-ion irradiations. The new multi-ion irradiation facility JANNUS which is in completion at CEA Saclay and CNRS Orsay will be described in details and the future irradiation experiments on ODS alloys will be discussed. <sup>1</sup>T.R. Allen et al., J. Nucl. Mater. 375, 2008, pp. 26-37.

**3:20 PM**

**Effect of Grain Size on the Radiation Resistance of Materials:** *Steven Zinkle*<sup>1</sup>; <sup>1</sup>Oak Ridge National Laboratory

Creation of a high density of point defect sinks in the form of nanoscale grain boundary interfaces offers a potentially attractive solution to the problem of developing radiation-resistant materials for fusion and Generation-IV fission energy systems, where the structural materials may be exposed to unprecedented high displacement damage levels. This presentation summarizes experimental observations on several materials that demonstrate the effectiveness of small grain sizes on inhibiting defect cluster nucleation and growth during irradiation. Whereas nanoscale grain dimensions may be very effective in improving radiation damage resistance, grain dimensions on the order of 100-5000 nm may under some conditions produce an acceleration of radiation damage. This enhanced retention of radiation damage can occur for example if the grain size is intermediate between the mean diffusion lengths for vacancy and interstitial type defects. Several caveats to using fine-grained materials will be noted, including the potential for radiation-enhanced grain coarsening.

**3:40 PM Break****4:00 PM Invited**

**Density Functional Based Modeling of FeCr Alloys:** *Par Olsson*<sup>1</sup>; <sup>1</sup>EDF R&D

FeCr alloys have garnered renewed interest during the last years, due to the foreseen use of Ferritic/Martensitic steels of high Cr content in future nuclear installations. Especially interesting as a model system is the binary FeCr since the Cr content has a major influence on the evolution of the mechanical properties in irradiated Ferritic/Martensitic alloys. Experimentally, these alloys have been studied for over 40 years, but for a long time the understanding of many observed effects was lacking. Already 20 years ago calculations appeared that indicated the relevance of the concentration, in terms of the inversion of short range ordering around 10% Cr. However, these studies were not extensively followed up until recently. Here we will discuss the latest developments in the modeling, based on density functional theory, of thermodynamics and defect properties in FeCr alloys and how the understanding of the microscopic origins of macroscopic effects is evolving.

**4:30 PM**

**Heavy-Ion Irradiation Damage in Fe-Cr Alloys:** *Sen Xu*<sup>1</sup>; Zhongwen Yao<sup>1</sup>; Mike Jenkins<sup>1</sup>; <sup>1</sup>University of Oxford

Bulk Fe-Cr specimens (of thickness about 100  $\mu\text{m}$  and with Cr contents ranging from 0-12%) were irradiated with dual-energy iron ions (0.5 and 2 MeV) at Surrey Ion Beam Centre at temperatures of 300°C and 500°C to doses up to 7dpa. TEM experiments showed that the radiation damage took the form of dislocation loops of interstitial nature with sizes up to 100nm. The average loop size was about four times larger at the higher irradiation temperature. In Fe-Cr alloys, both  $b = \langle 100 \rangle$  and  $b = \frac{1}{2}\langle 111 \rangle$  loops were present in roughly equal proportions at both temperatures. However, in the pure Fe,  $b = \frac{1}{2}\langle 111 \rangle$  loops predominated at 300°C whilst  $b = \langle 100 \rangle$  loops predominated at 500°C. Comparisons of this work with parallel in-situ experiments in which ion irradiations were performed on TEM specimens in the form of thin foils will also be reported.

**4:50 PM**

**Cluster Dynamics Modeling of Microstructural Evolution of Ferritic Martensitic Steels under High Energy Ion Irradiation:** *Donghua Xu*<sup>1</sup>; Francois Gallet<sup>1</sup>; Brian Wirth<sup>1</sup>; <sup>1</sup>University of California, Berkeley

The design goals of higher temperatures, higher radiation doses and higher energy neutron spectrum for future fission and fusion reactors demand new advanced materials with superior resistance to irradiation damages. Typical irradiation damages such as hardening, embrittlement, swelling, creep, precipitation etc., are all closely related to the generation and clustering of point and small fragmented defects, the fundamental reason for microstructural changes and subsequent mechanical property degradation under irradiation. Here we present our rate theory based modeling of cluster evolution in both compositional and geometric spaces under high energy ion irradiation. Particularly, we calculate the concentrations of interstitial loops and voids as a function of multiple variables including time, number of interstitials/vacancies, spatial position, dislocation densities, temperature, dose and dose rate, impurities and so on. Our calculations are compared with coordinated in-situ transmission electron microscopy irradiation studies performed by others.

**5:10 PM**

**Microstructure Evolution of Fe-9Cr-0.1C and Fe-12Cr-0.1C Model Martensitic Steels Ion-Irradiated In-Situ in a TEM:** *Djamel Kaoumi*<sup>1</sup>; Arthur Motta<sup>1</sup>; Mark Kirk<sup>2</sup>; <sup>1</sup>The Pennsylvania State University; <sup>2</sup>Argonne National Laboratory

Two model martensitic steels of compositions Fe9Cr0.1C and Fe12Cr0.1C are irradiated with 1 MeV Kr ions at 400°C to doses of 10 dpa in-situ in a TEM. These model materials have been processed to exhibit lath microstructures similar to those found in commercial steels. The microstructure evolution under irradiation –black dot density, nature and number density of defect clusters present, and stability of as-fabricated microstructure – is followed and characterized using weak-beam dark-field imaging and g.b analysis. The goal of the irradiations is to perform a direct determination of the spatial correlation of the time evolution of the irradiation-induced defect structures with the pre-existing alloy microstructure including lath boundaries, network dislocations and carbides, for comparison with computations. These results will be summarized in this paper.

**5:30 PM**

**In-Situ Ion Irradiations of Iron-Chromium Alloys:** *Carolyn Tomchik*<sup>1</sup>; Mark Kirk<sup>2</sup>; Maria Okuniewski<sup>3</sup>; James Stubbins<sup>1</sup>; Stuart Maloy<sup>4</sup>; <sup>1</sup>University of Illinois at Urbana-Champaign; <sup>2</sup>Argonne National Laboratory; <sup>3</sup>Idaho National Laboratory; <sup>4</sup>Los Alamos National Laboratory

Iron-chromium alloys are used as a model to study the microstructural evolution of defects in irradiated structural steel components of a nuclear reactor. We examine the effects of temperature and chromium concentration on the defect evolution, segregation behaviour, and second phase precipitation in the early stages of damage. In-situ irradiations are conducted at the IVEM-Tandem facility at Argonne National Laboratory at 300°C, 450°C, and 550°C with 150keV Fe ions in single crystal Fe14Cr and Fe19Cr bicrystal to doses of 2E15 ions/cm<sup>2</sup>. The microstructures of the irradiated iron-chromium alloys are characterized by analysis of TEM micrographs and compared with those of pure iron.

**Nanocomposite Materials: Polymer Nanocomposites**

Sponsored by: The Minerals, Metals and Materials Society, TMS Structural Materials Division, TMS Electronic, Magnetic, and Photonic Materials Division, TMS/ASM: Composite Materials Committee, TMS: Materials Characterization Committee, TMS: Nanomaterials Committee

Program Organizers: Jonathan Spowart, US Air Force; Judy Schneider, Mississippi State University; Bhaskar Majumdar, New Mexico Tech; Benji Maruyama, Air Force Research Laboratory

Monday PM

February 16, 2009

Room: 3020

Location: Moscone West Convention Center

Session Chairs: Karen Winey, University of Pennsylvania; Judy Schneider, Mississippi State Univ

**2:00 PM Introductory Comments****2:05 PM Invited**

**Inside Polymer Nanocomposites – Interphases, Gradients and Percolation:** *Catherine Brinson*<sup>1</sup>; Rui Qiao<sup>1</sup>; Supinda Watcharotone<sup>1</sup>; <sup>1</sup>Northwestern University

Polymers with small loadings of nanoparticles exhibit dramatic changes in thermomechanical properties, in large part due to the development of interphase zones of altered polymer properties near the interfaces. Given the enormous surface-to-volume ratio for nanoparticles, the interphase volume fraction can dwarf that of the inclusions and percolate through the composite. Experimental evidence of the existence of this interphase region is presented for several nanofiller types via local and global glass transition changes and microscopy. By properly controlled functionalization of the nanoscale inclusions, we can impact the properties of the interphase region and the nanocomposites. The nature of the properties of this interphase region and the gradient in properties away from the nanofiller is probed by novel nano-DMA experiments on model nanocomposite systems. In conjunction with the experimental results, the concept of percolated interphase is investigated by a finite element approach which accounts for an interphase region of gradient properties.

**2:30 PM**

**In Situ FTIR Studies on Double Wall Carbon Nanotube Composites of High Volume Percent:** *Scott Brownlow*<sup>1</sup>; Alexander Morvasky<sup>2</sup>; Nikolai Kalugin<sup>1</sup>; Bhaskar Majumdar<sup>1</sup>; <sup>1</sup>New Mexico Tech; <sup>2</sup>MER Corporation

While carbon nanotube (CNT) based polymer composites have drawn attention in recent years, the potential has been limited by the low volume fraction and poor load transfer to the nanotubes. Here, we have utilized functionalized mats of double walled nanotubes (DWNT) to develop strong epoxy based composites with 10 - 13 weight percent DWNT. In addition, we utilized the FTIR technique using in situ loaded specimens to monitor the changes in vibrations, with the goal of understanding load transfer behavior. Tests with neat epoxy and composite samples show that the stretching of epoxy bonds is greatly reduced in the composite at equal stress. We will attempt to show that in situ FTIR using current instruments and analysis procedures provides a means to tap this understanding and improve CNT composites. Our work is complemented with in situ Raman studies of the embedded DWNT that also shed insight on load sharing behavior.

2:50 PM

**Magnet-Polymer Nanocomposites for Shape Changing Structures:** *Raju Ramanujan*<sup>1</sup>; *V Nguyen*<sup>1</sup>; <sup>1</sup>Nanyang Technological University

There is an urgent need for intelligent shape changing structures for energy, biomedical and structural health monitoring applications. However, current materials either have low strains or are too slow for many practical applications. MAGPOL, a composite containing MAGnetic nanoparticles in a soft POLYmer matrix is capable of large deformation and fast response, hence is very attractive for novel shape changing structures. An external magnetic field can be used to apply forces on the particles, leading to fast shape change of the composite in contraction, elongation, deflection and torsion modes. The extent of shape deformation as a function of magnetic field strength was found to be highly nonlinear, large stress and strain was achieved with MAGPOL. MAGPOL can also act as a sensor, the resistance of composites at percolation concentration is a strong function of the actuation strain. Novel nanocomposite systems can be built by exploiting this unique combination of properties.

3:10 PM

**Nucleation and Growth of Hierarchical Structures and Phases in Pressure-Induced Crystallization of Polymer Nanocomposites:** *Qiang Yuan*<sup>1</sup>; *Devesh Misra*<sup>1</sup>; <sup>1</sup>University of Louisiana

The objective of the presentation is to elucidate the basic physical mechanisms underlying the evolution of hierarchical structures and phases during pressure-induced crystallization of polymers containing dispersion of nanoparticles. The phase selection in the polymers is normally dictated by pressure and temperature, however, the introduction of nanoparticles can dramatically alter the kinetics of the formation of the phases via nanoparticle interface driven nucleation. Thus, by controlling pressure and crystallization temperature, a high degree of phase selection and structural control may be achievable, which has profound effect on mechanical properties.

3:30 PM Break

3:45 PM Invited

**Electrical Conductivity and Polymer Diffusion in Polymer Nanocomposites:** *Karen Winey*<sup>1</sup>; <sup>1</sup>University of Pennsylvania

Both electrical conductivity and polymer diffusion in polymer nanocomposites are dominated by the presence of a nanotube network. This talk will present three-dimensional simulations of electrical conductivity above the filler percolation threshold for composites containing conductive, finite-sized rods with various orientations. The random resistor network model was used to calculate the electrical conductivity of these simulated composites. The observed trends compare favorably with our earlier experimental results. In addition, polymer tracer diffusion in single wall carbon nanotube / polymer nanocomposites is reported. Polymer diffusion is suppressed at low SWCNT loadings to a surprising extent and recovers at higher loadings. A new phenomenological trap model is used to discuss these results. This fundamental study provides insight to polymer dynamics in nanostructured environments and furthers the understanding of melt processing in polymers with nanoscale, high-aspect ratio fillers that form networks.

4:10 PM

**Solvent Studies on Submicron-Sized Aluminum/Epoxy Composites:** *S. Johnson*<sup>1</sup>; *Jared Boock*<sup>1</sup>; *Christopher Crouse*<sup>2</sup>; *C. Michael Lindsay*<sup>1</sup>; *Jennifer Jordan*<sup>1</sup>; *Jonathan Spowart*<sup>2</sup>; <sup>1</sup>Air Force Research Laboratory, Munitions Directorate, Eglin Air Force Base; <sup>2</sup>Air Force Research Laboratory, Materials and Manufacturing Directorate, Wright-Patterson Air Force Base

Composite materials processing often employs binders of polymeric epoxy systems that are highly viscous at lower temperatures. One processing technique utilized to reduce the viscosity of the polymer matrix is that of using solvents to facilitate incorporation of higher percentages of solids into the epoxy binder. This processing technique has been widely employed in the preparation of many types of composite samples without the benefit of comparing the properties of the composite materials processed both with and without solvents. Epoxy/Al composite materials obtained from commercially available epoxy resins and micron-/ nanometer-sized aluminum powders were prepared by decreasing mix viscosity with solvents of varying functional groups and volatilities. This study evaluates the impact of various solvents on the properties of the resultant composite materials. The chemical and mechanical properties of the resultant composites were evaluated and are reported.

## Neutron and X-Ray Studies of Advanced Materials: Diffuse Scattering

Sponsored by: The Minerals, Metals and Materials Society, TMS Structural Materials Division, TMS/ASM: Mechanical Behavior of Materials Committee, TMS: Advanced Characterization, Testing, and Simulation Committee, TMS: Titanium Committee  
Program Organizers: *Rozaliya Barabash*, Oak Ridge National Laboratory; *Yandong Wang*, Northeastern University; *Peter Liaw*, The University of Tennessee; *Jaimie Tiley*, US Air Force

Monday PM

February 16, 2009

Room: 3016

Location: Moscone West Convention Center

*Session Chairs:* *Rozaliya Barabash*, Oak Ridge National Laboratory; *Patrice Turchi*, Lawrence Livermore National Lab

2:00 PM Invited

**X-Ray Diffuse Scattering for The Study of the Size Distributions of Clustered Defects in Crystalline Materials:** *Bennett Larson*<sup>1</sup>; <sup>1</sup>Oak Ridge National Laboratory

The diffuse scattering near Bragg reflections arising from defect clusters in crystalline materials contains detailed signatures of the size, type, size-distribution, and the internal structure of clusters. In this presentation, the fundamental aspects of diffuse scattering from lattice defects will be considered within the coherent wave theory and the local-Bragg scattering interpretation in the so-called "asymptotic" diffuse scattering regime will be discussed. Detailed measurements of separate size distributions for vacancy and interstitial loops in neutron irradiated Cu and for coherent Co precipitates as a function of thermal aging in Cu(1%)Co single crystals will be presented. In addition, the use of submicron diameter x-ray microbeams to perform depth-resolved diffuse scattering measurements of vacancy and interstitial loop distributions in 10 MeV self-ion implanted silicon single crystals will be discussed. Research at ORNL supported by the DOE Office of Science, Basic Energy Sciences, Division of Materials Sciences and Engineering.

2:20 PM Invited

**Huang-Scattering as a Probe of Local Defect Structure:** *Branton Campbell*<sup>1</sup>; <sup>1</sup>Brigham Young University

Point-like crystal defects often give rise to anisotropic diffuse-scattering distributions that are centered around intense Bragg peaks in electron, x-ray and neutron diffraction data. These anisotropic Huang-scattering distributions are directly related to the long-range strain-fields extending outward from the defect core. By relating these strain fields to the atomic displacements within the defect core via the elastic dynamical matrix, Huang scattering can be used to indirectly probe local defect structure. We will present a convenient method of extracting local displacements from 3D Huang-scattering data that is sufficiently general to handle both arbitrary crystal symmetry and arbitrary defect symmetry. It involves first invoking the linear-continuum elastic approximation to characterize the strain fields, which are then used to extrapolate approximate local atomic displacements. In addition to exploring the strengths and limitations of this approach, we will demonstrate its application to the quantitative analysis of experimental diffuse scattering data.

2:40 PM

**Statistical Theory of Diffuse Scattering by Crystals with Nonrandom Precipitates:** *Rozaliya Barabash*<sup>1</sup>; *Gene Icel*<sup>1</sup>; <sup>1</sup>Oak Ridge National Lab

The statistical kinematical theory of diffuse scattering from precipitated alloys is reviewed. Nonperiodic potentials are used to model the scattering from different defect distributions. Fluctuating parts of the potential, resulting in diffuse scattering, is analyzed in the framework of the fluctuation wave method. Interaction of distortion fields from precipitates often causes their self-organization and nonrandom distribution. A comparison with the single defect approximation approach is performed for correlated/uncorrelated precipitates. Correlation and layered precipitates distribution in preferred crystallographic planes, results in specific features of the diffuse scattering intensity. The shape function of coherent precipitates is discussed. Experimental and simulated diffuse scattering intensity maps are used to perform quantitative characterization of the defects structure and distribution. Research is sponsored by the Division of Materials Sciences and Engineering, Office of Basic Energy Science U.S. Department of Energy.



**2:55 PM Invited****Elastic Diffuse Scattering of Binary Alloys with a Large Atomic-Size Difference:** *Bernd Schönfeld*<sup>1</sup>; <sup>1</sup>ETH Zurich

Alloys with local order and a relatively large difference in atomic sizes have continued to attract interest of theoreticians and experimentalists. Here, two such alloys, Ni-Re and Ni-Pt, were investigated experimentally. Not much is known on the microstructure in Ni-Re though its fraction in Ni-based superalloys has been steadily increased. From diffuse x-ray scattering of Ni-9.4 at.% Re in combination with small-angle neutron scattering it was now established that local order is present, characterized by 1/2 diffuse maxima. For the system Ni-Pt the superstructures Ni<sub>3</sub>Pt and NiPt are known; on the Pt-rich side, however, ordered structures are unknown. A diffuse x-ray scattering experiment of Ni-87.8 at.% Pt was undertaken to investigate the possible presence of NiPt<sub>7</sub>, suggested by electronic-structure calculations. With the interaction parameters obtained, Monte-Carlo simulations indicated that no NiPt<sub>7</sub> superstructure is to be expected. Species-dependent static atomic displacements also determined will be compared with values from the literature.

**3:15 PM Invited****Atomic Displacements on a Si-Ge Si Rich Single Crystal:** *Jose Rodriguez*<sup>1</sup>; *S. Moss*<sup>2</sup>; *J. Robertson*<sup>3</sup>; *Rozaliya Barabash*<sup>3</sup>; *J. Copley*<sup>4</sup>; *D. Neumann*<sup>4</sup>; <sup>1</sup>University of Maryland/National Institute of Standards and Technology; <sup>2</sup>University of Houston; <sup>3</sup>Oak Ridge National Laboratory; <sup>4</sup>National Institute of Standards and Technology

Si-Ge alloys have received a great deal of attention because of the possibility of faster devices that might employ them. However, the lattice mismatch between the two elements has made the growth of epitaxial homogeneous thin films quiet difficult and various strategies have been employed to overcome this. Le Bolloc'h et al. reported phonon measurements on a Si-Ge Si Rich single crystal. He also distinguishes in a radial scan of the elastic neutrons from the alloy the size effect displacement scattering. Using the Disk Chopper Spectrometer (DCS) at NIST we have measured the (110) and (001) planes which clearly shows the Huang Diffuse Scattering (HDS) and Size Effect scattering (SE) due to atomic displacements. The data also shows no SRO contribution. The data permits the extraction of HDS and SE displacements parameters. Phys. Rev. B 63, 035204 (2001).

**3:35 PM Invited****Structure and Dynamics of a Si-Rich SiGe Solid Solution:** *J. Robertson*<sup>1</sup>; <sup>1</sup>Oak Ridge National Lab

The SiGe system has been intensively studied because the carrier mobility is much higher than in pure silicon and this gives rise to considerable gains in electronic device performance. SiGe alloys have been the subject of intense investigation for several years. Several theoretical studies which are supported by a previous experiment on a polycrystalline solid solution predict a miscibility gap in the Si-Ge system. On the contrary, several long-range ordered structures have been reported in thin films although these were under either compressive or tensile strain as well as an XAFS study on SiGe thin films that indicates complete randomness. Thus, the study of the local atomic environments in this alloy is of fundamental importance. In this talk I will present the results of neutron and X-ray measurements on a homogeneous bulk crystal of Si<sub>92</sub>Ge<sub>8</sub> and discuss the nature of its structural disorder and dynamics.

**3:55 PM Invited****Small-Angle Scattering of X-Rays and Neutrons - Advances and Challenges:** *Gernot Kostorz*<sup>1</sup>; <sup>1</sup>ETH Zurich

Some applications of small-angle scattering in the field of materials science will be discussed. Emphasis will be on experiments pushing the spatial and temporal resolution limits of both types of radiation, exploiting their individual characteristics and their complementarity. Inhomogeneities on a scale from a few interatomic distances to several micrometers and their evolution can be studied in the bulk and at/near surfaces with good accuracy. These experiments serve to develop and test models of micro- and nanostructural features in materials.

**4:15 PM Break****4:25 PM Invited****"Small-Angle Scattering for Every Microstructure and Every Problem?" – A Critical Review of Advanced Small-Angle Scattering Techniques:** *Jan Ilavsky*<sup>1</sup>; <sup>1</sup>Argonne National Laboratory

Number of small-angle scattering tools and techniques – for both X-ray or neutrons – is available today. Since some of these were developed in the last years,

they may not be discussed in commonly available textbooks. Therefore many non-SAS expert researchers may not be aware of their advanced capabilities. Further, to learn these new tools and methods, one has to make use of original manuscripts, sometimes with sketchy techniques description and often-specific materials oriented. Therefore it may be difficult to generalize and apply these novel techniques to wider range of material science problems. This presentation will review different X-ray and neutron small-angle scattering techniques, such as anisotropic Porod scattering, anisotropic multiple scattering, and various types of ultra-small angle scattering. Examples of results, ranging from thermal barrier coatings to hierarchical polymer structures, will be given and applicability to assorted engineering material science problems will be discussed.

**4:45 PM Invited****Chemical Order in Alloys: Current Status and Prospect:** *Patrice Turchi*<sup>1</sup>; <sup>1</sup>Lawrence Livermore National Lab

The prediction of ordering trends in alloys provides valuable insight on phase formation, phase stability, and phase diagrams. In this context, neutron and X-ray scattering experiments can play a critical role in the verification and validation process, and also challenge theory. After a brief critical review of the quantum-mechanical-based approaches that are currently available for studying short-range order in alloys, examples of predictions will be discussed. They will include: transient ordering phenomenon, ordering in complex alloys such as A15 and sigma, pressure effect on chemical order, and ordering trends in some fcc and bcc-based alloys. This work was performed under the auspices of the U.S. Department of Energy by Lawrence Livermore National Laboratory under Contract DE-AC52-07NA27344.

**5:05 PM Invited****Phase Transitions in Ionic Liquid Based Mixtures Studied by Simultaneous X-Ray Diffraction and DSC Measurement:** *Hiroshi Abe*<sup>1</sup>; *Yusuke Imai*<sup>1</sup>; *Takefumi Goto*<sup>1</sup>; *Yukihiro Yoshimura*<sup>1</sup>; <sup>1</sup>National Defense Academy

Ionic liquids (ILs) are well known to be new solvents in "green chemistry". The curious nature of ILs is represented in almost zero vapor pressure. Recently, we found anomalous domain growth in [DEME][BF<sub>4</sub>]-H<sub>2</sub>O mixtures. Here, three different types of the domain structures were formed with a small content of H<sub>2</sub>O. In spite of a variety of domain formations, crystal structures are the same as pure [DEME][BF<sub>4</sub>]. In addition, boundaries between complicated domain structures could not provide intrinsic strains. Subsequently, complicated phase diagram is obtained from 0 to 12 mol% H<sub>2</sub>O. By simultaneous X-ray diffraction and DSC measurements, various kinds of phase transitions and phases are determined systematically. One of important solid phases is pure amorphous phase around 6 mol%. In Raman spectrum, there are "two dynamic components" in pure amorphous phase. Moreover, cold crystallization with some exothermal peak is observed upon heating above 4 mol%. The results are based on anomalous behaviors of water molecules. Y. Imai *et al.*, J. Phys. Chem. B (2008), in press. Y. Imai *et al.*, Chem. Phys. (2008), in press.

**5:25 PM Invited****From Average to Local Structure: A Structural Study of Zeolite-NdY/Se System:** *A. M. Milinda Abeykoon*<sup>1</sup>; *W. Donner*<sup>2</sup>; *M Brunelli*<sup>3</sup>; *A. J. Jacobson*<sup>1</sup>; *S. C. Moss*<sup>1</sup>; <sup>1</sup>University of Houston; <sup>2</sup>Darmstadt University of Technology; <sup>3</sup>European Synchrotron Radiation Facility (ESRF)

A challenging problem in crystal structure determination is the characterization of the atomic short-range order as observed in the diffuse scattering. The long-range order is characterized by a careful analysis of the sharp Bragg positions and intensities to obtain average atomic positions and equilibrium atom displacements. The short-range order appears as weak diffuse scattering widely distributed throughout the reciprocal space. Since many important crystalline materials have a significant disorder on the atomic scale, a method which is capable of modeling the structure of these materials is necessary. We emphasize the need of two techniques: the Pair Distribution Function (PDF) and the Rietveld method to model the structures of such systems. We will use our results of x-ray studies on zeolite-NdY/Se system to demonstrate this.

**5:45 PM****Small Angle X-Ray Scattering Studies of the Pore Structure in Metal and Metal Oxide Foams:** *Tony van Buuren*<sup>1</sup>; *Trevor Willey*<sup>1</sup>; *Alex Hamza*<sup>1</sup>; *Ted Baumann*<sup>1</sup>; *John Kinney*<sup>1</sup>; *James Stoken*<sup>1</sup>; *Jan Ilavsky*<sup>2</sup>; <sup>1</sup>Lawrence Livermore National Laboratory; <sup>2</sup>Advanced Photon Source

Although a great amount of study has been devoted to the physical properties of porous structures, it is not clear whether the theoretical models developed

to date can be extended to nanoscopic length scales. Our goal is to quantify the microstructure of highly porous metals and metal oxides to determine how processing of the porous material relates to the structure and ultimately to the mechanical behavior. We will quantify structural changes with a combination of small angle x-ray scattering (SAXS) and high-resolution x-ray imaging. Finite element modeling, using the structures determined above, will be used to study the effects of mechanical loading on the cell structures, and to map out relationships between processing, density, and strength. This work is supported by the US-DOE, under contract DE-AC52-07NA27344, LLNL. APS is supported by the U.S. DOE, BES, Office of Science under contract No. W-31-109-ENG-38.

## Pb-Free Solders and Emerging Interconnect and Packaging Technologies: Electromigration Reliability

Sponsored by: The Minerals, Metals and Materials Society, TMS Electronic, Magnetic, and Photonic Materials Division, TMS: Electronic Packaging and Interconnection Materials Committee

Program Organizers: Sung Kang, IBM Corp; Iver Anderson, Iowa State University; Srinivas Chada, Medtronic; Jenq-Gong Duh, National Tsing-Hua University; Laura Turbini, Research In Motion; Albert Wu, National Central University

Monday PM  
February 16, 2009

Room: 2020  
Location: Moscone West Convention Center

Session Chairs: C Robert Kao, National Taiwan University; Albert Wu, National Central Univ

### 2:00 PM Invited

#### Stress-Migration Induced by Electromigration in Flip Chip Pb-Free Solder Joints: King-Ning Tu<sup>1</sup>; <sup>1</sup>University of California

Abstract: Due to the unique line-to-bump configuration of flip chip, current crowding occurs at the location where the current enters or leaves the solder bump. At the anode, a concentration of compressive stress occurs due to electromigration. The concentrated compressive stress can squeeze out a Sn whisker or hillock, even at temperatures above 100°C. To investigate the stress-migration driven by electromigration, x-ray diffraction by micro beam synchrotron radiation has been performed. Transient stress build-up in the Sn matrix was detected. Since Cu diffuses interstitially in Sn and is much faster than self diffusion of Sn in Sn, intermetallic compound (IMC) formation of Cu-Sn in the anode region has been found. While the IMC may increase the compressive stress, it also may block the diffusion of Sn and slow down the growth of whisker and hillock.

### 2:20 PM

#### In Situ Study of Electromigration-Induced Orientation Evolution in Pb-Free Solder Joint by Synchrotron Microdiffraction: Kai Chen<sup>1</sup>; Nobumichi Tamura<sup>1</sup>; King-Ning Tu<sup>2</sup>; Yi-Shao Lai<sup>3</sup>; <sup>1</sup>Lawrence Berkeley National Laboratory; <sup>2</sup>UCLA; <sup>3</sup>Advanced Semiconductor Engineering

The rotation of Sn grains in Pb-free flip chip solder joints hasn't been reported in literature so far although it has been observed in Sn strips. In this letter, we report the detailed careful study of the grain orientation evolution induced by electromigration by synchrotron radiation based white beam X-ray microdiffraction. It is found that the grains in solder joint rotate much slower than in Sn strip even if under higher current density. On the other hand, based on our estimation, the reorientation of the grains in solder joints also results in the reduction of electric resistivity, similar to the case in Sn strip, although the change is not detected experimentally. We will also discuss the reason why the electric resistance decreases much more in strips than in the Sn-based solders, and the different driving force for the grain growth in solder joint than in thin film interconnect lines.

### 2:35 PM

#### The Direct Measurement of Stress Distribution on Silicon under Thermal Effect and Electromigration in Flip Chip: Albert Wu<sup>1</sup>; Chun-Yang Tsai<sup>1</sup>; <sup>1</sup>National Central University

The reliability of the flip chip is affected by electromigration or thermal stress. The variation of stress on silicon chip was directly measured by in-situ synchrotron X-ray. The minute variation of stress level in the solder strips could be resolved by high brightness synchrotron source. The flip chip samples were

stressed under various temperatures and current densities. At the edge of the silicon chip, the stress level is the highest at the center than at the edge. The simulation results is provided for the discussion in this paper.

### 2:50 PM

#### Electromigration in Tin-Copper, Tin-Silver, and Eutectic Tin-Lead Flip Chip Solder Joints: Luhua Xu<sup>1</sup>; Jarrett Liang<sup>1</sup>; Jung-Kyu Han<sup>1</sup>; Yi-Shao Lai<sup>2</sup>; K.N. Tu<sup>1</sup>; <sup>1</sup>University of California, Los Angeles; <sup>2</sup>Advanced Semiconductor Engineering

A comprehensive study of the electromigration reliability of SnCu, SnAg, and eutectic SnPb flip chip solder joints with and without thick UBM at the chip side is reported. The samples were stressed at multiple high temperatures and current densities. The polarity effects on intermetallic compound (IMC) growth and metallization consumption were characterized for both powered and un-powered solder joints. The un-powered solder joints exhibited slower growth in IMCs as well as minor consumption of copper metallization. However, due to thermal gradient from chip to substrate, it also shows polarity phenomena. The powered joints exhibited microstructural changes consistent with a directional diffusion guided by electron wind. Namely, the copper metallization at the cathode experienced accelerated consumption. The propagation of pancake voids was observed in detail, from initiation under the passivated area, to partially propagating across the aluminum line opening, and to complete propagation.

### 3:05 PM

#### Effects of Current Density, Environment, and Temperature on Adhesion and Debonding Kinetics of Cu / Barrier Interfaces: Ryan Biringier<sup>1</sup>; Roey Shaviv<sup>2</sup>; Reinhold Dauskardt<sup>1</sup>; <sup>1</sup>Stanford University; <sup>2</sup>Novellus Systems Inc.

It is widely accepted that electromigration in modern Cu interconnects is closely related to adhesion and bonding between the Cu line and the top capping layer. While four-point bend thin-film adhesion techniques are commonly used to characterize adhesion in Cu / barrier layer interfaces, the kinetics of sub-critical interface debonding in these films has been largely ignored. In the present study, we propose a new technique for characterizing the kinetics of EM void growth. The method is based on modified versions of well-known thin-film adhesion techniques and is used to quantify sub-critical debonding between Cu and selected barrier layers in the presence of variable current density through the film, environment, and temperature. Selected barrier materials include SiC, SiN, and CoWP. The sub-critical debonding kinetics of these barrier films are largely influenced by the environment, and the sub-critical debonding mechanisms present in ambient, forming gas, and noble gas environments are compared.

### 3:20 PM

#### The Study of Flip Chip Electromigration under Extra High Current Density: Yu-Wei Lin<sup>1</sup>; Jia-Hong Ke<sup>1</sup>; C. Kao<sup>1</sup>; Yi-Shao Lai<sup>2</sup>; <sup>1</sup>National Taiwan University; <sup>2</sup>Advanced Semiconductor Engineering, Inc.

The electromigration failure mechanism in flip chip solder joints under extra high current density ( $>1 \times 10^4$  A/cm<sup>2</sup>) was studied. It is known that the joint temperature under current stressing is strongly associated with the applied current density due to Joule heating effect. Hence, the heat generation and dissipation was found to be a very important factor on the final failure mechanism. In this study, two experimental setups were used. One was with a cooling system to make the chip temperature constant, and the other was not. Without cooling, the temperature increased while increasing the applied current. When the current density was up to  $5 \times 10^4$  A/cm<sup>2</sup>, rapid failure was caused by excessive Joule heating. With cooling, more time to failure was experience at the same current density. Therefore, this method provided a way to de-couple the applied current density and the device temperature.

### 3:35 PM

#### Effect of UBM on Electromigration Lifetime of SnAg Solder Joints: Hsiao-Yun Chen<sup>1</sup>; Chih Chen<sup>1</sup>; <sup>1</sup>NCTU

Electromigration in flip chip solder joints is investigated under current stressing at 135, 150 and 165°C. By using Kelvin probe, the failure time can be defined as bump with current stressing down by increasing 20% of its original value, therefore direct comparison between 3- $\mu$ m Cu and 5- $\mu$ m Cu/3- $\mu$ m Ni UBM systems can be accomplished. Additionally, by using Al trace TCR effect, it is possible to measure the real stressing temperature. It is found that the solder joints with the 5- $\mu$ m Cu/3- $\mu$ m Ni UBM have longer electromigration lifetime. The Ni layer may retard the electromigration failure since it is a good diffusion barrier for Cu. Furthermore, the Ni layer may relieve the current crowding effect.

Three-dimensional simulation on current density distribution has been carried out for these two systems and the results will be presented in the conference.

### 3:50 PM Break

### 4:05 PM Invited

**Comprehensive Studies on Microstructural Evolution from Current Stressing:** Y.C. Lee<sup>1</sup>; Cheng-En Ho<sup>2</sup>; K. Subramanian<sup>1</sup>; Andre Lee<sup>1</sup>; <sup>1</sup>Michigan State University; <sup>2</sup>Yuan Ze University

Imposition of high current densities causes material migration due to momentum transfer between electrons and atoms/ions. A clear quantitative understanding of the events that occur under such conditions, especially in multi-phase materials, is far from complete due to several geometry related constraints. Recently, our group has developed a realistic joint configuration to avoid unnecessary complications due to current crowding with the ability to impose a well-described thermal environment. Using these joints effects of current density and temperature on microstructural evolution in two-phase electronic solder joints were studied by Synchrotron X-rays and by Confocal Laser Scanning, Optical, and Scanning Electron Microscopies. These studies have provided unique opportunities to address materials movement, microstructure evolution, as well as solid-state reactions, due solely to the influence of current stressing. Critical current densities at various temperatures for evolution and extents of such events, under various current stressing scenarios were evaluated.

### 4:25 PM

**In-Situ Observation of Stress Evolution on Solder Strips under Electromigration:** Albert Wu<sup>1</sup>; Ciao-Nan Siao<sup>1</sup>; <sup>1</sup>National Central University

Synchrotron radiation x-ray diffraction was employed for in-situ observation of stress evolution on solder thin film strips under various temperatures and current densities. The minute variation of stress level in the solder strips could be resolved by high brightness synchrotron X-ray. The tensile stress at the cathode and the compressive stress at the anode degraded with time. The kinetics of the atomic diffusion under electron wind forces and the consequent stress distribution is measured; the relationship between the variation of morphology and the changes in the stress level is discussed in this paper.

### 4:40 PM

**Electromigration-Induced Failures at Cu/Sn/Cu Flip-Chip Joint Interfaces:** Hua-wei Tseng<sup>1</sup>; Chengyi Liu<sup>1</sup>; <sup>1</sup>National Central University

EM-induced failure modes at Cu/Sn/Cu solder joint interfaces were studied. Since the geometry of the flip-chip solder joint, the current density would vary in the both joint interface. Depending on the current-stressing density, different EM-induced failure modes were observed at the cathode joint interface; EM-induced dissolution at the high current stressing site and voiding at the low current stressing site. At the opposite anode interface, Kirkendall void formation also varies with the current distribution. At current crowding site, the current exiting corner, a serious Kirkendall voiding coalesced into a gap between the Cu<sub>3</sub>Sn/Cu interface. The Cu consumption activation energy without current stressing was determined in this work. With current stressing, the Cu consumption activation energy decreased. We believe that the enhancement of Cu consumption by current stressing is due to the Cu atoms dissolved in the Sn to electromigrate instantaneously toward the anode side.

### 4:55 PM

**Study of Electromigration Phenomena in Ultra-Thin Lead-Free Solder Joints:** Cheng-En Ho<sup>1</sup>; Wei-Hsiang Wu<sup>1</sup>; <sup>1</sup>Yuan Ze University

Traditional flip-chip solder joints have a line-to-bump configuration consisting of a solder bump with ~100 microns in height and electric circuits with few microns in thickness. Because of the huge divergence in the cross-section between circuit/bump and the electric current takes a ~90-degree turn at the contact, there will be a significant current crowding at the cathode side of solder, where a localized high current density induced a massive electromigration may occur. Failures in the joints resulted from such the current crowding effect mainly included void nucleation and propagation, local melting of solder, and rapid dissolution of metallization pads. To minimize the damages, modification of Cu pillars with ultra-tin solder bumping (20 microns) is being attempted by industry recently. However, little research has been devoted to evaluate its reliability. This study is aimed at gaining a better understanding of electromigration behaviors in lead-free solder joints with ultra-tin solder thicknesses.

### 5:10 PM

**Study of Electromigration-Induced Failures on Ni/Cu Bi-Layer Bond Pad:** Yu-Hsiang Hsiao<sup>1</sup>; Chengyi Liu<sup>1</sup>; <sup>1</sup>National Central University

EM (electromigration) on Sn(Cu)/Ni/Cu solder joints under 104 A/cm<sup>2</sup> at 160° were studied. For the pure Sn/Ni/Cu case, the interfacial compound layer is mainly Cu<sub>6</sub>Sn<sub>5</sub> compound phase. Under EM effect, the interfacial compound Cu<sub>6</sub>Sn<sub>5</sub> compound phase layer would suffer serious EM-induced dissolution. (2) Sn(Cu) alloys, i.e., Sn<sub>0.7</sub>Cu and Sn<sub>3.0</sub>Cu, formed a (Cu,Ni)<sub>6</sub>Sn<sub>5</sub> interfacial layer at the joint interfaces. The interfacial (Cu,Ni)<sub>6</sub>Sn<sub>5</sub> compound layer shows a stronger resistance to the EM-induced dissolution. The interfacial (Cu,Ni)<sub>6</sub>Sn<sub>5</sub> compound layer grows with the current stressing time in the Sn<sub>0.7</sub>Cu/Ni/Cu case.

### 5:25 PM

**In-Situ Studies of Electrical Current Induced Whiskers:** Andre Lee<sup>1</sup>; K. Subramanian<sup>1</sup>; Cheng-En Ho<sup>2</sup>; Wenjun Liu<sup>3</sup>; <sup>1</sup>Michigan State University; <sup>2</sup>Yuan Ze University; <sup>3</sup>Argonne National Laboratory

Use of high Sn solders for removing Pb from electronic packages has brought about concerns due to the spontaneous growth of metallic whiskers. Although Sn is known to spontaneously form whiskers, the formation and growth of Sn whiskers have never been observed in-situ, due to lack of knowledge of the exact causes and conditions for their formation and growth. Our recent studies on electrical current induced material movements have led us to design a package to study spontaneous formation and growth of Sn whiskers. This package facilitates formation of optically visible whiskers with a constant current of 0.2 amps at room temperature within 3 hours. Such conditions enable in-situ investigations of whisker formation and growth. Micro diffraction X-rays at APS was used to examine the evolution of grain structure, strain distribution during whisker growth in matte Sn coatings at various amplitudes of externally applied electric current and temperatures.

### 5:40 PM

**Electromigration Study of Eutectic SnPb Flip-Chip Solder Joints on Ceramic Substrates:** Chung Kuang Lin<sup>1</sup>; Chih Chen<sup>1</sup>; <sup>1</sup>National Chiao Tung University

This study investigates electromigration study of eutectic SnPb flip-chip solder joints on ceramic substrates. The under bump metallization (UBM) structure consists of 5- $\mu$ m Cu / 3- $\mu$ m Ni under bump metallization (UBM). Under the current stressing by 0.9A at 150°C, we did not find void formation but a large amount of intermetallic compound (IMC) of Cu<sub>6</sub>(Sn,Ni)<sub>5</sub> were formed when the bump resistance increased 10 m $\Omega$ . Three-dimensional electrical simulation by finite element analysis was carried out to simulate the current density distribution in solder joints with slit Cu traces. It is found that the current density was almost uniformly distributed in solder joint for this structure. It is found that the bump resistance only increases 0.07m $\Omega$  when half of the solder bump was transformed into Cu<sub>6</sub>Sn<sub>5</sub> IMC. The reason for the low crowding effect in the solder joints will be discussed in the conference.

### 5:55 PM

**Effective Charge of Electromigration from the Perspective of Electromagnetism:** Peng Zhou<sup>1</sup>; William Johnson<sup>2</sup>; <sup>1</sup>University of California Irvine; <sup>2</sup>University of Virginia

The mechanism of electromigration is discussed from the perspective of electromagnetism, other than from the traditional view of momentum exchange owing to the collision between electrons and diffusing atoms. It is suggested that the energy associated with electromigration is related to the work done by the electromagnetic fields, and conversion of the non-electrostatic energy, which is transferred by the Poynting's vector from the electric power source, into the chemical energy of the diffusion system. It is also suggested that the momentum transferred to the diffusing atoms is related to the Maxwell stress; at low temperatures, the momentum is transferred via Maxwell stress to the chemical impurities and crystal imperfections to give rise to the "polarity effect". It is shown from the perspective of electromagnetism, the effective driving force of electromigration has a square dependence on the current density; therefore, the effective charge number is linearly related to the current density.



## Peirce-Smith Converting Centennial Symposium: Operational Aspects

Sponsored by: The Minerals, Metals and Materials Society, TMS Extraction and Processing Division, TMS: Pyrometallurgy Committee  
Program Organizer: Joël Kapusta, Air Liquide

Monday PM  
February 16, 2009

Room: 2009  
Location: Moscone West Convention Center

Session Chairs: Anthony Warner, WorleyParsons HGE; Phillip Mackey, Xstrata Nickel

### 2:00 PM Keynote

#### A Century of Converter Operation in Vale Inco's Ontario Operations: Samuel Marcuson<sup>1</sup>; <sup>1</sup>Vale Inco Ltd

Smelting of nickel-copper sulfide ores at Vale Inco's Sudbury operations commenced in 1888 and the first converting plant went into operation in 1892. As the demand for nickel grew, the smelting operations expanded and by the 1960's the Copper Cliff Smelter featured the longest converter aisle in the world with space for nineteen Peirce-Smith converters. During this long period, different converting techniques and vessels were employed. The evolution of converting is reviewed with special emphasis on the modifications made to the Peirce-Smith vessel to accommodate the metallurgical and process needs of the changing times.

### 2:30 PM

#### Converting and Casting at Boliden's Rönnskär Smelter 2009 - An Update: Peter Olsson<sup>1</sup>; Magnus Ek<sup>1</sup>; <sup>1</sup>Boliden Mineral AB

The Rönnskär Smelter has been faithful to Peirce Smith Converting during its 79 years of existence. Though a visitor to our smelter museum will easily find out that a lot has happened since the beginning – and development continues. In this paper an update on Converting and Casting at the Rönnskär Smelter is presented. Recent developments include an investment into converter process gas handling, but also day-to-day operational aspects such as converter aisle productivity and flexibility, but also minimal EH&S impact.

### 2:50 PM

#### Environmental Situation and Enhanced Productivity at Norddeutsche Affinerie AG: Thomas Buenger<sup>1</sup>; <sup>1</sup>Norddeutsche Affinerie AG

The Hamburg smelter of Norddeutsche Affinerie AG is situated near downtown of the city of Hamburg and is therefore a special subject to fulfill environmental requirements according to the German legal regulations. Therefore are investments into increased concentrate throughput every time linked to packages to enhance the emission situation of the smelter. This connection in between environment protection and productivity enhancement should be explained by the example of the Peirce-Smith converter plant of the Hamburg smelter. As an outstanding investment this can be shown on hand of the transition of scrap charging via boot from the front side to a fully automatic and completely sucked scrap charging system.

### 3:10 PM

#### Evolution of the Converter Aisle at Xstrata Nickel's Sudbury Smelter: Bryan Salt<sup>1</sup>; Enrico Cerilli<sup>1</sup>; <sup>1</sup>Xstrata Nickel

Xstrata Nickel's Sudbury Smelter has systematically developed its converting aisle from a single stage to a counter current multi stage converting process. This has required the development of two unique converters: the slag cleaning vessel and the slag make converter. This has resulted in a unique three stage converting process that enables treatment of secondary materials as well as resulting in a slag that can be discharged without further treatment. The paper will also discuss future changes currently being considered to further improve environmental, plant hygiene and productivity performance.

### 3:30 PM Break

### 3:50 PM

#### Recent Operation and Improvement at the Sumitomo Toyo Peirce-Smith Converters: Kazuhiro Mori<sup>1</sup>; Katsuhiko Nagai<sup>1</sup>; Kosei Morita<sup>1</sup>; Osamu Nakano<sup>1</sup>; <sup>1</sup>Sumitomo Metal Mining Company, Ltd.

The Sumitomo Toyo Smelter and Refinery commenced operations in 1971 with three Peirce-Smith (PS) converters in operation. At the time, a "2 hot1

blowing" sequence was adopted (two vessels hot, one blowing and the third unit under repair), with in-stack times reaching 90%, producing five charges per day. Under the 2001 expansion program at the plant, a new "2 hot-2 blowing" operational pattern was adopted at the converters along with the installation of additional converter blowers and crane. In 2005, a fourth converter was installed and a "3 hot-2 blowing" operation commenced. Along with improvements in the anode department, the converters now produce over eight charges per day. The control of sulphur dioxide fugitive gas at the converters has also advanced, and the sulphur fixation rate at Toyo now exceeds 99.9%. This paper discusses the Toyo converter operation and describes improvements in environmental management techniques used at the plant.

### 4:10 PM

#### Changing Reality: Continuous Production Control for Optimized Productivity: Wilhelm Wendt<sup>1</sup>; Willy Persson<sup>1</sup>; <sup>1</sup>Semtech Metallurgy AB

With rising price of raw materials and increasing energy and environmental restrictions the optimization of pyrometallurgical processes beyond what can be achieved via modelling and operator experience has come more and more into focus and led to a quest for methods for dynamic process control. Independent of the details of the control mechanism it has to be based on real-time information on the status of the process. Since mid 1990s Semtech OPC Systems are in routine use at a number of smelters to provide continuous on-line information on the instantaneous status of converting processes in Peirce-Smith converters. This information offers an opportunity for the operators to maintain / bring back the process to the desired route. This presentation will discuss experiences from applications to converting of copper and nickel in Peirce-Smith converters. Special emphasis will be laid on de-bottlenecking, e.g., in concentrate injection, revert accumulation, magnetite handling and oxide-skim transfer.

### 4:30 PM

#### The Use of Injection Tuyeres Clad Welding with Anti-Abrasive in the Teniente Converter: Luis González M.<sup>1</sup>; Juan C. Davis C.<sup>1</sup>; Guillermo Guzman D.<sup>1</sup>; <sup>1</sup>Ventanas Smelter and Refinery, Codelco-Chile

The Teniente converter (CT) of the Ventanas Smelter and Refinery of Codelco-Chile has two tuyeres for dry concentrate injection directly into the melt. The diluted phase injection system can feed 15 to 20 kg of concentrate for 1 kg of air, which creates a very abrasive solid/gas phase. The tuyeres commonly used lasted for about 3.5 days due to the accelerated decay of the shell, and 1.5 hours were necessary for the replacement of new ones in the reactor. Tests were carried out with common shell tuyeres with a tungsten based welding cover, and a life span of 28 days was reached, increasing the Teniente converter operational continuity between 1.5 to 2 %.

### 4:50 PM

#### Full Utilization of the Matte Converting Process Energy for Operating Conditions of the RTB Bor: Bogdan Petkovic<sup>1</sup>; Boban Todorovic<sup>1</sup>; <sup>1</sup>RTB Bor, TIR Bor, Topionica

In the early 90's a completely unknown problem was encountered at the converter Department: it was a chronic shortage of the cold copper charge needed for the second operating period. A high temperature operating regime was caused which further provoked a chain of consequences such as a drastic drop of the number of operations in campaigns. The consumption of repair bricks reached the quantity of 8.3955 kg / tonne of anode Cu. In 1994, we won the process of cold material smelting during the "copper" blowing [2]. The number of operations per campaign reached 180-200 again. Also in 1994 we won the process of smelting cold materials to obtain "tin" blowing with the purpose of completing their processing cycle [2]. During the period 1994 – 2007 a total of 107,845 tonnes of cold material were remelted to make copper and 56,794 tonnes were re-smelted to obtain "tin". Upon synthesizing these two processes, a completely new model was achieved in 2005, by Bogdan Petkovic, which entirely utilized all available energy of the Peirce-Smith (PS) converters of the Bor Copper Smelter and now represents the basis of the time cycle. The cold material now enters the converter plant, copper recovery is increased and the method itself is environmentally friendly.

### 5:10 PM

#### Recent Operations of Peirce-Smith Converters in Pirdop Smelter: Evgeni Marinov<sup>1</sup>; Ivailo Vasilev<sup>1</sup>; Dimo Kirilov<sup>1</sup>; <sup>1</sup>Cumerio

The Pirdop Smelter was privatized by the Bulgarian government in September 1997. Since then, an investment program has been implemented to increase capacity to 290,000 tpy of copper, while improving the environmental

performance. A significant part of this investment program involved reconstruction of the three Peirce-Smith converters and gas handling system. Between June 2000 and April 2002, converter capacity was increased and primary gas collection systems at the Converters Section were upgraded. The result was a significant reduction in emissions. From 2002 until present, a continuous improvement of operating and environmental performance has been achieved. In 2005, Pirdop received from the Bulgarian Government the Complex Permit under the EU IPPC criteria. An Environmental Compliance Program was accordingly defined aiming for reduction in secondary emissions. In November 2007, a Secondary Gases Cleaning plant was put into operation. This paper describes these projects and the challenges faced by the company.

## Phase Stability, Phase Transformations, and Reactive Phase Formation in Electronic Materials VIII: Session II

Sponsored by: The Minerals, Metals and Materials Society, TMS Electronic, Magnetic, and Photonic Materials Division, TMS: Alloy Phases Committee  
 Program Organizers: Chih-ming Chen, National Chung-Hsing University; Srinivas Chada, Medtronic; Sinn-wen Chen, National Tsing-Hua University; Hans Flandorfer, University of Vienna; A. Lindsay Greer, University of Cambridge; Jae-ho Lee, Hongik University; Daniel J. Lewis, Rensselaer Polytechnic Institute; Kejun Zeng, Texas Instruments; Wojciech Gierlotka, AGH University of Science and Technology; Yee-wen Yen, National Taiwan University of Science and Technology

Monday PM Room: 2022  
 February 16, 2009 Location: Moscone West Convention Center

Session Chairs: Hans Flandorfer, University of Vienna; Wojciech Gierlotka, AGH University of Science and Technology

### 2:00 PM Invited 2009 Hume Rothery Award Recipient

**Alloy Phase Metastability and Microstructure:** *John Perepezko*<sup>1</sup>; <sup>1</sup>University of Wisconsin

Alloy phase stability is usually analyzed on the basis of the most stable structure for a given composition as guided by the Hume-Rothery rules and recent first principle calculations. However, some of the most interesting and useful phase reactions involved in microstructure development are based upon metastable structures. Metastability can develop in many processing routes where the initial phase is subjected to high supersaturation, pressure, undercooling or high defect concentration conditions that are encountered in nucleation processes. In these cases, the initial microstructure phase selection is directed by metastable phases and their relaxation towards equilibrium. While metastable structures are often not retained in the final microstructure in bulk volumes, they can still play a role as precursor structures and can be dominant in nanoscale volumes. Several examples from solidification, interface controlled reactions, precipitation and severe plastic deformation are discussed to illustrate the role of metastable alloy phases in microstructure development.

### 2:20 PM Invited

**Development of Thermodynamic Database for Cu-Base Alloy Systems and Micro-Solders:** Ikuo Ohnuma<sup>1</sup>; Yoshikazu Takaku<sup>1</sup>; Cui Ping Wang<sup>2</sup>; Xing Jun Liu<sup>2</sup>; Kiyohito Ishida<sup>1</sup>; <sup>1</sup>Tohoku University; <sup>2</sup>Xiamen University

The thermodynamic database for Cu-base alloys and micro-solders have been constructed by the CALPHAD (Calculation of Phase Diagrams) method. Based on the thermodynamic assessments on the Cu-X binary and Cu-X-Y ternary systems, the phase diagrams and thermodynamic properties of Cu-base multi-components systems which includes eleven elements of Cu, B, C, Cr, Fe, Ni, P, Si, Sn, Ti and Zn can be calculated. The solder database for eight elements of Ag, Bi, Cu, In, Pb, Sb, Sn and Zn have also been developed, which can be utilized for all combinations of elements and all composition ranges. The elements of Al, Au and Ni are also available for the calculation in the limited composition ranges. The typical examples of the calculations and applications will be presented.

### 2:40 PM

**Au-Sn-Based Lead-Free Solder Alloys:** *Leszek Zabdyr*<sup>1</sup>; Anna Wierzbicka-Miernik<sup>1</sup>; Joanna Wojewoda-Budka<sup>1</sup>; Pawel Zieba<sup>1</sup>; <sup>1</sup>Polish Academy of Sciences

Three invariant transition reactions were found among other features of the calculated poly-thermal projection of the liquidus surface close to Sn-corner of the

system at temperatures: 252, 289 and 305C, respectively. That and the relatively low gold content makes them the potential candidates as high-temperature lead-free solder materials. Alloy samples of three invariant compositions were prepared, and temperatures of solid-liquid equilibria were determined by DSC and DTA to confirm results of calculations. Structure and chemical composition were then examined using SEM-EDS device. Surface tension was calculated for the invariant liquids using Butler approach. Solid alloys of compositions under accord were used to prepare solder joints on copper substrates. Shear test and microhardness measurements were performed, and cross-section through the joints were analysed by SEM-EDS to give an idea about structural characteristic of joint material and possible interaction with substrate material.

### 2:55 PM

**Thermodynamic Modeling Studies of the Cu-In and Sn-In-Cu Systems:** *Wojciech Gierlotka*<sup>1</sup>; Sinn-wen Chen<sup>2</sup>; Shih-kan Lin<sup>2</sup>; <sup>1</sup>AGH University of Science and Technology; <sup>2</sup>National Tsing Hua University

Sn-Cu-In ternary system is of interests for lead-free solder applications. A thermodynamic model of this ternary system is developed using the CALPHAD method based on the experimental results in the literature as well as those obtained in this study. In addition to the terminal phases and binary compounds, at 160°C there are one continuous solid solution formed between the  $\eta$ -Cu<sub>6</sub>Sn<sub>5</sub> and  $\eta$ -Cu<sub>2</sub>In, and the  $\delta$  1-Cu<sub>41</sub>(Sn,In)<sub>11</sub> phase. The binary Cu-In system has been remodeled and the homogeneity ranges of the compounds have been described by the sublattice models similar to those used in the Cu-Sn system. Results of the calculation in the ternary system, such as thermodynamic properties of liquid and solid phases, isothermal and isopleths sections, and liquidus projections are compared with the experimental data.

### 3:10 PM

**Size and Substrate Effects upon Undercooling of Pb-Free Solders:** *Yu-chih Huang*<sup>1</sup>; Kuang-siang Wu<sup>1</sup>; Sinn-wen Chen<sup>1</sup>; <sup>1</sup>National Tsing Hua University

The melting and solidification temperatures of solders and solders on substrates are determined using differential scanning calorimetry. The solders are Sn, Sn-0.7wt%Cu, Sn-3.5wt%Ag and Sn-3.8wt%Ag-0.7wt%Cu solders, and the substrates are Ni, Cu and Ag. The heating and cooling rates are 10°C/min. The solders are of two different sizes, 5mg and 1mg. With repeated DSC measurements, the statistical distributions of degrees of undercooling are determined. The degrees of superheating are less than 2 degrees at 10°C/min heating rate and are negligible comparing with the degrees of undercooling which could be as significant as 56 degrees. Undercooling is more significant and variation is larger when the solders are of smaller sizes. The undercooling of solders on substrates is less significant than that of solders alone. Among the three kinds of substrates, solders on Ni are with the least undercooling.

### 3:25 PM Break

### 3:45 PM Invited

**Experimental Methods to Determine Thermodynamic Properties:** *Adolf Mikula*<sup>1</sup>; <sup>1</sup>University of Vienna

For phase stability, phase transformation the thermodynamic properties of the materials involved, must be known. No calculation of phase diagrams, viscosity, surface tension can be carried out without the knowledge of the partial or integral thermodynamic properties. In this lecture it will be demonstrated what type of experimental methods are available and what kind of data we get from different experiments and how reliable these data are. On a few examples it will be shown, how these data are used to calculate different properties of electronic materials.

### 4:05 PM Invited

**Solidification Behavior of Cu-Ni-Sn:** *Hans Flandorfer*<sup>1</sup>; Clemens Schmetterer<sup>1</sup>; Herbert Ipser<sup>1</sup>; <sup>1</sup>University of Vienna

Knowledge about the intermetallic system Cu-Ni-Sn is highly important for nickel-bronze alloys with additions of tin and for lead-free soldering as it concerns the majority of solder/substrate interactions of hitherto used lead-free solders. Detailed information to the solidification and formation of ternary phases is a crucial point for the control of the microstructure and texture of alloys and alloy interfaces. The system Cu-Ni-Sn was investigated by means of XRD, DTA and metallography including EPMA techniques. The occurrence of ordering phenomena at Cu<sub>2</sub>NiSn along (Ni<sub>x</sub>Cu<sub>1-x</sub>)<sub>3</sub>Sn and at Cu<sub>4</sub>Ni<sub>2</sub>Sn<sub>5</sub> along (Ni<sub>x</sub>Cu<sub>1-x</sub>)<sub>6</sub>Sn<sub>5</sub> has been described in literature. The enthalpy of formation of alloys along these sections was determined by tin solution calorimetry. Ordering should be indicated by a significant deviation from linearity of the respective

delta $\tau$  versus xCu (or xNi) curves. According to our results no such behavior could be observed.

#### 4:25 PM

**Investigation of Various Properties of Lead Free Solders:** *Michael Hindler*<sup>1</sup>; Sabine Knott<sup>1</sup>; Zuoan Li<sup>2</sup>; Clemens Schmetterer<sup>1</sup>; Peter Terzieff<sup>1</sup>; Adolf Mikula<sup>1</sup>; <sup>1</sup>Universitaet Wien; <sup>2</sup>University of Oslo

Different properties of various lead free solders have been investigated. The wetting angles, viscosity, surface tension and thermodynamic properties of Ag-Cu-Sn, Ag-Bi-Sn, Ag-Au-Sn, Au-Cu-Sn and Pd-Sn-Zn have been determined. The thermodynamic properties of the ternary Ag-Au-Sn, Au-Cu-Sn, and Pd-Sn-Zn systems have been determined with the EMF method with a liquid electrolyte as well as with a Calvet type calorimeter. With the data obtained by the calorimetric method the viscosity of the Ag-Au-Sn system has been calculated using the model of Iida et al. The surface tension of the Ag-Bi-Sn and the Ag-Au-Sn system was calculated and will be presented. Additional results of the wetting angle of the Ag-Cu-Sn alloy with various compositions on copper and nickel substrate, as well as the temperature dependency of the wetting angles and some intermetallic structures will be presented.

#### 4:40 PM

**Development of Pb-Free Heat Resistant Joints Using Sn-Bi and Ag Powders:** *Yoshikazu Takaku*<sup>1</sup>; Yuki Sakurada<sup>2</sup>; Ikuo Ohnuma<sup>1</sup>; Kiyohito Ishida<sup>1</sup>; <sup>1</sup>CREST-JST, Tohoku University; <sup>2</sup>Tohoku University

TLPS (Transient Liquid Phase Sintering) is a candidate method of heat-resistant jointing, which makes use of the reaction between low-melting temperature powder (P1) and reactive powder (P2). During heat treatment above the melting temperature of P1, the molten P1 reacts rapidly with the solid P2, which results in the formation of intermetallic compound (IMC). In this study, the TLPS properties of a combination of eutectic Sn-Bi and Ag powder were investigated. During differential scanning calorimetry measurement, an endothermic reaction occurred at the eutectic temperature of the Sn-Bi (139°C), followed by an exothermic reaction at about 220°C, which was caused by the formation of the Ag<sub>3</sub>Sn IMC and Bi-rich solid solution phases. After the overall measurement, the reactant contained the Ag<sub>3</sub>Sn and Bi-rich phases, which melt above 270°C, with a small amount of residual Sn-Bi eutectic phase. These results suggest that the TLPS process can be applied for Pb-free heat-resistant soldering.

#### 4:55 PM

**Phase Behavior of Sn- and Zr-Doped Alpha-Al<sub>2</sub>O<sub>3</sub> upon Solution Annealing:** *Liu Lumg*<sup>1</sup>; Lu Jer-Han<sup>1</sup>; Shen Pouyan<sup>1</sup>; <sup>1</sup>University of NSYSU

$\alpha$ -Al<sub>2</sub>O<sub>3</sub> powders mixed with 8 mole % SnO<sub>2</sub> versus ZrO<sub>2</sub> were sintered and then solution annealed in air at specified temperatures in order to study the expulsion of a small amount of aliovalent and size-mismatch solute. X-ray diffraction and analytical electron microscopic observations indicated that the Sn-doped alpha-Al<sub>2</sub>O<sub>3</sub> sintered at 1500°C and then annealed at 1000°C contains disk-like Guinier-Preston (G.P.) zones, which are parallel to (0001), (-12-10) and (10-10) planes of the host lattice. By contrast, the Zr-doped alpha-Al<sub>2</sub>O<sub>3</sub> shows (0001) and {01-12}-specific distortion planes in association with coherent defect clusters when sintered (1600°C) and then solution annealed at higher temperatures (1200 and 1350°C) for effective diffusion. The precipitation of (hkil)-specific G.P. zones and lattice distortion of the corundum-type structure upon exsolution of a rather limited amount of Sn<sup>4+</sup> and Zn<sup>4+</sup>, respectively can be rationalized by structure anisotropy and defect chemistry of the hexagonal close packed oxide.

## Recent Advances in Thin Films: Applications

Sponsored by: The Minerals, Metals and Materials Society, TMS Electronic, Magnetic, and Photonic Materials Division, TMS: Thin Films and Interfaces Committee  
Program Organizers: Nugehalli Ravindra, New Jersey Institute of Technology; Gregory Krumbick, Argonne National Laboratory; Choong-un Kim, University of Texas; Narsingh Singh, Northrop Grumman, ES

Monday PM

Room: 3011

February 16, 2009

Location: Moscone West Convention Center

*Session Chairs:* Narsingh Singh, Northrop Grumman Corp ES; Gregory Krumbick, Argonne National Laboratory

### 2:00 PM Introductory Comments

#### 2:05 PM Keynote

**Mechanisms of Crystallization and Grain Growth of Amorphous Si Thin Films by Metal-Initiated Crystallization:** *Nugehalli Ravindra*<sup>1</sup>; *Bhushan Sopori*<sup>2</sup>; Vishal Mehta<sup>1</sup>; Peter Rupnowski<sup>2</sup>; A. Rangappan<sup>2</sup>; <sup>1</sup>New Jersey Institute of Technology; <sup>2</sup>National Renewable Energy Lab

The mechanisms of crystallization and grain growth of amorphous silicon thin films by metal-initiated crystallization are described in relation to silicon solar cell fabrication.

#### 2:35 PM Invited

**Rare Earth Impurity Centers in Silicon for Enhancement of Light Emission and Improving Photovoltaic Efficiency:** *Sufian Abedrabbo*<sup>1</sup>; Anthony Fiory<sup>1</sup>; Nugehalli Ravindra<sup>1</sup>; <sup>1</sup>New Jersey Institute of Technology

While silicon is intrinsically an inefficient light emitter, there is considerable interest in improving its optical emission efficiency through materials modification by incorporation of rare-earth metals. Impurity centers will modify the silicon bandgap enabling an improved solar response when acting as photovoltaic devices. In this work, rare-earth metals impurity centers in silicon are investigated. Erbium is co-evaporated with silicon on silicon substrates along with other proper dopants. The processed samples are investigated optically by photoluminescence and structurally by Rutherford backscattering.

#### 3:05 PM

**An Integrated Optical and Electronic Method to Measure Nano deflections in a Silicon Diaphragm:** *Ivan Padron*<sup>1</sup>; Anthony T. Fiory<sup>1</sup>; N.M. Ravindra<sup>1</sup>; <sup>1</sup>New Jersey Institute of Technology

The introduction of an embossed diaphragm in the fabrication of a pressure sensor facilitates in the fabrication of a Fabry-Perot optical sensor that permits to measure nano deflections in a silicon diaphragm. A piezoresistive based electronic sensor is introduced as a Q-point stabilization method. An analytical and experimental analysis to study the behavior and performance of the Fabry-Perot pressure sensor is presented.

#### 3:25 PM

**Effect of Gas Flow Rate on the Formation of Aligned Nanorods in ZnO Thin Films:** *Nugehalli Ravindra*<sup>1</sup>; *Sudhakar Shep*<sup>2</sup>; Kwang-Soon Ahn<sup>2</sup>; Yanfa Yan<sup>2</sup>; John Turner<sup>2</sup>; Mowafak Al-Jassim<sup>2</sup>; <sup>1</sup>New Jersey Institute of Technology; <sup>2</sup>National Renewable Energy Laboratory

ZnO thin films are deposited in mixed Ar and N<sub>2</sub> gas ambient at substrate temperature of 500°C by rf sputtering ZnO targets. We find that the presence of optimum N<sub>2</sub> to Ar ratio in the deposition ambient promotes the formation of well aligned ZnO nanorods. ZnO thin films grown at 25 % N<sub>2</sub> gas flow rate promoted aligned nanorods along c-axis exhibit significantly enhanced photoelectrochemical response, as compared to ZnO thin films grown at other N<sub>2</sub> to Ar gas flow ratios. Our results suggest that chamber ambient is very important for the formation of aligned nanostructures, which offer potential advantages for improving the efficiency of photoelectrochemical water splitting for H<sub>2</sub> production.



3:45 PM

**Modeling Epitaxial Quantum Dots Formation and Growth Using Finite Difference Method:** *Solmaz Torabi*<sup>1</sup>; Peng Zhou<sup>1</sup>; Shuwang Li<sup>2</sup>; Steven Wise<sup>3</sup>; Axel Voigt<sup>4</sup>; John Lowengrub<sup>1</sup>; <sup>1</sup>University of California; <sup>2</sup>Illinois Institute of Technology; <sup>3</sup>University of Tennessee; <sup>4</sup>Technische Universität Dresden

Self-assembly semiconductor nanostructures such as quantum-dots are a promising inexpensive and effective approach to manufacture novel nanoscale electronic devices. The main goal is the production of large numbers of spatially ordered nanostructures with narrow size distribution via a controlled self-assembly process. Consequently, we need to have a fundamental understanding of the self-organization process (nucleation, growth and coarsening) during epitaxial growth to achieve this goal. For this reason we study the influence of elastic, surface energies and kinetics on heteroepitaxial thin film growth. Numerical studies in 2D and 3D are presented that complement experimental investigations. Here, we present a new approach for modeling strongly anisotropic crystal and epitaxial growth using regularized, anisotropic Cahn-Hilliard-type equations as a model for the growth and coarsening of thin films. A key feature of the new approach is that the interface thickness is independent of crystallographic orientation. We use an adaptive nonlinear multigrid finite-difference method.

4:05 PM

**Opto-Electronic Properties of Phthalocyanines:** *Fiorella Fuentes*<sup>1</sup>; Nuggehalli Ravindra<sup>1</sup>; Parth Patel<sup>1</sup>; <sup>1</sup>NJIT

An overview of the opto-electronic properties of phthalocyanines is presented in this study. This overview is based on the application of Wemple-DiDomenico and Penn-like models to understand the opto-electronic properties of phthalocyanines in relation to their band structure. The utility of Phthalocyanines to various medical applications is summarized.

4:25 PM Break

4:40 PM Invited

**Al and N Co-Doped ZnO Films with Significantly Reduced Bandgap and Enhanced Photoelectrochemical Responses:** *Nuggehalli Ravindra*<sup>1</sup>; *Sudhakar Shet*<sup>2</sup>; Kwang-Soon Ahn<sup>2</sup>; Yanfa Yan<sup>2</sup>; John Turner<sup>2</sup>; Mowafak Al-Jassim<sup>2</sup>; <sup>1</sup>New Jersey Institute of Technology; <sup>2</sup>National Renewable Energy Laboratory

We present results on bandgap narrowing and photoelectrochemical (PEC) response of Al and N co-doped ZnO thin films. The ZnO:(Al,N) thin films were deposited by sputtering at substrate temperature of 100°C and followed by postannealing at 500°C in air for 2 hours. We found that ZnO:(Al,N) thin films exhibited significantly enhanced crystallinity as compared to ZnO, Al doped ZnO (ZnO:Al), and N doped ZnO (ZnO:N) at the same growth conditions. Furthermore, ZnO:(Al,N) thin films exhibited enhanced N-incorporation and resulted in much reduced bandgap. As a result, ZnO:(Al,N) thin films achieved improved PEC response, as compared to ZnO, ZnO:Al, and ZnO:N thin films. Our results suggest a general way to reduce the bandgap and improve PEC response for wide-bandgap oxides.

5:10 PM Invited

**Enhanced Ferroelectric Properties and the Integrated Growth of Hf-Doped Bismuth Titanate Thin Films on GaN Substrates:** *Jun Zhu*<sup>1</sup>; Yanrong Li<sup>1</sup>; <sup>1</sup>State Key Laboratory of Electronic Thin Films and Integrated Devices, University of Electronics Science and Technology of China

Hf-doped BIT (BTH) thin films were fabricated on SrRuO<sub>3</sub>/SrTiO<sub>3</sub>/TiO<sub>2</sub> buffered GaN substrates by pulsed laser deposition. As confirmed by x-ray photoelectron spectroscopy investigation, the oxygen bonded to B-site ions became much stronger after Hf substitution. X-ray diffraction scans, including  $\theta$ - $2\theta$  and  $p$ -scans, showed that both films were highly (104)-oriented. Compared to the BIT films, the BTH films have significantly enhanced electrical properties with 3 times larger remanent polarization ( $2P_r=45.7\mu\text{C}/\text{cm}^2$ ), 0.7 times smaller coercive field ( $2E_c=184\text{ kV}/\text{cm}$ ) and better fatigue endurance (11.4% degradation). These results showed that equal-valence B-site Hf-substitution is effective to improve the electrical properties of BIT. By inserting effective buffer layers, BIT film can epitaxially deposited on GaN substrates. The integration growth of ferroelectric films with GaN may supply a possible way to realize multifunctional electronic devices.

5:40 PM

**Synthesis and Characterization of ZnO:GaN Thin Films for Photoelectrochemical Water Splitting:** *Nuggehalli Ravindra*<sup>1</sup>; *Sudhakar Shet*<sup>1</sup>; Kwang-Soon Ahn<sup>2</sup>; Yanfa Yan<sup>2</sup>; John Turner<sup>2</sup>; Mowafak Al-Jassim<sup>2</sup>; <sup>1</sup>New Jersey Institute of Technology; <sup>2</sup>National Renewable Energy Laboratory

ZnO:GaN thin films with significantly reduced bandgaps were synthesized by using ZnO and GaN targets at 100°C followed by postdeposition annealing at 500°C in ammonia for 4 hr. All the films were synthesized by rf magnetron sputtering on F-doped tin oxide-coated glass. We found that ZnO:GaN thin films exhibited narrowed bandgap, as a result showed improved PEC response, as compared to ZnO thin film. Furthermore, ZnO:GaN thin films with various bandgap were realized by varying the N<sub>2</sub> mass flow rate in mixed N<sub>2</sub> and O<sub>2</sub> chamber ambient.

## Recycling of Electronic Wastes: Mechanical Recycling and Pyrometallurgical Recycling

Sponsored by: The Minerals, Metals and Materials Society, TMS Extraction and Processing Division, TMS Light Metals Division, TMS Materials Processing and Manufacturing Division, TMS: Recycling and Environmental Technologies Committee  
Program Organizers: Lifeng Zhang, Missouri University; Fay Hua, Intel Corp; Oladele Ogunseitan, University of California, Irvine; Gregory Krumdick, Argonne National Laboratory

Monday PM

Room: 2024

February 16, 2009

Location: Moscone West Convention Center

Session Chairs: Oladele Ogunseitan, University of California-Irvine; Fay Hua, Intel Corp

2:00 PM Introductory Comments

2:05 PM

**Green Combustion of Waste Printed Circuit Boards:** *Lifeng Zhang*<sup>1</sup>; Xiangjun Zuo<sup>1</sup>; <sup>1</sup>Missouri University of Science and Technology

In this paper, the pyrometallurgical recycling of Printed Circuit Boards (PCB) was executed. The mechanisms of thermal degradation and combustion were investigated using TG/DTA and MS. Some chemical powders, such as Na<sub>2</sub>CO<sub>3</sub>, NaHCO<sub>3</sub>, NaOH and CaCO<sub>3</sub> were used to control the exhausted toxic gas, such as Br<sub>2</sub>. Finally a green combustion process for the recycling of waste PCB was proposed.

2:25 PM Question and Answer Period

2:35 PM

**Industrial Recycling of Electronic Scrap at Boliden's Rönnskär Smelter:** *Theo Lehner*<sup>1</sup>; Hans Henriksson<sup>1</sup>; <sup>1</sup>Boliden Mineral AB

Recycling plays a central part in supplying the smelters with raw materials. Boliden has developed proprietary technology to extract metal values from complex secondary raw materials with minimal impact on the environment as well as on the workers health and safety. Recycling plays also a central part in the political and public perception of our business. Secondary raw materials collected on a global scale include secondary metal concentrates, metal scrap, electronic scrap; to mention a few. In the presentation the operations and performance will be presented and the challenges as well as opportunities along the road map will be discussed.

2:55 PM Question and Answer Period

3:05 PM

**Size-Dependent Melting Characteristics of Lead-Free Solder Alloys in Microelectronics:** *Rami Chukka*<sup>1</sup>; NRMR Bhrargava<sup>1</sup>; <sup>1</sup>A U College of Engineering

Reduction of melting point for lead free solder alloys helps (Sn–Ag–Cu, Sn–Cu and Sn–Ag alloys) to work efficiently for soldering of modern fine pitch electronic component design. Because lead free solders generally have liquidus points of 220°C or higher, compared to the 183°C melting point of eutectic tin-lead solder, that much of heat certainly damage electronic devices. Present work involves in size reduction of Tin based alloys to nano scale level in order to increase the surface area of crystalline materials it eventually results in lowering melting point. Nanoparticles of Sn<sub>3.5</sub>Ag<sub>0.5</sub>Cu, Sn<sub>3.5</sub>Ag and Sn<sub>0.7</sub>Cu lead free

solder alloys were produced by mechanical attrition using high energy planetary ball mill. The melting temperature depression due to nano size effect was calculated with differential scanning calorimeter (DSC) analysis and particle size is analyzed by using XRD data.

### 3:25 PM Question and Answer Period

### 3:35 PM

**Thermal Behavior of Mixed Household Portable Batteries:** Denise Espinosa<sup>1</sup>; Jorge Tenório<sup>1</sup>; <sup>1</sup>University of São Paulo

The recycling of waste of electric and electronic equipment (WEEE) is one of the main modern challenges. Among the variety of WEEE, batteries can be set apart due to their composition and their growing demand along with portable devices. The objectives of this work are to characterize the thermal behavior of a sample of mixed types of batteries using a thermobalance (TGA). The results of tests showed that Cd evaporated up to 800°C, Zn evaporation occurred mainly above 900°C and manganese oxides were prereduced to MnO at temperatures above 900°C.

### 3:55 PM Break

### 4:15 PM Invited

**Preparation of Cadmium Ingot and Nickel Powder from Spent Cd-Ni Batteries:** Li Changdong<sup>1</sup>; Xu Shengming<sup>2</sup>; Huang Guoyong<sup>1</sup>; Zhang Lifeng<sup>3</sup>; Xu Gang<sup>2</sup>; Tan Jingjin<sup>1</sup>; <sup>1</sup>Foshan Brunp Nickel & Cobalt Technology Co., Ltd; <sup>2</sup>Tsinghua University; <sup>3</sup>Missouri University of Science and Technology

Cadmium ingot and Nickel powder were synthesized by high-temperature distillation, solvent extraction and liquid phase reducing method with Spent Cd-Ni Batteries as raw material. The impacts of the temperature in the distilling stage, the concentration of H<sub>2</sub>SO<sub>4</sub> in the leaching stage, the pH value in the extracting stage and the dosage of hydrazine in the reducing stage were discussed respectively; moreover, the samples were characterized by the means of X-ray diffraction (XRD), scanning electron microscopy (SEM), atomic absorption spectrometry (AAS) and inductively coupled plasma-atomic emission spectrometry (ICP-AES). The results showed that the recovering efficiencies of Cd and Ni reach 99.5% and 99.3%; and the purities of Cd ingot and Nickel powder are higher than 99.90% and 99.80% respectively.

### 4:35 PM Question and Answer Period

### 4:45 PM

**Materials Recovery from Electronics Scrap via Mechanical Separation and Froth Flotation Technology:** Joseph Pomykala<sup>1</sup>; Bassam Jody<sup>1</sup>; Jeffrey Spangenberg<sup>1</sup>; Edward Daniels<sup>1</sup>; <sup>1</sup>Argonne National Laboratory

Argonne National Laboratory has developed a two-stage process for recovering materials from end of life electronics. The electronics are first mechanically processed to recover the residual metals and to produce a concentrated polymer fraction. Applying a developed froth flotation technology to the concentrated polymer fraction resulted in the separation and recovery of various polymers. This technology, which separates overlapping density materials from one another in an aqueous solution, has been successful in the separation and recovery of polymers such as acrylo-nitrile-butadiene-styrene (ABS) from polystyrene. This work was sponsored by the U.S. Department of Energy Office of Energy Efficiency and Renewable Energy. This paper describes three case studies of different sourced materials processed through the Argonne National Laboratory pilot plant facility. Results indicated that over 90% of the metals were recovered, the polystyrene was recovered at high concentrations and the ABS polymers could be recovered at concentrations greater than 95%.

### 5:05 PM Question and Answer Period

## Shape Casting: Third International Symposium: Processes

Sponsored by: The Minerals, Metals and Materials Society, TMS Light Metals Division, TMS: Solidification Committee, TMS: Aluminum Processing Committee  
Program Organizers: John Campbell, University of Birmingham; Paul Crepeau, General Motors Corp; Murat Tiryakioglu, Robert Morris University

Monday PM

Room: 2011

February 16, 2009

Location: Moscone West Convention Center

Session Chair: Alan Druschitz, University of Alabama at Birmingham

### 2:00 PM Introductory Comments

### 2:05 PM

**Influence of Hydrogen Content and Bifilm Index on Feeding Behaviour of Al-7Si Alloy:** Derya Dispinar<sup>1</sup>; Arne Nordmark<sup>1</sup>; Jorunn Voje<sup>2</sup>; Lars Arnberg<sup>3</sup>; <sup>1</sup>SINTEF; <sup>2</sup>Elkem Aluminium; <sup>3</sup>Norwegian University of Science and Technology

The relationship between 'hydrogen-porosity' and 'Sr modification-porosity' has long been investigated. In this study, this phenomenon has been investigated in terms of bifilm content. A feeding test with deliberately inadequate feeding to promote some degree of shrinkage porosity has been used to compare feeding and porosity of Al-7Si alloy in gravity die casting. A melt with three different hydrogen contents was prepared by degassing first and then upgassing to low, mid and high hydrogen levels (0.1, 0.2 and 0.3 respectively) with Ar-10%H<sub>2</sub> mixture. Reduced pressure test samples were taken for bifilm index calculation and 10 tensile test bars were cast into sand moulds for mechanical testing. The results showed that feedability was increased with B-grain refining (SiBloy alloy) than the conventional Ti-B grain refined. However, pore distribution was scattered in both cases when the alloys were Sr-modified.

### 2:30 PM

**Oxide Entrainment Structures in Horizontal Running Systems:** Carl Reilly<sup>1</sup>; Mark Jolly<sup>1</sup>; Nick Green<sup>1</sup>; <sup>1</sup>The University of Birmingham

During the transient phase of filling a casting running system surface turbulence can cause the entrainment of oxide films into the bulk liquid. Research has shown that these are detrimental to the material's integrity. Common mechanisms for this entrainment include returning waves, arising during filling of the runner bar, and plunging jets, found when pouring into a basin. One of these, the returning wave, has been studied in greater depth, using real-time X-ray and process modelling techniques alongside the application of physical principals. It has been concluded that when developed, returning waves cannot attain the more stable and less entraining tranquil flow regime desirable in the running system of castings.

### 2:55 PM

**Degassing: A Critical Stage in the Manufacturing of Al-Si-Cu Alloys for Automotive Castings:** Eulogio Velasco<sup>1</sup>; Rocio Valdes Lopez<sup>2</sup>; Jose Nino<sup>2</sup>; <sup>1</sup>Texas State University; <sup>2</sup>NEMAK

In the manufacturing of aluminum blocks for automotive engines, porosity requirements on sealing surfaces and other critical areas are so stringent that special controls and special processes are required to remove hydrogen and inclusions from the molten aluminum. Several trials and adjustments in the degassing parameters and melting practices were evaluated at a production foundry. To evaluate the degassing process, density measurements were performed and to evaluate the inclusion content, fluidity and PreFil™ measurements were performed. Additionally, the mechanical properties of the casting in the heat treated condition were determined. The relationship between the density as determined by the reduced pressure test (RPT) and actual hydrogen content as determined by an AlScan unit was established for A319 aluminum alloy. The results of the mechanical property tests showed a direct relation with the metal quality of the alloy.

3:20 PM

**Heat Treatment of A356.2 Aluminum Alloy: Effect of Quench Rate and Natural Ageing:** Manickaraj Jeyakumar<sup>1</sup>; Mohamed Mousa<sup>1</sup>; Mohamed Hamed<sup>1</sup>; Sumanth Shankar<sup>1</sup>; <sup>1</sup>LMCRC-McMaster University

A356.2 aluminum alloy is a popular commercial alloy used for structural shaped castings in automotive applications. The heat treatment of this alloy is critical to obtain the desired mechanical and performance properties. The three stages of heat treatment include, solutionizing, quenching and artificial ageing. In this study, the effect of quenching in water at 80°C and forced air at 33.5 m/s velocity is quantified. Further, the effect of natural ageing treatment prior to the artificial ageing is also quantified. It is observed that the mechanical properties of the castings are significantly affected by both the rate of quenching and the natural ageing treatment. Mechanical properties and hardness values are presented for standard tensile test specimen cast using gravity permanent mold process and subjected to various heat treatment conditions.

3:45 PM Break

3:55 PM

**Process Parameters Study for Net-Shape Steel Casting:** Von Richards<sup>1</sup>; Simon Lekakh<sup>1</sup>; Darryl Kline<sup>1</sup>; K. Chandrashekhara<sup>1</sup>; Jian Chen<sup>1</sup>; <sup>1</sup>Missouri University of Science & Technology

The objective of this research was the experimental study and computational modeling of process parameters of net-shape steel casting with complicated geometry. Gas permeability, burst pressure (pressurize water), and mechanical and physical properties at room and high temperatures for ceramic shells were evaluated for different ceramics. The experimental data was used to simulate stresses in the ceramic shell, mold filling, and solidification using ABAQUS and MAGMA software. Models were verified by pouring steel into ceramic molds of differing geometries and monitoring with electrical sensors and thermopiles connected to a high-speed DAQ. The results will be used for the optimization of an industrial process.

4:20 PM

**Improving Build Speed in Rapid Freeze Prototyping through Increase of Heat Transfer:** Ming Lew<sup>1</sup>; Sriram Isanaka<sup>1</sup>; Von Richards<sup>1</sup>; <sup>1</sup>Missouri University of Science and Technology

The heat transfer in the Rapid Freeze Prototyping (RFP) process has been significantly increased for improvement of build speed and part accuracy. RFP is a solid freeform fabrication process in which water droplets are deposited and solidified layer-by-layer to form three-dimensional ice patterns for investment casting. A mechanism has been devised to cool the substrate to as low as -140°C. Chilling plates were developed to enable effective transfer of heat with the aid of conduction. To ensure that deposited water does not freeze to the chilling plate, various surface coats were investigated. The most effective interface material was identified using contact angles measured using high resolution digital photography. The experimental results were substantiated with model based simulations performed using Fluent and Gambit. The improvements in build speed and dimensional accuracy after incorporating the above changes were measured and presented.

4:45 PM

**Cooling Properties of Frozen Sand Molds for Casting of Lead Free Bronze:** Hiroyuki Nakayama<sup>1</sup>; Shuji Tada<sup>1</sup>; Toshiyuki Nishio<sup>1</sup>; Keizo Kobayashi<sup>1</sup>; <sup>1</sup>National Institute of Advanced Industrial Science and Technology

A frozen mold is an advanced sand mold provided by freezing the mixture of sand and water. Bronze cast plates, which had dimensions of 30x150x5 mm, were produced through the frozen mold casting process. The temperature transition of the cast plates just after pouring were measured at three positions, near the gate, the center and the far side, by high speed recorder with sampling time of 1 ms. The temperature rapidly decreased on the initial stage. Subsequently, the slight temperature raise was observed in the near side of the gate. However, this phenomenon was not observed in the far side, where the temperature of melt was already decreased. In contrast, the above temperature raise was not observed at any positions in the casting by a green sand mold.

## Structural Materials Division Symposium: Advanced Characterization and Modeling of Phase Transformations in Metals in Honor of David N. Seidman on his 70th Birthday: Thermodynamics of Phase Transformations

Sponsored by: The Minerals, Metals and Materials Society, TMS Structural Materials Division, TMS: Advanced Characterization, Testing, and Simulation Committee, TMS: Chemistry and Physics of Materials Committee

Program Organizers: Robert Averback, University of Illinois, Urbana-Champaign; Mark Asta, University of California, Davis; David Dunand, Northwestern University; Ian Robertson, University of Illinois at Urbana-Champaign; Stephen Foiles, Sandia National Laboratories

Monday PM

Room: 3000

February 16, 2009

Location: Moscone West Convention Center

Session Chair: Mark Asta, University of California, Davis

2:00 PM Invited

**The Early Years:** David Brandon<sup>1</sup>; <sup>1</sup>Israel Institute of Technology

David Seidman has had a remarkably successful career, marrying atomistic studies of phase stability to kinetics and thermodynamics. But David's seminal years were spent at the university of Illinois, completing his doctorate under the leadership of Bob Balluffi, and at Cornell, 'learning' field-ion microscopy and developing the expertise that would later allow him to build his first atom probe and then expand these facilities at Northwestern, to create the world's leading international center for atom probe tomography. I met David Seidman when he was a graduate student at Illinois, where his room-mate was a former student of mine, Piers Bowden. My last 'professional' interaction with him was when I spent three weeks at Cornell, as a rather ineffectual 'consultant' on field-ion microscopy. Our shared interests in microstructural characterization would not have sufficed to maintain our friendship, but our shared interest in the State of Israel certainly has.

2:25 PM Invited

**Thermodynamic Properties of Grain Boundaries from Atomistic Simulations:** Jeffrey Hoyt<sup>1</sup>; D.L. Olmsted<sup>2</sup>; S. Jindal<sup>3</sup>; M. Asta<sup>3</sup>; A. Karma<sup>4</sup>; B.B. Laird<sup>5</sup>; <sup>1</sup>McMaster University; <sup>2</sup>Sandia National Laboratories; <sup>3</sup>University of California, Davis; <sup>4</sup>Northeastern University; <sup>5</sup>University of Kansas

Molecular dynamics (MD) and Monte Carlo simulations on an embedded atom method model of pure Ni have been used to study two thermodynamic properties of grain boundaries at elevated temperatures. First, premelting of a high energy  $\Sigma 9$  twist boundary has been investigated and, in agreement with the classic experiment of Hsieh and Balluffi, premelting has been observed at temperatures very close to the bulk melting point. In addition, by monitoring the width of the liquid-like layer over the course of lengthy MD runs, the disjoining potential between the two solid-liquid boundaries is derived. In agreement with phenomenological models, the disjoining potential was found to decay exponentially with the premelted layer width. Second, a lattice switch Monte Carlo technique has been used to compute the excess boundary free energy as a function of temperature for the  $\Sigma 3$  coherent twin.

2:55 PM Invited

**Chemical Short-Range Ordering in Liquid-Phase Ni Alloys:** Dallas Trinkle<sup>1</sup>; Mark Asta<sup>2</sup>; Christopher Woodward<sup>3</sup>; <sup>1</sup>University of Illinois, Urbana-Champaign; <sup>2</sup>University of California, Davis; <sup>3</sup>Air Force Research Laboratory

First-principles modeling provides new predictive capabilities and atomistic-scale insight into the behavior of alloys in the liquid phase. In support of a current effort aimed at the development of validated mathematical criteria for predicting the formation of solidification defects in Ni-based superalloys, ab-initio molecular dynamics (AIMD) simulations have been performed for elemental, binary and ternary alloys of Ni with Al, W, Re, and Ta, as well as a RENE-N4 multi-component superalloy, to compute equations of state, measure diffusion, and quantify short-range chemical and structural order at temperatures of 1830 and 1750 K. Structural analysis based on radial distribution functions augmented with common-neighbor analysis and bond angle distributions reveal a strong tendency for icosahedral short range order for Ni-W and Ni-Re alloys.



Finally, short-range chemical ordering and neighbor distances for solutes are compared with elemental liquids for binary, ternary, and complex alloys.

### 3:25 PM Break

### 3:45 PM Invited

**Atomistic Modeling of Interfacial Thermodynamics:** *Y. Mishin*<sup>1</sup>; T. Frolov<sup>1</sup>; <sup>1</sup>George Mason University

We present thermodynamic relations for the free energy, stress, strain, formation volume, segregation and other excess properties of interfaces in non-hydrostatically stressed solid phases in forms convenient for their atomistic calculations. Cahn's method of determinants permits easy access to all interface properties from "raw" atomistic data without having to compute the interface profiles. The equations are applied to examine the temperature and composition dependencies of interface free energy, interface stress, interface strain and interface segregation for a few free surfaces, grain boundaries, coherent phase boundaries and solid/liquid interfaces with different crystallographic orientations. The method is also used to study surface pre-melting and the orientation dependence of the solid/liquid interface stress by molecular dynamics and grand-canonical Monte Carlo methods. Extensions of the method to multi-component systems with the substitutional, interstitial and mixed solubility mechanisms are discussed.

### 4:15 PM

**Modeling of Diffusion along Triple Junction Lines:** *T. Frolov*<sup>1</sup>; *Y. Mishin*<sup>1</sup>; <sup>1</sup>George Mason University

It has long been believed that diffusion along triple junction lines in metals is much faster than grain boundary diffusion. The anomalously high diffusivity in some nano-crystalline materials was sometimes attributed to a contribution of triple junctions. There have been very few experimental measurements and no atomistic calculations of triple-junction diffusion. As a result, no reliable self-diffusion coefficients along triple junctions in metals are currently available. We present results of molecular dynamics simulations of triple-junction and grain-boundary diffusion in copper over a wide temperature range. The unexpected result is that, although the diffusion coefficients in triple junctions are larger than in high-angle boundaries, they are of the same order of magnitude at all temperatures studied (700-1320 K). Thus the role of triple-junction diffusion in polycrystalline materials might be overestimated. Possible consequences of this finding are discussed. We have also studied pre-melting of triple-junctions and its effect on the diffusivity.

### 4:30 PM Invited

**Computational Approach to Phase Transformations at the Nanoscale:** *Alfredo Caro*<sup>1</sup>; Paul Erhart<sup>1</sup>; Babak Sadigh<sup>1</sup>; Magdalena Caro<sup>1</sup>; <sup>1</sup>LLNL

The computational study of phase transformations is today a standard approach that provides detailed pictures of complex processes at scales going from the continuum down to the electronic structure. Since modeling phase transformation at the nanometer scale requires atomic resolution, there is an increasing interest on developing models for atomic interactions that translate the information obtained at the electronic scale into reliable classical potentials, able to carry information about thermodynamics of multicomponent systems. Concurrently, adequate tools to resolve the time and length scales required for these studies are being developed. Codes for massively parallel Metropolis Monte Carlo algorithm are available today and provide insight into equilibrium properties. The situation is not yet so developed for massively parallel kinetic Monte Carlo that would also provide kinetic information. In this talk I will review our work in nanophase alloys, from small clusters to bulk nanophases, developing potentials for alloys and codes for large systems, and our applications for grain boundary and surface segregation, corrosion, and radiation damage in steels.

### 5:00 PM Invited

**Free Energy Calculations for Reactions of Lithium-Ion-Battery Electrode Materials in Acid:** *Li(1+x+y)Mn(2-x)O<sub>4</sub> Spinel:* *Roy Benedek*<sup>1</sup>; <sup>1</sup>Argonne National Laboratory

The lithiated transition metal oxides employed as cathodes in lithium-ion batteries react with aqueous acid by dissolving, or exchanging protons for lithium. We have previously developed a method to calculate free energies for reactions in acid of lithiated transition metal oxides by applying first principles calculations for the solid phases and tabulated thermochemical data for aqueous species. In the present work, this approach is applied to calculate the reactions of LiMn<sub>2</sub>O<sub>4</sub> spinel, as a function of excess or deficiency of lithium. Our results show that, as expected, the dissolution reaction driving force is maximum for Li<sub>2</sub>Mn<sub>2</sub>O<sub>4</sub>,

for which all Mn is available for disproportionation to divalent and tetravalent states. We find however, that the driving force for dissolution decreases less for overlithiated compositions than might be expected if disproportionation were the only factor involved. Unlike the dissolution reaction, protonation is unfavorable at almost any composition.

### 5:30 PM

**Antiferromagnetic Transition and Martensitic Transformation in Mn-Rich g-MnFe Alloy:** *Ji Zhang*<sup>1</sup>; <sup>1</sup>Shanghai Jiao Tong University

This paper attempts to pay attention to research the effect of antiferromagnetic transition on martensitic transformation. Observation of Transmission Electron Microscopy (TEM) and the measurement from Dynamic Mechanical Analysis (DMA) showed that there are (011) fct twins of martensitic transformation in the alloy. Experiments of electrical resistance and Differential Scanning Calorimeter (DSC) show that the martensitic transformation temperature (M<sub>s</sub>) and reverse martensitic transformation temperature (A<sub>f</sub>) in the Mn-rich g-MnFe alloy is closed to each other or almost coincide, and direct and reverse martensitic transformation are similar to the second order typed-continuous transition. Because there is the coupling between first order martensitic transformation and second order antiferromagnetic transition, the temperature shape memory effect of the alloy showed a hysteresis-free characteristics in dilatation measurement. And there also is a magnetic-field induced shape strain (MFIS) under applied magnetic field and the maximum MFIS reached 1.6% at the applied field of 3.8 T.

### 5:45 PM

**Rigorous Simulations of Kirkendall Effects in Polycrystalline Solids:** *Hui-Chia Yu*<sup>1</sup>; Anton Van der Ven<sup>1</sup>; Katsuyo Thornton<sup>1</sup>; <sup>1</sup>University of Michigan

The Kirkendall effect stems from the biased interdiffusion in which the two atomic species have different exchange rates with vacancies that mediate diffusion. The vacancy injection/annihilation at their sources/sinks result in the so-called Kirkendall shift and deformation. In this study, we investigate the effect of grain boundaries acting as vacancy sources and sinks on the Kirkendall effect through computer simulations. The vacancy source effects on biased diffusion due to net vacancy flux and intermixing are analyzed. The result shows a new mechanism for the enhanced grain boundary diffusion. Furthermore, phase field simulations are employed to study the Kirkendall deformation based on the treatment that assumes grain boundaries to be discretely distributed vacancy sources/sinks. The results demonstrate the local expansion and contraction near grain boundaries lead to a different deformation pattern from the conventional model that assumes a continuous vacancy source/sink within the bulk of solids.

## Synergies of Computational and Experimental Materials Science: Three-Dimensional Materials Science II

Sponsored by: The Minerals, Metals and Materials Society, TMS Materials Processing and Manufacturing Division, TMS/ASM: Computational Materials Science and Engineering Committee

Program Organizers: Katsuyo Thornton, University of Michigan; Henning Poulsen, Risoe National Laboratory; Mei Li, Ford Motor Co

Monday PM

Room: 3003

February 16, 2009

Location: Moscone West Convention Center

Session Chairs: Jonathan Madison, The University of Michigan; Peter Voorhees, Northwestern Univ

### 2:00 PM Invited

**Combining Serial Sectioning, EBSD Analysis, and Image-Based Finite Element Modeling:** *Alexis Lewis*<sup>1</sup>; David Rowenhorst<sup>1</sup>; Andrew Geltmacher<sup>1</sup>; George Spanos<sup>1</sup>; <sup>1</sup>Naval Research Laboratory

Recent work combining 3D data obtained from serial sectioning, electron backscatter diffraction (EBSD), and finite element modeling (FEM) of materials microstructures has led to new advances in the fundamental understanding of structure-property relationships in three dimensions. Current techniques, both experimental and computational, will be described, with emphasis on imaged-based FE methods which use experimental data from these 3D reconstructions as the initial input conditions for simulations of the mechanical response of

3D microstructures to various externally applied loading conditions. Specific examples from work on a beta-Titanium alloy are utilized to illustrate the capabilities of these experimental and modeling techniques, the challenges and the solutions associated with these methods, and the types of results and analyses that can be obtained by the close integration of experiments and simulations.

#### 2:40 PM

**Modeling the Influence of Microstructure on Flow Stress in Ti-6Al-4V Alloy by Neural Networks:** *N. S. Reddy*<sup>1</sup>; C. H. Park<sup>2</sup>; Y. H. Lee<sup>3</sup>; Y. I. Son<sup>4</sup>; C. S. Lee<sup>2</sup>; <sup>1</sup>Alternative Technology Laboratory, Pohang University of Science and Technology; <sup>2</sup>Department of Materials Science and Engineering, Pohang University of Science and Technology; <sup>3</sup>Wire Rod Research Group; <sup>4</sup>Agency for Defence Development

Neural networks (NN) were used to model flow stress in Ti-6Al-4V alloy with equiaxed, martensite and Widmanstätten microstructure as initial microstructures. Continuous compression tests were performed over a wide range of temperatures (700-1100°C) with strain rates of 0.001-100 s<sup>-1</sup> and true strains of 0.1-1.4. These tests have been focused to obtain flow stress data under varying conditions of strain, strain rate, temperature, and initial microstructure to train NN model. The feed-forward neural network consisted of two hidden layers with a sigmoid activation function and back propagation training algorithm used. The NN model was successfully trained across ( $\alpha$ + $\beta$ ) to  $\beta$  phase regimes and across different deformation domains. Sensitivity analysis was carried on trained model to study the quantitative effect of microstructure on flow stress. Results show that the NN model can correctly reproduce the flow stress in the sampled data and it can predict well with the non-sampled data.

#### 3:00 PM

**Microstructural Analyses Using 3D Image-Based Finite Element Modeling:** *Andrew Geltmacher*<sup>1</sup>; Alexis Lewis<sup>1</sup>; Muhammed Qidwai<sup>2</sup>; David Rowenhorst<sup>1</sup>; George Spanos<sup>1</sup>; <sup>1</sup>Naval Research Laboratory; <sup>2</sup>SAIC

Image-based finite element (FE) models derived from 3D reconstructions of real material microstructures have been used to simulate the mechanical response in several advanced engineering alloys. In the work presented here, 3D image-based FE modeling of a single-phase beta Titanium alloy was used to determine the relationships between microstructure, crystallography, grain morphology, and mechanical response. Initial simulations show high stress concentrations at particular grain boundaries and junctions, and the combined 3D microstructural and crystallographic information at these areas of high local stress is used to determine correlations between the measured microstructure and the simulated response. Results will be presented for a number of representative volumes sampled from a larger reconstructed volume which contains thousands of grains. The effects of volume sampling size, simulation parameters, and mesh generation techniques on the observed material response will also be discussed.

#### 3:20 PM

**Numerical and Experimental Investigation of Deformation Behavior of a Duplex Microstructure of a  $\gamma$ -TiAl Alloy Using Crystal Plasticity and Two Scale Modeling Approach:** *Mohammad Rizviul Kabir*<sup>1</sup>; Liudmila Chernova<sup>1</sup>; Nikolay Zotov<sup>2</sup>; Marion Bartsch<sup>1</sup>; <sup>1</sup>German Aerospace Center; <sup>2</sup>Ruhr-Universität Bochum

The 3-dimensional microstructure of a duplex  $\gamma$ -TiAl has been modeled in a parameterized FE-model using a two scale approach (FE2-approach) for micro and macro coupling. The most important microstructural features, such as  $\alpha_2$  and  $\gamma$ -phases, their volume percents, orientations, lamellar and globular arrangements, were representatively incorporated. The microstructure information was experimentally determined by SEM, TEM and EBSD analysis. For describing the micromechanics of the phases a continuum based crystal plasticity model was used. The model parameters were validated on the microscopic level by nano-indentation testing and on the macroscopic level by tensile tests at room temperature. The global deformation behavior was explained fairly well by the slip interactions, the local stresses, and the local strains predicted by the modeling approach. The model can be used for optimizing the microstructure of polycrystalline materials for components.

#### 3:40 PM Break

#### 4:00 PM Invited

**Combined 3D X-Ray Microscopy and Dislocation Dynamics Simulation Investigation of the Fundamental Aspects of Deformation in Copper:** *Bennett Larson*<sup>1</sup>; Jie Deng<sup>2</sup>; Anter El-Azab<sup>2</sup>; <sup>1</sup>Oak Ridge National Laboratory; <sup>2</sup>Florida State University

Submicron resolution 3D x-ray microscopy measurements have been combined with dislocation dynamics simulations to initiate an investigation of the fundamental aspects of deformation in metals. 3D x-ray microscopy measurements of local plastic deformation were performed with 0.5  $\mu$ m resolution (~0.3  $\mu$ m beam size) on initially dislocation free Cu single crystals that were deformed in compression to strains varying from 1% to 7.6% along the [100] direction. Dislocation dynamics simulations were performed for [100] axial deformation of fcc Cu for strain values ranging up to 1.6%. The overlapping strain magnitudes for the measurements and simulations provide a direct and quantitative link between nondestructive 3D x-ray microscopy measurements and first principles simulations of deformation. Quantitative comparisons between the measured and simulated local lattice curvatures will be presented in graphical and statistical form. Research supported by the US DOE Office of Science, Basic Energy Sciences, Division of Materials Sciences and Engineering.

#### 4:40 PM

**X-Ray Synchrotron Tomography for Three Dimensional (3D) Microstructure Visualization and Modeling of Deformation in Metal Matrix Composites:** *Flavio Silva*<sup>1</sup>; Jason Williams<sup>1</sup>; Nikhilesh Chawla<sup>1</sup>; Pedro Portella<sup>2</sup>; Bernd Mueller<sup>2</sup>; <sup>1</sup>Arizona State University; <sup>2</sup>Federal Inst for Mat Rsch & Testing BAM

Current analytical and numerical techniques simplify the complex and heterogeneous microstructure of composite materials. These simplifications make modeling and analysis more efficient and straightforward, but fail to accurately predict the effective properties and local damage behavior which are inherently dependent on microstructure. We report on a novel methodology that addresses the critical link between microstructure and deformation behavior, by using a three-dimensional (3D) virtual microstructure as the basis for a robust model to simulate damage caused by deformation. The approach involves capturing the microstructure by novel and sophisticated x-ray tomography techniques, followed by image analysis, 3D reconstruction of the microstructure, and incorporation into a powerful finite element modeling code for simulation. We will present a case study based on uniaxial tensile deformation of SiC particle reinforced Al alloy matrix composites. In particular, the damage in the form of particle fracture will be described.

#### 5:00 PM

**Assessing the Sensitivity of FEM-Based Crystal Plasticity Models to Microstructures: A Multi-Scale Crystal Plasticity Model Combined with Experimental Methods:** *Remi Dingreville*<sup>1</sup>; Corbett Battaile<sup>1</sup>; Luke Brewer<sup>1</sup>; Elisabeth Holm<sup>1</sup>; <sup>1</sup>Sandia National Laboratories

In this paper, we examine the effect of the microstructure on the elastoplastic response of polycrystals by combining a non-local crystal plasticity simulations with experimental microscale characterization. The morphology and deformation behavior of polycrystals are characterized using electron back scatter diffraction (EBSD) and in situ tensile testing, and finite element simulations of the deformation are performed using an augmented kinematics framework and a non-local crystal plasticity constitutive treatment allowing a natural description of microstructure by featuring low angle sub-grain boundaries and high angle grain boundaries. Comparisons between experimental observations and computational simulations are provided at the macroscopic and microscopic scale. The contrasts between the experimental investigations and modeling technique highlight the strong and weak points of the theoretical framework used.

#### 5:20 PM

**A Failure Surface Calibrated with Mechanical Testing, Finite Element Analyses, and Metallography:** *Matthew Hayden*<sup>1</sup>; Xiaosheng Gao<sup>2</sup>; Charles Roe<sup>1</sup>; <sup>1</sup>Naval Surface Warfare Center; <sup>2</sup>The University of Akron

Ductile fracture is a complex phenomenon currently implemented in structural codes as empirical fits of material testing. Most often, these fits do not fully capture the effects of stress state, nor are they tied to material microstructure. This study develops a three-dimensional failure surface calibrated to 5083-H116

aluminum with a suite of tension, torsion, and compression tests over a broader range of stress states. Finite element models coupled to material microstructural topology analyze each specimen geometry to calculate local stress state and failure strain at the region of failure initiation.

## Transformations under Extreme Conditions: A New Frontier in Materials: Melting and Solidification II

Sponsored by: The Minerals, Metals and Materials Society, ASM International, ASM Materials Science Critical Technology Sector, TMS Materials Processing and Manufacturing Division, TMS/ASM: Phase Transformations Committee  
 Program Organizers: Vijay Vasudevan, University of Cincinnati; Mukul Kumar, Lawrence Livermore National Laboratory; Marc Meyers, University of California-San Diego; George "Rusty" Gray, Los Alamos National Laboratory; Dan Thoma, Los Alamos National Laboratory

Monday PM Room: 3001  
 February 16, 2009 Location: Moscone West Convention Center

Session Chairs: Robert Hixson, Naval Postgraduate School; Jorg Wieszorek, University of Pittsburgh

### 2:00 PM Invited

**Dynamics of Ultrafast Melting and Solidification in Metals:** *Robert Averback*<sup>1</sup>; Wai-Lun Chan<sup>1</sup>; David Cahill<sup>1</sup>; Yinon Ashkenazy<sup>2</sup>; <sup>1</sup>University of Illinois; <sup>2</sup>The Hebrew University of Jerusalem

Melting and solidification in metals have been investigated using a combination of experimental and simulation methods. The experimental work measures the velocity of the advancing melt front in Ag following excitation with a femtosecond laser and the subsequent resolidification as a function of undercooling. The liquid-solid transitions are followed using third harmonic generation of light. Critical to understanding these experiments is the thermal transport of energy under such extreme conditions. MD simulations were used to examine resolidification behavior as a function of undercooling in a number of metals, both FCC and BCC. We illustrate that the interface kinetics can be divided into three temperature regimes, with the lowest being controlled by diffusion. We also demonstrate a correlation in the low-temperature regime between the migration process controlling the crystallization and equilibrium point defect properties.

### 2:35 PM

**Microstructural Changes in Al Thin Films during Pulsed Laser Induced Rapid Lateral Solidification:** *Andreas Kulovits*<sup>1</sup>; *John Leonard*<sup>1</sup>; *Jorg Wieszorek*<sup>1</sup>; <sup>1</sup>University of Pittsburgh

Sputtered Al films (70-140nm thick) with and without silica cap-layers were melted using a single excimer laser (KrF) pulse with 28ns duration. SEM and TEM studies revealed RS microstructures consisting predominantly of through-film thickness high aspect ratio grains (~10-20µm long, 1µm wide) with an in-film-plane columnar structure, containing a variety of crystal defects. XRD and SEM EBSD measurements were used to quantify texture changes. Theoretically estimated re-solidification times of 100 to 500ns imply extremely fast solidification front velocities (~102m/s). The thin film sample geometry we successfully used for pulsed laser melting of Al and also Cu, Ag, Cr, Ni is suitable for dynamic in-situ experimentation using a novel in-situ TEM instrument or Dynamic TEM (DTEM). The DTEM uniquely offers the combination of nanoscale temporal and spatial resolution critically required for studying directly by experiment the dynamics associated with these unique and extremely rapid phase transformations.

### 2:55 PM

**A Computational Model for Thermal Response of Semi-Transparent Materials to Laser Processing:** *Jeffrey Colvin*<sup>1</sup>; *James Stölkén*<sup>1</sup>; <sup>1</sup>Lawrence Livermore National Lab

Lasers are widely used to modify the internal structure of semi-transparent materials for a wide variety of applications, including waveguide fabrication and laser glass damage healing. The diffusion approximation used in past models to describe radiative cooling is not adequate for these materials, particularly near the heated surface layer. In this paper we describe a new computational model based upon solving the radiation transport equation by the Pn method with ~1000 photon energy bands. The model accounts for the temperature-dependent

absorption of infrared laser light and subsequent redistribution of the deposited heat by both radiative and conductive transport. We present representative results for fused silica irradiated with 1-2 W for 10 s pulse durations. This work was performed under the auspices of the US Department of Energy by Lawrence Livermore National Laboratory under contract No. DE-AC52-07NA27344, with support received from LDRD Project #08-ERD-057.

### 3:15 PM Invited

**Experimental and Theoretical Research on Shock-Induced Phase Transformation in LSD:** *Wenjun Zhu*<sup>1</sup>; *Jianbo Hu*<sup>1</sup>; *Xianmin Zhou*<sup>1</sup>; *Jun Li*<sup>1</sup>; *Xinlin Cui*<sup>1</sup>; *Chenda Dai*<sup>1</sup>; *Hongliang He*<sup>1</sup>; <sup>1</sup>Laboratory for Shock Wave and Detonation Physics Research

Shock-wave has advantage to generate high pressure condition, where materials can undergo rich pressure-driven phase transformations. However, it is critical to measure the phase transformation pressure and to determine the new phase structure as well as phase boundaries due to very short time. We present three examples to show recent experimental and theoretical progresses on shock-induced phase transformation in our lab (LSD). (1) The classic configuration of reverse-impact experiments has been modified to enhance the accuracy of high-pressure sound velocity measurements. The shock induced bct to bcc phase transformation with slight change of volume in tin is distinctly detected through sound velocity measurements. (2) The phase transformation pressure for LiTaO3 and the structure have been determined by combination methods of shock velocity (D) versus particle velocity (Up) relation measurements and first-principle calculations. (3) Effects of defects to shock-induced phase transformation in iron have been investigated by molecular dynamics (MD) simulations.

### 3:50 PM Break

### 4:05 PM Invited

**Shock Wave Exploration of the High Pressure Phases of Carbon:** *Marcus Knudson*<sup>1</sup>; *Mike Desjarlais*<sup>1</sup>; *Dan Dolan*<sup>1</sup>; <sup>1</sup>Sandia National Laboratories

The high energy density response of diamond has gained interest of late due to its relevance to planetary astrophysics and the possible use of diamond an ablator material in inertial confinement fusion capsules. Recently, experiments utilizing an ultra-high flyer plate capability at the Sandia Z accelerator were performed to determine the Hugoniot and the shock melting properties of polycrystalline diamond. Composite aluminum/copper flyer plates were used to shock load diamond samples to pressures ranging from 5 to 14 Mbar. Multiple samples and fast diagnostics provided Hugoniot measurements with ~1% accuracy in density. This work provides compelling evidence for the existence of a diamond-bc8-liquid triple point along the coexistence region of the Hugoniot, at a pressure and density of ~850 GPa and ~6.5-6.6 g/cc. These high precision Hugoniot measurements at multi-Mbar pressures allow for high fidelity comparisons with recent quantum molecular dynamics calculations, and provides the first experimental evidence of a high pressure solid phase of carbon beyond that of diamond.

### 4:40 PM Invited

**Dynamic Solidification of Water under Quasi-Isentropic Compression: Heterogeneous Nucleation and Beyond:** *Daniel Dolan*<sup>1</sup>; <sup>1</sup>Sandia National Laboratories

Solidification is well established under static compression, but has proven elusive under dynamic compression. Creating solidification states with dynamic compression is challenging, and these states are short lived, whereas freezing is generally a slow phase transition. Using quasi-isentropic compression, it is possible to bring liquid water from ambient conditions to states deep within the ice VII domain on nanosecond time scales. Under these conditions, water can be made to solidify in two ways. If an appropriate nucleator is present, metastable water transforms to a mixed phase over the course of 10-100 ns. Much faster solidification occurs if compressed water is driven beyond its metastable limit. Both types of transformation have been observed experimentally in water, and will be discussed in this presentation. Sandia is a multiprogram laboratory operated by Sandia Corporation, a Lockheed Martin Company, for the United States Department of Energy's National Nuclear Security Administration under contract DE-AC04-94AL85000.



5:15 PM

**Liquid-Solid, Pressure-Induced Phase Transition for Water: Simulations:***Daniel Orlikowski<sup>1</sup>; Jeff Nguyen<sup>1</sup>; Neil Holmes<sup>1</sup>; <sup>1</sup>Lawrence Livermore National Laboratory*

Hydrodynamic simulations of liquid water undergoing a pressure-induced phase transition into ice VII are presented. From initial ambient conditions, the liquid system is quasi-isentropically compressed into its solid phase. To develop this modeling effort, we have used unique quasi-isentropic, light-gas gun data for water that have measured a phase-fraction along this path. Combining this information with the equilibrium equation of state (EOS), we have evaluated a possible kinetic model for its liquid to solid phase transition. Specifically, the simulations use two tabular single phase EOS's. To mitigate between the single phase EOS's during the mixed-phase intervals, a thermodynamic linear mixing scheme is used to compare to a simple kinetic model containing a time constant determined from experiment. The simulation models in one dimension the entire experimental setup, accounting for the wave interactions throughout the impactor and target, which are compared with experiment.

5:35 PM

**Transient Ionization of Shock Compressed Water Near Planetary Isentropes:***Nir Goldman<sup>1</sup>; Evan Reed<sup>1</sup>; Will Kuo<sup>1</sup>; Laurence Fried<sup>1</sup>; Christopher Mundy<sup>2</sup>; Alessandro Curioni<sup>3</sup>; <sup>1</sup>LLNL; <sup>2</sup>Pacific Northwest National Laboratory; <sup>3</sup>IBM Research*

We report herein first principles simulations of water under shock loading near the isentropes of Neptune and Uranus. Accurate description of the chemical mechanism for the ionic conductivity at high pressures and temperatures is of particular importance to models of the planetary dynamo mechanism in these planets. Using a novel simulation technique for shock compression, we are able to make excellent comparison to the experimental results for the Hugoniot pressure, temperature and density final states. Our simulations resolve controversy by showing that a unimolecular mechanism for electric conduction dominates at high pressures along the shock Hugoniot. Near the approximate intersection of the Hugoniot and the planetary isentrope we observe high concentrations of negatively charged species that contribute electronic states near the band gap. Our results provide a microscopic picture of the chemistry at planetary depths of ca. 6000 km and greater.

## 2009 Functional and Structural Nanomaterials: Fabrication, Properties, and Applications: Nanoscale Oxides: Synthesis and Applications

Sponsored by: The Minerals, Metals and Materials Society, TMS Electronic, Magnetic, and Photonic Materials Division, TMS Materials Processing and Manufacturing Division, TMS: Nanomaterials Committee, TMS: Nanomechanical Materials Behavior Committee

Program Organizers: Gregory Thompson, University of Alabama; Amit Misra, Los Alamos National Laboratory; David Stollberg, Georgia Tech Research Institute; Jiyoung Kim, University of Texas at Dallas; Seong Jin Koh, University of Texas at Arlington; Wonbong Choi, Florida International University; Alexander Howard, Air Force Research Laboratory

Tuesday AM Room: 3018  
February 17, 2009 Location: Moscone West Convention Center

Session Chairs: Alexander Howard, Air Force Research Laboratory; Jiyoung Kim, University of Texas at Dallas

### 8:30 AM

**Solution-Processed Nanostructured ZnO Electrodes for Photovoltaics:** *Rodrigo Noriega-Manez*<sup>1</sup>; *Ludwig Goris*<sup>1</sup>; *Sujay Phadke*<sup>1</sup>; *Greg Kusinski*<sup>2</sup>; *Alberto Salleo*<sup>1</sup>; <sup>1</sup>Stanford University; <sup>2</sup>Clemson University

Zinc oxide (ZnO) is a strong candidate for replacing indium tin oxide in solar cell electrodes and transparent electronics, provided that a high quality material with optimized properties can be obtained with a low-cost and high-throughput process. With this in mind, aluminum- and gallium-doped ZnO nanowires were synthesized using a low-temperature solution-based process, improving their electrical conductivity without affecting optical transparency. The resulting nanowires were characterized with electron microscopy (SEM, TEM), XRD, and composition-sensitive techniques (AES, XPS, EDS); the electrical properties were observed with a four-terminal probe. The dependence of sheet resistance with temperature and doping was studied. In-plane alignment of the nanowires allowed us to observe the effect of morphology in the film's resistivity, and single-wire measurements provided insight into their electronic characteristics. Early attempts to achieving uniform dopant incorporation are presented, as well as their effect on device performance.

### 8:45 AM

**Zinc Oxide Nanostructure Devices: Effect of Surface Cleaning by UV Radiation:** *Ved Verma*<sup>1</sup>; *Santanu Das*<sup>1</sup>; *Minnhyon Jeon*<sup>2</sup>; *Wonbong Choi*<sup>1</sup>; <sup>1</sup>Florida International University; <sup>2</sup>Inje University

We have studied the effect of surface cleaning on device performance of zinc oxide thin films transistors (ZnO-TFTs) and zinc oxide nanowire field effect transistors (ZnO-FETs). Ultraviolet irradiation at high temperature (~400 K) and under high vacuum (~4.0 × 10<sup>-4</sup> Torr) conditions enhances the device performance by removing the adsorbed oxygen species from the surface of nanostructures. 1 wt% Ga-doped ZnO-TFTs demonstrate mobility of 5.7 cm<sup>2</sup>/Vs at low operation voltage (<5V), with a low turn-on voltage of 0.5 V and sub-threshold-swing of 85 mV/decade. In case of ZnO-FETs this surface cleaning increases the source-drain current value upto ~7 μA from ~0.4 μA at a bias voltage of 3 V. ZnO-FETs fabricated in this study exhibits mobility of ~28 cm<sup>2</sup>/Vs and a high on-off ratio of ~10<sup>6</sup>. As fabricated FETs show a large hysteresis of ~5.0 to 8.0 V which is significantly reduced to ~1.0 V by surface treatment process.

### 9:00 AM

**Synthesis of Nanostructured Anatase and Its Grain Size Effect on Catalytic Properties:** *Francisco Robles Hernandez*<sup>1</sup>; *Leonardo Gonzalez-Reyes*<sup>2</sup>; *Isaias Hernández-Pérez*<sup>3</sup>; *Hector Dorantes Rosales*<sup>2</sup>; *Elsa Arce Estrada*<sup>2</sup>; <sup>1</sup>University of Houston; <sup>2</sup>Instituto Politécnico Nacional; <sup>3</sup>Universidad Autónoma Metropolitana

In the present paper are given the results of sono-synthesis of anatase nanoparticles that was heat treated at different times and temperatures to coarsen and investigate the effect of grain size and purity effects on catalytic properties of anatase. Pure anatase was coarsened from 6.2 nm to 28.3 nm and in a mix of anatase and rutile anatase reached a grain size of 89 nm, while pure rutile reaches a grain size of 232 nm. The coarsening kinetics of anatase and rutile show behaviors similar to those of described by the LSW theory. In this work

is proposed an algorithm to predict the surface characteristics of pure anatase based on the X-Ray diffraction results. Results of electro and photo catalysis are presented and are related to the surface characteristics of nanometric anatase. Anatase and/or rutile were characterized by means of: TEM, SEM, XRD, BET, UV-vis, Raman, Infrared, photo- and electro-catalysis.

### 9:15 AM

**ZnO Nanowires Doped with Al and Ga Synthesized by a Low-Temperature Solution-Based Process:** *Greg Kusinski*<sup>1</sup>; *Pooja Puneet*<sup>1</sup>; *Rodrigo Noriega-Manez*<sup>2</sup>; *L Goris*<sup>2</sup>; *Alberto Salleo*<sup>2</sup>; <sup>1</sup>Clemson University; <sup>2</sup>Stanford University

Zn-based oxides, due to the great natural abundance and low toxicity of Zn, are attractive replacement materials for indium tin oxide as transparent electrode in thin-film solar cells. ZnO can be made conductive by doping with group III elements. In this study, a solution-based chemistry was used to synthesize intrinsic, Al-doped and Ga-doped ZnO nanostructures. The nanowires were grown at 300°C in triethylamine by dissolving zinc acetate. The amount of dopant atoms was modulated by controlling the dopant salt (Aluminum acetate or Gallium nitrate) concentration in the solution to obtain the desired Al:Zn or Ga:Zn ratio. Different doping conditions gave rise to different nanoscale morphologies. The effect of a surfactant (oleic acid) was also investigated. An electron microscopy (TEM, HRTEM, EDS, EELS) study correlating the morphology, aspect ratio, surface roughness and doping of the individual ZnO wires to the electrical properties of the spin coated films is presented.

### 9:30 AM

**Synthesis of Titanium Oxide Nanotubes with Sonoelectrochemical Method:** *Saleh Nowrouzi*<sup>1</sup>; *Mehdi Attarchi*<sup>1</sup>; *S.K. Sadrnejad*<sup>1</sup>; *Behnam Gohari*<sup>1</sup>; <sup>1</sup>Material and Energy Research Center

Titanium oxide nanotubes have many important applications, for example in biomaterial, solar cell, hydrogen storage or gas sensing. Synthesis of these nanotubes are carried out upon applying electrical potentials, ranging from 20-150 v at various acidic solutions such as phosphoric acid and hydrofluoric acid. Sonoelectrochemical method is a new strategy for synthesis which shows very good results. The purpose of this investigation is synthesis of these nanotubes regarding the optimization of such parameters as solution composition, anodizing potential and ultrasound optimum situation in order to attain significant synthesis output.

### 9:45 AM

**Sonochemical Synthesis of TiO<sub>2</sub> Nanoparticles and the Effect on the Structural and Morphological Evolution under Thermal Treatment and Their Electrochemical Properties:** *Leonardo Gonzalez-Reyes*<sup>1</sup>; *Isaias Hernandez-Perez*<sup>1</sup>; *Hector Dorantes-Rosales*<sup>1</sup>; *Jose de Jesus Rivera*<sup>2</sup>; *Francisco Carlos Robles-Hernandez*<sup>3</sup>; <sup>1</sup>Instituto Politécnico Nacional; <sup>2</sup>UASLP; <sup>3</sup>Transportation Technology Center Incorporated

TiO<sub>2</sub> with an average grain size of 6 nm and BET surface area of 300 m<sup>2</sup>g<sup>-1</sup>, has been synthesized by Sonochemical method. The structure and particle size were determined by XRD and TEM. The stability of TiO<sub>2</sub> was studied in the range of 400 to 900°C. The TEM study elucidates porous spheres. Heat treated was accompanied by a change on the BET from 300m<sup>2</sup>g<sup>-1</sup> to 25 m<sup>2</sup>g<sup>-1</sup>. The electrochemical properties shows singularities that could be explain for the complex network of an original sample and quantum size effects. The influence of the size dependent and structure phase on store charge and current density, respectively. In fact, the highest current-charge magnitude is presented in the sample with a heat treatment of 450°C. It means that there is an optimal size, with its structural and morphological properties, to improve electro-reduction process. These analyses has been demonstrated and reported herein.

### 10:00 AM Break

### 10:15 AM

**Formation of Zirconia Coatings by Laser Ablation:** *Maxim Pugachevsky*<sup>1</sup>; *Alexander Kuz'menko*<sup>2</sup>; *Victor Zavodinsky*<sup>3</sup>; *Sergey Pyachin*<sup>3</sup>; <sup>1</sup>Institute of materials of Khabarovsk scientific centre of Far Eastern Branch of the Russian academy of Sciences; <sup>2</sup>Pacific national university; <sup>3</sup>Institute of Materials of Khabarovsk Scientific Centre of Far Eastern Branch of the Russian Academy of Sciences

Zirconia coatings were formed on monocrystalline silicon substrate by laser ablation. Zirconia monoclinic powder alloyed by CO<sub>2</sub> laser was used as a source. The pulsed radiation (YAG: Nd<sup>3+</sup>) was used with pulses up to 1ms and power up to 1 kWatt. The maximal size of particles deposited on the substrate was limited by the special filter. The SEM, TEM, AFM and X-ray analyses have shown that

the coating consists of particles of the cubic phase. A probable mechanism for cubic ordering of the ablated ZrO<sub>2</sub> is thermal stabilization.

#### 10:30 AM

**Fabrication and Characterization of Single TiO<sub>2</sub> Nanotube for Chemical and Bio Sensor Applications:** *Mingun Lee*<sup>1</sup>; Dongkyu Cha<sup>1</sup>; Hyunjung Shin<sup>2</sup>; M.J. Kim<sup>1</sup>; Jiyoung Kim<sup>1</sup>; <sup>1</sup>University of Texas at Dallas; <sup>2</sup>Kookmin University

Focus has been placed on TiO<sub>2</sub> nanotubes as a material for emerging applications particularly chemical and biological sensors. It is nontoxic and provides not only a large surface to volume ratio but also an open capped hollow structure. The nanotubes also exhibited n-type semiconductor behavior and show electrical conductance modulation under different environments. This implies the feasibility of using TiO<sub>2</sub> nanotubes for chemical sensors. Additionally, we explore their applications as biomaterial detectors. The surface of the nanotubes was functionalized by SAM (Self Assembly Monolayer) compounds with various terminal functional groups, such as carboxylic and alkoxyl groups, to detect other species selectively. In this study, we will present the viability of functionalized TiO<sub>2</sub> nanotubes for bio-sensors with selective detection. This research was supported by a grant (code #: M105KO010026-05K1501-02611) from 'Center for Nanostructured Materials Technology' under '21st Century Frontier R&D Programs' of the Ministry of Science and Technology, Korea.

#### 10:45 AM

**The Photocatalytic and Antimicrobial Activity of Cotton Fabrics Treated with Silver-Doped Titanium Dioxide Nanocrystals:** Guoliang Li<sup>1</sup>; Bing Peng<sup>1</sup>;

<sup>1</sup>School of Metallurgical Science and Engineering, Central South University

Cotton fabrics were treated with silver-doped titanium dioxide nanocrystals in self-made finishing agent and general non-iron finishing agent to provide the photocatalytic and antimicrobial properties for cotton fabrics by linking of silver-doped titanium dioxide to cellulose structure. The concentration of silver-doped TiO<sub>2</sub> nanocrystals in the finishing agents as well as the treatment conditions significantly affected the properties of treated cotton fabrics. The treated cotton fabrics showed fine photocatalytic activity to enhance the decolorization, degradation of methyl orange under UV light irradiation, good antimicrobial activity against *Escherichia coli*, and strong time effectiveness of photocatalytic and antimicrobial properties which was characterized by the standard test to washing. The optimal property was obtained when the cotton fabrics were first treated with general non-iron finishing agent, then self-made finishing agent including 3% silver-doped TiO<sub>2</sub> nanocrystals, predried at 80° for 5 min, and cured at 120° for 3min.

#### 11:00 AM

**The Photocatalytic Activity of N-Doped TiO<sub>2</sub> under Sunlight:** Liqiang Liu<sup>1</sup>; Bing Peng<sup>1</sup>; *Liyuan Chai*<sup>1</sup>; <sup>1</sup>School of Metallurgical Science and Engineering, Central South University

In order to utilize sunlight in a photocatalytic reaction, yellow N-doped titania was prepared by calcination of a mixture of the hydrolysis product (H<sub>2</sub>TiO<sub>3</sub>) of TiOSO<sub>4</sub> and urea. The catalysts were characterized by XRD, SEM and UV-Vis absorption spectra. The results showed that all catalysts were anatase, and the doping of nitrogen could extend the absorption spectra from UV light to the visible light region. The photocatalytic activity of N-doped TiO<sub>2</sub> was also characterized by degradation of methyl orange. The results further showed that the photocatalytic activity was affected by calcination temperature, time, Ti/N ratio, pH and concentration of titania. The photocatalytic reaction rate of N-doped TiO<sub>2</sub> was more rapid than the pure titania. There existed an optimal Ti/N ratio for the catalysts calcined at 400°, which resulted in the highest photocatalytic activity.

#### 11:15 AM

**Erosion-Corrosion Resistance of Plasma Sprayed Nanostructured Titanium Dioxide Coating:** Abdul B. Jabbar<sup>1</sup>; *Ahmad Zaki*<sup>1</sup>; <sup>1</sup>KFUPM

Nanostructured Titanium Dioxide (n-TiO<sub>2</sub>) thermal sprayed coatings have demonstrated a superior strength and durability compared to conventional TiO<sub>2</sub> coatings. Whereas some studies on the corrosion resistance of plasma air sprayed n-TiO<sub>2</sub> coatings have been conducted in the past, data on the erosion-corrosion behavior of these coatings is seriously lacking. Nanostructured powder (99% min purity) from METCO; AE9340, AE9342, and AE9303 were used to make agglomerates. Powder AE9342 was spray dried and densified, whereas powder AE9303 was chemically precipitated and spray dried. A high density polyvinyl chloride (HDPVC) was constructed for erosion-corrosion studies. AE9342 showed a dense oxide layer and elongated oxide covered lamellae with a spherical

morphology and a very narrow inter-lamellar zone. AE9303 showed an uneven surface morphology and high pore density. The specimens were subjected to a maximum velocity of 4 ms<sup>-1</sup> in a NaCl-polystyrene slurry. Specimen AE9342 dried and densified showed a lower sensitivity to erosion-corrosion compared to AE9303 (dried and sintered n-TiO<sub>2</sub> coating). No appreciable difference between the corrosion resistance of conventional TiO<sub>2</sub> coated (standard) and n-TiO<sub>2</sub> coated (AE9342 was observed). The erosion-corrosion resistance of plasma sprayed microstructure TiO<sub>2</sub> coating depends mainly on the characteristic of the feed powder, dispersion of slurry, reconstituted nano-powder and the control of key spraying parameters. The resistance of the nanostructured coatings to erosion-corrosion may further be improved by using impervious sealants and bond coatings with greater adhesion with the substrate.

#### 11:30 AM

**Corrosion Behavior of Nanostructured Titanium Dioxide Coating in Neutral Sodium Chloride Solutions:** *Ahmad Zaki*<sup>1</sup>; Abdul B. Jabbar<sup>1</sup>; <sup>1</sup>KFUPM

Studies were undertaken to determine erosion corrosion resistance of plasma air sprayed nanostructured and conventional titanium dioxide coatings (n, TiO<sub>2</sub>) in a sodium chloride polystyrene slurry. Nanostructured powder (99% min purity) from METCO; AE9342, and AE9303 were used to make agglomerates. Powder AE9342 was spray dried and densified, whereas powder AE9303 was chemically precipitated and spray dried. Erosion corrosion studies were conducted in a customized loop. Specimen AE9342 showed a spherical surface morphology and very narrow inter-lamellar zone whereas AE9303 showed an uneven surface morphology and high pore density. Specimen AE9342 showed lower sensitivity to erosion-corrosion compared to AE9303. No appreciable difference between erosion corrosion resistance of conventional TiO<sub>2</sub> coated specimens and n-TiO<sub>2</sub> coated was found. It was observed that the erosion-corrosion resistance of plasma sprayed microstructure TiO<sub>2</sub> coating was dependent on the characteristic of feed powder, dispersion of slurry, reconstitution of nanopowder and control of key spraying parameters.

### Alumina and Bauxite: Bauxite Ore Handling and Benefication

Sponsored by: The Minerals, Metals and Materials Society, TMS Light Metals Division, TMS: Aluminum Committee

Program Organizers: Everett Phillips, Nalco Co; Sringeri Chandrashekar, Dubai Aluminum Co

Tuesday AM

Room: 2002

February 17, 2009

Location: Moscone West Convention Center

Session Chair: Songqing Gu, Zhengzhou Light Metal Research Institute

#### 8:30 AM Introductory Comments

#### 8:35 AM

**Mining Scheduling at Paragominas Bauxite Mine:** *Octavio Guimaraes*<sup>1</sup>; Henrique Santos<sup>1</sup>; Flavio Zelante<sup>1</sup>; Leonardo Alves<sup>2</sup>; <sup>1</sup>Vale; <sup>2</sup>Runge do Brasil

The chain of the bauxite and alumina business in terms of quality, costs and longevity is critical for the mine and refinery installations. This paper describes the impact of the size of the mine according to the bauxite quality required by the Refinery, the influence of level of knowledge of the deposit on the life of the mine, and finally, some scenarios changing the some economic factors, such as price on the bauxite. So, there are several scenarios, which could help the decision maker to get the best solution joining the financial, quality and other strategic issues. Beside this, each scenario results gives a better understanding of the business risks and opportunities to improve the results.

#### 9:00 AM

**Transformation of Sodalite to Cancrinite under High Temperature Bayer Digestion Conditions:** Peter Smith<sup>1</sup>; *Bingan Xu*<sup>1</sup>; Christine Wingate<sup>1</sup>; <sup>1</sup>CSIRO

Cancrinite forms in high silica bauxite digestion at high temperature and is important to the Bayer process owing to its capacity to sequester impurities. Transformation conversion of sodalite (SOD) to CAN in synthetic pregnant liquor at 250°C was measured by using a quantitative XRD method on residues. The effect of sodium carbonate in liquor, lime charge, lime type and reaction time was investigated on the transformation. It was found that the proportion of cancrinite increased with the concentration of Na<sub>2</sub>CO<sub>3</sub> in the absence of lime.



Lime dramatically promoted the transformation which was largely complete in a few minutes. Lime charge and type had little effect on the amount of total CAN (both sodium and calcium type) but was related to the fraction of total CAN that was calcium substituted. Formation of tri-calcium aluminate and calcite consumed a large portion of the added lime, reducing the efficiency of CAN formation. Silica concentration in Bayer green liquor decreased with increasing CAN, suggesting CAN formation is beneficial to alumina quality and scaling control. Soda reduction in DSP is directly related to calcium content in CAN, indicating that the mechanism of soda reduction is the substitution of calcium for sodium in cancrinite cage.

**9:25 AM**

**Desilication of Bauxite Ores Bearing Multi-Aluminosilicates by Thermochemical Activation Process:** *Guanghai Li<sup>1</sup>; Tao Jiang<sup>1</sup>; Na Sun<sup>1</sup>; Xiaohui Fan<sup>1</sup>; Guanzhou Qiu<sup>1</sup>; <sup>1</sup>Central South University*

The bauxite ores are relatively abundant in China, but most of them are disopore type, which is characterized as high aluminum, high silicon content, and low A/S ratio in comparison with gibbsite ores. Silica minerals mainly occur as aluminosilicates such as kaolinite, pyrophyllite, illite etc. It is difficult to remove SiO<sub>2</sub> from the ores and to increase A/S ratio by physical processing methods. As the three aluminosilicate minerals can be activated and form active amorphous SiO<sub>2</sub> by thermal treatment, thermochemical activation (TCA) process followed alkali-leaching was developed to remove SiO<sub>2</sub> from the ores. By the process, a concentrate with 11 A/S ratio and 50% desilication has been achieved for a raw bauxite ore of 5.88 A/S ratio, with 12.5% illite, 6.0% pyrophyllite, 3.2% kaolinite under the optimum conditions of thermal activation and alkali leaching. Chemical principle of thermochemical activation of aluminosilicates has also been investigated in this paper.

**9:50 AM**

**Reductive Roasting and Magnetic Separation of Greek Bauxite Residue for Its Utilization in Iron Ore Industry:** *Anthimos Xenidis<sup>1</sup>; Charalabos Zografidis<sup>1</sup>; Ioannis Kotsis<sup>1</sup>; Dimitrios Boufounos<sup>2</sup>; <sup>1</sup>NTUA; <sup>2</sup>Aluminium of Greece SA*

The treatment of Greek bauxite residue through reduction roasting and magnetic separation is investigated. A sample of Greek bauxite residue, hematite being the predominant iron carrier mineral, is subjected to reduction roasting to produce a calcine with intense magnetic properties, where magnetite or metallic iron are the main iron mineral phases. The calcine is then subjected to wet magnetic separation so that the magnetic product can be utilized as a feed for sponge or cast iron production. The effect of parameters such as temperature, intensity of reducing conditions, intensity of magnetic field or dispersing agent addition rate on the result of both processes is investigated. It was indicated that reductive roasting at 500°C followed by wet magnetic separation of the calcine produced at low current intensity (0.04 A) and simultaneous addition of a dispersant resulted in the production of a magnetic product with iron content as high as 36%. The obtained results regarding iron recovery were very promising providing input for further research on the optimization of the proposed method.

**10:15 AM Break**

**10:35 AM**

**Reaction Behavior of Sulphur Existed in Diasporic Bauxite in Bayer Digestion Process:** *Zhonglin Yin<sup>1</sup>; Wu Guobao<sup>1</sup>; Li Xinhua<sup>1</sup>; Lu Peiqian<sup>1</sup>; <sup>1</sup>Zhengzhou Research Institute, CHALCO*

The reaction behavior of sulphur in Diasporic bauxite in Bayer digestion process is studied in this essay. The reaction extent of sulphur in Diasporic bauxite is enhanced along with the increase of the lime dosage in Bayer digestion process. The majority of the sulphur contained in the bauxite was leached into digestion liquor with in the form of S<sup>2-</sup> and the percentage of the sulphur which would be in the red mud is about 20-30%. Only a little sulphur can be removed when the bauxite is calcined at some conditions. The main form of sulphur in the digestion liquor is SO<sub>4</sub><sup>2-</sup> and about 50-60% sulphur in the bauxite will come into the red mud, the Na<sub>2</sub>S concentration in the digested liquor is less than 0.05g/L after the bauxite is calcined.

**11:00 AM**

**Roasting Pretreatment of High Sulfur Bauxite of China:** *Guozhi Lv<sup>1</sup>; Ting-an Zhang<sup>1</sup>; Li Bao<sup>1</sup>; Yan Liu<sup>1</sup>; Zhihe Dou<sup>1</sup>; Yan Li<sup>1</sup>; Xiaochang Cao<sup>1</sup>; Jicheng He<sup>1</sup>; <sup>1</sup>Northeastern University*

Effects of roasting temperature and roasting time on sulfur content of bauxite, digestion performance and settling performance of high sulfur bauxite by roasting pretreatment using Rotary tube furnace were studied. Changes of microscopic

appearance and crystal structure were analyzed by SEM and XRD. The results indicate that the sulfur content are successfully discharged as gas form through roasting, sulfur content of high sulfur bauxite meets the industrial standard at the conditions roasting temperature of 750° and holding time of 60min. The digestion rate of alumina is above 97% at the condition of digestion temperature of 220° and holding time of 60min. Roasting pretreatment make the apparent of red mud loose and porous, and transformed goethite into hematite, the settling performance were improved, particles size of red mud became smaller greatly. The digestion slurry of roasting ore in Rotary tube furnace has better settling performance than head ore.

**11:25 AM Concluding Comments**

## Aluminum Alloys: Fabrication, Characterization and Applications: Processing and Properties

Sponsored by: The Minerals, Metals and Materials Society, TMS Light Metals Division, TMS: Aluminum Processing Committee

Program Organizers: Weimin Yin, Williams Advanced Materials; Subodh Das, Phinix LLC; Zhengdong Long, Kaiser Aluminum Company

Tuesday AM  
February 17, 2009

Room: 2004  
Location: Moscone West Convention Center

*Session Chair:* Gyan Jha, ARCO Aluminum Inc

**8:30 AM**

**Multiple Extrusion and Consolidation of Al-4Mg-1Zr:** *Daniel Aguilar Garcia<sup>1</sup>; Richard Dashwood<sup>2</sup>; Martin Jackson<sup>3</sup>; David Dye<sup>1</sup>; <sup>1</sup>Imperial College; <sup>2</sup>University of Warwick; <sup>3</sup>University of Sheffield*

In the continued quest for metallic alloys with better properties, metallurgists have employed a variety of thermo-mechanical processing routes and non-conventional methods. While steady progress has been made in this area, recent work promises to produce alloys with a step change in properties via severe plastic deformation (SPD) techniques. Several SPD techniques are now being studied such as Equal-Channel Angular Pressing (ECAP), High Pressure Torsion (HPT) and Accumulative Roll Bonding (ARB). In this paper a new SPD technique is applied to a novel experimental alloy, Al-4Mg-1Zr. The alloy has been subjected to six passes of conventional extrusion. The mechanical properties and the microstructure was studied after each pass. Analysis showed that after the each pass the microstructure has been refined, the primary Al<sub>3</sub>Zr particles were broken down and the hardness increased slightly. However, the yield stress and the ultimate strength increased significantly after the first pass and decreased for the following passes.

**8:50 AM**

**Al-Zn-Mg for Extrusion - Hot Workability:** *Hugh McQueen<sup>1</sup>; Paola Leo; Emanuela Cerri<sup>2</sup>; <sup>1</sup>Concordia University; <sup>2</sup>University of Salento*

Al-Zn-Mg alloys (without Cu: lower strength, less quench sensitivity) are useful for terrestrial applications due to good extrudability. As-cast Al-5.5Zn-1.2Mg was torsion tested over 250 - 500°C and 10-2 to 5 s-1. The peak strength fell markedly from 300 to 400°C and then slowly up to 500°C; it was lower for lower strain rates. In the aged starting material, this is indicative of more rapid precipitate coalescence and solution at higher temperature. The ductility rose rapidly from 300 to 400°C and with decreasing strain rate, but a 500°C, it was high but inconsistent. The constitutive analysis by the sinh equation gave Q, 165 kJ/mol; n = 1. Elongated grains exhibited larger subgrains at higher temperature. In hot tensile tests, flow curve shapes are similar, peak stresses are fairly consistent (218 kJ/mol; n, 1.75) and ductility (fivefold less) varies similarly. Comparison is made to 7004, 7020, 7075 and 7012 alloys.

**9:10 AM**

**Microstructural Control through Heat Treatment Process in an Aerospace Aluminum Alloy:** *Zainul Huda<sup>1</sup>; <sup>1</sup>University of Malaya*

The 2017 aerospace aluminum alloy was characterized through metallographic investigations. A series of precipitation strengthening and age-hardening heat treatment processes involving solution treatment at 550°C followed by quenching (and tempering for various time-durations) were conducted for the 2017 alloy. Microstructural characterization of the heat-treated samples showed effective distribution of fine θ' particles in the α-matrix of the aluminum alloy; these

microstructural features enable us to develop proper precipitation strengthening and age-hardening heat-treatment process parameters for the 2017 aluminum alloy for aerospace application.

9:30 AM

**Microstructure and Mechanical Properties of Cast Hypereutectic Al-Si Alloys with High Magnesium Content:** *Animesh Mandal*<sup>1</sup>; M.M. Makhlof<sup>1</sup>; <sup>1</sup>Worcester Polytechnic Institute

Magnesium in excess of the quantities typically found in commercial hypereutectic Al-Si alloys can produce alloys with enhanced microstructure and attractive mechanical properties. With addition of Mg to hypereutectic Al-Si alloys, the primary silicon phase is suppressed and is replaced with a fine dispersion of small Si particles. However, an abundance of large Mg<sub>2</sub>Si particles with Chinese script morphology also forms in the microstructure and unfavorably influence the tensile properties of the alloy. Efforts were made to overcome the negative effects of these particles by manipulating their size and morphology. Several additives were made to a hypereutectic Al-Si-Mg alloy and their effect on the cast alloy was determined. The alloy treated with Misch Metal and Strontium showed promising results. The Mg<sub>2</sub>Si particles that formed in castings made from this alloy were very small and almost spherical; and the room temperature tensile and yield strengths of cast bars were remarkably high.

9:50 AM

**Electron Microscopy of Commercial Purity Al-2024 (Al-Mg-Cu) after Accumulative Roll-Bonding:** *Andreas Kulovits*<sup>1</sup>; Bryan Webler<sup>1</sup>; Anirudha Deshpande<sup>1</sup>; Jorg Wiezorek<sup>1</sup>; <sup>1</sup>University of Pittsburgh

Al-2024 has been severely plastically deformed using accumulative roll bonding (ARB), which increased the hardness from a value equivalent to a tensile strength of about 410MPa (HV=138) prior to deformation to about 720MPa (HV=225). Changes in the microstructure have been investigated using imaging, diffraction and analytical methods of transmission electron microscopy (TEM). Two morphologically different regions, namely an ultra-fine grained (UFG) region that contains elongated grains and regions comprised of equiaxed nanocrystalline (NC) grains, have been observed in the ARB product. Electron diffraction analysis showed that the same phases were present prior to and after severe plastic deformation by ARB in the UFG regions. In the NC region, however, evidence of dynamic solid-state reactions has been observed experimentally. The application of high strains in conjunction with dynamic microstructural transformations facilitates grain refinement beyond the UFG regime into the NC size regime for this commercial purity Al-alloy.

10:10 AM

**Annealing Behavior of an Heavily Deformed Aluminum Alloy in 20 Tesla Magnetic Field:** *Samuel Adedokun*<sup>1</sup>; <sup>1</sup>FAMU-FSU College of Engineering

A plate of aluminum alloy 6061 was given 85% deformation by cold rolling. Samples from the rolled specimen were heat treated for different times and at different temperatures in a 20 tesla resistive magnetic field. The effect of time and temperature on the heavily deformed specimens under 20 Tesla magnetic field was examined with the use of an Environmental Scanning Electron Microscopy equipped with an Orientation Imaging Microscopy (OIM) to study the changes in the grain size distribution and the grain boundary misorientation of the samples tested. The results indicate that the magnetic field of 20 Tesla increased the average grain size of the Aluminum alloy 6061 when compared with the aluminum alloy heat treated when the magnetic field was turned off. No effect on the grain boundary misorientation was noticed.

10:30 AM Break

10:45 AM

**Effects of Ultrasonic Treatment on Microstructures of Hypereutectic Al-23%Si Alloys:** *Haikuo Feng*<sup>1</sup>; <sup>1</sup>Jilin University

Microstructures and properties of Al-23%Si alloys were gained with and without ultrasonic treatment in a novel horn crucible designed specially for this experiment. Evolution, morphology and distribution of microstructure of alloys were investigated. The results show that the size of primary Si particulates decreased from 500µm to 180µm and the morphology of α-Al phase had been changed from dendritic crystal to equiaxial crystal under the ultrasonic treatment. However eutectic phase was coarser than that without ultrasonic treatment. In addition the ultimate tensile strength and the wear resistance of Al-23%Si alloy with ultrasonic treatment were better than that without ultrasonic treatment. The key on better properties of alloys treated by ultrasonic were discussed.

11:05 AM

**Distribution of Trace Elements in Sr-Modified and Grain Refined Hypoeutectic Al-Si Alloy:** M. Faraji<sup>1</sup>; L. Katgerman<sup>2</sup>; *Amir Masoud Akbari Pazooki*<sup>2</sup>; <sup>1</sup>M2i/ Delft University; <sup>2</sup>Delft University of Technology

The nucleation process of a commercial hypoeutectic Al-Si foundry alloy (Al-7Si-0.4Mg) unmodified, Sr-modified, grain-refined and Sr-modified + grain-refined has been investigated using optical microscopy and scanning electron microscopy (SEM). The results showed that adding strontium increased the number of eutectic silicon particles sensibly; however, the size of particles did not change considerably. Additionally, the results showed that grain refiner (AlTiB) reduced the incidence and size of porosities in both grain-refined and combined modified and grain-refined specimens compared to untreated condition. To study solidification and responsible mechanism of nucleation and modification in this alloy, electron probe microanalysis technique (EPMA) was used and the distribution of trace elements such as titanium, boron, phosphorus and strontium in the microstructure was analysed. Using EPMA, the negative interaction of strontium and AlTiB was closely examined and the optimised level of addition is suggested as 20 ppm boron (present in Al-3Ti-B) and 200 ppm strontium.

11:25 AM

**Effects of Zn on the Microstructures and Mechanical Properties of Al-Mg-Mn-RE Alloys:** *Hua Shen*<sup>1</sup>; Guangchun Yao<sup>1</sup>; Weidong Yang<sup>1</sup>; <sup>1</sup>School of Materials and Metallurgy Northeastern University

Al-2.3,4wt%Mg-0.6wt%Mn-0.3wt%RE alloys were prepared and effects of different Zn contents on the microstructures and mechanical properties of Al-Mg-Mn-RE alloys were studied in this work. Microstructures mechanism thinks that intensifying phase MgZn<sub>2</sub> could be formed while adding Zn and Mg simultaneously to aluminum, so intensifying action produced obviously to alloys. Mechanical tests were carried out at room temperature. The results showed that Al-Mg-Mn-Zn-RE alloys were of resisting crazing stress and enough intension when Zn/Mg ratio was 2.7. Rigidity tests results showed that these series of alloys were harder than pure aluminum.

11:45 AM

**Solidification and Processing of Aluminum Based Immiscible Alloys:** *Hiren Kotadia*<sup>1</sup>; Jayesh Patel<sup>1</sup>; Zhongyun Fan<sup>1</sup>; Evelyn Doernberg<sup>2</sup>; R. Schmid-Fetzer<sup>2</sup>; <sup>1</sup>Brunel University, West London; <sup>2</sup>Clausthal University of Technology

The Al-Sn based immiscible alloys have significant potential for bearing and superconducting applications. However, the mixing and understanding of solidification process for immiscible alloys have been long standing challenges for their development. This paper presents solidification, microstructural evolution of the Al-Sn-Cu alloys and describes the mechanism of effective mixing by the intensive shearing. The solidification path of Al-Sn-Cu alloys was systematically investigated with differential scanning calorimeter and compared with the calculated phase diagrams. The experimental work was also focused on analyzing the effects of shear rate, temperature and time on Sn-rich droplet size and their distribution. Mechanical properties of solidified Al-Sn-Cu alloys have been investigated. Experimental results suggest that the intensive shearing process produces homogeneous, finely dispersed Sn-rich droplets and improves mechanical properties.

## Aluminum Hot Rolling: Session I

Sponsored by: The Minerals, Metals and Materials Society, TMS Light Metals Division, TMS: Aluminum Processing Committee  
Program Organizer: Kai Karhausen, Hydro Aluminium

Tuesday AM

Room: 2010

February 17, 2009

Location: Moscone West Convention Center

*Session Chair:* Kai Karhausen, Hydro Aluminium

### 8:30 AM Introductory Comments

#### 8:35 AM Keynote

**Through-Process Texture and Microstructure Modeling of Aluminum Alloys from Hot Rolling through Final Annealing:** *Guenter Gottstein*<sup>1</sup>; Carmen Schaefer<sup>1</sup>; Volker Mohles<sup>1</sup>; Olga Sukhopar<sup>1</sup>; <sup>1</sup>RWTH Aachen

An improved through-process modeling scheme is proposed for the prediction of recrystallization textures and microstructures during sheet processing. The

deformation behavior is modeled by the advanced deformation texture model GIA-3IVM+, which is based on a multi-grain approach and incorporates the work hardening behavior in terms of the dislocation density evolution. The recrystallization model utilizes a spatially resolved adaptive cellular automaton code CORE, which also considers orientation dependent recovery on a grain level. Since the treatment of recovery in CORE is consistent with the formulation in GIA-3VM+ this enables the consequent tracking of changes in dislocation densities throughout the whole process. Nucleation is accounted for by separate nucleation models which allow for different nucleation mechanisms to become active. The final microstructure after recrystallization depends sensitively on the nucleus frequencies and on the amount of prior recovery. The presented modeling setup allows an improved prediction of final recrystallization textures and grain sizes.

## 9:15 AM

**Modeling Hot Rolling of Al-705X Alloys:** *Margaret Koker*<sup>1</sup>; Jonathan Dantzig<sup>2</sup>; Armand Beaudoin<sup>1</sup>; <sup>1</sup>University of Illinois At Urbana-Champaign; <sup>2</sup>University of Illinois at Urbana-Champaign

We present a model for texture, damage and recrystallization evolution during hot rolling of Al-705X alloys. A constitutive model, based on experimental hot compression tests, is implemented as a non-Newtonian fluid. The rolling process is then simulated through multiple passes at user-specified draft and speed, and the results are used as input to a viscoplastic self-consistent model for texture evolution to predict the final texture as a function of position in the slab. The model is calibrated using measured temperatures, textures, roll torque, and other process features. We also predict damage in the rolled slab using a model that combines shear rate and temperature. The model is conveniently packaged into a graphical user interface. We present several case studies to show how the model can be used to improve rolling practices.

## 9:35 AM

**Property Control during Aluminum Sheet Fabrication Using the Through Process Modelling (TPM) Approach:** *Nitin Singh*<sup>1</sup>; Nicolas Kamp<sup>2</sup>; Richard Hamerton<sup>1</sup>; <sup>1</sup>Novelis Global Technology Centre; <sup>2</sup>Novelis Deutschland GmbH

The importance of linking fabrication process steps with microstructural evolution within the Aluminium Rolling industry is widely recognized and work has progressed in alliance with universities in developing process informed microstructural models. The aim is to gain an in-depth understanding of the link between certain process steps e.g. casting, homogenization, rolling etc. and the material microstructure. This knowledge becomes particularly important when new alloys and new processes are being introduced on an industrial scale. Novelis uses the physically based models developed by IMM, RWTH University, Aachen in their TPM efforts. In this presentation, our experience with successes and difficulties in calibrating these models to specific alloys and their implementation in predicting microstructures would be discussed. A comparison would be made with certain in-house models developed over many years to suggest directions for further development of these models.

## 9:55 AM

**Profile Optimization on a Duo Hot Mill:** *Kai Karhausen*<sup>1</sup>; Ioannis Neitzel<sup>1</sup>; Luca Francescutti<sup>1</sup>; <sup>1</sup>Hydro Aluminium

Although state of the art hot rolling mills are usually in quarto-design, equipped with computer controlled profile and shape control actuators, older duo mill stands are still in operation in some locations. Such mills are either limited in their product range or have only limited possibilities to control the strip profile for a larger variety of product qualities. Essentially only the ground work roll crown combined with a suitable pass schedule can be changed to affect the strip profile. In the present paper, a duo mill has been analyzed with the aim of finding an operating window for a given target profile covering a large spectrum of alloys and strip widths. By a series of profile/shape simulations on the whole production spectrum, the thermo-mechanical behavior of the stand was characterized and the sensitivity of the main factors for the profile generation was determined. Finally an optimum set of differently ground work roll crowns was determined by computer simulation to achieve a defined strip profile for the whole production spectrum.

## 10:15 AM Question and Answer Period

## 10:25 AM Break

## 10:40 AM

**Evaluation of Recovery Kinetics of the Aluminum Alloy AA3103 Using Stress Relaxation and Double Tension Tests:** *Sheila Bhaumik*<sup>1</sup>; Günter Gottstein<sup>1</sup>; Volker Mohles<sup>1</sup>; <sup>1</sup>IMM

The softening processes, recovery and recrystallization, are of significant scientific and technological relevance especially for materials with high stacking fault energy. Since recovery is always connected to recrystallization, there is an urgent need to advance our understanding of recovery in particular with regard to through process modeling. Within the scope of the project stress relaxation and double tension tests at elevated temperatures were conducted on a commercial aluminum alloy 3103. The recorded stress-time evolution based on the stress relaxation and double tension tests were compared to gain a better understanding of the mechanisms governing the recovery processes and to obtain a reliable evaluation of recovery kinetics as well. This comparison enables to verify whether the low cost stress relaxation measurements can, in principle, replace the more laborious double compression tests. Furthermore, the obtained parameters for recovery were analyzed in terms of temperature dependency etc.

## 11:00 AM

**Patterns of Deformation and Associated Recrystallization in Warm/Hot Deformed AA6022:** *S. Raveendra*<sup>1</sup>; S. Mishra<sup>1</sup>; H. Weiland<sup>2</sup>; I. Samajdar<sup>1</sup>; <sup>1</sup>IIT Bombay; <sup>2</sup>ALCOA

Microstructural developments during hot-rolling of aluminum alloys significantly impact the forming process. In a deformation simulator, AA6022 samples were plane strain compressed (equivalent to hot-rolling) at different temperatures and strain rates to strains of 1 and 2. The deformed samples contain finite percentage of static recrystallization. The deformed/recrystallized regions were partitioned based on in-grain misorientation developments and grain size. Zener Holloman parameter (Z), which ties deformation temperature and strain rate had clear effects on microstructure and textural changes. At lower Z, i.e. at higher deformation temperatures, there is increase in deformed Cube {001} <100> (with increase in strain), which is due to the thickening of deformed Cube bands. Such a pattern cannot be explained from Taylor type deformation texture simulations, incorporating both octahedral and non-octahedral slip systems. These, in turn, strongly affected the associated recrystallization behavior – including relative contributions from particle stimulated nucleation and contributions from deformed grains/bands of different ideal orientations.

## 11:20 AM

**Pore Evolution during the Homogenization and Rolling of Direct Chill Cast Al-6Mg Alloy:** *Richard Dashwood*<sup>1</sup>; Anirut Chaijaruwanich<sup>2</sup>; Hiromi Nagaumi<sup>3</sup>; Peter Lee<sup>4</sup>; <sup>1</sup>University of Warwick; <sup>2</sup>King Mongkut's Institute of Technology; <sup>3</sup>Nippon Light Metal Company Ltd; <sup>4</sup>Imperial College London

The evolution of porosity during homogenisation and rolling (with a low reduction per pass) was quantified using two-dimensional metallography and three-dimensional X-ray microtomography (XMT) techniques. This paper will demonstrate the misinterpretations that can take place when only considering metallographic evidence. For example the metallographic evidence implied that the mean pore size increased during homogenisation and also in the centre of the plate during the initial rolling passes. However XMT demonstrated that intra-pore Ostwald ripening of the tortuous pore networks formed during DC casting was the key mechanism driving the evolution of pore morphology. Finite element modelling showed that during the initial low reduction ratio rolling passes the central region of the plate experienced a tensile, rather than a compressive, hydrostatic stress, explaining the initial pore ripening. A relationship between the roll geometry and the hydrostatic stress has been derived and the critical geometry identified.

## 11:40 AM

**Effect of Homogenization Treatment on Microstructural Evolution of 1050 and 1200 TRC Aluminium Alloys:** *Aziz Dursun*<sup>1</sup>; Beril Corlu<sup>1</sup>; Canan Inel<sup>1</sup>; Murat Dundar<sup>1</sup>; S. Levent Aktuđ<sup>1</sup>; <sup>1</sup>Assan Aluminium

Homogenization in twin roll casting (TRC) is an essential annealing treatment in order to obtain desired mechanical and microstructural properties like deep drawability in heat shield (1050) and matte surface appearance in packaging foil (1200) applications. Gradients in solification rates developed during TRC results in concentration gradients throughout the thickness with a supersaturated region of alloying elements near the surface. In order to minimize the influence



of concentration gradients on material performance and ensure homogeneously distributed particles, a series of homogenization treatments between 520 and 580 °C at different holding time were performed on 1050 and 1200 aluminium alloys. Size, distribution and composition of secondary particles were determined using an optical and scanning electron microscope. Microstructural evolution were monitored by hardness and tensile tests results. The results showed that a critical homogenization temperature and holding time lead to significant coarsening and more uniform particle size distribution thereby superior properties for both alloys.

### 12:00 PM

#### **Characterization of Edge Cracking Using a Crystal Plasticity Model with Damage Evolution:** *Soondo Kweon*<sup>1</sup>; Armand Beaudoin<sup>1</sup>; Russell J. McDonald<sup>1</sup>;

<sup>1</sup>University of Illinois at Urbana Champaign

A challenge to the analysis of edge cracking in aluminum rolling industry lies in the nature of the stress state at the side of the slab: traditional models for damage evolution are dependent on the state of tensile hydrostatic stress, whereas edge cracking is developed at free surfaces and in the presence of shear. Recent research efforts have augmented traditional models for damage to include the effect of shear, through the Lode parameter. These models are generally applied through use of J2 plasticity. In this study, we focus on thermo-mechanical conditions leading to edge cracks, giving attention to the mesoscale process of grain-to-grain interaction. A polycrystal, modeled using finite elements, is subjected to different loading conditions. Hydrostatic stresses develop through grain interaction, even with "average" deformations of pure shear. The development of damage in the polycrystal, both with and without use of the Lode parameter, is contrasted with experimental results.

### 12:20 PM Question and Answer Period

#### **Aluminum Reduction Technology: Potline Performances and Vision**

Sponsored by: The Minerals, Metals and Materials Society, TMS Light Metals Division, TMS: Aluminum Committee  
Program Organizers: Gilles Dufour, Alcoa Canada, Primary Metals; Martin Iffer, Trimet Aluminium AG; Geoffrey Bearne, Rio Tinto Alcan; Jayson Tessier, Alcoa Deschambault

Tuesday AM Room: 2001  
February 17, 2009 Location: Moscone West Convention Center

*Session Chair:* Jules Côté, Aluminerie Alouette Inc

### 8:30 AM Introductory Comments

#### **8:35 AM Panel Discussion**

*Representatives from eight smelters around the world are invited to present performances achieved at their smelters.*

### 11:15 AM Question and Answer Period

*The smelter representatives will answer questions from the audience.*

#### **Biological Materials Science: Drug Delivery and Imaging**

Sponsored by: The Minerals, Metals and Materials Society, TMS Structural Materials Division, TMS Electronic, Magnetic, and Photonic Materials Division, TMS: Biomaterials Committee, TMS/ASM: Mechanical Behavior of Materials Committee  
Program Organizers: Ryan Roeder, University of Notre Dame; John Nychka, University of Alberta; Paul Calvert, University of Massachusetts Dartmouth; Marc Meyers, University of California

Tuesday AM Room: 3014  
February 17, 2009 Location: Moscone West Convention Center

*Session Chairs:* John Nychka, University of Alberta; Paul Calvert, University of Massachusetts

### 8:30 AM Keynote

**Lipid-Modified Polymers as Biomimetic Nucleic Acid Carriers:** *Hasan Uludag*<sup>1</sup>; Vanessa Incani<sup>1</sup>; Artphop Neammark<sup>1</sup>; Orawan Suwanton<sup>1</sup>; <sup>1</sup>University of Alberta

Cationic polymers are utilized to deliver anionic plasmid DNA into cells. The polymer condense string-like DNA molecules into compact structures for passage through the plasma membrane. The cationic polymers, however, are effective only at doses where significant toxicities on cells are observed. Our research program aims to utilize naturally-occurring lipids to enhance the ability of polymers for DNA delivery into primary cells. Using lipid conjugates, we obtained polymers that were capable of condensing plasmid DNA effectively into 100-200 nm particles. The particle sizes were effectively controlled by the hydrophobic substitution on the polymer, achieving lower particle sizes with more hydrophobic polymers. The hydrophobic polymer were capable of enhancing the delivery of plasmid DNA into the cells by ~10-fold. Using a model gene (GFP), the designed polymers enabled improved GFP expression in primary cells. Structure-function relationships on the effectiveness of designed cationic polymers will be presented.

### 9:10 AM Invited

**Cell Membrane Penetrating Nanoparticles:** *Francesco Stellacci*<sup>1</sup>; <sup>1</sup>MIT

Non biological materials when in contact with cells are either endocytosed or created transient pores that allow cell entrance but are cytotoxic. Cell penetrating peptides on the other hand have the property of permeating cell membranes without generating transient pores. We will show that gold nanoparticles coated with a mixture of hydrophobic and hydrophilic ligand molecules are simply endocytosed when these molecules have no special arrangement but behave as cell penetrating peptides when the molecules are arranged in an ordered fashion.

### 9:40 AM

**Exploring Transferrin-Receptor Mediated Nanoparticle Cell Interactions at Single-Molecule Level during Cellular Uptake:** *Abhilash Vincent*<sup>1</sup>; Suresh Krishna Moorthy<sup>1</sup>; Eric Heckert<sup>1</sup>; William Self<sup>1</sup>; Christopher Reilly<sup>2</sup>; Sudipta Seal<sup>1</sup>; <sup>1</sup>University of Central Florida; <sup>2</sup>Virginia Tech

Recent studies indicate that cerium oxide nanoparticles (Cerium NPs) can function as biological antioxidants due to their ability to switch between different oxidation states. Hence Cerium NPs show tremendous potential in cancer therapeutics and it is important to develop Cerium NPs supported chemotherapeutics drugs that can target cancerous cells and destroy them without affecting neighboring healthy cells. This is achieved by bioconjugating Cerium NPs with targeting agents that can bind to the over expressed receptors on the target cancer cell. In this work we are focusing on understand the cellular uptake mechanism of Transferrin protein coated Cerium NPs by A549 lung cancer cell. Single Molecule Force Spectroscopy (SMFS) was used to study the interaction force between Transferrin protein coated Cerium NPs and cancer cells. Inductively Coupled Mass Spectrometer (ICPMS) results indicates A549 cells treated with Transferrin coated Cerium NPs showed better uptake compared to the cells treated with uncoated NPs.

10:00 AM

**Controlled Release of Bovine Serum Albumin Protein Using Calcium Phosphate Nanocarriers:** Sudip Dasgupta<sup>1</sup>; Amit Bandyopadhyay<sup>1</sup>; Susmita Bose<sup>1</sup>; <sup>1</sup>Washington State University

Calcium phosphate (CaP) based ceramics are of significant interest due to their bioactivity and chemical similarity with inorganic component of bone. Bovine serum albumin (BSA) protein release behavior from  $\beta$ -tricalcium phosphate ( $\beta$ -TCP) and calcium deficient hydroxyapatite (CDHA) nanoparticles (NP) were studied. Both surface adsorption and chemical synthesis route were used to make protein loaded CaP nanocarriers. Pure and Zn<sup>2+</sup>/Mg<sup>2+</sup> doped hydroxyapatite (HA)-BSA NPs were synthesized by in situ co-precipitation technique. BSA release rate from ex situ synthesized  $\beta$ -TCP-BSA NPs found to be faster compared to that from CDHA-BSA NPs. Pure HA-BSA NPs showed slower BSA release compared to doped HA-BSA NPs. The presentation will focus on the effect of doping, crystallinity and synthesis process on BSA release behavior from CaP based nanocarriers.

10:20 AM Break

10:30 AM Invited

**Characterization of Implantable Drug Delivery Bioceramics Using Magnetic Resonance Imaging (MRI):** Joshua Bray<sup>1</sup>; Mark Filiaggi<sup>1</sup>; Steven Beyea<sup>2</sup>; <sup>1</sup>Dalhousie University; <sup>2</sup>National Research Council of Canada

While novel and innovative interventions in regenerative medicine hold great promise, such methods are only as effective as the ability to develop an empirical and mechanistic understanding of how/why they work. One such example is the use of resorbable bioceramics, which have potential to provide large, sustained concentrations of therapeutic agents to a specific tissue, while not exceeding the minimum toxic concentration in other tissues. Optimization of resorbable bioceramic design requires methods that will permit the non-invasive and non-destructive study of the spatially and temporally varying physicochemical changes that occur due to material degradation. The study of drug delivery biomaterials using Magnetic Resonance Imaging (MRI) therefore has the potential to significantly improve our understanding of the performance of such devices. A host of complimentary MRI techniques (e.g. microscopy, diffusometry and relaxometry) were used to study changes in CPP bioceramics due to initial material processing and subsequent degradation.

11:00 AM

**Modeling Bio-Scaffolds: Structural and Fluid Transport Characterization Based on 3D Imaging Data:** Liang Hao<sup>1</sup>; David Raymont<sup>1</sup>; Bruno Notarberardino<sup>1</sup>; Philippe Young<sup>1</sup>; Ash Harkara<sup>1</sup>; <sup>1</sup>University of Exeter

Bio-scaffolds - which are commonly open celled porous structures - are increasingly used for tissue engineering and regenerative medicine. Numerical studies exploring the influence of architecture on structural and flow characteristics of porous media have been carried out assuming an idealized repeating unit cell approach. However, a number of studies have shown that the bulk properties of such irregular structures are poorly modeled using idealized unit cell approaches. High resolution three dimensional imaging techniques such as Micro-CT allow realistic porous structures to be straightforwardly and accurately scanned with sub-micron image resolutions. Combined with novel meshing techniques, these imaging techniques allow for robust conversion of the 3D data into models suitable for physics-based simulations. A number of studies will be shown which demonstrate the ease with which fidelic models can be generated and parametric studies will be presented which explore both fluid flow and structural properties of a range of bio-scaffolds.

11:20 AM

**Imaging Microdamage in Bone Using a Barium Sulfate Contrast Agent:** Matthew Landrigan<sup>1</sup>; Huijie Leng<sup>1</sup>; Ryan Ross<sup>1</sup>; Carl Berasi<sup>1</sup>; Xiang Wang<sup>1</sup>; Glen Niebur<sup>1</sup>; Ryan Roeder<sup>1</sup>; <sup>1</sup>University of Notre Dame

Accumulation of microdamage in bone tissue can lead to increased fracture susceptibility, including stress fractures in active individuals and fragility fractures in the elderly. However, clinically relevant damage and failure mechanisms remain poorly understood, in part, due to limitations imposed by current methods for imaging microdamage, which are inherently destructive, tedious and two-dimensional. Therefore, micro-computed tomography (micro-CT) has been investigated using a precipitated barium sulfate contrast agent to label damaged tissue. For proof-of-concept, the presence, spatial variation and accumulation of microdamage in cortical and trabecular bone specimens was nondestructively detected using micro-CT after staining with barium

sulfate. Damage quantification using micro-CT with a barium sulfate stain was further validated against conventional histological methods. Opportunities and limitations for the new imaging technique will be discussed.

11:40 AM

**Molecular Surface Modification of Gold Nanoparticles to Impart Specificity to Damaged Bone Tissue:** Ryan Ross<sup>1</sup>; Ryan Roeder<sup>1</sup>; <sup>1</sup>University of Notre Dame

The accumulation of microdamage in bone tissue can lead to increased fracture susceptibility. However, there are currently no non-invasive methods to detect damage in bone tissue. Therefore, gold nanoparticles (Au NPs) are being investigated as a potential damage-specific X-ray contrast agent due to their biocompatibility, ease of surface functionalization and high X-ray attenuation. Au NPs were synthesized by citrate reduction to a mean particle size of 20 nm and surface functionalized with either glutamic acid, 2-aminoethyl-phosphonic acid, or 2-aminethyl dihydrogenphosphate, to impart either carboxylic acid, phosphonate or phosphate functionality to the particle surface. The particle size distribution and stability of as-synthesized and functionalized Au NPs was confirmed using DLS, TEM and UV-vis spectroscopy. Functionalized Au NPs exhibited specificity for artificially damaged regions on the surface of cortical bone tissue as shown by SEM and EDS. The binding affinity of functionalized Au NPs on hydroxyapatite crystals and was quantified using ICP-OES.

## Bulk Metallic Glasses VI: Structures and Mechanical Properties I

Sponsored by: The Minerals, Metals and Materials Society, TMS Structural Materials Division, TMS/ASM: Mechanical Behavior of Materials Committee

Program Organizers: Peter Liaw, The University of Tennessee; Hahn Choo, The University of Tennessee; Yanfei Gao, The University of Tennessee; Gongyao Wang, University of Tennessee

Tuesday AM

February 17, 2009

Room: 3007

Location: Moscone West Convention Center

Session Chairs: Takeshi Egami, University of Tennessee; Daniel Miracle, US Air Force

8:30 AM Keynote

**Statistical Mechanics of Glasses and Liquids:** Takeshi Egami<sup>1</sup>; Valentin Levashov<sup>1</sup>; Rachel Aga<sup>2</sup>; James Morris<sup>2</sup>; <sup>1</sup>University of Tennessee; <sup>2</sup>Oak Ridge National Lab

In crystals the atomic vibrations are described by phonons, and the statistical mechanics can be formulated with phonons as the bases. In liquids and glasses, however, phonons are strongly scattered and have a very short lifetime, and cannot form the basis for statistical mechanics. We found recently that the atomic dynamics are so localized in high temperature liquids that the dynamics of an atom and its nearest neighbor shell can be an excellent basis for the analysis of the atomic dynamics. They were found to obey the equipartition law for the potential energy,  $U = (3/2)kT$ . We show how this leads to calculating the glass transition temperature, structural relaxation and other thermodynamic quantities. This research has been sponsored by the Division of Materials Sciences and Engineering, Office of Basic Energy Sciences, U.S. Department of Energy under contract DE-AC05-00OR-22725 with UT-Battelle.

8:55 AM Invited

**Size Effect in the Deformation and Failure of Metallic Glasses:** Ju Li<sup>1</sup>; <sup>1</sup>University of Pennsylvania

Recent experimental and theoretical works have suggested possible size effect in the plasticity and failure resistance of metallic glasses. While bulk metallic glasses manifest negligible tensile ductility, nanoscale metallic glasses show significant ductility under tension (PNAS 104, 11155). Nanopillar compression experiments also show intriguing behavioral differences sensitive to pillar size. Multiple reasons could contribute to size dependence: (a) proliferation of amorphous-crystal interfaces or surfaces that directly mediate plasticity, as well as indirectly alter the glass structure, (b) Weibull-like statistics for the nucleation of a runaway flow defect from the condensation of shear transformation zones in a finite volume, and (c) intrinsic lengthscales such as the glue zone width in the aged-rejuvenation-glue-liquid model of a runaway shear band (Acta Mater. 54,

4293). A “Hall-Petch” like relation may exist with respect to the metallic glass sizescale, but for the useful tensile or compressive ductility instead of strength (Phys. Rev. B 77, 155419).

#### 9:10 AM Invited

**Assessment of Binary and Ternary Metallic Glasses:** *Daniel Miracle*<sup>1</sup>; Dmitri Louzguine<sup>2</sup>; Larissa Louzguina<sup>3</sup>; <sup>1</sup>US Air Force; <sup>2</sup>Advanced Institute of Materials Research; <sup>3</sup>Institute of Materials Research

It has long been suggested that metallic glass stability is influenced by atomic structure, but it has been difficult to systematically explore this idea in detail until recently. The efficient cluster packing (ECP) model gives a simple approach to specify the structure and topology of metallic glasses. In this work, the ECP model was used to establish binary and ternary metallic glass structures. A broad assessment was conducted, collecting information from the literature on 167 different binary metallic glass systems and many dozens of ternary systems. Where available, characteristic temperatures (T<sub>g</sub>, T<sub>x</sub>, T<sub>l</sub>) were extracted from the literature, and parameters characterizing the thermal stability (T<sub>g</sub>/T<sub>l</sub>, T<sub>x</sub>/T<sub>l</sub>, ΔT<sub>x</sub> and γ) were computed. Structural parameters of these glasses obtained by analysis using the ECP model were correlated with thermal stability and glass-forming ability. The results from the structural assessment and from the correlations with thermal stability will be presented and discussed.

#### 9:25 AM

**Characterization of Local Deformation during Low and High Strain Rate Joining of Bulk Metallic Glasses:** *Nicholas Hutchinson*<sup>1</sup>; Yuan Zhang<sup>1</sup>; Glenn Daehn<sup>1</sup>; Katharine Flores<sup>1</sup>; <sup>1</sup>The Ohio State Univ

Previous work has demonstrated the viability of solid state joining techniques for bulk metallic glasses. However, optimization of these techniques requires detailed study of mechanical and diffusive mechanisms operative near the joint interface and their dependence on surface roughness and stress state. Recently, we characterized two solid state joining techniques which rely on mechanical work and plastic deformation at mating interfaces: a high strain rate electromagnetic impact process and a quasi-static electro-thermo-mechanical process. Interface strengths of ½ the bulk strength have been obtained with the electro-thermo-mechanical process, while the electromagnetic process has produced glass to crystalline joints exhibiting apparent interface strengths that exceed the strength of the crystalline material. In the present work, interface geometry is varied to evaluate the effect of stress state and roughness on deformation at the interface during joining. Interface failure is characterized, and cross sections and failure surfaces are examined using SEM and TEM.

#### 9:35 AM Invited

**Anelasticity in a Metallic Glass and Local Flow at Shear Bands:** *Michael Atzmon*<sup>1</sup>; Adam Ganuza<sup>1</sup>; Dongchan Jang<sup>1</sup>; Koteswararao Rajulapati<sup>1</sup>; <sup>1</sup>University of Michigan

Our recent indentation experiments have suggested that rolled amorphous Al86.8Ni3.7Y9.5 undergoes time-dependent deformation at room temperature. This result has motivated a detailed study of time-dependent deformation in this alloy. We used a combination of bend stress relaxation measurements and cantilever bending with a nanoindenter. Anelastic, i.e., time dependent and reversible, deformation is dominant at room temperature. We observe at least four distinct anelastic sites, in contrast with the common assumption that only two such site types exist. In order to observe local deformation at shear bands, we have created samples with a small number of shear bands by forming kinks in a melt-spun ribbon. These samples were then subjected to low, prolonged, stress. Using ex situ atomic-force microscopy, we have observed the change in offset at the intersection of individual shear bands with the surface. The results will be interpreted by considering the residual stress profile in the sample.

#### 9:50 AM Invited

**Relaxation Behavior of Ca-Based Bulk Metallic Glasses:** *Oleg Senkov*<sup>1</sup>; Daniel Miracle<sup>2</sup>; <sup>1</sup>UES Inc; <sup>2</sup>US Air Force Research Laboratory

The temperature dependence of the Maxwell relaxation time of three Ca-based bulk metallic glasses (BMGs), Ca<sub>65</sub>Mg<sub>15</sub>Zn<sub>20</sub>, Ca<sub>50</sub>Mg<sub>20</sub>Cu<sub>30</sub>, and Ca<sub>55</sub>Mg<sub>18</sub>Zn<sub>11</sub>Cu<sub>16</sub> was studied in the super-cooled liquid range, near the glass transition temperature, using a differential scanning calorimetry (DSC) method. The relaxation behavior of Ca<sub>65</sub>Mg<sub>15</sub>Zn<sub>20</sub> was found to be similar to that of SiO<sub>2</sub>. The behavior of two other Ca-based BMGs was more fragile, but they were stronger than the Zr- and Mg- based BMGs. The strong liquid behavior of the Ca-based BMGs was concluded to be one of the reasons of their excellent glass forming ability.

#### 10:05 AM Break

#### 10:15 AM Invited

**Atom Probe Analysis of Phases in a Zr-Based Bulk Metallic Glass with the Expectation Maximization Algorithm:** *Michael Miller*<sup>1</sup>; Xun-Li Wang<sup>1</sup>; Daniel Haley<sup>2</sup>; Michael Moody<sup>2</sup>; Simon Ringer<sup>2</sup>; <sup>1</sup>Oak Ridge National Laboratory; <sup>2</sup>Australian Key Centre for Microscopy and Microanalysis

Atom probe tomography has been used to characterize the local structure and the phases present in a Zr<sub>52.5</sub>Cu<sub>17.9</sub>Ni<sub>14.6</sub>Al<sub>10</sub>Ti<sub>3</sub> bulk metallic glass. The atom probe data from materials in the as-quenched condition and after a heat treatment of 3.5 h at 658 K were analyzed with the Expectation Maximization algorithm and other standard techniques to decompose underlying phase information. The Expectation Maximum method provides the statistically most likely number of phases present and the fraction of each phase by calculating the nearest neighbor histograms in the atom probe data and then applying a maximum likelihood method. These results will be compared to the results from other traditional atom probe tomography phase analysis techniques. Research at the Oak Ridge National Laboratory SHaRE User Facility was sponsored by Basic Energy Sciences, U.S. Department of Energy.

#### 10:30 AM

**Contribution to a New Understanding of Deformation-Induced Ductility in Bulk Metallic Glasses (BMG):** *Denise Beitelshmidt*<sup>1</sup>; Simon Pauly<sup>1</sup>; Min Lee<sup>2</sup>; Uta Kuehn<sup>1</sup>; Jürgen Eckert<sup>1</sup>; <sup>1</sup>IFW Dresden; <sup>2</sup>Korea Institute of Industrial Technology

Most BMGs show very limited plastic strain. In order to achieve a reliable process to enhance the plastic properties it is necessary to improve the understanding of atomic order in deformed samples. The change of mechanical behaviour of BMGs under different deformation conditions as pre-load, compressive or tensile stress is investigated. Different alloys are tested with regard to their mechanical properties: as-cast, after preload or deformation. Many (rolling-)deformed samples show series of shearbands with characteristic enhancement of the plastic properties. In order to get a better understanding a detailed investigation program with special interest in the shearbands' cross-over spots was performed. Furthermore the effect of structural changes under compressive pre-load below yield strength is investigated to obtain structural knowledge about materials with pre-load enhanced plasticity and the predicted non-lowered fatigue strength. Different investigations are presented leading to new concepts concerning the role of free volume in the mechanically treated samples.

#### 10:40 AM Invited

**Fragile to Strong Transitions in Zr- Based Alloys:** *Ralf Busch*<sup>1</sup>; <sup>1</sup>Saarland University

The viscosities of six bulk metallic glass forming Zr-based melts of different complexity have been measured in the equilibrium liquid state. The viscosity vs. shear rate behaviour of the three quinary (Vitrelloy105, Vitrelloy106, Vitrelloy106a), two quaternary (Vitrelloy101, Zr65Cu17.5Ni10Al7.5) and one ternary (Zr60Cu25Al15) alloys have been studied above their respective liquidus temperatures in a custom built Couette concentric cylinder viscosimeter. Earlier, in the Be bearing Vitrelloy 1, shear thinning behavior as well as a strong to fragile transition in the undercooled liquid had already been observed.<sup>1</sup> The actual study shows that for all tested alloys a fragile state was present above the liquidus temperature, like in Vitrelloy 1 with fragility parameters of about D\* = 10 and a weak shear thinning behavior. Results from parallel low temperature studies by three point beam bending show that they are much stronger liquids in the vicinity of the glass transition with D\* higher than 20, this being a strong indication for a strong to fragile transition between the glass transition and the liquidus temperature also in these alloys. Comparable to the behavior of the fragile state of Vitrelloy1 shear thinning exponents varying between 0.8 and 1 have been found for the tested alloys. To directly confirm the strong to fragile transition, studies are done in the supercooled liquid regions of the respective alloys. However, like in Vitrelloy 1 the fragile to strong transition seems to also promote crystallisation and only a small temperature and time window is available to observe the transition in the supercooled liquid directly. <sup>1</sup>C. Way, P. Wadhwa and R. Busch, Acta Mater. 55, 2977 (2007).



10:55 AM Invited

**Structural Changes in Metallic Glasses Induced by Mechanical Deformation:**

*Wojciech Dmowski<sup>1</sup>; Takeshi Egami<sup>1</sup>; Andrew Chuang<sup>1</sup>; Yoshihiko Yokoyama<sup>2</sup>; Akihisa Inoue<sup>2</sup>; Yang Ren<sup>3</sup>; Bogdan Palosz<sup>4</sup>; <sup>1</sup>University Tennessee/MSE; <sup>2</sup>Institute for Materials Research/Tohoku University; <sup>3</sup>Advanced Photon Source/ANL; <sup>4</sup>Institute of High Pressure Physics/PAS*

Glass deformation is accompanied by local rearrangement of atoms to accommodate shear strain. Disordered nature of the glass and small deformation volumes make it difficult to observe experimentally. However, the use of area detectors and high flux/energy X-rays makes such studies practical. We have examined structural changes induced by high temperature creep, axial tension, high temperature isostatic compression and high pressure torsion. Axial deformation leads to small but observable structural anisotropy, which can be analyzed in terms of the anisotropic components of the pair distribution function. We found that mechanical deformation involved rearrangement in clusters of atoms by local bond exchange that supported structural anisotropy in the deformed state. Structural changes induced by high pressure annealing were isotropic and affected chemical ordering. High pressure torsion resulted in isotropic but inhomogeneous changes in the local atomic structure. Work supported by the U.S. DOE under DE-AC05-00OR-22725.

11:10 AM

**Structural Influences on Metallic Glass Relaxation:** *Garth Wilks<sup>1</sup>; Daniel Miracle<sup>1</sup>; <sup>1</sup>Air Force Research Laboratory*

Variations in constitution and processing route (cooling rate and subsequent annealing) in ribbons made from the Al-La-Ni system are used to probe the deformation activation spectra for several conditions via bend stress relaxation. Deviations in spectra between conditions are rationalized in terms of "defect" states predicted by the Efficient Cluster Packing model that contribute to local free volume fluctuation and act as sites for unit shear process nucleation.

11:20 AM

**The Effects of Partial Crystallinity on the Hydrogen Permeation Properties of Bulk Amorphous Metallic Systems:** *Kyle Brinkman<sup>1</sup>; Elise Fox<sup>1</sup>; Paul Korinko<sup>1</sup>; Thad Adams<sup>1</sup>; <sup>1</sup>Savannah River National Laboratory (SRNL)*

It is recognized that hydrogen separation membranes are a key component of the emerging hydrogen economy. Potentially exciting materials for membrane separations are bulk metallic glass materials due to their low cost, high elastic toughness and resistance to hydrogen "embrittlement" compared to crystalline Pd-based membrane systems. However, at elevated temperatures and extended operation times structural changes including partial crystallization (devitrification) may appear in these amorphous metallic systems. A systematic evaluation of the impact of partial crystallization/devitrification on the diffusivity and solubility (i.e., permeability) behavior in multi-component Metallic Glass materials would provide great insight into the potential of these materials for hydrogen applications. This study will report on the impact of phase transformations occurring under different gas environments. This thermodynamic data as well the calorimetric determined crystallization rate will be used to intentionally crystallize a given material to varying degrees. Measurements of the hydrogen permeation flux as a function of phase composition have been performed and structure/property effects will be presented for commonly available Zr and Fe/Co based Metallic Glass materials.

11:30 AM Invited

**Formation, Structure and Crystallization Behavior of Cu-Based Bulk Glass-Forming Alloys:** *Dmitri Louzguine<sup>1</sup>; Guoqiang Xie<sup>2</sup>; Song Li<sup>2</sup>; Qingsheng Zhang<sup>2</sup>; Wei Zhang<sup>2</sup>; C. Suryanarayana<sup>3</sup>; Akihisa Inoue<sup>1</sup>; <sup>1</sup>Tohoku University, WPI Advanced Institute for Materials Research; <sup>2</sup>Institute for Materials Research, Tohoku University; <sup>3</sup>University of Central Florida*

We studied the structure and properties of Cu-Zr-based alloys having exceptionally high glass-forming ability and investigate the influence of Ag addition on their structure and crystallization behavior. Some bulk glassy alloy samples studied by high-resolution TEM were found to contain well developed medium-range order zones and nanoparticles. Some glassy alloys are also found to be highly sensitive to electron-beam irradiation. The crystallization kinetics of Cu55Zr45, Cu50Zr50, Cu55-xZr45Agx (x = 0, 10, 20), Cu45Zr45Al5Ag5 and Cu36Zr48Al8Ag8 glassy alloys was also analyzed and will be discussed based on classical nucleation theory. Cu35Zr45Ag20 alloy was found to exhibit possible phase separation upon heating within a supercooled liquid region. An influence of the cooling rate on the structure and properties of the Cu-based glassy alloys on heating was also studied. Some differences in the crystallization

kinetics and phase composition of the ribbon-shape and bulk glassy samples of Cu36Zr48Al8Ag8 alloys will be presented.

11:45 AM

**Fabrication and Mechanical Properties of Metal Particulates Reinforced Ni-Based Bulk Metallic Glass Composites by Spark Plasma and Microwave Sintering:** *Guoqiang Xie<sup>1</sup>; Dmitri V. Louzguine-Luzgin<sup>1</sup>; Song Li<sup>1</sup>; Akihisa Inoue<sup>1</sup>; <sup>1</sup>Tohoku University*

The lack of ductility limits the number of applications of bulk metallic glasses. The most common method to overcome this problem is to introduce nano- or micro-scale crystalline phases into glassy matrix leading to the formation of multiple shear bands and an enhanced plasticity. In this study, using the mixed powders of gas-atomized Ni-based glassy powder blend with nano- or micro-scale metal (W, Cu, etc.) powders, we fabricated large-size glassy alloy composites (GACs) with ultra-high strength and enhanced ductility by a spark plasma sintering process. The microstructure of the sintered compacts and the interface between powder particles were characterized by SEM and HRTEM. The good bonding state among the particulates and the glassy matrix was recognized. The additional metal particulates causing deviation, branching and multiplication of shear bands should be responsible for good mechanical properties of the fabricated bulk GACs. Microwave-induced sintering behavior of the mixed powders was also investigated.

**Cast Shop for Aluminum Production: Environment, Health and Safety**

Sponsored by: The Minerals, Metals and Materials Society, TMS Light Metals Division, TMS: Aluminum Committee

Program Organizers: Pierre Le Brun, Alcan CRV; Hussain Alali, Aluminium Bahrain

Tuesday AM

Room: 2005

February 17, 2009

Location: Moscone West Convention Center

Session Chair: Seymour Epstein, Aluminum Association

**8:30 AM Introductory Comments**

8:35 AM

**Sustainability and the Aluminum Industry: Future Strength:** *Steve Larkin<sup>1</sup>; <sup>1</sup>The Aluminum Association*

We live today in an increasingly constrained world. Both as individual consumers, and as representatives of the manufacturing sector, we live and operate our businesses in the midst of record commodity, energy, and now food prices. This paper will discuss the opportunities these constraints present to the aluminum industry, and how sustainability has become the dominant paradigm through which customers will judge performance. Key metrics for measuring the success of the industry are used to highlight aluminum's strength versus competing materials.

8:55 AM

**Meeting Environmental Challenges in the Casthouse:** *Corleen Chesonis<sup>1</sup>; Edward Williams<sup>1</sup>; David DeYoung<sup>1</sup>; <sup>1</sup>Alcoa Inc*

Sustainability has become an important issue to the aluminum industry in recent years. Environmental regulations have become more stringent and societal pressures to reduce the environmental footprint of our operations have increased. In U.S. casthouses, the Secondary MACT regulations set specific limits on gaseous and particulate emissions from both furnaces and in-line metal treatment units. These concerns have led to efforts to reduce or eliminate the use of chlorine gas in metal treatment while maintaining metal quality and meeting environmental regulations. The steady progress made in Alcoa over the last twenty years can be characterized as a series of step changes in technology, both in processes and in equipment. These step changes have included mixed gas tube fluxing, bagged salt addition, bath carryover reduction, rotary gas fluxing, and rotary salt fluxing. The effectiveness of these methods and their impact on emissions levels will be summarized.

9:15 AM

**Life Cycle Assessment (LCA) – A System Approach to Product Environmental Management:** *Jinlong Marshall Wang*<sup>1</sup>; <sup>1</sup>The Aluminum Association

Life Cycle Assessment (LCA) is a method for assessing environmental impacts of products and services. It takes a system approach and life cycle thinking on product's environmental impacts and it is extensively used for decision making, learning/exploration, and/or communication purposes. However, this environmental management tool is not only expensive and time consuming, but also has the potential to be manipulated or completely misinterpreted. This article gives a brief introduction to LCA, and some of the key aspects of conducting and interpreting LCA. In particular, it explores the use of LCA as a tool, among other environmental assessment tools, to help promote the sustainability of aluminum among its producers, consumers, and policy makers.

9:35 AM

**Beryllium in Dross Produced during Aluminum Melting:** *David DeYoung*<sup>1</sup>; *Jon Peace*<sup>1</sup>; <sup>1</sup>Alcoa Inc

Beryllium has historically been used in various aluminum alloys and is still used today in certain alloys. During the melting of scrap that contains beryllium, some portion of the beryllium reports to the dross; it potentially can even concentrate in the dross. Since dross handling can produce respirable dust, it is important to understand the beryllium content of the dross. A method to analyze beryllium in dross has been developed and was used to measure its distribution between the alloy and the dross. To overcome the inherent non-homogeneous nature of dross the method involved analysis of relatively large sample sizes. This method was used to analyze dross produced from alloys with varying concentrations of beryllium, and the data was then used to model potential beryllium exposure during dross handling.

9:55 AM Break

10:15 AM

**Molten Metal Explosions Are Still Occurring:** *Seymour Epstein*<sup>1</sup>; <sup>1</sup>Aluminum Association

The Aluminum Association continues to collect reports on explosions occurring in the aluminum industry around the world. Since the program began in 1985 more than 2500 reports have been received and entered into an ongoing database of molten metal incidents. A summary of the incidents will be presented, the causes will be discussed and several recent incidents will be detailed.

10:45 AM

**Safety Coatings to Prevent Molten Aluminum-Water Explosions:** *Joe Roberts*<sup>1</sup>; *Alex Lowery*<sup>2</sup>; <sup>1</sup>Pyrotek Inc; <sup>2</sup>Wisechem, LLC

Safety coatings to prevent molten aluminum-water explosions: A brief history and application guides. All the coatings require clean, oil free surfaces and must be mixed and applied properly for adhesion to steel or concrete substrates. There are a variety of ways to clean and apply these coatings

11:05 AM

**The Role of Automation in Explosion Prevention in Sheet Ingot Casting:** *Denis Bernard*<sup>1</sup>; <sup>1</sup>Rio Tinto Alcan

Over the past decades, sheet ingot production has evolved from completely manual systems using float and diptube and steady-eddy metal level control to more sophisticated automatic systems that have primarily been introduced for improved safety and process consistency. The reliability of these systems have allowed to adopt in specific cases a complete "hands-off" cast start-up procedure which has completely eliminated the need for operators intervention during this critical phase of the cast. These systems have not only reduced the probability of explosion though less process variability during the start-up phase but have also decreased the possibility of injuries that could be caused by a DC explosion. This presentation will highlight the evolution of the use of automation for sheet ingot casting as well as the need to expand the "hands-off" approach to other casting processes such as billet and T ingot casting.

11:25 AM

**Benefits to Safety Performance at ALBA from Use of the Wagstaff AutoFlo™ System for Casting of Extrusion Ingot:** *Talib Al Ansari*<sup>1</sup>; *Hussain Hassan Al Ali*<sup>1</sup>; *Michael Jacobs*<sup>1</sup>; *Jalal Mohammed*<sup>1</sup>; *Mohammed Kadhem*<sup>1</sup>; *Garry Martin*<sup>1</sup>; <sup>1</sup>Aluminium Bahrain (ALBA)

The use of Wagstaff AirSlip® Air Casting Technology for casting of extrusion ingot results in enhancement of the ingot quality for improved extrusion

performance. The control of the airflow does require operator attention by manual adjustment during casting. Wagstaff (USA) has developed a new automated gas control system for Airslip tooling called AutoCast™ AutoFlo™ Automated Casting Gas Control. Aluminum Bahrain (ALBA), in the Kingdom of Bahrain, purchased and installed this new control system in 2007 to provide improved consistency in the casting of extrusion ingot and further reduce the risk to operators in the casting area whilst further optimizing production performance and quality of extrusion ingot. This paper details the use of the new automated gas control system from Wagstaff at ALBA and assesses its capability in providing an improved casting environment for enhancement of both operator safety and overall production performance including ingot quality.

## Characterization of Minerals, Metals and Materials: Characterization of Microstructure of Properties of Materials I

Sponsored by: The Minerals, Metals and Materials Society, TMS Extraction and Processing Division, TMS: Materials Characterization Committee, TMS/ASM: Composite Materials Committee

Program Organizers: Toru Okabe, University of Tokyo; Ann Hagni, Geoscience Consultant; Sergio Monteiro, State University of the Northern Rio de Janeiro - UENF

Tuesday AM

Room: 3009

February 17, 2009

Location: Moscone West Convention Center

Session Chairs: Donato Firrao, Politecnico Di Torino; Jian Li, Natural Resources Canada

8:30 AM

**Two- and Three-Dimensional Analyses of Martensitic Steels:** *George Spanos*<sup>1</sup>; *David Rowenhorst*<sup>1</sup>; *Jerry Feng*<sup>1</sup>; *Keith Knipling*<sup>1</sup>; *Rick Everett*<sup>1</sup>; *Gregory Olson*<sup>2</sup>; *Stephanie Chan*<sup>2</sup>; <sup>1</sup>Naval Research Laboratory; <sup>2</sup>Northwestern University

This presentation outlines progress made on both two dimensional (2D) and three dimensional (3D) studies of martensitic steels. The first part of this talk will be centered about 2D studies of martensite in low carbon steels, including HSLA-100 and a high (10%) Ni steel. In particular, findings will be presented on a 2D quantification scheme of lath martensite structures based on automated analyses of Electron Backscatter Diffraction (EBSD) scans. The second part of the talk will focus on 3D analyses of martensitic steels. This will include progress on two 3D reconstruction efforts, including a project which utilizes the dual beam Focused Ion Beam and EBSD to study martensite in low carbon steels, and an investigation of cracks and voids in a titanium modified 4330 steel. The latter study employs both serial sectioning and X-ray tomography techniques.

8:45 AM

**Development of Atmosphere-controlled Mass Spectrometry Equipment:** *Takashi Nagai*<sup>1</sup>; *Masao Miyake*<sup>1</sup>; *Masafumi Maeda*<sup>1</sup>; <sup>1</sup>The University of Tokyo

Mass spectrometry is a new method to measure thermodynamic properties at high temperature. In this method, vapor pressures of gaseous species in equilibrium with specimen can be measured. Although thermodynamic properties of metals and alloys have been reported by this method, it has not yet been employed for oxides and oxide systems, because of the difficulty in controlling oxygen potential in Knudsen cells. This is true despite this being one of the most important factors in the thermodynamic measurement of oxide systems. Equipment for mass spectrometry which has a mechanism to introduce directly gaseous reactant, such as carbon monoxide and carbon dioxide mixture, to the Knudsen cells to control oxygen potential in the cells has been developed in this study. The change of oxygen potential in the cells following introduction of the reactant was demonstrated, and the thermodynamic properties of oxide systems containing phosphorus, such as calcium phosphate, were investigated.

9:00 AM

**Quantitative Phase Analysis of a Dual Phase Steel Using Electron Backscatter Diffraction:** *Jun-Yun Kang*<sup>1</sup>; *Do Hyun Kim*<sup>1</sup>; *Sung-II Baek*<sup>1</sup>; *Young-Woon Kim*<sup>1</sup>; *Kyu Hwan Oh*<sup>1</sup>; *Hu-Chul Lee*<sup>1</sup>; <sup>1</sup>Seoul National University

Phase differentiation between ferrite and martensite in a dual phase (DP) steel was examined to automatically assess the volume fraction of each phase using

electron backscatter diffraction. A cold rolled and annealed sheet was prepared to have 27% of martensite fraction. As the symmetry in the diffraction pattern could not differentiate the two phases due to the crystallographic similarity, band contrast (BC) value which represents pattern clarity was used. Using grain-averaged value of BC, a reasonable martensite fraction of 25% could be obtained. Concerning the distribution of the grain-averaged BC, there were two peaks detected in the martensite regime, which signified two types of them, lath and plate martensite.

## 9:15 AM

**Defect Analysis Using Resonant Ultrasound Spectroscopy:** Kevin Flynn<sup>1</sup>; Miladin Radovic<sup>1</sup>; <sup>1</sup>Texas A&M University

This paper demonstrates the practicability of using Resonant Ultrasound Spectroscopy (RUS) in combination with Finite Element Analysis (FEA) to determine the size and location of defects in a material of known geometry and physical constants. Defects were analyzed by comparing the actual change in frequency spectrum measured by RUS to the change in frequency spectrum calculated using FEA. Based on the analysis of many FEA-generated frequency spectra, it is possible to develop the model to determine size and position of the defects from measured resonant frequency, and acceptance/rejection criteria for Non-Destructive Testing. Experiments conducted on various materials and geometries show that cracks can be detected by RUS, and their depth and location determined with reasonable accuracy. However, results also indicate that there are limits to the applicability of such a method, the primary one being a lower limit to the size of crack for which this method can be applied.

## 9:30 AM

**Applications of a Commercially Available BENCH TOP TXRF System:** Alexander Seyfarth<sup>1</sup>; Hagen Stosnach<sup>1</sup>; <sup>1</sup>Bruker AXS Inc.

Total reflection X-ray fluorescence (TXRF) spectroscopy is a well-established and versatile method for the trace element analysis in solid and liquid samples with manifold matrices. Introduced in March 2008, a new bench top TXRF system, the S2 PICOFOX, offers similar performance than ICP-OES or AA without the lengthy sample preparation and standardization. The analytical range is from ppb to % levels for the elements from Al to U. We will be describing the principle of TXRF, comparing to other methods, including XRF and detailing the fast and convenient sample preparation. We will show studies done by the application laboratory and customers ranging from the analysis of nano materials to exploration screening for metals. This new implementation enables the chemical laboratory to finally take advantage of TXRF.

## 9:45 AM

**Non-destructive Analysis of Dislocations in Bulk Samples Using ECCI:** Martin Crimp<sup>1</sup>; <sup>1</sup>Michigan State University

Electron channeling contrast imaging (ECCI) allows near surface dislocations and other crystal defects to be imaged and characterized with high spatial resolution using a field emission gun SEM. Using this approach, dislocations may be assessed using varying electron channeling conditions, allowing the crystallographic details to be characterized in a manner similar to that carried out with diffraction contrast TEM. Because the dislocations are imaged in bulk samples, ECCI has a number of advantages over other approaches for imaging defects including allowing for analysis over large areas/volumes, being non-destructive in many applications, and being very conducive to in-situ testing. This talk will review the fundamental issues and experimental parameters involved with imaging dislocations using channeling contrast. Case studies will be presented that illustrate the flexibility of ECCI for assessing dislocation structures and morphologies in both metallic and semiconductor materials.

## 10:00 AM Break

## 10:20 AM

**Identification of Corrosion Product on Corroded Rebar in Concrete:** Jian Li<sup>1</sup>; Gordon Gu<sup>1</sup>; Valery Guertsman<sup>1</sup>; Pei Liu<sup>1</sup>; <sup>1</sup>CANMET-Materials Technology Laboratory

Corrosion resistance of materials is highly dependent on the microstructure of the specific material. Apart from general corrosion rate measurement using techniques like linear polarization and A.C. impedance, microstructural investigations are frequently needed to identify the root cause of corrosion. Advanced techniques, including scanning electron microscopy (SEM) and transmission electron microscopy (TEM), have been well integrated into routine characterization studies. Other microscopy techniques, including electron probe micro-analyzer (EPMA), Auger, X-ray photon spectroscopy (XPS) and secondary

ion mass spectroscopy (SIMS), can provide detailed chemistry information on corrosion products. In recent years, focused-ion beam (FIB) microscopes have evolved into an important microstructural characterization instrument. In this study, corrosion of rebar encased in concrete was studied in great detail using advanced microscopy techniques. Corrosion product on the rebar surface was identified as ferrous oxide with relatively large crystal size. The morphology of this passive layer was thoroughly analyzed, and its formation mechanism is proposed.

## 10:35 AM

**Linear Measures for 3-D Microstructures:** Martin Glicksman<sup>1</sup>; Paulo Rios<sup>2</sup>; Daniel Lewis<sup>3</sup>; <sup>1</sup>University of Florida; <sup>2</sup>Universidade Federal Fluminense; <sup>3</sup>Rensselaer Polytechnic Institute

Linear microstructure measures, including the average caliper, C, and mean width, L, may be employed to characterize the geometric properties of polyhedral grains, including their areas, volumes, and face curvatures. Moreover, linear measures permit prediction of curvature-mediated grain growth rates, thereby providing an important connection between kinetic behavior, grain size, and shape. The authors' development of regular polyhedra to represent each topological class of grains found in well-annealed polycrystals was used to calculate exact C and L values. The behavior of these linear measures for polyhedra with different face numbers and shapes will be discussed. Limitations were found, including a surprising insensitivity to grain shape that might limit the use of linear measures for practical characterization of 3-D microstructures. Alternative predictors of kinetic behavior for annealed polycrystals will be proposed.

## 10:50 AM

**Particle Size and Shape Analysis with CILAS Instruments:** Nicolas Marchet<sup>1</sup>; <sup>1</sup>CILAS

The particle size determination using Laser Diffraction is becoming the most popular instrument to analyze polymers, ceramics or metallic particles in chemistry, pharmaceutical or building applications. CILAS particle size analyzers permit to measure particle size distributions by three fast ways, with laser diffraction in wet and dry mode and with the optical microscopy thanks to the shape analysis option. This last instrument calculates more than twenty shape factors with the Expert Shape Software which permit to characterize the morphology of particles in order to give important information about the quality process, physical and chemical powder properties. This presentation gives some examples of applications using CILAS instruments in particle size and shape characterizations. The ways of particle characterization are according to the needs of each user and each material and present a good accuracy and repeatability in agreement with the ISO standard.

## 11:05 AM

**Materials Characterization Analytical Techniques of Minerals, Metals and Materials:** Ann Hagni<sup>1</sup>; <sup>1</sup>Geoscience Consultant

This paper is an overview of current analytical techniques available for characterization of minerals, metals, and materials, emphasizing chemical techniques, phase identification, and phase quantification techniques. Applications, sample preparation, capabilities, as well as limitations of techniques will be addressed. New developments and advancements over the past few years will be discussed. Practical examples from industry, product development, process improvement, and research and development may be included. This will be an excellent basic primer for the younger scientists, as well as a good refresher with updated information for the experienced materials scientists.

## 11:20 AM

**Analysis of Microstructure Evolution during Cold Deformation of Air-hardening Steel LH800:** Olexandr Grydin<sup>1</sup>; <sup>1</sup>Leibniz University of Hanover

The evolution of grain and dislocation structures during cold deformation of the new steel LH800 of Salzgitter AG is investigated in the frame of this work. The main feature of this material is its ability to air-harden by carbon content of about 0.1%. The initial ferrite structure of the metal provides high plasticity at cold deformation and subsequent heat treatment increases tensile strength approximately two times. Described are results of in-situ tensile tests in the SEM. SEM and TEM analysis of grain and dislocation structures evolution in samples, which have been uniaxially deformed to certain strains, are carried out. After statistical evaluation of results the grain elongation against strain is determined. A microstructure of a deep drawn cup is analyzed by means of



SEM. A quantitative evaluation of grain elongation on the different cup zones and comparison of these data with prediction results based on tensile tests are carried out.

11:35 AM

**Comparison of Phase Identification of EBSD and TEM in TRIP-aided Steel:**

*Sung Il Baik*<sup>1</sup>; Jun-Yeun Kang<sup>1</sup>; Do-Hyeon Kim<sup>1</sup>; Kyu-Hwan Oh<sup>1</sup>; Hu-Chul Lee<sup>1</sup>; Young Woon Kim<sup>1</sup>; <sup>1</sup>Seoul National University

Electron Back-Scattered Diffraction (EBSD) is a convenient and powerful tool to identify the phases and orientations in multiphase steel. Transmission Electron Microscopy (TEM), on the other hand, provides an accurate determination of phases even with the drawbacks of small area of observation. Direct comparisons of phase distributions were made from the Transformation Induced Plasticity (TRIP)-aided steel, which is consisted of ferrite, bainite and retained austenite. Unlike ferrite and martensite, bainite was known as a challenging phase to identify in EBSD. Phase mapping was made using EBSD and then the individual phases were identified using TEM in same region of the sample. Discrepancies in phase identification were observed in the region containing bainite, grains with low-angle grain boundaries, and small grains with less than 3 $\mu$ m diameter.

11:50 AM

**Materials Characterization Applied to Nanoparticulate Environmental Pollutants:** *Lawrence Murr*<sup>1</sup>; <sup>1</sup>University of Texas

There is a great deal of interest in the health effects of environmental (particularly atmospheric) nanoparticulates, both natural and anthropogenic; including indoor and outdoor air and occupational environments. It is now well established that nanoparticulate matter is more toxic than fine or course particulate matter. Scanning and transmission electron microscopy along with energy-dispersive spectrometries provide very detailed characterization for these nanoparticulate materials. This paper provides a broad overview of atmospheric nanoparticulates: their speciation, morphologies, sizes and size distributions, crystal structures, fundamental nanostructures, and frequency of occurrence. The preponderant nanoparticulates in the atmosphere are carbonaceous-including black carbon, soots and multiwall carbon nanotubes. These carbonaceous species are aggregates composed of hundred to thousands of primary nanoparticulate spheroids. Complex aggregates of nano-silica particles, multiwall carbon nanotubes and multiconcentric fullerenes are also often observed. The comparative cytotoxicities of these nanoparticulate materials will also be presented.

**CO2 Reduction Metallurgy 2009: Mechanisms and Electrolysis**

Sponsored by: The Minerals, Metals and Materials Society, TMS Light Metals Division, TMS Extraction and Processing Division, TMS: Energy Committee  
Program Organizers: Neale Neelameggham, US Magnesium LLC; Ramana Reddy, The University of Alabama; Jiann-Yang Hwang, Michigan Technological University; Jean-Pierre Birat, Arcelor Mittal Research

Tuesday AM  
February 17, 2009

Room: 2012  
Location: Moscone West Convention Center

*Session Chairs:* Ramana Reddy, The University of Alabama; Jiann-Yang Hwang, Michigan Technological University

**8:30 AM Introductory Comments**

**8:35 AM Invited**

**Metal Cations in CO<sub>2</sub> Assimilation and Conversion by Plants:** *Sergey Shabala*<sup>1</sup>; <sup>1</sup>University of Tasmania

Green leaf tissues convert solar energy into the energy of chemical bonds of sugar molecules during the process of photosynthesis. The efficiency of this conversion is at least twice higher than efficiency of any of currently known silicon-based solar panels. Importantly, vast amounts of CO<sub>2</sub> are assimilated during this process. The efficiency of photosynthesis is critically dependent on the availability of a large number of nutrients, among which metal cations such as K, Ca, Mg, Cu, Zn, Fe, Mn, and Ni play a key role. In this talk I will summarize basic requirements and major functions for each of these essential nutrients in plant photosynthesis, both at the whole-plant and molecular level. I will talk about how these requirements may be affected by the global climate trends

and discuss the prospects of creating artificial photosynthetic "bioreactors" for efficient energy conversion and CO<sub>2</sub> assimilation.

9:05 AM

**Aluminum Industry and Climate Change — Assessment and Responses:**

*Subodh Das*<sup>1</sup>; John Green<sup>2</sup>; <sup>1</sup>Phinix LLC; <sup>2</sup>Secat Inc

The aluminum industry is a latecomer to the suite of industrial metals. This paper assesses the impact of the global aluminum industry on climate changes. Subsequently, this paper also suggests several proactive strategies in the broad areas of production, application, recycling and carbon trading to minimize the impact.

9:25 AM

**Effect of Electrode Surface Modification on Dendritic Deposition of Aluminum on Cu Substrate Using Emic-AlCl<sub>3</sub> Ionic Liquid Electrolytes:**

*Debabrata Pradhan*<sup>1</sup>; Ramana Reddy<sup>1</sup>; <sup>1</sup>The University of Alabama

Electrorefining of aluminum scrap was investigated from 1-Ethyl-3-methyl-imidazolium chloride (EMIC)-AlCl<sub>3</sub> (60 wt%) electrolyte using copper/aluminum cathodes at 90  $\pm$  3°C. The deposits were characterized using scanning electron microscope (SEM), energy dispersive spectroscopy (EDS) and X-ray diffraction (XRD). The study was focused to determine the effect of electrode surface modifications, anode and cathode materials, surface roughness of electrodes and deposition time on dendritic deposition of aluminum. Also, their effect on current density was investigated. It was shown that the surface modification of electrodes reduced the dendritic deposition of aluminum at higher overpotentials. Pure aluminum (>99%) was deposited for all experiments with current efficiency of 95-99%.

9:45 AM

**Room-Temperature Production of Ethylene from Carbon Dioxide:** *Kotaro Ogura*<sup>1</sup>; <sup>1</sup>Yamaguchi Univ

Ethylene has been produced in aqueous solution from CO<sub>2</sub> by the electrochemical reduction driven by a natural energy. This process is useful for storing a large amount of the natural energy. In the closed system, the conversion efficiency of CO<sub>2</sub> is almost 100%, and the maximum selectivity for the formation of ethylene is more than 70%. On the other hand, the current efficiency for the competitive reduction of water is less than 10%. The electrolysis is practicable under such special conditions as three-phase interface consisting of gas, solution and metal, concentrated solution of potassium halide, low pH and copper or copper halide-confined metal electrode. These conditions are thoroughly examined, and the grounds to reply upon are revealed. A series of chemical apparatuses including an electrolytic cell in a large scale are designed for the ethylene production, which allow us continuously to supply raw CO<sub>2</sub> and to extract the product.

10:05 AM Break

10:25 AM

**The Electrochemical Reduction of Carbon Dioxide in Ionic Liquids:** *Huimin Lu*<sup>1</sup>; Xiaoxiang Zhang<sup>1</sup>; Pengkai Wang<sup>1</sup>; <sup>1</sup>Beijing University of Aeronautics & Astronautics

In this paper, the authors studied an electrochemical reduction process of carbon dioxide in ionic liquids such as 1-n-butyl-3-methylimidazolium hexafluorophosphate (BmimPF<sub>6</sub>) as the electrolytes. The electrolysis experiments were carried out under current and potential controls. The cathode products contained carbon nanotubes, carbon nanofibers, nanographites, and amorphous carbon. To establish the actual current and potential ranges, the electroreduction of carbon dioxide dissolved in the ionic liquid was studied by cyclic voltammetry on glass-carbon (GC) electrode at a temperature range from 100 to 145°C. The electrochemical mechanism of carbon dioxide electroreduction was studied for explanation of all obtained results. As the last thing, Carbon dioxide in ionic liquids was electroreduced as metals oxides were electroreduced in molten salts.

10:45 AM

**Silicon Dioxide as a Solid Store for CO<sub>2</sub> Gas:** *Victor Zavadinsky*<sup>1</sup>; Sergey Rogov<sup>1</sup>; <sup>1</sup>Institute for Materials Science

Pseudopotential fully relaxed total energy calculations are used to predict a hypothetical Si<sub>1-x</sub>C<sub>x</sub>O<sub>2</sub> (x<0.5) compound formed from SiO<sub>2</sub>  $\beta$ -cristobalite by substitution of some SiO<sub>2</sub> complexes by CO<sub>2</sub> molecules. The simulation shows that the Si<sub>1-x</sub>C<sub>x</sub>O<sub>2</sub> compound can be quasi stable if the CO<sub>2</sub> content is less than fifty per cent. It is assumed that six-molecule Si<sub>6-n</sub>C<sub>n</sub>O<sub>12</sub> (n=3) rings can play a role of nucleuses for formation of the Si<sub>1-x</sub>C<sub>x</sub>O<sub>2</sub> compound from SiO<sub>2</sub> and CO<sub>2</sub>

molecules. Thus, silicon dioxide can be considered as a possible solid store for gaseous CO<sub>2</sub>.

**11:05 AM**

**Recent Developments in Carbon Dioxide Capture Materials and Processes for Energy Industry:** *Malti Goel*<sup>1</sup>; <sup>1</sup>Former Advisor and Senior Scientist, Ministry of Science & Technology

The cost-effective capture of CO<sub>2</sub> from the point sources for its reduction in the atmosphere offers many challenges in materials science. Novel CO<sub>2</sub> capturing approaches using chemical, physical and biological methods are in the research stage and are aimed to minimize the cost. Appropriate materials development which can withstand required temperature or pressure as the case may be for CO<sub>2</sub> emanating from coal gas or industrial waste gases form the minimum condition. Other requirements are recyclability of material and cost of separation. Nano-material composites can be more effective in selective capture of CO<sub>2</sub> and can offer solutions for large-scale separation process. Nano-porous material catalysis can enhance the reaction rate of CO<sub>2</sub> with other chemicals and thus help in faster removal of CO<sub>2</sub>. This paper reviews recent industrial scale developments. In the Indian context, R&D priority areas in CO<sub>2</sub> capture process development with a focus on energy industry are presented.

## Computational Thermodynamics and Kinetics: Functional Materials

Sponsored by: The Minerals, Metals and Materials Society, ASM International, TMS Electronic, Magnetic, and Photonic Materials Division, TMS Materials Processing and Manufacturing Division, ASM Materials Science Critical Technology Sector, TMS: Chemistry and Physics of Materials Committee, TMS/ASM: Computational Materials Science and Engineering Committee

Program Organizers: Long Qing Chen, Pennsylvania State University; Yunzhi Wang, Ohio State University; Pascal Bellon, University of Illinois at Urbana-Champaign; Yongmei Jin, Texas A&M

Tuesday AM

Room: 3002

February 17, 2009

Location: Moscone West Convention Center

*Session Chair:* Long Qing Chen, Pennsylvania State University

**8:30 AM Invited**

**Anhysteretic Response of Compositionally Heterogeneous Alloys with Displacive Phase Transformations:** *Armen Khachaturyan*<sup>1</sup>; *Yong Ni*<sup>1</sup>; <sup>1</sup>Rutgers University

According to the phase rule, any diffusionless (displacive) transformation of a homogeneous solid solution is a metastable reaction developing within a two-phase field of the equilibrium phase diagram. Therefore, a sufficiently long annealing near the diffusionless transformation line should always result in a partial decomposition that eventually produces a compositionally heterogeneous state. This decomposition and displacive transformation in such a system are considered. In particular, we discuss a strain response to the applied stress/electric/magnetic fields in the martensitic/ferroelectric/ferromagnetic systems. It will be shown that in all these cases the field-induced displacive transformation and/or reorientation of structural domains of the low symmetry phase generates the macroscopic deformation. Given the energetic preference of the initial structural state, a removal of the external field can result in a recovering of the initial undeformed state, which means that this deformation is a pseudo-elastic recoverable strain. The pseudo-elastic response of the body can be an anhysteretic (or slightly hysteretic). If the applied field is stress, the response is a pseudo-elastic effect accompanied by the extrinsic softening of the shear modulus. Application of the theory and modeling results to the ferroelectric solid solution with high piezoelectric response and to the Fe-Ga alloys with a giant magnetostriction is discussed.

**9:00 AM Invited**

**Domain Microstructures and Mechanisms in Morphotropic Phase Boundary Ferroelectrics: Phase Field Model and Simulation:** *Wei-Feng Rao*<sup>1</sup>; *Yu Wang*<sup>1</sup>; <sup>1</sup>Virginia Tech

Phase field model is employed to study underlying domain microstructures and mechanisms responsible for enhanced electromechanical properties near morphotropic phase boundaries (MPBs) in ferroelectric solid solutions. This talk will present some new insights gained into the phase-coexisting domain

microstructures and field-induced inter-ferroelectric phase transformations and their relations to the advanced piezoelectric properties around MPB. The modeling and simulation show that extrinsic domain mechanisms play dominant roles in the strong piezoelectricity around MPBs, and crystallographic domain engineering is effective to fully exploit the domain mechanisms for property enhancement. Together with crystallographic and diffraction analyses, the study reveals a nanodomain perspective of MPB ferroelectrics, where coherent scattering and interference effects produce an adaptive diffraction phenomenon, which is peculiar to nanodomain microstructures.

**9:30 AM**

**Grain Boundaries-Ferroelectric Domains Interactions in Polycrystalline Ferroelectrics:** *Eva Anton*<sup>1</sup>; *R. Edwin Garcia*<sup>2</sup>; *John Blendell*<sup>2</sup>; *Keith Bowman*<sup>2</sup>; <sup>1</sup>Darmstadt TU; <sup>2</sup>Purdue University

Ferroelectric Lead Zirconate Titanate (PZT) films display physical behavior that makes them an important candidate for random access memory applications. In such devices, ferroelectric domains are locally switched by the application of an electric field, thus fixing the state of a memory unit. Today's technological advancement, however, demands ever higher memory densities. Therefore, as the device size shrinks, the microstructural features become increasingly important and the spatial variation of the hysteretic behavior increases, making the memory unit potentially unreliable. The local crystallographic orientation and the local grain-grain interactions play an important role in determining the switching of domains. In particular, large spatial variations of the fields arise as a combined result of the stresses that develop due to the thermal expansion and lattice mismatch of the film-substrate system, the anisotropy of the properties of the involved materials, and the processing conditions.

**9:50 AM**

**Phase-Field Simulation of Domain Stabilities and Structures in Strained SrTiO<sub>3</sub> Thin Films:** *Guang Sheng*<sup>1</sup>; *Yulan Li*<sup>1</sup>; *Jingxian Zhang*<sup>1</sup>; *Samrat Choudhury*<sup>1</sup>; *Darrell Scholom*<sup>1</sup>; *Quanxi Jia*<sup>2</sup>; *Zi-Kui Liu*<sup>1</sup>; *Long-Qing Chen*<sup>1</sup>; <sup>1</sup>Pennsylvania State University; <sup>2</sup>Los Alamos National Laboratory

Strontium titanate (SrTiO<sub>3</sub>) is known as a classical example of a system with coupled structural and incipient ferroelectric instabilities. In this study, the antiferrodistortive transition and ferroelectric transition in a strained (100) SrTiO<sub>3</sub> thin film are analyzed using phase-field approach. Based on the simulation results, the misfit strain-temperature domain stability diagrams, graphical representation of stable ferroelectric and structural domain structures as a function of strains and temperature, are constructed. The misfit strain-misfit strain domain stability diagrams at several representative temperatures were also generated, and the corresponding domain structures were analyzed and compared with experimental studies. By taking into account the different domain structures obtained from the variations of Landau coefficients used in the simulation, it is expected that such diagrams will provide guidance for interpreting experimental measurements and observations as well as to the design of SrTiO<sub>3</sub> films with specified domain structures.

**10:10 AM Invited**

**Defects and Domain Walls in LiNbO<sub>3</sub>: Insights from Microscopic Simulation:** *Haixuan Xu*<sup>1</sup>; *Donghua Lee*<sup>1</sup>; *Jun He*<sup>1</sup>; *Venkatraman Gopalan*<sup>2</sup>; *Volkmar Dierolf*<sup>3</sup>; *Susan Sinnott*<sup>1</sup>; *Simon Phillpot*<sup>1</sup>; <sup>1</sup>University of Florida; <sup>2</sup>Pennsylvania State University; <sup>3</sup>Lehigh University

We use electronic-structure, density functional theory calculations integrated with thermodynamic calculations to determine the structure and stability of point defects and point defect clusters in LiNbO<sub>3</sub>. In particular, we identify the dominant defects at different temperatures, oxygen partial pressure, and compositions. In addition, we use classical molecular-dynamics simulation approaches to characterize the structure and energetic of domain walls in LiNbO<sub>3</sub>. A discussion of the interaction of domain walls and point defects is presented. This work is supported by the National Science Foundation under awards DMR-0602986 and DMR-0303279.

**10:40 AM Invited**

**Phase-Field Modeling of Defect Interactions in Active Materials:** *Chad Landis*<sup>1</sup>; <sup>1</sup>The University of Texas at Austin

A continuum thermodynamics framework is presented to model the evolution of domain structures in active/smart materials. In a departure from previous derivations of the phase-field equations, a set of micro-forces and governing balance laws are postulated and applied within the second law of thermodynamics to identify the appropriate material constitutive relationships. To investigate the

consequences of the theories, fundamental defect interactions are studied. A principle of virtual work is specified for the theory and is implemented to devise a finite element formulation. For ferroelectrics, the theory and numerical methods are used to investigate the interactions of 180° and 90° domain walls with arrays of charged defects and dislocations to determine how strongly domain walls are electromechanically pinned by the arrays of defects. For ferromagnetic shape memory alloys the interaction between a martensite twin boundary and magnetic domain wall is modeled to explain the finite blocking stress in these materials.

### 11:10 AM Invited

**Microstructure Evolution of Ferromagnetic Shape Memory Alloys:** *Jiangyu Li*<sup>1</sup>; <sup>1</sup>University of Washington

Magnetoelastic domains in ferromagnetic shape memory alloys (FSMA) evolve through either variant rearrangement or magnetization rotation, resulting in large or small magnetic field-induced strain depending on the magnitude of applied compressive stress. A mesoscopic theory is developed to study the magnetoelastic behavior of FSMA to account for both variants rearrangement and magnetization rotation. A multi-rank laminated domain configuration is constructed first under the constrained theory, which is then relaxed by allowing the magnetization to rotate away from its easy axis, resulting in incompatibility in both magnetization and magnetostrictive strain. It is observed that microstructure evolution of FSMA is dominated by rearrangement of variants when the applied stress is small, but such rearrangement is blocked when the applied stress is relatively large, under which magnetization rotation takes over as the dominant mechanism. A novel phase-field simulation is also carried out to verify the theoretical analysis.

### 11:40 AM

**Phase Field Simulation of Coupled Twin Boundary and Domain Wall Motions in Magnetic Shape Memory Alloys:** *Yongmei Jin*<sup>1</sup>; <sup>1</sup>Texas A & M University

Magnetic field-induced deformation in magnetic shape memory alloys (MSMAs) results from coupled ferromagnetic and ferroelastic domain evolutions. The coupling occurs through elastostatic and magnetostatic interactions as well as magnetocrystalline anisotropy, and is investigated by computer modeling and simulation. It reveals that the motions of twin boundaries and domain walls depend not only on external magnetic fields but also on internal domain configurations, leading to complex domain processes. It is demonstrated that twin boundary can continue its motion under decreasing magnetic field, or even reverse motion direction without changing magnetic field, producing peculiar magnetomechanical behaviors. Based on the simulations, domain microstructure-dependent driving forces for the coupled motions of martensite twin boundaries and magnetic domain walls in magnetic shape memory alloys are analyzed.

### 12:00 PM

**Phase Field Modeling of the Martensitic Transition: i) Comparison between Geometrically Linear and Non-Linear Elasticity, and ii) Microstructures in Ni-Ti-Pd Alloys with Special Lattice Parameters:** *Alphonse Finel*<sup>1</sup>; Umut Salman<sup>2</sup>; <sup>1</sup>ONERA; <sup>2</sup>CNRS

Martensitic transformations are characterized by large strain misfits between the martensite and the austenite, and also between the different orientational variants of the martensitic phase. The transitions are often athermal and microstructures dictated by strain accommodation and thermoelastic equilibrium. We analyze these microstructures using a Phase Field method that incorporates kinetic energy and a Ginzburg-Landau modeling of the elastic energy. We first discuss the differences between a geometrically non-linear (i.e. invariant by rotation, and thus exact) and the often-used linear (i.e. approximate) form of this elastic energy and show that the metastable states differ considerably between the two models. We also compare our numerical results to experimental observations. Finally, we present briefly an investigation of the martensitic microstructures in Ni-Ti-Pd alloys with special lattice parameters.

## Diffusion in Materials for Energy Technologies: Session I

Sponsored by: The Minerals, Metals and Materials Society, TMS Structural Materials Division, TMS Electronic, Magnetic, and Photonic Materials Division, TMS: Alloy Phases Committee, TMS: High Temperature Alloys Committee, TMS/ASM: Nuclear Materials Committee, TMS: Solidification Committee, ASM-MSCTS: Atomic Transport Committee  
Program Organizers: Jeffrey LaCombe, University of Nevada, Reno; Yongho Sohn, University of Central Florida; Carelyn Campbell, National Institute of Standards and Technology; Afina Lupulescu, GE; Ji-Cheng Zhao, Ohio State University

Tuesday AM

Room: 3006

February 17, 2009

Location: Moscone West Convention Center

Session Chairs: Jeffrey LaCombe, University of Nevada, Reno; Dennis Keiser, Idaho National Laboratory; Afina Lupulescu, GE

### 8:30 AM Invited

**Computation of Diffusion Coefficients: Current Capabilities and Perspectives:** *Erich Wimmer*<sup>1</sup>; Clive Freeman<sup>1</sup>; Hannes Schweiger; Walter Wolf<sup>1</sup>; Paul Saxe<sup>1</sup>; <sup>1</sup>Materials Design, Inc.

Fueled by the remarkable progress in hardware and software, computational materials science based on first-principles quantum mechanics is now becoming an integral part of industrial engineering. The present contribution focuses on diffusion processes, which are of particular importance for the performance and aging of materials for energy technologies. As illustrative example the diffusion of hydrogen isotopes in transition metals demonstrates that temperature-dependent diffusion coefficients can be computed from first-principles reaching an accuracy which is comparable with experiment. In the near future we can anticipate a dramatic growth of compute power in terms of number of processors. This will provide a fascinating opportunity to explore diffusion mechanisms in complex systems such as nano-structured and composite materials by carrying out thousands of simultaneous calculations. To harness this power, we will need highly automated and extremely robust computational schemes as well as sophisticated methods to cope with the wealth of data.

### 9:05 AM Invited

**Composition Dependent Diffusion Coefficients from First Principles:** *Anton Van der Ven*<sup>1</sup>; <sup>1</sup>University of Michigan

Diffusion in both interstitial and substitutional alloys is a complex kinetic process that depends on the nature of intrinsic defects, the energetically most favorable hop mechanisms and the degree of short and long-range order among the constituents of the alloy. In this talk, I will describe how these factors can be rigorously accounted for in the first-principles prediction of diffusion coefficients in non-dilute alloys. The approach relies on the evaluation of Kubo-Green expressions, which provide the link between macroscopic diffusion coefficients and atomic trajectories sampled in kinetic Monte Carlo simulations. A first-principles description of the thermodynamics of short and long-range order in multi-component solids is achieved with the cluster expansion formalism. As examples, I will describe recent work on the prediction of diffusion coefficients in the B2-NiAl compound used as bond coat in turbine blades and in Li ion battery electrode materials.

### 9:40 AM Invited

**New Paradigm in Developing Atomic Mobility Databases:** *Zi-Kui Liu*<sup>1</sup>; <sup>1</sup>Pennsylvania State Univ

Atomic diffusion is a common and important non-equilibrium process in solids that takes place at finite temperatures. To computationally simulate atomic diffusion processes, the thermodynamic and atomic mobility databases of the materials of interest are needed. The modeling technique of atomic mobility databases and related software has been becoming more and more matured in the last decades. However, the input data for the modeling is exclusively taken from experimentally measured tracer and chemical diffusion coefficients. In this presentation, a new modeling paradigm is presented which integrates quantum mechanics calculations, statistic analysis, and phenomenological modeling. Firstly, our recent progress in predicting self and dilute diffusion coefficients by quantum mechanics calculations will be discussed. Secondly, our approach to the unstable vibrational mode of transition states during diffusion will be outlined. Finally, the contribution to phenomenological modeling of atomic mobility will be presented.



## 10:15 AM Break

### 10:25 AM Invited

**Mechano-chemistry, Foundations and Modeling:** *Marek Danielewski*<sup>1</sup>; Bartek Wierzbna<sup>2</sup>; Jolanta Janczak<sup>2</sup>; Magdalena Pawelkiewicz<sup>1</sup>; <sup>1</sup>AGH University of Science and Technology; <sup>2</sup>EMPA

The volume continuity equation is used to define the material frame of reference in the multicomponent alloys. It allows to omit Darken postulate of constant molar volume, extends his method, defines frame of reference for diffusion and allows using Navier-Lamé equation of mechanics. Proposed form of conservation equations is self-consistent with the literature from classical Kirkendall experiments and their interpretation by Darken, Shimozaki and Onishi. The method allows for phenomenological description of multiscale phenomena and opens vast number of entirely new possibilities. We will show four series of Ni-Cu-Ag-Sn quaternary diffusion multiples of various geometries and distributions of elements in 3D fragments. Comparison of experimental and modeling results are reviewed. The new software and interpretation of experimental results will be presented.

### 11:00 AM Invited

**Modelling of Oxidation and Creep Resistance in Fe-Cr High-Temperature Steels:** *John Agren*<sup>1</sup>; Samuel Hallström<sup>1</sup>; Johan Jeppsson<sup>1</sup>; Lars Höglund<sup>1</sup>; <sup>1</sup>Royal Institute of Technology

Modelling, based on oxidation controlled by bulk and grain boundary diffusion through the alloyed oxide on the steel surface, is presented. The model for volume diffusion is based on a vacancy mechanism and mobilities and thermodynamic factors assessed by means of the Calphad type of analysis. The model is implemented in the DICTRA software and allows the calculation of oxide growth controlled by diffusion of metal ions as well as oxygen ions. The effect of porosity caused by a Kirkendall effect in oxides is discussed. The creep resistance is modeled by considering dislocation mechanisms that involve particle strengthening and solution hardening. The evolution of precipitate structure is predicted by kinetic calculations involving diffusion controlled phenomena such as growth and coarsening and also dissolution of less stable phases. Comparisons with experimental data are presented.

### 11:35 AM

**First-Principles Calculation on Impurity Diffusivities in Ferritic Iron:** *Shenyang Huang*<sup>1</sup>; Daniel Worthington<sup>2</sup>; Mark Asta<sup>3</sup>; Peter Liaw<sup>1</sup>; <sup>1</sup>University of Tennessee, Knoxville; <sup>2</sup>University of Texas, Austin; <sup>3</sup>University of California, Davis

To assist the alloy design for a creep-resistant ferritic Fe-based superalloy useful up to 1,033K, first-principles calculations have been applied to compute impurity diffusivities in the ferritic iron. To augment existing kinetic databases, which lack experimental measurements for a number of 4d and 5d solutes, diffusivities have been derived by incorporating first-principles calculated jump rate probabilities into a generalized five frequency model of vacancy mediated diffusion in the dilute limit. Using a transition-matrix approach with input parameters derived from the first-principles calculations, the correlation factors for solutes in ferritic iron have been determined. First-principles calculations were also conducted to calculate the induced magnetization of the impurity in the first and second neighbors, and thus, to investigate the relation between activation energies in ferromagnetic and paramagnetic states, employing an established empirical relation. This project is acknowledged by the Department of Energy Office of Fossil Energy Program, with Dr. Patricia Rawls.

### 11:55 AM

**Isotopic Diffusion Studies in Mg-Rich Light Metal Alloy Systems:** *Nagraj Kulkarni*<sup>1</sup>; Peter Todd<sup>2</sup>; Yongho Sohn<sup>3</sup>; <sup>1</sup>University of Tennessee; <sup>2</sup>Oak Ridge National Laboratory; <sup>3</sup>University of Central Florida

The development of an Integrated Computational Materials Engineering (ICME) framework for Mg-based light-weight alloys required for next-generation automotive materials will require a reliable diffusion database that can be integrated with other modeling activities. In this study, we focus on SIMS-based tracer diffusion studies in the Mg-Al-Mn system that are carried out using stable isotopes. The procedures and challenges involved in such studies will be discussed and preliminary results will be presented. Research sponsored by the U.S. Department of Energy, Assistant Secretary for Energy Efficiency and Renewable Energy, Office of Vehicle Technologies, as part of the Automotive Lightweighting Materials Program, under contract DE-AC05-00OR22725 UT-Battelle, LLC.

## 12:15 PM

**Variational Approach to the Boltzmann Matano Methods for Determination of the Diffusivity Coefficient:** *Alonso Jaques*<sup>1</sup>; Jeffrey LaCombe<sup>1</sup>; <sup>1</sup>University of Nevada

The Boltzmann-Matano method is used extensively in the determination of diffusivities in alloys. In the course of analyzing experimental data to determine D(C), numerical integrations and differentiations of the concentration profile are performed. With experimental data containing point-to-point noise, there are challenges related to calculating the slope (for example). Therefore, smoothing of the experimental data is often performed prior to analysis. This step can introduce numerical "artifacts" into the data and affects the confidence in the estimated parameters. We present here, an approach to the Boltzmann-Matano method that is based on a variational formulation for the numerical operations performed on the concentration data, avoiding the necessity of smoothing the data beforehand. This approach therefore, has the potential to be less subjective, and in numerical simulations, shows an increased accuracy in the estimated diffusion coefficients. The analysis method and accompanying publically-available analysis software used for this analysis will be discussed.

## Dislocations: 75 Years of Deformation Mechanisms: Effects of Obstacles, Surfaces, and Scale on Dislocation Generation and Motion

Sponsored by: The Minerals, Metals and Materials Society, TMS Materials Processing and Manufacturing Division, TMS Structural Materials Division, TMS/ASM: Mechanical Behavior of Materials Committee, TMS: Nanomechanical Materials Behavior Committee

Program Organizers: David Bahr, Washington State University; Erica Lilleodden, GKSS Research Center; Judy Schneider, Mississippi State University; Neville Moody, Sandia National Laboratories

Tuesday AM

Room: 3022

February 17, 2009

Location: Moscone West Convention Center

Session Chairs: Scott Mao, University of Pittsburgh; Neville Moody, Sandia National Laboratories

### 8:30 AM Invited

**Fluid Mechanics of Dislocations Moving in a Phonon Liquid:** *John Gilman*<sup>1</sup>; <sup>1</sup>University of California

At moderately high velocities, the Reynolds number for dislocations moving in a phonon liquid lie in the range (~50) at which vortices begin to form and be shed. Vortex shedding causes buffeting forces which in turn cause local cross-gliding of screw dislocations; particularly in bcc-metals. This effect is in addition to the drag caused by the phonon viscosity. The buffeting forces increase with increasing velocities and lead to turbulent flow. At temperatures below the Debye temperatures, the phonon density decreases, reducing the phonon drag, and increasing the maximum velocities at constant applied stress. This increases the average Reynolds number, and therefore the buffeting intensity which increases the cross-gliding rate, while the latter increases the deformation-hardening rate. It is suggested that these fluid dynamics phenomena account for the increase in the flow stress with decreasing temperature that is observed in pure bcc-metals.

### 9:00 AM

**The Role of Solute Segregation on the Evolution and Strength of Dislocation Junctions:** *Bulent Biner*<sup>1</sup>; Q. Chen<sup>1</sup>; X. Y. Liu<sup>2</sup>; <sup>1</sup>Ames Laboratory (USDOE); <sup>2</sup>Los Alamos National Laboratory

In this study, the role of solute segregation on the strength and the evolution behavior of dislocation junctions is studied by utilizing kinetic Monte Carlo and 3D dislocation dynamics simulations. The different solute concentrations and the character of the junctions are all included in the simulations in an effort to make a parametric investigation. The results indicate that the solutes have a profound effect on the strength of the junctions. Solute segregation can lead to both strengthening and weakening behavior depending upon the evolution of the dislocation junctions. The local solute concentration seems to be the more relevant parameter to characterizing the solute and dislocation interactions, due to the short-range stress field of solutes; and its bounds are set by the unconstrained volume dilatation. \* This work at the Ames Laboratory was

supported by the Department of Energy-Basic Energy Sciences under Contract No. DE-AC0207CH11358.

#### 9:20 AM

##### **On the Origin of Plastic Instability of Al-Mg Alloy 5052 during Stress Rate Change Test:** *Chen-ming Kuo*<sup>1</sup>; Chi-Ho Tso<sup>1</sup>; I-Shou Univ

Plastic instability or Portevin-Le Chatelier effect is observed during stress rate change test of Al-Mg alloy 5052 at room temperature. In the stress rate change experiments, strain retardation and plastic instability are observed, that is, although the applied stress rate changes, plastic strain is insignificant until the plastic instability occurs. By slightly increasing the final stress level, plastic instability is observed and modeled by the typical plastic deformation mechanism, that is, thermally activated kinetic flow theory coupled with structural evolution law. By changing the values of suitable parameters to simulate the microstructure change of instability, the origin of plastic instability could be understood.

#### 9:40 AM

##### **Serrated Flow and the Portevin-LeChatelier Effect in Austenitic Steel with Twinning Induced Plasticity:** *Louis Hector*<sup>1</sup>; Pablo Zavattieri<sup>1</sup>; Vesna Savic<sup>2</sup>; James Fekete<sup>2</sup>; <sup>1</sup>General Motors R&D Center; <sup>2</sup>General Motors Corporation

The twinning induced plasticity (TWIP) effect in high manganese austenitic steels leads to extreme strain hardening and elongation. Twinning helps retain the austenitic structure and twin boundaries act as barriers to dislocation motion. True stress-true strain curves exhibit step-like serrations beyond a critical strain suggesting the Portevin-LeChatelier (PLC) effect and negative strain rate sensitivity. Here, PLC band nucleation and propagation in TWIP steel were investigated with a digital image correlation (DIC) technique. Images of one surface of a tensile specimen were recorded with a variable framing rate high speed digital camera and custom image acquisition software. Post-processing of the data resulted in color strain and strain rate contour maps. Band nucleation, the direction of band propagation, and strain accumulation in the wakes of the bands were explored in the vicinity of individual serrations in flow curves. The present results are qualitatively compared with the PLC effect in Al-Mg alloys.

#### 10:00 AM

##### **Twinning Dislocations and Twin/Matrix Interfacial Structure in HCP Metals:** *Bin Li*<sup>1</sup>; Evan Ma<sup>1</sup>; <sup>1</sup>Johns Hopkins University

The double-layered structure of the twinning planes of HCP metals makes the twinning processes in HCP metals distinctly different from those in high-symmetry metals where the twinning plane is also the slip plane for dislocations. While a previous study suggests that a combination of  $\langle c+a \rangle$  and  $\langle a \rangle$  dislocations that spreads over a number of twinning planes (a zonal dislocation) can be the source of a twin embryo, we show that the actual configuration of the twinning dislocations is controlled by the energetics at the twinning plane. Instead of bonding two single crystals in the twinning orientation and then relaxing the twins, we investigate twin/matrix interface structure during deformation twinning in magnesium, using molecular dynamics and a simulation scheme different from previous studies. Valuable information regarding the configuration of the twinning dislocations and the twin/matrix interfacial structure is obtained.

#### 10:20 AM Break

#### 10:40 AM Invited

##### **Dislocation Micromechanisms and Scale-Free Flow in Microcrystals:** *Dennis Dimiduk*<sup>1</sup>; Christopher Woodward<sup>1</sup>; Paul Shade<sup>2</sup>; Michael Uchic<sup>1</sup>; Satish Rao<sup>3</sup>; Ed Nadgorny<sup>4</sup>; <sup>1</sup>US Air Force Research Laboratory; <sup>2</sup>Ohio State University; <sup>3</sup>UES, Inc.; <sup>4</sup>Michigan Technological University

Recent evidence shows that dislocation plasticity of crystals exhibits scale-free flow avalanches. However, there are relatively few experimental studies that reveal the dislocation mechanisms governing such behavior. Simulation studies suggest that long-range interactions between the ensemble of dislocations leads to their intermittent collective motion and the observed power law avalanche statistics. Those observations appear to be supported by slip step-height statistics and, indirect acoustic-emission experiments have been interpreted in a similar way. The present study examined the flow behavior of a variety of micrometer-sized single crystals deformed at room temperature via compression testing. The avalanche statistics have been examined as a function of material type and assessments of expected dislocation micromechanisms. The results of the study are discussed with attention to the nature of avalanches, their maximum size cut-off and the size-affected flow stress observed for such crystals.

#### 11:10 AM

##### **In-Situ Mechanical Testing at the Micro-Scale:** *Paul Shade*<sup>1</sup>; Robert Wheeler<sup>2</sup>; Michael Uchic<sup>3</sup>; Dennis Dimiduk<sup>3</sup>; Yoon-Suk Choi<sup>2</sup>; Hamish Fraser<sup>1</sup>; <sup>1</sup>The Ohio State University; <sup>2</sup>UES, Inc.; <sup>3</sup>Air Force Research Laboratory

Mechanical testing of micron-size samples provides distinct advantages over macroscopic testing for quantifying selected fundamental processes governing plastic flow, such as intrinsic size effects and direct, quantitative measures of strain heterogeneity and intermittency. We have developed a custom device for performing uniaxial mechanical tests on micron-scale samples that can operate inside a scanning electron microscope (SEM). When this device is employed within an SEM one can access both tensile and compressive test modes, and also directly observe the spatial distribution of deformation events through continuous recording of SEM images. The present study will highlight the effect that the device construction—in particular, the lateral stiffness of the compression platen or tensile grip—has on the resultant mechanical response of microcrystals that are oriented for single slip deformation. We also compare the observed deformation response to results obtained with crystal-plasticity finite element modeling of similar test structures.

#### 11:30 AM

##### **Focused Ion Beam Induced Damage Effects on the Plasticity of Nano- and Micro-Pillars:** *Jaafar El-Awady*<sup>1</sup>; Christopher Woodward<sup>2</sup>; Dennis Dimiduk<sup>2</sup>; Nasr Ghoniem<sup>1</sup>; <sup>1</sup>University of California, Los Angeles; <sup>2</sup>Air Force Research Laboratory

We present a computational study of the effects of radiation damage produced during focused ion beam (FIB) milling on the mechanical behavior of nano- and micro-pillars. We conduct three-dimensional dislocation dynamics simulations of cylindrical Ni single-crystals under compression, using the parametric dislocation dynamics coupled with the boundary element method. A strengthening effect due to the FIB induced damage layer is seen to become more prominent for sizes in the range between 0.5 and 1 micrometer, where the flow strength can increase by over 20%. As the size of the micropillar decrease the applied stress becomes high enough to overcome the effects of the damaged layer. Also, for larger diameters some cases of softening are observed. In addition, it is shown that the dislocation density can reach 3 times that computed when the effects of the damage layer are neglected.

#### 11:50 AM

##### **Analysis of the Hertzian Estimate of Dislocation Nucleation Stresses in Nanoindentation Experiments:** *Li Ma*<sup>1</sup>; Dylan Morris<sup>1</sup>; Stephanni Jennerjohn<sup>2</sup>; David Bahr<sup>2</sup>; Lyle Levine<sup>1</sup>; <sup>1</sup>NIST; <sup>2</sup>Washington State University

The dislocation nucleation stress of crystalline materials is frequently estimated from the maximum shear stress assuming Hertzian contact up to the first “pop-in” event, which is a sudden displacement burst during load-controlled nanoindentation. However, the irregular indenter tip shape will significantly change the stress distribution, and therefore the maximum shear stress from Hertzian estimation. In this work, the near-apex shape of two real Berkovich indenters, one lightly and another heavily used, were measured by SPM and directly input into FEA models for “virtual” nanoindentation experiments on  $\langle 100 \rangle$ -oriented single-crystal tungsten. Simultaneously, experiments were carried out using the same indenters. The load-displacement curves from FEA simulation show good agreement with those from the experiments. Hertzian-estimated radii for both indenters were significantly larger than those directly measured from the scanning-probe experiments and those obtained from FEA spherical indentation. The underestimation of the dislocation nucleation shear stress from both indenters is studied.

#### 12:10 PM

##### **Atomic-Scale Deformation Kinematics for Simulations of Dislocation Nucleation and Bicrystal Grain Boundary Evolution:** *Jonathan Zimmerman*<sup>1</sup>; Garritt Tucker<sup>2</sup>; David McDowell<sup>2</sup>; <sup>1</sup>Sandia National Laboratories; <sup>2</sup>Georgia Institute of Technology

We present a method for calculating an atomic-scale deformation gradient within atomistic simulation, and use this method to analyze a biaxially stretched thin film containing a surface ledge, an FCC metal loaded by a nanometer-scale indenter, and bicrystal grain boundaries subjected to shear loading. Our analyses compare this metric’s consistency with its continuum counterpart, which is known to have a zero curl for compatible deformations. Discontinuities in the deformation gradient indicate the presence of defects associated with plastic deformation, including dislocations and stacking faults. Our grain boundary simulations reveal pronounced deformation for small regions surrounding

the grain boundary, and demonstrate the influence of interfacial structure on mechanical behavior. Our research provides a useful tool for linking atomistic simulation results with continuum mechanics. Sandia is a multiprogram laboratory operated by Sandia Corporation, a Lockheed Martin Company, for the United States Department of Energy's National Nuclear Security Administration under contract DE-AC04-94AL85000.

---

## Electrode Technology for Aluminum Production: Special Session: Coke Quality Changes and Countermeasures

Sponsored by: The Minerals, Metals and Materials Society, TMS Light Metals Division, TMS: Aluminum Committee

Program Organizers: Barry Sadler, Net Carbon Consulting Pty Ltd; John Johnson, RUSAL Engineering and Technological Center LLC

Tuesday AM  
February 17, 2009

Room: 2003  
Location: Moscone West Convention Center

Session Chair: Alan Tomsett, Rio Tinto Alcan

---

### 8:30 AM Introductory Comments

#### 8:35 AM Invited

**Coal Tar Pitch: Past, Present, and Future:** John Baron<sup>1</sup>; Robert Wombles<sup>1</sup>; Stacey McKinney<sup>1</sup>; <sup>1</sup>Koppers Industries Inc

The first coal chemical recovery ovens were installed in the United States in 1893. By 1915, by-product ovens accounted for 97% of metallurgical coke produced. These by-product ovens produced coal tar as one of the major by-products. An industry developed around distillation of coal tar to produce various products. One of the major products produced is coal tar pitch. Since that time, coal tar pitch has become the binder of choice for the aluminum, commercial carbon, and graphite industries. A science has developed around defining the quality of a binder pitch based on its physical properties. Successful and unsuccessful efforts in this endeavor will be discussed. In addition some of the major changes in coal tar pitch properties as well as some of the successful and unsuccessful attempts to modify pitch properties will be discussed. Lastly, coal tar pitch supply and quality issues for the future will be addressed.

#### 9:00 AM Invited

**Refining Challenges and Opportunities for Anode Coke Quality:** Frank Cannova<sup>1</sup>; Yen Hoang<sup>1</sup>; Bernie Vitclus<sup>1</sup>; <sup>1</sup>BP Coke

Crude oil supply and quality has significant impact on petroleum refining as well as calcined coke availability and quality. Calcined coke quality is directly affected by the crude oil quality and refining conditions. The choice of crude to refine is mostly affected by crude price, availability and product yields. The current and future challenges for the aluminum smelting industry will be discussed from the perspective of an integrated coke producer. World crude oil impacts, challenges to anode grade coke supplies and projected calcined coke quality will be presented together with a discussion for aluminum smelter carbon plant anode options.

#### 9:25 AM Invited

**US Refining Economics – A Model Based Approach:** Todd Dixon<sup>1</sup>; <sup>1</sup>ConocoPhillips

The US refining industry has seen a shift over the last decade towards processing heavy, sour crude. These crudes generally translate into coke that is inferior for the production of anodes versus the lighter crudes. This trend can be understood by reviewing the economics of refining a light, sweet crude versus a heavy, sour crude. To do so, a simple model refinery was developed and the economics of processing different crude types will be presented using market indices for pricing. From this model, basic coke properties that are of importance to the manufacture of anodes will also be derived.

#### 9:50 AM Invited

**Changes in Anode Raw Material Quality in China - The Impact of Imported Crudes and Refinery Modifications:** Paul Adkins<sup>1</sup>; <sup>1</sup>AZ China Limited

China has long been a source for low-cost reasonable-quality carbon anodes for aluminium smelters. More recently however, China's green coke output has seen increasing sulphur levels. As China imports increasing amounts of crude

oil, the crude slate is changing inexorably. What is the future for Chinese anodes in terms of quality and price? How will China's thirst for oil impact exports of green coke, calcined coke and anodes?

#### 10:15 AM Break

#### 10:25 AM Invited

**Enhancing Coke Bulk Density through the Use of Alternative Calcining Technologies:** Kenneth Ries<sup>1</sup>; <sup>1</sup>Kenneth E Ries Consulting

The quality of petroleum coke used to make anodes for Aluminum production has declined in recent years and this trend is expected to continue. For example, high volatile green coke can result in low bulk density calcined coke leading to a corresponding low apparent density baked anode. This can have a serious negative impact on the smelting process. While most of the coke used in the industry is calcined using either rotary kilns or rotary hearth furnaces, there is a notable exception - the widespread use of shaft furnaces for coke calcining in China. These furnaces have some unique attributes that result in higher than expected calcined coke bulk densities. This paper will examine the potential for wider use of these shaft furnaces, and other alternative calcining technologies, to improve calcined coke density from available green cokes.

#### 10:50 AM Invited

**Anode Coating to Prevent Air Burn Oxidation in Aluminium Smelters:** Mahnaz Jahedi<sup>1</sup>; Anselm Oh<sup>1</sup>; Enzo Gulizia<sup>1</sup>; Stefan Gulizia<sup>1</sup>; Ali Jassim Malallah<sup>2</sup>; Maryam Al Jallaf<sup>2</sup>; Najeeba Al Jabri<sup>2</sup>; Ali Al Zarouni<sup>2</sup>; <sup>1</sup>CSIRO/Light Metals Flagship; <sup>2</sup>Dubai

Carbon anodes in Aluminum smelters are subjected to Air burn oxidation which shortens anode life and increases CO<sub>2</sub> emission. CSIRO Light Metals Flagship has developed a novel coating to protect carbon anodes from air burn oxidation without adversely affecting current production. This coating is a barrier coating with robust properties which satisfies demanding requirement of Aluminum smelters. The coating is easy to apply and resistant to damage during transport, installation and operation. The coating maintains integrity throughout the life of the anode without cracking or melting. The industry trials showed no safety issues. The laboratory tests and prototype anode trials results are presented. The performance of this coating is compared with molten Aluminum coating and The results showed this coating has 20-30 times better performance than molten Aluminum coating while it is cost effective. The industry trials so far have shown promising results.

#### 11:15 AM

**Minimizing Impact of Low Sulfur Coke on Anode Quality:** Angeliq Adams<sup>1</sup>; Roy Cahill<sup>1</sup>; Yves Belzile<sup>1</sup>; Katie Cantin<sup>1</sup>; Michel Gendron<sup>1</sup>; <sup>1</sup>Alcoa Inc

Approximately 95% of the SO<sub>2</sub> emissions generated by a smelter can be attributed to sulfur found in the incoming petroleum coke used in anode production. Efforts to reduce smelter SO<sub>2</sub> emissions have resulted in a number of plants shifting to lower sulfur coke. Shifting to lower sulfur concentrations in the anode has been demonstrated by others to negatively impact anode quality and potentially potroom performance by increasing the anodes susceptibility to reaction with carbon dioxide. In the following paper, we explore various methods to minimize this impact. These include, types of low sulfur cokes to be used in the coke blend, alterations in aggregate granulometry, and improved baking practices. The results from these studies are presented.

#### 11:40 AM Invited

**Mild Coal Extraction for the Production of Anode Coke:** Rodney Andrews<sup>1</sup>; David Jacques<sup>1</sup>; Terry Rantell<sup>1</sup>; <sup>1</sup>University of Kentucky

The quality and availability of petroleum coke used in the manufacture of carbon anodes for aluminum production is becoming of increasing concern to the industry. Coke quality and yields have progressively declined as changes in refinery practice and the move towards processing an increasing proportion of heavier sour crudes have affected coke properties, resulting in an increase in the metal impurities and sulfur content of the coke. An alternative supply of anode coke is required to supplement or eventually replace calcined petroleum coke. The significant domestic reserves of coal could represent a viable carbon resource for anode production, provided defined coke specifications can be met and at a cost that is economically viable. This paper will present an overview of the use of coal to substitute for pet coke, with a particular focus on recent efforts to producing anode grade coke through mild solvent extraction of coal.



## Emerging Applications of Neutron Scattering in Materials Science and Engineering: Microstructure Control

Sponsored by: The Minerals, Metals and Materials Society, TMS Electronic, Magnetic, and Photonic Materials Division, TMS: Chemistry and Physics of Materials Committee

Program Organizers: Xun-li Wang, Oak Ridge National Laboratory; Brent Fultz, California Institute of Technology; Hahn Choo, University of Tennessee

Tuesday AM  
February 17, 2009

Room: 3012  
Location: Moscone West Convention Center

Session Chairs: Jaime Fernandez-Baca, Oak Ridge National Laboratory; Baek Seok Seong, KAERI

### 8:30 AM Invited

**Small Angle Neutron Scattering (SANS) Studies of Nanostructures in Irradiated RPV Steels:** *G. Robert Odette*<sup>1</sup>; Brian Wirth<sup>1</sup>; Matthew Alinger<sup>1</sup>; Nicholas Cuninghame<sup>1</sup>; <sup>1</sup>University of California

The advantage of producing both nuclear and magnetic scattering up to high  $q$  have made SANS the dominant tool for characterizing the hardening-embrittling nano-scale features (NFs) in irradiated light water reactor pressure vessel (RPV) steels. The NFs are coherent Cu-Mn-Ni zones ranging from Cu rich to Mn-Ni rich precipitates (CRPs and MNPs). We summarize an extensive SANS database on the synergistic effects of alloy composition (Cu, Ni, Mn) and irradiation variables (flux, fluence and temperature) on the NFs, including Cu free MNPs that may result in severe but previously unanticipated embrittlement during extended RPV lifetimes. We also compare SANS results to other techniques, including atom probe tomography, which has historically suggested that there is a significant quantity of Fe in the NFs; however, this is inconsistent with that SANS data. We resolved this inconsistency by measuring the temperature dependence of magnetic scattering, demonstrating that the NFs contain little Fe.

### 9:00 AM Invited

**Behavior of Light Elements in Steels Studied by Small-Angle Neutron and X-ray Scattering:** *Masato Ohnuma*<sup>1</sup>; Jun-ichi Suzuki<sup>2</sup>; Mayumi Ojima<sup>3</sup>; F.G. Wei<sup>4</sup>; Syuji Narita<sup>5</sup>; Tetsuya Shimizu<sup>6</sup>; Kaneaki Tsuzaki<sup>1</sup>; Yo Tomota<sup>7</sup>; <sup>1</sup>National Institute for Materials Science; <sup>2</sup>JAEA; <sup>3</sup>Ibaraki University; <sup>4</sup>Yakin Kawasaki Co. Ltd.; <sup>5</sup>Daido Steel Co. Ltd.

Demanding on green materials with lower emission to the environment and saving natural resource, steel is now needed to be stronger by adding smaller amount of alloying elements. To achieve such requirement, quantitative characterization of size and volume fraction of precipitates is strongly required for the efficient use of them. Since Small-Angle Scattering (SAS) is one of the optimum techniques for quantitative characterization of microstructures, applications of SAS using both X-ray and neutron are now promoting in NIMS. In this talk, we show two results as examples. First is SAS characterization of nitrogen-enriched clusters formed during tempering of high nitrogen martensitic stainless steel in conjunction with hardness. In the second part, we show the detection of hydrogen (average concentration is 0.03 at% in the sample) trapped by nano-size NbC in steel by SANS.

### 9:30 AM

**Small Angle Neutron Scattering Study on the Cold Rolled Steel Sheet:** *Eun-jo Shin*<sup>1</sup>; Baek Seok Seong<sup>1</sup>; Shi-Hoon Choi<sup>2</sup>; Hu-Chul Lee<sup>3</sup>; Kye Hong Lee<sup>4</sup>; <sup>1</sup>Korea Atomic Energy Research Institute; <sup>2</sup>Sunchon National University; <sup>3</sup>Seoul National University

For low carbon steels, the effect of a cold rolling on a SANS pattern was investigated. Several cold rolled steel samples with different reduction rates and annealed samples after a cold rolling were measured by SANS. The cold rolled samples presented anisotropic 2-dimensional(2D) SANS patterns. From the 2D SANS patterns, two kinds of 1D patterns were calculated; one was for the Q RD(rolling direction), the other for the Q/RD. The scatterer sizes calculated from the 1D patterns by using a model fitting were increased with the reduction rates, only for the Q RD section. The annealed sample presented an isotropic SANS pattern. A crystal plasticity finite element method was employed to simulate the strain distribution around fine precipitates in the steels after cold

rolling deformation. Representative volume elements are used to capture the inhomogeneous deformation in ferrite matrix containing hard precipitates. The  $\langle 111 \rangle // ND$  fiber texture components were assumed as initial orientations.

### 9:50 AM

**Nano-Scale Solute Partitioning in Bulk Metallic Glasses:** Ling Yang<sup>1</sup>; Michael Miller<sup>2</sup>; Xun-li Wang<sup>2</sup>; Chain Liu<sup>2</sup>; Alexandru Stoica<sup>2</sup>; Dong Ma<sup>2</sup>; Jon Almer<sup>3</sup>; Donglu Shi<sup>1</sup>; <sup>1</sup>University of Cincinnati; <sup>2</sup>Oak Ridge National Laboratory; <sup>3</sup>Argonne National Laboratory

Fundamental understanding of composition variations and morphology of the nanoscale structure is essential for the development of advanced materials. A single experimental technique simply cannot provide all the answers. In this paper, we demonstrate an approach that leverages the power of several state-of-the-art characterization tools, from microscopy to x-ray and neutron scattering, to uncover the structure and phase transformation of nanocrystalline particles in devitrified bulk metallic glass. Nano-scale solute partitioning, due to strong chemical order, is revealed at an unprecedented detail by a new wide field of view atom probe. This level of details is crucial for understanding the interference peaks observed in small angle x-ray and neutron scattering experiments, a mystery that has lingered for more than a decade. The implications of our experimental results are discussed with regard to the stability of metallic glass alloys.

### 10:10 AM Break

### 10:30 AM

**Effect of Nano-Sized Precipitates on the Mechanical Properties of Low-Carbon Steels by Neutron Scattering Techniques:** *Baek Seok Seong*<sup>1</sup>; Eun-jo Shin<sup>1</sup>; Shi-Hoon Choi<sup>1</sup>; Kye Hong Lee<sup>1</sup>; <sup>1</sup>KAERI

SANS and powder diffraction techniques were applied to study the effect of nano-sized precipitates and a boron addition on the mechanical properties of low carbon steels quantitatively. Fine core-shell spherical precipitates with an average radius of ~ 5 nm like MnS surrounded by BN layers in boron-added steels were mainly observed. In boron added steels the number of boron-precipitates such as BN, Fe<sub>3</sub>(C, B) drastically increased at higher rolling temperature. The volume fraction of the fine precipitates of the boron added steels was higher than that of the boron free steels. The boron addition to the low carbon steels resulted in reducing the strength and improving the elongation, which is related to the reduction of the solute carbon and the nitrogen contents in the ferrite matrix caused by the precipitation of the BN as well the increase of the volume fraction of the cementites.

### 10:50 AM Invited

**In-Situ Time-Resolved Analyses of Microstructure in Advanced Materials under High Magnetic Fields Using Neutron Scattering:** *Jaime Fernandez-Baca*<sup>1</sup>; Gerard Ludtka<sup>1</sup>; Gail Ludtka<sup>1</sup>; Camden Hubbard<sup>1</sup>; John Wilgen<sup>1</sup>; Roger Kiser<sup>1</sup>; <sup>1</sup>Oak Ridge National Laboratory

We will present recent developments to conduct in-situ neutron scattering measurements of transformations that occur in materials when processed at high magnetic fields and elevated temperatures. An induction heater was designed to provide temperatures up to 1200 degrees C inside a 5-Tesla cryomagnet. The combination of this thermal magnetic system and the Wide Angle neutron Diffractometer (WAND at ORNL's High Flux isotope Reactor) allowed the time-resolved neutron diffraction study of the shift in equilibrium phase transformation temperatures that occur in an Fe-C binary alloy when a high magnetic field is applied at elevated temperatures. The use of the WAND enabled several diffraction peaks to be monitored simultaneously as the microstructure evolved under the influence of the external magnetic field. The WAND is a high-intensity, medium-resolution powder instrument operated jointly by ORNL and the Japan Atomic Energy Agency (Tokai, Japan) under the US-Japan Cooperative program on Neutron Scattering.

### 11:20 AM

**Overview of the High Resolution Powder Diffractometer at the High Flux Isotope Reactor:** *Ovidiu Garlea*<sup>1</sup>; <sup>1</sup>ORNL

The powder diffractometer HB2a at the High Flux Isotope Reactor is undergoing a major upgrade, being optimized to offer both high flux and high resolution. The instrument is equipped with a new vertically focused Ge wafer monochromator that provides one of three principal wavelengths: 2.41 Å, 1.54 Å, and 1.12 Å. A new detector shielding, more effective and more compact, gives access to a wide scattering angle range ( $-2^\circ < 2\theta < 164^\circ$ ). This diffractometer will provide high-throughput studies of nuclear and magnetic structures as a

function of intensive conditions. In addition to traditional Rietveld refinements, studies of phase transitions, thermal expansion, quantitative analysis, and ab-initio structure solution from powder data can be undertaken. This presentation will give an overview of the HB2a diffractometer and illustrate its capabilities with recent neutron scattering studies on new materials ranging from ternary rare earth-alloys to organometallic systems.

## Fatigue: Mechanisms, Theory, Experiments and Industry Practice: The Role of Microstructure in Fatigue

Sponsored by: The Minerals, Metals and Materials Society, TMS Structural Materials Division, TMS/ASM: Computational Materials Science and Engineering Committee, TMS/ASM: Mechanical Behavior of Materials Committee, TMS/ASM: Nuclear Materials Committee

Program Organizers: Koenraad Janssens, Paul Scherrer Institute; Corbett Battaile, Sandia National Laboratories; Brad Boyce, Sandia National Laboratories; Luke Brewer, Sandia National Laboratories

Tuesday AM Room: 3008  
February 17, 2009 Location: Moscone West Convention Center

Session Chairs: Corbett Battaile, Sandia National Laboratories; Luke Brewer, Sandia National Laboratories

### 8:30 AM Invited

**Selected Problems in the Fatigue Behavior of Titanium Alloys:** Adam Pilchak<sup>1</sup>; Amit Bhattacharjee<sup>1</sup>; James Williams<sup>1</sup>; <sup>1</sup>Ohio State Univ

Titanium alloys have fatigue strengths at  $10^6$  cycles that typically are  $\sim 0.6$  of the tensile yield strength ( $\sigma_y$ ). Since Ti alloys essentially contain no inclusions, the fatigue strength can be tailored according to the value of  $\sigma_y$  without concern for intervention of inclusions as crack initiation sites. High temperature Ti alloys such as Ti-6Al-2Sn-4Zr-2Mo(+Si) and IMI834 also can exhibit a significant reduction in fatigue life if the load is held at maximum value as compared to continuously cycled in a load controlled test. This effect is called dwell fatigue. Furthermore, local variations in the microstructure due to processing or other production related events can serve as early fatigue crack initiation sites. These variations must be either eliminated or accounted for in design data, the former being preferred. This talk will describe several aspects of the fatigue behavior of Ti alloys. The practical implications of this behavior will be discussed.

### 9:00 AM

**Deformation of Ti-6-4 at the Microstructural Scale: Experiments and Simulations:** Philip Littlewood<sup>1</sup>; Mario Nardone<sup>1</sup>; Fionn Dunne<sup>1</sup>; Angus Wilkinson<sup>1</sup>; <sup>1</sup>University of Oxford

Experiments and simulations have been conducted on the local response at the microstructural scale of the titanium alloy Ti-6-4, to imposed monotonic and cyclic deformation. Both textured and untextured material has been examined. Regions of approximately 100  $\mu\text{m}$  by 100  $\mu\text{m}$  have been marked on the surface using a FIB, and EBSD used to map the grain morphology and orientations before deformation. FIB was also used to generate finer surface markers in these regions. The displacements of these allow the local in plane deformation fields to be determined. EBSD measurements on the undeformed samples were used to construct a crystal plasticity finite-element simulations. Simulations were run with different combinations of allowed slip systems including a and c+a slip and basal and prismatic slip planes. The importance of these slip systems and the boundary conditions in the model are assessed through comparison between experimental observations and modelling predictions.

### 9:20 AM

**The Population of Databases Relating Microstructure and Fatigue in Ti-555:** John Foltz<sup>1</sup>; Brian Welk<sup>1</sup>; Peter Collins<sup>1</sup>; Rajagopalan Srinivasan<sup>1</sup>; James Williams<sup>1</sup>; Hamish Fraser<sup>1</sup>; <sup>1</sup>Ohio State Univ

It is well known that variations in the thermomechanical history of Ti-555 (Ti-5Al-5V-5Mo-3Cr-0.5Fe), and the corresponding changes in microstructural features of the alloy can significantly impact the resulting mechanical properties. While such variation includes the fatigue life, the exact nature of the microstructure-property relationship is not well understood. In order to explore the influence of the microstructural features present in Ti-555 on fatigue life, a database relating these to the fatigue life in four-point bend ( $R=0.1$  at 60 hertz)

tests has been populated. Precisely controlled variations in thermal histories were affected using a Gleeble(R) thermomechanical simulator. The resulting microstructures have been characterized using optical and electron microscopic techniques, and subsequently quantified. The fatigue life has been measured at a constant fraction of the experimentally measured yield strengths. Fatigue life will be discussed in reference to important microstructural features.

### 9:40 AM

**Effects of Microstructure and In Situ Development of Crack Closure on Fatigue in Self-Healing Composites:** Eric Brown<sup>1</sup>; <sup>1</sup>Los Alamos National Lab

A growing body of work in the literature is investigating a class of materials possessing the ability to self-healing in response to damage and crack growth. The first of these materials, as reported in Nature, employed ureaformaldehyde microcapsules containing a dicyclopentadiene healing agent and dispersed Grubbs' ruthenium catalyst in an epoxy matrix. This material has been demonstrated to recover over 90% of its virgin fracture properties and to exhibit significantly improved resistance to fatigue crack growth. The composite microstructure and inclusion of fluid filled microcapsules inhibit fatigue crack growth in the glassy epoxy. Self-healing functionality can lead to negative crack growth through healing under simply cyclic loading and complex loading histories. Finally, crack closure associated with the in situ self-healing mechanism is shown to arrest fatigue crack growth in high cycle fatigue loading. These fatigue mechanisms will be discussed in the initial self-healing material and subsequent variants.

### 10:00 AM

**Fatigue Cracking Mechanisms of F.C.C. Crystalline Materials:** Z. F. Zhang<sup>1</sup>; <sup>1</sup>Institute of Metal Research/Chinese Academy of Sciences

In the current study, fatigue cracking mechanisms of pure Cu bicrystals, polycrystalline and ultrafine-grained pure Cu, Cu-Al and Cu-Zn alloys were systematically investigated under cyclic loading. In pure Cu bicrystals, it was found that the large-angle grain boundaries (GBs) are always the preferential sites for fatigue cracking; however, we never found fatigue cracking along those low-angle GBs. In polycrystalline pure Cu, Cu-Al and Cu-Zn alloys, the large-angle GBs are still the preferential fatigue cracking sites. With the addition of Al or Zn, the surface slip bands become more homogeneous and display less localization after cyclic deformation. It is found that the annealing twin boundaries (TBs) gradually trend to produce fatigue cracks. With the grain refinement into ultra-fine level, plastic strain localization and fatigue cracking nucleated along shear bands (SB) at low strain amplitude but was changed to deformation bands (DBs) at high strain amplitude.

### 10:20 AM Break

### 10:40 AM Invited

**Microstructurally Small Crack Fatigue in Lightweight Engineering Alloys: Modeling and Experiments:** Mark Horstemeyer<sup>1</sup>; Haitham El Kadiri<sup>1</sup>; Yibin Anna Xue<sup>1</sup>; <sup>1</sup>Mississippi State Univ

Fatigue crack growth micromechanisms in Al7075-T651 and in four cast magnesium alloys AM50, AM60, AZ91 and AE44 were identified using fractography and in-situ SEM techniques, and predicted through a microstructurally multistage fatigue model. Namely, for magnesium alloys, the main fatigue crack initiated on shrinkage pores and to a lesser extent on large Mn-rich particles. Small cracks propagated along the a-Mg dendrite / eutectic interface, and then through the Al-rich eutectic. In the long crack regime, the crack advanced in a mix transdendritic-interdendritic mode along persistent slip bands spreading over several tens of dendrite cells. For Al7075, The fatigue crack nucleated at iron-rich intermetallics through either a debonding or crack transition from the particle into the matrix. Small cracks showed a step-like structure that changed from grain to grain. The long cracks advanced through individual damage lines along slipped planes ahead of the crack tip.

### 11:10 AM

**Low Cycle Fatigue Variability in Single Crystal Nickel-Base Superalloys Directionally Solidified with Liquid Metal Cooled and Conventional Bridgman Processes:** Clinique Brundidge<sup>1</sup>; Tresa Pollock<sup>1</sup>; <sup>1</sup>University of Michigan

Factors influencing the fatigue variability of a single crystal nickel-base superalloy tested at 538°C (1000°F) have been examined. The role of cooling rates during solidification has been investigated with the use of a liquid metal cooling (LMC) directional solidification process in comparison to a conventional Bridgman solidification technique. Additions of Tantalum to improve the

shearing resistance of precipitates have also been investigated. Increases in cooling rates during solidification significantly decrease primary and secondary dendrite arm spacings as well as decrease the size of solidification shrinkage pores. Increases in cooling rates improve fatigue life by as much as a factor of seven. Solidification variables had a stronger impact on fatigue life than minor changes in chemistry. The influence of various features of cast microstructure on fatigue variability will be discussed.

**11:30 AM**

**Influence of Grain Boundaries on the Cyclic Slip Activity of PSBs – A Comparison of Surface and Bulk Grains:** *Anja Weidner*<sup>1</sup>; Werner Skrotzki<sup>1</sup>; <sup>1</sup>TU Dresden

The slip activity and shear strain of persistent slip bands in polycrystalline nickel were studied after half-cycle deformation at different stages of fatigue life using the combination of atomic force microscopy and scanning electron microscopy. Recent studies on surface grains showed that the half-cycle slip activity of PSBs significantly depends on the stage of fatigue life, although the local shear strain is nearly independent on it. But up to now this behaviour is indistinct. Possible reasons could be a hardening effect due to secondary slip within PSBs, the appearance of micro structurally short cracks, the influence of grain boundaries or a surface effect solely. Therefore, the surface investigations of the half-cycle slip activity as well as the local shear strain of PSBs have been extended by detailed studies on bulk grains after removing surface layer. A comparison between the results on surface and bulk grains will be discussed.

**11:50 AM**

**The Role of Microstructural Heterogeneity on Fatigue Lifetime Variability in the Very High Cycle Regime:** *Christopher Szczepanski*<sup>1</sup>; Sushant Jha<sup>2</sup>; James Larsen<sup>3</sup>; J. Wayne Jones<sup>1</sup>; <sup>1</sup>University of Michigan; <sup>2</sup>Universal Technology Corp; <sup>3</sup>US Air Force

The very high cycle fatigue behavior of Ti-6246 has been investigated using ultrasonic fatigue techniques and lifetimes ranging from  $10^6$  to  $10^9$  cycles have been observed. In this regime of fatigue ( $0.4-0.6\sigma_{ys}$ ), only certain microstructural regions are susceptible to fatigue damage accumulation, and lifetimes are related to the distribution of these fatigue critical microstructural neighborhoods. In the current work, three distinct classes of fatigue failures have been identified; one surface initiation mechanism and two subsurface initiation mechanisms. Fatigue cracks initiate by facet formation within  $\alpha_p$  grains favorably oriented for basal slip in microtextured regions of the microstructure. The  $\alpha_p$  grains inherit their orientation from the prior  $\beta$  phase, but they do not strictly follow the Burgers orientation relationship upon transformation from the  $\beta$  phase. The orientation of the  $\alpha_p$  grains with respect to the parent  $\beta$  phase has been investigated to determine how these microstructural neighborhoods encourage fatigue damage accumulation.

**Friction Stir Welding and Processing-V: Session III**

Sponsored by: The Minerals, Metals and Materials Society, TMS Materials Processing and Manufacturing Division, TMS: Shaping and Forming Committee  
Program Organizers: Rajiv Mishra, Missouri University of Science and Technology; Thomas Lienert, Los Alamos National Laboratory; Murray Mahoney, formerly with Rockwell Scientific

Tuesday AM  
February 17, 2009

Room: 2014  
Location: Moscone West Convention Center

Session Chair: Thomas Lienert, Los Alamos National Laboratory

**8:30 AM Invited**

**An Experimental Framework for Advancing the Science Base of Friction Stir Processing:** *Carl Sorensen*<sup>1</sup>; <sup>1</sup>Brigham Young University

Friction Stir Processing is used as a method for changing material properties as well as for joining materials. Significant effort has been expended to determine the effects of process parameters on resulting properties. In the course of developing these relationships, a number of empirical methods for understanding friction stir processing have been developed. This paper presents a framework for research in friction stir processing. It explains the domains of interest in the process, including the independent process parameter domain (spindle speed, feed rate, and depth control parameter), the dependent process

parameter domain (spindle torque, process forces, power, and heat input), the microstructure domain (grain size, grain shape, texture, microstructural components), and the processed zone property domain. Research to advance the understanding of FSP should focus on the mappings between these domains. Examples of research for each of these mappings is presented.

**8:50 AM**

**Effects of Rotation Speed and Welding Speed on Material Flow and Stir Zone Formation during FSW/P:** *Zhan Chen*<sup>1</sup>; Song Cui<sup>1</sup>; <sup>1</sup>AUT University

In the first part of our study, the mode of material flow in and next to thread space which determines the mode of nugget zone formation was quantified. Using an Al-Si alloy, the deformation of dendrites before entering into thread space could be traced. Using this method, rapidly increases in strain and strain rate towards thread space can be observed with strain and strain rate estimated to be up to  $\sim 3.5$  and  $\sim 85$  s<sup>-1</sup>, respectively. In the second part of our study, how the mode of material flow affected by tool rotation speed and feed rate were studied. This series of experiments included the use of two very different alloys (an Al-7Si based an Al-4.5Cu based). Thus the effect of the different mechanical behaviors at peak temperatures on flow mode can be evaluated. Variations of welding forces associated with the mode of change will also be correlated.

**9:10 AM**

**Bending Limits in Friction Stir Processed 5083 Aluminum Plate:** *Michael Miles*<sup>1</sup>; Chris Smith<sup>2</sup>; Murray Mahoney<sup>3</sup>; Rajiv Mishra<sup>4</sup>; <sup>1</sup>Brigham Young University; <sup>2</sup>Friction Stir Link; <sup>3</sup>Formerly with Rockwell Scientific; <sup>4</sup>Missouri University of Science and Technology

Bending performance of aluminum plates at room temperature can be enhanced by friction stir processing (FSP), which can locally anneal and refine grain size at the pre-tensile side of the plate. Plates with thicknesses from 8 - 25 mm of AA 5083 have been friction stir processed and then bent into a v-die to investigate the increase in ductility that results from FSP. A finite element model was also developed to predict bending limits of the friction stir processed plate, as well as an unprocessed plate. The material property gradient in the friction stir processed plate was obtained by machining tensile specimens at various locations through the thickness of the plate and then testing the specimens to generate flow stresses for the model calculations. This approach allowed for good agreement between experiments and model prediction of plate bending limits.

**9:30 AM**

**Microstructure and Mechanical Properties of an Al-Mo In Situ Nanocomposite Produced by Friction Stir Processing:** *I. Shan Lee*<sup>1</sup>; P. W. Kao<sup>1</sup>; N. J. Ho<sup>1</sup>; <sup>1</sup>NSYSU

In this work, friction stir processing (FSP) was applied to produce aluminum based nanocomposites from powder mixtures of Al-Mo. This technique has combined hot working nature of FSP and exothermic reaction between Al and Mo. Fully dense Al-matrix composites with large amount of nanometer sized reinforcement particles, which were formed in-situ, can be fabricated by FSP without further consolidation process. The microstructure was characterized by the use of TEM, SEM and XRD. The Al-Mo intermetallic particles were identified as Al<sub>12</sub>Mo, which were formed in situ during FSP. These particles have an average size of  $\sim 200$ nm. Due to the fine dispersion of Al<sub>12</sub>Mo particles, the aluminum matrix has ultrafine-grained structure ( $\sim 1\mu\text{m}$ ). In addition, the reaction mechanism, and microstructure evolution during FSP, as well as the mechanical properties of the Al-Mo in situ composites will be presented.

**9:50 AM**

**The Effect of Friction Stir Process on Erosion Wear Behaviors of Al-14Si Alloy:** *Tun-Wen Cheng*<sup>1</sup>; Li-Hui Chen<sup>1</sup>; Truan-Sheng Lui<sup>1</sup>; <sup>1</sup>Natl. Cheng-Kung University

In this study, die-casting Al-14Si alloy including several kinds of second phase particles were selected as base metal. Friction Stir Process (FSP) was applied to make the second phase particles more spherical and distribute uniformly in the Al matrix. The effect of second phase particles was examined by erosion test. According to the results, the erosion resistance of stirred samples is higher than that of base metal. Therefore the erosion resistance can be improved via FSP due to the modified second phase particles.



10:10 AM

**Effect of Aging Treatments on Microstructure and Mechanical Properties of Friction Stir Processed 7075 Aluminum Alloy:** *Chung-Wei Yang*<sup>1</sup>; Truan-Sheng Lui<sup>1</sup>; Li-Hui Chen<sup>1</sup>; <sup>1</sup>National Cheng Kung University

Friction stir processing (FSP) is applied on 7075-T6 aluminum alloy. The aim of present study is to clarify the effect of natural aging with reversion process and artificial aging on the microstructural homogeneity and mechanical properties of FSP-7075-T6 at the stir zone. Results show that the tensile strength and ductility is reduced after 40°C natural aging for 96 hours. EPMA analysis shows the distribution of precipitates is asymmetrical after FSP. This phenomenon can be reduced with significant promotion in tensile strength and ductility by solid solution treatment before natural aging. The ductility can also be recovered with 200°C reversion process. The artificial aging for FSP-7075-T6 is performed at 220°C and 320°C for 1 hour. Microstructural observation represents that there is no apparent difference on grain size and texture at the stir zone. The tensile strength is decreased with increasing temperature, but the ductility is significantly increased for 320°C artificial aging.

10:30 AM Break

10:40 AM

**Control of Structure in Conventional Friction Stir Welds through a Kinematic Theory of Metal Flow:** *Haley Rubisoff*<sup>1</sup>; Judy Schneider<sup>1</sup>; Arthur Nunes<sup>2</sup>; <sup>1</sup>Mississippi State University; <sup>2</sup>NASA-Marshall Space Flight Center

Tracer studies were conducted to compare two friction stir weld (FSW) processes using a threaded pin. Conventional (C) FSWing is used primarily for longitudinal flat welds and uses a threaded pin and backing anvil. For circumferential welding, a self-reacting (SR) FSW is made by pinching the metal between two shoulders. Copper was deposited on the crown, root, or faying surfaces of AA2219 panels before welding, and tungsten wire was placed longitudinally along the faying surface to trace the material flow in the weld. The test matrix compared tool rotational speed, travel speed, load, and pin thread pitch to better understand how the weld parameters affect the material flow. Plan, longitudinal, and transverse section radiographs were examined to determine flow paths using the copper and tungsten as markers. The results were used to model how the metal flow varied between the two FSW processes as a function of the process parameters.

11:00 AM

**3-D Microstructure Modeling of Friction Stir Processed AZ31B Mg Alloy:** *Zhenzhen Yu*<sup>1</sup>; Hahn Choo<sup>1</sup>; <sup>1</sup>The University of Tennessee

We investigated the dependence of dynamically-recrystallized grain size (d) on friction stir processing (FSP) parameters in an AZ31B Mg alloy plate. First, a systematic microstructural examination was performed on a series of compression test specimens with different initial grain sizes at various testing temperatures and strain rates in order to obtain the empirical relationship between the final recrystallized grain size (d) and Zener-Hollomon parameter (Z). Second, the Z-d relationship was applied for the prediction of final grain size distribution throughout the FSP plate in combination with the profiles of temperature and strain rate obtained from a 3-D viscoplastic model using FLUENT software under various processing conditions. Finally, the model prediction was validated by comparing to the experimentally-measured thermal history and final grain size distribution after the FSP.

11:20 AM

**Producing Ultra Fine Microstructure in AZ 31 Magnesium Alloy by Submerged Friction Stir Processing:** *Ali Shahnam*<sup>1</sup>; Fatollah Karimzadeh<sup>1</sup>; Mohammad Golozar<sup>1</sup>; <sup>1</sup>Isfahan University of Technology

Ultra fine grain size (UFG) microstructures with an average grain size of 300-900 nm are achieved in solution hardened AZ31 magnesium alloy prepared by submerged friction stir processing. The mean hardness of the region reaches about 95 Hv, which is more than twice as high as that of the AZ31 matrix. The relationship between the resulting grain size and the applied working strain rate and temperature for friction stir processing in AZ31 systemically was examined. The grain refinement kinetics are analyzed and the results are self-consistent.

## Frontiers in Solidification Science III: Coupled Multiphase Growth Morphologies

Sponsored by: The Minerals, Metals and Materials Society, ASM International, TMS Materials Processing and Manufacturing Division, TMS/ASM: Computational Materials Science and Engineering Committee, TMS/ASM: Phase Transformations Committee, TMS: Solidification Committee, TMS: Chemistry and Physics of Materials Committee  
Program Organizers: Ralph Napolitano, Iowa State University; James Morris, Oak Ridge National Laboratory

Tuesday AM

Room: 2018

February 17, 2009

Location: Moscone West Convention Center

Session Chair: Mathis Plapp, Ecole Polytechnique

8:30 AM Invited

**Solidification Dynamics of Regular, Irregular and Locked Eutectics:** *Silvère Akamatsu*<sup>1</sup>; Sabine Bottin-Rousseau<sup>2</sup>; Gabriel Faivre<sup>1</sup>; <sup>1</sup>CNRS; <sup>2</sup>UPMC

A classification of eutectic microstructures into regular (periodic) and irregular (disordered) eutectics has been proposed a long time ago. According to it, regular eutectics correspond to fully nonfaceted alloys, whereas irregular eutectics arise when the interface between at least one of the solid phases and the liquid is faceted. We propose to amend this classification, on the basis of real-time observations in thin-sample directional solidification of nonfaceted, transparent and metallic alloys. We find that, in a given sample, regular eutectic grains coexist with a kind of irregular eutectic grains, within which the interphase boundaries are more or less locked onto a given direction. This direction can be strongly tilted with respect to the solidification axis, and does not vary when solidification conditions are changed. This locked dynamics signals a faceting of the interphase boundaries, independently of the properties of the solid-liquid interfaces.

8:50 AM Invited

**Spacing Selection by Curved Isotherms in Rod-Like Eutectic Solidification:** *Sabine Bottin-Rousseau*<sup>1</sup>; Mikael Perrut<sup>1</sup>; Silvère Akamatsu<sup>1</sup>; Gabriel Faivre<sup>1</sup>; <sup>1</sup>INSP

We report on a real-time experimental study of rod-like eutectic solidification fronts in bulk samples of a succinonitrile-camphor eutectic alloy. After a long directional-solidification time, rod-like eutectic patterns exhibit a local hexagonal order, but are neither steady nor uniform. However, the average spacing is more or less maintained constant at a value close to the minimum undercooling spacing. Simultaneously, we observe a continual drift of the rod tips towards the walls of the crucible. We assign this dynamics to a slight bulging of the front envelope, thus of the isotherms, and to the fact that rods grow perpendicular to the front envelope. After a transient, during which the pattern is stretched without rod branching, the dynamics is controlled by a balance between stretching and branching, and the system operates near the point of marginal stability for the branching instability.

9:10 AM

**Early Stage Dynamics in Eutectic Solidification:** *Melis Serefoğlu*<sup>1</sup>; Ralph Napolitano<sup>1</sup>; <sup>1</sup>Iowa State University

Early-stage selection dynamics in succinonitrile-(D)camphor organic transparent rod eutectic system is investigated experimentally using directional solidification with different specimen thicknesses. The effect of the initial single-phase boundary thickness, the single-phase layer on the seeding mechanism and the overall competition between onset mechanisms are examined. The shape of the solid/liquid interface, the specimen thickness, and the grain boundaries are all observed to influence the formation of eutectic morphology in a geometrically constrained system. Additionally, the formation of single phase layer is investigated with respect to its role in the establishment of initial conditions for directional eutectic growth.

9:30 AM

**Phase Field Simulation of Eutectic Microstructure Evolution with Faceting:** *Abhik Choudhury*<sup>1</sup>; *Gandham Phanikumar*<sup>1</sup>; <sup>1</sup>Indian Institute of Technology Madras

Several phase field models to simulate eutectic microstructure are now available. In this study, we have chosen the model by Wheeler et al. (1996) with modification to include faceting in one of the two solid phases. Numerical and

algorithmic details will be discussed. Results obtained for isotropic case will be compared to those available in the literature. Interesting features arising out of anisotropy for one of the phases will be highlighted.

#### 9:50 AM Invited

##### Solidification Morphologies in the Cu-Sn Peritectic System at Low Growth

**Rate:** *Michel Rappaz*<sup>1</sup>; *Frédéric Kohler*<sup>1</sup>; <sup>1</sup>Ecole Polytechnique Fédérale de Lausanne

Solidification at very low speed of peritectic alloys such as Fe-Ni has shown a great diversity of microstructures: alternated bands or islands of  $\gamma$  and  $\delta$ , coupled growth of  $\gamma'$  and  $\delta'$  lamellae as in eutectics. Similar phenomena have been observed recently in Cu-Sn alloys, which exhibit a much larger solidification interval. Although influenced by solutal convection, bands and lamellae structures of  $\alpha$  and  $\beta$  were shown to alternate in the specimen while being part of a continuous structure. Unlike the nucleation-growth mechanism proposed for Fe-Ni, the formation of bands in Cu-Sn seems to proceed by a 3D overgrowth mechanism similar to that occurring in the initial stage of eutectic coupled growth. During the overgrowth of one phase by the other, lateral instabilities can develop and lead to the cooperative growth of lamellar structures. These results and remaining open questions on peritectic solidification at low speed will be discussed.

#### 10:10 AM Break

#### 10:30 AM Invited

##### Two-Phase Microstructure Formation in Peritectic Systems: *Rohit Trivedi*<sup>1</sup>;

<sup>1</sup>Iowa State University

An overview of two-phase microstructure formation in Peritectic systems will be presented by examining experimental data in selected systems. Specific emphasis will be placed on the development of coupled growth in peritectic systems and on the formation of banded microstructures. The banded microstructure is shown to consist of alternate bands of primary and peritectic phases or as alternate bands of primary phase and the two-phase coupled growth. The role of nucleation site, nucleation undercooling and competitive growth of the two phases will be quantitatively examined, and shown to be critical in the formation of these two types of banded microstructures. The mechanism of coupled growth evolution and the conditions for the formation of the coupled growth under diffusive growth conditions will be presented. Experimental results on the effect of convection on the stabilization or destabilization of the coupled growth and the banded microstructures will be discussed.

#### 10:50 AM Invited

##### Microsegregation Modelling of Multiple Phase Transformations: *Charles-André Gandin*<sup>1</sup>; *Damien Tournet*<sup>1</sup>; <sup>1</sup>Ecole Des Mines

A multiple phase transformation microsegregation model for the solidification of alloys is developed based on an extension of a volume averaging method. It accounts for diffusion in all phases and for the undercooling and the growth kinetics of the solidifying microstructures. It considers the occurrence of several phase transformations taking place in the presence of liquid, including peritectic and eutectic reactions. Volume averaged conservation equations for the mass of species in each phase and at each interface are coupled with an isothermal heat balance of the domain. The composition at interfaces between phases follows thermodynamic equilibrium. The diffusion fluxes at the interfaces between phases are calculated through characteristic microstructural diffusion lengths for which analytical expressions are derived. The model predicts cooling curves, volume fractions and average compositions of phases. It predicts the occurrence of recalcences during the growth of microstructures, and the progress of peritectic transformations consuming previously formed phases.

## Magnesium Technology 2009: Alloys II: Calcium

Sponsored by: The Minerals, Metals and Materials Society, TMS Light Metals Division, TMS: Magnesium Committee

Program Organizers: Eric Nyberg, Pacific Northwest National Laboratory; Sean Agnew, University of Virginia; Neale Neelameggham, US Magnesium LLC; Mihriban Pekguleryuz, McGill University

Tuesday AM

Room: 2006

February 17, 2009

Location: Moscone West Convention Center

*Session Chair:* Norbert Hort, GKSS Research Center

#### 8:30 AM Introductory Comments

#### 8:35 AM

**Creep Resistant Mg-Al-Zn-Ca-Sr Alloy:** *Kinji Hirai*<sup>1</sup>; Tokuteru Uesugi<sup>2</sup>; Yorinobu Takigawa<sup>2</sup>; Kenji Higashi<sup>2</sup>; <sup>1</sup>Advanced Technologies, Inc.; <sup>2</sup>Osaka Prefecture University

Optimum composition for creep resistant Ca and Sr added AZ91 based magnesium alloys has been investigated. Selecting Ca and Sr for improvement of heat resistance, optimum amount of these elements added to AZ91 alloy was decided by investigating effects of these elements to structure of the alloys including formation of thermally stable inter-metallic compounds and physical properties. For analysis of tensile properties at elevated temperature, an improved constitutive equation was adopted adding stacking fault energy and constant  $A'$ .  $A'$  is a material constant that represents effects of a second phase skeleton structure, therefore,  $A'$  is an indicator of creep resistance at elevated temperature. By these investigations optimum composition of AZ91Ca1.0Sr0.5 was determined. This alloy retains the room temperature tensile properties of AZ91 while the creep resistance at elevated temperature corresponds to alloy AE41.

#### 8:55 AM

**Effect of Ca on the Fluidity of AS41B Magnesium Alloy:** *Yaqin Zhang*<sup>1</sup>; Tetsuichi Motegi<sup>1</sup>; Takanori Kojima<sup>1</sup>; <sup>1</sup>Chiba Institute of Technology

In this study the effect of Ca on the fluidity of AS41B magnesium alloy was studied using a spiral mold. The microstructures and the phases of the alloys with Ca added were characterized by SEM, EPMA and XRD. The change of liquidus temperature and solidus one were measured by Differential Thermal Analysis. The results indicate that adding a small amount of Ca degrades fluidity due to the increase of the coexistence temperature of solid and liquid. As more Ca is added, however, the fluidity improves because MgSiCa refines the crystal and the quantity of coarse Mg<sub>2</sub>Si reduces. When Ca addition exceeds 1.5%, the fluidity declines again. This can be explained by the formation of coarse MgSiCa phase.

#### 9:15 AM

**Evolution of Grain Boundary Precipitate Depleted Zones in Mg-Ca-Zn Alloy Stabilized by Zr Additions:** *Dmitry Shepelev*<sup>1</sup>; *Evgeniya Edelshtein*<sup>1</sup>; *Alexander Katsman*<sup>1</sup>; *Menachem Bamberger*<sup>1</sup>; <sup>1</sup>Technion - Israel Institute of Technology

The nanoscale mechanical properties of grain boundary precipitate depleted zones (PDZ's) in Mg-Ca-Zn alloy with 1 wt% Zr were analyzed using combined nanoindentation and atomic force microscopy (AFM). These mechanical properties were then correlated to the composition and precipitate distribution in PDZ's analyzed by TEM and SEM equipped with EDS. The width of PDZ's was examined after different solution treatments (ST) at 410°C and different exposures to 175°C. An increase in ST duration from 10 h to 96 h at 410°C resulted in expansion of PDZ's from ~0.75 $\mu$ m to ~3 $\mu$ m, while the following aging at 175°C for up to 24 h did not lead to detectable change in PDZ's. The lowest hardness was found in the region where Zn<sub>2</sub>Zr precipitates density was low, regardless of solute concentration. The nanohardness of Zn<sub>2</sub>Zr precipitate conglomerate is two times higher than the average nanohardness of the matrix.

#### 9:35 AM

**Flame Resistance Behaviors of AS, AE, MRI and AO Series Mg Alloys:** *Jin-Kyu Lee*<sup>1</sup>; *Shae Kim*<sup>1</sup>; <sup>1</sup>Korea Institute of Industrial Technology

Mg chips and burrs produced during cutting process and diecasting are rapidly burned and exploded when they are exposed to ambient atmosphere. In

order to solve these problems, flame retardation solution has been studied in development of new Mg alloys. It is well known that Ca is used. However, Ca is high cost and difficult to handle due to their high reactivity. More than that, Ca is prone to hot cracking and reduced fluidity. Recently, CaO added Mg have been developed to obtain the same properties, as Ca addition in Mg alloy. The flame resistance behavior of Al containing Mg alloys (3, 5 and 9wt.%) with CaO addition was investigated by DTA test under ambient atmosphere, dry air and nitrogen atmosphere. This study discussed the results of flame temperature of CaO added Mg alloys compared with other high temperature Mg alloys such as AE44, AS21 and MRI153 etc..

## 9:55 AM

**Microsegregation and Creep in Mg-Al-Ca-Based Alloys:** *Jessica TerBush*<sup>1</sup>; Raghavendra Adharapurapu<sup>1</sup>; J. Wayne Jones<sup>1</sup>; Tresa Pollock<sup>1</sup>; <sup>1</sup>University of Michigan

Die-cast MRI230D and AXJ530 have superior creep resistance to MRI153M, despite their similar microstructure, primary eutectic phase and dislocation substructure. In order to better understand this difference in creep resistance, solute in the primary  $\alpha$ -Mg in as-cast Mg-Al-Ca-based alloys has been examined using the electron microprobe along with a Scheil analysis. The amount of Al in solution in the primary  $\alpha$ -Mg is of particular interest since it is likely to significantly affect the creep behavior, due to precipitation and/or solid-solution strengthening. Despite having a higher bulk Al content, MRI230D has a similar Al concentration in the primary  $\alpha$ -Mg as AXJ530, which may explain their similarities in creep resistance. In order to systematically vary the amount of Al in solution, quaternary additions of up to 3wt% Sn have been made to Mg-5Al-3Ca. Microsegregation and creep behavior of these quaternary alloys will be compared to AXJ530 and MRI230D.

## 10:15 AM Break

## 10:30 AM

**Thermodynamic Assessment and Its Application of Ternary Mg-Zn-Ca System Using CALPHAD Method:** *JoonSeok Kyeong*<sup>1</sup>; Hyun Kyu Lim<sup>1</sup>; Hoo Dam Lee<sup>1</sup>; Won Tae Kim<sup>2</sup>; Do Hyang Kim<sup>1</sup>; Byeong Joo Lee<sup>3</sup>; <sup>1</sup>Yonsei University, Department of Metallurgy/NSM Laboratory; <sup>2</sup>Cheongju University; <sup>3</sup>POSTECH

Recently, it has been shown that Mg-Zn-Ca ternary system exhibits good creep resistance due to high temperature stability of Mg<sub>2</sub>Ca compound and solution hardening effect of Zn. However, detailed thermodynamic assessment for ternary Mg-Zn-Ca system has not been reported yet. In the present study, phase equilibrium and thermodynamic assessment on Mg-Zn-Ca system including two ternary compounds ( $\tau_1$ : Ca<sub>2</sub>Mg<sub>6</sub>Zn<sub>3</sub>,  $\tau_2$ : Ca<sub>2</sub>Mg<sub>5</sub>Zn<sub>13</sub>) have been investigated. In order to assess thermodynamic parameters of ternary compound  $\tau_2$ , isothermal section and isopleths surrounding the composition range of  $\tau_2$  have been suggested using DSC, DTA, XRD, SEM, and TEM. Calculated phase diagram of Mg-Zn-Ca ternary system have been studied with ternary compound parameters. The result of solidification simulation via Scheil equation has been discussed with the specimens in as-cast state and after heat treatment. In particular, the composition range for invariant reactions has been compared with that for the bulk glass formation.

## 10:50 AM

**The Influence of Calcium and Cerium Mischmetal on the Ignition Behavior of Magnesium:** *Hongjie Luo*<sup>1</sup>; Yihan Liu<sup>1</sup>; <sup>1</sup>Northeastern University

Magnesium and its alloys are very active and readily igniting during heating and melting, therefore their application is limited. In this study, some anti-ignition magnesium alloys were prepared by adding Ca or Ce mischmetal into molten magnesium and their ignition points were also measured. Meanwhile, the microstructure of oxidation film was observed and the anti-ignition mechanism was analyzed. The results showed that the ignition point of pure magnesium increases gradually with increasing Ca content. The ignition point reaches 824° when Ca content is 4.5%. It is higher than that of pure magnesium about 189°. Ca and Mg composite oxidation film is key to prevent burning in the molten magnesium surface. The ignition point of pure magnesium increases first and then decreases with increasing Ce mischmetal content. The ignition point reaches 690.5° when Ce mischmetal content is 0.9%. The flame-retarded effect of Ca is better than that of Ce mischmetal obviously.

## 11:10 AM

**Solidification Paths of Mg-rich Mg-Ca-Sn Alloys:** Hongbo Cao<sup>1</sup>; Youngki Yang<sup>1</sup>; Sindo Kou<sup>1</sup>; Y. Chang<sup>1</sup>; <sup>1</sup>University of Wisconsin

A recently developed thermodynamic description of Mg-Ca-Sn was coupled with the Scheil solidification model to calculate the solidification paths of Mg-rich Mg-Ca-Sn alloys. Based on the calculation, four representative Mg-rich alloys were selected and directionally solidified. The calculated solidification paths are as follows. Alloy #1 (Mg-3Sn-2Ca) and alloy #3 (Mg-5Sn-1Ca) start to solidify with the primary  $\gamma$ (Mg) while alloy #2 (Mg-1.5Sn-1.5Ca) and alloy #4 (Mg-5Sn-0.5Ca) with primary CaMgSn. Then, alloys #1 and #2 proceed towards the ternary eutectic invariant I<sub>2</sub>: L =  $\gamma$ (Mg) + Mg<sub>2</sub>Ca + CaMgSn while alloys #3 and #4 the ternary eutectic I<sub>1</sub>: L =  $\gamma$ (Mg) + Mg<sub>2</sub>Sn + CaMgSn. These paths were confirmed by examining the microstructure from directional solidification by both SEM and XRD.

## 11:30 AM

**Hot Tearing of Mg-Rich Mg-Ca-Sn Alloys:** Youngki Yang<sup>1</sup>; Hongbo Cao<sup>1</sup>; Y. Austin Chang<sup>1</sup>; Sindo Kou<sup>1</sup>; <sup>1</sup>University of Wisconsin

The susceptibility of Mg-rich Mg-Ca-Sn alloys was evaluated by constrained rod casting (CRC) in a steel mold, including alloy #1 (Mg-3Sn-2Ca), alloy #2 (Mg-1.5Sn-1.5Ca), alloy #3 (Mg-5Sn-1Ca) and alloy #4 (Mg-5Sn-0.5Ca). The hot tearing susceptibility of these alloys was determined based on the widths and locations of the cracks in the rods and compared with that of AZ91E Mg, which is known to have good resistance to hot tearing. These alloys were found much more hot-tearing susceptible than AZ91E Mg and, in fact, significantly more susceptible than the Mg-rich Mg-Al-Ca alloys investigated recently. The cast microstructure agreed with the calculated solidification paths calculated based on the thermodynamic description of the Mg-Ca-Sn system and the Scheil solidification model.

## Magnesium Technology 2009: Applications, Testing and Forming

Sponsored by: The Minerals, Metals and Materials Society, TMS Light Metals Division, TMS: Magnesium Committee

Program Organizers: Eric Nyberg, Pacific Northwest National Laboratory; Sean Agnew, University of Virginia; Neale Neelameggham, US Magnesium LLC; Mihriban Pekguleryuz, McGill University

Tuesday AM

February 17, 2009

Room: 2007

Location: Moscone West Convention Center

Session Chair: Wilhelmus Sillekens, TNO Science and Industry

## 8:30 AM Introductory Comments

## 8:35 AM

**A Life Cycle Assessment of a Magnesium Front-End Auto Part:** *Sujit Das*<sup>1</sup>; Alain Dubreuil<sup>2</sup>; Lindita Bushi<sup>3</sup>; Ambalavanar Thaurmarajah<sup>4</sup>; <sup>1</sup>Oak Ridge National Laboratory; <sup>2</sup>Natural Resources Canada; <sup>3</sup>GHG Measurement; <sup>4</sup>CSIRO/CAST-CRC

This paper focuses on the comparative life cycle assessment of a magnesium front end automotive part for a 2007 GM-Cadillac CST. The analysis framework is based on the consequential life cycle assessment approach, using an extensive life cycle inventory data collected for various magnesium manufacturing technologies including primary production, cast and wrought, and end-of-life. The recent magnesium market trend has been captured with the consideration of the latest technology developments made for the Chinese primary magnesium production. Life cycle comparative assessment includes energy, GHG emissions and selected other air emissions for the baseline steel front end and the magnesium alternative. It is estimated that both energy and GHG reductions with the magnesium front end compared to the base line scenario can be achieved only after several years of operation into vehicle life. Sustainable material management and technology improvements including recycling would further enhance the environmental benefit of magnesium use in automobiles.



8:55 AM

**Initial Evaluation of Advanced Powder Metallurgy Magnesium Alloys for Dynamic Applications:** *Tyrone Jones*<sup>1</sup>; *Katsuyoshi Kondoh*<sup>2</sup>; <sup>1</sup>US Army Research Laboratory; <sup>2</sup>Joining and Welding Research Institute

The U.S. Army Research Laboratory (ARL) is interested in assessing the performance of different magnesium alloys. The ARL and the Joining and Welding Research Institute (JWRI) conducted a joint effort to develop and evaluate advanced powder metallurgy magnesium alloys AZ31B and AMX602 (Mg-6Al-0.5Mn-2Ca/mass%) sheets. JWRI performed the mechanical and metallurgical analysis, while ARL performed the ballistic analysis. The thin gauge magnesium alloy sheets were ballistically evaluated against the 0.22-cal fragment simulating projectile (FSP). The powder magnesium alloys' mechanical properties and ballistic performance are compared to the conventionally processed AZ31B-H24.

9:15 AM

**Microstructural and Mechanical Aspects of Reinforcement Welds for Lightweight Components Produced by Friction Hydro Pillar Processing:** *Gustavo Pinheiro*<sup>1</sup>; *Jorge dos Santos*<sup>1</sup>; *Karl Kainer*<sup>1</sup>; *Norbert Hort*<sup>1</sup>; <sup>1</sup>GKSS-Forschungszentrum

The development of new local engineering methods is one possibility to overcome the disadvantages of poor high temperature creep properties of present magnesium alloys. Friction Hydro Pillar Processing, which is a relative new friction-based welding process, can be used to improve locally the high temperature properties of magnesium alloys. Mechanical and Metallurgical aspects of magnesium AZ91D-T6 reinforced with a Mg-Al-Ca-Sr alloy were investigated. Welded samples presented a complex joint formation mechanism with plasticized material flowing towards the rotational centre in a first stage of the process and outwards after the saturation of the central region. Dynamic recrystallization has occurred in the recrystallized zone resulting in fine, equiaxed and homogeneous grains. Temperature measurement indicates solidus temperatures in regions around the bonding line were transgressed during the welding. Mechanical tests have also demonstrated the feasibility of the process in producing high efficiency joints with strength values comparable with those of base material.

9:35 AM

**Die Forging of the Alloys AZ80 and ZK60:** *Gerrit Kurz*<sup>1</sup>; *Bob Clauw*<sup>2</sup>; *Wim Sillekens*<sup>3</sup>; *Dietmar Letzig*<sup>1</sup>; <sup>1</sup>GKSS Research Centre Geesthacht GmbH; <sup>2</sup>N.V. INOFER S.A.; <sup>3</sup>TNO Science and Industry

Overall goal of the MagForge project is to provide tailored and cost-effective technologies for the industrial manufacturing of magnesium forged components. Scientific and technological aspects are new alloys/feedstock materials with improved performance, forging process modeling and design tools with a satisfying level of predictability, machining technology for safe and rational finishing of the forgings, and typical demonstrator components to validate results. The targeted advancements are to enable high-volume applications of magnesium forgings. This paper gives an overview on the MagForge project and the first results. The commercial magnesium alloys AZ80 and ZK60 were investigated. With respect to the different microstructure of the alloys the mechanical properties of the feedstock, the parameters of the forging process and the mechanical properties of the forging parts will be presented and discussed. The results show that the magnesium alloys offer the possibility to produce parts with complex geometries similar to aluminum forging parts.

9:55 AM

**Ignition-Proof of Magnesium Alloy and Preparation of Magnesium Foam:** *Haibin Ji*<sup>1</sup>; *Guangchun Yao*<sup>1</sup>; *Letian Liu*<sup>1</sup>; *Yihan Liu*<sup>1</sup>; *Guoyin Zu*<sup>1</sup>; <sup>1</sup>Northeastern University

The magnesium is highly active during melting. So the Protection measures must be taken when we want to produce foam magnesium. In this experiment we used alloying method in order to prevent magnesium from burning. Mg-Al-Ca alloys were prepared. The contents of calcium were from 0.5% (wt) to 5.0% (wt) increasing by 0.5% (wt). The aluminum is 9.0% and the rest is magnesium. The result showed the magnesium alloy didn't burn when the content of Ga was 3.5% (wt). CO<sub>2</sub> decomposed by MgCO<sub>3</sub> can stay in the magnesium melt. So we used MgCO<sub>3</sub> and Mg-9% Al-3.5% Ca (wt) alloy to produce magnesium foam. The foaming experiment was operated at 620°C. Different size of MgCO<sub>3</sub> were added into melt to prepare magnesium foam. The result showed the size of bubble was influenced obviously by the size of MgCO<sub>3</sub>. we can change the size and content of MgCO<sub>3</sub> to produce magnesium foam with different density.

10:15 AM Break

10:30 AM

**Applicability of Existing Magnesium Alloys as Biomedical Implant Materials:** *Muge Erinc*<sup>1</sup>; *Wilhelmus Sillekens*<sup>1</sup>; *Raymond Mannens*<sup>1</sup>; <sup>1</sup>TNO Industrie en Techniek

Being biocompatible and biodegradable, magnesium alloys are considered as the new generation biomedical implant materials, such as for stents, bone fixtures, plates and screws. A major drawback is the poor chemical stability of metallic magnesium; it corrodes at a pace that is too high for most prospective implant applications. Requirements for biodegradable implants are biocompatibility, controlled biodegradability and sustainable mechanical properties. Various magnesium alloys containing Al, Zn, Y and rare-earth elements are analyzed in this respect. The alloys are compared on the basis of microstructure, tensile tests and potentio-dynamic polarization tests in simulated body fluid. The effects of semi-solid processing, hot extrusion, heat treatments and sterilization on corrosion resistance and tensile properties are investigated. AZ80 magnesium alloy with certain post-processing treatments fulfills the requirements best as a prospect implant material which has the potential for further improvement by trace alloying additions and surface modifications.

10:50 AM

**History of the Magnesium-Base Alloys Application in the Romanian Aeronautical Industry:** *Aurelian Buzaianu*<sup>1</sup>; *S. Oprisan*<sup>2</sup>; *A.F. Olteanu*<sup>3</sup>; *L. Rusu*<sup>4</sup>; <sup>1</sup>S.C.METAV - R&D S.A.; <sup>2</sup>STRAERO S.A.; <sup>3</sup>Research and Development National Institute for Metals and Radioactive Resources; <sup>4</sup>"Gh.Asachi" Technical University

The history of flight, of the design and building of modern flying machines, begins with the first airplane made by the Romanian Traian Vuia who achieved his first flight on 18 March 1906, with his later famous "Vuia 1" plane, in the fields of Montesson, nearby Paris, France. It was then said and written that the man who designed and flown the machine was French, an error that was corrected in the history of aeronautics as late as 1990. He was the inventor of the first airplanes with their own take off systems, propulsion units and landing gear. He registered his first invention on August 17, 1903 and received the French patent number 332.106 for his "Airplane-automobile design".

11:10 AM

**Cruciform-Shaped Specimen Geometries for Controlled Biaxial Tensile Testing:** *Fadi Abu-Farha*<sup>1</sup>; *Louis Hector*<sup>2</sup>; *Marwan Khraisheh*<sup>3</sup>; <sup>1</sup>Pennsylvania State University, Erie; <sup>2</sup>General Motors Corporation; <sup>3</sup>University of Kentucky

Plastic deformation of sheet materials is typically characterized in uniaxial tension despite the fact that multiaxial loading predominates in many forming processes. Controlled biaxial testing, which is an attractive alternative to uniaxial tension, has seen very limited development. Although testing instrumentation is complex, biaxial specimen designs that do not prematurely fail before a desired level of plastic deformation has been achieved are currently unavailable. Here, we report on a variety of AA5083 and MgAZ31 biaxial specimen designs that follow a cruciform geometry. Biaxial tests at 300°C were conducted with a computed-controlled testing fixture, developed at the University of Kentucky, which enabled pure biaxial stretching. We demonstrate that with certain specimen designs, it is possible to attain localized biaxial deformation that progresses to fracture through the center of the specimen gage section. Our results provide key insights into the influence of certain geometrical parameters on the degree of deformation-biaxiality

11:30 AM

**Electromagnetic Forming of Magnesium Alloy Sheet:** *Adi Ben-Artzy*<sup>1</sup>; *John Bradley*<sup>2</sup>; *Paul Krajewski*<sup>2</sup>; <sup>1</sup>Rotem Industries Ltd.; <sup>2</sup>General Motors Corp

High velocity Electromagnetic Forming (EMF) is well known as a potential means of increasing the formability of metals at high strain rates. EMF offers the potential to manufacture components of more complex shape, and to form low-ductility materials to higher strains, than is expected based on static tensile properties. The formability of various magnesium sheet materials under EMF conditions was investigated. Rolled magnesium ZM21, AZ31, AM50 and AZ61 sheets were formed using electromagnetic pulses at both room temperature and elevated temperature. The trials were conducted using circular and channel-shaped dies with a 10kJ energy source. The influence of magnetic energy and temperature was evaluated as well as the influence of the tempering condition of the samples. Magnesium alloy sheets were found to be formable during EMF

over a wide range of forming parameters. Low-aluminum-content magnesium alloys and annealed materials exhibited the highest formability during EMF.

## 11:50 AM

**Friction Stir Processing (FSP) of Thixomolded AM60 Mg Alloy to Minimize Porosity and Improve Warm Formability:** Bilal Mansoor<sup>1</sup>; Sibasish Mukherjee<sup>1</sup>; Amit Ghosh<sup>1</sup>; <sup>1</sup>University of Michigan

Typically thixomolded Mg alloys are molded in the form of part shapes, and not subjected to wrought processing to make sheets, or to stamping operation. In this work, severe deformation of the molded metal was attempted. Warm formability of same alloy was found to improve considerably by Friction Stir Processing of the Alloy. While investigating the reasons for this, thixomolded alloy was found to contain gas porosity and oxide particles. They are reduced or dispersed to a great degree during severe deformation imparted by FSP. Extensive surface blistering of thixomolded AM60 Mg was found under certain thermal exposure, is minimized by FSP possibly due to a mechanism of gas expulsion caused by the stirring action at high strain rates and elevated temperature. The origin of gas porosity is believed to result from surface hydration of granular Mg feedstock, gas not permitted to be expelled during thixomolding operation.

## Materials for High Temperature Applications: Next Generation Superalloys and Beyond: Refractory Alloys I

Sponsored by: The Minerals, Metals and Materials Society, TMS Structural Materials Division, TMS: High Temperature Alloys Committee, TMS: Refractory Metals Committee Program Organizers: Joseph Rigney, GE Aviation; Omer Dogan, National Energy Technology Laboratory; Donna Ballard, Air Force Research Laboratory; Shiela Woodard, Pratt & Whitney

Tuesday AM Room: 3010  
February 17, 2009 Location: Moscone West Convention Center

*Session Chairs:* Omer Dogan, National Energy Technology Laboratory; John Perepezko, University of Wisconsin

## 8:30 AM Invited

**Very High-Temperature Nb-Silicide Based Alloys:** Bernard Bewlay<sup>1</sup>; Laurent Cretegy<sup>1</sup>; P.R. Subramanian<sup>1</sup>; <sup>1</sup>GE

The present paper will describe progress in the development of Nb-silicide-based alloys with particular emphasis on the investment casting. These alloys are being developed for structural applications with service temperatures of up to 1350°C. These composites contain high-strength Nb silicides and they are toughened by a Nb solid solution. From a commercial perspective, investment casting of Nb-silicide alloys offers substantial potential because of its proximity to existing airfoil manufacturing practices. However, investment casting is not well developed for Nb-silicide composite airfoils. Furthermore, there is only limited understanding of the relationship between composition, processing technique, and properties. Alloying schemes have been developed for an excellent balance of room-temperature toughness, fatigue crack growth behavior, high-temperature creep performance, and oxidation resistance over a broad range of temperatures. Nb-silicide alloys will be described with emphasis on processing, microstructure, and performance.

## 8:55 AM Invited

**Computational Design of High-Temperature Alloys:** Gregory Olson<sup>1</sup>; <sup>1</sup>Northwestern University

A systems approach to computational materials design has integrated materials science, applied mechanics and quantum physics in the predictive-science-based creation of high-performance alloys. An ongoing NASA initiative extends the DARPA-AIM methodology of accelerated aeroturbine disc process optimization through high-fidelity computational thermodynamics based simulation of microstructural evolution, employing high-resolution microanalysis for calibration and validation of PrecipiCalc code predictions. A recent AFOSR initiative has employed extensive first-principles calculations in the accelerated design of niobium-based alloys demonstrating protective YAG scale formation for oxidation resistance at 1300C in advanced turbine blade applications.

## 9:20 AM

**Application of Phase Diagram Calculations to the Development of Nb-Silicide Based Alloys:** Ying Yang<sup>1</sup>; B. Bewlay<sup>2</sup>; S.-L. Chen<sup>1</sup>; F. Zhang<sup>1</sup>; Y. Chang<sup>3</sup>; <sup>1</sup>CompuTherm LLC; <sup>2</sup>General Electric Global Research; <sup>3</sup>University of Wisconsin-Madison

In-situ refractory metal intermetallic composites (RMICs) based on Nb-Silicides are candidate materials for ultra-high temperature applications (T>1200°C). To provide a balance of mechanical and environmental properties, Nb-Si composites are typically alloyed with Ti, Hf, and Cr. Phase diagrams of Nb-Si-Ti-Hf-Cr are critically needed as prerequisite knowledge for the development of this family of materials. In this study, a thermodynamic database that compiles the Gibbs energy functions of the phases in the Nb-Si-Ti-Hf-Cr system was developed. It was then coupled with Pandat software for the calculation of phase equilibria and solidification paths. The calculated results were validated using designed experiments. Phase diagram calculation based on the developed Nb-Si-Ti-Hf-Cr thermodynamic database can provide engineers with useful insights on the understanding of the as-cast and heat-treated microstructure of existing alloys. The phase diagram calculations also allow selection of compositions and heat-treatment schedules for promising new alloys.

## 9:40 AM

**First Principles Design of Ductile Refractory Alloys: Ductility Criterion:** Michael Gao<sup>1</sup>; Omer Dogan<sup>2</sup>; Paul King<sup>2</sup>; <sup>1</sup>National Energy Technology Laboratory/Parsons; <sup>2</sup>National Energy Technology Lab

Refractory alloys such as Cr and Mo hold the promises for advanced fossil power generation applications such as oxy-fuel gas turbines. However, improvements to their ductility at low homologous temperatures has been an area of intense interest for decades. Several ductility criteria have been proposed and controversy remains. In this work, we examine two criteria for bcc refractory alloys using first principles calculations: the Rice-Thomson parameter and Poisson ratio. The Rice-Thomson parameter refers to the ratio  $\mu^*b/\gamma$ , where  $\mu$  is the shear modulus of the material in the preferred slip plane;  $b$  is the Burgers vector of a dislocation in the preferred slip direction within the slip plane and  $\gamma$  is the surface energy of the fracture plane. Both Cr- and Mo-based binary alloys are theoretically examined. Alloying strategies to improve their intrinsic ductility are proposed and also compared with available experimental data.

## 10:00 AM Break

## 10:10 AM Invited

**Fracture and Fatigue of Advanced Nb-Si Alloys:** John Lewandowski<sup>1</sup>; <sup>1</sup>Case Western Reserve Univ

The fracture and fatigue behavior of a variety of Nb-Si alloys will be reviewed. Fracture experiments have been conducted on both notched and fatigue-precracked samples, while fatigue crack growth behavior has also been characterized over a range of test temperatures. Microstructures and fracture paths have been characterized via conventional metallography, SEM, and laser confocal microscopy. The mechanical behavior of these advanced Nb alloys will be compared to data available in the literature for a range of high temperature materials.

## 10:35 AM Invited

**NbTiSiMo-X Alloys – Composition, Microstructure Refinement and Properties:** Young-Won Kim<sup>1</sup>; Menon Sarath<sup>1</sup>; Christopher Woodward<sup>2</sup>; <sup>1</sup>UES Inc; <sup>2</sup>Air Force Research Laboratory

Advanced NbTiSi-X alloys have demonstrated very high RT strength levels (compressive yield strength around 1,800MPa) and excellent high-temperature strength retention (~1,200MPa at 1,000°C and over 500MPa at 1,200°C). Unfortunately, these alloys have a highly inhomogeneous size and spatial distribution of silicides, low fracture strength under tension (<350MPa) at all temperatures, and low oxidation resistance. The high volume fraction and non-uniform size distribution of silicides were considered to be responsible for the poor fracture resistance. In this work we attempt to refine the microstructure of cast alloys and to increase oxidation resistance by introducing Mo and adjusting other alloying additions. In focused efforts, we explored highly refined near-eutectic alloys modified with Mo additions, NbTiSiMo-Y, that showed excellent compression flow behavior. Further chemistry adjustments were made for balanced improvements, and cast alloys in homogenized material forms were evaluated for fracture and oxidation resistance. Results will be discussed.



11:00 AM

**High Temperature Oxidation Characteristics of Nb-10W-XCr Alloys:** *Maria Moricca*<sup>1</sup>; Shailendra Varma<sup>1</sup>; <sup>1</sup>University of Texas

The effect of Cr content on the static and cyclic oxidation resistance of Nb-10W-XCr alloys has been investigated. Experiments were conducted in air for 24 hours, over a range of temperatures from 700 to 1400°C using static and seven cycle screening tests. The phases present in the alloys and the oxide scales were characterized by XRD, SEM and EDS. Alloy's microstructure consists of Nb solid solution phase regions surrounded by a network of NbCr<sub>2</sub> laves phase. The oxidation kinetics follow a parabolic behavior; isothermal experiments indicate a trend of improvement in oxidation resistance with increase of the intermetallic phase with the exception of 30Cr alloy, suggesting the existence of a limit concerning the effective Cr content. The oxidation products are a mixture of Nb<sub>2</sub>O<sub>5</sub>, Cr<sub>2</sub>O<sub>3</sub> and CrNbO<sub>4</sub>. Results delineate the influence of microstructure and composition on oxidation mechanisms of these alloys that represent a promising base for high-temperature intermetallic alloy development.

11:20 AM

**Oxidation Behavior of Nb-15Si-20Mo-5B-20Ti and Nb-15Si-20Mo-5B-20Cr Alloys between 700 and 1300°C:** Benedict Portillo<sup>1</sup>; Shailendra Varma<sup>1</sup>; *Julieta Ventura*<sup>1</sup>; Rabintra Mahapatra<sup>2</sup>; <sup>1</sup>University of Texas at El Paso; <sup>2</sup>Naval Air Warfare Center

X-20Ti and X-20Cr (X = Nb-15Si-20Mo-5B and compositions are in atomic percents) alloys have been oxidized in air from 700 to 1300°C for (a) 24 hours (Short Term Oxidation, STO) and (b) cycles of 24 hours for 2 weeks (Long Term Oxidation, LTO). Weight gain per unit area as a function of time (LTO) and temperature (STO) have been used for characterizing the oxidation behavior. Oxidized two and three phase alloys, respectively, have been characterized by XRD, EDS on FESEM, and back scattered electron imaging. Results of oxides formation and phase transformations will be presented. Long term stability of the alloys will be characterized by TEM. The influence of Ti and Cr on Nb-15Si-20Mo-5B alloy will be analyzed.

11:40 AM

**Study of the Effects of Hf and Mo Additions on the Microstructure and Properties of Nb Silicide Based Alloys:** *Panayiotis Tsakiroopoulos*<sup>1</sup>; Jie Geng<sup>2</sup>; <sup>1</sup>The University of Sheffield; <sup>2</sup>University of Surrey

Niobium silicide based alloys could replace Ni superalloys in some structural applications at high temperatures. Their development is aiming to improve their oxidation and mechanical properties at room, intermediate, high and very high temperatures. Alloying and processing strategies are seeking to enhance the performance of the Nbss and to identify optimum microstructures, and to understand how these affect performance at different temperatures. We have studied the role of Hf and Mo in the microstructures of as-cast and heat-treated Nb-24Ti-18Si-5Al-5Cr (at %) based alloys. The phases observed were the Nbss, 3-1 and 5-3 silicides, and Laves phase. The role of Hf and Mo individually or simultaneously regarding the selection/stability of the Nb<sub>3</sub>Si silicide, the structure of the 5-3 silicide (beta, alpha or gamma), the formation of the Nbss + Nb<sub>3</sub>Si eutectic and the Laves phase, the betaNb<sub>5</sub>Si<sub>3</sub> + alphaNb<sub>5</sub>Si<sub>3</sub> + (Nb,Ti)<sub>ss</sub> transformation and the oxidation of the alloys will be discussed.

12:00 PM

**Study of the Effects of Sn and Ti Additions on the Microstructure of Nb-18Si Based Alloys:** *Panayiotis Tsakiroopoulos*<sup>1</sup>; Nikos Vellios<sup>2</sup>; <sup>1</sup>The University of Sheffield; <sup>2</sup>University of Surrey

The need to operate gas turbines at temperatures exceeding those in advanced aeroengines has motivated the development of new alloys. Niobium silicide based alloys are candidate new metallic materials but given the poor oxidation of Nb and its alloys alloy development seeks to improve their oxidation and mechanical properties at different temperatures. Ti and Sn additions improve the oxidation behaviour but little is known regarding their effect on microstructure. We studied the latter in Nb-18Si (at %) based alloys. The phases observed in as-cast and heat-treated alloys were the Nbss, Nb<sub>3</sub>Sn, and the 5-3 silicides alphaNb<sub>5</sub>Si<sub>3</sub> and betaNb<sub>5</sub>Si<sub>3</sub>. The effect of Sn and Ti on the stability of the Nb<sub>3</sub>Si silicide, on the structure of the 5-3 silicide and in particular on the formation and stability of Nbss + Nb<sub>5</sub>Si<sub>3</sub> eutectic and the betaNb<sub>5</sub>Si<sub>3</sub> + alphaNb<sub>5</sub>Si<sub>3</sub> + (Nb,Ti)<sub>ss</sub> phase transformations and the hardness of Nb<sub>3</sub>Sn and Nb<sub>5</sub>Si<sub>3</sub> will be discussed.

## Materials in Clean Power Systems IV: Clean Coal-, Hydrogen Based-Technologies, and Fuel Cells: High Temperature Materials for Power Generation

Sponsored by: The Minerals, Metals and Materials Society, ASM International, TMS Electronic, Magnetic, and Photonic Materials Division, TMS/ASM: Corrosion and Environmental Effects Committee, TMS: Energy Harvesting and Storage Committee  
Program Organizers: K. Scott Weil, Pacific Northwest National Laboratory; Michael Brady, Oak Ridge National Laboratory; Ayyakkannu Manivannan, US DOE; Z. Gary Yang, Pacific Northwest National Laboratory; Xingbo Liu, West Virginia University; Zi-Kui Liu, Pennsylvania State University

Tuesday AM

Room: 3005

February 17, 2009

Location: Moscone West Convention Center

*Session Chairs:* K. Scott Weil, Pacific Northwest National Laboratory; Ayyakkannu Manivannan, US DOE

### 8:30 AM Introductory Comments

### 8:35 AM Invited

**Fossil Energy's Advanced Research Materials Program:** *Patricia Rawls*<sup>1</sup>; <sup>1</sup>US DOE, NETL

Advanced materials are required for the cleaner, more efficient and more economic electricity power generating systems that are currently being developed. To that end, research is focused on developing high-temperature, corrosion-resistant alloys and protective coatings that are suitable for the extreme environments of the advanced energy systems that are currently being designed. The scope of the Materials Program addresses the need for new materials that can withstand higher temperatures and corrosive environments of advanced power generation technologies including ultrasupercritical steam cycle plants, oxy-fueled combustors, CO<sub>2</sub> sequestration, IGCC plants, synthesis-gas-fueled turbines and turbines. Fossil Energy's Advanced Research Materials Program, coordinated by the National Energy Technology Laboratory, is organized into five clusters including Breakthrough Concepts, New Alloys, Coatings and Protection of Materials, Ultrasupercritical Materials and Functional Materials and is implemented through partnerships with academia, industry, non-profit organizations and other national laboratories.

### 9:10 AM

**Chromium Free Nickel Alloys for Hot Sulfuric and Sulfur Environments:** *Joseph Newkirk*<sup>1</sup>; Richard Brow<sup>1</sup>; <sup>1</sup>Missouri University of Science & Technology

Resistance to attack by hot, corrosive gases or liquids is important in many energy applications. A new nickel-silicon material based on the intermetallic alloy Ni<sub>3</sub>Si has been developed which naturally forms an in-situ glass, amorphous silica, film during exposure to oxidizing conditions. The alloy has an excellent balance of mechanical properties and extremely low corrosion rates. The effects of alloying additions to Ni<sub>3</sub>Si on mechanical properties and corrosion resistance will be presented. The mechanisms for the creation of a passive film in oxidizing acids will also be presented. Understanding the film formation mechanism is leading to improved performance through modifications of the alloy chemistry. A total materials approach is necessary to produce an alloy and a film both with good properties, while matching important properties at the interface. Fabrication and welding of the alloy into components will also be addressed.

### 9:30 AM

**Refractory Degradation by Slag Attack in Coal Gasification:** Jimichiro Nakano<sup>1</sup>; Sridhar Seetharaman<sup>1</sup>; James Bennet<sup>2</sup>; *Kyei-Sing Kwong*<sup>2</sup>; Tyler Moss<sup>1</sup>; <sup>1</sup>Carnegie Mellon University; <sup>2</sup>National Energy Technology Laboratory

Refractory wear in air cooled slagging coal gasifiers has been identified as one of the top research needs of gasifier users to increase gasifier on line availability. This research investigates sessile drop interfacial reactions between two refractory materials (high chromia and alumina) and two slags [coal (51SiO<sub>2</sub>-24Al<sub>2</sub>O<sub>3</sub>-15Fe<sub>2</sub>O<sub>3</sub>-7CaO-3K<sub>2</sub>O) and petcoke (24SiO<sub>2</sub>-46V<sub>2</sub>O<sub>5</sub>-7Al<sub>2</sub>O<sub>3</sub>-11Fe<sub>2</sub>O<sub>3</sub>-11CaO-1K<sub>2</sub>O)]. Pulverized slag samples were placed at specific microstructure locations on refractory materials and heated to 1500°C at log(Po<sub>2</sub>) = -8. Cross-sections of the slag/refractory interface were evaluated using SEM-EDS for evaluating slag penetration into specific areas of the refractory and refractory grain dissolution into the slag. Initially, the slag



attacked grain boundaries and fine microstructure areas, freeing alumina grains into the slag. VOx formation in the petcoke was found to alter the overall slag composition and kinetic behavior.

## 9:50 AM Break

## 10:00 AM Invited

**Oxidation Behavior of a New Ni-Fe-Cr-Al Alloy for Elevated Temperature Applications:** *Vinay Deodeshmukh*<sup>1</sup>; *Steve Matthews*<sup>1</sup>; *Henry White*<sup>1</sup>; *Dwaine Klarstrom*<sup>1</sup>; <sup>1</sup>Haynes International

High temperature oxidation of chromia-forming alloys is considerably accelerated in the presence of water vapor in a variety of industrial application such as microturbines, solid oxide fuel cell, ultra super-critical power plants. Alumina-forming alloys may provide adequate long-term protection in harsh oxidizing environments. An issue is the fact that several alumina-forming alloys often encounter fabricability and formability problems due to gamma-prime-Ni<sub>3</sub>Al precipitation. A new Ni-based superalloy based on the Ni-Fe-Cr-Al system which has excellent fabricability and formability has been recently developed for applications in harsh oxidizing environments. It forms a continuous, adherent, and slow-growing alumina-based scale for high temperature protection. This alloy also exhibits an excellent thermal stability which is needed for long-term use at elevated temperatures. The oxidation behavior and mechanical properties of this alloy were studied and compared to several solid solution strengthened alloys. This paper will discuss some of the major characteristics and benefits of this alloy.

## 10:35 AM

**Controlling Thermal Diffusion by Manipulating Nanoscale Structural Arrangement and Doping in Nanocomposites for High Temperature Applications:** *Vikas Samvedi*<sup>1</sup>; *Vikas Tomar*<sup>1</sup>; <sup>1</sup>University of Notre Dame

Next generation ceramic nanocomposite coatings are required to have the least thermal conductance to prevent exposing the substrates to extreme temperatures. Controlling thermal diffusion and, therefore, thermal conduction is an important requirement in nanocomposites for high temperature applications. Thermal conduction in the nanocomposites occurs across a series of grain boundaries (GBs), second phase particles, and primary matrix phase grains. It is possible that by altering the nanostructural arrangement of GBs, the second phase, and the primary phase, desired control of thermal conduction can be obtained. In the presented research, such analyses for silicon carbide (SiC)-silicon nitride (Si<sub>3</sub>N<sub>4</sub>) nanocomposites using non equilibrium molecular dynamics scheme are performed. Analyses show that it is possible to control thermal conduction by manipulating the phase arrangement. Fundamental mechanism to such control is the change in phase arrangement correlated with changes in overall mean phonon wavelengths. Alternate phase arrangements based on biomimetic structures are also analyzed.

## 10:55 AM

**High Temperature Oxidation of Ti-Si Alloys in Humidified Air and Argon-Oxygen Gas Mixtures:** *Jie Yang*<sup>1</sup>; *Hugh Middleton*<sup>2</sup>; *Truls Norby*<sup>3</sup>; <sup>1</sup>University of Oslo; <sup>2</sup>University of Agder; <sup>3</sup>University of oslo

The oxidation behavior of Ti-Si based alloys with two different silicon contents (2wt.% and 8.5wt.%) were investigated and compared to pure titanium (grade 2). Isothermal oxidation took place in air-2.5% H<sub>2</sub>O and Ar-20% O<sub>2</sub>-2.5% H<sub>2</sub>O at 800°C and 1000°C for up to 72h. The scale growth kinetics, morphology and composition were studied by thermogravimetry in combination with SEM/EDAX. The oxidation of the Ti-Si alloys at 800 °C and 1000°C in both gas mixtures generally displayed parabolic behaviour as did pure titanium. Silicon plays a significant positive effect on the oxidation resistance. The oxidized scales are sub-layered; the existence of SiO<sub>2</sub> layer beneath the TiO<sub>2</sub> layer ensures better oxidation resistance. Nitriding of the Ti-Si alloys oxidized in air-2.5% H<sub>2</sub>O leads to the formation of titanium nitride which provides better oxidation resistance compared to Ar-20% O<sub>2</sub>-2.5% H<sub>2</sub>O; the diffusion of nitrogen into the oxidized layers decreases the dissolution of oxygen into the substrate.

## Materials Issues in Additive Powder-Based Manufacturing Processes: Additive Manufacturing Metals II

Sponsored by: The Minerals, Metals and Materials Society, TMS Materials Processing and Manufacturing Division, TMS: Powder Materials Committee  
Program Organizers: David Bourell, University of Texas; James Sears, South Dakota School of Mines and Technology; Pavan Suri, Mississippi State University

Tuesday AM  
February 17, 2009

Room: 3004  
Location: Moscone West Convention Center

*Session Chair:* James Sears, South Dakota School of Mines and Technology

## 8:30 AM

**Overview of Materials Processing with Laser Engineered Net Shaping:** *John Smugeresky*<sup>1</sup>; *Baolong Zheng*<sup>2</sup>; *Yuhong Xiong*<sup>2</sup>; *Jonathan Nguyen*<sup>2</sup>; *Yizhang Zhou*<sup>2</sup>; *Enrique Lavernia*<sup>2</sup>; *Julie Schoenung*<sup>2</sup>; <sup>1</sup>Sandia National Laboratories; <sup>2</sup>University of California, Davis

Laser Engineered Net Shaping (LENS®) has combined laser deposition and powder metallurgy technologies with advanced methodologies for rapid manufacturing, converting complex CAD models into functional structural components without the need for part-specific tooling. In addition to fabricating complex geometries of fully dense metals that require minimal finish machining, the rapid-solidification deposition mechanism has produced microstructures with mechanical properties that have typically been superior to those of components made by conventional processes. In this overview, recent research and progress associated with the LENS® process are reviewed, such as laser materials processing for rapid manufacturing; development of metal alloys and composites; the effect of process parameters on microstructure, properties, and build height; thermal behavior measurements, and numerical simulation. This paper is based upon work supported by the National Science Foundation under Grant No. DMI-0423695. Work by Sandia is supported by the U. S. Department of Energy under contract DE-AC04-94AL85000.

## 8:55 AM

**Metallic Parts Fabrication with the Selective Inhibition Sintering (SIS):** *Behrokh Khoshnevis*<sup>1</sup>; *Mahdi Yoozbashizadeh*<sup>1</sup>; *Yong Chen*<sup>1</sup>; <sup>1</sup>University of Southern California

The fundamentals of the SIS-Metal process based on microscopic mechanical inhibition are expolored. In the process, salt solution is printed in the selected area of each metal powder layer; the salt re-crystallizes when water evaporates; salt crystals decompose and grow rapidly prior to sintering; the generated salt particles spread between metal powder particles and prevent the fusing of these particles together, hence inhibiting the sintering process in the affected regions. The SIS-Metal process has numerous advantages including low cost, minimal shrinkage and deformation effects, and non-contamination of sintering furnace because of lack of polymeric binders.

## 9:20 AM

**The Influence of Power Type On Properties of Electron Beam Melted Components:** *Denis Cormier*<sup>1</sup>; <sup>1</sup>North Carolina State University

Gas atomization (GA) and plasma rotating electrode (PREP) are two common methods used to produce titanium powders for direct metal additive manufacturing processes. The production method affects the size distribution, the shape and flowability, and the porosity of the powder. These properties, in turn, significantly affect the mechanical properties and the cost of the resulting parts. While PREP powder is currently preferred for the freeform fabrication of critical aerospace components, the cost and availability of GA powder is at present much better than that of PREP. This paper will discuss an extensive study in which static properties as well as low cycle fatigue of coupons fabricated via the Electron Beam Melting (EBM) process using GA and PREP powders are compared. This study aims to determine whether or not parts produced with a finer GA powder can achieve equivalent mechanical properties as parts produced with standard PREP powder.

9:45 AM

**Experimental Analysis of Porosity Formation in Laser-Assisted Powder Deposition Process:** *Liang Wang*<sup>1</sup>; Phillip Pratt<sup>1</sup>; Sergio Felicelli<sup>1</sup>; Haitham Kadiri<sup>1</sup>; Paul Wang<sup>1</sup>; <sup>1</sup>Mississippi State University

Porosity has been investigated in samples produced by the Laser Engineered Net Shaping (LENS) process. Different powders were employed including stainless steel SS410, SS316, and carbon steel AISI 4140. The effects of process parameters (e.g. laser power and scanning speed) and the metallic powder characteristics on the porosity formation were studied. The volume fraction, number density, and size distribution of porosity were characterized with x-ray computed tomography and optical metallography. Both interlayer porosity due to lack of fusion and intralayer porosity are identified. The results demonstrate the sensitivity of process parameters and powder quality on the porosity formation. The mechanisms of porosity formation in LENS process are discussed in detail.

10:10 AM

**Impact of Physical Phenomena During Selective Laser Melting of Ferrous Powders:** *Marleen Rombouts*<sup>1</sup>; Jean-Pierre Kruth<sup>2</sup>; Ludo Froyen<sup>2</sup>; <sup>1</sup>VITO; <sup>2</sup>Katholieke Universiteit Leuven

Broadening the range of materials that can be processed by selective laser melting (SLM) to high-density parts in a more systematic way than by trial-and-error requires a fundamental knowledge of the process. In this study the impact of physical phenomena during SLM of ferrous powders has been examined by finite element modeling and experiments. The thermal model reveals the effect of process parameters and of the change in material properties upon melting - like thermal conductivity, density, laser absorptance and heat release - on the temperature profile and on the melt pool dimensions. Experiments have indicated that even small alloying additions like carbon, copper and deoxidizers such as silicon and titanium have a large impact on the melt pool behaviour during SLM. Their impact is evaluated by roughness, density and microscopic analysis after SLM.

10:35 AM Break

10:50 AM

**Materials Issues in Indirect Selective Laser Sintering and Post Processing of Ferrous Components:** Phani Vallabhajosyula<sup>1</sup>; *David Bourell*<sup>1</sup>; <sup>1</sup>University of Texas

Selective Laser Sintering (SLS) is an additive manufacturing process in which three dimensional parts may be created directly from a computer solid model using part powder and a scanning laser beam. In indirect SLS, powder is mixed with a transient binder. A model for infiltration of an SLSed tool steel part with a cast iron is presented. Included is prediction of the equilibrium solid fraction in the final part at the infiltration temperature based on carbon diffusion from the infiltrant into the brown part particulate. The effects of pre-sintering and excess infiltrant are also developed. The model was tested using Laserformtm A6 tool steel powder infiltrated with ASTM A532 white cast iron. In some cases guided by Ashby densification maps, pre-sintering of the tool steel green part was performed to increase the initial relative density of the solid metal. This research project was sponsored by NSF grant # DMI-0522176.

11:15 AM

**Development of Processing Parameters for New Metallic Alloys Built Using Additive Layered Manufacturing Techniques:** *Robert Deffley*<sup>1</sup>; Manuelle Carnot<sup>2</sup>; Robert Sudamore<sup>3</sup>; Iain Todd<sup>2</sup>; <sup>1</sup>University of Sheffield; <sup>2</sup>University Of Sheffield; <sup>3</sup>TWI: The Welding Institute

Additive layer manufacturing in metals and alloys offers much to the engineer in terms of design freedom but its application is, in practice, often restricted by the limited number of metallic materials available for use in the machines. In this paper we apply design of experiments (DOE) to the development of processing parameters for the nickel alloy 718 in order to speed up the definition of suitable processing conditions. The DOE is based on parameters developed by consideration of the fundamental expressions governing heat flow and solidification and the results of this work will be presented and discussed.

11:40 AM

**Spatial Control of Crystal Texture by Laser DMD Process:** *J. Choi*<sup>1</sup>; J. Mazumder<sup>2</sup>; B. Dutta<sup>1</sup>; <sup>1</sup>POM Group; <sup>2</sup>University of Michigan

Turbine blades with controlled textures such as directionally solidified and single crystalline have proven to have much improved ductility and longer thermal and fatigue life. It has been further reported that the benefits of single-crystal over conventionally cast as well as directionally solidified components

critically depend on avoiding the introduction of defects, such as stray grains, freckles, or deviations from the required crystal orientation. Laser-based direct metal deposition (DMD) process equipped with proper sensors and NC devices helps in overcoming those hurdles to fabricate the blades with controlled texture. It appears that thermal control to provide uniform heat flow as well as spatial control of crystal texture by process feedback control is essential. The paper discusses about how to establish process conditions and thermal control requirements, development of a laboratory scale DMD process for spatial control of crystal texture, and mechanical properties of texture-controlled Ni-based superalloy turbine blade components.

12:05 PM

**Thermal Behavior of WC-Co Cermets During the LENS® Process:** *Yuhong Xiong*<sup>1</sup>; William Hofmeister<sup>2</sup>; Zhao Cheng<sup>3</sup>; John Smugeresky<sup>4</sup>; Jean-Pierre Delplanque<sup>1</sup>; Baolong Zheng<sup>1</sup>; Jonathan Nguyen<sup>1</sup>; Enrique Lavernia<sup>1</sup>; Julie Schoenung<sup>1</sup>; <sup>1</sup>University of California, Davis; <sup>2</sup>University of Tennessee Space Institute; <sup>3</sup>Earth Mechanics Inc.; <sup>4</sup>Sandia National Laboratories

The Laser Engineered Net Shaping (LENS®) process has been used to fabricate a broad range of materials, including WC-Co cermets. To better explore the potential of this process to cermets, there is a need to understand their special thermal behavior and the relevant effects on the microstructure. In this study, dense WC-Co cermets were produced by the LENS® process. In-situ high-speed thermal imaging was applied to determine temperature gradients and cooling rates in the vicinity of the molten pool created by the laser. The experimental results were compared with finite element method simulation. The entire thermal behavior of this process was predicted by the finite element modeling. The thermal behavior study was also correlated to the microstructure of WC-Co cermets.

## Materials Processing Fundamentals: Deformation Processing

Sponsored by: The Minerals, Metals and Materials Society, TMS Extraction and Processing Division, TMS: Process Technology and Modeling Committee Program Organizer: Prince Anyalebechi, Grand Valley State University

Tuesday AM

Room: 2016

February 17, 2009

Location: Moscone West Convention Center

*Session Chair:* Prince Anyalebechi, Grand Valley State University

8:30 AM

**Enhancing Tensile Response of Sn Using Cu at Nano Length Scale and High Temperature Extrusion:** *Md. Alam*<sup>1</sup>; Manoj Gupta<sup>1</sup>; <sup>1</sup>National University of Singapore

In the present study, 1.1 volume percent of nano size copper was incorporated into pure tin using hybrid microwave sintering assisted powder metallurgy route. Microwave sintered samples were extruded both at room temperature and at 230 °C. Microstructural characterization studies were conducted on the extruded samples to investigate the distribution characteristics of secondary phase and grain morphology. Room temperature tensile test results revealed that hot extruded Sn-Cu samples exhibited higher strengths (~ 41%, in case of 0.2% yield strength and ~ 38%, in case of ultimate tensile strength) and ductility (~ 15%) when compared to room temperature extruded samples. On the contrary, the tensile properties of pure tin remained independent of extrusion temperature. An attempt is made in this study to correlate the effect of extrusion temperature on the microstructural evolution and tensile properties of Sn-Cu solder.

8:50 AM

**Deformation Induced Ferrite Transformation in Low Carbon Cr-V Steels:** *Martin Bühler*<sup>1</sup>; Teresa Perez<sup>1</sup>; Victoria Ramos<sup>1</sup>; <sup>1</sup>Tenaris Siderca R&D

The austenite to ferrite phase transformation kinetic of two low carbon steels containing Cr and different levels of V and N was studied. Different tests were performed on a Gleeble 3500 thermomechanical simulator in the temperature range 700°C-1100°C after solution treating. Strain induced transformation tests were performed in order to study the formation of ferrite at high temperatures. Dilatometric measurements were also carried out to analyze the phase transformation kinetic without deformation. DIFT was observed at very high

temperatures in the V-N microalloyed steel. The influence of this transformation on the hot ductility was analyzed.

**9:10 AM**

**Effects of Process Path on Texture and Microstructure in ECAE Processed and Rolled High Purity Nb:** *Shreyas Balachandran*<sup>1</sup>; Karl Hartwig<sup>1</sup>; Derek Baars<sup>2</sup>; Thomas Bieler<sup>2</sup>; <sup>1</sup>Texas A&M University; <sup>2</sup>Michigan State University

High purity Nb is used to fabricate advanced superconducting radio frequency cavities for future particle accelerators. One possible approach to forming cavities efficiently is to use equal channel angle processing to achieve a fine grain size and a desirable texture in the material. Different ECAE processing paths were used on medium and high purity Nb ingots to examine the effects of different ECAE processing routes on recrystallized textures of material rolled to 90% reduction. Three components of texture were commonly observed in widely differing volume fractions that depended on the processing history: a punctuated gamma fiber with 6 evenly spaced peaks, an orientation that is near rotated cube, but often split into two symmetric peaks, and symmetric orientations that are just off the alpha fiber. Correlations between the magnitude of shear in particular ECAE process orientations and resulting textures have been identified.

**9:30 AM**

**Elimination of Crystallinity in Fractured Surface of Medium Carbon Low Alloy Steel Plates through Process Improvement:** *Ram Avtar*<sup>1</sup>; Gangeshwar Singh<sup>1</sup>; <sup>1</sup>Steel Authority of India Ltd.

High tensile thick plates (>80mm) of medium carbon low alloy steel, when heat treated, manifested higher percentage of Crystalline area (>20%) in fractured surface. The genesis of higher Crystallinity in fracture was examined. It was observed that the thicker plate undergone with slower rate from Soaking Temperature to Ms Temperature on cooling after austenising during oil quenching and thereby quenched microstructure had upper bainites. During tempering of as quenched bainite, additional precipitation took place at the lath boundaries of bainite. This led to weakening of grain boundaries and aided easy crack propagation during fracture and resulted in formation of higher percentage of crystalline area in fractured surface. Enhancement in cooling rate of austenised plate by switching over from oil quenching to water quenching practice resulted in complete transformation of austenite into martensite and produced ductile fracture (zero Crystallinity). Plates conformed improvement in mechanical properties between 2-5%.

**9:50 AM**

**Challenges of Producing Quality Construction Steel Bars in West Africa: Case Study of Nigeria Steel Industry:** Sanmbo Balogun<sup>1</sup>; David Esezobor<sup>1</sup>; Samson Adeosun<sup>1</sup>; *Olatunde Sekunowo*<sup>1</sup>; <sup>1</sup>University of Lagos

The production of quality high-yield reinforcing steel bars has recently received worldwide attention due to its important contribution to GDP index. In developing country such as Nigeria, empirical studies have shown that bars produced through conventional rolling requires appropriate modification of its chemical composition in order to obtain the desired mechanical properties. However, the high cost factor involved in composition adjustment makes such approach unattractive. Rather, the application of the combination of controlled rolling and controlled cooling systems proves to be the best option. This system also, requires some variations in processing parameters to suit individual plant production peculiarities. In this paper attempt is made to study the production challenges and opportunities the steel millers are facing in Nigeria. Previous works in this area were also reviewed with a view to charting the way forward. Experimental studies and process monitoring were carried out at some designated rolling mills in Nigeria.

**10:10 AM Break**

**10:25 AM**

**Influence of Ta Microstructure on Co-Deformability of a Ta Layer Embedded in Cu:** *Shreyas Balachandran*<sup>1</sup>; Karl Hartwig<sup>1</sup>; Taeyoung Pyon<sup>2</sup>; Derek Baars<sup>3</sup>; Thomas Bieler<sup>3</sup>; <sup>1</sup>Texas A&M University; <sup>2</sup>Luvata; <sup>3</sup>Michigan State University

Ta sheets are used as diffusion barriers in some niobium-tin superconductors to prevent contamination of stabilizer copper by tin. The ideal diffusion barrier thickness of 2-3 microns is rarely achieved because of Cu-Ta interface instabilities that occur during wire drawing. These instabilities lead to premature thinning and fracture of the Ta layer resulting in poor superconductor performance. Ta sheets produced from ECAE processed Ta bars show improved Cu-Ta co-deformation characteristics leading to lesser interface roughness.

Ta with improved co-deformability enables fabrication of wires with thinner Ta layers and a reduction in the amount of Ta needed for the diffusion barrier component. The effects of initial and evolving Ta microstructure on Cu-Ta interface roughening phenomena will be discussed.

**10:45 AM**

**Microstructural Evolution during Spark Plasma Sintering of Ni and W:** *Matthew Luke*<sup>1</sup>; Jeffrey Perkins<sup>1</sup>; William Windes<sup>2</sup>; Darryl Butt<sup>1</sup>; Megan Frary<sup>1</sup>; <sup>1</sup>Boise State University; <sup>2</sup>Idaho National Laboratory

Spark plasma sintering (SPS) is a novel processing technique for consolidating metal powders. As compared to traditional sintering techniques (e.g., pressureless sintering and hot pressing), SPS can produce fully dense components at lower sintering temperatures and with significantly shorter sintering times. We have studied how processing parameters such as applied pressure, sintering temperature and hold time affect the densification and microstructural evolution in both nickel and tungsten. Electron backscatter diffraction is used to characterize the grain size, grain boundary types, and crystallographic texture of the both materials. The microstructures that result from SPS are found to vary significantly from those of other processing techniques. SPS processing parameters can be adjusted to achieve microstructures with different grain sizes and distributions of grain boundaries. Based on the results, spark plasma sintering can be used to create a wide variety of metal-matrix composite materials with tailored microstructural properties.

**11:05 AM**

**Preliminary Evaluation of Spark Plasma Extrusion:** K. Morsi<sup>1</sup>; A. El-Desouky<sup>1</sup>; <sup>1</sup>San Diego State University

The interest in spark plasma sintering has been growing considerable over the past few years. This has been brought about by the unique advantages of the process, which include reduced sintering temperatures and times and the production of materials with unique microstructures and properties. Despite its current reputation as an outstanding process that has solved major problems such as nanopowder consolidation, it has so far been largely limited to the manufacture of simple shapes, due to its inherent configuration. In this paper we present preliminary results on spark plasma "extrusion" that can allow the production of extended geometries via electric-current processing. Preliminary results on the processing and microstructure of spark plasma extruded aluminum is discussed.

**11:25 AM**

**The Effect of Cold Working on the Deformation Induced Martensite (DIM) and Degree of Sensitization (DOS) of Austenitic Stainless Steel:** *Anil Kumar*<sup>1</sup>; <sup>1</sup>National Institute of Foundry and Forge Technology

Stainless steel possesses good mechanical properties combined with a high corrosion resistant. The cold rolled stainless steel leads high dislocation densities, enhanced residual stress and strain and produced metastable martensite phase. The deformation induced martensite and degree of sensitization behavior of austenitic stainless steel (AISI 304) is greatly influenced by several metallurgical factors, such as the chemical composition, the degree of prior deformation, grain size, and the aging temperature and time. The percentage deformation induced martensite behavior of the austenitic stainless steel (AISI 304) has been investigated after aging at various temperatures from 500°C to 700°C for 1 to 30 hours and also evaluate the degree of sensitization behavior on the cold rolled reduction in thickness from 0% to 60% at 500°C for 30 hours of austenitic stainless steel (AISI 304). This paper investigates the co-relation between deformation-induced martensite and degree of sensitization.

**11:45 AM**

**Seeking Relation of Dislocation Substructure to Recrystallized Grain Orientation in High Purity Single Crystal Niobium:** *Derek Baars*<sup>1</sup>; Kai Wang<sup>1</sup>; Chris Compton<sup>2</sup>; Tom Bieler<sup>1</sup>; Wenjun Liu<sup>3</sup>; Rosa Barabash<sup>4</sup>; Gene Ice<sup>4</sup>; <sup>1</sup>Michigan State University; <sup>2</sup>National Superconducting Cyclotron Laboratory, Michigan State University; <sup>3</sup>Advanced Photon Source, Argonne National Laboratory; <sup>4</sup>Oak Ridge National Laboratory

Manufacturing superconducting radio frequency (SRF) cavities from single crystal niobium is being investigated as an alternative to polycrystalline niobium, as single crystal sheets may be cut directly from the purified ingot, eliminating the cost of forging and rolling ingots into polycrystalline sheet. Normal cavity forming steps are approximated with two groups of samples: 1) different crystal orientations deformed by uniaxial tension, cut, and welded, 2) the same crystal orientation rolled to various reductions and then incrementally heat treated.



Active slip systems, dislocation substructures, and recrystallization will be examined by depth-resolved x-ray and orientation imaging microscopy, compared to crystal plasticity model predictions, and the possible influence of dislocation substructure on the orientations of recrystallized grains investigated.

## Mechanical Behavior of Nanostructured Materials: Plasticity and Deformation Mechanisms at Small Length Scale I

Sponsored by: The Minerals, Metals and Materials Society, TMS Electronic, Magnetic, and Photonic Materials Division, TMS Materials Processing and Manufacturing Division, TMS Structural Materials Division, TMS: Chemistry and Physics of Materials Committee, TMS/ASM: Mechanical Behavior of Materials Committee, TMS: Nanomechanical Materials Behavior Committee

Program Organizers: Xinghang Zhang, Texas A & M University; Andrew Minor, Lawrence Berkeley National Laboratory; Xiaodong Li, University of South Carolina; Nathan Mara, Los Alamos National Laboratory; Yuntian Zhu, North Carolina State University; Rui Huang, University of Texas, Austin

Tuesday AM Room: 3024  
February 17, 2009 Location: Moscone West Convention Center

Session Chairs: Andrew Minor, Lawrence Berkeley National Laboratory; Brad Boyce, Sandia National Laboratory

### 8:30 AM Invited

**Plastic Flow in Nanoscale Pillars:** *Evan Ma*<sup>1</sup>; <sup>1</sup>Johns Hopkins University

We have conducted in situ tests of metallic pillars with nanoscale dimensions in a transmission electron microscope. This technique is capable of spatially and temporally resolving the plastic flow, correlating the measured force-displacement response (such as pop-in) at ~0.3  $\mu\text{N}$  and <1 nm resolutions with time-resolved TEM images (movies). Also, one observes the exact sample geometry and punch location, which is important for interpreting the test data. The metallic pillars we tested have nanocrystalline or even sub-nanometer (amorphous) internal structures, and the pillars themselves have dimensions in the nano-regime. We can then reveal what happens to strength and plasticity in such extreme “nanostructured” cases. In addition to the expected high strength, we also observed very large plastic strains, without catastrophic instability that often occurs in large samples and conventional tests. Insights regarding flow defects and flow mechanisms are discussed, together with hints from molecular dynamics simulations.

### 8:50 AM Invited

**Progress in Understanding the Size-Affected Flow Behavior of Microcrystals:** *Dennis Dimiduk*<sup>1</sup>; *Michael Uchic*<sup>1</sup>; *Ed Nadgorny*<sup>2</sup>; *Satish Rao*<sup>3</sup>; *Christopher Woodward*<sup>1</sup>; <sup>1</sup>US Air Force Research Laboratory; <sup>2</sup>Michigan Technological University; <sup>3</sup>UES, Inc

Recently, experimental studies revealed that micrometer-scale crystals show strengthening effects, even at high initial dislocation densities. Their flow behavior is qualitatively characterized by four distinct attributes: (i) a sharply rising flow stress with decreasing sample size that follows power-law scaling (scaling exponent approximately -0.4 to -1.0); (ii) stochastic variation in flow stress that exhibits wider scatter at smaller sample sizes; (iii) intermittent flow as revealed by either repeated load drops or constant-stress flow avalanches; and (iv) an extended (>1% strain) elastic-plastic transition characterized by an average strain-hardening rate,  $H > G/200$ , where  $G$  is the shear modulus. Explanations for these phenomena include “dislocation starvation”, formation of an excess dislocation density, strengthening of dislocation sources, size-limited dislocation generation, and a statistical alteration of dislocation forest mechanisms. The present work uses both three-dimensional dislocation simulations and experiments on microcrystals to evaluate the relevancy of these mechanisms to various materials and sample sizes.

### 9:10 AM

**Plastic Size Effects in Ni-W Nanocrystalline Nano-Pillars:** *Julia Greer*<sup>1</sup>; *Dongchan Jang*<sup>1</sup>; <sup>1</sup>California Institute of Technology

When microstructural features or sizes of materials are reduced to nanometer scale, they exhibit different behaviors from bulk. Typical example is “smaller is stronger” manifested by high strengths attained during deformation of nano-sized single crystals. While specific plasticity mechanisms remain controversial,

this strengthening is attributed to greater contribution of surfaces and interfaces. Conventional strengthening mechanisms such as Hall-Petch may not be valid at nanometer scale. In this study combined effect of internal nano-structure and sample size on plasticity is investigated. These factors have been investigated separately, combination of their effects has never been reported. We present results of uniaxial compression and tension of Ni-W nano-pillars with grain sizes of 60 nm and diameters down to ~100 nm fabricated using Focused Ion Beam (FIB). Pillars are compressed in in-situ nanoindenter inside SEM chamber under displacement rate control. Site-specific TEM analysis reveals microstructural changes occurring as a result of mechanical deformation.

### 9:25 AM Invited

**Size Effects in Micro-Pillar Compression and Nanoindentation:** *Hongbin Bei*<sup>1</sup>; *Sanghoon Shim*<sup>1</sup>; *Michael Miller*<sup>1</sup>; *George Pharr*<sup>1</sup>; *Easo George*<sup>1</sup>; <sup>1</sup>Oak Ridge National Lab

Size-dependent strength has been measured both in micro-pillar compression and nanoindentation. Most of the micro-pillars reported on in the literature are produced by focused ion beam (FIB) milling. We report here results on single-crystal micro-pillars produced by a different technique, directional solidification. Since our as-grown pillars behaved like dislocation-free materials and yielded at the theoretical stress, we were able to systematically pre-strain the pillars before compression and study the effects of initial dislocation density and pillar size on pillar behavior. The directionally solidified pillars are also compared to directionally solidified and FIBed pillars to evaluate possible effects of FIB damage. Finally, we discuss an interesting indentation size effect (ISE) that we discovered recently by studying pop-in behavior during nanoindentation with spherical indenters. This ISE is based not on the measured hardness, as in conventional ISE, but rather on the stress to initiate dislocation plasticity.

### 9:45 AM

**Uniaxial Compression of FCC Au Nano-Pillars: The Effects of Prestraining and Annealing:** *Seok-Woo Lee*<sup>1</sup>; *Seung Min Han*<sup>1</sup>; *William Nix*<sup>1</sup>; <sup>1</sup>Stanford University

The size dependence of the strength of FCC metals, as revealed by uniaxial compression of nano-pillars, suggests that plasticity is dislocation source-controlled, with fewer sources in smaller pillars producing a “smaller is stronger” effect. To further investigate this phenomenon we have studied the effects of prestraining and annealing on the deformation properties of [001] Au nano-pillars. By making pillars from an epitaxial film of [001] Au on [001] MgO, using focused ion beam machining, we are able to create both puck-shaped pillars that can be stably prestrained and pillars with a high aspect ratio, which can be tested in uniaxial compression. We find that prestraining dramatically reduces the flow strength of nanopillars while annealing restores the strength to the un-prestrained levels. These are unusual effects are not seen in bulk FCC metals, which behave in an opposite way. We discuss their possible causes in terms of dislocation densities.

### 10:00 AM

**Strength in Small Sized Single Crystals: Discrete Dislocation Dynamics Simulations Using ParaDiS:** *Meijie Tang*<sup>1</sup>; <sup>1</sup>Lawrence Livermore National Laboratory

The dislocation dynamics method is a numerical tool to quantitatively describe plasticity and strength in crystalline materials. Applications have been made using the LLNL large scale parallel dislocation simulator (ParaDiS) for both bulk and finite sized single crystal systems. In these applications, the dislocation dynamics simulations are found to be powerful tools to discover new microstructure [Nature, 440, p1174 (2006)], understand strength in bulk systems, and to explore mechanisms responsible for ‘the smaller, the stronger’ observation in micro- and sub micro- systems in recent experiments. Latest development in coupling ParaDiS with FEM approach to simulate the strength in micro-sized single crystal pillars will be presented in this talk.

### 10:15 AM Break

### 10:25 AM Invited

**Oxygen in Grain Boundaries of Aluminum: A Molecular Dynamics Study:** *Andreas Elsener*<sup>1</sup>; *Olivier Politano*<sup>2</sup>; *Peter Derlet*<sup>1</sup>; *Helena Van Swygenhoven*<sup>1</sup>; <sup>1</sup>Paul Scherrer Institut; <sup>2</sup>Université de Bourgogne, Dijon

One of the important differences between simulation and experiments in grain boundary dominated metallic structures is the lack of impurities such as oxygen in computational samples. A modified variable-charge-method (Modell. Simul. Mater. Sci. Eng. 16,025006(2008)), based on the Streitz and Mintmire approach

that incorporates local chemical potentials to efficiently simulate oxidation in a predominantly metallic Al environment is presented. The present work reports on the application of this method to investigate aluminum samples with dilute amounts of oxygen under load. In particular, using aluminum bicrystals with symmetrical tilt grain boundaries, the influence of the presence of Oxygen on coupled grain boundary migration is investigated. It is found that grain boundary migration requires a higher applied shear to activate when Oxygen atoms exist within the boundary. This result is rationalized in terms of the stress signature of the Oxygen within the boundary and the associated atomistic grain boundary migration mechanism.

**10:45 AM**

**Superior Corrosion Resistance of Nanocrystalline Materials: Possible Effect of Grain Boundary Orientation:** *Indranil Roy*<sup>1</sup>; Hsaio-Wie Yang<sup>2</sup>; Farghalli Mohamed<sup>2</sup>; <sup>1</sup>University of California, Irvine / Schlumberger; <sup>2</sup>University of California, Irvine

This paper presents observations and evidences of superior corrosion resistance of nanocrystalline (nc) materials. These evidences are illustrated by orientation imaging microscopy (OIM) performed to produce electron backscatter diffraction (EBSD) maps. It has been observed that grain boundaries in electrodeposited (ED) nc-Ni having an average grain size of 100 nm are predominantly coherent low sigma coincidence site lattice (CSL) boundaries of the Sigma3 character. Similar observations have been made for nc-Ni having an average grain size of 20 nm. We attribute this property of corrosion resistance to be a possible effect of the grain boundary orientation. Our results are discussed with reference to the relative frequencies of these special boundaries as a function of their misorientations and sigma values. The role of this large volume fraction of Sigma3 boundaries appears to be consistent with improving intergranular corrosion resistance of nanocrystalline materials in comparison to their coarse-grained counterparts.

**11:05 AM Invited**

**Correlation between the Deformation of Nanostructured Materials and the Model of Dislocation Accommodated Boundary Sliding:** *Farghalli Mohamed*<sup>1</sup>; <sup>1</sup>University of California

Very recently, a new model for deformation in nanocrystalline (nc) materials has been formulated. The development of the model was based on the concept that plasticity in nc-materials is the result of grain boundary sliding accommodated by the generation and motion of dislocations under local stresses. By analyzing experimental data on two nc-materials, Ni and Cu, it is shown that this model can account not only for the deformation behavior of both metals over wide ranges of conditions but also for the occurrence of nanoscale softening.

**11:25 AM**

**Micro-Scratch Characterization of Strength in Nano-Crystalline Metals:** Luke Nyakiti<sup>1</sup>; Alan Jankowski<sup>1</sup>; <sup>1</sup>Texas Tech University

Tensile testing can provide the detailed plastic behavior from deformation at yielding to the ultimate strength. The power-law dependence of strength on strain rate provides a measure of the rate sensitivity. In general, tensile strength increases for many cubic metals as grain size decreases from the micro-scale into the nano-scale regime. However, many nano-crystalline metals are prone to localized plastic deformation or even brittle failure. As such, tensile strengths may appear well below the true upper-bound values. This drawback can make a quantitative interpretation of the strain-rate sensitivity quite difficult. As an alternative, the method of micro-scratch testing is used to evaluate the upper bound strength through micro-hardness measurements. By varying the velocity of the indent test under constant load, the width of the scratch reveals the rate dependence of hardness. New test results are presented for nanocrystalline cubic metals as gold alloys with grain sizes less than 10 nm.

**11:40 AM**

**Study of Plasticity in Small Size Tensile Samples:** Rick Lee<sup>1</sup>; Amit Ghosh<sup>1</sup>; <sup>1</sup>University of Michigan

Investigation of tensile behavior of small size tensile samples were carried out using small tensile stage within the chamber of a scanning electron microscope. Sample cross sections in the range of 300 - 2,000  $\mu\text{m}^2$  were machined by FIB. The micron-size samples exhibited strain bursts of appreciable size in comparison to relatively smooth stress-strain curves for larger samples. The strain bursts were correlated with slip steps observed on sample surface. The surface emergence of slip steps, their arrest, followed by strain hardening, define an intermittent slip process for small size samples. This surface based slip leads

to large amount of strain hardening in Inconel 625 and moderate amount of hardening in Ti-1100, but greater than large size samples. The high hardening rate is attributed to increasing fraction of surface atoms in small size specimens to penetrate through during slip, the strength level in the nanoscale size range approaching theoretical strength.

**11:55 AM**

**Synthesis of Bulk Nanolaminate Materials with Accumulative Roll Bonding:** *Rainer Hebert*<sup>1</sup>; Girija Marathe<sup>1</sup>; Jyothi Suri<sup>1</sup>; <sup>1</sup>University of Connecticut

Severe plastic deformation techniques provide an opportunity to study the relationship between mechanical properties and microstructural length scales. During accumulative roll bonding (ARB) of metallic multilayers, for example, the individual layer thickness continuously decreases by as much as four orders of magnitude. Aside from the layer thickness, the microstructure within the layers defines a second length scale. Nanoindentation studies with ARB-processed as-received Mo foils reveal a cyclic hardness change during processing to equivalent strains of about -10. Cu-Ni multilayers reveal necking of the Ni layers that depends on the work-hardening behavior of the Cu and Ni layers. Necking of elemental layers renders the top-down synthesis of nanolaminate materials more difficult. A continuum mechanics model along with experimentally determined strain hardening data enable the prediction of the onset of diffuse necking. The results highlight the relation between mechanical properties and microstructure evolution for the ARB synthesis of bulk nanolaminate materials.

**12:10 PM**

**Tensile Deformation and Fracture Mechanism of Bimodal Al-Mg Alloy:** *Zonghoon Lee*<sup>1</sup>; Velimir Radmilovic<sup>1</sup>; Byungmin Ahn<sup>2</sup>; Enrique Lavernia<sup>3</sup>; Steven Nutt<sup>2</sup>; <sup>1</sup>Lawrence Berkeley National Laboratory; <sup>2</sup>University of Southern California; <sup>3</sup>University of California, Davis

Bimodal bulk Al-Mg alloys, which were comprised of nanocrystalline grains separated by coarse grains, achieved balanced mechanical properties of enhanced strength and reasonable ductility and toughness compared to conventional counterparts and other nanocrystalline metals. However, the underlying deformation and fracture mechanism of the bulk bimodal metals have not been fully elucidated because of lack of unambiguous evidence based on direct observations in various scale range. We investigated cross-sections of tensile fractures of bimodal Al-Mg alloys at the micro and macro-scale using TEM, SEM equipped with FIB and optical microscopy. The direct observation revealed nanoscale voids and preserved micro-cracks near the tensile fracture surfaces successfully. It is evident that the incorporation of ductile coarse grains effectively impedes propagation of micro-cracks and results in enhanced ductility and toughness while retaining high strength. The findings may provide insights of further design of bimodal and moreover multiscale microstructures in ultra-fine grained and nanoscale regime.

**12:25 PM**

**The Effect of Starting Microstructure on the Creation of Ultra-Fine Grained Ti-6Al-4V via Multi-Axis Forging:** *Richard Didomizio*<sup>1</sup>; Andrew Deal<sup>1</sup>; Judson Marte<sup>1</sup>; P.R. Subramanian<sup>1</sup>; Steve Buresh<sup>1</sup>; Radhakrishna Bhat<sup>1</sup>; <sup>1</sup>GE Global Research

Multi-axis forging (MAF) under near-isothermal conditions was used to produce ultra-fine grained (UFG) structures in Ti-6Al-4V alloys. Mill-annealed and globurized microstructures were used as the starting material for the MAF processing. The resulting ultra-fine grained structures were compared with high resolution scanning electron microscopy and electron backscatter diffraction (EBSD). Using EBSD, the evolution of colonies of the alpha phase and the texture of both the alpha and beta phases were tracked from the starting structure through final processing. The flow responses of the UFG materials were obtained in both tension and compression. The salient microstructural features and flow behavior will be presented, along with resulting implications for superplastic behavior of the UFG Ti-6Al-4V alloys.

## Microstructural Processes in Irradiated Materials: Advanced Oxide Dispersion Strengthened Ferritic Alloys

Sponsored by: The Minerals, Metals and Materials Society, TMS Structural Materials Division, TMS/ASM: Nuclear Materials Committee  
Program Organizers: Christophe Domain, Electricite De France; Gary Was, University of Michigan; Brian Wirth, University of California, Berkeley

Tuesday AM Room: 2008  
February 17, 2009 Location: Moscone West Convention Center

*Session Chairs:* Akihiko Kimura, Kyoto University; Brian Wirth, University of California, Berkeley

### 8:30 AM Invited

**Recent CEA Results on the Development of Nanoscale Oxide Dispersion Strengthened Ferritic Alloys for Nuclear Applications:** *Yann de Carlan*<sup>1</sup>; Mathieu Ratti<sup>1</sup>; Marie-Hélène Mathon<sup>1</sup>; Patrick Olier<sup>1</sup>; Cyril Cayron<sup>1</sup>; Joël Ribis<sup>1</sup>; Philippe Pareige<sup>2</sup>; Arnaud Monnier<sup>1</sup>; Laurent Forest<sup>1</sup>; Xavier Averty<sup>1</sup>; <sup>1</sup>CEA; <sup>2</sup>GPM

Ferritic/martensitic ODS alloys are considered as promising materials for different nuclear applications. They exhibit very low swelling under irradiation and very good creep properties. In the seventies, different alloys were developed to be used as cladding materials in Sodium Fast Reactors (SFR) but the qualification of this type of materials has appeared long and difficult. In the framework of the studies on GENIV reactors, important means are now dedicated at CEA for the development of new F/M ODS alloys. The aim of this paper is to present the design of these new materials, their manufacture and the dedicated program to assess them as cladding materials. It includes the basic studies on the formation mechanisms of nano-oxides, the definition and the optimization of the fabrication route, the welding studies to evaluate the different joining processes and also all the experiments to insure the stability of the materials under irradiation.

### 9:00 AM Invited

**Analytical Electron Microscopy of Nano-Structured Ferritic Alloys:** *James Bentley*<sup>1</sup>; David Hoelzer<sup>1</sup>; <sup>1</sup>Oak Ridge National Laboratory

At a scale intermediate to those of atom probe tomography and "bulk" techniques such as small-angle neutron scattering, analytical (transmission) electron microscopy (AEM) of mechanically alloyed nano-structured ferritic alloys (NFAs) has provided much useful information for structure-property-processing correlations. The NFAs include MA957, ORNL-developed 14YWT (Fe-14.2%Cr-1.95%W-0.22%Ti-0.25%Y<sub>2</sub>O<sub>3</sub>) and prototypical 12YWT (12%Cr). Energy-filtered transmission electron microscopy (EFTEM) methods have been emphasized for reliably characterizing the oxide nano-clusters (typically with diameters less than 4 nm and concentrations exceeding 10<sup>23</sup> m<sup>-3</sup>) that are responsible for the exceptional mechanical properties of these materials. X-ray microanalysis, especially spectrum imaging in the scanning transmission mode, has been a useful complement to EFTEM methods. AEM characterization of irradiated specimens and of tensile- and creep-tested specimens will be discussed along with the role of AEM in identifying undesirable processing conditions and aiding the selection of more optimum fabrication protocols.

### 9:30 AM

**Microstructural Characterization of Irradiated ODS and Fe-Cr Alloys:** *Vanessa de Castro*<sup>1</sup>; Sen Xu<sup>1</sup>; Sergio Lozano-Perez<sup>1</sup>; Emmanuelle Marquis<sup>1</sup>; Mike Jenkins<sup>1</sup>; <sup>1</sup>University of Oxford

Reduced activation ferritic-martensitic steels are candidate structural materials for fusion reactors. Strengthening the steel with a homogeneous dispersion of oxide nanoparticles such as Y<sub>2</sub>O<sub>3</sub> could help to rise the operating temperature of these materials and lower the rate of damage accumulation in the steel. These oxide dispersion strengthened steels (ODS) are produced by pulvimetallurgical routes which lead to complex microstructures. This work describes the microstructure after ion irradiation of an ODS/Fe12Cr and a reference Fe12Cr alloy, produced by pulvimetallurgy, with the microstructure present in a Fe11Cr alloy produced by casting. The alloys were irradiated at 300 and 500°C with 0.5 and 2 MeV Fe<sup>+</sup> ions up to doses of 10<sup>16</sup> ions/cm<sup>2</sup>. The distribution, size and density of the defects induced in these materials are compared. The stability of the oxide nanoparticles

dispersion is also discussed. This research has been supported by FP6 Euratom Research and Training Programme on Nuclear Energy.

### 9:50 AM

**Radiation Induced Segregation to Nano-Particles and Grain Boundaries in 9CrODS Steel after Low Dose Irradiation:** *Alicia Certain*<sup>1</sup>; Kevin Field<sup>1</sup>; Kumar Sridharan<sup>1</sup>; Todd Allen<sup>1</sup>; Jeremy Busby<sup>2</sup>; Mike Miller<sup>2</sup>; <sup>1</sup>University of Wisconsin-Madison; <sup>2</sup>Oak Ridge National Laboratory

9Cr ferritic-martensitic (F-M) alloys show promise for nuclear applications due to their resistance to void swelling compared to austenitic alloys and improved toughness compared to 12Cr F-M alloys. However, these alloys tend to have low creep strength. This can be circumvented by adding Y-Ti-O nanoclusters that act as pinning points for dislocations. A 9Cr oxide dispersion strengthened (ODS) steel was irradiated with protons to 1 dpa at 525°C to investigate oxide stability. The radiation-induced segregation response of the alloys was investigated using EDS and atom probe tomography along prior austenite grain boundaries and in the yttrium-titanium oxide nano-particles contained within the matrix of the ODS steel. No segregation was observed at the particle or grain boundary interfaces in the unirradiated condition, but Cr enrichment was observed at the particle-matrix interface for the 1 dpa irradiated steel.

### 10:10 AM Break

### 10:30 AM Invited

**Atomic Scale Characterization of ODS Steels by Atom Probe Tomography:** *Emmanuelle Marquis*<sup>1</sup>; <sup>1</sup>University of Oxford

Reduced activation ferritic and ferritic-martensitic steels (RAFMS) are promising structural materials for the first wall and blanket of future fusion reactors. In order to improve the high temperature properties of these steels, oxide-dispersion strengthened (ODS) versions were processed with the addition of oxide precipitates that provide dislocation pinning points and remain stable up to temperatures close to the melting point. Controlling material properties during irradiation requires detailed understanding of the role of the defect sinks, i.e. nanoscale particles, grain boundaries, dislocations, etc. which in turn implies a detailed knowledge about the internal structure, chemistry, and interfacial structure of these microstructural features. The role of atom probe tomography for the 3-D atomic scale characterization of ODS steels will be discussed, focusing on the internal structure of the nanoscale particles and grain boundary chemistry before and after irradiation in different ODS Fe-Cr alloys.

### 11:00 AM

**Irradiation of Nanoclusters:** *Michael Miller*<sup>1</sup>; David Hoelzer<sup>1</sup>; Kaye Russell<sup>1</sup>; Chong Long Fu<sup>1</sup>; <sup>1</sup>Oak Ridge National Laboratory

Atomic displacement cascades produced during neutron or ion irradiations can induce mechanisms that can potentially destabilize or destroy nanoclusters and precipitates, change the vacancy and interstitial atom distribution, and thereby degrade the desired properties of materials. Atom-probe tomography has been used to determine, with atomic scale resolution, the solute distribution associated with titanium-, oxygen-, and yttrium-enriched nanoclusters in mechanically-alloyed, nanostructured ferritic alloys before and after high dose irradiation. This is the initial stage towards a fundamental understanding of the remarkable stability of these alloys when exposed to extreme conditions. This research was sponsored by the U.S. Department of Energy, Division of Materials Sciences and Engineering; research at the Oak Ridge National Laboratory SHaRE User Facility was sponsored by the Scientific User Facilities Division, Office of Basic Energy Sciences, U.S. Department of Energy.

### 11:20 AM

**A Density Functional Theory Study of Formation of Y-Ti-O Nanoclusters in Nanostructured Ferritic Alloys:** *Yong Jiang*<sup>1</sup>; John Smith<sup>1</sup>; G. Robert Odette<sup>1</sup>; <sup>1</sup>University of California, Santa Barbara

Atom probe tomography shows that nanostructured ferritic alloys are dispersion strengthened by far from equilibrium Y-Ti-O nanostructures. The nanostructures and large excess quantities of dissolved O persist even after prolonged high temperature aging. Density functional theory (DFT) calculations were used to study the energies, structures and formation mechanisms of dissolved Y, Ti and O solutes and small Y-Ti-O nanoclusters (NC). Y and O dissolve during mechanical alloying of Y<sub>2</sub>O<sub>3</sub> with metal powders, requiring solution energies of about 4 eV/atom provided by the ball milling. Substitutional Ti and Y and interstitial O have high solution energies, but O-O, Y-O and Ti-O pairs are strongly bound, and constitute NC building blocks. The energy decreases upon further clustering and is about -5.1 eV for a Y<sub>2</sub>TiO<sub>3</sub> NC. NC formation can take



place without the energetic assistance of pre-existing vacancies. The O-O pairs and O-O-Y/Ti complexes also increase the solubility of O.

## 11:40 AM

**Comparison of Microstructures of Commercial ODS Alloys Using Local Electrode Atom Probe and Transmission Electron Microscopy for Irradiation Applications:** *Peter Hosemann*<sup>1</sup>; Erich Stergar<sup>2</sup>; Christiane Vieh<sup>2</sup>; Patricia Dickerson<sup>1</sup>; Nicholas Cunningham<sup>3</sup>; Robert Odette<sup>3</sup>; Harald Leitner<sup>2</sup>; Stuart Maloy<sup>1</sup>; <sup>1</sup>Los Alamos National Laboratory; <sup>2</sup>Montanuniversität Leoben; <sup>3</sup>University of California Santa Barbara

Nanostructured ferritic/martensitic alloys have been shown to be promising candidate materials for high dose irradiation applications. The main reason for these materials irradiation tolerance is a distribution of nanometer sized stable oxide particles in the material. The work presented here used Local Electrode Atom Probe (LEAP) and Transmission Electron Microscopy (TEM) to investigate the aluminum and chromium alloyed materials PM2000 (two different grain sizes) and MA956 as well as the chromium alloyed material MA957 and an experimental alloy. The exact composition of the nanostructured oxide particles as well as their shape and distribution are discussed and compared to LEAP and TEM measurements on conventional reactor steels like HT-9. The new knowledge of these measurements are discussed in relation to radiation tolerance in comparison with results from the literature. In addition LEAP results as measured on these same materials after an ion beam irradiation experiment (1dpa, room temperature) are discussed.

## 12:00 PM

**Effects of Atypical Particle Distributions on Grain Growth:** *Zachary Royer*<sup>1</sup>; Ralph Napolitano<sup>1</sup>; Richard Lesar<sup>1</sup>; <sup>1</sup>Iowa State University

The thermal stability of oxide dispersion strengthened (ODS) steels is highly dependent on the distribution of the oxides in the matrix. We employ 2-D phase-field simulation to examine the effects of atypical particle distributions on grain growth. By varying the initial concentration and distribution of particles relative to the initial grain structure, we are developing scaling relationships to describe the interrelationship of particle distribution and the evolution of the microstructure.

## Nanocomposite Materials: Characterization and Modeling of Nanocomposites I

Sponsored by: The Minerals, Metals and Materials Society, TMS Structural Materials Division, TMS Electronic, Magnetic, and Photonic Materials Division, TMS/ASM: Composite Materials Committee, TMS: Materials Characterization Committee, TMS: Nanomaterials Committee

Program Organizers: Jonathan Spowart, US Air Force; Judy Schneider, Mississippi State University; Bhaskar Majumdar, New Mexico Tech; Benji Maruyama, Air Force Research Laboratory

Tuesday AM

Room: 3020

February 17, 2009

Location: Moscone West Convention Center

*Session Chairs:* Nikhilesh Chawla, Arizona State University; Nathan Mara, Los Alamos National Laboratory

## 8:30 AM Introductory Comments

### 8:35 AM Invited

**Length-Scale Dependent Failure of Hierarchical Composites:** *Shailendra Joshi*<sup>1</sup>; Yeong Sung Suh<sup>2</sup>; K.T. Ramesh<sup>3</sup>; <sup>1</sup>National University of Singapore; <sup>2</sup>Hannam University; <sup>3</sup>Johns Hopkins University

Nature tends to design multi-scale microstructures, using growth mechanisms to develop several levels of hierarchy, and these microstructures are efficient (strong and ductile) from the structural viewpoint. Motivated by this concept, we define hierarchical composites as heterogeneous materials comprising two or more constituent phases where at least one phase is itself a composite at a finer scale. Using these bio-inspired concepts, coupled with recent advances in nanostructured materials, we present explicit finite element analyses of artificial microstructures with multiple elasto-plastic phases, accounting for length-scale effects. The results provide insight in to topological influences on the strengthening and failure of hierarchical microstructures.

## 9:00 AM

**A Multi-Scale Statistical Model of the Dynamic Mechanical Response of Natural Composites:** *Mark Jhon*<sup>1</sup>; Daryl Chrzan<sup>1</sup>; <sup>1</sup>University of California, Berkeley and Lawrence Berkeley National Laboratory

Nacre is a natural composite material consisting of brittle mineral platelets and an organic adhesive. It has a very high toughness relative to the properties of its component materials. The reason for this lies in nacre's rich hierarchy of structural features. For instance, individual molecules in the organic have been shown to unfold in discrete steps on the order of 10s of nanometers. In the present study, a multi-scale statistical model is introduced to address the consequences of such nanometer length-scale features on the deformation of the microstructure of nacre. A dynamic fiber-bundle model models the rate-dependent mechanical behavior of the organic, while a random fuse model connects the local and macroscopic mechanical response. Faster loading rates are found to increase the microscopic strength. Introducing microscopic hardening is found to spread the spatial extent of damage. This work was supported by the U.S. Department of Energy under Contract No. DE-AC02-05CH11231.

## 9:20 AM

**Electron Instabilities in Inhomogeneous Nanoclusters and Nanostructured Materials:** *Armen Kocharian*<sup>1</sup>; Gayanath Fernando<sup>2</sup>; Kalum Palandage<sup>2</sup>; James Davenport<sup>3</sup>; <sup>1</sup>California State University, Los Angeles; <sup>2</sup>University of Connecticut, Storrs; <sup>3</sup>Brookhaven National Laboratory, Upton

Exact calculations of thermodynamic properties in various cluster geometries yield level crossing degeneracies driven by interaction strength, coupling strength and temperature. The electronic configurations of the lowest energy levels control the physics of electronic instabilities and magnetic phase transitions. Rigorous conditions are found for phase transitions and crossovers which resemble a number of inhomogeneous, coherent and incoherent nanoscale phases seen recently in high Tc cuprates, manganites and CMR nanomaterials. Small bipartite and frustrated nanoclusters exhibit instabilities and phase diagrams in many respects typical for nano and heterostructured materials.<sup>1</sup> The calculated phase diagrams in various cluster geometries may be linked also to atomic scale tunneling experiments in high Tc cuprates, manganites and other transition metal oxides. <sup>1</sup>A.N. Kocharian, G.W. Fernando, K. Palandage, and J.W. Davenport, cond.-mat.: arXiv:0804.0958 (2008); Phys. Lett. A364, 57 (2007); Phys. Rev. B74, 024511 (2006).

## 9:40 AM

**Molecular Dynamic Simulations for Effect of Polymer Chain Morphology on Mechanical Properties of Carbon Nanotube-Polymer Composites:** *Zhongqiang Zhang*<sup>1</sup>; Don Ward<sup>1</sup>; Yibin Xue<sup>1</sup>; Hongwu Zhang<sup>2</sup>; Mark Horstemeyer<sup>1</sup>; <sup>1</sup>Mississippi State University; <sup>2</sup>Dalian University of Technology

The influence of chain length and morphology of polyethylene on the constitutive properties of single walled carbon nanotube (SWCNT) reinforced polyethylene composites is investigated using molecular dynamics simulations. Molecular models of nanocomposites are developed by embedding SWCNTs into both an amorphous and a semi-crystalline polyethylene matrix at the thermodynamic equilibrium state, in which the carbon nanotubes can be pristine or functionalized. The mechanical properties of bulk polyethylene and nanocomposites are evaluated by simulating a series of tension, compression and shear tests at various loading rates and temperatures. For pure polymer, the results show that an increase in chain length has induced non-linear proportional increases in tensile strength and Young's modulus; the elongation and viscoelastic hardening of the polymer are significantly enhanced with the increase in chain length; The crystalline morphology varies as the deformation increases, which is a novel observation in simulations and is consistent with the assumptions in open literature.

## 10:00 AM

**Modeling of Indentation Behavior in Nanolayered Al/SiC Composites:** *Guanlin Tang*<sup>1</sup>; *Yu-lin Shen*<sup>1</sup>; Danny Singh<sup>2</sup>; Nikhilesh Chawla<sup>2</sup>; <sup>1</sup>University of New Mexico; <sup>2</sup>Arizona State University

The indentation behavior of multilayered Al/SiC composites is studied numerically. The numerical model features the explicit composite structure on top of a Si substrate indented by a conical diamond indenter. Attention is devoted to the evolution of stress and deformation fields in the layered composite during the indentation loading and unloading processes. It is found that the layered composite, consisting of materials with distinctly different mechanical properties, results in unique deformation patterns. Significant tensile stresses can be generated locally along certain directions, which offers a mechanistic

rationale for the indentation-induced internal cracking observed experimentally. The unloading process also leads to an expansion of the tension-stressed area, as well as continued plastic flow in parts of the Al layers. Implications of these numerical findings to the nanoindentation response of metal-ceramic laminates will be discussed. Simulation results on microcompression of the pillar structure will also be presented.

#### 10:20 AM Break

#### 10:35 AM Invited

**Deformation and Failure Mechanisms of Cu/Nb Nanoscale Composites: Microstructural Analysis at the Nanoscale:** *Nathan Mara*<sup>1</sup>; Dhriti Bhattacharyya<sup>1</sup>; Pat Dickerson<sup>1</sup>; Richard Hoagland<sup>1</sup>; Amit Misra<sup>1</sup>; <sup>1</sup>Los Alamos National Laboratory

Cu/Nb nanoscale multilayered composites have shown ultra-high strength as well as high ductility using a variety of mechanical test methods (nanoindentation, tensile testing, and micropillar compression). Individual layer thicknesses tested range from 100 nm to 5 nm, with flow stresses (5 nm Cu/Nb case) of nearly 3 GPa, and deformation during micropillar compression exceeding 20%. Through the use of Focused Ion Beam (FIB) milling, post-deformed microstructures of micropillars are examined via Transmission Electron Microscopy (TEM). Shear banding, as well as homogeneous deformation of over 10% true strain is evident at individual layer thicknesses as low as 5 nm. The microstructure within the shear band exhibits large plastic deformation and grain rotation relative to the compression axis, and the layered structure remains continuous even after local strains in excess of 70%. Plastic behavior of nanolayered composites at large plastic strains will be discussed in terms of interfacial effects on dislocation motion.

#### 11:00 AM

**Mechanical Characterization of Nanolayered Al/SiC Composites through Indentation and Microcompression Testing:** *Danny Singh*<sup>1</sup>; *Nikhil Chawla*<sup>1</sup>; *Guan Lin Tang*<sup>2</sup>; *Yu-lin Shen*<sup>2</sup>; <sup>1</sup>Arizona State University; <sup>2</sup>University of New Mexico

Multilayered Al/SiC composites exhibit extremely high strength and toughness. In this paper we discuss the processing, microstructural characterization, and mechanical behavior of this novel system. The nanolaminates were processed by physical vapor deposition (PVD) using magnetron sputtering. Layer thickness and morphology was studied using a dual beam focused ion beam (FIB). The mechanical properties were characterized by nanoindentation and microcompression of "pillars." The pillars were fabricated and characterized by FIB. The effect of pillar size on the mechanical response of these materials was studied. Mechanical properties derived from microcompression were compared to conventional nanoindentation results. Finally, post-deformation microstructural analysis and modeling was carried out to provide insight into the observed deformation mechanisms.

#### 11:20 AM

**Nanomechanics of Cellulose Nanocrystal Composites:** *Reza Shahbazian Yassar*<sup>1</sup>; *Anahita Pakzad*<sup>1</sup>; *Patricia Heiden*<sup>1</sup>; <sup>1</sup>Michigan Technological University

Cellulose nanocrystals are theoretically estimated to have mechanical properties comparable to carbon nanotubes. Being one of the most abundant materials in the world, cellulose has several appealing characteristics such as low cost, eco-friendly, and low density. As such, cellulose nanocrystals have attracted scientists to devote considerable efforts in order to develop cellulose-based nanocomposite materials for automotive applications. Yet no direct experimental work has been performed to measure the mechanical properties of the individual cellulose nanocrystals. In this research, we use a novel in-situ nanomechanical testing based on atomic force microscope (AFM) that operates inside a transmission electron microscope (TEM) and as a result makes the simultaneous quantitative and qualitative analysis possible. By this method, for the first time, deformation parameters including the elastic modulus, total amount of deformation, the amount of strain prior to fracture, and failure mechanisms of cellulose nanocrystals are determined.

#### 11:40 AM

**Nanoscale near-Surface Deformation in Polymer Nanocomposites:** *Devesh Misra*<sup>1</sup>; *Qiang Yuan*<sup>1</sup>; <sup>1</sup>University of Louisiana

The objective of the presentation is to elucidate the nanoscale near-surface deformation response of two polymer nanocomposite systems with significant differences in ductility during nanoscratching with a Berkovich indenter. An

accompanying objective is to investigate the commonality in surface deformation behavior between nano- and microscale deformation to reinforce the underlying fundamental principles governing surface deformation. An understanding of surface deformation response is accomplished through determination of physical and mechanical properties, structural characterization and electron microscopy analysis of surface deformation tracks and residual plastically deformed structures. The deformation behavior is described in terms of physical and mechanical properties of materials notably percentage crystallinity and elastic recovery.

## Neutron and X-Ray Studies of Advanced Materials: Small Scale and Thin Film Studies

Sponsored by: The Minerals, Metals and Materials Society, TMS Structural Materials Division, TMS/ASM: Mechanical Behavior of Materials Committee, TMS: Advanced Characterization, Testing, and Simulation Committee, TMS: Titanium Committee  
Program Organizers: *Rozaliya Barabash*, Oak Ridge National Laboratory; *Yandong Wang*, Northeastern University; *Peter Liaw*, The University of Tennessee; *Jaimie Tiley*, US Air Force

Tuesday AM

February 17, 2009

Room: 3016

Location: Moscone West Convention Center

*Session Chairs:* *Paul Zschack*, Advanced Photon Source; *Carol Thompson*, NIU

#### 8:30 AM Keynote

**Micro-Mechanical Insights from In-Situ X-ray and Neutron Diffraction:** *Helena Van Swygenhoven*<sup>1</sup>; <sup>1</sup>Paul Scherrer Institute

With the high intensities of neutron and X-ray sources, new detector developments and X-ray micro-focusing techniques, time resolved studies of mechanical behavior of interface/surface dominated structures becomes one of the new powerful methods in materials science. In this talk recent results obtained from in-situ powder diffraction at the Swiss Light Source and at the Swiss neutron source are presented for a variety of nano-materials. In the second part of this talk, results obtained from the new in-situ Laue micro-compression device at the SLS to study the dynamics of single crystal plasticity in micron-sized single-crystals will be presented. In most studies it is assumed that the pillars made by the FIB method do not contain pre-existing strain gradients. In-situ Laue has however revealed the presence of strain gradients and misorientations at the pillar base extending well into the pillar body – all features that are known to contribute to classical hardening.

#### 9:00 AM Invited

**Cation Ordering in Thin LaSrCoO Films:** *Wolfgang Donner*<sup>1</sup>; <sup>1</sup>TU Darmstadt

Cathode materials for low-temperature solid oxide fuel cells should exhibit a high oxygen permittivity at low temperatures (< 500 centigrades). It has been found that the oxygen diffusion through the cathode can be enhanced by using cation-ordered perovskites. We will present a Synchrotron x-ray study of thin (40 nm) epitaxial films of LaSrCoO on SrTiO that has been carried out under variable temperature and oxygen partial pressure. We found that the La / Sr cations undergo chemical ordering under reduction. This cation ordering is not present in the bulk material and induced by epitaxial strain from the substrate.

#### 9:20 AM Invited

**3D Spatially-Resolved Measurements of Strain Gradients in Embedded and Free Standing Mo Micro-Pillars and NiAl Matrix:** *Rozaliya Barabash*<sup>1</sup>; *Hongbin Bei*<sup>1</sup>; *Gene Ice*<sup>1</sup>; *J. Tischler*<sup>1</sup>; *Wenjun Liu*<sup>2</sup>; *Easo George*<sup>1</sup>; <sup>1</sup>Oak Ridge National Laboratory; <sup>2</sup>Argonne National Laboratory

Spatially resolved strain distributions in the NiAl matrix and the ~550-nm Mo fibers of a NiAl-Mo eutectic were investigated by micro-beam X-ray diffraction. Position sensitive d-spacings for the individual phases were obtained from Laue patterns. For embedded Mo fibers, the measured elastic strain is consistent with the predicted thermal mismatch strain between the NiAl and Mo phases. However, when the NiAl matrix is etched back to expose Mo micro-pillars, the d-spacing increases to that of unconstrained Mo, indicating release of the compressive residual strain in the Mo fibers.

## 9:40 AM Invited

**Gold as a Model System for Nanoscale Interconnects: Hillocking, Temperature Dependent Strength and Low Temperature Ductility:** *Ralph Spolenak*<sup>1</sup>; <sup>1</sup>ETH Zurich

Diffusion barriers limit the downscaling of classical interconnect materials such as aluminum and copper. Gold, on the other hand, does not require passivating layers and can thus be scaled down further. With regards to probes for interaction with biological material gold is also well suited. We report an in-situ synchrotron based study on gold interconnects as narrow as 20 nm, and thin films of similar dimension. Whereas thicker films exhibit hillocking under compressive stress as investigated by Laue microdiffraction, nanoscale films show an unexpectedly strong dependence of yield strength on temperature. A high low temperature yield strength is found to be correlated to an improved ductility.

## 10:00 AM Invited

**Characterization of Group-III Nitrides with X-Ray Diffraction:** *Alois Krost*<sup>1</sup>; Juergen Blaesing<sup>1</sup>; <sup>1</sup>Magdeburg University

During the last 15 years group-III nitrides have developed one of the most important and technological relevant semiconductor family. Unfortunately, due to the lack of homoepitaxy, most of such layer structures are far from being perfect single crystalline films but exhibit strong mosaicity. In this talk it will be shown, how a lot of information on such layers can be gathered with conventional and advanced laboratory equipment. In order to get lateral resolution down to 1  $\mu\text{m}$  in the laboratory, we have designed a new convergent beam, concurrent detection diffractometer. The instrument was built by Bruker and is equipped with a rotating anode generator, a Johannson monochromator crystal for beam focusing, and a Soller slit arrangement in combination with a knife edge in front of the sample which defines the illuminated area on the sample. A large area detector from Vantec allows for rapid simultaneous detection of the diffracted intensity.

## 10:20 AM Break

## 10:30 AM Invited

**In-Situ Synchrotron X-Ray Studies of (In,Ga)N Growth:** *Gregory Stephenson*<sup>1</sup>; Marie-Ingrid Richard<sup>1</sup>; Fan Jiang<sup>1</sup>; Matthew Highland<sup>1</sup>; Tim Fister<sup>1</sup>; Carol Thompson<sup>2</sup>; Stephen Streiffer<sup>1</sup>; Paul Fuoss<sup>1</sup>; Ken Elder<sup>3</sup>; Anneli Munkholm<sup>4</sup>; <sup>1</sup>Argonne National Laboratory; <sup>2</sup>Northern Illinois University; <sup>3</sup>Oakland University; <sup>4</sup>Philips Lumileds Lighting Company

In-situ, time-resolved x-ray techniques can provide unique insight into the atomic-scale mechanisms occurring during materials synthesis and processing. In this talk we discuss studies of metal-organic chemical vapor deposition of (In,Ga)N thin films. While high In content is desirable for several applications, InN has a 10% lattice mismatch with the GaN substrate, and is metastable at ambient pressure, requiring a chemically active nitrogen species for growth. Using x-ray scattering and fluorescence, we have studied the coupled strain and composition changes that occur during (In,Ga)N film growth and relaxation. During InN growth, we observe that self-sustaining oscillations in phase stability can occur: islands of relaxed InN nucleate and grow; the InN islands collectively transform into elemental In droplets; the liquid In evaporates; and then another cycle of InN growth begins. These observations indicate key synthesis mechanisms for these metastable materials. Work supported by DOE under contract DE-AC02-06CH11357.

## 10:50 AM Invited

**Using X-Ray Microbeams to Assess Long Range Internal Stresses in Materials:** *Michael Kassner*<sup>1</sup>; Peter Geantil<sup>1</sup>; Lyle Levine<sup>2</sup>; Bennett Larson<sup>3</sup>; Jon Tischler<sup>3</sup>; Wenjun Liu<sup>4</sup>; <sup>1</sup>University of Southern California; <sup>2</sup>National Institute of Standards and Technology; <sup>3</sup>Oak Ridge National Laboratory; <sup>4</sup>Argonne National Laboratories

The presence of counterbalanced stresses within microscopic volumes in deformed materials was predicted more than two decades ago and inferred from numerous indirect experiments. Yet, direct proof of their existence had been elusive, as spatially resolved measurements of the stress magnitudes and distributions critical for testing theories and computer modeling were not possible until recently. Researchers using the intense submicron x-ray beams at the Advanced Photon Source made the first quantitative, spatially resolved measurements of elastic strains within dislocation cells in plastically deformed Cu single crystals. The measurements indicated that the dislocation cell interiors were under significant and variable long range internal stresses. Additional measurements are uncovering other aspects of these stresses such

as the statistical distribution of magnitudes. The most recent results of long range internal stress measurements in plastically deformed Cu single crystals as a function of position in the heterogeneous dislocation substructure will be presented.

## 11:10 AM Invited

**X-Ray Studies of Thin-Film Thermoelectric Materials:** *Paul Zschack*<sup>1</sup>; Colby Heideman<sup>2</sup>; Qiyin Lin<sup>2</sup>; Ngoc Nguyen<sup>2</sup>; Mary Smeller<sup>2</sup>; Clay Mortensen<sup>2</sup>; David Johnson<sup>2</sup>; <sup>1</sup>Argonne National Laboratory; <sup>2</sup>University of Oregon

Layered materials fabricated with the Modulated Elemental Reactant (MER) technique have demonstrated extremely low thermal conductivity and hold great promise for effective thermoelectric applications. These thin-films and multilayers incorporate ordered stacking of 2D hexagonal sheets that are highly textured with [00L] along the surface normal and random crystalline orientation in the plane parallel to the substrate. The extremely low thermal conductivity of these disordered, layered crystals is related to the nano-scale structural arrangement, due to enhanced interface scattering and the localization of lattice vibrations within the randomly distributed nano-crystalline regions. X-ray diffraction and imaging techniques at the Advanced Photon Source have been used to characterize the structures.

## 11:30 AM Invited

**In Situ, Time-Resolved X-Ray Scattering Studies of Morphology Evolution and Kinetic Relaxation during Layer-by-Layer Growth of Complex Oxides via Pulsed Laser Deposition:** *Gökhan Arıkan*<sup>1</sup>; John Ferguson<sup>1</sup>; Arthur Woll<sup>1</sup>; *Joel Brock*<sup>1</sup>; <sup>1</sup>Cornell University

Obtaining time-resolved, atomic-scale structural information of thin film deposition remains an on-going challenge. Here, we present recent studies of layer by layer (LBL) homoepitaxy of SrTiO<sub>3</sub> (001) via pulsed laser deposition (PLD). First, we discuss single shot specular reflectivity measurements using an avalanche photodiode which provide access to changes in the surface roughness with temporal resolution comparable to the plume duration (~50e-6 sec.). Next, we discuss diffuse scattering measurements using a CCD detector operating in streak-camera mode. We simultaneously capture both the specular reflectivity and the diffuse scattering parallel to the substrate with a temporal resolution of ~0.2 seconds. These rich data sets provide information on the surface roughness, coverage, island density and size as a function of time. For example, the time scale for interlayer transport grows over the course of the first 5-10 layers and is correlated with an increase in the average distance between islands.

## 11:50 AM Invited

**In Situ X-Ray Scattering Investigations into the Growth of Nanostructured Surfaces:** *Paul Miceli*<sup>1</sup>; Chinkyo Kim<sup>2</sup>; Shawn Hayden<sup>1</sup>; Michael Gramlich<sup>1</sup>; Edward Conrad<sup>3</sup>; Rui Feng<sup>3</sup>; Michael Tringides<sup>4</sup>; Myron Hupalo<sup>4</sup>; Craig Jeffrey<sup>1</sup>; Philip Ryan<sup>5</sup>; <sup>1</sup>University of Missouri-Columbia; <sup>2</sup>Kyung Hee University; <sup>3</sup>Georgia Institute of Technology; <sup>4</sup>Ames Laboratory; <sup>5</sup>MUCAT

Because it is sensitive to both the surface and the subsurface of a sample, x-ray scattering possesses unique capabilities for exploring atomic-scale mechanisms that control the growth and formation of nanostructures at surfaces. Using the in-situ scattering facility that we developed at the Advanced Photon Source, our research has revealed unexpected behavior. For example, the formation of large vacancy clusters was discovered during the homoepitaxial growth of noble metals. Despite intense interest in film-growth mechanisms, conventional "surface-only" tools have missed these buried defects. Their existence is important for understanding the atomic-scale growth-mechanisms. Our studies of nanoscale Pb islands on Si(111) reveal anomalously fast surface kinetics as well as novel coarsening due to the breakdown of classical ripening processes, all of which derive from quantum-size-effects. These studies will be presented for a general audience in order to illustrate the utility of in-situ x-ray scattering methods. Funding: NSF, PRF, DOE



## Pb-Free Solders and Emerging Interconnect and Packaging Technologies: Effects of Surface Finishes and Advances in Interconnects

Sponsored by: The Minerals, Metals and Materials Society, TMS Electronic, Magnetic, and Photonic Materials Division, TMS: Electronic Packaging and Interconnection Materials Committee

Program Organizers: Sung Kang, IBM Corp; Iver Anderson, Iowa State University; Srinivas Chada, Medtronic; Jenq-Gong Duh, National Tsing-Hua University; Laura Turbini, Research In Motion; Albert Wu, National Central University

Tuesday AM Room: 2020  
February 17, 2009 Location: Moscone West Convention Center

Session Chairs: Srinivas Chada, Medtronic; Fay Hua, Intel

### 8:30 AM Invited

**Electroless Ni Contamination Induced ENIG Corrosion:** *John Osenbach*<sup>1</sup>; John Delucca<sup>1</sup>; Frank Baiocchi<sup>1</sup>; Ahmed Amin<sup>1</sup>; <sup>1</sup>LSI Corporation

Corrosion of ENIG surface finish has been known for almost 2 decades. There has been significant progress toward eliminating this corrosion problem. However, corrosion, often referred to a black pad, is still sometimes found. Using FIB cross sectioning and STEM/EDS analysis we have identified a second phase particle contamination in the electroless Ni, Ni(P), layer on substrates that have corroded ENIG but not on substrates with non-corroded ENIG. To the authors knowledge it is the first reported observation of this effect. These particles are almost the same composition as the Ni(P) layer. When present, the particle leads to a modification in the growth habit of the Ni(P) layer which ultimately lead to a modification in the surface topology as well as creating low density interfaces. This change in topology and microstructure ultimately leads to Ni(P) corrosion. The data and corrosion model will be presented in the talk

### 8:50 AM

**Effect of Cu Surface Finishes of Printed Circuit Board on the Microstructure of Lead-Free Solder Joint:** *Dai-hong Xiao*<sup>1</sup>; <sup>1</sup>Central South University

Effect of Cu surface finishes, including organic solderability preservatives (OSP) and immersion Ag (I-Ag), on the microstructure of lead-free solder joint was investigated with scanning electron microscope and energy dispersive X-ray spectroscopy. It was found that Cu surface finishes affected the microstructure of lead-free solder joint. The thickness of intermetallic compounds (IMC) layer with OSP was higher than that of I-Ag. Comparing with OSP, there are more plate-like Ag<sub>3</sub>Sn intermetallic compounds between solder joints and Cu pad after I-Ag surface finishing. However, there are more voids found in the solder joints which distributed close to the solder interface and reduced the strength of solder joints after OSP surface finishing.

### 9:05 AM

**Fluxless Ultrasonic Lead-Free Soldering for Electronics Packaging Applications:** *Shankar Srinivasan*<sup>1</sup>; Tim Frech<sup>1</sup>; Karl Graff<sup>1</sup>; <sup>1</sup>Edison Welding Institute

Microstructure and mechanical properties of Sn-3.0Ag-0.5Cu (SAC305) solder joints fabricated using fluxless ultrasonic soldering is reported. Single-lap copper-copper joints with two different surface finishes, electroless nickel immersion gold (ENIG) and immersion silver (ImAg), were fabricated by ultrasonic soldering using SAC305. Tensile shear strengths of SAC305 in Cu/Cu, Cu/Cu-ENIG, and Cu/Cu-ImAg joints were similar to each other and in the range 30-35 MPa. Fractographic characterization indicated failure occurring through the solder, and exhibiting typical shear failure mechanism. Furthermore, the shear strength of SAC305 in the fluxless solder joints was similar to that obtained by conventional flux-based soldering. The results of the present study clearly demonstrate the potential for using ultrasonic soldering as a fluxless joining technology in electronics packaging applications requiring structural integrity of the joint.

### 9:20 AM

**OSP PCB Via Hole Crack Effect Factors Analysis and Improvement:** *Xie Na*<sup>1</sup>; Park ChangYong<sup>1</sup>; Jin Xing<sup>1</sup>; Chung Won Seok<sup>1</sup>; Guo Shi Da<sup>1</sup>; <sup>1</sup>Samsung Electronics(Suzhou) Semiconductor Co., Ltd.

OSP(Organic Solderability Preservative) PCB(Printed Circuit Board) has been widely used for its preferable character and more competitive cost. In the field

of semiconductor, OSP has taken place of ENIG (Electroless Nickel/Immersion Gold) gradually. However, because of the process difference between ENIG and OSP, OSP PCB is prone to cause via hole crack, it is a headache problem puzzled us very much which brings us and our customers many reliability troubles. In this paper, through thermal cycling test, analyze the defect samples and contrast the structure difference for OSP & ENIG, to find reasons why OSP PCB via hole crack. Another purpose of this paper is by the means of DOE to select the optimal parameter for important effect factors, after applying to OSP PCB relative manufacture process, make improvement, reduce OSP via hole crack defect rate and control the quality of our products.

### 9:35 AM

**Transverse Ultrasonic Bonding of Electrodes Coated with Pb-Free Solder between Rigid and Flexible Printed Circuit Board:** *Jong-Bum Lee*<sup>1</sup>; Ja-Myeong Koo<sup>1</sup>; Jong-Gun Lee<sup>1</sup>; Seung-Boo Jung<sup>1</sup>; <sup>1</sup>Sungkyunkwan University

Recently, electrical and electronic equipment manufacturers have shown more interest in the development of electrical and mechanical bonding techniques for electrodes between a flexible printed circuit board (FPCB) and a rigid PCB (RPCB). The transverse ultrasonic bonding has been used for connecting the electrodes between RPCB and FPCB. There are attractive aspects that are rapid, low temperature and environmentally friendly process. However, there are many voids and un-bonded areas that have caused the reliability problems. Pb-free solder on the electrodes of the FPCB was melted and reacted with those of RPCB by ultrasonic vibration at optimized bonding condition. Thermal cycle, high temperature storage and high temperature/humidity test was evaluated to understand if there was vulnerability. Cross-section features in a bonding interface were also inspected by using a high resolution transmission electron microscope.

### 9:50 AM

**Developing of Sn-Bi Eutectic Alloy Soldering Behavior by Al Addition:** *Huseyin Adanir*<sup>1</sup>; <sup>1</sup>New Mexico Tech.

Sn-Al eutectic added Sn-Bi eutectic-based alloy was investigated on soldering of Cu-Cu components. Sn-Bi eutectic alloyed with Sn-Al eutectic at 25, 50 or 75 weight percentages. Al amount was increased 1-to-3 weight percentages in final compositions of three alloy samples. X-ray diffraction (XRD), differential scanning calorimeter (DSC), metallography and hardness testing were used to characterize the solder alloys. The joining of Cu-to-Cu substrates was investigated at 300, 350 and 400°C. The specimens were successfully soldered in a butt joint configuration and four-point bend tests were applied to determined soldered joint strength. The solder alloy containing eutectic-eutectic composition in weight percentages 14.5Bi+82.5Sn+3Al and soldered at 350°C performed highest joint value, as 72 MPa, among solder alloys. XRD and Scanning Electron Microscopy (SEM) were used to characterize the fracture surfaces after the four-point bend tests.

### 10:05 AM

**Effect of Rare Earth Addition on Physical and Mechanical Properties of Sn-Bi-Ag Lead-Free Solders:** *Miguel Neri-Flores*<sup>1</sup>; Alberto Martinez-Villafañe<sup>1</sup>; Caleb Carreño-Gallardo<sup>1</sup>; <sup>1</sup>CIMAV, S.C.

The effect of rare earth element addition (Nd and Pr) on the Physical and mechanical properties of the Sn-Ag-Bi alloy was investigated, specially the wettability of the evaluated solders through the contact angle measurements, applied on a copper substrate using two different RMA fluxes, with a higher chemical activity. The melting points of the alloys were determined using the Differential Scanning Calorimetry Technique (DSC). The effect of rare earth addition on the microstructure and tensile strength of the alloy Sn-Ag-Bi was investigated. Addition of 0.5 weight percent of rare earth elements Nd and Pr, refines the microstructure of the modified alloy Sn-Ag-Bi, obtaining finer particles of the formed intermetallic compounds, uniformly distributed on the alloy. The Pr addition on the Sn-Ag-Bi alloy increase the tensile strength up to 113 MPa, meanwhile the Nd addition on the alloy increase the tensile strength to 97 MPa.

## 10:20 AM Break

### 10:35 AM

**Effects of Surface Pre-Treatment and Various Bonding Temperatures on Interfacial Toughness of Cu-Cu Direct Bonds:** *Eun-Jung Jang*<sup>1</sup>; Jae-Won Kim<sup>1</sup>; Sarah Pfeiffer<sup>2</sup>; Bioh Kim<sup>2</sup>; Thorsten Matthias<sup>2</sup>; Seungmin Hyun<sup>2</sup>; Hak-Joo Lee<sup>3</sup>; Young-Bae Park<sup>1</sup>; <sup>1</sup>Andong National University; <sup>2</sup>EV Group; <sup>3</sup>Korea Institute of Machinery & Materials

Cu-to-Cu thermo-compression bonds for three dimensional(3D) integrated circuits(ICs) have several advantages such as low electrical resistivity, high EM resistance, and reduced interconnect RC delay. However, the process temperature is limited up to 400° to prevent CMOS devices from being thermally damaged. High temperature bonding is a key bottleneck for 3D ICs applications due to a deadly impact on device reliability. Cu and Ti films were deposited by sputtering on thermally oxidized Si(100) wafers and then the deposited films were bonded by direct Cu-to-Cu thermo-compression bonding for evaluating the effect of the native oxide on the bonding toughness. The bonding toughness will be evaluated as a function of acid cleaning time on Cu surface with varying bonding temperatures. The effect of post-annealing under oxygen and nitrogen environment at 200, 300, 400 and 500°C on the bonding toughness at the Cu bonded interface will be evaluated by four point bending test.

### 10:50 AM

**Microstructure and Mechanical Properties of Density-Matched Particle Reinforced Composite Pb-Free Solder Joints:** *James Lucas*<sup>1</sup>; <sup>1</sup>Michigan State Univ

Mechanical properties of Pb-free solder joints were investigated using nanoindentation testing. Indentation elastic moduli and hardness properties were determined for matrix and intermetallic compounds phases. Functional-gradient particle reinforcement was used to attain better gravity matching with the base solder alloy density. Density matching between the matrix and reinforcement allows for more uniform and consistent particle distribution within the composite solder joint. To better achieve matrix/particle density matching, Cu, Ag and Ni coated particles were introduced into the solder matrix. Indentation creep properties were assessed in localized regions of the solder joint microstructure. The stress exponent, n, associated with secondary creep differs widely with the microstructure features probed. Early investigation of the mechanical properties of density-matched particle composite solder shows promise improved electronic packaging.

### 11:05 AM

**Interfacial Reaction of Sn-Based Solder/Cu System with Zn Addition after Heat Treatment:** *Chi-Yang Yu*<sup>1</sup>; Jeng-Gong Duh<sup>1</sup>; <sup>1</sup>National Tsing Hua Univ

Intermetallic compounds (IMCs), Cu<sub>6</sub>Sn<sub>5</sub> and Cu<sub>3</sub>Sn, usually formed at the interface between Sn-based solders and Cu substrate during reflow. After long time aging, the total thickness of IMCs increased and Kirkendall voids were in Cu<sub>3</sub>Sn layer. Recently, it was reported that addition of minor Zn in Sn-Ag-Cu solder could suppress the growth rate of Cu<sub>6</sub>Sn<sub>5</sub> and Cu<sub>3</sub>Sn. To understand the mechanism of Zn addition in the formation of IMCs, the experimental design was carried out to fabricate Sn-based solder/Cu joint with and without minor Zn addition. After reflow and long time aging, Zn atoms accumulated at the interface between IMCs and Cu substrate, and incorporated into Sn sublattice of Cu<sub>6</sub>Sn<sub>5</sub>. The specific composition and structure of IMCs were obtained with the aid of FE-EPMA and TEM. IMCs growth mechanism was correlated to the microstructure feature. Besides, the mechanical properties of the solder joint with Zn-content was investigated and discussed.

### 11:20 AM

**Characterization of the Effect of Ni-Ti Shape Memory Alloy on Solder Joint Reliability through Modeling and Testing:** *Chia-Yen Tan*<sup>1</sup>; Jeng-Gong Duh<sup>1</sup>; <sup>1</sup>National Tsing Hua Univ

Nowadays, the most common problem that surface mount technology faces is the warpage and the inelastic strain concentration accumulated in the solder joint during thermal cycling due to the mismatch of thermal expansion coefficient between package side and chip side. The NiTi shape memory alloy (SMA) UBM can suppress the inelastic strain in the solder joint. The objective of this research is to investigate how SMA applied in UBM can affect solder joint reliability during thermal cycling. A BGA component with silicon chip, deposited multi layer UBM, SAC305 solder ball, and the adhered PCB side was prepared and employed for thermal cycling test. Meanwhile, a finite element model of the exact component was also set up for simulation of stress and strain distribution

in the solder joint under different temperatures. Cross section observation of fracture in solder joint also provided the direct evidence of SMA effect on the tested component.

### 11:35 AM

**Intermetallic Formations in Rapidly Solidified Pb-Free Solder Bonds Formed via the Solder Jet Bonding Technique:** John Wagner<sup>1</sup>; Peter Ladwig<sup>1</sup>; Douglas Riemer<sup>1</sup>; Galen Houk<sup>1</sup>; <sup>1</sup>Hutchinson Technology

The majority of the research published on Pb-free solders is concerned with BGA or other applications where the reflow time allows significant solder to pad reaction time. The hard disk drive industry predominately uses solder jet bonding to electrically connect the read/write sensor. This technique does not use flux and has cooling times on the order of milliseconds. Therefore, the intermetallic formation is highly non-equilibrium and is localized near the pad interface. Surface finish thicknesses and compositions have a significant influence on the intermetallic phases and morphologies that are formed. The intermetallic microstructure, along with voids, can significantly impact joint reliability. This study highlights unique intermetallic formations that occur with rapid solidification and probes how these are influenced by underlying pad metallization. From this understanding, recommendations for ideal surface finishes for solder jet bonding can be made.

### 11:50 AM

**Reliability Examination of Mixed Assemblies:** *Rishi Kaila*<sup>1</sup>; Doug D. Perovic<sup>1</sup>; <sup>1</sup>University of Toronto

Two problems have become apparent in the use of Pb-free solders. First, suppliers of electronic components are producing RoHS compliant versions of some area array components with only certain Pb-free solder balls. In use, these may be mixed in forming a joint with solder paste of a different composition, thereby forming a joint with an altered microstructure with unknown properties. Second, it has been found that the new Pb-free solders are susceptible to failure under impact loading conditions. Metallographic samples will be made and their microstructure examined under the optical and scanning electron microscope. Microhardness characteristics and the effect of ageing on microstructure will also be examined. This study will allow choosing the parameters for successful reflow and rework processes and provide industrial guidance on how to manage through the issues and concerns with incorporating new components in Pb-free assemblies.

## Peirce-Smith Converting Centennial Symposium: Injection Techniques, Modeling and Process Control

Sponsored by: The Minerals, Metals and Materials Society, TMS Extraction and Processing Division, TMS: Pyrometallurgy Committee  
Program Organizer: Joël Kapusta, Air Liquide

Tuesday AM

Room: 2009

February 17, 2009

Location: Moscone West Convention Center

*Session Chairs:* William Imrie, Bechtel Corp; Albert Wraith, A.E. Wraith

### 8:30 AM Keynote

**Peirce-Smith Converting: Another 100 Years?:** Thomas Price<sup>1</sup>; Cameron Harris<sup>2</sup>; Skip (I.E.) Hills<sup>2</sup>; Wayne Boyd<sup>3</sup>; Albert Wraith<sup>4</sup>; <sup>1</sup>TKTV Technologies; <sup>2</sup>Worley Parsons M&M Toronto; <sup>3</sup>Worley Parsons Canada; <sup>4</sup>Retired

Most Peirce-Smith converters inject air through tuyeres, with nitrogen representing the majority of gas passing through the process. The nitrogen controls the temperature of the vessel by carrying away heat from the reactions, both globally and locally at the tuyere tip. However, nitrogen adds energy to the bath and contributes to splashing and limits the blowing rate. High oxygen smelting has made streams of gas containing high concentrations of sulphur dioxide commonplace, which can be used to substitute SO<sub>2</sub> for nitrogen and drastically changes Peirce-Smith converting (and all other smelting/ converting processes as well). Less SO<sub>2</sub> is required to carry away the same quantity of heat, which allows higher concentrations of oxygen and leads to the possibility of increased production. The paper investigates this substitution, its impact on converter productivity, and on the remainder of the plant.

9:00 AM

**Technology and Operational Improvements in Tuyère Punching, Silencing, Pyrometry and Refractory Drilling Equipment:** *Michael Marinigh<sup>1</sup>*; <sup>1</sup>Heath & Sherwood, Ltd.

Increased safety requirements, higher operational costs, greater environmental restrictions, and new competitive processing techniques are the challenges smelter operators must confront in order to remain economically viable. In converting furnaces which have tuyères such as the Noranda Reactor and the Teniente, Peirce-Smith and Hoboken converters, efficient tuyère line management is critical to optimizing blowing rates, increasing refractory life, and improving safety. This paper will describe recent improvements made to equipment used for tuyère punching, tuyère silencing, tuyère pyrometry and refractory drilling of tuyères and how the proper application of the equipment can lead to operational and safety improvements.

9:20 AM

**Increasing Capacity and Productivity in the Metals Markets through Pneumatic Conveying and Process Injection Technologies:** *Mark Coleman<sup>1</sup>*; Gavin Money<sup>1</sup>; <sup>1</sup>Clyde Materials Handling Ltd

Clyde Materials Handling is an established customer-driven solutions provider, which utilizes its knowledge, expertise and technologies to transform the production processes of its customers, who operate in the ferrous and non-ferrous metals industries. With over 30 years experience in the process improvement industry, Clyde Materials Handling has helped their global customer base transform the way in which they operate their processes, which has enabled them to generate sustainable economic benefit and maintain their positions as leaders in their respective markets. Clyde Materials Handling has supported operators within the metals market by developing and deploying pneumatic conveying and pneumatic injection technologies. These environmentally supportive and sustainable solutions have been used to transport raw materials within operating facilities, from storage to silo, as well as injecting these materials directly into the heart of production processes. Clyde Materials Handling has worked closely with their customers, such as Codelco in Chile, where their pneumatic solutions have been used to inject a consistent, pulseless and accurate flow of copper concentrate into a bath smelter, which has helped to fuel the operational capacity, availability and productivity. This paper will discuss and highlight the ways in which pneumatic injection technologies, created by Clyde Materials Handling, and applied in partnership with their customers, have helped to improve the operational performance of the production processes of operators across the non-ferrous metals markets with specific reference to applications in the Peirce Smith Converter. Clyde Materials Handling has applications injecting Electronic Scraps, Dusts, Reverts, and other additives to the Peirce Smith Converter. They also have experience of modified PS Units used for Slag Cleaning. There experience with the Codelco Teniente Converter is also directly related to this area of operation.

9:40 AM

**Decision-Making Software for the Incremental Improvement of Peirce-Smith Converters:** *Alessandro Navarra<sup>1</sup>*; Joël Kapusta<sup>2</sup>; <sup>1</sup>École Polytechnique de Montréal; <sup>2</sup>Air Liquide Canada

The cost-modeling software introduced by Ng et al. in 2005 [1] has been extended to consider the remelting of copper scrap and revert. The original model evaluated the operational costs of a Peirce-Smith converter; algebraic relationships were implemented with arrays (to represent matrices, vectors and scalar ratios). The new software brings flexibility to the underlying thermochemical balances, by using linked-lists instead of arrays. It is now possible to consider the blending of several feeds, including scrap and revert. The software computes the length of the converting cycle from the blowing capacity and the times required for other operations (charging, skimming and idle time). Downtime, labor, and materials for converter lining repair are also considered. The software is easily extended to examine the costs of alternative operating strategies or injection technologies such as high-pressure, shrouded injection. The cost benefits of changing operating procedures and technology are demonstrated through example calculations.

10:00 AM Break

10:20 AM

**Advanced Metallurgical Modeling of Ni-Cu Smelting at the Xstrata Nickel's Sudbury Smelter:** *Nagendra Tripathi<sup>1</sup>*; Pascal Coursol<sup>1</sup>; David Tisdale<sup>2</sup>; Phillip Mackey<sup>1</sup>; <sup>1</sup>Xstrata Process Support; <sup>2</sup>Xstrata Nickel

Xstrata Nickel's Sudbury smelter operation is based on fluid bed roasting of Ni-Cu sulphide concentrate, followed by electric furnace reductive smelting and Peirce-Smith converting to produce a Bessemer matte for electro refining, along with sulphuric acid produced from smelter gas. While the site dates back to the 1930s, the present smelter configuration has been operational since 1978, and currently has a nominal capacity of about 67,000 tpy of contained nickel and is investigating options to expand in future up to 85,000 tpy. As part of a review of plant capacity options, a new metallurgical model of the plant was developed in order to examine a number of processing alternatives. Based on the METSIM™ platform, the present model includes the ability to examine the impact of a number of plant parameters on potential plant performance including; for example, the following: percent of sulphur elimination in roasting, matte grade, degree of matte metallization, temperature, coke requirements, sulphuric acid production, CO<sub>2</sub> emissions and overall energy requirements. The process model also includes a number of special features adopted; for example, approaches to effectively model the complex Ni-Cu-Co-Fe-S-O matte system. This paper provides a description of the model and gives an overview of the results. As well as presenting the results of the present study, the applicability of this modeling approach to pyrometallurgical systems in general is also briefly discussed in the paper.

10:40 AM

**A Dynamic Simulation for the Validation Tests of the Codelco-Chile Continuous Converting Process:** Carlos Caballero<sup>1</sup>; Alex Moyano<sup>1</sup>; Pedro Morales<sup>1</sup>; Claudio Toro<sup>2</sup>; *Hugo Jara<sup>2</sup>*; Leandro Guzmán<sup>2</sup>; Rodrigo Díaz<sup>2</sup>; <sup>1</sup>Codelco; <sup>2</sup>IM2-Codelco

During 2007, Codelco-Chile carried out industrial tests to validate the Continuous Converting Process in the Teniente Converter of the Codelco Norte smelter. For planning and starting up the tests, a predictive, analytical and dynamic model was developed to support operational decisions. The dynamic model was developed using the METSIM® platform and dynamic data exchange (DDE) to operate smoothly with MS Excel®. The main feature of this real-time model was the on/off-line ability to work and gather data from either the smelter's PI system® or database, and simulate the operation with or without scheduled events and controls. The main model development aspects, which include thermodynamics, metallurgical and kinetic considerations, slag-type and on-line mass and heat balances of the process, as well as the successful validation of the model, are presented and discussed in the present paper.

11:00 AM

**Applications of Thermo-Chemical and Thermo-Physical Modeling in the Copper Converter Industries:** *Pengfu Tan<sup>1</sup>*; <sup>1</sup>Xstrata Copper

A thermo-chemical model of the copper P-S converter and a viscosity model for the converter slag have been developed to predict the behavior of magnetite in the converter slag, amounts of slag and matte, compositions of slag and matte, volume of the bath, bath temperature, slag blow endpoint determination, SEMTECH OPC signals, and the viscosity of converter slags. The predictions of bath temperature, slag and matte compositions, and magnetite content in the slag have been validated by the industrial data. The effects of fluxing strategy, returns and skim charges, oxygen enrichment, and temperature on the magnetite formation in the slag have been predicted and discussed. The effect of oxygen potential, SiO<sub>2</sub>/Fe in slag, detection of slag blow endpoint, and temperature on Fe<sub>3</sub>O<sub>4</sub> content in converter slag, slag viscosity, liquidus temperature of converter slag and skimming operation has been modeled and discussed as well. Some applications of the industrial operations have been presented.

11:20 AM

**Minimum Numerical Model of a Peirce-Smith Converter:** Adriana Cervantes-Clemente<sup>1</sup>; *Cesar Real-Ramirez<sup>1</sup>*; Manuel Palomar-Pardave<sup>1</sup>; Luis Hoyos-Reyes<sup>1</sup>; Marco Gutierrez-Villegas<sup>1</sup>; Jesus Gonzalez-Trejo<sup>1</sup>; <sup>1</sup>Universidad Autonoma Metropolitana - Azcapotzalco

Recent improvements on Peirce-Smith Converters (PSC) have combined numerical and physical simulations. However, most of the physical simulations have been carried out in cold-water models with only one tuyere. Several authors have proved that 2D numerical simulations do not reproduce the hydrodynamic



behavior observed in physical simulations. On the other hand, most of the 3D numerical models have used a PSC thin slice with only one tuyere, but symmetric boundary conditions on the virtual walls have been imposed in order to reproduce the behavior of the whole converter. Therefore, there is no coincidence with the rigid walls of the physical models. The aim of this work is to quantify the effect of the virtual walls boundary conditions of a PSC thin slice and to determine the minimum number of tuyers to characterize the fluid flow behavior of the entire converter.

## Phase Stability, Phase Transformations, and Reactive Phase Formation in Electronic Materials VIII: Session III

**Sponsored by:** The Minerals, Metals and Materials Society, TMS Electronic, Magnetic, and Photonic Materials Division, TMS: Alloy Phases Committee  
**Program Organizers:** Chih-ming Chen, National Chung-Hsing University; Srinivas Chada, Medtronic; Sinn-wen Chen, National Tsing-Hua University; Hans Flandorfer, University of Vienna; A. Lindsay Greer, University of Cambridge; Jae-ho Lee, Hongik University; Daniel J. Lewis, Rensselaer Polytechnic Institute; Kejun Zeng, Texas Instruments; Wojciech Gierlotka, AGH University of Science and Technology; Yee-wen Yen, National Taiwan University of Science and Technology

Tuesday AM                      Room: 2022  
 February 17, 2009              Location: Moscone West Convention Center

**Session Chairs:** Kejun Zeng, Texas Instruments Inc; Albert Tzu-Chia Wu, National Central University

### 8:30 AM Invited

**Dynamic Reactive Wetting of Sn-Ag-Cu Solder Alloys on Cu Substrates Coated by Ni and Au:** Joonho Lee<sup>1</sup>; Jong-Min Kim<sup>2</sup>; <sup>1</sup>Korea University; <sup>2</sup>Chung-Ang University

In the electronic components and device packaging process, the conductor Cu surface is generally coated by Au and Ni. Au coating is applied to protect the oxidation of the Cu surface and enhance the solderability, while Ni coating is applied as a diffusion barrier between the solder alloy and the Cu substrate to restrict the formation and growth of the intermetallic compound. Dynamic reactive wetting characteristics of Sn-Ag-Cu alloys are related to the properties of the coating materials. This presentation will report the observation results on the reactive wetting behavior of Sn-Ag-Cu alloys on Cu substrates coated by Ni and Au in millisecond scale.

### 8:50 AM Invited

**Phase Equilibria for Understanding the Reaction between Sn-Based Solders and Ni(P) Substrates:** Clemens Schmetterer<sup>1</sup>; Herbert Ipsen<sup>1</sup>; Simona Delsante<sup>2</sup>; Gabriela Borzone<sup>2</sup>; <sup>1</sup>University of Vienna; <sup>2</sup>Università degli Studi di Genova

Ni(P) coated substrates are widely used in the electronics industry due to their ease of production and their favorable properties. In order to understand the reactions that occur between such a substrate and Sn-based solders, knowledge on the phase equilibria is important, because ternary Ni-P-Sn compounds are brittle and detrimental to the joint quality. The ternary alloy system Ni-P-Sn and its sub-systems have thus been the subject of extensive investigations. Five ternary compounds are known to exist in the Ni-rich corner. The related phase equilibria are shown as a consistent set of isotherms, isopleths and a liquidus surface. Emphasis will be placed on the thermal behavior. Due to the experimental difficulties caused by phosphorus, CALPHAD modelling of this system is desirable. Therefore enthalpies of formation of binary Ni-P and ternary Ni-P-Sn compounds have been determined by Direct Reaction Calorimetry.

### 9:10 AM

**Effect of Cu Lead-Frame Microstructure on Solder/Cu Interfacial Reaction and Soldering Wettability:** Huang Kuan Chih<sup>1</sup>; Hsiao Yu Hsiang<sup>1</sup>; Lee Chih Ming<sup>1</sup>; Liu Cheng Yi<sup>2</sup>; Shieu Fuh Sheng<sup>1</sup>; <sup>1</sup>National Chung Hsing University; <sup>2</sup>National Central University

Cu, with a high thermal conductive property, is used as Lead Frame (LF) for high power IC bond pad. The wettability and interfacial reactions of solders highly affect the reliability of power IC on Cu LF. Our preliminary results show that the solder wettability significantly depend on the microstructure of Cu LF, such as, preferred orientation of Cu grains, and Cu grain size. In this study, the correlation between the soldering wettability and interfacial reaction on Cu

LF and the microstructure of Cu LF was investigated. The Cu LF having (220) preferred orientation show the best wettability, comparing to other preferred orientations. Also, we found microstructure of Cu LF greatly influences the solder/Cu interfacial reaction, for example, Cu dissolution during solder reflow. Different grain size and grain orientation of Cu LF materials were investigated. The correlation between soldering interfacial reaction and Cu LF microstructure will be present in this talk.

### 9:25 AM

**Interfacial Reactions on Pb-Free Solders with Pd/Au/Ni/Cu and Pd/Au/Ni/Brass Multilayer Substrates:** Yee-Wen Yen<sup>1</sup>; Yang-Kai Fang<sup>2</sup>; Chiapng Lee<sup>2</sup>; <sup>1</sup>Graduate Institute of Materials Science and Technology, National Taiwan University of Science and Technology; <sup>2</sup>Department of Chemical Engineering

Interfacial reactions on Sn, Sn-3.0Ag-0.5Cu, Sn-0.7Cu, Sn-58Bi and Sn-9Zn with Pd/Au/Ni/Cu and Pd/Au/Ni/Brass at 240-270° for 20 minutes to 20 hours were investigated. The experimental results present that the (Ni,Cu)<sub>3</sub>Sn<sub>4</sub> phase converted to the (Cu,Ni)<sub>6</sub>Sn<sub>5</sub> phase and the Cu<sub>3</sub>Sn was formed in the Sn/Pd/Au/Ni/Cu. In Sn-3.0Ag-0.5Cu/Au/Pd/Ni/Cu and Sn-0.7Cu/Au/Pd/Ni/Cu, the (Cu,Ni)<sub>6</sub>Sn<sub>5</sub> and Cu<sub>3</sub>Sn phase were observed. Only the Ni<sub>3</sub>Sn<sub>4</sub> phase was observed in the Sn-58Bi/ Pd/Au/Ni/Cu. In the Sn-9Zn/Au/Pd/Ni/Cu, the Pd<sub>2</sub>Zn<sub>9</sub> and NiZn phases were formed. The Pd<sub>2</sub>Zn<sub>9</sub>, NiZn, and Ni<sub>5</sub>Zn<sub>21</sub> phases were formed for 4 hours later. The (Cu,Ni)<sub>6</sub>Sn<sub>5</sub> and CuZn phase were found in Sn/Au/Pd/Ni/Brass, Sn-3.0Ag-0.5Cu/Au/Pd/Ni/Brass, and Sn-0.7Cu/Au/Pd/Ni/Brass. In the Sn-58Bi/Au/Pd/Ni/Brass, only the Ni<sub>3</sub>Sn<sub>4</sub> phase was observed. However, the (Ni,Cu)<sub>3</sub>Sn<sub>4</sub>, (Cu,Ni)<sub>6</sub>Sn<sub>5</sub>, and CuZn phases were formed after 8 hours later. In the Sn-9Zn/Au/Pd/Ni/Brass, the Pd<sub>2</sub>Zn<sub>9</sub> and Ni<sub>5</sub>Zn<sub>21</sub> phases were formed. Aging for 20 hours, the CuZn<sub>5</sub>, Pd<sub>2</sub>Zn<sub>9</sub>, Ni<sub>5</sub>Zn<sub>21</sub>, and Cu<sub>5</sub>Zn<sub>8</sub> phases were formed.

### 9:40 AM

**The Growth of Intermetallic Compounds between SnAgBiIn Pb-Free Solders and Copper Substrates during Reflow and Solid State Aging:** Albert Wu<sup>1</sup>; Ming-Hsun Chen<sup>2</sup>; <sup>1</sup>National Central University; <sup>2</sup>National Taipei University of Technology

SnAgBiIn solder systems are one of the Pb-free candidates to replace eutectic SnPb solder. The addition of indium can lower the melting point of the alloy but will not reduce the mechanical strength of the joints. In this study, liquid solders were reflowed on Cu substrates at different temperatures and times. In addition, the solder systems were solid state aged for up to 40 days. The interfacial reactions between the SnAgBiIn solders and Cu substrates of the systems were investigated; the composition of the compounds was studied by EPMA. In this paper, the kinetics of the growth of the intermetallic compounds is discussed.

### 9:55 AM

**Volume Effect on the Solid-State Reaction between Sn-Ag-Cu Solders and Ni:** Su-Chun Yang<sup>1</sup>; C. Robert Kao<sup>1</sup>; <sup>1</sup>National Taiwan Univ

With the continuous push for device miniaturization, solder volume effect in electronic devices should be taken into account. In our previous study, strongly volume effect during soldering had been reported. In this study, solid state reaction would be considered. Sn<sub>3</sub>Ag<sub>x</sub>Cu (x = 0.3, 0.5 and 0.7 wt.%) were soldered on Ni and aged at 160°C for 1000 hrs. Three different sizes of solder spheres (300, 500, and 760 micrometer diameter) were used. The study revealed that the type of intermetallic compound transformed from (Cu,Ni)<sub>6</sub>Sn<sub>5</sub> to (Ni,Cu)<sub>3</sub>Sn<sub>4</sub> as the residual Cu concentration in solder dropped below 2 wt.%. In addition, during soldering (Cu,Ni)<sub>6</sub>Sn<sub>5</sub> spalled massively from the interface under certain conditions, including the smaller joints and those with lower Cu concentration. However, the spalling was not observed during aging. The reason for these observations would be discussed in this talk.

### 10:10 AM Break

### 10:30 AM Invited

**Detailed Phase Evolution of Phosphorous-Rich Layer and Formation of Ni-Sn-P Compound in SnAgCu/Electroplated Ni-P Solder Joint:** Yung-Chi Lin<sup>1</sup>; Kai-Jheng Wang<sup>1</sup>; Jeng-Gong Duh<sup>1</sup>; <sup>1</sup>National Tsing Hua Univ

Interfacial microstructure of Sn-3Ag-0.5Cu/Ni-P with various phosphorous contents was investigated by TEM and FE-EPMA. It was revealed that as the Ni-Sn-P compound was formed between the solder matrix and Ni-P UBM, the conventionally so-called phosphorous-rich layer was transformed to a series of layer compounds, including Ni<sub>3</sub>P, Ni<sub>12</sub>P<sub>5</sub> and Ni<sub>2</sub>P. The relationship between Ni-Sn-P formation and evolution of P-rich layers was probed by electron microscopic characterization with the aid of the phase diagram of Ni-P. It was

also demonstrated that the thickness of Ni-P UBM would affect the Ni-Sn-P formation. On the basis of the TEM micrograph, selected area diffraction pattern as well as the FE-EPMA results, the detailed phase evolution of P-rich layers in the SnAgCu/Ni-P joint was revealed and proposed. Moreover, in consideration of the mechanical property for the joint, Ni-Sn-P phase formation and fabrication feasibility of Ni-P UBM, the phosphorous content and suitable thickness of Ni-P UBM were discussed.

#### 10:50 AM Invited

##### **Effect of Cu in SnAgCu Solder on Interfacial Reliability of Solder Joints:** *Kejun Zeng<sup>1</sup>; <sup>1</sup>Texas Instruments Inc*

Effect of Cu content in solder is studied on the interfacial reliability of SnAgCu solder joints on Ni/Au plated pads. Solder ball composition was Sn3.0Ag0.5Cu. Cold ball pull test was performed to assess the BGA joint reliability after ball attachment process and also after preconditioning reflows. Test after BGA assembly (one reflow) did not generate any interfacial failure, but after the three more reflows of preconditioning many joints showed the failure mode of interfacial cracking by pull test. Cracking occurred between IMC layers of Cu<sub>6</sub>Sn<sub>5</sub> and Ni<sub>3</sub>Sn<sub>4</sub>. Formation of the bilayer IMC structure is explained from the perspective of interfacial equilibrium. Its effect on interfacial reliability of solder joints is discussed. It is suggested that, if the Cu content in the SnAgCu solder is reduced to a certain level, formation of the Cu<sub>6</sub>Sn<sub>5</sub> layer can be avoided and thus the interfacial reliability is improved.

#### 11:10 AM

##### **Nano-Sized Induced Low Temperature Alloying Behaviour in Interconnection Applications:** *Tzu-Hsuan Kao<sup>1</sup>; Jenn-Ming Song<sup>2</sup>; In-Gann Chen<sup>1</sup>; Weng-Sing Hwang<sup>1</sup>; Teng-Yuan Dong<sup>3</sup>; <sup>1</sup>National Cheng Kung University; <sup>2</sup>National Dong Hwa University; <sup>3</sup>Kaohsiung Medical University*

A concept of nanosize induced liquid-solid reaction and thus interdiffusion behavior between NPD (nanoparticle deposition) and metallic substrates has been proposed recently. The supercooled liquid reacts with the substrate and provides a fast atomic mobility, which results in low temperature alloying between NPD and substrate materials. Even though the reaction duration is very short, this liquid-solid reaction has a considerable effect on the mutual interdiffusion between the NPD and substrates, leading to a firm bonding. This study investigates the low temperature alloying behavior in binary and ternary systems. Several kinds of NPs and substrate materials are chosen to investigate the effect of the differences in lattice mismatch and electronegativity between the elements. Experimental results of elemental distribution and phase identification by XPS and Nano-AES, as well as the evaluation of mechanical properties such as adhesion strength and nanoindentation, will be given in this presentation.

#### 11:25 AM

##### **Interfacial Reactions in the Sn-9Zn+Cu Solder with Ni Substrate:** *Wei-Kai Liou<sup>1</sup>; Yee-wen Yen<sup>1</sup>; <sup>1</sup>Graduate Institute of Materials Science and Technology, National Taiwan University of Science and Technology*

This study investigates the interfacial reactions between (Sn-9Zn)+xCu/Ni systems. The sequences of IMC evolutions in the (Sn-9Zn)+xCu/Ni system aged at 255° for 1-3 hours were: (i) Ni<sub>5</sub>Zn<sub>21</sub> and Zn phases at Sn-9Zn/Ni couples; (ii) Cu<sub>5</sub>Zn<sub>8</sub>, Cu<sub>5</sub>Zn<sub>8</sub> phases, as x (the Cu content) was 1 wt%; (iii) (Ni<sub>3</sub>Zn<sub>3</sub>)<sub>3</sub>Sn<sub>4</sub> and Cu<sub>5</sub>Zn<sub>8</sub> phases, as x was 4 wt%; (iv) (Cu<sub>3</sub>Ni)<sub>6</sub>Sn<sub>5</sub> and Cu<sub>5</sub>Zn<sub>8</sub> phases, as x was 7 wt%, and (v) Cu<sub>6</sub>Sn<sub>5</sub> and Cu<sub>5</sub>Zn<sub>8</sub> phases at Sn-9Zn+10wt%Cu/Ni couples. As the reaction time was prolonged from 5 to 24 hour, the Cu<sub>5</sub>Zn<sub>8</sub> phase would convert to the (Cu<sub>5</sub>Zn<sub>8</sub>+Ni<sub>5</sub>Zn<sub>21</sub>) mixture at interface, as x was 1 wt%. When 10 wt% Cu was added into the Sn-9Zn solder, the (Cu<sub>5</sub>Zn<sub>8</sub>+Cu<sub>6</sub>Sn<sub>5</sub>) replaced the Cu<sub>5</sub>Zn<sub>8</sub> phase in the solder. Experimental results indicate that IMCs formation in (Sn-9Zn)+xCu/Ni systems dramatically changes with various reaction time and Cu contents.

#### 11:40 AM

##### **Wetting Properties and Interfacial Reactions of Cu<sub>5</sub>Zn<sub>8</sub>-Bearing Pb-Free Solders on the Cu Substrate by Mechanical Alloying:** *Inyu Jung<sup>1</sup>; Moon Gi Cho<sup>1</sup>; Hyuck Mo Lee<sup>1</sup>; <sup>1</sup>KAIST*

Cu<sub>5</sub>Zn<sub>8</sub>-bearing solders are proposed to enhance the wetting properties of the Zn-doped solder alloys. The Cu<sub>5</sub>Zn<sub>8</sub>-bearing solder powders with a diameter of 50-70 μm were fabricated successfully by the mechanical alloying process in which the milling time, the rotational speed and the ball-to-powder weight ratio were controlled. Their composition was identified as Sn-0.31Cu-0.48Zn (in wt.%) by the inductively coupled plasma atomic emission spectroscopy (ICP-AES). After making the powders into a paste with a rosin activated type flux,

the wetting angles of the Cu<sub>5</sub>Zn<sub>8</sub>-bearing solder paste on the Cu substrate were compared with those of Sn-0.31Cu-0.48Zn and Sn-0.7Cu bulk solder alloys. As a result, the wetting properties of the Cu<sub>5</sub>Zn<sub>8</sub>-bearing solder paste were better than the bulk Sn-0.31Cu-0.48Zn and similar with the bulk Sn-0.7Cu. The reason of the enhanced wetting properties is explained through thermodynamic calculations, and interfacial reactions with Cu substrates are also discussed.

## Recent Advances in Thin Films: Metal Films and Integration Schemes

Sponsored by: The Minerals, Metals and Materials Society, TMS Electronic, Magnetic, and Photonic Materials Division, TMS: Thin Films and Interfaces Committee  
Program Organizers: Nugehalli Ravindra, New Jersey Institute of Technology; Gregory Krumbick, Argonne National Laboratory; Choong-un Kim, University of Texas; Narsingh Singh, Northrop Grumman, ES

Tuesday AM

Room: 3011

February 17, 2009

Location: Moscone West Convention Center

*Session Chairs:* Bhushan Sopori, National Renewable Energy Laboratory; Nugehalli Ravindra, New Jersey Institute of Technology

#### 8:30 AM Introductory Comments

#### 8:35 AM

##### **Study of Surface Electromigration in Au Thin Films:** *Liangshan Chen<sup>1</sup>; N. Michael<sup>1</sup>; C. U. Kim<sup>1</sup>; U. Chul<sup>2</sup>; J. S. Cho<sup>2</sup>; J. T. Moon<sup>2</sup>; <sup>1</sup>Department of Materials Science and Engineering, The University of Texas at Arlington; <sup>2</sup>MK Electron Co. Ltd*

The mechanism of electromigration in Au thin films is one of the most illusive subjects in the related field primarily because of vastly differing results presented by previous studies. While some studies present that electromigration in Au occurs by grain boundary migration in the direction of electrons, others state that it occurs by surface in the opposite direction. With technical importance of electromigration mechanism, especially for Au wirebond and interconnects used in electronic devices, it is important to understand how such varying results are possible. In our study, we investigate the nature of electromigration using "cross-strip" configuration. Our study finds that electromigration of Au occurs in two routes, grain boundaries and surface, with different directionality. This paper presents the results leading to such a conclusion and discusses their technological impacts.

#### 8:55 AM

##### **Texture Control during Growth of Copper Thin Films: Atomic-Scale Simulations:** *Moneesh Upmanyu<sup>1</sup>; Haiyi Liang<sup>2</sup>; Hanchen Huang<sup>3</sup>; <sup>1</sup>Colorado School of Mines; <sup>2</sup>Harvard University; <sup>3</sup>Rensselaer Polytechnic Institute*

We have performed molecular dynamics simulations of the <111>-<110> texture competition during low energy copper film growth. For an initially bi-textured thin film, we find that the competition can be controlled by optimizing three accessible deposition conditions: in-plane strain, deposition rate, and angle of deposition. The variables modify the interplay between thermodynamic and surface kinetic anisotropies in copper which directly affect the texture evolution. The evolving surface morphology is also sensitive to the form and rate of texture evolution. The control paradigm should be applicable for thin film texture control in metallic thin films in general.

#### 9:15 AM

##### **A Novel Method for Parallel Assembly of Microcomponents:** *Nugehalli Ravindra<sup>1</sup>; Rene Rivero<sup>1</sup>; Michael Booty<sup>1</sup>; Anthony Fiory<sup>1</sup>; <sup>1</sup>New Jersey Institute of Technology*

Pick and Place is the current industry standard for the heterogeneous assembly of microcomponents. However, because Pick and Place is a serial processing method, which requires significant expenditures of resources, it is not the most efficient way to assemble devices. Several alternative and parallel techniques have been proposed but those methods are limited by geometric, material, and statistical issues. The method outlined in this paper will be shown to circumvent the drawbacks that plague existing parallel assembly techniques; it represents a versatile and scalable method which is able to conform to any manufacturing situation and to produce a 100% yield.

## Recycling of Electronic Wastes: Hydrometallurgical Recycling

Sponsored by: The Minerals, Metals and Materials Society, TMS Extraction and Processing Division, TMS Light Metals Division, TMS Materials Processing and Manufacturing Division, TMS: Recycling and Environmental Technologies Committee  
 Program Organizers: Lifeng Zhang, Missouri University; Fay Hua, Intel Corp; Oladele Ogunseitan, University of California, Irvine; Gregory Krumdick, Argonne National Laboratory

Tuesday AM Room: 2024  
 February 17, 2009 Location: Moscone West Convention Center

Session Chairs: Lifeng Zhang, Missouri University Science Technology; Christina Meskers, Umicore

### 8:30 AM Introductory Comments

#### 8:35 AM

**Extraction and Separation of Metals Using LIX 84 and D2EHPA Diluted in Kerosene from Sulfate Solution:** *Vinay Kumar*<sup>1</sup>; Manoj Kumar<sup>1</sup>; Manis Jha<sup>2</sup>; Jae-chun Lee<sup>2</sup>; <sup>1</sup>National Metallurgical Laboratory, Jamshedpur, India; <sup>2</sup>Korea Institute of Geoscience & Mineral Resources

The disposal of large quantities of electronic scraps generated world wide is causing not only environmental problem but also loss of resources. Therefore, R&D efforts have been made to develop a suitable process for extraction and separation of metals viz. copper, zinc, cadmium and nickel expected from the leaching of e-scraps using solvent extraction process. Different process parameters viz. pH, A/O ratio, contact time, simulation studies to establish stage requirement for extraction in continuous mode etc have been studied to optimise the condition for metals separation. The studies showed selective extraction of copper after iron precipitation from the sulfate leach solution of printed circuit boards containing 1.0 g/L Cu and minor impurities with 2-hydroxy-5-nonylacetophenoneoxime (LIX 84) above pH 2.0 in single stage. A scheme for separation of cadmium, zinc and nickel has also been proposed using di(2-ethylhexyl) phosphoric acid (D2EHPA) under controlled pH of the aqueous solution.

### 8:55 AM Question and Answer Period

#### 9:05 AM

**Metal Recovery from Waste Electrical and Electronic Equipment (WEEE) by Leaching and Electrodeposition IV:** *Geoff Kelsall*<sup>1</sup>; Chun-ye Cheng<sup>1</sup>; Anna Robson<sup>1</sup>; <sup>1</sup>Imperial College London

A novel process is being developed to recover metals from waste electrical and electronic equipment (WEEE) and other secondary sources using acidic aqueous chloride electrolyte. Chlorine is generated at the anode of a membrane-divided electrochemical reactor, absorbed into the solution and used to dissolve metals (Ag, Au, Cu, Pd, Sn, Pb, etc.) from shredded WEEE in an external leach reactor. The metals are electrodeposited at the cathode, enabling their subsequent recovery and refining. Hence, the overall process involves inputting electrical energy to move the metals from WEEE to cathode and, in principle, additionally produces only de-metallised WEEE, for further processing. Finite element models were developed for a packed bed metal leach reactor and the effects computed of particle shape, liquid flow rate and reaction rate coefficients, on metal conversions and efflux chlorine concentrations. Predictions were validated against experimental data; metal conversions >0.9 were achieved in 8 hours.

### 9:25 AM Question and Answer Period

#### 9:35 AM

**Metals Recover of Obsolete Mobile Electronics:** *Viviane Tavares*<sup>1</sup>; Mariana Maioli<sup>1</sup>; Denise Espinosa<sup>1</sup>; *Jorge Tenorio*<sup>1</sup>; <sup>1</sup>Escola Politecnica da Universidade de São Paulo

The technology advance of mobile devices makes consumers of these equipment do more constant exchanges, with this the obsolete devices discarding becomes an environmental problem, due its landfill accumulation. In order to minimize the environmental impacts caused by these equipment there's the recycling necessity of polymers, ceramic and metallic materials. The main goal of this recycling's to study the printed circuit board of device mobile processing through ore treatment in order to recoup copper. Initially were processed printed circuit

in a knives mill, in order to liberate the ferrous material, after that was done the magnetic separation of the reduced residue. With the not magnetic fraction it was done the grain sized analysis and sulfuric acid and hydrogen peroxide leaching analysis. With the chemical analysis results done with the leaching aliquot it was possible to observe that the leaching method with sulfuric acid and hydrogen peroxide presented greater copper recovery

### 9:55 AM Question and Answer Period

#### 10:05 AM Invited

**Recovery of Components and Valuable Metals from Printed Circuit Boards:** *Young Park*<sup>1</sup>; *Robert Gibson*<sup>1</sup>; *Derek Fray*<sup>1</sup>; <sup>1</sup>University of Cambridge

Printed circuit boards, free of iron and aluminium, were submerged in fluoroboric acid, selectively dissolving the solder and allowing the components, in working order, to be harvested. The boards were then shredded and the copper dissolved in ammonia/ammonium carbonate and subsequently electrowon. Aqua regia was used to leach the remaining metals and 95 wt% of the silver, 93 wt% of the palladium and 97 wt% of the gold were recovered. Zinc and nickel were also recovered from the aqua regia solution.

### 10:25 AM Break

#### 10:45 AM

**Recovery of Metals from Electronic Scrap by Hydrometallurgical Route:** *Nikhil Dhawan*<sup>1</sup>; *Vinay Kumar*<sup>2</sup>; *Manoj Kumar*<sup>2</sup>; <sup>1</sup>Punjab Engineering College; <sup>2</sup>NML

Electronic waste is a collective name given to discarded electronic devices such as Television, Cellular Phones and Computers. Among the heterogeneous metals present in the e-waste are the base metals: copper, aluminium, nickel, tin, iron and precious metals: gold, silver and platinum apart from several hazardous and halogens metals. Hence there is a need to recover these metals by recycling and then re-use to meet large amount of metals demand. Hydrometallurgical processing was employed for the recovery of metals from TV PCB. Different lixiviants such as hydrochloric acid, Sulphuric acid, and nitric acid were used to understand the dissolution behavior of copper, iron and lead present in the TV PCB. Effect of increasing concentration of nitric acid was also studied. Selective recovery of tin over 95% in the form of tin oxide was precipitated and was identified by XRD technique. Tin oxide of purity more than 99.9% was obtained.

### 11:05 AM Question and Answer Period

#### 11:15 AM Invited

**Leaching Behaviour of Metals from Waste Printed Circuit Boards (PCBs) in Acidic Medium:** *Manis Jha*<sup>1</sup>; *Jae-chun Lee*<sup>1</sup>; *Nghiem Nguyen*<sup>1</sup>; *Kyoungkeun Yoo*<sup>1</sup>; *Jinki Jeong*<sup>1</sup>; <sup>1</sup>Korea Institute of Geosci & Min Resources

The leaching behaviour of metals from waste printed circuit boards (PCBs) in acidic medium has been reported. The waste PCBs obtained from personal computer (PC) contains Cu, Ni, Fe, Pb, Sn as major metallic constituents and precious metals as minor. Batch experiments were carried out to investigate the leaching behaviour of metals from crushed PCBs in various acidic medium viz. hydrochloric, nitric and sulphuric acids with hydrogen peroxide as additive. Further, studies have been carried out by varying various process parameters viz. temperature, particle size, leaching time, pulp density, acid concentration etc. Lead forms unstable complex with nitric acid during the leaching. Therefore, leaching and precipitation behaviour of Pb with nitric acid was also studied. The obtained leach liquor could be used for the recovery of valuables as metal or salt by electrolysis or crystallization, respectively.

### 11:35 AM Question and Answer Period

#### 11:45 AM

**A Recovery Technology of Ag from Composite Ag-Cu Electronic Wastes:** *Jinhui Li*<sup>1</sup>; *Xinhai Li*<sup>1</sup>; *Daoling Xiong*<sup>2</sup>; *Qiyang Hu*<sup>1</sup>; *Zhixing Wang*<sup>1</sup>; <sup>1</sup>Central South University; <sup>2</sup>Jiangxi University of Science and Technology

Silver is a very important metal used in a wide range of applications. It is necessary to recovery of Ag from electronic wastes for increasing of Ag price and circumstance protection. For separating and recycling Ag from Ag-Cu composite materials, thermodynamic data of reaction is calculated and some experiments have been proceeded with Ag-Cu composite material scraps, time, temperature, nitric-sulfuric mixed acid volume ratio and the volume ration of mixed acid vs. water have been discussed. The results show that the optimization conditions is that nitric-sulfuric mixed acid volume ratio 5:95, volume ration of



mixed acid vs. water 10:1, temperature 55°, time 25min. In the conditions, Ag can be selectively leached from Cu-based composite material, Cu base is not eroded nearly.

#### 12:05 PM Question and Answer Period

### Shape Casting: Third International Symposium: Characterization

Sponsored by: The Minerals, Metals and Materials Society, TMS Light Metals Division, TMS: Solidification Committee, TMS: Aluminum Processing Committee  
Program Organizers: John Campbell, University of Birmingham; Paul Crepeau, General Motors Corp; Murat Tiryakioglu, Robert Morris University

Tuesday AM Room: 2011  
February 17, 2009 Location: Moscone West Convention Center

Session Chairs: Sumanth Shankar, McMaster University; Srinath Viswanathan, University of Alabama

#### 8:30 AM Introductory Comments

##### 8:35 AM

**Oxide Film and Porosity Defects in Magnesium Alloy AZ91:** *Liang Wang*<sup>1</sup>; Hongjoo Rhee<sup>1</sup>; Sergio Felicelli<sup>2</sup>; Adrian Sabau<sup>3</sup>; John Berry<sup>2</sup>; <sup>1</sup>Center for Advanced Vehicular Systems, Mississippi State University; <sup>2</sup>Center for Advanced Vehicular Systems and Mechanical Engineering Department, Mississippi State University; <sup>3</sup>Metals and Ceramics Division, Oak Ridge National Laboratory

Porosity is a major concern in the production of light metal parts. This work aims to identify some of the mechanisms of microporosity formation during the gravity-poured castings of magnesium alloy AZ91. Two graphite plate molds and a ceramic cylindrical mold were selected to produce a wide range of cooling rates. Temperature data during cooling was acquired with type K thermocouples at 60 Hz in two locations of each casting. The microstructure of samples extracted from the regions of measured temperature was then characterized with x-ray computed tomography and optical metallography. The gathered data was analyzed to search for correlations between cooling rate, dendrite arm spacing, pore volume fraction and pore size. The experimental outcomes were compared with simulations performed with a finite element continuum model of dendritic solidification. The results of this study confirm some of the findings observed in similarly cast aluminum alloys.

##### 9:00 AM

**Assessing Casting Quality Using Computed Tomography with Advanced Visualization Techniques:** *Georg Geier*<sup>1</sup>; Joerdis Rosc<sup>1</sup>; Markus Hadwiger<sup>2</sup>; Laura Fritz<sup>2</sup>; Daniel Habe<sup>1</sup>; Thomas Pabel<sup>1</sup>; Peter Schumacher<sup>1</sup>; <sup>1</sup>Austrian Foundry Research Institute; <sup>2</sup>VRVis Research Center for Virtual Reality and Visualization, Ltd

Increasing demand for high quality castings has increased the importance of the use of computed tomography (CT) in the casting industry. The major advantages of computed tomography include its ability to cover the whole sample-volume with respect to apparent differences in density within the object and being able to determine their size and position in three dimensions. The possibility of the detection and quantification of varied casting defects makes it a valuable tool. This paper deals with the possibilities and limits of the use of computed tomography for quality control and assessment in the casting industry from the materials to finished castings. Considerable improvements can be achieved using volume rendering with novel multi-dimensional transfer functions for the visualization of the volume data. In particular the quantification of casting defects will be addressed and compared to standard metallographic procedures and common CT analysis-tools.

##### 9:25 AM

**Reconstruction, Visualization, and Quantitative Characterization of Multi-Phase Three-Dimensional Microstructures of Cast Aluminum Alloys:** Harpreet Singh<sup>1</sup>; *Arum Gokhale*<sup>1</sup>; Yuxiong Mao<sup>1</sup>; Asim Tewari<sup>2</sup>; <sup>1</sup>Georgia Institute of Technology; <sup>2</sup>General Motors Corporation

Serial sectioning technique is well known for reconstruction of three-dimensional microstructures of opaque materials. During the recent years, techniques have also been developed for reconstruction of high fidelity large volume segments

of three-dimensional microstructures using montage serial sections; robot assisted automated acquisitions of montage serial sections are also reported. Nonetheless, the past work of three-dimensional microstructure reconstruction from serial sections is restricted to microstructures containing at the most two phases, or in the multi-phase microstructures, the three-dimensional geometry of only one or two phases is reconstructed. In this contribution, we present three-dimensional reconstruction of multi-phase microstructures of a series of cast Al-alloys containing porosity, Si particles, and numerous intermetallic inclusion phases. All the phases are segmented and separately reconstructed, rendered, and quantitatively characterized in three-dimensions, which clearly brings out the complex three-dimensional morphologies of all phases. The technique is useful for characterization of any multi-phase three-dimensional microstructure.

##### 9:50 AM

**Correlation of Thermal, Tensile and Corrosion Parameters of Zn-Al Alloys with Columnar, Equiaxed and Transition Structures:** Alicia Ares<sup>1</sup>; Liliana Gassa<sup>2</sup>; Sergio Guejman<sup>3</sup>; *Carlos Schvezov*<sup>1</sup>; <sup>1</sup>CONICET/Univ De Misiones; <sup>2</sup>CONICET/INIFTA; <sup>3</sup>National University of Misiones

The columnar to equiaxed transition (CET) has been examined in different wrought and casting alloys for many years and the metallurgical significance of CET has been treated in several articles. Experimental observations in the literature have focused on thermal parameters like cooling rate, velocity of the liquidus and solidus fronts, local solidification time, temperature gradients and recalescence. The objective of the present research consist on studying the influence of solidification thermal parameters on the type of structure (columnar, equiaxed or with the CET); and on the dendritic spacing (primary and secondary) in Zn-Al alloys (Zn-1%Al to Zn-4wt%Al, weight percent). Also, correlate the thermal and structure parameters of these alloys with tensile and corrosion behaviour. The results show that the CET zone and the equiaxed structures presented a better tensile and corrosion resistance than the columnar zone.

##### 10:15 AM Break

##### 10:25 AM

**Solidification, Macrostructure and Microstructure Analysis of Al-Cu Alloys Directionally Solidified from the Chill Face:** Alicia Ares<sup>1</sup>; *Carlos Schvezov*<sup>1</sup>; <sup>1</sup>CONICET/Univ De Misiones

The understanding of the phenomenon of the columnar to equiaxed transition (CET) is very important for metallurgical applications. In the present study the CET was observed in aluminum-copper alloys of different compositions covering a range from 2wt%Cu to 33.2 wt%Cu, which were solidified directionally from a chill face. The main parameters analyzed include cooling rates, temperature gradients, solidification velocities of the liquidus and solidus fronts, recalescence, heat flow, grain size, primary and secondary dendritic arm spacing and eutectic spacing. The temperature gradient and the velocity of the liquidus front reach low critical values before the transition. These critical values are between 0.35 to 3.12 mm/s for the velocity and -0.44 to 0.17 K/mm for the temperature gradient. The temperature measurements indicate that solidification in the transition region is far from equilibrium given by the lever rule and the phase diagram.

##### 10:50 AM

**The Modification of Cast Al-Mg<sub>2</sub>Si In Situ MMC by Lithium:** *Raheleh Hadian*<sup>1</sup>; Mahmood Emamy<sup>2</sup>; John Campbell<sup>3</sup>; <sup>1</sup>Sharif University of Technology; <sup>2</sup>University of Tehran; <sup>3</sup>University of Birmingham

The effects of both Li modification and cooling rate on the microstructure and tensile properties of an in-situ prepared Al-15% Mg<sub>2</sub>Si composite were investigated. The size of Mg<sub>2</sub>Si particles was refined and tensile properties were improved as a result of both 300 ppm Li additions and cooling rate increases, and these effects were additive. The refinement by Li and enhanced cooling rate is discussed in terms of an analogy with the effect of Sr and cooling rate in Al-Si alloys, and is ultimately attributed with the effect of the alkali and alkaline earth metals deactivating extrinsic (entrained oxide bifilms) suspended in Al melts as favoured substrates for intermetallics.

##### 11:15 AM

**Effect of Strontium on Viscosity and Liquid Structure of Al-Si Eutectic Alloy:** Sumanth Shankar<sup>1</sup>; *Srirangam VS Prakash*<sup>1</sup>; Minhajuddin Malik<sup>1</sup>; Manickaraj Jeyakumar<sup>1</sup>; Michael Walker<sup>2</sup>; Mohamed Hamed<sup>1</sup>; <sup>1</sup>LMCRC - McMaster University; <sup>2</sup>General Motors

This study aims to present conclusive evidence that trace level addition of Sr in Al-Si hypoeutectic alloys change the liquid melt characteristics and alter the

nucleation environment of the eutectic phases. High temperature rheological experiments measuring viscosity of Al-Si eutectic melt with and without Sr addition show that Sr significantly alters the melt viscosities at various shear rate regimes. Further, liquid diffraction experiments have been carried out on Al-12.5wt%Si (eutectic) alloy using high-energy synchrotron X-ray beam source to determine the effect of Sr on various liquid structure parameters such as structure factor, pair distribution function and coordination numbers at various melt superheat temperatures. The analysis of the data suggests that Sr changes the nucleation environment of the eutectic Si phase. Further, the effect of Sr on the atomic arrangement of the Si atom with respect of Si and Al atoms in the liquid will be quantified and presented.

## 11:40 AM

**Characterization of the Melt Quality and Impurity Content of an LM25 Alloy:** Katharina Haberl<sup>1</sup>; Peter Schumacher<sup>2</sup>; Georg Geier<sup>3</sup>; Bernhard Stauder<sup>4</sup>; <sup>1</sup>University of Leoben; <sup>2</sup>University of Leoben and Austrian Foundry Research Institute; <sup>3</sup>Austrian Foundry Research Institute; <sup>4</sup>Nemak

The melt quality of an LM25 aluminium casting alloy has been examined using reduced pressure test (RPT) measurements, porous disc filtration analysis (PoDFA), and fatigue and tensile tests. The aim of this study was to determine existing melt quality and thus evaluate methods used with respect to monitoring and improving melt cleanliness. Special emphasis was given to the influence of oxides. It was found that the melt quality has varying degrees of effect on the tests used. Results in particular indicate, that it was necessary to distinguish between "new" oxides and "hard" inclusions in the melt, as new oxides impact porosity whilst hard inclusions impact on ductility. Based on the results of this study, suggestions for the measurement of the melt quality have been proposed.

## Structural Materials Division Symposium: Advanced Characterization and Modeling of Phase Transformations in Metals in Honor of David N. Seidman on his 70th Birthday: Structure Property Relationships

Sponsored by: The Minerals, Metals and Materials Society, TMS Structural Materials Division, TMS: Advanced Characterization, Testing, and Simulation Committee, TMS: Chemistry and Physics of Materials Committee

Program Organizers: Robert Averback, University of Illinois, Urbana-Champaign; Mark Asta, University of California, Davis; David Dunand, Northwestern University; Ian Robertson, University of Illinois at Urbana-Champaign; Stephen Foiles, Sandia National Laboratories

Tuesday AM Room: 3000  
February 17, 2009 Location: Moscone West Convention Center

Session Chair: Stephen Foiles, Sandia National Laboratories

## 8:30 AM Invited

**Mechanical Consequences of Grain Boundary Structure:** John Cahn<sup>1</sup>; V. Ivanov<sup>2</sup>; Y. Mishin<sup>3</sup>; <sup>1</sup>University of Washington; <sup>2</sup>George Mason University

Most moving grain boundaries (GBs), not just small-angle dislocation and twin boundaries, deform and rotate the material traversed with important consequences for such processes as grain growth and recrystallization. Applied stresses couple to these GBs, leading to their motion and the deformations. For any given GB the structure and bicrystal symmetry play important roles, but there always are multiple solutions for the GB dislocation content. GB structure is important for understanding the atomic mechanisms for the GB motions that are realized in molecular dynamics simulations, including for the multiple coupling modes and abrupt changes in the direction of the GB motion. We discuss recent progress in understanding the stress-driven GB motion and its role in mechanical behavior of materials.

## 9:00 AM Invited

**A New Paradigm for Designing Strong Ductile Alloys with High Peierls Stress:** Morris Fine<sup>1</sup>; Semyon Vaynman<sup>1</sup>; <sup>1</sup>Northwestern Univ

Interaction of coherent misfit centers with dislocations to locally lower the Peierls stress is the concept for making metals and alloys more ductile below a ductile to brittle transformation temperature such as occurs in steels. Hans Weertman, circa 1958 developed the basic theory. The misfit centers catalyze

the formation of double kinks such as in screw dislocations in iron at low temperatures. We used Han's theory to explain why low carbon ferritic steels with low nanoscale coherent Cu alloy precipitates can have outstanding ductility and high Charpy impact fracture energies at cryogenic temperatures, below the usual ductile to brittle transformation temperature. These ideas are being extended to very high strength steels and to other metals and alloys. David Seidman and his group did the precipitate characterization using atom probe tomography, a key part of the research.

## 9:30 AM Invited

**Grain Boundary Dissociation in Low Stacking Fault Energy Metals:** Douglas Medlin<sup>1</sup>; John Hamilton<sup>1</sup>; Gene Lucadamo<sup>1</sup>; <sup>1</sup>Sandia National Laboratories

Grain boundaries in metals that possess low stacking fault energies can reconstruct into three-dimensional configurations by the emission of stacking faults. An important question is how the arrangement of these faults, and hence the structure of the interfacial layer, depends on the orientational parameters of the interface. Here, we present electron microscopic observations and modeling of two boundary misorientations in gold that both reconstruct to form a nanometer-scale layer of hexagonal-close-packed (HCP) material. In both cases, the HCP layer and its relationship to the grain misorientation is directly explained and predicted by the arrangement of Shockley partial dislocations at the interface. A comparison of the two boundary structures, one of which has partials paired as full lattice dislocations and the other, which does not, provides insight concerning the formation of other stacking arrangements, such as 9R, that have been observed at other grain misorientations in low SFE FCC metals.

## 10:00 AM Break

## 10:15 AM Invited

**Modeling Point, Line, and Planar Defects in Metal Alloys:** Christopher Woodward<sup>1</sup>; <sup>1</sup>Air Force Research Laboratory

Often solution and precipitation strengthening strategies are used to optimize properties of structural materials for aerospace applications. Much can be learned about these alloys by studying defects in model simple, binary and ternary systems. We review first principles predictions of point, line and planar effects in simple bcc metals and several ordered intermetallics. These include: enthalpy of point defects in  $\gamma$ -TiAl-X and  $\gamma$ -Al<sub>3</sub>Sc-X; dislocation core structure in bcc and fcc metals (including solute-dislocation interactions), and interfacial boundaries (IFB) in Ni-Ni<sub>3</sub>Al and Al-Al<sub>3</sub>Sc. Using thermodynamics we can predict concentration and temperature dependence of ternary-solute site selection in the ordered intermetallics. Predicted solute-dislocation interactions in Mo-X alloys are used to develop new model of solution hardening and softening. Finally, cluster expansion and lattice gas methods are used to study composition profiles and free energies of IFB's. Results for Mg impurity segregation to (100)Al-Al<sub>3</sub>Sc IFB have been verified by atom probe tomography.

## 10:45 AM Invited

**Structural Stability Issues in Nanocrystalline, Ultrafine-Grain and Nano-Twinned Copper:** Carla Shute<sup>1</sup>; Kai Zhang<sup>1</sup>; Andrea Hodge<sup>2</sup>; Benjamin Myers<sup>1</sup>; Sujing Xie<sup>1</sup>; Julia Weertman<sup>1</sup>; <sup>1</sup>Northwestern University; <sup>2</sup>University of Southern California

The mechanical behavior of pure nanocrystalline and ultrafine-grain (UFG) materials are of interest because of likely changes in deformation mechanisms in these grain size regimes. However it is found that the internal structure is unstable, especially under stress. Localized stress has been found to increase average grain size by a factor of more than 5 in high-purity nanocrystalline Cu. Fatigue loading of UFG Cu increases the grain size by orders of magnitude. However aligned nano-twinning considerably stabilizes samples subjected to fatigue or localized stresses. Recent experiments on nano-twinned Cu will be discussed. Characterization was performed in the EPIC facility NUANCE Center, supported by NSF-NSEC, NSF-MRSEC, Keck Foundation, State of Illinois, and Northwestern University.

## 11:15 AM Invited

**Stability of Nanocrystalline Ni-W Electrodeposits:** Christopher Schuh<sup>1</sup>; T. Rupert<sup>1</sup>; T. Ziebell<sup>1</sup>; <sup>1</sup>Massachusetts Institute of Technology

Electrodeposited Ni-W alloys are used as coatings for improved mechanical performance, and derive their desirable properties from very fine nanoscale structures. This talk will survey our work to characterize the coating structure both in the as-deposited state, and after exposure to thermal treatment and mechanical deformation. In the as-deposited condition, these alloys exhibit tensile residual stresses, disordered grain boundaries, as well as some degree of

grain boundary segregation. For thermal exposures of technological relevance, we observe grain boundary relaxation and hardening without any other structural changes, including grain growth, additional segregation, or precipitation of second phases. Severe mechanical deformation imposed by wear and abrasion also leads to structural relaxation that has broad implications for the use of these coatings in wear applications.

### 11:45 AM Invited

#### **Defect Generation and Stabilisation as a Route to Nanostructured and Amorphous Materials:** *Reiner Kirchheim*<sup>1</sup>; <sup>1</sup>University of Goettingen

Willard Gibbs Adsorption Isotherm and Carl Wagner's definition of excess solute at surfaces and grain boundaries were both extended to include other crystalline defects like dislocations and vacancies [1]. Thus solute segregation to dislocations and vacancies and other crystalline defects gives rise to a reduction of their formation energies, too. The Gibbs Adsorption Isotherm remains to be unchanged by its generalization. Thus defect formation requires less energy for positive excess solute, i.e. attractive interaction between solutes and defects. In this context special attention is paid to the intriguing question whether defect energies might become zero or negative leading to metastable equilibrium or instable crystalline phases. However, the corresponding high chemical potentials may not be reached as solute A may precipitate as pure A or an A-rich compound [2]. [1] R. Kirchheim, *Acta Mater.* 55 (2007) 5129-5138 and 5138-5148. [2] R. Kirchheim, *Acta Mater.* 50 (2002) 413-419

### 12:15 PM

#### **Forced Chemical Mixing in Alloys at Elevated Temperatures:** *Nhon Vo*<sup>1</sup>; *Samson Odunuga*<sup>1</sup>; *Robert Averback*<sup>1</sup>; *Pascal Bellon*<sup>1</sup>; <sup>1</sup>University of Illinois

Severe plastic deformation of alloys at low temperatures generally leads to the homogenization of alloying components regardless of their thermochemical properties. At elevated temperatures this is no longer the case as thermally activated jumps of point defects act in competition with the shearing until a dynamic equilibrium is established. In the present work we investigate this behavior by using molecular dynamics computer simulation to calculate the response of a series of immiscible alloys to high shear-rate deformation as a function of temperature, deformation rate, and the heat of mixing. We demonstrate that systems with large heats of mixing indeed undergo phase separation at high temperatures. For the high strain rates employed, however,  $5 \times 10^8 - 5 \times 10^9 \text{ s}^{-1}$ , we find that point defects have only minor impact on the behavior and that the phase separation results directly from the shearing events, themselves.

## Synergies of Computational and Experimental Materials Science: Three-Dimensional Materials Science III

Sponsored by: The Minerals, Metals and Materials Society, TMS Materials Processing and Manufacturing Division, TMS/ASM: Computational Materials Science and Engineering Committee

Program Organizers: Katsuyo Thornton, University of Michigan; Henning Poulsen, Risoe National Laboratory; Mei Li, Ford Motor Co

Tuesday AM  
February 17, 2009

Room: 3003  
Location: Moscone West Convention Center

*Session Chairs:* Alexis Lewis, Naval Research Laboratory; David Rowenhorst, Naval Research Laboratory

### 8:30 AM Invited

#### **Experimental and Modeling Synergies in High Temperature Materials:** *Tresa Pollock*<sup>1</sup>; *Jonathan Madison*<sup>1</sup>; *Sara Johnson*<sup>1</sup>; <sup>1</sup>University of Michigan

High temperature materials experience complex, aggressive environments during processing and in service. Two examples of the benefits of a combined computational-experimental approach will be discussed for nickel base superalloys. In the first, three-dimensional serial sectioning of the growth front of a superalloy single crystal is utilized to provide a computational mesh of a realistic dendritic structure. This provides the basis for a 3-D fluid flow model that permits assessment of the permeability of the dendritic structure and the tendency for convective instabilities to develop during single crystal solidification. In the second example, materials thermodynamic and strengthening models are combined with a thermostructural code to search for

materials design solutions to the complex problem of actively cooled structural panels for hypersonic flight vehicles. New experimental materials motivated by this approach will be discussed.

### 9:10 AM Invited

#### **Integration of 3D Structure Information for a Ni-Base Superalloy into Computational Models for Behavior Prediction:** *Michael Groeber*<sup>1</sup>; *Dennis Dimiduk*<sup>2</sup>; *Michael Uchic*<sup>2</sup>; *Chris Woodward*<sup>2</sup>; <sup>1</sup>UTC/AFRL; <sup>2</sup>AFRL

There is a drive to utilize modern advances in computational power to expedite development and enhance utilization of materials. Thus, there is a demand for virtual representations of material structure. Predicting material response using computational tools demands that microstructure is accurately described, either statistically or explicitly. Additionally, descriptions of microstructure must be integrated with property simulators. Applications of any such characterization-representation framework may well span from material design to life prediction. This talk will focus on the experimental collection of the 3D structure information for a Ni-Base superalloy turbine blade. Further, the talk will present developments in the integration of this information within computational models. Details of the serial-section collection methods will be presented, followed by descriptions of tools used to identify and measure features of interest. Lastly, the development of computational tools to represent the microstructure both explicitly and statistically will be discussed

### 9:50 AM

#### **Modeling Fluid Flow Within an Experimentally Obtained Three-Dimensional Solid-Liquid Interface in Directionally Solidified Nickel-Base Superalloy:** *Jonathan Madison*<sup>1</sup>; *Jonathan Spowart*<sup>2</sup>; *David Rowenhorst*<sup>3</sup>; *Katsuyo Thornton*<sup>1</sup>; *Tresa Pollock*<sup>1</sup>; <sup>1</sup>The University of Michigan; <sup>2</sup>US Air Force; <sup>3</sup>Naval Research Lab

Convective flow within the mushy zone of directionally solidified superalloys can result in the formation of freckles and misoriented grains. These defects signal not only a disruption in the columnar or single crystal nature of the component but also a tendency toward reduction in life and performance. Approximations of the onset of convective flow in the mush have primarily used the Rayleigh criteria as a predictor for the occurrence of freckles. However, a detailed understanding of fluid flow at the scale of the dendritic structure is still lacking. This research utilizes 3-D dendritic structures obtained from the solid-liquid interface of directionally solidified nickel-base superalloys as direct inputs to fluid flow models. These models have been utilized to assess the permeability of the dendritic array. Implications of simulations will be discussed with reference to the Rayleigh criteria and freckle prediction.

### 10:10 AM

#### **3-D Moment Invariants for Description of Precipitate Morphology and Evolution in Nickel Based Superalloys:** *Jeremiah MacSlyne*<sup>1</sup>; *Marc DeGraef*<sup>1</sup>; <sup>1</sup>Carnegie Mellon Univ

The quantitative description of 3-D shapes is of fundamental importance to microstructural characterization. One method to describe a microstructure is to characterize the shapes of individual precipitates. This characterization has typically been limited to particle size, aspect-ratio, and qualitative descriptors. In general, these are insufficient and do not provide an adequate characterization in a way that allows for direct comparison between microstructures. This is evident during microstructure evolution when changes in precipitate morphology occur or when precipitates exhibit complex shapes. We will show how moment invariants (combinations of second order shape moments that are invariant w.r.t. affine or similarity transformations) can be used as sensitive shape discriminators in 3-D. As an application of 3-D moment invariants, we will examine the morphological evolution of gamma-prime precipitates in a Ru containing single crystal nickel-based superalloy. Experimental data has been collected using automated FIB-based serial sectioning for different aging times.

### 10:30 AM Break

### 10:50 AM

#### **Utility of Experimental 3D Microstructure Reconstructions for Simulations of Realistic 3D Microstructures:** *Arun Gokhale*<sup>1</sup>; *Youxiong Mao*<sup>1</sup>; *Harpreet Singh*<sup>1</sup>; *Arun Sreeranganathan*<sup>2</sup>; <sup>1</sup>Georgia Institute of Technology; <sup>2</sup>Stress Engineering Services, Inc.

Current methodologies for microstructure simulations involve idealized simple particle/feature shapes; uniform-random spatial distribution of microstructural features; and isotropic feature orientations. However, the corresponding "real" microstructures often have complex feature shapes/morphologies; non-



random/non-uniform spatial distributions; and partially anisotropic feature orientations. Consequently, such simulations do not capture these aspects of microstructural reality. In this contribution, we present a methodology that enables simulations of “realistic” 3D microstructures where feature shapes/morphologies, spatial arrangement, and feature orientations are statistically similar to those in the corresponding real microstructures. The realistic complex feature shapes/morphologies are obtained via experimental reconstructions of 3D microstructures from serial sections. The methodology is applied for simulations of realistic 3D microstructures discontinuously reinforced Al-alloy composites. The methodology enables generation of a set of “virtual” microstructures that cover a wide range of process conditions, which can be implemented in finite element (FE) based computations to simulate mechanical response of the corresponding virtual materials.

## 11:10 AM

**The Use of Correlation Functions to Identify Features in Ti-Based Alloys:** *Stephen Niezgodal<sup>1</sup>; Peter Collins<sup>2</sup>; David Turner<sup>1</sup>; Surya Kalidindi<sup>1</sup>; Hamish Fraser<sup>2</sup>; <sup>1</sup>Drexel University; <sup>2</sup>Ohio State University*

The need to robustly and automatically identify certain features within two-dimensional and three-dimensional titanium microstructures has led to the development of novel techniques, based on 2-point and higher order microstructure correlations (n-point statistics) and local neighborhood statistics calculated via fast Fourier transforms (FFT) and other fast integral transforms, including Radon and Hough transforms. These methodologies have been successfully used to automatically identify critical microstructural features from two-dimensional micrographs of different Ti-based alloys, including colony boundaries - an often difficult feature to automatically identify. Microstructural features such as chord length distributions and interface area, typically estimated by stereological techniques, can be directly calculated from these correlations. These methodologies have been applied to existing datasets of Ti-based alloys, including Ti-6Al-4V and Ti-5553 (Ti-5Al-5V-5Mo-3Cr). The results will be compared with those results obtained using traditional manual or semi-automated procedures.

## 11:30 AM

**Morphological Analysis of 3D Grain Topology in Ti-21S:** *David Rowenhorst<sup>1</sup>; Alexis Lewis<sup>1</sup>; George Spanos<sup>1</sup>; <sup>1</sup>Naval Research Laboratory*

Using serial sectioning, the 3D morphology of a statistically significant number of  $\beta$  grains was determined in Ti-21S. Over 200 sections were collected, with a total of 4700 grains within the collection volume. Using the 3D information, direct comparisons are made between this experimental data and theory and simulation of grain growth and topology. This will include discussions of traditional measurements such as grain size distribution, but also the relationships in the topology, including the number of faces and edges within the grains, and their relationship to the interfacial curvature. We will also show that this type of experimental data is ideal for inclusion into simulations (both FEM and Phase-Field Modeling) as initial conditions, removing many assumptions in the modeling process.

## 11:50 AM

**3D Phase Field Simulation on Beta” Precipitation Kinetics in Al-Mg-Si Alloys:** *Ruijie Zhang<sup>1</sup>; Mei Li<sup>1</sup>; John Allison<sup>1</sup>; Longqing Chen<sup>2</sup>; <sup>1</sup>Ford Motor Company; <sup>2</sup>The Pennsylvania State University*

Beta” precipitates always appear at the peak aging condition and act as the most effective strengthening phase during heat treatment process in Al-Mg-Si alloys. In this paper, a phase field model for studying the growth kinetics of beta” precipitates was developed. An experimental nucleation model was adopted to predict the nucleation behavior of beta” precipitates. The Gibbs energy for solid solution and solute diffusion behavior were obtained from thermodynamics and diffusion mobility database using CALPHAD method. The Gibbs free energy, interface energy and elastic constants of beta” precipitates were selected from the results of first-principles calculations. Because there is no direct experimental data on the interface mobility, this parameter was optimized by several published experimental results. Good agreements were achieved between predictions and experimental results, such as precipitate size and volume fraction. These parameters are key factors for the description of ageing behavior and for the mechanical properties predictions.

## Transformations under Extreme Conditions: A New Frontier in Materials: High Rate Deformation

Sponsored by: The Minerals, Metals and Materials Society, ASM International, ASM Materials Science Critical Technology Sector, TMS Materials Processing and Manufacturing Division, TMS/ASM: Phase Transformations Committee  
Program Organizers: Vijay Vasudevan, University of Cincinnati; Mukul Kumar, Lawrence Livermore National Laboratory; Marc Meyers, University of California-San Diego; George “Rusty” Gray, Los Alamos National Laboratory; Dan Thoma, Los Alamos National Laboratory

Tuesday AM

Room: 3001

February 17, 2009

Location: Moscone West Convention Center

*Session Chairs:* Marc Meyers, University of California; Naresh Thadhani, Georgia Institute of Technology

## 8:30 AM Invited

**A Path to Materials Science above 1000 GPa (10 Mbar) on the NIF Laser:** *Bruce Remington<sup>1</sup>; Hye-Sook Park<sup>1</sup>; Shon Prisbrey<sup>1</sup>; Stephen Pollaine<sup>1</sup>; Luke Hsiung<sup>1</sup>; Robert Rudd<sup>1</sup>; Robert Cavallo<sup>1</sup>; Stefan Hau-Riege<sup>1</sup>; Justin Wark<sup>2</sup>; Marc Meyers<sup>3</sup>; <sup>1</sup>Lawrence Livermore National Laboratory; <sup>2</sup>University of Oxford; <sup>3</sup>University of California, San Diego*

Solid state dynamics experiments at extreme pressures,  $P > 1000$  GPa (10 Mbar), and strain rates ( $1.e6-1.e8$  1/s) are being developed for the National Ignition Facility (NIF) laser, and offer the possibility for exploring new regimes of materials science. These extreme, solid state conditions can be accessed with a ramped pressure drive. Velocity interferometer measurements (VISAR) establish the high pressure conditions. Constitutive models for solid state strength under these conditions are tested by comparing 2D simulations with experiments measuring perturbation growth from the Rayleigh–Taylor or Richtmyer–Meshkov instabilities in solid state samples of V and Ta. Radiography techniques using synchronized bursts of 20–40 keV x-rays have been developed to diagnose this perturbation growth. Time resolved lattice response and phase can be measured with dynamic X-ray diffraction and modeled with large scale molecular dynamics (MD) simulations. Methods proposed for inferring deformation mechanism (slip vs. twinning vs. phonon drag) will also be discussed.

## 9:05 AM Invited

**Shock Deformation in Cubic Metals:** *Neil Bourne<sup>1</sup>; <sup>1</sup>AWE*

There is a current need to solve design problems experienced where structures experience dynamic and impact loading. To do this, requires valid, physically-based, analytical laws that describe the deformation behaviour of materials. Populating material descriptions found in such codes with suitable analytical descriptions, generally requires knowledge of operating physical mechanisms at the mesoscale. This work will attempt to provide an overview of present work concerning the shock response of metals focusing upon work done on cubic materials. The materials chosen are pure nickel, pure tantalum and the ordered fcc material Ni<sub>3</sub>Al. Additionally TiAl is also considered. A range of results from complementary techniques is presented casting light on the operating mechanisms giving rise to the observed phenomena. The behaviour of these metals is discussed in terms of the materials’ Peierl’s stress, stacking fault energy of the microstructure and twinning prevalence.

## 9:40 AM

**High Rate Plasticity under Pressure Using an Oblique-Impact Ramp Compression Experiment:** *Jeffrey Florando<sup>1</sup>; Louis Ferranti<sup>1</sup>; Grant Bazan<sup>1</sup>; Richard Becker<sup>1</sup>; Roger Minich<sup>1</sup>; Dave Lassila; Tong Jiao<sup>2</sup>; Steve Grunschel<sup>2</sup>; Rodney Clifton<sup>2</sup>; <sup>1</sup>Lawrence Livermore National Laboratory; <sup>2</sup>Brown University*

An experimental technique has been developed to study the strength of materials under conditions of moderate pressures and high strain rates. The technique is similar to the traditional pressure-shear experiments except that window interferometry is used to measure both the normal and transverse particle velocities at the sample-window interface. Additionally, the sample is impacted with a graded density impactor, which imposes a ramp compression wave and controls the strain rate to between  $10^4 - 10^6$ . Both simulation and experimental results on copper samples with a sapphire window will be presented to show the utility of the technique to measure the strength properties under dynamic loading conditions.

10:00 AM

**Material Strength and Microstructural Effects in Beryllium during Nanosecond Heating by Hard X-Rays:** *Eric Loomis*<sup>1</sup>; Scott Greenfield<sup>1</sup>; Shengnian Luo<sup>1</sup>; Randall Johnson<sup>1</sup>; Tom Shimada<sup>1</sup>; Jim Cobble<sup>1</sup>; David Montgomery<sup>1</sup>; <sup>1</sup>Los Alamos National Laboratories

Understanding material behavior at high strain-rates and high temperatures is a formidable problem, requiring complex simulations of dislocation kinetics or experiments. From the experimental standpoint, lasers are a useful tool for inducing such states due to their ability in producing extreme conditions on nanosecond timescales. I will present recent data showing the response of single and polycrystalline beryllium exposed to nanosecond hard x-rays produced by laser-irradiated gold foils. Velocity measurements showed that a suddenly established temperature profile through the target resulted in high temperature tensile ramped loading. Plastic flow played a diminished role in single crystals compared to lower temperature behavior where the plastic deformation is more anisotropic. A large difference in single crystal behavior compared to polycrystalline behavior was observed in velocity measurements as well as surface displacement measurements where anisotropic thermal expansion resulted in observable differential grain expansion at the free surface.

10:20 AM Break

10:35 AM Invited

**Characterization of Deformation Bands, Adiabatic Shear Bands, and Crack Formation and Propagation in Ti-6Al-4V Ballistic Plug Targets:** *Lawrence Murr*<sup>1</sup>; A. Ramirez<sup>2</sup>; S. Gaytan<sup>1</sup>; M. Lopez<sup>1</sup>; E. Martinez<sup>1</sup>; D. Hernandez<sup>1</sup>; E. Martinez<sup>1</sup>; <sup>1</sup>University of Texas

The microstructures and microstructure evolution associated with deformation bands and adiabatic shear band (ASB) formation in ballistic plugging in thick, Ti-6Al-4V targets impacted by cylindrical, flat-nose 4370 steel projectiles at velocities ranging from 633 m/s to 1027 m/s were investigated by optical and transmission electron microscopy. Deformation bands were composed of transformed alpha-prime (hcp) platelets with spacing decreasing with impact velocity. Horizontal ASB spacing decreased with impact velocity while the ASB width increased. The deformation band microindentation hardness increased with an increase in impact velocity while the ASB microindentation hardness, although 16% higher than the surrounding matrix, remained constant; indicative of a consistent dynamic recrystallization (DRX) grain structure. The deformation bands were not precursors to ASB formation, and cracks nucleated and propagated preferentially in the ASBs, with crack length (0.02 mm at 633 m/s to 10 mm at 1006 m/s) and crack density increasing with impact velocity.

11:10 AM Invited

**Influence of the Shock-Induced  $\alpha$ - $\epsilon$  Transition in Fe and the  $\alpha$ - $\omega$  Transitions in Ti and Zr on Post-Shock Substructure Evolution and Mechanical Behavior:** *George Gray*<sup>1</sup>; Ellen Cerreta<sup>1</sup>; <sup>1</sup>Los Alamos National Lab

Shock loading of materials is well known to induce a range of defects in metals and alloys, including dislocations, deformation twins, and point defects. In addition to the defects generated to accommodate the plasticity of impact loading, some materials exhibit additional structure / property changes due to a pressure-induced phase transition in the material. In this paper, the manner by which the shock-induced  $\alpha$ - $\epsilon$  transition in Fe and the  $\alpha$ - $\omega$  transition in Ti and Zr alters the post-shock substructure evolution and mechanical behavior will be presented. Enhanced defect generation and storage mechanisms, including deformation twinning, and a commensurate increase in shock hardening is shown to occur upon crossing both the  $\alpha$ - $\epsilon$  transition in Fe and the  $\alpha$ - $\omega$  in Ti and Zr. Shock recovery experiments are shown to provide an invaluable window, when coupled with "real-time" diagnostic techniques, into the defect generation and storage processes operative during shock loading of materials.

11:45 AM

**Laser Shock Induced Residual Stress and Microstructural Changes in Aero Engine Alloys:** Amrinder Gill<sup>1</sup>; Yixiang Zhao<sup>1</sup>; Vibhor Chaswal<sup>1</sup>; Ulrich Lienert<sup>2</sup>; Jonathan Almer<sup>2</sup>; Yang Ren<sup>2</sup>; David Lahrman<sup>3</sup>; Seetha Mannava<sup>1</sup>; Dong Qian<sup>1</sup>; *Vijay Vasudevan*<sup>1</sup>; <sup>1</sup>University of Cincinnati; <sup>2</sup>Argonne National Laboratory; <sup>3</sup>LSP Technologies, Inc.

Laser shock peening (LSP) is a novel surface treatment that generates deep compressive residual stresses and near-surface microstructural changes through shockwaves, thereby leading to dramatic improvements in fatigue strength and crack propagation resistance of aircraft engine parts. In this study, coupons of IN718 and Ti-6Al-4V were LSP-treated at a range of beam energies. Depth-

resolved characterization of the residual strains and stresses was achieved using high-energy synchrotron x-ray diffraction at the APS/ANL. The near-surface and through-the-depth changes in microstructure were studied using EBSD/OIM and by TEM of thin foils fabricated using the FIB method. Local property changes were examined using microhardness and micropillar compression tests. Finally, analytical and finite element modeling and simulation were utilized to predict the laser shock induced residual stress and spallation. The results showing the relationship between shock parameters and the residual strain/stress distributions, near-surface microstructure, mechanical properties and tendency for spallation are presented and discussed.

12:05 PM

**Microstructural Evolution of Ti-6Al-4V during High Strain Rate Conditions of Metal Cutting:** *Lei Dong*<sup>1</sup>; Judy Schneider<sup>1</sup>; <sup>1</sup>Mississippi State University

The microstructural evolution following metal cutting was investigated within the metal chips of Ti-6Al-4V. Metal cutting was used to impose a high strain rate on the order of  $\sim 10^5$  s<sup>-1</sup> within the primary shear zone as the metal was removed from the workpiece. The initial microstructure of the parent material (PM) was composed of a bi-modal microstructure with coarse prior  $\beta$  grains and equiaxed primary  $\alpha$  located at the boundaries. After metal cutting, the microstructure of the metal chips showed coarsening of the equiaxed primary  $\alpha$  grains and  $\beta$  lamellar. These metallographic findings suggest that the metal chips experienced high temperatures which remained below the  $\beta$  transus temperature.

12:25 PM

**A Technique for Yield-Strength Experiments at Ultra-High Pressure and Strain Rate Using High-Power Laser Pulses:** *Paul DeMange*<sup>1</sup>; J. Colvin<sup>1</sup>; H. Park<sup>1</sup>; S. Pollaine<sup>1</sup>; R. Smith<sup>1</sup>; <sup>1</sup>Lawrence Livermore National Laboratory

High-power laser systems have made it possible to achieve Mbar pressure and MHz strain-rate. A laser pulse drives a shock through a reservoir material which then unloads onto the target specimen. Laser velocimetry measurements at the back surface of the specimen are used to infer the material response. With the advent of this recent capability, a technique for material strength experiments has been proposed in which the pressure wave reverberates within the specimen. The velocity amplitude due to the reflections at the back surface is recorded and an amplitude decrease due to the cumulative resistance to compression by material strength is measured. In this work, a general approach for optimizing the reverberation technique is explored that also includes eliminating the risk of shock and spall. Hydrocode simulations are used to develop a direct-drive target design for yield strength experiments at ultra-high pressure and strain rate.

## 2009 Functional and Structural Nanomaterials: Fabrication, Properties, and Applications: Nanoscale Fabrication and Devices: Concepts, Approaches and Scale-Up

Sponsored by: The Minerals, Metals and Materials Society, TMS Electronic, Magnetic, and Photonic Materials Division, TMS Materials Processing and Manufacturing Division, TMS: Nanomaterials Committee, TMS: Nanomechanical Materials Behavior Committee

Program Organizers: Gregory Thompson, University of Alabama; Amit Misra, Los Alamos National Laboratory; David Stollberg, Georgia Tech Research Institute; Jiyoung Kim, University of Texas at Dallas; Seong Jin Koh, University of Texas at Arlington; Wonbong Choi, Florida International University; Alexander Howard, Air Force Research Laboratory

Tuesday PM  
February 17, 2009

Room: 3018  
Location: Moscone West Convention Center

Session Chairs: Amit Misra, Los Alamos National Laboratory; David Stollberg, Georgia Tech Research Institute

### 2:00 PM Invited

**Functional Nanomaterials and the Birth of Ionic Memory:** *Michael Kozicki*<sup>1</sup>; <sup>1</sup>Arizona State University

Scalable devices that switch between widely-separated non-volatile resistance states at extremely low power are highly desirable for applications in nanoscale memory and logic. One promising approach involves the use of nanostructured ion-conducting films. A mobile ion-containing electrolyte sandwiched between two electrodes can constitute a device which reversibly transitions between high and low resistance states. The resistance reduction occurs by the formation of a nanoscale conducting region created by redistribution of the ions. A reverse bias (or in some cases a forward bias) returns the device to its high resistance state. In addition to possessing the speed, endurance, retention, and CMOS compatibility required of future switching elements, such devices can also have excellent scaling prospects due to their low operational energy and demonstrated physical scalability. This paper reviews the materials and functionality of a variety of ionic memory technologies and shows how nanostructure is critical to device operation.

### 2:30 PM

**Diffuse-Interface Field Approach to Simulation of Self- and Guided-Assembly of Charged Particles of Various Shapes and Sizes:** *Paul Millet*<sup>1</sup>; Yu Wang<sup>2</sup>; <sup>1</sup>Idaho National Laboratory; <sup>2</sup>Virginia Tech

Recent advances in the ability to control the size, shape, and composition of nanoparticles has significantly broadened the possibilities to create novel mesoscale structures as a result of their "bottom-up" assembly. A particularly efficient approach to facilitate various assembly dynamics is to control the collective electrostatic interactions by tuning the particle charge density, dipole moment, and/or an external electric field. Here, we present a novel mesoscale simulation approach that utilizes diffuse interface fields to capture the dynamic assembly processes for arbitrarily shaped particles with arbitrary charge density and/or dipole moment. We will present results illustrating the method's ability to predict a wide variety of colloidal crystal structures, with a particular focus on binary lattices consisting of positively- and negatively-charged particles. We find that varying the shapes, relative charge density ratio, as well as the relative number density of each particle type results in vastly different assembly dynamics.

### 2:45 PM

**Large-Scale Fabrication of CMOS Based Single-Electron Transistors:** *Vishva Ray*<sup>1</sup>; Ramkumar Subramanian<sup>1</sup>; Pradeep Bhadrachalam<sup>1</sup>; Seong Jin Koh<sup>1</sup>; <sup>1</sup>The University of Texas at Arlington

We present a new scheme of fabricating room-temperature single-electron transistors on a large-scale, in parallel processing, and using CMOS based processes. The nanometer scale gap between the source and the drain electrodes, a critical requirement in single-electron devices, was created by employing a vertical electrode configuration. Coulomb islands (10 nm Au nanoparticles) were positioned in the gap between the source and the drain electrodes using a combination of colloidal and surface chemistry. Addressable gate electrodes were also incorporated to fabricate single-electron transistors in complete parallel

processing. Single-electron transport phenomena (Coulomb blockade/staircase and Coulomb oscillations) have been demonstrated at room temperature (295K) as well as at low temperature (10K). A shift in the Coulomb staircase due to application of a gate bias, a definitive signature of single-electron transistor behavior has also been demonstrated. Simulations based on the orthodox theory are in very good agreement with the experimental results. (NSF-CAREER(ECS-0449958), ONR(N00014-05-1-0030), THECB(003656-0014-2006).

### 3:00 PM

**Low Temperature Photonic Curing of Nano-Particles for Printed Electronic Conductors and Dielectrics:** *James Sears*<sup>1</sup>; Steve Smith<sup>1</sup>; Michael Carter<sup>1</sup>; Jeffery West<sup>1</sup>; <sup>1</sup>South Dakota School of Mines and Technology

Photonic Curing is being developed to cure or sinter metal nano-particle based films by exposing them to a brief, intense pulse of light from a xenon flash lamp. This photonic curing technology allows for rapid and selective heating that fuses nano-scale metallic ink particles into functional components. This technology allows the curing or sintering of nanoscale metallic ink patterns on low-temperature substrates including flexible circuit boards, flat panel displays, interconnects, RFID tags, and other disposable electronics without the use of heat. This paper reports on the results obtained after sintering conductive, magnetic, and dielectric nano-particle inks. Sintering was performed with the photonic curing technique developed by NovaCentrix, 2W frequency doubled Nd:YAG CW laser, and a conventional muffle furnace. Sample thickness, micro-structural details, resistivity, and sintering characteristics are also examined and compared for the sintering techniques.

### 3:15 PM

**Nano-Scale Trench Filling Using Atomic Layer Deposition:** *Tae Wook Kim*<sup>1</sup>; Jiyoung Kim<sup>1</sup>; Duncan MacFarlane<sup>1</sup>; <sup>1</sup>University of Texas at Dallas

Minimizing the distance needed to redirect a light wave is a key enabling technology for integrated photonic circuits; a recent photonic nanocoupler proposal aims to achieve this through splitting incident light by disrupting total internal reflection with a trench. Fabrication of the trench, requiring a sub-100nm width and a very high aspect ratio, becomes a manufacturing challenge. This constraint, however, is substantially alleviated by filling the trench with a metal oxide. Atomic layer deposition (ALD) is particularly well suited due to excellent conformality on structures with high aspect ratios, and its level of fine control on the film thickness. This study will explore the use of ALD to deposit conformal films consisting of several types of materials including Al<sub>2</sub>O<sub>3</sub> and HfO<sub>2</sub>, chosen for their high refractive indices necessary for the nanocoupler trenches. Emphasis will be placed on the effects of process parameters, such as cycle time and dose of precursors.

### 3:30 PM Break

### 3:45 PM Invited

**Rapid Formation Reactions in Nanolayered Foils: Scientific Studies and Commercial Applications:** *Timothy Weihs*<sup>1</sup>; <sup>1</sup>Johns Hopkins University

Over the last 15 years we have investigated exothermic formation reactions that self-propagate in nanolayered foils where the layers alternate between materials with negative heats of mixing. These exothermic reactions can reach temperatures as high as 3300 K and can travel at velocities greater than 30 m/s. Using results from ignition experiments, velocity and temperature measurements, and continuum modeling, the physical parameters that control the ignition and the propagation of the reactions will be identified for multiple material systems. Commercial applications of these reactive foils will also be described. Emphasis will be placed on the use of the foils as local heat sources that melt solder and metallurgically bond components without thermal damage. Examples such as the bonding of LEDs to PCBs and the bonding of large sputter targets to backing plates will be provided.

### 4:15 PM

**A Novel Ceramic High Secondary Yield Microchannel Plate:** *Raghunandan Seelaboyina*<sup>1</sup>; Indranil Lahiri<sup>1</sup>; Kinzy Jones<sup>1</sup>; Wonbong Choi<sup>1</sup>; <sup>1</sup>Florida International University

In this presentation we will present our recent results on a novel ceramic microchannel plate with high secondary electron yield. Microchannel plates are electron multipliers utilized primarily as an amplification element in various applications. We have employed this unique property of theirs to enhance the field emission current from carbon nanotube emitters. When the microchannel plate was placed above the nanotube cathode, an enhancement of ~18 times in field emission current was achieved. This is attributed to the



giant electron multiplication from our novel high secondary emission material inside the channels of the microchannel plate. A bright field emission image also confirmed the field emission enhancement. The current density achieved with the microchannel plate and the nanotube cathode system was  $\sim 7.1$  mA/cm<sup>2</sup>. We will also discuss our ongoing work to further improve the performance of our novel system

**4:30 PM**

**Precise Placement of Single Nanoparticles on a Large Scale:** *Pradeep Bhadrachalam*<sup>1</sup>; Hong-Wen Huang<sup>1</sup>; Vishva Ray<sup>1</sup>; Seong Jin Koh<sup>1</sup>; <sup>1</sup>University of Texas at Arlington

The capability of manipulating single nanoparticles with nanoscale precision is one of the key requirements for the fabrication of various nanoparticle-based devices and sensors. We present a novel technique to place exactly one single nanoparticle onto a desired substrate location with nanoscale precision. Importantly, the single-nanoparticle placement has been demonstrated by parallel processing over a large area with success rate over 90%. The 20nm gold nanoparticles were positioned onto the target locations through electrostatic guiding structure which was defined using CMOS-compatible technology. The electrostatic guiding structure was made by functionalizing the substrate using self-assembled monolayers (SAMs). The precision of the nanoparticle placement was measured to be  $\sim 12 \pm 7$  nm. We also theoretically studied the forces exerted on the nanoparticles that are responsible for single-nanoparticle placement. This was done by calculating electrostatic potential through numerically solving the non-linear Poisson-Boltzmann equation. Very good agreement was found between the calculations and experiments. (NSF-CAREER(ECS-0449958), ONR(N00014-05-1-0030), THECB(003656-0014-2006))

**4:45 PM**

**Piezoresistive Effect in Nickel Nanostrand - Polymer Composites:** *Calvin Gardner*<sup>1</sup>; Oliver Johnson<sup>1</sup>; George Hansen<sup>2</sup>; Brent Adams<sup>1</sup>; David Fullwood<sup>1</sup>; <sup>1</sup>Brigham Young University; <sup>2</sup>Metal Matrix Composites Corp

Piezoresistive effects are observed when using nickel nanostrands as a conductive additive to a polymer matrix. Nickel nanostrands are elemental crystalline filaments engineered with diameters ranging from 50-1000nm and typical aspect ratios exceeding 50:1, and, most importantly, an interconnected highly bifurcated structure. When combined with a pliable polymer, either by mixing or infusion, unique piezoresistive properties result. We present experimental data exploring the decrease in resistivity and its directional dependence under compressive and tensile strain. A nickel nanostrand-silicone matrix composite in particular demonstrated a very large piezoresistive effect, with resistivity decreasing three orders of magnitude under comparatively small strain. The piezoresistive effect alters with changes in temperature, the resistivity decreasing as temperature increases. Further, the impacts of changing the volume fraction, magnetic alignment of the filaments, and fatigue loading are each examined to characterize the distinctive effect. Additionally, we present a preliminary microstructure based finite element model for the piezoresistivity.

**5:00 PM**

**Ultrasonic Processing of Ultrafine Materials:** *Qingyou Han*<sup>1</sup>; Clause Xu<sup>2</sup>; <sup>1</sup>Purdue University; <sup>2</sup>Hans Tech

Ultrasonic vibration has been used to generate oscillating strain and stress fields in solid materials, and to introduce varying pressure fields in the liquids. This article reports novel techniques for producing nanostructures in bulk materials using ultrasonic vibrations. Two approaches were tested. The first one was to use ultrasonically induced plastic deformation to produce dislocations and vacancies in materials for the formation of nanostructures. This approach was similar to the production of nanostructures using severe plastic deformation. The second approach was to use ultrasonically induced oscillating stress fields to induce repeated phase transformations in the solid materials. Experiments were carried out in 1010 steel using these two approaches. Initial experimental results indicate both approaches led to the formation of nanostructures in bulk materials. The size of the nanostructures obtained using the first approach is smaller than 200 nm and possibly in the range of 100 nm.

**5:15 PM**

**Nano-Manufacturing by Electroforming - A near Net Forming Process for Manufacturing Complex Parts:** *Mohammad Hussain*<sup>1</sup>; <sup>1</sup>KACST

This paper describes the application of electroforming in the synthesis of nano-crystalline nickel coatings/components by very high movement of the electrolyte. A high speed plating equipment has been designed and constructed.

Nanocrystalline nickel coatings were formed at a speed of 600  $\mu$ m per hour, by high speed plating, the grain size of the electrodeposited nickel was considerably reduced by high speed movement of the plating solution. Other processes such as casting, forging, stamping, deep drawing and machining may serve well for most applications. However, when requirements specify high tolerances, complexity, lightweight and miniature geometry, electroforming is a serious contender and in certain cases may be the only economically viable manufacturing process. The electroplated nickel deposits were characterized using SEM, XRD and AFM. The focus of this study is primarily in the application of nano-composites in industrial gas turbines in the synthesis of TBC (Thermal Barrier Coatings).

---

## Alumina and Bauxite: Process Improvements and Experiences - Red Side

Sponsored by: The Minerals, Metals and Materials Society, TMS Light Metals Division, TMS: Aluminum Committee  
Program Organizers: Everett Phillips, Nalco Co; Sringeri Chandrashekar, Dubai Aluminum Co

Tuesday PM

Room: 2002

February 17, 2009

Location: Moscone West Convention Center

*Session Chair:* Ashish Jog, Dubai Aluminium Company

---

### 2:00 PM Introductory Comments

**2:05 PM**

**Advanced Process Control in Alumina Digestion Unit:** *Ayana Oliveira*<sup>1</sup>; Jefferson Batista<sup>1</sup>; Jedson Santos<sup>1</sup>; Márcia Ribeiro<sup>1</sup>; Rafael Lopes<sup>2</sup>; Jorge Charr<sup>3</sup>; <sup>1</sup>ALUNORTE - Alumina do Norte do Brasil S.A.; <sup>2</sup>Honeywell do Brasil; <sup>3</sup>Honeywell Venezuela

The most competitive environment generated the need for performance optimization, for this reason a new control technologies seems a challenges for increase yield in alumina plant, using existing infrastructure and requiring a reduced support team. Robust Multivariable Predictive Control Technology becomes one of the main tools to optimize this class of plants. This paper will discuss the application and benefits of this technology to alumina digestion units, implemented in 3 interconnected digesters. The APC philosophy is based on process variability reduction, and consequently operations optimization, against plant constraints. Since alumina - caustic ratio (A/C) is the key plant variable, it has a fundamental role in this variability reduction. The main challenge in this project was to coordinate the use of 5 grinders to the 3 digesters. The implementation for phase I and II, are finished, respectively, in eight and six months generated more than 1.00% increase in production, rather than A/C variability reduction.

**2:30 PM**

**The Red Mud Recycles on Bayer Process and Its Effect on the Iron Content on Liquor:** *Ayana Oliveira*<sup>1</sup>; Eliomar Ferreira<sup>2</sup>; Tamara Ribeiro<sup>2</sup>; Angela Avelar<sup>2</sup>; Dorival Santos Jr.<sup>3</sup>; <sup>1</sup>ALUNORTE - Alumina do Norte do Brasil S.A.; <sup>2</sup>VALE - Department of Mineral Project Development; <sup>3</sup>VALE - DIAL

It is well known that as the content of iron on the bauxite decreases its concentration on the liquor is increasing and, as a consequence, its content on alumina increases. It is believed that this soluble iron on the liquor could be due to the presence of Al-goethite and its transformation of hematite during the digestion process. In order to minimize the content of iron on the liquor (DBO), the digestion process was carried out with two bauxite samples with recycles of red mud, fine and coarse part, called sand, at different percentages to reach the Fe<sub>2</sub>O<sub>3</sub> grade from 10 to 15% at the process feed. The bauxite and red mud mixtures were digested at 145°C, during 60 minutes, with caustic soda concentration at 280g Na<sub>2</sub>CO<sub>3</sub>/L and initial an A/C of 0.38 and the final A/C reached the value of 0.74. The results demonstrated that fine red mud added to the bauxite did not contribute to a decrease in the iron content of the liquor, instead, the iron content increased. However, the coarse part of red mud, called sand, decreased the iron in the liquor from 0.027g/L to less than 0.004/L.

2:55 PM

**Effect of Lime Quality on Slaking:** *David Kirkpatrick*<sup>1</sup>; Don Williamson<sup>1</sup>; Lynn Blankenship<sup>1</sup>; Shawn Kostelak<sup>1</sup>; <sup>1</sup>Gramercy Alumina LLC

At Gramercy Alumina, both water and liquor-slaked lime are used in the Bayer Process. After laboratory slaking and filtration properties testing, two sources were approved as lime suppliers. In 2007, economics drove a change in the source ratio, and soon the slaking operation began experiencing problems with excessive scaling and large pebbles in the slaker discharge. These problems decreased the operational life of the slakers, consequently decreasing the amount of lime available to the process. Gramercy Alumina began investigating the lime properties by conducting laboratory analyses, site visits and plant trials to determine the cause of the scaling. Although standard lime testing could not highlight the problem, additional tests found hydrocarbon residue after slaking from one source. Plant trials determined the lime source of the excessive scaling and the proper blend of the two limes to obtain the best processing characteristics at the best economics.

3:20 PM

**Selection of Sedimentation Equipment for the Bayer Process - An Overview of Past and Present Technology:** *Tim Laros*<sup>1</sup>; Frank Baczek<sup>1</sup>; <sup>1</sup>FLSmith Minerals

The Bayer Process relies heavily on sedimentation Equipment in Desilication, Liquor Clarification, Residue Disposal, Tertiary Seed Classification, as well as Caustization and Oxalate Removal. Over the past 20 years, sedimentation equipment design and operating philosophies have changed dramatically with the advent of feed slurry dilution, new flocculants, and robotic descaling. This paper will present an overview of the progression of Bayer Process sedimentation technology and current equipment options available.

3:45 PM Break

4:05 PM

**A Novel Chemistry for Improved Aluminate Scale Control in Bayer Process:** *Jing Wang*<sup>1</sup>; Harry Li<sup>1</sup>; Kevin O'Brien<sup>1</sup>; <sup>1</sup>Nalco

In the Bayer Process for the production of alumina, auto-precipitation of alumina trihydrate in the decantation, security filtration, and wash circuit results in both alumina losses and problematic deposit buildup on vessel surfaces. Moreover, auto-precipitation is a key limiting factor in improving plant production by limiting the A/C ratio of digestion. As a result, reduction of this scaling and/or prevention of auto-precipitation in these vessels can significantly improve overall plant performance. While chemical methods to control scale formation, such as Nalco's SCFA (Scale Control Filtration Aid) programs, are well established and widely used within the industry, significant opportunity for additional improvement still remains. In this work, a new, more effective, polymer based chemistry for the prevention of trihydrate scale in thickeners, washers and filters has been developed. This paper provides details on this experimental chemistry to further reduce auto-precipitation without downstream effects in the Bayer process.

4:30 PM

**Using a Statistical Model in the Red Mud Filtration to Predict the Caustic Concentration in the Red Mud:** *Américo Borges*<sup>1</sup>; *Jorge Aldi*<sup>1</sup>; <sup>1</sup>Alunorte - Alumina do Norte do Brasil S.A

Alunorte began its operation in 1995 with a nominal capacity of 1.1 mtpy and after three expansions in a row the production in 2009 will be around 6.3 mtpy. Alunorte uses dry-stacking technology to dispose the red mud, deep-thickeners in the mud washing circuit and drum filters for mud filtration, reducing the caustic concentration from 65 g/L in the last washers down to 7 g/L at filters discharge. This paper aims to present a DOE program with two levels and five factors in the red mud filtration area. Dilution, rotation, condensate, level in the basin and vacuum has been considered as control variables. The output variable considered was the caustic concentration in the red mud. The program measured the magnitude of the control variables and the influences on the output variable, making possible to model the filtration process, controlling the caustic concentration in the red mud below the target of 7 g/L.

4:55 PM

**The Application of Nepheline in Alumina Industry:** *Zhanwei Liu*<sup>1</sup>; Wangxing Li<sup>1</sup>; Wenmi Chen<sup>2</sup>; Bin Liu<sup>1</sup>; <sup>1</sup>Zhengzhou Research Institute of CHALCO; <sup>2</sup>Central South University

The manufacturers of alumina and aluminum manage to make use of local resources to solve the problem of resource shortages because of the rapid increase of alumina productivity. There are amounts of nepheline resources distributed

widely in China, the future for nepheline resources is bright. If nepheline resources are exploited and utilized to produce alumina, the byproduct of potash and sodium salt can be attained, so we can get remarkable economic returns. The physicochemical property, geographical distribution and the application of nepheline in alumina industry are reported in this paper.

5:20 PM Concluding Comments

## Aluminum Alloys: Fabrication, Characterization and Applications: Formability and Texture

Sponsored by: The Minerals, Metals and Materials Society, TMS Light Metals Division, TMS: Aluminum Processing Committee

Program Organizers: Weimin Yin, Williams Advanced Materials; Subodh Das, Phinix LLC; Zhengdong Long, Kaiser Aluminum Company

Tuesday PM

February 17, 2009

Room: 2004

Location: Moscone West Convention Center

Session Chair: Subodh Das, Phinix LLC

2:00 PM

**Influence of Microstructure of 5754 Aluminum Sheet on Localization under Uniaxial Loading:** *SooHo Kim*<sup>1</sup>; Raja Mishra<sup>1</sup>; Anil Sachdev<sup>1</sup>; Asim Tewari<sup>2</sup>; Pinaki Biswas<sup>2</sup>; Swamydha Vijayalakshmi<sup>2</sup>; Shashank Tiwari<sup>2</sup>; <sup>1</sup>Materials & Processes Laboratory, General Motors R&D Center; <sup>2</sup>India Science Laboratory, General Motors R&D Center

This study compares the material characteristics and influence of microstructure on strain localization in four 5754 aluminum sheets made by direct chill (DC) casting, twin belt continuous casting (TBC) and twin roll casting (TRC). Yield and tensile strengths of the four alloys were essentially similar, but the fracture and forming strains of all sheets were different, decreasing in the order of DC, TBC, and TRC. The particle distribution in the four sheets varied considerably; stringers were observed throughout the sheet thickness in both the TBC and TRC sheets, while centerline segregation was observed only in the TRC sheets. The DC cast sheets showed only randomly distributed particles. The difference in fracture strain was correlated to the spatial distribution of the second phase intermetallic particles. The talk will also discuss grain size and texture differences in the various sheets, and compare actual forming behaviors.

2:20 PM

**Development of a Three-Point Bend Test to Evaluate Hemming Performance of Aluminum Sheet:** *Susan Hartfield-Wunsch*<sup>1</sup>; John Carsley<sup>1</sup>; <sup>1</sup>General Motors Corp

General Motors' mid-size car platform is the first attempt to manufacture a common, global aluminum hood. To enable the use of common materials, a new global specification was created based on performance rather than on composition. A new three-point bend test procedure was developed to evaluate aluminum sheet alloys in severe bending deformation analogous to hemming. This new three-point bend test was compared to a previously used wrap bend test, and both tests were effective for evaluating and categorizing different aluminum alloys. The three-point bend test offers several advantages including bending the sample to 180°, and automated testing with a controlled punch rate and load measurement. New aluminum sheet alloys with improved bending performance were compared to current production alloys. A pass-fail criterion was established based on visual inspection of bent samples.

2:40 PM

**Recrystallization and Texture Evolution in Al-Cu-Li Alloys:** *Soonwuk Cheong*<sup>1</sup>; <sup>1</sup>Alcoa Inc

Al-Li alloys have been studied for aerospace applications. Compared to the incumbent non Li containing 2xxx alloys, the Li containing alloys provides attractive density savings in comparable strength and damage tolerance. The present paper discusses the effect of crystallographic texture on the mechanical properties in Al-Cu-Li alloys. Brass texture has been known as a deformation texture component in Al-Cu-Li alloys. The present work introduces Brass texture in a recrystallized microstructure, which presents a better strength and fracture toughness combination compared to Goss textured material. The work also discusses the recrystallization and texture evolution occurring during thermal mechanical processes in Al-Cu-Li alloys for sheet applications.

3:00 PM

**Bending Performance of Al-Mg-Si Alloy after Interrupted and Delayed Quench:** *Cyrille Bezencon*<sup>1</sup>; Jean-Francois Despois<sup>1</sup>; Juergen Timm<sup>1</sup>; Alok Gupta<sup>2</sup>; Corrado Bassi<sup>1</sup>; <sup>1</sup>Novelis Switzerland SA; <sup>2</sup>Novelis Global Technology Centre, Kingston

The hemming performance of 6xxx alloys is a key requirement for automotive panels' application. This mechanical behaviour can be improved by optimizing the alloy composition and the heat-treatment procedure applied during the sheet rolling process. In this paper, the influence of cooling conditions after partial solutionizing heat-treatment on the bending performance of industrial Al-Mg-Si alloys is assessed. Quenching is performed through a water spray system, allowing to control the temperature at which water quench start or end. Three points bending tests and SEM microstructure analysis have been performed for a range of final quenching temperature (interrupted or step quench) and various waiting time before quenching (delayed quench). It is shown that the bendability is highly dependant on the quenching procedure over a critical temperature range and that bending performance can be correlated to grain boundary precipitation.

3:20 PM

**The Effect of Stress Triaxiality and Lode Angle on Failure Strain of 5083-H116 Plate:** *Matthew Hayden*<sup>1</sup>; Charles Roe<sup>1</sup>; Xioasheng Gao<sup>2</sup>; <sup>1</sup>Naval Surface Warfare Center; <sup>2</sup>The University of Akron

Increased performance demands on next-generation vehicles are driving the use of structural aluminum alloys. In addition to strength, designers must consider the limited ductility of these complex structural aluminum alloys. Recent literature suggests that stress triaxiality alone does not fully characterize material failure strain. This study presents the experimental measurements of mechanical deformation of aluminum alloy 5083-H116 plate at multiple stress triaxialities and Lode angles. From these experimental observations Johnson-Cook strength and fracture parameters are calibrated with the goal of developing a more comprehensive failure criterion. Shear components represented by the Lode angle exhibited significant effects on failure strain not previously reported.

3:40 PM

**The Effect of Microstructure on the Surface Finish of Extruded 6262 Aluminum Alloy Billet:** *Qingyou Han*<sup>1</sup>; <sup>1</sup>Purdue University

6262 aluminum alloy is essentially nominal 6061 alloy with additions of lead and bismuth for improved machinability. However, the hot extruded 6262 alloy products suffer a poor surface quality, which varies from ingot to ingot. The intent of this study focuses on the effect of microstructure on the surface quality of the extruded products. The microstructure of the extruded samples is characterized and the microstructure of a sample with a good surface is compared with those of poor surface quality. To our surprise, the extruded samples contain a large number of Mg<sub>3</sub>Bi<sub>2</sub> particles rather than lead-bismuth particles. The microstructure of a sample with a good surface is compared with those of poor surface quality. The volume fraction, size, and size distribution of the Mg<sub>3</sub>Bi<sub>2</sub> are measured. Initial results suggest that the larger the Mg<sub>3</sub>Bi<sub>2</sub> particles, the more negatively the surface quality of the extruded parts are affected.

4:00 PM Break

4:15 PM

**Deformation Textures and Plastic Anisotropy of AA6xxx at Warm Temperatures:** Manojit Ghosh<sup>1</sup>; Alexis Miroux<sup>1</sup>; Jurij Sidor<sup>1</sup>; Leo Kestens<sup>2</sup>; <sup>1</sup>M2i; <sup>2</sup>Delft University of Technology

Tensile and plane strain compression tests as well as deep drawing tests have been used to investigate the forming behaviour of Al-Mg-Si alloys from room temperature to 250°C. In addition to the expected reduction of yield strength with increasing temperature, it is found that temperature also significantly influences the plastic anisotropy of the sheets. The earing profile of drawn cups show a four-fold symmetry after drawing at room temperature and the r-value is minimum along a direction at 45° from RD. At higher temperature the earing profile presents a 2-fold symmetry and the r-value is minimum along RD. The analysis of the deformed microstructures shows that other slip systems than {111}<110> can be activated at higher temperature. Crystal plasticity calculations reveal that for an adequate combination of {hkl}<110> slip systems a good correspondence between the experimental and calculated r-value, yield locus and textures at different temperatures is obtained.

4:35 PM

**Formation of the {111}<110> and {111}<112> Shear Bands and the <111> Fiber Texture during Moderate and Heavy Wire Drawing of 5056 Al-Mg Alloy:** *Mohammad Shamsuzzoha*<sup>1</sup>; Fingling Liu<sup>1</sup>; <sup>1</sup>University of Alabama

Metallography, conventional transmission electron microscopy and x-ray diffraction Techniques have been applied to study the microstructure of moderately and heavily wire drawn 5056 Al-Mg alloy. Samples drawn moderately (~70% of the original value) have been found to be comprised of columnar grains with no evidence of any recrystallization and contain deformation bands. Deformation bands are made of closely spaced parallel slip bands, which lie on {111} and extends along a <110> and contribute to the development of a moderate <111> fiber texture. These samples also possess a high residual stress and show material decohesion normal to fiber axis. The matrix of the sample drawn heavily (> 45% of the original value) showed fibrous microstructure with very little evidence of recrystallization, but exhibit a strong <111> texture. And a high residual stress. Deformation bands in these samples have been found to lie on {111} planes but extend along <112>.

4:55 PM

**Micromechanics of Ductile Fracture of Aluminum 5083 as a Function of Material Stress State:** *Marc Zupan*<sup>1</sup>; Christopher Cheng<sup>1</sup>; Matthew Hayden<sup>2</sup>; Charles Roe<sup>2</sup>; <sup>1</sup>UMBC- University of Maryland, Baltimore County; <sup>2</sup>Naval Surface Warfare Center

The formation of voids, their growth, subsequent ductile rupture, and strain at failure are strongly affected by material element triaxiality. Specifically, investigation of Aluminum 5083 demonstrates promise for insertion into complex weight efficient structural components of vehicles resulting in loading conditions of varied triaxiality. This work will present a ductile fracture failure surface fractography database for Aluminum 5083 loaded monotonically in tension at quasi-static and dynamic strain rates with triaxialities ranging between 0 and 3. The affect of the stress matrix shear components is also evaluated resulting in a failure surface for this alloy. Failure mechanisms including void entourage shearing, cupping, and shear linking are identified. Surface topology measurements are used to evaluate local material strain within the material at the cascade failure event. Failure mechanism maps for the micromechanical failure of this material will be presented.

5:15 PM

**Pole Figure Characteristics of Annealed Aluminum Alloy 6061 in Different Magnetic Fields up to 30 Tesla:** *Samuel Adedokun*<sup>1</sup>; <sup>1</sup>FAMU-FSU College of Engineering

This work presents the changes in the pole figure characteristics of an aluminum alloy 6061 given 85% deformation by cold rolling and later heat treated at 400C in different magnetic fields of up to 30 Tesla for different periods of time. Pieces of samples from the rolled specimen were heat treated in a resistive magnet of 30 Tesla strength with 50 mm bore. The texture changes in the samples were quantified by carrying out texture measurements through an x-ray diffractometer equipped with a texture goniometer. Changes in the texture with the use of the inverse and complete pole figures indicate that the strength of the magnetic field had no effect on the strength of the texture of the material.

5:35 PM

**Comparison of Textures and Microstructures of AA3XXX Hot Bands from Two Different Casting Processes:** *Xiyu Wen*<sup>1</sup>; Yansheng Liu<sup>2</sup>; Zhengdong Long<sup>1</sup>; Shridas Ningileri<sup>3</sup>; Tongguang Zhai<sup>1</sup>; Zhong Li<sup>4</sup>; Subodh Das<sup>5</sup>; <sup>1</sup>University of Kentucky; <sup>2</sup>Secat Inc.; <sup>3</sup>Secat Inc.; <sup>4</sup>Aleris International Inc.; <sup>5</sup>Phinix LLC

Measurements of textures of AA3xxx hotbands made from two different casting routes (twin belt casting vs. the proprietary pellet cast process) by use of the orientation distribution function (ODF) method are carried out, respectively. Their microstructures are observed by use of optical and scanning electronic microscopes. The difference in textures and microstructures resulting from the two processing is studied and presented.



## Aluminum Reduction Technology: Joint Aluminum Reduction Technology and Electrode Technology Session: Coping with Changes in Coke Quality

Sponsored by: The Minerals, Metals and Materials Society, TMS Light Metals Division, TMS: Aluminum Committee

Program Organizers: Gilles Dufour, Alcoa Canada, Primary Metals; Martin Iffert, Trimet Aluminium AG; Geoffrey Bearne, Rio Tinto Alcan; Jayson Tessier, Alcoa Deschambault; Barry Sadler, Net Carbon Consulting Pty Ltd; John Johnson, RUSAL Engineering and Technological Center LLC

Tuesday PM Room: 2003  
February 17, 2009 Location: Moscone West Convention Center

Session Chair: Barry Sadler, Net Carbon Consulting Pty Ltd

See page 190 for program.

## Biological Materials Science: Biological Materials I

Sponsored by: The Minerals, Metals and Materials Society, TMS Structural Materials Division, TMS Electronic, Magnetic, and Photonic Materials Division, TMS: Biomaterials Committee, TMS/ASM: Mechanical Behavior of Materials Committee

Program Organizers: Ryan Roeder, University of Notre Dame; John Nychka, University of Alberta; Paul Calvert, University of Massachusetts Dartmouth; Marc Meyers, University of California

Tuesday PM Room: 3014  
February 17, 2009 Location: Moscone West Convention Center

Session Chairs: Robert Ritchie, University of California; Marc Meyers, University of California

### 2:00 PM Keynote

**Biological Materials: A New Frontier in MSE:** *Marc Meyers*<sup>1</sup>; <sup>1</sup>University of California, San Diego

Biological Materials Science is part of the evolution of MSE from synthetic inorganic materials to organic materials, and finally to biology. It is not a passing fad, but represents a new direction in MSE encompassing three distinct areas: Biological (or natural) materials; Biomaterials (functional and structural); Bioinspired synthesis and processing (biomimetics). MSE brings to bear its unique approach rooted in the structure-property connection. Biological materials are being investigated using a methodology and characterization/testing methods developed by MSE for synthetic materials. This approach is yielding surprisingly rich results and is elucidating the complex hierarchical structures found in nature. We illustrate this approach for shells, crab exoskeletons, bird beaks and feathers, teeth, and bones. Attachment devices used in nature that are inspiring researchers are also reviewed as is current research on biomaterials. Research funding: National Science Foundation Biomaterials Program (DMR).

### 2:40 PM

**Structure and Functional Morphology in Parasitic Wasps:** *John Nychka*<sup>1</sup>; C. Andrew Boring<sup>2</sup>; Michael J. Sharkey<sup>2</sup>; <sup>1</sup>University of Alberta; <sup>2</sup>University of Kentucky

The insects have evolved intricate structures regarding many solutions to challenges of their daily life: locomotion, predation, and species propagation to name a few. Interpretation of the morphology of insect structures has long been mysterious. Nonetheless, many engineering designs have been generated from insect design (e.g., anti-reflection coatings on solar panels based on fly eye geometry, and serrated hypodermic needles mimicking the mosquito's proboscis to reduce pain). On the most basic level, the insect cuticle is a mastery of materials design, exhibiting variable and gradient properties via genetic control. This paper will describe the functional morphology of two systems in parasitic wasps, *Homolobus truncator* (Hymenoptera: Ichneumonoidea: Braconidae), namely the ovipositor (for egg deposition in hosts), and the hamuli-retinaculum (the hook and rail system of the wings). These systems have a multitude of fascinating structures when analyzed with regard to materials science and engineering principles, especially with regard to energy minimization, surface roughness, adhesion, and specific strength.

### 3:00 PM

**Investigation on the Compressive Behavior of Turtle's Shell: Experiment, Modeling, and Simulation:** *Hongjoo Rhee*<sup>1</sup>; *Youngkeun Hwang*<sup>1</sup>; *Seong Jim Park*<sup>1</sup>; *Mark Horstemeyer*<sup>1</sup>; <sup>1</sup>Mississippi State University

Turtle shell is a possible candidate as armor material. We investigated the microstructure, chemical composition, and compressive behavior of the turtle shell through the nano-indentor tests, uniaxial compression testing, and a three point bending test. The obtained experimental data were analyzed and modeled using elastic and viscoelastic theory such as Prony series for a similar bone material. The geometry of turtle shell was digitized and converted into mesh for finite element analysis to simulate three-dimensional deformation of turtle shell under compressive condition based on the developed model.

### 3:20 PM

**Biological Composites: Mechanical and Structural Functions of Bird Beaks:** *Yasuaki Seki*<sup>1</sup>; *Sara Bodde*<sup>1</sup>; *Marc Meyers*<sup>1</sup>; <sup>1</sup>UCSD

The mechanical response and sandwich structure of Toco Toucan and Hornbill beaks were investigated. The rhamphotheca is composed of multiple layers of biological composite of keratin tiles. The orientation of intermediate filaments in keratin matrix was revealed by Transmission Electron Microscope (TEM). The diameter of the keratin filament is ~4 nm. The internal foam consists of closed-cell face of trabeculae is closed by lipid face. The mechanical properties of rhamphotheca were evaluated by tensile testing and indentation techniques. Computed Tomography (CT) was employed for characterizing macrostructure of the network of trabeculae. Visualization Toolkit (VTK) was used for creating three dimensional structure of foam. The created model was used for Finite Element, which were compared with experimental results. We have used Dawson and Gibson model in order to evaluate the optimization and stability of bird beaks.

### 3:40 PM

**Sharp Biological Materials:** *Yen-Shan Lin*<sup>1</sup>; *Eugene Olevsky*<sup>2</sup>; *Marc Meyers*<sup>1</sup>; <sup>1</sup>UCSD; <sup>2</sup>SDSU

Teeth represent an important natural mineral tissue composed of collagen fibrils and carbonate apatite mineral. Structure and mechanical properties of teeth of a broad range of species including shark, piranha, alligator and hippo are investigated. Hardness test results are compared and show the similar hardness values in different living species. The hardness of the enamel ranges from 1.2 to 1.7GPa and the hardness of the dentin is about 0.2 to 0.5GPa. Serrations are observed through SEM analysis for piranha and great white shark teeth with serration sizes of 25µm and 300µm, respectively. The conducted analysis indicates that serrations are used to optimize the biting mechanism. The compressive strength of the teeth was also investigated under longitudinal and transverse loading. The mechanical property of teeth are highly anisotropic due to collagen fibril. Human molar dentins are demineralized and deproteinized through chemical treatment to evaluate the microstructure and test them under compression.

### 4:00 PM Break

### 4:10 PM

**Effects of Moisturizers on the Biomechanics of Human Skin:** *Kemal Levi*<sup>1</sup>; *Ka Yiu Alice Kwan*<sup>2</sup>; *Sumil Thapa*<sup>1</sup>; *Reinhold Dauskardt*<sup>1</sup>; <sup>1</sup>Stanford University; <sup>2</sup>Wellesley College

Moisturizers are widely used in the treatment of skin disorders and their biophysical effects have received extensive attention. However, there remains a significant lack of understanding of how such treatments affect the biomechanical function and responses of human skin. Using a combination of thin-film substrate curvature and bulge techniques, we characterize the stress state of the outermost layer of human skin, stratum corneum (SC), after exposure to well known moisturizers and molecular components of moisturizing treatments. Different classes of moisturizing molecules showed distinctive stress profiles during drying directly demonstrating the efficacy of the treatment. Within the existing classification of moisturizers into humectants and occlusives, occlusives are shown to reduce residual drying stress in SC more effectively than humectants. Finally, the role of the molecules on the SC components including intercellular lipids and corneocyte proteins and their resulting effect on SC stress is examined.

4:30 PM

**Structure-Property Relationships in Bovine Meniscus Attachments:** *Animish Dande*<sup>1</sup>; Diego Villegas<sup>1</sup>; Tammy Haut Donahue<sup>1</sup>; Reza Shahbazian-Yassar<sup>1</sup>; <sup>1</sup>Michigan Technological University

The meniscus tissue plays a critical role in normal functioning of the knee, and various meniscal replacements have been designed for partial or total replacement of the tissue. The proper attachment of these replacements to the tibial plateau is critical and requires fundamental understanding of the nanomechanical properties of meniscal attachments. The insertion sites of the meniscal horn attachments typically contain four zones: subchondral bone, calcified fibrocartilage, uncalcified fibrocartilage and ligamentous zone. This study aimed to correlate mechanical properties of the various zones with their calcium contents. Bovine meniscus attachments were cut into blocks containing all four zones and characterized using quantitative backscattered electron (qBSE) imaging under the scanning electron microscope (SEM). The nanomechanical characterization was carried out by the atomic force microscopy to determine Young's modulus and Poisson's ratio along with topographical studies. A one-to-one correlation between the calcium content and nanomechanical data was made using the above approach.

4:50 PM

**Evolution of Load Partitioning during Creep of Bone Measured by High-Energy X-Ray Diffraction:** *Anjali Singh*<sup>1</sup>; Jonathan Almer<sup>2</sup>; Stuart Stock<sup>1</sup>; Dean Haeffner<sup>2</sup>; David Dunand<sup>1</sup>; <sup>1</sup>Northwestern University; <sup>2</sup>Advanced Photon Source

Bone is a biological composite composed of two intimately mixed solid phases – an organic (protein) matrix, and a discontinuously-distributed reinforcing phase of calcium hydroxyapatite (HaP). An externally applied stress is partitioned by load-transfer between these stiff inorganic particles and the soft organic matrix. By using high-energy X-ray scattering, we determined the bulk in-situ elastic strains in each phase under an applied stress. Compressive creep tests were performed on a bovine femur bone, at different temperatures and stresses. The resulting wide- and small-angle diffraction patterns were used to determine the average phase strains for the two phases. With increasing creep time and stress, the high initial load partitioning between the HaP and protein phases decays. This load-shedding mechanism is discussed in terms of the interplay of viscoelastic deformation of the protein matrix and interfacial damage.

5:10 PM

**Synergistic Effect between the Biomineral and Biopolymer Phases in Bone:** *Po-Yu Chen*<sup>1</sup>; Damon Toroian<sup>1</sup>; Fred Sheppard<sup>1</sup>; Yu Fu<sup>1</sup>; Paul Price<sup>1</sup>; Joanna McKittrick<sup>1</sup>; <sup>1</sup>University of California

Bone is a composite of two main components: a biopolymer, collagen, and a mineral phase, carbonated hydroxyapatite. The collagen fibrils alternate orientation in the concentric rings that surround the main blood vessels (osteons), and the minerals lie primarily within the collagen fibrils. The purpose of this work was to investigate the structural and mechanical properties of demineralized and deproteinated compact and cancellous bone and to compare to untreated bone. Optical microscope, SEM and TEM observations were made and CT scans were used to reconstruct the 3D structure of both demineralized and deproteinated samples. We found the concentric ring structure of the osteons to be undisturbed after demineralization. Compression tests on the compact bone showed that the sum of the stress-strain curves for demineralized and deproteinated bone was far lower than that of the untreated bone, indicating a strong molecular interaction between the two phases. (Support: National Science Foundation DMR 0510138).

## Bulk Metallic Glasses VI: Structures and Mechanical Properties II

Sponsored by: The Minerals, Metals and Materials Society, TMS Structural Materials Division, TMS/ASM: Mechanical Behavior of Materials Committee  
Program Organizers: Peter Liaw, The University of Tennessee; Hahn Choo, The University of Tennessee; Yanfei Gao, The University of Tennessee; Gongyao Wang, University of Tennessee

Tuesday PM  
February 17, 2009

Room: 3007  
Location: Moscone West Convention Center

*Session Chairs:* A. Greer, University of Cambridge; Katharine Flores, Ohio State University

2:00 PM Keynote

**Plastic Deformation of Bulk Metallic Glasses:** *A. Greer*<sup>1</sup>; <sup>1</sup>University of Cambridge

Some recent results on the room-temperature plastic deformation of bulk metallic glasses will be reviewed. Particular attention will be paid to the mechanisms of shear banding and to structural changes caused by deformation. There will also be consideration of the relationship of plastic deformation to the elastic properties of the glasses as revealed by resonant ultrasound spectroscopy (RUS).

2:25 PM

**Mechanical Properties of a  $Zr_{57.4}Cu_{17.9}Ni_{13.4}Al_{10.3}Nb_1$  Bulk Metallic Glass at 300-4.2 K:** *Elena Tabachnikova*<sup>1</sup>; Aleksey Podolskiy<sup>1</sup>; Sergey Smirnov<sup>1</sup>; Vladimir Bengus<sup>1</sup>; Peter Liaw<sup>2</sup>; Hongqi Li<sup>2</sup>; <sup>1</sup>B.Verkin Institute for Low Temperature Physics and Engineering of the National Academy of Sciences of Ukraine; <sup>2</sup>University of Tennessee

The mechanical behaviour of the alloy has been studied in a uniaxial compression at temperatures 300, 170, 145, 77 and 4.2 K with strain rate  $2 \cdot 10^{-3} s^{-1}$ . Temperature dependences of the yield stress ( $\sigma_{0.2}$ ), ultimate strength ( $\sigma_u$ ) and plastic deformation till failure ( $\epsilon_f$ ) have been measured. Monotonous increase of  $\sigma_{0.2}$ ,  $\sigma_u$  and  $\epsilon_f$  have been registered in 300-77 K temperature interval. Thus, value of strength ( $\sigma_u$ ) changes from 1640 MPa (at 300 K) to 1970 MPa (at 77 K), and  $\epsilon_f$  increases from 0.15% (at 300 K) to 3% (at 77 K). At temperature 4.2 K value of strength  $\sigma_u$  reaches 2010 MPa, but macroscopic plastic deformation have not been observed. At whole investigated temperature interval (down to 4.2 K) the failure of the specimens in the two pieces by sliding-off along planes inclined at 45° relative to the compression axis.

2:35 PM Invited

**Characterization of Flow and Fracture in Bulk Metallic Glasses:** *Katharine Flores*<sup>1</sup>; Y.C. Jean<sup>2</sup>; Wolfgang Windl<sup>1</sup>; <sup>1</sup>Ohio State University; <sup>2</sup>University of Missouri, Kansas City

In order for bulk metallic glasses to realize their potential as structural materials, mechanisms of plastic deformation and fracture must be understood and controlled. Prior positron lifetime studies have identified three types of open volume sites in several metallic glass families: inherent interstitial sites, flow defects, and sub-nanometer scale voids. These results have been related to topological models for glass structure, as well as the relative fracture toughnesses of the alloys. In the present work, the crack tip damage zone in a Zr-based bulk metallic glass is examined in an effort to better characterize the relationship between shear band formation and crack growth. These experimental observations are discussed in light of computational studies of flow defects in simulated glass structures under tensile, compressive, and shear loading. It has been observed that flow localization in these simulations requires a pre-existing inhomogeneity in the glass structure, such as a void.

2:50 PM

**Microstructural Characterization of a 200 nm Thick Glass-Forming Metallic Film for Fatigue-Property Enhancements:** Rong Huang<sup>1</sup>; Zhe Zhi Liang<sup>1</sup>; *Jinn P. Chu*<sup>2</sup>; Fengxiao Liu<sup>3</sup>; Peter K. Liaw<sup>3</sup>; <sup>1</sup>National Taiwan Ocean University; <sup>2</sup>National Taiwan University of Science and Technology; <sup>3</sup>University of Tennessee

A 200 nm thick glass-forming metal film,  $Cu_{51}Zr_{47}Al_{13}Ni_9$ , deposited on the 316L stainless steel substrate using magnetron sputtering, has been investigated by using high resolution transmission electron microscopy (HRTEM) coupled

with nanobeam energy x-ray dispersive spectroscopy. The fatigue life of the coated stainless steel is considerably improved by ~3,200%. In addition, the application of the sputtered film yields an increase of the fatigue limit by 30%. The HRTEM analyses are further used to establish the relationship between fatigue property improvement and microstructure. Persistent slip bands in the steel, when arriving the surface, can create a surface offset, which becomes the potential fatigue-crack-initiation site. Our coating film can prevent the surface offset because of its good adhesion, high ductility and strength, thus yielding an improved fatigue property. Consequently, the fatigue-crack initiation and propagation behavior in the nanocrystalline-containing amorphous thin film could be understood.

### 3:00 PM Invited

#### Characterization of Shear Transformation Zones for Plastic Flow of Bulk Metallic Glasses: *Mingwei Chen*<sup>1</sup>; <sup>1</sup>Tohoku University

The basic units of plastic flow of BMGs, in a form of atomic clusters known as shear transformation zones (STZs), are the key to establish a fundamental model of deformation of BMGs at low temperatures. However, despite of extensive theoretical predictions and MD simulations, a direct experimental portrayal of STZ volumes in BMGs is still missing due to their small length scales and diminutive time scales. Here we report an experimental characterization of STZ sizes by proposing an experimental approach based on a newly-developed cooperative shearing theory. The measured STZ volumes of a variety of BMGs are fairly consistent with those predicted by MD simulations. This study offers compelling evidence that the plastic flow of BMGs occurs through cooperative shearing of unstable atomic clusters activated by shear stresses, and provides a new way to gain a quantitative insight into the atomic-scale mechanisms of BMG mechanical behavior.

### 3:15 PM Invited

#### Structure – Mechanical Property Relationship in Metallic Glasses: *Evan Ma*<sup>1</sup>; <sup>1</sup>Johns Hopkins University

For monolithic BMGs with an internal structure that is completely and invariably amorphous, a clear understanding of how the amorphous structures influence mechanical properties (e.g., strength and ductility) remains elusive. Here we investigate typical BMG-forming systems such as Zr-Cu, and Zr-Cu-Al, which are the basis of many important multi-component BMGs. The relationship between the local structure, dynamics and plastic flow is uncovered. We report the structural disordering processes responsible for the initiation of plastic flow at room temperature. Fertile and resistant sites for carrying shear transformations, as well as their effects on shear banding, have been identified. The composition-dependent local order is monitored in a quantitative manner, in lieu of qualitative arguments from the standpoint of free volume. This structural perspective offers a new explanation to the observation of BMGs with large plasticity reported before.

### 3:30 PM Break

### 3:40 PM

#### Structural Characterization of a Bulk Metallic Glass under a Tensile Stress via In-Situ High Energy X-Ray Diffraction: *ChihPin Chuang*<sup>1</sup>; *W. Dmowski*<sup>1</sup>; *Peter K. Liaw*<sup>1</sup>; *J. H. Huang*<sup>2</sup>; *G. P. Yu*<sup>2</sup>; <sup>1</sup>University of Tennessee, Department of Materials Science and Engineering; <sup>2</sup>National Tsing-Hua University

In the present work, the microstructural response of a Zr-based metallic glass (BMG) (Zr<sub>52.5</sub>Cu<sub>17.9</sub>Ni<sub>14.6</sub>Al<sub>10</sub>Ti<sub>5</sub>) to a uniaxial tension stress was investigated using the in-situ high-energy x-ray scattering technique. The atomic-scale elastic strain was recorded accurately by the high-energy synchrotron radiation through different stress levels up to 80% of the yield stress at room temperature. The strains extracted directly from the normalized scattering spectrum and from pair-correlation functions were carefully compared. The corresponding mechanical parameters, such as Young's modulus and Poisson's ratio, were calculated from the strain tensor and were in good agreement with the results deduced from macroscopic measurements.

### 3:50 PM Invited

#### Shear Band Activity during Micropillar Compression Testing of Bulk Metallic Glasses: *Ashwini Bharathula*<sup>1</sup>; *Seok-Woo Lee*<sup>2</sup>; *Katharine M. Flores*<sup>1</sup>; *Wendelin Wright*<sup>3</sup>; <sup>1</sup>The Ohio State University; <sup>2</sup>Stanford University; <sup>3</sup>Santa Clara Univ

Micropillar compression experiments have been performed on Zr<sub>58.5</sub>Cu<sub>15.6</sub>Ni<sub>12.8</sub>Al<sub>10.3</sub>Nb<sub>2.8</sub> bulk metallic glass. The pillar diameters ranged from 200 - 3600 nm with taper angles of 2 - 5 degrees and nominal aspect ratios of 3:1. Discrete

displacement bursts become less pronounced as pillar size decreases, but shear bands were observed to form in all pillars in this size range. The yield strengths do not show a dependence on the size of the deformed volume. Correlations between pillar size, geometry, and shear band activity will be discussed.

### 4:05 PM

#### Short-Range Order of Cu<sub>100-x</sub>Zr<sub>x</sub>Al<sub>5</sub> Bulk Metallic Glasses: *Norbert Matern*<sup>1</sup>; *Hermann Franz*<sup>2</sup>; *Juergen Eckert*<sup>1</sup>; <sup>1</sup>Leibniz Institute IFW Dresden; <sup>2</sup>DESY Hamburg

The short-range order of rapidly quenched and copper mold cast Cu<sub>100-x</sub>Zr<sub>x</sub>Al<sub>5</sub> glasses was investigated by means of Synchrotron high energy X-ray diffraction and Extended X-ray Absorption Fine Structure measurements. The total atomic pair correlation function were determined as a function of Cu content (x= 30-65 at% ). Atomic structure models were developed by the reverse Monte Carlo method. The influence of Al on the atomic structure will be discussed in comparison with corresponding data of binary Cu-Zr glasses. The composition dependence of the mechanical properties of the Cu<sub>100-x</sub>Zr<sub>x</sub>Al<sub>5</sub> glasses were analyzed and compared with their structural behavior.

### 4:15 PM Invited

#### Sample Size Dependent Mechanical Behaviour of BMGs: *Yi Li*<sup>1</sup>; <sup>1</sup>National University of Singapore

In general, a smaller sample size with a corresponding higher cooling rate will induce more free volume and a larger degree of structural disordering in the as-quenched amorphous alloys. As a consequence, smaller samples should have lower strength and a higher malleability. On the other hand, as a brittle material, statistically, the strength of BMGs will decrease when the sample size increases. In this work, with low temperature annealing to minimize the free volume differences among different sized BMG samples, we discovered a sample size-dependent "malleable-to-brittle" transition in a Zr-based BMG. We attribute this transition mainly to the geometrical size effect rather than the structural effect. Accompanied with this transition, the strength of BMG also exhibited a sample size dependence, which was discussed by both the flaw sensitivity<sup>3</sup> and free volume viewpoints. Our results point out the needs to identify the critical sample size for the "malleable-to-brittle" transition in BMGs, especially under engineering consideration.

### 4:30 PM Invited

#### Indentation Deformation of a Zr<sub>50</sub>Cu<sub>37</sub>Al<sub>10</sub>Pd<sub>3</sub> Bulk Metallic Glass: Effect of the Shear Banding Zone: *Fuqian Yang*<sup>1</sup>; *Hongmei Dang*<sup>1</sup>; *Gongyao Wang*<sup>2</sup>; *Peter Liaw*<sup>2</sup>; *Yoshihiko Yokoyama*<sup>3</sup>; *Akihiisa Inoue*<sup>3</sup>; <sup>1</sup>University of Kentucky; <sup>2</sup>University of Tennessee; <sup>3</sup>Tohoku University

The dependence of plastic deformation of bulk metallic glasses on the deformation history has not been well studied. In this contribution, a fatigue test was first performed on a Zr<sub>50</sub>Cu<sub>37</sub>Al<sub>10</sub>Pd<sub>3</sub> bulk metallic glass, which created a shear banding zone near the crack surface in the direction parallel to the crack propagation. Nanoindentation then was used to characterize the indentation deformation of the Zr<sub>50</sub>Cu<sub>37</sub>Al<sub>10</sub>Pd<sub>3</sub> BMG in both the shear banding zone and the area far away from the shear banding zone. The material in the shear banding zone had different indentation hardness from that away from the shear banding zone, suggesting that the plastic deformation of bulk metallic glasses depends on the deformation history. The plastic energy dissipated in an indentation cycle was calculated as a function of the indentation load. Implications of this study in characterizing mechanical behavior of metallic glasses are discussed.

### 4:45 PM

#### Microscale Measurement of Residual Stress by the Slit Method in Zr-Based Bulk Metallic Glass (Zr<sub>50</sub>Cu<sub>40</sub>Al<sub>10</sub>) Subjected to Severe-Plastic Deformation: *Bartlomiej Winiarski*<sup>1</sup>; *R.M. Langford*<sup>1</sup>; *Jiawan Tian*<sup>2</sup>; *Yoshihiko Yokoyama*<sup>3</sup>; *Philip Withers*<sup>1</sup>; *Peter Liaw*<sup>2</sup>; <sup>1</sup>University of Manchester; <sup>2</sup>University of Tennessee; <sup>3</sup>Tohoku University

A surface-treatment process, which was used to generate severe-plastic deformation in the near-surface layer in crystalline materials, is applied on the Zr<sub>50</sub>Cu<sub>40</sub>Al<sub>10</sub> bulk metallic glasses (BMGs). The slit method is used to determine the local residual stress in the plastically-deformed BMG component. The method is based on the measurement of the displacements field arose when a slit is milled into the material under investigation. The displacement field is determined by digital image correlation (DIC) analysis of scanning electron microscope (SEM) images. The slit is milled using focused ion beam (FIB-SEM) workstation. The surface under investigation is decorate with Ytria-stabilized zirconium (YSZ) equiaxial particles of size 20-30 nm precipitated from ethanol



suspension. It is found that the average compressive residual stress is equal to  $-300 \pm 100$  MPa. Microstructures and the micro-hardness profile of the deformed samples are also discussed.

### 4:55 PM Invited

**Stability, Mobility and Sinks of Point Defects in Bulk Metallic Glasses:** *Yuri Petrusenko*<sup>1</sup>; Alexander Bakai<sup>1</sup>; Ivan Neklyudov<sup>1</sup>; Igor Mikhailovskij<sup>1</sup>; Peter Liaw<sup>2</sup>; Lu Huang<sup>2</sup>; Tao Zhang<sup>3</sup>; <sup>1</sup>National Science Center - Kharkov Institute of Physics & Technology; <sup>2</sup>Department of Materials Science and Engineering, The University of Tennessee; <sup>3</sup>Department of Materials Science and Engineering, Beijing University of Aeronautics and Astronautics

Point defects, dislocations and interfaces determine the mechanical properties, transport phenomena, and radiation resistance of solids. Due to the existence of ideal crystalline structures, the defects of crystals can be properly determined. The attempts to determine an ideal glass structure make no real sense because glasses are non-equilibrium, non-ergodic and unstable. Field-emission microscopy was used to investigate compositional and structural heterogeneities of Zr-based bulk metallic glasses (BMGs). It is revealed that the BMG consists of nanoclusters of  $\sim 10$  nm size. Stable intercluster boundaries are identified as well. Electron irradiation of BMGs of different composites at low temperatures and electrical resistance-recovery experiments allow us to identify the existence of stable and mobile defects, such as vacancies. The temperature range of the defect mobility is found. Ordering and disordering processes under electron irradiation are observed. Evidently, the intercluster boundaries are strongest sinks of point defects in BMGs.

### 5:10 PM

**Size Effect on the Mechanical Behavior of Amorphous Alloys:** *F. X. Liu*<sup>1</sup>; Y. F. Gao<sup>1</sup>; W. R. Chiang<sup>2</sup>; P. K. Liaw<sup>1</sup>; <sup>1</sup>The University of Tennessee; <sup>2</sup>Metal Industries Research & Development Center

At low temperatures and high strain rates, the plastic deformation of amorphous alloys usually occurs in narrow shear bands. This highly-localized inhomogeneous deformation results in premature fracture and poor ductility under unconfined conditions. When the size of the amorphous alloys ranges from millimeter to micrometer, the introduction of exterior and interior constraints will effectively confine the excessive propagation of individual shear bands and promotes multiple shear-band formation, resulting in enhanced plasticity. More recently, it has been reported that the amorphous alloys could undergo homogeneous deformation without shear-band formation when the deformation volume or the sample size is down to the nanometer scale. This obvious size effect on the mechanical behavior of amorphous alloys will be summarized and reviewed in this paper. The underlying deformation mechanism will be discussed and validated with micro-compression studies. The application potentials of amorphous alloys implicating from the size effect will be pointed out.

### 5:20 PM

**Crystallization Behavior of a Zr-Based Bulk Metallic Glass during Rapid Heating and Cooling:** *Sun Hongqing*<sup>1</sup>; Katharine Flores<sup>1</sup>; <sup>1</sup>Ohio State Univ

Laser deposition is a useful technique to create metallic glasses and other non-equilibrium microstructures. In this work,  $Zr_{58.5}Cu_{15.6}Ni_{12.8}Al_{10.3}Nb_{2.8}$  powder was deposited onto glassy substrates of the same nominal composition. Amorphous melt zones surrounded by crystalline heat-affected zones (HAZ) consisting of numerous crystal morphologies are observed via SEM and TEM and characterized as functions of the heat input. The thermal history of the HAZ was analyzed using a three-dimensional finite element model. Numerical simulation results indicate that crystallization occurs in regions where the peak temperature exceeds 900 K, while the heating and cooling rates are on the order of  $10^3$  K/s. This rapid heating appears to suppress nucleation, resulting in a critical crystallization temperature  $\sim 150$  K higher than that observed during DSC experiments. The short heating time ( $\sim 10^{-2}$  s) associated with the observed large crystal size ( $\sim 10$   $\mu$ m) also suggests that crystallization in the HAZ is dominated by growth.

## Cast Shop for Aluminum Production: Characterization and Furnace Operation

Sponsored by: The Minerals, Metals and Materials Society, TMS Light Metals Division, TMS: Aluminum Committee  
Program Organizers: Pierre Le Brun, Alcan CRV; Hussain Alali, Aluminium Bahrain

Tuesday PM  
February 17, 2009

Room: 2005  
Location: Moscone West Convention Center

Session Chair: Shridas Ningileri, Secat Inc

### 2:00 PM Introductory Comments

#### 2:05 PM

**A Review of Inclusion Detection Methods in Molten Aluminium:** *Steve Poynton*<sup>1</sup>; Milan Brandt<sup>1</sup>; John Grandfield<sup>2</sup>; <sup>1</sup>CAST CRC and Swinburne University; <sup>2</sup>Grandfield Technology and CAST CRC

Management of inclusions is an important part of quality control within the aluminium cast house. Inclusions including oxide films and particles, spinel, refractory particles and silica particles have a detrimental effect on many aluminium cast products. The ability to reliably detect inclusions in a timely fashion is an essential part of this process. There are a number of tools available for inclusion measurement based on different chemical, physical and electrical principles. This document reviews existing techniques for inclusion detection such as K-Mold, Podfa, Lais, Prefil, LiMCA and Ultrasound, and also examines new techniques which may have potential to offer improved inclusion detection.

#### 2:25 PM

**A New Methodology for Performance Evaluation of Melt Refinement Processes in the Aluminum Industry:** *Bernd Prillhofer*<sup>1</sup>; Holm Böttcher<sup>2</sup>; Helmut Antrekowitsch<sup>1</sup>; <sup>1</sup>University of Leoben; <sup>2</sup>AMAG Casting GmbH

To produce high quality alloys with very low impurity contents, melt quality must be improved from one process step to another. Accordingly, casthouses must analyze and optimize their production processes from the beginning to the end. There are several methods available for process evaluation. Concerning to the strong fluctuating initial inclusion content, the testing methods are not suitable for a single process step improvement at any step in the production chain, within the commercial accomplishment. Only the PreFil®-Footprinter has the potential and the flexibility for inclusion measurement at any place of the process chain, but there is a lack of methodologies for a clear efficiency assessment of metal cleaning steps. This paper presents a new proceeding for quick efficiency evaluation of metal cleaning by using the PreFil®-Footprinter for instance on some refinement steps of the standard cast-house processing for the alloy AA 7075.

#### 2:45 PM

**A Multiphase Model to Describe the Behaviour of Inclusions in LiMCA Systems:** *Xiaodong Wang*<sup>1</sup>; Mihaiela Isac<sup>1</sup>; Roderick Guthrie<sup>1</sup>; <sup>1</sup>McGill University

LiMCA (Liquid Metal Cleanliness Analyzer) is a technique for the in-situ detection of inclusions in liquid metals that is widely used in the aluminum industry. It relies on the Electric Sensing Zone (ESZ) principle. A multiphase flow numerical model is now proposed for describing the motion of inclusions passing through variously-shaped ESZ orifices. The predicted motions of these entrained second phase particles take into account the various forces acting on them, including standard drag forces, added mass, fluid acceleration, buoyancy, and, most significantly, electromagnetic forces. The implications of using parabolic, fluted, and cylindrical orifices are considered, for various metals. The influence of conditioning current operations, electric conductivities, plus the density and size of the inclusions, on their trajectories, is investigated. The numerical results are compared with recent industrial results.

#### 3:05 PM

**Hydrogen Measurement Practices in Liquid Aluminium at Low Hydrogen Levels:** *Mark Badowski*<sup>1</sup>; Werner Droste<sup>1</sup>; <sup>1</sup>Hydro Aluminium Deutschland GmbH

Today's most common measurement systems for hydrogen content in aluminium melt use the principle of a carrier gas and heat flux sensitivity

(thermal conductivity cell). Current publications indicate, that the ambient humidity might influence hydrogen readings due to diffusion of water into the measurement loop. New systems – using electrochemical sensors with a solid reference material of known hydrogen content– enter the market. A comparison of these newer and older ways to determine hydrogen levels in liquid aluminium in a low and normal hydrogen regime will be presented.

**3:25 PM**

**Accurate Measurement of Hydrogen in Molten Aluminium Using Current Reversal Mode:** *Matt Hills*<sup>1</sup>; Chris Thompson<sup>1</sup>; Mark Henson<sup>1</sup>; Andy Moores<sup>2</sup>; Carsten Schwandt<sup>3</sup>; Vasant Kumar<sup>3</sup>; <sup>1</sup>EMC Limited; <sup>2</sup>Foseco; <sup>3</sup>University of Cambridge

Indium doped calcium zirconate is a high temperature perovskite proton conductor suitable for application as the solid electrolyte in a hydrogen concentration cell in molten aluminium. However, prolonged exposure to the melt can result in the prevalence of oxide ion conduction leading to loss of accuracy. Current Reversal Mode (CRM) is an amperometric technique which involves measuring currents through an electrochemical cell at two different states of polarisation. It is capable of accurately determining the cell voltage of a solid electrolyte sensor, as well as providing important diagnostic information in the form of sensor resistance. In this study, CRM is applied to the ALSPEK H sensor for the measurement of hydrogen in molten aluminium. The CRM parameters of frequency and bias voltage for making accurate measurements are identified. Results are presented that demonstrate the application of CRM as a reliable diagnostic tool to ensure that the sensor is measuring accurately.

**3:45 PM Break**

**4:05 PM**

**Increasing the Surface Emissivity of Aluminum Shapes to Improve Radiant Heat Transfer:** *Richard Chandler*<sup>1</sup>; *P. Shull*<sup>2</sup>; <sup>1</sup>Pyrotek Inc; <sup>2</sup>Transmet Corporation

It is common in the aluminum industry to utilize radiant heat during all or part of a melt cycle to transform solid aluminum shapes such as ingots, sows and T-bars to the molten state. The rate of heat transferred into or out of an object by thermal radiation will be governed by, among other things, the surface emissivity of the object, which is equal to the absorption coefficient. Aluminum has a very low absorption coefficient, resulting in inefficient radiant heat transfer during melting. However, it is possible to easily and significantly improve the absorption coefficient of aluminum shapes, thereby increasing melt rates, reducing energy consumption, and reducing oxidation. This paper summarizes the heat transfer theory involved in this process, describes how the absorption coefficient of aluminum shapes can be increased significantly, and presents laboratory and field trials which demonstrate the effects of increased surface emissivity on the melting process.

**4:25 PM**

**Waste Heat Recovery in an Aluminium Cast House:** *Tom Schmidt*<sup>1</sup>; Jan Migchielsen<sup>1</sup>; <sup>1</sup>Thermcon Ovens B.V.

The current fuel price development gives new impulses to further development of waste heat recovery in industries like aluminium cast houses. Fuel is becoming the major cost in melting and casting aluminium. The recovery of waste heat in this industry becomes more and more interesting. This paper will address the various sources of waste heat and the potentials of re-using these sources in and around the aluminium cast house. Eventually an economic evaluation is given for predicting coming developments in the field of heat recovery.

**4:45 PM**

**Reducing Metal Loss in Side Well Charged Melters with Invisiflame Burner Technology:** *James Feese*<sup>1</sup>; Felix Lisin<sup>1</sup>; <sup>1</sup>Hauck Manufacturing

An aluminum side well melting furnace was equipped with state of the art Ultra Low NOx (Nitrogen Oxide) burners resulting in not only reduced emissions but extremely low level of dross formation. Detailed studies of the furnace were carried out to quantify melt efficiency, dross formation and losses, and NOx emissions. Experimental data clearly demonstrates dross losses from the main melt chamber to be very low and additional Fluent Computational Fluid Dynamic (CFD) theoretical modeling of the melt chamber complete with burners further validates the experimental findings. The ultra low NOx burner technology applied results in very low levels of oxygen on the bath surface as well as low and uniform bath surface temperature distribution suppressing dross formation and NOx emissions. Dross losses were quantified taking into account

typical operating practices resulting in savings of several hundred thousand dollars per year.

## Characterization of Minerals, Metals and Materials: Characterization of Microstructure of Properties of Materials II

Sponsored by: The Minerals, Metals and Materials Society, TMS Extraction and Processing Division, TMS: Materials Characterization Committee, TMS/ASM: Composite Materials Committee

Program Organizers: Toru Okabe, University of Tokyo; Ann Hagni, Geoscience Consultant; Sergio Monteiro, State University of the Northern Rio de Janeiro - UENF

Tuesday PM

Room: 3009

February 17, 2009

Location: Moscone West Convention Center

*Session Chairs:* Ann Hagni, Geoscience Consultant; Takashi Nagai, University of Tokyo

**2:00 PM**

**Characterization Of Shear Deformation In Iron:** *Ellen Cerreta*<sup>1</sup>; Amy Ross<sup>1</sup>; Mike Lopez<sup>3</sup>; George Gray<sup>1</sup>; John Bingert<sup>1</sup>; <sup>1</sup>Los Alamos National Laboratory

Through the utilization of a “tophat” shaped specimen, the influence of specimen geometry on forced shear testing has been examined. Seven different geometries have been quasi-statically loaded and sectioned for post mortem analysis. Traditional techniques for this analysis include: optical microscopy, scanning electron microscopy, electron back scattered diffraction, and transmission electron microscopy. However, even with such multi-scale investigations, quantifying the characteristics of shear deformation can be difficult. Here, we present a method that utilizes grain aspect ratio to determine the thickness of the shear affected zone and then utilize this method to quantitatively investigate the influence of geometry on shear deformation as well as provide data for model validation.

**2:15 PM**

**Characterization of the Phase Equilibria and Transformation Behavior of TiNiPt High Temperature Shape Memory Alloys:** *Grant Hudish*<sup>1</sup>; D. Diercks<sup>2</sup>; A. Garg<sup>3</sup>; R. Noebe<sup>3</sup>; Michael Kaufman<sup>1</sup>; O. Rios<sup>4</sup>; <sup>1</sup>Dept. of Metallurgical and Materials Engineering, Colorado School of Mines, Golden, CO; <sup>2</sup>Dept. of Materials Science and Engineering, University of North Texas, Denton, TX; <sup>3</sup>NASA Glen Research Center; <sup>4</sup>University of Florida

One factor limiting more widespread use of conventional NiTi shape memory alloys (SMAs) is their near room-temperature transformation temperatures. Increasing the transformation temperature of these alloys would allow for their use in higher temperature applications in such industries as aerospace, automotive, and power-generation. While Pt is known to cause the highest increases in transformation temperatures for NiTi-based alloys, its effects on microstructure, phase equilibria, mechanical properties, work output etc. are unknown. We will report our results on several TiNiPt alloys with content ratios of Ti/(Ni+Pt)>1, Ti/(Ni+Pt)<1, and Ti/(Ni+Pt)=1 obtained using SEM, EBSD, and TEM techniques. We will show that several phases not present on published Ti-Ni and Ti-Pt phase diagrams are observed allowing us to establish portions of the Ti-Ni-Pt phase diagram. DSC and resistivity methods were also employed to confirm the assumed phase equilibria. Finally, the effects and phases of interstitial elements, namely C and O, were also investigated.

**2:30 PM**

**Object Based Quantitative Analysis of Complex Microstructures in Steel:** *Martin Fischer*<sup>1</sup>; Florian Gerdemann<sup>1</sup>; Wolfgang Bleck<sup>1</sup>; <sup>1</sup>RWTH Aachen University

A new method for the quantitative image analysis of complex microstructures in steel is presented. Microstructures in modern steel grades show growing complexity and ever smaller constituents. It is therefore increasingly difficult or even impossible to access reliable quantitative information on ratios, shapes and spatial distributions of individual phases and constituents via traditional metallographic methods. The new analysis procedure works object-based. Its basic processing units are so-called “image objects” which reflect the pictured structures by merged groups of likely related pixels. Thus information on shape, surface texture and spatial distribution of the microstructural constituents becomes

processable. With these data available, the method is able to quantitatively analyse complex microstructures. This is demonstrated by its application to SEM images of different multiphase steel grades. As the analysis routine is fully automated, the analysis of large amounts of image data is possible and thereby the investigation of statistically relevant areas of microstructures.

**2:45 PM**

**Grain Boundary Engineering in Alloy 800H:** *Daniel Drabble*<sup>1</sup>; Milo Kral<sup>1</sup>; <sup>1</sup>University of Canterbury

Grain boundary engineering has recently shown promise in its ability to improve the mechanical properties of metals by modification of the grain boundary network. The aim of this work was to investigate the feasibility of using grain boundary engineering to improve the high-temperature properties (especially creep) of a common superalloy, alloy 800H/HT. Samples of 800H plate were thermo-mechanically processed using a range of conditions and subsequently analysed using Electron Backscatter Diffraction (EBSD). From this analysis, results such as grain size and grain boundary character were obtained. Grain boundary connectivity was also compared using a novel technique involving grain boundary pixel maps. The microstructural analysis has then been correlated with secondary creep rate, measured in uniaxial tension at high temperature, low-stress conditions to replicate common service parameters.

**3:00 PM**

**Microstructural and Mechanical Characterization of Copper Microsamples after Cold Drawing:** *Christopher Cheng*<sup>1</sup>; Marc Zupan<sup>1</sup>; S. Banovic<sup>2</sup>; <sup>1</sup>University of Maryland Baltimore County; <sup>2</sup>National Institute of Standards and Technology

Copper jackets used in ballistic applications are manufactured via a multi-step drawing process. Cold drawing process causes non-uniform deformation along the longitudinal direction of the jacket, resulting in microstructural and mechanical property anisotropy. This may lead to variation in the performance of the jacket during flight, therefore a need to quantitatively understand the types and scale of deviation in the material. Optical microscopy and X-ray diffraction techniques, in concert with nanoindentation and novel micro-tensile testing, were used to examine the structure-properties relationship of the deformed material. Metallographical analysis revealed high levels of cold working at all locations of the jacket. Deformation level was non-uniform and increased from the jacket tip to tail. This was evidenced by the changes in Young's modulus, yield strength, and ultimate tensile strength, as well as the evolving crystallographic texture, as a function of location. The drawing-crystallographic texture-mechanical properties relationship will be discussed in detail.

**3:15 PM**

**Plastic Localization Phenomena in a Mn-Alloyed Austenitic Steel:** *Giorgio Scavino*<sup>1</sup>; Fabio D'aiuto<sup>2</sup>; Paolo Matteis<sup>1</sup>; Pasquale Russo Spena<sup>1</sup>; *Donato Firrao*<sup>1</sup>; <sup>1</sup>Politecnico Di Torino; <sup>2</sup>Fiat Group Automobiles s.p.a.

A 0.5 wt.% C, 22 wt.% Mn austenitic steel, recently proposed for fabricating automotive body structures by cold sheet forming, due to favorable overall strength and ductility, exhibits plastic localizations during uniaxial tensile tests, but not during biaxial Erichsen tests. Full-thickness tensile and Erichsen specimens, cut from as-produced sheets, were polished and tested at different strain rates. During the tensile tests, the plastic localization phenomena consist first of macroscopic deformation bands traveling along the tensile axis, and then of series of stationary deformation bands, each adjacent to the preceding ones; both types of bands involve the full specimen width and yield macroscopically observable surface relief. No comparable surface relief was observed during the standard Erichsen tests. The stress state being known to influence plastic localization phenomena, reduced-width Erichsen tests were performed with 10 to 50 mm width polished specimens, in order to explore the transition from biaxial to uniaxial loading.

**3:30 PM Break**

**3:50 PM**

**Characterization Laser Shock Peened IN718 Superalloy:** *Amrinder Singh Gill*<sup>1</sup>; S.R. Mannava<sup>1</sup>; Vijay Vasudevan<sup>1</sup>; <sup>1</sup>University of Cincinnati

LSP enhances service lifetimes of critical metal parts like aircraft engine fans and compressor blades. LSP dramatically improves fatigue strength, life and crack propagation resistance with shock wave-induced generation of deep compressive residual stress and microstructural changes. This study aims to understand effects of LSP parameters on residual stress distributions and microstructural changes in an important aero-engine material, IN718. Coupons of alloy with and

without sacrificial layer were LSP-treated with varying energy densities using the GENIV system at GE Aircraft Engines. Depth-resolved characterization of macro residual strains and stresses and degree of cold work in peening direction and transverse to it was achieved using high-energy synchrotron x-ray diffraction at the Advanced Photon Source. Property changes were also studied using EBSD in SEM and TEM. Local property changes were examined using micro and nano-indentation measurements. Results show dominant effects of sacrificial layer and energy density on residual stress distributions and microstructure.

**4:05 PM**

**Effects of Long Term Aging on Creep Properties of HP Reformer Tubes:** *Karl Buchanan*<sup>1</sup>; Milo Kral<sup>1</sup>; <sup>1</sup>Canterbury University

The centrifugally cast HP series has become the dominant reformer tube material for the petrochemical industry. HP alloys with small additions of Nb and Ti are reported to have superior creep properties over standard HP alloys in accelerated testing. However, tubes removed after 3-5 years service exhibit lower remaining life than expected. The present work studies the effects of long-term laboratory aging, as well as exposure to laboratory simulated service conditions, on the creep performance of these alloys. HP-Nb and HP-Micro alloys were aged at 900-1100°C for 500-10,000 hours. Aged samples were then creep tested. Both post creep and post aging samples were characterized in detail using high resolution SEM and high resolution TEM, with special attention paid to the size and distribution to intragranular carbides and the intergranular carbide networks.

**4:20 PM**

**Microstructure and Residual Stress Distribution in Laser Shock Peening Processed Ti-6Al-4V Alloy:** *Yixiang Zhao*<sup>1</sup>; Seetha Mannava<sup>1</sup>; Ulrich Lienert<sup>2</sup>; Jon Almer<sup>2</sup>; Yang Ren<sup>2</sup>; David Lahrman<sup>3</sup>; Vijay Vasudevan<sup>1</sup>; <sup>1</sup>University of Cincinnati; <sup>2</sup>Argonne National Laboratory; <sup>3</sup>LSP Technologies

Laser shock peening (LSP) is a novel surface process that generates deep compressive residual stresses and microstructural changes and thereby dramatically improves fatigue strength of critical metal aircraft engine parts. The present study was undertaken to develop a basic understanding of the effects of LSP parameters on the residual stress distributions and microstructural changes in Ti-6Al-4V. Coupons of the alloy with and without a sacrificial/ablative layer were LSP-treated at GE Infrastructure Aviation and LSP Technologies. Depth-resolved characterization of the macro residual strains and stresses and was achieved using high-energy synchrotron x-ray diffraction and conventional x-ray diffraction. The near-surface and through-the-depth changes in strain, texture and microstructure were studied using EBSD/OIM and by TEM of thin foils fabricated from specific locations. Local property changes were examined using microhardness and nanoindentation measurements. The results showing the relationship between LSP processing parameters, microstructure, residual stress distributions and hardness are presented and discussed.

**4:35 PM**

**Interfacial Microstructure and Evolution of Magnetic Pulse Welded AA6061-T6 and Cu101 Plates:** *Yuan Zhang*<sup>1</sup>; Suresh Babu<sup>1</sup>; Glenn Daehn<sup>1</sup>; Michael Miller<sup>2</sup>; Kaye Russell<sup>2</sup>; <sup>1</sup>The Ohio State University; <sup>2</sup>Oak Ridge National Laboratory

Magnetic Pulse Welding was applied to lap joining AA6061-T6 and Cu101 plates. The microsecond-duration process introduced high-strain rate deformation into the plates. Tensile tests indicated that failure occurred in the base metal. Scanning electron microscopy indicated that the interface had a wavy morphology with discontinuous pockets of an intermetallic phase. Transmission electron microscopy revealed elongated subgrains, lamellar microbands, micro-twinning, dislocation cells, submicron and nano-crystal grains, and articulation teeth-like grains. The high dislocation density and large misorientation of grain boundaries accommodated the deformation. Atom probe tomography suggested that a rod-shaped eutectic phase formed on the intermetallic regions. These results suggest that the refined grain structure with large misorientation and eutectic phase are the origin of high bonding strength of the weld. Research at the Oak Ridge National Laboratory SHaRE User Facility was sponsored by the Scientific User Facilities Division, Office of Basic Energy Sciences, U.S. Department of Energy.



4:50 PM

**Development of New Ultra-High Strength Nb-Containing Q-P-T Steel:** Xiaodong Wang<sup>1</sup>; Ning Zhong<sup>1</sup>; Yonghua Rong<sup>1</sup>; Zuyao Xu<sup>1</sup>; <sup>1</sup>Shanghai Jiao Tong University

A new heat treatment process was developed and named quenching – partitioning – tempering (Q-P-T) based on the previous quenching & partitioning (Q&P) process which is proposed by J.G. Speer et al. And an ultra-high strength steel containing the combination of Nb and less than 0.2%C was obtained using Q-P-T process. The results show that the above Q-P-T steel possesses excellent mechanical properties: the tensile strength of over 1400MPa and the elongation of over 10%. In addition, the volume fractions of martensite and retained austenite were determined and the microstructures were characterized to discover the correlation between microstructures and mechanical properties in the Q-P-T steel.

5:05 PM

**Toughness Characterization of Recycled Polyethylene Composites Reinforced with Post-Used Jute Fabric:** Sergio Monteiro<sup>1</sup>; Amanda Lima<sup>1</sup>; Luis Augusto Terrones<sup>1</sup>; Leandro Marques<sup>1</sup>; <sup>1</sup>State University of the Northern Rio de Janeiro - UENF

Jute fabric obtained from discarded sackcloth is a promising low cost and post-used material being considered as reinforcement of polymeric matrix composites. In particular, the combination of this fabric with a recycled plastic constitutes an environmentally correct composite with both economical and environmental advantages. The present work investigates the toughness of recycled polyethylene composites reinforced with up to 40 wt% of post-used jute fabric extracted from discarded sackcloth. Standard Izod notched specimens were impact tested and the results showed an increase in toughness with the amount of jute fabric. Observation of the composite fracture by SEM revealed that the fabric weave, in spite of damages caused by the previous use of the sackcloth, act as an effective obstacle to crack propagation.

5:20 PM

**Characterization of the Toughness of Piassava Fiber Reinforced Epoxy Matrix by Izod Impact Test:** Sergio Monteiro<sup>1</sup>; Denise Cristina Nascimento<sup>1</sup>; Ludy Motta<sup>1</sup>; <sup>1</sup>State University of the Northern Rio de Janeiro - UENF

Natural lignocellulosic fibers are increasingly being used as polymeric matrix composite reinforcement owing to economical and environmental advantages as renewable and biodegradable materials. Among these, the piassava fiber extracted from a palm tree native of South America stands as one of the most rigid with a potential to be used as composite reinforcement. Therefore, the present work investigates the notch toughness behavior, by Izod impact tests, of epoxy composites reinforced with up to 40 % in volume of continuous and aligned piassava fibers. It was found that the incorporation of piassava fibers results in significant increase in the impact energy of the composite. Scanning electron microscopy analysis showed that the nature of the piassava fiber interface with the epoxy matrix is the major responsible for the superior toughness of the composite.

5:35 PM

**Pullout Tests of Curaua Fibers in Epoxy Matrix for Evaluation of Interfacial Strength:** Sergio Monteiro<sup>1</sup>; Ailton Ferreira<sup>1</sup>; Felipe Lopes<sup>1</sup>; <sup>1</sup>State University of the Northern Rio de Janeiro - UENF

The interface between the matrix and the reinforcing fiber plays an important role in the efficiency by which an applied load is transmitted through the composite structure. The shear stress at the fiber/matrix interface can be associated with this load transference and, consequently, affects the composite strength. In the present work, pullout tests were used to evaluate the interfacial shear stress of curaua fiber in epoxy matrix composites. A small critical length was found for the curaua fiber embedded in epoxy, which corresponds to a relatively weak fiber/matrix bond and lower interfacial strength.

## CO2 Reduction Metallurgy 2009: Ferrous and Titanium Metallurgy

Sponsored by: The Minerals, Metals and Materials Society, TMS Light Metals Division, TMS Extraction and Processing Division, TMS: Energy Committee  
Program Organizers: Neale Neelameggham, US Magnesium LLC; Ramana Reddy, The University of Alabama; Jiann-Yang Hwang, Michigan Technological University; Jean-Pierre Birat, Arcelor Mittal Research

Tuesday PM  
February 17, 2009

Room: 2012  
Location: Moscone West Convention Center

Session Chairs: Jean-Pierre Birat, Arcelor Mittal; Malti Goel, Former Advisor and Senior Scientist, Ministry of Science and Technology

2:00 PM Introductory Comments

2:05 PM

**Reduction of CO<sub>2</sub> Emissions in Steel Industry Based on LCA Methodology:** Ana-Maria Iosif<sup>1</sup>; Jean-Pierre Birat<sup>1</sup>; Olivier Mirgau<sup>2</sup>; Denis Ablitzer<sup>2</sup>; <sup>1</sup>ArcelorMittal R&D; <sup>2</sup>LSG2M-Nancy

Integrating environmental considerations into the product traditional process design is now the major challenge for steel industry. Life Cycle Assessment (LCA) is nowadays considered as an appropriate method for assessing environmental impact and selecting new technologies to reduce CO<sub>2</sub> emissions for steel industry. In this paper we propose a new methodological concept which combines LCA thinking with process simulation software in order to carry out the life cycle inventory of classical steelmaking process. Using Aspen Plus<sup>TM</sup> software, a physicochemical model has been developed for the integrated steelmaking route. This model gives the possibility to carry out life cycle inventories for different operational practices in order to optimise the use of energy, to calculate CO<sub>2</sub> and other emissions and to control the mass and the heat balances of processes. It is also shown that such approach can be used to design and assess new technologies for steelmaking, without large industrial application.

2:25 PM

**Electrolytic Reduction of Ferric Oxide to Yield Iron and Oxygen:** Antony Cox<sup>1</sup>; Derek Fray<sup>1</sup>; <sup>1</sup>University of Cambridge

Hematite pellets were electrolytically reduced to iron in molten sodium hydroxide at 530C to produce iron sponge, free of carbon and sulfur, with about 10 wt% oxygen. The cell was operated at 1.7V with a hematite cathode and an inert nickel anode. Control of the activity of sodium oxide in the melt allowed the cell to be operated below the decomposition potential of the electrolyte with the overall reaction being the ionisation of oxygen from the hematite, its subsequent transport to the anode and discharge, leaving iron at the cathode. A current density of 0.5 A/cm<sup>2</sup> was attained and the energy consumption was 2.8 kWh/kg of iron.

2:45 PM

**Enhanced Energy Efficiency and Emission Reduction through Oxy-Fuel Technology in the Metals Industry:** Dietrich Gross<sup>1</sup>; Mark Schoenfeld<sup>1</sup>; Thomas Weber<sup>1</sup>; Brian Patrick<sup>1</sup>; Norman Bell<sup>1</sup>; <sup>1</sup>Jupiter Oxygen Corporation

Jupiter Oxygen Corporation has an over ten year history of utilizing Oxy-Fuel technology to process aluminum scrap with melt rates in the range of 700-950 BTGU/pound. Recent events have led to consideration of the Jupiter patented process in steel mill furnaces also. A walking beam billet furnace at a major steel company is currently under consideration for conversion to this process to reduce fuel costs and increase production. In addition the firing alumina kilns with Oxy-Fuel is being considered. Jupiter is testing the use of their Oxy-Fuel system for boilers in the power industry with very good results. The process reduces carbon emissions and virtually eliminates NO<sub>x</sub> from the flue gas stream leaving a much smaller volume of gas for sequestration or reuse.

3:05 PM

**Suspension Ironmaking Technology with Greatly Reduced CO<sub>2</sub> Emission and Energy Requirement:** Hong Yong Sohn<sup>1</sup>; Moo Eob Choi<sup>1</sup>; Yao Zhang<sup>1</sup>; Joshua Ramos<sup>1</sup>; <sup>1</sup>University of Utah

A new technology for ironmaking based on direct gaseous reduction of iron ore concentrate is under development. This technology would drastically

lower CO<sub>2</sub> emission and reduce energy consumption by nearly 38% of the blast furnace requirements. Experiments were performed using iron oxide concentrate at 1150°C in a bench-scale facility, which was the highest temperature that could be reached in the facility. The reduction extent was determined at residence times of 3.5 - 5.5 seconds in which the reduction extent approached 43% with 0% excess H<sub>2</sub> and 95% with 860% excess H<sub>2</sub>. Separate kinetics measurements showed that the rate is much faster at 1200 - 1400°C. Experiments were also carried out using syngas (mixtures of H<sub>2</sub> + CO). About 90% reduction in 3.5 seconds at 860% excess hydrogen contained in the syngas demonstrated sufficiently fast reduction for a suspension process and the feasibility of using syngas instead of pure hydrogen.

### 3:25 PM Break

### 3:40 PM

#### Investigation of Carbonic Anhydrase Assisted Carbon Dioxide Sequestration Using Steelmaking Slag: Charles Rawlins<sup>1</sup>; Simon Lekakh<sup>2</sup>; Kent Peaslee<sup>2</sup>; Von Richards<sup>2</sup>; <sup>1</sup>Montana Tech; <sup>2</sup>Missouri S&T

Batch aqueous leaching and carbonation tests were conducted using industrial steelmaking slags to determine the effect of carbonic anhydrase enzyme as a catalyst. Calcium leaching is a strong function of particle surface area, and the extent can be expressed as a function of time and particle size. Carbonic anhydrase did not affect the calcium-leaching rate, however, it did catalyze calcium carbonate formation to achieve a neutralization time near the theoretical rate. Additionally, carbonic anhydrase modified the precipitate morphology due to accelerated particle nucleation. Time controlled tests in which the pH dropped to ~6 decreased the amount of carbonate produced, and this effect was exaggerated by carbonic anhydrase, while pH controlled tests (>8.5) exhibited the highest rate of carbonation. Because the leaching rate was ~50% faster than the carbonation rate, a further increase in the amount of carbonation may be realized by using carbonic anhydrase however pH must be >10.3.

### 4:00 PM

#### Novel Alkali Roasting of Titaniferous Minerals and Leaching for the Production of Synthetic Rutile: Animesh Jha<sup>1</sup>; Abhishek Lahiri<sup>1</sup>; <sup>1</sup>University of Leeds

We present a novel route for the production of high purity synthetic rutile (>95 wt% TiO<sub>2</sub>) via a two-step chemical process. In the first step, the titaniferous minerals are roasted with alkali in air below 900C. After roasting in air the quenched reaction product is leached in water for the separation of water-soluble alkali phases from the insoluble alkali titanate. After aqueous leaching the alkali titanate is further leached in an organic acid medium in N<sub>2</sub> atmosphere from which the synthetic rutile is derived. Alkali phase was recovered from the leach solution. The synthetic rutile derived from roasting and leaching was contained 95-97 wt% of TiO<sub>2</sub> and 3-5 wt% oxide/hydroxide impurities of Fe/Na/Al/Ca. The paper will present the physical chemistry of phase separation process in detail including recycling of CO<sub>2</sub>. We also discuss the suitability of this process for potential mineral beneficiation with virtually zero-process waste.

### 4:20 PM

#### Accelerated Electro-Reduction of TiO<sub>2</sub> to Metallic Ti in a CaCl<sub>2</sub> Bath Using an Intermetallic Inert Anode: Xiaobing Yang<sup>1</sup>; Abhishek Lahiri<sup>1</sup>; Animesh Jha<sup>1</sup>; <sup>1</sup>University of Leeds

Discovery of the FFC Cambridge process for the electro-reduction of metal oxides to metals using carbon anode has been thought to be novel means to produce reactive metals of high purity. In this paper we will discuss the mechanistic aspects of electro-reduction of TiO<sub>2</sub> in the presence of a CaCl<sub>2</sub> bath and an inert anode of alloy material. A remarkable reduction in time from the reported 24-96 hours to less than 10 hours has been achieved by accelerated dissociation of perovskite phase in the presence of alkali modifiers in the TiO<sub>2</sub> pellet. We also discuss the stability of anodes in chloride bath and means to enhance the longevity of such anode materials by monitoring reduction. The paper will discuss the thermodynamics and kinetics aspects of reactions and the steps that leads to rapid conversion of TiO<sub>2</sub> to Ti metal.

## Computational Thermodynamics and Kinetics: Defects

Sponsored by: The Minerals, Metals and Materials Society, ASM International, TMS Electronic, Magnetic, and Photonic Materials Division, TMS Materials Processing and Manufacturing Division, ASM Materials Science Critical Technology Sector, TMS: Chemistry and Physics of Materials Committee, TMS/ASM: Computational Materials Science and Engineering Committee  
Program Organizers: Long Qing Chen, Pennsylvania State University; Yunzhi Wang, Ohio State University; Pascal Bellon, University of Illinois at Urbana-Champaign; Yongmei Jin, Texas A&M

Tuesday PM

Room: 3002

February 17, 2009

Location: Moscone West Convention Center

Session Chair: Yunzhi Wang, Ohio State University

### 2:00 PM Introductory Comments

### 2:05 PM Invited

#### Coupling Crystalline Defects in Microstructure Modeling: Chen Shen<sup>1</sup>; Ju Li<sup>2</sup>; Yunzhi Wang<sup>3</sup>; <sup>1</sup>GE Global Research; <sup>2</sup>University of Pennsylvania; <sup>3</sup>Ohio State University

Microstructure formation in solids typically involves mutual interactions among different types of crystalline defects, such as precipitates, grain boundaries, and dislocations. These interactions can include both chemical (e.g., through diffusion) and mechanical (e.g., through long-range elastic strain field) interactions. A capability of treating them in a common computational framework helps understanding their synergetics in the microstructure formation. We will discuss this attempt in the framework of phase field method, where various defects are treated with different types of phase fields that are coupled in energetics and kinetics. We will show that the marriage of phase field method with other computational techniques, such as ab initio energetic calculations and nudged elastic band method, can expand the capability of the framework to new territories, with examples given on precipitation at defects, dislocation network formation, and interactions between dislocations and precipitate microstructure.

### 2:35 PM

#### Coupling Phase Field Models with Continuum Crystal Plasticity: Anaïs Gaubert<sup>1</sup>; Yann Le Bouar<sup>2</sup>; Alphonse Fine<sup>3</sup>; <sup>1</sup>DMSM, ONERA; <sup>2</sup>LEM, CNRS; <sup>3</sup>LEM, ONERA

The aim of this study is to propose a phase field model to describe microstructural evolutions in nickel-base superalloys during a creep loading. The misfit stresses, the elastic anisotropy, as well as the inhomogeneity in elastic constants between matrix and precipitates are taken into account. Plasticity in the gamma phase is introduced by the means of a viscoplastic law coupled with the phase field model. More precisely, a continuum crystal plasticity formulation is used to efficiently take into account the mechanical behavior of the gamma phase as well as its anisotropy arising from the underlying dislocation slip systems. Our model has been applied to the microstructural evolution in monocrystalline AM1 superalloys. Several experimental tests have been performed to fully determine the coefficients of the viscoplastic law. Finally, we will show that our model is able to describe in detail the rafting of the microstructure during a creep loading.

### 2:55 PM

#### Dislocation and Grain Boundary Melting: A Phase Field Crystal Study: Joel Berry<sup>1</sup>; K. R. Elder<sup>2</sup>; Martin Grant<sup>1</sup>; <sup>1</sup>McGill University; <sup>2</sup>Oakland University

Dislocation and grain boundary melting are studied in three dimensions using the phase field crystal method. Isolated dislocations are found to melt radially outward from their core as the localized excess elastic energy drives a power law divergence in the melt radius. Dislocations within low angle and intermediate angle grain boundaries melt similarly until an angle-dependent first order wetting transition occurs when neighboring melted regions coalesce. High angle boundaries are treated within a screening approximation, and issues related to ensembles, metastability, and grain size are discussed.

3:15 PM

**Grain Boundary Roughening Temperature for Ni is Predicted to Range from below 800K to above 1400K:** David Olmsted<sup>1</sup>; Stephen Foiles<sup>1</sup>; Elizabeth Holm<sup>1</sup>; <sup>1</sup>Sandia National Laboratories

Two dimensional interfaces change from being smooth at low temperatures because of energy considerations to being rough at high temperature because of entropic effects. While this is true of grain boundaries, not much attention has been paid to the fact, except for faceted boundaries. We used molecular dynamics to study grain boundary mobility in fcc Ni as a function of temperature and driving force for 388 crystallographically distinct boundaries. In many of these boundaries a roughening transition can be observed, with the roughening temperature varying from below 800K to above 1400K, i.e. from 0.51 to 0.89 of the melting temperature for the EAM potential used. The grain boundary mobility was found to be much larger above the roughening temperature than below. Thus we expect roughening to affect microstructural evolution substantially during metallurgical processing.

3:35 PM

**Influence of Stress Evolution on Nanotwin Formation in Copper by First Principles Calculations:** Di Xu<sup>1</sup>; Vinay Sriram<sup>1</sup>; Vidvuds Ozolins<sup>1</sup>; Jenn-Ming Yang<sup>1</sup>; K. N. Tu<sup>1</sup>; Gery Stafford<sup>2</sup>; Carlos Beauchamp<sup>2</sup>; <sup>1</sup>UCLA; <sup>2</sup>National Institute of Standards and Technology

High density nanotwins in Cu have been shown to improve the mechanical strength and maintain good ductility and electrical conductivity. The formation of nanotwin is believed to relate to stress evolution during deposition and has been studied using first principles calculations of the total crystal binding energy. Under biaxial stress, the total energy of strained Cu can be larger than that of strain-relaxed periodic nano-twinning Cu. We propose that, during the deposition, highly strained Cu can undergo recrystallization and grain growth to relax stress and form strain-relaxed nanotwins. In-situ stress measurements were performed and showed periodic change of stress and stress relaxation in high frequency pulse electrodeposition. First principles calculations were used to predict nanotwin spacing that can be formed with the measured stress followed by a complete stress relaxation. The calculation results are in good agreement with experimental data.

3:55 PM Break

4:10 PM Invited

**Palladium-Hydrogen Interaction in Dislocations: Trapping and Diffusion:** Dallas Trinkle<sup>1</sup>; <sup>1</sup>University of Illinois, Urbana-Champaign

Pd has a high H solubility, and a high diffusivity due to low binding energy in the bulk. However, experiments have shown that additional binding sites are available in single-crystal Pd with much higher binding energy, effectively storing residual H in the crystal after removal from high pressure H. The storage of H is believed to occur in dislocation cores, which act as nanoscale H traps. Electronic-structure calculations of an isolated Pd dislocation core using flexible boundary conditions, to accurately couple to the long-range elasticity solution, determine the binding energy of H to a dislocation core, the changes in local geometry and electronic structure. Local vibrational modes of H give information about dynamics and compare with neutron scattering measurements; together with energy barrier calculations, H pipe diffusion is compared with bulk diffusivity. These calculations help elucidate the physical ingredients to design more energetically favorable hydrogen storage traps in materials.

4:40 PM

**Atomistic Simulation of Diffusion along Dislocation Cores in Aluminum:** Ganga Purja Pun<sup>1</sup>; Yuri Mishin<sup>1</sup>; <sup>1</sup>George Mason University

Kinetics of many materials processes are controlled by dislocation core diffusion. Its experimental measurements are very difficult and atomistic calculations are rare and nontrivial. We have performed molecular dynamics simulations of self-diffusion along screw and edge dislocations, both isolated and assembled in low-angle grain boundaries, in aluminum using an embedded-atom potential. While vacancy migration is confirmed to be the most important diffusion mechanism, the interesting and unexpected finding is that diffusion can occur even without pre-existing point defects in the core. This “intrinsic” diffusion mechanism is mediated by dynamic vacancy-interstitial pairs (Frenkel defects) that constantly form and recombine in the core due to thermal fluctuations. The Frenkel-pair formation can be assisted by the formation and motion of thermal jogs, making the intrinsic mechanism the dominant one in

screw dislocations. The dislocation interactions in low-angle boundaries result in acceleration of dislocation diffusion.

5:00 PM

**Phase Field Modelling of Stacking Fault Shear in Ni-Base Superalloys:** Vassili Vorontsov<sup>1</sup>; Roman Voskoboinikov<sup>1</sup>; Catherine Rae<sup>1</sup>; <sup>1</sup>University of Cambridge

The “Phase-Field Microelasticity Theory” has been used to simulate dislocation propagation in nickel-base superalloys. In particular, the cutting of gamma-prime precipitates by matrix dislocations has been comprehensively studied with the aim of verifying the governing mechanisms of primary creep. Formation of nodes and networks has also been examined. The model demonstrates various dislocation reactions, such as recombination, reordering and annihilation. The formation and evolution of superlattice and complex stacking faults and anti-phase boundaries is achieved by incorporating fault energy data from Molecular Dynamics simulations. For the first time, a double-plane gamma-surface is used to incorporate extrinsic faults. The observed likelihood of stacking fault formation is found to exhibit strong stress dependence. The simulated stacking faults form less readily as the applied stress approaches the superalloy’s theoretical yield. This demonstrates why numerous stacking faults are observed in primary creep specimens and not in those subjected to a simple tensile test.

5:20 PM

**Interaction of He-Vacancy Clusters with Cr in FeCr Alloys from First Principles:** Enrique Martinez<sup>1</sup>; Chu Chun Fu<sup>1</sup>; Frederic Soisson<sup>1</sup>; Maylise Nastar<sup>1</sup>; <sup>1</sup>CEA-Saclay

FeCr alloys are nowadays the strongest candidates as structural materials for fusion applications. As it is well known experimentally, irradiation modifies the response of such an alloy reducing considerably its working lifetime. During irradiation with fast neutrons He is produced by transmutation. How this He affects the properties of the base material is not well understood. We have studied the interaction of He, vacancy and small He-vacancy complexes of very high binding energy, and their possible diffusion paths as a function of Cr concentration and Cr-cluster spacing within the Density Functional Theory. The accuracy from various pseudo-potential and basis sets approximations are discussed in detail. Formation, binding and migration energies have been calculated systematically. The resulting energetics will be used in Monte Carlo simulations to try to understand how He bubbles nucleate in the FeCr matrix as well as how  $\alpha'$  precipitates may be formed in the presence of He.

5:40 PM Invited

**Interfaces and the Behavior of Nanocomposites under Irradiation:** Michael Demkowicz<sup>1</sup>; <sup>1</sup>Los Alamos National Laboratory

Nanocomposites—both hetero- and homophase—contain a high volume fraction of interfaces that can heal radiation damage by absorbing and recombining radiation-induced Frenkel pairs. But are all interfaces equally effective at reducing radiation damage? This question is addressed by a diffusion-reaction analysis that models interfaces as surfaces where point defect properties such as formation energies, migration energies, and vacancy-interstitial recombination rates differ from those of the surrounding crystalline medium. The dependence of an interface’s response to irradiation with varying interface properties and irradiation conditions is investigated and opportunities for designing radiation-tolerant nanocomposites for nuclear energy applications are discussed. We are grateful for support from the LANL LDRD and Director’s Postdoctoral Fellowship programs as well as from DOE-OBES.



## Diffusion in Materials for Energy Technologies: Session II

Sponsored by: The Minerals, Metals and Materials Society, TMS Structural Materials Division, TMS Electronic, Magnetic, and Photonic Materials Division, TMS: Alloy Phases Committee, TMS: High Temperature Alloys Committee, TMS/ASM: Nuclear Materials Committee, TMS: Solidification Committee, ASM-MSCTS: Atomic Transport Committee  
Program Organizers: Jeffrey LaCombe, University of Nevada, Reno; Yongho Sohn, University of Central Florida; Carelyn Campbell, National Institute of Standards and Technology; Afina Lupulescu, GE; Ji-Cheng Zhao, Ohio State University

Tuesday PM Room: 3006  
February 17, 2009 Location: Moscone West Convention Center

Session Chairs: Yongho Sohn, University of Central Florida; Maria Okuniewski, University of Illinois at Urbana-Champaign

### 2:00 PM Invited

**Rapid Diffusion-Limited Pathways to CuInxGa1-xSe2 Thin Film Synthesis:** Timothy Anderson<sup>1</sup>; Carelyn Campbell<sup>2</sup>; <sup>1</sup>University of Florida; <sup>2</sup>National Institute of Standards & Tech

A systematic search for rapid reaction pathways for the formation of CuInxGa1-xSe2 thin films was performed using in-situ high temperature X-ray diffraction. Time-resolved high temperature X-ray diffraction data were collected using a position sensitive detector while the precursor film temperature was held constant or ramped. Reaction pathways under both inert and Se overpressure were examined for a variety of elemental and bilayer precursor film structures. The observed pathways are compared to those suggested by diffusion limited transport with equilibrium conditions at the interfaces. Analysis of the diffraction data was supported by high resolution structural and compositional measurements of synthesized absorbers. The results indicate absorber synthesis is a robust process with different precursor structures and operating conditions leading to CuInxGa1-xSe2 formation, often through formation of intermediate compounds. Other results also suggest that MoSe2 forms after complete formation of the absorber when using Mo/Glass substrates.

### 2:35 PM

**Diffusion and Reaction Kinetics in the Al<sub>2</sub>O<sub>3</sub>-TiO<sub>2</sub> System under Electric Field Application:** Dat Quach<sup>1</sup>; Joanna Groza<sup>1</sup>; <sup>1</sup>University of California, Davis

Materials processing under external electric field / electrical current applications is of great interests due to its high heating rates and possibly enhanced mass transport. Dense Al<sub>2</sub>TiO<sub>5</sub> ceramic is obtained from a powder mixture of Al<sub>2</sub>O<sub>3</sub> and TiO<sub>2</sub> in a few minutes using the novel field-assisted sintering technique (FAST). Under field application the reaction kinetics and diffusion in this ceramic system are studied via powder reaction and diffusion couple experiments at temperatures from 1370–1500°C. Results from FAST show enhanced nucleation and a different activation energy for reaction compared with conventional heating.

### 3:00 PM

**Silver Diffusion in Silicon Carbide:** Erich Friedland<sup>1</sup>; Nic Van der Berg<sup>1</sup>; Johan Malherbe<sup>1</sup>; Thulani Hlatshwayo<sup>1</sup>; <sup>1</sup>University of Pretoria

This study aims to obtain information on volume and grain boundary diffusion as well as on the influence of radiation damage. For this purpose 360 keV 109-Ag was implanted with a fluence of 2xE16 cm<sup>-2</sup> in poly and single crystalline SiC at temperatures ranging from room temperature to 900 K. Diffusion coefficients were obtained from implantation profile broadening after isochronal and isothermal annealing up to 1900 K, using RBS analysis combined with alpha-particle channeling spectrometry. Structural information was obtained by scanning and transmission electron microscopy. As the surface region of the room temperature implants was completely disordered, the initial broadening was used to study diffusion in amorphous silicon carbide. Comparison of results for annealed single and poly crystalline samples yielded information on the relative importance of volume and grain boundary diffusion. The influence of radiation damage was extracted by comparing results for implants done at room and elevated temperatures.

### 3:25 PM

**Microstructure and Annealed Effect of Sn-Sb-(Ni) Thin Films on the Charge-Discharge Capacity Characteristics:** Wu Chao-Han<sup>1</sup>; Fei-Yi Hung<sup>2</sup>; Lui Truan-Sheng<sup>1</sup>; Chen Li-Hui<sup>1</sup>; <sup>1</sup>Department of Materials Science and Engineering, Center for Micro/Nano Science and Technology, National Cheng Kung University; <sup>2</sup>Institute of Nanotechnology and Microsystems Engineering, Center for Micro/Nano Science and Technology, National Cheng Kung University

In this study, radio frequency magnetron sputtering was adopted to prepare Sn-Sb-(Ni) film anodes. The effects of the thickness of the film and its index of crystalline (IOC) on the charge-discharge capacity characteristics are discussed. Increasing the thickness of the film anode from 500nm to 2000nm, not only raised the IOC, but also improved the migration of lithium ions and electrons because of the lower resistivity. So, the cyclability of the as-adopted film was enhanced with increasing the film thickness. After recrystallization, the IOC rose and the resistivity fell. However, cracks on the film induced by thermal strain increased the area of the passive film, resulting in reduced cyclability. In addition, added micro-Ni into Sn-Sb matrix was able to enhance the charge-discharge capacities and the high temperature cyclability.

### 3:50 PM Break

### 4:05 PM Invited

**High-Pressure Hydrogen Permeation and Diffusion in Iron and Steels:** Zhili Feng<sup>1</sup>; Lawrence Anovitz<sup>1</sup>; Timothy Armstrong<sup>1</sup>; <sup>1</sup>Oak Ridge National Laboratory

Hydrogen induced mechanical property degradation is a primary concern for the safe operation of hydrogen delivery and storage systems made of metallic engineering materials such as ferritic steels. The degree of degradation is directly related to the amount of hydrogen in the metal. In this work, we investigated the hydrogen permeation and diffusion processes in pure iron and ferritic steels by means of high-pressure gaseous hydrogen permeation experiment (up to 2,000psi). The dependency of hydrogen diffusion on hydrogen charging pressure and temperature are obtained and will be discussed. In addition, the observed surface effects will be discussed in relation to the high-pressure hydrogen permeation test and their implications in controlling hydrogen into metal. Issues related to hydrogen transport under high-pressure hydrogen environment to ensure the long-term reliability of the hydrogen delivery infrastructure will be highlighted.

### 4:40 PM

**Hydrogen Permeation in Steels via Fractional Diffusion:** Alonso Jaques<sup>1</sup>; Jeffrey LaCombe<sup>1</sup>; <sup>1</sup>University of Nevada

Frequently, hydrogen diffusion is analyzed using electrochemical permeation per methods per ASTM G148-97, where the experimental setup (Devanathan-Stachurski) is established, but the analysis methods are still largely based on "traditional" diffusion theory. Ample experimental evidence published in the literature calls this analytical approach into question, as much of the reported data in the literature shows deviation from theoretical predictions. For example, discrepancies observed in hydrogen diffusion in steel show signs of so-called "anomalous diffusion", where the characteristic length scale for diffusion is not proportional to  $t^{1/2}$ , but rather to  $t^{\alpha}$ , where  $(1 \leq \alpha \leq 2)$ . The formal description of anomalous diffusion is expressed using fractional calculus. Preliminary analysis of published "problematic" data from the literature shows improved agreement with fractional diffusion when compared to analyses using the traditional square-root scaling. The fractional calculus approach to diffusion will be discussed here, including implementation of the method and discussion of the phenomenological foundations.

### 5:05 PM

**Magnetic and Electric Field Effects on Hydrogen Absorption and Mass Transfer at the Metal/Electrolyte Interface:** John Roubidoux<sup>1</sup>; Brajendra Mishra<sup>1</sup>; Joshua Jackson<sup>1</sup>; David Olson<sup>1</sup>; <sup>1</sup>Colorado School of Mines

The superposition of a uniform magnetic field during laboratory-scale electrochemical hydrogen charging of pipeline steels (X52, X70, X80, X100) indicates an increase in the measured hydrogen content compared to unmagnetized charging. Increased hydrogen absorption may be associated with the disturbance of the Gouy-Chapman Layer (GCL) and the Helmholtz Double Layer (HDL). The disturbance of the GCL and HDL may be due to the interaction of the large magnetic and electric fields, which results in an altering of the kinetics of the system. The rate of mass transfer to the working electrode

(steel sample) is also known to increase when a magnetic field is superimposed on the experimental system. The objectives of this research were to determine the mechanism by which hydrogen absorption occurs at the metal/electrolyte interface and determine what influence combined magnetic and electric fields have on the rates of mass transfer to the working electrode.

## 5:30 PM

**Aspen Plus Modeling of a Diffusion-Limited Three-Reaction Hydrogen Producing CuCl Thermochemical Cycle:** Alexandra Lupulescu<sup>1</sup>; John Prindle<sup>1</sup>; Victor Law<sup>1</sup>; <sup>1</sup>Tulane University

As the world continues to grow at a steadfast pace, an even bigger strain is placed on already limited energy resources. Consequently, the fossil supply must be replaced by new methods of producing energy. A promising field is hydrogen. In the current work, the Copper-Chloride thermochemical cycle has been studied due to its low temperature requirements and easy implementation as a result of minimal solids transfer. A three-reaction scheme has been proposed:  $2\text{CuCl} + 2\text{HCl} \cdot 2\text{CuCl}_2 + \text{H}_2$  (electrochemical)  $100^\circ\text{C}$ ;  $2\text{CuCl}_2 + \text{H}_2\text{O} \cdot \text{Cu}_2\text{OCl}_2 + 2\text{HCl}$  (vacuum)  $375^\circ\text{C}$ ;  $\text{Cu}_2\text{OCl}_2 \cdot 2\text{CuCl} + 0.5\text{O}_2$   $550^\circ\text{C}$ . For the first time, to our knowledge, the electrolyzer has been modeled in Aspen by a calculator block rather than a stoichiometric reactor. This was done in order to accurately depict the diffusion across the ionic membrane of the electrolyzer, which in turn determines the kinetic rate of the hydrogen producing reaction.

## Dislocations: 75 Years of Deformation Mechanisms: Nanostructured and Temperature Effects on Dislocations

Sponsored by: The Minerals, Metals and Materials Society, TMS Materials Processing and Manufacturing Division, TMS Structural Materials Division, TMS/ASM: Mechanical Behavior of Materials Committee, TMS: Nanomechanical Materials Behavior Committee

Program Organizers: David Bahr, Washington State University; Erica Lilleodden, GKSS Research Center; Judy Schneider, Mississippi State University; Neville Moody, Sandia National Laboratories

Tuesday PM Room: 3022  
February 17, 2009 Location: Moscone West Convention Center

Session Chairs: Judy Schneider, Mississippi State University; Jonathan Zimmerman, Sandia National Laboratories

## 2:00 PM Invited

**Dislocation Dynamics and Storage in Nanocrystalline Materials:** Scott Mao<sup>1</sup>; Zhiwei Shan<sup>1</sup>; <sup>1</sup>University of Pittsburgh

This talk focuses on dislocation dynamics and storage in nc materials through in-situ TEM and in-situ synchrotron tests. It is believed that the dynamics of dislocation processes during the deformation of nanocrystalline materials can only be visualized by computational simulations. Here we demonstrate that observations of dislocation processes during the deformation of nanocrystalline Ni with grain sizes as small as 10nm can be achieved by using a combination of in situ tensile straining and high-resolution transmission electron microscopy. In collaboration with Dr. Yang in Argonne National Laboratory, in situ synchrotron on nc and micron Ni under hydrostatic stress up to 57Gpa show that peak broadening increases during loading up to 45 Gpa in nc-Ni, which indicates high dislocation density storage, and no clear grain growth or texturing. The stored dislocations are reversible after unloading. In course grained sample, stored dislocations are not reversible.

## 2:30 PM

**Mechanical Behavior of Trimetallic Nanocomposites under Various Loading Conditions:** Ioannis Matorakos<sup>1</sup>; Hussein Zhib<sup>1</sup>; David Bahr<sup>1</sup>; Firas Akasheh<sup>2</sup>; <sup>1</sup>Washington State University; <sup>2</sup>Taskegee University

Nano-Metallic Material (NMM) composites represent a novel class of advanced engineering materials whose scientific significance and technological potential as high performance materials is just beginning to be explored. Presently, NMM composites are made of bimetallic systems and are typically classified into coherent (the two metals having the same crystal structure and a small lattice parameter mismatch) and incoherent systems (the two metals having different crystal structure and a large lattice parameter mismatch). While coherent systems are more ductile, incoherent systems are generally stronger. The purpose of this

work is to expand our understanding on the behavior of NMM by performing atomistic simulations on trimetallic systems. The simulated composite material is consisted of alternating layers of Ni/Cu/Nb, thus creating a combination of coherent/incoherent interfaces. The deformation behavior as well as the damage mechanisms of the triaxial systems are investigated under uniaxial, biaxial and fatigue loading.

## 2:50 PM

**Stress and Dislocation Core Controlled Plasticity of Graphene Based Nanostructures:** Shuo Chen<sup>1</sup>; Elif Ertekin<sup>2</sup>; Daryl Chrzan<sup>1</sup>; <sup>1</sup>Department of Materials Science and Engineering, UC Berkeley, CA; <sup>2</sup>Berkeley Nanoscience and Nanoengineering Institute, UC Berkeley, CA

Graphene based nanostructures are expected to be plastically deformed under certain loading conditions mediated by defects best described as two-dimensional dislocations. Here we explore a novel mechanism of plasticity unique to these systems. Specifically, stress relaxation is studied via kinetic Monte Carlo simulations (both at T=0 K and finite temperatures) based on the empirical Tersoff-Brenner potential. In contrast to the usual glide response in bulk materials, the stress relaxation is initially achieved by generating an array of dislocation dipoles (Stone-Wales defects). At lower stresses, the plastic deformation mechanism switches to conventional dislocation glide. The kinetic pathway is further analyzed within linear elasticity theory. It is revealed that the nature of the plasticity is closely related to the core structure of the two-dimensional dislocations which, in turn, is strongly affected by the local curvature and the local stress and strain fields.

## 3:10 PM

**Dislocation-Interface Interaction in Nanoscale Metallic Multilayers:** Sergey Medyanik<sup>1</sup>; Shuai Shao<sup>1</sup>; <sup>1</sup>Washington State University

Nanoscale multilayered metallic materials often exhibit very high strength levels, close to the theoretical strength limits. This strengthening phenomenon has been usually attributed to the presence of interfaces between dissimilar materials that serve as barriers to the gliding dislocations. In this work, we present results of atomistic simulations that demonstrate some of the mechanisms of dislocation interaction with interfaces. We employ nanoindentation model to generate dislocations at and near the surface and focus on investigating bi- and tri- metallic systems composed of Cu, Ni, and Nb. Interaction of propagating dislocations with three types of interfaces (coherent, semi-coherent, and incoherent) is analyzed. Specific mechanisms that cause strengthening in nanoscale multilayered metallic composites are investigated in detail.

## 3:30 PM

**Dislocation Dynamics (DD) Analysis of Strength in Heterogeneous Nanoscale Tri-Metallic Multilayered Composites:** Firas Akasheh<sup>1</sup>; Hussein Zhib<sup>2</sup>; Cory Overman<sup>2</sup>; Sreekanth Akarapu<sup>2</sup>; David Bahr<sup>2</sup>; <sup>1</sup>Tuskegee University; <sup>2</sup>Washington State University

In this work, multiscale DD-continuum analysis of plasticity in heterogeneous multilayered structure made of 3 different metals is studied. Typical DD analysis does not account for Kohler image forces due to elastic properties mismatch. Such forces become increasingly significant in the case of NMM composites, affecting the strength and dislocation interaction among themselves and with the interfaces. A methodology based on the concept of eigenstrain and superposition was implemented and validated to account for such effects. The channeling strength of layer-confined glide dislocations in different FCC-BCC material systems is estimated and Kohler forces are quantified as a function of the layer thicknesses and layering scheme.

## 3:50 PM Break

## 4:10 PM Invited

**The Importance of Reordering during the High Temperature Deformation of Ni-Base Superalloys:** Libor Kovarik<sup>1</sup>; Raymond Unocic<sup>1</sup>; Yunzhi Wang<sup>1</sup>; Ju Li<sup>2</sup>; Michael Mills<sup>1</sup>; <sup>1</sup>Ohio State University; <sup>2</sup>University of Pennsylvania

In order to improve the capabilities of polycrystalline gamma-prime (L12 structure) strengthened Ni-based superalloys for turbine disk applications, the rate-controlling deformation mechanisms must be fully understood, and robust theory/models developed that connect the microstructure to creep and fatigue properties. Dramatically different deformation mechanism can occur depending upon temperature, applied stress and initial precipitate structure in disk alloys. Most remarkably, in the range of 600-800°F extended faulting through precipitates and matrix, isolated shearing of gamma-prime precipitates and microtwinning are observed. While these mechanisms are distinct, we argue that

they are all connected and controlled by the same thermally-activated process of chemical reordering in the ordered precipitates after shearing by Shockley partial dislocations. The evaluation of key activation processes, suggested from direct experimental observations of the deformation mechanisms, is being conducted using a novel combination of atomic-scale and phase field dislocation modeling.

4:40 PM

**Introducing Dislocation Climb by Bulk Diffusion in Discrete Dislocation Dynamics Simulations:** *Dan Mordehai*<sup>1</sup>; Emmanuel Clouet<sup>2</sup>; Marc Fivel<sup>3</sup>; Marc Verdier<sup>3</sup>; <sup>1</sup>SRMP, CEA-Saclay, Department of Materials Engineering, Technion-Israel Institute of Technology; <sup>2</sup>SRMP, CEA-Saclay, France; <sup>3</sup>SIMaP, Grenoble INP, France

One of the computational tools to study dislocation microstructure and plasticity at the mesoscopic scale is Discrete Dislocation Dynamics (DDD) simulations, in which dislocations are treated as elastic entities. In this talk, we present a method to incorporate dislocation climb by bulk diffusion in Dislocation Dynamics simulations, by coupling this simulation technique with the diffusion theory of vacancies. We adapt the method to a 3-dimensional DDD simulation, in which dislocations are represented by pure edge and screw segments. The calculation is demonstrated by simulating the activation of a Bardeen-Herring climb source upon the application of an external stress or under vacancy supersaturation, as well as isolated dislocation prismatic loops shrinkage and expansion. The model is shown to reproduce the coarsening of dislocation loops in annealed bulk, where large dislocation loops expand on the expense of smaller ones. The processes observed in our simulations agree with experimental observations in fcc metals.

5:00 PM

**Characterization of Dislocations and Modeling of Creep Mechanisms in Zirconium Alloys:** *Benjamin Morrow*<sup>1</sup>; Robert Kozar<sup>2</sup>; Ken Anderson<sup>2</sup>; Michael Mills<sup>1</sup>; <sup>1</sup>Ohio State University; <sup>2</sup>Bechtel Bettis Inc

Zirconium alloys are used commonly for applications in nuclear reactors. Accurately predicting creep deformation of zirconium alloys throughout the lifecycle of a reactor depends on reliable deformation models. The Modified Jogged-Screw Model asserts that the motion of tall jogs in screw dislocations act as the rate controlling mechanism during creep in certain regimes. Previous studies have demonstrated the applicability of the Modified Jogged-Screw model to the thermal creep behavior of hcp metals. Scanning transmission electron microscopy (STEM) was used to directly observe and characterize the dislocation structure of creep tested Zircaloy-4 and quantify model parameters such as jog height, jog spacing, and dislocation density. Attempts to correlate dislocation density measurements using X-ray diffraction and STEM techniques will be reported. Thorough characterization will provide a better understanding of creep dislocations structures in zirconium alloys, which will ultimately result in more robust creep deformation predictions.

5:20 PM

**Shock Induced Deformation Substructures in a Copper Bicrystal:** *Fang Cao*<sup>1</sup>; Irene Beyerlein<sup>1</sup>; Bulent Sencer<sup>2</sup>; Ellen Cerreta<sup>1</sup>; George Gray<sup>1</sup>; <sup>1</sup>Los Alamos National Laboratory; <sup>2</sup>Idaho National Laboratory

Controlled shock recovery experiments have been conducted to assess the role of shock pressure and orientation dependence on the substructure evolution of a [100]/[01-1] copper bicrystal. Electron backscatter diffraction (EBSD) and transmission electron microscopy (TEM) were utilized to characterize orientation variation and substructure evolution of the post-shock specimens. Well defined dislocation cell structures were displayed in both grains and the average cell size decreases with increasing shock pressure. Twinning has been occasionally observed in the 5 GPa shocked [100] grain and becomes the dominant substructure at higher shock pressure. The stress and directional dependence of twinning in the bicrystal is analyzed in considering the energetically favorable dissociation of dislocations into Shockley partials and the stress-orientation effect on the partial width. Moreover, a critical 'tear apart' stress is proposed and the calculated value is in good agreement with the experimental observations.

5:40 PM

**Static Recovery of Pure Copper near Room Temperature:** *Chen-ming Kuo*<sup>1</sup>; Chih-Sheng Lin<sup>1</sup>; <sup>1</sup>I-Shou University

Static recovery experiments of pure copper near room temperature have been conducted via TEM, DSC, hardness and extensometer to explore the time and temperature dependent relationships. By using different strain rates, dislocation

density is generated differently. The recovery phenomenon is more significantly as time and temperature increase. Activation energy at initial static recovery is 48 kJ/mol, which is the energy for dislocation annihilation by glide or cross-slip, and varies linearly with static recovered strain. Once dislocation annihilation processes are exhausted, more energy is required for subgrains to form and then grow. The recovered strain is slowed down and eventually is saturated.

---

## Electrode Technology for Aluminum Production: Joint Aluminum Reduction Technology and Electrode Technology Session: Coping with Changes in Coke Quality

Sponsored by: The Minerals, Metals and Materials Society, TMS Light Metals Division, TMS: Aluminum Committee

Program Organizers: Barry Sadler, Net Carbon Consulting Pty Ltd; John Johnson, RUSAL Engineering and Technological Center LLC; Gilles Dufour, Alcoa Canada, Primary Metals; Martin Iffert, Trimet Aluminium AG; Geoffrey Bearne, Rio Tinto Alcan; Jayson Tessier, Alcoa Deschambault

Tuesday PM

Room: 2003

February 17, 2009

Location: Moscone West Convention Center

Session Chair: Barry Sadler, Net Carbon Consulting Pty Ltd

---

### 2:00 PM Introductory Comments

2:05 PM Invited

**Calcined Coke Quality in 2009 and Beyond – Adapting for the Future:** *Les Edwards*<sup>1</sup>; <sup>1</sup>Rain CII Carbon LLC

Numerous papers have been written over the last 20 years forecasting a deterioration in the quality of calcined petroleum coke for the aluminum industry. Until recently, average calcined coke quality has not changed significantly and the industry has had no problem sourcing low sulfur (<3%), low vanadium (<300ppm) cokes with good bulk densities. This situation is changing however, and 2008 represented a turning point. Demand for coke has increased rapidly with the growth in aluminum production and the trend towards processing heavier, higher sulfur crudes by the refining industry is having a significant impact on coke quality and availability. This paper presents an overview of the changes that have occurred and will continue into the future. The industry is adapting but the rate of adaptation will need to increase in the future towards the use of cokes with higher impurity levels, higher sulfur, lower bulk densities and more isotropic structures.

2:30 PM Invited

**Use of Under-Calcined Coke for the Production of Low Reactivity Anodes:** *Jérémie Lhuissier*<sup>1</sup>; Laïlah Bezamanifary<sup>1</sup>; Magali Gendre<sup>1</sup>; Marie-Josée Chollier<sup>1</sup>; <sup>1</sup>Rio Tinto Alcan

The quality of petroleum coke used for the production of anodes for the aluminum industry is declining, affecting both the density and the purity of the cokes. Anodes produced from these cokes will have higher reactivity resulting in higher carbon consumption in the smelter. Under-calcined coke can be used as a response to the higher anode reactivity. The coke has a similar structure to the binder phase (a mix of ultra fines and coal tar pitch), resulting in a more homogenous reactivity of all anode components following baking. The preferential consumption of the anode binder phase by the side reactions with oxygen or carbon dioxide in the cell is reduced. In this paper, the theory behind the performance of under-calcined coke will be reviewed. This will be followed by results from laboratory experiments and industrial tests. Examples of the benefits obtained by plants using under-calcined coke will be provided.

2:55 PM Invited

**Use of Shot Coke as an Anode Raw Material:** *Les Edwards*<sup>1</sup>; Franz Vogt<sup>1</sup>; Ric Love<sup>2</sup>; Tony Ross<sup>2</sup>; William Morgan<sup>3</sup>; Marilou McClung<sup>2</sup>; R.J. Roush<sup>2</sup>; Mike Robinette<sup>1</sup>; <sup>1</sup>Rain CII Carbon LLC; <sup>2</sup>Century Aluminium of West Virginia; <sup>3</sup>Century Aluminum of Kentucky

With the aluminum industry's rapidly growing demand for anode grade petroleum coke, supplies have become very tight and the industry has started using cokes not considered suitable as little as 5 years ago. Shot coke is available in large volumes and is currently used for fuel and TiO<sub>2</sub> applications. Rain CII Carbon and Century Aluminum started a project in 2004 to explore the use



of shot coke and other isotropic cokes for anode production. The project was intended to address anode grade coke shortages being felt by the industry today. The paper summarizes laboratory and plant test work completed and makes a strong case for routine incorporation of up to 30% of these cokes into anode blends. Depending on how it is used, shot coke can improve properties such as anode density and it offers a lower cost raw material in today's world of escalating raw material costs.

### 3:20 PM Invited

**Maintaining Consistent Anode Density Using Varying Carbon Raw Materials:** *Siegfried Wilkening*<sup>1</sup>; <sup>1</sup>Carbon, Graphite and Reduction-Technology Consultant

At first, fundamental structural properties such as real density, apparent density and porosity of the solid carbon raw materials as well as of the green and baked anode blocks will be discussed. In this context practical examples and correlations will be given, and a method for the important determination of the apparent density and total porosity of coke particles will be presented. A method and facility will further be described how to react in the control room of the paste plant to density changes of the particle fractions in the preparation plant. The up-to-date vibro-compactor is key equipment, which allows the immediate adjustment of the compaction and thus the forming density of the green anode. A major problem is currently to bake high-density anodes without cracks. A future high-temperature mixing and forming process will be outlined to overcome some quality deficiencies of the carbon raw materials.

### 3:45 PM Break

### 3:55 PM Invited

**Combating Anode Quality Trends in Potrooms:** *Mark Taylor*<sup>1</sup>; <sup>1</sup>University of Auckland

Three factors are conspiring to create greater challenges for anodes in smelters. Firstly the quality of raw materials is deteriorating – especially coke quality. Secondly the amperage on each cell technology is still increasing year on year, with substantial impacts on heat generation in anodes and electrolyte. And thirdly the impact of greenhouse policy is driving ever lower carbon consumption targets. This presentation describes practical measures which smelters can take to counteract the first two factors above, in order to achieve the third. Specifically the issue of anode temperature needs to be addressed in order to counteract coke reactivity trends. Similarly, anode/assembly induced stresses in the carbon must be tackled both from an assembly design viewpoint and from an anode cover and bath processing design perspective if systematic anode cracking is to be avoided. Lastly the impact of operating practice with anode cover and dressing is pervasive.

### 4:20 PM Invited

**The Origin and Abatement of SO<sub>2</sub> Emissions from Primary Aluminium Smelters:** *Stephan Broek*<sup>1</sup>; *Brian Rogers*<sup>1</sup>; <sup>1</sup>Hatch Ltd

Modern aluminium smelters use dry scrubbing technologies to clean the ventilation gases from electrolytic cells before they are emitted into the atmosphere. Particulate and fluoride emissions are typically very low but while this is an excellent achievement, focus is slowly shifting towards the one emission that remain untouched, which is SO<sub>2</sub> that originates from the sulphur in the coke. In this paper is discussed the sulphur balances of modern aluminium smelters to understand where and how sulfur in the form of SO<sub>2</sub> is emitted. It will provide insight in what the best strategy is to address the issue of reducing sulphur emissions. Technologies are available to provide effective emissions reductions and over recent years many have been reviewed for their effectiveness. The paper will show some of the readily available technologies as well as taking a peek at emerging technology that may help the smelters to further mitigate their emissions.

### 4:45 PM Invited

**The Downstream Consequences of Rising Ni and V Concentrations in Smelter Grade Metal and Potential Control Strategies:** *John Grandfield*<sup>1</sup>; *J.A. Taylor*<sup>2</sup>; <sup>1</sup>Grandfield Technology Pty Ltd; <sup>2</sup>University of Queensland

Technology for controlling smelter metal impurities post reduction has steadily improved. For example control of sodium has seen the reduction and in some plants elimination of chlorine gas. However, changes in the purity of cell feed materials such as anodes are giving rise to new challenges in impurity control; vanadium and nickel levels are for example an emerging problem. This paper reviews the important impurities and their effects on downstream casting, forming and final application properties. Methods of controlling these impurities

are also discussed and areas where new technology is needed also highlighted. In some cases it is not know where the tolerable limits of impurities are. There are a plethora of metal refining techniques used in the extraction of other metals which can be investigated for control of impurities in smelter grade aluminium.

### 5:10 PM Keynote

**Inert Anodes - The Status of the Materials Science, the Opportunities They Present and the Challenges That Need Resolving before Commercial Implementation:** *Barry Welch*<sup>1</sup>; <sup>1</sup>Welbank Consulting Ltd.

Arguments in favor of developing smelting technology with inert anodes include; capital saving by eliminating the need for anode fabrication, baking and rodding plant; potential capital saving in the smelter by enabling higher intensity production per unit volume of cells; elimination of a significant ongoing material cost; reduced greenhouse gas emissions; and even lowering the cell voltage. With an increasing proportion of electricity being generated from natural gas or coal, the environmental advantage is substantially diminished and that appeal is more confined to areas with substantial nuclear or hydropower. As the materials science for producing satisfactory electrodes has progressed two paths emerged -ceramic or cermet conducting electrodes which has been championed by Alcoa, and the so-called "metal anodes" developed by Moltech and protected by more than 80 patents. In reality these two types of the electrodes become extremely similar at the active interface with the electrolyte and ultimately the choice will probably be favoured by engineering considerations. Both groups can claim they appear to have conquered the materials science with respect to the primary criteria, and both have reported larger scale trials retrofitting conventional cell design. These trials have thrown up new challenges, especially in design that will enable high intensity production and withstand the new operating conditions. Retrofitting may not be the preferred path The materials science aspects will be summarized together with the engineering challenges and my more likely development paths from this point on.

## Emerging Applications of Neutron Scattering in Materials Science and Engineering: Phase Transformation

Sponsored by: The Minerals, Metals and Materials Society, TMS Electronic, Magnetic, and Photonic Materials Division, TMS: Chemistry and Physics of Materials Committee

Program Organizers: Xun-li Wang, Oak Ridge National Laboratory; Brent Fultz, California Institute of Technology; Hahn Choo, University of Tennessee

Tuesday PM

Room: 3012

February 17, 2009

Location: Moscone West Convention Center

*Session Chairs:* Brent Fultz, California Institute of Technology; Kenneth Kelton, Washington University

### 2:00 PM Invited

**Ordering in Liquids and the Influence on Phase Transitions:** *Kenneth Kelton*<sup>1</sup>; <sup>1</sup>Washington University

Recent developments in novel levitation methods have led to a renewed interest in the structures of equilibrium and supercooled liquids. Such investigations are also of practical note, allowing regions of the alloy phase diagram to be quickly and accurately determined. Employing the technique of electrostatic levitation, we have measured metallic and semiconductor liquid x-ray diffraction patterns as a function of supercooling. The liquid order was characterized in terms of a dominant local cluster and by Reverse Monte Carlo (RMC) fits to the diffraction data. The topologies of the RMC structures are expressed in terms of their bond orientational order parameters and Honeycutt-Andersen indices. Case studies are presented and discussed, focusing on the influence of liquid ordering on thermophysical properties and phase transitions. Evidence for icosahedral short-range ordering in transition metal liquids and its role in crystallization and the glass transition are discussed.

### 2:30 PM

**Structural Studies of Amorphous Materials:** *Joerg Neugefand*<sup>1</sup>; <sup>1</sup>Oak Ridge National Laboratory

Many structural materials are amorphous materials. While this name may suggest that these materials are structureless, they in fact do possess structure

but no long-range periodicity and their properties are intimately linked to that structure. Neutron and X-ray scattering provide complementary information to understand the structure and ultimately the properties of amorphous systems. Neutrons in particular offer high sensitivity to light elements, high penetration power, isotope substitution experiments and sensitivity to magnetic moments. The Nanoscale Ordered Materials Diffractometer (NOMAD) under construction at the Spallation Neutron Source in Oak Ridge and scheduled to be completed in 2010 will allow neutron scattering experiments with unprecedented speed. Recent examples of structural studies of amorphous materials including deformation studies and time-resolved experiments to access metastable structures will be given.

**2:50 PM**

**Neutron Diffraction Study of Amorphous Zr-Cu Alloys Using Isotopic Substitution:** *A.D. Stoica*<sup>1</sup>; Dong Ma<sup>1</sup>; X.-L. Wang<sup>1</sup>; M. Kramer<sup>2</sup>; <sup>1</sup>Oak Ridge National Laboratory; <sup>2</sup>Ames National Laboratory

The recent discovery of bulk metallic glasses in the binary Zr-Cu system sparks renewed interest in determining atomic structure of amorphous alloys. In this study, a series of amorphous Zr-Cu alloys have been investigated by time-of-flight neutron diffraction using isotopic substitutions with <sup>63</sup>Cu, <sup>65</sup>Cu and natural Cu, respectively. Partial structure factors and partial pair correlation functions were determined in terms of both Faber-Ziman and Bhatia Thornton formalisms. By linking the resolved structure factors with packing of atomic clusters, this study sheds light on the topological and chemical orders in amorphous structure.

**3:10 PM Invited**

**Dynamic Pair-Density Function Method for Neutron Scattering:** *Takeshi Egami*<sup>1</sup>; Wojciech Dmowski<sup>1</sup>; <sup>1</sup>University of Tennessee

In crystals the atomic vibrations are described by phonons, of which dispersion can be determined by inelastic scattering of neutrons and x-rays. In glasses, liquids and strongly disordered crystals, however, phonons are damped, scattered, and localized. The conventional triple-axis spectrometer is not suited to catching these local modes. The dynamic pair-density function (DPDF) method was invented to catch these local modes of lattice and spin dynamics [1]. The dynamic structure factor  $S(Q, E)$  is Fourier-transformed to obtain the DPDF,  $g(r, E)$ , that describes the atomic vibration at a distance  $r$ , with the frequency  $E/\hbar$ . In crystalline solids this method captures only the semi-localized modes near the Van Hove singularities. We demonstrate how the DPDF describes local vibrations of Pb in relaxor ferroelectric  $\text{Pb}(\text{Mg}1/3\text{Nb}2/3)\text{O}_3$ , and gives insight into the dynamic origin of the relaxor behavior. [1] W. Dmowski, et al., Phys. Rev. Lett. 100, 137602 (2008).

**3:40 PM Break****4:00 PM Invited**

**Lattice Dynamics and Structural Phase Transitions:** *Stephen Shapiro*<sup>1</sup>; Brookhaven National Laboratory

Inelastic neutron scattering is an ideal probe to study the lattice dynamics and their modifications due to external perturbations such as temperature, pressure, electric or magnetic field, etc. Of particular interest is the anomalous behavior of the lattice dynamics of advanced materials undergoing phase transitions such as martensitic transformations. The soft mode theory of structural phase transitions was developed nearly 50 years ago and successfully predicted that the energy of a specific lattice mode would go to zero as the transition is approached and the material would spontaneously transform to a different structure. In this talk I shall review how neutron studies of single crystals show that specific modes exhibit strong anomalies that are precursors to the transitions. These observations, coupled with first principles calculations of the interaction between the electrons and the lattice can explain the driving mechanism of the phase changes in several metallic systems undergoing martensitic transformations.

**4:30 PM Invited**

**Inelastic Neutron Scattering Studies of Material Dynamics and Thermodynamics:** *Brent Fultz*<sup>1</sup>; <sup>1</sup>California Institute of Technology

When neutron wavelengths match interatomic distances, the neutrons have energies typical of room temperature. This is lucky — with inelastic neutron scattering, thermal vibrations of atoms and electron spins can be studied with enough detail to reveal both their energies and their wavelengths. Because atom motions are where heat is stored in solids, vibrations generate entropy. Differences in vibrational entropy are now known to be big enough to alter the phase stabilities of different alloys. More recently, we have been studying how

vibrational frequencies change with temperature. There are numerous exceptions to the textbook story of how thermal expansion causes vibrational frequencies to decrease in a non-parabolic potential. In this talk I will show why phonon-phonon interactions and electron-phonon interactions, which change the textbook story, are big enough to alter the phase diagrams of materials at elevated temperatures, and how they are studied by inelastic neutron scattering.

**5:00 PM**

**Thermodynamics from Elementary Excitations: Combined Studies with Inelastic Neutron Scattering and First-Principles Simulations:** *Olivier Delaire*<sup>1</sup>; Matthew Lucas<sup>1</sup>; Max Kresch<sup>2</sup>; Jiao Lin<sup>2</sup>; Brent Fultz<sup>2</sup>; <sup>1</sup>Oak Ridge National Laboratory; <sup>2</sup>Caltech

Inelastic neutron scattering is the preferred experimental technique to measure phonons and magnons, but it has long been limited by the low flux available at neutron sources, which limited the range of practical experiments. The high neutron flux of the Spallation Neutron Source, combined with the large detector banks of new time-of-flight spectrometers, allows for a qualitative change in feasible inelastic scattering measurements. However, a difficulty in analyzing the neutron scattering results resides in the complexity of the experimental datasets. First-principles simulations of the phonon dynamics have now reached a level of reliability such that the full phonon  $S(Q, E)$  predicted from quantum mechanics can directly be compared to experimental data. I will present examples of phonon investigations in transition metal alloys, that have benefited from combined studies with inelastic neutron scattering and first-principles (density functional theory) calculations.

**5:20 PM Invited**

**Neutrons Probe Dynamics in Metals and Polymers:** *Kenneth Herwig*<sup>1</sup>; <sup>1</sup>Oak Ridge National Laboratory

With the recent construction of new facilities and major upgrades of existing sources, world-wide access to advanced neutron scattering instrumentation has never been better. Techniques which have been historically limited by low neutron fluxes will benefit greatly from the increased power of the new sources including the Spallation Neutron Source (SNS) at the Oak Ridge National Laboratory. This is particularly true for inelastic neutron scattering where a neutron exchanges energy with atoms in a sample conveying information on the motion of atoms. Neutrons are particularly adept at identifying the diffusive motions of hydrogen atoms. Examples include identifying the various states of water during the curing of cement pastes and the high temperature diffusion of hydrogen atoms in metals. This talk will briefly introduce inelastic and quasielastic neutron scattering, continue with applications, and conclude with a summary of the instrumentation available at the SNS for these types of measurements.

## Fatigue: Mechanisms, Theory, Experiments and Industry Practice: Fatigue in Engineering Components

Sponsored by: The Minerals, Metals and Materials Society, TMS Structural Materials Division, TMS/ASM: Computational Materials Science and Engineering Committee, TMS/ASM: Mechanical Behavior of Materials Committee, TMS/ASM: Nuclear Materials Committee

Program Organizers: Koenraad Janssens, Paul Scherrer Institute; Corbett Battaille, Sandia National Laboratories; Brad Boyce, Sandia National Laboratories; Luke Brewer, Sandia National Laboratories

Tuesday PM

Room: 3008

February 17, 2009

Location: Moscone West Convention Center

Session Chairs: Ryuichiro Ebara, Hiroshima Institute of Technology; Koenraad Janssens, Paul Scherrer Institute

**2:00 PM Invited**

**Residual Stress Profiles for Mitigating Fretting Fatigue in Gas Turbine Engine Disks:** *Kwai Chan*<sup>1</sup>; Michael Enright<sup>1</sup>; Patrick Golden<sup>2</sup>; Ramesh Chandra<sup>3</sup>; Alan Pentz<sup>3</sup>; <sup>1</sup>Southwest Research Institute; <sup>2</sup>Air Force Research Laboratory; <sup>3</sup>NAVAIR

The driving force for fretting fatigue in engine disks is the contact stresses generated by fretting of the blade and the disk surfaces in the attachment region. In this paper, we examine the use of different residual profiles to counteract

the undesirable effects of contact stresses and to mitigate fretting fatigue. A global finite-element analysis of the disk blade assembly is first performed. The contact pressure and shear traction at the attachment region are extracted from the FEM results and used to compute the contact stress distribution. The contact stresses are then combined with the residual stresses and the bulk stresses. The overall stress distribution is then utilized in a probabilistic crack growth model to predict the risk of disk failure for a military engine under simulated loading conditions. The results are used to identify the minimum residual stress profile for mitigating fretting fatigue in engine disks.

## 2:30 PM

### **Fatigue Life Improvement of C-130 Airplane Propeller Blade Roots by Cold Surface Rolling:** *Behzad Majidi*<sup>1</sup>; <sup>1</sup>Amirkabir University of Technology

In turboprop engines of C-130 aircrafts, the propeller assembly has an important contribution to the safety of the aircraft and its failure leads to catastrophic aircraft crash. Service life of propeller blades is increased by conducting cold surface rolling to generate near surface compressive stresses. In this study service loads of the propeller has been simulated and maximum service stresses was determined. Compressive stress gradients were calculated from finite element modeling of rolling process using ABAQUS/Explicit. Fatigue lives of blades with and without rolling process determined by Basquin method. Results showed that the surface rolling has a considerable effect on fatigue life of the blades and results in 20 times more fatigue life.

## 2:50 PM

### **Structural Prognosis during an EA-6B Outer Wing Panel Fatigue Test:** *John Papazian*<sup>1</sup>; Elias Anagnostou<sup>1</sup>; Stephen Engel<sup>1</sup>; Daniel Fridline<sup>1</sup>; John Madsen<sup>1</sup>; Jerrell Nardiello<sup>1</sup>; Robert Silberstein<sup>1</sup>; <sup>1</sup>Northrop Grumman

A full-scale fatigue test of a retired EA-6B outer wing panel was conducted to validate the functioning of the Northrop Grumman/DARPA Structural Integrity Prognosis System (SIPS). The panel had been retired from active service with a Fatigue Life Expended index of 185. Laboratory fatigue testing of the entire panel was performed to determine its remaining life, evaluate several sensor systems, evaluate the SIPS fatigue models, and validate the SIPS reasoning and prediction system. Phased array ultrasonics was used as a non-destructive inspection system to establish the starting state, and pitch-catch ultrasonics, eddy current and electrochemical fatigue sensors were used to monitor fasteners on rib 1 during the test. The entire system performed admirably, and the accuracy and precision of the remaining life predictions improved continuously during the test. This work sponsored by the Defense Advanced Research Projects Agency under contract HR0011-04-C-0003. Dr. Leo Christodoulou is the DARPA Program Manger.

## 3:10 PM

### **The Examination of Failure of Crankshaft Used in Tractors:** *Huseyin Adanir*<sup>1</sup>; <sup>1</sup>New Mexico Tech.

Failure of crankshaft samples that used in tractors were examined. The samples had been taken from real life and failure during service. Metallurgical factors, design and manufacturing process steps were investigated for crankshaft samples. Materials characterization such as chemical composition analysis of the samples, metallography, and hardness were investigated and SEM was used to examine fracture surfaces. As known that from design and manufacturing process of crankshaft, micro-alloyed steel used as crankshaft material and shaped by forging method. After forging process, normalization as a heat treatment and surface hardening by induction method were done. In the micrographs examination, due to Mn and S content in the steel chemical composition, occurring of MnS forms are discussed. Micro hardness testing with hardness vs depth scrutiny was investigated. Materials selection as a design criteria and manufacturing procedure of crankshaft were discussed and finally, some advices were given to prevent future crankshaft failures.

## 3:30 PM

### **Effect of Varying Elasticity of Helical Gear Teeth on Loading and Stressing:** *Ahmed Elkholy*<sup>1</sup>; <sup>1</sup>Kuwait University

The study presents an analytical model for the calculation of loads and stresses of helical gears due to machining and assembly errors. The model accommodates, tooth elastic deformation caused by contact loads and the varying meshing stiffness of engaged teeth due to material properties. Load sharing among meshing teeth is also determined throughout the contact from the elastic deformation and gear material properties. To check the validity of the model, the changes in maximum root stresses throughout the contact regions

have been compared with strain gauge measurement and finite element results. All results compared very well and the maximum deviation did not exceed 11%. The model, therefore, provides accurate load capacity rating of helical gear drives, and reduces computation time when compared with similar models available from literature.

## 3:50 PM Break

## 4:10 PM

### **Fatigue Life Estimation for Tank Vehicle Structures Subjected to Liquid Sloshing:** *Liming Dai*<sup>1</sup>; <sup>1</sup>University of Regina

Strength analysis of heavy vehicles carrying liquid cargo becomes complex because of the dynamic liquid behavior due to external excitations and operation maneuvers. The research work discussed in this article is on an investigation of the fatigue life estimation of the subframe of a B-Train tank vehicle. The effect of liquid sloshing inside the tank on the structure of the vehicle is determined through a newly developed approach. The stress and strain histories of the subframe subjected to the liquid slosh are quantified with the employment of numerical analyses. Various operating conditions of the tank truck, such as sway, turning, lane change, sudden acceleration and braking, are considered in the investigation. The research results generated will benefit the heavy vehicle industry in designing a sturdy structure and will decrease the time and cost in the design stage of such vehicles.

## 4:30 PM

### **Fatigue Susceptibility of Silicon Thin Films in Harsh Environments with and without Nanometer-Scale ALD Alumina Coatings:** *Michael Budnitski*<sup>1</sup>; Olivier Pierron<sup>1</sup>; <sup>1</sup>Georgia Institute of Technology

The present study investigates the fatigue degradation of 2-micron-thick polycrystalline silicon notched cantilever beam structures in a high-temperature (80C), high-humidity (90%RH) environment. In addition, some structures are coated with ~20nm of atomic-layer-deposited (ALD) alumina (Al<sub>2</sub>O<sub>3</sub>). The specimens are subjected to fully reversed sinusoidal loading at resonance (~40 kHz) with stress amplitudes ranging from 2.1 to 2.3 GPa, resulting in life-spans between 10<sup>6</sup> and 10<sup>9</sup> cycles. The degree and rate of degradation are assessed by monitoring the change in resonant frequency resulting from a change in compliance of the structure. It is found that the damage accumulation rate in the 80C, 90%RH environment exceeds the reference (30C and 50%RH) by two orders of magnitude and tends to increase towards failure, as opposed to decreasing rates at 30C, 50%RH. Preliminary data on ALD coated devices suggest a considerably decreased susceptibility to fatigue degradation.

## 4:50 PM

### **Effect of Load Ratio and Hydrogen Concentration on Crack Growth Rate in Zr-2.5Nb Tubes:** *Young Suk Kim*<sup>1</sup>; Vidas Makarevicius<sup>1</sup>; <sup>1</sup>Korea Atomic Energy Research Institute

Crack growth rates (CGRs) were determined under sustained and cyclic loads using 17 mm compact tension and cantilever beam specimens taken from the Zr-2.5Nb tubes charged to 6 to 100 ppm H. The cyclic load effect on the CGR was investigated at 250°C where load ratios, R changed from 0.13 to 1 with constant K<sub>max</sub>. Under sustained loads, the CGR of the Zr-2.5Nb tube increased with increasing supersaturation of hydrogen, deltaC and leveled off above 20 to 25 ppm H of the deltaC. Under cyclic loads with 1 cycle/min, the CGR at 250°C decreased with decreasing R: 3.2x10<sup>-8</sup> m/s at R=1 and 4.8x10<sup>-9</sup> m/s at R=0.13. The striation spacing, corresponding to the critical hydride length, decreased with decreasing R, indicating easier cracking of the hydrides under cyclic loads. The decreased CGR under cyclic loads and its dependence on the deltaC are discussed using Kim's delayed hydride cracking model.

## 5:10 PM

### **Effect of Conductivity and Dissolved Hydrogen on Environmental Fatigue Behaviors of Type 316LN Stainless Steel in Pressurized Water Reactor Environment:** *Hun Jang*<sup>1</sup>; Pyoung Cho<sup>1</sup>; Changheui Jang<sup>1</sup>; Hyunchul Cho<sup>2</sup>; <sup>1</sup>KAIST; <sup>2</sup>Corporate R&D Institute Doosan Heavy Industries and Construction Co., Ltd.

Low cycle fatigue damage was known as one of the main degradation mechanisms of structural materials in nuclear power plant. To investigate the environmental fatigue behaviors of type 316LN stainless steel, low cycle fatigue tests in a simulated pressurized water reactor environment at 310°C has been performed. Among many parameters affecting the fatigue resistance in such condition, the effects of conductivity and dissolved hydrogen are subject of interest in this paper. Conductivity and dissolved hydrogen may act



as environmental factors in role of environmental assisted cracking. In this regard, we are performing low cycle fatigue tests of type 316LN stainless steel in pressurized water reactor environment. And then, effects of conductivity and dissolved hydrogen on environmental fatigue behaviors of type 316LN stainless steel will be investigated from fractography analysis and by comparing current results with previous ones obtained in 310°C deoxygenated water environment.

### Friction Stir Welding and Processing-V: Session IV

Sponsored by: The Minerals, Metals and Materials Society, TMS Materials Processing and Manufacturing Division, TMS: Shaping and Forming Committee  
Program Organizers: Rajiv Mishra, Missouri University of Science and Technology; Thomas Lienert, Los Alamos National Laboratory; Murray Mahoney, formerly with Rockwell Scientific

Tuesday PM  
February 17, 2009

Room: 2014  
Location: Moscone West Convention Center

Session Chair: Dwight Burford, Wichita State University

#### 2:00 PM Invited

**Friction Stir Spot Welding of Advanced High Strength Steels:** *Yuri Hovanski*<sup>1</sup>; Michael Santella<sup>2</sup>; Glenn Grant<sup>1</sup>; <sup>1</sup>PNNL; <sup>2</sup>Oak Ridge National Laboratory

Friction stir spot welding was used to join two advanced high-strength steels using polycrystalline cubic boron nitride tooling. Numerous tool designs were employed to study the influence of tool geometry on weld joints produced in both DP780 and a hot-stamp boron steel. Tool designs included conventional, concave shouldered pin tools with several pin configurations; a number of shoulderless designs; and a convex, scrolled shoulder tool. Weld quality was assessed based on lap shear strength, microstructure, microhardness, and bonded area. Mechanical properties were functionally related to bonded area and joint microstructure, demonstrating the necessity to characterize processing windows based on tool geometry.

#### 2:20 PM

**Mechanical Evaluation of Friction Stir Spot Welded Advanced High Strength Steels:** *Jeff Rodelas*<sup>1</sup>; Raiv Mishra<sup>1</sup>; Greg Hilmas<sup>1</sup>; Wei Yuan<sup>1</sup>; <sup>1</sup>Missouri University of Science and Technology

Friction stir spot welding (FSSW) is a solid-state alternative to resistive spot welding (RSW) of advanced high strength steels (AHSS), such as dual phase (DP) and fully martensitic steels. By avoiding bulk melting, FSSW offers the benefit of avoiding weld solidification defects that tend to be problematic in AHSS. Steel sheets were joined using plunge-type FSSW with a cemented carbide tool. Lap shear strengths for DP 590 steel 2 to 3.5 times greater than existing RSW design guidelines were obtained using FSSW process parameters which maximized the bonded region. Additionally, the relationship between failure mode and lap shear strength was interpreted in the context of bonded area. Microstructures of the resulting welds and tool wear mechanisms will also be discussed.

#### 2:40 PM

**Metallurgical Characterization of Friction Stir Spot Welded Mg Alloy:** *Qi Yang*<sup>1</sup>; Sergey Mironov<sup>2</sup>; Yutaka Sato<sup>2</sup>; Kazutaka Okamoto<sup>3</sup>; <sup>1</sup>Hitachi American Ltd; <sup>2</sup>Tohoku University; <sup>3</sup>Hitachi, Ltd

Hook and metallurgical features such as microstructure and texture are directly related to the thermo-mechanical interaction between the material and welding tool, and they could significantly affect strength of a friction stir spot weld. In the present work, friction stir spot welding was carried out on AZ31 Mg sheets in lap configuration at various rotation speeds and plunge depths. Copper foil, pre-placed between the overlapped metal sheets, was used as a tracer to apparently monitor material flow in the vicinity of the tool during welding. Furthermore, electron backscatter diffraction was conducted to obtain the microstructures and preferred crystallographic orientations in the stir zone and the hook region, respectively. Using these two characterization approaches, an understanding of hook formation and microscopic features, especially texture, in Mg spot welds was attained. Finally, the effect of tool rotation speed on the strength of a friction stir spot weld was discussed.

#### 3:00 PM

**Study of Failure Modes in Friction Stir Swing Welded Lap Shear Specimens:** *Harsha Badarinarayan*<sup>1</sup>; Qi Yang<sup>1</sup>; <sup>1</sup>Hitachi America Ltd

Swing (Stitch) friction stir spot welding is an extension of the conventional friction stir spot welding. This process produces an elongated spot (hence, the presence of advancing and retreating sides). The main advantage of this process is that it gives appreciably higher strength. In this research, an attempt is made to understand the failure mechanism of stitch welds made in lap shear configuration. There are 4 possible ways (orientations) in which coupons can be welded to produce a lap shear specimen – 2 in transverse direction and 2 in longitudinal. The static strength of welds made with these orientations was found to be different. A fracture mechanics and finite element analysis approach is used to explain this variation in strength. It was seen that failure occurred quicker when spot welds were loaded on the retreating side or when the loading condition caused the stress concentration around the keyhole.

#### 3:20 PM

**Low Z-Force Friction Stir Spot Welds – Conventional Tool and Process Development Approach:** *Tze Jian Lam*<sup>1</sup>; Christian Widener<sup>1</sup>; Jeremy Brown<sup>1</sup>; Dwight Burford<sup>1</sup>; <sup>1</sup>Wichita State University

Low Z-force FSSW can be achieved by studying the relationships between pin tool features, geometries, processing parameters and the resultant strength of FSSW. The objective of this research paper is to study the effects of geometrical changes to the pin tool, such as shoulder and pin diameter without compromising the mechanical properties of the spot weld. A variety of pin tool features are included in this study in an effort to reduce the required Z-force. Two concave shoulder diameters and three probe designs were investigated. The probe features included flutes, threads, Trivex™ and flats. The process parameters included in the research are spindle speed, plunge depth, plunge load and plunge rate. Static ultimate tensile strength (UTS) and metallographic analysis are correlated with process parameters, process forces, static UTS and pin tool designs.

#### 3:40 PM

**Joining PPSU Thermoplastic to 6061 Aluminum Using the Refill Friction Stir Spot Welding Process:** *Adam Gladen*<sup>1</sup>; William Arbegast<sup>1</sup>; Michael West<sup>1</sup>; Bharat Jasthi<sup>1</sup>; <sup>1</sup>South Dakota School of Mines and Technology

This paper presents the results of a preliminary study to investigate the joining of polyphenylsulfone (PPSU) thermoplastic sheets to 6061 aluminum sheets in lap joint configurations using the Refill Friction Stir Spot Welding (RFSSW) process. Both the “pin first” and “shoulder first” RFSSW methods were investigated. The RFSSW process on these materials results in a “button” of extruded aluminum being formed within the PPSU sheet which contributes to a strength which exceeds 300 pounds per spot. Samples were prepared with and without a supersonic cold sprayed (SCS) copper (Cu) interlayer between the sheets to enhance the bonding to the PPSU surfaces. The effects of process parameters and interface coatings on the joint quality and strength are discussed. Lap shear test results per AMS-W-6858 are presented along with metallurgical examinations of the interface. Overall, these findings show that the RFSSW can result in mechanical joints between these two radically different materials.

#### 4:00 PM Break

#### 4:10 PM

**Friction Stir Form Welding of Aluminum Tubes:** *K. Gupta*<sup>1</sup>; Rajiv Mishra<sup>1</sup>; Y. Chen<sup>2</sup>; X. Gayden<sup>2</sup>; <sup>1</sup>Missouri University of Science and Technology; <sup>2</sup>GM R&D Center

This paper summarizes the results of different methods of joining 6063 rectangular section aluminum tubes by friction stir welding (FSW). FSW was evaluated for three tube configurations: unsupported, plug supported and unsupported with top sheet. In these runs, fixturing and process variables were kept fixed and variability was assessed only with respect to the joint configuration. Two different tool designs were used for making these runs. Metallurgical and mechanical properties evaluations were done for three weld configurations. Comparison of properties was done to demonstrate the best joining method for tubes. Unsupported welds exhibited best mechanical properties, with 65% weld efficiency. This work was performed under the NSF-IUCRC for Friction Stir Processing and the additional support of NSF and GM for the Missouri S&T site is acknowledged.

4:30 PM

**Friction Stir Spot Welding of AA6016 Aluminum Alloy:** *Wei Yuan*<sup>1</sup>; Rajiv Mishra<sup>1</sup>; Yen Lung Chen<sup>2</sup>; Xiaohong Gayden<sup>2</sup>; Glenn Grant<sup>3</sup>; <sup>1</sup>Center for Friction Stir Processing, Department of Materials Science and Engineering; <sup>2</sup>General Motors R&D Center; <sup>3</sup>Pacific Northwest National Laboratory

Friction stir spot welds of 6016-T4 aluminum alloy were made using conventional pin (CP) tool and off-center feature (OC) tool. Different tool rotation speeds were employed for maximizing bonded region: 1500 rpm for CP tool and 2500 rpm for OC tool. Effects of penetration depth and plunge speed on cross-tension failure load were investigated. Maximum failure load of about 1.8 kN was obtained. Results indicated cross-tension failure load did not change after paint-bake cycle for both tools. Two different failure modes were observed: debonding and pull-out under cross-tension loading condition. Based on the experimental observation of failure path, load-displacement curve and microhardness profile, the effect of paint-bake cycle on cross-tension strength and the failure mechanisms are discussed.

4:50 PM

**Refill Friction Stir Spot Weld Process Optimization for 2024, 6061, and 7075 Aluminum Lap Joints:** *Clark Oberembt*<sup>1</sup>; William Arbegast<sup>1</sup>; Dana Medlin<sup>1</sup>; Michael West<sup>2</sup>; <sup>1</sup>SDSM&T; <sup>2</sup>South Dakota School of Mines and Technology

This paper describes the optimization procedures and results for the refill FSSW of 2024, 6061, & 7075 Aluminum alloys in the 0.040", 0.060", 0.080", & 0.125" sheet thicknesses. Both the "pin first" and "shoulder first" process methods were evaluated using test coupons consistent with AMS-W-6858. Welds were conducted on the MTS ISTIR 10 FSW system with custom designed FSSW adapters. These results of several designed experiments which varied processing parameters and pin tool designs are presented along with the results of static strength testing and metallurgical evaluations. The effect of spot size on strength and failure mode is presented along with the compression test results of integrally stiffened compression test panels fabricated using the refill FSSW process.

5:10 PM

**Evaluation of Swept Friction Stir Spot Welding in 2219-T62:** Dwight Burford<sup>1</sup>; Christian Widener<sup>1</sup>; Jeremy Brown<sup>1</sup>; Ken Poston<sup>2</sup>; Gary Moore<sup>2</sup>; <sup>1</sup>Wichita State University; <sup>2</sup>Bombardier Aerospace Short Brothers, PLC

The purpose of this investigation was to evaluate the effects of swept Friction Stir Spot Welding (FSSW) on tensile strength and fatigue life in 2219-T62 material with a faying surface gasket compound. The sheets were 2.5 mm (0.100-in.) thick. The top sheet was chromic acid anodized while the bottom sheet was sulfuric acid anodized. A poly-urethane based non-setting and non-hardening gasket compound was placed at the faying surface. The first round of testing involved exploratory bounding of the process windows for three tools. The bounding spots were evaluated through macroscopic inspection of spot cross sections. One tool was eliminated in the first round; however, the remaining two tools were evaluated for coupon tensile strength. The coupons were pulled to failure in a single spot, unguided lap shear configuration. Weld parameters for each tool varied per a Box-Behnken design of experiment (DOE). Coupons were also produced for limited fatigue testing from the 3 best weld parameters for each tool. The coupons were made in the 100% load transfer configuration from the NASM 1312-21 specification. A single tool was then chosen to continue based on the previous tensile and fatigue results. Another set of DOEs were performed to evaluate tensile strength and fatigue life. These DOEs again used the NASM 1312-21 100% load transfer coupons. Select FSSW coupons were then compared to riveted coupons at equal fatigue load levels. The rivets used in this experiment were MS20426E5-7 flush countersink. The FSSW coupons were able to outperform the riveted coupons in regards to tensile strength and for fatigue life at high load levels. At lower load levels FSSW coupon results were comparable to riveted coupons.

5:30 PM

**Energy Generation during Friction Stir Spot Welding (FSSW) of Al 6061-T6 Plates:** *Mokhtar Awang*<sup>1</sup>; Victor Mucino<sup>2</sup>; <sup>1</sup>Universiti Teknologi Petronas; <sup>2</sup>West Virginia University

Effective and reliable computational models would greatly enhance the study of energy dissipation during friction stir spot welding (FSSW) process. Approaches for the computational modeling of the FSSW process, however, are still under development and much work is still needed, particularly the application of explicit finite element codes for a verifiable simulation. The objectives of this work are to develop a finite element modeling of FSSW of 6061-T6 aluminum

alloy and analyze energy generation during the welding process. In this work, a three dimensional (3-D) finite element (FE) coupled thermal-stress model of FSSW process has been developed in Abaqus/Explicit code. Rate dependent Johnson-Cook material model is used for elastic plastic work deformations. Temperature profile and energy dissipation history of the FE model have been analyzed. The peak temperature at the tip of the pin and frictional dissipation energy are in close agreement with an experimental work.

5:50 PM

**Refill Friction Stir Spot Weld Process Optimization for Magnesium AZ31B-H24 Lap Joints:** *Clark Oberembt*<sup>1</sup>; William Arbegast<sup>1</sup>; Dana Medlin<sup>1</sup>; Michael West<sup>1</sup>; <sup>1</sup>SDSM&T

This paper describes the optimization procedures and results for the Refill FSSW of AZ31B-H24 Magnesium sheet in lap joint configurations. Both the "pin first" and "shoulder first" process methods were evaluated using test coupons consistent with AMS-W-6858. Samples were prepared on the MTS ISTIR 10 FSW system with custom designed RFSSW adapters. The unguided lap shear, cross tension, T-peel, and fatigue test results are presented. Metallurgical and SEM analysis and microhardness testing results are presented with correlations to the effects of processing parameters and defect formations. High strength and high quality RFSSW spot welds were produced with the results compared to conventional resistance spot welds in this magnesium alloy.

## Frontiers in Solidification Science III: Prediction and Control of Solidification Behavior and Cast Microstructures

Sponsored by: The Minerals, Metals and Materials Society, ASM International, TMS Materials Processing and Manufacturing Division, TMS/ASM: Computational Materials Science and Engineering Committee, TMS/ASM: Phase Transformations Committee, TMS: Solidification Committee, TMS: Chemistry and Physics of Materials Committee  
Program Organizers: Ralph Napolitano, Iowa State University; James Morris, Oak Ridge National Laboratory

Tuesday PM

February 17, 2009

Room: 2018

Location: Moscone West Convention Center

*Session Chair:* Silvere Akamatsu, Institute Des Nanosciences De Paris

2:00 PM Invited

**Recent Advances in Phase-Field Modeling of Polycrystalline Solidification:** *Laszlo Granasy*<sup>1</sup>; Gyorgy Tegze<sup>1</sup>; Gyula Toth<sup>2</sup>; Laszlo Kornyei<sup>2</sup>; Tamas Pusztai<sup>2</sup>; <sup>1</sup>Brunel Centre for Advanced Solidification Technology; <sup>2</sup>Research Institute for Solid State Physics & Optics

Various aspects of polycrystalline solidification will be addressed in the framework of conventional and atomistic phase field approaches. Parameter-free predictions for the nucleation barrier from Ginzburg-Landau free energy based phase-field models are compared to results from Monte Carlo simulations and other nucleation models in the hard-sphere system of recently revised interface properties [1]. A similar approach is applied for competing fcc-bcc nucleation in the Fe-Ni system. Solidification in a phase separating liquid will also be addressed. A phase-field model of polycrystalline solidification that relies on quaternary fields in representing crystallographic orientation is applied for describing complex 3D solidification structures including multi-particle dendritic morphologies, columnar to equiaxed transition, and various types of spherulites. Preliminary results will be shown for nucleation and polycrystalline solidification in phase field crystal models.[1] R.L. Davidchack et al., J. Chem. Phys. 125, 094710 (2006).

2:20 PM

**Predicting the As-Cast Grain Structure with a Hybrid Stochastic-Deterministic Mathematical Model:** *Vinicius Biscuola*<sup>1</sup>; *Marcelo Martorano*<sup>1</sup>; <sup>1</sup>University of São Paulo

A hybrid stochastic-deterministic model has been implemented to predict the as-cast grain macrostructure formed during solidification of binary alloys. The model is a combination of deterministic macroscopic equations, derived from mass, energy, and species conservation principles, and the cellular automaton technique to predict the nucleation and growth of grains. An isothermal and a unidirectional solidification system were simulated with the model. In the

isothermal system, the grain macrostructure was obtained for either a log-normal or a normal distribution of nucleation undercoolings, allowing the calculation of the average grain size under different solidification parameters. In the unidirectional solidification system, the columnar-to-equiaxed transition was also obtained from the calculated macrostructure. The model results were compared with those from a pure deterministic and a pure stochastic model proposed in the literature.

**2:40 PM**

**Comparative Study of CET in Refined and Non Refined Al-Based Alloys Using In Situ and in Real Time X-Ray Synchrotron Imaging:** *Hyejin Jung*<sup>1</sup>; N. Mangelinck-Noël<sup>2</sup>; H. Nguyen-Thi<sup>2</sup>; N. Bergeon<sup>2</sup>; B. Billia<sup>2</sup>; G. Reinhart<sup>2</sup>; A. Buffet<sup>3</sup>; J. Baruchel<sup>3</sup>; <sup>1</sup>NFRI; <sup>2</sup>IM2NP; <sup>3</sup>ESRF

The control of the Columnar to Equiaxed microstructure Transition (CET) is needed to determine final desired products. The main objective of the study presented is to better elucidate the CET phenomenon with carefully defined experiments, In-situ and real-time observation of the solid-liquid interface is a fruitful method to reveal the dynamics of the solidification phenomena. Such experiments have been conducted at the European Synchrotron Radiation Facility (ESRF) using Synchrotron X-ray Radiography and Topography. Firstly, we focus on Al-3.5wt%Ni alloy adding refining particles to study CET when it mainly comes from heterogeneous nucleation of equiaxed grains on particles followed by the blocking of the columnar front by the growing equiaxed grains. Secondly, Al-7.0wt%Si alloy without refiners is carefully considered to study fragmentation from pre-existing dendrites as another origin for equiaxed grains. Thanks to this comparative study, valuable information on CET phenomena are yielded and related to the characteristics of each alloy.

**3:00 PM**

**Quantitative Simulation of Fe-Rich Intermetallics in Al-Si-Cu-Fe Alloys during Solidification:** *Junsheng Wang*<sup>1</sup>; Peter D. Lee<sup>1</sup>; <sup>1</sup>Imperial College

Fe-rich intermetallic phases (e.g.  $\beta$ -Al<sub>5</sub>FeSi) which form during the solidification of Al-Si-Cu-Fe alloys can have a detrimental effect on the mechanical properties of cast components. A thermodynamic database was combined with a numerical solution of the multicomponent diffusion solver to predict the formation of this phase. The growth kinetics and morphology was simulated using a combined Monte-Carlo algorithm to calculate the transformation frequency for each cell as a function of total free energy, with the faceted shapes replicated via a decentered needle/plate algorithm. The non-stoichiometric composition of both Fe and Si was simulated by changing the partition coefficient at the S/L interface according to local kinetic parameters such as growth velocity and effective diffusion. The model predicted phase fraction, size and morphology of Fe-rich intermetallic phases in type-319 alloys (Al-7.5wt.%Si-3.5wt.%Cu-0.2~0.8wt.%Fe) compared well to high resolution synchrotron tomography results.

**3:20 PM Invited**

**High Density Nanocrystal Formation in Marginal Glass Forming Alloys:** *Eren Kalay*<sup>1</sup>; Scott Chumbley<sup>1</sup>; Matthew Kramer<sup>1</sup>; Ralph Napolitano<sup>1</sup>; Iver Anderson<sup>1</sup>; <sup>1</sup>Ames Laboratory / Iowa State University

The rapid solidification products of Al-rich Al-RE and Al-TM-RE (TM: transition metals; RE: rare earth elements) marginal glass-forming alloys represent an interesting class of metallic glass due to their common observation of a very high density of nuclei embedded in the amorphous matrix. A mechanism to explain such high nanocrystal densities has not been identified. The Al-Sm system was chosen to investigate this nucleation phenomenon in an Al-RE alloy. Both liquid and rapidly solidified structures were analyzed using high energy X-ray diffraction (HEXRD). A medium range order (MRO) structure different from fcc-Al was resolved in the liquid and in as-quenched alloys within composition range where glass formation occurs. Results from a combined study of calorimetry, electron microscopy and HEXRD with RMC (Reverse Monte Carlo) simulations will be presented to discuss the effects of MRO structure on the formation of high nanocrystal density. Research supported by U.S. DOE under Contract No.DE-AC02-07CH11358.

**3:40 PM Break**

**4:00 PM**

**Microstructure of Undercooled Al-Fe-Nd Alloy:** *Walman Castro*<sup>1</sup>; Benedito Luciano<sup>1</sup>; <sup>1</sup>Universidade Federal de Campina Grande

Rapid Solidification Processing of metals and alloys, is establish by increasing of the undercooling applying high cooling rates (100 - 1000000 K/s) or by reduce nucleation sites using low cooling rates (1 K/s). Melt undercooling

opens new solidification pathways for new non-equilibrium phases and unusual microstructures. Several techniques have been developed to reduce nucleation sites and produce increased undercooling in metals and alloys including the fluxing technique. In this work, an Al<sub>96</sub>Fe<sub>2</sub>Nd<sub>2</sub> alloy was solidified, by fluxing technique, and its microstructure and microhardness investigated as a function of the undercooling level. The increasing undercooling level from 30 K to 109 K promotes change in morphology and on the microhardness of the Al<sub>96</sub>Fe<sub>2</sub>Nd<sub>2</sub> alloy.

**4:20 PM**

**Laser Aided Direct Metal Deposition of Inconel 625 Superalloy: Solidification Microstructure and Thermal Stability:** *Guru Prasad Dinda*<sup>1</sup>; Ashish Dasgupta<sup>2</sup>; Jyoti Mazumder<sup>1</sup>; <sup>1</sup>University of Michigan; <sup>2</sup>Focus: HOPE

Inconel-625 has been widely used for over 50 years in the aerospace, chemical, and marine applications. Direct Metal Deposition is a laser aided rapid manufacturing process for fabricating metal parts directly from CAD models. In the present study, a high-power continuous wave CO<sub>2</sub> laser beam was focused on the Inconel-625 substrate to create a melt pool into which the Inconel-625 powder was delivered through a special nozzle carried by an inert gas where the powder streams converge at the same point on the focused laser beam. The solidification microstructure of the laser deposited sample was investigated by optical microscopy, SEM and X-ray diffraction. The as-deposited microstructure is columnar dendrite in nature. However, the orientation of the primary dendrite varies with the direction of the deposition. This paper presents the important concepts necessary for any process control for epitaxial growth and the microstructural stability of the dendritic structure at high temperature.

**4:40 PM**

**Phase Diagram Studies in  $\gamma$ -TiAl Turbine Blade Alloys by In Situ Diffraction of Synchrotron Radiation:** *Olga Shuleshova*<sup>1</sup>; Dirk Holland-Moritz<sup>2</sup>; *Wolfgang Löser*<sup>1</sup>; <sup>1</sup>IFW Dresden; <sup>2</sup>DLR Köln

Solidification processes and high-temperature phase transformations of Ti-Al-Nb turbine blade alloys with compositions Ti-45 to 54 at.% Al-5 to 10 at.% Nb have been studied in situ using high-energy x-ray diffraction on electromagnetically levitated droplets. The direct determination of the solidification modes in conventional microstructure analysis methods of Ti-Al alloys is normally impeded by the melt reactivity at elevated temperatures and various post-solidification transformations. This has led to discrepancies between existing Ti-Al-Nb phase diagrams. Here it was proved that by Nb addition the  $\beta$ -Ti primary solidification range extends to higher Al contents than in previous assessments. The experimental observations of solidification modes and phase transformation sequences for selected compositions match well with a recent CALPHAD calculation of the Ti-Al-Nb system.

**5:00 PM**

**Near Net Shape Repair and Remanufacturing of High Value Components Using DMD:** *Bhaskar Dutta*<sup>1</sup>; Jyoti Mazumder<sup>1</sup>; Harshad Natu<sup>1</sup>; Guru Dinda<sup>2</sup>; <sup>1</sup>POM Group; <sup>2</sup>University of Michigan

Direct Metal Deposition (DMD) with patented close loop feedback system enables greater control of the deposition process as compared to other deposition processes. Its ability to deposit different material at different pixels with a given height directly from a CAD data opens up a new horizon in the materials processing and allows re-configuration of parts with better properties. This becomes particularly critical for repair and reconstruction of components that desire high quality. The current work focuses on application of DMD for high value components with a special emphasize on the defense applications. The presentation will review the DMD process, its material capabilities with particular emphasize on dissimilar material cladding process and properties of DMD materials. Properties of different engineering alloys under different processing condition as compared to wrought alloys will be presented. Finally, case studies involving reconstruction of expensive components made of Al-alloys and steels will be discussed.



## General Abstracts: Light Metals Division: Session I

Sponsored by: The Minerals, Metals and Materials Society, TMS Light Metals Division, TMS: Aluminum Committee, TMS: Aluminum Processing Committee, TMS: Energy Committee, TMS: Magnesium Committee, TMS: Recycling and Environmental Technologies Committee

Program Organizers: Anne Kvithyld, SINTEF; Alan Luo, General Motors Corp

Tuesday PM  
February 17, 2009

Room: 2001  
Location: Moscone West Convention Center

Session Chair: Alan Luo, General Motors Corp

### 2:00 PM

**A Homogenization Treatment Study for Twin Roll Cast 3003 and 8006 Aluminium Alloys:** Beril Corlu<sup>1</sup>; Aziz Dursun<sup>1</sup>; Canan Inel<sup>1</sup>; Murat Dündar<sup>1</sup>; <sup>1</sup>Assan Aluminium R S

High solidification rates in twin roll casting of aluminum alloys results in concentration gradients through the thickness having a supersaturated microstructure with very fine grains at the surface. Homogenization treatment is usually applied at higher gauges in order to remove those microstructural gradients. Current study is aimed at optimizing our homogenization treatment for TRC 3003 and 8006 aluminium alloys by applying a series of homogenization temperatures between 520 and 580°C at different holding times. Surfaces and through thickness microstructure of the specimens were investigated under optical and scanning electron microscope, and the mechanical properties have been discussed accordingly. It is found that required microstructural transformations can not be completed if temperature and time combination of homogenization treatment is not sufficient enough, even after following thermomechanical processes. This in turn results in anisotropy in mechanical properties which causes poor deep drawability and earing formation.

### 2:20 PM

**Aluminum as Windings in Transformers:** Joel Liebesfeld<sup>1</sup>; <sup>1</sup>James F. Valentine and Assoc Inc

The alloys of aluminum/aluminum wiring that have been used in the past, in certain transformer applications, seemingly have a high fault rate under certain conditions. Specifically, aluminum deployed as windings in step-down transformers that have been part of motive charger systems have faulted in ways that have caused fires. As an electrical investigator, that has examined these devices in fire situations, the faulting apparently results in the breakdown of aluminum with a rise in temperatures as it changes state and causes a sudden load increase on power sources. The explanation and clarification of the ambient/environmental conditions that cause such breakdown and result in catastrophic failures will be the subject of the paper's analysis.

### 2:40 PM

**Carbon Compound as Anode Material Electrode in Super Lithium Ion Capacitor:** Jie Li<sup>1</sup>; Yang Juan<sup>1</sup>; Yan-Qing Lai<sup>1</sup>; Zhi-An Zhang<sup>1</sup>; Xin Hao<sup>1</sup>; <sup>1</sup>Central South University

Series of carbon compounds as anode materials were prepared for super lithium ion capacitor using graphite and active carbon (AC) as raw materials. Their electrochemical properties were investigated by constant current charge-discharge test. The results showed that the compound anode had good capacitive performance as well as Li-ion battery performance. The potential of the capacitor could be as high as 3.5V vs Li/Li<sup>+</sup> when compared with 2.5V vs Li/Li<sup>+</sup> in the AC-AC capacitor, accordingly, the energy density increased from 21.7Wh/kg to 40.3Wh/kg. The compound anode also had excellent rate performance that as the current density increasing from 0.1A/g to 1A/g, the capacitance decreased only 1.3F/g, and good cycle performance that the capacitance holding remained 96.7% after 10 times cycles even at the highest potential of 3.5 V vs Li/Li<sup>+</sup>.

### 3:00 PM

**Comparative Analysis of the Effects of Acidified Vegetable Extracts on the Corrosion Behaviour of Al – Zn Alloy Systems:** Chinedu Ekuma<sup>1</sup>; Ndubuisi Idenyi<sup>2</sup>; Greg Avwiriri<sup>1</sup>; Israel Owate<sup>1</sup>; <sup>1</sup>University of Port Harcourt; <sup>2</sup>Ebonyi State University, Abakaliki

The effects of acidified extracts of vernonia amegdalina, pipernigrum and telferia occidentalis on the corrosion behaviour of Al – (1.0%, 2.0% and 3.0%) Zn alloy in varying molarities of HCl has been investigated. Preweighed samples

of the alloy were subjected to 0.5M and 1.0M HCl, each containing 50 cm<sup>3</sup> of the extracts respectively. The set-ups were allowed to stand for 28 days with a set of samples withdrawn weekly for corrosion rate characterization. The results obtained showed the usual corrosion trend of initial steep rise in corrosion rate followed by a gradual decline over exposure time, characteristic of most passivating metals. Expectedly, the vegetable extracts showed inhibition traits with pronounced effects at lower acid molarities but the inhibition potentials diminished with increase in the reinforcing phase. Comparatively, it was noticed that telferia occidentalis showed the best inhibition potentials followed by pipernigrum while vernonia amegdalina was the worst.

### 3:20 PM

**Homogenized Baking Quality:** Domenico DiLisa<sup>1</sup>; Hans-Peter Mnikoleiski<sup>1</sup>; Detlef Maiwald<sup>1</sup>; <sup>1</sup>Innovatherm

The quality of a baked anode is defined mainly by the heat treatment. Each anode in a pit has to reach overall a specific temperature for a specific time. The heat transfer is given by the temperature versus time curve of the surrounding flues. Due to physical design of an open top ring furnace less energy is introduced to the outer flues. Further, the pitch burn starts and ends at a later point then at the inner flues. This lack of heat transfer will be compensated at a later stage by the new extended firing index module. In addition to this module a control strategy has been developed to modulate the burner temperature target in correlation to the preheat area temperature development. The result of the improved temperature target modulation is a homogenized baking quality

### 3:40 PM

**Improving the Robotized GMAW Technique for Joining Light Aluminum Extrusions:** Michel Guillot<sup>1</sup>; Isabelle Bouchard<sup>1</sup>; <sup>1</sup>Laval University

Gaz metal arc welding is commonly used for joining large assemblies. Even for light assemblies, the GMAW technique is increasingly preferred despite limitations. In this paper, several parameters of the GMAW process and robot motion are investigated on joining AL6061-T6 extrusions. For different thicknesses and joint types, are found sets of parameters providing good and repeatable joint quality with minimal distortion and good appearance at relatively high travelling speeds. Simple extruded flat stocks of three thicknesses are tested with parameters like typical GMAW settings, joint preparation geometries, wire gages and alloys, gun positions and angles, robot speeds and accuracy of welding path. The geometric and positioning errors of the components mounted in the fixture are also studied. The repeatability of weld quality is tested. Finally, the best conditions are applied for joining and testing a floor panel made of several extrusions.

### 4:00 PM

**Mechanical Properties of Powder Metallurgy Titanium Alloys Dispersed with Carbon Nano Particles:** Katsuyoshi Kondoh<sup>1</sup>; Thotsaphon Threrujirapong<sup>1</sup>; Hisashi Imai<sup>1</sup>; Bunshi Fugetsu<sup>2</sup>; <sup>1</sup>Osaka University; <sup>2</sup>Hokkaido University

Titanium powders are uniformly coated with carbon nanotubes (CNTs) and nano-scale carbon black (CB) particles via wet process in using the surfactant solutions, and mixed by ball milling. The titanium composite powder are compacted by spark plasma sintering (SPS) process, and consolidated by hot extrusion. TiC particles synthesized by the reaction of carbon nano particles and titanium powders are necessary to improve mechanical properties of the powder metallurgy (P/M) composite materials. In this study, SPS temperature is decided by high-temperature XRD analysis which detects the synthesis of TiC during heating. When using pure titanium powders and SPS temperature of 1073K, their composite material with 1% CNTs shows UTS of 810 MPa and 21% elongation, which are superior to the wrought material including no CNT with 585MPa UTS and 30% elongation. The uniform distribution of both of CNTs and TiC particles is remarkably effective for the improvement of their mechanical properties.

### 4:20 PM

**The Effect of Trace Boron Addition on Grain Growth Kinetics of As-Cast Beta21S:** Balakrishna Cherukuri<sup>1</sup>; Raghavan Srinivasan<sup>1</sup>; Sesh Tamarisakandala<sup>2</sup>; Daniel Miracle<sup>3</sup>; <sup>1</sup>Wright State University; <sup>2</sup>FMW Composite Systems Inc; <sup>3</sup>US Air Force

Several primary ingot breakdown steps are typically carried out to reduce the as-cast grain size and thus improve processability / workability in titanium alloys. Obtaining finer grain size in as-cast condition would eliminate / reduce processing steps and thus result in cost savings. Addition of boron in trace amounts to Beta21S (Ti-15Mo-2.6Nb-3Al-0.2Si) resulted in significant grain

refinement in the as-cast condition. The presence of TiB particles along the grain boundaries in the boron modified alloy restricts the grain boundary mobility at elevated temperatures, thus providing microstructural stability during hot working. The grain growth exponents and activation energies were calculated to study the effect of trace boron additions on the kinetics of grain growth. The effect of volume fraction, aspect ratio and orientation of the TiB particles with respect to the grain boundary are modeled using modified Zener pinnig criteria. Results show good correlation between the predictions and experimental results.

**4:40 PM**

**Microstructural Uniformity in AZ31B and Its Impact on Further Processing and Properties:** *David Foley*<sup>1</sup>; Majid Al-Maharbi<sup>1</sup>; Ibrahim Karaman<sup>1</sup>; Laszlo Kecskes<sup>2</sup>; Suveen Mathaudhu<sup>2</sup>; Karl Hartwig<sup>1</sup>; <sup>1</sup>Texas A & M University; <sup>2</sup>U S Army Research

Recently there has been building interest in improving the strength and formability of Mg alloys by severe plastic deformation (SPD) via equal channel angular extrusion. While improvements have been made to commercial alloys by this technique, our experience has shown that chemical and microstructural uniformity can play a key role in improving the material by SPD. This study examines AZ31B starting with cast and rolled forms. For a given low-temperature strain and route, we demonstrate the influence of initial heterogeneity on post-processing microstructure and mechanical properties. Issues such as mechanical property variability and shear banding are compared to material subjected to a prior homogenization.

**5:00 PM**

**Processing Response of Boron Modified Ti-6Al-4V Alloy in ( $\alpha+\beta$ ) Working Regime:** *Shibayan Roy*<sup>1</sup>; Satyam Suwas<sup>1</sup>; S. Tamirisakandala<sup>2</sup>; R. Srinivasan<sup>3</sup>; D.B. Miracle<sup>4</sup>; <sup>1</sup>Indian Institute of Science; <sup>2</sup>FMW Composite Systems, Inc.; <sup>3</sup>Wright State University; <sup>4</sup>Air Force Research Laboratory, Materials and Manufacturing Directorate, Wright-Patterson AFB

Titanium alloys e.g. Ti-6Al-4V are the backbone materials for aerospace, energy, and chemical industries. Hypoeutectic boron addition to Ti-6Al-4V alloy produces a reduction in as-cast grain size by roughly an order of magnitude resulting in the possibility of avoiding ingot breakdown step and thereby reducing the processing cost. In the present study, ISM processed as-cast boron added Ti-6Al-4V alloy showed identical, although refined microstructure and largely randomized/weak texture compared to normal Ti-6Al-4V alloy. When deformed in ( $\alpha+\beta$ )-phase field,  $\alpha$ -lath bending and globularization seemed to be the dominating deformation mechanisms at lower and higher temperatures, respectively for both these materials. Wherein normal Ti-6Al-4V showed flow instabilities (cavitations, cracking etc.) at low temperatures, boron added materials possessed enhanced workability under all processing conditions. The texture evolved during deformation was, however, completely different in these two kinds of alloys, suggesting a difference in the operating deformation mode that produces the end stable orientations.

**5:20 PM**

**Production of the Composite from 6082 Al Alloy Chips and Fly Ash Particles by Hot Pressing:** *Harun Mindivan*<sup>1</sup>; Huseyin Cimenoglu<sup>2</sup>; *Eyup Kayali*<sup>2</sup>; <sup>1</sup>Ataturk University; <sup>2</sup>Istanbul Technical University

In the present experimental investigation, 6082 Al alloy machining chips as matrix material and up to 20 wt% of fly ash particulate composite was fabricated using hot pressing method. Characterization of the composites was made by structural examinations and mechanical tests (hardness and dry sliding wear tests). The results indicate that the wear resistance of the fly ash reinforced composite increased with increase in fly ash content and the composites reinforced with fly ash particle exhibited superior hardness and wear resistance compared to the unreinforced 6082 Al alloy.

**5:40 PM**

**Selenium Treatment Technologies and Case Studies:** *Karen Hagelstein*<sup>1</sup>; <sup>1</sup>TIMES Limited

This paper discusses recent selenium treatment technologies which have been applied to metal processing, mining, agricultural and other industrial wastewaters. Physical, chemical, and biological properties of selenium compounds are discussed as well as analytical procedures. The removal technologies include membrane processes, ion exchange, chemical precipitation, adsorption processes, and biologically-based technologies such as biological treatment plants, in-situ treatment, constructed wetlands, evaporation ponds, Biopass and other passive technologies. Some technologies require management of the residues

from treatment, such as brines or wash solutions from membrane filtration and ion exchange, or sludges resulting from iron precipitation. Best management practices for seleniferous wastes including pilot testing, process chemistry, source control, and water management are discussed relative to industry case studies. The selenium treatment technologies which have been tested at a pilot-scale facility, implemented as treatment processes, are cost effective for large volumes of wastewater and can potentially meet regulatory treatment objectives are highlighted.

**6:00 PM**

**Surface Chemical Analyses of the Anti-Wear Boundary Film on Oxygen-Diffusion Treated Titanium:** *Jun Qu*<sup>1</sup>; Harry Meyer<sup>1</sup>; <sup>1</sup>Oak Ridge National Laboratory

Previous work has demonstrated that oxygen diffusion (OD) can dramatically improve the tribological characteristics for titanium alloys by enabling the formation of an anti-wear boundary film in a lubricated environment. In this study, XPS surface chemical analyses were conducted to reveal the film chemical compositions and compounds. The 50 nm thick boundary film detected on the worn OD-treated titanium (OD-Ti) surface contains significant amount of Ti, Zn, Ca, S, P, N, and O, while no such film exists on either the unworn OD-Ti surface or the worn, untreated titanium surface. Shifts of bonding energy spectrum peaks for elements extracted from the lubricant additives as well as the elements from the OD-Ti surface imply that the additive molecules reacted with the OD-Ti surface and formed new compounds during the wear process. Further analyses using an Auger parameter plot for Zn confirmed the existence of ZnS and ZnO in the boundary film.

## Magnesium Technology 2009: Alloys III: Rare Earth (Cerium and Other)

Sponsored by: The Minerals, Metals and Materials Society, TMS Light Metals Division, TMS: Magnesium Committee

Program Organizers: Eric Nyberg, Pacific Northwest National Laboratory; Sean Agnew, University of Virginia; Neale Neelameggham, US Magnesium LLC; Mihriban Pekguleryuz, McGill University

Tuesday PM

Room: 2006

February 17, 2009

Location: Moscone West Convention Center

*Session Chair:* Mark Easton, Monash University

**2:00 PM Introductory Comments**

**2:05 PM**

**Microstructure and Mechanical Properties of an Mg-Rare Earth Based Alloy AM-SC1:** *Mark Gibson*<sup>1</sup>; Colleen Bettles<sup>2</sup>; Suming Zhu<sup>3</sup>; Mark Easton<sup>3</sup>; Jain-Feng Nie<sup>3</sup>; <sup>1</sup>CSIRO; <sup>2</sup>ARC Centre of Excellence for Design in Light Metals; <sup>3</sup>CAST CRC

AM-SC1 is a high temperature Mg alloy that was originally developed as a sand casting alloy for automotive powertrain applications. In order to be truly competitive in critical automotive applications, magnesium alloys need to have properties that are similar to, or better than, aluminium alloy counterparts and they need to be readily manufacturable. AM-SC1 is suitable for both sand casting and permanent mould casting with properties that have been proven for both the AVL Genios LE and the USCAR lightweight magnesium engine projects. This paper describes the interrelationship between the microstructure and the mechanical properties of AM-SC1. The microstructural features contributing to the creep resistance are both inter- and intra-granular in nature and are on length scales from nanometres to micrometres. The creep behaviour at 150°C and 177°C is diffusion controlled, with any contribution from the grain boundaries being negligible.

**2:25 PM**

**Interdependence between Cooling Rate, Microstructure and Porosity in Mg Alloy AE42:** *Liang Wang*<sup>1</sup>; Sergio Felicelli<sup>1</sup>; Adrian Sabau<sup>2</sup>; John Berry<sup>3</sup>; <sup>1</sup>Mississippi State University; <sup>2</sup>Oak Ridge National Laboratory

Porosity is a major concern in the production of light metal parts. This work aims to identify some of the mechanisms of microporosity formation during the gravity-poured castings of magnesium alloy AE42. Two graphite plate molds and a ceramic cylindrical mold were selected to produce a wide range of cooling

rates. Temperature data during cooling was acquired with type K thermocouples at 60 Hz in two locations of each casting. The microstructure of samples extracted from the regions of measured temperature was then characterized with x-ray computed tomography and optical metallography. The gathered data was analyzed to search for correlations between cooling rate, dendrite arm spacing, pore volume fraction and pore size. The experimental outcomes were compared with simulations performed with a finite element continuum model of dendritic solidification. The results of this study confirm some of the findings observed in similarly cast aluminum alloys.

## 2:45 PM

### Application of Neutron Diffraction in In-Situ Studies of Stress Evolution in High Temperature Creep Testing of Creep Resistant Magnesium Alloys:

*Dimitry Sediako*<sup>1</sup>; <sup>1</sup>National Research Council of Canada

In-Situ Studies of Stress Evolution in magnesium alloys developed for high temperature applications have been the major focus of this study. Several alloying groups have been analyzed representing Mg-Al-Rare Earth, Mg-Al-Sr, Mg-Al-Ca, and Mg-Zn-Rare Earth systems. The samples were cast in permanent mould and extruded, and then subjected to 200 hrs of creep under load of 50 MPa for duration of 200 hours. Two temperatures were used in the creep tests: 150°C and 175°C. Primary and secondary creep evolution was observed for the studied alloys. In-situ and creep-induced residual stresses were analyzed with application of neutron diffraction techniques at the Canadian Neutron Beam Centre in Chalk River, Ontario. The in-situ diffraction pattern clearly shows the consecutive responses of the crystallographic lattice to the sample heating, creep loading, unloading, and cooling. Correlation of the resultant elongation of the sample (creep) to residual stress has also been demonstrated for several crystallographic planes.

## 3:05 PM

### Influence of Rare Earth Elements on the Microstructure and Texture Development during Rolling of Magnesium Alloy Sheets:

*Jason Hadorn*<sup>1</sup>; Kerstin Hantzschke<sup>2</sup>; Joachim Wendt<sup>3</sup>; Karl Kainer<sup>3</sup>; Jan Bohlen<sup>2</sup>; Dietmar Letzig<sup>2</sup>; Sean Agnew<sup>1</sup>; <sup>1</sup>University of Virginia; <sup>2</sup>GKSS-Forschungszentrum; <sup>3</sup>Hamburg University of Technology

The addition of rare earth elements has been observed to weaken and alter the predominant basal texture which normally occurs in conventional rolled magnesium-zinc alloy sheets. This effect offers the possibility to alter the mechanical properties and, in particular, improve the formability. Preliminary results have suggested that the "rare earth effect" is due to changes in the recrystallization behaviour of the alloys. Results from laboratory rolling trials designed to examine the effects of solid solution alloying with zinc and rare earth elements on the microstructural development will be presented. X-ray diffraction is used to characterize the bulk texture evolution. Electron backscattered diffraction (EBSD) is used to reveal the unique nucleation and growth patterns during recrystallization. Transmission electron microscopy is used to examine the level of grain boundary solute segregation. Finally, the impact of the resulting microstructure and texture on mechanical properties will be shown and discussed.

## 3:25 PM

### The Intergranular Microstructure of Magnesium Based Die-Cast AE Alloys:

*Liu-Ying Wei*<sup>1</sup>; Kun Wei<sup>1</sup>; Richard Warren<sup>1</sup>; <sup>1</sup>Malmö University

A systematic investigation on microstructures of magnesium based die cast Mg-Al-RE alloys (AE alloys) has been performed by XRD, SEM and TEM. The alloys are with content of Al around 4wt% and various content of rare earth (RE). Samples of these alloys are in as-cast condition as well as in aged condition at 200°C and 250°C. The intergranular microstructure of the alloys has been studied in details. Three types' binary Al-RE phases were found intergranularly. Al11RE3 is predominant intergranular phase in the as cast alloys. Al3RE particles and small amount of Al2RE phase were found in alloys with high RE content. Thermal stability of the Al-RE phases in AE alloys was suggested to decrease in sequence: Al2RE → Al11RE3 → Al3RE. The Al/RE ratio of the die cast alloys determined their phase constitutions. Promising AE alloys for creep resistance is suggested to have an Al/RE ratio not higher than 1.8.

## 3:45 PM Break

## 4:00 PM

### Thermal-mechanical processes to achieve peak strength in Mg-Zn-RE alloys: *Alok Singh*<sup>1</sup>; Hidetoshi Somekawa<sup>1</sup>; Toshiji Mukai<sup>1</sup>; <sup>1</sup>National Inst for Materials Sci

Mg-Zn-RE alloys have interesting ternary phases which have been used for strengthening of magnesium alloys, especially the quasiperiodic icosahedral phase (i-phase). Dispersion of this phase in magnesium matrix by hot rolling or extrusion has been shown to result in a good combination of strength and ductility. In alloys of composition Mg<sub>93</sub>Zn<sub>6</sub>RE, tensile and compressive strengths of about 230 MPa and 170 MPa, respectively, can be achieved in grain sizes over 25µm by extrusion. In this study, combinations of thermal and mechanical processes have been used to obtain strengths of 300 MPa in tension and 220 MPa in compression in grain sizes of over 25µm, by dynamic precipitation of the i-phase and ageing. Evolution of phases during the process has been studied. Tensile yield strength responds faster to ageing than compression. Isotropic mechanical properties are obtained in grain sizes of about 5µm.

## 4:20 PM

### On the Microstructure and Texture Development of Magnesium Alloy ZEK100 During Rolling: *Joachim Wendt*<sup>1</sup>; Karl Ulrich Kainer<sup>1</sup>; Gurutze Arruebarrena<sup>2</sup>; Kerstin Hantzschke<sup>3</sup>; Jan Bohlen<sup>3</sup>; Dietmar Letzig<sup>3</sup>;

<sup>1</sup>Hamburg University of Technology; <sup>2</sup>Mondragon Goi Eskola Politeknikoa; <sup>3</sup>GKSS-Forschungszentrum GmbH

The usage of Magnesium sheets as light-weight structures is limited due to their poor formability - in particular at room temperature - resulting from the typical strong basal texture of commercial magnesium sheets. Recently, it was shown that the basal texture may be weakened by the addition of rare earth (RE) or other alloying elements. The responsible mechanisms, however, are not yet well understood. In the presented work a series of experiments has been performed to study in more detail the influence of RE-elements on the texture development during hot rolling. The experiments are performed in several rolling passes with subsequent heat treatment. The paper presents texture and microstructure development over the whole rolling process and shows the distinct influence of the rolling procedure and a subsequent heat treatment. The research provides basic knowledge for targeted modification of the alloy composition aiming at enhanced formability of wrought magnesium alloys.

## 4:40 PM

### The Fracture Behavior of B2 Magnesium-Rare Earth Intermetallics: *Rupalee Mulay*<sup>1</sup>; James Wollmershauser<sup>1</sup>; Sean Agnew<sup>1</sup>; <sup>1</sup>University of Virginia

Intermetallic compounds have many attractive properties. The main issue, which limits the practical application of these compounds, is that most are brittle at room temperature. Recently, however, a family of binary intermetallic compounds has been discovered which exhibit appreciable polycrystalline ductility. These compounds are composed of a rare earth metal and a main group or transition metal and they have the B2 crystal structure. We are presently investigating the possibility that B2 compounds composed of Magnesium and a rare earth element may also exhibit the ductilizing effect. The compounds we are studying are MgY, MgCe, MgNd and MgDy. We have discovered that these compounds are brittle, and have undergone primarily cleavage fracture. We have used a combination of SEM-based stereology (to determine the facet normal) and EBSD (to determine the grain orientation) to, in turn, characterize the cleavage plane crystallography. Results indicate that MgY tends to cleave along {100} planes.

## 5:00 PM

### Effects of Solid Solution Heat Treatment on the Microstructures and Mechanical Properties of Mg96.82Zn1Gd2Zr0.18 Alloy with 14H-Type LPSO Structure: *Y.J. Wu*<sup>1</sup>; *X.Q. Zeng*<sup>1</sup>; *D.L. Lin*<sup>1</sup>; *L. M. Peng*<sup>1</sup>; *W.J. Ding*<sup>1</sup>;

<sup>1</sup>Shanghai Jiao Tong University

In as-cast Mg96.82Zn1Gd2Zr0.18 alloy, the microstructure mainly consists of eutectic structure in which the second phase, β-phase, is (Mg,Zn)3Gd having fcc structure, and α'-Mg solid solution and fine-lamellae consisting of 2H-Mg and 14H-type long period stacking ordered (LPSO) structure. The LPSO structure has been firstly observed in as-cast Mg96.82Zn1Gd2Zr0.18 alloys. During solid solution heat treatment at 773K for 0.5h to 234h, the microstructure evolution, especially the evolution of 14H-type LPSO structure were studied. It is concluded that β-phase can transform into a novel lamellar X-phase with 14H-type LPSO structure. Furthermore, it is concluded that the alloy heat-treated at 773K for



10h exhibits higher tensile strength (246.21MPa) and larger elongation (11.79%) owing to the dissolution of the  $\beta$ -phase and the much dispersion of X-phase with 14H-type LPSO structure and the lamellar 14H-type LPSO structure in matrix.

5:20 PM

**First-Principles Study of Elastic and Phonon Anomalies of CeMg Compound:** *Shunli Shang*<sup>1</sup>; Louis Hector<sup>2</sup>; Yi Wang<sup>1</sup>; Hui Zhang<sup>1</sup>; Zi-Kui Liu<sup>1</sup>; <sup>1</sup>The Pennsylvania State University; <sup>2</sup>General Motors Research and Development Center

Cerium serves a crucial role in Mg alloys which are currently of considerable interest as light weight alternatives to Al and steel alloys in vehicle body structures. The mechanisms by which Ce additions leads to observed improvements in Mg alloys are poorly understood due to leaking of the fundamental Ce-Mg property. In the present work, elastic constants, phonon properties and phase stability of CeMg compound have been investigated in terms of first-principles calculations. CeMg is predicted to be antiferromagnetic with wavevector along the [110] direction and in particular elastic anomaly with elastic constants  $c_{44} > c_{11}$  is found in CeMg. This elastic anomaly is confirmed by phonon calculations, i.e., the predicted frequency of longitudinal acoustic branch along the Gamma-X direction is lower than those of the transverse branches due mainly to the negative stretching force constants between the second nearest-neighbor Mg-Mg atoms and the third nearest-neighbor Ce-Ce atoms.

## Magnesium Technology 2009: Deformation

Sponsored by: The Minerals, Metals and Materials Society, TMS Light Metals Division, TMS: Magnesium Committee

Program Organizers: Eric Nyberg, Pacific Northwest National Laboratory; Sean Agnew, University of Virginia; Neale Neelameggham, US Magnesium LLC; Mihriban Pekguleryuz, McGill University

Tuesday PM  
February 17, 2009

Room: 2007  
Location: Moscone West Convention Center

Session Chair: Kwang Seon Shin, Seoul National University

### 2:00 PM Introductory Comments

2:05 PM

**Influence of Alloying Additions on the Microstructure Development of Extruded Mg-Mn Alloys:** *Jan Bohlen*<sup>1</sup>; Jacek Swiostek<sup>1</sup>; Dietmar Letzig<sup>1</sup>; Karl Ulrich Kainer<sup>1</sup>; <sup>1</sup>GKSS Forschungszentrum

In this study the effect of different alloying elements on the microstructure development of magnesium-manganese alloys during extrusion will be examined. Using alloy M1, which contains up to 1 wt.% Mn in solid solution as a basis, further elements such as rare earth elements or zirconium are added to the melt and cast into billets for extrusion. The effect of the alloying addition is analysed during indirect extrusion trials by varying the extrusion speed. Characterisation of the microstructure before and after extrusion gives information on the microstructure evolution during extrusion. Uniaxial tension and compression tests at ambient temperature relate the microstructure to the mechanical properties. The results are discussed with respect to the influence of these alloying elements on the microstructure development as well as the deformation and recrystallisation behaviour during extrusion.

2:25 PM

**Texture Evolution in an AZ31 Mg Alloy during Direct and Indirect Extrusion Processes:** *Shi-Hoon Choi*<sup>1</sup>; Hyeong-Wook Lee<sup>1</sup>; Dae-Ha Kim<sup>1</sup>; Duk-Jae Yoon<sup>2</sup>; Sung-Soo Park<sup>3</sup>; Bong-Sun You<sup>3</sup>; <sup>1</sup>Sunchon National University; <sup>2</sup>Korea Institute of Industrial Technology; <sup>3</sup>Korea Institute of Materials Science

Direct and indirect extrusion processes for an AZ31 Mg alloy were performed at various ram speeds. A finite element (FE) analysis with DEFORMTM -2D V9.1 was conducted to evaluate the deformation gradient tensor during direct and indirect extrusions. The evolution of extrusion texture in an AZ31 Mg alloy has been simulated numerically using a visco-plastic self-consistent (VPSC) polycrystal model. In order to capture crystallographic rotation during extrusion deformation, four slip and a tensile twin systems were considered in the polycrystal model. From direct and indirect extruded specimens, macrotexture was measured using X-ray diffractometer. The experimental results were compared with the results predicted by the theoretical approach. The FE

analysis combined with the VPSC polycrystal model successfully predicted the inhomogeneous texture distribution through thickness direction in the extrusion specimens.

2:45 PM

**Microalloying and Deformation Modes of Age Hardened Mg-Zn Based Alloys:** *Joka Buha*<sup>1</sup>; <sup>1</sup>University of New South Wales

Age hardening response of Mg-Zn alloy was significantly improved by alloying using novel and uncommon alloying elements such as Ti, Cr, Ba and V. These elements increase the number density of the precipitates in the aged alloys and accelerate the kinetics of precipitation during artificial and natural ageing. Alloying with Ti and V also results in significant grain refinement. It was also found that natural ageing in Mg-Zn based alloys results in a highly favourable combination of mechanical properties: hardness nearly equal to that in the T6 condition; yield strength close to that in the T6 condition but with ductility being three times greater than in the T6 condition. The high ductility/deformability in the T4 condition was correlated with the formation of a high density of fully and partially coherent precipitates and clusters of solute atoms, which enable activation of non-basal slip during deformation at the expense of twinning.

3:05 PM

**Deformation Mechanisms in Magnesium Alloy Elektron 675:** *David Randman*<sup>1</sup>; W Rainforth<sup>1</sup>; Brad Wynne<sup>1</sup>; Bruce Davis<sup>2</sup>; <sup>1</sup>University of Sheffield; <sup>2</sup>Magnesium Elektron North America

Elektron 675 is a new, rare earth-based magnesium alloy developed by Magnesium Elektron Ltd. for wrought applications. Elektron 675 has superior mechanical properties relative to the current commercially available wrought alloys AZ31B, WE43, and ZK60. This work looks at the rolling deformation behaviour of the alloy through plane strain compression tests at a range of temperatures and strain rates. Constitutive equations of flow stress as a function of strain, strain rate and temperature have been developed, showing a peak stress followed by gradual softening. Microstructural analysis has been carried out and the softening has been attributed to a small amount of dynamic recrystallisation that is occurring in areas of high strain, forming a necklace structure around the grain boundaries. In both EBSD and TEM it is seen that fine planar slip bands form on standard slip systems. The correlation between microstructure and flow behaviour will be discussed.

3:25 PM

**Elevated Temperature and Varied Load Response of AS41 at Bolted Joint:** *Okechukwu Anopuo*<sup>1</sup>; Guowu Shen<sup>2</sup>; Su Xu<sup>2</sup>; Norbert Hort<sup>1</sup>; Karl Kainer<sup>1</sup>; <sup>1</sup>GKSS Research Centre; <sup>2</sup>CANMET-Material Technology Laboratory

The effective application of Mg alloys as automotive power train components is continuously challenged by the ability of magnesium to withstand fastener clamp load under service condition. The stiffness of a joint is strongly dependent on the elastic moduli of the members of the bolted joint. As deflections on loaded bolted steel components could be ignored at low and elevated temperature condition that of magnesium alloys cannot be overlooked. In this work Bolt load retention experiments are carried out on AS41 between stresses of 40 MPa to 70 MPa and temperature of 100°C to 175°C. A power law creep relationship coded in finite elemental program is used to describe the time dependent stress-strain response of AS41. The parameters in this relationship are obtained by fitting typical compressive creep test results. A comparison of the model and bolt load retention experiments using load cell measuring techniques shows good agreement.

3:45 PM Break

4:00 PM

**High Temperature Deformations and Microstructural Evolutions of Mg Alloy Laminated Composites Fabricated by ECAE:** *Xibo Liu*<sup>1</sup>; *Rongshi Chen*<sup>1</sup>; *Enhou Han*<sup>1</sup>; <sup>1</sup>Institute of Metal Research Chinese Academy of Sciences

The laminated composites of dissimilar Mg-5Y-4Nd/Mg-6Zn-1Y (WE54/ZW61), similar WE54/WE54 and ZW61/ZW61 pairs were fabricated by equal channel angular extrusion (ECAE). The high temperature deformation and microstructural evolution of dissimilar WE54/ZW61 composite were investigated at 400°C with different strain rates, and the superplasticity with a maximum elongation of 620% was obtained at 400°C and  $1 \times 10^{-3} \text{ s}^{-1}$ . In addition, under the optimum conditions of 400°C and  $1 \times 10^{-3} \text{ s}^{-1}$  for superplasticity, the dissimilar WE54/ZW61 composites were deformed with various strains of 0.1, 0.5, 1 and 1.5, subsequently, the cavities and microstructural evolutions after deformation were observed and compared to each other. On the other

hand, the studies were also extended to the similar WE54/WE54 and ZW61/ZW61 composites deformed under 400°C and  $1 \times 10^{-3} \text{ s}^{-1}$  in comparison with the dissimilar WE54/ZW61 composite.

#### 4:20 PM

**Effect of Precipitates on Deformation Mechanisms at Low-Temperature in an AZ80 Magnesium Alloy:** *Jayant Jain*<sup>1</sup>; Jianxin Zou<sup>1</sup>; Warren Poole<sup>1</sup>; Chadwick Sinclair<sup>1</sup>; <sup>1</sup>University of British Columbia

In this work, the operation of various slip and twin modes during the low-temperature deformation of a precipitate containing AZ80 magnesium alloy have been investigated. An AZ80 alloy of nearly random initial texture was aged and then deformed in uniaxial compression at 77K and 293K. Compression tests were stopped at intermediate strains for microstructural analysis aimed at identifying different deformation mechanisms. Both optical Nomarski microscopy and Electron backscattered diffraction (EBSD) have been employed to characterize the deformed sample. The slip markings on polished surfaces have been identified using slip trace analysis while the effect of precipitates on the nature of deformation twinning has been investigated using EBSD. The results obtained on aged samples are compared and contrasted with previously reported results obtained on the solution-treated AZ80 material.

#### 4:40 PM

**Low Temperature Processing of Pure Mg by Equal Channel Angular Extrusion:** *Suveen Mathaudhu*<sup>1</sup>; Majid Al-Maharbi<sup>2</sup>; David Foley<sup>2</sup>; Bin Li<sup>3</sup>; K. Hartwig<sup>2</sup>; Evan Ma<sup>3</sup>; Ibrahim Karaman<sup>2</sup>; Laszlo Kecskes<sup>1</sup>; <sup>1</sup>U.S. Army Research Laboratory; <sup>2</sup>Texas A&M University; <sup>3</sup>The Johns Hopkins University

Severe plastic deformation by equal channel angular extrusion (ECAE) has been shown to improve both strength and ductility of a number of Mg-alloys, but the majority of processing has been done at or near the recrystallization temperature of ~220° C. The high temperatures promote dynamic recrystallization, thus limiting the grain refinement and strengthening capabilities of ECAE. The research presented here will give the microstructure and mechanical behavior of cast, pure Mg processed by ECAE at 150° C and 200° C to multiple strain values. The ECAE-processed microstructures are composed of a bimodal-like microstructure composed of worked regions and partially recrystallized grains with average grain sizes of ~1 micrometer. Compression test results show anisotropic properties in the as-cast starting material, and concurrently high strength and ductility in the processed Mg. Microhardness values and x-ray texture maps will also be presented to quantify the improved properties.

#### 5:00 PM

**Mechanical Behavior of ZK60 Magnesium Alloy Processed by Equal Channel Angular Extrusion:** *Yanwen Wang*<sup>1</sup>; Rajiv Mishra<sup>1</sup>; Elhachmi Essadiqi<sup>2</sup>; Ravi Verma<sup>3</sup>; <sup>1</sup>Missouri University of Science and Technology; <sup>2</sup>MTL CANMET; <sup>3</sup>General Motors Corp

The use of magnesium alloys in wrought products has been limited due to the poor room temperature ductility and the compression/tension yield point asymmetry. These problems could be solved by grain refinement and weaker texture generated by shear band and recrystallization in these alloys processed by ECAE. In this study, ZK60 magnesium alloy was processed via ECAE at 523 K, with different extrusion speeds. Tension and compression tests were conducted for the samples with different orientations. The results show that after two-pass processing at the temperature of 523 K and extrusion rate of 5 mm/s, ZK60 exhibited the room temperature ductility of 38.7%, 23.2%, 23.6% and 37.6% , and the compression/tension yield point asymmetry ratio R of 0.87, 1.09, 1.07 and 0.78, with respect to the parallel, perpendicular, and ±45° inclined to the extrusion direction. These results are explained by correlating the evolution of microstructure and texture during the ECAE.

#### 5:20 PM

**Modeling Texture, Twinning, and Hardening Evolution during Strain Path Reloads in Pure Magnesium:** *Andrew Oppedal*<sup>1</sup>; George Kaschner<sup>2</sup>; Laurent Capolungo<sup>2</sup>; Rodney McCabe<sup>2</sup>; Sven Vogel<sup>2</sup>; Donald Brown<sup>2</sup>; Carlos Tome<sup>2</sup>; Mark Horstemeyer<sup>1</sup>; <sup>1</sup>Mississippi State University; <sup>2</sup>Los Alamos National Laboratory

We examine the relationship between deformation twinning and slip in hexagonal close packed (HCP) metals in experiments using high purity (99.95%) Magnesium (Mg). Simple compression samples from rolled Mg plate were pre-loaded in through thickness (TT) and in-plane (IP) orientations followed by re-loading in IP and TT orientations, respectively. Deformation twinning introduced during pre-load affects the reload response and reveals the role that

microstructure evolution has on hardening. Mechanical testing characterization, as well as texture measurements via neutron diffraction and electron back-scattered diffraction (EBSD) is compared with results from a viscoplastic self-consistent (VPSC) polycrystal model. The VPSC model uses a dislocation based hardening constitutive relation and composite grain model to predict texture evolution and mechanical behavior. Results from similar earlier experiments with Zirconium and Mg AZ31 are compared.

#### 5:40 PM

**Study on Rolling Process of Mg-9Li-2Zn Alloy Plate:** *Guoyin Zu*<sup>1</sup>; Tinggang Li<sup>1</sup>; Guangchun Yao<sup>1</sup>; <sup>1</sup>Northeastern University, School of Materials and Metallurgy

The Mg-9Li-2Zn alloy ingot with good microstructure and properties prepared by melting-casting method, the rolling process of alloy was studied, and the softening mechanism of Mg-9Li-2Zn alloy during annealing process were discussed. The results show that the smelting result was good by using LiCl + LiF covering flux. The optimum homogenization processes for Mg-9Li-2Zn alloy is at 250°C for 24h. The dynamic recrystallization has happened in the rolling process when the heating temperature beyond 200°C. The optimum heating temperature is 200°C~300°C, the best pass reduction of Mg-9Li-2Zn alloy plate is 20%~30%. The optimum annealing process should be at 300°C for 60min, under this condition, the total deformation rate of as-annealed Mg-9Li-2Zn alloy plate can reach 70%.

## Materials for High Temperature Applications: Next Generation Superalloys and Beyond: Refractory Alloys II

Sponsored by: The Minerals, Metals and Materials Society, TMS Structural Materials Division, TMS: High Temperature Alloys Committee, TMS: Refractory Metals Committee  
Program Organizers: Joseph Rigney, GE Aviation; Omer Dogan, National Energy Technology Laboratory; Donna Ballard, Air Force Research Laboratory; Shiela Woodard, Pratt & Whitney

Tuesday PM

February 17, 2009

Room: 3010

Location: Moscone West Convention Center

*Session Chair:* Bernard Bewlay, GE Global Research (K1-MB271)

#### 2:00 PM Invited

**Microstructural Designs for High Temperature Mo-Si-B Alloys:** *John Perepezko*<sup>1</sup>; Ridwan Sakidja<sup>1</sup>; Megan Jarosinski<sup>1</sup>; <sup>1</sup>University of Wisconsin

While existing high temperature alloys exhibit a remarkable performance, the prospects are limited for advances in high-temperature capability (>1400°C). Among the new systems that can enable a step change in performance, multiphase Mo-Si-B alloys are attractive in meeting the difficult challenges of high temperature performance. Systematic studies of the phase equilibria and diffusion have provided a foundation of understanding of the governing phase stability and microstructure evolution. The baseline microstructure with a Mo + Mo<sub>3</sub>Si + Mo<sub>5</sub>Si<sub>2</sub> (T<sub>2</sub>) phase mixture provides a good performance, but solidification processing is difficult. An alternate approach based upon alloy design is also available. Phase stability guidance allows the Mo<sub>3</sub>Si phase to be replaced by a Mo<sub>5</sub>Si<sub>3</sub> (T<sub>1</sub>) structure and provides access to a monovariant three-phase BCC + T<sub>2</sub> + T<sub>1</sub> eutectic reaction. Similarly, other alloy designs yield a BCC + T<sub>2</sub> + D<sub>88</sub> phase. The microstructure designs provide new directions for processing and new performance levels.

#### 2:25 PM

**Deformation Behavior of Mo<sub>5</sub>SiB<sub>2</sub>:** *Oleg Kontsevoi*<sup>1</sup>; Nadezhda Medvedeva<sup>2</sup>; Arthur Freeman<sup>1</sup>; John Perepezko<sup>3</sup>; <sup>1</sup>Northwestern University; <sup>2</sup>Institute of Solid State Chemistry; <sup>3</sup>University of Wisconsin

Multiphase Mo-Si-B alloys attract increasing attention as very promising materials for applications at temperatures above 1200°C; poor ductility is one of the main drawbacks. To analyze the fracture and deformation mechanisms for Mo<sub>5</sub>SiB<sub>2</sub>, we performed ab initio calculations of generalized stacking fault energies for possible directions on the {001}, {010}, {110} and {012} slip planes. A striking result was obtained that the three favorable systems, <100>(001), <110>(001) and [001]{010}, have almost equal unstable and stable stacking faults, and the preference among them cannot be established.

This finding explains a large variety of experimental data on the observed slip systems. The dislocations associated with these slips may dissociate into partials joined with stacking faults and separated by the large splitting width of 5-6 nm, as estimated from elasticity theory. The absence of a strong preference for a certain slip system suggests a path for enhancing ductility through operation of multiple systems.

**2:45 PM**

**Compressive Deformation Behavior of High Temperature Mo-Si-B Alloy:** *Xingshuo Wen*<sup>1</sup>; Padam Jain<sup>2</sup>; Joachim Schneibel<sup>3</sup>; K. Sharvan Kumar<sup>2</sup>; Vijay Vasudevan<sup>1</sup>; <sup>1</sup>University of Cincinnati; <sup>2</sup>Brown University; <sup>3</sup>Oak Ridge National Laboratory

Alloys based on Mo-Si-B ternary system are of interest for very high temperature structural applications. The compression behavior at 1200, 1300 and 1400°C of a nominally Mo-20Si-10B (in wt.%) alloy that was processed such as to yield varying  $\alpha$ -Mo volume fractions (from 5 to 46%), with the balance made up of Mo<sub>3</sub>Si and T2-Mo<sub>3</sub>SiB<sub>2</sub> phases, was studied. The results of constant strain rate compression tests showed that the stresses required to maintain a given strain rate increased with a decrease in temperature and  $\alpha$ -Mo volume fraction. The values of the stress exponents determined from the data ranged from ~3-9, depending on temperature and volume fraction of  $\alpha$ -Mo; the activation energy for creep was found to be in the range of ~200-600 kJ/mole depending on stress level and volume fraction of  $\alpha$ -Mo. These results were correlated with SEM and TEM observations of the damage processes, deformation structures and deformation mechanisms.

**3:05 PM**

**CALPHAD Based Thermodynamic Modeling of the Mo-W-Si-C System:** *Sujoy Kar*<sup>1</sup>; Swetha Ganeshan<sup>1</sup>; Don Lipkin<sup>2</sup>; Martin Morra<sup>2</sup>; <sup>1</sup>GE Global Research, Bangalore; <sup>2</sup>GE Global Research, Niskayuna

Composite refractory systems based on SiC with Mo and W silicides have been found suitable for high temperature applications in both oxidizing as well as partially reducing atmospheres. Understanding the phase stability in the Mo-W-Si-C system is critical for optimizing the composition and processing of these alloys for specific applications. A CALPHAD based technique has been employed to develop the Mo-W-Si-C quaternary thermodynamic database. Prior literature in this system does not reveal any ternary compounds in three of the four constituent ternary systems: Mo-W-Si, Mo-W-C, and W-Si-C. This indicates the sufficiency of the ideal solution assumptions for the respective ternary interaction parameters. However, it has been reported that the Mo-Si-C system has a ternary compound, namely the Nowotny phase (Mo<sub>5-6</sub>Si<sub>3</sub>C<sub>7</sub>). Consequently, the Mo-Si-C ternary database has been assessed. Details of the database development and examples of phase stability in these alloy systems are described.

**3:25 PM Break**

**3:35 PM Invited**

**Structural Molybdenum Borosilicides: Processing as the Key for an Optimum Balance of Properties:** *Martin Heilmaier*<sup>1</sup>; Manja Krüger<sup>1</sup>; Holger Saage<sup>1</sup>; Pascal Jehanno<sup>2</sup>; Mike Böning<sup>2</sup>; Heinrich Kestler<sup>2</sup>; Joachim Schneibel<sup>3</sup>; Easo George<sup>3</sup>; <sup>1</sup>Otto Von Guericke University; <sup>2</sup>Plansee SE; <sup>3</sup>Oak Ridge National Laboratory

We review the current development status of molybdenum borosilicide (Mo-Si-B) alloys for ultra-high temperature applications in excess of 1100°C in air. The assessment of several ingot and powder metallurgy approaches revealed that (i) the presence of a continuous Mo solid solution matrix is crucial for adequate fracture toughness near ambient temperatures and (ii) wrought processing of such alloys at temperatures typical for refractory metals requires an ultrafine (sub-micron) microstructure. Both prerequisites could be fulfilled using mechanical alloying (MA) as the crucial processing step [1]. However, the ductile-to-brittle transition temperature (DBTT), 800°C, was high due to grain boundary embrittlement by Si segregation. First results on the effect of different microalloying additions (e.g. Zr) on reducing this segregation will be presented and discussed. A short outlook on current industrial activities closes the presentation. [1] M. Krüger et al., *Intermetallics* 16, 933 (2008).

**4:00 PM**

**Microstructural Engineering of Mo-Si-B Alloys Produced Using Nitride-Based Reactions:** *Michael Middlemas*<sup>1</sup>; Joe Cochran<sup>1</sup>; Arun Gokhale<sup>1</sup>; <sup>1</sup>Georgia Institute of Technology

Mo-Si-B intermetallic composite alloys are of interest as next-generation, high-temperature materials. Three-phase alloys consisting of bcc-Mo and the intermetallic phases Mo<sub>3</sub>Si and Mo<sub>3</sub>SiB<sub>2</sub> have been investigated. The intermetallic phases enhance creep strength and oxidation resistance, but hinder fracture toughness due to crack propagation through the brittle intermetallics. For good mechanical properties, the intermetallic phases must be present as a fine dispersion in a continuous molybdenum matrix. This has been achieved using a powder metallurgy approach through the reaction of molybdenum, Si<sub>3</sub>N<sub>4</sub> and BN powders. The effect of different boron nitride reactant powders on the dispersion of the intermetallic phases has been investigated. Electron backscatter diffraction imaging has been used to map the location of individual phases. Two-point correlation functions were used to quantify microstructural parameters in order to examine the effect of processing on the resulting microstructure.

**4:20 PM**

**Cr-Base Alloys: Current Problems and Future Possibilities for High-Temperature Applications:** *Yuefeng Gu*<sup>1</sup>; H. Harada<sup>1</sup>; <sup>1</sup>NIMS

In search of new materials for use as components in gas turbine engines, considerable interest has been shown in chromium (Cr) and Cr-rich alloys because Cr has high melting point (1863°C) and good oxidation resistance. Its low density and high thermal conductivity (two to four times higher than most of Ni-base superalloys) are also attractiveness to the benefit of the increasing efficiency. However, the implementation Cr-rich alloys as a viable substitute for Ni-base alloys has been impeded by their poor ductility at ambient temperature and low strength at high temperature. Recently, we find that adding Ag to Cr can greatly improve its tensile ductility. Some Cr-rich binary alloys show improved tensile ductility at ambient temperature and adequate strength at high temperature. Therefore, new composition design and process would open absolute opportunity for Cr-base alloys as a structural material used at temperatures up to 1300°C.

**4:40 PM**

**Structure, Chemical Stability and Properties of NiAl-Al<sub>2</sub>O<sub>3</sub> Interface Modified by MAX-Phase Interlayer:** *Weiping Hu*<sup>1</sup>; Jia Song<sup>1</sup>; Yunlong Zhong<sup>1</sup>; Günter Gottstein<sup>1</sup>; <sup>1</sup>Institute of Physical Metallurgy and Metal Physics

H-phase (also called MAX-phase) with the common formula M<sub>2</sub>AX, where M is an early transition metal, A is a group IIIA or IVA element, and X is either C and/or N, has attractive properties which usually associated with metals and ceramics, e.g. good thermal and electrical conductivity, high modulus and high strength at elevated temperatures, good thermal stability and good machinability. For this reason it has been tried to utilize the MAX-phase as an interlayer for modifying the interface structure and properties of continuous single crystal Al<sub>2</sub>O<sub>3</sub> fiber (sapphire) reinforced NiAl composites. In present investigation two different MAX-phases, V<sub>2</sub>AlC and Cr<sub>2</sub>AlC, were used. NiAl composites were produced as following: single crystal Al<sub>2</sub>O<sub>3</sub> fibers with a diameter of about 130  $\mu$ m were firstly coated by PVD with V<sub>2</sub>AlC or Cr<sub>2</sub>AlC (about 1  $\mu$ m thick) and then PVD-coated with NiAl (about 20~30  $\mu$ m thick). After PVD-process the fibers were further diffusion bonded in a channel die at 1300 °C under 40 MPa pressure for 1 hour in vacuum ( $2 \times 10^{-3}$  Pa).

**5:00 PM**

**Mullite-Based Graded-Architecture Thermal Barrier Coatings for Mo-Si-B Turbine Materials:** *Joshua Jackson*<sup>1</sup>; Angelique Lasseigne<sup>2</sup>; David Olson; Brajendra Mishra<sup>1</sup>; <sup>1</sup>Colorado School of Mines; <sup>2</sup>National Institute of Standards and Technology

Advanced corrosion- and oxidation-resistant thermal barrier coatings are being developed for Mo-Si-B turbine materials to achieve higher operating temperatures and pressures. Numerous precursor coating deposition techniques have been assessed using systematic change of process variables. Pulsed organic electrolysis has been selected for further development. The processing to form a graded thermal barrier coating includes deposition of a precursor coating layer, annealing to form a graded compositional region, and high-temperature oxidation to form a protective thermal barrier coating. Two different coating architectures are being explored, including a graded-coating architecture or a diffusion-barrier architecture. Annealing to achieve graded coating architecture and high-temperature oxidation to achieve mullite formation has been utilized to achieve the correct process parameters. Careful analysis at the substrate-coating



interface to understand the stability, diffusion, and adhesion of the deposited thermal barrier coatings is being performed to determine the need for a diffusion barrier layer.

## Materials in Clean Power Systems IV: Clean Coal-, Hydrogen Based-Technologies, and Fuel Cells: Hydrogen Storage Materials

Sponsored by: The Minerals, Metals and Materials Society, ASM International, TMS Electronic, Magnetic, and Photonic Materials Division, TMS/ASM: Corrosion and Environmental Effects Committee, TMS: Energy Harvesting and Storage Committee  
 Program Organizers: K. Scott Weil, Pacific Northwest National Laboratory; Michael Brady, Oak Ridge National Laboratory; Ayyakkannu Manivannan, US DOE; Z. Gary Yang, Pacific Northwest National Laboratory; Xingbo Liu, West Virginia University; Zi-Kui Liu, Pennsylvania State Univ

Tuesday PM Room: 3005  
 February 17, 2009 Location: Moscone West Convention Center

Session Chair: Zhenguo "Gary" Yang, Pacific Northwest National Laboratory

### 2:00 PM Introductory Comments

#### 2:05 PM Keynote

**High Capacity Hydrogen Storage Based on Solid Amine Boranes:** *Chris Aardahl*<sup>1</sup>; <sup>1</sup>PNNL

In the current vision of the hydrogen economy, fuel cell vehicles using some form hydrogen fuel will replace automobiles relying on gasoline powered internal combustion engines. A wide range of candidate on-board hydrogen storage methods are being evaluated including pressurized hydrogen gas tanks, liquefied hydrogen, and a host carriers from which hydrogen gas can be desorbed and regenerated. A portion of the current research within the US DOE Center of Excellence for Chemical Hydrogen Storage focuses on solid ammonia borane (AB). Ammonia borane and its derivatives are promising hydrogen storage materials because they contain large fractions of releasable hydrogen with reasonable kinetics. The results discussed in this presentation will cover release of hydrogen from these materials as well as the chemical regeneration required to recycle the fuel. Technical focus will be on release mechanism, how to increase kinetics, and on novel approaches for reducing H-depleted boron centers to enable fuel regeneration.

#### 2:50 PM Invited

**Enhancing the Hydrogen Storage Capacity of Nanoporous Carbons:** *Nidia Gallego*<sup>1</sup>; *Cristian Contescu*<sup>1</sup>; *Vinay Bhat*<sup>1</sup>; <sup>1</sup>Oak Ridge National Laboratory

Efficient storage of hydrogen for use in fuel cell-powered vehicles is a challenge that is being addressed in different ways, including adsorptive, compressive, and liquid storage approaches. In this presentation we report on adsorptive storage in Palladium-doped nanoporous carbon fibers. Nanoparticles of Pd, when dispersed in activated carbon fibers (ACF), enhance the hydrogen storage capacity of ACF. The adsorption capacity of Pd-ACF increases with increasing temperature below 0.4 bar, and the trend reverses when the pressure increases. To understand the cause for such behavior, hydrogen uptake properties of Pd with different degrees of Pd-carbon contact are compared with Pd-sponge using in situ XRD under various hydrogen partial pressures (<10 bar). The results support the spillover mechanism (dissociative adsorption of H<sub>2</sub> followed by surface diffusion of atomic H). Research sponsored by the Division of Materials Sciences and Engineering, U.S. Department of Energy under contract with UT-Battelle, LLC.

#### 3:25 PM

**Structural Phase Transitions Under Pressure in Mg(BH<sub>4</sub>)<sub>2</sub>:** *Lyci George*<sup>1</sup>; *Vadym Drozd*<sup>1</sup>; *Maximilian Fichtner*<sup>2</sup>; *Surendra Saxena*<sup>1</sup>; <sup>1</sup>Florida International University; <sup>2</sup>Forschungszentrum Karlsruhe GmbH

The structural stability of Mg(BH<sub>4</sub>)<sub>2</sub>, a promising hydrogen storage material, under pressure has been investigated up to 21 GPa with combined synchrotron X-ray diffraction and Raman spectroscopy. The analyses show a structural phase transition around ~ 3.5-5.4 GPa and again around ~14 GPa. At ambient conditions Mg(BH<sub>4</sub>)<sub>2</sub> has a hexagonal structure (space group-P6<sub>1</sub>, a=10.1647(6) Å, c= 36.902(8) Å and V= 3301.9(8) Å<sup>3</sup>), which agrees well with early reports. The high pressure phase is found to have different structure from

theoretically determined structures; the structure also does not match with that of the high temperature phase. The high pressure phase is found to be stable on decompression similar to the case of high temperature phase.

#### 3:45 PM

**An Investigation of Hydrogen Capacity of Magnesium Powder:** *Hung-Yu Tien*<sup>1</sup>; *Mahesh Tanniru*<sup>1</sup>; *Chang-Yu Wu*<sup>2</sup>; *Fereshteh Ebrahimi*<sup>1</sup>; <sup>1</sup>Materials Science and Engineering, University of Florida; <sup>2</sup>Environmental Engineering Science, University of Florida

Ideally magnesium hydride has a total capacity of 7.6wt%. However, during hydrogenation of magnesium powders the saturation level achieved is lower than this maximum capacity. In this study the kinetics of hydrogenation of a commercial magnesium powder is investigated as functions of temperature, pressure and hydrogenation procedure. Ni was applied as catalyst using two different techniques. The nucleation and growth of magnesium hydride were characterized using cross-sectional electron microscopy. The results of this study revealed that the hydrogenation kinetics and the saturation level depend on the sequence of heating and pressurization. When the powder was heated after pressurization a lower saturation level was obtained. Furthermore, the dry method of applying Ni was found to render faster hydrogenation kinetics because of the additional change in the morphology of the powder. In this study mechanism of hydrogenation is discussed based on microstructural evaluation. The financial support by NSF (DMR-0605406) is greatly appreciated.

#### 4:05 PM Break

#### 4:10 PM Invited

**Synthesis of Alkali Amidoboranes for Hydrogen Production:** *Xiong Zhitao*<sup>1</sup>; *Wu Guotao*<sup>1</sup>; *Chen Ping*<sup>1</sup>; <sup>1</sup>Dalian Institute of Chemical Physics

Holding a hydrogen capacity of 19.6wt%, ammonia borane (NH<sub>3</sub>BH<sub>3</sub>) shows potential to be a hydrogen storage material. Though considerable amount of hydrogen evolves from NH<sub>3</sub>BH<sub>3</sub>, its decomposition also generates borazine, a volatile product highly poisoning to PEM fuel cell. In addition, relatively high kinetic barrier in dehydrogenation of this chemical hinders the release of hydrogen at acceptably low temperatures. Our recent effort in modifying NH<sub>3</sub>BH<sub>3</sub> by replacing one of its H with alkali metal successfully produced lithium amidoborane (LiNH<sub>2</sub>BH<sub>3</sub>) and NaNH<sub>2</sub>BH<sub>3</sub>. TPD and volumetric release showed amidoboranes evolved 2 equiv. H<sub>2</sub> in two steps; a burst was observed around 90C and a broad TPD signal centralized at 150C. Borazine was undetectable. DSC indicated mild exothermic nature of that burst and the second dehydrogenation process was nearly thermal neutral. Therefore, isothermally heating LiNH<sub>2</sub>BH<sub>3</sub> and NaNH<sub>2</sub>BH<sub>3</sub> at 91°C for 19h resulted in the evolution of 10.7wt% and 7.4wt% hydrogen, respectively.

#### 4:45 PM

**Nano Approaches to use Light Metals Magnesium and Aluminum in Hydrogen Storage:** *Rajeev Ahuja*<sup>1</sup>; <sup>1</sup>Uppsala University

A fundamental understanding of the role of catalysts in dehydrogenation of MgH<sub>2</sub> nanoclusters is provided by carrying out first principles calculations based on density functional theory. It is shown that the transition metal atoms Ti, V, Fe, and Ni not only lower desorption energies significantly but also continue to attract at least four hydrogen atoms even when the total hydrogen content of the cluster decreases. In particular, Fe is found to migrate from the surface sites to the interior sites during the dehydrogenation process, releasing more hydrogen as it diffuses. This diffusion mechanism may account for the fact that a small amount of catalysts is sufficient to improve the kinetics of MgH<sub>2</sub>, which is essential for the use of this material for hydrogen storage in fuel-cell applications. Further, we have also studied the role of catalysts in dehydrogenation of AlH<sub>3</sub>.

#### 5:05 PM

**Effect of Al Addition on Dehydrogenation Characteristics of MgH<sub>2</sub>:** *Mahesh Tanniru*<sup>1</sup>; *Jacob Jones*<sup>1</sup>; *Darlene Slatery*<sup>2</sup>; *Fereshteh Ebrahimi*<sup>1</sup>; <sup>1</sup>University of Florida; <sup>2</sup>Florida Solar Energy Center

Magnesium hydride, which has a theoretical hydrogen capacity of about 7.6wt%, is an attractive hydrogen storage material for fuel cell applications. The main shortcoming of employing MgH<sub>2</sub> is its high desorption temperature. Alloying has been shown to affect the stability of this hydride. In this study the effect of Al addition on the dehydrogenation characteristics of magnesium hydride was investigated. Mg-Al alloy powders were fabricated by an electrodeposition technique. Ni was added as a catalyst for promoting the hydrogenation of these alloy powders. Electron microscopy techniques were employed for microstructural and compositional analyses. Pressure-composition isotherms

were developed at different temperatures to evaluate the enthalpy of formation/dissociation of  $MgH_2$ . The evolution of phases during the dehydrogenation was investigated using an in-situ high temperature x-ray diffractometer. In this presentation the effects of Al addition on the stability of  $MgH_2$  will be discussed. The financial support by NSF (DMR-0605406) is greatly appreciated.

#### 5:25 PM

**The hydrogen storage behaviours of nanocrystalline and amorphous  $Mg_{20-x}La_xNi_{10}$  ( $x=0-6$ ) alloys prepared by melt-spinning:** *Huiping Ren*<sup>1</sup>; Baowei Li<sup>2</sup>; Zaiguang Pang<sup>2</sup>; Yanguan Zhang<sup>2</sup>; <sup>1</sup>Inner Mongolia University of Science and Technology; <sup>2</sup>Inner Mongolia University of Science and Technology

The  $Mg_2Ni$ -type  $Mg_{20-x}La_xNi_{10}$  ( $x=0, 2, 4, 6$ ) hydrogen storage alloys were prepared by melt-spinning technology. The microstructures and hydrogen storage performances as well as thermal stabilities of the alloys were studied in detail. The results shows that the no amorphous phase forms in the as-spun La-free alloy, but the as-spun alloys containing La hold a major amorphous phase, confirming that the substitution of La for Mg significantly heightens the glass forming ability of the  $Mg_2Ni$ -type alloy. Melt-spinning significantly improves the hydrogen storage behaviours of the alloys. When the spinning rate increases from 0 (As-cast was defined as spinning rate of 0 m/s) to 30 m/s, the hydrogen absorption capacity of the alloys ( $x=2$ ) at 200° and 1.5 MPa in 10 min rises from 1.26 to 2.60 wt%, and its discharge capacity rises from 197.23 to 406.5 mAh/g at a current density of 20 mA/g.

phase, due to an exposure of carbide particles to high temperature detonation flame during the spraying and rapid quenching followed. The results will be compared with the APT results of distribution of constituent elements in each phase.

#### 2:50 PM

**Cold Sprayed Aluminum and Aluminum Alloy Coatings:** *Shaodong Wang*<sup>1</sup>; Lijue Xue<sup>1</sup>; Jiaren Jiang<sup>1</sup>; <sup>1</sup>NRC-IMI (London)

A downstream radial powder injection cold spray process has been developed and validated using aluminum-based (Al, Al-12Si and Al-7075) powders. Numerical simulation is performed to simulate the gas flow and particle movement behavior in the spray nozzle. Particle velocities at the nozzle exit were measured using an optical diagnostic method. The numerical simulation agrees well with the particle velocity measurement results. Microstructures and microhardness of the aluminum coatings deposited on Al-6061 aluminum substrates were investigated and were compared with results from the literature using upstream axial powder injection cold spray systems.

#### 3:15 PM

**High Performance Titanium Osteoconductive Coatings for Medical Implant Applications:** James Sears<sup>1</sup>; Dana Medlin<sup>1</sup>; *Jacob Fuerst*<sup>1</sup>; <sup>1</sup>South Dakota School of Mines and Technology

Laser Additive Manufacturing (LAM) is being evaluated for an improved methodology for creating a grid surface coating on osteoconductive implants. Titanium powder was directed into a small molten bead on a Titanium substrate produced with a focused laser operating from 200 to 350 watts with a beam diameter of 600 microns in an inert Ar environment. Evaluation of the deposition showed near 50% void formation within 100% dense grid structure. Metallurgical analysis shows low total heat input and fast bead cooling rate result in a fine microstructure in the grid structure with a very thin heat affected zone in the substrate. Developments with finer powders (20 to 50 microns) and a narrower beam (100 microns) result in increased void area and a finer grid structure. The formation of titanium interlocking structures with this technology has also been explored.

#### 3:40 PM Break

#### 4:05 PM

**Electrically Insulating Phosphate Coatings for Iron Powder Based Electromagnetic Core Applications:** W. Rane Nolan<sup>1</sup>; Francis Hanejko<sup>2</sup>; Howard Rutz<sup>2</sup>; *Mitra Taheri*<sup>3</sup>; <sup>1</sup>Massachusetts Institute of Technology; <sup>2</sup>Hoeganaes Corporation; <sup>3</sup>Drexel University

Powdered metals, such as iron, are a common building block for electromagnetic cores. An iron powder was reacted with phosphoric acid to create an electrically insulating iron phosphate layer on each particle, which could lead to significant reductions in eddy current losses in alternating current applications. The electromagnetic properties of this phosphate-coated powder material were examined as a function of heat treatment. Additionally, SEM and EDS were used to analyze the particle interfaces and composition in compressed bar-shape samples that were heat treated at temperatures ranging from 315°C to 540°C. Initial results show that after high temperature treatments (required for stress reduction, sintering, increased magnetic permeability, and decreased coercivity), the bulk resistivity is reduced. Correlation of structure and composition with trends in resistivity is discussed. Ultimately, our analysis will aid in the development of high temperature coatings with ideal properties for electromagnetic core applications.

#### 4:30 PM

**Influence of Processing Conditions on the Microstructure and Mechanical Properties of a Polycrystalline Nickel Alloy Created by Powder Bed Laser Deposition:** Xinhua Wu<sup>1</sup>; Fude Wang<sup>1</sup>; *Daniel Clark*<sup>2</sup>; <sup>1</sup>University of Birmingham; <sup>2</sup>Rolls-Royce Plc

Developments in powder bed laser deposition process capability enable structures with efficient material utilisation in response to service loading. Systematic research has been carried on the influence of processing conditions on microstructure and mechanical properties of a polycrystalline nickel alloy, which was direct laser melted (DLMed) via a laser powder bed machine. The processing parameters: laser power, scan speed, scan spacing and nominal laser power density, were studied. Assessment was made of: density, dimension accuracy, surface roughness, cracking and top-surface concavity across a range of processing conditions. Tensile samples were tested in order to assess the difference in mechanical properties induced by the difference in build

## Materials Issues in Additive Powder-Based Manufacturing Processes: Coatings and Deposition

Sponsored by: The Minerals, Metals and Materials Society, TMS Materials Processing and Manufacturing Division, TMS: Powder Materials Committee  
Program Organizers: David Bourell, University of Texas; James Sears, South Dakota School of Mines and Technology; Pavan Suri, Mississippi State University

Tuesday PM Room: 3004  
February 17, 2009 Location: Moscone West Convention Center

Session Chair: Pavan Suri, Heraeus MTD

#### 2:00 PM

**Issue Involved with Applying WC MMC's to Tooling Surfaces through Laser Additive Manufacturing:** *James Sears*<sup>1</sup>; Casey Bergstrom<sup>1</sup>; <sup>1</sup>South Dakota School of Mines and Technology

Laser Additive Manufacturing (LAM) of tungsten carbide metal matrix composites (MMCs) has been evaluated for surface modification of: hot die forming tools, cutting edges, glass tooling, extrusion mandrels, and other abrasive wear applications. This work is focused on transitions from tool steel (H-13) to these MMCs through a single pass laser powder deposition operation. Issues related to the application of various metal powders and carbides used include: surface hardness, porosity, cracking and dilution. These issues along with factory results that were obtained during this project are discussed. This work was performed under a grant from the U.S. Department of Energy (DOE), Office of Industrial Technology under contract DE-PS07-03ID14425: Industrial Materials for the Future Program.

#### 2:25 PM

**Combined Analyses of TEM and Atom Probe Tomography for Superfine WC-Co Coatings:** *Nam Suk Lim*<sup>1</sup>; Seong Yong Park<sup>2</sup>; Chan Gyung Park<sup>1</sup>; M. C. Kim<sup>1</sup>; <sup>1</sup>Pohang University of Science and Technology (POSTECH); <sup>2</sup>Pohang University of Science and Technology (POSTECH) - and - currently at the University of Texas at Dallas

The microstructure of WC-Co coatings fabricated by using superfine (0.1~0.5µm) carbide particles and detonation gun spraying method has been investigated. In order to find exact phase and unique 3D distribution of constituent elements, ultra high-resolution analysis using transmission electron microscope (TEM) and 3 dimensional atom probe tomography (3D-APT) has been performed. The analytical samples of WC-Co powders and coatings were made by using the focused ion beam (FIB). The microstructure of WC-Co coating layers fabricated with superfine carbides was identified as the combined phases of unmelted, partially melted and fully melted regions. TEM results revealed clearly that WC phase was decomposed crystalline  $W_2C$ , W phase and complex amorphous

location. Some DLMed samples were HIPped(hot isostatic pressed). It has been found that nominal laser power density has the dominating effects on the above characteristics however the influence of scan spacing and scan speed can sometimes be significant on some of those characteristics.

#### 4:55 PM

**Uniform-Droplet Spray Forming of  $Mg_{97}Zn_1Y_2$  Alloy:** *Hiroki Fukuda*<sup>1</sup>; Pengtao Wang<sup>2</sup>; Hongwei Sun<sup>2</sup>; Peter Wong<sup>3</sup>; Charalabos Doumanidis<sup>4</sup>; Teiichi Ando<sup>1</sup>; <sup>1</sup>Northeastern University; <sup>2</sup>University of Massachusetts-Lowell; <sup>3</sup>Tufts University; <sup>4</sup>University of Cyprus

A  $Mg_{97}Zn_1Y_2$  alloy was spray-deposited using uniform (mono-size) droplet sprays produced by the controlled capillary jet breakup. Consisting of mono-size droplets of desired diameter chosen in the range of 500 - 1000  $\mu m$ , and no fine, pyrophoric droplets, the uniform droplet sprays permitted stringent control of the thermal state of depositing droplets while assuring safe spraying. The solidification of traveling droplets was simulated with a model that accounted for the rapid crystallization during recalescence. A level-set-method based numerical model was used to simulate the deformation and solidification of a depositing droplet. Mg-Zn-Y deposits produced under optimal spraying conditions had a uniform microstructure consisting of equiaxed grains of hcp Mg-rich solid solution and  $Mg_{12}ZnY$  precipitates. Subsequent rolling resulted in further microstructural refinement and improved mechanical properties.

## Materials Processing Fundamentals: Smelting and Refining

Sponsored by: The Minerals, Metals and Materials Society, TMS Extraction and Processing Division, TMS: Process Technology and Modeling Committee  
Program Organizer: Prince Anyalebechi, Grand Valley State University

Tuesday PM

Room: 2016

February 17, 2009

Location: Moscone West Convention Center

*Session Chair:* K. Morsi, San Diego State University

#### 2:30 PM

**Boron Production via Molten Salt Electrolysis:** *Judith Gomez*<sup>1</sup>; Patrick Taylor<sup>1</sup>; Edgar Vidal<sup>2</sup>; <sup>1</sup>Colorado School of Mines; <sup>2</sup>Brush Wellman, Inc.

Boron is an element that is difficult to isolate in its pure form and requires a substantial amount of energy. Typically, boron is synthesized by metallothermic reduction of its oxide with magnesium or sodium; reaction of boron halogenides with hydrogen; or, thermal decomposition of diborane. An alternative method using molten salt electrolysis has been evaluated in this work. A mixture of  $MgF_2$ -NaF-LiF- $B_2O_3$  salts was molten under an inert atmosphere, and the effect of different experimental parameters such as temperature, potential and current density were evaluated. Characterization of the material deposited and efficiency of the process is presented, as well as conclusions and recommendations for future work.

#### 2:45 PM

**XRF Analysis of EAF and LMF Type Slags:** *Alexander Seyfarth*<sup>1</sup>; Dan Pecard<sup>1</sup>; <sup>1</sup>Brucker AXS Inc.

Talk and manuscript will detail a case study based tutorial on how LMF and EAF slags are sampled, prepared and analyzed by XRF. We will compare the applicability of both ED and WD XRF. Data derived from the analysis can then be used to optimize the SLAG composition using different models. We will present and compare the easy study of an EDX Benchtop system at the furnace directly operated by the meltshop vs. a laboratory based WD XRF system operated by the QC group. This is aimed to teach the application of XRF and its limitations to enable discussion and application of results to the process.

#### 3:00 PM

**Effect of EAF Slag Carryover on Slag-metal Equilibrium Calculations for Ladle Degassing Process:** *Hamid Doostmohammadi*<sup>1</sup>; Margareta Andersson<sup>1</sup>; Karin Steneholm<sup>2</sup>; Pär Jönsson<sup>1</sup>; <sup>1</sup>KTH, Royal Institute of Technology; <sup>2</sup>Uddeholm Tooling AB

During the tapping of liquid steel from Electric Arc Furnace (EAF), some slag is carried over into the ladle. High levels of FeO and MnO in slag carryover increase the oxygen activity in steel melt leading to oxide inclusion formation during the ladle treatment. The demand on cleaner steels requires minimization

of carryover slag. In this work the effect of EAF slag carryover on ladle slag-steel equilibrium calculations for a hot working tool steel was studied. Steel and slag sampling were done at Uddeholm Tooling AB in Sweden. XRF and OES techniques were used to determine chemical composition of samples. The quantity of slag carryover was calculated by mass balance followed by thermodynamic calculations on metal-slag equilibrium for vacuum degassing process using Thermo-Calc software. The agreement with lab analysis will lead to the development of a prediction method for optimizing the production of other tool steel grades.

#### 3:15 PM

**Effects of Stoichiometry on Boron Carbide Production via Self Propagating High Temperature Synthesis:** *Murat Alkan*<sup>1</sup>; Bora Derin<sup>1</sup>; Seref Sonmez<sup>1</sup>; Onuralp Yucel<sup>1</sup>; <sup>1</sup>Istanbul Technical University

In this study, a self-propagating high-temperature synthesis (SHS) and following acid leaching techniques were carried out to produce boron carbide (B<sub>4</sub>C) powder. First, B<sub>2</sub>O<sub>3</sub> was obtained through calcinations of H<sub>3</sub>BO<sub>3</sub> at 1073 K for 2 hours. Then, the glassy B<sub>2</sub>O<sub>3</sub> obtained was crushed and sieved. In the SHS experiments, different amounts of B<sub>2</sub>O<sub>3</sub>, Mg and C black were used. The SHS product was obtained in the form of black, spongy solid. In the leaching step, the SHS product was leached in a HCl solution to eliminate the MgO and Mg<sub>3</sub>B<sub>2</sub>O<sub>6</sub>. The effect of acid concentration on the selective leaching was studied at different concentration range, solid/liquid (S/L) ratio, and temperature. The products obtained were characterised by using X-ray diffraction, chemical analysis and SEM techniques.

#### 3:30 PM

**Lime-Enhanced Carbothermic Reduction of Chalcopyrite:** *William Rankin*<sup>1</sup>; Terry Hall<sup>1</sup>; <sup>1</sup>CSIRO Minerals

Lime-enhanced reduction may provide an alternative treatment for chalcopyrite concentrates yet most research on lime-enhanced reduction has been on pure sulfides. In this study, Gibbs energy minimisation calculations were performed to establish the thermodynamic limits of reaction then preliminary experiments were carried out on natural chalcopyrite using a thermogravimetric system. Next, a series of small crucible tests was performed based on the preliminary results using chalcopyrite concentrate and, finally, a large crucible test was performed under the "best" conditions. The study demonstrated that chalcopyrite in a concentrate is reduced at moderate temperatures and in a reasonable time to form copper, iron and calcium sulfide. At lower temperatures, calcium ferrite formed preferentially but the reaction did not go to completion. The reaction mass was readily liberated into constituent phases; however, the iron and copper occurred together in relict particles of chalcopyrite. The process implications are discussed.

#### 3:45 PM

**Process and Practice of EAF with De-P Hot Metal Charging for Melting Stainless Steel:** *Fangyi Zhu*<sup>1</sup>; <sup>1</sup>Baosteel

The article introduce the process of Electric Arc Furnace with Dephosphorized hot metal charging for melting stainless steel in Baosteel stainless steel Branch. Based on the practice of production, The main factors affecting the process of EAF with De-P HM charging are theoretically analyzed, such as using oxygen, the material charging and making slag. The optimization of hot metal charging can advance the use of chemical and physical energy, reduce the consumption of power. The optimization of using oxygen can increase the use of chemical energy. The optimization of material charging can reduce the oxidation of Cr. Making foamy slag can advance the transformer capacity and the use of power. Based on the character of the process EAF with De-P HM charging for Melting Stainless Steel, EAF productivity increased were reached with application of integrated control theory on EAF process in Baosteel stainless steel branch.

#### 4:00 PM Break

#### 4:15 PM

**Study on a New Electrolysis Technology of Preparing High-Nb Bearing TiAl Alloy from Metal Oxides:** *Fanke Meng*<sup>1</sup>; *Huimin Lu*<sup>1</sup>; <sup>1</sup>Beijing University of Aeronautics and Astronautics

Electrolyzing oxides of titanium, aluminum and niobium could prepare high-Nb bearing TiAl alloy(Ti-45Al-8.5Nb) in the temperature between 1700°C and 1800°C. The chosen electrolysis voltage ranges from 2.3V to 2.5V, which is lower than reducing voltage (~4.7V) of electrolyte CaF<sub>2</sub>, but higher than that of titanium, aluminum and niobium oxides. The investigation shows that compared with traditional methods, this method for preparing high-Nb bearing TiAl alloy



is of many advantages such as few steps, friendly environment, low energy consumption, low cost and high current efficiency.

#### 4:30 PM

**A Study on Nickel Containing Iron Alloy Production from West Anatolian Region Lateritic Ores:** *Cem Colakoglu*<sup>1</sup>; Bora Derin<sup>1</sup>; Onuralp Yucel<sup>1</sup>; <sup>1</sup>Istanbul Technical University

In this study, nickel containing iron alloys were produced by Carbothermal reduction of lateritic nickel ores obtained from Manisa-Caldag region of Turkey. In the experiments, the lateritic ore containing 1.58 % Ni and 0.12 % Co was first calcined in a semi-pilot scale rotary furnace at 1100°C for 1 hour. Then, a mixture of calcined ore and metallurgical grade charcoal was reacted in sintered alumina crucibles using a graphite resistance tube furnace at different time (0- 60 min) and temperature (1450-1600°C). The raw materials, alloys and slags were characterized by using wet chemical analyses, XRD (X-Ray Diffractometry), and EPMA (Electron Probe Micro Analyzer) techniques.

#### 4:45 PM

**Manufacture of High Nitrogen Austenitic Stainless Steels by Pressurized Electro-Slag Remelting:** Jiang Zhouhua<sup>1</sup>; Cao Yang<sup>1</sup>; Li Huabing<sup>1</sup>; <sup>1</sup>Northeastern University

The attempt has been made to manufacture high nitrogen austenitic stainless steels by pressurized electro-slag remelting furnace with maximum nitrogen pressure of 7MPa. To obtain high nitrogen content in steels, the compound electrodes with different nitrogen sources (FeCrN, Si3N4) were prepared. Using the Si3N4 as the nitrogen alloying source, the silicon contents in ingots were prone to be out of the specification range, and the electric current fluctuated greatly and the surface qualities of the ingots were poor. The surface qualities of the ingots were improved using FeCrN as nitrogen alloying source. The sound and compact macrostructure ingot with the maximum nitrogen above 1.0wt% could be obtained. A series of high nitrogen austenitic stainless steels have been successfully developed by this method. The mechanical and pitting corrosion properties of high nitrogen austenitic stainless steels were investigated. The results show that the steels exhibit excellent mechanical and pitting corrosion resistance properties.

#### 5:00 PM

**An Efficient Method of Stirring Melt with a Modulated Traveling Magnetic Field:** Xiaodong Wang<sup>1</sup>; Rene Moreau<sup>2</sup>; Yves Fautrelle<sup>2</sup>; <sup>1</sup>McGill University; <sup>2</sup>EPM-SiMAP-CNRS

This study examines a liquid GaInSn metal flow generated by a magnetic field whose traveling direction is periodically reversed. Ultrasonic Doppler velocimetry probes the generated fluid flow. Depending on the modulation frequency, a number of characteristic flow features are exhibited. A transition frequency (~4 Hz) exists, below this transition point, the amplitude of the velocity oscillation increases and below  $f_m = 0.05$  Hz, it saturates around a value close to that observed without any modulation. The role of this electromagnetically driven flow is to transport the solute rejected by the solidifying interface at significant distances in the melt, and to periodically reverse its circulation such that macro-segregation is minimized. An analytical electromagnetic model and a flow dynamic model for the recirculating fluid flow are derived, assuming that in this central region the flow is quasi-parallel to the main axis. The analytical velocity field achieves a satisfactory agreement with the measurements.

#### 5:15 PM

**Carbothermic Reduction of Ilmenite Concentrate:** Chengjun Gao<sup>1</sup>; Na Hou<sup>1</sup>; Hongmin Zhu<sup>1</sup>; <sup>1</sup>Beijing University of Science & Tech

Carbon thermo-reduction of ilmenite were performed with various ratio of carbon, at temperatures up to 1600°C. The thermodynamic possibility of selective carbothermic reduction was discussed in detail. Experiments for testing the reduction order of the oxides of iron, titanium, silicon, and magnesium were carried out. The products were characterized by X-ray diffraction, scanning electron microscope and chemical analysis. The results showed that it is possible to reduce all iron oxide to metal, and titania to titanium carbide (TiC), or oxycarbide (TiC<sub>x</sub>O<sub>y</sub>), without the reduction of silica and magnesia. The separation of the reduction product of TiC<sub>x</sub>O<sub>y</sub>-Fe-MO<sub>x</sub> was also carried out.

### Mechanical Behavior of Nanostructured Materials: Strengthening Mechanisms at Small Length Scale

Sponsored by: The Minerals, Metals and Materials Society, TMS Electronic, Magnetic, and Photonic Materials Division, TMS Materials Processing and Manufacturing Division, TMS Structural Materials Division, TMS: Chemistry and Physics of Materials Committee, TMS/ASM: Mechanical Behavior of Materials Committee, TMS: Nanomechanical Materials Behavior Committee

Program Organizers: Xinghang Zhang, Texas A & M University; Andrew Minor, Lawrence Berkeley National Laboratory; Xiaodong Li, University of South Carolina; Nathan Mara, Los Alamos National Laboratory; Yuntian Zhu, North Carolina State University; Rui Huang, University of Texas, Austin

Tuesday PM

February 17, 2009

Room: 3024

Location: Moscone West Convention Center

Session Chairs: Rui Huang, University of Texas; Thomas Buchheit, Sandia National Laboratories

#### 2:00 PM Invited

**Mechanical Properties of Nanocrystalline Thin Films:** Daniel S. Gianola<sup>1</sup>; Yixiang Gan<sup>2</sup>; Tim Rupert<sup>3</sup>; John Sharon<sup>4</sup>; Kevin Hemker<sup>4</sup>; <sup>1</sup>Forschungszentrum Karlsruhe, Institute for Materials Research II; <sup>2</sup>Forschungszentrum Karlsruhe, Institute for Materials Research II; <sup>3</sup>Massachusetts Institute of Technology; <sup>4</sup>Johns Hopkins University

Microtensile testing techniques have been developed and employed to characterize the small-scale and scale-specific mechanical behavior of materials for MEMS and nanocrystalline thin films. Geometric concentrators can be used to introduce spatial variations in the stress and strain states in these films, providing insight on how deformation is accommodated. Combining microstructural analysis with continuum descriptions of stress and strain gradients allows one to decouple the effect of stress and strain on deformation processes, however, use of multiple stress concentrators will lead to wrinkling and must be accounted for. Here we describe experiments and finite element simulations of freestanding submicron Al thin films with patterned interior holes. Stretching these films induces periodic and symmetric wrinkling that is imaged directly during tensile testing and faithfully reproduced by the simulations. An example will be presented using these techniques that elucidated the mechanisms of mechanical grain growth in nanocrystalline Al thin films.

#### 2:20 PM

**Characterization of Nanostructured Films Synthesized by High Power Pulse Ion Ablation:** Thomas Buchheit<sup>1</sup>; Timothy Renk<sup>1</sup>; Somuri Prasad<sup>1</sup>; Paul Kotula<sup>1</sup>; <sup>1</sup>Sandia National Laboratories

A unique Repetitive High Energy Pulse Power (RHEPP-1) facility at Sandia National Laboratories offers the capability for deposition of low stress multilayer films with layer thicknesses less than 10 nm. The facility generates an intense ion-beam of 10 J/cm<sup>2</sup> that ablates alternating targets to synthesize the films, with a wide range of multilayer films possible. Driven by a previous study focused on MoS<sub>2</sub>-Ti nano-laminate films for tribological applications, this investigation broadened the scope of deposited Mo-based nanolayered films. Targets were chosen to produce Mo-bearing laminates with a wide range of characteristics, although particular focus was directed toward choosing target materials with a range of differing shear moduli. Nanolaminate films investigated include Mo-Ir, Mo-Ti, and Mo-W. Each film contained at least one hundred alternating layers and all were compared against a uniform Mo deposition. Subsequent material and mechanical characterization revealed series of hard, well-ordered, semi-crystalline bilayer films. Details will be discussed.

#### 2:35 PM

**Temperature Dependence of Mechanical Properties in Ultra Thin Au Films with and without Passivation:** Patric Gruber<sup>1</sup>; Sven Olliges<sup>2</sup>; Eduard Arzt<sup>3</sup>; Ralph Spolenak<sup>2</sup>; Oliver Kraft<sup>4</sup>; <sup>1</sup>Universität Karlsruhe, Institut für Zuverlässigkeit von Bauteilen und Systemen; <sup>2</sup>ETH Zurich, Laboratory for Nanometallurgy, Department of Materials; <sup>3</sup>INM Leibniz Institute for New Materials; <sup>4</sup>Forschungszentrum Karlsruhe, Institut für Materialforschung II

Mechanical testing of thin metallic films at elevated temperatures is difficult. Here, we present a systematic study of the mechanical properties of 80 to 500 nm thick polycrystalline Au films with and without SiN<sub>x</sub> passivation layers in the temperature range from 123 to 523 K. The films have been tested by

a novel synchrotron-based tensile testing technique. All film systems show a very strong temperature dependence of the flow stress. For passivated Au films the temperature dependence of the flow stress can be rationalized by thermally activated dislocation glide. For pure Au films on polyimide, an analysis on the basis of a model for grain-boundary diffusional creep of a freestanding foil gives values for the activation energy of 0.3 to 0.6 eV, which indicates that diffusional creep is strongly pronounced in these films. This is remarkable because the testing temperatures are at most 0.3 of the homologous temperature.

## 2:50 PM Invited

**Nanoscale Deformation in Multilayered Nanocomposite Thin Films: In-Situ and Ex-Situ TEM Analyses:** *Jeff DeHosson*<sup>1</sup>; *Changqiang Chen*<sup>1</sup>; *Yutao Pei*<sup>1</sup>; <sup>1</sup>University of Groningen

Although high-resolution transmission electron microscopy is the most direct method to observe the effects of a mechanical response at nanometer scales, a common problem encountered in the HRTEM examination of deformed amorphous or uniformly nanostructured materials is the lack of intrinsic markers tracing microstructural evolutions. We will demonstrate that nanocrystallites may serve as perfect interior markers for distinguishing various deformation patterns in MeC/DLC nanocomposite coatings. This paper concentrates on the nanoindentation behavior and corresponding deformation mechanisms of the nanocomposite coatings under depth sensing indentation, using combined ex situ nanoindentation followed by XTEM and also in situ TEM nanoindentations. Through the examination of the displacement of the nanocrystallites an interparticle deformation process involving rearrangement of TiC nanocrystallites and displacement of the DLC a-C matrix is demonstrated that dominates the deformation mechanism at length scales ranging from tens of nm down to 1 nm.

## 3:10 PM

**Microstructure – Property Relationships in TiN-Based Coatings on Steel Substrates Prepared by Pulsed Laser Deposition:** *Andreas Jahja*<sup>1</sup>; *Paul Mumroe*<sup>1</sup>; <sup>1</sup>University of New South Wales

A range of sub-micron thick TiN coatings were deposited on a H13 hot worked tool steel substrate via pulsed laser deposition as a function of processing conditions. The coatings were subject to detailed microstructural characterization, including FIB and cross-sectional TEM studies. Coatings prepared at high substrate temperatures (450°C) and reactive gas conditions exhibited very fine nanoscale grain sizes, whilst slightly coarser structures were prepared in inert environments. Mechanical behaviour was assessed through nanoindentation using a spherical indenter. The coatings exhibited high hardness values and significant resistance to cracking, even at high loads. Examination of the indented layers revealed intercolumnar cracks within the TiN coatings, together with shear steps at the coating-substrate interface, whilst inclined cracks were observed at the periphery of the indentations.

## 3:25 PM Invited

**Atomistic Simulations of Diffusional Creep in Nanocrystalline BCC Molybdenum:** *Paul Milette*<sup>1</sup>; *Vesselin Yamakov*<sup>2</sup>; *Tapan Desai*<sup>1</sup>; *Dieter Wolf*<sup>1</sup>; <sup>1</sup>Idaho National Laboratory; <sup>2</sup>National Institute of Aerospace

As grain sizes are reduced to nanocrystalline dimensions, the role of diffusional creep as a dominant deformation mechanism becomes important. In this work, molecular dynamics (MD) simulations are used to study diffusion-accommodated creep deformation in body-centered cubic nanocrystalline molybdenum. Columnar microstructures with a uniform grain size and grain shape are subjected to constant-stress loading at high temperatures (i.e.,  $T > 0.75T_{\text{melt}}$ ). Remarkably, the results show that both grain-boundary (GB) diffusion in the form of Coble creep and lattice diffusion in the form of Nabarro-Herring creep contribute to the overall deformation. Visual analysis confirms that the GBs serve as sources for lattice vacancies that emit into the grain interiors thus enabling lattice diffusion. We perform an in-depth analysis of the vacancy source/sink behavior of the GBs with and without applied stress. Finally, creep rates for systems with supersaturated vacancy concentrations, i.e., under irradiation conditions, are also examined.

## 3:45 PM Break

## 3:55 PM Invited

**Deformation of Nanotube Arrays for Contact Switches in MEMS:** *David Bahr*<sup>1</sup>; *Ryan Johnson*<sup>1</sup>; <sup>1</sup>Washington State Univ

The properties of large assemblages of CNTs are not controlled by the individual tubes, but by the collective topological behavior of the “turf”,

consisting of many CNTs attached to an inflexible substrate. This presentation focuses on a range of experimental efforts using nanoindentation (including ECR) and compression testing in situ in an SEM to assess the properties of turfs. The stress required to form a collective buckle structure in the turf is dependant only on the ratio of tangent modulus to applied stress, and not the aspect ratio of the structures. Adhesion to diamond is strong and metallic coatings dramatically reduce the adhesion between the CNTs and diamond indenter tip. The results will be used to demonstrate a low temperature thermocompression bonding technique that demonstrates the flexibility of these materials. The CNT data will be contrasted to silica nanowires and springs, which follow more macroscopic models of fiber based deformation.

## 4:15 PM

**Interfacial Fracture in Scandium Deuteride Films from Micro to Nano Scales:** *Marian Kennedy*<sup>1</sup>; *Neville Moody*<sup>2</sup>; *David Adams*<sup>2</sup>; *E. David Reedy*<sup>2</sup>; *Nancy Yang*<sup>2</sup>; *David Bahr*<sup>3</sup>; <sup>1</sup>Clemson University; <sup>2</sup>Sandia National Laboratories; <sup>3</sup>Washington State Univ

Performance and reliability are extremely important issues for scandium deuteride films used in neutron tube applications where high residual stresses during processing can lead to premature failure. As a result, we have begun a program combining small volume property and thin film fracture tests to determine fracture susceptibility in these film systems. Samples were fabricated following a two-step procedure to create films on fused silica monitors that ranged in thickness from 150 nm to 6  $\mu\text{m}$  with a uniform grain size of 400 nm. On cool-down, high thermal mismatch led to spontaneous delamination in the thick films at an interfacial fracture energy near 4 J/m<sup>2</sup>. Surprisingly these values matched four point bend results on the thinnest films tested. In this presentation, we will discuss how structure, properties, and stress affect interfacial fracture in these films from micro to nanoscales. This work supported by Sandia National Laboratories under USDOE contract DE-AC0494AL85000.

## 4:30 PM

**Mechanical Behavior of Single-Layer Graphene:** *Qiang Lu*<sup>1</sup>; *Rui Huang*<sup>1</sup>; <sup>1</sup>University of Texas at Austin

The unique structure and properties of single-layer graphene has drawn tremendous interests recently. This paper presents a theoretical study of the mechanical behavior of graphene and associated morphological structures. By combining atomistic and continuum modeling, lattice deformation of graphene sheets under both in-plane forces and bending moments is analyzed. The model predicts a nonlinear and anisotropic mechanical behavior of graphene under large strains. Using a two-atom unit cell, the theoretical strength of single-layer graphene under macroscopically homogeneous in-plane deformation is investigated. Heterogeneous deformation with characteristic strain localization is observed in large-scale atomistic modeling. It is found that the bending properties of single-layer graphene are fundamentally different from those predicted by continuum plate or shell models. Furthermore, a buckling instability is predicted by atomistic simulations for graphene sheets under compression or shearing, leading to a periodic morphology that depends on the size and boundary conditions.

## 4:45 PM

**Nano-Scale Tribology of Polycrystalline Silicon Structural Films in Ambient Air:** *Daan Hein Alsem*<sup>1</sup>; *Ruben van der Hulst*<sup>2</sup>; *Eric Stach*<sup>3</sup>; *Michael Dugger*<sup>4</sup>; *Jeff DeHosson*<sup>2</sup>; *Robert Ritchie*<sup>5</sup>; <sup>1</sup>Lawrence Berkeley National Laboratory; <sup>2</sup>University of Groningen; <sup>3</sup>Purdue University; <sup>4</sup>Sandia National Laboratories; <sup>5</sup>University of California, Berkeley

Dynamic coefficients of friction (COF), nano-scale wear volumes and morphology have been studied for polysilicon MEMS (Sandia SUMMiT V) in ambient air at different relative humidity (%RH). Half of the devices show an increase in the COF by a factor of three with increasing number of wear cycles with failure after  $\sim 10^5$  cycles. The other half of the devices displayed similar behavior, but after peaking reached a lower steady-state COF showing no failure after millions of cycles. In this regime increasing the %RH resulted in a linear increase of the COF. Additionally, the wear coefficient and surface roughness sharply increased in the first  $\sim 10^5$  cycles and then decayed to a lower value over several million cycles. Electron microscopy shows that abrasive wear is the governing mechanism, and failures are being attributed to differences in local surface morphology. Re-oxidation of worn polysilicon only affects the friction coefficient after periods of inactivity.

5:00 PM Invited

**In-Situ Atomic Scale Nanomechanics Enabled by a TEM-SPM Platform:**Jianyu Huang<sup>1</sup>; <sup>1</sup>Sandia National Laboratory

By using a sharp scanning tunneling microscopy (STM) probe integrated into a transmission electron microscopy (TEM), in-situ atomic scale nano mechanical studies can be achieved. In this talk, I will review our recent progress in using a TEM-STM platform to probe the atomic scale deformation mechanisms of carbon nanotubes and nanowires. It is postulated that nanotubes accommodate no plastic deformation even beyond the elastic limit or before breakage at room temperatures. I report here our recent discoveries of plastic deformation, as characterized by the superplastic elongation, kink motion, and dislocation climb, in carbon nanotubes at about 2000 °C. These discoveries indicate that there are rich nanomechanics in carbon nanotubes at high temperatures. I will also discuss our progress in using the TEM-SPM platform to probe the mechanical properties of nanowires, and designing a MEMS platform to enable in-situ thermal and thermoelectric measurements of carbon nanotubes and nanowires.

5:20 PM

**In-Situ Nanomechanical-Electrical Testing of One-Dimensional Materials:**Reza Shahbazian Yassar<sup>1</sup>; Chee Lee<sup>1</sup>; Jiasheng Wang<sup>1</sup>; Yoke Yap<sup>1</sup>; <sup>1</sup>Michigan Technological University

One-dimensional nanomaterials including nanotubes are building blocks for constructing various complex nanodevices. Boron nitride (BN) nanotubes with structure similar to carbon nanotube are known to have the highest mechanical strength among the insulators. In this work, deformation of an individual BN nanotube is performed inside a high-resolution transmission electron microscope (TEM) using a piezo-driven atomic force microscope (AFM) and scanning tunneling microscope (STM)-TEM holder. The electrical and mechanical properties of individual BN nanotubes are obtained from the experimentally recorded I-V and force-displacement curves.

5:35 PM

**Young's Modulus Measurement of Alkaline Earth Metal Hexaboride Nanowires with Atomic Force Acoustic Microscopy:**Xiaoxia Wu<sup>1</sup>; Terry Xu<sup>1</sup>; <sup>1</sup>University of North Carolina Charlotte

Young's moduli of alkaline earth metal hexaboride (MB<sub>6</sub>; M = Ca, Sr and Ba) nanowires, a new group of one-dimensional nanostructures for thermoelectric energy conversion, was studied by Atomic Force Acoustic Microscopy (AFAM). The AFAM, a promising technique for nondestructive test of nanoscale mechanical properties, utilizes the resonance frequency shifts of the AFM cantilever induced by the tip-sample interaction for quantitative mechanical property measurement of nanowires. In this study, factors including (1) diameter of MB<sub>6</sub> nanowires, and (2) substrates (e.g., SiO<sub>2</sub>/Si, Si) used for supporting the nanowires were investigated to examine their effects of Young's modulus measurement. Initial results show that (1) the Young's modulus of BaB<sub>6</sub> nanowire (measured on SiO<sub>2</sub>/Si substrate) decreases from 136 GPa to 90 GPa as diameter decreases from 170 nm to 60 nm; and (2) the 'Receding contacts' mechanics originally introduced by Keer et al can be adapted to study the substrate effect.

5:50 PM

**Deformation Processes in Bimodal Nanometric Nickel at Elevated**Temperatures: Troy Holland<sup>1</sup>; Amiya Mukherjee<sup>1</sup>; <sup>1</sup>University of Calif. Davis

Nanometer-scale grains in metallic materials have shown excellent strength characteristics but their toughness, expected strengths, and elevated temperature behaviors are less good. One approach to ameliorate these concerns is to produce a metal with a bimodal distribution of grain sizes. The interplay of deformation mechanisms in these bimodal metals is largely unclear, particularly at elevated temperatures. The use of strain rate jump tests at homologous temperatures 0.2-0.3T<sub>m</sub> allowed determination of the activation volumes and energies of deformation in Ni samples with varying amounts of 20nm and 200nm grain sizes. The grain size of the samples pre-testing, post-annealing, and post-straining were evaluated with TEM. Further observation of the deformation was performed on thinned TEM specimens in-situ while controlling for both temperature and strain rate. This investigation is supported by a grant from the US National Science Foundation Division of Materials Research.

**Microstructural Processes in Irradiated Materials: Radiation Effects III: He Effects on Microstructural Evolution and Deformation**

Sponsored by: The Minerals, Metals and Materials Society, TMS Structural Materials Division, TMS/ASM: Nuclear Materials Committee

Program Organizers: Christophe Domain, Electricite De France; Gary Was, University of Michigan; Brian Wirth, University of California, Berkeley

Tuesday PM

Room: 2008

February 17, 2009

Location: Moscone West Convention Center

Session Chairs: Yann de Carlan, CEA; Takeshi Toyama, Tohoku University

2:00 PM Invited

**Ab Initio Modeling of He and H in W:** Charlotte Becquart<sup>1</sup>; Christophe Domain<sup>2</sup>; <sup>1</sup>University of Sciences and Technologies of Lille; <sup>2</sup>Electricite De France, Research and Development

To model radiation damage in tungsten with He and H production in order to predict the evolution of the microstructure and the possibility of swelling or blistering, the elementary physical phenomena associated with the point defects created and their interaction with the He and H produced have to be characterised. The role of the impurities most commonly found in tungsten has also to be investigated and in particular the interactions they establish with point defects as well as with the light elements. We have thus used density functional theory based ab initio calculations and the VASP code to determine the interactions of He and H with point defects, impurities as well as with themselves in W. For both elements the most stable site in interstitial configuration is the same: the tetrahedral site, however their diffusion properties and their tendency to form clusters are completely different.

2:30 PM Invited

**Modeling of He Diffusion and Clustering in Irradiated  $\alpha$ -Fe:** Christophe J. Ortiz<sup>1</sup>; Maria José Caturla<sup>2</sup>; Chu Chun Fu<sup>3</sup>; François Willaime<sup>3</sup>; <sup>1</sup>CIEMAT; <sup>2</sup>Universidad de Alicante; <sup>3</sup>CEA/Saclay

High levels of He are expected to be produced in materials under fusion conditions. This element and vacancies generated during irradiation agglomerate into stable He-vacancy clusters that can deteriorate the mechanical properties of materials. Although ferritic/martensitic steels are good candidates for this application due to their low swelling rate, they suffer from embrittlement and the role of He is still not clear. Using a multi-scale strategy we studied the diffusion and clustering of He in the presence of defects and impurities in irradiated  $\alpha$ -Fe. Density Functional Theory (DFT) calculations were performed to investigate the migration mechanisms and to determine the migration and binding energies of defects. Rate Theory and kinetic Monte Carlo models were used to reproduce the He kinetics under different conditions of irradiation and temperature. The influence of impurities such as carbon on the migration of He and on the formation of small He-vacancy clusters was also studied.

3:00 PM

**Interfacial Stability of He Ion Irradiated and Annealed Cu/V Nanolayers:**Engang Fu<sup>1</sup>; Jesse Carter<sup>1</sup>; David Foley<sup>1</sup>; Amit Misra<sup>2</sup>; Lin Shao<sup>1</sup>; Haiyan Wang<sup>1</sup>; Xinghang Zhang<sup>1</sup>; <sup>1</sup>Texas A&M University; <sup>2</sup>Los Alamos National Laboratory

Sputtered Cu/V nanolayers with individual layer thickness (h) of 1 to 100 nm were subjected to helium ion irradiation with a peak dose of 0.5-10 dpa. In most cases, Cu/V interfaces retain after radiation. A similar hardening trend has been observed in specimens radiated at different doses, i.e., radiation hardening decreases with decreasing layer thickness. For specimens with h  $\geq$  5 nm, radiation hardening seems to reach saturation when peak dose approaches 5 dpa. Hardening is negligible for fine (h  $\leq$  2.5 nm) nanolayers at all dose levels. Potential mechanisms of interface-defect (induced by radiations) interactions under the context of length scale and growth of He bubbles will be discussed. In parallel we investigated the interfacial stability of as-deposited nanolayers annealed up to 600°C. Evolutions of microstructure and hardness after annealing are also investigated.



3:20 PM

**Modeling the Transport and Fate of Helium in Tempered Martensitic Steels (TMS) and Nanostructured Ferritic Alloys (NFA):** *Takuya Yamamoto*<sup>1</sup>; G. Robert Odette<sup>1</sup>; Brian Wirth<sup>2</sup>; Richard Kurtz<sup>3</sup>; <sup>1</sup>University of California, Santa Barbara; <sup>2</sup>University of California, Berkeley; <sup>3</sup>Pacific Northwest National Laboratory

Managing high helium concentrations is an absolute requirement for fusion alloys. Matrix helium bubbles act as nucleation sites for growing voids and helium on grain boundaries leads to severe degradation of fracture toughness at low temperatures and creep strength at high temperatures. Thus viable fusion alloys must trap helium in bubbles that are too small to be void nucleation sites and that also protect the boundaries from helium accumulation. The predictions of a rate theory cluster dynamics model of helium transport and fate in partitioning between and within various microstructural sites to form bubbles in both TMS and NFA are described. The master rate theory model is parameterized by atomistic submodels of helium diffusion and trapping. The model predictions of helium partitioning and bubble formation on dislocations and boundaries in TMS and on Y-Ti-O enriched nanostructures in NFA are in good agreement with the results of in-situ helium implantation studies.

3:40 PM Break

4:00 PM Invited

**An Assessment of Susceptibility to Helium Embrittlement of Nano-Scaled Oxide Dispersion Strengthened Steels:** *Akihiko Kimura*<sup>1</sup>; <sup>1</sup>Kyoto University

Microstructure processing has been investigated for ODS steels and a reduced activation ferritic steel (RAFS), which were irradiated with iron and helium ions simultaneously. The void swelling of ODS steels were remarkably smaller than that of the RAFS because of much smaller size and higher density of helium bubbles in the ODS steels. The impact test results after helium implantation (900 appm He) by cyclotron clearly indicated that the ODS steels have a high resistance to helium embrittlement, while the RAFS suffered considerable intergranular embrittlement. This is considered to be due to high trapping capacity for helium atoms at matrix/particles boundaries in the steels. A simulation study based on the experimental results on microstructure processing and fracture mode change from cleavage to intergranular cracking is conducted to estimate the overall helium trapping capacity of the ODS steels, which consists of fine elongated grains and nano-scaled oxide particles in high density. Present study includes the result of "R&D of corrosion resistant super ODS steel for highly efficient nuclear systems" entrusted to Kyoto University by the Ministry of Education, Culture, Sports, Science and Technology of Japan (MEXT).

4:30 PM

**Absorption of  $\frac{1}{2}\langle 111 \rangle$  and  $\langle 100 \rangle$  Dislocation Loops on Moving Dislocations in bcc Fe:** *Dmitry Terentyev*<sup>1</sup>; D.J. Bacon<sup>2</sup>; P. Grammatikopoulos<sup>2</sup>; Yu. N. Osetsky<sup>3</sup>; <sup>1</sup>SCK-CEN; <sup>2</sup>University of Liverpool; <sup>3</sup>Oak Ridge National Laboratory

Neutron-irradiated ferritic alloys typically contain interstitial dislocation loops with Burgers vector equal to either  $\frac{1}{2}\langle 111 \rangle$  or  $\langle 100 \rangle$ . Their presence obstructs motion of dislocations, leading to an increase in the yield stress and reduction in ductility, and the ability of dislocations to absorb loops assists in the formation of 'clean' channels. The mechanisms controlling dislocation-loop reaction are therefore important. MD simulations have been used to investigate reactions between  $\frac{1}{2}\langle 111 \rangle$  edge dislocations and  $\frac{1}{2}\langle 111 \rangle$  or  $\langle 100 \rangle$  loops at different locations with respect to the slip plane, with loop size varying from 0.5 to 10nm and temperature from 1 to 600K. Some reactions are complex, but all can be described in terms of conventional dislocation reactions in which Burgers vector is conserved. The fraction of interstitials absorbed varies from 0 to 100%. The nature of these reactions and of those requiring high applied stress for dislocation breakaway has been identified.

4:50 PM

**The Role of Irradiation Microstructure in Localized Deformation in Austenitic Alloys:** *Zhijie Jiao*<sup>1</sup>; Gary Was<sup>1</sup>; <sup>1</sup>University of Michigan

Localized deformation has emerged as a potential factor in irradiation assisted stress corrosion cracking of austenitic stainless steels in LWR environments. The degree of localized deformation is very likely controlled by the irradiation microstructure. Seven austenitic alloys with various Cr and Ni content were irradiated using 2-3 MeV protons to doses of 1 and 5 dpa at 360C. The irradiation microstructure consisting of dislocation loops, precipitates and voids was characterized using transmission electron microscopy (TEM). The degree of

localized deformation was characterized using atomic force microscope (AFM) on the deformed samples after the constant extension rate tension test performed in argon. The contribution of irradiation microstructure to localized deformation will be discussed.

5:10 PM

**Strain Induced Evolution of Grain Boundary Character and Taylor Factor in 316L Stainless Steel:** *Elaine West*<sup>1</sup>; Gary Was<sup>1</sup>; <sup>1</sup>University of Michigan

Irradiation assisted stress corrosion cracking depends on grain boundary structure and deformation mode. The character of a grain boundary describes the degree of alignment between two adjacent grains, and the Taylor factor describes the propensity of a grain to undergo slip, and both may affect IASCC susceptibility. Restricted grain deformation under tensile strain alters both the grain orientation and the misorientation across a grain boundary, causing both the grain boundary character and Taylor factor to evolve with strain. Samples of 316L stainless steel were irradiated with 2.0 MeV protons at 400°C to a dose of 7 dpa and strained in supercritical water at 400°C. EBSD analysis was used to determine how the grain boundary character distribution and the Taylor factors of grains in irradiated and unirradiated 316L stainless steel evolved with strain. EBSD analysis results will be presented in the context of potential mechanisms for stress corrosion crack nucleation.

5:30 PM

**Effects of Dynamic Strain Aging and Cyclic Loading on Fracture Behavior of A516 Grade 70 and Other Steels:** *Indrajit Charit*<sup>1</sup>; Chang-Sung Seok<sup>2</sup>; *Korukonda Murty*<sup>3</sup>; <sup>1</sup>University of Idaho; <sup>2</sup>Sungkyunkwan University; <sup>3</sup>North Carolina State University

Ferritic steels used for fabricating nuclear reactor pressure vessels and reactor supports exhibit ductile-brittle transition temperature (DBTT). These steels show radiation embrittlement in terms of decreased toughness and increased DBTT following exposure to neutron irradiation. Recent work revealed decreased toughness during dynamic strain aging (DSA) as well as during reverse-cyclic loading. These have important implications on reliability of these structures under seismic loading conditions. We summarize here our work on these aspects along with synergistic effects of interstitial impurity atoms and radiation-induced defects under certain test conditions. Effect of DSA on ductility and toughness were investigated in pure iron, Si-killed mild steel, reactor support (A516) and pressure vessel steels (A533B). Temperature dependence of fracture toughness revealed plateau during DSA in A516 steel while A533B steel exhibited distinct dips. The effects of load ratio on J versus load-line displacement curves for A516 steel indicated decreased JIC as load ratio is decreased.

## Nanocomposite Materials: Metallic Nanocomposites

Sponsored by: The Minerals, Metals and Materials Society, TMS Structural Materials Division, TMS Electronic, Magnetic, and Photonic Materials Division, TMS/ASM: Composite Materials Committee, TMS: Materials Characterization Committee, TMS: Nanomaterials Committee

Program Organizers: Jonathan Spowart, US Air Force; Judy Schneider, Mississippi State University; Bhaskar Majumdar, New Mexico Tech; Benji Maruyama, Air Force Research Laboratory

Tuesday PM  
February 17, 2009

Room: 3020  
Location: Moscone West Convention Center

Session Chairs: Rajarshi Banerjee, University of North Texas; Bhaskar Majumdar, New Mexico Tech

2:00 PM Introductory Comments

2:05 PM Invited

**Carbon Nanotube Reinforced Nickel Matrix Nanocomposites:** Junyeon Hwang<sup>1</sup>; Antariksh Singh<sup>1</sup>; Soumya Nag<sup>1</sup>; Jaimie Tiley<sup>2</sup>; *Rajarshi Banerjee*<sup>1</sup>; <sup>1</sup>University of North Texas; <sup>2</sup>Air Force Research Laboratory

Nanocomposites based on multi-walled carbon nanotubes (MWCNT) dispersed in a nickel matrix have been processed using the laser-engineered net shape (LENS) processing technique. The advantage of using LENS is that that while using a powder feedstock, the composites are processed via a liquid metal route involving rapid solidification. The present study focuses on the survivability of nanotubes during melt processing using LENS in a liquid

nickel matrix. Furthermore, the stability of MWCNT versus graphite powders in liquid nickel, processed under identical conditions, has been compared. These nanocomposites have been characterized in detail using scanning electron microscopy (SEM), transmission electron microscopy (TEM), 3D atom probe tomography, and, micro-Raman spectroscopy in order to determine the state of the nanotubes post processing as well as the nature of the nanotube/matrix interface. Preliminary results of wear and micro-mechanical testing of these MWCNT reinforced nanocomposites will also be discussed.

### 2:30 PM

#### **Reinforcement with Atom-Infiltrated Carbon Nanotubes in Aluminum Matrix Composites:** *Hyunjoon Choi<sup>1</sup>; Donghyun Bae<sup>1</sup>; Yonsei University*

Reinforcing effects of multi-walled carbon nanotubes (MWNTs) in aluminum-based composites have been investigated. The composites are produced by hot rolling of the ball-milled mixture of aluminum powders and MWNTs. We present a new fabrication approach in constructing tight bonding between the MWNTs and the metal matrix by infiltrating metal atoms into the MWNTs with a controlled mechanical milling process, producing the network structure of metal atoms around the MWNTs. Furthermore, each of MWNTs is dispersed and mainly located inside the metal powders, providing an easy route of consolidation via conventional hot rolling processes. The composites exhibit remarkably enhanced strength at room temperatures. The composite sheets containing 4.5 vol. % exhibit around 600 MPa of tensile strength with ductile failure. Reinforcing effects of MWNTs in tensile properties at elevated temperature, fracture toughness, and tribological properties will be also presented.

### 2:50 PM

#### **Strengthening Mechanisms in Tri-Modal 5083 Al Based Composite:** *Ying Li<sup>1</sup>; Yonghao Zhao<sup>1</sup>; Julie Schoenung<sup>1</sup>; Enrique Lavernia<sup>1</sup>; University of California Davis*

We have performed systematic investigations on the microstructural origin of the previously published super-high yield strength (up to 1065 MPa) of a bulk composite with 10 wt.% boron carbide (B<sub>4</sub>C), 50 wt.% coarse-grained (CG) and 40 wt.% ultrafine-grained (UFG) 5083 Al. In principle, the strength of this composite conforms well to the rule-of-mixtures prediction, an observation that is attributed to the presence of clean metallurgical interfaces as revealed by high-resolution transmission electron microscopy (HRTEM). The grain size and distribution of the 5083 Al matrix were characterized. Al<sub>6</sub>(Mn, Fe) precipitates have been observed in CG interiors and at both UFG boundaries and interiors by scanning TEM (STEM) and electron dispersive X-ray spectroscopy (EDX) mapping. The presences of grain refinements, precipitates in the 5083 Al matrix, B<sub>4</sub>C particles and a high density of dislocations in the CG region are thought to represent the four principal factors responsible for the reported strength levels.

### 3:10 PM

#### **An Investigation into the Thermal Stability of an Aluminum Based Nanocomposite:** *Leyla Hashemi<sup>1</sup>; Rustin Vogt<sup>1</sup>; Zhihui Zhang<sup>1</sup>; Enrique Lavernia<sup>1</sup>; Julie Schoenung<sup>1</sup>; University of California, Davis*

A nanocomposite of Al 5083-14.3%B<sub>4</sub>C has been prepared by mechanically milling powders of Al 5083 and B<sub>4</sub>C in liquid nitrogen medium; a process referred to as cryomilling. This material, when consolidated using conventional powder metallurgy techniques, is well known to exhibit high strength due to the nanocrystalline aluminum matrix and boron carbide reinforcement. It is also expected for this nanocomposite to show high thermal stability. The effect of nitrogen content on grain growth was taken into account by cryomilling powders in liquid nitrogen for different durations, while also cryomilling in argon as a benchmark data point. The cryomilled powders were characterized for homogeneity, grain size, and other microstructural features. They were then annealed at various times and temperatures and a comparison of grain growth behavior was made on the basis of nitrogen content.

### 3:30 PM

#### **Microstructural Characterization of Tri-Modal Aluminum Alloy Composites:** *Bo Yao<sup>1</sup>; Helge Heinrich<sup>1</sup>; Yongho Sohn<sup>1</sup>; Cory Smith<sup>2</sup>; Mark van den Bergh<sup>2</sup>; Kyu Cho<sup>3</sup>; University of Central Florida; <sup>2</sup>DWA Aluminum Composites; <sup>3</sup>US Army*

Tri-modal aluminum alloy composites exhibit excellent strength and impact resistance for a variety of end-uses including survivability related applications. We have examined the microstructural characteristics of commercially produced tri-modal Al-5083 composites reinforced with B<sub>4</sub>C particulates.

Mixtures of 5083 aluminum powder and boron carbide were processed with a commercial scale cryomill in liquid nitrogen and blended with coarse grain inert gas atomized 5083 aluminum powder to produce a trimodal 5083 aluminum composite. Billets were fabricated via hot-vacuum degassing followed by vacuum hot pressing. Samples were taken from the vacuum hot pressed billet for evaluation. X-ray diffraction, scanning electron microscopy, transmission electron microscopy, and related complementary analytical characterization techniques were employed for microstructural characterization with emphasis on the size, composition and distribution of microstructural features. Results and analysis from the microstructural analysis will be discussed with respect to processing conditions and variables of the trimodal aluminum alloy composites process sequence.

### 3:50 PM Break

### 4:05 PM

#### **Aluminum Coated Carbon Nanofibers Reinforced Metal Matrix Composites:** *Chitoshi Masuda<sup>1</sup>; Yu-suke Nishimiya<sup>1</sup>; Fumio Ogawa<sup>1</sup>; Seiji Itabashi<sup>1</sup>; Minoru Oda<sup>1</sup>; University of Waseda*

Carbon nanofibers and carbon nanotubes are very attractive reinforcements of composites. Nanotubes and nanofibers are very difficult to disperse in the metal matrix using ball mill. Now the surface active agents to disperse the carbon nanotubes and nano fibers were useful. After carbon nano fibers were coated by Al using CVD method, they were mixed with Al powders by ball mill under 200rpm in Argon atmosphere for 180 min. The mixed powders were consolidated by SPS method under 50 MPa in vacuum at 550 and 600°C. On the coated carbon nanofibers (about 150nm in diameter)examined by XRD the aluminum carbide was detected. The diameter of carbon nano fiber was about 300nm. Tensile strength of pure aluminum, Al+CNF(non-coated), Al+CNF(coated) consolidated at 600°C were 125, 185, 193MPa, respectively. On the tensile fracture surfaces many dimple patterns were observed and carbon nano fibers were also seen.

### 4:25 PM

#### **Consolidated Cryomilled Al Stabilized with Diamantane:** *Khinlay Maung<sup>1</sup>; James C. Earthman<sup>1</sup>; Farghalli A. Mohamed<sup>1</sup>; University of California Irvine*

Thermal stability has been one of the primary issues for cryomilled nanocrystalline (nc) materials. In this paper we will present the effect of high temperature exposures on the nano-scale grain size of cryomilled Al stabilized with diamantane, the second smallest naturally occurring diamondoid particle. As-cryomilled powders having an average grain size of 22 nm were hot isostatically pressed (HIP'd) for consolidation at 723K (0.7 T<sub>m</sub> of Al).The consolidated stabilized Al composite exhibited an average grain size of 50 nm. A very high grain growth exponent was estimated which was found to be consistent with Burke's model based on drag forces exerted by dispersion particles. The high value of n suggests the operation of strong pinning forces on boundaries during high temperature processing and HIPping. An examination of the microstructure by means of transmission electron microscopy (TEM) showed evidence for recovery of low angle boundaries during HIP process.

### 4:45 PM

#### **A Novel Method for Preparation of Metal Matrix Nanocomposites:** *Payodhar Padhi<sup>1</sup>; Hitech Medical College and Hospital*

Particulate metal matrix composites (MMCs) can involve ceramic particulates ranging in size from few nanometers to 500 μm. Particulates are added to the metal matrix for strengthening. In particular, addition of nanoparticles, even in quantities as small as 2 weight percent can enhance the hardness or yield strength by a factor as high as 2. Solidification processing is a relatively cheaper route. However, during solidification processing nanoparticulates tend to agglomerate. To overcome these difficulties a non-contact method, where the ultrasonic probe is not in direct contact with the liquid metal, was attempted to disperse nano-sized Al<sub>2</sub>O<sub>3</sub> particulates in aluminum matrix. From HRTEM studies it is seen that the Al<sub>2</sub>O<sub>3</sub> particles are distributed uniformly. Both hardness and micro hardness were measured at different locations. It was found that the variations in hardness from location to location are not so significant. In micro scale the hardness is uniform throughout the sample.

5:05 PM

**Friction Stir Processed Nanocomposite Surface Layers for Aluminum Alloys:** *Jun Qu*<sup>1</sup>; Hanbing Xu<sup>1</sup>; Zhili Feng<sup>1</sup>; D. Alan Frederick<sup>1</sup>; Peter Blau<sup>1</sup>; <sup>1</sup>Oak Ridge National Laboratory

Previous work has demonstrated the feasibility of using a friction stir process (FSP) to form a nanocomposite layer on a pure aluminum surface to improve the hardness and wear-resistance without sacrificing the bulk ductility and conductivity. This study applied this surface engineering technique to the Al 6061-T6511 alloy. Nano- or micro-sized reinforcement materials (Al<sub>2</sub>O<sub>3</sub>, SiC, TiO<sub>2</sub>, LaB<sub>6</sub>) in different shapes (particles or fibers) and sizes (30 nm – 5 μm) were friction stirred into the Al 6061 alloy surface to form a composite layer up to 3 mm thick. The concentration of the hard phase was in the range of 10-20 vol%. Compared with a non-processed Aluminum surface, the FSP-formed nanocomposite surface exhibited a moderate increase in hardness and a substantial improvement on wear-resistance by more than one order of magnitude when rubbed against a hardened bearing steel. A post-FSP heat treatment (T6) afforded further enhancement of the wear performance.

---

## Near-Net Shape Titanium Components: Casting, Welding and Beam Processes

Sponsored by: The Minerals, Metals and Materials Society, TMS: Titanium Committee

Program Organizers: Rodney Boyer, Boeing Company; James Colton, Boeing Co

Tuesday PM

Room: 2010

February 17, 2009

Location: Moscone West Convention Center

Session Chair: Rodney Boyer, Boeing Company

---

2:00 PM

**The Boeing Approach to More Cost Effective Ti Components:** *Rodney Boyer*<sup>1</sup>; Kevin Slattery<sup>1</sup>; Todd Morton<sup>1</sup>; James Cotton<sup>1</sup>; <sup>1</sup>Boeing Co

The competition in commercial airframes, the present economy (fuel prices) and the continuing technology development globally mandate the development of new alloys and technologies to reduce the cost of titanium hardware. Obviously this applies to all materials, but with the high cost of titanium it is even more imperative for this technology area. Reducing the cost of titanium embraces the entire value stream including raw materials, melt and meltless technologies, machining, and reduction of the buy-fly ratio. The latter could involve modeling, near-net shape forging, casting, extrusions, welding, etc. Some of the Boeing approaches to reducing the cost of titanium hardware will be discussed.

2:20 PM

**Development of Databases to Relate Composition, Microstructure, and Properties for the Production of near-Net Shape Functionally Graded a+β and B-Type Ti-Based Materials:** *Peter Collins*<sup>1</sup>; Dan Huber<sup>1</sup>; Brian Welk<sup>1</sup>; Hamish Fraser<sup>1</sup>; <sup>1</sup>Ohio State Univ

Functionally graded Ti-based components offer the potential to engineer location-specific properties in unitized structures. However, the microstructures and properties arising from composition landscape between the two terminal compositions will often remain largely unexplored. This work explores the microstructural evolution that can occur at various compositions along binary (Ti-xMo and Ti-xFe) and multi-component (e.g., Ti to Ti-1Al-8V-5Fe or Ti to Ti-1Al-7Fe) gradients produced using laser engineered net shaping (LENS<sup>TM</sup>) and begins to populate databases that may be probed to relate composition with microstructure and properties.

2:40 PM

**Advanced Titanium Welding Processes for Improved Material Utilization in Aerospace Manufacturing:** *Paul Edwards*<sup>1</sup>; Chris Swallow<sup>1</sup>; Dan Sanders<sup>1</sup>; Kevin Slattery<sup>1</sup>; Amy Helvey<sup>1</sup>; <sup>1</sup>The Boeing Company

The use of Titanium by the aerospace industry has recently been driven to unprecedented levels, which has resulted in price escalations and temporary supply shortages. Most titanium parts are machined out of plate, blocks, forgings or extrusions, which all result in wasted scrap material and unnecessarily high fabrication costs. In order to reduce the buy-to-fly ratio of titanium parts, more efficient manufacturing techniques must be implemented. Laser Welding, Linear Friction Welding and Friction Stir Welding of titanium 6Al-4V have all

been developed in order to produce low cost aerospace structural components. For each of these welding technologies, process parameters have been identified for producing very repeatable, high quality welds on a variety of material thicknesses and joint configurations. Extensive metallurgical examinations and preliminary mechanical property evaluations have been performed to qualify these process for fabricating structural aerospace parts.

3:00 PM

**Microstructure-Properties of Alloy Ti-5Al-5Mo-5V-3Cr Castings:** *E. Chen*<sup>1</sup>; L. Weihmuller<sup>2</sup>; D. Bice<sup>1</sup>; G. Hall<sup>2</sup>; W. Thomas<sup>2</sup>; <sup>1</sup>Transition45 Technologies Inc; <sup>2</sup>Bell Helicopter Textron

Alloy Ti-5Al-5Mo-5V-3Cr-0.5Fe (Ti-5553) is an emerging high-strength titanium alloy with improved static mechanical properties compared with the industry workhorse Ti-6Al-4V. Studies to date have shown that this material also has comparable or better fatigue properties to 4340 steel and Ti-6Al-4V, respectively, thus could be a replacement candidate for these alloys to achieve weight savings and/or enhanced durability. The ability to cast complex net shapes from a high strength titanium as this also offers the potential to save both cost and weight over traditionally forged components. This presentation covers work being conducted on characterizing the microstructure-properties of Ti-5553 castings. Mechanical properties covered here include tensile, toughness, and fatigue behavior for microstructures achieved under different thermo-mechanical processing conditions. The results show outstanding strength and fatigue properties relative to both wrought and cast Ti-6Al-4V. This work was supported by the Naval Air Warfare Center.

3:20 PM Break

3:40 PM

**Optimization of Layered Additive Manufacturing Processes:** *Raghavan Srinivasan*<sup>1</sup>; Anil Chaudhary<sup>2</sup>; Matthew Keller<sup>2</sup>; <sup>1</sup>Wright State University; <sup>2</sup>Applied Optimization Inc.

Layered additive manufacturing offers a flexible approach for the production of complex near-net- and net-shaped components by building up three dimensional objects by selectively adding material on successive two dimensional layers. A recently developed software based tool, SAMP ® (Simulation of Additive Manufacturing Processes) provides the opportunity to simulate laser (or electron beam) based powder deposition processes. Using Ti-6Al-4V as the model material, SAMP ® will be used to conduct a systematic study of the effect of parameters, such as laser power, beam traverse rate, powder flow rate, and deposition schedule on the predicted microstructure, and to optimize the layered manufacturing process. Optimization of the process schedule has several cost benefits, such as decreased certification costs resulting from a uniform microstructure, decreased “buy/fly” ratio, and more effective use manufacturing equipment. Several part geometries ranging from a simple thin wall on a plate to more complicated geometries, such as “T”, “D”, “H” or box shapes, will be investigated.

4:00 PM

**The Effect of Powder Production Process on Microstructure and Mechanical Properties of Electron Beam Deposited Ti6Al4V:** *Jonathan Nguyen*<sup>1</sup>; Baolong Zheng<sup>1</sup>; Troy Topping<sup>1</sup>; Yizhang Zhou<sup>1</sup>; Scott Gilley<sup>2</sup>; James Good<sup>3</sup>; Enrique Lavernia<sup>1</sup>; <sup>1</sup>University of California, Davis; <sup>2</sup>Tec Masters, Inc.; <sup>3</sup>Teledyne Brown Engineering

Arcam Electron beam melting (EBM) is an emerging technique that utilizes an electron beam to melt metal powder in a layered powder additive process. Samples produced are near net shaped as well as have comparable or superior mechanical properties, thereby reducing costs associated with machining time and post heat treatment processing, respectively. Currently, there have been no published results on the effects of the method of prealloyed powder production processes. In this article, square columns were fabricated at a voltage of 60 kV and a current of 9.1 mA, using gas atomized (GA) and plasma rotating electrode process (PREP) powders to evaluate the effects of the initial powder on microstructure and mechanical properties. The microstructure of the as-deposited columns was characterized using optical and scanning electron microscopy (SEM). The amount of porosity resulting from the type of prealloyed powder used and its implication on the mechanical properties will be discussed.



4:20 PM

**Research of TiAl Alloy Complex Component Precision Casting:** *Nan Hai*<sup>1</sup>;<sup>1</sup>Beijing Institute of Aeronautical Materials

In this paper the fluidity of TiAl alloy was compared with Ti6Al4V in the graphite mould. By wax pattern preparing, ceramic mould making, centrifugal casting, and microstructure and property analysing, TiAl alloy complex component precision casting technology was introduced. Turbo charger and increasing pressure case were cast. The smallest wall thickness is 1mm.

4:40 PM

**Effect of Microstructure Variations on Fatigue of Investment Cast Ti-6Al-4V:** *Adam Pilchak*<sup>1</sup>; James Ault<sup>2</sup>; James Williams<sup>1</sup>; <sup>1</sup>Ohio State University;<sup>2</sup>Precision Castparts Corp

Investment castings of titanium are being used in increasing numbers. In the cast and hot isostatic pressed condition the material has a coarse, fully lamellar microstructure characterized by poor fatigue crack initiation resistance, but excellent crack growth resistance. Friction stir (FS) processing can improve the crack initiation resistance of castings. These FS processed castings may be able to replace forged components resulting in cost reduction for parts with complex geometries. In the course of studying the effects of FS processing on fatigue, several microstructural variations have been observed. These include tungsten contamination from the FS tool and regions of equiaxed  $\alpha$  grains formed as a result of HIP pore closure. Furthermore, the effect of yttrium rich particles on fatigue crack initiation in cast and wrought Ti-6Al-4V has been examined. This talk will describe the sources of these microstructural variations and their effect on fatigue behavior.

**Neutron and X-Ray Studies of Advanced Materials: Advances in Line Profile**

Sponsored by: The Minerals, Metals and Materials Society, TMS Structural Materials Division, TMS/ASM: Mechanical Behavior of Materials Committee, TMS: Advanced Characterization, Testing, and Simulation Committee, TMS: Titanium Committee  
Program Organizers: Rozaliya Barabash, Oak Ridge National Laboratory; Yandong Wang, Northeastern University; Peter Liaw, The University of Tennessee; Jaimie Tiley, US Air Force

Tuesday PM  
February 17, 2009Room: 3016  
Location: Moscone West Convention Center

*Session Chairs:* Yan-Dong Wang, Northeastern University; Peter Liaw, University of Tennessee

2:00 PM Keynote

**Advances in Diffraction Line Profile Analysis of Nanocrystalline and Heavily Deformed Materials:** *Paolo Scardi*<sup>1</sup>; <sup>1</sup>University of Trento

In the past ten years diffraction line profile analysis evolved from single-peak methods, with more or less arbitrary steps to remove background and to separate overlapping peaks, to one-step full pattern modeling methods. In particular, the Whole Powder Pattern Modeling is a new paradigm for the analysis of diffraction line profiles, according to which the diffraction pattern from polycrystalline materials can be analyzed on the basis of physical models of the microstructure, without using arbitrary analytical profile functions. The present contribution shows recent advances in the study of nanocrystalline materials, where crystalline domain shapes and size distribution can be analyzed in detail, as well as of heavily deformed materials, where grain refinement and lattice defect type and density can be obtained. Results are compared with those by other approaches (e.g. based on Debye formula) and different techniques (e.g., TEM). The specific case of dislocation containing materials is discussed in detail.

2:30 PM Invited

**Your Synchrotron Powder Diffraction Instrument: 11-BM at the Advanced Photon Source:** *Brian Toby*<sup>1</sup>; <sup>1</sup>Argonne National Laboratory

Synchrotron powder diffraction has revolutionized powder diffraction in that it makes possible data collection with tremendous resolution and signal to noise, or allows for extremely rapid collection (<1 second) collection of entire, high quality, powder diffraction patterns. The high penetration and data sensitivity over wide Q range even allows synchrotrons to make inroads into territory that previously demanded neutrons: extreme sample environments and

site occupancy studies. The problem has been that access to synchrotrons has been difficult. The 11-BM synchrotron powder diffractometer at the APS now offers easy mail-in access with quick turnaround for routine structural analysis, providing truly first-quality data. This talk will present the capabilities of the instrument and how these kinds of data can solve real-world materials problems. Also to be discussed is how to obtain access.

2:50 PM Invited

**Defects and Strains by X-Ray and Neutron Diffraction: Modeling and Applications:** *Davor Balzar*<sup>1</sup>; <sup>1</sup>University of Denver

With the constant improvement of experimental techniques, especially with the advent of new-generation synchrotron and neutron sources with superior resolution, sometimes subtle effects of lattice strains and low defect concentrations on diffraction lines, become easier to study. Furthermore, modern analysis methods, such as Rietveld refinement, increasingly go beyond the determination of structural parameters and include refinable parameters with a physical significance within accurate line-broadening models. Some recent improvements in modeling of line broadening and line shift in Rietveld refinement will be discussed. In the second part, several examples will be presented. In particular, I will talk on the determination of a complete strain tensor from Rietveld refinements of multiple TOF neutron-diffraction spectra, size-strain round-robin results, and applications of line-broadening and line-shift analyses to several materials of technological interest.

3:10 PM

**Development of Intergranular Thermal Residual Stresses in Beryllium during Cooling from Processing Temperatures:** *Thomas Sisneros*<sup>1</sup>; Donald Brown<sup>1</sup>; Mark Bourke<sup>1</sup>; Bjorn Clausen<sup>1</sup>; Sven Vogel<sup>1</sup>; Brian Smith<sup>1</sup>; Steve Abeln<sup>1</sup>; Michael Steinzig<sup>1</sup>; <sup>1</sup>Los Alamos National Laboratory

The intergranular thermal residual stresses in randomly textured solid polycrystalline beryllium have been determined by comparison of crystallographic parameters in solid and powder samples measured by neutron diffraction during cooling from 800°C. The stresses have been calculated by an Eshelby type polycrystalline model for comparison. The internal stresses are not significantly different from zero above 575°C and increase nearly linearly below 525°C. At room temperature the c-axis perceives roughly -200MPa of compressive internal stress; the a-axis 100MPa of tensile stress.

3:25 PM Invited

**Defect-Related Physical-Profile Based X-Ray and Neutron Line Profile Analysis:** *Tamas Ungar*<sup>1</sup>; Levente Balogh<sup>1</sup>; Gábor Ribárik<sup>1</sup>; <sup>1</sup>Eotvos University

Diffraction line broadening is caused by different defects present in crystalline materials: (i) small coherent domains, (ii) dislocations, (iii) other types of microstrains, (iv) twin boundaries (v) stacking faults, (vi) chemical inhomogeneities and (vii) grain-to-grain second order internal stresses. Line profile analysis provides qualitative and quantitative information about defect types and densities, respectively. Line profiles can broaden, be asymmetric, can be shifted and these features can be anisotropic in terms of hkl indices. A few thumb rules help qualitative selection of lattice types. If the beradths are globally not increasing with hkl, the defects are of size type, i.e. either domain size is small or twinning or faulting, or both are present. Whenever the beradths increase globally, the defects produce microstrains. It will be shown that physically based profile functions can be determined for each defect type and the hkl anisotropy allows evaluation of the different defect types and density.

3:45 PM Break

4:00 PM Invited

**Microstructure of Ultrafine-Grained Metals after Severe Plastic Deformation and Its Thermal Stability Studied by XRD in Combination with PAS, EBSD and TEM:** *Radomir Kuzel*<sup>1</sup>; Miloš Janeček<sup>1</sup>; Jakub Čížek<sup>1</sup>; Milan Dopita<sup>2</sup>; <sup>1</sup>Faculty of Mathematics and Physics, Charles University; <sup>2</sup>Technical University Freiberg

Different samples of cubic (Cu, Ni, Fe, Nb) and hexagonal (Mg) metals and their alloys or composites deformed by equal-channel angular pressing (ECAP) and high-pressure torsion (HPT) were studied by XRD line profile analysis and back-scattering photos, transmission electron microscopy (TEM), electron backscatter diffraction (EBSD) and positron annihilation spectroscopy (PAS). XRD revealed changes in both dislocation density (line broadening) and dislocation correlations (line shape) with number of ECAP paths, abnormal grain growth and bimodal grain-size distribution for Cu samples with annealing, grain fragmentation for iron, in-depth and in-plane microstructural inhomogeneities

for HPT samples. TEM and EBSD indicated changes of grain boundaries with ECAP paths (transition from low angle to high angle grain boundaries). XRD and EBSD could characterize variation of the texture. PAS detected the presence microvoids and enabled determination of their size. PAS was also complementary with XRD for dislocation density determination (lower and higher values, respectively).

#### 4:20 PM

**Synchrotron X-Ray Study of Nanocrystalline Ni during Cold Rolling:** *Li Li<sup>1</sup>; Yan-Dong Wang<sup>2</sup>; Tamas Ungar<sup>3</sup>; Yang Ren<sup>4</sup>; Hahn Choo<sup>1</sup>; Peter Liaw<sup>1</sup>; <sup>1</sup>University of Tennessee; <sup>2</sup>Northeastern University; <sup>3</sup>Eötvös University; <sup>4</sup>Argonne National Lab*

Two foils of nanocrystalline Ni metal (with nominal grain size of 10 - 20 nm) were rolled at room temperature (RT) and liquid-nitrogen temperature (LNT), respectively. Synchrotron-based high-energy x-ray diffraction was employed in the undeformed and deformed specimens to study the microstructure evolution. Quantitative microstructures, such as the area-average mean crystallite size, dislocation density, and dislocation character, were investigated by the x-ray line-profile analysis. X-ray line profile analysis is especially useful to the study of submicron-grained or nano-grained materials where the x-ray line broadening becomes well pronounced, and the observation of defects with a very large density is often challenging using conventional TEM. Texture experiment was also performed in the experiment. This research is supported by NSF-IMI program (DMR-0231320) and NSF-MRI program (DMR-0421219).

#### 4:30 PM Invited

**Total Scattering: The Key to the Local and Medium Range Structure of Complex Materials:** *Thomas Proffen<sup>1</sup>; <sup>1</sup>Los Alamos National Laboratory*

Structural characterization is mainly based on the measurement of Bragg intensities and yields the average structure of the crystalline material. However, this approach ignores any defects or local structural deviations that manifest themselves as diffuse scattering. It also fails in case of disordered materials and nano-crystalline. The total scattering pattern, however, contains structural information over all length scales and can be used to obtain a complete structural picture of complex materials. Suddenly one has access to a new parameter, the real-space range of the refinement and structures can be analyzed as function of length scale straight forwardly. Here we present different applications of this technique including data taken on the high resolution neutron powder diffractometer NPDF located at the Lujan Neutron Scattering Center. This instrument is design for total scattering studies using the Pair Distribution Function (PDF) approach and length scales in excess of 200Å can be accessed.

#### 4:50 PM Invited

**X-Ray Microdiffraction Study of the Ni-Based Superalloys after Friction Stir Processing:** *Oleg Barabash<sup>1</sup>; Rozaliya Barabash<sup>1</sup>; Gene Ice<sup>1</sup>; Zhili Feng<sup>1</sup>; <sup>1</sup>Oak Ridge National Laboratory*

Advanced 3D polychromatic X-ray micro diffraction at the APS synchrotron was applied to study structural changes in the Ni-based superalloy caused by Friction Stir Processing (FSP). Spatially resolved 3D Laue diffraction allowed following the changes in dislocation arrangement with depth in different regions of the FSP alloys. X-ray diffraction results are complemented by SEM and EBSD. Formation of several specific zones was established: friction stir zone, and thermomechanically and heat affected zones. It was shown that FSP generates a large number of geometrically necessary dislocations. Anisotropy of all stir processing zones is demonstrated. Ultrafine grain size is observed in the stir zone. Research is sponsored by the Division of Materials Sciences and Engineering, Office of Basic Energy Science U.S. Department of Energy.

#### 5:10 PM Invited

**Dynamic Recrystallization and Grain Refinement in a Friction Stir Processed AZ31B Mg Alloy: An X-ray Line Profile Analysis:** *Hahn Choo<sup>1</sup>; Zhenzhen Yu<sup>1</sup>; Levente Balogh<sup>2</sup>; Tamás Ungár<sup>2</sup>; Zhili Feng<sup>3</sup>; <sup>1</sup>University of Tennessee; <sup>2</sup>Eötvös University; <sup>3</sup>Oak Ridge National Laboratory*

Friction stir processing (FSP) has a great potential as a novel method for the fabrication of bulk ultrafine-grained structural materials. While it is known that the combined effects of severe plastic deformation and temperature result in fine grain sizes through dynamic recrystallization (DRX) process during FSP, the exact mechanism of DRX and the detailed understanding of the resulting microstructure are still unclear. In this study, a series of FSP was performed on AZ31B magnesium alloy under different strain rate and temperature by varying the processing parameters. High-resolution x-ray line profile analysis was

used, in combination with electron microscopy, to investigate the dynamically recrystallized microstructure as a function of the processing parameters. The effects of changing the processing parameters on the resulting microstructures; such as grain size, sub-grain size, dislocation density, and texture; in the dynamically-recrystallized zone will be discussed in the context of deformation and recrystallization mechanisms.

#### 5:30 PM

**Grain Structure and Dislocation Densities in a Friction Stir Welded Aluminum Alloy Studied by X-Ray Line Profile Analysis:** *Wan Chuck Woo<sup>1</sup>; Levente Balogh<sup>2</sup>; Tamas Ungar<sup>2</sup>; Hahn Choo<sup>3</sup>; Zhili Feng<sup>1</sup>; <sup>1</sup>Oak Ridge National Laboratory; <sup>2</sup>Eötvös University; <sup>3</sup>University of Tennessee*

Severe plastic deformation and recrystallization process results in the dislocation-embedded 'grain structure'. The dislocation density and grain structure of a friction stir welded 6061-T6 aluminum alloy was examined as a function of distance from the weld centerline using high-resolution micro-beam x-ray diffraction. Theoretically simulated and directly measured diffraction patterns are compared to each other and determined the microstructural characteristics. The results of the x-ray peak profile analysis show that the dislocation density is about  $1.2 \times 10^{14} \text{ m}^{-2}$  inside,  $4.8 \times 10^{14} \text{ m}^{-2}$  outside of the weld region. The average subgrain size is about 180 nm in both regions. Compared to the base material, the dislocation density was significantly decreased in the dynamic recrystallized zone of the friction stir welds, which is in good correlation with the TEM observations. The influence of the dislocation density on the strain hardening behavior during tensile deformation is also discussed.

#### 5:45 PM

**The Effect of Welding Pressure on Microstructural Evolution in Dissimilar Steel Friction Welds Studied by Synchrotron X-Ray Diffraction:** *Richard Moat<sup>1</sup>; Michael Preuss<sup>1</sup>; Mallikarjun Karadge<sup>1</sup>; Martin Rawson<sup>2</sup>; Simon Bray<sup>2</sup>; <sup>1</sup>University of Manchester; <sup>2</sup>Rolls Royce Plc*

The 2D microstructural evolution across inertia friction welded high strength steels of Aermet 100 against S/CMV has been studied as a function of axial forging pressure. High energy synchrotron x-ray diffraction was used to record 2D maps of retained austenite within the heat affected zone (HAZ), identify the thermomechanically affected zone (TMAZ) from peak broadening maps and use peak shape analysis to identify regions of martensitic phase transformation. Since a number of complete diffraction rings were recorded, it was also possible to calculate the crystallographic texture at each measurement point. Results show that with increasing weld pressure the amount of martensite formed within the heat affected zone is reduced significantly while the amount of retained austenite seems to increase. The texture mapping allowed relating hardness troughs to recrystallised regions. The results are discussed in terms of consequences for residual stress generation during joining.

#### 6:00 PM

**Recovery of Ultra-Fine Grained Materials by Severe Plastic Deformation:** *Yonghao Zhao<sup>1</sup>; Thomas Ungar<sup>2</sup>; Y. Li<sup>3</sup>; Ruslan Valiev<sup>4</sup>; Yuntian Zhu<sup>5</sup>; Yizhang Zhou<sup>3</sup>; Enrique Lavernia<sup>3</sup>; <sup>1</sup>Los Alamos National Laboratory; <sup>2</sup>Eotvos University; <sup>3</sup>University of California, Davis; <sup>4</sup>UFA State Aviation Technical University; <sup>5</sup>North Carolina State University*

It is well known that ultrafine-grained (UFG) metals prepared by severe plastic deformation (SPD) have nearly zero uniform elongation due to their low dislocation accumulation capability which was consumed during SPD process. Recovery by low temperature annealing is an effective way to regain the lost strain hardening/dislocation accumulation and therefore the ductility. In this work, we employed X-ray diffraction (XRD) combined with transmission electron microscopy (TEM) techniques to systematically investigate the recovery processes of the UFG Cu, Al, CuZn30, UFG Ti by equal-channel-angular (ECAP) process. Evolutions of dislocation density and grain size during annealing were analyzed. Our work will provide basic guidance for optimize mechanical properties of UFG materials.

## Pb-Free Solders and Emerging Interconnect and Packaging Technologies: Tin Whisker Formation and Mechanical Properties

Sponsored by: The Minerals, Metals and Materials Society, TMS Electronic, Magnetic, and Photonic Materials Division, TMS: Electronic Packaging and Interconnection Materials Committee

Program Organizers: Sung Kang, IBM Corp; Iver Anderson, Iowa State University; Srinivas Chada, Medtronic; Jenq-Gong Duh, National Tsing-Hua University; Laura Turbini, Research In Motion; Albert Wu, National Central University

Tuesday PM Room: 2020  
February 17, 2009 Location: Moscone West Convention Center

Session Chairs: Laura Turbini, Research In Motion; K. Subramanian, Michigan State University

### 2:00 PM Invited

#### Structure-Property Evaluations in Sn-Based Solders with Nano-Structured Chemicals: K. Subramanian<sup>1</sup>; Deep Choudhuri<sup>1</sup>; Andre Lee<sup>1</sup>; <sup>1</sup>Michigan State University

The integrity of solder joints deteriorates with repeated thermal excursions due to stresses arising from mismatch of coefficient of thermal expansion between the entities present in the packages and the anisotropic nature of Sn. Impact of this thermomechanical fatigue (TMF) depends on parameters such as imposed temperature differences, dwell times, ramp-rates, etc. Our recent investigations have shown that it also depends on the temperature extremes experienced during TMF, since the deformation characteristics of Sn-based solders are highly temperature sensitive. Strongly-bonded inert nano-structured reinforcements significantly improve the TMF resistance of Sn-based electronic solder interconnects. During reflow, active radicals present at the surface of these nano-structured inert structures facilitate strong bonding with the solder. Such strongly bonded inert structures do not coarsen, or de-bond from solder matrix, during service. Roles of various active radicals on the reflowed microstructure, and the resultant performance of SAC 305 and eutectic Sn-Ag solder joints are presented.

### 2:20 PM

#### Grain Orientation Effects on the Temperature Cycling Stability of 180 $\mu$ m Pitch Pb-Free Bump Interconnects: John Osenbach<sup>1</sup>; Dongmei Meng<sup>1</sup>; Chris Richardson<sup>1</sup>; Patrick Variot<sup>1</sup>; Chris Richardson<sup>1</sup>; <sup>1</sup>LSI Corporation

The crystallographic orientation of Pb-free solder has been shown to impact the thermo-mechanical and possibly electromigration reliability of the joint. In this paper, results on the influence of crystallographic bump orientation on the temperature cycling performance of Pb-free-180 $\mu$ m pitch-flip chip joints are presented. EBSD results of individual 180 $\mu$ m pitch bumps indicate that individual bumps contain multiple grains. In many cases the grains are highly oriented, separated by low angle grain boundaries. This type of microstructure produces a bump that from a thermo mechanical perspective can, to first order, be treated as a single crystal bump. In this paper, we show that the crystallographic orientation of the bump strongly influences the stability of individual bumps on flip chip devices subjected to extensive temperature cycling testing at temperatures between -55C to +125C.

### 2:35 PM

#### The Performance and Fracture Behavior of Low Silver Lead-Free Solder Joints upon Micro-Impact Test: Ya Ling Huang<sup>1</sup>; Kwang Lung Lin<sup>1</sup>; D. S. Liu<sup>1</sup>; <sup>1</sup>National Cheng Kung University

Various low silver lead-free solder alloys were examined herein to investigate the joint strength, fracture energy, and fracture behavior with micro-impact test at impact velocity of 1m/sec. The solder investigated include Sn-1Ag-0.5Cu (SAC105), Sn-1.2Ag-0.5Cu-0.05Ni, Sn-1Ag-0.5Cu-0.05Ni, Sn-1Ag-0.5Cu-0.05Co, and Sn-1Ag-0.1Cu-0.02Ni-0.05In (SAC101). Most of the solder joints, except SAC105 and SAC101, exhibit mixed brittle (fracture at interface) and ductile (fracture in bulk solder) fracture modes. The morphology of intermetallic compounds were found to affect fracture behavior of the solder joints. Needle-type Ni<sub>3</sub>Sn<sub>4</sub> and (Cu,Ni)<sub>6</sub>Sn<sub>5</sub> intermetallic compounds were observed in SAC101 and SAC105 solder joints, respectively. The SAC101 exhibits ductile fracture behavior while the SAC105 exhibits brittle fracture

behavior. Layer-type intermetallic compounds were observed in the Sn-1.2Ag-0.5Cu-0.05Ni, Sn-1Ag-0.5Cu-0.05Co, and Sn-1Ag-0.5Cu-0.05Ni solder joints which exhibit mixed fracture behavior. The ductile fracture behavior has higher fracture energy, displacement and force than brittle fracture.

### 2:50 PM

#### Effects of Temperature and Strain Rate on Mechanical Properties of Lead-Free Solders: Hongtao Ma<sup>1</sup>; <sup>1</sup>Cisco Systems

Due to the high homologous temperature of solder alloys ( $T_h > 0.5T_m$ ), the mechanical properties of solder alloys are strongly temperature and strain rate dependent. The investigation of this dependence on temperature and strain rates is therefore important in order to fully understand the materials behavior of solder alloys, and accurately predict the reliability of solder joints. There have been various studies on the temperature and strain rate dependence. However, none of the currently available documented data has considered the possible room temperature contribution in their data. In our prior work on aging effects (Ma, et al., ECTC 2006), we demonstrated that the observed material behavior variations of SAC405 and SAC305 lead free solders during room temperature aging (25°C) were unexpectedly large and universally detrimental to reliability. In this study, in order to reduce any room temperature aging contribution, all specimen tested were preconditioned under the same conditions.

### 3:05 PM

#### Finite Element Analysis of Stress Evolution in Sn Films Due to Intermetallic Growth: Eric Buchovecky<sup>1</sup>; Nitin Jadhav<sup>1</sup>; Allan Bower<sup>1</sup>; Eric Chason<sup>1</sup>; <sup>1</sup>Brown University

Although mechanical stress induced by growth of an intermetallic phase has been shown to be an important driving force for the formation of whiskers in pure Sn coatings on Cu, the mechanisms by which stresses are generated and transmitted through the Sn film are not fully understood. In this study, we perform three-dimensional finite element simulations to quantitatively model the stress evolution due to elastic and plastic deformation coupled with stress-driven grain boundary diffusion (Coble creep) within a polycrystalline Sn film. We explore the effects of grain size, film thickness and microstructure in the Sn film, as well as the morphology, distribution and growth rate of the intermetallic particles. We find that both dislocation plasticity in the Sn immediately surrounding the intermetallic particles and mass transport along grain boundaries are necessary to produce stress histories in the Sn film consistent with experimental measurements from our lab.

### 3:20 PM

#### Stress Distribution in Sn-Cu Layers and Its Relation to Whisker Formation: Nitin Jadhav<sup>1</sup>; Vivett Fawal<sup>1</sup>; Evan Laprade<sup>2</sup>; Eric Buchovecky<sup>1</sup>; Jae Wook Shin<sup>1</sup>; Eric Chason<sup>1</sup>; <sup>1</sup>Brown University; <sup>2</sup>RPI

Stress is generally believed to be the driving force for Sn whisker formation so measuring its time evolution and its distribution through the layers is useful for understanding its role in whisker growth. We have used a real-time wafer curvature technique to monitor the evolution of stress in bilayers of Sn and Cu deposited on glass substrates. By monitoring a series of samples with different initial Sn and Cu layers thicknesses, we can estimate the distribution of stress through the Sn, Cu and IMC layers. We additionally measure the change in curvature when the Sn layer is removed by selective etching to separate the stress in the Sn from the Cu/IMC layers. Our results suggest that the Sn layers have a relatively uniform compressive stress, the Cu layers have tensile stress confined to a region near the Cu/Sn interface and the stress in the IMC layer is small.

### 3:35 PM

#### Failure Mechanisms in Pb-Free Interconnects Resulting from Temperature and Mechanical Cycling: Brent Fiedler<sup>1</sup>; Jared Fry<sup>1</sup>; Morris Fine<sup>1</sup>; <sup>1</sup>Northwestern University

The quantitative effects of temperature and mechanical cycling on failure mechanisms in Sn-4.0Ag-0.5Cu (SAC405) solder ball grid array (BGA) interconnects are examined at the component level. The microstructure and composition changes – due to mechanical and temperature cycling – in the lead-free solder BGA are studied by scanning electron microscopy (SEM) and energy-dispersive spectroscopy (EDS). The studies focus on the interface of the solder, intermetallic compounds (IMC) and Cu pad. Cracking from temperature cycling is most often observed at interfaces with IMC, while mechanical cycling primarily initiates cracks in the solder. In-situ crack initiation and propagation is evaluated using the resistance of the daisy-chained arrays for structural health monitoring (SHM) of interconnects.



## 3:50 PM Break

### 4:05 PM

**Metal Whisker Formation in Multiphase Electronic Solder Joints under Electromigration:** *Guangchen Xu*<sup>1</sup>; Mengke Zhao<sup>1</sup>; Hongwen He<sup>1</sup>; Fu Guo<sup>1</sup>; <sup>1</sup>Beijing University of Technology

Numerous electronic system failures have been attributed to short circuits caused by metal whiskers that bridge closely-spaced circuit elements maintained at high current density. Typically, in the single phase of interconnect atoms are driven from the cathode to the anode and a compressive stress built up at the anode end of the stripe form the hillocks. However, the electronic solders used in interconnects are multiphase materials where primary and secondary diffusion entities exist. In this study, various current densities and ambient temperatures were applied to multiphase solder joints to accelerate metal whisker growth. Either Sn or Bi whiskers was observed depending on the field parameters applied. Such service parameters also affect the site and length of the metal whiskers. It was found that whiskers of the primary diffusion entity tend to form at the anode side, while those of the secondary diffusion entity tend to form at the cathode side.

### 4:20 PM

**Mitigation of Tin-Whiskers Growth by Applying Multiple Ni/Sn Plating Prior to the Final Tin Finish:** *Aleksandra Dimitrovska*<sup>1</sup>; Dechao Lin<sup>1</sup>; Radovan Kovacevic<sup>1</sup>; <sup>1</sup>SMU

World-wide research on the formation of Sn-whiskers has agreed that presence of the compressive stresses built up in the Sn-film is one of the driving forces for Sn-whiskers growth which cause failures of various components in the electronic industry. Migration of Cu-element from the substrate to the Sn-film generates Sn-Cu inter-metallic compounds at the Sn/substrate interface and in the Sn-film which triggers the growth of the compressive stresses. To reduce this stress level a multiple composite Ni/Sn layering was developed in this study. A Ni-layer was first deposited onto the brass substrate and then followed by multiple Sn/Ni layers with the thickness of several microns each. Experimental results demonstrated that this new layering procedure on a brass substrate significantly reduces both the volume fraction of Sn-Cu inter-metallic compounds and the Cu content in the final tin finish, resulting in tin whisker's growth mitigation.

### 4:35 PM

**Competing Mechanism between Intermetallic Compounds Formation and Whisker/Hillock Growth in Pb-Free Solder Joints:** *Jung-Kyu Han*<sup>1</sup>; Luhua Xu<sup>1</sup>; King-Ning Tu<sup>1</sup>; <sup>1</sup>UCLA

Whisker/hillock is formed at the anode side in flip-chip solder joints due to the accumulation of Sn. Besides, the electromigration of Cu causes the formation of intermetallic compounds at the anode side in solder joints. In order to see the relationship between whisker/hillock growth and intermetallic compounds formation, the cross-sectioned flip-chip SnAgCu samples were studied with current stressing ( $1.41 \times 10^4$  A/cm<sup>2</sup>) at 150°C. As a result, whisker/hillock was formed at the anode side and was gradually grown at the beginning. The growth of whisker/hillock, however, was hindered by intermetallic compounds formation as time goes by. It seems that Cu which was migrated along the electron flow consumed Sn to form intermetallic compounds at the anode side and blocked Sn source for whisker/hillock growth. The schematic diagram and competing mechanism between intermetallic compounds formation and whisker/hillock growth is proposed.

### 4:50 PM

**Copper Dissolution and Tin Whisker Growth in Lead-Free Solders:** *Lizabeth Nielsen*<sup>1</sup>; *Dana Medlin*<sup>1</sup>; <sup>1</sup>South Dakota School of Mines and Technology

The purpose of this research was to study and understand the tin whisker growth mechanism and the issue of copper dissolution during thermal treatments of lead-free solders. A brief history of tin whiskers and a literature review of copper dissolution issues will also be discussed. An analysis of the tin whiskers was performed by electron backscatter diffraction (EBSD) on the individual whiskers and the base materials where the whiskers originated to determine the crystal orientation of both the whisker and the base material to determine the relationship between base material crystal orientation, residual stress and whisker origin. The EBSD analysis was also able to determine the tin phases for both the whiskers and the base solder material. Solder samples were analyzed through the use of traditional metallographic techniques and scanning electron microscopy to determine the amount of copper dissolution that was occurring with different printed circuit board process parameters.

### 5:05 PM

**Whiskers, Hillocks, and Film Stress Evolution in Electroplated Sn and Sn-Cu Films:** *Aaron Pedigo*<sup>1</sup>; Patrick Cantwell<sup>1</sup>; John Blendell<sup>1</sup>; Carol Handwerker<sup>1</sup>; <sup>1</sup>Purdue University

The spontaneous growth of surface defects, including whiskers and hillocks, on lead-free tin electroplated films is believed to be a stress relief phenomenon. Previous research has shown that it is possible to plate pure tin and observe only hillock growth. Whisker growth, however, can be biased over hillock growth with the addition of copper contamination to the electrolyte. In this work, hillock and whisker growth was correlated to measured stress in electroplated tin and tin-copper films using cantilever beams. Cross-sections and morphologies of these defects were observed using SEM and FIB. A transition in short-term film behavior between 0.5 and 1.3% copper in the film was characterized by an increase in plating stress, long-term stress, and propensity to whisker. A transition in hillock morphology was also observed. These results support a growth model where the ratio of surface uplift to grain boundary motion determines defect type.

### 5:20 PM

**IMC Formation to Block Whisker and Hillock Growth in Lead-Free Flip-Chip Solder Joints under Electromigration:** *Shih-Wei Liang*<sup>1</sup>; Chih Chen<sup>1</sup>; J. K. Han<sup>2</sup>; Luhua Xu<sup>2</sup>; K. N. Tu<sup>2</sup>; <sup>1</sup>National Chiao Tung University; <sup>2</sup>UCLA

In this study, the flip chip was cross-sectioned for in-situ observation. At current density of  $1.3 \times 10^4$  A/cm<sup>2</sup> and at 100°C, we observed that the hillock squeezed out at the board side was more serious than the whisker grew at the chip side. Accompanying the hillock growth, the Cu-Sn IMCs were spread and grown in the anode after long stressing time. The distribution of IMC was investigated by a second cross-sectioning of the flip chip sample. We speculate that the board side has supplied enough copper to react with tin to form Cu<sub>6</sub>Sn<sub>5</sub>. The IMC may create compressive stress to form the hillocks. However, the excess IMC formed in the tin grain boundaries may block the diffusion path of Sn and slow down the growth of tin whisker and hillock. Our results show that the more IMC formation, the slower hillock and whisker growth.

### 5:35 PM

**Stress-Strain Behavior of Pb-Free Solders over Strain Rates Ranging from 10<sup>-6</sup>/s to 10<sup>2</sup>/s:** *Xu Nie*<sup>1</sup>; Dennis Chan<sup>1</sup>; Weinong Chen<sup>1</sup>; Ganesh Subbarayan<sup>1</sup>; Indranath Dutta<sup>2</sup>; <sup>1</sup>Purdue University; <sup>2</sup>Washington State University

An important need in predicting the reliability of electronic systems is to quantitatively understand the mechanical response of Pb-free solder joints to external loads ranging from creep to shock. In this research, we describe mechanical tests on Pb-free solders over a strain-rate range from 10<sup>-6</sup>/s to 10<sup>2</sup>/s using both quasi-static mechanical testers and a modified split Hopkinson pressure bar. Loading conditions in the dynamic experiments were controlled to subject the specimens to desired (constant) strain rates. We compare the saturation stress resulting from high-strain rate tests to that from previously conducted low-strain rate tests. We describe creep and viscoplastic constitutive models fit to the experimental data over nine decades of strain rates with reasonable agreement.

### 5:50 PM

**Stress Relaxation Behavior in Sn and Pb-Sn Layers and Its Relation to Whiskering:** *Jae Shin*<sup>1</sup>; Eric Chason<sup>1</sup>; <sup>1</sup>Brown University

We have used real-time wafer curvature measurements to study the relaxation kinetics of thermally-induced stresses in Sn and Pb-Sn thin films. We find that the relaxation behavior in Sn is well-described by a power law creep mechanism, with an exponent similar to that found in bulk Sn. However, the yield stress of the thin film is much higher than that of the bulk material. Additionally, the relaxation kinetics are thickness dependent so that thick layers relax more quickly than thin layers. Pb-Sn layers exhibit even faster relaxation behavior than pure Sn layers. The implications of the relaxation kinetics for whisker formation and mitigation will be discussed.

## Peirce-Smith Converting Centennial Symposium: New Converting Technologies

Sponsored by: The Minerals, Metals and Materials Society, TMS Extraction and Processing Division, TMS: Pyrometallurgy Committee  
Program Organizer: Joël Kapusta, Air Liquide

Tuesday PM  
February 17, 2009

Room: 2009  
Location: Moscone West Convention Center

*Session Chairs:* Joël Kapusta, Air Liquide; Theo Lehner, Boliden Mineral AB

### 2:00 PM Keynote

**Continuous Converting of Copper Matte in Packed Bed Reactor:** *Andrzej Warczok*<sup>1</sup>; Gabriel Riveros<sup>1</sup>; Juan Vargas<sup>2</sup>; Roberto Saez<sup>2</sup>; Arturo Tapia<sup>3</sup>; <sup>1</sup>Universidad de Chile; <sup>2</sup>ENAMI; <sup>3</sup>PYROS INGENIEROS SA

The new process of continuous converting of copper matte directly to blister copper in a packed bed reactor is an attractive option due to its very low investment cost, flexibility of operation with a liquid, solid or liquid and solid copper matte charge. Based on fundamental measurements of the rate of matte oxidation, the mathematical model of matte converting in the ceramic packed bed has been developed. The alumino-olivine slag has been chosen because the auto-melting properties of the mix of fluxes: clay, quartz and lime. The results of tests in the laboratory demonstrative installation showed process feasibility and effective matte oxidation up to the production of over-oxidized copper. Currently, the installation of an industrial-pilot plant with a capacity of 5 t/h of copper matte is completed.

### 2:30 PM

**Scrap Melting in the Anode Furnace and the Development of Coherent Jet Technology in Copper Refining:** *Adrian Deneys*<sup>1</sup>; A. Enriquez<sup>2</sup>; <sup>1</sup>Praxair Inc; <sup>2</sup>Rio Tinto Kennecott Utah Copper

Kennecott Utah Copper Corporation and Praxair have worked to develop a new oxy-fuel burner and gas injection system for copper anode refining. The system provides the capability to melt 60 to 70 tons of scrap copper per heat with acceptable NOx emissions. This paper will describe the process concept, system development, plant design, laboratory testing, equipment hardware, full-scale implementation, and current operation of the new system.

### 2:50 PM

**Advantages of Continuous Copper Fire Refining in a Packed Bed:** *Gabriel Riveros*<sup>1</sup>; Andrzej Warczok<sup>1</sup>; Daniel Smith<sup>2</sup>; Ariel Balocchi<sup>2</sup>; <sup>1</sup>Universidad de Chile; <sup>2</sup>ENAMI

Blister copper from converting of copper matte is processed in fire refining prior to electrorefining. The fire refining consists of two steps: copper oxidation with impurities slagging and copper reduction. The classical batch process is carried out in vascular or reverberatory furnaces called anode furnace. The new process of continuous copper fire refining has been proposed. The copper flows through two reactors in cascade, where is oxidized and reduced. The flow of a liquid copper through a ceramic packed bed increases the surface area and the rate of oxidation as well as the rate of reduction in the packed bed of charcoal. Mathematical model allowed for design a laboratory scale demonstrating installation and industrial-pilot installation in Hernan Videla Lira Smelter (Paipote). The results demonstrated the process feasibility and flexibility in operation.

### 3:10 PM

**The Validation of the Codelco-Chile Continuous Converting Process:** *Alex Moyano*<sup>1</sup>; Carlos Caballero<sup>1</sup>; Claudio Toro<sup>2</sup>; Pedro Morales<sup>1</sup>; Jonkion Font<sup>2</sup>; <sup>1</sup>CODELCO - Chile; <sup>2</sup>IM2

Codelco-Chile in about a decade has carried out industrially-oriented research as an alternative to the traditional batch-type converting process. In a first stage, carried out preliminary evaluations in a rearranged PS converter, and then, an exploratory test in a CT (Teniente Converter) for the Codelco-Chile Continuous Converting Process. However, the validation test for this process in the CT, was delayed up to the second quarter of 2007 where the validation studies were started. Hence, the objective of this paper is to present the results of the campaign tests validating the Codelco-Chile Continuous Converting Process in the CT1 of the Codelco Norte smelter. The results of charging the solid or liquid matte or "white metal" by garr-gun, or by mouth of the 22 m x 5 m CT1 are presented.

Some features of the industrially validated process are discussed, and the pilot test results of the matte injection are also presented.

### 3:30 PM Break

### 3:50 PM

**Continuous Improvement in Peirce-Smith Converter Design - Kumera's Approach:** *Shaolong Chen*<sup>1</sup>; Hannu Mansikkaviita<sup>1</sup>; Markku Rytkonen<sup>1</sup>; Ilpo Kylmäkorpi<sup>1</sup>; <sup>1</sup>Kumera Technology Center

Though the Peirce Smith (P-S) converter is a traditional type of furnace, continuous improvement in its mechanical and electrical design is still Kumera's approach. Efforts are made particularly on the following aspects: converter head shape for easy fabrication and structural strengthening, oxidation air swivel joint for low pressure drop and low noise level, wind box for even air distribution to tuyeres, drive unit and its control for reliable and handy operation. These improvements have successfully been applied in recent P-S converter deliveries.

### 4:10 PM

**Operation of the Air Liquide Shrouded Injector (ALSI) Technology in a Hoboken Siphon Converter:** *Romeo Pagador*<sup>1</sup>; Noparut Wachgama<sup>1</sup>; Chumnoon Khuankla<sup>1</sup>; Joel Kapusta<sup>2</sup>; <sup>1</sup>Thai Copper Industries Public Company Limited; <sup>2</sup>Air Liquide Canada Inc

Thai Copper Industries (TCI) is a custom copper smelter and refinery in Rayong, Thailand, with an annual capacity of 165,000 tons of cathodes. It employs the El Teniente Technology as the primary smelting reactor to produce white metal from copper concentrates. The white metal is further treated in Hoboken Siphon Converters to produce blister copper then refined in anode furnaces before being cast into anodes for electro-refining in the on-site tankhouse. Thai Copper Industries is the first copper smelter to install and successfully operate on a commercial scale with the Air Liquide Shrouded Injection (ALSI™) Technology in the Hoboken converters with sonic injection of oxygen enriched air and nitrogen for cooling of the injector tip areas. Following commissioning and the establishment of operating practices, the performance of the Hoboken converters with ALSI™ Technology produced outstanding results. The unique combination of an El Teniente and Hoboken siphon converters, both of which are bath smelting operations, offers very high blowing and oxygen efficiencies. As a consequence, reverts recycling was accelerated with minimal build up on the mouth, end-plates or even below the siphon that is typical in Hoboken converters. These outstanding results in the Hoboken Siphon Converters with ALSI™ Technology helped the TCI Plant reach a production of about 75% of its capacity within four months despite the fact that the TCI staff is quite young and its converter know-how and experience are not yet fully developed.

### 4:30 PM

**Flash Converting - Sustainable Technology Now and in the Future:** *Ilkka Kojo*<sup>1</sup>; *Markku Lahtinen*<sup>1</sup>; Elli Miettinen<sup>1</sup>; <sup>1</sup>Outotec Oyj

The recent trends of decreasing energy consumption and environmental emissions and utilization of economies of scale are strong drivers favoring continuous copper converting processes. Flash Converting benefits from low off-gas volumes and low investment and operational costs for off-gas treatment. Separate matte and blister furnaces allow the adaptation to concentrate quality changes and flexibility in layout and maintenance. The stationary blister copper bath in Flash Converting furnace is less aggressive to the furnace linings than agitated processes, resulting in low refractory consumption, long campaign life and high on-line availability. Copper Flash Converting has been successfully applied in Kennecott with a campaign life now exceeding five years. A second FCF was started at Xiangguang Copper in China in 2007. The process itself is proven, as its features are similar to those in FSF, Direct-to-Blister and Direct Outotec Nickel Flash Smelting (DON), with one significant difference: it is the easiest of all to operate. The paper presents differences between continuous Flash Converting and conventional converting based on recent experiences and studies.

### 4:50 PM

**Ausmelt C3 Converting:** *Jacob Wood*<sup>1</sup>; Robert Matuszewicz<sup>1</sup>; Markus Reuter<sup>1</sup>; <sup>1</sup>Ausmelt Limited

Over the last 20 years, significant improvements in copper smelter productivity have been realized through the advent of continuous smelting processes. This progress has until recently however, not been carried through to copper converting. Peirce-Smith converting has been widely used by the copper industry for 100 years but is limited by its batch nature in achieving large scale

of production. A logical next step is therefore copper converting on a continuous basis with its inherent environmental benefits. A number of continuous converting technologies are currently in use or being developed within the copper industry, the majority of these operating with calcium-ferrite slags. A notable exception however is the Ausmelt Continuous Copper Converting (C3) technology which has focused on operation with ferrous-calcium-silicate or loosely called olivine type slags. This paper discusses the merits of the Ausmelt C3 process and the advantages offered in terms of operational flexibility and process control arising from the use of lime modified iron silicate slags. It also examines the effects of key process variables pertinent to continuous copper converting from both a theoretical and experimental/operational perspective.

## 5:10 PM

**ISACONVERT™ – TSL Continuous Copper Converting Update:** *Stanko Nikolic*<sup>1</sup>; James Edwards<sup>1</sup>; Alistair S. Burrows<sup>1</sup>; Gerardo R.F. Alvear<sup>1</sup>; <sup>1</sup>Xstrata Technology

The copper ISASMELT™ process has evolved over more than a quarter of a century and can now be considered mainstream, with single furnaces producing more than 340,000 tpa of copper in matte. The next evolutionary step for the ISASMELT™ technology is to directly challenge the dominance of the Peirce-Smith converter by the implementation of a continuous copper converting process on a commercial scale. The present work describes the status of the continuous converting process – ISACONVERT™. Continuous converting has been performed successfully in pilot scale ISACONVERT™ plants, where operating results have verified the predictions of fundamental research and reinforced the underlying confidence in the design parameters. From a matte feed rate of 250 kg/hr, a calcium ferrite slag and a low-sulfur blister have been produced. Design is now complete for the first commercial application of the ISACONVERT™ process. The present paper describes the status of ISACONVERT™ by summarising results of recent pilot plant tests and describing the first commercial plant design.

## 5:30 PM Keynote

**What Got Us Here Won't Get Us There!:** *Tony Eltringham*<sup>1</sup>; <sup>1</sup>BHP Billiton Base Metals

A brief look at the future interspersed with personal stories from the past.

## 6:00 PM Closing Remarks

## Phase Stability, Phase Transformations, and Reactive Phase Formation in Electronic Materials VIII: Session IV

Sponsored by: The Minerals, Metals and Materials Society, TMS Electronic, Magnetic, and Photonic Materials Division, TMS: Alloy Phases Committee  
 Program Organizers: Chih-ming Chen, National Chung-Hsing University; Srinivas Chada, Medtronic; Sinn-wen Chen, National Tsing-Hua University; Hans Flandorfer, University of Vienna; A. Lindsay Greer, University of Cambridge; Jae-ho Lee, Hongik University; Daniel J. Lewis, Rensselaer Polytechnic Institute; Kejun Zeng, Texas Instruments; Wojciech Gierlotka, AGH University of Science and Technology; Yee-wen Yen, National Taiwan University of Science and Technology

Tuesday PM  
 February 17, 2009

Room: 2022  
 Location: Moscone West Convention Center

*Session Chairs:* Clemens Schmetterer, University of Vienna; Yee-wen Yen, National Taiwan University of Science and Technology

## 2:00 PM Invited

**Interesting Phenomena Observed in the Sn/Co Interfacial Reactions:** *Sinn-wen Chen*<sup>1</sup>; Chao-hong Wang<sup>2</sup>; <sup>1</sup>National Tsing Hua University; <sup>2</sup>National Chung-Cheng University

The CoSn<sub>3</sub> phase was formed along the Sn/Co interface in the Sn/Co couples reacted at 150 to 200°C. The reaction layers grew linearly with reaction time in the early stage, and then it changed to a parabolic growth when the layer reached a critical thickness. However, at the corners of the Co substrates in the Sn/Co couples, the reaction phase was the CoSn<sub>4</sub> phase at 180°C; cracking was observed and there were no reaction phases at 200°C. The reaction phase layer showed a unique cruciform pattern. The cruciform pattern was formed either by cracking or transformation to the CoSn<sub>4</sub> phase at the corners where stress was

most intensified. With the passage of electric current from the Co toward the Sn side, the CoSn<sub>3</sub> phase was thicker than that without the passage of electric current. A significant Peltier effect has been observed which is responsible for the different reaction layer growth.

## 2:20 PM

**Solid/Solid Interfacial Reactions between Sn and Ni-Co Alloys:** *Chih-chi Chen*<sup>1</sup>; Jenq-Gong Duh<sup>2</sup>; Sinn-wen Chen<sup>2</sup>; <sup>1</sup>Chung Yuan Christian University; <sup>2</sup>National Tsing Hua University

Nickel is a commonly used barrier layer material of under bump metallurgy (UBM) in flip chip packaging because of its low reactivity with solders. Tin is the primary constituent element of solders. Recent investigations indicate cobalt is a potential diffusion barrier material for copper. Therefore, Ni-Co alloys are potential diffusion barrier materials of UBM for integrated circuits (I.C.) with Cu/low k process. There have been some studies upon Sn/Co and Sn/Ni-Co interfacial reactions. However, Sn/Ni-Co interfacial reactions at solid state have not been examined. This work investigates the interfacial reactions between Sn and Ni-Co alloys at solid state. Reactions at 120, 150 and 200°C are carried out, and the compositions of Ni-Co alloys examined are Ni-5at%Co, Ni-20at%Co and Ni-40at%Co, respectively. The preliminary experimental result shows that a meta-stable phase, Co<sub>3</sub>Sn<sub>7</sub>, is formed. Based on the available Sn-Ni-Co isothermal section, the reaction paths of the Sn/Ni-Co couples can be determined.

## 2:35 PM

**Interfacial Reaction between Sn Solder and NiCo UBM:** *JyunWei Cheng*<sup>1</sup>; Chengyi Liu<sup>1</sup>; <sup>1</sup>National Central University

Cu-based UBM has been widely used in the electronic package. During soldering, Cu would dissolve seriously into the molten solder, which would cause reliability issue of the solder joints. Therefore, a reaction barrier often requires to prevent the fast reaction between solder and Cu pad. Ni(P) is the one used as the reaction barrier layer for last decade. Ni(P) also cause many reliability issues, for example, black pad and Ni<sub>3</sub>P crystalline layer formation. In the work, we study soldering reaction between Ni-Co alloy layer and Sn Pb-free solders. Different Co concentrations in Ni-Co alloy layer were electroplated on Cu foils. Then, Sn solders were reflowed on the Ni-Co alloy layers to investigate the interfacial reactions. We found that different Co concentration in Ni-Co alloy layers will result in different the reaction phase at the interface. The formation kinetics of Ni-Co-Sn ternary intermetallic compound (IMCs) at the interface will be reported.

## 2:50 PM

**A Study of Interfacial Reaction between Molten Sn-Ag Solder and Te Substrate:** *Yen-Chun Huang*<sup>1</sup>; Chien-Neng Liao<sup>1</sup>; <sup>1</sup>National Tsing Hua University

Telluride-based thermoelements can react with Sn-contained solders and form SnTe intermetallic compounds that may deteriorate electrical and mechanical properties of soldered junctions. In addition to Ni barrier approach, we may also change the recipe of solder alloys to suppress or slow down the formation of SnTe compounds. In this study the effect of Ag addition (0.1, 1, 3.5, 5 wt%) in pure Sn on the interfacial reaction between molten solder and Te substrate is explored. It is found that the thickness of SnTe compound is reduced after soldering reaction when Ag is added into Sn solder. The suppression of SnTe compound formation may be associated to the presence of Ag<sub>3</sub>Te<sub>2</sub> and Ag-Sn-Te ternary compounds that are located in between the SnTe compound and the Te substrate. Besides, the thickness of the planar-type Ag<sub>3</sub>Te<sub>2</sub> compound is found to increase with increasing Ag content.

## 3:05 PM

**Effect of Cu Addition in Sn Solder on the Interfacial Reaction with Elemental Te Substrate:** *Ching-Hua Lee*<sup>1</sup>; Chien-Neng Liao<sup>1</sup>; <sup>1</sup>National Tsing Hua University

Conventional telluride based thermoelectric elements can easily react with Sn-contained solder and form SnTe intermetallic compounds. The interfacial compounds are rather brittle and may lead to the failures of the soldered junctions under normal heating-to-cooling operations. Thus, modification of solder alloy recipe may suppress the interfacial compound formation. In this study the reaction of pure Te elements with Sn(Cu) molten solder is explored. The preliminary results showed that a tiny amount of Cu addition can suppress the vigorous Sn/Te interfacial reaction effectively. Moreover, a compound phase, CuTe, tends to form in between the SnTe phase and the Te substrate. The effect



of Cu content in Sn(Cu) solder alloy on the growth mechanism of SnTe and CuTe interfacial compounds will be investigated. The influence of the interfacial compounds on the electrical properties of the soldered junction is also a subject of interests.

### 3:20 PM Break

### 3:40 PM Invited

**Interfacial Reactions and Microstructures of Sn-0.7Cu-xZn Solders with Ni-P UBM during Thermal Aging:** Moon Gi Cho<sup>1</sup>; Sung K. Kang<sup>2</sup>; Da-Yuan Shih<sup>2</sup>; Hyuck Mo Lee<sup>1</sup>; <sup>1</sup>Korea Advanced Institute of Science & Tech; <sup>2</sup>IBM T.J. Watson Research Center

The effects of Zn addition to Sn-0.7Cu are investigated, focusing on their interfacial reactions, microstructure and hardness when reacted with Ni-P. The Zn content in Sn-0.7Cu-xZn varies as 0.2, 0.4 and 0.8 (in wt %). In the reaction with Ni-P, (Cu,Ni)<sub>6</sub>Sn<sub>5</sub> intermetallic compounds(IMCs) are formed at the interface, regardless of the Zn content. As the Zn content increases, the growth of (Cu,Ni)<sub>6</sub>Sn<sub>5</sub> during aging is gradually reduced, yielding a reduction of 40-50% for 0.8% Zn. (Cu,Ni)<sub>6</sub>Sn<sub>5</sub> IMCs are also commonly observed in the solder matrix. In Sn-0.7Cu, (Cu,Ni)<sub>6</sub>Sn<sub>5</sub> particles coarsen largely during aging, while in the Zn-added solders, they are much smaller initially and resistant to growth. This explains the stable microhardness of the Zn-added solders during aging. To understand the (Cu,Ni)<sub>6</sub>Sn<sub>5</sub> IMCs formed in the Zn-added solders, TEM studies are conducted. The microstructure and hardness of the Zn-added solders are further discussed with thermodynamic calculations and analytical works.

### 4:00 PM

**TEM Observations of Cu<sub>3</sub>Sn Growth at SnBi/Cu Interface:** P. Shang<sup>1</sup>; Z. Liu<sup>1</sup>; J. Shang<sup>2</sup>; <sup>1</sup>Institute of Metal Research; <sup>2</sup>University of Illinois at Urbana-Champaign

Transmission electron microscopy (TEM) studies were made to observe the growth of Cu<sub>3</sub>Sn intermetallic phase at SnBi/Cu interface during reflow and solid-state aging process. Two types of Cu-Sn intermetallics, Cu<sub>6</sub>Sn<sub>5</sub> and Cu<sub>3</sub>Sn, were found at the interface after reflow. In the early stage of solid state aging, Cu<sub>3</sub>Sn assumed columnar growth grains along [100] direction of Cu. With further aging, new triangle Cu<sub>3</sub>Sn grains were uncleaned at the triple junction sites of Cu/Cu<sub>3</sub>Sn interface, resulting in two distinct Cu<sub>3</sub>Sn layers between Cu and Cu<sub>6</sub>Sn<sub>5</sub> layer. Along the Cu<sub>3</sub>Sn/Cu interface, Bi segregation was detected following prolonged solid-state aging.

### 4:15 PM

**Oscillatory Growth of the Ni<sub>3</sub>Si<sub>2</sub> Intermetallic Compound in Reactive Interdiffusion of Thin Ni film on Si substrate:** Delphine Borivent<sup>1</sup>; Bernard Billia<sup>1</sup>; <sup>1</sup>IM2NP

The formation of Ni<sub>3</sub>Si<sub>2</sub> in solid-state reactive diffusion of a Ni film deposited on a <100>-oriented silicon substrate was followed in time by Bragg-Brentano X-ray diffraction, and further investigated by X-ray microdiffraction, optical and scanning electron microscopy. Concentric rings form from nucleation centres in the lateral propagation of the Ni<sub>3</sub>Si<sub>2</sub> phase revealing an oscillatory growth velocity. Similar ripples have already been observed in the explosive crystallization of amorphous films of Si. Yet, the propagation of the Ni<sub>3</sub>Si<sub>2</sub> front is too slow for heat-transport control to hold, which suggests that it is rather the diffusion of chemical species that is driving the patterning of the Ni<sub>3</sub>Si<sub>2</sub> phase into concentric rings. The synthesis of the experimental data allows us to propose a model the Bradley's way (R.M. Bradley, J. Appl. Phys. 60 (1986) 3146) based on a source-sink mechanism for silicon possibly leading to oscillatory instability of disk growth of Ni<sub>3</sub>Si<sub>2</sub>.

### 4:30 PM

**Interfacial Reaction Effect on Mechanical and Electrical Reliability in Cu Pillar Bump:** Gi-Tae Lim<sup>1</sup>; Byoung-Joon Kim<sup>2</sup>; Ki-Wook Lee<sup>3</sup>; Jae-Dong Kim<sup>3</sup>; Young-Chang Joo<sup>2</sup>; Young-Bae Park<sup>1</sup>; <sup>1</sup>Andong National University; <sup>2</sup>Seoul National University; <sup>3</sup>Amkor Technology Korea, Inc.

Flip chip solder bump has been widely used as a key interconnection technology of high performance devices. As the integration of devices increased, the size of solder bump became smaller with fine pitch. And increase of current density due to miniaturization of solder bump size with fine pitch causes serious reliability issues. Cu pillar bump is one of candidates to solve reliability issues because it provides the fine pitch and uniform current distribution. However, excessive intermetallic compound and Kirkendall void growth in Cu pillar bump can degrade the mechanical reliability of solder joints. Therefore, it is necessary to understand the growth kinetics of intermetallic compound and Kirkendall

void of Cu pillar bump. In this work, intermetallic compound and Kirkendall void growth kinetics in Cu pillar bump have been studied using in-situ scanning electron microscope during annealing and electromigration. Also, their effects on the mechanical reliability will be discussed in detail.

### 4:45 PM

**Analysis of Sintering Aids for High Melting Rare Earth-Iron-Boron Magnet Alloys:** Nathaniel Oster<sup>1</sup>; Iver Anderson<sup>2</sup>; Wei Tang<sup>2</sup>; Yaqiao Wu<sup>2</sup>; Kevin Dennis<sup>2</sup>; Matthew Kramer<sup>2</sup>; R. McCallum<sup>2</sup>; <sup>1</sup>Iowa State University; <sup>2</sup>Ames Lab

Many Rare Earth (RE)-Iron-Boron magnet alloys display a relatively low-melting (650-700°C) ternary eutectic. Nd-Fe-B is among these. The liquid formed during the eutectic promotes sintering of the particulate through processing of aligned, fully-dense sintered magnets. However, several alternative RE-Fe-B magnet alloys, such as Dy-Fe-B, do not exhibit this low-melting eutectic. Since the dominant RE<sub>2</sub>Fe<sub>4</sub>B phase in such particulate is a brittle intermetallic that melts much higher (about 1250°C), solid state sintering is difficult. Cu-base, Al-base, and Nd-Fe alloys have been proposed as possible systems that could be added to the magnet particulate in order to aid sintering. The wetting, bonding, and diffusive interaction of these alloys with a RE-Fe-B magnet alloy particulate will be the object of microstructure analysis of the sintered compacts by SEM, X-ray diffraction, and electron microprobe. Additionally, magnetic properties of the sintered magnets will be measured. Supported by DOE-EERE-FCVT Office through Ames Lab contract DE-AC02-07CH11358.

## Recycling of Electronic Wastes: General Recycling

Sponsored by: The Minerals, Metals and Materials Society, TMS Extraction and Processing Division, TMS Light Metals Division, TMS Materials Processing and Manufacturing Division, TMS: Recycling and Environmental Technologies Committee  
Program Organizers: Lifeng Zhang, Missouri University; Fay Hua, Intel Corp; Oladele Ogunseitan, University of California, Irvine; Gregory Krumdick, Argonne National Laboratory

Tuesday PM

Room: 2024

February 17, 2009

Location: Moscone West Convention Center

Session Chair: Fay Hua, Intel Corp

### 2:00 PM Introductory Comments

### 2:05 PM

**Assessment of Public Health Impacts of Open Air Incineration of Electronic Wastes:** Kathleen Hibbert<sup>1</sup>; Oladele Ogunseitan<sup>1</sup>; <sup>1</sup>University of California, Irvine

Electronic waste (E-waste) is the fastest growing source of hazardous solid waste. Americans discarded about 2 million tons of E-waste annually. The U.S. lacks comprehensive federal policies to reduce toxic materials in electronics manufacturing or for E-waste disposal. Furthermore, the U.S. is not a signatory to international regulation of transboundary shipment of hazardous waste, posing risks in developing countries, where waste processing is decentralized. Studies conducted by US EPA suggested that incineration of e-waste emits polybrominated dibenzofurans (PBDFs), and toxic metals such as lead, cadmium, copper, manganese and beryllium. We are analyzing potentially toxic exposures from incineration of cellular phones because they contain analogous components for generic e-waste. A representative sample of 100 cellular phones is being tested under conditions simulating open-air incineration. Emitted gases and ash residue will be analyzed for priority pollutants according to Occupational Safety and Health Administration standards, and the Clean Air Act.

### 2:25 PM Question and Answer Period

### 2:35 PM

**Separation of Nickel, Cobalt and Magnesium from the Spent Mn-Ni and Cd-Ni Battery Anode Materials:** Xu Shengming<sup>1</sup>; Wang Gehua<sup>2</sup>; Zhang Lifeng<sup>3</sup>; Li Linyan<sup>2</sup>; Xu Gang<sup>2</sup>; Liu Xiaobu<sup>2</sup>; <sup>1</sup>Tsinghua University; <sup>2</sup>Tsinghua University; <sup>3</sup>Missouri University of Science and Technology

Reductive leaching kinetics of LiCoO<sub>2</sub> from spent lithium ion battery were investigated in sulfur acid solutions. The leaching efficiency of LiCoO<sub>2</sub> increased with increasing temperature, and concentration of H<sub>2</sub>SO<sub>4</sub>, but with increasing the ratio of liquid to solid. With the addition of H<sub>2</sub>O<sub>2</sub> or Na<sub>2</sub>SO<sub>3</sub> as a reducing agent, the leaching efficiency of Li and Co from LiCoO<sub>2</sub> can obtain over 95%

due to the reduction of Co<sup>3+</sup> to Co<sup>2+</sup> which can be readily dissolved. Apparent activation energies in the two reductive leaching systems were obtained for Co and Li, respectively.

## 2:55 PM Question and Answer Period

### 3:05 PM

**LCD (Liquid Crystal Display) Separation Aiming Recycling:** Viviane Tavares<sup>1</sup>; Jorge Tenório<sup>1</sup>; Denise Espinosa<sup>1</sup>; <sup>1</sup>Escola Politécnica da Universidade de São Paulo

The liquid crystal display (LCD) are currently known by its vast application in electro – electronic devices, amongst them can be detached the TV's devices, laptops, electronic date, calculators and even though the mobile. The mobiles are changed more frequent of the TV, this happens due to the technology advance. With the constantly mobile exchange, the batteries, printed circuit board and liquid crystal display accumulation its become an environmental problem. To minimize the environmental impacts caused by mobile telephones residues are considered the segregation process of the LCDs main components, to goal to recover the recycle material. This process involves the use of treatment ore techniques with disc, hammers and balls mills. The glass recovered can be used in the glass recycling and the sand substitution in the production of concrete blocks. Key words: liquid crystal display, recycling, electro-electronic.

## 3:25 PM Question and Answer Period

### 3:35 PM

**Evaluation of Alkaline Battery End-of-Life Strategies:** Elsa Olivetti<sup>1</sup>; Edgar Blanco<sup>1</sup>; Jeffrey Dahmus<sup>1</sup>; Jeremy Gregory<sup>1</sup>; Randolph Kirchain<sup>1</sup>; <sup>1</sup>MIT

Approximately 80% of batteries manufactured worldwide are so-called alkaline dry cells with a global annual production exceeding 10 billion units. Today, the majority of these batteries go to landfills at end-of-life. An increased focus on environmental issues related to battery disposal, along with recently implemented battery directives in Europe and Canada, has intensified discussions about end-of-life battery regulations globally. The logistics of battery collection are intensive given the large quantity retired annually, their broad dispersion, and the small size of each battery. Careful evaluation of the economic and environmental impacts of battery recycling is critical to determining the conditions under which recycling should occur. This work compares a baseline scenario involving landfilling of alkaline batteries as municipal solid waste with several collection schemes for battery recycling through pyrometallurgical material recovery. Network models and life cycle assessment methods enable the evaluation of various end-of-life collection and treatment scenarios for alkaline batteries.

## 3:55 PM Question and Answer Period

### 4:05 PM

**Green Recycling of EEE: Special and Precious Metal Recovery from EEE:** Christina Meskers<sup>1</sup>; Christian Hagelueken<sup>1</sup>; <sup>1</sup>Umicore

EEE contains a range of components made of a wide variation of metals, plastics and other substances. Over 40 elements can be found in complex electronic equipment: base metals, precious metals and special metals in circuit boards and batteries. Because of its amount WEEE represents a considerable metal resource with a higher special and precious metal content than found in ores. The Umicore integrated smelter and refinery recovers and supplies back to the market 17 different metals from EEE. Pre-treated materials enter state of the art, material and energy efficient metallurgical processes for environmentally sound recovery of metals and treatment of off gasses and hazardous substances. The organics in the feed function as reducing agent and alternative energy source during smelting for precious metal recovery. Lithium-ion batteries are treated using a dedicated process. As a result the environmental footprint of metals produced from EEE is much smaller than primary production.

## 4:25 PM Question and Answer Period

### 4:35 PM

**Research on the Recovery of Organic Acid from Cyclohexanone Waste:** Daowu Yang<sup>1</sup>; Linping Yu<sup>1</sup>; Ping Yu<sup>2</sup>; Yunbai Luo<sup>2</sup>; <sup>1</sup>Changsha University of Science and Technology; <sup>2</sup>Wuhan University

A simplified ED process was developed for organic acids recovery from cyclohexanone waste in this paper. In this regard, the one-stage ED was investigated directly without pretreatment, such as ion-exchange or nanofiltration to removal of foulants. The current efficiency and the energy consumption in the

ED process for the recovery of carboxylic acids from cyclohexanone waste is theoretically analyzed and experimentally tested. The concentration of recovered carboxylic acid is related to many parameters and still needs more work to be determined.

## 4:55 PM Question and Answer Period

## Shape Casting: Third International Symposium: Novel Methods and Applications

Sponsored by: The Minerals, Metals and Materials Society, TMS Light Metals Division, TMS: Solidification Committee, TMS: Aluminum Processing Committee  
Program Organizers: John Campbell, University of Birmingham; Paul Crepeau, General Motors Corp; Murat Tiryakioglu, Robert Morris University

Tuesday PM

Room: 2011

February 17, 2009

Location: Moscone West Convention Center

Session Chair: Mahi Sahoo, CANMET Materials Technology Laboratory

## 2:00 PM Introductory Comments

### 2:10 PM

**Ablation Casting Update:** John Grassi<sup>1</sup>; John Campbell<sup>1</sup>; Martin Hartlieb<sup>2</sup>; Fred Major<sup>2</sup>; <sup>1</sup>Alotech Limited; <sup>2</sup>Rio Tinto Alcan

Light alloy castings made in an aggregate mold are ablated with coolant to erode away the mold by dissolving the mold binder. The coolant thereby gains access to the surface of the casting prior to extensive solidification, avoiding normal limitations to heat transfer via the 'air gap', and thus confers otherwise unattainable rates of cooling. The process was first announced at the previous TMS Annual Congress, and is here updated after this additional year. The unique structures and properties are described.

### 2:35 PM

**The Nemak Cosworth Casting Process - Innovation:** Glenn Byczynski<sup>1</sup>; Robert Mackay<sup>2</sup>; <sup>1</sup>Nemak Europe GmbH; <sup>2</sup>Nemak Canada

The Cosworth Process is well recognized for its ability to produce high quality, dimensionally accurate aluminum castings. The process was designed from first principles with casting quality as the main focus. Ford transformed this process into a high volume production system in the early 1990's at its Windsor Aluminum Plant and this plant continues to manufacture world-class aluminum cylinder block castings today as Nemak Canada. The one drawback (if any) of the original process is the resultant microstructure due to the relatively slow solidification rate in heavy sections in the sand mould. The secondary dendrite arm spacing combined with typical automotive grade alloys limits the mechanical properties in certain areas of the casting. The innovation discussed in this paper is an augmentation of the original Cosworth Process to include an integral chill that increases local solidification rates and drives casting performance to new levels.

### 3:00 PM

**Development of an Aluminum Alloy for Elevated Temperature Applications:** Kumar Sadayappan<sup>1</sup>; David Weiss<sup>2</sup>; Mahi Sahoo<sup>1</sup>; Gerald Gege<sup>3</sup>; <sup>1</sup>CANMET - Materials Technology Laboratory; <sup>2</sup>Eck Industries; <sup>3</sup>Material and Process Technologies

The need to reduce the exhaust emissions of medium and heavy-duty diesel engines has lead to the use a two-stage series turbocharger design for the air system. The current single stage compressors run at an outlet air temperature of approximately 175°C at sea level. This is the approximate temperature limit for the currently used 354-T61 aluminum alloy impellers. The second stage outlet air temperatures are predicted to reach 260°C or higher at sea level conditions and this temperature will increase with altitude. The maximum operating temperature of most current structural aluminum alloys is about 200°C which is equal to their aging temperatures (approximately 200°C). Efforts were made to develop an Al-Cu alloy with scandium addition which is able to retain its strength at 250°C. The details of the alloy development and the results are presented and discussed in this publication.

3:25 PM

**Controlled Diffusion Solidification (CDS): Conditions for Non-Dendritic Primary Aluminum Phase Al-Cu Hypo-Eutectic Alloys:** Abbas Khalaf<sup>1</sup>; Peyman Ashtari<sup>1</sup>; Sumanth Shankar<sup>1</sup>; <sup>1</sup>LMCRC - McMaster University

Controlled Diffusion Solidification (CDS) is a novel process wherein a non-dendritic primary aluminum phase is obtained in Al-Cu hypo-eutectic alloys by controlled solidification of two precursor liquid alloys and casting the resultant alloy. In CDS, the non-dendritic primary Al phase will enable a continuous network of inter-dendritic liquid during solidification of the mushy zone, thereby mitigating the hot-tearing tendencies typically exhibited by Al-Cu alloys with low solute concentrations. Hence, the process will enable near-net shaped casting of Al-Cu based wrought alloy compositions which exhibit superior mechanical and performance properties. In this paper, a hypothesis explaining the complex mechanism of nucleation and growth of the primary Al phase to result in a non-dendritic morphology will be presented. Critical parameters such as temperatures, mass ratios and rate of mixing of the two precursor liquids to obtain various compositions of Al-Cu hypo-eutectic alloys will be presented to support the suggested mechanism.

3:50 PM Break

4:00 PM

**Favorable Alloy Compositions and Melt Temperatures to Cast 2XXX and 7XXX Al Alloys by Controlled Diffusion Solidification (CDS):** Peyman Ashtari<sup>1</sup>; Gabriel Birsan<sup>1</sup>; Sumanth Shankar<sup>1</sup>; <sup>1</sup>LMCRC-McMaster University

Controlled diffusion solidification (CDS) is an innovative rheocasting (Semi-solid) processing route to obtain a cast part with a non-dendritic morphology of the primary Al phase. The process involves mixing two alloy melts with specific individual compositions and temperatures to produce the desired final alloy by mixing and immediately casting in a mold. The process enables the shape casting of Al based wrought alloy along with their superior cast properties and performance. The present work defines process conditions to enable shaped casting of the 2XXX and 7XXX series of Al based wrought alloys, specifically, 2024, 7005 and 7075 alloys.

4:25 PM

**The Application of Positron Emission Particle Tracking (PEPT) to Study the Movement of Inclusions in Shape Castings:** William Griffiths<sup>1</sup>; Y. Beshay<sup>2</sup>; D. J. Parker<sup>1</sup>; X. Fan<sup>1</sup>; M. Hausard<sup>3</sup>; <sup>1</sup>University of Birmingham; <sup>2</sup>University of Birmingham - and - Beshay Steel; <sup>3</sup>Formerly of the University of Birmingham; currently at Centre de Calcul de l'Institut National de Physique Nucléaire et de Physique des Particules

Positron Emission Particle Tracking (PEPT) was used to track radioactive particles entrained into castings during mould filling. The purpose of these experiments was to test the technique for its application to the study of inclusion movement in castings, and so provide a method for validation of computer simulations of inclusion behaviour. Two types of experiments were carried out, one using Al alloy plate castings made in resin-bonded sand moulds, into which were entrained radioactive alumina particles of size 325 to 710  $\mu\text{m}$ . A second type of experiment used smaller alumina and resin particles, around 50 to 100  $\mu\text{m}$  in size, entrained into a low melting point In alloy, (Field's Metal), cast at 80°C into an acrylic die. In each experiment the particles locations were recorded in real time, using a positron detection camera. The particle paths were obtained for each casting and the reproducibility of the technique determined.

4:50 PM

**Microstructural and Surficial Characteristics of Lead Free Bismuth Bronze Produced through the Frozen Mold Casting Process:** Shuji Tada<sup>1</sup>; Hiroyuki Nakayama<sup>1</sup>; Toshiyuki Nishio<sup>1</sup>; Keizo Kobayashi<sup>1</sup>; <sup>1</sup>National Institute of Advanced Industrial Science and Technology

The frozen mold is a kind of sand mold which is produced by freezing the mixture of sand and water. The frozen mold casting process has the possibility to reduce the environmental load and the rapid cooling effect on cast products is expected. The effect of cooling rate on the microstructure of produced bronze cast was investigated. The frozen mold indicated better cooling property compared with conventional green sand mold. The microstructure of bronze cast produced through the frozen mold casting process was refined in the thinner sample but the quenching effect did not work well in the thicker sample. The surface condition of bronze cast was also examined. The surface of bronze cast produced using frozen mold consisting of only sand and water was rather rough. The surface roughness, however, was improved by adding colloidal silica solution into the sand mixture.

5:15 PM

**Pressure Mold Filling of Semi-Solid Ductile Cast Iron:** Bashir Heidarian<sup>1</sup>; Mahmoud Nili-Ahmadabadi<sup>1</sup>; Marzieh Moradi<sup>1</sup>; Jafar Rassizadeghani<sup>1</sup>; <sup>1</sup>University of Tehran

The processing of metals in the semi-solid state is becoming an innovative technology for the production of globular structure and high quality cast parts. Ductile irons because of spherical graphite have specific properties such as good mechanical properties, strength and toughness together and suitable castability. This engineering alloy along with growing application has several shortcoming which had limited its applications such as non-formability, dendritic structure and alloying element segregation, micro-porosity resulted from solidification mode and fabrication of thin section parts. It seems that replacing dendritic structure with globular structure and thixoforming, results in improving of mechanical properties, controlling of alloying element segregation, decreasing of micro-porosity and increasing of ability to thin section filling. In this paper high pressure mold filling of ductile iron contains Mn and Mo in semi-solid state has been investigated. Filling properties, fluidity, liquid segregation, alloying element segregation and defects like shrinkages holes and cracks were characterized.

## Structural Materials Division Symposium: Advanced Characterization and Modeling of Phase Transformations in Metals in Honor of David N. Seidman on his 70th Birthday: Kinetics of Phase Transformations I

Sponsored by: The Minerals, Metals and Materials Society, TMS Structural Materials Division, TMS: Advanced Characterization, Testing, and Simulation Committee, TMS: Chemistry and Physics of Materials Committee

Program Organizers: Robert Averback, University of Illinois, Urbana-Champaign; Mark Asta, University of California, Davis; David Dunand, Northwestern University; Ian Robertson, University of Illinois at Urbana-Champaign; Stephen Foiles, Sandia National Laboratories

Tuesday PM

Room: 3000

February 17, 2009

Location: Moscone West Convention Center

Session Chair: David Dunand, Northwestern University

2:00 PM Invited

**Coarsening Kinetics with Large Diffusional Mobility Disparity in Two Phases:** Guang Sheng<sup>1</sup>; Qiang Du<sup>1</sup>; Kegang Wang<sup>2</sup>; Zikui Liu<sup>1</sup>; Long Qing Chen<sup>1</sup>; <sup>1</sup>Pennsylvania State University; <sup>2</sup>Florida Institute of Technology

Precipitation is a basic process underlying the development of many engineering alloys ranging from high-temperature Ni-based superalloys to light-weight Al-alloys. It is generally known that the diffusion coefficients of elements responsible for coarsening are dramatically different in the precipitate phase and in the matrix. It has recently been suggested that such dramatic difference in diffusivities may result in fundamentally different coarsening kinetics. In this presentation, we will discuss our recent simulation results of coarsening kinetics with large diffusional mobility disparity using a variable-mobility Cahn-Hilliard equation. We study the coarsening kinetics of both interconnected two-phase microstructures and isolated precipitate particles embedded in a matrix. Our preliminary simulations for both interconnected morphologies and isolated particles suggest a coarsening power law with an time exponent of  $\sim 0.30$ , which is surprisingly close to that obtained by Seidman's group for the coarsening of gamma-prime precipitates in Ni-based alloys using the three-dimensional atom probe technique.

2:30 PM Invited

**High Resolution Electron Microscopy of Core/Shell Precipitates in Al-Based Alloys:** Ulrich Dahmen<sup>1</sup>; M. D. Rossell<sup>1</sup>; R. Erni<sup>1</sup>; M. Watanabe<sup>1</sup>; V. Radmilovic<sup>1</sup>; <sup>1</sup>National Center for Electron Microscopy, Lawrence Berkeley National Laboratory, University of California

Core-shell precipitate structures have recently been demonstrated in Al-based alloys with Sc and Zr. It was shown that a Zr rich shell surrounded an Al<sub>3</sub>Sc core, acting as a diffusion barrier that reduced the growth rate of the Sc rich core. In this work, we investigate the effect of Li addition to AlScZr alloys. Using aberration-corrected high resolution transmission electron microscopy,



the role of Li as a transient nucleating agent for Sc and Zr during heating was documented, and the formation of an Al<sub>3</sub>Li shell around (Sc,Zr)-rich particles was observed. It was possible to directly image Li atom columns in the shell from the phase of the exit surface wavefunction. Likewise, Sc and Zr-containing columns in the core could be seen directly using high-angle annular dark field imaging. Finally, combining a monochromated source with aberration-corrected energy-filtered imaging, we were able to obtain spectrum images of plasmon peaks that provided a map of Li concentration in these precipitates. Our observations are consistent with a multi-stage precipitation mechanism. Initially, spinodal decomposition serves as a barrier-free process to grow evenly-spaced Li-rich clusters by congruent ordering, acting as heterogeneous nucleation sites for the formation of Sc-rich precipitates at high temperature. During subsequent low-temperature annealing, Li forms a shell around these particles. The resulting microstructure is remarkably monodisperse. This approach to generating precipitate distributions can be applied to a range of alloys and could lead to new types of dispersion-strengthened materials.

### 3:00 PM

**Study of Precipitation Kinetics of Copper in HSLA Steel by TEM Small Angle Neutron Scattering (SANS):** *Chandra Pande*<sup>1</sup>; M. Ashraf Imam<sup>1</sup>; <sup>1</sup>Naval Research Laboratory

Precipitation kinetic of copper in a high strength low-carbon ferrous alloy has been studied in the past by Prof. Seidman using field ion microscopy. These precipitates are initially coherent with the matrix and hence are difficult to detect by conventional transmission electron microscopy (TEM). We have therefore used TEM in conjunction with small angle neutron scattering (SANS) to study copper precipitation. Direct measurement from TEM micrographs and integral transform of the SANS data was used to calculate the size distribution for a variety of aging conditions. Maximum entropy principle was used to refine the distribution obtained. The role of these precipitates in hardening of the material will also be considered.

### 3:15 PM Break

### 3:30 PM Invited

**The Topology and Morphology of Three-Dimensional Bicontinuous Interfaces:** A. Genau<sup>1</sup>; Y. Kwon<sup>2</sup>; K. Thornton<sup>3</sup>; *Peter Voorhees*<sup>1</sup>; <sup>1</sup>Northwestern University; <sup>2</sup>Samsung Electronics; <sup>3</sup>University of Michigan

We examine the topology and morphology of interfaces produced following phase separation via spinodal decomposition and phase ordering. We employ three-dimensional simulations to examine the evolution of these systems during coarsening. We quantify the morphology of these complex microstructures via the interfacial shape distribution, the probability of finding a patch of interface with a given pair of principle curvatures. We also characterize the spatial correlations of the interfacial curvature. This analysis has identified new characteristic length scales of these complex structures. In the structure produced following phase ordering, despite the local evolution law governing interfacial motion, long-range correlations develop that lead to a characteristic length scale associated with the distance between high-curvature tunnels. In the structure produced following spinodal decomposition the diffusional dynamics leads to a length scale that is related to correlations and anticorrelations between regions of curvature of opposite sign.

### 4:00 PM Invited

**Solute-Vacancy Interaction in Al and Mg Alloys:** *Christopher Wolverton*<sup>1</sup>; Dongwon Shin<sup>1</sup>; <sup>1</sup>Northwestern Univ

Solute-vacancy binding is a key quantity in understanding diffusion kinetics, and also can have a considerable impact on age hardening response in alloys. Previous efforts to understand solute-vacancy binding in alloys have been hampered by a scarcity of reliable, quantitative experimental measurements. Here, we report a large database of solute-vacancy binding energies determined from first-principles density functional calculations for both Al and Mg alloys. The calculated binding energies agree well with accurate measurements where available, and provide an accurate predictor of solute-vacancy binding in other systems. For both Al and Mg, we have explored the physical effects controlling solute-vacancy binding. We find that there is a strong correlation between binding energy and solute size, with larger solute atoms possessing a stronger binding with vacancies.

### 4:30 PM

**Solute Segregation and Thermal Stability of Ultra-Fine-Grained Al-Mg:** *Richard Karnesky*<sup>1</sup>; Nancy Yang<sup>1</sup>; Christopher San Marchi<sup>1</sup>; Enrique Lavernia<sup>2</sup>; <sup>1</sup>Sandia National Laboratories; <sup>2</sup>University of California, Davis

The effect of hot vacuum degassing, consolidation, and annealing on ultra-fine-grained (d≈200 nm) Al-7.5 wt. % Mg, produced from cryomilled, nanocrystalline (d≈50 nm) powders is studied by means of X-ray diffraction and local-electrode atom-probe tomography. Tomographic reconstructions of the powders, mounted and milled with a dual-beam SEM/FIB, show that the majority of grain growth and solute segregation to grain boundaries occurs during the thermal degassing prior to consolidation. The documented Mg segregation provides a possible explanation for the thermal stability of the materials, as the post-consolidated grain size and solute distribution changes very little when the alloy is annealed at 500 °C for 2 hours.

### 4:45 PM Invited

**Roles of Interface Width and Chemical Diffusion in Particle Coarsening:** *Alan Ardell*<sup>1</sup>; <sup>1</sup>University of California

Experiments conducted by David Seidman and his students and other co-workers have provided valuable insights into the nature of the interfaces between precipitate and matrix phases. In Ni-base alloys containing  $\gamma'$  precipitates, typified by Ni<sub>3</sub>Al in binary Ni-Al alloys but also including other binary as well as ternary alloys, the interfaces are not sharp, the composition across them changing over distances the order of 2 nm or so. Chemical diffusion across the interfaces influences the growth rates of individual precipitates, hence ultimately the kinetics of coarsening of the entire ensemble. Since chemical diffusion in the ordered precipitate phase is much slower than in the disordered solid solution, the interface acts as a diffusion bottleneck. A recent theory of coarsening takes into account diffusion across the interface. In this presentation extant data, including measurements originating in Professor Seidman's laboratory, will be examined in light of this new theory.

### 5:15 PM

**Probing the Early Stages of Elemental Partitioning during the Nucleation and Growth of Alpha Platelets in the Beta Matrix of Titanium Alloys:** Soumya Nag<sup>1</sup>; *Rajarshi Banerjee*<sup>1</sup>; Junyeon Hwang<sup>1</sup>; Srinivasan Rajagopalan<sup>2</sup>; Hamish Fraser<sup>2</sup>; <sup>1</sup>University of North Texas; <sup>2</sup>Ohio State University

The solid-state precipitation of the alpha phase within the beta matrix of titanium alloys involves both a structural bcc to hcp transformation as well as the diffusional partitioning of the alloying elements. Developments in advanced characterization techniques such as high-resolution scanning transmission electron microscopy (HRSTEM) and 3D atom probe (3DAP) tomography allow for unprecedented insights into the true atomic scale structure and chemistry changes associated with the precipitation of alpha as a function of heat-treatments. Such a coupling of 3DAP and TEM observations, on complex beta titanium alloys, indicate that the structural component of the beta to alpha transformation precedes the diffusional partitioning of the alloying elements. Thus, platelet-shaped alpha precipitates of a composition near that of the beta matrix, far from the equilibrium alpha composition, nucleate and grow by what appears to be a mixed mode (displacive + diffusive) transformation, similar to the bainite transformation in steels.

### 5:30 PM

**Partitioning and Site Preference of Transition Metals (Cr, Ta, Ru, Re) in Model Ni-Based Superalloys: An Atom-Probe Tomographic and First-Principles Study:** *Zugang Mao*<sup>1</sup>; Christopher Booth-Morrison<sup>1</sup>; Yang Zhou<sup>1</sup>; David Seidman<sup>1</sup>; <sup>1</sup>Northwestern University

The site substitution and partitioning behavior of transition metals (Cr, Ta, Re, Ru) in Ni<sub>3</sub>Al (L1<sub>2</sub>)  $\gamma'$ -precipitates of model Ni-Al-Cr superalloys are investigated by first-principles calculations and atom-probe tomography (APT). Measurements of the  $\gamma'$ -phase composition by APT suggest that the investigated transition metals prefer to occupy the Al sublattice-sites in the  $\gamma'$ -precipitates. The calculated substitutional energies of the solute atoms at the Ni and Al sublattice sites indicate that Ta, Re, and Ru have a strong preference for Al site, while Cr has a weak Al site preference. The significant decrease of the substitutional energies of Cr, Re and Ru from the  $\gamma'$ -phase to the  $\gamma$ -phase provide the driving force for the partitioning of these elements to the  $\gamma$ -matrix. In contrast, the substitutional energy of Ta increases from the  $\gamma'$ -phase to the  $\gamma$ -phase, leading to strong partitioning of Ta to the  $\gamma'$ -phase.

5:45 PM

**Coarsening in Al-Cu Solid-Liquid Mixtures:** *Julie Fife*<sup>1</sup>; Larry Aagesen<sup>1</sup>; Erik Lauridsen<sup>2</sup>; Marco Stampanoni<sup>3</sup>; Peter Voorhees<sup>1</sup>; <sup>1</sup>Northwestern University; <sup>2</sup>Risoe National Laboratory; <sup>3</sup>Paul Scherrer Institut

We examine, in-situ, the morphological evolution of solid-liquid mixtures in the Al-Cu system during isothermal coarsening, with increasing solid volume fraction and varying solidification techniques. Through x-ray tomography, real-time data is collected for the three-dimensional analysis of these complex structures. Phase-field calculations, using this data as initial conditions, are also employed. The morphology and topology of the microstructure are analyzed through interface shape distributions and genus, which determine the probability of finding a patch of interface with a given set of principal curvatures and the topological complexity of the microstructure, respectively. We find that the microstructure evolves in a manner that is strongly influenced by the initial conditions prior to coarsening and that the phase-field models provide important insight into the experimental results. We also examine the formation of topological singularities, specifically tubes of liquid that fission into liquid droplets. An analysis of this process will be discussed.

6:00 PM

**Microstructural Evolution during Thermal Aging of IN718 Plus Alloy:** *Vibhor Chaswal*<sup>1</sup>; S. Mannava<sup>1</sup>; Vijay Vasudevan<sup>1</sup>; <sup>1</sup>University of Cincinnati

IN718 Plus is the latest high temperature candidate material for aero-engine components having improved peak temperature strength and toughness over IN718 attributed to lower Nb, and Fe and higher Al contents which modify its precipitation behavior. Precipitation hardening is controlled by location and extent of  $\gamma'$ ,  $\gamma''$  and  $\delta$  precipitates in this alloy, and is strongly influenced by thermal aging during service. Hence, thermal aging studies between 650°C to 850°C have been conducted on a hot rolled IN718 Plus alloy used commonly in industry. Quantitative measurements of precipitate location, extent and evolution at grain boundaries and within the matrix were evaluated with respect to dislocation density and grain orientation by transmission electron microscopy (TEM), X-ray diffraction (XRD) and electron back-scattered diffraction (EBSD). The predictability of temperature-time dependence of  $\gamma'$ ,  $\gamma''$  and  $\delta$  phases, and corresponding micro-hardness results were compared with conventional Larson Miller Parameter (LMP) based approach and multi-scale computational method.

## Surface Structures at Multiple Length Scales: Surface Properties in Various Length Scales

Sponsored by: The Minerals, Metals and Materials Society, TMS Materials Processing and Manufacturing Division, TMS: Surface Engineering Committee  
Program Organizers: Arvind Agarwal, Florida International University; Sudipta Seal, University of Central Florida; Yang-Tse Cheng, University of Kentucky; Narendra Dahotre, University of Tennessee; Graham McCartney, University of Nottingham

Tuesday PM  
February 17, 2009

Room: 3011  
Location: Moscone West Convention Center

Session Chair: To Be Announced

2:00 PM Keynote

**Thin Film Epitaxy across the Misfit Scale and Its Implications on Integration of Solid State Devices:** *Jagdish Narayan*<sup>1</sup>; <sup>1</sup>North Carolina State Univ

A unified domain epitaxy model for thin film growth across the misfit scale is presented, specifically addressing phenomena related to dislocation nucleation and propagation and stress relaxation during thin film growth. Due to difficulty in dislocation nucleation and propagation in oxides with high lattice frictional stress, it is argued that it is more difficult to relax smaller misfit strains, particularly tensile strains. Under a compressive strain, surface step is lower which reduces dislocation nucleation barrier at free surfaces. Thus, oxides films, where critical thickness is less than a couple of monolayers, can be grown epitaxially and more relaxed on substrates having a large lattice misfit using the paradigm of domain matching epitaxy. In the domain matching epitaxy, integral multiples of lattice planes match across the film-substrate interface, and the misfit falling in between the integral multiples can be accommodated by the principle of domain variation.

2:40 PM

**Heteroepitaxial Diffusion of Cu Islands on Ag(111) by the Dislocation Glide Mechanism:** *Henry Wu*<sup>1</sup>; Dallas Trinkle<sup>1</sup>; <sup>1</sup>University of Illinois, Urbana-Champaign

Island diffusion dynamics play an important role in determining the morphology and structure of heteroepitaxial thin film growth. In systems with large lattice-mismatch such as Cu islands on Ag(111), we expect dislocation glide as a migration mechanism. To study the size and shape dependence of Cu island diffusion, we optimize an embedded atom method potential. We validate the potential by comparing Cu monomer, dimer, and trimer results with DFT and experiment. A systematic study of diffusion pathways for islands up to 20-atoms shows faster diffusion for islands with the dislocation mechanism than without. This gives a "magic size" effect: non-monotonic behavior of diffusion with island size. The dislocation mechanism is sensitive to surface strain, where neighboring islands break the directional symmetry in diffusion barriers by 10-20meV. A kinetic Monte Carlo model for the dislocation-glide mechanism including island interactions via strain is compared with experimental observations of fast island diffusion.

3:00 PM

**New Characteristic Length Scale on Surfaces:** *Hanchen Huang*<sup>1</sup>; <sup>1</sup>RPI

Surfaces have various well-established characteristic length scales, such as Mullins' wavelengths due to mass transport and atomic islands dimension in epitaxy. Following the discovery of three-dimensional Ehrlich-Schwoebel barrier, we have discovered a new length scale during surface processing such as synthesis. This presentation starts with the physics origin of such length scale, and continues with atomistic simulations demonstrating the variation of the length scale and validation experiments, and ends with design of nanosynthesis based on the knowledge of this new length scale & its experimental validation. It is interesting to note that this length scale is the very reason that nanorods synthesis is possible, even though nanorods had been realized long time ago (and it was patented a decade ago).

3:20 PM Break

3:40 PM Invited

**From Dynamic Surface Roughening to Dynamic Smoothing of Nanocomposite Films:** *Jeff DeHosson*<sup>1</sup>; Yutao Pei<sup>1</sup>; <sup>1</sup>University of Groningen

This paper reports some striking findings on the breakdown of dynamic roughening in film growth. With increasing energy flux of concurrent ion impingement during pulsed DC sputtering, a transition from dynamic roughening to dynamic smoothing is observed in the growth behavior of MeC/a-C DLC nanocomposite films. In the case of dynamic smoothing, TiC/a-C nanocomposite films exhibit a negative growth exponent and ultra-smoothness (RMS roughness ~0.2 nm at film thickness of 1.5  $\mu$ m). As an experimental indication of the impact-induced downhill flow model an amorphous front layer of 2 nm thickness has been observed with high resolution cross-sectional transmission electron microscopy, always covering the bulk nanocomposite film and consequently leading to ultrasmoothness. Roughness evolution has been described by the linear stochastic equation which contains the second- and fourth-order gradient terms. The predicted interface evolution is in a good agreement with the atomic force microscopy measurements of roughness evolution.

4:10 PM

**Understanding Strain Localization through Matrix-Based 3-D Surface Roughness Characterizations:** *Mark Stoudt*<sup>1</sup>; Joseph Hubbard<sup>1</sup>; <sup>1</sup>National Institute of Standards & Tech

Since stretch-forming limiting strains are typically determined with complex, deterministic numerical simulations that do not reliably predict true localization strain, a matrix-based, 3-dimensional surface analysis technique has been developed to improve characterizations of the morphological conditions that promote strain localization. This technique quantifies and then maps the changes that are contained in the surface roughness data produced by plastic deformation. The results of analyses on commercial aluminum sheet surfaces subjected to three in-plane stretching modes established that strain localization is dominated by stochastic processes that can be reliably predicted with Weibull statistics. This study also suggests that gross localization may involve a nucleation and growth process that requires regions of the surface to exceed a threshold roughness magnitude before localization occurs. The methodology developed for this approach and the potential impact on models used to predict limiting strains shall be presented and discussed.

4:30 PM

**Stochastic Finite Temperature Continuum Modeling with Applications to Film Evolution:** *Lawrence Friedman*<sup>1</sup>; <sup>1</sup>Pennsylvania State Univ

Evolution of surface structure is frequently modeled as an energy dissipating process triggered and augmented by thermal fluctuations. Until recently, a prescription for including general thermal fluctuations in phenomenological models has been lacking and in most instances, random fluctuations are neglected or random initial conditions are used as a surrogate for actual thermal fluctuations. However, Lau and Lubensky (Phys. Rev. E 76, 011123, 2007) showed how to construct finite temperature models using stochastic differential equations with general white noise terms. Their method ensures that an ensemble of systems approaches the Boltzmann distribution. Here, their method is extended to discretized stochastic partial differential equations and then applied to fluctuations in strained and unstrained film surfaces.

4:50 PM

**Hydrogen Transport in Fe/Ti Nanometer-Scale Multilayers during In-Situ Low Temperature Annealing:** *Z.L. Wu*<sup>1</sup>; B.S. Cao<sup>1</sup>; J. Gao<sup>1</sup>; T.X. Peng<sup>1</sup>; M.K. Lei<sup>1</sup>; <sup>1</sup>Surface Engineering Laboratory, School of Materials Science and Engineering, Dalian University of Technology

Hydrogen transport in the Fe/Ti nanometer-scale multilayers on Si(100) substrates during in-situ thermal annealing at 463 K was investigated by using x-ray diffraction (XRD), secondary ion mass spectrometry (SIMS), and cross-sectional transmission electron microscopy (XTEM). The Fe/Ti nanometer-scale multilayers constructed with thickness of alternating Fe and Ti sublayers of 16.2 nm and the sublayer thickness ratio of 1:1 were deposited by direct current magnetron sputtering. The composition modulation structure was still maintained in Fe/Ti nanometer-scale multilayers during thermal annealing. After annealing for 10 min, hydrogen permeated through the whole Fe/Ti nanometer-scale multilayers and localized in Ti sublayers to form TiH. With the annealing time increased to 30 min, the concentration of hydrogen increased in the Ti sublayer and TiH transformed to TiH<sub>2</sub>. It is found that composition modulation structure has a significant effect on the transport of hydrogen during thermal annealing.

5:10 PM

**Synthesis and Characterization of Boron Carbide Thin Films Grown by RF Sputtering:** *Tolga Tavsanoglu*<sup>1</sup>; Sid Labdi<sup>2</sup>; Michel Jeandin<sup>3</sup>; <sup>1</sup>Istanbul Technical University; <sup>2</sup>Université d'Evry Val d'Essonne, Laboratoire d'études des Milieux Nanométriques; <sup>3</sup>MINES ParisTech, Centre des Matériaux

Boron carbide (B<sub>4</sub>C) is the third hardest material at room temperature and it combines many other attractive properties such as, high modulus, good wear resistance, and high chemical and thermal stability. Boron carbide films are considered to be promising candidate as hard, protective coatings for cutting tools and other wear resistance applications. In the present study, boron carbide thin films of 500–700 nm were deposited by RF sputtering from a boron carbide target. The elemental composition of the deposited films was measured by EPMA. The mechanical properties, Young's modulus and hardness were determined by AFM coupled nanoindentation technique. FTIR analyses were conducted to evaluate bonding characteristics of boron carbide. The microstructure and crystallinity of the films were characterized by cross-sectional SEM and XRD analysis. Tribological properties were also investigated by pin-on-disc test measurements.

5:30 PM

**Nanotribological Properties of Carbon Nanotube Reinforced Plasma Sprayed Aluminum-Silicon Alloy Composite Coatings:** *Srinivasa Bakshi*<sup>1</sup>; Kantesh Balani<sup>1</sup>; Arvind Agarwal<sup>1</sup>; <sup>1</sup>Florida International University

Nanoscratch experiments have been carried out on plasma sprayed Al-Si coatings containing 5wt% and 10wt% carbon nanotubes (CNT) as well as Al-Si coating without nanotubes. The effect of CNTs on the wear resistance and friction properties are studied. Scratching has been done both under constant load and increasing load conditions. SEM and AFM have been used to image the wear track under both loading conditions. Microstructure of the coatings has been discussed to delineate the wear resistance mechanisms in CNT reinforced composites.

**Synergies of Computational and Experimental Materials Science: Synergies in Nanoscience**

Sponsored by: The Minerals, Metals and Materials Society, TMS Materials Processing and Manufacturing Division, TMS/ASM: Computational Materials Science and Engineering Committee  
Program Organizers: Katsuyo Thornton, University of Michigan; Henning Poulsen, Risoe National Laboratory; Mei Li, Ford Motor Co

Tuesday PM  
February 17, 2009

Room: 3003  
Location: Moscone West Convention Center

*Session Chairs:* Yunzhi Wang, Ohio State University; Ragnvald Mathiesen, NTNU

2:00 PM Invited

**Dislocation Mechanism in Nanocrystalline Metals: Atomistic Simulations and Experiments:** *Helena Van Swygenhoven*<sup>1</sup>; Christian Brandl<sup>1</sup>; Steven Van Petegem<sup>1</sup>; Peter Derlet<sup>1</sup>; <sup>1</sup>Paul Scherrer Institut

Molecular dynamics deformation studies of nanocrystalline metals suggest dislocations are nucleated at grain boundaries, travel through the grain to be finally absorbed in the surrounding grain boundaries. Dislocation propagation on the slip plane on which it was nucleated was observed to be hindered by stress intensities in the grain boundaries suggesting that propagation could not be excluded as a rate limiting process. Recent constant strain rate molecular dynamics simulations of nanocrystalline Al demonstrate that dislocations also exhibit cross-slip via the Fleischer mechanism. The grain boundary is found to strongly influence when and where cross-slip occurs, allowing the dislocation to avoid local stress concentrations that otherwise can act as pinning sites for dislocation propagation (PRL 100(2008)235501). In this talk the latest suggestions from molecular dynamics are discussed in terms of new experiments involving strain rate sensitivity measurements, stress dip test, creep studies and in-situ tensile and compressive testing during X-ray diffraction.

2:40 PM Invited

**Effects of Solute Concentrations on Kinetic Pathways in Ni-Al-Cr Alloys: Experiments and Simulations:** *David Seidman*<sup>1</sup>; Christopher Booth-Morrison<sup>1</sup>; Zungang Mao<sup>1</sup>; Chantal Sudbrack<sup>1</sup>; <sup>1</sup>Northwestern Univ

The kinetic pathways resulting from the formation of coherent gamma-prime precipitates from a gamma (fcc) matrix are studied for two alloys with similar gamma-prime (L12) precipitate volume fractions at 873 K. The phase decompositions of Ni-7.5 Al-8.5 Cr at.%, and Ni-5.2 Al-14.2 Cr at.%, for aging times 1/6 to 1024 hours are investigated by atom-probe tomography (APT), and they differ significantly. The morphologies of the gamma-prime precipitates of the alloys are similar, though the gamma-prime precipitate coagulation and coalescence differ. The temporal evolution of the gamma-prime precipitate average radii and the gamma-matrix supersaturations follow the predictions of classical coarsening models. The compositional trajectories of the gamma matrix phases of the alloys are found to follow the equilibrium tie-lines, while the trajectories of the gamma-prime precipitates do not, resulting in significant differences in the partitioning ratios of the solute elements. The experimental APT results are compared with lattice kinetic Monte Carlo simulations.

3:20 PM

**Computer Simulations of Precipitate Strengthening of Al-Zr-Sc, as Informed by Local-Electrode Atom-Probe Tomography:** *Richard Karnesky*<sup>1</sup>; Keith Knippling<sup>2</sup>; Volker Mohles<sup>3</sup>; David Dunand<sup>4</sup>; David Seidman<sup>4</sup>; <sup>1</sup>Northwestern University and Sandia National Laboratories; <sup>2</sup>Northwestern University and Naval Research Laboratory; <sup>3</sup>RWTH Aachen University; <sup>4</sup>Northwestern University

Local-electrode atom-probe tomography allows structural information about hundreds of nanoscale precipitates, including precipitate size, volume fraction, number density, and edge-to-edge interprecipitate distances, to be measured directly in three dimensions. These data can be used to generate glide planes for use in a continuum dislocation dynamics simulation that calculates the critical resolved shear stress based on the elastic interactions of dislocations with each other, themselves, and with precipitates. Within a single glide plane, some precipitate cross sections may be sheared (creating an antiphase boundary) while others are bypassed via Orowan dislocation looping. When isochronally-aged



to 300 °C, Al-0.1 Zr-0.1 Sc (at. %) forms a high number density of nanoscale, coherent L<sub>1</sub> Al<sub>3</sub>(Sc<sub>1-x</sub>Zr<sub>x</sub>) precipitates. As the aging temperature is increased to 400 °C, a Zr-rich precipitate shell grows, further strengthening the alloy. We compare the ambient-temperature microhardnesses as a function of aging treatment with the strength that is modeled.

### 3:40 PM Break

### 4:00 PM Invited

**Combined Phase-field Simulations and Experimental Studies of Nanoferroics:** *Long Qing Chen*<sup>1</sup>; Darrell G. Schlom<sup>2</sup>; Venkat Gopalan<sup>1</sup>; X. X. Xi<sup>1</sup>; C. B. Eom<sup>3</sup>; S. V. Kalinin<sup>4</sup>; R. Ramesh<sup>5</sup>; X. Q. Pan<sup>6</sup>; <sup>1</sup>Pennsylvania State University; <sup>2</sup>Cornell University; <sup>3</sup>University of Wisconsin; <sup>4</sup>Oak Ridge National Laboratory; <sup>5</sup>UC Berkeley; <sup>6</sup>University of Michigan

This presentation will discuss a number of successful examples of coupling phase-field simulations and experimental measurements in the area of nanoferroics with an emphasis on the phase transitions, domain structures, and properties of ferroelectric thin films. It will be shown that one can use phase-field simulations to not only help interpreting experimental observations but also provide guidance to achieve desirable transition temperatures, specific domain states, domain wall orientations, and domain wall mobility. Furthermore, phase-field modeling has also been combined with piezoelectric force microscopy to study the local ferroelectric domain switching. Examples to be discussed include several important oxide systems BaTiO<sub>3</sub>, PbZr<sub>x</sub>Ti<sub>1-x</sub>O<sub>3</sub>, BiFeO<sub>3</sub> and BaTiO<sub>3</sub>/SrTiO<sub>3</sub> superlattices.

### 4:40 PM

**Crystal Plasticity Modeling and Micro-Mechanical Experiments of Gamma-TiAl Based Microstructures:** *Claudio Zambaldi*<sup>1</sup>; Franz Roters<sup>1</sup>; Stefan Zaeferrer<sup>1</sup>; Dierk Raabe<sup>1</sup>; <sup>1</sup>Max-Planck-Institut für Eisenforschung

The deformation behavior of a gamma-TiAl based alloy is incorporated into a crystal-plasticity formulation coupled with a finite-element solver. The single-phase constitutive behavior is calibrated by nano-indentation experiments in single phase regions. For the discrimination of the orientational variants a newly developed high-precision indexing method for electron backscatter diffraction patterns was applied. Nano-indentation experiments are evaluated by a 3D model. The simultaneous activation of deformation mechanisms is used to assess their relative strengths and cross-hardening. The lamellar microstructure is analyzed in terms of kinematic constraints, which lead to pronounced plastic anisotropy. Secondly, the mechanical behavior of massively transformed microstructures is modeled by applying a lower degree of kinematic constraints. On a grain-scale, this results in less plastic anisotropy and possibly improved ductility. An attempt is described to include the significant micro stresses. The modeling is complemented and validated by mechanical characterization through small-scale tests.

### 5:00 PM

**Modeling the Drawing of Steel Wire with Nano-Engineered Composite Hardmetal Dies:** *Ivica Smid*<sup>1</sup>; Daniel Cunningham<sup>1</sup>; Erik Byrne<sup>1</sup>; John Keane<sup>2</sup>; <sup>1</sup>Pennsylvania State University; <sup>2</sup>Allomet Corporation

Wire drawing with a novel composite hardmetal comprised of hard Al<sub>2</sub>O<sub>3</sub> core particles encapsulated in a tough WC-Co shell has been studied. Dynamic fracture toughness testing shows that this is an excellent material for machining in the high strain rate environments of metal forming operations such as wire drawing. This material's ability to resist dynamic fracture is due to the toughening mechanisms of its microstructure, such as added binder ductility, crack interactions at core particles, and crack interactions at grain boundaries. Finite element modeling was used to model the microstructural interactions in wire drawing. Using non-linear material properties for steel, permanent strain of the wire due to plastic deformation was found as well as the stress states imposed by them. Future advances of these simulations will include predictions of wear lifetime as well as influence of temperature.

### 5:20 PM

**First-Principles Simulations and Inelastic Neutron Scattering in Thermodynamics Studies:** *Olivier Delaire*<sup>1</sup>; Matthew Lucas<sup>2</sup>; Max Kresch<sup>1</sup>; Jiao Lin<sup>1</sup>; Brent Fultz<sup>1</sup>; <sup>1</sup>California Institute of Technology; <sup>2</sup>Oak Ridge National Laboratory

In crystalline materials, low energy excitations around the average configuration of the ions and electrons can be thermally activated, providing entropy. As such, phonons, spin-waves, or electronic excitations can be subdivided into their own entropic contributions. Inelastic neutron scattering is the preferred experimental

technique to measure phonons and magnons, but a difficulty in analyzing the neutron scattering results resides in the complexity of the experimental datasets. First-principles simulations of the phonon dynamics have now reached a level of reliability such that the full phonon scattering function can be predicted from quantum mechanics, and compared to experimental data. The synergy between quantum mechanical calculations and experimental measurements has provided us with valuable insights. Fundamental relations between phonon excitations and the underlying electronic band structure are discussed, and in particular, we show that the electron-phonon interaction can influence the thermodynamics of metals to much higher temperatures than was previously assumed.

## Transformations under Extreme Conditions: A New Frontier in Materials: Extreme Deformation and Damage

Sponsored by: The Minerals, Metals and Materials Society, ASM International, ASM Materials Science Critical Technology Sector, TMS Materials Processing and Manufacturing Division, TMS/ASM: Phase Transformations Committee  
Program Organizers: Vijay Vasudevan, University of Cincinnati; Mukul Kumar, Lawrence Livermore National Laboratory; Marc Meyers, University of California-San Diego; George "Rusty" Gray, Los Alamos National Laboratory; Dan Thoma, Los Alamos National Laboratory

Tuesday PM

February 17, 2009

Room: 3001

Location: Moscone West Convention Center

Session Chairs: George Gray, Los Alamos National Laboratory; James Stolken, Lawrence Livermore National Laboratory

### 2:00 PM Invited

**A Statistical View of High-Rate Material Instability and Failure:** *Thomas Wright*<sup>1</sup>; K.T. Ramesh<sup>2</sup>; <sup>1</sup>US Army Research Laboratory; <sup>2</sup>Johns Hopkins University

All materials have defects distributed throughout their interior and surfaces due to processing, prior deformation, microstructure, etc. As a consequence any applied loading on the material will result in stress concentrations also being distributed throughout the interior and surfaces. In quasi-static loading it is well understood that the weakest locations in the material are at risk for initiating failures through material instabilities. In dynamic loading, however, especially extreme dynamic cases, the situation tends to be far more complex, and it may be necessary to give independent consideration to the processes of damage nucleation, growth, and communication with other sites, each process developing according to its own time scale. Clearly the interaction of all these processes and time scales must be modulated by the statistics of defects within the material. Concrete examples will be given to illustrate these interconnected events.

### 2:35 PM

**Characterization of Incipient Spall Damage in Monocrystalline Copper Targets Subjected to Laser-Driven Flyer Impacts:** *Stephan DiGiacomo*<sup>1</sup>; Sheng-Nian Luo<sup>2</sup>; Darrin Byler<sup>2</sup>; Rob Dickerson<sup>2</sup>; *Pedro Peralta*<sup>1</sup>; Scott Greenfield<sup>2</sup>; Aaron Koskelo<sup>2</sup>; Kenneth McClellan<sup>2</sup>; <sup>1</sup>Arizona State University; <sup>2</sup>Los Alamos National Laboratory

Monocrystalline copper was subjected to low pressure shocks (4 - 6 GPa) along the <100>, <110>, <111>, <123>, and <114> directions using laser-driven flyers. Values for spall strength as determined from pullbacks in the free-surface velocity histories are reported for each orientation. Characterization of untested <100> samples using electron backscatter diffraction (EBSD) revealed very-low-angle (~0.5-2 deg.) sub-grain boundaries that localized damage in shocked specimens, since numerous isolated voids clustered along boundaries oriented parallel to the shock direction. Furthermore, EBSD revealed high misorientation bands parallel to {111} traces. Spall damage was noted to occur at the intersections of these bands and the low-angle sub-grain boundaries. High-resolution EBSD analysis of isolated voids in shocked <100> samples revealed octahedral geometry of individual voids with a characteristic misorientation field. The lattice rotations surrounding the spall voids were analyzed with a kinematic crystal plasticity model to derive the effective plastic strain around the voids.

## 2:55 PM Invited

**Laser-Shock Induced Deformation and Spalling in Metals:** *Marc Meyers*<sup>1</sup>; Hussam Jarmakani<sup>1</sup>; Bimal Kad<sup>1</sup>; Bruce Remington<sup>2</sup>; Daniel Kalantar<sup>2</sup>; Brian Maddox<sup>2</sup>; Eduardo Bringas<sup>2</sup>; James McNaney<sup>2</sup>; <sup>1</sup>UC San Diego; <sup>2</sup>Lawrence Livermore National Laboratory

High-amplitude lasers producing shock and quasi-isentropic compression are a powerful tool to probe the generation and evolution of damage in metals under extreme pressure and strain rate conditions. Pressures higher than 100 GPa, strain rates in the range  $10^6$ - $10^9$  s<sup>-1</sup>, and durations on the order of  $10^{-9}$  seconds are achieved in a controlled and reproducible manner. Monocrystalline and polycrystalline copper, nickel, and vanadium were subjected to laser compression at the LLNL Jupiter facility and at the University of Rochester Omega facility (LLE). The generation of dislocations, mechanical twins, stacking faults, and voids was characterized, quantified, and modeled. The transition from slip to twinning is analysed through the constitutive behavior of the two mechanisms, the Rankine-Hugoniot relation, and the Swegle-Grady equation. Analytical predictions are compared with molecular dynamics results. In spalling experiments, experimentally obtained fragment sizes are compared with predictions from the Grady-Kipp model. Support: UCOP ILSA Program.

## 3:30 PM

**Spall (Dynamic Fracture) Strength and Deformation Microstructure of SS304 Alloy at High Strain Rate:** Keshaw Joshi<sup>1</sup>; R. Tewari<sup>1</sup>; G. Dey<sup>1</sup>; Satish Gupta<sup>1</sup>; *Srikumar Banerjee*<sup>1</sup>; <sup>1</sup>Bhabha Atomic Research Centre

Spall (dynamic fracture) strength and the deformation microstructure of SS304 alloy have been determined at high strain rate. Spall in SS304 plate has been achieved by impacting it with a parallel SS304 plate at velocity of 0.6 km/s; this impact introduced a shock wave of 11.9 GPa in both the target and the impactor. The interaction of tensile waves resulting from the reflection of shock wave from the target free surface and from the flyer free surface generated large tensile stress in the target which exceeded the spall strength causing spall fracture. The analysis of the velocity history of the target free surface recorded using VISAR reveals the dynamic yield strength of 0.8 GPa and spall strength of 2.6 GPa at strain rate of  $\sim 10^4$  /s. The microstructure examination of the area in proximity of the fractured surface using SEM and TEM revealed new deformation features.

## 3:50 PM

**Three-Dimensional Characterization of Spall Damage in Shock Loaded Metallic Multicrystals:** Leda Wayne<sup>1</sup>; Shima Hashemian<sup>1</sup>; Stephan DiGiacomo<sup>1</sup>; *Pedro Peralta*<sup>1</sup>; Heber D'Armas<sup>2</sup>; Shengnian Luo<sup>3</sup>; Scott Greenfield<sup>3</sup>; Dennis Paisley<sup>3</sup>; Robert Dickerson<sup>3</sup>; Darrin Byler<sup>3</sup>; Ken McClellan<sup>3</sup>; <sup>1</sup>Arizona State University; <sup>2</sup>Universidad Simon Bolivar; <sup>3</sup>Los Alamos National Laboratory

Correlations between damage and local microstructure were investigated in multicrystalline copper, nickel and titanium samples via impact tests conducted with laser-driven plates. All samples had a large grain size compared to the thickness, to isolate microstructure effects on local response. Velocity interferometry was used to monitor the response of the samples and spall failure. Cross-sectional Electron Backscattering Diffraction (EBSD) was used to relate crystallography to damage at features such as grain boundaries (GBs) and triple points. Preferred damage nucleation and localization sites were identified via statistical sampling in serial sectioned specimens and through 3-D reconstructions obtained from serial cross-sections. Damage distribution and connectivity along the spall plane in 3-D were correlated to GB misorientations, GB inclination to the shock and grain connectivity at particular locations. Results indicate that the tips of terminated twins and locations with high grain connectivity are the preferred locations for intergranular damage in these samples.

## 4:10 PM Break

## 4:25 PM Invited

**Emergence of Mesoscopic Length Scales through Self-Organization in Alloys Subjected to Severe Plastic Deformation:** *Pascal Bellon*<sup>1</sup>; Robert Averback<sup>1</sup>; Pavel Krasnochtchekov<sup>1</sup>; Samson Odunuga<sup>1</sup>; Alfredo Caro<sup>2</sup>; Jung Singh<sup>1</sup>; Wenjun Cai<sup>1</sup>; <sup>1</sup>University of Illinois; <sup>2</sup>Lawrence Livermore National Laboratory

Materials are often subjected to sustained and severe plastic deformation, for instance during extrusion, high-energy ball milling, or when experiencing frictional wear. We recently showed that the chemical mixing forced by dislocation-based plasticity in solids can be superdiffusive in some length scale range. In alloy systems comprised of immiscible elements, the dynamical

competition between this superdiffusive forced mixing and thermally activated decomposition can lead to self-organization of the composition, producing mesoscopic composites. We will establish via atomistic simulations, modeling and experiments the parameters that determine the characteristic length scale of these compositional patterns. Self-organization may also impart new and beneficial properties. We will illustrate this point by discussing the important role played by mechanically mixed layers in improving resistance to sliding wear.

## 5:00 PM

**Carbide Decomposition Induced by Severe Plastic Deformation:** *Xavier Sauvage*<sup>1</sup>; Yulia Ivanisenko<sup>2</sup>; <sup>1</sup>University of Rouen; <sup>2</sup>Institute of Nanotechnology

The strain induced carbide (cementite) decomposition in pearlitic steels is widely reported in the literature. It is indeed thought to be responsible of the formation of the extremely hard white etching layer on rail track surfaces and also to affect the ductility of heavily drawn steel cords. However, the driving force and the kinetic of this phase transformation are still under debate and there are still some doubts about the distribution of carbon atoms resulting from the carbide decomposition. In this report, recent Atom Probe Tomography showing both the strain induced transformation of the cementite and carbon atoms diffusion would be presented. These data demonstrate that the first step of the decomposition is the formation of a thin layer of under-stoichiometric cementite along the cementite/ferrite interface. The role of dislocations on the diffusion and the distribution of carbon atoms in the ferrite would be discussed also.

## 5:20 PM

**Nanocluster Formation in Mechanically-Alloyed Ferritic ODS Steels:** *Michael Miller*<sup>1</sup>; Chong Long Fu<sup>1</sup>; David Hoelzer<sup>1</sup>; Kaye Russell<sup>1</sup>; Chain Liu<sup>1</sup>; <sup>1</sup>Oak Ridge National Lab

Atom probe tomography of ball-milled powders of a 14YWT ferritic alloy has revealed that the solute atoms from the yttria particles are forced into solid solution during mechanical alloying and there is an excess of vacancies. First principle calculations have revealed a delicate balance between vacancies and the levels of Ti and Y for the formation of nanoclusters and too high levels will result in the formation of Y<sub>2</sub>Ti<sub>2</sub>O<sub>7</sub> or TiO<sub>2</sub>. Although micron size oxides are observed, the predominant microstructural feature is a high density of Ti-, O- and Y-enriched nanoclusters that form during extrusion. The nanoclusters are extremely resistant to coarsening at temperatures up to 1400°C. This research was sponsored by the U.S. Department of Energy, Division of Materials Sciences and Engineering; research at the Oak Ridge National Laboratory SHaRE User Facility was sponsored by the Scientific User Facilities Division, Office of Basic Energy Sciences, U.S. Department of Energy.

## 5:40 PM

**Atomic Scale Investigation of Strain Induced Interdiffusion in the Cu-Fe System:** *Xavier Sauvage*<sup>1</sup>; Xavier Queleunenec<sup>1</sup>; Florian Wetscher<sup>2</sup>; Jean Marie Le Breton<sup>1</sup>; Alain Menand<sup>1</sup>; <sup>1</sup>University of Rouen; <sup>2</sup>Erich Schmid Institute

Strain induced interdiffusion and supersaturated solid solutions are widely reported in the literature, especially for ball milled powders. However, little is known about the physical mechanisms leading to such non-equilibrium structures. Here, we report about specific experiments performed on the Cu-Fe system in the bulk state with an accurate control of the temperature and of the strain rate. A nanostructured Cu-Fe composite was processed by high pressure torsion up to extreme level of deformation. Atom Probe Tomography and Mössbauer spectroscopy reveal the progressive interdiffusion of Cu and Fe and finally the formation of a homogeneous solid solution. The contribution of strain induced vacancies would be discussed.

## 2009 Functional and Structural Nanomaterials: Fabrication, Properties, and Applications: Bulk Nanocrystalline Materials

Sponsored by: The Minerals, Metals and Materials Society, TMS Electronic, Magnetic, and Photonic Materials Division, TMS Materials Processing and Manufacturing Division, TMS: Nanomaterials Committee, TMS: Nanomechanical Materials Behavior Committee

Program Organizers: Gregory Thompson, University of Alabama; Amit Misra, Los Alamos National Laboratory; David Stollberg, Georgia Tech Research Institute; Jiyoung Kim, University of Texas at Dallas; Seong Jin Koh, University of Texas at Arlington; Wonbong Choi, Florida International University; Alexander Howard, Air Force Research Laboratory

Wednesday AM Room: 3018  
February 18, 2009 Location: Moscone West Convention Center

Session Chairs: Wonbong Choi, Florida International University; Gregory Thompson, University of Alabama

### 8:30 AM Invited

#### Bulk Nanostructured Materials via Severe Plastic Deformation: Issues and Scale up: *Yuntian Zhu*<sup>1</sup>; <sup>1</sup>North Carolina State Univ

Severe plastic deformation (SPD) is an approach that refines the grains and microstructures of metals and alloys via extremely large accumulative plastic strain. The most developed SPD techniques include equal channel angular pressing, accumulative roll bonding, high-pressure torsion, etc. The advantage of SPD techniques is that they can produce bulk nanostructured metals and alloys that are not only large enough for structural applications, but also 100% dense and contamination free. Therefore, the SPD has a great potential for commercial applications. This talk will first present issues on the mechanical properties of SPD-processed materials, especially the ductility, and then discuss technologies for the large-scale production of nanostructured materials via SPD. Potential applications of nanostructured materials produced by SPD will also be discussed.

### 9:00 AM

#### Role of Severe Plastic Deformation on the Formation of Nanograins and Nano-Sized Precipitates in an Fe-Ni-Mn Steel: *Mahmoud Nili Ahmadabadi*<sup>1</sup>; *Hassan Shirazi*<sup>1</sup>; *Hadi Ghasemi-Nanesa*<sup>1</sup>; *Tadashi Furuhashi*<sup>2</sup>; *Behrang Poorganji*<sup>2</sup>; *Syamak Hossein Nadjad*<sup>3</sup>; <sup>1</sup>University of Tehran; <sup>2</sup>Tohoku University; <sup>3</sup>Sahand University of Technology

In this research the effect of severe plastic deformation (SPD) on the formation of nano-scaled grains and precipitation of nano-sized particles which consequently control mechanical properties of Fe-Ni-Mn alloy, was investigated. Fe-Ni-Mn martensitic steels show excellent age hardenability but suffer from embrittlement after aging. Discontinuous coarsening of grain boundary precipitates, resulting in the formation of precipitate free zone (PFZ) along prior austenite grain boundaries, has been found as the main source of embrittlement in previous studies. In this paper, severe plastic deformation has been carried out on Fe-10Ni-7Mn steel to improve its mechanical properties. It is found that substantial improvement of tensile properties in cold-rolled steels occurs at thickness reductions larger than 60% where formation of ultra fine grains is realized. According to TEM observations, formation of nano-scaled grains less than one hundred nanometers along with the copious precipitation of nanometer-sized precipitates take place in the severely-deformed steels.

### 9:15 AM

#### Ti-Base Nano-/Ultrafine Eutectic Composites: Microstructure and Deformation: *Jayanta Das*<sup>1</sup>; *Jürgen Eckert*<sup>1</sup>; <sup>1</sup>IFW Dresden

High strength Ti-Fe-Sn nano-/ultrafine eutectic composites have been prepared through arc melting and cold crucible casting. The microstructure consists of a two phase nano-/ultrafine eutectic comprised of FeTi (Pm3m, B2) and  $\beta$ -Ti (I m3m, A2) phases. The influence of alloying, i.e., addition of Sn, to the Ti70.5Fe29.5 eutectic is assessed in terms of the microstructure variations such as the change of eutectic spacing, morphology, cell size and the resulting mechanical properties in terms of strength and plasticity. The mechanical properties (maximum strength,  $\sigma_m=1939$  MPa, fracture strain,  $\epsilon_f=13.5\%$ ) of the ternary Ti-Fe-Sn are considerably improved compared to the Ti70.5Fe29.5 binary alloy ( $\sigma_m=1733$  MPa,  $\epsilon_f=3.4\%$ ). The change in the morphology of the eutectic,

the microstructure refinement, structural fluctuations and supersaturation in the  $\beta$ -Ti phase, and the elastic properties of nano-phases are crucial factors for improving the plastic deformability of the nano-/ultrafine eutectic alloys without any additional micrometer-size toughening phase.

### 9:30 AM

#### A Tough Nanostructured Material: *J. B. Zhang*<sup>1</sup>; *A. Y. Chen*<sup>2</sup>; *H. W. Song*<sup>1</sup>; *J. Lu*<sup>3</sup>; <sup>1</sup>Baosteel Technology Centre, Baoshan Iron and Steel Company, Ltd.; <sup>2</sup>Baosteel Technology Centre, Baoshan Iron and Steel Company, Ltd. - and - School of Materials Science and Engineering, Shanghai Jiao Tong University; <sup>3</sup>The Hong Kong Polytechnic University

Strength and ductility are two key mechanical properties of materials with intense confictions. We describe a simple and cost-effective way to fabricate this type of material by integrating toughening strategies widely used in ceramics and recently proposed in nanostructured materials. An engineering material stainless steel AISI 304 was selected in this investigation for showing the extensibility of our approach. The surface mechanical attritions treatment (SMAT) is first exerted on the stainless steel sheets for surface nanocrystallization and then the sheet is thinned by warm co-rolling process. This new periodic micro-submicro-nano structured material may reach high strength with exceptional ductility. In contrast to the original counterparts, the yield strength is increased more than twofold with a slightly reducing ductility, and in contrast to the counterparts after work hardening to reach the same strength, the elongation to failure is drastically increased more than threefold.

### 9:45 AM

#### Microstructure Evolution of Nano-Structured Bainite Steel during Surface Mechanical Attrition Treatment: *Hongyan Li*<sup>1</sup>; *Xuejun Jin*<sup>1</sup>; <sup>1</sup>Shanghai Jiao Tong University

Very strong nano-structured bainite has attracted much attention recently for excellent mechanical properties due to the introduction of very thin bainite and films of retained austenite. It is interesting to look into the microstructure evolution of the mixture of such thin bainite and retained austenite under severe plastic deformation, such as the surface mechanical attrition treatment (SMAT). Experimental results show that with increasing the SMATed time retained austenite in the surface layer gradually transforms to martensite under repeated multidirectional loading at high strain rates. Three regions could be identified according to the morphology: nanocrystalline layer, work-hardened layer and the matrix. A distinct boundary between nanocrystalline layer and work-hardened layer was identified, while no visible boundary was observed between work-hardened layer and matrix material. The grain refinement process involves formation of large laths a phase in the work-hardened layer, and formation of randomly orientated equiaxed nanocrystallines in the nanocrystalline layer.

### 10:00 AM Break

### 10:15 AM Invited

#### Nanocrystalline Soft Magnets: Microstructure and Magnetic Properties: *Matthew Willard*<sup>1</sup>; *Maria Daniil*<sup>1</sup>; *Michael Rawlings*<sup>1</sup>; *Keith Knipling*<sup>1</sup>; *Ramasis Goswami*<sup>1</sup>; <sup>1</sup>US Naval Research Laboratory

Soft magnetic materials consisting of nanocrystallites surrounded by a residual amorphous matrix provide excellent properties, including both low coercivity and high magnetization. They are produced by rapid solidification processing with devitrification by isothermal annealing. Ultimately, to obtain the highest permeability and lowest core losses, the microstructure must be successfully optimized, with grain diameters less than 10 nm and retained amorphous matrix. Typically, this microstructure is developed during an isothermal anneal between 450 and 650°C. This study will examine the influence of composition, kinetics, and microstructure on the magnetic properties of (Fe,Co,Ni)-Zr-B-Cu alloys. Differential thermal analysis, thermomagnetic analysis, x-ray diffraction, and transmission electron microscopy will be used to describe the phase transformations and the resulting structure/property relationships.

### 10:45 AM

#### Energy Efficient Magnetic Nanomaterials: *Raju Ramanujan*<sup>1</sup>; *S. Bhami*<sup>1</sup>; *S. Viswanathan*<sup>1</sup>; *P. Deheri*<sup>1</sup>; *S. Shukla*<sup>1</sup>; *Y. Liu*<sup>1</sup>; *J. Law*<sup>1</sup>; *Z. Liu*<sup>2</sup>; <sup>1</sup>Nanyang Technological University; <sup>2</sup>South China University of Technology

There is an urgent need for energy efficient devices to mitigate climate change and to reduce energy consumption. Nanostructured magnetic materials are being intensively studied for energy efficient permanent magnet systems and novel solid state cooling devices. Ongoing studies on giant energy product magnetic nanomaterials and high temperature magnetocaloric materials will be described.



Melt spun rapidly solidified nanocrystalline RE-TM-B (RE=Nd, Pr, Dy, TM=Fe, Co) alloys with enhanced hard magnetic properties were studied, composition and microstructure dependent elevated temperature magnetic properties were investigated. Reducing grain size and Co or Dy substitution had a significant beneficial effect on thermal stability. Energy product greater than 100 kJ/m<sup>3</sup> was obtained in nanophase alloys, attractive low values of temperature coefficients of remanence and coercivity were realized in exchange coupled nanocomposites. Synthesis of rapidly solidified Fe based magnetocaloric materials with high refrigerant capacity was also studied, the magnetocaloric properties and the effect of nanocrystallization were determined.

## 11:00 AM

### Microstructure of Al-Mn in the Nanocrystalline to Amorphous Transition Regime: *Shiyun Ruan*<sup>1</sup>; Christopher Schuh<sup>1</sup>; <sup>1</sup>MIT

We study the microstructure of Al-Mn alloys electrodeposited from a chloroaluminate electrolyte at room temperature. Transmission electron microscopy and x-ray diffraction analyses show that as the Mn content increases across the range 7.5 to 8.0 at%, a single phase crystalline solid solution changes into a two-phase alloy, where a Mn-rich amorphous phase coexists with a Mn-depleted crystalline phase. Concomitant with the appearance of the amorphous phase at 8.0 at% Mn, the crystalline grain size decreases drastically from >1 μm to ~50 nm. Further increase in Mn content results in a further reduction in grain size to ~5 nm and an increase in the amorphous phase fraction. Scanning transmission electron microscopy analysis reveals some detail of the solute distribution in these unique structures, and nanoindentation results show that there is an optimum amorphous/nanocrystalline structure with a hardness exceeding 5 GPa.

## 11:15 AM

### Characterization of Electrodeposited Nanocrystalline Al-Mg Powders: *Fereshteh Ebrahimi*<sup>1</sup>; Mahesh Tanniru<sup>1</sup>; Sankara Sarma Tatiparti<sup>1</sup>; <sup>1</sup>University of Florida

Powders of Al-Mg alloys were fabricated by electrodeposition technique under conditions that encouraged dendritic growth. These powders can potentially be used for hydrogen storage applications. XRD analysis revealed that the as-deposited powders consisted of supersaturated fcc-Al(Mg) and/or hcp-Mg(Al). The maximum solubility of Mg in fcc-Al was found to be 20at%, however, up to 40%Al could be dissolved in hcp-Mg. Equilibrium intermetallic phases precipitated upon elevated temperature exposures of the supersaturated phases. The dendrites developed with two distinct morphologies. The feather-like morphology formed at lower Mg concentrations and slower deposition rates. TEM results revealed that the nanocrystalline structure of these dendrites was extensively textured. Majority of dendrites showed a "globular" morphology consisting of spherical units with randomly oriented nanocrystalline grains. In this presentation, the mechanisms responsible for different dendrite morphologies are discussed. The financial support by NSF (grant DMR-0605406) is greatly appreciated.

## 11:30 AM

### Spontaneous Growth of Novel Hexagonal Mn Nanowhiskers from Hydrogen Activated Laves Phase Alloys: *Erdong Wu*<sup>1</sup>; Xiumei Guo<sup>1</sup>; <sup>1</sup>Chinese Academy of Sciences

The spontaneous growth of metal whiskers is a well-established phenomenon. Owing to its significant importance either as a hidden peril for electronic devices or as a potential fabrication technique for complex microstructures, the phenomenon has been extensively studied for decades. However, only the whiskers of soft metals with relatively low melting points, such as Sn, Cd, Zn and In, and primarily on a micrometer diameter scale, can spontaneously grow at room temperature. With the aid of activation of repeated cycles of hydrogenation/dehydrogenation, the crystalline whiskers of transition metal Mn in the shape of nanorod can segregate and grow spontaneously from the crystals of Zr<sub>1-x</sub>Ti<sub>x</sub>MnCr Laves phase alloys at room temperature. Moreover, the Mn atoms in the nanowhiskers form a novel hexagonal structured allotrope. The morphology and structure of the Mn nanowhiskers are exhibited, and the mechanism and potential of the phenomenon are discussed.

## 11:45 AM

### Surface Oxide Selectivity of Nanostructured CoNiCrAlY and NiCoCrAlY Materials: *Dominic Mercier*<sup>1</sup>; George Kim<sup>2</sup>; Mathieu Brochu<sup>1</sup>; <sup>1</sup>McGill University; <sup>2</sup>Perpetual Technologies Inc.

MCrAlYs are used for high temperature application because of their excellent hot oxidation resistance provided by the Cr<sub>2</sub>O<sub>3</sub> oxide layers that develops on the surface. Nanostructured coatings, such as NiCrAlY, are known to promote the formation of the more stable Al<sub>2</sub>O<sub>3</sub>, which increases the oxidation resistance, when compared to conventional NiCrAlY. This work was aimed at investigating this phenomenon on other nanostructured MCrAlY systems, namely CoNiCrAlY and NiCoCrAlY. The nanostructured powders were fabricated using the cryomilling technique. The free-standing coatings, obtained by HVOF, were isothermally oxidized in air at 1000°C for 24, 48, 96 and 192 hours in order to monitor the oxide scale evolution. The phase analysis was carried out by XRD, SEM and TEM. The results show that the nanostructured coatings form a more continuous α-Al<sub>2</sub>O<sub>3</sub> layer with very small amount of Cr<sub>2</sub>O<sub>3</sub> and no mixed oxides compared to that of the conventional powders.

## Alumina and Bauxite: Methods - Bauxite Characterization, Bayer Chemistry, Alumina Quality

Sponsored by: The Minerals, Metals and Materials Society, TMS Light Metals Division, TMS: Aluminum Committee

Program Organizers: Everett Phillips, Nalco Co; Sringeri Chandrashekar, Dubai Aluminum Co

Wednesday AM

Room: 2002

February 18, 2009

Location: Moscone West Convention Center

Session Chair: David Kirkpatrick, Gramercy Alumina LLC

## 8:30 AM Introductory Comments

## 8:35 AM

### Characterisation of Iron Mineralogy in Jamaican Bauxite and Associated Aspects of Alumina and Soda Losses: *Luke Kirwan*<sup>1</sup>; Desmond Lawson<sup>2</sup>; Ab Rijkeboer<sup>3</sup>; Kieran Hodnett<sup>4</sup>; Austin Mooney<sup>2</sup>; Radcliffe Walker<sup>2</sup>; Keddon Powell<sup>4</sup>; <sup>1</sup>Aughinish Alumina Ltd; <sup>2</sup>Winalco; <sup>3</sup>Rinalco B.V.; <sup>4</sup>University of Limerick

The characterisation of bauxite ores, in particular the iron mineralogy, is critical when determining their processability. In this study, various Jamaican bauxite ores have been characterised by Rietveld X-ray powder diffraction (XRD) and Mössbauer spectroscopy. The only forms of iron minerals found are crystalline hematite and crystalline aluminogothite of relatively small crystallite size. Within digestion, the apatite structure formed is a sodium carbonate hydroxyapatite, and hence a source of soda loss. No evidence of boehmite reversion was found. Post-digestion, the specific surface area of the bauxite residue is strongly correlated with the goethite content, attributed to a decreased particle size, rather than variations in porosity or density. Possibilities for remediation have focussed on the transformation of goethite to hematite, with thermal treatment proving to be most encouraging to date.

## 9:00 AM

### Technological Characterization of Bauxite from Pará-Brazil: *Fernanda Silva*<sup>1</sup>; Francisco Garrido<sup>2</sup>; João Sampaio<sup>3</sup>; Marta Medeiros<sup>2</sup>; Rachel Santos<sup>1</sup>; Manuel Carneiro<sup>3</sup>; Lucimar S. Costa<sup>3</sup>; <sup>1</sup>IQ-UFRJ/CETEM; <sup>2</sup>IQ - UFRJ; <sup>3</sup>Centro de Tecnologia Mineral

The bauxite from Pará-Brazil is a mixture of minerals where the most important are: gibbsite (Al(OH)<sub>3</sub>), kaolinite (Al<sub>2</sub>[Si<sub>4</sub>O<sub>10</sub>](OH)<sub>2</sub>), quartz, hematite, goethite, rutile and octahedrite. In this work, a bauxite sample from Northeast of Pará-Brazil was crushed and ground in order to get the same size distribution at alumina production industry by Bayer process. After preparation, the sample (90%, < 0.21 mm and 40% < 43 μm) with reactive silica and alumina contents of 5.9 and 47.5%, respectively, was ground with water in a bar mill to 210 min. The ground samples were characterized infrared spectra (IR), X-ray diffraction (XRD), X-ray fluorescence (XRF) and scanning electron microscopy (SEM). Results show that no major bauxite bulk structure modification was observed as a consequence of the grinding process. An analytical method to quantify reactive silica and available alumina contents was also developed. The method is based

on alkaline bauxite digestion, potentiometric titration and atomic absorption spectrometry (F-AAS) techniques. The method accuracy and precision were checked by analysis of the IPT 131 certified bauxite reference.

**9:25 AM**

**Characterisation of Alumina and Soda Losses Associated with the Processing of Goethitic Rich Jamaican Bauxite:** *Keddon Powell*<sup>1</sup>; Luke Kirwan<sup>2</sup>; Desmond Lawson<sup>3</sup>; Ab Rijkeboer<sup>4</sup>; Kieran Hodnett<sup>1</sup>; <sup>1</sup>University of Limerick; <sup>2</sup>Aughinish Alumina Limited; <sup>3</sup>Winalco; <sup>4</sup>Rinalco B.V., Netherlands

Iron oxides occur in Jamaican bauxites predominantly in the mineral forms of goethite and hematite. The relative concentrations of these iron minerals, and their morphologies, in conjunction with the soluble phosphate and available alumina content, has a great impact on alumina refinery operations and associated operational costs. Of the iron minerals, goethite in the Bayer process is generally experienced as being adverse, facilitating alumina losses, sequestration of soda, and rendering the mud more difficult to settle. A fundamental knowledge of the components within Jamaican bauxite that contribute to alumina and soda losses is paramount to finding mitigating solutions. This study focuses on the various components of Jamaican bauxite residue material and examines their propensity to promote gibbsite reversion and their soda adsorption capacity.

**9:50 AM**

**Impact of Excess Synthetic Flocculent on Security Filtration:** *Jean-Marc Rousseaux*<sup>1</sup>; Pierre Ferland<sup>1</sup>; <sup>1</sup>Rio Tinto Alcan

Synthetic polymers derived from acrylic acid and acrylamide are used in the Bayer process to assist the separation of red mud residues from the liquor. These contemporary flocculants have replaced starch mainly because of their high efficiency found at relatively low dosage. However usage in excess of flocculant can lead to reduced performances in liquor filtration and/or operational problems due to build-up of compacted mud onto the vessel's internals such as the rake. This work outlines the results obtained from an intensive investigation carried out in one of RTA alumina refineries after the commissioning of the new high rate decanter and security filter facilities. The impact of carried-over flocculent and other operating parameters such as filteraid (TCA) dosage and total suspended solids (TSS) on liquor filterability have been evaluated and are discussed. The paper also includes the basis of a laboratory method to quantify flocculent in Bayer liquor at sub ppm level.

**10:15 AM**

**The Effects of Temperature, Hydrate Solids Concentration and Particle Size on Clarity in Laboratory Settling Tests:** *Scott Moffatt*<sup>1</sup>; Francis Bruey<sup>1</sup>; <sup>1</sup>Cytec Industries

An experiment with a full factorial design was carried out to estimate the effects of controlled changes in liquor temperature, solids concentration and particle size distribution on supernatant clarity in laboratory-scale settling tests, when the liquor is tested "as is" and after treatment with a flocculant. The experiment was carried out on two separate occasions to provide some information on the magnitude of experimental error in the test setup. Each of the factors had a statistically significant main effect on clarity when varied over a reasonable range such as could be encountered in practice; there were also some statistically significant interactions among the factors. Effect magnitudes and confidence intervals are reported, and the implications of the findings on the conduct and interpretation of laboratory testing and on the assessment of the performance of a plant scale hydrate classification circuit are discussed.

**10:40 AM Concluding Comments**

## Aluminum Alloys: Fabrication, Characterization and Applications: Materials Characterization

Sponsored by: The Minerals, Metals and Materials Society, TMS Light Metals Division, TMS: Aluminum Processing Committee  
Program Organizers: Weimin Yin, Williams Advanced Materials; Subodh Das, Phinix LLC; Zhengdong Long, Kaiser Aluminum Company

Wednesday AM

Room: 2004

February 18, 2009

Location: Moscone West Convention Center

*Session Chair:* Sooho Kim, General Motors

**8:30 AM**

**Influence of Heat Treatment on Low-Cycle Fatigue Behavior of an Extruded 6063 Aluminum Alloy:** Lijia Chen<sup>1</sup>; Chunyan Ma<sup>1</sup>; Yuxing Tian<sup>1</sup>; Xin Che<sup>1</sup>; Peter Liaw<sup>1</sup>; <sup>1</sup>Shenyang University of Technology

Low-cycle fatigue studies were performed under the total strain-amplitude-controlled mode for the extruded 6063 aluminum alloys with different heat-treatment states. The influence of heat treatment on the fatigue behavior of the alloy was determined. The experimental results show that the alloys with different heat-treatment conditions exhibit cyclic hardening, softening and stability. The solution plus aging treatment can increase the fatigue life of the alloy, while the solution treatment leads to a decrease in the fatigue life of the alloy. For the as-extruded 6063 alloy, a single-slope linear relation between the elastic-strain amplitude, or the plastic-strain amplitude, and reversals to failure is observed. However, for the extruded 6063 alloys subjected to both solution and solution plus aging treatments, the single-slope linear relation between the elastic-strain amplitude and reversals to failure is noted while a two-slope linear relation between the plastic-strain amplitude and reversals to failure is noted.

**8:50 AM**

**Coarsening Kinetics of Al-Li Alloys:** *Ben Fletcher*<sup>1</sup>; Martin Glicksman<sup>1</sup>; Kegang Wang<sup>2</sup>; <sup>1</sup>University of Florida; <sup>2</sup>Florida Institute of Technology

Phase coarsening in overaged Al-Li alloys is a diffusion-controlled process. Large particles grow by dissolution and mass transfer from smaller particles. Four binary Al-Li alloys were aged for times between 3-240 h at 225C, to yield various distributions of d' (Al<sub>3</sub>Li) precipitates. Transmission electron microscopy was used to image 10-100 nm diameter, spherical d' precipitates via centered dark-field techniques. TEM images were then autonomously analyzed using a novel Matlab® function to process and provide good statistical 3D results. Computer analysis provides objective characterization and fast image processing, allowing practical access to larger sample sizes. TEM results are compared with small angle X-ray scattering analysis. Results, including the particle size distribution and maximum particle size, agree with predictions from diffusion screening theory and a multi-particle diffusion model.

**9:10 AM**

**Multiple Scale FEM Simulation of Deformation and Damage of an Aluminum Alloy Sheet:** *Yansheng Liu*<sup>1</sup>; Xiyu Wen<sup>2</sup>; Randall Bowers<sup>1</sup>; Zhengdong Long<sup>2</sup>; Shridas Ningileri<sup>1</sup>; Subodh Das<sup>3</sup>; <sup>1</sup>SECAT Inc; <sup>2</sup>Center for Aluminum Technology, University of Kentucky; <sup>3</sup>Phinix LLC

Particles have significant influence on the formability of aluminum alloys. It is difficult to directly integrate the effect of particles into FEM model. In the current investigation, particle distribution in micro-scale was determined by optical microscope on multiple locations on the surface and along thickness direction of sheet metal. Material heterogeneity properties were derived based on micro-scale analysis and assembled as a macro-scale model to simulate deformation and damage. The result was used to explain some failure examples from industry operation.

**9:30 AM**

**Precipitation under Cyclic Strain in Solution-Treated Al-4wt%Cu I: Mechanical Behavior:** *Adam Farrow*<sup>1</sup>; Campbell Laird<sup>2</sup>; <sup>1</sup>Los Alamos National Laboratory; <sup>2</sup>University of Pennsylvania

Solution-treated Al-4wt%Cu was strain-cycled at ambient temperature and above, and the precipitation and deformation behaviors investigated by TEM. Anomalously rapid growth of precipitates appears to have been facilitated by a vacancy super-saturation generated by cyclic strain and the presence of a continually refreshed dislocation density to provide heterogeneous nucleation

sites. Texture effects as characterized by EBSD appear to be responsible for latent hardening in specimens tested at room temperature, with increasing temperatures leading to a gradual hardening throughout life due to precipitation. Specimens exhibiting rapid precipitation hardening appear to show a greater effect of texture due to the increased stress required to cut precipitates in specimens machined from rolled plate at an angle corresponding to a lower averaged Schmid factor. The accelerated formation of grain boundary precipitates appears partially responsible for rapid inter-granular fatigue failure at elevated temperatures, producing fatigue striations and ductile dimples coexistent on the fracture surface.

## 9:50 AM

**Precipitation under Cyclic Strain in Solution-Treated Al-4wt%Cu II: Precipitation Behavior:** Adam Farrow<sup>1</sup>; Campbell Laird<sup>2</sup>; <sup>1</sup>Los Alamos National Laboratory; <sup>2</sup>University of Pennsylvania

Solution-treated Al-4wt%Cu was strain-cycled at ambient temperature and above, and the precipitation behavior investigated by TEM. In the temperature range 100C to 200C, precipitation of theta-double-prime appears to have been suppressed, and precipitation of theta-prime promoted. Anomalously rapid growth of precipitates appears to have been facilitated by a vacancy supersaturation generated by cyclic strain, with a diminishing effect observed at higher temperatures due to the recovery of non-equilibrium vacancy concentrations. The theta-prime precipitates generated under cyclic strain are considerably smaller and more finely dispersed than those typically produced via quenching due to their heterogeneous nucleation on dislocations, and possess a low aspect ratio and rounded edges of the broad faces, due to the introduction of ledges into the growing precipitates by dislocation cutting. Frequency effects indicate that dislocation motion, rather than the extremely small precipitate size, is responsible for the observed reduction in aspect ratio.

## 10:10 AM

**A Continuous Cast AA2037 Al Alloy with Excellent High Cycle Fatigue Properties:** Qiang Zeng<sup>1</sup>; T. Zhai<sup>1</sup>; X. Y. Wen<sup>1</sup>; Z. Li<sup>2</sup>; <sup>1</sup>University of Kentucky; <sup>2</sup>Aleris International, Inc.

A continuous cast AA2037 Al-Cu alloy was precipitation heat treated at 470°C for 24 hrs before the final peak-aging. It was found that the alloy exhibited a fatigue strength of 210 MP, much higher than that (175 MP) of the same alloy peak-aged using a conventional age-hardening method for an Al-Cu alloy, while their tensile strengths were comparable, though the elongation was somewhat inferior to that of the conventionally peak-aged alloy. The superior high cycle fatigue strength of the alloy was likely to be due to the combination of precipitation hardening predominantly by T (Al<sub>20</sub>Cu<sub>2</sub>Mn<sub>3</sub>) phase and grain refinement by fast heating in salt-bath before the final peak-aging process. The results from this study indicate that it is advantageous to produce Al-Cu alloys with the continuous cast technology over the direct chill cast method, because of the high level of solid solution in the continuous cast Al hot band.

## 10:30 AM Break

## 10:45 AM

**Alloy Preparation Improvements at Alumar:** Fernanda Silva<sup>1</sup>; Jarbas Feitosa<sup>1</sup>; Affonso Bizon<sup>1</sup>; Sebastião Silva<sup>1</sup>; Cristino Campos<sup>1</sup>; <sup>1</sup>ALUMAR Consortium

To support Alumar's strategy of increase aluminum alloys production, process of preparing Al-Si alloy was investigated aiming for a higher efficiency on achieving the chemical composition, (measured as percentage of charges where the right chemical composition was obtained in first sample), lower master alloys consumption and reduction on furnace turnaround. The substitution of AlSr10% for AlSr15% on preparation of Al-Si modified alloys and tests regarding the use of cage for master alloy addition were discussed. Therefore, silicon pre-heating was evaluated aiming on a molten aluminum temperature loss reduction and consequently decrease on average furnace turnaround. The usage of copper scrap from anodes on Al-Cu alloys was also investigated showing considerable gains. This paper discusses the issues associated with "First Sample on Grade", and "Furnace Turnaround", for AlSi Alloy preparation, and examines the benefits that may be realized through a different approach to alloying, pre-heating process and standard preparation practice change.

## 11:05 AM

**Effect of Calcium on the Microstructure in Al-Si Alloys: Prediction of the Formation and Identification of Phases by EBSD:** Antonio Zaldivar-Cadena<sup>1</sup>; Alfredo Flores-Valdés<sup>2</sup>; Francois Brisset<sup>3</sup>; <sup>1</sup>Universidad Autónoma de Nuevo León; <sup>2</sup>CINVESTAV-IPN Unidad Saltillo; <sup>3</sup>CNRS - ONERA

Al-7Si-3Cu-Fe, Al-7Si-3Cu-Fe-0.5Mn, A319, A380 and Al-12Si-Mg-Ni-Cu-0.2Fe alloys containing 0.0020, 0.0040, 0.0080, 0.1 and 0.2 wt.% Ca were used in this research to study the effects of Ca additions on their microstructures and Brinell hardness. The Ca-containing A319 alloy was artificially aged using the T6 thermal treatment to verify the effect of calcium on the response of Al-Si alloys during heat treatment. Samples from the molten alloys were characterized by XRD, SEM/EDS and EBSD analysis. The path of phase formation was predicted using Thermo-Calc® software and validated with experimental results provided from Thermal Analysis DTA runs and microstructural characterization of the samples. Compounds which contain calcium-rich particles were consistent with that of the hexagonal CaAl<sub>2</sub>Si<sub>2</sub> intermetallic phase in all of the alloys used. Finally, it was found that Ca additions refined the eutectic silicon and coarsened the iron-rich intermetallics.

## Aluminum Reduction Technology: New Pot Technology and Pot Start-Up

Sponsored by: The Minerals, Metals and Materials Society, TMS Light Metals Division, TMS: Aluminum Committee

Program Organizers: Gilles Dufour, Alcoa Canada, Primary Metals; Martin Iffert, Trimet Aluminium AG; Geoffrey Bearne, Rio Tinto Alcan; Jayson Tessier, Alcoa Deschambault

Wednesday AM

Room: 2012

February 18, 2009

Location: Moscone West Convention Center

Session Chair: Ketil Rye, Elkem Aluminium ANS

## 8:30 AM

**Start-up of New Generation SY350/SY400 Pot:** Kangjian Sun<sup>1</sup>; Xiaodong Yang<sup>1</sup>; Yafeng Liu<sup>1</sup>; Jiaming Zhu<sup>1</sup>; <sup>1</sup>ShenYang Aluminium and Magnesium Institute (SAMI)

SAMI has designed a number of SY350/SY400 potlines in China in the last 6 years. One of them is the CHALCO Lanzhou branch smelter. Four out of six sections of the SY350 potline at Lanzhou smelter were started up in mid-2007, with the remaining two sections a year later using an improvised start-up method. Several more SY350/SY400 potlines will start-up before the end of this year. This paper will introduce the pre-heat and start-up method used at Lanzhou smelter, which will also be used to start-up other SY350/400 potlines.

## 8:50 AM

**The Hamburg Smelter – A Study of the Cathode Performance:** Till Reek<sup>1</sup>; <sup>1</sup>Trimet Aluminium AG

In December 2005 the Hamburg aluminum smelter was shut down. In 2006, Trimet Aluminum AG was able to purchase the assets and successfully restarted the potlines in 2007. In December 2007 the plant was operating at full capacity again, after facing serious supply limitation of lining materials throughout the year. To be able to reach full production at record time, unproven Ukrainian and Chinese cathodes had to be acquired. Until August 2008 45 pots with Ukrainian cathodes and 46 pots with Chinese cathodes were started. In addition to these, 149 old linings that had been idle for more than 1 year were restarted. This paper highlights operational experience with these different groups of pots and describes the success story of the first year of operation after the restart without losing a single pot.

## 9:10 AM

**Spent Si<sub>3</sub>N<sub>4</sub> Bonded SiC Sideline Materials in Aluminium Electrolysis Cell:** Zhaohui Wang<sup>1</sup>; Egil Skybakmoen<sup>2</sup>; Tor Grande<sup>1</sup>; <sup>1</sup>Norwegian University of Science and Technology; <sup>2</sup>SINTEF

Si<sub>3</sub>N<sub>4</sub> bonded SiC sideline materials with different ages in operation have been analyzed by X-ray diffraction, electron microscopy and chemical analysis. The chemical degradation of the upper and the lower part of the sideline has been demonstrated to be substantially different. The upper part of the sideline has been subjected to oxidation by the pot gas and the main degradation product



found was  $\text{Si}_2\text{ON}_2$ . The lower part was infiltrated by  $\text{Na(g)}$  diffusing from the carbon cathode resulting in formation of  $\text{Na}_2\text{SiO}_3$  as the main oxidation product. Chemical reactions are proposed based on the experimental findings. The diffusion of the degradation species into the side lining has been modeled by a finite element model. The degradation overtime results in the change of the thermal conductivity of the sidelining materials.

#### 9:30 AM

**2008: A Milestone in the Development of the DX Technology:** B. Kakkar<sup>1</sup>; Marc de Zelicourt<sup>1</sup>; Abdulla Zarouni<sup>1</sup>; Abdulla Kalban<sup>1</sup>; Maryam Al-Jallaf<sup>1</sup>; Ibrahim Baggash<sup>1</sup>; Kamel Alaswad<sup>1</sup>; <sup>1</sup>Dubal

From September to December 2005, five prototype DX Reduction Cells were commissioned at the Jebel Ali smelter. They were progressively brought from 325 kA to 345 kA with a current efficiency greater than 96%. In 2008, the DX technology entered the industrial phase of its history with the commissioning of the first commercial Potline of 40 improved DX Reduction Cells from February end to April. The start-up at 340 kA went very smoothly. The pots reached soon 350 kA with excellent operating parameters. The results achieved so far show that there is a potential for further improvement. Meanwhile, in Abu Dhabi, the steady progress of the construction of the 700 kt EMAL phase 1 smelter takes DUBAL latest technology closer to yet another milestone with its implementation on a very large scale.

#### 9:50 AM Break

#### 10:10 AM

**AP50 Performances and New Development:** Ben-Aissa Benkahla<sup>1</sup>; Oliver Martin<sup>1</sup>; T. Tomasio<sup>1</sup>; <sup>1</sup>Rio Tinto Alcan

After 3 years of continuous improvement toward the industrial version which will be implemented in Jonquière (Canada), the AP50 cell has achieved very good technical performances on the LRF platform in Saint Jean de Maurienne (France). The detailed technical results are presented: at the same time, high amperage and low energy consumption have been reached. The reliable ALPSYS control system has demonstrated low Anode Effect rates and tighten thermal control. Pending availability of the future Jonquière development platform, an upgraded new version of the AP50 able to cope with higher amperage has been developed. The results of the first prototype cell are very promising.

#### 10:30 AM

**HAL4e – Hydro's New Generation Cell Technology:** Asgeir Bardal<sup>1</sup>; Christian Droste<sup>1</sup>; Frank Øvstetun<sup>1</sup>; Elin Haugland<sup>1</sup>; Elmar Wedershoven<sup>1</sup>; Morten Liane<sup>1</sup>; Bjørn Erik Aga<sup>1</sup>; Sven Olof Ryman<sup>1</sup>; Albert Berveling<sup>1</sup>; Morten Karlsen<sup>1</sup>; Markus Fechner<sup>1</sup>; Tor Helge Vee<sup>1</sup>; <sup>1</sup>Hydro Aluminium Metal

HAL4e is Hydro's new generation cell technology. The first pilot cells have operated at 420 kA at the Årdal Test Centre since the summer of 2008. The paper covers selected topics of economics (capex and opex), modelling and cell development, early operational experience, as well as elements in the development pipeline, which will be included in future versions of the technology.

#### 10:50 AM

**The Advancement of New Generation SY350 Pot:** Zhu Jia Ming<sup>1</sup>; Yang Xiaodong<sup>1</sup>; Liu YaFeng<sup>1</sup>; Sun KangJian<sup>1</sup>; <sup>1</sup>Shenyang Aluminum and Magnesium Engineering and Research Institute (SAMI)

SAMI's high amperage SY350 pot technology was developed in 2002. Presently, there are three SY350 potlines in operation in China and nine more in design phase. Over the years, SAMI has made further improvement on the SY350 pot technology and has since increase the pot amperage up to 378kA. SAMI has also developed the SY400 pot technology and has installed a total of 16 trial pots at one of SAMI's latest designed potline. The trial pots are currently operating at 402kA and have been in operation successfully for more than 14 months. Good performance obtained from the trial pots with high current efficiency and low energy consumption. Presently, there are two SY400 potlines under design. This paper will introduce the SY350 pot technology and describe some of the key advancements of the technology to date, including aspects of the SY400 trial pots.

## Aluminum Reduction Technology: Process Control

Sponsored by: The Minerals, Metals and Materials Society, TMS Light Metals Division, TMS: Aluminum Committee

Program Organizers: Gilles Dufour, Alcoa Canada, Primary Metals; Martin Iffert, Trimet Aluminium AG; Geoffrey Bearne, Rio Tinto Alcan; Jayson Tessier, Alcoa Deschambault

Wednesday AM

Room: 2001

February 18, 2009

Location: Moscone West Convention Center

Session Chair: Gary Tarcy, Alcoa Inc

#### 8:30 AM

**Correlation between Anode Properties and Cell Performance:** Trond Eirik Jentoftsen<sup>1</sup>; Hogne Linga<sup>1</sup>; Bjørn Erik Aga<sup>1</sup>; Vidar Geir Christensen<sup>1</sup>; Frode Hoff<sup>1</sup>; Inge Holden<sup>1</sup>; <sup>1</sup>Hydro Aluminium

The performance of a cell operating at high current density depends on heat balance, interpolar distance, adaptive process control system etc. In addition control of the raw materials; alumina, covering material and anodes is necessary. Parallel with current increase Hydro has worked continuously with improving anode quality. To succeed one needs measuring techniques for anode quality which reflect the cell performance. The equivalent temperature, which has been presented earlier, reflects the baking level of the anodes. In addition an internal gravimetric method for measuring the CO<sub>2</sub> and air reactivity is applied. Material brushed off after analysis is used together with the weight loss from reactivity to calculate a dust index. Performance data for a modern high amperage cell is presented showing the dependence of current efficiency on equivalent temperature and dust index of anodes. The need for improved anode quality with decreased interpolar distance is also discussed.

#### 8:50 AM

**Multivariate Statistical Process Monitoring of Reduction Cells:** Jayson Tessier<sup>1</sup>; Thomas Zwirz<sup>2</sup>; Gary Tarcy<sup>3</sup>; Richard Manzini<sup>3</sup>; <sup>1</sup>Alcoa Deschambault; <sup>2</sup>Alcoa Inc., Massena West Smelter; <sup>3</sup>Alcoa Inc., Alcoa Technical Center

Modern smelting control systems have large amounts of available data. The information in this data is often underutilized due to inefficient information extraction from databases containing a large number of noisy and highly collinear measurements. The difficulties associated with analyzing such large databases can limit process engineers to analyze a few variables at a time using either univariate control charts or simple x/y correlations to assess the efficiency of reduction cells. Principal Component Analysis has shown the capability to cope with large messy databases (including collinearity, missing data points, and noisy measurements). This technique generates statistics to determine if a pot is in multivariate control by projecting the pot data onto a reference model. It is then possible to extract information that highlights variables with a significant impact on driving the out-of-control pot. Alcoa Inc. is using multivariate Principal Component techniques for potroom problem solving. Several applications will be discussed.

#### 9:10 AM

**Development of a Multivariate Process Control Strategy for Aluminium:** Marco Stam<sup>1</sup>; Mark Taylor<sup>2</sup>; John Chen<sup>2</sup>; Albert Mulder<sup>1</sup>; Renuka Rodrigo<sup>3</sup>; <sup>1</sup>Aluminium Delfzijl B.V.; <sup>2</sup>University of Auckland; <sup>3</sup>Heraeus Electro-Nite LLC.

Process intensification is used worldwide to maximize economic as well as sustainable operation of existing chemical plants. The aluminium reduction process has strong interactive multivariate characteristics with limited process observability and responses which are non-linear and vary over a wide range of time scales. Contrary to application of more compensating single input-single output loops, this paper describes a process control strategy based on passivated responses to common cell behaviours, advanced detection of abnormalities, cause-specific corrective or preventative control actions. Statistical multivariate control surfaces are identified for alumina feed, bath and liquidus temperature measurements. Online root cause analysis and subsequent quality of decision-making have been improved through soft sensors which fingerprint individual failure mechanisms. A module-based approach allows flexible configuration of the overall control philosophy, which has now been tested on industrial

scale resulting in significantly higher current efficiency and reduced energy consumption. These will be discussed in the paper.

## 9:30 AM

**New Feed Control for VSS Side Break Pots:** *Nilton Nagem*<sup>1</sup>; Carlos Braga<sup>1</sup>; João Fonseca Neto<sup>2</sup>; Rodrigo Batista<sup>3</sup>; Frenando Costa<sup>1</sup>; Gustavo Andrade<sup>2</sup>; <sup>1</sup>ALUMAR; <sup>2</sup>UFMA - Universidade Federal do Maranhão; <sup>3</sup>ALCOA - Poços de Caldas

Sustainable aluminum production should be achieved by reducing greenhouse gas emissions (GHG) due to anode effect decrease. Reducing anode effect frequency is only possible by improving potroom operations and controls. A new control design should be developed to improve alumina control. Alumina control for a Vertical Soderberg Side Break is a hard task. The actual feed adjustment for the pot is done on a manual daily basis and the feed cycle is every 2 hours, the new control will adjust automatically the amount poured into the pot for each cycle. The algorithm calculates the resistance curvature by a Least Square Regression and a delta from the resistance is calculated too. This information provides the amount of alumina that will be feeding in the next cycle without mucking the pot and avoiding anode effect.

## 9:50 AM

**Controlled Cooling of Aluminium Smelting Cell Sidewalls Using Heat Exchangers Supplied with Air:** *Sankar Namboothiri*<sup>1</sup>; Pascal Lavoie<sup>1</sup>; David Cotton<sup>1</sup>; Mark Taylor<sup>1</sup>; <sup>1</sup>Light Metals Research Centre

Aluminium pot shells have increased in temperature and heat flow in the recent years. Removal of heat from cell sidewalls for the purposes of temperature control and ledge maintenance in smelters presently takes the form of compressed air impingement directly on the shell. These air lances cool in a non-uniform way, are extremely energy inefficient, adversely impact on the workplace environment due to the associated noise and dust, and offer no opportunity for energy recovery in the future. The Light Metals Research Centre (LMRC) has developed a technology with the capability of providing controlled cooling to sidewalls using easily installed heat exchangers, with lower air consumption. LMRC has an in-house dedicated testing facility for the development and demonstration of sidewall cooling based on sidewall heat exchangers supplied with air. This paper reports the experimental results obtained in the testing facility and critically analyses the practicality of this technology.

## 10:10 AM Break

## 10:30 AM

**Challenges in Power Modulation:** *David Eisma*<sup>1</sup>; Pretesh Patel<sup>2</sup>; <sup>1</sup>Trimet Aluminium AG; <sup>2</sup>The Light Metals Research Centre, University of Auckland

Due to the increasing power prices and the increase in the spread between hourly power prices, various European smelters have started doing power modulation. Amperage is increased during the usually cheaper night hours, while it is lowered during the day. The maximum leverage for power modulation can be achieved by a constant anode-to-cathode distance (ACD) approach. However, this solution has the biggest negative impact on the cell thermal behaviour. Therefore, it is important to evaluate the effects of extreme scenarios, ranging between a "constant ACD" approach and a "constant heat" approach. Typically, reduction cell operations are tuned to near constant amperage, while the cell voltage is being used to adjust the power input into the cells. No matter what modulation approach is chosen, traditional voltage-based control should be replaced by a purely energy-based control. This paper outlines some of the challenges that TRIMET Essen encountered in this process.

## 10:50 AM

**Electrical Power Availability Optimization at Alcoa Deschambault's Smelter:** *Vincent Letellier*<sup>1</sup>; Norman Plante<sup>1</sup>; <sup>1</sup>Alcoa Canada

Today's energy scarcity affects technology and economic choices in most industries. Even if Quebec is a huge producer of hydro-electricity, Alcoa's plants located in this province, are facing the issue. This situation forces optimization of available power in order to increase plants productivity. One way to achieve this goal is to increase power utilization directly at the electrical input of the smelter, allowing a higher operating amperage in the potline which is translated into more aluminum production. Some modifications have been made to the electric control system, at the main substation of the plant. Those modifications allowed Alcoa Deschambault's smelter to use 1.6 MW of power over its previous average consumption, with the same contract allowance. The rebuilt control system results in an utilization factor (percentage of actual power usage over power contract) up to 99.8% on a monthly basis. A significant gain for a very low capital cost!

## 11:10 AM

**Increasing Electrolysis Pot Performances through New Crustbreaking and Feeding Solutions:** *Nicolas Dupas*<sup>1</sup>; <sup>1</sup>ECL

Crustbreaking and feeding devices are key elements of the modern aluminium reduction technology. While the crustbreaker's concept has been implemented since the 1970s, its maintainability, reliability and performance monitoring are becoming key subjects for smelters. Increasing cell temperatures and frozen bath crusts put growing strains on the crustbreakers. Their performance is a key factor of the smelter's efficiency and productivity. This is why specific control systems validating the crustbreaking function have been developed. But it is now necessary to go further as the mechanical components of the crustbreakers are submitted to the increasingly aggressive environment of the pot. New functions protecting the crustbreaker's chisel from the acidic attacks of the bath have been developed, also opening new possibilities for pot process control (anode effects frequency control or bath level measurement). The immediate gain is not only on productivity but also on pot operator's health and safety, and environmental impact reduction.

## Biological Materials Science: Cell-Biomaterial Interactions

Sponsored by: The Minerals, Metals and Materials Society, TMS Structural Materials Division, TMS Electronic, Magnetic, and Photonic Materials Division, TMS: Biomaterials Committee, TMS/ASM: Mechanical Behavior of Materials Committee  
Program Organizers: Ryan Roeder, University of Notre Dame; John Nychka, University of Alberta; Paul Calvert, University of Massachusetts Dartmouth; Marc Meyers, University of California

Wednesday AM  
February 18, 2009

Room: 3014  
Location: Moscone West Convention Center

*Session Chairs:* John Nychka, University of Alberta; Devesh Misra, University of Louisiana

## 8:30 AM Invited

**Modulated Delivery of Biomolecules for Manipulating Responses at the Cell-Biomaterial Interface:** *David Puleo*<sup>1</sup>; <sup>1</sup>University of Kentucky

The goal of many drug delivery devices has been to obtain zero-order release kinetics. Wound healing, however, is a dynamic process involving numerous biomolecules that trigger a sequence of cellular events, including chemotaxis, proliferation, and differentiation. For example, analysis of growth factor expression in callus during bone fracture healing has revealed a complex sequence of several biomolecules. Therefore, to achieve desired responses at the cell-biomaterial interface, modulated delivery of one or more bioactive agents is expected to generate the greatest effect. To this end, we have been developing different polymeric systems to vary the release profiles of osteotropic (bone-active) molecules. Release periods ranged from days through months, and the molecules delivered ranged from small molecule drugs through plasmid DNA. Results show that cell behavior can be manipulated by modulating the timing of one or more osteotropic biomolecules. Properly designed controlled release devices have the potential to enhance localized tissue repair.

## 9:00 AM

**Cell Behavior on Thickness Graded Polyacrylamide Hydrogels:** *James Dahlman*<sup>1</sup>; John Maloney<sup>1</sup>; Krystyn Van Vliet<sup>1</sup>; <sup>1</sup>Massachusetts Institute of Technology

Mechanically compliant substrata provide a model material system for investigating cellular responses to localized mechanical environments. Previous work has demonstrated strong correlations between cellular properties and substrate mechanics by varying properties such as chemical composition and crosslink density to obtain stiffness gradients. Though these approaches are effective, techniques capable of producing mechanical variation without chemical changes are also desired. Here we outline a processing technique by which hydrogel thickness gradients were generated while maintaining constant compositional properties as well as constant biomolecular ligand density. Changes in the thickness of constant-stiffness coatings are predicted to alter the effective stiffness detected by adherent, traction-exerting tissue cells. We evaluate these predictions by quantifying fibroblast cell behavior on thickness-graded polyacrylamide hydrogels.

9:20 AM

**Nanograin/Ultrafine-Grained Structures Formed by Phase Reversion in Austenitic Stainless Steel Improves Cellular Activity:** *Wah Wah Thein-Han*<sup>1</sup>; Devesh Misra<sup>1</sup>; Mahesh Somani<sup>2</sup>; Pentti Karjalainen<sup>2</sup>; <sup>1</sup>University of Louisiana; <sup>2</sup>University of Oulu

We describe here the combination of fundamental aspects of materials science and engineering with biological sciences in the modulation of cell-substrate response of pre-osteoblasts on ultra-fine grained (UFG)/nanograin (NG) austenitic stainless steels. UFG/NG austenitic stainless steel were processed by a novel procedure involving controlled phase reversion of strain-induced martensite in a cold rolled austenitic stainless steel. The cellular response of UFG/NG austenitic stainless steel is compared with conventional coarse-grained austenitic stainless steel. Interestingly, the proliferation, adhesion, morphology and spread of pre-osteoblasts were significantly different and enhanced on UFG/NG austenitic stainless steel in comparison to conventional coarse-grained austenitic stainless steel. This was implied by cell-density measurements and observations made using fluorescence microscopy and scanning electron microscopy. The improved cellular response ascribed to UFG/NG structures opens up a new avenue for nanostructured materials with combined benefits of biological and mechanical properties such as high strength/weight ratio.

9:40 AM Invited

**Biomimetics – Learning from Diamonds:** Andrei Sommer<sup>1</sup>; Dan Zhu<sup>1</sup>; Kai Brühne<sup>1</sup>; Hans Fecht<sup>1</sup>; <sup>1</sup>Ulm University

There is increasing observational evidence for an implication of the order of interfacial water layers in biology, for instance in processes of cellular recognition and during first contact events, where cells decide upon survival or entering apoptosis. Experimental methods allowing access to the order of interfacial water layers are thus crucial in biomedical engineering. Here we show that interfacial water structures can be nondestructively analysed on nanocrystalline diamond. Results open the gate to a new chapter in the design of biomaterials inspired by biomimetic principles. Recent results on the role of surface modifications and chemical surface termination of nanocrystalline CVD grown diamond layers for biocompatible and biomimetic materials will be discussed.

10:10 AM Break

10:30 AM Invited

**Inkjet Printing of Multilayer Structures of Biopolymers and Cells:** *Paul Calvert*<sup>1</sup>; Skander Limem<sup>1</sup>; <sup>1</sup>University of Massachusetts, Dartmouth

We are using inkjet printing to deposit patterns of silk, collagen and ionic complexes of polypeptides. These guide the growth of cells deposited on the patterns. Yeast has been printed onto agar and the effect of overprinted biopolymer layers on the growth of yeast is being studied. Human fibroblasts and mesenchymal stem cells can also be printed and subsequently grown. This allows organized structures of differing cells and biopolymers to be printed in order to study cell-cell interactions.

11:00 AM

**Functional Relationship of Collagen Based Biomimetic Composites with Integral Cell Membrane Proteins:** Devendra Dubey<sup>1</sup>; Vikas Tomar<sup>1</sup>; <sup>1</sup>University of Notre Dame

Integral cell membrane proteins play an important role in structural integrity as well as adhesion properties of eukaryotic cells. An additional function of integral proteins may be the determination of cell response based on interactions with external stimuli from biofunctional materials such as drug delivery nanoparticles etc. In the presented research analyses of the interaction of cell membrane proteins with tropocollagen (COL) based COL-hydroxyapatite (HAP) biomimetic composite structures are presented. The analyses are performed using molecular dynamics (MD) method in a combined quantum mechanical (QM)-molecular mechanics (MM) framework. The focus is on understanding the free energy change and entropic variation based interactions of the nanocomposites with the cell membrane proteins that ultimately lead to variation in cell membrane proteins' adhesion behavior as well as their molecular conformation. Literature experiments related to cell adhesion and protein-protein interactions are also analyzed in light of presented simulation results.

11:20 AM

**Interactions of Microbes with Semiconductor Oxides: Adsorption and Membrane Damage:** *Qi Li*<sup>1</sup>; P. Wu<sup>1</sup>; J. Shang<sup>1</sup>; <sup>1</sup>University of Illinois at Urbana-Champaign

Microbial interactions with semiconductor oxides were examined on nitrogen-doped titanium oxides (TiONs) by atomic force microscopy, scanning and electron microscopy, fluorescence microscopy, and cell culture analysis. MS-2 virus was found to strongly adsorb onto TiONs and the adsorption was primarily controlled by the electrostatic force between the TiON surface and MS-2 virus. Upon light illumination, charge transfer with water created oxidative radicals on the semiconductor surface. These radicals induced visible damages on the cell membrane in forms of membrane thinning and perforations, leading to cell deaths.

11:40 AM

**Quantitative Assessment of Antibacterial and Antifungal Activities of Copper Vermiculite:** *Bowen Li*<sup>1</sup>; Jiann-Yang Hwang<sup>1</sup>; Susan Bagley<sup>1</sup>; <sup>1</sup>Michigan Technological University

Copper vermiculite is an excellent antimicrobial agent. To assess the antimicrobial durability of copper vermiculite, the antibacterial and antifungal activities of copper vermiculite against *E. coli* and *Aspergillus niger* were quantitatively investigated. The minimum inhibitory concentration of copper vermiculite against *E. coli* and *Aspergillus niger* were also determined.

## Bulk Metallic Glasses VI: Fatigue and Other Properties

Sponsored by: The Minerals, Metals and Materials Society, TMS Structural Materials Division, TMS/ASM: Mechanical Behavior of Materials Committee  
Program Organizers: Peter Liaw, The University of Tennessee; Hahn Choo, The University of Tennessee; Yanfei Gao, The University of Tennessee; Gongyao Wang, University of Tennessee

Wednesday AM

February 18, 2009

Room: 3007

Location: Moscone West Convention Center

Session Chairs: Jurgen Eckert, IFW Dresden; Christopher Schuh, MIT

8:30 AM Invited

**How to Improve the Deformability of Bulk Metallic Glasses:** *Jurgen Eckert*<sup>1</sup>; <sup>1</sup>IFW Dresden

Metallic glasses have mechanical properties that make them attractive candidates for a variety of structural and functional applications. One drawback still limiting such applications is their tendency for shear localization upon deformation. To circumvent such limitations, concepts of creating heterogeneous materials with different type and length-scale of phases have been followed to control the mechanical properties by proper alloy and microstructure design. The recent developments along this line will be summarized and new results for different types of bulk metallic glasses and composites will be presented to illustrate how the mechanical properties can be tuned by appropriate phase and microstructure control. In all these cases the details of the metastable phase formation are closely linked with optimized processing conditions required to form the desired microstructure. The possible mechanisms that govern the deformation behavior will be discussed and linked with the overall plastic deformability and the fracture of the material.

8:45 AM Invited

**Optimized Adhesive Bonding to Bulk Metallic Glass Substrates:** *Reinhold Dauskardt*<sup>1</sup>; Jeffrey Yang<sup>1</sup>; Mark Oliver<sup>1</sup>; <sup>1</sup>Stanford University

A range of applications of bulk metallic glass alloys involve the need for high-performance adhesive bonds capable of reliably operating in harsh chemical, temperature and loading environments. These bonds cannot be formed with conventional epoxy bonds. We describe a range of strategies for forming strong adhesive bonds using a conditioned oxide on the metallic glass substrate, an optimized sol-gel layer designed to improve adhesion to both the oxide and the metallic glass, and a high-performance epoxy resin. We describe methods to characterize the adhesive properties and also techniques to simulate the metal oxide on silicon wafers so that the subsequent adhesive sol-gel layers and epoxy can be optimized without the need for metallic glass substrates. Adhesive



properties of the joint together with subcritical debonding behavior in moist environments and fatigue loading will be presented.

## 9:00 AM

**Corrosion and Fatigue Behavior of Zr-Based Bulk-Metallic Glasses:** *Aaron Wiesl<sup>1</sup>; Gongyao Wang<sup>2</sup>; Marios Demetriou<sup>1</sup>; Peter Liaw<sup>2</sup>; William Johnson<sup>1</sup>;* <sup>1</sup>California Institute of Technology; <sup>2</sup>University of Tennessee

The ZrTiBe + Late Transition Metals (LTMs) system was studied for corrosion resistance in chloride-containing acidic environments. The compositional dependence of mass loss versus time in 37% HCl was explored and an empirical parameter based on an average electronegativity was found to adequately correlate the corrosion performance. The best composition was free of LTMs and lost less mass than Ti-6Al-4V or 316L stainless steel. Two alloys with "good" corrosion resistance in 37% HCl were subjected to high cycle fatigue experiments in air and 0.6M NaCl using a compression-compression geometry at 10Hz. An improvement in the corrosion fatigue endurance limit was observed over previously tested Zr-based glasses and this improvement is attributed to the enhanced corrosion resistance of the tested alloys. This work is supported by the NSF International Materials Institutes Program DMR-0231320, with Dr. C Huber as the contract monitor, and by the Office of Naval Research ONR06-251 0566-22

## 9:10 AM Invited

**Cyclic Hardening in Metallic Glasses:** *Christopher Schuh<sup>1</sup>; Corinne Packard<sup>1</sup>; Naser Al-Aqeeli<sup>1</sup>;* <sup>1</sup>MIT

This talk will describe our recent systematic nano-scale studies of cyclic loading in metallic glasses, which contribute to a mechanistic understanding of fatigue damage. Using a nanoindenter, we apply load cycles in the elastic regime, and study the effect of their amplitude, rate, and number on the local structure and strength of the glass. In general, we find that such load cycling leads to a shift in the nanoscale strength distribution of the glass, requiring higher loads to initiate a shear band. Our observations also offer some explanation for a number of reported features of glass fatigue, including most notably the fatigue endurance limit and striation spacing. To understand the process of sub-critical cyclic strengthening, we consider the potential for shear transformation zone activation under the point of contact, and specifically along the shear band path. Efforts to directly observe structural changes in cyclically deformed specimens are also discussed.

## 9:25 AM

**Highly Toughened Metallic Glass In-Situ Matrix Composites:** *Maximilien Launey<sup>1</sup>; Douglas Hofmann<sup>2</sup>; Jin-Yoo Suh<sup>2</sup>; William Johnson<sup>2</sup>; Robert Ritchie<sup>1</sup>;* <sup>1</sup>Lawrence Berkeley National Laboratory & University of California Berkeley; <sup>2</sup>California Institute of Technology

The potential for catastrophic failure associated with rapid propagation of shear bands is a concern for the utilization of BMGs in structural applications. For more reliable application, shear banding must be controlled using design strategies that involve the introduction of second phases. The fracture and fatigue behavior of a new class of ZrTiNbCuBe BMG matrix composite with in-situ dendritic phase was examined. Semi-solid processing was used to optimize the volume fraction, morphology, and size of dendrites in order to constrain the initial deformation band to the same length scale (~1micron) as the composite microstructure. Toughening mechanisms result in resistance-curve characteristics with a maximum measurable fracture toughness of  $K_{IC} \sim 145 \text{ MPa} \cdot \text{m}^{1/2}$  based on thickness limitations, and a fatigue limit at stress amplitude ~25% of the tensile strength, comparable that of high-strength steel. Such results are considered in the context of understanding the salient mechanisms responsible for the impressive crack arrest capabilities.

## 9:35 AM

**Thermomechanical Behavior of a Cu50Hf41.5Al8.5 Bulk Metallic Glass Following Cyclic Elastic Compression:** *Rainer Hebert<sup>1</sup>; Arif Mubarak<sup>1</sup>;* <sup>1</sup>University of Connecticut

Cyclic elastic compression-compression tests have been conducted with amorphous Cu50Hf41.5Al8.5 rods. Test parameters include the strain amplitude, the number of elastic compression cycles, and the frequency. Experimental analyses have focused mainly on differential scanning calorimetry (DSC) and thermomechanical analysis (TMA). Modulated TMA allows for a separation of the reversing true thermal expansion from the non-reversing structural relaxation and viscous effects. Changes in the elastic constants at room temperature following all elastic deformation conditions remain within the uncertainty of the resonant ultrasound measurements. Changes in the isochronal DSC and non-

reversing TMA measurements, however, agree with an effect of the cyclic elastic deformation on the amorphous atomic configuration that emulates a sub-T<sub>g</sub> annealing. A phenomenological relation between the reduced free volume and the forcing parameters could be established based on the free volume theory. The results indicate that sustained elastic deformation offers a mechanical approach to modifying the amorphous atomic configuration.

## 9:45 AM Invited

**Stress Corrosion and Corrosion Fatigue Crack Growth in Zr-Based Bulk Metallic Glass:** *Yoshikazu Nakai<sup>1</sup>; Yasunori Yoshioka<sup>1</sup>;* <sup>1</sup>Kobe University

Crack propagation tests on a Zr-based bulk metallic glass were conducted either in aqueous sodium chloride solutions or high purity water. Crack growth experiments were conducted under cyclic loading at a stress ratio of 0.1 or 0.5 under a loading frequency of 20 or 1.0 Hz. The experiments were also conducted under a sustained load. Although the crack growth rate in high purity water was almost identical to that in air, the rate in NaCl solution was much higher than that in air even in a very low concentration of NaCl such as 0.01%. In 3.5% NaCl solution, the time-based crack propagation rate during cyclic loading, da/dt, was determined by the maximum stress intensity factor, K<sub>max</sub>, but was independent of the loading frequency and the stress ratio, and the rate was almost identical to that of environment-assisted cracking under a sustained load.

## 10:00 AM Break

## 10:10 AM

**Fatigue Characteristics of Metallic Glass Foam:** *Gongyao Wang<sup>1</sup>; Marios Demetriou<sup>2</sup>; Joe Schramm<sup>2</sup>; Peter Liaw<sup>1</sup>; William Johnson<sup>2</sup>;* <sup>1</sup>University of Tennessee; <sup>2</sup>California Institute of Technology

Metallic glasses are able to deform plastically when the specimen dimensions fall below a critical size. Metallic-glasses foams that consist of struts having thicknesses below this critical size demonstrate good plastic deformability and yet retain a considerable fraction of the amorphous metal strength. Metallic-glass foams are presently being considered as energy-absorbing structures to mitigate impact, and as scaffold material for biomedical implants. These considerations require the study of the fatigue behavior. Uniaxial compression-compression fatigue experiments were performed on Pd-based metallic glass foams. Because the strength of foams decreases with increasing porosity, the predicted yield strength is employed to normalize the applied maximum stress. A clear relationship between the ratio of the applied maximum stress to yield strength and the cycles to failure is found, which is similar to the fatigue S (applied stress) - N (lifetime) curves for monolithic BMGs. A mechanistic understanding of the fatigue behavior will be proposed.

## 10:20 AM Invited

**Intrinsic and Extrinsic Factors Affecting the Plasticity/Toughness of Bulk Metallic Glasses:** *John Lewandowski<sup>1</sup>;* <sup>1</sup>Case Western Reserve Univ

The flow and fracture behavior of bulk metallic glasses are affected by both intrinsic and extrinsic factors that affect the both the magnitude of mechanical properties as well as the scatter in mechanical properties measured. Examples will be chosen from the authors work as well as those from the literature in order to illustrate some of the various factors that can affect the mechanical properties of these emerging materials.

## 10:35 AM

**Electrochemical Behaviors of Nickel-Based Metallic Glasses in Aqueous Solutions:** *Lu Huang<sup>1</sup>; Shujie Pang<sup>1</sup>; Ruijuan An<sup>1</sup>; Peter Liaw<sup>2</sup>; Tao Zhang<sup>1</sup>;* <sup>1</sup>Beihang University; <sup>2</sup>University of Tennessee, Knoxville

Electrochemical behaviors of specific nickel-based metallic glasses including Ni<sub>61</sub>Zr<sub>28</sub>Nb<sub>7</sub>Al<sub>4</sub>, Ni<sub>40</sub>Cu<sub>5</sub>Ti<sub>6.5</sub>Zr<sub>28.5</sub>Al<sub>10</sub>, Ni<sub>59</sub>Zr<sub>16</sub>Ti<sub>13</sub>Si<sub>3</sub>Sn<sub>2</sub>Nb<sub>7</sub> and [(Ni<sub>0.6</sub>Fe<sub>0.4</sub>)<sub>0.75</sub>B<sub>0.2</sub>Si<sub>0.05</sub>]<sub>96</sub>Nb<sub>4</sub> (at.%) were studied in aqueous solutions. Amorphous ribbons were prepared by melt spinning. Potentiodynamic polarization tests and static-immersion tests were performed at room temperature in 0.5M H<sub>2</sub>SO<sub>4</sub>, 1M HCl, and 3 mass% NaCl. Surface morphologies after immersion tests were observed by the scanning-electron microscopy (SEM). It is found that the Ni<sub>59</sub>Zr<sub>16</sub>Ti<sub>13</sub>Si<sub>3</sub>Sn<sub>2</sub>Nb<sub>7</sub> amorphous alloy exhibited a poor corrosion resistance in different aqueous solutions. Both Ni<sub>61</sub>Zr<sub>28</sub>Nb<sub>7</sub>Al<sub>4</sub> and Ni<sub>40</sub>Cu<sub>5</sub>Ti<sub>6.5</sub>Zr<sub>28.5</sub>Al<sub>10</sub> amorphous alloys exhibited a good corrosion resistance in a 0.5M H<sub>2</sub>SO<sub>4</sub> solution, but susceptible to pitting corrosion in 1M HCl, and 3 mass% NaCl due to the existence of chlorine ion. [(Ni<sub>0.6</sub>Fe<sub>0.4</sub>)<sub>0.75</sub>B<sub>0.2</sub>Si<sub>0.05</sub>]<sub>96</sub>Nb<sub>4</sub> amorphous alloy possesses an excellent corrosion resistance in different solutions with wide passive regions and low passive current densities. This work is supported by IGERT,IMI, and NSFC.

10:45 AM

**Influence of Laser Melting on Microstructure and Properties of Amorphous Coatings Deposited by High Velocity Oxyfuel Deposition Method:** *Greg Kusinski<sup>1</sup>; Jan Kusinski<sup>2</sup>; <sup>1</sup>Clemson University; <sup>2</sup>AGH*

Amorphous coatings (Fe<sub>57</sub>Cr<sub>8</sub>Mo<sub>12</sub>W<sub>3</sub>C<sub>11</sub>B<sub>11</sub>) with thickness varying from 50-450µm were deposited onto 9Cr steel substrates by a high-velocity oxyfuel (HVOF) flame-spraying process. The Nd:YAG laser with a varied output energy was used to remelt the coatings. The microstructure-property relationship (hardness, wear resistance) was studied as a function of laser power and coating thickness. The as-deposited coatings were amorphous (XRD) and were characterized by a high porosity, poor bonding to the substrate and a presence of unmelted, spherical powder particles. The hardness values were ~1350-1450HV for the unmelted particles, ~900-1000HV deformed particles and ~550HV substrate. After laser melting, a completely dense coating layer was formed with a hardness of 1100-1300HV. When the coating was remelted with the substrate, the microstructure (layers were fully crystalline), chemical composition and hardness (lower than 1000HV) of re-crystallized layer was depended on Fe enrichment. However, for all conditions, laser treatment was found to improve the wear resistance.

10:55 AM

**Size Effect on the Fatigue Behavior of Bulk Metallic Glasses:** *Gongyao Wang<sup>1</sup>; Peter Liaw<sup>1</sup>; Yoshihiko Yokoyama<sup>2</sup>; Akihisa Inoue<sup>2</sup>; <sup>1</sup>University of Tennessee; <sup>2</sup>Tohoku University*

Rod Zr<sub>50</sub>Cu<sub>40</sub>Al<sub>10</sub> and Zr<sub>50</sub>Cu<sub>30</sub>Al<sub>10</sub>Ni<sub>10</sub> (in atomic percent) bulk-metallic glasses (BMGs) were fabricated by arc-melt tilt-casting technique. The X-ray diffraction and DSC results exhibited that these rod specimens were fully amorphous alloys. Four-point-bend fatigue experiments were performed on these zirconium (Zr)-based BMGs with different size in air. The experiments were conducted at a frequency of 10 Hz, using an electrohydraulic machine with a R ratio of 0.1, where  $R = \sigma_{min}/\sigma_{max}$ ,  $\sigma_{min}$  and  $\sigma_{max}$  are the applied minimum and maximum stresses, respectively. The fatigue-endurance limits of these larger size samples were higher than those of the smaller size samples. The result suggested that although BMGs with small size exhibited good ductility, the fatigue resistance of BMGs might degrade when the specimen size decreases. A mechanistic understanding of the fatigue behavior of these Zr-based BMGs is suggested. The present work is supported by the National Science Foundation (NSF).

11:05 AM

**Crystallization Phenomena in Novel Ti-Based Bulk Metallic Glasses:** *Hesham Khalifa<sup>1</sup>; Kenneth Vecchio<sup>1</sup>; <sup>1</sup>UC-San Diego*

A new glass forming alloy system with excellent thermal stability is introduced of the form Ti-Ni-Cu-Si-Sn. Low density Ti-based bulk metallic glasses have potential as implant materials in biomedical applications. The development of Ti-based BMG composites permits the modulus to be tuned to match that of the bones into which they may be implanted. A series of isothermal and continuous heating experiments were performed to probe nucleation kinetics. Devitrification of the glassy state, and alternative cooling rate-controlled processing from the molten state were used to identify nucleating phases and investigate the role played by microstructure on mechanical properties in BMG composites. Under certain, cooling rate controlled, processing conditions, Ti-Ni-Cu dendrites lead to marked enhancements in mechanical properties. An understanding of nucleation kinetics, phase formation, and microstructural evolution of new metallic glass forming alloys are critical for the advancement of low cost, bioimplantable BMG composites.

11:15 AM

**A Study on Mg Flakes in MgCuYZn Bulk Metallic Glass Composite:** *Lalu Robin<sup>1</sup>; Michael Ferry<sup>1</sup>; Greig Kurniawan<sup>1</sup>; Kevin Laws<sup>1</sup>; <sup>1</sup>University of New South Wales*

The formation and distribution of Mg flakes in the composites, Mg<sub>65-x</sub>(Cu<sub>0.667</sub>Y<sub>0.333</sub>)<sub>30-x</sub>Zn<sub>5</sub> ( 12, 14 and 16) were found to be dependent on composition and cooling rate by casting. Higher cooling rate (i.e. the faster the composites solidifies) and lower concentration of the compositions produce less Mg flakes and less likely for crystallisation and morphology change to occur. This was evidenced by the lower volume fraction near the core of the sample. In addition, there is a thickness difference of Mg flakes between in the centre and at the edge of the sample. Furthermore, crystallisation formation was observed in larger compositions (i.e. 14 and 16). More Mg flakes appears during annealing.

**Cast Shop for Aluminum Production: Molten Metal Cleanliness**

Sponsored by: The Minerals, Metals and Materials Society, TMS Light Metals Division, TMS: Aluminum Committee  
Program Organizers: Pierre Le Brun, Alcan CRV; Hussain Alali, Aluminium Bahrain

Wednesday AM  
February 18, 2009

Room: 2005  
Location: Moscone West Convention Center

Session Chair: Edward Williams, Alcoa Inc

**8:30 AM Introductory Comments****8:35 AM Keynote****Improvements in the Molten Metal Process Chain in the Cast House Based on Modeling - Achievements so Far and Challenges Left:** *Gerd Ulrich Gruen<sup>1</sup>; Andreas Buchholz<sup>1</sup>; <sup>1</sup>Hydro Aluminium Deutschland GmbH*

Steadily growing demands in productivity and final product quality together with rising prices for energy and basic materials require optimum process conditions within the whole cast house. Although numerical modelling support to the related mandatory continuous improvement of the DC casting process is known for quite some time, the simulation of critical steps in the prior molten metal processing within the cast house is a more recent development. This contribution will give a brief summary of the actual status of activities with respect to molten metal processing including application examples within the area of transport phenomena in the furnace, filtration and launder design. The achieved results and the related conclusions will be used to pinpoint the additional benefits of modelling of related processes. Eventually, still existing challenges for a complete modelling coverage of the molten metal process chain are pointed out and correspondingly necessary future developments are briefly discussed.

**9:05 AM****Aluminium Flotation in Stirred Reactor: A Mathematical Model and a Computer Simulation Coupling CFD and Population Balance:** *Olivier Mirgaux<sup>1</sup>; Jean-Pierre Bellot<sup>1</sup>; Emmanuel Waz<sup>2</sup>; Denis Ablitzer<sup>1</sup>; <sup>1</sup>LSG2M - University of Nancy; <sup>2</sup>Alcan Centre de Recherches de Voreppe*

Removing inclusions from molten aluminium by flotation in stirred reactors is widely used in liquid aluminium treatments. This process consists in gas injection into the liquid bulk using an impeller: inclusions are attached to the bubbles during their ascension in the liquid bulk and are released in the dross layer. With the aim both of a better understanding of the physical phenomena acting during flotation and of the optimization of the refining process, a mathematical model of the behaviour of the inclusions population has been built up. Transport phenomena, agglomeration of inclusions, sedimentation and flotation are investigated and modelled. The simulation couples Population Balance with convective transport of the inclusions, in the diphasic flow field, in order to predict the evolution of the size distribution of inclusions as a function of time. A laboratory scaled flotation vessel has been modelled and results of a 2D simulation are presented.

**9:25 AM****Development and Practical Performance Characteristics of a New Impeller for Metal Treatment in Casting/Holding Furnaces:** *Bernd Prillhofer<sup>1</sup>; Holm Böttcher<sup>2</sup>; Helmut Antrekowitsch<sup>1</sup>; <sup>1</sup>University of Leoben; <sup>2</sup>AMAG Casting GmbH*

There are several criteria which characterize melt cleanliness, e.g. hydrogen, alkali metal and the inclusion content. According to the increasing quality demand of materials for high end applications, melt cleanliness has to reach a certain level before starting to cast. Therefore metal treatment has also to be done already in the casting furnaces. Besides adding refining agents like fluxes, a gas purging treatment with an impeller is one of the efficient ways to increase metal cleanliness. Due to the fact, that commercial rotor types are mostly developed for small vessels, they do not operate well in furnaces. Because of this, impellers used in furnaces have to be custom-made. This paper presents a new impeller for a 33 metric ton channel induction furnace. Based on CFD-calculations a new geometry was developed and tested. The performance behavior regarding inclusion, hydrogen and alkaline metal of all impeller types will be discussed.

9:45 AM

**Operational Experience with a Large Capacity Integrated TAC (Treatment of Aluminium in a Crucible) and a Skimmer:** Bruno Maltais<sup>1</sup>; *Dominique Prive*<sup>1</sup>; Ahmed Al Hashimi<sup>2</sup>; <sup>1</sup>Société des Technologies de l'Aluminium du Saguenay Inc. (STAS Inc.); <sup>2</sup>Aluminium Bahrain

This paper will present a description of the TAC/Skimmer (Treatment of Aluminium in Crucible/Skimmer), the different layouts that are available and the latest operational results on sodium removal from a TAC user in the Middle East. Needs for the TAC technology have been increasing in aluminium smelters because of higher amperages in the pot rooms, where sodium levels could now exceed up to 200 ppm. With its chlorine-free technology using AlF<sub>3</sub> as a reacting agent, the TAC has proven to give process efficiencies in excess of 90% removal, and alkaline levels as low as 1 or 2 ppm can now be achieved. There have been significant improvements in the TAC design over the last couple of years, and one of them has led to the use of the TAC system in conjunction with an automatic skimming system which is used to remove bath before the TAC treatment as well as before the metal is transferred to the casthouse.

10:05 AM Break

10:25 AM

**Comments on the Capture Mechanisms and Surface Forces Acting during Liquid Aluminum Depth Filtration:** *Hervé Duval*<sup>1</sup>; Véronique Ghetta<sup>2</sup>; Emilie Laë<sup>3</sup>; Nathalie Ruscassier<sup>1</sup>; Jean Trubuil<sup>1</sup>; Franz Wheling<sup>1</sup>; Jean-Bernard Guillot<sup>1</sup>; <sup>1</sup>Ecole Centrale Paris; <sup>2</sup>LPSC; <sup>3</sup>Alcan CRV

Only a few studies dealing with adhesion forces between inclusions and filter inner walls are reported in the literature. Said studies, which are essentially theoretical ones, predict values of adhesion force which are several orders of magnitude larger than the drag force exerted by the fluid on the inclusions. These predictions are in contradiction with the release of inclusions which can be observed during liquid aluminium depth filtration. In order to understand the discrepancies between the theoretical findings and the industrial observations, a research program combining experiments and theoretical calculations has been presently set up. This paper presents the experimental results of said research program and further develop a detailed discussion around the following points: coexistence of two different populations of inclusions in the melt, massive ones and oxide skin pieces, experimental estimation of the adhesion force magnitude and comparison with recent theoretical calculations, chemical effect of the AT5B addition.

10:45 AM

**Wetting of Pure Aluminium on Filter Materials Graphite, AlF<sub>3</sub> and Al<sub>2</sub>O<sub>3</sub>:** *Sarina Bao*<sup>1</sup>; Anne Kvithyld<sup>2</sup>; Sean Gaal<sup>2</sup>; Thorvald Engn<sup>1</sup>; Merete Tangstad<sup>1</sup>; <sup>1</sup>Norwegian University of Science & Technology; <sup>2</sup>SINTEF

The wettability of pure aluminium on filter materials is believed to be an important factor affecting the filtration of aluminium. The contact angle of molten aluminium on graphite, alumina and AlF<sub>3</sub> has been measured in 1 atmosphere of argon with an oxygen partial pressure of about 10<sup>-17</sup> Pa in the temperature range of 1000-1800°C. Improved techniques to remove the aluminium oxide layer from a molten aluminium drop have been employed in a horizontal graphite tube furnace. The wettability of aluminium on graphite, alumina and AlF<sub>3</sub> has been discussed and compared with the aim to obtain "new" and more effective filter materials.

11:05 AM

**Trial Results with an Improved System of Filtration of Molten Aluminium Based on a Three Stage Reactor Employing a Cyclone as Its Final Stage:** *John Courtenay*<sup>1</sup>; Frank Reusch<sup>2</sup>; <sup>1</sup>MQP Limited; <sup>2</sup>Drache Umwelttechnik GmbH

The development of a new prototype multi stage filter was described at TMS 2008 in which a ceramic foam filter was applied in a first chamber operating in cake mode; grain refiner added in a second chamber and a cyclone deployed in a final chamber to ensure removal of any oxides or agglomerates arising from the grain refiner addition or release events from the foam filter. The first industrial prototype was installed at Trimet Aluminium at Essen in Germany in February 2008 and demonstrated that liquid metal could pass through the cyclone successfully without excessive turbulence or splash. The results of further refinement of the prototype and the initial trial results with respect to inclusion removal efficiencies and operational performance are reported.

11:25 AM

**Removal of Iron and Manganese in Aluminium Alloys by Adding Magnesium and Subsequent Centrifuging:** *Christian Simensen*<sup>1</sup>; Pierre Le Brun<sup>2</sup>; <sup>1</sup>SINTEF Group; <sup>2</sup>Alcan CRV

The content of Fe and Mn is critical for the final properties of several alloys. The feasibility of the removal of Fe and Mn by primary crystals precipitation has been studied. Different amount of magnesium was added to Al-1%Mn-1%Fe-1%Si melts. The content was varied from 0 to 17 wt% Mg. Then the melts were homogenized and slowly cooled to a temperature about 10°C above the liquidus temperature of Al-crystals and held for four hours. A series of intermetallic particles was formed during this treatment. These particles were separated from the melt by the subsequent centrifuging of the molten metal. Microprobe analysis of the particles showed large particles of α-Al(Mn,Fe)Si, Al<sub>6</sub>(Mn,Fe), φ-(Al,Si)<sub>10</sub>(Fe,Mn)<sub>3</sub> and Al<sub>13</sub>(Fe,Mn) of size 0.04-0.4 mm. The content of Mn and Fe in the purified metal was correspondingly reduced to 0.10 wt%Mn and 0.13 wt%Fe (X-ray fluorescence measurements) in metal containing more than 12 wt%Mg.

11:45 AM

**Molten Metal Quality and Productivity Improvements by Process Optimization in Continuous Casting:** *Volker Ohm*<sup>1</sup>; Peter Bauer<sup>2</sup>; Stefan Schormann<sup>1</sup>; Guido Jerusalem<sup>1</sup>; <sup>1</sup>HOESCH Metallurgie GmbH; <sup>2</sup>Friedrich von Neumann GmbH

Process optimization is of increasing importance in order to improve quality, increase production capacity and minimize overall costs for wrought and cast aluminum alloys. The following paper describes a procedure for process optimization in a medium sized casting operation. The first step was to carry out a detailed plant audit of the production process, raw materials, melt treatment efficiency and temperature profiles from furnace to caster. These measurements were carried out with the Prefil® Footprinter melt cleanliness analyzer and with the AISCAN™ Hydrogen analyzer. Based on the results of this detailed audit the second step was to develop recommendations to optimize the production process. The third and final step was to implement the changes and measure the achieved results against the original targets. In this case study the original targets were to improve quality regarding the hydrogen and inclusion levels to enable more demanding end quality markets to be targeted and to increase daily output by at least 15% to improve overall plant profitability. Both objectives were achieved through the process optimization approach.

## Characterization of Minerals, Metals and Materials: Characterization of Microstructure of Properties of Materials III

Sponsored by: The Minerals, Metals and Materials Society, TMS Extraction and Processing Division, TMS: Materials Characterization Committee, TMS/ASM: Composite Materials Committee

Program Organizers: Toru Okabe, University of Tokyo; Ann Hagni, Geoscience Consultant; Sergio Monteiro, State University of the Northern Rio de Janeiro - UENF

Wednesday AM  
February 18, 2009

Room: 3009  
Location: Moscone West Convention Center

Session Chairs: Jiann-Yang Hwang, Michigan Technological University; Sergio Monteiro, State University of the Northern Rio de Janeiro - UENF

8:30 AM

**Characterization of Copper Oxides by EDS-SEM Depth Profiling, EIS and XRD:** *David Cocke*<sup>1</sup>; Eric Peterson<sup>1</sup>; Jewel Gomes<sup>1</sup>; Dan Rutman<sup>1</sup>; Morgan Reed<sup>1</sup>; Mohammad Akhtar Hossain<sup>2</sup>; <sup>1</sup>Lamar University; <sup>2</sup>Texas A&M University

Study of surface and subsurface interfacial chemistry of metallic and similar systems has its enormous technological importance. Copper, for example, is a common component of many alloys and bulk amorphous systems. It is being increasingly studied today because of its use for electronic interconnect systems where processing is done below 200 °C. Since several types of copper oxides exist, and the degree of their formation is dependent on temperature, perhaps characterization by EDS-SEM depth profiling and EIS might delineate the structural and stoichiometric differences among them. In this paper, we described our work on transformation of copper oxides with temperature ranging from 70 to 350 °C and their characterization by SEM, EDS, and XRD.



We also showed the use of the phase angle portion of the impedance as a means to identify the predominant structure and the transition through Cu<sub>3</sub>O<sub>2</sub> between the predominant stable CuO and Cu<sub>2</sub>O.

**8:45 AM**

**Characterizing the Interfacial Properties of SiO<sub>2</sub>/Si and Hf-Based/Si Gate Stacks:** *S.Y. Tan*<sup>1</sup>; Ming-Yuan Wu<sup>1</sup>; Hsing-Hung Chen<sup>1</sup>; <sup>1</sup>Chinese Culture University

As CMOS devices are scaled down into nano-region, SiO<sub>2</sub> dielectric is approaching its physical and electrical limits. High-k materials are recently employed by exploiting the increased physical thickness at the same equivalent oxide thickness. HfO<sub>2</sub> and HfSiO were prepared by MOCVD for gate dielectric, we investigated crystal structures properties and thermal stability of materials at various PDA temperatures. The electrical characteristics of HfSiO thin films were explored in comparison with HfO<sub>2</sub>. In addition to surface treatment could decrease the interfacial trapping density and the incorporation of N could increase dielectric constant and HfO<sub>2</sub> film. The XRD was utilized to analyze crystallization of the thin films, and the XPS was applied for surface chemical bounding energy to identify the silicon and dielectric layers. Surface roughness was detected by using AFM. As results, the interfacial layer was grown during annealing processes, this phenomenon lead to capacitance of device decreasing and hysteresis of C-V, oppositely, HfSiO films show the superior performance on thermal stability and electron properties.

**9:00 AM**

**Determination of Low Atomic Number Elements Using SDD in Portable XRF Instrumentation:** Alexander Seyfarth<sup>1</sup>; John Patterson<sup>1</sup>; <sup>1</sup>Bruker AXS Inc.

In recent years great advances have been made in the capability of portable XRF instruments. This paper will discuss the latest advance – the incorporation of Silicon Drift Detectors. This detector technology provides improved resolution and extremely high count rate capabilities and better sensitivity for low atomic number elements. These capabilities allow the accurate determination of low atomic number elements like Mg, Al, Si, P and S in essentially all alloy families with no special atmosphere as well as the complete analyses of aluminum and titanium alloys not available with current detector technology. The current state of these analyses will be presented.

**9:15 AM**

**A TEM Study of the Transient Stage Scale on the Fe-22wt%Cr Alloy with Reactive Elements Addition:** *Jingxi Zhu*<sup>1</sup>; Laura Fernández Díaz<sup>2</sup>; G. Holcomb<sup>2</sup>; P. Jablonski<sup>2</sup>; D. Alman<sup>2</sup>; Sridhar Seetharaman<sup>1</sup>; <sup>1</sup>Carnegie Mellon University; <sup>2</sup>National Energy Technology Laboratory

The chromium-oxide scales formed on Fe-Cr alloys at high temperatures are considered limited in capability of resisting high-temperature-oxidation. Adding a small amount of RE elements (Y, Ce or La) greatly improves the oxidation resistance of the alloys. Yet the precise roles of these reactive elements in oxidation process and the precise mechanisms by which they are incorporated into the scale are not well-established. One difficulty encountered is the location and form of RE in chromium-oxide scales hasn't been extensively explored. Therefore, this paper aims at characterizing selective sites by TEM where the scale and RE particle are both present. Cross section specimens were made via NOVA600-DualBeam system from a Fe-22wt%Cr alloy with addition of elemental La and Ce. The alloy was oxidized at 800°C in dry air for 15 minutes (transient stage). Based on TEM observations, possible effects of elemental La and Ce and RE-oxide particles on oxidation are elucidated.

**9:30 AM**

**Automatic Rietveld Refinement Based Quantitative Phase Analysis using TOPAS Combined with Same Sample WD XRF:** *Alexander Seyfarth*<sup>1</sup>; Rainer Schmidt<sup>1</sup>; <sup>1</sup>Bruker AXS Inc.

The paper will give an introduction to quantitative phase analysis using the TOPAS software based on the Rietveld method. Case studies using examples from the cement industry and mining industry are shown where the method is used in a QC environment in conjunction with WD XRF. The fundamental parameter approach of the TOPAS software allows the creation of a sturdy "recipe" for the refinement which can be used to automate the analysis and also enables the unattended operation. Combined with automated sample preparation this allows for a fully automated QC operation.

**9:45 AM**

**Thermographic Monitoring of Damage Characterization in Thermosetting Plastic Materials:** *Jeongguk Kim*<sup>1</sup>; <sup>1</sup>Korea Railroad Research Institute

The thermosetting plastic materials, which are employed for rail pad in railway application, were selected to characterize the damage evolution during tensile testing. The materials, unsaturated polyester resin, are used to buffer the vibration and impact in rail structure. The materials have to possess enough strength and modulus to endure the instant impact and strength from rails. During tensile testing, a high-speed infrared (IR) camera was used to monitor the fracture behavior and failure mode. After final failure, the SEM microstructural analysis was employed for tensile fractured specimens. The SEM characterization results were comparable with in-situ monitored IR camera analysis results. In this investigation, an IR camera and SEM characterization were used to facilitate a better understanding of damage evolution and failure mode of thermosetting plastic materials during monotonic loadings.

**10:00 AM Break****10:20 AM**

**Structural Change of Mesoporous Carbons Studied in an In-Situ Transmission Electron Microscopy:** *Dafei Kang*<sup>1</sup>; Mark Aindow<sup>2</sup>; <sup>1</sup>Michigan State University; <sup>2</sup>University of Connecticut

Mesoporous carbons, also known as carbon aerogels, have been studied more commonly for their desirable physical properties such as low density/high porosity, high surface areas and good electrical conductivity, which in combination make this category of materials very promising for applications ranging from catalytic supports to electrodes in fuel cells, just to name a few. Until recently, the structural modification of mesoporous carbons has received little attention, but in this paper the authors would illustrate such modification on nano-meter scale in a transmission electron microscope (a JEOL 2010F running at 200kV) that also doubles as a source of electron irradiation. The finding is that the original highly tortuous microstructure of mesoporous carbons, upon contact with the energetic electrons, would transform into more ordered graphene-like structures that largely adopt the morphology of a nano-meter sized cage.

**10:35 AM**

**Room and Elevated Temperature Validation and Characterization of a Novel Electrothermal Mechanical Tester:** Benjamin Peterson<sup>1</sup>; *Peter Collins*<sup>1</sup>; Hamish Fraser<sup>1</sup>; <sup>1</sup>Ohio State University

The Electrothermomechanical Tester (ETMT) was developed by Instron and NPL and uses direct resistive heating of small rectangular geometries approximately 40x2x1 mm in tension at a wide range of temperatures, including room temperature. Direct resistive heating allows for rapid and accurate temperature control. The mechanical properties of various heat treatments of alpha/beta and beta processed Ti64 were compared in conventional tensile testing and an ETMT at several temperatures to determine a correlation between the two methods. Creep tests were also performed in the ETMT and compared with conventional methods. The ETMT is potentially a realistic alternative to traditional tensile testing due to the material and time saving advantages. Digital image correlation is also employed as the strain measurement system and is also used to characterize the local and macro strain distribution due to the inherent temperature variation along the length of the samples. The statistical variation between samples is discussed.

**10:50 AM**

**EBSD Characterization of Hot Deformed Microstructure in a Ti-Modified Austenitic Stainless Steel:** *Sumantra Mandal*<sup>1</sup>; P.V. Sivaprasad<sup>1</sup>; Baldev Raj<sup>1</sup>; V. Subramanya Sarma<sup>2</sup>; <sup>1</sup>Indira Gandhi Centre for Atomic Research; <sup>2</sup>IIT Madras

Hot deformed microstructure of a Ti-modified austenitic stainless steel was investigated using electron backscatter diffraction (EBSD). Hot compression tests were conducted in a Gleeble thermo-mechanical simulator at temperatures in the range 1173K-1373K with a strain rate 10 and 100 s<sup>-1</sup> to different strains. Microscopic examination of the samples revealed various kinds of deformation patterns inside the deformed grains. These were inferred as the development of geometrically necessary boundaries or formation of parallel set of micro-bands. Recrystallized grains were partitioned from the deformed grains employing grain orientation spread approach. Extent of dynamic recrystallization (DRX) was found to be minimal at 1173K. DRX was predominantly found to happen at and above 1273K which increases with increase in strain. DRX nucleation and development mechanisms were discussed with respect to bulging of the

parent grains and sub-grain rotation. Special emphasis was given on the role of annealing twins on DRX nucleation and subsequent expansion.

**11:05 AM**

**Detection of Hard Alpha Inclusions in a Titanium Alloy by Magnetic Sensing:** *Hector Carreon*<sup>1</sup>; <sup>1</sup>UMSNH

This paper presents experimental data for the magnetic field produced by thermoelectric currents around uncracked hard-alpha inclusions in a Ti-6Al-4V specimen under external thermal excitation for different nitrogen content ranging from 1.6% to 5.9%. According to our preliminary results, the magnetic flux density measurements were found to be rather sensitive to changes in nitrogen content with the exception of the intrinsic material background magnetic signal that affected deeply the detectability of inclusions and imperfections in non-contacting thermoelectric measurements. Hopefully, these preliminary results can help identify a non-destructive test method that can detect material inclusions with a level of nitrogen that could be detrimental to Ti-6Al-4V alloy components.

**11:20 AM**

**Development and Characterization Investigations of Mechanically Alloyed W-Ni/TiC Composites:** *Selim Coskun*<sup>1</sup>; *Mustafa Ovecoglu*<sup>1</sup>; *Aziz Genc*<sup>1</sup>; <sup>1</sup>Istanbul Technical University

In this study, tungsten matrix composites reinforced with 2 wt% TiC particles were mechanically alloyed for 1h, 3h, 6h, 12h and 24h. 1 wt% Ni is used as sintering aid which is added before and after mechanical alloying and the effect of the amount of mechanical alloying on the microstructural, mechanical and sintering properties were investigated. Microstructure and phase characterizations of composite powders and sintered samples were carried out via SEM and XRD analyses. Furthermore, density and hardness measurements of as-consolidated and sintered samples were carried out. The effect of the Ni addition at different times on the sintering properties of the powders was investigated by DSC experiments.

**11:35 AM**

**Effect of Microalloying Elements and Deformation Mechanisms on the TWIP Steels:** *Huseyin Aydin*<sup>1</sup>; *Havva Kazdal Zeytin*<sup>1</sup>; *Huseyin Cimenoglu*<sup>2</sup>; <sup>1</sup>TUBITAK MRC; <sup>2</sup>Istanbul Technical University

TWIP (Twinning-Induced Plasticity) steels have exceptionally good combinations of strength, ductility and damage tolerance which satisfy the requirements for automotive industries. Firstly, TWIP has the most beneficial effect on the work-hardening. It is believed that deformation twins increase the work-hardening rate by acting as obstacles for gliding dislocations. Moreover, TWIP steels have low to intermediate stacking fault energy and hence undergo extensive mechanical twinning during deformation, which in turn leads a good combination of both strength and ductility. To explain which are the main characteristics and the behavior of the TWIP steels we have been made some investigations and experiments that show the effects of microalloying elements and deformation mechanisms. In this study, three different compositions of TWIP steels have been produced. The microstructure and mechanical properties are characterized by using optical, electron microscopy and mechanical tests.

## Computational Thermodynamics and Kinetics: Integrated Thermodynamic and Kinetic Modeling

Sponsored by: The Minerals, Metals and Materials Society, ASM International, TMS Electronic, Magnetic, and Photonic Materials Division, TMS Materials Processing and Manufacturing Division, ASM Materials Science Critical Technology Sector, TMS: Chemistry and Physics of Materials Committee, TMS/ASM: Computational Materials Science and Engineering Committee

Program Organizers: Long Qing Chen, Pennsylvania State University; Yunzhi Wang, Ohio State University; Pascal Bellon, University of Illinois at Urbana-Champaign; Yongmei Jin, Texas A&M

Wednesday AM

Room: 3002

February 18, 2009

Location: Moscone West Convention Center

Session Chair: Yongmei Jin, Texas A & M University

### 8:30 AM Introductory Comments

**8:35 AM**

**Large-Scale Three-Dimensional Phase Field Simulation of  $\gamma$ -Rafting and Creep Deformation in Single Crystal Superalloys:** *Ning Zhou*<sup>1</sup>; *Chen Shen*<sup>2</sup>; *Michael Mills*<sup>1</sup>; *Yunzhi Wang*<sup>1</sup>; <sup>1</sup>The Ohio State University; <sup>2</sup>GE Global Research

Three-dimensional phase field modeling of coupled  $\gamma/\gamma'$  microstructural evolution and plastic deformation was carried at two different length scales. The relative contributions from elastic modulus inhomogeneity and  $\gamma$  channel plasticity were first quantified by the dislocation-level simulations, which showed that the latter plays the dominant role in controlling the rafting process. Then micrometer-scale simulations were carried out that takes into account plastic deformation in  $\gamma$  channels described by local channel dislocation densities from individual active slip systems. The rafting kinetics and the corresponding creep deformation were characterized at different values of applied stress, lattice misfit and precipitate volume fraction. The simulation results were compared with available experiment carried out for Ni-Al-Cr and quantitative agreement has been obtained. The models have the ability to make quantitative predictions to  $\gamma$  rafting and the corresponding creep deformation in new superalloys (such as the Co- and Pt-based alloys) that are currently under development.

**8:55 AM**

**Computational Modeling and Critical Experiment in High Strength and Toughness Stainless Steel Development:** *Ning Ma*<sup>1</sup>; *Patrick Ray*<sup>1</sup>; *Michael Schmidt*<sup>1</sup>; *Hamish Fraser*<sup>2</sup>; <sup>1</sup>Carpenter Technology Corp; <sup>2</sup>The Ohio State University

Martensitic precipitation-hardened (PH) stainless steel has high strength and toughness with good levels of resistance to both general corrosion and stress-corrosion crack. The objective of present study is to understand the strengthening mechanisms during aging and make possible a computer model of the age hardening kinetics based on existing theories. The alloy studied is strengthened by two types of precipitates, ordered NiAl and a close packed intermetallic phase. A systematic experimental study has been conducted to understand the precipitation and growth under various aging conditions. The dislocation/particle configurations and interaction subjected to tensile deformation was reported. A mechanistic precipitation and hardening model was developed based on experimental observation. The model predictions were validated against experimental results from various heat treatment schedules. The high resolution characterization in present study is conducted in the Center of Accelerated Maturation of Materials (Camm) at the Ohio State University under Camm characterization membership agreement.

**9:15 AM**

**Influence of Elasticity on Phase Diagrams and Microstructures of Binary Alloys Using Monte Carlo, Lattice Statics and Phase Field Methods:** *Celine Varvenne*<sup>1</sup>; *Mathieu Fevre*<sup>1</sup>; *Alphonse Finel*<sup>1</sup>; *Yann Le Bouar*<sup>2</sup>; <sup>1</sup>ONERA; <sup>2</sup>CNRS

The knowledge of phases stability as a function of temperature and composition is essential to improve metallic alloy performances. The competition between chemical and elastic effects results in various type of morphologies and microstructural evolutions, which must be taken into account in numerical models. At atomic scale, we use relaxed Monte Carlo simulations with a position

dependent potential to calculate “exact” phase diagrams for different atomic sizes in the case of phase separation and ordering transformations. These results are compared to those obtained with the lattice statics technique, where elastic effects are embedded into an effective Hamiltonian on a rigid lattice. In this case, the simulation boxes are large enough to reproduce microstructures with several billions of atoms. Finally these two methods are compared to a phase field approach, where calculated phase diagrams are used as input parameters and microstructural evolutions at large time and space scales can be investigated.

9:35 AM

**PANDAT Software with PanEngine, PanOptimizer and PanPrecipitation for Multi-Component Phase Diagram Calculation and Materials Property Simulation:** *Weisheng Cao*<sup>1</sup>; Shuanglin Chen<sup>1</sup>; Fan Zhang<sup>1</sup>; Kaisheng Wu<sup>1</sup>; Ying Yang<sup>1</sup>; Y. Chang<sup>2</sup>; <sup>1</sup>CompuTherm LLC; <sup>2</sup>University of Wisconsin

The PANDAT software package, with PanEngine for thermodynamic calculation, PanOptimizer for model parameter optimization and PanPrecipitation for precipitation simulation, provides an integrated workspace for phase diagram calculation and materials property simulation of multi-component systems based on CALPHAD (CALculation of PHase Diagram) approach. The simulation results including thermodynamic, kinetic, thermo-physical properties, and microstructure related information, are critically needed in materials design. In addition to the functionalities provided by PANDAT as a stand-alone program, its calculation engines (PanEngine, PanOptimizer and PanPrecipitation) are built as shared libraries. This simplifies their integration with user's code for broader applications in the framework of Integrated Computational Materials Engineering (ICME) such as phase field modeling, microscopic/macroscale solidification simulation and other applications where phase equilibrium information and thermodynamic/kinetic properties are needed.

9:55 AM

**PanROME: A Phase Field Modeling Tool for Practical Applications:** *Kaisheng Wu*<sup>1</sup>; Shuanglin Chen<sup>1</sup>; Fan Zhang<sup>1</sup>; Y. Chang<sup>2</sup>; <sup>1</sup>CompuTherm LLC; <sup>2</sup>University of Wisconsin

Phase field modeling has been demonstrating its powerful capability to simulate complicated microstructural evolutions. Unfortunately, attempts for semi-quantitative or quantitative calculations have been limited, especially for multi-component and multiphase systems, due to the difficulties in relating the energy functionals to the thermodynamic properties of the systems, as well as mobilities to kinetic properties of the alloy elements involved. A phase field modeling tool, PanROME (Research Of Microstructure Evolution), has been developed that offers capabilities to overcome these difficulties. By fully integrating with PanEngine, it is able to use the thermodynamic and kinetic databases that are built based on CALPHAD approach, making it suitable for the simulations in multi-component and multiphase systems. The model is based on Kim-Kim-Suzuki model which is able to carry out the simulation in a practical length scale while maintaining a reasonable interfacial energy. Several examples have been shown to demonstrate its functionalities.

10:15 AM Break

10:40 AM

**Virtual Dilatometer Curves and Effective Young's Modulus of a 3D Multiphase Structure Calculated by the Phase-Field Method:** *Markus Apell*<sup>1</sup>; Stefan Benke<sup>1</sup>; Ingo Steinbach<sup>2</sup>; <sup>1</sup>Access, RWTH-Aachen; <sup>2</sup>ICAMS, Ruhr-University Bochum

The multiphase-field method allows for the calculation of 3D microstructures in multicomponent and multiphase materials. However, for technical applications the microstructure itself is not of primary interest, but material properties like elastic modules, yield strength etc. In this work we will derive effective mechanical properties directly from phase-field calculations coupled to linear elasticity. We simulated the austenite to ferrite transformation in a Fe-C-Mn steel and calculated the response of the two-phase microstructure on an external load. From these calculations the effective Young's modulus can be derived as a function of the phase fractions which is a useful input for finite element calculations on a larger scale. Furthermore, the external volume change caused by the phase transformation was calculated which leads to virtual dilatometer curves. For constant transformation strains, i. e. neglecting thermal and composition dependent lattice expansion, the volume change depends linearly on the ferrite fraction.

11:00 AM

**Phase Field Modelling of Slag Solidification:** *Jeroen Heulens*<sup>1</sup>; Nele Moelans<sup>1</sup>; Frederik Verhaeghe<sup>1</sup>; Bart Blanpain<sup>1</sup>; Patrick Wollants<sup>1</sup>; <sup>1</sup>Katholieke Universiteit Leuven

Phase field modelling has proven itself very powerful for simulating microstructural evolutions in materials. In this research, a phase field model is employed to simulate the solidification behaviour of slags, i.e. liquid oxide systems from extractive metallurgy. The prediction of the solidified microstructure of slags is of crucial importance for the application of freeze linings and the slag recycling. The main difference with the well established solidification theory of metals is glass formation at low cooling rates and redox reactions occurring, depending on the oxygen presence in the atmosphere. The model is validated against directional solidification experiments in a Bridgman setup because of its well controlled boundary conditions. Currently, this research is focussed on CaO-Al<sub>2</sub>O<sub>3</sub>-SiO<sub>2</sub> slags because of the fully optimized phase diagram and this slag is furthermore the basis of nearly all metallurgical slags.

11:20 AM

**Ordering and Clustering Instabilities in FCC-Based Alloys: Importance of Second Nearest Neighbors:** *Nitin Singh*<sup>1</sup>; William Soffa<sup>1</sup>; David Laughlin<sup>2</sup>; <sup>1</sup>University of Virginia; <sup>2</sup>Carnegie Mellon University

In TMS 2008, we called attention to the importance of 2nd nearest neighbor interactions on the ordering and clustering instabilities in FCC-based alloys. The Bragg-Williams model including the second-, third- etc nearest neighbor interactions are very often used to describe the energetics and kinetics of precipitation of ordered phases in many FCC-based alloys such as Al-Li, Ni-Ti and Ni-Al. In the present set of results, we describe the synergism that exists between the thermodynamic first-order, ordering transition and spinodal decomposition in such alloys also including the occurrence of the so called conditional spinodal. Specific attention is drawn to the influence of 2nd neighbor interactions on the two-phase region in FCC alloys involving the precipitation of an ordered L1<sub>2</sub> phase within a supersaturated FCC solid solution. The salient features of the generalized Bragg-Williams model applied to FCC alloys (A1-L1<sub>2</sub>) will be further elucidated and compared to the BCC case (A2-B2).

11:40 AM

**Thermodynamic Modeling of the Cr-Ir Binary System Using the Cluster/Site Approximation (CSA) Coupling with First-Principles Energetic Calculation:** *Chuan Zhang*<sup>1</sup>; Jun Zhu<sup>1</sup>; Dane Morgan<sup>1</sup>; Fan Zhang<sup>2</sup>; Ying Yang<sup>2</sup>; Y. Austin Chang<sup>1</sup>; <sup>1</sup>UW-Madison; <sup>2</sup>CompuTherm LLC

A thermodynamic description of Cr-Ir was developed in this study by combining first-principles calculation with Calphad approach. The zero-kelvin enthalpies of formation of Cr<sub>3</sub>Ir (A15), e (hcp) as well as the ordered Cr<sub>x</sub>Ir<sub>1-x</sub> face-centered cubic (fcc) L1<sub>2</sub> compounds at x(Ir)=0.25 and 0.75 and L1<sub>0</sub> compound at x(Ir)=0.5 were obtained from first-principles calculation. They were used as the initial values for optimizing the Gibbs energies of the corresponding phases in the Cr-Ir system. The cluster/site approximation (CSA) model was employed to model the phases in the fcc family: ordered L1<sub>2</sub>, L1<sub>0</sub> and disordered A1 (they are also referred to as the three states of fcc phase). The phase boundaries and thermodynamic properties calculated from the current thermodynamic description are in good agreement with the experimental data as well as the first-principles calculation. The calculated fcc phase metalstable phase diagram using current description reasonably describe the order-disorder transition of L1<sub>2</sub>/A1 and L1<sub>0</sub>/A1.

12:00 PM

**A First Principles Study of Hydrogen Trapping by Yttrium in Iron:** *Sanket Desai*<sup>1</sup>; Neeraj Thirumalai<sup>1</sup>; Peter Gordon<sup>1</sup>; <sup>1</sup>ExxonMobil Research and Engineering

The interaction of hydrogen with alloying elements in steels has been well-explored experimentally by various groups over the years due to its relevance in hydrogen trapping. With advances in first-principles based modeling methods, it is now possible to complement these experimental studies with atomistic insights. In the 1980s, Myers<sup>1,2</sup> et al. reported that yttrium centers in iron can act as strong binding sites that trap hydrogen. In this talk, we use yttrium in iron as a model system to study its interaction with hydrogen from first-principles. Various interstitial positions around yttrium are examined as potential binding sites for hydrogen, and the calculated binding energies are compared with experimental observations of Myers et al.. The models help provide atomistic insights into their experimental observations. References: (1) Myers S.M., et al., Appl. Phys. Letter 37, 168 (1980) (2) Myers S.M., et al., Rev. Mod. Phys. 64, 559 (1992).



## Diffusion in Materials for Energy Technologies: Session III

Sponsored by: The Minerals, Metals and Materials Society, TMS Structural Materials Division, TMS Electronic, Magnetic, and Photonic Materials Division, TMS: Alloy Phases Committee, TMS: High Temperature Alloys Committee, TMS/ASM: Nuclear Materials Committee, TMS: Solidification Committee, ASM-MSCTS: Atomic Transport Committee  
Program Organizers: Jeffrey LaCombe, University of Nevada, Reno; Yongho Sohn, University of Central Florida; Carelyn Campbell, National Institute of Standards and Technology; Afina Lupulescu, GE; Ji-Cheng Zhao, Ohio State University

Wednesday AM Room: 3006  
February 18, 2009 Location: Moscone West Convention Center

Session Chairs: Ji-Cheng Zhao, The Ohio State University; Zhili Feng, Oak Ridge National Laboratory

### 8:30 AM Invited

**Challenges Associated with the Global Nuclear Energy Partnership Nuclear Fuels and Structural Materials:** *Maria Okuniewski*<sup>1</sup>; Steven Hayes<sup>1</sup>; Dennis Keiser<sup>1</sup>; Yongho Sohn<sup>2</sup>; Yunzhi Wang<sup>3</sup>; John Morral<sup>3</sup>; <sup>1</sup>University of Illinois at Urbana-Champaign; <sup>2</sup>University of Central Florida; <sup>3</sup>Ohio State University

The vision of the Global Nuclear Energy Partnership (GNEP) is to recycle nuclear fuel by utilizing proliferation-resistant technologies to recover more energy and reduce nuclear waste. To accomplish this mission GNEP is currently focused on utilizing sodium fast reactors (SFRs) to transmute actinides. This mission will require fuel compositions significantly different than traditional SFR irradiated to substantially higher burnup levels. Thus, there are a variety of new fuels and materials related issues to be addressed relative to this mission. This talk will focus on the challenges that will be faced in the nuclear fuels and structural materials development, with specific emphasis on the diffusion related problems. Examples of multi-scale modeling in nuclear fuels and structural materials will also be discussed. The objectives of these multi-scale models are to develop comprehensive, science-based, and predictive tools.

### 9:10 AM Invited

**Interdiffusion in U-Pu-Zr Alloys:** *Mysore Dayananda*<sup>1</sup>; <sup>1</sup>Purdue Univ

Concentration profiles of solid-solid diffusion couples investigated with (bcc) U-Pu-Zr alloys at 750°C by Petri and Dayananda in the mid-1990s are reanalyzed with the aid of the *MultiDiff* program developed at Purdue University for the evaluation of ternary interdiffusion coefficients from individual couples over selected composition ranges. The evaluated data on interdiffusion coefficients are utilized for the regeneration of concentration profiles of the diffusion couples. Also, the interdiffusion coefficients are compared with those determined at the common composition of a couple pair with intersecting diffusion paths. The appreciable diffusional interactions among the components exhibited by the relatively large cross coefficients are discussed in the light of uphill diffusion of U and zero-flux plane development for Zr observed in selected couples. Atomic mobilities of the individual components and vacancy wind effects in these alloys are also briefly discussed.

### 9:50 AM Invited

**Interdiffusion Behavior in U-Pu-Zr Alloy Versus Advanced Cladding Steel Couples Annealed at 700°C:** *Dennis Keiser*<sup>1</sup>; James Cole<sup>1</sup>; <sup>1</sup>Idaho National Laboratory

The Advanced Fuel Cycle Initiative is responsible for the development of advanced nuclear energy systems. One of these nuclear energy systems is the Sodium Fast Reactor (SFR). To maximize the performance of this type of nuclear reactor, it will be important to improve on the performance of the nuclear fuel, i.e., allow for higher fuel burnup and/or operation of the fuel at higher reactor operating temperatures. In order to investigate the compatibility of U-Pu-Zr alloys with what are considered advanced claddings, diffusion couples have been annealed at 700°C to investigate the development of diffusion structures at relatively high temperatures. This talk will describe the types of phases that develop in the interdiffusion zones, the partitioning behavior of the various constituents between these phases, and whether or not there is evidence of melting within the diffusion structures of couples annealed at the relatively high temperature of 700°C.

### 10:30 AM Break

### 10:45 AM

**Interdiffusion in U-Mo-X (X = Nb, Ti, Zr) vs. Al Diffusion Couples:** *Ashley Ewh*<sup>1</sup>; Emmanuel Perez<sup>2</sup>; Dennis Keiser<sup>2</sup>; Yongho Sohn<sup>1</sup>; <sup>1</sup>University of Central Florida; <sup>2</sup>Idaho National Laboratory

U-Mo alloys are used for metallic fuels in nuclear research and test reactors due to their high uranium density. However, a diffusional interaction occurs between the U-Mo and the Al cladding alloys producing intermetallic compounds, which may have deleterious effects on the performance and service life of the fuels. Ternary U-Mo-X alloys were examined with an aim to reduce the interdiffusion fluxes, and to attenuate this interaction. This study focused on three such ternary alloys whose compositions in wt.% are U-8Mo-3Nb, U-7Mo-3Ti, and U-7Mo-6Zr. Diffusion couples have been assembled between these U-Mo-X alloys and pure Al to examine the effects of the alloying addition on the intermetallic formation. Using optical and scanning electron microscopy, both the thickness and phase constituents of the interaction layers were determined, and compared to previous studies involving binary U-Mo alloys in order to assess the suitability of ternary U-Mo-X alloys as enhanced metallic fuels.

### 11:10 AM

**Interdiffusion and Microstructural Development of U-7Mo, U-10Mo and U-12Mo Alloys in Contact with Al, Al-2Si, Al-5Si, 6061Al and 4043Al Alloys at 550°C:** *Emmanuel Perez*<sup>1</sup>; Dennis Keiser<sup>2</sup>; Yongho Sohn<sup>1</sup>; <sup>1</sup>University of Central Florida; <sup>2</sup>Idaho National Laboratory

Interdiffusion and microstructural development in the U-Mo-Al system was examined using solid-to-solid diffusion couples consisting of U-7wt.%Mo, U-10wt.%Mo and U-12wt.%Mo vs. Al, Al-2wt.%Si, Al-5wt.%Si, 6061Al and 4043Al. These diffusion couples were annealed at 550°C for 1, 5 and 20 hours. Electron microscopy and microanalysis were employed to examine the development of a very fine multi-phase intermetallic layer. Gamma-to-alpha polymorphic transformation in the U-Mo alloys accelerated the interdiffusion in some diffusion couples. Diffusion couples with Si containing Al-alloys showed a decrease in the growth of multi-phase intermetallic layer regardless of polymorphic transformation in U-Mo alloys. Effects of composition (e.g., Mo, Si content and trace-element additions) and polymorphic transformation of U-alloy on the overall interdiffusion behavior are discussed.

### 11:35 AM

**Interdiffusion Microstructure of U-Mo vs. Al Diffusion Couples Annealed at 600°C for 24 Hours:** *Emmanuel Perez*<sup>1</sup>; Brian Kempshall<sup>1</sup>; Ashley Ewh<sup>1</sup>; Dennis Keiser<sup>2</sup>; Yongho Sohn<sup>1</sup>; <sup>1</sup>University of Central Florida; <sup>2</sup>Idaho National Laboratory

Electron microscopy and microanalysis were carried out for diffusion couples, U-7wt.%Mo, U-10wt.%Mo and U-12wt.%Mo vs. Al annealed at 600°C for 24 hours. While a slight variation in the thickness of the interdiffusion microstructure was observed as a function of Mo concentrations in the U-Mo alloys, all couples exhibited complex and layered multiphase microstructure. Compositional analysis of the interdiffusion microstructure by electron microprobe showed little variation in the average composition throughout. Transmission electron microscopy with electron diffraction was employed to examine the phase constituents and interdiffusion microstructure for the diffusion couple U-10 wt.% Mo vs. Al. Results are discussed with respect to the equilibrium phases, cubic-UAl<sub>3</sub>, orthorhombic-UAl<sub>4</sub>, hexagonal-U<sub>6</sub>Mo<sub>4</sub>Al<sub>3</sub> and diamond cubic-UMo<sub>2</sub>Al<sub>20</sub> on the Al-rich corner of U-Mo-Al system, which were determined experimentally in our previous study. Preliminary diffusion paths were constructed for the U-Mo vs. Al diffusion couples.

### 12:00 PM

**Phase Field Modeling of Microstructure Evolution under Applied Temperature Gradient:** *Rashmi Mohanty*<sup>1</sup>; Yongho Sohn<sup>1</sup>; <sup>1</sup>University of Central Florida

When a temperature gradient is applied to an alloy, a concentration gradient can develop and alter the local microstructure of the initially homogeneous alloy. Thermotransport or the Ludwig-Soret effect can be important in many applications including interconnects of electronic circuits, metallic nuclear fuels, gas turbine component, where a larger temperature gradient is imposed for higher efficiency and performance. A diffuse interface model was devised and employed to predict the effect of thermotransport in single-phase and multi-phase alloys of an ideal binary system. Simulation results show that an applied temperature gradient can cause significant redistribution of constituents

and phases in the alloy. The magnitude and the direction of the redistribution depend on the initial composition, the atomic mobility and the heat of transport of the respective elements. In multi-phase alloys, the thermomigration effect can cause the formation of single-element rich phases at the cold and hot ends of the alloy.

---

### Electrode Technology for Aluminum Production: Anode Production Operations - Focus on Baking

Sponsored by: The Minerals, Metals and Materials Society, TMS Light Metals Division, TMS: Aluminum Committee  
Program Organizers: Barry Sadler, Net Carbon Consulting Pty Ltd; John Johnson, RUSAL Engineering and Technological Center LLC

Wednesday AM Room: 2003  
February 18, 2009 Location: Moscone West Convention Center

Session Chair: Stephen Lindsay, Alcoa Inc

---

#### 8:30 AM Introductory Comments

##### 8:35 AM

**Anode Baking: The Underestimated Human Aspect:** Felix Keller<sup>1</sup>; Werner Fischer<sup>1</sup>; Peter Sulger<sup>1</sup>; <sup>1</sup>R&D Carbon Ltd.

As a result of carbon plant auditing, significant differences in the performance of bake furnaces with similar design were identified. Avoidable direct annual losses of one million USD and more per 100,000 tons of baking capacity have been identified. Most of the problems creating financial losses could have been avoided. The key question, therefore, is why were these opportunities not explored? We identified four main reasons creating these losses: 1) No well-defined objectives and goals set. 2) Persisting errors regarding anode baking and misunderstanding of cause-effect chain. 3) Organizational and motivational aspects underestimated. 4) Inadequate data and information presentation preventing optimum decision making. Propositions are made how losses can be avoided and how management can react in order to optimize bake furnace efficiency while minimizing cost.

##### 9:00 AM

**A New Concept for Baking Anodes – Initial Full Scale Test Results and Future Potential:** Rick Lazarou<sup>1</sup>; Wolfgang Leisenberg<sup>2</sup>; William Morgan<sup>3</sup>; Barry Sadler<sup>4</sup>; Kristen Watson<sup>1</sup>; Dennis Schubert<sup>5</sup>; <sup>1</sup>Lazar Anode Technologies; <sup>2</sup>Transtec Consultancy; <sup>3</sup>Century Aluminum – Hawesville Operations; <sup>4</sup>Net Carbon Consulting Pty Ltd; <sup>5</sup>ANH Refractories Co.

The concepts underpinning a new vertical shaft anode baking furnace technology have been proven and design options assessed in plant scale anode trials conducted continuously over several months. Following these successful trials, the consortium backing the furnace development is constructing a demonstration unit, capable of baking large plant anodes. The new furnace design has many inherent advantages over existing ring furnaces, including improved thermal efficiency, much reduced fuel consumption, lower CO<sub>2</sub> gas generation, lower capital costs, and a steady state temperature profile that enhances control of anode heat-up rates and gives longer refractory life. These advantages make the technology ideal for baking high density anodes made using high intensity Paste Plant technologies; such anodes can be difficult to bake without cracking in conventional baking furnaces. This paper outlines the furnace design basics, the concept proving trial results, and plans for the construction of the demonstration unit.

##### 9:25 AM

**Resistance Heating of Laboratory Scale Prebake Anodes:** Stein Rørvik<sup>1</sup>; Trygve Foosnæs<sup>2</sup>; Hogne Linga<sup>3</sup>; Arne Petter Ratvik<sup>4</sup>; <sup>1</sup>Sintef Materials and Chemistry; <sup>2</sup>Norwegian University of Science and Technology; <sup>3</sup>Hydro Aluminium; <sup>4</sup>Sintef Materials & Chemistry

Resistivity heating of prebaked anode samples has been done in a laboratory study. The samples were heated by passing electric current through the anodes in a cold nitrogen atmosphere. No external heating was applied. Temperature measurements were done on the samples using both thermocouples and an infrared camera to examine differences in the temperature distribution during heating. The samples were also electrically heated in an air atmosphere using the same setup to observe the oxidation of the anode surface. Microscopy

investigations were done after cooling to look for selective reactivity on the anode surface. The results are discussed with respect to their relevance to anode dusting problems.

##### 9:50 AM Break

##### 10:00 AM

**Which Strategy to Use When Sampling Anodes for Coring and Analysis? - Start with How the Data Will Be Used:** Keith Sinclair<sup>1</sup>; Barry Sadler<sup>2</sup>; <sup>1</sup>Sinclair Associates Inc.; <sup>2</sup>Net Carbon Consulting Pty Ltd.

Most Prebake Anode Aluminium Smelters take and test anode core samples, using the results for a range of purposes, including: ·Characterizing product quality going to the Potrooms; ·Historical anode performance troubleshooting; ·Analysis of raw materials, paste plant, or baking furnace performance issues. To generate the data consistent with each of these purposes, a specific approach to selecting the anodes for coring should be used. Unfortunately, only rarely is serious consideration given to these sampling strategies, and while a number of different approaches are used in the industry, in most cases these are not consistent with the information desired. This can lead to poor decision making and waste. This paper will outline appropriate sampling strategies and discuss the key issues to be considered when designing a sampling strategy appropriate for the intended use of anode core data.

##### 10:25 AM

**Simulation-Based Approach for Validating a Lean Anode Plant Configuration:** Robert Baxter<sup>1</sup>; Trevor Bouk<sup>1</sup>; Laszlo Tikasz<sup>1</sup>; Robert I. McCulloch<sup>1</sup>; <sup>1</sup>Bechtel

Bechtel's Aluminium Center of Excellence (ACE), in the Mining and Metallurgy Business Unit, intensively worked on developing advanced modeling tools for plant design and operation. Today, process modeling and simulation are integral parts of Bechtel Studies and Proposals on smelter projects. The present paper outlines the steps of applying lean techniques as continuous improvement effort to the anode handling/storing process. For the carbon area operation in a recent Study, sector models of anode fabrication, namely anode storage, anode baking, rodding and pallet storage models were linked to cover the overall anode handling process. Simulation scenarios were performed under projected normal and extreme operation conditions. Early findings were fed back to designers and measured and analyzed with lean criteria. Reduced storage spaces and still appropriate anode inventories were targeted and achieved. Results introduced to Client demonstrated robust plant operation and adequate green, baked and rodded anode inventories.

##### 10:50 AM

**Environmental Improvements during the Handling of Packing Coke at the Albras' Bake Furnaces:** Paulo Douglas Vasconcelos<sup>1</sup>; André Mesquita<sup>2</sup>; <sup>1</sup>Albras Alumínio Brasileiro S.A.; <sup>2</sup>Federal University of Pará

ALBRAS operates five open ring-type bake furnaces in two plants with a capacity of 285,000ton anodes/year. Each furnace is composed of sections made with six pits separated by partition flue walls through which the furnace is fired. The pits are about four meters deep and accommodate twelve anodes, around which petroleum coke is packed to avoid air oxidation and facilitate the heat transfer. During anode baking, about 20 kg of coke per baked anode are used. The placement and removal of this coke cause significant problems with a high generation of carbon dust causing consequent pollution in the workplace environment. This is a common "nuisance" problem faced by all aluminum smelters, and since 2004 Albras' Carbon Plant Engineering Department has been working on a solution. This paper presents the existing problem at Albras and shows the technical solutions that were implemented in 2006 to resolve the dusting problems.

## Emerging Applications of Neutron Scattering in Materials Science and Engineering: Deformation Behaviors

Sponsored by: The Minerals, Metals and Materials Society, TMS Electronic, Magnetic, and Photonic Materials Division, TMS: Chemistry and Physics of Materials Committee

Program Organizers: Xun-li Wang, Oak Ridge National Laboratory; Brent Fultz, California Institute of Technology; Hahn Choo, University of Tennessee

Wednesday AM  
February 18, 2009

Room: 3012  
Location: Moscone West Convention Center

Session Chairs: James Jones, Northern College of Applied Arts and Technology; Sheng Cheng, University of Tennessee

### 8:30 AM Invited

**Neutron Diffraction Study of the Strain Rate Dependent Development of Microstructure in Beryllium:** *Donald Brown*<sup>1</sup>; Thomas Sisneros<sup>1</sup>; Bjorn Clausen<sup>1</sup>; Saurabh Kabra<sup>1</sup>; Diana Donati<sup>1</sup>; <sup>1</sup>Los Alamos National Laboratory

Plastic deformation of hexagonal metals such as Be, Mg, and Zr occurs by a mix of slip and twinning mechanisms. Deformation slip and twinning are controlled by different mechanisms at the atomic scale, and thus respond differently to variations in strain rate. In general, deformation twinning is expected to be favored by high strain rate conditions. We have completed neutron diffraction studies of the evolution of the microstructure of strongly textured and random Be as a function of strain rate, from 0.0001/sec to 5000/sec. The yield point is rate insensitive over 7+ orders of magnitude of strain rate. The hardening, however, is strongly rate dependent, due to the increased role of twinning at increased strain rates. We measure texture to characterize the twin volume fraction, lattice strains to determine load partitioning between different grain orientations, and line profiles to monitor the defect characteristics, all as a function of strain rate.

### 9:00 AM

**Fatigue Deformation Mechanism of Nanocrystalline Metals Studied by Neutron and X-Ray Diffraction:** *Sheng Cheng*<sup>1</sup>; Peter Liaw<sup>1</sup>; Hahn Choo<sup>1</sup>; Xun-Li Wang<sup>2</sup>; <sup>1</sup>University of Tennessee; <sup>2</sup>Oak Ridge National Laboratory

Grain size of materials has a great influence on their deformation mechanism. It is also true for fatigue deformation. However, the deformation mechanism of nanocrystalline metals under fatigue was inadequately studied. We have recently performed fatigue studies on a range of materials with grain size from nanocrystalline to ultrafine-grained to conventional coarse-grained samples under both tensile and compressive loading modes. We used in situ and ex situ neutron diffraction and synchrotron X-ray diffraction to study the deformation mechanism during fatigue. Insightful information (including intergranular strain, texture evolutions, peak broadening etc) in connection with the microstructural change was examined during fatigue tests. From the critical information, we show distinctive deformation mechanism. These influential mechanisms will be discussed. This work is supported by the NSF International Materials Institutes (IMI) Program (DMR-0231320) and Major Research Instrumentation (MRI) Program (DMR-0421219) with Dr. C. Huber and Dr. C. Bouldin as the Program Directors, respectively.

### 9:20 AM

**Deformation in a Bulk Amorphous Alloy Investigated by Neutron Scattering:** *Dong Ma*<sup>1</sup>; A.D. Stoica<sup>1</sup>; X.-L. Wang<sup>1</sup>; Z.P. Lu<sup>2</sup>; D.W. Brown<sup>3</sup>; B. Clausen<sup>3</sup>; Th. Proffen<sup>3</sup>; <sup>1</sup>Oak Ridge National Laboratory; <sup>2</sup>University of Science and Technology of Beijing; <sup>3</sup>Los Alamos National Laboratory

An in-situ neutron scattering study of deformation in a Zr-based bulk amorphous alloy has been carried out on the Spectrometer for Materials Research at Temperature and Stress (SMARTS). By monitoring the evolution of the structure factor in the reciprocal space and representing microscopic strains in a q-dependent manner, our analysis of the diffraction data reveals distinct variation of strains on multiple length scales. This unusual behavior is interpreted as a manifestation of the interplay of two structural units in the amorphous metal, i.e., short-range order (SRO) and medium range order (MRO), in response to the stresses.

### 9:40 AM Invited

**In Situ Studies of Ferroelectrics Using Neutron Diffraction:** *Jacob Jones*<sup>1</sup>; <sup>1</sup>University of Florida

Ferroelectric materials are used in a variety of applications including diagnostic and therapeutic ultrasound, sonar, and vibration and displacement sensors. The electromechanical response in ferroelectric materials is comprised of both intrinsic (lattice strain) and extrinsic (e.g., domain switching) components that are expressed as characteristic changes in the diffraction pattern. This talk presents the results of three in situ techniques applied to a soft lead zirconate titanate (PZT) ceramic. First, the lattice strains and domain switching (texture) behavior is measured under uniaxial compressive stress using HIPPO at LANSCE. Next, a stroboscopic technique is applied using the instrument TASS at ANSTO to characterize the domain switching behavior under dynamic electric field loading. Finally, the lattice strains under dynamic electric field loading are characterized using the instrument ENGIN-X at the ISIS facility. These measurements provide a comprehensive picture of the constitute behavior of ferroelectrics. New techniques and instruments will also be reviewed.

### 10:10 AM Break

### 10:30 AM

**In-Situ Neutron Diffraction Study of Uniaxial Deformation of Nickel Based Anode Materials for Solid Oxide Fuel Cells:** *Ke An*<sup>1</sup>; Alexandru Stoica<sup>1</sup>; Bjorn Clausen<sup>2</sup>; Beth Armstrong<sup>1</sup>; Don Brown<sup>2</sup>; Xun-Li Wang<sup>1</sup>; <sup>1</sup>Oak Ridge National Laboratory; <sup>2</sup>Los Alamos National Laboratory

Anode-supported solid oxide fuel cells (SOFCs) allow lower operating temperature due to the substantially lower ohmic resistance of the thin electrolyte. Multi-physical integrity including the structural and mechanical properties plays an important role on the durability and reliability of anode-supported SOFCs performance. Cylindrical NiO-Y2O3 stabilized zirconia (YSZ) and Ni-YSZ specimens with different porosities are investigated by in-situ neutron diffraction under uniaxial loads at room and high temperatures. With in-situ neutron diffraction, the monotonic and creep deformation mechanisms at micro-structural level of each single phase, inter-granular strain/stress evolution between the two phases and the impact of porosity on the response are characterized. Redox effect on the deformation evolution of the Ni-YSZ anode is also investigated by neutron diffraction. The details of the experiments and results of this approach will be discussed.

### 10:50 AM

**Neutron Diffraction Measurements of Residual Stress in an Electron Beam Welded Uranium Tubular:** *Thomas Holden*<sup>1</sup>; D.W. Brown<sup>2</sup>; B. Clausen<sup>2</sup>; T. Sisneros<sup>2</sup>; J. Vaja<sup>3</sup>; <sup>1</sup>Northern Stress Technologies; <sup>2</sup>Los Alamos Neutron Science Center, Los Alamos National Laboratory; <sup>3</sup>AWE Aldermaston

Neutron diffraction measurements have been made of the stresses associated with electron-beam welding a uranium tube. The tube exhibits a large grain size and fairly strong crystallographic texture. To mitigate the effect of the large grain size the tube was rotated about its own axis during the measurements so the results obtained are circumferential averages. High hoop stresses (350±100MPa) were found in the center of the weld close to the outside diameter. A strong hoop stress gradient was observed between the outside, OD, and inside, ID, diameters such that hoop compression (-50±100MPa) was observed close to the ID in the weld center. Hoop compression was also observed away from the center of the weld for all through-thickness positions. An axial tensile stress (150±50MPa) was observed near the OD which decreases to zero at the ends of the tubular. There is also a gradient of axial stress from the OD to the ID. The radial stresses were found to be zero to within the experimental uncertainties. The stresses associated with the weld are conventional in form. However, the unequal coefficients of linear expansion, and the anisotropic elastic and plastic response of orthorhombic uranium means that thermal residual strains are expected as well as mechanically-induced type 2 strains in the weld region. The analysis must seek to minimize the effect of these strains on the derived stresses. The presence of strong crystallographic texture is helpful in this case.

### 11:10 AM

**Multistage Deformation in Uranium 6 Wt% Niobium:** *Catherine Tupper*<sup>1</sup>; Don Brown<sup>2</sup>; Bjorn Clausen<sup>2</sup>; Robert Field<sup>2</sup>; Dan Thoma<sup>2</sup>; Rajan Vaidyanathan<sup>1</sup>; <sup>1</sup>University of Central Florida; <sup>2</sup>Los Alamos National Laboratory

The uranium-niobium alloy system demonstrates shape memory behavior mechanistically similar to the nickel-titanium system. In both U-Nb and NiTi, the shape memory behavior is governed by the selection of martensitic variants



in the microstructure in response to enforced mechanical strain. Through in-situ neutron diffraction experiments, we have identified a second twin reorientation in uranium niobium in the post shape memory regime (4-8% strain) under tensile loading. The reorientation is identified through the use of inverse pole figures, which can each be calculated from one neutron diffraction pattern. The reflections are about the (010) plane or the (100) plane, and are only made possible by the monoclinic structure of the U6Nb alloy. This twin system would not be available in orthorhombic uranium because in the higher symmetry crystal structure, i.e. the (010) is a mirror plane.

## Fatigue: Mechanisms, Theory, Experiments and Industry Practice: Experimental Studies of Initiation and Growth in Structural Materials

Sponsored by: The Minerals, Metals and Materials Society, TMS Structural Materials Division, TMS/ASM: Computational Materials Science and Engineering Committee, TMS/ASM: Mechanical Behavior of Materials Committee, TMS/ASM: Nuclear Materials Committee

Program Organizers: Koenraad Janssens, Paul Scherrer Institute; Corbett Battaille, Sandia National Laboratories; Brad Boyce, Sandia National Laboratories; Luke Brewer, Sandia National Laboratories

Wednesday AM  
February 18, 2009

Room: 3008  
Location: Moscone West Convention Center

Session Chairs: Robert Ritchie, University of California; Brad Boyce, Sandia National Laboratories

### 8:30 AM Invited

#### Fatigue Crack Initiation and Propagation Behavior of Forging Die Steels: Ryuichiro Ebara<sup>1</sup>; <sup>1</sup>Hiroshima Institute of Technology

In this paper low cycle fatigue, thermal fatigue and gigacycle fatigue behavior of forging die steel is presented. First, the effects of temperature, hardness and surface treatment on low cycle fatigue strength of hot forging die steels are summarized. Fatigue crack initiation and propagation behavior is discussed with fracture surface morphology. Thermal fatigue crack initiation and propagation behavior of hot forging die steel is also presented with respect to fracture surface morphology. Then low cycle fatigue behavior of representative cold forging die steels is summarized. Fatigue crack initiation and propagation behavior of cold forging die steels is discussed with respect to stress concentration factor, hardness and surface roughness. Crack initiation behavior in very high cycle regime is also discussed for cold forging die steels with respect to the effect of surface roughness and heat treatment. Finally recommended study on fatigue of forging die steels is touched on briefly.

### 9:00 AM

#### Fatigue Crack Growth in Inhomogeneous Steel Components: Donato Firrao<sup>1</sup>; Paolo Matteis<sup>1</sup>; Pasquale Russo Spena<sup>1</sup>; Giovanni Mortarino<sup>1</sup>; <sup>1</sup>Politecnico Di Torino

Massive low-alloy high-strength steel components often exhibit microstructure variations from surface to core due to decreasing quenching rates when moving towards the interior. Since different steel constituents exhibit different Fatigue Crack Growth (FCG) behaviors, both the overall FCG rate and the crack shape are expected to be influenced by the microstructural changes. The case of slack-quenched components with simple geometries, having a surface flaw, and subjected to mode-I constant-force-amplitude fatigue, is first examined theoretically. The microstructural variations are hypothesized by considering medium steel hardenabilities and quench severities; thereafter the FCG is computed by considering (during each integration step) the stress-intensity-factor amplitude and the FCG behavior of different points of the crack front, the pointwise FCG properties being determined by the local steel constituents fractions. Simulation results are compared with experimental evidences from a recent failure occurred in a 90 mm diameter connection rod of a 2500 kW naval diesel generator.

### 9:20 AM

#### Determine of Fatigue Fracture Mechanisms and Modeling of P/M Heterogeneous Steels: Hamid Khorsand<sup>1</sup>; <sup>1</sup>K.N.Toosi University

Industrial parts manufactured by P/M process have found a wide spread use in a variety of applications so, investigation of mechanical properties and

determine of how improvement of them is very important, under different kinds of service conditions. In this research, mechanical properties of several low alloy steels have been studied. Specimens with different chemical compositions, metallurgical phases and densities were prepared. The green compacts were sintered at 1120 c and 1250 c in a H<sub>2</sub>-N<sub>2</sub> atmosphere for 35 minutes to densities in the range of 6.6 to 7.2. The formation of different metallurgical phases in the research samples with different densities was caused that the authors can present equations for prediction of mechanical properties of P/M steel parts.

### 9:40 AM

#### Effects of Processing Residual Stresses on Fatigue Crack Growth Behavior of Structural Materials: Christopher Lammi<sup>1</sup>; Diana Lados<sup>1</sup>; <sup>1</sup>Worcester Polytechnic Institute

Fatigue crack growth mechanisms of long cracks through fields with high and low residual stresses were investigated for various structural materials commonly used in transportation applications. Macro residual stresses were introduced within each material first by processing methods, and then replicated in both magnitude and distribution, through original mechanical/geometrical techniques. Residual stresses were measured/paired using microstructure-tailored X-ray diffraction techniques. Compact tension specimens were fatigue crack growth tested at room temperature and stress ratio, R=0.1. Residual stress corrections were done using the Restoring Force Model, and the results were compared to those generated by a real-time compliance correction technique. Qualitative and quantitative effects of residual stress on fatigue crack growth characteristics, such as fatigue crack growth threshold and fracture toughness, will be presented and discussed for each material/class. Recommendations are given for fatigue crack growth data collection and interpretation to facilitate consistent and accurate design in the presence of residual stress.

### 10:00 AM

#### Nominal and Local Effects of Surface Treatment on Fatigue Variability: Sushant Jha<sup>1</sup>; Reji John<sup>2</sup>; Dennis Buchanan<sup>3</sup>; James Larsen<sup>2</sup>; <sup>1</sup>Universal Technology Corp; <sup>2</sup>US Air Force Research Laboratory; <sup>3</sup>University of Dayton Research Institute

Incorporating surface-treatment induced residual stresses (RS) in life prediction has been hampered by the variability in the RS profile and relaxation, and a lack of physics-based measure of the benefit of RS on the lifetime. Towards this, the fatigue variability behavior of the alpha+beta titanium alloy, Ti-6Al-2Sn-4Zr-6Mo, under low stress ground (LSG) and two shot-peening (SP) intensities was studied at 260°C. It was found, that the competing roles of the nominal RS profile and the local, microstructure – surface-treatment-process interaction was the strongest determinant of the lifetime distribution. In particular, the probability of surface vs. subsurface failure, the predominant crack initiation mechanisms, and the corresponding crack-initiation sizes can be effectively understood in terms of these two competing effects. This hypothesis was applied in modeling the influence of the RS level and the variability in the profile on the lifetime distribution and the probabilistic lifetime limit in Ti-6Al-2Sn-4Zr-6Mo.

### 10:20 AM Break

### 10:40 AM Invited

#### Short Crack Effects in Extrinsic Toughened Materials: Jamie Kruzic<sup>1</sup>; <sup>1</sup>Oregon State Univ

Extrinsic toughening mechanisms (crack bridging, transformation toughening, etc.) are effective at providing crack propagation resistance in many materials and composites; however, these mechanisms result in a crack size dependence (i.e., "short crack effect") for the fatigue properties over the crack sizes where the extrinsic toughening zone forms and develops. This presentation examines how fatigue resistance curves (fatigue R-curve or fatigue threshold R-curve) may be used to understand and predict such crack size effects. Experimental results using compact tension, C(T), and/or beam specimens for several bridging materials (human bone, polycrystalline Al<sub>2</sub>O<sub>3</sub>, Si<sub>3</sub>N<sub>4</sub>) are presented, along with discussion of the role the material microstructure. Furthermore, it is demonstrated that the fatigue behavior can be predicted by characterizing the bridging zone and quantifying the effects of bridging using crack tip opening displacement, compliance, and/or Raman spectroscopy experiments. Experimentally measured small crack data agrees well with the predictions based on quantitative bridging zone characterization.

## 11:10 AM

### **Fatigue Crack Propagation in New Generation Aluminum-Lithium Alloys:** *Sébastien Richard*<sup>1</sup>; Christine Sarrazin-Baudoux<sup>1</sup>; Jean Petit<sup>1</sup>; <sup>1</sup>LMPM ENSMA

Aluminium alloys are widely used in aeronautical industry due to their good specific mechanical properties. Low-density third generation aluminum-lithium alloys are good candidates in view of reducing the fuel consumption. However, a better knowledge of damage properties is required for application. To answer this question, a study of fatigue crack growth behavior of three new aluminum lithium alloys in T8 temper was undertaken. Tests were performed at 20 Hz (CCT specimens) and 35 Hz (CT specimens), at stress ratios  $R=0.1$  and  $0.7$  under three environments: ambient air, simulated high atmosphere (dew point and temperature of 223K) and high vacuum as reference for an inert environment. Crack closure contribution was systematically evaluated. Experimental results are analyzed in terms of  $da/dN$  curves, crack path profiles and SEM examinations. Influence of specimen geometry, texture, stress ratio, environment and alloy composition is discussed in comparison with conventional alloys.

## 11:30 AM

### **The Influence of Shot Peening on Alpha-Case Formation and Microcracking in Titanium Alloys:** *Meurig Thomas*<sup>1</sup>; Trevor Lindley<sup>1</sup>; Martin Jackson<sup>2</sup>; <sup>1</sup>Imperial College London; <sup>2</sup>The University of Sheffield

Exposure of titanium alloys to air at high temperature leads to the formation of an all-alpha, oxygen-rich, embrittled surface layer termed the alpha-case. Whilst the deleterious effects of the alpha-case on component integrity such as fatigue behaviour have been identified, research examining the link between processing, microstructure and the propensity for alpha-case formation is limited. This paper seeks to explore the relationship between alloy chemistry, thermo-mechanical processing and surface treatments, (notably shot peening) and alpha-case growth kinetics. In addition, the metallurgical aspects of failure as a result of the alpha-case induced microcracking and approaches to improve aero-engine component life are also discussed.

## 11:50 AM

### **Combination of Safe Life and Fail Safe Concepts to Assess the Lifetime of Ti-6Al-4V Forgings:** *Bernd Oberwinkler*<sup>1</sup>; Heinz Leitner<sup>1</sup>; Martin Riedler<sup>2</sup>; <sup>1</sup>University of Leoben; <sup>2</sup>Böhler Schmiedetechnik GmbH & Co KG

Forged parts made of Ti-6Al-4V are generally used in aerospace industry, e.g. for engine mounts, pylon fitting and frame parts, housings, gear boxes, engine disks and so on. To achieve damage tolerant together with light weight design of such parts a combination of the safe life and the fail safe concept is necessary. The characterization of the fatigue behavior of Ti-6Al-4V with different microstructures has been done through low cycle and high cycle fatigue tests for different stress ratios and relative stress gradients (notches) as well as crack propagation tests for small and long cracks. Assuming the smallest detectable flaw size using non-destructive testing methods the residual lifetime can be estimated with fracture mechanics. To combine this fail safe concept with the safe life concept the crack initiation has to be taken into account. This approach has been validated using flawed specimens under high cycle fatigue loading.

## 12:10 PM

### **Fatigue Crack Growth Behavior of Long and Small Cracks in Structural Materials:** *Anastasios Gavras*<sup>1</sup>; Diana Lados<sup>1</sup>; <sup>1</sup>WPI

Fatigue crack propagation of long and small cracks was investigated for various structural materials. For each material, two microstructures were prepared and tested. Low residual stress was ensured during processing to shed light on microstructural effects on crack growth. Compact tension and single edge tension specimens were fatigue crack growth tested at room temperature and stress ratio,  $R=0.1$ . Microstructure related mechanisms were used to explain the near-threshold behavior and crack growth responses in Regions II and III for each material/microstructure. Threshold behavior of long cracks is attributed to closure-dependent mechanisms. In Regions II and III, the changes in crack growth mechanisms were explained by the extent of the plastic zone ahead of the crack tip. Threshold behavior of small cracks is explained through closure-independent mechanisms, specifically through the barrier effects of characteristic features specific to each material/microstructure. Recommendations for integrating materials knowledge in structural design for fatigue performance are given.

## **Friction Stir Welding and Processing-V: Session V**

Sponsored by: The Minerals, Metals and Materials Society, TMS Materials Processing and Manufacturing Division, TMS: Shaping and Forming Committee  
Program Organizers: Rajiv Mishra, Missouri University of Science and Technology; Thomas Liener, Los Alamos National Laboratory; Murray Mahoney, formerly with Rockwell Scientific

Wednesday AM  
February 18, 2009

Room: 2014  
Location: Moscone West Convention Center

*Session Chair:* William Arbegast, South Dakota School of Mines and Technology

## 8:30 AM Invited

### **Partitioning of Forces in Friction Stir Welding – Part 1:** *John Baumann*<sup>1</sup>; Abe Askari<sup>1</sup>; Robert Landers<sup>2</sup>; <sup>1</sup>The Boeing Company; <sup>2</sup>Missouri University of Science and Technology

In the FSW system built by Broetje Automation for The Boeing Company, retractable pin tool capability has been achieved with an arrangement that allows for independent positioning and force measurement / control of the shoulder and pin, along with radial loads and torque measurement / control capabilities. The goal of the work described is to characterize the weld envelopes for two pin-length regimes, to measure the loads and torques under changing process conditions, and to compare this collected data with predicted values from the Boeing-Sandia FSW modeling code, Cth. A previous paper described progress in refining that code, to be able to resolve the output into separate contributions from the shoulder and pin. This paper will cover the data collected on the Broetje system for the shoulder and pin tools, using a Design of Experiments approach, while making welds in 2024 Al, and complete the comparison with the model.

## 8:50 AM Invited

### **Boundary Condition Effects on Friction Stir Welds in 7050-T7 Sheet:** Piyush Uphadyay<sup>1</sup>; *Anthony Reynolds*<sup>1</sup>; <sup>1</sup>University of South Carolina

A series of friction stir welds was made in 6.4 mm thick 7050-T7 sheet. Thermal boundary conditions for the welds were varied by (1) using tools with different values of thermal diffusivity and (2) by varying the ambient thermal conditions. Tools with shoulders made from Nimonic 105, H13 tool steel, and Densimet (a tungsten based alloy) were used for welding. The thermal conductivities of the various shoulder materials vary by a factor of 12 (minimum for the Nimonic and maximum for the Densimet). Each tool was instrumented with thermocouples in the probe and at various locations in the shoulders and shanks. Welds were performed in room air and underwater and with varying levels of base plate pre-cooling. Weld response variables, hardness distributions, and nugget grain size were correlated with the thermal boundary conditions. Finite element simulations are used to enhance understanding of the observed phenomena.

## 9:10 AM Invited

### **Aging Weapons Systems Repair Using Friction Stir Welding:** *Bryan Tweedy*<sup>1</sup>; William Arbegast<sup>2</sup>; Robert Hrabec<sup>1</sup>; <sup>1</sup>H. F. Webster Inc.; <sup>2</sup>South Dakota School of Mines and Technology

Friction stir welding and processing (FSW&P) was identified in the FY07 Aging Aircraft Study conducted by the South Dakota School of Mines and Technology as a technology that is ready to enter into a qualification process for use as standard repair technique on aging weapons systems. FSW has been widely investigated as a manufacturing process with successes reported in the commercial and government sectors, however, little is reported in the literature on the qualification of FSW&P for repair applications. Preliminary analysis in this study utilizing FSP for repair of several components showed technical feasibility. In addition, the demonstration of FSP to refurbish an actual part was successful. Radiographic inspection showed that the volumetric defects and fatigue cracking were processed from the candidate component. The study produced a cost benefits analysis which estimated \$31.4M annual savings to the USAF alone.

9:30 AM

### **The Role of Friction Stir Welding in the Nuclear Fuel Plate Fabrication:**

*Douglas Burkes<sup>1</sup>; N. Hallinan<sup>1</sup>; Michael Chapple<sup>1</sup>; Jared Wight<sup>1</sup>; Pavel Medvedev<sup>1</sup>; Indrajit Charit<sup>2</sup>; Peter Wells<sup>2</sup>; Amit Amritkar<sup>3</sup>; <sup>1</sup>Idaho National Laboratory; <sup>2</sup>University of Idaho; <sup>3</sup>University of Utah*

The friction bonding process combines desirable attributes of both friction stir welding and friction stir processing. The development of the process is spurred on by the need to fabricate thin, high density, reduced enrichment fuel plates for nuclear research reactors. The work seeks to convert research and test reactors currently operating on highly enriched uranium to operate on low enriched uranium without significant loss in reactor performance, safety characteristics, or significant increase in cost. In doing so, the threat of global nuclear material proliferation will be reduced. Feasibility studies performed on the process show that this is a viable option for mass production of plate-type nuclear fuel. Adapting the friction stir weld process for nuclear fuel fabrication has resulted in the development of several unique ideas and observations. Potential areas in the nuclear field where friction stir welding could continue to play a significant role will be discussed.

9:50 AM

### **Effects of Parts and Fixture Geometric Errors and In-Process Deformations on the Quality of Friction Stir Welds:**

*Michel Guillot<sup>1</sup>; Sébastien Bédard<sup>1</sup>; Isabelle Bouchard<sup>1</sup>; <sup>1</sup>Laval University*

Although the friction stir technique is increasingly used for welding extrusions, aircraft and automotive components, its implementation is often delayed by a lack of understanding of the parameters involved. Among these parameters, the large forces exerted by the tool can induce deformations in the parts and in the fixture. Furthermore, this process appears to be very sensitive to any geometric error in the welding joint. In this paper, the effect on weld quality of geometric errors and in-process deformations is investigated on typical AL6063-T6 and AL6061-T6 extrusions. Butt and lap joints are produced in 6061-T6 samples using a stiff fixture with controlled geometric deviations and gaps. The effect of in-process deformations on weld quality is quantified. A method for improving fixture designs is proposed. Effect of heat transfer to the fixture is considered. Finally, this method is applied to improve the assembly of floor panels made of several extrusions.

10:10 AM

### **Friction Stir Welding of a AA2199 Al-Li Alloys:**

*Axel Steuwer<sup>1</sup>; Jens Altenkirch<sup>2</sup>; Myriam Dumont<sup>3</sup>; Philip Withers<sup>4</sup>; <sup>1</sup>ESS Scandinavia; <sup>2</sup>Institute Laue-Langevin; <sup>3</sup>Faculté des Sciences et Techniques de St-Jérôme; <sup>4</sup>University of Manchester*

In this paper we discuss friction stir welding of a novel low-density aluminium-lithium alloy AA2199, which is intended for use in the aerospace industry. Nine trial welds were produced to study the effect of varying welding parameters on residual stresses and microstructure with a view to optimising the welding process. The welds were characterised using a variety of techniques such as hardness measurements, SEM, TEM, DSC and SAXS, which allows a discussion of the effect of FSW on the precipitation kinetics, and its effect on residual stress. Additionally the in-situ global mechanical tensioning (GMT) was applied to produce nearly stress free welds in this alloy. Residual stresses of ~50% of the yield strength were found after weld parameter optimization, while the stress engineering technique (GMT) allowed producing stress free welds.

10:30 AM Break

10:40 AM

### **Corrosion in 2XXX-T8 Aluminum Alloys:**

*Christian Widener<sup>1</sup>; Tze Jian Lam<sup>1</sup>; Dwight Burford<sup>1</sup>; <sup>1</sup>Wichita State University*

This paper investigates the apparent trend in 2XXX-T8 aluminum alloys to possess excellent as-welded exfoliation corrosion resistance in the weld zone compared to the parent material. To evaluate this trend, friction stir welds were produced in 0.125 (3.2 mm) 2024-T81, 0.080-in. (2 mm) 2219-T87 and 0.153-in. (3.9 mm) 2198-T851 (Al-Li) material, and then tested in a standard and modified ASTM G34 exfoliation environment. Unlike welding in the -T3 or -T4 tempers, where the weld zone can become anodic to the parent metal and exhibit preferential corrosion, when welded in the -T8 starting temper the weld zone has been found to be relatively cathodic compared to the parent material exhibiting only mild evidence of corrosion attack.

11:00 AM

### **Correlation between Ultrasonic Phased Array and Feedback Force Analysis of Friction Stir Welds:**

*Pedro Gimenez Britos<sup>1</sup>; Christian Widener<sup>1</sup>; Dwight Burford<sup>1</sup>; <sup>1</sup>NIAR - WSU*

Ultrasonic phased array has been used as a powerful non-destructive test (NDT), well known for its capability to detect different kinds of FSW defects. A new NDT technique developed at the South Dakota School of Mines and Technology is a FSW Analysis Software, designed to analyze any specific section of the weld in almost real time using discrete Fourier transforms and phase space analysis. With this software, a trained user can detect where potential flaws may exist. The purpose of this study is to determine if the defects found using ultrasonic phased array inspection can be correlated with defects identified by the software. By correlating this software with an ultrasonic phased array inspection, the time and expense associated with 100% inspection of parts could be significantly reduced. The ultimate goal of this research is to support the development of real time quality control to minimize the cost of inspection through statistical process control methods.

11:20 AM

### **A Novel Artificial Neural Network Model for Evaluating Hardness in Stir Zone of Submerge Friction Stir Processed Al-6061-T6 Plate:**

*Abbas Ebnonnasir<sup>1</sup>; F. Karimzadeh<sup>1</sup>; M. H. Enayati<sup>1</sup>; <sup>1</sup>Isfahan University of Technology*

The aluminum (Al) alloy 6061-T6 was friction stir processed at submerged condition and different tool rotation speeds ( $\omega$ ) and processing speeds ( $V$ ). The effect of processing parameters on hardness of stir zone was investigated. In order to derive out the relationship between the hardness of stir zone and processing parameters and optimizing them, some test was done and a matrix of variation parameters of process was filled and used for training of an artificial neural network (ANN) model. A sensitivity analysis was carried out using the ANN model. It is shown that, among two process parameters, the processing speed ( $V$ ) is more important on stir hardness. In addition, a safe zone can be defined by ANN model in which superior hardness can be achieved.

11:40 AM

### **Corrosion and Fatigue Evaluation of Swept Friction Stir Spot Welding through Sealants and Surface Treatments:**

*Jeremy Brown<sup>1</sup>; Dwight Burford<sup>1</sup>; Christian Widener<sup>1</sup>; Walter Horn<sup>1</sup>; George Talia<sup>1</sup>; Bryan Tweedy<sup>2</sup>; <sup>1</sup>Wichita State University; <sup>2</sup>H.F. Webster Engineering*

This experiment investigates the capability of welding through sealants and surface treatments with swept Friction Stir Spot Welding (FSSW) in thin gauge 2024-T3 aluminum alloy. The aluminum sheets have a sealant applied and are pre-treated with various surface coatings. The uncured sealants were applied to the faying surface of the test coupons shortly before joining. The results are also compared to bare sheets in the untreated condition. Corrosion testing was performed through alternate immersion in a salt solution. The samples were evaluated through metallography and testing of residual strength. Fatigue testing was performed per the NASM 1312-21 specification. S-N data was collected for 5 load levels for each sample type. Riveted data has also been collected using this method. Work in this area is important to support increased implementation of FSSW in production applications as a replacement for other discrete fastening methods, like riveting and resistance spot welding.



## General Abstracts: Materials Processing and Manufacturing Division: Session I

Sponsored by: The Minerals, Metals and Materials Society, TMS Materials Processing and Manufacturing Division, TMS/ASM: Computational Materials Science and Engineering Committee, TMS: Global Innovations Committee, TMS: Nanomechanical Materials Behavior Committee, TMS/ASM: Phase Transformations Committee, TMS: Powder Materials Committee, TMS: Process Technology and Modeling Committee, TMS: Shaping and Forming Committee, TMS: Surface Engineering Committee

Program Organizers: Thomas Bieler, Michigan State University; Neville Moody, Sandia National Laboratories

Wednesday AM  
February 18, 2009

Room: 3022  
Location: Moscone West Convention Center

Session Chair: To Be Announced

### 8:30 AM

**Anisotropic Properties of Tantalum Processed by Equal Channel Angular Pressing:** Joel House<sup>1</sup>; Philip Flater<sup>1</sup>; James O'Brien<sup>2</sup>; William Hosford<sup>3</sup>; John Bingert<sup>4</sup>; Robert De Angelis<sup>5</sup>; <sup>1</sup>US Air Force; <sup>2</sup>O'Brien and Associates; <sup>3</sup>University of Michigan; <sup>4</sup>Los Alamos National Laboratory; <sup>5</sup>University of Florida/REEF

The current study examines the effect of severe plastic deformation on pure tantalum via equal channel angular pressing (ECAP). After processing, three metallurgical conditions were characterized: as worked, fine-grain annealed, and large-grain annealed. A series of low strain rate, split Hopkinson Pressure Bar, and Taylor Impact experiments were conducted to characterize the mechanical properties. These experiments revealed orientation dependence in mechanical strength as a result of the processing history. This paper will describe the initial microstructures to include grain size and texture. Data will be given on the mechanical properties relative to orientation. The recovered specimens were analyzed to provide in-sight into the evolution of texture for the various experimental conditions. These data sets will be discussed in the contexts of processing by severe plastic deformation and the resulting anisotropic material properties.

### 8:50 AM

**Corrosion Performance of Al/SiCP Composites with Multimodal Distribution under Humid Ambient and Aerated Chloride Solutions:** Miguel Montoya-Dávila<sup>1</sup>; Martin Pech-Canul<sup>1</sup>; Maximo Pech-Canul<sup>2</sup>; <sup>1</sup>Cinvestav-Salttillo; <sup>2</sup>Cinvestav-Merida

The effect of the multimodal distribution on the corrosion behavior of Al/SiCp composites was investigated. Composites with 0.6 volume fraction of reinforcements were prepared by the infiltration of preforms (silica-coated a-SiC powders of 10, 54, 86, and 146  $\mu\text{m}$ ) with the alloy Al-13.3Mg-1.8Si (wt. %) in Ar-N<sub>2</sub> at 1100°C for 60 min. Corrosion potential measurements were carried out in aerated 0.1M NaCl solutions; humidity tests were performed in 90±3% humidity chambers at 50 °C. Results show that weight gain augments with increase in particle size distribution. A possible explanation to this outcome is the formation of the unwanted Al<sub>4</sub>C<sub>3</sub>. Despite the weight gain registered, the composites show no evidence of degradation. Corrosion potential curves are characterized by two stages; in stage 1, E<sub>corr</sub> tends towards the corrosion potential for aluminum; in stage 2 and after 4.33 h, E<sub>corr</sub> oscillates within a well defined and approximately constant range.

### 9:10 AM

**Fast Epitaxial High Temperature Brazing of Single Crystalline Nickel Based Superalloys:** Britta Laux<sup>1</sup>; <sup>1</sup>Technische Universität Braunschweig

A new brazing technology has been developed for the repair of cracks in turbine components. Conventional diffusion bonding technologies work with nickel based braze alloys which are enhanced by fast diffusing melting point depressants (MPD) like boron or silicon. An epitaxial growth can be achieved by a diffusion controlled isothermal solidification. Due to the poor solubility of the MPD within nickel, entire diffusion of the MPD out of the braze gap is essential. Otherwise, brittle secondary phases form which results in deteriorating mechanical properties. Since the required hold times for epitaxial solidification are very long, new manganese containing alloys were developed as manganese is completely solvable within nickel. Brazing times being up to 100-times shorter

could be achieved. By the addition of aluminium, chromium and titanium a microstructure very similar to that of the base material was produced over a gap width of 300 $\mu\text{m}$ , whereas a complete epitaxial solidification occurred.

### 9:30 AM

**GTAW-Assisted Laser Welding of Galvanized High-Strength Steel in Gap-Free Lap Joint Configuration:** Shanglu Yang<sup>1</sup>; Radovan Kovacevic<sup>1</sup>; Robert Ruokolainen<sup>2</sup>; <sup>1</sup>Research Center for Advanced Manufacturing; <sup>2</sup>General Motors Corporation

Laser welding assisted by GTAW preheating is introduced for welding of galvanized DP 980 in gap-free lap joint configuration. The controlled heat management during the preheating by GTAW will transform the zinc coating at the top surface into the zinc oxides, which will dramatically improve the coupling of the laser power to the welded material. The keyhole is readily formed with the help of zinc oxides, which allows the high-pressurized zinc vapor to be vented out. The completely defect-free laser welds have been obtained. Furthermore, a CCD video camera is used to on-line monitor the molten pool. By the analysis of the video film, it is revealed that when the welding process is stable, the keyhole is kept open. However, the keyhole is readily collapsed when the welding process is instable. The results from the micro-hardness and shear tensile tests reveal that the high strength is obtained in the laser welds.

### 9:50 AM

**Uniform Metallic Coatings on High Conductivity Graphite Foams:** Ben Poquette<sup>1</sup>; Stephen Kampe<sup>2</sup>; <sup>1</sup>Keystone Materials LLC; <sup>2</sup>Virginia Tech

In the late 90's, a novel technique for fabricating high conductivity graphite foam was developed by Oak Ridge National Laboratory. With its unique properties, this foam has shown promise to revolutionize the performance of many commercial and defense related systems not limited to: high surface area electrodes and catalysts supports, power electronics cooling, personal cooling, evaporative cooling, radiators, nuclear reactor core, space radiator, brake and clutch cooling, high temperature bearings, EMI shielding, thermal and acoustic signature management. Until recently, difficulties in joining graphite foam to other materials have hindered its incorporation into current platforms. A technique was developed, through cooperation with ORNL and Virginia Tech, which allows a strongly adhered, uniform metallic coating to be applied throughout the thickness of graphite foam. These metal coatings should serve to both solve existing short-falls (brittleness, lack of joinability, etc.) as well as lend their properties (magnetic, catalytic, etc.) to graphitic foam.

### 10:10 AM

**Microstructural Evolution during Grain Boundary Engineering of Stainless Steel:** Benjiman Albiston<sup>1</sup>; Megan Frary<sup>1</sup>; <sup>1</sup>Boise State University

Grain boundary engineering (GBE) is a method for controlling the microstructure to improve the material properties. The purpose of GBE is to reduce the interconnection of general grain boundaries (i.e., those susceptible to intergranular degradation) and to increase the fraction of "special" boundaries (i.e., those resistant to attack). The objective of the present work project is to modify the microstructure of 316L stainless steel using GBE. An iterative processing technique involving cold working and annealing steps was developed and electron backscatter diffraction (EBSD) is used to characterize the resulting microstructures. The special boundary fraction was increased from 50% to 80%, effectively reducing the size of connected general boundary clusters. The reduced general boundary cluster size makes it more difficult for cracks to propagate through the material. By controlling the properties of the grain boundaries in the material, its performance can be enhanced by increasing its lifetime and reliability.

### 10:30 AM

**Modeling Uncertainty Propagation in Deformation Processes:** Nicholas Zabaras<sup>1</sup>; Babak Kouchmeshky<sup>1</sup>; <sup>1</sup>Cornell University

We will present a non-intrusive method for modeling the propagation of uncertainty in process conditions and initial microstructure on the final product properties and geometry in a deformation process. The stochastic multiscale deformation problem is modeled using a sparse grid collocation approach that allows the utilization of a deterministic simulator to build interpolants of the main solution variables in the stochastic support space. The ability of the method in estimating the statistics of the macro-scale properties such as ductility and hardness of the product of the metal forming process is shown through examples featuring randomness in initial texture and process parameters. Comparisons are made with the results obtained from Monte-Carlo method.

10:50 AM

**Phase Segregation in Semisolid Powder Processing of Micro-Features:** *Gap-Yong Kim<sup>1</sup>; Yufeng Wu<sup>1</sup>; Iver Anderson<sup>1</sup>; Thomas Lograsso<sup>1</sup>; <sup>1</sup>Iowa State University*

In near future, micromanufacturing is expected to play a key role in that it will bridge the macro- and nano-worlds. Increasing demand for miniature parts has attracted significant industrial and academic interests on near net-shape processing of complex, 3-D micro-parts. Among various techniques, the paper investigated the potential of metallic powder materials at semisolid state (i.e., "mush state") to fabricate micro-features. The unique behavior of solid and liquid phase mixture is expected to overcome challenges encountered by traditional net-shape methods when applied to micromanufacturing. Recent research results on semisolid powder forming (SPF) of microscale features will be presented. The work investigated phase segregation when semisolid powders were forced into micro-cavity through back-extrusion experiment. Results of microstructural analysis and hardness test will be presented. Finally, potentials of the SPF as a near net-shape micromanufacturing method are discussed.

11:10 AM

**Modeling the Critical Conditions for the Rolling of Seamless Pipes:** *Roman Pschera<sup>1</sup>; Jürgen Klarner<sup>2</sup>; Christof Sommitsch<sup>1</sup>; <sup>1</sup>University of Leoben; <sup>2</sup>voestalpine Tubulars*

The present work deals with the description of the material behavior in the feed region and in the rolling gap during cross roll piercing. Numerous previous investigations have shown that the "Mannesmann-Effect" (cyclic plastic deformation of the core of the billet before getting in contact with the plug) exists and has a negative impact on the quality of the pipes. In order to model this effect in the presence of the plug, a new empirical damage criterion was tested. This model takes into account the relative position of the middle principal stress with respect to the other principal stresses. In addition to it, a stress triaxiality function is suggested where negative values influence the damage process. The results agree with the theoretical assumptions giving reason to investigate the "Mannesmann-Effect" in more detail.

11:30 AM

**Sol-Gel Synthesis and Adsorption Properties Study of Spinel Manganese Oxide Lithium Ion-Sieves:** *Dong Li<sup>1</sup>; Qinghua Tian<sup>1</sup>; Rongyi Liu<sup>1</sup>; Xueyi Guo<sup>1</sup>; <sup>1</sup>School of Metallurgical Science and Engineering*

Two types of spinel manganese oxide lithium ion-sieves were derived from  $\text{LiMn}_2\text{O}_4$  and  $\text{Li}_{1.33}\text{Mn}_{1.67}\text{O}_4$  respectively, which were synthesized by a sol-gel method using an aqueous solution of lithium hydroxide and manganese acetate containing citric acid as a chelating agent. The two ion-sieves were compared in terms of physical characteristics and lithium adsorption properties. The maximum adsorption capacity in a 0.1 mol·L<sup>-1</sup> LiOH system by these ion-sieves were 25mg·g<sup>-1</sup> and 30mg·g<sup>-1</sup>, respectively. The mechanisms of adsorption by these two ion-sieves were discussed, indicating that the change of lattice constants in a lithium ion-sieve reaction is mainly caused by the change of manganese valence, rather than the extraction/insertion of lithium ions.

11:50 AM

**Surface Treatment by Variable-Polarity Arc to Promote the Energy Absorption in Laser Welding of Aluminum Alloy:** *Rouzbeh Sarrafi<sup>1</sup>; Dechao Lin<sup>1</sup>; Radovan Kovacevic<sup>1</sup>; <sup>1</sup>Southern Methodist Univ*

One of the major obstacles limiting the application of laser technology in the welding of aluminum alloys is the low energy absorption. In order to enhance the laser absorption, a practical technique in which a variable polarity arc is used to treat the surface prior to laser welding is introduced. Non-reflective surfaces on Al6061 were produced by using the mentioned technique. The objective was to investigate the effect of surface treatment by arc on both laser spot welding and continuous laser welding. To help understand the welding process, a machine vision system was integrated, and the molten pool images were captured in real time. Results demonstrated that the by surface treatment, deeper spot welds can be produced. However, it does not play a critical role in the continuous laser welding in keyhole mode since the laser beam mostly interacts with the molten pool, and not with the treated surface.

12:10 PM

**Synthesis of Oxide Coated Carbon Nano Fibers via CO Disproportionation in Mg/MgO System:** *Farhad Golestanifard<sup>1</sup>; Mohamad Sharif<sup>1</sup>; <sup>1</sup>Iran University of Science and Technology*

Synthesis of oxide coated CNFs via CO Disproportionation in Mg/MgO system was investigated. Mg metal and MgO was mixed with specific weight ratio and then heat treatment at 1000 C at in coke bed. the product was characterized using different method i. e. SEM, TEM, XRD, STA and Raman spectroscopy. The results showed that in this system CNFs can be formed and an oxide (MgO) coating cover outer surface of CNFs. aiding Raman spectroscopy and TEM observation high degree of crystallinity of CNFs was concluded and the arrangement of 2D graphene planes were detected parallel to growth axis of CNFs. oxide coated CNFs prepared via such a simple route showed high oxidation resistance and no weight loss related to oxidation of fibers was seen up to 1200 C.

12:30 PM

**In-Situ Fabrication of Metal Matrix Composites by Solidification Process under High Magnetic Fields:** *Qiang WANG<sup>1</sup>; Tie Liu<sup>1</sup>; Chunjiang Wang<sup>1</sup>; Changsheng Lou<sup>1</sup>; Donggang Li<sup>1</sup>; Jicheng He<sup>1</sup>; <sup>1</sup>Northeastern University*

High magnetic fields were used to in-situ fabricate metal matrix composites during the solidification processes of Mn-Sb, Mn-Bi and Al-Ni alloys. MnSb-MnSb/Sb-Sb and Mn-BiMn-Bi/BiMn functionally graded materials (FGMs) with gradient structures in morphology and composition have been successfully obtained by controlling magnetic gradients. And anisotropic Al-Al<sub>3</sub>Ni composites in which the Al<sub>3</sub>Ni crystals were oriented parallel to the imposed magnetic fields and the primary Al<sub>3</sub>Ni phases with their long axes were aligned perpendicular to the magnetic fields were also fabricated under uniform magnetic field conditions. The effects of both uniform and gradient high magnetic fields on the migration, crystalline orientation and phase alignment of the reinforced or functional phases during the solidification were examined. Furthermore, the physical properties and mechanical performances of these materials were investigated. The experimental results indicate that the high magnetic field is one of promising approaches in producing metal matrix composites with special performances.

## General Abstracts: Structural Materials Division: Session II

Sponsored by: The Minerals, Metals and Materials Society, TMS Structural Materials Division, TMS: Advanced Characterization, Testing, and Simulation Committee, TMS: Alloy Phases Committee, TMS: Biomaterials Committee, TMS: Chemistry and Physics of Materials Committee, TMS/ASM: Composite Materials Committee, TMS/ASM: Corrosion and Environmental Effects Committee, TMS: High Temperature Alloys Committee, TMS/ASM: Mechanical Behavior of Materials Committee, TMS/ASM: Nuclear Materials Committee, TMS: Refractory Metals Committee, TMS: Titanium Committee

Program Organizers: Robert Hanrahan, National Nuclear Security Administration; Eric Ott, GE Aviation

Wednesday AM

Room: 2018

February 18, 2009

Location: Moscone West Convention Center

Session Chair: To Be Announced

8:30 AM

**Analysis of Lattice Stress Direction Evolution in Copper Polycrystals Due to Mechanical Loading Using Crystal Yield Surface Vertex:** *Tong-Seok Han<sup>1</sup>; Jun-Sang Park<sup>2</sup>; Paul Dawson<sup>2</sup>; Matthew Miller<sup>2</sup>; <sup>1</sup>Yonsei University; <sup>2</sup>Cornell University*

Lattice stresses of a polycrystalline copper under uniaxial tension obtained from the x-ray diffraction experiment and the finite element simulation were compared in a crystal orientation space. The lattice stress distributions from experiment and simulation were in good agreement, and showed significant crystal orientation dependence. To provide insights on the mechanism behind the agreement, the preferred stress direction and its evolution during loading process were investigated using single crystal yield surface vertices. It was found that a lattice stress tends to move toward a vertex when the vertex is aligned or close to the loading direction as the plasticity develops. However, if the closest vertex

from the lattice stress direction is not closely aligned with the loading direction, the lattice stress finds its direction where it can accommodate the equilibrium and deformation of aggregates through grain interactions.

## 8:50 AM

**Compressive Properties of a Closed- Cell Aluminum Foam as a Function of Strain-Rate and Temperature:** *Carl Cady*<sup>1</sup>; Cheng Liu<sup>1</sup>; George Gray<sup>1</sup>; <sup>1</sup>Los Alamos National Lab

The compressive deformation behavior of a closed-cell Aluminum foam (ALPORAS) manufactured by Shinko Wire. Co. in Japan was evaluated under static and dynamic loading conditions as a function of temperature. High strain rate tests (1000 - 2000/s) were conducted using a split-Hopkinson pressure bar (SHPB). Quasi-static and intermediate strain rate tests were conducted on a hydraulic load frame. Little change in the flow stress behavior as a function of strain rate was measured. The deformation behavior of the Al-foam was however found to be strongly temperature dependent under both quasi-static and dynamic loading. Localized deformation and stress state instability during testing of metal foams will be discussed in detail since the behavior over the entire range of strain rates indicates non-uniform deformation. Additionally, investigation of residual stresses created during manufacturing was investigated.

## 9:10 AM

**Effects of Alloying Elements on Mechanical Properties of API X80 Linepipe Steels:** *Seung Youb Han*<sup>1</sup>; Sang Yong Shin<sup>1</sup>; Chang-hyo Seo<sup>1</sup>; Hakcheol Lee<sup>1</sup>; Jin-ho Bae<sup>2</sup>; Kisoo Kim<sup>2</sup>; Sunghak Lee<sup>1</sup>; Nack J. Kim<sup>1</sup>; <sup>1</sup>POSTECH; <sup>2</sup>Technical Research Laboratories, POSCO

This study aimed at investigating effects of alloying elements on mechanical properties of API X80 linepipe steels. Four kinds of steels were fabricated by varying Mo, Cr, and V additions, and their microstructures, tensile and Charpy impact properties, and effective grain size measurement were analyzed. Since the addition of Mo and V promoted to form fine acicular ferrite and granular bainite, while prohibiting the coarsening of granular bainite, it improved strengths and upper shelf energy, and decreased the energy transition temperature. The Cr addition promoted the formation of coarse granular bainite and hard secondary phases, which led to the increased effective grain size, energy transition temperature, and strength, and the decreased upper shelf energy. The steel containing 0.3 wt.% Mo and 0.06 wt.% V had best impact properties because it was composed of fine acicular ferrite and granular bainite, while tensile properties maintained excellent.

## 9:30 AM

**Finite Element Analysis of Viscoelastic Core Sandwich Structures:** Dan Watt<sup>1</sup>; *Xiaomin Li*<sup>1</sup>; <sup>1</sup>University of Windsor

The mechanical behavior of a sandwich panel depends on the face and core materials, and on its geometry. Polymers are sometimes used in the core. These viscoelastic materials are subject to creep and stress relaxation. Because many interactive factors have to be considered for designing sandwich constructions, an effective way to evaluate performance is to use FEA. The present work simulated 7 combinations of different materials based on their viscoelastic and elastic properties as given in the literature. The exception is that compression and shear test values for aluminum foam were obtained experimentally. The most important result is that viscoelastic creep in the polymeric sandwich core, which carries only a very small fraction of the applied load, can lead to large strains in the overall structure. This effect is apparently ignored in the literature, so others may not be aware of its significance.

## 9:50 AM

**Investigation on Microstructure and Properties of Ti-45Al-5.5(Cr, Nb, B, Ta) Alloy Prepared by Double Mechanical Milling (DMM) and Spark Plasma Sintering (SPS):** *Yuyong Chen*<sup>1</sup>; Hongbao Yu<sup>1</sup>; Deliang Zhang<sup>2</sup>; Fei Yang<sup>1</sup>; Shulong Xiao<sup>1</sup>; Fantao Kong<sup>1</sup>; Dezhong Wu<sup>1</sup>; <sup>1</sup>Harbin Institute of Technology; <sup>2</sup>The University of Waikato

In this paper, Ti-45Al-5.5(Cr, Nb, B, Ta) alloy with sub-microstructure was prepared successfully by DMM and SPS using element powders as starting materials. XRD patterns show that the as-milled powder is mainly composed of nanometer TiAl and TiAl<sub>3</sub> phases, and there is still Al<sub>3</sub>Ti and Ti phases to exist after DMM. The effect of sintering temperature on microstructure and properties of bulk Ti-45Al-5.5(Cr, Nb, B, Ta) alloy has been investigated. All of the samples sintered at different temperatures (900, 1000 and 1100°C) exhibit high density and same phase constitution ( plenty of TiAl phase and a small quantity of Ti<sub>3</sub>Al , Ti<sub>2</sub>Al and Ti<sub>2</sub>B phases). With the sintering temperature is

900°C, the sample shows good ductility, excellent yield strength and fracture strength, with the value of 5%, 1899MPa and 2229MPa, respectively. When the sintering temperature increases, the properties of the bulk Ti-45Al-5.5(Cr, Nb, B, Ta) alloy declined slightly.

## 10:10 AM

**Martensite in Quenched Fe-C Steels and the Engel-Brewer Electron Theory of Crystal Structures:** *Oleg Sherby*<sup>1</sup>; Jeffrey Wadsworth<sup>2</sup>; Chol Syn<sup>2</sup>; Donald Lesuer<sup>3</sup>; <sup>1</sup>Stanford University; <sup>2</sup>Battelle Memorial Institute; <sup>3</sup>Lawrence Livermore National Laboratory

The transformation step to form martensite in Fe-C steels has been thoroughly explored over the past 70 years. It is based on the formation of a body-centered-tetragonal phase containing retained FCC austenite. These phases are only observed at above 0.6 wt% C. In contrast, these two phases have not been observed below 0.6 wt% C and no transformation models have been proposed in this carbon range. The present authors propose a model based on two transformations taking place during the quenching process. The first step is from FCC austenite to an HCP phase, designated by the authors as hexagonite. The second step is from hexagonite to BCC ferrite containing a carbon rich phase. The 0.6 wt% C composition is interpreted as the maximum solubility of carbon in hexagonite. An electron-controlled mechanism is described, based on the Engel-Brewer theory of crystal structures that is shown to confirm the proposed transformation model.

## 10:30 AM

**Microstructure and Mechanical Behavior in High Strength Nanostructured Spinodal FeNiMnAl Alloys:** *Xiaolan Wu*<sup>1</sup>; Ian Baker<sup>1</sup>; Yifeng Liao<sup>1</sup>; Michael Miller<sup>2</sup>; <sup>1</sup>Thayer School of Engineering, Dartmouth College; <sup>2</sup>Oak Ridge National Laboratory

An ingot of Fe<sub>35</sub>Ni<sub>15</sub>Mn<sub>25</sub>Al<sub>25</sub> was drop cast and directionally solidified under Ar using a Bridgman furnace. TEM showed that the as-cast alloy had a periodic coherent microstructure consisting of alternating B2 and BCC phases. EDS showed that the BCC phase was rich in Fe and Mn, while the B2 phase was rich in Ni and Al, features confirmed by analysis using a Local Electrode Atom Probe. Hardness measurements were performed as a function of annealing time at 550°C. The directionally solidified alloy showed a steady increase in hardness from 437 HV with annealing time, but the as-cast alloy, which was initially harder at 523 HV, showed more complex behavior. The final hardness after 72 h anneals was very similar at 676 HV for the two initial conditions. The paper will relate the mechanical properties to the changes in microstructure. Research was supported by DOE Award #DE-FG02-07ER46392.

## 10:50 AM

**Neutron Scattering Characterization of TWIP Steels Deformed by Tensile Test:** *Jae Suk Jung*<sup>1</sup>; Yang Mo Koo<sup>1</sup>; Il-Kyung Jeong<sup>2</sup>; <sup>1</sup>POSTECH; <sup>2</sup>Pusan National University

TWIP steels have excellent tensile behavior. It is mainly due to planar faults formation during deformation. So, it is important to know the amount of planar-defects as strain increase. Conventionally there was a method to characterize this kind of defects using diffraction line profile analysis by examining the intensity, displacement and broadening of the Bragg peaks. But, there are some drawbacks to this approach such as the restriction of the quantitative analysis to the effects of faulting on the Bragg peaks only, ignoring the information in the diffuse scattering. So, we have attempted another technique to include both the Bragg peaks and diffuse scattering. we had increased planar defects using tensile tests and then performed neutron scattering experiment to analyse the defects of TWIP steels. With the scattering data, we conducted the Rietveld refinement and the PDF refinement. Using those refinement methods we've identified planar defects more effectively.

## 11:10 AM

**Relaxation of Shot Peened and Laser Shock Peened Residual Stresses in a Nickel-Base Superalloy:** *Dennis Buchanan*<sup>1</sup>; Reji John<sup>2</sup>; Michael Shepard<sup>2</sup>; <sup>1</sup>University of Dayton Research Institute; <sup>2</sup>Air Force Research Laboratory (AFRL/RXLMN)

Shot peening (SP) is a commonly used surface treatment that imparts compressive residual stresses into the surface of components. The shallow depth of compressive residual stresses, and the extensive plastic deformation associated with shot peening, has been overcome by modern approaches such as laser shock peening (LSP). LSP surface treatment produces compressive residual stress magnitudes that are similar to SP, that extend 4-5 times deeper,



and with less plastic deformation. Retention of compressive surface residual stresses is necessary to retard initiation and growth of fatigue cracks under elevated temperature loading conditions. This presentation compares the thermal relaxation behavior of SP and LSP residual stress profiles in a powder metal nickel-base superalloy (IN100) for a range of temperatures and exposure times. Results indicate that the LSP processing retains a higher percentage of the initial (as processed) residual stress profile over that of SP.

**11:30 AM**

**Surface Characteristics of Low-Temperature Gas Nitrided 316 Ti Austenitic Stainless Steels:** *Ozgur Celik*<sup>1</sup>; Eyup Sabri Kayali<sup>1</sup>; Huseyin Cimenoglu<sup>1</sup>; <sup>1</sup>Istanbul Technical University

Austenitic stainless steels are widely used in manufacturing of orthopedic implants due to their excellent corrosion resistance and fabricability. However, the application of austenitic stainless steel as a bearing surface is limited by poor wear and friction behaviour. It has been reported that, formation of nitrogen super saturated solid solution with distorted crystal lattice (expanded austenite) at the outer surface of austenitic stainless steel by low temperature plasma nitriding process (below 450 °C) results in a significant improvement in both tribological and corrosion properties besides surface hardness. In the present study, low temperature nitriding was applied to an AISI 316Ti quality austenitic stainless steel in fluidized bed to form nitrogen rich expanded austenite layer. The surface characteristics of nitrided alloy was examined through microstructural examinations, mechanical tests as well as biocompatibility tests and compared with those of Rex 734, which was recently produced austenitic stainless steel for manufacturing of implants.

**11:50 AM**

**The Role of Microstructure on the Fracture Behavior of Cast Ti-5Al-1V-1Zr-1Sn-0.8Mo (Ti-5111) Alloy:** *Jennifer Gaies*<sup>1</sup>; Amy Robinson<sup>2</sup>; <sup>1</sup>NSWC Carderock Division; <sup>2</sup>ARL Penn State

A set of heat treatments were developed and conducted on Ti-5111 castings. Critical microstructure features, including prior- $\beta$  grain size,  $\alpha$ -colony size,  $\alpha$ -lath length and thickness, and the volume fraction and composition of the  $\alpha$  and  $\beta$  phases were quantified for each heat treatment condition. Additionally, a series of mechanical tests, including tensile and fracture toughness tests, were conducted on each condition to correlate the critical microstructure features with the mechanical properties of the cast Ti-5111 alloy. Fracture surfaces of several tensile and fracture toughness specimens were examined and directly correlated to the microstructure to understand crack propagation and failure mechanisms of this alloy. Results showed significant scatter in ductility and toughness, even within the same casting set, which is a function of the large grain size. A grain refinement heat treatment was developed to optimize toughness and ductility, while decreasing scatter in the data.

## Magnesium Technology 2009: Refining and Surface Treatment

Sponsored by: The Minerals, Metals and Materials Society, TMS Light Metals Division, TMS: Magnesium Committee  
Program Organizers: Eric Nyberg, Pacific Northwest National Laboratory; Sean Agnew, University of Virginia; Neale Neelameggham, US Magnesium LLC; Mihriban Pekguleryuz, McGill University

Wednesday AM  
February 18, 2009

Room: 2006  
Location: Moscone West Convention Center

Session Chair: Susan Slade, US Magnesium LLC

### 8:30 AM Introductory Comments

**8:35 AM**

**On the Influence of Settling of  $(ZrB_2)_p$  Inoculants on Grain Refinement of Mg-Alloys: Experiment and Calculation:** *Robert Günther*<sup>1</sup>; Christian Hartig<sup>1</sup>; Norbert Hort<sup>2</sup>; Rüdiger Bormann<sup>1</sup>; <sup>1</sup>Hamburg University of Technology; <sup>2</sup>GKSS Research Centre

A simulation method for heterogeneous nucleation has been developed that enables the prediction of the resulting grain size in Mg-alloys as a function of the inoculant particle size distribution, cooling rate, alloy constitution and volumetric content of inoculants. Experiments with  $(SiC)_p$  and  $(Al_4C_3)_p$  have

been already successfully performed and verified the model assumptions. In view of the considerably smaller lattice mismatch between  $ZrB_2$  and Mg compared to  $SiC$  and  $Al_4C_3$ , respectively,  $(ZrB_2)_p$  should act even more as potent inoculant for grain refinement. However, the larger density of  $ZrB_2$  leads to sedimentation of the inoculants that greatly alters the particle size distribution and therefore the efficiency of grain refinement. A theoretical estimate for the final grain size under consideration of the settling effect has been performed and will be discussed in view of experimental results.

**8:55 AM**

**Grain Refining of AZ91E Alloy Using Ultrasonic Vibration:** *Sandeep Poola*<sup>1</sup>; Qingyou Han<sup>1</sup>; <sup>1</sup>Purdue University

Ultrasonic vibration has been used for grain refining in ingot of small sizes but it is unclear if the technique can be used for grain refining in larger ingots. This article discusses the effect of ingot size on grain refining using ultrasonic vibration. Techniques that combine ultrasonic processing of molten metal and grain refining using nano-particles are evaluated for grain refining. Experimental results indicate that ultra-fine globular grains can be obtained in small ingots using ultrasonic vibration alone. The grain refining effect using ultrasonic vibration decreases with increasing ingot size. Nano-particles that are dispersed into molten metal using ultrasonic vibration can serve as nuclei for grain refining of Mg alloys.

**9:15 AM**

**The Influence of  $\beta$ -(Mg<sub>17</sub>Al<sub>12</sub>) Phase Distribution on Corrosion Behavior of AM50 Alloy in NaCl Solution:** *Surender Maddela*<sup>1</sup>; Yar-Ming Wang<sup>2</sup>; Anil K. Sachdev<sup>2</sup>; Balasubramanian R<sup>3</sup>; <sup>1</sup>Missouri University of Science and Technology ; <sup>2</sup>GM Research and Development Center; <sup>3</sup>Indian Institute of Technology-Kanpur

The effect of  $\beta$  (Mg<sub>17</sub>Al<sub>12</sub>) phase distribution on the corrosion behavior of AM50 alloy in NaCl solution was studied using scanning vibrating electrode technique (SVET) in conjunction with potentiodynamic polarization scan. The  $\beta$  phase distribution was modified by casting AM50 alloy at different cooling rates. For all cooling rates, the following phases were present: primary magnesium ( $\alpha$ ), eutectic mixture of  $\alpha$  and  $\beta$  phase,  $\beta$  phase and  $Al_8Mn_3$  phase. In 0.17 wt% and 1.6 wt% NaCl solutions, the free corrosion potential (FCP) of the moderate cooled alloy was more noble than that for the fast and slow cooled alloy. The corrosion current densities calculated from SVET analysis at zero current potential (ZCP) were in agreement with that determined from potentiodynamic polarization method. This study clearly indicated that for a given magnesium alloy composition, the corrosion resistance of the alloy can be greatly affected by size and distribution of secondary phases.

**9:35 AM**

**Study of Cathodic Metal Transfer to Magnesium Surfaces in Aqueous Environments and Engine Coolant Formulations by Surface Analytic Methods:** *Zhiming Shi*<sup>1</sup>; Pankaj Mallick<sup>1</sup>; *Robert McCune*<sup>2</sup>; <sup>1</sup>University of Michigan-Dearborn; <sup>2</sup>Robert C. McCune and Associates

The corrosion performance of magnesium in the presence of aqueous engine coolants is one of the primary technical challenges in the development of magnesium engine blocks. In addition to the aqueous environment, the coolant loop is a source of dissolved metal ions such as Fe and Cu, which can potentially "plate out" on nascent magnesium surfaces, thereby aggravating corrosion as localized cathodes. The present study considers the composition and growth of the surface film produced on pure magnesium and AM-SC1 magnesium alloy due to transition metal transfer in ethylene glycol-water mixtures containing Fe<sup>2+</sup> and Cu<sup>2+</sup> ions in solution at 20 and 80°C. Surface compositional analysis was conducted using Rutherford Backscattering Spectroscopy (RBS) and Auger Electron Spectroscopy (AES). It was observed that metal ion transfer from the electrolyte to the magnesium surface created local galvanic corrosion cells on the magnesium surface and promoted higher rates of corrosion in localized areas.

**9:55 AM**

**New Surface Treatment for Developing Luster on AZ31 Magnesium Alloy in Industrial Scale:** *Miyoshi Ohara*<sup>1</sup>; Yorinobu Takigawa<sup>2</sup>; Kenji Higashi<sup>2</sup>; <sup>1</sup>Kasatani Corp.; <sup>2</sup>Department of Materials Science, Graduate School of Engineering, Osaka Prefecture University

Magnesium alloys are frequently used in the chassis of laptop computers and cellular phones. The surfaces of such chassis are generally characterized by their luster rather than by any geometrical figures. However, the metallic luster of magnesium alloys is lost by the exposure to air and by the application

of general surface treatment because magnesium alloys is active metal. We therefore, developed a new surface treatment, Mgbright, for producing a luster on the surface of AZ31 magnesium alloy. Mgbright consist of two processes, a chemical treatment process and a coating process, and has the characteristics of developing a primary luster on magnesium and imparting a high resistance to corrosion. We produced high quality chassis of the laptop computers by making use of the characteristics.

## 10:15 AM Break

## 10:30 AM

### **Characteristics of Phosphate Chemical Conversion-Coating on Magnesium Alloy:** *Yongfeng Jiang*<sup>1</sup>; *Yefeng Bao*<sup>1</sup>; *Fei Chen*<sup>1</sup>; <sup>1</sup>Hohai University

The characteristics of phosphate conversion coating on AZ91D magnesium alloy are investigated. Methods of SEM and EDX analysis, as well as salt spray test and potentiodynamic polarization in 5% NaCl solution, reciprocate erase test using alcohol-cotton and mini-ohm meter are employed to investigate mass transfer and structure transformation in surface layer. A compact and dense surface morphology with fine particles cluster of the oxalate coating is presented on magnesium alloy. The particles are homogeneously distributed over the surfaces of the coatings. The salt spray test of coating is evaluated as 9.5 degree according to ASTM B117. Polarization curves reveal that the anti-corrosion of the magnesium after phosphate treatment is better than the magnesium substrate. The reciprocate erase test using alcohol-cotton for the evaluation of adhesion is over 50 cycles, which achieved desires for adhesion in application. The electrical conductivity to substrate of phosphate chemical conversion coating is below 0.1 Ohm.

## 10:50 AM

### **Electroless Ni-P Plating on Magnesium-Lithium Alloy:** *Hongjie Luo*<sup>1</sup>; *Yihan Liu*<sup>1</sup>; <sup>1</sup>Northeastern University

A novel process of electroless Ni-P plating on Magnesium-Lithium alloy was discussed in this paper, by which nickel ions were provided by basic nickel carbonate and a new pretreatment method was introduced for obtaining good quality coating. The corrosion behavior of Magnesium-Lithium alloy without and with coating was compared and the bonding strength of the electroless Ni-P coating to the matrix was also measured. The results showed that the process of electroless Ni-P could easily occur on the intermediate layer and a compact Ni-P coating without flaws could be formed, accordingly the Ni-P coating was above 20  $\mu\text{m}$  thickness and its phosphorus content was about 10.501%. The corrosion potential of Magnesium-Lithium alloy containing the Ni-P coating increased obviously (-0.315V) during anodic polarization in 3.5 mass% NaCl solution and indicated an effective protection for the matrix. It was proved that the Ni-P coating combined closely with Magnesium-Lithium alloy through test.

## **Magnesium Technology 2009: Twin Roll Casting and Semi-Solid Processing**

Sponsored by: The Minerals, Metals and Materials Society, TMS Light Metals Division, TMS: Magnesium Committee

Program Organizers: Eric Nyberg, Pacific Northwest National Laboratory; Sean Agnew, University of Virginia; Neale Neelameggham, US Magnesium LLC; Mihriban Pekguleryuz, McGill University

Wednesday AM  
February 18, 2009

Room: 2007  
Location: Moscone West Convention Center

Session Chair: Michele Manuel, University of Florida

## 8:30 AM Introductory Comments

## 8:35 AM

### **NanoMag High Strength/Density Mg Alloy Sheet:** *Raymond Decker*<sup>1</sup>; *Sanjay Kulkarni*<sup>1</sup>; *Jack Huang*<sup>1</sup>; *Stephen LeBeau*<sup>1</sup>; <sup>1</sup>Thixomat, Inc

Thixomat has developed the Thixomolding Thermomechanical Processing (TTMP) process to generate high strength/density Mg alloy sheet, called NanoMag. The first step of the process is to Thixomold (T) sheet bar with low porosity containing isotropic fine grains - so obtained by the fast cooling rates inherent in near-liquidus molding. The second step is Thermomechanical Processing (TMP) in 1-2 fast passes of warm deformation designed to command

continuous dynamic recrystallization to micron grain size. At the same time coarse eutectic intermetallic phases are refined to nanometer dispersoids. The end result is increases in both yield strength and ductility.

## 8:55 AM

### **Magnesium Alloy Strips Produced by a Melt Conditioned Twin Roll Casting (MC-TRC) Process:** *I. Bayandorian*<sup>1</sup>; *Z. Bian*<sup>1</sup>; *Mingxu Xia*<sup>1</sup>; *H. Zhang*<sup>1</sup>; *Z. Fan*<sup>1</sup>; <sup>1</sup>BCAST

Twin roll casting (TRC) offers a promising route for economical production of Mg sheets. But unfortunately, it offers coarse and non-uniform microstructure and severe central line segregation as well. To address this problem, we developed a melt conditioned twin roll casting (MC-TRC) process. Compared with the conventional TRC process, MC-TRC process has the following features: (1) emphasizing on solidification control at the casting stage instead of on hot rolling in conventional TRC process. (2) solidification control achieved by melt conditioning under intensive forced convection prior to the TRC process, which allows an enhanced heterogeneous nucleation followed by equiaxed growth; (3) minimized central line segregation. In this paper we present MC-TRC process and the microstructures of Mg-alloy strip produced by the MC-TRC process. The discussion will be focused on the solidification behaviour of the intensively sheared liquid metal in the twin roll casting process.

## 9:15 AM

### **Microstructures of the Deforming Zone in Hot Rolling AZ31 Sheet:** *L. K. Fan*<sup>1</sup>; *L.M. Peng*<sup>1</sup>; *R. Wang*<sup>1</sup>; *J. Dong*<sup>1</sup>; *W.J. Ding*<sup>1</sup>; <sup>1</sup>National Engineering Research Center of Light Alloy Net Forming, Shanghai Jiao Tong University

The OM and SEM were used to investigate the microstructures of the deforming zone in hot rolling AZ31 sheet in present study. FEM was also used to analyze the deformation character. The experimental and simulation results show that the microstructure is nonuniform, which is correlated with the nonuniformities of stress and strain in deforming zone. However, the methods of large strain rolling and multiple pass rolling can enhance the uniformity of microstructure and the forming of twins is in favor of uniformity of microstructure.

## 9:35 AM

### **Effect of Warm Rolling and Heat Treatment on Microstructure and Mechanical Properties in Twin Roll Cast ZK60 Alloy Sheet:** *Suk-bong Kang*<sup>1</sup>; *Jaehyung Cho*<sup>1</sup>; *Hyoung Wook Kim*<sup>1</sup>; *Hongmei Chen*<sup>2</sup>; *Huashun Yu*<sup>2</sup>; *Guanghui Min*<sup>2</sup>; <sup>1</sup>Korea Institute of Machinery and Materials; <sup>2</sup>Shandong University

Microstructure and mechanical properties of ZK60 alloy sheets produced by twin roll casting (TRC) and warm rolling were investigated using OM, SEM, TEM and a standard universal testing machine. The microstructure of TRC ZK60 alloy strip consisted of dendrite structure, eutectics and intermetallic compounds located in the interdendritic region. Relatively higher density of shear bands was observable in TRC ZK60 alloy sheet and no obvious dynamic recrystallization was found after warm rolling. The warm rolling induced high strength and low elongation in the TRC ZK60 alloy sheets. Annealing treatment after warm rolling induced the decrease of strength and increase of elongation. Solution treatment at 3750C for 3 hours and subsequent artificial aging treatment at 1750C for 10 hours can be considered to be the optimum T6 treatment. The uniformity of tensile properties was improved and fine equiaxed structure was obtained at this optimum T6 treatment condition.

## 9:55 AM Break

## 10:10 AM

### **Development of Rolling Technology for Twin Roll Casted 1500mm Wide Magnesium AZ31 Alloy:** *Ozgur Duyugulu*<sup>1</sup>; *Selda Ucuncuoglu*<sup>1</sup>; *Gizem Oktay*<sup>1</sup>; *Deniz Temur*<sup>1</sup>; *Onuralp Yucel*<sup>2</sup>; *Ali Kaya*<sup>2</sup>; <sup>1</sup>TUBITAK MRC, Materials Institute; <sup>2</sup>Istanbul Technical University, Department of Metallurgical and Materials Engineering; <sup>3</sup>Mugla University, Engineering Faculty, Department of Metallurgy and Materials

Magnesium alloy AZ31 sheets of 4.5-6.5mm thick and 800 and 1500mm width were produced by twin roll strip casting first time in Turkey. Afterwards, sheets were hot and cold rolled down to less than 1mm both by laboratory and industrial scale rolls. Microstructure of the sheet was analyzed by optical microscope and scanning electron microscope. In addition, pole figures have been obtained by XRD studies. Mechanical properties were investigated by tensile tests and also hardness measurements. Anisotropy ratio of the rolled sheets has been studied. Annealing heat treatments were performed on the produced sheets. Forming trials and deep drawing tests have been done on the sheets having different thicknesses.

10:30 AM

**Development of 150cm Wide Wrought Magnesium Alloys by Twin Roll Strip Casting Technique in Turkey:** *Ozgur Duygulu*<sup>1</sup>; Selda Ucuncuoglu<sup>1</sup>; Gizem Oktay<sup>1</sup>; Deniz Temur<sup>1</sup>; Onuralp Yucel<sup>2</sup>; Ali Kaya<sup>3</sup>; <sup>1</sup>TUBITAK MRC, Materials Institute; <sup>2</sup>Istanbul Technical University, Department of Metallurgical and Materials Engineering; <sup>3</sup>Mugla University, Engineering Faculty, Department of Metallurgy and Materials

Magnesium alloy AZ31 sheet was produced by twin roll strip casting first time in Turkey. Sheets of 4.5-6.5mm thick and 800 and 1500mm width were successfully achieved. Microstructure of the sheet was analysed by optical microscope and scanning electron microscope, SEM from length, width, thickness and wedge views. Semi-quantitative analyses were performed by SEM-EDS. In addition, XRD studies were performed for both characterization and texture purposes. Mechanical properties were investigated by tensile tests and also hardness measurements. Tensile tests were performed at three different directions: rolling direction, 45 degrees to rolling direction and transverse direction. Moreover, micro Vickers and Brinell Hardness test measurements were done on different crosssection directions. Homogenization and annealing heat treatments were performed on the produced sheets.

## Materials for High Temperature Applications: Next Generation Superalloys and Beyond: Advanced Coatings I

Sponsored by: The Minerals, Metals and Materials Society, TMS Structural Materials Division, TMS: High Temperature Alloys Committee, TMS: Refractory Metals Committee Program Organizers: Joseph Rigney, GE Aviation; Omer Dogan, National Energy Technology Laboratory; Donna Ballard, Air Force Research Laboratory; Shiela Woodard, Pratt & Whitney

Wednesday AM  
February 18, 2009

Room: 3010  
Location: Moscone West Convention Center

*Session Chairs:* Gerald Meier, University of Pittsburgh; Bruce Pint, Oak Ridge National Laboratory

8:30 AM Invited

**Thermo-Mechanical Property Profiles Governing the Performance of Coated Airfoils Used in Aero-Turbines: Opportunities for Materials Innovation:** *Anthony Evans*<sup>1</sup>; <sup>1</sup>University of California, Santa Barbara

Oxides and Ni-alloys are present in the hot section of turbines used for propulsion and power generation. By designing and using these materials in optimal combinations, it has been possible to systematically increase the combustion temperature. In turn, enhancing the fuel efficiency. The utility of these materials is greatest in the high-pressure turbine, especially the airfoil. The technology has demonstrated how oxides can be used to protect load-bearing, Ni-based structural members that experience environmental extremes. It involves choices of materials and spatial configurations, as well as survivability upon extreme temperature cycling, without loss of functionality. The newest research on mechanisms governing durability has identified the combinations of material properties that dictate temperature capability. In turn, this identification has provided directions for materials innovation expected to further enhance fuel efficiency. These innovations are described and discussed.

8:55 AM Invited

**Opportunities and Trade-offs in Designing Next Generation TBCs:** Rafael Leckie<sup>1</sup>; Stephan Krämer<sup>1</sup>; Jessica Koschmeder<sup>1</sup>; Erin Donohue<sup>1</sup>; *Carlos Levi*<sup>1</sup>; <sup>1</sup>University of California, Santa Barbara

Zirconia partially stabilized with 7±1wt% Y<sub>2</sub>O<sub>3</sub> (7YSZ) has been the standard material for thermal barrier coatings (TBCs) since their commercial insertion, but it is becoming increasingly limited as engine temperatures continue to rise. Key durability concerns arise from accelerated sintering kinetics, loss of phase stability and attack by calcium-magnesium-alumino-silicate (CMAS) deposits. In addition, improved performance drives the search for materials with lower thermal conductivity. Numerous alternate compositions exist, but every design path involves improvements in some properties and detriment in others. Conceptual guidelines for design and the associated opportunities and trade-offs will be examined in this presentation in the context of current research on new compositions by the authors and their collaborators. Emphasis will be

on the interplay between phase stability, thermal conductivity and toughness, as well as on the implications for improved resistance to CMAS attack. Research sponsored by NSF (DMR-0605700) and ONR (N00014-08-1-0522).

9:20 AM

**Hf Addition by Sputtering in  $\beta$ -NiPtAl Bond Coating for TBC Systems and Its Effect on Thermal Cycling Behaviour:** *Aurélie Vande Put*<sup>1</sup>; Djar Oquab<sup>1</sup>; John Nicholls<sup>2</sup>; Daniel Monceau<sup>1</sup>; <sup>1</sup>CIRIMAT; <sup>2</sup>Cranfield University

During thermal cycling under oxidising conditions, thermal barrier systems undergo microstructural and morphological changes as well as stresses development. These evolutions initiate cracks whose propagation leads to spallation. Works by Streiff *et al.* and Pint *et al.* showed that Hf additions improve spallation resistance of nickel aluminide coatings/materials. Based on these results, Hf is added to a  $\beta$ -NiPtAl thermal barrier system. The chosen manufacturing process consists in depositing, onto the superalloy, alternative Hf and Pt layers by sputtering. A conventional diffusion treatment is performed before out-of-pack aluminising and a final heat treatment. To study the effect of Hf on TGO adherence and rumpling, the systems are thermally cycled, at 1100°C in air, in the same time as conventional Pt-modified nickel aluminide thermal barrier systems. After failure, TGO and bond coating microstructure and composition are analysed by SEM and compared to the "as-processed" systems.

9:40 AM

**Cyclic Oxidation Behavior of Multilayer NiCrAlYSi/Ru-Al Coatings on the DZ125 Superalloy:** Liang Chen<sup>1</sup>; Limin He<sup>2</sup>; *Qiang Feng*<sup>1</sup>; <sup>1</sup>University of Science & Technology Beijing; <sup>2</sup>Beijing Institute of Aeronautical Materials

Improvement in creep stress of the bond coat could extend the life time of thermal barrier coatings (TBCs). Recently, it was reported that RuAl had shown a superior creep resistance. However, limited research has been devoted to the influence of the addition of Ru to the NiCrAlY bond coat. In the present study, the fabrication of the Ru-Al modified multilayer NiCrAlYSi coatings was developed via arc ion plating technique (AIP), including the Ru-Al layer deposited by detonation spraying technology. The cyclic oxidation behavior of NiCrAlYSi coatings containing the Ru-Al multilayer in various positions has been investigated. The results indicated that the coatings with Ru-Al multilayer exhibited better oxidation resistance than the conventional NiCrAlYSi coatings. The evolution of the coating microstructure at various stages of cyclic oxidation and the relevant interdiffusion between the coating and substrate was studied. The corresponding mechanisms for different types of coatings were evaluated and discussed.

10:00 AM

**Development of Oxidation Resistant Pt-Based Coatings on  $\gamma$ -TiAl for High Temperature Applications:** *Maik Froehlich*<sup>1</sup>; Andrea Ebach-Stahl<sup>1</sup>; Christoph Leyens<sup>2</sup>; <sup>1</sup>DLR-German Aerospace Center; <sup>2</sup>Technical University of Brandenburg at Cottbus

Due to much lower density and excellent mechanical properties  $\gamma$ -TiAl alloys are promising candidates to replace the heavy steels and Ni-based superalloys typically applied in the field of aerospace and automotive industry. Protective coatings are necessary to exploit the full potential of  $\gamma$ -TiAl at temperatures higher than 750°C; however, so far no coating system tested has proven sufficient performance for long-term use. The paper is focused on the development of Pt-based coatings produced by magnetron sputtering. Two Pt containing systems with different aluminum contents - PtAl and PtAl<sub>2</sub> - were investigated aiming at the formation of a slow growing and protective Al<sub>2</sub>O<sub>3</sub> scale. The oxidation resistance of each coating system was tested under cyclic conditions at 950°C up to 1000 1h-cycles and compared to the oxidation behaviour of pure Pt deposited on  $\gamma$ -TiAl. Investigations of microstructure evolution will be presented observed by means of SEM and EDS analysis after exposure.

10:20 AM Break

10:30 AM

**Effects of Reactive Element and Silicon Additions on the High-Temperature Oxidation Behavior of  $\gamma$ -Ni+ $\gamma'$ -Ni<sub>3</sub>Al-Based Alloys:** *Zhihong Tang*<sup>1</sup>; Scott Chumbley<sup>1</sup>; Eren Kalay<sup>1</sup>; Brian Gleeson<sup>2</sup>; <sup>1</sup>Iowa State University; <sup>2</sup>University of Pittsburgh

The effects of Hf and/or Y additions on the isothermal and cyclic oxidation behavior in air of  $\gamma$ -Ni+ $\gamma'$ -Ni<sub>3</sub>Al-based alloys were investigated. It was found that Hf addition was more effective in slowing scale growth rate, while Y addition appeared to have a greater effect in improving scale adhesion. Co-



doping with Hf and Y significantly improved the cyclic oxidation resistance of alloys compared to single Hf or Y addition. This beneficial effect of co-doping was more apparent for cyclic oxidation to 1150°C than to 1000°C. Addition of Si to co-doped alloys further markedly improved the cyclic oxidation performance of  $\gamma$ -Ni+ $\gamma'$ -Ni<sub>3</sub>Al-based alloys. The oxidized alloys were characterized by SEM, TEM and STEM to study the scale structure, segregation behavior of Hf or Y on the alumina scale grain boundaries to explain the underlying mechanism of co-doping and Si additions.

## 10:50 AM

**Understanding the Role of Dopants in the Structural Evolution of YSZ:** *Jessica Koschmeder*<sup>1</sup>; Yan Gao<sup>2</sup>; Don Lipkin<sup>2</sup>; Carlos Levi<sup>1</sup>; <sup>1</sup>University of California at Santa Barbara; <sup>2</sup>GE Global Research, Niskayuna, NY

The evolution of the metastable  $t'$ -phase of air plasma sprayed yttria stabilized zirconia (YSZ) coatings was studied using high-resolution synchrotron x-ray diffraction data. In order to observe the phase evolution as a function of time and temperature, the coatings were subjected to a wide range of heat treatments characterized by a Larson Miller Parameter (LMP). Rietveld's refinement method was employed to develop more accurate structural models for Ti- and Ta-doped YSZ. Using this method phase fractions were also quantified enabling the calculation of the resulting tetragonal and cubic phase compositions.

## 11:10 AM

**Lifetime Prediction of Thermal Barrier Coatings Using Computational, Experimental and Non-Destructive Tools:** *Andre Luz*<sup>1</sup>; Daniel Balint<sup>1</sup>; Kamran Nikbin<sup>1</sup>; <sup>1</sup>Imperial College London

Thermal barrier coatings (TBCs) deposited on the superalloy turbine blades can lower the temperature of metallic substrate by 100-300°C, allowing an increase in the turbine inlet temperature. As a result, the engine efficiency is improved. However, the TBCs have durability problems due to the significant thermal mismatch between the coating and substrate, which leads to crack nucleation and propagation at the interface and subsequent coating delamination and loss of thermal protection. In order to understand the influence of several non-linear thermo-mechanical and microstructural parameters in the life of the TBC a new finite element model was developed and run in a high-performance distributed computing system. The evolution of material properties with thermal exposure was experimentally determined in collaboration with a number of international research centers and the results from several image- and laser-based non-destructive techniques were merged using a neural network to improve the lifetime prediction of TBCs.

## Materials for the Nuclear Renaissance: New Materials and Past Limitations

Sponsored by: The Minerals, Metals and Materials Society, TMS Structural Materials Division, TMS/ASM: Corrosion and Environmental Effects Committee, TMS/ASM: Nuclear Materials Committee, TMS: Refractory Metals Committee  
Program Organizers: Raul Rebak, GE Global Research; Robert Hanrahan, National Nuclear Security Administration; Brian Cockeram, Bechtel-Bettis Inc

Wednesday AM  
February 18, 2009

Room: 2009  
Location: Moscone West Convention Center

*Session Chairs:* Raul Rebak, GE Global Research; Robert Hanrahan, National Nuclear Security Administration

## 8:30 AM Invited

**Advanced Materials for Nuclear Reactor Systems: Overcoming Past Limitations:** *Jeremy Busby*<sup>1</sup>; Steven Zinkle<sup>1</sup>; <sup>1</sup>Oak Ridge National Lab

Advanced materials have the potential to improve reactor performance via increased safety margins, design flexibility, and fast reactor economics and can overcome traditional limitations. Increased strength and creep resistance can give greater design margins leading to improved safety margins, longer lifetimes, and higher operating temperatures. The use of advanced materials for component replacement in the existing light water reactor fleet may improve safety margins and reduce the frequency of component replacement. The use of advanced materials in nuclear reactor systems requires considerable development and licensing effort, however. Modern materials science tools such as computational thermodynamics and multiscale radiation damage computational models in

conjunction with rapid science-guided experimental validation may offer the potential for a dramatic reduction in the time period to develop and qualify structural materials. This paper will discuss the potential impacts of advanced materials on nuclear reactor systems and contrast those gains with the hurdles for alloy development.

## 9:10 AM

**Development of Ni-W-Cr Alloys for Gen IV Nuclear Reactor Applications:** *Thierry Auger*<sup>1</sup>; Rafael Cury<sup>2</sup>; Jean-Pierre Chevalier<sup>3</sup>; <sup>1</sup>Ecole Centrale de Paris; <sup>2</sup>CECM-CNRS; <sup>3</sup>Conservatoire National Des Arts Et Metiers

Whether for high temperature gas cooled or molten salt reactor designs, alloys are required to be oxidation and corrosion resistant, to have appropriate high temperature mechanical properties (creep resistance and yield stress) as well as acceptable room temperature toughness. For instance, a Ni based alloys like Hastelloy N was selected for the Oak Ridge National Laboratory experimental molten salt reactor. The related Ni-Cr-W system offers improvements over Ni-Cr-Mo alloys, such as a lower activation or diffusion of W with respect to Mo and potentially higher in-service temperature, while maintaining similar corrosion and oxidation resistance. Here we present results on ternary alloys, with special emphasis on short-range order (SRO), high temperature hardness, phase diagram determination, and oxidation behaviour. Using electron diffraction, the structural state (in terms of short and long range order) of the alloys as a function their composition (especially, the influence of Cr on SRO) will be presented.

## 9:30 AM

**Super ODS Steels R&D towards Gen-IV Systems:** *Akihiko Kimura*<sup>1</sup>; <sup>1</sup>Kyoto University

The development of high performance fuel cladding is essential for the realization of Gen-IV systems. The 9Cr-ODS martensitic steel was developed as the cladding material for sodium-cooled first breeder reactor in Japan, and the steel showed a good performance in sodium, while the corrosion resistance is poor in supercritical water (SCW) and lead-bismuth eutectics (LBE). High-Cr ODS steels added with Al showed a drastic improvement in the corrosion resistance in SCW and LBE. High-temperature strength, however, was reduced because of the characteristic changes in the dispersion morphology of aluminum oxide particles. Recently, "super ODS steels" have been developed by means of the third element alloying method, which results in an achievement of high-temperature strength even with Al addition, as well as high-resistance to corrosion in SCW and LBE. The strengthening mechanism of the super ODS steels is proposed on the bases of nano/meso structure observations and analyses by FE-TEM/EDS, FE-EPMA and FE-AES. Present study includes the result of "R&D of corrosion resistant super ODS steel for highly efficient nuclear systems" entrusted to Kyoto University by the Ministry of Education, Culture, Sports, Science and Technology of Japan (MEXT).

## 9:50 AM

**A Comparative Study of Uniform Corrosion of Refractory Alloys in Supercritical Water:** *Mickael Payet*<sup>1</sup>; Patrick Arnoux<sup>2</sup>; Olivier Raquet<sup>2</sup>; Jean-Pierre Chevalier<sup>1</sup>; <sup>1</sup>CNAM; <sup>2</sup>CEA-Saclay

Interest in supercritical water (SCW) for higher efficiency energy production, has led to the supercritical water-cooled reactor (SCWR) concept. SCWR designs lead to coolant temperatures until 620°C at 25MPa. Materials selection criteria concern high temperature yield stress, creep resistance, no embrittlement and resistance to both uniform corrosion and stress corrosion cracking. This paper presents results of a comparative study of uniform corrosion in SCW of several austenitic stainless steels and Ni-based alloys after exposure to deaerated SCW at 610°C and 25 MPa. Observations of cross-sections reveal that two-layer oxides were formed. Steels present thicker films but in some circumstances, thinner films are observed and may be related to surface preparation. Ni-based alloys present much thinner films with similar structures. Cation and anion diffusions would be responsible respectively of the outer and inner oxide layer growths. The effects of alloy composition and surface microstructure on the oxide films will be discussed.

## 10:10 AM Break

## 10:20 AM Invited

**Challenges of Materials Degradation in Light Water Reactors:** *Peter Andresen*<sup>1</sup>; <sup>1</sup>GE Global Research Center

Environmental degradation of materials in high temperature water has been a dominant factor in safe and economic operation of light water reactors. All structural materials, which are comprised of iron- and nickel-base materials, are

susceptible to phenomena such as stress corrosion cracking, corrosion fatigue, irradiation assisted SCC, environmental effects on fracture, and others. This talk summarizes these factors, emphasizing the common underlying factors that determine their response and the associated lifetime of components.

### 11:00 AM Invited

**Mitigation of Environmentally Assisted Cracking in Nuclear Power Plants:** *Aladar Csontos*<sup>1</sup>; Lee Fredette<sup>2</sup>; Paul Scott<sup>2</sup>; <sup>1</sup>U.S. Nuclear Regulatory Commission; <sup>2</sup>Battelle Memorial Institute

Environmentally assisted cracking of components in nuclear power plants is an area of continued focused research by the domestic and international nuclear power industry and regulatory bodies. Domestically, the U.S. Nuclear Regulatory Commission (NRC) is currently conducting several research programs evaluating environmentally assisted cracking in pressurized (PWR) and boiling water reactors (BWR) components. One of these programs indicated that residual stresses play a key role in the growth and arrest of stress corrosion cracks (SCC) in PWR piping components containing dissimilar metal butt welds. Residual stresses in these types of components typically arise from fabrication, fit up, joining, and repair processes. This talk will present the results of NRC research programs evaluating the effectiveness of SCC mitigation measures to include using engineered residual stresses to potentially limit SCC initiation and growth in PWR components.

### 11:40 AM

**A PWSCC Mechanism in Alloy 600:** *SungSoo Kim*<sup>1</sup>; *JoungSoo Kim*<sup>1</sup>; <sup>1</sup>Korea Atomic Energy Rsch Inst

A new explanation is proposed base on an order reaction in Alloy 600. Both the existence of order reaction in Alloy 600 and an activation energy for an order reaction in Alloy 600,  $Q \approx 46$  kcal/mole ( $\sim 190$  kJ/mole), are determined by a differential scanning calorimeter (DSC). The lattice contraction was confirmed by a high resolution neutron diffraction using a series of isothermally treated specimens at 400°C to accelerate the ordering reaction. The ordering reaction in Alloy 600 causes a lattice contraction and produces an additional stress, internally, in components made of Alloy 600 during a reactor operating condition. The stress level by the order reaction would be about 50 ~ 150 MPa according to the lattice planes. This stress level may be doubled by a certain combination of the neighboring grains. It seems that the basic process of a PWSCC is controlled by the additional stress due to an ordering.

steels that would be typically used for this cost-effective transport. Very little information is available on the embrittlement of pipeline steels exposed directly to high pressure hydrogen, and on the effect of microstructure on the extent of embrittlement. This presentation will highlight the effect of high pressure hydrogen on the mechanical properties of pipeline steels from the X-70/X-80 grade, with a ferritic-pearlitic microstructure, and a ferrite-acicular ferrite microstructure. This talk will review the effect of high pressure hydrogen on the mechanical properties of these steels measured in-situ in a hydrogen atmosphere with specific reference to hydrogen pressures, steel compositions, and microstructures. \*Research sponsored by the U.S. Department of Energy's Hydrogen, Fuel Cells and Infrastructure Technologies Program.

### 9:45 AM

**Development of a Non-Noble Metal Hydrogen Purification System:** *Paul Korinko*<sup>1</sup>; Thad Adams<sup>1</sup>; Kyle Brinkman<sup>1</sup>; George Rawls<sup>1</sup>; <sup>1</sup>Savannah River National Laboratory

High purity hydrogen is essential for the hydrogen economy to be viable as an alternative to fossil fuels. The development of advanced separation membranes to economically remove gas contaminants from hydrogen produced using coal gasification or as front end gas purifiers is needed. In addition, new gas purification devices are needed to replace tube type palladium based purifiers to reduce costs and maintain rapid throughput. While Pd-based systems are highly successful, they suffer from both the high costs of raw materials as well as the high costs associated with thin tube manufacturing. In this work, a multi-phase vanadium-nickel-titanium alloy has been tested for use as a hydrogen separation membrane. It exhibited acceptable permeability as a thin foil, therefore a scaled-up prototype reactor was designed and built. This presentation will discuss the design details and test data obtained from the prototype gas purifier.

### 10:05 AM Break

## Materials in Clean Power Systems IV: Clean Coal-, Hydrogen Based-Technologies, and Fuel Cells: Advanced Materials for PEM Fuel Cells and Batteries - Session I

Sponsored by: The Minerals, Metals and Materials Society, ASM International, TMS Electronic, Magnetic, and Photonic Materials Division, TMS/ASM: Corrosion and Environmental Effects Committee, TMS: Energy Harvesting and Storage Committee  
Program Organizers: K. Scott Weil, Pacific Northwest National Laboratory; Michael Brady, Oak Ridge National Laboratory; Ayyakkannu Manivannan, US DOE; Z. Gary Yang, Pacific Northwest National Laboratory; Xingbo Liu, West Virginia University; Zi-Kui Liu, Pennsylvania State University

Wednesday AM  
February 18, 2009

Room: 3005  
Location: Moscone West Convention Center

Session Chair: Zi-Kui Liu, Pennsylvania State University

### 10:10 AM Keynote

**The Science and Economics of Materials for Batteries, Capacitors, and Fuel Cells:** *Jay Whitacre*<sup>1</sup>; <sup>1</sup>Carnegie Mellon University

There is now an intense need for alternative clean energy technologies, a key aspect of which is the ability to generate, store and convert power for applications ranging from cell phones to power grid nodes. This talk will offer an overview of the state of the art in materials for energy storage systems for the transportation and stationary sector, as well as examination of the critical materials for fuel cells (both PEM and SOFC). An overview of the economics of scaled materials production for these technologies will be presented and a subsequent analysis of the most promising materials and systems to further focus on will be offered.

### 10:55 AM Invited

**Novel Fabrication Strategies for Control of Electrode Architectures:** *Peter Rieke*<sup>1</sup>; <sup>1</sup>Pacific Northwest National Laboratory

More than incremental increases in the energy and power densities of batteries and fuel cells will require improved electrode architectures and new techniques to fabricate those architectures. For example, optimal mass transport in fuel cells requires not only an integration of structural features from the nano to macro scales but also requires variation in structure across the plane of the electrode. As

## Materials in Clean Power Systems IV: Clean Coal-, Hydrogen Based-Technologies, and Fuel Cells: Materials for Hydrogen Production and Transport

Sponsored by: The Minerals, Metals and Materials Society, ASM International, TMS Electronic, Magnetic, and Photonic Materials Division, TMS/ASM: Corrosion and Environmental Effects Committee, TMS: Energy Harvesting and Storage Committee  
Program Organizers: K. Scott Weil, Pacific Northwest National Laboratory; Michael Brady, Oak Ridge National Laboratory; Ayyakkannu Manivannan, US DOE; Z. Gary Yang, Pacific Northwest National Laboratory; Xingbo Liu, West Virginia University; Zi-Kui Liu, Pennsylvania State University

Wednesday AM  
February 18, 2009

Room: 3005  
Location: Moscone West Convention Center

Session Chair: Zi-Kui Liu, Pennsylvania State University

### 8:30 AM Introductory Comments

### 8:35 AM Invited

**H2 Generation by Solar Water Splitting:** *Craig Grimes*<sup>1</sup>; <sup>1</sup>Pennsylvania State University

Abstract not available.

### 9:10 AM Invited

**Effect of Microstructure on Hydrogen Embrittlement of Pipeline Steels:** *Govindarajan Muralidharan*<sup>1</sup>; Joe Strizak<sup>1</sup>; Neal Evans<sup>1</sup>; Doug Stalheim<sup>2</sup>; Subodh Das<sup>3</sup>; <sup>1</sup>Oak Ridge National Laboratory; <sup>2</sup>DGS Metallurgical Solutions, Inc.; <sup>3</sup>Phinix LLC

High pressure transport through pipelines is one of the most economical methods for hydrogen delivery. However, hydrogen is known to embrittle

applied to polymer electrolyte membrane fuel cells, digital fabrication methods can be used to control structures from the micro to macro scales and result in improved performance and elimination of processing steps. In a second example, phase separation methods can be used to control porosity in high power lithium batteries on the nano to micro scales – using in the processing steps only the components needed for the electrolyte. This results in substantial simplification and cost saving in the fabrication of lithium batteries while improving power density. With new electrode architectures and new fabrication methods, batteries and fuel cells can meet the increased performance and cost criteria driven by increasing energy costs and demands for portable power.

## 11:30 AM

### **Effect of $\beta$ '-Alumina Electrolyte Thickness on the Performance of Na/NiCl<sub>2</sub> Cells:** Amin Mali<sup>1</sup>; Anthony Petric<sup>1</sup>; <sup>1</sup>McMaster University

Na/NiCl<sub>2</sub> batteries use  $\beta$ '-alumina solid electrolyte tubes 1-2 mm thick and operate at elevated temperatures. Reducing the  $\beta$ '-alumina electrolyte thickness offers significant advantages in battery performance due to the reduction in cell internal resistance. Different methods including electrophoresis, sol-gel and slip casting were used to fabricate  $\beta$ '-alumina tubes. Dense electrolyte tubes with reduced thickness of less than 100  $\mu$ m and supported on a porous substrate were successfully produced. The electrolyte microstructure was examined by scanning electron microscopy. The effect of electrolyte thickness on the performance of Na/NiCl<sub>2</sub> cells was investigated in sealed laboratory research cells.

## 11:50 AM

### **Synthesis and Electrochemical Properties of Al-Doped Li<sub>3</sub>V<sub>2</sub>(PO<sub>4</sub>)<sub>3</sub> Cathode Materials for Lithium Batteries:** Shengkui Zhong<sup>1</sup>; Zhoulan Yin<sup>1</sup>; Jiequn Liu<sup>1</sup>; Qiyuan Chen<sup>1</sup>; <sup>1</sup>Central South University

Al-doped Li<sub>3</sub>V<sub>2</sub>(PO<sub>4</sub>)<sub>3</sub> cathode materials were prepared by a carbothermal reduction(CTR) process. The properties of the Al-doped Li<sub>3</sub>V<sub>2</sub>(PO<sub>4</sub>)<sub>3</sub> were investigated by X-ray diffraction (XRD) and electrochemical measurements. XRD studies show that the Al-doped Li<sub>3</sub>V<sub>2</sub>(PO<sub>4</sub>)<sub>3</sub> has the same monoclinic structure as the undoped Li<sub>3</sub>V<sub>2</sub>(PO<sub>4</sub>)<sub>3</sub>. The Al-doped Li<sub>3</sub>V<sub>2</sub>(PO<sub>4</sub>)<sub>3</sub> samples were investigated on the Li extraction/insertion performances through charge/discharge, cyclic voltammogram (CV), and electrochemical impedance spectra(EIS). The optimal doping content of Al was that x=0.04 in the Li<sub>3</sub>V<sub>2</sub>-xYx(PO<sub>4</sub>)<sub>3</sub> samples to achieve high discharge capacity and good cyclic stability. The electrode reaction reversibility was enhanced, and the charge transfer resistance was decreased through the Al-doping. The improved electrochemical performances of the Al-doped Li<sub>3</sub>V<sub>2</sub>(PO<sub>4</sub>)<sub>3</sub> cathode materials are attributed to the addition of Al 3+ ion by stabilizing the monoclinic structure.

## 12:10 PM

### **Electroless Copper Plating on Microcellular Polyurethane Foam:** Qinghua Tian<sup>1</sup>; Xueyi Guo<sup>1</sup>; Qingming Feng<sup>1</sup>; Shengzhang Liu<sup>1</sup>; <sup>1</sup>Central South University

In order to get a good conductivity substrates for foam zinc materials used in zinc-air battery, a novel method for electroless copper plating on microcellular polyurethane foam with diameter of 0.2mm was proposed. A new salt-based palladium colloid activation solution was compared with conventional acid palladium colloid activation solution. The result show that the salt-based palladium colloid activation solution presented fairly high activity, all property parameters of it were better than acid palladium colloid activation solution. The stability of electroless copper plating solution has been studied in this paper. The effects of the components of the solution and the technological conditions on the stability and the sedimentation rate have been analyzed by experiments. The optimal prescription for the solution and the technological regulation for electroless copper plating on polyurethane foam have been determined.

## **Materials Processing Fundamentals: Powders, Composites, Coatings and Measurements**

Sponsored by: The Minerals, Metals and Materials Society, TMS Extraction and Processing Division, TMS: Process Technology and Modeling Committee  
Program Organizer: Prince Anyalebechi, Grand Valley State University

Wednesday AM

Room: 2016

February 18, 2009

Location: Moscone West Convention Center

Session Chair: Prince Anyalebechi, Grand Valley State University

## 8:30 AM

### **Preliminary Evaluation of the Processing of Carbon Nanotube Reinforced Aluminum Composites:** K. Morsi<sup>1</sup>; A. ESAWI<sup>2</sup>; P. Borah<sup>1</sup>; S. Lanka<sup>1</sup>; A. Sayed<sup>2</sup>; A. Gawad<sup>2</sup>; <sup>1</sup>San Diego State University; <sup>2</sup>American University in Cairo

Carbon nanotube (CNT) reinforced metallic composites have been recently generating significant scientific interest, due to their expected superior properties compared with other composites. Out of the metallic matrices investigated for reinforcement with CNTs, aluminum has received considerable attention. A major problem has been the dispersion of CNTs in metallic matrices. This paper discusses preliminary results on the mechanical dispersion of CNTs in aluminum powder, powder processing, stability and characterization of aluminum dispersed with CNTs at reinforcement levels equal to and below 5 wt.%.

## 8:45 AM

### **Synthesis of Nanosized Tungsten Powder by a Thermal Plasma Process and Its Sintering Behavior:** Taegong Ryu<sup>1</sup>; Kyu Sup Hwang<sup>1</sup>; Hong Yong Sohn<sup>1</sup>; Zhigang Fang<sup>1</sup>; <sup>1</sup>University of Utah

Nanosized tungsten powder was synthesized by the hydrogen reduction of ammonium paratungstate (APT) in thermal plasma. The effects of operating conditions on the product composition and particle size were investigated. The particle size of synthesized W powder was less than 30 nm in all cases tested. The sintering behavior of the synthesized powder (25 nm average size) was then investigated and compared with those of commercial W powder of 500 nm average size and W powder of 23 nm average size produced by milling the commercial powder. The sintering was done at 1400°C for 60 minutes. The hardness of the resulting compact from the synthesized W powder (315 VHN) was similar to that from the milled W powder (309 VHN), but the plasma-synthesized powder had a much lower tendency to form cracks. The compacts of both nanopowders were significantly harder than that of the commercial powder (192 VHN).

## 9:00 AM

### **Plasma-Assisted Chemical Vapor Synthesis of Tungsten Carbide and Cobalt Nanocomposite Powder:** Taegong Ryu<sup>1</sup>; Kyu Sup Hwang<sup>1</sup>; Hong Yong Sohn<sup>1</sup>; Zhigang Fang<sup>1</sup>; <sup>1</sup>University of Utah

A thermal plasma process was used to synthesize nanosized tungsten carbide - cobalt composite powder, in which ammonium paratungstate and cobalt oxide were reacted with a gas mixture containing CH<sub>4</sub>, H<sub>2</sub> and Ar. The reduction and carburization of vaporized precursors produced nanosized tungsten carbide (WC<sub>1-x</sub>) - cobalt composite powder, which sometimes contained small amounts of W<sub>2</sub>C and/or W phase. The effects of gas composition, plasma torch power, the flow rate of plasma gas, and the addition of secondary plasma gas (H<sub>2</sub>) on product composition and grain size were investigated. The grain size of synthesized tungsten carbide powder was less than 20 nm. The synthesized composite powders were also subjected to a hydrogen heat treatment to fully carburize WC<sub>1-x</sub>, W<sub>2</sub>C, and W phases to the WC phase as well as to remove excess carbon in the product. Finally nanosized WC-Co composite powder of grain size less than 50 nm was obtained.

## 9:15 AM

### **Highly Stable Modification of Silicon Carbide and Silicon Nitride Surfaces by Covalently Attached Organic Monolayers:** Han Zuilhof<sup>1</sup>; <sup>1</sup>Wageningen University

Silicon carbide and silicon nitride are both highly attractive materials due to their mechanical robustness and chemical "inertness". It is therefore of interest to be able to modify the surface of these materials by a stable organic monolayer (thickness: 1-2 nm) that persistently changes relevant surface properties. This paper discusses options to make these surfaces either hydrophobic or fully



protein-repelling via the attachment of tailor-made organic molecules (omega-functionalized-1-alkenes) at room temperature. These conditions allow a wide range of bio-functional moieties to be attached to the substrates. The synthesis and detailed characterization of these surfaces will be outlined (e.g. via XPS, IRRAS, contact angle). Subsequently the extremely high stability of the functionalized surfaces in hot acid and base will be discussed, and finally the protein repellence of oligoethylene oxide-functionalized monolayers.

**9:30 AM**

**Processing and Characterization of Hybrid Perform for Composites:** *Qiang Zhang*<sup>1</sup>; Henry Hu<sup>1</sup>; Lihong Han<sup>1</sup>; <sup>1</sup>University of Windsor

Hybrid composites are fabricated by adding two or more reinforcements into matrix materials so that the expected excellent properties can be achieved through the combined advantages of short fibers and whiskers and different size particles including nanoparticles, which provide a high degree of design freedom. In this paper, hybrid preforms were produced by mixing Al<sub>2</sub>O<sub>3</sub> short fiber with low volume fraction of micro Al<sub>2</sub>O<sub>3</sub> particles. The composites prepared with the hybrid preforms are characterized by optical and scanning electron microscopy. The results show that the reinforcements distribute homogeneously in the matrix materials.

**9:45 AM**

**In Situ Synthesis of Silicon-Silicon Carbide Composites from SiO<sub>2</sub>-C-Mg System via Self-Propagating High Temperature Synthesis:** *Sutham Niyomwas*<sup>1</sup>; <sup>1</sup>Prince of Songkla Univ

Silicon-Silicon Carbide (Si-SiC) composites were synthesized by self-propagating high temperature synthesis (SHS) from a powder mixture of SiO<sub>2</sub>-C-Mg. The reaction was carried out in a SHS reactor under static argon gas at a pressure of 0.5 MPa. The standard Gibbs energy minimization method was used to calculate the equilibrium composition of the reacting species. The effects of silica sources and carbon mole ratio in precursor mixture on the Si-SiC conversion were investigated using X-ray diffraction and scanning electron microscope technique. The as-synthesized products of Si-SiC-MgO powders were leached with 0.1M HCl acid solution to obtain the Si-SiC composite powders.

**10:00 AM Break****10:15 AM**

**Spark Plasma Sintering and Post-Sinter Annealing of Alumina:** *Lin Huang*<sup>1</sup>; Wenlong Yao<sup>1</sup>; Jing Liu<sup>1</sup>; Dongtao Jiang<sup>1</sup>; Amiya Mukherjee<sup>1</sup>; Julie Schoenung<sup>1</sup>; <sup>1</sup>University of California, Davis

Magnesia doped alumina has been synthesized via spark plasma sintering (SPS) in two-stage sintering schedules. The effects of both dopant contents and sintering conditions, including sintering temperature, heating rate, holding time on microstructure, such as grain size, porosity, and mechanical properties, such as microhardness, fracture toughness and strength have been investigated. In addition, the influences of select post-sinter annealing conditions, including a variety of annealing times and temperatures, on grain growth have also been considered. The concurrent hindrance on grain growth kinetics of dopants and the application of two-stage sintering has been studied using scanning electron microscopy (SEM) and phase transition studies using X-ray diffraction (XRD).

**10:30 AM**

**Effect of Sintering Temperature and Pressure on the Properties of ZrB<sub>2</sub>-SiC Composites Prepared by Spark Plasma Sintering:** *Ipek Akin*<sup>1</sup>; Mikinori Hotta<sup>2</sup>; Takashi Goto<sup>2</sup>; Filiz Sahin<sup>1</sup>; Gultekin Goller<sup>1</sup>; <sup>1</sup>Istanbul Technical University; <sup>2</sup>Tohoku University Institute for Materials Research

The ZrB<sub>2</sub>-SiC composites were prepared by the spark plasma sintering (SPS) technique. The SPS process was carried out at different sintering temperatures of 1800-2100°C for 180-300 s with a heating rate of 1.7°C/s in vacuum and uniaxial pressures of about 20 to 80 MPa were applied during the entire process. Densities of the composites were determined by the Archimedes' method and more than 99% relative density was obtained for the composites. The hardness of the composites was calculated as 15 to 26 GPa at the loads of 0.9 to 9.8 N and the fracture toughness was calculated from a half-length of crack formed around corners of indentation and the obtained results were in the range of 3.5 to 4.2 MPa•m<sup>1/2</sup> at the loads of 2.9 to 9.8 N.

**10:45 AM**

**Development of Powder Injection Molding Process for Sponge Ti Alloy:** Ozkan Gulsoy<sup>1</sup>; Pavan Suri<sup>2</sup>; *Seong Jin Park*<sup>3</sup>; Arockiasamy Antonyraj<sup>3</sup>; Randall German<sup>4</sup>; Paul Wang<sup>3</sup>; <sup>1</sup>Marmara University; <sup>2</sup>Heraeus; <sup>3</sup>Mississippi State University; <sup>4</sup>San Diego State University

Newly developed sponge Ti powder and its alloys have price competitiveness suitable for automotive application. In this study, the metal powder injection molding process was developed for sponge Ti alloyed with Fe and Zr. The effort included development of the alloy composition, binder system, mixing process, debinding process, and sintering process. All samples were analyzed in term of density, microstructure, and mechanical properties. The process simulation and microstructures analysis were performed to rationalize the effects of processing conditions on the sintered density and mechanical properties.

**11:00 AM**

**Migration and Interaction Behavior of Electrical-Insulating Particles in a Conductive Melt under Strong Magnetic Field with High Gradient:** *Zhi Sun*<sup>1</sup>; Muxing Guo<sup>1</sup>; Tadej Kokalj<sup>1</sup>; O. Vander Biest<sup>1</sup>; Bart Blanpain<sup>1</sup>; <sup>1</sup>Katholieke Universiteit Leuven

Magnetic fields have been used for inclusions removal from melt and preparation of materials with gradient compositions. Fundamental in these applications is that the induced magnetic forces on the particles/melt can enhance migration and change the interaction behavior. In the present paper, migration and interaction behavior of electrical-insulating particles in a conductive melt under strong magnetic field are theoretically analyzed. It is found that the migration can be considerably enhanced for micrometer sized particles by applying a strong magnetic field. In addition, two forces are involved in the interaction between two particles: the interparticle magnetic dipole-dipole attractive force due to magnetization and the repulsive force induced by flow of the melt. This theoretical analysis renders a better understanding of recent experimental results. Additionally, a new method by using strong magnetic field can be proposed to control the particle size distribution for the preparation of metal-matrix composites.

**11:15 AM**

**Investigation into the Effects of LF Bottom Blown Stirring by Two Nozzles:** *Zhigang Liang*<sup>1</sup>; <sup>1</sup>Northeastern University

Investigation into the mixing of 150t ladle furnace by two-nozzle jetting was performed through a physical simulation experiment with geometric similarity proportion of 1:4. The effects of nozzle arrangements including separation angle, radial position and asymmetry as well as tracer adding position on the mixing time were studied. The most favorable mixing is achieved under the condition of the two nozzles are symmetrically arranged at half radii in the ladle, with 45° separation angle. The empirical relationship between the mixing time and stirring power intensity has been established for two-nozzle jetting based on the present experimental results. In addition, the swelling above bath surface is also investigated with two-nozzle jetting. Finally, a plant test on industrial scale to compare the different refining effects, including the composition homogenization and desulphurization between the original and optimized nozzle arrangement was also carried out.

**11:30 AM**

**Preparation of a Carbon Free Precast Block for Ladle Lining:** *Zhigang Liang*<sup>1</sup>; <sup>1</sup>Northeastern University

A carbon free precast block was prepared by using high-alumina fused corundum as aggregate and fused magnesia, and ultra-fine Al<sub>2</sub>O<sub>3</sub> and ultra-fine SiO<sub>2</sub> powders as matrix materials. A small linear expansion for the precast block was achieved through spinel formation from the reaction of MgO with Al<sub>2</sub>O<sub>3</sub>. The precast block showed a lower apparent porosity, higher hot modulus of rupture and better slag corrosion resistance compared to the traditional Al<sub>2</sub>O<sub>3</sub>-MgO-C brick. Moreover, the practical application of the precast block to the ladle lining proved it to possess a better thermal insulation which could effectively prevent the temperature drop of molten steel during the refining process. It can be predicted that the carbon free precast block could possibly be used as a new type of ladle lining material for the production of low-carbon and ultra-low-carbon steel.

11:45 AM

**Vibratory Stress Relief in D-406A Aerospace Alloy:** *M. Bilal Khan*<sup>1</sup>; T. Iqbal<sup>1</sup>; <sup>1</sup>School of Chemical and Materials Engineering, National University of Science and Technology

Thermal stress relief by means of a typical heat treatment cycle (660 °C for one hr) is compared with the one achieved through vibratory stress relief at resonant and multiple resonant frequencies for the D-406 HSLA material. Our analysis of the data is based on the micro-hardness profiles measured for the entire length of scales, namely, base metal, heat affected zone (HAZ) and the weld bead itself. The profiles obtained using the two techniques mimic each other, for an equivalent 70% stress relief level. The data are further qualified by impact testing wherein the zone of interest is projected in the retention groove to provide impact by the pendulum striker in the Charpy mode. Higher equivalent energy absorption in the treated specimens confirms the efficacy of the vibratory method. The present work rectifies earlier anomaly where heat treatment has been reported at 310°C for the same material.

## Mechanical Behavior of Nanostructured Materials: Plasticity and Deformation Mechanisms at Small Length Scale II

Sponsored by: The Minerals, Metals and Materials Society, TMS Electronic, Magnetic, and Photonic Materials Division, TMS Materials Processing and Manufacturing Division, TMS Structural Materials Division, TMS: Chemistry and Physics of Materials Committee, TMS/ASM: Mechanical Behavior of Materials Committee, TMS: Nanomechanical Materials Behavior Committee

Program Organizers: Xinghang Zhang, Texas A & M University; Andrew Minor, Lawrence Berkeley National Laboratory; Xiaodong Li, University of South Carolina; Nathan Mara, Los Alamos National Laboratory; Yuntian Zhu, North Carolina State University; Rui Huang, University of Texas, Austin

Wednesday AM Room: 3024  
February 18, 2009 Location: Moscone West Convention Center

Session Chairs: Xiaodong Li, University of South Carolina; Ting Zhu, Georgia Institute of Technology

8:30 AM Invited

**Strength and Ductility of Nano-Grained Cu With Nano-Scale Twin Bundles:** *Y. Zhang*<sup>1</sup>; N.R. Tao<sup>1</sup>; *K. Lu*<sup>1</sup>; <sup>1</sup>Institute of Metal Research, Chinese Academy of Sciences

By means of dynamic plastic deformation (DPD, with high strain rates) at cryogenic temperature, bulk nanostructured Cu specimens have been prepared, consisting of nano-sized grains embedded with nano-scale twin bundles. The nanostructure characteristics including grain sizes, nano-twin concentration, and grain boundary structure, can be adjusted by subsequent mechanical and thermal treatments such as cold-rolling and annealing. Tensile properties of the as-prepared DPD samples, the cold-rolled samples, and the as-annealed samples have been systematically investigated to reveal the effects of grain size and twin density on strength and ductility. Experimental results revealed that thermal annealing of the cold-rolled DPD samples leads to a superior strength-ductility combination relative to the samples processed via other routes. Analysis of the enhanced tensile properties in these samples was made in terms of grain size effect and nano-twin effect on strength and ductility.

8:50 AM

**Epitaxial Nanotwinned Cu Films with High Strength and High Conductivity:** *Osman Anderoglu*<sup>1</sup>; Amit Misra<sup>2</sup>; Haiyan Wang<sup>1</sup>; Filip Ronning<sup>2</sup>; Michael Hundley<sup>2</sup>; Xinghang Zhang<sup>1</sup>; <sup>1</sup>Texas A&M University; <sup>2</sup>Los Alamos National Lab

We report on the synthesis of epitaxial (single-crystal like), nanotwinned Cu films via magnetron sputtering. Increasing the deposition rate from 1 to 4 nm/s, decreased the average twin lamellae spacing from 16 to 7 nm. These epitaxial nanotwinned Cu films exhibit significantly higher ratio of hardness to room temperature electrical resistivity than columnar-grain (nanocrystalline), textured, nanotwinned Cu films.

9:05 AM

**Nanomechanics of Surface and Interfacial Plasticity in Nanostructured Metals:** *Ting Zhu*<sup>1</sup>; Ju Li<sup>2</sup>; <sup>1</sup>Woodruff School of Mechanical Engineering, Georgia Institute of Technology; <sup>2</sup>Department of Materials Science and Engineering, University of Pennsylvania

Dislocation nucleation is central to our understanding of the plastic deformation in nanostructured metals. The free surface and nanostructure interface may act as effective sources of dislocation to initiate and sustain the plastic flow. Here, we develop an atomistic modeling framework to address the statistical nature of dislocation nucleation. Such an approach bridges the timescale gap between atomistic modeling and laboratory experiments by combining transition state theory and atomistic energy landscape exploration. We show dislocation mediated interfacial reactions is the rate-controlling mechanisms in nano-twinned copper, giving rise to an unusual combination of ultrahigh strength and high ductility. Our results also demonstrate a small activation volume associated with surface nucleation dislocation, leading to sensitive temperature and strain-rate dependence of the nucleation stress, and providing an upper bound to the size-strength relation in nanopillar compression experiments.

9:20 AM

**Deformation Twinning Behaviors in Al and Cu Single Crystals:** *Zhe-Feng Zhang*<sup>1</sup>; W. Han<sup>1</sup>; S. Wu<sup>1</sup>; S. Li<sup>1</sup>; <sup>1</sup>Institute of Metal Research

Twinning is one of the important plastic deformation modes in metals and alloys. The deformation twinning behaviors in various FCC metals and alloys, including pure Cu and Al single crystals, subjected to equal-channel angular pressing (ECAP), were systematically investigated by taking account of crystallographic orientation, stacking fault energy (SFE) and grain size. For Cu and Al single crystals, their orientations were specially designed with one of twinning systems to just match the macroscopic shear deformation of ECAP. For Al single crystal, no deformation twins were observed after one-pass ECAP although a preferential crystallographic orientation was selected for twinning, while for Cu single crystal, profuse deformation twins were found even strained at room temperature and low strain rate. The current experimental results provided clear and comprehensive evidences that SFE, crystallographic orientation have remarkable influence on the deformation twinning behaviors in Al and Cu single crystals.

9:35 AM

**Direct Evidence for Detwinning of Nano-Twinned Copper under Low Temperature Deformation:** *Yan-Dong Wang*<sup>1</sup>; Wen-Jun Liu<sup>2</sup>; Lei Lu<sup>3</sup>; Yang Ren<sup>2</sup>; Zhi-Hua Nie<sup>1</sup>; Jonathan Almer<sup>2</sup>; Sheng Cheng<sup>4</sup>; Yong-Feng Shen<sup>1</sup>; Peter K. Liaw<sup>4</sup>; Ke Lu<sup>3</sup>; <sup>1</sup>Northeastern University; <sup>2</sup>Argonne National Laboratory; <sup>3</sup>Institute of Metal Research; <sup>4</sup>The University of Tennessee

We report a new mechanism – detwinning, which is found to operate at low temperatures during the tensile deformation of the electrodeposited Cu with a high density of nano-sized growth twins. Both in-situ synchrotron X-ray diffraction methods, i.e., using the three-dimensional (3-D) X-Ray Microscopy with the submicron-resolution white beam and the high-energy X-ray diffraction with the monochromatic beam, provide the direct experimental evidences for detwinning at low temperatures and capture the rich information on the changes of the crystallographic orientation and stress of individual grains. The migration of twin-boundary and other high-angle boundaries under an extremely high stress at low temperatures is distinct from the twinning activity previously observed in metals deformed at low temperatures or during high-temperature annealing. We believe that the detwinning process, as an important deformation mechanism in nanostructured materials, may increase the capacity for accommodation of plastic strain and promote the homogeneous deformation of nanostructured materials.

9:50 AM Invited

**Evolution of Intrinsic Stresses in Thin Film Growth via Coupled Surface and Grain Boundary Diffusion:** Tanmay Bhandakkar<sup>1</sup>; Eric Chason<sup>1</sup>; *Huajian Gao*<sup>1</sup>; <sup>1</sup>Brown University

In order to explain experimental observations on the evolution of intrinsic stresses during Vomer-Weber growth of thin metal films of high surface mobility, Chason et al. (2002) have proposed a model based on the assumption that a higher chemical potential near the film surface during deposition provides a driving force for a flow of adatoms into the grain boundaries (GB). Here we build upon the previous models of Gao et al. (Acta Mat, 1999), Chason et al. (PRL, 2002) and Guduru et al. (JMPS, 2003) on coupled surface and GB diffusion and extend these models to include the effect of GB diffusion heterogeneity. Our model

considers a layer of active diffusion near the surface during deposition. Inside the active layer, both surface and GB diffusivities are assumed to be higher than their normal values. The simulation results show excellent comparisons with experimentally measured stress evolution in various films.

**10:10 AM**

**Nanoscale Plasticity at Elevated Temperatures in Tantalum (Ta) Single Crystals:** *Koteswararao Rajulapati<sup>1</sup>; Monika Biener<sup>2</sup>; Juergen Biener<sup>2</sup>; Andrea Hodge<sup>1</sup>;* <sup>1</sup>University of Southern California; <sup>2</sup>Lawrence Livermore National Laboratory

The deformation behavior of body centered cubic (BCC) materials is very complex and is relatively poorly understood by the scientific community. The main challenge is to understand the operation of the several slip systems active during the deformation in BCC materials. In this study we utilize instrumented nanoindentation in order to investigate the dislocation nucleation and nano scale plasticity of tantalum single crystals with different orientations. Tests were carried out at different loading rates and at different temperatures. The differences between the deformation behavior at room temperature and the deformation behavior at elevated temperatures will be addressed. The associated deformation mechanisms in single crystal tantalum will be explained with the aid of characteristic differences in load-displacement curves and the topographical features of the indents.

**10:25 AM Break****10:35 AM**

**Size-Dependence of Yield Stress in Twinned Gold Nanowires under Uniaxial Tension:** *Chuang Deng<sup>1</sup>; Frederic Sansoz<sup>1</sup>;* <sup>1</sup>University of Vermont

In this work, the mechanical properties of [111]-oriented cylindrical gold nanowires containing pre-grown twin boundaries are investigated by molecular dynamics simulations with an embedded-atom method potential. Wires with different diameters (4 nm to 32 nm) and twin-boundary spacings (1.4 nm to 24 nm) are investigated with up to 2 million atoms. We find strong size effects on the yield stress and maximum strength of twinned gold nanowires as a function of both sample diameter and twin boundary spacing. Defect-free nanowires are found to yield at a higher stress as the radius decreases. However, for twinned nanowires, we show that there exists a transition from a decrease to an increase in yield stress as the twin boundary spacing decreases. This crossover effect can provide guidance for the design of nanoscale devices.

**10:50 AM Invited**

**Structural Evolution and Mechanical Response of Nanoporous Noble Metals:** *Ye Sun<sup>1</sup>; Jia Ye<sup>2</sup>; Andrew Minor<sup>2</sup>; Thomas Balk<sup>1</sup>;* <sup>1</sup>University of Kentucky; <sup>2</sup>National Center for Electron Microscopy

Nanoporous noble metals exhibit a nanoscale structure of interpenetrating pores and ligaments at a length scale as small as 5 nm. This presentation will focus on microstructural characterization, thin film stress measurements and in-situ nanoindentation in the transmission electron microscope, and will investigate the effects of nanoscale geometric confinement on mechanical properties and dislocation-mediated plasticity. Although some nanoporous films exhibit macroscopic cracking, individual ligament deformation is completely ductile and clearly involves dislocation activity. The film stresses that evolve during thermal cycling correspond to bulk stresses that, according to scaling equations, approach the theoretical strength of the metal. Surprisingly, film stress exhibits a thickness dependence, although the smaller ligament width would presumably govern deformation. This may be due to the finite number of ligament/pore pairs that span the film thickness. These and other observations will be discussed in light of studies on the microstructure and mechanical behavior of nanoporous noble metals.

**11:10 AM Invited**

**Molecular Dynamics Simulations of Shock Compression of Nanocrystalline Nickel:** *Marc Meyers<sup>1</sup>; Hussam Jarmakani<sup>1</sup>; Bruce Remington<sup>1</sup>; Eduardo Bringa<sup>1</sup>; V. Nhon<sup>1</sup>;* <sup>1</sup>UC San Diego

Shock compression in nanocrystalline nickel (5 nm and 10 nm grain size) is simulated over a range of pressures (10-80 GPa) and compared with experimental results. Molecular Dynamics simulations are ideal, both in time and length scales, for comparing with laser-shock compression experiments and providing insight on deformation processes involved. Contributions to the net strain from the various mechanisms of plastic deformation such as partials, perfect dislocations, and twins were quantified in the nanocrystalline samples. The effect of release, a phenomenon often neglected in MD simulations, on dislocation behavior is also

studied. It is shown that a large fraction of the dislocations generated at the front are annihilated. An analytical model is applied to predict the critical pressures for the cell-stacking-faults transition in single-crystalline nickel and the onset twinning occurs in nanocrystalline nickel. The results resolve a disagreement consistently observed between MD computations and experimental results. Research funding: UCOP ILSA/LLNL.

**11:30 AM**

**High-Velocity Impact Behavior of Ultrafine Grained Tungsten:** *Laszlo Kecskes<sup>1</sup>; Lee Magness<sup>1</sup>; Brian Schuster<sup>1</sup>; Zhiliang Pan<sup>2</sup>; Qiuming Wei<sup>2</sup>; Eric Klier<sup>1</sup>;* <sup>1</sup>US Army Research Laboratory; <sup>2</sup>University of North Carolina at Charlotte

Compared to tungsten-based heavy alloy (WHA) penetrators, those fabricated from depleted uranium alloy (DUA) have greater penetration ability. The effectiveness of DUA is attributed to localized shear zones that sharpen its tip during penetration. Based on published evidence of a definite transition in deformation behavior of ultrafine grained (UFG) Fe and W, it was expected that ballistic tests would also reflect this transition from gross plastic to localized shear deformation. Sub-scale projectiles were fired into rolled homogeneous armor steel targets. The targets were sectioned to reveal the embedded projectile remnant, or 'residual', which was metallographically prepared for microhardness measurements, and optical and scanning electron microscopy. Differences in the deformation behavior of the pure UFG W to that of conventional WHA or DUA will be identified and demarcated.

**11:45 AM**

**Dislocation Nucleation Inside Nanoscale Ribbons in Composite Microwires and the Importance for Determining Composite Strength:** *David Morris<sup>1</sup>; Maria Muñoz-Morris<sup>1</sup>;* <sup>1</sup>CENIM CSIC

In situ fibre-reinforced composites are prepared by very heavy straining that elongates the ductile minor phase into very fine ribbons, producing extremely high strength. Examples are Cu-bcc metal mixtures and drawn pearlitic steel wires. Strengthening is explained using a rule-of-mixtures approach, modified to take account of the many geometrically-necessary dislocations introduced during formation of the fibre composite or by scale and barrier strengthening. This final term supposes high stresses for dislocation glide inside nanoscale regions and for dislocation sources inside neighbouring regions. Transmission electron microscopy studies have been carried out on a composite wire containing nanoscale Cr ribbons and ultrafine grain Cu matrix. The nanoscale ribbons are initially dislocation free in a matrix too fine to accommodate dislocation substructures. During deformation, dislocations nucleate in the ribbons at sources that are not ribbon size dependent, while randomly-arranged dislocations glide in the matrix. The implications for strengthening are considered.

**12:00 PM**

**Microstructure and Mechanical Property of Gradient Nanocrystalline Cobalt:** *Xiao-Lei Wu<sup>1</sup>;* <sup>1</sup>Institute of Mechanics, Chinese Academy of Sciences

A grain-size gradient surface layer on bulk cobalt was generated by means of the technique of surface mechanical attrition treatment. The process of nanocrystalline formation was systematically studied by transmission electron microscopy. The grain refinement was accompanied by the onset of deformation twinning, the operation of prismatic and basal slip, and the successive subdivision of grains to a finer and finer scale, resulting in the formation of highly misoriented nanocrystalline grains. The uniaxial tensile tests were conducted also for the understanding of the deformation mechanisms of gradient nanocrystalline materials.

**12:15 PM**

**Intelligent Viscoelastic Polyurethane Intrinsic Nano Composites:** *M. Bilal Khan<sup>1</sup>;* <sup>1</sup>NUST

Polyurethanes are multiphase systems comprising intrinsically variant nanodomains. The material properties can be tailored by adjusting the relative proportions and organizing the structure of the hard and soft segments akin to the spring-dashpot system in an automobile. The paper describes how an intelligent PU system is created to offer smart response to mechanical and vibrational stimuli. In this work unidirectional, dynamic (DMTA), acoustic and impact testing results are qualified with the unique viscoelastic character that determines the rate-temperature response of the nanocomposite. Attenuated total reflection infrared spectroscopy(ATR-IR) and DMTA offer logical explanation of the observed viscoelastic behavior in terms of the nanodomains. Acoustic and impact attenuation are correlated with the mechanical modulus.



## Microstructural Processes in Irradiated Materials: Ceramics and Fuels

Sponsored by: The Minerals, Metals and Materials Society, TMS Structural Materials Division, TMS/ASM: Nuclear Materials Committee  
Program Organizers: Christophe Domain, Electricite De France; Gary Was, University of Michigan; Brian Wirth, University of California, Berkeley

Wednesday AM Room: 2008  
February 18, 2009 Location: Moscone West Convention Center

*Session Chairs:* Gary Was, University of Michigan; Steven Zinkle, Oak Ridge National Laboratory

### 8:30 AM Invited

**Microstructural Evolution of SiC and ZrC under High Temperature Neutron Irradiation:** *Lance Snead*<sup>1</sup>; *Yutai Katoh*<sup>1</sup>; *Sosuke Kondo*<sup>1</sup>; *Hsin Wang*<sup>1</sup>; <sup>1</sup>Oak Ridge National Laboratory

SiC has been used for decades as the pressure vessel and fission product barrier in gas cooled fission reactor TRISO fuels. Under irradiation SiC is quite resilient, as proven by the successful TRISO fuel performance, and both historic and recent studies on the effects of irradiation and irradiation temperature on its mechanical properties. However, two limitations to the SiC-based TRISO system are its maximum temperature, and the poorly understood issue of silver migration through the SiC. ZrC has been suggested and developed as a possible substitute for SiC, or potentially an additive to SiC, to address these issues and to improve the fuel performance. However, the irradiation performance of ZrC is essentially unknown. This paper presents and contrasts microstructural and mechanical property data for high-purity neutron irradiated ZrC and SiC. Irradiations were carried out in the irradiation temperature and neutron dose range of 600-1500°C and 8 dpa, respectively.

### 9:00 AM

**Characterization of Changes in Mechanical Properties of Glassy Polymeric Carbon and Pyrolytic Carbon Following Ion Irradiation – A Comparison:** *Malek Abunaemeh*<sup>1</sup>; *Bopha Chhay*<sup>1</sup>; *Cydale Smith*<sup>1</sup>; *Claudiu Muntele*<sup>1</sup>; *Yanbin Chen*<sup>2</sup>; *R. Zhou*<sup>2</sup>; *Lumin Wang*<sup>2</sup>; *Gary Was*<sup>2</sup>; *Daryush Ila*<sup>1</sup>; <sup>1</sup>Alabama A&M University; <sup>2</sup>University of Michigan

The TRISO fuel that is planned to be used in some of the Generation IV nuclear reactor designs consists of a fuel kernel of UOX coated in several layers of materials with different functions. Pyrolytic carbon (PyC) is considered for some of these layers. In this study we investigate the possibility of using glassy polymeric carbon (GPC) as an alternative to PyC. GPC is used for artificial heart valves, heat-exchangers, and other high-tech products developed for the space and medical industries. This lightweight material can maintain dimensional and chemical stability in adverse environment and very high temperatures (up to 3000°C). Here we are looking at comparing the changes in physical properties and structures of GPC and PyC after different doses irradiation with 2 MeV proton, 3 MeV N and 5 MeV Si bombardment at 600 and 800 °C by using scanning electron microscopy, transmission electron spectroscopy, microindentation, and three-point bending.

### 9:20 AM

**Phase Stability of Nanostructurally-Stabilized Pure Cubic ZrO<sub>2</sub> under Ion Beam Irradiation:** *Jie Lian*<sup>1</sup>; *Jiaming Zhang*<sup>2</sup>; *Fereydoon Namavar*<sup>3</sup>; *Hani Haider*<sup>3</sup>; *Kevin Garvin*<sup>3</sup>; *Rodney Ewing*<sup>2</sup>; <sup>1</sup>Rensselaer Polytechnic Institute; <sup>2</sup>University of Michigan; <sup>3</sup>University of Nebraska

Zirconia polymorphs display extremely high radiation tolerance and demonstrate no amorphization in bulk sample even under extreme damage level. However, a transformation from monoclinic to tetragonal or cubic phases was induced by irradiation of bulk monoclinic zirconia. In this study, we first report the phase stability of nanostructurally-stabilized pure cubic ZrO<sub>2</sub> at room temperature upon 1 MeV Kr<sup>2+</sup> irradiation, and pure cubic zirconia was produced by ion beam assisted deposition (IBAD). Cross-sectional TEM examination indicated that there is an amorphous buffer layer (70 nm thick) between Si substrate and cubic nanocrystalline ZrO<sub>2</sub> film with an average grain size of 8 nm. Ion irradiation induced a cubic to tetragonal phase transformation for nanocrystalline ZrO<sub>2</sub>. Furthermore, tetragonal ZrO<sub>2</sub> nanocrystals were directly recrystallized from the amorphous layer upon irradiation. These results suggest that tetragonal phase of

nanocrystalline ZrO<sub>2</sub> are more energetically favorable upon ion irradiation as compared with cubic, monoclinic and amorphous phases.

### 9:40 AM

**Microstructural Evolution in SiC Irradiated above 1273 K in HFIR:** *Sosuke Kondo*<sup>1</sup>; *Yutai Katoh*<sup>1</sup>; *Lance Snead*<sup>1</sup>; <sup>1</sup>Oak Ridge National Laboratory

Very dense black spots and small loops, which are nano-sized aggregates of displaced Si and C atoms, are the dominating defect microstructures in SiC irradiated in a wide-temperature range of 573-1273K. However, accelerated defect development has been recently demonstrated by authors following neutron-irradiation at >1273K. With the defects which undergo unstable growth, progressive changes in various material properties may commence. This paper reports the recent results of the TEM studies on β-SiC irradiated at 1273-1733K in HFIR. The dominating defects in the temperature regime are faceted voids and interstitial-type Frank loops. Both the magnitude and the growth rate of void swelling were very limited (<~0.01%) below ~1573K, 9.3dpa, whereas the fluence and temperature dependent increase in the void swelling was observed clearly above ~1673K, and the maximum value was 0.25% at 1733K, 9.6dpa. Of interest results such as unidirectional formation of tetrahedral voids and interstitial diffusivity will also be discussed.

### 10:00 AM

**Structural Modifications in A<sub>2</sub>B<sub>2</sub>O<sub>7</sub> Pyrochlore Induced by Swift Heavy Ions with and without Pressure:** *Maik Lang*<sup>1</sup>; *Fuxiang Zhang*<sup>1</sup>; *Jie Lian*<sup>2</sup>; *Jiaming Zhang*<sup>1</sup>; *Christina Trautmann*<sup>3</sup>; *Rodney Ewing*<sup>1</sup>; <sup>1</sup>University of Michigan; <sup>2</sup>Rensselaer Polytechnic Institute; <sup>3</sup>Gesellschaft fuer Schwerionenforschung

Pyrochlore, A<sub>2</sub>B<sub>2</sub>O<sub>7</sub>, exhibit a variety of properties that find application in a number of different technologies, from electrolytes in solid oxide fuel cells to actinide-bearing compositions that are used as nuclear waste forms and inert matrix fuels. Ion beam irradiations (energy: GeV) have been used to systematically modify the Gd<sub>2</sub>Zr<sub>2-x</sub>Ti<sub>x</sub>O<sub>7</sub> binary at the nanoscale by radiation-induced phase transitions that include the crystalline-to-amorphous transition and an order-disorder structural transformation to a defect-fluorite structure. Synchrotron XRD, Raman spectroscopy, and TEM provide a consistent understanding of these results of the pure electronic excitation and ionization caused by the heavy ions. When pressure is included as an additional parameter, the response of the pyrochlore structure to these extreme conditions differs significantly. We show that the combination of relativistic ions and pressure can induce novel structural modifications in pyrochlore that cannot be obtained by irradiation or pressure applied separately (e.g., formation of a new phase).

### 10:20 AM Break

### 10:40 AM

**Effects of Irradiation on the Microstructures of Low-Enriched U-Mo Fuels:** *Dennis Keiser*<sup>1</sup>; *Jan Fong Jue*<sup>1</sup>; *Adam Robinson*<sup>1</sup>; <sup>1</sup>Idaho National Laboratory

The Reduced Enrichment for Research and Test Reactors (RERTR) program is developing low-enriched U-Mo alloy fuels for application in research and test reactors around the world. A big part of this development effort is actual irradiation testing of a variety of different fuel types in the Advanced Test Reactor (ATR). As part of this testing, microstructural characterization of dispersion and monolithic plate-type fuels is performed before and after irradiation using scanning electron microscopy to help determine the effects of irradiation on the microstructural stability of the different fuels. This talk will discuss the changes that occur in the microstructures of both dispersion and monolithic U-Mo fuel plates that have been fabricated using different techniques. Comments will be made on changes in fuel plate performance that have been observed as a function of changing matrix composition for dispersion fuel plates and changes in fuel/cladding interlayer composition for monolithic fuel plates.

### 11:00 AM

**Kr Ion Irradiation Study of the Depleted-Uranium Alloys:** *Jian Gan*<sup>1</sup>; *Dennis Keiser*<sup>1</sup>; *Brandon Miller*<sup>2</sup>; *Jeffery Rest*<sup>3</sup>; *Marquis Kirk*<sup>3</sup>; *Todd Allen*<sup>2</sup>; *Daniel Wachs*<sup>1</sup>; <sup>1</sup>Idaho National Laboratory; <sup>2</sup>The University of Wisconsin; <sup>3</sup>Argonne National Laboratory

Fuel development for the Reduced Enrichment Research and Test Reactor (RERTR) program is tasked with the development of new low enrichment uranium nuclear fuels that can be employed to replace existing high enrichment uranium fuels currently used in some research reactors throughout the world. Radiation stability of the fuel-cladding interaction product has a strong impact on fuel performance. Three depleted uranium alloys were successfully cast for the radiation stability studies of the fuel-cladding interaction product using Kr

ion irradiation to simulate radiation damage from fission products. SEM analysis indicates the presence of the phases of interest:  $U(Si,Al)_3$ ,  $(U,Mo)(Si,Al)_3$  and a mixture of  $UMo_2Al_{20}$ ,  $U_6Mo_4Al_{43}$ , and  $UAl_4$ . Irradiation of TEM disc samples with 500 keV Kr ions at 200°C to the doses of 1.0 and 10 dpa should provide insight to the microstructural stability of the phases relevant to fuel-cladding products anticipated to form in RERTR dispersion type fuel.

**11:20 AM**

**Microstructural Evolution in Irradiated Uranium-Bearing Delta-Phase Oxides:** *Ming Tang*<sup>1</sup>; Kiel Holliday<sup>2</sup>; Yongqiang Wang<sup>1</sup>; James Valdez<sup>1</sup>; Blas Uberuaga<sup>1</sup>; Ken Czerwinski<sup>2</sup>; Kurt Sickafus<sup>1</sup>; <sup>1</sup>Los Alamos National Laboratory; <sup>2</sup>University of Nevada, Las Vegas

Irradiation damage effects in uranium-bearing delta-phase oxides of  $A_6U_1O_{12}$  (A = rare earth cations) were characterized using grazing incidence X-ray diffraction and transmission electron microscopy. Polycrystalline  $Y_6U_1O_{12}$ ,  $Gd_6U_1O_{12}$ ,  $Ho_6U_1O_{12}$ ,  $Yb_6U_1O_{12}$ , and  $Lu_6U_1O_{12}$  samples were irradiated with 300 keV Kr<sup>++</sup> to fluences up to  $2 \times 10^{20}$  ions/m<sup>2</sup> at cryogenic temperature (100 K). The crystal structure of these compounds was determined to be an ordered, fluorite derivative structure, known as the delta phase, a rhombohedral symmetry belonging to space group R-3. Our preliminary results indicate that all these compounds are resistant to amorphization to a displacement damage dose of 50 displacements per atom. In these experiments, we sometimes observed an irradiation-induced order-to-disorder (O-D) phase transformation. We also will discuss the different tendencies of these compounds to experience the O-D transformation. Factors influencing the irradiation damage response of these compounds will be discussed in terms of cation radius ratio and defect formation.

**11:40 AM**

**Proton Irradiation Studies of Depleted-Uranium RERTR Fuels:** *Brandon Miller*<sup>1</sup>; Jian Gan<sup>2</sup>; Todd Allen<sup>1</sup>; Dennis Keiser<sup>2</sup>; Dan Wachs<sup>2</sup>; <sup>1</sup>University of Wisconsin-Madison; <sup>2</sup>Idaho National Laboratory

With the concern of fuel-cladding chemical interaction in RERTR dispersion fuels, three depleted uranium alloys were successfully cast to understand their microstructure during irradiation. These alloys simulate the phases that have been seen to form between the fuel and the Al-matrix in various neutron irradiated dispersion fuel experiments. The primary phases present in the three alloys are  $U(Si,Al)_3$  and  $(U,Mo)(Si,Al)_3$ , which are expected to respond well to irradiation, and  $UMo_2Al_{20}$ ,  $U_6Mo_4Al_{43}$ , and  $UAl_4$ , which are not expected to respond well to irradiation. Irradiations were conducted using 2.6 MeV protons at 200°C to doses of 0.1, 1.0, and 3.0 displacements per atom, dpa. TEM and XRD studies are being conducted to understand the radiation effects on the microstructure of these alloys. Initial benchmarking been completed and analysis on the proton irradiated alloys is currently being conducted.

**12:00 PM**

**Molecular Dynamics Study of Thermo-Migration of Voids in Single Crystal UO<sub>2</sub>:** *Tapan Desai*<sup>1</sup>; Paul Millett<sup>1</sup>; Dieter Wolf<sup>1</sup>; <sup>1</sup>Idaho National Laboratory

It is well known that within few hours after startup of a nuclear reactor, the temperature gradient within a fuel element causes migration of voids radially inwards to form a central hole. To understand the atomic processes that control thermomigration of voids, we performed molecular dynamics simulations on single crystal UO<sub>2</sub> with voids (d=2.2nm). Then, temperature gradient was applied across the simulation cell by supplying additional kinetic energy at the ends and removing it from the center. The system was equilibrated for 1ns at a temperature (T=2800K) well above the oxygen sub-lattice disordering. After a simulation run of 19ns, we found that the voids had moved towards the hot ends. The void mobility is shown to be controlled by the surface diffusion of uranium ions. As the voids migrate, the trailing region on the uranium sub-lattice is completely restored. This work was supported by the DOE-BES Computational Materials Science Network.

## Nanocomposite Materials: Characterization and Modeling of Nanocomposites II

Sponsored by: The Minerals, Metals and Materials Society, TMS Structural Materials Division, TMS Electronic, Magnetic, and Photonic Materials Division, TMS/ASM: Composite Materials Committee, TMS: Materials Characterization Committee, TMS: Nanomaterials Committee

Program Organizers: Jonathan Spowart, US Air Force; Judy Schneider, Mississippi State University; Bhaskar Majumdar, New Mexico Tech; Benji Maruyama, Air Force Research Laboratory

Wednesday AM  
February 18, 2009

Room: 3020  
Location: Moscone West Convention Center

Session Chairs: Nikhil Gupta, Polytechnic Institute of New York University; Nikhil Koratkar, Rensselaer Polytechnic Institute

**8:30 AM Introductory Comments**

**8:35 AM Invited**

**Quantitative Morphology Characterization of Polymer Nanocomposites through Electron Tomography:** *Lawrence Drummy*<sup>1</sup>; Hilmar Koerner<sup>1</sup>; Richard Vaia<sup>1</sup>; <sup>1</sup>Air Force Research Laboratory, Materials and Manufacturing Directorate

Polymer nanocomposites often display a hierarchical structure that can be accurately described only through the combination of quantitative results from multiple complimentary characterization techniques. Here we compare quantitative analysis of electron tomography results with results from small angle X-ray scattering (SAXS) from the same samples. Nanocomposites were processed by mixing of organically modified montmorillonite (MMT), a layered silicate material functionalized with an octadecylammonium surfactant, and epon 862 epoxy monomer. Electron tomographic reconstruction of HAADF-STEM tilt series data from the nanocomposites produced a fully segmented 3D data set. The analysis revealed good agreement between tomography and SAXS from the sub-nm regime up to a length scale of 1 micron, however, for certain samples, a representative volume element was not obtained in the electron tomography data. These results are expected to provide a basis for quantitative morphology analysis of nanocomposites and should be applicable to a wide range of materials.

**9:00 AM**

**Nano Holographic Interferometry for Characterization of Nano-Composites:** Cesar Sciammarella<sup>1</sup>; Luciano Lamberti<sup>1</sup>; *Federico Sciammarella*<sup>2</sup>; <sup>1</sup>Politecnico di Bari; <sup>2</sup>Northern Illinois University

Properties of nano-composite materials depend not only on the properties of their individual parents but also on their morphology and interfacial characteristics. Currently, a lot of effort is focused on the ability to obtain control of the nanoscale structures via innovative synthetic approaches. Moving down into this regime to measure characteristics to ensure the desired outcome requires the use of expensive and highly sophisticated equipment. A novel approach that uses a conventional far field microscope is presented here as an alternative for measuring nanoscale structures. Going beyond the resolution limits of traditional optics becomes feasible by the use of evanescent wave fronts as a source of illumination. The observed objects here are sodium-chloride nano-crystals. The mean absolute error on the nano-crystals dimensions is 3.06 nm and the standard deviation  $\pm 3.7$  nm. The measured lengths of the nano-crystals agree very well with integral numbers of the sodium-chloride elementary cell size.

**9:20 AM**

**Morphological and Dielectric Behavior of Carbon Nanotube-Ferroelectric Liquid Crystal Composite:** *Deepika Sharma*<sup>1</sup>; <sup>1</sup>Indian Institute of Technology Roorkee, India

The present study deals with the effect of dispersing carbon nano tubes in ferroelectric liquid crystal material. Carbon nanotube dispersed ferroelectric liquid crystals have high dielectric constant, fast switching response, large electro-optic coefficient which makes them ideal for memories, capacitors and display devices etc. An attempt has been made to understand the influence of carbon nanotubes on dielectric and morphological properties of ferro-electric liquid crystal and how the level (wt/wt %) of carbon nanotubes concentration effect the transition temperature of ferro-electric liquid crystal. Hot stage microscope was

used to investigate the texture and phase changes in the composite. Differential Scanning Calorimetry (DSC) confirmed these phase changes. The results are compared with the original ferro-electric liquid crystal material and showed that the dielectric losses are decreased to a great extent.

## 9:40 AM

**Nanocomposite Coatings for Structural Health Monitoring of Materials:** Nguyen Nguyen<sup>1</sup>; SengYoon Lee<sup>1</sup>; *Nikhil Gupta*<sup>1</sup>; <sup>1</sup>Polytechnic University

Conducting coatings, containing a network of carbon nanofibers, are developed for structural health monitoring of materials. These coatings can be applied to the material surface or on the structural elements as paints. Applied stress on the material results in strain in the coating and changes its resistance. The resistance of the coating is calibrated with respect to the applied stress. The coatings are optimized for thickness and nanofiber content. In the calibration and validation study the coatings are applied to fiber reinforced laminates. Effect of presence and growth of a crack in the laminate on the coating response is also studied. The results show that the use of nanofibers can provide a low cost and more efficient alternative to other conducting composites which rely on carbon nanotubes.

## 10:00 AM Break

## 10:15 AM Invited

**Suppression on Fatigue Crack Growth in Carbon Nanotube Composites:** *Nikhil Koratkar*<sup>1</sup>; <sup>1</sup>Rensselaer Polytechnic Institute

Fatigue is one of the primary causes for catastrophic failure in structural materials. Here we report an order of magnitude reduction in fatigue crack propagation rate for an epoxy system with the addition of 0.5% weight of carbon nanotube additives. Using fractography analysis and fracture mechanics modeling we show that the crack suppression is caused by crack bridging which results in an effective crack-closing stress due to the pull-out of nanotube-fibers in the wake of the crack tip. Using this model, we show that the suppression of crack growth can be further optimized by reducing the nanotube diameter, by increasing the number density of nanotubes that bridge the crack and by increasing the nanotube pull-out length. Control experiments with nanotubes of different diameters, lengths and dispersion confirmed the model predictions. These results demonstrate that carbon nanotubes can significantly enhance the fatigue-life of structural polymers that are susceptible to fatigue failure.

## 10:40 AM

**Effects of Core-Shell Rubber(CSR) Nanoparticles on the Cryogenic Fracture Toughness of CSR Modified Epoxies:** *Jun Wang*<sup>1</sup>; Seth Cannon<sup>1</sup>; Daniel Magee<sup>1</sup>; Judy Schneider<sup>1</sup>; <sup>1</sup>Mississippi State University

This study investigated the effects of core-shell rubber (CSR) nanoparticles on the mechanical properties and fracture toughness of an epoxy resin at ambient and liquid nitrogen (LN2) temperatures. Varying amounts of Kane Ace® MX130 and MX960 toughening agents were added to commercially available EPON 862/Epikure W epoxy resin. Elastic modulus was calculated using quasi-static tensile data. Fracture toughness was evaluated by the resulting breaking energy measured in Charpy impact tests conducted on an instrumented drop tower. The size distribution of the CSR nanoparticles was characterized using Transmission Electron Microscopy (TEM) and Small Angle X-ray Scattering (SAXS). Scanning Electron Microscopy (SEM) was used to study fracture surface morphologies. The addition of the CSR nanoparticles increased the fracture toughness with negligible change in elastic modulus. At ambient temperature the breaking energy increased with increasing additions of the CSR nanoparticles, while at LN2 temperatures, it reached a plateau at lower CSR concentration.

## 11:00 AM

**Effects of Annealing on the Microstructure of Cu-10vol% Alumina Nanocomposite Powders Prepared by High Energy Ball Milling:** *Charlie Kong*<sup>1</sup>; Paul Munroe<sup>1</sup>; Aamir Mukhtar<sup>2</sup>; Deliang Zhang<sup>2</sup>; <sup>1</sup>University of New South Wales; <sup>2</sup>University of Waikato

The effects of annealing on the microstructure of a copper matrix nanocomposite with a dispersion of 10vol% alumina nanoparticles prepared by high energy ball milling have been investigated using focused ion beam (FIB) microscopy and transmission electron microscopy (TEM). The ball milled powder was annealed in vacuum at temperatures up to 500°C. TEM studies of the microstructure of specimens cut from the powder particles using FIB showed no significant changes in the grain size of the copper matrix when annealed at 150°C, compared to the as-ball milled sample, presumably due to the pinning effects of the alumina nanoparticles, which are typically 20nm in diameter. The average grain size slightly increased from 50nm to 80nm as the annealing

temperature increased to 500°C. However, annealing to this temperature resulted in a significant decrease in dislocation density and the formation of annealing twins, consistent with reductions in the microhardness of the particles.

## 11:20 AM

**Effects of Plasmonic Electric Field in Nano-Metallic Cylinders Chains Lateral and Vertically Coupled on Quantum Dots:** *Juan Arias Castro*<sup>1</sup>; Angela Camacho Beltran<sup>1</sup>; <sup>1</sup>Universidad de los Andes

We are interested in the superficial plasmons propagation in a chain of nano-metallic cylinders by studying the size effect and the coupling between the cylinders. Particularly we focus on the main features of electric fields in the inter-cylinder regions due to their relationship with SERS (Surface-Enhanced Raman Scattering). Giant electric fields have been observed in spherical nanoparticles showing an enormous increasing of the cross section, which offers very interesting applications in molecular physics. We discuss the electric field features dependent on geometry and coupling of the nano-metallic particles and extend the results to possible SERS geometric effect. Furthermore, we propose to extend the SERS to quantum dots, which also allows us to study the effect of the plasmons on the quantum dot geometry.

## 11:40 AM

**Processing, Microstructural Characterization and Mechanical Properties of a Ti2AlC/Nanocrystalline Mg-Matrix Composite:** *Shahram Amiri*<sup>1</sup>; Michel Barsoum<sup>1</sup>; <sup>1</sup>Drexel University

We report on the processing and properties of Ti2AlC/nanocrystalline Mg-matrix composites fabricated by melt infiltration or hot pressing. XRD and TEM both confirmed the Mg grain size was ~35±15 nm. Some Mg was dissolved in the Ti2AlC confirming the existence of a (Ti1-xMgx)2AlC solid solution. A small amount of Ti (3±1 at. %) – postulated to be the nucleating agent of the Mg nano-grains – was also found in the Mg-matrix. This microstructure was also remarkably stable: annealing at 550 °C for 6h did not result in grain growth. At 350±40 and 700±10 MPa, the ultimate tensile and compressive stresses were significantly higher than those of Ti3SiC2-Mg and SiC-Mg composites, in which the Mg-matrix grains were not at the nanoscale. The composites exhibit exceptional damping capabilities. The energy dissipated per cycle per unit volume at 500MPa is believed to be the highest ever reported for a crystalline solid.

## Near-Net Shape Titanium Components: Powder Metallurgy I

Sponsored by: The Minerals, Metals and Materials Society, TMS: Titanium Committee

Program Organizers: Rodney Boyer, Boeing Company; James Cotton, Boeing Co

Wednesday AM  
February 18, 2009

Room: 2010  
Location: Moscone West Convention Center

Session Chair: James Cotton, Boeing Co

## 8:30 AM

**Powder Metallurgy Titanium Extrusion Billets for Rod Stock:** *Jane Adams*<sup>1</sup>; Vladimir Moxson<sup>2</sup>; Volodymyr Duz<sup>2</sup>; Jason Deters<sup>3</sup>; Craig Niese<sup>3</sup>; Christine Suminski<sup>3</sup>; <sup>1</sup>US Army Research Laboratory; <sup>2</sup>ADMA Products, Inc.; <sup>3</sup>General Dynamics Land Systems

Defense vehicle manufacturers use self-tapping threaded mechanical fasteners to mount various components onto the vehicle structure quickly. GDLS' Fredsert® is a unique design in that it has no fixed mechanical locking, which means replacement is easy. Each vehicle uses thousands of inserts that are currently made from aerospace-grade titanium alloys. A high volume powder metallurgy manufacturing process to produce titanium extrusion billets to make rod feedstock for threaded attachment inserts is under evaluation. These aspects will be discussed: 1) characterization of titanium and master alloy powders, 2) compaction of the powder into cylinders by cold iso-static pressing and vacuum sintering, 3) microstructure characterization and mechanical testing of performs and extruded bar stock, 4) insert performance comparative testing (tensile, torque, and breakaway) of inserts made from conventional melt-formed industrial titanium stock vs. powder metallurgy titanium, and 5) analysis of properties versus cost and processing factors.



**8:50 AM****Development of High Strength Titanium Alloy Bar Stock from TiH<sub>2</sub> Powder:**

*Curt Lavender*<sup>1</sup>; Yuri Hovanski<sup>1</sup>; K. Scott Weil<sup>1</sup>; Vladimir Moxson<sup>2</sup>; Volodymyr Duz<sup>2</sup>; Orest Ivasishin<sup>3</sup>; <sup>1</sup>Battelle - Pacific Northwest National Laboratory; <sup>2</sup>ADMA Products Inc.; <sup>3</sup>Institute for Metal Physics National Academy of Science Ukraine

A new method to produce TiH<sub>2</sub> for use in blended elemental powder metallurgy has been under development and has been synthesized into many alloys. This paper reports on the results of use the TiH<sub>2</sub> powder for the production of the 5Al15Mo5V3Cr and the difficult to cast 1Al18V5Fe alloys via cold iso-static pressing, sintering and rod rolling. Static and dynamic mechanical properties of the as rolled and heat treated materials were characterized by room temperature tensile, compression and fatigue tests. Elastic constants were determined by ultrasonic techniques. This paper will summarize the characterization of the material and discuss the suitability for use in automotive suspension applications.

**9:10 AM**

**Canless Extrusion Process Development for Blended Elemental Powder-Based Titanium Ti-6Al-4V Alloy:** *Sami El-Soudani*<sup>1</sup>; Oscar Yu<sup>2</sup>; Fusheng Sun<sup>2</sup>; Michael Campbell<sup>3</sup>; Joshua Phillips<sup>3</sup>; Tony Esposito<sup>3</sup>; Vladimir Moxson<sup>4</sup>; Vlad Duz<sup>4</sup>; <sup>1</sup>The Boeing Company; <sup>2</sup>RTI International Metals Inc.; <sup>3</sup>Plymouth Engineered Shapes; <sup>4</sup>ADMA

The feasibility of canless extrusion in ambient environment of hydride/dehydride blended elemental Ti-6Al-4V ADMA-processed powder previously direct-consolidated by cold isostatic pressing (CIP), followed by vacuum sintering has been successfully demonstrated. Extrusion of these billets was conducted at both RTI International Metals, Inc. and Plymouth Engineered Shapes, Inc. The extrusion processing sequence and parameters were derived separately based on prior extrusion experience at both RTI and Plymouth Engineered Shapes, but were found to be essentially similar to those used for wrought ingot-based Ti-6Al-4V material. Laboratory analysis showed that the canless powder-based billet extrusion processing step conducted in air added no more than 200 ppm oxygen to the as-vacuum-sintered billet oxygen content. Preliminary tensile properties of the blended-elemental ADMA powder-based extrusions of a Ti-6Al-4V composition processed both in the beta or alpha-beta ranges of extrusion temperatures showed equivalent or superior tensile properties as compared to identically processed wrought, ingot-based and extruded Ti-6Al-4V.

**9:30 AM**

**Developments in Die Pressing Strategies for Low-Cost Titanium Powders:** *Yuri Hovanski*<sup>1</sup>; K. Scott Weil<sup>1</sup>; Curt Lavender<sup>1</sup>; <sup>1</sup>Battelle - Pacific Northwest National Laboratory

Recent developments in the production of low-cost titanium powders have rejuvenated interest in manufacturing titanium powder metallurgy components by direct press and sinter techniques. However excessive friction typically observed during titanium powder pressing operations leads to numerous problems ranging from non-homogeneous green densities of the compacted powder to excessive part ejection forces and reduced die life due to wear and galling. An instrumented double-acting die press was developed to both investigate the mechanics of titanium powder pressing (particularly for the new low-cost powder morphologies) and to screen potential lubricants that could reduce frictional effects. As will be discussed, the instrument was used to determine friction coefficients and to evaluate a number of candidate lubricants. These results were then used to optimize the lubricant system to reduce die-wall stresses and improve part density uniformity.

**9:50 AM Break****10:10 AM**

**A CIP-HIP Method for the Production of Near Net Shaped Titanium Components:** *Richard Dashwood*<sup>1</sup>; Fatos Derguti<sup>2</sup>; Martin Jackson<sup>3</sup>; David Dye<sup>2</sup>; Malcolm Ward-Close<sup>4</sup>; <sup>1</sup>University of Warwick; <sup>2</sup>Imperial College London; <sup>3</sup>University of Sheffield; <sup>4</sup>QinetiQ

The emergence of a number of novel low cost production methods for titanium alloy powders has stimulated significant interest in the near net shape production of titanium components via powder metallurgy. This paper describes work on new route for titanium parts based on a multi-stage forming and consolidation process using both cold and hot isostatic pressing. Commercial purity titanium and Ti-6Al-4V powders of varying particle size distributions were subjected

to cold isostatic pressing at a number of compaction pressures using various bagging materials. The resulting compacts were then subject to a special indirect hot isostatic pressing process intended to achieve full material density without the need for expensive metal cans. Different secondary pressing media (SPM) were used to improve pressure transmission and heat transfer and the optimum SPM/workpiece ratio was investigated. The benefits of this process with respect to the microstructure and properties of the final product will be presented.

**10:30 AM**

**LENS™ Deposition of  $\alpha_2+\gamma+\beta_2$  Structures Based on Ti-Al-Fe:** Brian Welk<sup>1</sup>; Peter Collins<sup>1</sup>; Mark Gibson<sup>2</sup>; Colleen Bettles<sup>3</sup>; Hamish Fraser<sup>1</sup>; <sup>1</sup>Ohio State University; <sup>2</sup>CSIRO; <sup>3</sup>Monash Univ

Laser Engineered Net Shaping (LENS™) has been used to explore the  $\alpha_2+\gamma+\beta_2$  of the Ti-Al-Fe system. Three composition gradients have been produced and subsequently heat-treated to effect variations in microstructure. The properties have been measured along the gradients. State of the art characterization tools, including SEM, FIB, (S)TEM, EDS and EELS, have been used to explore the microstructural variations as a function of composition. The results are correlated with alloy composition.

**10:50 AM**

**Enhancement of Densification Kinetics of Ti-6Al-4V Powders by Thermal Cycling:** Bing Ye<sup>1</sup>; Marc Matsen<sup>2</sup>; Wesley Crow<sup>2</sup>; Lee Firth<sup>2</sup>; *David Dunand*<sup>1</sup>; <sup>1</sup>Northwestern University; <sup>2</sup>Boeing Co

The densification of Ti-6Al-4V powders is investigated in uniaxial die pressing experiments carried out isothermally at 1000 C (in the beta-field of the alloy) and during thermal cycling between 800 and 1000 C (about the alpha/beta phase transformation range of the alloy). Thermal cycling enhances densification kinetics because transformation-mismatch plasticity becomes the dominant densification mechanism, replacing dislocation creep active for isothermal densification. Cyclic and isothermal hot-pressing densification data for various processing parameters (temperature range, thermal cycling rate and compaction pressure) are compared with analytical and numerical finite-element models of powder densification. The microstructure and mechanical properties of the fully densified Ti-6Al-4V samples are also studied and compared to baseline values.

---

## Neutron and X-Ray Studies of Advanced Materials: Phase Transition

Sponsored by: The Minerals, Metals and Materials Society, TMS Structural Materials Division, TMS/ASM: Mechanical Behavior of Materials Committee, TMS: Advanced Characterization, Testing, and Simulation Committee, TMS: Titanium Committee Program Organizers: Rozaliya Barabash, Oak Ridge National Laboratory; Yandong Wang, Northeastern University; Peter Liaw, The University of Tennessee; Jaimie Tiley, US Air Force

Wednesday AM

Room: 3016

February 18, 2009

Location: Moscone West Convention Center

*Session Chairs:* Dean Haefner, Argonne National Laboratory; Ralph Gilles, TU München

---

**8:30 AM Keynote**

**Characterization of Structure and Dynamics in Metallic Glasses by Scattering:** *Takeshi Egami*<sup>1</sup>; <sup>1</sup>University of Tennessee

Whereas the structure of glasses can be modeled by a computer, understanding the salient and relevant features of the model requires a special consideration. But we have not gone much beyond using the nearest neighbor distance, coordination number and the topology of the local clusters, and it is not easy to link them to real properties. In this talk I propose to consider the width of the first peak of the atomic pair-density function (DPF) and its anisotropy as an important measurable parameter. It is related to the local atomic-level strains, and we now know how it depends upon temperature. The relations to structural relaxation, glass transition, mechanical deformation and other properties will be demonstrated. This research has been sponsored by the Division of Materials Sciences and Engineering, Office of Basic Energy Sciences, U.S. Department of Energy under contract DE-AC05-00OR-22725 with UT-Battelle.

## 9:00 AM Invited

**Probing the Relationship of Ordering in Antiphase Nanodomain FeCo Alloys with Ternary Additions Using Neutron Diffraction:** *Ralph Gilles*<sup>1</sup>; Michael Hofmann<sup>1</sup>; Yan Gao<sup>1</sup>; Frank Johnson<sup>2</sup>; Luana Iorio<sup>2</sup>; Markus Hoelzel<sup>3</sup>; Bruno Barbier<sup>4</sup>; <sup>1</sup>TU München; <sup>2</sup>GE Global Research; <sup>3</sup>TU Darmstadt / FRM II; <sup>4</sup>Universität Bonn

FeCo alloys are industrially important engineering materials due to their very high saturation magnetization and Curie temperature. These alloys play an important role in applications requiring soft magnetic materials, such as electrical generators, motors and transformers. For many industrial applications, the challenge involves increasing the tensile strength and ductility of FeCo alloys while maintaining magnetic performance. Methods used to meet this challenge include alloy design (eg. addition of certain ternary metals such as Ni, V, Nb, Ta, Cr, Mo etc.), annealing, and advanced deformation processing. However, modern applications require even better mechanical and magnetic performance. The effects of alloying FeCo with Pt, Pd, Mn, Ir, and Re have been investigated using neutron diffraction as part of this work. In the composition range of about 30% - 70% Co, FeCo alloys undergo a continuous order-disorder phase transformation at a maximum temperature of 730°C at the equiatomic composition.

## 9:20 AM Invited

**Polarization Switching in Ultrathin Ferroelectric Film by Changing the Chemical Environment:** *Carol Thompson*<sup>1</sup>; Matthew Highland<sup>2</sup>; Dillon Fong<sup>2</sup>; Jeffrey Eastman<sup>2</sup>; Paul Fuoss<sup>2</sup>; Timothy Fister<sup>2</sup>; Stephen Streiffer<sup>2</sup>; G. Brian Stephenson<sup>2</sup>; <sup>1</sup>Northern Illinois University; <sup>2</sup>Argonne National Laboratory

We have used grazing-incidence x-ray scattering to show that polarization orientation in an ultrathin ferroelectric film can be switched through control of the chemical environment above the surface. Monodomain epitaxial PbTiO<sub>3</sub> films of typical 5 nm thickness are grown by metal-organic chemical vapor deposition onto conducting SrRuO<sub>3</sub>/SrTiO<sub>3</sub> (001) substrates. Our experiments have found that changing the partial pressure of oxygen in the gas above the film can induce inversion in the sign of the polarization. At lower temperatures in thicker films, switching occurs by the mechanism of nucleation and growth of 180° domains, while at higher temperatures in thinner films the polarization switching is continuous; i.e., the polarization magnitude decreases to zero and changes sign uniformly without domain formation. Work supported by the U. S. Department of Energy under Contract No. DE-AC02-06CH11357.

## 9:40 AM

**Multi-scale Analysis during the Mechanically-Induced Martensite Phase Transformation by Synchrotron X-Ray Radiation and Neutron Diffraction:** *Benoit Malard*<sup>1</sup>; Guillaume Geandier<sup>2</sup>; Jon Wright<sup>3</sup>; Sophie Berveiller<sup>4</sup>; Etienne Patour<sup>3</sup>; <sup>1</sup>Institute of Physics; <sup>2</sup>LMP - SP2MI; <sup>3</sup>ESRF; <sup>4</sup>LPMM

Martensitic transformation in Shape Memory Alloys (SMAs) can be induced and controlled by external stress and temperature. The transformation is accompanied by the reversible evolution of large high successive inelastic strains. This paper summarizes three in-situ experimental studies of the superelastic behaviour associated to stress induced martensite transformation in Cu-12%Al-0.5%Be [wt. %] polycrystalline samples with the complementarities between synchrotron X-ray radiation and neutron diffraction on three different length scales: 1. The macroscopic scale involves the analysis of small-grain alloys. A new experimental method to determine in-situ the deformation average strain will be explained. 2. The mesoscopic scale takes us down to in the grain to measure the evolution of the rotation in individual grains with different orientations with the 3DXRD method. 3. In the microscopic scale, the changes of grain orientation inside the austenite between two martensitic variants were studied by synchrotron x-ray microdiffraction.

## 9:50 AM

**High Pressure Deformation of Zirconium:** Sven Vogel<sup>1</sup>; Donald Brown<sup>1</sup>; N. Nishiyama<sup>2</sup>; Helmut Reiche<sup>1</sup>; Thomas Sisneros<sup>1</sup>; Heather Volz<sup>1</sup>; Yanbin Wang<sup>2</sup>; Yusheng Zhao<sup>1</sup>; *David Weldon*<sup>1</sup>; <sup>1</sup>Los Alamos National Laboratory; <sup>2</sup>Argonne National Laboratory

In situ deformation studies using diffraction have become routine for materials stable at ambient conditions. However, some materials only exist in extreme conditions, leaving in situ devices the only means to study their structure and mechanical properties. Here, we report results of uni-axial deformation studies of zirconium at hydrostatic pressures of several GPa. The experiments were performed at the BM13 beam line at the Advanced Photon Source. The deformation-DIA apparatus generates a confining hydrostatic pressure causing

a phase change ( $\alpha$ -Zr to  $\omega$ -Zr). Uniaxial deformation is superposed on the hydrostatic pressure to obtain the mechanical response at pressure. The applied stress is measured from the lattice response while the macroscopic strain is determined from radiography. Deviations from Debye rings from circular allow for determination of the full stress tensor, that is de-convolution of the hydrostatic and uniaxial components and intensity variations along the ring allow quantitative texture analysis.

## 10:05 AM

**In-Situ Study on Phase Transition of NiMnGa Alloy under Magnetic Field by Synchrotron High-Energy X-Ray Diffraction:** *Gang Wang*<sup>1</sup>; Yandong Wang<sup>1</sup>; Yang Ren<sup>2</sup>; Yandong Liu<sup>1</sup>; Liang Zuo<sup>1</sup>; <sup>1</sup>Northeastern University; <sup>2</sup>Argonne National Laboratory

Full information on crystallographic aspects during phase transition under magnetic field is essential for understanding the effect of magnetic field on the 'memory' characteristics in the ferromagnetic shape-memory alloys (FSMA) related to texture and stress. In the present paper, the detailed local information of the microstructural evolution of NiMnGa alloy under magnetic field was measured in-situ on the high energy synchrotron beam line 11-ID-C of APS. The transformation between parent phase and martensitic phase was traced by means of the instantaneously recorded 2D images of diffraction results. According to these results, the mechanism of phase transition of NiMnGa under magnetic field is concluded, which can enrich our knowledge for controlling the microstructure and performances of FSMA.

## 10:20 AM Break

## 10:25 AM Invited

**Industrial Applications of X-Ray Characterization for Advanced Materials:** *Assunta Vigilante*<sup>1</sup>; <sup>1</sup>Bruker-AXS

Films of few nanometers thicknesses, quantum dots, quantum wires are the basis of the modern electronic industry and X-ray diffraction techniques is starting to play a very important role as a basic characterization tool for determining the detailed structural information of ultra-thin film such as: the evolution of strain relaxation, defect formation, interfacial properties between film/substrate, the effects of the reduced dimensionality and their correlation to the electrical properties. Materials of technological interests are: high and low K dielectric materials which will substitute SiO<sub>2</sub>, materials for interconnects, new materials for memory storage, materials for spintronics. Traditional optical and opto-acoustic metrology methods, which have been used in industry for decades, are being strongly challenged to meet the new characterization requirements of complex materials. In this talk, I will give an overview of the state-of-the-art of commercial laboratory instrumentation and applications to the electronic industry.

## 10:45 AM

**Atomic-Scale Studies of Phase Transition in Ni-Mn-In Nanoparticles:** *Zhihua Nie*<sup>1</sup>; Dongmei Liu<sup>1</sup>; Yang Ren<sup>2</sup>; Yandong Wang<sup>1</sup>; Gang Wang<sup>1</sup>; Dennis Brown<sup>3</sup>; Liang Zuo<sup>1</sup>; <sup>1</sup>Northeastern University, Key Laboratory for Anisotropy and Texture of Materials (MOE); <sup>2</sup>X-ray Science Division, Argonne National Laboratory; <sup>3</sup>Department of Physics, Northern Illinois University

The Ni-Mn-In ferromagnetic shape-memory alloys have received great interest due to their potential applications as magnetic-field-driven actuators or sensors. The shape memory effect, large magnetoresistance and magnetocaloric effect have been reported in the ternary or Co-doped quaternary alloy systems, which is due to the magnetic field-driven reversible transition from martensite to Heusler parent phase, associated with a ferro- to antiferro- magnetic transformation. The NiMnIn nanoparticles were prepared by a high-energy ball-milling method. The atomic-scale study of phase transition in Ni<sub>50</sub>Mn<sub>34</sub>In<sub>16</sub> nanoparticles were carried out using the high-energy X-ray diffraction and the atomic pair distribution function (PDF) method. Our results show that the as-milled nanoparticles were of highly disordered cubic structure at room temperature, which can dramatically change to the ordered Heusler structure at 523 K with a large heat-release. This disorder-to-order transition is highly temperature sensitive and the annealed nanoparticles are tailored to 14M modulated structure at room temperature.

11:05 AM

**Precipitation Behaviour of Fe-25wt%Co-15wt%Mo Investigated by In-Situ SANS and Complementary Methods:** *Elisabeth Eidenberger*<sup>1</sup>; Erich Stergar<sup>1</sup>; Thomas Schmöler<sup>1</sup>; Harald Leitner<sup>2</sup>; Peter Staron<sup>3</sup>; Helmut Clemens<sup>1</sup>; <sup>1</sup>Montanuniversität Leoben; <sup>2</sup>CD Laboratory "Early Stages of Precipitation"; <sup>3</sup>GKSS Research Centre Geesthacht

The precipitation of a nano-scaled intermetallic phase in a martensitic Fe-25wt%Co-15wt%Mo alloy was investigated by in-situ small-angle neutron scattering (SANS). Solution annealed samples were heated to 700°C using different heating rates while successively measuring the scattered intensity. The size distribution and volume fraction of precipitates as well as the ratio of nuclear and magnetic scattering cross-section, sensitive to changes in the chemical composition of precipitates, were analyzed. Differential scanning calorimetry (DSC) was performed using identical heating rates to gain knowledge of the kinetics of the precipitation reaction. Complementary, three-dimensional atom probe (3DAP) measurements were conducted to characterize size, shape, and chemical composition of the precipitates. A combination of the results obtained by SANS, DSC, and 3DAP leads to a thorough understanding of the precipitation reaction in the investigated alloy. Specifically, the question if spinodal decomposition takes place in this alloy is addressed.

11:15 AM

**In-Situ Synchrotron Investigations and Finite Element Modeling of Microstrains and Mesoscopic Phase Interfaces During Localized Deformation of Pseudoelastic NiTi Shape Memory Alloys:** *Martin Wagner*<sup>1</sup>; Marcus Young<sup>1</sup>; Christian Grossmann<sup>1</sup>; Jan Frenzel<sup>1</sup>; Susanne Gollerthan<sup>1</sup>; Mahamudul Hasan<sup>2</sup>; Wolfgang Schmah<sup>2</sup>; Gunther Eggeler<sup>1</sup>; <sup>1</sup>Ruhr-University Bochum; <sup>2</sup>Ludwig-Maximilians-University Munich

NiTi Shape memory alloys are used in various biomedical and actuator applications. Pseudoelastic materials (in particular wires that possess favorable textures) can recover macroscopic strains of the order of 10 % by virtue of a reversible stress-induced martensitic phase transformation. We report on an in-situ synchrotron diffraction study during tensile straining of pseudoelastic NiTi, where the deformation is associated with the formation of distinct transformation bands. The diffraction data allow documenting how localization of transformation / deformation is related to the macroscopic stress-strain behavior. Moreover, we characterize microstrains in transformation bands and in the adjacent austenitic regions, and we perform a detailed analysis of shapes and widths of boundaries between martensitic bands and austenite. Synchrotron data and complementary finite element simulations of these mesoscopic phase interfaces demonstrate how phase fractions and strain gradients change more sharply in the bulk of a specimen than near the surface.

11:30 AM Invited

**Modeling Ductility and Failure Modes of Dual Phase Steels Using Phase Properties Characterized by In-Situ High Energy X-Ray Diffraction:** *Xin Sun*<sup>1</sup>; Kyoo Sil Choi<sup>1</sup>; Yang Ren<sup>2</sup>; Yandong Wang<sup>3</sup>; <sup>1</sup>Pacific Northwest National Laboratory; <sup>2</sup>Argonne National Laboratory; <sup>3</sup>Northeastern University

Ductile failure of dual phase steels is predicted in the form of plastic strain localization resulting from the incompatible deformation between the harder martensite phase and the softer ferrite matrix. Failure modes and ultimate ductility of two dual phase steels are analyzed based on the actual steel microstructures. The plastic work hardening properties for the constituent phases are determined by the in-situ synchrotron-based high-energy X-ray diffraction technique. Under different loading conditions, different failure modes and ultimate ductility are predicted in the form of plastic strain localization. It is found that the local failure mode and ultimate ductility of DP steels are closely related to the stress state. Under plane stress condition with free lateral boundary, one dominant shear band develops and leads to final failure of the material. However, if the lateral boundary is constrained, splitting failure perpendicular to the loading direction is predicted with much reduced ductility.

11:50 AM Invited

**The Effect of Secondary Gamma-Prime on the Primary Creep Behavior of Single Crystal, Ni-Base Superalloys:** *Gerhard Fuchs*<sup>1</sup>; Brandon Wilson<sup>1</sup>; <sup>1</sup>University of Florida

Some second, third and fourth generation single crystal Ni-base superalloys (i.e., Re-containing alloys) have demonstrated a propensity for excessive primary creep at intermediate temperatures. This behavior has been attributed to the presence of secondary gamma-prime precipitates in the gamma matrix channels, as well as on the Re content of the alloys. This investigation examined creep

behavior for a common first generation alloy, PWA 1480, a common second generation alloy, PWA 1484, as well as an modified first generation alloy, PWA 1480 with 3 weight percent rhenium added. Additionally, two different aging heat treatments were given to each alloy to either precipitate or prevent the formation of, fine (nm scale) secondary gamma-prime in the gamma channels. The microstructures of these samples were characterized by SEM, TEM, XRD and LEAP. The role of the fine scale microstructure and the alloy composition on primary creep deformation will be discussed.

12:10 PM

**Stress-Induced Martensitic-Transformation Behaviors in Ni-Co-Mn-In-Polymer Composites:** *Dongmei Liu*<sup>1</sup>; Zhihua Nie<sup>1</sup>; Yang Ren<sup>2</sup>; Guoshuai Zhou<sup>1</sup>; Peter K. Liaw<sup>3</sup>; Yandong Wang<sup>1</sup>; <sup>1</sup>Northeastern University; <sup>2</sup>X-ray Science Division, Argonne National Laboratory; <sup>3</sup>The University of Tennessee

The ferromagnetic shape-memory composite has been prepared with the Ni-Co-Mn-In particles embedded in a polymer matrix. Ni<sub>46</sub>Co<sub>3</sub>Mn<sub>36.6</sub>In<sub>13.4</sub> particles ~30 μm were obtained by a mechanical ball-milling process. The martensitic phase-transformation temperature of the composite is around room temperature. The stress-induced martensitic transformation in the composite was studied by the in-situ high-energy synchrotron x-ray diffraction technique under the uniaxial compressive deformation. After a stress of 50 MPa was applied, the textured martensite with the 14 M modulated structure appeared, and the volume fraction raised with increasing the stress, characterized by preferred distributions of martensitic twin variants with the (0 4 0) and (0 4 14) crystallographic planes parallel to the loading direction (LD) and the (1 3 0) and (0 1 23) planes perpendicular to the LD. The applied magnetic field can certainly lead to the revised phase transition from the martensite to parent phase in the deformed Ni-Co-Mn-In composite.

## Pb-Free Solders and Emerging Interconnect and Packaging Technologies: Reliability and Microstructure Development

Sponsored by: The Minerals, Metals and Materials Society, TMS Electronic, Magnetic, and Photonic Materials Division, TMS: Electronic Packaging and Interconnection Materials Committee

Program Organizers: Sung Kang, IBM Corp; Iver Anderson, Iowa State University; Srinivas Chada, Medtronic; Jenq-Gong Duh, National Tsing-Hua University; Laura Turbini, Research In Motion; Albert Wu, National Central University

Wednesday AM  
February 18, 2009

Room: 2020  
Location: Moscone West Convention Center

Session Chairs: Iver Anderson, Iowa State University; Darrel Frear, Freescale Semiconductor

8:30 AM Invited

**Microstructure and Reliability Comparison of Different Pb-Free Alloys Used for Wave Soldering and Rework:** *Polina Snugovskiy*<sup>1</sup>; Craig Hamilton<sup>1</sup>; Zohreh Bagheri<sup>1</sup>; <sup>1</sup>Celestica

This paper will describe the results of a intensive microstructural and reliability study of PTH and SMT components which were wave solder assembled using various Pb-free alloys. Both primary attach and reworked solder connections using solder fountain and hand rework were studied. The PTH connector types and SMT resistors were assembled on a test vehicle using the Sn-Ag-Cu, Sn-Cu-Ni-Ge, Sn-Ag-Cu-Bi, Sn-Cu-X, and Sn-Pb solders. Accelerated thermal cycling was conducted at 0 to 100°C. The difference in microstructures, intermetallic formation, Cu dissolution, grain coarsening, and crack formation will be shown. The influence of the microstructure after assembly and rework on Weibull plot parameters and failure mode will be described. Interconnect defects such as non-uniform phase distribution, and void formation will be discussed. Recommendations on alloy applications will also be given.

8:50 AM

**Effect of Surface Finish, Package Size, and Rework on Pb-free Solder Ball Grid Arrays During Thermal Cycling:** *Fengjiang Wang*<sup>1</sup>; Matt O'Keefe<sup>1</sup>; <sup>1</sup>Missouri University of Science and Technology

The current transition to Pb-free solders raises issues for high reliability applications, such as military and aerospace, where there is a lack of long



term field service data to predict performance lifetime. This work focused on the performance of Sn-3.0Ag-0.5Cu (SAC) Pb-free solder ball grid array (BGA) packages soldered to a high T<sub>g</sub> polyimide printed circuit board during temperature cycling. Parameters varied included of the board surface finish, electroless nickel immersion gold (ENIG) vs. Sn-Pb hot air solder level (HASL), the size and location of the BGA components on the board, and whether the BGAs were as-reflowed or removed and replaced (reworked). Results indicate there was no measurable difference in performance with surface finish but SAC, as-assembled, larger BGAs had fewer failures than Sn-Pb, reworked, and smaller BGAs. After thermal cycling assemblies were cross-sectioned to determine failure mechanisms and changes in microstructure.

## 9:05 AM

**Effects of Sn Orientation on Stress Evolution during In-Situ Thermal Cycling of SAC Ball Grid Array Solder Joints from Synchrotron Measurements:** *Thomas Bieler*<sup>1</sup>; *Tae-Kyu Lee*<sup>2</sup>; *Kuo-Chuan Liu*<sup>2</sup>; <sup>1</sup>Michigan State University; <sup>2</sup>Cisco Systems, Inc.

The stress-strain histories in each joint in a lead-free solder joint array in a package differs depending on the Sn crystal orientations and the location within the array. A slice containing a single row of solder joints was thermally cycled from 0 to 100°C in a period of about an hour with concurrent acquisition of Laue patterns using synchrotron radiation, which indicated that most joints are single or multi-crystals with no more than a few Sn grain orientations. Laue patterns were analyzed using Fit2D, Maud, and Beartex to obtain orientation distribution functions as well as the state of stress in each orientation, allowing the volume fraction and stress history to be tracked in each Sn grain. The same specimens were subsequently given several hundred additional thermal cycles and measured in the synchrotron again to assess how the stress history, volume fraction of Sn phases, and precipitate size evolved.

## 9:20 AM

**A Phenomenological Study of the Effect of Microstructural Evolution on Pb-Free Solder Joint Fatigue Resistance:** *Richard Coyle*<sup>1</sup>; *Claire Ryan*<sup>2</sup>; *Steven Kummerl*<sup>3</sup>; *Peter Read*<sup>1</sup>; *Michael Reid*<sup>2</sup>; <sup>1</sup>Alcatel-Lucent; <sup>2</sup>Stokes Institute, Limerick University; <sup>3</sup>Texas Instruments

This paper presents a phenomenological study of the relationship between the initial Sn-Ag-Cu (SAC) solder joint microstructure, the evolving microstructure, and the thermal fatigue performance during accelerated temperature cycling (ATC). Commercial SMT components with different SAC alloy compositions are evaluated using daisy chained test vehicles. The initial microstructures are altered by varying the solder joint cooling rate, using a single or double pass SMT reflow, and with isothermal preconditioning. Different ATC temperature extremes and dwell times are used to vary the rate of microstructural evolution during testing. The microstructural evolution is tracked and characterized with optical metallography and scanning electron microscopy. Unlike SnPb solders, the thermal fatigue reliability of the SAC solders is influenced significantly by both the initial and evolving microstructures. These results could have practical implications in terms of limiting the ability to develop acceleration factors and effective strain-based models for predicting Pb free solder joint life.

## 9:35 AM

**The Effect of Ni Additions on the Impact Strength of Tin-Copper and Tin-Silver-Copper Lead-free Solders:** *Keith Sweatman*<sup>1</sup>; *Shoichi Suenaga*<sup>1</sup>; *Masuo Koshi*<sup>1</sup>; *Tetsuro Nishimura*<sup>1</sup>; <sup>1</sup>Nihon Superior Co., Ltd.

The problem of failure of near eutectic SnAgCu alloy joints to area array components when portable devices such as cell phones are accidentally dropped has prompted consideration of alloys with lower Ag levels with and without microalloying additions. The authors report a study of a range of lead-free alloys that explore these options including SAC305+Ni, SAC1205, SAC1205+Ni and Sn-0.7Cu-0.05Ni+Ge in high speed shear and pull testing. The results for these alloys are benchmarked against those for the tin-lead eutectic and SAC305. 0.5mm spheres were reflow soldered to solder-mask-defined pads on OSP and ENIG substrates and fracture energies measured in shear at speeds up to 2000mm/sec and in tension at speeds up to 200mm/sec. Failure modes were characterised by the fracture surfaces and overall performance correlated with the joint microstructure. Impact strength was found to be sensitive to both the alloy composition and the substrate.

## 9:50 AM

**The Microstructure and Crystal Orientation of Sn-Ag and Sn-Cu Solders Affected by their Interfacial Reactions with Cu and Ni(P):** *Sun Kyoung Seo*<sup>1</sup>; *Sung K. Kang*<sup>2</sup>; *Moon Gi Cho*<sup>1</sup>; *Da-Yuan Shih*<sup>2</sup>; *Hyuck Mo Lee*<sup>1</sup>; <sup>1</sup>KAIST; <sup>2</sup>IBM T.J. Watson Research Center

Recently, it has been reported that the crystal orientation and grain size of the β-Sn phase in Sn-rich solders have profound effects on the reliabilities of Pb-free solder joints, such as thermo-mechanical fatigue, electromigration, and among others. It is also known that the microstructure of Sn-rich solders is strongly affected by their alloy composition. In this study, the grain size and orientation of the β-Sn phase are investigated in terms of their alloy composition and interfacial reactions with two different under bump metallurgy (UBM), Cu vs. Ni(P). The Cu content investigated varies from 0.5 to 2.0wt% in Sn-Cu, while the Ag content varies from 0.5 to 3.5wt% in Sn-Ag. After reflowed at 250°C for 2min, the microstructure of solder joints is analyzed by cross polarization light microscopy and electron backscatter diffraction (EBSD). In addition, the microstructure changes of both solders are examined after aging at 150°C for 1000h.

## 10:05 AM

**Heterogeneous Intragranular Inelastic Behaviour of an SnAgCu Alloy:** *Jicheng Gong*<sup>1</sup>; *Paul Conway*<sup>2</sup>; *Changqing Liu*<sup>2</sup>; *Vadim Silberschmidt*<sup>2</sup>; <sup>1</sup>University of Oxford; <sup>2</sup>Loughborough University

Sub-100µm scale SnAgCu joints may be formed with only one or a few grain. Its mechanical behaviour shifts from polycrystalline aggregate to single crystal. The latter exhibits anisotropic properties since the β-Sn matrix has a contracted body-centred tetragonal structure. Shear tests have shown one slip system is activated in each grain, indicating lattice-dependent inelastic behaviour. The simple shearing may not be the only mechanism for intragranular behaviour. To capture the intragranular deformation principles, micromechanical behaviour has been investigated for SnAgCu grains under low loading. A reflowed alloy is machined to a block of 25x5x2mm. One surface is ground, polished and examined under polarized light to characterize the structure. FIB milling is used to prepare microspecimens that are tested on an Instron 5848 with a low loading rate. TEM is employed to study crystallographic characteristics within a grain to examine the evolution of the substructure and dislocations.

## 10:20 AM Break

## 10:35 AM

**Impact Behavior of Thermomechanically Fatigued Sn-Based Solder Joints:** *K. Subramanian*<sup>1</sup>; *Andre Lee*<sup>1</sup>; *T. Kobayashi*<sup>1</sup>; <sup>1</sup>Michigan State University

Most of the accidental impact loading of electronic packages occurs after they have experienced different extents of thermal, electrical and mechanical field influences encountered during service. In order to evaluate the effects of thermal field influences on the impact behavior of Sn-based solders with and without Pb, studies were carried out after subjecting these joints to isothermal aging at different temperatures, and thermomechanical fatigue in different temperature regimes. Roles of the microstructural features and thickness/morphology of interface IMC layers resulting from imposed thermal field influences, and the type of loading, on failures resulting from impact were evaluated to understand the effects of such fields on the impact reliability of electronic components.

## 10:50 AM

**The Effects of Nucleation and Solidification on the Fatigue Life of Pb-free Solders:** *Babak Arfaei*<sup>1</sup>; *Yan Xing*<sup>1</sup>; *Peter Borgesen*<sup>2</sup>; *Jim Woods*<sup>1</sup>; *Jeremy Wolcott*<sup>1</sup>; *Pushkraj Tumne*<sup>1</sup>; *Eric Cotts*<sup>1</sup>; <sup>1</sup>Binghamton University; <sup>2</sup>Unovis Solutions

Variations in the nucleation behavior of near eutectic Sn-Ag-Cu alloys result in significant differences in both the Sn grain and precipitate morphologies of solidified solder joints. These microstructural factors profoundly affect the thermomechanical response of SnAgCu Pb free solder alloys. The present study utilized differential scanning calorimetry to examine the nucleation behavior of Pb-free solders of various compositions and sizes, on different metallizations and substrates. Individual solder balls were tested in a load controlled shear fatigue test. The microstructure of cross sectioned samples was characterized by means of electron backscattered diffraction in a scanning electron microscope. The effect of solidification temperature and number of reflows on the number of precipitates and grain orientation was studied. The variations of fatigue life of SnAgCu solder joints with both Sn grain size and orientation, and with secondary precipitate size and number, are reported.

11:05 AM

**Influence of Thermal Cycling on Thermal Resistance of Solder Interfaces:** J. Guo<sup>1</sup>; H. Guo<sup>1</sup>; J. Shang<sup>2</sup>; <sup>1</sup>Institute of Metal Research; <sup>2</sup>University of Illinois at Urbana-Champaign

Solder alloys are attractive thermal interface materials for thermal management in microprocessors because of their excellent thermal conductivity. However, solder interfaces with the device metallization or heat spreader are prone to damage by thermal cycling. In this study, the effect of thermal cycling on thermal resistance of solder interfaces was investigated by comparing interface thermal resistance at various stages of thermal cycling. The thermal resistance was found to increase with thermal cycling. The increase was related to formation of the interfacial defects.

11:20 AM

**Improvement of Thermal Fatigue at Sn-Ag-Cu System Alloy by Addition of Bi:** Minoru Ueshima<sup>1</sup>; <sup>1</sup>Senju Metal Industry Co. Ltd.

The Sn-3Ag-0.5Cu alloy have been already put to practical use, and the development of high reliability solder alloy is expected for automobile. Indeed the crack penetrate the Sn-3Ag-0.5Cu solder fillet of 6432 chip resister (6.4mm length, 3.2mm width) after the thermal fatigue of 2000 cycles between -55 and +125 degrees centigrade at 30 minutes holding. And then the fine needle Ag3Sn became coarse at the crack neighborhood. In this study the crack generation after the thermal fatigue at Sn-Ag-Cu system Alloy is restricted by addition of Bi and then the mechanical properties of Sn-Ag-Cu-Bi system alloys are researched at the room temperature and +125 degrees centigrade. At Sn-3Ag-1Cu-3Bi alloys, the crack doesn't penetrate the solder fillet after 3000 cycles and the weibull distribution of the shear strength is equivalent to that of Sn-3Ag-0.5Cu alloy after 1000 cycles. Sn-3Ag-1Cu-3Bi alloy is recommended for automobile and the power device.

11:35 AM

**The Influence of Solder Composition on the Impact Strength of Lead-Free Solder BGA Joints:** Hideaki Tsukamoto<sup>1</sup>; Kazuhiro Nogita<sup>1</sup>; Stuart McDonald<sup>1</sup>; Tetsuro Nishimura<sup>2</sup>; Shoichi Suenaga<sup>2</sup>; Keith Sweatman<sup>2</sup>; <sup>1</sup>University of Queensland; <sup>2</sup>Nihon Superior Co. Ltd.

At the interface between Sn-based solders and substrates, intermetallic compounds (IMCs) form and grow during soldering operations and subsequent use. Such IMCs provide a metallurgical bond, and their interface microstructure has a critical effect on solder joint mechanical reliability. In the present study, the impact strength of BGA solder joints between (i) Cu substrates and Sn-Cu solders and (ii) Cu substrates and Sn-Cu-Ni solders has been evaluated using shear and tensile ball tests and Finite Element Modelling. In both tests, connections made using Sn-Cu-Ni solders show consistently better properties than those made using Sn-Cu solders, particularly at high displacement rates. Microstructural analysis and fractography are used to interpret the results and develop the FEM.

11:50 AM

**Mechanism Solder Joint Failure under Cyclic Bending Fatigue:** Woong Ho Bang<sup>1</sup>; Liang-Shan Chen<sup>1</sup>; Choong-Un Kim<sup>1</sup>; Tae-Kyu Lee<sup>2</sup>; Kuo-Chuan Liu<sup>2</sup>; <sup>1</sup>University of Texas at Arlington; <sup>2</sup>Cisco Systems

The mechanical stability of a solder joint is one of the primary concerns in microelectronics as it determines the reliability of assembled devices and thus has been extensively investigated. Such studies have examined various factors affecting solder joint stability, including joint metallurgy, joint geometry and testing conditions. Recently, there is a growing research interest on new types of load conditions that impart significant impact to solder reliability. One of such is the fatigue incurred by cyclic loading on solder joints. We have investigated the failure mechanics of solder joint under cyclic bending fatigue, and part of our results will be presented in this presentation. Particular focus of this study is the dependence of fatigue failure on bending cycle frequency (at high speed regime) and the mechanics leading to such a dependency.

12:05 PM Invited

**Mechanical Shock of Environmentally-Benign Pb-Free Solders:** Kyle Yazzie<sup>1</sup>; Jason Williams<sup>1</sup>; Nikhilesh Chawla<sup>1</sup>; Hanqing Jiang<sup>1</sup>; <sup>1</sup>Arizona State Univ

Pb-free solder alloys are routinely subjected to mechanical shock and drop conditions in service. While these solder alloys are somewhat susceptible to dynamic loading, a fundamental understanding of mechanical shock and vibration fatigue is lacking. Existing methods developed to probe this strain-rate

regime do not provide a direct and local measurement of strain in the solder. Quantifying the contributions of intermetallic thickness and solder microstructure to the mechanical shock behavior of the solder specimen is extremely important and needs to be studied. In this study the mechanical shock behavior of pure Sn and Sn-3.5Ag-0.7Cu solders was systematically quantified. Intermetallic thicknesses and solder microstructures of individual solder specimens were varied to elucidate their individual contributions to mechanical shock resistance. The strain distribution and evolution was measured using a novel high-speed camera. Multiscale modeling of the complex stress state experienced by the solder during mechanical shock was conducted and will be discussed.

12:25 PM

**Reliability Assessment of Interconnects by an Accelerated Mechanical Fatigue Testing Technique:** Golta Khatibi; Witold Wroczewski<sup>1</sup>; Agnieszka Betzwar Kotas<sup>1</sup>; Brigitte Weiss<sup>1</sup>; Thomas Licht<sup>2</sup>; <sup>1</sup>University of Vienna; <sup>2</sup>Infinitec Technologies AG

A mechanical fatigue testing method is presented for rapid evaluation, lifetime determination and early failure detection of interconnects consisting of a special experimental set-up in combination with an ultrasonic fatigue testing system and laser doppler vibrometry. This technique allows testing various interconnect types under shear, tension-compression and combined loading modes. Validity of the mechanical fatigue testing as an alternative to time consuming thermal cycling is demonstrated. Using this technique lifetime curves up to 10<sup>9</sup> cycles for Al wire bonded interconnects in high power electronic devices were determined which showed a good correlation to thermal fatigue life of similar bonds obtained by power cycling tests. In conformity with the main failure mechanism of power cycling tests, wire bond lift-off could be reproduced. Application of the system in combination with vibrational analysis of the bonds for early failure detection is as well demonstrated and confirmed by the micro-sections of tested interconnects.

## Peirce-Smith Converting Centennial Symposium: Short Course on Injection Phenomena in the Peirce-Smith Converter

Sponsored by: The Minerals, Metals and Materials Society, TMS Extraction and Processing Division, TMS: Pyrometallurgy Committee  
Program Organizer: Joël Kapusta, Air Liquide

Wednesday AM Room: Exhibit Hall  
February 18, 2009 Location: Moscone West Convention Center

Session Chair: Joël Kapusta, Air Liquide

1. Introduction to Fluid Dynamics
  - a. Definitions
  - b. Compressible Versus Incompressible Flows
  - c. Continuity and Momentum Equations
  - d. Sonic Flow
2. Single-Pipe Tuyere Injection
  - a. Background - Bubbling Versus Jetting Regime
  - b. Injection Under Bubbling Regime
  - c. Injection Under Jetting Regime
3. Shrouded Sonic Injection
  - a. Shrouded Injection Fundamentals
  - b. Trials and Implementation in Cu and Ni Converters
  - c. Shrouded Injector Design
  - d. Shrouded Injector Modes of Operation

## Phase Stability, Phase Transformations, and Reactive Phase Formation in Electronic Materials VIII: Session V

Sponsored by: The Minerals, Metals and Materials Society, TMS Electronic, Magnetic, and Photonic Materials Division, TMS: Alloy Phases Committee  
 Program Organizers: Chih-ming Chen, National Chung-Hsing University; Srinivas Chada, Medtronic; Sinn-wen Chen, National Tsing-Hua University; Hans Flandorfer, University of Vienna; A. Lindsay Greer, University of Cambridge; Jae-ho Lee, Hongik University; Daniel J. Lewis, Rensselaer Polytechnic Institute; Kejun Zeng, Texas Instruments; Wojciech Gierlotka, AGH University of Science and Technology; Yee-wen Yen, National Taiwan University of Science and Technology

Wednesday AM Room: 2022  
 February 18, 2009 Location: Moscone West Convention Center

Session Chairs: Jenn-Ming Song, National Dong Hwa University; Jae-Ho Lee, Hong Ik University

### 8:30 AM

#### Electropolishing of Overplated Copper for the Planarization of Copper through Via: Suk-Ei Lee<sup>1</sup>; Jae-Ho Lee<sup>1</sup>; <sup>1</sup>Hong Ik University

Planarization of copper thin films by electropolishing has great challenges due to the minimum amount copper to be removed. In this research the effects of current density, electrolytes and additives on the electropolishing of 50 and 20 $\mu$ m diameter copper via were investigated to eliminate thickness disparity during overplated copper removal in 3D SiP through via. The termination time was determined with analysis of applied potential on anode and cathode to avoid excess electropolishing. Acetic acid played a role of accelerator and glycerol played a role of inhibitor in phosphoric acid electrolytes. The overplated copper on the through via was effectively electropolished by applying proper current density in the phosphoric electrolytes with acetic acid and glycerol addition. The electropolishing was terminated at the point of abrupt change of applied potential to remove only overplated copper on the through via.

### 8:45 AM Invited

#### Fabrication of Copper and Tin Bump Using Electropolishing and Electroless Plating Methods in 3D SiP: Seong-Hun Kim<sup>1</sup>; Yun-Sung Moon<sup>1</sup>; Suk-Ei Lee<sup>1</sup>; Yeong-Kwon Ko<sup>1</sup>; Jae-Ho Lee<sup>1</sup>; <sup>1</sup>Hong Ik University

In conventional flip chip interconnection, CMP and lithographic processes were used in Cu/Sn bumps fabrication. During CMP process, copper via substrates were easily damaged and lithographic process is high-cost process. Series of electropolishing, electroless copper plating, electroless tin plating followed by reflow were suggested to replace CMP and lithographic process. The 50 and 20 $\mu$ m diameter copper via were fabricated by electroplating method. Overplated copper were successfully removed by electropolishing method in suppressor and accelerator added phosphoric acid. Copper bumps with 5 $\mu$ m height were formed on electropolished via by electroless plating method. Suppressor added electroless copper bath can promote selectivity of copper bump formation on via after proper acid cleaning. Tin bumps with 9 $\mu$ m height were formed on electroless copper bump. Finally uniform sized Cu/Sn bumps were fabricated after reflow process.

### 9:05 AM

#### 15 nm Ru Diffusion Barrier on NiSi/Si for Sub-45-nm Cu Contact Plug: Jia-Huei Lin<sup>1</sup>; Chen-Sheng Hsu<sup>1</sup>; Jau-Shiung Fang<sup>1</sup>; <sup>1</sup>National Formosa University

This study aims at evaluating Ru barrier on NiSi/Si for Cu contact metallization. The films were deposited by magnetron sputtering using Ni, Ru and Cu targets. Low resistivity NiSi film was firstly obtained by carefully optimizing the conditions of rapid thermal annealed Ni/Si, then Ru and Cu films were sequentially deposited onto NiSi/Si substrate. The diffusion barrier properties of the studied films were elucidated using four-point probe (FPP), x-ray diffraction (XRD), scanning electron microscopy (SEM), Auger electron spectroscopy (AES) and transmission electron microscopy (TEM). The failure temperatures of 600°C (Cu/NiSi/Si) and 650°C (Cu/Ru/NiSi/Si) have been demonstrated. Structural analysis revealed that the failure mechanisms of the studied film involved the Cu penetrating through Ru/NiSi stack film, inducing the accelerated dissociation of the NiSi. Interposing a Ru layer remarkably improved thermal stability and barrier performance in the Cu/NiSi/Si stack films; which can be an effectively diffusion barrier for sub-45-nm Cu contact plug.

### 9:20 AM

#### Thermal Stability Properties of Various Vopper Alloy Films Used in Advanced Barrierless Cu Metallization: Jinn P. Chu<sup>1</sup>; Chon-Hsin Lin<sup>2</sup>; Wean-Kuan Leau<sup>3</sup>; Dung-Yuan Yu<sup>1</sup>; <sup>1</sup>Graduate Institute of Materials Science and Technology, National Taiwan University of Science and Technology; <sup>2</sup>Chin-Min Institute of Technology; <sup>3</sup>Institute of Materials Engineering, National Taiwan Ocean University

Owing to its low resistivity and high electromigration resistance, Cu is increasingly being used as an interconnect material in Si-based devices. Unfortunately, Cu diffuses rapidly in Si, thus deteriorating the device properties. To prevent device failure, a diffusion barrier must be placed between Cu and Si. However, with a decrease in the feature size, the barriers cause many problems. Therefore, barrier-free Cu metallization is proposed in this study. A Cu seed layer is prepared by alloying Cu with insoluble substances such as RuN to improve the thermal stability of the seed layer; the layer acts as a barrier and minimizes Cu/Si interdiffusion. The seed layer is characterized using X-ray diffraction, a focused ion beam, secondary ion mass spectroscopy, transmission electron microscopy, the film resistivity, and current-voltage measurements. The results indicate the enhancement of the thermal stability of the Cu film, with no apparent interaction between Cu and Si.

### 9:35 AM

#### Failure Behavior of Electroless CoWP Film as a Diffusion Barrier between Electroless Cu and Si: Ting Tsai<sup>1</sup>; Jiing Lee<sup>1</sup>; Sin Wu<sup>2</sup>; Jau Fang<sup>1</sup>; <sup>1</sup>National Formosa University; <sup>2</sup>National Taiwan University of Science and Technology

The electroless CoWP film with 89.4 at.% Co, 2.4 at.% W and 8.2 at.% P was deposited on silicon substrate as diffusion barrier for electroless Cu and Si. The Cu/CoWP/Si stacked samples with 100 nm electroless CoWP films were prepared and annealed in a rapid thermal annealing (RTA) furnace. The failure behavior of electroless CoWP film in Cu/CoWP/Si has been investigated by transmission electron microscopy (TEM), scanning electron microscopy (SEM), energy dispersive X-ray spectrometer (EDS), X-ray diffraction (XRD) and sheet resistance measurement. The failure temperature of Cu/CoWP/Si is 650° and its failure is caused by the interdiffusion of Co and Cu. The cobalt penetrates through the copper film to form granular grains on the copper film and the copper penetrates through the electroless CoWP film to form the Cu<sub>3</sub>Si faceted-like grains in the silicon. Finally, Co reacts with Cu<sub>3</sub>Si to form cobalt silicide on the top of Cu<sub>3</sub>Si.

### 9:50 AM Break

### 10:10 AM

#### Investigations of the Interfacial Properties in Ni-FUSI/Hf-Based/Si and Ni-FUSI/SiO<sub>2</sub>/Si Stacks by I-V and XPS Techniques: S.Y. Tan<sup>1</sup>; Ming-Yuan Wu<sup>1</sup>; Hsing-Hung Chen<sup>1</sup>; <sup>1</sup>Chinese Culture University

Metal gate and high-k gate dielectric are widely believed to be necessary for 45 nm CMOS node. Hf-based film is a promising candidate to replace SiO<sub>2</sub> as gate dielectric, due to its much higher dielectric constant and stability. The combination of Ni-FUSI gate electrodes and high-k gate dielectrics is one of the most promising gate stacking structures. In this work, we established an effective way to identify the phase transformations by some nondestructive techniques. Furthermore, the aim of this work is to carry-out a comparative electrical and physical characterization of Ni-FUSI/Hf-based/Si and Ni-FUSI/SiO<sub>2</sub>/Si Stacks. The thermal stability, phase and interface uniformity of Ni-silicide are some key issues for Ni-FUSI technology. Lot of concerns on phase and interface uniformity of nickel silicide and electrical active defects caused by rapid Ni diffusion. We investigated the phase and interface properties of Ni-silicides formed by Ni-Si solid-state reaction and will be characterized by XRD, XPS and I-V techniques.

### 10:25 AM

#### Enhancement in Conductivity and Transmittance of Zinc Oxide Prepared by Chemical Bath Deposition: Wei-Hsiang Luo<sup>1</sup>; Ting-Kan Tsai<sup>1</sup>; Jau-Shiung Fang<sup>1</sup>; <sup>1</sup>National Formosa University

Low resistivity and high transparency ZnO thin films were prepared on cleaned Corning Eagle<sup>2000</sup> glass substrate by chemical bath deposition (CBD) and the effect of deposition parameters on the structural, electrical and optical properties of the films were investigated. Using CBD to prepare ZnO film has the benefits of low cost and low temperature process, which make it potential to be used on a roll-to-roll process. The electrical properties were correlated with the structure of the film, and detail structural characterization was performed using



x-ray diffraction and field emission scanning electron microscopy. Experimental results indicated that the studied thin film had a low resistivity of  $2.9 \times 10^{-2} \Omega$  cm and high transmittance above 80% in the visible range when the film was annealed under  $\text{Ar} + \text{H}_2$  ambient. The results revealed that low resistivity and high transmittance ZnO film can be prepared using chemical bath deposition by carefully adjusting the deposition conditions.

**10:40 AM**

**The Study on the Solubility of TiO-TiC System:** Na Hou<sup>1</sup>; Chengjun Gao<sup>1</sup>; Xiaohui Ning<sup>1</sup>; Xiaotong Hu<sup>1</sup>; Hongmin Zhu<sup>1</sup>; <sup>1</sup>Beijing University of Science & Tech

The solubility of TiO-TiC system was studied by heating conversion and X-ray diffraction analysis (XRD). Pellets of the mixture of titanium monoxide (TiO) and titanium carbide (TiC) were heated under vacuum up to 1700°C. The results of XRD indicated that all the samples with various compositions had the single phase with NaCl-typed structure, which is the same of TiC and beta-TiO. The lattice parameter of the sample changes continuously with the change of the component. All the samples after the heat conversion showed high electronic conductivity.

**10:55 AM**

**Dynamic Study on Formation Processes and Thermal Stability of Nickel Germanides by Using *In Situ* Transmission Electron Microscopy:** Jae-Wook Lee<sup>1</sup>; Kwan-Woo Song<sup>1</sup>; Jee-Hwan Bae<sup>1</sup>; Min-Ho Park<sup>1</sup>; Han-Byul Kang<sup>1</sup>; Hyungsub Kim<sup>1</sup>; Cheol-Woong Yang<sup>1</sup>; <sup>1</sup>Sungkyunkwan University

Ge MOSFET has been considered as one of the promising devices for future high-speed CMOS technology due to higher carrier mobility than Si. However, the NiGe shows a poorer thermal stability than NiSi. It has been reported that the thermal stability of Ni-germanide improved through the addition of an alloying element, such as Ta or Zr. In this study, the formation and morphological evolution of metal (Ni, Ni-Ta, Ni-Zr) germanides as a function of temperature was investigated by *in situ* annealing of 15 nm-thick metal/Ge systems in the TEM with a specimen heating holder. Through the addition of alloying elements, Ni germanide grain growth was retarded and the surface morphology of the Ni germanide layer improved. Eventually, the agglomeration of Ni germanides was retarded and the thermal stability of the Ni germanides formed from the Ni alloys became superior to that formed from the pure Ni.

**8:45 AM**

**Effective Recovery of Aluminium from Aluminum Dross by Selective Grinding and Air Classification:** Euisup Shin<sup>1</sup>; Sujeong Lee<sup>1</sup>; SangBae Kim<sup>1</sup>; Wantae Kim<sup>1</sup>; Hosung Yoon<sup>1</sup>; *Sung-Baek Cho*<sup>1</sup>; <sup>1</sup>Korea Institute of Geoscience & Mineral Resources

Physical separation containing selective grinding and air classification were carried out to effectively recover aluminium from the aluminium dross. The aluminium dross sample used in this work contained about 12-18wt.% of metal aluminium and the metal content was varied in the fractions prepared by crushing and sieving. Aluminum metal is ductile and easily enlarged when a compressive force is engaged, whereas, oxide forms of aluminium can be easily broken and their resultant sizes are reduced after grinding. Since +5mm product is mainly aluminum metal, it was recovered by sieving and then -5mm product was ground by rod mill or steel ball mill for various periods and then air classified. The results showed that aluminium metals can be effectively recovered by air classification after milling using steel ball mill rather than rod mill. Thus recovered aluminum was leached out by various solvent to synthesize a alum, alumina and Al-alkoxide.

**9:00 AM**

**The Energy and Environmental Implications of Recovering Salt Flux from Salt Slag Generated by the Aluminum Industry:** John Hryn<sup>1</sup>; <sup>1</sup>Argonne National Laboratory

Recycling aluminum at secondary smelters usually involves the use of salt fluxes to improve aluminum recovery. Unfortunately, the use of salt fluxes results in the generation of a salt slag (or salt cake) waste stream. Attempts at developing a viable salt cake recycling technology to date have been unsuccessful, primarily due to the high energy cost of recovering a usable salt fraction from salt cake, and the lack of a suitable market for placing the residual non-metallic products, NMP. This presentation outlines the overall negative energy and environmental implications of attempting to recover salt flux from salt cake for reuse by the aluminum industry. From an energy and environmental perspective, the best practice today is to maximize aluminum recovery from salt cake and dispose the salt and NMP fractions in a controlled landfill.

**9:20 AM**

**Recycling of Aluminum Metal Matrix Composite Reinforced with Zircon Sand:** Sanjeev Das<sup>1</sup>; <sup>1</sup>Thapar University

In the present investigation, recycling of an aluminum alloy (Al-4.5 wt% Cu) from zircon sand reinforced aluminum metal matrix composite was done by simple melting and casting route. It is possible to separate molten matrix metal from zircon particles in the composite scrap by remelting, holding and casting. The scarp generated during casting of the composites was remelted at 800°C in a resistance furnace. It was observed that due to high difference in densities of the zircon sand and aluminum alloy, zircon readily settles down at the bottom of the crucible. About 50-70 wt%. of the matrix metals was separated from the composite reinforced with zircon particles of different amount and particle size. Minimum holding time of melt was evaluated for complete settling in which maximum amount of aluminum alloy was recovered.

**9:35 AM**

**Selective Enrichment of Ti Components in Ti-Bearing Blast Furnace Slag and Coarsening of Perovskite Phase during Dynamic Oxidation:** Li Zhang<sup>1</sup>; Yang Cao<sup>1</sup>; Tai Lou<sup>1</sup>; Zhi Sui<sup>1</sup>; <sup>1</sup>Northeastern University

The analysis of processing mineralogy on Ti-bearing blast furnace slag shows that most Ti components enrich in perovskite phase. Air was blown into the molten slag as oxygen resource during dynamic oxidation. It was found that the oxidation is not only in favour of Ti components into perovskite phase, but also the increase of slag temperature and decrease of slag viscosity during dynamic oxidation promote the precipitation and growth of perovskite phase, average crystal size of perovskite phase is 40 µm. The experimental result realizes the selective enrichment of Ti components and coarsening of perovskite phase, perovskite phase can be separated by mineral dressing method.

**9:55 AM**

**The Recovery of Valuable Metals Containing in the Slag of Jamesonite Smelting in the Blast Furnace:** Xie Zhaofeng<sup>1</sup>; Yang Tianzu<sup>1</sup>; Liu Wei<sup>1</sup>; Xia Wentang<sup>2</sup>; Liu Weifeng<sup>1</sup>; <sup>1</sup>Central South University; <sup>2</sup>Chongqing University of Science and Technology

A new recovery process of the valuable metals containing in the blast furnace slag of jamesonite was studied. In this process, the valuable metals such as Pb,

**Recycling—General Session: Session I: Metals**

Sponsored by: The Minerals, Metals and Materials Society, TMS Extraction and Processing Division, TMS Light Metals Division, TMS: Recycling and Environmental Technologies Committee

Program Organizer: Joseph Pomykala, Argonne National Laboratory

Wednesday AM  
February 18, 2009

Room: 2024  
Location: Moscone West Convention Center

Session Chair: Joseph Pomykala, Argonne National Laboratory

**8:30 AM**

**Structure and Features of Slag from the Aluminum and Aluminum Alloys Melting and the Consequences:** Sergey Novichkov<sup>1</sup>; Anatoliy Zholnin<sup>1</sup>; <sup>1</sup>Mosoblprommontazh

The influence of the flux structure upon the consistence of hot slag was investigated on basis of the earlier published model of aluminum slag structure. The aim of the investigation was to receive an experimentally proved conclusion which ensued from the described model. A practical consequence of the realized investigation was the detection of additives minimizing the flux consumption required to achieve the pre-determined consistence of hot slag. Two possible ways for decreasing of flux consumption ensue from the suggested model: a) use of additives which decrease the surface tension of melted flux; b) use of fluoride additives which reduce to fragments the oxide scales as principal thickener of melted flux. The investigations were realized with slag from salt-free remelting of aluminum scrap. As basic flux the equiposited mixture of sodium chloride and potassium chloride was used. The possibility of the substantial decreasing of flux consumption was obtained.

Sb, Zn and In etc. were fumed and volatilized and enriched in the dust firstly and then the dust was leached by sulfuric acid. In the leaching procedure, Zn and In in the dust entered into the leaching solution and were separated from Pb and Sb which remained in the residue. The volatilization rates of Pb, Sb, Zn and In are 95%, 92%, 86% and 75% respectively. The leaching rates of Zn and In are 98.5% and 95.2% respectively. The experimental results shows that the valuable metals in the dust can be recovered and separated effectively by this process and their recovery efficiencies are as follows: Pb94%, Sb91%, Zn84% and In69%.

## 10:15 AM Break

## 10:30 AM

### Impact of Recycling on Materials Availability: A Case Study of Platinum:

Elisa Alonso<sup>1</sup>; Frank Field<sup>1</sup>; Randolph Kirchain<sup>1</sup>; <sup>1</sup>MIT

Recycling is generally a more sustainable alternative to landfilling. However, recycling can be difficult to justify on the basis of simple cost recovery. As a consequence, significant amounts of even precious metals, such as platinum, can end up unrecovered. When one considers the risks of supply disruptions for firms that require scarce materials, recycling may serve to mitigate firm risk exposure, thus increasing its strategic value. This paper explores elements of this question, using a System Dynamics simulation model that strives to capture the dynamics of platinum market supply, demand and price. The detailed structures of supply and demand are key features of the model. Results show that since the secondary supply of platinum depends on a supply chain separate from primary extraction, recycling can diversify the risks of primary supply instabilities and reduce the impact of price fluctuations upon firms.

## 10:50 AM

### Substance Flow Analysis of Lead in China: Xueyi Guo<sup>1</sup>; Juya Zhong<sup>1</sup>; Qinghua Tian<sup>1</sup>; Yu Song<sup>1</sup>; <sup>1</sup>Central South University

The method of Substance Flow Analysis (abbreviated as SFA) provides a helpful tool for the study of the industrial metabolism of a certain metal within a regional level. In this work, the flow of lead in China, 2006, was traced within the STAF model, and the situation of production, consumption and recycling of lead resources in China were introduced. The SFA is performed on lead flows during its one year life cycle in detail. As one of the biggest producer and consumer of lead in the world, China is facing a severe depletion of lead resources. How to increase the resource efficiency is a significant issue for lead industry of China. Based on the result, several advices were proposed in the paper, aiming to contribute important reference information for the industrial metabolism and resource management and recycling of lead industry in China.

## 11:05 AM

### High Performance Recycling of Agricultural Wastes: Rice Husk Silica Used as Reinforcements of Magnesium Sintered Materials: Katsuyoshi Kondoh<sup>1</sup>; Junko Umeda<sup>1</sup>; <sup>1</sup>Osaka University

The utilization of silica particles originated in rice husks as reinforcements of magnesium composites is discussed. A reactivity of magnesium with silica particles in solid state to synthesize Mg<sub>2</sub>Si is investigated. Finer silica particles are more effective to be reacted with magnesium at low temperature due to the increase of their surface area contacted with magnesium. Amorphous silica is more useful for the reaction than crystalline one. The reactivity of rice husk silica is superior to the conventional mineral silica because of not only its amorphous structure but larger specific surface area by the porous structures. In the case of green compacts of the elemental mixture of silica particles and Mg powder, the silica particle size is not effective on the reactivity because the coarse particles are fractured into fine ones by cold compaction. The distribution of Mg<sub>2</sub>Si intermetallics of magnesium powder composites consolidated by SPS process is investigated.

## 11:25 AM

### Treatment of Residues during Aluminum Recycling: Bernd Prillhofer<sup>1</sup>; Ramona Prillhofer<sup>1</sup>; Helmut Antrekowitsch<sup>1</sup>; <sup>1</sup>University of Leoben

Salt slag is a waste product, produced by the recycling of aluminum. In Europe the landfill disposal of this waste is forbidden, because the slag contains soluble salts and these represents a potential source of pollution to the surface and groundwater. Additionally, consisting metal and some compounds in the salt slag can react with water and resulting from this, noxious gases are generated. Recovery of useful materials from these wastes is according to this, both environmentally necessary and economically feasible. This study describes a complete recycling-process for the salt slag, which includes a leaching-crystallization-step to obtain the oxidic residue, a pyrometallurgical-

step to treat the oxidic residue and final an extensive characterization of the achieved products. Due to the increasing price of raw materials, the utilization of the oxidic residue into commercial products was investigated and application possibilities are discussed.

## 11:45 AM

### Recovery of Nickel and Cobalt by Pyrometallurgical Process of Waste from Producing Program of Nickel Metal Hydride Batteries: Hui Wang<sup>1</sup>; Huimin Lu<sup>1</sup>; <sup>1</sup>Beijing University of Aeronautics & Astronautics

With the great increasing use of nickel metal hydride batteries recently, the waste of this kind batteries have been paid for close consideration. For the main reason that the waste of the batteries contained precious metals and lanthanide which cost great lose. This paper introduces the pyrometallurgical process of recovering nickel and cobalt from the waste of the nickel metal hydride batteries. Particularly, the waste for the process was from factory during the producing program. The use of designed solvent to divide nickel and cobalt in melted state from the waste is described. Also, the result of the nickel and cobalt and melted gangue that mainly consist of lanthanide oxide are included in details. The aim of the paper is to find out a simple and feasible way to reuse waste from nickel metal hydride batteries.

## 12:00 PM

### Recovery of Ni, Co and Mn from Spent Battery Material: Jinhui Li<sup>1</sup>; Xinhai Li<sup>1</sup>; Yunhe Zhang<sup>1</sup>; Qiyang Hu<sup>1</sup>; Zhixing Wang<sup>1</sup>; Fangming Fu<sup>1</sup>; <sup>1</sup>Central South University

Recovery of Ni, Co and Mn from spent battery material not only protects the environment but also increases the utilization of resources and decreases the cost of battery material. With contrast of sulfate acid and hydrochloric acid, the results show that it has higher solubility and faster leaching rate in hydrochloric system than that in sulfate system, and hydrochloric acid can be recycled in the circuit. The experiments results show that the dissolution yields of Ni, Co and Mn can be 95% at least in hydrochloric system, the optimal conditions are that hydrochloric acid is 6mol/L and the particle size of waste is 120 $\mu$ m at least, temperature is about 60 $^{\circ}$ , Liquid/Solid ratio=8:1, and the leaching time is 2 hour. The process seems to be able to claim economic recovery of base metals from waste, and which is reliable and feasible.

## Shape Casting: Third International Symposium: Modeling

Sponsored by: The Minerals, Metals and Materials Society, TMS Light Metals Division, TMS: Solidification Committee, TMS: Aluminum Processing Committee  
Program Organizers: John Campbell, University of Birmingham; Paul Crepeau, General Motors Corp; Murat Tiryakioglu, Robert Morris University

Wednesday AM  
February 18, 2009

Room: 2011  
Location: Moscone West Convention Center

Session Chair: Christof Heisser, MAGMA Foundry Technologies, Inc.

## 8:30 AM Introductory Comments

## 8:35 AM

### Prediction of Columnar to Equiaxed Transition in Alloy Castings with Convective Heat Transfer and Equiaxed Grain Transportation: Wajira Mirihanage<sup>1</sup>; Shaun McFadden<sup>1</sup>; David Browne<sup>1</sup>; <sup>1</sup>University College Dublin

A macroscopic, non-equilibrium model of the Columnar to Equiaxed Transition (CET) in alloy shape casting is presented. Convective heat transfer in the liquid metal and equiaxed grain transportation by fluid flow is included in the model. Nucleation from mould walls is used as the mechanism for columnar grain initiation. Nucleation from inoculants in undercooled liquid-ahead of the columnar front is considered for equiaxed grain formation. The front tracking model computes the advancement of the columnar front while the average growth of the equiaxed grain envelopes is simultaneously simulated. Latent heat release is incorporated in the model. The columnar mush and the coherent equiaxed dendrites are treated as porous media for convective flow. When equiaxed fraction is sufficient, no further advancement of the columnar front is permitted and the CET position is determined. CET is simulated for solidification of an aluminum-silicon alloy along with predictions of average equiaxed grain sizes.

9:00 AM

**Prediction of Deformation and Hot Tear Formation Using a Viscoplastic Model with Damage:** M. G. Pokorny<sup>1</sup>; Charles Monroe<sup>1</sup>; *Christoph Beckermann*<sup>1</sup>; <sup>1</sup>Department of Mechanical and Industrial Engineering, University of Iowa

A three-phase model is presented that predicts solid deformation as well as melt pressure, feeding flow and shrinkage porosity during casting. A viscoplastic constitutive theory with material damage is used to model the solid deformation. The damage created by mechanically induced voiding is proposed as a new hot tear criterion. The liquid feeding and shrinkage porosity model is coupled to the solid deformation model, which enables the final damage prediction to be more accurate than previous hot tear criteria. Novel steel casting experiments have been performed to measure the deformations and forces from solidification to shakeout. The measured and predicted deformations and forces show good agreement with the simulation results. Furthermore, the damage predictions show good correspondence with hot tear indications on radiographs of the test castings.

9:25 AM

**A Diffusing Runner for Gravity Casting:** *Fu-Yuan Hsu*<sup>1</sup>; Huey-Jiuan Lin<sup>1</sup>; <sup>1</sup>National United University

In gravity casting, the quality of an aluminium alloy casting relies on, among other things, the design of the runner system in which the gate velocity into the mould cavity should be controlled under a critical velocity close to 0.5 m/s. In this study a diffuser was proposed to reduce the velocity of liquid metal to below the critical value while the flow rate being almost unchanged. Flow separation and dead-zone in the diffuser design are avoided. A computational modeling package and real casting experiment (water analogy method) were employed for exploring and verifying the new design. The efficient of the diffuser is quantified by the measurement of coefficient of discharge, Cd.

9:50 AM

**Process Modelling and Microstructure Prediction in Gravity Die Aluminium Castings with Sand Cores:** Rosario Squatrito<sup>1</sup>; *Luca Tomesani*<sup>1</sup>; Ivan Todaro<sup>1</sup>; <sup>1</sup>University Bologna

The gravity die casting process for aluminium engine heads is one of the most complex of the casting industry, with high geometrical complexity, highest mechanical properties, lowest porosity levels. In the design of such a process by means of numerical methods, two kinds of problems arise: the first is the correctness of the boundary conditions of the thermal problem, the second is the availability of algorithms for predicting microstructural features, by which the final mechanical properties can be assessed. To assess this problems, a full numerical analysis has been carried out on an 8 cylinders A356 engine head which is in current production, by carefully replicating all the available process monitoring data: die temperatures and gradients, alloy composition and gas content, casting temperature, filling strategy and cooling times. An advanced microstructure module was then run to evaluate the porosity distribution throughout the casting; predicted and experimental values were finally compared.

10:15 AM Break

10:25 AM

**Autonomous Optimization in Casting Process Simulation:** *Christof Heisser*<sup>1</sup>; <sup>1</sup>MAGMA Foundry Technologies, Inc.

Computer processing speed has changed dramatically in the last 10 years. Traditional casting process modeling is based on "what-if" scenarios, requiring the user to make a decision, implement changes and start simulation. To gain the most advantage out of computer advances casting process modeling is now combined with genetic autonomous optimization tools, which produce a simulation based on a range of parameters rather than specific design points. Besides the optimization of designs, process parameters, as well as mechanical properties, can be optimized too. The production of high quality castings depends on many factors. As state-of-the-art simulation tools consider many of these factors, multi-objective autonomous optimization opens a whole new level of accuracy. Input parameters and thermophysical properties can be optimized to characterize the specific melt of a foundry or production line. This paper will show the back ground of genetic optimization tools and examples of optimized castings utilizing this technology.

10:50 AM

**Modeling the Formation of Porosity during Low Pressure Die Casting (LPDC) of Aluminum Alloy A356:** *Ehsan Khajeh*<sup>1</sup>; XinMei Shi<sup>1</sup>; Daan Maijer<sup>1</sup>; <sup>1</sup>The University of British Columbia

In this study, a coupled thermo-fluid flow model for predicting the position and the size of macro-shrinkage in low pressure die cast (LPDC) of A356 alloy has been developed using the Finite Volume Method (FVM). By solving the conservation equations, the interdendritic flow due to the change in density associated with phase transformation has been obtained. In order to satisfy continuity, the volume contraction must be accommodated by introduction of additional melt based on total volumetric strain rate. By studying the role of permeability, as the critical factor in determining pressure drop, feedability of mushy zone and the formation of macro-shrinkage in isolated zones have been determined. In order to validate the current method, the model has been applied to examine the evolution of shrinkage pores in a casting trial.

11:15 AM

**Predicting Residual Stresses Caused by Heat Treating Cast Aluminum Alloy Components:** *Chang-Kai Wu*<sup>1</sup>; Makhlof Makhlof<sup>1</sup>; <sup>1</sup>WPI/MPI

A mathematical model that enables the prediction of the effects of heat treatment on cast aluminum alloy components has been developed. The model uses the commercial software ABAQUS to predict residual stresses in heat treated components. An extensive database has been developed for A356 aluminum alloy and includes the mechanical, physical, and thermal properties of the alloy as functions of temperature. In addition, boundary conditions – in the form of heat transfer coefficients for each of the heat treatment steps – have been obtained from measurements performed with a specially designed quenching system. The database and boundary conditions were used to predict the response of a typical A356 cast component to a standard commercial heat treating cycle and the model predictions were found to be in good agreement with their measured counterparts.

11:40 AM

**Internet-Based Casting CAE System:** *Tao Jing*<sup>1</sup>; Baicheng Liu<sup>1</sup>; <sup>1</sup>Tsinghua University

Numerical simulation of solidification process has become a valuable tool for evaluating and optimizing casting pattern and rigging design to dramatically reduce the cost of reaching a satisfactory design. This paper presented the development of a Web-based Casting CAE System. The major competitive advantage of a Web-based casting CAE system, compared to a stand alone system, lies in its capability to share the limited resources through Internet within quite a lot of foundries, especially those medium and small scale foundries which may have difficulties to set up their own system alone. Java-based multi-tier architecture, CORBA-based distributed computing technology and Java Applet, Swing and Java Severlet technology are used for the implementation of the system.

---

### Solar Cell Silicon: Production and Recycling: Session I

Sponsored by: The Minerals, Metals and Materials Society, TMS Extraction and Processing Division, TMS Light Metals Division, TMS: Recycling and Environmental Technologies Committee  
Program Organizer: Anne Kvithyld, SINTEF

Wednesday AM

Room: 3004

February 18, 2009

Location: Moscone West Convention Center

Session Chair: Anne Kvithyld, SINTEF

---

8:30 AM

**Generation of Lustrous Carbon for Silicon Production:** Valery Bogomolov<sup>1</sup>; Alexey Kozhan<sup>1</sup>; *Vladyslav Sokolov*<sup>1</sup>; Boris Bondarenko<sup>1</sup>; <sup>1</sup>Gas Institute NASU

The obvious way for increasing of efficiency of the solar grade Si production is lowering the amount of detrimental admixtures in its feedstock. The high purity raw materials should be applied in the charge to be smelted in reduction conditions. A unit for production of the correspondent semi-finished product has been designed, manufactured and put into operation. The applied novel technology is based on high temperature electro-thermal method of generation



of lustrous carbon on the surface of silica fines. The silica reduction process should be facilitated in comparison with application of more traditional carbon black in terms of more intimate contact between the reacting matters in the charge. Very promising results were got earlier in production of silicon carbide by the technology. The current productivity of the unit is 35 kg silicon in semi-finished product per hour. The options for its increase are discussed.

## 8:55 AM

**Settling of Particles in Molten Silicon before Directional Casting of a Solar Grade Silicon Ingot:** *Arjan Cifjja*<sup>1</sup>; Eivind Øvrelid<sup>2</sup>; Merete Tangstad<sup>1</sup>; Thorvald Engh<sup>1</sup>; <sup>1</sup>Norwegian University of Science & Technology; <sup>2</sup>Sintef – Materials and Chemistry

Due to shortage of SoG-Si feedstock in the recent years, there has been a lot of effort to find alternative routes for the manufacturing of SoG-Si for solar cells. The development of cheaper processes for the production of SoG-Si has been subject of recent research worldwide. In this work, settling of inclusions in molten silicon is investigated. The material used is multi-crystalline silicon produced from a metallurgical route named Sunsilc. A 12kg directional-crystallisation furnace is used to cast metallurgical grade silicon with an addition settling step. The idea is to let SiC particles settle and then cast the ingot. Samples from the cast multi-crystalline silicon ingots are investigated by light microscope. The results show that the majority of particles remain at a depth of 2mm from the bottom of the cast ingot. The rest of inclusions are found along the whole height of the ingot but at much lower concentrations.

## 9:20 AM

**Effects of Some Conditions on Si Growth from Si-Al Melts:** *Yuuki Nishi*<sup>1</sup>; Kazuki Morita<sup>1</sup>; <sup>1</sup>University of Tokyo

In order to develop a new silicon refining process for solar cells, "solidification refining of silicon with Si-Al melt at low temperature" has been investigated in our research group. This process was considered to be more effective than conventional solidification refining from thermodynamic prediction. However, refined Si with needle-like shape was highly dispersed in a directional solidification refining and a bulk Si crystal could hardly be obtained. In this study, the solidification conditions to obtain bulk Si crystal were investigated. The shape variation of the interface between Si and Si-Al melt was observed with various temperature gradients and cooling rates. Bulk Si crystal was found to be obtained under the condition when the flat interface was observed. For better understanding of the Si growth condition, zone melting growth was also carried out and the condition to obtain facet Si growth was discussed.

## 9:45 AM

**Refining of Silicon by Directional Solidification:** *Eivind Øvrelid*<sup>1</sup>; Mari Juel<sup>1</sup>; Benjamin Tuffour<sup>2</sup>; Martin Bellman<sup>2</sup>; <sup>1</sup>Sintef; <sup>2</sup>NTNU

In all new processes for upgrading of metallurgical feedstock to solar grade, directional solidification is used as the last step to remove the last traces of impurities. In this work we have investigated the possibility to optimize the refining efficiency by modification of the fluid flow pattern by the Accelerating Crucible Rotation Technique (ACRT). We have made experiments in a furnace for directional solidification with and without ACRT, and characterised the material. Numerical modelling has been used to support the experiments. We have seen that the rotation gives a positive effect on the refining and we believe the results can be used to optimize industrial systems.

## 10:10 AM Break

## 10:20 AM

**Simulation of Silicon Casting Process for Photovoltaic (PV) Application:** Bei Wu<sup>1</sup>; *Sam Scott*<sup>2</sup>; Nathan Stoddard<sup>1</sup>; Roger Clark<sup>1</sup>; Adi Sholapurwalla<sup>2</sup>; <sup>1</sup>BP Solar; <sup>2</sup>ESI Group NA

Multicrystalline silicon ingot casting is widely used in Photovoltaic industry due to its feedstock tolerance, low cost, simple processes and equipment and high throughputs. To achieve high solar cell efficiency, crystal defects must be minimized and grain structure must be controlled. These crystal qualities strongly depend on temperature gradient and thermal history during casting processes. In order to better understand the casting process, numerical simulation is used to predict the temperature distributions and resulting crystal structure under different growth processes. Direct Solidification System (DSS), a common casting process in the solar industry, will be simulated using ProCAST, a commercial software primarily used for metal casting simulation. The software may be adapted to simulate the transient temperature field of the DSS station and the solidification process, including grain growth. The simulation results focus

on the effects of insulation movement on crystallization initiation and grain structure with comparisons to cast silicon ingots.

## 10:45 AM

**The Removal Rate of Phosphorus from Molten Silicon:** *Takayuki Kemmotsu*<sup>1</sup>; Hisao Kimura<sup>1</sup>; Takashi Nagai<sup>1</sup>; Masafumi Maeda<sup>1</sup>; <sup>1</sup>The University of Tokyo

The production of solar cell is increasing rapidly and the shortage of silicon for solar cell becomes a serious problem. Developing a low-cost production process for solar grade silicon is required. An electron beam remelting technique under high vacuum is known to be effective for the removal of phosphorus from silicon. In this process, phosphorus can be removed preferentially from molten silicon because the vapor pressure of phosphorus is higher than that of silicon. However, the removal rate of phosphorus from silicon is not sufficient in this process. In this research, a more efficient removal process of phosphorus from silicon by an electron beam remelting technique was studied. Experiments showed that the removal rate of phosphorus from silicon increased with electron beam power. This indicated that raising temperature of molten silicon was effective for high-rate purification.

## Structural Materials Division Symposium: Advanced Characterization and Modeling of Phase Transformations in Metals in Honor of David N. Seidman on his 70th Birthday: Kinetics of Phase Transformations II

Sponsored by: The Minerals, Metals and Materials Society, TMS Structural Materials Division, TMS: Advanced Characterization, Testing, and Simulation Committee, TMS: Chemistry and Physics of Materials Committee

Program Organizers: Robert Averback, University of Illinois, Urbana-Champaign; Mark Asla, University of California, Davis; David Dunand, Northwestern University; Ian Robertson, University of Illinois at Urbana-Champaign; Stephen Foiles, Sandia National Laboratories

Wednesday AM

Room: 3000

February 18, 2009

Location: Moscone West Convention Center

*Session Chair:* Robert Averback, University of Illinois

## 8:30 AM Invited

**Effect of Rare-Earth Elements Additions on Microstructure and Mechanical Properties of Al-Sc Alloys:** *David Dunand*<sup>1</sup>; Matt Krug<sup>1</sup>; Alexandra Werber<sup>2</sup>; Marsha van Dalen<sup>3</sup>; Richard Karnesky<sup>4</sup>; David Seidman<sup>1</sup>; <sup>1</sup>Northwestern University; <sup>2</sup>Stuttgart University; <sup>3</sup>Momentive Performance Materials; <sup>4</sup>Sandia National Laboratories

Al-Sc alloys display a high number density of nanosize Al<sub>3</sub>Sc precipitates which are coherent with the Al matrix. Al-Sc-RE alloys (where RE is one of ten rare-earth elements: Y, Sm, Gd, Tb, Dy, Ho, Er, Tm, Yb or Lu) were studied by local-electrode atom-probe (LEAP) tomography. All RE segregate to the core of the Al<sub>3</sub>(Sc,RE) precipitates and some RE accelerate the kinetics of precipitation. The precipitate sizes and composition profiles are studied as a function of aging time at 300 °C and correlated with mechanical properties at ambient and elevated temperature. RE replacement of Sc, which reduces the cost of the alloys, does not increase their hardness, since the Orowan mechanism of precipitate bypass by dislocations is controlling strength at ambient temperature. RE replacement of Sc however improves creep resistance, which is explained by the increased matrix/precipitate lattice mismatch resulting in enhanced elastic interactions with matrix dislocations.

## 9:00 AM

**Investigation of Alloying Effects on the Kinetics of Ni<sub>3</sub>Cr Formation in Nickel-Chromium Alloys:** George Young<sup>1</sup>; Reza Najafabadi<sup>1</sup>; James Vollmer<sup>1</sup>; Steven Attanasio<sup>1</sup>; *Julie Tucker*<sup>1</sup>; Mikael Christensen<sup>2</sup>; Walter Wolf<sup>2</sup>; Erich Wimmer<sup>2</sup>; <sup>1</sup>Lockheed Martin; <sup>2</sup>Materials Design

Isothermal aging experiments and first principles modeling were used to better understand the effects of alloying elements on the tendency of nickel-chromium alloys to undergo long range ordering (i.e., Ni<sub>3</sub>Cr formation). Ordering is a concern in engineering alloys because it can increase residual stresses, lower the toughness, and degrade environmentally assisted cracking resistance. Long range order in both model and commercially produced alloys was assessed via

heat treatments at 475°C for times between 100 and 10,000 hours. The degree of ordering was quantified via lattice parameter contraction as determined by x-ray diffraction. Furthermore, the intrinsic effects of iron, niobium, and molybdenum on the stability of the Ni<sub>2</sub>Cr structure were investigated via density functional theory. These results are used to assess the tendency for ordering in high chromium nickel-based alloys and to develop strategies to mitigate long range order.

#### 9:15 AM

**Atom-Probe Tomography in Materials Design:** *Jason Sebastian*<sup>1</sup>; Gregory Atom<sup>2</sup>; <sup>1</sup>QuesTek Innovations, LLC; <sup>2</sup>Northwestern University

In honor of Prof. Seidman's birthday, we present a review of the role of atom probe tomography (APT) in materials design. Research efforts at Northwestern University and alloy development work at QuesTek Innovations have relied heavily on the ability of atom probe tomography to answer questions about the nanoscale structure and chemistry of engineering materials. Topics to be presented include the design of high strength intermetallic- and carbide-strengthened steels (including QuesTek's Ferrium@S53 corrosion resistant high strength landing gear steel), Ni superalloy design, aluminum alloy design, and high strength copper alloy design (QuesTek's Cuprium™ alloys). In all cases, APT allows for validation of important model predictions including phase compositions (as predicted by CALPHAD techniques), precipitate morphologies and size/spatial distributions, and segregation phenomena. Overall trajectories of nanoscale precipitate evolution under equilibrium and non-equilibrium conditions can be investigated experimentally via APT, and compared to model predictions.

#### 9:35 AM

**Phase Transformations in Pulsed Laser Deposited (PLD) FePd Thin Films:** *Andreas Kulovits*<sup>1</sup>; John Leonard<sup>1</sup>; Jorg Wiezorek<sup>1</sup>; <sup>1</sup>University of Pittsburgh

We study the complex phase transformation behavior of off-stoichiometric Fe-rich and stoichiometric metastable FCC solid solution g-(Fe,Pd) and amorphous Fe-Pd thin films fabricated by pulsed laser deposition (PLD) on crystalline and amorphous substrates. We thoroughly characterized the microstructures of the as deposited films on the nanoscale using transmission electron microscopy (TEM) and X-ray diffraction (XRD). Upon equilibration the metastable FePd thin films undergo various different solid-state phase transformations, including crystallization, disorder-order transformation and phase separation reactions. We investigated solid-state transformation induced microstructural changes in grain size, morphology and local misorientation using HREM and TEM and changes in global texture using XRD after ex situ heat treatments. Furthermore we conducted in-situ heating TEM experiments to directly observe phase transformation sequences for the different metastable starting conditions.

#### 9:50 AM Break

#### 10:10 AM Invited

**Dynamic Transmission Electron Microscope: Studying Nanoscale Material Processes with Nanosecond Time Resolution:** *Thomas LaGrange*<sup>1</sup>; Geoffrey Campbell<sup>1</sup>; Bryan Reed<sup>1</sup>; Nigel Browning<sup>1</sup>; Judy Kim<sup>1</sup>; Mitra Taheri<sup>2</sup>; James Evans<sup>1</sup>; Wayne King<sup>1</sup>; <sup>1</sup>Lawrence Livermore National Laboratory; <sup>2</sup>Drexel University

There have been many efforts in the past decades to improve the spatial resolution of transmission electron microscopes but little in way of improving the temporal resolution of in situ transmission electron microscopy. Most materials dynamics occur at rates much faster than can be captured with standard video rate acquisition methods. Thus, there is a need to increase temporal resolution in order to capture and understand salient features of these rapid materials processes. To meet the need for studying fast dynamics in material processes, we have constructed a nanosecond dynamic transmission electron microscope (DTEM) at Lawrence Livermore National Laboratory to improve the temporal resolution of in-situ TEM observations. The DTEM consists of a modified JEOL 2000FX transmission electron microscope that provides access for two pulsed laser beams. One laser drives the photocathode (which replaces the standard thermionic cathode) to produce the brief electron pulse. The other strikes the sample, initiating the process to be studied. A series of pump-probe experiments with varying time delays enable, for example, the reconstruction of the typical sequence of events occurring during the rapid phase transformation. This presentation will discuss the core aspects of the DTEM instrument and how the DTEM has been used to study rapid solid-state phase transformations and chemical reactions. Work was performed under the auspices of the U.S. Department of Energy by the Lawrence Livermore National Laboratory and

supported by the Office of Science, Office of Basic Energy Sciences, Division of Materials Sciences and Engineering, of the U.S. Department of Energy under contract No. DE-AC52-07NA27344.

#### 10:40 AM

**Precipitation of Nano-Sized Nitrides in Nitrided Low-Alloy Steels:** *Tadashi Furuhashi*<sup>1</sup>; Yuusaku Tomio<sup>1</sup>; Keiichiro Oh-ishi<sup>2</sup>; Kazuhiro Hono<sup>2</sup>; Goro Miyamoto<sup>1</sup>; <sup>1</sup>Tohoku University; <sup>2</sup>National Institute for Materials Science

Nitriding becomes more important as a surface hardening heat treatment in wear resistant steels. High surface hardness is achieved by adding nitride-forming alloying elements because precipitation of fine alloy nitrides occurs. During nitriding, various kinds of metastable and stable nitrides precipitate depending upon alloying elements added. In this presentation, precipitation behavior of alloy nitrides during plasma nitriding of Fe-M(-C) alloys is described. Particularly, results of phase identification of nitrides and quantification of particle distribution made experimentally by means of advanced characterization methods, such as HRTEM, EFTEM and 3DAP, are shown.

#### 10:55 AM

**Segregation of W at  $\gamma'$  (L12) /  $\gamma$  (f.c.c.) Interfaces in a Ni-Based Superalloy: An Atom-Probe Tomographic and First-Principles Study:** *Yaron Amoyal*<sup>1</sup>; Zungang Mao<sup>1</sup>; David Seidman<sup>1</sup>; <sup>1</sup>Northwestern University

Owing to their excellent mechanical behavior at high temperatures, Ni-based superalloys are utilized for turbine blades in aeronautical jet engines and land-based electricity generators, which are the most technologically-advanced energy conversion devices. Investigating the heterophase interfaces (HIs) of these alloys is essential for improving their high-temperature performances.  $\gamma'$  (L12) /  $\gamma$  (f.c.c.) HIs in a Ni-based superalloy are investigated using atom-probe tomography and first-principles calculations. {100} interfaces exhibit a Gibbsian interfacial excess of tungsten,  $\Gamma_w = 1.2 \pm 0.2 \text{ nm}^{-2}$ , corresponding to a 5 mJ/m<sup>2</sup> decrease in interfacial energy. First-principles calculations for a W-alloyed Ni-Al system with a {100} HI have a similar decrease in interfacial energy when a W atom is placed as close as 1-3 atomic planes from it. Conversely, no measurable segregation of W is detected at general HIs. Indeed, similar calculations for {110} and {111} HIs predict an increase of 1 and 9 mJ/m<sup>2</sup> in their energies, respectively.

#### 11:10 AM

**Structure and Composition of  $\gamma/\gamma'$  Interfaces in the Ni-Base Superalloy Rene88DT:** *Srinivasan Rajagopalan*<sup>1</sup>; Rajarshi Banerjee<sup>2</sup>; Gopal Viswanathan<sup>1</sup>; Junyeon Hwang<sup>2</sup>; Soumya Nag<sup>2</sup>; Jaimie Tiley<sup>3</sup>; Dennis Dimiduk<sup>3</sup>; Hamish Fraser<sup>1</sup>; <sup>1</sup>The Ohio State University; <sup>2</sup>University of North Texas; <sup>3</sup>Air Force Research Laboratory

The interfacial structure and composition in Ni-base superalloys can play a substantial role in determining several physical and mechanical properties. Of primary interest are the order-disorder transition, and the overall compositional transition from from the  $\gamma'$  to the  $\gamma$  phase. Using techniques such as aberration-corrected High Resolution Scanning Transmission Electron Microscopy (HRSTEM) and 3-Dimensional Atom Probe (3DAP) Tomography, this structural and compositional transition across the interface has been investigated at atomic resolution. Additionally, the effect of factors such as cooling rate (from a supersolvus annealing treatment) and aging time on the structural and compositional parameters affecting the interface are explored. Comparisons with atomistics-based modeling and implications for materials properties will be discussed.

#### 11:25 AM

**The Micromechanisms of Heterogeneous Phase Formation in Ti-Mo Alloys:** *Robert Williams*<sup>1</sup>; Peter Collins<sup>1</sup>; Gopal Viswanathan<sup>1</sup>; Rajarshi Banerjee<sup>2</sup>; Srinivasan Rajagopalan<sup>1</sup>; Hamish Fraser<sup>1</sup>; <sup>1</sup>The Ohio State University; <sup>2</sup>University of North Texas

Ti-Mo alloys constitute an ideal model binary monotectoid system, providing the opportunity to gain insights into several microstructural processes that can be translated to the more complex  $\beta$ -Ti alloys. This study focuses on the observation and rationalization of key phase transformations in Ti-Mo alloys of varying compositions (8-18 wt% Mo). Of particular interest are the formation and growth of the  $\omega$  phase, and the compositional dependence of the mechanics of  $\alpha$ -phase nucleation. Employing techniques such as HRTEM, HRSTEM and EELS in an aberration corrected microscope, an attempt is made to capture the initial and later stages of phase formation and growth. Finally, an attempt is made

to rationalize the nucleation of  $\alpha$ -phase in Ti-Mo alloys, and extend applicability of the rationale to other  $\beta$ -Ti alloy systems.

**11:40 AM**

**The Temporal Evolution of the Nanostructures of a Low-Supersaturation Ni-Al-Cr Superalloy:** *Christopher Booth-Morrison*<sup>1</sup>; *Yang Zhou*<sup>1</sup>; *Zugang Mao*<sup>1</sup>; *Ronald Noebe*<sup>2</sup>; *David Seidman*<sup>1</sup>; <sup>1</sup>Northwestern University; <sup>2</sup>NASA Glenn Research Center

The early stages of phase decomposition of a low-supersaturation Ni-6.5 Al-9.5 Cr at.% alloy, via the formation of coherent  $\gamma'(L1_2)$ -precipitates from the  $\gamma$ -matrix, are studied by atom-probe tomography. The  $\gamma'$ -precipitate morphologies, radii, volume fractions, number densities, and interprecipitate spacing are measured, providing a complete description of the nanostructure during aging at 873 K. Additionally, the composition profiles across the heterophase  $\gamma$ -matrix/ $\gamma'$ -precipitate interfaces are quantified, providing information about elemental partitioning and the interfacial width. Experimental results are compared with the predictions of classical nucleation, growth and coarsening models, and are found to differ from these mean-field descriptions. The temporal evolution of the  $\gamma'$ -precipitate average radii and the  $\gamma$ -matrix supersaturations, however, follow the predictions of classical coarsening models. APT results are complemented by computational modeling employing Grand Canonical and Lattice Kinetic Monte Carlo simulation, and Thermo-Calc, DICTRA and PrecipiCalc, to elucidate the kinetic pathways that lead to phase decomposition in this alloy.

**11:55 AM**

**Dependence of Deformation Induced Martensitic Transformation on Crystallographic Orientation in a Metastable Austenitic Stainless Steel:** *Jongbae Jeon*<sup>1</sup>; *Young Won Chang*<sup>1</sup>; <sup>1</sup>Pohang University of Science & Technology

Deformation induced martensitic transformation (DIMIT) has been reported to depend on the amount of plastic strain, strain rate, chemical composition, and loading temperature. The strain distribution during plastic deformation is, however, inherently inhomogeneous due to different crystallographic orientation of each grain, so that each grain should exhibit different transformation behavior. It is therefore attempted in the present study to investigate the effects of crystallographic orientation on the DIMIT behavior in a meta-stable austenitic stainless steel by means of an in-situ electron backscattered diffraction (EBSD) technique. The early stage of nucleation and growth of martensite phase induced by plastic deformation can be observed semi-directly from this in-situ EBSD method. Metastable austenite grains having the preferable crystallographic orientations for DIMIT is more likely to nucleate first and grow into martensite phase. The nucleation sites are observed to be the intersections of thin shear bands e.g. localized dislocation bands, twins, or epsilon (HCP) bands.

---

## Surface Structures at Multiple Length Scales: Bio Coatings and Nanoscale Characterization

Sponsored by: The Minerals, Metals and Materials Society, TMS Materials Processing and Manufacturing Division, TMS: Surface Engineering Committee  
Program Organizers: Arvind Agarwal, Florida International University; Sudipta Seal, University of Central Florida; Yang-Tse Cheng, University of Kentucky; Narendra Dahotre, University of Tennessee; Graham McCartney, University of Nottingham

Wednesday AM  
February 18, 2009

Room: 3011  
Location: Moscone West Convention Center

Session Chair: To Be Announced

**8:30 AM Invited**

**Nanoindentation of Biomaterials - The Evolution of Soft Material Testing:** *Michelle Dickinson*<sup>1</sup>; <sup>1</sup>Hysitron Inc.

Nanoindentation is an established method for obtaining the nanomechanical properties such as hardness and modulus of traditional, elastic-plastic homogenous materials. Recently, the technique has moved into the biological field, which has created new challenges due to their inherent viscoelastic behavior and stringent environmental requirements. As biomaterials research progresses into smaller scale structures, new challenges such as time dependent analysis, heterogeneity and hydration become important considerations. Following a brief introduction on elastic-plastic indentation, the current paper reviews new techniques available

for indentation analysis of viscoelastic and other non-standard materials. Recent works from nanoindentation of highly diverse biomaterials ranging from thin protein films, individual cells and insect exoskeletons to teeth, bones and replacement devices will be given with a discussion on the challenges and models used for each.

**9:00 AM**

**Bioactivity and Biocompatibility of Laser Textured Ca-P Coatings for Hard Tissue Replacement:** *Sameer Paital*<sup>1</sup>; *Narendra Dahotre*<sup>1</sup>; <sup>1</sup>University of Tennessee

As the interaction between the cells and tissues with biomaterials at the tissue implant interface is a surface phenomenon, surface engineered biomaterials aimed at modifying the surface properties while still maintaining the bulk properties of the implant are the design of current interest. In the present work a novel laser based direct writing technique is being explored to synthesize Ca-P coatings on Ti-6Al-4V substrate. Four samples with distinct patterned surfaces were obtained from two varying laser power conditions. Bioactivity of the coated samples was proved by the formation of an apatite like layer following immersion in SBF. Adhesion and proliferation of fibroblast and osteoblast like cells cultured on the coated samples further proved its biocompatibility. Elemental and phase analysis of the coated samples were studied by using both XRD and EDS. SEM and CLSM microscopy was used to study the morphology and focal contacts of the cell cultured samples.

**9:20 AM**

**Interaction of Proteins with Primary Packaging Containers:** *Rajendra Redkar*<sup>1</sup>; <sup>1</sup>SCHOTT North America, Inc.

Advances in the biotechnology industry have resulted in increased development of therapeutic protein drugs. Although Type I glass is the standard primary packaging container, the role played by the primary packaging material in destabilizing drug is not clearly understood. SCHOTT is interested in understanding the contribution of glass in inducing physical instabilities. A series of experiments involving treatment of glass vials to different buffers and other pharmaceutically relevant treatments were employed to evaluate how structural modifications can affect protein adsorption and aggregation over a period of time. In addition, the role of charge on the protein and surface charge on protein adsorption/aggregation will be presented. For syringes, the role of silicone oil in inducing protein aggregation and alternatives to the silicone oil, i.e. silicone-free lubricant system will be discussed. Finally, SCHOTT's approaches in mitigating other critical problems faced by the pharmaceutical industry through surface modifications will be presented.

**9:40 AM Break**

**9:50 AM Invited**

**Laser Processing of Microstructured and Nanostructured Biomaterials:** *Roger Narayan*<sup>1</sup>; <sup>1</sup>University of North Carolina - and - North Carolina State University

Lasers may serve to create novel medical devices with unique biological functionalities. For example, lasers offer a unique opportunity for microscale and nanoscale processing of biomaterials. We have recently developed microstructured and nanostructured biomaterials with unique biological functionalities using pulsed laser deposition, laser direct writing, and stereolithography processes. Laser processing of nanocomposite thin films, tissue substitutes, microstructured medical devices, and nanostructured medical devices will be discussed.

**10:20 AM**

**Corrosion Control by Plant-Derived Agents in Silicone Coatings on Mild Steel Exposed to Seawater:** *Sandy Tran*<sup>1</sup>; *James Earthman*<sup>1</sup>; <sup>1</sup>University of California, Irvine

Protective coatings are typically applied to improve corrosive and fouling resistance but often do not satisfactorily prevent localized corrosion. Immersion testing with nicotine and caffeine in simulated seawater solution was performed to evaluate the potential effectiveness of common plant-derived alkaloids for controlling corrosion. Relative to a control sample of mild steel, the most favorable results indicate that mild steel coated with silicone and exposed to seawater containing nicotine exhibit corrosion rates that are roughly 10-fold smaller than that for the same silicone coating in unaltered seawater. Coatings containing 4% and 10% wt. nicotine resulted in lower reductions in corrosion rate by comparison which was attributed to the effect of nicotine on the ability of the coating to adhere to the steel substrate. Similarly, seawater containing 1%



wt. caffeine in solution resulted in a reduction in corrosion rate by a factor of approximately 14 for samples coated with silicone.

### 10:40 AM Invited

**Quantitative Deformation Tests inside TEM:** Z. W. Shan<sup>1</sup>; A. Minor<sup>2</sup>; S. A. Syed Asif<sup>1</sup>; O. Warren<sup>1</sup>; <sup>1</sup>Hysitron Inc.; <sup>2</sup>Lawrence Berkeley National Laboratory and University of California, Berkeley

We report the current progress in the application of a unique TEM apparatus that enables to build a one-to-one relationship between the mechanical data and the evolving microstructure of the probed materials with a time resolution same as that of the recorded movies. For the indentation tests on submicron-sized Al grains, we found that even noise-level-force can nucleate dislocations from perfect Al grains and theoretical-level-stress can be achieved in grains with high density defects (Minor et al, Nat. Mat., 2006). Most recently, this device was used to perform compression tests on Ni pillars containing large amount initial defects. Surprisingly, the defects density was reduced dramatically upon the applied stress and in some cases, even resulted in a defect-free crystal. This phenomenon, termed as "mechanical annealing", can find its general application in interpreting the unusual mechanical behaviors that accompany the micro- and nano- structured crystals (Shan et al, Nat. Mat., 2008).

## Synergies of Computational and Experimental Materials Science: Synergies in Integrated Computational Materials Engineering

Sponsored by: The Minerals, Metals and Materials Society, TMS Materials Processing and Manufacturing Division, TMS/ASM: Computational Materials Science and Engineering Committee

Program Organizers: Katsuyo Thornton, University of Michigan; Henning Poulsen, Risoe National Laboratory; Mei Li, Ford Motor Co

Wednesday AM                      Room: 3003  
February 18, 2009                      Location: Moscone West Convention Center

Session Chairs: Mei Li, Ford Motor Co; Baicheng Liu, Tsinghua University

### 8:30 AM Invited

**The Importance of Experiments in Integrated Computational Materials Engineering (ICME):** John Allison<sup>1</sup>; <sup>1</sup>Ford Motor Company

Integrated Computational Materials Engineering (ICME) is the integration of materials information, captured in computational tools, with engineering product performance analysis and manufacturing-process simulation. While computational models provide the basic means of capturing and delivering quantitative processing-structure-property relationships to the engineering community, much of this knowledge relies critically on comprehensive experimental results. Despite important theoretical advances, processing-structure-property relationships are sufficiently complex and phenomenological that experiments are central to the development and calibration of these models and for filling information gaps in situations where theoretical models are not available. Experiments are also important for model validation. Virtual Aluminum Castings is an ICME method developed at Ford to improve the development process in the design of cast aluminum powertrain components. This talk will provide examples of the importance of a strong synergy between experiments and modeling in the development of Virtual Aluminum Castings.

### 9:00 AM Invited

**An Integrated Multiscale Model for the Prediction of the Fatigue Life of Cast A356 Components as a Function of Solidification Microstructures:** Peter Lee<sup>1</sup>; Pavel Ramirez Lopez<sup>1</sup>; Trevor Lindley<sup>1</sup>; Junsheng Wang<sup>1</sup>; <sup>1</sup>Imperial College

A multiscale, through process model is developed to predict the impact of using high Fe-content secondary A356 alloy on the fatigue life of safety critical automotive components. The formation of Fe-rich intermetallics and microporosity is determined as a function of casting conditions and alloy composition at microstructural level in Al-Si-Mg alloys due to increased recycled scrap content. The final fatigue life is predicted by integrating the microstructural prediction into a macroscopic model of the casting, machining and final service of an automotive component. A second microstructural model was used to relate the maximum pore and intermetallic size, as well as stress state, to final fatigue life.

In situ x-ray radiography experiments using synchrotron and laboratory sources were performed to quantify the nucleation and growth kinetics of the different microstructural features to inform and validate the models. The resulting living predictions showed good correlation to experimental measurements.

### 9:30 AM

**Developing Local Mechanical Property Model for A319-Type Aluminum Alloys through Integrated Computational Materials Engineering (ICME) Approach:** Mei Li<sup>1</sup>; Ruijie Zhang<sup>1</sup>; John Allison<sup>1</sup>; <sup>1</sup>Ford Motor Co.

In recent years, aluminum alloys have been increasingly used in automotive industry to replace cast iron for powertrain applications to reduce weight and emission. To provide high-quality blocks and heads at the lowest possible cost, products and manufacturing methods need to be developed and implemented in record time. The use of robust computational models in up-front analysis has proven to play an increasingly important role. This talk describes an ICME approach to develop local yield strength model for A319-type alloys which captures the influence of the manufacturing process history. The local yield strength model links a micro-model for solidification microstructures, a 3D phase field model for precipitation evolution morphology and kinetics and a micromechanical model for precipitation strengthening. The developed model was applied to a v6 engine block and the predicted local yield strength shows good agreement with the experimental measurement.

### 9:50 AM

**Optimizing Aluminum Alloys for Multiple Objectives by Combining an Optimization Algorithm and FactSage Software:** George Dulikravich<sup>1</sup>; Marcelo Colaco<sup>2</sup>; Carlos Velez<sup>1</sup>; <sup>1</sup>Florida International University; <sup>2</sup>Military Institute of Engineering (IME)

A novel concept of simultaneous optimization of several properties of aluminum alloys was developed and demonstrated. The method utilizes a commercially available software FactSage capable of predicting multiple alloy properties when provided with concentrations of each of the alloying elements. This alloy design method also utilizes a multi-objective evolutionary optimization algorithm that simultaneously extremizes several properties of the alloy. In order to accelerate the alloy design optimization process, an accurate and robust multi-dimensional response surface algorithm based on polynomial radial basis functions was utilized. The entire concept was successfully proven by the authors on H-type steels, Ni-based superalloys, Ti-based alloys and Hf-based bulk metallic glasses during the past six years. This paper presents an application of this design optimization methodology to Al-based alloys. Dulikravich and Egorov-Yegorov: Chemical Composition Design of Superalloys for Maximum Stress, Temperature and Time-to-Rupture Using Self-Adapting Response Surface Optimization. Materials and Manufacturing Processes. 20 (3) 2005, 569-590.

### 10:10 AM Break

### 10:30 AM Invited

**Developing Micromechanism-Based Models to Assist in Alloy Design through an Integrated Experimental and Simulation Approach:** Ning Zhou<sup>1</sup>; Chen Shen<sup>2</sup>; Ju Li<sup>3</sup>; Michael Mills<sup>1</sup>; Yunzhi Wang<sup>1</sup>; <sup>1</sup>Ohio State University; <sup>2</sup>GE Global Research; <sup>3</sup>University of Pennsylvania

To develop detailed understanding of dislocation-precipitate interactions in multi-phase alloys and to incorporate the most relevant deformation mechanisms in materials models, we have adopted an approach that integrates advanced experimental characterization with multi-scale computer simulations. Using Ni-base superalloys as examples we demonstrate (a) how computer simulations have helped in resolving a long-standing issue concerning the mechanisms of rafting in blade alloys and (b) how experimental characterizations have motivated and focused simulation studies of deformation mechanisms in disk alloys. In the former, defect-level simulations assisted in identifying the dominant mechanisms, upon which a micrometer-scale model was developed that makes quantitative predictions of rafting kinetics and the corresponding creep deformation at experimentally relevant length and time scales. In the latter, the activation energies associated with each individual deformation mechanisms suggested by experiment were calculated using a combination of ab initio informed microscopic phase field model and NEB method.

## 11:00 AM Invited

**Solder Joint Lifetime Prediction via a Combined Experimental and Computational Approach:** Michael Neilsen<sup>1</sup>; Paul Vianco<sup>1</sup>; *Elizabeth Holm*<sup>1</sup>; <sup>1</sup>Sandia National Laboratories

Because solders operate at high homologous temperatures, microstructural evolution, cracking, and failure can occur during service. Since circuit boards must function reliably for thousands of thermal cycles in applications such as aircraft and satellites, lifetime prediction is critical for product design and maintenance. We have developed a combined experimental and computational approach to predict both aging (crack initiation) and failure (open circuit) during thermomechanical cycling of lead-tin solder joints. A unified creep plasticity model, which includes contributions from microstructural parameters, predicts failure initiation during thermomechanical fatigue for a variety of solder joint geometries; in a blind study, model results are in excellent agreement with experimental observations of cycles to crack initiation. By adding element death to the model, crack propagation was captured over several thousand fatigue cycles; both crack location and morphology are in agreement with experiments. At each step, experiments inform and benefit from model predictions.

## 11:30 AM Invited

**Macro and Micro Modeling of Conventional and Unidirectionally Solidified Investment Castings:** Dong Pan<sup>1</sup>; Qingyan Xu<sup>1</sup>; Jing Yu<sup>1</sup>; *Baicheng Liu*<sup>1</sup>; Akihiko Kimatsuka<sup>2</sup>; Yasunoi Kuroki<sup>2</sup>; Yuriko Saito<sup>2</sup>; <sup>1</sup>Tsinghua University; <sup>2</sup>Ishikawajima-Harima Heavy Industry Co. Ltd

An integrated model for the three dimensional simulation of the solidification process both for conventional and unidirectionally solidified investment castings was developed. It was applied to industries to investigate the temperature distribution and shrinkage porosity, and to predict the grain growth and grain structure of the shaped castings. A ray tracing method was used to deal with the complex heat radiation transfer, and the micro structure evolution was simulated based on MCA method. In addition, a layer-by-layer calculation method was developed to couple the macro and micro model together and to save large computation memory as well. Experiments for titanium alloy turbine wheel casting produced by conventional investment process and nickel-based superalloy turbine blade casting by unidirectional solidification process were carried out, and the cooling curves, shrinkage porosity and microstructure during solidification were compared with the simulated results. Finally, some further recommendations were proposed.

## 12:00 PM

**Genetic Computational Design of Novel High Strength Stainless Steels: Model Description and First Experimental Validation:** *Wei Xu*<sup>1</sup>; P.E.J. Rivera Diaz del Castillo<sup>2</sup>; Sybrand van der Zwaag<sup>2</sup>; <sup>1</sup>Materials Innovation Institute and Delft University of Technology, the Netherlands; <sup>2</sup>Faculty of Aerospace Engineering, Delft University of Technology

A computational alloy design approach for precipitation hardened stainless steels coupling thermodynamic and kinetic calculations with a genetic optimization algorithm is presented. The alloys are designed so as to display desired microstructures, which include controlled densities of fine precipitates resulting from optimized composition and heat treatment aimed at maximizing the precipitation strengthening contribution. Alloy systems leading to MX carbide and/or Cu, NiAl and Ni<sub>3</sub>Ti intermetallic precipitates while keeping undesirable phases and Cr depletion at a minimum level were favored. Four novel alloys were fabricated and subjected to several heat treatment scenarios. The microstructures and resulting mechanical properties were evaluated and compared to model predictions as well as those of existing alloys.

## Transformations under Extreme Conditions: A New Frontier in Materials: Solid-Solid Transformations and In Situ Diagnostics I

Sponsored by: The Minerals, Metals and Materials Society, ASM International, ASM Materials Science Critical Technology Sector, TMS Materials Processing and Manufacturing Division, TMS/ASM: Phase Transformations Committee  
Program Organizers: Vijay Vasudevan, University of Cincinnati; Mukul Kumar, Lawrence Livermore National Laboratory; Marc Meyers, University of California-San Diego; George "Rusty" Gray, Los Alamos National Laboratory; Dan Thoma, Los Alamos National Laboratory

Wednesday AM  
February 18, 2009

Room: 3001  
Location: Moscone West Convention Center

*Session Chairs:* Vijay Vasudevan, University of Cincinnati; James Belak, Lawrence Livermore National Laboratory

## 8:30 AM Invited

**The Shock Properties of Mild and Bainitic Steels - Phase Transformation and Strength:** *W.G. Proud*<sup>1</sup>; R.I. Hammond<sup>2</sup>; S.M. Walley<sup>1</sup>; D.J. Chapman<sup>1</sup>; <sup>1</sup>Fracture and Shock Physics Group, Cavendish Laboratory; <sup>2</sup>Fracture and Shock Physics Group, Cavendish Laboratory - and - currently at TWI Ltd.

Bainitic steels are ferrous alloys produced through the careful control of the cooling regime and are of potential interest in ballistic applications. An upper and a lower bainitic steel were studied. Whilst, superficially, the Hugoniot were found to be similar, the materials display important differences. The upper bainitic steel was recovered whole or in a few fragments, whilst the lower bainitic steel exhibited substantial brittle fracture. A further and interesting difference was that while the ferrite in the lower temperature Bainite underwent a pressure induced phase transition, the upper Bainite showed no evidence of such a transition. To study the transformation in detail, the lateral shock strength of the materials was measured. The gauges used required extensive protection in the region of the phase transition, a factor which affects the fidelity of the measurements. The properties of these alloys are compared with that of a well-characterised mild steel.

## 9:05 AM Invited

**Atomistic Calculations of Shock Induced Phase Transformations and the Mechanical Properties of the Shocked Material:** *Michael Baskes*<sup>1</sup>; <sup>1</sup>Los Alamos National Laboratory and University of California, San Diego

Shock waves in materials produce a number of interesting phenomena including phase transformations. This presentation will discuss calculations of this phenomenon at the atomic level using an embedded atom method potential for fcc Ni. Using standard flyer-plate geometry, molecular dynamics (MD) calculations at room temperature were performed. In summary: (1) the fcc crystal transforms to a bcc-like crystal structure just behind the shock front; (2) after a period of time, the bcc structure transforms to a layered hcp/fcc material; and (3) when the reflected shock wave traverses this material, the system mostly transforms back to fcc leaving twins and stacking faults (SFs) as the prominent defects. A small sample of the highly defective material was then tested using MD under a variety of loading conditions at high strain rate. The strength of the shocked material depends sensitively upon loading condition. The strengthening and weakening mechanisms will be discussed.

## 9:40 AM Invited

**Kinetics of the Shock-Induced  $\alpha$ - $\epsilon$  Phase Transition in Solid Iron:** *Timothy Germann*<sup>1</sup>; Kai Kadau<sup>1</sup>; Brad Holian<sup>1</sup>; <sup>1</sup>Los Alamos National Laboratory

Previously we have demonstrated that molecular dynamics (MD) simulations can provide unique insight into the atomic-scale mechanisms of shock-induced solid-solid phase transformations. In situ dynamic x-ray diffraction studies have shown excellent agreement with these simulations, for thin foils of single crystal iron subjected to laser shock. However, the rapid kinetics observed in these studies is orders of magnitude faster than that observed in traditional macroscopic shock experiments (e.g. gas gun), including recent experiments with single crystal targets as thin as 100  $\mu\text{m}$ . Moreover, these latter experiments indicate a three-wave structure, with bcc plasticity evident ahead of the phase transformation wave, unlike the smaller-scale MD simulations and laser-shock experiments. After reviewing this earlier work, we will present the results of a series of very-large-scale MD simulations of single crystal and polycrystal iron

samples (as long as 10  $\mu\text{m}$ ), subject to both shock and ramp wave loading, to explore these discrepancies.

#### 10:15 AM Break

#### 10:30 AM Invited

**Studying Dynamic Material Response under Dynamic Compression: The Intersection of Experiment and Simulation:** *Hector Lorenzana*<sup>1</sup>; Eduardo Bringa<sup>1</sup>; Bassem El-Dasher<sup>1</sup>; James Hawreliak<sup>1</sup>; Daniel Kalantar<sup>1</sup>; Giles Kimminau<sup>2</sup>; James McNaney<sup>1</sup>; Despina Milathianaki<sup>1</sup>; Warren MoberlyChan<sup>1</sup>; Babak Sadigh<sup>1</sup>; Michael Surh<sup>1</sup>; Damian Swift<sup>1</sup>; Anthony Van Buuren<sup>1</sup>; Justin Wark<sup>2</sup>; <sup>1</sup>Lawrence Livermore National Laboratory; <sup>2</sup>Oxford University

Understanding the dynamic lattice response of solids under extreme conditions of pressure, temperature and strain rate is a topic of broad scientific and technological interest. Critical to developing this understanding is the ability to probe and simulate the spatial and temporal evolution of phase transformations, material microstructure, and related properties at the characteristic timescale of the physical phenomena driving these processes—down to picoseconds. We will present studies exploiting new generation of bright and fast x-ray sources to investigate the real-time physical evolution of dynamically compressed materials. Specifically, we will discuss laser-based in situ x-ray diffraction measurements of phase transformations and lattice relaxation in single crystal and polycrystalline systems and results of post-processed large-scale molecular dynamics simulations that calculate physical observables and couple to experiment at similar temporal scale. This work performed under the auspices of the U.S. Department of Energy by Lawrence Livermore National Laboratory under Contract DE-AC52-07NA27344.

#### 11:05 AM

**Phase Transformation under Pressure: Studies Combined Synchrotron High Energy X-Ray Diffraction and 3D Microtomography Techniques:** *Luhong Wang*<sup>1</sup>; Haozhe Liu<sup>1</sup>; Xianghui Xiao<sup>2</sup>; Peter Lee<sup>2</sup>; <sup>1</sup>Harbin Institute of Technology; <sup>2</sup>Argonne National Laboratory

Application of new high-pressure synchrotron diamond anvil cell microtomography and high energy x-ray diffraction techniques has uncovered unexpected dynamics and volume expansion associated with pressure-induced crystallization of amorphous Se. The unusual volume expansion phenomenon under pressure associated with the recrystallization of 'over-pressurization' of a metastable phase may be more common than previously believed. Moreover, tuning relative densities and energetics of phases in this way may provide a new route for creating new structures from highly metastable states. Finally, the new microtomographic technique developed here could find widespread use in accurate determinations of the equation of state of glasses and melts up to megabar pressures, which is crucial to many problems in earth and materials sciences. The results demonstrate the importance of using new time- and spatially- resolved high-pressure x-ray diffraction and imaging techniques to understand the kinetics of structural transformations in materials under extreme conditions far from equilibrium.

#### 11:25 AM

**Measuring Plastic Response of Materials during Shock Compression Using In-Situ X-Ray Diffraction:** *James Hawreliak*<sup>1</sup>; Bassem El-Dasher<sup>1</sup>; Andrew Higginbotham<sup>2</sup>; Giles Kimminau<sup>2</sup>; James McNaney<sup>1</sup>; Despina Milathianaki<sup>3</sup>; William Murphy<sup>2</sup>; Damian Swift<sup>1</sup>; Justin Wark<sup>2</sup>; Hector Lorenzana<sup>1</sup>; <sup>1</sup>LLNL; <sup>2</sup>University of Oxford; <sup>3</sup>University of Texas

The relaxation of a material from a uniaxially compressed state to a more hydrostatic state during shock compression through the generation and propagation of defects is a scientifically rich but relatively unexplored area of material science. Using in-situ x-ray diffraction to probe during the shock compression gives the ability to look at the lattice relaxation during shock compression. We discuss in-situ probing techniques and recent results looking at the plastic response of single and poly crystalline iron shock at pressure around the alpha to epsilon phase transition. This work performed under the auspices of the U.S. Department of Energy by Lawrence Livermore National Laboratory under Contract DE-AC52-07NA27344.

#### 11:45 AM Invited

**Prospects for Validation of Crystal Level Phase Transformation Models:** *Nathan Barton*<sup>1</sup>; Joel Bernier<sup>1</sup>; <sup>1</sup>Lawrence Livermore National Laboratory

We explore prospects for validation of a crystal level model of phase transformation and twinning. The model treats the formation of distinctly orientated crystalline domains during polymorphic phase transformation and

twinning, and allows for plastic deformation by crystallographic slip in each variant. In cases involving concurrent transformation and crystallographic slip, complexity of both the experimental material response and the model details have limited validation efforts. Work on carefully chosen materials and loading conditions has enabled validation of certain aspects of the model, and this work will be reviewed. New work focuses on the prospects for more extensive validation using recently developed in situ diffraction based techniques. Preliminary results will be presented for twinning in magnesium, and we will discuss the outlook for validation using in situ measurements under elevated pressure conditions. This work performed under the auspices of the US DOE by Lawrence Livermore National Laboratory under Contract DE-AC52-07NA27344 (LLNL-ABS-405264).

#### 12:20 PM

**Transforming Graphite to Diamond: An Ab Initio Molecular Dynamics Study of Graphite under Shock Compression:** *Nir Goldman*<sup>1</sup>; I.-F. W. Kuo<sup>1</sup>; Evan J. Reed<sup>1</sup>; Laurence E. Fried<sup>1</sup>; C. J. Mundy<sup>2</sup>; Alessandro Curioni<sup>3</sup>; <sup>1</sup>Lawrence Livermore National Laboratory; <sup>2</sup>Pacific Northwest National Laboratory; <sup>3</sup>IBM Research, Zurich Research Laboratory

We present an extremely large scale ab initio calculation of the transformation of graphite to diamond under shock compression utilizing Car-Parrinello Molecular Dynamics (CPMD) in conjunction with the Multi-Scale Shock Method (MSSM). Our results indicate that the transition from graphite to diamond is Martensitic, in agreement with experimental observations. We find that a shock of 12 km/s forms a short-lived layered diamond phase which eventually relaxes to a cubic diamond state. Moreover, access to the electronic structure allows the computation the x-ray absorption spectra (XAS) to characterize the final states. The XAS spectra and wide angle x-ray scattering spectra (WAXS) confirm the presence of a cubic diamond final state.

## 2009 Functional and Structural Nanomaterials: Fabrication, Properties, and Applications: Nanoscale Phenomena: Mechanics, Phase Stability and Properties

Sponsored by: The Minerals, Metals and Materials Society, TMS Electronic, Magnetic, and Photonic Materials Division, TMS Materials Processing and Manufacturing Division, TMS: Nanomaterials Committee, TMS: Nanomechanical Materials Behavior Committee

Program Organizers: Gregory Thompson, University of Alabama; Amit Misra, Los Alamos National Laboratory; David Stollberg, Georgia Tech Research Institute; Jiyoung Kim, University of Texas at Dallas; Seong Jin Koh, University of Texas at Arlington; Wonbong Choi, Florida International University; Alexander Howard, Air Force Research Laboratory

Wednesday PM

February 18, 2009

Room: 3018

Location: Moscone West Convention Center

Session Chairs: Jiyoung Kim, University of Texas at Dallas; Seong Jin Koh, University of Texas at Arlington

#### 2:00 PM Invited

**3-D Compositional Imaging at the Nano-Scale:** *David Larson*<sup>1</sup>; <sup>1</sup>Imago Scientific Instruments

Atom-probe tomography can provide 3-D atomic-scale structural and compositional analysis of materials which is difficult to duplicate using other high-performance techniques such as transmission electron microscopy and secondary ion mass spectroscopy. Recent specimen fabrication techniques using focused-ion beam instruments with in-situ manipulation now allows a variety of nanoscale materials with site-specific features to be prepared and analyzed in the atom probe. This talk will address the fabrication and atom probe analysis, as well as comparison to other characterization techniques, of dopant profiling and defect ring structures in semiconductor transistors materials. Additionally, microstructural analysis of nanoscale laminates in magnetic and quantum-well layered features will be described.



2:30 PM

**Advanced Production of Nanobased Photocatalytic Surfaces:** *Christian Wögerer*<sup>1</sup>; Robert Katzensteiner<sup>1</sup>; Thomas Placzek<sup>1</sup>; Georg Waldner<sup>2</sup>; Norica Godja<sup>3</sup>; <sup>1</sup>Profactor Research and Solutions GmbH; <sup>2</sup>Austrian Research Center; <sup>3</sup>CEST GmbH

The paper describes a continuous wet-chemical production of photocatalytic nanoparticles technology with different direct connected coating processes including necessary pre- and aftertreatment for photocatalytic-surfaces on different substrates. A newly developed nozzle-technique based on a simple precipitation process will be used to establish a continuous particle production capable for Up-Scaling without having to deal with the typical problems of "conventional" precipitation. The most important facts in this matter are: continuous operation, controllable particle characteristics, easy Up-Scaling, pcnp's in colloidal solution, cheap precursors combined with simple plant design resulting in a cost effective production method. For an advanced coating procedure new developed coating techniques will be implemented by establishing a "tandem plant" which will be able to produce pcnp's and deposit them on substrates within one single device or depositing the pcnp's in a subsequent device apart from the production ("ambulant coating"). Both methods will lead to prototype plants/devices capable to be commercialised.

2:45 PM

**Characterization and Hydrogen Cycling Behavior of Nanoporous Palladium Alloy Thin Films:** *Wen Chung Li*<sup>1</sup>; T. John Balk<sup>1</sup>; <sup>1</sup>University of Kentucky

Nanoporous palladium (np-Pd) films were prepared by dealloying of co-sputtered Pd alloy precursors on Si substrates. Film stress, microstructure and composition were tracked during dealloying using wafer curvature, electron microscopy, x-ray diffraction and energy-dispersive spectroscopy. Np-Pd films exhibit a uniform porous structure with pores and ligaments as small as 5 nm, yielding a high amount of surface area for possible hydrogen sensing applications. To test this capability, hydrogen cycling experiments were performed in the wafer curvature system with a hydrogen-containing atmosphere (partial pressure of hydrogen gas varied from 0 to 760 torr) over a range of temperatures (-50 to 200 degrees Celsius). Various np-Pd alloy films were compared and found to exhibit quicker hydrogen sensing than dense Pd films of comparable thickness. Finally, the elastic and plastic deformation components of np-Pd alloy film behavior were analyzed in relation to film microstructure and stability.

3:00 PM

**Metastable Phases in Sputtered Fe-C Thin Films:** *Arnaud Weck*<sup>1</sup>; Chad Sinclair<sup>1</sup>; Colin Scott<sup>2</sup>; Christian Maunders<sup>3</sup>; <sup>1</sup>The University of British Columbia; <sup>2</sup>Arcelormittal; <sup>3</sup>McMaster University

Vapor deposition as a continuous technique for modifying the surface of sheet metals provides rich opportunities for the development of novel functional and mechanical properties in metallurgical systems. In this work, we focus on the wealth of metastable structures that can be obtained in the iron-carbon system when thin films are deposited by sputtering with and without an applied substrate bias (ion plating). Various characterization techniques (e.g. EELS, HRTEM, APFIM) have been employed to characterize the as-deposited structures which range from amorphous to highly faulted nanocrystalline carbides (e.g. Fe<sub>7</sub>C<sub>3</sub>). The results suggest the possibility of colossal carbon supersaturation in bcc Fe under particular conditions of deposition, not inconsistent with previous observations of carbon supersaturation resulting from other far from equilibrium processes.

3:15 PM

**Phase Diagram of the Ag-Pd Bimetallic Nano Cluster:** Hyun You Kim<sup>1</sup>; Da Hye Kim<sup>1</sup>; *Hyuck Mo Lee*<sup>1</sup>; <sup>1</sup>KAIST

We report on the complete phase diagram of 135Ag-16Pd bimetallic nano cluster that is widely used as a selective hydrogenation catalyst. The solid to liquid transition region was investigated using molecular dynamics simulations with an improved collision method, and the solid state region of the phase diagram was explored with the combination of molecular dynamics, modified basin hopping Monte Carlo, and density functional theory. The solid state structure of the 135Ag-16Pd cluster is discussed in a viewpoint of over-stability of the meta-stable structure. Because the properties of the clusters are a kind of manifestation of their structures, our phase diagram will serve as a brief guidance for practical application of the Ag-Pd catalysts.

3:30 PM Break

3:45 PM

**A Mimetic NanoPorous Carbon Model by Quench Molecular Dynamics Simulation:** *Yunfeng Shi*<sup>1</sup>; <sup>1</sup>Rensselaer Polytechnic Institute

Despite extensive applications in many fields and even greater prospects in the future, the structure of nanoporous carbon is poorly understood at the atomic level. Due to the difficulty in its structural determination experimentally, many virtual carbon models have been put forth with various physical and chemical details. In this talk, a mimetic porous carbon model is generated using quench molecular dynamics simulations that reproduces experimental radial distribution functions of activated carbon. The quench conditions are systematically varied and the final porous structure is scrutinized in terms of its pore size distribution, pore connectivity and fractal dimension. It is found that the initial carbon density affects the fractal dimension but only causes a minor shift in the pore size distribution. On the other hand, the quench rate affects the pore size distribution but only causes a minor shift in the fractal dimension.

4:00 PM

**Scale-Dependent Performance of Piezo-Composites:** *Nelson Pinilla*<sup>1</sup>; Kishore Pochiraju<sup>1</sup>; <sup>1</sup>Stevens Institute of Technology

Composites reinforced with piezoelectric fibers are used in smart structures and high performance sensors. Piezo-composites act as both sensing and actuation elements in smart material applications with embedded closed loop control. However, response time delay between strain development and electrical signal detection may be significant; the response time delay lowers the control loop frequency and limits the performance of the composite when subjected to high frequency impact or shock loading. This paper investigates the fiber size dependence on the response time delay of piezo-composites. Nanoscale fibers have the potential to reduce the time delay and increase the control loop frequencies. This paper presents a characterization of model piezo-composites reinforced with fibers with varying diameters. Processing and electrical interconnections of the piezo composites are quite challenging; a unique experimental setup has been used to determine the response delays of the composites. Model-based, performance, and experimental results would be presented in this paper.

4:15 PM

**Plastic Flow Stability of Nanotwinned Cu Films:** *Osman Anderoglu*<sup>1</sup>; Amit Misra<sup>2</sup>; Xinghang Zhang<sup>1</sup>; <sup>1</sup>Texas A&M University; <sup>2</sup>Los Alamos National Laboratory

We have room temperature rolled sputtered deposited, (111) textured, nanotwinned Cu foils up to 50% thickness reduction. X-ray pole figure measurements indicate no significant out-of-plane rotation of the grains. No significant change in the average twin lamellar thickness is seen although the height of the columnar grains was reduced by a factor of two after rolling. Transmission electron microscopy was used to elucidate the stored dislocation content at twin boundaries. A dislocation mechanism is developed to explain the plastic flow stability of nanotwins to large strains.

4:30 PM

**Influence of Crystallization on Sheet Resistivity Associated with the Size Effect of AgInSbTe Chalcogenide Films:** *Chung-Wei Yang*<sup>1</sup>; Tuan-Sheng Lui<sup>1</sup>; Chien-Chih Chou<sup>1</sup>; <sup>1</sup>National Cheng Kung University

The as-deposited AgInSbTe (AIST) chalcogenide films with different thickness were prepared with using a series of power, pressure and sputtering durations by RF-sputtering process. The quasi-crystallized structure of as-deposited films can be recognized according to evidences of grazing-incidence x-ray diffraction analysis and transmission electron microscopy. Through the estimation of crystal size, a higher sputtering power and a longer sputtering duration can result in a larger extent of atomic rearrangements. The sheet resistivity measurement of amorphous films reveals that the relationship between the sheet resistivity and thickness of amorphous films is against the common known size effect. The low carrier mobility in the amorphous films is due to the effect of its disorder microstructure from the measurement of Hall coefficients to the as-deposited and crystallized films.

4:45 PM

**Electrical Transport Behavior of Nanoscale Ga-Doped ZnO Film in Low Temperature Regime:** *Young Gun Ko*<sup>1</sup>; *Byung Du Ahn*<sup>2</sup>; *Hyun Jae Kim*<sup>2</sup>; *Dong Hyuk Shin*<sup>3</sup>; <sup>1</sup>Massachusetts Institute of Technology; <sup>2</sup>Yonsei University; <sup>3</sup>Hanyang University

This paper deals with the electrical response of nanoscale Ga:ZnO thin films fabricated through pulsed laser deposition method and the transporting mechanisms associated with electrical conduction and scattering behavior with respect to temperature tested within the range of 300 to 10 K. All films that contain the degenerate band due to heavy doping process itself exhibit the metallic characteristics except those observed below 100 and 60 K, respectively when deposited at 298 and 773 K, respectively. This metal-semiconductor transition here is explained based on the role of weakly localized electrons found in a disorder conductor. As for scattering behavior of the present films, governing mechanism is thought to be ionized-impurity scattering below metal-semiconductor transition temperature. Depending on grain size, however, matrix and grain boundary will act as a barrier to inhibit the motion of electrons in a regime above metal-semiconductor transition temperature.

5:00 PM

**Interfacial Effects in the Relaxation Dynamics of Silver Nanometal-Glass Composites Probed by Transient Grating Spectroscopy:** *José Jiménez*<sup>1</sup>; *Sergiy Lysenko*<sup>1</sup>; *Valentin Vikhnin*<sup>1</sup>; *Huimin Liu*<sup>1</sup>; <sup>1</sup>University of Puerto Rico at Mayagüez

The relaxation dynamics of silver nanoparticles (NPs) in phosphate glass have been studied by picosecond time-resolved transient grating spectroscopy. Glasses were prepared by melting and heat treatment (HT) processes where two different metal-glass interfaces were presumably produced. The first is a glass system containing silver and tin in which Ag NPs are embedded in the matrix upon HT. The second is a heat-treated silver-doped glass with spectroscopic indications of Ag<sup>+</sup>-Ag<sup>0</sup> pairs located at/or near the metal-glass interface. The time evolution of the light-induced transient diffraction grating for the Ag/Sn-doped glass shows an uncommon relaxation in the nanosecond time scale. Such behaviour is explained in terms of energy transfer processes between polaronic and/or excitonic states in the near-interface region of the glass matrix and NPs. In contrast, a faster monotonic relaxation is observed for the Ag-doped nanocomposite. This result is attributed to Ag NP → Ag<sup>+</sup>-Ag<sup>0</sup> plasmon resonance energy transfer.

growth and it was found that the dominant mechanism of the crystal of gibbsite growth was single particle growth.

2:30 PM

**Effect of  $\alpha$ -Alanine on the Seeded Precipitation of Sodium Aluminate Solution:** *Baolin Lv*<sup>1</sup>; *Qiyuan Chen*<sup>1</sup>; *Zhoulan Yin*<sup>1</sup>; *Huiping Hu*<sup>1</sup>; *Xing Chen*<sup>1</sup>; <sup>1</sup>Central South University

The effect of  $\alpha$ -alanine on the seeded precipitation of sodium aluminate solution was investigated. The relative concentrations of Al<sub>2</sub>O(OH)<sub>2</sub><sup>2-</sup> with the absorption band at about 530cm<sup>-1</sup> or polynuclear complex with the absorption bands at about 885cm<sup>-1</sup> and 635cm<sup>-1</sup> and the stability of sodium aluminate solution were determined using semi-quantitative method of FT-IR spectrum and 27Al NMR spectra, respectively. All the results show that compared to the blank,  $\alpha$ -alanine at proper dosages reduces the precipitation ratios of sodium aluminate solution during the initial reaction time, then accelerates precipitation process, which may result from the break of dynamic balance among aluminate specieses present in sodium aluminate solution or from the variation of the stability of sodium aluminate solution due to the transformation of some new aluminate specieses which could be beneficial for the formation of growth unit in sodium aluminate solution.

2:55 PM

**Effects of Four Aromatic Carboxylic Acids as Inhibitors on the Seeded Precipitation Ratios of Sodium Aluminate Solutions and the Agglomeration Efficiency of Gibbsite:** *Baolin Lv*<sup>1</sup>; *Qiyuan Chen*<sup>1</sup>; *Zhoulan Yin*<sup>1</sup>; *Huiping Hu*<sup>1</sup>; <sup>1</sup>Central South University

The effects of four aromatic carboxylic acids as inhibitors on precipitation ratios of sodium aluminate solutions, particle size distribution (PSD) of gibbsite were investigated using titration method, particle size analyzer, respectively. The net charges of oxygen atoms in the four aromatic carboxylic anions and the dipole moments of the four aromatic carboxylic anions were calculated by GGA-PW91 in Module-Dmol3 of Materials Studio and B3LYP/6-31G of Gaussian, respectively. Results show that the inhibitory effects on precipitation ratio decrease in the order of p-toluic acid>benzoic acid>m-toluic acid>o-toluic acid. The negative effects on agglomeration efficiency of gibbsite decrease in the order of m-toluic acid>benzoic acid>p-toluic acid>o-toluic acid. All the phenomena correlate with the net charges of oxygen atoms in the four aromatic carboxylic anions and the dipole moments of the four aromatic carboxylic anions. Therefore, a possible electrostatic adsorption-polarization mechanism about the interaction between these inhibitors and gibbsite surfaces is proposed.

3:20 PM

**Effect of Ultrasound on Particle Size Distribution of Al(OH)<sub>3</sub> in Seeded Precipitation of Sodium Alumina Solution:** *Yusheng Wu*<sup>1</sup>; *Li Mingchun*<sup>1</sup>; *Bi Shiwen*<sup>2</sup>; *Yang Yihong*<sup>2</sup>; <sup>1</sup>Shenyang University of Technology; <sup>2</sup>Northeastern University

To solve the problem of periodically explosive attenuation of Al(OH)<sub>3</sub> particles in seeded precipitation process of sodium aluminate solution, a systematic study was made of the effect and mechanism of ultrasound on particle size distribution of Al(OH)<sub>3</sub> crystals in seeded precipitation. The results indicate that ultrasound significantly enhance growth of Al(OH)<sub>3</sub> crystals, and optimize the particle size distribution. For instance, with ultrasound, the mean particle size of Al(OH)<sub>3</sub> increases by 4.37 $\mu$ m. The crystal morphologies show that the ultrasounds enhance the agglomeration process and second nucleation process.

3:45 PM Break

4:05 PM

**Effect of Carbonization Seeds on Seeded Precipitation of Sodium Aluminate Solution:** *Yusheng Wu*<sup>1</sup>; *Shiwen Bi*<sup>2</sup>; *Yihong Yang*<sup>2</sup>; <sup>1</sup>Shenyang University of Technology; <sup>2</sup>Northeastern University

To solve the problem of periodically explosive attenuation of Al(OH)<sub>3</sub> particles in seeded precipitation process of sodium aluminate solution, the effect of carbonization seeds on seeded precipitation were investigated under industrial conditions modeled in laboratory. The results show that adding carbonization seeds to Bayer process can enhance precipitation rate, reduce fluctuation of particle size and improve the intensity of Al(OH)<sub>3</sub>. Analysed the physical chemistry characteristic of Al(OH)<sub>3</sub> crystals, high quality Al(OH)<sub>3</sub> product can be obtained with 200g/L carbonization seeds. SEM photomicrographs shows that carbonization seeds transformed inlay structure during seed precipitation of sodium aluminate solution.

## Alumina and Bauxite: Alumina Precipitation

Sponsored by: The Minerals, Metals and Materials Society, TMS Light Metals Division, TMS: Aluminum Committee  
Program Organizers: Everett Phillips, Nalco Co; Sringeri Chandrashekar, Dubai Aluminum Co

Wednesday PM  
February 18, 2009

Room: 2002  
Location: Moscone West Convention Center

Session Chair: Jorge Aldi Lima, Alunorte

### 2:00 PM Introductory Comments

2:05 PM

**Kinetics of Super-Fine Aluminum Hydroxide Precipitation from Sodium Aluminate Solutions with Gel-Seed:** *Jianli Wang*<sup>1</sup>; *Qiyuan Chen*<sup>2</sup>; *Wangxing Li*<sup>1</sup>; *Zhoulan Yin*<sup>2</sup>; <sup>1</sup>Zhengzhou Research Institute of Chalco; <sup>2</sup>Central South University

Effect of precipitation temperature, sodium hydroxide concentration and seed ratio on super-fine aluminum hydroxide precipitation from sodium aluminate solutions with gel-seed was studied and the kinetics model was proposed. According to this model, super-fine aluminum hydroxide precipitation follows second order reaction kinetics, however, its rate constant is larger than the rate constant of metallurgical grade aluminum hydroxide precipitation. Both the precipitation temperature and the gel seed ratio affected the precipitation rate and the particle size. Compared with metallurgical gibbsite precipitation, the reaction rate was faster, the precipitation rate could reach about 40% when precipitation time was 8 hours. The gel seeds were dissolved partly first and then new aluminum hydroxide was precipitated and grew on the surface of the seeds. Dynamic light scattering was used to characterize super-fine gibbsite particle

4:30 PM

**Effect of Cationic Polyacrylamide on the Seeded Agglomeration Process of Sodium Aluminate Liquors:** *Jianguo Yin<sup>1</sup>; Qiyuan Chen<sup>2</sup>; Zhoulan Yin<sup>2</sup>; Wangxing Li<sup>1</sup>; Zhonglin Yin<sup>1</sup>; <sup>1</sup>Zhengzhou Research Institute of Chalco; <sup>2</sup>School of Chemistry and Chemical Engineering of Central South University*

Effect of cationic polyacrylamide (PAM) on the seeded agglomeration of sodium aluminate liquors was investigated, conclusions were drawn as follows. Cationic PAM can increase precipitation ratio of sodium aluminate liquors and it is 2.5% higher than the blank at the dosage of 2.5 ppm. It can also improve particle size distribution (PSD) of gibbsite products. Average size of the products is 4.6  $\mu\text{m}$  larger and particles less than 45 $\mu\text{m}$  is 21% less than the blank at the dosage of 10 ppm. Gibbsite agglomerates with the addition of cationic PAM are made up of median size crystallines which are filled with many crystallines of 5  $\mu\text{m}$  or so, and there fills with even less ones among 5  $\mu\text{m}$  crystallines. That is to say, cationic PAM is beneficial to get products of higher intensity. Cationic PAM is expected to be a crystal growth modifier (CGM) or be one component of CGM.

4:55 PM

**Model on Batch Seeded Gibbsite Precipitation from Bayer Liquor:** *Jibo Liu<sup>1</sup>; Wangxing Li<sup>1</sup>; Yadong Wang<sup>1</sup>; Zhiming Liu<sup>2</sup>; <sup>1</sup>Zhengzhou Research Institute; <sup>2</sup>Zhengzhou Research Institute - and - Central South University*

A mathematical model incorporating concepts of various parameters evolution has been developed to predict the alumina hydrate productivity of batch seeded gibbsite precipitation process. The model is based on the theoretical concepts rather than on empirical basis, and considers the evolution of liquor composition, solid content and crystal surface area. The relationship of kinetic constant and other important parameters versus reaction conditions were determined by the laboratory experiments, these parameters can also be used in the practical process model. The value estimated by the model is well fitted with the data that detected in practical precipitation system, and the ratio of data that the error lower than 5% is exceed 95%.

5:20 PM **Concluding Comments**

## Aluminum Alloys: Fabrication, Characterization and Applications: Modeling and Corrosion

Sponsored by: The Minerals, Metals and Materials Society, TMS Light Metals Division, TMS: Aluminum Processing Committee

Program Organizers: Weimin Yin, Williams Advanced Materials; Subodh Das, Phinix LLC; Zhengdong Long, Kaiser Aluminum Company

Wednesday PM  
February 18, 2009

Room: 2004  
Location: Moscone West Convention Center

Session Chair: Yansheng Liu, SECAT Inc

2:00 PM

**Modelling Homogenization Heat Treatment of AA3003 Alloy:** *Qiang Du<sup>1</sup>; Warren Poole<sup>1</sup>; Mary Wells<sup>2</sup>; <sup>1</sup>University of British Columbia; <sup>2</sup>University of Waterloo*

The homogenization treatment of AA3003 involves the growth and dissolution of inter-granular constituent particles and intra-granular dispersoids. It is a multi-scale problem involving the long-range diffusions (~10  $\mu\text{m}$ ) and short-range diffusions (~0.1 to 1  $\mu\text{m}$ ) of all of the alloying elements (Fe, Mn and Si). In this paper a comprehensive model is proposed to simulate these phenomena. It consists of 1D pseudo front tracking method for inter-granular constituent particles and a multi-precipitate growth model for dispersoids. The multi-precipitate model is developed based on a variational approach and it could capture the influence of precipitate size distribution on the overall precipitate kinetics. The abilities of the multi-precipitate growth model will be demonstrated by comparing with existing models in the literature. The comparison of the simulation results with the experimental measurement for an industrial practice of this homogenization treatment will be also be conducted.

2:20 PM

**Evaluation of AA5083 Constitutive Models for Elevated-Temperature Bulge Forming Simulations under QPF Conditions:** *Eric Taleff<sup>1</sup>; Louis Hector<sup>2</sup>; Paul Krajewski<sup>2</sup>; <sup>1</sup>University of Texas; <sup>2</sup>General Motors R&D Center*

Finite-element (FE) predictions of dome pole height and pole thickness in gas-pressure bulge forming of fine-grained AA5083 sheet under quick plastic forming (QPF) conditions are compared with experimental bulge data. We examine four material constitutive models constructed from tensile tests. These include a single-mechanism model without temperature dependence commonly used to simulate SPF processes and a single-mechanism model that accounts for temperature. A pair of two-mechanism models that account for the independent creep mechanisms observed in QPF are also investigated. One includes the effect of threshold stress and the other does not. Based upon our results, a recommendation is made as to which of the four models should be used in FE simulations of QPF processes. The applicability of material models based upon uniaxial tensile data to predictions for forming under balanced-biaxial tension is addressed in detail, and suggestions for future improvements to the existing models are offered.

2:40 PM

**A Monte Carlo Simulation of Grain Refinement during Thermomechanical Processing of an Al-Mg-Si-Cu Alloy:** *Panthea Sepherband<sup>1</sup>; Shahrzad Esmaeili<sup>1</sup>; Haiou Jin<sup>2</sup>; <sup>1</sup>University of Waterloo; <sup>2</sup>Novelis Global Technology Centre*

The grain refinement of a 6000 series aluminum alloy during a newly developed thermomechanical processing route has been simulated using the Monte Carlo technique. Based on the TEM studies on the as-deformed state of the alloy, the initial microstructure of the simulation is generated considering deformation inhomogeneities around large particles as well as within the heavily deformed grains. Subsequently, the simulation is formulated based on a concurrent recovery-recrystallization process and the pinning effect of precipitates. The technique provides simulated microstructures and predictions for the recrystallized fraction, grain size and grain size distribution at different stages of annealing. EBSD tests on thermomechanically processed samples are used to validate the simulation results.

3:00 PM

**Microstructure and Stress Corrosion Cracking of Al-5083:** *Ramasis Goswami<sup>1</sup>; Peter Pao<sup>2</sup>; George Spanos<sup>2</sup>; Ronald Holtz<sup>2</sup>; <sup>1</sup>SAIC; <sup>2</sup>Naval Research Laboratory*

Commercial Al 5XXX alloys have been used for marine applications because they exhibit excellent resistance to corrosion. However, these alloys become susceptible to stress corrosion cracking (SCC) when exposed to temperatures in the range of 50-200°C for many days. The present investigation focuses on the effect of corrosive environments on crack propagation in Al-5083 exposed to 175°C for 10 days. Pre-cracked double cantilever beam specimens, treated with a dropwise exposure to 3.5% NaCl, were bolt loaded with a constant crack opening displacement. The microstructure, chemistry and dislocation structures at the grain boundary and inside the grains have been investigated using transmission electron microscopy (TEM) just below the crack surface. TEM reveals a large number of precipitates in the matrix, while most of the grain boundaries are covered with Al<sub>3</sub>Mg<sub>2</sub>. The correlation between the microstructure, dislocations and the stress corrosion cracking behavior will be discussed.

3:20 PM

**Welding Techniques and Corrosion Behavior of 5xxx Alloy for Marine Structural Application:** *Zhengdong Long<sup>1</sup>; Subodh Das<sup>2</sup>; John Kaufman<sup>3</sup>; Shridas Ningileri<sup>3</sup>; Yufu Wang<sup>3</sup>; <sup>1</sup>Center for Aluminum Technology, University of Kentucky; <sup>2</sup>Phinix LLC; <sup>3</sup>Secat Inc*

Al-Mg 5xxx aluminum alloys are broadly used in naval ship structures due to their superior strength-to-weight ratio and generally excellent salt-water corrosion resistance. However, the strength and corrosion properties are significantly affected by joining with the traditional gas metal arc welding (GMAW) process. The large heat affected zone resulting from the GMAW has relatively low strength and is susceptible to intergranular corrosion. The Navy has experienced both intergranular corrosion (IGC) and exfoliation corrosion of Al-Mg alloys used in long-term exposure in equatorial environments. The friction stir welding (FSW) technique provides less heat input, potentially providing improvement in this condition, and therefore was investigated in this study. The welding efficiency, microstructure, microhardness and corrosion resistance of FS and GMAW joints in a representative 5456-H116 plate were



compared. The FSW provides higher weld strength efficiency and may also have improved corrosion resistance.

### 3:40 PM

**Hydrogen Generation by Aluminum-Water Reactions:** *Paul Rozenak*<sup>1</sup>; *Ester Shani*<sup>1</sup>; <sup>1</sup>Hydrogen Energy Batteries LTD

The aluminum-water surface reaction in the alkaline dissolution of aluminum was studied by secondary ion mass spectroscopy (SIMS) and transmission electron microscopy (TEM). In our experiments, hydrogen (deuterium) absorption in the aluminum surface after reaction with an alkaline solution was characterized. We suggest the interpretation that anodic oxidation during the first anodic scan irreversibly converts the active hydride-covered Al surface to a passive oxide-covered surface. The result suggests that, at least in alkaline solutions, the Al dissolution pathway proceeds through a hydride oxidation step. Hydride may be formed by the etching of Al and hydrogen gas generated cathodically on the surface. Various densities and distributions of hemispherical bubbles, ranging in size from large (some micrometers in diameter) to very small (a few nanometers in diameter) were obtained in the surface hydroxide layers of aluminum. The principles of the production of gaseous hydrogen are described.

### 4:00 PM Break

### 4:15 PM

**Effect of Scandium Addition on Microstructure and Corrosion Properties of Al-Cu-Mg-Ag Alloys:** *D. H. Xiao*<sup>1</sup>; *K.H. Chen*<sup>1</sup>; <sup>1</sup>Central South University

The Al-Cu-Mg-Ag alloys with different scandium contents were prepared by ingot metallurgy technology. Effect of scandium addition on microstructure and corrosion properties of an Al-5.3Cu-0.8Mg-0.6Ag-0.2Zr alloy were investigated using optical microscope, scanning electron microscopy (SEM), transmission electron microscopy (TEM), intercrystalline corrosion and exfoliation corrosion. It has been shown that 0.3~0.5%Sc addition refines the grains of the casting alloys and the average grain size decrease from over 300 μm to 60 μm. Increasing Sc content from 0.1 to 0.3 wt% increased corrosion-resistance properties. However, the coarsening Al<sub>3</sub>(Sc,Zr) compounds in alloys with 0.5%Sc decrease corrosion-resistant properties seriously.

### 4:35 PM

**Splitting Water with Al Rich Alloys: Structure and Reaction Kinetics:** *Go Choi*<sup>1</sup>; *Jerry Woodall*<sup>1</sup>; *Jeffrey Ziebarth*<sup>1</sup>; *Charles Allen*<sup>1</sup>; *J-H Jeon*<sup>1</sup>; *Deborah Sherman*<sup>1</sup>; *Robert Kramer*<sup>1</sup>; <sup>1</sup>Purdue University

Solid alloys of aluminum, gallium, indium and tin are capable of reacting with water at room temperature to form hydrogen, alumina, and heat. The alloys are shown to contain a phase of solid aluminum-rich grains with small amounts of gallium. In and Sn have nearly zero solid solubility in Al, and energy dispersive x-ray (EDX) analysis found In and Sn to be in the grain boundaries together with Al and Ga. It is believed that the grain boundary phase becomes liquid at or near room temperature and as a result enables reaction with water. When these alloys react with water or oxidize in air, EDX results show that the reaction occurs at or near the grain boundary. Current research efforts focus on studying the reaction mechanisms for alloy compositions containing 50 wt% and 95 wt% Al, with 95 wt% Al alloys being the more interesting of the two from an economics standpoint.

## Aluminum Reduction Technology: Fundamentals

Sponsored by: The Minerals, Metals and Materials Society, TMS Light Metals Division, TMS: Aluminum Committee

Program Organizers: Gilles Dufour, Alcoa Canada, Primary Metals; Martin Iffert, Trimet Aluminium AG; Geoffrey Bearne, Rio Tinto Alcan; Jayson Tessier, Alcoa Deschambault

Wednesday PM  
February 18, 2009

Room: 2012  
Location: Moscone West Convention Center

Session Chair: Alton Tabereaux, Consultant

### 2:00 PM

**Alumina Dissolution in Aluminum Smelting Electrolyte:** *Xiangwen Wang*<sup>1</sup>; <sup>1</sup>Alcoa Inc

Alumina dissolution rate in cryolitic electrolytes has been a subject of intensive studies, and its relation to the alumina physical properties had been attempted

through various studies over past decades as reported in the open literature. The findings from these reported lab studies have been proved to be difficult to relate alumina solubility in industrial operating cells due to lack of similarities between the two settings. Alcoa has been using a different experimental approach to measure alumina dissolution rate to monitor ore quality changes for providing necessary information to our smelting operations. This paper briefly describes the background for alumina dissolution studies, experimental setup and procedures for measuring dissolution rate. Some comparison results of typical good and bad alumina ores in term of dissolution rate are presented.

### 2:20 PM

**Alumina Dissolution and Current Efficiency in Hall-Heroult Cells:** *Bjørn Lillebuen*<sup>1</sup>; *Marvin Bugge*<sup>1</sup>; *Helge Høie*<sup>1</sup>; <sup>1</sup>Hydro Aluminium

The dissolution and distribution of alumina can be described as a coupled heat- and mass transport process, with intermediate formation of solid cryolite. Current Efficiency(CE) can be evaluated by means of the rate equations for the back reaction between dissolved metal and carbon dioxide gas. Solid cryolite may be formed close to the metal pad, under certain conditions in the cell. The bath superheat, and the mass transfer coefficient at the bath/metal interface, will be important parameters for the maximization of CE. In some cells, there is a clear correlation seen between CE and the sodium content in the metal, indicating that mass transfer is the dominant factor. In other cells, sodium levels can be quite low even at high CE, which can indicate that cryolite formation plays a significant role, making superheat the dominant factor.

### 2:40 PM

**The Behaviour of Moisture in Cryolite Melts:** *Karen Osen*<sup>1</sup>; *Christian Rosenkilde*<sup>2</sup>; *Asbjørn Solheim*<sup>1</sup>; *Egil Skybakmoen*<sup>1</sup>; <sup>1</sup>SINTEF Materials and Chemistry; <sup>2</sup>Hydro Aluminium AS

HF emissions are still an environmental challenge for the aluminium industry. Hydrogen fluoride is generated when fluorides present in the bath and in the vapour phase react with moisture. It has been established that the main sources of water are structural hydroxyl contained in the primary alumina and humidity in the air. The objective of the present work was to study the behaviour of moisture in cryolite melts. Argon saturated with water vapour was bubbled through the melt, while gas analysis with respect to HF and H<sub>2</sub>O as well as electrochemical measurements on a gold electrode were performed. The results from the gas analysis and the electrochemical measurements demonstrate that one or several hydrogen-containing species are soluble in the melt. The results also showed that these species exhibit long residence times, i.e. they remained in the melt long after the water supply was terminated.

### 3:00 PM

**Physical-Chemical Properties of the KF-NaF-AlF<sub>3</sub> Molten System with Low Cryolite Ratio:** *Olga Tkatcheva*<sup>1</sup>; *Alexei Apisarov*<sup>1</sup>; *Alexander Dedyukhin*<sup>1</sup>; *Alexander Redkin*<sup>1</sup>; *Elena Nikolaeva*<sup>1</sup>; *Yurii Zaiikov*<sup>1</sup>; *Pavel Tinghaev*<sup>1</sup>; <sup>1</sup>IHTE

The development of low temperature aluminum electrolysis makes possible to reduce the consumption of energy and raw materials per unit of final product and to increase the electrochemical cell lifetime. The supposed operating temperature range of this technology is 750-850oC that corresponds to the KF-NaF-AlF<sub>3</sub> electrolyte compositions at cryolite ratio 1,3-1,7. The liquidus temperature, electrical conductivity, density and alumina solubility in the KF-NaF-AlF<sub>3</sub> molten mixtures at the [KF]/([KF]+[NaF]) ratio from 0 to 1 and ([KF]+[NaF])/[AlF<sub>3</sub>] ratio equal to 1,3; 1,5 and 1,7 have been measured. There is a maximum on the liquidus curves in KF-rich region and a minimum in NaF-rich region at constant CR. The electrical conductivity increases but alumina solubility decreases with potassium fluoride substitution by sodium fluoride.

### 3:20 PM

**Aspects of Crust Formation from Today's Anode Cover Material:** *Tatiana Grouso*<sup>1</sup>; *Mark Taylor*<sup>1</sup>; *Anthony Hudson*<sup>2</sup>; <sup>1</sup>Light Metal Research Centre, The University of Auckland; <sup>2</sup>Kempe Engineering

The structure and composition of different anode cover materials were analyzed by XRD and examined by SEM. SEM images have shown that slow sintering of alumina was a cause to conversion of transition alumina phases to alpha plates and XRD showed corundum content reached 40-45%. However, the morphology of the alpha alumina has not previously been observed and gave both the anode cover and partially crushed bath samples particular properties of hardness and resistance to crushing. Specifically, crushed bath agglomerates have "keyed" into the corundum platelets. For many agglomerates, the fused chiolite formed a casing surrounding the interlocked alpha plates. The resulting

agglomerates are prevented from breaking in normal brittle fracture through the multiple interlocked corundum "gluing" phases. The amount of chiolite increases from the bottom of the crust to the top which also increased the propensity for formation of these hard agglomerates towards the top of the crust material.

## 3:40 PM Break

### 4:00 PM

**Sidededge in Aluminium Cells: The Trench at the Metal-Bath Boundary:** *Asbjørn Solheim*<sup>1</sup>; Henrik Gudbrandsen<sup>1</sup>; Sverre Rolseth<sup>1</sup>; <sup>1</sup>SINTEF

The paper sums up some observations concerning sidededge in industrial aluminium cells. Some laboratory experiments using a gas-cooled cylinder (coldfinger) immersed into bath and metal are also reported. The freeze formed on the coldfinger when it was located in the bath did not melt away when it was lowered deep into the metal; this is in accordance with a recently suggested hypothesis concerning sidededge facing the metal. It appeared, however, that the freeze melted away rapidly at a zone near the metal-bath interface, even though stirring or wave motion was not applied. This observation gave rise to a new interpretation of the conditions at the ledge-metal-bath boundary. It is suggested that the trench formed at that zone is caused by a high heat transmission coefficient between metal and ledge at the meniscus formed at the ledge-metal-bath boundary.

### 4:20 PM

**Inert Anode: Challenges from Fundamental Research to Industrial Application:** Vittorio de Nora<sup>1</sup>; *Thinh Nguyen*<sup>1</sup>; <sup>1</sup>Moltech Invent SA

To overcome the thermodynamic penalties in cell voltage and heat generation, higher current density should be operated with oxygen evolving inert anodes retrofitted in conventional Aluminum reduction cells. Being semiconductor metallic oxides the electrochemical characteristics of inert anode active layer may be modified by diffusion interactions, oxygen activity and composition balance. Unstable cell voltage regimes have been observed with metallic inert anodes operating at high current densities; the formation of n-p semiconductor junctions may be a possible hypothesis. Several questions are still open; further fundamental research should be investigated for better understanding prior to the industrial application of oxygen evolving inert anodes.

### 4:40 PM

**Studies on the Possible Presence of an Aluminum Carbide Layer or Bath Film at the Bottom of Aluminum Electrolysis Cells:** Sverre Rolseth<sup>1</sup>; *Egil Skybakmoen*<sup>1</sup>; Henrik Gudbrandsen<sup>1</sup>; Jomar Thonstad<sup>2</sup>; <sup>1</sup>Sintef Materials & Chemistry; <sup>2</sup>Norwegian University of Science and Technology

The background of this work is the hypothesis that an aluminium carbide layer will be formed at the interface between the liquid aluminium and the carbon cathode at the bottom of aluminium electrolysis cells. It is assumed that the formation and dissolution of aluminium carbide is one of the crucial steps of the wear mechanism of carbon cathode blocks in industrial electrolysis cells. The electrical potential between liquid aluminium and the carbon cathode was measured during current interruption using specially designed probes, both in laboratory and on industrial scale. A potential difference corresponding to the theoretical aluminium carbide formation cell was found in small laboratory cells, but not in industrial cells. It is believed that when the contact area is so large as in an industrial cell, it is unlikely that a permanent coherent aluminium carbide containing layer can be established that covering the entire contact area.

### 5:00 PM

**Solid State Carbothermal Reduction of Alumina:** Dongsheng Liu<sup>1</sup>; *Guangqing Zhang*<sup>1</sup>; Jiuqiang Li<sup>1</sup>; Oleg Ostrovski<sup>1</sup>; <sup>1</sup>The University of New South Wales

The Hall-Heroult process, the only commercial technology for aluminium production requires high energy and is a major origin of perfluorocarbons and green house gases. A promising alternative process, carbothermal reduction of alumina to metallic aluminium has advantages of lower capital cost, less energy consumption, and lower emission of green house gases. Carbothermal reduction processes under development are based on formation of aluminium carbide-alumina melts at high temperatures. Solid state carbothermal reduction of alumina is possible at reduced CO partial pressure. This paper presents results of experimental study of carbothermal reduction of alumina into aluminium carbide in Ar, He and H<sub>2</sub> atmospheres at 1500-1700\176C. The reduction rate of alumina increases with increasing temperature, and is significantly faster in He and H<sub>2</sub> than in Ar. Increasing gas flow rate and decreasing pressure favours the reduction.

### 5:20 PM

**In-Situ Analysis Methods for Electrowinning in Chloride and Fluoride Baths:** *Kathie McGregor*<sup>1</sup>; Graeme Snook<sup>1</sup>; Andrew Urban<sup>1</sup>; Marshall Lanyon<sup>1</sup>; Nicola Scarlett<sup>1</sup>; Ian Madsen<sup>1</sup>; <sup>1</sup>CSIRO

The in-situ analysis of electrode and cell materials in their functional states, i.e., during electrolysis, is highly desirable. Such methods eliminate the possibility of experimental artifacts brought about by changes during sample preparation. This is particularly challenging, however, for electrochemical processes conducted at high temperatures in molten salts. In this paper, several new in-situ techniques, and their challenges and limitations, will be described: (1) Dynamic measurements of resistance and capacitance obtained simultaneously during electrolysis; (2) An innovative Fast Fourier Transform Current Pulse technique to investigate anode bubble resistance; (3) Synchrotron X-ray diffraction phase-mapping for a model inert anode material via Tomographic Energy Dispersive Diffraction Imaging (TEDDI). Application of these techniques to aluminium and titanium reduction cells will be discussed. This work was conducted as part of the CSIRO Light Metals Flagship and CSIRO Emerging Science Initiative (Synchrotron Science).

## Aluminum Reduction Technology: Operational Improvements

Sponsored by: The Minerals, Metals and Materials Society, TMS Light Metals Division, TMS: Aluminum Committee

Program Organizers: Gilles Dufour, Alcoa Canada, Primary Metals; Martin Iffert, Trimet Aluminium AG; Geoffrey Bearne, Rio Tinto Alcan; Jayson Tessier, Alcoa Deschambault

Wednesday PM

February 18, 2009

Room: 2001

Location: Moscone West Convention Center

*Session Chairs:* Mohd Mahmood, Aluminium Bahrain; Jean Crépeau, Rio Tinto Alcan

### 2:00 PM

**AP30 toward 400 kA:** *Oliver Martin*<sup>1</sup>; Laurent Fiot<sup>1</sup>; Claude Ritter<sup>1</sup>; Renaud Santerre<sup>2</sup>; Herman Vermette<sup>1</sup>; <sup>1</sup>Rio Tinto Alcan; <sup>2</sup>Alcan Primary Metal

After an intensive development program, two new versions of the AP30 have been developed. The AP37 cell, today available in its industrial version, is able to cope with more than 370 kA and to guarantee reliable technical and environmental performance. Industrial test has been carried out on the Alma (Canada) boosted section in order to validate the AP37 technology. The technical results of the Alma trial are presented in detail. The advantages of the new AP37 compared with the previous version of the AP30 on a greenfield project are presented. The AP39 will soon be able to cope with 400 kA without degradation of the specific energy consumption. The Saint Jean de Maurienne (France) industrial test has demonstrated reliable operation above 390 kA and gives confidence to industrialize the AP39 in high performance industrial package for future greenfield projects.

### 2:20 PM

**Evolution of CD20 Reduction Cell Technology towards Higher Amperage Plan at Dubai:** *Maryam Al-Jallaf*<sup>1</sup>; Ali Hussain Ahmed Mohamed Al Zarouni<sup>1</sup>; Arvind Kumar<sup>1</sup>; Mohammad Shabbir Ali<sup>1</sup>; <sup>1</sup>Dubai Aluminium Company Limited

Dubai Aluminium and Comalco (now part of Rio Tinto Alcan) jointly developed the CD20 reduction cell technology, with the first cells commissioned in 1996 at 190 kA and now currently running at 233 kA. DUBAL has since pursued an ambitious programme to optimise the cell design and its successor, the D20 cell technology, for higher amperage and production. The D20 has been continually developed over the past five years to enable this increase in amperage and production. The main changes were in lining design, anode design and operational practices i.e. anode cover thickness, bath/metal height, control of excess AlF<sub>3</sub>, AEF detection and termination and improved HF gas recovery. This paper summarises the evolution of the CD20 cell technology through to the development of the D20 cell technology, which is currently operating at 248 kA with current efficiency over 96%.

2:40 PM

**Development of D18 Cell Technology at Dubai:** *Daniel Whitfield*<sup>1</sup>; Abdulmunim Al-Moniem Said<sup>1</sup>; Maryam Mohamed Al-Jallaf<sup>1</sup>; Ali Mohamed Al Zarouni<sup>1</sup>; <sup>1</sup>Dubai Aluminium Company Limited

Despite the development and construction of new pot technologies at Dubai Aluminium, development and improvement of the original D18 cell technology has been sustained, and continues to play a significant part of the growth and expansion of the company. This paper summarises the progress of the original D18 cell technology at Dubai over the past few years, and its contribution towards the goal of 1 million tonnes plant annual (hot metal) production. Amperage has increased from an original design target of 155kA up to 196kA in 2008. To ensure adequate pot performance is maintained with this increase in production, there has been significant development of the cell alumina, bath chemistry and heat balance control. Other changes such as anode size increase, modifications to the cathode and measures to ensure busbar integrity have allowed for further planned amperage and production increase over the next five years.

3:00 PM

**ACD Measurement and Theory:** *Marianne Jensen*<sup>1</sup>; Kjell Kalgraf<sup>1</sup>; Tarjei Nordbø<sup>2</sup>; Tor Bjarne Pedersen<sup>1</sup>; <sup>1</sup>Elkem Aluminium ANS; <sup>2</sup>Elkem Research

People generally assume that the ACD is constant nearly all the time in prebake pots. The argument is that the anode consumption will soon bring any deviations in the ACD to zero because the current will increase where the ACD is lower and vice versa. Measurements, however, show that there are great variations in the ACD between the different anodes in the same pot. Differences of 2 cm are not uncommon, and there are also more regular variations along the pot side depending on the position in the anode set cycle. This is because anodes are being replaced, and the ACD is therefore never in equilibrium, but always in a transient state. The current distribution and the magnetic field are constantly changing and affecting the ACD distance. Findings agree with modeled results. A method was developed to measure the ACD.

3:20 PM Break

3:40 PM

**Improved Cell Operation by Redistribution of the Alumina Feeding:** *Bjorn Moxnes*<sup>1</sup>; Asbjorn Solheim<sup>2</sup>; Morten Liane<sup>3</sup>; Anveig Halkjelsvik<sup>1</sup>; Ellen Svinsås<sup>1</sup>; <sup>1</sup>Hydro Aluminium Sunndal; <sup>2</sup>SINTEF Materials Technology; <sup>3</sup>Hydro Aluminium Technology Centre Årdal

The local anode-cathode distance in aluminium cells, as well as the local superheat, depend strongly on the local concentration of alumina in the bath. Based on the idea that it is beneficial to have a uniform alumina concentration, a measurement campaign aiming at a redistribution of the alumina feeding was undertaken at the SU4 potline, Hydro Aluminium Sunndal. By using AIF<sub>3</sub> as a tracer, the path of each alumina dosis could be followed by measuring the current pick-up at each individual anode. This enabled mapping of the connection between each of the alumina feeders and the anodes. Based on the measurements, the rate of each individual alumina feeder was optimised in test cells. The change turned out to be highly successful with respect to improved operational results, such as higher current efficiency, reduced anode effect frequency, and less anode problems. Optimised alumina feeding has now been implemented in the entire potline.

4:00 PM

**Improving Anode Cover Material Quality at Nordural – Quality Tools and Measures:** *Halldor Gudmundsson*<sup>1</sup>; <sup>1</sup>Nordural

Anode cover material (ACM) composition and granulometry determines the properties of the anode cover. This paper describes the experience Nordural has had with a new ACM mixing station employing autogeneous milling and dense phase to convey the material to the potrooms. The pros and cons of this system for delivering the required granulometry is discussed by showing the evolution of the ACM granulometry before and after the commissioning of the new mixing station. To evaluate the effect of the conveying system the granulometry of the material at the output of the mixing station is compared with the granulometry of the material on the anodes. The automated XRD/XRF method for bath analysis has been used to evaluate the alumina- and chiolite composition of the ACM which can impact the bath mass balance and cover structural stability. Finally, heat flux data is shown as one measure of quality.

4:20 PM

**Comparison of Bubble Noise of Søderberg Pots and Prebake Pots:** *Kjell Kalgraf*<sup>1</sup>; Marianne Jensen<sup>1</sup>; Tor Pedersen<sup>1</sup>; Tarjei Nordbø<sup>1</sup>; <sup>1</sup>Elkem Aluminium Research

In previous work we analyzed the relationship between bubble noise, bath height, and anode quality with data mostly from Søderberg pots. We have now acquired additional data for both Søderberg pots and for prebake pots. From an accidental current increase from 127 to 145 kA over 2 days at a Søderberg plant, we can see both the immediate increase of bubble noise proportional to the square of the current, and the gradual decline of bubble noise due to increasing crack area in the anode. For prebakes, however, the response is different. In the short run the bubble noise is increasing when bath height goes up, because of increased adhesion when pressure goes up, but after 1-2 hours the bubble noise has fallen to a value lower than before the bath height went up. This happens because less current flows in the central regions when there is more gas there, and more current flows further away from the central region, giving a steeper slope of the anode closer to the boundary. In fact, the long term decline of bubble noise for prebake pots is very similar to the decline found for Søderberg pots when bath height goes up. Because of the opposite short term and long term response, the correlation between bath height and bubble noise of prebake pots can be positive for rapid height changes and negative for height changes with a bigger time spacing.

### Applicable Computing Technologies in Heat Treating: Numerical Modeling and Simulation for Heat Treatment

Sponsored by: TMS Materials Processing and Manufacturing Division, TMS/ASM: Computational Materials Science and Engineering Committee

Program Organizers: Lei Zhang, Scientific Forming Technologies Corporation (SFTC); Yiming Rong, Worcester Polytechnic Institute

Wednesday PM

Room: 3000

February 18, 2009

Location: Moscone West Convention Center

Session Chairs: Yiming Rong, Worcester Polytechnic Institute; Lei Zhang, Scientific Forming Technologies Corporation

2:00 PM Introductory Comments

2:05 PM

**Modeling of Carbon Behaviors during Hot and Cold Rolling in Low Carbon Steels:** *Kyung Jong Lee*<sup>1</sup>; J.M. Choi<sup>1</sup>; J.Y. Lee<sup>1</sup>; K.S. Lee<sup>1</sup>; K.J. Lee<sup>1</sup>; <sup>1</sup>Hanyang University

It is very important to understand interstitial carbon behaviors in cold rolled steel to get the good formability as well as the high strength. In low carbon steel, most of carbons are consumed by the formation of grain boundary cementite during cooling. During heating and holding between Ae1 and Ae3, cementite is dissolved and consequently carbon enriched austenite is formed. In this study, the effect of heating rate and holding temperature on carbon by the formation and dissolution of cementite and austenite are modeled by nucleation and growth, diffusion and dissolution. Partitioning of substitutional elements is also considered.

2:25 PM Question and Answer Period

2:30 PM

**Microstructure-Based Models for the Austenitization of Steels during Industrial Heat-Treatment Processes:** *Ramanathan Krishnamurthy*<sup>1</sup>; Narendra Singh<sup>1</sup>; Amy Clarke<sup>1</sup>; <sup>1</sup>Caterpillar Inc

Reliable predictions of property changes in steels during industrial heat treatment processes require accurate descriptions of the kinetics of associated solid state phase changes, and accompanying changes in microstructure, over a specimen of macroscopic dimensions. Here, we describe such a model for the kinetics of austenitization of a ferritic-pearlitic steel. Nucleation of austenite grains, cementite platelet decomposition, and carbon-diffusion driven ferrite-austenite transition are all included in the model. The effect of the initial ferritic-pearlitic microstructure on austenitization is included through the effect of the various length scales characterizing it. Temperature gradient effects and temperature and carbon concentration dependent carbon diffusivities



are also included. Model predictions compare well with continuous heating transformation curves generated from dilatation experiments. We show model predictions for spatial and temporal variations in the progress of austenitization obtained by integrating the current model within a full-scale simulation of an induction heat treatment process, to demonstrate its efficacy.

## 2:50 PM Question and Answer Period

### 2:55 PM

**Multiphase Flow Model of Porosity Formation for Casting Process of Aluminum Alloy:** Gang Wang<sup>1</sup>; Yiming Rong<sup>1</sup>; Shoumei Xiong<sup>2</sup>; <sup>1</sup>Worcester Polytechnic Institute; <sup>2</sup>Tsinghua University

An integrated model for the casting process of binary aluminum alloy has been implemented on CFD prediction in this paper. The model, which uses much of the multicomponent multiphase fluid architecture as a comprehensive system, involves solid-liquid change, latent heat term, Darcy-based flow in mushy zone, and entrapped air shift. It can predict the formation derived from air entrapment, and the morphology and distribution of porosity. The model is demonstrated on a representative 2-D aluminum shape casting example, in which it produces reasonable results and describes generation and distribution of porosities with detailed flow structure.

## 3:15 PM Question and Answer Period

### 3:20 PM Break

### 3:35 PM

**Problems in Assessing Thermal Diffusivity of Steel Constituents for Quench Simulation:** Donato Firrao<sup>1</sup>; Paolo Matteis<sup>1</sup>; Chiara Pozzi<sup>1</sup>; Elena Campagnoli<sup>1</sup>; Giuseppe Ruscica<sup>1</sup>; Ion Vasile<sup>1</sup>; Marian Miculescu<sup>2</sup>; <sup>1</sup>Politecnico Di Torino; <sup>2</sup>Universitatea Politehnica Bucuresti

In developing a finite-elements thermo-metallurgical model of the quench of carbon and low-alloy steels, a significant improvement can be obtained from the knowledge of the thermal diffusivity of each metallographic constituent possibly involved in the process (martensite, bainite, pearlite, stable and metastable austenite), as a function of temperature. Two medium-carbon steels designed for quenching and tempering and one low-carbon precipitation hardening steel, all employed to fabricate large plastic molds, were examined. Standard flash measurements were performed at increasing temperatures on each steel constituent and on as-received mixed-microstructure material. Non-standard measurements were performed on metastable austenite during continuous cooling, to avoid the phase transformation. The thermal diffusivity was determined by fitting the whole thermal transient data with analytical models. Two separate testing apparatuses, equipped with different vacuum furnaces, pulse sources (flash lamp, pulse laser) and temperature detectors (infrared pyrometer, thermocouple), yielded significantly different results, which are thoroughly compared and discussed.

## 3:55 PM Question and Answer Period

### 4:00 PM

**Modelling of Precipitation Hardening in Aluminium Alloys with the KWN Model:** W. George Ferguson<sup>1</sup>; Linda Wu<sup>1</sup>; <sup>1</sup>University of Auckland

Phase separation in supersaturated metastable solid solution is often assumed to occur in three distinct steps: nucleation, growth and coarsening. However, recent studies have shown that these processes significantly overlap which leads to the formation of a particle population that can be described by the particle size distribution (PSD). The Kampmann and Wagner Numerical (KWN) model is a powerful method for dealing with concomitant nucleation, growth and coarsening and for predicting the evolution of the size distribution. In the present work, the precipitation kinetics are modeled by the KWN method, and a strength model is used to evaluate the resulting change in strength at room temperature by taking into account contributions from the lattice resistance, solid solution hardening and precipitation hardening. The modeling is applied to isothermal and non-isothermal heat treatments and is validated by comparison with experimental results.

## 4:20 PM Question and Answer Period

### 4:25 PM

**A Thermal-microstructure Model to Predict the Grain Growth of a Dual-phase Steel DP980 in Laser Heat-treatment:** Fanrong Kong<sup>1</sup>; Soundarapandian Santhanakrishnan<sup>1</sup>; Dechao Lin<sup>1</sup>; Radovan Kovacevic<sup>1</sup>; <sup>1</sup>Research Center for Advanced Manufacturing

A coupled model combining an experiment-based finite element analysis with Monte Carlo method was developed to study the grain evolution in the heat-affected zone (HAZ) of heat treated dual phase steel DP 980 by direct diode laser. In this study, an energy distribution model matching the peculiarity of direct diode laser beam was considered to obtain the temperature field. In addition, the Monte Carlo method was applied to simulate the grain growth in the HAZ based on the calculated temperature history of heating and cooling process. The martensite decomposition in the HAZ of DP 980 has also been involved into consideration. The results show that temperature gradient in the HAZ decreases with an increased scanning speed for the fixed laser power. Thereby, the mean grain size of HAZ becomes finer and the percentage of martensite decomposition in the HAZ will be smaller with increase in the laser scanning speed.

## 4:45 PM Question and Answer Period

### 4:50 PM

**Surface Modification of Tool Steel AISI S7 by Using High-Power Direct Diode Laser:** Soundarapandian Santhanakrishnan<sup>1</sup>; Fanrong Kong<sup>1</sup>; Dechao Lin<sup>1</sup>; Radovan Kovacevic<sup>1</sup>; <sup>1</sup>Southern Methodist University

Key components used in die making industries require high quality molds with superior surface quality and mechanical properties. Tool steel AISI S7 has found an application in this area since it is characterized with shock and impact-resistance. To retain the core property and to produce a hardened surface, laser surface hardening technique can be used. The objective of this work is to determine the surface hardening conditions by using a high power direct diode laser. Compared to other lasers, direct diode laser has several unique properties for localized heat treatment such as a rectangular (12x1 mm) beam footprint and shorter wavelength (808 nm). Results show that the treated area includes a melted zone and a heat affected zone (HAZ), and their geometry depends on the process parameters. A machine vision system including a high speed camera and an optical filter was developed to monitor the treated area in real-time.

## 5:10 PM Question and Answer Period

### 5:15 PM

**Study of Natural Convection in a Closed Square Cavity:** Xiang-mei Li<sup>1</sup>; Jie-yu Zhang<sup>1</sup>; Wei-hua Qi<sup>1</sup>; Bo Wang<sup>1</sup>; <sup>1</sup>Shanghai University

Natural convection flow analysis in closed cavities has many thermal engineering applications, such as cooling of electronic devices, energy storage systems and the process of solidification. In particular, natural convection in the thermally driven closed cavity is one of the classical problems. In this paper, the feasibility of the investigation of heat and momentum transfer by using CALCOSOFT software was testified in comparison with some reported results. Simultaneously, numerical solutions were presented by studying the influences of Rayleigh number on the streamlines, isotherms, and the variation of velocity, temperature and Nusselt numbers. With the increase of Rayleigh number, the heat transfer mechanism was changed from heat conductivity to natural convection, and boundary layer began to form near the sidewalls. Dimensionless velocity in the midpoint of the cavity was equivalent to zero while dimensionless temperature was equal to 0.5. And Nusselt and Rayleigh numbers possibly abides by a certain rule.

## 5:35 PM Question and Answer Period

### 5:40 PM

**Solution on the Heat Transfer Coefficients during the Heat Treatment Process of a Turbine Disk:** Jiafeng Zhang<sup>1</sup>; Jinwu Kang<sup>1</sup>; Baicheng Liu<sup>1</sup>; Jinwen Zou<sup>2</sup>; Shunquan Liu<sup>2</sup>; <sup>1</sup>Tsinghua University; <sup>2</sup>Institute of Aeronautical Materials

Heat treatment, as one of the most important processes of manufacturing P/M superalloy turbine disk, determines its final microstructure and properties. It is necessary to understand the cooling potential of the quenching media and the actual cooling rate of the disk to ensure fast and even cooling and avoid defects such as deformation and cracks. In this paper, a series of quenching experiments of a sample turbine disk were carried out. Thermal couples were placed at center of the disk with different depth. And only the measured surface was exposed

while the other surfaces were insulated to ensure one dimensional heat transfer. Based on the cooling curves of the measured points, the heat transfer coefficient was calculated by the inverse heat transfer method. The heat transfer coefficients of the top and bottom surfaces were obtained during forced air cooling and oil quenching.

## Biological Materials Science: Implant Biomaterials II - Scaffolds

Sponsored by: The Minerals, Metals and Materials Society, TMS Structural Materials Division, TMS Electronic, Magnetic, and Photonic Materials Division, TMS: Biomaterials Committee, TMS/ASM: Mechanical Behavior of Materials Committee  
Program Organizers: Ryan Roeder, University of Notre Dame; John Nychka, University of Alberta; Paul Calvert, University of Massachusetts Dartmouth; Marc Meyers, University of California

Wednesday PM Room: 3014  
February 18, 2009 Location: Moscone West Convention Center

Session Chairs: Ryan Roeder, University of Notre Dame; Paul Calvert, University of Massachusetts

### 2:00 PM Keynote

**PEEK Biomaterials: From Isoelastic Hip Stems to Bone Scaffolds:** *Steven Kurtz*<sup>1</sup>; <sup>1</sup>Drexel University and Exponent

Developed in the 1980s, Polyetheretherketone (PEEK) is a relatively new structural biomaterial that is gaining increased acceptance for use in orthopedic and spine implants. With over a decade of clinical experience, PEEK composites can be tailored with elastic moduli ranging from titanium alloy, at the high end, to cortical and cancellous bone, at the low end of the spectrum. Used initially in spinal cages due to its MRI-compatibility, recent PEEK research has been focused on isoelastic hip stems, thin orthopedic bearings, and bioactive composites. This talk will provide researchers with an overview of current orthopedic and spinal applications for PEEK biomaterials, a primer on the biocompatibility and biotribology of PEEK, as well as and recent advances in bioactive PEEK composites.

### 2:40 PM

**In-Vitro Bioactivity and Mechanical Properties of a Novel Implantable Biomaterial: Nano-Tricalcium Phosphate-Silicone Rubber Nanostructured Composite:** *Jinesh Shah*<sup>1</sup>; *Wah Wah Thein-Han*<sup>1</sup>; *Qiang Yuan*<sup>1</sup>; *Devesh Misra*<sup>1</sup>; <sup>1</sup>University of Louisiana

An excellent vehicle to achieve the objective of good cell attachment and proliferation of fibroblast and osteoblast in conjunction with the desired mechanical properties in an implant is to consider compounding a bioactive material with the superior mechanical properties of a scaffold. The approach to accomplish this objective involves the synthesis of tricalcium phosphate (TCP) nanoparticles using the concept of reverse micelle, which are dispersed via shear mixing and ultra-sonication, followed by cryo-compounding with silicone rubber (SR) and pressure-induced solidification. Experiments using the approach have confirmed that high strength-at-break and undiminished intrinsic ductility of silicone rubber and high cytocompatibility are achieved by uniquely combining the high-extensibility of silicone rubber with bioactive and bone-bonding properties of nano-TCP. Such composites represent a new class of biomaterials for biomedical implants and scaffolds, where ultra-fine surface features are used to modulate cell-substrate interactions and to ensure the long term stability of the implant.

### 3:00 PM

**Mechanical Behavior of Hydroxyapatite Whisker Reinforced Collagen Scaffolds:** *Robert Kane*<sup>1</sup>; *Ryan Roeder*<sup>1</sup>; <sup>1</sup>University of Notre Dame

Hydroxyapatite-collagen composite scaffolds have been investigated as a tissue engineering scaffold that mimics the extra-cellular matrix of bone tissue. While numerous hydroxyapatite-collagen scaffolds have been fabricated, the effects of hydroxyapatite addition on the mechanical properties of the scaffolds have not been systematically investigated. Freeze-dried collagen scaffolds were fabricated with equiaxed or unidirectional pore structures, three hydroxyapatite whisker reinforcement levels (1:1, 2:1, and 4:1 mass ratio of hydroxyapatite to collagen), and cross-linked by heating to 105°C for 24 h under vacuum. HA whiskers were observed to be aligned within each collagen strut. Unconfined

uniaxial compression tests showed that increased levels of hydroxyapatite resulted in an increased apparent elastic modulus and strength for scaffolds with either an equiaxed and unidirectional pore structure.

### 3:20 PM

**Pre-Osteoblast Response of Biomimetic Chitosan/Nano-Hydroxyapatite Composite Scaffolds for Bone Tissue Engineering:** *Wah Wah Thein-Han*<sup>1</sup>; *Devesh Misra*<sup>1</sup>; <sup>1</sup>University of Louisiana

We describe here three dimensional biodegradable chitosan-nanohydroxyapatite (nHA) composite scaffold with improved mechanical, physico-chemical, and biological properties compared to pure chitosan scaffolds for bone tissue engineering. High and medium molecular weight chitosan scaffolds with 0.5, 1, and 2 wt.% fraction of nHA were fabricated by freezing and lyophilization. The nanocomposite scaffolds were characterized by a highly porous structure with interconnected pores and the pore size was similar for the scaffolds with varying content of nHA. The nanocomposite scaffolds exhibited greater compression modulus, slower biodegradation rate and reduced water uptake, but the water retention ability was similar to pure chitosan scaffolds. Favorable biological response of pre-osteoblast (MC 3T3-E1) on nanocomposite scaffolds includes improved cell adhesion, higher proliferation, and well spreading morphology in relation to pure chitosan scaffold. The study underscores chitosan-nHA composite as a potential scaffold material for bone regeneration.

### 3:40 PM Break

### 3:50 PM

**Genetically Engineered Inorganic-Binding Peptides for Medical Applications:** *Candan Tamerler*<sup>1</sup>; *Mehmet Sarikaya*<sup>2</sup>; <sup>1</sup>Istanbul Technical University; <sup>2</sup>University of Washington

We utilize peptides and protein constructs as molecular building blocks in synthesizing, assembling, and fabricating materials systems. The major components in this approach are inorganic binding polypeptides which are selected through combinatorial biology methods and tailored for their functionality through post selection engineering approaches. Here, we will explain how genetic engineering tools can be employed for tailoring functionality, and then present examples from different medical application areas by describing their use: i. On calcium phosphate materialization with controlled morphology. ii. As molecular films and scaffolds in developing biocompatible materials, including testing engineered peptide effects on cell proliferation, adhesion and toxicity. Here, we will summarize our work on the induced mineralization on scaffolds prepared by hydroxyapatite-binding peptides conjugated with peptide hydrogels. The results show that combinatorially selected peptides may be used to tailor morphogenesis of calcium phosphate in restoration or regeneration of hard tissues such as those in teeth and bone.

### 4:10 PM

**Creation of Ovalbumin Based Porous Scaffolds for Bone Regeneration:** *Gabrielle Farrar*<sup>1</sup>; *Justin Barone*<sup>2</sup>; *Abby Morgan*<sup>1</sup>; <sup>1</sup>Materials Science and Engineering, Virginia Tech; <sup>2</sup>Biological Systems Engineering, Virginia Tech

Despite recent discoveries in tissue engineering, there is still a need for bio-based materials due to synthetic polymer failure. 3D porous bio-based scaffolds have been made in the past; however ovalbumin has not been researched. Ovalbumin is a natural protein, therefore, ovalbumin cross-linked with glutaraldehyde was the focus in this research. Salt leaching and freeze drying were used to create interconnected porous structures needed for tissue formation. Mechanical properties were determined using compression tests and DMA. Thermal properties were investigated using DSC and beta sheet formation using FTIR spectroscopy. Scaffolds were sterilized with ethylene oxide prior to seeding. WST-1, von Kossa and live/dead assays were used to examine proliferation, calcium deposits and glutaraldehyde toxicity on cells. OPN and ALP levels were also tested to determine cell differentiation and mineralization. Biodegradability was investigated to determine mass loss. This work demonstrated the use of ovalbumin scaffolds for bone tissue engineering applications.

### 4:30 PM

**Templated Precipitation and Growth of Calcium Phosphate Nanocrystals on Self-Assembling Ionic Block Copolymers:** *Yusuf Yusufoglu*<sup>1</sup>; *Mathumai Kanapathipillai*<sup>1</sup>; *Aditya Rawal*<sup>2</sup>; *Yanyan Hu*<sup>1</sup>; *Yunus Kalay*<sup>1</sup>; *Klaus Schmidt-Rohr*<sup>1</sup>; *Surya Mallapragada*<sup>1</sup>; *Mufit Akinc*<sup>1</sup>; <sup>1</sup>Iowa State University; <sup>2</sup>University of California, Santa Barbara

In an effort to imitate the growth of natural bone, polysulfobetaine-based zwitterionic and poly acrylic acid-based self-assembling ionic pentablock

copolymers were employed as templates for growth of calcium phosphate nanocrystals from aqueous solutions. Calcium and phosphate ions were dissolved in block-copolymer micellar dispersion at low temperatures and hierarchically assembled nanocomposite calcium phosphate-copolymer gels were prepared at pH ~5. As the ions were driven into the interstitial cavities of polymer micelle structures by aging at ambient temperature, inorganic nanoparticles were formed at the polymer-inorganic interface, presumably nucleated by ionic interactions. XRD experiments revealed that calcium phosphate in the zwitterionic copolymer gel was natural brushite, while the one in PAA-based pentablock gel was synthetic brushite. TEM, solid-state NMR and SAXS studies showed that calcium phosphate precipitated on and interacted with the polymer micelles forming approximately 15 nm diameter nanospheres. Further, inorganic fraction of the nanocomposite was around 30 wt% of dried hydrogel.

## Bulk Metallic Glasses VI: Joint Session of Mechanical Behavior of Nanostructured Materials and Bulk Metallic Glasses VI: Mechanical Behavior of Nano and Amorphous Materials

Sponsored by: The Minerals, Metals and Materials Society, TMS Structural Materials Division, TMS/ASM: Mechanical Behavior of Materials Committee

Program Organizers: Peter Liaw, The University of Tennessee; Hahn Choo, The University of Tennessee; Yanfei Gao, The University of Tennessee; Gongyao Wang, University of Tennessee; Xinghang Zhang, Texas A & M University; Andrew Minor, Lawrence Berkeley National Laboratory; Xiaodong Li, University of South Carolina; Nathan Mara, Los Alamos National Laboratory; Yuntian Zhu, North Carolina State University; Rui Huang, University of Texas, Austin

Wednesday PM Room: 3012  
February 18, 2009 Location: Moscone West Convention Center

Session Chairs: Nathan Mara, Los Alamos National Laboratory; Julian Raphael, Columbus McKinnon

### 2:00 PM Keynote

**Micromechanisms for Plastic Flow in Nanocrystalline and Amorphous Metals:** *Frans Spaepen*<sup>1</sup>; <sup>1</sup>Harvard University

Amorphous or glassy metals can be considered the ultimate nanostructure, in that their microstructural length scale is the atomic one. Correspondingly, their strength approaches the theoretical strength of the material. In the absence of lattice periodicity, plastic deformation of glassy metals can not occur by the motion of dislocation. Instead, the deformation occurs by sequential shear of equiaxed pockets of atoms. It has recently become possible to observe this process directly by confocal tracking of the particles in a colloidal glass. Nanocrystalline materials, even with very small grain size, still have a structure that is fundamentally different from that of a glass. It is interesting, therefore, to compare the mechanical properties and flow mechanisms in the two types of materials.

### 2:30 PM Invited

**Systematic Studies of the Hall-Petch Breakdown:** *Christopher Schuh*<sup>1</sup>; Jason Trelewicz<sup>2</sup>; <sup>1</sup>MIT

The breakdown of Hall-Petch scaling in the finest nanocrystalline metals has been the subject of speculation and controversy for some time. With recent advances in techniques to synthesize nanocrystalline alloys and control their grain size, new possibilities have emerged for systematic experimental exploration of the Hall-Petch breakdown. In this talk, our work on binary nanocrystalline alloys with grain sizes ranging from 2-200 nm is discussed. The scaling of strength, as well as its rate-, pressure-, and temperature-dependence are systematically revealed across the entire range of the Hall-Petch breakdown. Activation energies, activation volumes, and pressure coefficients are revealed through the regime of mechanistic changes. Additionally, the effects of annealing, relaxation, and alloy composition are addressed. Some points of confusion in the literature are clarified through these data, such as the presence vs. absence of "inverse Hall-Petch" scaling, the role of alloy composition, and the tendency for shear localization.

### 2:50 PM

**Atomic Scale Study of Plastic-Yield Criterion in Nanocrystalline Metals Using Molecular Dynamics Simulations:** *Avinash Dongare*<sup>1</sup>; A. Rajendran<sup>2</sup>; B. LaMattina<sup>2</sup>; M. Zikry<sup>1</sup>; Donald Brenner<sup>1</sup>; <sup>1</sup>North Carolina State University; <sup>2</sup>Army Research Office

The plastic deformation mechanisms of nanocrystalline materials depend on the interplay between dislocation and grain boundary processes. A reduction in grain size results in an increase in yield strength of materials, a relation known as the Hall-Petch effect. Recent studies indicate that the increase in strength with decreasing grain size reaches a maximum after which further a decrease in the grain size (less than ~ 15 nm) results in the weakening of the metal due to the shift in the dominating mechanism of plastic deformation from dislocation induced plasticity in the case of coarse grained materials to grain boundary sliding in the case of ultra-small grain sizes. The commonly used yield criteria for polycrystalline metals and alloys are the Tresca and the von Mises criteria. These criteria are based on the maximum shear stress during loading, and the fact that the deformation of the metals is primarily due to the motion of dislocations. As a result, it can be expected that the yield criterion needs to be modified to account for the change in deformation mechanisms at the ultrafine grain size (= 10 nm) of nanocrystalline metals. The plastic-yield surface (three-dimensional) for these ultra-fine grain sized nanocrystalline Cu during multi-axial loading at room temperature will be presented. In addition we will discuss the inclusion of a normal stress dependence in addition to the maximum shear stress in the criterion to predict the yield surface for nanocrystalline metals.

### 3:05 PM

**Microstructure and Wear Resistance of Vacuum Hot Pressed Ti-Based Bulk Metallic Glass Composites:** *Pee-Yew Lee*<sup>1</sup>; Chih-Feng Hsu<sup>1</sup>; Hong-Ming Lin<sup>2</sup>; <sup>1</sup>National Taiwan Ocean University; <sup>2</sup>Tatung University

In the present study, Ti<sub>50</sub>Cu<sub>28</sub>Ni<sub>15</sub>Sn<sub>7</sub> metallic glass composite powders were successfully synthesized by mechanical alloying of powder mixtures of pure Ti, Cu, Ni, Sn, and carbon after 8 h of milling. The metallic glass composite powders were found to exhibit a large supercooled liquid region before crystallization. The thermal stability of the glassy matrix is affected by the presence of the carbon particles. Bulk metallic glass composite compact discs were obtained by consolidating the 8 h as-milled composite powders by a vacuum hot pressing process. Although the hardness of carbon/Ti<sub>50</sub>Cu<sub>28</sub>Ni<sub>15</sub>Sn<sub>7</sub> bulk metallic glass composites is increased with carbon addition, the wear resistance of the composites is not commensurate with their high hardness. The residual porosity and in situ-formed hard TiC particles inside the matrix of composites may be related to the increase in wear rate of Ti<sub>50</sub>Cu<sub>28</sub>Ni<sub>15</sub>Sn<sub>7</sub> bulk metallic glass composites with high carbon content.

### 3:20 PM Break

### 3:30 PM

**Electron Irradiation Induced Amorphization and Crystallization in Metallic Materials:** *Takeshi Nagase*<sup>1</sup>; <sup>1</sup>Osaka University, Research Center for Ultra-High Voltage Electron Microscopy

Atom-displacement mediated phase transitions between a glass phase and a crystal phase, namely, solid-state amorphization and crystallization not by thermal process but by mechanical process, can be induced by various techniques such as electron-irradiation (E-IR), severe plastic deformation (SPD), mechanical milling (MM), shot peening and so on. Among these processes, E-IR is an attractive technique because in-situ observations of the transition can be achieved without heavy contamination, or change in chemical composition, and with negligible temperature rise. Recently a unique disordering-ordering phase transition in metallic glass alloys driven by mechanical atom-displacement was found to take place during the MM and E-IR processes: a cyclic crystalline-amorphous (Cyclic-CA) transformation during MM, and a crystal-to-amorphous-to-crystal (C-A-C) transition during E-IR. In the present study, the electron irradiation induced C-A-C transition in metallic glasses will be reviewed. Materials discussed here include metallic glasses such as binary Zr-based, ternary Fe-Nd-B and Fe-Zr-B alloys.

### 3:45 PM

**Co-Deformed Metallic Glass/Light Alloy (MEGA) Sandwiches:** Jennifer Ragani<sup>1</sup>; Antoine Volland<sup>1</sup>; Sebastien Gravier<sup>1</sup>; *Jean-Jacques Blandin*<sup>1</sup>; Michel Suery<sup>1</sup>; <sup>1</sup>Grenoble Institute of Technology

MEtallic Glass / light Alloys (MEGA) multilayered materials were elaborated by high temperature co-deformation of the glass and the light alloy. The produced



multimaterials associate a zirconium based bulk metallic glass to light alloys (i.e. aluminium or magnesium alloys). Co-deformation was performed above the onset glass transition of the glass and the process conditions were selected on the one hand from the rheologies of both the metallic glass and the light alloys and on the other hand from information related to the thermal stability of the glass. After elaboration, structural and mechanical characterisations of the sandwiches were carried out. The effect of the ratio of the strains undergone by the glass and the light alloy during the process has been investigated. It was concluded that the quality of the bonding depends strongly upon the strain undergone by the glass during the process.

#### 4:00 PM Invited

**Strain Softening and Sample Size Effects in Bulk Metallic Glasses:** *Hongbin Bei<sup>1</sup>; S Xie<sup>2</sup>; S Shim<sup>1</sup>; Easo George<sup>1</sup>; <sup>1</sup>Oak Ridge National Laboratory; <sup>2</sup>The University of Tennessee*

Plastic deformation in crystalline metals occurs by the motion and multiplication of dislocations. In contrast, BMGs deform by highly localized shear bands. Therefore, there is much interest in understanding the relationships between shear band formation and mechanical properties. In this talk, first we will discuss shear banding induced softening in a Zr-based BMG. Systematic strain-induced softening was observed in the BMG, which contrasts sharply with the hardening typically observed in crystalline metals. Second, we will discuss how sample size affects mechanical behavior in both compression and indentation tests. In compression, even at the millimeter scale, stable shear band propagation and extensive plastic deformation can be achieved in small specimens in contrast to large specimens which fail catastrophically after limited plastic deformation. In indentation, it is found that the maximum shear stress to initiate plasticity in a Zr-based BMG is almost constant when the indenter radius is smaller than 70  $\mu\text{m}$ .

#### 4:20 PM

**Fatigue and Fracture Behavior of a Ca-Based Bulk Metallic Glass:** *Julian Raphael<sup>1</sup>; Gongyao Wang<sup>2</sup>; Peter Liaw<sup>2</sup>; Oleg Senkov<sup>3</sup>; Daniel Miracle<sup>4</sup>; <sup>1</sup>Columbus McKinnon Corporation; <sup>2</sup>University of Tennessee; <sup>3</sup>UES, Inc.; <sup>4</sup>Air Force Research Laboratory*

The compression and fatigue behavior of a  $\text{Ca}_{65}\text{Mg}_{15}\text{Zn}_{20}$  bulk-metallic glass (BMG) was studied in air at room temperature. During the preparation of cubical samples of the  $\text{Ca}_{65}\text{Mg}_{15}\text{Zn}_{20}$  for compression and fatigue investigations, small spherical cavities were found. Under both monotonic and cyclic compression loadings of the samples, fractures initiated in these cavities and propagated in a direction parallel to the loading axis. Finite element analysis (FEA) was used to model the fracture behavior. The FEA of a centrally located spherical void showed that under compression loading large tensile stresses evolved in the cavities. The orientation of the maximum principal stress was normal to the direction of crack propagation. FEA of a void located near the loaded surfaces was also performed and the influence of void location in the cubical sample on the fracture behavior was quantitatively discussed. GYW and PKL are very grateful for the support of NSF IMI Program.

#### 4:35 PM Invited

**Fracture and Strength of Bulk Metallic Glasses:** *Z. F. Zhang<sup>1</sup>; R. T Qu<sup>1</sup>; <sup>1</sup>Institute of Metal Research*

Tension and compression tests were systematically applied to various bulk metallic glassy (BMG) materials at room temperature for comprehensive understanding of their fracture and strength behavior. It is found that the fracture behavior of metallic glasses is strongly affected by the loading mode. Based on the experimental results, we propose an ellipse criterion as a new failure criterion to unify the four classical criteria above and apply it to exemplarily describe the tensile fracture behavior of BMGs as well as a variety of other materials. It is suggested that each of the classical failure criteria can be unified by the present Ellipse criterion depending on the difference of the ratio  $\alpha = \tau_v/\sigma_v$ . In addition, we designed some new tests to prove that the Ellipse criterion is better than the Mohr-Coulomb criterion. Furthermore, we developed the Ellipse criterion into a more general case through introducing a new parameter  $\beta$ .

#### 4:55 PM

**The Investigation of the Correlation between the Structure Evolution in the Elastic Region and the Plasticity of CuZrAl Bulk-Metallic Glasses with In-Situ Synchrotron X-Ray Measurement:** *Feng Jiang<sup>1</sup>; Yandong Wang<sup>2</sup>; Yang Ren<sup>3</sup>; Lu Huang<sup>4</sup>; Yan Li<sup>4</sup>; Tao Zhang<sup>4</sup>; Taleshi Egami<sup>1</sup>; Peter Liaw<sup>1</sup>; Hahn Choo<sup>1</sup>; <sup>1</sup>University of Tennessee; <sup>2</sup>Northeastern University; <sup>3</sup>Argonne National Laboratory; <sup>4</sup>Beijing University Aeronautic and Astronautic*

In the  $(\text{Cu}_{50}\text{Zr}_{50})_{100-x}\text{Al}_x$  ( $x = 4, 5, 6, \text{ and } 8$ ) glass-forming alloys, it has been found that minor deviations in composition can drastically change the plasticity of the alloys. The anisotropy in the structure function,  $S(q)$ , and the atomic pair density function,  $g(r)$ , was measured at ambient temperature with an in-situ high-energy synchrotron x-ray diffraction facility equipped with a loading device. The changes in the peak width of  $S(q)$  of  $(\text{Cu}_{50}\text{Zr}_{50})_{100-x}\text{Al}_x$  ( $x = 4, 5, 6, \text{ and } 8$ ) alloys indicate that the more homogeneous the atomic-level behavior, the better the plasticity.

#### 5:10 PM Invited

**New ZrCuNiAl Bulk Metallic Glasses with Superhigh Glass-Forming Ability:** *Jun Shen<sup>1</sup>; <sup>1</sup>Harbin Institute of Technology*

Three new Zr-Cu-Ni-Al bulk metallic glasses were developed through appropriate mixing of three binary eutectics Zr44Cu56, Zr51Al49 and Zr64Ni36. By suppressing solidification of competing crystalline phases, a new glass forming alloy  $\text{Zr}_{50.7}\text{Cu}_{28}\text{Ni}_{9}\text{Al}_{12.3}$  with the critical diameter of up to 14 mm is obtained. Structural analysis identified by Synchrotron radiation high energy X-ray diffraction (HEXRD) shows the first peaks for the three new alloys in the atomic pair distribution function curves all split into two sub-peaks. Based on D.B. Miracle's theoretical model, we consider substitution of smaller Cu atoms for Zr in the three investigated alloys is a very comfortable path to stabilize the ECP structure, which lead to an increased GFA.

#### 5:30 PM Invited

**Glass-Forming Ability and the Competitive Crystalline Phases for the Light-Weighted Ti-Be Based Alloys:** *Yong Zhang<sup>1</sup>; WeiGui Zhang<sup>1</sup>; JunPin Lin<sup>1</sup>; GuoJian Hao<sup>1</sup>; GuoLiang Chen<sup>1</sup>; <sup>1</sup>University of Science and Technology Beijing*

The glass forming ability (GFA) for the Ti-Be based alloys in the Ti-Be-Zr ternary alloy system was systematically studied. It is found that the best GFA obtained at a composition of  $\text{Ti}_{47}\text{Be}_{34}\text{Zr}_{19}$  in the Ti-Be-Zr ternary alloy system, and the bulk metallic glass (BMG) rod samples with diameter of 5 mm were fabricated by conventional Cu-mold casting. The competitive crystalline phases around the composition of the best GFA were determined by scanning electron microscopy (SEM) and X-ray diffractometer (XRD). The GFA of the ternary alloys were further improved by addition of a small amount of Vanadium. The largest supercooled liquid region  $\Delta T_x$  ( $\Delta T_x = T_x - T_g$ ,  $T_g$  is the glass transition temperature and  $T_x$  the crystallization temperature) in the ternary alloy system reaches 110 K for the  $\text{Ti}_{35}\text{Be}_{32}\text{Zr}_{33}$  alloy.

### Bulk Metallic Glasses VI: Structures and Modeling

Sponsored by: The Minerals, Metals and Materials Society, TMS Structural Materials Division, TMS/ASM: Mechanical Behavior of Materials Committee  
Program Organizers: Peter Liaw, The University of Tennessee; Hahn Choo, The University of Tennessee; Yanfei Gao, The University of Tennessee; Gongyao Wang, University of Tennessee

Wednesday PM

February 18, 2009

Room: 3007

Location: Moscone West Convention Center

Session Chairs: Mo Li, Georgia Institute of Technology; Wendelin Wright, Santa Clara University

#### 2:00 PM Invited

**Mechanical Response and Atomic Structure Characterization of Model Metallic Glasses:** *Mo Li<sup>1</sup>; <sup>1</sup>Georgia Institute of Technology*

Mechanical responses of several model metallic glasses under various external loadings are investigated using extensive molecular dynamics simulations, including shear, tension, compression, hydrostatic pressure, and bending. The structure changes associated with the mechanical deformation are characterized. In particular, the volume dilatation is seen to occur almost universally in all samples with the metallic bonding under these deformation modes, which is

closely related to the atomic packing and neighbor change. Of particular interest is the behavior of the model metallic glasses under compression. The systematic structure evolution is presented with an emphasis on the thermodynamic mechanism of stability and first-principle calculations.

**2:15 PM**

**Experimental Characterization of Shear Transformation Zones for Plastic Flow of Bulk Metallic Glasses:** *Mingwei Chen*<sup>1</sup>; <sup>1</sup>Tohoku University

The basic units of plastic flow of BMGs, in a form of a small cluster of randomly close-packed atoms known as shear transformation zones (STZs), are the key to establish a fundamental model of deformation of BMGs at low temperatures. However, despite of extensive theoretical predictions and MD simulations, a direct experimental portrayal of STZ volumes in BMGs is still missing due to their small length scales and diminutive time scales. Here we report an experimental characterization of STZ sizes by proposing an experimental approach based on a newly-developed cooperative shearing theory and traditional deformation thermodynamics. By determining the strength and its rate sensitivity, we measured STZ volumes of a variety of BMGs, which offers compelling evidence that the plastic flow of BMGs occurs through cooperative shearing of unstable clusters of atoms activated by shear stresses. This study offers a new way to gain a quantitative insight into the atomic-scale mechanisms of BMG mechanical behaviour and has implications for characterizing the physical processes in the dynamics and rheology of noncrystalline solids.

**2:25 PM Invited**

**Structure of Metallic Glasses: Beyond Pair Correlation Functions:** *Todd Hufnagel*<sup>1</sup>; <sup>1</sup>Johns Hopkins University

Traditional scattering techniques can reveal some aspects of the atomic short-range order of metallic glasses (through pair correlation functions) but cannot provide information about higher-order (three- and four-body) correlation functions or about structure over longer length scales (so-called "medium range order"). Here, we discuss the application of fluctuation electron microscopy to structural characterization of metallic glasses. We show that models of atomic-scale structure that are consistent with highly constrained pair correlation data from Pd-Ni-P metallic glasses are not improved by adding variable coherence fluctuation electron microscopy data as an additional constraint. This implies that the fluctuation signal is largely determined by the pair correlations, and is not the result of additional medium-range order. We discuss the implications of this finding for our understanding of metallic glass structure, as well as prospects for future progress.

**2:40 PM**

**Elementary Shear Banding in Model Metallic Glasses:** *Craig Maloney*<sup>1</sup>; *Anael Lemaitre*<sup>2</sup>; <sup>1</sup>Carnegie Mellon University; <sup>2</sup>Institut Navier

We present results on an extensive set of computer simulations on simple model atomistic amorphous solids in 2D. The deformation which results is shown to consist of avalanches of plastic activity which localize onto elementary shear bands, similar to those observed in analog macroscopic laboratory models such as bubble rafts and foams. These elementary shear bands have widths on the order of atomic dimensions and their role in the formation of the much larger-scale shear bands which are observed experimentally is currently a crucial open question. Key results are the emergence of a quantum of slip analogous to a Burgers vector and a universal value of the yield strain in good agreement with experiment.

**2:50 PM Invited**

**Molecular Dynamics Simulations of Poisson Ratio Effects in Metallic Glasses:** *James Morris*<sup>1</sup>; *Rachel Aga*<sup>1</sup>; *Takeshi Egami*<sup>2</sup>; *Valentin Levashov*<sup>2</sup>; <sup>1</sup>Oak Ridge National Laboratory; <sup>2</sup>University of Tennessee

Recent studies have indicated correlations between the Poisson ratio of a metallic glass and its properties. We provide direct evidence for this, using a new atomistic model that allows us to tune the Poisson ratio without changing the cohesive energy, lattice parameter, or bulk modulus of the crystalline phase. An increase in the Poisson ratio (from ~0.25 to ~0.3) dramatically stabilizes the disordered phase. The melting temperature drops nearly 30%, due in large part to a lower enthalpy of the liquid phase. The diffusion barrier drops by a comparable amount. We demonstrate the importance of shear fluctuations in the liquid properties, and that changes in this are correlated with changes in the liquid's structure and viscosity. Experimentally observable effects will be discussed. This research has been sponsored by the Division of Materials

Sciences and Engineering, Office of Basic Energy Sciences, U.S. Department of Energy under contract DE-AC05-00OR-22725 with UT-Battelle.

**3:05 PM Invited**

**Bond Deficiency Defects Assisted Flow in Amorphous Metals:** *Aiwu Zhu*<sup>1</sup>; *Gary Shiflet*<sup>1</sup>; *Joseph Poon*<sup>1</sup>; <sup>1</sup>University of Virginia

Atomic bond deficiency (BD), as characteristic defects, is considered to assist atomic rearrangement for mass transports in amorphous metals. Plastic strain (flow) response to external shear stress is attributed to local cooperative movements of multiple adjacent atoms that are facilitated by the aggregated BD defects. This complements the STZ model and can be formulated to reproduce observed features of steady-state flows. Additionally, it explains one of the puzzles concerning the density of expected defects for flow which is only the square of that for diffusion.

**3:20 PM Break**

**3:30 PM**

**Nanoindentation of Amorphous Alloys with Various Indenter Tips:** *Jae-il Jang*<sup>1</sup>; *Young-Wook Park*<sup>1</sup>; *So-Jung Kwon*<sup>1</sup>; *Byoung-Wook Choi*<sup>1</sup>; *Byung-Gil Yoo*<sup>1</sup>; <sup>1</sup>Hanyang University

In this study, we critically evaluated the influence of indenter geometry on the nanoindentation-induced elastic/plastic deformation of amorphous alloys which are known to exhibit an elastic-perfectly-plastic deformation and (arguably) no indentation size effect and thus are good for the analysis on the basis of classical contact mechanics theories. After performing nanoindentation experiments with a series of triangular pyramidal indenters having different centerline-to-face angles as well as various spherical indenters having different radii, we carefully compared the mechanical responses from spherical indentations to those from geometrically self-similar sharp indentations. Results are discussed in terms of the relationship between the constraint factor and the plasticity index. \* This work was sponsored by Hanyang Fusion Materials Program funded by Ministry of Education, Science and Technology, Korea.

**3:40 PM Invited**

**Molecular Dynamics Simulation of Structure and Liquid-Glass Transition in Cu-Zr Alloys:** *Mikhail Mendeleev*<sup>1</sup>; *Ryan Ott*<sup>1</sup>; *Matthew Kramer*<sup>1</sup>; *Daniel Sordelet*<sup>1</sup>; <sup>1</sup>Ames Laboratory

The diffraction experiments provide only information about pair correlations in non-crystalline materials and even these data are averaged over different types of atoms. Therefore, atomistic computer simulation is required for detailed analysis of structure. In this talk, we will discuss how semi-empirical interatomic potentials can be developed to provide an excellent agreement between molecular dynamics (MD) simulation and diffraction data for Cu-Zr alloys. Next we present the results of MD simulation of the structure and thermodynamics properties of these alloys. A special attention will be paid to the concentration dependences of liquid diffusivities and their relation to the best glass forming composition in this system. Finally, we will show how these properties depend on the cooling rate which varies in our simulations from 1e14 K/s to 5e9 K/s. Work at the Ames Laboratory was supported by the Department of Energy, Office of Basic Energy Sciences, under Contract No. DE-AC02-07CH11358.

**3:55 PM Invited**

**Experimental Studies of the Amorphous and Liquid Structures in the Cu<sub>1-x</sub>Zr<sub>x</sub> Binary System:** *Matthew Kramer*<sup>1</sup>; <sup>1</sup>Iowa State University

The short-range order of the bulk metallic glasses has been postulated to be dominated by icosahedral order. High energy X-ray scattering studies have been performed on compositions in the Cu<sub>1-x</sub>Zr<sub>x</sub> binary system to explore the relationship between the topological and chemical order in the liquid state and the amorphous state. In all compositions studied, the first diffuse scattering peak sharpens and shifts to a higher Q with undercooling. However, the most notable change in the S(Q) in the deeply undercooled state is a sharpening in the low Q side of the 2nd diffuse scattering peak which shifts to a lower Q with increasing undercooling. While the amorphous alloys show a clear bifurcation in the second diffuse peak, this is not observed in the undercooled liquid. The changes in the short range order will be discussed in light of molecular dynamics simulations using ab initio and embedded atom methods.

**4:10 PM Invited**

**Molecular-Dynamics Study of Shear Band Formation and Propagation in Zr-Based Metallic Glass under Indentation:** *Yun-Che Wang*<sup>1</sup>; Hong-Chang Lin<sup>1</sup>; Chun-Yi Wu<sup>1</sup>; Fengxiao Liu<sup>2</sup>; Chi-Chung Hwang<sup>1</sup>; Jinn Chu<sup>3</sup>; Yanfei Gao<sup>2</sup>; Peter Laiw<sup>2</sup>; <sup>1</sup>National Cheng Kung University; <sup>2</sup>The University of Tennessee; <sup>3</sup>National Taiwan University of Science and Technology

Formation and propagation of shear bands in metallic glasses dominate their mechanical properties. In this paper, the molecular dynamics models of the Zr-based metallic glass are first deposited with simulated sputtering processes. Then, the as-deposited films are used as initial structures for subsequent nano-indentation simulations. For the deposition simulations, a many-body, tight-binding potential is adopted for interatomic interactions among the multiple species of atoms. Interactions between metallic atoms and working gas (Ar+) are modelled with the pair-wise Molier potential. As for indentation simulations, a right-angle conical indenter tip is adopted, and homogeneous flow occurs to form pile-ups on the surface of the metallic glass; a signature for amorphous materials under indentation. Both three-dimensional stress and strain calculations reveal the formation and propagation of shear bands under the indenter tip and near the film-substrate interfaces. In addition, effects of loading rate are investigated.

**4:25 PM Invited**

**The Effects of Crystalline Phases on the Deformation and Fracture Behaviors of Fe-Based Bulk Metallic Glassy Alloys:** *Ke-Fu Yao*<sup>1</sup>; Chang-Qing Zhang<sup>1</sup>; Feng-Juan Liu<sup>1</sup>; <sup>1</sup>Tsinghua University

Different from the traditional glassy alloy which possesses limited whole plasticity, recently it has been found that some bulk metallic glasses exhibit high plasticity despite that the reason has not well been understood. Then investigating the factors influencing the deformation behavior of metallic glasses is meaningful and important, both for the understanding the deformation mechanism and for improving the mechanical properties of the glassy alloys. Here, we report that the in-situ formed nanocrystalline phases possess significant influence on the deformation ability and fracture behavior of bulk metallic glasses. For an Fe-based alloy, the full glassy alloy exhibits good plasticity, while with the increase of the crystalline phases, the whole plasticity of the alloys decreases greatly and the fractographical morphology changes significantly. The effects of the crystalline phases on the deformation and fracture behaviors of the glassy alloys have been discussed.

**4:40 PM**

**Structural Changes during Deformation of Zr-Based Metallic Glasses:** *Ashwini Bharathula*<sup>1</sup>; Weiqi Luo<sup>2</sup>; Wolfgang Windl<sup>1</sup>; Katharine Flores<sup>1</sup>; <sup>1</sup>Ohio State University

Flow defects in metallic glasses are commonly associated with locally increased free volume. Indeed, positron annihilation measurements reveal a trimodal distribution of open volume in several metallic glasses, suggesting that some regions are more open than others. This distribution shifts with deformation. However, a detailed description of the flow defect structure and operation is lacking. In the present study, the mechanical responses of simulated Zr-Cu and Zr-Cu-Al glasses under tension, compression and shear are investigated using large-scale molecular dynamics simulations. Fluctuations in the electron density distribution are examined to characterize the evolution of low atomic density regions with deformation. The computational results are compared with experimental results for a Zr-based glass. TEM investigations reveal that homogeneous flow in tension results in nanocrystallization, which is not observed during annealing at the same temperature. Evolution of the experimental glass structure with deformation is characterized using DSC, TEM, EELS, and positron annihilation spectroscopy.

**4:50 PM Invited**

**The Oxygen-Induced Degradation of Cu- and Zr-Based Bulk Glassy Alloys:** *Wu Kai*<sup>1</sup>; P. C. Kao<sup>1</sup>; P. K. Liaw<sup>2</sup>; <sup>1</sup>National Taiwan Ocean University; <sup>2</sup>Department of Materials Science and Engineering, The University of Tennessee

Cu- and Zr-based bulk metallic glasses (BMGs) have been extensively developed during the past two decades. These BMGs generally possess excellent mechanical properties and good corrosion resistance in various aqueous solutions. However, one important challenge to use them for certain applications is to retain their amorphous structure involved in thermal-activated processes at ambient atmospheres. In this study, the effect of oxygen on the degradation of several BMG systems near the glass transition temperature (T<sub>g</sub>) was discussed. In general, the degradation can be catalogued at three different cases, consisting of the first case of pre-oxidation, and then, followed by the substrate crystallization,

while a reverse situation was occurred for the second case. In addition, the third case was composed of the simultaneous oxidation and crystallization.

---

**Cast Shop for Aluminum Production: Casting Structure vs. Process**

Sponsored by: The Minerals, Metals and Materials Society, TMS Light Metals Division, TMS: Aluminum Committee

Program Organizers: Pierre Le Brun, Alcan CRV; Hussain Alali, Aluminium Bahrain

Wednesday PM

Room: 2005

February 18, 2009

Location: Moscone West Convention Center

*Session Chair:* Michel Rappaz, Swiss Federal Institute of Technology

---

**2:00 PM Introductory Comments****2:05 PM Keynote**

**Recovery vs Structure Driven DCCasting Process Optimisation:** *Philippe Jarry*<sup>1</sup>; <sup>1</sup>ALCAN Centre de Recherches de Voreppe

DCC has to be optimised along internal criteria as well as external to the casthouse. Oftentimes parameters have an influence both on the casting recovery and on the metallurgical structure of the slabs or billets, therefore certain heredity in the downstream fabrication schedule. Trade-offs are thus necessary. Distribution systems, casting recipes, grain refinement strategies, etc. will be successively reviewed at the light of both recent academic findings and industrial experience under this dual perspective. Most relevant issues will be pointed out and research avenues for the future will be suggested.

**2:35 PM**

**3D Modeling of the Flow and Heat Transfer during DC Casting with a Combo Bag:** Florin Ilinca<sup>1</sup>; Jean-François Héту<sup>1</sup>; *André Arsenault*<sup>2</sup>; Daniel Larouche<sup>2</sup>; Sylvain Tremblay<sup>3</sup>; <sup>1</sup>National Research Council, Industrial Materials Institute; <sup>2</sup>Laval University; <sup>3</sup>Pyrotek Inc

The goal of this study is to determine the influence of combo bag on the velocity and temperature fields in the liquid metal pool during the DC casting of aluminum ingots. For this, a 3D finite element solution algorithm is used to compute the flow and heat transfer phenomena. The solution approach is able to deal with high Reynolds number turbulent flows, buoyancy effects and flow through combo bag meshed openings. An isothermal study with turbulence modeling quantifies the effect of the combo bag on the flow and an effective viscosity is determined for the respective flow conditions. The coupled flow and heat transfer during ingot formation are solved for forced convection conditions (no buoyancy) and by including the natural convection terms. It will be shown that the flow is driven by the inlet flow rate in the vicinity of the combo bag and by natural convection outside this region.

**2:55 PM**

**Advanced CFD Modeling of DC Casting of Aluminum Alloys:** *Maimul Hasan*<sup>1</sup>; Kamal Ramadan-Ragel<sup>1</sup>; <sup>1</sup>McGill University

A 3-D CFD model for the simulation of vertical direct chill (DC) slab casting of aluminum alloys is developed. The basis of the model is the 3D time-averaged turbulent transport equations. An in-house developed CFD code is used to solve the modeled equations. The model is qualitatively and quantitatively verified by comparing the computed results with a physical water model and a real casting experiment of independent researchers. Each of the comparisons showed a good agreement. A parametric study has been carried out for a DC slab caster of aspect ratio 2.0 fitted with a combo bag for melt distribution from the nozzle. The primary and the secondary cooling zones are simulated by changing the heat transfer coefficient on the slab surface. An in-depth understanding is gained of some behaviors of the melt flow and solidification profile in the steady state operational phase of the commercial DC casting process.

**3:15 PM**

**Mathematical Modeling of DC Cast Sheet Ingots Using a Semi-Solid Tensile Constitutive Behaviour for Hot Tearing Prediction:** *Daniel Larouche*<sup>1</sup>; Dung-Hanh Nguyen<sup>1</sup>; Steven Cockcroft<sup>2</sup>; André Larouche<sup>3</sup>; <sup>1</sup>Laval University;

<sup>2</sup>University of British Columbia; <sup>3</sup>Rio Tinto Alcan

Hot tearing occurs generally during the last stages of solidification, especially near the solidus where the fraction solid is very high and the metal is under



tensile loading. When the deformation is too high for the strength of the semi-solid microstructure, rupture occurs and a defect appears if the liquid metal cannot feed the void created by the rupture. A stress-strain based theory has been developed previously and was applied based on tensile curves obtained with a direct chill surface simulator. The constitutive model built from the results represents the tensile behaviour of the alloy in the mushy zone. This constitutive behaviour was implemented in a 3D thermal-stress model of the direct chill casting process created within ABAQUS. Stresses calculated in zones where hot tearing occurs in DC casting were found to be close to the failure stresses found when the fraction solid lies in the interval 0.9 - 0.95.

### 3:35 PM

**A Comparison of Hot Tear Testing and Hot Tensile Testing of Al – Cu Alloys:** *David Viano*<sup>1</sup>; *Mary Wells*<sup>2</sup>; *David StJohn*<sup>3</sup>; <sup>1</sup>CSIRO; <sup>2</sup>University of Waterloo; <sup>3</sup>CAST

The determination of mechanical property data in the semi-solid region is vital for developing hot tearing numerical models. The mechanical properties are measured either during cooling from the fully liquid state or during reheating from the fully solid state. An experimental program was conducted comparing the two techniques on AA196, Al – 0.5wt%Cu and Al – 2wt%Cu alloys. Hot tear experiments were conducted using the CAST Hot Tear rig which measures load development during solidification. The same alloys were tested in an apparatus developed to test reheated alloys at temperatures above the solidus. A model was used to estimate the effect of solid state diffusion during the reheating test. Load development from the hot tear test and maximum stress from hot tensile tests were compared as a function of fraction solid. The results of this comparison and challenges faced in conducting these types of tests are discussed in this paper.

### 3:55 PM Break

### 4:15 PM

**Influence of Iron and Manganese on Structure and Microporosity of the DC Cast AA5083 Alloy:** *Carmen Stanica*<sup>1</sup>; *Petru Moldovan*<sup>2</sup>; *Gheorghe Dobra*<sup>3</sup>; *Cristian Stanescu*<sup>1</sup>; *Dionezie Bojin*<sup>2</sup>; <sup>1</sup>ALRO; <sup>2</sup>Politechnic University Bucharest

The AA5083 alloy is one of the most common alloys in the AA5XXX series wrought aluminum alloys. The effect of iron and manganese content intermetallics on the microstructure and microporosity has been studied by optical microscopy (OM), scanning electron microscopy (SEM) and energy – dispersive X-ray analysis (EDS). It was clear underlined that micropores formation is well connected with iron and manganese intermetallics, which cause blockage in the interdendritic channels which can hinder feeding and hence promote porosity.

### 4:35 PM

**Influence of Ultrasonic Melt Treatment on Structure Formation in Aluminum Alloys with High Amount of Transition Metals:** *Tetyana Atamanenko*<sup>1</sup>; *Dmitry Eskin*<sup>2</sup>; *Laurens Katgerman*<sup>1</sup>; <sup>1</sup>TU Delft; <sup>2</sup>Materials Innovation Institute

In the casting of aluminum, ultrasonics can be used to promote the formation of a fine, uniform, non-dendritic grain structure. From previous investigations it is known that main condition for obtaining fine equiaxed grain structure is a combined action of grain refiners and an intense ultrasound inducing developed cavitation on a solidifying melt. Additions of transition metals (Zr, Ti etc.) can significantly increase the number of nucleation sites in the melt without using an Al-Ti-B master alloy. Many commercial wrought aluminum alloys contain these elements because they also prevent recrystallization. The paper describes the results on the influence of zirconium and titanium in hypo- and hyperperitectic concentrations on structure formation during ultrasonic melt treatment (UST) in liquid state. In separate experiments, model binary Al-Zr and Al-Ti alloys are solidified with and without UST. The final microstructure is analyzed in terms of grain size and formation of intermetallics.

### 4:55 PM

**Ultrasonic Treatment of a Solidifying Al-Cu Melt in the Presence of Micron-Sized Hydrogen Bubbles:** *Mainul Hasan*<sup>1</sup>; *Ali-Reza Naji-Meidani*<sup>1</sup>; <sup>1</sup>McGill University

The possibility of dynamic grain refinement of aluminum alloys using high-powered ultrasonic waves in the presence of small hydrogen bubbles in the melt is explored. In this regard, a mathematical model is developed to simulate the dynamic behavior of a hydrogen bubble present in the mushy region of a solidifying aluminium-3.4 wt pct copper alloy melt under various applied ultrasonic pressure fields. Due to violent collapse of a small gas bubble, the melt pressure surrounding the bubble increases very rapidly. If the pressure in

the vicinity of the dendrites exceeds a threshold value, dendrite fracturing can take place. Dendrite fragments then can act as nuclei during metal crystallization process. This can lead to refined crystalline structure of the metal. This study demonstrates that even far from the bubble's surface, the melt pressure can be sufficiently high to fracture the dendrite arms and produce nuclei for equiaxed crystal growth.

### 5:15 PM

**Silicon Crystal Formation during DC Casting of Aluminium-Silicon Alloys:** *Torbjorn Carlberg*<sup>1</sup>; <sup>1</sup>Mid Sweden University

During brazing of automotive heat exchangers, aluminium alloys containing 7-12% silicon is used as filling material. Although these alloys are hypoeutectic, polyhedral silicon crystals, of a type similar to primary precipitation in hypereutectic alloys, can form before to the growth of the eutectic silicon. This occurs during casting of the alloys, which is done by the DC casting process. If these crystals are too large they can cause problems during the brazing. The polyhedral silicon crystal formation has been studied both in industrial ingots and in simulation experiments in a Bridgman furnace. It was found that the nucleation temperature and the cooling rate were important factors influencing the amount and size of the polyhedral crystals. Modelling of diffusion controlled growth of the silicon phase in this type of aluminium-silicon alloys shows how the nucleation temperature influences the morphology of the precipitated silicon, and how large crystals can be avoided.

### 5:35 PM

**Effect of Application of out-Phase Electromagnetic Field on Horizontal Direct Chill Casting of 7075 Aluminum Alloy:** *Qingfeng Zhu*<sup>1</sup>; *Zhihao Zhao*<sup>1</sup>; *Jianzhong Cui*<sup>1</sup>; *Yubo Zuo*<sup>1</sup>; <sup>1</sup>Key Laboratory of Electromagnetic Processing of Materials, Ministry of Education, Northeastern University

The effect of application of the out-phase electromagnetic field in HDC on the process and the metallurgical quality of ingots of 7075 alloy was investigated in detail. The results show that when out-phase electromagnetic field was applied, the effect of gravity on the HDC casting process was eliminated effectively, the temperature distribution in the pool become more uniform, cooling difference between upper surface and bottom surface and depth of sump was reduced, the sump shape was changed to be more symmetric about geometrical center of the mold, the thickness of segregation layer decreased and the surface quantity and the microstructures of the ingots were improved, the area of feathery grains decreased and the area of equiaxed grains increased, the equiaxed grains were refined and the floating grains eliminated so that the quality of the ingots was improved.

---

## Characterization of Minerals, Metals and Materials: Characterization of Microstructure of Properties of Materials IV

Sponsored by: The Minerals, Metals and Materials Society, TMS Extraction and Processing Division, TMS: Materials Characterization Committee, TMS/ASM: Composite Materials Committee

Program Organizers: Toru Okabe, University of Tokyo; Ann Hagni, Geoscience Consultant; Sergio Monteiro, State University of the Northern Rio de Janeiro - UENF

Wednesday PM

Room: 3009

February 18, 2009

Location: Moscone West Convention Center

*Session Chairs:* Dafei Kang, Michigan State University; Jeongguk Kim, Korea Railroad Research Institute

### 2:00 PM

**Structural Investigations of the Orientation Patterning in Plastically Deformed Single Crystals:** *Olga Dmitrieva*<sup>1</sup>; *Dierk Raabe*<sup>1</sup>; <sup>1</sup>Max-Planck-Institute for Iron Research

In this contribution we present the investigations of the orientation patterning on single crystals after a plastic shear deformation. The digital image correlation applied during the shear experiments allowed determining both the macroscopic deformation and the local strain distribution during the plastic deformation of the sample. The microstructure of the deformed crystals was investigated by high resolution electron backscattered diffraction (EBSD). By comparing the strain data to microstructure, orientation patterning effects such as the formation

of microbands can be correlated to the local rotation and shearing of the sample. The orientation pattern observed in high resolution EBSD experiments revealed local lattice rotations up to  $3^\circ$  within the microbands. The spatial distribution of the microbands was investigated using the combination of a focused ion beam with a high resolution EBSD analysis. This work was supported by the Deutsche Forschungsgemeinschaft.

#### 2:15 PM

**Quantification of the Mineral Phases in Sintered Ores from Gray Histogram of Micrograph:** *Xuwei Lv*<sup>1</sup>; *Lifeng Zhang*<sup>1</sup>; *Shaojiang Deng*<sup>2</sup>; *Chenguang Bai*<sup>2</sup>; <sup>1</sup>Missouri University of Science and Technology; <sup>2</sup>Chongqing University

An intelligent recognition and quantification system for the micrographs sintered ores was developed in the current paper. The average distribution parameters in a gray histogram of minerals were obtained using the Gaussian gray distribution model. The feature curves of the gray histogram of two minerals were achieved by combining the two density functions. The feature indexes, such as the number and position of the peaks and the valleys of two minerals in different ratios, were quantified by differentiating the distribution functions. This algorithm is able to extract the feature of the minerals adequately and accurately for recognizing the composition and phases of the minerals intelligently.

#### 2:30 PM

**Green Rust: Its Electrochemical Generation, Characterization, and Implications:** *Jewel Gomes*<sup>1</sup>; *David Cocke*<sup>1</sup>; *Hector Moreno*<sup>2</sup>; *Doanh Tran*<sup>1</sup>; *Appel Mahmud*<sup>1</sup>; *Kamol Das*<sup>1</sup>; *Mallikarjuna Guttula*<sup>1</sup>; <sup>1</sup>Lamar University; <sup>2</sup>Instituto Tecnológico de la Laguna

Green rust is an important intermediate in oxidative transformation of Fe(II) phase. This unstable compound contains a mixture of ferrous and ferric hydroxides that belong to a family of minerals known as layered double hydroxides (LDH). This brucite-type LDH contains anions such as chloride, carbonate and sulfate, and also water molecules filling the interlayers. In addition, either the bivalent or the trivalent iron can be replaced by other trivalent or bivalent metal ions. It was first identified as corrosion product, later in soils as a product of interactions between microbes and metals in soils. Due to its high reactivity, it is used in the reduction of organic and inorganic compounds, As removal, and the treatment of acid mine drainage. In this paper, we described the method of electrochemical generation of green rust and its characterization by XRD, SEM and FT-IR. We also illustrated its implications to electrocoagulation.

#### 2:45 PM

**Antimicrobial Property of Copper Stamp Sand:** *Jiann-Yang Hwang*<sup>1</sup>; *Domenic Popko*<sup>2</sup>; *Bowen Li*<sup>1</sup>; *Jaroslav Drelich*<sup>1</sup>; *Susan Bagley*<sup>1</sup>; <sup>1</sup>Michigan Technological University; <sup>2</sup>Lesktech Ltd.

Mining of native copper was active in the Upper Peninsula of Michigan in the last century. Stamp sand is the mining waste left behind after separating copper from the crushed rock fragments. It is estimated that there are about 500 million tons of stamp sands left in the area. Since the separation of copper was not complete in the early days, there are copper left in the stamp sand. Copper is an element that has the antimicrobial property. Therefore, a study to determine if the stamp sand has the antimicrobial property was carried out and the results are reported.

#### 3:00 PM

**Numerical Modeling of Liquid Flow Permeability on 3D Microtomographic Geometry of Al-Cu Alloys:** *Ehsan Khajeh*<sup>1</sup>; *Daan Maijer*<sup>1</sup>; <sup>1</sup>The University of British Columbia

Modeling the formation of defects related to the flow of interdendritic liquid, requires a good knowledge of the way in which permeability changes with local geometry of interdendritic channels. In this study, the permeability of Al-15.5wt%Cu and Al-19.5wt%Cu has been modeled by solving the full Navier-Stokes equations on real 3D geometries of interdendritic channels obtained by X-ray microtomography (XMT). The samples for XMT were obtained from different positions in directionally solidified cylinders in order to produce different microstructure for each composition. The flow has been solved using a 2nd-order accurate Finite Volume Method (FVM) approach. Marching-cube triangulation method was necessary to produce an accurate surface and unstructured volume meshes. Calculated values of permeability for this range of solid fraction show partial agreement with previous experiments and the Carman-Kozeny expression for flow through granular beds. Observed deviations are analyzed and attributed to the experimental difficulties of permeability measurements.

#### 3:15 PM Break

#### 3:35 PM

**Mechanical Behavior of Polyester Composites Reinforced with Alkali Treated Coir Fibers:** *Sergio Monteiro*<sup>1</sup>; *Hélvio Santafé Jr.*<sup>1</sup>; *Lucas da Costa*<sup>1</sup>; <sup>1</sup>State University of the Northern Rio de Janeiro - UENF

Polymeric matrix composites reinforced with coir fibers are being used in many industrial applications such as automobile interior panels and cushions. These composites have relatively low mechanical strength due to the weak fiber/matrix interface. The objective of the present work was to investigate the effect of a surface alkali treatment of the curaua fiber on the mechanical behavior of polyester composites with different amounts of these fibers. The treatment, also known as mercerization, was performed with distinct concentrations, 0.1 and 10% of NaOH at 1 min and 1 hour, before incorporation of the coir fibers into the polyester composite. The results showed no significant change in comparison to similar untreated coir fiber composites. A microstructure analysis revealed that, in addition to reducing the hydrophilic characteristic of the fiber, the treatment also affects the surface morphology and impairs the fiber/matrix interfacial strength.

#### 3:50 PM

**Characterization of the Mechanical Behavior of Epoxy Matrix Composites Reinforced with Ramie Fibers:** *Sergio Monteiro*<sup>1</sup>; *Frederico Margem*<sup>1</sup>; *Luiz Fernando dos Santos Jr.*<sup>1</sup>; <sup>1</sup>State University of the Northern Rio de Janeiro - UENF

Fibers extracted from the ramie plant have been traditionally used in textile and are now being considered as polymeric composite reinforcement owing to their superior strength. Recently the mechanical behavior of ramie fiber reinforced polyester composites was investigated but no significant improvement was found. Therefore, the objective of this work was to carry out a similar investigation by changing the type of polymeric matrix. Specimens with up to 30% in volume of ramie fibers incorporated into epoxy were bend tested until fracture. The results showed a moderate improvement with a tendency of decreasing stress for higher amounts of ramie fibers due to the weak interface developed with the epoxy matrix.

#### 4:05 PM

**Characterization of Clays from Campos Dos Goytacazes, State of Rio De Janeiro, Brazil:** *Carlos Maurício Vieira*<sup>1</sup>; *Sergio Monteiro*<sup>1</sup>; <sup>1</sup>State University of the Northern Fluminense

The main characteristics and physical and mechanical properties of clays from the county of Campos dos Goytacazes, located at the northern part of the State of Rio de Janeiro, Brazil, are presented. The characterization included mineralogical composition, chemical composition and particle size distribution. The properties related to water absorption, linear shrinkage and flexural rupture strength were obtained in samples that were prepared by 20 MPa uniaxial pressing and fired at 950, 1100 and 1250°C. The results showed that the clays are predominantly kaolinitic with high percentage of clay minerals. The kaolinitic structure associated with a small amount of fluxes confers a refractory behavior which makes difficult the sinterization and impairs the ceramic consolidation.

#### 4:20 PM

**Effect of the Particle Size of Incorporated Grog on the Properties and Microstructure of Clayey Bricks:** *Carlos Maurício Vieira*<sup>1</sup>; *Sergio Monteiro*<sup>1</sup>; <sup>1</sup>State University of the Northern Fluminense

The brick industry generates a significant amount of residues composed of broken pieces that can be recycled, after crushing, as a particulate type of waste called grog. In the present work a grog screened at two different particle size, 840 and 420  $\mu\text{m}$ , was reintroduced in the process in mixtures with clays to make bricks. The effect of the grog addition up to 20 wt.% on the properties and microstructure of bricks fired at 700°C was evaluated. The results indicated that both the particle size and the amount of grog addition changed the fired properties of the clayey body. Additions above 5 wt.% of grog, with the coarser particle size, decreased the mechanical strength of both the dry body and the fired ceramic pieces. By contrast, the finer particle size grog may be used up to 10% wt. without impairing the properties and corresponding microstructure of the clayey body.

4:35 PM

**Characterization of the Critical Length of Sisal Fibers for Polyester Composite Reinforcement:** *Sergio Monteiro*<sup>1</sup>; Wellington Inácio<sup>1</sup>; Felipe Perissé Lopes<sup>1</sup>; Lucas da Costa<sup>1</sup>; Luiz Fernando dos Santos Jr.<sup>1</sup>; <sup>1</sup>State University of the Northern Rio de Janeiro - UENF

From the leaves of the sisal plant (*Agave sisilana*) a relatively strong fiber can be extracted and is nowadays being investigated as a possible reinforcement for polymeric matrix composites. For this purpose, it is important to determine the critical length of the fiber with respect to the matrix to be reinforced. This has never been properly done for sisal fibers in polyester matrix. Therefore, this work characterized the critical length of sisal fibers, with different sizes, embedded in polyester capsules by means of pullout tests. The critical length obtained allowed the sisal fiber/polyester matrix interface shear stress to be calculated. The relevance of these values for polyester composites reinforcement with sisal fibers is discussed.

## Computational Thermodynamics and Kinetics: Thermodynamics

Sponsored by: The Minerals, Metals and Materials Society, ASM International, TMS Electronic, Magnetic, and Photonic Materials Division, TMS Materials Processing and Manufacturing Division, ASM Materials Science Critical Technology Sector, TMS: Chemistry and Physics of Materials Committee, TMS/ASM: Computational Materials Science and Engineering Committee

Program Organizers: Long Qing Chen, Pennsylvania State University; Yunzhi Wang, Ohio State University; Pascal Bellon, University of Illinois at Urbana-Champaign; Yongmei Jin, Texas A&M

Wednesday PM Room: 3002  
February 18, 2009 Location: Moscone West Convention Center

Session Chair: Raymundo Arroyave, Texas A & M University

2:00 PM Invited

**Massively Parallel Architectures and Alloy Theory:** *Axel Van De Walle*<sup>1</sup>; <sup>1</sup>California Institute of Technology

Numerous materials problems demand large-scale computational resources and Alloy theory problems are no exception. This talk discusses two specific computationally-intensive problems and their solutions: (i) the calculation of multicomponent alloy phase diagrams and (ii) the automated determination of structure-property relationships in crystals. The proposed methods rely on input from first principles electronic structure calculations and employ the so-called cluster expansion formalism (which, in some applications, must be generalized to handle tensors). The key insight is the realization that these problems can be cast into the form of a large number of smaller-scale weakly coupled ab initio calculations. To ensure efficiency, these tasks need to be dynamically created based upon earlier calculation output, thus requiring flexible scheduling schemes that are nevertheless compatible with existing queuing systems. We explain how these calculations can be efficiently carried out on shared large-scale supercomputers, such as the ones available via the Teragrid infrastructure.

2:30 PM

**Thermodynamic Description of the System Cu-Sn-P - Computational Thermodynamics and Experimental Investigation on the Systems CuSn and CuP:** *Monika Grasser*<sup>1</sup>; Florian Mayer<sup>1</sup>; Andreas Ludwig<sup>1</sup>; Johann Riedle<sup>2</sup>; Udo Hofmann<sup>2</sup>; <sup>1</sup>Montanuniversität of Leoben; <sup>2</sup>Wieland-Werke AG

Technical bronzes are based on Cu-Sn-P alloys. Sn and P tend to form microsegregations and macrosegregations during DC-casting why the involved phase diagrams are of great interest for industry. The paper shows experimental investigations with Differential Scanning Calorimetric measurements for the binary Cu-Sn and

Cu-P system and diffusion experiments. Besides, numerical calculations have been performed. The DSC measurements allow the identification of phase transformation temperatures. For the identification of the phase distribution, SEM investigations are applied. Most of the phases were detected. Diffusion experiments have been performed for two binary diffusion partners, namely CuSn<sub>20</sub> and CuP<sub>8.3</sub>, with a cylindrical geometry. Here information has been gained about diffusion coefficients of Sn and P under specific conditions. Besides, numerical calculations have been performed with ThermoCalc based on a user defined database. As a final step already published phase diagram data, resent experimental data, and numerical assessment work are compared.

2:50 PM

**First Principles Study of the Thermodynamics of Carbynes:** *W. Luo*<sup>1</sup>; *Wolfgang Windl*<sup>1</sup>; <sup>1</sup>OSU

Many years ago, a third solid carbon allotrope has been suggested to exist besides diamond and graphite called carbyne, consisting of linear carbon chains. Carbynes were suggested to form at high temperatures under pressure and have been suggested to be detrimental to the high-temperature performance of carbon materials. Even today, their existence is still under discussion, and no atomic structure for pure-carbon carbyne has been resolved. In this paper, we propose a structural model for carbynes, combining elements from previous work. Structural optimization within density functional theory shows that the crystallography of these structures agrees well with previous experimental results. The free energy of the proposed carbyne structures is calculated within wide ranges of temperature and pressure (1000 to 4000 K and 0 to 180 kbar) and is higher than that of graphite in the whole studied region. However, our calculations confirm that additional elements can stabilize carebynes.

3:10 PM

**Graphical Representation for Isothermal Kinetics of Non-Equilibrium Grain-Boundary Segregation and Its Applications:** *Tingdong Xu*<sup>1</sup>; <sup>1</sup>Central Iron and Steel Research Institute

A recent model for non-equilibrium solute segregation at the grain-boundary is expressed with graphs for the isothermal ageing at various temperatures after quenching from a solution temperature. Some new characteristics are found using the graphical representations. For the samples aged for a certain time at various temperatures, an ageing temperature exists at which solute concentration at grain boundaries reaches a maximum value and the critical time of the non-equilibrium segregation at the ageing temperature will be equal or close to the ageing time. These findings have important consequences for the analysis of grain boundary segregation during the common thermal cycles. A number of diverse and sometimes conflicting experimental results from a number of different labs are rationalized on the graphical representation. As the application of these new characteristics, a non-equilibrium grain-boundary segregation mechanism for intermediate temperature brittleness of metals and alloys is proposed.

3:30 PM

**Thermodynamic Assessment of Ce-Cr, Cr-La and Cr-Y Systems:** *Wren Chan*<sup>1</sup>; Michael Gao<sup>2</sup>; Omer Dogan<sup>2</sup>; Paul King<sup>2</sup>; <sup>1</sup>Carnegie Mellon University; <sup>2</sup>National Energy Technology Laboratory

In order to improve ductility and creep resistance, early rare earth elements are added to refractory metal based alloys to absorb residual oxygen in the alloy and form dispersion strengthening oxides. In this work, three binary systems, Ce-Cr, Cr-La and Cr-Y, were thermodynamically assessed based on available experimental data in the literature. The PARROT module of Thermo-Calc package was used to optimize the systems. Self-consistent and reasonable thermodynamic descriptions for all three systems were obtained.

3:50 PM Break



4:15 PM

**Thermodynamic Calculations Predicting MgO Saturated EAF Slag for Use in EAF Steel Production:** *Kyeising Kwong*<sup>1</sup>; James Bennett<sup>1</sup>; Rick Krabbe<sup>1</sup>; Arthur Petty<sup>1</sup>; Hugh Thomas<sup>1</sup>; <sup>1</sup>NETL, USDOE

The use of foamy slags is widely practiced in EAF steel production resulting in energy savings, productivity improvements, and enhanced refractory service life. Foamy slag requires the control of slag viscosity to sustain gas bubbles during processing. This is accomplished through the precipitation of magnesium wustite particles in the slag at the operating temperature. A thermodynamic program, Factsage®, was utilized to study the quaternary oxide system of MgO-CaO-FeO-SiO<sub>2</sub>, to predict the dual and MgO saturated EAF slag chemistry under different oxygen partial pressures, temperatures, and slag basicity. These predictions indicate a linear relationship between oxide components and slag basicity, from which an accurate prediction of the optimum slag chemistry can be made. The results of the Factsage® calculations will be compared to models developed by other researchers and experimental data. Also discussed will be how these results can be used from practical slag management during EAF steel production.

4:35 PM

**Thermodynamic Model as Double Function of Temperature and Molar Fraction for Aluminum-Tin Alloys:** *Cristian-Aurelian Popescu*<sup>1</sup>; Dragos Taloi<sup>1</sup>; Liana Vladutiu<sup>1</sup>; <sup>1</sup>University POLITEHNICA Bucharest

In this paper, a new thermodynamic model developed as double function of temperature and molar fraction for characterization of thermodynamic behavior of aluminum-tin alloys is presented. The model offers the advantage of computing thermodynamic functions of the aluminum-tin alloys in every composition and temperature desired. The proposed model is a polynomial model having sixteen interactions parameters which were determined using the least squares method based on three sets of data: own experimental results, equilibrium diagram and literature data. The experimental data were obtained in our laboratory using electrochemical measurements of activity. Using the model developed the molar thermodynamic functions and partial molar functions were computed. The comparison of the results computed using the model and the experimental and literature data have shown a very good correlation.

4:55 PM

**Estimation of Formation Enthalpies Using an Extended Miedema Approach:** *Pratik Ray*<sup>1</sup>; Mufit Akinc<sup>1</sup>; Matthew Kramer<sup>2</sup>; <sup>1</sup>Iowa State University; <sup>2</sup>Ames Laboratory

Formation enthalpy, which is an indicator of phase stability, is an important parameter in materials research. A number of methods can be used to calculate enthalpy. Ab-initio calculations can often give highly precise results, but are time intensive. Models based on solution thermodynamics, like CALPHAD, are based on expressing the thermodynamic variables as a polynomial function of temperature. These approaches are fast; but they require a prior extensive database. Semi-empirical models like Miedema's method can be used for extremely fast calculation of enthalpies in situations where a large number of alloys have to be considered in absence of a prior thermodynamic database. While the original Miedema's model was postulated for binary alloys, in this paper we attempt to extend it to ternary systems and use it for estimating formation enthalpies of a large number of Ni based ternary alloys.

5:15 PM

**Thermodynamic Calculation of CaSO<sub>4</sub>-Ca(OH)<sub>2</sub>-H<sub>2</sub>O System Phase Equilibria:** Xiaoyu Peng<sup>1</sup>; Yunyan Wang<sup>1</sup>; <sup>1</sup>Central South University

Pitzer theory was applied to calculate solubility in the ternary brine system of CaSO<sub>4</sub>-Ca(OH)<sub>2</sub>-H<sub>2</sub>O, and the phase diagram has been drawn at 298.15K. This diagram consists of one single-phase region and three two-phase regions. The single-phase region is the unsaturated solution zone, and three two-phase regions include the crystallization zone of CaSO<sub>4</sub>•2H<sub>2</sub>O, the crystallization zone of Ca(OH)<sub>2</sub> and the coexist zone of CaSO<sub>4</sub>•2H<sub>2</sub>O and Ca(OH)<sub>2</sub>. The interaction characteristics between the solubility of CaSO<sub>4</sub>(s) and Ca(OH)<sub>2</sub>(s) was also obtained. The results would provide a theoretical basis for the treatment and reuse of industrial wastewater, especially for the wastewater containing sulfate which would be treated by lime-milk neutralization.

5:35 PM

**Computing the Phase Diagram of the FeCr Binary Alloy by Path-Sampling Techniques:** *Gilles Adjanor*<sup>1</sup>; Manuel Athènes<sup>2</sup>; <sup>1</sup>EDF R&D; <sup>2</sup>CEA

Due to their potential application as structural material for fusion and Generation IV reactors, high-chromium ferritic/martensitic steels have recently received considerable interest. Ab initio results have shown that due to magnetism the sign of the mixing enthalpy of the Fe-Cr system changes at low temperature. One of the most challenging tasks is now to establish how this effect influences the phase diagram of the system. In a recent study, Monte-Carlo simulations in the semi-grand canonical ensemble and the thermodynamic integration method were applied, with their respective limitations. We report on the first attempt to apply a path-sampling method on this system. This method can be seen as a combination of the former methods in the limiting cases of fast and slow switching rates respectively. In addition, the analysis of path histograms yields a built-in criterion for diagnosing the convergence of thermodynamic potential estimates.

## Diffusion in Materials for Energy Technologies: Session IV

Sponsored by: The Minerals, Metals and Materials Society, TMS Structural Materials Division, TMS Electronic, Magnetic, and Photonic Materials Division, TMS Alloy Phases Committee, TMS High Temperature Alloys Committee, TMS/ASM Nuclear Materials Committee, TMS Solidification Committee, ASM-MSCTS Atomic Transport Committee  
Program Organizers: Jeffrey LaCombe, University of Nevada, Reno; Yongho Sohn, University of Central Florida; Carelyn Campbell, National Institute of Standards & Tech; Afina Lupulescu, GE; Ji-Cheng Zhao, Ohio State University

Wednesday PM  
February 18, 2009

Room: 3006  
Location: Moscone West Convention Center

*Session Chairs:* Carelyn Campbell, National Institute of Standards and Technology; Jeffrey LaCombe, University of Nevada, Reno

2:00 PM Invited

**Determination of the Diffusivity for Point Defects in Passivation Layer on NiTi and NiTiAl Thin Films:** K. T. Liu<sup>1</sup>; *Jeng-Gong Duh*<sup>1</sup>; <sup>1</sup>National Tsing Hua University

The shape memory NiTi and NiTiAl alloys are widely used in the biomedical application. In the electrolyte, the passivation layer is formed on the NiTi and NiTiAl. A Point Defect Model (PDM) based on the movement of cation and anion defects in an electrostatic field was carried out to explain the growth or dissolution behavior of a passivation layer on a NiTi and NiTiAl thin films. The potential drop was related to the barrier film/electrolyte interface on the applied voltage and to estimate the diffusivity of defect. The calculated value of diffusivity was in range of 10<sup>-16</sup> – 10<sup>-17</sup> cm<sup>2</sup>/s. This value was extracted from the potential relationship between the donor density and the film formation voltage. Besides, the Mott-Schottky (M-S) analysis also indicated that the movement of the major defect was contributed by the oxygen vacancy. The defect of oxygen vacancy revealed that the passivation film was an n-type semiconductor. Analysis has shown that the doping level within a passive film was rather large and in the order of 10<sup>20</sup> - 10<sup>21</sup> cm<sup>-3</sup> film. In the electrochemical reaction, the lower donor density and the lower diffusion coefficient retarded the movement of defect in the passivation layer and improved the stability of the passive film during corrosion.

2:30 PM

**Kinetic Monte Carlo Formation of Hollow Nanospheres Using the Kirkendall Effect:** Alexander Evtsev<sup>1</sup>; Elena Levchenko<sup>1</sup>; Irina Belova<sup>1</sup>; *Graeme Murch*<sup>1</sup>; <sup>1</sup>University of Newcastle

The experimental formation in 2004 of hollow nanospheres using the Kirkendall effect has attracted a great deal of interest because of the possible applications of these structures in a very wide range of technologies. An in-depth theoretical understanding of the phenomenon is lacking. Results of kinetic Monte Carlo simulations of the formation of a hollow nanosphere by interdiffusion from a core-shell binary system are presented. The faster diffusing species is located in the core whilst the slower diffusing species forms the shell. With its self-generated vacancies all stages of the hollow sphere formation process are observed in this model: interdiffusion, the supersaturation of the core of the

nanosphere by vacancies, precipitation of pores and eventual void formation. Results confirm the experimental conclusions that interdiffusion accompanied by the Kirkendall effect and Kirkendall porosity is one of the mechanisms responsible for the formation of hollow nano-objects.

## 2:50 PM

**Molecular Dynamics Study of Surface Segregation in Bimetallic Ag-Ni Core-Shell Nanoparticles:** Alexander Evteev<sup>1</sup>; Elena Levchenko<sup>1</sup>; Irina Belova<sup>1</sup>; Graeme Murch<sup>1</sup>; <sup>1</sup>University of Newcastle

Bimetallic nanoparticles have received considerable attention for their importance in catalysis and nanotechnology. Much of the research has focussed on binary metal systems that form ordered or random bulk alloys. But in another type of binary metal system such as Ag-Ni the two metal components do not mix appreciably in the bulk. Ag-Ni nanoparticles are expected to possess the surface character of Ag and the magnetic properties of Ni and have applications in many fields. At the nano-level, in addition to the tendency for phase separation, surface segregation of Ag is expected since it has a lower surface energy. Molecular dynamics is used to investigate the effect of surface segregation on the structure and atomic distribution of an initial Ag-Ni core-shell nanoparticle. It is found that Ag atoms diffuse through the Ni shell until they have completely covered the outer surface of this nanoparticle with a well-defined surface monolayer.

## 3:10 PM

**Ab Initio Study of Reordering in Microtwinning Deformation Mechanism in Ni Base Superalloys:** Libor Kovarik<sup>1</sup>; Ju Li<sup>2</sup>; Raymond Unocic<sup>1</sup>; Michael Mills<sup>1</sup>; <sup>1</sup>Ohio State University; <sup>2</sup>University of Pennsylvania

Microtwinning is an important deformation mechanism at intermediate temperature, low stress and low strain rate conditions in Ni base superalloys. The rate limiting process of the microtwinning deformation mechanism is the diffusion-controlled reordering in  $\gamma'$  phase. It is shown that reordering requires very simple, vacancy-mediated exchange between Al and Ni atoms. The energy barriers for the different pathways that lead to vacancy-mediated exchanges have been studied using ab initio calculations. Based on the results it is possible to predict the most favorable reordering pathways. The current results indicate that the diffusion coefficient for reordering should be similar to that for Ni self-diffusion considering an ideal Ni<sub>3</sub>Al system. The currently investigated alloy Rene 104 is a multi-elemental system. It will be discussed that other factors such as segregation of heavy elements at the twin interface may have a significant influence on the kinetics of reordering.

## 3:35 PM Break

## 3:50 PM Invited

**Interdiffusion Coefficients Extraction from Multicomponent Diffusion Couple Data:** Liang Jiang<sup>1</sup>; Shamik Chaudhuri<sup>2</sup>; Jack Madelone<sup>1</sup>; <sup>1</sup>GE Global Research; <sup>2</sup>GE Bangalore Engineering Center

The behavior of multicomponent diffusion can be complex due to the interdependence of diffusion among multiple elements. Interdiffusion coefficients are critical to characterize diffusion in multicomponent systems. Multicomponent diffusion couples are typically used to extract the interdiffusion coefficient. In the present study, various interdiffusion coefficients determination procedures are reviewed and a numerical inverse method is proposed. The numerical inverse method along with others is utilized to extract interdiffusion coefficients from experimental data of multicomponent diffusion couples. In this approach we are using an analytical diffusion solver to predict diffusion profiles and try to minimize the difference of the predicted profile and the experimental profile to estimate diffusion coefficients.

## 4:20 PM

**Accounting for Transient Ostwald Ripening in Creep Models of Multi-Modal Nickel-Base Superalloys:** James Coakley<sup>1</sup>; Hector Basoalto<sup>2</sup>; David Dye<sup>1</sup>; <sup>1</sup>Imperial College; <sup>2</sup>QinetiQ

Traditionally aero and industrial gas-turbine disc materials have been developed to ensure high resistance to fatigue cracking and propagation, as well as high yield strength, tensile strength, ductility and fracture toughness. Creep resistance has been given less emphasis due to the lower operating temperatures, but as operating temperatures increase over the years, disc components are being pushed into regimes where significant creep can occur. However, at these temperatures the microstructure may not be stable; significant diffusion-controlled coarsening of the, potentially multi-modal, precipitate distribution often occurs. An expansion of the Dyson microstructure-based creep model is presented in this talk that accounts for these effects using a modified LSW

model to account for the evolution of the precipitate distribution. Creep data and microscopy of the precipitate distribution obtained for the multi-modal nickel superalloy Nimonic 115 is compared to model predictions.

## 4:45 PM

**Thermal Stability of Ta-Based Diffusion Barriers:** Julien Nazon<sup>1</sup>; Bernard Fraisse<sup>1</sup>; Marie-Hélène Berger<sup>2</sup>; Jean-Claude Tedenac<sup>1</sup>; Nicole Fréty<sup>3</sup>; <sup>1</sup>Institut Charles Gerhardt - Université Montpellier II; <sup>2</sup>Centre des Matériaux P.M. Fourn - Ecole des Mines de Paris; <sup>3</sup>Institut Charles Gerhardt - Université Montpellier II

There has been recently an increasing interest in the development of diffusion barriers against electrical wiring copper used in the thermoelectric and microelectronic device technologies. In this context, the barrier efficiency of TaN(50 nm)/Ta(50 nm)/TaN(50 nm) multilayers against copper diffusion has been investigated and was compared with that of TaN(150 nm) single layers. Tantalum-based and copper thin layers were successively deposited using the sputtering process. The thermal stability of these Ta-based thin layers was experimentally studied from high temperature in-situ Glancing Angle X-ray Diffraction experiments, which were conducted in the temperature range of 773 to 973 K. The diffusion coefficient of Cu through the TaN single layer was calculated from these experiments. These analyses were associated to a microstructural characterization using Scanning and Transmission Electron Microscopies. The TaN/Ta/TaN barrier appeared to be more efficient in preventing Cu diffusion than the TaN single layer.

## 5:10 PM

**Site Preference and Diffusion in Ni<sub>3</sub>Al Alloyed with Ir, Ta or Re at 1200°C:** Narayana Garimella<sup>1</sup>; Yongho Sohn<sup>1</sup>; <sup>1</sup>University of Central Florida

Diffusion in L1<sub>2</sub>-Ni<sub>3</sub>Al with ternary alloying additions of Ir, Ta and Re was investigated at 1200°C using solid-to-solid diffusion couples, and examined with respect to site preference in ordered intermetallic compound. Average effective interdiffusion coefficients were determined directly from the experimental concentration profiles. Ni has the largest magnitude of average effective interdiffusion coefficient, followed by Al, Ir, Re and Ta. The average effective interdiffusion coefficients for Ir, Re and Ta are much smaller than those for Ni and Al. Tracer diffusion coefficients determined by extrapolation technique, and available literature also followed the same trend. The relative tendency of Ni, Al, Ir, Re and Ta to occupy the  $\alpha$ -Ni and  $\beta$ -Al sites are correlated to these diffusion coefficients, with due consideration for diffusion mechanisms as well as the size and coordination of atoms.

## 5:35 PM

**Isothermal Oxidation of  $\gamma$  (fcc) Ni-Cr-X and  $\gamma$  (fcc) Fe-Ni-Cr-X (X = Al, Si, Ge or Pd) Alloys at 800°C:** Narayana Garimella<sup>1</sup>; Michael Brady<sup>2</sup>; Yongho Sohn<sup>1</sup>; <sup>1</sup>University of Central Florida; <sup>2</sup>Oak Ridge National Lab

Isothermal oxidation of several  $\gamma$  (fcc) Ni-Cr-X and Fe-Ni-Cr-X (X = Al, Si, Ge or Pd) alloys was examined to assess the influence of alloying additions, Al, Si, Ge or Pd, with respect to ternary and quaternary interdiffusion behavior in these alloys. Alloys having various compositions in Ni-Cr-X and Fe-Ni-Cr-X (X = Al, Si, Ge or Pd) systems were arc-melt, chill-cast, and homogenized for 168 hours at 900°C. Isothermal oxidation was carried out in air at 800°C up to 1,008 hours. Change in specimen weight, microstructure of oxide scale and compositional changes in the alloy underneath the oxide scale were examined by using thermogravimetric analysis, X-ray diffraction, scanning electron microscopy, energy dispersive spectroscopy and electron probe microanalysis. The results from isothermal oxidation are discussed and related to our previous studies on ternary and quaternary interdiffusion studies where the influence of alloying additions were quantitatively reported via multicomponent interdiffusion analysis.

## Electrode Technology for Aluminum Production: Electrode Connections and Cathode Studies

Sponsored by: The Minerals, Metals and Materials Society, TMS Light Metals Division, TMS: Aluminum Committee

Program Organizers: Barry Sadler, Net Carbon Consulting Pty Ltd; John Johnson, RUSAL Engineering and Technological Center LLC

Wednesday PM  
February 18, 2009

Room: 2003  
Location: Moscone West Convention Center

Session Chair: Marilou McClung, Century Aluminum Co

### 2:00 PM Introductory Comments

#### 2:05 PM

**FEM Analysis of Voltage Drop in the Anode Connector Assembly:** *Hugues Fortin*<sup>1</sup>; Mario Fafard<sup>1</sup>; Nedelcho Kandevo<sup>2</sup>; Patrice Goulet<sup>1</sup>; <sup>1</sup>Laval University; <sup>2</sup>IREQ

During their service life, steel stubs are exposed to an extremely aggressive environment involving thermomechanical stresses and chemical attacks, causing their shape to change. These phenomena affect the thermo-electro-mechanical contact at carbon/cast-iron/steel interfaces and have a significant effect on anode voltage drop. To estimate this voltage drop, a 3D finite element model (FEM) of a whole anode was developed and solved with the in-house code FESh+. Different models of stub shapes representing degradation were compared with a new stub to determine variations in voltage drop. The analyzed parameter was diameter of the steel stubs.

#### 2:30 PM

**Electrical Losses in the Stub-Anode Connection: Computer Modeling and Laboratory Characterization:** *Nedelcho Kandevo*<sup>1</sup>; Hugues Fortin<sup>1</sup>; <sup>1</sup>Hydro-Quebec

The Joule heat dissipated in the anode connection is an important part of the anode power losses and it should be minimized. In this work, the electrical losses in the anodic connector were investigated through laboratory tests, microscope analysis and simple electrical 3D finite elements model (FEM). The electrical resistivity and the thermal expansion have been characterized for the three constitutive materials (steel, cast iron, carbon) as a function of the temperature. Special attention has been paid to the impact of the phase transition period on the electrical resistivity and the thermal expansion for steel and cast-iron. The interfacial contact resistance between the steel stubs and cast-iron has also been studied in the laboratory as a function of the temperature in the range from ambient to cell operating temperature. Ideas for reduction of anodic losses are suggested in this paper to improve the power efficiency of the aluminium reduction process.

#### 2:55 PM

**Challenges in Stub Hole Optimisation of Cast Iron Rodded Anodes:** *Daniel Richard*<sup>1</sup>; Patrice Goulet<sup>2</sup>; Olivier Trempe<sup>2</sup>; Marc Dupuis<sup>3</sup>; Mario Fafard<sup>2</sup>; <sup>1</sup>Hatch; <sup>2</sup>Aluminium Research Centre - REGAL; <sup>3</sup>GéniSim Inc.

Reduction of cell voltage through redesign of the stub holes of cast iron rodded anodes is an attractive idea. In practice, stub hole optimisation is not an easy task and in situ trials may yield what seem to be counter-intuitive results. A closer examination reveals a complex behaviour of the steel stub - cast iron - carbon joint. It was shown in previous work to be a non-linear thermal-electrical-mechanical coupled system. Minimisation of the stub-to-carbon voltage drop is a balancing act between contact surface area and electrical contact resistance. To gain insights into the merits of different designs, a finite element demonstration model was built using the in-house code FESh++. In order to take into account the rodding shop productivity, alternative configurations with a constant volume of cast iron were studied. The impact of cast iron mean thickness is also examined. Potential industrial applications are discussed.

#### 3:20 PM

**New Solutions for Stub-Anode Connection at Egyptalum:** *Adel Nofal*<sup>1</sup>; Mohamed Waly<sup>1</sup>; Mahmoud Agour<sup>2</sup>; Shaher Mohamed<sup>2</sup>; <sup>1</sup>CMRDI; <sup>2</sup>Aluminium Company of Egypt

This work studies the possibility of replacing the high phosphorus cast iron with other cast iron grades for casting of stub-anode connection collars

in the aluminum electrolytic cells to avoid the harmful effect of phosphorus on electrical resistivity of cast iron and contamination of primary aluminum. Bench scale measurements on the steel stub/cast iron collars/anode carbon combinations were conducted using different cast iron alloys such as high-and low-phosphorus grey irons and ductile iron with low and high carbon equivalents as well as other alloyed irons. The electrical resistivity and voltage drop values were measured at different temperatures and times. The alloy with the best performance was used in actual production conditions over a complete life cycle of the anode up to 850 °C and the results compared with the current situation.

#### 3:45 PM Break

#### 3:55 PM

**Use of Cell Autopsy to Diagnose Potlining Problems:** *Richard Jeltsch*<sup>1</sup>; <sup>1</sup>Jeltsch Consulting

The technique of cell autopsy, commonly used to determine the mode of failure of a single reduction cell, can be used to dig more deeply into potlining problems. Identification of such problems in a timely manner is important due to the long time horizon for implementation of the solutions. In this paper examples of problems with lining design, materials, cell construction, cell startup and cell operations found through the cell autopsy technique are described and illustrated.

#### 4:20 PM

**Autopsies of Spent Refractory Pot Linings – A Revised View:** *Kati Tschöpe*<sup>1</sup>; Christian Schöning<sup>2</sup>; Tor Grande<sup>1</sup>; <sup>1</sup>NTNU; <sup>2</sup>SINTEF

Cathode autopsies performed after pot failures or shutdowns of cells have frequently been used to investigate pot failure and degradation of cathode lining. The sequence of materials observed from the cathode to the non-reacted refractory lining has been assumed to reflect the situation before the pot was taken out of service. Here we demonstrate that this is not necessary the case. Based on annealing experiments, X-ray diffraction and electron microscopy we propose that the thermal gradient in the lining is reversed during cooling and that the physical appearance of the lining reflects a combination of cooling and operation of the cell. The presence of molten phases below the carbon cathode may therefore solidify from the top rather than towards the bottom of the lining. Finally, we show experimental evidence that Na (g) infiltrate the refractory lining and is the main attacking chemical specie in the reaction front.

#### 4:45 PM

**Energy Recovery and Amperage Increase in Aluminium Cells by Active Cooling of the Anode Yokes:** *Asbjørn Solheim*<sup>1</sup>; Bjørn Moxnes<sup>2</sup>; Kristin Vamraak<sup>3</sup>; Elin Haugland<sup>2</sup>; <sup>1</sup>SINTEF; <sup>2</sup>Hydro Aluminium

The anode stubs and yoke assembly acts as an important heat sink in aluminium electrolysis cells. Removing heat by cooling the yokes gives increased heat flow out of the cell. Experiments in an industrial cell indicated that 2.5-3.0 kW could be removed from each anode by using compressed air supplied to channels at the outside of the yoke, and there were positive correlations between air flow, amount of heat collected, and heat loss through the stubs. By covering the yoke with thermal insulation, 4.3 kW was collected at a temperature of 320°C, which is interesting with a view to electricity production from waste heat. Besides the inherent potential for amperage increase and energy recovery, a number of benefits can be anticipated, such as improved cell control (new manipulated variable), lower exhaust gas temperature, and improved electrical conductivity of the steel parts of the anode assembly due to lower temperature.

#### 5:10 PM

**Modelling of Collector Bar Sealing in Cathode Blocks with Cast-Iron:** *Benedicte Allard*<sup>1</sup>; Serge Lacroix<sup>1</sup>; Jean-Philippe Noyel<sup>2</sup>; Loig Rivoaland<sup>1</sup>; <sup>1</sup>Carbone Savoie; <sup>2</sup>Ecole Catholique des Arts et Métiers

Cast iron rodding is the most spread technique of collector bar sealing in the cathode blocks for the aluminium electrolysis cells. This operation needs to be carefully mastered, either because of all the safety issues involved in the operation, or because of the quality impact of the rodding on the future electrical performance of the cathode blocks in the pots. During cast-iron sealing the cathode blocks are submitted to thermomechanical stresses that can be very important and that may induce block cracking. A model has been developed with ANSYS® software to describe firstly the thermal distribution inside the cathode blocks and secondly the resulting stresses. The influence of different parameters related to the contact between the different products and to the thermal transfer mechanism is studied. First results on the thermal validation of the model and the level of stresses obtained in different types of conditions are also presented.



5:35 PM

## Evaluation of Contact Resistance in Electrodes of Hall-Heroult Process:

Laszlo Kiss<sup>1</sup>; Lyne St-Georges<sup>1</sup>; Mathieu Rouleau<sup>1</sup>; <sup>1</sup>University of Quebec

In the Hall-Heroult cells, the electrodes are made of carbon blocks where steel inserts are sealed with cast iron. The contact resistance between these solids influence the energy efficiency of the process and potentially the life of the cell. An experimental device has been developed where the thermal and electrical contact resistances are determined simultaneously from room temperatures up to 1000°C under mechanical loads corresponding to those in the real cell. Special attention is paid to the fabrication of the test samples to reproduce realistic cast-iron/carbon and cast-iron/steel interfaces. A procedure representative of industrial cathode and anode sealing is used for the fabrication of the contact surfaces. The conditions of friction (static and dynamic) between the two solids can also be analysed. Using an inverse mathematical method, the evolution of the friction mechanism as a function of the relative displacement between the samples can be followed.

## Fatigue: Mechanisms, Theory, Experiments and Industry Practice: Fatigue at High-Temperature and in Harsh Environments

Sponsored by: The Minerals, Metals and Materials Society, TMS Structural Materials Division, TMS/ASM: Computational Materials Science and Engineering Committee, TMS/ASM: Mechanical Behavior of Materials Committee, TMS/ASM: Nuclear Materials Committee

Program Organizers: Koenraad Janssens, Paul Scherrer Institute; Corbett Battaile, Sandia National Laboratories; Brad Boyce, Sandia National Laboratories; Luke Brewer, Sandia National Laboratories

Wednesday PM

Room: 3008

February 18, 2009

Location: Moscone West Convention Center

Session Chair: Brad Boyce, Sandia National Laboratories

2:00 PM Invited

## Low-Cycle Fatigue Properties of Single-Crystal Silicon Films in Harsh Environments: Pierre-Olivier Theillet<sup>1</sup>; Olivier Pierron<sup>1</sup>; <sup>1</sup>Georgia Institute of Technology

Understanding the mechanisms for fatigue crack initiation and propagation in micron-scale silicon is of great importance to improve MEMS reliability in harsh environments. Accordingly, this investigation studies the low-cycle fatigue properties of single-crystal Si films using kHz-frequency resonating structures. The influence of resonant frequency (4 vs. 40 kHz) and environment (30C/50%RH vs. 80C/90%RH) on the resulting S-N curves and resonant frequency evolution is monitored. During each fatigue test, consisting of successive bursts of cycles at large stresses, the resonant frequency is precisely measured (0.01Hz resolution) at low stress between bursts. We observe a continuous, monotonic decrease in resonant frequency for each fatigue test. The damage accumulation rates are not significantly influenced by the environment for fatigue lives shorter than 10<sup>7</sup> cycles, although they clearly are for longer fatigue lives. The underlying mechanism for the low-cycle fatigue behavior of single-crystal Si films is discussed in light of these experimental data.

2:30 PM

## The Effect of Processing, Microstructure, and Texture on the Elevated-Temperature Fatigue and Creep Behavior of Ti-6Al-4V-xB Alloys: Wei Chen<sup>1</sup>; Carl Boehlert<sup>1</sup>; Andrew Payzant<sup>2</sup>; Seshacharyulu Tamarisakandala<sup>3</sup>; Daniel Miracle<sup>4</sup>; <sup>1</sup>Michigan State University; <sup>2</sup>Oak Ridge National Laboratory; <sup>3</sup>FMW Composite Systems Inc.; <sup>4</sup>US Air Force

The effect of nominal boron additions on the elevated-temperature fatigue and creep deformation behavior of Ti-6Al-4V was evaluated. The alloys were evaluated in the as-cast and cast-then-extruded conditions. The creep resistance of the as-cast alloys significantly improved with increased B concentration, where almost an order of magnitude decrease in the secondary creep rate was observed between the Ti-6Al-4V-1B(wt.%) and Ti-6Al-4V(wt.%) as-cast alloys. For the same nominal B contents, the cast-then-extruded alloys exhibited significantly greater creep and fatigue resistance than the as-cast alloys. This was explained to be an effect of the TiB phase and  $\alpha$ -phase texture, and the decreased lath width in the cast and extruded alloys compared with the as cast alloys. The cast-then-

extruded alloys exhibited four times smaller lath widths than the as-cast alloys, and the  $\alpha$ -phase basal plane normal and TiB whisker axis were preferentially oriented parallel to the extrusion axis.

2:50 PM

## Effects of Microstructure on Fatigue Crack Growth Rate of Alloy 10 at Elevated Temperatures: Gilbert Mora<sup>1</sup>; Pete Kantzos<sup>1</sup>; <sup>1</sup>Honeywell International

The effects of microstructure on fatigue crack growth rate (FCGR) behavior have been studied in a powder metal, Alloy 10. It was processed in two ways, As-Hip and extruded and isothermal forge, and given subsolvus and supersolvus heat treatments to obtain a variety of microstructures. FCGR testing was performed using a triangular waveform at 20 cycles per minute. Dwell FCGR testing was performed using a 90 second dwell at max load. Test temperatures ranged from 315 to 760C. Fractography and metallography was used to document failure modes and microstructures. The biggest overall driver controlling dwell and non-dwell FCG was grain size, with coarse grain supersolvus microstructures displaying better FCGR behavior. Under dwell and non-dwell conditions, the failure mode for subsolvus microstructures was intergranular above 649C. For supersolvus microstructures the transition from mixed mode to intergranular was between 649 and 760C. These transitions were accompanied by an increase in FCGR.

3:10 PM

## Mechanistic Studies on Fatigue of Steels Welded with IN625 Alloy: Neeraj Thirumalai<sup>1</sup>; Raghavan Ayer<sup>1</sup>; Cary Marzinsky<sup>1</sup>; Russell Mueller<sup>1</sup>; Dan Lillig<sup>2</sup>; Mark Crawford<sup>2</sup>; Geoff Dunn<sup>2</sup>; Thomas Gnaupel-Herold<sup>3</sup>; <sup>1</sup>ExxonMobil Research & Engineering Co; <sup>2</sup>ExxonMobil Development Company; <sup>3</sup>NIST Center for Neutron Research

Superior fatigue performance of welded structures is critical for offshore applications in the oil and gas industry. Recently, it was shown that X-65 (65 ksi yield strength) steel tubulars joined with IN625 weld metal illustrated superior fatigue performance compared to those welded with carbon steel weld metal. The current study was initiated to understand the mechanisms underlying the difference in the fatigue performance in these two systems. We have conducted weld and base metal fatigue crack growth studies, microstructural analysis and full-scale residual stress measurements by neutron scattering, in steels welded with carbon steel and IN625 weld metals. In this presentation we will discuss the results of this study.

3:30 PM

## The Effect of Grain Boundary Microstructure on Hold-Time Crack Growth in Allvac 718Plus Superalloy: Leif Viskari<sup>1</sup>; Thomas Hansson<sup>2</sup>; Krystyna Stiller<sup>1</sup>; <sup>1</sup>Chalmers University of Technology; <sup>2</sup>Volvo Aero Corporation

High temperature Low Cycle Fatigue (LCF) tests incorporating a hold-time at maximum tensile load have shown to increase Crack Growth Rate (CGR) in Ni-base superalloys. For Allvac 718Plus, hold-time crack propagation has been shown to be predominantly intergranular. It is thus of interest to investigate any correlation between grain boundary microstructure and hold-time crack growth. Two conditions of 718Plus were investigated; a lean condition with very low amount of grain boundary phases and a rich condition with higher amount of grain boundary phases. The phases were characterized by Transmission Electron Microscopy (TEM) and Scanning Electron Microscopy (SEM) with Energy Dispersive X-ray (EDX) analyses. Hold-time testing was performed at 704°C using a load cycle of 10Hz with intermittent hold-times of 100s at maximum tensile load. The obtained microstructural characterization results were then correlated to results from hold-time fatigue testing.

3:50 PM Break

4:20 PM Invited

## High Temperature Fatigue of Nickel-Base Superalloys Single Crystals: Bernard Fedelich<sup>1</sup>; Rainer Sievert<sup>1</sup>; Hellmuth Klingelhöffer<sup>1</sup>; Birgit Skrotzki<sup>1</sup>; Pedro Portella<sup>1</sup>; <sup>1</sup>BAM

Due to their relatively simple microstructure, single crystal superalloys allow a useful insight into deformation mechanisms. On the other hand their intrinsic anisotropy can pose difficult questions to the measurement and interpretation of strain. In this paper we describe the mechanical response of uncoated specimens of different superalloys to fatigue loading including thermo-mechanical and biaxial fatigue. The concomitant changes in the gamma / gamma prime microstructure as well as the damage evolution are presented and set into relation to the observed mechanical behavior. On the basis of this extensive experimental

basis, a viscoplastic anisotropic model was developed and calibrated for different alloys. Finally, some practical applications are considered.

### 4:50 PM

**Investigation of Fatigue Crack Growth Mechanisms in a Monocrystalline Ni-Based Superalloy:** *Clarissa Yablinsky*<sup>1</sup>; Katharine Flores<sup>1</sup>; Michael Mills<sup>1</sup>; James Williams<sup>1</sup>; <sup>1</sup>Ohio State University

Historically, the critical design parameter for Ni-based superalloy turbine blades has been creep resistance. Recently, because of modern airfoil designs, the focus has broadened to include fatigue resistance, resulting in the need to better understand fatigue behavior. In this study, compact tension specimens of monocrystalline Ni-based superalloy René N5 were tested under cyclic loading conditions. Test temperature and frequency (0.5 Hz / 10 Hz) were varied in order to examine the effects of plastic zone size, recovery, and other time dependent processes on crack growth. Fracture surfaces and microstructures were characterized using a scanning electron microscope in order to examine crack path selection and the  $\gamma/\gamma'$  morphology along the crack wake and in the bulk material. Dislocation arrangements were characterized via transmission electron microscopy using conventionally prepared and site-specific foils prepared by focused ion beam techniques, in order to understand the damage mechanisms active during fatigue crack growth.

### 5:10 PM

**Microstructural Effects on Fatigue Behavior of Nickel-based Superalloy René 88DT at 593°C:** *Jiashi Miao*<sup>1</sup>; Tresa Pollock<sup>1</sup>; J Jones<sup>1</sup>; <sup>1</sup>University of Michigan

Fatigue behavior of polycrystalline nickel-based superalloy, René 88 DT, was investigated at 593°C using an ultrasonic fatigue testing apparatus. Within the testing stress range of 500 - 760MPa, all fatigue failures initiated internally. Critical microstructural features controlling fatigue crack initiation and early stage of small crack growth were identified by the combination of serial sectioning, orientation imaging microscopy (OIM) and quantitative fractographic analysis. Cyclic deformation substructures were characterized by transmission electron microscopy. Fatigue cracks initiated and propagated along {111} slip planes. Twin boundaries within favorably oriented large grains are important sources for cyclic damage in this alloy at 593°C. The influence of different microstructural factors on fatigue crack initiation and the fatigue life variability of this alloy will be described.

### 5:30 PM

**Creep Fatigue Behavior at High Temperature of a Udimet 720 Nickel-Base Superalloy:** *Thomas Billor*<sup>1</sup>; Patrick Villechaise<sup>1</sup>; Mustapha Jouiad<sup>1</sup>; José Mendez<sup>1</sup>; <sup>1</sup>LMPM ENSMA

Nickel-base superalloys employed for components in the hot parts of aircraft engines are subjected to both steady and fluctuating stresses due to high temperature, centrifugal force and high frequency vibrations. The present study concerns a polycrystalline cast and wrought Udimet 720 elaborated and forged by Aubert & Duval corp. and provided by Turbomeca. It focuses on the interaction between creep and fatigue at 700°C. For that, tests have been performed with a trapezoidal signal and a dwell time ranges from 1 to 50 seconds. Results are compared to "pure" creep and fatigue tests. The damage process relative to the different loadings is described from SEM observation. Deformation mechanisms (dislocations structures) have been studied by TEM. A special attention is paid on the role of the hold period to investigate the transition of mechanical behaviour and durability from the "pure" creep to the fatigue testing conditions.

## Friction Stir Welding and Processing-V: Session VI

Sponsored by: The Minerals, Metals and Materials Society, TMS Materials Processing and Manufacturing Division, TMS: Shaping and Forming Committee  
Program Organizers: Rajiv Mishra, Missouri University of Science and Technology; Thomas Lienert, Los Alamos National Laboratory; Murray Mahoney, formerly with Rockwell Scientific

Wednesday PM  
February 18, 2009

Room: 2014  
Location: Moscone West Convention Center

*Session Chair:* Anthony Reynolds, University of South Carolina

### 2:00 PM Invited

**Microstructure Development of Friction Stir Welded Joints in a AlMgSc Alloy:** Cesar Weis Olea<sup>1</sup>; *Jorge dos Santos*<sup>1</sup>; Telmo Strohaecker<sup>2</sup>; <sup>1</sup>GKSS Forschungszentrum; <sup>2</sup>UFRGS

Scandium is well known due formation of a large second phase Al<sub>3</sub>Sc which is responsible for significant microstructural control, promoting a high increase in material strength added to recrystallization inhibition. In this work, AlMgSc alloy 4 mm thick plates developed and provided by Airbus were joined by friction stir welding (FSW). Mechanical behaviour and local properties of the weld seam were evaluated by microhardness measurements, conventional tensile tests and, microflat tensile tests. Structural changes and precipitation features were investigated mainly using transmission electron microscopy, in order to understand microstructural evolution in the weld zones and to establish the relationships with mechanical behaviour. The Al<sub>3</sub>Sc precipitates present in the base material were very stable and the thermal cycle produced during welding was not able to deteriorate significantly the strengthening effect as evidenced by the mechanical testing. The AlMgSc joints presented in general similar mechanical behaviour to the base material.

### 2:20 PM

**Monotonic and Cyclic Deformation Behavior of Friction Stir Welded (FSW) Mg/Mg- and Al/Mg-Joints:** *Guntram Wagner*<sup>1</sup>; Dietmar Eifler<sup>1</sup>; Otmar Klag<sup>1</sup>; <sup>1</sup>University of Kaiserslautern

In this research project the friction stir weldability of die casted AZ31 and AZ91 was investigated. The FSW system was equipped with a measurement unit to record online temperatures and welding forces. In monotonic tensile tests with AZ31/AZ31-joints and AZ91/AZ91-joints a tensile strength at the value of the parent materials could be realized. By light microscopical investigations and two-dimensional hardness measurements it could be demonstrated that the FSW process leads to an extreme grain refinement of about 85% compared to the parent status. Furthermore lower hardness values and a significantly higher ductility was measured in the joining area. To describe the cyclic deformation behavior of the AZ31/AZ31- and AZ91/AZ91-joints, high resolution stress-strain-hysteresis as well as temperature and electrical resistance measurements were performed. As a result of the grain refinement and the higher ductility of the joints the cyclic deformation curves are characterized by cyclic hardening until macro crack growth.

### 2:40 PM

**Effect of Interface Characteristics on Transverse Tensile Strength of Dissimilar Metal Al-Mg Friction Stir Welds:** Perumal Venkateswaran<sup>1</sup>; Y. Chen<sup>2</sup>; *Anthony Reynolds*<sup>1</sup>; <sup>1</sup>University of South Carolina; <sup>2</sup>General Motors R&D

A series of friction stir welds was made between AZ31 magnesium alloy and 6063 aluminum alloy sheets. Weld quality was assessed via metallographic analysis, fractography, and transverse tensile testing. Transverse tensile strengths varied between 80 and 120 MPa; however, the ductility of all welds was low. Al-Mg intermetallic phases were identified by XRD and were observed to form a continuous film at the interface between the base metals. Transverse tensile strength was correlated to several interface features including: (1) maximum intermetallic layer thickness, (2) actual interface length, (3) extent of interpenetration between the aluminum and magnesium base materials, and (4) area fraction of micro-void coalescence on the fracture surfaces. Results indicate that maximizing the extent of interpenetration, promoting mechanical interlocking between the metallic phases, is the key to attaining reasonable transverse strength in Al-Mg dissimilar metal welds.

3:00 PM

**Dissimilar Friction Stir Welding of AA2024-T3 and AA7075-T6 Aluminium Alloys:** *Antonio Monaco da Silva*<sup>1</sup>; *Egoitz Aldanondo*<sup>1</sup>; *Pedro Alvarez*<sup>2</sup>; *Ainhoa Lizarralde*<sup>1</sup>; *Alberto Echeverría*<sup>1</sup>; <sup>1</sup>Centro de Investigación en Tecnologías de Unión LORTEK

The scope of this investigation is to evaluate the effect of joining parameters on the mechanical and microstructural properties of dissimilar aluminium alloys (3 mm thick AA2024-T3 and AA7075-T6 sheets) joints produced by friction stir welding. Material flow under different parameters and the effect of the location of the base materials during welding on the flow pattern have also been investigated. Microstructural features have been analysed; while mechanical performance has been investigated in terms of hardness and tensile testing. Onion ring formation has been associated with high rotational speeds; while at low rotational speeds the boundary between both base materials is clearly delineated. Failure of tensile specimens always occurs at the 2024 side (independent of the material location related to the pin rotation and welding direction). Microstructural observation has revealed the development of a recrystallised fine-grained stir zone, with two different grain sizes resulting from the two different base materials.

3:20 PM

**Fatigue Behavior of Friction Stir Welded (FSW) Aluminium Joints:** *Guntram Wagner*<sup>1</sup>; *Dietmar Eifler*<sup>1</sup>; *Markus Gutensohn*<sup>1</sup>; *Masahiro Endo*<sup>2</sup>; <sup>1</sup>University of Kaiserslautern; <sup>2</sup>Fujioka University

For the application of FSW in monotonically and cyclically loaded components, a detailed knowledge of the deformation behavior of the joints is required. The present work provides an overview of the deformation behavior of aluminium 5454 FSW-joints. In monotonic tensile tests the yield strength of the friction stir welded joints reaches up to 90% of the value of the parent material. In fatigue tests high-resolution plastic strain amplitude and electrical resistance measurements were performed to describe the cyclic deformation. With FSW-joints welded at different welding forces single step tests were carried out at constant stress amplitudes. With higher welding forces the plastic deformation during the first cycles increases as a result of the increasing size of the softened process zone and simultaneously the fatigue life of the joints increases. The development of the change in electrical resistance correlates in detail with the fatigue life as function of the welding force.

3:40 PM **Invited**

**Time-Dependent Variations of Residual Stresses in a Friction Stir Welded 6061-T6 Al Alloy:** *Wan Chuck Wool*<sup>1</sup>; *Zhili Feng*<sup>1</sup>; *Xun-li Wang*<sup>1</sup>; *Ke An*<sup>1</sup>; *Camden Hubbard*<sup>1</sup>; *Stan David*<sup>1</sup>; <sup>1</sup>Oak Ridge National Laboratory

We report the time-dependent variations of residual stresses observed in a friction stir welded (FSW) 6061-T6 aluminum alloy using neutron diffraction. 6.5-mm thick FSW Al alloy samples were prepared and installed in the residual stress diffractometer (NRSF2) at High Flux Isotope Reactor, Oak Ridge National Laboratory. The residual stress measurements were performed as a function of time from 2 to 10,000 hours after welding at 17 locations at different distances from the weld centerline along the mid-thickness of the plate. The results show that the tensile longitudinal stress noticeably decreased from 100 to 60 MPa near the weld centerline within about 50 hours after FSW. Causes of such time-dependent behavior could be attributed to the natural aging phenomenon of precipitates and the low temperature creep process in FSW Al alloys.

4:00 PM **Break**

4:10 PM

**Friction Stir Welding of Sc-Modified Al-Zn-Mg-Cu Alloy Extrusions:** *Carter Hamilton*<sup>1</sup>; *Stanislaw Dymek*<sup>2</sup>; *Oleg Senkov*<sup>3</sup>; <sup>1</sup>Miami University; <sup>2</sup>AGH University of Science and Technology; <sup>3</sup>UES, Inc.

Small additions of Sc to Al-Zn-Mg-Cu 7000 series alloys can significantly improve mechanical properties and augment the strength retention at low and elevated temperatures. This research program evaluates the residual mechanical and corrosion properties of Sc-modified Al-Zn-Mg-Cu alloy extrusions joined through friction stir welding. SSA038-T6 extrusions were friction stir welded at 175, 225, 250, 300, 350 and 400 RPM (weld velocity and force were held constant). Mechanical tests demonstrated that the highest joint efficiency was achieved at 250 RPM, but that the exfoliation corrosion resistance was lowest for this weld condition. Microstructural investigations through light, scanning electron and transmission electron microscopy correlate the residual properties of the welded alloy with the microstructure in each of the unique weld regions.

4:30 PM

**Friction Stir Welding Characterization of Double-Welded Al-7075 Joints:** *Meysam Mirazizi*<sup>1</sup>; *Amir Hosein Kokabi*<sup>1</sup>; <sup>1</sup>Sharif University of Technology

Double-welded friction stir welding of 7075 aluminium alloy was performed to investigate the effects of the second pass of weld on the microstructure of first pass and microstructure of final weld. Also the effect of pin length that influences the amount of overlapping of two stir zones was studied. Furthermore, the effect of heat input on microstructure of weld investigated by using various rotating speeds and welding travel speeds that results to various amount of heat input (hot, average, cold). Tensile test and shear punch test (SPT) were conducted to determine mechanical properties of joints. Experimental results indicated that second pass of weld and amount of heat input had significant effects on microstructure of weld. Somewhat overlapping of two passes in the middle of joint improved the mechanical properties of joint.

4:50 PM

**Reducing Tool Axial Stresses in HSLA-65 during the Plunge:** *Kenneth Ross*<sup>1</sup>; <sup>1</sup>Brigham Young University

Using friction stir welding to join high-carbon steels would be more common if the PCBN tool had a longer tool life. Because PCBN tools appear to fail due to normal loading, reducing normal stress in the tool should increase tool life. The highest stresses occur during the plunge. A broad study of z stresses during the plunge, first in Aluminum 7075 then in HSLA-65 steel, was conducted. In aluminum the lowest stresses were produced using pilot holes and a force control program. In HSLA-65 steel pilot holes greatly reduced stresses. It was discovered that increasing weld power decreases z-stress while the pin is engaged. When the shoulder is engaged increasing power increases z stress. A statistical analysis was performed and equations were derived to model stress during the plunge. Parameters are given for running a plunge with the least possible stress. Other findings are also discussed.

5:10 PM

**Material Flow and Texture Analysis of Friction Stir Welded Aluminum Alloys:** *Suk Hoon Kang*<sup>1</sup>; *Kee Bum Kim*<sup>2</sup>; *Heung Nam Han*<sup>1</sup>; *Kyu Hwan Oh*<sup>1</sup>; *Jae-Hyung Cho*<sup>1</sup>; *Chang Gil Lee*<sup>1</sup>; *Sung-Joon Kim*<sup>1</sup>; <sup>1</sup>Seoul National University

Friction Stir Welding (FSW) is an intricate process because threaded tool rotates and moves forward at the same time. Many researches on numerical flow simulations and direct flow visualization have been conducted for understanding the material flow behavior during the FSW process. In this study, material flow of Al6061-T651 sheet joined by FSW was investigated by electron backscattered diffraction (EBSD). It was confirmed that the forward movement of the tool pin resulted in a loose contact between the tool pin and the receding material during FSW. The amount of incompletely rotated material due to the loose contact was estimated from the tilt angle of the shear texture which could be obtained from a pole figure.

5:30 PM

**Investigation of a Donor Material in Friction Stir Welding:** *Justin Rice*<sup>1</sup>; *Saptarshi Mandal*<sup>1</sup>; *Abdelmageed Elmustafa*<sup>1</sup>; <sup>1</sup>Old Dominion University

Excessive tool wear caused during the plunge phase of friction stir welding (FSW) is hindering the application of FSW of hard materials such as steel. This research uses a finite element model of the Johnson-Cook material constitutive law to investigate the shear stresses and axial forces experienced by the tool during the entire plunge stage of FSW. The model in this research consists of both a deformable workpiece and a deformable tool. By implementing the concept of using a donor material, we are able to have localized pre-heating and minimize the forces throughout the tool, therefore reducing tool fracturing and production costs. The numerical simulation data supports the concept of using a donor material to reduce tool wear and the need to implement this concept to experimental work for further verification.

5:50 PM

**Tool Degradation during Friction Stir Welding of Aluminum:** *Kazutaka Okamoto*<sup>1</sup>; *Akihiro Sato*<sup>1</sup>; *Seung Hwan Park*<sup>1</sup>; *Satoshi Hirano*<sup>1</sup>; <sup>1</sup>Hitachi, Ltd

Friction stir welding is well matured process and already implemented to aluminum alloys in various industries especially of transportation. Tool steel is a common material for the welding tool, which demonstrates acceptable performance as well as cost impact. However, tool failure such as pin snap off is sometimes observed even in aluminum welding. In this study, tool degradation is discussed considering several fundamental aspects; fatigue damage, thermal damage (tempering), chemical damage (Al diffusion) and impact damage.



## General Abstracts: Electronic, Magnetic and Photonic Materials Division: Session I

Sponsored by: TMS: Alloy Phases Committee, TMS: Biomaterials Committee, TMS: Chemistry and Physics of Materials Committee, TMS: Electronic Materials Committee, TMS: Electronic Packaging and Interconnection Materials Committee, TMS: Energy Committee, TMS: Nanomaterials Committee, TMS: Superconducting and Magnetic Materials Committee, TMS: Thin Films and Interfaces Committee  
 Program Organizers: Long Qing Chen, Pennsylvania State University; Mark Palmer, Kettering University; Sung Kang, IBM Corp

Wednesday PM Room: 2022  
 February 18, 2009 Location: Moscone West Convention Center

Session Chair: To Be Announced

### 2:00 PM

**Alumina Coated Steels by the Sol Gel Method for a New Lamellar Soft Magnetic Composite:** *Patrick Lemieux*<sup>1</sup>; *Roderick Guthrie*<sup>1</sup>; *Mihaiela Isac*<sup>1</sup>; <sup>1</sup>McGill University

A new soft magnetic composite has been developed. It is produced by sintering or forging lamellar particles of steel obtained from a cut ribbon. Prior to cutting, the steel ribbon is coated with a Sol-Gel solution to form a refractive dielectric. The composition, viscosity and concentration of the sol Gel solution must be adapted to the coating process (spray or dip) and to the overall soft magnetic composite process and application. An alumina-PVP composite sol-gel solution was developed in order to coat ribbons at high speed and to give a final 0.5  $\mu\text{m}$  thick layer of refractive electrical insulator. Final properties of the soft magnetic composite obtained are reviewed.

### 2:20 PM

**Correlation between the Morphological and Electrochemical Properties IrO<sub>2</sub> Based DSA<sup>®</sup> Anodes:** *Ozgenur Kahvecioglu*<sup>1</sup>; *Servet Timur*<sup>1</sup>; <sup>1</sup>Istanbul Technical Univ

In this study, IrO<sub>2</sub> was coated onto titanium anodes both by thermal and sol-gel procedures. Surface morphology of these coatings was investigated by SEM and the phase determination was carried out by thin film XRD analysis. The electrodes were electrochemically characterized by means of applying potentiodynamic polarization tests in 1.0 M H<sub>2</sub>SO<sub>4</sub> solution. Although the surfaces of the electrodes obtained with two coating procedures show variant morphologies (nano-structured, mud crack, nodular based flats) and it was expected that these electrodes show radical variation in the electrochemical activation due to having different *S* (active site), no difference was seen. That is to say, *a* (materials coefficient) and *b* (Tafel slope) values of the materials didn't demonstrate a radical change with the morphology. Increasing current densities resulted in an increase in the Tafel slope from 59 mV/dec to 90 mV/dec. Keywords: IrO<sub>2</sub>, DSA<sup>®</sup>, Electrochemical Activation

### 2:40 PM

**Hetero and Homoepitaxy of ZnO by Metalorganic Chemical Vapor Phase Epitaxy:** *Tommy Ive*<sup>1</sup>; *Tammy Ben-Yaacov*<sup>1</sup>; *Chris Van de Walle*<sup>1</sup>; *Umesh Mishra*<sup>1</sup>; *Steven DenBaars*<sup>1</sup>; *James Speck*<sup>1</sup>; <sup>1</sup>University of California, Santa Barbara

Thin films of Zn-face ZnO(0001) were grown by metalorganic chemical vapor epitaxy on Si(111), Al<sub>2</sub>O<sub>3</sub>(0001), GaN(0001) and on high quality ZnO(0001) substrates. The focus of our study was on homoepitaxy which yielded excellent results. Atomic force microscopy revealed that our homoepitaxial films exhibited monolayer steps on the surface. The root-mean-square roughness was 0.09-0.15 nm for a 20 $\times$ 20  $\mu\text{m}^2$  area. The x-ray rocking curve full-width-at-half-maximum was  $\leq 36$  arcsec across both the (0002) and the (20-21) reflections. These full widths are comparable to the corresponding values for the bare ZnO bulk substrates. We found that a growth temperature  $>950^\circ\text{C}$  was needed to obtain a smooth two-dimensional surface. Samples grown below 950 $^\circ\text{C}$  exhibited a very rough three-dimensional surface morphology. This indicates that with respect to the comparatively low growth temperatures reported in the literature, much higher growth temperatures might be needed in order to obtain a smooth two dimensional surface morphology.

### 3:00 PM

**Nonvolatile Memory Property of WSi<sub>2</sub> and TiSi<sub>2</sub> Nano-Particles in SiO<sub>2</sub> Dielectrics:** *Ki Bong Seo*<sup>1</sup>; *Seung Jong Han*<sup>1</sup>; *Dong Uk Lee*<sup>1</sup>; *Seon Pil Kim*<sup>1</sup>; *Eun Kyu Kim*<sup>1</sup>; <sup>1</sup>Hanyang University

We have studied nonvolatile nano-floating gated memory (NFGM) device with WSi<sub>2</sub> and TiSi<sub>2</sub> nano-particles, and characterized electrical properties such as threshold voltage, endurance, and retention time. Silicide films with thickness of 5 ~ 10 nm were deposited by dc sputter on tunnel oxide layer with 4.5-nm-thickness, which was grown by thermal oxidation process. Then, the silicide nano-particles were formed by RTA process at temperature range of 600 to 1000 $^\circ\text{C}$  for 1 min under nitrogen gas ambient. Finally, SiO<sub>2</sub> control oxide layer with 30-nm-thickness was sputtered and then an Al gate electrode was evaporated. These nano-floating gate capacitors with nano-particles in SiO<sub>2</sub> dielectrics were characterized by capacitance-voltage and current-voltage measurements. The memory windows were ranged from 1 V to 4 V by applying the gate voltages from  $\pm 3$  V to  $\pm 7$  V. Then, the programming and erasing speeds were measured about 50 ms and 600 ms, respectively.

### 3:20 PM Break

### 3:40 PM

**Quantum Dots Shape Effects on Surface Plasmons Propagating in Chains:** *Jimena Vergara Mojica*<sup>1</sup>; *Angela Camacho*<sup>1</sup>; <sup>1</sup>Universidad de Los Andes

We are interested in the study of collective excitations in quantum dot chains because these can be used to effectively transmit information at nano scale and to control spontaneous and stimulate electromagnetic emission in the quantum dots. [1] This work is centered in the study of semiconductor and metallic one-dimensional quantum dot arrays. We analyze how the geometry of the dot affects the collective oscillation of charge and its propagation. Furthermore, we introduce the Coulomb interaction between charges and compare our results with the ones where this interaction is neglected. We find out that Coulomb interaction plays an important role in these systems, which are good candidates to be used as nanometric devices. [1] A.V.Akimov, A.Mukherjee, C.L. Yu, D.E Chang, A.S.Zybrov, P.R. Hemmer, H Park and M.D Lukin, Generation of Single optical plasmons in metallic nanowires coupled to quantum dots, Nature 450, 402 (2007).

### 4:00 PM

**Study of Properties in MgB<sub>2</sub> Doped with NbB<sub>2</sub> by High Energy Ball Mill (Spex 8000D):** *Yenny Cardona-Quintero*<sup>1</sup>; *Richard Perez*<sup>1</sup>; *Oswald Uwakweh*<sup>1</sup>; *Eric Hellstrom*<sup>2</sup>; *David Larbalestier*<sup>2</sup>; <sup>1</sup>University of Puerto Rico-Mayaguez; <sup>2</sup>Florida State University

The doping of Magnesium Diboride (MgB<sub>2</sub>) by the addition of Niobium Diboride (NbB<sub>2</sub>) at 5 at% is carried out by high-energy ball milling at 60, 120, 180 and 300 minutes of milling. All the samples are processed in SPEX 8000D followed by cold and hot isostatic pressing. The obtained samples are characterized by measuring critical current density (*J<sub>c</sub>*), critical temperature transition (*T<sub>c</sub>*) and critical magnetic field (*H<sub>c2</sub>*), while structural characterization will be undertaken with X-ray diffraction. The values of these properties will be compared with the ones obtained in previous studies carried out on bulk and doped MgB<sub>2</sub>. In addition, doping with other transition metal diborides such as Titanium Diboride (TiB<sub>2</sub>), Chromium Boride (CrB<sub>2</sub>) and Tantalum Boride (TaB<sub>2</sub>) will be carried out. The results of this work will be an important contribution towards the development of improved superconductors with better *J<sub>c</sub>* capable of performing at higher *T<sub>c</sub>*.

### 4:20 PM

**Ultraviolet Photoconductive Properties of TiO<sub>2</sub> Nanotubes Grown by Atomic Layer Deposition:** *Yung-Huang Chang*<sup>1</sup>; *Chih Chen*<sup>1</sup>; <sup>1</sup>National Chiao Tung University

Self-organized TiO<sub>2</sub> nanotubes are grown on Si substrates using anodic aluminum oxide as a template and atomic layer deposition (ALD) for the deposition of TiO<sub>2</sub>. With the aid of the ALD, the deposition temperature can be as low as 400 $^\circ\text{C}$  and no any metal catalysts or seed layers are needed. Each nanotube is perpendicular to the Si substrate. We controlled the deposited cycles of ALD to modify the morphology of TiO<sub>2</sub> nanotube arrays. The structure of the TiO<sub>2</sub> appears to be polycrystalline, and their grain size become larger as deposited cycles increase. The Ultraviolet (UV) photoconductive properties of TiO<sub>2</sub> nanotubes were investigated to obtain the best transformation efficiency for the application of UV detector. The results of photoluminescence, transmission

electron microscope, and the performances of UV photoconduction for the TiO<sub>2</sub> nanotube arrays will be presented in the conference.

## General Abstracts: Materials Processing and Manufacturing Division: Session II

Sponsored by: The Minerals, Metals and Materials Society, TMS Materials Processing and Manufacturing Division, TMS/ASM: Computational Materials Science and Engineering Committee, TMS: Global Innovations Committee, TMS: Nanomechanical Materials Behavior Committee, TMS/ASM: Phase Transformations Committee, TMS: Powder Materials Committee, TMS: Process Technology and Modeling Committee, TMS: Shaping and Forming Committee, TMS: Surface Engineering Committee

Program Organizers: Thomas Bieler, Michigan State University; Neville Moody, Sandia National Laboratories

Wednesday PM Room: 3022  
February 18, 2009 Location: Moscone West Convention Center

Session Chair: To Be Announced

### 2:00 PM

**Bulk Nanoscale Hydroxyapatite Structures Using Microwave Sintering:** Sudip Dasgupta<sup>1</sup>; Amit Bandyopadhyay<sup>1</sup>; Susmita Bose<sup>1</sup>; <sup>1</sup>Washington State University

Nanostructured hydroxyapatite (HA) is of significant interest because of the nanoscale feature of the inorganic part of natural bone. In our research, nanostructure HA compacts were processed with below 200 nm average grain size using microwave sintering which showed improved mechanical and biological properties. Nano HA compacts showed compressive strength of 395 ± 36 MPa, indentation hardness of 8.4 ± 0.4 GPa and indentation fracture toughness of 2.0 ± 0.1 MPa m<sup>1/2</sup>. These numbers are significantly higher compared to pure HA compacts with micron size grains. Nano HA compacts were assessed for cell material interaction using SEM, MTT and immunochemistry assays using protein expression studies with human osteoblast cell line for 1, 5 and 11 days. These studies show better cell material interaction on nano grain HA compared to compacts with larger grains. The presentation will focus on processing and characterization of microwave sintered HA compacts.

### 2:20 PM

**Dilatometric and Differential Scanning Studies of Cryogenic Treatment Methods and Cryogenically Treated Samples:** Harish Sivasankaran<sup>1</sup>; Bensely Albert<sup>2</sup>; Mohan Lal D.<sup>2</sup>; Nagarajan G.<sup>2</sup>; <sup>1</sup>Arizona State University; <sup>2</sup>College of Engineering Guindy

Even though cryogenic treatments are widely used as strengthening mechanisms for metals, especially tool steels, the underlying metallurgical principles of the same have remained unexplained. The present investigation aims at determining the actual metallurgical metamorphosis during the cryogenic treatment of a case hardened gear material, En353. A differential scanning calorimeter (DSC) and a thermomechanical analyzer (TMA) are used and the relevant parameters are measured during the course of the treatment procedure itself. Simultaneous measurement by DSC and TMA enables the comparison of the cryogenic treatment methods, namely Deep Cryogenic Treatment (DCT) and Shallow Cryogenic Treatment (SCT) and the data obtained is studied. Possible means of reducing the retention time for Deep Cryogenic Treatment (DCT) process is discussed. Quantitatively, the values from TMA are used to validate the treatment procedures.

### 2:40 PM

**Effect of Pulse Magneto Oscillation on the Solidification Structure of Pure Aluminum During Crystal Growth Stage:** Yongyong Gong<sup>1</sup>; Qijie Zhai<sup>1</sup>; <sup>1</sup>Shanghai Univ

The effect of Pulse Magneto Oscillation (PMO) on solidification structures of pure aluminum at different solidification stages has been researched and the refinement mechanism has been analyzed. The previous experimental results show that PMO can not refine the solidification structure of pure aluminum when it is only applied to high temperature liquid metal. However, the solidification structures are significantly refined when PMO is applied from the end of nucleation till beginning of crystal growing. But if cooling ability of the mold

and treatment frequency of PMO are increased, the solidification structures are also greatly refined when PMO is applied during the stage of crystal growth.

### 3:00 PM

**Finite Element Analysis and Experimental Investigation of the Effect of Spatial Energy Distribution on Dual-Beam Welding of Aluminum Alloys:** Rouzbeh Sarrafi<sup>1</sup>; <sup>1</sup>Southern Methodist University

The effect of beam splitting on the laser welding of aluminum in conduction and keyhole modes is studied through a FEM model as well as experiments. For the conduction mode, four types of energy distribution were compared, 1) single laser beam, 2) the same laser beam split into two equal beams, 3) laser beam split unequally and the weaker beam leads, and 4) laser beam split unequally and the stronger beam leads. The results showed the variation of molten pool profile with the spatial energy distribution. Furthermore, the setup with strong beam ahead can reduce porosities in the weld since it provides a notably slower cooling rate for the molten pool before solidification compared to the other cases of spatial energy distribution. The analysis results showed reasonable agreement with experiments. In addition, the effect of spatial energy distribution on keyhole laser welding of aluminum alloys was experimentally investigated.

### 3:20 PM

**Lamellar Decomposition in U-Nb Alloys:** Robert Hackenberg<sup>1</sup>; Heather Volz<sup>1</sup>; Robert Dickerson<sup>1</sup>; Pallas Papin<sup>1</sup>; Robert Forsyth<sup>1</sup>; Ann Kelly<sup>1</sup>; Tim Tucker<sup>1</sup>; Robert Field<sup>1</sup>; <sup>1</sup>Los Alamos National Laboratory

Lamellar decomposition products result when U-Nb alloys are transformed between about 300C and the 650C monotectoid temperature. As such microstructures give undesirable properties, TTT diagrams were generated for U-5.6 wt% Nb and U-7.7 wt% Nb alloys. Detailed kinetic studies of these reactions were undertaken to better understand their mechanisms. The relevant parameters for the initial discontinuous precipitation as well as the succeeding discontinuous coarsening reactions were investigated via light microscopy, X-ray diffraction, SEM, and TEM. These results will be compared with theory. Attention will be paid to the rates and degrees to which these various aging reactions drive the system toward its final equilibrium state.

### 3:40 PM

**Monitoring of Spatters by Using Microphone during Gas Tungsten Arc Welding of Galvanized High-Strength Steel DP980:** Wei Huang<sup>1</sup>; Shanglu Yang<sup>1</sup>; Dechao Lin<sup>1</sup>; Radovan Kovacevic<sup>1</sup>; <sup>1</sup>Southern Methodist University, Research Center for Advanced Manufacturing

Galvanized high-strength steels have broad applications in automobile industry. However, during the welding process, many spatters are produced due to a lower boiling point of zinc coat (907°) than the melting point of steel (over 1300°). Since spatters greatly deteriorate the quality of welds, it is necessary to monitor the presence of spatters and achieve quality control. In this paper, a microphone was used to acquire the airborne acoustic signals during gas tungsten arc welding of galvanized high-strength steel DP980. The signals were denoised by spectral subtraction and analyzed in wavelet domain. The results show that by applying noise reduction, spatters can be detected in a noisy environment. In addition, the wavelet analysis shows a good correlation between the signals in the frequency range [0:100 Hz] and the quality of welds, which can be explained by the frequency characteristic of the oscillation behavior of molten pool.

### 4:00 PM

**Porous and Permeable Metal Membranes from Slurry Precursors:** Kevin Hurysz<sup>1</sup>; Jason Nadler<sup>1</sup>; <sup>1</sup>Georgia Tech Research Institute

Oxide slurries present a unique opportunity for fabricating thin, porous and permeable metal structures. Powder raw material precursors are mixed with a binder and solvent into a viscous slurry. Air is then introduced into the structure via high shear mixing. By employing traditional tape casting and doctor blading techniques, thicknesses of 100 μm can be achieved. The tape is then dried and fired in a controlled atmosphere to form a metal membrane. The advantage to this process is that feature sizes can be substantially decreased through shrinkage: evaporation of the solvent, binder burnout, reduction shrinkage, and sintering of the structure. Thicknesses of 30 μm with pore sizes on the order of 10 – 50 μm have been achieved.

### 4:20 PM

**Rapid Materials Processing and Surface Sculpting Using Electron Beam and Laser Processes:** Bruce Dance<sup>1</sup>; <sup>1</sup>TWI Ltd

For up to fifty years high energy density power beams have been used in many industrial processes. More recently, 'Surfi-Sculpt®' processing has been

developed. This novel process typically uses a focused energy beam to displace material in the liquid phase. By means of controlled and usually repeated movements of the beam with overlapping or intersecting paths, extraordinarily complex 3-D geometries may be generated rapidly and precisely. The Surf-Sculpt process can be implemented using electron beams and laser beams, in materials ranging from metals to polymers. Feature sizes from tens of mm to tens of  $\mu\text{m}$  may be created quickly and efficiently. Novel materials thus processed are under evaluation for a wide range of applications including composite to metal 'Comeld®' bonding, materials for enhanced heat transfer and flow control, as well as biocompatible/bone ingrowth materials. Examples of different types of treatments are presented, together with some recent developments.

#### 4:40 PM

**Solidification Structure Transformation of Bearing Steel under Electric Current Pulse:** Ma Jianhong<sup>1</sup>; Li Jie<sup>1</sup>; Gao Yulai<sup>1</sup>; Chen Zhongxin<sup>2</sup>; Li Zheng<sup>2</sup>; Zhai Qijie<sup>1</sup>; <sup>1</sup>Shanghai University; <sup>2</sup>Special Steel Branch, Baoshan Iron & Steel Co., Ltd, P.R. China

The solidification structure transformation of bearing steel with different patterns of electric current pulse (ECP) was carried out. The results showed that the ratio of equiaxed dendrites could only be slightly increased and little reduction of the primary dendritic arm was obtained under the effect of high voltage and low discharge frequency of ECP. In contrast, high ratio of equiaxed dendrites and large reduction of the primary dendritic arm were generated by low voltage and high discharge frequency of ECP. It was deemed that grain refinement could be attributed to the heterogeneous nucleus formed on the top surface and their falling by the agitation resulted from the ECP. For high voltage ECP, non-crowded agitation and lower accumulated heat were generated and therefore little nucleus dissociated from the top surface. Contrarily, much more nucleus falling due to combined action of dense agitation and more accumulated heat by employing low voltage ECP.

#### 5:00 PM

**The Effect of Feedstock Composition on Defect Evolution in Powder Injection Molded Ceramic Microarrays:** Sachin Laddha<sup>1</sup>; Sundar Atre<sup>2</sup>; Kevin Simmons<sup>1</sup>; <sup>1</sup>Pacific Northwest National Laboratory; <sup>2</sup>Oregon State University

Powder injection molding is a cost-effective to manufacture Microchannel arrays (MCA), which are used as the major component and design feature for many microsystems in a large variety of applications, such as microfluidics, micro optics, etc. In this paper, characterization of feedstock consisting of alumina nanopowder (average particle size of 400nm) with ethylene-propylene/wax and polyacetal binder systems for micro-powder injection molding is reported. It is found that the wax-based binder system performs the lowest viscosity and heat capacity as well as greater pseudo-plasticity than the polyacetal binder system. However, the results from Moldflow simulations inferred that the polyacetal-based system, though having a higher viscosity than wax-based system at higher shear rate, fills the microcavities (50 $\mu\text{m}$ ) in a more efficient way. Also, a design of experiments involving variations in powder injection molding conditions were carried out to map the homogeneity at the macroscale (part level) and microscale (particle level) in MCA.

#### 5:20 PM

**Viscosity – Structure Relationships in Copper Foams:** Kevin Hurysz<sup>1</sup>; Jason Nadler<sup>1</sup>; <sup>1</sup>Georgia Tech Research Institute

Metallic foams can be constructed by mixing oxide precursors with a binder and solvent, introducing air into the resulting slurry by mechanical mixing, drying, and heat treating in controlled atmospheres. Slurry viscosity plays a key role in the ability to form a green porous structure. The combined action of drainage, coalescence, and Ostwald ripening among bubbles will cause foams made from fluids of low viscosity to collapse. High viscosity slurries will not foam because mixing that is turbulent enough to incorporate air into the structure is impossible to achieve. A critical target viscosity range for foaming clearly emerges: 1 000 to 5 x 10<sup>5</sup> cP. This paper will investigate the structure of thin, tape cast foams made from slurries of cuprous oxide (Cu<sub>2</sub>O), polyvinyl alcohol (PVA), and water.

## General Abstracts: Structural Materials Division: Session III

Sponsored by: The Minerals, Metals and Materials Society, TMS Structural Materials Division, TMS: Advanced Characterization, Testing, and Simulation Committee, TMS: Alloy Phases Committee, TMS: Biomaterials Committee, TMS: Chemistry and Physics of Materials Committee, TMS/ASM: Composite Materials Committee, TMS/ASM: Corrosion and Environmental Effects Committee, TMS: High Temperature Alloys Committee, TMS/ASM: Mechanical Behavior of Materials Committee, TMS/ASM: Nuclear Materials Committee, TMS: Refractory Metals Committee, TMS: Titanium Committee

Program Organizers: Robert Hanrahan, National Nuclear Security Administration; Eric Ott, GE Aviation

Wednesday PM  
February 18, 2009

Room: 2018  
Location: Moscone West Convention Center

Session Chair: To Be Announced

#### 2:00 PM

**A New Microstructure-Sensitive Crystallographic Constitutive Model for Creep of Ni-Base Single -Crystal Blade Alloys:** Yoon Suk Choi<sup>1</sup>; You-Hai Wen<sup>1</sup>; Triplicane Parthasarathy<sup>1</sup>; Christopher Woodward<sup>2</sup>; Dennis Dimiduk<sup>2</sup>; <sup>1</sup>UES Inc; <sup>2</sup>Air Force Research Laboratory

We developed a microstructure-sensitive, mechanism-based crystallographic constitutive model to predict creep behavior of Ni-base single-crystal blade alloys over a wide range of stress and temperature. The new creep constitutive model accommodated major slip-system-based dislocation micro-mechanisms to predict primary and secondary creep, and adopted a phenomenological creep formulation to predict tertiary creep. In particular, the new model was directly linked to a  $\gamma'$ -rafting model, which predicts the evolution of the  $\gamma'$ -precipitate morphology during creep, in order to update the microstructural information at every time step of the creep simulation. We implemented the new creep model into the FEM package ABAQUS through the User MATerial subroutine (UMAT) and performed creep simulations for selected stress and temperature regimes with the microstructural information as variables. The model predictions were primarily intended to clarify the effect of the microstructural heterogeneity on the creep variability for various stress and temperature regimes.

#### 2:20 PM

**Characterisation of Microplasticity in TiAl Based Alloys:** Francisco Garcia-Pastor<sup>1</sup>; Hui Jiang<sup>2</sup>; David Hu<sup>2</sup>; Xinhua Wu<sup>2</sup>; Michael Loretto<sup>2</sup>; Michael Preuss<sup>1</sup>; Philip Withers<sup>1</sup>; <sup>1</sup>The University of Manchester; <sup>2</sup>The University of Birmingham

Three different microstructural variants (nearly fully lamellar, fully lamellar and duplex) of two-phase ( $\alpha_2+\beta$ ) Ti-44Al-8Nb-1B (at%) have been studied by in-situ loading, coupled with acoustic emission and image correlation, electron backscatter diffraction and transmission electron microscopy. The observations show that the onset of microyielding occurs at different stress levels: the lamellar materials yielding at the lowest stress and duplex material withstanding the highest stress before any microplasticity was observed. The early microyielding observed in the lamellar microstructures is explained by the strong strain heterogeneity seen at early stages during loading using image correlation and post-mortem TEM analysis. It was possible to relate the level of microyielding to the orientation of the lamellae in respect of the loading direction. In contrast, duplex microstructures show no strain heterogeneity until its macroscopic yield point. This strain heterogeneity may lead to stress concentrations and early cracking detected by acoustic emission.

#### 2:40 PM

**Effect of Strain Rate, and Deformation Temperature on the Microstructure of an Equal Channel Angular Extrusion (ECAE) Processed Ti-6Al-4V Alloy:** Rabindra Mahapatra<sup>1</sup>; Shankar Sastry<sup>2</sup>; <sup>1</sup>Naval Air Systems Command; <sup>2</sup>Washington University

The Ti-6Al-4V alloy was ECAE processed to produce ultra-fine grains of 1-2 $\mu\text{m}$ . The uni-axial compression experiments to simulate forging parameters subsequent to ECAE processing were carried out to elucidate whether, the ultra-fine grained microstructure of the alloy can be sustained after the deformation. The ECAE processed Ti-6Al-4V alloy showed no significant grain growth when



deformed at 750°C, at a strain rate of 0.1"/sec., where as when deformed at same temperature, a strain rate of 0.001"/sec., both the recovery and grain growth were observed.

### 3:00 PM

**Quasi-Static and Dynamic Torsional Deformation Behavior of API X70 and X80 Linepipe Steels:** *Yongjin Kim*<sup>1</sup>; Yanggon Kim<sup>1</sup>; Sunghak Lee<sup>1</sup>; <sup>1</sup>Pohang University of Science & Technology

This study aimed at investigating quasi-static and dynamic torsional deformation behavior of three API X70 and X80 linepipe steels fabricated by varying alloying elements and hot-rolling conditions. Quasi-static and dynamic torsional tests were conducted on these steel specimens, which had different grain sizes and volume fractions of acicular ferrite and polygonal ferrite, using a torsional Kolsky bar, and then the test data were compared via microstructures, tensile properties, fracture mode, and adiabatic shear band formation. The dynamic torsional test results indicated that the steels rolled in the single phase region had the higher maximum shear stress and fracture shear strain than the steel rolled in the two phase region because their microstructures were composed of acicular ferrite. Particularly in the X80 steel rolled in the single phase region, the increased dynamic torsional properties could be explained by the decrease in the overall effective grain size.

### 3:20 PM

**High-Temperature Surface Stability and Creep Behavior of Ni-Based Alloys in Impure-He Environment:** *Raghavendra Adharapurapu*<sup>1</sup>; Deepak Kumar<sup>1</sup>; Chris Torbet<sup>1</sup>; Tresa Pollock<sup>1</sup>; J Jones<sup>1</sup>; Gary Was<sup>1</sup>; <sup>1</sup>University of Michigan

The high-temperatures and long lifetimes expected in the very high temperature reactor (VHTR) for the Next Generation Nuclear Plant (NGNP) necessitate the use of alloys with good surface stability as well as corrosion and creep resistance. However, the understanding of alloy stability and creep strength in an environment of helium containing impurities such as CO+CO<sub>2</sub> is currently insufficient for long term predictions of crucial properties. New alloying strategies to improve strength and creep resistance over Alloy 617 through the addition of solution hardening elements such as Re and W are presented. Laboratory air cyclic oxidation behavior at 1000°C is described for a set of 11 experimental alloys. Creep behavior and the surface stability of selected alloys exposed to an impure helium environment (in carburization, decarburization atmospheres) at 1000°C is also examined.

### 3:40 PM

**Low Torsional Ductility Induced by Shear Deformation Localization of a High Strength Steel Wire:** *Youshi Hong*<sup>1</sup>; Xiaolei Wu<sup>1</sup>; Zhijia Wang<sup>1</sup>; <sup>1</sup>Institute of Mechanics, Chinese Academy of Sciences

Adequate torsional ductility is required by high strength steel wire products because the wires are inevitably subjected to cabling and brunching in applications. The torsional ductility of the wire is characterized by the number of twists in torsion test with a given gauge length. In this investigation, the values of torsional ductility for a high strength steel wire with different heat-treatment states were tested and examined. Torsion deformation characteristics, i.e. the values of shear strain along the longitudinal axis of the wire specimen were measured. Torsion rupture modes and fracture surfaces of the wire specimens were examined. A numerical simulation was performed to illustrate the temperature field of wire cross section. The results indicate that the low torsional ductility of the wire originates from shear deformation localization due to nonuniform microstructure distribution resulted from nonuniform temperature field, which eventually leads to delamination and final fracture of the wire specimen.

### 4:00 PM

**Microstructural Characterization Of High-Explosive Driven Tantalum:** *Veronica Livescu*<sup>1</sup>; John Bingert<sup>1</sup>; Thomas Mason<sup>1</sup>; <sup>1</sup>Los Alamos National Laboratory

Three-dimensional high-explosive (HE) shock loading results in a triangular wave profile. While shock wave interaction in three-dimensions is a complex phenomenon, post-mortem interrogation and quantification of damaged microstructures provides insight towards the understanding of dynamic damage evolution. This work investigates microstructural damage and deformation in Tantalum specimens tested in HE drive experiments. Volumetric reconstruction of the damage field revealed substantial differences compared to the damage structure observed in plate-impact experiments on equivalent material. Electron Backscatter Diffraction (EBSD) was used to capture microstructural changes due to shock loading, for identification and quantification of twinning, and for

characterization of potential orientation-related phenomena contributing to void nucleation processes. These results offer insight on the variables affecting damage features, which is essential to the validation of predictive damage models.

### 4:20 PM

**Modeling the Room Temperature Deformation Behaviour of a Commercial Ti-6Al-4V Alloy for Low and High Strain Rates:** *Frederik Coghe*<sup>1</sup>; Luc Rabet<sup>1</sup>; Paul Van Houtte<sup>2</sup>; <sup>1</sup>Royal Military Academy; <sup>2</sup>Katholieke Universiteit Leuven

This work will show some results on the modeling of the plastic deformation behaviour of a Ti-6Al-4V alloy. Cylindrical specimens, originating out of a rod in the mill-annealed condition and machined along different sample orientations, were compressed (at room temperature) at low and high strain rates using a servo-hydraulic testing machine and a Split Hopkinson Pressure Bar setup. The texture of the specimens before and after deformation was determined by the use of XRD and EBSD techniques. The Visco-Plastic Self-Consistent plasticity code (VPSC7) was used in order to try to simulate the texture evolution during deformation and to identify the active slip and twinning systems as a function of initial texture and strain rate. This work will focus in particular on the determination of the active twinning systems and on the influence of twinning on the overall deformation behaviour.

### 4:40 PM

**Studies on Transient-Stage-Scale Growth on Fe-22 wt.% Cr Alloys Containing 120 ppm La + 270 ppm Ce:** Laura Maria Fernandez Diaz<sup>1</sup>; Jingxi Zhu<sup>1</sup>; G.R. Holcomb<sup>2</sup>; P.D. Jablonski<sup>2</sup>; D.E. Alman<sup>2</sup>; Sridhar Seetharaman<sup>1</sup>; <sup>1</sup>National Energy Technology Laboratory - Carnegie Mellon University; <sup>2</sup>National Energy Technology Laboratory

Reactive elements (RE), such as Ce, La or Y, are known to improve oxidation resistance of Fe based alloys that form Cr<sub>2</sub>O<sub>3</sub> scales. The current investigation aims to characterize the oxide scale in a Fe-22 wt.% Cr alloy containing 120 ppm La and 270 ppm Ce (added during melt-stage processing) as a function of oxidation times (at 800C in dry air) during the transient stage of scale formation. The surface oxidation processes were imaged in-situ through a Confocal Scanning Laser Microscope (CSLM). The results are correlated with post-experiment characterization through FEG-SEM and dual beam FIB-SEM. The evolution of the reactive-elements-containing scale, its morphology and composition are determined.

### 5:00 PM

**Development and Ballistic Testing of a New Class of Autotempered High Hard Steels under Military Specification MIL-DTL-46100E:** *William Gooch*<sup>1</sup>; Dwight Showalter<sup>1</sup>; Matthew Burkins<sup>1</sup>; Jonathan Montgomery<sup>1</sup>; Richard Squillacioti<sup>1</sup>; Andrew Nichols<sup>2</sup>; Larry Martin<sup>2</sup>; Ronald Bailey<sup>2</sup>; Glenn Swiatek<sup>2</sup>; <sup>1</sup>US Army Research Laboratory; <sup>2</sup>Allegheny Technologies Inc

The US Army Research Laboratory (ARL) was directed to expand current steel armor plate production as the large military demand for armor plate exceeded the production capacity at US steel facilities for quench and tempered high hard(HH)steel armor plate. The solution was to expand the availability of HH steels under the current military specification to include a new class of air-quenched, autotempered steels that do not use existing water quench and temper facilities. Allegheny Technologies Incorporated (ATI) developed the autotempered steel alloy ATI500 that has physical and mechanical properties that meet the HH specification. ARL procured sufficient amounts of ATI500 plate to allow acceptance testing and certification of ATI500 as complying with First Article requirements in a new MIL-DTL-46100E specification. This paper documents the development of ATI500 and subsequent ballistic testing and inclusion into the specification as Class 2 auto-tempered HH armor steel.

## Magnesium Technology 2009: Alloys IV: Yttrium and Tin

Sponsored by: The Minerals, Metals and Materials Society, TMS Light Metals Division, TMS: Magnesium Committee  
 Program Organizers: Eric Nyberg, Pacific Northwest National Laboratory; Sean Agnew, University of Virginia; Neale Neelameggham, US Magnesium LLC; Mihriban Pekguleryuz, McGill University

Wednesday PM Room: 2006  
 February 18, 2009 Location: Moscone West Convention Center

Session Chairs: Menachem Bamberger, Israel Institute of Technology; Alan Luo, General Motors Corp

### 2:00 PM Introductory Comments

#### 2:05 PM

#### Microstructure and Mechanical Properties of Mg-Al-Mn and Mg-Al-Sn Alloys: Alan Luo<sup>1</sup>; Anil Sachdev<sup>1</sup>; <sup>1</sup>General Motors Corp

The Mg-Al-Mn (AM) based cast alloys were optimized for balanced tensile properties (strength and ductility) and reasonable response to heat treatment. 1-3% tin addition was found to be effective in strengthening the AM alloys due to the precipitation of Mg<sub>2</sub>Sn phase in the Mg-Al-Sn (AT) alloys. The new AT72 (Mg-7%Al-2%Sn) offers a well balanced strength and ductility as well as good corrosion resistance. T5 (artificial aging after as-cast condition) is recommended for additional strengthening effect of AM and AT alloys.

#### 2:25 PM

#### Directionally Controlled Precipitation on Twin-Boundaries in Mg-Zn-Y Alloys: Julian Rosalie<sup>1</sup>; Hidetoshi Somekawa<sup>1</sup>; Alok Singh<sup>1</sup>; Toshiji Mukai<sup>1</sup>; <sup>1</sup>National Institute for Materials Science

Precipitation strengthening in Mg-Zn(-X) alloys occurs via the formation of a fine dispersion of  $\beta_1'$  rods aligned parallel to the hexagonal axis. In this study, controlled deformation has been used to alter the precipitation behaviour in a Mg-2.8at%Zn-0.4at%Y alloy. The resulting microstructures were studied via conventional and high-resolution transmission electron microscopy. Texture was developed through extrusion at 300°C, followed by controlled room-temperature deformation to generate microstructures where yield occurred either with, or without, twinning. The ageing response was monitored using hardness testing. Both compressive and tensile deformation accelerated the ageing response. Compression parallel to the extrusion axis also generated a high volume fraction of twins. Precipitates on the twin boundaries assumed a low aspect-ratio morphology different from the usual high-aspect ratio rods. The change in precipitate morphology was due to the reduced matrix symmetry at the twin boundary.

#### 2:45 PM

#### Effect of Extrusion Temperature on the Microstructure and Mechanical Properties of Mg97Y2Zn1 Alloy: Bin Chen<sup>1</sup>; Xiaoqin Zeng<sup>1</sup>; Dongliang Lin<sup>1</sup>; <sup>1</sup>SJTU

The microstructure and mechanical properties of as-cast and extruded Mg-Y-Zn alloys were investigated. It was found that the addition of yttrium and zinc not only influence the microstructure of Mg-Y-Zn alloys but also their mechanical properties. With increasing yttrium or yttrium and zinc total alloy content, the amount of secondary phases is also increased. The long-period stacking (LPS) structure was observed at both as-cast and extruded Mg-Y-Zn alloys. The formation of LPS structure in matrix was attributed to the dissolution of a certain amount of Y and Zn. The yttrium and zinc addition play very important role in mechanical properties of extruded Mg-Y-Zn alloys. The extruded Mg-Y-Zn alloys exhibit excellent mechanical properties at both ambient temperature and elevated temperature. Their excellent mechanical properties were thought due to the strengthening by the grain refinement, solid solution, formation of LPS structure and distribution of fine Mg<sub>24</sub>Y<sub>5</sub> phase.

#### 3:05 PM

#### Effect of Trace Elements on Age Hardening Behavior of Mg-Sn Alloy: Do Hyung Kim<sup>1</sup>; Hyun Kyu Lim<sup>1</sup>; Joon Seok Kyeong<sup>1</sup>; Won Tae Kim<sup>2</sup>; Do-hyang Kim<sup>1</sup>; <sup>1</sup>Yonsei University; <sup>2</sup>Cheongju University

Mg-Sn alloy system is well known as one of precipitation hardening type Mg-based alloys due to high solubility of Sn at high temperature. In the present study, to improve age hardening response of Mg-Sn alloy, 0.2at% of various trace elements such as Si, Ge, Ca, Ti and Zr are added in Mg-1.5at%Sn alloy. All of trace elements remarkably improve the yield strength level of Mg-Sn binary alloy after aging treatment. From the result of TEM analysis, the strength improvement is attributed to the formation of higher number of density of Mg<sub>2</sub>Sn precipitates. However, their hardening mechanisms are different each other. It is considered that the trace elements of Si, Ge and Ca suppress the growth of Mg<sub>2</sub>Sn precipitates by reducing lattice mismatch between  $\alpha$ -Mg and Mg<sub>2</sub>Sn phase, while the trace elements of Ti and Zr encourage the increase of nucleation site of Mg<sub>2</sub>Sn phase.

#### 3:25 PM

#### Effects of Sb Additions on the Microstructure and Mechanical Properties of As-Cast Mg-5%Sn Alloy: Ghazal Nayyeri<sup>1</sup>; Reza Mahmudi<sup>1</sup>; <sup>1</sup>Tehran University

Mg-Sn based alloys have great potential for creep resistance because of the formation of thermally stable phase Mg<sub>2</sub>Sn in the as cast condition. In the present investigation, for further enhancement of the creep resistance 0.15, 0.4 and 0.7 wt.% of Sb was added to the base Mg-5%Sn alloy. The dendritic structure of the base alloy was refined after the addition of Sb, the effect being more pronounced in Mg-5%Sn-0.4%Sb. EDS analysis of the phases indicated that in addition to Mg<sub>2</sub>Sn, the new Mg-Sn-Sb rich particles are formed along grain boundaries. Impression creep tests were carried out at 175°C under constant stresses of 300 and 350 MPa. The Mg-5%Sn-0.4%Sb alloy had the lowest creep rates and thus the highest creep resistance among all materials tested. This is attributed to the higher volume fraction of Mg-Sn-Sb rich second phase precipitates which acts as the main strengthening agent in the investigated system.

#### 3:45 PM Break

#### 4:00 PM

#### Thermodynamic Modeling and Its Applications to Mg-Sn Based Alloy Development: In-Ho Jung<sup>1</sup>; D.H. Kang<sup>2</sup>; Nack J. Kim<sup>2</sup>; Woo-Jin Park<sup>3</sup>; SangHo Ahn<sup>3</sup>; <sup>1</sup>McGill University; <sup>2</sup>POSTECH; <sup>3</sup>RIST (Research Institute of Industrial Science and Technology)

Recently an Mg-Sn based alloy system has been investigated actively in order to develop new Mg alloys which have a stable structure and good mechanical properties at high temperatures. In the present study, thermodynamic modeling of the Mg-Sn-Al-Mn-Sb-Si-Zn system has been performed based on available thermodynamic, phase equilibria and phase diagram data. With the aid of the optimized database, unexplored complex phase equilibria/phase diagrams and Scheil cooling solidifications in multicomponent system can be readily calculated. It shows that the microstructural evolutions of Mg-Sn-Al-Zn alloys with additions of Si and Sb can be well explained by the thermodynamic calculations, which proves the applicability of thermodynamic calculations for new Mg alloy design. All calculations were performed using FactSage thermochemical software.

#### 4:20 PM

#### Strengthening Mechanisms in Mg-Al-Sn Based Alloys: Shaul Avraham<sup>1</sup>; Menachem Bamberger<sup>1</sup>; <sup>1</sup>Technion

Intermetallic phases in Mg alloys determine the elevated temperature mechanical properties. Alloying elements dissolved in the  $\alpha$ -Mg matrix, thermally stable intermetallics in the matrix and at the grain boundaries can hinder plastic deformation by solid solution strengthening, dispersion hardening and pinning of the grain boundaries respectively. Thermodynamics, X-ray diffraction and electron microscopy analysis indicate that the formation of  $\gamma$ -Mg<sub>17</sub>Al<sub>12</sub>, creep resistance deteriorating phase, is suppressed. The presence of different types of precipitates (Al-X) at the grain boundaries may serve as a source for grain boundary pinning. Nucleation of thermally stable intermetallics (Mg<sub>2</sub>Sn) in the matrix can serve as obstacles for dislocation motion. The correlation between the microstructure evolution, hardening mechanisms and mechanical behavior will be discussed.

4:40 PM

**Relation between the Microstructure and the Plastic Deformation Behavior in Mg<sub>12</sub>ZnY with the LPSO Structure:** *Koji Hagihara*<sup>1</sup>; Akihito Kinoshita<sup>1</sup>; Yuya Sugino<sup>1</sup>; Naoyuki Yokotani<sup>1</sup>; Michiaki Yamasaki<sup>2</sup>; Yoshihito Kawamura<sup>2</sup>; Yukichi Umakoshi<sup>1</sup>; <sup>1</sup>Osaka University; <sup>2</sup>Kumamoto University

In the recent development of some high-strength Mg alloys, the role of Mg<sub>12</sub>ZnY strengthening phase with long-period stacking ordered (LPSO) structure is focused. Some ideas to explain the strengthening mechanism with the LPSO phase have been reported, but the detail is not enough clarified yet. Recently we investigated the plastic deformation behavior of 18R LPSO phase by using the directionally solidified single-phase crystals, and clarified that the (0001)<11-20> basal slip is dominantly operative in it. In compression at the loading orientation where the Schmid factor for the basal slip is negligible, on the other hand, the deformation proceeds accompanied by the formation of deformation kink. These results indicate that the LPSO phase exhibits strong plastic anisotropy. In this study, some LPSO single-phase alloys with different microstructures were prepared by casting, extrusion and heat-treatment under several conditions, and the variation in plastic deformation behavior depending on microstructure was examined.

5:00 PM

**Effect of Rare Earth Elements Addition and T6 Heat Treatment on Creep Properties of Mg-Al-Zn Alloy:** *Kaveh Meshinchi Asl*<sup>1</sup>; Farzad Khomamizadeh<sup>2</sup>; <sup>1</sup>Clemson University; <sup>2</sup>Sharif University of Technology

This paper focuses on creep properties of Mg-Al-RE and heat treated AZ91 magnesium alloy. The influence of heat treatment and rare earth elements addition on microstructure and mechanical properties were also investigated. The steady state creep rates were measured and for the AZ91 alloy, the results indicate a mixed mode of creep behavior, with some grain boundary effects contributing to the overall behavior. However for the cerium rich misch metal added samples, the sliding of grain boundaries was greatly suppressed due to morphological changes and the dislocation climb controlled creep was the dominant deformation mechanism at high temperatures. As a result, the grain boundaries were less susceptible for grain boundary sliding at higher temperatures. Effect of decreasing Al content on creep resistance of Mg-Al-RE alloys was also investigated. It was found that by decreasing the Al content to 4 wt%, the steady state creep rate was even decreased.

5:20 PM

**Influence of RE Elements on Microstructure and Mechanical Properties of the quaternary Mg-Zn-Y-RE systems:** *Jonghyun Kim*<sup>1</sup>; Yoshihito Kawamura<sup>2</sup>; <sup>1</sup>Kumamoto Technology & Industry foundation; <sup>2</sup>Kumamoto University

Magnesium alloys are known for their light weight and specific stiffness which are greatly attractive to the automotive and aerospace industries. However, the application of the Mg alloys is limited due to their lower mechanical properties. Recently, Kawamura et al. have developed the Mg-Zn-Y (at. %) alloys with LPSO phase. These alloys have the excellent mechanical properties. The investigation reported here focused on the influence of RE elements, which were also effective in strengthening Mg-Zn-Y alloys, on the microstructure and mechanical properties of the Mg-Zn-Y-RE alloys. The microstructure of the Mg<sub>96</sub>Zn<sub>2</sub>Y<sub>2</sub>-xREx alloys (RE= La, Ce, and Yb) with RE content in the range 0.1 to 1.0 at. % was composed of α-Mg, compounds and LPSO phases. However, Mg<sub>96</sub>Zn<sub>2</sub>Y<sub>1</sub>RE<sub>1</sub> alloys (RE= Nd, Pr, and Sm) not detected LPSO phase. The tensile yield strength of Mg<sub>96</sub>Zn<sub>2</sub>Y<sub>2</sub>-xREx alloys with LPSO phase was higher than that of Mg<sub>96</sub>Zn<sub>2</sub>Y<sub>2</sub>-xREx alloys without LPSO phase.

5:40 PM

**Changes in Microstructure and Mechanical Properties of Mg-Zn-Y Alloy with Long Period Stacking Ordered Structure during Annealing:** *Masafumi Noda*<sup>1</sup>; Yoshihito Kawamura<sup>2</sup>; <sup>1</sup>Kumamoto Technology and Industry Foundation; <sup>2</sup>Kumamoto University

Changes in the mechanical properties and structure of extruded Mg-Zn-Y alloy with a long period stacking ordered structure on annealing at various temperatures were examined. The grain size of the extruded alloy increased to 9.4 μm on annealing between 473K and 773K for 3.6ks. However, the long period stacking ordered structure in the α-Mg matrix inhibited grain growth, and alloy annealed at 573K had similar mechanical properties to the extruded alloy, showing that the annealed alloy retained its strength.

## Magnesium Technology 2009: Wrought Alloys

Sponsored by: The Minerals, Metals and Materials Society, TMS Light Metals Division, TMS: Magnesium Committee

Program Organizers: Eric Nyberg, Pacific Northwest National Laboratory; Sean Agnew, University of Virginia; Neale Neelameggham, US Magnesium LLC; Mihriban Pekguleryuz, McGill University

Wednesday PM

Room: 2007

February 18, 2009

Location: Moscone West Convention Center

*Session Chairs:* Tyrone Jones, US Army Research Laboratory; Chamini Mendis, National Institute for Materials Science

## 2:00 PM Introductory Comments

2:05 PM

**Age Hardening Response and Microstructures of ZK60 Alloy with Li Additions:** *Chamini Mendis*<sup>1</sup>; Keiichiro Oh-ishi<sup>1</sup>; Kazuhiro Hono<sup>1</sup>; <sup>1</sup>National Institute for Materials Science

Mg-Zn based ZK60 alloy is a widely used wrought magnesium alloy that has a good combination of strength and ductility. However, only a small increment in strength is achieved by precipitation hardening due to the formation of coarse MgZn<sub>2</sub> rod-like precipitates parallel to [0001]<sub>Mg</sub>. In this work, we have found that systematic additions of 1-3at%Li to the ZK60 alloy enhanced the age hardening response and the peak hardness is doubled compared to that of Li free alloy. TEM investigations have revealed that the improved age hardening is attributed to the refinement of the precipitates and the increase of their aspect ratio, thereby hindering the motion of basal dislocations. The precipitates remain MgZn<sub>2</sub> phase. The role of Li in increasing the aspect ratio and number density of precipitates will be discussed.

2:25 PM

**High Temperature Deformation Behavior of Three Rolled Sheets of Magnesium Alloy AZ31:** *Ravi Verma*<sup>1</sup>; Jon Carter<sup>1</sup>; Paul Krajewski<sup>1</sup>; <sup>1</sup>General Motors Corp

Magnesium AZ31 sheet alloys from three different sources, 2 DC (Direct-Chill) and 1 CC (Continuous-strip cast), were assessed for elevated temperature formability by tensile testing. Both monotonic and step-strain tensile tests were conducted at several different temperatures and strain rates. The paper discusses the relationship between initial sheet microstructure and tensile deformation behavior in terms of ductility to failure, strainrate sensitivity of flow stress, necking characteristics, and failure modes. The three alloys exhibit very different deformation behaviors, suggesting microstructural features in addition to the grain size influencing the deformation behaviors.

2:45 PM

**Physical Metallurgy of Mg AZ80 Alloys for Forging Applications:** Chris Sager<sup>1</sup>; Igor Yakubtsov<sup>2</sup>; William MacDonald<sup>3</sup>; *Scott Shook*<sup>4</sup>; Brad Diak<sup>1</sup>; Marek Niewczas<sup>2</sup>; <sup>1</sup>Queen's University; <sup>2</sup>McMaster University; <sup>3</sup>Canmet MTL; <sup>4</sup>Timminco Corp.

The Dow Chemical Company originally developed Mg AZ80 alloy in the 1950's for forging applications. The physical metallurgy and microstructural makeup of AZ series alloys can be quite varied and are dependent on alloy content, casting parameters, cooling rate, heat treatment, and thermomechanical processing. Early attempts to improve the ductility of this alloy focused on reduction of the as-cast grain size and volume fraction of brittle second phase particles. We have studied mechanical properties and the microstructure of Mg AZ80 alloys after different thermomechanical processing and assessed its suitability for the forging applications. The stability of secondary phases was evaluated in this alloy by modeling phase equilibria and examining its microstructure using a range of experimental approaches. The recrystallization behaviour of the alloy was studied to optimize homogenization treatments, deformation processing and the microstructure of the as-cast billets to achieve the full potential of AZ80 in applications for automotive wheels.



3:05 PM

**Effects of Alloying Elements on Texture and Mechanical Properties of Extruded Mg-Zn-Al Alloys:** *Jung Woo Choi*<sup>1</sup>; Ji Hoon Hwang<sup>1</sup>; Kwang Seon Shin<sup>1</sup>; <sup>1</sup>Seoul National University

Mechanical properties of magnesium alloys are significantly influenced by their microstructure and texture. In recent years, there have been numerous attempts to improve the mechanical properties by controlling microstructure and texture using different manufacturing processes. Little study, however, has been carried out to examine the effects of alloying elements on texture in magnesium alloys. In the present study, the changes in texture and mechanical properties were examined in the extruded magnesium alloys with different Zn and Al contents. The effects of Zn and Al on the texture of magnesium alloys were examined systematically using the X-ray diffraction method. The effects of Zn and Al on the mechanical properties were examined by tensile and compressive tests. Using these experimental results, simulations were conducted based on a visco-plastic self-consistent model in order to predict the changes in major deformation modes and textures during tensile and compressive tests.

3:25 PM

**Formability of Magnesium Sheet:** *Dietmar Letzig*<sup>1</sup>; Lenka Fuskova<sup>1</sup>; Kerstin Hantzsche<sup>1</sup>; Gerrit Kurz<sup>2</sup>; Sangbong Yi<sup>1</sup>; Jan Bohlen<sup>1</sup>; <sup>1</sup>GKSS Forschungszentrum

Processing of magnesium and its alloys such as sheet-rolling causes significant changes in microstructures, especially in their crystallographic texture. Further, these changes influence on the mechanical properties such as strength, formability as well as the anisotropic behaviour. Rolled AZ31 alloy sheets typically have a strong basal texture, which limits their formability especially at room temperature. On the other hand, aluminium-free magnesium alloys with additions of rare-earth-elements exhibit different crystallographic texture, in terms of main texture component and its strength. Thus, the improvement in sheet formability can be achieved in rare-earth-elements added alloys, comparing to AZ31 alloy. In this study the formability of both AZ31 and ZE10 alloys at different temperatures is examined. Based on the present results, the influence of texture on the mechanical behaviour is discussed. It will be shown how the formability can be improved by weakening the crystallographic texture by means of alloy modification.

3:45 PM Break

4:00 PM

**Application of Incremental Forming Technique to Mg-AZ31 Sheet:** *Jong Park*<sup>1</sup>; <sup>1</sup>Hongik University

Magnesium alloy has a good strength-to-weight ratio. However, the material is so brittle that its application is limited to casting. Recently, as the formability of the material was found to be improved at warm temperatures, various sheet-metal forming techniques such as incremental forming and deep drawing at warm temperatures have been applied to this material. In the present study, the incremental forming technique was applied to Mg-AZ31 sheet in order to form various shapes, including cones, pyramids and curved surfaces. During forming, the sheet was continuously heated by hot-air blowers to keep the temperature to be consistent. As a result, these shapes were found to be successfully formed that were almost impossible by other forming techniques. Methodologies to utilize the material's formability, to overcome the forming limit and to compensate the springback were explored.

4:20 PM

**Grain Size Effect on Hot Forging of Mg Alloys:** *Yong Nam Kwon*<sup>1</sup>; <sup>1</sup>Korea Institute of Machinery and Materials

Magnesium alloys still have a lot of technical challenges to be solved for more applications. In the present study, effect of grain size on hot forging characteristics of Mg alloys using both cast and extruded forging stocks. For this purpose, three different Mg alloys such as AZ31, AZ61 and ZK60 were used. A general deformation behavior was gathered through a conventional compression test with the variation of strain rate and temperature. Both numerical and experimental works have been carried out on a model which contains both upsetting and extrusion geometries. Forgeability of magnesium alloys was found to depend greatly on grain size. Also, forging speed seemed to be more influential than temperature.

4:40 PM

**Deformation Mechanisms in AZ31 Magnesium Alloy Tube Bending:** *Wenyun Wu*<sup>1</sup>; Li Jin<sup>1</sup>; Shoushan Yao<sup>1</sup>; Alan Luo<sup>2</sup>; Anil Sachdev<sup>2</sup>; <sup>1</sup>Shanghai Jiao Tong University; <sup>2</sup>General Motors Research & Development Center

Abstract: This paper investigates the plastic deformation mechanisms of AZ31 magnesium alloy tubes under a rotary bending process at room and warm temperatures. The results suggest extensive twinning occurred at both intrados and extrados, leading to crack initiation and limited bendability at room temperature. With increasing bending temperature, less twinning is evident and the dislocation slip became more important in the bending deformation. When the bending temperature is too high, dynamic recrystallization occurs at the prior grain boundary and results in softening which leads to plastic instability and premature failure by cavity linkage.

5:00 PM

**Elevated-Temperature Gas-Pressure Bulge Forming of Magnesium AZ31 Sheet: Theory and Experiment:** *Eric Taleff*<sup>1</sup>; Ravi Verma<sup>2</sup>; Louis Hector<sup>2</sup>; Jung-Kuei Chang<sup>1</sup>; John Bradley<sup>2</sup>; Paul Krajewski<sup>2</sup>; <sup>1</sup>University of Texas; <sup>2</sup>General Motors R&D Center

Accurate prediction of strain fields and cycle times for fine-grained Mg alloy sheet forming at high temperatures (400-500°C) is limited by a lack of accurate material constitutive models. This paper details a first step toward addressing this issue by evaluating material constitutive models, developed from tensile data, for high-temperature plasticity of a fine-grained Mg AZ31 sheet material. The finite element method was used to simulate gas pressure bulge forming experiments at 450°C using four constant gas pressures. The applicability of the material constitutive models to a balanced-biaxial stress state was evaluated through comparison of simulation results with bulge forming data. Simulations based upon a phenomenological material constitutive model developed using data from both tensile elongation and strain-rate-change experiments were found to be in favorable accord with experiments. These results provide new insights specific to the construction and use of material constitutive models for hot deformation of wrought, fine-grained Mg alloys.

### Materials for High Temperature Applications: Next Generation Superalloys and Beyond: Advanced Coatings II and Intermetallics

Sponsored by: The Minerals, Metals and Materials Society, TMS Structural Materials Division, TMS: High Temperature Alloys Committee, TMS: Refractory Metals Committee  
Program Organizers: Joseph Rigney, GE Aviation; Omer Dogan, National Energy Technology Laboratory; Donna Ballard, Air Force Research Laboratory; Shiela Woodard, Pratt & Whitney

Wednesday PM

February 18, 2009

Room: 3010

Location: Moscone West Convention Center

*Session Chairs:* Brian Gleeson, University of Pittsburgh; Patrick Martin, Air Force Research Laboratory

2:00 PM Invited

**High-Temperature, Environmental-Resistant Coatings for Current and Future Alloys:** *Bruce Pint*<sup>1</sup>; <sup>1</sup>Oak Ridge National Laboratory

The implementation of current and new high-temperature materials is often hampered by their lack of oxidation or environmental resistance, particularly due to ever-increasing performance demands. Environmental-resistant coatings can increase service lifetime but often perform best on alloys with some inherent environmental resistance. So-called "prime-reliant" coatings that could prevent catastrophic degradation of substrates optimized for high-temperature strength are a noble research goal, however, there is considerable risk associated with inevitable coating defects and reliability in general. Further, other properties that high-performance coatings must demonstrate, such as chemical and mechanical compatibility with the substrates, assume greater importance as operating temperatures are increased. Examples are given for conventional alloys, superalloys and advanced materials in a variety of power generation applications.

## 2:25 PM Invited

**Hot Corrosion Degradation of Alumina-Forming Coatings on Ni-Base Superalloys:** *Gerald Meier*<sup>1</sup>; Frederick Pettit<sup>1</sup>; Brian Gleeson<sup>1</sup>; Michael Task<sup>1</sup>; <sup>1</sup>University of Pittsburgh

The components of gas turbine engines operating in many environments are susceptible to deposit-induced accelerated attack. In this study, relevant coatings and bulk alloys are being studied under conditions that are representative of Type I and Type II aggressive hot corrosion environments and cyclic oxidation. Experiments are also being performed to evaluate the effects of intermittent hot corrosion exposures on cyclic oxidation resistance of the alloys and coatings. The coatings and base alloys are relevant to current state-of-the-art systems. In order to examine the degradation of these systems without the complication of coating-substrate interactions, bulk alloys with the coatings compositions are also being studied. The effects of coating composition and phase distribution on the relative resistance to the various exposure environments and corresponding degradation mechanisms will be described.

## 2:50 PM

**Industrially Prepared EQ Coating Systems for Advanced Ni-Base Superalloys:** *Rudder Wu*<sup>1</sup>; Kyoko Kawagishi<sup>2</sup>; Kazuhide Matsumoto<sup>2</sup>; Hiroshi Harada<sup>2</sup>; <sup>1</sup>Imperial College London; <sup>2</sup>National Institute for Materials Science, Japan

"EQ coating" as a new coating system, has been introduced by NIMS-Japan in 2006. In this system, phases in thermodynamic equilibrium with the substrate (i.e.  $\gamma'$  phase) are used as coating materials to improve oxidation-resistance of substrates and suppress the formation of secondary reaction zone (SRZ). In our latest study, two EQ systems (standard and Pt-containing EQ) for the TMS-138A superalloy have been industrially prepared. The systems have further been coated by an electron beam-physical vapour deposited (EB-PVD)  $ZrO_2/7wt\% Y_2O_3$  (YSZ) top coat. Thermal-cycling experiments have shown that standard EQ systems can offer performances comparable to industrially used thermal barrier coatings (TBC). By the addition of Pt in the EQ system, the spallation-resistance of the YSZ coated system have been increased by approximately three times and exceed the majority of the current leading bond coat materials. Characterization of the coating cross-sections after spallation has confirmed the substrate-coating thermodynamic compatibility.

## 3:10 PM

**Fluorine Treatment for Improved Adherence of Eb-Pvd Thermal Barrier Coatings on TiAl Alloys:** *Alexander Donchev*<sup>1</sup>; Reinhold Braun<sup>2</sup>; Michael Schütze<sup>1</sup>; <sup>1</sup>DECHEMA; <sup>2</sup>German Aerospace Center

TiAl-alloys are promising candidates for high temperature applications in e.g. aero turbines. The capability of TiAl to withstand high temperature environmental attack is limited to temperatures of about 800°C. The fluorine effect is one possibility to enhance the oxidation resistance of TiAl alloys by forming a protective alumina scale. This scale can work as a bond layer for thermal barrier coatings (TBCs). To investigate the potential of the fluorine treatment in combination with ceramic YSZ-coatings (yttria stabilised zirconia) disk-shape specimens were treated with fluorine and preoxidised in air to form an Al<sub>2</sub>O<sub>3</sub>-scale. On these samples a ceramic YSZ top coat was deposited by electron-beam physical vapour deposition (EB-PVD). The oxidation resistance of these samples was studied performing cyclic oxidation tests for up to 2400 1-h cycles between 60°C and 900°C, 950°C or 1000°C in air. The TBCs exhibited good adhesion to the pre-treated specimens. Failure only occurred on those areas which had not been protected by the F- treatment before the EB-PVD process.

## 3:30 PM

**Resistance of Y<sub>2</sub>SiO<sub>5</sub> to CMAS Degradation by Apatite Formation:** *Kendra Grant*<sup>1</sup>; Stephan Kramer<sup>1</sup>; Carlos Levi<sup>1</sup>; <sup>1</sup>University of California, Santa Barbara

Environmental barrier coatings (EBCs) protect ceramic matrix composites (CMCs) from volatilization in high temperature combustion environments containing water vapor. Degradation of EBCs by siliceous deposits known as CMAS may limit the durability of these coatings. Yttrium monosilicate, a candidate EBC, has been shown to dissolve into molten CMAS and re-precipitate as a Ca:Y Apatite phase, with minor additional crystalline phases. The formation of a dense Apatite layer along the CMAS/EBC interface offers promise as a barrier to protect the underlying Y<sub>2</sub>SiO<sub>5</sub> from further chemical reaction with the CMAS melt. These results are particularly significant in light of earlier findings that EBCs based on barium-strontium-alumino-silicate (BSAS) do not form a reaction product with similar protective potential, and are susceptible to CMAS

penetration along grain boundaries to substantial depths below the interface. No such penetration has been observed in Y<sub>2</sub>SiO<sub>5</sub>. The observations, underlying mechanisms and implications for EBC durability are discussed.

## 3:50 PM Break

## 4:00 PM Invited

**Development Pathways to Engineering "Beta Gamma TiAl" Alloys:** *Young-Won Kim*<sup>1</sup>; Sang-Lan Kim<sup>1</sup>; Dennis Dimiduk<sup>2</sup>; Christopher Woodward<sup>2</sup>; <sup>1</sup>UES Inc; <sup>2</sup>AFRL

"Beta gamma" alloys are a new class of TiAl alloys that may offer improved processibility, refined microstructures, and increased strength without loss of ductility. The alloy design concept selected for the present investigations was to determine alloy compositions that are beta solidified but yield gamma- and beta-phase volume fractions of >85% and <5%, respectively, below 1000°C. Such alloys were found to exist within compositional ranges of Ti-(42-45)Al-(2-6)Nb-(1-6)(Cr, Mn, Mo, V)-(0.2-0.4)(B,C) in the proximity of the ternary phase field ( $\gamma + \beta/B2 + \alpha/\alpha_2$ ). Employing various processing methods and analytical tools, together with phase diagram constructions, the results showed that this alloy system exhibits the desired attributes and improvements, at least for medium-scale ingot processing. However, there are numerous issues/challenges that need to be overcome for beta gamma alloys to become viable as high-temperature structural materials. This presentation reports our ongoing development pathways toward beta gamma materials technology, and discusses the challenges.

## 4:25 PM

**Damage Evolution and Fatigue after Impact of the TiAl-Alloy TNBV3B:** *Susanne Gebhard*<sup>1</sup>; P.W.M. Peters<sup>1</sup>; Dan Roth-Fagaraseanu<sup>2</sup>; Heinz Voggenreiter<sup>1</sup>; <sup>1</sup>German Aerospace Center; <sup>2</sup>Rolls-Royce Germany

TiAl-alloys show a low ductility, which limits their application especially in components prone to impact damage like turbine blades or vanes. Therefore, the influence of impact damage on the mechanical behavior of a cast and a forged TNBV3B alloy has been investigated. Ballistic tests were performed with impact energies up to several joules. In order to approach the impact situation with real blades or vanes, a blade-like geometry was chosen for the specimen edges. The caused damage has been evaluated as a function of the impact speed, the particle weight and the impact location. Fatigue experiments at different temperatures were performed to determine the threshold for crack growth as a function of the impact damage size. For these tests, specimens showing cracks with lengths up to some millimeters on the specimen back side as well as specimens showing other damages like blow-outs were chosen.

## 4:45 PM

**Development of Ti-Al-Nb Intermetallic Alloys from Accumulative Roll Bonding and Reaction Annealing:** *Peng Qu*<sup>1</sup>; Viola Acoff<sup>1</sup>; <sup>1</sup>University of Alabama

The TiAl intermetallic compound has long been considered as a next-generation structural material and a replacement for traditional Ni-based superalloy not only for its high oxidation resistance, creep strength and excellent mechanical properties at elevated temperatures, but also because of its low density and light weight. In this paper, a ternary Ti-46Al-9Nb intermetallic alloy (at. %) was produced by accumulative cold roll bonding (ARB) followed by reaction annealing. X-ray diffraction (XRD), scanning electron microscopy (SEM) equipped with energy dispersive spectroscopy (EDS), and microhardness testing were used to characterize the phases that appeared after subjection to a two-stage annealing process. The diffusion mechanism for the first annealing stage was studied. The final lamellar structure that was obtained after the two-stage annealing process resulted in desirable properties.

## 5:05 PM

**The Effects of Cooling Rates on Phase Transformation and Microstructural Evolution in Ti-44Al-4Nb-4Zr Alloy:** *Hongwei Yang*<sup>1</sup>; <sup>1</sup>Delaware St Univ

Phase transformation and microstructural evolution has been studied in Ti-44Al-4Nb-4Zr-0.2Si-0.1B alloys that were cooled from the alpha + beta phase region with various cooling rates. It has been shown that the cooling rates have different influence on the morphology of the transformation products for three phase transformations studied, alpha -> alpha 2, B2 -> omega and alpha -> gamma. In furnace-cooled samples all three transformations are fulfilled completely, while in water-cooled samples, B2 -> omega is partially retained and a diffuse omega phase forms as metastable phase, and alpha -> gamma is completely suppressed, which support that the gamma lamellae formation is diffusion-controlled.

5:25 PM

**Beyond Near-Gamma Alloys: Development of Gamma+Sigma Alloys:** *Fereshteh Ebrahimi*<sup>1</sup>; Michael Kesler<sup>1</sup>; Sonalika Goyal<sup>1</sup>; Hans Seifert<sup>2</sup>; <sup>1</sup>University of Florida; <sup>2</sup>Freiberg University of Mining and Technology

The performance of aircrafts can be significantly improved by reducing the weight of their engines. Two-phase ( $\gamma$ -TiAl+ $\alpha$ -Ti<sub>3</sub>Al) near-gamma alloys with densities less than half of Ni-based superalloys are presently being developed but their application is limited due to their low creep resistance at high temperatures. We have developed alloys based on Ti-Al-Nb-X (X = Cr, Mo, W) system with  $\gamma$ -TiAl+ $\sigma$ -Nb<sub>2</sub>Al microstructures, which exhibit superior creep resistance. One of the shortcomings of gamma phase is its low ductility. In the presents study ductility improvement is achieved through significant refinement of the gamma grains, whose sliding at high temperatures is inhibited by the presence of a fine distribution of the hard sigma-phase. In this presentation, microstructural evolution in alloys based on Ti-Al-Nb-X systems is discussed and the dependency of toughness on microstructural scale and volume fraction of phases is elucidated. The support by NSF/AFOSR under grant number DMR-0605702 is greatly appreciated.

## Materials for the Nuclear Renaissance: Materials: Applications and Characterization

Sponsored by: The Minerals, Metals and Materials Society, TMS Structural Materials Division, TMS/ASM: Corrosion and Environmental Effects Committee, TMS/ASM: Nuclear Materials Committee, TMS: Refractory Metals Committee  
Program Organizers: Raul Rebak, GE Global Research; Robert Hanrahan, National Nuclear Security Administration; Brian Cockeram, Bechtel-Bettis Inc

Wednesday PM  
February 18, 2009

Room: 2009  
Location: Moscone West Convention Center

*Session Chairs:* Brian Cockeram, Bechtel-Bettis Inc; Raul Rebak, GE Global Research

2:00 PM

**Beryllium Use in Commercial Nuclear Reactors:** *Edgar Vidal*<sup>1</sup>; <sup>1</sup>Brush Wellman, Inc.

Beryllium has unique nuclear properties that make it an attractive metal for use in commercial nuclear reactors. Beryllium has been extensively used in advanced test reactors around the world as both a moderator and reflector of neutrons. Published work report that the use of beryllium improves the "neutron efficiency" of power generating nuclear reactors, thus reducing the fuel enrichment requirements in light water reactors, and heavy water inventory in heavy water reactors. Beryllium in solid form, like many industrial materials, poses no special health risk if safe handling practices are followed.

2:20 PM

**Hydride Redistribution and Delayed Hydride Cracking in Spent Fuel Rods during Dry Storage:** *Young Suk Kim*<sup>1</sup>; <sup>1</sup>Korea Atomic Energy Research Institute

The aim of this work is to investigate the effect of thermal creep during vacuum drying of the spent fuel rods on redistribution of hydrides and their delayed hydride cracking (DHC) susceptibility. To this end, we analyzed Tsai's thermal creep results of irradiated Zircaloy-4 cladding segments from two pressurized water reactors and Simpson and ELLS's observation where zirconium alloy cladding tube failed during a long-term storage at room temperature. On cooling the spent fuel rods, it is found that hydrogen moves from the peak temperature regions toward the cooler parts such as both ends of the cladding tubes, causing DHC cracks to grow there. When the spent fuel rods are cooled to below 180°C during their dry storage, this study demonstrates that according to Kim's DHC model spent fuel rods may fail by DHC only if the stressed regions with a higher tensile stress are present inside them.

2:40 PM

**In-Situ Studies and Modeling the Fracture of Zircaloy-4:** *Brian Cockeram*<sup>1</sup>; K. Chan<sup>2</sup>; <sup>1</sup>Bechtel Bettis Inc; <sup>2</sup>Southwest Research Institute

In-situ fracture studies were performed on non-irradiated Zircaloy-4 using tensile specimens and pre-cracked Compact Tension (CT) specimens to clarify the mechanism for fracture initiation in the constrained and non-constrained state. Similar approaches have been reported in the literature to understand

the role of hydrides on the fracture of Zircaloy-4, but hydride-free Zircaloy-4 has received little study. Both annealed and beta-treated Zircaloy-4 were tested in the longitudinal, transverse, and short-transverse orientations to study the role of microstructure and orientation. Unstable crack extension is shown to occur under plastic constraint by a process of void nucleation, growth, and coalescence initiating from the Laves phase particles in the microstructure. A micromechanical model is developed for ductile tearing by void growth and coalescence. Excellent agreement between the model and experiments are observed. Aspects of the fracture mechanism and model are discussed.

3:00 PM

**Influence of Grain Boundary Character on Creep Void Formation in Alloy 617:** *Thomas Lillo*<sup>1</sup>; James Cole<sup>1</sup>; Megan Frary<sup>2</sup>; Scott Schlegel<sup>2</sup>; <sup>1</sup>Idaho National Laboratory; <sup>2</sup>Boise State Univ

Alloy 617, a high temperature creep-resistant, nickel-based alloy, is in the process of being code qualified for the primary heat exchanger for the Next Generation Nuclear Plant (NGNP) which will operate at temperatures above those for materials listed in ASME Boiler and Pressure Vessel Code for nuclear power applications. Orientation imaging microscopy (OIM) is used to characterize the grain boundaries in the vicinity of creep voids that develop during high temperature creep tests terminated at relatively low creep strains (800-1000°C at creep stresses ranging from 20-85 MPa) so only the sites most prone to void formation are present. Grain boundary character of the boundaries comprising triple junctions, the primary location for creep void nucleation, is reported. Also, the grain boundary character of triple junctions that appear to be resistant to void formation, as indicated by the absence of voids during creep tests carried out to fracture, are surveyed.

3:20 PM

**Precipitate Redistribution during Creep of Alloy 617:** Scott Schlegel<sup>1</sup>; Thomas Lillo<sup>2</sup>; James Cole<sup>2</sup>; Sharla Hopkins<sup>1</sup>; Evan Young<sup>1</sup>; *Megan Frary*<sup>1</sup>; <sup>1</sup>Boise State University; <sup>2</sup>Idaho National Laboratory

The next-generation nuclear plant (NGNP) will require materials that can operate at very high temperatures (e.g., in heat exchangers). Alloy 617 is known for its high temperature strength and corrosion resistance; however, during creep, carbides that are supposed to retard grain boundary motion are found to dissolve and re-precipitate on boundaries in tension. To quantify the redistribution, we have used electron backscatter diffraction and energy dispersive spectroscopy to analyze the microstructure of 617 after creep testing. The data were analyzed with respect to location of the carbides (e.g., intergranular vs. intragranular), grain boundary character, and precipitate type (i.e., Cr-rich or Mo-rich). We find that grain boundary character is the most important factor in carbide distribution; some evidence of preferential distribution to tensile boundaries is also observed. If the role of grain boundary character on redistribution can be determined, materials could be engineered to have microstructures resistant to carbide redistribution.

3:40 PM Break

3:50 PM

**Microstructural and Corrosion Characteristics of Austenitic Stainless Steels Containing Silicon:** Peter Andresen<sup>1</sup>; Martin Morra<sup>1</sup>; Peter Chou<sup>2</sup>; *Raul Rebak*<sup>1</sup>; <sup>1</sup>GE Global Research; <sup>2</sup>Electric Power Research Institute

Austenitic stainless steels (SS) core internals components in nuclear light water reactors are susceptible to irradiation assisted stress corrosion cracking (IASCC). One of the effects of irradiation is the hardening of the SS and a change in the dislocation distribution in the alloy. Irradiation also alters the local chemistry of these austenitic alloys, for example in the vicinity of grain boundaries. The segregation or depletion phenomena at near grain boundaries may enhance the susceptibility of these alloys to environmentally assisted cracking (EAC). The objective of the present work was to perform laboratory tests in order to better understand the role of Si on microstructure, electrochemical behavior and susceptibility to EAC. Experimental results are presented for two main types of especially prepared stainless steels: (1) Type 304L SS + 1-5% added Si and (2) 12% Cr Steel + 5% added Si.



4:10 PM

**On Processing and Orientation Effects on the Viscoplastic Constitutive Laws of Nanostructured Ferritic Alloys:** Michael Salston<sup>1</sup>; G. Robert Odette<sup>1</sup>; Charles Eisel<sup>2</sup>; Kurt Van Nugtrent<sup>1</sup>; <sup>1</sup>University of California, Santa Barbara; <sup>2</sup>Forschungszentrum Karlsruhe

The creep strength of nanostructured ferritic alloys (NFA) is controlled by a high density of Y-Ti-O nanofeatures, dislocations and grain structures that depend on alloy composition and thermomechanical processing treatments. Extruded NFA have strong axial and weak transverse orientations. High temperature viscoplastic properties are evaluated for a range of NFA and different orientations using strain rate jump (SRJ) creep tests: a low strain rate is imposed until the stress reaches steady-state, exhausting the primary creep strain, followed by a series of increases in the imposed strain-rates and corresponding steady-state stresses. The creep data are fitted to a threshold stress model. The creep rates vary for the different NFA and orientations, but the threshold stresses are found to be significant fractions of the at-temperature yield stress. The NFA SRJ data are compared to those for 9Cr tempered martensitic steels (TMS) including constant stress creep data.

4:30 PM

**Titanium Aluminides for Advanced Fission Plants?:** Wolfgang Hoffelner<sup>1</sup>; Jiachao Chen<sup>1</sup>; Per Magnusson<sup>1</sup>; <sup>1</sup>Paul Scherrer Institute

Titanium aluminides are well accepted elevated temperature materials. In conventional applications their poor oxidation resistance limits the maximum operating temperature. Advanced reactor environments operate in non-oxidizing environments which could widen the applicability of these materials to higher temperatures. The behaviour of a cast gamma-alpha-2 TiAl in was investigated under thermal and irradiation conditions. Irradiation creep was studied in-beam using helium and proton irradiation. Thin strip samples of 100 micrometer thickness were investigated in a temperature range of 300-500 C under irradiation and significant creep strains were detected. At temperatures above 500 C thermal creep becomes the predominant mechanism. Thermal creep was investigated at temperatures up to 950 C with non-irradiated and irradiated material. No significant effect of sample geometry was detected. Irradiation induced damage and creep damage were studied with the transmission electron microscope. The results are compared with similar tests performed with a ferritic oxide dispersion strengthened material.

4:50 PM

**Effect of Grain Boundary Engineering on Microstructure and Properties of Alloy 800H:** Lichen Tan<sup>1</sup>; Loic Rakotojaona<sup>2</sup>; Kumar Sridharan<sup>1</sup>; Todd Allen<sup>1</sup>; <sup>1</sup>University of Wisconsin; <sup>2</sup>Mines ParisTech

Grain boundary engineering (GBE) has been demonstrated as an effective technique to improve the properties of polycrystalline metals. This technique essentially increases the population of low-sigma coincidence site lattice boundaries (CSLBs) with sigma less than 29 and interrupts the connectivity of general/random boundaries, by means of a carefully designed thermomechanical processing route. GBE has been successfully applied to Incoloy alloy 800H in this study. The supercritical water exposure and cyclic air oxidation tests showed significant improvement in oxide scale integrity with limited oxide exfoliation on the GBE-treated samples. The tensile and impact tests showed enhancement in strength at room and elevated temperatures. The microstructural evolution including precipitates and dislocations induced by the GBE treatment has been characterized by transmission electron microscopy and atomic force microscopy. This study provides insights on the property improvements due to the microstructural evolution induced by the GBE treatment.

5:10 PM

**Advanced Finite Element Flaw Growth Analysis of Stress Corrosion Cracks in Dissimilar Metal Butt Welds:** Aladar Csontos<sup>1</sup>; David Rudland<sup>2</sup>; Do-Jun Shim<sup>2</sup>; <sup>1</sup>U.S. Nuclear Regulatory Commission; <sup>2</sup>Engineering Mechanics Corporation of Columbus

On October 13, 2006, Wolf Creek Nuclear Operating Corporation performed inspections on the pressurizer surge, spray, relief, and safety nozzle-to-safe end dissimilar metal (DM) welds. The inspection identified five circumferential indications in the surge, relief, and safety DM welds that were attributed to primary water stress corrosion cracking (PWSCC). These indications were significantly larger than previously seen in commercial pressurized water reactors. As a result of the initial U.S. Nuclear Regulatory Commission (NRC) flaw evaluation study, the nuclear power industry agreed to complete pressurizer nozzle DM weld inspections on an accelerated basis. The industry

then conducted an advanced finite element analyses (AFEA) using more realistic assumptions to address NRC's concerns regarding the potential for rupture without leakage from circumferentially oriented PWSCC. This talk will discuss the modeling approach and a comparison of the industry's AFEA results to the NRC's confirmatory AFEA research program.

---

## Materials in Clean Power Systems IV: Clean Coal-, Hydrogen Based-Technologies, and Fuel Cells: Advanced Materials for PEM Fuel Cells and Batteries - Session II

Sponsored by: The Minerals, Metals and Materials Society, ASM International, TMS Electronic, Magnetic, and Photonic Materials Division, TMS/ASM: Corrosion and Environmental Effects Committee, TMS: Energy Harvesting and Storage Committee  
Program Organizers: K. Scott Weil, Pacific Northwest National Laboratory; Michael Brady, Oak Ridge National Laboratory; Ayyakkannu Manivannan, US DOE; Z. Gary Yang, Pacific Northwest National Laboratory; Xingbo Liu, West Virginia University; Zi-Kui Liu, Pennsylvania State University

Wednesday PM

Room: 3005

February 18, 2009

Location: Moscone West Convention Center

Session Chair: Xingbo Liu, West Virginia University

---

2:00 PM Introductory Comments

2:05 PM Invited

**Atomic-Scale Structural and Compositional Characterization of Alloy Catalyst Particles for PEM Fuel Cell Cathodes:** Karren More<sup>1</sup>; Lawrence Allard<sup>1</sup>; K. Reeves<sup>1</sup>; <sup>1</sup>Oak Ridge National Laboratory

High angle annular dark field (HAADF)-STEM (Z-contrast) imaging with sub-Å resolution is being used to image individual Pt-alloy catalyst particles having catalytically-relevant surface features, i.e., crystallographic/atomic ordering, surface faceting, surface 'skin' or 'skeleton' structures, and core-shell morphologies. In this study, several Pt-alloy catalysts, such as Pt-Co, Pt-Cr, Pt-Ti, and Pt-W, have been characterized by HAADF-STEM, high-resolution analytical TEM, and X-ray diffraction, in order to identify the crystallographic structures and predominant particle shapes and to correlate these observations with cathode durability and performance. Results from in-situ heating experiments of Pt-alloy catalysts, used to assess durability, will be discussed. Research sponsored by the U.S. Department of Energy, Office of Hydrogen, Fuel Cells, and Infrastructure Technologies Program, under contract DE-AC05-00OR22725 with UT-Battelle, LLC. Research conducted at ORNL's SHaRE User Facility was sponsored by the Division of Scientific User Facilities, Office of Basic Energy Sciences, U.S. Department of Energy.

2:40 PM

**A Novel Non-Platinum Group Electrocatalyst for PEM Fuel Cell Application:**

Jin Yong Kim<sup>1</sup>; K. Scott Weil<sup>1</sup>; <sup>1</sup>Pacific Northwest National Laboratory

Recent economic studies conducted indicate that cost of PEMFC stacks can be reduced dramatically by decreasing or eliminating the amount of platinum required in the cell electrodes; the largest quantity of which is employed in the cathode where it catalyzes the oxygen reduction reaction (ORR). While substantial progress has been made in understanding why platinum is such an effective catalyst for the ORR and in explaining the catalyst degradation mechanisms that currently limit the operational lifetimes of PEMFCs, less success has been achieved in identifying promising alternative electrocatalysts. We have recently completed a series of preliminary experiments on a composite material that shows promise as an alternative ORR electrocatalyst, in partial or full replacement of platinum. We will present the synthesis approach used in preparing the material, describe results from half-cell measurements, and discuss the reasons for the observed high catalytic activity based on current interpretations of supporting microstructural data.

3:00 PM Invited

**Metallic Bipolar Plates for Direct Methanol Fuel Cells:** Christian Trappmann<sup>1</sup>; Martin Mueller<sup>1</sup>; Juergen Mergel<sup>1</sup>; Detlef Stolten<sup>1</sup>; <sup>1</sup>Forschungszentrum Juelich

The results of the current research into design and development of novel metallic bipolar plates for direct methanol fuel cells (DMFCs) will be presented. The bipolar plate is one of the most important components of the fuel cell. In

conventional DMFCs the bipolar plates fabricated from graphite based materials are used. Since such plates mainly contribute more than 70% to the entire size and weight of the cell, the investigations into possibilities to utilize alternative metallic materials and advanced manufacturing methods are crucial for the reduction of the size and weight of the cell. The anodic and cathodic flow fields in the metallic bipolar plates recently developed at Forschungszentrum Juelich (IEF-3) are shaped into a 0.1 mm thick foil material by a hydroforming process. Various ways to enhance the corrosion stability of the plates are discussed. To reduce the contact resistance full or partially coating of the active areas is utilized.

**3:35 PM**

**Effect of Annealing on Microstructures of Nb-Clad 304LSS and Nb-Clad 434 SS for PEMFC Bipolar Plates:** Sung-tae Hong<sup>1</sup>; K. Scott Weil<sup>2</sup>; Jung Pyung Choi<sup>2</sup>; <sup>1</sup>University of Ulsan; <sup>2</sup>Pacific Northwest National Laboratory

Two different Niobium (Nb)-clad stainless steels (SS) manufactured by cold rolling are currently under consideration for use as bipolar plate materials in polymer electrolyte membrane fuel cell (PEMFC) stacks. In the manufacturing process of Nb-clad SS, annealing was needed to reduce the springback induced by cold rolling. Two different annealing conditions were required due to the two different SS substrates. For Nb-clad 304L SS, the annealing developed an interfacial layer between the Nb cladding and the SS core and the interfacial layer plays a key role in the failure of the Nb-clad 304L SS as reported earlier. For Nb-clad 434 SS, the development of interfacial layer was insignificant even though the recovered ductility was similar. For Nb-clad 304L SS, the effect of interfacial layer on the bulk electrical resistance was investigated.

**3:55 PM Break**

## Materials in Clean Power Systems IV: Clean Coal-, Hydrogen Based-Technologies, and Fuel Cells: Solid Oxide Fuel Cell Materials, Session I: Membranes, Electrodes, and Seals

Sponsored by: The Minerals, Metals and Materials Society, ASM International, TMS Electronic, Magnetic, and Photonic Materials Division, TMS/ASM: Corrosion and Environmental Effects Committee, TMS: Energy Harvesting and Storage Committee  
Program Organizers: K. Scott Weil, Pacific Northwest National Laboratory; Michael Brady, Oak Ridge National Laboratory; Ayyakkannu Manivannan, US DOE; Z. Gary Yang, Pacific Northwest National Laboratory; Xingbo Liu, West Virginia University; Zi-Kui Liu, Pennsylvania State University

Wednesday PM                      Room: 3005  
February 18, 2009                      Location: Moscone West Convention Center

*Session Chairs:* Ayyakkannu Manivannan, US DOE; Xingbo Liu, West Virginia University

**4:00 PM Invited**

**Reliability Prediction of SOFCs Anode Material Exposed to Fuel Gas Contaminants: Modeling & Experiment:** Gulfam Iqbal<sup>1</sup>; Huang Guo<sup>1</sup>; Bruce Kang<sup>1</sup>; <sup>1</sup>West Virginia University

Solid Oxide Fuel Cells (SOFCs) operate under harsh environment which deteriorate anode material properties and reduce its service life. In addition to electrochemical performance, structural integrity of SOFCs anodes is essential for long-term operation. SOFCs anodes are subjected to stresses at high temperature, thermal/redox cyclic effects, and coal syngas contaminants. These mechanisms can degrade anode microstructure and decrease electrochemical performance and structural properties. In this research a anode material degradation model is developed and implemented in FE analysis. The model takes into account thermo-mechanical and coal syngas contaminants degradation mechanisms for prediction of long-term structural integrity of SOFC anode. The model will be validated using a NexTech Probestat™ SOFC button cell test apparatus integrated with a Sagnac optical setup and infrared thermometer. The setup is capable of in-situ surface deformation and temperature measurement while measuring electrochemical performance of button cells under hydrogen or simulated coal syngas environment at operating conditions.

**4:35 PM**

**First-principles Calculations and CALPHAD Thermodynamic Modeling of Defects in  $\text{La}_{1-x}\text{Sr}_x\text{CoO}_{3-d}$ :** James Saal<sup>1</sup>; Venkateswara Rao Manga<sup>1</sup>; Mei Yang<sup>1</sup>; Zi-Kui Liu<sup>1</sup>; <sup>1</sup>Penn State University

To fully exploit the properties of  $\text{La}_{1-x}\text{Sr}_x\text{CoO}_{3-d}$ , a comprehensive and quantitative description of its defects is necessary. The parameters of the Gibbs free energy that make up thermodynamic models for defects in ionic systems are usually evaluated by fitting to experimental measurements, such as d. Such an approach reproduces experiments but is not always capable of uniquely describing the thermodynamic properties of the material. We report the progress in overcoming this difficulty by incorporating first-principles data, which allows us to predict not only measurable quantities but also properties that are difficult to determine experimentally, such as the valences of cobalt. This technology development has been supported in part by the U.S. Department of Energy under Contract No. DE-FC26-98FT40343. The Government reserves for itself and others acting on its behalf a royalty-free, nonexclusive, irrevocable, worldwide license for Governmental purposes to publish, distribute, translate, duplicate, exhibit and perform this copyrighted paper.

**4:55 PM Invited**

**Development of Chromium Barrier Layers for Solid Oxide Fuel Cells:** Dilip Chatterjee<sup>1</sup>; Samir Biswas<sup>1</sup>; <sup>1</sup>Corning Incorporated

Development of robust barrier layers is of prime interest for efficient operation of SOFC. High chromium content of ferritic stainless steels in electrolyte supported SOFC form gaseous oxides/hydroxides at the operating temperature and condense on various components of the stack, particularly on cathodes, resulting in performance degradation. Ideal barrier layer properties should include low diffusivity of chromium species in it, low thermal expansion mismatch of this layer with that of the substrate, durable at operating temperature, and most importantly, the preferred interface between the steel substrate and barrier layer should be continuous in nature. Primarily, two types of barrier layer were designed, produced and optimized for an electrolyte supported SOFC stack. These barrier layers were produced by diffusional and non-diffusional processes. This presentation will describe various barrier coatings, barrier properties provided by those coatings, and the transpiration measurements adopted to evaluate the efficiency of those coatings.

**5:30 PM**

**Evaluation of Thermal Stresses in Intermediate and High Temperature Solid Oxide Fuel Cells as a Function of Thermo-Mechanical Properties of Conventional and Advanced Anode, Cathode and Electrolyte Materials:** T. Manisha<sup>1</sup>; Miladin Radovic<sup>1</sup>; Nina Orlovskaya<sup>2</sup>; Beth Armstrong<sup>3</sup>; <sup>1</sup>Texas A & M University; <sup>2</sup>University of Central Florida; <sup>3</sup>Oak Ridge National Laboratory

Distribution of mechanical stresses in Solid Oxide Fuel Cells (SOFCs) is a complex function of geometry, temperature distribution, residual thermal stresses, external mechanical loads, etc. In the present work, we report on evaluation and distribution of thermal stresses as a function of thermo-mechanical properties of constituent materials at various temperatures for high temperature and intermediate temperature SOFCs. The materials studied include Ni-Y0.8Zr0.92O2 and Ni-Sc0.1Ce0.01Zr0.89O2, as anode materials, LaMnO3, (La0.7Sr0.3)0.98 MnO3, and La0.6Sr0.4Fe0.8Co0.2O3 as the cathode material and Yt0.08Zr0.2, Sc0.1Ce0.01Zr0.2, and Gd0.2Ce0.8O2 as the electrolyte materials. The thermo-mechanical properties namely coefficient of thermal expansion and elastic and shear moduli were determined in 25-900°C temperature range using thermal mechanical analyzer and resonant ultrasound spectroscopy in nitrogen and air atmosphere respectively. These thermo-mechanical properties have been used to estimate and model the distribution of thermal stresses at different temperatures in the anode, electrolyte and cathode assembly of intermediate and high temperature fuel cells.

**5:50 PM**

**Microstructure Design of Solid Oxide Fuel Cell Electrodes:** Kei Yamamoto<sup>1</sup>; R. Edwin Garcia<sup>1</sup>; <sup>1</sup>Purdue University

The effects of connected porosity and functionally graded electrode material are analyzed for a typical YSZ/LSM SOFC cells. Optimal microstructure electrodes are proposed by identifying microstructural mechanisms that control the transport of oxygen in the porous cathode electrode. For the selected material parameters simulations show that a decrease in the spacing of interconnected porosity improves power delivery at moderate and high current densities. Microstructural mechanisms, such as self-induced starvation and the effect of the tortuosity of the LSM network to power generation are assessed.

Microstructures where LSM with engineered particle density gradients and directly connected porosity networks are described.

## Materials Processing Fundamentals: Aqueous and Liquid Processing

Sponsored by: The Minerals, Metals and Materials Society, TMS Extraction and Processing Division, TMS: Process Technology and Modeling Committee  
Program Organizer: Prince Anyalebechi, Grand Valley State University

Wednesday PM Room: 2016  
February 18, 2009 Location: Moscone West Convention Center

Session Chair: Sutham Niyomwas, Prince of Songkla University

### 2:00 PM

**A Study on the Mechanism of Magnetite Formation Based on Iron Isotope Fractionation:** *Payman Roonasi*<sup>1</sup>; Allan Holmgren<sup>1</sup>; <sup>1</sup>Luleå University of Technology

Having knowledge of mechanism of magnetite formation is essential in a number of industrial processes including magnetite synthesis and corrosion of iron. In this study, magnetite nano-particle was synthesized via two different ways; coprecipitation of iron (II) and (III) and oxidation of ferrous hydroxide. The samples were characterized using X-ray diffraction (XRD), Mid-Far IR spectroscopy, scanning electron microscopy (SEM), chemical analysis for determination of FeII/FeIII ratio and ICP-MS for iron isotopic ratio (<sup>56</sup>Fe/<sup>54</sup>Fe) measurement. Since fractionation of iron isotopes depends on reaction rate and bonding strength, interpretation of the isotopic data with respect to the possible mechanisms is discussed. No fractionation of iron isotopes was observed for the magnetite synthesized by coprecipitation, whilst magnetite formed from ferrous hydroxide showed higher abundance of <sup>54</sup>Fe compared to <sup>56</sup>Fe in the beginning of reaction, implying the significance of the following reaction:  $\text{Fe}(\text{OH})_2(\text{solid}) \rightleftharpoons [\text{Fe}(\text{OH})]^{+}(\text{aq}) + \text{OH}^{-}$ .

### 2:15 PM

**Kinetic Studies of Hydrochloric Acid Leaching Process of Ilmenite for Rutile Synthesis:** *Zengjie Wang*<sup>1</sup>; *Jilai Xue*<sup>1</sup>; Haibei Wang<sup>2</sup>; Xunxiang Jiang<sup>2</sup>; <sup>1</sup>University of Science & Tech Beijing; <sup>2</sup>Beijing General Research Institute of Mining and Metallurgy

Kinetic study of hydrochloric acid leaching of Panzhihua ilmenite from China is presented. The leaching process is found to follow the spherical model  $f(a)=1-(1-a)^{1/3}$  and the apparent activation energy is 47.21 KJ/mol. The dissolving behaviors varied in different kinetic stages. At the beginning stage the dissolved amount of Fe and Ti increased monotonically with leaching time, while about 15 minutes later the dissolved Ti in the form of TiOCl<sub>2</sub> began hydrolyzed into TiO<sub>2</sub> powder reunited on the ilmenite ore surface, as observed by SEM and EDS. With the unreacted ilmenite particles covered by a layer of hydrolyzed TiO<sub>2</sub>, the leaching seemed as a selective leaching of iron and other impurities because Ti dissolved and hydrolyzed rapidly. The leaching process can end 4 hour later when most of Fe and other impurities have been dissolved and TiO<sub>2</sub> remains as residues. The effects of acid concentration and leaching temperature were also investigated.

### 2:30 PM

**Studies on the Anodic Dissolution Behavior of TiC<sub>x</sub>O<sub>y</sub> in Alkali Chloride Melt:** *Xiaohui Ning*<sup>1</sup>; Hengyang Liu<sup>1</sup>; Hongmin Zhu<sup>1</sup>; <sup>1</sup>Beijing University of Science & Tech

The chemical and electrochemical anodic dissolution behavior of TiC<sub>x</sub>O<sub>y</sub>, which were prepared through carbothermic reduction of titanium dioxide, was investigated in alkali chloride melt. A mass spectrometer was used to on-line detect the anodic gas generated during the dissolution. The results showed that TiC<sub>x</sub>O<sub>y</sub> can dissolve by electrochemical way but not chemical dissolution. During the electrochemical dissolution, titanium dissolves as Ti<sup>2+</sup> ion into the molten salt melt and carbon and oxygen form carbon oxide (CO, CO<sub>2</sub>) simultaneously. The influence of ratio of O/C in TiC<sub>x</sub>O<sub>y</sub> on the dissolution behavior, as well as the gas component was also studied in detail. It is very interesting that the components of anodic gas changed with the change of ratio of O/C in TiC<sub>x</sub>O<sub>y</sub>. When the ratio of O/C is 1:1, the carbon monoxide was main production. And as the ratio of O/C in TiC<sub>x</sub>O<sub>y</sub> is more than 1, CO<sub>2</sub> was also detected.

### 2:45 PM

**Synthesis and Chlorination of Titanium Oxycarbide:** *Guangqing Zhang*<sup>1</sup>; Mohammad Dewan<sup>1</sup>; Andrew Adipuri<sup>1</sup>; Oleg Ostrovski<sup>1</sup>; <sup>1</sup>The University of New South Wales

Chlorination of titanium oxycarbide has an advantage over chlorination of titanium dioxide as it occurs at much lower temperatures. The paper presents results of a systematic study of synthesis of titanium oxycarbide and its chlorination. Titanium oxycarbide was produced by carbothermal reduction of titania in hydrogen, argon and helium. Formation of titanium oxycarbide started at 1200°C in all gases. The reduction was the fastest in hydrogen. Formation of titanium oxycarbide in hydrogen was close to completion in 120 min at 1300°C, 60 min at 1400°C and less than 30 min at 1500°C. Reduction in argon and helium progressed similarly and reached 90-95% after 300 min at 1400-1500°C. The chlorination of titanium oxycarbide was ignited at 150-200°C. Chlorine partial pressure and gas flow rate strongly affected the chlorination rate. Chlorination of titanium oxycarbide produced with carbon to titania molar ratio 2.5 at 235-400°C was close to 100% in 30 min.

## Mechanical Behavior of Nanostructured Materials: Joint Session of Mechanical Behavior of Nanostructured Materials and Bulk Metallic Glasses VI: Mechanical Behavior of Nano and Amorphous Materials

Sponsored by: The Minerals, Metals and Materials Society, TMS Structural Materials Division, TMS/ASM: Mechanical Behavior of Materials Committee

Program Organizers: Peter Liaw, The University of Tennessee; Hahn Choo, The University of Tennessee; Yanfei Gao, The University of Tennessee; Gongyao Wang, University of Tennessee; Xinghang Zhang, Texas A & M University; Andrew Minor, Lawrence Berkeley National Laboratory; Xiaodong Li, University of South Carolina; Nathan Mara, Los Alamos National Laboratory; Yuntian Zhu, North Carolina State University; Rui Huang, University of Texas, Austin

Wednesday PM Room: 3012  
February 18, 2009 Location: Moscone West Convention Center

Session Chairs: Nathan Mara, Los Alamos National Laboratory; Julian Raphael, Columbus McKinnon

See page 283 for program.

## Mechanical Behavior of Nanostructured Materials: Plasticity and Deformation Mechanisms at Small Length Scale III

Sponsored by: The Minerals, Metals and Materials Society, TMS Electronic, Magnetic, and Photonic Materials Division, TMS Materials Processing and Manufacturing Division, TMS Structural Materials Division, TMS: Chemistry and Physics of Materials Committee, TMS/ASM: Mechanical Behavior of Materials Committee, TMS: Nanomechanical Materials Behavior Committee

Program Organizers: Xinghang Zhang, Texas A & M University; Andrew Minor, Lawrence Berkeley National Laboratory; Xiaodong Li, University of South Carolina; Nathan Mara, Los Alamos National Laboratory; Yuntian Zhu, North Carolina State University; Rui Huang, University of Texas, Austin

Wednesday PM Room: 3024  
February 18, 2009 Location: Moscone West Convention Center

Session Chairs: Nathan Mara, Los Alamos National Laboratory; Zhiwei Shan, Hysitron Inc

### 3:30 PM Invited

**Creep, Superplasticity and Fracture Toughness in Nanocrystalline Ceramics:** *Dongtao Jiang*<sup>1</sup>; Dustin Hulbert<sup>1</sup>; *Amiya Mukherjee*<sup>1</sup>; <sup>1</sup>University of California

A three-phase alumina based nanoceramic composite demonstrated superplasticity at a surprisingly lower temperature and at a higher strain rate. An alumina-carbon nanotube-niobium nanocomposite demonstrated fracture



toughness values that are three times higher than that for pure nanocrystalline alumina. It was possible to take advantage of both fiber-toughening and ductile-metal toughening in this investigation. A silicon nitride/silicon carbide nanocomposite, produced by pyrolysis and liquid polymer precursor, demonstrated one of the lowest creep rates reported so far in ceramics. This was primarily achieved by avoiding oxynitride glassy phase at the intergrain boundaries. One important factor in the processing of these nanocomposites was the use of electrical field assisted sintering method. This allowed the sintering to be completed at significantly lower temperatures and at much shorter times. These improvements in mechanical properties will be discussed in the context of results from microstructural investigations. Work supported by grants from ARO and ONR.

**3:50 PM**

**Phase Transformation and Recrystallization during Creep of a Nanostructured Intermetallic TiAl Alloy:** *Fritz Appel*<sup>1</sup>; Jonathan Paul<sup>1</sup>; Michael Oehring<sup>1</sup>; <sup>1</sup>GKSS Research Centre Geesthacht

The creep behavior of a novel type of nanostructured TiAl alloys with a modulated morphology has been investigated. The constitution and microstructure of the alloy result from decomposition reactions of the high-temperature  $\beta/\beta_2$  phase. The characteristic constituents are structurally modulated laths that are comprised of several stable and metastable phases. Tensile creep tests have been correlated with characterization by high-resolution transmission electron microscopy. The creep behavior of the material is mainly limited by the early onset of tertiary creep at higher stresses and temperatures. The processes associated with this behavior are several phase transformations towards thermodynamic equilibrium, dynamic recrystallization and the relaxation of constraint stresses that exist between misfitting phases.

**4:05 PM**

**Investigation of Creep Behaviour with a New Innovative Nanoindentation Tester:** *Nicholas Randall*<sup>1</sup>; <sup>1</sup>CSM Instruments

Nanoindentation testing is particularly appropriate for creep and stress relaxation tests because it can measure materials whose properties are highly viscoelastic. However, the main drawback of nanoindentation tests is linked to the low thermal stability of most instruments. These instabilities introduce an uncontrollable penetration drift superimposed to the viscoelastic deformation of the sample. For some polymers thermal expansion of the instrument frame can be quite significant. The recent development of a new innovative instrument (the Ultra Nanoindentation Tester) has allowed such drawbacks to be avoided, and has allowed precise investigation of the creep behaviour of samples using very long duration tests. This results in almost complete elimination of the thermal drift in the measurement head. This study demonstrates that nanoindentation testing, when performed in good conditions with appropriate apparatus, constitutes a reliable tool to study the time dependent mechanical properties of materials.

**4:20 PM Break****4:40 PM**

**Examining Nanomechanical Properties through Quantitative In Situ TEM Compression Testing:** *Jia Ye*<sup>1</sup>; Raja Mishra<sup>2</sup>; Andrew Minor<sup>1</sup>; <sup>1</sup>Lawrence Berkeley National Laboratory; <sup>2</sup>General Motors R&D Center

In situ TEM nanocompression testing gives us insight into size effects in nanoscale volumes and also the ability to systematically measure the mechanical properties of small, well-defined single crystals. Using this technique, we have studied the origins of ductility in Aluminum alloys and the twinning process in Mg. In the first system, an AA6063 alloy was found to exhibit very different plastic deformation characteristics depending on the solute concentration in the matrix. For the second system, we studied Mg nanopillars. Due to their hexagonal structure, we will show that knowing the orientation of the Mg samples is particularly important. During in situ nanopillar compression testing the pure Mg demonstrated basal plane sliding and extensive twinning behavior. Importantly, our in situ technique allows for the stress state at the point of twin nucleation and during the progression of the twinning process to be measured directly.

**4:55 PM**

**Modeling the In Situ TEM Deformation of CdS Nanospherical Shells:** *Matthew Sherburne*<sup>1</sup>; Hillary Green<sup>1</sup>; D. Chrzan<sup>2</sup>; <sup>1</sup>University of California, Berkeley; <sup>2</sup>Materials Sciences Division, Lawrence Berkeley National Laboratory

Experiments performed by Shan et al. indicate that hierarchically structured CdS nanospherical shells, composed of multiple nanograins, can be compressed

up to 20% of their diameters before brittle fracture occurs. A finite element model was used to analyze the stress state within the shells; the shear stresses within the shell approach 2.2 GPa at the point of failure. The ideal shear stress for CdS was computed using density functional based total energy method. The computed ideal shear strength for CdS is 3.1 GPa. The stresses within the shell approach 71% of the ideal strength of the material. This unusual strength is attributed to the hierarchical structure of the nanospheres. Research supported by the Director, Office of Science, Office of Basic Energy Sciences (BES), of the US Department of Energy under Contract No. DE-AC02-05CH11231 and National Science Foundation under Grant No. DMR 0304629. Z. W. Shan et al., submitted for publication

**5:10 PM**

**Systematic Study of Strain Rate Sensitivity of Nanostructured Pd Alloys Using Nanoindentation:** *Insuk Choi*<sup>1</sup>; Ruth Schwaiger<sup>1</sup>; Anna Castrup<sup>1</sup>; Julia Ivanisenko<sup>1</sup>; Horst Hahn<sup>1</sup>; Oliver Kraft<sup>1</sup>; <sup>1</sup>Forschungszentrum Karlsruhe

Nanostructured metals have shown a strong strain rate sensitivity at room temperature. In this study, we performed nanoindentation tests with different strain rates to provide more quantitative and systematic understandings of the mechanisms behind this strain rate sensitivity by studying nanostructured metal alloys. Pd alloys with grain size ranging from a few nm to 150 nm were prepared, with Ag and Zr as alloying additions, by High Pressure Torsion (HPT), and by R.F. magnetron sputtering. For Pd based alloys, stacking fault energy varies with respect to the Ag content and is likely to affect deformation mechanisms. Furthermore, grain boundary sliding may be controlled by Zr, which segregates to the grain boundaries. For Pd-Ag alloys, the sensitivity becomes dramatically weaker with increasing Ag alloying content. Furthermore, the strain rate sensitivity itself was observed to be stronger for smaller strain rates indicating that different mechanisms are active in different strain rate regimes.

**5:30 PM**

**Isostatic Pressing of a Nanocrystalline Al Alloy Powder:** *Byungmin Ahn*<sup>1</sup>; Andrew Newbery<sup>2</sup>; Enrique Lavernia<sup>2</sup>; Steven Nutt<sup>1</sup>; <sup>1</sup>University of Southern California; <sup>2</sup>University of California, Davis

When consolidating nanocrystalline powder, it is important to obtain full densification without losing the beneficial microstructure. Although cryomilled Al alloy powder typically has very high thermal stability, the time at extended temperature and pressure during consolidation by hot isostatic pressing (HIP) results in moderate grain growth and reduction in the strength. In the work described in this paper, we carry out the isostatic pressing of cryomilled Al-5083 powder at lower temperatures, either by cold isostatic pressing (CIP) or by HIPping at low temperature. The effect of increasing CIP pressure was also investigated. The density and microstructure of the consolidated billets were characterized. A nearly 100% dense billet can be obtained at temperatures within the range of what is termed warm isostatic pressing. The resultant microstructure has much reduced grain size relative to material produced using previous HIP conditions. Mechanisms of hardening as well as microstructural development during processing were investigated.

**5:45 PM**

**Mechanical Behavior of Fine-Grained Ductile Films on Polymer Substrates:** *Megan Cordill*<sup>1</sup>; Gerhard Dehm<sup>1</sup>; F. Fischer<sup>2</sup>; <sup>1</sup>Erich Schmid Institute of Materials Science; <sup>2</sup>Institute of Mechanics, Montanuniversitaet Leoben

Adhesion has been shown to be an important parameter in increasing the stretchability of flexible electronic devices. These devices are made on polymer substrates where the adhesion energies of the ceramic transistors and metal lines are difficult to determine. These interfaces need to be able to stretch as well as compress while maintaining good electrical conductivity. Common methods to measure adhesion energies of films on hard substrates (stressed overlayers, nanoindentation, and four point bend) cannot be easily implemented due to the compliance of the substrate. Cu films deposited onto polyimide are examined using an in-situ tensile test inside the scanning electron microscope to induce fracture and delamination of the films for measuring adhesion energies. Two interlayers, Cr and Ti, will also be studied to determine which increases the adhesion at the polyimide-metal interface.

**6:00 PM**

**Hypersensitive Moisture-Assisted Debonding along Sol-Gel Coupled Oxide/Epoxy Interfaces:** *Mark Oliver*<sup>1</sup>; Reinhold Dauskardt<sup>1</sup>; <sup>1</sup>Stanford University

Thin (~100nm) metal/epoxysilane sol-gel coupling layers exhibit excellent adhesive and cohesive fracture properties and have the potential to enable

new technologies that require high-performance epoxy/oxide interfaces. We demonstrate the existence of a new mechanism of moisture-assisted subcritical crack growth involving cohesive fracture of the sol-gel coupling layer wherein the crack growth kinetics exhibit a hypersensitivity to the moisture content of the environment at low growth rates. Rather than a threshold below which crack growth is dormant, persistence debonding is observed at growth rates below ~10 nm/sec. Existing models of moisture-assisted cracking, which have been successfully applied to numerous materials and interfaces, are unable to capture the observed behavior. A new model for moisture-assisted crack growth in hybrid organic-inorganic thin films will be proposed. Strategies for eliminating this behavior will be presented along with the implications of these findings for the reliability of sol-gel materials in general.

## Nanocomposite Materials: Nanocomposites for Energy Conversion and Storage

Sponsored by: The Minerals, Metals and Materials Society, TMS Structural Materials Division, TMS Electronic, Magnetic, and Photonic Materials Division, TMS/ASM: Composite Materials Committee, TMS: Materials Characterization Committee, TMS: Nanomaterials Committee

Program Organizers: Jonathan Spowart, US Air Force; Judy Schneider, Mississippi State University; Bhaskar Majumdar, New Mexico Tech; Benji Maruyama, Air Force Research Laboratory

Wednesday PM Room: 3020  
February 18, 2009 Location: Moscone West Convention Center

Session Chairs: Terry Tritt, Clemson University; Michael Durstock, US Air Force

### 2:00 PM Introductory Comments

### 2:05 PM Invited

**Nanostructured Materials for Energy Harvesting and Storage Devices:** *Michael Durstock*<sup>1</sup>; <sup>1</sup>Air Force Research Laboratory, Materials and Manufacturing Directorate

The development of low-cost, lightweight, and flexible energy harvesting and storage devices are an enabling technology for many different types of applications. The fabrication of highly efficient conversion and/or storage devices with a high power and energy density, have yet to be achieved. In general, poor charge transport in organic and nanoparticle-hybrid devices is one of these factors and can result from low electronic charge carrier mobilities, relatively random thin film morphologies, and/or limited ionic intercalation and conduction pathways. Our efforts to address these issues for a variety of devices (including photovoltaics and battery electrode materials) include developing materials and fabrication methodologies that result in highly ordered structures to permit enhanced charge transport. This talk will discuss a number of these approaches including the fabrication and utilization of vertically aligned TiO<sub>2</sub> and carbon nanotubes, as well as the assembly of mixtures of electroactive discotic liquid crystals.

### 2:30 PM

**Electrochemical Lithium Storage of Li-Doped Titanate Nanotube:** *Yi-Heon Jeong*<sup>1</sup>; *Sun-Jea Kim*<sup>2</sup>; *Kyung Sub Lee*<sup>1</sup>; <sup>1</sup>Hanyang University; <sup>2</sup>Sejong University

Li-doped titanate nanotubes were synthesized by hydrothermal lithium ion exchange processing from titanate nanotube precursor. To prepare the Li-doped titanate nanotubes, titanate nanotubes powder that had been treated with NaOH was mixed with LiOH aqueous solution and the resulting suspension was placed in a Ni-lined stainless-steel autoclave at 120°C for 24hrs, and subsequently fired at 100-500°C in vacuum to remove the hydrate in the nanotube. The electrochemical tests were performed by cycle voltammetry and galvanostatic method on a coin-type cell assembled with working electrode/separator/reference electrode (metallic lithium). The electrolyte solution was 1M LiBF<sub>4</sub> dissolved in a propylene carbonate (PC). Galvanostatic charge-discharge tests were performed at constant current density (10mA/g), with cutoff voltage of 1.0 to 3.0V. Systematic studies of effect of Li dopant and residual Na<sup>+</sup> in the nanotube on lithium ion storage have been presented.

### 2:50 PM

**Evaluation of Single-Wall Carbon Nanotube/Poly-(p-Naphthaleneethynylene)-Based Composite Electronic Materials for Supercapacitor Applications:** *Maria Abreu-Sepulveda*<sup>1</sup>; *Mariem Rosario-Canales*<sup>2</sup>; *Pravas Deria*<sup>3</sup>; *Michael Therien*<sup>3</sup>; *Jorge Santiago-Avilés*<sup>2</sup>; <sup>1</sup>University of Puerto Rico at Humacao; <sup>2</sup>University of Pennsylvania; <sup>3</sup>Duke University

Although substantial improvement in capacitance, energy densities, and discharge times has been achieved for redox supercapacitors over last several years, important challenges remain. These include high series resistance which limits the ability to quickly discharge these devices, excessive heat generation, and the coupled thermoelastic strain field which tends to deform the device materials. High stability composites based upon conjugated polymers that wrap single-wall carbon nanotubes (SWNTs) provide a platform to develop materials that can broadly impact these issues. This work discusses the preparation, characterization, and testing of new electrode materials based on polymer-wrapped SWNTs for the construction of supercapacitors. These polymer-wrapped SWNT composites exploit rigid, polyanionic poly(aryleneethynylene)s which provide unusual solubility and dispersion characteristics for carbon nanotubes in several solvents. Testing of the PNES/SWNT materials was done in sulfuric acid and potassium hydroxide aqueous solutions and in propylene carbonate-based solutions containing either tetrabutylammonium perchlorate or the ionic liquid 1-ethyl-3-methylimidazolium bis(trifluoromethylsulfonyl)imide.

### 3:10 PM

**Novel Activated Carbon Based Nanocomposites for Electrochemical Supercapacitors:** *Prabeer Barpanda*<sup>1</sup>; <sup>1</sup>Rutgers University

Activated carbons are dominating electrode materials for commercial electrochemical supercapacitors. It majorly stores electrostatic charge via non-faradaic ionic double-layer formation at electrode-interface. The overall capacitance of activated carbons can be improved by modifying the surface morphology (specific surface area, porosity distribution etc) and improving the space charge capacitance in carbon. The current work is an attempt to combine these two routes to modify activated carbons, which has been achieved by in-situ gr-VII halides (iodine and bromine) doping via high-energy milling. The highly electronegative halides induce strong charge transfer reaction in carbon, thereby improving its electrical conductivity. As a result of halidation, a homogeneous carbon-halide nanocomposites is obtained which shows dramatic improvement in gravimetric (~100% rise) and volumetric capacity (~300% rise). The structural and electrochemical properties of these nanocomposites will be presented using a suite of techniques like XRD, DSC, BET, XRF, XPS, TEM, Raman spectroscopy and electrochemical measurements.

### 3:30 PM Break

### 3:45 PM Invited

**Overview of Thermoelectric Properties of Bulk Nano-Composite Thermoelectric Materials:** *Terry Tritt*<sup>1</sup>; *Xiaohua Ji*<sup>1</sup>; *Jian He*<sup>1</sup>; *Bo Zhang*<sup>1</sup>; *Nick Gothard*<sup>1</sup>; *Paola Alboni*<sup>1</sup>; *Zhe Su*<sup>1</sup>; <sup>1</sup>Clemson University

Recently, there has been an ever-increasing research effort on thermoelectric nanocomposite materials. Composites using a mixture of bulk thermoelectric materials with nanoparticles incorporated with the bulk are of specific interest. One of the main goals is to have additional design or tuning parameters for materials in order to manipulate and control the phonon scattering mechanisms, without significantly deteriorating the electrical transport properties. The ability to decouple the electron and phonon scattering mechanisms is very important in the development of higher efficiency thermoelectric (TE) materials, wherein the figure of merit, ZT, can be greater than unity. New opportunities are being explored in order to improve existing TE materials and significantly increase ZT. The role of phonons may be one of the most important parameters to understand in these novel materials. A review of recent results in nanocomposite TE materials from several research groups will be presented.

### 4:10 PM

**ErAs Nanoparticles Embedded in (InGaAs)<sub>1-x</sub>(InAlAs)<sub>x</sub> for Thermoelectric Power Conversion:** *Gehong Zeng*<sup>1</sup>; *Hong Lu*<sup>2</sup>; *Je-Hyeong Bahk*<sup>1</sup>; *Ashok Ramu*<sup>1</sup>; *Arthur Gossard*<sup>2</sup>; *John Bowers*<sup>1</sup>; <sup>1</sup>Electrical and Computer Engineering Department, University of California, Santa Barbara; <sup>2</sup>Materials Department, University of California, Santa Barbara

Erbium arsenide metallic nanoparticles are incorporated into InGaAlAs to create scattering centers for middle and long wavelength phonons, provide charge carriers, and form local potential barriers for electron filtering. The

thermoelectric properties of  $\text{ErAs}:(\text{InGaAs})_{1-x}(\text{InAlAs})_x$  were characterized by variable temperature measurements of thermal conductivity, electrical conductivity and Seebeck coefficient from 300 K to 800 K. The results show that the material's ZT is greater than 1.2 when the temperature is above 700 K. Generator modules of  $\text{Bi}_2\text{Te}_3$  and  $\text{ErAs}:(\text{InGaAs})_{1-x}(\text{InAlAs})_x$  segmented elements were fabricated and an output power over 6 W was measured. Device modeling shows that the performance of thermoelectric generator modules can further be enhanced by the improvement of the thermoelectric properties of the materials, and reducing the electrical and thermal parasitic losses.

#### 4:30 PM

**Enhancement of Surface Morphology and Optical Properties of ZnO-Ag-ZnO Used as Transparent Conductive Thin Films:** *Wen-Long Wang*<sup>1</sup>; Fei-Yi Hung<sup>1</sup>; S. J. Chang<sup>2</sup>; K. J. Chen<sup>2</sup>; Z. S. Hu<sup>3</sup>; <sup>1</sup>Institute of Nanotechnology and Microsystems Engineering, Center for Micro/Nano Science and Technology, National Cheng Kung University; <sup>2</sup>Institute of Microelectronics and Department of Electrical Engineering, Center for Micro/Nano Science and Technology, National Cheng Kung University; <sup>3</sup>Institute of Electro-Optical Science and Engineering, Center for Micro/Nano Science and Technology, National Cheng Kung University

Sputtered ZnO-Ag-ZnO films (100nm/30nm/100nm) on the quartz glass were used to investigate the effect of crystallized mechanism on their surface morphology, electrical properties and optical properties. The thin films were heated at 400°C~500°C for 1 hour in vacuum and in  $6.9 \times 10^{-1}$  Torr with pure O<sub>2</sub>. The analyzed results were also compared to investigate the interface structure, and the relation between oxygen atom concentration and optical characteristics. From XRD and FIB analysis, the ZnO-Ag-ZnO (ZAZ) thin films possessed the hexagonal structures and the Ag diffused layer was observed. After O<sub>2</sub> annealed, the ZAZ not only raised the index of crystalline, but also reduced the electrical resistivity. Notably, increasing O<sub>2</sub> concentration can improve the transparent effect of Ag diffused layer. For the PL spectra, both the interface structure and the index of crystalline increasing of ZAZ thin film made a strong UV emission band and a blue-shift.

#### 4:50 PM

**New WC-Co Electrode Materials with Additives of Al<sub>2</sub>O<sub>3</sub> Nanopowder:** *Sergey Nikolenko*<sup>1</sup>; Sergey Pyachin<sup>1</sup>; <sup>1</sup>Institute of Materials, Khabarovsk Scientific Centre, Far Eastern Branch, Russian Academy of Sciences

Hard alloys based on tungsten carbide with cobalt are used usually as electrode materials for the forming of strengthening coatings by electro-spark alloying (ESA). The ESA method can be improved using nanocrystalline materials. We have produced WC-8%Co alloys with 1-5% additives of Al<sub>2</sub>O<sub>3</sub> nanopowder applied as a inhibitor of grain growth. Powders have been compacted at a pressure of 150 MPa. Sintering of compacted electrodes was performed in vacuum at temperature 1450°C for 60 min. The microstructure investigation of obtained alloys showed that Al<sub>2</sub>O<sub>3</sub> additives from 1 to 5 wt% decreases the grain size of tungsten carbide from 2.5 to 1 micron. In our work, physicomechanical properties of coatings formed by ESA method with new electrode materials have been studied. The microhardness increased in 2 times and the wear resistance grown in 3-4 times in comparison with a coating produced using WC-Co alloy.

#### 5:10 PM

**Effect of Nb Addition on Magnetic Properties and the Microstructure of Fe<sub>3</sub>B / Nd<sub>2</sub>Fe<sub>14</sub>B Nanocomposite Permanent Magnets:** *Junhua You*<sup>1</sup>; <sup>1</sup>Northeastern University

The microalloying effect of Niobium on the microstructure and magnetic properties of Fe<sub>3</sub>B / Nd<sub>2</sub>Fe<sub>14</sub>B nanocomposite permanent magnet has been investigated. As a result, Niobium addition stabilizes the amorphous phase and hinders the kinetics of the crystallization of the Fe<sub>3</sub>B particles. Niobium added in combination with Cu reduces grain size of Fe<sub>3</sub>B particles more remarkably than that without Niobium; with Niobium addition enhances magnetic properties of the alloy, but the amount must be suitable. Optimum magnetic properties with  $B_r=1.15\text{T}$ ,  $jH_c=467\text{kA/m}$  and  $(BH)_{\text{max}}=132.7\text{kJ/m}^3$  were obtained by annealing a melt-spun Nd<sub>5.5</sub>Fe<sub>70.0</sub>Co<sub>5</sub>Cu<sub>0.5</sub>Nb<sub>0.5</sub>B<sub>18.5</sub> amorphous ribbon at 670°C for 40 min.

### National Academies Propulsion Materials Study Community Town Hall Meeting: National Academies Propulsion Materials Study Community Town Hall Meeting

Sponsored by: National Academy of Sciences  
Program Organizer: Erik Svedberg, National Academy of Sciences

Wednesday PM Room: 3010  
February 18, 2009 Location: Moscone West Convention Center

Session Chair: Erik Svedberg, National Academy of Sciences

#### 6:00 PM Town Hall Meeting

### Near-Net Shape Titanium Components: Deformation and Machining Processes

Sponsored by: The Minerals, Metals and Materials Society, TMS: Titanium Committee

Program Organizers: Rodney Boyer, Boeing Company; James Cotton, Boeing Co

Wednesday PM Room: 2010  
February 18, 2009 Location: Moscone West Convention Center

Session Chair: John Fanning, TIMET

#### 2:00 PM

**Heat Treat and Cold Worked ATI-425® Properties:** *John Hebda*<sup>1</sup>; <sup>1</sup>ATI Wah Chang

Early after the discovery that ATI-425® was cold workable, trials were also conducted to examine the heat treat response for strengthening via solution treatment and aging. While the alloy demonstrated capability for strengthening via STA, a full matrix of heat treat cycles and anneals had not been performed. This presentation examines the mechanical properties and microstructure from a matrix of four solution temperatures, three cooling rates, and six aging or annealing temperatures. The mechanical properties are compared to cold worked material in the cold worked state, various stress relief cycles, and fully annealed. In general, there exist a variety of opportunities to utilize ATI-425® to optimize strength and ductility.

#### 2:20 PM

**Hot Stretch Forming of Near Net Shape Titanium Profiles:** *Martin Moffatt*<sup>1</sup>; <sup>1</sup>Cyril Bath Company

The development of Hot Stretch Forming was motivated by the need to design and manufacture Titanium airframe structures for new aircraft with carbon fiber fuselage skins. These structures are contoured to fit against the inside radius of the fuselage curvature. By combining traditional stretch forming technology with hot metal forming techniques, the new technology of Hot Stretch Forming (HSF) was developed by the Cyril Bath Company. This new forming technology allows design engineers to develop a variety of Titanium structure profiles at reduced buy to fly costs. The HSF technology is cost effective, repeatable, and available to be used for immediate production in volumes to meet aircraft build rates, now and in the future. The process saves both material and machining time; serious cost issues for today's aircraft budgets. The benefits of this process in controlling and minimizing residual stress allowing consistent machining will be discussed.

#### 2:40 PM

**Property Evolution of ATI 425®: From Ingot through Final Tubing:** *Melissa Martinez*<sup>1</sup>; John Hebda<sup>1</sup>; <sup>1</sup>ATI Wah Chang

ATI 425® alloy (4Al-2.5V-0.2Fe-0.25O) is a cold workable titanium alloy showing similar properties to Ti 6Al-4V. Previous work on sheet has shown the alloy to have improved fatigue properties over alloys such as Ti 6Al-4V Super ELI and Ti 3Al-2.5V. The improved properties make the alloy a good candidate for a higher pressure hydraulic system with a reduced wall thickness and weight resulting in cost savings. Microstructure and mechanical properties are examined at various stages in processing from ingot to final sized hydraulic



tubing of ATI 425® alloy including: ingot breakdown, extrusion and rocking. Properties are compared to Ti 3Al-2.5V at various stages.

### 3:00 PM

**Superplastic Formability of Ti-5Al-4V-0.6Mo-0.4Fe Alloy (TIMETAL®54M):** *Yoji Kosaka*<sup>1</sup>; Phani Gudipati<sup>1</sup>; Vasishth Venkatesh<sup>1</sup>; <sup>1</sup>TIMET

Ti-5Al-4V-0.6Mo-0.4Fe alloy (Ti-54M) was developed at TIMET recently. The alloy exhibits superior machinability in most of machining conditions and strength comparable to that of Ti-6Al-4V. This is believed to be due to its lower flow stresses at elevated temperatures. The alloy has commercially been produced with Electron Beam Single Melt process for automotive forgings applications. Since the beta transus of Ti-54M is lower than Ti-6Al-4V, and the alloy contains iron, a fast diffuser, it is of interest to examine superplastic formability of the alloy. This paper will introduce and discuss preliminary results of SPF evaluation of Ti-54M sheets produced in a laboratory scale.

### 3:20 PM

**A New Method of Laser Milling of Titanium for Rapid Manufacture of 3D Parts:** *Gareth Littlewood*<sup>1</sup>; Lin Li<sup>1</sup>; Zhu Liu<sup>1</sup>; Malcolm Ward-Close<sup>2</sup>; <sup>1</sup>University of Manchester; <sup>2</sup>QinetiQ

A new method of rapid manufacture of near net shape Ti components has been developed based on laser ablation. The majority of current methods of rapid manufacture using lasers are based on additive techniques in which a part is built up layer-by-layer. The new method is faster than the current additive laser based rapid manufacture techniques and uses lower laser powers than the current laser milling processes. This is achieved through the choice of experimental conditions and laser parameters. Thin walls and delicate structures have been demonstrated which are possible as the process is non-contact and deep, high aspect ratio holes have also been produced which have been difficult to produce by mechanical rapid manufacture techniques. This raises the possibility of application of the technique in the areas of medical and aerospace component manufacture.

### 3:40 PM

**Machining Advantages of Ti-54M:** *Rodney Boyer*<sup>1</sup>; James Cotton<sup>1</sup>; Stacey Nakayana<sup>2</sup>; John Fanning<sup>2</sup>; Megan Harper<sup>1</sup>; <sup>1</sup>Boeing Co; <sup>2</sup>TIMET

TIMET has developed an alloy referred to as 54M (Ti-5Al-4V-0.6Mo-0.4Fe) which has demonstrated the potential for a significant advantage in the cost of machining over Ti-6Al-4V, and has properties slightly lower than those of Ti-6Al-4V, but comparable. TIMET first noted an advantage in the number of holes which could be drilled with a single tool in comparison to Ti-6Al-4V. Boeing has studied the milling characteristics of the alloy and found a noteworthy advantage in this area for some machining modes. The mechanism(s) behind this improvement are not well understood, but are assumed to include such factors as changes in microstructure, flow and fracture stresses, and chemistry; these will be discussed.

## Neutron and X-Ray Studies of Advanced Materials: Advanced Imaging and Bio-Inspired Studies

Sponsored by: The Minerals, Metals and Materials Society, TMS Structural Materials Division, TMS/ASM: Mechanical Behavior of Materials Committee, TMS: Advanced Characterization, Testing, and Simulation Committee, TMS: Titanium Committee  
**Program Organizers:** Rozallya Barabash, Oak Ridge National Laboratory; Yandong Wang, Northeastern University; Peter Liaw, The University of Tennessee; Jaimie Tiley, US Air Force

Wednesday PM Room: 3016  
 February 18, 2009 Location: Moscone West Convention Center

**Session Chairs:** Emil Zolotoyabko, Technion-Israel Institute of Technology; Yang Ren, Argonne National Laboratory

### 2:00 PM Invited

**The Structure of Natural Bio-Composites: Combined X-Ray and Neutron Diffraction Study of Mollusk Shells:** *Emil Zolotoyabko*<sup>1</sup>; <sup>1</sup>Technion-Israel Institute of Technology

Formation of natural bio-composites with superior characteristics attracts growing attention of researchers focusing on deeper understanding and potential mimicking of biomineralization. Organic macromolecules, supplied by organisms, play a crucial role in this sophisticated "processing". Our recent

studies using high-resolution x-ray and neutron powder diffraction showed that the interaction between organic substance and ceramic mineral influences even the atomic structure of biogenic crystals. Specifically, we found that the unit cells in both mollusk-made aragonite and calcite are anisotropically distorted as compared to their geological counterparts. These distortions are the result of local forces imposed on mineral crystallites by intra-crystalline organic macromolecules. These forces also influence atomic positions in biogenic aragonite and calcite and, hence, atomic bonds, which are probed by neutron diffraction. For example, we found significant changes in the aplanarity of carbonate groups in biogenic aragonite, which are well correlated with frequency shifts in the Raman spectra.

### 2:20 PM Invited

**Diffraction X-Ray Tracking (DXT) for Super Accurate Dynamic Observations of Single Molecular Motions:** *Yuji Sasaki*<sup>1</sup>; <sup>1</sup>Spring-8/JASRI, JST/CREST Sasaki-Team

Recent progress in in-vivo or in-vitro observations of individual single protein molecules has been achieved with several single-molecular techniques and systems. However, it is difficult to measure intramolecular structural changes of single proteins molecules using visible lights due to the lack of monitoring precision and stability of the signal intensity in physiological conditions. One of the methods for the improvement of the positional decision accuracy is to shorten wavelength, for example, X-rays, electrons, and neutron. Recently, we succeeded picometer-scale slow Brownian motions of individual protein membranes (Bacteriorhodopsin (BR) and Potassium channel KcsA) in aqueous solutions from time-resolved Laue observations. In this single molecular detection system with X-rays, which we call Diffracted X-ray Tracking (DXT), we observed the rotating motions of an individual nanocrystal, which is labeled to the specific site in individual protein molecules.

### 2:40 PM Invited

**Monte Carlo Simulation Study of Diffuse Scattering in Pb(Zr,Ti)O<sub>3</sub> (PZT):** *T. R. Welberry*<sup>1</sup>; R.L. Withers<sup>1</sup>; K.Z. Baba-Kishi<sup>2</sup>; <sup>1</sup>Australian National University; <sup>2</sup>The Hong Kong Polytechnic University

Transverse polarized diffuse streaks have been observed in diffraction patterns of Pb(Zr<sub>1-x</sub>Ti<sub>x</sub>)O<sub>3</sub> ceramics for compositions ranging from x=0.3 (rhombohedral phase) to x=0.7 (tetragonal phase) including the important MPB region (x = 0.48). The streaks correspond to diffuse planes of scattering in 3D and these are oriented normal to the (cubic) <111> directions. A Monte Carlo (MC) model has been developed that convincingly reproduces the observed diffraction patterns. In this the displacements of Pb ions running in chains along each of the <111> directions are directed along the chain and are strongly correlated from cell to cell. There is no evidence of lateral correlation. Neighbouring chains are essentially independent. At this stage it is not clear what role the local order revealed by the scattering might play in governing the exceptional piezo-electric properties of the material but its presence requires the currently accepted models for the average structure to be reassessed.

### 3:00 PM Invited

**High-Density Resolution Microtomography Using Synchrotron Radiation for Materials Science Applications:** *Felix Beckmann*<sup>1</sup>; <sup>1</sup>GKSS-Research Center Geesthacht

The GKSS-Research Center Geesthacht is operating the user experiments for microtomography using synchrotron radiation at DESY, Hamburg, Germany. At the GKSS HARWI II wiggler beamline at DORIS III an intense and large X-ray beam in the photon energy range from 20 to 250 keV is available. Tomograms with high spatial resolution together with high density resolution are now routinely be obtained. Several applications for the characterizing new materials for light weight construction and new welding techniques will be shown. Furthermore, the perspectives for micro- and nanotomography at the new undulator beamlines the imaging beamline (IBL) and the high energy materials science beamline (HEMS) at the new PETRA III storage ring will be given.

### 3:20 PM Invited

**Mapping 3D Shape, Orientation and Strain State of Individual Grains in Polycrystals by X-Ray Diffraction Contrast Tomography:** *Wolfgang Ludwig*<sup>1</sup>; Andrew King<sup>2</sup>; Peter Reischig<sup>3</sup>; Sabine Rolland du Roscoat<sup>3</sup>; Erik Lauridsen<sup>4</sup>; <sup>1</sup>Mateis, CNRS; <sup>2</sup>Manchester University; <sup>3</sup>ESRF; <sup>4</sup>Technical University of Denmark

X-ray diffraction contrast tomography (DCT) is a synchrotron based imaging technique that enables the mapping of 3D shape, orientation and the elastic strain

state of individual grains in the bulk of polycrystalline materials. The sample is illuminated using a monochromatic X-ray beam and both the direct and the diffracted beams are captured simultaneously on a single detector positioned closely behind the sample. The scanning and analysis procedure are based on the acquisition of Friedel pairs of diffraction spots - a concept enabling the implementation of robust indexing and accurate strain determination procedures. The shapes of the individual grains are obtained by tomographic reconstruction from the observed diffraction spots, employing algebraic reconstruction techniques (ART). The talk will illustrate the current possibilities and limitations of the technique with the help of some selected applications, including the analysis of stress-corrosion and fatigue crack propagation, grain growth and elastic deformation in metallic alloys.

### 3:40 PM Break

### 3:50 PM

**X-Ray Micro-Tomography Imaging of Crack Propagation in Biological Samples Using an In Situ Mechanical Testing Device:** *Holly Barth*<sup>1</sup>; *Alastair MacDowell*<sup>2</sup>; *Robert Ritchie*<sup>1</sup>; <sup>1</sup>University of California, Berkeley; <sup>2</sup>Lawrence Berkeley National Laboratory

Many extrinsic mechanisms are activated in a biological structure during crack growth on the length scale of a micrometer. The x-ray microtomography beamline at the Advanced Light Source allows for non-destructive three-dimensional imaging at this length scale. The process takes 2D projections and through a filtered back projection algorithm the images are reconstructed into a 3 dimensional image, which is representative of the sample's absorption. Using this technique the crack path is visualized as it interacts with the biological sample's microstructure. However, to really visualize the interactions it is important to do the crack growth in real time. The in situ mechanical testing device allows for the stable crack growth of these specimens as the tomographic 3-dimensional imaging is being done using either three point bending or tension. The specimens observed in the in situ device have included human cortical bone, bovine cortical bone, and dentin.

### 4:05 PM Invited

**Properties of Dislocation Microstructures during Deformation under Single Slip:** *Patrick Veyssiere*<sup>1</sup>; <sup>1</sup>LEM, CNRS-Onera

In a first part of this talk, effects of test temperature on dislocation organization will be examined in fcc-based ordered alloys such as TiAl and Ni<sub>3</sub>Al. It will be shown that TEM provides unique information on dislocation behavior that would remain unnoticed under indirect diffraction methods. The second part will be devoted to dislocation self-organization into entanglements. The property that dislocations of a given slip system are able to spontaneously engender obstacles to their own propagation has been the object of constant attention since the early 1950's. Entanglements are believed to stem from the sweeping of prismatic loops by mobile dislocations. Little is known though on the origin and organization of the prismatic loops and on the mechanism by which stable multipolar entanglements are formed. The present investigation concentrates on selected aspects related to self-organization under single slip in an effort to clarify its various constituents.

### 4:25 PM Invited

**Study of Biomineralization of Fish Bone Using X-Ray Diffraction Microscopy:** *Huaidong Jiang*<sup>1</sup>; *Changyong Song*<sup>2</sup>; *Kevin Raines*<sup>1</sup>; *Rui Xu*<sup>1</sup>; *Bagrat Amirbekian*<sup>1</sup>; *Yoshinori Nishino*<sup>2</sup>; *Tetsuya Ishikawa*<sup>2</sup>; *Jianwei Miao*<sup>1</sup>; <sup>1</sup>University of California, Los Angeles; <sup>2</sup>RIKEN SPring-8 Center

X-ray diffraction microscopy is a newly developed imaging modality that extends the methodology of X-ray crystallography to allow the structural determination of noncrystalline specimens. Herein, the biomineralization and development of 3D architecture of Alewife herring bone were investigated by using X-ray diffraction microscopy. To study the spatial relationships of mineral crystals to the collagen matrix of the fish bone, we performed nanoscale imaging of the mineral crystals inside collagen fibrils at different stages of mineralization. The origin and distribution of mineral crystals inside the collagen matrix has been identified. Based on the experimental results, we proposed a dynamic structural model of bone to account for the nucleation and growth of mineral crystals in the collagen matrix with maturation of bone. These results will not only contribute to understand the biomineralization mechanism of fish bone, but also provide important design principles for hard tissue engineering and the development of biocompatible materials.

### 4:45 PM

**The EDXRF Analysis of Components in Electric and Electronic Instruments in Accordance with RoHS Standard:** *Denis Negrea*<sup>1</sup>; *Catalin Ducu*<sup>1</sup>; <sup>1</sup>University of Pitesti

The use of Cd, Pb, Hg and hexavalent Cr in electric and electronic products is limited within the framework of the RoHS directives. The limiting value for Cd is 100 mg/kg, for Hg, Pb, hexavalent Cr and the brominated flame retardants PBB and PBDE is 1000 mg/kg. The values must be below these limits for all components in an instrument, making regular monitoring necessary. An electronic circuit board was mapped using an EDXRF spectrometer and a Fundamental Parameters algorithm. Based on the obtained map, a point scan was done for Cd, Pb, Hg, Cr and Br in the highest intensity spots in order to obtain their highest concentrations within the analyzed sample area. In the end it was verified the compliance of the circuit board subjected to the analysis with the RoHS standard.

### 5:00 PM

**An Analysis of Solidification Porosity in Atomized Al-Cu and Al-Fe Powders:** *Stephane Ablitzer*<sup>1</sup>; *Jon Johansson*<sup>1</sup>; *Denise Thornton*<sup>1</sup>; *Maryia Maizlin*<sup>1</sup>; *Hani Henein*<sup>1</sup>; <sup>1</sup>University of Alberta

Porosity is a defect encountered in numerous casting operations. There are numerous efforts still underway to model this porosity formation. However, porosity in castings can occur due to numerous causes such as solidification shrinkage or poor feeding. Experimental data of solidification shrinkage porosity has not been easily available to date. X-ray tomography using synchrotron radiation with 0.27 micron beam resolution at the European Synchrotron Radiation Facility was used to generate three-dimensional (3-D) images for rapidly solidified Al-Cu and Al-Fe atomized droplets. The 3D image of the solidified droplets was observed and the porosity in these droplets were isolated. The volume fraction, interconnectivity and position of the porosity in the droplets was analyzed. The effect of gas in the atomizing chamber as well as particle size and alloy chemistry will be discussed.

### 5:15 PM Invited

**High-Energy Synchrotron X-Ray Diffraction for Materials Research under Complex Sample Environments:** *Yang Ren*<sup>1</sup>; <sup>1</sup>Argonne National Laboratory

The availability of synchrotron photons generated in high-flux and with energies much greater than 60 keV has significantly advanced the field of materials research because of the great penetration and low absorption. Obtaining high angular resolution for high-energy x-ray scattering provides still further research opportunities, especially in the study of bulk samples for both fundamental research and practical applications. Here we present a user facility, at the APS high-energy x-ray beamline 11-ID-C, where we combine a 2D and a point detector for both rapid and high-resolution x-ray diffraction studies. Both powder and single crystal samples can be studied in confined and complex sample environments with combined tunable external parameters (for example, combinations of temperature, pressure, stress, magnetic and electric fields). We will present the technical details and scientific research opportunities for this facility, as well as some recent results obtained with this instrument in different research areas.

### 5:35 PM Invited

**Diffuse Scattering from Molecular Crystals:** *Darren Goossens*<sup>1</sup>; <sup>1</sup>Australian National University

Diffuse scattering is a probe of the local ordering in a crystal, whereas Bragg peaks are descriptive of the average long-range ordering. This long-range average is made up of numerous local configurations whose population cannot be determined from analysis of the Bragg peaks. Diffuse scattering allows examination of this population and so offers a way to look at crystal structures in great detail. This is particularly the case when making use of the three-dimensional distribution of diffuse scattering. However, diffuse scattering is very weak and broad and often of similar intensity to experimental background, so data collection is demanding. Further, disorder can take on many forms and local configurations are not constrained by the average crystallographic symmetry. Here, the modelling of diffuse scattering from molecular crystals will be discussed, with particular reference to an X-ray study of pentachloronitrobenzene (C<sub>6</sub>Cl<sub>5</sub>NO<sub>2</sub>) and a neutron diffraction study of *para*-terphenyl, C<sub>18</sub>H<sub>14</sub>.

## Pb-Free Solders and Emerging Interconnect and Packaging Technologies: Microstructure, Modeling and Test Methods

Sponsored by: The Minerals, Metals and Materials Society, TMS Electronic, Magnetic, and Photonic Materials Division, TMS: Electronic Packaging and Interconnection Materials Committee

Program Organizers: Sung Kang, IBM Corp; Iver Anderson, Iowa State University; Srinivas Chada, Medtronic; Jenq-Gong Duh, National Tsing-Hua University; Laura Turbini, Research In Motion; Albert Wu, National Central University

Wednesday PM Room: 2020  
February 18, 2009 Location: Moscone West Convention Center

Session Chairs: Carol Handwerker, Purdue University; Fu Guo, Beijing University of Technology

### 2:00 PM Invited

**Nucleation Control of Near-Eutectic Sn-Ag-Cu+X Solder Joints by Alloy Design:** Iver Anderson<sup>1</sup>; Jason Walliser<sup>1</sup>; Joel Harringa<sup>1</sup>; Alfred Kracher<sup>1</sup>; <sup>1</sup>Iowa State Univ

Selecting a general purpose Sn-Ag-Cu (SAC) reflow solder remains a quandary. Instead of a eutectic microstructure found in Sn-Pb, the difficulty of Sn nucleation in typical SAC joint solidification promotes increased undercooling and Sn dendrites in normal reflow or, in slow cooling (e.g., BGA reflow), pro-eutectic Ag<sub>3</sub>Sn “blades” can form that may embrittle joints. SAC alloy designs with low Cu (0.5 wt.%) and very low Ag, down to 1%Ag (SAC105) have been proposed to promote Sn nucleation and inhibit nucleation of Ag<sub>3</sub>Sn, but this results in higher melting (226C liquidus) and decreased strength. Alternatively, this work focused on avoiding Ag<sub>3</sub>Sn blades with near-eutectic SAC3595 solder (220C liquidus) by promoting Sn nucleation with 4th elements (X=Zn, Mn, Al, and Fe) at low concentrations (<0.21%). These were selected by alloy design rules to form pro-eutectic intermetallic “seeds” that can reform during multiple reflows. Supported by Nihon-Superior through Ames Lab (contract no. DE-AC02-07CH11358).

### 2:20 PM

**A Novel Solder Based on Metallic Nanoparticle Inks for Low-Temperature Packaging Technology:** Teymur Bakhishev<sup>1</sup>; Vivek Subramanian<sup>1</sup>; <sup>1</sup>University of California, Berkeley

A novel solder technology based on gold (Au) nanoparticle ink was investigated. Inks consisted of surfactant passivated nanoparticles dissolved in a solvent. Optimized gold inks are able to sinter at temperatures as low as 120°C and achieve conductivities of up to 70% of bulk. Once sintered, the metallic structure reverts to bulk-like properties and approaches bulk reliability and performance. Thus nanoparticle-based solders would operate at much lower homologous temperatures as compared to alloy-based solders. Nanoparticle inks under investigation were sintered at 180°C. These inks showed no significant contact resistance due to surfactant or solvent contamination. Electromigration studies were carried out and time to failure was investigated as a function of temperature. Electromigration activation energy was calculated through Black’s equation to be 0.52eV, which is consistent with grain boundary diffusion. Nanoparticle inks are promising candidates as next-generation solders.

### 2:35 PM

**Utilizing the Thermodynamic Nanoparticle Size Effects for Low Temperature Pb-Free Solder Applications:** John Koppes<sup>1</sup>; Kevin Grossklaus<sup>1</sup>; Anthony Muza<sup>1</sup>; R. Rao Revur<sup>2</sup>; Suvankar Sengupta<sup>2</sup>; Hong-Sik Hwang<sup>3</sup>; Eric Stach<sup>1</sup>; Carol Handwerker<sup>1</sup>; <sup>1</sup>Purdue University; <sup>2</sup>MetaMateria Partners; <sup>3</sup>Indium Corporation of America

Development of lead-free solders with melting temperatures near traditional eutectic Pb/Sn solder is needed to limit damage to heat sensitive microelectronic components and devices. A possible method for reducing the melting temperature of Pb-free solders is by using nanoparticle solder pastes, in which the nanoparticles melt at temperatures far below their bulk counterparts due to the thermodynamic size effect. Particles with 5 nm diameters, observed to melt at temperatures below traditional Pb/Sn solder, are combined with flux (organic rosin used to prevent and remove oxide layers) to produce nanosolder pastes. The prototype nanosolder pastes display nanoparticle coalescence, in some

cases to sizes with “bulk” melting temperatures, as characterized by differential scanning calorimetry (DSC).

### 2:50 PM

**Novel Liquid Phase Sintered Solders for Next Generation Thermal Interface Materials and Interconnect Applications:** Praveen Kumar<sup>1</sup>; C Nagaraj<sup>2</sup>; Indranath Dutta<sup>1</sup>; Rishi Raj<sup>2</sup>; Mukul Renavikar<sup>3</sup>; <sup>1</sup>Naval Postgraduate School; <sup>2</sup>University of Colorado; <sup>3</sup>Intel Corporation

At present, there is significant interest in low-temperature solders for thermal interface material and interconnect applications for packaging thermally sensitive next-generation devices. In this paper, we report on the processing and characterization of novel liquid phase sintered solders (LPSS), based on the Sn-In and Cu-In systems. The LPSS microstructure comprises grains of a majority high melting phase which is highly thermally and electrically conductive, and a minority low melting phase which gives the solder very high mechanical compliance. For the Sn-In system, solders with flow stresses close to that of In were obtained with 30-50 vol.% In, along with electrical and thermal conductivities which are about half those of In. Sintering characteristics, artifacts, and property evolution as a function of material parameters will be discussed. Preliminary results on the Cu-In system will also be reported. Finally, a phenomenological model for the thermal conductivity of the LPSS will be presented.

### 3:05 PM

**Measurement Method of Liquidus Temperature of Lead-Free Solder Using Differential Scanning Calorimetry Curves:** Hiroshi Nishikawa<sup>1</sup>; Yoshihito Hamada<sup>2</sup>; Tadashi Takemoto<sup>1</sup>; <sup>1</sup>Osaka University; <sup>2</sup>Uchihashi Estec Co., Ltd.

In general, liquidus temperature of lead-free solder is measured using cooling curve of differential scanning calorimetry (DSC). However, small amount of crystallization is not reflected in the cooling curve. Since DSC was essentially able to measure small amount of heat transfer, extrapolated end temperatures of endothermic peaks were measured in several heating rates in this study. As a result, the extrapolated end temperature of endothermic peak was a linear function of square root of the heating rate. It was found that intercept at a temperature axis of the linear function was concluded to be liquidus temperature.

### 3:20 PM

**Modeling Reactive Wetting in Bi-Sn System:** Shun Su<sup>1</sup>; Bruce Murray<sup>1</sup>; Ying Sun<sup>1</sup>; <sup>1</sup>Binghamton University

Reactive wetting, referred to as a liquid spreading on a substrate with reaction or diffusion, is involved in soldering, brazing, printing, and many other materials joining processes. In this work, a diffusive transport model is employed to study the dynamic behavior of Bi-Sn alloy drops wetting and spreading on Bi substrates. The simulations are performed on a millimeter scale in order to model experiments that are part of a collaborative study. The kinetics of the triple junction, the shape of the dissolution boundary and the final equilibrium stage are investigated as a function of initial Sn concentration, total contact angle, and diffusion coefficient. Also, the experimentally determined mobility relationship (i.e., contact angle versus contact line velocity) is incorporated into the model to better understand the solid/liquid interface evolution (i.e., dissolution depth and contact angle as a function of time). The impact of convective transport is investigated as well.

### 3:35 PM

**Kinetics of Copper Dissolution in Liquid Lead Free Solders in Static and Dynamic Conditions:** Nader Dariavach<sup>1</sup>; Jin Liang<sup>1</sup>; Vernorris Kelly<sup>1</sup>; Dongkai Shangguan<sup>2</sup>; <sup>1</sup>EMC Corp; <sup>2</sup>Flextronics

During lead free wave soldering for through hole components, high rate copper dissolution may occur to printed wired boards. Sn-Ag-Cu lead-free alloys, the most popular alloys in the electronic industry for surface mount technology (SMT), has more than twice the rate of copper dissolution compared to the Sn-Pb eutectic (63Sn-37Pb) solder alloy. In this study, copper dissolution was evaluated with four lead free alloys at temperatures from 245 up to 300°C with time duration from 20 up to 600 seconds. Results show that K100LD and SN100C have the lowest rate of copper dissolution. A unique dynamic copper dissolution test was performed to investigate the effect of liquid solder flow speed, time and temperature on dissolution kinetics at motion speeds from 2 up to 15 ft/min. Obtained test results show that alloy selection and process window definition are critical for lead free soldering for through hole component assembly and repair operation.



## 3:50 PM Break

## 4:05 PM

**Three-Dimensional (3D) Visualization and Modeling of Reflow Porosity in Pb-Free Solder Joints:** *Martha Dudek*<sup>1</sup>; Stephen Kranz<sup>1</sup>; Aaron Hilger<sup>1</sup>; Jason Williams<sup>1</sup>; Nikhilesh Chawla<sup>1</sup>; Luke Hunter<sup>2</sup>; S. Lau<sup>2</sup>; <sup>1</sup>Arizona State University; <sup>2</sup>XRadia Corporation

In this paper we describe a non-destructive x-ray tomography technique for visualization of the microstructure of Sn-3.9Ag-0.7Cu/Cu joints. The system had a high resolution (1  $\mu\text{m}$ ) which was used to visualize the three-dimensional (3D) characteristics of reflow porosity. A set of experiments were conducted to examine the effect of several key reflow parameters, including flux activation, temperature, and time, on porosity in the joints. Flux activation temperature and time were varied between 170-210°C and 30-120s, respectively. Solder joints were first visualized using the lab-scale x-ray microtomography system, followed by monotonic shear tests. The effect of pore fraction, size, distribution, and interconnectivity on the mechanical integrity of the solder joints will be discussed.

## 4:20 PM

**Multi-Phase Field Simulation of Intermetallic Compound Growth during Lead Free Soldering:** *Min Soo Park*<sup>1</sup>; Raymundo Arroyave<sup>1</sup>; <sup>1</sup>Texas A&M University

A multi-phase field simulation of the morphological evolutions of the intermetallic compounds (IMCs) formed during reaction between liquid Sn-based solder and copper substrate is presented. Cu-substrate, Cu<sub>3</sub>Sn layer, Cu<sub>6</sub>Sn<sub>5</sub> grains, and the Sn-liquid phase are considered. In order to determine the diffuse interface structure, we assume that all components of coexisting phases within the interfacial region have equal chemical potential, which is calculated from CALPHAD thermodynamic databases. Fast grain boundary diffusion in the IMC layer, the IMC grain coarsening along the IMC growth, and the dissolution of Cu from the substrate and IMC layer will be discussed and compared to previous works. The simulation will address the kinetics of the IMCs during soldering and the influence of fast GB diffusion and the concurrent coarsening (Cu<sub>3</sub>Sn and Cu<sub>6</sub>Sn<sub>5</sub>) rate of the IMC grains. The kinetic behavior of the substrate/IMC/solder system as a function of model parameters will also be presented.

## 4:35 PM

**Diffusion Multiples Technique in Studying the Mechano-Chemistry of Ni-Cu-Ag-Sn Solders:** *Marek Danielewski*<sup>1</sup>; Magdalena Pawelkiewicz<sup>1</sup>; Bartek Wierzba<sup>1</sup>; Nick Bosco<sup>2</sup>; Jolanta Janczak<sup>3</sup>; <sup>1</sup>AGH University of Science and Technology; <sup>2</sup>National Renewable Energy Laboratory; <sup>3</sup>EMPA

Using the HIP technique four series of Ni-Cu-Ag-Sn quaternary diffusion multiples of various geometries were prepared. The kinetics of formation for selected intermetallic compounds and distributions of elements in 2D and 3D fragments are presented. The volume velocity is a unique frame of reference for the mass diffusion and allows the use of mass and momentum continuity equations to model reactive interdiffusion. This presented method allows for a self-consistent phenomenological description of multiscale phenomena and opens a vast number of entirely new possibilities. Comparison of experimental and modeling results are reviewed.

## 4:50 PM

**Thermodynamic Studies of Liquid Cu-Sn-Sb Alloys Using e.m.f and Calorimetric Measurements:** *Dominika Jendrzyszczak-Handzlik*<sup>1</sup>; Boguslaw Onderka<sup>1</sup>; Krzysztof Fitzner<sup>1</sup>; <sup>1</sup>AGH University of Science and Technology

The results of metal/oxide experiments proved that in the Sn-Sb-O system liquid alloy remains in equilibrium with pure, solid SnO<sub>2</sub>. The thermodynamic properties of the liquid Cu-Sb-Sn alloys were determined using the following galvanic cell: Re+kanthal, Cu<sub>x</sub>-In<sub>y</sub>Sn<sub>(1-x-y)</sub>, SnO<sub>2</sub>/ZrO<sub>2</sub>+Y<sub>2</sub>O<sub>3</sub>/Ni, NiO, Pt in the temperature range from 1000 to 1200K. Activities of tin were determined from the measured e.m.f's along chosen cross sections with the ratio  $x_{\text{Cu}}/x_{\text{Sb}}$  kept constant. The cell performance was checked by comparing Gibbs free energy change of the reaction of formation of SnO<sub>2</sub> taken from the literature with that determined from our experiments:  $\Delta G_{\text{L,SnO}_2}^0 = -567902.68 + 200.33 T$  (J/mole) in the temperature range from 773K to 1198K. Additionally, to work out precise description of the properties of the liquid phase with Redlich-Kister-Muggianu formula, calorimetric measurements of the heat of mixing were done. Phase relations in the ternary system were calculated and compared with the available experimental data.

## 5:05 PM

**Novel Microprobe Test Metrology to Assess the Mechanics of Complex Multilayer Interconnect Structures:** *Alexander Hsing*<sup>1</sup>; Reinhold Dauskardt<sup>1</sup>; <sup>1</sup>Stanford University

Advanced semiconductor technology nodes require the integration of heterogeneous multilayer thin-film structures with vastly different mechanical properties. Quantitative characterization techniques for understanding the mechanical behavior of the overall multilayer stack structure to allow complex packaging is of critical importance but almost completely lacking. We describe a novel test metrology based on a micron-scale diameter probe and a piezoelectric actuator to accurately measure a range of key mechanical properties of multilayer thin-film device structures, including stack compliance, strength characteristics, fracture behavior, and fatigue resistance. With accurate microprobe positioning, we also demonstrate mapping of material properties over the entire die area and the ability to resolve stiffness and strength differences across a given die and between different dies. Micron-scale soldering enables localized tensile loading of the underlying multilayer interconnect structure. Deformation and defect evolution due to local tensile and compressive monotonic and cyclic contact stresses will also be considered.

## 5:20 PM

**Microtensile Testing of Sn-Cu and Sn-IMC-Cu Lead Free Solder Films for Packaging Applications:** *Zi-Yi Wang*<sup>1</sup>; Chi-Jia Tong<sup>1</sup>; *Ming-tzer Lin*<sup>1</sup>; <sup>1</sup>National Chung Hsing University

As the miniaturization continues, the reduced dimensions of soldering materials potentially play a greater role in defining the overall mechanical behavior of the interconnects. In practical, many of the leading solder alloy candidates for replacement of Pb-Sn solders are based on the Sn-Cu system. Therefore, the mechanical properties of Sn-Cu based intermetallics plays a significant role in determining the reliability in joints. Here, we had conducted the uniaxial tensile testing for the mechanical characterization of freestanding Pb-free solders films. We measured the elastic modulus and mechanical properties of intermetallics compounds commonly formed in reactions of Sn-IMC-Cu solder with Cu metallizations resulted in the formation of intermetallics as those formed in electronic joints. The experiments provide a useful database of mechanical properties of lead free Sn-based intermetallics, in terms of deformation mechanisms and reliability concerns in solder joints for the mechanical behavior of thin Pb-free solders film materials use for package technologies.

## Progress in Computational Materials Science and Engineering Education: Session I

Sponsored by: The Minerals, Metals and Materials Society, TMS: Education Committee

Program Organizers: Gregory Olson, Northwestern University; Anter El-azab, Florida State University; Katsuyo Thornton, University of Michigan; Laura Bartolo, Kent State University

Wednesday PM

Room: 3003

February 18, 2009

Location: Moscone West Convention Center

*Session Chairs:* Gregory Olson, Northwestern University; Laura Bartolo, Kent State University

## 2:00 PM Invited

**Status of Computational Materials Education in the US: Results of Recent Surveys:** *Mark Asta*<sup>1</sup>; Katsuyo Thornton<sup>2</sup>; R. Edwin Garcia<sup>3</sup>; <sup>1</sup>University of California; <sup>2</sup>University of Michigan; <sup>3</sup>Purdue University

This talk will describe results of recently completed surveys investigating the status of computational materials education at leading research universities in the US. The survey includes results such as number and types of courses taught, the extent to which computational tools are being integrated into core curricula and the perspectives of employers concerning future needs. The results of the survey will be presented along with examples exemplifying approaches taken to including computational material into both undergraduate and graduate courses.

## 2:25 PM Invited

**Integrated Computational Materials Engineering: Opportunities and Needs for Educating Future Materials Engineers and Scientists:** *John Allison*<sup>1</sup>; <sup>1</sup>Ford Research and Advanced Engineering, Ford Motor Company

Integrated Computational Materials Engineering (ICME) is considered a new discipline within the materials profession. ICME is the integration of materials information, captured in computational tools, with engineering product performance analysis and manufacturing-process simulation. As an emerging discipline, it is important that the education of future materials engineers and scientists includes an understanding of the potential of ICME and aptitude in use of the tools that are required for its development and utilization. Equally important is motivating their involvement in the design and development of the tools that will be required by this emerging discipline. This talk will attempt to provide an industrial perspective on these educational needs and opportunities. It will also report on findings of a recent National Academies study on ICME which identifies a number of critical needs for change in MSE curricula.

## 2:50 PM Invited

**Computational Materials Science: From NIST to the Academy:** *James Warren*<sup>1</sup>; *Laura Bartolo*<sup>2</sup>; <sup>1</sup>National Institute of Standards and Technology; <sup>2</sup>Kent State University

While NIST's mission is to deliver the highest quality measurement science tools to our customers in industry, other government laboratories and academia, NIST maintains an abiding interest in also transferring these tools to the classroom. In the case of Computational Materials Science, this transfer both enables the training of students in state-of-the-art software tools and, upon their transition to the workforce, the use of these tools by industry, where they can have a direct impact. The NIST Center for Theoretical and Computational Materials Science has been involved in this transfer through a joint effort a number of academic partners to develop Matforge, a repository for computational materials science software, data, and information exchange. In this talk I will discuss our current efforts to use Matforge and the associated tools to help achieve the CTCMS mission.

## 3:15 PM Invited

**Computational Materials Science Education and Training at the University of Florida:** *Simon Phillpot*<sup>1</sup>; *Susan Sinnott*<sup>1</sup>; <sup>1</sup>University of Florida

The integrated program of formal, in-class education and research-driven training in computational materials science at the University of Florida is presented. A review of the computational materials science components in the undergraduate and graduate curricula is given. An analysis is also given of the strengths and weaknesses of the two core classes in graduate computational materials science that are offered. Our approach to research-driven training, including peer-to-peer education at all levels from high school to postdoctoral, is also discussed. Lastly, the computational materials science program is put into the context of education and research on computational methods in other engineering disciplines and in physical sciences. This work is supported by the National Science Foundation (DMR-0426870).

## 3:40 PM Break

## 3:50 PM

**Public Domain Simulation Tools for the Thermodynamics and Kinetics of Materials Education:** *R. Edwin Garcia*<sup>1</sup>; *Michael Waters*<sup>1</sup>; *Matthew Kasenga*<sup>1</sup>; <sup>1</sup>Purdue University

In order to prepare future engineers to tackle increasingly complex technological problems and develop physical intuition that leads to a clear understanding on the Thermodynamics and Kinetics of Materials, teaching modules were developed to enrich the undergraduate curricula at Purdue University. The educational modules are learned sequentially by sophomores and juniors in an increasingly sophisticated level of expertise, so that at the end of the semester the student understands the intricacies of real thermodynamic and kinetic systems. Through the development of easy-to-use graphical user interfaces, driving forces, nanosize length scales, and multiphysical contributions on the thermodynamic equilibrium of materials are understood. Given the mathematical intricacies of the state function equations and the time constraints imposed by a classroom setting, these tools have provided the students with a simple interface where they focus on understanding the physical aspects and behavior of matter, instead of dealing with the mathematics.

## 4:15 PM

**From Passive Learners to Active Model-Builders: A Case Study in Computational Materials Science Education:** *Paulo Blikstein*<sup>1</sup>; *Uri Wilensky*<sup>1</sup>; <sup>1</sup>Northwestern University

For the past 4 years, I have developed and tested in classrooms "MaterialSim", a undergraduate-level Computational Materials Science curriculum. In this paper, I investigate: (a) the cognition of students engaging in scientific inquiry through interacting with simulations; (b) the effects of students programming simulations as opposed to only interacting with ready-made simulations; (c) the characteristics, advantages, and trajectories of scientific content knowledge that is articulated in epistemic forms and representational infrastructures unique to Computational Materials Science, and (d) the principles which govern the design of computational agent-based learning environments in general and for materials science in particular. Data sources for the evaluation of these studies include classroom observations, interviews with students, videotaped sessions of model-building, questionnaires, and analysis of artifacts. Results suggest that by becoming 'model-builders,' students develop deeper understanding of core concepts in Materials Science, and learn how to better identify unifying principles and behaviors in the field.

## 4:40 PM Invited

**Computational Materials Science and Engineering Curriculum at Penn State:** *Zi-Kui Liu*<sup>1</sup>; *Long-Qing Chen*<sup>1</sup>; *Coray Colina*<sup>1</sup>; *Vincent Crespi*<sup>1</sup>; *Tarasankar DebRoy*<sup>1</sup>; *Evangelos Manias*<sup>1</sup>; *Jorge Sofo*<sup>1</sup>; <sup>1</sup>Pennsylvania State Univ

In the last few years, a number of new computational based courses have been developed at the department of materials science and engineering at Penn State along with the insertion of computational approaches to several existing undergraduate graduate and courses. These courses primarily are focused on thermodynamic and kinetic aspects of materials based on faculty expertise in the department. A range of computational approaches are introduced to students through class lectures, hand-on exercises, and individual and team projects. In this presentation, the overview of our course portfolio will be presented on several core courses. The connection between teaching and research activities in the department will also be briefed.

## 5:05 PM

**Coaching Technical Design Teams in Materials Design Course:** *Shengjun Zhang*<sup>1</sup>; *Gregory Olson*<sup>1</sup>; <sup>1</sup>Northwestern University

The materials design course at Northwestern University is comprised of lectures, computational labs, homework, a midterm and a final design project. The primary goal of the course is to teach design practices grounded in materials science through active learning in a group design project. Each junior-level team is coached by a graduate student or post-doctoral research associate who is performing research in that area. The Terminator 4 is a long term project which has been carried out in one team per year for more than 15 years. The Terminator 4 project leveraged an ongoing research project utilizing a post-doctoral research associate coach to develop a high specific-strength Mg-based alloy composite for aerospace applications that can self-heal. Through thermodynamic calculations, the team designed high performance Mg alloys with thermodynamically compatible shape memory alloy (SMA) wires, which demonstrates yield strengths greater than a commonly used Mg-based alloy.

## Computational Materials Research and Education Luncheon Roundtable: FiPy

Sponsored by: National Science Foundation  
Program Organizer: Laura Bartolo, Kent State University

Wednesday PM Room: 3003  
February 18, 2009 Location: Moscone West Convention Center

Session Chair: Laura Bartolo, Kent State University

## 12:45 PM Panel Discussion

## Recycling—General Session: Session II: Waste Utilization

Sponsored by: The Minerals, Metals and Materials Society, TMS Extraction and Processing Division, TMS Light Metals Division, TMS: Recycling and Environmental Technologies Committee

Program Organizer: Joseph Pomykala, Argonne National Laboratory

Wednesday PM  
February 18, 2009

Room: 2024  
Location: Moscone West Convention Center

Session Chair: Joseph Pomykala, Argonne National Laboratory

### 2:00 PM

**Properties of Clay-Based Ceramics Added with Construction and Demolition Waste:** *Wilson Acchar*<sup>1</sup>; Ana Segadaes<sup>2</sup>; Sonia Castanho<sup>3</sup>; Juliana Silva<sup>1</sup>; <sup>1</sup>Federal University of Rio Grande do Norte; <sup>2</sup>University of Aveiro, Portugal; <sup>3</sup>Institute of Energy and Nuclear Research

The accelerated growth of urbanization processes and current environmental concerns brought to light the existing enormous quantity of construction and demolition waste (C&DW). Considering the frequent lack of adequate landfill areas available for the disposal of these materials, their use in the manufacture of ceramic products has been attracting a growing interest from researchers and is becoming common practice, with the consequent relief in public administration concerns for the appropriate C&DW management. This work describes the study of clay-based products added with C&DW collected directly from the building industry. Samples containing up to 50 wt.% C&DW were uniaxially pressed and sintered in air in an electric furnace (950-1150°C, 1 hour). Sintered test pieces were characterized by X-ray diffraction, apparent density, open porosity and flexural strength. The results showed that up to 50 wt.% C&DW can be added into the clay material, with no degradation in the final product properties.

### 2:20 PM

**Characterization and Recycling of Paper Sludge Waste into Clay Bricks – Industrial Test:** *Carlos Maurício Vieira*<sup>1</sup>; Rubén Sánchez<sup>1</sup>; Sergio Monteiro<sup>1</sup>; Regina Pinheiro<sup>1</sup>; <sup>1</sup>State University of the Northern Fluminense

This work has for objective to both characterize a waste generated in the form of sludge during the treatment of the effluent of a paper making industry and to evaluate the effect of its incorporation in the amount of 10 wt.% on the properties and microstructure of a clayey brick. The characterization of the waste was done by X-ray diffraction, X-ray fluorescence, differential thermal analysis and thermogravimetric analysis. The physical and mechanical properties evaluated of the bricks fired at 750°C were water absorption and compression strength. The microstructure of the fired ceramic was evaluated by optical microscopy. The environmental evaluation was made by solution test and atmospheric emission by monitoring the release of SO<sub>2</sub>, NO<sub>x</sub> and particulate material. The results showed that it is possible to recycle this type of waste with energy saving during the firing stage.

### 2:40 PM

**Synthesis of Mullite from the Residue of Kaolin by Microwave:** *Lisiane Santana*<sup>1</sup>; Maria Brasileiro<sup>1</sup>; Gelmires Neves<sup>1</sup>; Helio Lira<sup>1</sup>; Romualdo Menezes<sup>1</sup>; Heber Ferreira<sup>1</sup>; <sup>1</sup>UFCEG

The production of waste for ore industry is a problem that is intensifying nowadays because of high productivity. The kaolin processing industries produce residue rich in Al<sub>2</sub>O<sub>3</sub> and SiO<sub>2</sub>, oxides that are precursors to produce mullite. So, the aim of this work is to use the residue from the kaolin improvement industry to produce mullite ceramics bodies. In this study it was used as raw materials: alumina and residue from the kaolin industry. The powder compacts were prepared by uniaxial pressing at 30 MPa. The material was drying and after sintering in the microwave oven. The ceramics bodies formed by the microwave reaction were characterized by X-ray diffraction and scanning electron microscopy. The flexural strength was measured by the three point bending technique. Based on these results it was concluded that is possible the production of the mullite bodies using high quantity of the waste.

### 2:55 PM

**Recycling of Steelmaking Slag Aiming at the Production of Thermo-Acoustic Insulation:** *Joner Alves*<sup>1</sup>; Denise Espinosa<sup>1</sup>; Jorge Tenório<sup>1</sup>; <sup>1</sup>Universidade de São Paulo - USP

The aim of this work was to study the use of steelmaking slag as raw material to the production of rock wool and glass wool. Firstly, the chemical composition of the slag was analyzed. These results were used to infer the amount of additives to assemble the charge for the experiments. A laboratory-scale electric furnace was used to melt the mixtures used as charge. The melt material were turned into a water filled recipient, this process was performed in order to impose a fast freezing that is a characteristic of mineral wool production. Finally, with the rest of the melt material it was performed the Herty Viscosity Test. Samples of the produced material were characterized by different analyses. The results found in this research may lead to a technological innovation, because they indicate that the use of steelmaking slag to produce rock wool and glass wool is possible.

### 3:15 PM Cancelled

**Moving Business to Clean Production and Triple the Bottom Line:** *J. Michael Huls*<sup>1</sup>; <sup>1</sup>California Take It Back Partnership

### 3:30 PM

**Production of High-Grade Potassium Chloride from a Sinter Plant Baghouse Dust:** *Naiyang Ma*<sup>1</sup>; <sup>1</sup>Arcelor Mittal

A sinter plant baghouse dust has been treated as a hazardous solid waste, and disposed at a very high price. A series of leaching tests were conducted to examine the possibility to produce high grade potassium chloride from the solid waste. It is found that around 50% of the solid wastes can dissolve into water. By taking step precipitation, a deposit with more than 95% KCl can be produced.

### 3:50 PM

**Life Cycle Inventory Analysis of Municipal Solid Wastes Management:** *He Dewen*<sup>1</sup>; Song Dan<sup>1</sup>; Liang Dingming<sup>1</sup>; Du Lu<sup>1</sup>; <sup>1</sup>Central South University

Based on the principle of life cycle assessment (LCA), municipal solid waste management (MSWM) was analyzed by life cycle inventory method. According to the system expansion and substitution method, the content and frame of life cycle analysis is summarized and applied to municipal solid waste. On the basis of feasibility research of life cycle analysis on MSWM, the paper put forwards complete and concrete "three changes" measures under life cycle analysis on MSWM. Some aims of MSWM can be achieved under above conditions of LCA on MSWM: to improve the current system efficiency of MSWM; to enhance the serve quality of MSWM, to increase recycle garbage from MSW; to reduce waste amount and reach minimization and innocuity aim of MSWM; to help the departments of MSWM to get over all difficulties to realize their ideal goals.

### 4:10 PM Break

### 4:30 PM

**Study on Selectively Separating Iron Constituents in Copper Smelting Slags:** *Hongyang Cao*<sup>1</sup>; Li Zhang<sup>1</sup>; Cigong Wang<sup>1</sup>; Nianxin Fu<sup>1</sup>; Zhitong Sui<sup>1</sup>; Naixiang Feng<sup>1</sup>; <sup>1</sup>Northeastern University

The iron constituents selectively separated from the modified copper slags by magnetic separation and flotation were studied. The results of magnetic separation for modified copper smelting slags show that the grinding size, current intensity and dispersant agent had great influence on grade, and recovery ratio of TFe in preparation concentrate; The results of flotation for magnetic concentrate show that the positive flotation of sodium oleate negatively upgrade the grade of magnetic concentrate, but the reverse flotation of lauryl amine and soluble starch are effective. The grade of TFe can reach 54% and the recovery ratio can reach about 90% in magnetic concentrate, when the grinding size is 45.8µm and the current intensity is 2.5A. The optimal effect is obtained by using lauryl amine as collector and soluble starch as depressant to reverse floatate magnetic concentrate, and the grade of TFe be upgraded 2.37%.

### 4:50 PM

**Preparation of Iron Oxide Red Pigment Powders from Pyrite Cinders by Hydrothermal Method:** *Zhaocheng Liu*<sup>1</sup>; Yajie Zheng<sup>1</sup>; <sup>1</sup>Central South University

Iron oxide red pigment powders of high quality were prepared from pyrite cinders. Iron oxide red pigment powders were prepared by hydrothermal method from the precursor of Fe(OH)<sub>3</sub> and Fe(OH)<sub>2</sub> colloid, which were obtained after ammonia solution reacted with acidic leaching solution produced by the reaction



of pyrite cinders with sulfuric acid. Effects of reaction concentration, reaction temperature, reaction time, pH value and  $n(\text{Fe}^{2+})/n(\text{Fe}^{3+})$  on main properties of oxide iron red were studied by experiments. The prepared particles were characterized by means of X-ray diffraction (XRD) and scanning electron microscope (SEM). The results revealed that the prepared iron oxide red particles were  $\alpha\text{-Fe}_2\text{O}_3$  and pseudocubic with particle size of 0.50–0.75  $\mu\text{m}$ . Furthermore, iron oxide red pigment powders reached the first grade of China standard (GB1863-89).

## 5:10 PM

**Research on Treatment Project of Municipal Solid Waste of Changsha City:** *He Dwen*<sup>1</sup>; Liang Ding-ming<sup>1</sup>; Du Lu<sup>1</sup>; Qin Yan<sup>1</sup>; <sup>1</sup>Central South University

The municipal solid waste is a by-product of the daily life of urban residents. The quantity and ingredients of municipal solid waste has exceeded the current management and disposal ability, which has done a great harm to municipal environment and sanitation quality and threatened people's health. On the basis of analysis on the amounts and main elements of municipal solid waste of Changsha City, the sanitation landfill, incineration, composting, reclamation and utilization technology of household waste were compared specifically in this paper. Based on the concrete conditions of Changsha City, the paper has proposed an disposal proposal combined with reclamation and landfill of municipal solid waste of Changsha City, and the environmental benefit, social benefit and economical benefit of the prepared processing routes were also analyzed in the paper

## 5:30 PM

**Separation for Recycling of Spent Potlining by Froth Flotation:** Chuanlin Fan<sup>1</sup>; Yongfeng Chang<sup>1</sup>; *Xiuqing Zhai*<sup>1</sup>; Yan Fu<sup>1</sup>; Binchuan Li<sup>1</sup>; <sup>1</sup>Northeastern University

The process of flotation separation and recycling of spent potlining (SPL) was described. On the basis of the laboratory investigations, the effects of influencing factors in froth flotation process, such as grain size, flotation agent dosage, pH value, pulp density, and dissolved components concentration, etc. were carefully studied. And the influence on environment of the process was also discussed. It was found that flotation separation can be used as an environment-friendly method for treatment of SPL residue. Carbon and other compounds (include cryolite, sodium fluoride, calcium fluoride and diaoyudaonite, etc.) from SPL were separated and recycled as flotation products respectively.

---

## RPV Embrittlement and Fusion Materials: Measuring, Modeling and Managing Irradiation Effects: RPV Embrittlement: Technical Contributions of Professor G. Robert Odette

Sponsored by: The Minerals, Metals and Materials Society, TMS Structural Materials Division, TMS/ASM: Nuclear Materials Committee

Program Organizers: Matthew Alinger, GE Global Research; Kurt Edsinger, Electric Power Research Institute; Roger Stoller, Oak Ridge National Laboratory; Brian Wirth, University of California, Berkeley

Wednesday PM  
February 18, 2009

Room: 2008  
Location: Moscone West Convention Center

*Session Chairs:* Brian Wirth, University of California, Berkeley; Roger Stoller, Oak Ridge National Laboratory

---

## 2:00 PM Invited

**An Evolution of Understanding of Reactor Pressure Vessel Steel Embrittlement:** *Glenn Lucas*<sup>1</sup>; <sup>1</sup>University of California, Santa Barbara

This paper will attempt to summarize the lifetime contributions of Prof. G. Robert Odette to our understanding of the effects of neutron irradiation on reactor pressure vessel steel embrittlement. These contributions span the entire range of phenomena that contribute to embrittlement, from the production and evolution of fine scale features by radiation damage processes, to the effects of this damage microstructure on mechanical properties. They include the development and application of unique and novel experimental tools (from Seebeck Coefficient to Small Angle Neutron Scattering to confocal microscopy/fracture reconstruction), the design and implementation of large multi-variable experimental matrices, the application of multi-scale modeling to understand

the underlying mechanisms of defect evolution and property change, and the development of predictive methodologies employed to govern reactor operations. The ideas and discoveries have provided guidance worldwide to improving the safety of operating nuclear reactor pressure vessels.

## 2:20 PM Invited

**The Development of Mechanistic Understanding of RPV Embrittlement:** *Colin English*<sup>1</sup>; <sup>1</sup>Nexia Solutions

Professor G. Robert Odette has and continues to make significant technical contributions to understanding of the mechanisms controlling the embrittlement of thermally aged and irradiated RPV steels and the application of such understanding to the development of physically-based models that predict the embrittlement of RPV steels. In recognition of the 65th birthday of Professor Odette this paper highlights these technical contributions; in particular his role in the founding of IGRDM and his seminal contribution to developing an accepted framework of the mechanisms of RPV embrittlement. In the latter it will be emphasised how his work ensured a proper debate on the effects of irradiation parameters, such as flux, and material parameters, such as composition and in particular the role of Mn and Ni in the formation of irradiation-induced solute clusters in low Cu RPV steels.

## 2:40 PM Invited

**RPV Embrittlement Models: The Technical Contribution of Professor G. R. (Bob) Odette:** *Timothy Williams*<sup>1</sup>; <sup>1</sup>Rolls-Royce plc

In the 1960s and 1970s irradiation embrittlement of RPV steels was predicted using simple trend curves based on statistical fits to the available surveillance data. In general, the models were empirical and the important variables and interactions were deduced by visual or statistical assessment of the data. Bob Odette was responsible for introducing three major advances, which transformed embrittlement modelling and continue to do so. The first was an insistence that model formulation and development be based on sound physical understanding. Second, that important gaps in understanding must be filled by careful, systematic experiments, and the results and insights of these experiments should be used to guide the development of the models fitted to the surveillance data. Third, the continued development of physical models of irradiation damage was also vital to provide insights about the irradiation damage process and to enable better data interpretation.

## 3:00 PM Invited

**Prediction of Irradiation Damage Effects in RPV Steels in the Frame of the PERFECT Project:** *Christophe Domain*<sup>1</sup>; Bernard Marini<sup>2</sup>; David Lidbury<sup>3</sup>; Stéphane Bugat<sup>1</sup>; Jean-Paul Massoud<sup>1</sup>; <sup>1</sup>EDF R&D; <sup>2</sup>CEA; <sup>3</sup>Serco Assurance

A multi-scale numerical modelling tools has been developed within the EURATOM project PERFECT to simulate the effects of neutron irradiation on the mechanical, fracture and corrosion properties of the Reactor Pressure Vessel and internal structures in Light Water Reactors (LWR). The models are based on the physics and mechanics at the scale where it can be described with well defined parameters and concepts. They were carefully validated at the relevant scales with dedicated experiments and investigations. PERFECT addresses both the microscopic effects of irradiation, which are manifested by changes in the microstructure and basic properties of the materials, as well as the mechanical properties, which influence the behaviour of reactor components. The simulation tools can be used to predict long-term projections and help the understanding of the phenomena leading to degradations design experimental programs. At the same time the models contribute to explore conditions outside existing experimental databases.

## 3:20 PM Invited

**Characterization of the Early Stages of Solute Clustering in A508 Gr4N Steels and a 1 Ni – 1.3 Mn Weld:** *M. Burke*<sup>1</sup>; Jonathan Hyde<sup>2</sup>; R. M. Boothby<sup>2</sup>; Colin English<sup>2</sup>; William Server<sup>2</sup>; <sup>1</sup>Bettis Laboratory; <sup>2</sup>Nexia Solutions

During the last decade there have been significant improvements in microstructural techniques that can be used to characterise the damage caused by neutron irradiation and this has led to improvements in the mechanistic understanding of embrittlement. However, it is clear that no single technique can currently provide a complete description of the microstructural changes that occur as a result of neutron damage. Furthermore, despite advances in techniques and mechanistic understanding, many questions still persist and the detailed interpretation of microstructural data obtained remains open to academic debate. In this paper the authors examine the early stages of irradiation-induced clustering in a low Cu (0.03wt.%), high Ni (~1wt.%) weld and A508 Gr 4N

steels. The materials were irradiated at very high dose rate and then examined by atom probe (Energy-Compensated Optical Position Sensitive Atom Probe-ECOPoSAP) with supporting microstructural information obtained by small angle neutron scattering (SANS).

#### 3:40 PM Break

#### 4:00 PM Invited

**Atom Probe Tomography Characterizations of Neutron Irradiated Pressure Vessel Steels:** *Michael Miller*<sup>1</sup>; Kaye Russell<sup>1</sup>; <sup>1</sup>Oak Ridge National Laboratory

Atom-probe tomography has provided unique information on the effects of neutron irradiation on the microstructure of reactor pressure vessel steels and related model alloys including the formation and dissolution of ultra-fine copper-enriched precipitates in copper-containing steels and nickel-, manganese-, and silicon-enriched nanoclusters in low copper and copper-free steels; solute segregation to and precipitation on dislocations; and solute segregation to grain boundaries. A review of the quantification of the solute distribution in the microstructure of several different pressure vessel steels after post weld stress relief heat treatments, neutron irradiation, and post irradiation annealing treatments, as determined by atom probe tomography, will be presented. Research at the Oak Ridge National Laboratory SHaRE User Facility was sponsored by Basic Energy Sciences, U.S. Department of Energy and by the Office of Nuclear Regulatory Research, U. S. Nuclear Regulatory Commission, under inter-agency agreement 1886-N695-3W and under contract DE-AC05-00OR22725 with UT-Battelle, LLC.

#### 4:20 PM Invited

**On the Composition of Cu-Mn-Ni Precipitates in Irradiated Reactor Pressure Vessel Steels:** *Brian Wirth*<sup>1</sup>; G. Robert Odette<sup>2</sup>; Michael Miller<sup>3</sup>; Takuya Yamamoto<sup>2</sup>; R. D. Klingensmith<sup>2</sup>; J.M. Smith<sup>2</sup>; <sup>1</sup>University of California, Berkeley; <sup>2</sup>University of California, Santa Barbara; <sup>3</sup>Oak Ridge National Laboratory

Irradiation embrittlement of reactor pressure vessel (RPV) steels results from formation of a high density of nm-scale precipitates. In RPV steels with >0.1%Cu the dominant hardening features are copper-rich precipitates (CRPs) alloyed with manganese, nickel and silicon. But as theoretically predicted long ago, manganese-nickel rich precipitates (MNPs) can form in both copper bearing and copper free alloys, containing large amounts of these elements. Large volume fractions of these late blooming MNPs (LBP), cause severe hardening and embrittlement. The presence of LBP-MNPs and large hardening in low copper and copper free alloys has been demonstrated by a variety of techniques. We present results and comparisons from several complementary microanalytical characterization techniques used to investigate the nanoscale precipitates, including small angle neutron scattering, atom probe tomography, positron annihilation spectroscopy, and electrical resistivity – Seebeck coefficient measurements. The results are discussed in context of extended operation of light water reactors.

#### 4:40 PM Invited

**Fundamental Modeling of Radiation Effects:** *Roger Stoller*<sup>1</sup>; <sup>1</sup>Oak Ridge National Laboratory

Radiation damage in structural materials involves a complex range of phenomena with influence over many time and spatial scales. Considerable research during the past 60 years has provided a good understanding of these phenomena, with the most significant progress obtained when well designed experiments were analyzed on the basis of sound physical models. The computational advances of recent years have provided the opportunity to advance the theory and modeling of radiation effects, taking advantage of the dramatic improvements in the tools and techniques for microstructural and mechanical characterization. The fundamental models used to investigate radiation effects at length scales ranging from the atomistic to the macroscopic will be discussed, with an emphasis on the methods that have been developed and applied by Professor Odette and his co-workers.

#### 5:00 PM Invited

**Dose Dependence of Irradiation Hardening of Fe-Cu and Fe-Mn Model Alloys:** *Akihiko Kimura*<sup>1</sup>; <sup>1</sup>Kyoto University

The amount of irradiation hardening of iron-copper alloys is significantly larger than those of the other iron base alloys, indicating that copper cluster is a higher potential hardener. The contribution of copper cluster to the hardening is rather large but almost similar to the hardening caused by interstitial dislocation

loops. The microvoids are not the high potential hardener. Another high potential hardener is manganese. The iron-manganese model alloys suffer a remarkable hardening as large as those in iron-copper alloys. Since manganese atoms do not cluster like copper atoms and the number density of interstitial loops increases significantly, it is considered that manganese enhances the formation interstitial loops and causes large hardening. The dependence of irradiation hardening on irradiation dose is discussed on the bases of the previous our irradiation data and hardening mechanisms shown above.

#### 5:20 PM Invited

**Atomic-Scale Modeling of Hardening Due to Cu-Precipitates in Iron:** *Yuri Osetsky*<sup>1</sup>; Roger Stoller<sup>1</sup>; David Bacon<sup>2</sup>; <sup>1</sup>Oak Ridge National Laboratory; <sup>2</sup>University of Liverpool

A vast contribution to mechanical properties depends on the direct interaction between dislocation and obstacles that depends on the particular atomic-scale structure of the both moving dislocation core and obstacle. In this work we present recent progress in large-scale modeling of edge dislocation dynamics in iron containing Cu-precipitates initially coherent with the bcc matrix. Interactions with precipitates of different size were studied over a wide temperature and strain rate ranges. Special attention was paid to structural instability of precipitates, phase transformation during interactions and factors affecting this (temperature, strain rate, vacancy concentration inside precipitates). It was concluded that structural transformation is responsible for the precipitate size dependence of temperature dependent Cu-precipitate hardening.

#### 5:40 PM Invited

**Reactor Pressure Vessel Embrittlement and Fracture Mechanics Contributions of Prof. G. Robert Odette:** *Randy Nanstad*<sup>1</sup>; <sup>1</sup>Oak Ridge National Laboratory

Current regulations require reactor pressure vessels (RPV) to maintain conservative margins of fracture toughness during both normal operation and accident transients. Neutron irradiation degrades fracture toughness through the evolution of nanoscale features in RPV steels which are linked to key embrittlement variables and how they mediate embrittlement through the micromechanics of the ductile-to-brittle transition temperature shift. Advances have been made in fracture mechanics that permit determination of the transition temperature using relatively small specimens, e.g., the fracture toughness master curve. Professor G. R. Odette and co-workers at UCSB have made significant contributions to many aspects of fracture technology through a combination of experiments, modeling and microstructural studies, including development of models that link fundamental mechanisms of radiation damage with kinetic embrittlement models for prediction of RPV steels frangibility. These studies have provided significant insights into the nature of fracture in RPV steels that enable major advances in RPV embrittlement predictability.

## Solar Cell Silicon: Production and Recycling: Session II

Sponsored by: The Minerals, Metals and Materials Society, TMS Extraction and Processing Division, TMS Light Metals Division, TMS: Recycling and Environmental Technologies Committee

Program Organizer: Anne Kvithyld, SINTEF

Wednesday PM

Room: 3004

February 18, 2009

Location: Moscone West Convention Center

Session Chair: Anne Kvithyld, SINTEF

#### 2:00 PM

**Recycling of Solar Cell Silicon: An Overview:** *Lifeng Zhang*<sup>1</sup>; Xuewei Lv<sup>1</sup>; <sup>1</sup>Missouri University of Science and Technology

The recycling of solar cells include three parts: recycling of the top-cut solar cell silicon, recycling of the sawing slurry generated during wafer cutting, and recycling the used solar cell modules. This paper extensively reviewed the current state-of-the-art of these three kinds of recycling of solar cell silicon. The most recent research on this topic at Missouri S&T was also summarized: a) the new filtration process removed 99% of the inclusions in the top-cut silicon scraps without introducing any pollution to the silicon; b) a design for the recycling of silicon sawing slurry was proposed, and was welcomed by several industries;

c) remelting of waste solar cell modules was also proposed with a new non-contaminative technology.

## 2:30 PM

**Electrorefining of Silicon in Molten Chloride Electrolytes:** *Geir Haarberg*<sup>1</sup>; Ole Kongstein<sup>2</sup>; Shuihua Tang<sup>1</sup>; Shulan Wang<sup>3</sup>; <sup>1</sup>Norwegian University of Science & Tech; <sup>2</sup>SINTEF Materials and Chemistry; <sup>3</sup>Northeastern University

Electrochemical studies and electrolysis experiments were carried out in molten chloride electrolytes to develop a process for the electrorefining of metallurgical grade silicon to produce solar grade silicon. The molten electrolyte was based on calcium chloride containing some sodium chloride, calcium oxide and dissolved silicon. The experiments were carried out under dry argon at 850°C. Metallurgical grade silicon was mixed with copper and prepared in separate experiments to produce the alloy for the anode (38 - 62 mol% Si - Cu). Molybdenum and high purity silicon were used as cathode substrates, while Ag/AgCl placed in a mullite tube was used as the reference electrode. Electrochemical studies showed that silicon can be anodically dissolved and cathodically deposited from electrolytes based on molten calcium chloride. Analyses of the silicon deposits were made by EDS and ICP. Promising electrorefining results for some key elements were obtained in recent experiments.

## 3:00 PM

**Pre-Electrolysis of Electrolyte for Silicon Electrorefining:** Ji-guang Yi<sup>1</sup>; Yan-qing Lai<sup>2</sup>; Zhong-liang Tian<sup>1</sup>; Ming Jia<sup>1</sup>; Jian-feng Yan<sup>1</sup>; Ye-xiang Liu<sup>1</sup>; <sup>1</sup>Central South University

The pre-electrolysis of Na<sub>2</sub>AlF<sub>6</sub>-K<sub>2</sub>SiF<sub>6</sub> melt was carried out and the metallurgical silicon was electrorefined in the pre-electrolyzed bath with liquid electrodes. The results show that the appropriate current density of pre-electrolysis is 20 mA/cm<sup>2</sup> at 1000°. The contents of impurities and moisture are reduced after pre-electrolysis process. The purity of the electrolyte is a key factor to obtain high pure silicon, and the silicon of the purity 99.99 % can be obtained by controlling the electrolysis condition.

## 3:30 PM

**Production of High Purity Silicon for Solar Cell with Three-Layer Process Method:** Liang Pang<sup>1</sup>; Huimin Lu<sup>1</sup>; <sup>1</sup>Beijing University of Aeronautics & Astronautics

At present, polysilicon with 99.9999% purity has been used to solar cell raw. The traditional method of producing polysilicon is improved SIEMENS method. In this paper, the authors explored a new molten salt electrolysis method for purify industrial silicon. Electrolytic process for purify the industrial silicon was called the three-layer process, in which silicon is refined from a lower anodic molten layer of impure silicon, via an intermediate electrolyte layer of molten salts, to a top cathodic layer of pure silicon. The electrolytic process was carried out at temperature 1450 - 1500°C. The industrial silicon fed into the cell may be electrolytically refined to high purity silicon but impurities as Al, Fe, Ca, B, P decreased obviously with ICP-AES test.

## State of the NSF Metallic Materials and Nanostructures (MMN) Program: Session I

Sponsored by:

Program Organizer: Alan Ardell, University of California

Wednesday PM  
February 18, 2009

Room: 2002  
Location: Moscone West Convention Center

Session Chair: Alan Ardell, University of California

## 12:30 PM

**Materials Research Support at the National Science Foundation:** *Alan Ardell*<sup>1</sup>; <sup>1</sup>Program Director, Metallic Materials & Nanostructures Division of Materials Research, Directorate of Mathematical and Physical Sciences, National Science Foundation, Arlington, VA 22230

The NSF perspective on needs and opportunities in materials research and education will be presented. The National Science Foundation invests approximately \$400 million annually in this field, supporting people, ideas, and tools primarily through awards to the nation's colleges and universities. A major focus for this activity is NSF's Division of Materials Research (DMR), but there is also substantial support for materials and materials-related research and

education from other areas of NSF. Specific new opportunities and directions - including a relatively new program in biomaterials to focus DMR support for the study of biologically related materials and phenomena - will be described. There are also opportunities for collaborative research, nationally and internationally, via different types of block funding programs. For additional information, visit the DMR Web page at <<http://www.nsf.gov/mps/divisions/dmr/>>. For general inquiries please feel free to contact me, email: aardell@nsf.gov or Dr. Bruce MacDonald, DMR Expert, email: bmacdona@nsf.gov

## Surface Structures at Multiple Length Scales: Processing of Novel Surfaces

Sponsored by: The Minerals, Metals and Materials Society, TMS Materials Processing and Manufacturing Division, TMS: Surface Engineering Committee

Program Organizers: Arvind Agarwal, Florida International University; Sudipta Seal, University of Central Florida; Yang-Tse Cheng, University of Kentucky; Narendra Dahotre, University of Tennessee; Graham McCartney, University of Nottingham

Wednesday PM

Room: 3011

February 18, 2009

Location: Moscone West Convention Center

Session Chair: To Be Announced

## 2:00 PM Invited

**Functional Nanostructures through Nanosecond Laser-Induced Dewetting:** *Ramki Kalyanaraman*<sup>1</sup>; <sup>1</sup>University of Tennessee, Knoxville

Techniques of processing nanoscale metallic structures with spatial order and tunable physical characteristics, such as size and microstructure, are paramount to realizing applications in the areas of magnetism, optics and sensing. Here we discuss how pulsed laser melting of ultrathin films can be a powerful but simple and cost-effective technique to fabricate functional nanostructures. Ultrathin metal films (1 to 100 nm) on inert substrates like SiO<sub>2</sub> are generally unstable, with their free energy resembling that of a spinodal system. Such films can spontaneously evolve into predictable nanomorphologies with well-defined length scales. Here we review this laser-based experimental technique and provide examples of resulting robust nanostructures that can have applications in magnetism and optics.

## 2:30 PM

**Novel Infrared-Processed Titanium Composite Coatings for High Temperature Galling Resistance:** *Evan Ohriner*<sup>1</sup>; Peter Blau<sup>1</sup>; <sup>1</sup>Oak Ridge National Laboratory

Titanium alloys offer high strength-to-weight ratios for elevated temperature use but are susceptible to wear and galling in applications in which metal to metal contact occurs. A series of titanium composite coatings are being developed that contain significant volume fractions of refractory hard particles, such as carbides and nitrides. The coatings are applied by a novel method of infrared heating using a plasma arc lamp to provide a metallurgical bond to the coating and minimize dilution of the coatings by the substrate. The effects of coating composition and processing parameters on the microstructures of the coatings are discussed. Research sponsored by the Laboratory Directed Research and Development Program of Oak Ridge National Laboratory, managed by UT-Battelle, LLC, for the U. S. Department of Energy.

## 2:50 PM

**Reducing Crack Initiation and Propagation in Coatings Containing Suspended Brittle Particles:** Steven Bianculli<sup>1</sup>; Jack Beuth<sup>2</sup>; <sup>1</sup>US Steel Research and Technology Center; <sup>2</sup>Carnegie Mellon University

In this talk, modeling research is presented for determining optimal sizes and shapes of brittle particles suspended in otherwise ductile coatings to increase coating fracture resistance. Although this research is inspired by strain-induced cracking problems in steel coating systems, results are applicable to the general problem of a coating containing brittle particles. In many such systems, coating cracking is linked to the formation of cracks in brittle particles, which then propagate through the coating thickness with additional applied strain. This research considers the separate problems of particle cracking and subsequent propagation of the crack from the particle. This leads to the identification of optimal particle shapes and sizes to reduce crack initiation and propagation, as a function of the ratio of coating matrix and particle stiffnesses.



3:10 PM

**Microstructure and Mechanical Properties of 316L/Polymer/316L Sandwich Systems:** Adele Carrado<sup>1</sup>; Heinz Palkowski<sup>2</sup>; <sup>1</sup>IPCMS; <sup>2</sup>Clausthal University of Technology

Sandwich systems (SMs) - as hybrid materials - offer significant opportunities for enhancement of product performance in terms of strength, stiffness combined with low density. SMs are used in industrial applications such as automotive-, building-, transport-, chemical-, aerospace- and airplane industry. Nevertheless there is a lack of understanding in the interaction between the mono-materials and their behaviour as hybrids, especially in processing. This paper deals with the development of functionally adapted and for customers' use designed SMs produced by press joining rolling process and heating press process. For surface layers austenitic high-grade steel (316L) sheets were used and for the cores different thermoplastic and/or thermoset polymers (also fibre reinforced). Beside the mechanical tests stretch, deep drawing and adhesive tests with different simple geometries were done. Various morphological observations were performed in order to connect them with the mechanical response.

3:30 PM Break

3:40 PM Invited

**Synthesis, Elastic Properties and Chemical Stability of MAX Phases:** Jochen Schneider<sup>1</sup>; <sup>1</sup>RWTH Aachen

A strategy towards knowledge based materials selection for Al<sub>2</sub>O<sub>3</sub>/NiAl based composites for efficient energy conversion is presented. Theoretical and experimental elasticity and phase stability data are considered for a design proposal including a MAX phase interlayer along the Al<sub>2</sub>O<sub>3</sub>/NiAl interface. The major challenges that need to be addressed here are: a) chemical stability at temperatures up to 1300°C and b) stress management during cooling of Al<sub>2</sub>O<sub>3</sub>/NiAl, where NiAl has a 1.6 larger thermal expansion coefficient than Al<sub>2</sub>O<sub>3</sub>. Based on bulk modulus,  $c_{44}$  to bulk modulus ratio, ductility models, and results of our theoretical stress strain analysis, we expect sufficient stiffness and ductility of the MAX phase interlayer to accommodate mechanical loading during operation and cooling down. Our calorimetric data indicate the formation of a stable Al<sub>2</sub>O<sub>3</sub>/V<sub>2</sub>AlC/NiAl composite to be realized at T < 1499°C.

4:10 PM

**Microstructure Evolution and Thermal Stability of an Fe-Based Amorphous Alloy Powder and Thermally Sprayed Coatings:** K. Chokethawai<sup>1</sup>; P. H. Shipway<sup>1</sup>; Graham McCartney<sup>1</sup>; <sup>1</sup>University of Nottingham

High velocity oxy-fuel (HVOF) thermal spraying was used to deposit coatings of a multi-component Fe-based amorphous alloy (Fe<sub>43</sub>Cr<sub>16</sub>Mo<sub>16</sub>C<sub>15</sub>B<sub>10</sub>) approximately 300 μm thick onto a steel substrate. The microstructures of the feedstock powder and the coatings before and after heat treatments were investigated by a combination of X-ray diffraction, scanning and transmission electron microscopy and differential scanning calorimetry (DSC). The as-sprayed coatings and gas atomised feedstock powders both had fully amorphous structures. The coatings had layered morphologies due to the deposition and solidification of successive molten or semi-molten slats but only a small amount of oxide formed during the spraying process. The thermal stability and crystallization behaviour of the powders and the coatings were investigated by DSC and XRD techniques. A comparison of the results of XRD and DSC measurements shows that crystallization in the samples is largely a single stage processes. The enthalpy of crystallization and its activation energy were calculated from the DSC data. Broadly, powders and coatings showed identical behaviour with only small differences in crystallization peak shapes.

4:30 PM

**Structure-Property Correlation of ZnO Thin Films Grown on Sapphire(0001) by a Two-Step Process by Pulsed Laser Deposition:** Punam Pant<sup>1</sup>; Jagdish Narayan<sup>1</sup>; <sup>1</sup>North Carolina State University

We have investigated growth of ZnO on sapphire(0001) by a two-step growth process, where the LT buffer grows two-dimensionally via domain-matching epitaxy and therefore it is expected to play a critical role in defect reduction and in turn in improving the device properties of the film. The measured surface roughness(rms) of the films is ~1nm. Smooth surface morphology of the film is critical for high performance of LEDs and other optical devices. High-Resolution theta-2theta scans through ZnO(0002) and (10-11) give values of 5.217A and 3.244A for the c and a-lattice parameters. These values of the lattice constants signify that films are fully relaxed as expected from the domain matching paradigm. These results will be supplemented by HRTEM, electrical and optical

characterization of the films to further understand the role of the buffer layer in strain relaxation and defect reduction mechanism in the grown film for improved heteroepitaxy of ZnO on sapphire.

4:50 PM

**Developing Reversible Surface Structures on Shape Memory Alloys:** Xueling Fei<sup>1</sup>; Yang-Tse Cheng<sup>2</sup>; David Grummon<sup>1</sup>; <sup>1</sup>Michigan State University; <sup>2</sup>General Motors Corporation

Reversible surface structures are desirable for many applications, ranging from friction control to information storage. In this paper, we present our method of indentation-planarization to create various reversible surface structures on NiTi shape memory alloys with feature sizes ranging from nano to millimeters. Specifically, we show that a shallow indent, made under a spherical tip, can fully recover upon austenitization. Deep spherical indents, made in the martensite, show pronounced two-way cyclic depth changes, for an unlimited number of thermal cycles. Upon planarization, two-way cyclic depth changes are converted to reversible surface protrusions. Various surface protrusions were made using this indentation-planarization method to achieve a variety of basic forms (such as lines and circles). We believe that these "thermo-topodynamic" surfaces at the micro and nano scales have many potential applications for micro-electrical-mechanical systems (MEMS), nano-scale sensors and actuators, variable friction surfaces, information storage devices, and controllable optical devices.

5:10 PM

**Formation of Regular Nanostructures on Surfaces of Copper Foils under Electric Discharge:** Sergey Pyachin<sup>1</sup>; Victor Zavodinsky<sup>1</sup>; Maxim Pugachevsky<sup>1</sup>; Alexander Burkov<sup>1</sup>; <sup>1</sup>Institute of Materials of Khabarovsk Scientific Centre of Far Eastern Branch of the Russian Academy of Sciences

We have studied the regular structure formation on the metal surface under a single electric discharge. 60-120-microns-thick copper foils were used as cathodes. As the anode, a copper sharpened rod was used. The electric discharging current was equal to 10-40 A and the pulse duration was varied in the range of 0.05-1.2 ms. The copper foil is melted by heat, releasing at the electric discharge region. The melting area has a radial symmetry. In regions located approximately 100 microns from the centre of the melting area, a regular cell structure is seen distinctly with periodicity of 0.5-1 micron. The AFM studies have shown that cells consist of small crystallites with lateral size of 50-200 nm. The Fourier analysis of AFM images of the copper surface has shown that the arrangement of cells aspires mainly to the hexagonal packing.

5:30 PM

**Structure Formation in Covering Layer at Low-Voltage Electrospark Processing:** Sergey Khimukhin<sup>1</sup>; Marja Teslina<sup>1</sup>; Tatjana Khimukhina<sup>2</sup>; <sup>1</sup>Institute of Materials of Khabarovsk Scientific Centre of Far Eastern Branch of Russian Academy of Sciences; <sup>2</sup>Pacific National University

Electrospark alloying (ESA) is one of the deposition coating methods with the use of concentrated energy streams. EAS is based on using the electric spark occurring between the anode and the cathode. To investigate the above mentioned basic laws copper and its alloys have been used as the material for the electrodes. Two main mechanisms of covering layer structure formation have been discovered. In one case in the absence of the defects the covering structure consists of a number of basaltiform crystal grains normally oriented towards the layer surface along its whole thickness and equiaxed grains being in the middle. In the other case, the layerwise oriented basaltiform crystal grains are divided by the defects. To reduce or to eliminate the defects and to obtain the required covering layer structure it is necessary to warm up the cathode in the course of electrospark processing to the temperature of 50°C.

## Transformations under Extreme Conditions: A New Frontier in Materials: Pressure/Stress-Induced Transformations and In Situ Diagnostics II

Sponsored by: The Minerals, Metals and Materials Society, ASM International, ASM Materials Science Critical Technology Sector, TMS Materials Processing and Manufacturing Division, TMS/ASM: Phase Transformations Committee  
**Program Organizers:** Vijay Vasudevan, University of Cincinnati; Mukul Kumar, Lawrence Livermore National Laboratory; Marc Meyers, University of California-San Diego; George "Rusty" Gray, Los Alamos National Laboratory; Dan Thoma, Los Alamos National Laboratory

Wednesday PM Room: 3001  
 February 18, 2009 Location: Moscone West Convention Center

*Session Chairs:* Dan Thoma, Los Alamos National Laboratory; Timothy Weihs, Johns Hopkins University

**2:00 PM Invited**  
**Studying Nanoscale Material Processes under Extreme Conditions with High Time Resolution Electron Microscopy:** *Thomas LaGrange*<sup>1</sup>; Geoffrey Campbell<sup>1</sup>; Patrice Turchi<sup>1</sup>; Bryan Reed<sup>1</sup>; Nigel Browning<sup>1</sup>; Wayne King<sup>1</sup>; <sup>1</sup>Lawrence Livermore National Laboratory

Often material's macroscopic properties and behavior under external stimuli can be described through observation of its microstructural features and dynamical behavior. Materials models and computer simulations that are used to predict material behavior in different environments, e.g., phase transformation kinetics under high pressure loading, typically require experimental data for validation or interpretation of simulated quantities. However, most materials dynamics are extremely rapid, making it difficult to capture transient, fine-scale features of the material process, especially on the length and time scale relevant for most simulations. In effort to meet the need for studying fast dynamics in material processes, we have constructed a nanosecond dynamic transmission electron microscope (DTEM) at Lawrence Livermore National Laboratory to improve the temporal resolution of in-situ TEM observations. The DTEM consists of a modified JEOL 2000FX transmission electron microscope that provides access for two pulsed laser beams. One laser drives the photocathode (which replaces the standard thermionic cathode) to produce the brief electron pulse. The other strikes the sample, initiating the process to be studied. A series of pump-probe experiments with varying time delays enable, for example, the reconstruction of the typical sequence of events occurring during rapid phase transformations. This presentation will discuss the core aspects of the DTEM instrument with particular focus on how it has been used to study martensitic phase transformations in Ti and "superheated" crystallization processes in amorphous NiTi films. Work was performed under the auspices of the U.S. Department of Energy by the Lawrence Livermore National Laboratory and supported by the Office of Science, Office of Basic Energy Sciences, Division of Materials Sciences and Engineering, of the U.S. Department of Energy under contract No. DE-AC52-07NA27344.

**2:35 PM**  
**Coherent Electromagnetic Radiation Emission from Phase Transformations in Shocked CdSe: A New Ultrafast Materials Diagnostic:** *Evan Reed*<sup>1</sup>; <sup>1</sup>Lawrence Livermore National Laboratory

Using molecular dynamics simulations coupled to Maxwell's equations, we show that the ultrafast transformation of wurtzite CdSe to the rocksalt phase under shock compression is accompanied by detectable electromagnetic radiation emission. The wurtzite to rocksalt transition can be accompanied by a change in static macroscopic material polarization which generates electrical currents that radiate. The radiation is in the 100 GHz frequency range, corresponding to the timescale of the onset of the phase transformation. The radiation amplitude is sufficiently large to be detected several mm away from the shocked material using existing THz frequency detection techniques. This work was performed in part under the auspices of the U.S. Department of Energy by Lawrence Livermore National Laboratory under Contract DE-AC52-07NA27344.

**2:55 PM**  
**Study of Crystallization of Amorphous Silicon Using Dynamic Transmission Electron Microscopy:** *Shona McGowan*<sup>1</sup>; Liliya Nikolova<sup>2</sup>; Federico Rosei<sup>2</sup>; Bradley Siwicki<sup>1</sup>; Mitra Taheri<sup>3</sup>; <sup>1</sup>McGill University; <sup>2</sup>Institut National de la Recherche Scientifique; <sup>3</sup>Drexel University

Amorphous silicon is an important material of particular interest in the context of thin film transistors. It also provides an ideal model system for the study of crystallization dynamics, and to this end we have investigated the crystallization of a thin amorphous silicon film in the Dynamic Transmission Electron Microscope (DTEM) at Lawrence Livermore National Laboratory. Crystallization is initiated by a laser pulse that deposits sufficient heat into the system to activate the transition. A variable time delay after this initiation pulse, the sample is probed by a short photoelectron pulse in the TEM, generating a diffraction pattern or image with nanosecond temporal resolution. Thus, using the DTEM we can gain access to the kinetics of crystallization and details of the nucleation mechanism in-situ through time-resolved diffraction patterns and images of the specimen. Results of this study will be presented.

**3:15 PM**  
**FIB and Electron Microscopy Movies of Extreme Materials Dynamism:** *Warren MoberlyChan*<sup>1</sup>; Bassem El-Dasher<sup>1</sup>; Luis Zepada-Ruiz<sup>1</sup>; Graham Bench<sup>1</sup>; Scott Tumey<sup>1</sup>; Thomas Felner<sup>1</sup>; Alex Gash<sup>1</sup>; Hector Lorenzana<sup>1</sup>; <sup>1</sup>Lawrence Livermore National Lab

FIB and 2-beam-tools enable site-specific serial-sectioning at nanometer-scale. Movies and 3D-image-collection are versatile, but collection remains slower than sub-microsecond-timescales for extreme experiments. Piecing together nanostructural changes in 3D illuminates how nanosecond events occurred. The analogy is quenching series capturing thermal reactions by metallography. What happens when loading is so fast and so hard that <1 nanosecond is insufficient time for deformation mechanisms to engage? How can self-sustaining reactions, propagating >nanometer/nanosecond in an energetic material, be "stopped"? The reverse reaction always present on a free energy diagram, is statistically irrelevant at the macroscale but paramount at the picoscale, so what happens when the reverse reaction of deposition catches up to the primary reaction of erosion? Or the reverse? To understand and control processing at the nanoscale, materials metrology needs picosecond and picometer resolution. But until we achieve extreme in situ capabilities, FIB/EM movies help answer these extreme questions. (DOE-LLNL Contract-#-DE-AC52-07NA27344-UCRL-ABS-405723).

**3:35 PM Break**  
**3:50 PM Invited**  
**Interface Mobility for Ti Alpha to Omega Transformation:** *Dallas Trinkle*<sup>1</sup>; <sup>1</sup>University Illinois, Urbana-Champaign

While the shock-induced Ti alpha (hcp) to omega martensitic transformation has been studied extensively experimentally, atomistic-scale simulations of the transformation mechanism have only recently added new insight. Ab initio work generated and sorted through homogeneous transformations to find the TAO-1 pathway with an energy barrier more than four times lower than other transformations. Now, a new atomistic potential for Ti accurately describes phonons, surface and stacking fault energies for the alpha, omega, and beta (bcc) phases, as well as homogeneous transformation barriers for alpha to omega. The new potential determines the structure and mobility of glissile disconnections (interfacial line defects) in the alpha/omega interface for different transformation pathways under pressure. This provides crucial insight into the dynamics of the shock-induced transformation, and the important role of interfacial kinetics in strongly driven transformations. The transformation of alpha interstitial sites to omega helps elucidate the atomistic-scale behavior of oxygen on the transformation.

**4:25 PM**  
**Omega Phase Transition in Zirconium Based Alloys under High Pressure:** *Raghvendra Tewari*<sup>1</sup>; Jyoti Gyanchandani<sup>1</sup>; Dinesh Srivastava<sup>1</sup>; Srikumar Banerjee<sup>1</sup>; Gautam Dey<sup>1</sup>; <sup>1</sup>Bhabha Atomic Research Centre

The  $\omega$  phase under high pressure exists as an equilibrium phase in Group 6 metals. However, with pressures exceeding 30 GPa the  $\omega$ -phase transforms to the  $\beta$ -phase in pure-Zr. This observation establishes the transformation sequence  $\alpha$ - $\beta$ - $\omega$  with increasing pressure. This paper reports that the formation of the  $\omega$  phase in a  $\beta$  stabilized zirconium alloy under shock pressure condition. The plate shape morphology of the  $\omega$  phase in the  $\beta$  matrix is akin to the martensitic phase. The mechanism for the formation of the plate shaped  $\omega$  phase is explained on the

basis of a shear on  $\langle 112 \rangle$  planes of the bcc lattice and the mechanical instability of the  $\beta$  phase. Similar platelet morphology of the  $\omega$  phase was observed when pure-Zr was also subjected to shock pressure whereas the granular morphology was observed under static pressurization. Different mechanisms have been proposed to explain differences in the morphology.

**4:45 PM**

**Dislocation Patterning and Formation of Omega Phase in Shocked Tantalum:** *Luke Hsiung*<sup>1</sup>; Geoffrey Campbell<sup>1</sup>; <sup>1</sup>Lawrence Livermore National Lab

We present the results obtained from transmission electron microscopy studies of shocked tantalum, a group V transition metal that exhibits no clear solid-state phase transformation under static-pressure conditions, to investigate and verify the occurrence of shock-induced phase transformation under peak pressures above 30 GPa. Since the omega phase domains are frequently found in regions containing high-density dislocations with no cell-wall formation, we suggest that the shock-induced phase transformation in tantalum is nucleated through the catalysis of dislocations with a unique patterning configuration when the dynamic recovery process for cell-wall formation becomes suppressed under dynamic conditions. A strain-rate dependent dislocation mechanism based upon the clustering of closely spaced dislocation loops generated from a jogged screw dislocation is proposed to rationalize the shock-induced phase transformation. This work was performed under the auspices of the U. S. Department of Energy by the University of California, Lawrence Livermore National Laboratory under Contract No. W-7405-Eng-48.

**5:05 PM**

**The Influence of the Shape Memory Transformation on the Shock Dynamic Behavior and Phase Stability of U-6Nb:** *Dan Thoma*<sup>1</sup>; Robert Field<sup>1</sup>; Ellen Cerreta<sup>1</sup>; Darcie Dennis-Koller<sup>1</sup>; George Gray<sup>1</sup>; Heather Volz<sup>1</sup>; Ann Kelly<sup>1</sup>; Robert Hackenberg<sup>1</sup>; Jason Lashley<sup>1</sup>; <sup>1</sup>Los Alamos National Laboratory

U-6wt%Nb is a disordered alloy that exhibits a thermoelastic phase transition at approximately 100°C during cooling and associated shape-memory behavior. Shock loading of the material using a variety of techniques, including explosive charges with water capture and gas gun testing, results in two distinct effects: 1) the high temperature austenitic phase is stabilized, even after soft capture, and 2) the material does not readily display a Hugoniot elastic limit. Dynamic gas gun testing has been performed at different temperatures to reveal the characteristics of the phase transition under various loading conditions. The phase stability in the virgin and recovered samples has been investigated through x-ray diffraction, TEM, and thermal analysis techniques. The results suggest that reversion of the martensite masks the Hugoniot elastic limit and that the high temperature phase is stabilized by residual strains under extreme (explosive) loading conditions.

**5:25 PM**

**Phase Transformation and Microstructural Evolution of a NiTi Shape Memory Alloy at High Strain Rates:** *Xiuhua Zheng*<sup>1</sup>; Shukui Li<sup>1</sup>; Benqiang Zhu<sup>1</sup>; <sup>1</sup>Beijing Institute of Technology

To get a better understanding of phase transformation and microstructural evolution of NiTi SMAs occurring during dynamic loading, an experimental investigation into the stress-strain response of a NiTi shape memory alloy with different specimen geometry was conducted using Split Hopkinson Pressure Bar (SHPB). The microstructures of tested specimens were studied using SEM, TEM and XRD. The influence of strain rate and specimen geometry on phase transformation behavior of the material at high strain rate was discussed and compared with the behavior at quasi-static strain rates.

**5:45 PM**

**Stress-Induced Phase Transformation in Nanocrystalline UO<sub>2</sub>:** *Tapan Desai*<sup>1</sup>; Blas Uberuaga<sup>2</sup>; Paul Millett<sup>1</sup>; Dieter Wolf<sup>1</sup>; <sup>1</sup>Idaho National Laboratory; <sup>2</sup>Los Alamos National Laboratory

We have performed Molecular Dynamics (MD) simulations using an empirical potential to study stress-induced phase transformation in nanocrystalline UO<sub>2</sub> at T=1000K. The columnar UO<sub>2</sub> microstructure consists of 6 grains of identical hexagonal shape and diameter (d=20 nm) in a three-dimensional periodic simulation cell. Under constant-stress tensile loading conditions, we found a phase transformation from the fluorite to a-PbO<sub>2</sub> structure. The heterogeneous nucleation process of this new phase (a-PbO<sub>2</sub>) occurs at the grain boundaries and the new phase then grows toward the interior of the grain. To verify that this phase transformation seen in MD simulations is physically reasonable, density functional theory (DFT) calculations were performed. The DFT calculations

agree that the a-PbO<sub>2</sub> structure is energetically favored over the fluorite structure under certain tensile conditions. According to our knowledge, experimental validation of this phase transformation is not yet available. This work was supported by the DOE-BES Computational Materials Science Network.



## 2009 Functional and Structural Nanomaterials: Fabrication, Properties, and Applications: Nanoscale Powders: Materials, Synthesis and Applications

Sponsored by: The Minerals, Metals and Materials Society, TMS Electronic, Magnetic, and Photonic Materials Division, TMS Materials Processing and Manufacturing Division, TMS: Nanomaterials Committee, TMS: Nanomechanical Materials Behavior Committee

Program Organizers: Gregory Thompson, University of Alabama; Amit Misra, Los Alamos National Laboratory; David Stollberg, Georgia Tech Research Institute; Jiyoung Kim, University of Texas at Dallas; Seong Jin Koh, University of Texas at Arlington; Wonbong Choi, Florida International University; Alexander Howard, Air Force Research Laboratory

Thursday AM  
February 19, 2009

Room: 3018  
Location: Moscone West Convention Center

Session Chair: Gregory Thompson, University of Alabama

### 8:30 AM

#### Mono-Dispersed Nano-Crystalline Aggregated Nickel Powders Obtained by Using Hydrazine in the Presence of Sodium Dodecyl Sulphate: *Mohammad Hussain*<sup>1</sup>; <sup>1</sup>KACST

A range of aggregated mono-dispersed nano-crystalline nickel powders has been synthesized by chemical reduction process using hydrazine as a reducing agent at 600C. The rate of reaction was further accelerated as the temperature was increased to 800C. Under reflux conditions at 1000C, the rate of reaction was much faster and even finer powders were obtained. The aggregated powders were characterized by XRD, SEM and TEM. The results showed the presence of nickel particles which were less than 20nm in diameter. The particle size of the synthesized metal powders was also measured at room temperature (RT) using Nano ZS Particle Sizer instrument (Malvern Instrument), which utilizes the technique of dynamic light scattering (DLS). Further thermodynamic measurements were carried out using Differential Scanning Calorimeter (DSC) and Thermal Gravimetric Analyser (TGA) to establish any differences in the energy levels of the powders synthesized by different methods. These results are further discussed.

### 8:45 AM

#### Nano-Powders of Ni<sub>3</sub>N and Ni Metal Prepared through Liquid Ammonia Solution: Zhao Han<sup>1</sup>; *Hailong Qiu*<sup>1</sup>; Hongmin Zhu<sup>1</sup>; <sup>1</sup>Beijing University of Science and Technology

Nickel nitride(Ni<sub>3</sub>N) nano-powders were synthesized through chemical reduction, of NiCl<sub>2</sub> by sodium in liquid ammonia at -45°C. The produced Ni<sub>3</sub>N nano-powders were heat-treated and subsequently converted to nickel metal nano-powders at 300°C. The crystal structures and particle morphologies of the products were characterized by X-ray powder diffraction(XRD) and field emission scanning electron microscope(SEM). The results indicated that the products were hexagonal Ni<sub>3</sub>N and cubic nickel metal powders, with average particle size of 21 nm and 19 nm, respectively. The possible mechanisms of the reactions were also discussed.

### 9:00 AM

#### Consolidation of Gas Atomized Precursor Alloy Powder for the Formation of an Oxide Dispersion Strengthened Ferritic Stainless Steel Microstructure: *Joel Rieken*<sup>1</sup>; I. Anderson<sup>2</sup>; M. Kramer<sup>2</sup>; Y. Wu<sup>2</sup>; J. Anderegg<sup>2</sup>; <sup>1</sup>Iowa State University; <sup>2</sup>Ames Laboratory

Gas atomization reaction synthesis (GARS) was used as an innovative route for the fabrication of precursor oxide dispersion strengthened ferritic stainless steel powder. During this process the as-atomized powder particles, with a nominal chemical composition of Fe-(12.5-15.0)Cr-(0.5-1.0)Y-(0.0-0.54)Ti-(0.0-3.0)W wt.%, were reacted in situ forming a thin surface oxide. The surface oxide of the particles is intended to act as an internal oxygen supply reservoir for the formation of nano-metric yttrium-enriched oxide dispersoids. The formation of the nano-metric dispersoids occurs during elevated temperature consolidation of the powders and is driven by an oxygen exchange reaction between the initial surface oxide (e.g., chromium oxide) and yttrium metal. Microstructure phase evaluation was performed using scanning electron microscopy and transmission electron microscopy. Elevated temperature tensile testing was used to examine the initial strength of the as-consolidated specimens. Support from the DOE-FE

(ARM program) through Ames Laboratory contract no. DE-AC02-07CH11358 is gratefully acknowledged.

### 9:15 AM

#### Synthesis of Nano-Scale Fibrous Ni/Co Alloy Powders from Complex Nickel-Cobalt Oxalate Containing Ammonia: Zhan Jing<sup>1</sup>; Zhang Chuanfu<sup>1</sup>; Huang Boyun<sup>1</sup>; He Yuehui<sup>1</sup>; *Fan Youqi*<sup>1</sup>; <sup>1</sup>Central South University

A nickel-cobalt oxalate complex precursor containing ammonium for the synthesis of nano-scale fibrous nickel cobalt powder was obtained by coordination coprecipitation technique under suitable conditions. The experimental conditions including feeding methods, precipitation temperature, reactant concentration, surfactant, washing method and pH value of solution that influence the morphology, average particle size and the dispersion of the precursor have been studied in detail. SEM, XRD pattern, thermal analysis and IR spectroscopy were used in the characterization and the evaluation of some aspects of the formation mechanism of fibrous morphology of the precursor. The crystallinity, purity, and surface morphology of the as-prepared Ni<sub>x</sub>Co<sub>1-x</sub> fibers were investigated by XRD, SEM, respectively. The X-ray photoelectron spectroscopic(XPS) data have confirmed that the nickel and cobalt in the bimetallic nano-scale fibre are in the zero-valence state.

### 9:30 AM

#### Optical and Magnetic Properties of Transition Metal-Doped ZnO Nanoscale Powders Synthesized by Chemical Method: *M. Khan*<sup>1</sup>; <sup>1</sup>Center for Advanced Mathematics and Physics

We report the results of a detailed investigation of sol-gel-synthesized nanoscale (Co,Mn) co-doped ZnO powders processed at 600°C in forming gas (Ar95%+H5%) to understand how the structural, optical and magnetic properties of ZnO are modified by doping, in addition to searching for the theoretically predicted ferromagnetism. X-ray diffraction results indicate a purely single phase. The diffused reflectance spectroscopy revealed many characteristic absorption bands correspond to the Co<sup>+2</sup> ions and Mn<sup>+2</sup> ions in tetrahedral symmetry, indicating that dopants (Co, Mn) are well substituted in ZnO lattice. Magnetic measurements showed a paramagnetic when the samples annealed in air. However a weak ferromagnetic behaviour was observed for the sample containing Mn (4at%) while Co varied x = 0.00-0.02. One the other hand a relatively strong ferromagnetic coupling observed in the samples containing Co (4at%) with Mn variation. The mechanism of ferromagnetic behavior can be interpreted in light of F-center exchange (FCE) model.

### 9:45 AM

#### Synthesis and Crystallization of Amorphous Nano-Sized Si-B-N Powders: *Hailong Qiu*<sup>1</sup>; Mei Yang<sup>1</sup>; Zhao Han<sup>1</sup>; Hongmin Zhu<sup>1</sup>; <sup>1</sup>Beijing University of Science and Technology

Si-B-N ceramic powders were prepared through chemical reduction of SiCl<sub>4</sub> and BBr<sub>3</sub> by sodium in liquid ammonia. The products obtained were characterized by X-ray diffraction (XRD), transmission electron microscopy (TEM), and selected area electron diffraction (SAED). The results indicated that the products were amorphous phase with the particle size less than 50nm. The powders were heat-treated under vacuum at various temperatures. Up to 1500°C, the powder remained in amorphous phase. When the powders were heated at temperatures higher than 1500°C, crystallites of silicon nitride and boron nitride appeared from the matrix phase.

## Alumina and Bauxite: Process Improvements and Experiences - White Side

Sponsored by: The Minerals, Metals and Materials Society, TMS Light Metals Division, TMS: Aluminum Committee  
Program Organizers: Everett Phillips, Nalco Co; Sringeri Chandrashekar, Dubai Aluminum Co

Thursday AM Room: 2002  
February 19, 2009 Location: Moscone West Convention Center

Session Chair: Carlos Suarez, Hatch Associates Inc

### 8:30 AM Introductory Comments

#### 8:35 AM

**Electrocatalytic Oxidation of Organics in Bayer Liquor:** *Anthony Perrotta*<sup>1</sup>; Fred Williams<sup>2</sup>; <sup>1</sup>Pennsylvania State University; <sup>2</sup>CMIS Corp

Electrochemical oxidation for chemical bleaching of wood pulp was developed by the Dow Chemical Company. The present work used the Dow approach to electrochemically oxidize organics in a Kwinana spent liquor by the in situ cathodic reduction of oxygen to peroxide using only air as feed. Significant oxidation of the organics, relative to steel electrodes, was achieved using platinum, and platinum alloyed with 10% rhodium. The TOC reduction showed a decrease from 22g/l to 18g/l, 12g/l, and 7g/l for the steel, platinum, and platinum-10%rhodium electrodes, respectively. The electrocatalytic oxidation, obtained with the Pt-10Rh electrode shows, in accord with enhanced TOC reduction, the sodium carbonate concentration increasing from 50g/l to 150g/l. In comparison, the sodium oxalate concentration remained essentially unchanged. In conclusion, electrocatalytic oxidation is shown to be effective in a spent plant liquor in the presence of liquor impurities.

#### 9:00 AM

**The Influence of Moisture in the Attrition Index of Alumina:** *Jorge Lima*<sup>1</sup>; Joaquim Ribeiro<sup>1</sup>; Cleto Júnior<sup>1</sup>; Clauderino Batista<sup>1</sup>; <sup>1</sup>ALUNORTE

Attrition index is one of the most important physical parameter to define smelting grade alumina quality. Several papers have been correlated alumina morphology with strength. The present paper has the main objective to investigate the moisture influence in the attrition index measurement and the alumina strength. Alumina has a high capacity to absorb water from the environment, due to high surface area available to water absorption. It is very well known that water content can affect the alumina performance during the pot room operations, i.e. handling, HF control and formation of geysers and volcanoes, but fewer papers make relations between moisture and attrition index or strength. Presently, we discuss the attrition index analytical method, water adsorption and how they correlate each other, using particle size distribution, moisture, LOI and surface area analysis.

#### 9:25 AM

**The World's Largest Hydrate Pan Filter: Engineering Improvements and Experiences:** *Birger Petersen*<sup>1</sup>; *Manfred Bach*<sup>2</sup>; Rolf Arpe<sup>1</sup>; <sup>1</sup>Aluminium Oxid Stade GmbH; <sup>2</sup>FLSmidth Dorr-Oliver Eimco GmbH

FLSmidth Dorr-Oliver Eimco GmbH (FLS) and Aluminium Oxid Stade GmbH (AOS) present the latest engineering highlights and details of the operation of the world's largest hydrate pan filter at AOS. The various features of the pan filter with a filtration area of 71m<sup>2</sup> have resulted in AOS's decision to use FLS technology for product filtration. A track record is provided that deals with experiences of the filter operation. This covers the major process features and the operating procedures, which have been developed to maximize the availability and performance of the filtration system. Comments are made concerning a comparison with the operation of hydrate drum filters used before the commissioning of the 71m<sup>2</sup> pan filter. The production of high quality hydrate is discussed in relation to filtration parameters and optimization measures which have been practiced since the startup of the filter.

### 9:50 AM Break

#### 10:10 AM

**Superior Arguments for Most Modern Filtration Technologies in High Capacity Alumina Refineries:** *Reinhard Bott*<sup>1</sup>; Thomas Langeloh<sup>1</sup>; Juergen Hahn<sup>1</sup>; <sup>1</sup>BOKELA GMBH

In the last years capacity of alumina plants steadily increased leading to high capacity alumina refineries with annual production rates up to 3 Mt/y and even more. Before this background requirements on filtration technologies increased and great importance is placed on factors such as performance capacity, improved operation control, availability of equipment, reliability of operation, ease of maintenance or impact of the filtration process on downstream processing. The paper highlights characteristics in the design, construction and operation control of modern filtration technologies which are decisive to meet these increased requirements, by exemplary focusing of backflush filters for polishing filtration and pan filters for product filtration.

#### 10:35 AM

**Energy Efficiency in Gas Suspension Calciners (GSC):** *Susanne Wind*<sup>1</sup>; Benny Raahaug<sup>1</sup>; <sup>1</sup>FLSmidth Minerals A/S

Since commissioning three 4500 tpd. GSC units, the world's largest calciner installation at Queensland Alumina Limited in 2004, FLSmidth Minerals has introduced its new generation Gas Suspension Calciner Technology in order to obtain enhanced performance. The new generation Gas Suspension Calciners include the installation of a Fluidised Holding Vessel in the Furnace Cyclone after the Calciner Furnace, now being introduced into several new GSC units under design and construction. In addition to the Holding Vessel, a Forced Draft fan can be added to existing installations to increase capacity and provide enhanced operation. The paper will present the new generation Gas Suspension Calciner from FLSmidth Minerals and will focus on energy efficiency, alumina quality and upgrade possibilities of existing units.

#### 11:00 AM

**Increased Availability and Optimization of Calciner Performance Due to Automation:** *Michael Missalla*<sup>1</sup>; Jan Jarzembowski<sup>1</sup>; Roger Bligh<sup>1</sup>; Hans-Werner Schmidt<sup>1</sup>; <sup>1</sup>Outotec GmbH

In the last 30 years, Outotec has installed more than 50 calciners worldwide. Over the years the operation was improved significantly and thus also availability was raised. Real costs for instrumentation and control systems have also reduced over this period, thus encouraging the installation of more instrumentation, data analysis and better process monitoring. More recently, the trend has been towards full automation of activities like capacity load changes while maintaining other performance and product quality related parameters within specification. Other examples of improved automation are the use of advanced control loops with multiple input, while preheating and shut down of the calcination plant can be achieved with just the push of a button. The benefits of improved automation include improved availability through avoidance of operator error, reduction in manpower for process control related tasks and reduced requirement for field adjustment in potentially hazardous areas. The implementation of multivariable control strategies in recently commissioned plants and comprehensively engineered control concepts are described. Furnace temperature feed forward control, automated pre-heating, start-up, gas and solids purge, equipment protection monitoring, and automated protective measures for operational stability and plant trip prevention are presented.

#### 11:25 AM Concluding Comments

## Aluminum Alloys: Fabrication, Characterization and Applications: Composite and Foam

Sponsored by: The Minerals, Metals and Materials Society, TMS Light Metals Division, TMS: Aluminum Processing Committee

Program Organizers: Weimin Yin, Williams Advanced Materials; Subodh Das, Phinix LLC; Zhengdong Long, Kaiser Aluminum Company

Thursday AM  
February 19, 2009

Room: 2004  
Location: Moscone West Convention Center

Session Chair: Zhengdong Long, Kaiser Aluminum Company

### 8:30 AM

**Joining of Aluminum 5754 Alloy to Carbon Fiber Reinforced Polymers (CFRP) by Ultrasonic Welding:** *Frank Balle<sup>1</sup>; Guntram Wagner<sup>1</sup>; Dietmar Eifler<sup>1</sup>;* <sup>1</sup>University of Kaiserslautern, Institute of Materials Science and Engineering, Germany

Ultrasonic metal welds were performed to realize aluminum alloy/carbon fiber reinforced polymer (CFRP) – joints. Important advantages of ultrasonic welding are welding times less than three seconds and welding temperatures below 450°C. Important steps of the process are the softening and displacing of the polymer out of the welding zone by the ultrasonic shear oscillation. In the following, in contrast to conventional joining processes a direct contact between the aluminum surface and the carbon fibers takes place. The bonding mechanisms can be shown in detail by scanning electron microscopy. In a first step shear strengths of about 30 MPa were realized for AA5754/CF-PA66 – joints. By special surface pre-treatments of the metal, for example shot peening or etching, the joint strength could be increased up to 60%. Finally, the cyclic deformation behavior of these hybrid joints and the influence of aging in selected climates will be discussed.

### 8:50 AM

**Study of Particle-Matrix Interaction in Al/AIB2 Composite Material via Nanoindentation:** *Zenon Melgarejo<sup>1</sup>; Pedro Resto<sup>1</sup>; Donald Stone<sup>1</sup>; Marcelo Suárez<sup>2</sup>;* <sup>1</sup>University of Wisconsin; <sup>2</sup>University of Puerto Rico-Mayagüez

The tribological performance of functionally graded Al/AIB2 composites produced by centrifugal casting has demonstrated the suitability of these materials for lightweight, high wear resistance components. Hard AIB2 particles embedded in the composites promote wear strength, which is also critically dependent on the Al matrix-particle interaction. To measure AIB2 properties and understand the particle-matrix interaction nanoindentation experiments were performed on 3-10 µm diameter AIB2 particles embedded in the aluminum matrix of an Al-5 wt%B gravity cast alloy. Elastic modulus and hardness were obtained by separating out the effects of the surrounding aluminum matrix. Orientation-dependence of the mechanical properties of the AIB2 particles was assessed using electron backscattered diffraction. Under large nanoindentation loads, AIB2 particles could be pushed into the matrix. On a per-area basis smaller particles were more difficult to push in than larger particles. Strain gradient plasticity theory was used to explain the size dependence of the push-in force.

### 9:10 AM

**Study of Microstructure-Mechanical Properties Relationship in Accumulative Roll Bonding Processed Al6016 Alloy:** *Suhash Dey<sup>1</sup>; Juliane Hüttenrauch<sup>1</sup>; Klemens Reuther<sup>1</sup>; Werner Skrotzki<sup>1</sup>;* <sup>1</sup>Technische Universität Dresden

Ultrafine grained (UFG), less than 1 micrometer, metals and alloys provide more strength to the material than coarser grained (more than 1 micrometer). Severe plastic deformation is one way to generate UFG materials and there exists several ways to perform for eg. equal-channel angular extrusion/pressing, accumulative roll bonding (ARB), high pressure torsion, etc. ARB technique looks promising as one can achieve UFG materials in the form of bulk sheets. ARB is the process which bonds two material surfaces while rolling simultaneously. This is a relatively new technique and requires comprehensive microstructural-textural-mechanical properties studies on different materials. In the conference, ARB performed on AA6016 alloy would be presented with its microstructure-mechanical properties relationship in full details.

### 9:30 AM

**Sintering Response of Aluminum Alloys with and without Addition of Si and SiC By Powder Metallurgy:** *Antonyraj Arockiasamy<sup>1</sup>; Seong J. Park<sup>1</sup>; Randall M. German<sup>2</sup>; Pavan Suri<sup>3</sup>; Paul Wang<sup>1</sup>;* <sup>1</sup>Mississippi State University; <sup>2</sup>San Diego State University; <sup>3</sup>Heraeus

The demand for lightweight automotive components from aluminum and its alloys is turning to powder metallurgy (P/M) for optimal combinations of strength and creep, especially when the properties are required beyond that possible from a cast ingot route. This paper describes the die compaction and sintering response of aluminum with and without the addition of Si and SiC. A design of sintering experiments involving three sintering temperatures, hold times, and heating rates based on the Taguchi method was employed to isolate the optimum processing sintering cycle. Besides the mechanical properties, phase transformation and microstructure are investigated using hardness testing, compression-tension testing, dilatometry, thermogravimetric analysis coupled with differential scanning calorimeter and scanning electron microscopy with energy dispersive spectroscopy. A comparison study has also been made to analyze the strength and weakness of sintered aluminum alloys and ranked in terms of the effectiveness of the alloys based on their mechanical properties.

### 9:50 AM

**Impact Properties and Microstructural Evolution of Weldable and Unweldable Aluminum-Scandium (Al-Sc) Alloys:** *Woei-Shyan Lee<sup>1</sup>; Tao-Hsing Chen<sup>1</sup>;* <sup>1</sup>National Cheng Kung University

This study employs a compressive split-Hopkinson pressure bar to investigate the impact properties of two weldable and unweldable Al-Sc alloys at strain rates ranging from  $1.2 \times 10^3 \text{ s}^{-1}$  to  $5.9 \times 10^3 \text{ s}^{-1}$  and temperatures of  $-100^\circ$ ,  $25^\circ$  and  $300^\circ$ , respectively. The results indicate that for both alloys, the impact properties are found to be significantly dependent on both the strain rate and temperature. Moreover, the flow stress, work hardening rate and strain rate sensitivity are higher in the unweldable Al-Sc alloy than in the weldable alloy. In describing the plastic deformation behaviour of the two Al-Sc alloys using the Zerilli-Armstrong fcc constitutive model. The TEM observations reveal that in both alloys, the dislocation density increases with increasing strain rate, but decreasing with increasing temperature. Furthermore, it is found that the dislocation density of the unweldable Al-Sc alloy is higher than that of the weldable Al-Sc alloy.

### 10:10 AM Break

### 10:30 AM

**An Investigation into the Mechanical Behaviour of 7075-Al Based Composites:** *Indumati Deshmunya<sup>1</sup>; G. K. Purohit<sup>1</sup>;* <sup>1</sup>Poojya Doddappa Appa College of Engineering, Gulbarga

Metal matrix composite (MMC) materials are finding applications in various fields ranging from cutting tools to aero-space materials because of their high strength-to-weight ratios, high wear resistance and easy manufacturability. Extensive research work on the feasibility of these composites is undertaken by the authors. A knowledge of their mechanical behaviors is believed to enhance their applicability. This paper presents the results of a study on the mechanical behavior of 7075-AL alloys with  $\text{Al}_2\text{O}_3$  reinforcing produced by stir casting. Factorial design techniques and ANOVA have been used to develop models. Of these, 7075-Al alloy composites are of particular importance because of their suitability in wear resistant, corrosion resistant and fracture resistant environment hardness and impact strength (Charpy-V) have been performed on specimens, which are carefully extracted from the cast material. The effect of particle size (100m-400m), of reinforcement (5% to 12% by weight), sintering temperature and holding time on the selected mechanical properties are reported. An attempt is made to correlate the results with microstructural studies.

### 10:50 AM

**Effect of Aging on the Mechanical and Corrosion Performance of 7012 Al Matrix SiC Particle Reinforced Composites:** *Harun Mindivan<sup>1</sup>; Eyup Kayali<sup>2</sup>;* *Huseyin Cimenoglu<sup>2</sup>;* <sup>1</sup>Ataturk University; <sup>2</sup>Istanbul Technical University

In this study mechanical and corrosion properties of 7012 aluminum alloy matrix 50 vol.% SiC particle reinforced composites produced with a squeeze casting technique has been examined in as-cast and T6 tempered states. Mechanical properties of the composites were determined by hardness measurements, impact tests and wear tests. Corrosion tests were carried out according to ISO 11846 standard by immersing the composites in a "30g/l NaCl + 10 ml/l HCl" solution for 24 hours. T6 tempering improved the hardness, wear resistance and corrosion resistance while reducing the impact toughness.



11:10 AM

**Fabrication Process of Hybrid Porous Structured Aluminum:** *Young Ik Seo*<sup>1</sup>; Chang Won Park<sup>1</sup>; Dae-Gun Kim<sup>1</sup>; Kyu Hwan Lee<sup>2</sup>; Young Do Kim<sup>1</sup>; <sup>1</sup>Hanyang University; <sup>2</sup>Korea Institute of Science and Technology

Porous materials can be applied to products with various functions such as energy absorption systems, light weight structures, and air/water filtration systems. Especially, the filtration system using the metallic membrane should have good permeability and excellent filtration efficiency. In this study, a hybrid porous structure was created by styrofoam for macropore network and surface modification for nanoporous surface. A mixture of Al powder, styrofoam and PVP solution was formed in an Al tube and then was dried in oven at 60°C for 1 hour. Styrofoam and binder were removed at 450°C for 2 hours and were subsequently heated up to over 600°C. The fabricated macroporous Al body was surface-modified in dilute alkali solution with different concentrations. The optical microscopy and scanning electron microscopy were employed to investigate the microstructure. The characteristics of pores were confirmed through the porosimeter and Brunauer-Emmett-Teller method.

## Aluminum Reduction Technology: Modelling

Sponsored by: The Minerals, Metals and Materials Society, TMS Light Metals Division, TMS: Aluminum Committee

Program Organizers: Gilles Dufour, Alcoa Canada, Primary Metals; Martin Iffert, Trimet Aluminium AG; Geoffrey Bearne, Rio Tinto Alcan; Jayson Tessier, Alcoa Deschambault

Thursday AM

Room: 2012

February 19, 2009

Location: Moscone West Convention Center

*Session Chairs:* Daniel Richard, Hatch Associates Ltd; Marc Dupuis, GeniSim Inc

8:30 AM

**Busbar Arrangement Optimization for End Cells:** *Donald Ziegler*<sup>1</sup>; Yimin Ruan<sup>1</sup>; <sup>1</sup>Alcoa Inc

Cells at the ends of potrooms have magnetic environments different from those in the rest of the potline. Their lack of close neighbors on one side and the effects of the crossover or rectifier bus can cause these cells to have serious magnetic problems if they are not appropriately compensated. We use examples of this problem to further examine the possibilities of automated optimization of magnetic fields in Hall cells. We discuss an objective function that takes partial account of the effect of the steel in the end cells.

8:50 AM

**Heat Transfer Considerations for DC Busbars Sizing:** *Andre Schneider*<sup>1</sup>; Tom Plikas<sup>2</sup>; Daniel Richard<sup>1</sup>; Lowy Gunnewiek<sup>2</sup>; <sup>1</sup>Hatch; <sup>2</sup>Hatch, Sheridan Science & Technology Park

The main DC busbars connecting the rectifiers to the potrooms or connecting the potrooms of a potline often consist of several naturally cooled parallel bars. To reduce cost, sizing of the bars is usually based on the minimum bar cross-section at the maximum allowable bar temperature. An adequate representation of the heat transfer characteristics of the bar system is therefore required for an efficient design of both busbars (preventing excessive costs or overheating) and expansion joints. A discussion on radiation and natural convection heat losses of the bars to the ambient is made using detailed Computational Fluid Dynamics (CFD) simulations. The effects of bar geometry, bar-to-bar spacing, ambient conditions and current density are discussed. Finally, a simplified calculation methodology based on semi-empirical convection correlations and analytical radiation view factors is proposed. Potential industrial applications, for example increasing the line amperage of existing potlines, are discussed.

9:10 AM

**The Effect of Channel Width under Different Bath Forces on the Aluminium Reduction Cell Current Efficiency:** *Mohamed Ali*<sup>1</sup>; Mohamed Doheim<sup>1</sup>; Abdel Fattah El-Kersh<sup>1</sup>; <sup>1</sup>Egyptalum

A two-dimensional mathematical model is used to study the effect of changing channel width on current density, bath circulation and current efficiency. The current density decreases towards the side wall carbon blocks and this is more pronounced as the channel width increases. The gas bubbles induced force is more effective compared with electromagnetic forces (EMFs). The bath velocity

values under various driving forces, bubble, EMFs, and the combined effect, were increased with reducing the channel widths. The reduction in channel width by 10 cm for the conditions representing the actual situation of the cell leads to increase the current efficiency by 0.4 %.

9:30 AM

**The Impact of Cell Ventilation on the Top Heat Losses and Fugitive Emissions in an Aluminium Smelting Cell:** *Haiam Abbas*<sup>1</sup>; Mark Taylor<sup>1</sup>; Mohammed Farid<sup>2</sup>; John Chen<sup>1</sup>; <sup>1</sup>Light Metals Research Center, University of Auckland; <sup>2</sup>Chemical and Materials Engineering, University of Auckland

Problems associated with aluminium smelting cell ventilation, caused by leakage of fume gases through pots superstructure gaps into the potroom, are normally solved by increasing the fume suction rate (draught) above certain levels. It is also known that, fugitive emissions are associated with reducing the draught below certain critical levels. Top heat losses are increasing in smelting cells as line amperage is raised. This drives further fugitive emissions through greater buoyancy of the fume/air mixture. A quantitative understanding of the relationship between fugitive emissions, superstructure tightness, top heat loss, and cell draught is crucial in the environmental context. It is also important if this top heat loss could be recovered for re-use. This problem is studied here computationally using the ANSYS-CFX software. Possibilities to improve cell ventilation and to decrease fugitive emissions are analysed for a typical industrial cell. The computed cell emissions and temperatures are compared with measured values. The impact of draught on ventilation and heat loss is also discussed.

9:50 AM

**A Modelling Approach to Estimate Bath and Metal Heat Transfer Coefficients:** *Dagoberto Severo*<sup>1</sup>; Vanderlei Gusberti<sup>1</sup>; <sup>1</sup>PCE Ltd

The heat transfer coefficients between the cell cavity and the liquids (bath and metal) are important parameters in order to achieve correct thermal calculations of the electrolytic cell's behavior. Traditionally, the wall heat transfer coefficients are adjusted with help of thermal measurements done in the real existent cells. However, this procedure cannot be done in a new project. The present work aims to show numerical procedures for estimation of the local heat transfer coefficients, at the liquid bath regions, independent of previous measurements. These results can be compared with the values obtained by experimental correlation formulae developed using physical models with similar fluids. The influence of anode-ledge channel width, interanode channels width, anode width, slots and anode immersion depth as well the current density passing through the anodes on heat transfer coefficients are investigated by numerical experiments.

10:10 AM Break

10:30 AM

**Comparison of Two Different Numerical Methods for Predicting the Formation of the Side Ledge in an Aluminium Electrolysis Cell:** Clement Bertrand<sup>1</sup>; Marc-Andre Marois<sup>1</sup>; *Martin Desilets*<sup>1</sup>; Marcel Lacroix<sup>1</sup>; Marie-Michelle Coulombe<sup>1</sup>; <sup>1</sup>Sherbrooke University

The solid-liquid phase change problem that takes place on the inside walls of an aluminium reduction cell has been modelled using two numerical approaches. In the first approach, called the single phase method, the phase change is not modelled explicitly, i.e., the solidification front is estimated by tuning cleverly the thermophysical properties of the liquid electrolyte. In the second approach, the phase change is modelled with an enthalpy method. In this case, heat transfer in all phases is calculated and the phase change is taken into account via a liquid fraction for the melt. Both methods are tested and compared to a benchmark problem from the literature. In spite of the fact that both methods are fairly robust and accurate for predicting the steady state condition, only the enthalpy method can predict the time-varying shape of the side ledge in situations like the cell cooling during a potline power interruption.

10:50 AM

**Solutions for the Metal-Bath Interface in Aluminium Electrolysis Cells:** *Valdis Bojarevics*<sup>1</sup>; Koulis Pericleous<sup>1</sup>; <sup>1</sup>University of Greenwich

The dynamic MHD modelling package is applied to the simple test case presented recently by Dagoberto, et al. in Light Metals 2008. It is compared to the derived analytical solution for a variation of boundary conditions. The interface stability is tested and compared to previously published analytical solutions. The problem is extended by a simple busbar design in order to run the universal busbar design tool and to apply it for the dynamic simulations of the electromagnetic fields, the interface waves and the velocity field.

11:10 AM

**Fluid Flow and Bubble Behavior in the Aluminum Electrolysis Cell:** *Lifeng Zhang*<sup>1</sup>; Yufeng Wang<sup>1</sup>; Xiangjun Zuo<sup>1</sup>; <sup>1</sup>Missouri University of Science and Technology

A full scale water model was established to investigate the phenomena in aluminum reduction cells. The behavior of bubbles under the anode is analyzed by both directly observation and camera recording. Bubble under the anode has a thick bubble front and a thin, long trail portion. With 0° tilted angle, hardly can the bubbles move forward, but form a gas film under the anode. With non-zero tilted angle, bubble motion under the anode is driven by the buoyancy force, thus bubbles are easy to escape through the curved end of the anode. LDV was used to investigate the fluid flow pattern. The LDV measurements reveal a recirculation flow pattern in side channel, similar to the observation of the tracer dispersion. Larger tilted angle and larger gas flow rate generate larger velocity and bigger turbulent energy, especially in the region close to the end of the anode and the top surface.

---

## Aluminum Reduction Technology: Potroom Operation and Maintenance

Sponsored by: The Minerals, Metals and Materials Society, TMS Light Metals Division, TMS: Aluminum Committee

Program Organizers: Gilles Dufour, Alcoa Canada, Primary Metals; Martin Iffert, Trimet Aluminium AG; Geoffrey Bearne, Rio Tinto Alcan; Jayson Tessier, Alcoa Deschambault

Thursday AM

Room: 2001

February 19, 2009

Location: Moscone West Convention Center

Session Chair: Michel Reverdy, Dubai

---

8:30 AM

**Alcoa Maintenance Best Practices: To Achieve Excellence in Planning, Scheduling, Autonomous Maintenance and Reliability:** *Maurice Beaudry*<sup>1</sup>; Marco Plante<sup>1</sup>; <sup>1</sup>Alcoa-Deschambault Aluminum Smelter

At Alcoa Aluminum smelter in Deschambault, Quebec, planning, scheduling, autonomous maintenance and reliability are already established. This abstract is to show the importance of a good planned maintenance on the production and profit to the plant. How to maintain a high equipment reliability level to improve the client satisfaction to a higher level (production), to reduce our production cost, reduce maint. cost by reducing our unplanned jobs (emergencies) and maintain a good operational availability (oa). Our success is based on our culture and values. In 2002, this Alcoa plant won the North American Maintenance Excellence Award (Name) who is an annual program conducted by the foundation for Industrial maintenance Excellence to recognize North American companies that excell in performing the maintenance process. The program not only covers maintenance, but the entire organizational structure. The main benefit and not the less was to be acknowledged as a world leader in maintenance.

8:50 AM

**Reliability and Maintenance Excellence from "Cradle to Grave":** *Serge Mathieu*<sup>1</sup>; <sup>1</sup>ABB Inc

Energy costs and metal prices have increased, environmental and safety have become Sr management main concerns. Industry must change the way major projects are delivered. Have you ever, as a production mgr or a maintenance mgr been given a new equipment, a new line or a new plant and been told "Now it is yours, operate and/or maintain it". As production or maintenance managers, yours objectives are to accelerate the start-up and get a sustainable uptime asap. Reliability and Maintenance began at the design phase of a project. This presentation will demonstrate how we can deliver a Reliable project to the production and maintenance manager by integrating the Reliability concepts and the maintenance best practices right at the design phase, through the commissioning and start-up.

9:10 AM

**Pure Metal Production and Methodology: The Alcoa Deschambault Experience:** *Stephen Lindsay*<sup>1</sup>; Patrice Doiron<sup>2</sup>; <sup>1</sup>Alcoa Primary Metals; <sup>2</sup>Alcoa Deschambault

Since 2005, Alcoa Aluminerie de Deschambault as kept iron level under 850 ppm. Many tools and trial has been developed and tested to achieve this performance. In this presentation, we will share methodology used, success key item, trial result and best practice that help plant achieve and maintain those result.

9:30 AM

**A Simple Method for Alumina Homogenization in Large Silos:** Geir Wedde<sup>1</sup>; Ketil Rye<sup>2</sup>; Gaute Nyland<sup>2</sup>; <sup>1</sup>Alstom Norway AS; <sup>2</sup>Elkem Aluminium ASA

In many silo systems for the aluminium industry little emphasis was laid on the way the alumina was fed into the silos. Simply one point of entry at center of top of silo was widely used. As the powder drops to the top of the alumina level inside the silo the powder segregates with effects when discharged into downstream systems such as dry scrubbers, alumina transport and pot feeding systems. Sampling of alumina discharged from an enriched alumina silo at the Elkem Mosjoen smelter demonstrated systematic large differences in the fines fraction being fed the pots. Typically, one potroom received twice as much fines as the other. An anti-segregation system was integrated in the silo with a challenge on restricted heights and space. Immediately after connecting up the anti-segregation system sampling of the two alumina discharge spouts consistently demonstrated a homogenous alumina with equal fractions of fines and fluoride content.

9:50 AM

**Issues Arising from the Back EMF in Potlines:** *Ali Mohamed*<sup>1</sup>; Arvind Kumar<sup>1</sup>; Maryam Al Jallaf<sup>1</sup>; <sup>1</sup>Dubai Aluminium Co Ltd

In a rapidly collapsing line current to zero, the cells are known to have an electrode potential which stays on during zero load situation. It is termed as back electromotive force (back emf). During this period, the cells behave as a battery since anodes have partially discharged intermediates in a thin region on its surface. Back emf decays with time from a high value of ~1.7 to ~1.0 volt. It plays a pivotal role during a power outage period and during power restoration. Safety issues and 'earthing' a potline circuit are of paramount importance when working on cut out pots. This paper covers a study of back emf during planned power outages at DUBAL and work practices evolved as a result to handle such a situation. The paper also covers the importance of deploying a portable 'earth' when working on cut out cells.

10:10 AM Break

10:30 AM

**Electrolysis Pots Anode Changing Automation: Impact on Process and Safety Performances:** *Nicolas Dupas*<sup>1</sup>; <sup>1</sup>ECL

The anode changing of the electrolysis pots is a recurring procedure in the aluminium smelter. Traditional methods involve a floor operator and a Pot Tending Machine to conduct the task. The precise vertical positioning of the new anode bottom surface with respect to the molten aluminium is critical to the stability of the electrolysis pot, to its overall performance, and therefore to the productivity of the smelter. The anode changing process is a determining factor in the safety and productivity of the potlines. By developing unique technical solutions and implementing a high level of automation in this process, it is possible to not only greatly increase its precision and repeatability, but also to alleviate the associated safety risks for pot floor operators. Such new solutions have been implemented in a renowned North American smelter, allowing a complete study of its benefits and progression margin.

10:50 AM

**Automated Stub Inspection System for Söderberg Technology:** *Jean-Pierre Gagne*<sup>1</sup>; René Minville<sup>1</sup>; Denys Bérubé<sup>2</sup>; Leonardo Paulino<sup>3</sup>; Gilles Dufour<sup>4</sup>; <sup>1</sup>STAS; <sup>2</sup>Alcoa Aluminerie de Baie-Comeau; <sup>3</sup>Alumar; <sup>4</sup>Alcoa Aluminerie de Deschambault

In the Söderberg process, steel stubs – inserted directly into the anode paste of the electrolysis cell – have to be changed every 15-18 days. Their shape and length are critical to ensure good electrical distribution and avoid anode breakage. After each cycle, stubs are cleaned and manually inspected by operators to determine whether they will be sent back to production or to the repair area. Stubs with improper lengths are rejected using a Go gauge; those with improper shapes are rejected according to the operators' judgment, thus with highly variable

results. Furthermore, some eroded shapes that could cause the anode block to crack during stub extraction are difficult to spot. The Alcoa-STAS R&D team has developed an automated stub inspection system that measures and classifies stubs. The information is saved in a database used to characterize stub population, prepare schedules and forecast costs of stub repairs.

### 11:10 AM

**Logistic Simulation of Discrete Material Flow and Processes in Aluminum Smelters:** Anton Winkelmann<sup>1</sup>; Ingo Eick<sup>1</sup>; Christian Droste<sup>1</sup>; Martin Segatz<sup>1</sup>; <sup>1</sup>Hydro Aluminium

Aluminium production depends on a multitude of different operations requiring discrete transport of materials more than twice as much as metal produced. The efficient integration of additional transport and process demand due to capacity creep or brownfield expansion into the existing infrastructure is intricate. Hydro Aluminium has a long history in solving the logistic challenges using simulation tools. Limitations of the existing models concerning model set-up and control logic suggested the development of a more flexible, modular and powerful simulation tool. The targeting range of applications includes the evaluation of transport logistics of existing smelters, but also the optimization of new mega smelter designs, new potroom operating concepts and support of investment decisions. The paper outlines the relevant discrete material flows, processes and procedures and some details of the model architecture. Examples highlight the range of applications and illustrate the outcome and gain of the systematic simulation approach.

### 11:30 AM

**Potroom Metal Treatment by Charcoal Filtration - Removing Lithium and Other Alkaline Metals from the Aluminum:** André Abbe<sup>1</sup>; <sup>1</sup>TRIMET ALUMINIUM AG

The Hamburg smelter, which was started in 1974, is now operated by TRIMET ALUMINIUM AG since December 2006. The potlines are equipped with 180 kA side-by-side Reynolds P19 cells. The electrolyte was lithium modified to reduce the liquidus temperature and increase the bath conductivity. The lithium content in the bath of roughly 3 wt% caused a lithium contamination of the aluminum of 20 ppm. This level is harmful to special products in the casthouse and metal treatment was essential. The metal filtration was done using a charcoal filter to reduce the lithium content of the aluminum by 50%. This approach was successful but to the expense of metal loss in the order of 0.3 wt%. Therefore TRIMET started changing the electrolyte composition to eliminate lithium contamination and eliminate the filtration. This paper discusses the charcoal filtration process and reflects the challenges when switching the electrolyte from lithium to non-lithium bath.

## Biological Materials Science: Biological Materials II - and - Implant Biomaterials III

Sponsored by: The Minerals, Metals and Materials Society, TMS Structural Materials Division, TMS Electronic, Magnetic, and Photonic Materials Division, TMS: Biomaterials Committee, TMS/ASM: Mechanical Behavior of Materials Committee  
Program Organizers: Ryan Roeder, University of Notre Dame; John Nychka, University of Alberta; Paul Calvert, University of Massachusetts Dartmouth; Marc Meyers, University of California

Thursday AM  
February 19, 2009

Room: 3014  
Location: Moscone West Convention Center

*Session Chairs:* Marc Meyers, University of California; Po-Yu Chen, University of California, San Diego

### 8:30 AM Invited

**Nanomechanics of Biological Systems — What Can We Learn from Nature about the Principles of Hierarchical Materials?:** Huajian Gao<sup>1</sup>; <sup>1</sup>Brown University

Mechanics of hierarchical materials inspired by nature may provide useful hints for materials engineering. Some questions of interest include: what are the roles and principles of structural hierarchy? What determines the size scales in a hierarchical material system? Is it possible to design hierarchical materials with designated mechanical and other properties/behaviors? The present talk will be focused on the basic mechanics principles behind hierarchical materials. We perform detailed analyses on two idealized, self-similar models of hierarchical

materials, one mimicking the mineral-protein composite structure of bone and bon-like materials, and the other mimicking gecko's attachment system, to demonstrate that structural hierarchy leads to simultaneous enhancement/optimization of multiple mechanical properties/functions such as stiffness, toughness, flaw tolerance and work of adhesion.

### 9:00 AM

**Hierarchy Correlations in Atomistic Mechanics of Collagen Hydroxyapatite Biomimetic Composites:** Devendra Dubey<sup>1</sup>; Vikas Tomar<sup>1</sup>; <sup>1</sup>University of Notre Dame

One of the motivations in developing biomimetic materials is the use of complex structural hierarchy to obtain materials with fault tolerance. Another interest is in using hierarchy to couple with additional functional properties. In this work, we present our extensive atomistic hierarchical analyses of tropocollagen (COL) and hydroxyapatite (HAP) nanocomposite interfaces. Focus is on understanding the role of hierarchy in peak interfacial strength for fracture and in determining the extent of the localization of peak fracture stress. We find that the crystalline orientation, supercell dimensions, collagen residue sequence, and volume fraction are important factors crucial to the overall hierarchical fault tolerant design. We also analyzed COL-HAP nanocomposites in three different chemical environments: vacuum, water, and calcinated water. Simulations show a clear correlation between the concentration of the surrounding environment and the predicted mechanical properties. We also found that environment could be coupled with multitude of functional properties in such bio-nanocomposites.

### 9:20 AM

**Advanced Characterization of Biological Materials via Microstructure Correlation Functions:** Stephen Niezgod<sup>1</sup>; David Turner<sup>1</sup>; Haviva Goldman<sup>1</sup>; Ulrike Wegst<sup>1</sup>; Surya Kalidindi<sup>1</sup>; <sup>1</sup>Drexel University

The internal structure of biological materials has been optimized by evolution and is primarily responsible for the unmatched combination of properties seen in materials such as wood, shell and bone. For many bio-materials this internal structure is extremely complex exhibiting structural anisotropies and heterogeneities that span several length scales. The challenges posed by biomimetic design require a more complete structure description than volume fraction based metrics such as pore size distributions and more advanced homogenization relationships than simple rule-of-mixtures bounds. To this end we present a mathematically rigorous description of internal structure based on a hierarchy of higher-order statistical functions (n-point correlations). In particular we will demonstrate the utility of 2-point correlation functions in characterizing the inherent variability in a materials structure and properties, generating representational volume elements and quantification of the similarities or differences between materials and samples on a range of biological materials including cancellous bone and wood.

### 9:40 AM

**Traumatic Brain Injury: Constitutive Modeling of the Porcine Brain under Large Deformation:** Raj Prabhu<sup>1</sup>; Mark Begonia<sup>2</sup>; Jean-Luc Bouvard<sup>1</sup>; Lakiesha Williams<sup>2</sup>; Jun Liao<sup>2</sup>; Esteban Marin<sup>1</sup>; Doug Bammann<sup>1</sup>; Mark Horstemeyer<sup>1</sup>; <sup>1</sup>Center for Advanced Vehicular Systems, Mississippi State University; <sup>2</sup>Department of Agricultural and Biological Engineering, Mississippi State University

Brain is one of the most critical organs of the human body during life-threatening and injury sustaining accidents. According to Center for Disease Control reports, Traumatic brain injury (TBI) is a leading cause of death and life-long disability in the United States. Current finite element (FE) models lack accurate descriptions of the mechanical behavior of the brain. Without an accurate representation of the history-based constitutive models of various components, predictive capabilities of these FE models are limited. The primary goal of this research effort is to develop a history-based internal state variable constitutive model for the mechanical behavior of porcine brain. The constitutive model equations are framed in a thermodynamics setting using large deformation kinematics that accounts for history dependence and microstructure-property relations for damage. The parameters of the model have been calibrated using stress-strain responses obtained from both quasi-static and high rate tests performed on porcine brain samples.



## 10:00 AM Break

### 10:10 AM

#### Field-Assisted Sintering of Nanocrystalline Hydroxyapatite for Biomedical Applications:

*Tien Tran*<sup>1</sup>; James Shackelford<sup>1</sup>; Joanna Groza<sup>1</sup>; <sup>1</sup>University of California

A recognized bioactive ceramic, hydroxyapatite (HA) is an excellent candidate in biomaterials selection. By reducing grain sizes to the nanocrystalline level, protein adsorption and cell adhesion are enhanced while strength, hardness, and wear resistance are improved. Unfortunately, the low phase stability, poor sinterability, and tendency towards exaggerated grain coarsening make it difficult to isolate the fracture toughness-grain size relationship from porosity effects by conventional sintering methods. The field-assisted sintering technique (FAST) is capable of heating rates up to 1000°C/min, thereby minimizing the low temperature exposure time of the powders when grain coarsening is active, but densification is minimal. Fully dense, transparent nanocrystalline HA has been consolidated by FAST in fewer than 20 minutes. While no decomposition was detected by XRD, the degree of dehydroxylation was assessed by simulated body fluid immersion tests. Fracture toughness was measured by both microindentation and single-edge v-notch bend (SEVNB) testing.

### 10:30 AM

#### Synthesis of Hydroxyapatite Nanopowders Using Induction Plasma Spray:

Mangal Roy<sup>1</sup>; Amit Bandyopadhyay<sup>1</sup>; *Susmita Bose*<sup>1</sup>; <sup>1</sup>Washington State University

Calcium phosphate (CaP) materials, especially hydroxyapatite (HAp) and tricalcium phosphate (TCP), gained significant importance as bone substitutes, fillers and coating materials due to their compositional similarities with natural bone. Nanoscale CaP materials has the ability to promote intimate bone growth and improve mechanical properties of dense compacts. In our work, HAp nanopowder was synthesized using inductively coupled radio frequency solution plasma spray with HAp sol as precursor. HAp sol was axially fed into the RF plasma jet at different plasma powers between 20 and 30kW. Particle size, surface area, morphology and phase composition of the synthesized powders were characterized using TEM, XRD, FTIR, particle size analyzer and BET surface area. High purity spherical HAp nanopowders were synthesized in large scale with particle size in the range of 40-80 nm. The presentation will focus on influence of induction plasma spray parameters on HAp nanopowder synthesis and process yield.

### 10:50 AM

#### Influence of Citric Acid on the Formation of Hydroxyapatite Powders:

*Chang Qing*<sup>1</sup>; Ru Hongqiang<sup>1</sup>; Yu Liang<sup>1</sup>; Zhang Xiantie<sup>1</sup>; Li Jiguang<sup>1</sup>; <sup>1</sup>Northeastern University

Citric acid (CA) is known as a strong chelating agent for metallic ions. Our purpose is to study the influence of CA on the formation mechanism and properties of hydroxyapatite (HA). The nano-HA powders were synthesized by a simple sol-gel method using Ca(NO<sub>3</sub>)<sub>2</sub>·4H<sub>2</sub>O and P<sub>2</sub>O<sub>5</sub> as precursors, with CA as an additive. For comparison, gels without CA were also prepared. The addition of CA promoted HA formation, and the powders calcined at 320°C contained the HA phase, though exhibiting low crystallinity. Under identical calcination conditions, the gel without CA showed an intense XRD peak of CaO, but that with CA showed major peaks of HA and a very weak CaO peak. Thus CA played an active role in reducing CaO content. Results also showed that the synthesized HA powders from gels with CA were finer than those without CA.

### 11:10 AM

#### Design and Fabrication of Nanocomposites for Biomedical Applications:

*Iris Rivero*<sup>1</sup>; <sup>1</sup>Texas Tech University

Materials for biomedical applications, such as orthopedic implants, must be designed with several criteria in mind: 1) biocompatibility, 2) mechanical properties resembling those of bones, and 3) and efficient processing. Overall, nanocomposites can provide increased strength, improved toughness, higher thermal expansion coefficient, with reduced elastic modulus and density. For orthopedic implants it is expected that nanocomposites will improve osteoblast and osteoclast functions, and decrease fibroblast functions, in comparison with microstructured materials. This research will consider titanium and hydroxyapatite as constituents for the suggested biocompatible nanocomposites. Fabrication of the biomedical nanocomposites will be achieved by means of ball mill grinding at room temperature. Fabrication of the nanocomposites will be followed by characterization of the resultant grain size, morphology, and

composition of the material. At the end, this research will identify the effect of processing parameters as milling temperature, time, and volume proportion of titanium and hydroxyapatite on resultant grain size.

## Bulk Metallic Glasses VI: Structures and Mechanical Properties III

Sponsored by: The Minerals, Metals and Materials Society, TMS Structural Materials Division, TMS/ASM: Mechanical Behavior of Materials Committee

Program Organizers: Peter Liaw, The University of Tennessee; Hahn Choo, The University of Tennessee; Yanfei Gao, The University of Tennessee; Gongyao Wang, University of Tennessee

Thursday AM

Room: 3007

February 19, 2009

Location: Moscone West Convention Center

*Session Chairs:* Yoshihiko Yokoyama, Institute of Materials Research; Tohru Yamasaki, University of Hyogo

### 8:30 AM Invited

#### Ordered Cluster and Free Volume in a Zr-Ni Metallic Glass: X. J. Liu<sup>1</sup>; G. L. Chen<sup>1</sup>; X. Hui<sup>1</sup>; Z. P. Lu<sup>1</sup>; <sup>1</sup>University of Science and Technology Beijing

In this work, the atomic arrangement of a model metallic glass (MG) Zr<sub>2</sub>Ni was studied by extended x-ray absorption fine structure and x-ray scattering experiments combined with reverse Monte Carlo (RMC) simulation imposed an additional potential constraint. By an approach to calculate the free volume (FV) on atomic level, we have found a connection between the coordination number and FV, and then revealed that the atomic structure of Zr<sub>2</sub>Ni MG is essentially an association of ordered clusters and FV. The ordered clusters about 1.5 nm consist of a densely packed core (i.e., icosahedral-type packing) and the surrounding loosely packed clusters with large FV. The decreasing potential energy during RMC simulation proves that the associated structure is a more stable structure. This finding not only will facilitate the understanding of atomic structure of MGs, but also may provide fundamental insights into the explanation of their unique mechanical behaviors.

### 8:45 AM

#### Fracture of (Cu<sub>50</sub>Zr<sub>50</sub>)<sub>100-x-z</sub>Al<sub>x</sub>Y<sub>z</sub> Bulk Metallic Glasses: Paolo Matteis<sup>1</sup>;

Pasquale Russo Spena<sup>1</sup>; Chiara Pozzi<sup>1</sup>; *Donato Firrao*<sup>1</sup>; Tanya Baser<sup>2</sup>; Marcello Baricco<sup>2</sup>; Jurgen Eckert<sup>3</sup>; Livio Battezzati<sup>2</sup>; Jayanta Das<sup>3</sup>; <sup>1</sup>Politecnico Di Torino; <sup>2</sup>Università di Torino; <sup>3</sup>IFW Dresden

The interplay between chemical composition, plastic behavior, and fracture modes of (Cu<sub>50</sub>Zr<sub>50</sub>)<sub>100-x-z</sub>Al<sub>x</sub>Y<sub>z</sub> (x=4, 5, 7 and z=0, 5) bulk metallic glasses was investigated by compression test and fracture surfaces analyses, to explore the possibilities of coupling physical, chemical and hardness properties, on one side, with adequate macroscopic compression plasticity, on the other side. Compression cylindrical test samples, having a height-to-diameter ratio equal to 2, were machined and ground from as-cast bars, and were loaded between lubricated plates, the displacement being measured by a clip-gage inserted between the plates. As a function of Al and Y content, the engineering stress-strain curves may show a plastic behavior consisting of successive sudden stress drops and linear reloading segments (evident in the absence of Y). These features, as well as the number of serrations, were statistically examined. Rupture surfaces were observed by SEM to ascertain the influence of composition on the varying fracture mechanisms.

### 8:55 AM Invited

#### Viscous Flow Behaviours of Zr-Cu-Al-(Ni) Bulk Metallic Glasses over the

**Entire Temperature Range:** *Tohru Yamasaki*<sup>1</sup>; Yosuke Tanimoto<sup>1</sup>; Yoshihiko Yokoyama<sup>2</sup>; Takehiko Ishikawa<sup>3</sup>; Akihisa Inoue<sup>2</sup>; <sup>1</sup>University of Hyogo; <sup>2</sup>Tohoku University; <sup>3</sup>Japan Aerospace Exploration Agency

Viscous flow behaviors of Zr<sub>55</sub>Cu<sub>30</sub>Al<sub>10</sub>Ni<sub>5</sub> and Zr<sub>55-x</sub>Cu<sub>35+x</sub>Al<sub>10</sub>(x=0, 5, 10 at. %) bulk metallic glasses over the entire temperature range containing supercooled liquid region and the equilibrium liquid region has been examined. Viscosity has been measured by using a penetration viscometer under various heating rates in the supercooled liquid region and a containerless electrostatic levitation method in the equilibrium liquid region. In the supercooled liquid region, the viscosity decreased with increasing the heating rate and tended to saturate at the heating rate of 200°C/min and above. So, acceptable results were obtained at the heating

rate of 200°C/min and above. This may partly reflect a decrease in the oxygen contamination. In the equilibrium liquid region, the viscosity exhibited very low values that are about  $1 \times 10^{10}$  times lower than that of the supercooled liquid. The viscosity of these Zr-Cu-Al-(Ni) supercooled liquids and equilibrium liquids has been fitted by a Vogel-Fulcher-Tammann (VFT) relationships.

#### 9:10 AM

**Strain Distribution in Bulk Metallic Glasses Investigated by In-Situ Tensile Tests under Synchrotron Radiation:** *Mihai Stoica*<sup>1</sup>; Jayanta Das<sup>1</sup>; Jozef Bednarcik<sup>2</sup>; Wei Hua Wang<sup>3</sup>; Jürgen Eckert<sup>4</sup>; <sup>1</sup>IFW Dresden; <sup>2</sup>HASYLAB Hamburg; <sup>3</sup>Institute of Physics, Chinese Academy of Sciences

We report on the evolution of the atomic-scale strain tensor of ductile Zr<sub>64.13</sub>Cu<sub>15.75</sub>Ni<sub>10.12</sub>Al<sub>10</sub> bulk metallic glass under tensile loading by using x-ray synchrotron radiation. The same kind of samples was previously investigated under compressive loading and revealed yielding at 1690 MPa together with large deformability of up to 160% strain. In tension the samples fracture at a lower stress, 1500 MPa, with no sign of yielding or plastic deformation. With no macro-plasticity observed under tension, large differences in the elastic constants obtained from the strain tensor and from ultrasonic sound velocity measurements are revealed. The work presents in detail the measuring procedure as well as the calculation of the tensile tensor and pair distribution functions of Zr<sub>64.13</sub>Cu<sub>15.75</sub>Ni<sub>10.12</sub>Al<sub>10</sub> at different stages of deformation. The results are discussed in comparison with other reported data obtained from x-ray diffraction measurements using synchrotron radiation.

#### 9:20 AM Invited

**Solid State Bonding of Zr Based and Cu Based BMG:** *Shing-Hoa Wang*<sup>1</sup>; Pei-Hung Kuo<sup>2</sup>; Peter K. Liaw<sup>3</sup>; Guo-Jiang Fan<sup>3</sup>; Hsiao-Tsung Tsang<sup>4</sup>; Dongchun Qiao<sup>5</sup>; Feng Jiang<sup>6</sup>; <sup>1</sup>Department of Mechanical Engineering, National Taiwan Ocean University; <sup>2</sup>Institute of Materials Engineering, National Taiwan Ocean University; <sup>3</sup>Department of Materials Science and Engineering, The University of Tennessee; <sup>4</sup>Chung-Shan Institute of Science and Technology

Limitations and difficulties with the welding and joining of bulk metallic glasses (BMGs) are caused by cracks formed by brittle recrystallization compounds produced during welding of interfacial zones of joints. The previous research works of the welding on Bulk Metallic Glass will be reviewed. A fully amorphous phase of similar S1(Cu60Zr30Ti10)/S1(Cu60Zr30Ti10) and S3(Zr52.5Cu17.9Ni14.6Al10Ti5)/S3(Zr52.5Cu17.9Ni14.6Al10Ti5) BMGs joints and a dual-amorphous phase of dissimilar S1(Cu60Zr30Ti10)/S3(Zr52.5Cu17.9Ni14.6Al10Ti5) BMGs joints have successfully been developed at the interface. Furthermore BMG with Sc addition (Zr55Cu30Ni5Al10)99.98Sc0.02 shows an excellent stable glass forming ability (GFA). The fusion zone of BMG (Zr55Cu30Ni5Al10)99.98Sc0.02 remains in the same amorphous state as that of the amorphous base metal when the weld is cooled with accelerated cooling.

#### 9:35 AM

**Mechanical Properties of Mg58Cu31Y6Nd5 BMG Composites with the Porous Mo Dispersion:** *Hsieh Pei-Jui*<sup>1</sup>; Su Hsiao-Chun<sup>1</sup>; <sup>1</sup>I-Shou University

The base alloys of Mg58Cu31Y6Nd5 BMG rods are made by injection casting. Vickers indentation and compression test are performed for the mechanical properties measuring. The fracture toughness is ~8 MPa m<sup>1/2</sup> and the fracture behavior of the compressive tests is brittle. For the mechanical properties promotion, the Mo particles are selected to be an additive in the base alloy. Then the results of the compressive tests for Mg58Cu31Y6Nd5-Mo BMG composites revealed that the plastic strain is improved with the addition of Mo particles (~5.2%). Vein-patterns are spread on the fracture surface. The fracture toughness is also improved (~25 MPa m<sup>1/2</sup> for Mg58Cu31Y6Nd5 -20 vol% Mo). SEM observation of BMG composites reveals that the addition of Mo particle for resisting the shear bands and cracks propagation is contributive. Shear bands are stopped at the Mo particles and secondary shear bands are formed during the plastic deformation process.

#### 9:45 AM

**Chemical Composition Effect on the Mechanical Behaviour of Zr-Based BMG:** *Yannick Champion*<sup>1</sup>; Sophie Nowak<sup>1</sup>; Patrick Ochin<sup>1</sup>; Alexander Pasko<sup>1</sup>; <sup>1</sup>Centre National De La Research Sci

Metallic glasses are known for exhibiting strong stress-strain localisation in shear bands which gives rise to absence of macroscopic ductility. The mechanisms of initiation and propagation of shear bands have been described by the monatomic free volume model proposed by Spaepen and subsequently by its extension to group of atoms developed by Argon. This can be examined experimentally

through the activation volume (or more precisely “apparent activation volume” since it depends on the type of testing), which is the thermally activated volume of matter involved in the rate controlling process. Shear band initiation and then mechanical behaviour should be dependant on, and then controlled by average atomic bonding energy. Variation of the activation volume was analysed using nano-indentation with respect to the chemical composition in order to evaluate local effect of various atoms such as W, Ta, Sn on the mechanical behaviour of Zr-based BMG.

#### 9:55 AM Break

#### 10:05 AM

**Size Effect on the Deformation and Yield Strength of Zr50Cu37Al10Pd3 Metallic Glass Micro-Pillars:** *Yong Yang*<sup>1</sup>; <sup>1</sup>the Hong Kong Polytechnic University

We report our recent experimental findings, in the micro-compression tests at a constant strain rate, of the size effect on the deformation and yield strength of the Zr-based metallic glass micro-pillars. At a fixed pillar's height, the reduction of the pillar's diameter from the micron to submicron scale led to a gradual transition of the plastic deformation modes from successive to intermittent shear banding, and eventually to homogeneous deformation at the pillar's diameter of ~700 nm. Accompanying the deformation mode transition, an increase in the apparent initial yield strengths was also observed.

#### 10:15 AM

**Correlation of Atomic Structure with Kinetic and Elastic Properties in Zr- and Cu Based Bulk Metallic Glasses:** *Xidong Hui*<sup>1</sup>; Guoliang Chen<sup>1</sup>;

<sup>1</sup>University of Science and Technology Beijing

Ab initio molecular dynamics(AIMD) calculations were performed on the atomic configuration, kinetic properties and elastic constants of Zr-Ti-Cu-Ni-Be and Cu-Zr-Al bulk metallic glass. The local structures were characterized in terms of structure factors, pair correlation functions, coordinate numbers, bond pairs and Voronoi polyhedra. The glass transition temperature, generalized PCF and SF predicated by AIMD were compared with experimental data. Short- and medium-range orders are extracted from the atomic configurations. The diffusion coefficients and viscosities of the undercooled liquid, and the elastic constants of these two bulk metallic glasses were calculated. Based on these calculation results, the correlations of atomic structure with the elastic property, fragility and glass forming ability were discussed in detail.

#### 10:25 AM

**Size Dependence of Compressive Strength of a Zr-Based BMG:** *W.F. Wu*<sup>1</sup>; Yi Li<sup>1</sup>; <sup>1</sup>National University of Singapore

A sample size dependence of the compressive strength has been established for a Zr-based bulk metallic glass (BMG) with a statistical method. Two competing factors, namely, free volume effect and flaw-sensitivity effect were found to affect the apparent strength of BMGs with different specimen sizes. As a result, there was a critical size with which the strength of BMG reached a maximum. In addition, a size dependence of Weibull modulus was observed which is attributed to the fact that the resulted BMG samples possessed various structural configurations due to the different size dependence cooling rate. The decrease in Weibull modulus as the sample size increases indicates a deterioration of mechanical reliability for larger-sized BMG component.

#### 10:35 AM Invited

**Thermodynamic Calculation and Microstructure Evolution in Phase Separating Metallic Glass Alloys:** H. J. Chang<sup>1</sup>; E. S. Park<sup>2</sup>; W. Yook<sup>3</sup>; J. S. Kyeong<sup>4</sup>; W. T. Kim<sup>4</sup>; *Do-hyang Kim*<sup>3</sup>; <sup>1</sup>Division of Humantronics Information Materials, Yonsei University; <sup>2</sup>Harvard University; <sup>3</sup>Yonsei University; <sup>4</sup>Cheongju University

In the present study, various types of microstructures resulted from phase separation in liquid state have been investigated in melt spun Gd-(Zr/Ti)-Al-(Co/Cu) alloys. The existence of miscibility gaps and spinodal decomposition curve in the liquid Gd-Ti-Al-Co/Cu systems were examined by thermodynamic calculation using CALPHAD method. Considering the thermodynamic information, we can control the microstructure depending on the processing parameters (undercooling) and alloy chemistry; i.e. i) droplet and interconnected structure in terms of morphology, and ii) amorphous+amorphous phases or amorphous+crystalline phases in terms of crystallinity. Interestingly, it was found that droplet of β-Ti phase was present in Gd-rich amorphous matrix in the Gd30Ti25Al25Cu20 alloy, and GdCu phase was present with Ti-rich amorphous phase in a complicated interconnected network structure in

the Gd<sub>30</sub>Zr<sub>25</sub>Al<sub>25</sub>Cu<sub>20</sub> alloy. The present result suggests that using phase separation in the liquid state, a new type of amorphous-crystalline composite structure in the form of droplet/interconnected structure can be fabricated.

## 10:45 AM Invited

### Research Activities of Bulk Metallic Glasses at Zhejiang University: *Jianzhong Jiang*<sup>1</sup>; <sup>1</sup>Zhejiang University

In this talk, we report research activities of bulk metallic glasses (BMGs) at Zhejiang University within the last four years (2004-2008). (1) We report composition optimization, thermal and physical properties of new families of La-based bulk metallic glasses with high glass forming ability (GFA) based on a ternary La<sub>62</sub>Al<sub>14</sub>Cu<sub>24</sub> alloy. By refining (Cu, Ag)/(Ni, Co) and La/(Cu, Ag) ratios in La-Al-(Cu, Ag)-(Ni, Co) pseudo quaternary alloy system, formation of 35 mm in diameter of LaAl(CuAg)(NiCo) BMG alloy is achieved by using Cu-mold casting; (2) We report the use of in situ high energy X-ray diffraction to detect the tensile behavior of two Zr- and La-based BMGs. Based on the diffraction data, the tensile elastic modulus and Poisson's ratio can be accurately evaluated; (3) Atomic structures of bulk glass-forming Cu<sub>64.5</sub>Zr<sub>35.5</sub> and the eutectic composition Cu<sub>61.8</sub>Zr<sub>38.2</sub> metallic glasses (MGs) have been studied by a combination of state-of-the-art experimental techniques and computational methods.

## 11:00 AM

### Characterization of Amorphous and Crystalline ZrCuAgAl Thin Films Deposited by Magnetron Sputtering: *Chia-Cheng Tsai*<sup>1</sup>; J. H. Huang<sup>1</sup>; G. P. Yu<sup>1</sup>; ChihPin Chuang<sup>2</sup>; Peter K Liaw<sup>2</sup>; <sup>1</sup>National Tsing-Hua University; <sup>2</sup>University of Tennessee, Department of Materials Science and Engineering

Amorphous and crystalline ZrCuAgAl films were deposited on p-type (100) Si and 304 stainless steel substrates by unbalanced magnetron sputtering (UBMS). The influence of structures on the mechanical, electrical, and corrosion properties of the thin films were studied. Results showed that the ZrCuAgAl thin film deposited at room temperature was in an amorphous form, while that deposited at 400°C possessed a good crystalline structure with major phases consisting of Cu<sub>10</sub>Zr<sub>7</sub> and CuZr<sub>2</sub>. The electrical resistivity of the films was about 160 μΩ-cm. The crystalline thin films had higher hardness and elastic constants compared with the amorphous counterparts. The residual stresses for the films deposited on the Si exhibited large differences for the crystalline and amorphous forms. The stress of the crystalline film was more than 8 times higher than that for the amorphous one. On the other hand, the amorphous thin films had better corrosion resistance than the crystalline films.

---

## Cast Shop for Aluminum Production: Casting Technology

Sponsored by: The Minerals, Metals and Materials Society, TMS Light Metals Division, TMS: Aluminum Committee

Program Organizers: Pierre Le Brun, Alcan CRV; Hussain Alali, Aluminium Bahrain

Thursday AM  
February 19, 2009

Room: 2005  
Location: Moscone West Convention Center

Session Chair: Robert Wagstaff, Novelis

---

## 8:30 AM Introductory Comments

## 8:35 AM Keynote

### Remelt Ingot Production Technology: *John Grandfield*<sup>1</sup>; <sup>1</sup>Grandfield Technology Pty Ltd

The technology related to the production of remelt ingots (small ingots, sows and T-Bar) is reviewed. Open mould conveyors, benching, sow casters, and VDC and HDC casting of T-Bar are described and compared. Process economics, capacity and product quality issues are listed. Trends in casting machine technology such as longer open mould conveyor lines are highlighted. Safety issues related to the operation of open mould conveyor casting machines for production of remelt alloy ingots are discussed. The potential hazards are listed. One of the main risks is the potential for molten metal ejections during mould filling. The advantages and disadvantages of the various machine configurations and options such as dry filling with the mould out of water and wet filling with the mould in water are discussed. The effect of mould design on machine productivity, mould cracking and mould life is also examined.

## 9:05 AM

### Nanotechnology Breakthrough Optimises Casting Process: *Volker Hofmann*<sup>1</sup>; <sup>1</sup>ItN Nanovation AG

With Nanotechnology it is possible to create a ceramic coat by using process given temperatures. A suspension containing nanoscale particles, sprayed thinly on the substrate, sinters to a robust and heat resistant ceramic by 300-400°C (600 – 750°F). It is not required to sinter the coat in a pre heating process. Sintering while melt contact leads to the expected result. So the robustness of a ceramic applies to moulds launders and dies. This can be achieved by simple maintenance operation on the shop floor. High service time provided by a very thin coat avoids coat build-up and leads to process stability.

## 9:25 AM

### A Simplified Method to Characterize Mold Cooling Heat Transfer and an Experimental Study of Impacts of Water Temperature on Ingot Casting: *Sebastien Bolduc*<sup>1</sup>; Ho Yu<sup>2</sup>; Laszlo Kiss<sup>1</sup>; <sup>1</sup>University of Quebec; <sup>2</sup>Alcoa Technical Center

The heat transfer characteristics of mold cooling water are of great interest in ingot casting. A question often arises, when there is a bleed-out or cracking problem, is how much cooling water should one increase or decrease to correct the problem. To characterize the cooling water heat transfer of a mold is time consuming. It usually needs numerous heat transfer measurements in an experimental setup under different cooling water conditions, e.g. flow rate, water temperature and chemistry, etc. This paper presents a unique method to characterize the cooling water heat transfer of a mold. The method determines the Leidenfrost temperatures, reducing greatly the amount of effort needed to generate the mold heat transfer correlations. The correlations can then be used as guidelines to adjust cooling water flow rate or as boundary conditions for an ingot mathematical model. As an example, the effects of water temperature on ingot casting are presented.

## 9:45 AM

### Advances in Cooling Water Deposit Control for Direct Chill Ingot Casting: *Yves Lefebvre*<sup>1</sup>; Caroline Sui<sup>1</sup>; Wilson Whitekettle<sup>1</sup>; <sup>1</sup>GE Water and Process Technologies

In aluminium DC casting, maintaining the integrity of heat transfer at the mould-water interface is of utmost importance from a productivity and surface quality standpoint. Heat extraction is critical and the focus of cooling water treatment is to keep this high temperature surface free of deposits. This paper discusses two new-generation products that have been recently developed to control two very troublesome types of deposits as far as resistance to heat transfer: biofilms and mineral scales. Furthermore, biofilms are a health concern as they provide favourable conditions for growth of the Legionella bacteria. The first product is a non-foaming biofilm remover, the second one is a polymer to control phosphate, iron and aluminium deposits. Laboratory data using cooling tower simulation equipment will be presented along with preliminary field applications.

## 10:05 AM Break

## 10:25 AM

### Heat Transfer During Rod Casting: *Laurent Cottignies*<sup>1</sup>; Vincent Duhoux<sup>1</sup>; Soizic Blais<sup>1</sup>; Celio Duran<sup>1</sup>; <sup>1</sup>RioTinto Alcan

This work contains the description of a heat transfer model which was specially developed for the aluminium rod casting process. A two dimensional finite element formulation was used to describe the temperature field within the solidifying bar, the copper mould and the steel belt. The focus of this work was on heat transfer coefficients at interfaces. Heat fluxes at aluminium-mould and mould-water interfaces were estimated by inverse heat transfer analysis, using dedicated temperature measurements. Significant differences were registered between various locations along the aluminium-mould interface. Thermo mechanical calculations and experimental characterizations of the casting surfaces were used to understand in more detail the factors controlling heat transfer.

## 10:45 AM

### Prevention of Starting Cracks in Al-Billets: Feasible Methods for Float and Spout DC-Casting: *Marcel Rosefort*<sup>1</sup>; Thomas Koehler<sup>1</sup>; Hubert Koch<sup>1</sup>; <sup>1</sup>Trimet Aluminium AG

Hot crack formation especially starting crack formation in butts of DC cast extrusion billets often causes rejections, in particular while casting high-alloyed aluminum. The prevention of such starting cracks can reduce the rejection rate



noticeable. Crack formation is well investigated in theory and many techniques for crack prevention are used in practice. Nevertheless starting cracks are a problem in DC casting. This paper presents an investigation on methods to prevent starting cracks in Al-billets production using float and spout DC-casting. Starting with the results of former investigations and practical experience these methods are tested for their suitability for crack prevention. The main focus was to apply all technologies to the float and spout DC-casting. The paper presents the research methods, the results of crack prevention and the real implementation in practice.

**11:05 AM**

**Improving the Surface of AA6111 Sheet Material, Cast at High Speeds, through the Use of Macroscopically Textured Substrates:** *Donghui Li*<sup>1</sup>; Luis Calzado<sup>1</sup>; Mihaiela Isac<sup>1</sup>; Roderick Guthrie<sup>1</sup>; <sup>1</sup>McGill Metals Processing Centre

The surface topography and coating materials of water cooled belts greatly affect interfacial heat flows, strip surface quality, and as-cast microstructures, for thin strips cast on high speed horizontal single belt casting machines (HSBC). The purpose of this paper was to investigate the surface quality of the strip by casting Aluminum AA6111 alloy on an HSBC simulator using a copper mould with different macroscopic surface textures and coatings. The transient interfacial heat flows were measured by thermocouples embedded in the copper mould. Ab-initio heat flows between the melt and the mould were predicted by mathematical modeling and favorably compared with experimental heat fluxes. It was found that the mould surface texture and coatings could be optimized to mitigate casting defects caused by air pockets entrained at the interface between the melt and rapidly moving mould. Attendant improvements in as-cast microstructures were obtained.

**11:25 AM**

**Reinventing Twin Roll Casting for the 21st Century:** *Enrico Romano*<sup>1</sup>; Chris Romanowski<sup>1</sup>; <sup>1</sup>Fata Hunter

The invention of twin roll casting in 1956 profoundly influenced the Western aluminum industry. The original twin roll casters were low cost machines that economically converted a variety of common alloys into sheet and foil products for the rapidly growing post-war consumer market. To meet market demand for an ever increasing range of alloys and widths, twin roll casters then became progressively bigger, more complex and costly. In recent years the economic growth in developing markets such as India has produced a surge in demand for low cost aluminum products that mirrors the Western post-war economic boom. To meet the requirements of these markets, FATA Hunter has developed a low cost casting machine that combines the low capital and operating costs of the original 1950s casters, with the latest in twin roll casting technology. The design features of this new caster are described and contrasted with a typical large machine.

**11:45 AM Concluding Comments**

### Characterization of Minerals, Metals and Materials: Characterization of Microstructure of Properties of Materials V

Sponsored by: The Minerals, Metals and Materials Society, TMS Extraction and Processing Division, TMS: Materials Characterization Committee, TMS/ASM: Composite Materials Committee  
Program Organizers: Toru Okabe, University of Tokyo; Ann Hagni, Geoscience Consultant; Sergio Monteiro, State University of the Northern Rio de Janeiro - UENF

Thursday AM Room: 3009  
February 19, 2009 Location: Moscone West Convention Center

*Session Chairs:* Lawrence Murr, University of Texas; Sergio Monteiro, State University of the Northern Rio de Janeiro - UENF

**8:30 AM**

**Data Driven Reduced Order Models for the Representation of Polycrystalline Microstructures:** *Nicholas Zabaras*<sup>1</sup>; Baskar Ganapathysubramanian<sup>2</sup>; <sup>1</sup>Cornell University; <sup>2</sup>Iowa State University

The stochastic analysis of a system requires the availability of appropriate input models of the uncertain variables. Constructing reliable input stochastic

models from limited data/information is therefore an important prerequisite for the realistic analysis of complex systems. This is particularly true during physical process modeling in polycrystalline microstructures where the amount of microstructural data is limited or only available in coarse-grained form. We investigate various dimensionality reduction strategies to construct compact, data-driven reduced order models of polycrystalline microstructures. In particular, we compare and analyze features of linear model reduction strategies based on Principal Component Analysis as well as non-linear model reduction strategies based on ideas from manifold learning.

**8:45 AM**

**Development of a Portable Load-Depth Sensing Indentation System for Online Material Characterization:** *Chuanyu Feng*<sup>1</sup>; Jared Tannenbaum<sup>1</sup>; *Bruce Kang*<sup>1</sup>; Mary Anne Alvin<sup>2</sup>; <sup>1</sup>West Virginia University; <sup>2</sup>National Energy Technology Laboratory

Indentation technique has a unique position for online material characterization. However, due to the complexity of the indentation depth and/or contact area measurement, current portable indentation instruments are solely developed for the purpose of hardness measurement. Powerful load-depth sensing indentation can be performed only in the lab. Due to this, a load-based indentation technique suitable for field applications has been developed, which does not need any direct measurement of the contact area or depth of indentation. The new technique bears the same theoretical background as traditional load-depth sensing indentation. Additionally, by applying a multiple-partial unloading procedure, the indentation system developed using this technique involves much less cost compared to current commercial products. To demonstrate the feasibility, a portable indentation system suitable for online material characterization has been developed. Excellent measurement results have also been obtained.

**9:00 AM**

**Safety Characterization of Electrical Systems in Diesel Electric Locomotive:** *Jeongguk Kim*<sup>1</sup>; Chang-Young Lee<sup>1</sup>; Seung-Koo Baek<sup>1</sup>; Sung Cheol Yoon<sup>1</sup>; <sup>1</sup>Korea Railroad Research Inst

In diesel electric locomotives, which were used for over 25 years, the characterization of electrical system was conducted for deterioration and safety evaluation through insulation resistance measurement, degradation testing, and infrared thermography method. Especially an infrared camera and thermocouples were employed for the evaluation. The thermocouples were attached on high-voltage cables connected to traction motors, for in-situ measurement of abnormal heating during test running. After test running, the thermographic images were obtained for the inspection of high-voltage cables using the infrared camera. The thermographic results were quantitatively analyzed, and compared with temperature changes during running. In this investigation, various analysis techniques for the safety characterization of diesel electric locomotives have been introduced, and the analysis results have been used to provide the deterioration or wear information in current locomotive systems.

**9:15 AM**

**Characterization of Hot Spots Generation in Railway Brake Disc:** *Jeongguk Kim*<sup>1</sup>; Byung Choon Goo<sup>1</sup>; Sung Cheol Yoon<sup>1</sup>; Sung-Tae Kwon<sup>1</sup>; <sup>1</sup>Korea Railroad Research Inst

The generation of hot spots on railway brake disc was investigated using the infrared thermography method. In brake system, the hot spots on the surface of brake disc have been considered as thermal distortions with high thermal gradient, and the control of hot spots has been an important issue for the lifetime extension of brake disc. In this investigation, a brake disc with gray cast iron, which is currently used in Korea, was employed. A high-speed infrared (IR) camera was used to measure the surface temperature of brake disc as well as for in-situ monitoring of hot spot evolution during braking operation. From the thermographic images, the observed hot spots and thermal damage of railway brake disc during braking operation were qualitatively analyzed. Moreover, the previous experimental and theoretical studies on hot spots phenomenon were reviewed, and the current experimental results were introduced and compared with theoretical prediction.

9:30 AM

**Mechanical Properties and Fracture Toughness Evaluation of Structural Steel with the Emerging Ball Indentation Technique and Its Numerical Validation:** *Sabita Ghosh*<sup>1</sup>; Mita Tarafder<sup>1</sup>; S Sivaprasad<sup>1</sup>; Soumitra Tarafder<sup>1</sup>; <sup>1</sup>National Metallurgical Laboratory

Among various small specimen and minimally invasive techniques to determine mechanical properties of materials, the ball indentation technique (BIT) has proved to be advantageous. BIT is used when a tensile test cannot be performed: on welded joints or components under service. The present work highlights the applicability of BIT to evaluate flow behaviour of engineering structural steels. Mechanical properties like ultimate tensile strength, yield stress, strain hardening coefficient evaluated for steels with varying heat treatment and mechanical working conditions. To determine fracture toughness from the flow curve, non linear damage models have been utilized. Attempt has been made to model the crack initiation, propagation and finally the fracture behaviour at different aging conditions using the results generated by the BIT. These results are compared with the same obtained by conventional tests. Validation of the BI test results has been carried out by Finite Element Modelling using ABAQUS software package.

9:45 AM

**Characterization of Cantera Stone from Hidalgo State, México: Viability Study for Recycling and Reusing of Wastes:** *Eleazar Salinas*<sup>1</sup>; Juan Hernández<sup>1</sup>; Francisco Patiño<sup>1</sup>; Eduardo Cerecedo<sup>1</sup>; Marius Ramírez<sup>1</sup>; Martín Reyes<sup>1</sup>; Miguel Pérez<sup>1</sup>; <sup>1</sup>Universidad Autónoma del Estado de Hidalgo

This work is related with a whole characterization of cantera stone, to establish its characteristics that can give it an additional value for its reuse and reutilization of dust, slurries and small pieces of stone which can be treated as wastes. The obtained results reflects that the residues studied can be used as substitutes of feldspars in the production of pieces of ceramic, and also in the elaboration of paints for the same pieces according to the mixes that can be made with the variation of Na<sub>2</sub>O, CaO and K<sub>2</sub>O. According to the humidity proofs and specific gravity done, this material can be proposed as a soil improver into hydroponics systems, leading so an important alternative for food production in zones leaking of water. In the same way, it was found the possibility of use this material as a seal 3A in processes of asphaltting of roads, highways and streets.

10:00 AM Break

10:20 AM

**Izod Impact Energy of Polyester Matrix Composites Reinforced with Aligned Curaua Fibers:** *Sergio Monteiro*<sup>1</sup>; Ailton Ferreira<sup>1</sup>; Felipe Lopes<sup>1</sup>; <sup>1</sup>State University of the Northern Rio de Janeiro - UENF

Polymer matrix composites have been applied in components such as helmets and shieldings for which toughness is a major requirement. Natural fiber present interfacial characteristics with polymeric matrices that favor a high impact energy absorption by the composite structure. The objective of this work was then to assess the Izod impact resistance of polymeric composites reinforced with different amounts, up to 30% in volume, of a promising high strength natural fiber from the Amazon region known as curaua. The results showed a remarkable increase in the notch toughness with the amount of incorporated curaua fibers. This can be attributed to a preferential debonding of the fiber/matrix interface, which contributes to an elevated absorbed energy.

10:35 AM

**Statistical Analysis to Characterize the Uniformity of Mechanical Properties of Buriti Fibers:** *Sergio Monteiro*<sup>1</sup>; Felipe Lopes<sup>1</sup>; Ludy Motta<sup>1</sup>; Leandro Marques<sup>1</sup>; <sup>1</sup>State University of the Northern Rio de Janeiro - UENF

Lignocellulosic fibers obtained from plants like cotton, flax, hemp, sisal, jute and many others are natural materials used, since long time, in basic items such as textile, baskets, roofing and carpets. These traditional natural fibers as well as some new ones are nowadays replacing synthetic fibers as composite reinforcement owing to environmental advantages. The heterogeneous characteristic of lignocellulosic fibers is, however, a limitation for application in composites. The buriti fiber, extracted from a tropical plant tree, is recently being investigated as a possible reinforcement for polymeric matrix composites but no complete information exists regarding its mechanical behavior. The objective of this work was then to carry out a statistical analysis on the mechanical properties' uniformity of buriti fibers. By precise dimensional measurements in association with tensile tests, it was found that the mechanical properties depend on the range of the fibers' dimension.

10:50 AM

**Coating Characterization in CrN Deposited by Magnetron Sputtering Method on AISI 316 Steel:** *Isaías Hilerio*<sup>1</sup>; <sup>1</sup>UAM AZCAPOTZALCO

Chromium nitride (CrN) thin films were deposited on steel AISI 316 substrates by radio frequency (rf) magnetron sputtering method using sputtering of a Cr target in nitrogen ambient. CrN films were produced by varying the deposition temperature, nitrogen partial pressure and rf power density. The films coated were characterized by X ray diffraction method, quantitative energy dispersive and scanning electron microscopy. These techniques were employed to characterize their phases, chemical composition and microstructure. Additionally, micro hardness was evaluated. The results show that the mechanical properties can be varied by changing the deposition conditions.

11:05 AM

**Effect of Molybdenum on the Microstructure and Thermal Expansion of Ductile Iron:** *Francisco Patiño*<sup>1</sup>; Juan Hernández Ávila<sup>1</sup>; Eleazar Salinas Rodríguez<sup>1</sup>; Francisco Patiño Cardona<sup>1</sup>; Isauro Rivera Landero<sup>1</sup>; <sup>1</sup>Centro de Investigaciones en Materiales y Metalurgia, Universidad Autónoma del Estado de Hidalgo

This work studies the Molybdenum effect on the microstructure and mechanical properties of an as-cast ductile iron. For this study five ductile irons with different amounts of Molybdenum each were made in an induction furnace. In this material, nodule count and nodularity are affected by the Molybdenum additions. The iron's matrix, nodules and the phase were analyzed using scanning electron microscopy detecting Molybdenum only in the matrix. Mechanical properties, such as hardness, microhardness, tensile strength and yield strength, show increments as the Molybdenum amount is increased. In the same way, ferrite and pearlite phases display a variation in their percentage as the contents of the alloy element increase. This element has a marked influence on the pearlite interlamellar spacing. From the obtained results we conclude that Molybdenum in these quantities dissolves in solid ferrite solution during the solidification process, improving the material's mechanical properties.

11:20 AM

**Removal Fe (III) from Dilute Solutions Containing Zn (II) by Ion Flotation Techniques:** Martín Reyes Perez<sup>1</sup>; Francisco Patiño Cardona<sup>1</sup>; Miguel Perez Labra<sup>1</sup>; Francisco Tavera Miranda<sup>2</sup>; Ramiro Escudero Garcia<sup>2</sup>; Eduardo Cerecedo Saenz<sup>1</sup>; *Eleazar Salinas Rodriguez*<sup>1</sup>; <sup>1</sup>UAEH; <sup>2</sup>UMSNH

Iron concentration by ion flotation techniques, from sulfate solutions in presence of zinc was studied, in a laboratory flotation column by continuous mode; using a synthesized sand shell plate sparged, an anionic collector, promoters, and surfactant propilenglicol 400. Effects of experimental parameters, such as the concentration of reagent, potassium amyl xanthate, dithiophosphate, superficial gas velocity, and superficial liquid velocity, were studied in terms of the recovery and enrichment of Fe (III). The results founded, shown that the iron elimination from solution in the presence and absence of zinc (II) are 59 % and 72 % respectively. The flotation efficiencies decrease with an increase of the concentration of xanthate, and air flow rate. A best recovery was achieved, at Jg 0.1 cm/s, JI 0.72 cm/s and a mixture of xanthate and dithiophosphate as promoter. Also was demonstrated that is possible selectively separate and concentrate iron (III) from solution containing zinc.

## Computational Thermodynamics and Kinetics: Grain Growth and Recrystallization

Sponsored by: The Minerals, Metals and Materials Society, ASM International, TMS Electronic, Magnetic, and Photonic Materials Division, TMS Materials Processing and Manufacturing Division, ASM Materials Science Critical Technology Sector, TMS: Chemistry and Physics of Materials Committee, TMS/ASM: Computational Materials Science and Engineering Committee

Program Organizers: Long Qing Chen, Pennsylvania State University; Yunzhi Wang, Ohio State University; Pascal Bellon, University of Illinois at Urbana-Champaign; Yongmei Jin, Texas A&M

Thursday AM Room: 3002  
February 19, 2009 Location: Moscone West Convention Center

Session Chair: Yu Wang, Virginia Tech

### 8:30 AM Introductory Comments

#### 8:35 AM Invited

**Quantifying the Solute-Drag Effect in Al-Mg Alloys:** *Moneesh Upmanyu*<sup>1</sup>; Branden Kappes<sup>1</sup>; Anthony Rollett<sup>2</sup>; Seth Wilson<sup>2</sup>; C Roberts<sup>2</sup>; <sup>1</sup>Colorado School of Mines; <sup>2</sup>Carnegie Mellon University

Quantifying the effect of solutes on grain boundary kinetics is a multiscale challenge because the characteristic length scale for boundary-solute interaction is a few nanometers, as opposed to the micron scale for most grain growth problems. We present the results of combined approach that uses Monte-Carlo for quantifying solute interactions at the atomistic scale and phase field/level set for modeling grain growth at the mesoscale. The interaction energies between Al grain-boundaries and individual Mg solute atoms are reported for various high angle, tilt grain boundaries. Our results reveal large variations in the form of these interactions, in stark contrast to the typical triangular profiles assumed in most previous theoretical frameworks. Using these interaction energies as inputs in the meso-scale simulations allows us to quantify solute drag effect in the low velocity, loaded regime. The results are compared with existing experimental data on Mg concentration dependence of Al grain boundary mobilities.

#### 8:55 AM

**The Topological Evolution of Anisotropic Three-Dimensional Grain Growth:** *Ian McKenna*<sup>1</sup>; Mogadala Gururajan<sup>1</sup>; Peter Voorhees<sup>1</sup>; <sup>1</sup>Northwestern University

Phase field simulations are a well accepted method for modeling the evolution of various microstructures, of particular interest is polycrystalline grain growth. Many of these systems exhibit anisotropic behavior during grain growth. Therefore, it is imperative that this behavior is included in phase field models in order to accurately describe the evolution. The model employed incorporates all five macroscopic degrees of freedom, grain boundary plane and grain misorientation, dependence of the grain boundary energy. To overcome the large resource requirements for calculating the evolution of three-dimensional polycrystals with thousands of grains a finite-difference sparse-matrix algorithm was developed. The calculations illustrate the important effects that anisotropy can have on three-dimension grain growth. We compare the topological evolution of grains in both isotropic and anisotropic systems.

#### 9:15 AM

**Kinetics of Copper Precipitation in Iron: Thermal Ageing and Irradiation Effects:** *Frederic Soisson*<sup>1</sup>; <sup>1</sup>CEA Saclay

The kinetics of copper precipitation in iron is modeled by ab initio calculations, Monte Carlo simulations and cluster dynamics methods. Ab initio calculations are used to compute the point defect jump frequencies of vacancies and self-interstitial atoms with dumbbell configurations. These jump frequencies are used to parameterize atomistic Monte Carlo simulations which take into account the dependence of the jump frequencies on the local atomic configuration. The simulations of copper precipitation during thermal ageing are compared with experimental studies. They reveal that copper diffusion occurs not only by migration of isolated copper atoms, but also by small copper clusters. Cluster dynamics are used to study the effect of this mechanism on the long term precipitation behavior. Under irradiation, we focus on the coupling between point defects and copper fluxes, which lead to radiation induced segregation of

copper at point defects sinks. We study its consequences for the precipitation kinetics.

#### 9:35 AM

**Kinetics of Formation and Thermal and Mechanical Properties of Char Obtained by Ultra-High Temperature Pyrolysis of Polyethylene via Molecular Dynamics Simulations:** *Maxim Makeev*<sup>1</sup>; Deepak Srivastava<sup>1</sup>; <sup>1</sup>NASA Ames Research Center

We present a molecular-dynamics simulation study of ultra-high temperature pyrolysis of polyethylene, leading to char formation via hydrogen removal and collapse of carbon network. The kinetics aspect of the study includes computations of rates of hydrogen removal and temporal evolution of carbon network via Voronoi tessellation analysis. The kinetics of dehydrogenation is quantified in terms of kinetic rate behavior as a function of pyrolysis temperature. The resultant char samples are investigated for thermal and mechanical behavior and their relation to microstructure. The thermal conductivity of char samples is studied between 10K and 500K for microstructures with different coordination numbers and ring statistics. The behavior of thermal conductivity as a function of char microstructure is explained via vibrational spectral analysis of char samples. Finally, the mechanical properties of char are studied within the framework of random network paradigm and the simulation results are compared with reported data on amorphous carbon.

#### 9:55 AM

**Numerical Investigation of Deformation-Induced Dynamic Transformation in Fe-C Alloy Using a Q-State Potts Monte Carlo Model:** *Dianzhong Li*<sup>1</sup>; Namin Xiao<sup>1</sup>; <sup>1</sup>Institute of Metal Research

The deformation induced dynamic transformation (DIDT) of a Fe-C alloy above Ae3 temperature is simulated using a Q-state Potts Monte Carlo (MC) model. The austenite-to-ferrite transformation, dynamic recrystallization (DRX) of austenite and ferrite and the ferrite-to-austenite reverse transformation can be simulated simultaneously in one MC model by building suitable MC transition rules. Meanwhile, an affine transformation model based on vector operation is also coupled with the MC model for the first time for tracking the changes in grain shape during dynamic transformation. The influence of deformation parameters, including temperature and strain rate, on the microstructure evolution and the stress-strain curves are discussed. The simulation results show that the competition between the DRX of austenite and austenite-to-ferrite transformation causes the different microstructures and changes the shape of the stress-strain curves for the different deformation parameters.

#### 10:15 AM Break

#### 10:30 AM

**CFD Modelling of Gas Injections in Top Submerged Lance Smelting:** *Nazmul Huda*<sup>1</sup>; Jamal Naser<sup>1</sup>; Geoffrey Brooks<sup>1</sup>; *Markus Reuter*<sup>2</sup>; Robert Matusewicz<sup>2</sup>; <sup>1</sup>Swinburne University of Technology; <sup>2</sup>Ausmelt Limited

A Computational Fluid Dynamic modelling of gas injections in a top submerged lance smelting unit was developed and the effect of lance submergence was investigated. The CFD software used for this purpose was FIRE 8.52. The simulation result was validated against the experimental data by comparing the velocity fields and generation of turbulence in the bath. Water was used as the modelling fluid and air was used as the injected gas to have an understanding of the mixing process and the effect of lance submergence. The simulation results showed that deeply submerged lance provide better mixing of the bath.

#### 10:50 AM

**Computational Tools for the Design of Weldable and Creep Resistant Superalloys:** *Franck Tancret*<sup>1</sup>; <sup>1</sup>Polytech Nantes

One drawback of many nickel-base superalloys is their poor weldability. In particular, cracking can occur in the mushy zone during solidification, in the so-called Brittle Temperature Range (BTR). Another type of cracking is due to the formation of intergranular liquid films, by the liquation of low melting point phases like carbides and/or intermetallics. In this work, CALPHAD-type computing tools (Thermo-Calc, DICTRA) are used to predict the occurrence of these types of cracking, and to design Ni base alloys by minimizing both the BTR and the risk of  $\gamma'$  liquation cracking, while keeping a good phase stability and good mechanical properties in the expected service temperature range. Among others, the creep rupture resistance is estimated through the multivariate regression of existing data, using artificial neural networks or Gaussian processes. Predictions are first compared to data in the case of existing alloys, and then used to propose new weldable and creep-resistant superalloys.



11:10 AM

**A Mechanism of Non-Equilibrium Grain Boundary Segregation for Intermediate Temperature Brittleness in Metals:** *Tingdong Xu<sup>1</sup>; Kai Wang<sup>1</sup>;*  
<sup>1</sup>Central Iron and Steel Research Institute

The graphical representation of non-equilibrium grain segregation of impurity offers a clear solution to an outstanding fundamental scientific mystery, intermediate temperature brittleness in metals, a problem which leading researchers in the field have struggled to explain for the past 100 years. For the elevated temperature tension tests of metallic materials a test temperature must exist at which a concentration peak of non-equilibrium grain boundary segregation of impurity and a relevant ductility minimum occur. The test temperature has a critical time of non-equilibrium grain boundary segregation of impurity to be equal or close to the test isothermal time at this tension test temperature. A number of diverse experimental results from a number of different labs can be rationalized on the new mechanism of intermediate temperature brittleness suggested in present paper. Main References: [1] Xu Tingdong, Cheng Buyuan, Prog. Mater. Sci., 2004; 49(2): 109-208.

11:30 AM

**A Simulation of Recrystallization on a Magnesium Alloy Using Phase Field Method for Real Time and Size in Industry Scale:** *Mingtao Wang<sup>1</sup>;* B.Y. Zong<sup>1</sup>; Yan Wu<sup>1</sup>; Xiangang Zhang<sup>1</sup>; <sup>1</sup>Northeastern University

A model has been established to simulate the realistic spatio-temporal microstructure evolution in recrystallization of a magnesium alloy using the phase field approach. Rules have been proposed to decide the reasonable value of all the parameters in the model with physical background discussion. The thermodynamic software THERMOCALC is applied to determine the local chemical free energy of the alloy and strain energy is added to the free energy density of the grains before recrystallization. A concept of boundary range is suggested to decide the gradient parameters in addition of fitting to the experimental boundary energy value. The parameter values can be regarded as a database for other similar simulations and the model is easy to adapt to other alloy systems. The simulated results show a good agreement with reported experimental measurement of the alloy at the temperatures from 300° to 400° for up to 100 minutes.

## Electrode Technology for Aluminum Production: Electrode Technology - Cathodes and Inert Anodes

Sponsored by: The Minerals, Metals and Materials Society, TMS Light Metals Division, TMS: Aluminum Committee  
Program Organizers: Barry Sadler, Net Carbon Consulting Pty Ltd; John Johnson, RUSAL Engineering and Technological Center LLC

Thursday AM  
February 19, 2009

Room: 2003  
Location: Moscone West Convention Center

Session Chair: To Be Announced

8:30 AM Introductory Comments

8:35 AM

**Formation and Dissolution of Aluminium Carbide in Cathode Blocks:** *Kristin Vasshaug<sup>1</sup>;* Trygve Foosnæs<sup>2</sup>; Geir Haarberg<sup>2</sup>; Arne Ratvik<sup>3</sup>; Egil Skybakmoen<sup>3</sup>; <sup>1</sup>Hydro Aluminium; <sup>2</sup>Norwegian University of Science and Technology; <sup>3</sup>SINTEF Materials and Chemistry

Today, failure of aluminium reduction cells due to wear of carbon cathode blocks is one of the main factors limiting the lifetime of the cell. Formation and dissolution of aluminium carbide plays an important role in the wear process, but the mechanisms are poorly understood. Electrolysis tests were performed, and the cathode samples were analyzed by SEM and optical microscopy to study the formation of Al<sub>4</sub>C<sub>3</sub> at the surface and/or in the pores of the sample. Samples from industrial cells were also included in the study. The results showed that in areas exposed to bath, dissolution of Al<sub>4</sub>C<sub>3</sub> was faster than formation, as no Al<sub>4</sub>C<sub>3</sub> could be seen on the surface. On surfaces covered by sintered alumina or aluminium, a thin non-coherent layer of Al<sub>4</sub>C<sub>3</sub> was observed, as well as in pores close to the cathode surface. Transport mechanisms of aluminium carbide related to the wear process will be discussed.

9:00 AM

**Resistivity Change of Cathode Graphite during and after Electrolysis in Alumina Molten Salt:** *Noboru Akuzawa<sup>1</sup>;* Morio Chiwata<sup>2</sup>; Manabu Hagiwara<sup>2</sup>; Yoshinori Sato<sup>1</sup>; Hiroshi Imagawa<sup>1</sup>; <sup>1</sup>SEC Corp; <sup>2</sup>Tokyo National College of Technology

Change of electrical resistivity of cathode graphite during and after electrolysis in alumina molten salt was determined at different temperatures between 870 and 980°C. Resistivity of cathode graphite decreased remarkably in the initial stage of electrolysis and then became almost constant for further electrolysis. On the other hand, resistivity increased with time by interrupting electrolysis. Just after the interruption, resistivity increased rapidly with time, followed by a characteristic plateau, and again increased towards a final steady value. Repeating of this cycle resulted in remarkable enlargement of resistivity. It should be noted that a large increasing ratio of resistivity of cathode graphite before and after electrolysis was observed at relatively low temperature such as 870°C. This observation suggested intercalated sodium is stabilized at lower temperature and the amount of sodium uptake increased during electrolysis. Correspondingly, the electrolysis at lower temperature provides an effective way for evaluation on degradation of cathode graphite.

9:25 AM

**Study of Aluminum Carbide Formation in Hall-Heroult Electrolytic Cells:** *Abdelhalim Zoukel<sup>1</sup>;* Patrice Chartrand<sup>2</sup>; *Gervais Soucy<sup>1</sup>;* <sup>1</sup>Universite de Sherbrooke; <sup>2</sup>Ecole Polytechnique de Montreal

The trend in the aluminum reduction industry today is that of operating cells, using graphitized carbon cathode blocks; increased current density and bath chemistry with an AlF<sub>3</sub> excess. The resulting problem is that of accelerated wear of the graphitized cathode blocks, which is thought to be caused by the formation and subsequent dissolution of the aluminum carbide at the cathode surface. This is now recognized as one of the factors limiting the cell lifetime. We will discuss a literature review. A special laboratory test method has been also developed to elucidate the mechanism of the aluminum carbide formation. The following operational parameters are varied: current density, electrolysis with or without aluminum thin film being added during start-up and time of electrolysis. The aluminum carbide formation has been studied, using X-ray photoelectron spectroscopy, X-ray diffraction and scanning electron microscopy. The analysis of the preliminary results will be presented in this paper.

9:50 AM

**The Effect of Potassium Cryolite on Construction Materials under Electrolysis Condition:** *Yurii Zaikov<sup>1</sup>;* Alexander Kataev<sup>1</sup>; Alexander Chuikin<sup>1</sup>; Nikolai Shurov<sup>1</sup>; *Alexander Redkin<sup>1</sup>;* Anton V. Frolov<sup>2</sup>; Alexander O. Gusev<sup>2</sup>; <sup>1</sup>Institute of High Temperature Electrochemistry; <sup>2</sup>Engineering-Technological Center, RUS-Engineering LLC, Rusal

Laboratory study of interaction SiC-Si<sub>3</sub>N<sub>4</sub> with low melting electrolyte based on potassium cryolite at temperature 800°C are presented. The investigation has been carried out by two techniques: 1) thermal gravimetric - continuous weighing of the sample in molten salt; 2) 100-hours electrolysis test. The values of the corrosion rate were obtained and the interaction mechanism of the material with electrolyte was proposed. Recommendations for applicability of the SiC-Si<sub>3</sub>N<sub>4</sub> composite in potassium containing electrolyte as lining bricks in the aluminum electrolysis cell were made.

10:15 AM Break

10:25 AM

**Mechanically Alloyed Cu-Ni-Fe Based Materials as Inert Anode for Aluminium Production:** *Badr Assouli<sup>1</sup>;* Martial Pedron<sup>1</sup>; Sebastien Helle<sup>1</sup>; Daniel Guay<sup>1</sup>; Lionel Roue<sup>1</sup>; Ambre Carrere<sup>1</sup>; <sup>1</sup>Institut National de la Recherche Scientifique

High-energy ball milling has been successfully applied to the synthesis of various materials with improved chemical, physical and mechanical properties for many applications including high-temperature corrosion resistance materials. It consists of inducing at room temperature a solid state reaction between the components of a powder mixture by repeated cold welding and fractures caused by ball-to-powder collisions. In the present study, it is demonstrated that nanostructured and monophased fcc CuxNi(85-x)Fe15 materials (with x varying from 0 to 55 wt.%) can be prepared by mechanical alloying. The study of their oxidation behaviour in air at 750°C indicates that the composition, the thickness and the growth kinetics of the oxide layer vary with the Cu content in the alloy. Aluminium electrolysis tests conducted at 700°C in 45 wt.% KF + 50 wt.% AlF<sub>3</sub>

+ 5 wt.% Al<sub>2</sub>O<sub>3</sub> electrolyte show that the electrode stability and aluminium purity are strongly dependent on the alloy composition.

**10:50 AM****Effects of Pitches Modification on Properties of TiB<sub>2</sub>-C Composite Cathodes:**

*Liu Xiaojun*<sup>1</sup>; Xu Jian<sup>1</sup>; Lai Yanqing<sup>1</sup>; Li Jie<sup>1</sup>; Fang Zhao<sup>1</sup>; Shi Yan<sup>1</sup>; Liu Yexiang<sup>1</sup>;

<sup>1</sup>School of Metallurgical Science and Engineering, Central South University

Pitches were modified by the heat-treated method, and the properties of pitches modified at different treatment temperatures were studied. Furthermore, the effects that modified pitches used as binder on properties of TiB<sub>2</sub>-C composite cathodes were investigated. The results showed that the coke yield and the viscosity of modified pitches increased as the treatment temperature increased. When the treatment temperature increased from 220°C to 420°C, the viscosity increased from 506 mPa·s to 27500 mPa·s and the coke yield increased from 47.21% to 69.64%. As the treatment temperature increased, the variation of cathode bulk density ( $\Delta\rho_p = \rho_{\text{Baked}} - \rho_{\text{Green}} / \rho_{\text{Green}}$ ) increased and the electrolysis expansion first decreased then increased. When pitches modified at 340°C, the electrolysis expansion reached the minimum and decreased by 14.01% compared to cathodes of primitive pitches. However, when pitches modified at 420°C, it increased by 3.82%.

---

**General Abstracts: Electronic, Magnetic and Photonic Materials Division: Session II**

Sponsored by: TMS: Alloy Phases Committee, TMS: Biomaterials Committee, TMS: Chemistry and Physics of Materials Committee, TMS: Electronic Materials Committee, TMS: Electronic Packaging and Interconnection Materials Committee, TMS: Energy Committee, TMS: Nanomaterials Committee, TMS: Superconducting and Magnetic Materials Committee, TMS: Thin Films and Interfaces Committee  
 Program Organizers: Long Qing Chen, Pennsylvania State University; Mark Palmer, Kettering University; Sung Kang, IBM Corp

Thursday AM

Room: 2022

February 19, 2009

Location: Moscone West Convention Center

Session Chair: To Be Announced

**8:30 AM****Control of Texture and Improvement of Magnetic Properties of Fe-6.5wt%Si by Directionally Recrystallization:**

*Z. W. Zhang*<sup>1</sup>; *G. Chen*<sup>2</sup>; *H. Bei*<sup>3</sup>; *F. Ye*<sup>4</sup>; *G. L. Chen*<sup>5</sup>; *C. T. Liu*<sup>6</sup>; *E. P. George*<sup>6</sup>; <sup>1</sup>Nanjing University of Science and Technology; <sup>2</sup>Nanjing University of Science and Technology, Oak Ridge National Laboratory; <sup>3</sup>Oak Ridge National Laboratory; <sup>4</sup>USTB; <sup>5</sup>Nanjing University of Science and Technology, USTB; <sup>6</sup>Oak Ridge National Laboratory and University of Tennessee

Fe-6.5%Si alloy is a high-silicon material with superior magnetic properties. However, it is difficult to be produced with controlled grain orientations by traditional processes. This research work reports for the first time that the grain orientation in the Fe-6.5%Si alloy can be controlled through directional recrystallization, and the coercivity force in the direction of 60°C along the growth direction of directional recrystallization can be reduced by 5 times than that without texture control. The significance of this work is that it not only makes it possible to produce grain-oriented Fe-Si alloys with high silicon content but also proves a unique way to control the orientation of magnetic materials magnetic property improvement. This work was supported by the Creative-Research-Foundation for PhD candidates of Jiangsu province, partially by the key project of China Natural Science Foundation (50431030) and by the U.S. Department of Energy, Materials Sciences and Technology Division.

**8:50 AM****Electrodeposition of Ni-CNT Electrode Using Pulse-Reversal Current Technique:**

*Saleh Nowrouzi*<sup>1</sup>; *Mehdi Attarchi*<sup>1</sup>; *S.K. Sadrejad*<sup>1</sup>; <sup>1</sup>Material and Energy Research Center

Ni electrode has been desired and applied by electrochemistry researchers because of its good properties. Several electrochemical applications of this material beside its good mechanical properties have persuaded to examine new methods of this material's synthesis. One of important electrochemical properties is surface area of this material which particularly is of great important in batteries. With co-deposition synthesis of Ni and carbon nano tubes (CNTs) it is possible to create nucleation centres on nanotubes and increase the surface area

of Ni considerably. With pulse-reverse technique (PRC) which is an effective way to improve the performance of coating, co-deposition of these two materials better carried out. In this study with investigation of various parameters of PRC technique, the optimum statuses of this technique are found out.

**9:10 AM****Examination of Charge Transport Mechanisms in Vanadium Oxide Thin Films for Infrared Imaging:**

*Bharadwaja Srowthi*<sup>1</sup>; *C. Venkatasubramanian*<sup>1</sup>; *N. Fieldhouse*<sup>1</sup>; *S. Ashok*<sup>1</sup>; *M. Ashok*<sup>1</sup>; <sup>1</sup>The Pennsylvania State University

Current commercial uncooled infrared focal plane arrays rely on vanadium oxide (VO<sub>x</sub>) thin films as the sensitive imaging layer. To date, however, very little is understood about the conduction mechanism that enables cameras to resolve temperature differentials approaching 10 mK. In this work, charge transport mechanisms in the VO<sub>x</sub> films deposited using a pulse dc sputtering were analyzed in terms of band and hopping mechanisms. The resistivity and temperature coefficients of resistance values of the films varied between 0.1-100 ohm-cm and -1.1% to -2.4% K<sup>-1</sup> respectively by varying composition via processing conditions. High temperature resistivity vs. temperature response of these films seems consistent with a band type conduction mechanism whereas, the origins of low temperature charge transport was due to charge hopping phenomena. These differences in electrical properties were due to variations in the density of states and statistical shift in the Fermi energy level due to temperature dependent disorder.

**9:30 AM****Giant Magnetoresistance and Microstructure of CuCo Granular Prepared by Electrodeposition:**

*Zhao Lin*<sup>1</sup>; <sup>1</sup>Northeastern University

CuCo granular films were prepared by electrodeposition on semiconductor Si. We studied the microstructure of the granular films during electrodeposition and elements distribution of the granular film after annealing. The maximum value of GMR was obtained at Cu<sub>80</sub>Co<sub>20</sub> film after annealing at 450° for 1h, with increasing the temperature of annealing, the electrical resistivity was dropped. Surface scanning for elements analysis and XRD show that the separation of Co grain was occurred during annealing, and part Co-rich regions was appeared. It was contribution to improved the value of GMR by resistance measure. The value of the GMR was decreased after annealing at higher temperature. The saturation magnetization M<sub>s</sub> coercive force H<sub>c</sub> remanence magnetization M<sub>r</sub> were increased with improved the annealing temperature by magnetization measure.

**9:50 AM Break****10:10 AM****Optical Properties of Molybdenum Oxide Thin Films Deposited by Chemical Vapor Transport of MoO<sub>3</sub>(OH)<sub>2</sub>:**

*Young Jung Lee*<sup>1</sup>; *Hee Young Jeon*<sup>1</sup>; *Chang Won Park*<sup>1</sup>; *Dae-gun Kim*<sup>1</sup>; *Young Do Kim*<sup>1</sup>; <sup>1</sup>Hanyang University

MoO<sub>3</sub> thin films have been extensively investigated in the electrochromic (EC) device field due to its superior optical properties; electrochromism is simply defined as a color change caused by an applied bias. Recently, many deposition techniques to deposit Mo oxide thin films have been developed including chemical vapor deposition (CVD), evaporation, sol-gel coating, RF magnetron sputtering, and pulsed laser deposition (PLD). In this study, MoO<sub>2</sub> thin films was homogeneously deposited by the chemical vapor transport (CVT) of MoO<sub>3</sub>(OH)<sub>2</sub> during reduction of MoO<sub>3</sub> powder in H<sub>2</sub>. Subsequently, a MoO<sub>3</sub> thin film was obtained by annealing of the deposited MoO<sub>2</sub> at 400°C for various holding times in O<sub>2</sub>. As annealing commenced, the optical transmittance of the films increased due to the crystallinity resulting from phase change and subsequent reduced oxygen vacancy.

**10:30 AM****Study of Failure Mechanism by Electromigration in Au/Al Wire Bond:**

*Emil Zin*<sup>1</sup>; *Nancy Michael*<sup>1</sup>; *S. H. Kang*<sup>2</sup>; *K.H. Oh*<sup>2</sup>; *U. Chul*<sup>3</sup>; *J. S. Cho*<sup>3</sup>; *J. T. Moon*<sup>3</sup>; *Choongun Kim*<sup>1</sup>; <sup>1</sup>University of Texas at Arlington; <sup>2</sup>Seoul National University; <sup>3</sup>MK Electron Co. Ltd.

This study investigates the mechanism of contact failure in Au/Al wirebond under the influence of electromigration. Conventionally, wirebond failure has been largely attributed to the formation of intermetallic compounds that increases contact resistance by itself as well as through formation of voids. However, there is a growing concern in microelectronics that electromigration may impart added influence on the contact reliability because wires used in modern and future devices should carry high density current, enough to induce electromigration. In our study, electromigration reliability of Au/Al wirebond is conducted at varying temperature, current density and Au compositions. Our study finds that

electromigration do influence the failure mechanism, perhaps more significantly than was previously believed, and that it is affected by alloying elements. This paper present supporting evidences along with understanding made from the failure analysis.

## 10:50 AM

**Synthesis and Characterization of Superparamagnetic Co and CoNi Particles:** *Maitreyee Bhattacharya*<sup>1</sup>; M. Ghosh<sup>1</sup>; S.K. Das<sup>1</sup>; B. Mahato<sup>1</sup>; <sup>1</sup>National Metallurgical Laboratory

Magnetic nano particles are presently the object of intensive research for their interest from fundamental and technological point of view. The special magnetic properties of iron, cobalt, nickel and alloys find promising use in various applications. Magnetic nano particles Co and CoNi were prepared by the reduction of synthesized Co<sub>2</sub>NiO<sub>4</sub> and Co<sub>3</sub>O<sub>4</sub> nano particles. A homogenous carbonate precipitation method was adopted for the synthesis of Co<sub>2</sub>NiO<sub>4</sub> and Co<sub>3</sub>O<sub>4</sub> nanocrystalline particles. Hydrogen gas was used to study the reduction behavior of Co<sub>2</sub>NiO<sub>4</sub> and Co<sub>3</sub>O<sub>4</sub> in the temperature range 250-550°C. The characteristics and properties of the particles were studied by transmission electron microscopy, scanning electron microscopy, XRD and magnetic measurements by Vibration Sample Magnetometer. Co and CoNi nano particles show single domain at temperature >500°C. Hydrogen reduction using synthesized metal oxides is effective to obtain a superparamagnetic Co and CoNi powder. The process is novel and cheap to produce superparamagnetic particles.

## 11:10 AM

**Ultraviolet Photoconductive Properties of ZnO Thin Film/Nanowell Grown by Using Atomic Layer Deposition:** *Chia-Ling Lu*<sup>1</sup>; Chih Chen<sup>1</sup>; <sup>1</sup>National Chiao Tung University

Self-organized ZnO thin film/nanowells are grown on Si/glass substrates by using an anodic aluminum oxide template and atomic layer deposition (ALD) to deposit ZnO. By using ALD, the deposition temperature can be as low as room temperature and there is no need for metal catalysts or seed layers. The nanowells are highly ordered and grew perpendicularly to the Si/glass substrates. We controlled the morphology of ZnO nanowell arrays by modifying ALD deposition processes. The microstructure of the ZnO appears to be polycrystalline, with a grain size that increases with increasing number of deposited cycles. Because of its relevance in UV detector applications, the UV photoconductive properties of ZnO thin film/nanowells were investigated to obtain the best transformation efficiency. Results to be presented at the conference will include photoluminescence, SEM and TEM images, and UV photoconduction data for the ZnO thin film/ nanowell arrays will be presented in the conference.

## 11:30 AM

**Properties of the Long-Term Ordered Semiconductors:** *Sergei Pyshkin*<sup>1</sup>; John Ballato<sup>2</sup>; George Chumanov<sup>2</sup>; Michael Bass<sup>3</sup>; Giorgio Turri<sup>3</sup>; <sup>1</sup>Academy of Sciences; <sup>2</sup>Clemson University; <sup>3</sup>University of Central Florida

Periodical monitoring since 1960th of optical and mechanical properties of the chosen III-V and Si crystals shows that the stimuli for long-term improvement of crystal quality prevail over those which lead to its degradation due to intensification of heterogenic distribution of impurities and defects. Evolution of optical and mechanical properties partly presented at international conferences testifies that now in GaP doped by N, impurity is a regular element of the new crystal lattice - it increases the forbidden gap, and at relevant concentration and level of optical excitation creates a bound excitonic crystal. CdIn<sub>2</sub>S<sub>4</sub>, now having the perfect normal (instead of partly inverted) spinel crystal lattice, as well as GaP with evenly distributed impurities, dislocations, and increased microhardness demonstrate new stable and bright luminescent phenomena, including stimulated emission and "hot" luminescence at room temperature. Existing technologies help us to reproduce artificially these naturally ordered structures for application in optoelectronics.

## General Abstracts: Materials Processing and Manufacturing Division: Session III

Sponsored by: The Minerals, Metals and Materials Society, TMS Materials Processing and Manufacturing Division, TMS/ASM: Computational Materials Science and Engineering Committee, TMS: Global Innovations Committee, TMS: Nanomechanical Materials Behavior Committee, TMS/ASM: Phase Transformations Committee, TMS: Powder Materials Committee, TMS: Process Technology and Modeling Committee, TMS: Shaping and Forming Committee, TMS: Surface Engineering Committee

Program Organizers: Thomas Bieler, Michigan State University; Neville Moody, Sandia National Laboratories

Thursday AM  
February 19, 2009

Room: 3022  
Location: Moscone West Convention Center

Session Chair: To Be Announced

## 8:30 AM

**Analysis of Anisotropy Behavior in UOE Forming for X80 HSLA Steel:** *Sadegh Moenifar*<sup>1</sup>; <sup>1</sup>Azad University

Anisotropy can potentially affect the integrity of the line pipes, such as their buckling and collapse resistance. Tensile and impact fracture toughness samples selected from 90 and 180° of pipe in longitudinal and transverse directions. The microstructures of the rolled plate have a fine acicular ferrite microstructure with some (M/A) that dispersed in the matrix phase. Tensile properties in 90° (transverse) are highest. Yield strength is about 6% higher than before UOE forming. Minimum amount of Charpy impact appears in 90° (transverse) that amount of toughness decrease is about 5.5% in this orientation. Test temperature decrease from 0°C to -50°C show toughness impact energy decrease about 0.4-0.9% related to degree and orientation of samples. Therefore impact fracture toughness in all degree and orientation low dependent to decrease in temperature up to -50°C in X80 HSLA steel after UOE forming.

## 8:50 AM

**Slurry Erosive Wear Behaviour of Laser Surface Alloyed 13Cr-4Ni Steel for Hydroturbine Applications:** *R. C. Shivamurthy*<sup>1</sup>; M. Kamaraj<sup>1</sup>; R. Nagarajan<sup>1</sup>; S. M. Shariff<sup>2</sup>; G. Padmanabham<sup>2</sup>; <sup>1</sup>Indian Institute of Technology; <sup>2</sup>ARCI Hyderabad

13Cr-4Ni steels are extensively used as guide vanes, runners and nozzles in hydroturbine systems for power generation. These components normally found to undergo severe silt erosion during service. Laser surface modification with hardfacing alloys like Colmonoy 88 and Stellite 6 are proved to improve erosion resistance. In the present work, erosion behaviour of river sand is compared with commercial silica sand on laser surface alloyed steel at varying impact angles and constant slurry velocity. The erosion test result indicates that silica sand is found to be more aggressive in its erosion behaviour compared to river sand at all impact angles. The chemical analysis of erodents indicates that the river sand is an admixture of silica, alumina and several other oxides, where as commercial sand is pure silica. This indicates that the erosion rates are highly influenced by the volume fraction of hard silica particles within the erodent type.

## 9:10 AM

**Effect of Al Contents on Recrystallization Kinetics of High Manganese Steel:** *Hyuk-Jin An*<sup>1</sup>; Yang-Mo Koo<sup>1</sup>; Jae-Sang Lee<sup>1</sup>; Gyo-Sung Kim<sup>2</sup>; <sup>1</sup>Pohang University of Science & Technology; <sup>2</sup>POSCO Technical Laboratory

High Manganese steel is extensively studied for the application of high performance automotive steel. In this work, recrystallization kinetics of high-manganese steel was studied. To observe the kinetics of recrystallization of cold rolled specimen, Vickers hardness tests and microstructure observation were performed with varying Al contents and annealing condition, and Vickers hardness was analyzed by using the Avrami equation. The textures of hot rolled, cold rolled and fully re-crystallized specimen were analyzed by electron back scattering microscopy (EBSD). And the effects of Al contents on texture of high-manganese steel will be discussed.



9:30 AM

**Effect of Small Additions of Boron on Shape Memory Properties and Grain Refinement of Cu-Al-Mn SMAs:** *Sampath Vedamanickam*<sup>1</sup>; U.S. Mallik<sup>2</sup>; <sup>1</sup>Department of Metallurgical and Materials Engineering, Indian Institute of Technology Madras; <sup>2</sup>Department of Mechanical Engineering, Siddaganga Institute of Technology

Cu-12.5wt.% Al-5.0wt.% Mn shape memory alloys with varying amounts of boron (0.05-0.2wt.%) were prepared by the casting route in an induction furnace under argon atmosphere. The Al and Mn contents of the alloys were maintained constant, while that of B was varied. The ingots obtained were homogenized followed by step quenching them to obtain a fully martensitic structure. The alloys were then characterized by subjecting them to compositional analysis, DSC and microstructural examination. The shape memory effect and superelasticity of the alloys were determined by bend and tensile tests. The study reveals that B acts as a good grain refiner, leading to a decrease in grain size of about 80%. Moreover, it increases the transformation temperatures by ~ 10°C, while at the same time decreasing the strain recovery by shape memory effect by 4%, and superelasticity by ~ 2%. Experimental results are presented and discussed in detail in this paper.

9:50 AM

**Hydroxyapatite Coating on Titanium Using Induction Plasma Spray:** *Mangal Roy*<sup>1</sup>; *Amit Bandyopadhyay*<sup>1</sup>; *Susmita Bose*<sup>1</sup>; <sup>1</sup>Washington State University

Plasma sprayed hydroxyapatite (HAP) coatings are widely used in orthopedic and dental applications. Most of these applications demand strong adhesion with the substrate and in vivo stability. To maintain long term stability, high level of crystallinity is necessary in HAP coatings, since resorption rate of amorphous HAP is significantly higher than its crystalline form. During plasma spray, partially melted particles dissipate heat to the substrate and cool at a very high rate. Rapid cooling increases amorphicity in HAP coatings. Therefore most of the coating at or near the interface is amorphous in nature. We have explored the influence of a thermal barrier layer to improve coating crystallinity. XRD results show that the surfaces of the coatings are highly crystalline with insignificant phase decomposition. The presentation will include interface microstructure, crystallinity, hardness, adhesive strength, flexural strength and wear properties of induction plasma spray HAP coatings on Ti substrate.

10:10 AM

**Modeling Anisotropic Deformation of Tantalum Processed by Equal Channel Angular Pressing:** *Michael Nixon*<sup>1</sup>; *Joel House*<sup>1</sup>; *Philip Flater*<sup>1</sup>; <sup>1</sup>Air Force Research Laboratory/Munitions Directorate

This study describes the computational modeling of the dynamic deformation of a commercially pure tantalum material after it was processed by equal channel angular pressing. Three variations were tested and simulated: as worked, fine-grain annealed, and large-grain annealed. Due to the processing, the materials display transverse isotropic behavior. Comparisons are shown between the well known Hill model of 1948 and a recent anisotropic description involving both the second and third invariants of the stress deviator. The test results also show a clear correlation between grain structure and macroscopic deformation that is captured by both models.

10:30 AM

**Performance of Improved Autocatalytic Nickel Boron Coating System as a Potential Replacement for Chrome Plating in Aerospace Applications:** *Kevin Garing*<sup>1</sup>; <sup>1</sup>Praxair Surface Technologies

There has long been interest in nickel boron plating, primarily because of unique deposit properties that generate a surface with good wear resistance and low coefficient of friction. The coating has found limited use due to the difficulties in maintaining the complex bath chemistry and poor performance against corrosion. This paper discusses a new, stabilized nickel boron process and its pairing with base coats and sealants for improved performance. The preferred morphology is identified and evaluated as a baseline, and then evaluated as part of a complete coating system that will provide lubricity, wear resistance, and corrosion protection. The link between tightly controlled process parameters, coating structure, and performance is demonstrated, and efforts to improve performance by changing the deposit morphology are discussed. A comparison to chrome and other coatings commonly used in low-friction and wear-resistant applications is provided along with a discussion of other potential uses.

10:50 AM

**A Novel Process for Preparing Strontium Carbonate with Celestite Concentrate:** *Mudan Liu*<sup>1</sup>; *Tao Jiang*<sup>1</sup>; *Guanghui Li*<sup>1</sup>; *Guangzhou Qiu*<sup>1</sup>; <sup>1</sup>Central South University

Preparation of high-purity strontium carbonate from celestite flotation concentrate by agglomeration-roasting process is studied. It is indicated that, by the results of SME and natural ballability analysis, celestite concentrates are difficult to agglomerate as they possess flat and silky surface, high viscosity and strong hydrophobicity. Lignin xanthate is added to improve the ballability, and the drop strength of green pellet is 7 times $\times(0.5m)^{-1}$  when the dosage is 0.5%. Roasting results show that the SrSO<sub>4</sub> conversion of celestite pellet is 82~83%, which is 10% higher than celestite lump under the same conditions, as different structure causes different reaction kinetics conditions between them. The high-purity strontium carbonate with the SrCO<sub>3</sub> content of 98.25% and CaCO<sub>3</sub> content of 0.3% are obtained under the conditions of leaching temperature of 92° and time of 8h, carbonation temperature of 60° and time of 60min, ratio of NH<sub>4</sub>HCO<sub>3</sub> and Sr(OH)<sub>2</sub> of 1/1.

11:10 AM

**Severe Deformation by Linear Flow Splitting of Low Alloyed Steels:** *Enrico Bruder*<sup>1</sup>; *Tilman Bohn*<sup>1</sup>; *Felix Rullmann*<sup>1</sup>; *Clemens Müller*<sup>1</sup>; <sup>1</sup>TU Darmstadt

The innovative linear flow splitting process enables the continuous production of bifurcated profiles from plain sheet metal without lamination, joining of material or heating of the semi-finished product. The modified roll forming process uses obtuse angled splitting rolls and supporting rolls to form flanges out of the band edge which involves severe plastic deformation in the process zone. The necessary formability of the material is constituted by high hydrostatic compressive stresses, resulting in the formation of an ultrafine grained microstructure. Thereby a steady state is reached in the process zone where increasing deformation leads no more to significant changes in microstructure and mechanical properties. The present paper outlines for different low alloyed steels the evolution of linear flow split profiles by finite element simulation and by microstructural observations in the process zone.

11:30 AM

**Surface Modification and Characterization of Commercially Available Nylon-6,6 Fibers for Electroless Nickel Deposition:** *Gina Bunster*<sup>1</sup>; *Jason Nadler*<sup>1</sup>; <sup>1</sup>Georgia Tech Research Institute

An electroless nickel plating process has been developed that employs commercially available polymer fibers. Commonly experienced challenges are addressed in this work, which include finding a suitable polymer substrate, determining an effective etching method, and relating substrate surface area to the effectiveness of catalyst adsorption. Numerous studies testing the suitability of oxidizing and dissolution agents as etchants for nylon-6,6 (polyhexamethylene diamide) resulted in the formulation of a 25 vol % 2-chlorophenol solution in toluene. Measurements of the resulting etched surface area were obtained using atomic force microscopy (AFM) in conjunction with quantitative image analysis. Etching increased exposed surface area and is correlated to the initial deposition rate of nickel.

11:50 AM

**The Study of Droplet Impact Behavior on Different Surface Roughnesses:** *KuZilati KuShaari*<sup>1</sup>; <sup>1</sup>Universiti Teknologi PETRONAS

The understanding of the behavior of a droplet impinging a flat surface is important in knowledge development in many engineering disciplines, such as spray coating, ink-jet printing and plasma coating. The focus of this work is to investigate the maximum spreading diameter or the spreading factor, of a single droplet on metal surfaces, namely stainless steel and etched silicon, having different surface roughnesses. A CCD high-speed camera with framing rate of 2,000, attached to a microscope, was used to capture the phenomena. The results of the stainless steel surfaces show that the rougher the surface the lower the spreading factor. All of the droplets on these surfaces also demonstrate that a droplet with a higher spreading factor gives a lower bouncing factor. However, the results of the etched silicon surfaces with the range of roughness used in this work, does not show a significant different in their spreading factors.

## General Abstracts: Materials Processing and Manufacturing Division: Session IV

Sponsored by: The Minerals, Metals and Materials Society, TMS Materials Processing and Manufacturing Division, TMS/ASM: Computational Materials Science and Engineering Committee, TMS: Global Innovations Committee, TMS: Nanomechanical Materials Behavior Committee, TMS/ASM: Phase Transformations Committee, TMS: Powder Materials Committee, TMS: Process Technology and Modeling Committee, TMS: Shaping and Forming Committee, TMS: Surface Engineering Committee

Program Organizers: Thomas Bieler, Michigan State University; Neville Moody, Sandia National Laboratories

Thursday AM Room: 3008  
February 19, 2009 Location: Moscone West Convention Center

Session Chair: To Be Announced

### 8:30 AM

**Weldability of Advanced High Strength Steels (AHSS) Martensitic Type by Resistance Spot Welding (RSW): An Optimization Model to the Automotive Industry Components:** Arturo Reyes-Valdes<sup>1</sup>; Victor Lopez-Cortes<sup>1</sup>; <sup>1</sup>Corporacion Mexicana de Investigacion en Materiales

When joining AHSS Martensitic Type with Resistance spot welding the correct welding schedule is an important production process part for successful assembly. Automotive manufacturers require optimized weld schedules that meet the customer quality requirements to obtain the best weld performance during the life vehicle. In certain instances modifications to welding parameters like current, pressure and time are made and the welding performance of the spot weld change and the mechanical and metallurgical properties are modified. This paper presents the results of the variables impact of Spot Welding Process in the weldability, welding metallurgy and quality characteristics of the AHSS Martensite Type welds. The microstructure, hardness and mechanical tensile properties were evaluated according with the different process condition. In order to know the multivariate correlation, a statistical and neural network models were obtained. A comparative study between these models was analyzed to apply at real condition.

### 8:50 AM

**Changes in Microstructure and Mechanical Properties of CIP-Processed Tungsten Rods during Rotary-Swaging and Stretching Operations:** Ismail Duman<sup>1</sup>; Duygu Agaogullari<sup>1</sup>; <sup>1</sup>Istanbul Technical University

The microstructure of the in rotary swagers hammered rods is gradually transformed from sintered to compact metallic. In order to gain a high quality product, it is essential to optimize the wire draft production conditions and to control the recrystallization (inductive annealing) process particularly. Tensile strength of swaged rods (wire drafts) is determinative for the next step i.e. stretching by turn-tables. In this study, as a part of the complete process for thin wire ( $\phi < 10$  micron) production, changes in microstructure (grain size and grain population density) and mechanical properties (density, porosity, hardness and tensile strength) during swaging and stretching of tungsten to 400 micron are investigated. The mentioned wire is obtained using industrial scale equipments by passing the rod ( $\phi$  16 mm) through three rotary-swagers ( $\phi$  7.6 mm, 4 mm, 3 mm respectively), intermediate annealing (2400°C) and through three stretching machines (turn-tables) each with  $H_2/N_2$  protected heating furnaces.

### 9:10 AM

**Dynamic Recrystallization Texture in Nickel Superalloys 718 and 718plus:** James Baird<sup>1</sup>; Haitham El Kadiri<sup>1</sup>; Hongjoo Rhee<sup>1</sup>; Abel Lowry<sup>1</sup>; Mark Horstemeyer<sup>1</sup>; Paul Wang<sup>1</sup>; <sup>1</sup>The Center for Advanced Vehicular Systems

We studied the effect of dynamic recrystallization on the deformation texture generated by simple compression in two grades of Nickel super alloy; 718 and 718plus. The texture was analyzed through Electron Backscattered Diffraction (EBSD) technique. The Compression tests were carried out on cylindrical and double cone samples at three different temperatures, two different strain rates and several dwelling times after deformation. The double cone compression tests were performed to examine the effect of a strain gradient on texture. The dynamic recrystallization showed different trends for the two alloys and induced a quite different texture through deformation.

### 9:30 AM

**Effect of Si/Mg Molar Ratio on the Electrochemical Behavior of Al/SiCp Composites with Bimodal Distribution of Reinforcements:** Miguel Montoya-Dávila<sup>1</sup>; Martin Pech-Canul<sup>1</sup>; Maximo Pech-Canul<sup>2</sup>; <sup>1</sup>Cinvestav-Saltillo; <sup>2</sup>Cinvestav-Mérida

The effect of the Si/Mg molar ratio - in the raw aluminum alloy - on the electrochemical behavior of Al/SiCp composites was investigated. Composites were fabricated by reactive infiltration of porous preforms with 0.6 volume fraction of silica-coated SiC with particle sizes of 10 and 146  $\mu$ m, in the particle size ratio 1:5, correspondingly. Four experimental Al-Mg-Si alloys with Si/Mg molar ratios of 0.12, 0.49, 0.89, and 1.05, were used to infiltrate the preforms in argon followed by nitrogen, at 1100°C for 60 min. The composites were characterized by X-ray diffraction (XRD) and scanning electron microscopy (SEM) before and after electrochemical tests, measuring the corrosion potential (E<sub>corr</sub>) and cyclic polarization in aerated and de-aerated 0.1M NaCl solutions, respectively. Results show that pitting potential (E<sub>pit</sub>) becomes less negative with decrease in the Si/Mg molar ratio, thus enhancing the corrosion resistance. By contrast, E<sub>corr</sub> tends to similar values after two hours of immersion.

### 9:50 AM

**Functionally Graded Boron Carbide and Aluminum Composites with Tubular Geometries Using Pulsed Electric Current Sintering:** Troy Holland<sup>1</sup>; Dustin Hulbert<sup>2</sup>; Amiya Mukherjee<sup>1</sup>; <sup>1</sup>University of California, Davis; <sup>2</sup>Nanosolar, Inc.

Functionally graded boron carbide (B4C) with precipitous property and microstructural gradients has been synthesized using pulsed electric current sintering (PECS) in tubular shape forms. This processing route results in a material with very promising inner diameter properties while blending smoothly into those of cast aluminums on the outside. During PECS the amorphous powders react and partially consolidate forming a density gradient. Modeling results support the presence of a large radial temperature gradient sufficient to produce B4C in smoothly varying densities from inside to outside. This material and geometry is both novel and of particular use in applications requiring a cylinder of differing surface structures that transition smoothly into a metallic substructure or assembly.

### 10:10 AM

**Hybrid Monte Carlo/Vertex Simulation of Strain-Induced Grain Growth:** Corentin Guebels<sup>1</sup>; Benjamin Fell<sup>1</sup>; Tien Tran<sup>1</sup>; Joanna Groza<sup>1</sup>; Jean-pierre Delplanque<sup>1</sup>; <sup>1</sup>University of California

The prediction of microstructural evolution and abnormal grain growth phenomena during high-temperature creep requires an accurate description of recrystallization. A two dimensional Monte Carlo - Vertex (MC-V) model is presented which characterizes grain-growth kinetics during strain-induced recrystallization. The MC-V model presents a powerful means to incorporate strain affects into Monte Carlo grain growth simulations. The current approach tracks strain-induced microstructural phenomena at grain boundary junctions, as well as within the grain, to capture grain sliding and rotation events, diffusion along grain boundaries, and plastic work. By capturing these realistic geometrical constraints, combined with a dynamically reorganizing numerical lattice, the model provides a flexible, physics-based methodology to investigate external influences on the microstructural evolution. The simulation results clarify the influences of deforming microstructure on grain growth kinetics.

### 10:30 AM

**Model of Thermal Physics in Plasma-Sprayed Coatings and Calculation of Residual Stress:** Liping Niu<sup>1</sup>; Ting-an Zhang<sup>1</sup>; Jicheng He<sup>1</sup>; Zhihe Dou<sup>1</sup>; Yan Liu<sup>1</sup>; Guanyong Shi<sup>1</sup>; Xiaochang Cao<sup>1</sup>; <sup>1</sup>Northeastern University

Different thermophysical properties of the substrate and coating materials and different spraying parameters deduce the residual internal stress induced in thermally-sprayed coating composite materials during deposition. In this paper, thermal physic model of temperature field at the plasma spraying processe based on analysis of particle's deposition process is established. Spraying process parameters and mechanical and thermal properties of sprayed materials are considered. Regarding the formation of coating as superimposed n sub-coatings with thickness h<sub>min</sub>, the change of temperature can be described by a two-step calculation model: at the initial step temperature doesn't exceed 20% corresponding spraying material melting point; at the final step substrate and coating are bound and led to the formation of residual stress when both of them achieve the highest temperature of system. This model has made it possible to evaluate the components of residual stresses.

10:50 AM

**Residual Stress Reduction for Air Plasma Sprayed Al-Si Abradable Coating:***Jon Tucker*<sup>1</sup>; Terry Alford<sup>1</sup>; <sup>1</sup>School of Materials, Arizona State University

Air plasma spray is a common process used to apply abradable coatings. However the large residual stresses make the layers prone to delamination. Therefore it is important to elucidate the mechanisms of the high residual stresses. To determine an effective method to reduce the residual stresses present in the coating, heat treatments were performed to better understand the effects that a post-deposition heat treatment has on the microstructure and subsequent stress levels in the abradable coating. The microstructure and stress analyses included x-ray diffraction, energy dispersive x-ray spectroscopy, and secondary electron microscopy. Analysis of the microstructure and residual stress of the heat treated samples revealed that a key factor in the reduction of residual stress is formation of silicon precipitates.

11:10 AM

**Porous NiTi Shape Memory Alloy Structures Using Laser Engineered Net Shaping:** Vamsi Balla<sup>1</sup>; Susmita Bose<sup>1</sup>; Amit Bandyopadhyay<sup>1</sup>; <sup>1</sup>Washington State University

Porous NiTi alloy samples were fabricated with 12 to 36% porosity from equiatomic NiTi alloy powder using Laser Engineered Net Shaping (LENS). LENS processed porous NiTi samples showed high amount of cubic B2 phase compared to feed stock powder. Moreover, high cooling rates associated with laser processing increased the reverse transformation temperature due to thermally induced stresses and defects. Transformation temperatures were found to be independent of pore volume, while high pore volume in the samples decreased the maximum recoverable strain from 6% to 4%. Porous NiTi samples with 12 to 36% porosity exhibited low Young's modulus between 2 and 18 GPa as well as high compressive strength and recoverable strain. These porous samples are thus promising biomaterials for different applications including hard tissue replacements. This talk will focus on process-structure-property correlation of these porous NiTi alloy samples.

11:30 AM

**Surface Hardening of Titanium and Ti-6Al-4V Using near- Atmospheric Pressure Plasma Generated by CO<sub>2</sub> Laser Irradiation:** Ravindra Kumar Akarapu<sup>1</sup>; Dana Scott<sup>1</sup>; Abdalla Nassar<sup>1</sup>; Stephen Copley<sup>1</sup>; Judith Todd<sup>1</sup>; <sup>1</sup>Penn State University

Titanium and its alloys are widely used in the aerospace industry due to their high specific strength and good corrosion resistance. Tribological coatings may be required for high wear resistance applications. Surface coating processes such as plasma nitriding or chemical vapor deposition (CVD) require vacuum environments and yield low coverage rates. This paper discusses a near-atmospheric pressure surface hardening process, developed using plasma generated by CO<sub>2</sub> laser irradiation of titanium and Ti-6Al-4V alloy in the presence of shielding gas mixtures (Ar + N<sub>2</sub>, Ar + CO<sub>2</sub>) to yield nitrides, oxynitrides and oxycarbides. The effect of mole fraction of Ar on the active species in the plasma was studied by optical emission spectroscopy. Optimized parameters for deposition of near-stoichiometric titanium nitride will be discussed.

11:50 AM

**The Structure and Properties of Glass-Coated Amorphous FeCoSiB Micro-Wire:** Zhihao Zhang<sup>1</sup>; Chengduo Wang<sup>1</sup>; Fengmei Wang<sup>1</sup>; Jianxin Xie<sup>2</sup>; <sup>1</sup>Advanced Materials and Technologies Institute, University of Science and Technology Beijing; <sup>2</sup>State Key Laboratory for Advanced Metals and Materials, University of Science and Technology Beijing

Because of the excellent performance, glass-coated amorphous metallic micro-wires get comprehensive application in many regions, such as sensor devices, forgery prevention label and electromagnetic shielding materials. In this paper, the glass-coated Fe<sub>69</sub>Co<sub>10</sub>Si<sub>8</sub>B<sub>13</sub> amorphous micro-wires with various glass coating thickness and metallic core diameter are fabricated through adjusting casting rate and cooling water position. The relationships between the microstructure and mechanical properties of the micro-wire with casting rate, cooling condition and annealing process are analyzed. The critical casting rate for preparing amorphous micro-wire is determined. The influences of the ratio between core diameter and coating thickness as well as the annealing process on the remanence ratio, coercive force and large Barkhausen effect are investigated.

**Magnesium Technology 2009: Modeling**

Sponsored by: The Minerals, Metals and Materials Society, TMS Light Metals Division, TMS: Magnesium Committee

Program Organizers: Eric Nyberg, Pacific Northwest National Laboratory; Sean Agnew, University of Virginia; Neale Neelameggham, US Magnesium LLC; Mihriban Pekguleryuz, McGill University

Thursday AM

Room: 2006

February 19, 2009

Location: Moscone West Convention Center

Session Chairs: Eric Nyberg, Pacific Northwest National Laboratory; Sean Agnew, University of Virginia

**8:30 AM Introductory Comments**

8:35 AM

**Blind Study of the Effect of Processing History on the Constitutive Behavior of Alloy AZ31B:** Cyrus Dreyer<sup>1</sup>; F. Polesak<sup>1</sup>; Thomas Shultz<sup>2</sup>; Sean Agnew<sup>1</sup>; <sup>1</sup>University of Virginia; <sup>2</sup>Hampden-Sydney College

The discipline of materials science is founded upon the structure-property paradigm, and yet it is often held that the full processing history must be known in order to predict material properties. The latter is in conflict with the fundamental premise. The present study probes these philosophical issues within the context of a blind study of AZ31B sheet tensile properties. Four sheets were processed by different vendors and by different approaches, including strip casting and more conventional direct chill ingot casting followed by hot rolling. The experimentalists do not know which sheets were subjected to a given processing history. Property distinctions between the sheets, such as flow strengths, anisotropies, and propensities for dynamic recrystallization and cavitation, are explained in terms of observable structural quantities: grain size and shape, texture, and particle distributions. The results provide sheet producers with microstructure guidelines to augment current property targets.

8:55 AM

**New Microalloyed Magnesium with Exceptional Mechanical Performance:** Anja Hänzl<sup>1</sup>; Timo Ebeling<sup>2</sup>; Rüdiger Bormann<sup>2</sup>; Peter Uggowitzer<sup>1</sup>; <sup>1</sup>ETH Zürich; <sup>2</sup>Hamburg University of Technology

New Mg-Zn alloys have been developed according to the microalloying concept and in consideration of growth restriction during alloy casting and forming. After extrusion (30:1) they reveal very fine grains (< 10 μm), excellent ductility (uniform elongation: 17-20%) at considerable strength (UTS: 250-270 MPa) and homogeneous distribution of intermetallic particles, which suppress grain growth even at comparably high temperatures. The new alloys exhibit also very low tension-compression asymmetry ( $R_{p,tension} / R_{p,compression} \sim 1$ ). This phenomenon is not only ascribed to the weak texture but also to the fine-grained structure, which enables activation of complimentary deformation processes (non-basal slip) at RT. Indeed, simulations of the deformation modes indicate very soft prismatic slip. Furthermore they explicitly point to activation of tension twinning {10-12}<10-11>, which is rather unusual for fine-grained Mg alloys. Due to the choice of only biocompatible alloying elements, the new alloys are very promising for applications in a broad range.

9:15 AM

**A New Approach for Inverse Parameter Calculations of the Plastic Deformation Behavior of AZ31 Magnesium Alloy:** Timo Ebeling<sup>1</sup>; Christian Hartig<sup>1</sup>; Rüdiger Bormann<sup>1</sup>; <sup>1</sup>Hamburg University of Technology

In order to improve the mechanical properties of magnesium wrought alloys, a better understanding of the texture evolution and anisotropic behavior is necessarily needed. The approach is a detailed investigation of the deformation mechanisms by model calculations. Therefore, room temperature tensile tests of AZ31 hot rolled sheets have been performed and the stress-strain behavior as well as the r-value-function has been measured. An inverse parameter calculation yielding information about deformation mode activities, texture evolution and mechanical properties was performed using a viscoplastic self-consistent model. The first objective function of the inverse parameter calculation was the macroscopic hardening. Additionally the r-value, which reacts strongly on changes of the yield surface, was introduced into the modeling as a second objective function. The additional input of experimental r-values can result in a better understanding of the mostly disregarded latent hardening of the deformation modes.



9:35 AM

**Dislocations and Their Configurations in Mg and Mg Alloys:** *Bin Li*<sup>1</sup>; Evan Ma<sup>1</sup>; K. T. Ramesh<sup>1</sup>; <sup>1</sup>Johns Hopkins University

Mg and Mg alloys have attracted significant attention in recent years. Despite extensive investigations on the deformation mechanisms in Mg over the past several decades, specifics of dislocation slip during deformation remains controversial, partly due to the complicated slip systems. There are three possible Burgers vectors that differ significantly in magnitude,  $\langle a \rangle$ ,  $\langle c \rangle$  and  $\langle c+a \rangle$ , and the identification of the dislocations by TEM is not trivial. Consequently, there are misunderstandings and misinterpretations about the dislocations in Mg and Mg alloys, especially the  $\langle c+a \rangle$  dislocation for pyramidal slip. We present TEM observations on the dislocations and stacking faults in deformed Mg and Mg alloys with various plastic strain levels (2%, 4% and 8%). We show that using an appropriate zone axis  $\langle 01-10 \rangle$  and the weak-beam-dark-field (WBDF) technique, we can determine the Burgers vectors of the dislocations with clarity. We also show TEM observations of the  $\langle c+a \rangle$  dislocations and the stacking faults.

9:55 AM

**Lattice Reconstruction – A Crystallographic Model for Grain Reorientation in HCP Magnesium:** *Bin Li*<sup>1</sup>; Evan Ma<sup>1</sup>; <sup>1</sup>Johns Hopkins University

We present a new model to describe the crystallographic reorientation in HCP Mg during deformation. In this model, the original lattice can be reoriented by 90 degrees, by reconstructing new basal planes from the existing lattice points on the  $\{10-10\}$  prismatic planes, such that the new basal planes are parallel to the loading axis (possibly also relevant to texture formation in deformed polycrystalline Mg). The structural deviation between the original and the new lattices is so small (much shorter than any known Burgers vectors) that it can be accommodated by a simple shear. We show that this minor structural deviation can be compensated by either elastic shear strain or plastic strain to establish the correct stacking sequence. Molecular dynamics simulations are performed to investigate the mechanism of lattice reorientation in single crystal Mg during shear and tensile deformation.

10:15 AM Break

10:30 AM

**Microstructural Investigation of Twins under the Fracture Surface in AZ31 Mg Alloys:** *Daisuke Ando*<sup>1</sup>; Junichi Koike<sup>1</sup>; <sup>1</sup>Tohoku University, Department of Materials Science

Magnesium alloys form many types of twins which play important roles on deformation and failure. Reed-Hill and others suggested that double twins are the origin of poor ductility. Recently, we experimentally showed that double twins accompany large surface relieves and cracks. However, the current knowledge does not provide an undisputable evidence of the double twins being the major reason for premature failure. In this work, we performed detailed observation and analysis of the underlying microstructure on fractured surface. The sample was a rolled AZ31 sheet. Tensile test was performed at room temperature. A number of facets were observed on fractured surface. Cross-sectional TEM samples were prepared by FIB from these facets. TEM observation showed the formation of double twins underneath the facet. The presence of fine recrystallized grains indicates substantial dislocation activity related to the double twins. These results indicate the relation between localized large deformation and macroscopically brittle failure.

10:50 AM

**Mechanisms of Deformation and In Situ 3D Damage Analyses during High Temperature Deformation of an AZ31 Mg Alloy:** *Jean-Jacques Blandin*<sup>1</sup>; Luc Salvo<sup>1</sup>; Remi Boissiere<sup>1</sup>; Jerome Adrien<sup>2</sup>; Eric Maire<sup>2</sup>; <sup>1</sup>Grenoble Institute of Technology; <sup>2</sup>INSA Lyon

Large elongations to fracture ( $> 300\%$ ) can be obtained during high temperature deformation of the AZ31 Mg alloy. This capacity results from the ability to activate deformation mechanisms displaying a high value of the strain rate sensitivity parameter and from the resistance to strain induced damage. In this work, the effect of strain rate and temperature on the rheology of a fine grained AZ31 alloy was investigated and experimental domains for which a high plastic stability is expected were identified. A particular attention was also given to the quantification of damage during high temperature deformation. A 3D damage characterisation was performed thanks to the use of X-ray microtomography for imaging the cavities. Post mortem investigations were performed but an in situ characterisation was also attempted thanks to a specifically dedicated device

allowing concomitant high temperature deformation and fast acquisition X-ray micro tomography analysis.

11:10 AM

**New Crystal Plasticity Constitutive Model for Large Strain Phenomena in HCP Metals:** *Adel Izadbakhsh*<sup>1</sup>; Kaan Inal<sup>1</sup>; Raja Mishra<sup>2</sup>; Sanjeev Bedi<sup>1</sup>; <sup>1</sup>University of Waterloo; <sup>2</sup>General Motors

Secondary twinning systems are important deformation mechanisms in pure magnesium and its alloys. For a given texture of these metals in certain loading paths, these microscopic deformation mechanisms account for a significant amount of macroscopic strain. The existing crystal plasticity based constitutive models do not account for the kinematics of these deformation mechanisms. To address this limitation, a crystal plasticity based constitutive model that individually simulates the slip-induced shear in the matrix, primary and secondary twinned regions, and twin-induced shear in the primary and secondary twinned regions has been developed for Hexagonal Closed-Packed (HCP) metals. Separate resistance evolution functions for the primary, secondary, and tertiary slip systems, as well as primary and secondary twinning systems have been considered. The model tracks the texture evolution in the matrix, primary, and secondary twinned regions. Numerical simulations have been performed for HCP single crystals and the effects of model parameters have been investigated.

11:30 AM

**Application of a Finite Strain Elastic-Plastic Self-Consistent Model to Deformation of Magnesium:** *Bjørn Clausen*<sup>1</sup>; C Neil<sup>2</sup>; Sean Agnew<sup>2</sup>; Donald Brown<sup>1</sup>; Carlos Tomé<sup>1</sup>; <sup>1</sup>Los Alamos National Laboratory; <sup>2</sup>University of Virginia

The traditional elastic-plastic self-consistent (EPSC) model, which is a small strain formulation that does not take into account lattice rotations, has been applied with great success to simulations of metals at low degrees of plastic deformation. The application of the EPSC model to low symmetry materials, such as magnesium, is only approximate as texture evolution due to both slip and twinning can be pronounced even in the early stages of plastic deformation. Recently, a finite strain version of the EPSC model has been developed which includes grain reorientation due to twinning and slip. With the new finite strain model in hand, we can now account for the effect of slip and twinning reorientation upon the evolution of internal stress and peak intensities during plastic deformation. The new model has been used to explain the observed texture and internal stress changes measured in-situ using neutron diffraction during compressive loading of extruded magnesium.

11:50 AM

**Test Results and FEA Predictions from Magnesium AM30 Extruded Beams:** *David Wagner*<sup>1</sup>; Steve Logan<sup>2</sup>; Kathy Wang<sup>3</sup>; Tim Skrzek<sup>4</sup>; Christopher Salisbury<sup>5</sup>; <sup>1</sup>Ford Motor Company; <sup>2</sup>Chrysler LLC; <sup>3</sup>General Motors Corp; <sup>4</sup>Cosma International; <sup>5</sup>University of Waterloo

Load versus displacement measurements are compared to finite element analysis (FEA) predictions of the component behavior of magnesium AM30 extruded beams. Results from quasi-static four-point bend, quasi-static axial crush and high-speed axial crush tests of extruded magnesium AM30 beams show the beam's behavior over a range of loadings and responses. The extrude AM30 beams showed significant cracking and splitting in the tests. LS-DYNA material model MAT124 captures the extruded magnesium AM30 constitutive behavior over a range of strain rates and accommodates different responses in tension and compression. Examinations of various element sizes and failure criterion show the sensitivity and robustness of the predicted beam behavior. The boundary conditions in the FEA predictions closely mimic the loading and constraint conditions in the component testing. LS-DYNA explicit FEA predictions of the tests agree to differing degrees with the test results.

## Materials for High Temperature Applications: Next Generation Superalloys and Beyond: Ceramic Composites and Other Technologies

Sponsored by: The Minerals, Metals and Materials Society, TMS Structural Materials Division, TMS: High Temperature Alloys Committee, TMS: Refractory Metals Committee  
Program Organizers: Joseph Rigney, GE Aviation; Omer Dogan, National Energy Technology Laboratory; Donna Ballard, Air Force Research Laboratory; Shiela Woodard, Pratt & Whitney

Thursday AM Room: 3010  
February 19, 2009 Location: Moscone West Convention Center

Session Chairs: Michael Cinibulk, Air Force Research Laboratory; Donna Ballard, Air Force Research Laboratory

### 8:30 AM Invited

**Ceramic Composites Development for Air and Space Applications:** *Michael Cinibulk*<sup>1</sup>; <sup>1</sup>Air Force Research Laboratory

Constant demands of greater high-temperature chemical and environmental stability, mechanical performance, durability, service life, and affordability continue to be made on materials systems for air and space applications. Next generation turbine and space propulsion systems continue to require higher operating pressures and temperatures, which require higher performing materials and systems than are currently available. Ceramics, both monoliths and composites, have achieved the level of development that is enabling their use as components in the combustor, turbine, and exhaust sections of demonstration turbine engines. However, their durability to ensure long life in actual production systems is lacking. Current thermal protection systems are projected to greatly limit the readiness and potential of "aircraft-like capabilities" of future reusable space launch vehicles; but, again, improvements in durability of the friable materials upon which these systems are based is required. The desire for aerospace vehicles to operate at hypersonic speeds is dependent upon dramatic improvements in high-temperature ceramics. This presentation will summarize work on ceramics development being targeted for air and space applications. A brief review of the recent research that is being conducted in our laboratory will also be provided.

### 8:55 AM

**A Study on Flow Behaviors of Alloy IC10 over a Wide Range of Temperatures and Strain Rates:** Hongjian Zhang<sup>1</sup>; Weidong Wen<sup>1</sup>; Haitao Cui<sup>1</sup>; Ying Xu<sup>1</sup>; <sup>1</sup>Nanjing University of Aeronautics and Astronautics

IC10 is a newly developed Ni<sub>3</sub>Al-based superalloy, with its nominal composition (wt%): 0.07-0.12% C 11.5-12.5% Co 6.5-7.5% Cr 5.6-6.2% Al 4.8-5.2% W 1.0-2.0% Mo 6.5-7.5% Ta 1.3-1.7% Hf 0.01-0.02% B and Bal. Ni. To investigate flow behaviors of IC10, tensile experiments were conducted over a wide range of temperatures (293~1073K) and strain rates (0.00001~0.01/s) on Material Test System. Experiments show that: (1) flow behaviors are not sensitive to strain rates over the wide range of temperatures; (2) flow behaviors varies slightly with the temperature at the same strain rate. Z-A model, one of the most widely used models, is employed in describing the flow features of IC10. Normally, the parameters in Z-A model are regarded as constants in whole deforming process, which isn't agree with the actual process and will decrease its predicted accuracies. In order to improve the predicted accuracies, the parameters in Z-A model are modified by introducing the evolution function. The modified model is used to predict flow behaviors of IC10 under different experiment conditions. The results show that it is valid.

### 9:15 AM

**A TEM Study of the Evolution of Deformation Mechanisms Following LCF of a Ni-Base Superalloy:** *Patrick Phillips*<sup>1</sup>; Raymond Unocic<sup>1</sup>; Libor Kovarik<sup>1</sup>; Michael Mills<sup>1</sup>; <sup>1</sup>Ohio State University

The effect of microstructure on the high temperature low cycle fatigue deformation mechanisms of an advanced Ni-base disk superalloy was studied using TEM characterization methods. In order to track the evolution of these mechanisms, specimens were interrupted after a limited number of cycles and were not run to failure. Both fine and coarse precipitate microstructures were examined, corresponding to a fast or slow cool, respectively, from the gamma prime solvus temperature. Various microstructural attributes, such as smooth

or serrated grain boundaries and precipitate size scale and morphology were correlated with the operative deformation mechanisms, which included stacking faults, dislocation bands, and microtwins. The evolution of the operative mechanisms with number of cycles will also be discussed.

### 9:35 AM

**Advances in Non-Contact Measurement of Creep Properties:** *Robert Hyers*<sup>1</sup>; Stacy Canepari<sup>1</sup>; Erica Bischoff White<sup>1</sup>; Laurent Cretegy<sup>2</sup>; Jan Rogers<sup>3</sup>; <sup>1</sup>University of Massachusetts; <sup>2</sup>General Electric Co; <sup>3</sup>NASA MSFC

As the required service temperatures for superalloys increases, so do the demands on testing for development of these alloys. Non-contact measurement of creep of refractory metals using electrostatic levitation has been demonstrated at temperatures up to 2300 C using samples of only 20-40 mg. These measurements load the spherical specimen by inertial forces due to rapid rotation. However, the first measurements relied on photon pressure to accelerate the samples to the high rotational rates of thousands of rotations per second, limiting the applicability to low stresses and high temperatures. Recent advances in this area extend this measurement to higher stresses and lower-temperatures through the use of an induction motor to drive the sample to such high rotational speeds. Preliminary results on new measurements on new materials will be presented.

### 9:55 AM

**Study of Precious Metal Modified Ni-Based Superalloys Using the Calphad Approach:** *Fan Zhang*<sup>1</sup>; Shuanglin Chen<sup>1</sup>; Weisheng Cao<sup>1</sup>; Ying Yang<sup>1</sup>; Kaisheng Wu<sup>1</sup>; Y. Chang<sup>2</sup>; <sup>1</sup>CompuTherm LLC; <sup>2</sup>University of Wisconsin

Precious metal modified nickel-based super alloys have recently been under development due to their excellent properties of high temperature oxidation and hot corrosion resistance. To improve the performance of precious metal modified nickel-based superalloys, alloy composition need to be carefully adjusted to promote the formation of desired phases and microstructure, while avoiding the formation of deleterious phases. This requires detail knowledge of phase equilibria in the multi-component nickel-based alloy systems. In this study, Calphad approach is used to develop a multi-component thermodynamic database which contains Pt, Ir and Ru. Using this database, effects of a variety of alloying elements on the materials properties, such as liquidus, solidus, gamma\_prime solvus, gamma\_prime phase fraction, elemental partitioning, and so on, can be predicted. Such information provides valuable guidance in the design and development of nickel-based superalloys. In this presentation, calculated results for a wide range of compositions will be discussed.

### 10:15 AM Break

### 10:25 AM

**Exploring the 3D Nanospace of Defects Formed in Ni-Based Superalloys Using Atom-Probe Tomography Assisted by Dual-Beam Focused Ion-Beam Microscopy:** *Yaron Amoyal*<sup>1</sup>; David Seidman<sup>1</sup>; <sup>1</sup>Northwestern University

Chains of misoriented grains are common defects occurring during the directional solidification of nickel-based superalloy single-crystals used for turbine blades in jet engines. These so-called freckles cause degradation in a turbine blade's mechanical properties at high-temperatures. Eliminating the formation of freckles is a compelling technological challenge, which can be achieved by characterizing an alloy's microstructure and composition at the micrometer to nanometer length scales. Transmission and scanning electron microscopic observations of multi-component (>10 elements) Ni-based superalloys reveal a microstructure comprising dendritic and inter-dendritic regions that are present in both the freckles and single-crystalline matrix. All four regions differ in their compositions. We employ the lift-out technique in the dual-beam focused ion-beam (FIB) microscope to prepare selectively samples for APT analyses in the form of sharply pointed tips (edge radius < 50 nm). Thus, we determine the roles played by different alloying elements in the formation of freckles.

### 10:45 AM

**Development of Heat Treatment for a Powder Metallurgy Nickel-Base Superalloy:** *Gaofeng Tian*<sup>1</sup>; Chengchang Jia<sup>1</sup>; Fazhang Yin<sup>1</sup>; Benfu Hu<sup>1</sup>; <sup>1</sup>University of Science and Technology Beijing

Nickel-base superalloys should have excellent high temperature performance to challenge the improved operating temperatures in advanced aircraft engines. An important approach to meet this goal to modify the heat treatment for these alloys, this could control the characteristic microstructures including grain size and the distribution of gamma prime phases, and hence, determine the mechanical properties. In this study, a new heat treatment was developed for

a powder metallurgy nickel-base superalloy, mechanical property testing was performed to assess the new heat treatment. The results of this investigation have shown that the new heat treatment can obviously improve the high temperature plasticity without sacrificing strength: elongation increases 33%, reduction in area increases 57%.

## 11:05 AM

### **Application of Advanced Creep Modeling Incorporating Damage to Nickel Based Superalloy:** Nicola Bonora<sup>1</sup>; Luca Esposito<sup>1</sup>; <sup>1</sup>University of Cassino

The increasing demand of reliable creep design for longer lives requires model formulation in which the contribution of different creep and damage mechanisms should be accounted for. Recently, the authors (Bonora and Esposito, Proc. of ASMEPVP, 2008) proposed a creep model which takes into account the resulting action of both diffusional and dislocation type creep and damage effects associated with microvoids/cracks. In this work, the model has been extended to nickel-based superalloy. The following features has been addressed: a) the possibility to accurately predict the minimum creep rate over a wide range of stress/temperature; b) the extension to primary creep stage; c) the extension to damage mechanisms associated with microstructural changes that may occurs during long term high temperature exposure. The model has been implemented into FEM code and used to predict creep response of laboratory samples and components. Model application examples to MAR and Rene nickel-based superalloys are presented.

## 11:25 AM

### **Effects of Cr on the Stress Rupture of Ni-Based Single Crystal Superalloys:** J. Y. Chen<sup>1</sup>; B. Zhao<sup>1</sup>; L. M. Cao<sup>2</sup>; Qiang Feng<sup>1</sup>; <sup>1</sup>University of Science & Technology Beijing; <sup>2</sup>Beijing Institute of Aeronautical Materials

Chromium is beneficial to hot corrosion resistance and oxidation resistance of Ni-based superalloys. However, Cr additions significantly promote the formation of TCP phases and degrade mechanical properties. In the current study, single crystal superalloys with various levels of Cr-additions (0-5.7wt.%) were investigated. It is very interesting to note that the Cr addition significantly improved the life of stress rupture at 1100°/140MPa from 30h in the Cr-free alloy to 138h in the alloy containing high levels of Cr additions. Meantime, the  $\gamma'$  morphology changed from spherical to cuboidal with the decrease of the precipitate size, and the volume fraction of  $\gamma'$  precipitates increased with increasing Cr additions. In order to understand the strengthening mechanism under the influence of Cr additions, the investigations on microstructure, partitioning behaviour of alloying elements, lattice misfit and stress rupture properties will be conducted, and the relationship among them will be discussed.

## 11:45 AM

### **Microstructure and Mechanical Properties of Directionally Solidified Castings Processed by HRS and LMC:** Wenshu Tang<sup>1</sup>; Shen Jian<sup>1</sup>; Jian Zhang<sup>1</sup>; Langhong Lou<sup>1</sup>; Dawei Wang<sup>1</sup>; <sup>1</sup>Institute of Metal Research, Chinese Academy of Sciences

Large castings were directionally solidified (DS) using high rate solidification (HRS) and liquid metal cooling (LMC) techniques. The as cast microstructural features such as primary dendrite arm spacing, and size and fraction of eutectic and porosity were characterized as a function of the distance from casting chill. The heat treatment was also studied according to the measured incipient melting points. Room temperature tensile properties, creep rupture as well as low cycle fatigue properties of specimens sectioned at different position of the large castings were examined. Microstructure and mechanical properties of alloys with deliberately added Sn were also studied. A much finer and more homogenous structure along the DS direction was achieved by LMC process. A higher fraction of residual eutectics was found in HRS samples after heat treatment. No properties degradation was found in the present DS alloy containing up to 1200ppm Sn addition.

## **Materials for the Nuclear Renaissance: Materials: Manufacturing and Testing**

Sponsored by: The Minerals, Metals and Materials Society, TMS Structural Materials Division, TMS/ASM: Corrosion and Environmental Effects Committee, TMS/ASM: Nuclear Materials Committee, TMS: Refractory Metals Committee  
Program Organizers: Raul Rebak, GE Global Research; Robert Hanrahan, National Nuclear Security Administration; Brian Cockeram, Bechtel-Bettis Inc

Thursday AM  
February 19, 2009

Room: 2009  
Location: Moscone West Convention Center

*Session Chairs:* Raul Rebak, GE Global Research; Brian Cockeram, Bechtel-Bettis Inc

## 8:30 AM

### **The Fracture Toughness and Toughening Mechanism of Commercially Available Unalloyed Molybdenum and ODS Molybdenum with an Equiaxed, Large Grain Structure:** Brian Cockeram<sup>1</sup>; A. Mueller<sup>1</sup>; <sup>1</sup>Bechtel Bettis Inc

Commercially available molybdenum and ODS molybdenum produced by Powder Metallurgy (PM) methods are subject to fracture toughness testing and examination of the toughening mechanism. Both PM molybdenum and ODS molybdenum are shown to have an equiaxed grain size that is larger in scale than wrought products. Although the grain size for PM molybdenum is large and the oxygen content is relatively high, and these attributes tend to embrittle molybdenum, the transition temperature and fracture toughness values are comparable to those for wrought molybdenum. Crack initiation at grain boundaries and the center of grains where pores are present was observed to leave ligaments for the PM molybdenum that are similar in size to those observed for wrought molybdenum. This is a similar toughening mechanism to the ductile laminate mechanism observed for wrought molybdenum. The impact of grain size, grain shape, and oxide particles on the toughening mechanism and properties is discussed.

## 8:50 AM

### **Powder Diffraction Characterization of Reactor Materials:** Heather Volz<sup>1</sup>; Christopher Stanek<sup>1</sup>; Samantha Yates<sup>1</sup>; Erik Luther<sup>1</sup>; John Dunwoody<sup>1</sup>; Kenneth McClellan<sup>1</sup>; Sven Vogel<sup>1</sup>; Sally Tracy<sup>1</sup>; <sup>1</sup>Los Alamos National Laboratory

Characterization studies of materials are important to many aspects of nuclear energy research. In this talk, an overview of recent work will be presented with a focus on powder diffraction studies as validation of UO<sub>2</sub> defect modeling. As an example from transmutation fuel development associated with closing the fuel cycle, changes in the lattice parameter due to lanthanide impurities in the UO<sub>2</sub> crystal structure may be related to cracking during the sintering process. Therefore, samples were prepared with various lanthanides in differing concentrations to validate atomistic simulations of various defect mechanisms in UO<sub>2</sub>. Preliminary laboratory X-ray diffraction data show differences in lattice parameters as a function of lanthanide concentration that suggest the creation of U<sup>5+</sup> ions predominate in Ln:UO<sub>2</sub>, contracting the unit cell. Time-of-flight neutron data from HIPPO at LANSCE's Lujan Center were also collected, and will be discussed.

## 9:10 AM

### **Microstructural Evolution and Multi-Scale Characterization of Sintered ZrN as a Surrogate for PuN Fuel Pellets:** Kirk Wheeler<sup>1</sup>; Pedro Peralta<sup>1</sup>; <sup>1</sup>Arizona State University

ZrN was studied as a possible surrogate for PuN under the Global Nuclear Energy Partnership (GNEP) program. The mechanical properties of sintered ZrN pellets were examined at elevated temperatures to investigate the effects that sintering temperatures and post-sintering heat treatments have on structural integrity. Uniaxial compression testing was performed on ZrN pellets in a gettered ultra-high purity Argon atmosphere at various temperatures (25°C, 800°C, 1200°C). Post-Mortem fractography was performed using scanning electron microscopy (SEM). In addition, nano-indentation and nano-compression testing was performed on ZrN as well as nano-pillars that were produced using Focused Ion Beam milling. The failure modes of the pellets and their mechanical properties are evaluated in terms of the initial microstructure. Applicability of the results to the understanding of the structural reliability of nitride fuel pellets is discussed. Work supported under DOE/NE Agreement # DE-FC07-05ID14654.



9:30 AM

**Development of a Ceramic-Lined Crucible for the Separation of Salt from Uranium:** *Brian Westphal*<sup>1</sup>; Ken Marsden<sup>1</sup>; JC Price<sup>1</sup>; <sup>1</sup>Idaho National Laboratory

As part of the spent fuel treatment program at the Idaho National Laboratory, alternate crucible materials are being developed for the processing of uranium and salt. The separation of salt (LiCl/KCl based) from uranium is performed in an inductively-heated furnace capable of distillation under vacuum conditions. Historically, salt and uranium have been processed in graphite crucibles coated with a zirconia mold wash. Although the coated crucibles have performed adequately considering the reactive nature of salt and uranium at high temperature, the operations required for multiple use of the crucibles are quite labor intensive. Thus, an alternate ceramic-lined crucible has been developed to eliminate the interim operations. Two ceramic-lined crucibles have been tested using irradiated materials to verify their compatibility and determine an ultimate life-cycle. Results from the testing program will be presented on crucible deterioration and other cumulative effects.

9:50 AM

**Microscopic and Spectroscopic Characterization of Aluminosilicate Waste Form with Cs/Sr Loaded Using SEM, TEM and XRD:** *Gary Cerefice*<sup>1</sup>; Longzhou Ma<sup>1</sup>; <sup>1</sup>University of Nevada Las Vegas

The goal of this work is the characterization of an aluminosilicate waste form for the storage and ultimate disposal of an isolated cesium and strontium waste stream. The aluminosilicate waste forms with/without Cs/Sr loading were synthesized from bentonite clay at different sintering temperatures to examine the impact of fabrication temperature on waste form. TGA and DTA analysis for the synthesized waste forms were conducted, identifying the temperatures where interstitial water is driven from the waste former matrix. Microscopic and spectroscopic characterization of the synthesized waste forms was conducted using SEM, TEM and XRD. The SEM analysis results show the sponge-like morphology of the synthesized materials. Further analysis by TEM, HRTEM and XRD indicates that the waste stream components are actually segregated into discrete phases, and that these discrete, sub-micron particles are distributed throughout the matrix. EDX examination was also performed to identify the chemical composition of these particles and substrate.

10:10 AM Break

10:20 AM

**Quantification of Microstructurally Induced Variability on the Thermo-mechanical Response of Nitride Nuclear Fuels through Finite Element Models:** *Manuel Parra Garcia*<sup>1</sup>; Pedro Peralta<sup>1</sup>; Kirk Wheeler<sup>1</sup>; Ken McClellan<sup>2</sup>; <sup>1</sup>Arizona State University; <sup>2</sup>Los Alamos National Laboratory

A two-dimensional (2D) finite element model of a cylindrical fuel pellet has been formulated to investigate the variability of the thermo-mechanical response due to microstructure heterogeneity within a Representative Volume Element (RVE). Microstructural information was obtained from sintered ZrN as a surrogate for PuN, processed under conditions similar to those used in actinide bearing fuels. The 2-D RVE obtained from microstructural characterization, which includes pore and grain geometry as well as grain orientation, is surrounded by "effective material" and located at different positions in the model to evaluate variations in stresses strains, and temperature fields within the RVE. The models account for different boundary conditions, as well as creep, thermal expansion and radiation swelling. This effort is directed towards the formulation of a framework that can be translated into characterization and modeling of actual fuels to improve simulations of fuel performance. Work supported under DOE/NE Agreement # DE-FC07-05ID14654.

10:40 AM

**Miniaturized Specimen Testing of Monolithic Fuels and Structural Materials:** *Ramprashad Prabhakaran*<sup>1</sup>; James Cole<sup>1</sup>; Douglas Burkes<sup>1</sup>; Jian Gan<sup>1</sup>; Indrajit Charit<sup>2</sup>; <sup>1</sup>Idaho National Laboratory; <sup>2</sup>University of Idaho

Efforts are ongoing to develop new nuclear fuels to enable research and test reactors to use low-enriched uranium fuels instead of high-enriched uranium fuels, without significant loss in performance. Hence, a new monolithic fuel type, where the fuel region consists of a single U-Mo (Uranium-Molybdenum) foil encased inside aluminum cladding, is being developed. Understanding fuel foil mechanical properties and fuel/cladding bond strength in monolithic plates is of paramount importance. Efforts are also underway to investigate advanced structural/cladding materials for the next generation reactors. The irradiated

materials currently being studied include MA 754, MA 957, 800H and T122. Hence, in this study, the mechanical properties of monolithic fuel foils and irradiated structural materials were evaluated using small-scale specimen testing techniques such as shear punch, micro-hardness and sub-size tensile testing. Optical microscopy, SEM and TEM were used to study the microstructural characteristics.

**Materials in Clean Power Systems IV: Clean Coal-, Hydrogen Based-Technologies, and Fuel Cells: Solid Oxide Fuel Cell Materials, Session II: Interconnects**

Sponsored by: The Minerals, Metals and Materials Society, ASM International, TMS Electronic, Magnetic, and Photonic Materials Division, TMS/ASM: Corrosion and Environmental Effects Committee, TMS: Energy Harvesting and Storage Committee  
Program Organizers: K. Scott Weil, Pacific Northwest National Laboratory; Michael Brady, Oak Ridge National Laboratory; Ayyakkannu Manivannan, US DOE; Z. Gary Yang, Pacific Northwest National Laboratory; Xingbo Liu, West Virginia University; Zi-Kui Liu, Pennsylvania State Univ

Thursday AM

Room: 3005

February 19, 2009

Location: Moscone West Convention Center

Session Chairs: Gordon Xia, Pacific Northwest National Laboratory; Ayyakkannu Manivannan, US DOE

8:30 AM Introductory Comments

8:35 AM Invited

**Ferritic Steel Interconnects for SOFC Systems: Corrosion and Protection:** *Paul Gannon*<sup>1</sup>; Max Deibert<sup>1</sup>; Preston White<sup>1</sup>; Richard Smith<sup>1</sup>; <sup>1</sup>Montana State University

Ferritic stainless steels with and without protective coatings have been developed for solid oxide fuel cell (SOFC) interconnect applications (~800°C). The effects of alloy and coating composition and morphology on SOFC interconnect-relevant performance are reviewed. Minor differences in alloy composition are associated with significant differences in surface corrosion behavior. Differences in coating composition and mode of deposition can also significantly influence protection capacity. Observations and interpretations are discussed in context of developing inexpensive and durable SOFC interconnects.

9:10 AM

**Thermal and Electrical Stability of New Aluminizing Process in Planar SOFC Stacks:** *Jung Pyung Choi*<sup>1</sup>; K. Scott Weil<sup>1</sup>; <sup>1</sup>Pacific Northwest National Laboratory

The list of candidate high-temperature alloys considered applicable in SOFCs includes those that form a stable, protective chromium-, silicon-, or aluminum oxide scale in-situ during use. However both chromia and silica volatility occur at high temperature (>600°C), particularly in water vapor bearing environments. Additionally these species preferentially adsorb at the cathode/electrolyte interfaces of cells and cause continual degradation in the overall power output of the fuel cell system. This presentation will discuss the development of a new process (reactive air aluminizing) that results in a stable, Cr-free oxide coating. The process is a powder-based technique that employs diffusion between stainless steel and aluminum in an air environment. The basic concept will be outlined and results (including Cr volatility, thermal expansion, and ASR testing) obtained on aluminized Crofer 22APU will be described. In addition, a mechanism of how the process provides oxidation and Cr volatility protection will be discussed.

9:30 AM

**High Temperature Studies on the Ag-CuO Air Braze Filler Metal System:** *Jens Darsell*<sup>1</sup>; K. Scott Weil<sup>1</sup>; <sup>1</sup>Pacific Northwest National Laboratory

A series of high-temperature studies have been conducted on the Ag-CuO system to understand its viability in creating long-lasting, oxidation ceramic-ceramic and ceramic-metal joints for various electrochemical applications (e.g. solid oxide fuel cells, gas separation devices, and high-temperature sensors). These studies include: an investigation of phase equilibria in the Ag-CuO system using a combination of thermal, microstructural and compositional analyses, high-temperature wetting experiments, and in-situ observations of wetting transitions between select Ag-CuO compositions and various substrates. Taken as

a whole, the results from each series of experiments exhibit an interesting set of interrelated relationships. We will present and discuss these findings specifically as they pertain to investigating potential compositional modifications to the Ag-CuO system and more broadly as possible tools for exploring high-temperature wetting phenomena in other liquid-solid phase material systems.

## 9:50 AM Break

## 9:55 AM Invited

**Exploration of Alloy 441 Chemistry for SOFC Interconnect Application:** Paul Jablonski<sup>1</sup>; Christopher Cowen<sup>1</sup>; <sup>1</sup>NETL

Alloy 441ss is being considered for application as an SOFC interconnect. There are several advantages to this selection: First and foremost this production alloy is low cost and readily available. Second, the coefficient of thermal expansion (CTE) is compatible with ceramic components of the fuel cell. Third, this alloy forms Laves phase at SOFC operating temperatures. Laves phase has been shown to preferentially consume the Si in the alloy thus avoiding the formation of electrically resistive Si rich oxide subscales which have been shown to be detrimental to SOFC operation. In this paper we will explore the alloy 441ss metallurgy through the use of computational thermodynamics and discuss them with regards to Laves phase formation under SOFC operating conditions. We find that special care must be employed in alloy specification to insure that Laves phase is available to remove Si from the matrix and thus insure useful SOFC operation.

## 10:30 AM

**Comparison of MnCo Coated SS430 and T441 for SOFC Interconnect:** Junwei Wu<sup>1</sup>; Christopher Johnson<sup>2</sup>; Xingbo Liu<sup>1</sup>; Randall Gemmen<sup>2</sup>; Yinglu Jiang<sup>1</sup>; <sup>1</sup>West Virginia University; <sup>2</sup>National Energy Technology Lab

Ferritic stainless steel SUS430 and T441 are one of the most promising candidate for SOFC interconnect. With the addition of Nb, Ti in T441, the formation of continuous silica sub-layer can be avoided, which is attributed to Nb and Si rich secondary phase formation to stabilize silicon. However, it is not clear how the secondary phase affect the diffusion of substrate elements, Mn, Cr and Fe. Electrodeposition of MnCo alloys with the following oxidation has been proved to be effective for interconnects coating. In this work, MnCo coated SUS 430 and T441 by pulse plating has been oxidized at 800°C for different times. Then surface and cross-section SEM/EDX test are used to study the elements diffusion and secondary phase effect. Furthermore, uncoated and MnCo coated SUS430 and T441 interconnect on button cell test has been conducted to compare the cell performance degradation.

## 10:50 AM

**Mixed Conductive Coatings on Metallic Interconnects in SOFCs:** Zhenguo "Gary" Yang<sup>1</sup>; Gordon Xia<sup>1</sup>; Josh Templeton<sup>1</sup>; Zimin Nie<sup>1</sup>; L. Shari Li<sup>1</sup>; Chong-Min Wang<sup>1</sup>; Jeff Stevenson<sup>1</sup>; Prabhakar Singh<sup>1</sup>; <sup>1</sup>Pacific Northwest National Laboratory

In intermediate-temperature planar SOFC stacks, stainless steels are used as promising candidates for construction of interconnects, that electrically connect neighboring cells and hermetically separate fuel at the anode-side and air at the cathode-side. For long-term operation at temperatures that are allowed by current cell materials and technologies however, further improvement is required in their surface stability and the electrical resistance arising from the oxide scale growth. For this purpose, the ferritic stainless steels are surface-modified via application of a conductive oxides protection layer. In the past couple of years, PNNL has been conducting this investigation and developing the protection layers and fabrication approaches. This paper will give an update on our efforts in this area.

## 11:10 AM

**Development of MnCoO Coating with New Aluminizing Process for Planar SOFC Stacks:** Jung Pyung Choi<sup>1</sup>; K. Scott Weil<sup>1</sup>; Yeong-Shyung Chou<sup>1</sup>; Jeffry W. Stevenson<sup>1</sup>; Zhenguo "Gary" Yang<sup>1</sup>; Prabhakar Singh<sup>1</sup>; <sup>1</sup>Pacific Northwest National Lab

Low-cost, chromia-forming steels find widespread use in SOFCs at operating temperatures below 800°C, because of their low thermal expansion mismatch and low cost. However volatile Cr-containing species originating from this scale poison the cathode material in the cells and subsequently cause power degradation in the devices. To prevent this, a conductive manganese cobaltite coating has been developed. However this coating is not necessarily compatible with forming hermetic seals between the interconnect or window frame component and ceramic cell. Thus, a new aluminizing process has been developed for the

sealing regions in these parts, as well as for other metallic stack and balance-of-plant components. This paper will present the basic processes used in each coating technique and discuss some of the compatibility issues that arise when integrating both coatings into the same component.

## 11:30 AM

**Development of Electrical Contacts between Cathodes and Metallic Interconnects in SOFCs:** Gordon Xia<sup>1</sup>; Zhenguo "Gary" Yang<sup>1</sup>; Josh Templeton<sup>1</sup>; Jeff Stevenson<sup>1</sup>; <sup>1</sup>Pacific Northwest National Lab

In SOFCs, electrical contacts or contact layers are applied between electrodes (anode or cathode) and interconnects to promote electrical contact and facilitate stack assembling. Particularly the electrical contact at the cathode-side is essential to offer a low resistant electron transport bridge that connects a metallic interconnect and perovskite cathode. One promising group of materials for the contact layers are conductive oxides that nevertheless often demonstrate an inferior sintering activity for this particular applications. PNNL has searched suitable materials and developed approaches to fabricate the contact layers with emphasis on improving the materials sintering activity. This paper will present details of this work.

## Nanocomposite Materials: Nanocomposite Processing

Sponsored by: The Minerals, Metals and Materials Society, TMS Structural Materials Division, TMS Electronic, Magnetic, and Photonic Materials Division, TMS/ASM: Composite Materials Committee, TMS: Materials Characterization Committee, TMS: Nanomaterials Committee

Program Organizers: Jonathan Spowart, US Air Force; Judy Schneider, Mississippi State University; Bhaskar Majumdar, New Mexico Tech; Benji Maruyama, Air Force Research Laboratory

Thursday AM

February 19, 2009

Room: 3020

Location: Moscone West Convention Center

Session Chairs: Jonathan Spowart, US Air Force; Francisco Robles Hernandez, University of Houston

## 8:30 AM Introductory Comments

## 8:35 AM Invited

**Consolidation of Bulk Nanocomposites Using Current Activated Densification:** Javier Garay<sup>1</sup>; <sup>1</sup>University of California, Riverside

Nanocrystalline ceramics display significantly different properties than their microcrystalline counterparts, yet they have been difficult to produce in bulk sizes. The versatile material processing technique of current-activated pressure assisted densification has proven effective in densifying nano-ceramic powders into bulk nanomaterials. Results on large-sized, fully dense oxide ceramics with crystal sizes much less than 100nm will be presented. In particular we will focus on our recently developed processing technique that leverages metastability to partially transform phases producing nanocomposites with very clean epitaxial-like interfaces. These materials display unique functional and structural properties. Properties discussed include improved visible light transmittance and novel magnetic properties.

## 9:00 AM

**Development of Nanostructured Polyurethanes Materials for Anticorrosive Coatings:** Ariosvaldo Sobrinho<sup>1</sup>; Luiz Pontes<sup>2</sup>; Rejane Dantas<sup>2</sup>; André Rodrigues<sup>1</sup>; Edjânio Araujo<sup>2</sup>; <sup>1</sup>CCT / Materials; <sup>2</sup>UFPPB

Nanocomposites based on Polyurethane/organophilic clay solutions were obtained using methyl ethyl ketone (MEK) like organic solvent. Various organo-modified clays were prepared in solution and their morphology, adhesive force, shock-resistant toughness, densification of lacquer surface and anti-corrosion were evaluated in coating anticorrosive applications. For better performance of solvent-based polyurethane for anticorrosive coatings applications, they were modified either by varying polyurethane microstructures or by dispersing inorganic fillers, especially by incorporating nanosized layered silicates within the polyurethane continuous matrix. The main objectives of this work were the synthesis of solvent-based polyurethane using organophilic clay and their study by TGA, morphology, adhesive force, shock-resistant toughness, densification and anti-corrosion properties. The most significant feature of this investigation

is the improve of adhesive force, shock-resistance toughness and anti-corrosion of various chemical media so that it is possible to resolve various problems in materials applied to petroleum applications industry.

9:20 AM

**Dispersing of Nano-Particles in Molten Aluminum Using High-Intensity Ultrasonic Vibrations:** Clause Xu<sup>1</sup>; Lu Shao<sup>1</sup>; *Qingyou Han*<sup>2</sup>; <sup>1</sup>Hans Tech; <sup>2</sup>Purdue University

The most inexpensive method for processing particle reinforced aluminum matrix composites involves the use of a stirrer for dispersing particles in molten metal. The method is successful in making composites containing particles larger than a few microns but is difficult in dispersing particles in the nano-size range (<100 nm). This article discusses an enabling technology for dispersing nanoparticles in molten metal using high-intensity ultrasonic processing technology. The use of high-intensity ultrasonic vibration breaks up the nanoparticle clusters and disperses the individual nanoparticles into the melt. The resultant nanocomposites are of superior mechanical properties especially tensile and creep resistance at elevated temperature. Issues associated with the dispersing of nano-particles are addressed.

9:40 AM

**Influence of Dispersed Carbon Nano-Fibers/Carbon Nano-Tubes in Al Matrix Composite:** Minoru Oda<sup>1</sup>; Chitoshi Masuda<sup>1</sup>; Fumio Ogawa<sup>1</sup>; Seiji Itabashi<sup>1</sup>; Toshiyuki Nishimura<sup>2</sup>; <sup>1</sup>Waseda University; <sup>2</sup>National Institute for Materials Science

CNT and CNF are cohered by Van der Waals force, and the cohesion of CNT and CNF deteriorates the properties of the composite material such as strength, elastic modulus remarkably. First, the influence of surfactant is examined by comparing dispersed CNT, CNF and without dispersed ones. The dispersion state is observed by TEM and SEM. Secondly, mechanical properties of composites made by using surfactant are also examined and compared with those ones made without using surfactant. CNT and CNF are dispersed by using ultrasonic shaker and dried in homoiothermal chamber. Next, dispersed ones are mixed with Al powder (30µm) in ball mill for 3 hours by rotating at 200 rpm. After that, mixed powders are sintered by SPS. The pressure of SPS is held at 200MPa and the hold time is 5 minutes. Mechanical properties of composites made using above two methods will be measured.

10:00 AM

**Influence of Solvent on Dispersion State of the Reinforcement in Magnesium Matrix Composites:** Seiji Itabashi<sup>1</sup>; Chitoshi Masuda<sup>1</sup>; Fumio Ogawa<sup>1</sup>; Minoru Oda<sup>1</sup>; Toshiyuki Nishimura<sup>2</sup>; <sup>1</sup>Waseda University; <sup>2</sup>National Institute for Materials Science

Carbon nanotubes (CNT) and carbon nanofibers (CNF) have superior characteristic, such as high strength, high Young's modulus. However, CNT and CNF are cohered by Van der Waals force and the cohesion of CNT and CNF deteriorates the properties of the composite material such as strength remarkably. Primarily, influence of solvent on composite material is examined by dispersing CNT and CNF using surfactant. For comparison, it is examined without solvent. Secondly, mechanical properties of composites produced using above solvent are also examined and compared with that of one produced without solvent. CNT and CNF are dispersed in solvents using ultrasonic shaker and the solvent is dried in homoiothermal chamber. Next, the carbon powder is mixed with magnesium powder (180µm) in the ball mill. After mechanical alloying, mixed powder is sintered using SPS. Mechanical properties of composites produced using two methods, mechanical and physical properties will be measured.

10:20 AM Break

10:35 AM

**Production of Metal Matrix Composites with CFullerene and CGraphite Reinforcements:** *Francisco Robles Hernandez*<sup>1</sup>; Hector Calderon Benavides<sup>2</sup>; <sup>1</sup>University of Houston; <sup>2</sup>Instituto Politécnico Nacional

In the present work are reported the results of the production of nanostructured Al and Fe matrix composites with reinforcements of CGraphite or CFullerene (C60 + C70 + CSoot) sintered by means of Spark Plasma Sintering (SPS) and characterized by means of XRD, SEM and TEM. CFullerene withstands longer mechanical milling or alloying showing better control agent characteristics when compared to CGraphite. The SPS method preserves the nanometric nature of the composites and the full transformation of CFullerene into Al4C3. For the Fe-CFullerene composite the CFullerene is not affected by mechanical alloying SPS processes; an apparent transformation of the CSoot into CFullerene and

Orthogonal CFullerene are identified; followed by a transformation to diamond by thermomechanical means. The sintered, by SPS, products showed an increase in hardness for in the final composites being the composites with CFullerene the ones with higher hardness.

10:55 AM

**Ultrafine-Grained Aluminum Alloy and Boron Carbide Composite Extrusions:** *Rustin Vogt*<sup>1</sup>; Zhihui Zhang<sup>1</sup>; Troy Topping<sup>1</sup>; Enrique Lavernia<sup>1</sup>; Julie Schoenung<sup>1</sup>; <sup>1</sup>University of California, Davis

Ultrafine-grained aluminum alloys have shown significant increases in strength with addition of ceramic particulate reinforcement. In the present study, boron carbide (B4C) particulate (1-7 micron) was cryomilled together with Al 5083 to form a nanocrystalline composite powder (i.e. grain size ~27 nm). The nanocomposite powder was blended with un-milled Al 5083 powder and processed by different consolidation routes to form ultra-fine grained bulk composites. The processing effects of hot isostatic and cold isostatic pressing as well as dynamic and quasi-static extrusion rate have been investigated on basis of the resulting microstructure, mechanical properties and fracture behavior of the final extrusions.

11:15 AM

**Thermal Stability of a Lamellar Nanocomposite Al/AlMg3 Prepared by Accumulative Roll Bonding:** *Margarita Slamova*<sup>1</sup>; Peter Slama<sup>2</sup>; Petr Homola<sup>1</sup>; Jaromir Uhlir<sup>1</sup>; Miroslav Cieslar<sup>3</sup>; <sup>1</sup>COMTES FHT, Ltd.; <sup>2</sup>VUK Panenske Brezany, Ltd.; <sup>3</sup>Charles University in Prague

High strength ultrafine-grained (UFG) materials can be prepared by accumulative roll bonding (ARB). Their low ductility however represents a grave drawback in many applications. The ductility problem can be resolved in materials with bimodal grain size distributions with good yield strength and fairly large uniform elongation. A lamellar composite with grains of submicrometer size was prepared by ARB from Al and AlMg3 sheets. The thermal stability of the UFG structure was investigated in the temperature range 150-350°C. The grain size was evaluated by various microscopy methods, including EBSD. AlMg3 composite layers remained unrecrystallized up to 250°C, whereas the Al layers started recrystallizing at much lower temperature. Bimodal grain size distributions shifted to smaller sizes with increasing ARB cycles were observed in the annealed materials. The evolution of strength with number of cycles and temperature was monitored by hardness and tensile tests. The composite was compared with mono-material ARB sheets.

11:35 AM

**Mg Matrix Nano Composites:** *Ari Erman*<sup>1</sup>; Joanna Groza<sup>1</sup>; Xiaochun Li<sup>2</sup>; Guoping Cao<sup>2</sup>; Hong-seok Choi<sup>2</sup>; Prashant Soni<sup>3</sup>; <sup>1</sup>University of California, Davis; <sup>2</sup>University of Wisconsin-Madison; <sup>3</sup>Indian Institute of Technology Bombay

Mg matrix nanocomposites, reinforced with SiC nanoparticles, have been cast by ultrasonic cavitation based dispersion methods. Microstructural studies of as cast specimens are done to characterize the grain and dislocation structure and SiC particle size and distribution. We plan to carry out low cycle fatigue experiments of Mg-SiC nano composites.

## Near-Net Shape Titanium Components: Powder Metallurgy II

Sponsored by: The Minerals, Metals and Materials Society, TMS: Titanium Committee

Program Organizers: Rodney Boyer, Boeing Company; James Cotton, Boeing Co

Thursday AM  
February 19, 2009

Room: 2010  
Location: Moscone West Convention Center

Session Chair: M. Ashraf Imam, Naval Research Laboratory

8:30 AM

**Cost-Effective Titanium Alloy Powder Production and Consolidation for Near-Net Shaped Component Manufacturing:** *Deliang Zhang*<sup>1</sup>; Stiliانا Raynova<sup>1</sup>; Vijay Nadakuduru<sup>1</sup>; Brian Gabbitas<sup>1</sup>; Barry Robinson<sup>2</sup>; <sup>1</sup>University of Waikato; <sup>2</sup>South Auckland Forging Engineering Ltd (SAFE)

This paper will first briefly introduce a newly developed cost-effective titanium alloy powder production process, the TiPro process, which utilises



relatively low cost TiO<sub>2</sub> and Al powders and other reactants as raw materials, and involves solid-liquid separation and powder purification. Findings from a study on the effects of thermomechanical consolidation conditions on the defects, microstructure and mechanical properties of the consolidated samples of titanium and Ti-Al based alloys such as Ti-6wt%Al-4wt%V alloy will also be presented and discussed. At this stage of the project, the major aim of the research is to develop a novel thermomechanical powder consolidation process that can be used to produce semi-finished titanium alloy products such as forged blocks and rolled plates cost effectively. The longer term goals of the research on powder consolidation also include development of cost-effective powder consolidation processes for manufacturing titanium alloy near-net shaped components for various applications.

## 8:50 AM

**Development and Manufacturing of the Near Net Shape Parts from Ti Alloys with the Reduced “Buy to Fly” Using PM HIP Route Based on the Process Modeling:** *Victor Samarov<sup>1</sup>; C. Barre<sup>1</sup>; D. Poor<sup>2</sup>; <sup>1</sup>Synertech PM; <sup>2</sup>Kittyhawk Products Inc*

The general task of HIP modeling is in designing the initial shape of the HIP tooling providing the final “net” or “near net shape” part after HIP consolidation of powder. The core of modeling is the description of the mutual deformation of the compressible (powder) and non-compressible (HIP tooling) materials. The paper presents the results of development efforts providing adequate description of the HIP deformation for parts from Ti alloys of the different geometrical complexity and physical non-uniformity mainly used for the aerospace applications. Such process modeling associated with the novel design of the HIP tooling enables to manufacture “selectively net shape” and “near net complex shape” parts for different static and rotating applications requiring no or minimal machining of the critical (and difficult to machine) surfaces and cutting down substantially the buy-to-fly ratio for various aerospace components.

## 9:10 AM

**Fabrication of Titanium Shrouded Impellers for Rocket Engine Liquid Hydrogen Pumps:** *Cliff Bampton<sup>1</sup>; Victor Samarov<sup>2</sup>; John Wooten<sup>3</sup>; <sup>1</sup>Pratt & Whitney Rocketdyne; <sup>2</sup>Synertech Inc.; <sup>3</sup>CalRAM Inc.*

A case study is presented for competing methods of fabricating titanium alloy shrouded impellers. These are critical components in liquid hydrogen fueled rocket engines. The shrouded impeller design, optimized for pump performance, makes conventional fabrication - machining of die forgings - difficult and expensive with long cycle times. Three alternate net and near-net shaping processes are compared: Investment casting; Powder metal hot isostatic pressing; Powder metal additive layered build by electron beam melting. Attributes and limitations of each process are demonstrated and discussed.

## 9:30 AM

**New Possibilities of Enhancing Mechanical Properties and Microstructure for Conventional Ti Alloys via the PM HIP near Net Shape Route:** *I. Polkin<sup>1</sup>; Victor Samarov<sup>2</sup>; <sup>1</sup>VILS; <sup>2</sup>Synertech PM*

It is acknowledged today that Ti parts obtained via PM HIP route have better uniformity and homogeneity compared to cast and wrought material, however the latter still keeps the advantages in mechanical properties. The paper presents the results of the development work on PM HIP of near net shape parts from Ti alloys with the enhanced micro-structure and mechanical properties. These new advantages are gained due to the exceptionally fine and uniform micro-structure that can be achieved as a result of the special processing including encapsulation and HIP. The results obtained for the complex shape parts from the conventional grades of Ti alloys are compared to the micro-structure and mechanical properties of the parts made via conventional forging of billets. It is demonstrated that the mechanical properties of PM HIPed material are at the same level or even higher than those of the cast and wrought material with substantial reduction of the processing steps to produce them to the desired shape.

## 9:50 AM Break

## 10:10 AM

**Study of Sintering Behavior of Ultrafine Titanium Powders:** *Hongtao Wang<sup>1</sup>; Zhigang Fang<sup>1</sup>; <sup>1</sup>University of Utah*

The near net shape (NNS) capability of powder metallurgy (PM) techniques can dramatically reduce the cost of titanium components. It is well known that sintering behaviour of a metal powder is related to its particle size, and the sintering can be significantly enhanced via the refinement of powder size. In this investigation, the size-dependent sintering behaviour of titanium powders

has been studied by sintering of different-sized titanium powders (coarse and ultrafine) using a dilatometer. The ultrafine powders were produced via high-energy mechanical milling. The results show that the sintering temperature of ultrafine titanium powder decreases remarkably compared to that of the sintering of conventional coarse powder, and as a result, better sintering densification is achieved by using ultrafine titanium powder. Dilatometric data are used to study the difference of sintering process and kinetics between coarse Ti powder and ultrafine Ti powder, and the mechanisms of densification will also be discussed.

## 10:30 AM

**Low Temperature Compaction of Titanium Alloy Powder by Equal Channel Angular Extrusion with Back Pressure:** *Rimma Lapovok<sup>1</sup>; Dacian Tomus<sup>1</sup>; <sup>1</sup>Monash University*

It is shown that the use of Equal Channel Angular Extrusion (ECAE) with applied back pressure for compaction of powder allows significantly decrease the temperatures of consolidation compare to those used in conventional practice. The possibility to lower the processing temperature would give a cost-effective method to produce a cheaper product as well as minimise the contamination of powder and compact with gaseous constituents known to be harmful to resultant properties. The novelty of the approach arises from the notion that severe shear deformation triggers several physical mechanisms contributing to improved compaction. The compacts produced from CP-Ti at temperatures in the range from room temperature to 300°C by ECAE with back pressure have a relative density above 99.5%. Efficient consolidation of pre-alloyed (PA) Ti-6Al-4V (HDH) powder at temperatures of 400°C and below, achieving relative densities of 98.3-98.6% and green strengths up to 750 MPa has been performed.

## 10:50 AM

**Stress-Corrosion Cracking and Fatigue Crack Growth of Consolidated Powder of Ti-6Al-4V:** *Peter Pao<sup>1</sup>; M. Ashraf Imam<sup>1</sup>; Robert Bayles<sup>1</sup>; Jerry Feng<sup>1</sup>; <sup>1</sup>Naval Research Laboratory*

Ti-6Al-4V plates, consolidated from powders, manufactured from Armstrong-process and hydride-process were studied. The Armstrong-process allows direct production of titanium powder in a single step in-situ reaction whereas the hydride-process uses the hydrogenation of the ore. Both processes result into considerable savings when compared to converting sponge to powder. The yield strengths of these plates are about 920 MPa. The oxygen content from hydride-process is higher compared to the Armstrong-process (0.3 vs. 0.2 wt%). Preliminary fatigue crack growth study indicates that, in the as-received condition, the threshold stress intensities of Armstrong-process and hydride-process approaches to that of the conventional cast-ingot of Ti-6Al-4V. The stage II fatigue crack growth rates of hydride-process are substantially higher than that of the Armstrong-process and the conventional cast-ingot-cast. The mechanism of the fatigue crack growth rates difference, fracture toughness, and stress-corrosion cracking resistance of Ti-6Al-4V will be discussed.

## 11:10 AM

**Use of Rapid Solidification to Affect Ultra-Refined Microstructures in Near-Net Shape Materials:** *Peter Collins<sup>1</sup>; Jonathan Orsborn<sup>1</sup>; Hamish Fraser<sup>1</sup>; <sup>1</sup>Ohio State University*

Directed laser deposition techniques, such as laser engineered net shaping (LENS<sup>TM</sup>), will often exhibit solidification and cooling rates approaching rapid solidification ( $\Delta T \sim 1000^\circ\text{C}/\text{sec}$ ). It is possible to exploit the resulting ultra-refined microstructures to control properties. Using both conventional processing and LENS<sup>TM</sup> processing, ultrafine distributions of alpha-precipitates will be affected in Ti-6Al-4V, Ti-6-2222, and model alloy based on the Ti-Al-Mo system. The mechanical properties of these materials will be probed and correlated with microstructural length scale.

## Neutron and X-Ray Studies of Advanced Materials: Neutron Diffraction and Modeling of Materials Behavior

Sponsored by: The Minerals, Metals and Materials Society, TMS Structural Materials Division, TMS/ASM: Mechanical Behavior of Materials Committee, TMS: Advanced Characterization, Testing, and Simulation Committee, TMS: Titanium Committee  
Program Organizers: Rozaliya Barabash, Oak Ridge National Laboratory; Yandong Wang, Northeastern University; Peter Liaw, The University of Tennessee; Jaimie Tiley, US Air Force

Thursday AM Room: 3016  
February 19, 2009 Location: Moscone West Convention Center

Session Chairs: Judy Pang, Oak Ridge National Laboratory; Jaimie Tiley, US Air Force

### 8:30 AM Keynote

**In-Situ Neutron Scattering Studies of Multi-Ferroids under Stress, Temperature and Magnetic Fields:** *Donald Brown*<sup>1</sup>; <sup>1</sup>Los Alamos National Laboratory

Multi-ferroic materials, such as shape memory alloys, ferro-electrics, and ferromagnetic shape memory alloys have been studied heavily recently. Despite being driven by distinct stimuli, such as stress or magnetic field, the underlying physics of multi-ferroic materials is similar. Relatively large and recoverable dimensional changes are achieved by either large scale crystal reorientation (variant selection) or phase transformation. Time-of-Flight (TOF) neutron diffraction is uniquely suited to study multi-ferroids because neutrons penetrate into the bulk and the TOF technique allows us to record the entire diffraction pattern (0.5-4Å) simultaneously. This talk will highlight the technique and our efforts to study various multi-ferroic materials including shape memory alloys, such as U6Nb and NiTi, magnetic shape memory alloys, such as Ni2MnGa, and ferro-electrics under conditions of monotonic and cyclic loading, elevated temperature, and applied magnetic field on the SMARTS diffractometer at the Lujan Center.

### 9:00 AM Invited

**Advances in Modeling Internal Strain Evolution of Aggregates:** *Carlos Tome*<sup>1</sup>; Bjorn Clausen<sup>1</sup>; John Neil<sup>2</sup>; Sebastian Merkel<sup>3</sup>; <sup>1</sup>Los Alamos National Laboratory; <sup>2</sup>University of Virginia; <sup>3</sup>University des Sciences et Technologies de Lille

Polycrystal models are used for simulating and interpreting in-situ internal strain measurements done with neutron and X-ray diffraction. Our Elasto-Plastic Self-Consistent (EPSC) model has proven effective not only in providing interpretation of experimental results, but also insight into the crystallographic mechanisms responsible for plasticity. In this presentation we discuss new capabilities of our EPSC approach and how they impact our understanding of polycrystal plasticity. First, accounting for texture evolution allows us to address the large strain regime; results for Cu and stainless steel will be discussed. A second modeling advance allows us to account for twin reorientation and for the stress relaxation associated with it; experimental and modeling results will be presented for Mg AZ31. Finally, the interpretation of results for Co (hcp) tested to 50 GPa pressure, reveals the role played by plasticity in controlling stress build-up under high pressure.

### 9:20 AM

**Characterization of Gamma and Gamma Prime Phases in Nickel Base Superalloys Using Neutron Diffraction and XRD Techniques:** *Jaimie Tiley*<sup>1</sup>; R. Srinivasan<sup>2</sup>; R. Banerjee<sup>3</sup>; Hamish Fraser<sup>2</sup>; B. Viswanathan<sup>3</sup>; <sup>1</sup>US Air Force; <sup>2</sup>Ohio State University; <sup>3</sup>University of North Texas

Gamma and Gamma Prime precipitates in a nickel base superalloy were characterized using advanced neutron diffraction and x-ray diffraction techniques. Specifically, volume fraction, chemical composition, residual stresses, and lattice parameters were determined and used in Rietveld refinements to determine lattice site occupancies of alloying elements. Rene88 material was treated to three different cooling rates and then aged up to 200 hours to provide different microstructures. Material parameters were measured as a function of cooling rates and aging times. In addition, samples were heated in situ to obtain neutron

diffraction data at temperatures up to 600°C. Results link microstructures to heat treatment conditions and compare different characterization techniques.

### 9:40 AM

**Evolution of Crystallographic Texture of TRIP Steel after Multi-Axial Deformation:** *Adam Creuziger*<sup>1</sup>; Thomas Gnaeupel-Herold<sup>1</sup>; Timothy Foecke<sup>1</sup>; Mark Iadicola<sup>1</sup>; Stephen Banovic<sup>1</sup>; <sup>1</sup>NIST

TRIP (Transformation Induced Plasticity) steel is a high strength, high ductility steel alloy being investigated as a replacement for conventional steel used in outer body panels and internal structure of automobiles. In this study, as received TRIP 780 steel sheets were deformed under a variety of in plane multi-axial conditions and the elastic and plastic strains were measured in-situ. After deformation the phase fraction of the deformed material and crystallographic texture was determined using neutron and x-ray diffraction. The results of the samples deformed under multi-axial loads will be compared to uniaxial tension tests and the experimentally determined effect of loading path on deformation, phase fraction and texture will be discussed.

### 9:55 AM

**In-situ Neutron Diffraction of the Anomalous Ductility of CoTi and CoZr B2 Intermetallics:** *James Wollmershauser*<sup>1</sup>; C. Neil<sup>1</sup>; Sean Agnew<sup>1</sup>; <sup>1</sup>University of Virginia

Fully-ordered B2 compounds, CoTi and CoZr, are examined by in-situ neutron diffraction during compression testing at room temperature. Previous studies have shown that both alloys can accommodate appreciable elongation, up to 20% in CoZr, while TEM studies have shown only dislocations with <100> Burgers vectors, which suggests that there are insufficient independent slip systems to accommodate arbitrary strains at the grain level. Such anomalous ductility is similar to that reported of B2 compounds composed of rare earth elements in combination with late transition elements, such as AgY and CuDy. Modeling of the measured internal strain evolutions using the elastoplastic self-consistent (EPSC) polycrystal plasticity code is used to explore the mechanisms of plastic deformation and the results are compared to an earlier neutron diffraction study of a rare earth-containing compound, AgCe, and conventional intermetallics, NiAl and CuZn.

### 10:05 AM

**Effects of Overload and Underload on the Residual Stress, Crack-Opening Load, and the Crack-Growth Behavior:** *Soo Yeol Lee*<sup>1</sup>; *Peter Liaw*<sup>1</sup>; Hahn Choo<sup>1</sup>; Ronald Rogge<sup>2</sup>; Michael Gharghour<sup>2</sup>; <sup>1</sup>University of Tennessee; <sup>2</sup>Chalk River Laboratories

Various fatigue-loading conditions (i.e., fatigued, tensile overloaded, compressive underloaded, tensile overloaded-compressive underloaded, and compressive underloaded-tensile overloaded) were introduced to study the crack-growth retardation/acceleration mechanisms during fatigue crack growth. First, the spatially-resolved neutron-strain mapping was performed to measure three principal residual-strain components developed near a crack tip under the various loading conditions, and then residual-stress distributions were calculated as a function of the distance from the crack tip. Second, the electric-potential technique was employed to determine the crack-opening load associated with the crack-tip driving force at different crack-growth stages. Finally, the relationship among the residual stress, crack-opening load, and the crack-growth rate is investigated, and the mechanisms concerning the overload/underload effects are suggested.

### 10:15 AM

**Formation of Deformation Textures in F.C.C. Materials Studied by In-Situ Neutron Diffraction and Self-Consistent Model:** *Nan Jia*<sup>1</sup>; Yandong Wang<sup>1</sup>; Ru Peng<sup>2</sup>; X. Zhao<sup>1</sup>; <sup>1</sup>Northeastern University; <sup>2</sup>Linköping University

Polycrystalline f.c.c. materials usually deform in a variety of slip, twinning and shear banding modes and exhibit marked plastic anisotropy at the grain level. This causes the evolution of preferred grain orientation distribution (crystallographic texture) that affects again the distribution of heterogeneous stresses within materials. In the current work, in-situ neutron diffraction experiments were employed on f.c.c. metals (copper, aluminium and brass) with different stacking fault energy. The evolution of microstresses in each metal was traced under the stress field. Based on the grain-boundary-mediated activities that were experimentally characterized as the lattice strain distributions of multiple reflections, deformation textures of the different materials were simulated with an Elastic-Plastic Self Consistent (EPSC) model. The featured slip systems and stress/stain states were selected according to the accommodation of misfits

among grains. Such an approach thus provides an unambiguous understanding of the micromechanics of texture development in various f.c.c. materials under external load.

## 10:30 AM Break

## 10:40 AM Invited

### High-Pressure Studies of Various Materials by Synchrotron-Based X-Ray Diffraction: *Haozhe Liu*<sup>1</sup>; Luhong Wang<sup>1</sup>; <sup>1</sup>Harbin Institute of Technology

The study of polymorphism and polyamorphism in pressure domain will undoubtedly broaden our horizons and perspectives of the states of matter in general, and may have a significant impact on the existing theories about the structure, formation, and evolution of crystal and amorphous materials. The synchrotron x-ray diffraction and diamond anvil cell techniques were used to study these subjects. One typical powder sample, zinc oxide from NIST standards, was selected to study its phase transition mechanism under high pressure and low temperature conditions. Two types of metallic glass were selected to test the pressure induced polyamorphism. The procedure of the pressure-induced amorphous state to crystalline state is another subject in this talk. These will provide new insight on the nature of phase transition, provide new invitation for the electronic theoretical studies for the phase stability, and improve our understanding of the kinetic process of the common pressure induced crystallization.

## 11:00 AM

### Fundamental Studies of Intergranular Strains Evolution in a Zircaloy-4 Alloy with Random Texture: *Elena Garlea*<sup>1</sup>; Bjorn Clausen<sup>2</sup>; Sven Vogel<sup>3</sup>; Judy Pang<sup>3</sup>; Hahn Choo<sup>4</sup>; <sup>1</sup>B&W Y-12 National Security Complex / University of Tennessee; <sup>2</sup>Los Alamos National Laboratory; <sup>3</sup>Oak Ridge National Laboratory; <sup>4</sup>University of Tennessee / Oak Ridge National Laboratory

A Zircaloy-4 alloy with Basketweave - Widmanstätten type microstructure and random texture has been used to study the deformation systems responsible for the polycrystalline plasticity at the grain level. The evolution of internal strains and bulk texture is investigated using neutron diffraction and an elasto-plastic self-consistent (EPSC) modeling scheme. The macroscopic stress-strain behavior and intergranular (hkil-specific) strain development, parallel and perpendicular to the loading direction, were measured in-situ during uniaxial tensile loading. Then, the EPSC model was employed to simulate the experimental results. This modeling scheme accounts for the thermal anisotropy; elastic-plastic properties of the constituent grains; and activation, reorientation, and stress relaxation associated with twinning. The agreement between the experiment and the model will be discussed as well as the critical resolved shear stresses (CRSS) and the hardening coefficients obtained from the model.

## 11:15 AM

### Neutron and X-Ray Diffraction Study of Residual Stress in Creep Deformed Single Crystal Superalloy: *Erdong Wu*<sup>1</sup>; Jinchao Li<sup>1</sup>; Guangai Sun<sup>2</sup>; Bo Chen<sup>2</sup>; V. Ji<sup>3</sup>; V. Klosek<sup>4</sup>; M.H. Mathon<sup>4</sup>; <sup>1</sup>Chinese Academy of Sciences; <sup>2</sup>Institute of Nuclear Physics and Chemistry, CAEP; <sup>3</sup>LEMHE/ICMMO, UMR 8182, Université Paris-Sud 11; <sup>4</sup>Laboratoire Léon Brillouin, CEA Saclay

The redistribution of residual stress state and loss of coherency between the matrix and precipitates are strongly associated with the creep deformation of the single crystal superalloys. However, although estimations have been made, the quantitative measurements on the residual stress are still rare, as the stress measurements on single-crystal are much more complicated than that on poly-crystal sample. In this work, the residual stresses in crept single crystal superalloys were measured by neutron and X-ray diffraction. The evolutions of residual stress and associated lattice distortion and microstrain during the creep deformation were revealed from the analysis of diffraction profiles. A remarkable increase in compressive stress indicating a built-up of residual stress occurred during the low straining stage of creep. The development of the tetragonal lattice distortion for both phases and the greater microstrain along the loading axis associated with stress state change and dislocation were observed.

## 11:30 AM

### Texture and Microstrain Evolution during the Dynamic Recrystallization of Fe: *Tien Tran*<sup>1</sup>; Donald Brown<sup>2</sup>; Benjamin Fell<sup>1</sup>; Joanna Groza<sup>1</sup>; <sup>1</sup>University of California; <sup>2</sup>Los Alamos National Laboratory

Dynamic recrystallization (DRX) during power-law creep is explored as a means to produce large single crystals of alpha-iron by abnormal grain growth (AGG). The current *in situ* neutron diffraction studies focus on the temporal evolution of microstrain and texture during DRX. Typically, recrystallization

events during constant-stress creep are inferred from fluctuations in the strain rate. Furthermore, any information obtained from *post mortem* metallography may be contaminated by metadynamic recrystallization. The Spectrometer for Materials Research at Temperature and Stress (SMARTS) at the Los Alamos Neutron Science Center (LANSCE) is a neutron diffractometer designed to study the behavior of bulk materials under extreme loads and temperatures. Creep tests were conducted at various stresses and temperatures to investigate the rate of strain energy accumulation as it relates to grain orientation and the onset of recrystallization. Preferential nucleation/growth leading to texture development was explored as a possible AGG-inducing occurrence.

## 11:40 AM

### Texture Effect and the Role of Deformation Twinning on the Cyclic Deformation of a Rolled Magnesium Alloy, AZ31B: *Liang Wu*<sup>1</sup>; Sean Agnew<sup>2</sup>; Yang Ren<sup>3</sup>; Donald Brown<sup>4</sup>; Bjorn Clausen<sup>4</sup>; Feng Jiang<sup>1</sup>; Peter Liaw<sup>1</sup>; <sup>1</sup>University of Tennessee; <sup>2</sup>University of Virginia; <sup>3</sup>Argonne National Laboratory; <sup>4</sup>Los Alamos National Laboratory

Neutron and synchrotron diffraction has been employed to study the cyclic deformation of a rolled magnesium alloy, AZ31B, loaded, respectively, along the rolling direction (RD), transverse direction (TD), and normal direction (ND) at a fully reversed total constant strain amplitude of 3% at room temperature, starting with compression. The initial preferred orientation with the basal poles in most grains aligned along ND favors extensive twinning under in-plane compression or through-thickness tension, and detwinning during the subsequent loading reversals. In-situ neutron diffraction indicates that the twinning and detwinning alternates with the cyclic loading. The texture measurements using synchrotron diffraction suggest the initial texture is completely reversed once detwinning capability is exhausted, concurrent with the disappearance of twin bands. The cyclic deformation behavior is similar for the RD and TD loadings due to the in-plane texture symmetry, while the macroscopic hysteresis under the ND loading is distinct from those under in-plane loadings.

## 11:50 AM

### Continuous Pole Figure Measurement with Neutron Radiation: *Ulf Garbe*<sup>1</sup>; Christian Randau<sup>2</sup>; Christian Hesse<sup>3</sup>; Michael Hofmann<sup>3</sup>; Heinz-Guenter Brokmeier<sup>2</sup>; <sup>1</sup>ANSTO; <sup>2</sup>TU-Clausthal; <sup>3</sup>FRM II

Samples for texture analyses are often coarse grained or samples with sharp texture. Measurements with neutron radiation in a typically 5x5 degree grid will not represent the existing texture. Continuous pole figure measurement instead of step wise technique, will lead to better results with coarse grained material, because every grain is under reflection condition. This technique also decreases beam time for high resolution pole figures, caused on shorter positioning time for the sample orientation. Here we present first results of continuous texture measurements on different type of samples.

## 12:05 PM

### X-Ray Scattering Studies of Orbital Correlations and Quasi-3D Ordered Lattice Modulations in Bilayer Ruthenates with No Long-Range Orbital Order: *Zahirul Islam*<sup>1</sup>; <sup>1</sup>Argonne National Laboratory

X-ray scattering studies of the role of structural correlations across the phase diagram of bilayered ruthenate ( $Sr_{1-x}Ca_xRu_2O_7$  compounds (SCRO) are presented. While the pure Ca end member is an antiferromagnetic insulator, pure Sr compound is an itinerant metamagnet. Bulk measurements reveal disorder-induced unconventional quantum critical behaviors in these materials, in particular, near  $x=0.3$ . X-ray scattering studies revealed that robust 2-unit-cell periodic lattice modulations that are characterized by (1/2,0,0) and (0,1/2,0), respectively, even at room temperature, exist at  $x=0.3$  and in the pure Sr compound, but absent in the Ca end member of the series. These modulations are transversely polarized and quasi-3D ordered in that they are fully coherent in the basal plane with c-axis correlations at least one unit cell in extent. These modulations are due to correlated displacements of the O atoms.



## Open Source Tools for Materials Research and Engineering: Session I

Sponsored by: The Minerals, Metals and Materials Society, TMS Materials Processing and Manufacturing Division, TMS/ASM: Computational Materials Science and Engineering Committee, TMS: Process Technology and Modeling Committee  
Program Organizers: Adam Powell, Opennovation; Kim Ferris, Pacific Northwest National Laboratory

Thursday AM Room: 3000  
February 19, 2009 Location: Moscone West Convention Center

*Session Chairs:* Adam Powell, Opennovation; Kim Ferris, Pacific Northwest National Laboratory

### 8:30 AM Introductory Comments

#### 8:40 AM Invited

##### NSDL MatDL's MatForge: Open Efforts for Computational Materials Research and Education: *Laura Bartolo*<sup>1</sup>; <sup>1</sup>Kent State University

The Materials Digital Library Pathway (MatDL) is an NSF-supported National Science Digital Library (NSDL) Pathway project to create community-centered, user-tailored access for broad dissemination in the materials community. MatDL is a consortium of organizations including: Kent State University, MIT, National Institute of Standards and Technology, University of Michigan, Purdue University, and Iowa State University. MatDL's MatForge (<http://matforge.org>), is a Subversion/TRAC workspace for open source development of modeling and simulation codes, serving as a branded, trusted, non-commercial, and neutral site. It hosts mature research code projects, including: FiPy administered by MSEL/NIST code developers and newly launched projects such as OpenThermo, endorsed by the TMS Committee on Integrated Computational Materials Engineering (ICME). As a centralized site with integrated services for developers of team-based materials code projects, MatForge contributes to awareness and use of codes in research and teaching to facilitate development of next generation users in academe and industry.

#### 9:05 AM Invited

##### The Development of a Public Repository of Interatomic Potentials for Atomistic Simulations: *Chandler Becker*<sup>1</sup>; <sup>1</sup>National Institute of Standards and Technology

With the increasing demand and use of atomistic simulation techniques in materials research and design, the need for a repository of interatomic potentials and the means to compare them becomes ever more important. This is especially true given the sometimes widely different properties calculated using interatomic potentials that are nominally for the same element or alloy. Here we will focus on the development of a public repository to provide a source for vetted interatomic potentials, as well as reference experimental and ab-initio data for comparison. The development of standard evaluation methods (including thermodynamic, kinetic, and mechanical properties) and distribution methods will also be addressed.

#### 9:30 AM

##### Cyberinfrastructure for Integrated Computational Material Engineering: *Tomasz Haupt*<sup>1</sup>; <sup>1</sup>Mississippi State University

ICME is an approach to design products and materials that comprise them by linking material models at multiple length scales. The complexity of the new generation of simulation codes demands the employment of high-performance computing platforms. Currently, it is a very tedious and error-prone manual effort by the designer to submit, monitor and coordinate hundreds of jobs in heterogeneous distributed environments which requires the designer to learn the arcana of ever-changing IT technologies such as operating systems, batch systems, storage systems, networking, and security. This presentation demonstrates the use of the modern information infrastructure based on Service Oriented Architecture (SOA), Web Services and Grid computing streamlining of the process of gathering experimental results, and deriving the material properties for a particular material model and employing the material model in finite element analysis in the process of building validated metamodels and design optimizations.

#### 9:55 AM Break

#### 10:15 AM Invited

##### An Integrated Open Source Stack for Thermodynamics and Phase Field Simulations: *Adam Powell*<sup>1</sup>; <sup>1</sup>Opennovation

A public repository of packages for Ubuntu Linux at [www.opennovation.org/ubuntu](http://www.opennovation.org/ubuntu) provides several open source engineering software packages for that operating system. This talk will focus on the subset of packages comprising a software stack for integrated computational materials engineering (ICME) calculations. This stack consists of four tools: abinit for DFT energy calculations; ATAT for automating DFT, cluster expansion and Monte Carlo software for calculating the free energy functions of low-energy phases in a system; Ternary for calculating ternary phase diagrams from such free energy functions; and a finite element phase field code for microstructure prediction. The public repository provides full source code for all of these tools, except for ATAT which one must download from its website at CalTech (due to license restrictions), though a package on the repository automates that download and compile process. A demonstration in two ternary alloy systems illustrates the capabilities of this open source stack.

#### 10:40 AM Invited

##### FiPy: An Open Source Finite Volume PDE Solver Implemented in Python: *Jonathan Guyer*<sup>1</sup>; *Daniel Wheeler*<sup>1</sup>; *James Warren*<sup>1</sup>; <sup>1</sup>National Institute of Standards and Technology

FiPy <<http://www.ctcms.nist.gov/fipy>> is an object oriented, partial differential equation (PDE) solver, written in Python, based on a standard finite volume (FV) approach. FiPy is particularly tailored to phase transformation simulations, focusing on the phase field and level set methods. The solution of coupled sets of PDEs is ubiquitous to the numerical simulation of science problems. Numerous PDE solvers exist, using a variety of languages and numerical approaches. Many are proprietary and difficult to customize. As a result, scientists spend considerable resources repeatedly developing limited tools for specific problems. Our approach, combining the FV method and Python, provides a tool that is extensible, powerful and freely available. A significant advantage to Python is the existing suite of Open Source tools for array calculations, sparse matrices and data rendering. We will discuss our recent efforts to integrate FiPy with one particular tool, the PyTrilinos parallel sparse solvers.

#### 11:05 AM Invited

##### Implementing an Open-Source Integrated Framework for Ab Initio Thermodynamics Using Python as a Glue Language: *Raymundo Arroyave*<sup>1</sup>; *Michael Williams*<sup>1</sup>; <sup>1</sup>Texas A & M University

In this talk, I will present some recent experiences regarding the implementation of an integrated framework for ab initio calculations of thermodynamic and structural properties of crystals using Python. The open-source tools being developed are capable of seamlessly integrating a wide range of packages and programs within a single input-file based framework. Pre and post-processing of ab initio calculations using either commercial or open-source density functional theory are linked to higher level alloy thermodynamic tools, such as the ATAT Alloy Thermodynamics package, developed by Axel van de Walle to fully automate the prediction of thermodynamic and structural properties of crystals, including thermal and configurational effects. The talk will mostly consist of a brief description of the tools developed as well as their impact on the productivity of ab initio thermodynamic calculations.

#### 11:30 AM

##### The 3D Materials Atlas: An Interactive Database for Materials Research: *Andrew Geltmacher*<sup>1</sup>; *Donald Boyce*<sup>2</sup>; *Paul Dawson*<sup>2</sup>; *Matt Heying*<sup>3</sup>; *Kristina Taylor*<sup>3</sup>; *Krishna Rajan*<sup>3</sup>; *William Pearlman*<sup>4</sup>; *George Spanos*<sup>1</sup>; <sup>1</sup>Naval Research Laboratory; <sup>2</sup>Cornell University; <sup>3</sup>Iowa State University; <sup>4</sup>Rensselaer Polytechnic Institute

The 3D Materials Atlas is an interactive, web-based repository for 3D material microstructure and property data. It has been developed as part of the ONR/DARPA "D 3-D Digital Structure" program. The goal of the atlas is to provide materials scientists the ability to store and access 3D datasets for materials research, including scientific visualization, analysis, and simulation of microstructural evolution. The atlas consists of compressed data files of experimental and computational data, a relational database, and Input/Output and plug-in interfaces used for data transfer and visualization. Examples of data currently stored in the database include 3D reconstructions of actual microstructures, statistically-based microstructural representations, material

property measurements, and computationally-derived simulation results. Novel data compression routines are used for storage and transfer of large datasets. The relational database is written using Python and PostgreSQL and allows for easy recall and search functions on any of the database fields.

## 11:55 AM Concluding Comments

### Pb-Free Solders and Emerging Interconnect and Packaging Technologies: Electromigration, Microstructure, and Mechanical Properties

Sponsored by: The Minerals, Metals and Materials Society, TMS Electronic, Magnetic, and Photonic Materials Division, TMS: Electronic Packaging and Interconnection Materials Committee

Program Organizers: Sung Kang, IBM Corp; Iver Anderson, Iowa State University; Srinivas Chada, Medtronic; Jenq-Gong Duh, National Tsing-Hua University; Laura Turbini, Research In Motion; Albert Wu, National Central University

Thursday AM Room: 2020  
February 19, 2009 Location: Moscone West Convention Center

Session Chair: Nikhilesh Chawla, Arizona State University

## 8:30 AM

**In Situ Electromigration-Induced Transient Stress in Pb-Free Sn-Cu Solder Joints Measured by Synchrotron Radiation:** *Kai Chen*<sup>1</sup>; Nobumichi Tamura<sup>1</sup>; King-Ning Tu<sup>2</sup>; Yi-Shao Lai<sup>3</sup>; <sup>1</sup>Lawrence Berkeley National Laboratory; <sup>2</sup>UCLA; <sup>3</sup>Advanced Semiconductor Engineering

Electromigration-induced elastic hydrostatic stress in Pb-free SnCu solder joints has been studied by using in situ synchrotron X-ray white beam microdiffraction. The elastic stress within two different grains, one located at the anode end and the other at the cathode end, was analyzed based on the anisotropy of the  $\beta$ -Sn crystal structure. The stress at the cathode end was almost constant except for temperature fluctuation, while the compressive stress at the anode end was build-up as a function of time in electromigration until a steady state was reached. The effective charge number of  $\beta$ -Sn was estimated to be in good agreement with the calculated value. The measured compressive stress gradient is much larger than that needed in pushing Sn whisker growth.

## 8:45 AM

**Effects of Current Stressing on Shear Properties of Sn-3.8Ag-0.7Cu Solder Joints:** X. Wang<sup>1</sup>; Q. Zeng<sup>1</sup>; Q. Zhu<sup>1</sup>; Z. Wang<sup>1</sup>; J. Shang<sup>2</sup>; <sup>1</sup>Institute of Metal Research; <sup>2</sup>University of Illinois at Urbana-Champaign

Effects of electric current on the microstructure and shear properties of SnAgCu joints were investigated by lap shear of ball joints at a current density of  $1.1 \times 10^3 \text{ A/cm}^2$  and a working temperature of  $83^\circ\text{C}$ . It was found that the maximum shear load depended strongly on the current stressing time. For short durations of current stressing, only a slight decrease in the maximum shear load was observed. However, as the duration of current stressing lengthened, the maximum shear load was drastically reduced. The reductions were related to softening of the solder alloy without much loss of plasticity for the intermediate durations of current loading, and to brittle interfacial fracture at very long current loading.

## 9:00 AM

**Direct Measure the Current Crowding Effect in Flip-Chip Solder Joints:** *Shih-Wei Liang*<sup>1</sup>; Chih Chen<sup>1</sup>; K. N. Tu<sup>2</sup>; <sup>1</sup>National Chiao Tung University; <sup>2</sup>UCLA

As the electronic devices were concerned to have higher performance, the I/O capability should be increased. For this purpose, the numbers of solder joints need to raise and the size of solder joints need to reduced. The electromigration in the solder bumps would become an important reliability issue for this technology due to carrying high current density. The current crowding effect in flip-chip solder bumps has been reported several simulation studies. There are no experimental data to show out relation of the current crowding effect and the atom movement. In this paper, flip-chip solder bump with markers is adopted to distinguish the movement during electromigration due to current crowding effect. The marker velocity is proportional to the current density. The marker moved faster under higher current density. Also, the  $DZ^*$  was obtained to be  $3.34 \times 10^{-12} \text{ cm}^2/\text{s}$ .

## 9:15 AM

**The Effect of an Imposed Current on the Creep Rates of Sn-Ag-Cu Ball Grid Array Solder Joints:** *Christopher Kinney*<sup>1</sup>; Tae-Kyu Lee<sup>2</sup>; J.W. Morris<sup>1</sup>; <sup>1</sup>University of California, Berkeley; <sup>2</sup>Cisco Systems

This study examines the effect of an imposed current on the steady state creep behavior of PBGA chips. These devices are subjected to loads and carry current during operational use; therefore it is important to characterize the behavior of the chip under current. The chip interconnects consist of a  $4 \times 4$  grid of 610  $\mu\text{m}$  diameter 96.5-Sn 3.0-Ag 0.5-Cu solder balls. Different sample treatments were employed: as received, thermally aged and electromigrated. The PBGA chips were tested in creep under constant load at 20C, 75C and 100C. These conditions were repeated with the samples placed under an imposed current density to ascertain the influence of an imposed current on the creep rate. Optical and electron microscopy were used to characterize the materials before and after the tests.

## 9:30 AM

**Electrical Conductivity Changes in Eutectic Sn-Based Solder Reaction Couples during Electromigration:** Fu Guo<sup>1</sup>; *Jia Sun*<sup>1</sup>; Guangchen Xu<sup>1</sup>; <sup>1</sup>Beijing University of Technology

Electrical conductivity of electronic interconnects made with Sn-based solders undergo a significant amount of deterioration during service. With the electromigration impact, the metal atoms/ions migrated towards the direction of electron wind flow. The accumulation of atoms/ions at the anode interface could cause the hillock formation, while the depletion of atoms/ions at the cathode interface could cause the valley formation. In addition, the different  $\alpha$ -rich and  $\beta$ -rich phases in a binary eutectic system was found to separate in the bulk region of the Sn-based solders. Such mass movement will induce electrical conductivity changes at different stages of electromigration. A LabVIEW® controlled software was programmed to quantitatively measure the instantaneous electrical conductivity values after the electrical current was applied. The current study investigates the roles of different parameters, such as current density, ambient temperatures, etc., on the deterioration of electrical conductivities during the electromigration process.

## 9:45 AM

**Microstructure and Orientation Evolution of the Sn Phase as a Function of Position in Ball Grid Arrays in Sn-Ag-Cu Solder Joints:** *Tae-Kyu Lee*<sup>1</sup>; Kuo-Chuan Liu<sup>1</sup>; Thomas Bieler<sup>2</sup>; <sup>1</sup>Cisco; <sup>2</sup>Michigan State University

The Thermal fatigue performance of SAC305 solder alloy joints are studied and the microstructure evolution is observed focused on Sn grain orientation during thermal cycling on thermally aged Plastic Ball Grid array (PBGA) packages. Thermally cycled PBGA packages after various pre-conditions with 196 full array solder joints are used in this study. Each selected PBGA package is polished to view the solder joints from the top by both Polarized Optical microscopy and Orientation Imaging Microscopy. The observations reveal different patterns of single and multi-grained Sn microstructure distribution as a function of position in the package depending on their pre-condition and thermal cycle history. Overall a faster degradation of thermal cycling performance is observed after aging at  $100^\circ\text{C}$  aging, compared to both non-aged and  $150^\circ\text{C}$  aged PBGAs. The difference of the distribution at different pre-conditions and evolution of the grain structures during thermal cycling are discussed.

## 10:00 AM

**Mechanical Behavior and Corresponding Microstructural Characterization of Solder Materials:** *Fang Cao*<sup>1</sup>; Ellen Cerreta<sup>1</sup>; George Gray<sup>1</sup>; <sup>1</sup>Los Alamos National Laboratory

Enhanced need for electronic devices to survive and function in extreme environments, such as conditions of stress and/or temperatures fluctuations, requires knowledge of the mechanical properties of solder materials in a wide range of temperatures and strain rates. Currently information on the dynamic response of solder alloys is limited. The focus of this study is, therefore, to investigate the mechanical behavior of three solder alloys: Sn63Pb37, Sn62Pb36Ag2, and Sn96.5Ag3Cu0.5 (wt%) at a variety of temperatures (77 ~ 298 K) and strain rates (10<sup>-3</sup> ~ 10<sup>3</sup>) by conducting quasi-static and dynamic compression tests. Microstructural characterization of these materials prior to and after testing was carried out by scanning electron microscopy (SEM) to correlate observed properties with developing microstructures. The effects of the Sn grain morphology and orientation, precipitate microstructure and corresponding substructural changes on the mechanical response of these solder alloys were studied and discussed in detail.

**10:15 AM Break****10:30 AM**

**Effect of Microstructure Evolution on the Mechanical Properties of SAC Solder Joints:** *Yan Xing*<sup>1</sup>; James Woods<sup>1</sup>; Pushkraj Tumne<sup>1</sup>; Michale Meilunas<sup>2</sup>; Peter Borgesen<sup>2</sup>; Eric Cotts<sup>1</sup>; <sup>1</sup>Suny-Binghamton; <sup>2</sup>Unovis Solutions

We examine the effect of the evolution of solder joint microstructure (Sn dendrite and precipitate size, Sn grain size and orientation) on the mechanical properties of SnAgCu solder joints. Solder joints (500 micron SAC205 balls on Cu/OSP pads) were subjected to thermal cycling or room temperature shear fatigue tests. Variations in sample lifetime with initial (as-solidified) microstructure, dwell time and evolution of microstructure were examined. Crack initiation and growth were examined as a function of dwell time, or number of shear fatigue cycles. Correlations between solder joint lifetime and microstructure were studied. We found that Sn dendrite, precipitate and grain size was all coarsened due to thermal cycling aging. The degree of recrystallization also changed as a function of dwell time. The results of both tests show that although recrystallization may help cracks propagate, cracks can form before recrystallization occurs.

**10:45 AM**

**Effects of Microstructure on Creep of Sn-3.5Ag Solder:** *Sung Bum Kim*<sup>1</sup>; Yu Jin<sup>1</sup>; <sup>1</sup>KAIST

Understanding the mechanism of creep deformation is an important element of estimating the solder joint life time accurately. However, in real life, creep data of Pb-free solder alloys vary widely even for a given composition. A main culprit is differences in the solder microstructure ( $\beta$ -Sn granular size and volume fraction, grain size, Ag<sub>3</sub>Sn particle size and spacing), which are dependent of solidification conditions. Varying microstructures are obtained from various cooling rates from melt, steady maintaining temperatures and times during solidification process. Primary  $\beta$ -Sn granule is surrounded by walls of creep resistant eutectic region which is a mixture of  $\beta$ -Sn and precipitates of Ag<sub>3</sub>Sn. In the present work, creep tests were conducted under uniaxial tension by using the Sn-3.5Ag alloy with varying microstructures. Based on nano-indentation measurement of  $\beta$ -Sn and eutectic region, a model is also presented here, which explains effects of solder microstructure.

**11:00 AM**

**Effects of Solder Cu Concentrations on the Formation of Micro Voids:** *Yi-Wun Wang*<sup>1</sup>; C. Robert Kao<sup>1</sup>; <sup>1</sup>National Taiwan University

In the reactions between Sn-based solders and Cu substrate, the formation of micro voids within the Cu<sub>3</sub>Sn layer had been reported by many research groups. These micro voids raise the potential of brittle interfacial fracture of the solder joints. In this study, the effect of Cu concentration in solders on the micro voids formation was studied. The solder compositions used were SnxCu (x=0~0.8 wt.%). The reflow temperature profile had a peak temperature of 235°C. The reaction times were 90 s and 30 s. The samples were then subjected to solid-state aging at 160°C for 500, 1000 or 2000 hrs. The experimental results show that the Cu concentration in solder can influence the micro voids formation. High Cu concentration in solder retards the micro voids formation.

**11:15 AM**

**Low Stress Creep in SAC Solder:** *Kathryn Baldwin*<sup>1</sup>; Chris Kinney<sup>1</sup>; Tae-kyu Lee<sup>2</sup>; Weidong Xie<sup>2</sup>; John Morris<sup>1</sup>; <sup>1</sup>University of California, Berkeley; <sup>2</sup>Cisco Systems

It is well known that behavior and governing equations for creep change in the low stress regime. There is also a paucity of data for Pb-free solders in the low stress creep regime. The work reported here characterizes the creep behavior for two commercially important SnAgCu solders in the low stress regime and explores the governing constitutional equations. The solder specimens were tested using constant mechanical loads under various conditions in a double-shear configuration. Both as-cast and aged specimens were tested.

**11:30 AM**

**Effect of Strain Rate and Temperature on Tensile Properties of Sn-8.5Zn-0.5Ag-0.01Al-0.1Ga Solder:** *Teng-Chun Hsuan*<sup>1</sup>; Kwang-Lung Lin<sup>1</sup>; <sup>1</sup>National Cheng Kung University

This study investigated the tensile properties of Sn-8.5Zn-0.5Ag-0.01Al-0.1Ga (5-e) solder alloy under various temperatures (25°C~180°C) and strain rates (8.33×10<sup>-4</sup> s<sup>-1</sup>~3.33×10<sup>-2</sup> s<sup>-1</sup>). The yield stress and ultimate tensile strength increase while the ductility reduces with an increase in strain rate or a lowering in temperature. Most of the fracture surfaces of 5-e alloy appear to

show dimple morphology except for the case with strain rate of 3.33×10<sup>-2</sup> s<sup>-1</sup> at 25°C whence existing a fracture transition from ductile to brittle. During tensile test at 180°C and 8.33×10<sup>-4</sup> s<sup>-1</sup>, the grain growth of  $\beta$ -Sn caused the ductility reduction of 5-e alloy. An increase in strain rate and the lowering in temperature result in reduction in the dimension of the fracture dimple. With temperature increasing from 25 to 180°C, the strain hardening exponent (n) of 5-e solder alloy reduces gradually but the strain rate sensitivity exponent (m) increases rapidly.

**11:45 AM**

**Re-Precipitation of Cu<sub>6</sub>Sn<sub>5</sub> onto Ni Substrate during Thermal Aging of Solder Joints:** *Bo-Mook Chung*<sup>1</sup>; Joo-Youl Huh<sup>1</sup>; <sup>1</sup>Korea University

In electronic packaging, SnAgCu (SAC) solders are commonly used to produce solder joints with Ni/Au-finished substrates. In this study, the Cu/Sn/Ni and Cu/Sn/Cu/Sn/Ni diffusion couples were employed to examine the re-precipitation of Cu<sub>6</sub>Sn<sub>5</sub> particles in the bulk of a SAC solder onto the Ni substrate during solid-state aging. Pure Sn (27  $\mu$ m) and Cu (0.8  $\mu$ m) layers were sequentially electrodeposited on thick Ni substrates to produce the diffusion couples. The diffusion couples were aged at 200°C for different periods of time. At the early stage of aging, all the Cu layers were completely transformed into (Cu<sub>1-y</sub>Ni<sub>y</sub>)<sub>6</sub>Sn<sub>5</sub> and a ternary (Cu<sub>1-x</sub>Ni<sub>x</sub>)<sub>6</sub>Sn<sub>5</sub> compound layer formed at the Sn/Ni interface. The thickness and Ni content of the (Cu<sub>1-y</sub>Ni<sub>y</sub>)<sub>6</sub>Sn<sub>5</sub> and (Cu<sub>1-x</sub>Ni<sub>x</sub>)<sub>6</sub>Sn<sub>5</sub> layers were monitored as functions of the aging time. In this presentation, we will also discuss the formation and growth of a (Ni,Cu)<sub>3</sub>Sn<sub>4</sub> layer at the (Cu<sub>1-x</sub>Ni<sub>x</sub>)<sub>6</sub>Sn<sub>5</sub>/Ni interface.

**12:00 PM**

**Shear and Pull Testing of Sn3.0Ag0.5Cu Solder with Ti/Ni(V)/Cu UBM during Aging:** *Kai-Jheng Wang*<sup>1</sup>; Jeng-Gong Duh<sup>1</sup>; <sup>1</sup>National Tsing Hua Univ

The Ti/Ni(V)/Cu under bump metallization is widely used in the flip chip technology today. During reflow or aging, Sn atoms would diffuse to Ni(V) layer to form the Sn-rich phase, as the so-called "Sn-patch". However, the literatures about relationship between Sn-patch and mechanical property of solder joint were limited. In this study, the sputtered Ti/Ni(V)/Cu UNM was reflowed with Sn3.0Ag0.5Cu solder, and then the solder joint was aged at 125 and 200C, respectively, for 500h, 1000h, and 2000h. (Cu,Ni)<sub>6</sub>Sn<sub>5</sub> and (Cu,Ni)<sub>3</sub>Sn<sub>4</sub> formed and grew gradually at interface between solder and Ni(V) during aging at 125C. In contrast, Sn-patch replaced Ni(V) layer, and another (Ni,Cu)<sub>3</sub>Sn<sub>4</sub> formed between (Cu,Ni)<sub>6</sub>Sn<sub>5</sub> and Sn-patch at 200C for 1000h. After different heat treatment, the solder joints were tested by a XYZTEC bonding tester. The effects of the aging temperature and Sn-patch formation on mechanical property of the solder joint would be probed and discussed.

**12:15 PM**

**Strain Localization in Pb-Free Solder Joints Due to Rate-Dependent Solder Behavior:** *Dennis Chan*<sup>1</sup>; Xu Nie<sup>1</sup>; Ganesh Subbarayan<sup>1</sup>; Indranath Dutta<sup>2</sup>; <sup>1</sup>Purdue University; <sup>2</sup>Washington State University

Increasingly, it is necessary to understand Pb-free solder response under conditions from quasi-static office use environment to drop/shock conditions. Significant existing research is focused on SnAgCu solder behavior at low strain rates (10<sup>-6</sup> to 10<sup>-3</sup>s<sup>-1</sup>). In a companion paper we presented data characterizing behavior at high strain rates and constitutive models valid across nine decades of strain rate. This study uses that data to numerically model strain localization in solder joints from rate-dependent loading. We demonstrate at low strain rates, plastic damage accumulation and failure is in the solder near its interface with the intermetallic compound. Consistent with experimental observations, use of rate dependent solder behavior predicts increasing load localization at the interface with increasing loading rate. We use cohesive zone fracture models embedded in finite element models to characterize rate-dependent failure at the interface. We simulate ball shear and ball pull tests to demonstrate rate-dependent behavior effects of solder.



## Progress in Computational Materials Science and Engineering Education: Session II

Sponsored by: The Minerals, Metals and Materials Society, TMS: Education Committee

Program Organizers: Gregory Olson, Northwestern University; Anter El-Azab, Florida State University; Katsuyo Thornton, University of Michigan; Laura Bartolo, Kent State University

Thursday AM  
February 19, 2009

Room: 3003  
Location: Moscone West Convention Center

*Session Chairs:* Anter El-Azab, Florida State University; Katsuyo Thornton, University of Michigan

### 8:30 AM Invited

**Molecular Simulation Modules in Undergraduate and Graduate Education: Examples from Molecular Engineering:** *Aaron Keys*<sup>1</sup>; Christopher Iacovella<sup>1</sup>; Sharon Glotzer<sup>1</sup>; <sup>1</sup>University of Michigan

We discuss the use of molecular simulation modules developed using the Glotzilla simulation API in undergraduate and graduate courses teaching fundamental concepts in thermodynamics, kinetics, and molecular interactions. The API enables easy creation of MC and MD simulation modules, realtime 2-d and 3-d rendering tools, and analysis methods. The modules are coordinated with a Wiki and link to the Materials Digital Library (MATDL) Soft Matter Wiki and digital library repository ([www.matdl.org](http://www.matdl.org)). This provides students with relevant linked material including definitions of key terms, explanations of algorithms, research examples, and links to relevant literature. As examples, we show modules on phase separation, crystallization, liquid-crystalline ordering, and polymer dynamics designed for an undergraduate course in molecular engineering at the University of Michigan. *The molecular engineering course was developed and taught by M.J. Solomon and M.A. Burns. MatDL is a collaboration between the University of Michigan and Kent State University (NSF DUE-0532831).*

### 8:55 AM Invited

**Crystal Growth: Experimental and Mathematical/Computer Modeling Courses in Beauty, Symmetry and Complexity:** *John Lowengrub*<sup>1</sup>; Daniel Mumm<sup>1</sup>; Katsuyo Thornton<sup>2</sup>; <sup>1</sup>University of California, Irvine; <sup>2</sup>University of Michigan

In this talk, we discuss two month-long courses on crystal growth we developed for high-school students as part of the California State Summer School for Mathematics and Science (COSMOS) at the University of California, Irvine. The first course dealt with concepts and characterization of crystal growth using physical theory and experiments. In this course, we discussed the underlying science of why crystals take their shape as well as the basics of thermodynamics, the role of atomic structure and how, together with environmental conditions, these determine the symmetry and shape of crystals. The second course focused on modeling and simulation of crystal growth at the micro and nano scales. The students applied the computer models to develop their own virtual crystals with remarkable shapes and symmetries. The students took both courses at the same time, and working in teams, produced a research project which involved both experimental and modeling components.

### 9:20 AM Invited

**Computational Materials Science Course for Soft Matter Physicists:** *Robin Selinger*<sup>1</sup>; <sup>1</sup>Kent State University

Computer simulation plays an important role in the study of soft matter, including both fundamental research and engineering applications. We describe a Computational Materials Science course at Kent State's Liquid Crystal Institute, with a focus on modeling liquid crystals and other soft materials. Topics covered include: random walks and diffusion in disordered media; Monte Carlo methods and lattice models; simulated annealing; modeling microstructure and defects in liquid crystal cells; and off-lattice molecular simulation. Models and computational algorithms are discussed in class, along with techniques for data analysis and visualization. Students then independently write their own simulation codes "from scratch" in the programming language of their choice. The final few weeks of the course are devoted to individual research projects.

We present examples of lesson units with associated homework exercises, and discuss the course's long-term impact on student achievement.

### 9:45 AM Invited

**Enhancing Materials Science and Engineering Curricula through Computation:** *John Kieffer*<sup>1</sup>; <sup>1</sup>University of Michigan

Our goal is to devise a more effective instructional process by incorporating computation and cyber infrastructure (CI) throughout materials science and engineering (MSE) undergraduate curriculum. We expect students to gain a better fundamental understanding of materials science concepts and principles, and to advance their computational thinking and proficiency. To this end we are developing instructional modules that (i) visually present fundamental concepts in materials science, thereby increase student comprehension; (ii) actively engage students in computer-based experimentation; and (iii) concentrate student attention on algorithmic thinking and concepts in scientific computation. Modules are based on visualization, simulation, and numerical problem solving approaches. Currently we are establishing proof of concept in the context of the MSE Thermodynamics course by evaluating student learning before and after introducing these modules. In this presentation we demonstrate examples of such modules and report on the impact this effort has had to date.

### 10:10 AM Break

### 10:20 AM

**The Role of Coaching in Facilitating Computational Materials Science Education:** *Michele Manuel*<sup>1</sup>; McKenna Ann<sup>2</sup>; <sup>1</sup>University of Florida; <sup>2</sup>Northwestern University

Introduction of computational tools in the undergraduate curriculum is a daunting task. A new coaching model has been implemented in a junior-level materials science and engineering course that integrates computational tools within the framework of traditional capstone design. This model utilizes graduate students as coaches to serve as a technical resource and role model for the undergraduate design teams, producing learning experiences that are at a high technical level. Results show that successful coaching provides greater individualized attention for the undergraduate design teams and professional development opportunities for the graduate student coaches.

### 10:45 AM

**Computational Materials Science Education as Part of a Degree Program in Computational Science:** *Anter El-Azab*<sup>1</sup>; Sachin Shanbhag<sup>1</sup>; Max Gunzburger<sup>1</sup>; <sup>1</sup>Florida State University

This talk summarizes an effort to establish a Computational Materials Science (CMS) subfield in a wider-scope interdisciplinary computational science program at Florida State University, with both undergraduate and graduate components. The talk addresses the conceptual and scientific challenges that must be dealt with in order to develop and implement CMS curricula in a traditional university environment. These challenges include (i) creating the right level of synergy between CMS and other programs in engineering, chemistry, physics and computational mathematics and scientific computing, (ii) striking the right balance between various CMS program components, (iii) developing and teaching CMS curricula in way that integrates materials theory and computational techniques, and (iv) performing the task of CMS education at the undergraduate level. The relevant issues will be illustrated by three examples: advanced Monte Carlo modeling of materials, continuum models of microstructure evolution in materials, and multiscale modeling methods.

### 11:10 AM

**Multiyear Computational Materials Design Education:** *Gregory Olson*<sup>1</sup>; <sup>1</sup>Northwestern University

The Bodeen-Lindberg Materials Design Studio serves as a central teaching facility for computational MSE in the undergraduate materials curriculum at Northwestern. Software tools introduced throughout core courses are integrated in a required junior-level Materials Design course. Through an integration of education activities of the Segall Design Institute with funded design research activities of the Materials Technology Laboratory, coaching by graduate students and post-doctoral researchers facilitates cross-disciplinary concurrent computational engineering of materials and structures in engineering schoolwide "institute projects" involving multidisciplinary undergraduate teams spanning freshman to senior level. Project examples include "Civil Shield" addressing materials and structures for civilian anti-terrorism bomb mitigation, and "Smart Stent" integrating high-performance shape memory alloys in endovascular stent designs.

### Computational Materials Research and Education Luncheon Roundtable: Gibbs: A Multi-Component Thermodynamics Calculation and Visualization Suite

Sponsored by: National Science Foundation

Program Organizer: Laura Bartolo, Kent State University

Thursday PM

Room: 3003

February 19, 2009

Location: Moscone West Convention Center

*Session Chairs:* Adam Powell, Opennovation; Edwin Garcia, Purdue University; Raymundo Arroyave, Texas A & M University

### 12:00 PM Panel Discussion

### Recycling—General Session: Session III: Aqueous Processing

Sponsored by: The Minerals, Metals and Materials Society, TMS Extraction and Processing Division, TMS Light Metals Division, TMS: Recycling and Environmental Technologies Committee

Program Organizer: Joseph Pomykala, Argonne National Laboratory

Thursday AM

Room: 2024

February 19, 2009

Location: Moscone West Convention Center

*Session Chair:* Jeffrey Spangenberg, Argonne National Laboratory

### 8:30 AM

**Fundamental Aspects of Electrocoagulation: Removal of Oily Wastewaters from the Metallurgical Industry:** *Mauricio Torem*<sup>1</sup>; Antonio Merma<sup>1</sup>; Rodolfo Rangel<sup>1</sup>; Roberto de Carvalho<sup>1</sup>; Lorgio Gonzales<sup>1</sup>; <sup>1</sup>Catholic University of Rio de Janeiro PUC-Rio

In this work, the electrocoagulation technique was studied in order to treat chemically stabilized concentrated oil-water emulsions. This study was mainly focused on the effects of operating parameters such as initial pH, current density, reaction time, ionic strength, electrode distance and inlet concentration on the separation of oil as measured by the chemical oxygen demand (COD) method. The synthetic emulsion was prepared from Shell - Talpa 30 oil (3g.L<sup>-1</sup>) and sodium dodecyl sulfate (1.0 g.L<sup>-1</sup>), having a Zeta potential around -70 mv at pH 8.7. The process was carried out in an electrocoagulation cell with a set of four parallel monopolar electrodes. This set consisted of two aluminum plate anodes and two 316L stainless steel plate cathodes. Kinetic curves showed that the electrocoagulation process exhibits three phases. The results showed that the period to reach the reactive phase decreased as the current density increased and the pH values decreased.

### 8:50 AM

**Biosorption Removal of Aluminum Species from Wastewaters Streams:** *Mauricio Torem*<sup>1</sup>; Javier Basurco<sup>1</sup>; <sup>1</sup>Catholic University of Rio de Janeiro PUC-Rio

In this work, a gram-positive bacteria was used as biosorbent to elucidate the aluminum load capacity under different conditions related to metallurgical and chemical plants. The sorption data followed the Langmuir, Freundlich, Temkin, Dubinin-Radushkevich isotherms. In order to determine the best isotherm fit, three error analysis methods were used to assess the data: correlation coefficient (R<sup>2</sup>), residual root mean square error (RMSE) and Chi-square test. The error analysis established that the Freundlich model fits better the aluminum biosorption data. The maximum sorption capacity was found to be 41.59 mg.g<sup>-1</sup>. The maximum removal of aluminum was 95% at pH around 5. Thermodynamic parameters have also been evaluated and the results show that the sorption process was spontaneous and exothermic in nature. The experimental kinetics data was evaluated considering three models (pseudo-second order, pseudo-first order and intraparticle diffusion). This study indicated that the *R. opacus* is an environmental friendly biosorbent.

### 9:10 AM

**Biosorption of Cadmium from Aqueous Solutions by Waste Microzyme:** *Chen Yunnen*<sup>1</sup>; <sup>1</sup>Jiangxi University of Science and Technology

The test and use of natural materials as biosorbents for the removal of heavy metals from industrial wastewater is under constant development. Consequently this work concerns the study of cadmium biosorption by means of pretreated waste microzyme. The cadmium removal study has been carried out batchwise where the influence of physico-chemical key parameters such as the pH value of solution, the temperature, the agitation speed, the contacting time, the dosage of adsorbent and initial cadmium ions concentration have been considered. The maximum percent removal was attained at the pH 7.0 after about 30 min. The adsorbent can be effectively regenerated using 0.1M HCl and reused. The experimental results provided evidence for ion exchange as the major biosorption mechanisms for binding the divalent metal ions to the waste microzyme. Waste microzyme was a potential biosorbent for the removal of Cd(II) from the effluent of electroplating industry.

### 9:30 AM

**Effects of Organic Acids on Extraction of Cr(III) in Soils Contaminated by Chromium-Containing Slag:** Youze Xu<sup>1</sup>; *Liyuan Chai*<sup>1</sup>; Zhihui Yang<sup>1</sup>; Shunhong Huang<sup>1</sup>; <sup>1</sup>Institute of Environmental Science and Engineering, School of Metallurgical Science and Engineering, Central South University

The effect of oxalic acid, acetic acid, citric acid and EDTA on extraction of Cr(III) in soils contaminated by chromium-containing slag were investigated using a batch of incubation experiment. The results show that the pH value decreases more obvious with the increase of the amount of organic acid. The amount of Cr(III) extracted increases with increasing the amount of organic acid. When the ratio of organic acids to total Cr(III) was 5:1, citric acid revealed the highest extraction effectiveness, followed by EDTA, oxalic acid and acetic acid, respectively. The amounts of Cr(III) extracted by citric acid, EDTA, oxalic acid and acetic acid increased by 439%, 244%, 215% and 162%.

### 9:50 AM

**Leaching and Reduction of Cr(VI) by Indigeous Microorganism in the Contaminated Soils:** Youze Xu<sup>1</sup>; *Liyuan Chai*<sup>1</sup>; *Zhihui Yang*<sup>1</sup>; Shunhong Huang<sup>1</sup>; Changqing Su<sup>1</sup>; Bing Wang<sup>1</sup>; <sup>1</sup>Central South University

The leaching and reduction of Cr(VI) in soils contaminated by chromium-containing slag were investigated with column experiments. The results showed that Cr(VI) concentration in leachate decreased from 988 mg L<sup>-1</sup> to 407 mg L<sup>-1</sup> after 7 days when water was used as leaching agent. However, Cr(VI) in leachate in culture medium treatment was not detected at above periods. In comparison, Cr(VI) concentration in leachate from autoclaved soil remained 398 mg L<sup>-1</sup> at the end of experiment. The results indicated that the indigenous microorganism was capable of reducing Cr(VI). The amount of Cr(VI) reduction was 335 mg at the whole experiment period and the reduction rate was 67.09 mg d<sup>-1</sup>. Carbon supply showed minor effect on Cr(VI) reduction. However the reduction capability of Cr(VI) could be improved by combination of the carbon and the nitrogen. The optimal quantity was 5 g L<sup>-1</sup> of yeast extract and 4 g L<sup>-1</sup> of glucose.

### 10:10 AM

**Effects of the Mixed Surfactants on Detoxification of Chromium-Containing Slag by *Achromobacter* sp. CH-1:** Lijuan Chen<sup>1</sup>; *Liyuan Chai*<sup>1</sup>; Yan Huang<sup>1</sup>; Yude Shu<sup>1</sup>; <sup>1</sup>School of Metallurgical Science and Engineering, Central South University

During the detoxification of chromium-containing slag by *Achromobacter* sp. CH-1, anionic surfactant Sodium Dodecyl Sulphate(SDS) and its mixed systems with different Tween surfactants(Tween 20, Tween 60 and Tween 80) were used to promote the interaction between the bacteria and the chromium-containing slag and the rate of acid-soluble Cr(VI) leached from the slag. The effects were evaluated by the surface tension, the pH of the leaching solution and the leaching rate of total Cr(VI) from the slag. The results showed that the surfactants systems improved Cr(VI) leaching and its detoxification of chromium-containing slag. The mixed surfactants of SDS combined with Tween surfactant revealed better effectiveness of detoxification than SDS only. When the mass ratio of SDS to Tween 80 was 1:1, the rate of Cr(VI) leached from the slag increased by 12%.

### 10:25 AM Break

10:40 AM

**Adsorption of Copper from Aqueous Solution by Chemically Modified Orange Peel:** Sha Liang<sup>1</sup>; Ningchuan Feng<sup>1</sup>; Qinghua Tian<sup>1</sup>; Xueyi Guo<sup>1</sup>; <sup>1</sup>School of Metallurgy Science and Technology

In this study, adsorption of copper by chemically modified orange peel was investigated. A conspicuous change occurs in the surface morphology of the biomass due to modification, which is depicted by SEM images. Equilibrium isotherms and kinetics were obtained, and the effects of various factors, including solution pH, contact time, initial metal ions concentration and temperature, were studied by batch experiments. Equilibrium was better described by Langmuir isotherms rather than Freundlich isotherms, and maximum adsorption capacity was 70.67mg•g<sup>-1</sup>. With increase of temperature, adsorption efficiency decreased. The biosorbent was suitable for repeated use for more than five cycles.

10:55 AM

**Adsorption of Copper Ions in Aqueous Solution by a Submersed Aquatic Macrophyte *Potamogeton Pectinatus* L:** Licheng Zhou<sup>1</sup>; Liyuan Chai<sup>1</sup>; <sup>1</sup>Central South University

The use of aquatic plants for the removal of heavy metals from wastewater has gained high interest. In this study, batch experiments were conducted to evaluate the adsorption of copper ions in aqueous solution by *P. pectinatus* L. under various conditions of contact time, initial pH of the solution, metal concentration and adsorbent dosage. The results showed that the maximum adsorption amount of copper ions by *P. pectinatus* L. was 22.60 mg g<sup>-1</sup> when the initial copper ions concentration was 98.41mg L<sup>-1</sup> at pH 4.5. The Langmuir and Freundlich models were used to describe the adsorption equilibrium of copper ions on *P. pectinatus* L. and the adsorption followed the Langmuir isotherm. The adsorption kinetic was well-fitted with pseudo-second-order sorption equations.

11:10 AM

**Novel Technology for Treatment of Acidic Wastewater Containing Mercury in Zinc Smelter by Biologics:** Qingwei Wang<sup>1</sup>; Liyuan Chai<sup>1</sup>; Yunyan Wang<sup>1</sup>; Qingzhu Li<sup>1</sup>; Yude Shu<sup>1</sup>; <sup>1</sup>School of Metallurgy Science and Engineering, Central South University

This study focused on acidic wastewater from producing sulfuric acid system in zinc smelter containing mercury 21.48mg/L, zinc 55.85mg/L, lead 38.50mg/L, copper 1.68mg/L, cadmium 10.25mg/L, As 29.86mg/L treated by biologics. The factors of pH value, the ratio of biologics to mercury, complexing time, hydrolytic time and temperature was studied in this paper. Experimental results indicated that at pH value 10, quantity of biologics to mercury ratio was 16, complexing time 30min, hydrolyzation time 20min, temperature at 40°, concentration of mercury in treated water was removed to 22.15µg/L. At same time heavy metals such as Zn, Pb, Cu, Cd, As was removed by biologics, the remained concentration in treated water was Zn 0.53mg/L, Pb 0.12mg/L, Cu 0.01mg/L, Cd low to 0.01mg/L and As 0.023mg/L. According to EDAX analysis, mercury content in complexing sediment reached 28.49% easily to recycle as raw material and low concentration of heavy metals in hydrolytic sediment easily to dispose and treat.

11:25 AM

**Removal of Hg(II) from Aqueous Solutions Using Spent Grain:** Liyuan Chai<sup>1</sup>; Qingzhu Li<sup>1</sup>; <sup>1</sup>Central South University

In this study, spent grain was used as an adsorbent for the removal of Hg(II) from aqueous solutions, the process parameters such as contact time, solution pH, adsorbent dose, and initial Hg(II) concentration were studied in batch experiments. The initial adsorption process was fast, 91.08% of adsorption occurred within 5 min and equilibrium was reached at around 30min. Adsorption process was found to follow pseudo-second-order kinetics. The equilibrium data were better fitted to Langmuir isotherm than Freundlich isotherm with the maximum adsorption capacity 41.36 mg/g. The structure and component of spent grain before and after adsorption of Hg(II) were investigated using scanning electron microscope(SEM) and energy dispersive X-ray analysis(EDAX), these analysis also confirmed the adsorption of Hg(II) onto spent grain. The results indicated that spent grain had potential as a new inexpensive adsorbent for Hg(II) removal from aqueous solutions.

11:40 AM

**Adsorption and Recovery of Ag(I) from Aqueous Solutions Using Spent Grain:** Qingzhu Li<sup>1</sup>; Liyuan Chai<sup>1</sup>; <sup>1</sup>Central South University

The brewing industry byproduct, spent grain(SG), was evaluated for its ability to adsorb Ag(I) from aqueous solutions. Ag(I) adsorption was dependent

on solution pH, contact time, adsorbent dose, initial Ag(I) concentration and temperature. The kinetic data was well described by pseudo-second-order kinetic model, indicating that chemical adsorption was the rate-controlling step. The equilibrium data followed Freundlich isotherm rather than Langmuir isotherm, suggesting heterogeneity of the adsorption sites on spent grain. Ag(I) desorbed from Ag(I)-loaded spent grain was also evaluated in this study. HCl, NaOH, Na<sub>2</sub>S<sub>2</sub>O<sub>3</sub> and ultrapure water were chosen as eluants and desorbed Ag(I)-loaded spent grain for 30min, Ag(I)-loaded spent grain desorbed in 0.1M Na<sub>2</sub>S<sub>2</sub>O<sub>3</sub> exhibited higher elution efficiency as compared with other eluants. The results indicated that application of spent grain for adsorption and recovery of silver from aqueous solutions was feasible.

11:55 AM

**Treatment of Wastewater Containing Benzene by Technology Combined Blow-off with Fenton Reagent Oxidation:** He Dewen<sup>1</sup>; Qin Yan<sup>1</sup>; Liang Dingming<sup>1</sup>; Wang Wei-liang<sup>1</sup>; Du Lu<sup>1</sup>; <sup>1</sup>Central South University

The influence of wastewater containing benzene from chemical industry by technology combined blow-off with Fenton reagent oxidation was experimentally studied. The present results suggest that the technology combined blow-off with Fenton reagent oxidation can effectively remove benzene pollutant in wastewater. The main factors that influence the removal benzene such as temperature and blowing time and volume, pH and reagent dosage of H<sub>2</sub>O<sub>2</sub> and Fe<sup>2+</sup> are studied and the optimal experimental conditions are as follows: time 20min, temperature 40°, air-blowing volume 0.4L/min, pH value 5, and H<sub>2</sub>O<sub>2</sub> and Fe<sup>2+</sup> dosage 2mL/L and 200mg/L respectively. Under the above conditions, benzene pollutant can be removed up to 97%. Compared to other removal ways of wastewater containing benzene, the technology combined blow-off with Fenton reagent oxidation is more effective and has the advantage of high speed.

12:10 PM

**Removal of Zinc and COD from Electroplating Effluent Using Sawdust:** Chen Yunnen<sup>1</sup>; Jiangxi University of Science and Technology

This work concerns the removal of zinc(II) and COD by means of sawdust obtained as a by-product from locally used wood. The zinc(II) and COD removal study has been carried out batchwise where the influence of physico-chemical key parameters such as tree species, the pH value of solution, the temperature and the contacting time and dosage of adsorbent have been considered. The maximum percent removal was attained at pH 9.0 all for Zn(II) and COD after about 30 min. The adsorbent can be effectively regenerated using 0.1M HCl. The experimental results provided evidence for ion exchange as the major adsorption mechanisms for binding the divalent metal ions to the sawdust. Pine sawdust was a potential adsorbent for the removal of Zn(II) from the effluent of electroplating industry.

## RPV Embrittlement and Fusion Materials: Measuring, Modeling and Managing Irradiation Effects: Fusion Reactor Materials: Technical Contributions of Professor G. Robert Odette

Sponsored by: The Minerals, Metals and Materials Society, TMS Structural Materials Division, TMS/ASM: Nuclear Materials Committee

Program Organizers: Matthew Alinger, GE Global Research; Kurt Edsinger, Electric Power Research Institute; Roger Stoller, Oak Ridge National Laboratory; Brian Wirth, University of California, Berkeley

Thursday AM

February 19, 2009

Room: 2008

Location: Moscone West Convention Center

Session Chairs: Matthew Alinger, GE Global Research; Kurt Edsinger, Electric Power Research Institute

8:30 AM Invited

**Great Footprints toward Viable Fusion Materials: The Roadmap of Professor Bob Odette:** Hideki Matsui<sup>1</sup>; <sup>1</sup>IAE Kyoto University

UCSB is recognized worldwide for materials science excellence, and Professor Bob Odette is the main engine in nuclear materials. My interactions and collaborations with Prof. Odette have focused on the development of vanadium-based alloys for fusion reactor materials, the development of small specimen test technology to minimize the volume of materials to be irradiated



in the International Fusion Materials Irradiation Facility, and the evaluation of the Master Curve Shifts Method for predicting shift of the Ductile to Brittle Transition Temperature. These are just a small fraction of his accomplishments. More recently, he developed the "Injector Foil" experiment for helium effects in ferritic steels. His success is not only in the technical but also in education, including mentoring a number of brilliant young Japanese and European Scientists. It is difficult to cover all aspects of his influence but I will highlight some of his important accomplishments related to fusion materials.

### 8:50 AM Invited

#### **Integration of Modeling and Experimental Validation in Fusion Materials Research:** *Steven Zinkle*<sup>1</sup>; <sup>1</sup>Oak Ridge National Laboratory

Throughout his distinguished research career, Bob Odette has been a champion for utilization of tightly integrated physics-based models and experimental tests of model alloy systems. This efficient scientific methodology has proved particularly useful for investigating fundamental radiation effects mechanisms for materials exposed to the intense high-energy neutron irradiation environment of proposed future fusion energy systems. In this talk, a brief overview will be given to summarize current understanding of physical mechanisms responsible for void swelling and fracture toughness embrittlement of potential structural materials systems for fusion energy. The key role of the high transmutant helium generation levels in the deuterium-tritium fusion reaction environment will be discussed. Due to limited volumes of material or irradiation space, it is often essential to utilize innovative miniaturized specimen test techniques to extract the maximum useful information from nonstandard specimen geometries.

### 9:10 AM Invited

#### **Understanding and Managing the Effects of Helium on Fusion Structural Material Properties:** *Richard Kurtz*<sup>1</sup>; <sup>1</sup>Pacific Northwest National Laboratory

A unique aspect of the fusion neutron environment is substantial production of gaseous transmutation products such as helium and hydrogen. Helium is particularly detrimental to mechanical performance because it is insoluble in materials and can agglomerate at grain boundaries. Professor G. Robert Odette has made substantial contributions for almost 40 years to the understanding of how helium interacts with microstructural features and to the creation of more helium tolerant materials. This paper highlights his many technical contributions to understanding and managing helium effects, among which are models of the transport and fate of helium and prediction of the critical bubble size for break-away void swelling, design and implementation of novel irradiation effects experiments, including a 'helium-implanter layer' technique that enables exploration of microstructural evolution at fusion relevant He/dpa ratios, and development of advanced nanostructured ferritic alloys that offer the potential for improved radiation resistance and tolerance for high helium concentrations.

### 9:30 AM Invited

#### **In Situ He Implanter Studies of the Transport and Fate of Helium at Fusion Relevant Helium to Displacement Per Atom Ratios:** *Takuya Yamamoto*<sup>1</sup>; G. Robert Odette<sup>2</sup>; Danny Edwards<sup>2</sup>; Pifeng Miao<sup>1</sup>; Richard Kurtz<sup>2</sup>; Peter Hosemann<sup>3</sup>; Stuart Maloy<sup>3</sup>; <sup>1</sup>University of California, Santa Barbara; <sup>2</sup>Pacific Northwest National Laboratory; <sup>3</sup>Los Alamos National Laboratory

Thermal neutron 58-Ni reactions in NiAl layers irradiated in the JP26 and 27 HFIR experiments were used to implant alpha particles into a large matrix of iron based alloys to a depth of 6 to 8  $\mu\text{m}$ . Fast neutrons generated displaced atoms at a He/dpa ratio that was controlled by the thickness of the NiAl layer for irradiations from 300 to 500°C up to over 20 dpa and 1000 appm He. We summarize some initial TEM results from these experiments, with particular emphasis on comparisons of 9 Cr tempered martensitic steels (TMS) and nanostructured ferritic alloys (NFA). A bimodal distribution of bubbles and voids is observed in the TMS. The bubbles primarily nucleate on dislocations, interfaces and grain boundaries; the bubble concentration increases at higher dislocation densities. In contrast the bubbles are much smaller in NFA and primarily form on Y-Ti-O enriched nanofeatures, rather than dislocations or interfaces.

### 9:50 AM Invited

#### **Experiments and Modeling of Thermal Desorption of Helium-Implanted Iron in a Broad Temperature Regime:** *Donghua Xu*<sup>1</sup>; Brian Wirth<sup>1</sup>; <sup>1</sup>University of California, Berkeley

Helium effects on the microstructural evolution and mechanical properties of structural materials are among the most challenging issues facing fusion materials research. Thermal helium desorption spectroscopy, through measuring He surface outflux as a function of temperature (or time), provides indirect

information about the kinetics and energetics of helium transport and trapping which is important for developing a predictive model for the life performance of fusion reactors. Nevertheless, the experiments and the data interpretation are not straightforward, particularly when a wide temperature range is concerned. In this work, we present desorption data for single and polycrystalline iron implanted with 4He under varying conditions. We also present a temporally and spatially dependent rate theory model, which incorporates diffusion, trapping, detrapping, and cluster coalescence kinetics during both implantation and post-implantation thermal annealing. Both the experiments and simulations are performed over a broad temperature regime from room temperature up to BCC-FCC transformation.

### 10:10 AM Invited

#### **Atomistic Modeling of Helium Interactions with Dislocations, Grain Boundaries and Coherent/Semi-Coherent Interfaces in Alpha-Iron:** *Howard Heinisch*<sup>1</sup>; Richard Kurtz<sup>1</sup>; Fei Gao<sup>1</sup>; <sup>1</sup>Pacific Northwest National Laboratory

Neutron capture reactions in fusion reactor structural materials will produce high concentrations of helium that may severely degrade their creep-rupture and fracture properties if it aggregates at grain boundaries to a sufficiently high level. Mitigation of deleterious helium effects by alloy design requires detailed knowledge of the transport and fate of helium to sinks. To address these issues atomic-scale modeling methods are being used to study the fate of helium in the neighborhood of dislocations, grain boundaries and coherent/semi-coherent interfaces in alpha-iron. Results of molecular statics models show that the binding energies of helium to these defects are strongly correlated with excess atomic volume. Long-time molecular dynamics and the dimer saddle point search method indicate that interstitial helium atoms and helium-vacancy complexes are attracted to and easily migrate within dislocations and grain boundaries. The effects on the results of using different interatomic potentials will also be discussed.

### 10:30 AM Break

### 10:50 AM Invited

#### **Nanostructured Ferritic Alloys: The Technical Contributions of Professor G.R. Odette:** *Matthew Alinger*<sup>1</sup>; <sup>1</sup>GE Global Research

Oxide dispersion strengthened (ODS) ferritic/martensitic steels, have long been considered candidates for advanced fusion and fission reactor structural materials. Extensive studies in the US breeder reactor program showed that ODS alloy MA957 has high tensile and creep strengths and unusual resistance to radiation damage. Further investigation revealed that MA957 contains ultrahigh densities of stable, nm-scale features (NFs). Building on a career dedicated to understanding the causes and consequences of irradiation damage, Odette was responsible for realizing the unique opportunity to design a microstructure with the 'key ingredients' for irradiation-resistance: a) high, stable dislocation sink strengths and large numbers of stable, nm-scale features trapping He in fine-scale bubbles, b) high creep strength. Thus, research focused on understanding alloy and processing variables to optimize NF formation, mechanical properties and, thermal and irradiation stability NFs. This international effort has led to the emergence of a new class of materials, Nanostructured Ferritic Alloys (NFAs).

### 11:10 AM Invited

#### **Analysis of Hardening Limits in Oxide Dispersion Strengthened Steel:** *Amuthan Ramar*<sup>1</sup>; Robin Schaeublin<sup>1</sup>; <sup>1</sup>CRPP - EPFL

Oxide dispersion strengthened (ODS) ferritic / martensitic (F/M) steels are considered as promising materials for high temperature applications in the future fusion reactor. Oxide dispersion in steel increases the strength of the matrix at the expense of its ductility. In this paper, the hardening due to the dispersed oxide particles as a function of particle size and spatial distribution in EUROFER97 matrix were investigated. Also the impact of the alloy production steps such as ball milling and HIPping over the alloy hardening were investigated in detail. Ti addition helps in refining the size of the dispersed yttria particle by the formation of Y-Ti oxide particles. During TEM in-situ heating up to 1000°C yttria dispersion remains unaltered, whereas dissolution is observed in the case Ti is added. Analysis of hardening using the dispersion barrier-strengthening model shows that hardening due to dislocations overcomes the one of oxides, depending on the heat treatment.

### 11:30 AM Invited

#### **Constitutive Behavior Modeling of bcc Metals and Alloys before and after Neutron Irradiation:** *Philippe Spatig*<sup>1</sup>; <sup>1</sup>CRPP-EPFL

In this paper we will review the development and current state of the physically-based models of plastic deformation of bcc metals and structural

alloys for nuclear applications, including the low-alloyed reactor pressure vessel steels, the high-chromium tempered martensitic steels and vanadium alloys. We will focus on the evolution of the plastic flow properties associated with the neutron irradiation temperature regime leading to hardening. The models developed to rationalize the synergistic effects of the irradiation parameters (temperature, flux, fluence) and of the metallurgical variables (chemical composition, thermo-mechanical processing) will be presented. The multi-scale nature and complexity of the processes controlling the plastic flow in technical alloys will be highlighted starting from the production and accumulation of irradiation-induced defect clusters in the matrix, followed by the interaction of the moving dislocations with those defects, leading ultimately to changes in the macroscopic plastic flow curves and subsequent degradation of the associated fracture properties.

## 11:50 AM Invited

**Micromechanical Testing of Self-Ion Irradiation Effects in Fe-Cr Alloys:** Fiona Halliday<sup>1</sup>; Laurence Whyatt<sup>1</sup>; David Armstrong<sup>1</sup>; Steve Roberts<sup>1</sup>; <sup>1</sup>University of Oxford

Fe-Cr alloys up to 12% Cr were irradiated using Fe ions to damage levels up to 5.5dpa. The effects of irradiation on mechanical properties were studied by nanoindentation and by a micro-mechanical test technique. Micron-scale cantilever test specimens were cut from the radiation-damaged surface layers, and tested in bending using an AFM/nanoindenter as an imaging/loading device. Nanoindentation tests found increases in near-surface hardness due to irradiation. The micromechanical tests found significant changes in elastic modulus, yield stress and work-hardening behaviour, varying strongly with irradiation dose and chromium content. Results will be reported, and the applicability and interpretation of these test methods discussed.

## 12:10 PM Invited

**The Dose Dependence of Fracture Toughness of F82H Steel:** Mikhail Sokolov<sup>1</sup>; Hiroyasu Tanigawa<sup>2</sup>; G. Robert Odette<sup>3</sup>; Takuya Yamamoto<sup>3</sup>; Takanori Hirose<sup>2</sup>; Nariaki Okubo<sup>2</sup>; <sup>1</sup>Oak Ridge National Laboratory; <sup>2</sup>Japan Atomic Energy Agency; <sup>3</sup>University of California, Santa Barbara

The advanced ferritic-martensitic steel F82H is a primary candidate low-activation material for fusion applications. Fracture toughness specimens of this steel were irradiated in High-Flux Isotope Reactor to a wide range of doses from 3.5 to 25 dpa. The range of irradiation temperature was from 250C to 500C. This paper summarizes the changes in fracture toughness transition temperature and decrease in the ductile fracture toughness as result of various irradiation conditions. It is shown that in the 3.5 to 25 dpa dose range, irradiation temperature plays the key role in determination of the shift of the transition temperature. At a given irradiation temperature, shift of the fracture toughness transition temperature increases slightly with dose within the studied dose range. It appears that main gain in transition temperature shift occurred during initial ~5 dpa of irradiation. The present data are compared to the available published trends.

## Surface Structures at Multiple Length Scales: Surface Deposition and Properties

Sponsored by: The Minerals, Metals and Materials Society, TMS Materials Processing and Manufacturing Division, TMS: Surface Engineering Committee  
Program Organizers: Arvind Agarwal, Florida International University; Sudipta Seal, University of Central Florida; Yang-Tse Cheng, University of Kentucky; Narendra Dahotre, University of Tennessee; Graham McCartney, University of Nottingham

Thursday AM  
February 19, 2009

Room: 3011  
Location: Moscone West Convention Center

Session Chair: To Be Announced

## 8:30 AM

**Modulated Epitaxial Growth of Fe/Cu Nanometer-Scale Multilayers on Si Substrates Deposited by Magnetron Sputtering:** J. Gao<sup>1</sup>; Z.P. Zhang<sup>1</sup>; Z.L. Wu<sup>1</sup>; M.K. Lei<sup>1</sup>; <sup>1</sup>Surface Engineering Laboratory, School of Materials Science and Engineering, Dalian University of Technology

Fe/Cu nanometer-scale multilayers of nominal modulation wavelength of 5 nm were deposited by magnetron sputtering on Si(100) substrates. Microstructure

and morphology of the multilayers were examined by small/wide angle x-ray diffraction (SA/WAXRD) and cross-sectional transmission electron microscopy (XTEM), respectively. The Fe(110) and Cu(111) textures formed in the multilayers with the modulation wavelength of about 5 nm. The sharp interfaces in the epitaxial multilayers were obtained with no interfacial phase. The metastable f.c.c.-Fe and b.c.c.-Cu under the duplex modulation in composition and structure coexisted in the multilayers due to an alternatively growth by order of b.c.c.-Fe/b.c.c.-Cu/f.c.c.-Cu/f.c.c.-Fe. A critical point in the phase stability diagram as a function of modulation wavelength and atomic volume fraction was found to predict the phase states of Fe/Cu multilayers. The interface roughness and the constraint of underlayer atoms led to the phase transformation of Fe and Cu from bulk stable to metastable in Fe/Cu multilayers.

## 8:50 AM

**Preparation of Carbon Foam Electrodeposited with Lead for the Application on Positive Current Collector for Lead Acid Batteries:** Li-Wen Ma<sup>1</sup>; Bai-Zhen Chen<sup>1</sup>; Ya Chen<sup>1</sup>; Yong Pan<sup>1</sup>; <sup>1</sup>Central South University

Carbon foam may be used as current collector for lead acid batteries and reduce the weight of them. Because of the premature oxygen evolution on it, carbon foam is unable to serve as positive current collector. To use this novel carbon foam as positive current collector for lead acid batteries, the modification of lead electrodeposition is necessary. A complex system and a fluoborate system are suggested, respectively, to acquire a dense and uniform lead coating which can restrain the oxygen evolution. The morphology of lead deposit show that adopting a fluoborate system, the qualified lead deposit can be obtained. The experimental parameters like lead concentration, temperature and current density in the preparation of lead electrodeposited carbon foam from fluoborate system, have been investigated. A lead acid battery with the lead electrodeposited carbon foam as positive current collector can exhibit favorable performance.

## 9:10 AM

**Study of Nano-TiN Composite Coating on Aluminum Alloys Strengthened by Plasma Arc:** Shiqiang Qian<sup>1</sup>; <sup>1</sup>Shanghai University of Engineering Science

Using a combination of high speed jet electrodeposition and plasma arc quenching, a nano-TiN composite coating can be produced. The coating possess high hardness, distinctive corrosion-resistance, high bond strength and well oxidization-resistance at high temperature. Nano-TiN composite coating with fine and uniform microstructure could be prepared by the optimal process. The hardness of the nano-TiN composite coating after scanned by plasma arc was increased. The influences of TiN content on the bone strength of nano-TiN composite coating also increased because of plasma arc scanning. After scanned by plasma arc the coating's bone strength was enlarge as nano-TiN content heighten in composite coating. The plasma arc scanning also change the influences of TiN content on the corrosion resistance of nano-TiN composite coating. The corrosion resistance of coating is enhanced after scanned by plasma arc but it was on the contrary before scanned.

## 9:30 AM

**Electroless Nickel Plating on Mg-Li Alloy by Two-Step Process:** Binna Song<sup>1</sup>; Guangchun Yao<sup>1</sup>; Hongjie Luo<sup>1</sup>; Yihan Liu<sup>1</sup>; Zhongsheng Hua<sup>1</sup>; <sup>1</sup>Northeastern University

This paper introduces two-step process for electroless plating technology of Mg-Li alloy by nickel which purpose is to avoid the corrosion of SO42- to Mg-Li alloy and reduce the cost. Firstly, the samples pre-treated were pre-plated in NiCO3•2Ni(OH)2•4H2O solution, and then plated in the solution with NiSO4•6H2O as the main salt to form a thin film of Ni-P alloy plate. The surface morphology, structure and corrosion resistance of the coatings were studied. Results showed that a flat, bright and compact plating layer well-combined with the base metal was obtained. The P content reached 13.56wt.%. The hardness value of the Ni-P coatings was about 549HV. Polarization curve showed that the open-circuit potential for the Ni-P film had reached -0.249V(SCE). Long passivation region was found on the polarization curve, which showed excellent anti-corrosion property of the film.

## 9:50 AM

**Surface Morphology of Precious-Metal Free Copper Electroless Plating Process Carbon Fiber:** Dehui Che<sup>1</sup>; Wei Kang<sup>1</sup>; Guangchun Yao<sup>1</sup>; Zhuokun Cao<sup>1</sup>; Hua Zhang<sup>1</sup>; <sup>1</sup>Northeastern University

This paper studied different Surface morphology of carbon fiber in the process on the nickel salt activated carbon fiber electroless copper plating. Before electroless plating, the pretreatment of carbon fiber is a very important

aspect. The pretreatment processing of carbon fiber including to degumming, to coarsening, to activation, to reducing four steps. In the first stage unglued studied on the tensile-strength of carbon fiber changes, with different temperature and different heating time. The Surface morphology of carbon fiber was characterized by scanning electron microscope (SEM). The results showed that carbon fiber in more than 400°C heat, Surface morphology seriously damaged. And the tensile strength decreased significantly. In the activation process, studied the formation mechanism of nickel particles on the carbon fiber. The Surface morphology of copper coating was characterized by scanning electron microscope (SEM) and Infrared Spectrometer. Further identify the nickel seeds are catalyzer for electroless plating process.

#### 10:10 AM Break

#### 10:20 AM

**Synthesis and Electrochemical Characteristics of SnO<sub>2</sub>-Coated LiNi<sub>1/3</sub>Co<sub>1/3</sub>Mn<sub>1/3</sub>O<sub>2</sub> Cathode Materials for Lithium Ion Batteries:** Ping Yang<sup>1</sup>; Chuang-fu Zhang<sup>1</sup>; Jing Zhan<sup>1</sup>; You-qi Fan<sup>1</sup>; Jian-hui Wu<sup>1</sup>; <sup>1</sup>Central South University

LiNi<sub>1/3</sub>Co<sub>1/3</sub>Mn<sub>1/3</sub>O<sub>2</sub> cathode materials have been coated with SnO<sub>2</sub> (3% wt) by heterogeneous nucleation process to improve its electrochemical performances and the physical and electrochemical properties were studied. The scanning electron microscope (SEM) images show that there is a uniform coating on the modified materials and the X-ray diffraction (XRD) patterns show that the structure of LiNi<sub>1/3</sub>Co<sub>1/3</sub>Mn<sub>1/3</sub>O<sub>2</sub> is not affected by the SnO<sub>2</sub> coating. The electrochemical tests indicate that the SnO<sub>2</sub>-coated LiNi<sub>1/3</sub>Co<sub>1/3</sub>Mn<sub>1/3</sub>O<sub>2</sub> improves the cyclic performance and rate capability comparing the bare LiNi<sub>1/3</sub>Co<sub>1/3</sub>Mn<sub>1/3</sub>O<sub>2</sub>. The electrochemical impedance spectroscopy (EIS) studies suggest that the presence of a thin SnO<sub>2</sub> layer could suppress the reaction between the cathode and electrolyte, and remarkably decreases the charge transfer resistance, which is attributed to the improvement in electrochemical performances.

#### 10:40 AM

**The Effect of Pre-Phosphating of Stainless Steel 316L on Adhesion of Alumina Coating:** Ali Akbar Oskuei<sup>1</sup>; Abdollah Afshar<sup>1</sup>; <sup>1</sup>Sharif University of Technology

In this study stainless steel 316L has been pre-phosphated by electrochemical method and then a multi-layer coating of alumina has applied on them from a sol prepared by Yoldas process. It was believed that pre-phosphating would give a rougher surface and so a stronger physical bond between the subsequent ceramic layers would be formed. Our research reveals that although pre-phosphating produces a more cracked surface compared to the untreated steel, it improves the adhesion of the ceramic layer to the substrate. SEM, EDS, nano scratch test, and potentiodynamic corrosion tests were used to assess the effects of the prephosphating on alumina coating applied on stainless steel substrate.

#### 11:00 AM

**Three Cation Phosphating of Mild Steel:** Mohammad Zareii<sup>1</sup>; Abdollah Afshar<sup>1</sup>; <sup>1</sup>Sharif University of Technology

In this study the effects of addition of calcium and nickel ions have been studied on low zinc phosphating process of St14 steel. Firstly the composition of the bath was optimized along with the temperature and pH of the bath. Then nickel nitrite has been introduced to produce the three cation phosphated layer. In this research weight of the phosphate layer and its thickness was measured in different bath compositions. For chemical and structural analysis SEM, EDX, XRD and atomic absorption was used. To prove the beneficial effects of the three cation coating compared to two cation and single cation phosphates corrosion tests has performed on the samples. Nickel and calcium ions on one hand increase the corrosion resistance of the steel and on the other hand give out a smoother phosphated layer which is a better substrate for electrophoretic painting.

#### 11:20 AM

**Evolution of Zinc-Nickel Alloy Electrodeposited Coatings with DC and Pulse Currents:** Masoud Toghraie<sup>1</sup>; Mohammad Mosavie Khoei<sup>1</sup>; Gholamreza Heidari<sup>1</sup>; <sup>1</sup>Amirkabir University of Technology

New electrodeposition processes of zinc-nickel alloys such as pulsed electrodeposition have been producing deposits with better physical and anti-corrosion characteristic. In this research chloride bath was used and Zn-Ni alloy deposits were obtained using direct and pulse currents. The taguchi statistical method was used for experiment planning and optimization. Pulse current seems to increase brightness and percentage of nickel in the deposits. In addition, the polarization curve of zinc-nickel deposits with pulse current is shifted to positive

potentials in comparison with direct current curves. The morphology of surface coatings was examined by means of metallography observations and scanning electron microscopy methods. The temperature of plating bath had a very strong effect on the composition and microhardness of coating. Frequency had a little effect on chemical composition but considerable effect on CCE.

## Transformations under Extreme Conditions: A New Frontier in Materials: Driven Reactions

Sponsored by: The Minerals, Metals and Materials Society, ASM International, ASM Materials Science Critical Technology Sector, TMS Materials Processing and Manufacturing Division, TMS/ASM: Phase Transformations Committee  
Program Organizers: Vijay Vasudevan, University of Cincinnati; Mukul Kumar, Lawrence Livermore National Laboratory; Marc Meyers, University of California-San Diego; George "Rusty" Gray, Los Alamos National Laboratory; Dan Thoma, Los Alamos National Laboratory

Thursday AM

Room: 3001

February 19, 2009

Location: Moscone West Convention Center

Session Chairs: Vijay Vasudevan, University of Cincinnati; Mukul Kumar, Lawrence Livermore National Laboratory

#### 8:30 AM Invited

**In Situ XRD Studies of Self-Propagating Formation Reactions in Steep Thermal and Chemical Gradients:** Timothy Weihs<sup>1</sup>; <sup>1</sup>Johns Hopkins University

Exothermic formation reactions are known to self-propagate in multilayer foils with nanoscale layers. These foils typically contain hundreds or thousands of nanoscale layers, and the layers alternate between materials with large, negative heats of mixing. Ni/Al, Ti/B, Nb/Si and Ti/C are some simple examples. The exothermic reactions can travel at velocities greater than 30 m/s and they can reach temperatures as high as 3300 K. The combination of rapid propagation and high temperatures produces extremely fast heating rates (~10<sup>7</sup> K/s) within the reaction front, while the nanoscale layers provide very steep chemical gradients. Here we investigate the impact of both extremes (heating rate and chemical gradient) using ex situ and in situ X-ray diffraction experiments on Ni/Al and Ni/Zr multilayer foils. The sequences of phase transformations that appear under fast and slow (~1 K/s) heat rates are shown to be different and the impact of steep chemical gradients is assessed.

#### 9:05 AM Invited

**Intermetallic Reactions under Extreme Strain Rate Conditions: Instrumented Experiments and Meso-Scale Simulations:** Naresh Thadhani<sup>1</sup>; <sup>1</sup>Georgia Institute of Technology

The occurrence of intermetallic reactions in powder mixture compacts and laminates of foils, under extreme strain-rate conditions generated with uniaxial strain and uniaxial stress gas gun experiments will be described. The discussion will be based on in-situ time-resolved measurements employing stress gauges, velocity interferometry, and high-speed digital imaging to measure the stress profiles, shock velocity, and transient deformation states. Meso-scale simulations of shock-wave propagation through discretely represented constituents (with imported microstructures) performed using CTH code to investigate the effects of reactant morphology on deformation and mixing of reactants in dense powder compacts and foils, will also be described. The results reveal the heterogeneous nature of shock waves propagating through the reactants of dissimilar physical and mechanical properties, and resulting in localized flow, jetting, and vortex formation, prior to reaction initiation. The information generated is useful for understanding the reaction mechanisms and controlling their initiation and resulting energy release.

#### 9:40 AM

**Reaction of Ni-Al Laminate Composites by Laser Shock Compression and Spalling:** Chung-Ting Wei<sup>1</sup>; Marc Meyers<sup>1</sup>; Vitali Nesterenko<sup>1</sup>; Brian Maddox<sup>2</sup>; Timothy Weihs<sup>3</sup>; <sup>1</sup>University of California, San Diego; <sup>2</sup>Lawrence Livermore National Laboratory; <sup>3</sup>Johns Hopkins University

A new reactive laminate material was developed, which consists of alternate layers of Ni and Al with bi-layer thickness of 8.3 and 48 μm. Their potential in tailoring the energy release upon impact was investigated by extreme laser loading. The laser energy was varied between 100J (initial estimated pressure



P~140 GPa) and 400 J (P~350 GPa) with an initial duration of 3 ns. SEM, EDX and optical microscopy were carried out on the samples to study the damage induced, failure modes, and spall due to the laser interaction. It was found that the 8.3  $\mu\text{m}$  laminate exhibited localized interfacial reaction at both laser energies. Potential reaction products of Ni and Al are Ni<sub>3</sub>Al, NiAl<sub>3</sub>, Ni<sub>2</sub>Al<sub>3</sub>, and amorphous Ni-Al structure, analyzed by X-Ray diffraction pattern. The cooling rate is  $5.7 \times 10^5$  K/s and cooling time is 2.1 ms approximately, by calculating from the secondary dendrite arm spacing of the reaction products.

## 10:00 AM

**Explosive Consolidation of Ti-6Al-4V Powder: A Structure-Property Reference for Rapid-Layer Manufacturing Using Ti-6Al-4V Powder:** *Noe Alba-Baena*<sup>1</sup>; Lawrence Murr<sup>2</sup>; Carlos Ramirez<sup>3</sup>; José Olivares Pro<sup>1</sup>; <sup>1</sup>Universidad Autonoma de Ciudad Juarez; <sup>2</sup>University of Texas; <sup>3</sup>Delphi

Rapid-layer manufacturing or rapid prototyping (RP) based upon liquid-phase sintering or melting of metal or alloy powders by electron or laser beams features the prospect for performance optimization through process-determined structure-property optimization. In contrast to wrought or cast Ti-6Al-4V where yield strengths average ~1 GPa with elongations ranging from 4-14%, RP technologies produce products with yields strengths above 1.2 GPa and elongations as high as 25%. Hardnesses have been observed to vary from HRC 36 to 50 in contrast to wrought hardnesses of HRC 37. But shock loaded, bulk Ti-6Al-4V has demonstrated hardnesses in excess of HRC 50. In this research RP Ti-6Al-4V powder (~30  $\mu\text{m}$ ) was explosively consolidated into a monolithic rod from which tensile specimens and hardness coupons were extracted along with sections utilized for optical and electron microscopy. The microstructures and mechanical properties were compared with those for electron beam RP for the same Ti-6Al-4V powder.

## 10:20 AM

**High-Energy-Density Structural Energetic Materials Using Linear Cellular Alloy Exoskeletons:** *Naresh Thadhani*<sup>1</sup>; *Joe Cochran*<sup>1</sup>; *Tammy McCoy*<sup>1</sup>; *Anthony Fredenburg*<sup>1</sup>; <sup>1</sup>Georgia Institute of Technology

We are investigating the design, fabrication, and evaluation of high-We are investigating the design, fabrication, and evaluation of high-energy-density structural energetic materials, based on coupling of intermetallic- and thermite-forming reactive powder mixtures with Linear Cellular Alloys (LCAs). The LCAs, made as honeycomb structures from powder extrusion and reactive sintering, are used as aerodynamic casings (exoskeletons) for ballistic delivery of energetic materials. LCA casings are being made from high-strength steels, high-density Ta and Ta matrix composites. The honeycomb casings are to be filled with highly-exothermic intermetallic (ie Ti, Si) and thermitic (e.g., Ta+Fe<sub>2</sub>O<sub>3</sub>) micro- and nano-scale powder mixtures. The focus is on manipulating the LCA material and channel design, in concert with the reactive material characteristics, such that the transfer of shear stresses from the casing walls to the energetic filler provides control of reaction initiation and energy release characteristics. Coupling of the resulting chemical and kinetic energies will provide tunable performance, enabling control of reactivity and sensitivity of the energetic material. The rate of energy release in reactive powder mixtures is limited by the rates of mass transport; thus design of cell wall geometry will be critical in facilitating controlled mechanochemical reaction initiation conditions and attaining maximized energy density.

## 10:40 AM Break

## 10:55 AM Invited

**The Observation of Phase Changes in Metal Alloys under Irradiation:** *Stuart Maloy*<sup>1</sup>; <sup>1</sup>Los Alamos National Laboratory

The extreme environment of irradiation and its effects on core materials is a central problem to the lifetime of these materials in the core of a reactor. This environment encompasses irradiation to doses greater than 200 dpa at temperatures from 400-600C. Materials undergo many changes under this extreme environment including embrittlement from agglomeration of defects, phase transformations, radiation induced segregation and helium embrittlement. Observations of phase changes include, dissolution of strengthening phases, precipitation of embrittling phases and amorphization of precipitates. In this talk, many examples of such observed phase changes will be discussed from previous studies at LANL in connection with plans for future work in these areas.

## 11:30 AM

**Irradiation Damage on Iron-Related Defects Using Molecular Dynamics:** *Hyejin Jung*<sup>1</sup>; *S. Oh*<sup>1</sup>; <sup>1</sup>NFRI

Reduced Activation Ferritic Martensitic Steels (RAFMS) is one of the prime industrial candidates for next fusion reactor. For several decades, impressive experiments on RAFMS have been conducted but not under the irradiation condition. A parallel attempt has to be required to obtain the material properties under this extreme environment using theoretical modelling and computer simulation. In this study, we review the influence of fusion environment on the nucleation of various point defects, these defect diffusions and local stress around the atomic cascade as changing Primary Knock-on Atom (PKA) Energy values and temperatures in pure Fe and in Fe-Cr alloy. The configurations of voids, Self-Interstitial Atoms (SIA) and stress fields which affect material swelling effect are dynamically investigated using Parallel Molecular Dynamics modelling. Furthermore, the irradiation effects in vicinity on the grain boundary are additionally examined in poly-Fe.

## 11:50 AM

**Microstructural Evolutions during Very High Temperature Transients in Ni-Based Single Crystal Superalloys:** *Jonathan Cormier*<sup>1</sup>; *Michaël Arnoux*<sup>1</sup>; *Xavier Milhet*<sup>1</sup>; *Florence Hamon*<sup>1</sup>; *José Mendez*<sup>1</sup>; <sup>1</sup>ENSMA/LMPM

During operating conditions, aircraft turbine blade can experiment a short and abrupt temperature increase due to engine failure (One Engine Inoperative ratings). To mimic these conditions, a specific burner rig, enabling heating and cooling rates close to 60-80°C/s between 1050 and 1200°C, was used to characterize high and very high temperature evolutions of the  $\gamma'$ -phase of Ni-based single crystal superalloys. A great impact of the heating and cooling rates on the mechanical properties is observed.  $\gamma'$  phase dissolution, precipitation and coalescence processes in relation with both the dislocation activity and the local chemistry are responsible for the observed creep behavior under isothermal and non-isothermal conditions. Therefore, both the  $\gamma'$ -phase area fraction and morphology can be used as a local temperature/stress probe. Interaction between the precipitates evolutions and the deformation mechanism will be especially highlighted.

## 12:10 PM

**Resistive Properties of the Shape Memory Alloy AuZn under an Applied High Magnetic Field:** *Alyssa Maich*<sup>1</sup>; <sup>1</sup>Los Alamos National Laboratory

AuZn undergoes a shape memory transition that varies with composition. Shape memory alloys are applied in many aspects of society today; from stents, in the biomedical field, to temperatures switches, orthodontic arch wires, and sunglass frames. AuZn is an excellent candidate for studying electronic properties of martensitic transformations because of the high degree of order in the system and extremely low transition temperature. Both single and polycrystalline samples of AuZn at various compositions were tested in a superconductive magnet and subjected to magnetic fields from 0-15T. A change in magneto resistance from negative to positive, on either side of the martensitic transition, was found in the 48%Au single crystal sample. The 48%Au polycrystalline sample showed history dependence with magnetic cycling.

## 12:30 PM Concluding Comments

## General Poster Session

Sponsored by: The Minerals, Metals and Materials Society, TMS Electronic, Magnetic, and Photonic Materials Division, TMS Extraction and Processing Division, TMS Light Metals Division, TMS Materials Processing and Manufacturing Division, TMS Structural Materials Division

Program Organizers: Mark Palmer, Kettering University; Christina Raabe, TMS

Mon AM-Wed PM  
February 16-18, 2009

Room: 2nd/3rd Floor Foyers  
Location: Moscone West Convention Center

### 3-D FEM Simulation and a Physics Model of Thermal Proximity Effect of Phase-Change Random Access Memory: *Ke Sun*<sup>1</sup>; <sup>1</sup>University of California, Los Angeles

Thermal proximity effect of phase-change random access memory (PcRAM) is studied by 3-D finite element simulation. Results show that there is no essential worsening of thermal proximity issue as the device feature size scales down to ultra small dimension. A physics model has been developed to explain the underlying physics of this phenomenon and demonstrates that, to the first order approximation, the profile of temperature distribution will be scaled together with the device dimension.

### 3-D Finite Element Simulation of a Phase-Change Random Access Memory Cell with a Novel Self-Insulated Structure: *Ke Sun*<sup>1</sup>; <sup>1</sup>University of California, Los Angeles

In this work, we proposed a phase-change random access memory (PCRAM) cell with a novel self-insulated structure (SIS), which is expected to have better thermal efficiency than the conventional structures. 3-D finite element simulation is used to study the most power consuming RESET process for both SIS and conventional normal bottom contact (NBC) cells driven by a MOSFET. Instead of programming current, power consumption is investigated to give a more fundamental comparison between the two structures. Thermal proximity effect for both kinds of cells is directly analyzed by simulating a 3x3 device array. The potential slow-quenching issue of SIS is also discussed.

### A Description of an Urgent Pot Cut out and Restarting Process at Alcoa Pocos: *Roberta Camilli*<sup>1</sup>; *Flávio Silva*<sup>1</sup>; *Andre Abreu*<sup>1</sup>; <sup>1</sup>Alcoa Alumínio S.A.

Through January 2008 the Brazil's energy scenario was critical impacting the prices involved. Due this, Alcoa Pocos de Caldas Smelter Team has done a significant effort to cut out and restarted 15 pots out of 288 pots in a short period of time. This paper will describe how these pots were effectively restarted in this short period of time. This description will detail: the procedure elaborated to cut out 15 pots in 3 days without delayed tapping and stubbing operation; the process control adjustments to minimize the lost of current efficiency at neighborhood pots; and the potlining activities in order to re-use cathodes from old pots successfully.

### A Linear Multiple-Degree-of-Freedom Ultrasonic Motor Using Bi2O3 and Fe2O3 Co-Doped PMN-PZT Piezoelectric Ceramics: *Ying Yang*<sup>1</sup>; *Qian Li*<sup>1</sup>; *Jiamei Jin*<sup>1</sup>; <sup>1</sup>Nanjing University Aeronautics and Astronautics

A linear multiple-degree-of-freedom ultrasonic motor was fabricated using Bi2O3 and Fe2O3 co-doped PMN-PZT piezoelectric ceramics. The electrical driving properties of the motor were investigated. It is found that the motor has large output force, easy to miniaturize. Because of the designed symmetrical position of piezoelectric ceramics, the motor has the advantage of fabrication simplicity. A combination of Bi2O3 and Fe2O3 was selected as a flux to sinter 0.375Pb (Mg1/3Nb2/3)O3-0.625Pb(Zr0.4Ti0.6)O3 ceramics at low temperature condition (lower than 1000°). The piezoelectric properties were determined as well according to the IEEE standard. It is justified that the Bi2O3 and Fe2O3 co-doping is very effective on the low temperature sintering of piezoelectric ceramics without degrading their performance.

### A Research Study on the High Strength API Steel

**Production for Sour Gas Pipelines:** *Shahrokh Pourmostadam*<sup>1</sup>; <sup>1</sup>Mobarakeh Steel Company

With regard to the achievement of the latest global Technologies for Pipe transportation of natural gas, containing substantial amounts of H2S (sour gas) is becoming increasingly common. Transportation of sour gas through HSLA pipelines can lead to failure from two mechanisms, hydrogen induced cracking (HIC) and sulfide stress corrosion cracking (SSCC). Over the years, suitable

measures in alloy design, steelmaking technology and downstream processing has resulted in sour gas resistant linepipe steels. To ensure better weldability, steels are today designed with lower carbon and carbon equivalent levels. The strength is derived through controlled rolling, resulting in a fine ferrite grain size. Grain refinement is the only strengthening mechanism which increases the strength and toughness properties concurrently.

### AC Induced Corrosion of 13 Cr Super Martensitic Line Pipe Steel in Seawater: *Jenny Collins*<sup>1</sup>; *David Olson*<sup>1</sup>; <sup>1</sup>Colorado School of Mines

Alternating current (AC) corrosion in buried pipelines has been reported in the literature; especially common is the influence of overhead transmission power lines inducing current in the pipe. The mechanism of AC corrosion, however, remains not fully characterized and described. A number of possible AC corrosion mechanistic models are being considered and tested. These models will be presented. Isolation of the physical phenomena is being achieved through laboratory testing. Emphasis is centered on assessing the change in susceptibility to localized corrosion with and without high AC current densities. Pitting and environmental cracking, including hydrogen assisted cracking, are also being analyzed. Impedance probe measurements are being used to assess for extra-induced stirring in the near electrolyte region of the stainless steel. Asymmetry of AC current due to a difference in anodic and cathodic behavior at the metal-environment interface is also being explored as a possible cause of a potential self-bias, resulting in accelerated anodic and/or cathodic (hydrogen ingress) behavior, and will be described. Preliminary laboratory results to date have shown pitting in seawater of a 13 Cr Super Martensitic Stainless Steel pipeline sample under an AC current density of 3800 A/m<sup>2</sup> after ten days, while a specimen in seawater under no applied AC had no evidence of pitting after 17 days. Furthermore, initial results show that seawater pH increased by 0.23, from 8.17 to 8.40 after testing with an applied AC, which is preliminary evidence in support of an AC corrosion model involving alkalization of the environment. Data and correlations of a full battery of tests will be presented and mechanistic interpretations will be given.

### Addition of Nitrogen and Nickel in the Fusion Zone of Plasma Transferred arc Weldments in UNS 32760 Super Duplex Stainless Steel: Effect on the Microstructure and on the Pitting Corrosion Resistance: *Kostas Migiakis*<sup>1</sup>; *George Papadimitriou*<sup>1</sup>; <sup>1</sup>National Technical University of Athens

Super duplex stainless steels present excellent combination of strength and corrosion resistance due to their strict composition control and ferrite-austenite phase balance. This microstructural balance in the fusion zone and the HAZ of the weldments is often disturbed because of the rapid cooling rates. These changes in microstructure lead to the loss of the good corrosion and mechanical properties of duplex steels. The scope of this work is to study the effect of nitrogen addition in the plasma operation gases and the addition of higher nickel content in the filler metal, on the microstructure and pitting corrosion resistance of super duplex stainless steels welded by the plasma transferred arc technique. Results have shown that nitrogen addition in the plasma operation gases and higher nickel content in the filler metal has positive effects on the phase balance and the pitting corrosion resistance of the weldments.

### Al-Based Complex Metallic Alloys: *Jean-Marie Dubois*<sup>1</sup>; <sup>1</sup>Institut Jean Lamour

Complex Metallic Alloys (CMA) comprise a broad family of crystalline compounds most often made of aluminum alloyed with transition metals, rare earths or metalloids, and characterized by huge crystal unit cells containing tens, when not hundreds, of atoms. As a result, properties are different, often surprisingly, from the properties of the pure constituents. An example is given by the low thermal, and electronic, conductivity of the icosahedral Al-Fe-Cu compound. The talk will pay special attention to the selection mechanisms of such complex phases forming from metals that form especially simple crystal architectures when pure. Resulting properties will be reviewed as well as potential applications, such as e.g. preparation of composites, thermal barriers, catalysts, etc. The effort going on in Europe on such complex intermetallics in the frame of the FP6 Network of Excellence called CMA will be illustrated.

### Al<sub>2</sub> Particle Segregation in Al-Cu-Mg Composites by Means of Centrifugal Casting: *Hermes Calderón*<sup>1</sup>; *Giovanni Sandoval*<sup>1</sup>; *Carla Príncipe*<sup>1</sup>; *O. Marcelo Suárez*<sup>1</sup>; <sup>1</sup>University of Puerto Rico

In certain applications, a gradual variation of mechanical properties throughout a mechanical part is required. For example, gear teeth need a good wear resistance on and near the surface as well as a ductile core. In aluminum

matrix composites (AMCs) this is achieved by increasing the volume fraction of hard particles at the surface with respect to inner regions or core. The goal of this work has been to obtain functionally-graded AMCs inducing particle volume fraction variation through the matrix. The particle segregation occurs by centrifugal forces acting on denser  $AlB_2$  dispersoids. To control the process several variables have been taken into account: Melt pouring temperature, mold temperature, centrifugal force (via rotation speed), solidification rate, volume fraction of particles and particle density. Adjusting the variables, complete  $AlB_2$  particle segregation at the surface can be obtained in an Al-Cu-Mg matrix. The procedure can be used to fabricate specimens for flexural tests.

**An Investigation on Growth Mechanism of Nano-Boric Acid Structures:** Mehmet Isik<sup>1</sup>; Servet Timur<sup>1</sup>; <sup>1</sup>Istanbul Technical University

Nano-boric acid is being used in traditional lubrication oils due to providing low friction coefficient while it is friendly to environment. Also, recently it is shown that it improves motor performance when used in diesel fuels. In this study, growth mechanism of nano-boric structures were investigated and characterized by SEM and XRD. In the first stage bamboo shaped hollow structures (length: 25  $\mu m$ , diameter: 1  $\mu m$ , wall thickness less than 10 nm) are formed. By boric acid transfer in time, hexagonal like head (diameter: 5  $\mu m$ , wall thickness: 25 nm) emerges and the shape becomes like a tadpole. After that growing occurs in 3-D and hexagonal head grows in bowl form, with nucleation of new particles (d: 10 nm) inside. Finally bowl-shaped structures are closed and coalesced.

**Analysis of Boron Distribution in Low Carbon Steel by Neutron Autoradiography:** Dong Jun Mun<sup>1</sup>; Kyung Chul Cho<sup>1</sup>; Eun Joo Shin<sup>2</sup>; Yang Mo Koo<sup>1</sup>; <sup>1</sup>Pohang University of Science and Technology; <sup>2</sup>Korea Atomic Energy Research Institute

It is well known that a very small amount of boron in steel is hard to be detected with electron spectroscopy because of its low atomic value, so that a delicate and special technique is necessary to observe boron distribution in steel. So, in this present study, characteristics of boron distribution with variation of cooling rate after austenitization were investigated in low carbon steel employing Neutron Autoradiography method. The composition of the steel used in this study are 0.042C-0.059Si-0.530Mn-0.016P-0.013S-0.028Al-0.040Mo-with 23ppm of B. The technique applied was based on the detection of 1.53MeV alpha-particles from the thermal neutron  $^{10}B(n,\alpha)^7Li$  reaction. It was observed that, when samples are fast cooled (20°/s) from 1350° to holding temperature, boron are mainly segregated along grain boundaries. However, when samples are slow cooled (1°/s) from 1350° to holding temperature, boron are uniformly distributed over the whole specimen without segregated regions along grain boundaries.

**Analysis of Dendritic Growth in Casting Alloys A356 with Cu and Modified with Sr, by: Optical Microscopy, Poles Figures and Thermal Analysis:** Francisco Esteves-Alcazar<sup>1</sup>; Alejandro Garcia-Hinojosa<sup>1</sup>; Aline Hernandez-Garcia<sup>1</sup>; <sup>1</sup>Univ Nacional Autonoma De Mexico

One factor that defines the properties of a metal such as aluminium is the plane or direction of growth, because this is done anisotropically. In the case of the A356 alloy (Al-7Si-0.3Mg) in casting conditions this presents a dendritic morphology with precipitates of Si (eutectic) in acicular or plaques forms, which influence in conjunction with the grain size properties end of the alloy. The matrix will be very important as it is the largest fraction of the microstructure, so in the case of a piece of casting if not done a check on growth unidirectional, submit a piece growth in many directions, with some preference toward extraction of heat direction. But not only the eutectic Si determines the direction of preferential growth, it is also important the presence of alloying elements as well as the modification of silicon eutectic caused the addition of Sr.

**Analysis of Mechanical Properties of Low Carbon Hot Rolled Steel with Composition and Process Parameters: Neural Networks Approach:** N. S. Reddy<sup>1</sup>; Jae Sang Lee<sup>1</sup>; <sup>1</sup>Alternative Technology Lab

An artificial neural network (ANN) model is developed for the analysis and simulation of the correlation between the mechanical properties of low alloy steels and composition and processing temperatures. The input parameters of the model consist of alloy composition and process parameters. The outputs of the ANN model include property parameters namely ultimate tensile strength, yield strength, and percentage elongation. Good performance of the ANN model is achieved. The model can be used to calculate properties of low alloy steels as a function of alloy composition and process parameters. The individual and the combined influence of inputs on properties of low alloy steels is simulated using the model. The results are in agreement with experimental knowledge.

Explanation of the calculated results from the metallurgical point of view is attempted. The developed model can be used as a guide for further alloy development.

**AUMUND Cooling Conveyor for Hot Bath Material:** Christian Niedzwiedz<sup>1</sup>; Frank Reddemann<sup>1</sup>; <sup>1</sup>AUMUND Foerdertechnik GmbH

The AUMUND company supplies equipment for raw material handling in cement, iron and steel as well as in primary aluminium industry. In these industries, the handling of hot and abrasive bulk materials demands tailor-made solutions of the conveying technique. For primary aluminium industry AUMUND has designed a cooling conveyor for defined cooling of hot bath material. The bath material will be charged out of pots into a crusher, make SMV, which will feed the cooling conveyor. Subsequently, the bath material will cool down from 850°C to below 300°C or 100°C. The outlet temperature will depend on the following process. HF gases will not be emitted into the environment by application of a special cooling hood connected to the existing dry scrubbing system. The cooling conveyor is operating successfully in several European smelters. The biggest of them will be installed in the UAE in the near future.

**Bridgman Growth and Characterization of Ga1-xNixSb Crystal: A Magnetic Semiconductor:** Sushanta Kamilla<sup>1</sup>; B.K. Samanta<sup>2</sup>; S. Basu<sup>2</sup>; <sup>1</sup>Institute of Technical Education and Research; <sup>2</sup>Indian Institute of Technology

The present work, high purity Ga, Ni and Sb in required proportions were vacuum sealed in quartz ampoule and melted inside a vertical Bridgman furnace with well defined temperature profile. Subsequent pulling by a low speed motor produced ingots of 3 cm length and 0.7 cm diameter. The formation of Ga1-xNixSb ternary alloys with different concentrations of Ni was confirmed by XRD, a linear lattice parameter-composition relation, as postulated by Vegard's Law. The electrical properties of the grown sample were studied at different temperatures from 78K to 300K by Hall Effect measurements using van der Pauw configurations. The positive sign of Hall coefficient confirmed p-type conductivity. The magnetoresistance studies at different magnetic fields (<10kG) and in the temperature range 78K to 300K showed positive magnetoresistance and indicate low Curie temperature (<78K), which was confirmed by AC susceptibility study.

**Carbon-Metal Composite Foams for Increased Catalytic Activity, Electron Transfer, and Heat Recovery:** Ben Poquette<sup>1</sup>; Stephen Kampe<sup>2</sup>; <sup>1</sup>Keystone Materials LLC; <sup>2</sup>Virginia Tech

In the late 90's, a novel technique for fabricating high conductivity graphite foam was developed by Oak Ridge National Lab. With its unique properties, this foam has shown promise to revolutionize the performance of many commercial and defense related systems not limited to: high surface area electrodes, catalysts supports, useful heat recovery. Until recently, difficulties in joining graphite foam to other materials have hindered its incorporation into current platforms. A technique was developed, through cooperation with ORNL and Virginia Tech, which allows a strongly adhered, uniform metallic coating to be applied throughout the thickness of graphite foam. These metal coatings should serve to both solve existing short-falls (brittleness, lack of joinability, etc.) as well as lend their properties (magnetic, catalytic, solderability, etc.) to graphitic foam.

**Characteristics of Friction Stir Welding on 6061-T6 Al Alloy for Upper Structure of Leisure Ship:** Kim Seong-jong<sup>1</sup>; Jang Seok-Ki<sup>1</sup>; Kim Jong-Shin<sup>1</sup>; Lee Seung-Jun<sup>1</sup>; <sup>1</sup>Mokpo Maritime University

Recently, there has been a new appreciation of aluminum alloys as materials that are capable of reducing the environment load. Therefore, this study investigated the on characteristics in friction stir welded condition of 6061-T6 alloy for leisure ship. In friction stir welded by using probe diameter of 5mm for 6061-T6 with various traveling speed at the rotation speed conditions of 210 ~ 1800 RPM and 220~720mm/min., the best characteristics presented in traveling speed of 507mm/min and rotation speed 1100RPM. The maximum tensile strength and yield strength increased with the increasing of traveling speed. This research was financially supported by MOCIE and KOTEF through the Human Resource Training Project for Regional Innovation.

**Characteristics of MIG Welding by ROBOT on 6061-T6 Al Alloy for Upper Structure of Leisure Ship:** Kim Seong-jong<sup>1</sup>; Jang Seok-Ki<sup>1</sup>; Han Min-Su<sup>1</sup>; Park Jae-Cheul<sup>1</sup>; <sup>1</sup>Mokpo Maritime University

If aluminum were used as a substitute for FRP in ships, the result would be more environmentally friendly vessels that are easy to recycle. This study investigated the on characteristics in welded by ROBOT for 6061-T6 alloy with



the factor of welding materials. The hardness of heat affected zone is lower than those of welding and base metal. At the result of tensile test, the specimen welded with ER5183 presented excellent property compared with ER5556. The corrosion current density in base metal is the lowest value more than those of two welding materials. Acknowledge; This research was financially supported by MOCIE and KOTEF through the Human Resource Training Project for Regional Innovation.

**Characterization Microstructural and Corrosion Performance Heat Treated in a New Al-Mg-Zn Alloy by: Optic Microscopy, SEM, Corrosion Test and Microstructural Predictions Using Thermocalc:** Aline Hernandez-Garcia<sup>1</sup>; Bernardo Campillo-Illanes<sup>1</sup>; Edgar Onofre<sup>1</sup>; *Francisco Esteves-Alcazar*<sup>1</sup>; Sergio Serna<sup>1</sup>; Socorro Valdez<sup>1</sup>; <sup>1</sup>National Autonomous University of Mexico

All over the world the aluminum alloys applications has been increased over the last decade, principally due to its weight/strength ratio in aircraft and transport industry. The Al-Mg-Zn alloys has been used as sacrificial anodes for cathodic protection, in the present work the characterization of two new Al-Mg-Zn alloys, with modification on Mg and Zn contents, were performed. Several heat treatments were carried to modify the foundry microstructure. Corrosion tests and metallographic quantification of phases were performed, to find the sample with best heat treatment condition suitable for be an option to be used as anode sacrifice. Additionally we conducted a prediction of stable phases using Thermocalc software and comparing with experimental quantification.

**Characterization of Heat Treatment of Aging Applied to a Steel API X-52, Aged at Different Times, by SEM, Optical Microscopy, Prediction and Analysis by Thermocalc:** Adair Jimenez-Nieto<sup>1</sup>; Bernardo Campillo-Illanes<sup>1</sup>; Aline Hernandez-Garcia<sup>1</sup>; *Francisco Esteves-Alcazar*<sup>1</sup>; Sergio Serna<sup>1</sup>; <sup>1</sup>National Autonomous University of Mexico

It is important to be able to characterize and to consider optimal times of heat treatments for steel, API-X52 that in the last 50 years has increased significantly their use in the industry, mainly for pipes. The process of manufacture of these pipes diminishes their mechanical properties, reason why a study of several times of treatment sets out to be able to have one more an ampler vision of what it would be adapted to use. Two alloys of the serie API-X52 would be used for this study, the X52-E and the X-52PS, to which it analyzed its mechanical properties, their microstructure by means of optical microscopy, SEM and prediction of phases by the software Thermocalc.

**Characterization of Microstructure, Mechanical Properties and Corrosion Resistance of Welded Joints of 2205 Duplex Stainless Steel:** *Yefeng Bao*<sup>1</sup>; Xuco Song<sup>2</sup>; Ruhong Zhang<sup>3</sup>; Yun Zhou<sup>4</sup>; <sup>1</sup>Hohai University; <sup>2</sup>Provincial Key Laboratory of Advanced Welding Technology of Jiangsu University of Science and Technology; <sup>3</sup>United Offshore Construction Co. CONHW; <sup>4</sup>China Office of SAF

2205 stainless steel pipes were welded by flux-cored arc welding (FCAW) and shielded metal arc welding (SMAW). The microstructures and the ratio of phase of the base metal, heat affected zone (HAZ) and weld metal were examined by optical microscopy. The mechanical properties in the variable zones were also determined. Corrosion properties were evaluated by cyclic voltammetry and polarization tests in 3.5% NaCl solution. The results showed that the weld microstructures were ferrite/austenite duplex structure. The hardness of the filler passes of both two welded joints was lower than that of the root passes for the effect of the welding heat cycle. The toughness of SMAW joint was higher than the FCAW joint due to the high austenite content. The two welding joints had the similar corrosion mechanism, but the FCAW joint had better corrosion resistance than SMAW joint, as it present an adequate ferrite:austenite proportion.

**Characterization of Oxides in Low-Carbon GMAW Weld Deposits for High Speed Applications:** *Germán León*<sup>1</sup>; Jorge Acevedo Dávila<sup>1</sup>; Mauricio Garza<sup>1</sup>; Mario Trejo<sup>1</sup>; <sup>1</sup>COMIMSA

GMAW equipment is one of the most widely applied for automatic and semiautomatic processes due to the high speed that can be achieved. Trend is to generate high speed deposits with high heat inputs, taking care of weld penetration. Purpose of this work is to verify decrease of the mechanical properties of the weld deposits made under these conditions. In order to accomplish this purpose test coupons were made at different speeds with constant heat input to evaluate weld penetration by the characterization of present oxides. Results show that the amount of oxides increase with speed and microstructure changed. A neural network approach is done to determine critical speed for oxides growth.

**Characterization of the NiAl-xFe<sub>2</sub>-xO<sub>4</sub> Catalyst Obtained by the Combustion Reaction:** *Lucianna Vieira*<sup>1</sup>; Patrícia Tatiana Santos<sup>1</sup>; Ruth Kiminami<sup>2</sup>; Heloysa Andrade<sup>3</sup>; Ana Cristina Costa<sup>1</sup>; <sup>1</sup>University Federal of Campina Grande; <sup>2</sup>University Federal of São Carlos; <sup>3</sup>University Federal of Bahia

The water-gas shift reaction (WGS) is one of the key steps involved in the automobile exhaust processes, converting CO with water to hydrogen and carbon dioxide and including the produced hydrogen as a very effective catalyst for NO<sub>x</sub> removal. The objective of this work is synthesized and characterizes NiAl<sub>x</sub>Fe<sub>2</sub>-xO<sub>4</sub> catalyst by combustion reaction used urea as fuel. To synthesis used a vitreous silica crucible on a hot plate at 480°C. The resulting powders were characterized by XRD, FTIR, adsorption of nitrogen for BET and catalytic measures. The results show that the catalyst presents crystalline phase of inverse spinel and trace of NiO and two stretching bands below 1000cm<sup>-1</sup>. NiAl<sub>x</sub>Fe<sub>2</sub>-xO<sub>4</sub> with x = 0, 0.5, 1, 1.5 e 2 moles Al<sup>3+</sup>, presented value of superficial area 25; 31; 28; 41; 88 m<sup>2</sup>/g, respectively. The catalyst with x = 1.5 presented CO/CO<sub>2</sub> conversion major of 91% and activity of 49.5 mmol-g<sup>-1</sup>.h<sup>-1</sup>.

**Chemical Species Quantification and Oxide Film Measurements of Metal Surfaces by X-Ray Photoelectron Spectroscopy (XPS):** *Mark Biesinger*<sup>1</sup>; L.W.M. Lau<sup>1</sup>; A. Gerson<sup>1</sup>; R.St.C. Smart<sup>1</sup>; <sup>1</sup>University of South Australia / University of Western Ontario

Improvements in X-ray photoelectron spectroscopy (XPS) technology and data processing procedures have allowed for significant improvements in our ability to quantify the oxide and hydroxide structures on the surface of metals. Significant progress in the analysis of the transition metals, which are complicated by a number of spectral phenomena, has been achieved. As well, calculations allowing for a more precise measurement of passive oxide/hydroxide thicknesses have been developed and improved upon, particularly for Al, Fe and Ni species. Examples from a range of metal surfaces will be shown.

**Combined Experimental-Numerical Approach to Study the Diffusion and Dissolution of Al<sub>2</sub>O<sub>3</sub> in CaO-Al<sub>2</sub>O<sub>3</sub>-SiO<sub>2</sub> Liquid:** *Frederik Verhaeghe*<sup>1</sup>; Muxing Guo<sup>1</sup>; Junhu Liu<sup>1</sup>; Bart Blanpain<sup>1</sup>; Patrick Wollants<sup>1</sup>; <sup>1</sup>Katholieke Universiteit Leuven

Dissolution phenomena and, more generally, interactions between solids and fluids are ubiquitous in materials science and engineering. In this work we focus on the dissolution behavior of solid Al<sub>2</sub>O<sub>3</sub> in CaO-Al<sub>2</sub>O<sub>3</sub>-SiO<sub>2</sub> liquids, a system with applications in metallurgy, e.g., for the removal of inclusions, the addition of fluxes, and the degradation behavior of refractory materials. We compare experimental observations using confocal scanning laser microscopy with numerical simulations to analyse the dissolution behavior, leading to the identification of a diffusion-controlled dissolution mechanism and an estimation of the effective diffusion coefficient of Al<sub>2</sub>O<sub>3</sub> and its activation energy in this system.

**Comparison between Theoretically Predicted and Experimentally Observed Microstructures in Alloys from Nb-W-Cr System:** *Krista Amato*<sup>1</sup>; Benedict Portillo<sup>1</sup>; Julieta Ventura<sup>1</sup>; Shailendra Varma<sup>1</sup>; <sup>1</sup>University of Texas at El Paso

The experimentally observed microstructures of Nb-20W-5Cr and Nb-20W-10Cr, wt.%, alloys have been compared with theoretically obtained isotherms from the Nb-W-Cr phase diagram. The isotherms were obtained from a commercially available Pandat™ program and are based on the recent thermodynamic data from the literature. The predicted microstructures for these alloys based on the calculated isotherms from this source and Metals Handbook are different. The microstructural dependence on the oxidation behavior of the two alloys in a range of temperature from 700 to 1400° C will be presented.

**Comparison of Short and Long Crack Growth for Titanium and Aluminum Alloys:** *Bernd Oberwinkler*<sup>1</sup>; Christian Oberwinkler<sup>1</sup>; Wilfried Eichlseder<sup>1</sup>; <sup>1</sup>University of Leoben

To estimate the lifetime of flawed components with the aid of fracture mechanics it's essential to know the crack growth behavior. Therefore the crack propagation has been characterized for short and long cracks in two different light metals, namely Ti-6Al-4V and AlSi9Cu3, respectively. The measurement of long crack propagation has been done on single-edge-bending specimens via potential drop method to determine the crack length. To investigate the short crack growth plane tension/compression specimens have been provided with initial cracks. The growth of the crack has been observed with a high resolution camera. The results of these experiments provide a basis for a correlation with S/N-curves, determined with specimens from high pressure die casts and forgings.

They include casting inhomogeneities (AlSi9Cu3) and surface flaws (Ti-6Al-4V) respectively which act as initial cracks.

**Composites of Polyamide6/Ferrite for Absorbers of Electromagnetic Radiation:** *Daniella Bezerra*<sup>1</sup>; Keila Machado de Medeiros<sup>1</sup>; <sup>1</sup>UFCG

Composite consists of a mixture or combination of the two or more, micro or macro constituents that differ in shape and chemical composition and, in essence, are insoluble in one another. The polyamide is a polymer that presents dimensional stability, good resistance to impact without notch and excellent chemical resistance. Already the ferrites are absorbers of electromagnetic radiation and have versatility to be used as a composite of ferrites. The composite of polyamide6/ferrite was obtained by mixing 10, 20, 30% of ferrite added to polyamide6 in a blender internal Haake. The objective of this work was to develop composites of polyamide6/ferrite to achieve superior properties or better in some aspects regarding the properties of each of its components. The results were very promising, with a good interaction between the ferrite and polyamide6, to be used as absorbers of electromagnetic radiation.

**Computer Aided Design for Metal Strip Coil Shape Corrector Machine:** *Mohamed Elsalawy*<sup>1</sup>; M Mokhtar<sup>2</sup>; A Wifi<sup>2</sup>; <sup>1</sup>Kandil Steel Complex; <sup>2</sup>Faculty of Engineering, Cairo University

This thesis presents a new approach to the selection and design of metal strip coil shape correcting machine. Coil defects as well as coil properties are categorized and relevant required machines, namely, levelers, straighteners or flatteners are specified. These approaches are fed to a specially devised computer technique in order to calculate the required power for leveling process, the number of rolls, rolls dimensions and configurations. For a given fully specified machine specifications, a decision could be taken to either to purchase or to construct the machine. In case, the decision is to purchase; the computer program introduces steps for selection out of data base of machine suppliers. On the other hand, in case, it's decided to design a new machine, the computer program has been so arranged to couple with this decision and the full design is achieved. The design procedure has been herein explained.

**Constitutive Parameter Determination Using Instrumentation and Simulation of Electromagnetic Ring Expansion Experiment:** *Anupam Vivek*<sup>1</sup>; Glenn Daehn<sup>1</sup>; Jason Johnson<sup>1</sup>; Yuan Zhang<sup>1</sup>; Geoff Taber<sup>1</sup>; Pierre L'Elpattienier<sup>2</sup>; Gregg Fenton<sup>3</sup>; <sup>1</sup>Ohio State University; <sup>2</sup>LSTC; <sup>3</sup>Applied Research Associates

The modeling problem of electromagnetic forming is often dominated by inertial acceleration by a magnetic field which is a much better posed problem than the traditional ones that are dominated by complex 3-D constitutive behavior and frictional effects. However, important aspects of the problem are dominated by the constitutive properties of the material, and often electromagnetic forming is performed in a high-strain-rate regime where reliable material strength data is scarce. Also, there is little or no data in cases where temperature rises significantly over very short times (tens of micro-seconds). This rapid temperature rise is very important to the material response because the short time scales largely preclude the material from recovery and recrystallization processes. This presentation will show how advanced instrumentation, particularly the *Photon Doppler Velocimeter (PDV)* can be coupled with electromagnetic ring expansion and provide avenues to characterize material and to critically validate numerical models of electromagnetic forming.

**Conventional Windmills Integrated with Generator Based on Magnetically Augmented Rotational System:** *Nuggehalli Ravindra*<sup>1</sup>; *Rohit Chauhan*<sup>1</sup>; *Gaurav Devrani*<sup>1</sup>; *Fiorella Fuentes*<sup>1</sup>; *Tony Chow*<sup>1</sup>; *Howard Helfgott*<sup>1</sup>; <sup>1</sup>New Jersey Institute of Technology

A normal approach for the design and implementation of magnetic engine for potential power generation is described. The engine comprises a flywheel that is driven by utilization of a large number of magnetic field sources. Wind power is considered to be a promising and encouraging alternative for power generation because of its tremendous environmental and social benefits, together with public support and government incentives. The wind, however, is variable, site specific and an intermittent source of energy. The application for this magnetic engine for variety of pollution free power generating schemes is described.

**Corrosion and Mechanical Properties of Electro Plasma Deposited Zn-Ni Coatings:** *Pratheesh George*<sup>1</sup>; Edward Daigle<sup>1</sup>; Danila Ryabkov<sup>1</sup>; <sup>1</sup>CAP Technologies LLC

Electro Plasma Technology (EPT) is a hybrid technology which employs plasma process in an aqueous electrolytic cell for cleaning, coating and surface modification of metals. Coatings can be deposited at a very high rate of 1 µm per

second using environmentally friendly chemicals and has unique characteristics to it such as nano sized grains which imparts excellent corrosion resistance and mechanical properties. The salt fog testing under ASTM B117 specification and wet/dry cycle testing of Zn-Ni coatings deposited using this technology has shown excellent resistance against corrosion. The process fundamentals, microstructural characteristics and corrosion test results of coatings deposited using EPT will be presented. Hydrogen Embrittlement and Fatigue tests have confirmed the superior nature of these coatings and these results will be also discussed. These properties make it an excellent replacement choice for cadmium and hexavalent chromium based coatings.

**Crystallization Kinetics and Thermal Stability of Amorphous Cu50Zr50 Alloy:** *Ilkay Kalay*<sup>1</sup>; Yunus Kalay<sup>1</sup>; Matthew Kramer<sup>1</sup>; Ralph Napolitano<sup>1</sup>; <sup>1</sup>Ames Laboratory / Iowa State University

The Cu-Zr binary system is well known to have a wide composition range of glass forming ability, but yet a complex devitrification behavior. In the present study, the crystallization kinetics and thermal stability of the Cu50Zr50 amorphous alloys were investigated using a combined study of differential scanning calorimetry (DSC), in-situ high energy X-ray diffraction (HEXRD) and transmission electron microscopy (TEM) in isochronal and isothermal annealing conditions. The amorphous Cu50Zr50 alloy was found to devitrify into the orthorhombic Cu10Zr7, tetragonal Zr2Cu (C11b) and cubic CuZr (B2) phases simultaneously. The results from TEM at different stages of crystallization accompanied with calorimetry analysis will be presented to discuss the mechanism of crystallization kinetics in amorphous Cu50Zr50.

**Crystallization of a Marginal Glass Forming Alloy with DSC and Kinetic Analysis:** *Charley Yeager*<sup>1</sup>; Yunus Kalay<sup>2</sup>; Scott Chumbley<sup>2</sup>; Iver Anderson<sup>2</sup>; <sup>1</sup>University of Rolla; <sup>2</sup>Ames Laboratory of DOE/Iowa State University

A kinetic analysis was done for the crystallization of the marginal glass former AlSm10at%. Undercooling yields an amorphous bulk phase with quenched-in fcc Al nano-crystals at a density of 10<sup>22</sup>/m. Ribbons melt spun at 30 m/sec wheel speed were isothermally crystallized using DSC. TEM analysis was performed at different stages of crystallization to validate kinetic analysis results. Two simultaneous thermal events are seen in DSC due to crystallizations of the quenched in fcc Al and the primitive-cubic intermetallic. To analyze these separate events a deconvolution was performed on the DSC trace taken at 178 °C. JMA kinetics were used to approximate these events as well as other models. JMA kinetics describe the fcc event well for site saturated nucleation and interface controlled growth. The cubic event was modeled best with steady state nucleation and interface controlled growth. Peak deconvolution was viable, supported by kinetic analysis and TEM observation agreement.

**Density Measurement of Hugoniot End States in Polycrystalline Materials Using Dynamic X-Ray Diffraction:** *D. Milathianaki*<sup>1</sup>; J. Hawreliak<sup>1</sup>; B. S. El-Dasher<sup>1</sup>; J. M. McNaney<sup>1</sup>; T. Ditmire<sup>2</sup>; H. E. Lorenzana<sup>1</sup>; <sup>1</sup>Lawrence Livermore National Laboratory; <sup>2</sup>University of Texas at Austin

Measuring material density under extreme conditions of pressure and temperature induced by shock waves is important in identifying the state of the compressed solid and potential phase transformations such as melt. In addition, knowledge of density together with a shock wave parameter such as particle velocity can provide information on the material equation-of-state. We present an x-ray diffraction technique that has yielded promising results in the density determination of polycrystalline materials of a wide Z range. Specifically, we report on the density measurement of shock compressed states in polycrystalline Cu along with particle velocity measurement using velocimetry (VISAR). The potential of this technique in absolute equation of state determination is discussed. This work performed under the auspices of the U.S. Department of Energy by Lawrence Livermore National Laboratory under Contract DE-AC52-07NA27344.

**Design and Application of Variable Contact Roll Contour on Backup Roll of Finishing Stand at a Hot Strip Mill:** *Xiaodong Wang*<sup>1</sup>; Quan Yang<sup>2</sup>; Fei Li<sup>1</sup>; Ming Li<sup>3</sup>; Wei Yu<sup>3</sup>; Bin Li<sup>3</sup>; Baohui Zhang<sup>3</sup>; <sup>1</sup>Research Institute of Technology, Shougang Steel Corporation; <sup>2</sup>National Engineering Research Center for Advanced Rolling Technology, University of Science and Technology Beijing; <sup>3</sup>Qian'an Iron and Steel Company of Shougang Steel Corporation

Hot strip rolling has a feature of severe and complex working condition. There are many disturbing factors affecting strip shape control, and all of them can be expressed concentratedly to be rolling force fluctuation and roll contour change during hot rolling process. VCR backup roll, with a contour curve of



six order polynomial expression, was designed and applied on a hot strip mill of Shougang Corporation to reduce the influences of rolling force fluctuation and roll shape change on strip shape control for improving the shape control performance. This kind contour curve of backup roll can make the contact length between backup roll and work roll adapt with the width of strip rolled under the function of rolling force, eliminate or reduce the adverse contact areas between rolls, enhance the cross rigidity of loaded roll gap and then increase the shape control performance of hot strip mill.

**Design of Experiment to Minimize Fluoride and Particulate Emissions at Alumar:** *Eliezer Batista*<sup>1</sup>; *Nilton Nagem*<sup>1</sup>; *Valerio Gomes*<sup>1</sup>; *Edson Montoro*<sup>1</sup>; *Paulo Miotto*<sup>1</sup>; *Luicano Souza*<sup>1</sup>; <sup>1</sup>Alcoa

Most of Aluminum plants have been minimizing the fluoride and particulate emissions at the main source, which is the pot rooms, in order to reduce the environmental impacts. Many actions and studies are in place currently at Alumar. A quantitative study was done to map and determine the impact of each operation in the fugitive fluoride emissions (HF) in the pot rooms. Then, this full factorial experiment 2k was run in order to identify the main factors and their impacts on fluoride and particulate emissions. The statistical model is showing that the fluoride emission has been affected mainly by pot draft, pot dressing, and usage of compressed air for housekeeping with R2 at 82%. Based on the models, it was recommended some actions which will minimize both of these emissions. In addition, this paper describes, step by step, how this kind of experiment can be applied in the Aluminum industry.

**Determination of Strain Field and Inhomogeneity in Radial Forging of Tube Using FEM and Microhardness Test:** *Mehdi Sanjari*<sup>1</sup>; *Saeed Tamimi*<sup>2</sup>; *Ali Taheri*<sup>1</sup>; <sup>1</sup>Sharif University; <sup>2</sup>Tehran Polytechnic University

Utilizing the FEM, the strain field in the radial forging process of tube is calculated at different process conditions and compared with the experimental results achieved using the microhardness test. The effect of various process parameters such as friction, axial feed, back push and front pull forces and die angles on the strain field are investigated. Using the results of the analysis, it is shown that the deformation inhomogeneity, introduced by an Inhomogeneity Factor (IF), is the highest in the internal surface of tube, while the maximum and minimum effective strains are appeared at the internal surface of tube and about the core of the tube thickness, respectively.

**Development of Nanocomposites Based on Polyamide 6 and Polyethylene Blends:** *Pankaj Agrawal*<sup>1</sup>; *André Rodrigues*<sup>1</sup>; *Edcleide Araújo*<sup>1</sup>; *Tomás Mélo*<sup>1</sup>; <sup>1</sup>Universidade Federal de Campina Grande

In this work, Nanocomposites based on Polyamide 6 (PA6) and Low Density Polyethylene (LDPE) blends were developed using organically modified clay(organoclay). EMA-GMA terpolymer was used as compatibilizer. The nanocomposites were prepared in an intensive batch mixer Rheomix 600 attached to a HAAKE System 90 torque rheometer equipped with roller blades, at 50rpm and 240°C for 15 minutes under air atmosphere. Initially, a Masterbatch containing 50 % (wt) of organoclay and 50% (wt) of LDPE was prepared. The mixing time was 10 minutes. Afterwards the following compositions were prepared: PA6/LDPE; PA6/LDPE/Organoclay, PA6/LDPE/EMA-GMA, and PA6/LDPE/Organoclay/EMA-GMA. The degree of dispersion of the clay in the polymer (PA6 or LDPE) was evaluated through X-Ray Diffraction (XRD). The results showed that the clay was dispersed and exfoliated predominantly in the PA6 phase.

**Development of Revabratory Furnace in Egyptian Copper Works (ECW) by Using Reformed Natural Gas:** *Mohamed A.Kawy Hamad*<sup>1</sup>; <sup>1</sup>Central Metallurgical Research and Development Institute

In ECW, revabratory furnace which used for smelting of scrape of copper and residual anodes and cathodes from the next stages which carried out in copper after casting from this furnace. In this time, deoxidation process carrying out by wood as a resource of reduction gases such carbon monoxide, hydrogen and methane. That is the problem, using of wood causes the following: 1- Pollution of medium of copper melting (forming soot of smock above furnace); 2-low efficiency in removal of oxygen from copper and more contamination in copper matta causes in rising of heat to remove of it and increasing in cost and time of casing of copper; 3-high expencive this problem was solved by using of reformed natural gas as a source of reduction gases (CO+ H<sub>2</sub>), this led to the following.

**Effect of Coating Thickness on the Structure and Properties of C/2024 Alloy Composites:** *Linli Wu*<sup>1</sup>; *Guangchun Yao*<sup>1</sup>; <sup>1</sup>School of Material and Metallurgy, Northeastern University

Carbon fiber surface metallization is designed to increase the wettability between carbon fiber and aluminum alloy matrix, but at the same time, coating thickness will affect the structure and properties of composite materials. Thick coating will change the components of the matrix alloy and change the performance of the base alloy. Otherwise, thin coating will not achieve the role of connections. In this paper, different thickness of the nickel-plated carbon fiber was selected to reinforce alloy 2024. The microstructure and mechanical properties of the composite materials was studied to determine the more appropriate thickness of the layer nickel plating. When the coating thickness was 0.7μm, carbon fiber and matrix alloy had a better interface, the mechanical properties of composite materials also was the best.

**Effect of Cooling Rate on Linear Contraction Rate and Hot Cracking Trend of T10 Steel:** *Zhijun Li*<sup>1</sup>; *Quanzhi Sun*<sup>1</sup>; *Zhengqi Xu*<sup>1</sup>; *Honggang Zhong*<sup>1</sup>; *Jianping Liang*<sup>1</sup>; *Qijie Zhai*<sup>1</sup>; <sup>1</sup>Materials Science & Engineering, Shanghai University

The effects of cooling rate ranging from 6°C/s to 1°C/s on the linear contraction and hot cracking of T10 steel are investigated. The results show that, on one hand, the linear contraction rate of T10 steel can hardly vary with the cooling rate decreasing. On the other hand, the cooling rate influences the hot cracking trend of T10 steel. The hot cracking always appears in the surface of T10 steel sample when the cooling rate decreases from 6°C/s to 2°C/s. However, as 1°C/s of cooling rate, there isn't the hot cracking in the surface of T10 steel sample. Meanwhile, the hot cracking force increases with the cooling rate decreasing, which means to the decrease in the hot cracking trend of T10 steel.

**Effect of Deposition Conditions on the Optical and Chemical Properties of SiO<sub>2</sub> Films:** *Xiaoyan Xu*<sup>1</sup>; *Sergey Nikishin*<sup>1</sup>; *Vladimir Kuryatkov*<sup>1</sup>; *Ayrton Bernussi*<sup>1</sup>; <sup>1</sup>Texas Tech University

Thin SiO<sub>2</sub> films were deposited by plasma enhanced chemical vapor deposition (PECVD) in N<sub>2</sub>O/SiH<sub>4</sub> plasma. The influences of chamber pressure, substrate temperature, and RF power on growth rate, refractive index (RI), and etching rate of SiO<sub>2</sub> films are investigated. When the thickness of film increases from 21.8 nm to 88.5 nm the RI increases from 1.273 to 1.463 corresponding to the RI of bulk SiO<sub>2</sub>. P-etch (15 HF:10 HNO<sub>3</sub>:300 H<sub>2</sub>O) experiments performed on these films show a decreasing etching rate with increasing film thickness, indicating that films with a lower RI also have a lower density and more pores. From the temperature dependence of SiO<sub>2</sub> growth rate the apparent activation energy of 600 cal/mol was estimated for the surface reactions. The species and pathways of the surface reactions as well as the effect of He and Ar plasma dilution on PECVD are also discussed.

**Effect of Heat Treatment on Two New IGT Superalloys:** *James Staley*<sup>1</sup>; *Chuck Biondo*<sup>1</sup>; <sup>1</sup>Alstom/PSM

Industrial gas turbine (IGT) engine buckets are made from creep and elevated temperature tensile and fatigue resistant investment cast nickel-based superalloys. Superalloys with improved mechanical properties can increase efficiency and lower emissions and engine life cycle costs. Power Systems Mfg, LLC (PSM), a subsidiary of Alstom Power Inc., has developed two new, proprietary superalloys, which exhibit higher mechanical properties than some current IGT superalloys. Specimens were solution heat treated at different temperatures followed by precipitation heat treatment. Heat treated specimens were tensile, low cycle fatigue and stress rupture tested. Properties to date showed a significant increase when the solution heat treatment temperature was increased to above the gamma prime solutioning temperature. The highest solution heat treatment temperature conducted so far rendered the highest mechanical properties. It is expected that even higher solution heat treatment temperatures below the eutectic melting temperature would result in higher properties.

**Effect of Nitrogen Contents on Stacking Fault Energy in TWIP Steel Using TEM:** *Tae-Young Ahn*<sup>1</sup>; *Sung-II Baik*<sup>1</sup>; *Yeon-Seung Jung*<sup>2</sup>; *Young-Kook Lee*<sup>2</sup>; *Young-Woon Kim*<sup>1</sup>; <sup>1</sup>Seoul National University; <sup>2</sup>Yonsei University

Twin-induced plasticity (TWIP)-aided steel is widely studied as a next-generation structural materials because of its exceptional plasticity and high strength. Stacking fault energy (SFE) is known as the key parameter to control the deformation and strengthening of high-Mn TWIP steel. Nitrogen was incorporated in the Mn-TWIP steel to reduce the Mn content and the change of SFE was measured with the content of nitrogen. SFE values were obtained in



TEM by measuring the curvature of direct extended 3-fold node of dislocation network. As Mn contents was reduced from 18 to 15 wt% , SFE was changed from 34.5 to 13.9 mJ/m<sup>2</sup>. When nitrogen was added, however, SFE increased up to 17.4 mJ/m<sup>2</sup> with 0.09wt% of nitrogen in the alloy. It was confirmed from the X-ray diffraction that the addition of the nitrogen in the Fe-15Mn TWIP steel alloy suppressed the formation of the  $\epsilon$ -hcp phase.

**Effect of Probe Shape with Traveling Speed in Friction Stir Processing for 5456-H116 Al Alloy:** *Kim Seong-jong*<sup>1</sup>; Park Jong-Seek<sup>1</sup>; Han Min-Su<sup>1</sup>; Park Jae-Cheul<sup>1</sup>; <sup>1</sup>Mokpo Maritime University

This paper investigated friction stir processing with probe traveling speed to improve mechanical characteristics. From result of experiment with probe screw, the case of existence of probe screw considers that has good material characteristics because of by plastic flow by heat which comes from high friction heat. In full screw probe, the material characteristics decrease with traveling speed increase and the best characteristics is 15 mm/min. It was shown the best characteristic when experimental conditions are 800 RPM, 15 mm/min. And then this case has hardness, which advancing side is higher than retreating side and heat-material effected zone has the lowest one. Acknowledge: This research was financially supported by MOCIE and KOTEF through the Human Resource Training Project for Regional Innovation.

**Effect of Residual Sodium Contents on the Structure and Morphology of Titanate Nanotubes for Hydrogen Storage:** *Bora Lee*<sup>1</sup>; Sun Jae Kim<sup>2</sup>; Chang Hee Lee<sup>1</sup>; Kyung Sub Lee<sup>1</sup>; <sup>1</sup>Hanyang University; <sup>2</sup>Sejong University

The titanate nanotubes synthesized by hydrothermal method using rutile powder in NaOH solution usually show a small amounts of sodium in the structure. In this work, the sodium contents have been controlled by changing the pH levels in the washing condition. The three samples with different contents of residual sodium were prepared and fired from 200°C to 800°C. Under relatively higher pH, the titanate nanotubes without annealing had the structure of A<sub>2</sub>Ti<sub>2</sub>O<sub>5</sub>•H<sub>2</sub>O (A=Na or H), the shape remained tubular upto 400°C and finally converted to Na<sub>2</sub>Ti<sub>6</sub>O<sub>13</sub> of rod-like shape at 800°C. However, the sample at a lower pH (no residual sodium) was converted to anatase in the granular form at 400°C. The rod-like shape absorbed a relatively higher capacity than the tubular shape. The relationship between the hydrogen storage, the structure and morphology of nano titanate was discussed.

**Effect of the Addition of Two Alkaline Activators on the Hydraulic Behavior of Composites Cements with Ground Granulated Blast Furnace Slag, Fly Ash and Geothermal Waste:** *Javier Lozano*<sup>1</sup>; Lauren Gómez-Zamorano<sup>2</sup>; <sup>1</sup>IPN-ESIQIE, Programa de Maestría en Ciencias en Ingeniería Metalúrgica; <sup>2</sup>Universidad Autónoma de Nuevo León, Facultad de Ingeniería Mecánica y Eléctrica, Programa Doctoral de Ingeniería de Materiales

The mechanical properties and the hydraulic behavior of environmentally friendly cement pastes of ground granulated blast furnace slag (GGBFS) - fly ash (FA) - geothermal waste (GW) and Portland cement (PC) were investigated. The replacement materials were activated with 1, 4 and 7% of Na<sub>2</sub>O using NaOH and water glass. The pastes were cured up to 90 days at 20°C. The results indicated that the mechanical properties were improved with the activator load and with the use of water glass; nevertheless the latter reduced the workability of the pastes. The FA addition reduced the properties but increased the workability of the pastes. Moreover the increase on GGBFS and GW load enhanced the compressive strength and the formation of hydration products as analyzed by SEM and an important consumption of clinker phases and calcium hydroxide were also found by XRD, indicating a contribution of the replacement materials on the hydration reactions.

**Effect of the Matrix Viscosity on the Morphology and Mechanical Properties of Polypropylene /Brazilian Organoclay Nanocomposites:** *André Rodrigues*<sup>1</sup>; Tomás Melo<sup>1</sup>; *Edcleide Araujo*<sup>1</sup>; Pankaj Agrawal<sup>1</sup>; <sup>1</sup>Universidade Federal de Campina Grande

In this work, the effect of Polypropylene (PP)viscosity and the Brazilian organically modified clay (organoclay) on the morphology and the mechanical properties of PP/Organoclay Nanocomposites was investigated. The nanocomposites were prepared using a co-rotating twin screw extruder. Two grades of PP with different viscosities were used as a matrix and PP-g-MA was used as a compatibilizer. The nanocomposites were characterized by X-Ray Diffraction (XRD), Transmission Electron Microscopy (TEM) and Mechanical Properties. XRD results showed that a predominantly intercalated nanocomposites were formed. The nanocomposites formation was not affected

by the PP viscosity. These results were confirmed by TEM. Mechanical properties results showed that the elastic modulus and the tensile strength were improved.

**Effect of Thermo-Mechanical Processes on Alloy 909 Stress-Rupture Properties:** *Octavio Covarrubias*<sup>1</sup>; Osvaldo Elizarraras<sup>1</sup>; <sup>1</sup>Frisa Aerospace

Alloy 909 is a Ni-Fe-Co alloy which properties make it useful for gas turbines and rocket-engine applications. Several turbine-engine components, like casings, seals and others can be made from this alloy by ring-rolling processes. This alloy is a precipitation hardenable material which properties are result of forging procedures and heat-treatment processes. As most materials processed for industrial purposes, components made of this alloy shall be mechanically and microstructurally tested to validate promoted properties: stress-rupture is a key characteristic to be evaluated. From an industrial standpoint, this job summarizes the effects on stress-rupture properties when several alloy 909 forgings are produced according to different ring-rolling and heat-treatment variables. Experimentation results are complemented by light microscopy and SEM evaluations, allowing determination of production parameters to promote best alloy properties. It must be mentioned, since implementation of proposed production parameters, no deviation due to metallurgical causes was reported.

**Effects of a Tantalum Addition on the Morphological and Compositional Evolution of a Model Ni-Al-Cr Superalloy:** *Christopher Booth-Morrison*<sup>1</sup>; David Seidman<sup>1</sup>; <sup>1</sup>Northwestern University

The effect of a 2.0 at.% addition of Ta to a model Ni-Al-Cr superalloy aged at 1073 K is assessed using scanning electron microscopy and atom-probe tomography. The addition of Ta is found to result in appreciable strengthening, and the morphology is found to evolve from a bimodal distribution of spheroidal precipitates, to cuboidal precipitates aligned along the elastically soft <001>-type directions. Tantalum is observed to partition preferentially to the  $\gamma'$ -precipitate phase and suppresses the mobility of Ni in the  $\gamma$ -matrix sufficiently to cause an accumulation of Ni on the  $\gamma$ -matrix side of the  $\gamma'$ -precipitate/ $\gamma$ -matrix heterophase interface.

**Effects of V and C Additions on the Mechanical Properties of High Strength Invar Base Alloy:** *Ae-Cheon Yun*<sup>1</sup>; Jin-Hwa Song<sup>2</sup>; Tae-Kwon Ha<sup>3</sup>; *Kee-Ahn Lee*<sup>1</sup>; <sup>1</sup>Andong National University; <sup>2</sup>RIST; <sup>3</sup>Kangnung National University

The Fe-Ni based Invar alloys usually have relatively low strength and hardness. This study sought to examine the effect of V & C additions on the mechanical properties of the high strength invar type alloy. By using the FactSage program for thermodynamic equilibrium phase simulation, base alloy represents the Mo<sub>2</sub>C carbide can be formed as main precipitate. V<sub>2</sub> alloy (V+C additions) indicated to appear Mo<sub>2</sub>C+(V,Mo)C carbides. It was apparent in mechanical results that the vanadium carbide can improve hardness and strengths of high strength invar type alloy. The tensile fractography of V<sub>2</sub> alloy represented ductile transgranular fracture mode and voids were initiated between the vanadium carbide particle and matrix. Superior properties of high strength and low CTE could be obtained by (V,Mo)C precipitation in the V<sub>2</sub> alloy. By examining appropriate condition for cold rolling and heat treatment, the high strength of 1.556GPa could be successfully obtained in V<sub>2</sub> alloy.

**Elastic Moduli and Mechanical Properties of Some Bulk Metallic Glasses:** *John Plummer*<sup>1</sup>; I. Todd<sup>1</sup>; I. A. Figueroa<sup>1</sup>; R. J. Hand<sup>1</sup>; H. A. Davies<sup>1</sup>; <sup>1</sup>University of Sheffield

The relationships between the elastic moduli and response to deformation of bulk metallic glasses were investigated. Five bulk metallic glasses were prepared from high purity elements via suction casting. The results confirm that there exists a correlation between energy absorbed to failure during compression testing and the bulk to shear modulus ratio. This finding is developed such that it corresponds only to the elastic component of energy absorption, and so is not capable of predicting extensive plasticity. Instead, the ideas of the shoving model are applied to plastic deformation, identifying new criteria for the relationship between shear and bulk moduli and plasticity. This idea is subsequently tied into the widely considered apparent dependency of free volume to plastic flow. The importance of structural features frozen in during the glass transition is therefore isolated meaning that it is suitable to consider the effect of glass fragility. Therefore, it may be possible to specify different criteria to maximise elastic and plastic energy absorption separately, opening new possibilities with regard to engineering the mechanical response of bulk metallic glasses.

**Electrochemistry Study on Epoxy Resin to Anti-Corrosion Performance of Reinforced Bar in the Concrete:** *Daowu Yang*<sup>1</sup>; *Chengfeng Wang*<sup>1</sup>; *Zhongliang Xiao*<sup>1</sup>; <sup>1</sup>Changsha University of Science and Technology

Corrosion behavior of reinforced bar in concrete was studied by simulating the 4×4 array wire-beam electrode in this paper. These reinforced concretes have been coated respectively in different ways: blank, iron wire with coating resin in surface, concrete with coating resin in surface, concrete and iron wire with coating resin. By measuring open-circuit potential of iron wire, the impact of different ways of coating were studied on the corrosion of concrete. The result showed that it is the best protection way to coat resin on the surface of concrete, which keep the open-circuit potential within the passivation range all the time, so as to ensure the integrity of the passivation membrane.

**Evaluated of the Structure and Morphology of the NiAl<sub>2</sub>O<sub>4</sub> Catalysts Obtained by Combustion Reaction Using Glycine as Fuel:** *Lucianna Vieira*<sup>1</sup>; *Ana Cristina Costa*<sup>1</sup>; *Elvia Leal*<sup>1</sup>; *Normanda Freitas*<sup>1</sup>; *Hélio Lira*<sup>1</sup>; <sup>1</sup>University Federal of Campina Grande

NiAl<sub>2</sub>O<sub>4</sub> is an oxide well known by its great thermal stability and chemical inertia, for this reason, is very used as catalysts, catalysts support and optical layers. The synthesis of these catalysts is based on combustion reaction using the thermodynamic concepts from propellants chemical. The aim of this work is to evaluate the influence of the glycine fuel when it was used in the stoichiometric proportion and with the excess of 10% and 20% in the preparation of NiAl<sub>2</sub>O<sub>4</sub> by combustion reaction. The powders were characterized by DRX, nitrogen adsorption for BET, granulometric distribution, and infrared spectroscopy. The results show the presence of NiAl<sub>2</sub>O<sub>4</sub> as major phase and traces of NiO and Ni for all studied powders. The size of the crystallites was 22, 17 and 9 nm to the stoichiometric composition, 10% and 20% in excess of glycine, respectively. The powders presented morphology with agglomerates of irregular plates shape.

**Evaluation of Characteristics in Slow Strain Rate Test for Solution Heat Treated Al-Mg Alloy:** *Kim Seong-jong*<sup>1</sup>; *Han Min-Su*<sup>1</sup>; *Kim Jong-Shin*<sup>1</sup>; *Jang Seok-Ki*<sup>1</sup>; <sup>1</sup>Mokpo Maritime University

The Al alloy specimen was carried out to prevent corrosion with solution heat treatment. The optimal heat treatment over the range from 10 to 240 min. involved heating specimens for 120 minutes at 420°C and then cooling them in water. The SSRT in sea water revealed that heat treatment under optimal conditions produced improved elongation, time-to-fracture and amount of dimples compared with the as-received specimen. The optimum cathodic protection range in slow strain rate test presented -1.4V~-0.7V. The characteristics of stress corrosion cracking and hydrogen embrittlement by solution heat treatment at optimum condition are improved 10.20 and 9.51 percent, respectively. Acknowledge: This research was financially supported by MOCIE and KOTEF through the Human Resource Training Project for Regional Innovation.

**Evaluation of Structural Strength in Body Structure of Container Freight Car:** *Sung Cheol Yoon*<sup>1</sup>; <sup>1</sup>Korea Railroad Research Institute

This paper describes a carbody structural analysis and the result of its loading test. The purpose of this study is to evaluate the safety and functionality of the A carbody operating under maximum load. The freight car was designed with SM490YA steel and SM490Y steel for the railway transportation. The carbody of rolling stock is a principal structure supporting major equipment of underframe, and container freight. So, the strength evaluation of this structure is important and can be the core technique in rolling stock analysis. Both structural analysis and loading test were performed under the loading condition. Prior to the evaluation, finite element method software was used for structural analyses on stress distribution in a carbody of freight car. The strain gages were attached on the carbody based on the FEM results. The test results showed that the carbody is safe and stable under the condition of designed load.

**Evaluation of Toughness Deterioration by an Electrochemical Method in an Isothermally-Aged N-Containing Austenitic Stainless Steel:** *Maribel Saucedo-Muñoz*<sup>1</sup>; *Victor Lopez-Hirata*<sup>1</sup>; <sup>1</sup>Instituto Politecnico Nacional

This work shows the evaluation of the cryogenic toughness deterioration by means of an electrochemical method in a N-containing austenitic stainless steel aged at temperatures of 700, 800 and 900°C for times from 10 to 1000 minutes. The aging process at 700 and 800°C caused the decrease in the Charpy V-Notch impact energy at -196°C because of the intergranular precipitation of carbides. The scanning electron microscope fractographs of the Charpy V-Notch test specimens showed the presence of intergranular brittle fracture. The degree of sensitization was determined by the ratio of the maximum density current

generated by the reactivation scan to that of the anodic scan, Ir/Ia using the double-loop electrochemical potentiokinetic reactivation test. The Charpy V-Notch impact energy decreased with the increase in the Ir/Ia ratio. This relation enables to estimate the deterioration of cryogenic toughness because of the thermal aging in this type of steel.

**Evolution of the Microstructure of As-Rolled Ti-43Al-9V-Y Alloy with Different Heat Treatments:** *Fantao Kong*<sup>1</sup>; *Yuyong Chen*<sup>1</sup>; <sup>1</sup>Harbin Institute of Technology

Microstructures developed in TiAl intermetallics sheet after heat treatments in the  $\alpha$ ,  $\alpha+\gamma$  and  $\alpha+\beta$  regions of the Ti-Al phase diagram have been studied. The Ti-43Al-9V-Y alloy sheet material investigated had a starting microstructure consisting of equiaxed  $\gamma$  grains with a small volume fraction of B2 phase mainly located in  $\gamma$  grain boundaries. Samples were heat treated at different temperatures ranging from 1250°C up to 1320°C. After different heat treatment, the equiaxed  $\gamma$  grain size of the sheet does not increase dramatically but precipitation of B2 phase lamellas in equiaxed  $\gamma$  grains is observed upon furnace cooling. Furthermore, microstructure of Ti-43Al-9V-Y alloy sheet transferred from  $\gamma$ +B2 phase microstructure to DP microstructure after the heat treatment of 1300°/30min. The identification of the various phases present in the microstructures was made with the help of XRD, which also helped to understand the nature of the phase transformation in Ti-43Al-9V-Y alloy.

**Evolution of Zn + NaCl Foams, Characterization and Interconnection in Open Cell:** *Said Casoleo*<sup>1</sup>; <sup>1</sup>Tecnológico de Monterrey

The structure and hardness of a Zn+ NaCl prepared with sintering process. It established parameters for the synthesis of metal foam with high porosity. The consolidation process consisted of the alloy powders mechanic of Zn and a foaming agent NaCl purity make to at room temperature, were conducted three different compositions that are: 80% Zn 20% NaCl, 60% Zn 40% NaCl and 50% Zn 50% NaCl. The mechanical properties were determined from trials of hardness and mechanical strength in a universal machine. It was determined that the best is the composition of 80% Zn 20% NaCl with a maximum load of 146 MPa. The energy absorption of 72% and a hardness of 50 HV0.5. The effect of Zn weight fraction are significant for different applications with potential use in the aerospace, automotive and biomedical applications.

**Experimental Phase Studies in the TeO<sub>2</sub> - WO<sub>3</sub> System:** *Ercin Ersundu*<sup>1</sup>; *Miray Çelikkibilek*<sup>1</sup>; *Günkut Karaduman*<sup>1</sup>; *Nuri Solak*<sup>1</sup>; *Suheyla Aydin*<sup>1</sup>; <sup>1</sup>Istanbul Technical University

Tellurite glasses are of great importance in fiber optic amplifying applications and as laser hosts. Comparing with silicate, borate and phosphate glasses, tellurite glasses have superior properties, such as low-phonon energy, high refractive index, high dielectric constant, good corrosion resistance, thermal and chemical stability. TeO<sub>2</sub> is the main but the conditional glass former; therefore, addition of a secondary component, such as heavy metal oxides, increases the glass forming ability. The present study aims investigation of the phase equilibria in the TeO<sub>2</sub>-WO<sub>3</sub> system. Three different compositions, (1-x) TeO<sub>2</sub> - x WO<sub>3</sub> (x = 0.10, 0.15, 0.20 in molar ratio) were prepared. The samples were heated in a platinum crucible for 30 minutes at 750°C, then were quenched and crushed. TG/DTA, XRD and SEM techniques were used to investigate the samples.

**Exploring the 3D Nanospace of Defects Formed in Ni-Based Superalloys Using Atom-Probe Tomography, Electron Microscopy, and Dual-Beam Focused Ion-Beam Microscopy:** *Yaron Amouyal*<sup>1</sup>; *David Seidman*<sup>1</sup>; <sup>1</sup>Northwestern University

Turbine blades utilized in aeronautical jet engines and land-based power generators are fabricated from single-crystal Ni-based superalloys, which offer superior strength and creep resistance at high temperatures. However, the formation of freckles as chains of misoriented grains along the solidification direction of the alloy results in the degradation of the blades. We employ atom probe tomography (APT) in combination with scanning and transmission electron microscopies to investigate the microstructure and chemistry of freckles in multi component Ni-based alloys at all pertinent length scales. This powerful combination of techniques provides us with high detectability (< 10 at. ppm) analysis extending from the 10 nm to 10 mm length scales. Additionally, we apply site-specific measurements using the dual-beam focused ion-beam (FIB) microscope to lift-out samples for APT from specific regions of interest. Thus, we determine the roles played by different low-concentration (<500 at. ppm) alloying elements in the formation of freckles.



**Fabrication and Characterization of Squeezed Cast Aluminum Matrix Composites with Boride Reinforcements:** *Lilia Olaya-Luengas*<sup>1</sup>; Elvin Estremera<sup>1</sup>; O.M. Suárez<sup>1</sup>; <sup>1</sup>University of Puerto Rico

Aluminum-copper alloys reinforced with borides were successfully fabricated by a squeeze casting technique employing squeezing pressures from 0 to 100 MPa. The distribution of reinforcements on composite was determined and the effect of pressure on density and hardness of composites was established. Besides, the borides stability was analyzed while the composites were heat treated. The pressure responses in the composites squeezed were investigated by optical microscopy, Vickers microhardness testing, Thermal Differential Analysis (DTA) and X-Ray Diffraction (XRD) advanced techniques.

**Failure Analysis in a Total Knee Prosthesis Metal-Polyethylene Implanted in an Active Patient:** *Marco Hernandez-Rodriguez*<sup>1</sup>; Arturo Juarez-Hernandez<sup>1</sup>; Alan Castillo<sup>1</sup>; Jose Diabb<sup>1</sup>; Alberto Perez-Unzueta<sup>1</sup>; <sup>1</sup>UANL FIME

One of the most important problems with total joint prosthesis is the early wear. The present work is about a metal-polyethylene total knee prosthesis that failed in service prematurely within 5 months by severe wear in a 50 year old female active patient with natural bony misalignment in her legs. In order to determine the origin of the failure, the prosthesis components were analyzed by means of visual inspection, optical microscopy, scanning electronic microscope (SEM), energy dispersive spectroscopy (EDS), chemical analyses, roughness test, Fourier transformer infrared (FTIR), gel penetration chromatography (GPC) and differential scanning calorimeter (DSC). The studies showed that the failure was due to a degraded UHMWPE resulting in low mechanical and tribological properties, along with an unbalanced high stress by an uncorrected surgery collocation, lead an atypical accelerated wear failure.

**Finite Element Model of Compression of a Polycrystalline Layer Showing Banding Behavior:** *Ryan Quarforth*<sup>1</sup>; Md. Zakaria Quadir<sup>2</sup>; Michael Ferry<sup>2</sup>; Lori Bassman<sup>1</sup>; <sup>1</sup>Harvey Mudd College; <sup>2</sup>University of New South Wales

Finite element models were developed for compression and rolling of metal sheet. The model uses experimentally-determined polycrystalline grain structures with orientation-dependent material properties. Specifically, anisotropic Young's modulus values are included and orientation-dependent yield stresses are calculated based on the Schmid factor with respect to the normal direction. The model shows bands of increased localized shear strain, and the geometry of the bands is a product of the grain structure. Areas of increased shear strain can lead to localized flow in the microstructures in the form of microbands and shear bands. Their inclination in the model at approximately 40 degrees relative to the rolling direction and initiation at the grain boundaries is consistent with experimental findings in conventionally rolled material and in layered aluminum-alloy structures.

**Formation, Structure and Deformation Behavior of High Strength Ti-Based Alloys with Fe:** *Dmitri Louzguine*<sup>1</sup>; Larissa V. Louzguina-Luzgina<sup>1</sup>; Akihisa Inoue<sup>1</sup>; <sup>1</sup>WPI Advanced Institute for Materials Research, Tohoku University

The high-strength metastable eutectic and hypereutectic Ti-Fe, Ti-Fe-Co, Ti-Fe-Cu, Ti-Fe-Co-Sn and Ti-Fe-Cu-Sn alloy ingots were produced by arc-melting. The structure of these Ti-based alloys containing about 20-40 at.% LTM (LTM-late transition metals, here Co or Cu) at high enough Fe/Co or Fe/Cu ratio (=1) is found to consist of the primary dendrites of an ordered cP2 intermetallic (IM) compound having a rounded dendritic morphology and an eutectic consisting of the cP2 IM compound and a disordered supersaturated cI2  $\beta$ -Ti solid solution. On compressive test at room temperature these Ti-based alloys exhibit a high ultimate mechanical strength values (some of them exceeding 2000 MPa) and a plastic deformation of 4-24%. The formation of a composite-like structure with a hard carcass of the IM phase in the relatively soft eutectic matrix enabled both high strength and ductility. The deformation behavior and the fractography of these Ti-based alloys were also studied.

**Fundamental Study on the Diffusion of PbSn Eutectic Solder Electroplated on 95Pb5Sn High-Lead Solder:** *Chun-Cheng Lin*<sup>1</sup>; Chih Chiang Chang<sup>1</sup>; C. Robert Kao<sup>1</sup>; <sup>1</sup>National Taiwan University

Many of the flip-chip solder joints were composed of the 95Pb5Sn solder bump, and the PbSn eutectic pre-solder. In order to understand the interfacial reaction behavior, 95Pb5Sn/37Pb63Sn diffusion couples were used. The diffusion couples was processed high temperature storage tests at various temperatures (100, 130, 150, and 175°C) for 100~2000 hrs. It is found that the grain growth in the initially fine eutectic PbSn microstructure is the key microstructural evolution during the interdiffusion.

**Gas Injection System for Ion Beam Induced Deposition and Etching:** *Andrew Madison*<sup>1</sup>; Donovan Leonard<sup>1</sup>; Anuj Dhawan<sup>2</sup>; Phillip Russell<sup>2</sup>; <sup>1</sup>Appalachian State University; <sup>2</sup>Duke University

The versatility of focused ion beam (FIB) nanofabrication has been well established for tasks such as TEM sample preparation and circuit or mask repair. We report the added capability of material deposition and etching, using ion beam induced chemistry, made possible by mating a commercial gas injection system (GIS) with a FIB. Deposition parameters relative to several organometallic gases including, C<sub>9</sub>H<sub>16</sub>Pt, (CO)<sub>6</sub>W, and gold precursor will be discussed in the context of the development of novel nanostructures. In exhibition of the enhanced capability realized with FIB/GIS, the fabrication of templates for bio-related plasmonic sensing will be presented. Experimental protocols for the nanofabrication of binary Pt/W metallic nanowires will be included along with variables for beam induced XeF<sub>2</sub> etching of HfO<sub>2</sub> thin films for microelectronic device cross section decoration.

**Gas Sensing Properties of MoO<sub>3</sub> Thin Film Deposited Using Chemical Vapor Transport of MoO<sub>3</sub>(OH)<sub>2</sub>:** *Young Jung Lee*<sup>1</sup>; Young Moon Kim<sup>1</sup>; Han Seob Kim<sup>1</sup>; Dae-gun Kim<sup>1</sup>; Young Do Kim<sup>1</sup>; <sup>1</sup>Hanyang University

MoO<sub>3</sub> thin film has strongly attracted attention as a conductance-type gas sensor because of high sensitivity to various gases such as NO<sub>x</sub>, CO, H<sub>2</sub>, and NH<sub>3</sub> in the temperature range of 300-600°C. There are many deposition techniques for MoO<sub>3</sub> film such as thermal evaporation, sputtering, chemical vapor deposition, and pulsed laser deposition. Characteristics of films are dominated by deposition technique and its parameters, so that a challenge of new approach is required as well as extensive studies of structural and physical properties to obtain enhanced sensing properties. In this study, a new fabrication technique of MoO<sub>3</sub> film for a gas sensor is suggested. MoO<sub>2</sub> film was deposited at 500°C in H<sub>2</sub> by chemical vapor transport of MoO<sub>3</sub>(OH)<sub>2</sub> during hydrogen reduction of MoO<sub>3</sub> powder and the deposited film was annealed at 400°C in O<sub>2</sub> to fabricate MoO<sub>3</sub> phase. Gas sensing properties of the films were discussed relating with microstructural evaluations.

**Growth of  $\beta$ -Ga<sub>2</sub>O<sub>3</sub> Nanowires and Nanobelts Prepared by Physical GaAs Evaporation:** *Hee-Suk Chung*<sup>1</sup>; Seoung-Bum Son<sup>1</sup>; Tae Jun Ko<sup>1</sup>; Seul Cham Kim<sup>1</sup>; Do Hyun Kim<sup>1</sup>; Kyu Hwan Oh<sup>1</sup>; <sup>1</sup>Seoul National University

Nano-structured materials can perform unique optical, electronic, and structural properties as compared to their bulk forms on account of quantum confinement effects and a high fraction of chemically similar surface sites. One-dimensional (1D) nanostructures have drawn extensive attractions due to their distinguished properties resulting from their unique size and dimensionality. Among various 1D nanostructures, monoclinic( $\beta$ )-Ga<sub>2</sub>O<sub>3</sub>, a wide-band gap compound with a band gap of approximately 4.9eV at room temperature, is a promising transparent conductor for the coming generation of optoelectric devices in the deep-ultraviolet wavelength region. Recently,  $\beta$ -Ga<sub>2</sub>O<sub>3</sub> have been fabricated via arc discharge, laser ablation, powder evaporation, etc. However, little literature is only available with regard to understanding the vapour-liquid-solid via oxygen atmosphere on  $\beta$ -Ga<sub>2</sub>O<sub>3</sub> nanowires synthesis. In this letter, we report fabrication and characterization of  $\beta$ -Ga<sub>2</sub>O<sub>3</sub> nanowires synthesized through GaAs physical evaporation. As-synthesized nanowires were characterized with scanning electron microscopy, transmission electron microscopy, X-ray diffraction.

**High-Pressure/High-Temperature Raman Studies on Thermal Storage Materials –Neopentylglycol (NPG):** *Vamsi Krishna Kamisetty*<sup>1</sup>; Juan Carlos Fallas<sup>1</sup>; Wen-Ming Chien<sup>1</sup>; Dhanesh Chandra<sup>1</sup>; Erik Emmons<sup>2</sup>; Aaron Covington<sup>1</sup>; Raja Chellappa<sup>3</sup>; <sup>1</sup>University of Nevada, Reno; <sup>2</sup>U.S. Army Edgewood Chemical Biological Center; <sup>3</sup>Carnegie Institute of Washington

Pressure-Temperature phase diagrams for the materials neopentylglycol (NPG) were determined using high-pressure/high-temperature Raman scattering experiments. The presence of thermal transitions between orientational order and disorder in this material make it important and has been suggested for use as thermal storage materials. At room temperature there is no phase change observed upon increasing the pressure up to ~10 GPa, but at 0.5 GPa and above 50°C there is a orientational order/disorder transition in which NPG goes into  $\gamma$ -phase. Similar phase change into  $\gamma$ -phase is seen again at 1.16 GPa and above 126°C. Further Increasing the pressure to 2.08 GPa and at 151°C the order/disorder transition shows that NPG enters into a new  $\gamma$ -phase. Pressure-Temperature phase diagram of NPG has been determined based on the temperature-dependent and pressure-dependent Raman data acquired.



**High-Temperature Microstructures of ZrB<sub>2</sub>-SiC Composites Prepared by Spark Plasma Sintering:** *Ipek Akin*<sup>1</sup>; Filiz Sahin<sup>1</sup>; Onuralp Yucel<sup>1</sup>; Takashi Goto<sup>2</sup>; Gultekin Goller<sup>1</sup>; <sup>1</sup>Istanbul Technical University; <sup>2</sup>Tohoku University

In this study, ZrB<sub>2</sub>-SiC composites were produced using SPS at high temperatures, above 2100°C, and microstructural features were investigated. The temperature of the die increased at 0.8°C/s in vacuum under a pressure of 10 MPa. Pulsed direct current (60 ms/on, 10 ms/off) was applied during the SPS process. The temperature of the die was measured by an optical pyrometer and the shrinkage of the specimens was continuously monitored during the process. The microstructure of ZrB<sub>2</sub>-SiC composites containing 40 mass% SiC sintered at 2200°C consisted of irregular texture composed of ZrB<sub>2</sub> and fine a-SiC grains in addition to the elongated a-SiC grains. For the ZrB<sub>2</sub>-80 mass% SiC composite, porous structure was detected. The decomposition of SiC may have caused the formation of large pores at higher temperatures, 2280°C, 2300°C and 2360°C.

**High Pressure Raman and X-Ray Studies of Tris(Hydroxymethyl)Amino methane (TRIS):** *Vamsi Krishna Kamisetty*<sup>1</sup>; Wen-Ming Chien<sup>1</sup>; Juan Carlos Fallas<sup>1</sup>; Dhanesh Chandra<sup>1</sup>; Erik Emmons<sup>1</sup>; Aaron Covington<sup>1</sup>; Raja Chellappa<sup>1</sup>; Simon Clark<sup>1</sup>; <sup>1</sup>University of Nevada, Reno

Organic thermal energy storage materials are useful for thermal energy storage due to the presence of solid-state phase transition where the latent heat can store energy. The effects of temperature and pressure on X-ray diffraction patterns and Raman spectra of tris(hydroxymethyl) aminomethane (TRIS) (C(CH<sub>2</sub>OH)<sub>3</sub>NH) were measured. DSC and in-situ X-ray diffraction results show the solid-state ( $\alpha$ -orthorhombic to  $\gamma$ -BCC) phase transition of TRIS occurs at 133.7°C at ambient pressure (1 atm). At room temperature, high pressure synchrotron X-ray diffraction patterns and Raman spectra using Diamond Anvil Cell (DAC) show TRIS undergoes a phase transition ( $\alpha$  to  $\beta$ ) at ~1 GPa. A new high pressure  $\beta$ -phase was observed from ~1 GPa to 9.3 GPa. The effects of hydrogen bonding on the broad OH and sharp NH stretching modes will be discussed. Detail results of temperature dependent effects on high pressure Raman spectra and Pressure-Temperature (P-T) phase diagram of TRIS will be presented.

**High Strength FeCo-Based Multiphase Composite Alloys with Good Magnetic Properties:** *Ran Li*<sup>1</sup>; Mihai Stoica<sup>1</sup>; Gang Liu<sup>1</sup>; Jürgen Eckert<sup>1</sup>; <sup>1</sup>Leibniz-Institute of Solid State and Materials Research (IFW) Dresden

It is well known that near-equiatomic FeCo-based alloys offer exceptional magnetic properties. However, notorious brittleness of this alloy obstructs its industrial application. By controlling rapid-solidification condition and designing multicomponent alloying, we produced a family of FeCo-based multiphase composite alloys with good mechanical and magnetic properties. Comparing with equiatomic FeCo binary alloy, the “designing” alloys exhibit 3~4 times improvement of yield stress and obvious plastic deformation of 5~20% during compressive test. The structural analysis indicated that homogeneous fined grains, induced by the control of liquid solidification, and morphologic construction of multiphase composite, designed by the choice of alloying elements, endow these alloys with good mechanical properties. Furthermore, although the alloying decreased the saturation magnetization of resulting alloys, it still remains ~ 2 T as high as the result of pure iron. These FeCo-based multiphase composite alloys combining with advantages of structural materials and functional materials have a good potential application.

**High Temperature Corrosion Behavior of Sputtered K38 Nanocrystalline Coating with Yttrium Additions in Molten Sulfate:** *Fuhui Wang*<sup>1</sup>; Wen Wang<sup>1</sup>; Ping Yu<sup>1</sup>; <sup>1</sup>Institute of Metal Reserach, Chinese Academy of Sciences

A two-dimension nanostructured coating, which chemical composition is similar to the Ni-based substrate alloy, was deposited by sputtering technique. The influence of various amounts of yttrium addition on high temperature corrosion behavior of the sputtered coating in the presence of molten 75wt.% Na<sub>2</sub>SO<sub>4</sub>+25wt.% K<sub>2</sub>SO<sub>4</sub> at 1173K was investigated. The results indicated that nanocrystallization for superalloys increased the corrosion resistance significantly through the rapid formation of continuous exclusive alumina scale. The addition of yttrium further improved the corrosion resistance of the nanocrystalline coating by increasing the stability of the alumina scale. The synergetic effects of nanocrystallization and yttrium addition on the high temperature corrosion behavior in molten sulfate were discussed.

**High Temperature Oxidation of Steels in Air and Co<sub>2</sub>-O<sub>2</sub> Atmosphere:** *SangHwan Bak*<sup>1</sup>; DongBok Lee<sup>1</sup>; <sup>1</sup>Sungkyunkwan University

Three kinds of hot rolled steel slabs, viz. high strength steel, bake hardened steel and low carbon steel, were oxidized isothermally between 1100 and 1250°C

for up to 2 hr in 1 atm of air and an 85%N<sub>2</sub>-10%CO<sub>2</sub>-5%O<sub>2</sub> gas mixture. The steels oxidized in a similar fashion in both atmospheres. The oxidation process followed an initial linear rate law, which then gradually transformed to a nearly parabolic rate law. Thick, porous and nonadherent scales formed rapidly, due to the high oxidation temperature. The scales formed consisted of Fe<sub>2</sub>O<sub>3</sub>, (Fe<sub>2</sub>O<sub>3</sub>+Fe<sub>3</sub>O<sub>4</sub>), (Fe<sub>3</sub>O<sub>4</sub>+Fe<sub>2</sub>O<sub>3</sub>+FeO) and (FeO+Fe<sub>3</sub>O<sub>4</sub>) from the outer surface. The presence of supersaturated oxygen beneath the scale resulted in grain boundary oxidation and the formation of internal oxide precipitates.

**Impact of the Brazing Process Variables in the Reduction of Porosity of Copper Alloys with Copper and Silver Filler Material:** *Misael Hernández*<sup>1</sup>; Jorge Acevedo<sup>1</sup>; Mauricio Garza<sup>1</sup>; <sup>1</sup>Corporación Mexicana de Investigación en Materiales S.A. de C.V., Ciencia y Tecnología

In this study the relation between welding time, temperature and filler material variables were studied in copper tubes used in the freezing system and welded by brazing. The most important variables were the welding time and the cleaning treatment. The best result were found with 350°C and 11 seconds with cleaning treatment, reducing the porosity in the welding zone but the base material started to recrystallize. The result found at 350°C and 7 seconds without cleaning treatment was more porosity.

**Impression Creep of a Thermo-Stable PMR-15 Polyimide:** *Rong Chen*<sup>1</sup>; Fuqian Yang<sup>1</sup>; Y. C. Lu<sup>1</sup>; G. P. Tandon<sup>2</sup>; G. A. Schoeppner<sup>3</sup>; <sup>1</sup>University of Kentucky; <sup>2</sup>University of Dayton Research Institute; <sup>3</sup>Air Force Research Laboratory/RXBC

Polyimides based on the polymerization of monomeric reactants (PMR) approach have the potential for high temperature applications in aircraft engines. The performance of the PMR-based structures depends on the mechanical durability of the PMR at high temperatures, such as creep and stress relaxation. In this work, the creep behavior of PMR-15 polyimide was studied, using the impression technique in the temperature range of 250 to 300°C and the impression stress of 111 to 277 MPa. The impression stress corresponded to about 3.5 time of the compressive stress, i.e. 31.7 to 79.1 MPa. It was found that there existed a steady state creep for the creep tests with temperatures of 280°C and higher, from which a constant impression velocity was calculated. The steady state impression velocity increased with temperature and the impression stress with a stress exponent of about 2.5.

**Improvement of Tensile Ductility of Heavily Rolled and Recovery Annealed Aluminum Alloy Sheet:** *Ni-Hsing Lee*<sup>1</sup>; Jyun-Hao Chen<sup>1</sup>; T. Tseng<sup>2</sup>; P. W. Kao<sup>1</sup>; <sup>1</sup>National Sun Yat-sen University; <sup>2</sup>China Steel Corporation

For non-heat treatable aluminum alloys, strength can be achieved by heavy cold working, but poor ductility is often accompanied. In order to restore some ductility, a low temperature recovery annealing may be applied, in which the annealing is carried out at a temperature below the onset of recrystallization. The recovery annealing often produces yield drop, which is followed by flow localization, early onset of necking, and poor ductility. In this work, Al-Fe-Mn alloy sheets produced by heavy cold rolling (>95%) followed by recovery annealing were investigated. Anisotropic tensile tests were carried out with stress axis along the directions of 0°, 45°, and 90° from rolling direction. It was observed that the presence of Mn in solid solution could improve both the tensile strength and ductility of the recovery annealed aluminum alloy sheet. Microscopic observations were also performed and related to the tensile properties.

**Indentation Creep Properties of Self-Similar Indenters:** S. V. Thube<sup>1</sup>; P. Kumar<sup>1</sup>; A. Elmustafa<sup>2</sup>; <sup>1</sup>Applied Research Center-Old Dominion University-Jefferson Laboratory; <sup>2</sup>Old Dominion University

Finite element analysis is used to simulate indentation creep experiments with variable indenter tips. Indentation creep simulations of self-similar indenters i.e., cone, pyramid, and berkovich are presented. The purpose of the analysis is to identify the relationship between the strain rate sensitivity of the hardness,  $v_H$ , and that of the flow stress,  $v\sigma$  in materials with variable elastic-plastic properties. The results from the pyramidal and berkovich indenter tips will be compared with results already published for a conical indenter tips to complete the set of analysis for self-similar indenters. Previously it was asserted that  $v_H$  differs from  $v\sigma$ , but the ratio  $v_H/v\sigma$  is found to be a unique function of where H is the hardness and  $\nu$  is the modulus relevant to Hertzian contact. Due to self-similarity, it is expected that this result will hold for the other two indenters tips (pyramidal and Berkovich).

**Influence Local Use of Ageing Effects in Multiphase Steels for Designing Local Properties of Constructional Elements:** *Heinz Palkowski<sup>1</sup>; Mehdi Asadi<sup>1</sup>; <sup>1</sup>TU Clausthal*

The investigations deal with processes leading to local effects of strengthening in multiphase steels, being characterized by good formability, continuous yielding, high strength and a strong bake hardening and ageing effect. Dual phase and complex phase steels are under investigation to examine the effect of thermo-mechanical processing parameters on local ageing ability. For this purpose local heat treatment by laser are studied, as well as stability of local ageing on the adjusted strength. The local heat treatment leads to an increase of hardness and strength and to local strengthening of the material. The stability of the local strengthening effect could be confirmed. Partial heat treatment of multiphase steels by laser can open a new field of application for the local use of the bake hardening effect. Chance is given to influence only relevant areas, thus representing a potential for energy-saving.

**Influence of Additives on Immobilization Process of Heavy-Metal Containing Waste Residues Using Elemental Sulfur:** *Liyuan Chai<sup>1</sup>; Li Wang<sup>1</sup>; Xiaobo Min<sup>1</sup>; Yu Wu<sup>1</sup>; Yunyan Wang<sup>1</sup>; <sup>1</sup>Central South University*

In this paper, three additives, namely sodium hydroxide, calcium hydroxide and sodium carbonate, were used to enhance the immobilization of cadmium and zinc in sulfuration neutralization sludge using elemental sulfur. The results showed that the pH of the leachate increased as the addition rate of these three additives increased. Both NaOH and Ca(OH)<sub>2</sub> greatly improved the performance of immobilization. Na<sub>2</sub>CO<sub>3</sub> also enhanced the immobilization of cadmium and zinc, however, to a less extent. After analyzing the products of metal oxides mixed with sulfur and additives or without any additive at 413K, the results revealed that metal sulfuration did not occur during the sulfur immobilization process without any additive. However, with the addition of NaOH, cadmium sulfide and zinc sulfide were produced. Other two additives could not promote metal sulfuration, while they enhanced the immobilization of cadmium and zinc simply by increasing the pH value of the leachate.

**Influence of Heat Input on Microstructure and Mechanical Properties of Laser Beam Welded Superalloy Inconel 718:** *Akin Odabasi<sup>1</sup>; Necip Ünlü<sup>1</sup>; Gültekin Göller<sup>1</sup>; Niyazi Eruslu<sup>1</sup>; <sup>1</sup>Istanbul Technical University*

The effect of heat input from laser beam welding (LBW) on the microstructural and mechanical properties of superalloy Inconel 718 were investigated. Four different heat input produced to evaluate the geometry of weld seams. Full penetration was achieved in all weld experiments. The analysis of optical and field emission scanning electron microscopy together with micro-hardness based on ISO 9015-2:2003(E) were performed. Increasing the amount of heat input from 74.5 J/mm through 126.5 J/mm changed the resulting weld shape from a wine glass shape to a stemless wine glass shape with wider surface bead widths. The effect of heat input was significantly clear at the widths of the mid- and upper-side of the weld seam. It was observed that the differences of the heat input affected the solidification rate. The secondary dendrite arm spacing increased with increasing heat input.

**Influence of Processing Conditions on Development of PE/PE-g-MA/Organoclay Nanocomposites:** *Luana Kojuch<sup>1</sup>; Renata Barbosa<sup>1</sup>; Edcleide Araújo<sup>1</sup>; Tomas Melo<sup>1</sup>; <sup>1</sup>Universidade Federal de Campina Grande*

Nanocomposites developed with silicates in layers represent an alternative to the composites developed with conventional filler, because they use minimum levels of nanofiller. In this work, polyethylene/PE-g-MA/organoclay nanocomposites were produced in a Torque Rheometer Haake in these conditions: 190°C, 60 and 120rpm, for 7 and 14 minutes. The systems were characterized by X-ray diffraction (XRD). The obtained results indicated that the PE/PE-g-MA/organoclay nanocomposites presented intercalated and/or partially exfoliated structures for the 120 rpm and 7 minutes, probably due to bigger number of intercalation of polyethylene molecules between the layers of the organoclay. For the time of 14 minutes, the material showed a little degradation probably due to excessive time in the mixer.

**Influence of Submerged Tandem Arc Welding on HAZ Toughness of X80 Micro Alloy:** *Sadegh Moeinifar<sup>1</sup>; <sup>1</sup>Azad University*

X80 HSLA steel is a high grade microalloy steel that is used for this research. Tandem SAW with two or excess electrode is an economic process for joining microalloy steels components. welding process is done with four wires but lowering in heat affected zone toughness for high grade microalloy steels. Toughness in heat affected zone (fusion line, coarse grain HAZ and fine grain

HAZ) studied. Welding done in different amount of heat input. Microstructure and Impact energy with CVN (charpy V notch) studied in -50°C. Heat affected zone in microalloy steels is complex due to many phases (polygonal ferrite, quasi polygonal ferrite, widmanstatten ferrite, acicular ferrite, granular ferrite, bainite, M/A, inclusions). Impact energy changes with heat input up to optimum and increased about fifty percent. Microstructure study with SEM shown that M/A island, austenite grain growth and ferrite side plate is a major factor in CGHAZ toughness.

**Interfacial Bonding Characteristics of Cu Thin Film on FR-4 Substrate for Chip-in-Substrate Applications:** *Kyoung-Jin Min<sup>1</sup>; Sung-Cheol Park<sup>1</sup>; Ki-Wook Lee<sup>2</sup>; Jae-Dong Kim<sup>2</sup>; Do-Geun Kim<sup>3</sup>; Gun-Hwan Lee<sup>3</sup>; Young-Bae Park<sup>1</sup>; <sup>1</sup>Andong National University; <sup>2</sup>Amkor Technology Korea Inc; <sup>3</sup>Korea Institute of Materials Science*

Chip Embedding is increasingly adopted as future electronics technology due to its trend of high density and high performance. One responsible technology is to embedded active device into a dielectric substrate by build-up process, for example, chip in substrate (CiS) structure. This embedding of active devices technology needs Cu metallization of micro-via for contacts I/O pad on embedded chip with outer layers, however, the poor interfacial adhesion between Cu via and dielectric substrate can lead to limitation of interfacial reliability at actual using conditions. In this study, we investigated the effects of the ion-beam treatment conditions on chemical bonding of FR-4 substrate surface and also on the interfacial adhesion of Cu via to FR-4 systems in order to understand the interfacial bonding mechanism. Extensive interface analyses using FE-SEM, AFM and XPS were performed to understand the fundamental interfacial bonding mechanism and to find the optimum conditions of ion-beam treatment, respectively.

**Investigation of Intermetallides, Obtained in Ti-Al System under Shock Wave Loadings:** *Nikoloz Chikhradze<sup>1</sup>; George Oniashvili<sup>1</sup>; Mikheil Chikhradze<sup>1</sup>; <sup>1</sup>Mining Institute of Georgia*

The paper describes the results of investigations of the reactions in Ti-Al system induced on shock wave front developed during the chemical explosions. Experiments were conducted in the cylindrical and normal mode of shock-wave configuration. Theoretically calculated the energetic characteristics and stress tensor components in steel container containing the Ti-Al reaction mixture. The phase constitution of obtained samples, microstructure and mechanisms of intermetallides formation are investigated depending on the initial ratio of components in reaction mixture. Welding zone of intermetallides and cylindrical surface of steel ampoule were studied and determined the micro-hardness distribution in structure. The above mentioned and structure/properties relationships are discussed in the paper.

**Investigation of the Influence of Silver and Tin on Trivalent Europium Ions in Aluminophosphate Glass:** *José Jiménez<sup>1</sup>; Sergiy Lysenko<sup>1</sup>; Huimin Liu<sup>1</sup>; Esteben Fachini<sup>2</sup>; Oscar Resto<sup>2</sup>; Carlos Cabrera<sup>2</sup>; <sup>1</sup>University of Puerto Rico at Mayagüez; <sup>2</sup>University of Puerto Rico at Río Piedras*

The spectroscopic properties of Eu<sup>3+</sup> ions in aluminophosphate glass containing silver and tin have been studied. Glasses were prepared by the melt-quenching technique in which Ag nanoparticles (NPs) were embedded upon heat treatment (HT), and studied by optical absorption, photoluminescence (PL) spectroscopy, X-ray photoelectron spectroscopy, and transmission electron microscopy. An enhanced Eu<sup>3+</sup> ions emission was observed for non-resonant excitation near 270 nm. Optical measurements suggest that light absorption occurs at isolated Ag<sup>+</sup> ions and/or twofold-coordinated Sn centers followed by energy transfer to Eu<sup>3+</sup>. The PL properties and decay characteristics of silver, tin and europium in the host have been assessed in order to elucidate the nature of energy transfer. The effect of HT on Eu<sup>3+</sup> ions is discussed along with likely Ag NP-Eu<sup>3+</sup> interactions in the nanocomposite.

**Joining of TiAl with Reactive Multilayer Thin Films and TiNi Thin Foils:** *Sónia Simões<sup>1</sup>; Filomena Viana<sup>1</sup>; Ana Ramos<sup>2</sup>; Maria Vieira<sup>2</sup>; Manuel Vieira<sup>1</sup>; <sup>1</sup>Faculdade de Engenharia, Universidade do Porto; <sup>2</sup>Faculdade de Ciências e Tecnologia, Universidade de Coimbra*

TiAl application in aerospace components depends not only on the alloy design but also on the processing, surface modification and joining. In this work, we join gamma-TiAl with Ni/Al multilayer thin films; TiNi foils were used as a braze alloy to fill the bond gap. The multilayers were deposited into TiAl samples by d.c. magnetron sputtering with periods of 5, 14 and 30 nm. Joining experiments were performed under a pressure of 50 MPa at 800, 900 and 1000°C



for 1 hour in a vertical furnace, with a vacuum level better than 10-4 mbar. The microstructure of the cross-sections of bond interface was analysed by energy dispersive X-ray spectroscopy (EDS) and characterized by scanning electron microscopy (SEM) and high resolution transmission electron microscopy (HRTEM). Sound joints are obtained with a combination of reactive multilayer thin films and TiNi thin foils. Several NiAlTi intermetallic compounds are formed in the interface region.

**Large Cold Deformation Behavior of a High Strength Ti-Alloy:** *Yongqing Zhao*<sup>1</sup>; Zhengping Xi<sup>1</sup>; <sup>1</sup>Northwest Institute for Nonferrous Metal Research

How to reduce the cost is one of the main research directions in the Ti field. Ti26 is a new high strength Ti alloy with tensile strength over 1250MPa developed by Northwest Institute for Nonferrous Metal Research. After large cold deformation, its yield strength increases quickly, its tensile strength and elongation also increases with the increase of deformation amount. The observations of microstructure show that the grains size is not well distribution and big grains are exist with not so large deformation, and the grains are fine with the increase of deformation amount. The evolution of its microstructure undergoes two processes, that is deformation and recrystallization, after large cold deformation and solution. After solution, its microstructure becomes equiaxed grains through recrystallization. The large cold deformation mechanism of Ti-26 alloy is twin and slip.

**Laser-Co2 Process Optimization to Stainless Steels in the Manufacture of Control Emission System in the Automotive Application:** Arturo Novales<sup>1</sup>; Arturo Reyes<sup>1</sup>; <sup>1</sup>Corporacion Mexicana De Investigacion En Materiales

This paper shows the results to the investigation project to evaluate the impact of the variables of laser-CO2 process, apply in the manufacture of control emission system in the automotive industry. The impact of the energy power, velocity and shielding gas in the microstructure, tensile properties and microhardness was evaluated. The data had been treated to obtain a multivariate statistical model to the process optimization. The model was validated and it has been applying in the real process, increasing the productivity and use to other technological projects.

**Latest State of Continuous Carbon Paste Preparation with Buss Kneader Technology:** *Hans-Ulrich Siegenthaler*<sup>1</sup>; Joel Stampfli<sup>1</sup>; Peter Franz<sup>1</sup>; <sup>1</sup>Buss AG

The "Buss Kneader" is since over 50 years the leading technology of continuous anode paste mixing. The main obstacles of anode manufacturers today are the rising costs of pitch and coke, followed by their deteriorating quality. Intensified mixing process together with micro dispersion of the pitch is the answer to this dilemma. These specific process requirements have been analysed and converted to the latest generation of Buss Kneaders, having improved mixing performance. For this development Buss AG used the experiences of the recent year's development of the advanced Buss technology. A systematic process oriented approach was one of the key elements for reaching the ambitious goals. This paper will present the latest state of the developments to mix green carbon paste with specific focus on high production capacities and for achieving the processing and economic advantages as requested by the anode producers today and tomorrow.

**Lorentz Force Flowmeter in Industrial Application:** *Vitaly Minchenya*<sup>1</sup>; Christian Karcher<sup>1</sup>; Yuri Kolesnikov<sup>1</sup>; Andre Thess<sup>1</sup>; <sup>1</sup>Ilmenau University of Technology

Lorentz force velocimetry is an innovative technique for non-contact measurement of the flow rate and accumulated mass of moving conductive fluids like high-temperature liquid metal alloys. In this work we present the results of industrial tests of the Lorentz force flowmeter (LFF) in a secondary aluminum production plant. The measurements were carried out in an open channel within which the primary melt is transported from the rotary furnace to the holding furnace. The uncertainty of measurement is obtained by comparing the measured accumulated mass with the results of preliminary weighting of the alloy components.

**Magnetic Properties and High Frequency Characteristics of FeCoZrO/ZrO2 Multilayered Thin Film:** *Kai-Xin Liu*<sup>1</sup>; Jeng-Gong Duh<sup>1</sup>; <sup>1</sup>National Tsing Hua Univ

During last decade, the IT technology has offered huge application of soft magnetic films for high frequency devices, like power converters. Fe-Co alloy thin film exhibits very large saturation magnetization. Thin films with fine grains with size smaller than ferromagnetic exchange length and with multilayer

structure lead to low coercivity. In this study, multilayered soft magnetic thin films of FeCoZrO/ZrO2 were deposited by DC reactive magnetron sputtering. Zr and O were added to refine the grain size and to increase the resistivity, respectively. The field annealing was followed by film deposition to release internal stress and to induce uniaxial anisotropy. The composition, the static magnetic properties and the complex permeability of films was determined by EPMA, VSM and permeameter, respectively. The resistivity was measured by conventional four-point method. The effect of multilayered structure and the addition of Zr and O on magnetic softness would be probed and discussed.

**Manufacturing of Copper Foam by Electro-Deposition:** *Jun Li*<sup>1</sup>; Qinghua Tian<sup>1</sup>; Ling Huang<sup>1</sup>; Xueyi Guo<sup>1</sup>; <sup>1</sup>Central South University

A novel method for preparing porous copper foam was proposed in which the polyurethane foam as substrate was processed by degreasing process, roughening process, conductive treatment and copper electrodeposition. Influence of different solution compositions and operation conditions on factors such as current efficiency and cell voltage was discussed. Optimum experiment conditions were got by optimizing the factors.

**Mechanical and Microstructural Observations during Creep of Fine-Grained Ti-45Al-5Nb-0.2B-0.2C:** *Dennis Peter*<sup>1</sup>; Gopal Babu Viswanathan<sup>2</sup>; Martin Wagner<sup>1</sup>; Gunther Eggeler<sup>1</sup>; <sup>1</sup>Ruhr University Bochum; <sup>2</sup>The Ohio State University

Constant load creep experiments were conducted on the hot-extruded Ti-45Al-5Nb-0.2B-0.2C (at.-%) alloy in the 700°C-800°C temperature range. The material exhibits a fine-grained duplex microstructure consisting of equiaxial  $\gamma$  grains of about 2.5  $\mu\text{m}$  grain size, as well as lamellar  $\alpha_2/\gamma$  colonies. Microstructures before and after creep were analyzed using scanning electron microscopy (SEM), transmission electron microscopy (TEM), electron back scatter diffraction (EBSD) measurements, and a complementary specimen preparation technique with focused ion beams (FIB). TEM analysis after creep reveals that dislocation creep and some twin activity occurs in the lamellar colonies. In contrast, only few deformation substructures are found in the equiaxial grains. These results and surface observations of FIB tracer lines on specimens crept under high purity Argon atmosphere indicate that the equiaxial  $\gamma$  grains (representing 65-75 vol.-% of the material) may well deform by grain boundary sliding.

**Mechanochemical Synthesis and Characterization of Titanium Diboride Powder:** *Duygu Agaogullari*<sup>1</sup>; Fikret Aynibal<sup>1</sup>; Osman Cihan Demirhan<sup>1</sup>; Ismail Duman<sup>1</sup>; <sup>1</sup>Istanbul Technical University

Titanium diboride classified as advanced ceramic is commonly produced using high temperature technologies. In this study, TiB<sub>2</sub> powder was produced at room temperature by mechanochemical process providing magnesiothermic reduction of TiO<sub>2</sub> (anatase) and native anhydrous B<sub>2</sub>O<sub>3</sub> which were employed in stoichiometric amount. Following the synthesis of TiB<sub>2</sub> in multi-axial ball mills in constant ball-to-powder weight ratio (10:1), the intermediate products will be refined by HCl leaching. In experimental studies, the parameters in milling and leaching which affect the microstructure of final product and the efficiency of process, such as milling type (Spex and Platenery ball mill), milling time (1-40 hours), PCA (% 2 stearic acid) and excess Mg (5%-20%) addition, leaching duration (from 3 minutes to 2 hours) and acid concentration (1M - 3M) will be examined. The intermediate and final products were characterized by Particle Analyzer, XRD, SEM/EDS and DTA analyses. Also, leaching solutions were analyzed by AAS.

**Methane in Syngas Conversion over Ni/A-Al2O3/ ZnO Catalyst:** *Lucianna Vieira*<sup>1</sup>; Laedna Neiva<sup>1</sup>; Heloysa Andrade<sup>2</sup>; Ruth Kiminami<sup>3</sup>; Ana Cristina Costa<sup>1</sup>; <sup>1</sup>University Federal of Campina Grande; <sup>2</sup>UFBA; <sup>3</sup>UFSCar

This work has as aim the development Ni catalyst supported in a-Al<sub>2</sub>O<sub>3</sub>/ZnO, to be applied in the reaction of steam reforming of the methane. The Al<sub>2</sub>O<sub>3</sub>/ZnO catalytic support was obtained by synthesis method of the combustion reaction. The catalytic support was characterized by X-ray diffraction, textural analysis by BET method, SEM and TEM. The support was submitted to impregnation with Ni by humid method. After of the impregnation the catalyst was characterized by adsorption/desorption of N<sub>2</sub> for BET, XRD and submitted to catalytic test in laboratory. Al<sub>2</sub>O<sub>3</sub>/ZnO catalytic support presents crystalline structure and nanosize particles with crystallite size of 55 nm and similar morphologic aspect to of the  $\alpha$ -Al<sub>2</sub>O<sub>3</sub> pure. The Ni impregnations promoted an alteration textural in the structure porosity of the catalyst. The result of catalytic test showed that the



developed catalyst in this work is extremely efficient in the obtainment of the syngas from the methane.

**Microstructure and Mechanical/Electrical Properties of Nanostructured High-Strength, High-Conductivity (HSHC) Cu Material:** *Timothy Lin<sup>1</sup>; Chunhu Tan<sup>1</sup>; Bob Liu<sup>1</sup>; <sup>1</sup>Aegis Technology Inc.*

With continual size shrinking of microelectronic systems, the electrical wires, circuit leads, contacts, and interconnects in these systems are desired to possess both good electrical conductivity, and high mechanical strength. Commercially pure Cu is a traditional material of choice for these components, which however suffers the limitations of low mechanical strength. Recent investigations suggested that the formation of a special class of nanocrystalline microstructure would provide the opportunity to achieve both high strength and high conductivity (HSHC), in contrast with conventional nanocrystalline Cu materials generally featured with high strength and yet substantially reduced electrical conductivity. Aegis Technology has successfully demonstrated the fabrication of bulk HSHC Cu materials by using a cost-effective synthesis and consolidation process that can be scaled up for mass production. In this presentation, we will report the microstructure, mechanical/electrical properties and their correlations of this HSHC Cu material.

**Microstructures and Mechanical Properties of Copper Alloyed Austempered Ductile Irons:** *Usanee Kitkamthorn<sup>1</sup>; Ittipon Diewwanit<sup>2</sup>; <sup>1</sup>Suranaree University of Technology; <sup>2</sup>Chulalongkorn University*

Microstructures and mechanical properties of copper alloyed austempered ductile iron were investigated. The standard tensile specimens were austenitized at 900°C for 60 minute and then austempered at 300°C and 340°C for a range of 60-6000 seconds. Results showed that amounts of bainitic ferrite and retained austenite increase with increasing austempering time. The transformation of the higher content of copper alloyed iron shows significantly the difference of microstructure between eutectic cell and intercellular boundary. The yield strength and ultimate tensile strength and %elongation increase with an increase of austempering time. The mechanical properties of austempered ductile irons satisfied the high strength grade of standard ASTM A897M:1990 when austempering was carried out at 300°C. However, the austempering at 340°C can not produce the more ductile grade. The microstructure revealed that the amounts of bainitic ferrite, martensite and retained austenite are in good agreement with the tensile properties.

**Microstructures of Electron Beam Melted (EBM) Biomaterial Ti-6Al-4V:** *Adnan Safdar<sup>1</sup>; Liu-Ying Wei<sup>1</sup>; <sup>1</sup>Malmö University*

Ti-6Al-4V alloy is an attractive material to be considered as biomaterial. The current work evaluates the microstructures by SEM/EDX and optical microscopy of the solid and net-shape Ti-6Al-4V alloy produced by Electron Beam Melting (EBM). The microstructures are influenced by the cooling rate, processing parameters in EBM system and re-heating of the existing layer during the melting of subsequent layer. Layer structure and occasional columnar beta grains have been observed, with growing direction parallel to built direction. The interior of  $\beta$  grains consists of alternating  $\alpha$  /  $\beta$  phases. The  $\beta$  phase in the colonies resembles rod shape embedded in the plates. Along the  $\beta$  grain boundaries more or less continuous  $\alpha$  layers were observed. In comparison to solid samples uneven surfaces and pores were observed in the net shape structure. Microhardness evaluation of the EBM produced alloys were also carried out and compared with conventionally produced alloys.

**Mixture of Calcium Hydrides and Lithium Borohydrides for Hydrogen Storage Materials:** *Hongwei Yang<sup>1</sup>; Andrew Goudy<sup>1</sup>; <sup>1</sup>Delaware St Univ*

Destabilization of lithium borohydrides for reversible hydrogen storage materials has been studied by using calcium hydrides as a destabilizer. In our experimental work, mechanically milled mixtures of LiBH<sub>4</sub> and CaH<sub>2</sub> are shown to store about 13 wt% hydrogen. The equilibrium pressures of absorption and desorption at the different temperature are measured and a van's Hoff diagram is plotted, which are compared to those for pure LiBH<sub>4</sub>. In addition, the kinetics of absorption and desorption of destabilized LiBH<sub>4</sub> will be discussed.

**Modelling the Influence of the Temperature on the Subsurface Deformation of an Aluminum Pin during a Wear Test:** *Mario Rosenberger<sup>1</sup>; Elena Forlerer<sup>2</sup>; Carlos Schvezov<sup>1</sup>; <sup>1</sup>UNaM; <sup>2</sup>UA Materiales - GIDAT-GAEN. CNEA.*

During the wear of aluminum pins under dry sliding it is normally observed a lot of plastically deformed material placed on the ending borders. This deformation is located mainly in the subsurface. The influence of the temperature on the subsurface deformation was studied using finite element analysis. A

three-dimensional model was employed, and temperature dependent properties were assumed. Loads were applied simulating a test performed in a pin-on-ring machine. An elasto-plastic model was employed with small deformation in the plastic range. A sudden subsurface deformation was observed when the tangential load achieves a well determined value defined as the critical load. This critical load increases when the temperature diminishes. The comparison of these results with experiments performed on A1060 alloys reinforced with 15% alumina particles shows little deviation between predictions and experiments which may be attributed to the difference of mechanical properties between the alloys.

**Modification of Cast IN738LC Alloy Microstructure:** *Nader El-Bagoury<sup>1</sup>; Mohamed Waly<sup>1</sup>; Adel Nofal<sup>1</sup>; <sup>1</sup>CMRDI*

The microstructure of cast polycrystalline Inconel 738LC (IN738LC) under different heat treatment conditions was investigated. The cast microstructure of this alloy consists of austenitic  $\gamma$  matrix,  $\gamma'$  precipitates, MC carbide and  $\gamma/\gamma'$  eutectic. The microstructure of the conventional solution treatment, 1120°C/2h/ accelerated air cooling (AAC), contains a bimodal  $\gamma'$  precipitate. Solution treatment at several temperatures of: 1120, 1180, and 1220°C for 1.5 h as well as 1180°C/1.5h + 1220°C/2h has been carried out under argon atmosphere. Accelerated air cooling (AAC) and water quenching (WQ) were applied after solution treatment. Moreover, aging treatment at 845°C was carried out for all solutioning conditions followed by WQ. Solution treatment at 1180°C/1.5h + 1220°C/2h gives the best homogeneity for different alloying elements and a uniform size for the fine  $\gamma'$  precipitates. AAC increases the volume fraction and tends to agglomerate  $\gamma'$  precipitates compared to WQ.

**Nanotechnology Education: Pennsylvania's National Model:** *Robert Ehrmann<sup>1</sup>; <sup>1</sup>Pennsylvania State Center for Nanotechnology Education and Utilization*

Pennsylvania has been working on meeting the critical need for nano-scale trained workers for the last ten years. The NSF Advanced Technology Education (ATE) Center at Penn State University and its partner institutions prepare students to work in any industry that uses micro- and nanotechnology. The Center's curriculum and facilities enable partner colleges across Pennsylvania to offer more than 35 associate degree programs in nanotechnology. The key feature of these degree programs in nanotechnology is the PA Nanofabrication Manufacturing Technology (NMT) Capstone Semester consisting of six hands-on courses taught three times per year. The Center's faculty, staff, and facilities provide an immersive experience in nanotechnology fabrication and characterization, for the community college and university students who come to Penn State University from their home colleges for the Capstone Semester. Capstone semester graduates are employed in micro- and nanotechnology jobs at nearly 100 companies from a wide variety of industries.

**Novel Method for Identifying Low-Angle Sub-Grain Boundaries:** *Kevin King<sup>1</sup>; Benyue Liu<sup>1</sup>; Md. Zakaria Quadir<sup>2</sup>; Michael Ferry<sup>2</sup>; Lori Bassman<sup>1</sup>; <sup>1</sup>Harvey Mudd; <sup>2</sup>University of New South Wales*

Post-processing of EBSD slice data for 3D reconstruction of crystallographic volumes requires boundary identification for regions of interest. In the case of subgrain structures such as microbands, these boundaries are low-angle, and automatic, accurate identification of regions presents a number of challenges. In commercial software, misorientations between individual pixels are used to identify boundaries; however, with subgrains there are instances of gradual orientation change. By using a novel method that combines a color quantization algorithm and misorientation between pixels, we can more accurately identify regions. Minimum variance color quantization identifies a specified number of major components within an inverse pole figure to create a quantized map. This method provides an alternative way to group similar orientations. As an example, we applied this method to microbands in deformed IF steel. The 3D reconstruction allows us to gather statistical data for local normals corresponding to slip systems active in the deformation process.

**Novel Method for Physical Simulation of Solidification Process in Slab Continuous Casting:** *Jianping Liang<sup>1</sup>; Yulai Gao<sup>1</sup>; Renxing Li<sup>1</sup>; Qijie Zhai<sup>1</sup>; <sup>1</sup>Shanghai University*

Physical and numerical simulations of continuous casting processes are general approaches to avoid costly and heavy experiments on full-scale production lines. In the present work, a novel approach based on improved Bridgeman method is presented to physically simulate the solidification process of slab continuous casting. Attributing to the similarity of the heat transfer between unidirectional

solidification and practical slab continuous casting process, the Bridgeman setup was improved with real time controlling of draw speed, heating temperature and cooling rate, then growth velocity of crystals and overheat of melt were online controllable. During the simulation, the solidification parameters were set according to that of the practical slab continuous casting, by which the so called physical simulation was performed. Utilizing this novel method, the slab solidification process of AISI 321 stainless steel was simulated, showing good agreement with the practical production in solidification structure.

**Numerical Simulation of Phase Decomposition during Aging in Cu-Ni Based Alloys:** Erika Avila-Davila<sup>1</sup>; Victor Lopez-Hirata<sup>1</sup>; Dulce Melo-Maximo<sup>1</sup>; Maribel Saucedo-Muñoz<sup>1</sup>; Orlando Soriano-Vargas<sup>1</sup>; Jorge Gonzalez-Velazquez<sup>1</sup>; <sup>1</sup>Instituto Politecnico Nacional

The microstructure simulation of spinodal decomposition was carried out in the isothermally-aged Cu-Ni and Cu-Ni-Fe alloys using the phase field method. The calculated results were compared to those determined by atom-probe field ion microscope analyses of the solution treated and aged alloys. The numerically simulated results of the concentration profiles and microstructure showed a good agreement with the experimental ones in both alloy systems. A slow growth kinetics of phase decomposition was observed to occur in the early stages of aging in both alloys. The morphology of decomposed phases consisted of an irregular shape with no preferential alignment in any crystallographic direction at the early stages of aging in the aged alloys. In the case of the aged Cu-Ni-Fe alloys, a further aging caused the change of initial morphology to an equiaxial shape of the decomposed Ni-rich phase aligned in the elastically-softest crystallographic direction  $\langle 100 \rangle$  of Cu-rich matrix.

**Numerical Simulations of the Crimping Process:** Tobias Rist<sup>1</sup>; <sup>1</sup>Fraunhofer Institute for Mechanics of Materials IWM

Crimping is an important process to manufacture electrical connectors by deforming one or more metals to hold together. The increasing number of electrical components in automobiles makes crimp connections very important parts, the reliability of which must be assured. Simulation of process and operation is an efficient tool to optimize crimped connectors and to reduce the amount of expensive testing during development of new crimps. A three dimensional FE-Model validated with crimp experiments is used to simulate the crimp process. Therefore tensile tests on clip and wire material were performed to determine the parameters of the material models employed in the process simulations. The Calculations lead to various process dependent results like crimp force, contact pressure and resulting stress state that give information about the crimp performance. Thus, a significant reduction in cost and development time can be achieved.

**Nylon 6/Brazilian Clay Nanocomposites: Evaluation of Thermal Behavior by Differential Scanning Calorimetry and Heat Distortion Temperature:** Rene Paz<sup>1</sup>; Amanda Melissa Leite<sup>1</sup>; Edcleide Araújo<sup>1</sup>; Tomas Melo<sup>1</sup>; <sup>1</sup>Universidade Federal de Campina Grande

Recently, investigation of nanocomposites made from polymers and silicate/layers has received significant attention because often they exhibit improved mechanical properties, thermal, optical and physical when compared with conventional or polymer composites. In this work, nanocomposites were prepared using Brazilian clay and a quaternary ammonium salt. The used nylon6 matrix was with three different molecular weight and the thermal properties were evaluated. The results of DSC showed discrete changes in temperature and enthalpy than that nylon 6. In general, the nanocomposites exhibited bigger degree of crystallinity compared to pure nylon 6. The heat distortion temperature (HDT) of the nanocomposites was around 550°C and the nylon6 around 490°C. This increase was attributed to good dispersion of the layers of silicate in the nylon6 matrix.

**Nylon6/Ferrite Composites for Absorbers of Electromagnetic Radiation:** Daniella Bezerra<sup>1</sup>; Keila Machado de Medeiros<sup>1</sup>; Taciana Regina de Gouveia<sup>1</sup>; Edcleide Maria Araújo<sup>1</sup>; Ana Cristina Figueiredo de Melo Costa<sup>1</sup>; <sup>1</sup>UFCG

Composite consists of a mixture or combination of the two or more, micro or macro constituents that differ in shape and chemical composition and, in essence, are insoluble in one another. The nylon is a polymer that presents dimensional stability, good resistance to impact without notch and excellent chemical resistance. Already the ferrites are absorbers of electromagnetic radiation and have versatility to be used as a composite of ferrites. The nylon6/ferrite composite was obtained by mixing 10, 20, 30% of ferrite added to nylon6 in a blender internal Haake. The objective of this work was to develop nylon6/ferrite

composite to achieve superior properties or better in some aspects regarding the properties of each of its components. The results were very promising, with a good interaction between the ferrite and nylon6, to be used as absorbers of electromagnetic radiation.

**Observation of Solid-State Wetting Morphology in Abnormally Growing Grain of Fe-3%Si Steel:** Kyung Jun Ko<sup>1</sup>; Jong Tae Park<sup>2</sup>; Jae Kwan Kim<sup>2</sup>; Anthony D. Rollett<sup>3</sup>; Nong Moon Hwang<sup>1</sup>; <sup>1</sup>Seoul National University; <sup>2</sup>POSCO; <sup>3</sup>Carnegie Mellon University

In this study, we suggest a new approach to the growth advantage of abnormal grain growth (AGG) by solid-state wetting. If the energy sum of the two grain boundaries is lower than the energy of the other grain boundary in contact at the triple junction, the high energy grain boundary will be replaced by the two low energy grain boundaries through the wetting process. The experimentally-observed abnormally growing grain by solid-state wetting has the microstructural feature of AGG such as the formation of numerous island and peninsular grains. Very high frequency of island and peninsular grains formed at or near the growth front of abnormally growing grains could be best explained by solid-state wetting. 3-sided or 4-sided grains with negative curvatures, which are formed near the growth front of abnormally growing grains, are the two-dimensional section vertical to the triple junction wetting in three-dimensional polycrystalline structure.

**Optimization of Machine Parameters for an A487 Steel Welding Process:** Armando Garcia<sup>1</sup>; Mario Trejo<sup>1</sup>; Mauricio Garza<sup>1</sup>; Jorge Acevedo<sup>1</sup>; <sup>1</sup>Corporación Mexicana de Investigación en Materiales S.A. de C.V., Ciencia y Tecnología

Aim of this work is to show relation between machine parameters in a GMAW process and weld depth on an A-487 steel. Industrial application of this steel is well known for heavy work. Artificial intelligence and statistical approaches are carried to find optimal parameters for deep weld penetration.

**Optimization of Milling Conditions for the Production of Fine Silver Powders:** H. Kübra Yumakgil<sup>1</sup>; Hasan Gökçe<sup>1</sup>; Burak Özkal<sup>1</sup>; Sebahattin Gürmen<sup>1</sup>; M. Lütfi Öveçoglu<sup>1</sup>; <sup>1</sup>ITU

High energy milling of ductile metals is difficult because of their flattening tendency under milling deformation. These powders are easily cold welded to each other and get flattened. Therefore to ensure their continues fragmentation is a complex process which needs optimization of milling parameters and in most cases it is necessary to add process control agents. Silver is a good example having above mentioned difficulties. In this study high energy milling behavior of Ag powders were studied under different milling conditions. Milled powders were characterized via XRD, BET, LPS measurements and SEM observations for the optimization of the milling conditions for achieving continues fragmentation Ag powders leading fine powders.

**Oxidation Behavior of Low Carbon Steel in Oxygen and/or Water Vapor at 500-700°C:** Jei-Pil Wang<sup>1</sup>; W.D. Cho<sup>1</sup>; <sup>1</sup>University of Utah

The oxidation behavior of low carbon steel was investigated at 500-700°C in the oxidizing atmosphere with or without water vapor. The effects of temperature, oxygen pressure, and water vapor contents on the oxidation of the steel were studied. The morphology and microstructure of oxide formed in dry or moist oxygen was examined and analyzed by XRD, SEM, and EDX. The oxidation mechanism was discussed based on the study of diffusion, oxide defects, and microstructure between the substrate and oxide layer.

**Partial Oxidation on Methane on Ni/Ceria-Based Materials:** Maria Salazar-Villalpando<sup>1</sup>; <sup>1</sup>National Energy Technology Laboratory

Partial oxidation of methane (POM) was studied over Ni/(Ce<sub>0.56</sub>Zr<sub>0.44</sub>)O<sub>2-x</sub>, Ni/(Ce<sub>0.91</sub>Gd<sub>0.09</sub>)O<sub>2-x</sub>, Ni/(Ce<sub>0.71</sub>Gd<sub>0.29</sub>)O<sub>2-x</sub> and Ni/(Ce<sub>0.88</sub>La<sub>0.12</sub>)O<sub>2-x</sub>. The effect of catalyst reducibility and redox cycles was investigated. It was found that the type of doped-ceria support and its reducibility played an important role in the catalyst activity. It was also observed that redox cycles had a positive influence on H<sub>2</sub> production, which was enhanced as the number of redox cycle increased. Results of carbon formation are discussed as a function of ionic conductivity. Temperature programmed reduction (TPR) profiles, and XRD patterns were determined to characterize catalysts. Experimental tests to determine the catalytic activity revealed that of the materials tested, Ni/(Ce<sub>0.56</sub>Zr<sub>0.44</sub>)O<sub>2-x</sub> was the most active material for the production of syngas, which correlates with its TPR profile. It was observed that doping CeO<sub>2</sub> with Zr, rather than with La or Gd caused an enhanced reducibility of Ni/supported-ceria catalysts.

**Photocatalytic Reduction of CO<sub>2</sub>: A Review:** *Maria Salazar-Villalpando<sup>1</sup>; Bryan Reyes<sup>1</sup>*; <sup>1</sup>National Energy Technology Laboratory

The transformation of CO<sub>2</sub> to hydrocarbons using sunlight is one of best routes to produce renewable energy. State of the art of the photo catalytic reduction of CO<sub>2</sub> with H<sub>2</sub>O will be discussed here. Several types of catalysts have been used to study this reaction, for example: Ruthenium dye-sensitized TiO<sub>2</sub>-based catalysts; TiO<sub>2</sub>/SO<sub>4</sub><sup>2-</sup> photo catalyst; copper-doped Titania catalysts, etc. The discussion of results will include identifying the effect of type catalyst and type of reactor on composition of products and yield of reaction. Main reaction pathways will be reviewed; thermodynamic and kinetics effects will be discussed. Recommendations to improve the yield of reaction will be included.

**Pilot Experiments of Low Temperature (700 ~ 800°C) Aluminum Electrolysis in a 5kA Aluminum Reduction Cell:** *Huimin Lu<sup>1</sup>; Hengchao Zhao<sup>1</sup>; Pengkai Wang<sup>1</sup>*; <sup>1</sup>Beijing University of Aeronautics & Astronautics

In this paper, pilot experiments of the new technique of low temperature (700 ~ 800°C) electrolysis in a 5kA aluminum reduction cell are conducted. The electrolyte is the Na<sub>3</sub>AlF<sub>6</sub>-AlF<sub>3</sub>-BaF<sub>2</sub>-CaF<sub>2</sub> bath system. The experiment results indicate that the Na<sub>3</sub>AlF<sub>6</sub>-AlF<sub>3</sub>-BaF<sub>2</sub>-CaF<sub>2</sub> bath system is promising. These pilot experiments lay a good foundation for industrial application. In the meantime, the physico-chemical properties of Na<sub>3</sub>AlF<sub>6</sub>-AlF<sub>3</sub>-BaF<sub>2</sub>-CaF<sub>2</sub> bath system were systematically studied based on experiments designed using three-factor quadratic orthogonal regressive method. The cathodic current efficiency of the new low temperature aluminum electrolysis is up to 94% and DC power consumption 12000kWh/t aluminum in 5kA experiments cell.

**Polymer-Based TNT Sensor Using Initiated Chemical Vapor Deposition:** *Lucas McIntosh<sup>1</sup>*; <sup>1</sup>Missouri University of Science and Technology

Current techniques for the detection of nitroaromatic high explosives such as 2,4,6-trinitrotoluene (TNT) are considered inadequate for their expense and/or inconvenience in field operations. Our goal is to develop a mechanically robust, low power, highly sensitive and selective polymer-based TNT sensor that can be incorporated into a field-ready detection system. Such a system would rely on the polymer swelling as a result of absorption or reaction with TNT, thus closing a DC electrical circuit. Various homo- and co-polymers hypothesized to interact with the aromatic ring and nitro groups of TNT were deposited on silicon wafers using a novel polymerization technique – initiated chemical vapor deposition (iCVD). Using in situ interferometry to monitor swelling, samples were found to swell by as much as 800% in the presence of TNT analogues such as 4-nitrotoluene at a concentration of 187 ppm. Samples did not interact with controls such as water, nitrogen, and cyclohexane.

**Post-Consumption Decoloration Oil Application as Biofuel Using Brazilian Clay:** *Elaine Araújo<sup>1</sup>; Edcleide Araújo<sup>1</sup>; Marcus Fook<sup>1</sup>; Renata Barbosa<sup>1</sup>; Sara Oliveira<sup>1</sup>*; <sup>1</sup>UFCG

Since the ancient times, clays were used as decolorant material for various types of oils. These clays were called “decolorant clay”. They have the property to decolor dye materials present in mineral oils, plants and animals. Biofuel is a fuel derived from biomass of live organisms. As biodiesel is produced from renewable sources, the generation of employment due to industrial scale production may cause a reduction in the dependence on foreign diesel importing, as well as the reduction of air pollution by the addition of biodiesel to diesel. This study aimed to develop a technological process to decolor post- consumption oil to be applied as biofuel. The clays and oils were characterized by XRD (X-ray Diffraction), FTIR (Fourier Transform Infrared) and X-ray fluorescence. It was observed that the post-consumption oils presented a higher decoloration result after treatment with the Brazilian clay.

**Precipitation during Ausaging and Composition Design for Ferromagnetic Shape Memory Effect of Fe-Ni-Co-Ti Alloys:** *Jin Mingjiang<sup>1</sup>; Jin Xuejun<sup>1</sup>*; <sup>1</sup>ShangHai Jiao Tong University

Fe-Ni-Co-Ti alloys have received attention for its potential magnetically induced shape memory effect (MISME) with high output power and excellent mechanical properties. Present study is concerning on optimizing composition and ausaging technique to obtain the thin-plate-martensite at room temperature, which is critical for promising MISME, through the adjustment of transformation temperature and matrix strength. Morphology of martensite in different composition and ageing process were presented and the influence of component in alloy was investigated. Hardness and MS temperature are also tested as a function of ageing time. Results show that nickel is the sensitive

element on morphologies of martensite and MS temperature. With Ni content of 29~32wt% and appropriate aging treatment, the thin plate martensite could be obtained at room temperature. Ti plays an important role in improving hardness in the process of precipitation, while Co accelerates the Ni<sub>3</sub>Ti precipitate. The impact of precipitation on martensitic transformation is also discussed.

**Precipitation Kinetic of AlMgSi Alloy Added with Ag:** *S. Valdez<sup>1</sup>; Said R. Casolco<sup>1</sup>*; <sup>1</sup>ICF-UNAM

AlMgSi alloy is widely attractive due to their physical, mechanical and chemical properties, such as corrosion, formability, weldability, etc. However, a study detailed on the kinetic precipitation with Ag addition has not been carried out yet. In addition, the Ag content could be exerting a marked effect on their mechanical properties and dimensional stability. The present work reports the silver effect on the hardenable AlMgSi (6xxx) alloy. In addition, the age hardening capability and their relationship with the Ag-alloying addition influence, has been studied. The results describe the kinetic of precipitate formation and cluster dissolution during the ageing. The phase transformation was observed by differential scanning calorimetry (DSC) and X-ray diffraction XRD. The formation of atomic clusters was identified before the GP-zone and precipitate formation. A β-phase precipitates were formed during the age at 190°C. The silver added improves the precipitation kinetic and microhardness value.

**Precipitation Kinetics in Cerium Nitrate Precursor Droplets Heated by Monochromatic Irradiation:** *Saptarshi Basu<sup>1</sup>; Abhishek Saha<sup>1</sup>; Sudipta Seal<sup>1</sup>; Virendra Singh<sup>1</sup>*; <sup>1</sup>University of Central Florida

Generation of nanoceria coating from liquid cerium nitrate precursors involves injection of precursor containing droplets into a high temperature plasma environment. Upon vaporization, nucleation, precipitation and shell fracture the final microstructure of the coating is attained. To investigate the precipitation mechanism for cerium nitrate precursors, they were heated by a CO<sub>2</sub> laser to simulate the rapid heating condition the droplets encounter in a plasma. Ex-situ analysis of the laser-heated samples were carried out using SEM and XPS. In situ analysis involved high speed imaging to study the morphological changes in the droplet before and after precipitation. It is seen that depending on the solute loading concentration, laser heating of the droplets can give rise to very dense to porous type of precipitates. The high speed imaging show the evolution of the droplet morphology which included contraction in size, instability in the liquid phase, vapor bubble formation, nucleation and precipitation.

**Precision Forging of a Two Cylinder Crankshaft:** *Sven Muller<sup>1</sup>*; <sup>1</sup>Institut für Integrierte Produktion

Precision forging is defined as a flashless near net shape forging. A quality in the tolerance class from IT 8 to IT 10 can be achieved. The flashless precision forging offers an integrated heat treatment with the forging heat, because a clipping process is not necessary. After the forging and heat treatment often only a final fine machining of the functional surface with small chip volume is required. In the collaborative research project SFB 489 a two-cylinder-crankshaft is selected as an example for complex flat long pieces with a characteristic mass distribution along the longitudinal axis. The continuative development considers the thermal and mechanical tool stresses, which are also as complex as the crankshaft itself. Further on a parameter study on a bi-directional forging tool is made. The tests of the forging sequence, tools, cooling systems and measuring technology of the developed process are finished now.

**Prediction of Microstructural Changes in Drawing of Pearlitic Steel Wires:** *Yong-Shin Lee<sup>1</sup>; W-J Nam<sup>1</sup>; Kyung-Tae Park<sup>2</sup>*; <sup>1</sup>Kookmin University; <sup>2</sup>Hanbat University

It is well known that fully pearlitic steel wire manufactured by cold drawing exhibits very high strength. However, its ductility is often limited by the internal defects during drawing. It is generally accepted that interlamellar spacing is the most important factor to control ductility and strength of pearlitic steels, simultaneously. It is attempted to predict the microstructural changes during drawing of a pearlitic steel wire. First, finite element simulations for wire drawing are performed to trace the deformation histories of material points in a steel wire. Then, a couple of algorithms developed in this work are applied to predict changes of microstructures such as orientation, shape, and thickness of a cementite. The predictions will be compared to those reported in the literature. Also, the difference of microstructural evolution according to the depth from the surface in the cross-section of the wire will be carefully investigated.



**Preparation and Characterization of Assymmetric Membranes Obtained of Nylon6/Brazilian Clay Nanocomposites:** Amanda Melissa Leite<sup>1</sup>; Larissa Maia<sup>1</sup>; Edcleide Araújo<sup>1</sup>; Hélio Lira<sup>1</sup>; <sup>1</sup>Universidade Federal de Campina Grande

A membrane is an interphase between two adjacent phases acting as a selective barrier, regulating the transport of substances between the two compartments. The main advantages of membranes technology as compared with other unit operations in chemical engineering are related to this unique separation principle, i.e. the transport selectivity of the membrane. Separations with membranes do not require additives, and they can be performed isothermally at low temperatures and compared to other thermal separation processes-at low energy consumption. In this work, asymmetric membrane of Nylon6/Brazilian clay nanocomposites using quaternary ammonium salts were obtained by phase inversion method. The membranes were characterized by SEM. The results showed that there is a significant difference in size and distribution of pores between pure nylon 6 membranes and membranes obtained from nanocomposites.

**Preparation and Characterization of NiCo2O4 Fibre by Coordination Coprecipitation-Thermal Decomposition Method:** Zhan Jing<sup>1</sup>; Zhang Chuanfu<sup>1</sup>; Bai Meng<sup>1</sup>; Wu Jianhui<sup>1</sup>; <sup>1</sup>Central South University

The spinel NiCo<sub>2</sub>O<sub>4</sub> fibers with diameters less than 1µm were prepared by thermal decomposition of nickel-cobalt oxalate complex precursor containing ammonium, which were obtained by coordination coprecipitation technique. The effects of different Ni/Co ratios, decomposition temperature and decomposition time on the phase constitute of final product were addressed in detail. The crystallinity, purity, and surface morphology of the as-prepared NiCo<sub>2</sub>O<sub>4</sub> fibers were investigated by XRD, IR, SEM, respectively. Finally, Structure of nickel cobaltite spinel examined by X-ray absorption spectroscopy (XPS) indicates, as expected, that Ni occupies the octahedral sites of the spinel structure while Co occupies both tetrahedral and octahedral sites. The result of the surface examination by xps shows that the surface composition is different from nominal bulk composition.

**Preparation of Fibrous Nickel Powder by Complexing Precipitation-Thermal Decomposition Method:** Jianhui Wu<sup>1</sup>; Chuanfu Zhang<sup>1</sup>; Jing Zhan; Youqi Fan<sup>1</sup>; Baiyun Huang<sup>1</sup>; Yuehui He<sup>1</sup>; <sup>1</sup>Central South University

Fibrous nickel powder was prepared by complexing precipitation - thermal decomposition method. The composition and morphology of the powder were characterized by the analysis methods of XRD and SEM. The effects of temperature, concentration, pH value and surfactant on the morphology and the dispersion of the precursor and the conditions of the thermal decomposition on the morphology and the dispersion of the nickel powder have been studied. The results indicate that the nickel powder is fibrous and well dispersive, and can be prepared by thermal decomposition of the precursor, which is obtained under conditions as proposed: precipitation temperature is 60~70°, the nickel ion concentration is 0.5~0.8 mol·L<sup>-1</sup>, pH value is 8.4~8.8 and adding PVP as surfactant.

**Preparation of Zinc Oxide Nanostructures from Zinc Sulfate and Zinc Nitrate Precursor:** Sebahattin Gurmen<sup>1</sup>; Burcak Ebin<sup>1</sup>; Burak Ozkal<sup>1</sup>; <sup>1</sup>Istanbul Technical University

Over the past decades, zinc oxide nanostructures have attracted great interest due to its unique physical and chemical properties including optical transparency, electric conductivity, and light emission. However, size and morphology are important parameters to determine the physicochemical features of ZnO nanostructures. Ultrasonic spray pyrolysis method, suitable for formation of spherical particle morphology, was used to prepare nanostructure ZnO particles from zinc sulfate and zinc nitrate solution. The size and shape of the ZnO particles were controlled by the reaction conditions, temperature, selection of precursors, frequency of ultrasonic atomizer, carrier gas kind and flow rate. Effects of temperature and precursor concentration on products were investigated in this study under constant gas flow rate and frequency. Characterization studies were conducted on not only size and shape morphologies, but also crystalline structure, and phase determination. Obtained particles size increases with elevated reaction temperature, and particle morphology strongly depends feature of precursor.

**Preparation of ZrB2-ZrC Composites by Spark Plasma Sintering:** Filiz Sahin<sup>1</sup>; Ipek Akin<sup>1</sup>; Onuralp Yucel<sup>1</sup>; Takashi Goto<sup>2</sup>; Gultekin Goller<sup>1</sup>; <sup>1</sup>Istanbul Technical University; <sup>2</sup>Tohoku University Institute for Materials Research

The ZrB<sub>2</sub>-ZrC composites were prepared by the spark plasma sintering (SPS) at temperatures of 1800 to 2000°C for 300 under a pressure of 50 MPa. Densification, crystalline phases, microstructure and mechanical properties of the ZrB<sub>2</sub>-ZrC composites were investigated. Fully dense ZrB<sub>2</sub>-ZrC composites containing 20 to 80 wt% ZrC with a relative density of more than 98% were obtained at 1900°C for 300 s. The all characteristics peaks of ZrB<sub>2</sub> and ZrC were identified and chemical reaction was not detected between ZrB<sub>2</sub> and ZrC for all compositions at 1800 to 2000°C. Vickers hardness of dense ZrB<sub>2</sub>-SiC composites containing 80 wt% ZrC sintered at 1900 and 2000°C had the maximum value of 18.7 GPa. The highest fracture toughness of 3.5 MPa·m<sup>1/2</sup> was observed for ZrB<sub>2</sub>-ZrC composite containing 80 wt% ZrC sintered at 1900°C.

**Processing of a TiAl Alloy by Powder Metallurgy and Hot Working:** Rao Kamineni<sup>1</sup>; Y.V.R.K. Prasad<sup>1</sup>; <sup>1</sup>City University of Hong Kong

Titanium aluminides have superior high temperature properties and are attractive for gas turbine applications. Cast titanium aluminides have large grain sizes which reduce hot workability. Alternately, powder metallurgy technique is explored by mixing of elemental powders for 2 hrs to prepare 46Ti-46Al-4Nb-2Cr-2Mn followed by Hot Isostatic Pressing (HIP) at 1150°C for 4 hrs under a pressure of 150 MPa. In addition to the formation of TiAl solid solution, the microstructure showed a small volume fraction of Nb-rich phase. The HIP'ed billets were compressed at temperatures and strain rates in the ranges of 850-1050°C and 0.0001-10 s<sup>-1</sup>. The flow curves exhibited continuous flow softening at strain rates lower than 0.1 s<sup>-1</sup> while fracture has occurred at higher strain rates. The hot workability was good at temperatures higher than 1000°C and the flow stress at different temperatures and strain rates follows the kinetic rate equation.

**Production and Characterization of Soda-Lime Photosensitive Glasses:** Arca Iyiel<sup>1</sup>; Suheyly Aydin<sup>2</sup>; Onuralp Yucel<sup>2</sup>; <sup>1</sup>Turkiye Sise ve Cam Fabrikalari A.S.; <sup>2</sup>Istanbul Technical University

Photosensitive glasses can be produced by conventional methods but contain alkali halide silver (AgX), alkali oxide, fluorine and at least one of the group consisting of chlorine, bromine and iodine, after an exposure to high energy or actinic radiations following a unique heat treatment. In this study, previously known sodium silicate photosensitive glass composition was modified to conventional soda-lime float glass composition which contains silver, alkali oxide, fluorine and halide group elements. Then by means of the applied UV radiation microstructural and optical properties have been controlled with the aid of the additives. The effect of lanthanides at colorless level, on the photosensitive glasses are studied. The present study shows the effects of addition of lanthanides such as Ho<sub>2</sub>O<sub>3</sub>, Er<sub>2</sub>O<sub>3</sub>, Pr<sub>2</sub>O<sub>3</sub>, Nd<sub>2</sub>O<sub>3</sub> for first time. Optical characterization has been also performed before and after UV exposure. Microstructural changes after the photochemical process were observed clearly.

**Production and Characterization of ZrB2-ZrC-SiC Composites:** Gultekin Goller<sup>1</sup>; Ipek Akin<sup>1</sup>; Filiz Sahin<sup>1</sup>; Onuralp Yucel<sup>1</sup>; Takashi Goto<sup>2</sup>; <sup>1</sup>Istanbul Technical University; <sup>2</sup>Tohoku University

In this study, the production of ZrB<sub>2</sub>-ZrC-SiC composites using spark plasma sintering (SPS) technique was studied. Sintering of powder mixtures was carried out at 1850 and 1900°C for 180 to 300 s under a uniaxial pressure of 50 MPa in vacuum atmosphere. The temperature of the die was increased at 1.7°C/s. Shrinkage of the specimens during SPS process was continuously monitored. Densities of the composites were determined by the Archimedes' method and more than 98% relative density was obtained for the composites. The crystalline phases of the specimens were identified by X-ray diffractometry. Vickers hardness (HV) was measured under loads of 0.98 to 9.80 N and fracture toughness (KIC) were evaluated by a microhardness tester. The fracture toughness was calculated from a half length of crack formed around the indentations.

**Properties and Consolidation of Nanostructured MoSi<sub>2</sub> from Mechanically Reacted Powder by Rapid Sintering:** In-Jin Shon<sup>1</sup>; Jeong-Hwan Park<sup>1</sup>; Kee-Do Woo<sup>1</sup>; Jin-Kook Yoon<sup>2</sup>; <sup>1</sup>Division of Advanced Materials Engineering, the Research Center of Industrial Technology, Chonbuk National University; <sup>2</sup>Advanced Functional Materials Research Center, Korea Institute of Science and Technology

MoSi<sub>2</sub> has been investigated as potential material for high temperature structural applications and for application in the electronics industry. Its properties provide a desirable combination of a high melting temperature (2020°C), high modulus (440 GPa), good oxidation resistance in air, a relatively low density (6.24 g/cm<sup>3</sup>). A dense nanostructured MoSi<sub>2</sub> was sintered by the high-frequency induction heating method within 1 minute from high energy ball milled powder of MoSi<sub>2</sub>. Highly dense MoSi<sub>2</sub> with relative density of up to 97% was produced under simultaneous application of a 60 MPa pressure and the induced current. The average grain size of MoSi<sub>2</sub> was about 100 nm. The hardness and fracture toughness values obtained were 1203 kg/mm<sup>2</sup> and 4.2 MPa•m<sup>1/2</sup>, respectively. These fracture toughness and hardness values of nanostructured MoSi<sub>2</sub> are higher than those (fracture toughness; 2.58 MPa.m<sup>1/2</sup> hardness; 8.7MPa) of micronstructured MoSi<sub>2</sub>.

**Rapid Synthesis and Consolidation of Nanocrystalline 1.5Ti-Al<sub>2</sub>O<sub>3</sub> from Mechanically Activated Powders:** Dae Ho Rho<sup>1</sup>; In-Jin Shon<sup>2</sup>; Byung-Ryang Kim<sup>3</sup>; Kee-Do Woo<sup>3</sup>; Jin-Kook Yoon<sup>4</sup>; <sup>1</sup>Department of Metal Processing Research Center, Korea Institute of Science and Technology; <sup>2</sup>Division of Advanced Materials Engineering, the Research Center of Industrial Technology, Chonbuk National University; <sup>3</sup>Division of Advanced Materials Engineering and Research Center for Advanced Materials Development, Engineering College, Chonbuk National University; <sup>4</sup>Advanced Functional Materials Research Center, Korea Institute of Science and Technology

Interest in cermet of Ti-Al<sub>2</sub>O<sub>3</sub> has increased significantly in recent years because of their potential application as aeronautical and automotive materials. This combination of metal and ceramic has good properties, such as adequate creep resistance at high temperature, low density, excellent oxidation and corrosion resistance, good wear resistance and high hardness. Dense nanocrystalline 1.5Ti-Al<sub>2</sub>O<sub>3</sub> composite was synthesized by pulsed current activated combustion synthesis(PCACS) method within 2 min in one step from mechanically activated powders of 1.5TiO<sub>2</sub> and 2Al. Highly dense 1.5Ti-Al<sub>2</sub>O<sub>3</sub> with relative density of up to 99% was simultaneously synthesized and consolidated under application of a 60 MPa pressure and the pulsed current. The average grain sizes of Ti and Al<sub>2</sub>O<sub>3</sub> in the composite were 282nm and 65 nm, respectively. The hardness and fracture toughness of the composite were 1207 kg/mm<sup>2</sup> and 7 MPa.m<sup>1/2</sup>, respectively.

**Rapid Transient-Liquid-Phase Bonding of Al<sub>2</sub>O<sub>3</sub> Ceramics:** Thomas Reynolds<sup>1</sup>; Sung Hong<sup>1</sup>; Christopher Bartlow<sup>1</sup>; Andreas Glaeser<sup>1</sup>; <sup>1</sup>University of California-Berkeley

In engineered devices, dissimilar materials must often be joined to attain desired properties. Transient-liquid-phase (TLP) bonding is an elegant method of joining materials at reduced temperatures to protect fragile microstructures, but it often requires multi-hour isothermal holds. In the present work, the processing time to join high-purity Al<sub>2</sub>O<sub>3</sub> is significantly reduced using Ni/Nb/Ni multilayer interlayers that form thin transient-liquid films. We demonstrate that ultrahigh strengths, averaging ≥ 500 MPa, are attainable with isothermal holds as short as 5 min at 1400°C. The wetting behavior of the TLP on Al<sub>2</sub>O<sub>3</sub>, the rapid redistribution of Ni within the interlayer, and the joint fracture characteristics are described. Using multilayer interlayers with similar thermokinetic properties, it should be possible to extend this joining technology to other materials.

**Relaxed Grain Cluster Homogenization Scheme for Polycrystals:** Denny Tjahjanto<sup>1</sup>; Philip Eisenlohr<sup>1</sup>; <sup>1</sup>Max-Planck Institut für Eisenforschung

We develop an efficient and accurate homogenization scheme, namely relaxed grain cluster (RGC). The scheme is based on the generalization of the relaxed constraints Taylor model. A cluster consisting of eight uniform hexahedral grains is considered. The relaxation of local deformation of individual grains is described by means of interface relaxation vectors. The kinematic of the relaxation is formulated within a finite deformation framework. An penalty associated with deformation incompatibility at interfaces is computed in analogy to the concept of geometrically-necessary dislocations. The relaxation vectors are determined in accordance with the minimization of the total energy, which leads to the condition of the stress equilibrium at the interfaces. Several elementary simulations have been performed. The predictions of the relaxed grain cluster

model in terms of the effective stress-strain response is analyzed. In addition, the RGC scheme is used to simulate texture evolution during rolling.

**Removal of Impurity Elements from the Molten Aluminum: Modeling and Validation:** Xuwei Lv<sup>1</sup>; Lifeng Zhang<sup>1</sup>; Chenguang Bai<sup>2</sup>; <sup>1</sup>Missouri University of Science and Technology; <sup>2</sup>Chongqing University

In order to remove the impurity elements from the molten aluminium, many processes, such as using the inert gas, reactive gas, reactive powders, unreactive powders, slag, vapor pressure, or their combinations, have been used during recent thirty years. In the current paper, mathematical models for these refining methods were developed. The removal of impurity elements for batch and continuous reactor were investigated. The modeling was validated by the industrial measurement. The effect of the parameters, such as the refining temperature, gas flow rate, powder injection rate, stirring power, removal efficiency of the impurity elements were discussed.

**Removal of Pb, Cd and Cl from Waelz Oxide via Pyrometallurgical Process:** Hakan Morcali<sup>1</sup>; Bora Derin<sup>2</sup>; Adnan Aydin<sup>1</sup>; Onuralp Yucel<sup>2</sup>; <sup>1</sup>Marmara University; <sup>2</sup>Istanbul Technical University

In this study, removal of residue such as, chlorine, lead and cadmium was carried out via pyrometallurgical process by using collected condensed powder (Waelz oxide). In the previous study, Waelz oxide (containing 66.24 wt. % Zn, 0.18 wt. % Fe, 5.55 wt. % Pb, 0.0859 wt. % Cd, and 4.99 wt. % Cl) was collected through carbothermic reduction of EAF dust at 1100°C for 90 minutes. In the experimental series, a temperature controlled pilot scale rotary furnace was utilized. Temperature (1000, 1100, 1150, and 1200°C) and time (0-120 minutes) were selected as reaction parameters. It was observed that the amount of lead, cadmium and chlorine in the Waelz oxide decreased with increased both time and temperature. The optimum conditions for the removal of Pb, Cd and Cl were achieved at 1200°C for 120 minutes. As a conclusion, zinc oxide with 99.04% purity was obtained after the refinement by volatilization process. The products obtained were characterized by X-Ray diffraction and chemical analysis techniques.

**Removal of Sr (II) from Aqueous Solutions by Using Bentonite as Natural Adsorbent:** Siavash Nikfar<sup>1</sup>; Saeed Milani<sup>2</sup>; Sharyar Mirhakimi<sup>1</sup>; <sup>1</sup>Arak Azad University; <sup>2</sup>Nuclear Science Research School, Nuclear Science and Technology Research Institute

In the present study, the ability of bentonite (clay ,as natural adsorbent) to remove strontium ions from aqueous solutions has been investigated. Batch method was carried out during adsorption process. The effect of various parameters such as contact time, initial concentration, PH, particle size and existence of competing metal ions has been studied. Kinetic of adsorption showed that the uptake of strontium ions is very rapid during first thirty minutes and equilibrium time is independent of initial strontium concentration. Simple kinetic and thermodynamic models have been applied to the rate and isotherm sorption data and the relevant kinetic and thermodynamic parameters were determined from the graphical presentation of these models.

**Semiconducting Properties of Passive Films and Pitting Corrosion Resistance of Nickel Free High Nitrogen Austenitic Stainless Steels:** Huabing Li<sup>1</sup>; Zhouhua Jiang<sup>1</sup>; Yan Yang<sup>1</sup>; Yang Cao<sup>1</sup>; <sup>1</sup>Northeastern University

The semiconducting property of passive films of nickel free high nitrogen austenitic stainless steel was investigated in chloride solution by electrochemical impedance spectroscopy. The structure, chemical composition of passive films and the pitting corrosion of the steels have been investigated. The capacitance results show that the passive films behave as n-type and p-type semiconductors in the potential range above and below the flat band. The donor density, acceptor density and the flat band decrease with increasing nitrogen. The thickness of the space charge layer of n-type semiconductor increases with increasing nitrogen. The steels exhibit excellent pitting corrosion resistance, and their pitting potentials and critical pitting temperature increase with increasing nitrogen in steels. The XPS results show that the beneficial effect of nitrogen on improving pitting corrosion resistance are attributed to the enrichment of nitrogen in passive films to form the ammonium ions and the synergy effect between molybdenum and nitrogen.

**Semiconducting Properties of Passive Films of Nickel Free High Nitrogen Austenitic Stainless Steels:** Huabing Li<sup>1</sup>; Jiang Zhouhua<sup>1</sup>; Yang Yan<sup>1</sup>; <sup>1</sup>Northeastern University

The semiconducting property of passive films of nickel free high nitrogen austenitic stainless steel was investigated in 3.5% wt NaCl solution by

electrochemical impedance spectroscopy (EIS). The capacitance results show that the passive films behave as n-type and p-type semiconductors in the potential range above and below the flat band (EFB). The donor density (ND), acceptor density (NA) and the EFB decrease with increasing the nitrogen content in steels. The thickness of the space charge layer(W) of n-type semiconductor increases with increasing the nitrogen content. The XPS results show that the passive films are composed of an inner region of a mixed chromium-iron oxide and an outer region of iron oxide. The nitrogen enriches on the out layer of passive films as the form of CrN, NH<sub>3</sub>, N(atom) and NH<sub>4</sub><sup>+</sup>. The synergism effect between molybdenum and nitrogen improves greatly the pitting corrosion resistance of the high nitrogen stainless steels.

**Sheared Slugs for Precision Forging – Improved Shear Zone Quality by an Oscillating Shear Cutter:** *Michael Lücke*<sup>1</sup>; *Karsten Müller*<sup>1</sup>; <sup>1</sup>IPH - Institute for Integrated Production Hannover

Closed-die-forging requires constant process provisions. One of the most important factors of influence by forging without flash is the mass constancy of the billet. Because of large reachable quantities and low costs is the shearing of bar stock an established proceeding in the forging industry. Furthermore offers this method a nearly lossless process. Drawbacks of shearing are shearing faults and the inconstant volume of the sheared billets. For flashless forging in closed dies is the constancy of billet-geometry and -volume essential. Hence the IPH – Institute for Integrated Production worked in research projects on methods to enhance the cutting-plane-quality. A previous working of IPH shows that an oscillating cutter can improve the shearing output. In this study a provisional experimental set-up was used. To evidence these results, a new oscillating unit will be implanted into the shear. The existing solution interrupts the outgoing oil flow to 40 times per second.

**SiC Particulate Reinforced Iron Matrix Composites Processed by Specimen Current Heating Hot Press Sintering:** *Wang Yaomian*<sup>1</sup>; *Zong B. Y.*<sup>1</sup>; *Yang Yufang*<sup>1</sup>; *Li Jie*<sup>1</sup>; <sup>1</sup>Northeastern University

Specimen current heating hot press sintering is one kind of efficient technology to fabricate metal matrix composites. By use of Joule heat and hot pressing while intense current passing through the specimen, powder compact can be consolidated quickly. The whole sintering process is finished within a few minutes, thus the severe reaction between particle reinforcement and matrix is avoided. The results demonstrate that the two-stage sintering of this technology can improve material properties significantly comparing with the previous single stage sintering. The heating up time and holding time have important influence on the material properties during the two-stage sintering. The 10v% SiCp/Fe composites processed by the two-stage sintering with 100 seconds heating and 200 seconds holding can be achieved a density nearly to the theoretical value, the Brinell hardness to 477HB and the tensile strength being up to 915MPa.

**Sintering Advances in Consolidating W and Its Alloys:** *Avijit Mondal*<sup>1</sup>; *Anish Upadhyaya*<sup>1</sup>; *Dinesh Agrawal*<sup>2</sup>; <sup>1</sup>Indian Institute of Technology Kanpur; <sup>2</sup>The Pennsylvania State University

Microwave processing has been emerging as an innovative and highly effective sintering method offering many advantages over conventional methods for consolidation. It is recognized for its various advantages, such as: time and energy saving, very rapid heating rates, considerably reduced processing cycle time and temperature, fine microstructures and improved mechanical properties, better product performance, etc. Major constraints in conventional sintering of refractory material such as tungsten and its alloys, normally require high sintering temperatures, long soaking times favoring abnormal grain growth which finally leads to poor mechanical properties. This problem gets further aggravated at smaller (submicron and nano) tungsten powder sizes. This study describes recent research findings wherein pure tungsten and its alloys have been successfully consolidated using microwave heating which resulted in an overall reduction of sintering time of up to 80%. This sintering time compression restricts grain coarsening and results in superior mechanical properties.

**Solute Concentration Effect on the Dendritic Orientation of Al-Sn Binary Alloy:** *Jeong Yun Choi*<sup>1</sup>; *Paul Matlage*<sup>1</sup>; *Ralph Napolitano*<sup>1</sup>; <sup>1</sup>Iowa State University

On the pattern formation of the solidification, the solute concentration is recently regarded as a possible factor which can largely affect on the orientation of growing phases. This leads the control of the orientation of solidification morphologies is possible by adjusting the concentration in the melt phase, whereas the solid phase has been believed to grow along with the primary

crystallographic orientations. In this work, to clarify the quantitative effect of solute content on the anisotropy of the intrinsic properties of the interface between the growing crystalline phase and the melt phase, the dendritic growth orientations of Al-Sn binary alloy with different concentrations are observed using experimental directional solidification, and computationally simulated using the phase-field model. By comparing the anisotropy of the equilibrated phases with that of growing phases with different growth velocities, the effect of concentration on the anisotropy of the kinetic factor of the interfacial properties is examined.

**Structural Strength Evaluation of a Carbody by Structural Analysis and Load Test:** *Sung Cheol Yoon*<sup>1</sup>; *Jeongguk Kim*<sup>1</sup>; *Chang Sung Jeon*<sup>1</sup>; *Won Kyung Kim*<sup>1</sup>; <sup>1</sup>Korea Railroad Research Institute

This paper describes a carbody structural analysis and the result of its loading test. The purpose of this study is to evaluate the safety and functionality of the body structure operating under maximum load. Aluminum alloy was used as the body structure's material. The carbody of rolling stock is a principal structure supporting major equipment of underframe, roof, interior and passenger. So, the strength evaluation of this structure is important and can be the core technique in rolling stock analysis. Both structural analysis and loading test were performed under the condition based on "Performance Test Standard for Electrical Multiple Unit" with the reference code JIS E 7105. The test results showed that the body structure is safe and stable under the condition of designed load.

**Structure Changes during Tempering of Quenched Fe-C Steels as Assessed by Electrical Resistivity Studies:** *Donald Lesuer*<sup>1</sup>; *Oleg Sherby*<sup>2</sup>; *Chol Syn*<sup>1</sup>; <sup>1</sup>Lawrence Livermore National Laboratory; <sup>2</sup>Stanford Univ

Electrical resistivity measurements are a powerful experimental tool for understanding the structure of Fe-C steels. It is shown that the electrical resistivity of fully annealed Fe-C steel is solely dependent on the amount of iron carbide independent of its distribution. During tempering of quenched Fe-C materials, however, significant changes are observed. Resistivity changes with carbon content show distinctly different behavior above and below 0.6 wt% C. These changes are attributed to the different martensitic products that form and their differences in tempering response. In the high carbon region, the data has been analyzed in terms of a time-temperature parameter  $t\text{-exp}(-Q/RT)$ . The activation energy for tempering was found to be 150 kJ/mole which is related to Fe atom interaction with carbide particles. The results also show significant influence of substitutional solute atoms and retained austenite on the tempering response. Results provide insight into the mechanisms of tempering.

**Structure Refinement of 12wt.%Cr Ferritic Stainless Steel by Pulse Current:** *Changjiang Song*<sup>1</sup>; *Jianping Liang*<sup>1</sup>; *Qijie Zhai*<sup>1</sup>; <sup>1</sup>Shanghai University

Due to low Cr and Ni content, 12wt.%Cr ferritic stainless steel is a cheap stainless steel but still has good corrosion resistance. Therefore, it will have good potential applications in many filed, such as automotive industry and chemistry industry, because of low cost. To improve its mechanical properties, this paper investigated the effects of pulse current on solidification structure of a 12wt.%Cr ferritic steel. Experimental results show that during the solidification course of 12wt.%Cr ferritic stainless steel, employing of pulse current can significantly increase the area ratio of equiaxed crystal and decrease the grain size. Moreover, increasing the frequency and density of pulse current can improve refinement effect.

**Study of Effect of Silicon Resin over Capacitance on TaMnO<sub>2</sub> Devices under Room and Humid Environments:** *Miguel Esquivel-Aguirre*<sup>1</sup>; *Héctor Barrientos*<sup>1</sup>; *Sandra Padrón*<sup>1</sup>; *Juan Torres*<sup>1</sup>; *Juan Pérez-Medina*<sup>1</sup>; *Pablo Ruiz*<sup>1</sup>; <sup>1</sup>Kemet De Mexico

Silicon resins have a wide usage in electronics industry, especially on passive components prone to absorb moisture from the environment. TaMnO<sub>2</sub> capacitors molded with epoxy compound are not hermetically sealed and can be affected by the conditions in the environment. Significant changes on capacitance (~ 5% of capacitance reduction) happen when the silicon resins are added to the cathode of the capacitors. The effects of the silicon layers on the cathode are discussed in this paper. The efficiency of the moisture protection was analyzed based on silicon resin nature at different concentrations and studied using fluorescent inks. The microstructure has been characterized with Scanning Electron Microscope. The effects on capacitance and other electrical properties were measured using Frequency Scan Techniques. The stability of the electrical properties was measured after Humidity 85% / 85 °C Test with and without voltage.



**Study of Properties Enhancement of Magnesium Diboride (MgB<sub>2</sub>) by TaB<sub>2</sub> Doping via High Energy Ball Milling:** *Richard Perez*<sup>1</sup>; Yenny P Cardona Quintero<sup>1</sup>; Pedro Vargas<sup>1</sup>; Oswald Uwakweh<sup>1</sup>; Eric E Hellstrom<sup>1</sup>; David Larbalestier<sup>2</sup>; Durval Rodrigues Jr.<sup>3</sup>; <sup>1</sup>University of Puerto Rico; <sup>2</sup>Florida State University; <sup>3</sup>University of San Paulo, Brazil

The study of superconductivity properties enhancement on MgB<sub>2</sub> due to TaB<sub>2</sub> doping at 2 and 5 at. % levels were carried out. High energy ball milling was used for the purposes of fostering mechanical alloying, generation of nanometer sized particles, and strain inducements respectively. SPEX processed materials revealed smaller particle size and higher strains in comparison to the Pulverisette-4 processed ones. The 5 at. % TaB<sub>2</sub> doped MgB<sub>2</sub> yielded the highest critical current density (J<sub>c</sub>) corresponding to 474.1 kA/cm<sup>2</sup> at 2 T, while 344.4 kA/cm<sup>2</sup> for SPEX and Pulverisette-4 materials. Correspondingly, the values of the flux pinning (F<sub>p</sub>) deduced for the 5 at. % TaB<sub>2</sub> doped MgB<sub>2</sub> processed with the SPEX mill was 7.58 GN/m<sup>3</sup> while for same level of doping processed with the Pulverisette-4 processed material was 6.90 GN/m<sup>3</sup>. The irreversibility field (H<sub>irr</sub>) was 8.50 T for the 5 at. % doped MgB<sub>2</sub>, while for Pulverisette-4 was 7.11 T.

**Study of the Pitting Corrosion under Insulation of Duplex Stainless Steels:** Khalil Alahmadi<sup>1</sup>; *Joanna Groza*<sup>1</sup>; <sup>1</sup>UC-Davis

Duplex Stainless Steel (DSS) is a class of stainless steel that has two-phase structure, namely, ferrite (α) and austenite (γ) with around equal amounts of the two phases. DSS offers an attractive combination of mechanical properties and corrosion resistance. Corrosion under insulation (CUI) of this material has not been discussed thoroughly in the past as per the author's knowledge. This paper discusses the CUI (particularly the pitting CUI) of two grades of this material, namely, 2205 and 2507 at different temperatures. Further, results and conclusions will be fully available by the time of the subject meeting.

**Study on a New Process for Recovery Rhenium and Producing Ammonium Rhenium from Reduction Solution of Process Copper Smelting:** Bai Meng<sup>1</sup>; *Zhan Jing*<sup>1</sup>; Zhang Chuanfu<sup>1</sup>; Wu Jianhui<sup>1</sup>; Fan Youqi<sup>1</sup>; <sup>1</sup>Central South University

Rhenium is a kind of rare metal with its content in the earth shell only at about 7 × 10<sup>-8</sup> %, so it is very meaningful to recover it. The paper describes distribution of rhenium in copper concentrate ore during the process of copper smelting. Aiming at particularity of reduction solution with peracid, high concentration of arsenic, more impurity and low content of rhenium and problem of avoiding changing property of reduction solution during recovery of ammonium rhenium, a new process for recovery of rhenium and producing ammonium rhenium from reduction solution of process copper smelting, namely, solvent extraction- strip extraction-purification-crystallization. The process has low operation cost and high economic efficiency. Percentage extraction and stripxtraction of rhenium are more than 98%. Direct recovery of rhenium is more than 85% and grade of ammonium rhenium product is more than 99%.

**Study on Effects of Cement Additives on Properties of Cement by Using the Calorimeter Method:** *Daowu Yang*<sup>1</sup>; Chengfeng Wang<sup>1</sup>; Zhongliang Xiao<sup>1</sup>; <sup>1</sup>Changsha University of Science and Technology

In this paper the used technique to study affect of cement additions on properties of cement was conduction calorimeter. The affect of cement added to one of the three additions (lignosulfonate, citric acid, DBS) and the cement added to all on the pure cement was measured using the TAM Air calorimeter instrument which owns eight channels made by Sweden. And eight curves of heat dissipation of cement hydration was determined. The value of heat dissipation of hydration and the hydration rate was get from the curves. And the affect of additions on the cement was analyzed. Result shows that: the chemical additions such as water reducer(lignosulfonate), set retarder(citric acid) can decrease the value of cement hydration and the increasing temperature differently, also it can delay the time when the curve of heat dissipation appears. Air training admixture DBS affect the heat of hydration and the increasing temperature little.

**Study on Electric Conductivity of AlCl<sub>3</sub>/Benzyltrimethylammonium Chloride Room Temperature Ionic Liquids:** Liu Quan<sup>1</sup>; Liu Kui-ren<sup>1</sup>; Han Qing<sup>1</sup>; Tu Gan-feng<sup>1</sup>; <sup>1</sup>Northeastern University

This paper studied influences of organic solvents (ethanol, acetone, ethyl acetate, tetrahydrofuran, toluene and benzene), composition and temperature on electric conductivity of Benzyltrimethylammonium Chloride and anhydrous aluminum chloride (TMBAC/AlCl<sub>3</sub>) ionic liquids, optimized the aluminum reduction process and characterized Al deposition prepared by using the methods of SEM, XRD and EIS. Except that benzene could significantly improve the electric conductivity, the other solvents were detrimental to this

system. The electric conductivity of ionic liquids increased with increasing benzene concentration, and when the concentration of benzene was 50% (vol.), the electric conductivity reached the maximum. The relation curves between temperature and electric conductivity were found to obey Arrhenius equation in the lower temperature range. In the TMBAC/AlCl<sub>3</sub> ionic liquids with benzene concentration 50% (vol.), silvery aluminum deposition with dense surface was prepared and had a excellent corrosion resistance.

**Study on Phosphorus Recovery from Rare Earth Minerals Containing Apatite by Citric Acid Coordination:** *Bian Xue*<sup>1</sup>; *Wu Wenyuan*<sup>1</sup>; <sup>1</sup>Northeast University

Phosphorus is intergeneration and unreplacement resource. The phosphorus minerals will dry up in middle period of this century in world. The recovery of phosphorus from rare earth minerals containing apatite is meaningful. In this paper, the coordination of citric acid (H<sub>3</sub>cit) is used to recover phosphorus and separate it with rare earth using the coordination of citric acid. The relationship among the ratio of phosphorus recovery, citric acid addition, pH, temperature, and time was studied, and then the regression equation was obtained. The optimum process conditions of phosphorus recovery were obtained as follows: citric acid concentration 0.05mol•L<sup>-1</sup>, pH=9, and time 20min, the ratio phosphorus recovery 99.8%, rare earth loss 0.98%. This research gives the support to recover phosphorus from rare earth minerals containing apatite.

**Study on the Surface Filming of Magnetic Modified Carbon Fiber:** *Xiaozhong Huang*<sup>1</sup>; *Zuojuan Du*<sup>1</sup>; <sup>1</sup>Central South University

In this paper, the surface filming of the carbon fiber for iron Sol was studied. IR analysis of the iron Sol showed that there are a large number of hydroxyl, carboxyl and other organic groups in the iron Sol, which implies a good infiltration with carbon fiber. The unglued process of the carbon fiber and the heat treatment technology of carbon fiber coating iron Sol were investigated. The carbon fibers are unglued under the protection of N<sub>2</sub> and 800°C temperature. The analysis of DTA showed that the heat treatment technology of carbon fiber coating iron Sol is divided into two stages: the first stage of temperature control in the 120°C and the second phase of temperature control in the 300°C. The magnetic modified carbon fibers were prepared by coating thin and uniform iron Sol.

**Surface Modification of a Biometallic Aisi 316L Stainless Steel by Means of Pulsed Electron Beam Treatment:** *Kemin Zhang*<sup>1</sup>; <sup>1</sup>Shanghai University of Engineering Science

Low energy high current pulsed electron beam (LEHCPEB) is a fairly new technique for surface modifications. The pulsed electron irradiation induces (i) very rapid heating, melting, solidification and cooling of the surface together with (ii) the formation of thermal stress waves. As a result, improved surface properties of the material, often unattainable with conventional surface treatment techniques, can be obtained fairly easily. This is particularly true for corrosion and tribological properties. In the present work, LEHCPEB was applied on two kinds of bio-metallic materials, 316L stainless steel and Ni(50.6 at%)Ti alloy. It was demonstrated that the corrosion resistance and the biocompatibility of the two alloys were significantly improved after the LEHCPEB treatment. The improvement in properties can be attributed to the microstructure and chemical modifications in surface layers induced by LEHCPEB.

**Surface Modification of Ti6Al4V Alloy by Pack Boriding:** Erdem Atar<sup>1</sup>; Eyup Kayali<sup>2</sup>; *Huseyin Cimenoglu*<sup>2</sup>; <sup>1</sup>Gebze Institute of Technology; <sup>2</sup>Istanbul Technical University

Titanium and its alloys have been widely used in aerospace, chemical and biomedical industries because of their low density, high dynamic and static strengths and excellent corrosion resistance. However, they suffer from poor tribological performance especially when used in wear related engineering applications. In fact poor wear resistance is inherent characteristics of titanium alloys and can only be improved by surface treatment. In the present study surface hardening of an extensively used Ti6Al4V alloy through boriding was investigated. Boride layer composed of TiB and TiB<sub>2</sub> phases were formed on the surface by using pack boriding technique. The hardness of the boride layer was over 2000 HV and caused considerable improvement wear resistance.

**Surface Rumppling of Pt-Modified Aluminide Coating with the Thickness of the Pre-Deposited Pt during Fabrication:** *Seokjun Hong*<sup>1</sup>; Yongnam Ko<sup>1</sup>; Sunggoon Kang<sup>1</sup>; <sup>1</sup>Hanyang University

Pt-modified aluminide coatings were prepared with various thicknesses of pre-deposited Pt on CM247LC by heat treatment and low-activity high-temperature (LAHT) pack aluminizing. After heat treatment, thicknesses of interdiffused area

were individually different with thicknesses of pre-deposited Pt. Also, thicknesses of pre-deposited Pt affected the surface roughening. When the Pt atom and the Ni atom were interdiffused each other, surface morphology was affected because of internal stress and the differential atomic radiuses. After pack auminizing, Pt-modified aluminide coating consisted of a two-phase, a one-phase and an interdiffusion layer. The two-phase layer was increased with increasing thickness of pre-deposited Pt. Also, from 2 to 8  $\mu\text{m}$ , surface roughness was increased with increasing thickness of pre-deposited Pt. However, surface roughness of Pt-modified aluminide coating which was fabricated with pre-deposited Pt of 12  $\mu\text{m}$  was relieved because of crowded PtAl<sub>2</sub> phase nearby the coating surface.

**Synthesis and Characterization of Novel Biomaterials:** *Nikhil Dhawan*<sup>1</sup>; <sup>1</sup>Punjab Engineering College

Biomaterials are widely used in the field of medical science as prosthetics. Metallic biomaterials, in spite of good mechanical properties, suffer from poor corrosion resistance as well as release of toxic elements in the body and cause implant failure, inflammation and body allergies. This problem has been overcome by coating their surface with ceramic biomaterials. The present work deals with some newly synthesized bioactive materials like Hydroxyapatite and Ca-P bioactive glass. HAp and HAp- Bioactive glass composite has been synthesized through powder metallurgy technique and has been characterized for their structure and phase composition using XRD and SEM techniques. Also corrosion resistance has been tested in vitro keeping the biomaterials in simulated body fluids at body temperature. It is expected that these materials, apart from being non-toxic, will exhibit better bonding characteristics to bone tissue.

**Synthesis of Meso-Porous CaCO<sub>3</sub> Particles by a Spray Drying Method:** *Hee Dong Jang*<sup>1</sup>; *Kuk Cho*<sup>1</sup>; *Hankwon Chang*<sup>1</sup>; *Kikuo Okuyama*<sup>2</sup>; <sup>1</sup>Korea Institute of Geoscience & Mineral Resources; <sup>2</sup>Hiroshima University

Synthesis of nanostructured spherical CaCO<sub>3</sub> particles having mesopores was investigated using a spray drying method with colloidal suspension of CaCO<sub>3</sub> nanoparticles. The CaCO<sub>3</sub> nanoparticles ranged from 20 nm to 100 nm in primary particle size were prepared from 3  $\mu\text{m}$  of the particles by ultrafine grinding using a bead mill. Average particle size of the synthesized porous particles was around 1  $\mu\text{m}$  in diameter. The porous CaCO<sub>3</sub> particles showed pore size distribution consisting of mesopores ranged from 2 nm to 30 nm. As the primary particle size of CaCO<sub>3</sub> nanoparticles increased, mesopores size increased due to a reduction in packing rates of primary CaCO<sub>3</sub> nanoparticles composing the walls of nanostructured porous particles. As the surfactant concentration increased in the colloid, smoother surface particles were prepared but major diameter of mesopores decreased. Mesopores of the particles disappeared when the furnace temperature was higher than 400°C.

**The Analog Simulation of Three-Layer Electrolysis Cell for Refining of Aluminum:** *Hengchao Zhao*<sup>1</sup>; *Huimin Lu*<sup>1</sup>; <sup>1</sup>Beijing University of Aeronautics and Astronautics

In the paper, the commercial simulation software ANSYS is used to build the three-dimensional model of refining aluminum cell. According to the relative parameters of the existing 85kA three-layer electrolysis cells as well as reasonable boundary condition hypotheses, the analog simulation computations to electric, temperature and magnetic fields in different production time are carried on, their results tally well with this actual production situation. The feasibility and the accuracy are confirmed in applying these models to analog simulation in the existing cells. Then, using the multiple elements and multiple properties of ANSYS software, the responsibility of 100kA three-layer electrolysis cells for refining aluminum is also checked.

**The Annealing and Aging Effect on Irradiated ZnO:Al Film by Cs-137:** *Meliha Tekin*<sup>1</sup>; *Eyup Kayali*<sup>1</sup>; *Huseyin Cimenoglu*<sup>1</sup>; *Nilgun Baydogan*<sup>1</sup>; *Hande Sengel*<sup>2</sup>; *Fehiman Akmaz*<sup>2</sup>; *Ates Parlar*<sup>2</sup>; <sup>1</sup>Istanbul Technical University; <sup>2</sup>Sisecam

ZnO:Al thin film was prepared using spin coating technique. Annealing effect on ZnO:Al thin film was evaluated at different temperatures. Annealing temperature was effected the structure of ZnO:Al film. For the determination of aging effect of sun on ZnO:Al film, the ultraviolet light source with double beam was used. The beams of UV light source have at 366 nm as long wave UV light and at 254 nm as short wave UV light. Besides, Cs-137 radioisotope with 9.5  $\mu\text{Ci}$  activity was used to accelerate the aging effect on ZnO:Al thin film. Cs-137 with 662 KeV photon energy was an appropriate source to decrease the aging time. Therefore it can be possible to compare the changes of the optical properties after the irradiation of ZnO:Al thin film with a UV light photons and with gamma rays.

**The Effect of Sintering Temperature and Pinning Elements on the Superconducting Properties of Spark Plasma Sintered MgB<sub>2</sub>:** *In Shup Ahn*<sup>1</sup>; *Su Gun Lim*<sup>1</sup>; *Dong Woong Kim*<sup>1</sup>; *Deuk Kyun Kang*<sup>1</sup>; <sup>1</sup>Gyeongsang University

Many researches on the MgB<sub>2</sub> have been carried out because of high critical temperature(Tc) and current density. In this study, the Mg and B powders of equivalent composition of MgB<sub>2</sub> and pinning element of carbon were mixed or milled for 9 hours maximum at argon atmosphere. The MgB<sub>2</sub> bulk was fabricated at the various temperatures by Spark Plasma Sintering. The formation of MgB<sub>2</sub> phase was confirmed at the temperature of 550°, and the formation temperature decreased to 350° in case of milled powder for 9hours. The relative density of sintered MgB<sub>2</sub> was over 99%, which increased as the sintering temperature increases. The densification was proceeded with solid phase and liquid phase sintering behavior step by step without abnormal grain growth. In the PPMS result, the Tc was about 37K in case of carbon pinning element addition. The MgB<sub>2</sub> grains size effect on the Tc change was not obtained.

**The Effect of Temperature on In-Situ Intrinsic Stress Behavior in Cu Thin Films:** *Moohyun Cho*<sup>1</sup>; *Sang Ryu*<sup>1</sup>; *Youngman Kim*<sup>1</sup>; <sup>1</sup>Chonnam National University

The intrinsic stress in thin film evolves during nucleation and growth of atoms on the substrate. Cu thin films, which grow in Volmer-Weber type, have unique stress behavior of three stages, such as initial compressive, tensile and incremental compressive. The tensile stress evolution was reported from the volume contraction though island coalescence. The mechanism of compressive stress is still in controversy even though extensive research efforts are being made. Incremental compressive stress may be related to the mobility of adatom on the substrate. To control the mobility of depositing Cu atoms, the substrate temperatures are changed from room temperature to 250° during deposition. We observed the in-situ stresses behavior of Cu thin films during deposition using multi-beam curvature measurement system attached to a thermal evaporation device. When temperature of substrate increased, the thickness at tensile maximum and the slope of incremental compressive stress showed a tendency to decrease.

**The Effect over Capacitance Properties of Surfactants Used in Mn(NO<sub>3</sub>)<sub>2</sub> Impregnation Process in High Charge Tantalum Powders:** *Juan Torres-Castañón*<sup>1</sup>; *Miguel Esquivel-Aguirre*<sup>1</sup>; *Héctor Barrientos*<sup>1</sup>; *Ana Pimentel*<sup>1</sup>; *Cristina Mota-Caetano*<sup>1</sup>; *Juan Pérez-Medina*<sup>1</sup>; <sup>1</sup>Kemet De Mexico

The manganese dioxide has been used since several years ago like a counter electrode in the tantalum capacitor fabrication. It has been reported that the additions of surfactants reduce the interfacial tension (liquid/solid interface) and help to improve the impregnation process. The impregnation with a non-ionic surfactant in tantalum pellets made from high CV powders was investigated at 30-60°C and concentrations of 0,01-0,1% wt. The influence of the surfactant in the MnO<sub>2</sub> structure was electrically characterized and phase distribution was analyzed with Scanning Electron Microscopy. A recovery in capacitance (~10%) was detected for under treatment part types with 100 and 320  $\mu\text{F}$ . The surfactant concentration into the solution is the main factor for the capacitance recovery and the electrical performance. The best capacitance recovery and electrical performance was obtained with 0.05% wt. of surfactant.

**The Effects of Finish Cooling Temperature on Yield Strength 800MPa Heavy Steel Plate Subjected to Direct Quenching Process:** *LianDeng Yao*<sup>1</sup>; *Sixin Zhao*<sup>1</sup>; *Xiaoting Zhao*<sup>1</sup>; *Hongbin Li*<sup>1</sup>; <sup>1</sup>Baosteel Technology Center

A kind of low carbon micro-alloyed heavy steel plates with thickness 40mm and low susceptibility to welding crack which yield strength exceed 800MPa, tensile strength exceed 950MPa, -40°C; charpy V-notch impact energy exceed 120J was produced by direct quenching process. The structure constitutions of heavy plates are bainitic ferrite plates which thickness less than 1 $\mu\text{m}$  and M/A constitute decorating at bainitic plates boundaries. Bainitic ferrite plates composed by sub-plate become thinner with the finish cooling temperature decreasing. The charpy V-notch impact energy at -40°C; of the plate direct quenching to 350°C; is lower than that direct quenching to room temperature but higher than that direct quenching to 250°C. Bainitic ferrite plate of experimental steel plates with various finish cooling temperature have high density dislocation. The bainite nucleation and growth process of experimental steel can be explained reasonably by diffusional mechanism.

**The Effects of Probe Diameter on Optimum FSW Conditions of 5456-H116 Alloy for Leisure Ship:** *Kim Seong-jong*<sup>1</sup>; *Lee Seung-Jun*<sup>1</sup>; *Han Min-Su*<sup>1</sup>; *Park Jong-Seek*<sup>1</sup>; *Park Jae-Cheul*<sup>1</sup>; <sup>1</sup>Mokpo Maritime University

This investigated the optimum FSW conditions of 5456-H116 alloy for leisure ship. Moreover, in probe diameter of 6mm with 15mm/min, the rough surface and



void with insufficiency of heat input due to low rotation speed were observed at 170-210RPM. However, a lot of chip due to excessive heat input is observed in 1100-2500RPM. In addition, the effect of heat input is prominently presented at the bottom side. In 15mm/min increased with the increasing of rotation speed due to heat input increase by increasing friction. The mechanical characteristics are decreased by accelerating softening of base metal due to increasing of heat input. Acknowledge: This research was financially supported by MOCIE and KOTEF through the Human Resource Training Project for Regional Innovation.

**The Electrochemical Leaching of the Chalcopyrite Concentrate in Acid Solution:** *Izolda kakhmishvili*<sup>1</sup>; Archil Benashvili<sup>1</sup>; <sup>1</sup>R.Agladze Institut of Inorganic Chemistry and Electrochemistry

The anodic dissolution of the suspension electrode made of Madneuli chalcopyrite concentrate in 30 g/l H<sub>2</sub>SO<sub>4</sub> solution was investigated using platinum and chalcopyrite probes. The experimental results suggest that the anodic dissolution of the chalcopyrite suspension electrode occurs not only when the electrode comes into contact with the current fitter but also in solution. The anodic oxidations of chalcopyrite concentrate proceeds in acidic solution in the presence of NaCl. It was established the optimal parameters of the processes.

**The Evaluation of Densified Layer Formation Mechanism and Thickness during Dry Sliding Wear of Porous Powder Metallurgy Steels:** *Shaahin Amini*<sup>1</sup>; Kavan Hazeli<sup>2</sup>; <sup>1</sup>University of California, Riverside; <sup>2</sup>Iran Test and Research Auto Company (ITRAC)

When a porous powder metallurgy part is worn by a counterbody, intense shear stresses are exerted on the surface and subsurface owing to the both normal load and tangential load (i.e. friction). Hence, the pores near the surface are closed owing to intense plastic deformation in this area and a hardened densified layer is formed. This densified layer has the thickness in which applied stresses are more than the yield stress of the matrix. In this research a porous Distaloy AE material which is a partially alloyed steel powder was worn by AISI 52100 steel in a reciprocating manner. Then subsurface stresses derived from normal and tangential load were calculated. The thickness of densified layer was obtained by comparing these stresses with yield stress of the matrix. The results compare with the metallographic photos and the differences are discussed.

**The Investigation of Microstructural Changes in ZnO:Al Thin Film by Beta Irradiation:** Hande Tugral<sup>1</sup>; Huseyin Cimenoglu<sup>1</sup>; *Nilgun Baydogan*<sup>1</sup>; Hande Sengel<sup>2</sup>; Fehiman Akmaz<sup>2</sup>; Ates Parlar<sup>2</sup>; <sup>1</sup>Istanbul Technical University; <sup>2</sup>Sisecam

ZnO:Al thin film was prepared using spin coating technique. After the coating process the texture of ZnO:Al film was exposed to Sr-90 radioisotope. It was found that the texture of the film can be affected with beta radiation. The microstructural changes using Sr-90 is critical with the charge trapping of radiolytic electrons or holes and the formation of defect centers and radiolytic electrons or holes. Beta radiation at ZnO:Al film led to a change in the physical properties such as colour when the beta radiation penetrated into the film. The evaluation of colour changes of irradiated ZnO:Al film is possible using the colour system. The changes of dominant wavelength, brightness and excitation purity of ZnO:Al transparent film were evaluated. Colour co-ordinates were used for the determination of dominant wavelength and excitation purity of ZnO:Al thin film in the CIE tristimulus system.

**The Microstructure and Mechanical Properties of As-HIP FGH 95 P/M Superalloy for High Pressure Turbine Blade Retainers:** *Yu Tao*<sup>1</sup>; Jian Jia<sup>1</sup>; Jiantao Liu<sup>1</sup>; Yiwen Zhang<sup>1</sup>; <sup>1</sup>CISRI

FGH 95 is a powder metallurgy (P/M) processed superalloy, which was developed in the 1980s in China. One of the applications of FGH 95 is for high pressure turbine blade retainers. The manufacturing processes used to produce FGH 95 blade retainers consist of atomization by plasma rotating electrode process (PREP), hot isostatic pressing (HIP) and a heat treatment with sub-solvus solution. The material has a equiaxed grain structure (about ASTM 7) with a fine dispersion of gamma prime and carbide precipitates. Batch production statistics of the mechanical properties for FGH 95 blade retainers were investigated. The as-HIP FGH95 blade retainers show high strength in room temperature and 650°, excellent creep resistance and stress rupture strength in 650°.

**The Reheating Behavior and Extrudability of Al-Zn-Mg Alloy Billet with Added Scandium:** *Sung-Yong Shim*<sup>1</sup>; Dae-Hawn Kim<sup>1</sup>; In-Sub Ahn<sup>1</sup>; Su-Gun Lim<sup>1</sup>; <sup>1</sup>Gyeongsang National University

The grain growth behavior under reheating process and extrudability of Al-Zn-Mg-(Sc) alloy fabricated by cooling plate method were evaluated. When Sc was added in aluminum alloy, the formed Al<sub>3</sub>Sc precipitation performed grain-

boundary pinning, which enabled the reheating process for Thixo-extrusion to reduce the grain growth. With the addition of Sc, the reheating behavior of the Al-Zn-Mg alloy was observed by optical microscope and EMPA after being heated to solid-liquid temperatures. The extrudability was evaluated by examining the surface cracking under extrusion conditions such as ram speed, billet heating temperature and extrusion ratio. The grain growth was significantly reduced when the Sc content exceeded 0.1 wt.% and the grain size of the Al-Zn-Mg+0.1wt.%Sc alloy was maintained at about 70° after 30 minutes at 600°. The extrudability was superior to that of conventional billets because the semi-solid materials have the advantage of having a low shear stress that allows deformation.

**The Role of Iron Addition on the Fire Assay of Pyritic Ores:** *Ahmet Turan*<sup>1</sup>; Hakan Morcali<sup>1</sup>; Onuralp Yucel<sup>1</sup>; <sup>1</sup>Istanbul Technical University

Fire assay is the most reliable and essential method which is employed to accurately analyse the precious metal content of ores. The avoiding from lead containing matte formation is the necessity for the fire assay of pyritic ores. Therefore iron is added on the smelting stage of pyritic ores in order to reduce lead from matte. In this study, experiments were conducted to understand the effects of different quantities of additional iron on the gold and silver recovery from pyritic ores. Specimens were fused by using fluxes and PbO, which accumulates precious metals, with various quantities of iron. AAS was used to analyze the precious metals obtained. Correlation between the quantity of additional iron and the recovery of gold and silver was investigated.

**The Shock Wave in High Velocity Compaction of Iron Powders:** *Haiqing Yin*<sup>1</sup>; Xuanhui Qu<sup>1</sup>; Shengyu Zhou<sup>1</sup>; Jianzhong Wang<sup>1</sup>; Mingjun Yi<sup>1</sup>; Sharon Elder<sup>2</sup>; <sup>1</sup>University of Science and Technology Beijing; <sup>2</sup>Pennsylvania State University

High velocity compaction of iron powder in both single impact and multiple impacts was investigated. The shock wave of the impact force and the green density were studied. The shock wave showed the characteristics of shock wave discontinuity during compaction. The shock wave of the initial impact was observed as saw-tooth waves. The compaction velocity and density prior to compaction were key factors affecting value and shape of the shock wave. With the increase of the compaction velocity, the working duration of the initial impact on the powder shortened. And the secondary wave on the initial wave became steeper with a greater peak force on the powder. Further, the saw-tooth shape of the shock wave disappeared with the increasing density prior to the last impact in double and triple impacts. In double impacts, the green density was found to be greater than those in single and triple impacts.

**The Thermal Decomposition Behaviour of Ammonium Heptamolybdate Tetrahydrate:** *Kemal Can Kevser*<sup>1</sup>; Aliye Arabaci<sup>1</sup>; Ibrahim Yusufoglu<sup>1</sup>; <sup>1</sup>University of Istanbul

In this study, the thermal decomposition of ammonium heptamolybdate tetrahydrate (AHM) in different heating rates and under different air and nitrogen gas flow rates was investigated. Therefore, analysis techniques like TGA, DTA and EGA were used. In the thermal decomposition of AHM three well-defined steps were observed and the intermediate and final products of each decomposition step were characterized by using XRD and FTIR analysis techniques and their morphologies were determined by SEM analysis. The characterization of the products and thermogravimetric analyses showed that AHM decomposes as (NH<sub>4</sub>)<sub>6</sub>Mo<sub>7</sub>O<sub>24</sub>·4H<sub>2</sub>O · (NH<sub>4</sub>)<sub>4</sub>Mo<sub>5</sub>O<sub>17</sub> + (NH<sub>4</sub>)<sub>2</sub>Mo<sub>2</sub>O<sub>7</sub> · (NH<sub>4</sub>)<sub>2</sub>Mo<sub>4</sub>O<sub>13</sub> · MoO<sub>3</sub> in air and as (NH<sub>4</sub>)<sub>6</sub>Mo<sub>7</sub>O<sub>24</sub>·4H<sub>2</sub>O · (NH<sub>4</sub>)<sub>4</sub>Mo<sub>5</sub>O<sub>17</sub> + (NH<sub>4</sub>)<sub>2</sub>Mo<sub>2</sub>O<sub>7</sub> · (NH<sub>4</sub>)<sub>2</sub>Mo<sub>4</sub>O<sub>13</sub> · MoO<sub>3</sub>-x in nitrogen gas. The activation energy values were calculated in air and nitrogen gas atmospheres for the each decomposition step observed in TGA diagrams by applying Ozawa method.

**Theoretical Investigation of Sulfur Adsorption on Fe (100):** *Weimin Cao*<sup>1</sup>; Anna Delin<sup>1</sup>; Taishi Matsushita<sup>1</sup>; Seshadri Seetharaman<sup>1</sup>; <sup>1</sup>Royal Institute of Technology (KTH)

Electronic and structural properties of the atomic sulfur adsorbed on the iron surface (100) are examined by using the density functional theory (DFT). The sulfur coverage is considered from a quarter to two monolayers (MLs). The adsorption energy and work function are calculated for three different adsorption sites of sulfur. The calculated results indicate that the most likely site for S adsorption is the hollow site on Fe (100), which is in agreement with experiment. In addition, the work function increased after the S adsorption on the Fe (100) surface, which implies the charge transfer from the surface to sulfur. The present results are in agreement with the other theory calculations.



**Thermodynamic Study on Complex System Co (II)-C2O4<sup>2-</sup>-NH<sub>3</sub>-NH<sub>4</sub><sup>+</sup>-H<sub>2</sub>O for Preparation of Fibrous Cobalt Powder Precursor:** *Zhan Jing*<sup>1</sup>; Zhang Chuanfu<sup>1</sup>; Wu Jianhui<sup>1</sup>; Yang Ping<sup>1</sup>; <sup>1</sup>Central South University

Based on the principles of simultaneous equilibrium and mass balance, a series of thermodynamic equilibrium equations of Co(II)-C<sub>2</sub>O<sub>4</sub><sup>2-</sup>-NH<sub>3</sub>-NH<sub>4</sub><sup>+</sup>-H<sub>2</sub>O system at ambient temperature are deduced theoretically and the logarithm concentration versus pH (log<sub>c</sub>-pH) diagrams at different solution compositions are drawn. The results show that when pH is above 8.0, cobalt ions coordinate with ammonia and the precipitation proceeds slowly accompanying with the release of cobalt ions from the multicoordinated Co(NH<sub>3</sub>)<sub>n</sub><sup>2+</sup> (n=1, 2, ..., 6), the morphology of cobalt powder precursor is fibrous; when pH is below 8.0, cobalt ions directly react with C<sub>2</sub>O<sub>4</sub><sup>2-</sup>, the morphology of cobalt powder precursor is cubic-shape. According to thermodynamics analysis and calculation, some experiments were done to validate the relation between the total concentration of cobalt ions and pH in this study.

**Ti-6Al-4V Alloy for Tooling Applications in Semi-Solid Processing:** Kemal Korkmaz<sup>1</sup>; *Yücel Birol*<sup>1</sup>; <sup>1</sup>TÜBITAK-Marmara Research Center

The processing of metals in the semi-solid state offers the opportunity of manufacturing complex structural parts in near-net shape. The process temperatures are usually in the semi solid area of metals, thus it is possible to decrease cost and save energy. However, tool dies for semi-solid forming are subjected to extreme conditions and life time of the tool dies is restricted by thermo-mechanical load cycles. The purpose of the present study is to investigate Ti-6Al-4V alloy as tool die materials. In this study, a ceramic layer is formed on Ti-6Al-4V alloy by micro-arc oxidation (MAO) in solutions of Na<sub>3</sub>PO<sub>4</sub> and NaAlO<sub>2</sub>. MAO is mainly promising a new surface technology for Ti-6Al-4V alloys, where thick and hard ceramic oxide layers can be formed. After MAO process, the wear, heat and corrosion resistance of these alloys can significantly be improved.

**Tin Recovery from Printed Circuit Boards of Obsolete Computers Using a Hydrometallurgical Approach:** *Afonso Martins*<sup>1</sup>; <sup>1</sup>Universidade Federal de Minas Gerais

This paper presents the preliminary experimental results for leaching of printed circuit boards from obsolete computers aiming at extraction of tin and recovery it by precipitation. Printed circuit boards were disassembled, cut off in small pieces and fed into a cylinder mill. The powder obtained was leached using aqueous solutions 2,18N H<sub>2</sub>SO<sub>4</sub>, 2,18N H<sub>2</sub>SO<sub>4</sub>+3,0N HCl, 3,0N HCl or 3,0N HCl+1,0N HNO<sub>3</sub>. The lowest values for percent of extraction were obtained for the 2,18N H<sub>2</sub>SO<sub>4</sub> (2.7% Sn). Meanwhile, the leach system 3,0N HCl+1,0N HNO<sub>3</sub> exhibited 98% Sn. Precipitates were obtained at different pH values by neutralization of the leach liquors using NaOH. The leach system 3,0N HCl+1,0N HNO<sub>3</sub> presented the highest recovery values from the powder feed (84.1% Sn) and from the leach liquor (85.8% Sn).

**Titanium Extraction by Electrochemical Reduction of TiO<sub>2</sub>:** *Chaganti Nagesh*<sup>1</sup>; <sup>1</sup>DMRL

Titanium extraction by electrochemical reduction of titanium dioxide (TiO<sub>2</sub>) is emerging as a potential alternate for titanium sponge production, owing to its several advantages resulting in cost and energy savings. In this work, the electrochemical reduction process has been studied on a laboratory scale of 100-200 grams per batch. Experimental work involving conversion of titanium dioxide granules into titanium metal by subjecting them to a cathodic treatment in a molten calcium chloride bath at a temperature of 950C, and using graphite anode. After the experiment, the sponge granules are thoroughly washed with water, acetic acid and dilute HCl. Excellent metallization has been found in granules which was confirmed by metallurgical characterization techniques viz. metallography, SEM, EDAX, EPMA etc. Attempts have also been made to evolve a theoretical kinetic model that describes the metallization process during the electrochemical reduction.

**Titanium Sponge Production in India:** *Chaganti Nagesh*<sup>1</sup>; Brahmendra Kumar Gummadi<sup>1</sup>; Sitaraman TS<sup>1</sup>; Ramachandran CS<sup>1</sup>; <sup>1</sup>DMRL

India possesses large and rich reserves of ilmenite (FeOTiO<sub>2</sub>), an important mineral of titanium. Defence Metallurgical Research Laboratory, Hyderabad, India (DMRL) has successfully developed the technology for production of titanium sponge by high temperature magnesium reduction of pure titanium tetrachloride followed by vacuum distillation of reduced mass employing a 'Combination unit'. This development work includes (i) development of distillation columns for TiCl<sub>4</sub> purification, (ii) design, development and operation of equipment for conducting Reduction and Vacuum distillation processes in a batch size of 3000 kg of sponge and (iii) development of equipment and

tooling for titanium sponge grading, cutting and quality evaluation to prepare homogenous lots of high quality sponge. This paper brings out salient features of DMRL technology and results of the technology development program including the improved understanding of the metal production process. The country's first commercial titanium sponge plant is coming up with this technology.

**Toolcoatings as Thermocouple for Chipping:** *Klaus Pantke*<sup>1</sup>; Heilmann Markus<sup>1</sup>; Dirk Biermann<sup>1</sup>; <sup>1</sup>University of Dortmund

The acknowledgement of temperature influences onto the cutting edge and workpieces achieves a growing relevance. Particularly with regards to the cutting material-, coating-, and cooling lubricant selection, the knowledge of appearing temperatures is essential. Up to now, the action-close thermo measurement at the cutting edge is conducted by video-thermographic recordings, pyrometers or according to the principle of resistance-measurements. Modern coating technology offers new options. Already established measuring methods allow the detection of temperature and wear following the principle of conductivity variation by close meshed conductor structures plated on the cutting inserts. An improved method utilizing an alternative physical principle now allows to implicate coatings for temperature measurements by means of the so-called "Seebeck-Effect". Applying the principle of thermo electricity just as in conventional thermo couples, different metals are affiliated with each other and exposed to an temperature gradient, so that a measurable voltage results.

**Two-Step Sintering of Nd-Fe-B Powder:** *Se Hoon Kim*<sup>1</sup>; Hoon Sup Kim<sup>1</sup>; Min Suh Park<sup>1</sup>; Ji Hoon Seo<sup>1</sup>; Young Do Kim<sup>1</sup>; <sup>1</sup>Hanyang University

Sintered Nd-Fe-B magnets have been widely used due to their excellent magnetic properties. However, heterogeneous microstructure of Nd-Fe-B magnet is an important factor limiting their magnetic property. Therefore, modifying a sintering process has been an important method for better homogeneous microstructure. In this study, Nd-Fe-B powder was fabricated by strip-casting and jet milling. The powder was compacted in a magnetic field. After that, the green compact was sintered at temperature between 1050°C and 1150°C as first-step, then, second-step was sintered at temperature between 900°C and 1000°C. Two-step process was employed for the sintering of Nd-Fe-B powder to obtain homogeneous grain size in bulk part. Densification over 99% could be obtained by the two-step sintering of Nd-Fe-B powder with 5 μm in Nd<sub>2</sub>Fe<sub>14</sub>B phase and the Nd-rich phase was homogeneously distributed. Moreover, the two-step sintering process led to uniform grain size distribution with the improvement of magnetic properties.

**Uniform Depth of Cladding through Vision-Based Monitoring of VP GTAW Cladding of Aluminum Alloys:** *Rouzbeh Sarrafi*<sup>1</sup>; <sup>1</sup>Southern Methodist University

Variable-polarity GTAW (VP-GTAW) process is capable of producing sound clads on aluminum alloys due to the real-time removal of oxide layers. However, heat accumulation in the workpiece during the cladding causes non-uniform depth of clads, making heat management a big challenge to the application of VP-GTAW for cladding of aluminum alloys. In this research, a machine-vision system was integrated to monitor the molten pool width during cladding. The image of the bright arc plasma has been almost eliminated by an illumination/ filtering technique. A low-resolution CCD camera was used to capture the images in real-time. The results showed that by this method, clear images of the molten pool boundary are obtained so that they can be subsequently integrated to a control system. In addition, it is experimentally shown that by controlling the width of molten pool by altering current or travel speed, a uniform depth of clad can be achieved.

**Upgrading Titaniferous Metallurgical Slag by Activation -Acid Leaching Process:** *Tao Jiang*<sup>1</sup>; Haigang Dong<sup>1</sup>; Yufeng Guo<sup>1</sup>; Guanghui Li<sup>1</sup>; Yongbin Yang<sup>1</sup>; <sup>1</sup>Central South University

Large reserve of vanadium-titanium magnetite ore has been found in China. Currently, Ilmenite concentrate with 47% TiO<sub>2</sub> has been obtained from the ore by beneficiation. By electrical furnace smelting, the concentrate is processed into the titanium-rich slag with 73% TiO<sub>2</sub>, which is still not suitable for the production of titanium white by chlorination process due to its high content of impurities, such as CaO, MgO, etc. This work has developed a new process to upgrade the slag. The slag is first activated by roasting at a temperature of 700°C to 900°C with addition of alkali metal salts. The activated slag is then leached by sulphuric acid and the leached slag is calcined at a temperature of 900°C. By this process, the Ti-rich product with 92% TiO<sub>2</sub> is obtained. The mechanism of activation-acid leaching is studied by XRD analysis and thermodynamic investigation.

- A**
- A.Kawy Hammad, M.....364
- Aagesen, L.....80, 102, 222
- Aalund, R.....88
- Aardahl, C.....203
- Abanades, A.....29
- Abassi, M.....101
- Abbas, H.....326
- Abbe, A.....328
- Abd Elrahman, A.....48
- Abderrahim, A.....113
- Abe, H.....116
- Abedrabbo, S.....121
- Abeln, S.....212
- Abeykoon, A.....116
- Ablitzer, D.....185, 234
- Ablitzer, S.....312
- Abreu, A.....360
- Abreu-Sepulveda, M.....309
- Abu-Farha, F.....152
- Abunaemeh, M.....29, 257
- Acchar, W.....316
- Acevedo, J.....368, 372
- Acevedo Dávila, J.....362
- Acharya, A.....99
- Acoff, V.....303
- Acosta G., F.....53
- Ada, E.....106
- Adams, A.....145
- Adams, B.....176
- Adams, D.....207
- Adams, J.....259
- Adams, T.....137, 252
- Adanir, H.....164, 193
- Adedokun, S.....132, 178
- Adeosun, S.....157
- Adharapurapu, R.....21, 151, 299
- Adiga, S.....38
- Adipuri, A.....307
- Adjanor, G.....290
- Adkins, P.....145
- Adrien, J.....341
- Afshar, A.....358
- Aga, B.....230
- Aga, R.....51, 135, 285
- Agaogullari, D.....339, 370
- Agarwal, A.....222, 223, 271, 319, 357
- Ager III, J.....66
- Aghaie-Khafri, M.....24
- Agnew, S.....20, 57, 58, 104, 105, 150,  
151, 198, 199, 200, 248, 249,  
300, 301, 340, 341, 348, 349
- Agour, M.....292
- Agrawal, A.....87
- Agrawal, D.....376
- Agrawal, P.....364, 365
- Agren, J.....143
- Aguilar-Sanchez, M.....34
- Aguilar Garcia, D.....131
- Ahmad-Bitar, R.....18
- Ahn, B.....25, 28, 159, 276, 308
- Ahn, I.....378, 379
- Ahn, K.....121, 122
- Ahn, S.....300
- Ahn, T.....364
- Ahuja, R.....203
- Aindow, M.....236
- Aini Abd Majid, N.....16
- Ajerssch, F.....90
- Akamatsu, S.....149, 195
- Akarapu, R.....340
- Akarapu, S.....189
- Akasheh, F.....189
- Akbari Pazooki, A.....132
- Akbarzadeh, A.....43
- Akin, I.....254, 368, 374
- Akinc, M.....282, 290
- Akman, F.....30
- Akmaz, F.....378, 379
- Akogwu, O.....27
- Aksit, M.....22
- Aksoy, M.....17
- Aktaa, J.....64
- Aktuð, S.....133
- Akuzawa, N.....335
- Al-Aqeeli, N.....233
- Al-Bermani, S.....109
- Al-Jallaf, M.....230, 279
- Al-Jassim, M.....121, 122
- Al-Maharbi, M.....58, 198, 201
- Al-Moniem Said, A.....280
- Alahmadi, K.....377
- Alali, H.....89, 137, 182, 234, 286, 331
- Alam, M.....71, 156
- Alankar, A.....95
- Al Ansari, T.....138
- Alaswad, K.....230
- Alayavalli, K.....62
- Alba-Baena, N.....359
- Albert, B.....297
- Albiston, B.....245
- Alboni, P.....309
- Alboussièrè, A.....22
- Aldanondo, E.....295
- Aldi, J.....83, 177
- Alevizos, K.....31
- Alexander, J.....64
- Alford, T.....340
- Al Hashimi, A.....235
- Ali, M.....48, 279, 326
- Alinger, M.....65, 146, 317, 355, 356
- Alizadeh, M.....110
- Al Jabri, N.....145
- Al Jallaf, M.....86, 145, 327
- Alkan, M.....205
- Allaire, C.....90
- Allard, B.....292
- Allard, L.....305
- Allen, C.....278
- Allen, T.....29, 160, 257, 258, 305
- Alley, E.....99
- Allison, J.....35, 173, 272, 315
- Alman, D.....236, 299
- Almer, J.....29, 31, 146, 174, 180, 184, 255
- Alonso, E.....267
- Alsem, D.....207
- Altenkirch, J.....244
- Altman, K.....17
- Alvarenga, J.....37
- Alvarez, P.....295
- Alvear, G.....217
- Alves, J.....316
- Alves, L.....130
- Alvin, M.....60, 332
- Al Zaroni, A.....86
- Al Zarouni, A.....145, 279, 280
- Amancio-Filho, S.....41
- Amato, K.....362
- Ames, M.....64
- Ames, N.....50
- Amin, A.....164
- Amini, S.....259, 379
- Amirbekian, B.....312
- Amouyal, Y.....42, 270, 342, 366
- Amritkar, A.....244
- An, H.....337
- An, K.....241, 295
- An, R.....233
- An, Z.....93
- Anagnostou, E.....99, 193
- Anami, T.....84
- Anderegg, J.....323
- Anderoglu, O.....255, 275
- Andersen, K.....46, 47
- Anderson, I.....31, 46, 71, 117, 164, 196,  
214, 218, 246, 262, 313, 323, 351, 363
- Anderson, K.....190
- Anderson, T.....188
- Andersson, J.....22
- Andersson, M.....205
- Ando, D.....341
- Ando, T.....205
- Andrade, G.....231
- Andrade, H.....362, 370
- Andresen, P.....251, 304
- Andrews, R.....145
- Ang, J.....23
- Ann, M.....353
- Anopuo, O.....200
- Anovitz, L.....188
- Anselmino, E.....80
- Anton, E.....141
- Antonyraj, A.....254
- Antrekowitsch, H.....182, 234, 267
- Anumalasetty, V.....104
- Anyalebechi, P.....17, 62, 63, 109,  
156, 205, 253, 307
- Aoyama, A.....30
- Apel, M.....238
- Apisarov, A.....278
- Appel, F.....48, 308
- Ara, K.....14
- Arabaci, A.....379
- Araujo, E.....345, 365, 372
- Araújo, E.....364, 369, 372, 373, 374
- Arbegas, W.....54, 194, 195, 243, 245, 246
- Arce Estrada, E.....129
- Ardell, A.....221, 319
- Ares, A.....170
- Aretz, H.....85
- Arfaei, B.....263
- Arias Castro, J.....259
- Arikan, G.....163
- Armstrong, B.....241, 306
- Armstrong, D.....357
- Armstrong, T.....188
- Arnberg, L.....80, 123
- Arnoux, M.....61, 359
- Arnoux, P.....251
- Arockiasamy, A.....325
- Arpe, R.....324
- Arroyave, R.....289, 314, 350, 354
- Arruebarena, G.....199
- Arsenault, A.....286
- Arslan, C.....82
- Arzt, E.....206
- Asadi, M.....369
- Ashbrook, M.....17
- Ashkenazy, Y.....127
- Ashok, M.....336
- Ashok, S.....336
- Ashtari, P.....220
- Asim, K.....59
- Askari, A.....243
- Aslani, M.....18

Asokan, K .....	47	Balla, V .....	39, 340	Bearne, G .....	16, 41, 86, 134, 179, 190, 229, 230, 278, 279, 326, 327
Assouli, B .....	335	Ballard, D .....	22, 60, 107, 108, 153, 201, 250, 302, 342	Beauchamp, C .....	187
Asta, M .....	52, 78, 92, 124, 143, 171, 220, 269, 314	Ballato, J .....	337	Beaudoin, A .....	99, 133, 134
Atamanenko, T .....	287	Balle, F .....	325	Beaudry, M .....	327
Atar, E .....	377	Balocchi, A .....	216	Becker, R .....	350
Athènes, M .....	290	Balogh, L .....	112, 212, 213	Becker, R .....	173
Atre, S .....	298	Balogun, S .....	157	Beckermann, C .....	51, 80, 101, 268
Attallah, M .....	26	Balzar, D .....	212	Beckman, J .....	53
Attanasio, S .....	269	Bambach, M .....	85	Beckmann, F .....	41, 311
Attarchi, M .....	129, 336	Bamberger, M .....	150, 300	Becquart, C .....	29, 66, 208
Atzmon, M .....	136	Bammann, D .....	328	Bédard, S .....	244
Auger, T .....	251	Bampton, C .....	108, 347	Bedi, S .....	341
Ault, J .....	212	Bandyopadhyay, A .....	39, 109, 135, 297, 329, 338, 340	Bednarcik, J .....	330
Avelar, A .....	176	Banerjee, R .....	209, 221, 270, 348	Begonia, M .....	328
Averback, R .....	66, 78, 79, 124, 127, 171, 172, 220, 225, 269, 271	Banerjee, S .....	18, 80, 81, 225, 321	Behi, M .....	108
Averty, X .....	160	Banerji, A .....	90	Bei, H .....	158, 162, 284, 336
Ávila, J .....	333	Bang, W .....	264	Beitelschmidt, D .....	136
Avila-Davila, E .....	372	Banovic, S .....	184, 348	Belak, J .....	81, 273
Avraham, S .....	300	Bao, L .....	131	Bell, N .....	185
Avtar, R .....	157	Bao, S .....	235	Bellman, M .....	269
Awiriri, G .....	197	Bao, Y .....	249, 362	Bellmann, M .....	80
Awang, M .....	195	Bao, Z .....	87	Bellon, P .....	43, 66, 79, 92, 113, 141, 172, 186, 225, 237, 289, 334
Aydin, A .....	375	Bar - Ziv, S .....	19	Bellot, J .....	234
Aydin, H .....	237	Barabash, O .....	213	Belova, I .....	290, 291
Aydin, S .....	366, 374	Barabash, R .....	69, 70, 115, 116, 157, 162, 212, 213, 260, 311, 348	Belt, C .....	47, 97, 98
Ayer, R .....	293	Barbier, B .....	261	Belzile, Y .....	145
Aynibal, F .....	370	Barbosa, R .....	369, 373	Ben-Artzy, A .....	152
<b>B</b>					
B. Jabbar, A .....	130	Bardal, A .....	230	Ben-Yaacov, T .....	296
Baars, D .....	157	Bardt, J .....	89	Benashvili, A .....	379
Baated, A .....	74	Baricco, M .....	329	Bench, G .....	321
Baba-Kishi, K .....	311	Barker, S .....	84	Benedek, R .....	125
Babu, S .....	184	Baron, J .....	95, 145	Bengus, V .....	26, 180
Bach, M .....	324	Barone, J .....	282	Benkahla, B .....	230
Bäckström, J .....	73	Barpanda, P .....	82, 309	Benke, S .....	238
Bacon, D .....	209, 318	Barre, C .....	347	Bennet, J .....	154
Baczek, F .....	177	Barrientos, H .....	376, 378	Bennett, J .....	290
Badarinarayan, H .....	194	Barry, S .....	90	Benson, D .....	94
Badillo, A .....	66	Barsoum, M .....	259	Bentley, J .....	23, 65, 160
Badowski, M .....	182	Barth, H .....	312	Berasi, C .....	135
Bae, D .....	21, 210	Bartlow, C .....	375	Bergeon, N .....	102, 196
Bae, G .....	21	Bartolo, L .....	314, 315, 350, 353, 354	Berger, M .....	75, 291
Bae, J .....	21, 32, 247, 266	Barton, N .....	274	Berghmans, A .....	56
Baek, S .....	138, 332	Bartsch, M .....	126	Bergner, F .....	30
Baena Murillo, E .....	91	Baruchel, J .....	102, 196	Bergstrom, C .....	204
Baggash, I .....	230	Baser, T .....	329	Bermek, H .....	17
Bagheri, Z .....	262	Baskes, M .....	273	Bernard, D .....	138
Bagley, S .....	232, 288	Basoalto, H .....	291	Bernath, J .....	50, 100
Bahk, J .....	309	Bass, M .....	337	Bernhard, C .....	109
Bahr, D .....	44, 45, 94, 143, 144, 189, 207	Bassi, C .....	178	Bernier, J .....	70, 274
Bai, C .....	288, 375	Bassman, L .....	367, 371	Bernussi, A .....	364
Baik, S .....	140, 364	Basu, S .....	361, 373	Berry, J .....	170, 186, 198
Bailey, R .....	299	Basurco, J .....	354	Bertolo, J .....	87
Bailey, W .....	96	Batista, C .....	324	Bertrand, C .....	326
Bainbridge, I .....	105	Batista, E .....	364	Bérubé, D .....	327
Baiocchi, F .....	164	Batista, J .....	176	Berveiller, S .....	261
Baird, J .....	339	Batista, R .....	231	Berveling, A .....	230
Bak, S .....	368	Battaille, C .....	48, 99, 126, 147, 192, 242, 293	Berzansky, J .....	83
Bakai, A .....	182	Battezzati, L .....	329	Beshay, Y .....	220
Baker, I .....	247	Bauer, P .....	98, 235	Bestyzev, N .....	64
Bakhishev, T .....	313	Baumann, J .....	243	Bettles, C .....	198, 260
Bakshi, S .....	223	Baumann, T .....	116	Betzwar Kotas, A .....	264
Balachandran, S .....	157	Baxter, R .....	240	Beuth, J .....	109, 319
Balani, K .....	223	Bayandorian, I .....	105, 249	Bewlay, B .....	153, 201
Balasubramaniam R .....	248	Baydogan, M .....	17	Beyea, S .....	135
Baldwin, K .....	352	Baydogan, N .....	30, 378, 379	Beyerlein, I .....	190
Balint, D .....	251	Bayles, R .....	347	Bezamanifary, L .....	190
Balk, T .....	27, 256, 275	Bazan, G .....	173	Bezencon, C .....	178
		Beals, R .....	104	Bezerra, D .....	363, 372
				Bhadrachalam, P .....	175, 176
				Bhame, S .....	226



- Bhandakkar, T ..... 255  
 Bharathula, A ..... 181, 286  
 Bhargava, S ..... 84  
 Bhat, R ..... 65, 159  
 Bhat, V ..... 203  
 Bhattacharjee, A ..... 54, 147  
 Bhattacharya, M ..... 337  
 Bhattacharyya, D ..... 35, 65, 80, 162  
 Bhaumik, S ..... 133  
 Bhrargava, N ..... 122  
 Bhujang Mutt, G ..... 92  
 Bhujang Mutt, S ..... 92  
 Bi, S ..... 276  
 Bian, Z ..... 105, 249  
 Bianculli, S ..... 319  
 Bice, D ..... 211  
 Bidylo, M ..... 26  
 Bieler, T ..... 35, 94, 157, 245,  
 ..... 263, 297, 337, 339, 351  
 Biener, J ..... 256  
 Biener, M ..... 256  
 Bierman, M ..... 70  
 Biermann, D ..... 85, 380  
 Biesinger, M ..... 362  
 Bigault, T ..... 47  
 Billia, B ..... 102, 196, 218  
 Billot, T ..... 294  
 Biner, B ..... 143  
 Bingert, J ..... 111, 183, 245, 299  
 Biondo, C ..... 364  
 Birat, J ..... 140, 185  
 Birol, Y ..... 380  
 Birozca, S ..... 48  
 Birringer, R ..... 64, 117  
 Birsan, G ..... 220  
 Bischoff White, E ..... 342  
 Biscuola, V ..... 195  
 Biswas, P ..... 177  
 Biswas, S ..... 306  
 Bizon, A ..... 229  
 Blackmore, M ..... 109  
 Blaesing, J ..... 163  
 Blais, S ..... 331  
 Blanco, D ..... 76  
 Blanco, E ..... 53, 219  
 Blandin, J ..... 283, 341  
 Blankenship, L ..... 177  
 Blanpain, B ..... 34, 80, 238, 254, 362  
 Blau, P ..... 211, 319  
 Blawert, C ..... 104  
 Bleck, W ..... 35, 183  
 Blendell, J ..... 141, 215  
 Bligh, R ..... 324  
 Blikstein, P ..... 315  
 Bodde, S ..... 179  
 Boehlert, C ..... 293  
 Boettinger, W ..... 51, 92  
 Boettner, H ..... 56  
 Boggs, B ..... 96  
 Bogomolov, V ..... 268  
 Bohlen, J ..... 58, 199, 200, 302  
 Bohn, T ..... 338  
 Boissiere, R ..... 341  
 Bojarevics, V ..... 326  
 Bojin, D ..... 287  
 Bolduc, S ..... 331  
 Bonarski, B ..... 111  
 Bondarenko, A ..... 30  
 Bondarenko, B ..... 268  
 Böning, M ..... 202  
 Bonora, N ..... 343  
 Boock, J ..... 68, 115  
 Booth-Morrison, C ..... 54, 221, 223, 271, 365  
 Boothby, R ..... 317  
 Booty, M ..... 168  
 Bor, H ..... 22  
 Borah, P ..... 253  
 Borbely, A ..... 42, 69  
 Borges, A ..... 177  
 Borgesen, P ..... 263, 352  
 Boring, C ..... 179  
 Borisevich, A ..... 113  
 Borivent, D ..... 218  
 Bormann, R ..... 248, 340  
 Borzone, G ..... 167  
 Bosáček, V ..... 46  
 Bosco, N ..... 314  
 Bose, S ..... 39, 109, 135, 297, 329, 338, 340  
 Bossuyt, S ..... 88  
 Bott, R ..... 324  
 Böttcher, H ..... 182, 234  
 Bottin-Rousseau, S ..... 149  
 Bouchard, G ..... 95  
 Bouchard, I ..... 197, 244  
 Bouchard, V ..... 86  
 Boufounos, D ..... 131  
 Bouk, T ..... 240  
 Boulanger, C ..... 95  
 Bourell, D ..... 61, 62, 108, 155, 156, 204  
 Bourke, M ..... 212  
 Bourne, G ..... 89  
 Bourne, N ..... 173  
 Boutin, B ..... 96  
 Bouvard, J ..... 328  
 Bower, A ..... 214  
 Bowers, J ..... 309  
 Bowers, R ..... 228  
 Bowman, K ..... 141  
 Boyce, B ..... 48, 99, 147, 158, 192, 242, 293  
 Boyce, D ..... 350  
 Boyd, W ..... 165  
 Boyer, R ..... 31, 211, 259, 310, 311, 346  
 Boyun, H ..... 323  
 Bozek, J ..... 99  
 Bradley, J ..... 59, 106, 152, 302  
 Brady, M ..... 154, 203, 252, 291, 305, 306, 344  
 Braga, C ..... 231  
 Brandes, M ..... 70  
 Brandl, C ..... 223  
 Brandon, D ..... 124  
 Brandt, M ..... 182  
 Brar, H ..... 20  
 Brasileiro, M ..... 316  
 Braun, R ..... 303  
 Bray, J ..... 135  
 Bray, S ..... 213  
 Breault, R ..... 96  
 Brenner, D ..... 283  
 Brewer, L ..... 48, 99, 126, 147, 192, 242, 293  
 Bright, M ..... 90  
 Bringa, E ..... 94, 225, 256, 274  
 Brinkman, K ..... 137, 252  
 Brinson, C ..... 114  
 Brisset, F ..... 229  
 Brocchi, E ..... 16  
 Brochu, M ..... 227  
 Brock, J ..... 163  
 Broek, S ..... 191  
 Brokmeier, H ..... 349  
 Brooks, G ..... 334  
 Brow, R ..... 154  
 Brown, D ..... 96, 201, 212, 241, 261, 341, 348, 349  
 Brown, E ..... 147  
 Brown, J ..... 194, 195, 244  
 Brown, S ..... 110  
 Browne, D ..... 267  
 Browning, N ..... 42, 270, 321  
 Brownlow, S ..... 114  
 Bruder, E ..... 338  
 Bruey, F ..... 228  
 Brühne, K ..... 232  
 Brundidge, C ..... 147  
 Brunelli, M ..... 116  
 Buazza, O ..... 15  
 Buchanan, D ..... 242, 247  
 Buchanan, K ..... 184  
 Buchanan-Vega, J ..... 82  
 Buchheit, T ..... 206  
 Buchholz, A ..... 234  
 Buchovecky, E ..... 214  
 Budai, J ..... 70  
 Budnitzki, M ..... 193  
 Buenger, T ..... 119  
 Buffet, A ..... 102, 196  
 Bugat, S ..... 317  
 Bugge, M ..... 278  
 Buha, J ..... 200  
 Bühler, M ..... 156  
 Bulatov, V ..... 67, 113  
 Bunn, J ..... 96, 97  
 Bunster, G ..... 338  
 Buresh, S ..... 159  
 Burford, D ..... 194, 195, 244  
 Burke, M ..... 317  
 Burkes, D ..... 244, 344  
 Burkins, M ..... 299  
 Burkov, A ..... 320  
 Burrows, A ..... 217  
 Busby, J ..... 160, 251  
 Busch, R ..... 136  
 Bushi, L ..... 151  
 Buslaps, T ..... 42  
 Buta, D ..... 52  
 Butt, D ..... 157  
 Buzaianu, A ..... 152  
 Byczynski, G ..... 77, 219  
 Byler, D ..... 224, 225  
 Byrne, E ..... 224  
 Byun, K ..... 31
- ## C
- Caballero, C ..... 166, 216  
 Cabrera, C ..... 369  
 Caceres, C ..... 104  
 Cady, C ..... 247  
 Cahill, D ..... 127  
 Cahill, R ..... 145  
 Cahn, J ..... 171  
 Cai, J ..... 65  
 Cai, W ..... 225  
 Cai, Y ..... 87  
 Calderón, H ..... 360  
 Calderon Benavides, H ..... 346  
 Calvert, P ..... 16, 38, 87, 134,  
 ..... 179, 231, 232, 282, 328  
 Calzado, L ..... 332  
 Camacho, A ..... 296  
 Camacho Beltran, A ..... 259  
 Camilli, R ..... 360  
 Campagnoli, E ..... 281  
 Campbell, A ..... 28  
 Campbell, B ..... 115  
 Campbell, C ..... 56, 142, 188, 239, 290  
 Campbell, G ..... 270, 321, 322  
 Campbell, J ..... 77, 78, 123, 170, 219, 267

Campbell, M	260	Chan, T	25	Cheng, Z	156
Campillo-Illanes, B	362	Chan, W	127, 289	Chenguang, B	53
Campos, C	229	Chandler, R	183	Cheng Yi, L	167
Candic, M	34	Chandra, D	46, 367, 368	Chengyong, D	92
Canepari, S	342	Chandra, R	192	Cheong, S	177
Can Kevser, K	379	Chandrasekar, S	65	Chernova, L	126
Cannon, S	259	Chandrashekar, S	83, 130, 176, 227, 276, 324	Cherukuri, B	197
Cannova, F	95, 145	Chandrashekhara, K	124	Chesonis, C	137
Cantin, K	145	Chang, C	74, 113, 367	Chevalier, J	251
Cantwell, P	215	Chang, H	330, 378	Chhay, B	29, 257
Cao, B	223	Chang, J	302	Chiang, W	182
Cao, F	190, 351	Chang, S	310	Chiba, A	45, 49, 55
Cao, G	346	Chang, Y	151, 153, 238, 271, 296, 317, 342	Chien, W	367, 368
Cao, H	151, 316	Changdong, L	123	Chih Ming, L	167
Cao, J	14	ChangYong, P	164	Chikhradze, M	369
Cao, L	44, 105, 343	Chao, H	53	Chikhradze, N	369
Cao, W	23, 238, 342, 379	Chao-Han, W	188	Chinella, J	84
Cao, X	131, 339	Chapman, D	273	Chinh, N	27
Cao, Y	266, 375	Chapple, M	244	Chiwata, M	335
Cao, Z	357	Charest, G	96	Cho, H	112, 193
Capdevila, C	79	Charette, A	95	Cho, I	26
Capolungo, L	35, 201	Charit, I	32, 101, 209, 244, 344	Cho, J	168, 249, 295, 336
Cardona, F	333	Charr, J	176	Cho, K	69, 210, 361, 378
Cardona Quintero, Y	296, 377	Chartrand, P	335	Cho, M	168, 218, 263, 378
Carlberg, T	287	Chason, E	214, 215, 255	Cho, P	193
Carlile, C	46	Chaswal, V	174, 222	Cho, S	266
Carlsson, P	46	Chatterjee, D	306	Cho, W	372
Carneiro, M	227	Chatterjee, S	24, 26	Choate, W	98
Carnot, M	156	Chaudhary, A	211	Choi, B	285
Caro, A	125, 225	Chaudhuri, S	291	Choi, E	63
Caro, M	125	Chauhan, M	28	Choi, G	278
Caron, A	26	Chauhan, R	363	Choi, H	210, 346
Carrado, A	320	Chavali, S	32	Choi, I	308
Carreño-Gallardo, C	164	Chawla, N	49, 126, 161, 162, 264, 314, 351	Choi, J	47, 69, 156, 280, 302, 306, 344, 345, 376
Carreon, H	237	Che, D	357	Choi, K	262
Carrere, A	335	Che, X	228	Choi, M	185
Carsley, J	177	Che-Ming, C	76	Choi, S	146, 200
Carter, J	208, 301	Chee, S	79	Choi, W	14, 37, 82, 129, 175, 226, 274, 323
Carter, M	175	Cheeseman, B	95	Choi, Y	14, 16, 82, 144, 298
Casolco, S	366, 373	Chellappa, R	367, 368	Chokethawai, K	320
Castanho, S	316	Chen, A	226	Chollier, M	95, 190
Castillejos, A	53	Chen, B	19, 300, 349, 357	Choo, H	26, 39, 46, 88, 96, 135, 146, 149, 180, 191, 213, 232, 241, 283, 284, 307, 329, 348, 349
Castillo, A	367	Chen, C	32, 33, 68, 70, 74, 75, 89, 117, 118, 120, 167, 207, 215, 217, 265, 296, 337, 351	Chou, C	275
Castro, W	196	Chen, E	211	Chou, H	108
Castrup, A	308	Chen, F	16, 249	Chou, P	304
Caturla, M	208	Chen, G	103, 284, 329, 330, 336	Chou, Y	42, 345
Cavallaro, J	70	Chen, H	117, 236, 249, 265	Choudhuri, D	214
Cavallo, R	173	Chen, I	168	Choudhury, A	149
Cayron, C	160	Chen, J	16, 52, 63, 124, 230, 305, 326, 343, 368	Choudhury, S	67, 141
Ceder, G	44	Chen, K	70, 117, 278, 310, 351	Chow, T	363
Cederqvist, L	50	Chen, L	42, 43, 81, 92, 141, 148, 149, 168, 173, 186, 220, 224, 228, 237, 250, 264, 289, 296, 315, 334, 336, 354	Christ, H	48
Celik, O	248	Chen, M	39, 88, 110, 167, 181, 285	Christ, R	49
Çelikbilek, M	366	Chen, P	180, 328	Christensen, M	269
Cerecedo, E	333	Chen, Q	143, 253, 276, 277	Christensen, V	230
Cerecedo Saenz, E	333	Chen, R	57, 200, 368	Chrzan, D	66, 161, 189, 308
Cerefice, G	344	Chen, S	72, 74, 120, 153, 167, 189, 216, 217, 238, 265, 342	Chu, G	26
Cerilli, E	119	Chen, T	82, 91, 325	Chu, H	56
Cerjak, H	100	Chen, W	25, 38, 177, 215, 293	Chu, J	72, 88, 180, 265, 286
Cerreta, E	174, 183, 190, 322, 351	Chen, X	276	Chuanfu, Z	92, 323, 374, 377, 380
Cerri, E	131	Chen, Y	28, 29, 43, 155, 194, 195, 247, 257, 294, 357, 366	Chuang, A	137
Certain, A	29, 160	Chen, Z	63, 148	Chuang, C	181, 331
Cervantes-Clemente, A	166	Cheng, C	169, 178, 184	Chuang, H	72
Cha, D	130	Cheng, J	34, 217	Chuanquan, Z	57
Chada, S	31, 71, 74, 117, 120, 164, 167, 214, 217, 262, 265, 313, 351	Cheng, S	241, 255	Chui, A	335
Chahine, G	88	Cheng, T	148	Chukka, R	122
Chai, L	16, 92, 130, 354, 355, 369	Cheng, Y	89, 222, 271, 319, 320, 357	Chul, U	168, 336
Chaijaruwanch, A	133			Chumanov, G	337
Champion, Y	330			Chumbley, S	196, 250, 363
Chan, D	32, 215, 352			Chung, B	352
Chan, K	192, 304				
Chan, S	138				

- Chung, H.....367  
 Chung, P.....76  
 Chung, Q.....31  
 Chuvilin, A.....26  
 Cieslar, M.....346  
 Ciftja, A.....269  
 Cimenoglu, H.....17, 30, 198, 237,  
 .....248, 325, 377, 378, 379  
 Cinibulk, M.....342  
 Ciobanu, C.....37  
 Cízek, J.....212  
 Clappier, T.....88  
 Clark, D.....110, 204  
 Clark, R.....269  
 Clark, S.....368  
 Clarke, A.....280  
 Clausen, B.....96, 212, 241, 341, 348, 349  
 Clauw, B.....152  
 Clemens, H.....262  
 Clifton, R.....173  
 Clitheroe, S.....96  
 Clouet, E.....190  
 Coakley, J.....291  
 Cobble, J.....174  
 Cochran, J.....62, 202, 359  
 Cochran, R.....109  
 Cockcroft, S.....286  
 Cocke, D.....53, 235, 288  
 Cockeram, B.....31, 251, 304, 343  
 Coghe, F.....299  
 Colaco, M.....272  
 Colakoglu, C.....206  
 Cole, J.....101, 239, 304, 344  
 Coleman, M.....166  
 Colina, C.....315  
 Collins, J.....360  
 Collins, P.....36, 42, 147, 173,  
 .....211, 236, 260, 270, 347  
 Colvin, J.....127, 174  
 Compton, C.....157  
 Conrad, E.....163  
 Contescu, C.....203  
 Conway, P.....263  
 Cooksey, M.....47, 97  
 Cooper, K.....108  
 Cooper, M.....34  
 Copley, J.....116  
 Copley, S.....340  
 Cordill, M.....308  
 Corlu, B.....133, 197  
 Cormier, D.....155  
 Cormier, J.....359  
 Coskun, S.....237  
 Costa, A.....362, 366, 370  
 Costa, F.....231  
 Costa, L.....227  
 Côté, J.....134  
 Cottignies, L.....331  
 Cotton, D.....231  
 Cotton, J.....31, 211, 259, 310, 311, 346  
 Cotts, E.....263, 352  
 Coulombe, M.....326  
 Coursol, P.....166  
 Courtenay, J.....90, 235  
 Covarrubias, O.....365  
 Covington, A.....367, 368  
 Cowen, C.....345  
 Cox, A.....185  
 Cox, M.....39  
 Coyle, R.....263  
 Cravens, R.....48  
 Crawford, M.....293  
 Crawford, P.....110  
 Crépeau, J.....279  
 Crepeau, P.....77, 123, 170, 219, 267  
 Crespi, V.....315  
 Creteigny, L.....153, 342  
 Creuziger, A.....348  
 Crimp, M.....20, 35, 94, 139  
 Crouse, C.....68, 115  
 Crow, W.....260  
 Cruz Rivera, J.....92  
 CS, R.....380  
 Csontos, A.....252, 305  
 Cui, H.....342  
 Cui, J.....105, 287  
 Cui, S.....148  
 Cui, X.....127  
 Cuningham, N.....146  
 Cunningham, D.....224  
 Cunningham, N.....30, 65, 161  
 Curioni, A.....128, 274  
 Curtiss, L.....38  
 Cury, R.....251  
 Custódio da Silva, O.....76  
 Czerwinski, A.....112  
 Czerwinski, K.....258
- D**
- D'aiuto, F.....184  
 D'Armas, H.....225  
 Dabbs, T.....98  
 da Costa, L.....288, 289  
 Daehn, G.....35, 59, 136, 184, 363  
 Daghfal, J.....72  
 Daguang, L.....53  
 Dahlman, J.....88, 231  
 Dahmen, U.....220  
 Dahmus, J.....77, 219  
 Dahotre, N.....39, 222, 271, 319, 357  
 Dai, C.....127  
 Dai, L.....193  
 Dai, X.....18, 19  
 Dai, Y.....38  
 Daigle, E.....363  
 Dalgard, E.....51  
 Dalgarno, K.....109  
 Damiano, J.....47  
 Dan, S.....316  
 Dance, B.....297  
 Dande, A.....180  
 Dando, N.....86, 87  
 Dang, H.....181  
 Dangelewicz, A.....111  
 Danielewski, M.....143, 314  
 Daniels, E.....123  
 Daniels, J.....49  
 Daniil, M.....226  
 Dantas, R.....345  
 Dantzig, J.....133  
 Dariavach, N.....313  
 Darsell, J.....106, 344  
 Das, J.....15, 226, 329, 330  
 Das, K.....53, 288  
 Das, S.....48, 62, 84, 129, 131,  
 .....140, 151, 177, 178, 228,  
 .....252, 266, 277, 325, 337  
 Dasgupta, A.....101, 196  
 Dasgupta, S.....135, 297  
 Dashwood, R.....31, 131, 133, 260  
 Dauskardt, R.....24, 60, 106, 117, 179, 232, 308, 314  
 Davenport, J.....161  
 David, B.....46  
 David, S.....96, 295  
 Davies, H.....88, 365  
 Davis, B.....53, 105, 200  
 Davis C., J.....119  
 Dawson, P.....246, 350  
 Dayananda, M.....239  
 Deal, A.....65, 159  
 De Angelis, R.....245  
 DeRoy, T.....315  
 de Carlan, Y.....29, 160, 208  
 de Carvalho, R.....354  
 de Castro, V.....160  
 Decker, J.....47  
 Decker, M.....106  
 Decker, R.....249  
 Dedyukhin, A.....278  
 Deffley, R.....156  
 DeFouw, J.....59  
 de Gouveia, T.....372  
 DeGraef, M.....172  
 Deheri, P.....226  
 Dehm, G.....308  
 DeHosson, J.....207, 222  
 Deibert, M.....344  
 Dejiang, L.....57  
 Delaire, O.....192, 224  
 Delaleau, P.....80  
 Delgado, L.....20  
 Delin, A.....379  
 Delplanque, J.....156, 339  
 del Rio, E.....29  
 Delsante, S.....167  
 Delucca, J.....164  
 DeMange, P.....174  
 de Medeiros, K.....372  
 de Melo Costa, A.....372  
 Demetriou, M.....40, 88, 89, 233  
 Demiray, Y.....105  
 Demirhan, O.....370  
 Demkowicz, M.....187  
 DenBaars, S.....296  
 Deneys, A.....216  
 Deng, C.....256  
 Deng, J.....94, 126  
 Deng, S.....288  
 Dennis, K.....218  
 Dennis-Koller, D.....322  
 de Nora, V.....279  
 Deodeshmukh, V.....155  
 Derenzo, S.....20  
 Derguti, F.....260  
 Deria, P.....309  
 Derin, B.....105, 205, 206, 375  
 Derlet, P.....158, 223  
 Desai, S.....238  
 Desai, T.....207, 258, 322  
 Deshmanya, I.....325  
 Deshpande, A.....132  
 Deshpande, V.....55  
 Desilets, M.....326  
 Desjarlais, M.....127  
 Despois, J.....178  
 Deters, J.....259  
 DeVasConCellos, P.....39  
 Devincre, B.....44  
 Devlin, E.....53  
 Devrani, G.....363  
 Dewan, M.....307  
 Dewen, H.....54, 316, 317, 355  
 Dey, G.....18, 225, 321  
 Dey, S.....66, 325  
 DeYoung, D.....41, 137, 138



de Zelicourt, M.....	230
Dhawan, A.....	367
Dhawan, N.....	169, 378
Dheda, S.....	43
Diabb, J.....	367
Diak, B.....	301
Dianzhong, L.....	111
Díaz, R.....	166
Diaz de la Rubia, T.....	78
Dickerson, M.....	87
Dickerson, P.....	65, 161, 162
Dickerson, R.....	224, 225, 297
Dickinson, M.....	271
Didomizio, R.....	65, 159
Diercks, D.....	183
Dierolf, V.....	141
Diewwanit, I.....	371
DiGiacomo, S.....	224, 225
DiLeo, R.....	37
DiLisa, D.....	197
Dimiduk, D.....	144, 158, 172, 270, 298, 303
Dimitrovska, A.....	33, 215
Dinda, G.....	196
Ding, G.....	63
Ding, R.....	50
Ding, W.....	199, 249
Dingming, L.....	54, 316, 317, 355
Dingreville, R.....	99, 126
Dispinar, D.....	123
Ditmire, T.....	363
Dixit, V.....	36, 42
Dixon, T.....	145
Dlouhá, M.....	46
Dmitrieva, O.....	287
Dmowski, W.....	137, 181, 192
Do, E.....	14
Dobra, G.....	287
Doernberg, E.....	132
Dogan, O.....	22, 60, 107, 153, 201, 250, 289, 302, 342
Doheim, M.....	326
Doiron, P.....	327
Dolan, D.....	127
Domack, M.....	84, 109
Domain, C.....	28, 29, 66, 67, 113, 160, 208, 257, 317
Donati, D.....	241
Donchev, A.....	303
Donev, A.....	67
Dong, H.....	380
Dong, J.....	249
Dong, L.....	174
Dong, T.....	168
Dongare, A.....	283
Donner, W.....	116, 162
Donohue, E.....	250
Doostmohammadi, H.....	205
Dopita, M.....	212
Dorantes Rosales, H.....	129
Dorr, M.....	81
dos Santos, J.....	41, 152, 294
dos Santos Jr., L.....	288, 289
Dou, Z.....	131, 339
Doubell, P.....	100
Doumanidis, C.....	205
Drabble, D.....	184
Drelich, J.....	288
Dresselhaus, M.....	103
Dreyer, C.....	340
Droste, C.....	230, 328
Droste, W.....	182
Drozd, V.....	203
Druffel, T.....	15
Drummy, L.....	258
Druschitz, A.....	78, 123
Du, Q.....	220, 277
Du, Z.....	377
Duan, Z.....	27
Dubey, D.....	232, 328
Dubois, J.....	360
Dubreuil, A.....	151
Dubuisson, P.....	29
Ducu, C.....	312
Dudek, M.....	314
Dufour, G.....	16, 41, 86, 134, 179, 190, 229, 230, 278, 279, 326, 327
Dugger, M.....	207
Duh, J.....	31, 71, 72, 117, 164, 165, 167, 214, 217, 262, 290, 313, 351, 352, 370
Duhoux, V.....	331
Dulikravich, G.....	272
Duman, I.....	339, 370
Dumont, M.....	244
Dumoulin, S.....	28
Dunand, D.....	39, 59, 78, 124, 171, 180, 220, 222, 223, 260, 269
Dundar, M.....	133
Dündar, M.....	197
Dunn, G.....	293
Dunne, F.....	147
Dunwoody, J.....	343
Dupas, N.....	231, 327
Dupuis, M.....	292, 326
Duran, C.....	331
Durstock, M.....	309
Dursun, A.....	133, 197
Dutrizaç, J.....	91
Dutta, B.....	156, 196
Dutta, I.....	32, 215, 313, 352
Duval, H.....	235
Duygulu, O.....	249, 250
Duz, V.....	259, 260
Dye, D.....	31, 131, 260, 291
Dymek, S.....	295
Dyroy, A.....	86
Dziencial, K.....	42
<b>E</b>	
Earthman, J.....	210, 271
Eastman, J.....	261
Easton, M.....	198
Ebach-Stahl, A.....	250
Ebara, R.....	192, 242
Ebeling, T.....	340
Ebin, B.....	82, 374
Ebling, D.....	56
Ebnonnasir, A.....	244
Ebrahimi, F.....	203, 227, 304
Echeverría, A.....	295
Echlin, M.....	35
Eck, S.....	110
Eckert, C.....	97
Eckert, J.....	15, 136, 181, 226, 232, 329, 330, 368
Edelshtein, E.....	150
Edney, W.....	78
Edsinger, K.....	317, 355
Edwards, D.....	32, 356
Edwards, J.....	217
Edwards, L.....	190
Edwards, P.....	50, 211
Egami, T.....	135, 137, 192, 260, 284, 285
Eggeler, G.....	262, 370
Ehrmann, R.....	371
Eichseder, W.....	78, 362
Eick, I.....	328
Eidenberger, E.....	262
Eifler, D.....	294, 295, 325
Eiselt, C.....	30, 305
Eisenlohr, P.....	35, 94, 375
Eisma, D.....	231
Ek, M.....	119
Ekuma, C.....	197
El-Awady, J.....	144
El-Azab, A.....	67, 76, 94, 126, 314, 353
El-Bagoury, N.....	371
El-Dasher, B.....	274, 321, 363
El-Desouky, A.....	157
El-Kersh, A.....	326
El-Soudani, S.....	260
Elam, J.....	38
Elder, K.....	163, 186
Elder, S.....	379
Eleruja, M.....	27
Eliezer, S.....	29
Elizarraras, O.....	365
El Kadiri, H.....	147, 339
Elkhodary, K.....	95
Elkholy, A.....	193
Elmustafa, A.....	295, 368
Elsalmawy, M.....	363
Elsener, A.....	158
Eltringham, T.....	72, 217
Emamy, M.....	170
Emmons, E.....	367, 368
Enayati, M.....	244
Endo, M.....	295
Engel, S.....	193
Engh, T.....	235, 269
English, C.....	317
Enikeev, N.....	111, 112
Enright, M.....	192
Enriquez, A.....	216
Enzinger, N.....	100
Eom, C.....	224
Epstein, S.....	137, 138
Erhart, P.....	125
Erinc, M.....	152
Erman, A.....	346
Erni, R.....	220
Ernst, E.....	87
Ersundu, E.....	366
Ertekin, E.....	189
Ertorer, O.....	25, 113
Eruslu, N.....	369
Es-Said, O.....	85
ESAWI, A.....	253
Escudero Garcia, R.....	333
Esezobor, D.....	157
Eskin, D.....	287
Esmaeili, S.....	84, 277
Esola, S.....	109
Espinosa, D.....	123, 169, 219, 316
Esposito, L.....	343
Esposito, T.....	260
Esquivel-Aguirre, M.....	376, 378
Essadiqi, E.....	201
Esteves-Alcazar, F.....	361, 362
Estremera, E.....	367
Estrin, Y.....	112
Eumann, M.....	46
Evans, A.....	108, 250
Evans, J.....	107, 110, 270
Evans, N.....	252
Evans, T.....	55

- Everett, R ..... 138  
 Evtcev, A ..... 290, 291  
 Ewh, A ..... 239  
 Ewing, R ..... 257
- F**
- Fachini, E ..... 369  
 Fafard, M ..... 292  
 Faivre, G ..... 149  
 Fallas, J ..... 367, 368  
 Fan, C ..... 317  
 Fan, G ..... 330  
 Fan, L ..... 249  
 Fan, X ..... 35, 131, 220  
 Fan, Y ..... 18, 19, 358, 374  
 Fan, Z ..... 104, 105, 108, 132, 249  
 Fang, J ..... 265  
 Fang, Y ..... 87, 167  
 Fang, Z ..... 253, 347  
 Fanning, J ..... 310, 311  
 Farahany, S ..... 24  
 Faraji, M ..... 132  
 Farid, M ..... 326  
 Farmer, S ..... 15  
 Farrar, G ..... 282  
 Farrow, A ..... 228, 229  
 Farson, D ..... 17  
 Fattebert, J ..... 81  
 Fautrelle, Y ..... 206  
 Fawal, V ..... 214  
 Fechner, D ..... 104  
 Fechner, M ..... 230  
 Fecht, H ..... 26, 65, 89, 232  
 Fedelich, B ..... 293  
 Feese, J ..... 183  
 Fei, X ..... 320  
 Fei-Shuo, H ..... 76  
 Feitosa, J ..... 229  
 Fekete, J ..... 144  
 Felicelli, S ..... 110, 156, 170, 198  
 Fell, B ..... 339, 349  
 Felter, T ..... 321  
 Feng, C ..... 50, 332  
 Feng, H ..... 132  
 Feng, J ..... 138, 347  
 Feng, L ..... 83  
 Feng, N ..... 106, 316, 355  
 Feng, Q ..... 15, 250, 253, 343  
 Feng, R ..... 163  
 Feng, W ..... 53  
 Feng, Z ..... 96, 188, 211, 213, 239, 295  
 Fenton, G ..... 35, 363  
 Ferguson, J ..... 163  
 Ferguson, W ..... 281  
 Ferland, P ..... 83, 228  
 Fernandez-Baca, J ..... 146  
 Fernandez Diaz, L ..... 236, 299  
 Fernando, G ..... 161  
 Ferracane, J ..... 38  
 Ferranti, L ..... 173  
 Ferreira, A ..... 185, 333  
 Ferreira, E ..... 176  
 Ferreira, H ..... 316  
 Ferri, E ..... 55  
 Ferris, K ..... 350  
 Ferry, M ..... 234, 367, 371  
 Fevre, M ..... 237  
 Fichtner, M ..... 203  
 Fiedler, B ..... 214  
 Field, D ..... 76, 95  
 Field, F ..... 267  
 Field, K ..... 29, 160  
 Field, R ..... 241, 297, 322  
 Fieldhouse, N ..... 336  
 Fife, J ..... 80, 102, 222  
 Figueiredo, R ..... 111  
 Figueroa, I ..... 88, 365  
 Filiaggi, M ..... 135  
 Findley, K ..... 44  
 Fine, M ..... 61, 171, 214  
 Finel, A ..... 142, 186, 237  
 Fiory, A ..... 121, 168  
 Fiot, L ..... 279  
 Firrao, D ..... 138, 184, 242, 281, 329  
 Firth, L ..... 260  
 Fischer, F ..... 308  
 Fischer, M ..... 183  
 Fischer, W ..... 95, 240  
 Fister, T ..... 163, 261  
 Fitzgerald, T ..... 17  
 Fitzner, K ..... 17, 314  
 Fitzpatrick, M ..... 96  
 Fivel, M ..... 190  
 Fjeld, A ..... 62  
 Flandorfer, H ..... 74, 120, 167, 217, 265  
 Flater, P ..... 245, 338  
 Fleming, G ..... 103  
 Fleurial, J ..... 55, 103  
 Florando, J ..... 173  
 Flores, K ..... 17, 136, 180, 181, 182, 286, 294  
 Flores-Valdés, A ..... 229  
 Flynn, K ..... 139  
 Foecke, T ..... 348  
 Foiles, S ..... 78, 124, 171, 187, 220, 269  
 Foley, D ..... 58, 198, 201, 208  
 Foltz, J ..... 147  
 Fonda, R ..... 50  
 Fong, D ..... 261  
 Fonseca Neto, J ..... 231  
 Font, J ..... 216  
 Fook, M ..... 373  
 Foosnaes, T ..... 240, 335  
 Forest, L ..... 160  
 Forgan, T ..... 46  
 Forlerer, E ..... 371  
 Forsmark, J ..... 55, 103  
 Forster, R ..... 96  
 Forsyth, R ..... 297  
 Forsyth, T ..... 46  
 Fortier, L ..... 89  
 Fortin, H ..... 292  
 Fox, E ..... 137  
 Fraisse, B ..... 291  
 Francescutti, L ..... 133  
 Frankel, P ..... 70  
 Franz, H ..... 181  
 Franz, P ..... 370  
 Franzén Byttner, K ..... 60  
 Frary, M ..... 157, 245, 304  
 Fraser, H ..... 36, 42, 55, 144, 147, 173, 211,  
 ..... 221, 236, 237, 260, 270, 347, 348  
 Fray, D ..... 169, 185  
 Frear, D ..... 71, 262  
 Frech, T ..... 164  
 Fredenburg, A ..... 359  
 Frederick, D ..... 211  
 Fredette, L ..... 252  
 Fredholm, S ..... 77  
 Freeman, A ..... 201  
 Freeman, C ..... 142  
 Frei, G ..... 97  
 Freitas, N ..... 366  
 Frenzel, J ..... 262  
 Fréty, N ..... 75, 291  
 Fridline, D ..... 193  
 Fried, L ..... 128, 274  
 Friedland, E ..... 188  
 Friedman, L ..... 223  
 Fritz, L ..... 170  
 Froehlich, M ..... 250  
 Frolov, A ..... 335  
 Frolov, T ..... 92, 125  
 Froyen, L ..... 156  
 Fry, J ..... 214  
 Fu, C ..... 160, 187, 208, 225  
 Fu, E ..... 208  
 Fu, F ..... 267  
 Fu, J ..... 83  
 Fu, N ..... 316  
 Fu, P ..... 57  
 Fu, Y ..... 180, 317  
 Fuchs, G ..... 22, 262  
 Fuentes, F ..... 122, 363  
 Fuerst, J ..... 204  
 Fugetsu, B ..... 197  
 Fuh Sheng, S ..... 167  
 Fujita, K ..... 40  
 Fujiyoshi, M ..... 75  
 Fukuda, H ..... 205  
 Fukuhara, M ..... 49  
 Fullwood, D ..... 176  
 Fuloria, D ..... 102  
 Fultz, B ..... 46, 96, 146, 191, 192, 224, 241  
 Fuoss, P ..... 163, 261  
 Furrer, D ..... 31  
 Furuhashi, T ..... 226, 270  
 Fuskova, L ..... 58, 302
- G**
- Gaal, S ..... 235  
 Gabb, T ..... 107  
 Gabbitas, B ..... 346  
 Gagne, J ..... 327  
 Gagnon, A ..... 95  
 Gagnon, M ..... 86  
 Gaies, J ..... 248  
 Galenko, P ..... 51  
 Gallego, N ..... 203  
 Gallerneault, M ..... 84  
 Gallet, F ..... 114  
 Gamweger, K ..... 98  
 Gan, J ..... 257, 258, 344  
 Gan, M ..... 66  
 Gan, Y ..... 206  
 Gan-feng, T ..... 377  
 Ganapathysubramanian, B ..... 93, 332  
 Gandin, C ..... 150  
 Ganesan, K ..... 22  
 Ganeshan, S ..... 202  
 Gang, X ..... 123, 218  
 Ganguly, S ..... 96  
 Gannon, P ..... 344  
 Ganuza, A ..... 136  
 Gao, B ..... 106  
 Gao, C ..... 206, 266  
 Gao, F ..... 356  
 Gao, H ..... 255, 328  
 Gao, J ..... 223, 357  
 Gao, L ..... 57  
 Gao, M ..... 153, 289  
 Gao, X ..... 126, 178  
 Gao, Y ..... 38, 39, 57, 88, 135,  
 ..... 180, 182, 232, 251, 261,  
 ..... 283, 284, 286, 307, 329, 371

Garay, J.....	345	Gill, D.....	61	Grande, T.....	229, 292
Garbe, U.....	349	Gilles, R.....	260, 261	Grandfield, J.....	105, 182, 191, 331
García, A.....	372	Gilley, S.....	211	Grant, G.....	50, 194, 195
García, E.....	359	Gilman, J.....	55, 143	Grant, K.....	303
García, R.....	141, 306, 314, 315	Gilman, P.....	56	Grant, M.....	186
García-Barriocanal, J.....	113	Gimenez Britos, P.....	244	Grasser, M.....	289
García-Hinojosa, A.....	361	Gipson, B.....	42	Grassi, J.....	219
Garcia-Pastor, F.....	298	Girault, G.....	87	Gravier, S.....	283
Garcia-Sanchez, E.....	27	Giulietti, M.....	20	Gray, G.....	80, 127, 173, 174, 183, 190, 224, 247, 273, 321, 322, 351, 358
Gardner, C.....	176	Gladen, A.....	194	Green, H.....	308
Gareth, S.....	30	Glaeser, A.....	375	Green, J.....	140
Garg, A.....	183	Glavicic, M.....	31	Green, N.....	123
Garimella, N.....	291	Gleeson, B.....	107, 250, 302, 303	Greenfield, S.....	174, 224, 225
Garing, K.....	338	Glicksman, M.....	139, 228	Greer, A.....	74, 120, 167, 180, 217, 265
Garlea, E.....	349	Glosli, J.....	81	Greer, J.....	158
Garlea, O.....	146	Glotzer, S.....	52, 353	Gregory, J.....	77, 219
Garrido, F.....	227	Gnaeupel-Herold, T.....	348	Greving, D.....	107
Garvin, K.....	257	Gnaeupel-Herold, T.....	293	Grewer, M.....	64
Garza, M.....	362, 368, 372	Goddin, H.....	74	Griffin, J.....	78
Gasca, P.....	67	Godja, N.....	275	Griffin Roberts, K.....	113
Gash, A.....	321	Goel, M.....	141, 185	Griffiths, W.....	220
Gassa, L.....	170	Gohari, B.....	129	Grimes, C.....	252
Gatenby, K.....	84	Gökçe, H.....	372	Grinfeld, M.....	76
Gaubert, A.....	186	Göken, M.....	24	Groeber, M.....	172
Gavras, A.....	243	Gokhale, A.....	170, 172, 202	Gross, D.....	185
Gawad, A.....	253	Golden, P.....	192	Grosse, K.....	68
Gayda, J.....	107	Goldman, H.....	328	Grossklaus, K.....	313
Gayden, X.....	194, 195	Goldman, N.....	128, 274	Grossmann, C.....	262
Gaytan, S.....	109, 174	Golestanifard, F.....	246	Groutso, T.....	278
Geandier, G.....	261	Gollapudi, S.....	32	Groza, J.....	188, 329, 339, 346, 349, 377
Geantil, P.....	70, 94, 163	Goller, G.....	254, 368, 374	Gruber, P.....	206
Gebhard, S.....	303	Göller, G.....	369	Gruen, G.....	234
Gegel, G.....	78, 219	Gollerthan, S.....	262	Grumon, D.....	320
Gehua, W.....	218	Golozar, M.....	149	Grunschel, S.....	173
Geier, G.....	170, 171	Golubov, S.....	30	Grydin, O.....	139
Gelles, D.....	67	Gomes, J.....	53, 235, 288	Gu, G.....	139
Geltmacher, A.....	125, 126, 350	Gomes, V.....	364	Gu, J.....	57
Gemmen, R.....	345	Gomez, J.....	205	Gu, S.....	83, 130
Gemmer, B.....	98	Gómez-Zamorano, L.....	365	Gu, Y.....	202
Genau, A.....	102, 221	Gong, J.....	263	Guay, D.....	335
Genc, A.....	237	Gong, Y.....	297	Gudbrandsen, H.....	279
Gendre, M.....	190	Gonzales, L.....	354	Gudipati, P.....	311
Gendron, M.....	145	Gonzalez-Reyes, L.....	129	Gudmundsson, H.....	280
Geng, H.....	43	Gonzalez-Trejo, J.....	34, 64, 166	Guebels, C.....	339
Geng, J.....	154	Gonzalez-Velazquez, J.....	372	Guedou, J.....	60
George, E.....	158, 162, 202, 284, 336	González M., L.....	119	Gueijman, S.....	170
George, L.....	203	Goo, B.....	332	Guertsman, V.....	139
George, P.....	363	Gooch, W.....	299	Guillot, J.....	235
Gerard, R.....	113	Good, J.....	211	Guillot, M.....	197, 244
Gerdemann, F.....	183	Goodridge, R.....	62	Guimaraes, O.....	130
German, R.....	254, 325	Goossens, D.....	312	Gulizia, E.....	145
Germann, T.....	273	Gopalan, V.....	141, 224	Gulizia, S.....	145
Gershenson, M.....	87	Gordon, P.....	44, 238	Gulsoy, O.....	254
Gerson, A.....	69, 70, 362	Goris, L.....	129	Gummadi, B.....	380
Gesing, A.....	104	Gorni, D.....	19	Gunaydin, H.....	43
Gharghour, M.....	348	Gossard, A.....	309	Gunnewiek, L.....	326
Ghasemi-Nanesa, H.....	226	Goswami, R.....	226, 277	Günther, R.....	248
Ghassemi Armaki, H.....	23	Gothard, N.....	309	Gunyuz, M.....	17
Ghetta, V.....	235	Goto, A.....	84	Gunzburger, M.....	353
Ghoniem, N.....	30, 144	Goto, T.....	116, 254, 368, 374	Guo, C.....	18
Ghorbani, M.....	15	Gottstein, G.....	22, 132, 133, 202	Guo, F.....	31, 33, 215, 313, 351
Ghosh, A.....	101, 153, 159	Goudy, A.....	371	Guo, H.....	264, 306
Ghosh, G.....	61	Goulet, P.....	292	Guo, J.....	74, 264
Ghosh, M.....	178, 337	Gourdon, O.....	47	Guo, M.....	254, 362
Ghosh, S.....	333	Gourlay, C.....	31	Guo, Q.....	15
Gianola, D.....	206	Goyel, S.....	304	Guo, W.....	102
Gibson, M.....	198, 260	Grady, D.....	35	Guo, X.....	15, 56, 227, 246, 253, 267, 355, 370
Gibson, R.....	169	Gräfe, M.....	83	Guo, Y.....	380
Gierlotka, W.....	74, 120, 167, 217, 265	Graff, K.....	164	Guo, Z.....	97
Gigliotti, M.....	61	Gramlich, M.....	163	Guobao, W.....	131
Gil, O.....	90	Grammatikopoulos, P.....	209	Guotao, W.....	203
Gill, A.....	174, 184	Granasy, L.....	51, 52, 195		



- Guoyong, H ..... 123  
 Gupta, A ..... 178  
 Gupta, K ..... 194  
 Gupta, M ..... 71, 156  
 Gupta, N ..... 258, 259  
 Gupta, S ..... 81, 225  
 Gupta, V ..... 32  
 Gupta, Y ..... 80  
 Gurmen, S ..... 82, 374  
 Gürmen, S ..... 372  
 Gururajan, M ..... 334  
 Guruswamy, S ..... 55, 103  
 Gusberti, V ..... 326  
 Gusev, A ..... 335  
 Gutensohn, M ..... 295  
 Guthrie, R ..... 182, 296, 332  
 Gutierrez-Villegas, M ..... 166  
 Guttula, M ..... 53, 288  
 Guyer, J ..... 15, 350  
 Guzman, J ..... 66  
 Guzmán, L ..... 166  
 Guzman D., G ..... 119  
 Gyanchandani, J ..... 321
- H**
- Ha, S ..... 32  
 Ha, T ..... 365  
 Haarberg, G ..... 319, 335  
 Haataja, M ..... 93  
 Habe, D ..... 170  
 Haberl, K ..... 171  
 Hackenberg, R ..... 297, 322  
 Hadian, R ..... 170  
 Hadorn, J ..... 199  
 Hadwiger, M ..... 170  
 Haeffner, D ..... 180, 260  
 Hafley, R ..... 109  
 Hagelstein, K ..... 198  
 Hagelueken, C ..... 76, 219  
 Hagen, M ..... 96  
 Hagihara, K ..... 301  
 Hagiwara, M ..... 335  
 Hagni, A ..... 18, 41, 91, 138, 139, 183, 235, 287, 332  
 Hague, R ..... 62  
 Hahn, H ..... 308  
 Hahn, J ..... 324  
 HAI, N ..... 212  
 Haider, H ..... 257  
 Haines, C ..... 68  
 Haj-Taieb, M ..... 64  
 Haley, D ..... 136  
 Halikia, I ..... 53  
 Halkjelsvik, A ..... 280  
 Hall, G ..... 211  
 Hall, J ..... 17, 84  
 Hall, T ..... 205  
 Haller, E ..... 66  
 Halliday, F ..... 357  
 Hallinan, N ..... 244  
 Hallström, S ..... 143  
 Hamada, Y ..... 313  
 Hamasaki, K ..... 74  
 Hamed, M ..... 124, 170  
 Hamel, G ..... 96  
 Hamer, S ..... 89  
 Hamerton, R ..... 133  
 Hamilton, C ..... 262, 295  
 Hamilton, J ..... 171  
 Hamilton, R ..... 102  
 Hammond, R ..... 273  
 Hamon, F ..... 359
- Hamza, A ..... 116  
 Han, B ..... 40  
 Han, E ..... 57, 200  
 Han, G ..... 14  
 Han, H ..... 295  
 Han, J ..... 75, 117, 215  
 Han, L ..... 20, 254  
 Han, Q ..... 176, 178, 248, 346  
 Han, S ..... 158, 247, 296  
 Han, T ..... 246  
 Han, W ..... 255  
 Han, Z ..... 41, 323  
 Hand, R ..... 365  
 Handwerker, C ..... 34, 215, 313  
 Handzlik, P ..... 17  
 Hanejko, F ..... 204  
 Haneman, B ..... 83  
 Hanley, P ..... 90  
 Hann, B ..... 107  
 Hanrahan, R ..... 54, 246, 251, 298, 304, 343  
 Hansel, M ..... 73  
 Hansen, G ..... 176  
 Hansson, T ..... 293  
 Hantzsche, K ..... 199, 302  
 Hänzi, A ..... 340  
 Hao, G ..... 284  
 Hao, L ..... 135  
 Hao, X ..... 197  
 Harada, H ..... 107, 202, 303  
 Hardin, R ..... 47, 97  
 Hardwick, D ..... 60, 107  
 Hari Babu, N ..... 104  
 Harkara, A ..... 27, 135  
 Harper, M ..... 311  
 Harrell, J ..... 82  
 Harringa, J ..... 313  
 Harris, C ..... 165  
 Harris, J ..... 82  
 Hartfield-Wunsch, S ..... 84, 177  
 Hartig, C ..... 248, 340  
 Hartlieb, M ..... 219  
 Hartmann, H ..... 51  
 Hartwig, J ..... 102  
 Hartwig, K ..... 39, 157, 198, 201  
 Hasan, M ..... 22, 24, 262, 286, 287  
 Hasegawa, M ..... 113  
 Hasegawa, T ..... 60, 106  
 Hashemi, L ..... 210  
 Hashemian, S ..... 225  
 Hassan Al Ali, H ..... 138  
 Hatkevich, S ..... 59  
 Hattingh, D ..... 100  
 Hau-Riege, S ..... 173  
 Haugland, E ..... 230, 292  
 Haupt, T ..... 350  
 Hausard, M ..... 220  
 Haut Donahue, T ..... 180  
 Hawreliak, J ..... 274, 363  
 Haxhimali, T ..... 52  
 Hay, R ..... 45  
 Hayashi, N ..... 84  
 Hayden, M ..... 126, 178  
 Hayden, S ..... 163  
 Hayes, S ..... 239  
 Hazel, B ..... 61  
 Hazeli, K ..... 379  
 He, H ..... 127, 215  
 He, J ..... 131, 141, 246, 309, 339  
 He, L ..... 250  
 He, Y ..... 374  
 Hebda, J ..... 310  
 Hebert, R ..... 159, 233
- Heckel, T ..... 48  
 Heckert, E ..... 134  
 Heckl, A ..... 60  
 Hector, L ..... 45, 81, 144, 152, 200, 277, 302  
 Heering, C ..... 85  
 Heidari, G ..... 358  
 Heidarian, B ..... 220  
 Heideman, C ..... 163  
 Heiden, P ..... 162  
 Heidloff, A ..... 107  
 Heilmaier, M ..... 202  
 Heinisch, H ..... 356  
 Heinrich, H ..... 69, 210  
 Heintze, C ..... 30  
 Heisser, C ..... 267, 268  
 Helfgott, H ..... 363  
 Helle, S ..... 335  
 Hellstrom, E ..... 296, 377  
 Helvey, A ..... 211  
 Hemker, K ..... 64, 206  
 Hemrick, J ..... 47, 48  
 Henein, H ..... 52, 55, 312  
 Henke, S ..... 76  
 Henriksson, H ..... 122  
 Henry, H ..... 52  
 Henson, M ..... 183  
 Herlach, D ..... 51  
 Hernandez, D ..... 109, 174  
 Hernández, J ..... 333  
 Hernández, M ..... 368  
 Hernandez-Garcia, A ..... 361, 362  
 Hernandez-Mayoral, M ..... 30  
 Hernandez-Perez, I ..... 129  
 Hernandez-Rodriguez, M ..... 27, 367  
 Heroux, L ..... 46, 47  
 Herwig, K ..... 192  
 Heshmati-manesh, S ..... 23  
 Hesse, C ..... 349  
 Hetu, J ..... 90  
 Héту, J ..... 286  
 Heulens, J ..... 238  
 Heying, M ..... 350  
 Hibbert, K ..... 218  
 Higashi, K ..... 150, 248  
 Higginbotham, A ..... 274  
 Highland, M ..... 163, 261  
 Highsmith, A ..... 59  
 Hilerio, I ..... 333  
 Hilger, A ..... 314  
 Hillier, C ..... 109  
 Hills, M ..... 183  
 Hills, S ..... 165  
 Hilmas, G ..... 62, 194  
 Hindler, M ..... 121  
 Hirai, K ..... 150  
 Hirano, S ..... 100, 295  
 Hirose, T ..... 357  
 Hirt, G ..... 85  
 Hiwarkar, V ..... 18  
 Hixson, R ..... 81, 127  
 Hlatshwayo, T ..... 188  
 Ho, C ..... 118  
 Ho, N ..... 148  
 Hoagland, R ..... 65, 162  
 Hoang, Y ..... 145  
 Hochhalter, J ..... 99  
 Hodge, A ..... 171, 256  
 Hodges, J ..... 46, 47  
 Hodnett, K ..... 227, 228  
 Hoelzel, M ..... 261  
 Hoelzer, D ..... 65, 160, 225  
 Hoff, F ..... 230

Hoffelner, W.....	305	Hua, F .....	76, 122, 164, 169, 218	Inel, C .....	133, 197
Hofmann, D.....	39, 40, 88, 233	Hua, Z .....	357	Ingraffea, A.....	99
Hofmann, M.....	97, 261, 349	Huabing, L.....	206	Inoue, A.....	40, 88, 137, 181, 234, 329, 367
Hofmann, U.....	289	Huang, B.....	374	Inoue, K.....	113
Hofmann, V.....	331	Huang, E.....	25, 70	Inzunza, E.....	20
Hofmeister, C.....	69	Huang, H.....	67, 168, 176, 222	Iorio, L.....	261
Hofmeister, W.....	156	Huang, J.....	181, 208, 249, 331	Iosif, A.....	185
Höglund, L.....	143	Huang, L.....	182, 233, 254, 284, 370	Ippolito, S.....	84
Høie, H.....	278	Huang, R.....	24, 64, 111, 158, 180, 206, 207, 255, 283, 307	Ipser, H.....	120, 167
Holby, E.....	43	Huang, S.....	35, 61, 143, 354	Iqbal, G.....	306
Holcomb, G.....	236, 299	Huang, W.....	297	Iqbal, T.....	255
Holden, I.....	230	Huang, X.....	377	Isaac, A.....	42
Holden, T.....	241	Huang, Y.....	104, 120, 214, 217, 354	Isac, M.....	182, 296, 332
Holian, B.....	273	Huang, Z.....	17, 63	Isanaka, S.....	124
Holland, T.....	208, 339	Hubbard, C.....	96, 97, 146, 295	Ishida, K.....	120, 121
Holland-Moritz, D.....	51, 196	Hubbard, J.....	222	Ishikawa, T.....	312, 329
Hollang, L.....	66	Huber, D.....	42, 55, 211	Isik, M.....	361
Holliday, K.....	258	Huda, N.....	334	Isiksacan, C.....	17
Holm, E.....	99, 126, 187, 273	Huda, Z.....	131	Islam, Z.....	349
Holmes, N.....	128	Hudish, G.....	183	Itabashi, S.....	210, 346
Holmgren, A.....	307	Hudson, A.....	278	Ivanisenko, J.....	26, 65, 308
Holt, N.....	86	Hufnagel, T.....	285	Ivanisenko, Y.....	89, 225
Holtz, R.....	277	Huh, J.....	352	Ivanov, V.....	92, 171
Holzleithner, C.....	112	Hui, X.....	329, 330	Ivasishin, O.....	260
Home, A.....	90	Hulbert, D.....	307, 339	Ive, T.....	296
Homola, P.....	346	Huls, J.....	316	Iyiel, A.....	374
Hong, S.....	58, 59, 306, 375, 377	Humadi, H.....	52	Izadbakhsh, A.....	341
Hong, Y.....	299	Hundley, M.....	255	Izumi, T.....	107
Hongqiang, R.....	329	Huner, P.....	17	Izuta, G.....	71
Hongqing, S.....	182	Hung, F.....	76, 188, 310		
Hono, K.....	270, 301	Hung, Y.....	75	<b>J</b>	
Hooks, D.....	45	Hunter, L.....	314	Jablonski, P.....	236, 299, 345
Hopkins, S.....	304	Hupalo, M.....	163	Jackson, J.....	188, 202
Horn, W.....	244	Huq, A.....	46, 47	Jackson, M.....	31, 131, 243, 260
Horstemeyer, M.....	99, 147, 161, 179, 201, 328, 339	Hurysz, K.....	297, 298	Jacobs, M.....	138
Hort, N.....	104, 150, 152, 200, 248	Hussain, M.....	176, 323	Jacobson, A.....	116
Hosemann, P.....	65, 161, 356	Hutchinson, N.....	136	Jacques, D.....	145
Hosford, W.....	59, 245	Hüttenrauch, J.....	325	Jacquot, A.....	56
Hossain, M.....	235	Hwang, C.....	286	Jadhav, N.....	214
Hossein Nedjad, S.....	226	Hwang, H.....	313	Jae-Cheul, P.....	361, 365, 378
Hotta, M.....	254	Hwang, J.....	140, 185, 209, 221, 232, 235, 270, 288, 302	Jahani, B.....	23
Hou, N.....	206, 266	Hwang, K.....	253	Jahazi, M.....	51
Houk, G.....	165	Hwang, N.....	372	Jahedi, M.....	145
Houk, K.....	43	Hwang, W.....	168	Jahja, A.....	207
House, J.....	245, 338	Hwang, Y.....	179	Jain, J.....	21, 201
Hovanski, Y.....	51, 194, 260	Hyde, J.....	317	Jain, P.....	202
Howard, A.....	14, 37, 82, 129, 175, 226, 274, 323	Hyers, R.....	103, 342	Jaiswal, A.....	98
Howard, H.....	34	Hyun, S.....	165	Jakobsen, B.....	69
Hoyos-Reyes, L.....	34, 166			James, A.....	22
Hoyt, J.....	52, 101, 124	<b>I</b>		James, J.....	96
Hrabe, R.....	243	Iacovella, C.....	353	James, M.....	100
Hryn, J.....	266	Iadicola, M.....	348	Janczak, J.....	143, 314
Hsia, J.....	56	Ice, G.....	47, 69, 70, 94, 115, 157, 162, 213	Janecek, M.....	212
Hsiao, H.....	33	Idenyi, N.....	197	Jang, C.....	193
Hsiao, Y.....	118	Iffert, M.....	16, 41, 86, 134, 179, 190, 229, 230, 278, 279, 326, 327	Jang, D.....	136, 158
Hsiao-Chun, S.....	330	Ikhmayies, S.....	18	Jang, E.....	165
Hsing, A.....	314	Ila, D.....	29, 257	Jang, H.....	193, 378
Hsin Jay, W.....	39	Ilavsky, J.....	29, 116	Jang, J.....	32, 67, 285
Hsiung, L.....	173, 322	Ilinca, F.....	286	Jang, S.....	88
Hsu, C.....	265, 283	Illinca, F.....	90	Jankowski, A.....	64, 159
Hsu, F.....	268	Imagawa, H.....	335	Jannasch, E.....	85
Hsu, Y.....	59	Imai, H.....	197	Janssens, K.....	48, 99, 147, 192, 242, 293
Hsuan, T.....	352	Imai, Y.....	116	Jaques, A.....	143, 188
Hu, B.....	38, 342	Imam, M.....	221, 346, 347	Jara, H.....	166
Hu, D.....	298	Imrie, W.....	165	Jarmakani, H.....	225, 256
Hu, H.....	20, 21, 254, 276	Inácio, W.....	289	Jarosinski, M.....	201
Hu, J.....	127	Inal, K.....	341	Jarry, P.....	286
Hu, Q.....	169, 267	Inceni, V.....	134	Jarzebowski, J.....	324
Hu, W.....	22, 202			Jassim Malallah, A.....	145
Hu, X.....	21, 106, 266			Jasthi, B.....	194
Hu, Y.....	282			Jean, Y.....	180
Hu, Z.....	76, 310				

- Jeandin, M.....223  
 Jee, Y .....71  
 Jeffrey, C .....163  
 Jehanno, P .....202  
 Jein-Wein, L .....39  
 Jelen, E .....56  
 Jeltsch, R .....292  
 Jenabali Jahromi, S .....110  
 Jendrzeczyk-Handzlik, D .....314  
 Jenkins, M .....30, 114, 160  
 Jenn-Ming, Y .....27  
 Jennerjohn, S .....144  
 Jensen, D .....80  
 Jensen, M .....280  
 Jentoftsen, T .....230  
 Jeon, C .....376  
 Jeon, H .....336  
 Jeon, J .....271, 278  
 Jeon, M .....129  
 Jeong, I .....247  
 Jeong, J .....169  
 Jeong, Y .....32, 309  
 Jeppsson, J .....143  
 Jer-Han, L .....121  
 Jerusalem, G .....235  
 Jeyakumar, M .....124, 170  
 Jha, A .....186  
 Jha, G .....131  
 Jha, M .....169  
 Jha, S .....100, 148, 242  
 Jhon, M .....161  
 Ji, H .....152  
 Ji, V .....349  
 Ji, X .....309  
 Jia, C .....342  
 Jia, F .....40  
 Jia, J .....379  
 Jia, M .....319  
 Jia, N .....348  
 Jia, P .....89  
 Jia, Q .....141  
 Jia, R .....60  
 Jia, Z .....82  
 Jia Ming, Z .....230  
 Jian, S .....343  
 jian, X .....336  
 Jiang, D .....254, 307  
 Jiang, F .....163, 284, 330, 349  
 Jiang, H .....264, 298, 312  
 Jiang, J .....204, 331  
 Jiang, L .....291  
 Jiang, Q .....16, 43  
 Jiang, T .....131, 338, 380  
 Jiang, X .....307  
 Jiang, Y .....160, 249, 345  
 Jiang, Z .....69, 105, 375  
 Jianhong, M .....298  
 Jianhui, W .....92, 374, 377, 380  
 Jianxin, C .....19  
 Jiao, T .....173  
 Jiao, Z .....29, 67, 209  
 Jie, D .....57  
 Jie, L .....18, 298, 336, 376  
 Jiguang, L .....329  
 Jiménez, J .....276, 369  
 Jimenez-Nieto, A .....362  
 Jin, H .....84, 277  
 Jin, J .....360  
 Jin, L .....302  
 Jin, S .....37, 70  
 Jin, X .....226  
 Jin, Y .....43, 92, 141, 142,  
 186, 237, 289, 334, 352  
 Jindal, S .....124  
 Jing, T .....268  
 Jing, Z .....92, 323, 374, 377, 380  
 Jingjin, T .....123  
 Jo, C .....14  
 Jo, T .....23  
 Jody, B .....123  
 Joël, R .....113  
 Jog, A .....176  
 Johansson, J .....312  
 John, R .....242, 247  
 Johnson, C .....345  
 Johnson, D .....163  
 Johnson, F .....261  
 Johnson, J .....20, 59, 95, 145, 179,  
 190, 240, 292, 335, 363  
 Johnson, O .....176  
 Johnson, R .....174, 207  
 Johnson, S .....68, 115, 172  
 Johnson, W .....39, 40, 88, 89, 118, 233  
 Jolly, M .....123  
 Jonas, J .....51  
 Jones, E .....56  
 Jones, H .....50  
 Jones, J .....21, 148, 151, 203, 241, 294, 299  
 Jones, K .....175  
 Jones, T .....152, 301  
 Jong-Seek, P .....365, 378  
 Jong-Shin, K .....361, 366  
 Jonkman, K .....17  
 Jönsson, P .....205  
 Joo, Y .....31, 63, 218  
 Jordan, J .....68, 115  
 Jorjani, E .....18  
 Joshi, K .....81, 225  
 Joshi, S .....161  
 Jouiad, M .....294  
 Joung, J .....32, 247  
 Juan, Y .....18, 197  
 Juarez-Hernandez, A .....367  
 Jue, J .....257  
 Juel, M .....269  
 Juhas, M .....50  
 Jung, H .....32, 58, 102, 196, 359  
 Jung, I .....168, 300  
 Jung, J .....31  
 Jung, S .....32, 164  
 Jung, Y .....364  
 Júnior, C .....324  
 Júnior, D .....20  
 Jyothi, R .....53
- K**
- Kabir, M .....126  
 Kabra, S .....241  
 Kad, B .....225  
 Kadau, K .....273  
 Kadhém, M .....138  
 Kadiri, H .....156  
 Kaftelen, H .....55  
 Kagawa, Y .....27  
 Kahler, D .....56  
 Kahvecioglu, O .....296  
 Kai, J .....25  
 Kai, W .....286  
 Kaila, R .....165  
 Kainer, K .....57, 58, 104, 152, 199, 200  
 kakhniashvili, I .....379  
 Kakkar, B .....230  
 Kalantar, D .....225, 274  
 Kalay, E .....196, 250  
 Kalay, I .....363  
 Kalay, Y .....282, 363  
 Kalban, A .....230  
 Kalgraf, K .....280  
 Kalidindi, S .....173, 328  
 Kalinin, S .....224  
 Kalugin, N .....114  
 Kalyanaraman, R .....319  
 Kamaraj, M .....337  
 Kamer, A .....24  
 Kamilla, S .....361  
 Kamineni, R .....374  
 Kamisetty, V .....367, 368  
 Kamp, N .....133  
 Kampe, S .....245, 361  
 Kanapathipillai, M .....282  
 Kandev, N .....292  
 Kane, R .....282  
 Kaneta, Y .....43  
 Kang, B .....306, 332  
 Kang, D .....20, 21, 236, 287, 300, 378  
 Kang, H .....21, 32, 266  
 Kang, J .....42, 138, 140, 281  
 Kang, N .....21  
 Kang, S .....31, 37, 71, 117, 164,  
 214, 218, 249, 262, 263,  
 295, 296, 313, 336, 351, 377  
 Kang, W .....21, 357  
 KangJian, S .....230  
 Kantzos, P .....107, 293  
 Kao, C .....72, 74, 117, 167, 352, 367  
 Kao, P .....113, 148, 286, 368  
 Kao, T .....168  
 Kaoumi, D .....114  
 Kapias, P .....54  
 Kapoor, D .....68  
 Kappes, B .....29, 334  
 Kapusta, J .....72, 119, 165, 166, 216, 264  
 Kar, A .....14  
 Kar, M .....85  
 Kar, S .....202  
 Karadge, M .....213  
 Karaduman, G .....366  
 Karaman, I .....58, 198, 201  
 Karcher, C .....370  
 Karhausen, K .....85, 132, 133  
 Karimzadeh, F .....149, 244  
 Karjalainen, P .....39, 112, 232  
 Karlsen, M .....86, 230  
 Karlsson, M .....46  
 Karma, A .....102, 124  
 Karnesky, R .....113, 221, 223, 269  
 Kaschner, G .....201  
 Kasenga, M .....315  
 Kassner, M .....70, 94, 163  
 Kataev, A .....335  
 Katgerman, L .....132, 287  
 Katoh, Y .....257  
 Katsman, A .....150  
 Katzensteiner, R .....275  
 Kaufman, J .....277  
 Kaufman, M .....89, 183  
 Kawagishi, K .....303  
 Kawamura, Y .....58, 301  
 Kaya, A .....249, 250  
 Kaya, M .....77  
 Kayali, E .....17, 198, 248, 325, 377, 378  
 Kazama, H .....84  
 Kazdal Zeytin, H .....237  
 Kazimirov, A .....49



Kazmerski, L.....	103	Kinoshita, M.....	43	Korkmaz, K.....	380
Ke, J.....	117	Kinsella, M.....	108	Kornyei, L.....	195
Keane, J.....	224	Kirchain, R.....	77, 219, 267	Korsunsky, A.....	97
Keck, W.....	109	Kirchheim, R.....	172	Korzekwa, D.....	110
Keckes, L.....	39, 58, 198, 201, 256	Kirilov, D.....	119	Kosaka, Y.....	311
Keiser, D.....	142, 143, 239, 257, 258	Kirk, M.....	30, 114, 257	Koschmeder, J.....	250, 251
Keiser, J.....	47	Kirkpatrick, D.....	177, 227	Koshi, M.....	263
Keller, F.....	240	Kirwan, L.....	227, 228	Koskelo, A.....	224
Keller, M.....	211	Kisner, R.....	146	Kostelak, S.....	177
Kelly, A.....	297, 322	Kiss, L.....	293, 331	Kostorz, G.....	116
Kelly, T.....	79	Kistler, M.....	47, 97	Kotadia, H.....	132
Kelly, V.....	313	Kitkamthorn, U.....	371	Kotsis, I.....	131
Kellsall, G.....	169	Kizil, H.....	22	Kotula, P.....	206
Kelton, K.....	191	Klag, O.....	294	Kou, S.....	151
Kemmotsu, T.....	269	Klarner, J.....	246	Kouchmeshky, B.....	110, 245
Kempshall, B.....	239	Klarstrom, D.....	155	Kovacevic, R.....	33, 88, 215, 245, 246, 281, 297
Kennedy, M.....	207	Klauber, C.....	83	Kovarik, L.....	189, 291, 342
Kerber, M.....	24	Klein, C.....	22	Kozar, R.....	190
Kerckhofs, G.....	62	Klepeis, J.....	81	Kozhan, A.....	268
Kesler, M.....	304	Klier, E.....	256	Kozicki, M.....	175
Kestens, L.....	85, 178	Kline, D.....	124	Krabbe, R.....	290
Kestler, H.....	202	Klingelhöffer, H.....	293	Kracher, A.....	313
Keys, A.....	52, 353	Klingensmith, R.....	318	Krachler, R.....	75
Khachatryan, A.....	141	Klösch, G.....	105	Kraft, O.....	206, 308
Khajeh, E.....	268, 288	Klosek, V.....	349	Krajewski, P.....	152, 277, 301, 302
Khalaf, A.....	220	Knaak, U.....	85	Kral, M.....	184
Khalifa, H.....	234	Knafling, K.....	50, 138, 223, 226	Kramer, M.....	192, 196, 218, 285, 290, 323, 363
Khan, M.....	255, 256, 323	Knott, S.....	75, 121	Kramer, R.....	278
Kharicha, A.....	110	Knudson, M.....	127	Kramer, S.....	303
Khatibi, G.....	264	Knutson, D.....	56	Krämer, S.....	250
Khimukhin, S.....	320	Ko, K.....	372	Kranz, S.....	314
Khimukhina, T.....	320	Ko, T.....	367	Krasnochtchekov, P.....	79, 225
Khomamizadeh, F.....	301	Ko, Y.....	112, 265, 276, 377	Krempaszky, C.....	97
Khorsand, H.....	242	Kobayashi, K.....	76, 124, 220	Kresch, M.....	192, 224
Khoshnevis, B.....	155	Kobayashi, T.....	263	Krishna, B.....	109
Khounsary, A.....	69	Koch, C.....	64	Krishna Moorthy, S.....	134
Khraisheh, M.....	152	Koch, H.....	331	Krishnamurthy, R.....	93, 280
Khuankla, C.....	216	Kocharian, A.....	161	Krishnan, K.....	113
Kieback, B.....	56	Kockelmann, W.....	97	Kroger, N.....	87
Kieffer, J.....	353	Kodambaka, S.....	37	Krost, A.....	163
Kim, B.....	27, 165, 218, 375	Koduri, S.....	36, 42	Krug, M.....	269
Kim, C.....	75, 121, 163, 168, 264, 336	Koehler, T.....	331	Krüger, M.....	202
Kim, D.....	23, 25, 26, 138, 140, 151, 200, 275, 300, 326, 330, 336, 367, 369, 378, 379	Koerner, H.....	258	Krumdick, G.....	75, 76, 121, 122, 168, 169, 218
Kim, E.....	296	Koh, S.....	14, 37, 82, 129, 175, 176, 226, 274, 323	Kruth, J.....	62, 156
Kim, G.....	227, 246, 337	Kohler, F.....	150	Kruzic, J.....	38, 242
Kim, H.....	249, 266, 275, 276, 367, 380	Koike, J.....	341	Kuan Chih, H.....	167
Kim, J.....	14, 21, 32, 37, 63, 72, 82, 129, 130, 165, 167, 175, 218, 226, 236, 252, 270, 274, 287, 301, 305, 323, 332, 369, 372, 376	Koike, M.....	88	Kubin, L.....	45
Kim, K.....	21, 71, 74, 247, 295	Kojima, T.....	150	Kuehn, U.....	136
Kim, M.....	130, 204	Kojo, I.....	216	Kuhn, T.....	78
Kim, N.....	21, 247, 300	Kojuch, L.....	369	Kui-ren, L.....	377
Kim, S.....	71, 74, 150, 177, 228, 252, 265, 266, 295, 296, 303, 309, 352, 365, 367, 380	Kokabi, A.....	295	Kulkarni, N.....	143
Kim, T.....	25, 26, 175	Kokalj, T.....	254	Kulkarni, S.....	249
Kim, W.....	25, 26, 151, 266, 300, 330, 376	Kokawa, H.....	100	Kulovits, A.....	25, 45, 127, 132, 270
Kim, Y.....	22, 23, 31, 71, 138, 140, 153, 193, 299, 303, 304, 326, 336, 364, 367, 378, 380	Koker, M.....	133	Kumar, A.....	86, 157, 279, 327
Kimatsuka, A.....	273	Kolb, C.....	50	Kumar, D.....	299
Kiminami, R.....	362, 370	Kolesnikov, Y.....	370	Kumar, K.....	202
Kimminau, G.....	274	Koley, G.....	82	Kumar, M.....	80, 127, 169, 173, 224, 273, 321, 358
Kimura, A.....	160, 209, 251, 318	Kolozhvari, E.....	60	Kumar, N.....	51
Kimura, H.....	40, 55, 269	Kolwyck, J.....	96	Kumar, P.....	313, 368
King, A.....	311	Kondo, S.....	257	Kumar, V.....	169, 183
King, K.....	371	Kondoh, K.....	152, 197, 267	Kumbeshwara, M.....	92
King, P.....	153, 289	Kong, C.....	112, 259	Kummerl, S.....	263
King, W.....	270, 321	Kong, F.....	247, 281, 366	Kunc, V.....	42
Kinney, C.....	351, 352	Kongstein, O.....	319	Kunz, M.....	70
Kinney, J.....	116	Konno, T.....	45	Kuo, C.....	22, 24, 33, 144, 190
Kinoshita, A.....	301	Kontsevoi, O.....	201	Kuo, I.....	274
		Koo, J.....	164	Kuo, P.....	330
		Koo, Y.....	247, 337, 361	Kuo, S.....	71
		Kopp, R.....	85	Kuo, W.....	128
		Koppes, J.....	313	Kuramoto, S.....	66
		Koratkar, N.....	258, 259	Kurmanaeva, L.....	26
		Korinko, P.....	137, 252	Kurniawan, G.....	234

- Kuroki, Y.....273  
 Kurtz, R.....209, 356  
 Kurtz, S.....282  
 Kuryatkov, V.....364  
 Kurz, G.....152, 302  
 KuShaari, K.....338  
 Kusinski, G.....129, 234  
 Kusinski, J.....234  
 Kuz'menko, A.....129  
 Kuzel, R.....212  
 Kvithyld, A.....197, 235, 268, 318, 319,  
 .....335, 336, 337, 339, 357  
 Kwabi, D.....27  
 Kwan, K.....179  
 Kweon, S.....134  
 Kwon, S.....285, 332  
 Kwon, Y.....221, 302  
 Kwong, K.....154, 290  
 Kyeong, J.....151, 300, 330  
 Kylmäkorpi, I.....216
- L**
- L'Elpattener, P.....363  
 Labdi, S.....223  
 LaCombe, J.....142, 143, 188, 239, 290  
 Lacroix, M.....326  
 Lacroix, S.....292  
 Laddha, S.....298  
 Lados, D.....35, 242, 243  
 Ladwig, P.....165  
 Laé, E.....235  
 Lafuente, A.....29  
 Lagacé, C.....95  
 LaGrange, T.....270, 321  
 Lahiri, A.....186  
 Lahiri, I.....175  
 Lahrman, D.....174, 184  
 Lahtinen, M.....216  
 Lai, Y.....75, 117, 197, 319, 351  
 Laird, B.....124  
 Laird, C.....228, 229  
 Laiw, P.....286  
 Lal D, M.....297  
 Lam, C.....77  
 Lam, T.....194, 244  
 LaMattina, B.....283  
 Lamberti, L.....258  
 Lambrakos, S.....108  
 Lamm, M.....44  
 Lammi, C.....35, 242  
 Landero, I.....333  
 Landers, R.....62, 243  
 Landi, B.....37  
 Landis, C.....141  
 Landrigan, M.....135  
 Lang, M.....257  
 Langdon, T.....27, 111  
 Langeloh, T.....324  
 Langford, R.....181  
 Lanka, S.....253  
 Lanyon, M.....279  
 Lapovok, R.....112, 347  
 Laprade, E.....214  
 Larbalestier, D.....296, 377  
 Larkin, S.....137  
 Laros, T.....177  
 Larouche, A.....286  
 Larouche, D.....286  
 Larsen, J.....100, 148, 242  
 Larson, B.....69, 70, 94, 115, 126, 163  
 Larson, D.....274
- Lashley, J.....322  
 Lashmore, D.....68  
 Lasseigne, A.....202  
 Lassila, D.....173  
 Lattis, M.....15  
 Lau, L.....362  
 Lau, S.....314  
 Laughlin, D.....238  
 Launey, M.....233  
 Lauridsen, E.....80, 102, 222, 311  
 Laux, B.....245  
 Lavender, C.....68, 260  
 Lavernia, E.....16, 25, 28, 40, 41, 43, 111, 113, 155,  
 .....156, 159, 210, 211, 213, 221, 308, 346  
 Lavoie, P.....231  
 Law, J.....226  
 Law, V.....189  
 Laws, K.....89, 234  
 Lawson, D.....227, 228  
 Lazarou, R.....240  
 Lazono-Perez, S.....65  
 Le, Q.....105  
 Leal, E.....366  
 Leau, W.....265  
 LeBeau, S.....249  
 Le Bouar, Y.....186, 237  
 Le Breton, J.....225  
 Le Brun, P.....89, 137, 182, 234, 235, 286, 331  
 Leckie, R.....250  
 Lee, A.....118, 214, 263  
 Lee, B.....14, 67, 151, 365  
 Lee, C.....58, 126, 167, 208, 217, 295, 332, 365  
 Lee, D.....112, 141, 296, 368  
 Lee, E.....85  
 Lee, G.....33, 369  
 Lee, H.....28, 31, 138, 140, 146, 151,  
 .....165, 168, 200, 218, 247, 263, 275  
 Lee, I.....148  
 Lee, J.....31, 32, 58, 74, 75, 120, 150, 164,  
 .....167, 169, 217, 265, 266, 280, 337, 361  
 Lee, K.....21, 32, 146, 218, 280, 309, 326, 365, 369  
 Lee, M.....130, 136  
 Lee, N.....368  
 Lee, P.....89, 102, 133, 196, 272, 274, 283  
 Lee, R.....159  
 Lee, S.....14, 21, 31, 158, 181, 247,  
 .....259, 265, 266, 299, 348  
 Lee, T.....263, 264, 351, 352  
 Lee, W.....95, 325  
 Lee, Y.....43, 118, 126, 336, 364, 367, 373  
 Lee, Z.....159  
 Lefebvre, Y.....331  
 Legris, A.....67  
 Lehman, E.....97  
 Lehmann, E.....97  
 Lehner, T.....73, 122, 216  
 Lei, M.....223, 357  
 Leisenberg, W.....240  
 Leite, A.....372, 374  
 Leitner, H.....78, 161, 243, 262  
 Lekakh, S.....64, 124, 186  
 Lelièvre-Berna, E.....46  
 Lemaitre, A.....285  
 LeMaster, R.....96  
 Lemieux, P.....296  
 Leng, H.....135  
 Leo, P.....131  
 Leon, C.....113  
 León, G.....362  
 Leonard, D.....367  
 Leonard, J.....127, 270  
 Lepage, D.....95
- Le Sar, R.....44  
 Lesar, R.....161  
 Lesuer, D.....247, 376  
 Letellier, V.....231  
 Letzig, D.....58, 152, 199, 200, 302  
 Leu, M.....62, 124  
 Levashov, V.....135, 285  
 Levchenko, E.....290, 291  
 Levi, C.....250, 251, 303  
 Levi, K.....179  
 Levine, L.....70, 94, 144, 163  
 Levy, R.....19  
 Lewandowski, J.....153, 233  
 Lewis, A.....125, 126, 172, 173  
 Lewis, D.....74, 120, 139, 167, 217, 265  
 Leyens, C.....250  
 Lhuissier, J.....190  
 Li, B.....45, 102, 144, 201, 204,  
 .....232, 288, 317, 341, 363  
 Li, D.....15, 35, 38, 246, 332, 334  
 Li, F.....36, 363  
 Li, G.....15, 130, 131, 338, 380  
 Li, H.....26, 56, 105, 177, 180, 226, 375, 378  
 Li, J.....15, 34, 41, 44, 75, 127,  
 .....135, 138, 139, 142, 169, 186, 189,  
 .....197, 255, 267, 272, 279, 291, 349, 370  
 Li, L.....213, 311, 345  
 Li, M.....34, 35, 65, 79, 104, 125,  
 .....172, 173, 223, 272, 284, 363  
 Li, Q.....232, 355, 360  
 Li, R.....368, 371  
 Li, S.....76, 122, 137, 255, 322  
 Li, T.....201  
 Li, W.....20, 27, 69, 177, 275, 276, 277  
 Li, X.....17, 24, 63, 64, 82, 85, 111, 158, 169,  
 .....206, 247, 255, 267, 281, 283, 307, 346  
 Li, Y.....16, 24, 25, 28, 40, 41, 43,  
 .....44, 69, 74, 111, 113, 122,  
 .....131, 141, 181, 210, 213, 284, 330  
 Li, Z.....121, 178, 229, 364  
 Li-Hui, C.....188  
 Li-ling, H.....39  
 Lian, J.....257  
 Liane, M.....230, 280  
 Liang, H.....168  
 Liang, J.....117, 313, 364, 371, 376  
 Liang, S.....75, 215, 351, 355  
 Liang, Y.....329  
 Liang, Z.....63, 69, 180, 254  
 Liao, C.....25, 56, 66, 217  
 Liao, J.....328  
 Liao, Y.....247  
 Liaw, P.....25, 26, 39, 40, 61, 69, 70,  
 .....88, 115, 135, 143, 162, 180,  
 .....181, 182, 212, 213, 228, 232, 233,  
 .....234, 241, 255, 260, 262, 283, 284,  
 .....286, 307, 311, 329, 330, 331, 348, 349  
 Licht, T.....264  
 Lidbury, D.....317  
 Liebesfeld, J.....197  
 Lienert, T.....49, 100, 148, 194, 243, 294  
 Lienert, U.....49, 69, 70, 174, 184  
 Lifeng, Z.....123, 218  
 Lillebuen, B.....278  
 Lilleodden, E.....44, 94, 143, 189  
 Lillig, D.....293  
 Lillo, T.....304  
 Lim, G.....218  
 Lim, H.....58, 151, 300  
 Lim, N.....204  
 Lim, S.....77, 378, 379  
 Lima, A.....185

Lima, J	276, 324	Lou, L	343	Madsen, C	53
Limem, S	232	Lou, T	266	Madsen, I	279
Lin, C	72, 75, 118, 190, 265, 367	Louzuina, L	136	Madsen, J	193
Lin, D	17, 33, 199, 215, 246, 281, 297, 300	Louzuina-Luzgina, L	367	Maeda, M	138, 269
Lin, H	32, 89, 268, 283, 286	Louzuine, D	136, 137, 367	Magee, D	259
Lin, J	192, 224, 265, 284	Louzuine-Luzgin, D	137	Magness, L	68, 256
Lin, K	71, 214, 352	Love, R	190	Magnusson, P	305
Lin, M	314	Lowengrub, J	76, 93, 122, 353	Mahajan, B	87
Lin, Q	163	Lowery, A	138	Mahapatra, R	154, 298
Lin, S	120	Lowry, A	339	Mahato, B	337
Lin, T	106, 371	Lozano, J	365	Mahmood, M	279
Lin, Y	56, 71, 75, 117, 167, 179	Lozano-Perez, S	160	Mahmud, A	288
Lin, Z	336	Lu, C	337	Mahmudi, R	34, 300
Lindley, T	243, 272	Lu, D	54, 316, 317, 355	Mahoney, M	49, 100, 101, 148, 194, 243, 294
Lindsay, C	68, 115	Lu, H	140, 205, 267, 309, 319, 373, 378	Mai, L	38
Lindsay, S	87, 240, 327	Lu, J	226	Maia, L	374
Linga, H	230, 240	Lu, K	255	Maich, A	359
Linyan, L	218	Lu, L	255	Maijer, D	268, 288
Liou, F	108	Lu, Q	207	Maioli, M	169
Liou, K	56	Lu, Y	59, 368	Maire, E	341
Liou, W	168	Lu, Z	241, 329	Maiwald, D	90, 197
Lipkin, D	202, 251	Lucadamo, G	171	Maizlin, M	312
Lippold, J	50	Lucas, G	317	Majidi, B	86, 193
Lira, H	316, 366, 374	Lucas, J	165	Major, F	219
Lisin, F	183	Lucas, M	192, 224	Majumdar, B	68, 114, 161, 209, 258, 309, 345
Littlewood, G	311	Luciano, B	196	Makarevicius, V	193
Littlewood, P	147	Lücke, M	376	Makaya, A	40
Liu, B	106, 177, 268, 272, 273, 281, 371	Ludlow, A	83	Makeev, M	334
Liu, C	33, 61, 68, 74, 118, 146, 217, 225, 247, 263, 336	Ludtka, G	146	Makhlouf, M	132, 268
Liu, D	214, 261, 262, 279	Ludwig, A	62, 289	Malard, B	261
Liu, F	178, 180, 182, 286	Ludwig, W	311	Malcolm, E	87
Liu, G	368	Lui, T	148, 149, 275	Malherbe, J	188
Liu, H	62, 274, 276, 307, 349, 369	Luke, M	157	Mali, A	253
Liu, J	82, 253, 254, 277, 362, 379	Lung, L	121	Mali, S	39, 112
Liu, K	14, 263, 264, 290, 351, 370	Luo, A	197, 300, 302	Malik, M	170
Liu, L	16, 63, 130, 152	Luo, H	151, 249, 357	Mallapragada, S	282
Liu, M	112, 338	Luo, S	174, 224, 225	Mallick, P	248
Liu, P	139	Luo, T	14, 82	Mallik, U	338
Liu, Q	20, 106	Luo, W	113, 265, 286, 289	Maloney, C	285
Liu, R	18, 246	Luo, Y	219	Maloney, J	231
Liu, S	109, 253, 281	Lupini, A	113	Maloy, S	114, 161, 356, 359
Liu, T	33, 246	Lupulescu, A	142, 143, 188, 189, 239, 290	Maltais, B	235
Liu, W	16, 26, 43, 54, 69, 70, 82, 94, 118, 157, 162, 163, 255	Luther, E	343	Maltais, J	86
Liu, X	17, 120, 143, 154, 200, 203, 252, 305, 306, 329, 344, 345	Luton, M	44	Mandal, A	132
Liu, Y	16, 25, 131, 151, 152, 178, 226, 228, 229, 249, 261, 277, 319, 339, 357	Luz, A	251	Mandal, S	236, 295
Liu, Z	74, 81, 141, 142, 154, 177, 200, 203, 218, 220, 226, 252, 277, 305, 306, 311, 315, 316, 344	Lv, B	276	Mangelinck-Noel, N	102, 196
Livescu, V	299	Lv, G	131	Manias, E	315
Lizarralde, A	295	Lv, X	288, 318, 375	Maniruzzaman, M	110
Lloyd, D	84	Lysenko, S	276, 369	Manisha, T	306
Lo, W	73	<b>M</b>		Manivannan, A	154, 203, 252, 305, 306, 344
Lobovsky, A	108	Ma, C	228	Mannava, S	174, 184, 222
Logan, S	341	Ma, D	146, 192, 241	Mannens, R	152
Lograsso, T	246	Ma, E	45, 89, 144, 158, 181, 201, 341	Mannweiler, U	95
Loic, B	113	Ma, H	214	Mansikkaviita, H	216
Long, Z	48, 84, 131, 177, 178, 228, 277, 325	Ma, L	21, 144, 344, 357	Mansoor, B	153
Loomis, E	174	Ma, N	237, 316	Manuel, M	20, 249, 353
Lopes, F	185, 289, 333	MacDonald, W	301	Manzini, R	230
Lopes, R	176	MacDowell, A	312	Mao, S	66, 143, 189
Lopez, M	174, 183	MacFarlane, D	175	Mao, Y	170, 172
Lopez-Cortes, V	339	Machado de Medeiros, K	363	Mao, Z	221, 223, 270, 271
Lopez-Hirata, V	366, 372	Mackay, R	219	Mara, N	24, 64, 65, 111, 158, 161, 162, 206, 255, 283, 307
Lorentsen, O	86	Mackey, P	73, 119, 166	Marathe, G	159
Lorenzana, H	274, 321, 363	MacSleyne, J	172	Marchet, N	139
Loretto, M	298	Maddela, S	248	Marcuson, S	119
Löser, W	196	Maddox, B	225, 358	Margem, F	288
Lou, C	246	Madec, R	45	Marin, E	328
		Madelone, J	291	Marini, B	317
		Mader, E	28	Marinigh, M	166
		Madison, A	367	Marinov, E	119
		Madison, J	125, 172	Markmann, J	26, 64
				Marks, J	86



- Markus, H ..... 380  
 Marois, M ..... 326  
 Marques, L ..... 185, 333  
 Marquis, E ..... 65, 160  
 Marsden, K ..... 344  
 Marshall, P ..... 35  
 Marte, J ..... 65, 159  
 Martin, D ..... 68  
 Martin, G ..... 78, 138  
 Martin, L ..... 299  
 Martin, M ..... 90  
 Martin, O ..... 230, 279  
 Martin, P ..... 108, 302  
 Martinez, E ..... 29, 109, 174, 187  
 Martinez, M ..... 310  
 Martinez-Val, J ..... 29  
 Martinez-Villafañe, A ..... 164  
 Martinez Sanchez, R ..... 92  
 Martins, A ..... 380  
 Martorano, M ..... 195  
 Maruyama, B ..... 68, 114, 161, 209, 258, 309, 345  
 Marzinsky, C ..... 293  
 Masiel, D ..... 42  
 Mason, D ..... 35  
 Mason, T ..... 299  
 Masset, P ..... 61  
 Massoud, J ..... 317  
 Mastorakos, I ..... 95, 189  
 Masuda, C ..... 210, 346  
 Matejczyk, D ..... 108  
 Mathaudhu, S ..... 39, 58, 198, 201  
 Mathiesen, R ..... 79, 80, 223  
 Mathieu, S ..... 327  
 Mathon, M ..... 160, 349  
 Matlage, P ..... 376  
 Matsen, M ..... 260  
 Matsui, H ..... 355  
 Matsumoto, H ..... 45  
 Matsumoto, K ..... 303  
 Matsushita, T ..... 379  
 Matteis, P ..... 184, 242, 281, 329  
 Mattern, N ..... 181  
 Matthews, S ..... 155  
 Matthias, T ..... 165  
 Matuszewicz, R ..... 216, 334  
 Maunders, C ..... 275  
 Maung, K ..... 210  
 Maxey, E ..... 46  
 Mayer, F ..... 289  
 Mazumder, J ..... 156, 196  
 McCabe, R ..... 35, 80, 201  
 McCallum, R ..... 218  
 McCartney, G ..... 222, 271, 319, 320, 357  
 McClellan, K ..... 224, 225, 343, 344  
 McClintock, D ..... 65  
 McClung, M ..... 190, 292  
 McCoy, T ..... 359  
 McCulloch, R ..... 240  
 McCune, R ..... 248  
 McDevitt, E ..... 23  
 McDonald, R ..... 134  
 McDonald, S ..... 31, 264  
 McDowell, D ..... 99, 144  
 McFadden, S ..... 267  
 McGowan, K ..... 48  
 McGowan, S ..... 321  
 McGregor, K ..... 279  
 McIntosh, L ..... 373  
 McIntyre, G ..... 46  
 McIntyre, S ..... 70  
 McKay, B ..... 105  
 McKenna, I ..... 80, 334  
 McKindra, T ..... 91  
 McKinney, S ..... 95, 145  
 McKittrick, J ..... 180  
 McLaughlin, S ..... 56  
 McLean, K ..... 105  
 McNaney, J ..... 225, 274, 363  
 McNelley, T ..... 49  
 McQueen, H ..... 94, 131  
 Mede, M ..... 88  
 Medeiros, M ..... 227  
 Medina, F ..... 109  
 Medlin, D ..... 56, 171, 195, 204, 215  
 Medvedev, P ..... 244  
 Medvedeva, N ..... 201  
 Medyanik, S ..... 189  
 Mehta, V ..... 121  
 Meier, G ..... 250, 303  
 Meilunas, M ..... 352  
 Melendez, A ..... 101  
 Melgarejo, Z ..... 325  
 Mellenthin, J ..... 52  
 Melo, T ..... 365, 369, 372  
 Mélo, T ..... 364  
 Melo-Maximo, D ..... 372  
 Menand, A ..... 225  
 Mendeleev, M ..... 285  
 Mendez, J ..... 61, 294, 359  
 Mendis, C ..... 301  
 Mendoza, M ..... 16  
 Menezes, R ..... 316  
 Meng, B ..... 374, 377  
 Meng, D ..... 214  
 Meng, F ..... 205  
 Menon, S ..... 49  
 Meoslang, A ..... 30  
 Mercier, D ..... 227  
 Meressi, T ..... 87  
 Mergel, J ..... 305  
 Merkel, S ..... 348  
 Merma, A ..... 354  
 Merrill, J ..... 37  
 Meshinchi Asl, K ..... 301  
 Meskers, C ..... 76, 169, 219  
 Mesquita, A ..... 240  
 Meyer, H ..... 198  
 Meyer, M ..... 87  
 Meyers, M ..... 16, 38, 80, 87, 94, 127,  
 134, 173, 179, 224, 225, 231,  
 256, 273, 282, 321, 328, 358  
 Miao, J ..... 294, 312  
 Miao, P ..... 65, 356  
 Miceli, P ..... 163  
 Michael, N ..... 168, 336  
 Michel, K ..... 43  
 Michiel, M ..... 42  
 Miculescu, M ..... 281  
 Middlemas, M ..... 202  
 Middleton, H ..... 155  
 Midhuri, S ..... 27  
 Miettinen, E ..... 53, 54, 216  
 Migchielsen, J ..... 183  
 Migiakis, K ..... 360  
 Mikami, M ..... 76  
 Mikhailovskij, I ..... 182  
 Mikula, A ..... 120, 121  
 Mikulowski, B ..... 111  
 Milani, S ..... 375  
 Milathianaki, D ..... 274, 363  
 Miles, M ..... 59, 106, 148  
 Milhet, X ..... 61, 359  
 Miller, B ..... 257, 258  
 Miller, M ..... 49, 70, 79, 136, 146, 158,  
 160, 184, 225, 246, 247, 318  
 Millett, P ..... 67, 175, 207, 258, 322  
 Mills, M ..... 70, 108, 189, 190,  
 237, 272, 291, 294, 342  
 Min, G ..... 249  
 Min, K ..... 32, 369  
 Min, X ..... 369  
 Min-Su, H ..... 361, 365, 366, 378  
 Minchenya, V ..... 370  
 Mindivan, H ..... 198, 325  
 Mingchun, L ..... 276  
 Mingjiang, J ..... 373  
 Mingler, B ..... 111  
 Minich, R ..... 173  
 Minor, A ..... 24, 64, 66, 111, 158,  
 206, 255, 256, 272, 283, 307, 308  
 Minville, R ..... 327  
 Miotto, P ..... 364  
 Miracle, D ..... 88, 135, 136, 137, 197, 198, 284, 293  
 Miranda-Tello, R ..... 64  
 Mirazizi, M ..... 63, 295  
 Mirgaux, O ..... 185, 234  
 Mirhakimi, S ..... 375  
 Mirihanage, W ..... 267  
 Mirkovic, D ..... 104  
 Mironov, S ..... 194  
 Miroux, A ..... 80, 85, 178  
 Mishin, Y ..... 92, 125, 171, 187  
 Mishra, B ..... 15, 47, 188, 202  
 Mishra, R ..... 49, 51, 100, 101, 148, 177,  
 194, 195, 201, 243, 294, 308, 341  
 Mishra, S ..... 133  
 Mishra, U ..... 296  
 Misra, A ..... 14, 37, 65, 82, 129, 162, 175,  
 208, 226, 255, 274, 275, 323  
 Misra, D ..... 38, 39, 112, 115, 162, 231, 232, 282  
 Missalla, M ..... 324  
 Mittal, J ..... 71  
 Miwa, K ..... 40, 104  
 Miyake, M ..... 138  
 Miyamoto, G ..... 270  
 Miyano, T ..... 55  
 Miyauchi, A ..... 91  
 Miyazaki, T ..... 76  
 Mizushima, K ..... 84  
 Mnikoleiski, H ..... 197  
 Moat, R ..... 70, 213  
 Moats, M ..... 53  
 MoberlyChan, W ..... 274, 321  
 Moeinifar, S ..... 337, 369  
 Moelans, N ..... 34, 80, 238  
 Moffat, M ..... 310  
 Moffatt, S ..... 228  
 Mohamed, A ..... 327  
 Mohamed, F ..... 28, 159, 210  
 Mohamed, H ..... 110  
 Mohamed, M ..... 94  
 Mohamed, S ..... 292  
 Mohamed Al-Jallaf, M ..... 280  
 Mohammed, J ..... 138  
 Mohanty, R ..... 239  
 Mohapatra, B ..... 47  
 Mohapatra, R ..... 47  
 Mohles, V ..... 132, 133, 223  
 Mohsenzadeh, M ..... 15  
 Mokhtar, M ..... 363  
 Molaison, J ..... 47  
 Moldovan, P ..... 287  
 Monaco da Silva, A ..... 295  
 Monceau, D ..... 250  
 Mondal, A ..... 376  
 Money, G ..... 166

Monnet, G.....	44	Mukhtar, A.....	112, 259	Nassar, A.....	340	
Monnet, I.....	29	Mulay, R.....	199	Nastar, M.....	187	
Monnier, A.....	160	Mulder, A.....	230	Natu, H.....	101, 196	
Monroe, C.....	268	Müller, C.....	338	Navarra, A.....	166	
Monteiro, S.....	18, 41, 91, 138, 183, 185, 235, 287, 288, 289, 316, 332, 333	Müller, K.....	376	Nayak, B.....	15, 47	
Montgomery, D.....	174	Muller, S.....	373	Nayak, S.....	39, 112	
Montgomery, J.....	299	Mumm, D.....	353	Nayyeri, G.....	300	
Montoro, E.....	364	Mun, D.....	361	Nazon, J.....	75, 291	
Montoya, J.....	91	Mundy, C.....	128, 274	Neamnark, A.....	134	
Montoya-Dávila, M.....	245, 339	Munhutu, A.....	27	Neelameggham, N.....	20, 57, 58, 104, 105, 140, 150, 151, 185, 198, 200, 248, 249, 300, 301, 340	
Moody, M.....	136	Munkholm, A.....	163	Negrea, D.....	312	
Moody, N.....	44, 94, 143, 189, 207, 245, 297, 337, 339	Muñoz-Morris, M.....	256	Neil, C.....	341, 348	
Moon, D.....	50	Munroe, P.....	112, 207, 259	Neil, J.....	348	
Moon, J.....	168, 336	Muntele, C.....	29, 257	Neilsen, M.....	273	
Moon, M.....	27	Mupidi, T.....	92	Neitzel, I.....	133	
Moon, Y.....	265	Muralidharan, G.....	252	Neiva, L.....	370	
Mooney, A.....	227	Muralidharan, S.....	93	Neklyudov, I.....	30, 182	
Moore, G.....	195	Murashkin, M.....	112	Nelson, B.....	101	
Moore, A.....	183	Murayama, Y.....	55	Nelson, T.....	101	
Mora, G.....	293	Murch, G.....	290, 291	Neri-Flores, M.....	164	
Moradi, M.....	220	Murphy, W.....	274	Nesterenko, V.....	358	
Morales, P.....	166, 216	Murr, L.....	109, 140, 174, 332, 359	Neu, R.....	99	
Morcali, H.....	375, 379	Murray, B.....	313	Neuefeind, J.....	191	
Mordehai, D.....	25, 78, 190	Murty, K.....	32, 209	Neumann, D.....	116	
More, K.....	305	Muza, A.....	34, 313	Neumann, J.....	107	
Moreau, R.....	206	Myers, B.....	171	Neumann, S.....	85	
Moreno, H.....	288	Mysore, K.....	32	Neumeier, S.....	24	
Morgan, A.....	282	<b>N</b>			Neves, G.....	316
Morgan, D.....	28, 42, 43, 67, 238	Na, X.....	164	Newbery, A.....	308	
Morgan, E.....	17	Nadakuduru, V.....	346	Newbery, P.....	28	
Morgan, W.....	190, 240	Nadgorny, E.....	144, 158	Newby, M.....	100	
Mori, K.....	119	Nadler, J.....	297, 298, 338	Newkirk, J.....	108, 154	
Mori, T.....	56	Nag, S.....	209, 221, 270	Ngayam-Happy, R.....	29	
Moricca, M.....	154	Nagai, K.....	119	Nguyen, D.....	286	
Morita, K.....	91, 119, 269	Nagai, T.....	138, 183, 269	Nguyen, J.....	128, 155, 156, 211	
Morra, M.....	202, 304	Nagai, Y.....	113	Nguyen, N.....	163, 169, 259	
Morrall, J.....	24, 239	Nagaraj, C.....	313	Nguyen, T.....	279	
Morris, D.....	144, 256	Nagarajan, R.....	337	Nguyen, V.....	105, 115	
Morris, J.....	51, 65, 66, 101, 135, 149, 195, 285, 351, 352	Nagarajan G.....	297	Nguyen-Thi, H.....	102, 196	
Morrow, B.....	190	Nagase, T.....	283	Nhon, V.....	256	
Morsi, K.....	157, 205, 253	Nagaumi, H.....	133	Ni, Y.....	141	
Mortarino, G.....	242	Nagem, N.....	231, 364	Nicholls, J.....	250	
Mortensen, C.....	163	Nagesh, C.....	380	Nichols, A.....	299	
Morton, T.....	211	Nagle, M.....	105	Nie, J.....	198	
Morvasky, A.....	114	Nai, S.....	71	Nie, X.....	20, 215, 352	
Mosavie Khoei, M.....	358	Najafabadi, R.....	269	Nie, Y.....	21	
Moscicki, M.....	69	Naji-Meidani, A.....	287	Nie, Z.....	255, 261, 262, 345	
Moses, B.....	37	Nakai, Y.....	233	Niebur, G.....	135	
Moss, S.....	116	Nakamura, K.....	100	Niedzwiedz, C.....	361	
Moss, T.....	154	Nakano, J.....	154	Niehoff, T.....	98	
Mota-Caetano, C.....	378	Nakano, O.....	119	Nielsen, B.....	100	
Motegi, T.....	150	Nakayama, H.....	124, 220	Nielsen, L.....	215	
Motta, A.....	114	Nakayama, K.....	88	Niese, C.....	259	
Motta, L.....	185, 333	Nakayana, S.....	311	Niewicz, M.....	301	
Mourer, D.....	108	Nam, W.....	373	Niezgoda, S.....	173, 328	
Mousa, M.....	124	Namavar, F.....	257	Nikbin, K.....	251	
Moxnes, B.....	280, 292	Namboothiri, S.....	231	Nikfar, S.....	375	
Moxson, V.....	259, 260	Nanstad, R.....	318	Nikishin, S.....	364	
Moyano, A.....	166, 216	Napolitano, R.....	51, 101, 149, 161, 195, 196, 363, 376	Nikles, D.....	82	
Mubarak, A.....	233	Naranjo, R.....	98	Nikolaeva, E.....	278	
Mucino, V.....	195	Narayan, J.....	222, 320	Nikolenko, S.....	310	
Mueller, A.....	343	Narayan, R.....	38, 87, 271	Nikolic, S.....	217	
Mueller, B.....	126	Nardiello, J.....	193	Nikolova, L.....	321	
Mueller, M.....	305	Nardone, M.....	147	Nili Ahmadabadi, M.....	17, 23, 220, 226	
Mueller, R.....	293	Narita, S.....	100, 146	Ning, X.....	266, 307	
Mueller, T.....	44	Narula, M.....	30	Ninglieri, S.....	48, 84, 178, 182, 228, 277	
Mukai, T.....	199, 300	Nascimento, D.....	185	Nino, J.....	123	
Mukherjee, A.....	208, 254, 307, 339	Naser, J.....	334	Nishi, Y.....	269	
Mukherjee, S.....	101, 153	Nasihatkon, S.....	110	Nishikawa, H.....	313	
				Nishimiya, Y.....	210	

- Nishimura, T ..... 31, 263, 264, 346  
 Nishino, Y ..... 312  
 Nishio, T ..... 124, 220  
 Nishiyama, N ..... 261  
 Niu, L ..... 339  
 Nix, W ..... 158  
 Nixon, M ..... 338  
 Niyomwas, S ..... 254, 307  
 Noda, M ..... 301  
 Noebe, R ..... 54, 183, 271  
 Nofal, A ..... 292, 371  
 Nogita, K ..... 31, 264  
 Nolan, W ..... 204  
 Noori, H ..... 34  
 Norby, T ..... 155  
 Nordbø, T ..... 280  
 Nordmark, A ..... 123  
 Noriega-Manez, R ..... 129  
 Noskova, N ..... 25, 26  
 Notarberardino, B ..... 27, 135  
 Novales, A ..... 370  
 Novichkov, S ..... 266  
 Nowak, S ..... 330  
 Nowrouzi, S ..... 129, 336  
 Noyel, J ..... 292  
 Nunes, A ..... 149  
 Nutt, S ..... 25, 28, 159, 308  
 Nuzzo, R ..... 56  
 Nyakiti, L ..... 159  
 Nyberg, E ..... 20, 57, 58, 104, 105, 150,  
 ..... 151, 198, 200, 248, 249, 300, 301, 340  
 Nychka, J ..... 16, 38, 87, 134, 179, 231, 282, 328  
 Nyland, G ..... 327
- O**
- O'Brien, J ..... 245  
 O'Brien, K ..... 177  
 O'Keefe, M ..... 91, 262  
 Oberembt, C ..... 195  
 Oberwinkler, B ..... 243, 362  
 Oberwinkler, C ..... 78, 362  
 Ochin, P ..... 330  
 Oda, M ..... 210, 346  
 Odabasi, A ..... 369  
 Odette, G ..... 28, 30, 65, 146, 160,  
 ..... 209, 305, 318, 356, 357  
 Odette, R ..... 161  
 Odunuga, S ..... 172, 225  
 Oehring, M ..... 308  
 Ogawa, F ..... 210, 346  
 Ogunseitán, O ..... 76, 77, 122, 169, 218  
 Ogura, K ..... 140  
 Oh, A ..... 145  
 Oh, C ..... 71  
 Oh, K ..... 63, 138, 140, 295, 336, 367  
 Oh, S ..... 22, 32, 113, 359  
 Oh, T ..... 27  
 Oh, Y ..... 32  
 Oh-ishi, K ..... 270, 301  
 Ohara, M ..... 248  
 Ohm, V ..... 235  
 Ohnuma, I ..... 120, 121  
 Ohnuma, M ..... 146  
 Ohriner, E ..... 319  
 Oi, T ..... 91  
 Ojima, M ..... 146  
 Okabe, T ..... 18, 41, 88, 91, 138, 183, 235, 287, 332  
 Okamoto, I ..... 84  
 Okamoto, K ..... 100, 194, 295  
 Oktay, G ..... 249, 250  
 Okubo, N ..... 357  
 Okuniewski, M ..... 114, 188, 189, 239  
 Okuyama, K ..... 378  
 Olakanmi, E ..... 109  
 Olaya-Luengas, L ..... 367  
 Olevsky, E ..... 179  
 Olier, P ..... 160  
 Olivas Pro, J ..... 359  
 Oliveira, A ..... 176  
 Oliveira, S ..... 373  
 Oliver, E ..... 97  
 Oliver, M ..... 232, 308  
 Olivetti, E ..... 77, 219  
 Olliges, S ..... 206  
 Olmsted, D ..... 124, 187  
 Olson, D ..... 188, 202, 360  
 Olson, G ..... 138, 153, 270, 314, 315, 353  
 Olsson, P ..... 29, 114, 119  
 Olteanu, A ..... 152  
 Onderka, B ..... 314  
 Oniashvili, G ..... 369  
 Onofre, E ..... 362  
 Oppedal, A ..... 201  
 Oprea, G ..... 73  
 Oprisan, S ..... 152  
 Oquab, D ..... 250  
 Orduña-Martinez, R ..... 34  
 Orlikowski, D ..... 128  
 Orlovskaya, N ..... 306  
 Orsborn, J ..... 347  
 Ortiz, C ..... 208  
 Ortiz-Cuellar, E ..... 27  
 Osbourne, M ..... 97  
 Osen, K ..... 278  
 Osenbach, J ..... 164, 214  
 Osetsky, Y ..... 209, 318  
 Oskuie, A ..... 358  
 Oster, N ..... 218  
 Ostrovski, O ..... 279, 307  
 Ott, E ..... 54, 246, 298  
 Ott, R ..... 285  
 Ou, W ..... 20  
 Öveçoğlu, L ..... 55  
 Ovecoglu, M ..... 237, 372  
 Overfield, K ..... 98  
 Overman, C ..... 189  
 Ovrelid, E ..... 269  
 Øvrelid, E ..... 269  
 Øvstetun, F ..... 230  
 Owate, I ..... 197  
 Ozaki, K ..... 76  
 Ozdemir, O ..... 30  
 Ozkal, B ..... 374  
 Özkal, B ..... 372  
 Ozolins, V ..... 43, 92, 187
- P**
- Pabel, T ..... 170  
 Packard, C ..... 233  
 Packer, S ..... 101  
 Padhi, P ..... 210  
 Padmanabham, G ..... 337  
 Padron, I ..... 121  
 Padrón, S ..... 376  
 Pagador, R ..... 216  
 Paik, D ..... 16  
 Paisley, D ..... 225  
 Paital, S ..... 39, 271  
 Pakzad, A ..... 162  
 Pal, J ..... 22, 24  
 Palandage, K ..... 161  
 Palkowski, H ..... 320, 369  
 Palm, M ..... 46  
 Palmer, M ..... 296, 336, 360  
 Palomar-Pardave, M ..... 34, 64, 166  
 Palosz, B ..... 137  
 Pan, D ..... 273  
 Pan, J ..... 59  
 Pan, T ..... 59, 106  
 Pan, X ..... 24, 29, 224  
 Pan, Y ..... 357  
 Pan, Z ..... 256  
 Pande, C ..... 221  
 Pang, H ..... 23  
 Pang, J ..... 348, 349  
 Pang, L ..... 319  
 Pang, S ..... 233  
 Pang, Z ..... 204  
 Pant, P ..... 18, 320  
 Pantelides, S ..... 113  
 Pantke, K ..... 85, 380  
 Pantleon, W ..... 69, 94  
 Pao, P ..... 50, 277, 347  
 Papadimitriou, G ..... 360  
 Papazian, J ..... 49, 193  
 Papin, P ..... 297  
 Pareige, P ..... 160  
 Parikh, N ..... 30  
 Park, C ..... 42, 126, 204, 326, 336  
 Park, E ..... 330  
 Park, H ..... 21, 106, 173, 174  
 Park, J ..... 21, 23, 25, 26, 49, 246, 302, 372, 375  
 Park, K ..... 373  
 Park, M ..... 32, 266, 314, 380  
 Park, S ..... 23, 32, 58, 100, 179,  
 ..... 200, 204, 254, 295, 325, 369  
 Park, W ..... 300  
 Park, Y ..... 31, 32, 165, 169, 218, 285, 369  
 Parker, D ..... 220  
 Parlar, A ..... 30, 378, 379  
 Parra Garcia, M ..... 344  
 Parthasarathy, T ..... 298  
 Partin, K ..... 44  
 Pasco, A ..... 99  
 Pasko, A ..... 330  
 Patel, J ..... 132  
 Patel, P ..... 122, 231  
 Patiño, F ..... 333  
 Patiño Cardona, F ..... 333  
 Patoor, E ..... 261  
 Patrick, B ..... 185  
 Patrick, T ..... 113  
 Patterson, J ..... 236  
 Paul, J ..... 308  
 Paulino, L ..... 327  
 Pauly, S ..... 15, 136  
 Pawelkiewicz, M ..... 143, 314  
 Payet, M ..... 251  
 Payne, J ..... 49  
 Payton, E ..... 108  
 Payzant, A ..... 293  
 Paz, R ..... 372  
 Peace, J ..... 138  
 Pearlman, W ..... 350  
 Peaslee, K ..... 186  
 Pecard, D ..... 205  
 Pech-Canul, M ..... 245, 339  
 Pedersen, T ..... 280  
 Pedigo, A ..... 215  
 Pedron, M ..... 335  
 Pei, F ..... 92  
 Pei, Y ..... 207, 222  
 Pei-Ju, H ..... 330  
 Peiqian, L ..... 131



Pekguleryuz, M.....	20, 57, 58, 104,	Pinilla, N.....	275	Ptschelinzew, N.....	89
.....	105, 150, 151, 198, 200,	Pint, B.....	250, 302	Pugachevsky, M.....	129, 320
.....	248, 249, 300, 301, 340	Pinto, H.....	69	Pujari, P.....	18
Pelletier, A.....	73	Placzek, T.....	275	Puleo, D.....	231
Pellin, M.....	38	Plante, M.....	327	Punet, P.....	129
Peng, B.....	15, 16, 130	Plante, N.....	231	Purja Pun, G.....	187
Peng, C.....	72	Plapp, M.....	52, 149	Purohit, G.....	325
Peng, J.....	106	Pletcher, B.....	228	Pusztai, T.....	51, 195
Peng, L.....	51, 57, 58, 199, 249	Phikas, T.....	326	Puzyrev, Y.....	47
Peng, R.....	348	Plummer, J.....	365	Pyachin, S.....	129, 310, 320
Peng, T.....	223	Pochiraju, K.....	275	Pyczak, F.....	24
Peng, X.....	290	Podolskiy, A.....	26, 180	Pyon, T.....	157
Peng, Y.....	35	Poirier, S.....	96	Pyshkin, S.....	337
Penisten, J.....	29, 67	Pokorny, M.....	268	Pyun, Y.....	26
Pennycook, S.....	113	Polatidis, E.....	70	Pyzalla, A.....	42, 69
Pentz, A.....	192	Polesak, F.....	340		
Penumadu, D.....	42, 97	Politano, O.....	158	<b>Q</b>	
Peralta, P.....	49, 224, 225, 343, 344	Polkin, I.....	347	Qi, W.....	281
Perepezko, J.....	120, 153, 201	Pollaine, S.....	173, 174	Qi, Y.....	38
Perez, E.....	239	Pollock, T.....	21, 35, 60, 61, 108,	Qian, D.....	174
Pérez, M.....	333	.....	147, 151, 172, 294, 299	Qian, L.....	19
Perez, R.....	296, 377	Pomykala, J.....	123, 266, 316, 354	Qian, S.....	357
Perez, T.....	156	Pontes, L.....	345	Qiao, D.....	330
Pérez-Medina, J.....	376, 378	Poola, S.....	248	Qiao, R.....	114
Perez-Unzueta, A.....	367	Poole, W.....	201, 277	Qidwai, M.....	126
Perez Labra, M.....	333	Poon, J.....	285	Qijie, Z.....	298
Pericleous, K.....	326	Poor, D.....	347	Qin, Z.....	19
Perkins, J.....	157	Poorganji, B.....	226	Qing, C.....	329
Perlado, M.....	29	Popescu, C.....	290	Qing, H.....	377
Perovic, D.....	165	Popko, D.....	288	Qiu, G.....	131, 338
Perrotta, A.....	324	Poquette, B.....	107, 245, 361	Qiu, H.....	323
Perruchoud, R.....	95	Portella, P.....	126, 293	Qu, J.....	198, 211
Perrut, M.....	149	Porter, J.....	43	Qu, P.....	303
Persson, W.....	119	Portillo, B.....	154, 362	Qu, R.....	284
Peter, D.....	370	Poston, K.....	195	Qu, X.....	379
Peters, K.....	47, 48	Potapov, A.....	25	Quach, D.....	188
Peters, P.....	303	Poulsen, H.....	34, 69, 79, 125, 172, 223, 272	Quadir, M.....	367, 371
Petersen, B.....	324	Poulsen, N.....	87	Quan, L.....	377
Peterson, B.....	236	Pourmostadam, S.....	360	Quarforth, R.....	367
Peterson, E.....	235	Pouyan, S.....	121	Quek, S.....	103
Peterson, R.....	97, 98	Powell, A.....	350, 354	Queennec, X.....	225
Petit, J.....	243	Powell, K.....	227, 228	Querin, J.....	50, 51
Petkovic, B.....	119	Power, G.....	83	Quillien, C.....	60
Petri, N.....	104	Poynton, S.....	182	Quinones, S.....	109
Petric, A.....	253	Pozzi, C.....	281, 329		
Petrov, R.....	85	Prabhakaran, R.....	101, 344	<b>R</b>	
Petrusenko, Y.....	30, 182	Prabhu, R.....	328	Raabe, D.....	224, 287
Petry, W.....	97	Pradhan, D.....	140	Raahauge, B.....	324
Pettingill, J.....	105	Pradhan, N.....	47	Rabet, L.....	299
Pettit, F.....	303	Prahl, U.....	35	Rabkin, E.....	19, 25
Petty, A.....	290	Pramann, Z.....	100	Radmilovic, V.....	66, 159, 220
Pfeiffer, S.....	165	Prasad, S.....	206	Radovic, M.....	139, 306
Phadke, S.....	129	Prasad, Y.....	374	Rae, C.....	23, 187
Phanikumar, G.....	149	Prasannavenkatesan, R.....	99	Raffaella, R.....	37
Pharr, G.....	158	Pratt, P.....	156	Ragan, R.....	14
Phillion, A.....	102	Prentice, L.....	105	Ragani, J.....	283
Phillips, E.....	83, 130, 176, 227, 276, 324	Preuss, M.....	70, 213, 298	Raghavan, P.....	85
Phillips, J.....	260	Price, J.....	344	Raines, K.....	312
Phillips, P.....	342	Price, P.....	180	Rainforth, W.....	200
Phillpot, S.....	141, 315	Price, T.....	165	Raj, B.....	236
Piao, K.....	58	Prillhofer, B.....	182, 234, 267	Raj, R.....	313
Picraux, S.....	37	Prillhofer, R.....	267	Rajagopalan, S.....	221, 270
Pierer, R.....	109	Príncipe, C.....	360	Rajan, K.....	350
Pierron, O.....	193, 293	Prindle, J.....	189	Rajendran, A.....	283
Pike, L.....	25	Prisbrey, S.....	173	Rajgarhia, R.....	112
Pilchak, A.....	50, 147, 212	Prive, D.....	235	Rajulapati, K.....	136, 256
Pilotek, S.....	68	Proffen, T.....	213, 241	Rakotojaona, L.....	305
Pimentel, A.....	378	Proud, W.....	273	Ramachandran, M.....	93
Ping, C.....	203	Proust, G.....	35	Ramadan-Ragel, K.....	286
Ping, Y.....	380	Pruitt, L.....	38	Ramanujan, R.....	115, 226
Pinheiro, G.....	152	Przybyla, C.....	99	Ramar, A.....	30, 356
Pinheiro, R.....	316	Pschera, R.....	246		

- Ramesh, K.....161, 224, 341  
Ramesh, R.....224  
Ramirez, A.....174  
Ramirez, C.....73, 359  
Ramirez, M.....333  
Ramirez lopez, P.....272  
Ramos, A.....369  
Ramos, J.....185  
Ramos, K.....45  
Ramos, V.....156  
Ramu, A.....309  
Ramulu, M.....50  
Randall, N.....308  
Randau, C.....349  
Randman, D.....200  
Rangappan, A.....121  
Rangel, R.....354  
Rankin, W.....205  
Rantell, T.....145  
Rao, S.....144, 158  
Rao, W.....141  
Rao Manga, V.....306  
Raphael, J.....283, 284, 307  
Rappaz, M.....150, 286  
Raquet, O.....251  
Rashkeev, S.....113  
Rassizadeghani, J.....220  
Rath, B.....103  
Ratti, M.....160  
Ratvik, A.....240, 335  
Raveendra, S.....133  
Ravindra, N.....75, 121, 122, 168, 363  
Rawal, A.....282  
Rawlings, M.....226  
Rawlins, C.....186  
Rawls, G.....252  
Rawls, P.....154  
Rawson, M.....213  
Ray, P.....237, 290  
Ray, V.....175, 176  
Raymont, D.....135  
Raynova, S.....346  
Read, P.....263  
Reade, N.....104  
Ready, W.....82  
Real-Ramirez, C.....34, 64, 166  
Rebak, R.....251, 304, 343  
Reddemann, F.....361  
Reddy, N.....126, 361  
Reddy, R.....59, 93, 106, 140, 185  
Redkar, R.....271  
Redkin, A.....278, 335  
Reed, B.....81, 270, 321  
Reed, E.....128, 274, 321  
Reed, M.....235  
Reedy, E.....207  
Reek, T.....229  
Reeves, K.....305  
Reiche, H.....261  
Reid, M.....263  
Reilly, C.....123, 134  
Reinhart, G.....102, 196  
Reischig, P.....311  
Remington, B.....173, 225, 256  
Ren, H.....204  
Ren, Y.....137, 174, 184, 213, 255,  
.....261, 262, 284, 311, 312, 349  
Ren, Z.....103  
Renavikar, M.....313  
Renk, T.....206  
Renou, S.....103  
Renshaw, C.....54  
Renusch, D.....61  
Repper, J.....97  
Rest, J.....257  
Resto, O.....369  
Resto, P.....325  
Restrepo, O.....91  
Reusch, F.....235  
Reuter, M.....216, 334  
Reuther, K.....66, 325  
Reverdy, M.....327  
Revur, R.....313  
Reyes, A.....370  
Reyes, B.....373  
Reyes, M.....333  
Reyes-Valdes, A.....339  
Reyes Perez, M.....333  
Reynolds, A.....50, 243, 294, 296, 297, 298  
Reynolds, T.....375  
Rezai, B.....18  
Rezaiyan Deloei, M.....15  
Rhee, H.....170, 179, 339  
Rhee, K.....112  
Rho, D.....375  
Ribárik, G.....212  
Ribeiro, J.....324  
Ribeiro, M.....176  
Ribeiro, T.....176  
Ribis, J.....29, 160  
Rice, D.....107  
Rice, J.....295  
Richard, D.....292, 326  
Richard, M.....163  
Richard, R.....24  
Richard, S.....243  
Richards, D.....81  
Richards, V.....124, 186  
Richardson, C.....214  
Riedle, J.....289  
Riedler, M.....243  
Rieke, P.....252  
Rieken, J.....323  
Riemer, D.....165  
Ries, K.....145  
Rigby, J.....73  
Rigney, J.....22, 60, 107, 153, 201, 250, 302, 342  
Rijkeboer, A.....227, 228  
Rimoshevsky, S.....64  
Ringer, S.....136  
Rios, O.....183  
Rios, P.....139  
Rist, T.....372  
Ritchie, R.....179, 207, 233, 242, 312  
Ritter, C.....279  
Rivera, J.....129  
Rivera Diaz del Castillo, P.....273  
Rivero, I.....329  
Rivero, R.....168  
Riveros, G.....73, 216  
Rivoaland, L.....292  
Roberts, C.....334  
Roberts, J.....138  
Roberts, S.....27, 357  
Robertson, D.....64  
Robertson, I.....78, 124, 171, 220, 269  
Robertson, J.....116  
Robin, L.....234  
Robinette, M.....190  
Robinson, A.....248, 257  
Robinson, B.....346  
Robles Hernandez, F.....129, 345, 346  
Robson, A.....169  
Rodelas, J.....51, 101, 194  
Rodopoulos, C.....96  
Rodrigo, R.....230  
Rodrigues, A.....345, 364, 365  
Rodrigues Jr., D.....377  
Rodríguez, E.....333  
Rodríguez, F.....90  
Rodríguez, J.....116  
Rodríguez M., E.....53  
Rodríguez Torres, I.....92  
Roe, C.....126, 178  
Roeder, R.....16, 38, 87, 134,  
.....135, 179, 231, 282, 328  
Rogers, B.....191  
Rogers, J.....342  
Rogge, R.....348  
Rogov, S.....140  
Roh, H.....71  
Rokhlin, S.....54  
Rokkam, S.....67  
Rolland du Roscoat, S.....311  
Rollett, A.....334, 372  
Rolseth, S.....279  
Romano, E.....332  
Romanosky, R.....60  
Romanowski, C.....332  
Rombouts, M.....156  
Romero-Romo, M.....34  
Rong, Y.....93, 185, 280, 281  
Ronning, F.....255  
Roonasi, P.....307  
Rørvik, S.....240  
Rosalie, J.....300  
Rosario-Canales, M.....309  
Rosc, J.....170  
Rosefort, M.....331  
Rosei, F.....321  
Rosen, D.....62  
Rosenberger, A.....107  
Rosenberger, M.....371  
Rosenkilde, C.....278  
Ross, A.....183  
Ross, F.....37  
Ross, J.....86  
Ross, K.....295  
Ross, R.....135  
Ross, T.....190  
Rossell, M.....220  
Roters, F.....224  
Roth-Fagaraseanu, D.....303  
Roubidoux, J.....188  
Roue, L.....335  
Rouleau, M.....293  
Roush, R.....190  
Rousseaux, J.....228  
Roven, H.....28, 112  
Rowan, M.....109  
Rowenhorst, D.....80, 125, 126, 138, 172, 173  
Roy, A.....22, 24  
Roy, I.....159  
Roy, M.....329, 338  
Roy, S.....198  
Royer, Z.....161  
Rozenak, P.....278  
Ruan, S.....227  
Ruan, Y.....326  
Rubal, M.....50  
Rubisoff, H.....51, 149  
Rudd, R.....173  
Rudland, D.....305  
Rugg, D.....31  
Ruiz, P.....376  
Rullmann, F.....338

Ruokolainen, R .....	245	Sanders, D .....	50, 211	.....	114, 143, 149, 161, 174, 189,
Rupert, T .....	171, 206	Sandhage, K .....	87	.....	209, 258, 259, 309, 320, 345
Rupnowski, P .....	121	Sandoval, G .....	360	Schoenfeld, M .....	185
Ruscassier, N .....	235	Sanjari, M .....	364	Schoenung, J .....	16, 77, 113, 155, 156, 210, 254, 346
Ruscica, G .....	281	Sankar, J .....	107	Schoepfner, G .....	368
Russell, K .....	79, 160, 184, 225, 318	San Marchi, C .....	113, 221	Scholom, D .....	141
Russell, P .....	367	Sansoz, F .....	256	Schönfeld, B .....	116
Russo Spena, P .....	184, 242, 329	Santafé Jr., H .....	288	Schøning, C .....	292
Rusu, L .....	152	Santamaría, J .....	113	Schormann, S .....	235
Rutman, D .....	235	Santana, L .....	316	Schramm, J .....	89, 233
Rutz, H .....	204	Santella, M .....	194	Schroers, J .....	40, 88
Ruz, P .....	73	Santerre, R .....	279	Schrooten, J .....	62
Ryabkov, D .....	363	Santhanakrishnan, S .....	281	Schubert, D .....	240
Ryan, C .....	263	Santiago-Avilés, J .....	309	Schuh, C .....	171, 227, 232, 233, 283
Ryan, P .....	163	Santos, A .....	20	Schulson, E .....	54
Rye, K .....	229, 327	Santos, H .....	130	Schumacher, P .....	105, 170, 171
Ryman, S .....	230	Santos, J .....	176	Schuster, B .....	256
Rytkonen, M .....	216	Santos, P .....	362	Schütze, M .....	61, 303
Ryu, S .....	22, 378	Santos, R .....	227	Schvezov, C .....	170, 371
Ryu, T .....	253	Santos Jr., D .....	176	Schwaiger, R .....	308
<b>S</b>					
S. Aghamiri, S .....	17	Saphores, J .....	77	Schwandt, C .....	183
Saage, H .....	202	Sarahan, M .....	42	Schweiger, H .....	142
Saal, J .....	306	Sarath, M .....	153	Schwen, D .....	66
Sabau, A .....	170, 198	Sarikaya, M .....	282	Schwub, S .....	24
Sabri, Y .....	84	Sarma, V .....	236	Sciammarella, C .....	258
Sachdev, A .....	177, 248, 300, 302	Sarrafi, R .....	246, 297, 380	Sciammarella, F .....	258
Sadayappan, K .....	219	Sarrazin-Baudoux, C .....	243	Scott, C .....	275
Sadek, A .....	26	Sarveswara Rao, K .....	47	Scott, D .....	340
Sadigh, B .....	125, 274	Sasaki, M .....	58	Scott, J .....	59
Sadler, B .....	20, 95, 145, 179, 190, 240, 292, 335	Sasaki, S .....	55	Scott, P .....	252
Sadrnejad, S .....	129, 336	Sasaki, Y .....	311	Scott, S .....	269
Saez, R .....	216	Sastry, S .....	298	Seal, S .....	134, 222, 271, 319, 357, 373
Safdar, A .....	371	Sato, A .....	100, 295	Sears, J .....	61, 108, 155, 175, 204
Sager, C .....	301	Sato, H .....	55	Sebastian, J .....	270
Saha, A .....	373	Sato, Y .....	100, 194, 335	Sediako, D .....	199
Saha, P .....	20	Saucedo-Muñoz, M .....	366, 372	Seelaboyina, R .....	175
Sahin, F .....	254, 368, 374	Sauvage, T .....	75	Seetala, N .....	82
Sahoo, K .....	26	Sauvage, X .....	225	Seetharaman, S .....	63, 154, 236, 299, 379
Sahoo, M .....	219	Savard, G .....	95	Segadaes, A .....	316
Sahoo, S .....	18	Savic, V .....	144	Segatz, M .....	328
Sahu, R .....	26	Sawyer, W .....	89	Seidman, D .....	42, 54, 221, 223, 269,
Saikaya, M .....	87	Saxe, P .....	142	.....	270, 271, 342, 365, 366
Saito, J .....	14	Saxena, A .....	107, 112	Seifert, H .....	304
Saito, Y .....	273	Saxena, S .....	203	Seki, Y .....	179
Sakamoto, M .....	91	Sayed, A .....	253	Sekunowo, O .....	157
Sakidja, R .....	201	Saylor, D .....	15	Self, W .....	134
Sakurada, Y .....	121	Scamans, G .....	105	Selinger, R .....	353
Sakurai, T .....	88	Scardi, P .....	212	Semenova, O .....	75
Salageheh, N .....	99	Scarlett, N .....	279	Semiatin, L .....	31, 108
Salazar-Villalpando, M .....	372, 373	Scavino, G .....	184	Sencer, B .....	190
Saldana, C .....	65	Schaefer, R .....	132	Sengel, H .....	30, 378, 379
Salem, H .....	26	Schaeublin, R .....	30, 356	Sengupta, S .....	313
Saliba, C .....	90	Schaffer, P .....	80	Senkov, O .....	136, 284, 295
Salinas, E .....	333	Schafler, E .....	111	Seo, C .....	247
Salinas Rodriguez, E .....	333	Schauerman, C .....	37	Seo, J .....	380
Salisbury, C .....	341	Schenk, T .....	102	Seo, K .....	296
Salleo, A .....	129	Schlegel, S .....	304	Seo, S .....	263
Salman, U .....	142	Schlom, D .....	224	Seo, Y .....	326
Salston, M .....	30, 305	Schmahl, W .....	262	Seok, C .....	209
Salt, B .....	119	Schmetterer, C .....	120, 121, 167, 217	Seok-Ki, J .....	361, 366
Salvo, L .....	341	Schmid-Fetzer, R .....	104, 132	Seol, J .....	42
Samajdar, I .....	18, 133	Schmidt, H .....	324	Seong, B .....	16, 146
Samantaay, B .....	361	Schmidt, J .....	56	Seong-jong, K .....	361, 365, 366, 378
Samarov, V .....	108, 347	Schmidt, M .....	237	Sepehrband, P .....	277
Samir, J .....	110	Schmidt, R .....	236	Serbruyns, A .....	34
Sampaio, J .....	227	Schmidt, T .....	183	Serefoglu, M .....	149
Samuelsson, C .....	73	Schmidt-Rohr, K .....	282	Serna, S .....	362
Samvedi, V .....	155	Schmitz, T .....	89	Server, W .....	317
Sánchez, R .....	316	Schmölzer, T .....	262	Setman, D .....	24
		Schneibel, J .....	202	Seung-Jun, L .....	361, 378
		Schneider, A .....	326	Severo, D .....	326
		Schneider, J .....	44, 50, 51, 68, 94,	Seyfarth, A .....	139, 205, 236



- Shabala, S ..... 140  
 Shackelford, J ..... 329  
 Shade, P ..... 144  
 Shah, J ..... 282  
 Shah, M ..... 38  
 Shahbazian Yassar, R ..... 162, 180, 208  
 Shahnam, A ..... 149  
 Shakoorian, H ..... 23  
 Shamsuzzoha, M ..... 106, 178  
 Shan, Z ..... 189, 272, 307  
 Shanbhag, S ..... 353  
 Shang, J ..... 72, 74, 218, 232, 264, 351  
 Shang, P ..... 74, 218  
 Shang, S ..... 81, 200  
 Shangguan, D ..... 313  
 Shani, E ..... 278  
 Shankar, R ..... 65  
 Shankar, S ..... 124, 170, 220  
 Shanping, L ..... 111  
 Shao, L ..... 208, 346  
 Shao, S ..... 189  
 Shao-Horn, Y ..... 43  
 Shapiro, A ..... 77  
 Shapiro, S ..... 192  
 Sharafat, S ..... 30  
 Sharif, M ..... 246  
 Shariff, S ..... 337  
 Sharkey, M ..... 179  
 Sharma, D ..... 258  
 Sharon, J ..... 206  
 Sharp, A ..... 21  
 Sharp, I ..... 66  
 Shaviv, R ..... 117  
 Shen, C ..... 186, 237, 272  
 Shen, G ..... 200  
 Shen, H ..... 132  
 Shen, J ..... 284  
 Shen, Q ..... 16  
 Shen, Y ..... 161, 162, 255  
 Sheng, G ..... 141, 220  
 Sheng, W ..... 43  
 Shengming, X ..... 123, 218  
 Shenoy, R ..... 84  
 Shepard, M ..... 247  
 Shepelev, D ..... 150  
 Sheppard, F ..... 180  
 Sherburne, M ..... 308  
 Sherby, O ..... 247, 376  
 Sherman, D ..... 278  
 Shet, S ..... 121, 122  
 Shi, D ..... 146  
 Shi, G ..... 339  
 Shi, X ..... 19, 268  
 Shi, Y ..... 36, 44, 275  
 Shi, Z ..... 106, 248  
 Shian, S ..... 87  
 Shi Da, G ..... 164  
 Shifler, D ..... 60  
 Shiftlet, G ..... 285  
 Shih, D ..... 218, 263  
 Shim, D ..... 305  
 Shim, S ..... 158, 284, 379  
 Shimada, T ..... 174  
 Shimizu, T ..... 100, 146  
 Shin, B ..... 21  
 Shin, D ..... 112, 221, 276  
 Shin, E ..... 16, 146, 266, 361  
 Shin, H ..... 130  
 Shin, J ..... 214, 215  
 Shin, K ..... 58, 200, 302  
 Shin, S ..... 66, 247  
 Shinde, A ..... 14  
 Shipway, P ..... 320  
 Shirayama, S ..... 91  
 Shirazi, H ..... 226  
 Shivamurthy, R ..... 337  
 Shiwen, B ..... 276  
 Sholapurwalla, A ..... 269  
 Shon, I ..... 23, 27, 375  
 Shook, S ..... 301  
 Showalter, D ..... 299  
 Shrestha, T ..... 32  
 Shu, D ..... 69  
 Shu, Y ..... 92, 354, 355  
 Shukla, S ..... 226  
 Shuleshova, O ..... 196  
 Shull, P ..... 183  
 Shultz, T ..... 340  
 Shurov, N ..... 335  
 Shute, C ..... 171  
 Siao, C ..... 118  
 Sickafus, K ..... 258  
 Sidor, J ..... 85, 178  
 Siegenthaler, H ..... 370  
 Sievert, R ..... 293  
 Sigworth, G ..... 78  
 Silberschmidt, V ..... 263  
 Silberstein, R ..... 193  
 Sillekens, W ..... 151, 152  
 Silva, E ..... 20  
 Silva, F ..... 126, 227, 229, 360  
 Silva, J ..... 316  
 Silva, S ..... 229  
 Simensen, C ..... 235  
 Simmons, K ..... 298  
 Simões, S ..... 369  
 Sinclair, C ..... 21, 201, 275  
 Sinclair, K ..... 240  
 Singer, R ..... 60  
 Singh, A ..... 52, 72, 199, 209, 300  
 Singh, D ..... 85, 161, 162  
 Singh, G ..... 157  
 Singh, H ..... 170, 172  
 Singh, J ..... 225  
 Singh, N ..... 55, 56, 75, 121, 133, 168, 238, 280  
 Singh, P ..... 345  
 Singh, V ..... 373  
 Singhal, A ..... 180  
 Singler, T ..... 32  
 Sinn-wen, C ..... 39  
 Sinnott, S ..... 141, 315  
 Sisneros, T ..... 96, 212, 241, 261  
 Sisson, R ..... 110  
 Sivaprasad, P ..... 236  
 Sivaprasad, S ..... 333  
 Sivasankaran, H ..... 297  
 Siwick, B ..... 321  
 Sjöberg, G ..... 22  
 Sket, F ..... 42  
 Skrotzki, B ..... 293  
 Skrotzki, W ..... 66, 95, 148, 325  
 Skrzek, T ..... 341  
 Skybakmoen, E ..... 229, 278, 279, 335  
 Slade, S ..... 57, 248  
 Slama, P ..... 346  
 Slamova, M ..... 346  
 Slattery, D ..... 203  
 Slattery, K ..... 108, 211  
 Smart, R ..... 362  
 Smeller, M ..... 163  
 Smid, I ..... 224  
 Smirnov, S ..... 26, 180  
 Smith, B ..... 212  
 Smith, C ..... 29, 69, 148, 210, 257  
 Smith, D ..... 83, 216  
 Smith, J ..... 160, 318  
 Smith, P ..... 130  
 Smith, R ..... 31, 174, 344  
 Smith, S ..... 175  
 Smugeresky, J ..... 55, 61, 108, 155, 156  
 Snead, L ..... 31, 257  
 Snook, G ..... 279  
 Snugovsky, P ..... 262  
 Soboyejo, W ..... 27  
 Sobrinho, A ..... 345  
 Soderlind, P ..... 81  
 Soffa, W ..... 238  
 Sofo, J ..... 315  
 Sohn, H ..... 185, 253  
 Sohn, S ..... 25, 26  
 Sohn, Y ..... 69, 142, 143, 188, 189, 210, 239, 290, 291  
 Soisson, F ..... 187, 334  
 Sokolov, M ..... 65, 357  
 Sokolov, V ..... 268  
 Sokolowski, J ..... 104  
 Solak, N ..... 366  
 Solheim, A ..... 278, 279, 280, 292  
 Solórzano Naranjo, G ..... 16  
 Somani, M ..... 39, 112, 232  
 Somekawa, H ..... 52, 72, 199, 300  
 Sommariva, M ..... 46  
 Sommer, A ..... 232  
 Sommitsch, C ..... 34, 246  
 Son, I ..... 112  
 Son, S ..... 367  
 Son, Y ..... 126  
 Song, B ..... 357  
 Song, C ..... 312, 376  
 Song, H ..... 226  
 Song, J ..... 22, 33, 168, 202, 265, 365  
 Song, K ..... 58, 266  
 Song, M ..... 19  
 Song, X ..... 362  
 Song, Y ..... 267  
 Soni, P ..... 346  
 Sonmez, S ..... 205  
 Sopori, B ..... 121, 168  
 Sordelet, D ..... 285  
 Sordo, F ..... 29  
 Sorensen, C ..... 100, 101, 148  
 Sorhuus, A ..... 87  
 Soriano-Vargas, O ..... 372  
 Sosa, J ..... 42  
 Soucy, G ..... 335  
 Southwick, L ..... 72, 73  
 Souza, L ..... 364  
 Spaepen, F ..... 283  
 Spangenberg, J ..... 123, 354  
 Spanos, G ..... 125, 126, 138, 173, 277, 350  
 Spatig, P ..... 356  
 Spatschek, R ..... 102  
 Spearot, D ..... 112  
 Specht, E ..... 42  
 Speck, J ..... 296  
 Spolenak, R ..... 163, 206  
 Spowart, J ..... 68, 114, 115, 161, 172, 209, 258, 309, 345  
 Squatrito, R ..... 268  
 Squillacioti, R ..... 299  
 Sreeranganathan, A ..... 172  
 Sridharan, K ..... 160, 305  
 Srinivasan, R ..... 55, 147, 197, 198, 211, 348  
 Srinivasan, S ..... 59, 164  
 Sriram, V ..... 33, 187  
 Srivastav, D ..... 18

Srivastava, D.....	321, 334	Sugar, J.....	56	Tamimi, S.....	364
Srivastava, S.....	107	Sugino, Y.....	301	Tamirisakandala, S.....	198, 293
Srolowitz, D.....	25, 93	Sugui, T.....	19	Tamura, N.....	70, 71, 117, 351
Srowthi, B.....	336	Suh, C.....	26	Tamura, T.....	40, 104
St-Georges, L.....	293	Suh, J.....	40, 71, 88, 233	Tan, C.....	106, 165, 371
Stach, E.....	37, 65, 207, 313	Suh, M.....	31	Tan, L.....	305
Stafford, G.....	187	Suh, Y.....	161	Tan, P.....	166
Stål, R.....	90	Sui, C.....	331	Tan, S.....	236, 265
Staley, J.....	364	Sui, Z.....	266, 316	Tanaka, Y.....	27
Stalheim, D.....	252	Sukhopar, O.....	132	Tancret, F.....	334
Stam, M.....	230	Sukla, L.....	47	Tandon, G.....	368
Stampanoni, M.....	80, 102, 222	Sulger, P.....	240	Tang, G.....	161, 162
Stampfli, J.....	370	Suminski, C.....	259	Tang, M.....	158, 258
Stanek, C.....	343	Sun, D.....	52	Tang, S.....	319
Stanescu, C.....	287	Sun, F.....	260	Tang, W.....	35, 218, 343
Stanica, C.....	287	Sun, G.....	349	Tang, Z.....	107, 113, 250
Staron, P.....	262	Sun, H.....	205	Tangstad, M.....	235, 269
Stauder, B.....	171	Sun, J.....	351	Tanigawa, H.....	357
Steel, R.....	101	Sun, K.....	75, 229, 360	Tanimoto, Y.....	329
Stein, F.....	46	Sun, N.....	131	Tannenbaum, J.....	332
Steinbach, I.....	102, 238	Sun, P.....	111, 113	Tanniru, M.....	203, 227
Steinzig, M.....	212	Sun, Q.....	364	Tao, J.....	19
Stellacci, F.....	134	Sun, S.....	37	Tao, N.....	255
Stenholm, K.....	205	Sun, W.....	61	Tao, X.....	82
Stephenson, G.....	163, 261	Sun, X.....	262	Tao, Y.....	379
Stergar, E.....	65, 161, 262	Sun, Y.....	32, 256, 313	Tapia, A.....	216
Steuwer, A.....	49, 97, 100, 244	Sun, Z.....	20, 254	Tarafder, M.....	333
Stevenson, J.....	345	Suominen Fuller, M.....	70	Tarafder, S.....	333
Stewart, D.....	98	Suresha, S.....	64	Tarcy, G.....	230
Stiller, K.....	293	Surh, M.....	274	Task, M.....	303
StJohn, D.....	287	Suri, J.....	159	Tatiparti, S.....	227
Stock, S.....	180	Suri, P.....	61, 108, 155, 204, 254, 325	Tavares, V.....	169, 219
Stoddard, N.....	269	Suryanarayana, C.....	137	Tavazza, F.....	70, 94
Stoffel, D.....	98	Suslov, S.....	65	Tavera Miranda, F.....	333
Stoica, A.....	146, 192, 241	Suwantong, O.....	134	Tavsanoglu, T.....	223
Stoica, M.....	330, 368	Suwas, S.....	198	Taylor, J.....	191
Stoken, J.....	116	Suzuki, A.....	60, 61	Taylor, K.....	350
Stolken, J.....	224	Suzuki, J.....	146	Taylor, M.....	16, 191, 230, 231, 278, 326
Stölken, J.....	127	Svedberg, E.....	310	Taylor, P.....	205
Stollberg, D.....	14, 37, 82, 129, 175, 226, 274, 323	Svinsås, E.....	280	Teale, R.....	49
Stoller, R.....	30, 317, 318, 355	Swallow, C.....	211	Tedenac, J.....	75, 291
Stolten, D.....	305	Swaminathan, S.....	49	Tegze, G.....	52, 195
Stone, D.....	325	Sweatman, K.....	263, 264	Tekin, M.....	378
Stone, H.....	23	Swiatek, G.....	299	Telesman, J.....	107
Stosnach, H.....	139	Swift, D.....	274	Templeton, J.....	345
Stotler, T.....	50, 100	Swiostek, J.....	200	Temur, D.....	249, 250
Stoudt, M.....	222	Swoboda, B.....	28, 67	Teng, Z.....	61
Streiffer, S.....	163, 261	Syed Asif, S.....	272	Tenorio, J.....	169
Streitz, F.....	81	Syn, C.....	247, 376	Tenório, J.....	123, 219, 316
Strizak, J.....	252	Szczepanski, C.....	148	TerBush, J.....	151
Strohaecker, T.....	294			Terentyev, D.....	209
Stubbins, J.....	29, 114	<b>T</b>		Terrones, L.....	185
Stumphy, B.....	79	Tabachnikova, E.....	26, 180	Tersoff, J.....	37
Su, C.....	354	Taber, G.....	35, 59, 363	Terzieff, P.....	121
Su, J.....	49	Tabereaux, A.....	278	Teslina, M.....	320
Su, S.....	313	Tada, S.....	124, 220	Tessier, J.....	16, 41, 86, 134, 179, 190, 229, 230, 278, 279, 326, 327
Su, Z.....	309	Tadano, S.....	45	Tewari, A.....	170, 177
Suarez, C.....	324	Tafforeau, P.....	102	Tewari, R.....	225, 321
Suarez, M.....	90	Taheri, A.....	364	Thadhani, N.....	173, 358, 359
Suárez, M.....	325	Taheri, M.....	204, 270, 321	Thapa, S.....	179
Suárez, O.....	360, 367	Tai, C.....	22	Thaurmarajah, A.....	151
Subbarayan, G.....	32, 34, 215, 352	Tai, Y.....	88	Theillet, P.....	293
Subjeck, J.....	34	Takacs, P.....	47	Thein-Han, W.....	232, 282
Subramanian, K.....	47, 118, 214, 263	Takaku, Y.....	120, 121	Therien, M.....	309
Subramanian, P.....	65, 153, 159	Takemoto, T.....	313	Thess, A.....	370
Subramanian, R.....	175	Takigawa, Y.....	150, 248	Thirumalai, N.....	44, 238, 293
Subramanian, V.....	14, 313	Taleff, E.....	277, 302	Thoma, D.....	80, 127, 173, 224, 241, 273, 321, 322, 358
Sudamore, R.....	156	Talia, G.....	244	Thomas, B.....	109
Sudbrack, C.....	223	Taloi, D.....	290	Thomas, H.....	290
Suenaga, S.....	31, 263, 264	Tamarisakandala, S.....	197	Thomas, M.....	243
Suery, M.....	283	Tamerler, C.....	282		
Suganuma, K.....	71, 74				

- Thomas, W ..... 211  
Thome, M ..... 85  
Thompson, B ..... 50, 100  
Thompson, C ..... 162, 163, 183, 261  
Thompson, G ..... 14, 37, 82, 129, 175, 226, 274, 323  
Thonstad, J ..... 279  
Thornton, D ..... 312  
Thornton, K ..... 34, 79, 125, 172,  
221, 223, 272, 314, 353  
Threrurirapapong, T ..... 197  
Thube, S ..... 368  
Tian, B ..... 34  
Tian, G ..... 342  
Tian, J ..... 181  
Tian, Q ..... 15, 246, 253, 267, 355, 370  
Tian, Y ..... 228  
Tian, Z ..... 319  
Tianzu, Y ..... 53, 266  
Tien, H ..... 203  
Tikasz, L ..... 240  
Tilak, R ..... 89  
Tiley, J ..... 69, 115, 162, 209,  
212, 260, 270, 311, 348  
Timm, J ..... 178  
Timur, S ..... 296, 361  
Tin, S ..... 107  
Tinghaev, P ..... 278  
Tiryakioglu, M ..... 77, 78, 123, 170, 219, 267  
Tischler, J ..... 69, 70, 94, 162, 163  
Tisdale, D ..... 166  
Tiwari, R ..... 18  
Tiwari, S ..... 177  
Tjahjanto, D ..... 375  
Tkatcheva, O ..... 278  
Toby, B ..... 212  
Todaro, I ..... 268  
Todd, I ..... 88, 109, 156, 365  
Todd, J ..... 340  
Todd, P ..... 143  
Todorovic, B ..... 119  
Toghraie, M ..... 358  
Tomar, V ..... 66, 155, 232, 328  
Tomasino, T ..... 230  
Tomaswick, K ..... 63  
Tomchik, C ..... 114  
Tome, C ..... 80, 201, 348  
Tomé, C ..... 341  
Tomesani, L ..... 268  
Tomio, Y ..... 270  
Tomota, Y ..... 146  
Tomozawa, M ..... 76  
Tomsett, A ..... 145  
Tomus, D ..... 112, 347  
Tong, C ..... 314  
Tong, M ..... 34  
Topping, T ..... 25, 28, 40, 41, 111, 113, 211, 346  
Torabi, S ..... 122  
Torbet, C ..... 21, 299  
Torem, M ..... 354  
Toro, C ..... 166, 216  
Toroian, D ..... 180  
Torrents Cabestany, A ..... 28  
Torres, J ..... 376  
Torres-Castañón, J ..... 378  
Tosta, R ..... 20  
Toth, G ..... 195  
Tourret, D ..... 150  
Toyama, T ..... 113, 208  
Tracy, S ..... 343  
Traiviratana, S ..... 94  
Tran, D ..... 53, 288  
Tran, S ..... 271  
Tran, T ..... 329, 339, 349  
Trappmann, C ..... 305  
Trautmann, C ..... 257  
Traxler, G ..... 42  
Treimer, R ..... 73  
Trejo, M ..... 362, 372  
Trelewicz, J ..... 283  
Tremblay, S ..... 286  
Trempe, O ..... 292  
Tribyshevsky, V ..... 64  
Tringides, M ..... 163  
Trinkle, D ..... 45, 124, 187, 222, 321  
Tripathi, N ..... 166  
Tritt, T ..... 309  
Trivedi, R ..... 150  
Troczyński, T ..... 73  
Troppeano, A ..... 90  
Truan-Sheng, L ..... 76, 188  
Trubuil, J ..... 235  
TS, S ..... 380  
Tsai, A ..... 52, 72  
Tsai, C ..... 117, 331  
Tsai, M ..... 74  
Tsai, T ..... 265  
Tsakirooulos, P ..... 23, 154  
Tsang, H ..... 330  
Tsao, C ..... 41  
Tsao, W ..... 33  
Tsay, C ..... 89  
Tschöpe, K ..... 292  
Tseng, H ..... 118  
Tseng, T ..... 368  
Tso, C ..... 144  
Tsujimoto, M ..... 74  
Tsukamoto, H ..... 31, 264  
Tsuzaki, K ..... 146  
Tu, K ..... 33, 42, 71, 75, 117, 187, 215, 351  
Tuck, C ..... 62  
Tucker, G ..... 144  
Tucker, J ..... 28, 34, 67, 269, 340  
Tucker, T ..... 297  
Tuffour, B ..... 269  
Tugral, H ..... 379  
Tulk, C ..... 47  
Tumey, S ..... 321  
Tumne, P ..... 263, 352  
Tuppen, S ..... 110  
Tupper, C ..... 241  
Turan, A ..... 379  
Turbini, L ..... 31, 71, 117, 164, 214, 262, 313, 351  
Turchi, P ..... 81, 115, 116, 321  
Turner, D ..... 173, 328  
Turner, J ..... 121, 122  
Turri, G ..... 337  
Turski, M ..... 96  
Tweedy, B ..... 243, 244  
Tyagi, S ..... 68  
Tzamtzis, S ..... 104
- U**
- Uberuaga, B ..... 258, 322  
Uchic, M ..... 144, 158, 172  
Ucisik, A ..... 17  
Ucuncuoglu, S ..... 249, 250  
Ueshima, M ..... 264  
Uesugi, T ..... 150  
Uffelman, D ..... 84  
Uggowitzzer, P ..... 340  
Uhlir, J ..... 346  
Ulbricht, A ..... 30  
Uludag, H ..... 134
- Umakoshi, Y ..... 301  
Umeda, J ..... 267  
Ungar, T ..... 212, 213  
Ungár, T ..... 112, 213  
Ünlü, N ..... 55, 369  
Unocic, R ..... 189, 291, 342  
Upadhyaya, A ..... 376  
Uphaday, P ..... 243  
Upmanyu, M ..... 29, 37, 168, 334  
Urban, A ..... 279  
Usta, M ..... 17  
Uthaisanguk, V ..... 35  
Utke, O ..... 104  
Uwakweh, O ..... 296, 377
- V**
- Vaia, R ..... 258  
Vaidyanathan, R ..... 241  
Vainik, R ..... 90  
Vaja, J ..... 241  
Valdes Lopez, R ..... 123  
Valdevit, L ..... 108  
Valdez, J ..... 258  
Valdez, S ..... 362, 373  
Valero Rocha, M ..... 92  
Valiev, R ..... 26, 111, 112, 213  
Vallabhajosyula, P ..... 156  
Vamraak, K ..... 292  
Van Bael, S ..... 62  
Van Benthem, K ..... 113  
Van Buuren, A ..... 274  
van Buuren, T ..... 116  
van Dalen, M ..... 269  
van den Bergh, M ..... 69, 210  
Vandenbroucke, B ..... 62  
Vande Put, A ..... 250  
Van der Berg, N ..... 188  
Vander Biest, O ..... 254  
van der Hulst, R ..... 207  
Van der Ven, A ..... 28, 44, 125, 142  
van der Zwaag, S ..... 80, 273  
Van De Walle, A ..... 289  
Van de Walle, C ..... 296  
Van Houtte, P ..... 299  
Van Nugtren, K ..... 305  
Van Petegem, S ..... 223  
van Putten, K ..... 85  
Van Sluytman, J ..... 108  
Van Swygenhoven, H ..... 158, 162, 223  
Van Tyne, C ..... 44  
Van Vliet, K ..... 231  
van Walle, E ..... 113  
Varela, M ..... 113  
Vargas, J ..... 216  
Vargas, P ..... 377  
Variot, P ..... 214  
Varma, S ..... 154, 362  
Varvenne, C ..... 237  
Vasconcelos, P ..... 240  
Vasile, I ..... 281  
Vasilev, I ..... 119  
Vasshaug, K ..... 335  
Vasudevan, V ..... 80, 127, 173, 174, 184,  
202, 222, 224, 273, 321, 358  
Vaynman, S ..... 171  
Vecchio, K ..... 234  
Vedamanickam, S ..... 338  
Vee, T ..... 230  
Veilleux, M ..... 99  
Velasco, E ..... 123  
Velez, C ..... 272



Vellios, N.....	23, 154	Walker, M.....	170	Weidemann, C.....	69
Venkatasubramanian, C.....	336	Walker, R.....	50, 109, 227	Weidner, A.....	95, 148
Venkatesh, V.....	311	Walleser, J.....	313	Weifeng, L.....	53, 266
Venkateswaran, P.....	294	Walley, S.....	273	Weihmuller, L.....	211
Ventura, J.....	154, 362	Walmsley, J.....	28	Weih, T.....	175, 321, 358
Verdier, M.....	190	Waly, M.....	292, 371	Weil, K.....	68, 154, 203, 252,
Vergara Mojica, J.....	296	Wang, B.....	31, 281, 354	.....	260, 305, 306, 344, 345
Verhaeghe, F.....	238, 362	Wang, C.....	36, 63, 72, 74, 120, 217,	Weil, S.....	59, 106
Verma, R.....	201, 301, 302	.....	246, 316, 340, 345, 366, 377	Weiland, H.....	133
Verma, V.....	129	Wang, D.....	343	Weinberger, T.....	100
Vermaak, N.....	108	Wang, F.....	204, 262, 340, 368	Weis Olea, C.....	294
Vermette, H.....	279	Wang, G.....	14, 39, 40, 61, 88, 108,	Weiss, B.....	264
Vettier, C.....	46	.....	110, 135, 180, 181, 232, 233,	Weiss, D.....	78, 219
Veysiere, P.....	312	.....	234, 261, 281, 283, 284, 307, 329	Weissgaerber, T.....	56
Viana, F.....	369	Wang, H.....	37, 45, 208, 255, 257, 267, 307, 347	Weissmüller, J.....	65
Vianco, P.....	34, 273	Wang, J.....	82, 138, 177, 196, 208,	Welberry, T.....	311
Viano, D.....	287	.....	259, 272, 276, 372, 379	Welch, B.....	191
Vidal, E.....	47, 97, 205, 304	Wang, K.....	157, 167, 220, 228, 335, 341, 352	Weldon, D.....	261
Vieh, C.....	161	Wang, L.....	29, 35, 69, 94, 156,	Welk, B.....	147, 211, 260
Vieira, C.....	288, 316	.....	170, 198, 257, 274, 349, 369	Wells, M.....	277, 287
Vieira, L.....	362, 366, 370	Wang, M.....	335	Wells, P.....	244
Vieira, M.....	369	Wang, P.....	140, 156, 205, 254, 325, 339, 373	Welsh, G.....	49
Vigliante, A.....	261	Wang, Q.....	57, 246, 355	Wen, C.....	37
Vijayalakshmi, S.....	177	Wang, R.....	249	Wen, W.....	342
Vikhnin, V.....	276	Wang, S.....	21, 59, 204, 319, 330	Wen, X.....	178, 202, 228, 229
Vild, C.....	90	Wang, W.....	86, 310, 330, 368	Wen, Y.....	298
Villarreal, T.....	49	Wang, X.....	14, 17, 46, 96, 105,	Wenchao, D.....	111
Villechaise, P.....	294	.....	135, 136, 146, 182, 185, 191,	Wendt, J.....	199
Villegas, D.....	180	.....	192, 206, 241, 278, 295, 351, 363	Wendt, W.....	119
Vincent, A.....	134	Wang, Y.....	18, 24, 43, 59, 69, 81, 82,	Wentang, X.....	53, 266
Viskari, L.....	293	.....	92, 106, 108, 113, 115, 141,	Wenyuan, W.....	377
Viswanathan, B.....	348	.....	162, 175, 186, 189, 200, 201, 212,	Werber, A.....	269
Viswanathan, G.....	270, 370	.....	213, 223, 237, 239, 248, 255, 258,	Werner, E.....	97
Viswanathan, S.....	20, 170, 226	.....	260, 261, 262, 272, 277, 284, 286, 289,	West, E.....	209
Vitchus, B.....	145	.....	290, 311, 327, 334, 348, 352, 355, 369	West, J.....	175
Vivek, A.....	35, 363	Wang, Z.....	21, 52, 103, 106, 169,	West, M.....	194, 195
Vladutiu, L.....	290	.....	229, 267, 299, 307, 314, 351	Westphal, B.....	344
Vo, N.....	172	Warczok, A.....	73, 216	Wetscher, F.....	225
Vogel, F.....	61	Ward, D.....	161	Wheeler, D.....	51, 350
Vogel, S.....	46, 201, 212, 261, 343, 349	Ward-Close, M.....	260, 311	Wheeler, K.....	343, 344
Voggenreiter, H.....	303	Wark, J.....	173, 274	Wheeler, R.....	144
Vogler, T.....	35	Warner, A.....	119	Wheling, F.....	235
Vogt, F.....	190	Warren, J.....	15, 51, 315, 350	Whitacre, J.....	252
Vogt, R.....	113, 210, 346	Warren, O.....	272	White, H.....	155
Voigt, A.....	76, 122	Warren, R.....	199	White, P.....	344
Voje, J.....	123	Was, G.....	28, 29, 66, 67, 113,	Whitekettle, W.....	331
Volland, A.....	283	.....	160, 208, 209, 257, 299	Whitfield, D.....	280
Vollmer, J.....	269	Watanabe, M.....	220	Whitis, D.....	108
Volz, H.....	261, 297, 322, 343	Watcharotone, S.....	114	Whyatt, L.....	357
Voorhees, P.....	52, 80, 102, 125, 221, 222, 334	Waters, M.....	315	Wicker, R.....	109
Vorontsov, V.....	23, 187	Watson, K.....	240	Wickett, M.....	81
Voskoboynikov, R.....	187	Watt, D.....	247	Widderburn, I.....	100
Vratislav, S.....	46	Wawrzynek, P.....	99	Widener, C.....	194, 195, 244
VS Prakash, S.....	170	Wayne, L.....	225	Wierzba, B.....	143, 314
		Waz, E.....	234	Wierzbicka-Miernik, A.....	120
<b>W</b>		Weatherspoon, M.....	87	Wiest, A.....	40, 88, 233
Wachgama, N.....	216	Webb, E.....	37	Wiezorek, J.....	25, 45, 127, 132, 270
Wachs, D.....	257, 258	Weber, T.....	185	Wifi, A.....	363
Wachter, L.....	54	Webler, B.....	132	Wight, J.....	244
Wadsworth, J.....	247	Weck, A.....	275	Wikoff, D.....	98
Wagner, B.....	56	Wedde, G.....	87, 327	Wilensky, U.....	315
Wagner, D.....	341	Wedershoven, E.....	230	Wilgen, J.....	146
Wagner, G.....	294, 295, 325	Weertman, J.....	171	Wilkening, S.....	191
Wagner, J.....	165	Wegst, U.....	328	Wilkinson, A.....	48, 94, 147
Wagner, M.....	262, 370	Wei, C.....	19, 22, 33, 358	Wilkosz, D.....	59
Wagner, W.....	96, 97	Wei, D.....	108	Wilks, G.....	137
Wagoner, R.....	58	Wei, F.....	146	Willaime, F.....	208
Wagstaff, R.....	331	Wei, K.....	199	Willard, M.....	226
Walczak, B.....	60	Wei, L.....	53, 101, 199, 266, 371	Willey, T.....	116
Waldner, G.....	275	Wei, Q.....	256	Williams, C.....	62
Walker, B.....	27, 50	Wei-lian, W.....	54	Williams, E.....	98, 137, 234
		Wei-liang, W.....	355	Williams, F.....	324

- Williams, J .....50, 54, 126, 147, 212, 264, 294, 314  
Williams, L.....328  
Williams, M .....350  
Williams, R .....270  
Williams, S.....98  
Williams, T.....317  
Williamson, D .....177  
Wilson, B .....262  
Wilson, S .....334  
Wilt, D .....37  
Wimmer, E .....142, 269  
Wind, S .....324  
Windes, W .....157  
Windl, W .....180, 286, 289  
Winey, K .....114, 115  
Wingate, C .....130  
Winiarski, B .....181  
Winkelmann, A.....328  
Winter, G.....34  
Wirth, B.....28, 31, 66, 67, 113,  
.....114, 146, 160, 208, 209,  
.....257, 317, 318, 355, 356  
Wise, S .....76, 93, 122  
Withers, P.....96, 181, 244, 298  
Withers, R .....311  
Withey, E.....66  
Wögerer, C.....42, 275  
Wojewoda-Budka, J .....120  
Wolcott, J .....263  
Wolf, D .....67, 207, 258, 322  
Wolf, W .....142, 269  
Wolfson, N .....40  
Woll, A .....163  
Wollants, P .....34, 80, 238, 362  
Wollmershauser, J .....199, 348  
Wolverton, C .....43, 221  
Wombles, R.....95, 145  
Wong, K .....67  
Wong, P .....205  
Won Seok, C .....164  
Woo, K .....23, 27, 375  
Woo, W .....96, 213, 295  
Wood, J .....216  
Woodall, J.....278  
Woodard, S.....22, 60, 107, 153, 201, 250, 302, 342  
Woodfield, A.....54  
Woods, J .....263, 352  
Woodward, C .....124, 144, 153, 158,  
.....171, 172, 298, 303  
Wooten, J.....347  
Worthington, D.....143  
Wraith, A.....73, 165  
Wright, J.....261  
Wright, T.....224  
Wright, W.....181, 284  
Wroczewski, W .....264  
Wu, A .....31, 71, 75, 117, 118,  
.....164, 167, 214, 262, 313, 351  
Wu, B .....269  
Wu, C .....81, 203, 268, 286  
Wu, D .....33, 92, 247  
Wu, E .....227, 349  
Wu, H .....222  
Wu, J .....19, 345, 358, 374  
Wu, K .....120, 238, 342  
Wu, L .....281, 349, 364  
Wu, M .....236, 265  
Wu, P .....232  
Wu, Q .....87  
Wu, R .....14, 303  
Wu, S .....255, 265  
Wu, W .....42, 118, 302, 330  
Wu, X .....29, 106, 204, 208, 247, 256, 298, 299  
Wu, Y .....59, 199, 218, 246, 276, 323, 335, 369  
Wu, Z .....223, 357  
Wynne, B.....200
- X**
- Xenidis, A.....131  
Xi, X .....224  
Xi, Y .....63  
Xi, Z .....370  
Xia, G .....344, 345  
Xia, M .....105, 249  
Xia, X .....54  
Xiangyang, Z.....18  
Xiantie, Z .....329  
Xianyu, B .....19  
Xiao, D .....21, 93, 164, 278  
Xiao, H .....92  
Xiao, N .....334  
Xiao, S .....247  
Xiao, X .....274  
Xiao, Z .....36, 44, 366, 377  
Xiaobu, L .....218  
Xiaodong, Y .....230  
Xiaojun, L .....336  
Xiaoqin, Z .....57  
Xie, G .....40, 88, 137  
Xie, J .....340  
Xie, S .....171, 284  
Xie, W .....352  
Xin, H .....18  
Xing, J .....164  
Xing, Y .....263, 352  
Xingmin, C.....63  
Xinhua, L .....131  
Xiong, D .....169  
Xiong, S .....281  
Xiong, Y.....155, 156  
Xu, B .....130  
Xu, C .....27, 176, 346  
Xu, D .....33, 45, 75, 114, 187, 356  
Xu, G .....215, 351  
Xu, H .....19, 141, 211  
Xu, J .....89  
Xu, L .....33, 75, 117, 215  
Xu, N .....70  
Xu, Q .....273  
Xu, R .....312  
Xu, S .....114, 160, 200  
Xu, T .....208, 289, 335  
Xu, W .....86, 273  
Xu, X .....364  
Xu, Y .....342, 354  
Xu, Z .....107, 185, 364  
Xue, B .....377  
Xue, J .....20, 307  
Xue, L .....204  
Xue, W .....39  
Xue, Y .....99, 147, 161  
Xuejun, J .....373
- Y**
- Yablinsky, C .....294  
Ya Feng, L .....230  
Yakubtsov, I.....301  
Yamagishi, H.....49  
Yamakov, V.....207  
Yamamoto, K .....306  
Yamamoto, T.....28, 209, 318, 356, 357  
Yamasaki, M .....58, 301  
Yamasaki, T.....329  
Yan, J .....319  
Yan, Q .....317, 355  
Yan, S .....336  
Yan, Y .....121, 122, 375  
Yanada, I .....74  
Yang, B .....41, 92  
Yang, C .....32, 72, 113, 149, 206, 266, 275  
Yang, D .....36, 219, 366, 377  
Yang, F .....38, 106, 181, 247, 368  
Yang, H .....28, 41, 43, 159, 303, 371  
Yang, J .....33, 34, 155, 187, 232  
Yang, K .....26  
Yang, L .....146  
Yang, M .....306, 323  
Yang, N .....113, 207, 221  
Yang, P .....18, 19, 358  
Yang, Q .....74, 194, 363  
Yang, R .....45  
Yang, S .....21, 31, 64, 106, 167, 245, 297  
Yang, T .....26, 54  
Yang, W .....132  
Yang, X .....186, 229  
Yang, Y .....18, 22, 29, 35, 42,  
.....52, 59, 94, 151, 153, 238,  
.....276, 330, 342, 360, 375, 380  
Yang, Z .....154, 203, 252, 305, 306, 344, 345, 354  
Yann, d .....113  
Yanqing, L.....18, 336  
Yao, B .....69, 210  
Yao, G .....132, 152, 201, 357, 364  
Yao, K .....286  
Yao, L .....378  
Yao, S .....302  
Yao, W .....254  
Yao, Y .....110  
Yao, Z .....30, 114  
Yaomian, W .....376  
Yaowei, Y .....53  
Yap, Y .....208  
Yasi, J .....45  
Yasunaga, K .....84  
Yates, S .....343  
Yavari, A.....40  
Yazzie, K.....264  
Ye, B .....260  
Ye, F .....336  
Ye, J .....60, 66, 106, 256, 308  
Yeager, C .....363  
Yen, Y .....74, 120, 167, 168, 217, 265  
Yexiang, L .....336  
Yi, D .....66  
Yi, J .....319  
Yi, M .....379  
Yi, S .....302  
Yihong, Y .....276  
Yim, C .....21  
Yim, J .....63  
Yin, F .....342  
Yin, H .....110, 379  
Yin, J .....277  
Yin, W .....84, 131, 177, 228, 277, 325  
Yin, Z .....83, 131, 253, 276, 277  
Yiping, Z .....18  
Yiyi, L .....111  
Yokotani, N .....301  
Yokoyama, Y.....40, 88, 137, 181, 234, 329  
Yoo, B .....285  
Yoo, K .....169  
Yoo, S .....87  
Yook, W .....330  
Yoon, C .....62, 76  
Yoon, D .....200

Yoon, H	266	Zhai, Q	297, 364, 371, 376	Zhu, A	285
Yoon, J	23, 375	Zhai, T	178, 229	Zhu, B	322
Yoon, S	332, 366, 376	Zhai, X	317	Zhu, D	232
Yoon, Y	63	Zhan, D	105	Zhu, F	205
Yoozbashizadeh, M	155	Zhan, J	18, 19, 358, 374	Zhu, G	14, 16, 38
Yoshimura, Y	116	Zhan, X	36, 44	Zhu, H	206, 266, 307, 323
Yoshioka, Y	233	Zhang, B	309, 363	Zhu, J	20, 122, 229, 236, 238, 299
You, B	21, 200	Zhang, C	18, 19, 238, 286, 358, 374	Zhu, M	102
You, J	14, 310	Zhang, D	54, 112, 247, 259, 346	Zhu, Q	287, 351
Young, B	16	Zhang, F	153, 238, 257, 342	Zhu, S	198
Young, E	304	Zhang, G	279, 307	Zhu, T	255
Young, G	269	Zhang, H	81, 104, 105, 161, 200, 249, 342, 357	Zhu, W	127
Young, M	262	Zhang, J	92, 125, 141, 226, 257, 281, 343	Zhu, Y	24, 64, 111, 158, 206, 213, 226, 255, 283, 307
Young, P	27, 135	Zhang, K	171, 377	Zieba, P	120
Young, S	42	Zhang, L	16, 76, 102, 122, 169, 218, 266, 280, 288, 316, 318, 327, 375	Ziebarth, J	278
Youqi, F	92, 323, 377	Zhang, Q	20, 88, 137, 254	Ziebell, T	171
Yu, C	113, 165	Zhang, R	33, 173, 272, 362	Ziegler, D	326
Yu, D	265	Zhang, S	35, 97, 315	Zikry, M	95, 283
Yu, G	181, 331	Zhang, T	131, 182, 233, 284, 339	Zimmerman, J	144, 189
Yu, H	55, 125, 247, 249, 331	Zhang, W	40, 137, 284	Zin, E	336
Yu, J	63, 71, 72, 86, 273	Zhang, X	24, 40, 64, 79, 111, 140, 158, 206, 208, 255, 275, 283, 307, 335	Zinkle, S	113, 251, 257, 356
Yu, L	36, 219	Zhang, Y	19, 35, 136, 150, 184, 185, 204, 255, 267, 284, 363, 379	Zografidis, C	53, 131
Yu, O	260	Zhang, Z	40, 41, 105, 113, 147, 161, 197, 210, 255, 284, 336, 340, 346, 357	Zolotoyabko, E	311
Yu, P	219, 368	Zhao, B	343	Zong, B	335, 376
Yu, W	363	Zhao, F	336	Zotov, N	126
Yu, Z	149, 213	Zhao, H	373, 378	Zou, J	21, 201, 281
Yu-Fu, L	27	Zhao, J	142, 188, 239, 290	Zoukel, A	335
Yuan, C	66	Zhao, L	110	Zschack, P	70, 162, 163
Yuan, Q	115, 162, 282	Zhao, M	215	Zschau, H	61
Yuan, W	101, 194, 195	Zhao, P	84	Zu, F	63
Yuan, Y	19	Zhao, R	33	Zu, G	86, 152, 201
Yucel, O	105, 205, 206, 249, 250, 368, 374, 375, 379	Zhao, S	378	Zuilhof, H	83, 253
Yueh-Tse, L	39	Zhao, X	348, 378	Zuo, L	261
Yuehui, H	323	Zhao, Y	25, 43, 46, 57, 111, 174, 184, 210, 213, 261, 370	Zuo, X	122, 327
Yue Qin, Q	19	Zhao, Z	287	Zuo, Y	287
Yueqin, Q	19	Zhaofeng, X	266	Zupan, M	178, 184
Yufang, Y	376	Zhen, Z	104	Zwirz, T	230
Yu Hsiang, H	167	Zheng, B	41, 155, 156, 211		
Yulai, G	298	Zheng, L	298		
Yumakgil, H	372	Zheng, W	36, 44		
Yun, A	365	Zheng, X	322		
Yun, T	19	Zheng, Y	316		
Yunnen, C	354, 355	Zheng, Z	44		
Yusufoglu, I	379	Zhengrong, Z	53		
Yusufoglu, Y	282	Zhian, Z	18		
Yves, S	113	Zhihong, L	19		
		Zhitao, X	203		
<b>Z</b>		Zholnin, A	266		
Zabaras, N	93, 110, 245, 332	Zhong, H	364		
Zabdyr, L	120	Zhong, J	267		
Zaefferer, S	224	Zhong, N	185		
Zaikov, Y	278, 335	Zhong, S	253		
Zaki, A	130	Zhong, Y	202		
Zaldivar-Cadena, A	229	Zhongxin, C	298		
Zambaldi, C	224	Zhou, C	24		
Zareii, M	358	Zhou, G	32, 262		
Zarouni, A	230	Zhou, J	20		
Zavattieri, P	144	Zhou, L	355		
Zavodinskiy, V	129	Zhou, M	82		
Zavodinsky, V	140, 320	Zhou, N	237, 272		
Zbib, H	189	Zhou, P	93, 118, 122		
Zeenberg, D	89	Zhou, R	28, 29, 257		
Zehetbauer, M	24, 111, 112	Zhou, S	379		
Zelante, F	130	Zhou, X	127		
Zeng, G	309	Zhou, Y	20, 40, 41, 111, 155, 211, 213, 221, 271, 362		
Zeng, K	74, 120, 167, 168, 217, 265	Zhouhua, J	206, 375		
Zeng, Q	229, 351				
Zeng, X	199, 300				
Zepada-Ruiz, L	321				
Zevgolis, E	53				



# TMS

## **Who We Are**

The Minerals, Metals & Materials Society (TMS) is the professional organization encompassing the entire range of materials science and engineering, from minerals processing and primary metals production to basic research and the advanced applications of materials. The Society's broad technical focus covers light metals; electronic, magnetic and photonic materials; extraction and processing; materials processing and manufacturing; and structural materials.

## **Our Members**

Included among TMS professional members are metallurgical and materials engineers, scientists, researchers, educators and administrators who work in industry, government and academia, as well as students. They hail from more than 70 countries on six continents.

## **Our Mission**

The mission of TMS is to promote the global science and engineering professions concerned with minerals, metals and materials. The Society works to accomplish its mission by providing technical learning and networking opportunities through interdisciplinary and specialty meetings; continuing education; publications, including four journals and proceedings; and its Web site.

**To learn more, visit [www.tms.org](http://www.tms.org) or [www.materialstechnology.org](http://www.materialstechnology.org).**

## **TMS**

184 Thorn Hill Road

Warrendale, PA 15086-7514 USA

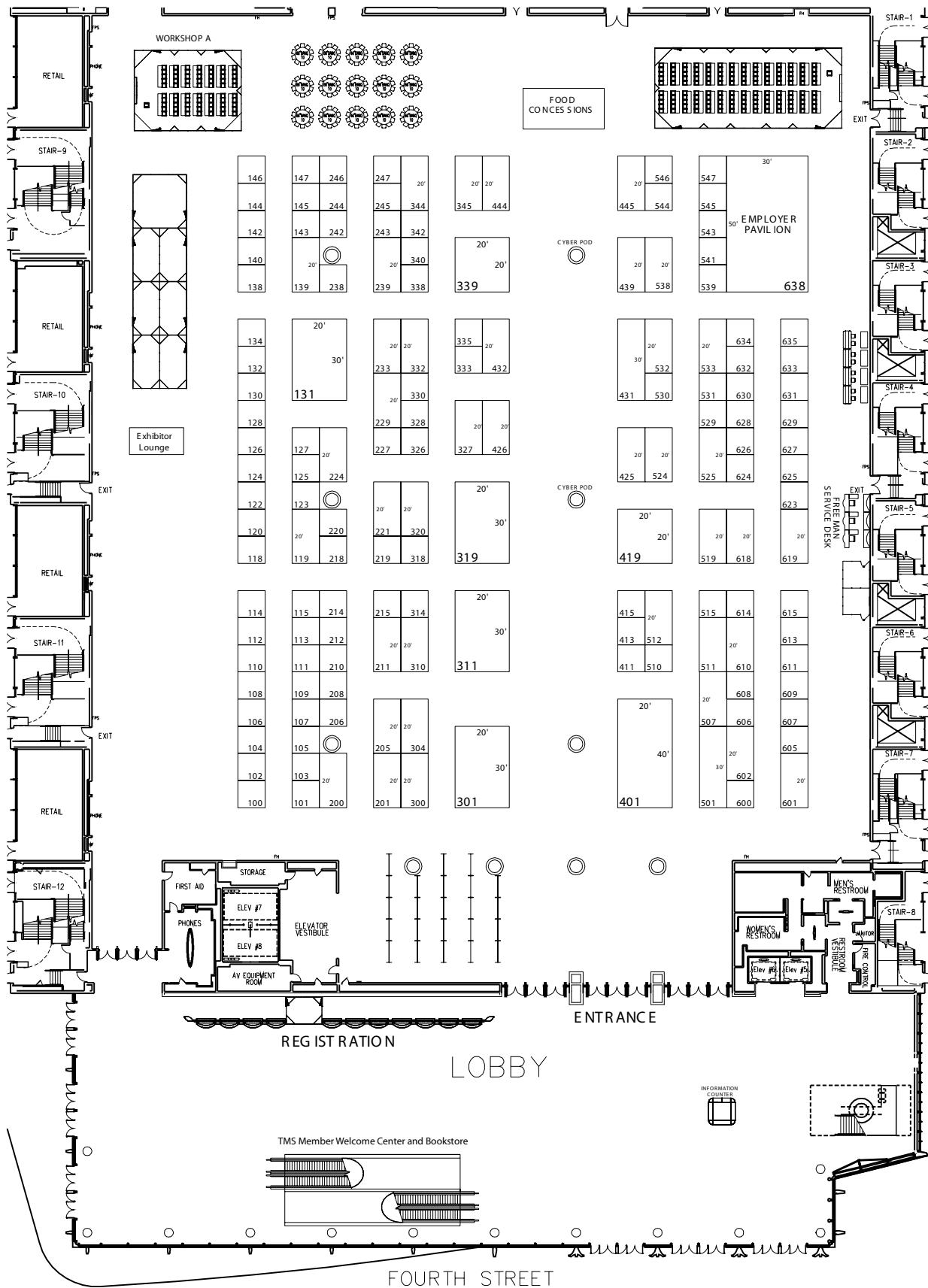
Telephone: (724) 776-9000 • (800) 759-4TMS

Fax: (724) 776-3770

E-mail: [tmsgeneral@tms.org](mailto:tmsgeneral@tms.org)



## Moscone Center West Hall - Level One

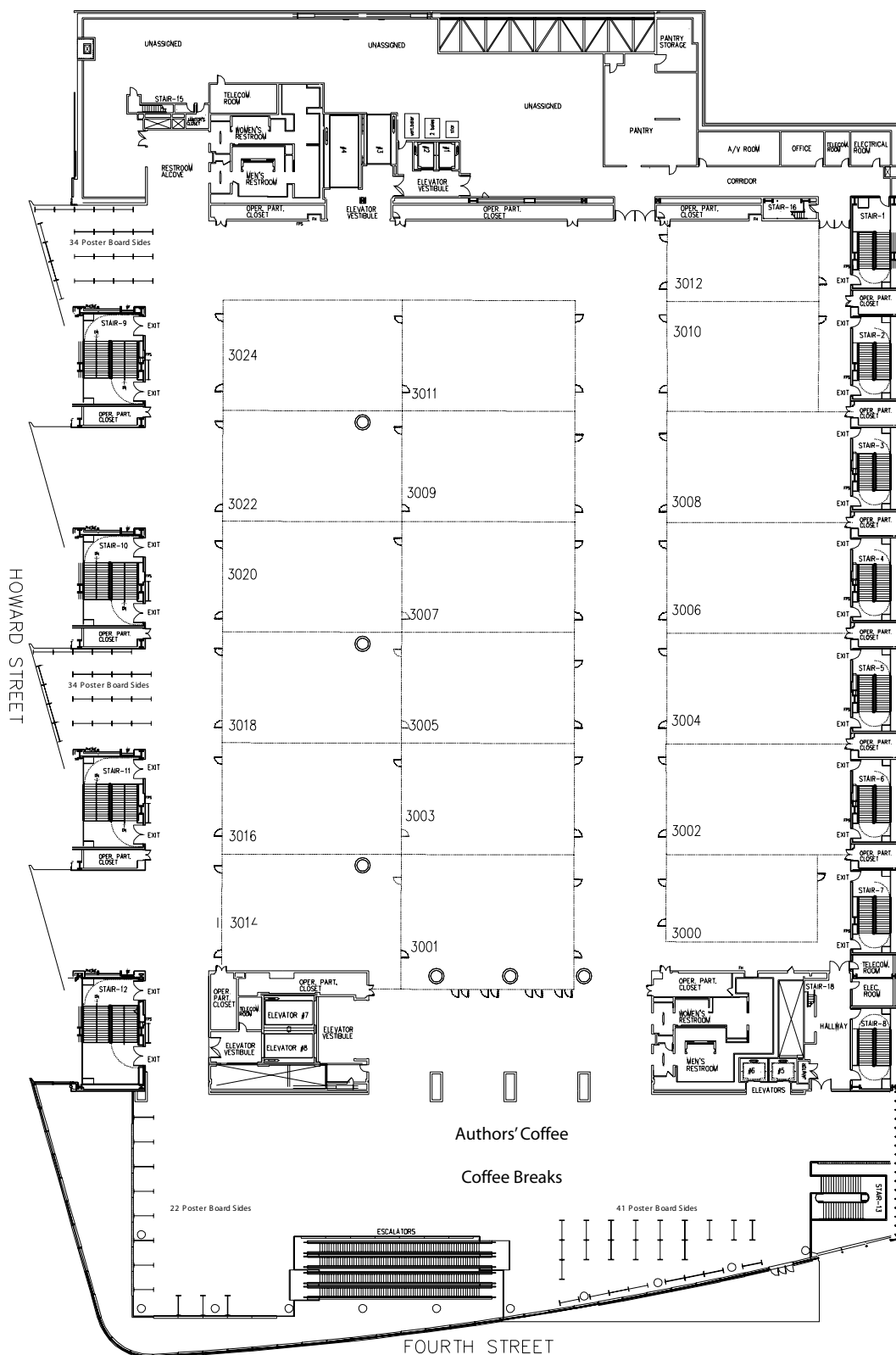




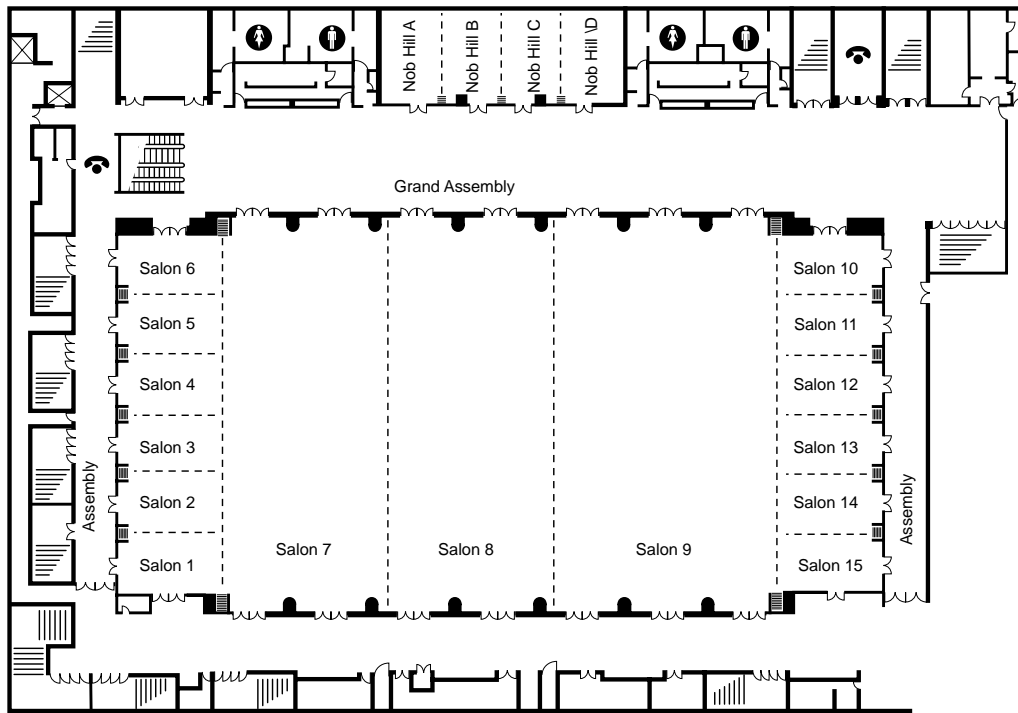


## Moscone Center West Hall - Level Three

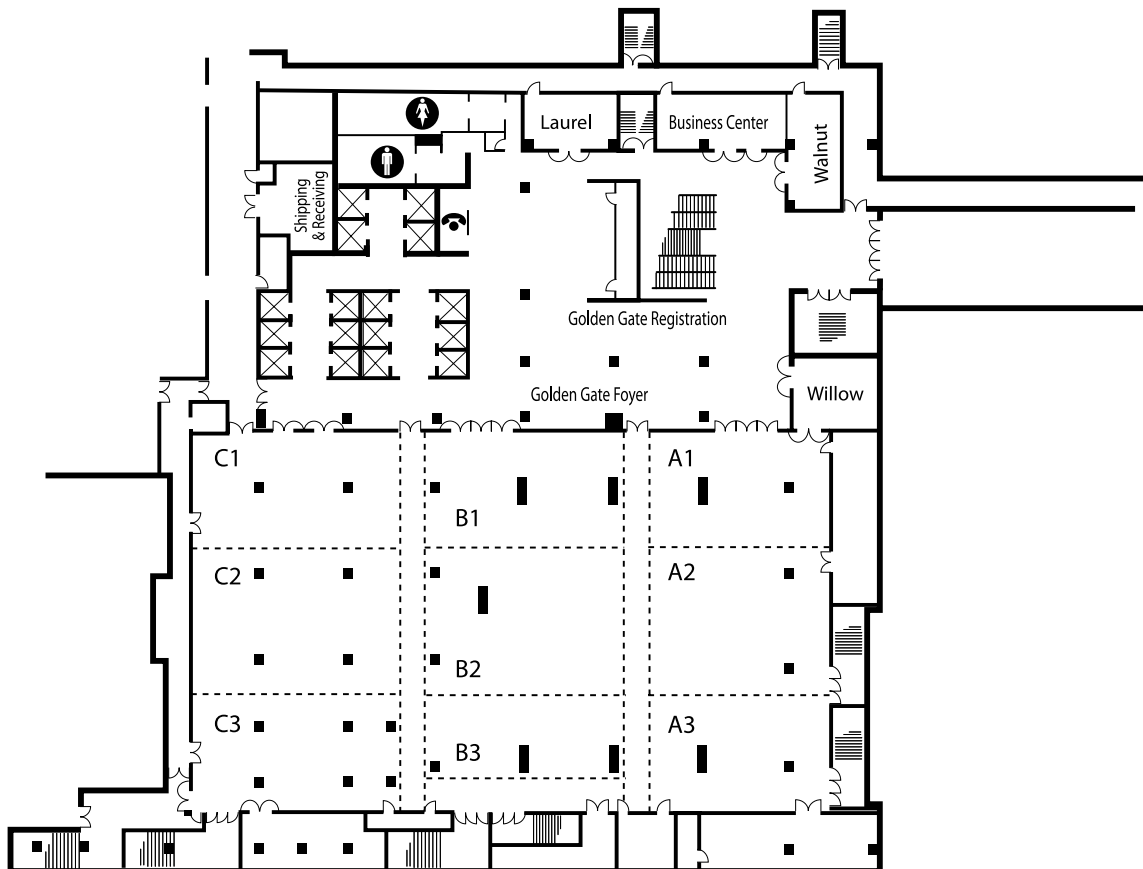
SCALE IN FEET



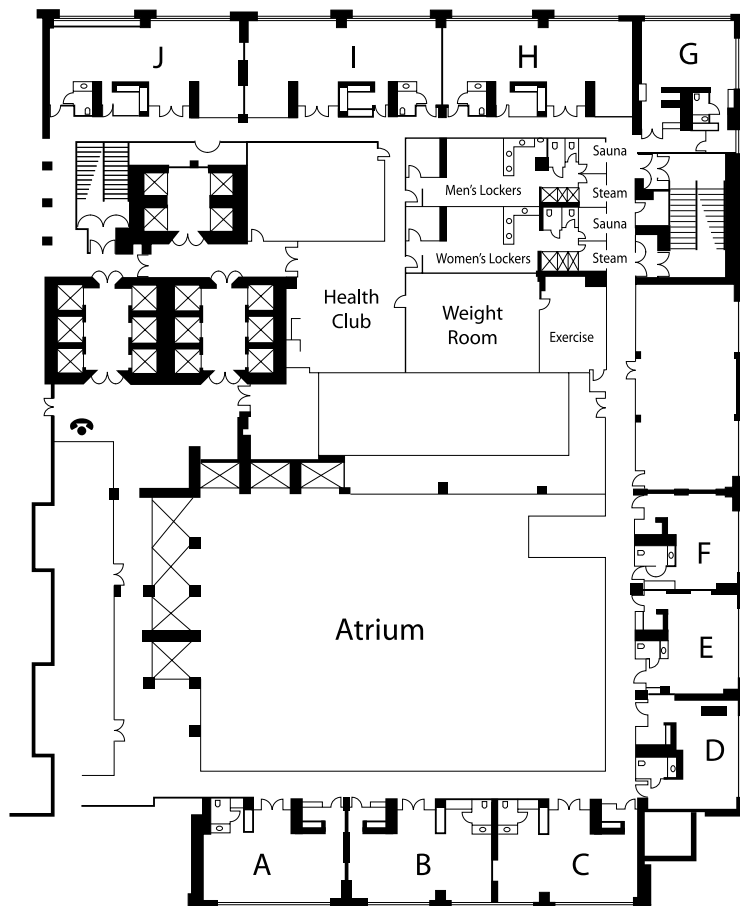
## San Francisco Marriott Yerba Buena Ballroom - Lower B2 Level



## San Francisco Marriott Golden Gate Hall - B2 Level



## San Francisco Marriott Pacific Floor - Fourth Floor



## San Francisco Marriott Sierra Floor - Fifth Floor

